Advances in Photosynthesis and Respiration
Volume 24

Photosystem I

The Light-Driven Plastocyanin:Ferredoxin Oxidoreductase

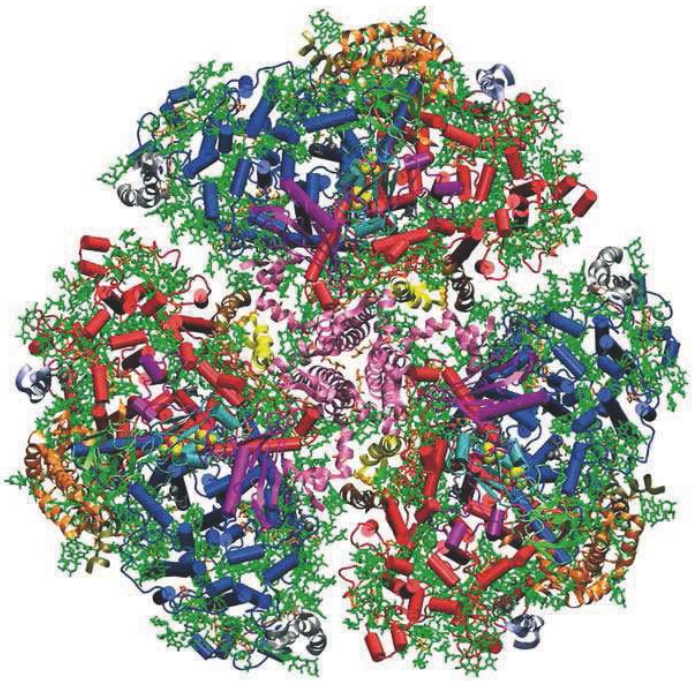

Edited by
John H. Golbeck

Springer

Photosystem I

The Light-Driven Plastocyanin:Ferredoxin Oxidoreductase

Advances in Photosynthesis and Respiration

VOLUME 24

The scope of our series, beginning with volume 11, reflects the concept that photosynthesis and respiration are intertwined with respect to both the protein complexes involved and to the entire bioenergetic machinery of all life. *Advances in Photosynthesis and Respiration* is a book series that provides a comprehensive and state-of-the-art account of research in photosynthesis and respiration. Photosynthesis is the process by which higher plants, algae, and certain species of bacteria transform and store solar energy in the form of energy-rich organic molecules. These compounds are in turn used as the energy source for all growth and reproduction in these and almost all other organisms. As such, virtually all life on the planet ultimately depends on photosynthetic energy conversion. Respiration, which occurs in mitochondrial and bacterial membranes, utilizes energy present in organic molecules to fuel a wide range of metabolic reactions critical for cell growth and development. In addition, many photosynthetic organisms engage in energetically wasteful photorespiration that begins in the chloroplast with an oxygenation reaction catalyzed by the same enzyme responsible for capturing carbon dioxide in photosynthesis. This series of books spans topics from physics to agronomy and medicine, from femtosecond processes to season long production, from the photophysics of reaction centers, through the electrochemistry of intermediate electron transfer, to the physiology of whole orgamisms, and from X-ray crystallography of proteins to the morphology or organelles and intact organisms. The goal of the series is to offer beginning researchers, advanced undergraduate students, graduate students, and even research specialists, a comprehensive, up-to-date picture of the remarkable advances across the full scope of research on photosynthesis, respiration and related processes.

The titles published in this series are listed at the end of this volume and those of forthcoming volumes on the back cover.

Photosystem I

The Light-Driven Plastocyanin:Ferredoxin Oxidoreductase

Edited by

John H. Golbeck
The Pennsylvania State University, USA

Springer

A C.I.P. Catalogue record for this book is available from the Library of Congress.

ISBN-10 1-4020-4256-6 (e-book)
ISBN-13 978-1-4020-4256-0 (e-book)

ISBN-10 1-4020-4255-8 (HB)
ISBN-13 978-1-4020-4255-3 (HB)

Published by Springer,
P.O. Box 17, 3300 AA Dordrecht, The Netherlands.

www.springer.com

Cover Figure Image. The trimeric structure of Photosystem I from cyanobacteria; the view direction is from the stromal side onto the membrane plane. The 12 proteins are shown in a backbone representation (PsaA, blue; PsaB, red; PsaC, pink; PsaD, turquoise; PsaE, light blue; PsaF, yellow; PsaI, dark pink; PsaJ, green; PsaK, gray; PsaL, brown; PsaM, orange and PsaX, light pink). The head groups of the chlorophylls are shown in yellow, their phytyl-tails have been omitted for clarity; the carotenoids are depicted in gray and the lipids in dark turquoise. Figure courtesy of Petra Fromme.

Printed on acid-free paper

From the Series Editor

Advances in Photosynthesis and Respiration

Volume 24, Photosystem I: The Light-Driven Plastocyanin: Ferredoxin Oxidoreductase

I am delighted to announce the publication, in *Advances in Photosynthesis and Respiration* (AIPH) Series, of ***Photosystem I: The Light-Driven Plastocyanin:Ferredoxin Oxidoreductase***, a book integrating biochemistry, biophysics and molecular biology of this photosystem that provides the necessary reducing power for carbon fixation in plants, algae and cyanobacteria. This volume was edited by a leading World authority John H. Golbeck of The Pennsylvania State University, University Park, PA, USA. Several earlier AIPH volumes (particularly Volume 10, authored by Bacon Ke) did include a good discussion of Photosystem I; however, the current book integrates all known aspects of this system, including its evolution. The current volume follows the 23 volumes listed below.

Published Volumes (1994–2005)

- *Volume 1:* ***Molecular Biology of Cyanobacteria*** (28 Chapters; 881 pages; 1994; edited by Donald A. Bryant, from USA);
- *Volume 2:* ***Anoxygenic Photosynthetic Bacteria*** (62 Chapters; 1331 pages; 1995; edited by Robert E. Blankenship, Michael T. Madigan and Carl E. Bauer, from USA);
- *Volume 3:* ***Biophysical Techniques in Photosynthesis*** (24 Chapters; 411 pages; 1996; edited by the late Jan Amesz and the late Arnold J. Hoff, from The Netherlands);
- *Volume 4:* ***Oxygenic Photosynthesis: The Light Reactions*** (34 Chapters; 682 pages; 1996; edited by Donald R. Ort and Charles F. Yocum, from USA);
- *Volume 5:* ***Photosynthesis and the Environment*** (20 Chapters; 491 pages; 1996; edited by Neil R. Baker, from UK);
- *Volume 6:* ***Lipids in Photosynthesis: Structure, Function and Genetics*** (15 Chapters; 321 pages; 1998; edited by Paul-André Siegenthaler and Norio Murata, from Switzerland and Japan);
- *Volume 7:* ***The Molecular Biology of Chloroplasts and Mitochondria in Chlamydomonas*** (36 Chapters; 733 pages; 1998; edited by Jean David Rochaix, Michel Goldschmidt-Clermont and Sabeeha Merchant, from Switzerland and USA);
- *Volume 8:* ***The Photochemistry of Carotenoids*** (20 Chapters; 399 pages; 1999; edited by Harry A. Frank, Andrew J. Young, George Britton and Richard J. Cogdell, from USA and UK);
- *Volume 9:* ***Photosynthesis: Physiology and Metabolism*** (24 Chapters; 624 pages; 2000; edited by Richard C. Leegood, Thomas D. Sharkey and Susanne von Caemmerer, from UK, USA and Australia);
- *Volume 10:* ***Photosynthesis: Photobiochemistry and Photobiophysics*** (36 Chapters; 763 pages; 2001; authored by Bacon Ke, from USA);
- *Volume 11:* ***Regulation of Photosynthesis*** (32 Chapters; 613 pages; 2001; edited by Eva-Mari Aro and Bertil Andersson, from Finland and Sweden);
- *Volume 12:* ***Photosynthetic Nitrogen Assimilation and Associated Carbon and Respiratory Metabolism*** (16 Chapters; 284 pages; 2002; edited by Christine Foyer and Graham Noctor, from UK and France);
- *Volume 13:* ***Light Harvesting Antennas*** (17 Chapters; 513 pages; 2003; edited by Beverley Green and William Parson, from Canada and USA);
- *Volume 14:* ***Photosynthesis in Algae*** (19 Chapters; 479 pages; 2003; edited by Anthony Larkum, Susan Douglas and John Raven, from Australia, Canada and UK);
- *Volume 15:* ***Respiration in Archaea and Bacteria: Diversity of Prokaryotic Electron Transport Carriers*** (13 Chapters; 326 pages; 2004; edited by Davide Zannoni, from Italy);
- *Volume 16:* ***Respiration in Archaea and Bacteria 2: Diversity of Prokaryotic Respiratory Systems***

(13 chapters; 310 pages; 2004; edited by Davide Zannoni, from Italy);

- *Volume 17:* ***Plant Mitochondria: From Genome to Function*** (14 Chapters; 325 pages; 2004; edited by David A. Day, A. Harvey Millar and James Whelan, from Australia);
- *Volume 18:* ***Plant Respiration: From Cell to Ecosystem*** (13 Chapters; 250 pages; 2005; edited by Hans Lambers, and Miquel Ribas-Carbo, 2005; from Australia and Spain);
- *Volume 19:* ***Chlorophyll a Fluorescence: A Signature of Photosynthesis*** (31 Chapters; 817 pages; 2004; edited by George C. Papageorgiou and Govindjee, from Greece and USA);
- *Volume 20:* ***Discoveries in Photosynthesis*** (111 Chapters; 1304 pages; 2005; edited by Govindjee, J. Thomas Beatty, Howard Gest and John F. Allen, from USA, Canada and Sweden (& UK));
- *Volume 21:* ***Photoprotection, Photoninhibition, Gene Regulation and Environment Photosynthesis*** (21 Chapters; 380 pages; 2005; edited by Barbara Demmig-Adams, Willam Adams III and Autar K. Mattoo, all from USA);
- *Volume 22:* ***Photosystem II: The Light-Driven Water:Plastoquinone Oxidoreductase*** (34 Chapters; 786 pages; 2005; edited by Thomas J. Wydrzynski and Kimiyuki Satoh, from Australia and Japan, respectively);
- *Volume 23:* ***Structure and Function of the Plastids*** (27 Chapters; 576 pages; 2005; edited by Robert Wise and J. Kenneth Hoober, both from USA)

The next volume in the AIPH Series, also scheduled for publication in 2006, is:

- *Volume 25:* ***Chlorophylls and Bacteriochlorophylls: Biochemistry, Biophysics, Functions and Applications*** (37 Chapters; number of pages not yet available; edited by Bernhard Grimm, Robert Porra, Wolfhart Rüdiger and Hugo Scheer, from Germany and Australia)

Further information on these books and ordering instructions can be found at <http://www. springeronline. com> under the Book Series 'Advances in Photosynthesis and Respiration'. Table of Contents of the earlier volumes (1–19) may be found at <http://www.life. uiuc.edu/govindjee/photosynSeries/ttocs.html>. Special discounts are available to members of the International Society of Photosynthesis Research, ISPR (<http://www.photosyn-thesisresearch.org/>).

About Volume 24: Photosystem I: The Light-Driven Plastocyanin:Ferredoxin Oxidoreductase

This book summarizes, in 40 authoritative chapters, the advances made in the last decade in the biophysics, biochemistry, and molecular biology of the enzyme known as Photosystem I, the light-driven plastocyanin:ferredoxin oxidoreductase. Photosystem I participates along with Photosystem II in harvesting solar energy to supply photosynthetic organisms with stored chemical energy in the form of ATP and stored reducing power in the form of NADPH for processes such as metabolism, growth, and reproduction. This volume is a unique compilation of chapters that include information on molecular architecture, protein-pigment interactions, excitation and electron transfer dynamics, protein-cofactor interactions, kinetics of electron transfer and bioassembly of proteins and cofactors. The volume begins with a series of historical perspectives that provide a solid background to the field, and ends with information on modelling of light-harvesting and electron transfer reactions, and the evolution of the reaction center. Particular attention is paid to spectroscopy, including the theory of the measurement and the interpretation of the data. The book is intended to be a comprehensive and up-to-date source of background information on the Photosystem I reaction center for seasoned researchers, those who are just entering the field, Ph.D. students, researchers and undergraduates in the fields of biophysics, biochemistry, microbiology, agriculture, and ecology.

This book complements "Photosystem II: The Light-Driven Water:Plastoquinone Oxidoreductase" edited by Thomas J. Wydrzynski and Kimiyuki Satoh. Electrons are transferred from water to plastoquinone by Photosystem II. Plastoquinol transfers electrons to Photosystem I via the cytochrome b_6f complex, and Photosystem I then reduces $NADP^+$.

Photosystem I: The Light-Driven, Plastocyanin: Ferredoxin Oxidoreductase is divided into the following topics: Historical Perspectives (4 chapters); Molecular Architecture (4 chapters); Pigment-Protein Interactions (3 chapters); Excitation Dynamics and Electron Transfer Processes (2 chapters); Modification of the Cofactors and their Environments (2 chapters); Spectroscopic Studies of the Cofactors (8 chapters); Kinetics of Electron Transfer (6 chapters); Biosynthetic Processes (3 chapters); Modeling of Photosystem I Reactions (4 chapters); Cyclic Photophosphorylation (1 chapter); Photoinhibition (1 chapter); and Evolution

(2 chapters). For details see Table of Contents (pp. xi–xxiii) of this extraordinary book.

This book is written by 80 international authorities from 13 countries. It is my privilege to publicly express my thanks to all of them (listed in alphabetical order):

Mikhail **A**ntonkine; James **B**arber; Roberto Bassi; Adam Ben-Shem; Thomas Bibby; Robert Blankenship; Egbert Boekema; Jacques Breton; Donald Bryant; Sergey K. **C**hamorovsky; Roberta Croce; Jan **D**ekker; Bruce A. Diner; Fredrich Drepper; James Duncan; P. Leslie Dutton; Alexander **F**ish; Petra Fromme; John H. **G**olbeck; Carlos Gómez–Moreno; Ingo Grotjohann; Anna **H**aldrup; Toshiharu Hase; Gary Hastings; Manuel Hervás; Michael Hippler; John K. Hurley; Poul Erik **J**ensen; Giles Johnson; Anne Joliot; Pierre Joliot; Navassard **K**arapetyan; Bacon Ke; David Knaff; Konstantin Kogan; Gerd Kothe; Roman Kouřil; Wolfgang **L**ubitz; Richard **M**alkin; Mahir D. Mamedov; Paul Mathis; David Mauzerall; Milagros Medina; Fernando P. Molina-Heredia; Tomas Morosinotto; Christopher C. Moser; José A. **N**avarro; Rachel Nechushtai; Nathan Nelson; Jon Nield; Oleg **P**oluektov; Velupillaimani M. **R**amesh; Fabrice Rappaport; Jason Raymond; Kevin Redding; Thomas Renger; Jean-David Rochaix; Miguel de la Rosa; Yumiko **S**akuragi; Anthony San Pietro; Kenneth Sauer; Sergei Savikhin; Henrik Vibe Scheller; Eberhard Schlodder; Peter Schürmann; Alexey Yu. Semenov; Pierre Sétif; Gaozhong Shen; Vladimir Shinkarev; Anatoli Ya. Shkuropatov; Vladimir A. Shuvalov; Kintake Sonoike; Dietmar Stehlik; Marion **T**hurnauer; Gordon Tollin; Arthur **v**an der Est; Rienk van Grondelle; L. G. Vasilieva; Andrew **W**ebber; and Andrei G. **Y**akovlev

The URL for this book is at:
http://www.life.uiuc.edu/Govindjee/newbook/Volume%2024.html

A Bit of History – From there to here

Just to give a flavor of history, I list below some discoveries. [For historical perspectives, I refer the readers to chapters 1–4 (Anthony San Pietro; Richard Malkin; Bacon Ke; and Paul Mathis & Kenneth Sauer) in this volume.]

- *Discovery of P700, reaction center of Photosystem I (PS I) in The Netherlands.* Bessel Kok (1918–1978; see Kok, Biochim. Biophys. Acta 22: 399–401, 1956), while in Wageningen, The Netherlands, discovered, in several photosynthetic organisms, a light-induced absorbance decrease that had its highest long-wavelength peak at 700 nm (labeled as P700).
- *Two-Light Effects in USA in Baltimre (MD) and Urbana (IL); hypothesis in Cambridge, UK*. Kok and George Hoch, from Baltimore, MD presented in 1960 (see McElroy WD and Glass B (eds) (1961) A Symposium on Light, and Life, pp 397–423. The Johns Hopkins Press, Baltimore, MD), a two-light reaction scheme at about the time Robin Hill and Fay Bendall, in UK, were publishing his now famous Z-scheme (Nature 186: 136–137, 1960). Kok (Plant Physiol. 34: 184–192, 1959) had already shown, in cyanobacteria, that red light oxidized P700 and orange light reduced oxidized P700. He had already related this two-light effect to the Emerson Enhancement effect, discovered earlier by Emerson et al. (Proc. Natl. Acad. Sci., USA, 43: 133–143, 1957).
- *Naming of Photosystem I in Leiden, The Netherlands*. Louis N. M. Duysens et al. (Nature, 190: 510–511, 1961) provided the crucial evidence for the two light reaction two-pigment system scheme, working in series. In the red alga *Porphyridium cruentum*, red light absorbed by chlorophyll *a* oxidized a cytochrome. When green light, absorbed by phycoerythrin, was superimposed, the oxidized cytochrome became reduced. Duysens et al. called the red light 'light 1,' and the chlorophyll *a*-containing system, 'system 1.' The other light, they had called 'light 2,' was absorbed by 'system 2.'
- *Crystal structure of Photosystem I in Berlin, Germany*. P. Jordan et al. (Nature, 411: 909–917, 2001) were the first to resolve the X-ray crystallographic structure of Photosystem I of a thermophilic cyanobacterium for a 3D structure at 2.5 Å resolution.

(For a time-line on oxygenic photosynthesis, see Govindjee and David Krogmann (2004) Photosynthesis Research 80: 15-57.)

Future AIPH Books

The readers of the current series are encouraged to watch for the publication of the forthcoming books (not necessarily arranged in the order of future appearance):

- **Biophysical Techniques in Photosynthesis II** (Editors: Thijs J. Aartsma and Jörg Matisyk);

- **Photosynthesis: A Comprehensive Treatise; Physiology, Biochemistry, Biophysics and Molecular Biology**, **Part 1** (Editors: Julian Eaton-Rye and Baishnab Tripathy); and
- **Photosynthesis: A Comprehensive Treatise; Physiology, Biochemistry, Biophysics and Molecular Biology, Part 2** (Editors: Baishnab Tripathy and Julian Eaton-Rye)
- **The Purple Photosynthetic Bacteria** (Editors: C. Neil Hunter, J. Thomas Beatty, Fevzi Daldal and Marion Thurnauer)

In addition to these contracted books, we are in touch with prospective Editors for the following books:

- Sulfur Metabolism in Photosynthetic Systems
- Molecular Biology of Cyanobacteria II.
- ATP Synthase
- Genomics and Proteomics
- Hydrogen Evolution
- Molecular Biology of Stress
- Global Aspects, Parts 1 and 2
- Artificial Photosynthesis

Readers are encouraged to send their suggestions for these and future volumes (topics, names of future editors, and of future authors) to me by E-mail (gov@uiuc.edu) or fax (1-217-244-7246).

In view of the interdisciplinary character of research in photosynthesis and respiration, it is my earnest hope that this series of books will be used in educating students and researchers not only in Plant Sciences, Molecular and Cell Biology, Integrative Biology, Biotechnology, Agricultural Sciences, Microbiology, Biochemistry, and Biophysics, but also in Bioengineering, Chemistry, and Physics.

Acknowledgments

I take this opportunity to thank and congratulate John H. Golbeck for his outstanding and painstaking editorial work. I thank all the 80 authors (see the list above) of volume 24 of the AIPH Series: without their authoritative chapters, there would be no such volume. We owe thanks to Jacco Flipsen, Noeline Gibson and André Tournois (both of Springer) for their friendly working relation with us that led to the production of this book. I thank Seema Koul (of Techbooks, New Delhi) for her outstanding work on this book; she communicated wonderfully well at every step of the process. Thanks are also due to Jeff Haas (Director of Information Technology, Life Sciences, University of Illinois at Urbana-Champaign, UIUC), Evan DeLucia (Head, Department of Plant Biology, UIUC) and my dear wife Rajni Govindjee for their constant support.

January 26, 2006

Govindjee
Series Editor, *Advances in Photosynthesis and Respiration*
University of Illinois at Urbana-Champaign,
Department of Plant Biology
Urbana, IL 61801-3707, USA
E-mail: gov@uiuc.edu;
URL: http://www.life.uiuc.edu/govindjee

A photograph of **Govindjee** (taken in 2004) with a letter box in the Department of Botany, University of Allahabad; this letter box was used by Govindjee during his pre-PhD days (1952–1956).

Govindjee, the Series Editor of 'Advances in Photosynthesis and Respiration', uses only one name; he was born on October 24, 1932, in Allahabad, India. His father, along with other reformers of that time, belonging to the 'Arya Samaj Movement', dropped their family names, since they reflected the 'caste' of the person. The family name was 'Asthana', a member of the 'Kayastha', who were mostly professionals, including being teachers. Govindjee (whose name was then written as Govind Ji) obtained his B.Sc. (Chemistry, Biology) and M.Sc. (Botany, Plant Physiology) in 1952 and 1954, from the University of Allahabad, India, both in the first division. He came to USA in September, 1956 to work with Robert Emerson; after Emerson's death on February 4, 1959, he became a graduate student of Eugene Rabinowitch, receiving his Ph.D. (Biophysics), in 1960, from the University of Illinois at Urbana-Champaign (UIUC), IL, U.S.A. He has since focused his research mainly on the function of "Photosystem II" (PS II, the water:plastoquinone oxidoreductase), particularly primary photochemical events, the unique role of bicarbonate on the acceptor side of PS II, and the mechanism of 'photoprotection' in plants and algae, using lifetime of chlorophyll a fluorescence measurements. His research on Photosystem I (the topic of this book) has included low temperature fluorescence spectroscopy (1963–1970), and one of the first measurements on its primary photochemistry (J.M. Fenton, M.J. Pellin, Govindjee, and K. Kaufmann (1979) Primary Photochemistry of the Reaction Center of Photosystem I. FEBS Lett. 100: 1–4.; and M.R. Wasielewski, J.M. Fenton, and Govindjee (1987) The Rate of Formation of P700 [$^{+}$]-Ao[$^{-}$] in Photosystem I Particles from Spinach as Measured by Picosecond Transient Absorption Spectroscopy. Photosynth. Res. 12: 181–190.). For further details, on his discoveries and research, see his biography in earlier Advances in Photosynthesis and Respiration volumes. His current focus, however, is on the "History of Photosynthesis Research" and in 'Photosynthesis Education'. He has served the UIUC as an Assistant Professor, Associate Professor and Professor (1961–1999). Since 1999, he has been Professor Emeritus of Biochemistry, Biophysics and Plant Biology at the UIUC. His honors include: Fellow of the American Association of Advancement of Science (1976); Distinguished Lecturer of the School of Life Sciences, UIUC (1978); Fellow and Life Member of the National Academy of Sciences (Allahabad, India, 1978); President of the American Society for Photobiology (1980–1981); Fulbright Senior Lecturer (1996–1997); and Honorary President of the 2004 International Photosynthesis Congress (Montréal, Canada).

Contents

Preface

Photosystem I: The Light-Driven, Plastocyanin:Ferredoxin Oxidoreductase is the 24th volume in the series Advances in Photosynthesis and Respiration (Series Editor, Govindjee). It is one of the two volumes that deal with the photosynthetic reaction centers in oxygenic photosynthetic organisms. The other, Volume 22, is Photosystem II: The Light-Driven Water:Plastoquinone Oxidoreductase, edited by Thomas J. Wydrzynski and Kimiyuki Satoh.

The realization that two independent photochemical reactions are required in oxygenic photosynthesis came about through a series of biophysical observations, particularly with the discovery of the Enhancement Effect in oxygen evolution by Robert Emerson in 1957 that culminated in the codification of the 'Z-scheme' by Robin Hill and Fay Bendall in 1960. The terminology in use today was coined by Lou Duysens, who, in 1961, proposed a hypothetical scheme for photosynthesis composed of two photochemical pigment systems that were termed 'system I' and 'system II'. In the banner year of 1956, three components of what we know as Photosystem I were discovered: Bessel Kok found an absorption change at 700 nm that is now attributed to the oxidation of the primary donor, P700; Mordhay Avron and André Jagendorf isolated a $TPNH_2$ diaphorase, a soluble enzyme that is now known as $NADP^+$:ferredoxin oxidioreductase; and Anthony San Pietro and Helga Lang purified a soluble protein termed PPNR (photosynthetic pyridine nucleotide reductase), a soluble enzyme that is now known as ferredoxin (a story told in detail in Chapter 1). The last soluble component associated with Photosystem I was discovered in 1961 when Sakae Katoh and colleagues isolated plastocyanin, which was then proposed to function as a redox carrier in the Hill reaction and is now known to function as the soluble electron donor to $P700^+$. The physical separation from the membrane of the Photosystem I reaction center as a discrete pigment-protein complex was accomplished by Keith Boardman and Jan Anderson who, in 1964, made use of the detergent digitonin to isolate the 'D-144 particle'. This advance set the stage for dealing with Photosystem I as a distinct pigment-protein complex. By 1970, the focus had switched to the bound cofactors, and the race was on to find the primary electron acceptor, the story of which is provided by the original investigators in Chapters 2 through 4 of this volume.

This book comprises 40 chapters, authored by 80 international experts in the field. The highly diverse nature of Photosystem I is evident in the multiplicity of skills and techniques that have proven necessary to understand how the energy of a photon of visible light is converted into the stable products of oxidized plastocyanin (or cytochrome c_6) and reduced ferredoxin (or flavodoxin). This book is arranged into 11 sections. Following a section on '*Historical Perspectives*', the book is divided into sections that deal with '*Molecular Architecture*', '*Pigment-Protein Interactions*', '*Excitation Dynamics and Electron Transfer Processes*', '*Modification of the Cofactors*', '*Spectroscopic Studies of the Cofactors*', '*Kinetics of Electron Transfer*', '*Biosynthetic Processes*', '*Modeling of Photosystem I Reactions*', '*Related Processes*', and '*Evolution of Photosystem I*'.

The volume covers Photosystem I in sufficient depth so that it is useful not only for molecular biologists, biochemists and biophysicists, but also for plant physiologists, ecologists and those interested in applying lessons learned from natural photosynthesis to artificial photosynthetic systems. I had asked each author to provide an in-depth introduction so that each topic is accessible to the beginners. I had also asked that each author provide sufficient depth so that each of the topics is of value to seasoned researchers. I fully expect that the book will be a source of information not only for undergraduate and graduate students but also for postdoctoral scientists and those who are entering the field for the first time.

I have made no attempt, beyond the most cursory, to enforce a common nomenclature of the proteins or cofactors that comprise Photosystem I. Conventions establish themselves by consensus over time, and to large degree this has happened in this field. Nevertheless there are sub-discipline norms, and a note is made in the 'nomenclature' footnote of those chapters where the nomenclature differs from convention. This volume is not meant to be a textbook in the sense that authors of textbooks strive to give the final word, and to achieve closure, on a topic. On the contrary, no attempt is made to achieve a forced reconciliation or synthesis of controversial issues. Instead, the reader is shown exactly where the points of disagreement lie, and hence, where the boundary of the research frontier is drawn. Such is the nature of a thriving, dynamic discipline. Indeed, it is my hope that this book will stimulate not only the research necessary to solve these problems, but for others to enter this exciting field.

I would like to take this opportunity to acknowledge the authors for providing uniformly excellent chapters. Each author is a leading authority in his/her field, and each has generously offered the time and effort to make this book a success. I thank Petra Fromme for the striking view of the X-ray crystal structure of cyanobacterial Photosystem I which appears on the front cover. I would like to thank my mentors, Anthony San Pietro and Bessel Kok, and my closest colleagues and collaborators, Joseph Warden, Parag Chitnis, Lee McIntosh, Alyosha Semenov, Art van der Est, Dietmar Stehlik and (especially) Don Bryant, all of whom have contributed to the field as well as to my development as a research scientist. I wish to thank my students and postdoctoral scientists for their hard work on Photosystem I over the past 20 years. In particular, I would like to single out Ilya Vassiliev, with whom I have published 30 papers. Ilya was tragically struck by a car and died as this book was being sent to press. Finally, I very much appreciate the support my wife, Carolyn Wilhelm, who (as always) provides assistance and encouragement in all of my endeavors.

I also acknowledge the help received from Noeline Gibson and Jacco Flipson (of Springer, Dordrecht, The Netherlands), from Seema Koul (of TechBooks, New Delhi, India) and from Govindjee (of the University of Illinois at Urbana-Champaign).

John H. Golbeck
Department of Biochemistry and Molecular Biology
and Department of Chemistry
The Pennsylvania State University
University Park, PA 16802, USA
E-mail: jhg5@psu.edu

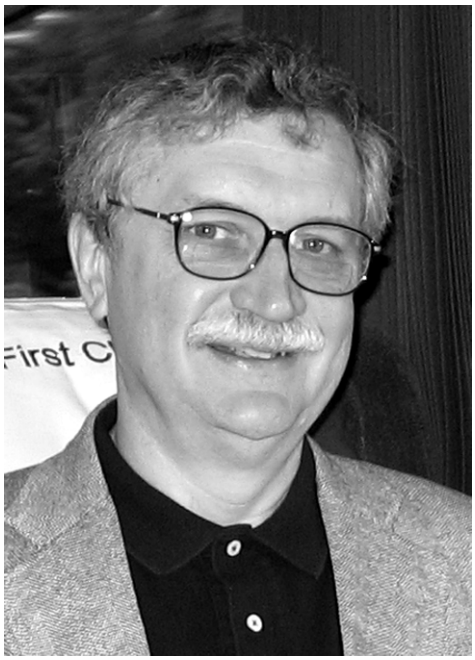

John H. Golbeck

John H. Golbeck is Professor of Biochemistry and Biophysics and Professor of Chemistry at The Pennsylvania State University (Penn State), University Park, PA. John's research interests lie in the assembly, structure, function, and modification of Type I reaction centers. John was born in Wisconsin in 1949. He received his Ph.D. in Biological Chemistry from Indiana University, Bloomington IN, under the supervision of Anthony San Pietro for work related to the bound Fe/S clusters in Photosystem I. His postdoctoral studies at Martin Marietta Laboratories, Baltimore, MD, with Bessel Kok centered around the identification of F_X (A_2) as a third bound Fe/S cluster in Photosystem I. After a five year (ad)venture into industrial research, John went back to university life as Professor in the Chemistry Dept. at Portland State University, Portland, OR, where he focused on isolating the P700-F_X core and on the resolution and reconstitution of the stromal ridge proteins, PsaC, PsaD and PsaE. In 1990, he moved to the Biochemistry Department at the University of Nebraska, Lincoln, NE, where he worked to identify the ligands to the F_A and F_B clusters of PsaC. Six years later, he accepted a position in the Dept. of Biochemistry and Molecular Biology at Penn State, where he studied quinone biosynthetic pathway mutants as a means to biologically introduce novel quinones into Photosystem I. Since 2004, he has held an appointment in the Department of Chemistry at Penn State. John spent sabbatical leaves at Rensselaer Polytechnic Institute (1984), the Centre d'Etudes Nucléaires de Saclay (1992), and most recently at the Freie Universität, Berlin (2002/2003). He has published 120 articles in refereed journals and 10 invited reviews and book chapters. His current research interests involve the genes and proteins that assemble the bound Fe/S clusters, the protein factors that confer redox potentials to organic and inorganic cofactors, and the structural makeup of Type I reaction centers from anaerobic bacteria. His long-term goal lies in modifying Photosystem I to produce H_2. John is a member of the American Society for Biochemistry and Molecular Biology, the Biophysical Society of America, and the International Society for Photosynthesis Research. He presently serves as Secretary for the International Society for Photosynthesis Research. Further information on him and his work can be found at his web site: http://www.bmb.psu.edu/faculty/golbeck/golbeck.html

Dedication: A Tribute to Lee McIntosh

Lee McIntosh (1950–2004)

With the death of Lee McIntosh on June 18, 2004, the scientific community lost an esteemed and valued colleague. Lee's passion for science was apparent to whomever he met, and it never wavered, even through the 5 years that he suffered from chronic lymphocytic leukemia. Lee was born in Los Angeles in 1950. He received his Ph.D. from the University of Washington, Seattle, WA, with Bastiaan J.D. Meeuse and he performed postdoctoral research at Harvard University, Boston, MA, with Laurie Bogorad, where he was a Maria Moors Cabot Postdoctoral Research Fellow. In 1983, Lee worked at the University of Geneva, Switzerland, under a European Molecular Biology Fellowship, and in 1981, he joined the Plant Research Laboratory at Michigan State University, East Lansing, MI. Lee received the Distinguished Faculty award in 2002. At the time of his passing, he was a Distinguished Professor of Biochemistry and Molecular Biology.

Lee's scientific accomplishments were many and varied. He was one of the pioneers in applying the techniques of modern molecular biology to understanding the biochemical mechanisms of photosynthesis. In a wonderful achievement at the time, Lee and his collaborators used directed mutagenesis to identify the electron donor to $P680^+$ as Tyr161 on the D1 polypeptide. Lee's primary interest was focused on plant mitochondria, particularly in the genetics and function of the alternative oxidase (AOX) in plant respiration. His work on Photosystem I involved modifying the ligands to the bound Fe/S clusters as a means of establishing the pathway of electron transfer through F_X, F_B, and F_A. A suppressor mutation of a cysteine mutant to F_A led to his last scientific paper, the identification of a gene that codes for a transcriptional repressor that controls the biosynthesis of Fe/S clusters in cyanobacteria.

Lee's long-term goal was to determine how organelles communicated with each other, particularly how signals were transduced from the mitochrondrion to the nucleus as a way of regulating mitochondrial energy and carbon metabolism. His discoveries were always made in the context of the larger picture, which was to understand at the molecular level the control of energy and carbon flow in plants. His approach was to modify specific proteins and to create new transgenic plant lines in the attempt to dissect the pathways by which nuclear genes are regulated by organelles. These transgenic plants allowed him to study the function of specific nuclear-encoded mitochondrial genes as well as the means by which the mitochondrion signals the nucleus.

Lee was a scientist of uncommon skill and uncompromising integrity. He never tired of pointing out that genetics (and not biochemistry or biophysics) is the engine for making new discoveries in biology. His favorite saying (uttered when a particularly bad idea was put forward) was '*you know, you really don't want to go down that path*'. Lee enjoyed his farm, Walnut Rise, where he and his son Angus Robin raised 30 to 40 Shetland sheep as breeding stock, and for their fleece.

His loss is mourned by all of us who had the pleasure of working with him.

Author Index

Color Plates

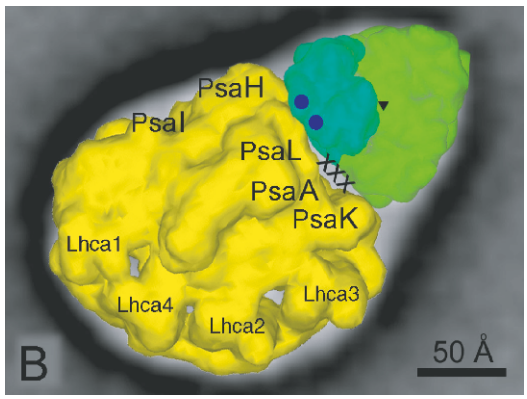

Fig. 1. Model of the PSI-LHCII complex. Assignment of the supercomplex by fitting of the high-resolution structures of PS I (yellow) and trimeric LHCII (green). One LHCII monomer is indicated in blue-green, blue dots mark the spots where the ends of the helices A and B are closest to PS I in projection and the center of the trimer is indicated by a triangle. The part of subunits PSI-A, -H, -I, -K and -L closest to the LHCII trimer has been indicated. Open space in the interfaces of PS I and LHCII is marked by crosses. (Modified from Kouřil et al., 2005.) See Chapter 5, p. 43.

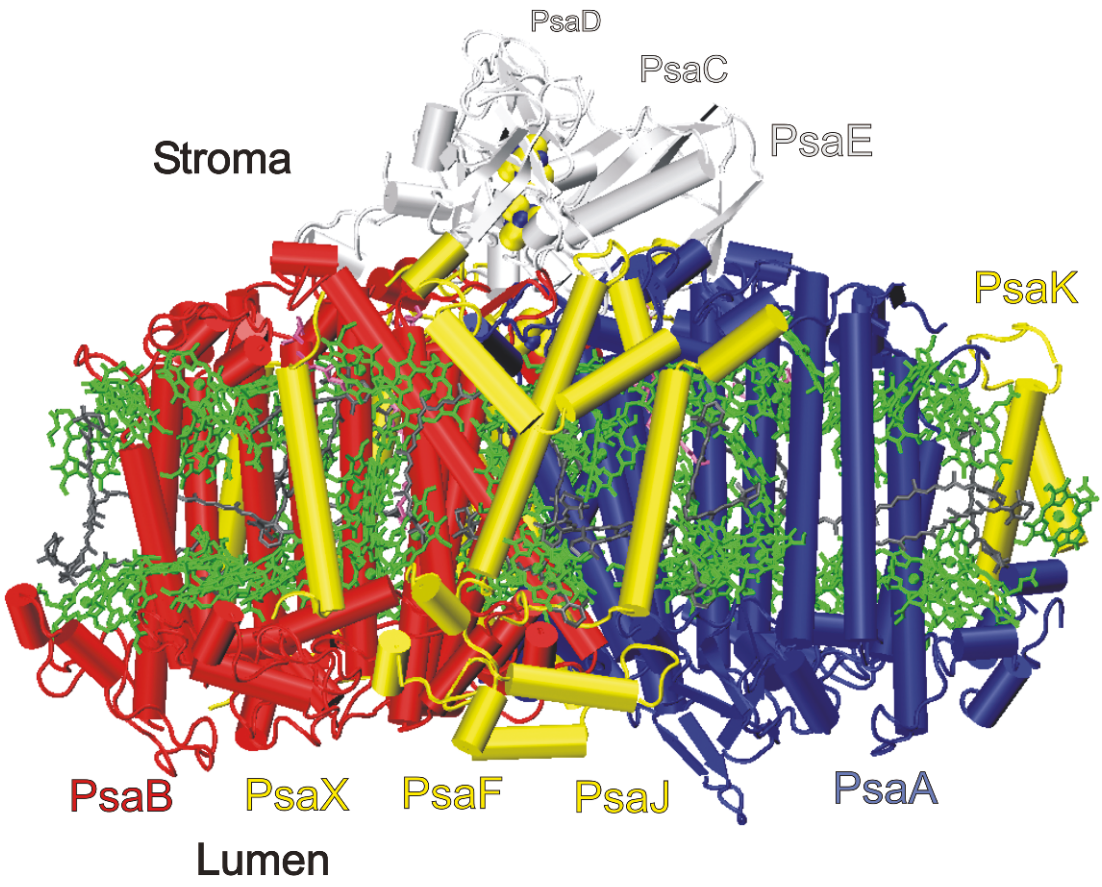

Fig. 2. Photosystem I. PS I with all cofactors as seen from within the membrane plane. The view leads from the distal side into the trimerization site. PsaA is shown in blue, PsaB in red, the small subunits with transmembrane helices in yellow, the stromal subunits in white, chlorophylls in green, carotenoids in grey, lipids in mauve, and Fe/S clusters with yellow/blue spheres. (P. Fromme and I. Grotjohann, unpublished.) See Chapter 6, p. 50.

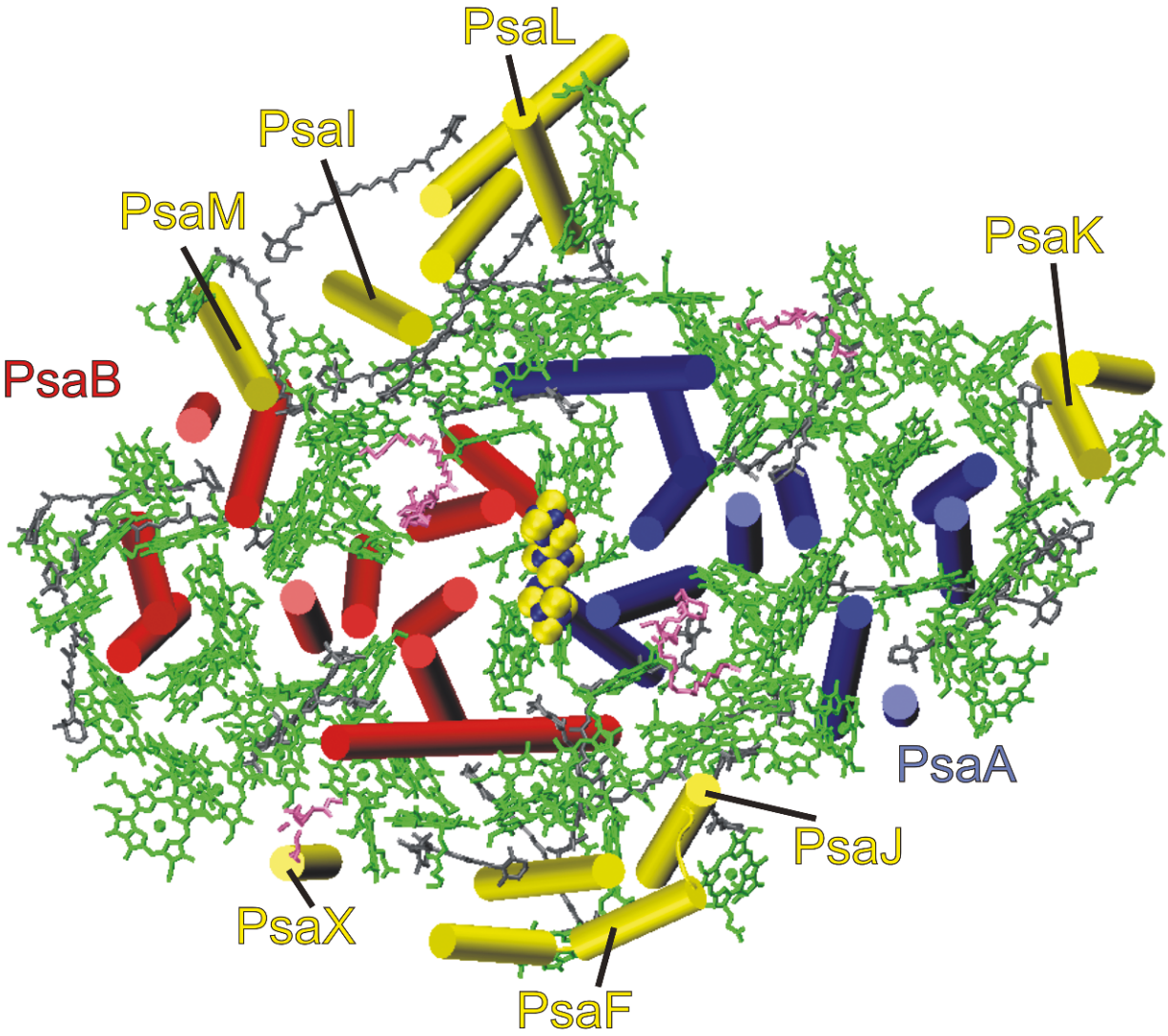

Fig. 2. (*cont.*) Photosystem I. View of the transmembrane helices of the protein backbone with all cofactors as seen from the stroma. The trimerization site can be found on the top of the picture. PsaA is shown in blue, PsaB in red, the small subunits with transmembrane helices in yellow, the stromal subunits in white, chlorophylls in green, carotenoids in grey, lipids in mauve, and Fe/S clusters with yellow/blue spheres. (P. Fromme and I. Grotjohann, unpublished.) See Chapter 6, p. 51.

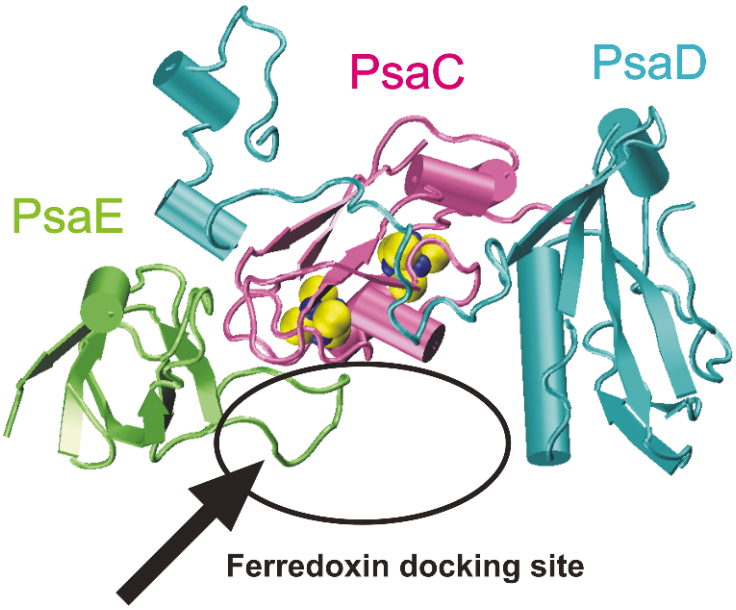

Fig. 1. The stromal subunits of Photosystem I. View from the stromal side of the thylakoid membrane. The subunits PsaC, PsaD, and PsaE form a protein cluster on the stromal side of PS I, which harbors the terminal part of the electron transfer chain. PsaC coordinates the Fe/S clusters F_A and F_B. PsaC is depicted in mauve, PsaD in cyan, and PsaE in lime. The docking site for ferredoxin is indicated. (P. Fromme and I. Grotjohann, unpublished.) See Chapter 6, p. 54.

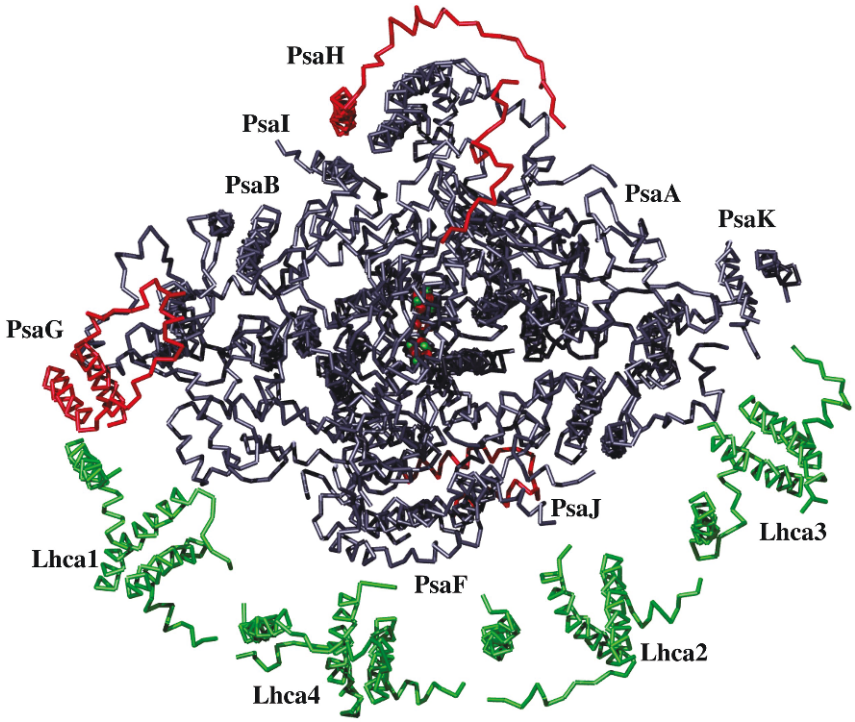

Fig. 2. The Cα backbone model of plant Photosystem I at 4.4 Å resolution. View from the stromal side of the thylakoid membrane. The four light-harvesting proteins are in green (Lhca1-4). Novel structural elements within the RC (core) not present in the cyanobacterial counterpart are colored red, the conserved features of the RC are in grey. The three [4Fe-4S] clusters are depicted as red (Fe) and green (S) balls. Subunits A, B, F, G, H, I, J and K of the RC are indicated. The assignment of the four different Lhca proteins is shown. (Modified from Ben-Shem et al., 2003.) See Chapter 7, p. 73.

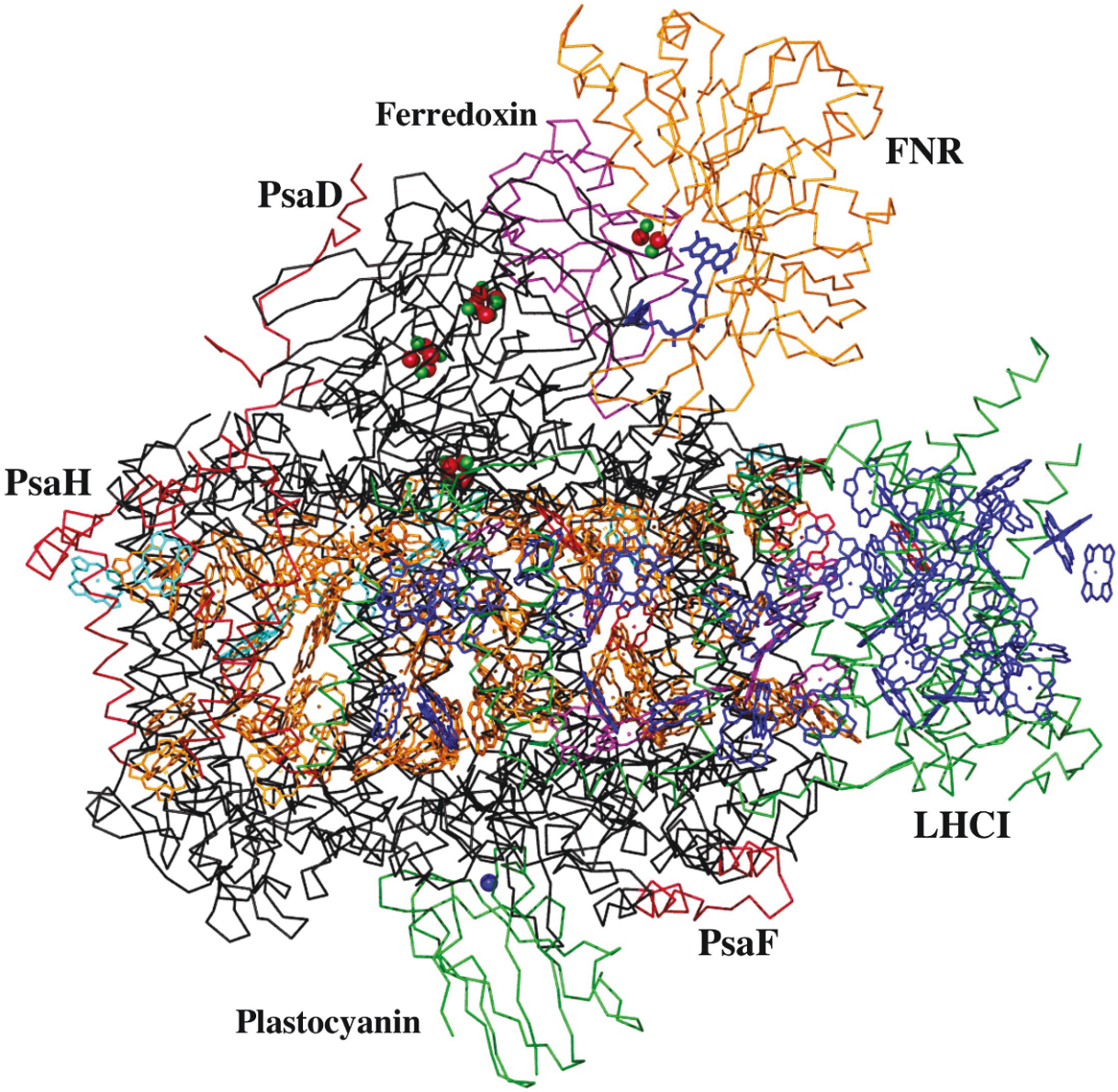

Fig. 1. A model of the side view of putative interactions between plant PS I, platocyanin and ferredoxin-FNR complex. The color code of the Cα-backbone of PS I is as in Color Plate 3, Fig. 2. Chlorophylls are depicted in colors corresponding to their assignments as previously described (Ben-Shem et al., 2003b). Plastocyanin is in green and its copper atom in blue. Ferredoxin in magenta and its [2Fe-2S] cluster is in red and green balls. FNR is in orange and its FAD is in blue. The positions of subunits D, F and H are indicated. (A. Ben-Shem and N. Nelson, unpublished.) See Chapter 7, p. 74.

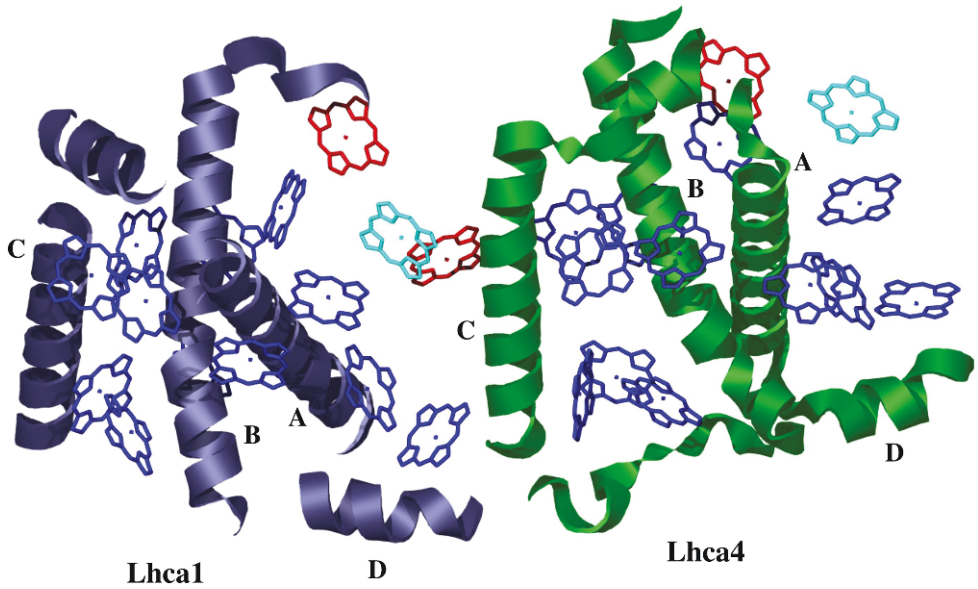

Fig. 1. Dimer formation between Lhca1 and Lhca4. The close contact between helix D of Lhca1 (grey) and both the lumenal region of helix C and the lumenal loop connecting helices B and C of Lhca4 (green), is shown. Chlorophyll molecules that were previously assigned as part of the Lhca molecule are in blue. The novel chlorophyll (Liu et al., 2004) that corresponds to a missing chlorophyll (in Kuhlbrandt et al., 1994) is in green. This chlorophyll was previously assigned as a linker chlorophyll (Ben-Shem et al., 2003b). Linker chlorophylls are in red. (Modified from Ben-Shem et al., 2003.) See Chapter 7, p. 75.

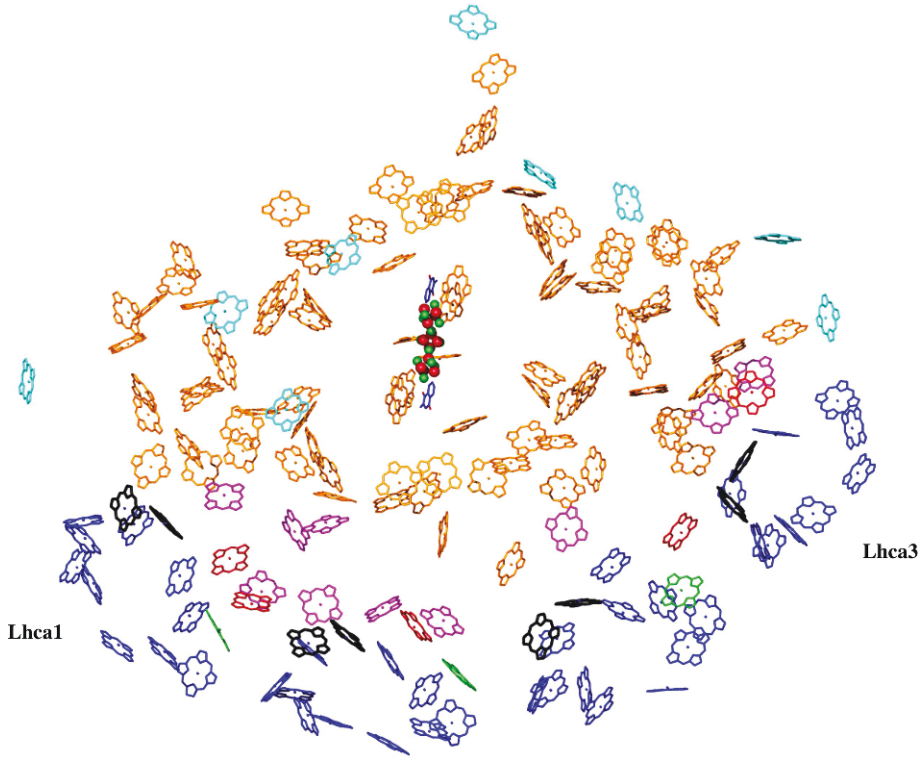

Fig. 2. The arrangement of chlorophyll molecules of plant PS I. Color code used: yellow – plant RC chlorophylls that are present in cyanobacteria, cyan – RC chlorophylls unique for plants, blue – chlorophylls bound to the Lhca monomers, black – chlorophylls bound to the Lhca monomers that may form the "red chlorophylls", red – LHCI "linker" chlorophylls between Lhca monomers, magenta – chlorophylls positioned in the cleft between LHCI and the RC. (Modified from Ben-Shem et al., 2003.) See Chapter 7, p. 76.

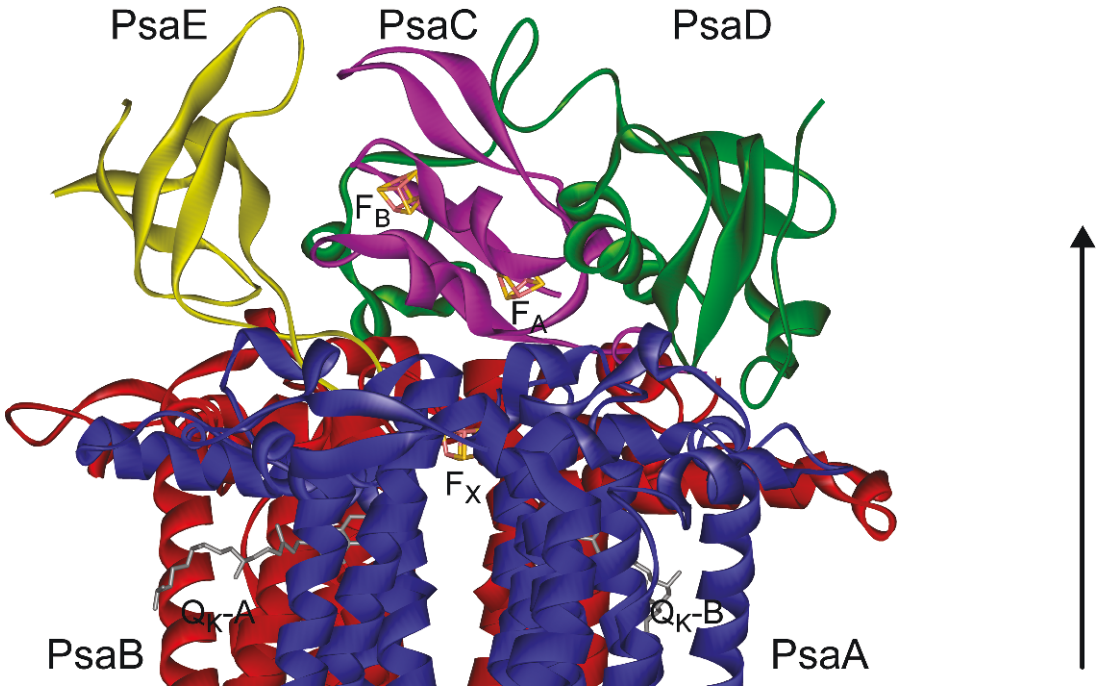

Fig. 1. The X-ray structure of cyanobacterial PS I at 2.5 Å resolution (PDB entry 1JB0) (Jordan et al., 2001). Detail of the structural model of the PS I monomer. View is parallel to the membrane plane. The complete backbones of the stromal subunits PsaC, PsaD and PsaE are depicted, as well as their respective arrangement on the stromal surface of the PsaA/PsaB heterodimer. PsaA is shown in blue, PsaB in red, PsaC in magenta, PsaD in green, PsaE in gold; peripheral proteins are omitted for clarity; [4Fe-4S] iron-sulfur clusters F_X, F_A and F_B are shown as cubes in which the yellow corners indicate the positions of the sulfur atoms and the light-brown corners the position of the iron atoms; quinones Q_K-A and Q_K-B are shown as "stick" models, both represent the acceptor A_1 bound to PsaA and PsaB respectively. The position of the trimer C_3-symmetry axis is indicated by an arrow. (From Antonkine et al., 2003.) See Chapter 8, p. 81.

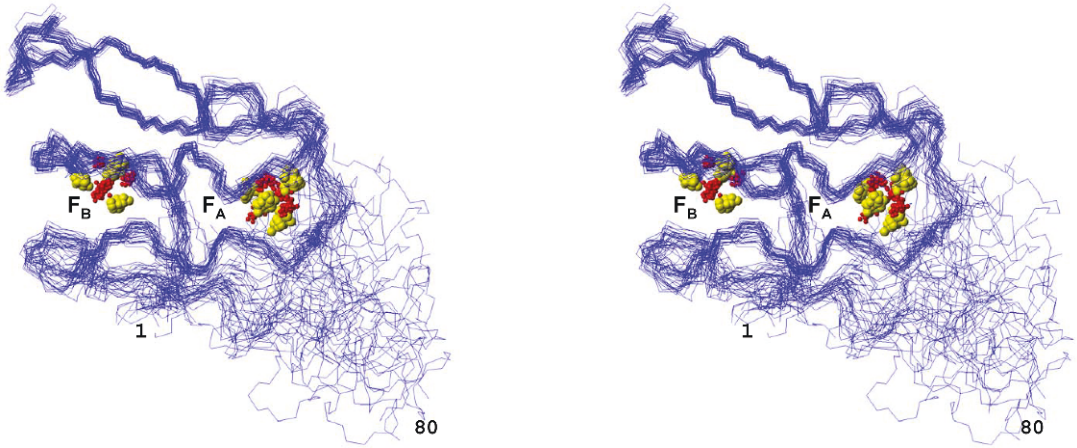

Fig. 2. Solution structures of the unbound PsaC subunit of PS I (PDB entry 1K0T) depicting backbone stereo drawings of 30 superimposed DYANA structures. The iron and sulfide ions of the [4Fe-4S] clusters of each of the 30 DYANA structures are shown with iron atoms as red spheres and sulfur atoms as yellow spheres. The protein backbone is shown in blue. The direction of the view is perpendicular to the F_A/F_B connecting axis and parallel to the stromal membrane plane of the assembled PS I complex. This figure was prepared using MOLMOL (Koradi et al., 1996). (From Antonkine et al., 2002.) See Chapter 8, p. 86.

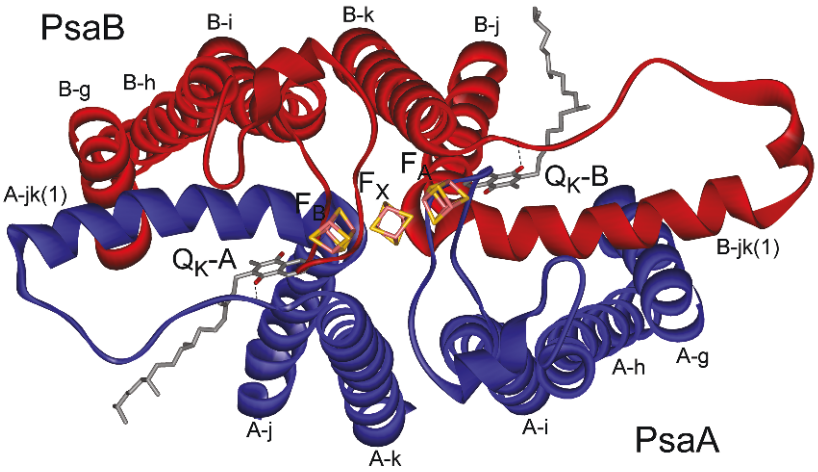

Fig. 1. Detail of the structural model of the PS I monomer. The position of the trimer C_3-symmetry axis is indicated by the triangle. View on the PsaA/PsaB heterodimer along the membrane normal from the stromal side. Of PsaA and PsaB only the central transmembrane α-helices g, h, i, k, j are shown, and the stromal surface α-helices A-jk(1) and B-jk(1) including the return loop to respective α-helix k as well as the complete stromal loops connecting α-helices h and i. The sole hydrogen bond between the quinone and protein backbone is shown (dashed line). (From Antonkine et al., 2003.) See Chapter 8, p. 88.

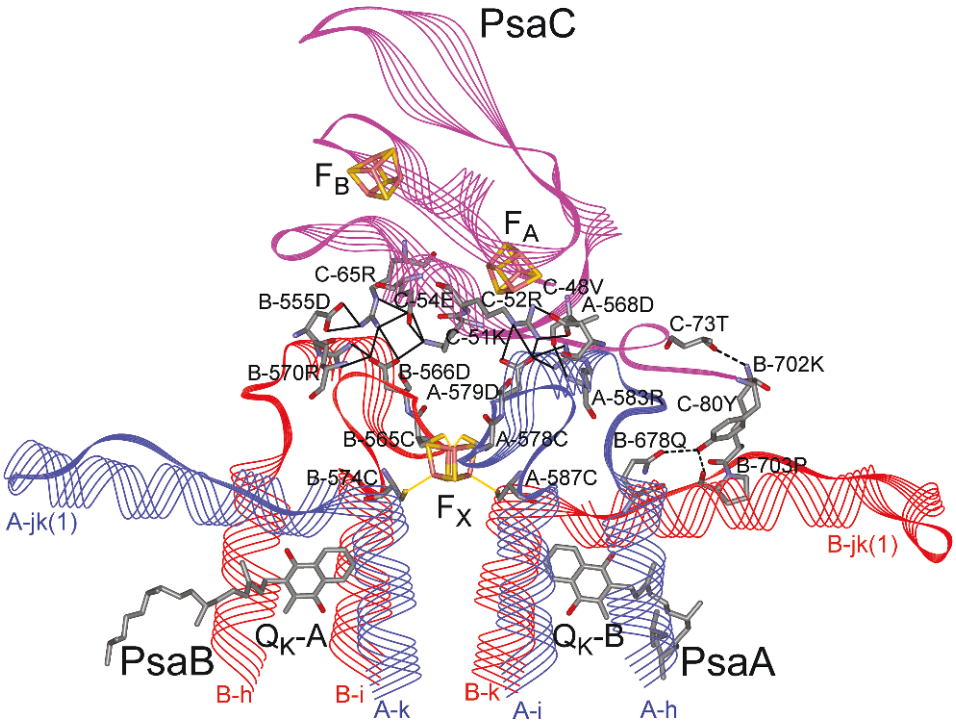

Fig. 2. The PsaC contact area with PsaA and PsaB from the PS I structure (PDB entry 1JB0) (Jordan et al., 2001). Stromal surface α-helices A-jk(1) and B-jk(1), and part of transmembrane α-helices A-h, A-i, A-k and B-h, B-i, B-k are shown, and are labeled in the same colors as the respective polypeptide chain. Amino acids participating in inter- and intra-polypeptide H-bond and ionic contacts and cysteines ligating interpolypeptide [4Fe-4S] cluster F_X are shown as "stick" models and are identified by their number in the protein sequence; ionic bonds are indicated by a solid line; hydrogen bonds are indicated by a dashed line; bonds between cysteines and irons of the F_X cluster are identified by a solid yellow line. View direction is parallel to the membrane plane and is perpendicular to the triangular plane of the [4Fe-4S] clusters. (From Antonkine et al., 2003.) See Chapter 8, p. 90.

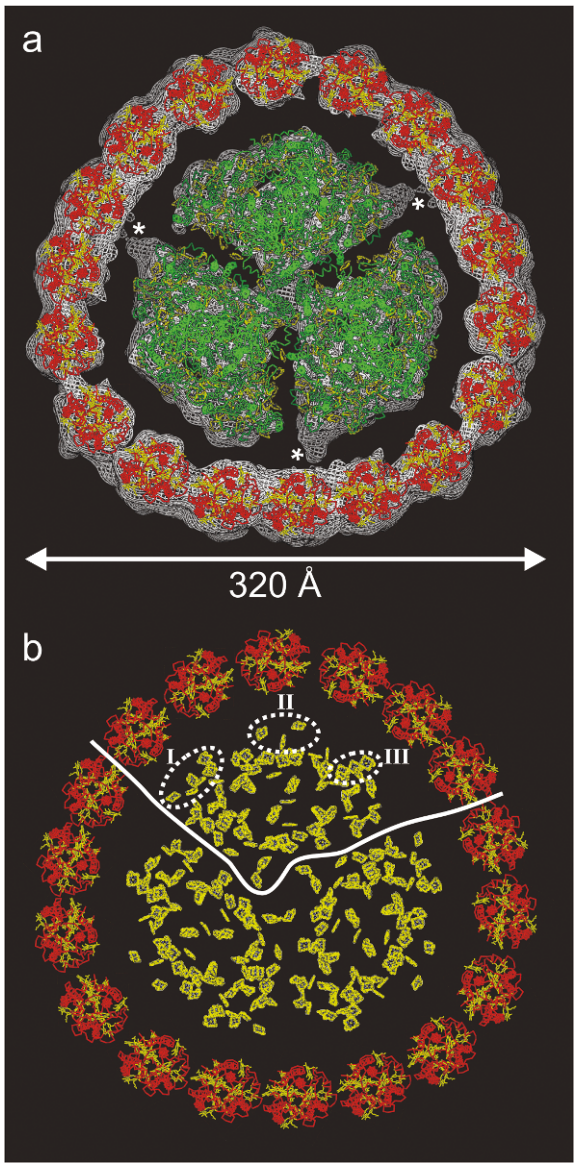

Fig. 1. Interpretation of the cryo-EM 3D structure of the IsiA–PS I supercomplex of *Synechocystis* sp. PCC 6803. (a) Modeling of the C_α-backbone and chlorophylls of the PS I trimer and CP43 using data derived from X-ray diffraction studies for PS I (Jordan et al., 2001) and PS II (Ferreira et al., 2004), overlaid onto the molecular envelope of the 3D cryo-EM map, viewed from the stromal side. The white stars indicate areas of density that are not present in the X-ray structure of PS I and might represent linker regions between the PS I RC and the IsiA antenna ring. (b) Modeling of Chl organization using coordinates from the X-ray structures of PS I (Jordan et al., 2001) and PS II (Ferreira et al., 2004) viewed from the stromal side. The three ringed areas (I–III) highlight regions where the peripheral Chls of the PS I RC monomer are closest to the Chls within the IsiA ring. The modeling assumed that helices V and VI of IsiA are adjacent to the surface of the PS I RC. (Modified from Nield et al., 2003.) See Chapter 9, p. 105.

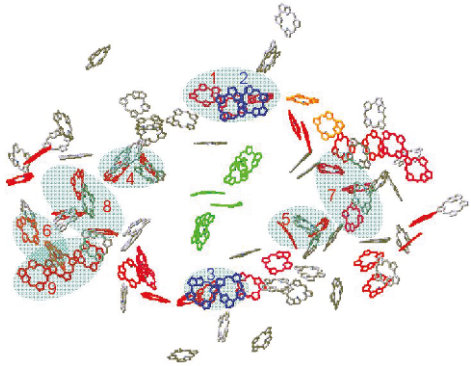

Fig. 1. The arrangement of Chls in one PS I monomer of *T. elongatus*. Only the ring planes of the Chls are shown for clarity. The strongest coupled Chls with an interaction energy ≥ 100 cm^{-1} are depicted in color. See Chapter 13, p. 183.

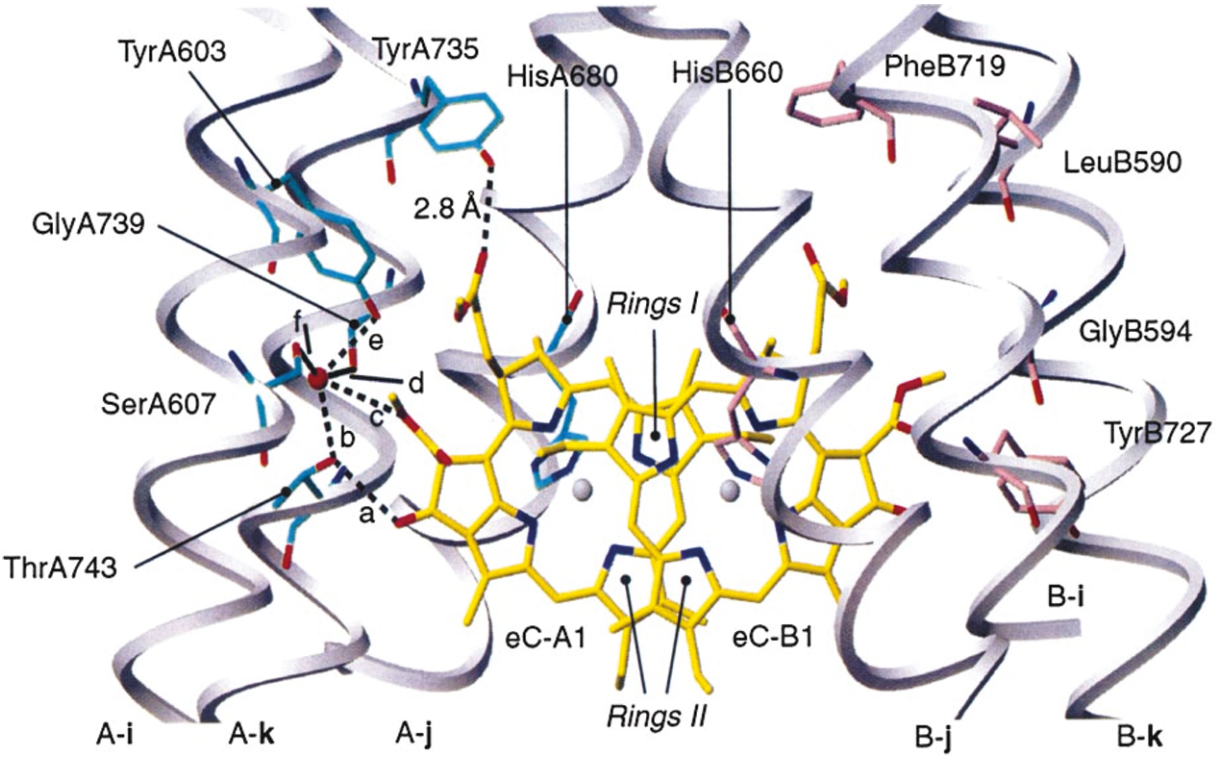

Fig. 2. The primary donor P_{700} and its protein environment. The helices surrounding the two chlorophylls eC-A1 and eC-B1 (yellow) are shown as grey ribbons. Residues of PsaA involved in hydrogen bonds (dashed black lines) to the water molecule (red sphere) or eC-A1 are colored blue. The corresponding amino acid residues of PsaB are colored pink. All six possible hydrogen bonds in the vicinity of ring V of eC-A1 are labeled with letters a to f. (Modified from Fromme et al., 2001.) See Chapter 14, p. 194.

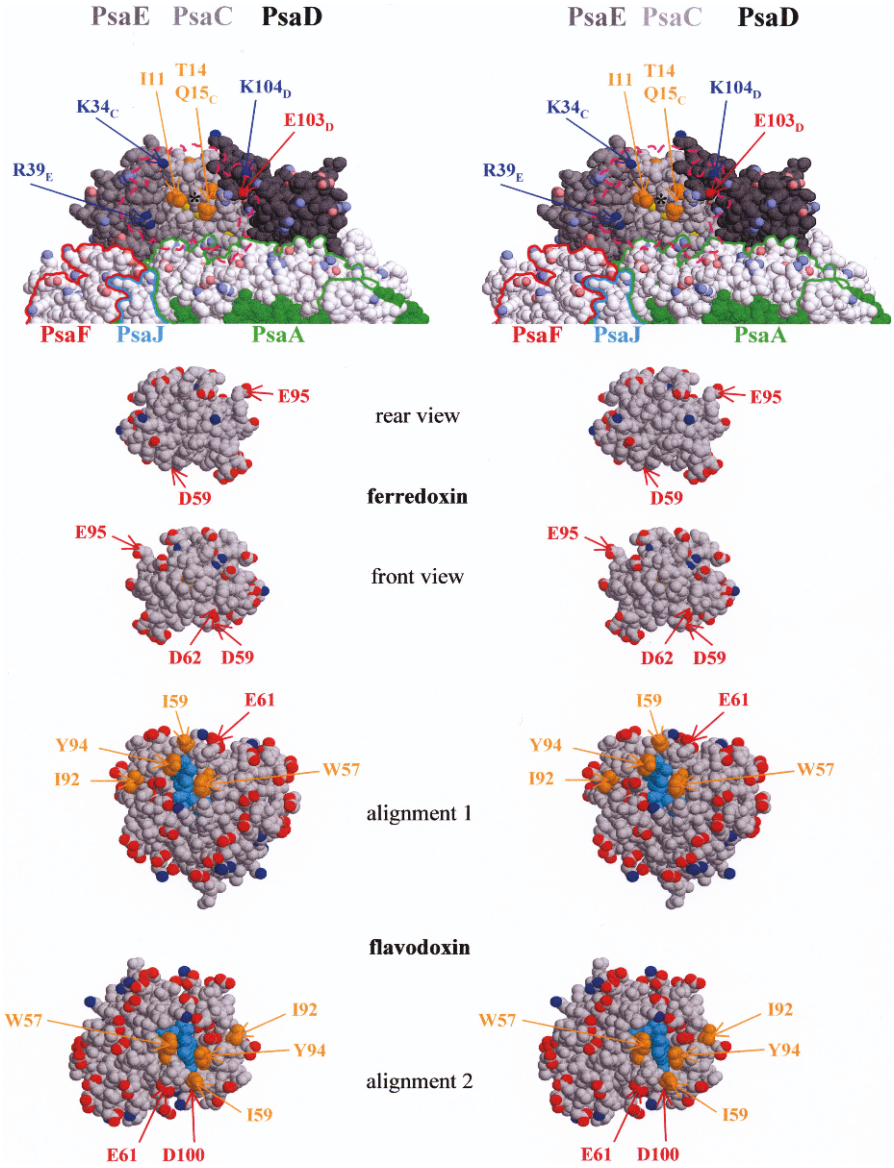

Fig. 1. Stereo views of photosystem I, ferredoxin and flavodoxin (crossed eyes). Upper part: This stereo side view shows PS I parallel to the membrane plane. The PS I residues which have been found to give the largest effects on K_d (shaded areas; see Table 3) are arrowed and numbered according to the *T. elongatus* structure (Jordan et al., 2001). Residue K104 of PsaD is also arrowed (see text). Color coding: different shades of grey have been used for different polypeptides. From the darkest to the clearest: PsaD, PsaE, PsaC, all other polypeptides; The contours of PsaA, PsaF and PsaJ are shown in green, red and cyan, respectively; Chlorophylls are green-colored; The oxygen atoms of the carboxylic groups of glutamate and aspartate residues are colored in light red; The nitrogen atoms of the lysine and arginine side chains are colored in light blue; Dark colors are used for acidic and basic residues which are arrowed; The side chains of I11, T14 and Q15, and the alpha carbon of G36 of PsaC are colored in orange. The β carbon of C13 of PsaC is indicated by an asterisk. The Fd contour corresponding to the rear view is superimposed on the proposed Fd binding region (dashed pink). Middle part: the Fd structure from *S. platensis* (Fukuyama et al., 1995) is shown in a rear view and front view, related to the rear view by a 180° rotation about a vertical axis. In both views, the reducible iron of Fd is located approx. in the middle, facing the viewer in the front view. The oxygen atoms of the carboxylic groups of glutamate and aspartate residues are colored in dark red. The nitrogen atoms of the lysine and arginine side chains are colored in dark blue. The side chains of the residues which give large changes in Fd reduction upon mutation are arrowed (Table 4). Lower part: the Fld structure from *Anabaena* sp. PCC 7120 (Burkhart et al., 1995) is shown in two orientations which can be compared with the front view of Fd, using the two alignments between Fd and Fld derived in (Ullmann et al., 2000). FMN is colored in cyan. Same colors as Fd for acidic and basic residues. The side chains of the residues which give large changes in Fld reduction upon mutation are arrowed (Table 5). The side chains of W57, I59, I92 and Y94 are colored in orange. (P. Sétif, unpublished.) See Chapter 26, p. 449.

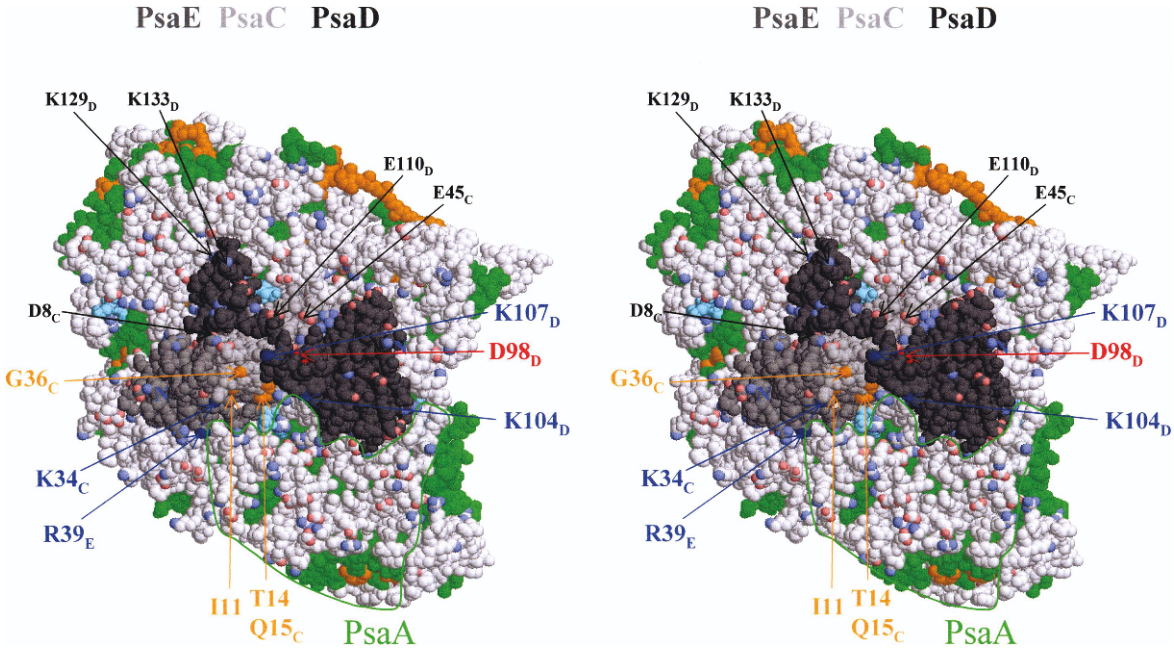

Fig. 1. Stereo top view of Photosystem I. This stereo view (crossed eyes) shows PS I from the stromal side perpendicularly to the membrane plane. Same color coding as in Color Plate 10, Fig. 1. Carotenes are colored in orange; lipids are colored in cyan. Black arrows indicate side chains of PsaC and PsaD residues which have been mutated without significant change of the affinity of Fd for PS I. (P. Sétif, unpublished.) See Chapter 26, p. 450.

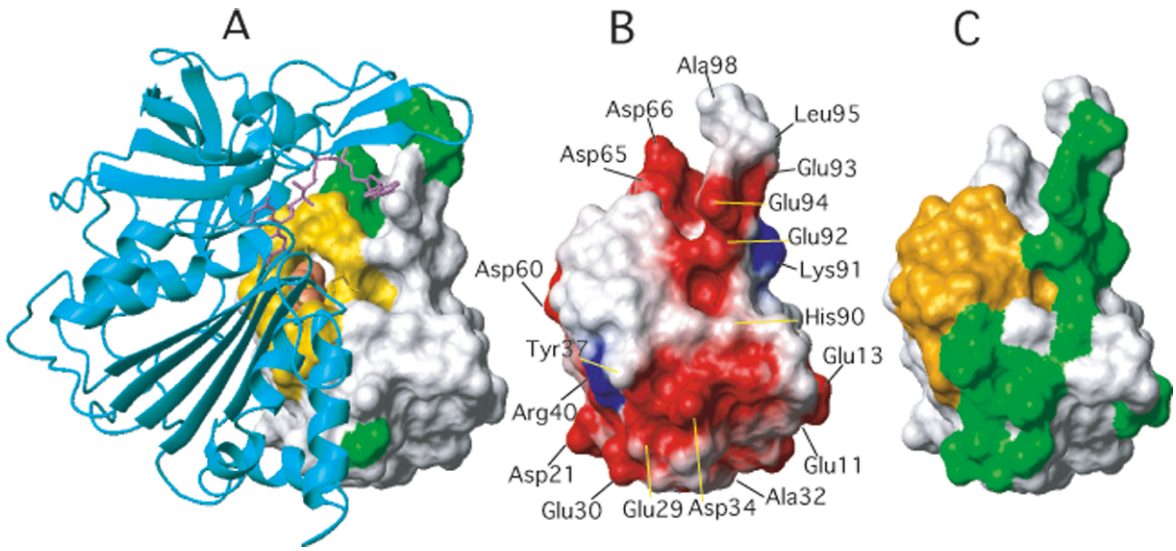

Fig. 2. NMR chemical shift perturbation of Fd upon complex formation with FNR or SiR determined by measuring 2D ^{1}H-^{15}N HSQC spectra of ^{15}N labeled Fd. (A) Structure of the maize leaf Fd/FNR complex determined by the x-ray crystallography (Kurisu et al., 2001). FNR is shown in a ribbon diagram format, with its FAD prosthetic group drawn in a wire format in purple. Fd is shown in a space-filling format with its [2Fe-2S] prosthetic group shown in brown. The Fd residues that exhibit significant changes in NMR chemical shift on complex formation with FNR, all of which are located at the contact interface between the two proteins shown in green in the 3D structure of Fd. Signals for Ser 38-Ala 48 and Thr 76-His 78 of Fd, shown in yellow, are not observed due to the paramagnetic nature of [2Fe-2S] cluster. (B) Surface electrostatic potential distribution of Fd. Negative and positive potential regions are depicted in red and blue, respectively. (C) Fd residues with significant chemical shift changes in the complex with SiR are show in green. Gene bank accession numbers are maize leaf Fd (Fd I) (P27787), leaf FNR (L-FNR1) (AB035644) and SiR (D50679), and atomic coordination of Fd-FNR complex is 1GAQ. (T. Hase, P. Schürmann and D. Knaff, unpublished.) See Chapter 28, p. 479.

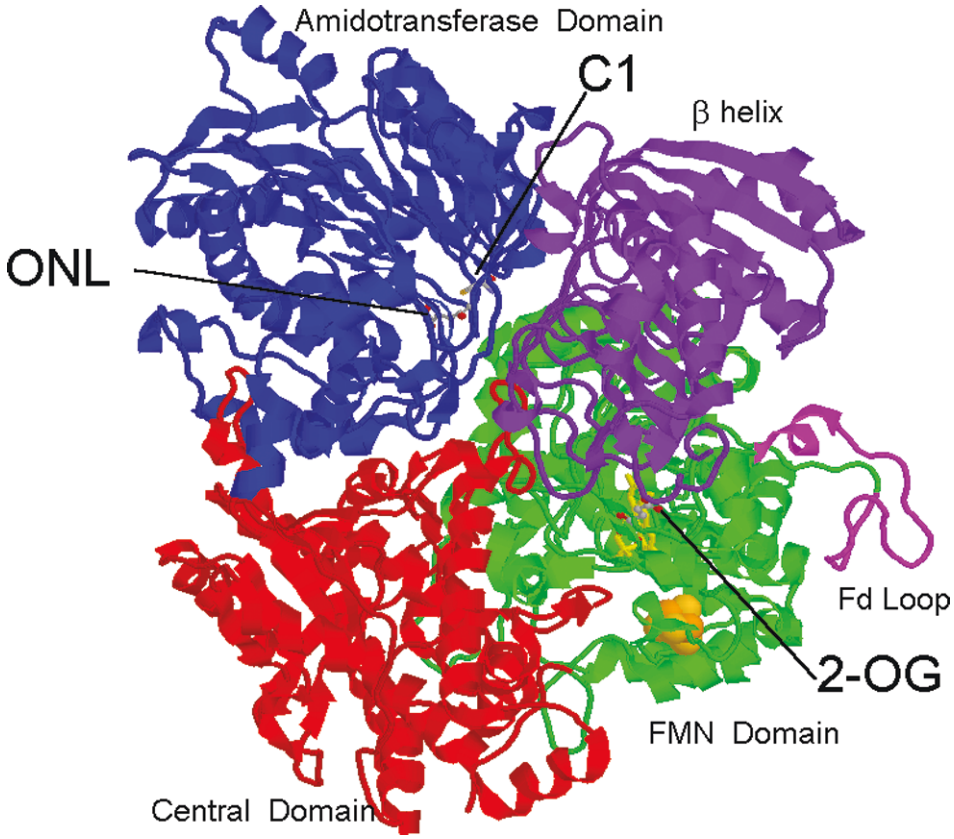

Fig. 1. The structure of the Fd-dependent glutamate synthase from the cyanobacterium *Synechocystis* sp. PCC 6820. Ribbon diagram of subunit A of *Synechocystis* sp. PCC 6820 Fd-GltS in complex with 5-oxo-L-norleucine and 2-oxoglutarate. The ligands, C1 and FMN are in sticks; the [3Fe-4S] center is represented in a space-filling format. The color coding is: blue, the glutamine amidotransferase domain; red, central domain; green, synthase domain containing the FMN cofactor (shown in yellow) and the [3Fe-4S]$^{0,+1}$ cluster (shown in orange, along with its ligating cysteine residues, Cys1137, Cys1143 and Cys1148); purple, C-terminal β helix. (From Vanoni et al. 2005.) See Chapter 28, p. 487.

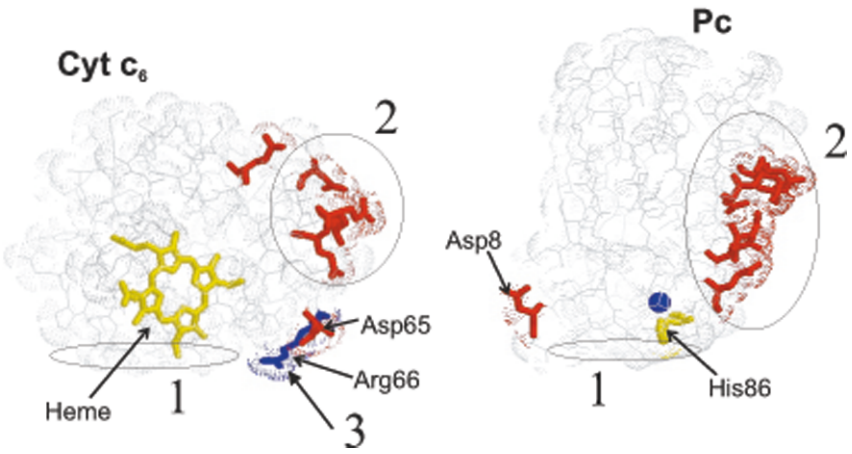

Fig. 2. Crystal structures of *Chlamydomonas reinhardtii* Cyt c_6 at a resolution of 1.6 Å (Kerfeld et al. 1995) and Pc at 1.5 Å (Redinbo et al. 1994). The recognition sites of both donors that are important for the interaction with PS I are indicated. 1. The flat "northern face" interacts with the PsaA/B heterodimer, the electron transfer occurs via this side. 2. Acidic patches on the "eastern side" are required for the electrostatic interaction with the positive patches on PsaF. 3. The cyanobacterial Pc or Cyt c_6 possess a positively charged amino acid at position of Arg66 of Cyt c_6 of *C. reinhardtii*, which is missing in eukaryotic plastocyanin. (M. Hippler, and F. Drepper, unpublished.) See Chapter 29, p. 501.

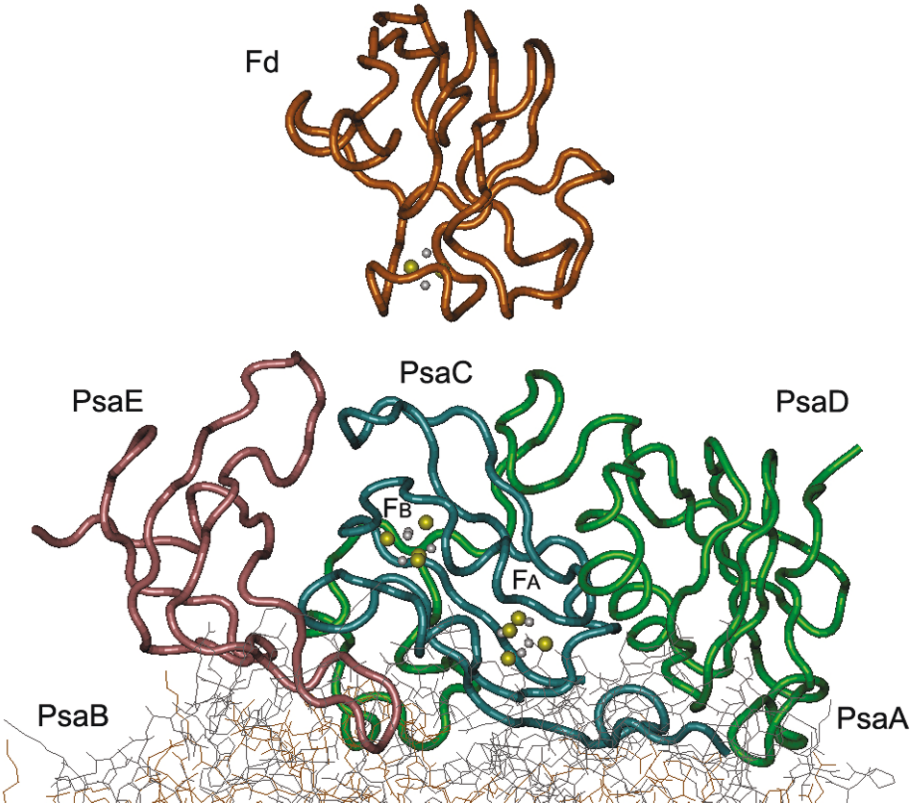

Fig. 1. Structural representation of the subunits of PS I reducing site and their electron acceptor, Fd. The structures of the PsaC, PsaD and PsaE subunits of PS I structure were taken from *Synechococcus elongatus* (PDB code 1JB0) where PsaA, PsaB, PsaC, PsaD and PsaE are colored gray, ochre, cyan, green and pink, respectively. For details please refer to Jordan et al. (2001). The Fd structure of *Aphanothece sacrum* (PDB code 1FXI) is colored orange, for details please refer to Tsukihara et al. (1990). Iron-sulfur (Fe/S) clusters F_A, F_B of PsaC and Fd are shown in ball representation where the Fe and S atoms are colored gray and yellow, respectively. The presented model was constructed using the graphics program VMD (Humphrey et al. 1996). (A. Fish, K. Kogan and R. Nechushtai, unpublished.) See Chapter 32, p. 554.

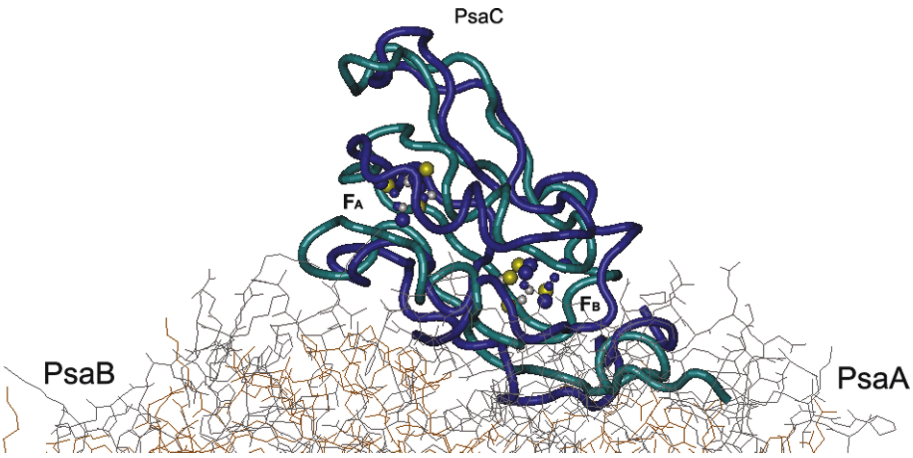

Fig. 2. Association of PsaC with the PS I complex. The NMR structure of free/soluble PsaC (colored blue) of *Synechococcus sp.* PCC 7002 (PDB code 1K0T), (for details please refer to Antonkine et al. (2002)). This structure is superpositioned on the structure of bound PsaC (colored cyan) in the assembled-PS I structure from *Synechococcus elongatus* (PDB code 1JB0) (for details please refer to Jordan et al. (2001)). F_A, F_B of PsaC are shown in ball representation where the Fe and S atoms of assembled PsaC are colored gray and yellow, respectively. The Fe and S atoms of free PsaC are colored blue. The presented model was constructed using the graphics program VMD (Humphrey et al. 1996). (A. Fish, K. Kogan and R. Nechushtai, unpublished.) See Chapter 32, p. 559.

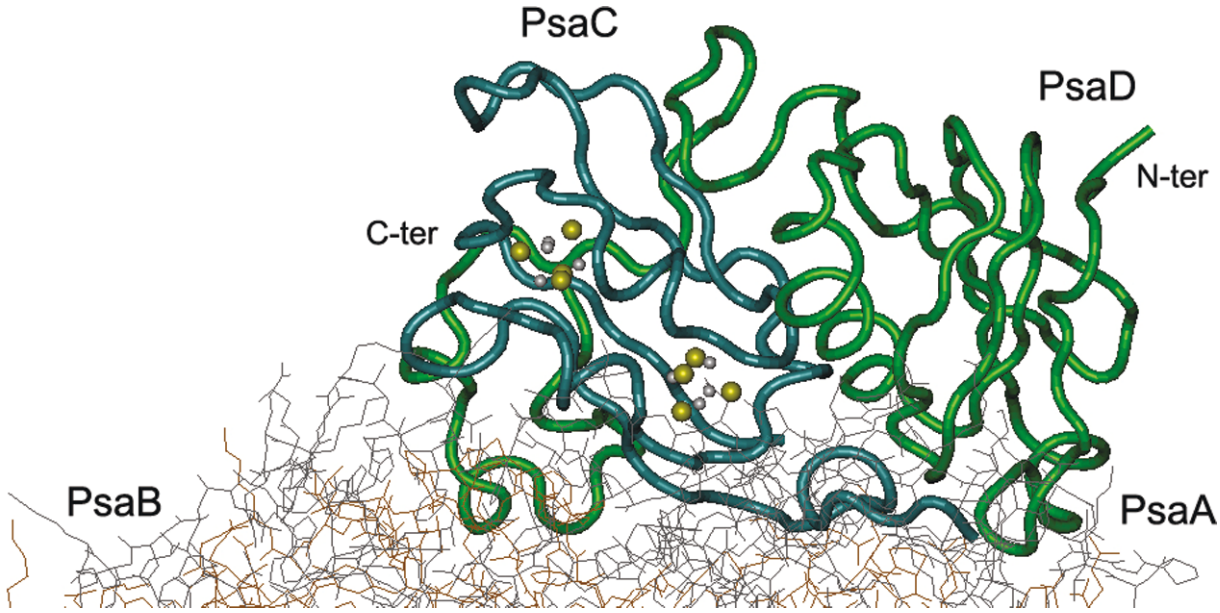

Fig. 1. Assembly of PsaD in the PS I complex. The different subunits of PS I structures were taken from *Synechococcus elongatus* (PDB code 1JB0) PsaA, PsaB, PsaC and PsaD, colored gray, ochre, cyan and green, respectively (for details please refer to Jordan et al. (2001)). The presented model was constructed using the graphics program VMD (Humphrey et al. 1996). (A. Fish, K. Kogan and R. Nechushtai, unpublished.) See Chapter 32, p. 561.

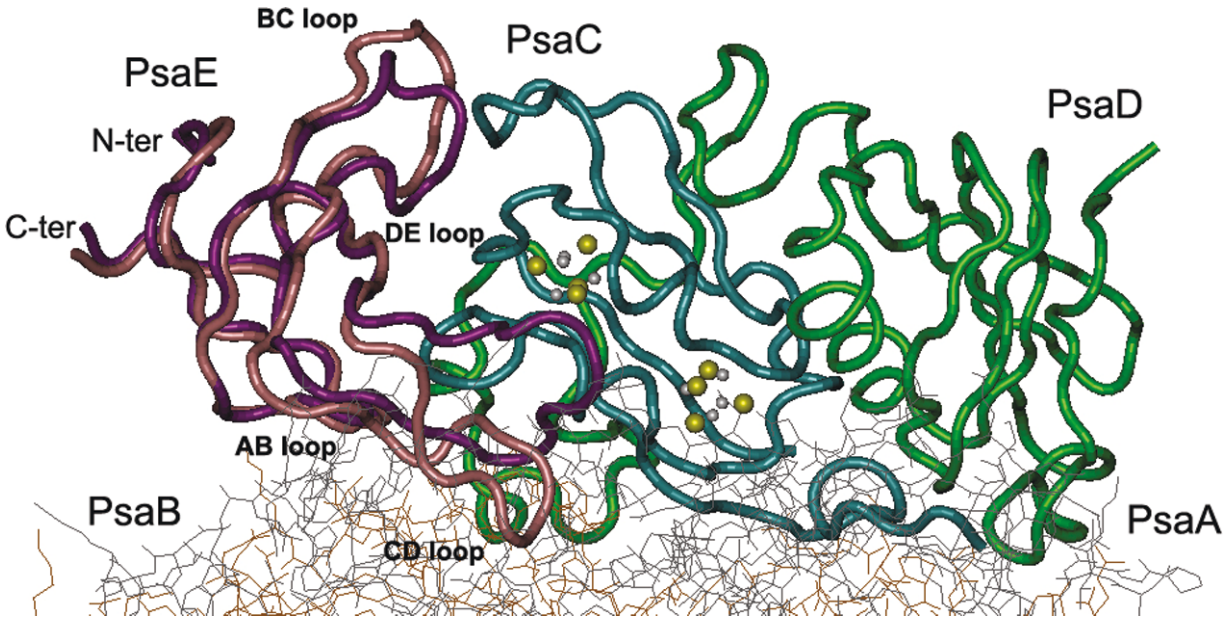

Fig. 2. Association of PsaE with the PS I complex. The NMR structure of free/soluble PsaE (colored purple) of *Synechococcus sp. PCC 7002* (PDB code 1PSF) for details please refer to Falzone et al. (1994), was superpositioned with the structure of PsaE in the assembled-PS I structure (colored pink) from *Synechococcus elongatus* (PDB code 1JB0), (for details please refer to Jordan et al. (2001)). The subunits of PS I structure PsaA, PsaB, PsaC and PsaD, colored gray, ochre, cyan and green, respectively. F_A, F_B of PsaC are shown in ball representation where the Fe and S atoms are colored gray and yellow, respectively. The presented model was constructed using the graphics program VMD (Humphrey et al. 1996). (A. Fish, K. Kogan and R. Nechushtai, unpublished.) See Chapter 32, p. 563.

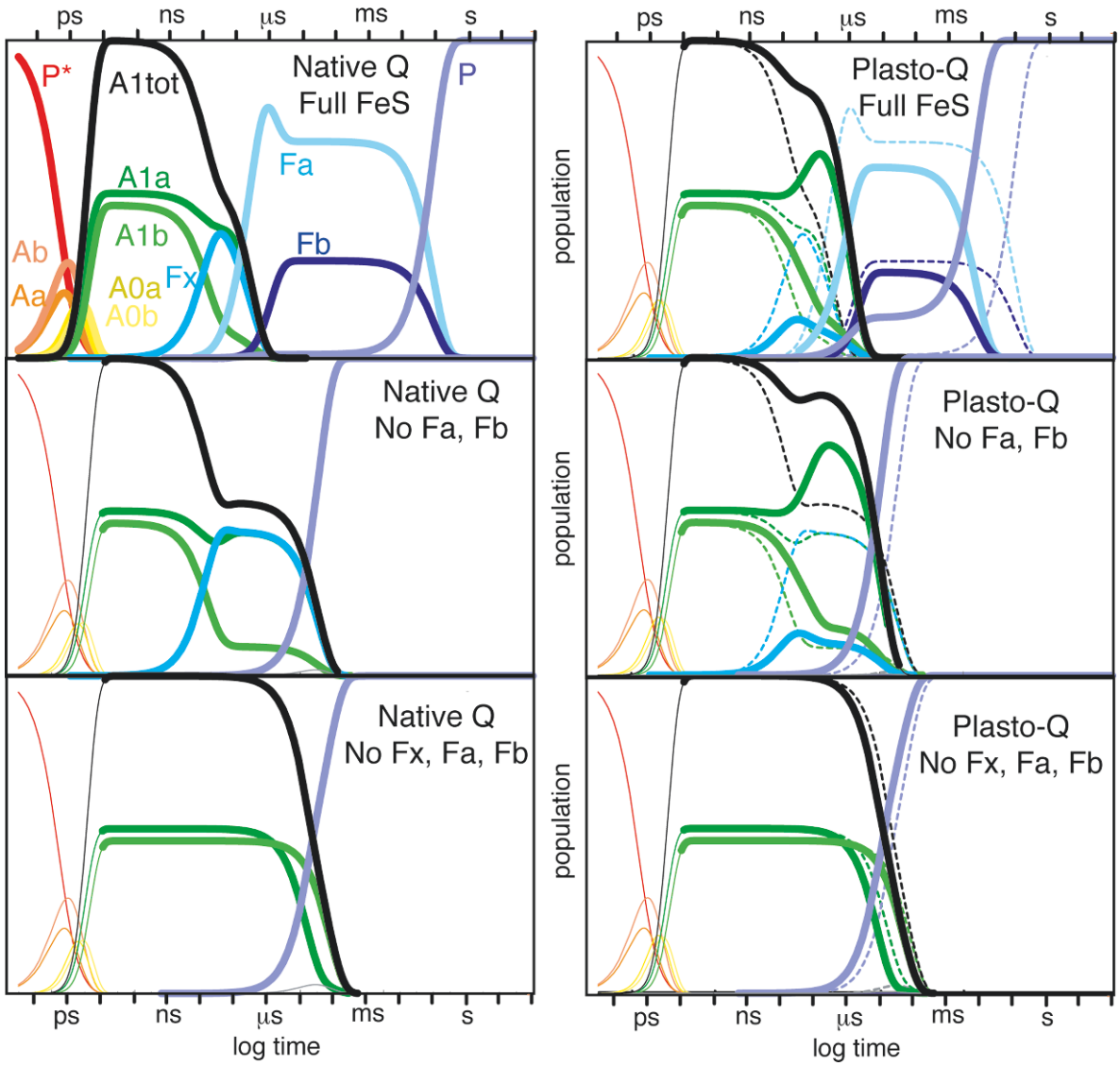

Fig. 1. Electron tunneling kinetics with different complements of Fe/S and different quinones using electron tunneling parameters described in the text. On the right, a comparison of native phylloquinone (dashed) with plastoquinone (solid). (C. Moser and L. Dutton, unpublished.) See Chapter 34, p. 591.

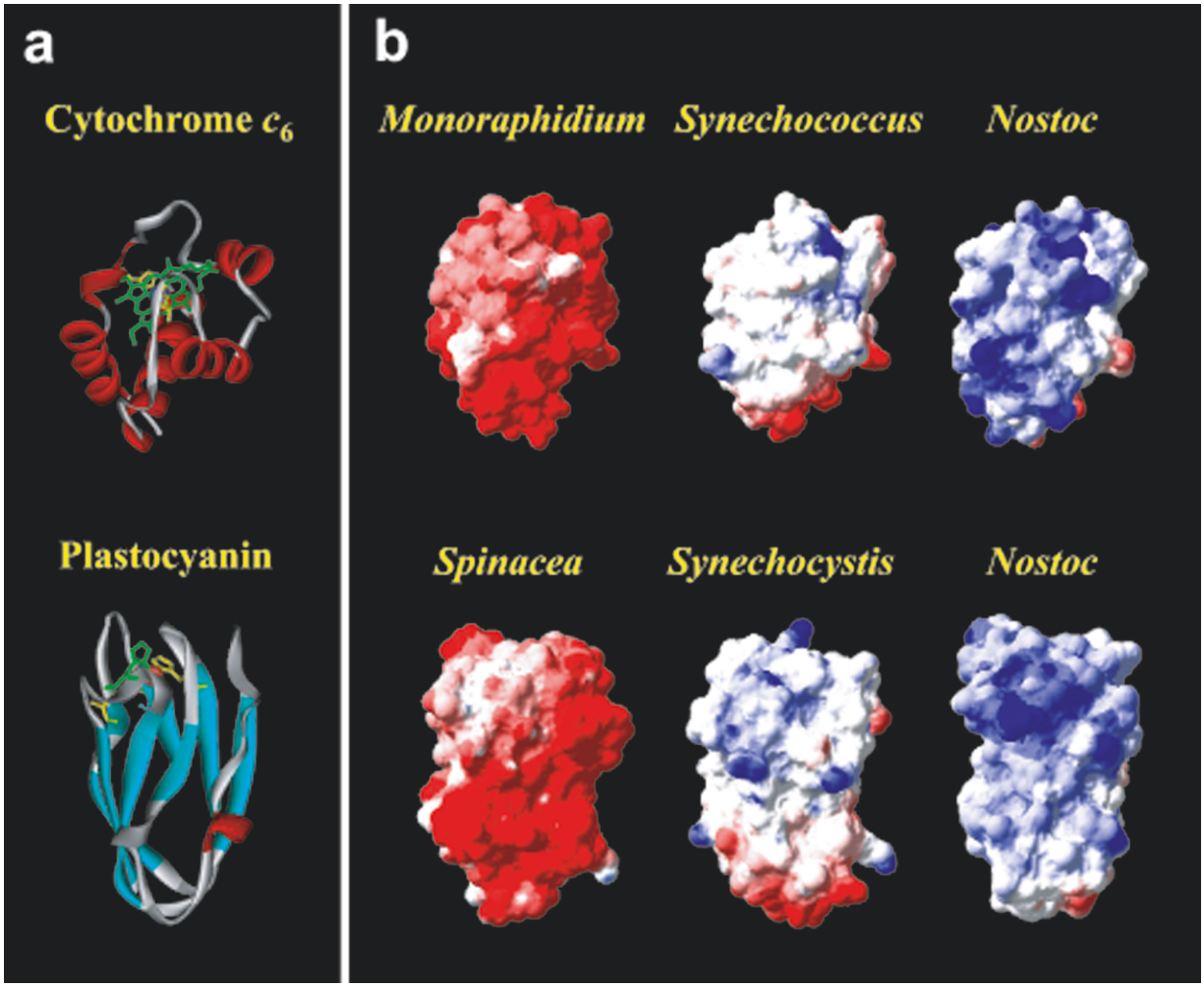

Fig. 1. Overall folding (a) and surface electrostatic potential distribution (b) of Cytochrome c_6 (*upper*) and Plastocyanin (*lower*) from different organisms. Iron and copper atoms are in space-filling representations, porphyrin ring and metal ligands in sticks, and polypeptide chains in flat ribbons. Positively and negatively charged areas are in blue and red, respectively, with the surface electrostatic potential being calculated at 40 mM ionic strength and pH 7. In all cases, the two molecules are similarly oriented with their sites 1 and 2 at the top and front, respectively. (M. De la Rosa, F. Molina-Heredia, M. Hervás and J. Navarro, unpublished) See Chapter 40, p. 687.

Chapter 1

A Personal Historical Introduction to Photosystem I: Ferredoxin + FNR, the Key to NADP$^+$ Reduction

Anthony San Pietro*
Department of Biology, Indiana University, 1001 East Third Street, Bloomington, IN 47405-3700, USA

Summary

The system concerned with reduction of the pyridine nucleotide coenzymes depends on two proteins: a non-heme iron protein associated closely with the photochemical reaction center (Photosystem I) and a flavoprotein that functions as a reductase. The non-heme iron protein, previously known as the "methemoglobin reducing factor (MRF)," as "photosynthetic pyridine nucleotide reductase (PPNR)," and as the "TPN[1] reducing factor (TRF)," is recognized as a member of a class of proteins now called "ferredoxin (Fd)." The FAD-containing flavoprotein known now as "Fd:NADP$^+$ oxidoreductase (FNR)" was known previously as "TPNH diaphorase," as "pyridine nucleotide transhydrogenase," and as "TPN reductase." An abbreviated review of the investigations leading to the isolation and characterization of these two proteins that have extended over a number of years and in a number of different laboratories is presented herein. This has unavoidably led to a synonymy and I describe here my personal recollection of how this came about.

I. Prologue

The reduction of pyridine nucleotides by illuminated chloroplasts was demonstrated independently in three different laboratories in 1951 (Arnon, 1951; Tolmach, 1951; Vishniac and Ochoa, 1951). In these experiments, the formation of reduced pyridine nucleotides was demonstrated *indirectly* by coupling the photochemical reaction with a suitable dehydrogenase and measuring the formation of the product of the dehydrogenase system. In the absence of the coupling system, no directly measurable reduction of pyridine nucleotides was observed. The inability of pyridine nucleotides to undergo directly measurable photochemical reduction was considered to be a consequence of their low oxidation–reduction potential (E'_0 at pH 7 $= -0.32$ V) since most of the substances that were effective as oxidants in the Hill reaction have high oxidation–reduction potentials (E'_0 at pH 7 $= +0.1$ to $+0.4$ V).

* Author for correspondence, email: sanpietr@indiana.edu

[1] NAD and NADP were known earlier as Coenzymes I and II and then later as DPN and TPN

Abbreviations: ATP – adenosine triphosphate; DPN – dinucleotide phosphate; FAD – flavin adenine dinucleotide; Fd – ferredoxin; MRF – methemoglobin reducing factor; NADP$^+$ – nicotinamide dinucleotide phosphate; PPNR – photosynthetic pyridine nucleotide reductase; TPN – trinucleotide phosphate; TRF – TPN reducing factor.

John H. Golbeck (ed): Photosystem I: The Light-Driven Plastocyanin:Ferredoxin Oxidoreductase, 1–8.

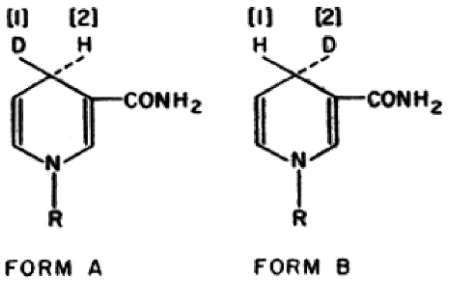

Fig. 1. Stereoisomers of reduced deuteriopyridine nucleotides.

As an extension of my interest in hydrogen transfer reactions in biological systems,[2] I began an investigation of the reduction of pyridine nucleotides by illuminated grana (thylakoids) because of their important and well-known physiological role as coenzymes in enzyme-catalyzed reactions. In light of the proposed redox limitation indicated above, the initial approach, also *indirect*, was to measure the turnover of the pyridine nucleotides; i.e., photoreduction followed by reoxidation assayed as deuterium incorporation from the medium. This approach was valid independent of which of the two possible stereoisomers of reduced pyridine nucleotide (Fig. 1) was formed initially and so long as the subsequent oxidation was of opposite stereospecificity. The expectation was that the information obtained in this study would permit determination as to whether the reduction was enzymatic or chemical in nature. *An unexpected but very important finding ensued.* As expected, there was incorporation of deuterium from the medium into the oxidized pyridine nucleotide and the deuterium was present at the site at which the pyridine nucleotides underwent enzymatic reversible oxidation–reduction (San Pietro and Lang, 1956, 1957). The *unexpected* result was the observation that at high grana (chlorophyll) concentration, there was an accumulation of the reduced form of the coenzyme. At low grana (chlorophyll) concentration, there was no indication of the reduced coenzyme. I remember vividly to this day the excitement Helga Lang and I experienced when we noted a small, but meaningful, decrease ($\Delta A = 0.044$) in absorbance at 340 nm upon addition of yeast alcohol dehydrogenase and acetaldehyde to the reaction mixture.

II. Ferredoxin

This chance observation prompted Helga Lang and I to investigate the conditions under which the photochemical reduction of pyridine nucleotides could be demonstrated directly. It was shown that when either dinucleotide phosphate (DPN) or trinucleotide phosphate (TPN)[3] is incubated with chlorophyll grana in the light, either aerobically or anaerobically, reduced pyridine nucleotide accumulates in the medium (San Pietro and Lang, 1956).

In these studies, however, it was necessary to employ fairly high concentrations of grana and pyridine nucleotides. More significant in this connection was the relationship between the grana concentration and the amount of pyridine nucleotide reduced. At low grana concentrations there was no reduction of pyridine nucleotide; at higher grana concentrations there was a linear relationship between the grana concentration and the amount of reduced pyridine nucleotide formed. This is shown graphically in Fig. 2; experimental conditions were as described in San Pietro and Lang (1956).

These results suggested that a naturally occurring factor or catalyst was required for the reduction of pyridine nucleotides. To test this hypothesis, a soluble extract of chloroplasts was prepared. The addition of the soluble extract to a system containing a low concentration of grana restored the pyridine nucleotide reduction activity (San Pietro and Lang, 1956). This finding allowed for the direct and rapid measurement of the initial rate of pyridine nucleotide reduction since the reduction could be assayed spectrophotometrically by the

[2] From 1952 to 1954, I was a Post-Doctoral Fellow in Biology and the McCollum Pratt Institute, the Johns Hopkins University. During this period my research centered on elucidation of the structure of reduced pyridine nucleotides with M. E. Pullman and S. P. Colowick and on elucidation of the mechanism and stereospecificity of the pyridine nucleotide transhydrogenase reaction in *Pseudomonas fluorescens* with N. O. Kaplan and S. P. Colowick. In addition, I was interested in the stereospecificity of enzymatic pyridine nucleotide reduction by various dehydrogenases: i.e., was only one, or both, of the two possible stereoisomers of the reduced pyridine nucleotide formed during dehydrogenase activity. It was shown previously that yeast alcohol dehydrogenase (ADH) is stereospecific with respect to both the alcohol and the pyridine nucleotide (Form A in Fig. 1). The stereospecificity of the transhydrogenase reaction in *P. fluorescens* is opposite (Form B in Fig. 1) to that of yeast ADH Thereafter, the stereospecificities of a number of additional pyridine nucleotide-linked dehydrogenases were elucidated relative to that exhibited by yeast ADH.

In 1954, I joined the faculty and began the study of photosynthetic electron/hydrogen transfer reactions.

[3] The use of DPN rather than TPN in our initial experiments was dictated by cost. If my memory is correct, the cost of TPN was about $1,000 per gram; in contrast, the cost of DPN was only about $50 per gram.

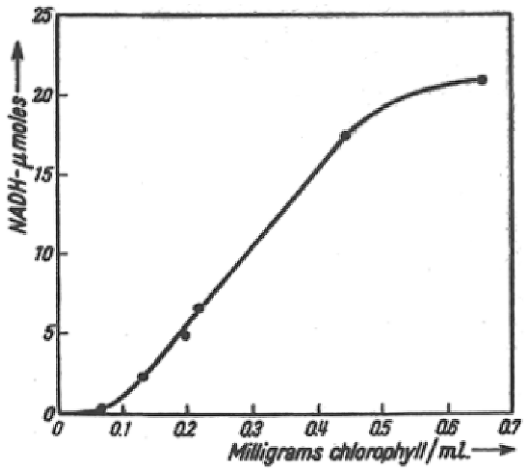

Fig. 2. Relationship between chlorophyll concentration and accumulation of DPNH. Source: San Pietro and Lang (1956).

increase in absorbance at 340 nm of the reaction mixture without the prior removal of the grana.[4] Furthermore, the heat lability of the soluble factor supported our earlier assumption that the reduction of pyridine nucleotides by illuminated grana was enzymatic in nature rather than chemical.

Soon thereafter, Arnon et al. (1957) reported evidence in agreement with our findings. They demonstrated that the reduction of TPN by illuminated chloroplasts was made possible by the addition of an aqueous extract of whole chloroplasts. The reduction process was not specific for TPN since DPN was also reduced but at a slower rate.

In 1958, San Pietro and Lang reported the isolation and partial purification of a soluble protein that catalyzed the reduction of pyridine nucleotides by illuminated chloroplasts or grana. They suggested that this protein be named Photosynthetic Pyridine Nucleotide Reductase (PPNR). In agreement with Arnon et al. (1957), the partially purified PPNR was not specific for TPN as DPN was also reduced but at a slower rate. The specificity for TPN was observed when the PPNR was further purified. It must be noted that the first demonstration that a soluble factor can be added back to chloroplasts to reconstitute their overall electron transport reaction must be attributed to Robin Hill and his colleagues. The following statement taken from Hill (1951) summarizes their findings. "We have found that untreated chloroplast suspensions from many plants show an active capacity for reducing muscle methemoglobin in light. When the chloroplast suspension is diluted, the activity (in terms of chlorophyll present) falls off in a way showing the presence of a soluble factor. The washed chloroplasts were incapable of reducing methemoglobin in light, but addition of the soluble fraction of the leaf juice restored the activity. The soluble *methemoglobin reduction factor* (MRF) is thermolabile." Helga Lang and I were unaware of the prior work on the methemoglobin reducing factor when we reported our observations in 1956. In 1962, Tagawa and Arnon described this protein under the name of spinach (or chloroplast) ferredoxin. This change in nomenclature was based on the chemical and functional similarities of the proteins isolated from plants and bacteria. Bacterial ferredoxin was discovered by Mortenson et al. (1962) at the DuPont Laboratories.[5] It is interesting that in spite of the similarities, the proteins isolated from these two sources differ in their absorption spectra, in their iron contents, in their molecular weights and in their amino acid analyses. The redox potentials, however, of the plant and bacterial proteins are similar.

In the same year Gewitz and Volker (1962) reported the purification from *Chlorella* of a red protein and described a flavoprotein. The absorption spectrum of the red protein was similar to those of PPNR and MRF shown in Fig. 3. Furthermore, both the red protein and the flavoprotein were required for the maximal rate of TPN reduction and oxygen evolution.

Both MRF and PPNR were extensively purified and shown to be homogeneous by electrophoresis, by

[4] The availability of a rapid assay procedure and the easy accessibility of large amounts of starting material provided for a biochemical approach to the elucidation and function of the unknown factor(s) as well as the mechanism of the photobiological coenzyme reduction process.

[5] That which follows is my personal recollection of the genesis of the descriptive name ferredoxin. Following the discovery of the bacterial protein there was a contest at DuPont to provide an appropriate name for this new bacterial redox factor. The winner of the contest was David Wharton and his derivation of ferredoxin was:

fer	**redox**	**in**
iron-containing	**oxidation–reduction**	**protein**

Thereafter, ferredoxin became the generic name for this new group of non-heme iron and labile sulfide containing redox proteins.

Although the ferredoxin terminology was universally accepted, most investigators were unaware of the Wharton derivation. Piqued by curiosity, Harold Davenport, in typical scholarly fashion, sought help from the dictionary and mentioned to me personally in 1965 in Yellow Springs, OH, clearly with tongue in cheek, an alternative derivation; namely,

ferre	**doxin(doxy)**
iron	**(woman) of low morals**

Table 1. Correlation of absorbance in the visible region and iron content

Protein	Source	Wavelength (mμ) 330	420	465
PPNR	Spinach	6.70	4.95	4.45
Red enzyme	*Chlorella*	7.37	5.29	4.89
Ferredoxin	Spinach	6.95	5.16	4.65
MRF	Parsley	6.83	5.18	4.67

The values are presented as the absorbance of a solution of protein containing 1 μmol of iron per milliliter. Source: Hill and San Pietro (1963).

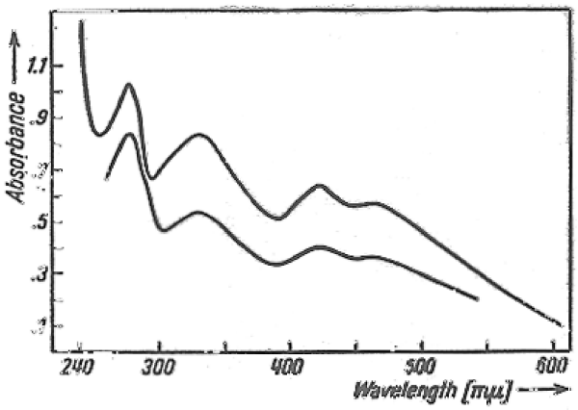

Fig. 3. Absorption spectra of methemoglobin reducing factor from parsley and PPNR from spinach. Upper curve: methemoglobin reducing factor, 0.77 mg of protein per milliliter; lower curve: PPNR, concentration equivalent to 0.081 μmol of iron per milliliter. Source: Hill and San Pietro (1963).

column chromatography, and by ultracentrifugation. The absorption spectra of PPNR from spinach and MRF from parsley are very similar as shown in Fig. 3; the major difference between them is the relationship of the absorption in the visible region to that in the ultraviolet (Table 1). Although the absolute values for PPNR are lower than those for MRF, yet the relationship between the three visible maxima to the ultraviolet peak is similar for each protein. The difference in the absolute values is very likely due to the presence of 1 mol of tryptophan in PPNR and its absence in MRF.

In view of the difference in tryptophan content a comparison of the absolute absorption spectra of these proteins is not meaningful. However, when the relative absorbance per unit of iron at 330, 420, and 465 nm due to the chromophoric group was calculated, the data obtained was essentially identical for PPNR, MRF, the Red Enzyme, and spinach ferredoxin (Table 1). The implication was that the chromophoric group in these proteins was the same (Hill and San Pietro, 1963).

Fry and San Pietro (1962) reported that PPNR contains "labile sulfide" in an amount stoichiometric to the iron content that is liberated as hydrogen sulfide upon acidification. Similar results were reported for the red protein of *Chlorella*, for spinach ferredoxin, and for the crystalline Clostridial ferredoxins. In a personal discussion with Philip Handler, I learned that three iron flavoproteins, dihydroorotic dehydrogenase, aldehyde oxidase, and xanthine oxidase also contain an amount of "labile sulfide" equivalent to their iron content. Hill and San Pietro (1963) stated in their review that this appears to be a property common to all non-heme iron proteins that undergo reversible oxidation–reduction. It is most likely that the iron is involved in electron transport catalyzed by these proteins and undergoes a reversible change in valence state. The redox potentials of spinach ferredoxin (Tagawa and Arnon, 1962), of Clostridial ferredoxin (Tagawa and Arnon, 1962) and of PPNR (Hill and San Pietro, unpublished data) are similar and close to that of the hydrogen electrode at neutral pH. It seems reasonable to assume that there is a correlation between the low redox potential of these proteins and the fact that they contain non-heme iron and "labile sulfide" in equivalent amounts.

Table 2. Correlation between extent of photobleaching and reduction of iron

Illumination time (min)	% Bleaching 420 mμ	460 mμ	% Total iron in ferrous state	% Fe^{++}/average % bleaching
0.5	34	32	19	0.58
1.0	74	74	33	0.45
3.0	97	97	44	0.45

Source: Fry et al. (1963).

Although it was inferred that the reduction of non-heme proteins correlated with a change in the valence state of the metal, definitive proof in support of this correlation was lacking. Nor was it known whether all, or only part, of the metal underwent reversible oxidation–reduction during the electron donation activity. Fry et al. (1963) provided answers to both questions when they reported that one half of the iron in PPNR underwent a valence change when the protein was reduced by illuminated chloroplasts. In the oxidized state, all of the metal was in the ferric iron state. Following illumination of the protein and the blocking of sulfhydryl groups to prevent further reduction of the remaining ferric iron, the amount of ferrous iron present was assessed spectrally as the ferrous-orthophenanthroline complex at 510 nm (see Table 2 below).

It was important to demonstrate further the reversibility of the oxidation–reduction cycle and restoration of the original spectrum and activity. When the photobleached PPNR was reoxidized by TPN in the presence of chloroplasts, there was essentially

Table 3. Amount of ferrous iron after photobleaching followed by reoxidation with TPN

Illumination iron in time (min)	% Bleaching		TPN	% Restoration of original spectrum		% Total ferrous state
	420 mμ	460 mμ		420 mμ	460 mμ	
2	38	40	+	98	98	7
5	85	86	+	93	92	9
8	93	95	+	94	93	11
5	87	88	−			43

Each reaction mixture contained 2.6 mg PPNR (equivalent to 0.237 μmol iron), chloroplasts equivalent to 18.4 μg chlorophyll, 0.5 mg glucose oxidase, 10 mg glucose, and 135 μmol Tris–HCl buffer, pH 7.45, in a total volume of 2.8 ml. Where indicated, 1.1 μmol TPN was added after illumination. In a dark control in the absence of TPN, 6% of the total iron was in the ferrous state. The data presented above have been corrected for this value. Source: Fry et al. (1963).

Table 4. Reversal of photobleaching by TPN and recovery of enzymatic activity

Illumination time, min	% Bleaching		Time, min, in dark before TPN	% Restoration of original spectrum		% Original activity
	420 mμ	460 mμ		420 mμ	460 mμ	
5	85	86	5	93	94	92
5	81	81	10	92	91	93
5	77	80	25	91	91	89

Source: Fry et al. (1963).

complete restoration of the original spectrum of the protein (see Tables 3 and 4). In a control experiment, water was added in place of the TPN solution (Table 3, last row), and the absorbance change observed was negligible.

It is seen that in the control mixture to which TPN was not added, 43% of the total iron was in the ferrous state (Table 3). After reoxidation with TPN, the percentage of iron in the ferrous state is greatly decreased (Table 3).

The photobleached PPNR was stable when kept in the dark up to 25 min before addition of TPN (Table 4). The enzymatic activity of the PPNR used in these experiments was again determined after photobleaching and subsequent reoxidation by TPN. It is seen that there was very little loss in enzymatic activity (Table 4, last column).

Finally, since PPNR was inferred to function as an electron carrier between the photosystem and $NADP^+$ reduction, it was important to demonstrate that the kinetics of PPNR reduction (and reoxidation) were equal to, or faster than, the kinetics of $NADP^+$ reduction. When PPNR was purified to a degree sufficient for optical tests Chance and San Pietro (1963) demonstrated that the rate of the light-induced bleaching was sufficient to explain the rate of $NADP^+$ reduction. In brief, it was important to know whether or not the spectroscopically identifiable change is part of the action of PPNR. As seen in section A of Fig. 4, the reduction of PPNR began almost immediately upon illumination.

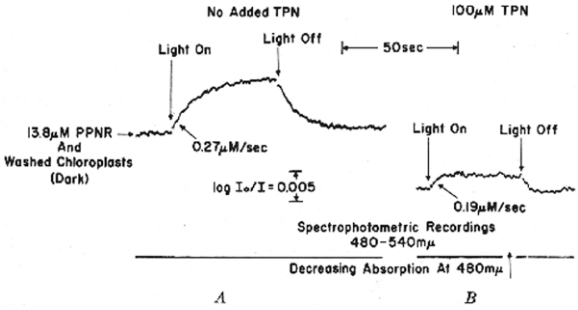

Fig. 4. (A) Kinetics of bleaching of 13.8 μM PPNR in the presence of chloroplast (2.5 μg chlorophyll/ml) but in the absence of $NADP^+$. The time and absorbancy scales are indicated on the diagram. A decrease of absorbancy at 480 mμ with respect to 540 mμ corresponds to an upward deflection of the trace. The moments at which the lights turn on and off are marked on the figure. (B) An experiment identical to that of Fig. 3A except that 100 μM $NADP^+$ is present. Source: Chance and San Pietro (1963).

The initial rate of reduction was 0.27 μM/sec and the amplitude of the effect corresponds to 3.9 μM oxidized or 28% of the 13.8 μM PPNR. In this case the activity of the chloroplasts in reducing PPNR was measured directly, without added $NADP^+$. The rate corresponds to 390 μmol of PPNR reduced/mg chlorophyll/h at 260 °C.

The chloroplast–PPNR system was tested in the same concentration of $NADP^+$ used in Fig. 4 and the rate of $NADP^+$ reduction measured at 340 nm was

0.1 μM/sec. This value is about one half of the rate of PPNR reduction in the presence of $NADP^+$ (section B of Fig. 4) and one third of the rate observed in the absence of $NADP^+$. The overall activity corresponded to 140 μmol $NADP^+$ reduced/mg chlorophyll/h at 260 °C.

The observation that PPNR is reduced more rapidly than $NADP^+$ shows that the reduced form has the potentiality of acting as an electron carrier between the chloroplasts and $NADP^+$.

III. Ferredoxin:$NADP^+$ Oxidoreductase

San Pietro and Lang (1958) found that the partially purified PPNR catalyzed the reduction of both TPN and DPN. In these studies the initial rate of reduction of DPN was about 70% of the rate observed with TPN. However, when PPNR was further purified, it catalyzed the reduction of only TPN; DPN was not reduced. These observations were explained on the basis that the PPNR is specific for TPN; the reduction of DPN was thought to require a second protein in addition to PPNR. It was suggested that this second protein that was present in the partially purified PPNR, but absent in the purified PPNR, would exhibit pyridine nucleotide transhydrogenase activity. Arnon et al. (1957) explained their observation that DPN was as effective as TPN in stimulating photosynthetic phosphorylation, provided either a large amount of chloroplast material or an excess of chloroplast extract was used, in a similar manner. However, at that time the presence of pyridine nucleotide transhydrogenase in spinach had not been demonstrated. Avron and Jagendorf (1956) reported the isolation and purification of a TPNH diaphorase[6] from washed spinach chloroplasts.[7] In the discussion of this paper they state that the diaphorase preparation catalyzed the reduction of the acetylpyridine analogue of TPN by TPNH. The similar analog of DPN did not serve as a hydrogen acceptor. The significance of this observation was recognized when the pyridine nucleotide transhydrogenase was purified and shown to be identical to the TPNH diaphorase of Avron and Jagendorf.

The occurrence of pyridine nucleotide transhydrogenase in a partially purified preparation of PPNR was reported by Keister and San Pietro (1959). The further purification of the partially purified PPNR was accomplished by the precipitation of the enzyme with protamine sulfate. It is during this purification step that the transhydrogenase and PPNR activities separate and that the specificity of PPNR for TPN reduction becomes apparent. The transhydrogenase was purified by Keister et al. (1960) and certain of its properties studied. The enzyme is specific for TPN with respect to the hydrogen donor and acceptor and the absorption spectrum of the purified enzyme is typical of a flavin. In addition, the flavin constituent of the enzyme has been shown to be flavin adenine dinucleotide (FAD). The protein was obtained in crystalline form in 1963 by Shin et al., from spinach under the name of TPN reductase.

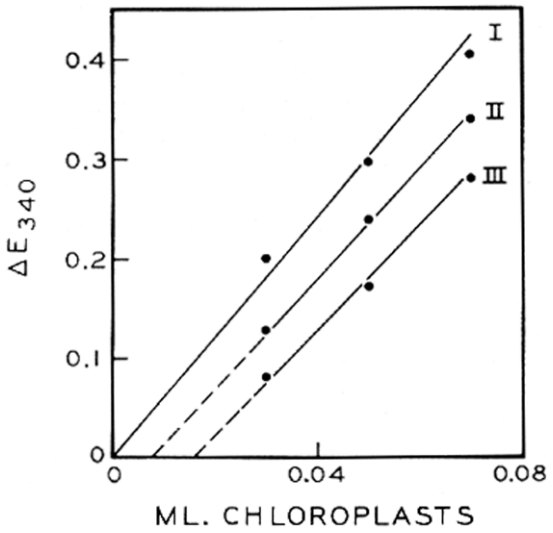

Fig. 5. Effect of antibody on photochemical reduction of TPN. The antibody preparation contained 17.4 mg protein/ml. Curve I: no antibody; curves II and III: 0.004 and 0.008 ml antibody, respectively. Time of illumination: 2.5 min. Source: Keister et al. (1962).

It was found that the reduction of TPN, as well as DPN, by illuminated chloroplasts requires both PPNR and transhydrogenase (Keister et al., 1962).

The experimental approach used to demonstrate the requirement for transhydrogenase was to prepare an antibody to the purified protein. The antibody inhibited the reduction of both pyridine nucleotides and the inhibitory effect of the antibody could be alleviated by the addition of purified transhydrogenase. The inhibitory effect of the antibody on TPN reduction, as well as the other activities catalyzed by this protein, is shown in Figs. 5 and 6.

Using the antibody technique it was possible to estimate that chloroplasts equivalent to 1 mg of chlorophyll contain sufficient transhydrogenase to catalyze the reduction of 120 μmol of TPN per hour. It is understandable, therefore, that the photochemical reduction

[6] Diaphorase catalyzes the oxidation of TPNH (NADPH) in the presence of an electron acceptor.

[7] In 1956, Andre Jangendorf and I were colleagues in the Biology Department of the Johns Hopkins University.

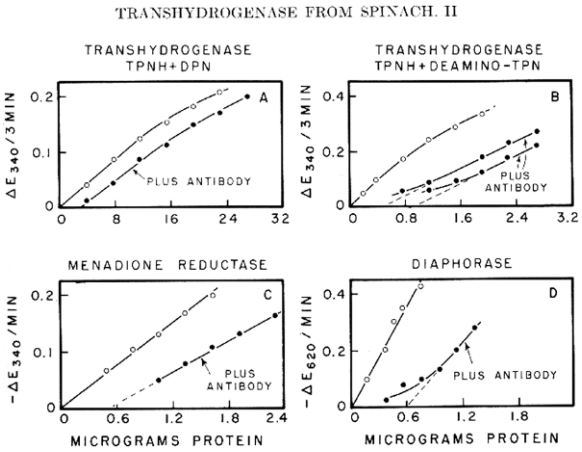

Fig. 6. Inhibitory effect of antibody. The antibody preparation contained 17.4 mg protein/ml. The volume of antibody used was: A, 0.03 ml; B, 0.005 ml for the middle curve and 0.01 ml for the lower curve; C and D, 0.005 ml. Source: Keister et al. (1962).

of TPN could be observed in the absence of added transhydrogenase and was thought originally to require only PPNR.

Tagawa and Arnon (1962) and Shin et al. (1963) reported similar results using two different experimental approaches. First, they reasoned that it should be possible to use hydrogen and hydrogenase in place of illuminated chloroplasts to provide the reducing potential necessary for the reduction of TPN. According to expectation, the reduction of TPN by hydrogen and hydrogenase was shown to occur only when both spinach ferredoxin and TPN reductase were present. The second approach used by them was to extract the TPN reductase from the chloroplasts. The extracted chloroplasts were unable to photoreduce TPN in the presence of only added spinach ferredoxin; TPNH formation was observed upon the subsequent addition of TPN reductase.

IV. Epilogue

Some four decades ago it was known that the reduction of pyridine nucleotides by illuminated chloroplasts requires the presence of two proteins, Fd and Fd:$NADP^+$ oxidoreductase, which are of prime importance in the conversion of electromagnetic energy into useful chemical free energy in the form of NADPH and adenosine triphosphate (ATP).[8] Very fortunately, the coenzymes, NAD and $NADP^+$, have in their reduced states the important property of not being oxidized directly by molecular oxygen at an appreciable rate. This property of the reduced pyridine nucleotides allowed for the study of a partial system derived from green plants under aerobic conditions. Provided that the two specific proteins are present, chloroplasts will catalyze the following reaction in absorbed light:

$$\mathrm{Pi} + \mathrm{ADP} + \mathrm{NADP^+} + \mathrm{H_2O} \leftrightarrow \mathrm{NADPH} + \mathrm{H^+} + \mathrm{ATP} + 1/2\mathrm{O_2}$$

The energy generated, together with additional ATP formed by cyclic photophosphorylation, is used for cell growth and reproduction.

As detailed in subsequent chapters, some 40 years later we realize how simplistic was our view of the electron transport pathway involving Photosystem I. At what time in the future will today's views suffer the same fate?

V. Addendum

A. Role of Non-Heme Proteins in Energy Conversion

The ubiquity of the non-heme iron, labile sulfide-containing proteins in biological systems and their role in energy conversion processes was only beginning to be realized in the mid-1960s. The initial discovery of the bacterial and plant ferredoxins in the 1950s focused primarily on their role in electron transport. The bacterial and plant ferredoxins are relatively simple proteins of low molecular weight (<20,000) and have no other detectable cofactors. The discovery of more complex non-heme iron proteins with higher molecular weights (>20,000) and which contains cofactors such as flavins, Coenzyme Q, etc., was coincident with their role in energy conserving processes. By the mid-1960s, non-heme iron proteins were shown to function in mitochondrial electron transport and nitrogen fixation as well as photosynthetic electron transport. Clearly, the importance of non-heme iron proteins was beginning to approach that of the heme proteins. I believe the current view is that they are equally important.

I was fortunate to convene a symposium in 1965 entitled "Non-Heme Iron Proteins: Role in Energy Conversion." Prior to the time of this symposium the problem of energy conversion was hardly even mentioned mainly because the focus earlier (1950s) had been on the simple bacterial and plant proteins. The more recent (early 1960s) research dealt with complex non-heme

[8] Although not discussed herein, photosynthetic electron transport from water to NADP results in ATP production stoichiometric to pyridine nucleotide reduction.

iron proteins such as aldehyde oxidase, which contains ubiquinone-Coenzyme Q, flavin, iron, labile sulfide, and molybdenum. This enzyme was proposed as a model for the electron transport chain in mitochondria because its susceptibility to inhibitors such as amytal, antimycin, and oligomycin is reminiscent of oxidative phosphorylation in mitochondria.

The late Professor Efriam (Ef) Racker, a preeminent biochemist, chaired the last session of the symposium and ended his Chairman's Remarks as follows: "This morning we shall hear from Dr. Butow that there is a non-heme iron linked electron transport system in mitochondria which appears to be closely linked to the process of oxidative phosphorylation. Indeed, it begins to look as if non-heme iron (NHI) may become almost as important to studies of energy conversions as NIH. The remarkable vision of the organizer of this symposium, who selected the title before a direct relationship between non-heme iron proteins and energy conversion was established must be admired." As the sole organizer of that symposium, I was, and will always be, grateful to Ef Racker for his kind and gracious remark!

References

Arnon DI (1951) Extracellular photosynthetic reactions. Nature 167: 1008–1010

Arnon DI, Whatley FR and Allen MB (1957) Triphosphopyridine nucleotide as a catalyst of photosynthetic phosphorylation. Nature 180: 182–185

Avron M and Jagendorf AT (l956) A TPNH diaphorase from chloroplasts. Arch Biochem Biophys 65: 475–490

Chance B and San Pietro A (1963) On the light-induced bleaching of photosynthetic pyridine nucleotide reductase in the presence of chloroplasts. Proc Natl Acad Sci USA 49: 633–638

Fry KT and San Pietro A (1962) Studies on photosynthetic pyridine nucleotide reductase. Biochem Biophys Res Commun 9: 218–221

Fry KT, Lazzarini RA and San Pietro A (1963) The photoreduction of iron in photosynthetic pyridine nucleotide reductase. Proc Natl Acad Sci USA 50: 652–657

Gewitz HS and Volker FR (1962) On the respiratory enzyme of *Chlorella*. Z Physiol Chem 330: 124–131

Hill R (1951) Oxidoreduction in chloroplasts. Symp Soc Exp Biol 5: 222

Hill R and San Pietro A (1963) Hydrogen transport with chloroplasts. Z Naturforsch 186: 677–682

Keister DL and San Pietro A (1959) Pyridine nucleotide transhydrogenase from spinach. Biochem Biophys Res Commun 1: 110–114

Keister DL, San Pietro A and Stozenbach FE (1960) Pyridine nucleotide transhydrogenase from spinach: I. Purification and properties. J Biol Chem 235: 2989–2996

Keister DL, San Pietro A and Stolzenbach FE (1962) Pyridine nucleotide transhydrogenase from spinach: II. Requirement of enzyme for photochemical accumulation of reduced pyridine nucleotides. Arch Biochem Biophys 98: 235–244

Mortenson LE, Valentine RC and Carnahan JE (1962) An electron transport factor from *Clostridium pasteurianum*. Biochem Biophys Res Commun 7: 448–452

San Pietro A and Lang HM (1956) Accumulation of reduced pyridine nucleotides by illuminated grana. Science 124: 118–119

San Pietro A and Lang HM (1957) Incorporation of deuterium into oxidized pyridine nucleotides by illuminated grana. J Biol Chem 227: 483–493

San Pietro A and Lang HM (1958) Photosynthetic pyridine nucleotide reductase: I. Partial purification and properties of the enzyme from spinach. J Biol Chem 231: 211–229

Shin M, Tagawa K and Arnon DI (1963) Crystallization of ferredoxin-TPN reductase and its role in the photosynthetic apparatus of chloroplasts. Biochem Z 338: 84–96

Tagawa K and Arnon DI (1962) Ferredoxins as electron carriers in photosynthesis and in the biological production and consumption of hydrogen gas. Nature 195: 537–543

Tolmach LJ (1951) Effects of triphosphopyridine nucleotide upon oxygen evolution and carbon dioxide fixation by illuminated chloroplasts. Nature 167: 946–948

Vishniac W and Ochoa S (1951) Photochemical reduction of pyridine nucleotides by spinach grana and coupled carbon dioxide fixation. Nature 167: 768–769

Chapter 2

The Discovery of Bound Iron–Sulfur Clusters in Photosystem I by EPR Spectroscopy

Richard Malkin*
Department of Plant and Microbial Biology, University of California, Berkeley, 111 Koshland Hall, Berkeley, CA 94720-3102, USA

Summary

The discovery of bound iron–sulfur proteins in chloroplast membranes was made in 1971 using EPR spectroscopy. This chapter describes the events leading up to that discovery and the conclusions drawn concerning the structure and function of these proteins.

I. Ferredoxins and Laccase

I was introduced to iron–sulfur proteins shortly after I came to graduate school in the Department of Biochemistry at UC Berkeley in 1962. Although I had a strong interest in enzyme mechanisms, I chose to work in the laboratory of Jesse Rabinowitz, a microbial biochemist who was involved in studies of metabolic processes in the anaerobic bacteria, Clostridia. In the early 1960s, the laboratory had become involved with a new group of electron transfer proteins, the ferredoxins, which were required for a variety of biochemical reactions in Clostridia, including pyruvate oxidation and nitrogen fixation. Ferredoxin from *Clostridium pasteurianum* was first discovered by Mortenson et al. (1962) and was subsequently shown to be present in a number of anaerobic bacteria as well as photosynthetic bacteria. Subsequently, ferredoxins were also discovered in chloroplasts of plants and in other oxygen-evolving photosynthetic organisms where they played a key role in the photosynthetic light reactions (see San Pietro, Chapter 1 of this volume). Little was known about the chemical nature of these proteins, other than they contained non-heme iron and an unusual form of sulfur, usually known as "acid-labile sulfur" or "inorganic sulfide," which was released from the protein as H_2S upon acidification. In the Rabinowitz lab, two postdoctoral fellows, Bob Buchanan and Walt Lovenberg, were leading the investigations of the chemical properties of Clostridial ferredoxin and showed this protein contained equivalent amounts of iron and sulfide. In this case, the Clostridial protein contained 8 mol of iron per mole of protein and 8 mol of inorganic sulfide per mole of protein. My initial thesis project, however, did not deal with the chemistry of ferredoxin but rather dealt with the question of how the protein was synthesized, and my official thesis title was "The Biosynthesis of Ferredoxin." Before even beginning this project, two reports came out from Bayer et al. (1965) and Bayer and Parr (1966), which claimed that the inorganic sulfide in ferredoxin originated from the cysteine residues in the protein. Upon seeing this report, my efforts were immediately redirected toward testing this proposal and attempting to define the source of the sulfide in ferredoxin. A major breakthrough came when I discovered conditions for the reconstitution of ferredoxin from

* Author for correspondence, email: dickm@nature.berkeley.edu

Abbreviations: EPR – electron paramagnetic resonance; PS I – Photosystem I.

John H. Golbeck (ed): Photosystem I: The Light-Driven Plastocyanin:Ferredoxin Oxidoreductase, 9–14.

an isolated apoferredoxin, totally free of iron and sulfide (Malkin and Rabinowitz, 1966). If ferredoxin was treated with a mercurial compound, the iron and inorganic sulfide were released from the protein and an apoprotein could be isolated. The apoprotein, which still contained eight cysteine residues, could be reconstituted by the addition of iron and Na_2S in the presence of a thiol compound, such as 2-mercaptoethanol. The reconstituted ferredoxin was indistinguishable from the native protein with respect to enzymatic activity, spectra, and iron and sulfide content. This experiment proved conclusively that the inorganic sulfide in ferredoxin did not originate from cysteine residues but rather existed in a different form that could be resolved from the protein independent of the sulfur-containing amino acids in the polypeptide chain.

I digressed to this discussion of my first experiments with Clostridial ferredoxin because this was my introduction to this class of electron carriers, and little did I know at the time that the broader group of iron–sulfur proteins would be the focus of my research career over the next 40 years. In 1967, I finished my Ph.D. work with a thesis entitled "Studies on the Chemical Nature of Bacterial Ferredoxin," never having faced the problem of biosynthesis. Toward the end of my graduate school days, it became apparent to me that various spectroscopic techniques were powerful tools for studying the structure and function of metalloproteins. For example, Helmut Beinert and his colleagues at the University of Wisconsin used electron paramagnetic resonance (EPR) spectroscopy as a technique that allowed the study of iron–sulfur proteins in mitochondrial membranes and submitochondrial particles. Wanting to continue to study metalloproteins, I decided to do postdoctoral work in a laboratory that would allow me to learn more about EPR, and my final choice turned out to be an excellent one. In 1969 I moved to the Department of Biochemistry at the University of Göteborg in Sweden to join the laboratory of Professor Bo Malmström. The Malmström lab included both biochemists and biophysicists, the latter using EPR to study copper-containing proteins. After a short time in the lab, I decided to work on the so-called "blue" copper-containing oxidase, laccase. Laccase was an unusual oxidase that contained four copper atoms per mole of protein, including a single "blue" copper atom with unusual spectroscopic properties. The enzyme catalyzed the four-electron reduction of oxygen to water. This protein was ideal for biophysical characterization because it could be prepared in large quantities in a pure state. Collaborating with another American in the lab, Jim Fee, we were able to characterize the multiple copper atoms in the enzyme and provide details on the mechanism of the oxidase reaction. EPR was particularly useful with this protein because two of the four copper atoms, known as type 1 and type 2 cupric atoms, could be readily differentiated on the basis of their EPR properties. We also discovered that the remaining two copper atoms in the protein, although formally in the cupric state, were EPR-silent because of a proposed spin coupling mechanism (Fee et al., 1969).

II. Photosynthesis and Fe/S Clusters

In 1969, I had the opportunity to return to Berkeley as a staff member in the Department of Cell Physiology, chaired by Daniel Arnon. At that time, the department was more like a research institute, the focus of the program being biochemical aspects of photosynthesis. The department was comprised of a highly professional group of Ph.D. level scientists, supported by a skilled group of technicians. Among the scientists were Bob Buchanan, who moved from the Department of Biochemistry and was engaged on studies of ferredoxins in photosynthetic systems and Dave Knaff, who had come to Berkeley shortly before me to study photosynthetic processes in plants. As a physical biochemist, Dave introduced me to the intricacies of redox potentiometry, a technique that we both used extensively in characterizing metalloproteins in biological systems. I came to Cell Physiology because of my familiarity with copper-containing proteins and the great interest in plastocyanin, a blue copper-containing protein that was a presumed member of the chloroplast electron transport chain.

In addition to my new colleagues in Cell Physiology, I also had the opportunity to become reacquainted with Alan Bearden upon my return to Berkeley. I had met Alan at a Gordon Conference on Metal Ions in Biology in 1968, at which time Alan was a faculty member at UC San Diego where he had studied the structure of iron–sulfur proteins using Mössbauer spectroscopy. He moved to the Donner Laboratory on the Berkeley campus shortly before my arrival in 1969 and had initiated a project using EPR spectroscopy to study the role of metals in biological systems. Alan's familiarity with biophysical aspects of iron–sulfur proteins and EPR complemented my background, which was more along the biochemical direction. In early discussions, Alan and I decided to look at a perplexing problem that existed in our understanding of plant photosynthesis. Two EPR signals had been identified in plants, known

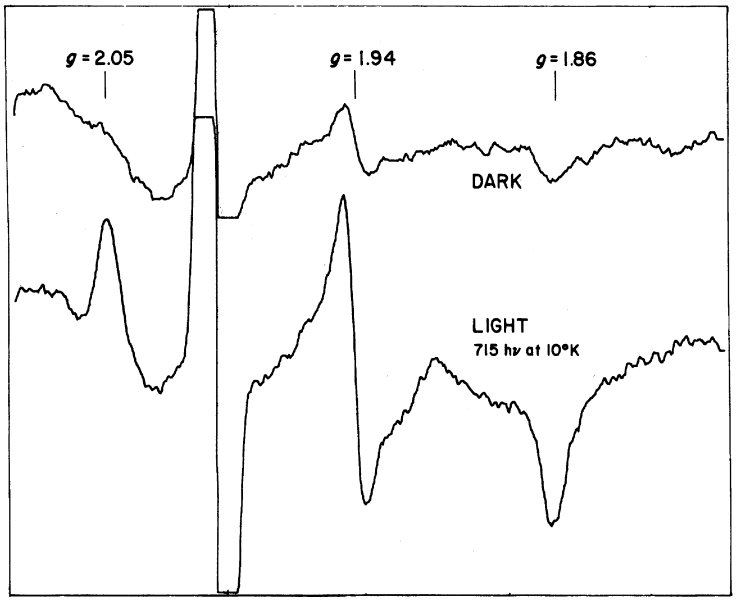

Fig. 1. Photoreduction of a bound iron–sulfur center in intact chloroplasts after illumination at 10 K with far-red (715 nm) light. The EPR spectrum was recorded at 20 K. Source: Malkin R and Bearden AJ (1971).

as Signal I and Signal II (Commoner et al., 1956). The first of these was associated with Photosystem I (PS I) and a number of studies had shown that this narrow free-radical signal was associated with the oxidized form of P700 (Beinert et al., 1962). The second signal, Signal II, was associated with Photosystem II (PS II) and its origin was much more controversial but was finally shown to arise from an oxidized tyrosine residue involved in water oxidation (Barry and Babcock, 1987). Signal I shared a common feature with other components known to function as reaction center chlorophylls – these molecules underwent photooxidation at cryogenic temperatures, that is, temperatures as low as that of liquid helium (4.2 K). The reasoning behind the temperature-insensitive nature of this photooxidative reaction was that the reaction only involved photon capture and did not involve chemical diffusion of molecules, and thus the so-called "primary reaction of photosynthesis" was independent of temperature. The perplexing result, however, was that although the photooxidation of the chlorophyll species involved in the primary reaction could be demonstrated by EPR through the detection of a free-radical species resulting from the loss of an electron from the chlorophyll, no paramagnetic reduced species had been identified by EPR, although we knew the electron lost from P700 had to be transferred to another component, making it an additional paramagnetic species. We reasoned that one possible reason the reduced component had not been identified by EPR was that the reduced species might be a transition metal ion whose EPR signal could only be detected at very low temperatures. For example, it was known from the early EPR studies of ferredoxins that these iron–sulfur proteins had characteristic EPR signals in the reduced state (the so-called $g = 1.94$ EPR signal), but these were only observable at or near liquid helium temperatures and that these signals broadened at higher temperatures and became undetectable.

Our first EPR experiments were rather simple. I isolated intact spinach chloroplasts and took these preparations to the Bearden laboratory in the Donner Laboratory where the EPR equipment resided. We then incubated a chloroplast sample in the dark in the presence of ascorbate, which was followed by freezing in liquid nitrogen. The sample was then illuminated in an unsilvered Dewar at 77 K with a strong 1000-W light source. Our first illuminations were for fairly long times (minutes) because of the inefficiency of the illumination setup and the high concentrations of chlorophyll being used. The chloroplast sample was then analyzed in the dark by EPR, recording spectra at 10–20 K. A typical result with intact chloroplasts is shown in Fig. 1. After illumination at 77 K, there was an increase in EPR intensity at g-values of 2.05, 1.94, and 1.86. The large signal in the $g = 2.00$ region came from chloroplast free-radical signals and were not associated with the iron–sulfur signals. A comparison of the signal

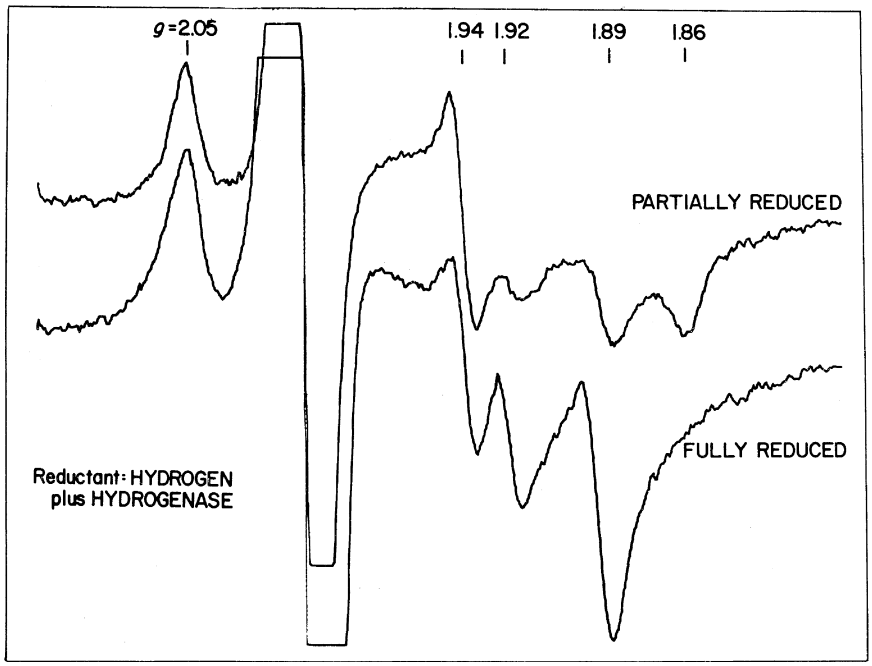

Fig. 2. EPR spectra of the iron–sulfur centers in intact chloroplasts after reduction in the dark with hydrogen and hydrogenase in the presence of methyl viologen. The EPR spectrum was recorded at 20 K. Source: Malkin R and Bearden AJ (1971).

observed in chloroplasts with that of purified soluble chloroplast ferredoxin (*g*-values of 2.05, 1.94, and 1.89) indicated a close similarity in *g*-values, although the chloroplast signals were considerably sharper than those from the soluble protein.

The light-induced signal in chloroplasts was consistent with other known EPR signals from reduced ferredoxin-type proteins from a variety of sources. To eliminate the possibility that we were simply observing the soluble ferredoxin in intact chloroplasts, we repeated this experiment with washed, broken chloroplasts, which were primarily composed of thylakoid membranes and were free of all soluble components, such as ferredoxin. The signals observed after low-temperature illumination were identical to those seen with whole chloroplasts, indicating these signals arose from a membrane-bound component. Another important observation at this time was that chemical reduction of chloroplast membranes in the dark by the addition of strong reducing agents, such as sodium dithionite or hydrogen gas, produced a more complicated EPR spectrum than that observed after illumination at cryogenic temperatures. As shown in Fig. 2, the EPR spectrum of a fully chemically reduced sample showed four *g*-values (2.05, 1.95, 1.93, and 1.89), and the *g*-value at 1.86 observed on photoreduction was absent in the fully chemically reduced sample. It was initially proposed that the chemical reduction spectrum consisted of two overlapping sets of *g*-values from two components, one with *g*-values of 2.05, 1.95, and 1.89 and a second with *g*-values of 2.05, 1.93, and 1.89. The *g*-value at 1.86 had apparently shifted to 1.89 upon reduction of the second component, and this is supported by the EPR spectrum of a partially reduced sample shown in Fig. 2. This complex spectrum could arise from the presence of two different iron–sulfur clusters in a single protein, with only one cluster undergoing photochemical reduction at cryogenic temperature, but both centers being capable of chemical reduction in the dark.

In our first report (Malkin and Bearden, 1971), we discussed our findings in terms of a "bound ferredoxin," not knowing whether chloroplast membranes contained a bound form of soluble ferredoxin or a new species. Our findings led to the conclusion that "this protein is either a primary electron acceptor or part of an electron acceptor complex in which electrons can be transferred directly to the ferredoxin at 77 K." This statement turned out to be prophetic as future studies led to a more complicated picture of the electron acceptor complex in PS I. After our initial report, our work was confirmed and extended by other workers, most notably by Mike Evans and coworkers in London (Evans et al., 1972) and by Bacon Ke and Helmut Beinert (Ke and Beinert,

1973) in a collaborative effort in Wisconsin and Ohio. We also continued to follow up our initial observations by showing that the photoreducible bound iron–sulfur protein was associated with PS I, using monochromatic illumination techniques and studies with enriched PS I fragments (Bearden and Malkin, 1972a,b). This series of experiments led to the concept that PS I contained two iron–sulfur clusters, known as Centers A and B,[1] one of which (Center A) was photoreduced at cryogenic temperatures. Our initial proposal, however, that the photoreducible Center A was the primary electron acceptor of PS I required further modification as more experimental work was done on these centers. The key observation that led to a modification of our proposal was the finding by McIntosh et al. (1975) that P700 oxidation at cryogenic temperatures could still occur under conditions where both iron–sulfur Centers A and B were fully reduced prior to illumination, leading to the conclusion that there was an electron acceptor in PS I that preceded Centers A and B. This led to the detection of an additional iron–sulfur center, Center X,[2] that preceded Centers A and B in the PS I electron acceptor complex. The *g*-values of Center X (2.08, 1.88, and 1.78) were sufficiently different from those of Centers A and B so that EPR detection, although experimentally difficult, was possible. Thus, a model for the PS I electron acceptor complex emerged in the mid-1970s that included three different iron–sulfur clusters, A, B, and X, with Center X being the first reducible cluster and Center A being the terminal acceptor of the complex.

While the biophysical aspects of the PS I electron acceptor complex were clarified in the 1970s, biochemical characterization of these components lagged. Finally, in the 1980s, we were able to isolate an iron–sulfur protein from chloroplast membranes by acetone extraction of well-washed membranes to remove soluble chloroplast ferredoxin (Wynn and Malkin, 1988). Matsubara and coworkers in Japan also isolated the same protein using a similar procedure (Oh-Oka et al., 1988). The isolated bound protein had properties that were reminiscent of bacterial-type ferredoxins, with a broad absorption band in 390 nm spectral region. The EPR spectrum of the isolated protein showed a complex signal that indicated the presence of two [4Fe–4S] clusters, presumably associated with Centers A and B, respectively. Amino acid sequence analysis of this isolated protein identified it as the product of the *PsaC* gene, which codes for a 9-kDa-polypeptide subunit in PS I. The protein contained eight cysteine residues in a pattern that was identical to those found in other bacterial-type ferredoxins, and it is known that two clusters of four cysteines coordinate with two [4Fe–4S] clusters in these proteins. An interesting discovery aside from our work on the isolation of the bound iron–sulfur protein of PS I was that we also found a second-bound iron–sulfur protein during our purification procedure, and the characterization of this protein resulted in its identification as the Rieske high-potential iron–sulfur protein, a component of the chloroplast cytochrome $b_6 f$ complex (Malkin and Aparicio, 1975).

The culmination of the structural work on the bound iron–sulfur centers in PS I came more recently from the elegant work of the German group of Witt–Saenger on the X-ray crystallographic structure of a PS I complex from *Synechococcus elongatus* (Schubert et al., 1997), now at a resolution of 2.5 Å (Jordan et al., 2001), and more recently, from the structure of the plant PS I complex by Ben-Shem et al. (2003) in Israel at a resolution of 4.4 Å. These structural analyses provided the details of the organization of the two iron–sulfur clusters in the PsaC protein and documented the unusual bonding of the [4Fe–4S] cluster of Center X by the PsaA and PsaB subunits of the reaction center complex. It has taken almost 30 years to move from the first spectroscopic signals of the iron–sulfur centers detected in whole chloroplasts to the molecular details of the structure of these centers and one can take some consolation that most of the predictions made from the biophysical and biochemical studies have been confirmed by the structural biologists.

Acknowledgments

This chapter is dedicated to the memory of two friends and colleagues with whom I had the pleasure of collaborating for a number of years: Alan Bearden and Philip Thornber. Alan and I worked together on various projects in photosynthesis in a creative and productive relationship that blended biophysics and biochemistry for over 20 years. Phil Thornber was a special friend who was also a collaborator with whom I shared thoughts on PS I over many years, both in Berkeley and in Los Angeles. I would also like to dedicate this chapter to my son, Daniel Malkin, whose passing at an early age left a personal void that can never be filled. His memory continues with two wonderful granddaughters. There are many other collaborators with whom I have had the pleasure to do science over the course of my career, including my students and postdoctoral

[1] Now known as F_A and F_B.
[2] Now known as F_X.

fellows, and although not naming them individually, they know they have contributed, and I am indebted to them. And, of course, my wife, Carole, has been an essential part of all of this. Finally, the work on PS I in my laboratory was exclusively supported by the Biophysics program of the National Science Foundation without which we could not have had any successes.

References

Barry B and Babcock GT (1987) Tyrosine radicals are involved in the photosynthetic oxygen-evolving system. Proc Natl Acad Sci USA 84: 7099–7103

Bayer E and Parr W (1966) Elimination of hydrogen sulfide from ferredoxin and cysteine methyl ester. Angew Chem Int Ed Engl 5: 840–841

Bayer E, Parr W and Kazamaier B (1965) Aufbau des ferredoxins des wirkstoffes der assimilations-vorgange. Arch Pharm 298: 196–201

Bearden AJ and Malkin R (1972a) Quantitative EPR studies of the primary reaction of photosystem I in chloroplasts. Biochim Biophys Acta 283: 456–468

Bearden AJ and Malkin R (1972b) The bound ferredoxin of chloroplasts: a role as the primary electron acceptor of photosystem I. Biochem Biophys Res Commun 46: 1299–1305

Beinert H, Kok B and Hoch G (1962) The light-induced paramagnetic resonance signal of photocatalyst P700. Biochem Biophys Res Commun 7: 209–212

Ben-Shem A, Frolow F and Nelson N (2003) Crystal structure of plant photosystem I. Nature 426: 630–635

Commoner B, Heise J and Townsend J (1956) Light-induced paramagnetism in chloroplasts. Proc Natl Acad Sci USA 42: 710–718

Evans MCW, Telfer A and Lord AV (1972) Evidence for the role of a bound ferredoxin as the primary electron acceptor of photosystem I in spinach chloroplasts. Biochim Biophys Acta 267: 530–537

Fee JA, Malkin R, Malmström BG and Vanngard T (1969) Anaerobic oxidation–reduction titrations of fungal laccase – evidence for several high potential electron-accepting sites. J Biol Chem 244: 4200–4207

Jordan P, Fromme P, Witt HT, Klukas O, Saenger W and Krauß N (2001) Three-dimensional structure of cyanobacterial photosystem I at 2.5Å resolution. Nature 411: 909–917

Ke B and Beinert H (1973) Evidence for the identity of P430 of photosystem I and chloroplast-bound-iron sulfur protein. Proc Natl Acad Sci USA 70: 2941–2945

Malkin R and Aparicio P (1975) Identification of a $g = 1.90$ high-potential iron–sulfur protein in chloroplasts. Biochem Biophys Res Commun 63: 1157–1160

Malkin R and Bearden AJ (1971) Primary reactions of photosynthesis: photoreduction of a bound chloroplast ferredoxin at low temperatures as detected by EPR spectroscopy. Proc Natl Acad Sci USA 68: 16–19

Malkin R and Rabinowitz JC (1966) The reconstitution of clostridial ferredoxin. Biochem Biophys Res Commun 23: 822–827

McIntosh AR, Chu M and Bolton JR (1975) Flash photolysis electron spin resonance studies of the electron acceptor species at low temperatures in photosystem I of spinach subchloroplast particles. Biochim Biophys Acta 376: 308–314

Mortenson LE, Valentine RC and Carnahan JE (1962) An electron transport factor from *Clostridium pasteurianum*. Biochem Biophys Res Commun 7: 448–452

Oh-Oka H, Takahashi Y, Kuriyama K, Saeki K and Matsubara H (1988) The protein responsible for centers A/B in spinach photosystem I: isolation with iron–sulfur cluster(s) and complete sequence analysis. J Biochem 103: 962–968

Schubert W-D, Klukas O, Krauß N, Saenger W, Fromme P and Witt HT (1997) Photosystem I of *Synechococcus elongatus* at 4Å resolution: comprehensive structure analysis. J Mol Biol 272: 741–769

Wynn RM and Malkin R (1988) Characterization of an isolated chloroplast membrane Fe–S protein and its identification as the photosystem I Fe–S_A/Fe–S_B binding protein. FEBS Lett 229: 293–297

Chapter 3

The Discovery of P430 and Work on Photosystem I Electron Acceptors FeS-X and A_0 at the Charles F. Kettering Research Laboratory

Bacon Ke*
6100 Horsemans Canyon Drive, Walnut Creek, CA 94595, USA

Summary

This article presents a brief historic account of the discovery of the electron acceptor P430 of green-plant Photosystem I (PS I) by optical spectroscopy. The spectro-kinetic and redox properties of P430 are described. A brief description of the recently-discovered P430 analogs, C-P430, in green-sulfur bacteria (Kusumoto et al., 1995) and its spectro-kinetic properties are also included. As an aid to the discussion, the PS I reaction center containing the primary donor (P700) and the series of electron acceptors is written as $\{P700\bullet A_0\bullet A_1\bullet FeS\text{-}X\bullet FeS\text{-}A/B(P430)\}Fd$. The chronological order of the discovery of the PS I electron acceptors is related to the fact that the slower decaying species are farther removed from the primary donor and technically more readily detected and thus discovered earlier. The sequence of electron transfers along the electron-acceptor chain in PS I is included here as a frame of reference to aid the discussion.

I. Introduction

Photosystem I (PS I) is a part of the photosynthetic apparatus of green plants, algae, and cyanobacteria. Light-induced charge separation in PS I is coupled with Photosystem II (PS II) through Cyt b_6f, resulting in oxygen evolution at PS II and $NADP^+$ reduction at

* Author for correspondence, email: baconke@comcast.net

Abbreviations: EPR – electron paramagnetic resonance; FeS-X – iron–sulfur cluster now known as F_X; FeS-A/B – iron–sulfur clusters now known as F_A and F_B; MV – methyl viologen; TMPD – N,N,N',N'-tetramethyl-phenylenediamine; PS I – Photosystem I.

John H. Golbeck (ed): Photosystem I: The Light-Driven Plastocyanin:Ferredoxin Oxidoreductase, 15–29.

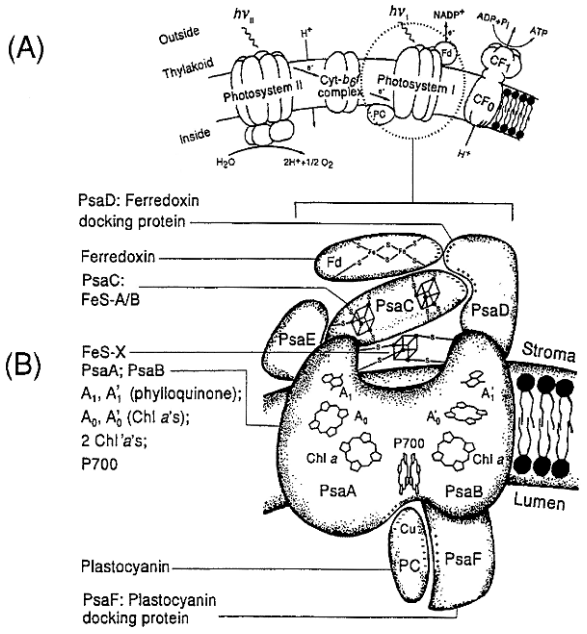

Fig. 1. Schematic representation of PS I. (A) Major components of the green-plant thylakoid. (B) Composite figure for PS I. (Adapted from Bruce et al., 1989 and Schubert et al., 1997).

PS I. The NADPH provides the reducing power for CO_2 fixation. A schematic representation of the photosynthetic thylakoid membrane in green plants is shown in Fig. 1A and an expanded view of PS I consisting of various structural polypeptides, pigment proteins, and redox cofactors is shown in Fig. 1B.

II. The Discovery of P430, the Optic-Spectroscopic Form of FeS-A/B

A. The Prelude

Various views on the electron acceptor in photosynthesis were considered since the late 1940s. Katz (1949) developed a physical model resembling charge separation in a barrier photocell; this model was further elaborated by Calvin (1961). In this model, the photoexcited porphyrin donates an electron to an acceptor to produce a species with a high reducing level that eventually reduces CO_2, with the electron or H-atom ultimately coming from water. The net result is the transfer of hydrogen from H_2O to CO_2.

The concept of chlorophyll serving as the primary electron acceptor was initiated by Kamen (1961) with a chlorophyll-dimer model. The energy of an absorbed photon removes an electron from one Chl of the [Chl•Chl] pair and places it on the other Chl to form [Chl^+•Chl^-]. Kamen's concept was prophetic and pertinent to the future developments of the concept of photosynthetic reaction centers.

Considering that ferredoxin is present in all photosynthetic cells investigated and also the physiological reductant with the most negative redox potential formed during photosynthesis, Arnon (1965) called it the "crucial" electron acceptor in the primary photochemical act. Vernon and Ke (1966) further suggested two possibilities with regard to ferredoxin reduction: (a) ferredoxin reacts directly with the photoexcited chlorophyll and gains an electron through a charge-transfer reaction; or (b) it reacts with a reduced chlorophyll produced by a preceding charge-transfer reaction.

During the mid-1960s, three groups of investigators, Zweig and Avron (1965), Kok et al. (1965), and Black (1966) found that chloroplasts could reduce highly electronegative viologen dyes with redox-potential values lying between −500 and −700 mV, which is considerably more negative than that of ferredoxin. These new findings therefore indicated that ferredoxin might not be the *initial* reductant produced photochemically in PS I. In the meantime, other new candidates emerged, which included the naturally occurring, low-potential (∼−0.7 V), unconjugated pteridine (Fuller and Nugent, 1969), a flavin-like compound (Wang, 1970). Three additional compounds were isolated from green-plant chloroplasts and algae, and all of which were suggested to be involved in the reduction of the primary electron acceptor of PS I. They included the "cytochrome *c* reducing substance," or CRS (Fujita and Myers, 1966), the "ferredoxin reducing substance" or FRS (Yocum and San Pietro, 1969), and a water-soluble factor released from lyophilized chloroplasts after treatment with diethylether, designated as "$S_{L,eth}$" (Regitz et al., 1970).

The search for the PS I primary electron acceptor eventually reached a turning point, with the discovery of the membrane-bound iron–sulfur proteins by Malkin and Bearden (1971) and the simultaneous discovery of the optic-spectral species "P430" by Hiyama and Ke (1971a). These two independent and apparently closely related investigations began to open up an active area of research for the PS I reaction center.

B. The Discovery of P430 by Optical Spectroscopy

The optic-spectral species P430 was discovered as a result of an observation by Tetsuo Hiyama, who was my postdoctoral associate at the time, of a visually

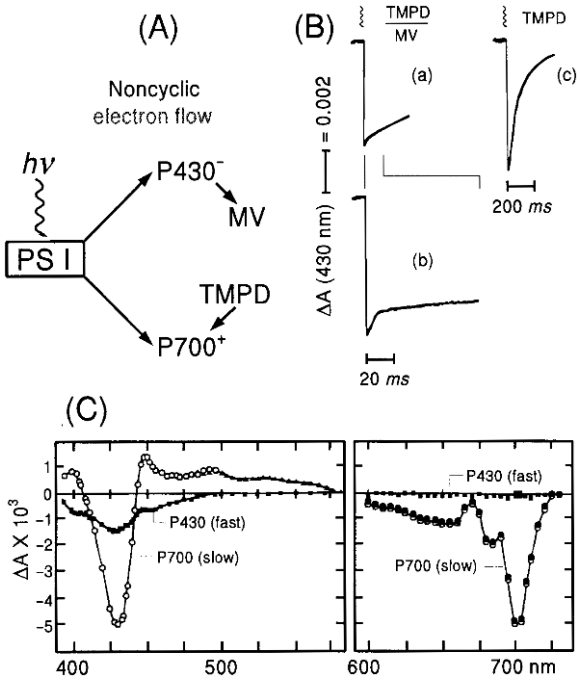

Fig. 2. (A) The scheme for "noncyclic electron flow" in PS I with reduced TMPD and methyl viologen serving as the artificial electron donor and acceptor, respectively. (B) Flash-induced absorbance changes at 430 nm due to noncyclic electron flow in digitonin-fractionated spinach PS I particles (D144) measured at two different time resolutions [(a) and (b)] and in the presence of reduced TMPD alone (c). (C) Difference spectra of P700 and P430 derived from kinetic plots made from the slow and rapid-decaying signals obtained in the light-induced noncyclic reaction as shown in (B)-(b). Source: Hiyama and Ke (1971a) and Ke (1973).

missing kinetic component in the flash-induced transient absorbance change produced by a PS I subchloroplast fragment (D-144) in a "noncyclic" electron-transport pathway (Hiyama and Ke, 1971a). The reaction medium contained *N*,*N*,*N*′,*N*′-tetramethylphenylenediamine (TMPD) plus ascorbate as an electron donor, and methyl viologen as an electron acceptor (Fig. 2A). At a relatively low time resolution [Fig. 2B-(a)], only a slow decay was observed. At a higher time resolution, an additional small and rapid-decaying signal could also be seen [Fig. 2B-(b)]. The slower phase with a decay time of ~600 msec and the small, rapid phase with a decay time of only a few ms were, respectively, attributed to the reduction of $P700^+$ by TMPD and the reoxidation of the presumed "primary" electron acceptor, later called "P430" (see below), by methyl viologen (MV) in a so-called "noncyclic electron flow" in the dark phase. In the presence of only TMPD [Fig. 2B-(c)], $P700^+$ and $P430^-$ recombine ("charge recombination") showing only a single kinetic component with a decay $t_{1/2}$ of ~40 msec. At the measuring wavelength of 430 nm, the amplitude of the absorbance change of the single kinetic component in charge recombination is, as expected, equal to the sum of the rapid and slow decay components due to ($P700^+ \rightarrow$ P700) and ($P430^- \rightarrow$ P430), respectively, in the noncyclic reaction.

The spectral profile of the primary donor P700 and the presumed PS I "primary" acceptor can then be obtained by plotting the amplitudes of the slow and rapid decay phases in the presence of reduced TMPD and MV, as shown in Fig. 2C. The difference spectrum constructed from the slow-decaying changes closely resembles that of P700 and represents the reduction of photooxidized $P700^+$ by the artificial donor TMPD. The difference spectrum constructed from the rapid-decaying changes mainly shows a broad band around 430 nm with minor absorbance changes elsewhere in the 400–500 nm region and the component responsible for it was therefore called "P430." Little or no absorbance changes in the red region could be found, which had the rapid kinetics corresponding to those in the blue region. Similar difference spectra were also obtained from Triton-fractionated particles from spinach and three kinds of P700-enriched particles prepared from cyanobacteria (Hiyama and Ke, 1971b).

C. Five Reaction Pathways in PS I

There are five possible fates for the photooxidized $P700^+$ and the photoreduced $P430^-$ formed in the photochemical charge separation in PS I, depending on reaction conditions. In addition to "charge recombination" and the "noncyclic electron flow" just described, the kinetic profiles of $P700^+$ and $P430^-$ in "cyclic electron flow," and in the "photoaccumulations" of either $P700^+$ or $P430^-$, were also demonstrated (Ke, 1973). The five reaction pathways of P700 and P430 in PS I are summarized in Fig. 3.

Soon after the discovery of P430, its "spectral profile" led Hiyama and Ke (1971a,b) and also Shuvalov et al. (1976) to suggest P430 to be closely related to an iron–sulfur protein on the basis of the resemblance of its difference spectrum to that of an iron–sulfur protein, presumably FeS-A/B. This suggestion was subsequently confirmed by Oh-oka et al. (1990) who isolated the native FeS-A/FeS-B protein and found its absorption spectrum to closely resemble the difference spectrum of P430 shown above.

When P430 was initially found, it was thought to be the "closest" reaction partner of P700, i.e., the

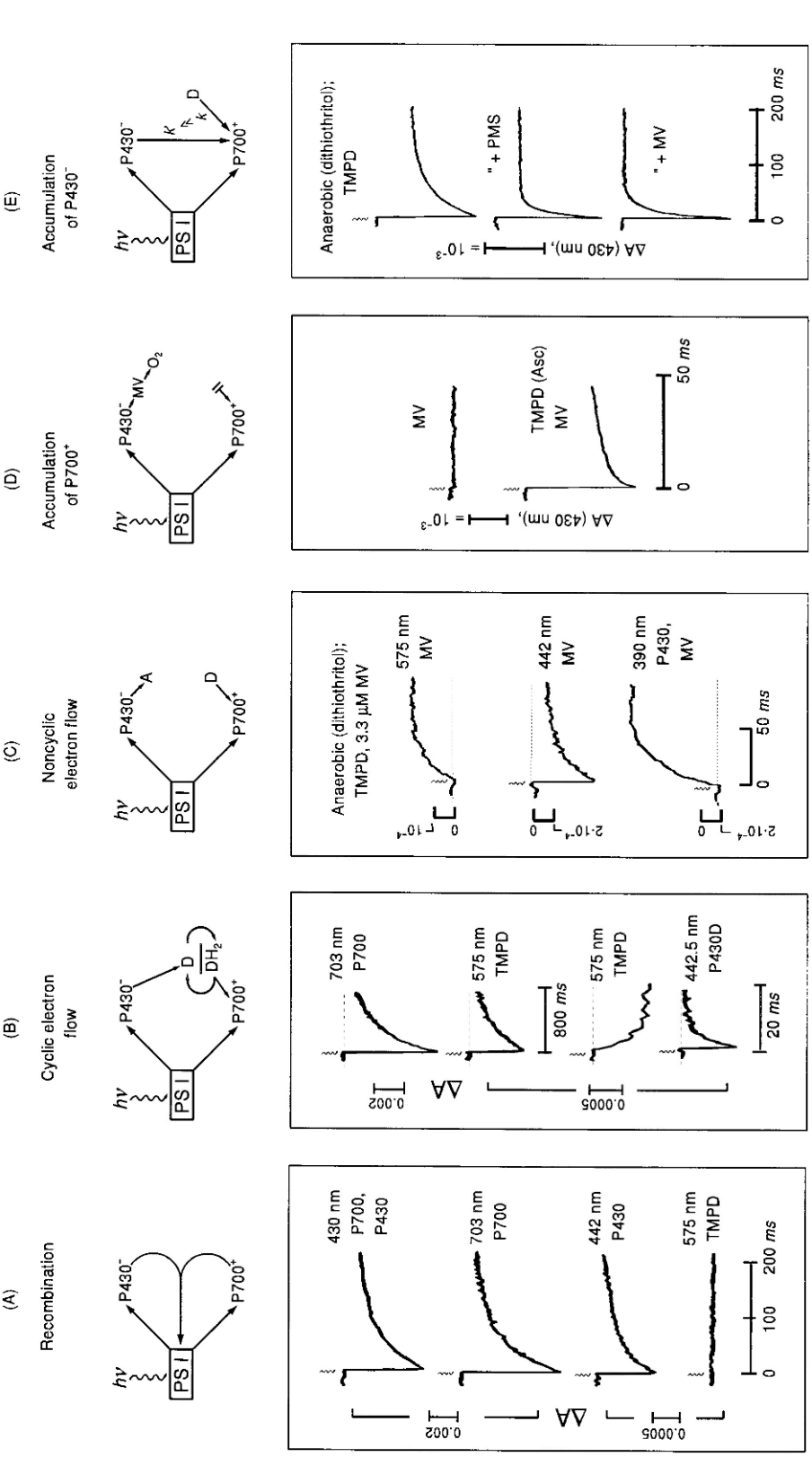

Fig. 3. Five possible fates of the primary oxidant, $P700^+$, and the primary reductant, $P430^-$, formed in the photochemical reaction in PS I. (A) Charge recombination. (B) Cyclic electron flow. (C) Noncyclic electron flow. (D) Photoaccumulation of $P700^+$. (E) Photoaccumulation of $P430^-$. Each case is illustrated with experimental results with PS-I D144 particles. Source: Ke (1973).

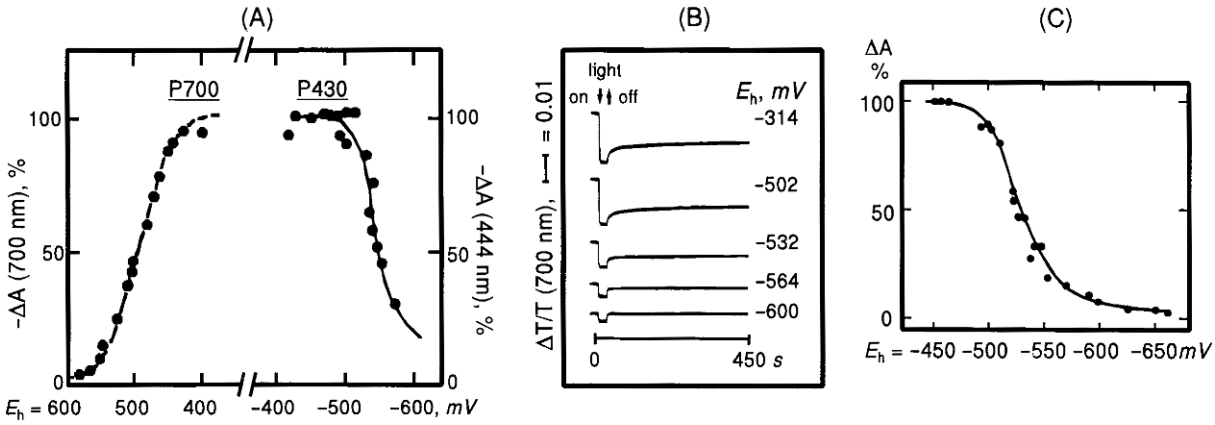

Fig. 4. (A) Dependence of the amplitude of light-induced absorbance changes due to P430 reduction (and also P700 oxidation) on redox potential. (B) Redox titration of PS-I particles (TSF-I) at pH 11 monitored by light-induced P700 absorbance changes at 86 K. (C) Plot of the slow decay component at 700 nm in (B) vs. the imposed potential. Source: (A) from Shuvalov et al. (1976); (B, C) from Ke et al. (1977).

"primary" electron acceptor, of PS I. As we know now, however, P430 is preceded by several earlier acceptors (A_0, A_1, and FeS-X), which undergo even faster electron transfers.

D. Correlation of P430 with FeS-A/B by Freeze-Quenching EPR and Redox Potentiometry

A definitive identification of P430 discovered by optic spectroscopy with FeS-A/B discovered by EPR spectroscopy could best be made by spectro-kinetic measurements. However, since the EPR signals of FeS-A/B are detectable only at ca. 15 K, the decay time of $(FeS\text{-}A/B)^-$ is prohibitively long, and no meaningful direct correlation is practicable. Low-temperature EPR spectroscopy showed that the onset times of P700 photooxidation and FeS-A photoreduction are both rapid and essentially not resolvable. Ke et al. (1974) carried out "freeze-quenching" experiments in an attempt to correlate P430 and FeS-A. A dark-adapted PS I particle cooled to 13 K was first illuminated to produce $P700^+$ and $FeS\text{-}A^-$. The sample was then rapidly brought to a higher temperature ranging from 75 to 225 K for various time periods, and then very rapidly quenched to 13 K for EPR analysis. In all cases, the extent of recovery, i.e., amount of P700 rereduced and FeS-A reoxidized, was equivalent. The decay behavior found in this fashion also agreed with that subsequently obtained from light-induced optical absorbance changes in PS I at low temperatures (Ke et al., 1977).

P430 and FeS-A/B may be correlated on the basis of their redox potentials. At first, the approximate E_m value of P430 at room temperature was estimated to be between −500 and −600 mV by Hiyama and Ke (1971b) on the basis of its ability to reduce certain exogenous electron carriers, including low-potential viologen dyes. The E_m values of FeS-A/B were directly determined by redox potentiometry and monitored by EPR spectroscopy (Ke et al., 1973); the midpoint potentials of FeS-A and FeS-B were estimated to be −530 and −570 mV, respectively.

Shuvalov et al. (1976) later determined the redox potential of P430 at room temperature by directly monitoring the amplitude of its light-induced absorbance changes at 444 nm (near the isosbestic point of P700) as a function of the imposed potential on a PS I particle (DT175). As shown by the titration curve in Fig. 4A, the absorbance-change amplitude due to P430 remained unchanged when the potential was decreased to −500 mV, but began to decrease below −500 mV, with just about 50% of the signal remaining at −550 mV, agreeing with the E_m value directly determined for FeS-A by EPR-potentiometry (Ke et al., 1973).

Subsequently, Ke et al. (1977), in an attempt to correlate P430 with FeS-A/B, measured the light-induced changes in both the optical and EPR spectra of P700 at 86 K as a function of the imposed potential. As shown in Fig. 4B, the biphasic decay consists of ∼20% rapid-decaying phase, which stayed constant over a wide range of potentials, plus an irreversible phase whose amplitude was dependent on the imposed redox potential. At the most negative potential of ≤−600 mV, the residual signal was exclusively of the rapidly decaying type. The titration curve constructed from the amplitude of the irreversible signal vs. potential is shown in Fig. 4C. The midpoint potential for the

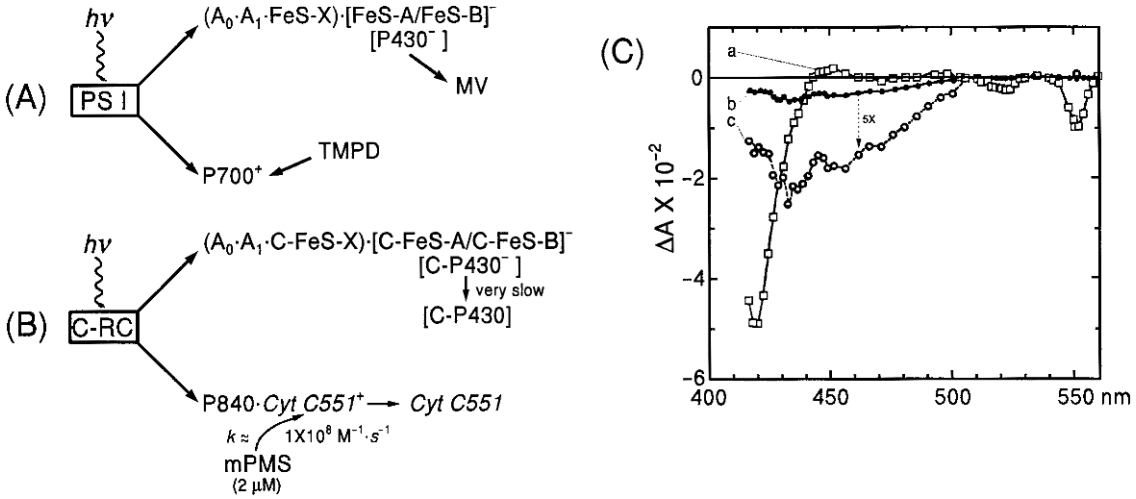

Fig. 5. Schemes representing the components in the FeS-type reaction centers in PS I (A) and the *Chlorobium* reaction center (C-RC) (B). (C) Difference spectra constructed from the recombination between $C551^+$ and C-$P430^-$ (a) and that for the accumulated C-$P430^-$ (b); spectrum (c) is (b) magnified fivefold. See text for details. Source: (C) from Kusumoto et al. (1995).

species being chemically reduced and thus unavailable to participate as an electron acceptor was estimated to be ~530 mV, in close agreement with the value obtained by direct EPR titration of FeS-A (Ke et al., 1973).

E. P430 Analog in Green-Sulfur Bacteria, C-P430

As noted earlier and illustrated in Fig. 5A,B, green-sulfur bacteria and heliobacteria also contain the FeS-type electron acceptors. The green-plant and green-bacterial systems, however, differ in that while the secondary donor to $P700^+$, plastocyanin, is readily solubilized, the electron donor to $P840^+$ in the green-sulfur bacterium, cytochrome C551, is membrane-bound and can rapidly donate an electron to $P840^+$. The oxidized $C551^+$ then rapidly recombines with C-$(FeS\text{-}A/B)^-$ or C-$P430^-$. However, $C551^+$ and C-$P430^-$ cannot be spectroscopically or kinetically differentiated in the $\{[C551^+ - C551] + [C\text{-}P430^- - C\text{-}P430]\}$ spectrum [Fig. 5C-(a)]. Kusumoto et al. (1995) devised a reaction pathway for accumulating C-$P430^-$ by using mPMS (1-methoxy-5-methylphenazonimmethosulfate) as an efficient reductant for $C551^+$, whereby reoxidation of C-$P430^-$ by $C551^+$ is prevented and the difference spectrum $\Delta A[C\text{-}P430^- - C\text{-}P430]$ for C-$P430^-$ accumulation could be obtained, as shown in Fig. 5C-(b) and (c).

III. The Iron–Sulfur Center FeS-X

In 1974, McIntosh et al. observed a small, reversible, light-induced absorbance change due to P700 in spinach PS I subchloroplasts, where the terminal electron acceptor(s) FeS-A/FeS-B were fully chemically reduced beforehand. While a reversible, light-induced EPR-signal change involving P700 interacting with FeS-A/FeS-B was not expected under these conditions, a reversible light-induced EPR signal with prominent *g*-values of 1.75 and 2.07 was detected at 6 K. The observation led McIntosh et al. to suggest that this unknown EPR species may possibly represent an earlier electron acceptor that precedes FeS-A/B in PS I.

Furthermore, collaborative studies of Jim Bolton with Evans et al. (1975) clarified the nature of the new EPR species by using PS I particles treated with dithionite at pH 9 to reduce the membrane-bound FeS-A/B before freezing it in the dark. EPR spectra measured first in the dark and then under illumination showed nearly the same spectra of the chemically reduced iron–sulfur proteins FeS-A/B. But there was also a light-induced, reversible free-radical signal at $g = 2.0$, suggesting that $P700^+$ was formed in the light and then disappeared in the dark, thus another electron acceptor that precedes FeS-A/B must be present. Under these conditions, a new EPR signal with *g*-value of 1.76 could be detected under illumination but disappeared after light was turned off. These results and those reported earlier by McIntosh et al. (1974) indicate that the

EPR spectrum at $g = 1.76$ represents an intermediary electron acceptor (called "X" then) that is presumably located closer to P700 than the bound FeS-A/B and serves as the electron acceptor for $P700^+$. The light-induced reaction is shown below:

$$[P700 \cdot\bullet\cdot\bullet\cdot \text{FeS-X}] \cdot (\text{FeS-A/FeS-B})^- + h\nu \rightarrow [P700^+ \cdot\bullet\cdot\bullet\cdot \text{FeS-X}^-] \cdot (\text{FeS-A/FeS-B})^-$$

where the dots ($\cdot\bullet\cdot\bullet\cdot$) in the [P700$\cdot\bullet\cdot\bullet\cdot$ FeS-X] formulation for the PS I core complex are used to represent two other earlier acceptors A_0 and A_1, whose existence was not yet known at the time. In the absence of any other effective reductant for P700, FeS-X^- would be expected to recombine with $P700^+$ in the dark, i.e.:

$$[P700^+ \cdot\bullet\cdot\bullet\cdot \text{FeS-X}^-] \cdot (\text{FeS-A/FeS-B})^- \rightarrow [P700 \cdot\bullet\cdot\bullet\cdot \text{FeS-X}] \cdot (\text{FeS-A/FeS-B})^-$$

A. The Absorption Spectrum of FeS-X

Sauer et al. (1978) and Vladimir Shuvalov, who was a visiting scientist at the author's laboratory, and coworkers (1979a) independently examined the absorption spectra and kinetic behavior of PS I particles under various reducing conditions. Sauer et al. showed that when FeS-A/B was chemically reduced beforehand, the ~40 msec recombination time between $P700^+$ and $[\text{FeS-A/B}]^-$ or $P430^-$ was replaced by a much faster time of ~250 μsec, presumably due to recombination between $P700^+$ and a photoreduced, earlier acceptor. The authors were able to construct a light-minus-dark difference spectrum, which appeared to consist of changes due to photooxidation of P700 plus a component resembling P430, which they designated as "A_2."

Shuvalov et al. (1979b) provided an optic-spectroscopic confirmation for assigning the EPR spectrum to an iron–sulfur center by isolating the difference spectrum of FeS-X. It was found that when the TSF-I particles were poised at −625 mV in the dark to chemically reduce FeS-A/B, subsequent illumination at room temperature caused a direct *photoaccumulation* of the reduced form of the earlier electron acceptor FeS-X:

$$[P700 \cdot\bullet\cdot\bullet\cdot \text{FeS-X}] \cdot (\text{FeS-A/FeS-B})^- + h\nu \rightarrow [P700^+ \cdot\bullet\cdot\bullet\cdot \text{FeS-X}^-] \cdot (\text{FeS-A/FeS-B})^- + e^- \rightarrow [P700 \cdot\bullet\cdot\bullet\cdot \text{FeS-X}^-] \cdot (\text{FeS-A/FeS-B})^-$$

The difference spectrum, obtained by 10-sec illumination in a phosphoroscopic photometer (Ke et al., 1985) would then represent that due to the photoaccumulation of FeS-X^-, as shown in Fig. 6A. The spectral profile, with broad bleaching from 400 to ~550 nm is typical of the reduction of an iron–sulfur protein and reminiscent of P430. In the reducing environment, P700 remained in the reduced state. The relatively small absorbance changes in the 670–720 nm region likely reflect an electrochromic shift in the absorption spectrum of chlorophyll induced by the electric field associated with FeS-X^-. A similar electrochromic shift in the 420-nm region may have caused some distortion of part of the FeS-X spectrum. It was also shown that when TSF-I particles poised at −625 mV were frozen to 5 K in the dark, subsequent illumination with 710-nm dye-laser flashes produced absorbance changes near 700 nm with a biphasic decay, one part of which decayed with a $t_{1/2}$ of ~130 msec and attributed to recombination of $P700^+$ with FeS-X^-, which was presumed to correspond to the species "A_2" of Sauer et al. (1978) that decayed with $t_{1/2}$ of 250 μs at ambient temperature.

Subsequently, Koike and Katoh (1982) and Parrett et al. (1989) carried out similar measurements. Koike and Katoh measured light-induced absorbance changes in membrane fragments of the thermophilic cyanobacterium *Synechococcus* sp. in the presence of dithionite at pH 10 and observed absorption changes with a decay $t_{1/2}$ of ~300 μsec at room temperature. The results were ascribed to P700 photooxidation and FeS-X photoreduction. The authors obtained the difference spectrum of [FeS-X^- − FeS-X] in Fig. 6B indirectly by subtracting the difference spectrum of [$P700^+$ − P700] from the total difference spectrum. The difference spectrum ascribed to FeS-X shows a broad bleaching between 410 and 475 nm, with negative bands at 420, 440, and 460 nm and a very slight positive change at 480 nm. For reference purpose, the difference spectrum for [$P700^+$ − P700] is shown separately in all three panels.

In 1989, Parrett et al. measured the difference spectrum of FeS-X using a PS I core complex isolated from the cyanobacterium *Synechococcus* sp. PCC 6301 (*Anacystis nidulans*) from which FeS-A/B had been removed. In the core complex, the role of the terminal electron acceptor is played by FeS-X, and $P700^+$ recombines with FeS-X^- in 1.2 msec at room temperature. In this PS I complex, methyl viologen also appears capable of intercepting electrons from the photoreduced FeS-X^- and channeling them to oxygen, leaving $P700^+$ accumulated. The difference spectrum of FeS-X obtained in this manner is shown in Fig. 6C; it appears typical of an iron–sulfur protein, with broad bleaching between 400 and 500 nm, and the main band centered at ~430 nm. Considering the difference spectra obtained by workers from three different laboratories, it

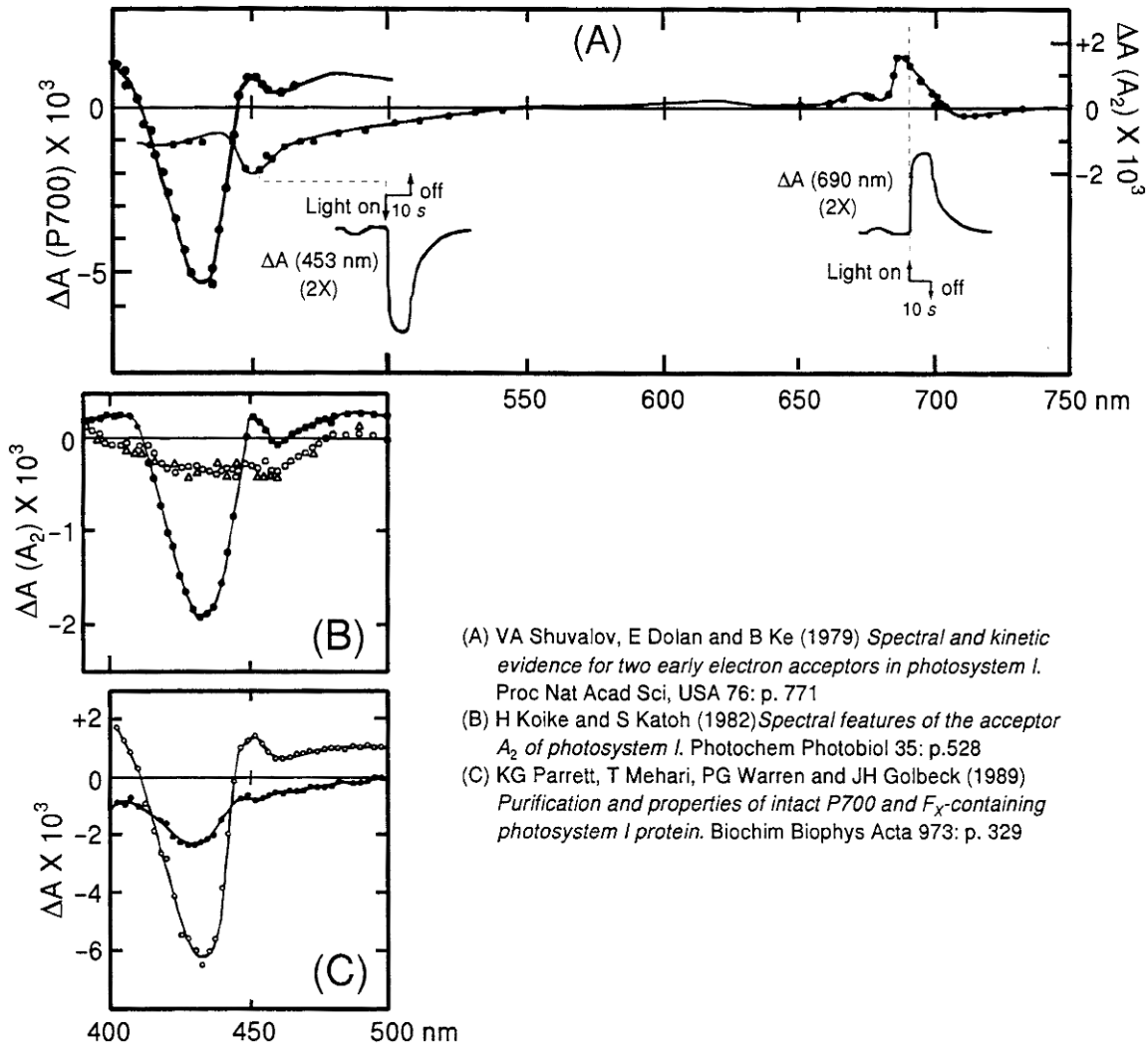

Fig. 6. (A) Room-temperature, light-minus-dark difference spectrum (small dots) obtained by photoaccumulation of FeS-X$^-$ in TSF-I particles poised at −625 mV. As a reference, the difference spectrum for P700 photooxidation is also shown (larger dots). (B) Difference spectrum of FeS-X (open symbols) obtained by subtracting the difference spectrum for P700 oxidation from that for P700 photooxidation *plus* FeS-X photoreduction. (C) Difference spectrum (solid dots) for FeS-X obtained using the PS-I core complex that is devoid of FeS-A/B by subtracting the P700 difference spectrum from the composite spectrum consisting of both P700 and FeS-X changes. Source: Shuvalov (1979a), Koike and Katoh (1982), and Parrett et al. (1989).

is worth noting that, besides some possible distortion of the spectrum by electrochromic shifts in one case, the three difference spectra assigned to FeS-X are very similar, with only minor variations in the spectral profile.

B. EPR Spectro-Kinetic Correlation Between P700 and FeS-X

Spectro-kinetic correlation between P700 and FeS-X was also made by comparing the EPR signals of P700$^+$ and FeS-X$^-$. Taking the previously measured flash-induced optical absorbance-change signal near 700 nm with a decay time of 130 msec at 5 K as that due to P700$^+$•FeS-X$^-$ recombination, then the kinetics of formation and decay of the EPR signals of FeS-X$^-$ at $g = 1.78$ could also be used to confirm its role, as reported by Shuvalov et al. (1979b). Figure 7A top shows the light-minus-dark EPR spectrum in the $g = 1.78$ region characteristic of FeS-X$^-$, produced under continuous illumination at 9 K in TSF-I particles poised at −625 mV. The lower part of the figure shows the flash-induced EPR changes at $g = 1.78$, representing FeS-X → FeS-X$^-$, measured with an instrument-limited response time of 200 μsec. The

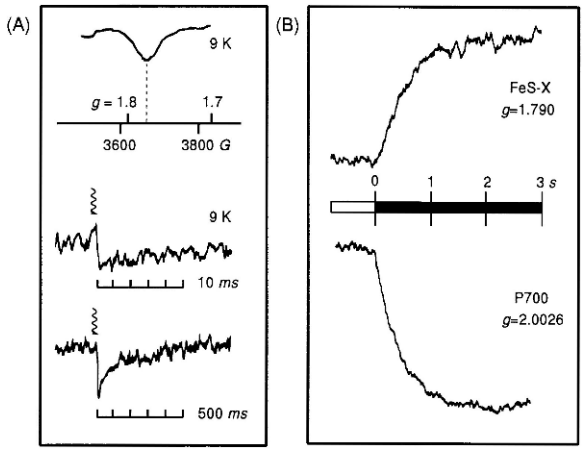

Fig. 7. (A) Top: light-minus-dark EPR spectrum of TSF-I particles poised at −625 mV and 9 K in the $g = 1.78$ region ([FeS-X^- − FeS-X] spectrum); middle and bottom: kinetics of flash-induced EPR-signal at $g = 1.78$ on two different timescales. (B) Kinetics of the dark decay of the EPR signal of FeS-X^- at $g = 1.79$ (top) and of $P700^+$ at $g = 2.0026$ (bottom) in an LDS-fractionated PS-I core complex from spinach. Source: (A) from Shuvalov et al. (1979a); (B) from Warden and Golbeck (1986).

change in EPR signal on two different timescales shows a single decay component with $t_{1/2}$ of 130 msec, which is identical to that of the optical absorbance-change signal for $P700^+$ rereduction described above.

A correlation between the $g = 2.0026$ EPR signal of $P700^+$ and the $g = 1.78$ signal of FeS-X^- was reported by Warden and Golbeck (1986) using a PS I core complex free of FeS-A/B. Even though the EPR signals of reduced FeS-A/B was not expected during or after illumination at 19 K, a large, reversible signals due to $P700^+$ at $g = 2.0026$ and one representing FeS-X^- at $g = 1.79$ were observed upon illumination at 8 K. The authors demonstrated that when the $P700^+$ and FeS-X^- were generated by continuous illumination first and then allowed to decay in the dark, both decays showed an identical kinetics with a $t_{1/2}$ of 300 msec (Fig. 7B).

C. The Redox Potential of FeS-X

FeS-X, being an earlier electron acceptor, would be expected to have a more negative redox potential than FeS-A/B, and its determination would help to understand its functional role. Ke et al. (1977) reported an indirect electrochemical titration of FeS-X. Under ambient redox conditions, the light-induced ΔA signal of $P700^+$ at 86 K shows a large irreversible fraction, which then decreased as the potential became more negative, reflecting a decrease in the amount of FeS-A/B available for photoreduction. When all the FeS-A/B had been chemically reduced, the EPR signal of P700 became completely reversible, reflecting light-induced charge separation between P700 and FeS-X, followed by their recombination in the dark. The amplitude of the (reversible) $P700^+$ signal also decreased gradually when the imposed potential was made more negative than ∼−700 mV. Thus the change in amplitude of the reversibly-decaying $P700^+$ signal would serve as an indirect reductive titration of FeS-X. The titration yielded an E_m of ∼−730 mV.

In 1982, Chamorovsky and Cammack determined the redox potential of FeS-X directly by monitoring the appearance of the EPR line at $g = 1.76$ as a function of the imposed potential. The titration was carried out electrochemically using a number of viologen dyes as redox mediators. As in the titration of Ke et al. (1977), even electrochemical titration could not produce sufficiently negative potential to completely reduce FeS-X. However, additional illumination of any partially titrated sample can bring about the maximum EPR signal of FeS-X^-. The titration curve constructed from data of combined redox titration plus supplementary illumination yielded a midpoint potential of −705 mV for FeS-X/FeS-X^-, and consistent with the Nernst equation for $n = 1$. Note that this E_m value is still over a hundred millivolts more negative than those of FeS-A/B.

In 1989, Parrett et al. also determined the redox potential of FeS-X indirectly in a PS I core complex by monitoring the amplitude of the optical ΔA signal of P700. The room-temperature kinetics of $P700^+$/FeS-X^- recombination are much faster than those between $P700^+$ and [FeS-A/FeS-B]$^-$, having a $t_{1/2}$ of 1.2 msec, rather than 30–40 msec for the latter. The redox potential of FeS-X determined by these workers was −670 mV, which is more positive than the values found by Ke et al. (1977) or Chamorovsky and Cammack (1982). The more positive redox-potential value of FeS-X is consistent with the experimentally measured slower backreaction of FeS^- in the absence of PsaC.

D. Establishment of the Position of FeS-X in the Electron-Transfer Sequence

As FeS-X is located closer to P700 than FeS-A/B in the electron-transfer chain, its functional role is of interest but the problem is difficult because all their spectra appear similar, making differentiation difficult, in spite of adequate time resolution of optical spectroscopy. And, even though the three iron–sulfur proteins have

characteristically different EPR spectra, the EPR technique itself does not lend adequate time resolution to allow the needed kinetic information to be obtained and, furthermore, EPR technique is not usable for these species at physiological temperatures.

Initially, examination of the decay profile of the photooxidized $P700^+$ was used to gain indirect information on the nature of its reacting partner(s). The multiple-flash-excitation protocol of Sauer et al. (1978) and the more recent work of Vassiliev et al. (1997, 1998) in examining $P700^+$ decay at 830 nm over a wide time domain have offered promising approaches and given evidence for several components recombining with each of the photoreduced, electron acceptors, including FeS-A/B. However, there is still a lack of spectral differentiation or unique kinetic parameters for the species involved. In spite of these inherent difficulties, Lüneberg et al. (1994) and Franke et al. (1995) independently measured the minute differences in the spectra of the FeS's, and identified FeS-X as the intermediary electron acceptor located between A_1 and FeS-A/B, and also confirmed the electron transfer from FeS-X to FeS-A/B.

As the charge recombination between $P700^+$ and the reduced terminal acceptor in the PS-I complex, $\{P700^+ \bullet A_0 \bullet A_1 \bullet \text{FeS-X} \bullet [\text{FeS-A/B}]^-\}$ and the PS I core complex, $\{P700^+ \bullet A_0 \bullet A_1 \bullet \text{FeS-X}^-\}$ is expected to be different, Lüneberg et al. (1994) measured the reaction kinetics in a PS-I complex of the thermophilic cyanobacterium *Synechocystis* sp. treated with urea to gradually remove its PsaC (FeS-A/B), PsaD, and PsaE subunits. The intact complex showed a decay phase with a $t_{1/2}$of 25 msec, very close to that for recombination between $P700^+$ and $P430^-$ or $[\text{FeS-A/B}]^-$. With increasing incubation, the decay time gradually decreased to only 750 msec, suggesting $P700^+$ was recombining with FeS-X^-. The nature of the partner recombining with $P700^+$ was further identified from the difference spectra of the two complexes. Although the major portion of the difference spectra was accounted for by the oxidation of P700, the very small absorbance changes in the wing region reflect the involvement of FeS-A/B in the PS I complex and FeS-X in the core complex.

Lüneberg et al. also measured the absorbance change at 384 nm to monitor the kinetics of the redox change involving the earlier acceptor A_1 that precedes FeS-X. Interestingly, both the PS I complex and the core complex showed the same kinetics, with a rise time of ~5 nsec and a decay phase with $t_{1/2}$ of 180 nsec. Since the 180-nsec decay phase of $A_1^- \rightarrow A_1$ is linked to $\text{FeS-X} \rightarrow \text{FeS-X}^-$, and since the kinetics are identical and almost independent of the presence or absence of the FeS-A/B acceptor, the results unambiguously showed that FeS-X is an obligatory intermediary carrier in the normal forward electron-transfer pathway in PS I.

Franke et al. (1995) also examined the electron-transfer pathway on the reducing side of PS I by comparing the difference spectra of $\Delta A[\text{FeS-X}^- - \text{FeS-X}]$ and $\Delta A[(\text{FeS-A/B})^- - (\text{FeS-A/B})]$ (or $\Delta A[P430^- - P430]$). The difference spectrum for P430, the optic-spectroscopic form of FeS-A/B, was measured using the procedures of Hiyama and Ke (1971a,b) with an intact PS I complex isolated from *Synechococcus* sp. PCC 6301 while that of FeS-X was measured with the PS I core complex. The minute but significant differences shown in Fig. 8A were used to examine the electron-transfer sequence in PS I. The light-minus-dark, or reduced-minus-oxidized difference spectra for FeS-X and P430 both show minima in the 420–430 nm region; the differential molar absorptivities were estimated to be $13{,}000 \pm 500$ and $15{,}000 \pm 500\ M^{-1} \cdot cm^{-1}$ for P430 and FeS-X, respectively. Furthermore, the difference spectrum of P430 differs from that of FeS-X by a narrow shoulder in the 410–418 nm region and a diminished absorbance above ~450 nm (see Fig. 8A).

Figure 8B shows the flash-induced, absorbance changes at 430 and 416 nm in the intact PS I complex, and changes at both wavelengths are dominated by a bleaching due to P700 photooxidation. Absorbance changes involving the iron–sulfur centers at these wavelengths are probably at the level of instrument sensitivity. The 453-nm transient measured with the intact PS I complex $\{P700 \bullet A_0 \bullet A_1 \bullet \text{FeS-X} \bullet [\text{FeS-A/B}]\}$ in Fig. 8C, top, on the other hand, shows a rapid increase followed by a nearly total relaxation on the timescale of the experiment. The transient positive absorbance change was ascribed to the formation of the $[P700^+ \bullet \text{FeS-X}^-]$ state. The change relaxed by 10–25% of the initial amplitude in ~800 nsec. The relative extent of this absorbance change appeared to be consistent with the difference in molar absorptivity between FeS-X and P430 (FeS-A/B) in the 450-nm region of the difference spectra shown in Fig. 8A. The 800-nsec decay was therefore considered to reflect electron transfer from FeS-X^- to FeS-A/B.

The assignment of the 800-nsec kinetic component was further corroborated by comparing the 453-nm kinetics of the intact PS I complex, [P700• FeS-A/B] with that of the PS I core complex, [P700• FeS-X]. As expected, removal of the terminal FeS-A/B acceptors should result in the elimination of the 800-nsec

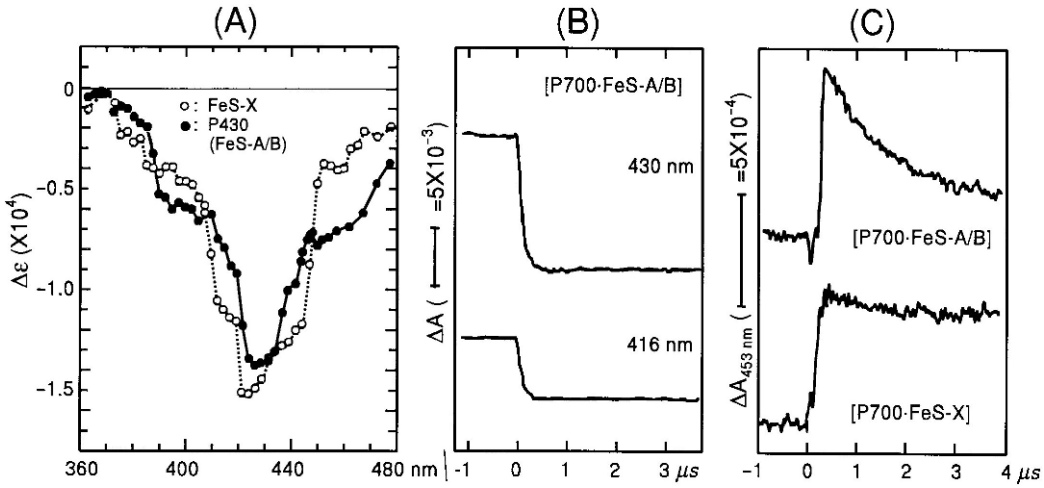

Fig. 8. (A) Absorbance-difference spectra, plotted as differential molar absorptivity, $\Delta\varepsilon$, for FeS-X and P430 from flash-induced transients with intact PS-I complex $\{P700{\cdot}A_0{\cdot}A_1{\cdot}FeS\text{-}X{\cdot}[FeS\text{-}A/B]\}$ and the PS I core complex $\{P700{\cdot}A_0{\cdot}A_1{\cdot}FeS\text{-}X]$. (b) Kinetic traces of flash-induced absorbance changes at 430 and 416 nm for the intact PS I complex. (C) Kinetic traces of flash-induced absorbance changes at 453 nm for the intact PS I complex (top trace) and the PS-I core complex (bottom trace). Note the ~10-fold difference in ΔA scale between (B) and (C). Source: Franke et al. (1995).

decay component. In the transient signal of the PS I core complex shown in Fig. 8C bottom, the relaxation is much slower, making the 800-nsec component contingent on the presence of the terminal acceptors FeS-A/B. The 800-nsec electron-transfer time from FeS-X to FeS-A/B also agrees with the PsaC reduction time of ca. 1 msec reported independently by Sigfridsson et al. (1995) using photovoltage measurements.

IV. Early Optic-Spectroscopic Studies of A_0

In the late 1970s, two working groups, those of Mathis in Saclay and the Kettering Laboratory in Yellow Springs had used optical spectroscopy to measure the spectrum of A_0, i.e., $\Delta A[A_0^- - A_0]$. Initially, Mathis et al. (1978) "isolated" the charge separation between P700 and A_0 spectroscopically in the CP1 complex. That the reaction was considered to involve P700 and the primary acceptor was based on the rapid rate of recombination and the makeup of the CP1 complex, although the nature of the acceptor was largely unknown. The difference spectrum constructed from the absorbance-change transients essentially resembles that of P700. Subsequent measurements utilized PS I particles that had undergone photoaccumulation under very low redox potential so that all secondary acceptors were photochemically reduced and remained so at cryogenic temperatures. With such a sample, charge separation between P700 and A_0 would be expected to take place upon illumination:

$$\{P700{\bullet}A_0{\bullet}A_1^-{\bullet}FeS\text{-}X^-{\bullet}[FeS\text{-}A/FeS\text{-}B]^-\} + h\nu \rightarrow \{P700^+{\bullet}A_0^-{\bullet}A_1^-{\bullet}FeS\text{-}X^- {\bullet}[FeS\text{-}A/FeS\text{-}B]^-\}$$

The difference spectrum of A_0 reduction may then be obtained by subtracting that for P700 photooxidation from the experimentally measured composite difference spectrum $\Delta A\{[P700^+{\bullet}A_0^-] - [P700{\bullet}A_0]\}$. Sauer et al. (1978) and Shuvalov et al. (1979b) used this approach to maintain TSF-I particles at ~ -0.62 V with dithionite plus either neutral red or background illumination to keep the iron–sulfur centers in the reduced state.

On the assumption that the difference spectrum is a composite consisting of contributions by P700 and A_0, i.e., $\Delta A[P700^+ - P700]$ and $\Delta A[A_0^- - A_0]$, Shuvalov et al. subtracted the separately measured difference spectrum of $[P700^+ - P700]$ from the composite spectrum to yield $\Delta A[A_0^- - A_0]$ alone. While the latter spectrum resembles that of $[P700^+ - P700]$, it is also very similar to that for the formation of Chl *a* anion radical in solution as reported by Fujita et al. (1978), except red-shifted. Subsequently, several groups also tried to obtain the difference spectrum of A_0^- by photoaccumulation under *steady* illumination. Swarthoff et al. (1982) placed TSF-1 particles maintained at a redox potential of -625 mV, and obtained absorbance-change transients by 3-sec illumination. As the oxidized $P700^+$ formed under illumination is continually rereduced, the

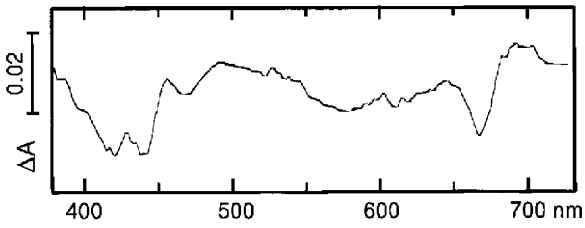

Fig. 9. Difference spectrum representing $\Delta A[A_0^- - A_0]$ in PS I obtained directly with a P700-enriched, PS I particle in a conventional, commercial spectrophotometer (Hitachi Model 557) in the light-minus-dark mode. Source: Ikegami and Ke (1984).

difference spectrum thus obtained, with negative bands at 420 and 670 nm and positive bands at 460 and 690 nm, would represent $\Delta A[A_0^- - A_0]$.

A. Photoaccumulation of Reduced of A_0 by Steady Illumination

Isamu Ikegami, and Ke (1984) isolated the difference spectrum of A_0^- from a highly enriched particle containing 10–15 chlorophylls and also ~12 Fe- and S-atoms per P700, but devoid of phylloquinone as a result of extraction during its preparation. The difference spectrum measured at 77 K from photoaccumulation of A_0^- showed absorbance decreases at 420, 440, and 670 nm and increases at 455 and 700 nm (Fig. 9). This spectrum agrees quite well with that of Swarthoff et al. (1982) but displayed more details in the blue region. The illuminated sample was examined separately by EPR spectroscopy and a 14-*G* wide free-radical signal at $g = 2.0$ was obtained. The optical and EPR spectra strongly support the notion that the photoaccumulated A_0^- is a chlorophyll anion radical, with spectral characteristics similar to that reported by Fujita et al. (1978). It is worth noting that, because of the enriched PS I particle used, it was possible to measure the difference spectrum of A_0 in a conventional commercial spectrophotometer.

Note that the position of the red band obtained for A_0^- by steady illumination is at 670 nm (Fig. 9), while flash excitation produced one near 694 nm. This discrepancy was explained by Mathis et al. (1988) that steady illumination under a strongly reducing condition may have caused a neighboring 670 nm-absorbing Chl *a*, possibly the bridging Chl *a*, to be reduced by the initially formed A_0^-. Brettel (1997) put forward two alternative suggestions: either the spectral properties of A_0 are being modified by the harsh reducing conditions used during photoaccumulation or some, as yet unknown, electrochromic band-shift exerted by either $P700^+$ or A_0^- could have caused a blue shift in the band maximum of $\Delta A[A_0^- - A_0]$.

B. Early Picosecond Measurements of Spectra and Reaction Kinetics of A_0

After the initial rapid-spectroscopic studies of PS I by Shuvalov et al. (1979a), even faster spectroscopic methods became needed for examining the extremely short lifetimes of the charge-transfer state $[P700^+ \bullet A_0^-]$.

The first picosecond measurements on PS I were made independently by Fenton et al. (1979) and by Shuvalov et al. (1979b). Fenton et al. examined a spinach PS I particle with 8-psec, 528-nm excitation pulses and found that P700 was photooxidized within 10 psec, and a reduced electron acceptor formed within 10 psec was reoxidized in tens of picoseconds.

Shuvalov et al. (1979b) used TSF-I particles (Chl/P700 ~26) and single, ~50-psec ruby-laser (694.3 nm) pulses for excitation. A portion of the laser pulse, directed by a beam splitter and optically delayed, served as the monitoring beam. As shown in Fig. 10A, with the PS I particle poised at ~200 mV and a time resolution of 60 psec, a bleaching at 694.3 nm was observed with an amplitude approximately twice that attributable to P700 photooxidation alone and decayed to the steady-state level with a $t_{1/2}$ of ~200 psec. The 200 psec decay was interpreted as due to reoxidation of the reduced primary acceptor by the next acceptor along the electron-transfer chain. When P700 was preoxidized by continuous background illumination, the absorbance change was diminished ~10-fold (Fig. 10B). When the PS I particle was maintained at ~−625 mV to prereduce the secondary acceptors, picosecond-pulse excitation produced the same initial absorbance decrease, but the signal decay had an initial $t_{1/2}$ of ~10 nsec and it extended into the ms domain (Fig. 10C). The initial rapid absorbance decrease was interpreted as due to the formation of the radical pair $[P700^+ \bullet A_0^-]$, and the 10-nsec decay as reflecting recombination of the radical pair plus some interconversion into a triplet state that decayed in 3 msec (1.3 msec at 5 K).

As only 694.3-nm light was available for the above experiments, spectral information on the primary electron acceptor was limited, this work was extended over a broader spectral range at Pushchino [Shuvalov et al. (1979c)] by using excitation pulses of 30-psec at 689 and 708 nm generated as stimulated Stokes Raman emission by passing a frequency-doubled

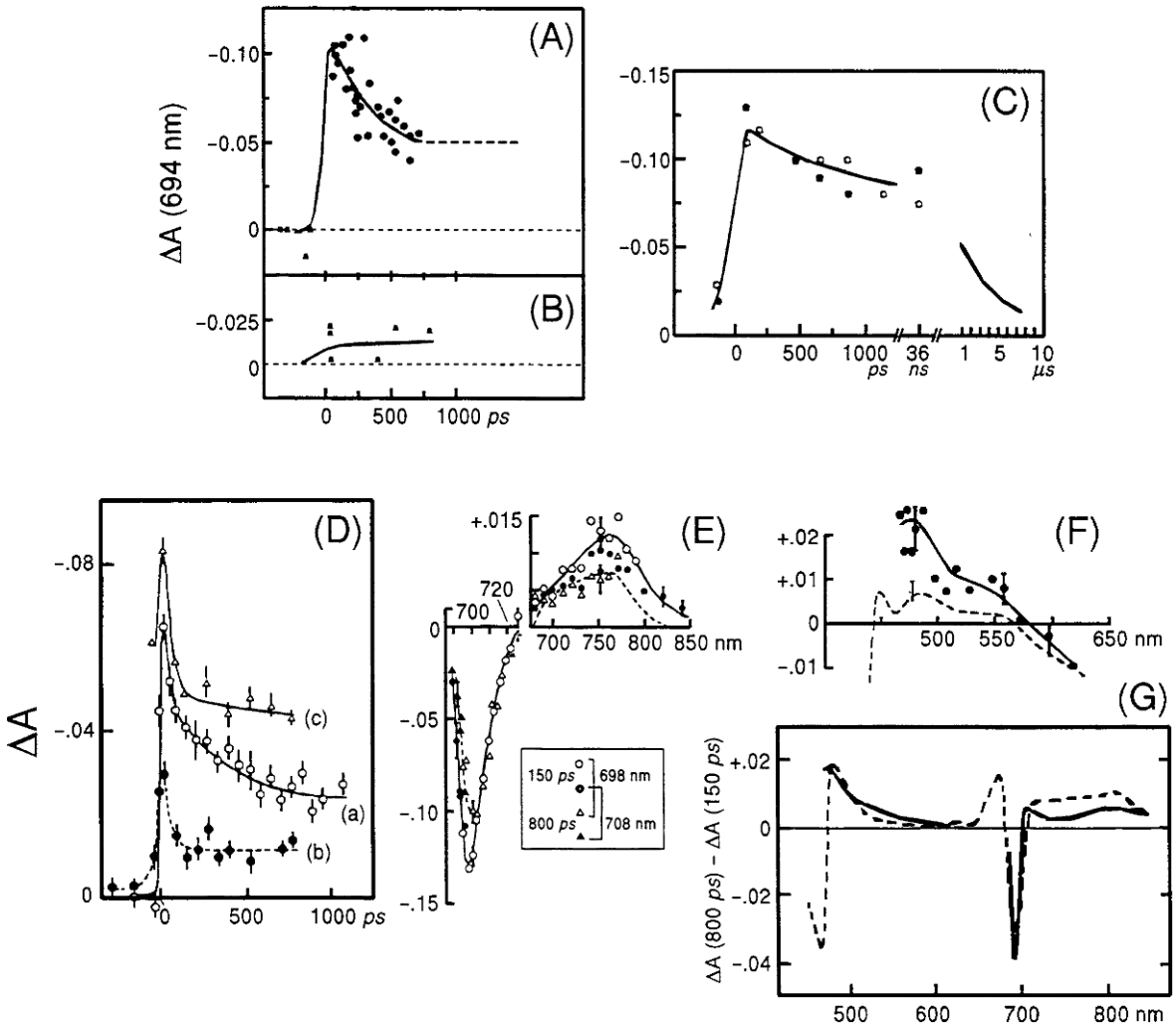

Fig. 10. (A) ΔA measured at 694 nm in TSF-I particles poised at ~200 mV and excited by 50-psec flashes at 694.3 nm and (B) that measured in TSF-I particles with P700 preoxidized by background illumination. (C) ΔA measured at 694 nm in TSF-I particles poised at −625 mV. (D) ΔA at 694 nm measured in TSF-I particles (a) poised at ~200 mV, (b) P700 preoxidized by continuous illumination, and (c) heat treated to inactivate the bound iron–sulfur centers. (E) ΔA (red region) measured in TSF-I particles 150 and 800-psec after the flash; 30-psec flashes at either 708 or 689 nm were used [see data-point code in the inset]; note also the different absorbance scales used. (F) ΔA (450–600 nm) induced by 30-psec, 689-nm flashes. (G) Solid trace is the difference between ΔA measured at 150 and 800 psec; the dashed trace is the *in vitro* difference spectrum for Chl *a* anion radical, shifted toward the red by ~25 nm. Source: (A)–(C) from Shuvalov et al. (1979a); (D)–(G) from Shuvalov et al. (1979b).

Nd-YAG pulse through deuterated ethanol. Part of the Nd-YAG pulse was also used to generate a picosecond continuum in D_2O, from which monitoring light of selected wavelengths was isolated by a monochromator.

Figure 10D shows ΔA at 694 nm produced by a 708-nm excitation pulse in TSF-I particles poised at ~200 mV. The ΔA reached a maximum in <30 psec and decayed in two phases with lifetimes of ~45 and 210 psec, respectively, to a level corresponding to P700 photooxidation alone, as shown in Fig. 10D-(a). The 210-psec phase was greatly diminished in a sample in which P700 was photooxidized by prior illumination while the 45-psec phase was unaffected [trace (D)-(b)]. PS I particles heated to inactivate the bound iron–sulfur proteins gave an enhanced 45-psec phase and another phase that decayed in a time longer than 210 psec [trace (D)-(c)]. The 45-psec phase, which was observed mostly below 690 nm and apparently unaffected by prior oxidation of P700, was attributed to excited antenna chlorophylls.

Figure 10E shows the spectra of light-induced absorbance changes measured 150 and 800 psec after excitation by 708- or 689-nm flashes. The 150-psec spectrum shows an absorbance increase in the 750-nm region; the 800-psec difference spectrum coincides well with the difference spectrum of [$P700^+ - P700$], shown as a dashed curve. The flash-induced ΔA spectrum in the 450–600 nm region was also similar to that of P700, as shown in Fig. 10E. Assuming that the 150-psec difference spectrum consists of changes due to primary-donor photooxidation and primary-acceptor photoreduction and the 800-psec difference spectrum consists of changes due to the photooxidized P700 only, it should be possible to obtain the difference spectrum of the photoreduced primary acceptor, i.e., $\Delta A[A_0^- - A_0]$, as a temporal difference in the absorbances, as represented by the solid trace in Fig. 10G. Not surprisingly, the plotted $\Delta(\Delta A)$ also resembles closely that reported by Fujita et al. (1978) for the Chl *a* anion radical formed *in vitro*, and almost coincides with it when the latter is shifted by ~25 nm toward the red. Furthermore, as shown in more detail in Fig. 10F, the flash-induced ΔA spectrum in the 450–600 nm region is also similar to that of P700. From the above results, the millimolar extinction coefficient ε of A_0 at its red maximum was estimated to be 46 $mM^{-1}cm^{-1}$, using 64 $mM^{-1}cm^{-1}$ as the ε value for P700.

Acknowledgments

I thank John Golbeck, editor of this volume in Kluwer's "*Advances in Photosynthesis*" Series, for asking me to contribute a "*Historical Introduction to Photosystem I*: *The Discovery of the Electron Acceptors by Optical Spectroscopy*," for the volume. I have taken the liberty to describe works on several PS I electron acceptors carried out over the years at the Charles F. Kettering Research Laboratory. I want to again express my sincere thanks for the contributions my former colleagues, associates, and friends, Bob Breeze (deceased), Helmut Beinert, Sandor Demeter, Ed Dolan, Fred Hawkridge, Tetsuo Hiyama, Isamu Ikegami, Vladimir Shuvalov, Elwood Shaw, Kiyoshi Sugahara, Bill Treharne, and Leo Vernon have made in the research areas described in this article. For the sake of integrity of the article, I have also taken the liberty of including some works carried out by colleagues from other laboratories that have a close logical relationship to our own work. Finally, I wish to express my sincere gratitude to the Charles F. Kettering Research Laboratory, the United States National Science Foundation and the United States National Institutes of Health for their generous support that made our work possible. This article is dedicated to my former colleagues and associates for their valuable contributions to photosynthesis research.

References

Arnon D (1965) Ferredoxin and photosynthesis. Science 149: 1460–1469

Black CC (1966) Chloroplast reactions with dipyridyl salts. Biochim Biophys Acta 120: 332–340

Brettel K (1997) Electron transfer and arrangement of redox cofactors in photosystem I. Biochim Biophys Acta 1318: 322–373

Bruce BD, Malkin R, Wynn RM and Zilber A (1989) Structure organization and function of polypeptide subunits in photosystem I. In: Barber J and Malkin R (eds) Techniques and New Developments in Photosynthesis, NATO Adv Sci Inst Ser Sec A Life Sci, p. 76

Calvin M (1961) Some photochemical and photophysical reactions of chlorophyll and its derivative. In: McElroy WD and Glass B (eds) Light and Life, pp 317–355

Chamorovsky SK and Cammack R (1982) Direct determination of the midpoint potential of the acceptor X in chloroplast photosystem I by electrochemical reduction and ESR spectroscopy. Photobiochem Photobiophys 4: 195–200

Evans MCW, Sihra CK, Bolton JR and Cammack R (1975) Primary electron acceptor complex of photosystem I in spinach chloroplasts. Nature 256: 669–670

Fenton JM, Pellin MJ, Govindjee and Kaufmann KJ (1979) Primary photochemistry of the reaction center of photosystem I. FEBS Lett 100: 1–4

Franke JE, Ciesla L and Warden JT (1995) Kinetics of PsaC reduction in photosystem I. In: Mathis P (ed) Photosynthesis: from Light to Biosphere, Vol. II, pp 75–78. Kluwer, Dordrecht

Fujita I and Myers J (1966) Cytochrome *c* redox reactions induced by photochemical system 1 in sonicated preparations of *Anabaena cylindrica*. Arch Biochem Biophys 113: 730–737

Fujita I, Davis MS and Fajer J (1978) Anion radicals of pheophytin and chlorophyll a: their role in the primary charge separations of plant photosynthesis. J Am Chem Soc 100: 6280–6282

Fuller RC and Nugent NA (1969) Pteridines and the function of the photosynthetic reaction center. Proc Natl Acad Sci USA 63: 1311–1318

Hiyama T and Ke B (1971a) A new photosynthetic pigment, "P430": its possible role as the primary electron acceptor of photosystem I. Proc Natl Acad Sci USA 68: 1010–1013

Hiyama T and Ke B (1971b) A further study of 430: a possible primary electron acceptor of photosystem I. Arch Biochem Biophys 147: 99–108

Ikegami I and Ke B (1984) A 160-kilodalton photosystem-I reaction-center complex. Low temperature absorption and EPR spectroscopy of the early electron acceptors. Biochim Biophys Acta 764: 70–79

Kamen M (1961) Comments on the function of haem proteins as related to primary photochemical processes in photosynthesis. In: McElroy WD and Glass B (eds) Light and Life, pp. 483–488. Johns Hopkins Press, Baltimore

Katz E (1949) Photosynthesis in Plants, pp. 287–293. Iowa State College Press, Ames

Ke B (1973) The primary electron acceptor of photosystem I. Biochim Biophys Acta 301: 1–33

Ke B, Hansen RE and Beinert H (1973) Oxidation–reduction potentials of bound iron–sulfur proteins of photosystem I. Proc Natl Acad Sci USA 70: 2941–2945

Ke B, Sugahara K, Shaw ER, Hansen RE, Hamilton WD and Beinert H (1974) Kinetics of appearance and disappearance of light-induced EPR signals of $P700^+$ and iron–sulfur protein(s) at low temperature. Biochim Biophys Acta 368: 401–408

Ke B, Dolan E, Sugahara K, Hawkridge FM, Demeter S and Shaw ER (1977) Electrochemical and kinetic evidence for a transient electron acceptor in the photochemical charge separation in photosystem I. In: Photosynthetic Organelles [Plant Cell Physiol (special issue no. 3)], pp 187–199

Ke B, Breeze RH, Dolan E and Vore D (1985) Versatile spectrophotometer for photosynthesis (light-induced changes in absorbance and fluorescence yield, circular and linear dichroism) and other biophysical measurements. Rev Sci Instrum 56: 26–31

Koike H and Katoh S (1982) Spectral features of the bound electron acceptor A_2 of photosystem I. Photochem Photobiol 35: 527–531

Kok B, Rurainski HJ and Owens OVH (1965) The reducing power generated in photoact I of photosynthesis. Biochim Biophys Acta 109: 347–356

Kusumoto N, Inoue K and Sakurai H (1995) Spectroscopic studies of bound cytochrome *c* and an iron–sulfur center in a purified reaction-center complex from the green sulfur bacterium *Chlorobium tepidum*. Photosynth Res 43: 107–112

Lüneberg J, Fromme P, Jekow P and Schlodder E (1994) Spectroscopic characterization of PS I core complexes from thermophilic *Synechococcus* sp. Identical reoxidation kinetics of A_1^- before and after removal of the iron–sulfur clusters F_A and F_B. FEBS Lett 338: 197–202

Malkin R and Bearden AJ (1971) Primary reaction of photosynthesis: photoreduction of bound chloroplast ferredoxin at low temperatures as detected by EPR spectroscopy. Proc Natl Acad Sci USA 68: 16–19

Mathis P, Sauer K and Remy R (1978) Rapidly reversible flash-induced electron transfer in a P-700 chlorophyll–protein complex isolated with SDS. FEBS Lett 88: 275–278

Mathis P, Ikegami I and Sétif P (1988) Nanosecond flash studies of the absorption spectrum of the photosystem I primary acceptor A_0. Photosynth Res 16: 203–210

McIntosh AR, Chu M and Bolton JR (1975) Flash photolysis electron spin resonance studies of the electron acceptor species at low temperatures in photosystem I of spinach subchloroplast particles. Biochim Biophys Acta 376: 308–314

Oh-oka H, Itoh S, Saeki K, Takahashi Y and Matsubara H (1990) FA/FB protein from the spinach photosystem I complex: isolation in a native state and some properties of the iron–sulfur centers. Plant Cell Physiol 32: 11–17

Parrett KG, Mehari T, Warren PG and Golbeck JH (1989) Purification and properties of the intact P-700 and F_X-containing Photosystem I core protein. Biochim Biophys Acta 973: 324–332

Regitz G, Berzborn R and Trebst A (1970) On a water soluble factor neutralizing antibodies against primary acceptor in photosynthetic electron transport of chloroplasts. Planta 91: 8–17

Sauer K, Mathis P, Acker S and van Best J (1978) Electron acceptors associated with P-700 in Triton-solubilized photosystem I particles from spinach chloroplasts. Biochim Biophys Acta 503: 120–134

Schubert W-D, Klukas O, Krauß N, Saenger W, Fromme P and Witt HT (1997) Three-dimensional crystal of photosystem I of *Synechococcus elongatus* at 4 Å resolution: comparative structure analysis. J Mol Biol 272: 741–769

Shuvalov VA, Klimov VV and Krasnovsky AA (1976) Primary photoprocesses in light fragments of chloroplasts. Mol Biol 10: 326–339

Shuvalov VA, Dolan E and Ke B (1979a) Spectral and kinetic evidence for two early electron acceptors in photosystem I. Proc Natl Acad Sci USA 76: 770–773

Shuvalov VA, Ke B and Dolan E (1979b) Kinetic and spectral properties of the intermediary electron acceptor A_1 in photosystem I. Subnanosecond spectroscopy. FEBS Lett 100: 5–8

Shuvalov VA, Klevanik AV, Sharkov AV, Kryukov PG and Ke B (1979c) Picosecond spectroscopy of photosystem I reaction centers. FEBS Lett 107: 313–316

Sigfridsson K, Hansson O, and Brzezinski P (1995) Electrogenic light reactions in photosystem I: resolution of electron-transfer rates between iron–sulfur centers. Proc Natl Acad Sci USA 92: 3458–3462

Swarthoff T, Gast P, Amesz J and Buisman HP (1982) Photoaccumulation of reduced primary electron acceptors of photosystem I of photosynthesis. FEBS Lett 146: 129–132

Vassiliev IR, Jung YS, Mamedov MD, Semenov AY and Golbeck JH (1997) Near-IR absorbance changes and electrogenic reactions in the microsecond-to-second time domain in photosystem I. Biophys J 72: 301–315

Vassiliev IR, Jung YS, Yang F and Golbeck JH (1998) PsaC subunit of photosystem I is oriented with iron–sulfur cluster F_B as the immediate electron donor to ferredoxin and flavodoxin. Biophys J 74: 2029–2035

Vernon LP and Ke B (1966) Photochemistry of chlorophyll in vivo. In: Vernon LP and Seely GR (eds) The Chlorophylls, pp 569–607. Academic Press, New York

Wang JH (1970) Oxidative and photosynthetic phosphorylation mechanisms. Science 167: 25–30

Warden JT and Golbeck JH (1986) Photosystem I charge separation in the absence of centers A and B. II. ESR spectral characterization of 'X' and correlation with optical signal 'A_2.' Biochim Biophys Acta 849: 25–31

Yocum CF and San Pietro A (1969) Ferredoxin-reducing substance (FRS) from spinach. Biochem Biophys Res Commun 36: 614–620

Zweig G and Avron M (1965) On oxidation–reduction potential of the photoreduced reductant of isolated chloroplasts. Biochem Biophys Res Commun 19: 397–400

Chapter 4

Historical Introduction to Photosystem I: The Discovery of the A_1 and $A_2(F_X?)$ Acceptors by Time-Resolved Optical Spectroscopy

Paul Mathis
Service de Bioénergétique, DBJC, CEA/Saclay, 91191 Gif-sur-Yvette Cédex, France
Present address: 6, avenue Jean Perrin, 92330 Sceaux, France

Kenneth Sauer*
Chemistry Department, University of California and Calvin Laboratory, Lawrence Berkeley National Laboratory, Berkeley, CA 94720-5230, USA

Summary

This chapter summarizes some of the results obtained by the authors, in a collaborative work done in 1976–1977, about the Photosystem I electron acceptors. The results are placed in a historical perspective and discussed in the light of the present knowledge on the Photosystem I reaction center.

I. Introduction

In the middle of the 1970s, the two authors undertook with their colleagues to explore the path of Photosystem I (PS I) electron transfer, especially on the acceptor side of P700. In the days before any high-resolution X-ray diffraction structure was available, the obvious way to carry out such an exploration was to use available spectrometric tools [optical absorption changes, electron paramagnetic resonance (EPR)] in time-resolved

* Author for correspondence, email: sauer@cchem.berkeley.edu

Abbreviations: A (A_0, A_1, A_2) – electron acceptors; A_2 – Fe/S cluster now known as F_X; CD – circular dichroism; EPR – electron paramagnetic resonance; PS I – Photosystem I; PS II – Photosystem II; RC – reaction center; Q_A – primary quinone acceptor of PS II; Q_B – secondary quinone acceptor of PS II; P430 – optical designation of Fe/S clusters now known as F_A and F_B; P700 – primary electron donor of PS I; P680 – primary electron donor of PS II.

John H. Golbeck (ed): Photosystem I: The Light-Driven Plastocyanin:Ferredoxin Oxidoreductase, 31–40.

kinetic studies. Prior research in many laboratories had resulted in knowledge of how physically to separate PS I from PS II and other chloroplast components and in the characterization of the electrochemical properties (redox potentials) of P700 and several electron acceptors. Techniques for achieving time resolution in the millisecond range for small optical absorption changes under a variety of experimental conditions were essential to the ultimate success of the project. Fortunately, apparatus sufficient to meet this challenge was assembled by one of the coauthors (Paul Mathis) and his associates at CEN-Saclay coincident with the granting of a year of sabbatical leave from UC Berkeley for the other coauthor (Ken Sauer) and the award of a fellowship from the Guggenheim Foundation. The research to be described was accomplished during approximately 1 year spanning 1976–1977 in the laboratories in Saclay and was described in four publications that appeared in 1977–1979.

II. Status of Knowledge of PS I in 1976

In 1976, when we started our work, several properties of the PS I reaction center (RC) were well-established. Basically, following light absorption, the primary electron donor, P700, is brought to an excited state and transfers an electron to a bound iron–sulfur center. The reduced iron–sulfur center then reduces ferredoxin, and $P700^+$ is rereduced by plastocyanin. It was also established that two iron–sulfur centers, named F_A and F_B, are present in the RC and can be photoreduced irreversibly at low temperature. When F_A and F_B are chemically prereduced, illumination at low temperature induces the reduction of another electron acceptor, named F_X. This is followed by a slow back-reaction, with a $t_{1/2}$ of several hundred milliseconds. Most of these data were obtained by EPR, at temperatures below 77 K. At physiological temperatures, flash absorption spectroscopy showed that a species named P430 behaves as a "primary electron acceptor," and it was equated with F_A or F_B or both of them. For all these discoveries, key references are Malkin and Bearden (1971), Hiyama and Ke (1971), Evans et al. (1972, 1974, 1975), Ke and Beinert (1973), and McIntosh et al. (1975). Reviews were published by Ke (1973) and by Bearden and Malkin (1975). Many of these aspects are discussed in this book by Bacon Ke (Chapter 3), Richard Malkin (Chapter 2), and Anthony San Pietro (Chapter 1).

With respect to our work, let us mention a few of the problems that we faced. The first was that there was no consensus on the functional role of F_X (see for instance Bearden and Malkin, 1976). Concerning "primary acceptors," some thought that F_A or F_B was playing that role, while supporters of F_X thought they had discovered the "real" primary acceptor. Studies at physiological temperature indicated only P430 as primary acceptor and provided no evidence for F_X. If P430 could be equated with the bound iron–sulfur centers detected by EPR, was it F_A or F_B, or could it be both of them? And of course, there was no indication for electron acceptors more primary than F_X. So, many things were known, but many essential questions also remained.

III. Motivation and Rationale for Our Work

In approaching this problem, each of us brought some experience from working on PS I. Ken Sauer with John Biggins had investigated excitation spectra for electron transport to $NADP^+$ by reactions that involved both PS I and PS II light reactions with water as the electron donor, or that involved only PS I using ascorbate and dichlorophenolindophenol ($DCPIPH_2$) as donor together with an inhibitor of PS II (Sauer and Biggins, 1965). The increased quantum efficiency for the PS I-only reaction at the red edge of the chlorophyll absorption (700 nm and greater) was found to be consistent with the pronounced red-drop in efficiency of the reaction involving both light reactions, owing to a fall-off in absorption of pigments transferring excitation to PS II in the far red. Studies carried out by Jeff Kelly showed that an analogous PS I reaction using cytochrome *c* as electron acceptor occurred with a quantum yield close to 1.0 in the far red region (Kelly and Sauer, 1965) and that a pigment antenna consisting of more than 400 chlorophyll molecules feeds PS I in spinach (Kelly and Sauer, 1968). Similar high-quantum yields were found by Alex Sun in the PS I reaction leading to $NADP^+$ reduction (Sun and Sauer, 1971). These were some of the first quantitative measurements of the PS I light reactions and they were done using spectrophotometric monitoring of substrate reduction. Spectrometric investigations of PS I-enriched particles using circular dichroism (CD) provided evidence to support the participation of two chlorophyll molecules in the primary electron donor, P700. Light-minus-dark difference CD spectra were consistent with the presence of a pair of chlorophylls in P700 that are coupled by an excitonic interaction that disappeared upon its oxidation to $P700^+$ (Philipson et al., 1972). The assignment of P700 to a chlorophyll dimer had been proposed the previous year on the basis of the linewidth of the EPR

spectrum from $P700^+$ (Norris et al., 1971). EPR studies carried out subsequently in Berkeley revealed the occurrence of transient electron spin polarization associated with PS I in broken chloroplasts (Blankenship et al., 1975). The attribution of the spin polarization to a "triplet mechanism" was later revised to a radical-pair origin upon more extensive measurements using membrane samples that were oriented in a hydrodynamic flow gradient. The anisotropy of the spin tensor showed that the radical-pair interaction occurred between $P700^+$ and F_X^-, but that the amplitude observed required interaction with an electron acceptor closer to P700 and with an isotropic spin tensor (Dismukes et al., 1978). We shall see that this picture is in good accord with the optical studies that were being carried out at Saclay.

Paul Mathis, on his side, was mostly experienced in flash absorption kinetics that he had used first to study the transient states of carotenoids and then a few properties of Photosystem II, mainly the kinetic properties of $P680^+$ using its absorption band in the near-infra-red. Following the observation made *in vitro* (Borg et al., 1970) that the chlorophyll *a* cation radical has a well-defined absorption band around 820 nm (a spectral region in which neutral chlorophyll has no absorption), it was inferred that 820 nm would be a good wavelength for studying $P680^+$ because a strong measuring light can be used without having an actinic effect, allowing an improved signal-to-noise ratio. In a first study (Mathis and Vermeglio, 1975), following flash excitation of chloroplasts at 103 K, $P680^+$ was detected by its absorption band around 825 nm. It decays with a half-time of about 3 msec, following multiple paths that are dominated by electron donation from cytochrome b_{559} and electron return from the Q_A acceptor (also named C-550 at that time). Haveman and Mathis (1976) studied chloroplasts in which oxygen evolution was inhibited by Tris washing or by a treatment at low pH. At room temperature, $P680^+$ (again detected by its absorption at 820 nm) is formed by a flash and it decays by a back-reaction with reduced Q_A, with a half-time of 120 μsec. After Tris washing, $P680^+$ was detected only after preillumination, indicating that at least one fast (undetected) electron donor is still working after Tris washing (later shown to be Tyr_Z).

These results led to the conclusion that new tools would be useful to improve the signal-to-noise ratio and the time resolution, particularly with the use of Si photodiodes (detectors) and laser diodes (emitters) that became commercially available. Starting September 1976, new flash absorption set-ups were built in P. Mathis's laboratory in Saclay, by J. van Best, a Dutch postdoc trained in Duysens's lab in Leiden. Rapidly, results were obtained, giving an entirely new view of the donor side of PS II where electron donation to $P680^+$ appeared to be a thousand times faster than previously assumed (van Best and Mathis, 1978). It seemed worthwhile to also reexamine PS I kinetics, measuring the state of $P700^+$ primarily by its near-IR absorption band.

Our rationale for the kinetic study of acceptors through $P700^+$ was to extend what had been done by Hiyama and Ke (1971) (See Ke, this volume, Chapter 3). With PS I subchloroplast particles when no electron donor is present, $P700^+$ formed by a short flash is reduced by electrons coming back from acceptors. Transfer of electrons to soluble artificial acceptors (such as viologens) leads to a very slow rereduction of $P700^+$. If electrons stop at the level of P430,[1] the back-reaction has a half-time of about 30 msec. If P430 is prereduced, electrons should stop at the level of the preceding acceptor (if any) and come back—but at which rate? If the earlier acceptor is itself prereduced, charge separation can take place only if a still more primary acceptor is present, and the back-reaction will be even faster; etc. This should make it possible to determine the number of electron acceptors connected to one P700 and their chemical nature, if the difference spectra are good enough.

Forward movement of electrons can be blocked by reduction of remote acceptors (with the implicit assumption that they have sufficiently less negative midpoint reduction potentials). Blockage can also be induced by low temperature or by specific inhibitors such as the herbicides that act between Q_A and Q_B in PS II and in purple bacteria; that method, however, has been much less successful with PS I. Biochemical treatments that remove some acceptors were used later on, with great success, by John Golbeck and his colleagues by manipulation of polypeptides, and by several groups with the selective extraction of phylloquinone. Already at that time, it was known that PS I particles prepared by treatment of membranes with sodium dodecylsulfate (SDS) appear to be devoid of secondary electron acceptors. Are they also devoid of primary ones?

IV. A Brief Account of Our Results

Our results, acquired between September 1976 and July 1977, were published in four papers (Sauer et al., 1977, 1978, 1979; Mathis et al., 1978). These report the

[1] F_A and F_B in current terminology.

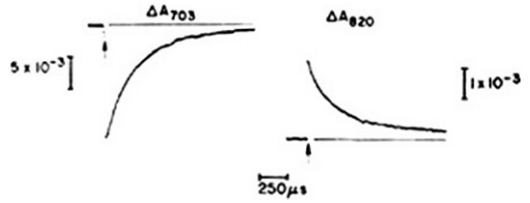

Fig. 1. Absorption transients at 703 nm (left) and 820 nm (right) induced by a ruby laser flash (10 nsec duration) incident on a sample of Triton-solubilized PS I particles. Anaerobic reaction mixture contains $Na_2S_2O_4$ (2 mg/ml), Triton (0.015%), glycine (0.2 M, pH 10), and particles sufficient to give $A_{672nm} = 1.61\ cm^{-1}$. The vertical bars indicate ΔA at each wavelength. At 703 nm, $t_{1/2} = 270$ μsec (96%); at 820 nm, $t_{1/2} = 245$ μsec (90%); the remaining signal at each wavelength was a slower component. No background illumination (Fig. 1; from Sauer et al., 1978).

results of absorption kinetic studies following excitation by a short laser flash of several biological materials: broken spinach chloroplasts, PS I subchloroplast particles prepared with Triton X-100 or with SDS. Various simple chemical treatments were used to bring the PS I electron acceptors to a desired state of reduction. That objective was also reached by a controlled use of preillumination by continuous light or by a sequence of single-turnover flashes. A cryostat was used to study the effects of low temperature on reaction kinetics. We do not wish here to repeat a detailed account of our published results, but instead we will focus on three salient aspects.

1. When P430 is prereduced (before flash excitation), $P700^+$ formed by a flash is rereduced with a half-time of 250 μsec. This result was obtained at room temperature with Triton subchloroplast particles in which P430 was apparently functional, according to the data of Ke and coworkers (back-reaction with a $t_{1/2}$ of about 30 msec, under mildly reducing conditions). After addition of dithionite at pH 10 and in the absence of air, to decrease the ambient redox potential, $P700^+$ was formed to the same extent in response to a short flash, but the 30-msec phase was replaced by a nearly monoexponential phase with a $t_{1/2}$ about 250 μsec (Fig. 1) The difference spectrum was not significantly modified, indicating formation of $P700^+$ and possibly the reduction of a species analogous to P430; however, our spectra between 400 and 500 nm were not accurate enough to be very conclusive on the chemical nature of the partner in the back-reaction with $P700^+$. The conclusion of that study supported the presence of an electron acceptor preceding P430 and fully active when P430 is prereduced (Sauer et al., 1978). We named this acceptor A_2 for reasons that will appear soon below. In view of the proposal that the species named F_X was "the" primary electron acceptor at low temperature, we proposed that A_2, the electron acceptor preceding P430 and operative at room temperature, was F_X (which had been detected only by EPR at low temperature).

2. When P430 was oxidized before illumination, and an electron donor provided to rereduce $P700^+$ much faster than electrons can come back from $P430^-$, two preflashes were necessary to induce the appearance of the 250-μsec phase. In these experiments, also done with Triton subchloroplast particles at room temperature, reduced phenazine methosulfate was added in the medium at a concentration permitting its reduction of $P700^+$ in about 2 msec; that is, faster than the back-reaction with P430 but slower than the 250-μsec back-reaction. The excitation flash given to obtain the rereduction kinetics of $P700^+$ was preceded by 0, 1, 2, or 3 single-turnover flashes, to provide a known number of electrons to the P430 species. We found that the rereduction of $P700^+$ was slow after 0 or 1 preflash; the 250-μsec decay appeared to a full extent after two or three preflashes (Fig. 2). We concluded that P430 can accommodate two electrons (Sauer et al., 1978). Because two Fe/S centers are known to be present (F_A and F_B, on the basis of EPR measurements), these two centers function as a pool hosting two electrons.

3. A much faster signal due to P700 was elicited, at the expense of slower phases, under two conditions: (1) By forcing electrons into the pool of acceptors by illumination under reducing conditions, in the presence of a good electron donor. The signal, with a half-time of return of about 3 μsec, was found with Triton PS I subchloroplast particles and with broken chloroplasts. (2) With CP1, a particle prepared with SDS and commonly assumed to be devoid of photoinduced electron transfer. Mildly reducing conditions were sufficient, and the decay $t_{1/2}$ was about 7 μsec. We found no effect of oxygen on the signal decay, and we thus eliminated the hypothesis of a triplet state. The decay becomes

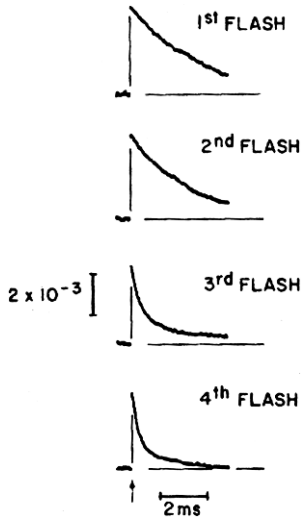

Fig. 2. Absorption transients at 820 nm for Triton-solubilized PS I particles induced by a saturating dye laser flash (λ = 605 nm, 1.0 μsec halfwidth) preceded by zero to three saturating preillumination flashes (not shown in the traces) from a xenon flash lamp; spacing 30 msec between flashes. Anaerobic mixture contains dithionite (1 mg/ml), Triton (0.005%), phenazine methosulfate (30 μM), tricine (0.02 M, pH 7.6), and sufficient particles to give $A_{673nm} = 1.11\ cm^{-1}$. Top curve, laser flash only; $t_{1/2} = 2.4$ msec (>95%). Second curve, one preillumination flash; $t_{1/2} = 1.9$ msec (>95%). Third curve, two preillumination flashes; $t_{1/2} = 0.32$ msec (90%). Bottom curve, three preillumination flashes; $t_{1/2} = 0.26$ msec (75%). The response to only the last (dye laser) flash is shown (Fig. 6; from Sauer et al., 1978).

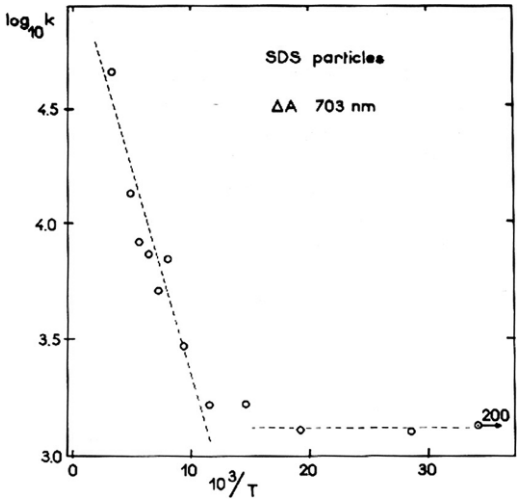

Fig. 3. Arrhenius plot for the flash-induced decay of ΔA_{703nm} in a frozen suspension of SDS PS I particles (200 μl thawed sample) + ascorbate (40 μl, 100 mM) + dichlorophenolindophenol (40 μl, 1 mM) + Tris (200 μl, 50 mM, pH 8.2) + glycerol (650 μl). At each temperature the decay has been decomposed into two exponential phases. The rate constant, k, of the major (fast) phase is reported in the plot (Fig. 5; from Mathis et al., 1978).

slower when temperature decreases; below 80 K, it is temperature-independent with $t_{1/2}$ = 0.55 msec (Fig. 3). We assumed that this signal is the same under the two sets of conditions (with slightly different kinetics), and we attributed it to charge separation between P700 and an electron acceptor named A_1 (this is why the electron acceptor giving rise to the 250-μsec phase was named A_2). The interpretation was that a back-reaction between $P700^+$ and A_1^- was taking place when A_2 was lost (in CP1 particles) or prereduced, in Triton particles and in chloroplasts, under very reducing conditions (Mathis et al., 1978).

So, we believed that we had made a good progress toward elucidation of electron transfer in the PS I RC. In the conclusion of our paper (Sauer et al., 1978), we wrote: "This chain of (four) acceptors must serve to produce a substantial and very rapid separation of charges across the photosynthetic membrane." This was anticipatory of the present view that efficient and fast electron transfer in RCs is permitted by a complex sequence of electron transfer relays. However, we were far from thinking that two additional relays participate in one branch (or that there is a second electron transfer branch, which might also be functional!).

The situation in PS I is much more complicated than we anticipated. The 250-μsec phase can probably be attributed to the back-reaction between $P700^+$ and one electron added to the couple (F_X–phylloquinone). Our attribution of the 3–10 μsec phase was dramatically wrong, because it was probably due to the triplet state of P700, although it correctly indicated the presence of another acceptor. Let us now discuss our results in the light of the present knowledge of the PS I RC.

V. A Brief Description of the Present View of PS I Electron Acceptors

The recent availability of a well-resolved 3D structure for the PS I RC (Jordan et al., 2001) permits a description of light-induced electron transfer that is compatible with the arrangement of redox-active components. For what concerns us here, the RC is made essentially of two homologous large protein subunits (PsaA and PsaB) that bear most of the redox cofactors and also of one small subunit (PsaC) that bears the Fe/S centers F_A and F_B. Like other RCs, PS I has a nearly symmetrical

structure, with a pseudo-C_2 axis that runs from the primary donor, P700 (a dimer of chlorophylls), to F_X, a [4Fe–4S] center, which is borne by the two large subunits and has a very central location. The redox cofactors are organized as two branches. Starting from P700, each branch includes two chlorophyll *a* molecules, the first assumed to be simply a relay in electron transfer, and the second a real intermediate, named A_0, where an electron arrives in about 1 psec after excitation of P700. The next acceptor is a phylloquinone A_1 (reached in 30 psec), from where the electron goes to F_X. Two [4Fe–4S] centers, F_A and F_B, are located downstream. In less than 1 msec, an electron reaches F_B, which is the last species located integrally in the RC. These electron acceptors are arranged roughly in order of increasing midpoint redox potentials, presumably with two exceptions: A_1 and F_X may have nearly equal midpoints, and F_B is 60 mV more negative than F_A. The species from P700 to F_X are all carried by a protein complex made of the two closely associated large subunits, PsaA and PsaB, while F_B and F_A are carried by the small PsaC polypeptide. Once reduced, F_B can donate an electron to the terminal acceptor, ferredoxin or flavodoxin, both of which are small water-soluble proteins that interact with the RC thanks to polypeptides PsaD and PsaE. Rates of back-reaction will be discussed together with our data. Concerning forward electron transfer, the major uncertainty is the contribution of each structural branch. Relying on a similarity with the RC of purple bacteria, it was usually assumed that only one branch was active, but recent data indicate that the two branches may be almost equally active in *Chlamydomomas reinhardtii* (Guergova-Kuras et al., 2001).

VI. Our 3–10 ms Phase: The Triplet State of P700?

Following flash excitation, we observed a microsecond absorption signal under two conditions: with CP1 particles under mildly reducing conditions, and with more intact materials (Triton particles and broken chloroplasts) after forcing electrons through P700 by illumination at a low redox potential, a treatment intended to reduce secondary electron acceptors.

Let us start with CP1 particles (Mathis et al., 1978), which at that time were supposed to display no photoinduced electron transfer (Shiozawa et al., 1974). Our results indicated that some sort of electron transfer was taking place, but our signal could have been due either to a radical pair lasting a few microseconds, or to a triplet state formed as a product of rapid charge recombination in the radical pair. We chose the first hypothesis because we found no effect of oxygen on the lifetime of the signals, whereas it is known that oxygen usually accelerates the decay of triplet states. We made, however, the wrong choice: Our signal was due to the triplet state of P700, as later shown conclusively by a more detailed analysis of absorption change transients (Sétif et al., 1981) and by flash kinetic EPR (Sétif et al., 1982), and as proposed also for our signal to account for the properties of a steady-state light-induced spin-polarized triplet signal (Rutherford and Mullet, 1981). The lack of an oxygen effect is still not understood, as far as we know, but it is a general property for the triplet state of the primary donor in all kinds of photosynthetic RCs.

There has now been a wealth of studies showing that, in PS I, the P700 triplet state is formed as a product of the back-reaction, with a $t_{1/2}$ of about 30 nsec, between $P700^+$ and A_0^-, where A_0, the true primary acceptor, is a molecule of chlorophyll *a* (review by Brettel, 1997). In all kinds of RCs, the spin-polarized triplet state of the primary donor P is formed by a similar mechanism, where the primary radical ($P700^+A_0^-$ in the case of PS I) is initially formed as a singlet state and then oscillates between a triplet and a singlet state. The charge recombination gives rise either to the triplet state or to the vibrationally excited singlet ground state of P, according to the state of the radical pair at the time of charge recombination [see Hoff (1981) for a general reference on the radical-pair mechanism for the formation of triplet states in RCs].

In fact, our attention should have been drawn to the triplet state by the peculiar effect of temperature on the kinetics: a temperature region with a thermal activation between room temperature and 100 K, and a temperature-independent decay below 80 K. A strikingly similar behavior had been reported for the state named P^R in the RC of purple bacteria (Parson et al., 1975), and shown to be the triplet state of P (Parson and Monger, 1976). This state, however, was found at ambient temperatures only in carotenoid-less RCs (such as *Rb. sphaeroides* R26), while PS I is full of β-carotene. From the detailed 3D structure of PS I (Jordan et al., 2001), it now seems that no carotene molecule is close enough to P700 to allow triplet–triplet energy transfer.

We also found a microsecond signal in more intact materials, and we assumed that we were observing the same species (Sauer et al., 1978). Was it a correct assumption? A spin-polarized triplet state has indeed been observed under conditions similar to ours by Frank et al. (1979). But the mechanism of triplet P700 formation is probably different. Sétif and coworkers (Sétif and Bottin, 1989; Sétif and Brettel, 1990) have

shown that it is possible to prepare PS I RCs in a state where all iron–sulfur centers are reduced and A_1 is still oxidized (this is not a highly stable situation because A_1 tends to become fully reduced to the hydroquinone state). Following light excitation, the radical pair ($P700^+A_1^-$) is formed and recombines with a half-time of about 250 nsec, leading to the formation of $^3P700$ with a yield close to 100%. This efficient triplet formation from the secondary radical seems rather surprising, but it is consistent with the energetics of charge separated states in PS I (Polm and Brettel, 1998). In our 1977 experiments, it cannot be excluded, however, that the phylloquinone A_1 became fully reduced as studied by Sétif and Bottin (1989), in which case the triplet state of P700 is formed from the back-reaction in the primary radical pair $P700^+A_0^-$. But the state where phylloquinone is fully reduced recovers very slowly, whereas the state giving rise to a 3-μsec signal in our early experiments (Sauer et al., 1978) disappears quickly after a background illumination.

To conclude with the signal with a $t_{1/2}$ of 3–10 μsec at room temperature, it appears that we were wrong in attributing it to a radical-pair state because, whatever its mechanism of formation, it is due to $^3P700$. But we were right in concluding that it indicated the existence of a new, very primary, electron acceptor.

VII. Two Electrons in P430

Our experiments (Sauer et al., 1978) in which the rereduction of $P700^+$ was measured after a number of saturating preflashes led very simply to the conclusion that two electrons could be accumulated in the species named P430 (Ke, 1973). EPR experiments at low temperature had shown the existence of two iron–sulfur centers, F_A and F_B. Our conclusion was thus rather straightforward that F_A and F_B also function at ambient temperature and together make up what had been called P430. F_A and F_B have respective redox midpoint potentials of about −530 and −580 mV. Thus, they were supposed to be positioned in the RC structure in such a way that electrons coming from P700 would go first to F_B, and then to F_A. That was shown not to be the case: F_A is reached first, and there is an uphill electron transfer from the reduced F_A to F_B. This has been shown by a conjunction of spectroscopic and photovoltage experiments (Diaz-Quintana et al., 1998), and confirmed by the 3D structure (Jordan et al., 2001).

The redox equilibrium between F_A and F_B is certainly reached in less than 1 μsec, and there should be no difficulty for placing two electrons in the F_A/F_B pool (P430). We heard subsequently that some people had problems in reproducing our preflash experiments. We were presumably lucky in finding the proper redox conditions, as well as in using the most appropriate PS I subchloroplast particles.

VIII. Origin of Our 250 μs Phase

Our finding of a 250-μsec back-reaction between $P700^+$ and a reduced acceptor that we named A_2 (Sauer et al., 1978) was experimentally straightforward, but it required a large number of subsequent experiments to be correctly interpreted. We observed the back-reaction at room temperature under conditions where F_A and F_B were prereduced. Previous low-temperature EPR experiments had shown that, in PS I, a species named F_X behaves like an electron acceptor more primary than F_A and F_B (McIntosh et al., 1975; Evans et al., 1975). We thus naturally equated our A_2 with F_X.

Time-resolved EPR experiments had shown that reduced F_X recombines with $P700^+$ with a half-time of a few hundred milliseconds below 20 K. We thus thought that it should be straightforward to show that the 250-μsec back-reaction slows down progressively to hundreds of milliseconds, when temperature decreases. That was the rationale for our flash absorption studies at temperatures from 294 K to nearly 4 K (Sauer et al., 1979). However, we were not able to verify our prediction, and things were revealed to be much more complex than we expected. We now know that this complexity has several origins: first, what we named A_2 is in fact made of two successive acceptors, the phylloquinone A_1 and the iron–sulfur center F_X; and secondly, most electron transfer reactions (either forward or reverse) in PS I become strongly multiphasic at low temperature. Two other features add to the complexity: Recombination kinetics are influenced by the redox state of downstream electron acceptors (perhaps because of electrostatic repulsion); and the triplet state of P700 is formed in many experiments, adding unwanted (and sometimes unrecognized) kinetic phases. We will discuss a few of these aspects only briefly, referring largely to Brettel (1997) for a detailed discussion.

Compared to our results, the first important progress was made by Golbeck et al. (1978) who showed that the A_2 phase disappears when PS I particles are treated to denature iron–sulfur clusters, supporting the idea that A_2 is an iron–sulfur center, presumably F_X. This proposal was further supported by the results of Golbeck and Cornelius (1986), who were able to selectively remove F_A and F_B from PS I particles by a controlled

treatment with lithium dodecyl sulfate. After this treatment, flash excitation induces a charge separation that recombines with a half-time of 1.2 msec. This was interpreted as the back-reaction between $P700^+$ and F_X^-. The decay is not far from that of our 250-μsec signal, reinforcing the hypothesis that A_2 is F_X. The lengthening from 250 μsec to 1.2 msec might be due to a minor perturbation of the structure between P700 and F_X or to the disappearance of negative charges on F_A and F_B (which were reduced in our studies and absent in Golbeck's).

To identify A_2, it is also possible to analyze the difference spectrum of the state ($P700^+$ A_2^-). Our own study revealed that A_2 could be an iron–sulfur center, but our spectra were not accurate enough. Detailed spectral studies were conducted by Brettel (1989), with PS I particles from cyanobacteria, in which F_A and F_B were chemically reduced. He found that the difference spectrum fitted poorly with A_2 being an iron–sulfur center, but fitted much better with a phylloquinone (since in the meanwhile many indications were obtained for the presence of a phylloquinone, named A_1, as intermediate electron acceptor between P700 and F_X) (Brettel et al., 1986). Brettel thus proposed that the 250-μsec back-reaction takes place between $P700^+$ and A_1^-.

What can we learn from studies versus temperature, which have been numerous? In our work with Triton PS I particles (Sauer et al., 1978) we found at low temperature a back-reaction of less than 1 msec, under conditions where we expected a back-reaction of $P700^+$ with F_X^- in hundreds of milliseconds (although we should remember that the light-induced formation of F_X^-, in low-temperature experiments where F_A and F_B were prereduced, always indicated a small extent of reaction). A next step was really surprising, since Mathis and Conjeaud (1979) found that, with chloroplasts below 77 K, a large part of $P700^+$ formed by a flash is rereduced by a back-reaction with a half-time of 122 μsec, without any prereduction of iron–sulfur centers. That result was totally against the "dogma" of a highly efficient irreversible photooxidation of P700 at low temperature (see, e.g., Bearden and Malkin, 1976), but it has been largely confirmed by later studies (see for instance Sétif et al., 1984b; Schlodder et al., 1998). Detailed studies have shown that a dominant back-reaction with a $t_{1/2}$ between 100 and 200 μsec, observed in various PS I preparations, at low temperature, is due to the state ($P700^+$ A_1^-), where A_1 is a phylloquinone (Brettel et al., 1986; Brettel and Golbeck, 1995; Schlodder et al., 1998). It was also shown that the back-reaction between $P700^+$ and A_1^- is multiphasic and nearly temperature-independent (Sétif et al., 1984a; Brettel and Golbeck, 1995; Schlodder et al., 1998).

All of these data tend to support the idea that our 250-μsec phase may well be a back-reaction between $P700^+$ and phylloquinone, and that what we named A_2 may be the phylloquinone (now called A_1) rather than F_X. As a matter of fact, as discussed in detail by Brettel (1997), the redox midpoint potentials of the phylloquinone A_1 and of F_X are probably very close and, when F_A and F_B are either removed or prereduced, there is a rapid equilibrium between the states ($P700^+A_1^-$) and ($P700^+F_X^-$), in which each state contributes significantly, with a weight that depends on the biological material. Brettel (1997), however, recognizes that the question is not fully settled. Until now, our discussion has not integrated the idea that the two phylloquinones of PS I may be active. What we named A_1 may in fact be constituted of both molecules. This may be a reason for the complexity of the kinetic behavior of the PS I acceptors, since the parameters controlling the rates of electron transfer (distances, driving force, reorganization energies) might be different for the two quinones and their partners.

IX. Concluding Remarks

In photosynthetic systems spectroscopic studies, including steady-state, light-minus-dark and flash-induced transients, typically precede the determination of molecular structure using crystallographic diffraction analysis. This was true for purple bacteria RCs, for PS I and for PS II, as well as for many chlorophyll–protein antenna complexes. In general, many conclusions from spectroscopic studies were confirmed by the structural information. However, crystallography has also provided new insights that were not evident from the spectroscopy, such as the two parallel paths of electron transfer cofactors that occur in RCs. Once structural data are available, additional experiments are indicated on the basis of features that had not been anticipated. Refined spectroscopic studies are now providing answers to many of these issues. This synergy of methodologies is still proving extremely valuable in ongoing investigations of the photosynthetic reactions.

References

Bearden AJ and Malkin R (1975) Primary photochemical reactions in chloroplast photosynthesis. Quart Rev Biophys 7: 131–177

Bearden AJ and Malkin R (1976) Chloroplast photosynthesis: the RC of Photosystem I. Brookhaven Symp Biol 28: 247–266

Blankenship R, McGuire A and Sauer K (1975) Chemically induced dynamic electron polarization in chloroplasts at room temperature: evidence for triplet state participation in photosynthesis. Proc Natl Acad Sci USA 72: 4943–4947

Borg DC, Fajer J, Felton RH and Dolphin D (1970) The π-cation radical of chlorophyll a. Proc Natl Acad Sci USA 67: 813–820

Brettel K (1989) New assignment for the 250 μs kinetics in Photosystem I: P-700$^+$ recombines with A1$^-$ (not F_X^-). Biochim Biophys Acta 976: 246–249

Brettel K (1997) Electron transfer and arrangement of the redox cofactors in photosystem I. Biochim Biophys Acta 1318: 322–373

Brettel K and Golbeck JH (1995) Spectral and kinetic characterization of electron acceptor A_1 in a Photosystem I core devoid of iron–sulfur centers F_X, F_B and F_A. Photosynth Res 45: 183–195

Brettel K, Sétif P and Mathis P (1986) Flash-induced absorption changes in photosystem I at low temperature: evidence that the electron acceptor A_1 is vitamin K_1. FEBS Lett 203: 220–224

Diaz-Quintana A, Leibl W, Bottin H and Sétif P (1998) Electron transfer in Photosystem I RCs follows a linear pathway in which iron–sulfur cluster F_B is the immediate electron donor to soluble ferredoxin. Biochemistry 37: 3429–3439

Dismukes GC, McGuire A, Blankenship R and Sauer K (1978) Electron spin polarization in photosynthesis and the mechanism of electron transfer in Photosystem I. Biophys J 21: 239–256

Evans MCW, Telfer A and Lord AV (1972) Evidence for the role of a bound ferredoxin as the primary electron acceptor of Photosystem I in spinach chloroplasts. Biochim Biophys Acta 267: 530–537

Evans MCW, Reeves SG and Cammack (1974) Determination of the oxidation–reduction potential of the bound iron–sulphur proteins of the primary electron acceptor complex of Photosystem I in spinach chloroplasts. FEBS Lett 49: 111–114

Evans MCW, Sihra CK, Bolton JR and Cammack R (1975) Primary electron acceptor complex of photosystem I in spinach chloroplasts. Nature 256: 668–670

Frank HA, Mc Lean MB and Sauer K (1979) Triplet states in photosystem I of spinach chloroplasts and subchloroplast particles. Proc Natl Acad Sci USA 76: 5124–5128

Golbeck JH and Cornelius JM (1986) Photosystem I charge separation in the absence of centers A and B. I. Optical characterization of center "A_2" and evidence for its association with a 64-kDa peptide. Biochim Biophys Acta 849: 16–24

Golbeck J, Velthuys BR and Kok B (1978) Evidence that the intermediate electron acceptor, A_2, in Photosystem I is a bound iron–sulfur protein. Biochim Biophys Acta 504: 226–230

Guergova-Kuras M, Bourdeaux B, Joliot A, Joliot P and Redding K (2001) Evidence for two active branches for electron transfer in Photosystem I. Proc Natl Acad Sci USA 98: 4437–4442

Haveman J and Mathis P (1976) Flash-induced absorption changes of the primary donor of Photosystem II at 820 nm in chloroplasts inhibited by low pH or Tris treatment. Biochim Biophys Acta 440: 346–355

Hiyama T and Ke B (1971) A new photosynthetic pigment, "P430": its possible role as the primary electron acceptor of Photosystem I. Proc Natl Acad Sci USA 68: 1010–1013

Hoff AJ (1981) Magnetic field effects on photosynthetic reactions. Q. Rev. Biophys. 14: 599–665

Jordan P, Fromme P, Witt HT, Klukas O, Saenger W and Krauß N (2001) Three-dimensional structure of cyanobacterial photosystem I at 2.5 Å resolution. Nature 411: 909–917

Ke B (1973) The primary electron acceptor of Photosystem I. Biochim Biophys Acta 301: 1–33

Ke B and Beinert H (1973) Evidence for the identity of P430 of Photosystem I and chloroplast-bound iron–sulfur protein. Biochim Biophys Acta 305: 689–693

Kelly J and Sauer K (1965) Action spectrum and quantum requirements for the photoreduction of cytochrome c with spinach chloroplasts. Biochemistry 4: 2798–2802

Kelly J and Sauer K (1968) Functional photosynthetic unit sizes for each of the two light reactions in spinach chloroplasts. Biochemistry 7: 882–890

Malkin R and Bearden AJ (1971) Primary reactions of photosynthesis: photoreduction of a bound chloroplast ferredoxin at low temperature as detected by EPR spectroscopy. Proc Natl Acad Sci USA 68: 16–19

Mathis P and Conjeaud H (1979) Rapid reduction of P-700 photooxidized by a flash at low temperature in spinach chloroplasts. Photochem Photobiol 29: 833–837

Mathis P and Vermeglio A (1975) Chlorophyll radical cation in Photosystem II of chloroplasts. Millisecond decay at low temperature. Biochim Biophys Acta 369: 371–381

Mathis P, Sauer K and Rémy R (1978) Rapidly reversible flash-induced electron transfer in a P700 chlorophyll–protein complex isolated with SDS. FEBS Lett 88: 275–278

McIntosh AR, Chu M and Bolton JR (1975) Flash photolysis electron spin resonance studies of the electron acceptor species at low temperatures in Photosystem I of spinach subchloroplast particles. Biochim Biophys Acta 376: 308–314

Norris JR, Uphaus RA, Crespi HL and Katz JJ (1971) Electron spin resonance of chlorophyll and the origin of Signal I in photosynthesis. Proc Natl Acad Sci USA 68: 625–628

Parson WW and Monger TG (1976) Interrelationships between excited states in bacterial RCs. Brookhaven Symp Biol 28: 195–212

Parson WW, Clayton RK and Cogdell RJ (1975) Excited states of photosynthetic RCs at low redox potentials. Biochim Biophys Acta 387: 265–278

Philipson KD, Sato VL and Sauer K (1972) Exciton interaction in the Photosystem I RC from spinach chloroplasts. Absorption and circular dichroism difference spectra. Biochemistry 11: 4591–4595

Polm M and Brettel K (1998) Secondary pair charge recombination in Photosystem I under strongly reducing conditions: temperature dependence and suggested mechanism. Biophys J 74: 3173–3181

Rutherford AW and Mullet JE (1981) RC triplet states in Photosystem I and Photosystem II. Biochim Biophys Acta 635: 225–235

Sauer K and Biggins J (1965) Action spectra and quantum yields for nicotinamide adenine dinucleotide phosphate reduction by chloroplasts. Biochim Biophys Acta 102: 55–72

Sauer K, Acker S, Mathis P and van Best J (1977) Optical studies of Photosystem I particles: evidence for the presence of multiple electron acceptors. In: Packer L, Papageorgiou GC and Trebst A (eds) Bioenergetics of Membranes, pp 351–359. Elsevier/North Holland Biomedical Press, Amsterdam

Sauer K, Mathis P, Acker S and van Best J (1978) Electron acceptors associated with P700 in Triton-solubilized Photosystem I particles from spinach chloroplasts. Biochim Biophys Acta 503: 120–134

Sauer K, Mathis P, Acker S and van Best J (1979) Absorption changes of P700 reversible in milliseconds at low temperature in Triton-solubilized Photosystem I particles. Biochim Biophys Acta 545: 466–472

Schlodder E, Falkenberg K, Gergeleit M and Brettel K (1998) Temperature dependence of forward and reverse electron transfer from A_1^-, the reduced secondary electron acceptor in Photosystem I. Biochemistry 37: 9466–9476

Sétif P and Bottin H (1989) Identification of electron-transfer reactions involving the acceptor A_1 of Photosystem I at room temperature. Biochemistry 28: 2689–2697

Sétif P and Brettel K (1990) Photosystem I photochemistry under highly reducing conditions: study of the P700 triplet state formation from the secondary radical pair ($P700^+$-A_1^-). Biochim Biophys Acta 1020: 232–238

Sétif P, Hervo G and Mathis P (1981) Flash-induced absorption changes in Photosystem I: radical pair or triplet state formation? Biochim Biophys Acta 638: 257–267

Sétif P, Quaegebeur JP and Mathis P (1982) Primary processes in Photosystem I. Identification and decay kinetics of the P700 triplet state. Biochim Biophys Acta 681: 345–353

Sétif P, Mathis P, Lagoutte B and Duranton J (1984a) Electron acceptors in PS-I: comparison of A_2 and F_X. In: Sybesma C (ed) Advances in Photosynthesis Research, Vol I, pp. 589–592, Martinus Nijhoff/Dr W Junk Publishers, The Hague

Sétif P, Mathis P and Vänngård T (1984b) Photosystem I photochemistry at low temperature. Heterogeneity in pathways for electron transfer to the secondary acceptors and for recombination processes. Biochim Biophys Acta 767: 404–414

Shiozawa JA, Alberte RS and Thornber JP (1974) The P700-chlorophyll *a*–protein. Arch Biochem Biophys 165: 388–397

Sun ASK and Sauer K (1971) Pigment systems and electron transport in chloroplasts I. Quantum requirements for the two light reactions in spinach chloroplasts. Biochim Biophys Acta 234: 399–414

Van Best J and Mathis P (1978) Kinetics of reduction of the oxidized primary electron donor of Photosystem II in spinach chloroplasts and in Chlorella cells in the microsecond and nanosecond time ranges following flash excitation. Biochim Biophys Acta 503: 178–188

Chapter 5

Association of Photosystem I and Light-Harvesting Complex II during State Transitions

Egbert J. Boekema* and Roman Kouřil
Department of Biophysical Chemistry, GBB, University of Groningen, Nijenborgh 4, 9747 AG Groningen, The Netherlands

Jan P. Dekker
Division of Physics and Astronomy, Faculty of Sciences, Vrije Universiteit, De Boelelaan 1081, 1081 HV Amsterdam, The Netherlands

Poul Erik Jensen
Plant Biochemistry Laboratory, Department of Plant Biology, The Royal Veterinary and Agricultural University, 40 Thorvaldsenvej, Frederiksberg C DK-1871, Denmark

Summary

Green plant photosystem I (PS I) not only binds a chlorophyll *a*/*b*-binding, membrane-intrinsic antenna complex (LHCI) that is associated with the PS I core complex under almost all physiological conditions, but it can also transiently bind the major chlorophyll *a*/*b*-binding light-harvesting complex (LHCII), when the light conditions favor excitation of photosystem II (PS II) and the photosynthetic apparatus is in the so-called state 2. Recently, a low-resolution structure was obtained of a PS I–LHCII supercomplex from *Arabidopsis thaliana*. We describe here some of the structural features of this transient complex, and discuss the role of small PS I subunits that are involved in the binding of LHCII. We also discuss structural features of the PS I complex of the green algae *Chlamydomonas reinhardtii*, which has a larger LHCI antenna and shows a more pronounced difference between state 1 and state 2.

I. Introduction

One of the ways by which plants adapt to changing light conditions is to change the direction of part of the absorbed light to either PS I or PS II. The response of the photosynthetic apparatus to such light fluctuations is called a state transition (Allen and Forsberg,

* Author for correspondence, email: e.j.boekema@rug.nl

Abbreviations: EM – electron microscopy; LHCI – light-harvesting complex I; LHCII – light-harvesting complex II; PS I – photosystem I; PS II – photosystem II; PS I-A to PS I-O – alternative higher plant nomenclature for PS I polypeptides.

John H. Golbeck (ed): Photosystem I: The Light-Driven Plastocyanin:Ferredoxin Oxidoreductase, 41–46.

2001; Haldrup et al., 2001; Wollman, 2001). State transitions occur in three main steps. The first step is the initiation of a signal transduction leading to the activation of kinases. This activation is brought about by the reduced state of the plastoquinone (PQ) pool and the cytochrome b_6f complex, induced by preferential excitation of PS II (Vener et al., 1997; Zito et al., 1999). The second step is the phosphorylation, by the activated kinases, of light-harvesting complex II (LHCII). In plants, the major LHCII proteins consist of three closely related chlorophyll *a*/*b*-binding proteins encoded by the *Lhcb1–3* genes (Jansson, 1994; see also Croce et al., this volume, Chapter 10). Two kinase families are proposed to be involved in LHCII phosphorylation: TAK kinases (Snyders and Kohorn, 1999, 2001) and STT7 kinases in *Chlamydomonas reinhardtii* (Depège et al., 2003) and its homolog in *Arabidopsis* STN7 (Bellafiore et al., 2005). Mutants without those kinases cannot perform phosphorylation of LHCII and have impaired state transitions. The phosphorylation of LHCII is thought to cause a conformational change, which allows LHCII to diffuse from the grana to PS I in the stromal parts of the thylakoid membrane, constituting the last step in the state transition (Allen and Forsberg, 2001). The binding of phosphorylated LHCII to PS I brings the system to state 2 and allows a redistribution of the light energy between the two photosystems and a balancing of linear electron flow. This association between PS I and LHCII is reversible. Preferential excitation of PS I leads to oxidation of the plastoquinol pool, a dephosphorylation of LHCII, and a release of LHCII from the PS I–LHCII complex (state 1).

The three main steps in the state transitions are rather similar in green plants and green algae such as *C. reinhardtii*, but in some respects these systems are very different. The extent of the state transition is much larger in *C. reinhardtii*, in which 80% of LHCII may migrate between PS II and PS I (Delosme et al., 1996), whereas in plants only 10–20% of LHCII migrates between PS II and PS I (Allen, 1992). The differences in the extent of the state transitions may relate to the amount of stacking, which is much lower in *C. reinhardtii*. A less tight stacking may result in a greater accessibility of LHCII for the kinases and a larger proportion of LHCII that can migrate to PS I (Dekker and Boekema, 2005). In *C. reinhardtii*, the transition from state 1 to state 2 is accompanied by an increase of cyclic electron transfer around PS I (Finazzi et al., 2002), whereas in *Arabidopsis thaliana*, no change in cyclic electron transfer occurs upon state transitions (Lunde et al., 2003). Furthermore, the structure of the PS I–LHCI complex is different in both types of organisms. LHCI of green plants consists of four chlorophyll *a*/*b*-binding proteins, encoded by the *Lhca1–4* genes (Jansson, 1994), while LHCI of *C. reinhardtii* consists of nine proteins of the Cab gene family (Takahashi et al., 2004). The structure of the PS I–LHCI complex from pea is known at 4.4 Å resolution (Ben-Shem et al., 2003), and shows that the four LHCI proteins are located in a row at the PS I-FJ side of the complex between the PS I-G and PS I-K subunits. A low-resolution structure of the PS I–LHCI complex from *C. reinhardtii* was obtained by single-particle electron microscopy (Germano et al., 2002; Kargul et al., 2003). It was suggested that four of the additional LHCI proteins are bound in a second row flanked by the PS I-G and PS I-K proteins, and that a single LHCI protein is bound at the other side of the complex between PS I-H, PS I-A, and PS I-K (Dekker and Boekema, 2005).

Despite intensive search, no structural information on the putative PS I–LHCII complex in state 2 was available until very recently. On the basis of both cross-linking experiments and the structures of the green plant PS I–LHCI and LHCII complexes, Ben-Shem and Nelson proposed a location of LHCII at the PS I-A side between PS I-H and PS I-K (Ben-Shem and Nelson, 2005). Recently, we obtained a structure of the top view of a PS I–LHCII complex from *Arabidopsis* in state 2 (Kouřil et al., 2005), in which the LHCII is slightly displaced compared to the suggestion of Ben-Shem and Nelson. The new structure gives new information on the interaction between PS I–LHCI and LHCII, and forms the main topic of this chapter.

II. Structure of the PS I–LHCII Complex

Thylakoid membranes of *A. thaliana* were prepared in state 1 or state 2 by red or orange light treatment, respectively, as described by Zhang and Scheller (2004). The membranes were solubilized with the very mild detergent digitonin, and immediately without further purification analyzed by electron microscopy (Kouřil et al., 2005). This procedure prevents disassembly of the particles as much as possible, and allows a statistical analysis of the numbers of the various complexes in the membranes. Figure 1 shows a typical electron micrograph of the solubilized material. Many of the projections can be recognized because of their particular size and shape, such as ATPase, $C_2S_2M_2$ PS II–LHCII supercomplexes (Yakushevska et al., 2001), and PS I–LHCI particles (Boekema et al., 2001). All projections from particles with a size similar or larger than that of the PS I–LHCI complex (see also Nelson and

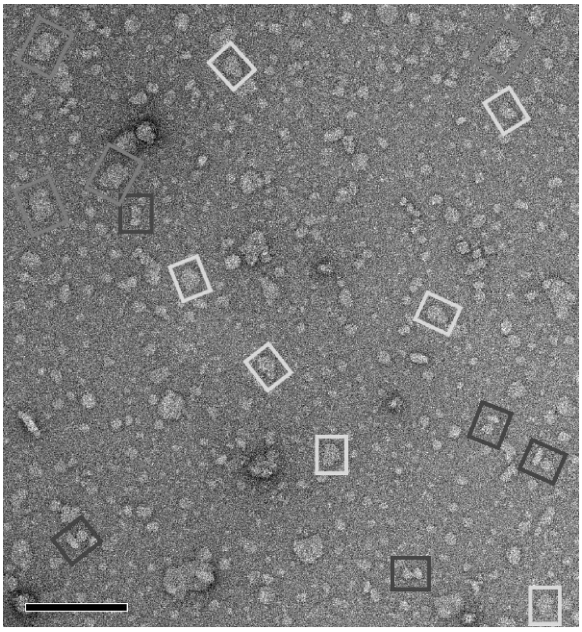

Fig. 1. Part of an electron micrograph of nonpurified single particles from digitonin solubilized thylakoid membranes of *Arabidopsis thaliana* in state 2. Projections of PSI/PSI–LHCII, PSII, and ATPases are indicated by white, gray, and black boxes, respectively. The scale bar equals 100 nm. (Modified from Kouřil et al., 2005.)

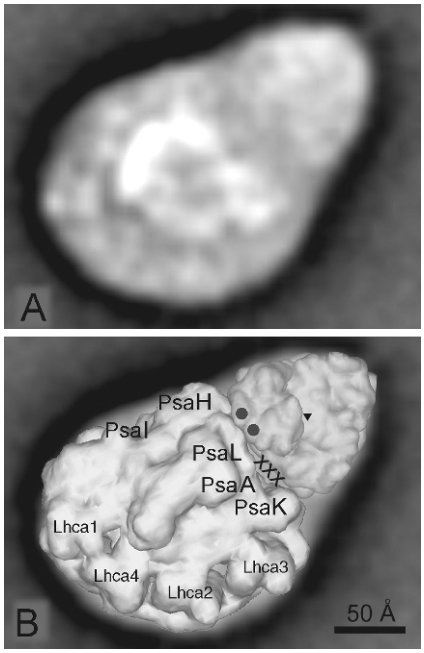

Fig. 2. Model of the PSI–LHCII supercomplex. (A) Final projection map at 16 Å. (B) See Color Plate 1, Fig. 1.

Ben-Shem, this volume, Chapter 7) were selected and subjected to multivariate statistical analysis. The results showed that the majority of the analyzed PS I projections from state 2 membranes belong to classes of oval-shaped PS I–LHCI particles, or to novel pear-shaped particles (Fig. 2A), representing a supercomplex of PS I and trimeric LHCII (see below). The same projections were obtained from state 1 membranes, but with the pear-shaped particles in much smaller numbers.

The results obtained by Kouřil et al. (2005) have a number of implications. One implication is that at least the majority of LHCII that binds to PS I is trimeric. More than 90% of the analyzed PS I particles could be attributed to either the normal PS I–LHCI complex, or to the same complex with associated trimeric LHCII, which excludes the occurrence of significant amounts of supercomplexes of PS I and monomeric LHCII. In older literature (see, e.g., Bassi et al., 1988) it was suggested that the migrating LHCII could be monomeric, but in these papers the "state 2" was obtained by high light, which is not an appropriate way to induce the state transition. High light can, for instance, induce monomerization of LHCII (Garab et al., 2002), so the earlier proposed involvement of monomeric LHCII may be the result of the applied illumination protocol. It was also suggested that phosphorylation induces conformational changes of LHCII, one of which is a trimer-to-monomer transition (Nilsson et al., 1997). Our results show that a trimer-to-monomer transition is not required for binding to PS I and that the amount of bound monomers in state 2 is very small.

Another implication is that the binding of PS I and LHCII is specific. If the binding of LHCII to PS I was not specific, the final image (Fig. 2A) would have been more blurred, or there would have been more than one class of projections with differences in the LHCII area. A final fitting of the atomic PS I and LHCII structures into the electron microscopy projection map (Fig. 2B) clearly resembles the proposal of Ben-Shem and Nelson (2005) based on the fits of the intermediate-resolution structures of PS I and LHCII, though the LHCII in our image is slightly displaced toward the PS I-K subunit.

III. Role of Small PS I Subunits in State Transitions

Earlier work has shown that plants without PS I-H and PS I-L (Lunde et al., 2000) and without PS I-O (Jensen et al., 2004) are highly deficient in state transitions (Zhang and Scheller, 2004). In addition, cross-links could be established between LHCII and PS I-I, PS I-H,

and/or PS I-L. The new PS I–LHCII structure shows that the LHCII trimer is attached at a defined position between subunits PS I-A, -H, -L, and -K (Fig. 2B). The involvement of PS I-H and PS I-L in the binding of LHCII is expected in view of the role of these subunits in the state transitions and of the detected cross-link to LHCII. The involvement of PS I-K in the binding of LHCII is however surprising, because the absence of PS I-K by the addition of an antisense construct does not impair state transitions to any great extent (Jensen et al., 2000) and a cross-link between PS I-K and LHCII was not detected (Zhang and Scheller, 2004). The absence of PS I-K even resulted in a slightly enhanced binding of LHCII (Zhang and Scheller, 2004), which can be explained by a small shift of LHCII toward PS I-A. This is possible because in the presence of PS I-K there seems to be a small gap between PS I-A and LHCII (indicated as XXX in Fig. 2B). It is not known where the PS I-O subunit is located. This protein was not found in the PS I–LHCI crystal structure, but without this protein the state transitions are 50% impaired (Jensen et al., 2004). A cross-link with LHCII was not found, but particles isolated from mutants without PS I-O have smaller amounts of attached LHCII (Zhang and Scheller, 2004), which indicates that this protein is at least indirectly involved in the binding of LHCII. Recently the discovery of a new subunit of PS I was reported (Khrouchtchova et al., 2005). This subunit, which is denoted PS I-P, appears to be associated with PS I-L in the proximity of PS I-O and -H and it is likely that PS I-P also is involved in the interaction with LHCII. The exact role of these small membrane-intrinsic subunits in state transitions need further functional characterization.

Figure 2B also shows that the observed cross-link between PS I-I and LHCII (Zhang and Scheller, 2004) is hard to explain by the structure of the current PS I–LHCII complex. It is possible though that there is a second binding site of LHCII, which is even weaker than the first and therefore can be missed in our analysis. Cross-linking will prevent the detachment of the cross-linked complex, so in this type of analysis such a binding might be revealed. If a second binding site exists, it may be present at the symmetry-related position covered by the PS I-H, -I, -B, and -G subunits. Further work is needed to clarify this point.

IV. Origin of LHCII Bound to PS I

The results of Kouřil et al. (2005) show that solubilization of state 2 membranes results in slightly lower numbers of PS II–LHCII supercomplexes with four bound LHCII complexes and somewhat higher numbers of supercomplexes with three bound LHCII complexes. This suggests that among the LHCII complexes that move from the grana to PS I there are at least some that originate from the so-called M-LHCII, the LHCII that is bound to the PS II core dimer at the site of the CP29 and CP24 units (Dekker and Boekema, 2005). However, it is hard to make quantitative statements on the origin of the LHCII that migrates to PS I. It is possible that some LHCII arises from supercomplexes that were completely disintegrated during the state transition, because the remaining complexes are too small to be picked up and analyzed by our EM analysis. It is also possible that a considerable part of the migrating LHCII originates from LHCII-only parts of the grana (Boekema et al., 2000).

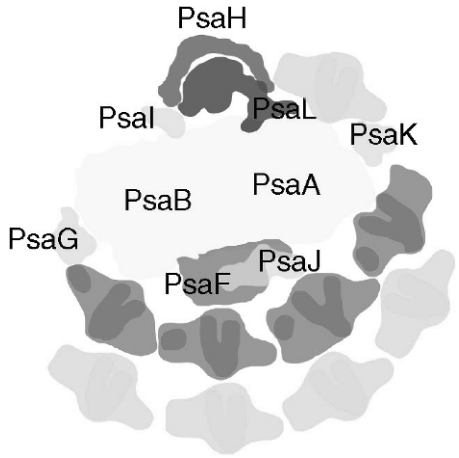

Fig. 3. Model of the PSI–LHCI complex of *Chlamydomonas reinhardtii* with an inner row of four peripheral LHCI proteins (darker shade), and with four LHCI proteins in a second row (lighter shade) plus one single LHCI protein (lighter shade) at the position of the LHCII trimer in green plants. (Modified from Dekker and Boekema, 2005.)

V. State Transitions in *C. reinhardtii*

It is now well-established that the PS I–LHCI complex from the green alga *C. reinhardtii* is larger than that of green plants (Germano et al., 2002; Kargul et al., 2003). In this organism, PS I binds nine monomeric LHCI subunits (Takahashi et al., 2004), eight of which are most likely bound at the PS I-FJ side of the complex in two rows between the PS I-G and PS I-K (Fig. 3), and one at the other side of the complex between PS I-H and PS I-K. This is the same position at which

trimeric LHCII binds in state 2 in *A. thaliana* (see above). An analysis of *n*-dodecyl-β-D-maltoside solubilized PS I–LHCII particles from *C. reinhardtii* prepared in state 1 or state 2 revealed no differences in the positions of the nine LHCI proteins (A. E. Yakushevska, unpublished observations). This suggests that the binding site of LHCII on green plant PS I is always occupied by a monomeric LHC type of protein in PS I of *C. reinhardtii*. This also suggests significant differences in the binding of LHCII to PS I in both types of organisms.

However, there may be a relation between a relatively small mass at the tip of the complex, near the PS I-H protein, and state transitions. Multivariate statistical analysis of single-particle projections from PS I–LHCI particles prepared in a state between a pure state 1 and a pure state 2 (Germano et al., 2002) revealed two types of complexes with a small size difference near PS I-H. The difference is too small for the binding of one additional trimeric LHCII complex in the larger complex, but fits more or less that of a monomeric LHCII-type of complex. Preliminary results indicate that the smaller complex is more abundant in state 1 (in agreement with Kargul et al., 2003), and that the larger complex is more abundant in state 2. However, the additional mass in the larger particle is much too small to explain the large extent of the state transition in *C. reinhardtii*. It is in this respect interesting to note that PS II–LHCII super- and megacomplexes could only be isolated from *C. reinhardtii* membranes grown in state 1, but not in state 2 (A. E. Yakushevska, unpublished observations), suggesting that the association of PS II and LHCII is less tight in state 2 than in state 1. So, the disintegration of majority of the PS II–LHCII supercomplexes could form a major contributor to the state transition in this organism. Digitonin solubilization and an immediate analysis of all solubilized complexes, as done for *Arabidopsis* (Kouřil et al., 2005) should provide more information on the possible presence of a PS I–LHCII complex in *C. reinhardtii* in state 2.

Acknowledgment

This work was supported by the European Union, Grant HPRN-CT-2002-00248 (PSICO network).

References

Allen JF (1992) Protein phosphorylation in regulation of photosynthesis. Biochim Biophys Acta 1098: 275–335

Allen JF and Forsberg J (2001) Molecular recognition in thylakoid structure and function. Trends Plant Sci 6: 317–326

Bassi R, Giacometti GM and Simpson DJ (1988) Changes in the organization of stroma membranes induced by in vivo state-1–state-2-transition. Biochim Biophys Acta 935: 152–165

Bellafiore S, Barneche F, Peltier G and Rochaix JD (2005) State transitions and light adaptation require chloroplast thylakoid protein kinase STN7. Nature 433: 892–895

Ben-Shem A and Nelson N (2005) System biology of photosystem I – formation of supercomplexes. In: Van der Est A and Bruce D (eds) Photosynthesis: Fundamental Aspects to Global Perspectives, pp 770–772. Alliance Communications Group, Lawrence, Kansas

Ben-Shem A, Frolow F and Nelson N (2003) Crystal structure of plant photosystem I. Nature 426: 630–635

Boekema EJ, van Breemen JFL, van Roon H and Dekker JP (2000) Arrangement of photosystem II supercomplexes in crystalline macrodomains within the thylakoid membrane of green plant chloroplasts. J Mol Biol 301: 1123–1133

Boekema EJ, Jensen PE, Schlodder E, van Breemen JFL, van Roon H, Scheller HV and Dekker JP (2001) Green plant photosystem I binds light-harvesting complex I on the side of the complex. Biochemistry 40: 1029–1036

Dekker JP and Boekema EJ (2005) Supramolecular organization of thylakoid membrane proteins in green plants. Biochim Biophys Acta 1706: 12–39

Delosme R, Olive J and Wollman F-A (1996) Changes in light energy distribution upon state transitions: an *in vivo* photoacoustic study of the wild type and photosynthetic mutants from *Chlamydomonas reinhardtii*. Biochim Biophys Acta 1273: 150–158

Depège N, Bellafiore S and Rochaix JD (2003) Role of chloroplast protein kinase Stt7 in LHCII phosphorylation and state transition in *Chlamydomonas*. Science 299: 1572–1575

Finazzi G, Rappaport F, Furia A, Fleischmann M, Rochaix J-D, Zito F and Forti G (2002) Involvement of state transitions in the switch between linear and cyclic electron flow in *Chlamydomonas reinhardtii*. EMBO Rep 3: 280–285

Garab G, Cseh Z, Kovacs L, Rajagopal S, Varkonyi Z, Wentworth M, Mustardy L, Der A, Ruban AV, Papp E, Holzenburg A and Horton P (2002) Light-induced trimer to monomer transition in the main light-harvesting antenna complex of plants: thermo-optic mechanism. Biochemistry 41: 15141–15149

Germano M, Yakushevska AE, Keegstra W, van Gorkom HJ, Dekker JP and Boekema EJ (2002) Supramolecular organization of photosystem I and light-harvesting complex I in *Chlamydomonas reinhardtii*. FEBS Lett 525: 121–125

Haldrup A, Jensen PE, Lunde C and Scheller HV (2001) Balance of power: a view of the mechanism of photosynthetic state transitions. Trends Plant Sci 6: 301–305

Jansson S (1994) The light-harvesting chlorophyll *a*/*b* proteins. Biochim Biophys Acta 1184: 1–19

Jensen PE, Gilpin M, Knoetzel J and Scheller HV (2000) The PSI-K subunit of photosystem I is involved in the interaction between light-harvesting complex I and the photosystem I reaction center core. J Biol Chem 275: 24701–24708

Jensen PE, Haldrup A, Zhang S and Scheller HV (2004) The PSI-O subunit of plant photosystem I is involved in balancing the excitation pressure between the two photosystems. J Biol Chem 279: 24212–24217

Kargul J, Nield J and Barber J (2003) Three-dimensional reconstruction of a light-harvesting complex I-photosystem

I (LHCI-PSI) supercomplex from the green alga *Chlamydomonas reinhardtii* – insights into light harvesting for PSI. J Biol Chem 278: 16135–16141

Khrouchtchova A, Hansson M, Paakkarinen V, Vainonen JP, Zhang S, Jensen PE, Scheller HV, Vener AV, Aro E-M and Haldrup A (2005) A previously found thylakoid membrane protein of 14 kDa (TMP14) is a novel subunit of plant photosystem I and is designated PSI-P. FEBS Lett 29: 4808–4812

Kouřil R, Zygadlo A, Arteni AA, de Wit CD, Dekker JP, Jensen PE, Scheller HV and Boekema EJ (2005) Structural characterization of a complex of photosystem I and light-harvesting complex II in *Arabidopsis thaliana*. Biochemistry 44: 10935–10940

Lunde C, Jensen PE, Haldrup A, Knoetzel J and Scheller HV (2000) The PSI-H subunit of photosystem I is essential for state transitions in plant photosynthesis. Nature 408: 613–615

Lunde C, Jensen PE, Rosgaard L, Haldrup A, Gilpin MJ and Scheller HV (2003) Plants impaired in state transitions can to a large degree compensate for their defect. Plant Cell Physiol 44: 44–54

Nilsson A, Stys D, Drakenberg T, Spangfort MD, Forsén S and Allen JF (1997) Phosphorylation controls the three-dimensional structure of plant light-harvesting complex II. J Biol Chem 272: 18350–18357

Snyders S and Kohorn BD (1999) TAKs, thylakoid membrane protein kinases associated with energy transduction. J Biol Chem 274: 9137–9140

Snyders S and Kohorn BD (2001) Disruption of thylakoid-associated kinase 1 leads to alteration of light harvesting in Arabidopsis. J Biol Chem 276: 32169–32176

Takahashi Y, Yasui T-A, Stauber EJ and Hippler M (2004) Comparison of the subunit compositions of the PSI–LHCI supercomplex and the LHCI in the green alga *Chlamydomonas reinhardtii*. Biochemistry 43: 7816–7823

Vener AV, van Kan PJ, Rich PR, Ohad I and Andersson B (1997) Plastoquinol at the quinol oxidation site of reduced cytochrome bf mediates signal transduction between light and protein phosphorylation: thylakoid protein kinase deactivation by a single-turnover flash. Proc Natl Acad Sci USA 94: 1585–1590

Wollman FA (2001) State transitions reveal the dynamics and flexibility of the photosynthetic apparatus. EMBO J 20: 3623–3630

Yakushevska AE, Jensen PE, Keegstra W, van Roon H, Scheller HV, Boekema EJ and Dekker JP (2001) Supermolecular organization of photosystem II and its associated light-harvesting antenna in *Arabidopsis thaliana*. Eur J Biochem 268: 6020–6028

Zhang S and Scheller HV (2004) Light-harvesting complex II binds to several small subunits of photosystem I. J Biol Chem 279: 3180–3187

Zito F, Finazzi G, Delosme R, Nitschke W, Picot D and Wollman FA (1999) The Qo site of cytochrome $b(6)f$ complexes controls the activation of the LHCII kinase. EMBO J 8: 2961–2969

Chapter 6

Structural Analysis of Cyanobacterial Photosystem I

Petra Fromme* and Ingo Grotjohann
Department of Chemistry and Biochemistry, Arizona State University, P.O. Box 871604, Tempe, AZ 85287-1604, USA

Summary

Photosystem I is a large membrane protein complex that catalyzes the first step of oxygenic photosynthesis. It can be regarded as a solar energy converter that captures the light from the sun through a large core-antenna system of chlorophylls and carotenoids and transfers the energy into the center of the complex, where the energy is used to catalyze the light-driven transmembrane electron transfer from plastocyanin to ferredoxin. Photosystem I from

* Author for correspondence, email: pfromme@asu.edu

John H. Golbeck (ed): Photosystem I: The Light-Driven Plastocyanin:Ferredoxin Oxidoreductase, 47–69.

cyanobacterial origin consists of 12 protein subunits, to which 127 cofactors are noncovalently bound. This chapter describes the structure and function of the cyanobacterial Photosystem I as revealed from the X-ray structure at 2.5 Å resolution.

I. Introduction

Oxygenic photosynthesis is the main process on Earth that converts the light energy from the sun into chemical energy. The process supplies all higher life on earth with food and produces all of the oxygen in the atmosphere. Two large membrane protein complexes – Photosystem I (PS I) and Photosystem II (PS II) that are embedded in this membrane – catalyze the initial steps of photosynthesis, the light-induced charge separation. A pool of plastoquinones, the cytochrome b_6f complex, and plastocyanin or cytochrome c_6 functionally couple both photosystems.

Cyanobacterial PS I consists of 12 protein subunits to which 127 cofactors are noncovalently bound. It catalyzes the light-driven electron transfer from the soluble Cu-containing protein plastocyanin on the lumenal side (i.e., the inside of the thylakoids) to ferredoxin at the stromal side (outside) of the thylakoid membrane. Cyanobacteria can also use the heme-containing soluble protein cytochrome c_6 as an alternate or unique electron donor to PS I. There is also some flexibility concerning the electron acceptor. In the case of iron deficiency, flavodoxin can act as the electron acceptor instead of ferredoxin.

The first step of the whole process is the light capturing, performed by the large antenna system, which consists of 90 antenna chlorophylls and 22 carotenoids. The energy is transferred to the center of the complex, where the electron transport chain is located. When the energy excites a special pair of two chlorophylls, located in the center of the complex, the "action" takes place and charge separation occurs. Due to its absorption maximum at 700 nm, this pair of chlorophylls was named P700. The electron is transferred from P700 across the membrane by a chain of electron carriers. These electron carriers had been previously identified by spectroscopic investigations, and their historical names have been maintained. The electron transport chain consists of five steps. The electron is stepwise transferred from P700 to A (a Chl *a* molecule), A_0 (also a Chl *a* molecule), A_1 (a phylloquinone molecule) and from there to the three [4Fe–4S] clusters, F_X, F_A, and F_B. After the docking of the soluble electron carrier ferredoxin, the electron is transferred from PS I to ferredoxin, which subsequently leaves the docking site to bring the electron to the enzyme ferredoxin:$NADP^+$-reductase, which then finally reduces $NADP^+$ to NADPH. After this process has occurred once, $P700^+$ has to be rereduced to complete the reaction cycle. There is a docking site for soluble electron carrier proteins located at the lumenal site of the complex, just underneath P700. In plants, reduced plastocyanin docks to this site and reduces $P700^+$, whereas cytochrome c_6 can substitute plastocyanin in cyanobacteria.

Detailed structural information is available from the X-ray structure of cyanobacterial PS I from the thermophilic cyanobacterium *Synechococcus elongatus* (now renamed *Thermosynechococcus elongatus*) at 2.5 Å resolution (Jordan et al., 2001) and will be described in this chapter. The structure of plant PS I has been determined at 4.4 Å resolution from pea (Ben-Shem et al., 2003) and will be described in Chapter 7 of this volume.

II. General Architecture of PS I

In cyanobacteria, PS I can exist in trimeric and monomeric forms (Hladik and Sofrova, 1991). In *S. elongatus*, the total amount of PS I and its oligomeric organization depends on the environmental conditions. At low-light intensity, the PS I trimer is the most abundant protein in the thylakoid membrane. The amount of PS I exceeds the amount of PS II by a factor of eight. Under these low-light conditions essentially all PS I exists in the membrane in trimeric form. The formation of intact trimers is essential for the growth of the cells at low-light intensity (Fromme et al., 2003). The trimer has a molecular weight of 1,056,000 Da; this PS I trimer has been isolated and crystallized (Fromme 1998, Fromme et al., 2003). PS I is the largest and the most complex membrane protein for which the structure has been determined.

Figure 1 shows a simplified picture of the trimeric complex, pointing out the complex organization of

Abbreviations: Chl – chlorophyll; ENDOR – electron nuclear double resonance; EPR – electron paramagnetic resonance; ET – electron transport; Fe/S – iron–sulfur cluster; FNR – ferredoxin-$NADP^+$-oxidoreductase; pBRC – purple bacterial reaction center; PS I – Photosystem I; PS II – Photosystem II.

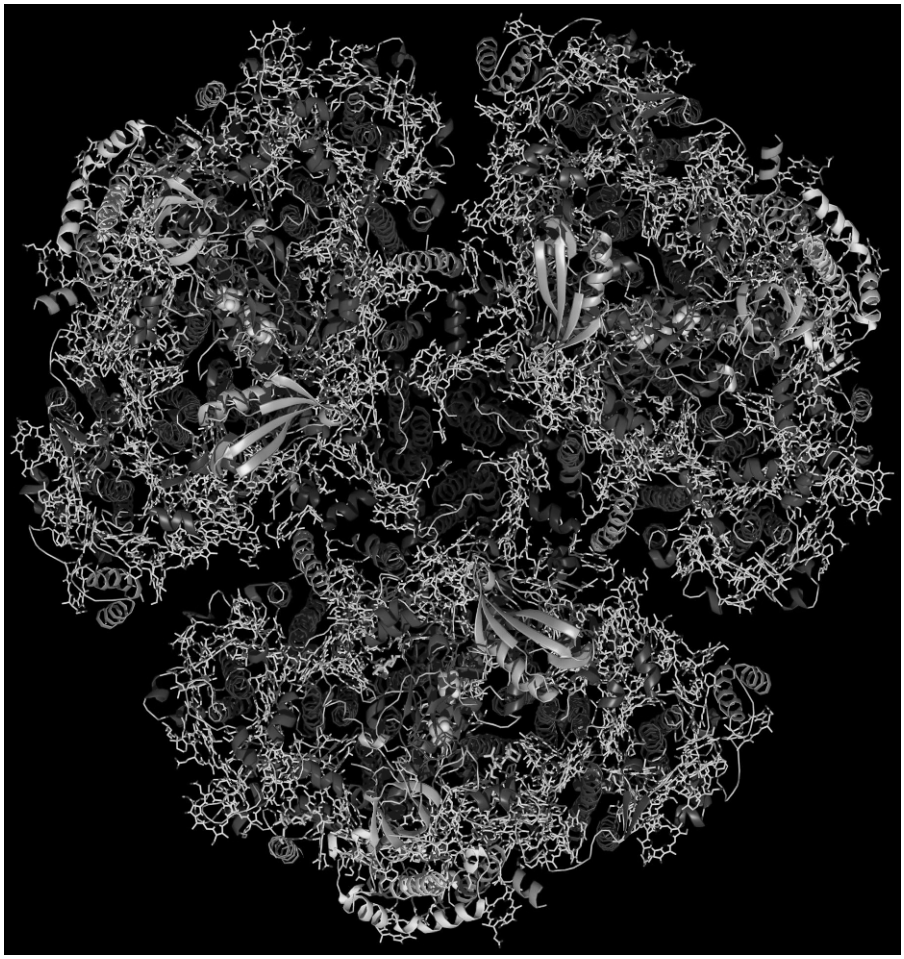

Fig. 1. The trimeric structure of Photosystem I from cyanobacteria; the view direction is from the stromal side onto the membrane plane. The 12 proteins are shown in a backbone representation. The phytyl tails of the chlorophylls have been omitted for clarity. See also Cover Picture.

this nano-biosolar system. The 12 subunits are shown in a ribbon representation. Each monomeric unit contains 12 proteins, 96 chlorophylls, 22 carotenoids, 3 [4Fe–4S] clusters, 2 phylloquinone molecules, and 4 lipids. This picture of the trimeric PS I visualizes a further remarkable feature of PS I: the high content of cofactors. Thirty percent of the total mass of PS I consists of cofactors, which are therefore not only important for the function of the protein but also play an essential role in the assembly and structural integrity of PS I.

One monomeric unit of the cyanobacterial PS I consists of 12 different proteins (PsaA, PsaB, PsaC, PsaD, PsaE, PsaF, PsaI, PsaJ, PsaK, PsaL, PsaM, and PsaX) to which 127 cofactors are noncovalently bound. In plants, the system contains at least four additional subunits whose functions are still under investigation (see Nelson and Ben-Shem, this volume, Chapter 7; Haldrup et al., this volume, Chapter 11 for a detailed description of the plant PS I).

It is known that the main proteins, including all cofactor-binding sites, are well conserved between plants and cyanobacteria, whereas PsaX and PsaM may be unique to cyanobacteria, even if the homologous gene for PsaM has been identified in liver moss (Ohyama et al., 1986).The structure of the plant PS I confirms the absence of PsaM and PsaX in higher plants (Ben-Shem et al., 2003).

Figure 2A shows the organization of protein subunits in PS I. The two most important proteins are the large subunits PsaA and PsaB. They harbor most of the antenna system as well as most of the cofactors of the electron transport chain from P700 to the first Fe/S cluster, F_X.

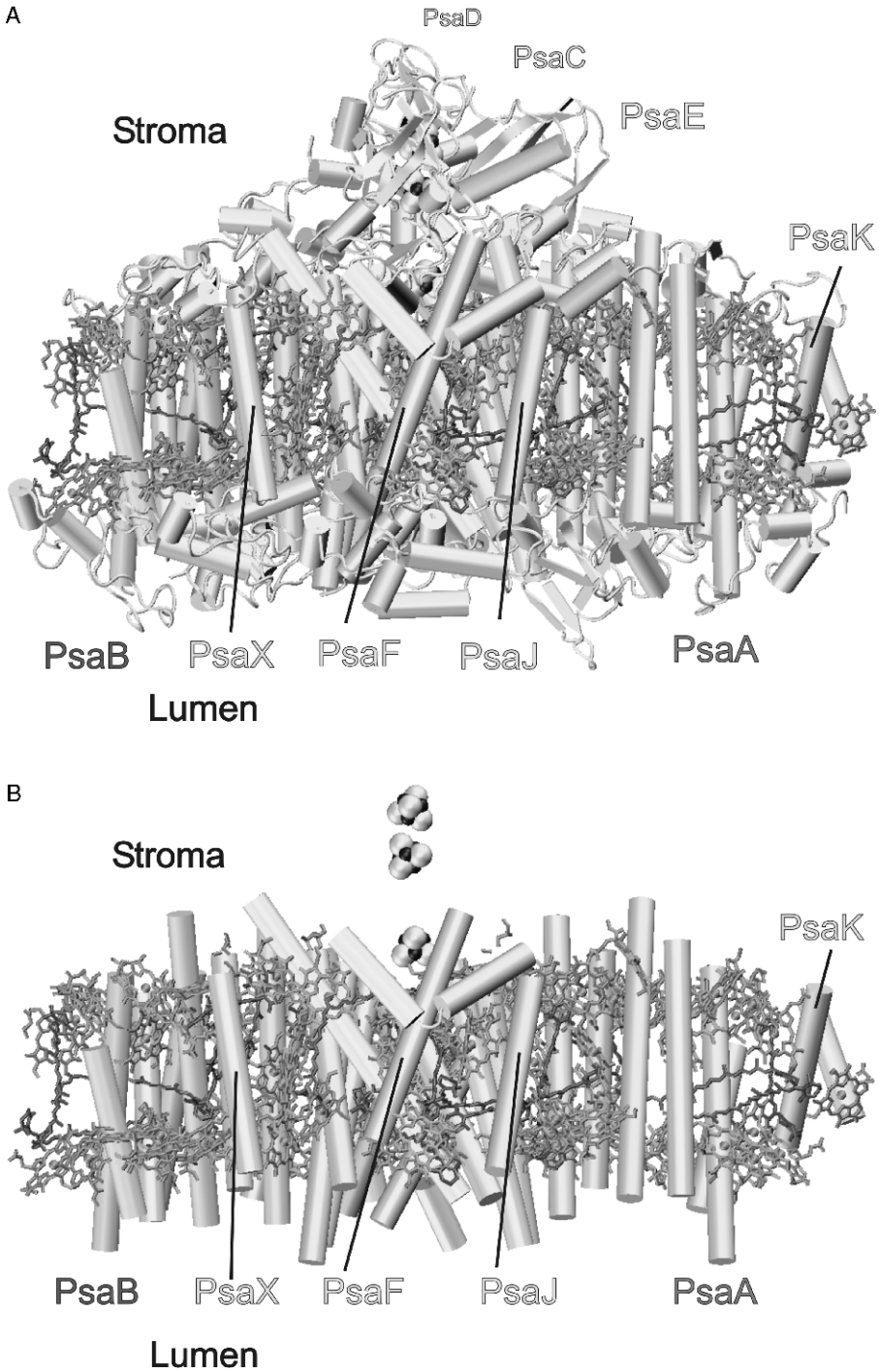

Fig. 2. Photosystem I. (A) PS I with all cofactors as seen from within the membrane plane. The view leads from the distal side into the trimerization site. (B) The same view as in (A), but only the transmembrane helices of the protein backbone are shown. See Color Plate 1, Fig. 2.

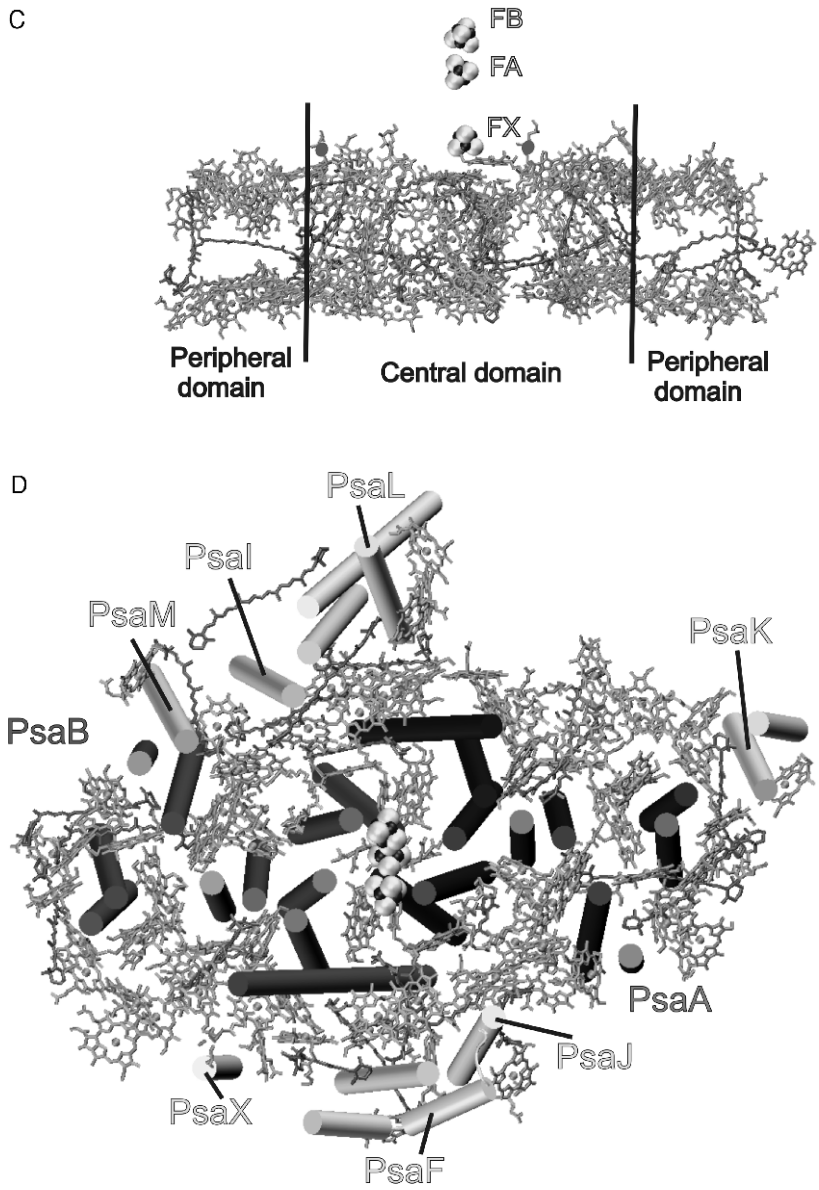

Fig. 2. (*cont.*) Photosystem I. (C) Same view as in Panels A and B, but only the cofactors are shown. (D) View of the transmembrane helices of the protein backbone with all cofactors as seen from the stroma. See Color Plate 2, Fig. 2.

All of the small subunits are located peripheral to PsaA and PsaB. The subunits PsaC, PsaD, and PsaE do not contain transmembrane helices. They form the stromal hump of PS I, which extends the membrane by approximately 90 Å. PsaC carries the two terminal Fe/S clusters, F_A and F_B.

The remaining small subunits contain between one and three transmembrane helices and are located at the periphery of PsaA and PsaB. They are in quite different environments. The subunits PsaL and PsaI are located in the center of the trimeric complex and form the "trimerization domain," while PsaM is located at the interface between the monomers. PsaJ and PsaF, as well as PsaK and PsaX, are located at the membrane exposed surface of the trimeric PS I complex. They stabilize the core-antenna system of PS I and may also be involved in the interaction of PS I with its external antenna systems (see also Barber et al., this volume, Chapter 9; Croce et al., this volume, Chapter 10).

III. The Protein Subunits

First, we will examine the structure and function of the protein subunits in PS I, starting with the large subunits PsaA and PsaB.

A. The Core: The Large Subunits PsaA and PsaB

The major subunits of PS I, PsaA, and PsaB, show a large homology to each other and are suggested to have evolved via gene duplication. Each of them contains 11 transmembrane helices as evidenced from sequence alignment and folding predictions (Golbeck, 1994; Pakrasi, 1995). The arrangement of transmembrane helices in PS I is depicted in Fig. 2B,D. The field of transmembrane helices for PsaA/PsaB can be divided into two domains: The five C-terminal α-helices (g–j) surround the electron transport chain, whereas the N-terminal six helices flank the central region at both sides, forming an arrangement of "trimers of helix-pairs," where the pairs are formed by transmembrane helices a/b, c/d, and e/f. The N-terminal domain of PsaA/B is connected to the C-terminal domain by hydrophobic interactions of helix f with helix i, by the fg loop and interaction between the loops, as well hydrophobic interactions mediated by the cofactors (chlorophylls, carotenoids, and lipids). The C-terminal domain shows some similarity to the arrangement of the L and M proteins in bacterial reaction centers (Deisenhofer et al., 1995) and the D1 and D2 proteins in PS II (Zouni et al., 2001; Kamiya and Shen, 2003; Ferreira et al., 2004), whereas the N-terminal domain of PsaA and PsaB shows a striking similarity to the arrangement of helices in the core-antenna proteins of PS II (PsbB and PsbC) and the peripheral antenna protein IsiA, expressed under iron deficiency (Bibby et al., 2001; Boekema et al., 2001; Nield et al., 2003; see also Barber et al., this volume, Chapter 9). It is therefore very likely that all photoreaction centers have evolved from a common ancestor and the genes for PsaA and PsaB have evolved by a gene fusion of an ancient reaction center protein containing five transmembrane helices and an antenna protein consisting of six transmembrane helices, as suggested earlier (Schubert et al., 1998).

Whereas the transmembrane helices nearly perfectly match the twofold symmetry between PsaA and PsaB, some of the loops show striking differences in sequence, length, and secondary structure elements, making the system more asymmetric. The functional reason for this asymmetry is its ability to attach the stromal hump and the small membrane intrinsic subunits at a proper position to the core of PS I. It is interesting that nearly neither hydrogen bonds nor any salt bridges exist between PsaA/PsaB and the small subunits in the transmembrane regions of PS I (Loll et al., 2003). Therefore, analysis of these interactions does not give an answer to the question how PS I may be assembled. Instead, the peripheral membrane intrinsic subunits are attached by hydrophobic interactions with the cofactors and by specific interactions (salt bridges and H-bonds) within the asymmetric parts of the loops of PsaA and PsaB.

PsaA and PsaB coordinate the majority of the cofactors of the electron transport chain (P700, A, A_0, A_1, and F_X) and 79 of the 90 antenna chlorophylls in PS I. In addition, most of the carotenoids show hydrophobic interactions with either PsaA or PsaB. Most, but not all, of the chlorophylls are coordinated by histidines. It is very interesting that most of the coordination sites were conserved over millions of years during the evolution between plants and cyanobacteria. The cofactors of the electron transport chain from P700 to F_X are coordinated by the C-terminal region of PS I between the end of transmembrane helix h (corresponding to the eighth transmembrane helix) and start of transmembrane helix k (corresponding to the 10th transmembrane helix). Details of the ligandation of P700, A, and A_1 are discussed extensively below.

The helices of the two large subunits are related to each other by a local twofold symmetry axis running through the Fe/S cluster F_X. The iron–sulfur cluster, F_X, is coordinated by two cysteines of the conserved sequence motif of the large subunits PsaA and PsaB. It is a rare example of an inter-protein iron–sulfur cluster. This loop is not only responsible for the coordination of F_X, but also plays an important role in the attachment of PsaC and the whole assembly of the stromal hump (see Antonkine et al., 2003; Antonkine and Golbeck, this volume, Chapter 8).

PsaA and PsaB also play an essential role in the docking of the soluble electron donors to PS I. Plastocyanin and cytochrome c_6 bind to PS I at an indentation at the lumenal side to rereduce the primary electron donor, $P700^+$. The major interaction site is formed by two helices in the loop between helices i and j, located at the lumenal indentation close to $P700^+$. They provide a hydrophobic docking site for plastocyanin and cytochrome c_6. Figure 3 shows a view of the potential docking site for plastocyanin and cytochrome c_6.

Both plastocyanin and cytochrome c_6 have hydrophobic faces that match the hydrophobic docking site of PS I (Frazao et al., 1995). Mutants that

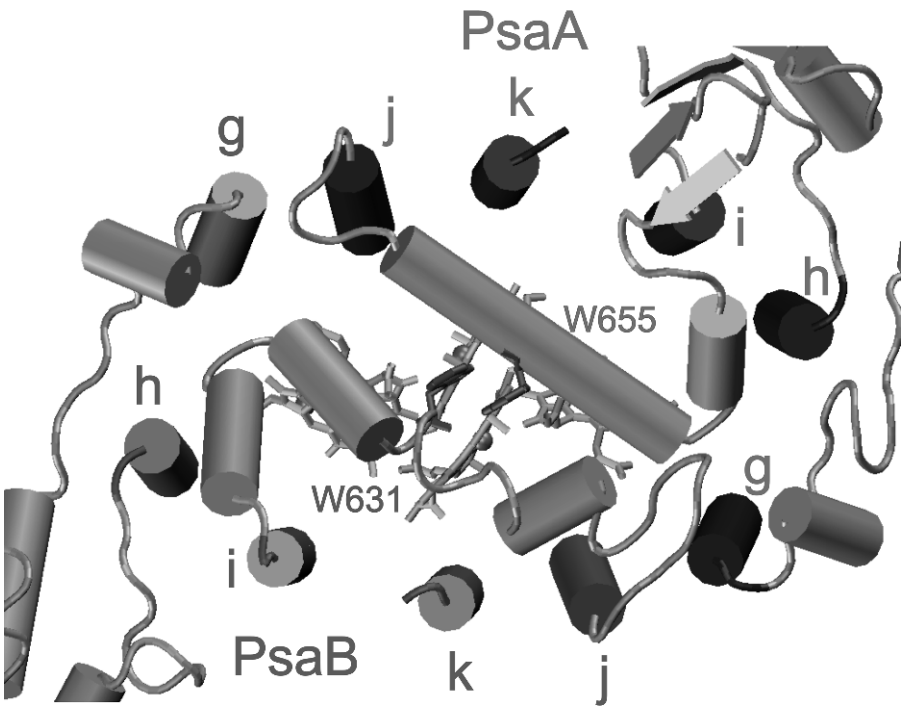

Fig. 3. Plastocyanin/cytochrome c_6 docking site at the luminal side of Photosystem I. The lumenal five amino acids of the transmembrane helices of the reaction center core of PsaA and PsaB together with their lumenal loops are shown. The two tryptophans (dark bond structures) have been shown to be essential for the docking.

disturb this site are impaired in binding and electron transfer (Molina-Heredia et al., 1999). A further increase in affinity can be provided by positively charged patches of both plastocyanin and cytochrome c_6 that may electrostatically drive their attractive movement toward PS I (Molina-Heredia et al., 1999). Two tryptophan residues that are partially exposed to the aqueous phase are further prominent features of the docking site (Fig. 3). They may form an important part of the recognition site for the soluble electron donors and may even be involved in the electron transfer from plastocyanin/cytochrome c_6 to P700. Experimental evidence for this hypothesis was provided by mutagenesis studies on one of these tryptophan (Sommer et al., 2002).

In contrast to cyanobacteria, where only PsaA and PsaB are involved in the docking of plastocyanin, in plants PsaF may also play an important role in the docking of plastocyanin (see below).

B. The Stromal Hump of PS I: PsaC, PsaD, and PsaE

Three subunits (PsaC, PsaD, and PsaE) are located at the stromal side of PS I and are involved in the docking of ferredoxin. The structure of the three subunits in the stromal hump and the potential docking site of ferredoxin are shown in Fig. 4A,B.

1. Subunit PsaC

Subunit PsaC (8.9 kDa) carries the two terminal Fe/S clusters F_A and F_B. Both clusters are of the [4Fe–4S] type. They are defined by distinct lines in the EPR spectra of PS I (Evans et al., 1974). The gene of PsaC contains two conserved sequence motifs CXXCXXCXXXCP in which the cysteines provide the ligands to the Fe atoms. A homology of subunit PsaC to bacterial ferredoxins also containing two [4Fe–4S] clusters was suggested from strong sequence similarity and homology models (Golbeck, 1993; Dunn et al., 1988) and was confirmed by the similarity of both structures (Adman et al., 1973; Jordan et al., 2001). The structure of PsaC is shown in Fig. 4A,B.

The central part of PsaC consists of two short α-helices connecting the two Fe/S clusters. This part is very similar in PsaC and ferredoxin. The preeminent deviations between the two structures are the C- and N-termini, elongated by 14 and 2 residues in PsaC, respectively, and an extension of 10 residues pointing toward the putative ferredoxin/flavodoxin docking site

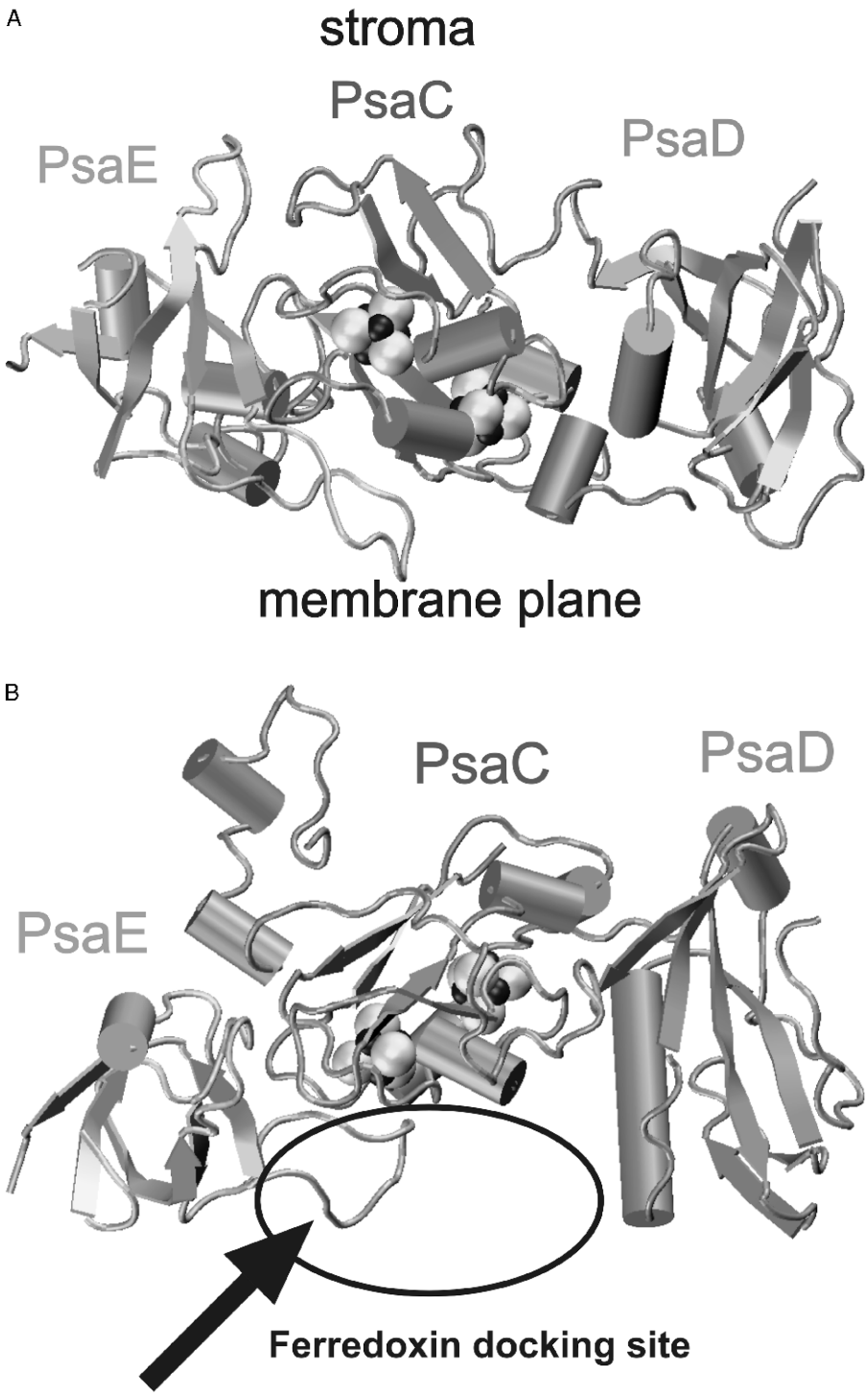

Fig. 4. The stromal subunits of Photosystem I. The subunits PsaC, PsaD, and PsaE form a protein cluster on the stromal side of PS I, which harbors the terminal part of the electron transfer chain. PsaC coordinates the Fe/S clusters F_A and F_B. (A) Side view into the binding site of F_A and F_B. (B) View from the stroma on all three stromal subunits of PS I. The docking site for ferredoxin is indicated. See Color Plate 3, Fig. 1.

in the internal loop region exposed to the stromal surface of the PS I complex.

The C-terminus of PsaC is very important for the correct docking of PsaC to the PS I core (for more details see Antonkine et al., 2003; Antonkine and Golbeck, this volume, Chapter 8).

2. Subunit PsaD

Subunit PsaD is essential for the electron transfer from PS I to ferredoxin (V. P. Chitnis et al., 1996, 1997; Barth et al., 1998; Sétif, 2001; Sétif et al., 2002). It is located at the stromal hump, close to the "connecting domain."

The main part of PsaD consists of a large antiparallel four stranded β-sheet. The fourth β-strand is connected to the only α-helix of PsaD by a short loop. This helix forms interactions both with PsaC and with PsaA. A short antiparallel β-sheet follows the helix in the sequence and is followed by a very prominent and remarkable feature of PsaD: its stromal clamp consisting of the sequence region between D95 and D123. This part of PsaD wraps around PsaC, forming several contacts between PsaD and both PsaC and PsaE.

This stromal clamp confirms the important function of PsaD as a critical stabilization factor of the electron acceptor sites in PS I and its important role in holding PsaC in its correct orientation (Li et al., 1991; Lagoutte et al., 2001).

The C-terminal part of PsaD is in close vicinity to PsaB and PsaL. The close vicinity of PsaD and PsaL was already suggested from cross-linking and mutagenesis results (Xu et al., 1994a; Janson et al., 1996). This interaction may also play an important role in the stabilization of PS I, as the deletion of subunit PsaL destabilizes subunit PsaD in cyanobacteria (Armbrust et al., 1996). The C-terminal region of subunit PsaD is exposed on the stromal surface of PS I. This fact was already suggested previously by work on the protease accessibility, NHS-biotin labeling as well as investigations on mutant PS I lacking the 24 residues from the carboxyl terminus of PS I (Xu et al., 1994a; P. Chitnis et al., 1995).

In addition to its stabilizing function, PsaD is actively involved in the docking of ferredoxin. The direct interaction of these two proteins was shown by chemical cross-linking (Zanetti and Merati, 1987; Zilber and Malkin, 1988; Lelong et al., 1994). In the work of Lelong et al. (1994) it was shown that the cross-linked complex is fully competent in the transfer of electrons from PS I to ferredoxin. The position of ferredoxin in these cross-linked complexes was identified by electron microscopy (Lelong et al., 1996). The same docking site was also found for flavodoxin (Mühlenhoff et al., 1996a,b). This docking site is indicated in Fig. 4B. The negatively charged ferredoxin may be guided toward by the basic patch provided mainly by PsaD and PsaC. It is also very remarkable that overexpressed PsaD can still bind ferredoxin (Pandini et al., 1999). Cocrystals between PS I and ferredoxin have been reported which may serve as a basis for a structure of the PS I–ferredoxin complex (Fromme et al., 2002).

3. Subunit PsaE

The structure of subunit PsaE (8 kDa) in solution was determined by ^{1}H and ^{15}N NMR (Falzone et al., 1994a,b). It shows a compact structure of five antiparallel stranded β-sheets. The core structure of PsaE, consisting of five β-strands is essentially the same in solution and in PsaE attached to the PS I complex. The main difference between the free and bound PsaE are the conformations of the loops and the C- and N-terminus. The flexible loop connecting the β-sheets β3 (C) and β4 (D) were not well resolved in the NMR structure and therefore seems to be flexible and involved in the interaction with the PsaA/PsaB core. This loop has a different conformation and is twisted when PsaE binds to the core complex. The twist of this loop already was reported at 4 Å (Klukas et al., 1999) and is fully confirmed in the structural model at 2.5 Å resolution (Zouni et al., 2000). This loop is involved in interactions with PsaA, PsaB, and PsaC, suggesting a change of the loop conformation during assembly of the PS I complex. Recent studies show that PsaE can assemble into the PS I complex without help of assembly factors and that it is driven by electrostatic interactions (Lushy et al., 2002).

The first evidence for the location of subunit PsaE at the periphery of the stromal hump came from electron microscopy of a mutant lacking the gene of PsaE in cyanobacteria (Kruip et al., 1997). This was confirmed by the 4 and 2.5 Å structural models of PS I (Klukas et al., 1999; Jordan et al., 2001).

The loop E-β2β3 (BC-loop) connecting strands E-β2 (B) and E-β3 (C), which points toward the putative docking site of ferredoxin, is close to the loop insertion of PsaC. Interactions between PsaE (loop β1/β2) (AB) and the C-terminal region of the partially membrane integral subunit PsaF also exist, in good agreement with mutagenesis and cross-linking studies (Xu et al., 1994a,b,c). The interactions of PsaE with PsaC and PsaD are relatively weak, which explains the finding that the geometry of the stromal structure formed by PsaC and PsaD is not dramatically

changed in the absence of PsaE (Barth et al., 1998). However, the C-terminal region of PsaD, which forms a clamp surrounding PsaC, is in direct contact with PsaE (loop β2/β3), confirming previous cross-linking studies (Mühlenhoff et al., 1996a,b).

Different functions have been reported for PsaE. Subunit PsaE is directly involved in the anchorage of ferredoxin (Sonoike et al., 1993; Strotmann and Weber, 1993; Rousseau et al., 1993) plays a role in cyclic electron transport (Yu et al., 1993) and can be cross-linked in barley with FNR, via its N-terminal extension (Andersen et al., 1992). Site-directed mutagenesis on subunit E in *Synechocystis* shows that the C-terminal eight amino acids are necessary for precise anchorage of subunit C into PS I. Furthermore, several mutants on PsaE have a dramatic effect on the binding of ferredoxin (for detailed discussion on the function of subunit E see Sétif, 2001; Sétif et al., 2002). The fact that PsaE is involved in docking of ferredoxin and flavodoxin (Mühlenhoff et al., 1996a,b; Meimberg et al., 1998) was questioned by the finding that PsaE deletion mutants are still able to grow photoautotrophically. This contradiction was solved by the discovery that PsaE deletion mutants increased the level of ferredoxin in the cells by orders of magnitude to compensate defects caused by the lack of PsaE (van Thor et al., 1999).

C. The Monomer–Monomer Interface: PsaL, PsaI, and PsaM

PsaL, PsaI, and PsaM are located in the region where the adjacent monomers face each other in the trimeric PS I complex. PsaL and PsaI are located in the trimerization domain, whereas PsaM is located at the monomer–monomer interface.

1. Subunit PsaL

The location of PsaL in the trimerization domain was first proposed by mutagenesis studies, because no trimers can be detected in PsaL deletion mutants of cyanobacteria (V. P. Chitnis et al., 1993). PsaL is located close to the C_3 axis in the "trimerization domain." It forms most of the contacts between the monomers. Furthermore, PsaL coordinates three antenna Chl *a* and forms hydrophobic contacts with carotenoids and may be therefore important for the excitation energy transfer between the monomers.

The structure of PsaL is shown in Fig. 5A. This subunit contains three transmembrane helices, named L-d, L-e, and L-g with L-d and L-e forming hydrophobic contact sites between the monomers within the trimer. Most of the further contact sites between the monomers in the trimerization domain are provided by hydrogen bonds and electrostatic interactions within the loop regions. The N-terminal loop is located on the stromal side, harboring three small β-strands and one α-helix. This loop forms various contacts with loop regions of PsaA and is also in contact with PsaD, thereby attaching PsaL to the core of PS I. A short lumenal loop connects the first and second transmembrane α-helices. Correspondingly the second and third transmembrane α-helices are connected by a short stromal loop. The C-terminus is folded into a short α-helix located in the lumen. The electron density map suggests that a metal ion, possibly a Ca^{2+}, is coordinated by amino acid side chains of PsaL in two adjacent PS I monomers and by PsaA. Possibly, it could be required for stabilization of the PS I trimer, in agreement with observations in *Synechocystis* sp. PCC 6803 that the addition of Ca^{2+} stimulates formation of PS I trimers (P. Chitnis and J. Kruip, personal communication). PsaL forms hydrophobic contacts with three carotenoids, two are located at the interface between PsaL and PsaA and PsaI, the third one is located at the monomer–monomer interface in the trimerization domain. The latter carotenoid may also play an important role in the stabilization of the trimeric PS I complex.

2. Subunit PsaI

PsaI is shown in Fig. 5A. It contains one transmembrane helix. It does not bind Chl *a*, but forms hydrophobic interactions with carotenoid molecules and forms few contacts with the adjacent monomer. PsaI is located between PsaL and PsaM; the close vicinity of PsaL and PsaI was first suggested by mutagenesis experiments, where PsaI was deleted. Schluchter et al. (1996) showed that the deletion of PsaI influences the stability of these two subunits in the PS I complex in *Synechococcus* sp. PCC 7002. These mutants were comprised of only 10% trimeric PS I, indicating that PsaI stabilizes PsaL. A close interaction of PsaL and PsaI was also reported for *Synechocystis* sp. PCC 6803 (Xu et al., 1995) and barley (Janson et al., 1996). The crystal structure showed that PsaI forms various contacts with PsaL, but also forms contacts with PsaM, as already suggested by Schluchter in 1996. The existence of close interactions of PsaI and PsaL in higher plants suggests that the arrangement of these small subunits is a motif that is conserved during evolution (Andersen and Scheller, 1993; Janson et al., 1996). Recently, the structure of higher plant PS I has been determined at 4.4 Å resolution (Ben-Shem et al., 2003). Even if the

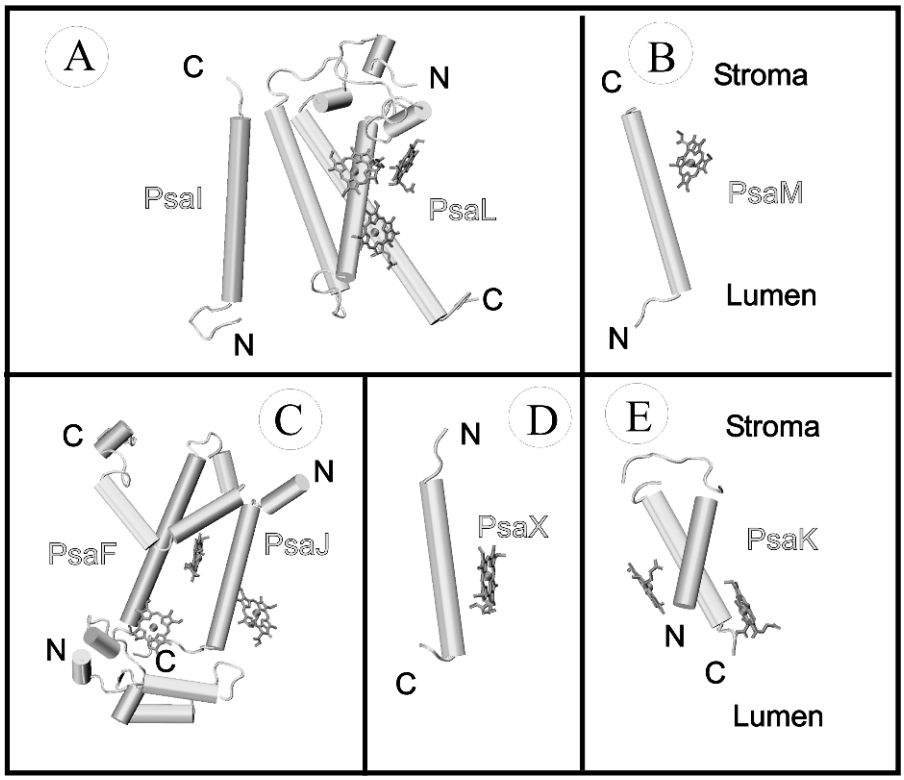

Fig. 5. The small transmembrane subunits of Photosystem I as seen from within the membrane plane. All subunits are shown with the chlorophylls they coordinate, if any, and the position of the N- and C-termini are depicted.

sequence was not assigned due to the limited resolution, the structure shows that PsaI and PsaL also form close contacts in plant PS I. This is remarkable, taking into account the fact that plant PS I is a monomer and the region of PsaI and PsaL (and PsaH) may function in forming interactions with the light harvesting complex II (LHCII) (Andersen and Scheller, 1993; Janson et al., 1996; Scheller et al., 2001). This raises the question of the function of the trimer in cyanobacteria. Mutants of *Synechococcus elongatus*, which lack PsaL (Mühlenhoff et al., 1996a,b), show normal growth at high light intensity, whereas growth under low light was decreased by a factor of 10 compared to wild type (Fromme, 1998). These results suggest that the trimer is essential for optimal light capturing in cyanobacteria. In plants, an additional subunit (PsaH) is located in close vicinity to PsaI and PsaL (Ben-Shem et al., 2003). This region may be the contact site between PS I and the LHCII complex (Zhang and Scheller, 2004). The idea can be put forward that PsaL stabilized by PsaI might form an entrance gate for the excitation energy from the external antenna complexes in plants. This would correspond to excitation energy transfer between the monomers in the trimeric PS I. Significant excitation energy transfer between monomers have been spectroscopically determined (Karapetyan et al., 1999, 2004) and was also found by theoretical studies (Sener et al., 2004, 2005).

3. Subunit PsaM

PsaM (3.4 kDa) is the smallest subunit of PS I. It is shown in Fig. 5B. This subunit contains only one transmembrane α-helix as predicted by (Mühlenhoff et al., 1993). This subunit is unique to cyanobacterial PS I. Although an open reading frame for this subunit was also found in the liverwort chloroplast genome (Ohyama et al., 1986), this subunit was not identified thus far in any preparation of plant PS I and is also not present in the 4.4 Å structure of pea PS I (Ben-Shem et al., 2003). PsaM is located close to the monomer–monomer interface, in the neighborhood of PsaI and PsaB (see Fig. 2D). The N-terminus is located in the lumen, the C-terminus in the stroma. PsaM forms hydrophobic contacts with a carotenoid molecule and is involved in the coordination of one Chl *a*. This chlorophyll (M-1)

may play an important role in excitation energy transfer between monomers. It is strongly functionally coupled to chlorophylls of the neighboring monomer, i.e., functionally may be considered to be part of the clustered network of this adjacent monomeric unit (Sener et al., 2004). In this respect, it is remarkable that the protein side chains of PsaM do not form direct contacts between monomers. However, it may play a role in the stabilization of the trimeric structure by forming hydrophobic interaction with the carotenoid that is involved in trimerization.

D. The Membrane Exposed Subunits: PsaF, PsaJ, PsaK, and PsaX

Four hydrophobic protein subunits, PsaF, PsaJ, PsaK, and PsaX, are located at the detergent exposed surface of PS I. PsaF and PsaJ are located symmetrically to the trimerization domain and form various contacts with PsaA, PsaB, and PsaE, whereas PsaX is only in contact with PsaB and PsaK is located at the periphery of PsaA. All four proteins are involved in the stabilization of the core-antenna system of PS I and may play an additional important role in forming interactions with the membrane intrinsic peripheral antenna system, the IsiA ring (see also Barber et al., this volume, Chapter 9).

1. Subunit PsaF

With regards to its structure, function, and import pathway, PsaF is the most astonishing subunit in PS I. For a long time, it was thought that subunit PsaF was an extrinsic subunit located at the lumenal side of PS I. This assumption was mainly based on the fact that plant PsaF contains two presequences: one for the import into the chloroplast and a second for import into the thylakoid lumen. It was shown that this protein is imported by the same pathway used for the import of plastocyanin (the soluble lumenal electron carrier) (Karnauchov et al., 1994; Scott et al., 1994; Hugosson et al., 1995). It is still unknown why PsaF, as a transmembrane protein, can be translocated by the Sec pathway.

The structure of subunit PsaF (see Fig. 5C) consists of three domains. The N-terminal domain is located in the lumen, followed by a transmembrane domain with one transmembrane helix and two short helical pieces in a V-shaped arrangement. The C-terminus is located in the stroma and is sandwiched between PsaA and PsaE. The N-terminal domain is located at the lumenal side of the complex, with α-helices F-c and F-d being the most prominent features. These hydrophilic α-helices are parallel to the membrane plane and are located at approximately 15 Å distance to the putative docking site of cytochrome c_6. The function of the N-terminal domain of PsaF is different in plant and cyanobacterial PS I. In plants and green algae subunit PsaF contains an insertion of 25 amino acids in its lumenal domain, which is responsible for the formation of a tight complex between plastocyanin and PS I (Hippler et al., 1996, 1998). This structural region forms an extension of the two lumenal α-helices F-c and F-d in plants (Ben-Shem et al., 2003). This insertion of PsaF may explain why PsaF is involved in the docking of plastocyanin in plants (Haehnel et al., 1994; Farah et al., 1995; Hippler et al., 1997, 1998), but not in cyanobacteria (Xu et al., 1994c). Although cyanobacterial PsaF is not directly involved in electron transfer from plastocyanin/cytochrome c_6 to P700, this part of PsaF could play an important role in the stabilization of the lumenal surface of PS I.

The membrane intrinsic domain of PsaF contains only one transmembrane α-helix F-f, followed by a short hydrophilic helix F-g and two shorter hydrophobic α-helices, F-h and F-i. This region of PsaF is very unusual. α-Helix F-h enters the membrane from the stromal side and ends in the first third of the membrane. It is followed after a crease by α-helix F-i, running back to the stromal side, where the C-terminus is located and forms contacts with PsaE, PsaA, and also PsaB. PsaF does not axially coordinate chlorophylls, but forms hydrophobic interactions with chlorophylls and several carotenoids. A possible role of the transmembrane part of PsaF could be a shielding of the carotenoids and of chlorophylls from the lipid phase. A possible further function of PsaF in cyanobacteria could be its structural and functional interaction with the external antenna system of IsiA and the phycobilisomes. Deletion of PsaF in *Synechococcus elongatus* leads to a growth defect at low-light intensity, accompanied by a dramatic increase of allophycocyanin, giving the whole cell suspension a turquoise color (P. Jordan and P. Fromme, unpublished), which may support the suggestion that PsaF plays a role in the interaction of the PS I core with the phycobilisomes. Recently, mutants lacking PsaJ and PsaF have been investigated and it was found that the acceptor site of PS I was impaired and the cells showed signs of oxidative damage. Furthermore, IsiA is induced in these mutants even in the presence of iron (Jeanjean et al., 2003). Boekema and coworkers investigated mutants lacking PsaF and PsaJ under iron deficiency by electron microscopy (Kouřil et al., 2003). The mutants form large aggregates of IsiA; however, some PS I–IsiA complexes can still be isolated that

contain 17 instead of 19 IsiA proteins attached to the PS I complex. These results show that PsaF and PsaJ are important but are not absolutely essential for the interaction of PS I with the IsiA ring.

In plants, a direct contact of PsaF with the plant light harvesting systems has been suggested by experiments, in which plant subunit PsaF was isolated as a chlorophyll–protein complex with LHCI proteins (Anandan et al., 1989). Interaction sites between PsaF and the LHCI proteins were also identified in the structure of PS I from pea (Ben-Shem et al., 2003).

2. Subunit PsaJ

PsaJ contains one transmembrane α-helix. It binds three chlorophylls and is in hydrophobic contact with carotenoids. The structure is shown in Fig. 5C.

A location of PsaJ close to PsaF was predicted by mutagenesis and cross-linking experiments on the cyanobacterial (Xu et al., 1994a,b) and plant PS I (Janson et al., 1996; Fischer et al., 1999a,b). The N-terminus of PsaJ is located in the stroma; the C-terminus is located in the lumen. In addition to the coordination of three antenna chlorophylls, PsaJ may play an important role in the stabilization of PsaF and the pigment clusters located at the interface between PsaJ/PsaF and the PsaA/PsaB core. The three chlorophylls, that are coordinated by this subunit are supposed to play an important role in the excitation energy transfer from the IsiA ring to the PS I core.

3. Subunit PsaX

A single transmembrane helix in the neighborhood of PsaF was identified as PsaX, a 12th subunit of PS I. It coordinates one chlorophyll and forms hydrophobic contacts with several carotenoid molecules and one of the lipids. The structure of PsaX is shown in Fig. 5D. Because it is present at the membrane exposed surface of PS I, one can speculate that PsaX may also play a role in the interaction of PS I with the IsiA antenna ring, formed under iron deficiency. This protein is not present in plant PS I, as recently shown by the 4.4 Å structure of the PS I from the pea (Ben-Shem et al., 2003). PsaX has been identified so far only by N-terminal sequencing in PS I from the thermophilic cyanobacteria *Thermosynechococcus vulcanus* and *Anabaena variabilis* (Koike et al., 1989; Ikeuchi et al., 1991) and in the single crystals from *Thermosynechococcus elongatus*. The structural model of PsaX contains 29 residues. The six stromally located N-terminal amino acids were not identified in the structure, possibly because this part of the structure is flexible. It is remarkable that no gene was assigned to PsaX in the complete genomic sequence of *Thermosynechococcus elongatus* (Nakamura et al., 2002). The reason could be that the sequence was just not assigned to be an open reading frame. Also, no gene sequence for PsaX has yet been assigned in the mesophilic cyanobacterium *Synechocystis* sp. PCC 6803. The question as to whether PsaX is a unique subunit of thermophilic cyanobacteria, necessary for stability of the PS I complex at higher temperatures, has still to be answered.

4. Subunit PsaK

Subunit PsaK (Fig. 5E), which contains two transmembrane α-helices, as predicted from the sequence (Mühlenhoff et al., 1993) was found to be located at the periphery of the PS I complex. It only forms protein contacts with PsaA. This subunit seems to be the least ordered subunit in the PS I complex, as indicated by high-temperature factors, so that an unambiguous sequence assignment was not possible and the structure was modeled with polyalanine. The two helices are connected in the stroma, so that both the C- and N-terminus are located in the lumen. This topology is also supported by insertion studies, performed on *in vitro* expressed PsaK (Mant et al., 2001) and meets the "positive inside rule" (Gavel et al., 1991), which was based on the finding that highly positively charged loops connecting transmembrane α-helices are rarely translocated through the membrane during the insertion and assembly of membrane proteins. The protein coordinates two chlorophylls and forms contacts with carotenoids. It may also play an important role in the interaction with the IsiA antenna ring under iron deficiency. In plants, PsaK has been shown to interact with the LHCI proteins. Furthermore, a role of PsaK in state transitions has been suggested (Varotto et al., 2002).

Cyanobacterial PS I, in contrast to plant PS I, does not contain a subunit corresponding to PsaG, a plant PS I subunit which shows sequence homology to PsaK. These proteins have the same genetic origin (Kjaerulff et al., 1993) and PsaG has evolved via gene duplication. The 4.4 Å structure of pea PS I shows that this subunit is located at a position symmetrically to PsaK in the vicinity of PsaB. It is the only subunit of the plant PS I core that forms direct contacts via a transmembrane helix with the light harvesting complex I (Lhca1) (Ben-Shem et al., 2003).

IV. The Electron Transport Chain

The electron transport chain is located in the center of the PS I complex, representing the heart of PS I. Figure 6 shows the structural organization of the cofactors of the electron transport chain. It consists of six chlorophylls, two phylloquinones and three [4Fe–4S] clusters. The organic cofactors (i.e., the chlorophylls and the phylloquinones) of the electron transport chain are arranged in two branches. They are named the A- and B-branches, because most – but not all – cofactors of the A-branch and B-branch are coordinated by PsaA and PsaB, respectively. Most of the molecules involved in electron transfer were first identified by spectroscopy and the names, given to them by spectroscopy, have been maintained. One of the most exciting questions is whether one or both branches are active in electron transfer. First, we want to discuss the structure and function of the individual cofactors and then come back to the question of whether one or two branches are active when the function of the phylloquinones is discussed.

A. P700: The Primary Electron Donor

The pair of chlorophylls assigned to P700 is located close to the lumenal surface of PS I. It consists of two chemically different chlorophyll molecules. The chlorophyll on the B-branch is the "common" Chl *a* molecule, chemically identical to all the other 95 chlorophylls in PS I, whereas the chlorophyll at the A-branch is Chl *a*′, the epimer at the C^{13} position of the chlorin ring system. The existence of at least one Chl *a*′ molecule was first suggested by Watanabe and coworkers (Watanabe et al., 1985; Maroc and Tremolieres, 1990; Maeda et al., 1992) on the basis of chlorophyll extraction experiments, but their pioneering findings were questioned until the existence of a Chl *a*/Chl *a*′ heterodimer was verified by the 2.5 Å crystal structure of cyanobacterial PS I (Jordan et al., 2001).

The chlorophyll on the B-branch of P700 (eC-B1) is axially coordinated to His B660. No hydrogen bonds are formed between the surrounding protein and the chlorin head group of eC-B1. The chlorophyll on the A-branch of P700 (eC-A1) is the Chl *a*′ molecule; it is axially coordinated by His A680. This Chl *a*′ forms three hydrogen bonds to the side chains of transmembrane α-helices A-i and A-k and a water molecule.

The distance between the Mg^{2+} ions of the two chlorophylls assigned to P700 is 6.3 Å, which is shorter than the corresponding distance between the bacteriochlorophylls in the special pair of the purple bacterial reaction center (pBRC). The planes of eC-A1 and eC-B1 are oriented perpendicularly to the membrane plane and parallel to each other with an interplanar distance of 3.6 Å. The overlap between the ring systems differs between P700 in PS I and the special pair of the pBRC. In the bacteriochlorophyll ring system in the special pair, the rings I overlap perfectly (Deisenhofer et al., 1995), whereas rings I and II of the chlorophylls only partially overlap in P700. ENDOR studies in solution (Kass et al., 1995) and on single crystals of PS I (Kass et al., 2001) showed that the spin density in P700 is asymmetric, with more than 85% of the spin density located on the B-branch Chl*a* of P700. Molecular orbital studies of the electronic structure of P700, based on semiempirical density functional calculations on the 2.5 Å structure show that the two chlorophylls are tightly coupled and P700 is a super-molecule (Plato et al., 2003). The asymmetry of the spin density can be explained by the interplay between the asymmetric hydrogen bonding, differences in the protein environment and the chemically different nature of the two chlorophyll molecules. Whether the asymmetry is essential for the function of PS I is still to be proven; however, the fact that Chl *a*′ is a constituent in cyanobacterial, algal, and plant PS I may suggest Chl *a*′ as having an essential role in the function of PS I. It may be speculated that the asymmetrical spin density distribution could be responsible for the "gating" of the electron along the two cofactor branches; however, there is thus far no experimental proof for this suggestion. The question of how the Chl *a*′ is assembled into the PS I complex or if it may be isomerized by PS I in a photoactivated process also remains unanswered.

B. A: The Initial Electron Acceptor

Three pairs of chlorophylls are present in the electron transport chain. In the X-ray structural model of PS I at 2.5 Å resolution. From P700 (represented by the first pair of chorophylls) the electron is transferred via one of the chlorophylls from the second pair chlorophylls (A) to the first stable electron acceptor A_0, which may be located on one of the chlorophylls located in the middle of the membrane (see Fig. 6). These first steps of electron transport occur in less than 3 psec (3/1,000,000,000 parts of a second) so that the second pair of chlorophylls has not been detected by spectroscopy so far.

The chlorophylls of the second pair (eC-B2 and cC-A2) are often named misleadingly accessory chlorophylls. They have a center-to-center distance of approximately 12 Å to the chlorophylls of P700 and represent

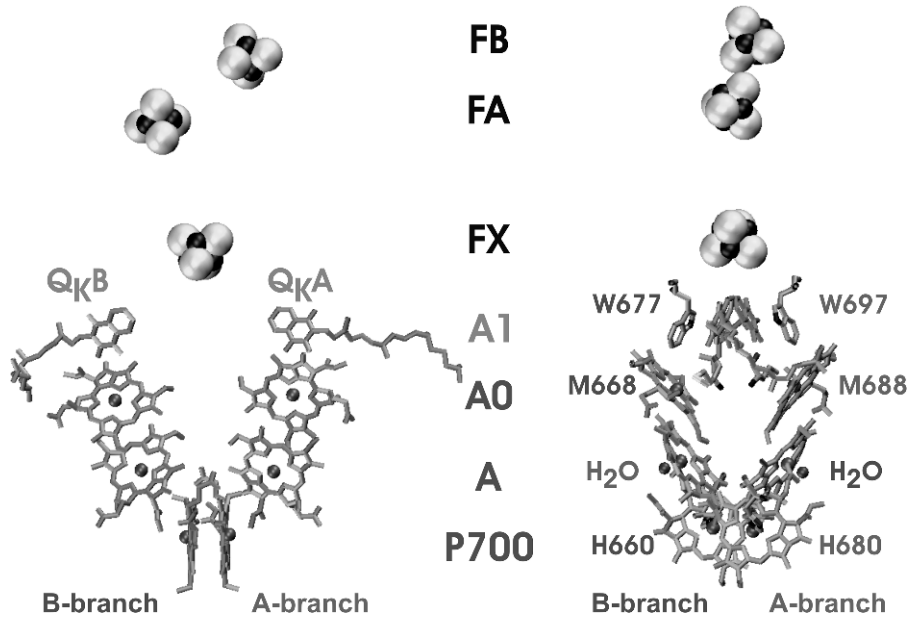

Fig. 6. The electron transfer chain of Photosystem I. Left panel: The view depicts chain B at the left and chain A at the right side. Right panel: The view is slightly turned compared to the left panel. In addition to the chlorophylls, phylloquinones, and Fe/S clusters of the electron transfer chain, the coordinating amino acids and water molecules are indicated.

the first electron acceptor in PS I. These two chlorophylls are the only cofactors of the electron transport chain, in which the coordinating subunit of the A-branch is PsaB and *vice versa*. In both branches, a water molecule provides the fifth ligand to the central Mg^{2+} ion of the second pair of chlorophylls. The water molecule, which serves as the axial ligand to the Chl*a* at the A-branch, is hydrogen bonded to asparagine residue AsnB591; thus this chlorophyll molecule is named eC-B2. The binding pocket of the corresponding chlorophyll in the B-branch is similar, so that AsnA604 is hydrogen bonded to the water molecule, which axially ligands the chlorophyll eC-A2. Remarkable differences are observed in the orientation and coordination of the second pair of chlorophylls/bacteriochlorophylls ["accessory (bacterio) chlorophylls"] between PS I and the pBRC, in which histidines provide the fifth ligand for the Mg^{2+} (Jordan et al., 2001). It is remarkable that the "accessory" chlorophylls in PS II match the pBRC with respect to the orientation but may match the coordination with PS I, because they are not coordinated by a His side chain (Ferreira et al., 2004). The structure of PS I at 2.5 Å resolution strongly supports the idea that the chlorophylls eC-A2 and eC-B2 may be directly involved in electron transfer from P700 to A_0. Recent results of Holzwarth and coworkers suggested that the charge separation may start from the accessory chlorophyll at the B-branch instead of P700 (Muller et al., 2003) but this is still a matter of debate.

C. A_0: The First Stable Electron Acceptor

The second pair and third pair of chlorophylls are located in close vicinity to each other in PS I (3.8 Å), with a roughly parallel orientation of the chlorin rings of eC-B2 ⇔ eC-A3 and eC-A2 ⇔ eC-B3. Even if eC-A3 and eC-B3 are supposed to correspond to the spectroscopically identified electron acceptor A_0 it is very likely that the spectroscopic and redox properties of eC-A3 and eC-B3 may be influenced by eC-B2 and eC-A2, respectively. The finding supports the suggestion that the difference spectrum $A_0/A_0^{-\cdot}$ contains contributions from more than one chlorophyll (Hastings et al., 1995).

EC-A3 and eC-B3 are located in the middle of the membrane at a position which roughly shows similarities to the position of pheophytin both in the pBRC (Deisenhofer et al., 1995) and in PS II (Ferreira et al., 2004). Both chlorophylls constitute one hydrogen bond to the tyrosines A696 and B676, which are direct neighbors to the Trp residues W697 of PsaA and W677 of PsaB which π-stack with the quinone electron acceptor (see below). The axial ligands of eC-A3 and eC-B3 are unusual. The sulfur atoms of methionine residues A688 and B668 provide the fifth "ligands" of the Mg^{2+} ions. This structural result is remarkable, because the

concept of hard and soft acids and bases predicts only weak interactions between the hard acid Mg^{2+} and methionine sulfur as a soft base. The mutation of the methionine AMet688 to AHis688 provides a strong ligand to Mg^{2+} and thereby blocks the electron transfer chain along the A-branch (Fairclough et al., 2003). It is remarkable that the cells are not strongly affected in autotrophic growth by this mutation, whereas the mutation of BMet668 into BHis668 lead to severe growth deficits of the green algae, even if the electron transfer along the B-branch is not completely blocked. Recent results of Webber and coworkers (Ramesh et al., 2004) who investigated the mutation of the methionines in both branches also found a more pronounced phenotype for the B-site mutation, but both mutants still show some limited photoautotrophic growth. These findings lead to the suggestion that the A-branch is less important than the B-branch – at least in green algae. Mutagenesis studies on the cyanobacterial PS I from *Synechocystis* sp. PCC 6803 (which involves a Leu mutant) favor the A- over the B-branch (Cohen et al., 2004), so that the question of the two-versus-one active branch in PS I is still the most controversially discussed topic in PS I. It may even be the case that the branching of the electron along the two chains may differ between different organisms.

A sequence comparison between PS I complexes from cyanobacteria, green algae, and higher plants reveals that all amino acids that are involved axial coordination or hydrogen bonding to the second and third Chl *a* pairs of the electron transfer chain are strictly conserved. The conservation of the differences in the axial coordination and hydrogen bonding between the three pairs of chlorophyll molecules throughout evolution could suggest that these protein–chlorophyll interactions are essential for the physico-chemical properties (e.g., the redox potentials) of these cofactors. However, the question as to whether the very low redox potential of the electron acceptor, A_0, (−1,050 mV) is caused by lack of a strong fifth ligand to the Mg^{2+} atom of these chlorophylls, remains to be answered.

D. A_1: The Phylloquinone

In the next step of the electron transfer chain, the electron is further transferred from A_0 to one of the phylloquinones, which represent the electron acceptor "A_1." The two phylloquinones, Q_KA and Q_KB, which may represent A_1, are located at the stromal side of the membrane. The binding pockets are identical on both sites but differ significantly from all other quinone-binding pockets found in proteins so far. Both quinones are π-stacked with a tryptophan residue and both show asymmetrical hydrogen bonding: only one of the two oxygen atoms forms a H-bond to an NH backbone group, whereas the other oxygen atom is not hydrogen bonded at all. This could lead to a protein-induced asymmetry in the distribution of the unpaired electron in the radical state $A_1^{-\cdot}$. This may answer the question of why A_1 has the most negative redox potential (−770 mV) of all quinones so far found in nature. The electron proceeds from A_1 to the Fe/S cluster, F_X (van der Est et al., 1994). This is the rate limiting step of the electron transfer in PS I. Still, a lively scientific discussion continues regarding the question of whether one or both branches are active.

There is experimental evidence that the electron transfer can proceed along both branches, but with different rates. In the green algae *Chlamydomonas reinhardtii*, the electron transfer is about a factor of 50 slower on the A- than on the B-branch (Boudreaux et al., 2001; Guergova-Kuras et al., 2001). This could be the result of a higher activation energy barrier on the A- compared to the B-branch. This finding raises the question of the structural reason for this functional difference. There is not a significant difference concerning the protein environment in both branches, but there are two lipid molecules located close to the pathway from A_1 to F_X that could be responsible for the asymmetry. A negatively charged phospholipid is located on the slower A-branch and the electron has to be transferred against this negative charge, whereas on the faster B-branch a neutral galactolipid has replaced the phospholipid. This is the most reasonable explanation for the higher activation energy barrier of the electron transfer between Q_KA and F_X compared to the electron transfer between Q_KB and F_X. Another factor, which could lead to a difference in reorganization energy between the two branches, are differences in the water clusters that are located between the quinone-binding site and F_X. There are five water molecules located in a pocket at the A-branch, which show a nonspecific arrangement. In contrast, five of the total of six water molecules located between the quinone-binding pocket and F_X at the B-branch phylloquinone form the structure of a hexagon, which is a well-defined low energy arrangement of a water cluster (Akhmatskaya et al., 1999). Thereby, the hexagon structure of the water cluster at the B-branch may also contribute to the lowering of the reorganization energy and the activation energy barrier at the B-branch. One possible explanation was provided for the faster electron transfer along the B-branch compared to the A-branch by results of Ishikita and Knapp. They calculated the redox potentials of the two electron

transfer active quinones in PS I by evaluating the electrostatic energies from the solution of the Poisson–Boltzmann equation based on the crystal structure. The calculated redox potentials are −531 mV for Q_KA and -686 mV for Q_KB, which would lead to an uphill electron transfer from Q_KA to F_X (Ishikita and Knapp, 2003). However, these results have to be taken with a grain of salt as electron transfer is still possible from A_1 to F_X in core PS I samples lacking F_A and F_B (Lüneberg et al., 1994; van der Est et al., 1994), which would not be possible if the ET from Q_KA to F_X were energetically uphill. In summary the burning questions of the structural and functional differences of the two branches and their function in PS I are still controversial and further experiments have to be performed to unravel the reason for the observed differences in electron transfer rates.

E. F_X: The First Fe/S Cluster

F_X is a rare example of an inter-protein Fe/S cluster. Histidine ligands are provided by Cys578 and Cys587 of PsaA and Cys565 and Cys574 of PsaB. The ligands are located in the loop connecting helices h and i. This loop is very highly conserved and essentially identical in all PS I species from plants, algae, and cyanobacteria. It contains two cysteines in the highly conserved sequence (FP**C**DGPGRGGT**C**XXSAWDH). In the 1980s, this site was already suggested to be the coordination site for the first [4Fe–4S] cluster F_X (Fish et al., 1985), which was experimentally supported by mutagenesis studies (Hallahan et al., 1995; Vassiliev et al., 1995). The structure of cyanobacterial PS I at 2.5 Å resolution confirmed this assignment (Jordan et al., 2001; Fromme et al., 2001).

The electron transfer from the quinone to F_X is slower than the ET from F_X to F_A, therefore F_X is difficult to detect in intact PS I complexes and was therefore mainly studied in complexes depleted of the extrinsic subunits or where the terminal Fe/S clusters are prereduced. Both of these procedures can alter the physical chemical parameters of F_X, therefore the values given for the redox potential of F_X (−710 mV) have to be treated with caution.

In addition to its functional role in electron transfer, F_X also plays an important role in the stabilization and assembly of the PS I complex. The PS I complex cannot assemble without the help of proteins that are not a part of PS I, but can be found to be attached to the monomeric PS I during assembly. A mutant was described and spectroscopically characterized that lacks the open reading frame for a rubredoxin (*rubA*) (Shen et al., 2002). Shen et al. showed striking evidence that this protein is involved in the assembly of F_X. The mutant PS I assembles all membrane intrinsic subunits but lacks F_X and the extrinsic subunits PsaC, PsaD, and PsaE. The assembly of the whole stromal hump may therefore depend on the functional assembly of F_X.

F. F_A and F_B: the Terminal Fe/S clusters

The two terminal Fe/S are bound to the extrinsic subunit PsaC. A long time question was whether F_A or F_B is the terminal Fe/S cluster that transfers the electron to ferredoxin. Mutagenesis in combination with EPR investigations (Zhao et al., 1992; Mehari et al., 1995) showed that the cluster in close proximity to F_X (center-to-center distance 14.9 Å), coordinated by the cysteine residues C21, C48, C51, and C54 represents F_A, whereas the distal cluster, coordinated by the cysteine residues C11, C14, C17, and C58, represents the distal cluster F_B (Yu et al., 1995a,b). Thereby F_B is the terminal Fe/S cluster with a center-to-center distance of 22 Å to F_X. A sequential electron transport from F_X to F_A to F_B is also confirmed by a large number of spectroscopic and biochemical studies (Fischer et al., 1999a,b; Lakshmi et al., 1999; Golbeck, 1999 and references therein; for a more detailed discussion of F_A and F_B see also Antonkine and Golbeck, this volume, Chapter 8).

V. The Antenna System

The antenna system of PS I consists of 90 Chl *a* molecules and 22 carotenes. The arrangement of the pigments is shown in Fig. 2C,D. The function of the antenna chlorophylls (shown in green) is to capture light and transfer the excitation energy to the center of the complex, where the electron transfer is located. The quantum efficiency of the excitation energy transfer is very high. After excitation of any of the antenna chlorophylls the chance that the energy is successfully transferred to P700 and subsequent charge separation occurs is 99.98% at room temperature.

A. The Chlorophylls

The arrangement of the antenna chlorophylls in PS I is unique. The chlorophylls form a clustered network instead of a symmetric ring surrounding the reaction center core, as it is in the light harvesting systems of purple bacteria (McDermott et al., 1995). Each of the chlorophylls has several neighbors at a distance of less than 15 Å, so energy can be efficiently transferred in

multiple pathways to the center of the complex. The system can be somewhat compared to the nerve-network system in the brain, where multiple connections are responsible for the high efficiency of information transfer. The antenna system in PS I is highly optimized for efficiency and robustness (Sener et al., 2004). The side view along the membrane plane (Fig. 2C) shows that the core-antenna system of PS I can be divided into a central domain, which surrounds the electron transfer chain, and two peripheral domains, flanking the core on both sides. In the peripheral domains, the antenna chlorophylls are arranged in two layers, one close to the stromal surface of the membrane and the other close to the lumenal surface of the membrane. When a peripheral antenna chlorophyll is excited the energy will be first transferred from this "two-dimensional" layer to the central domain. In the central domain, chlorophylls are distributed over the full depths of the membrane, i.e., the excitation energy can be exchanged between the two layers. The excitation energy is then transferred from the chlorophylls of the central domain to the electron transfer chain. There are two chlorophylls (named "connecting chlorophylls") that seem to structurally link the antenna system to the electron transfer chain. Recently, mutagenesis experiments were performed on the ligands of these connecting chlorophylls (Gibasiewicz et al., 2003). The mutants show minor alterations in the trapping of the excitation energy, but the question as to whether they play a crucial role in energy transfer is still not resolved.

A very exciting topic in PS I is the question of the location and function of the pigments that absorb at wavelength >700 nm. They are called "red" or "long-wavelength" chlorophylls. There are several reasons that can cause a red-shift of the chlorophyll absorption: strong excitonic coupling with neighboring chlorophylls may provide the strongest contribution, but the protein environment may also play an important role as the red-shift can also be caused by variation of the fifth ligand of the Mg^{2+} or electrostatic fields provided by the protein. The long-wavelength chlorophylls may function in increasing the spectral width of the light absorbed by PS I that can be used in charge separation. Another function of the "red" chlorophylls may be the "funneling" of the excitation energy to the center of the PS I complex. The latter function may be provided by chlorophylls that absorb between 685 and 705 nm, which are present in all PS I complexes from plants, algae, and cyanobacteria. One of the very exciting questions is about the location of the "red" chlorophylls in the PS I complex. Flemming and coworkers calculated the effective Hamiltonian for chlorophyll Q_y excitations, enabling tentative assignment of red chlorophylls and calculation of the absorption spectrum of PS I (Damjanovic et al., 2002; Yang et al., 2003). The calculations show that the strongly coupled chlorophylls must not be the ones that absorb at the longest wavelength.

The PS I composition concerning the pigments absorbing at longer wavelength vary between organisms. The PS I core in cyanobacteria contains more chlorophylls that absorb at wavelength >705 nm than the core of the plant systems, but the variation between different cyanobacterial species is as high as between plants and cyanobacteria, so that a directed evolution from cyanobacteria toward replacement of the long-wavelength chlorophylls as suggested recently (Ben-Shem et al., 2004), seems to be questionable. It is much more likely that cyanobacteria have adapted to low-light conditions and concurrence from aquatic photosynthetic organisms by the development of pigments absorbing at longer wavelength. On the basis of the structure of PS I, several theoretical studies investigated the excitation energy transfer and trapping in PS I. These studies show that the excitation energy transfer in PS I is trap limited and is highly optimized for robustness and efficiency (Palsson et al., 1998; Byrdin et al., 2002; Sener et al., 2004).

B. The Carotenoids

Twenty-two carotenoids have been identified in the cyanobacterial structure of PS I. The carotenoids fulfill three functions in PS I. They play a structural role, function as additional antenna pigments, and prevent the system from damage by over-excitation caused by excess light (photoinhibition). The latter function is very critical for the whole system. Chlorophylls are in principle dangerous and reactive molecules. Over-excitation can lead to the formation of chlorophyll triplets (Chl^3), which can react with oxygen to form the highly toxic singlet oxygen, a very dangerous cell poison. Multiple interactions can be observed between the carotenoids and the chlorophylls of the antenna system. The carotenoids are distributed over the whole antenna system and prevent photodamage by the quenching of chlorophyll triplet states. The energy from the triplet chlorophylls is transferred to the carotenoids that form the triplet state Car^3. The energy of the Car^3 is too low to react with O_2. When the carotenoids return to the ground state they dissipate the energy as heat, thereby preventing photodamage. The system works very efficiently, even under high light conditions, as the Chl^3 triplet state cannot be detected in the intact PS I.

Despite the important role of carotenoids in photoprotection, structural integrity, and light capturing, they might not be directly involved in the electron transfer process. Mutants that completely lack the carotenoids (Romer et al., 1995) still contain some PS I and charge separation can be detected. Samples in which all carotenoids are extracted with organic solvents lack the quinones but are still able to perform electron transfer from P700 to A_0 (Ikegami et al., 2000).

An important and still unanswered question is why 17 of the carotenoids are in *all-trans* configuration, whereas five carotenoids contain one or two *cis*-double bonds. The easiest explanation would be that simple "fit-into-space" considerations lead to the incorporation of the *cis*-carotenoids. However, other possibilities may also have to be taken into account, as there may be a different efficiency for quenching for the *cis*- and *trans*-carotenoids because the energy level for the *trans* form is lower than for the *cis*-carotenoids. The investigation of the role of the *cis*-carotenoids is a very interesting subject for further investigations.

VI. The Lipids

Four lipids have been identified in the structure of PS I at 2.5 Å resolution: three molecules of phosphatidylglycerol (PG) and one molecule of monogalactosyldiacylglycerol (MDGD). Two of these lipids are located close to the electron transfer chain. They must be incorporated into PS I at a very early stage of the assembly process, because their head groups are not solvent accessible but are covered by the loops of PsaA and PsaB and the three stromal subunits PsaC, PsaD, and PsaE. They are located close to the electron transport chain and may even play an important role in the difference in the rates of electron transfer between the two different branches. Recently, mutants have been described that are impaired in the synthesis of PG (Domonkos et al., 2004). These mutants grow only in the presence of externally added PG, i.e., PG is essential for photoautotrophic growth. When the mutants are depleted of PG, at first PS II activity is inhibited, probably due to the much higher turnover of PS II compared to PS I. In the PG-depleted PS II, the ET from Q_A to Q_B is blocked. This finding is very exciting and raises the question as to whether there might also be lipids in PS II located in a similar position as in PS I. The long time depletion (>10 days) finally leads to the loss of PS I function, which parallels the starvation of the cells, which show that PS I is nonfunctional or cannot be assembled without the lipids.

The two other PG molecules are located at the periphery of PS I, one at the monomer–monomer interface, the other at the membrane exposed surface of PS I in tight interaction with PsaX. The interaction between PsaX and PG are mainly hydrophobic but both molecules interact so tightly that the role of this PG might be the stabilization of PsaX within the complex. The lipid at the monomer–monomer interface coordinates one chlorophyll (named PL1). This chlorophyll may contribute to the excitation energy transfer between different monomeric units.

Recently, it was reported that PG may also be involved in trimerization of PS I and interacts with PsaL (Domonkos et al., 2004). The electron density map of PS I at 2.5 Å resolution indeed showed a lipid-like structure close to PsaL, with the lipid-head group located in the lumen (Jordan et al., unpublished). However, the electron density was not clearly identified as a PG molecule (it looks more like a lipid with four fatty acids chains). Due to the unclear assignment, the "fifth" lipid was not included in the published X-ray structure. So, the function of lipids in PS I is still an exciting topic with new discoveries and surprises still on the way.

References

Adman ET, Sieker LC and Jensen LH (1973) The structure of a bacterial ferredoxin. J Biol Chem 248: 3987–3996

Akhmatskaya EV, Cooper MD, Burton NA, Masters AJ and Hillier IH (1999) Monte Carlo simulations of water clusters on a parallel computer using an *ab initio* potential. Int J Quantum Chem 74: 709–719

Anandan S, Vainstein A and Thornber JP (1989) Correlation of some published amino acid sequences for photosystem I polypeptides to a 17 kDa LHCI pigment–protein and to subunits III and IV of the core complex. FEBS Lett 256: 150–154

Andersen B and Scheller HV (eds) (1993) Structure, Function and Assembly of Photosystem I. Academic Press, San Diego

Andersen B, Scheller HV and Moller BL (1992) The PSI-E subunit of photosystem I binds ferredoxin:$NADP^+$ oxidoreductase. FEBS Lett 311: 169–173

Antonkine ML, Jordan P, Fromme P, Krauß N, Golbeck JH and Stehlik D (2003) Assembly of protein subunits within the stromal ridge of photosystem I. Structural changes between unbound and sequentially PS I-bound polypeptides and correlated changes of the magnetic properties of the terminal iron sulfur clusters. J Mol Biol 327: 671–697

Armbrust TS, Chitnis PR and Guikema JA (1996) Organization of photosystem I polypeptides examined by chemical crosslinking. Plant Physiol 111: 1307–1312

Barth P, Lagoutte B and Sétif P (1998) Ferredoxin reduction by photosystem I from *Synechocystis* sp. PCC 6803: toward an understanding of the respective roles of subunits PsaD and PsaE in ferredoxin binding. Biochemistry 37: 16233–16241

Ben-Shem A, Frolow F and Nelson N (2003) Crystal structure of plant photosystem I. Nature 426: 630–635

Ben-Shem A, Frolow F and Nelson N (2004) Evolution of photosystem I – from symmetry through pseudo-symmetry to asymmetry. FEBS Lett 564: 274–280

Bibby TS, Nield J and Barber J (2001) Iron deficiency induces the formation of an antenna ring around trimeric photosystem I in cyanobacteria. Nature 412: 743–745

Boekema EJ, Hifney A, Yakushevska AE, Piotrowski M, Keegstra W, Berry S, Michel KP, Pistorius EK and Kruip J (2001) A giant chlorophyll–protein complex induced by iron deficiency in cyanobacteria. Nature 412: 745–748

Boudreaux B, MacMillan F, Teutloff C, Agalarov R, Gu F, Grimaldi S, Bittl R, Brettel K and Redding K (2001) Mutations in both sides of the photosystem I reaction center identify the phylloquinone observed by electron paramagnetic resonance spectroscopy. J Biol Chem 276: 37299–37306

Byrdin M, Jordan P, Krauß N, Fromme P, Stehlik D and Schlodder E (2002) Light harvesting in photosystem I: modeling based on the 2.5-Å structure of photosystem I from *Synechococcus elongatus*. Biophys J 83: 433–457

Chitnis PR, Xu Q, Chitnis VP and Nechustai R (1995) Function and organization of photosystem I polypeptides. Photosynth Res 44: 23–40

Chitnis VP, Xu Q, Yu L, Golbeck JH, Nakamoto H, Xie D-L and Chitnis PR (1993) Target inactivation of the gene *psaL* encoding a subunit of photosystem I of the cyanobacterium *Synechocystis* PCC 6803. J Biol Chem 268: 11678–11684

Chitnis VP, Jungs YS, Albee L, Golbeck JH and Chitnis PR (1996) Mutational analysis of photosystem I polypeptides. Role of PsaD and the lysyl 106 residue in the reductase activity of the photosystem I. J Biol Chem 271: 11772–11780

Chitnis VP, Ke A and Chitnis PR (1997) The PsaD subunit of photosystem I. Mutations in the basic domain reduce the level of PsaD in the membranes. Plant Physiol 115: 1699–1705

Cohen RO, Shen G, Golbeck JH, Xu W, Chitnis PR, Valieva AI, van der Est A, Pushkar Y and Stehlik D (2004) Evidence for asymmetric electron transfer in cyanobacterial photosystem I: analysis of a methionine-to-leucine mutation of the ligand to the primary electron acceptor A_0. Biochemistry 43: 4741–4754

Damjanovic A, Vaswani HM, Fromme P and Fleming GR (2002) Chlorophyll excitations in photosystem I of *Synechococcus elongatus*. J Phys Chem B 106: 10251–10262

Deisenhofer J, Epp O, Sinning I and Michel H (1995) Crystallographic refinement at 2.3 Å resolution and refined model of the photosynthetic reaction centre from *Rhodopseudomonas viridis*. J Mol Biol 246: 429–457

Domonkos I, Malec P, Sallai A, Kovacs L, Itoh K, Shen G, Ughy B, Bogos B, Sakurai I, Kis M, Strzalka K, Wada H, Itoh S, Farkas T and Gombos Z (2004) Phosphatidylglycerol is essential for oligomerization of photosystem I reaction center. Plant Physiol 134: 1471–1478

Dunn PP, Packman LC, Pappin D and Gray JC (1988) N-terminal amino acid sequence analysis of the subunits of pea photosystem I. FEBS Lett 228: 157–161

Evans MCW, Reeves SG and Cammack R (1974) Determination of oxidation–reduction potential of bound iron–sulfur proteins of primary electron-acceptor complex of photosystem-I in spinach-chloroplasts. FEBS Lett 49: 111–114

Fairclough WV, Forsyth A, Evans MC, Rigby SE, Purton S and Heathcote P (2003) Bidirectional electron transfer in photosystem I: electron transfer on the PsaA side is not essential for phototrophic growth in *Chlamydomonas*. Biochim Biophys Acta 1606: 43–55

Falzone CJ, Kao YH, Zhao J, Bryant DA and Lecomte JT (1994a) Three-dimensional solution structure of PsaE from the cyanobacterium *Synechococcus* sp. strain PCC 7002, a photosystem I protein that shows structural homology with SH3 domains. Biochemistry 33: 6052–6062

Falzone CJ, Kao YH, Zhao J, MacLaughlin KL, Bryant DA and Lecomte JT (1994b) ^{1}H and ^{15}N NMR assignments of PsaE, a photosystem I subunit from the cyanobacterium *Synechococcus* sp. strain PCC 7002. Biochemistry 33: 6043–6051

Farah J, Rappaport F, Choquet Y, Joliot P and Rochaix JD (1995) Isolation of a *psaF*-deficient mutant of *Chlamydomonas reinhardtii*: efficient interaction of plastocyanin with the photosystem I reaction center is mediated by the PsaF subunit. EMBO J 14: 4976–4984

Ferreira KN, Iverson TM, Maghlaoui K, Barber J and Iwata S (2004) Architecture of the photosynthetic oxygen-evolving center. Science 303: 1831–1838

Fischer N, Boudreau E, Hippler M, Drepper F, Haehnel W and Rochaix JD (1999a) A large fraction of PsaF is nonfunctional in photosystem I complexes lacking the PsaJ subunit. Biochemistry 38: 5546–5552

Fischer N, Sétif P and Rochaix JD (1999b) Site-directed mutagenesis of the PsaC subunit of photosystem I. F(b) is the cluster interacting with soluble ferredoxin. J Biol Chem 274: 23333–23340

Fish L, Kück U and Bogorad L (1985) Two partially homologous adjacent light-inducible maize chloroplast genes encoding polypeptides of the P700 chlorophyll a protein complex of photosystem I. J Biol Chem 260: 1413–1421

Frazao C, Soares CM, Carrondo MA, Pohl E, Dauter Z, Wilson KS, Hervas M, Navarro JA, De la Rosa MA and Sheldrick GM (1995) *Ab initio* determination of the crystal structure of cytochrome c_6 and comparison with plastocyanin. Structure 3: 1159–1169

Fromme P (1998) Crystallization of Photosystem I for Structural Analysis. Habilitation. Technical University Berlin, Berlin, Germany

Fromme P, Jordan P and Krauß N (2001) Structure of photosystem I. Biochim Biophys Acta 1507: 5–31

Fromme P, Bottin H, Krauß N and Sétif P (2002) Crystallization and EPR characterization of a functional complex of photosystem I with its natural electron acceptor ferredoxin. Biophys J 83: 1760–1763

Fromme P, Melkozernov A, Jordan P, Krauß N (2003) Structure and function of photosystem I. Interaction with its soluble electron carriers and external antenna system. FEBS Lett 555, 40–44

Gavel Y, Steppuhn J, Herrmann R and von Heijne G (1991) The "positive inside rule" applies to thylakoid membrane proteins. FEBS Lett 282: 41–46

Gibasiewicz K, Ramesh VM, Lin S, Redding K, Woodbury NW and Webber AN (2003) Excitonic interactions in wild-type and mutant PSI reaction centers. Biophys J 85: 2547–2559

Golbeck JH (1993) The structure of photosystem I. Curr Opin Struct Biol 3: 508–514

Golbeck JH (1994) Photosystem I in cyanobacteria. In: Bryant DA (ed) Advances in Photosynthesis: The Molecular Biology of Cyanobacteria, Vol 1, pp 319–360. Kluwer Academics, Dordrecht, The Netherlands

Golbeck JH (1999) A comparative analysis of the spin state distribution of *in vitro* and *in vivo* mutants of PsaC. Photosynth Res 61: 107–144

Guergova-Kuras M, Boudreaux B, Joliot A, Joliot P and Redding K (2001) Evidence for two active branches for electron transfer in photosystem I. Proc Natl Acad Sci USA 98: 4437–4442

Haehnel W, Jansen T, Gause K, Klosgen RB, Stahl B, Michl D, Huvermann B, Karas M and Herrmann RG (1994) Electron transfer from plastocyanin to photosystem I. EMBO J 13: 1028–1038

Hallahan B, Purton S, Ivison A, Wright D and Evans MCW (1995) Analysis of the proposed FeSx binding region of photosystem I by side directed mutation of PsaA in *Chlamydomonas rheinhardtii*. Photosynth Res 46: 257–264

Hastings G, Hoshina S, Webber AN and Blankenship RE (1995) Universality of energy and electron transfer processes in photosystem I. Biochemistry 34: 15512–15522

Hippler M, Reichert J, Sutter M, Zak E, Altschmied L, Schroer U, Herrmann RG and Haehnel W (1996) The plastocyanin binding domain of photosystem I. EMBO J 15: 6374–6384

Hippler M, Drepper F, Farah J and Rochaix JD (1997) Fast electron transfer from cytochrome c_6 and plastocyanin to photosystem I of *Chlamydomonas reinhardtii* requires PsaF. Biochemistry 36: 6343–6349

Hippler M, Drepper F, Haehnel W and Rochaix JD (1998) The N-terminal domain of PsaF: precise recognition site for binding and fast electron transfer from cytochrome c_6 and plastocyanin to photosystem I of *Chlamydomonas reinhardtii*. Proc Natl Acad Sci USA 95: 7339–7344

Hladik J and Sofrova D (1991) Does the trimeric form of the photosystem-1 reaction center of cyanobacteria *in vivo* exist. Photosynth Res 29: 171–175

Hugosson M, Nurani G, Glaser E and Franzen LG (1995) Peculiar properties of the PsaF photosystem I protein from the green alga *Chlamydomonas reinhardtii*: presequence independent import of the PsaF protein into both chloroplasts and mitochondria. Plant Mol Biol 28: 525–535

Ikegami I, Itoh S and Iwaki M (2000) Selective extraction of antenna chlorophylls, carotenoids and quinones from photosystem I reaction center. Plant Cell Physiol 41: 1085–1095

Ikeuchi M, Nyhus KJ, Inoue Y and Pakrasi HB (1991) Identities of four low-molecular-mass subunits of the photosystem I complex from *Anabaena variabilis* ATCC 29413. Evidence for the presence of the *psaI* gene product in a cyanobacterial complex. FEBS Lett 287: 5–9

Ishikita H and Knapp EW (2003) Redox potential of quinones in both electron transfer branches of photosystem I. J Biol Chem 278: 52002–52011

Janson S, Andersen B and Scheller HV (1996) Nearest-neighbor analysis of higher-plant photosystem I holocomplex. Plant Physiol 112: 409–420

Jeanjean R, Zuther E, Yeremenko N, Havaux M, Matthijs HC and Hagemann M (2003) A photosystem 1 *psaFJ*-null mutant of the cyanobacterium *Synechocystis* PCC 6803 expresses the *isiAB* operon under iron replete conditions. FEBS Lett 549: 52–56

Jordan P, Fromme P, Klukas O, Witt HT, Saenger W and Krauß N (2001) Three-dimensional structure of cyanobacterial photosystem I at 2.5 Å resolution. Nature 411: 909–917

Kamiya N and Shen JR (2003) Crystal structure of oxygen-evolving photosystem II from *Thermosynechococcus vulcanus* at 3.7-Å resolution. Proc Natl Acad Sci USA 100: 98–103

Karapetyan NV (2004) The dynamics of excitation energy in photosystem I of cyanobacteria: transfer in the antenna, capture by the reaction site, and dissipation. Biofizika 49: 212–226

Karapetyan NV, Shubin VV and Strasser RJ (1999) Energy exchange between the chlorophyll antennae of monomeric subunits within the photosystem I trimeric complex of the cyanobacterium *Spirulina*. Photosynth Res 61: 291–301

Karnauchov I, Cai D, Schmidt I, Herrmann RG and Klosgen RB (1994) The thylakoid translocation of subunit 3 of photosystem I, the *psaF* gene product, depends on a bipartite transit peptide and proceeds along an azide-sensitive pathway. J Biol Chem 269: 32871–32878

Kass H, Bittersmannweidlich E, Andreasson LE, Bonigk B and Lubitz W (1995) ENDOR and ESEEM of the N-15 labeled radical cations of chlorophyll-*a* and the primary donor P-700 in photosystem-I. Chem Phys 194: 419–432

Kass H, Fromme P, Witt HT and Lubitz W (2001) Orientation and electronic structure of the primary donor radical cation $P\text{-}700^+$ in photosystem I: a single crystals EPR and ENDOR study. J Phys Chem B 105: 1225–1239

Kjaerulff S, Andersen B, Nielsen VS, Møller BL and Okkels JS (1993) The PSI-K subunit of photosystem I from barley (*Hordeum vulgare* L.). Evidence for a gene duplication of an ancestral PSI-G/K gene. J Biol Chem 268: 18912–18916

Klukas O, Schubert WD, Jordan P, Krauß N, Fromme P, Witt HT and Saenger W (1999) Photosystem I, an improved model of the stromal subunits PsaC, PsaD, and PsaE. J Biol Chem 274: 7351–7360

Koike K, Ikeuchi M, Hiyama T and Inoue Y (1989) Identification of photosystem I components from the cyanobacterium *Synechococcus vulcanus* by N-terminal sequencing. FEBS Lett. 253: 257–263

Kouřil R, Yeremenko N, D'Haene S, Yakushevska AE, Keegstra W, Matthijs HC, Dekker JP and Boekema EJ (2003) Photosystem I trimers from *Synechocystis* PCC 6803 lacking the PsaF and PsaJ subunits bind an IsiA ring of 17 units. Biochim Biophys Acta 1607: 1–4

Kruip J, Chitnis PR, Lagoutte B, Rögner M and Boekema EJ (1997) Structural organization of the major subunits in cyanobacterial photosystem 1. Localization of subunits PsaC, -D, -E, -F, and -J. J Biol Chem 272: 17061–17069

Lagoutte B, Hanley J and Bottin H (2001) Multiple functions for the C terminus of the PsaD subunit in the cyanobacterial photosystem I complex. Plant Physiol 126: 307–316

Lakshmi KV, Jung YS, Golbeck JH and Brudvig GW (1999) Location of the iron–sulfur clusters F_A and F_B in photosystem I: an electron paramagnetic resonance study of spin relaxation enhancement of P700+. Biochemistry 38: 13210–13215

Lelong C, Sétif P, Lagoutte B and Bottin H (1994) Identification of the amino acids involved in the functional interaction between photosystem I and ferredoxin from *Synechocystis* sp. PCC 6803 by chemical cross-linking. J Biol Chem 269: 10034–10039

Lelong C, Boekema EJ, Kruip J, Bottin H, Rögner M and Sétif P (1996) Characterization of a redox active cross-linked complex between cyanobacterial photosystem I and soluble ferredoxin. EMBO J 15: 2160–2168

Li N, Warren PV, Golbeck JH, Frank G, Zuber H and Bryant DA (1991) Polypeptide composition of the photosystem I complex and the photosystem I core protein from *Synechococcus* sp. PCC 6301. Biochim Biophys Acta 1059: 215–225

Loll B, Raszewski G, Saenger W and Biesiadka J (2003) Functional role of Cα-HΛO hydrogen bonds between transmembrane α-helices in photosystem I. J Mol Biol 328: 737–747

Lüneberg J, Fromme P, Jekow P and Schlodder E (1994) Spectroscopic characterization of PS I core complexes from thermophilic *Synechococcus* sp. – Identical reoxidation kinetics of A_1- before and after removal of the iron–sulfur clusters F_A and F_B. FEBS Lett 338: 197–120

Lushy A, Verchovsky L and Nechushtai R (2002) The stable assembly of newly synthesized PsaE into the photosystem I complex occurring via the exchange mechanism is facilitated by electrostatic interactions. Biochemistry 41: 11192–11199

Maeda H, Watanabe T, Kobayashi M and Ikegami I (1992) Presence of two chorophyll *a′* molecules at the core of photosystem I. Biochim Biophys Acta 1099: 74–80

Mant A, Woolhead CA, Moore M, Henry R and Robinson C (2001) Insertion of PsaK into the thylakoid membrane in a "Horseshoe" conformation occurs in the absence of signal recognition particle, nucleoside triphosphates, or functional albino3. J Biol Chem 276: 36200–36206

Maroc J and Tremolieres A (1990) Chlorophyll *a′* and pheophytin *a*, as determined by HPLC, in photosynthesis mutants and double mutants of *Chlamydomonas reinhardtii*. Biochem Biophys Acta 1018: 67–71

McDermott G, Prince SM, Freer AA, Hawthornthwaite-Lawless AM, Papiz MZ, Cogdell RJ and Isaacs NW (1995) Crystal-structure of an integral membrane light-harvesting complex from photosynthetic bacteria. Nature 374: 517–521

Mehari T, Qiao F, Scott MP, Nellis DF, Zhao J, Bryant DA and Golbeck JH (1995) Modified ligands to F_A and F_B in photosystem I. I. Structural constraints for the formation of iron–sulfur clusters in free and rebound PsaC. J Biol Chem 270: 28108–28117

Meimberg K, Lagoutte B, Bottin H and Mühlenhoff U (1998) The PsaE subunit is required for complex formation between photosystem I and flavodoxin from the cyanobacterium *Synechocystis* sp. PCC 6803. Biochemistry 37: 9759–9767

Molina-Heredia FP, Diaz-Quintana A, Hervas M, Navarro JA and De La Rosa MA (1999) Site-directed mutagenesis of cytochrome c(6) from *Anabaena* species PCC 7119. Identification of surface residues of the hemeprotein involved in photosystem I reduction. J Biol Chem 274: 33565–33570

Mühlenhoff U, Haehnel W, Witt H and Herrmann RG (1993) Genes encoding 11 subunits of photosystem-I from the thermophilic cyanobacterium *Synechococcus* sp. Gene 127: 71–78

Mühlenhoff U, Kruip J, Bryant DA, Rögner M, Sétif P and Boekema E (1996a) Characterization of a redox-active cross-linked complex between cyanobacterial photosystem I and its physiological acceptor flavodoxin. EMBO J 15: 488–497

Mühlenhoff U, Zhao J and Bryant DA (1996b) Interaction between photosystem I and flavodoxin from the cyanobacterium *Synechococcus* sp. PCC 7002 as revealed by chemical cross-linking. Eur J Biochem 235: 324–331

Muller MG, Niklas J, Lubitz W and Holzwarth AR (2003) Ultrafast transient absorption studies on photosystem I reaction centers from *Chlamydomonas reinhardtii*. 1. A new interpretation of the energy trapping and early electron transfer steps in photosystem I. Biophys J 85: 3899–3922

Nakamura Y, Kaneko T, Sato S, Ikeuchi M, Katoh H, Sasamoto S, Watanabe A, Iriguchi M, Kawashima K, Kimura T, Kishida Y, Kiyokawa C, Kohara M, Matsumoto M, Matsuno A, Nakazaki N, Shimpo S, Sugimoto M, Takeuchi C, Yamada M and Tabata S (2002) Complete genome structure of the thermophilic cyanobacterium *Thermosynechococcus elongatus* BP-1. DNA Res 9: 123–130

Nield J, Morris EP, Bibby TS and Barber J (2003) Structural analysis of the photosystem I supercomplex of cyanobacteria induced by iron deficiency. Biochemistry 42: 3180–3188

Ohyama K, Fukazawa H, Kohchi T, Shirai H, Tohru S, Sano S, Umesono K, Shiki Y, Takeuchi M, Chang Z, Aota SI, Inokuchi H and Ozeki H (1986) Chloroplast gene organization deduced from complete sequence of liverwort *Marchantia polymorpha* chloroplast DNA. Nature 322: 572–574

Pakrasi HB (1995) Genetic analysis of the form and function of photosystem I and photosystem II. Annu Rev Genet 995: 755–756

Palsson LO, Flemming C, Gobets B, van Grondelle R, Dekker JP and Schlodder E (1998) Energy transfer and charge separation in photosystem I: P700 oxidation upon selective excitation of the long-wavelength antenna chlorophylls of *Synechococcus elongatus*. Biophys J 74: 2611–2622

Pandini V, Aliverti A and Zanetti G (1999) Interaction of the soluble recombinant PsaD subunit of spinach photosystem I with ferredoxin I. Biochemistry 38: 10707–10713

Plato M, Krauß N, Fromme P and Lubitz W (2003) Molecular orbital study of the primary electron donor P700 of photosystem I based on a recent X-ray single crystal structure analysis. Chem Phys 294: 483–499

Ramesh VM, Gibasiewicz K, Lin S, Bingham SE and Webber AN (2004) Bidirectional electron transfer in photosystem I: accumulation of A_0- in A-side or B-side mutants of the axial ligand to chlorophyll A_0. Biochemistry 43: 1369–1375

Romer S, Senger H and Bishop N (1995) Characterization of the carotenoidless strain of *Scenedesmus oliquus*, mutant C-6E, a living photosystem I model. Bot Acta 108: 80–86

Rousseau F, Sétif P and Lagoutte B (1993) Evidence for the involvement of PSI-E subunit in the reduction of ferredoxin by photosystem I. EMBO J 12: 1755–1765

Scheller HV, Jensen PE, Haldrup A, Lunde C and Knoetzel J (2001) Role of subunits in eukaryotic photosystem I. Biochim Biophys Acta 1507: 41–60

Schluchter WM, Shen G, Zhao J and Bryant DA (1996) Characterization of *psaI* and *psaL* mutants of *Synechococcus* sp. strain PCC 7002: a new model for state transitions in cyanobacteria. Photochem Photobiol 64: 53–66

Schubert WD, Klukas O, Saenger W, Witt HT, Fromme P and Krauß N (1998) A common ancestor for oxygenic and anoxygenic photosynthetic systems: a comparison based on the structural model of photosystem I. J Mol Biol 280: 297–314

Scott MP, Nielsen VS, Knoetzel J, Andersen R and Møller BL (1994) Import of the barley PSI-F subunit into the thylakoid lumen of isolated chloroplasts. Plant Mol Biol 26: 1223–1229

Sener M, Park S, Lu DY, Damjanovic A, Ritz T, Fromme P and Schulten K (2004) Excitation migration in trimeric cyanobacterial photosystem I. J Chem Phys 120, 11183–11195

Sener MK, Jolley C, Ben-Shem A, Fromme P, Nelson N, Croce R and Schulten K (2005) Comparison of the light-harvesting networks of plant and cyanobacterial photosystem I. Biophys J 8–9, 1630–1642

Sétif P (2001) Ferredoxin and flavodoxin reduction by photosystem I. Biochim Biophys Acta 1507: 161–179

Sétif P, Fischer N, Lagoutte B, Bottin H and Rochaix JD (2002) The ferredoxin docking site of photosystem I. Biochim Biophys Acta 1555: 204–209

Shen GZ, Antonkine ML, van der Est A, Vassiliev IR, Brettel K, Bittl R, Zech SG, Zhao JD, Stehlik D, Bryant DA and Golbeck JH (2002) Assembly of photosystem I. II. Rubredoxin is required for the *in vivo* assembly of F_X in *Synechococcus* sp PCC 7002 as shown by optical and EPR spectroscopy. J Biol Chem 277: 20355–20366

Sommer F, Drepper F and Hippler M (2002) The luminal helix l of PsaB is essential for recognition of plastocyanin or cytochrome c_6 and fast electron transfer to photosystem I in *Chlamydomonas reinhardtii*. J Biol Chem 277: 6573–6581

Sonoike K, Hatanaka H and Katoh S (1993) Small subunits of photosystem I reaction center complexes from *Synechococcus elongatus*. II. The *psaE* gene product has a role to promote interaction between the terminal electron acceptor and ferredoxin. Biochim Biophys Acta 1141: 52–57

Strotmann H and Weber N (1993) On the function of PsaE in chloroplast photosystem I. Biochim Biophys Acta 1143: 204–210

Van der Est A, Bock C, Golbeck JH, Brettel K, Sétif P and Stehlik D (1994) Electron transfer from the acceptor A_1 to the iron–sulfur centers in photosystem I as studied by transient EPR spectroscopy. Biochemistry 33: 11789–11797

van Thor JJ, Geerlings TH, Matthijs HC and Hellingwerf KJ (1999) Kinetic evidence for the PsaE-dependent transient ternary complex photosystem I/Ferredoxin/Ferredoxin:$NADP^{(+)}$ reductase in a cyanobacterium. Biochemistry 38: 12735–12746

Varotto C, Pesaresi P, Jahns P, Lessnick A, Tizzano M, Schiavon F, Salamini F and Leister D (2002) Single and double knockouts of the genes for photosystem I subunits G, K, and H of Arabidopsis. Effects on photosystem I composition, photosynthetic electron flow, and state transitions. Plant Physiol 129: 616–624

Vassiliev IR, Jung YS, Smart LB, Schulz R, McIntosh L and Golbeck JH (1995) A mixed-ligand iron–sulfur cluster ($C556S_{PsaB}$ or $C565S_{PsaB}$) in the F_X binding site leads to a decreased quantum efficiency of electron transfer in photosystem I. Biophys J 69: 1544–1553

Watanabe T, Kobayashi M, Hongu A, Nakazato M and Hiyama T (1985) Evidence, that a chlorophyll *a′* dimer constitutes the photochemical reaction centre 1 (P700) in photosynthetic apparatus. FEBS Lett 235: 252–256

Xu Q, Jung YS, Chitnis VP, Guikema JA, Golbeck JH and Chitnis PR (1994a) Mutational analysis of photosystem I polypeptides in *Synechocystis* sp. PCC 6803. Subunit requirements for reduction of $NADP^+$ mediated by ferredoxin and flavodoxin. J Biol Chem 269: 21512–21518

Xu Q, Odom WR, Guikema JA, Chitnis VP and Chitnis PR (1994b) Targeted deletion of *psaJ* from the cyanobacterium *Synechocystis* sp. PCC 6803 indicates structural interactions between the PsaJ and PsaF subunits of photosystem I. Plant Mol Biol 26: 291–302

Xu Q, Yu L, Chitnis VP and Chitnis PR (1994c) Function and organization of photosystem I in a cyanobacterial mutant strain that lacks PsaF and PsaJ subunits. J Biol Chem 269: 3205–3211

Xu Q, Hoppe D, Chitnis VP, Odom WR, Guikema JA and Chitnis PR (1995) Mutational analysis of photosystem I polypeptides in the cyanobacterium *Synechocystis* sp. PCC 6803. Targeted inactivation of psaI reveals the function of *psaI* in the structural organization of *psaL*. J Biol Chem 270: 16243–16250

Yang M, Damjanovic A, Vaswani HM and Fleming GR (2003) Energy transfer in photosystem I of cyanobacteria *Synechococcus elongatus*: model study with structure-based semi-empirical Hamiltonian and experimental spectral density. Biophys J 85: 140–158

Yu L, Zhao J, Mühlenhoff U, Bryant DA and Golbeck JH (1993) PsaE Is required for *in vivo* cyclic electron flow around photosystem I in the cyanobacterium *Synechococcus* sp. PCC 7002. Plant Physiol 103: 171–180

Yu L, Bryant DA and Golbeck JH (1995a) Evidence for a mixed-ligand [4Fe–4S] cluster in the C14D mutant of PsaC. Altered reduction potentials and EPR spectral properties of the F_A and F_B clusters on rebinding to the P700-F_X core. Biochemistry 34: 7861–7868

Yu L, Vassiliev IR, Jung YS, Bryant DA and Golbeck JH (1995b) Modified ligands to F_A and F_B in photosystem I. II. Characterization of a mixed ligand [4Fe–4S] cluster in the C51D mutant of PsaC upon rebinding to P700-F_X cores. J Biol Chem 270: 28118–28125

Zanetti G and Merati G (1987) Interaction between photosystem I and ferredoxin. Identification by chemical cross-linking of the polypeptide which binds ferredoxin. Eur J Biochem 169: 143–146

Zhang SP and Scheller HV (2004) Light-harvesting complex II binds to several small subunits of photosystem I. J Biol Chem 279: 3180–3187

Zhao J, Li N, Warren PV, Golbeck JH and Bryant DA (1992) Site-directed conversion of a cysteine to aspartate leads to the assembly of a [3Fe–4S] cluster in PsaC of photosystem I. The photoreduction of F_A is independent of F_B. Biochemistry 31: 5093–5099

Zhao J, Snyder WB, Mühlenhoff U, Rhiel E, Warren PV, Golbeck JH and Bryant DA (1993) Cloning and characterization of the *psaE* gene of the cyanobacterium *Synechococcus* sp. PCC 7002: characterization of a *psaE* mutant and overproduction of the protein in *Escherichia coli*. Mol Microbiol 9: 183–194

Zilber M, Malkin R (1988) Ferredoxin cross-links to a 22 kDa subunit of photosystem I. Plant Physiol 88: 810–814

Zouni A, Jordan R, Schlodder E, Fromme P and Witt H (2000) First photosystem II crystals capable of water oxidation. Biochim Biophys Acta 1457: 103–105

Zouni A, Witt HT, Kern J, Fromme P, Krauß N, Saenger W and Orth P (2001) Crystal structure of photosystem II from *Synechococcus elongatus* at 3.8 Å resolution. Nature 409: 739–743

Chapter 7

Structure, Function, and Regulation of Plant Photosystem I

Nathan Nelson* and Adam Ben-Shem
Department of Biochemistry, The George S. Wise Faculty of Life Sciences, Tel Aviv University, Tel Aviv 69978, Israel

Summary

The recently determined structure of plant photosystem I (PS I) provides the first relatively high-resolution structural model of a supercomplex containing a reaction center and its peripheral antenna. The peripheral antenna of PS I (LHCI) is composed of four gene products (Lhca1–4) that are unique among the chlorophyll a/b binding proteins in their pronounced long-wavelength absorbance and their assembly into dimers. We describe some of the structural features responsible for the unique properties of LHCI and its interaction with the reaction center. The possible architecture of the docking sites for plastocyanin, ferredoxin, ferredoxin:$NADP^+$ reductase, and LHCII are discussed.

I. Introduction

Like all the other protein complexes that carry out oxygenic photosynthesis, PS I is present in cyanobacteria, algae, and plants. Plant PS I is composed of a reaction center (RC) of up to 14 subunits and a membranal antenna complex (LHCI) that captures light and guides its energy to the RC. Plant PS I contains approximately 200 cofactors, and is much larger than its cyanobacterial counterpart (Mullet et al., 1980; Ben-Shem et al., 2003a,b). As was shown by the crystal structures of cyanobacterial (see Fromme and Grotjohann, this volume, Chapter 6) and plant PS I, the bulk of the reaction center is built of two homologous, large subunits (PsaA and PsaB), which harbor most of its pigments and all the cofactors that are involved in light-induced electron transfer from the special chlorophyll pair (P700) to the electron acceptor F_X (Jordan et al., 2001; Ben-Shem et al., 2003b). The structure of plant PS I revealed the interactions between the two loosely coupled subcomplexes of the RC and LHCI (see Croce et al., this volume, Chapter 10). Essentially, plant PS I is not only the first structure of a plant membrane protein that was solved by X-ray crystallography but also it represents the first membrane supercomplex that was solved by this method.

II. Crystal Structure of Plant PS I at 4.4 Å Resolution

A complete PS I isolated from pea seedlings (*Pisum sativum* var. Alaska), was purified in an active form

* Author for correspondence, email: nelson@post.tau.ac.il

Abbreviations: FNR – ferredoxin:$NADP^+$ reductase; LHCI – light-harvesting chlorophyll in PS I; Lhca1, Lhca2, Lhca3, and Lhca4 – the four gene products that comprise LHCI; LHCII – light-harvesting chlorophyll in PS II; PS I – Photosystem I; PS II – Photosystem II; RC – reaction center.

John H. Golbeck (ed): Photosystem I: The Light-Driven Plastocyanin:Ferredoxin Oxidoreductase, 71–77.

and crystallized (Ben-Shem et al., 2003a). We noted several factors that should be considered for successful preparation and crystallization of membranal supercomplexes. They are listed below bearing in mind that no proper control experiments were performed to render them scientifically sound: (1) The variety of pea (*Pisum sativum* var. Alaska) seemed to be important since at least two other varieties did not yield high-quality crystals. (2) The pea seeds had to be germinated under sunlight and grown under controlled conditions of cool-white fluorescent light (90–130 $\mu Em^{-2}s^{-1}$) in a 16 h light, 8 h darkness cycle beneath a cover that still let in some daylight. (3) There was a seasonal effect (perhaps substitution of Lhca1–4 with other Lhca proteins), and only during the autumn and the beginning of the winter were good diffracting crystals obtained. (4) Clean thylakoids (membranes) have to be prepared prior to solubilization by detergents. (5) Negative purification by treatment with low detergent concentrations is very useful. (6) During solubilization, the membrane protein concentration should be kept high and the detergent concentration as low as it is sufficient for solubilizing the specific protein complex. (7) The purification procedure has to be as brief as possible and the protein concentration should be kept high throughout the purification procedure. (8) Use primitive ion exchange columns driven by gravitation and not fast protein liquid chromatography (FPLC) with fancy high-capacity resins. (9) During the purification reduce the detergent concentration as low as possible, provided that it keeps your complex soluble and gets rid of unnecessary material. (10) Finally, try to crystallize your protein with low detergent concentrations such that in the presence of the proteins the level of free detergent is below the critical micelle concentration. (11) Good luck.

By following these rules we obtained PS I crystals that diffracted up to 4 Å at the ESRF beamline ID14-4 and solved the structure to 4.4 Å using heavy atom derivative data sets (Ben-Shem et al., 2003a,b). The cyanobacterial reaction center (Jordan et al., 2001) Cα backbone (without subunits X and M) could be fitted into the MIRAS (Multiple Isomorphous Replacement Anomalous Signal) derived electron density map very well. It required no modification in the membrane section and served as an initial model for the core moiety. The 15 additional transmembrane helices that could be found in the MIRAS map were first modeled by Cα backbone of idealized α-helical geometry and then adjusted to better fit the map. Some secondary structure elements in solvent-exposed regions could also be added to the model, which was then completed by identifying 167 chlorophylls, 3 Fe/S centers, and 2 phylloquinones (per PS I monomer) in the MIRAS map. Sections of somewhat diffuse electron density that are situated within the membrane may correspond to additional eight chlorophylls that are not included in the model (Table 1). Figure 1 shows all the polypeptides and cofactors that were included in the model of plant PS I.

Table 1. Chlorophylls and transmembrane helices in PS I of cyanobacteria and higher plants. About eight potential densities that are likely be of chlorophyll molecules make a total of about 175 chlorophylls molecules in plant PS I

	Cyanobacterial PS I	Plant PS I
Chlorophylls		
Core (reaction center)	96	101
Lhca1–4	–	50
Contacts	–	16
	96	167
	Transmembrane helices	
Subunits		
A	11	11
B	11	11
F	1	1
I	1	1
J	1	1
K	2	2
L	3	3
M	1	–
X	1	–
G	–	2
H	–	1
Lhca1	–	3
Lhca2	–	3
Lhca3	–	3
Lhca4	–	3
	32	45

The model of plant PS I contains four LHCI chlorophyll–proteins (Lhca1–4). In all four LHCI proteins, we were able to trace all transmembrane domains and most of the lumenal exposed regions. Our model of the reaction center moiety (the core) is missing only very few solvent-exposed regions, most notably the stromal loop connecting the two transmembrane helices of PsaK (Ben-Shem et al., 2004a,b). We find an electron density that probably corresponds to this region but cannot make a definite assignment. SDS–PAGE and mass-spectrometer analysis confirm that plant PS I crystals contain four different LHCI proteins, namely Lhca1–4 (Jansson et al., 1996; Croce et al., 2002; Ben-Shem et al., 2003b).

The main difference between cyanobacterial and plant PS I-RC is that the latter is monomeric both *in vitro* and *in vivo* (Scheller et al., 2001). This opens up the possibility for lateral interactions with other membrane proteins in an asymmetric fashion (Ben-Shem et al., 2004a). A view from the stroma of the plant PS I

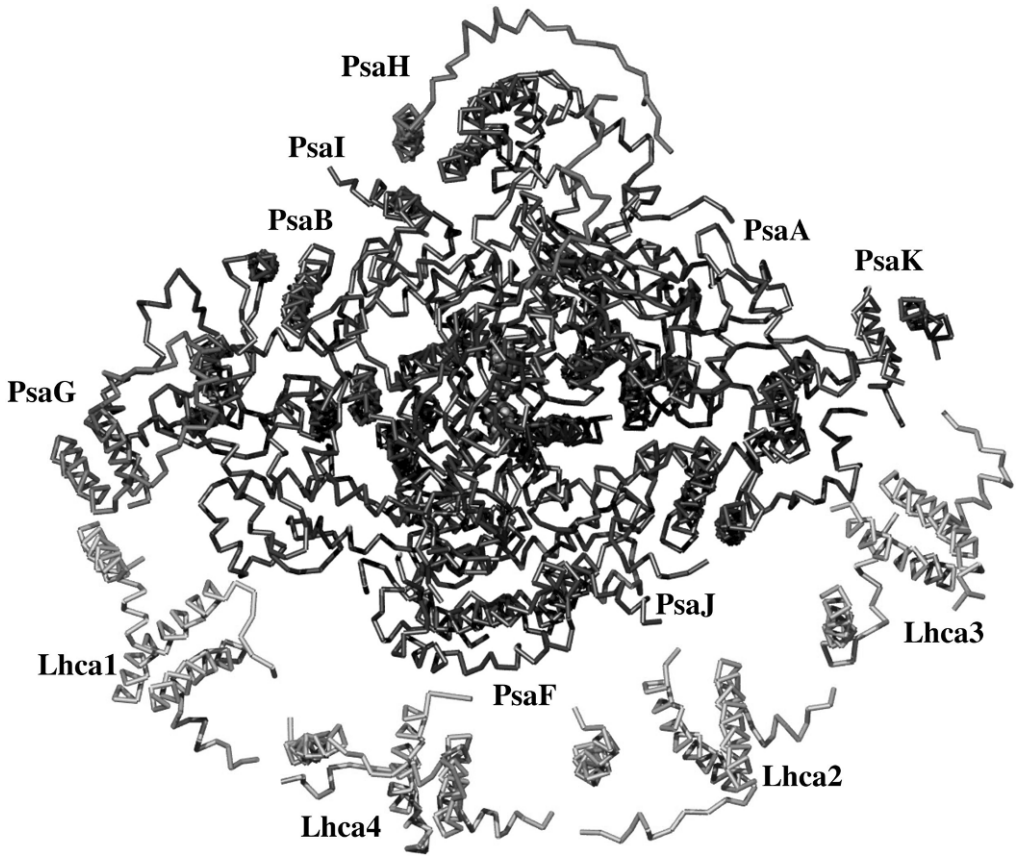

Fig. 1. The Cα backbone model of plant photosystem I at 4.4 Å resolution. See Color Plate 3, Fig. 2.

(Fig. 1) reveals that the RC and LHCI form two distinct and loosely associated moieties, with a deep cleft between them. The four antenna proteins assemble into two dimers, arranged in a series, creating a half-moon shaped belt which docks to the RC's subunit F side. The LHCI belt, with its associated chlorophylls, is the plant's (and green algae's) most prominent addition to PS I structure. The LHCI belt, contributes a mass of 150 kDa out of approximately 525 kDa. LHCI is composed of four nuclear gene products (Lhca1–4), which are 20–24 kDa polypeptides belonging to the LHC family of chlorophyll a/b binding proteins. The archetype of this family and the most abundant membrane protein in nature is the major LHCII protein (Lhcb1) whose structure was elucidated by electron crystallography at 3.4–4.9 Å resolution and recently by X-ray crystallography at 2.7 Å (Kuhlbrandt et al., 1994; Liu et al., 2004).

III. The Core Complex

The core complex (RC) of plant PS I contains approximately 100 chlorophyll molecules (Bengis and Nelson, 1995, 1997). The vast majority of them maintained an almost identical position as in cyanobacterial PS I (Ben-Shem et al., 2003b). The plant RC retains the location and orientation of the electron transfer components and all cyanobacterial transmembrane helices, except those of subunits X and M that are not present in plants. In addition, two RC proteins are exclusively present in plants and green algae (subunits G and H). Subunits G (PsaG) and H (PsaH) are 10 kDa membrane proteins where PsaH contains a single transmembrane helix adjacent to PsaL (Fig. 1). The position and shape of PsaH conforms well to its proposed role as a docking site for LHCII (Lunde et al., 2000). On the opposite side of the RC, PsaG with its two tilting transmembrane helices, contributes most of the contact surface area for association with LHCI (Ben-Shem et al., 2003b). On the lumenal side, the most noticeable distinction between plant and cyanobacterial reaction centers is the helix–loop–helix motif contributed by the longer N-terminus domain of plant PsaF (Fig. 2). This domain enables the more efficient plastocyanin binding in plants and, as a result, two orders of magnitude faster electron transfer from this copper protein to P_{700} (Ben-Shem et al., 2003b).

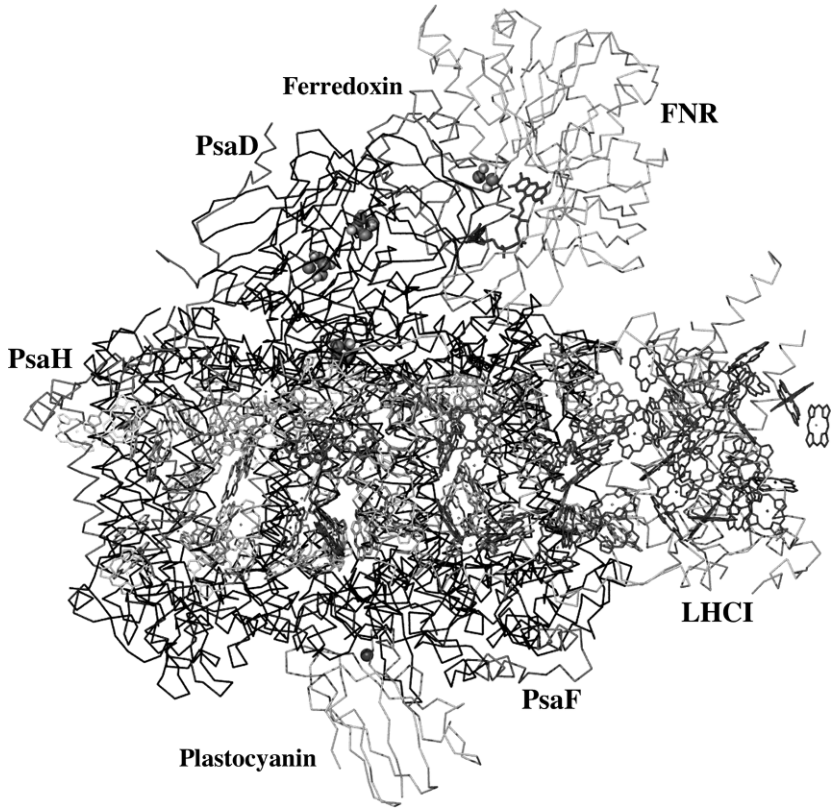

Fig. 2. A model of the side view of putative interactions between plant PS I, plastocyanin and the ferredoxin–FNR complex. See Color Plate 4, Fig. 1.

The two new eukaryotic subunits PsaG and PsaH were probably crucial for the evolution of algae that inhabited the surface of the oceans starting about 1.2 billion years ago and eventually the evolution of plants that settled on land. In addition, modification of PsaL played a role in the advancement toward monomeric PS I (Ben-Shem et al., 2004a). The protruding C-terminus of cyanobacterial PsaL is essential for the PS I trimer formation (Chitnis et al., 1993; Jordan et al., 2001). A forced model of trimeric plant PS I showed that not only this part of PsaL is missing in plants but also that the added subunit H prevents any possibility of forming trimeric structure (Ben-Shem et al., 2004a). Concomitantly with the shortening of PsaL and the emerging of PsaH, PsaK underwent gene duplication to form the eukaryotic PsaK and PsaG (Fig. 1). The new subunit (PsaG) found a binding site on the opposite side of the RC and served as a template for the evolving LHCI complex. Few more slight changes in the eukaryotic RC made it ready for vertical interactions with LHCII and probably also with cytochrome b_6f complex as well as for efficient horizontal interactions with plastocyanin and ferredoxin (Nelson and Ben-Shem, 2004).

Binding of LHCI to the RC is asymmetric, namely much stronger on the G-pole than on the K-pole of the core (Fig. 1). Lhca1 is strongly attached to the core through the helix bundle formed between its transmembrane helix C and the two tilted helices of PsaG, and due to the close interaction of its stromal loop with the novel Loop 1 of PsaB (Fig. 3). The other LHCI proteins interact with the core mainly through small binding surfaces at their stromal exposed regions (Fig. 1). Lhca4 binds to PsaF, Lhca2 associates weakly with PsaJ, and Lhca3 interacts with an unassigned electron density, which is probably attributable to the stromal loop of PsaK (on the lumenal side Lhca3 binds weakly to PsaA).

IV. Light-Harvesting Complex of Higher Plants

Even though the light-harvesting chlorophyll a/b binding proteins that constitute the peripheral antennas

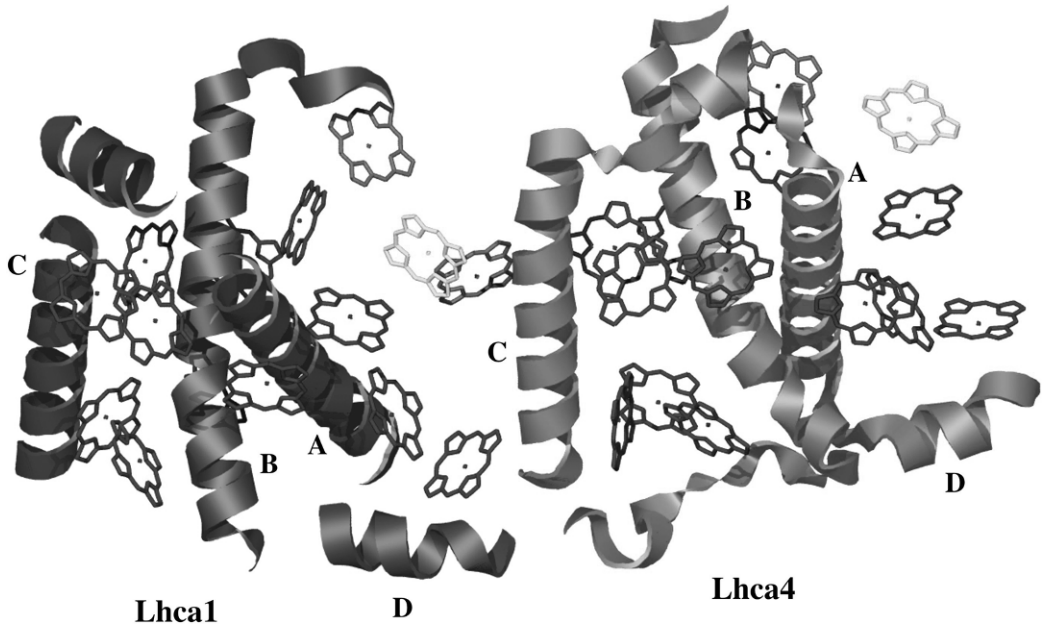

Fig. 3. Dimer formation between Lhca1 and Lhca4. See Color Plate 5, Fig. 1.

of PS I and PS II (LHC) share sequence and structural homology, their oligomeric states vary considerably. Whereas LHCI proteins assemble into dimers, the light-harvesting proteins that associate with PS II form either trimers (LHCII) or monomers as minor antenna members CP24, CP26, and CP29 (Barber, 2002). The recently determined structure of plant PS I and that of LHCII provide a first opportunity to analyze the need for various oligomeric states of antenna proteins in the eukaryotic photosynthetic apparatus (Ben-Shem et al., 2003b; Liu et al., 2004). Both Lhca1–4 and LHCII, bind around 13 chlorophyll a + b molecules each and possess the LHCII general fold (Durnford et al., 1999; Ben-Shem et al., 2003b; Liu et al., 2004). The absorption peak of the "bulk" chlorophylls of LHCI proteins is also shifted to lower energies in comparison with LHCII (Ben-Shem et al., 2003b, 2004b; Morosinotto et al., 2002). Dimerization in LHCI is mediated by relatively small contact surfaces at the luminal side by the C-terminus and at the stromal side the N-terminal domain of the Lhca proteins (Fig. 3; Ben-Shem et al., 2003b). Thus a rather weak head-to-tail assembly is formed that does not involve any interactions within the membrane. A similar mode of association is observed between LHCI dimers. This allows all LHCI proteins to have their wider side turn to the reaction center enabling the maximal number of chlorophylls to face the core (Ben-Shem et al., 2004b). This arrangement results in relatively long distances between the membrane domains of adjacent monomers. Two chlorophylls bridging between monomers facilitate the efficient energy-transfer along the LHCI belt. Originally we regarded these two pigments as "linker chlorophylls" unique to LHCI since they are absent in the electron crystallography model of LHCII (Kuhlbrandt et al., 1994; Ben-Shem et al., 2003b). In view of the recent X-ray crystallography structure of LHCII (Liu et al., 2004), we find that one of them is not unique to LHCI and appear also in LHCII (Fig. 3). This chlorophyll is coordinated by the N-terminus of each LHCI monomer and is probably stabilized by the interactions between LHCI monomers. The second chlorophyll site is indeed unique to LHCI proteins Lhca4 and Lhca3. We do not find this additional chlorophyll in Lhca2 because it is not present between the two heterodimers. The dimeric form stabilizes to some extent the binding of monomers to the reaction center and the interaction between the two heterodimers is also important for Lhca2–3 association with PS I (Ganeteg et al., 2001; Ben-Shem et al., 2004b). A high degree of flexibility may be important for assembling LHCI proteins in its half-moon shape. This may contribute to the efficient energy-transfer along the LHCI belt and between it and the RC. It is remarkable that PS I exhibits a quantum yield of nearly 1 (Trissl and Wilhelm, 1993), and every captured photon is eventually trapped and results in electron translocation.

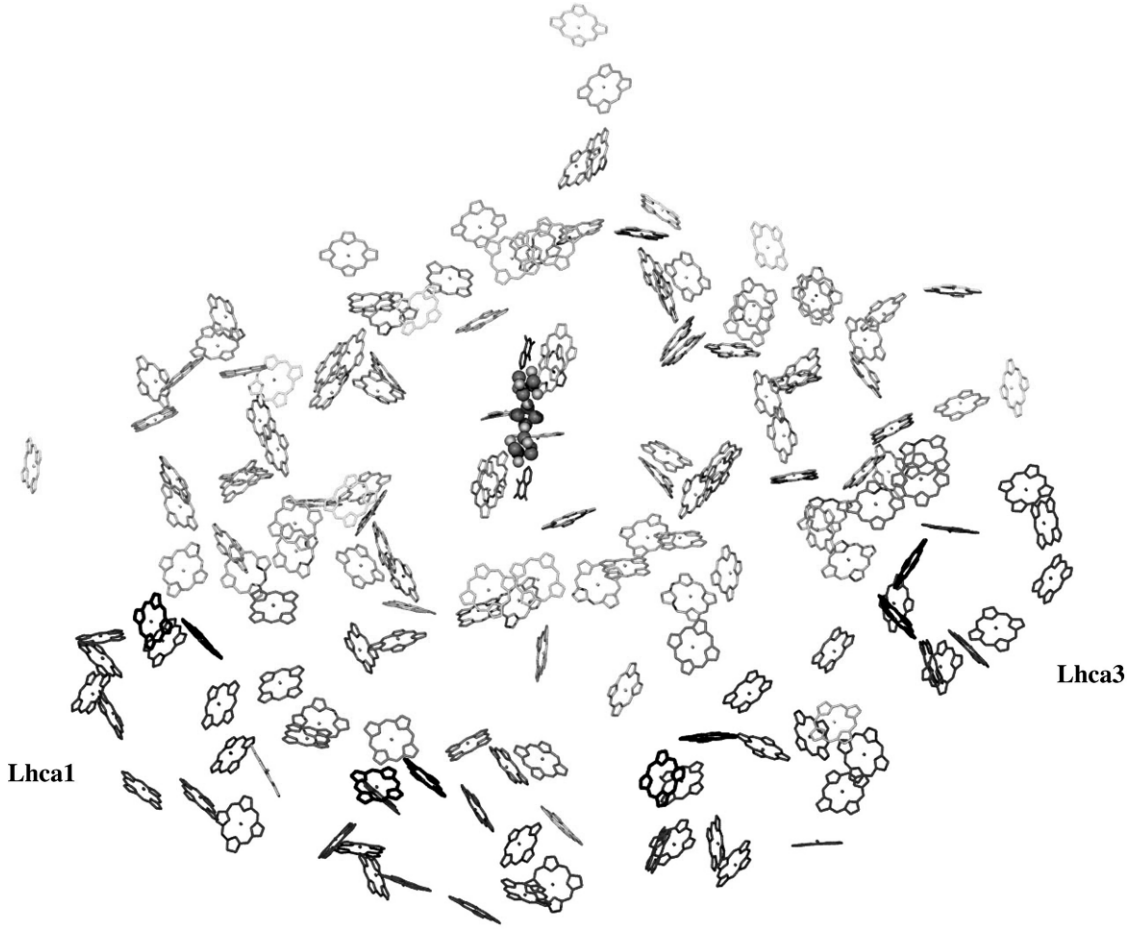

Fig. 4. The arrangement of chlorophyll molecules of plant PS I. See Color Plate 5, Fig. 2.

A top view of chlorophyll arrangement within the plant holo-complex (Fig. 4) reveals that most LHCI chlorophylls are contained within a narrow belt with Mg–Mg distances of 20–30 Å from the nearest RC chlorophyll. However, there are three "contact regions," where much smaller inter-pigment distances (10–15 Å) are observed. The denser "contact regions" are located at the two poles of the LHCI belt near PsaK and PsaG with an additional minor one located at the center of the LHCI belt in the vicinity of PsaF. The half-moon shape of LHCI and the relatively loose and flexible coupling among its monomers may serve two important functions. One would be to get the most efficient light-harvesting and excitation migration. The second is to provide the basis for coping with ever-changing light intensities. Increased light intensities result in sharp decrease in antenna size associated with the vulnerable PS II (Chow et al., 1990; Park et al., 1997). However, such an affect was not observed in LHCI. The composition rather than the size of this peripheral antenna varies with intensity (Bailey et al., 2001). The 4.4 Å resolution model of PS I–LHCI provides the structural basis for understanding how this flexibility is achieved but it does not tell us how it serves the purpose of responding to the different light intensities (Ben-Shem et al., 2003b). Possibly, replacing Lhca2–3 heterodimer with an Lhca3–3 dimer results in longer trapping times, decreased efficiency in energy migration to the RC and dissipation of energy localized on Lhca3 by carotenoids.

Figure 2 depicts a model for the interaction of plant PS I and its electron donor and acceptors. Plastocyanin (Xue et al., 1998) was fitted at the donor side as previously described (Ben-Shem et al., 2003b). The solved structure of the ferredoxin–FNR complex (Kurisu et al., 2001) was fitted at the most likely binding site upon the plant PS I. Crystal structures of supercomplexes of PS I with its electron donor and acceptors will be one of the

future avenues for better understanding the mechanism of oxygenic photosynthesis.

V. Future Studies

The goal of 2 Å resolution in plant PS I that we set up for quenching our curiosity (Nelson and Ben-Shem, 2002) appeared to be much farther in the horizon of what we anticipated. We will happily settle, for the time being, with 3.5 Å resolution that proved to be highly valuable for cyanobacterial PS II (Ferreira et al., 2004). This will allow the precise assignment of all the cofactors that are involved in the structure and function of PS I and the tracing of most of the amino acid side chains. We have to bear in mind that plant PS I is a supercomplex and that the known technology may not be sufficient for achieving the goal of 3.5 Å resolution with this supercomplex. We and others presented structural models for the horizontal interactions between PS I and LHCII or cytochrome b_6f and the vertical interactions with plastocyanin and ferredoxin and/or FNR (Nelson and Ben-Shem, 2004). These models have to be examined by cocrystallization of PS I with soluble and membrane factors that interact with PS I during its activity in oxygenic photosynthesis and cyclic photophosphorylation.

References

Bailey S, Walters RG, Jansson S and Horton P (2001) Acclimation of *Arabidopsis thaliana* to the light environment: the existence of separate low light and high light responses. Planta 213: 794–801

Barber J (2002) Photosystem II: a multisubunit membrane protein that oxidises water. Curr Opin Struct Biol 12: 523–530

Bengis C and Nelson N (l975) Purification and properties of the photosystem I reaction center from chloroplasts. J Biol Chem 250: 2783–2788

Bengis C and Nelson N (l977) Subunit structure of chloroplast photosystem I reaction center. J Biol Chem 252: 4564–4569

Ben-Shem A, Nelson N and Frolow F (2003a) Crystallization and initial X-ray diffraction studies of higher plant photosystem I. Acta Crystallogr D 59: 1824–1827

Ben-Shem A, Frolow F and Nelson N (2003b) The crystal structure of plant photosystem I. Nature 426: 630–635

Ben-Shem A, Frolow F and Nelson N (2004a) Evolution of Photosystem I – from symmetry through pseudosymmetry to asymmetry. FEBS Lett 564: 274–280

Ben-Shem A, Frolow F and Nelson N (2004b) Light-harvesting features revealed by the structure of plant photosystem I. Photosynth Res 81: 239–250

Chitnis VP, Xu Q, Yu L, Golbeck JH, Nakamoto H, Xie DL and Chitnis PR (1993) Targeted inactivation of the gene *psaL* encoding a subunit of photosystem I of the cyanobacterium *Synechocystis* sp. PCC 6803. J Biol Chem 268: 11678–11684

Chow WS, Melis A and Anderson JM (1990) Adjustments of photosystem stoichiometry in chloroplasts improve the quantum efficiency of photosynthesis. Proc Natl Acad Sci USA 87: 7502–7506

Croce R, Morosinotto T, Castelletti S, Breton J and Bassi R (2002) The Lhca antenna complexes of higher plants photosystem I. Biochim Biophys Acta 1556: 29–40

Durnford DG, Deane JA, Tan S, McFadden GI, Gantt E and Green BR (1999) A phylogenetic assessment of the eukaryotic light-harvesting antenna proteins, with implications for plastid evolution. J Mol Evol 48: 59–68

Ferreira KN, Iverson TM, Maghlaoui K, Barber J and Iwata S (2004) Architecture of the photosynthetic oxygen-evolving center. Science 303: 1831–1838

Ganeteg U, Strand A, Gustafsson P and Jansson S (2001) The properties of the chlorophyll a/b-binding proteins Lhca2 and Lhca3 studied *in vivo* using antisense inhibition. Plant Physiol 127: 150–158

Jansson S, Andersen B and Scheller HV (1996) Nearest-neighbor analysis of higher-plant photosystem I holocomplex. Plant Physiol 112: 409–420

Jordan P, Fromme P, Witt HT, Klukas O, Saenger W and Krauß N (2001) Three-dimensional structure of cyanobacterial photosystem I at 2.5 Å resolution. Nature 411: 909–917

Kuhlbrandt W, Wang DN and Fujiyoshi Y (1994) Atomic model of plant light-harvesting complex by electron crystallography. Nature 367: 614–621

Kurisu G, Kusunoki M, Katoh E, Yamazaki T, Teshima K, Onda Y, Kimata-Ariga Y and Hase T (2001) Structure of the electron transfer complex between ferredoxin and ferredoxin-NADP(+) reductase. Nat Struct Biol 8: 117–121

Liu Z, Yan H, Wang K, Kuang T, Zhang J, Gui L, An X and Chang W (2004) Crystal structure of spinach major light-harvesting complex at 2.2 Å resolution. Nature 428: 287–292

Lunde CP, Jensen PE, Haldrup A, Knoetzel J and Scheller HV (2000) The PS I-H subunit of photosystem I is essential for state transitions in plant photosynthesis. Nature 408: 613–615

Morosinotto T, Castelletti S, Breton J, Bassi R and Croce R (2002) Mutation analysis of Lhca1 antenna complex low energy absorption forms originate from pigment–pigment interactions. J Biol Chem 277: 36253–36261

Mullet JE, Burke JJ and Arntzen CJ (1980) Chlorophyll proteins of photosystem I. Plant Physiol 65: 814–822

Nelson N and Ben-Shem A (2002) Photosystem I reaction center: past and future. Photosynth Res 73: 193–206

Nelson N and Ben-Shem A (2004) The complex architecture of oxygenic photosynthesis. Nat Rev Mol Cell Biol 6, 818–818

Park Y, Chow WS and Anderson JM (1997) Antenna size dependency of photoinactivation of photosystem II in light-acclimated pea leaves. Plant Physiol 115: 151–157

Scheller HV, Jensen PE, Haldrup A, Lunde C and Knoetzel J (2001) Role of subunits in eukaryotic Photosystem I. Biochim Biophys Acta 1507: 41–60

Trissl H-W and Wilhelm C (1993) Why do thylakoid membranes from higher plants form grana stacks? Trends Biochem Sci 18: 415–419

Xue Y, Okvist M, Hansson O and Young S (1998) Crystal structure of spinach plastocyanin at 1.7 Å resolution. Protein Sci 7: 2099–2105

Chapter 8

Molecular Interactions of the Stromal Subunit PsaC with the PsaA/PsaB Heterodimer

Mikhail L. Antonkine*
Max-Planck-Institut für Bioanorganische Chemie, Stiftstr. 34-36, Mülheim an der Ruhr D-45470, Germany; Institut für Experimentalphysik, Freie Universität Berlin, Arnimallee 14, D-14195 Berlin, Germany; On leave from the Photochemistry Center of the Russian Academy of Sciences, Novatorov St. 7a, 117421 Moscow, Russia

John H. Golbeck
Department of Biochemistry and Molecular Biology, Department of Chemistry, The Pennsylvania State University, University Park, PA 16802, USA

Summary

The X-ray crystal structure of cyanobacterial Photosystem I (PS I) has been solved to atomic resolution (PDB entry 1JB0). It provides a structural model for the subunits PsaC, PsaD, and PsaE that comprise the stromal ridge of PS I. Independently, the three-dimensional solution structures of unbound, recombinant PsaC (PDB entry 1K0T) and PsaE (PDB entries 1PSF, 1QP2, and 1GXI) have been solved using NMR spectroscopy. Unbound, recombinant PsaD was also studied by NMR; in solution it contains only a few elements of secondary structure and no

* Author for correspondence, email: antonkin@physik.fu-berlin.de

John H. Golbeck (ed): Photosystem I: The Light-Driven Plastocyanin:Ferredoxin Oxidoreductase, 79–98.

stable three-dimensional structure. The availability of structural information on the unbound and bound forms of all three stromal ridge proteins has allowed a scenario to be envisioned for the assembly of the stromal ridge of PS I. The key step in the assembly of all three stromal ridge proteins is the binding of PsaC onto the PsaA/PsaB heterodimer. Details of the three-dimensional structures of unbound PsaC, bacterial dicluster ferredoxins, and PS I-bound PsaC are compared and contrasted. This is followed by a discussion of the ionic and hydrogen bond interactions between PsaC and the PsaA/PsaB heterodimer in the fully assembled PS I complex. C_2-symmetry in the binding of PsaC to the PS I core is discussed, and a mechanism is proposed of how the ambiguity in binding is resolved in nature. The assembly of PsaC onto the PsaA/PsaB heterodimer, which is accompanied by altered properties of the PsaC-bound [4Fe–4S] clusters F_A and F_B, can serve as a model for the assembly of other multicofactor, multisubunit membrane-protein complexes.

I. Overview of the Stromal Subunits

Photosystem I (PS I) is an obligatory component of the photosynthetic electron transfer chain in all oxygen-evolving organisms. The X-ray crystal structure of cyanobacterial PS I has been solved to a resolution of 2.5 Å (Jordan et al., 2001; see also Fromme and Grotjohann, this volume, Chapter 6), and the X-ray crystal structure of plant PS I is available at a resolution of 4.4 Å (Ben-Shem et al., 2003; see also Nelson and Ben-Shem, this volume, Chapter 7). PsaC, PsaD, and PsaE are termed the "stromal ridge proteins" of PS I (Fig. 1); their masses are: 9.3, 15.2, and 8 kDa, respectively. The PsaC subunit binds two [4Fe–4S] clusters F_A and F_B, making it one of three PS I subunits that binds electron transfer cofactors. F_A and F_B are indispensable components of the electron transfer chain in PS I. Spectroscopic studies have shown that F_A is the cofactor that accepts an electron from F_X, and F_B is the cofactor that donates an electron to soluble ferredoxin on the stromal side of the membrane (Jung et al., 1995; Diaz-Quintana et al., 1998; Mamedov et al., 1998; Vassiliev et al., 1998; Lakshmi et al., 1999; Shinkarev et al., 2000; reviewed in Vassiliev et al., 2001). The linear arrangement of $F_X \rightarrow F_A \rightarrow F_B$ is supported by the X-ray crystallographic structure of cyanobacterial PS I (Jordan et al., 2001).

Abbreviations: EPR – electron paramagnetic resonance; F_A – [4Fe–4S] cluster bound by cysteines 20, 47, 50, and 53 of the PsaC subunit of Photosystem I, equivalent to cluster 2 in bacterial ferredoxins containing two [4Fe–4S] clusters; F_B – [4Fe–4S] cluster bound by cysteines 10, 13, 16, and 57 of the PsaC subunit of Photosystem I, equivalent to cluster 1 in bacterial ferredoxins containing two [4Fe–4S] clusters; F_X – interpolypeptide [4Fe–4S] cluster bound to the PsaA and PsaB subunits of Photosystem I; NMR – nuclear magnetic resonance; NOE – nuclear Overhauser effect; P700 – primary electron donor of Photosystem I; P700-F_X core – PS I preparation in which stromal polypeptides PsaC, PsaD, and PsaE, together with [4Fe–4S] clusters F_A and F_B, have been removed and the final electron acceptor is the [4Fe–4S] cluster F_X; PS I – Photosystem I.

II. Prerequisites for an Investigation of the Assembly of the Stromal Ridge Proteins

In the late 1980s, a method was developed for removing the stromal ridge proteins by treating isolated PS I complexes with chaotropic agents such as 6.8 M urea or 2 M sodium iodide (Golbeck et al., 1988; Parrett et al., 1989; Li et al., 1991b). Shortly thereafter, it was found that the [4Fe–4S] clusters F_A and F_B could be re-inserted into apo-PsaC by procedure similar to that used for reconstitution of iron–sulfur clusters into soluble ferredoxins (Lovenberg et al., 1963; Mehari et al., 1991). This procedure involves incubation of the apo-protein with excess of iron salt and sodium sulfide in the presence of 2-mercaptoethanol, which functions both as a reductant and as a transiently-bound ligand. Reconstituted PsaC rebinds to P700-F_X cores without the involvement of chaperons or the expenditure of ATP (Mehari et al., 1991). However, the EPR linewidths of F_A and F_B remain broadened, and little or no ferredoxin can be reduced by the reconstituted P700-F_X/PsaC complex in the light. We refer to the complex between PsaC and P700-F_X cores as a P700-F_X/PsaC or PsaC(only) core. The stable binding of PsaC to PS I depends on the presence of PsaD (Zhao et al., 1990; Li et al., 1991a). PsaD, however, can be rebound to P700-F_X cores only after PsaC is bound. In the presence of both PsaC and PsaD, the wild-type EPR spectra of F_A and F_B are restored and the reconstituted PS I complex regains the ability to photoreduce ferredoxin. PsaE can also be rebound to P700-F_X/PsaC cores, but the magnetic properties of F_A and F_B remain unchanged in the absence of PsaD, and the reconstituted PS I lacks the ability to photoreduce ferredoxin (J. H. Golbeck, unpublished results).

In the 1990s, mutants of the stromal ridge proteins were constructed in cyanobacteria, allowing study of PS I cores from *psaC* (Yu et al., 1995), *psaD* (Chitnis et al., 1996), and *psaE* deletion strains (Rousseau et al., 1993; Zhao et al., 1993). Deletion of the *psaC* gene

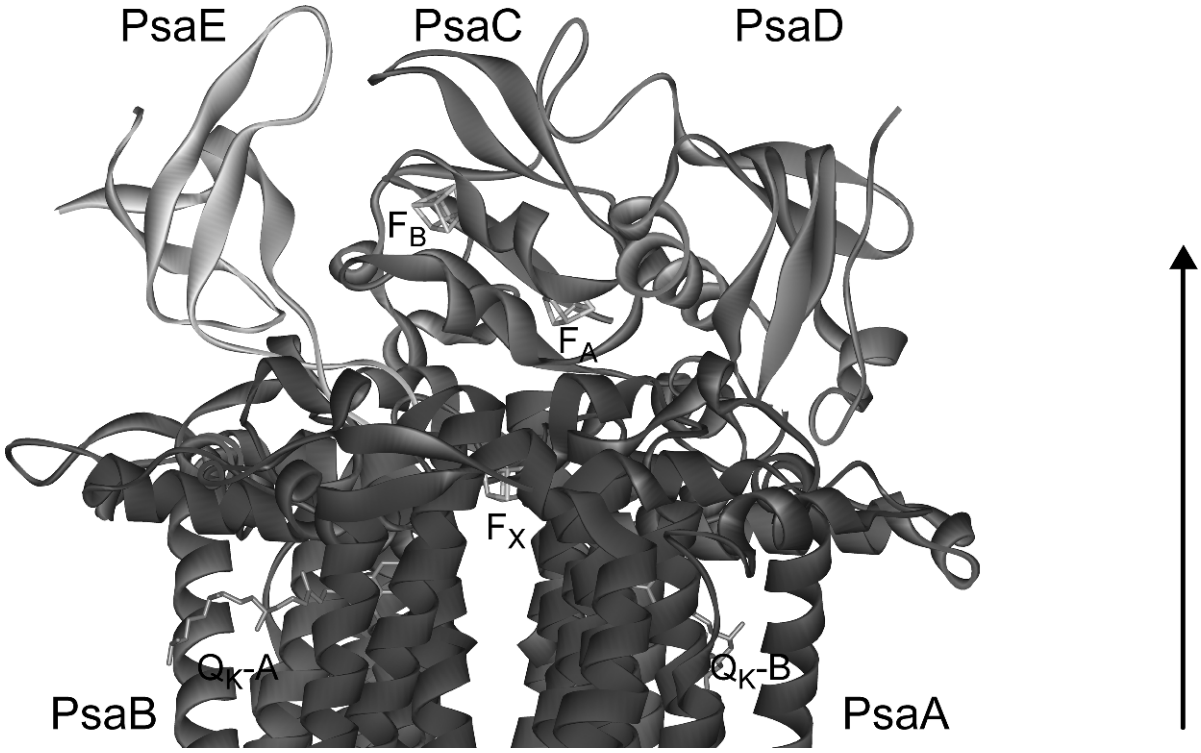

Fig. 1. The X-ray structure of cyanobacterial PS I at 2.5 Å resolution. Detail of the structural model of the PS I monomer (PDB entry 1JB0) (Jordan et al., 2001). See Color Plate 6, Fig. 1.

results in a PS I core similar to a P700-F_X core prepared chemically *in vitro*. Thus, PsaC, along with the [4Fe–4S] clusters, F_A and F_B, and the PsaD and PsaE subunits (Yu et al., 1995) are missing from these PS I cores. The interpolypetide [4Fe–4S] cluster F_X was not affected by the loss of the stromal ridge proteins, and its function as an electron acceptor was retained as shown by low-temperature EPR spectroscopy and room temperature optical kinetic spectroscopy. Deletion of the *psaD* gene (Chitnis et al., 1996) results in a PS I core similar to a P700-F_X/PsaC/PsaE core prepared *in vitro*. Thus, only PsaD is absent in the *psaD* deletion strain. The magnetic properties of F_A and F_B in PS I cores isolated from the *psaD* deletion strain are similar to those of the *in vitro* reconstituted P700-F_X/PsaC/PsaE cores (Li et al., 1991a; Chitnis et al., 1996). Notably, PsaE cannot substitute for PsaD in the *psaD* deletion strain in conferring wild-type magnetic properties to F_A and F_B (Chitnis et al., 1996). The steady-state rates of ferredoxin reduction remain negligible in PS I cores isolated from the *psaD* deletion strain (Xu et al., 1994), and the reduction of ferredoxin by PS I in a single-turnover flash is inefficient (Sétif, 2001). In short, both *in vivo* and *in vitro* studies show that PsaD is necessary to restore the wild-type properties of the PsaC-bound [4Fe–4S] clusters F_A and F_B. Deletion of the *psaE* gene results in a PS I core similar to the reconstituted P700-F_X/PsaC/PsaD core prepared *in vitro*. Thus, only PsaE is absent in the *psaE* deletion strain. The magnetic properties of F_A and F_B in PS I cores isolated from the *psaE* deletion strain are indistinguishable from the wild-type. Thus, PsaE cannot be responsible for conferring wild-type magnetic properties of F_A and F_B (Li et al., 1991a; Chitnis et al., 1996). Deletion mutants of *psaE* in cyanobacteria are characterized by lower growth rates in low light and near wild-type growth rates in high light (Zhao et al., 1993), and are associated with a reduced efficiency for reduction of ferredoxin by PS I assayed on a single-turnover flash (Sétif, 2001). Thus in the absence of PsaE, ferredoxin binding and/or reduction is diminished, but not so much as to affect viability of the organism at high light intensities.

The availability of recombinant PsaC, PsaD, and PsaE *via* an efficient overproduction system in *Escherichia coli* allowed the large-scale production and selective isotopic labeling of all three proteins. *In vitro* studies showed that recombinant PsaC, PsaD, and PsaE proteins are equivalent to natively-isolated proteins in re-establishing a functional PS I *via* reconstitution

Table 1. Summary of available experimental facts regarding the intermediate assembly steps of PS I core complexes. (Reprinted from Antonkine et al., 2003; Table 2. © 2003, with permission from Elsevier.)

	Three-dimensional structure available		Complex formation established	
Core abbreviation	NMR	X-Ray	*in vitro*	*in vivo*
P700-F_X/PsaC *or* PsaC(only)	–	–	Yes	–
P700-F_X/PsaC/PsaE	–	–	Yes	PsaD-less
P700-F_X/PsaC/PsaD	–	–	Yes	PsaE-less
P700-F_X/PsaC/PsaD/PsaE *or* PsaC(PS I)	–	Yes	Yes	wild-type
Isolated subunit PsaC(free)	Yes	Structures of related ferredoxins containing two [4Fe–4S] clusters	PsaC/PsaD; PsaC/PsaE; PsaD/PsaE or PsaC/PsaD/PsaE subunit precomplexes not reported thus far	
Isolated subunit PsaD(free)	Natively unfolded Protein	–		
Isolated subunit PsaE(free)	Yes	–		

experiments (Zhao et al., 1990; Li et al., 1991a). These developments allowed investigation of the three-dimensional solution structures of all three stromal ridge proteins by NMR (Falzone et al., 1994; Xia et al., 1998; Mayer et al., 1999; Antonkine et al., 2002; Barth et al., 2002) at or around the same time the structure of the fully-assembled cyanobacterial PS I became available by X-ray crystallography (Fromme et al., 2001; Jordan et al., 2001; Saenger et al., 2002). A detailed comparison of the structures of the unbound and bound proteins provided key information for our understanding of the assembly of the stromal subunits of PS I and the fine tuning of the magnetic properties of the [4Fe–4S] clusters F_A and F_B (Antonkine et al., 2003).

In hindsight, several prerequisites must be in-place for a successful investigation of the assembly and molecular interactions of PsaC, PsaD, and PsaE with PS I: first, the ability to remove and to rebind all three stromal ridge proteins *in vitro*; second, the availability of deletion mutant strains of all three proteins, which provided the first clues for an assembly sequence; third, the availability of the overexpression system in *E. coli* for the three proteins, which allowed production in large quantities necessary for the structural studies; fourth, investigation of the solution structure of all three stromal proteins by NMR in the unbound form; and fifth, the availability of a high-resolution X-ray structure of PS I.

On the basis of available experimental evidence, three assembly stages of stromal subunits of PS I can be deduced: PsaC(free), PsaC(only), PsaC(PS I) (Antonkine et al., 2003). The biochemical and structural information regarding different stages of PS I assembly is summarized in Table 1. Because the binding of PsaC is a decisive step in the assembly of stromal ridge proteins of PS I, in the following sections we will focus on the changes in the three-dimensional structure of PsaC upon binding to PS I and on the interprotein interactions that determine specificity of PsaC binding to PS I. For more details of the interactions of PsaD and PsaE with PsaA/PsaB/PsaC core and with each other see (Antonkine et al., 2003).

III. PsaC

A. The Amino Acid Sequence of PsaC

The amino acid sequences of plant and cyanobacterial PsaC are nearly identical within each class and are strikingly similar between each class (Golbeck and Bryant, 1991). A lesser degree of similarity is found between PsaC and small, dicluster bacterial ferredoxins. Here, the similarity is largely restricted to the iron–sulfur binding motifs and their immediate proximity (Fig. 2). Both PsaC and dicluster ferredoxins contain two [4Fe–4S] cluster binding motifs consisting of the consensus sequence C(I)xxC(II)xxC(III)xxxC(IV)P, where C is cysteine, P is proline, and x are other noncysteine amino acids. Cysteines I, II, and III of the first binding site ligate the first [4Fe–4S] cluster, while cysteine IV of the first binding site ligates the second [4Fe–4S] cluster; cysteines I′, II′, and III′ of the second binding site ligate the second [4Fe–4S] cluster, while cysteine IV′ of the second binding site ligates the first [4Fe–4S] cluster. The distance between the two [4Fe–4S] clusters is predetermined by the distance between Cys(III/III′) and Cys(IV/IV′) in the binding sites

```
                        10  13 16  20                          47 50 53  57
C. acidi urici  --AYVINEACISCGACEPECPVNAIS--------SGDDRYVIDADTCIDCGACAGVCPVD
C. pasteurianum --AYKIADSCVSCGACASECPVNAIS--------QGDSIFVIDADTCIDCGNCANVCPVG
P. aerogenes    --AYVINDSCIACGACKPECPVNIQ---------QG-SIYAIDADSCIDCGSCASVCPVG
Synechococcus   SHSVKIYDTCIGCTQCVRACPLDVLEMVPWDGCKAGQIASSPRTEDCVGCKRCETACPTD
                  .  * ..*. *  *   **.             *       .. *. *  *   **

C. acidi urici  APVQA---------------
C. pasteurianum APVQE---------------
P. aerogenes    APNPED--------------
Synechococcus   FLSIRVYLGAETTRSMGLAY
```

Fig. 2. Sequence alignment of PsaC from *Synechococcus* sp. PCC 7002 and dicluster bacterial ferredoxins from *Clostridium pasteurianum*, *Clostridium acidi urici*, and *Peptococcus aerogenes*. The cysteines that coordinate the [4Fe–4S] clusters are indicated by bold underlined letters and their numbers in the sequence of PsaC from *Synechococcus* sp. PCC 7002 are shown at the top. The sequences were aligned with CLUSTALW (1.60). Conserved amino acids are indicated by an asterisk, conservative substitutions by a dot. (Reprinted from Antonkine et al., 2000; Fig. 1. © 2000, with permission from Springer.)

because they are separated by a rigid one-turn *a*-helix and they always ligate different [4Fe–4S] clusters. Through site-directed mutagenesis studies of PsaC, it has been shown that in cysteines 10, 13, 16, and 57 ligate F_B and cysteines 47, 50, 53, and 20 ligate F_A (Zhao et al., 1992; reviewed in Golbeck, 1999). The numbering of the PsaC sequence in this review corresponds to that used in the NMR structure of the protein (Antonkine et al., 2002) and in the crystal structure of PS I (Jordan et al., 2001); it assumes that the N-terminal methionine has been cleaved.

B. Bacterial Dicluster Ferredoxins as a Models for the Structure of PsaC

1. Similarities Between Bacterial Dicluster Ferredoxins and PsaC

Several high-resolution X-ray and NMR structures are available for the bacterial dicluster ferredoxins [PDB entries 1FDX (now replaced with 1DUR), 1CLF, 1FDN, 2FDN, 1BLU, 1FCA, 5FD1, 1BC6, 1BQX, 1RGV] (Adman et al., 1973, 1976; Stout, 1993; Duee et al., 1994; Bertini et al., 1995; Tranqui and Jesior, 1995; Moulis et al., 1996; Dauter et al., 1997; Aono et al., 1998a,b; Unciuleac et al., 2004; see also reviews Sticht and Rosch, 1998; Bentrop et al., 2001). A comparison of the NMR and X-ray structures of these ferredoxins shows that the structural details change very little between the solution and crystal phases. The two-stranded antiparallel β-sheet arrangement of N- and C-termini and the two [4Fe–4S] clusters separated by a single α-helical turn are typical features of all bacterial dicluster ferredoxins known thus far. In PsaC and bacterial dicluster ferredoxins, both [4Fe–4S] cluster binding motifs and the clusters themselves exhibit a local pseudo-C_2-symmetry. These central structural features are common to all dicluster ferredoxins characterized thus far and have proven to be a good structural model for the iron–sulfur core of PsaC.

The presumed structural similarity between the environment of the [4Fe–4S] clusters in PsaC and the environment of the [4Fe–4S] clusters in bacterial ferredoxins was used in the interpretation of NMR resonances derived from the cysteines that ligate F_A and F_B in the reduced and oxidized states (Bentrop et al., 1997; Antonkine et al., 2000). To illustrate how close is this similarity let us consider details of the investigation of reduced PsaC (Antonkine et al., 2000). The aim of the study was to determine the preferential position of the mixed-valence and equal-valence pairs of the reduced [4Fe–4S] clusters F_A and F_B. They can be inferred by ^{1}H NMR investigation from a study of the temperature dependence of the contact-shifted resonances of the protons belonging to the cysteines that ligate the [4Fe–4S] clusters. For this, a sequence-specific assignment of the NMR resonances of the βCH_2 protons ligating the iron–sulfur clusters is required. Assignment transfer from the oxidized to the reduced state by the usual method of saturation transfer *via* intermediate reduction states turned out to be not possible in PsaC due to the fast electron exchange between iron–sulfur clusters F_A and F_B. As a consequence, the oxidized and two-electron reduced protein had to be studied

independently (Bentrop et al., 1997; Antonkine et al., 2000). The ^{1}H NMR spectra of reduced, unbound PsaC was recorded and an unique assignment of all 18 observable hyperfine-shifted signals was obtained through a *de novo* 1D NOE analysis (Antonkine et al., 2000). The resonances from three of the four cysteines ligating each of the two reduced [4Fe–4S] clusters were assigned sequence-specifically.

The key to the assignment of the contact-shifted NMR signals of PsaC was the NOE between protons of cysteines III and III′ in two consensus iron–sulfur binding sites that ligate either F_B and F_A clusters respectively (Antonkine et al., 2000). Similar intercluster NOE is present in all dicluster ferredoxins studied by NMR thus far. Other structural arguments based on the sequence similarity between PsaC and dicluster ferredoxins were also used, such as the relative orientation of Hα and HN protons of cysteines I(I′) and IV(IV′) with respect to the [4Fe–4S] cluster(s).

The preferential localization of mixed-valence and equal-valence pairs in F_A^- and F_B^- was obtained from these measurements. It was shown that equal- and mixed-valence pairs are ligated by homologous cysteines of the consensus iron–sulfur-binding site in PsaC and dicluster ferredoxins. Regarding F_B^- the mixed-valence pair is ligated by cysteines 10(I) and 16(III), and the equal-valence pair is ligated by cysteines 13(II) and 57(IV′). Regarding F_A^-, the mixed-valence pair is ligated by cysteines 47(I′) and 53(III′), and the equal-valence pair is ligated by cysteines 20(IV) and 50(II′) (Antonkine et al., 2000). These studies showed that the ferredoxin structures are good models for the structure of the iron–sulfur core of PsaC [PDB entries 1FDX (now replaced with 1DUR), 1CLF, 1FDN, 2FDN, 1BLU, 1FCA, 5FD1, 1BC6, 1BQX, 1RGV] (Adman et al., 1973, 1976; Stout, 1993; Duee et al., 1994; Bertini et al., 1995; Tranqui and Jesior, 1995; Moulis et al., 1996; Dauter et al., 1997; Aono et al., 1998a,b; Unciuleac et al., 2004; see also reviews Sticht and Rosch, 1998; Bentrop et al., 2001). The structural similarity between the iron–sulfur core of PsaC and dicluster ferredoxins has been confirmed by the structure of PS I-bound PsaC in the X-ray crystal structure of PS I (Klukas et al., 1999; Jordan et al., 2001) and of unbound PsaC in solution (Figs. 1, 4, 6; Antonkine et al., 2002; see section III.C).

2. Differences Between Bacterial Dicluster Ferredoxins and PsaC

The amino acid sequence of PsaC differs from bacterial dicluster ferredoxins in three regions, a minor extension of the N-terminus (2 residues), an insertion of 8 residues in the middle of the loop connecting the two consensus iron–sulfur binding motifs, and a C-terminal extension of 14 or 15 residues (Fig. 2). However, the amino acid sequence pre-C-terminus of PsaC is quite different from amino acid sequence C-terminus of bacterial dicluster ferredoxins.

The logical assumption is that differences in the amino acid composition of PsaC and bacterial dicluster ferredoxins owe their origin to function. While this is generally correct, an interesting case is the ferredoxin from *Thauera aromatica*, which is exactly the same size as PsaC (80 amino acids) (PDB entry 1RGV) (Unciuleac et al., 2004). Similar to PsaC it has a sequence insertion between the two consensus [4Fe–4S] cluster sites and a sequence extension at the C-terminus. A structural comparison between this dicluster ferredoxin and PsaC in unbound and PS I-bound forms will be discussed below (see section III.C). Note, however, that this ferredoxin is not involved in photosynthetic electron transfer.

The amino acids in the loop insertion region of PsaC are considered to be involved in ferredoxin/flavodoxin binding (Fischer et al., 1998, 1999) and those in the C-terminus in binding of PsaC to the PsaA/PsaB core and to other stromal subunits. As will be discussed below (section V.B) the N- and C-termini of PsaC play a key role in the specific interactions between PsaC and the PsaA/PsaB heterodimer (Jordan et al., 2001; Antonkine et al., 2003). Another significant sequence difference concerns the F_A-binding site, which has an increased number of charged amino acids as compared to the binding sites of [4Fe–4S] clusters in bacterial ferredoxins or to the F_B-binding site. These amino acids are well conserved in all PsaC sequences available thus far (Golbeck, 1994), which emphasizes their significance. They form salt bridges with the PsaA/PsaB heterodimer of PS I (Antonkine et al., 2003); this key feature of the F_A-binding site will be discussed below (section V).

C. The Structure of Unbound PsaC in Solution; Comparison with the Structure of PS I-Bound PsaC and Structures of Bacterial Dicluster Ferredoxins

Given the different magnetic properties of F_A and F_B between unbound and PS I-bound PsaC (Li et al., 1991a; reviewed in Vassiliev et al., 2001), significant differences were anticipated between the unbound and PS I-bound structures of PsaC. Thus far, PsaC is one of the few membrane-associated proteins to be

studied in both the bound and unbound states. Determination of NMR solution structure of protein that contain iron–sulfur clusters, such as PsaC or a bacterial dicluster ferredoxin, presents a particular challenge. The ground state of an oxidized low-potential [4Fe–4S] cluster ($[4Fe–4S]^{2+}$) is diamagnetic; however, at room temperature excited paramagnetic states are partially populated and certain paramagnetic character therefore comes about. In such a small protein nearly all parts are affected by this paramagnetism.

The NMR solution structure of oxidized unbound PsaC (PDB entry 1K0T) (Antonkine et al., 2002) is shown in Figs. 3 and 4A, and the X-ray structure of PsaC solved as a part of the overall X-ray structure of PS I is shown in Figs. 4B and 5 (PDB entry 1JB0) (Jordan et al., 2001). Individual structural elements of unbound PsaC are shown in Fig. 3B–E and discussed below. Details of the NMR solution structure of PsaC are compared to the X-ray structure of PS I-bound PsaC (Fig. 4) and to NMR and X-ray structures of bacterial dicluster ferredoxins [PDB entries 1FDX (now replaced with 1DUR), 1CLF, 1FDN, 2FDN, 1BLU, 1FCA, 5FD1, 1BC6, 1BQX, 1RGV] (Adman et al., 1973, 1976; Stout, 1993; Duee et al., 1994; Bertini et al., 1995; Tranqui and Jesior, 1995; Moulis et al., 1996; Dauter et al., 1997; Aono et al., 1998a,b; Unciuleac et al., 2004; see also reviews Sticht and Rosch, 1998; Bentrop et al., 2001).

For simplicity of presentation PsaC is separated into five structural sub-domains. Each is shown in Fig. 3: the iron–sulfur core of the protein (Fig. 3B); the PsaC-specific sequence insertion (Fig. 3C); the N- and pre-C-termini, which have unusual orientations with respect to each other (Fig. 3D); and the C-terminus, which assumes a helical structure in solution (Fig. 3E).

Figure 3B shows the [4Fe–4S] clusters F_A and F_B and the backbone of amino acids belonging to respective iron–sulfur cluster binding sites on PsaC. As predicted from sequence similarity (see section III.B.1) the iron–sulfur core of PsaC is very similar to bacterial dicluster ferredoxins. Both the F_A- and F_B-binding site have a fold typical of iron–sulfur cluster binding sites in bacterial dicluster ferredoxins. Each of the two sites is followed by a single α-helical turn, with the fourth cysteine of the consensus iron–sulfur binding site ligating the other cluster. This feature of PsaC assures a fixed distance between cluster 1 (F_B) and cluster 2 (F_A). Within the accuracy of the determination, the overall structure of the iron–sulfur core of PsaC is identical in unbound (PDB entry 1K0T) (Antonkine et al., 2002) and in PS I-bound forms (1JB0) (Fig. 4; Jordan et al., 2001).

In the NMR solution structure of PsaC a larger disorder is found for the polypeptide chain surrounding the binding motif of F_A, which results in a significant deviation in the position of the [4Fe–4S] cluster itself within the final family of 30 NMR structures. This structural disorder cannot be explained simply by the influence of the paramagnetic iron–sulfur center because the environments of the [4Fe–4S] cluster F_B in the NMR structure of PsaC and the environments of the [4Fe–4S] clusters in the NMR solution structures of bacterial dicluster ferredoxins (PDB entries 1CLF, 1BC6, 1BQX (Bertini et al., 1995; Aono et al., 1998a,b) are well defined. In the NMR structures of dicluster ferredoxins from *Clostridium pasteurianum* and *Clostridium acidi urici* (PDB entries 1CLF, 2FDN) (Bertini et al., 1995; Dauter et al., 1997) as well as in the crystal structure of PS I-bound PsaC, the binding sites of cluster 2 and F_A, respectively, are in close contact with the N-terminus of the protein. In the NMR structures of bacterial dicluster ferredoxins the long-range NOEs between the amino acids of the N-terminus and the cluster 2 binding site (equivalent to F_A) provide the constraints necessary to define its position. In the NMR solution structure of unbound PsaC, the N-terminus is located far away from the F_A site (see below) and no interaction between them could be observed, which results in the lack of long-distance constraints and leads to larger disorder in F_A site. Due to the larger disorder in the F_A site, the α-helix that follows it also shows a higher degree of disorder (Figs. 3 A,B and 4A) as compared to the better defined α-helix that follows the F_B site.

An intriguing feature of PsaC is the larger number of charged amino acids in the vicinity of the F_A site. These amino acid play a crucial role in binding PsaC to PS I (section V). Unfortunately, the positions of amino acids Lys 51 and Arg 52, which form key contacts between PsaC and PsaA/PsaB heterodimer (Fig. 6 and Table 2; Jordan et al., 2001; Antonkine et al., 2003), are not defined in the NMR solution structure due to the lack of constraints. Only the backbone amide protons were assigned for these amino acids. Most likely this is due to both the lack of packing contacts with other parts of the protein as well as to the vicinity of the paramagnetic center.

The PsaC-specific sequence insertion between the two iron–sulfur cluster binding sites forms two strands of an antiparallel β-sheet connected by a turn (Fig. 3C). This structural feature distinguishes PsaC from most bacterial dicluster ferredoxins [PDB entries 1FDX (now replaced with 1DUR), 1CLF, 1FDN, 2FDN, 1BLU, 1FCA, 5FD1, 1BC6, 1BQX] (Adman et al., 1973, 1976; Stout, 1993; Duee et al., 1994; Bertini

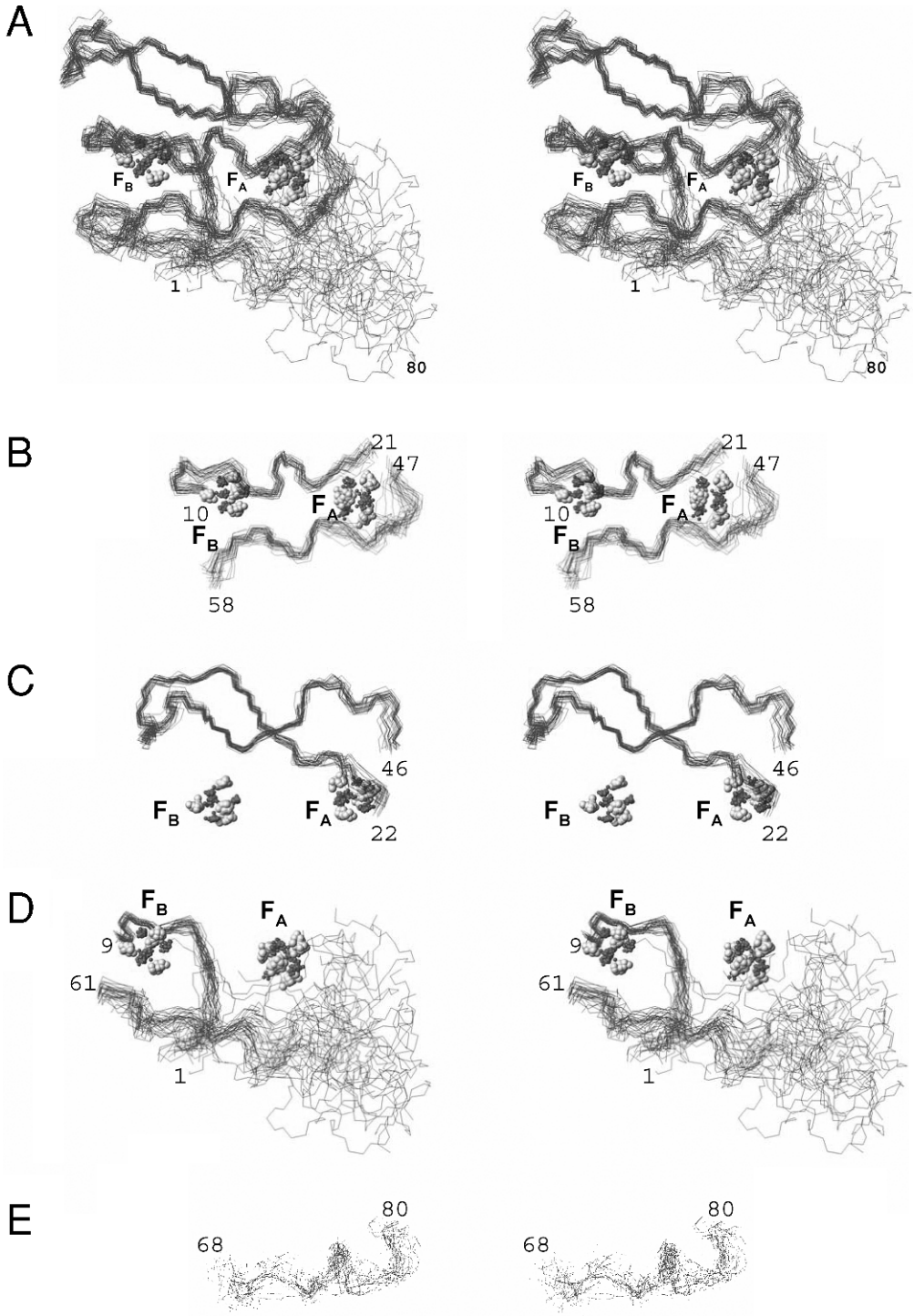

Fig. 3. Solution structures of the unbound PsaC subunit of PS I (PDB entry 1K0T) (Antonkine et al., 2002) depicting backbone stereo drawings of 30 superimposed DYANA structures. In (A)–(D) a family of 30 DYANA structures is shown in a superposition of amino acids 5–67. In (B)–(D) the [4Fe–4S] clusters are shown for each of the 30 structures, iron atoms as dark grey small and sulfur atoms as light grey large spheres. In (B)–(E) selected structural elements of unbound PsaC are shown. (A) See Color Plate 6, Fig. 2. (B) The two iron–sulfur clusters together with their conserved CxxCxxCxxxCP binding motifs, i.e. the backbone of amino acids 10–21 and 47–58 are shown. (C) The loop region of PsaC between the two iron–sulfur binding motifs, i.e. the backbone of amino acids 22–33 in the back and 34–46 in front. (D) N-terminus (1–9), pre-C-terminus (61–67) and disordered C-terminus (68–80); note the close contact between amino acids 2–5 and 65–67 and the position of the N-terminus between the iron–sulfur core of PsaC and the loop formed by amino acids 63–68. (E) The backbone of amino acids 68–80 in the family of 30 PsaC structures is shown in superposition of solely the amino acids 68–80. The helical secondary structure at the C-terminus is clearly revealed. This figure was prepared using MOLMOL (Koradi et al., 1996). (From Antonkine, et al., 2002.)

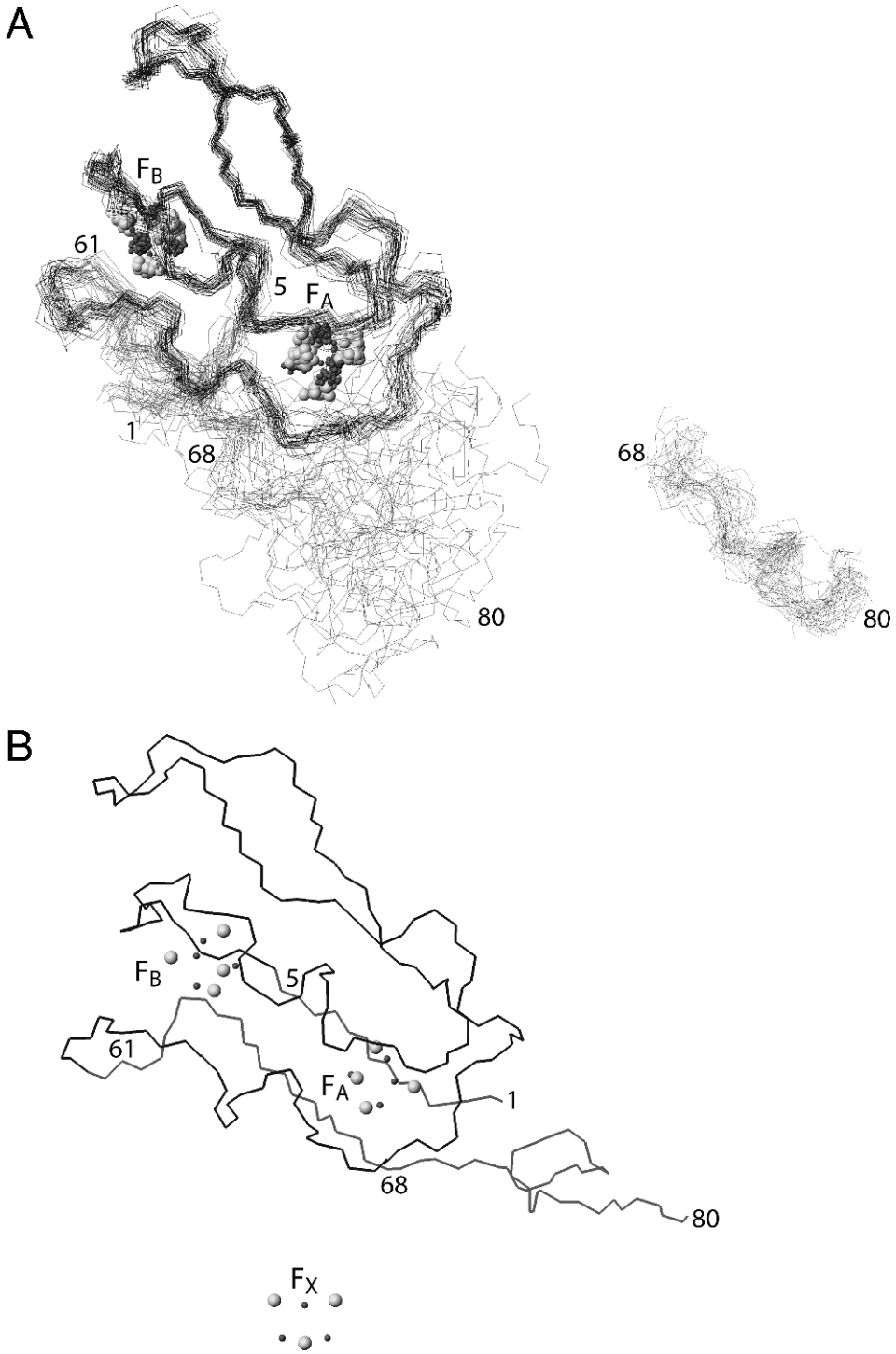

Fig. 4. Comparison of the NMR solution structure of unbound PsaC (PDB entry 1K0T) (Antonkine et al., 2003) with bound PsaC as part of the 2.5 Å X-ray structure of PS I (PDB entry 1JB0) (Jordan et al., 2001). The regions where the two structures show significant differences are identified by the lighter tint. [4Fe–4S] clusters are shown; iron atoms as dark grey small and sulfur atoms as light grey large spheres. (A) Backbone drawing of the final family of 30 superimposed structures of unbound, oxidized PsaC from *Synechococcus* sp. PCC 7002 determined by solution NMR (Antonkine et al., 2003). The backbone of the family of 30 structures is shown in a superposition of residues 5–67. The iron and sulfur atoms of the [4Fe–4S] clusters of each of the 30 structures are shown. The view direction is equivalent to the membrane plane of the assembled PS I complex (see Fig. 1). The inset shows the backbone of residues 68–80 in the same family of 30 PsaC structures. Superposition of solely the residues 68–80 reveals the helical secondary structure of the C-terminus. (B) Structure of PS I-bound PsaC taken from the PS I X-ray structure at 2.5 Å X-ray resolution (PDB entry 1JB0) (Jordan et al., 2001). The polypeptide backbone and iron–sulfur clusters F_A and F_B are shown. F_X is included to indicate the position and the correct orientation of PsaC on PS I. This figure was prepared using MOLMOL (Koradi et al., 1996).(Reprinted from Antonkine et al., 2003; Fig. 2a,b. © 2003 with permission from Elsevier.)

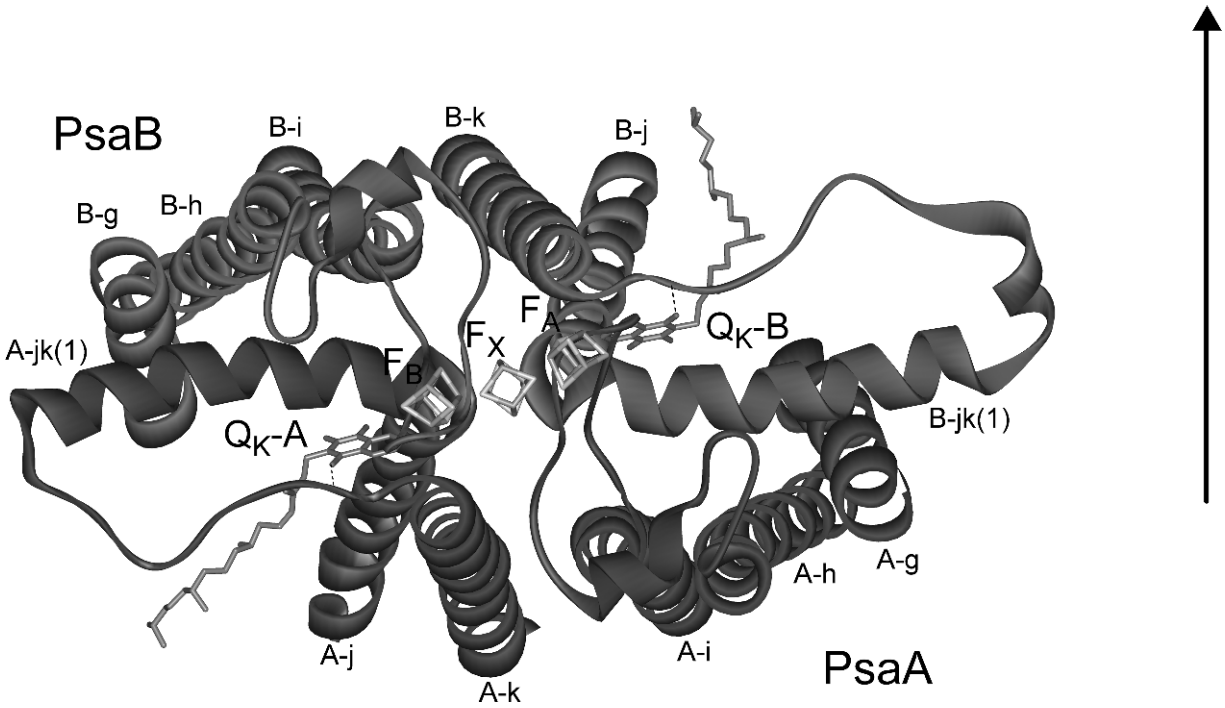

Fig. 5. Detail of the structural model of the PS I monomer. See Color Plate 7, Fig. 1.

et al., 1995; Tranqui and Jesior, 1995; Moulis et al., 1996; Dauter et al., 1997; Aono et al., 1998a,b). The only exception is ferredoxin from *Thauera aromatica* (PDB entry 1RGV) (Unciuleac et al., 2004), where a similar sequence insertion also forms an antiparallel β-sheet connected by a turn. In PsaC, the loop between F_A and F_B is reported to be involved in the binding of ferredoxin/flavodoxin. (Fischer et al., 1998, 1999). The secondary structure and position of the loop in unbound PsaC are identical to those in PS I-bound PsaC (Fig. 4; Jordan et al., 2001; Antonkine et al., 2002, 2003).

One of the most striking features of NMR solution structure of unbound PsaC is the intricate and unusual arrangement of the N-, pre-C-, and C-termini of PsaC (Figs. 3A,D,E and 4A). These are the three regions of PsaC that undergo conformational changes upon binding to PS I (see below). Let us now focus on their conformation and respective arrangement in solution.

The position of the first two amino acids at the N-terminus of PsaC is not very well defined, which is typical for many protein NMR solution structures. However, the overall N-terminus (amino acids 3–9) is well defined. The N-terminus of PsaC in solution is bent as compared to the N-terminus of PS I-bound PsaC (Antonkine et al., 2002), with a turn comprised of Val4, Lys5, and Ile6. The pre-C-terminus of PsaC, which is comprised of amino acids 63–68, forms a short and shallow loop around the N-terminus (amino acids 63–68) (Fig. 3D). The N- and C-termini in all known structures of bacterial dicluster ferredoxins are arranged in an antiparallel β-sheet structure, which is positioned in the vicinity of cluster 2 (analogous to F_A). The N- and pre-C-termini of PS I-bound PsaC are also arranged as an antiparallel β-sheet (Figs. 4B and 6) (β-sheets β_{1A} and β_{4A} in PDB entry 1JB0) (Jordan et al., 2001), and are positioned in the vicinity of F_A. Thus, the special cross-over arrangement between the N- and pre-C-termini and their position far away from F_A, is unique structural feature of unbound PsaC in solution and distinguishes it both from structures of bacterial dicluster ferredoxins and PS I-bound PsaC. The binding of PsaC to PS I must be accompanied by a conformational change in the N- and pre-C-termini of PsaC, thereby establishing their antiparallel β-sheet arrangement and moving them much closer toward the F_A site (Antonkine et al., 2002).

In unbound PsaC, the N- and pre-C-termini are located much further from F_A site, leaving the iron–sulfur cluster exposed to the solution. This, most likely, explains oxygen-sensitivity of unbound PsaC. In contrast, in PS I-bound PsaC the N- and pre-C-termini are arranged as an antiparallel β-sheet and are positioned much closer to F_A site, thereby shielding the iron–sulfur

cluster from oxygen and from the aqueous phase. As a result PS I-bound PsaC is insensitive to degradation by atmospheric oxygen. Furthermore, a change in solvent accessibility should contribute to a change in the redox potential of the iron–sulfur cluster(s) between the unbound and PS I-bound states of PsaC.

The C-terminus of PsaC has a disordered structure (Figs. 3A,D and 4A); the helical secondary structure of C-terminus is revealed only when the family of 30 NMR structures is superimposed based solely on those amino acids belonging to C-terminus (68–80) [Figs. 3E and 4A (inset)] (Antonkine et al., 2002). A significant number of medium range NOE constraints, which define the secondary structure of the protein, and no long-distance NOE constraints, which define the tertiary structure of the protein, are observed for amino acids 69–80 of the C-terminus of PsaC (Fig. 1A in Antonkine et al., 2002). As a result, this region of PsaC has a secondary structure; however, it has no packing interactions with the rest of the protein, and its position is undetermined within the family of NMR structures. The resolution of the NMR structure of PsaC is insufficient to determine what type of helix is formed by the C-terminus. On the basis of indirect experimental evidence, it was proposed in (Antonkine et al., 2002) that the C-terminus of PsaC is mobile or at least has intrinsically higher mobility than other parts of the protein. While such a suggestion has significant implications for the assembly of PsaC onto PS I, thus far there are no strong experimental evidence either for or against this idea.

The helical structure of the C-terminus of unbound PsaC is dramatically different from an extended coil, with a single α-helical turn, a conformation that is reported for PS I-bound PsaC (Jordan et al., 2001; Antonkine et al., 2002; Fig. 4). Thus, the binding of PsaC to PS I must be accompanied by unwinding of the C-terminus of the protein (Antonkine et al., 2002).

Most bacterial dicluster ferredoxins are 25–30 amino acids shorter than PsaC and have no equivalent of the longer C-terminus or the sequence insertion between iron–sulfur clusters. However, ferredoxin from *Thauera aromatica* is exactly the same size as PsaC (80 amino acids) (PDB entry 1RGV) (Unciuleac et al., 2004) and provides an interesting point of comparison. Similarly to PsaC it has a sequence extension at the C-terminus (see section III.B.2), which is a well-defined three turn α-helix (Unciuleac et al., 2004). This is longer than the one-turn α-helix in bound PsaC (Jordan et al., 2001) and somewhat similar to the helical conformation of C-terminus in unbound PsaC (Antonkine et al., 2002).

In summary, three important features of unbound PsaC structure are quite clear. Firstly, the iron–sulfur core of unbound PsaC is very similar to PS I-bound PsaC and to bacterial dicluster ferredoxins. Secondly, the structure and spatial arrangement of the N-, pre-C-, and C-termini of PsaC are significantly different from equivalent regions of bacterial dicluster ferredoxins. Thirdly, they are also very different from PS I-bound PsaC. Therefore, during the transition from unbound to PS I-bound PsaC, the N-, pre-C-, and C-termini of the protein need to undergo large-scale structural rearrangements (Fig. 4; Antonkine et al., 2002, 2003). This is in good agreement with the results obtained much earlier by EPR (Li et al., 1991a). The change in the EPR spectra of F_A and F_B implied that that environment of iron–sulfur clusters changed upon binding to PS I. In the broader context the interesting issue is that PS I-bound PsaC is structurally much more similar to soluble dicluster ferredoxins than is unbound PsaC in solution. This implies that PsaC evolved to be different from ferredoxins in solution, but similar to them in the PS I-bound form.

IV. The F_X-Binding Site is also the Main Binding Site for PsaC

F_X is the interpolypeptide iron–sulfur cluster bound between the PsaA and PsaB subunits of PS I (Fig. 6). EXAFS and Mössbauer spectroscopic studies of a P700-F_X core devoid of F_A and F_B unambiguously identified F_X as a [4Fe–4S] cluster (McDermott et al., 1989; Petrouleas et al., 1989). The midpoint potential of F_X was found to be −730 (Ke et al., 1977) and −705 mV (Chamorovsky and Cammack, 1982) in PS I particles with prereduced F_A and F_B. This makes F_X one of the most reducing, functional [4Fe–4S] clusters known in biology. The binding site of F_X was first proposed based on the amino acid sequences of the PsaA and PsaB polypeptides that comprise the membrane-bound PS I heterodimer (Fish et al., 1985; Cantrell and Bryant, 1987). The site consists of two identical amino acids sequences, FPCDGPGRGGTC, which are located in loops connecting helices *h* and *i* on PsaA and PsaB (Figs. 5 and 6). Each of these sequences provides two conserved cysteine ligands to the cluster; thus F_X represents a highly unusual instance of a [4Fe–4S] cluster bound between a protein heterodimer. The high-resolution crystal structure of cyanobacterial PS I shows that negatively-charged amino acids within the conserved F_X-binding sequences on PsaA and PsaB provide a set of ionic contacts for the binding of

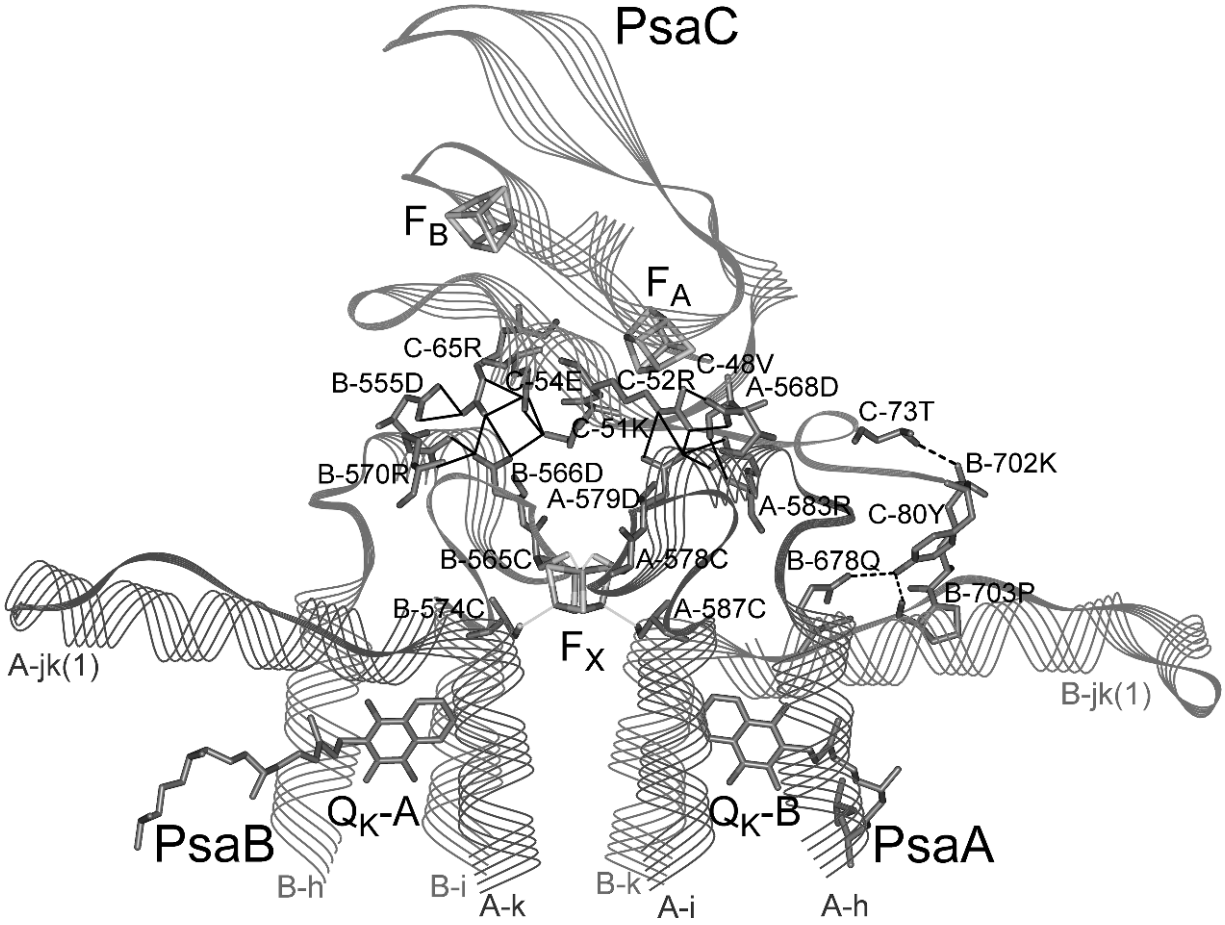

Fig. 6. The PsaC contact area with PsaA and PsaB from the PS I structure. See Color Plate 7, Fig. 2.

positively-charged amino acids on PsaC (Jordan et al., 2001; Antonkine et al., 2003; see section V). The F_X-binding sequences on both PsaA and PsaB are parts of large, extramembrane loops that have a completely C_2-symmetric three-dimensional structure (Fig. 5). For understanding of assembly of stromal subunits subunits PsaC, PsaD, and PsaE this is both the most unusual and the most important feature of the F_X-binding site.

In addition to providing ligands for F_X, these extramembrane loops serve several additional functions such as forming the ionic contacts with PsaC and shielding the F_X cluster from molecular oxygen (Antonkine et al., 2003). F_X is additionally shielded by α-helices that comprise the core of the PsaA/PsaB heterodimer. The iron protein of nitrogenase [for example PDB entry 1CP2 (Schlessman et al., 1998)] and 2-hydroxyglutaryl-CoA dehydratase component A [PDB entry 1HUX (Locher et al., 2001)] are the only other proteins with available three-dimensional structure that have an interpolypeptide [4Fe–4S] cluster. However, the environments of these [4Fe–4S] clusters are significantly different: each subunit of these homodimeric proteins has two fully-conserved cysteines that are located far apart from each other in the amino acid sequence. Hence, in these proteins, there is no short consensus binding sequence for the [4Fe–4S] cluster as exists for F_X on PsaA and PsaB subunits of PS I. It follows that properties of these interpolypeptide [4Fe–4S] clusters are also very different from F_X. The [4Fe–4S] clusters bound to these proteins have midpoint potentials of −420 to −430 mV (i.e., 280 to 300 mV more oxidizing than F_X); this range is more typical for low potential [4Fe–4S] clusters in monocluster and dicluster bacterial ferredoxins. Moreover, the [4Fe–4S] clusters in nitrogenase and 2-hydroxyglutaryl-CoA dehydratase component A are highly sensitive to oxygen, probably because the binding site of the interpolypeptide [4Fe–4S] cluster is open and accessible. In contrast, F_X is not oxygen sensitive as was shown by the ability to isolate functional P700-F_X cores under aerobic

conditions (Golbeck et al., 1988; Parrett et al., 1989). The requirement for oxygen-insensitivity may come about because P700-F_X cores are likely to be assembled as an intermediate step during the biogenesis of PS I in the functional (i.e., oxygen-evolving) thylakoid membrane.

V. Assembly of PsaC onto the PsaA/PsaB Heterodimer

A. Ionic and Hydrogen Bond Contacts of PsaC to the Surface of the PsaA/PsaB Heterodimer

Figure 6 presents a view of the contact area between PsaC and the PsaA/PsaB heterodimer. The hydrogen and ionic bond contacts that are found in the X-ray crystal structure of PS I between PsaC and PsaA/PsaB heterodimer are listed in Table 2A. The nomenclature in this review uses the first letter name of the PS I subunit, separated by a dash from the number of the amino acid in the sequence, which is specified by its single amino acid code. For example C-52R refers to the Arg 52 of PsaC subunit of PS I. All amino acid numbers in this section refer to the amino acid sequence of polypeptides in *Synechococcus elongatus*.

1. C_2-Symmetric Contacts Between the Iron–Sulfur Core of PsaC and the F_X-binding loops on PsaA/PsaB

The F_X-binding stromal loops on PsaA and PsaB have a completely C_2-symmetric three-dimensional structure and provide most hydrogen and ionic bond contacts for PsaC binding (see section IV). The amino acids of PsaC that take part in these contacts belong to different structural elements of the protein, namely the F_A-binding site and the pre-C-terminus (β-strand β_{4a} in PS I-bound PsaC).

Let us focus on the main contact network connecting PsaC to the PsaA/PsaB heterodimer. Two equivalent contact systems exist, PsaA–PsaC–PsaA (left) and PsaB–PsaC–PsaB (right), both of which employ the identical contact scheme Asp-Arg-Asp (Fig. 6). Another key contact between PsaC and PsaB is the C-51K, which forms an ionic bond to B-566D. Note, that neighboring amino acids C-51K and C-52R form ionic bonds with PsaB and PsaA, respectively (Table 2A).

The PsaC–PsaA and PsaC–PsaB inter-subunit contacts are further stabilized by intra-subunit contacts, as well as by the local protein environment. A-579D and B-566D, key contacts on PsaA and PsaB respectively (Table 2A subsets α and β), have intra-subunit contacts with A-568R and B-555R, respectively. These ionic bonds contacts are further stabilized by the presence of nearby hydrophobic patches. The headgroups of A-579D and B-566D, and their ionic bonds to a C-52R and C-65R, are in the highly packed region with Gly residues on either side of A-583R and B-570R [Fig. 6 and Table 1 of Antonkine et al. (2003)]. The PsaC inter-subunit contacts are also stabilized by intra-subunit ones (Table 2A subset γ). The pre-C-terminus of PsaC changes its conformation upon binding to PS I. It carries Arg 65, which participates in key PsaC–PsaB contacts. C-54E forms an ionic bond with C-65R and a hydrogen bond with C-66V, thus stabilizing proper conformation of pre-C-terminus and PsaC–PsaB contacts. C-54E also forms an ionic bond with C-51K, another important PsaC–PsaB contact.

C-51K, C-52R, and C-54K all belong to the F_A-binding site, which contain an increased number of charged amino acids as compared to the F_B-binding site or the binding sites of [4Fe–4S] clusters in bacterial dicluster ferredoxins (see section III.A). It is clear that all of these charged amino acids, including C-46D (PsaC–PsaD contact), play an important role in binding of PsaC within the fully assembled PS I complex.

Rotation of PsaC by 180° around the C_2-symmetry axis of the PsaA/PsaB heterodimer results in the perfect overlay of C^{ζ}-atoms of C-52R and C-65R, while the lines connecting the respective N^{η} atoms are nearly perpendicular to each other (Antonkine et al., 2003). Moreover, out of ten ionic and one hydrogen bonds formed between iron–sulfur core of PsaC and PsaA/PsaB heterodimer eight ionic and one hydrogen bond can be formed equally well by 180° rotated PsaC (Table 2B). Therefore, the iron–sulfur core of PsaC binds symmetrically to the PsaA/PsaB hetrodimer and forms a C_2-symmetric contact area with it. The larger issue here is the overall assembly of PsaC, in which this inherently asymmetric protein is assembled asymmetrically onto its perfectly C_2-symmetric main binding site on the PsaA/PsaB heterodimer.

2. Contacts Between the C-terminus of PsaC and PsaB. Symmetry Breaking During PsaC Binding

The only symmetry-breaking contacts that form upon binding of PsaC to PsaA/PsaB are the contacts of the C-terminus of PsaC to PsaB. C-80Y forms hydrogen bonds with B-678Q and B-703P; whereas C-73T forms a hydrogen bond with B-702K. These contacts

Table 2. (A) Inter-(or intra-)protein contacts (ionic and H-bond) between the PsaA/PsaB heterodimer and the PsaC subunit. The arrangement of the participating PsaA and PsaB amino acids reflects perfect C_2-symmetry on this part of the stromal surface. This table consists of three subsets – α: Contacts of PsaC with the PsaA stromal surface. β: Contacts of PsaC with the PsaB stromal surface. Note the C_2-symmetry is reflected in equivalent stromal surface contacts of PsaC with PsaA and PsaB, with the exception of those contacts of the C-terminus of PsaC with PsaB at the end of subset β. γ: Intra PsaC contacts stabilizing the tertiary structure. α and β subsets present contacts between the iron–sulfur core of PsaC and the F_X-binding loops of PsaA and PsaB. (B) Contacts corresponding to those in part A except that PsaC is rotated around the quasi-C_2-symmetry axis of the PsaA/PsaB core. This table consists of two subsets – α: Contacts of rotated PsaC with the PsaA stromal surface. β: Contacts of rotated PsaC with the PsaB stromal surface. α and β subsets present contacts between the iron–sulfur core of PsaC and the F_X-binding loops of PsaA and PsaB. (C) Contacts and clashes between the the C-terminus of rotated PsaC and the PsaA stromal surface. The PS I structure involves a close contact between C-terminus of PsaC and its PsaB-specific binding site. If rotated, the same conformation of the C-terminus would produce clashes with the PsaA surface. Thus, the conformation of the C-terminus of PsaC would need to change to allow binding. (Reprinted from Antonkine et al., 2003; Table 3. © 2003, with permission from Elsevier.)

Remarks	Polypeptide	Residue	Dist. (Å)/type		Residue	Polypeptide	Remarks
A. Inter-(or intra-)protein contacts (ionic and H-bond) between the PsaA/PsaB heterodimer and the PsaC subunit							
α							
(i)	PsaC	Arg 52 $N^{\eta 1}$	3.22	I	$O^{\delta 2}$Asp 568	PsaA	(1)
(i)	PsaC	Arg 52 $N^{\eta 2}$	2.84	I	$O^{\delta 1}$Asp 568	PsaA	(1)
(i)	PsaC	Arg 52 $N^{\eta 2}$	2.77	I	$O^{\delta 1}$Asp 579	PsaA	(2A)
(i)	PsaC	Arg 52 N^{ε}	3.04	I	$O^{\delta 1}$Asp 579	PsaA	(2A)
(i)	PsaC	Arg 52 N^{ε}	3.07	I	$O^{\delta 2}$Asp 579	PsaA	(2A)
	PsaA	Arg 583 $N^{\eta 2}$	2.95	I	$O^{\delta 1}$Asp 579	PsaA	Intra PsaA (3)
	PsaA	Arg 583 $N^{\eta 1}$	3.24	I	$O^{\delta 1}$Asp 579	PsaA	Intra PsaA (3)
(ii)	PsaC	Val 48 O	2.84	H	N Arg 583	PsaA	
β							
(i)	PsaC	Lys 51 N^{ζ}	2.6	I	$O^{\delta 1}$Asp 566	PsaB	(2B)
(iii)	PsaC	Arg 65 $N^{\eta 1}$	3.11	I	$O^{\delta 1}$Asp 555	PsaB	(1)
(iii)	PsaC	Arg 65 $N^{\eta 1}$	2.98	I	$O^{\delta 2}$Asp 555	PsaB	(1)
(iii)	PsaC	Arg 65 $N^{\eta 2}$	3.06	I	$O^{\delta 1}$Asp 566	PsaB	(2B)
(iii)	PsaC	Arg 65 $N^{\eta 2}$	2.63	I	$O^{\delta 2}$Asp 566	PsaB	(2B)
	PsaB	Arg 570 $N^{\eta 1}$	3.15	I	$O^{\delta 2}$Asp 566	PsaB	Intra PsaB (3)
	PsaB	Arg 570 $N^{\eta 2}$	2.67	I	$O^{\delta 2}$Asp 566	PsaB	Intra PsaB (3)
(iv)	PsaC	Thr 73 $O^{\gamma 1}$	2.96	H	N^{ζ}Lys 702	PsaB	(4)
(iv)	PsaC	Tyr 80 O^{η}	3.18	H	$O^{\varepsilon 1}$Gln 678	PsaB	(4)
(iv)	PsaC	Tyr 80 O^{η}	2.67	H	O Pro 703	PsaB	(4)
γ							
	PsaC	Lys 51 N^{ζ}	3.08	I	$O^{\varepsilon 1}$Glu 54	PsaC	Intra PsaC (5)
	PsaC	Lys 51 N^{ζ}	3.20	I	$O^{\varepsilon 2}$Glu 54	PsaC	Intra PsaC (5)
	PsaC	Arg 65 $N^{\eta 2}$	3.08	I	$O^{\varepsilon 2}$Glu 54	PsaC	Intra PsaC (5)
	PsaC	Arg 65 N^{ε}	3.15	I	$O^{\varepsilon 2}$Glu 54	PsaC	Intra PsaC (5)
	PsaC	Glu 54 $O^{\varepsilon 2}$	2.79	H	N Val 66	PsaC	Intra PsaC (5)
B. Contacts corresponding to those in Table 2A but when PsaC is rotated around the quasi-C_2-symmetry axis of the PsaA/PsaB core							
α							
(i)	PsaC	Lys 51 N^{ζ}	2.93	I	$O^{\delta 2}$Asp 579	PsaA	(2A)
(ii)	PsaC	Arg 65 $N^{\eta 1}$	2.64	I	$O^{\delta 1}$Asp 568	PsaA	(1)
(ii)	PsaC	Arg 65 $N^{\eta 1}$	2.52	I	$O^{\delta 2}$Asp 568	PsaA	(1)
(ii)	PsaC	Arg 65 $N^{\eta 2}$	2.74	I	$O^{\delta 1}$Asp 579	PsaA	(2A)
(ii)	PsaC	Arg 65 $N^{\eta 2}$	2.96	I	$O^{\delta 2}$Asp 579	PsaA	(2A)
	PsaA	Asp 579 $O^{\delta 1}$	2.95	I	$N^{\eta 2}$Arg 583	PsaA	Intra PsaA
	PsaA	Asp 579 $O^{\delta 1}$	3.24	I	$N^{\eta 1}$Arg 583	PsaA	Intra PsaA
β							
(i)	PsaC	Arg 52 $N^{\eta 2}$	2.67	I	$O^{\delta 2}$Asp 566	PsaB	(2B)
(i)	PsaC	Arg 52 N^{ε}	2.99	I	$O^{\delta 2}$Asp 566	PsaB	(2B)
(i)	PsaC	Arg 52 N^{ε}	3.36	I	$O^{\delta 1}$Asp 566	PsaB	(2B)
(iii)	PsaC	Val 48 O	3.25	H	N Gly 571	PsaB	
	PsaB	Asp 566 $O^{\delta 2}$	3.15	I	$N^{\eta 1}$Arg 570	PsaB	Intra PsaB (3)
	PsaB	Asp 566 $O^{\delta 2}$	2.67	I	$N^{\eta 2}$Arg 570	PsaB	Intra PsaB (3)

Table 2. (*cont.*)

Remarks	Polypeptide	Residue	Dist. (Å)/type		Residue	Polypeptide	Remarks
C. Contacts and clashes between the C-terminus of PsaC (rotated) and the PsaA stromal surface							
	PsaC	Thr 73 $O^{\gamma 1}$	2.83	H	O Gln 43	PsaA	
	PsaC	Tyr 80 O^{η}	2.97	H	$N^{\varepsilon 2}$Gln 698	PsaA	
	PsaA	Pro 719 O	0.88		O^{η}Tyr 80	PsaC	CLASH
	PsaA	Pro 719 C	2.12		O^{η}Tyr 80	PsaC	CLASH
	PsaA	Gln718 C^{γ}	1.43		O Tyr 80	PsaC	CLASH
	PsaA	Gln718 C^{δ}	1.18		O Tyr 80	PsaC	CLASH
	PsaA	Arg 720 $N^{\eta 1}$	1.59		$C^{\delta 2}$ Leu 78	PsaC	CLASH
	PsaA	Arg 720 $N^{\eta 1}$	1.24		C^{β} Leu 78	PsaC	CLASH
	PsaA	Arg 720 $N^{\eta 2}$	1.51		C^{γ} Leu 78	PsaC	CLASH
	PsaA	Arg 720 $N^{\eta 2}$	1.60		C^{β} Leu 78	PsaC	CLASH
	PsaA	Arg 720 C^{ζ}	0.25		C^{γ} Leu 78	PsaC	CLASH
	PsaA	Arg 720 C^{ζ}	1.55		$C^{\delta 2}$ Leu 78	PsaC	CLASH
	PsaA	Arg 720 C^{ζ}	1.49		C^{β} Leu 78	PsaC	CLASH
	PsaA	Arg 720 N^{ε}	1.88		$C^{\delta 1}$ Leu 78	PsaC	CLASH
	PsaA	Arg 720 N^{ε}	1.30		C^{γ} Leu 78	PsaC	CLASH

(i) Amino acid found in the pair of equally charged residues between the second and third cysteine in the F_A binding motif.
(ii) Backbone of the F_A binding motif.
(iii) Center of the β_{4a}-sheet in the pre-C-terminus of PsaC.
(iv) C-Terminus of PsaC.
(1) Middle of conserved PDK triplet preceding the hi(1) helix turn in PsaA and PsaB.
(2A) Next to A-578Cys ligating F_X.
(2B) Next to B-565Cys ligating F_X.
(3) Intra F_X-binding loop stabilizing the (2A) and (2B) contacts.
(4) PsaB-Specific binding site of PsaC C-terminus.
(5) Intra PsaC contacts involving C-54Glu in the center of the short α-helix connecting F_A to the F_B binding motif.
The letter H following the distance indicates that this contact is a hydrogen bond. The letter I following the distance indicates that this contact is an ionic bond.

are included in Fig. 6 and are listed at the end of subset β in Table 2A. Formation of these three contacts requires a major conformational change of the C-terminus of PsaC upon binding to the PsaA/PsaB heterodimer. Namely, the helical C-terminus of PsaC in solution must unwind to allow these contacts with PsaB to be established (Antonkine et al., 2002, 2003; Fig. 4 see section III.C). In succeeding assembly stages, the extended conformation of the C-terminus of PsaC and the interactions between the C-terminus of PsaC and PsaB are stabilized by the binding of PsaD (Jordan et al., 2001; Antonkine et al., 2003).

When PsaC is rotated 180° around the C_2-symmetry axis, a certain number of clashes are found between the C-terminus of PsaC and PsaA (Table 2C). This is the only part of the contact area between rotated PsaC and PsaA/PsaB heterodimer where clashes occur. To avoid these clashes, the C-terminus would need to assume a different conformation from that of the nonrotated PS I-bound PsaC and/or from unbound PsaC. Namely, a different set of contacts would need to be made between amino acids of the C-terminus of rotated-PsaC and the PsaA/PsaB heterodimer. Thus, the binding of the PsaC terminus is specific to the nonrotated orientation of PsaC on PsaA/PsaB heterodimer. The contacts between the C-terminus of PsaC and PsaB are the sole symmetry-breaking element of PsaC binding to the P700-F_X/PsaC core. Note, however, that only a few hydrogen bonds on the C-terminus of PsaC are involved (Table 2A). It is difficult to believe that these few contacts qualify as a sufficiently strong symmetry-breaking driving force to determine in which of the two equivalent orientations PsaC binds to PS I. Of particular relevance here is the highly hydrophobic PVAL sequence block next to the PsaC-binding pocket on PsaB (residues 703–706), which would add stability to the H-bonds of the C-terminus binding of PsaC. Indeed, C-80Y sits in a highly hydrophobic pocket surrounded by the side chains of B-685V, B-703P, B-704V, C18-L, C-19A, and C-78L as well as by the carbon tails of B-682E and B-702K. This highly hydrophobic environment likely contributes to the free energy of binding and further strengthens the hydrogen bonds formed by C-terminus of PsaC. We can expect a very large entropic contribution to the free energy of binding simply because the large number of relatively immobile water molecules that are expected to line these hydrophobic residues would become freed when PsaC binds.

In summary, a PsaB-specific binding pocket for the C-terminus of PsaC can be clearly identified (Jordan et al., 2001; Antonkine et al., 2003). Thus, breaking of C_2-symmetry during PsaC binding is possible. However, it is difficult to believe that the formation of just three hydrogen bonds in the PsaB-specific binding pocket of PsaC can qualify as a sole driving force for an overall asymmetric binding of PsaC.

B. What Determines the Specificity of PsaC Binding to the PsaA/PsaB Heterodimer?

The overall pseudo-C_2-symmetry of the PsaA/PsaB heterodimer is clearly broken upon binding of PsaC. How PsaC assembles asymmetrically raises intriguing questions that concern the interplay between the near-perfect C_2-symmetry of the PsaA/PsaB core, including its stromal interface, which is in contact with the completely nonsymmetrical PsaC that undergoes significant conformational changes during its assembly onto PsaA/PsaB core.

The completely C_2-symmetric binding of the iron–sulfur core region of PsaC to its main binding site on the PsaA/PsaB heterodimer presents several problems. There exist two possible solutions for the stepwise assembly of PsaC: (1) In the "iron–sulfur core binds first" hypothesis, PsaC initially forms the main body of ionic contacts between the iron–sulfur core and the F_X site on the PsaA/PsaB heterodimer; i.e., PsaC binds strongly, but nonspecifically with a C_2-ambiguity; (2) In the "C-terminus binds first" hypothesis, PsaC initially forms contacts between the C-terminus and its PsaB-specific binding site; thus it binds weakly, but specifically, and this is followed by a strong binding of the iron–sulfur core region to the PsaA/PsaB heterodimer; i.e., PsaC binds in only one of two orientations. We need to analyze these two cases in depth.

The "iron–sulfur core binds first" hypothesis can be expected to result in a C_2-ambiguity in the binding of PsaC; i.e., one-half of PsaC binds to the P700-F_X core correctly, and one-half of PsaC binds to the P700-F_X core incorrectly. Because only one orientation of PsaC is known experimentally, one would need to propose that prior to the assembly of the stromal ridge proteins, i.e., binding of PsaD and PsaE, incorrectly-bound PsaC would need to become unbound. If the same C_2-symmetry binding of PsaC continues to occur on repeated cycles of unbinding and binding, one can envision an asymptotic assembly of correctly-bound PsaC. This presupposes a finite equilibrium constant for the binding of incorrectly-bound PsaC to the PsaA/PsaB heterodimer. Correctly-bound PsaC would raise the equilibrium binding constant (tighter binding) and would presumably be further stabilized by the binding of the C-terminal region. One problem with this hypothesis is that it is a seemingly inefficient and highly inelegant way to build asymmetric stromal ridge of PS I. Another is that at least eight ionic bonds and one hydrogen bond would need to be broken for the unbinding of PsaC to occur. This contradicts earlier studies that showed the reconstitution of PsaC to P700-F_X cores was spontaneous *in vitro*, i.e., that the equilibrium constant was far in the direction of binding due to a large binding constant (Li et al., 1991a). One might propose that a chaperone may be involved in unbinding of PsaC *in vivo*, relying on ATP hydrolysis to supply energy, but this idea is invalidated by the fact that the *in vitro* reconstitution experiments invariably result in the correctly bound form of PSI-bound PsaC. In principle, correctly and incorrectly bound PsaC can be distinguished by the EPR spectra of F_A and F_B. PsaD will not be able to bind to the P700-F_X/PsaC cores with incorrectly-bound PsaC (Antonkine et al., 2003); therefore, the resonances of F_A and F_B will remain broadened as compared to the sharp resonance in PS I-bound PsaC (Li et al., 1991a). In fact, this is not observed during *in vitro* reconstitution of P700-F_X cores with PsaC and PsaD, and only one form of PsaC is detected (Li et al., 1991a).

The "C-terminus binds first" hypothesis can be expected to result in the binding of only one of the two C_2-symmetric forms of PsaC, the correctly bound form. In this scenario, the mobile C-terminus of PsaC finds the hydrophobic binding pocket on PsaB during the initial stages of assembly. When it is locked in place by establishing H-bonds, the C-terminus unwinds, thereby allowing the core region of PsaC to assemble on the PsaA/PsaB heterodimer. As PsaC binds, water molecules are excluded as the ionic bonds in the iron-sulfur core region are formed. Clearly, once the C-terminus finds its PsaB-specific binding pocket, the binding of PsaC to the P700-F_X core is very specific, which solves the C_2-ambiguity in PsaC binding. This is a very simple and attractive scenario because it ensures specificity of PsaC binding right from the beginning of the assembly process. However, this hypothesis presumes that not even a small percentage of the core region can be allowed to bind prior to the C-terminus, which may be a difficult undertaking. Obviously, something must prevent the formation of the main body of contacts between the iron–sulfur core of PsaC and the F_X-binding site on the PsaA/PsaB heterodimer

prior to the specific binding of the C-terminus to PsaB.

Because the information for one preferred orientation of PsaC resides exclusively in the amino acid sequences, and hence, three-dimensional structures of PsaA, PsaB, and PsaC, we need to look for additional differences between the three-dimensional structures of unbound and PS I-bound PsaC. Indeed, there is one and only one factor that hasn't yet been brought into the equation: the altered orientation of the N-terminus. Comparison of structures of PS I-bound and unbound PsaC (see section III.C) shows that the N-terminus of unbound PsaC is bent as compared to PS I-bound PsaC (Antonkine et al., 2002, 2003; Fig. 4). The backbone of the bent N-terminus in unbound PsaC occupies the position of the C-65R side chain in PS I-bound PsaC (see section III.C). C-65R forms one of the key contacts between iron–sulfur core of PsaC and the F_X-binding site on the PsaA/PsaB heterodimer (see Table 2). C51K, another key contact, is also displaced, though to the lesser degree, in unbound PsaC. A side-by-side comparison of the unbound and PS I-bound forms of PsaC shows that when viewed from the underside, i.e., the region that binds F_X, the bent N-terminus pushes the polypeptide chain from residue 61 to 68 away from the core region, changing dramatically the location of C-65R and altering the orientation of the side chains of C-51K, C-52R as well. Thus the bent N-terminus forces PsaC to assume a dramatically different three-dimensional structure in the key binding region that includes these three important basic residues (see section III.C). This alteration would serve to prevent the binding of the iron–sulfur core region of PsaC to the F_X-binding site of PsaA/PsaB heterodimer prior to binding of the C-terminus.

In summary, the "C-terminus binds first" hypothesis is supported by the experimental data. On binding, the C-terminal region is expected to partially lose its helical propensity, allowing the body of PsaC to be in proximity with the ionic residues on PsaA/PsaB. The C-52R residue is the least affected by the changes in PsaC conformation, and it may serve as the initial contact with A-568D and A-579. Concomitantly, the N-terminus would swing around to position itself to be in H-bond contact with part of the pre-C-terminus. This would allow C-65R and C51K to make contact with B-555D and B-566D. Therefore, after the C-terminus of PsaC binds, structural changes occur that correspond to a concerted movement of the N- and pre-C-termini toward the F_A-binding site. This establishes the conformation of P700-F_X/PsaC. Although experimental evidence is currently unavailable to either support or refute such a detailed scenario, on paper, it looks highly plausible.

The conformation of PS I-bound PsaC is further influenced by PsaD binding (Li et al., 1991a). However, these changes do not affect specificity of PsaC binding to PsaA/PsaB heterodimer.

In conclusion, the simple evolutionary adaptation of allowing the the N-, pre-C-, and C-termini to concertedly change their conformation upon binding of PsaC to PS I shows how a relatively small change in the structure of PsaC may have evolved to serve as a key conformational switch that uniquely determines the specificity of binding and its orientation on the P700-F_X core. This is important because PsaC binding is the decisive step for an assembly of all three subunits of the PS I stromal ridge.

VI. Outlook

The discovery of an 8 kDa protein named PshB, which is the functional analogue of PsaC in homodimeric reaction center of *Heliobacterium modesticaldum* (Heinnickel et al., 2005) opens new avenues for investigation of the assembly of Type I reaction centers. PshB can be removed from the heliobacterial reaction center by mild salt treatment. In comparison, it is necessary to use chaotropic agents in significant concentration to remove PsaC from PS I (Heinnickel et al., 2005). Therefore, it is likely that PshB is bound more weakly to the PshA homodimer than PsaC is to the PsaA/PsaB heterodimer. Another interesting feature of this protein is that the EPR spectra of the PshB-bound [4Fe–4S] clusters do not change upon removal of the protein from the reaction center. This implies that, unlike PsaC, PshB does not undergo a significant change in its conformation upon binding to the reaction center core. More importantly, for understanding of assembly of Type I reaction centers, investigation of the Heliboacterial center presents a unique opportunity to compare and contrast the assembly of heterodimeric and homodimeric reaction center proteins. This investigation awaits determination of the 3-dimensional structures of both PshB and the Helibacterial reaction center as whole.

Another area where progress can be made in the near future is further investigation of the assembly of PsaC and the other stromal subunits by TROSY-based (Transverse Relaxation Optimized Spectroscopy) NMR techniques (Pervushin et al., 1997). Application of TROSY

allows the study large protein complexes comparable in size to PS I (Fiaux et al., 2002) by NMR in solution. Furthermore, this technique has already been applied to the investigation investigation of interactions between PS I and the soluble electron carrier cytochrome c_6 (Diaz-Moreno et al., 2005). Application of TROSY to PS I makes it possible to test our assembly scenario of the stromal subunits by solution NMR. Data obtained on PsaC (Antonkine et al., 2002) and PsaE (Falzone et al., 1994; Mayer et al., 1999; Barth et al., 2002), where assignments of the NMR signals of the unbound protein in solution is available, will be used as the starting point in these studies.

VII. Conclusions

PsaC is the unique example of an iron–sulfur protein whose structure is known to be different in the bound and unbound forms. The binding of PsaC is a decisive step in the assembly of all three of the stromal subunits (PsaC, PsaD, and PsaE). PsaC changes its conformation upon binding to PS I. Structural changes occur in the secondary structure and in respective arrangements of the N-, pre-C-, and C-termini of the protein. Our hypothesis is that during the assembly of PsaC onto the PsaA/PsaB heterodimer, the C-terminus of PsaC binds first, establishing the hydrogen bonds and hydrophobic contacts with a PsaB-specific binding pocket. This specific binding at the very first step assures overall binding of PsaC in the "correct" orientation. The formation of the main body of contacts between the iron sulfur core region of PsaC and the F_X-binding site on the PsaA/PsaB heterodimer protein follows. Prior to the binding of the C-terminus of PsaC to its PsaB-specific binding pocket, formation of the key contacts between iron–sulfur core of PsaC and F_X-binding site on PsaA/PsaB heterodimer is prevented by the bent conformation of N-terminus of unbound PsaC. The binding of PsaC to PS I serves as an excellent example of the sequential assembly of a multisubunit protein complex accompanied by the modulation of the properties of the protein-bound cofactors.

Acknowledgments

This work was supported generously by the Max-Planck Society, the Russian Academy of Sciences (M. L. Antonkine), the Sfb 498 (project A3 to D. Stehlik), and the US National Science Foundation (MCB-0117079 to J. H. Golbeck). Many thanks to Irina Koryagina, Jens Niklas, Dietmar Stehlik, and Oksana Gopta for critically reading the manuscript.

References

Adman ET, Sieker LC and Jensen LH (1973) The structure of a bacterial ferredoxin. J Biol Chem 248: 3987–3996

Adman ET, Siefker LC and Jensen LH (1976) Structure of *Peptococcus aerogenes* ferredoxin. Refinement at 2 Å resolution. J Biol Chem 251: 3801–3806

Antonkine ML, Bentrop D, Bertini I, Luchinat C, Shen GZ, Bryant DA, Stehlik D and Golbeck JH (2000) Paramagnetic ^{1}H NMR spectroscopy of the reduced, unbound Photosystem I subunit PsaC: sequence-specific assignment of contact-shifted resonances and identification of mixed- and equal-valence Fe-Fe pairs in [4Fe-4S] centers F_A^- and F_B^-. J Biol Inorg Chem 5: 381–392

Antonkine ML, Liu GH, Bentrop D, Bryant DA, Bertini I, Luchinat C, Golbeck JH and Stehlik D (2002) Solution structure of the unbound, oxidized Photosystem I subunit PsaC, containing [4Fe-4S] clusters F_A and F_B: a conformational change occurs upon binding to Photosystem I. J Biol Inorg Chem 7: 461–472

Antonkine ML, Jordan P, Fromme P, Krauß N, Golbeck JH and Stehlik D (2003) Assembly of protein subunits within the stromal ridge of Photosystem I. Structural changes between unbound and sequentially PS I-bound polypeptides and correlated changes of the magnetic properties of the terminal iron sulfur clusters. J Mol Biol 327: 671–697

Aono S, Bentrop D, Bertini I, Cosenza G and Luchinat C (1998a) Solution structure of an artificial Fe_8S_8 ferredoxin: the D13C variant of *Bacillus schlegelii* Fe_7S_8 ferredoxin. Eur J Biochem 258: 502–514

Aono S, Bentrop D, Bertini I, Donaire A, Luchinat C, Niikura Y and Rosato A (1998b) Solution structure of the oxidized Fe_7S_8 ferredoxin from the thermophilic bacterium *Bacillus schlegelii* by ^{1}H NMR spectroscopy. Biochemistry 37: 9812–9826

Barth P, Savarin P, Gilquin B, Lagoutte B and Ochsenbein F (2002) Solution NMR structure and backbone dynamics of the PsaE subunit of Photosystem I from *Synechocystis* sp. PCC 6803. Biochemistry 41: 13902–13914

Ben-Shem A, Frolow F and Nelson N (2003) Crystal structure of plant Photosystem I. Nature 426: 630–635

Bentrop D, Bertini I, Luchinat C, Nitschke W and Mühlenhoff U (1997) Characterization of the unbound 2[Fe_4S_4] ferredoxin-like Photosystem I subunit PsaC from the cyanobacterium *Synechococcus elongatus*. Biochemistry 36: 13629–13637

Bentrop D, Capozzi F and Luchinat C (2001) Iron-sulfur proteins. In: Bertini I, Sigel A and Sigel H (eds) Handbook on Metalloproteins, pp 357–460. Marcel Dekker, New York

Bertini I, Donaire A, Feinberg BA, Luchinat C, Piccioli M and Yuan HP (1995) Solution structure of the oxidized 2[4Fe-4S] ferredoxin from *Clostridium pasteurianum*. Eur J Biochem 232: 192–205

Cantrell A and Bryant DA (1987) Molecular-cloning and nucleotide-sequence of the *psaA* and *psaB* genes of the cyanobacterium *Synechococcus* sp. PCC 7002. Plant Mol Biol 9: 453–468

Chamorovsky SK and Cammack R (1982) Direct determination of the midpoint potential of the acceptor X in chloroplast

Photosystem I by electrochemical reduction and ESR spectroscopy. Photobiochem Photobiophys 4: 195–200

Chitnis VP, Jung YS, Albee L, Golbeck JH and Chitnis PR (1996) Mutational analysis of Photosystem I polypeptides – role of PsaD and the Lysyl 106 residue in the reductase activity of photosystem I. J Biol Chem 271: 11772–11780

Dauter Z, Wilson KS, Sieker LC, Meyer J and Moulis JM (1997) Atomic resolution (0.94 Å) structure of *Clostridium acidi urici* ferredoxin. Detailed geometry of [4Fe-4S] clusters in a protein. Biochemistry 36: 16065–16073

Diaz-Moreno I, Diaz-Quintana A, Molina-Heredia FP, Nieto PM, Hansson O, De la Rosa MA and Karlsson BG (2005) NMR analysis of the transient complex between membrane Photosystem I and soluble cytochrome c_6. J Biol Chem 280: 7925–7931

Diaz-Quintana A, Leibl W, Bottin H and Sétif P (1998) Electron transfer in Photosystem I reaction centers follows a linear pathway in which iron-sulfur cluster F_B is the immediate electron donor to soluble ferredoxin. Biochemistry 37: 3429–3439

Duee ED, Fanchon E, Vicat J, Sieker LC, Meyer J and Moulis JM (1994) Refined crystal structure of the 2[4Fe-4S] ferredoxin from *Clostridium acid urici* at 1.84 Å resolution. J Mol Biol 243: 683–695

Falzone CJ, Kao YH, Zhao JD, Bryant DA and Lecomte JTJ (1994) Three-dimensional solution structure of PsaE from the cyanobacterium *Synechococcus* sp. strain PCC 7002, a Photosystem I protein that shows structural homology with SH3 domains. Biochemistry 33: 6052–6062

Fiaux J, Bertelsen EB, Horwich AL and Wuthrich K (2002) NMR analysis of a 900K GroEL-GroES complex. Nature 418: 207–211

Fischer N, Hippler M, Sétif P, Jacquot JP and Rochaix JD (1998) The PsaC subunit of photosystem I provides an essential lysine residue for fast electron transfer to ferredoxin. EMBO J 17: 849–858

Fischer N, Sétif P and Rochaix JD (1999) Site-directed mutagenesis of the PsaC subunit of Photosystem I. F_B is the cluster interacting with soluble ferredoxin. J Biol Chem 274: 23333–23340

Fish L, Kück U and Bogorad L (1985) Two partially adjacent light-inducible maize chloroplast genes encoding polypeptides of the P700 chlorophyll *a* protein complex of Photosystem I. J Biol Chem 260: 1413–1421

Fromme P, Jordan P and Krauß N (2001) Structure of Photosystem I. Biochim Biophys Acta 1507: 5–31

Golbeck JH (1994) Photosystem I in cyanobacteria. In: Bryant DA (ed) The Molecular Biology of Cyanobacteria, pp 179–220. Kluwer Academic Publishers, The Netherlands

Golbeck JH (1999) A comparative analysis of the spin state distribution of *in vitro* and *in vivo* mutants of PsaC – a biochemical argument for the sequence of electron transfer in Photosystem I as $F_X \rightarrow F_A \rightarrow F_B \rightarrow$ ferredoxin/flavodoxin. Photosynth Res 61: 107–144

Golbeck JH and Bryant DA (1991) Photosystem I. In: Lee CP (ed) Current Topics in Bioenergetics, Vol 16, pp 83–177. Academic Press, Inc., San Diego

Golbeck JH, Parrett KG, Mehari T, Jones KL and Brand JJ (1988) Isolation of the intact Photosystem I reaction center core containing P700 and iron-sulfur center F_X. FEBS Lett 228: 268–272

Heinnickel M, Shen G, Agalarov R and Golbeck J (2005) Resolution and reconstitution of a bound Fe-S protein from the photosynthetic reaction center of *Heliobacterium modesticaldum*. Biochemistry 44: 9950–9960

Jordan P, Fromme P, Witt HT, Klukas O, Saenger W and Krauß N (2001) Three-dimensional structure of cyanobacterial Photosystem I at 2.5 Å resolution. Nature 411: 909–917

Jung YS, Yu L and Golbeck JH (1995) Reconstitution of iron-sulfur center F_B results in complete restoration of $NADP^+$ photoreduction in Hg-treated Photosystem I complexes from *Synechococcus* sp PCC 6301. Photosynth Res 46: 249–255

Ke B, Dolan E, Sugahara K, Hawkridge FM, Demeter S and Shaw ER (1977) Electrochemical and kinetic evidence for a transient electron acceptor in the photochemical charge separation in Photosystem I. In: Photosynthetic Organelles [Plant Cell Physiol (Special Issue no. 3)] pp 187–199

Klukas O, Schubert WD, Jordan P, Krauß N, Fromme P, Witt HT and Saenger W (1999) Photosystem I, an improved model of the stromal subunits PsaC, PsaD, and PsaE. J Biol Chem 274: 7351–7360

Koradi R, Billeter M and Wuthrich K (1996) MOLMOL: a program for display and analysis of macromolecular structures. J Mol Graph 14: 29–32, 51–55

Lakshmi KV, Jung YS, Golbeck JH and Brudvig GW (1999) Location of the iron-sulfur clusters F_A and F_B in Photosystem I: an electron paramagnetic resonance study of spin relaxation enhancement of P700+. Biochemistry 38: 13210–13215

Li N, Zhao J, Warren PV, Warden JT, Bryant DA and Golbeck JH (1991a) PsaD is required for the stable binding of PsaC to the Photosystem I core protein of *Synechococcus* sp. PCC 6301. Biochemistry 30: 7863–7872

Li N, Warren P, Golbeck J, Frank G, Zuber H and Bryant D (1991b) Polypeptide composition of the Photosystem-I complex and the Photosystem-I core protein from *Synechococcus* sp. PCC 6301. Biochim Biophys Acta 1059: 215–225

Locher KP, Hans M, Yeh AP, Schmid B, Buckel W and Rees DC (2001) Crystal structure of the *Acidaminococcus fermentans* 2-hydroxyglutaryl-CoA dehydratase component A. J Mol Biol 307: 297–308

Lovenberg W, Rabinowitz JC and Buchanan BB (1963) Studies on chemical nature of clostridial ferredoxin. J Biol Chem 238: 3899–3913

Mamedov MD, Gourovskaya KN, Vassiliev IR, Golbeck JH and Sememov AY (1998) Electrogenicity accompanies photoreduction of the iron-sulfur clusters F_A and F_B in Photosystem I. FEBS Lett 431: 219–223

Mayer KL, Shen GZ, Bryant DA, Lecomte JTJ and Falzone CJ (1999) The solution structure of Photosystem I accessory protein E from the cyanobacterium *Nostoc* sp. strain PCC 8009. Biochemistry 38: 13736–13746

McDermott AE, Yachandra VK, Guiles RD, Sauer K, Klein MP, Parrett KG and Golbeck JH (1989) EXAFS structural study of F_X, the low-potential Fe-S center in Photosystem I. Biochemistry 28: 8056–8059

Mehari T, Parrett KG, Warren PV and Golbeck JH (1991) Reconstitution of the iron-sulfur clusters in the isolated F_A/F_B protein: EPR spectral characterization of same-species and cross-species Photosystem I complexes. Biochim Biophys Acta 1056: 139–148

Moulis JM, Sieker LC, Wilson KS and Dauter Z (1996) Crystal structure of the 2[4Fe-4S] ferredoxin from *Chromatium vinosum*: evolutionary and mechanistic inferences for [3/4Fe-4S] ferredoxins. Protein Sci 5: 1765–1775

Parrett KG, Mehari T, Warren PG and Golbeck JH (1989) Purification and properties of the intact P700 and F_X-containing Photosystem I core protein. Biochim Biophys Acta 973: 324–332

Pervushin K, Riek R, Wider G and Wuthrich K (1997) Attenuated T_2 relaxation by mutual cancellation of dipole-dipole coupling and chemical shift anisotropy indicates an avenue to NMR structures of very large biological macromolecules in solution. Proc Natl Acad Sci USA 94: 12366–12371

Petrouleas V, Brand JJ, Parrett KG and Golbeck JH (1989) A Mössbauer analysis of the low-potential iron-sulfur center in Photosystem I – spectroscopic evidence that F_X is a 4Fe-4S cluster. Biochemistry 28: 8980–8983

Rousseau F, Sétif P and Lagoutte B (1993) Evidence for the involvement of PSI-E subunit in the reduction of ferredoxin by Photosystem I. EMBO J 12: 1755–1765

Saenger W, Jordan P and Krauß N (2002) The assembly of protein subunits and cofactors in Photosystem I. Curr Opin Struct Biol 12: 244–254

Schlessman JL, Woo D, Joshua-Tor L, Howard JB and Rees DC (1998) Conformational variability in structures of the nitrogenase iron proteins from *Azotobacter vinelandii* and *Clostridium pasteurianum*. J Mol Biol 280: 669–685

Sétif P (2001) Ferredoxin and flavodoxin reduction by Photosystem I. Biochim Biophys Acta 1507: 161–179

Shinkarev VP, Vassiliev IR and Golbeck JH (2000) A kinetic assessment of the sequence of electron transfer from F_X to F_A and further to F_B in Photosystem I: the value of the equilibrium constant between F_X and F_A. Biophys J 78: 363–372

Sticht H and Rosch P (1998) The structure of iron-sulfur proteins. Prof Phys Mol Biol 70: 95–136

Stout CD (1993) Crystal structures of oxidized and reduced *Azotobacter vinelandii* ferredoxin at pH 8 and pH 6. J Biol Chem 268: 25920–25927

Tranqui D and Jesior JC (1995) Structure of the ferredoxin from *Clostridium acidi urici* – model at 1.8 Å resolution. Acta Crystallogr D Biol Crystallogr 51: 155–159

Unciuleac M, Boll M, Warkentin E and Ermler U (2004) Crystallization of 4-hydroxybenzoyl-CoA reductase and the structure of its electron donor ferredoxin. Acta Crystallogr D Biol Crystallogr 60: 388–391

Vassiliev IR, Jung YS, Yang F and Golbeck JH (1998) PsaC subunit of Photosystem I is oriented with iron-sulfur cluster F_B as the immediate electron donor to ferredoxin and flavodoxin. Biophys J 74: 2029–2035

Vassiliev IR, Antonkine ML and Golbeck JH (2001) Iron-sulfur clusters in type I reaction centers. Biochim Biophys Acta 1507: 139–160

Xia ZC, Broadhurst RW, Laue ED, Bryant DA, Golbeck JH and Bendall DS (1998) Structure and properties in solution of PsaD, an extrinsic polypeptide of Photosystem I. Eur J Biochem 255: 309–316

Xu Q, Jung YS, Chitnis VP, Guikema JA, Golbeck JH and Chitnis PR (1994) Mutational analysis of Photosystem I polypeptides in *Synechocystis* sp. PCC 6803 – subunit requirements for reduction of $NADP^+$ mediated by ferredoxin and flavodoxin. J Biol Chem 269: 21512–21518

Yu JP, Smart LB, Jung YS, Golbeck J and Mcintosh L (1995) Absence of PsaC subunit allows assembly of Photosystem I core but prevents the binding of PsaD and PsaE in *Synechocystis* sp PCC 6803. Plant Mol Biol 29: 331–342

Zhao J, Warren PV, Li N, Bryant DA and Golbeck JH (1990) Reconstitution of electron transport in Photosystem I with PsaC and PsaD proteins expressed in *Escherichia coli*. FEBS Lett 276: 175–180

Zhao J, Li N, Warren P, Golbeck J and Bryant D (1992) Site-directed conversion of a cysteine to aspartate leads to the assembly of a [3Fe-4S] cluster in PsaC of Photosystem I – the photoreduction of F_A is independent of F_B. Biochemistry 31: 5093–5099

Zhao J, Snyder WB, Mühlenhoff U, Rhiel E, Warren PV, Golbeck JH and Bryant DA (1993) Cloning and characterization of the *psaE* gene of the cyanobacterium *Synechococcus* sp. PCC 7002 – characterization of a *psaE* mutant and overproduction of the protein in *Escherichia coli*. Mol Microbiol 9: 183–194

Chapter 9

Accessory Chlorophyll Proteins in Cyanobacterial Photosystem I

James Barber*, Jon Nield, and James Duncan
Wolfson Laboratories, Division of Molecular Biosciences, S. Kensington Campus, Imperial College London, London SW7 2AZ, UK

Thomas S. Bibby
National Oceanographic Centre, University of Southampton, SO14 3ZH, UK

Summary

The IsiA protein accumulates in many cyanobacteria under conditions of iron starvation. It is a Chl *a*-binding protein, which is closely related to the six-transmembrane α-helical antenna family typified by CP43 of PS II. One of its functions is to provide an efficient accessory light harvesting system for Photosystem I (PS I) by forming a ring of 18 IsiA subunits around the trimeric reaction center core. This response is probably to compensate for a drop in the PS I level relative to Photosystem II (PS II) and, the level of phycobiliproteins, in response to iron deficiency. A similar accessory light harvesting system for PS I has been shown to occur in cyanobacteria that do not contain phycobiliproteins, often termed prochlorophytes. This light harvesting system is composed of Pcb proteins that are closely related to IsiA but bind Chl *b* as well as Chl *a*. Unlike IsiA, Pcb proteins can also provide accessory light harvesting systems for PS II. Some cyanobacteria contain phycobiliproteins and Pcb proteins, where both are able to function as light harvesting systems. In one case the Pcb protein seems to bind only Chl *a* (*Fischerella muscicola*) while in another they bind Chl *d* (*Acaryochloris marina*). Sequence analysis indicates that the IsiA/Pcb proteins have very similar pigment binding sites to those of CP43 and to a lesser extent to the other reaction center proteins of this family and have the capacity to accommodate several different forms of Chl. The six-transmembrane α-helical Chl-binding proteins, of which IsiA and Pcb are members, seem to have evolved from a basic evolutionary building block providing both internal and accessory light harvesting systems for a wide range of photosynthetic organisms.

* Author for correspondence, email: j.barber@impertial.ac.uk

John H. Golbeck (ed): Photosystem I: The Light-Driven Plastocyanin:Ferredoxin Oxidoreductase, 99–117.

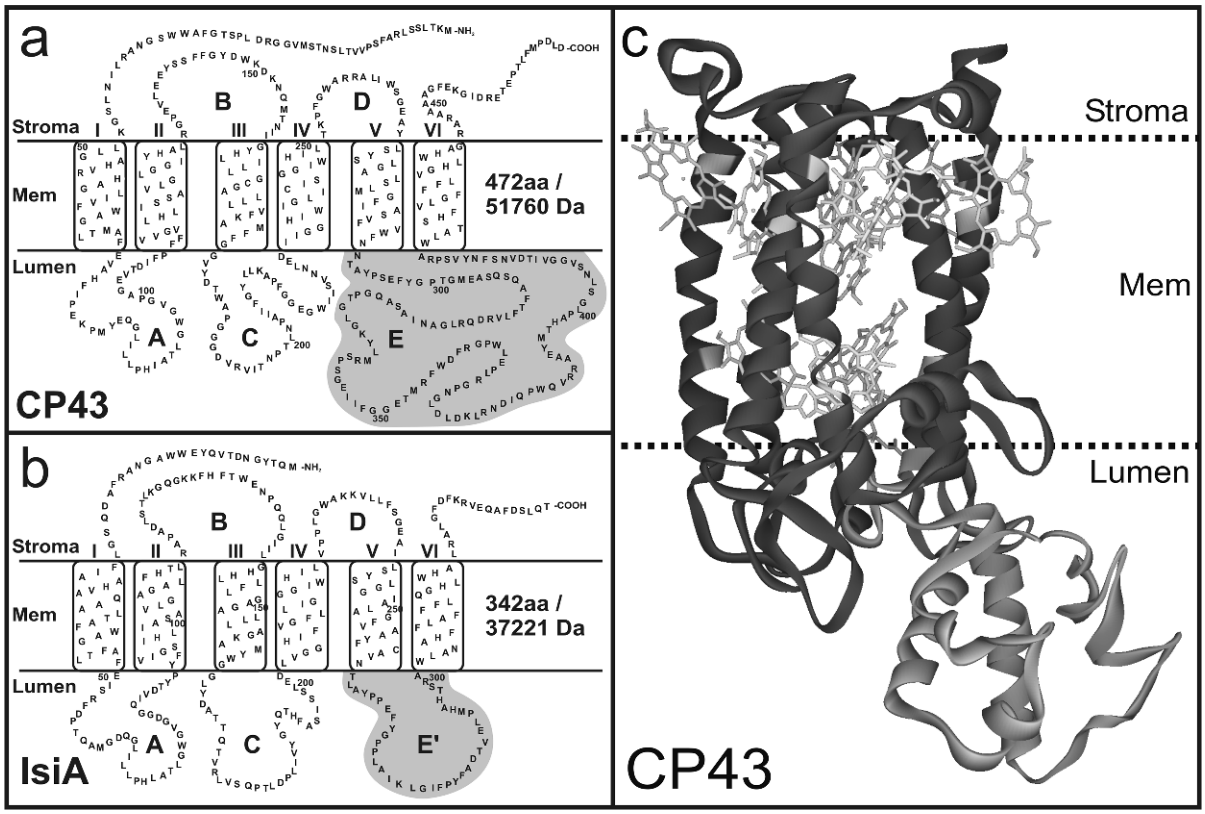

Fig. 1. Structure of CP43 and IsiA proteins. (a) and (b) Diagrammatic representations of CP43 and IsiA proteins (based on the sequence of *Synechocystis* sp. PCC 6803) emphasizing their structural similarities and differences. Also highlighted are the histidine residues (H) of CP43 and IsiA. In CP43 of *Thermosynechococcus elongatus*, these histidines provide 10 ligands for the 14 Chls bound to this PS II protein (Ferreira et al., 2004), which are almost entirely conserved in IsiA. (c) X-ray model of CP43 from Ferreira et al. (2004) emphasizing the structure of the large extrinsic loop joining transmembrane helices V and VI. Also shown are some of the Chls bound to this protein.

I. Overview of Light Harvesting Systems

All types of oxygenic photosynthetic organisms contain a chlorophyll (Chl)/carotenoid (Car)-based internal light harvesting system that is tightly associated with the reaction center (RC) domains of photosystem I (PS I) and photosystem II (PS II) core complexes. In the case of PS II the internal antenna system is composed of two homologous proteins, CP43 and CP47, which bind 14 and 16 Chl *a* molecules, respectively (Ferreira et al., 2004) with the majority ligated to histidine residues. They are composed of six-membrane spanning α-helices characterized by having large lumenal extrinsic loops joining helices V and VI (see Fig. 1). Their structures have been fully elucidated (Ferreira et al., 2004) and as predicted (Schubert et al., 1998) were found to be remarkably similar to the N-terminal portion of the PS I RC proteins PsaA and PsaB (Rhee et al., 1998; Zouni et al., 2001; Kamiya and Shen, 2003; Ferreira et al., 2004). However, in the case of the PS I proteins there are no equivalent large lumenal loops (Jordan et al., 2001). The number of Chls bound to the N-terminal domain of PS I is approximately the same as for CP43 and CP47, but unlike PS II, there is a cluster of Chl *a* molecules bound at the interface between the N-terminal and C-terminal regions of the PsaA and PsaB proteins (Jordan et al., 2001). Therefore, the PS I light harvesting domain binds a total of 90 Chl *a* molecules while that of the PS II binds only 30 light harvesting Chl *a* molecules with the other six Chls of each photosystem bound to the RC domain.

Abbreviations: Car – carotenoid; Chl – chlorophyll; CP43 – chlorophyll-binding protein encoded by *psbC* gene; Cyt – cytochrome; EM – electron microscopy; Isi A – iron-stress-induced chlorophyll-binding protein; LHC – light harvesting complex; Pcb – prochlorophyte chlorophyll-binding protein; PS I – Photosystem I; PS II – Photosystem II; RC – reaction center.

In plants and all types of algae, the light harvesting capacity of PS I and PS II is further enhanced by outer accessory light harvesting systems. Plants and green algae use Chl *a*/Chl *b* light harvesting complexes (LHC) encoded by *cab* genes where LHCII and LHCI service PS II and PS I, respectively (Green and Durnford, 1996). The LHC proteins have three transmembrane helical domains and also act as light harvesting systems in brown algae and diatoms, but in these cases they bind Chl *a* and Chl *c* (Grossman et al., 1995). Dinoflagellate algae also use Chl *c* as an outer light harvesting pigment but at relatively low levels compared with the unusual carotenoid, peridinin, acting as the major antenna pigment in this class of organisms (Grossman et al., 1995).

Although red algae use Chl *a*-binding LHCI as an antenna for PS I (Wolfe et al., 1994) they differ from the above oxygenic organisms in that PS II has as its outer light harvesting system, the water soluble phycobiliproteins assembled into phycobilisomes bound to the stromal surface of PS II (Glazer, 1985).

Until recently the situation in classical cyanobacteria seemed to be simpler, with phycobilisomes being the only type of accessory light harvesting system. This extrinsic light harvesting antenna mainly transfers energy to PS II but seems to provide some light harvesting function for PS I (Mullineaux, 1994). However, it is now clear that cyanobacteria can also use Chl as an accessory light harvesting system. It was the discovery of *Prochloron didemni* by Lewin (1975, 1976, 1977), which indicated for the first time that some cyanobacterial-like oxygenic prokaryotic organisms employ Chl *a* and Chl *b* rather than phycobilins as pigments for accessory light harvesting systems. *Prochloron* is symbiotic with didemnid ascidians of tropical water (Newcomb and Pugh, 1975) and as yet there is no report of its existence as a free-living organism. Originally*Prochloron* and the related free-living Chl *a*/Chl *b*-containing oxygenic prokaryotes *Prochlorothrix hollandica* (Burger-Wiersma et al., 1986) and *Prochlorococcus marinus* (Chisholm et al., 1988) were given their own classification as prochlorophytes. Today, based on 16S rRNA analyses (Turner et al., 1999; Ting et al., 2002; Ernst et al., 2003) they are well located within the cyanobacterial clade (see Fig. 2). For this reason this chapter will not only review the Chl-containing accessory light harvesting systems of classical cyanobacteria but also of prochlorophytes and the recently characterized prochlorophyte-like cyanobacteria, *Fischerella muscicola* (Geiss et al., 2001), and *Acaryochloris marina* (Miyashita et al., 1996).

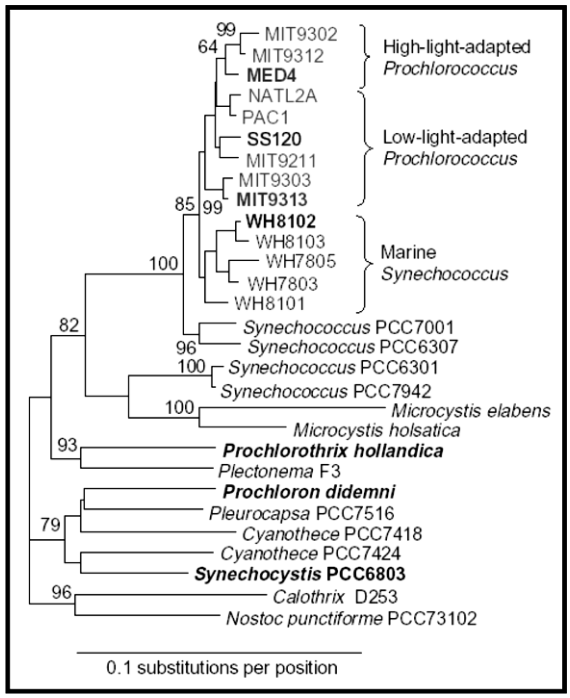

Fig. 2. A phylogenetic tree constructed from 16S RNA sequences showing that the three prochlorophytes, *Prochloron*, *Prochlorothrix*, and *Prochlorococcus* are distributed within the cyanobacterial clade and are not directly related to each other being positioned on different branches of the cyanobacterial radiation. (Modified from Ting et al., 2002.)

II. Response to Iron Deficiency

Iron is the fourth most common element and also the most abundant transition metal on Earth. It is an absolute requirement for cyanobacteria and other organisms to flourish. Iron concentrations in the aquatic environment can fluctuate and they are often limited to picomolar levels (Martin et al., 1994). This is due in part to the fact that in the presence of oxygen iron exists in its ferric (Fe^{3+}) state. At physiological pH, Fe^{3+} forms insoluble hydroxides, severely reducing the availability of iron to aquatic organisms, thus the level of available iron may be insufficient to support high phytoplankton biomass and maximal growth rates in the oceans (de Baar et al., 1995; Falkowski et al., 1998; Behrenfeld and Kolber, 1999).

As a response to low levels of available iron, cyanobacteria have evolved a number of strategies for survival (Straus, 1994). These include responses that reduce the demand for iron in the cell including: (i) A reduction in the number of photosynthetic complexes, all of which incorporate iron (Guikema and Sherman,

1983); (ii) An increase in the ratio of PS II RCs to PS I RCs (Guikema and Sherman, 1983). PS I binds six times more iron than PS II and by specifically reducing the number of PS I RCs per cell, the cells demand for iron is reduced; (iii) A reduction in the amount of phycobilisomes that rely on iron-binding complexes for their synthesis (Sherman and Sherman, 1983).

In culture, iron starved cyanobacteria can maintain a normal growth rate for a while and recover rapidly from their stressed state when iron is introduced into the growth medium (Sherman and Sherman, 1983). It is, therefore, apparent that cyanobacteria can acclimatize to conditions where iron concentrations are low. Here we will restrict the discussion to a response that induces the formation of a Chl *a*-based accessory light harvesting system for PS I.

Under iron-deficient conditions the spectral characteristics of cyanobacterial cells in culture, such as *Synechocystis* sp. PCC 6803 or *Synechococcus* sp. PCC 7942, can change: the maximal red Chl *a* absorption peak shifts dramatically to the blue from 680 to 675 nm (Öquist, 1971, 1974a). This characteristic absorption shift is coincident with the appearance of a dominant 77 K fluorescence emission peak at 685 nm (Öquist, 1974b). It has been shown that these responses are linked to the expression of the "iron-stress-induced" gene, *isiA* (Burnap et al., 1993).

In most but not all cyanobacteria studied to date, the *isiA* gene is the first of two genes on the *isiAB* operon. The *isiA* gene encodes a 34 kDa protein, called the IsiA protein throughout this chapter. It has an amino acid sequence homologous to that of CP43 of PS II (Pakrasi et al., 1985a) and for this reason is also referred to as CP43′. The second gene, *isiB*, encodes flavodoxin which, under conditions of iron deficiency, functionally replaces the iron-containing ferredoxin as the electron acceptor of PS I (Fitzgerald et al., 1977; Sétif, 2001). The *isiAB* operon is transcribed into two messages, a monocistronic message containing only the *isiA* transcript and a dicistronic message that also contains the *isi*B gene (Laudenbach et al., 1988).

The IsiA protein is predicted by hydropathy analysis to have six transmembrane helices and judging by the conservation of histidine residues (see Fig. 1), it is likely to bind about the same number of Chl *a* molecules as CP43. The major difference is that IsiA lacks the large hydrophilic loop that joins the lumenal ends of helices V and VI of CP43 (see Fig. 1). For this reason, it consists of about 340 amino acids rather than 470, which typically make up CP43, a fact reflected in the difference in their molecular masses (34 kDa as compared with 52 kDa). Under severe iron stress the IsiA becomes an abundant Chl *a*-binding protein in some cyanobacteria and is the cause of the large spectral changes associated with iron deficiency (Öquist, 1971, 1974a; Riethman and Sherman, 1988). Isolated IsiA has a room temperature maximum at 670 nm while that of PS I is 680 nm (Bibby et al., 2001b).

Although the discovery of the IsiA protein was made some time ago (Guikema and Sherman, 1983, 1984), its function as a discrete light harvesting system has only recently been proven. Prior to this there had been at least four postulates for its function.

(i) IsiA aids the recovery of cells from their stressed condition by acting as a Chl store for when iron becomes readily available in the environment (Riethman and Sherman, 1988). Support for this is in part based on the observation that even in the presence of inhibitors of chlorophyll synthesis, CP43 and CP47 are synthesized during recovery from iron stress.

(ii) IsiA protects PS II from photo-induced damage by acting as a dissipater of excitation energy. Indeed, it has been reported that iron-stressed cyanobacterial cells are more resistant to photoinhibition of photosynthesis than normal cells (Park et al., 1999; Sandstrom et al., 2001; Michel and Pistorius, 2004).

(iii) IsiA may act as a light harvesting complex under iron-stress conditions, mainly for PS II (Pakrasi et al., 1985b; Riethman and Sherman, 1988) but also for PS I (Tetenkin et al., 1998) and in that way compensate for the decreased level of phycobiliproteins.

(iv) IsiA could provide a functional replacement for CP43 in PS II during iron starvation (Straus, 1994). This would generate a PS II complex that lacks the large extrinsic loop of CP43. This loop plays an important role in stabilizing the extrinsic subunits of the oxygen-evolving complex (OEC) (De Las Rivas and Barber, 2004) and also provides a ligand (CP43-Glu354) to one of the Mn ions of the catalytic center of the OEC (Ferreira et al., 2004). It can, therefore, be speculated that this modified form of PS II would no longer have a functional OEC and could extract electrons from alternative substrates to water. In fully functional PS II the extrinsic OEC subunits create the environment in which water is oxidized at the catalytic manganese cluster and provide steric hindrance to

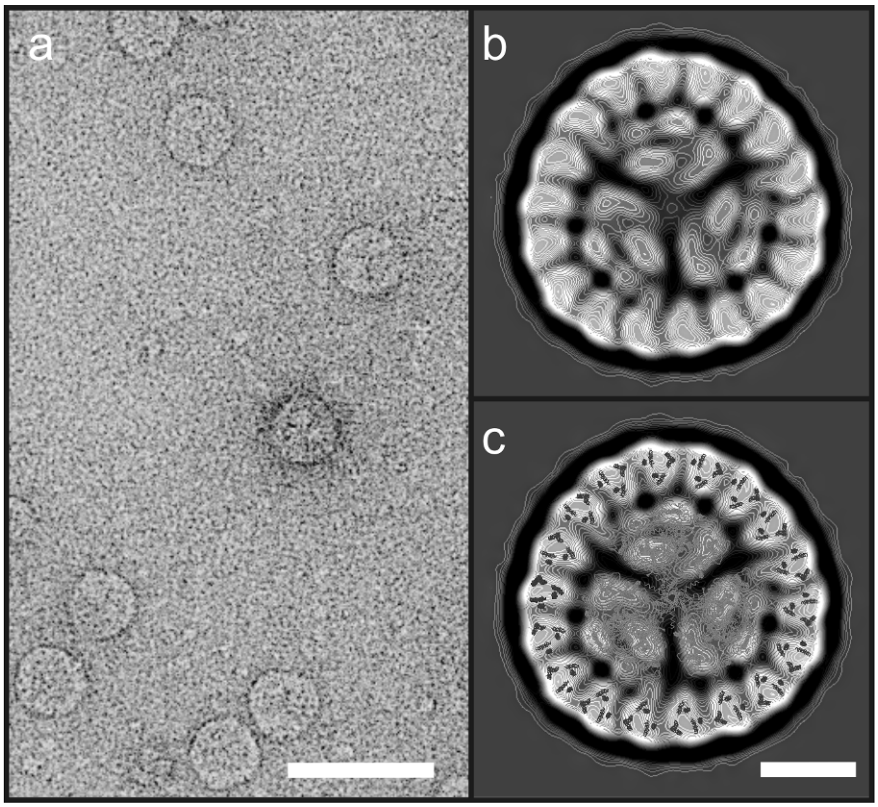

Fig. 3. Structure of the IsiA–PS I supercomplex of *Synechocystis* sp. PCC 6803 deduced by electron microscopy and single particle analysis of negatively stained preparations presented as a projection map viewed from the stromal surface. (a) Raw electron micrograph. Bar represents 500 Å. (b) After image processing of 3,000 particles. (c) The overlay of the X-structure of trimeric PS I as a C_α-trace (Jordan et al., 2001) and six transmembrane helices of CP43 (Zouni et al., 2003). Bar represents 100 Å. (Modified from Bibby et al., 2001a.)

prevent other substrates being oxidized by the primary electron donor $P680^+$. A PS II complex having CP43 replaced by IsiA and lacking the extrinsic OEC proteins could in principle obtain electrons from alternative substrates such as plastocyanin. In this way a pathway of cyclic electron flow around PS II and the cytochrome (cyt) b_6f complex might occur in a similar fashion to that found in photosynthetic purple bacteria where cyt *c*, reduced by the cyt *bc* complex, acts as a donor to the Type II reaction center (Nogi and Miki, 2001). Cyclic electron flow around PS II has been suggested previously (Arnon, 1995) and could represent a method by which the iron-stressed cyanobacteria could generate a proton gradient for driving ATP synthesis and thus compensate for the reduction of cyclic electron flow mediated by PS I. However, till date there is no report of the isolation of this modified form of PS II.

III. IsiA as a Light Harvesting Protein

Electron microscopy (EM) and single particle analysis showed that 18 copies of the IsiA protein associates with the PS I trimeric RC core complex of *Synechocystis* PCC 6803 (Bibby et al., 2001a). As shown in Fig. 3, this arrangement was emphasized by modeling into the structure the X-ray data obtained for the PS I RC (Jordan et al., 2001) and CP43 (Zouni et al., 2001) of *Thermosynechococcus elongatus* assuming the expected structural homology between CP43 and IsiA. A similar IsiA–PS I supercomplex was also isolated from *Synechococcus* sp. PCC 7942 grown in low iron conditions by Boekema et al. (2001).

The isolated IsiA–PS I supercomplex has a molecular mass of about 2,000 kDa and assuming that the IsiA protein binds 14 Chl as does CP43, then the antenna size of PS I increases from 90 per P700 to 174, an increase of about 100%. That the additional light harvesting system composed of IsiA can transfer energy efficiently

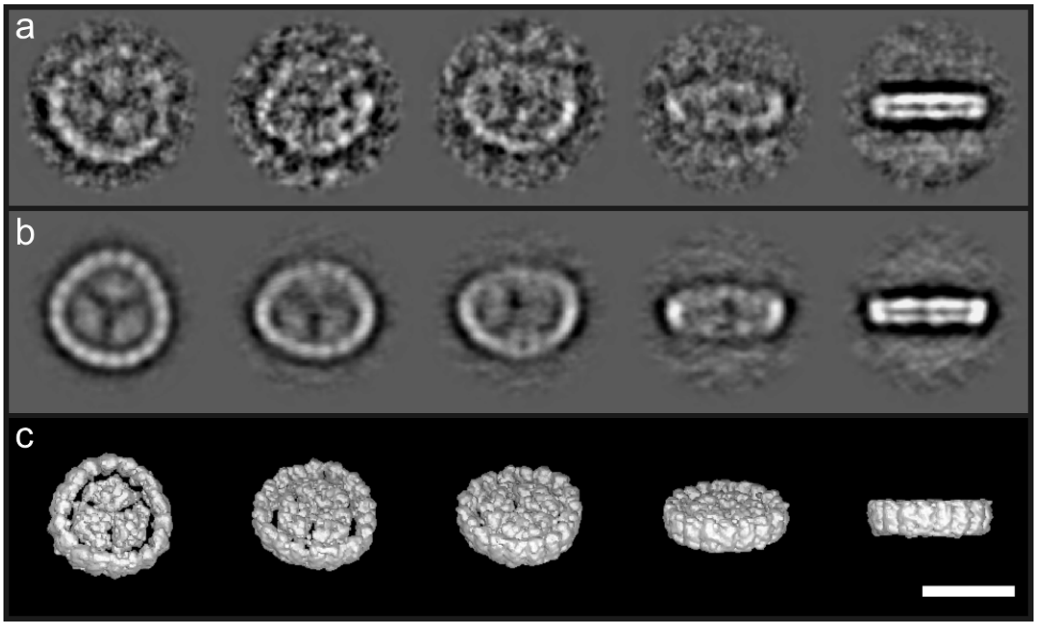

Fig. 4. 3D reconstruction of the IsiA–PS I supercomplex of *Synechocystis* sp. PCC 6803 obtained by electron cryomicroscopy. (a) A selection of typical class averages used for the 3D reconstruction. (b) Re-projections from the 3D map in orientations identical to those corresponding to the class averages in panel (a). (c) Surface representation of the final 3D map viewed in the same orientations. Bar represents 300 Å. (Modified from Nield et al., 2003.)

to the PS I RC has been shown by steady-state room temperature (Bibby et al., 2001b) and low-temperature (Andrizhiyevskaya et al., 2002) fluorescence studies and also by measuring the relative quantum yield for the oxidation of P700 (Boekema et al., 2001). The validity of this conclusion was substantiated and extended by time resolved fluorescence and absorption spectroscopy (Melkozernov et al., 2003; Andrizhiyevskaya et al., 2004). All these studies concluded that the 18-mer ring of IsiA increases the absorption cross-section for light absorption by the PS I RC by about 100%. The time resolved studies concluded that energy transfer within the ring occurs in sub-psec times. Transfer from the ring to the PS I RC core also seems to be very fast, occurring within 10 psec. The efficiency of energy transfer from the antenna ring to the PS I RC core gives rise to a short excitation lifetime for the IsiA–PS I supercomplex measured to be in the region of 40 psec. This value is longer than the 25 psec measured for the cyanobacterial PS I trimer but in line with the essential doubling of the antenna size.

The images shown in Fig. 3 were derived from EM of samples stained with uranyl acetate, which enhances the contrast of the images facilitating initial structural analyses. This heavy metal staining, however, can cause artifacts such as variable flattening of the 3D structure brought about by dehydration and granulation due to differential penetration of the stain (Ruprecht and Nield, 2001). To overcome these stain-induced artifacts, EM and image analyses were conducted on samples rapidly frozen in vitreous ice in the absence of stain (Nield et al., 2003). This approach also ensures that the particles are frozen in a variety of orientations, which is required for producing an isotropically resolved 3D model.

Figure 4 shows five typical class averages of the IsiA–PS I supercomplex derived from electron cryomicroscopy (cryo-EM) which, together with further class averages, were used to calculate the 3D structure depicted in Fig. 4c. This 3D structure has a resolution of about 20 Å and provides a more reliable framework for modeling the most complete X-ray structures of PS I RC and CP43 of *T. elongatus* (Jordan et al., 2001; Ferreira et al., 2004). The modeling is shown in Fig. 5a as an overlay onto the molecular envelope of the 3D map. It can be seen that the 18-mer ring is not a true circle and that much of it is not directly attached to the surface of PS I RC core trimer. There is, however, a linking density for each monomer, which is outside the density corresponding to the X-ray structures. This seems to suggest that a "linker protein" is induced under low iron conditions, but the nature of this protein is

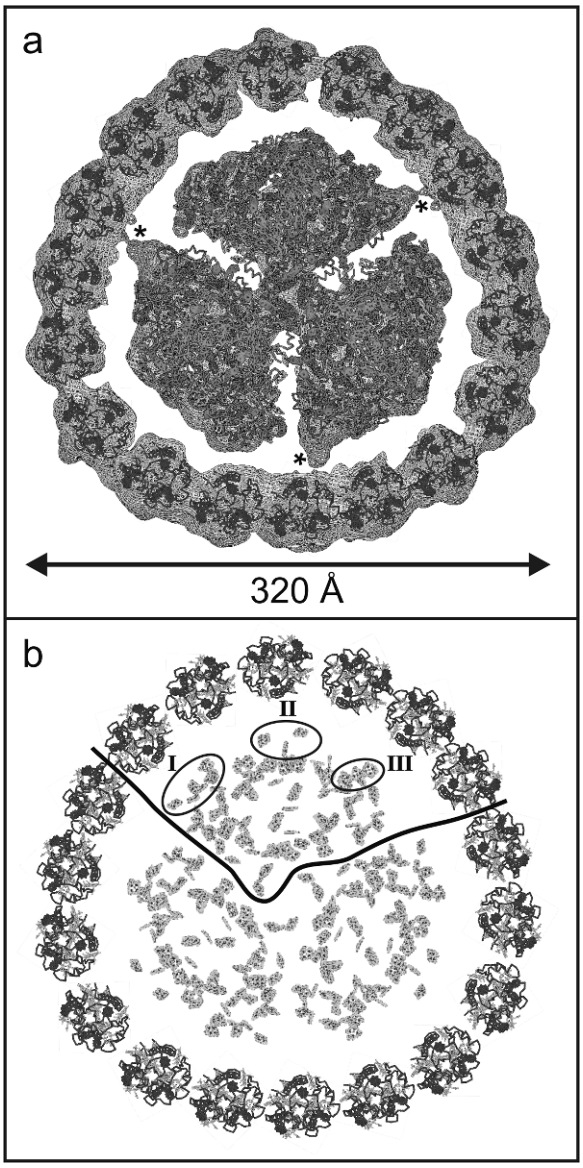

Fig. 5. Interpretation of the cryo-EM 3D structure of the IsiA–PS I supercomplex of *Synechocystis* sp. PCC 6803. (a) Modeling of the C_α-backbone and chlorophylls of the PS I trimer and CP43 using data derived from X-ray diffraction studies for PS I (Jordan et al., 2001) and PS II (Ferreira et al., 2004), overlaid onto the molecular envelope of the 3D cryo-EM map, viewed from the stromal side. The white stars indicate areas of density that are not present in the X-ray structure of PS I and might represent linker regions between the PS I RC and the IsiA antenna ring. (b) Modeling of Chl organization using coordinates from the X-ray structures of PS I (Jordan et al., 2001) and PS II (Ferreira et al., 2004) viewed from the stromal side. The three ringed areas (I–III) highlight regions where the peripheral Chls of the PS I RC monomer are closest to the Chls within the IsiA ring. The modelling assumed that helices V and VI of IsiA are adjacent to the surface of the PS I RC. (Modified from Nield et al., 2003). See Color Plate 8, Fig. 1.

unknown. A recent X-ray structure of the LHCI–PS I supercomplex of higher plants (Ben-Shem et al., 2003, 2004) also has a linker protein in a similar position. It has been suggested that the protein linking LHCI subunits to the PS I RC is PsaG. It is, therefore, conceivable that a "PsaG-like" protein, expressed in response to iron deficiency, links the IsiA antenna system to the PS I RC.

The remaining interactions that stabilize the six IsiA subunits associated with each monomeric PS I RC seem to be via interactions to the IsiA themselves, which as can be seen in Fig. 5 are tightly packed. A similar conclusion has been reached for the Lhca proteins of LHCI (Ben-Shem et al., 2003).

Further support for the idea that the IsiA antenna is a self-assembling system involving interactions between adjacent IsiA subunits coupled with a specific binding to the PS I RC via a linker protein comes from studies with a *psaL*-less mutant of *Synechocystis* sp. PCC 6803 (Aspinwall et al., 2004). The PsaL protein is located in the trimerization domain of the cyanobacterial PS I trimer. The deletion of the *psaL* gene inhibits trimer formation (Chitnis and Chitnis, 1993). When this mutant was grown under iron limiting conditions it was found that IsiA associated with monomeric PS I along the same surface as with normal PS I trimers. In the majority of cases, there were six IsiA subunits per RC but also seven IsiA subunits could be found in a subpopulation of the data set. Chlorophyll fluorescence measurements indicated that these IsiA subunits were functionally coupled to the RC. Clearly these results show that the association of IsiA with PS I does not depend on the trimeric conformation of RCs. Moreover, that more than six subunits could be identified in some particles reinforces the view that it is interactions between adjacent IsiA proteins that stabilize the light harvesting system. We will return to this point later.

IV. Organization of Chls in the IsiA–PS I Supercomplex

The improved 3D structural model for the IsiA–PS I supercomplex derived from cryo-EM (Nield et al., 2003) has provided an opportunity to identify Chls, which may be involved in energy transfer from the IsiA ring to the PS I RC. Figure 5b shows a model for the distribution of Chl in the supercomplex derived from the X-ray data. When viewed from the lumenal surface three regions (I, II, and III) at the periphery of each monomer of the PS I RC trimer can be identified where the Chls are located closer to those in the IsiA

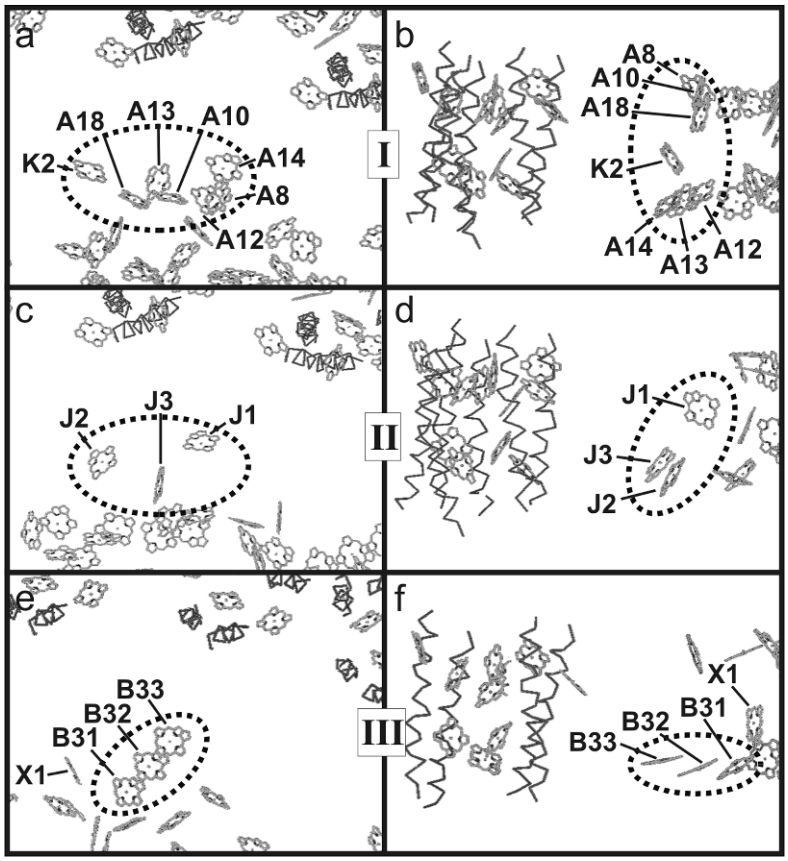

Fig. 6. Organization of Chls in regions I–III of Fig. 5. Close up top views from the stromal surface (a, c, and e) and side views (b, d, and f). The Chls are numbered according to the nomenclature of Byrdin et al. (2002). (From Nield et al., 2003, with permission.)

ring. The closest distances between the IsiA Chls and those of the PS I RC are 20–30Å edge-to-edge. These distances do not vary much if the IsiA subunit is rotated within the density (Nield et al., 2003). However, it seems likely that helices V and VI of IsiA are located adjacent to the PS I RC surface given that this is the arrangement of the transmembrane helices of CP43 in the PS II RC core (Kamiya and Shen, 2003; Ferreira et al., 2004).

Figure 6 shows the three regions in more detail. The numbering of these Chls is in accordance with the literature (Byrdin et al., 2002). The first circled region (region I) contains a cluster of seven Chls, of which three are distributed toward the stromal surface, A8, A10, and A18, and three toward the lumenal surface, A12–A14. All are located within the transmembrane helices of the PsaA protein, spanning the region from A-Gly170 to A-Gly320, and all are ligated to histidines. Interestingly, the seventh Chl *a* of this cluster, K2, is coordinated with the small subunit PsaK at residue K-His67. The central cluster (region II) contains three Chls: J1–J3, which are associated with the small subunit PsaJ; Chl J2 is ligated to J-Glu28; and J3 to J-His39. The other Chl, J1, is ligated to a water molecule also coordinated with the PsaJ protein. The cluster of Chls identified in region III is composed of three Chl *a* molecules, B31–B33, each separated by ∼8 Å, lying almost in the plane of the membrane toward the lumenal side. All are directly or indirectly ligated to a large lumenal loop of the PsaB protein stretching from residue B-Phe465 to B-Gly510. Chlorophyll B31 is ligated to B-His470, and the other Chls, B32, and B33, are coordinated to water molecules. However, there is some uncertainty whether this cluster of Chls exists in *Synechocystis* sp. PCC 6803.

If it is assumed that the PS I structure of *T. elongatus* applies for *Synechocystis* sp. PCC 6803, it seems likely that the three clusters of Chls identified in regions I–III could facilitate energy transfer from the IsiA antenna ring to the PS I RC. Although some of these Chls are bound within the PsaA and PsaB RC proteins, some are associated with the small subunit located on the

peripheral edge of the trimer. This is clearly the case for all three Chls associated with PsaJ and similarly for one of the Chls indirectly coordinated with PsaK. There is, however, the possibility that other "linker Chls" are present in the IsiA–PS I supercomplex, which are in addition to those resolved by X-ray crystallography for the PS I complex (Jordan et al., 2001) or for CP43 (Ferreira et al., 2004). Such linker Chls have been identified in the higher plant LHCI–PS I supercomplex (Ben-Shem et al., 2003).

The functional importance of PsaJ has been investigated using a PsaJ/PsaF double null-mutant of *Synechocystis* sp. PCC 6803 (Kouril et al., 2003). This mutant expressed the *isi*A gene, not only in response to low iron but also under oxidative stress due to impairment of electrons on the acceptor side of PS I (Jeanjean et al., 2003). A similar effect was observed in wild-type *Synechocystis* when methyl viologen was added to facilitate superoxide radical formation. A follow-up study showed that the PsaJ/PsaF null-mutant, when iron stressed, formed an IsiA–PS I supercomplex, but in this case IsiA antenna ring was composed of 17 subunits (Kouril et al., 2003). Consequently the diameter of this 17-mer supercomplex was 295 Å compared with 324 Å for the normal 18-mer equivalent. This work clearly shows that neither PsaJ nor PsaF is required to form the IsiA accessory antenna system around PS I. Presumably the reduction in the size of the PS I RC complex due to the absence of PsaF and PsaJ allows the IsiA ring to form with a smaller diameter having one less subunit than the wild-type. This clearly breaks the symmetry and it will require more detailed work to understand how under these circumstances the IsiA subunit specifically interacts with the surface of the PS I RC. In this context it has recently been shown, using WT *Synechocystis* sp. PCC 6803 as well as the PsaJ/PsaF null-mutant, that after prolonged growth in iron depleted media, when the IsiA protein accumulates to a high level, it assembles into a variety of structures which are in addition to those where it forms an accessory light harvesting system for trimeric PS I RC (Yeremenko et al., 2004). These mainly take the form of multilayer rings of IsiA. Some of these multilayer rings surround a central mass attributed by the authors to be monomeric PS I RC. The physiological significance of these structures is unclear since the cyanobacteria were subject to severe iron deprivation over a long period of time. It was suggested that structures not associated with the PS I RC could play a role in photoprotection in line with earlier suggestions that IsiA can function in this way (Park et al., 1999; Sandström et al., 2001). The multilayers around the PS I monomer may be legitimate light harvesting systems under very extreme conditions.

All the studies to date seem to indicate that IsiA is a rather promiscuous protein which, by interactions with itself, can form a host of structures, some of which involve association with PS I to form a functional light harvesting unit, while others are not involved in energy transfer to the PS I RC. Given this conclusion it is surprising that there is no report of the IsiA protein associating with PS II.

V. Pcb Light Harvesting Proteins

The discovery of *Prochloron didemni* (Lewin, 1975; Newcomb and Pugh, 1975) provided evidence that not all prokaryotic oxygenic organisms contain phycobilins. Indeed, the finding that its accessory light harvesting system was composed of Chl *a*- and Chl *b*-binding proteins that were intrinsic to the membrane gave rise to the general belief that *Prochloron*, like higher plants and green algal chloroplasts, contained Cab proteins. It was, therefore, suggested that *Prochloron* was a living example of the precursor to the modern chloroplast assumed to be derived from an endosymbiotic event involving a Chl *a*/Chl *b*-containing prokaryote (Lewin, 1984; Walsby, 1986). This theory was given further credibility with the discovery of two types of free-living "*Prochloron*-like" or prochlorophyta, *Prochlorothrix hollandica* (Burger-Wiersma et al., 1986), and *Prochlorococcus marinus* (Chisholm et al., 1988).

A number of studies suggested that the Chl *a*/*b*-binding proteins of prochlorophytes differed from Cab proteins of higher plants and green algae (Matthijs et al., 1994). The uncertainty was clarified in 1996 when the genes encoding the Chl *a*/*b* proteins of *Prochlorothrix* and *Prochloron* were sequenced (La Roche et al., 1996). This sequencing clearly showed that genes of these prochlorophytes, now known as *pcb* genes (prochlorophyte chlorophyll-binding genes), were not related at all to *cab* genes but closely related to *isiA* genes of cyanobacteria. This conclusion explains the results of Bullerjahn et al. (1987), where an immunological relatedness between the Pcb proteins of *Prochlorothrix* and the IsiA protein was found and that immunological cross-reaction between Pcb and Cab proteins could not be observed (Hiller and Larkum, 1985; Bullerjahn et al., 1990).

In the case of *Prochloron*, one *pcb* gene (*pcbA*) was sequenced (La Roche et al., 1996) but recently a second *pcb* gene (*pcbC*) has been identified (Chen et al., 2004).

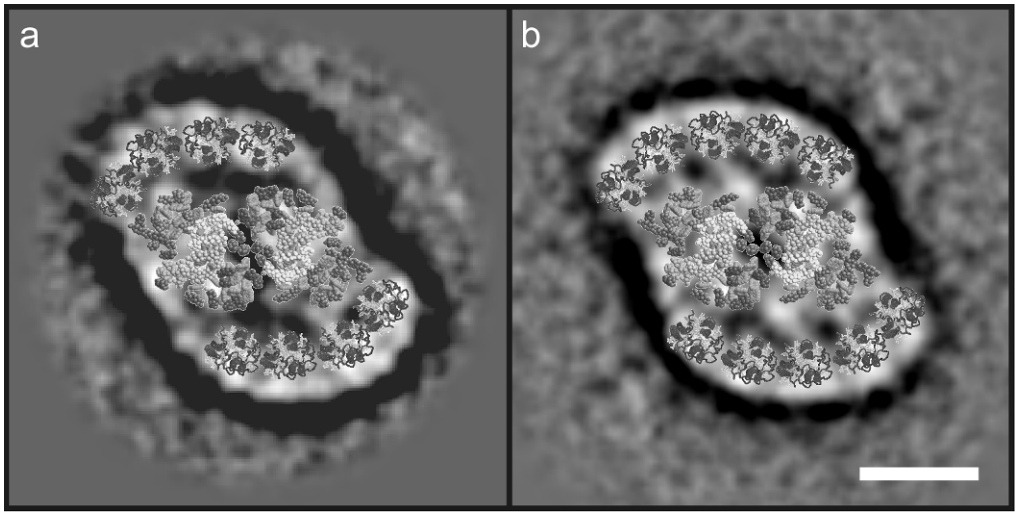

Fig. 7. Association of Pcb proteins with dimeric PS II as identified by EM and single particle analysis of negatively stained preparations shown as a projection map viewed from the lumenal surface. (a) Pcb–PS II supercomplex of *Prochlorococcus marinus* SS120 having four Pcb subunits located on each side of the dimeric PS II. (Modified from Bibby et al., 2003a.) (b) Pcb–PS II supercomplex of *Prochloron didemni* with five Pcb subunits on each side of the PS II dimer. (Modified from Bibby et al., 2003b.) The X-ray structures of the PS II dimer and CP43 (Ferreira et al., 2004) are overlaid on the projection maps of both supercomplexes. Bar represents 100 Å.

Prochlorothrix was found to contain three *pcb* genes denoted A, B, and C where *pcbA* and *pcbB* are closely related to each other with the *pcbC* gene more distant (van der Staay and Staehelin, 1994; van der Staay et al., 1998). The highly abundant marine picoplankton *Prochlorococcus*, has been found to have varying numbers of *pcb* genes dependent on the strain. The high light strain MED4 has just one *pcb* gene (*pcbA*) while the moderate light strain, MIT9313, has two *pcb* genes (*pcbA* and *pcbB*). In contrast the low light strain SS120, has eight *pcb* genes (A–H) (Partensky and Garczarek, 2003).

Soon after the discovery of the 18-mer IsiA ring around the cyanobacterial PS I it was shown that *Prochlorococcus* SS120 also had a similar light harvesting structure around its PS I trimeric RC core (Bibby et al., 2001c). In this case, however, the 18-mer Pcb-antenna ring contained a high level of Chl *b* as well as Chl *a*.

The high level of Chl *b* allows this low light adapted strain to utilize blue light, which becomes enriched at increasing depths in the oceans (Partensky et al., 1999). N-terminal sequencing indicated that the Pcb protein forming the accessory antenna ring around the trimeric PS I RC of *Prochlorococcus* SS120 was the product of the *pcbG* gene (Bibby et al., 2003a). This therefore raised the question about the function of the other *pcb* genes of SS120 and also suggested that other strains of *Prochlorococcus* as well as other prochlorophytes may have a similar PS I accessory light harvesting system.

A study to address the question posed above was directed at comparing *Prochlorococcus,* strains MED4, MIT9313, and SS120 (Bibby et al., 2003a). Although the 18-mer Pcb ring around PS I was induced under normal growth conditions, where iron was present in the case of SS120, no such antenna ring around PS I was observed with MED4 or MIT9313. In fact, all three strains of *Prochlorococcus* were found to have Pcb proteins attached to PS II. EM and single particle analyses indicated that four Pcb proteins attached to each side of the PS II dimeric complex (i.e., eight Pcb subunits per dimer) (see Fig. 7a). Again, assuming that each Pcb subunit binds 14 Chls, then the antenna size of each PS II monomer within the dimer increased from 30 Chls to 86 Chls. If Chls of the Pcb proteins can efficiently transfer energy to PS II, then they increase the absorption cross-section of PS II by about 200%. Clearly in the case of MED4, given its one *pcb* gene, the PS II Pcb protein must be encoded by the *pcbA* gene of this strain. In the case of MIT9313 it was shown that the PS II antenna protein was also the product of its *pcbA* gene. This finding with MIT9313 correlated with the fact that the expression of its *pcbB* gene under iron replete conditions was very low compared with that of the *pcbA* gene. However, when MIT9313 was grown in

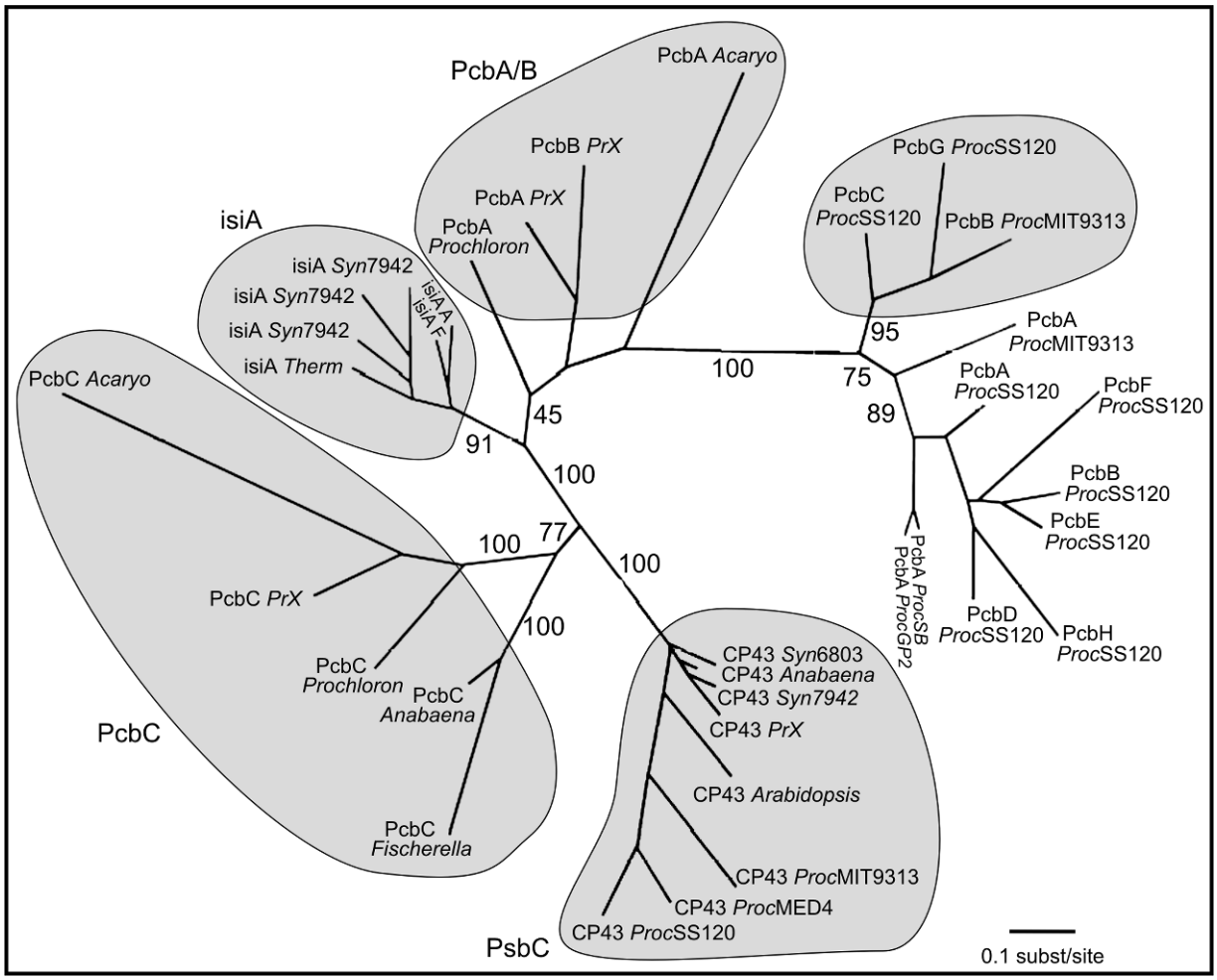

Fig. 8. Phylogenetic distance tree of the IsiA, Pcb, and CP43 proteins of cyanobacteria, prochlorophytes, and prochlorophyte-like cyanobacteria. (Modified from Chen et al., 2004.) Acary – *Acaryochloris marina*; PrX – *Prochlorothrix hollandica*; Prochloron – *Prochloron didemni*; Syn – *Synechococcus* or *Synechocystis*; Therm – *Thermosynechococcus elongatus*; Anabaena – *Anabaena* PCC 7120; *Fischerella* – *Fischerella muscicola*; Proc – *Prochlorococcus*.

an iron-deficient medium, the *pcbB* gene was upregulated and biochemical and structural studies indicated that the PcbB protein associated with PS I to form the 18-mer antenna ring (Bibby et al., 2003a).

From these results it was concluded that *pcb* genes of *Prochlorococcus* encode Chl *a*/Chl *b*-containing proteins, which are either targeted to PS II or PS I. In the case of SS120, the *pcbG* [and possibly the closely related *pcbC* gene, which is upregulated under low iron conditions (Bibby et al., 2003a)] are targeted to PS I to form the 18-mer antenna system. Although not yet investigated in detail it seems likely that the remaining *pcb* genes of SS120 (Itoh et al., 2001), which are closely related (*pcbA*, *B*, *D*, *E*, *F*, *H*), are targeted to PS II. In the case of MIT9313 and MED4 the situation is much clearer. PcbA of both strains forms an antenna system for PS II and PcbB of MIT9313 acts like an IsiA protein and forms the 18-mer antenna ring around PS I when iron levels are lowered. Interestingly, a phylogenetic analysis (Fig. 8) of *isiA* and *pcb* genes indicates that the products of *Prochlorococcus pcb* genes that seem to be targeted to PS I (C and G of SS120 and B of MIT9313) are closely related.

It has also been shown by EM studies (Bibby et al., 2003b) that *Prochloron* has a Pcb–PS II supercomplex, but differs from that of *Prochlorococcus* in that it has five subunits associated on each side of the PS II core dimer (10 Pcb subunits per dimer) (see Fig. 7b). Chlorophyll *b* fluorescence studies indicated that these Pcb proteins are functionally coupled to PS II.

Although isolated PS I of *Prochloron* is trimeric no Pcb–PS I supercomplex has been found. Whether such a structure forms in response to low iron levels is difficult to test since *Prochloron* has not been successfully cultured as a free-living organism. However, it remains to be determined whether the two *pcb* genes (*pcbA* and *pcbC*) in this organism are differentially expressed and targeted to different RCs. There is also evidence that *Prochloron* contains an *isiA* gene (La Roche et al., 1996) and if true then clearly this organisms would have the potential to form an IsiA–PS I supercomplex.

Several studies have indicated that Pcb proteins provide an accessory light harvesting system for PS II of *Prochloron* (Hiller and Larkum, 1985; Schreiber et al., 1997). Despite this it has also been suggested that Pcb proteins might associate with the PS I RC of *Prochloron* (Schuster et al., 1984; Bullerjahn et al., 1987; Post et al., 1993). However, as Fig. 8 shows, the *pcbC* gene of *Prochloron* is not closely related to the *Prochlorococcus* genes that are providing an antenna for PS I (SS120 *pcbG*/*C*, MIT 9313 *pcbB*). Moreover, there is no evidence that *Prochloron* can undergo state transitions involving possible association of Pcb proteins with PS I although it has been shown that its Pcb proteins are permanently phosphorylated (Schuster et al., 1984).

As mentioned above, in the case of *Prochlorothrix,* phylogenetic analyses indicate that its *pcb*A and *pcb*B genes are closely related, while its *pcb*C gene is divergent (van der Staay et al., 1998) (see Fig. 8). As in the case of *Prochloron*, there are several studies indicating that Pcb proteins provide an accessory light harvesting system for PS II (van der Staay, 1992; Matthijs et al., 1994). However, in the case of this organism it was shown that it could undergo state transitions implying functional association of Pcb proteins with PS I and that reversible N-terminal phosphorylation of Pcb proteins was involved in the regulatory process (Burger-Wiersma and Post, 1989; van der Staay, 1992; Post et al., 1993; Post and Bullerjahn, 1994). It was concluded from further work (van der Staay and Staehelin, 1994) that the phosphoprotein was the largest of the Pcb proteins of *Prochlorothrix,* having an apparent molecular mass of 38 kDa, later concluded to be the product of the *pcbC* gene (van der Staay et al., 1998). However, unlike the PcbA and PcbB proteins of *Prochlorothrix*, which have threonines in their N-terminal domains, the PcbC protein does not (see Fig. 9). Thus a scheme recently suggested by Partensky and Garezarek (2003) implying that the PcbC is the mobile phosphoprotein bringing about state transitions in *Prochlorothrix* seems unlikely. Presumably PcbA or PcbB or both, are more likely to function in this way.

VI. Cyanobacterial-Like Prochlorophytes

Although *Prochloron*, *Prochlorothrix*, and *Prochlorococcus* have been called prochlorophytes, there is no doubt that based on 16S rRNA analyses (Turner et al., 1999; Ernst et al., 2003), they belong to the cyanobacterial clade (see Fig. 2). Indeed *Prochlorococcus* SS120 not only contains *pcb* genes but also genes that encode for the α- and β-subunits of phycoerythrin (Hess et al., 1996). However, the contribution of this pigment to light harvesting in this organism is believed to be low (Steglich et al., 2003). In fact, as shown in Fig. 2, phylogenetic analyses indicate that *Prochloron*, *Prochlorothrix*, and *Prochlorococcus* are more distantly related than previously thought, being positioned on different branches of the cyanobacterial radiation. For example, *Prochlorococcus* is more phylogenetically related with certain marine *Synechococcus* species (e.g., WH8102) than with the other prochorophytes.

The inter-relationship of prochlorophytes and cyanobacteria has recently become even more obvious. It was shown that the cyanobacteria *Fischerella muscicola* and *Anabaena* sp. PCC 7120 not only contained phycobilin genes but also have *pcb* genes (Geiss et al., 2001; Kaneko et al., 2001). In *Fischerella* the *pcb* gene is on the same operon as its *isiA* gene and therefore must also be influenced by iron levels. The *pcb* gene of *Fischerella* is similar to the *pcbC* gene of *Prochlorothrix* (see Fig. 8). Using EM it was found that the PS I RC complex of *Fischerella* is monomeric and that under iron-stress conditions it has an accessory antenna of 8–10 Chl *a*-binding IsiA or Pcb subunits (Duncan and Barber, 2004). It has yet to be clarified whether the iron-stress-induced antenna of *Fischerella* is a mixture of IsiA and Pcb proteins or contains just one of these proteins. As in the case of *Synechocystis* sp. PCC 6803, no evidence has yet been found for association of IsiA or Pcb subunits with PS II.

The most recently discovered cyanobacterial-like prochlorophyte is *Acaryochloris marina* (Miyashita et al., 1996), which contains both *pcb* genes (Chen et al., 2002, 2004) and genes encoding for phycobiliproteins (Marquardt et al., 1997). This organism does not contain Chl *b* but is rich in Chl *d* (Chen et al., 2002). Despite the presence of Chl *a*, albeit at a low level, this organism uses Chl *d* as the primary electron donor of PS I (Hu et al., 1998a). It has a red-shifted absorption maximum at 740 nm (P740) as compared with P700. It

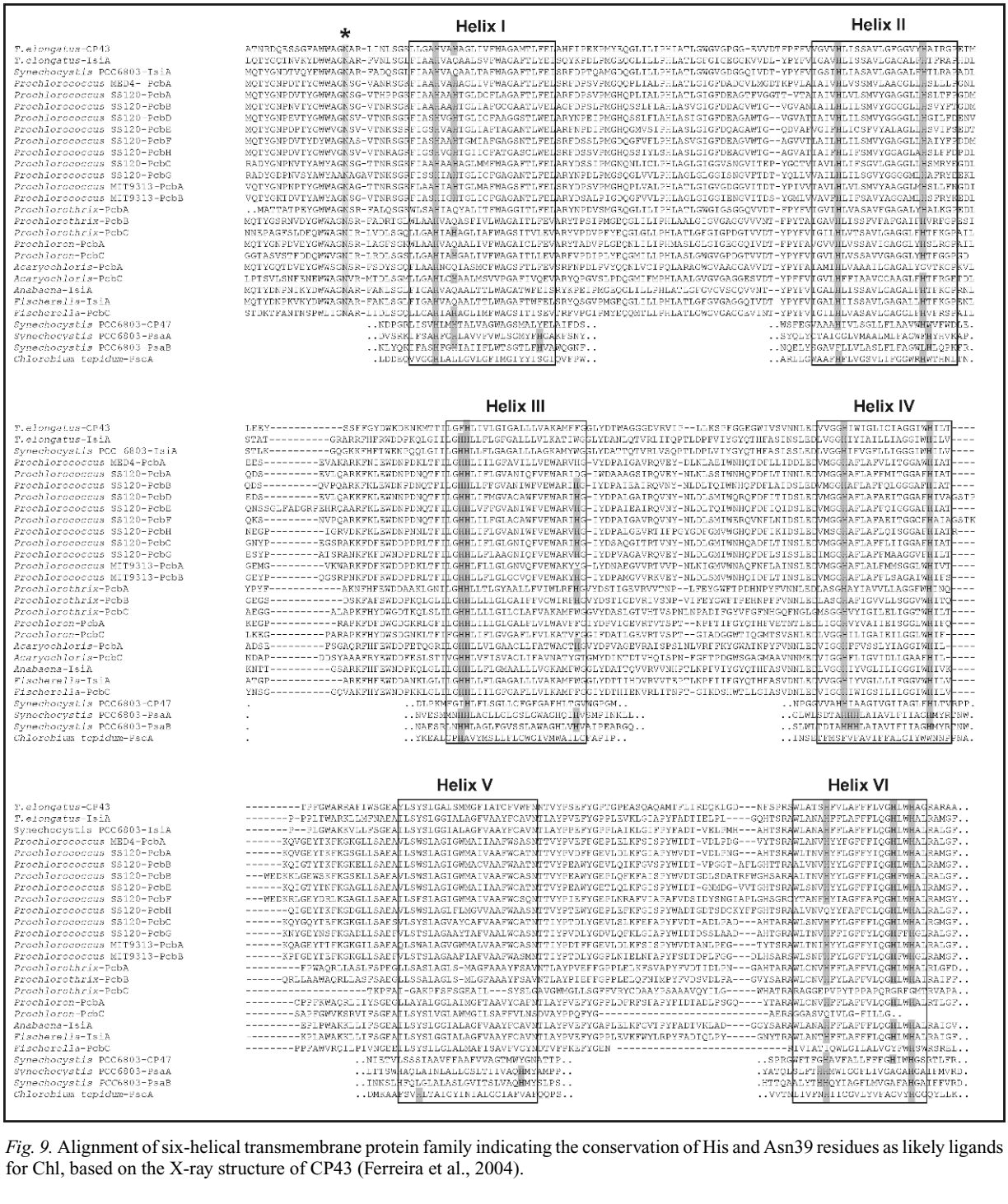

Fig. 9. Alignment of six-helical transmembrane protein family indicating the conservation of His and Asn39 residues as likely ligands for Chl, based on the X-ray structure of CP43 (Ferreira et al., 2004).

remains a matter of debate whether the primary donor of PS II is composed of Chl *a* or Chl *d* (Mimuro et al., 1999, 2004; Itoh et al., 2001).

In *Acaryochloris* the phycobiliproteins form a single $4\alpha_6\beta_6$ rod, which provides a light harvesting antenna for PS II (Hu et al., 1998b; Marquardt et al., 2000). Pcb proteins are also produced under iron-replete conditions and associate with PS II (Chen et al., 2002). Electron microscopy has shown that the Pcb–PS II supercomplexes of *Acaryochloris* are made up of two

end-to-end PS II dimers with four Pcb protein subunits along the side of each dimer (Chen et al., 2005a). It seems likely that these Pcb–PS II supercomplexes are located in the stacked regions of the *Acaryochloris* thylakoids, while those PS II having phycobiliprotein rods are restricted to the unstacked regions (Hu et al., 1998b; Marquardt and Morschell, 1999). *Acaryochloris* contains two *pcb* genes, A and C (Chen et al., 2005a), and recent studies have shown that *pcb*A is targeted to PSII. The *pcb*C gent, like the *pcb*B gene of *Prochlorococcus* MIT9313 is upregulated under iron depletion and forms an 18 mer ring around PSI (Chen et al., 2005b).

VII. Pigments of IsiA and Pcb Proteins

Till date all known examples of IsiA bind only Chl *a*, whose ligation is likely to involve the histidines that are conserved between IsiA and CP43 (see Figs. 1 and 9). The X-ray structure of CP43 has shown that of the 14 Chls bound to this protein, 10 are ligated by histidine while 1 is ligated to asparagine (Asn39). The remaining three Chls are not ligated directly by amino acid side chains and assignment of one of these is uncertain. Interestingly, the Asn is conserved in IsiA and also in Pcb proteins (see Fig. 9). Although the IsiA protein naturally binds Chl *a* a recent study has shown that when the *cao* gene (Chl *a* oxidase gene of Arabidopsis) is cloned into *Synechocystis* sp. PCC 6803, enabling the conversion of some Chl *a* to Chl *b* (Satoh et al., 2001), the effect of iron deficiency leads to the incorporation of some Chl *b* into its IsiA protein (Duncan et al., 2003).

The result obtained with the *cao-Synechocystis* mutant is consistent with the fact that the Pcb proteins of prochlorophytes bind both Chl *a* and Chl *b*. The relative ratio of these two Chl species varies considerably with different growth conditions and in different species. For example, the Chl *a*/*b* ratio of *Prochlorothrix* cells can vary from 10 to 18 depending on the light intensity to which they have adapted [30 and 100 $\mu Em^{-2}s^{-1}$, respectively (Matthijs et al., 1994)]. In general, the Chl *b* level of *Prochloron*, *Prochlorothrix*, and certain strains of *Prochlorococcus*, like MED4, falls in the region of 5–20% (Lewin and Withers, 1975; Matthijs et al., 1989; Garczarek et al., 1998). However, in the low light, adapted *Prochlorococcus* strain SS120, the Chl *b* level can be as high as 65%, which exceeds the levels of Cab proteins. Although *Prochloron* and *Prochlorothrix* bind Chl *a* and Chl *b* to their Pcb proteins, *Prochlorococcus* contains only divinyl derivatives of Chl *a* and Chl *b* that are unique to this genus. It has also been reported that *Prochloron* contains a low level (4–15% total Chl) of

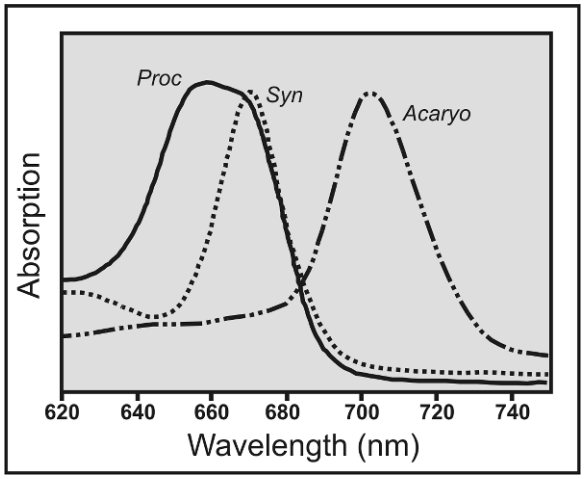

Fig. 10. Long wavelength room temperature absorption spectrum of the Chl *a*-binding IsiA protein of *Synechocystis* sp. PCC 6803 (Syn, dotted trace), Chl *a*/Chl *b*-binding Pcb protein of *Prochlorococcus marinus* SS120 (Proc, solid line), and Chl *d*-binding Pcb protein of *Acaryochloris marina* (Acaryo, dashed line). (T Bibby and J Barber, unpublished).

a Chl *c*-like pigment similar to magnesium-3,8-divinyl pheoporphyrin a_5 monomethyl ester and that this is involved in light harvesting (Larkum et al., 1994). In the case of *Fischerella*, no Chl *b* is present despite this organism containing a *pcb* gene, a finding probably explained by the absence of Chl oxidase enzyme. Perhaps the most remarkable Pcb protein is that of *Acaryochloris*, which binds Chl *d* (Chen et al., 2002). Figure 10 shows the long wave absorption spectra for the IsiA protein of *Synechocystis*, Pcb protein of *Prochlorococcus* SS120, and the Pcb protein of *Acaryochloris*. The high divinyl Chl *b* level relative to divinyl Chl *a* of the Pcb of *Prochlorococcus* SS120 is clearly seen as is the significant shift of the Chl *d* absorption maximum to 705 nm from Chl *a* absorption maximum of the IsiA protein is at 670 nm.

The IsiA protein also binds β-carotene as does CP43. According to the recent X-ray structure of CP43 there are three β-carotene molecules bound to the surface of this protein. The Pcb proteins of *Prochloron* and *Prochlorothrix* also seem to bind β-carotene (Withers et al., 1978; Pearl et al., 1984; Omata et al., 1985; Foss et al., 1987) while those of *Prochlorococcus* and *Acaryochloris* probably contain α-carotene (Goericke and Repeta, 1992; Miyashita et al., 1997; Garczarek et al., 1998).

According to sequence comparison shown in Fig. 9, the majority of the ligands for IsiA and Pcb proteins are conserved. It therefore seems that this six-membrane spanning α-helical family is versatile in its ability to bind different pigments and therefore, provides a light harvesting system with spectral properties, which are

compatible with the habitat of the organism whether it be at great depths in the ocean, as for *Prochlorococcus* SS120 (Partensky et al., 1999), or screened by Chl *a*-containing organisms, as in the case of *Acaryochloris* (Murakami et al., 2004).

VIII. Evolution of the Six-Membrane Spanning α-Helical Chl-Binding Protein Family

Above we have described and discussed how IsiA and Pcb proteins can act as Chl-based accessory light harvesting systems for cyanobacterial PS I. They are members of a six-helical transmembrane protein family, which are found in all types of oxygenic photosynthetic bacteria. The family is characterized by its versatility to bind different types of Chl and provide either "internal" or "outer/accessory" light harvesting systems. It has been suggested that this basic unit may have evolved from an 11-helical transmembrane protein (typical of Type I RCs) by gene fission to form the six plus five arrangement of the transmembrane helices now found in the CP43/D1 or CP47/D2 pairing of PS II (Mulkidjanian and Junge, 1997). Alternatively, the six-helical transmembrane protein could have been a basic building block for the light harvesting systems of present day RCs, as shown in Fig. 11.

In the case of Type I RCs, this six-helical basic building block may have fused during evolution with the five-helical RC core before undergoing gene duplication to produce the homodimeric RCs of present day green sulfur bacteria and heliobacteria. Subsequent gene modification would have had to occur to produce the heterodimeric RC of PS I. On the other hand, a gene fusion giving rise to the large extrinsic loop between helices V and VI of modern CP43 and CP47 and the association of this modified six-helical chlorophyll-binding protein to the primitive five-helical RC may have initiated the first steps toward the evolution of the Type II RC. As suggested for the evolution of Type I RCs, gene duplication and modification would need to have occurred to arrive at the present day water splitting PS II RC with its heterodimeric structure consisting of the D1 and D2 proteins flanked, but not fused with, the CP43 and CP47 proteins. This nonfused arrangement would be beneficial for carrying out the repair processes of PS II due to photodamage, whereby the D1 protein is degraded and replaced. Figure 11 also shows a diagrammatic representation of the Pcb–PS II and Pcb/IsiA–PS I supercomplexes emphasizing how the Pcb/IsiA proteins form an accessory light harvesting system, which is an extension of those contained within the PS I and

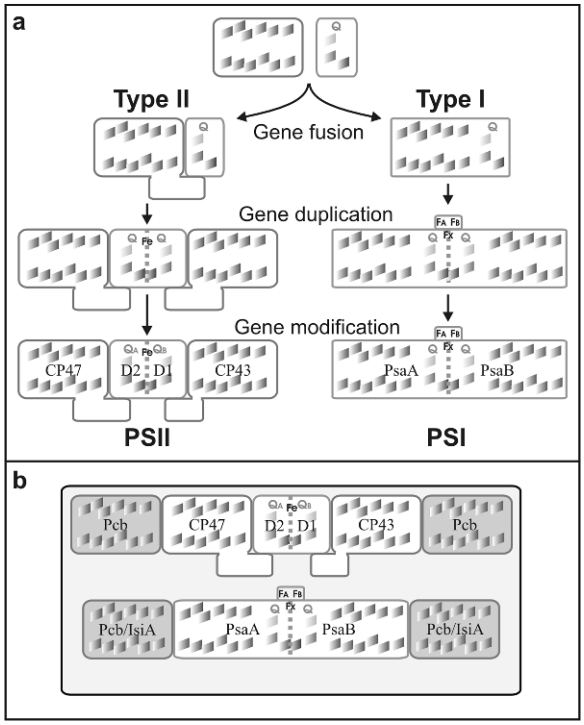

Fig. 11. A diagrammatic scheme, emphasizing the distribution and possible evolutionary importance of the six-transmembrane helical Chl-binding protein superfamily. Members of the six-transmembrane α-helical family are depicted as having two layers of light harvesting Chls. The five-transmembrane α-helical proteins that make up RC cores of Type I and Type II photosystems are indicated by their cofactors including the quinine (Q) electron acceptor (see text).

PS II RC cores. However, intriguingly one of the major cyanobacterium in the ocean, *Synechococcus* sp. WH8102 has neither *pcb* nor *isiA* genes (Palenik et al., 2003) indicating that Chl accessory light harvesting systems are not an obligatory requirement for all types of cyanobacteria.

References

Andrizhiyevskaya EG, Schwabe TM, Germano M, D'Haene S, Kruip J, van Grondelle R and Dekker JP (2002) Spectroscopic properties of PS I–IsiA supercomplexes from the cyanobacterium *Synechococcus* PCC 7942. Biochim Biophys Acta 1556: 265–272

Andrizhiyevskaya EG, Frolov D, Van Grondelle R and Dekker JP (2004) Energy transfer and trapping in the Photosystem I complex of *Synechococcus* PCC 7942 and in its supercomplex with IsiA. Biochim Biophys Acta 1656: 104–113

Arnon DI (1995) Unconventional pathways of photosynthetic electron transport: the autonomous oxygenic and anoxygenic photosystems. In Barber J, Medrano H and Guerrero MC (eds) Trends in Photosynthesis Research, pp 47–71. Intercept Limited, UK

Aspinwall CL, Duncan J, Bibby T, Mullineaux CW and Barber J (2004) The trimeric organisation of photosystem I is not necessary for the iron-stress induced CP43′ protein to functionally associate with this reaction centre. FEBS Lett 574: 126–130

Behrenfeld MJ and Kolber SZ (1999) Widespread iron limitation of phytoplankton in the South Pacific Ocean. Science 283: 840–843

Ben-Shem A, Frolow F and Nelson N (2003) Crystal structure of plant photosystem I. Nature 426: 630–635

Ben-Shem A, Frolow F and Nelson N (2004) Evolution of photosystem I – from symmetry through pseudo-symmetry to asymmetry. FEBS Lett 564: 274–280

Bibby TS, Nield J and Barber J (2001a) Iron deficiency induces the formation of an antenna ring around trimeric photosystem I in cyanobacteria. Nature 412: 743–745

Bibby TS, Nield J and Barber J (2001b) Three-dimensional model and characterization of the iron stress-induced CP43′–photosystem I supercomplex isolated from the cyanobacterium *Synechocystis* PCC 6803. J Biol Chem 276: 43246–43252

Bibby TS, Nield J, Partensky F and Barber J (2001c) Oxyphotobacteria. Antenna ring around photosystem I. Nature 413: 590

Bibby TS, Mary I, Nield J, Partensky F and Barber J (2003a) Low-light-adapted *Prochlorococcus* species possess specific antennae for each photosystem. Nature 424: 1051–1054

Bibby TS, Nield J, Chen M, Larkum AW and Barber J (2003b) Structure of a photosystem II supercomplex isolated from *Prochloron didemni* retaining its chlorophyll *a*/*b* light-harvesting system. Proc Natl Acad Sci USA 100: 9050–9054

Boekema EJ, Hifney A, Yakushevska AE, Piotrowski M, Keegstra W, Berry S, Michel KP, Pistorius EK and Kruip J (2001) A giant chlorophyll–protein complex induced by iron deficiency in cyanobacteria. Nature 412: 745–748

Bullerjahn GS, Matthijs HC, Mur LR and Sherman LA (1987) Chlorophyll–protein composition of the thylakoid membrane from *Prochlorothrix hollandica*, a prokaryote containing chlorophyll *b*. Eur J Biochem 168: 295–300

Bullerjahn GS, Jensen TC, Sherman DM and Sherman LA (1990) Immunological characterization of the *Prochlorothrix hollandica* and *Prochloron* sp. chlorophyll *a*/*b* antenna proteins. FEMS Microbiol Lett 55: 99–105

Burger-Wiersma T and Post AF (1989) Functional analysis of the photosynthetic apparatus of *Prochlorothrix hollandica* (Prochlorales), a chlorophyll *b* containing prokaryote. Plant Physiol 91: 770–774

Burger-Wiersma T, Veenhuis M, Korthals HJ, van der Weil CCM and Mur LR (1986) A new prokaryote containing chlorophylls *a* and *b*. Nature 320: 262–264

Burnap RL, Troyan T and Sherman LA (1993) The highly abundant chlorophyll–protein complex of iron-deficient *Synechococcus* sp. PCC 7942 (CP43′) is encoded by the *isiA* gene. Plant Physiol 103: 893–902

Byrdin M, Jordan P, Krauß N, Fromme P, Stehlik D and Schlodder E (2002) Light harvesting in photosystem I: modeling based on the 2.5Å structure of photosystem I from *Synechococcus elongatus*. Biophys J 83: 433–457

Chen M, Bibby TS, Nield J, Larkum AW and Barber J (2005a) Iron deficiency induces a chlorophyll d-binding Pcb antenna around photosystem I in *Acaryochloris marina*. Biochim Biophys Acta 1708: 367–374

Chen M, Bibby TS, Nield J, Larkum AW and Barber J (2005b) Structure of a large photosystem II supercomplex from *Acaryochloris marina*. FEBS Lett 579: 1306–1310

Chen M, Quinnell RG and Larkum AW (2002). The major light-harvesting pigment protein of *Acaryochloris marina*. FEBS Lett 514: 149–152

Chen M, Hiller RG, Howe CJ and Larkum AW (2004) Unique origin and lateral transfer of prokaryotic chlorophyll-*b* and chlorophyll-*d* light-harvesting systems. Mol Biol Evol, 22: 21–28

Chisholm SW, Olsen RJ, Zettler ER, Waterbury JB, Goericke R and Welschmeyer N (1988) A novel free living prochlorophyte abundant in the oceanic euphotic zone. Nature 334: 340–343

Chitnis VP and Chitnis PR (1993) PsaL subunit is required for the formation of photosystem I trimers in the cyanobacterium *Synechocystis* sp. PCC 6803. FEBS Lett 336: 330–334

de Baar HJW, de Jong JTM, Bakker DCE, Loscher BM, Veth C, Bathmann UV and Smetacek V (1995) Importance of iron for plankton blooms and carbon dioxide drawdown in the southern ocean. Nature 373: 412–415

De Las Rivas J and Barber J (2004) Analysis of the structure of the PsbO protein and its implications. Photosynth Res 81: 329–343

Duncan J and Barber J (2004) Isolation and structural analysis of the photosynthetic antenna complexes in the cyanobacterium *Fischerella muscicola* PCC 73103, In: Photosynthesis, Fundamental Aspects to Global Perspectives, Eds. D. Bruce and A. van der Est, Allen Press, Lawrence KS (2005) vol 1, pp. 146–148

Duncan J, Bibby T, Tanaka A and Barber J (2003) Exploring the ability of chlorophyll *b* to bind to the CP43′ protein induced under iron deprivation in a mutant of *Synechocystis* PCC 6803 containing the *cao* gene. FEBS Lett 541: 171–175

Ernst A, Becker S, Wollenzien UI and Postius C (2003) Ecosystem-dependent adaptive radiations of picocyanobacteria inferred from 16S rRNA and ITS-1 sequence analysis. Microbiology 149: 217–228

Falkowski PG, Barber RT and Smetacek V (1998) Biogeochemical controls and feedbacks on ocean primary production. Science 281: 200–206

Ferreira KN, Iverson TM, Maghlaoui K, Barber J and Iwata S (2004) Architecture of the photosynthetic oxygen-evolving center. Science 303: 1831–1838

Fitzgerald MP, Husain A, Hutber GN and Rogers LJ (1977) Studies on the flavodoxins from a cyanobacterium and a red alga. Biochem Soc Trans 5: 1505–1506

Foss P, Lewin RA and Liaaen-Jensen S (1987) The carotenoids of *Prochloron* sp. (Prochlorophyta). Phycologia 26: 142–144

Garczarek L, van der Staay G, Thomas JC and Partensky F (1998) Isolation and characterisation of photosystem I from two strains of the marine oxychlorobacterium *Prochlorococcus*. Photosynth Res 56: 131–141

Geiss U, Vinnemeier J, Schoor A and Hagemann M (2001) The iron-regulated *isiA* gene of *Fischerella muscicola* strain PCC 73103 is linked to a likewise regulated gene encoding a Pcb-like chlorophyll-binding protein. FEMS Microbiol Lett 197: 123–129

Glazer AN (1985) Light harvesting by phycobilisomes. Annu Rev Biophys Biophys Chem 14: 47–77

Goericke R and Repeta DL (1992) The pigments of *Prochlorococcus marinus*: the presence of divinyl chlorophyll *a* and *b* in a marine prokaryote. Limnol Oceanogr 37: 425–433

Green B and Durnford D (1996) The chlorophyll carotenoid proteins of oxygenic photosynthesis. Annu Rev Plant Physiol Plant Mol Biol 47: 685–714

Grossman AR, Bhaya D, Apt KE and Kehoe DM (1995) Light-harvesting complexes in oxygenic photosynthesis: diversity, control, and evolution. Annu Rev Genet 29: 231–288

Guikema JA and Sherman LA (1983) Organisation and function of chlorophyll in membranes of cyanobacteria during iron starvation. Plant Physiol 73: 250–256

Guikema JA and Sherman LA (1984) Influence of iron deprivation on the membrane composition of *Anacystis nidulans*. Plant Physiol 74: 90–95

Hess WR, Partensky F, van der Staay GW, Garcia-Fernandez JM, Borner T and Vaulot D (1996) Coexistence of phycoerythrin and a chlorophyll *a*/*b* antenna in a marine prokaryote. Proc Natl Acad Sci USA 93: 11126–11130

Hiller RG and Larkum AWD (1985) Chlorophyll–protein complexes of *Prochloron* (Prochlorophyta). Biochim Biophys Acta 806: 107–115

Hu Q, Miyashita H, Iwasaki II, Kurano N, Miyachi S, Iwaki M and Itoh S (1998a) A photosystem I reaction center driven by chlorophyll *d* in oxygenic photosynthesis. Proc Natl Acad Sci USA 95: 13319–13323

Hu Q, Ishikawa T, Inoue Y, Iwasaki II, Miyashita H, Kurano N, Miyachi S, Iwaki M, Itoh S, Marquardt J and Morschel E (1998b) Heterogeneity of chlorophyll *d*-binding photosystem I reaction centers from the photosynthetic prochlorophyte *Acaryochloris marina*. In: Garab G (ed) Photosynthesis: Mechanism and Effects. Kluwer Academic Publishers, The Netherlands

Itoh S, Iwaki M, Noguti T, Kamamori A and Mino H (2001) Photosystem I and II reaction centers of a new oxygenic organism *Acaryochloris marina* that use chlorophyll *d*. In: PS2001 Proceedings: 12th International Congress on Photosynthesis. CSIRO Publishing, Melbourne, Australia, S6-28–30

Jeanjean R, Zuther E, Yeremenko N, Havaux M, Matthijs HC and Hagemann M (2003) A photosystem 1 *psaFJ*-null mutant of the cyanobacterium *Synechocystis* PCC 6803 expresses the *isiAB* operon under iron replete conditions. FEBS Lett 549: 52–56

Jordan P, Fromme P, Witt HT, Klukas O, Saenger W and Krauß N (2001) Three-dimensional structure of cyanobacterial photosystem I at 2.5 Å resolution. Nature 411: 909–917

Kamiya N and Shen JR (2003) Crystal structure of oxygen-evolving photosystem II from *Thermosynechococcus vulcanus* at 3.7 Å resolution. Proc Natl Acad Sci USA 100: 98–103

Kaneko T, Nakamura Y, Wolk CP, Kuritz T, Sasamoto S, Watanabe A, Iriguchi M, Ishikawa A, Kawashima K, Kimura T, Kishida Y, Kohara M, Matsumoto M, Matsuno A, Muraki A, Nakazaki N, Shimpo S, Sugimoto M, Takazawa M, Yamada M, Yasuda M and Tabata S (2001) Complete genomic sequence of the filamentous nitrogen-fixing cyanobacterium *Anabaena* sp. strain PCC 7120. DNA Res 8: 205–213

Kouril R, Yeremenko N, D'Haene S, Yakushevska AE, Keegstra W, Matthijs HC, Dekker JP and Boekema EJ (2003) Photosystem I trimers from *Synechocystis* PCC 6803 lacking the PsaF and PsaJ subunits bind an IsiA ring of 17 units. Biochim Biophys Acta 1607: 1–4

Larkum AW, Scaramuzzi C, Cox GC, Hiller RG and Turner AG (1994) Light-harvesting chlorophyll *c*-like pigment in *Prochloron*. Proc Natl Acad Sci USA 91: 679–683

La Roche J, van der Staay G, Partensky F, Ducret A, Aebersold R, Li R, Golden SS, Hiller RG, Wrench P, Larkum AW and Green B (1996) Independent evolution of the prochlorophyte and green plant chlorophyll *a*/*b* light harvesting proteins. Proc Natl Acad Sci USA 93: 15244–15248

Laudenbach DE, Reith ME and Straus N (1988) Isolation, sequence analysis and transcriptional studies of the flavodoxin gene from *Anacystis nidulans* R2. J Bacteriol 170: 258–265

Lewin RA (1975) A marine *Synechocystis* (Cyanophyta, Chlorococcales) epizoic on ascidians. Phycologia 14: 153–169

Lewin RA (1976) Prochlorophyta. A proposed new division of algae. Nature 261: 697–698

Lewin RA (1977) *Prochloron*, type genus of the Prochlorophyta. Phycologia 16: 217

Lewin RA (1984) *Prochloron* – a status report. Phycologia 23: 203–208

Lewin RA and Withers NW (1975) Extraordinary pigment composition of a prokaryotic alga. Nature 256: 735–737

Marquardt J and Morschel E (1999) The photosynthetic apparatus of *Prochloron*-like cyanobacteria. In: Argyroudi-Akoyunoglou JH and Senger H (eds) The Chloroplast: From Molecular Biology to Biotechnology, pp 41–46. Kluwer Academic Publishers, The Netherlands

Marquardt J, Senger H, Miyashita H, Miyachi S and Morschel E (1997) Isolation and characterization of biliprotein aggregates from *Acaryochloris marina*, a *Prochloron*-like prokaryote containing mainly chlorophyll *d*. FEBS Lett 410: 428–432

Marquardt J, Morschel E, Rhiel E and Westermann M (2000) Ultrastructure of *Acaryochloris marina*, an oxyphotobacterium containing mainly chlorophyll *d*. Arch Microbiol 174: 181–188

Martin JH, Coale KH, Johnson KS, Fitzwater SE, Gordan RM, Tanner SJ, Hunter CN, Elrod VA, Nowicki JL, Coley TL, Barber RT, Lindley S, Watson CJ, Van Scoy K, Law CA, Liddicoat MI, Ling R, Stanton T, Stockel J, Collings C, Anderson A, Bidigare R, Ondrusek M, Tatasa M, Millero FJ, Lee K, Yao W, Zhang JZ, Friederich G, Sakamoto C, Chavez F, Buck K, Kolber Z, Green R, Falkowski P, Chisholm SW, Hoge F, Swift R, Yungel J, Turner S, Nightingale P, Hatton A, Liss P and Tindale NW (1994) Testing the iron hypothesis in ecosystems of the equatorial Pacific. Nature 371: 123

Matthijs HC, van der Staay G, van Amerongen H, van Grondelle R and Garab G (1989) Structural organization of chlorophyll *b* in the prochlorophyte *Prochlorothrix hollandica*: lack of chlorophyll *b* eximer circular dichroism bands. Biochim Biophys Acta 975: 185–187

Matthijs HC, van der Staay G and Mar LR (1994) Prochlorophytes: the 'other' cyanobacteria. In: Bryant DA (ed) The Molecular Biology of Cyanobacteria. Kluwer Academic Publishers, The Netherlands

Melkozernov AN, Bibby TS, Lin S, Barber J and Blankenship RE (2003) Time-resolved absorption and emission show that the CP43′ antenna ring of iron-stressed *Synechocystis* sp. PCC 6803 is efficiently coupled to the photosystem I reaction center core. Biochemistry 42: 3893–3903

Michel KP and Pistorius EK (2004) Adaptation of the photosynthetic electron transport chain in cyanobacteria to iron deficiency: the function of IdiA and IsiA. Physiol Planta 120: 36–50

Mimuro M, Akimoto S, Yamazaki I, Miyashita H and Miyachi S (1999) Fluorescence properties of chlorophyll *d*-dominating

prokaryotic alga, *Acaryochloris marina*: studies using time-resolved fluorescence spectroscopy on intact cells. Biochim Biophys Acta 1412: 37–46

Mimuro M, Akimoto S, Gotoh T, Yokono M, Akiyama M, Tsuchiya T, Miyashita H, Kobayashi M and Yamazaki I (2004) Identification of the primary electron donor in PSII of the Chl *d*-dominated cyanobacterium *Acaryochloris marina*. FEBS Lett 556: 95–98

Miyashita H, Ikemoto H, Kurano N, Adachi K, Chihara M and Miyachi S (1996) Chlorophyll *d* as a major pigment. Nature 383: 402

Miyashita H, Adachi K, Kurano N, Ikemoto H, Chihara M and Miyachi S (1997) Pigment composition of a novel oxygenic photosynthetic prokaryote containing chlorophyll *d* as the major chlorophyll. Plant Cell Physiol 38: 274–281

Mulkidjanian AY and Junge W (1997) On the origin of photosynthesis as inferred from sequence analysis – a primordial UV-protector as common ancestor of reaction centres and antenna proteins. Photosynth Res 51: 27–42

Mullineaux CW (1994) Excitation energy transfer from phycobilisomes to photosystem I in a cyanobacterial mutant lacking photosystem II. Biochim Biophys Acta 1185: 71–77

Murakami A, Miyashita H, Iseki M, Adachi K and Mimuro M (2004) Chlorophyll *d* in an epiphytic cyanobacterium of red algae. Science 303: 1633

Newcomb EH and Pugh TD (1975) Blue-green algae associated with ascidians of the Great Barrier Reef. Nature 253: 533–534

Nield J, Morris EP, Bibby TS and Barber J (2003) Structural analysis of the photosystem I supercomplex of cyanobacteria induced by iron deficiency. Biochemistry 42: 3180–3188

Nogi T and Miki K (2001) Structural basis of bacterial photosynthetic reaction centers. J Bacteriol (Tokyo) 130: 319–329

Omata T, Okada M and Murata N (1985) Separation and partial characterization of membranes from *Prochloron sp*. Plant Cell Physiol. 26: 579–584

Öquist G (1971) Changes in pigment composition and photosynthesis induced by iron-deficiency in the blue-green alga *Anacystis nidulans*. Physiol Plant 25: 188–191

Öquist G (1974a) Iron deficiency in the blue-green alga *Anacyctis nidulans*: changes in pigmentation and photosynthesis. Physiol Plant 30: 30–37

Öquist G (1974b) Iron deficiency in the blue-green alga *Anacystis nidulans*: fluorescence and absorption spectra recorded at 77 K. Physiol Plant 31: 55–58

Pakrasi HB, Goldenberg A and Sherman LM (1985a) Membrane development in the cyanobacterium *Anacystis nidulans*, during recovery from iron-starvation. Plant Physiol 79: 290–295

Pakrasi HB, Riethman HC and Sherman LA (1985b) Organisation of pigment proteins in the photosystem II complex of the cyanobacterium *Anacystis nidulans* R2. Proc Natl Acad Sci USA 82: 6903–6907

Palenik B, Brahamsha B, Larimer FW, Land M, Hauser L, Chain P, Lamerdin J, Regala W, Allen EE, McCarren J, Paulsen I, Dufrense A, Partensky F, Webb EA and Waterbury J (2003) The genome of a motile marine *Synechococcus*. Nature 424: 1037–1042

Park YI, Sandstrom S, Gustafsson P and Oquist G (1999) Expression of the *isiA* gene is essential for the survival of the cyanobacterium *Synechococcus* sp. PCC 7942 by protecting photosystem II from excess light under iron limitation. Mol Microbiol 32: 123–129

Partensky F and Garczarek L (2003) The photosynthetic apparatus of Chlorophyll *b*- and *d*-containing oxychlorobacteria. In: Larkum AW, Douglas SE and Raven JA (eds) Photosynthesis in Algae, pp 29–62. Kluwer Academic Publisher, The Netherlands

Partensky F, Hess WR and Vaulot D (1999) *Prochlorococcus*. A marine photosynthetic prokaryote of global significance. Microbiol Mol Biol Rev 63: 106–127

Pearl HW, Lewin RA and Cheng L (1984) Variations in chlorophyll and carotenoid pigmentation among *Prochloron* (Prochlorophyta) symbionts in diverse marine ascidians. Bot Mar 27: 257–264

Post AF and Bullerjahn GS (1994) The photosynthetic machinery of prochlorophytes: structural properties and ecological significance. FEMS Microbiol Rev 13: 393–414

Post AF, Ohad I, Milbauer KM and Bullerjahn GS (1993) Energy distribution between PSI and PSII in the photosynthetic prokaryote *Prochlorothrix hollandica* involves a chlorophyll *a*/*b* antenna associated with PSI. Biochim Biophys Acta 1144: 374–384

Rhee KH, Morris EP, Barber J and Kuhlbrandt W (1998) Three-dimensional structure of the plant photosystem II reaction centre at 8 Å resolution. Nature 396: 283–286

Riethman HC and Sherman LA (1988) Purification and characterisation of an iron stressed-induced chlorophyll–protein from the cyanobacterium *Anacystis nidulans* R2. Biochim Biophys Acta 935: 141–151

Ruprecht J and Nield J (2001) Determining the structure of biological macromolecules by transmission electron microscopy, single particle analysis and 3D reconstruction. Prog Biophys Mol Biol 75: 121–164

Sandström S, Park YI, Öquist G and Gustafsson P (2001) CP43′, the *isiA* gene product, functions as an excitation energy dissipator in the cyanobacterium *Synechococcus* sp. PCC 7942. Photochem Photobiol 74: 431–437

Satoh S, Ikeuchi M, Mimuro M and Tanaka A (2001) Chlorophyll *b* expressed in Cyanobacteria functions as a light-harvesting antenna in photosystem I through flexibility of the proteins. J Biol Chem 276: 4293–4297

Schreiber U, Gademann R, Ralph PJ and Larkum AW (1997) Assessment of photosynthetic performance of *Prochloron* in *Lissoclinum patella* by in situ and in hospite chlorophyll fluorescence measurements. Plant Cell Physiol 38: 945–951

Schubert WD, Klukas O, Saenger W, Witt HT, Fromme P and Krauß N (1998) A common ancestor for oxygenic and anoxygenic photosynthetic systems: a comparison based on the structural model of photosystem I. J Mol Biol 280: 297–314

Schuster G, Owens CG, Cohen Y and Ohad I (1984) Thylakoid polypeptide composition and light independent phosphorylation of chlorophyll *a*,*b* protein in *Prochloron*, a prochlorophyte exhibiting oxygenic photosynthesis. Biochim Biophys Acta 767: 596–605

Sétif P (2001) Ferredoxin and flavodoxin reduction by photosystem I. Biochim Biophys Acta 1507: 161–179

Sherman DM and Sherman LA (1983) Effect of iron deficiency and iron restoration on ultrastructure of *Anacystis nidulans*. J Bacteriol 156: 393–401

Steglich C, Mullineaux CW, Teuchner K, Hess WR and Lokstein H (2003) Photophysical properties of *Prochlorococcus marinus* SS120 divinyl chlorophylls and phycoerythrin in vitro and in vivo. FEBS Lett 553: 79–84

Straus N (1994) Iron deprivation: physiology and gene regulation. In: Bryant DA (ed) The Molecular Biology of Cyanobacteria, pp 731–750. Kluwer Academic Publishers, The Netherlands

Tetenkin VL, Golitsin VM and Gulyaev BA (1998) Stress protein of cyanobacteria CP36: interaction with photoactive complexes and formation of supermolecular structures. Biochemistry (Moscow) 63: 584–591

Turner S, Pryer KM, Miao VPW and Palmer JD (1999) Investigating deep phylogenetic relationships among cyanobacteria and plastids by small subunit rRNA sequence analysis. J Eukaryot Microbiol 46: 327–338

Ting CS, Rocap G, King J and Chisholm SW (2002). Cyanobacterial photosynthesis in the oceans: the origins and significance of divergent light-harvesting strategies. Trends Microbiol 10: 134–142

van der Staay GW (1992) Functional localization and properties of the chlorophyll *b*-binding prochlorophyte *Prochlorothrix hollandica*. PhD Thesis. Universiteit van Amsterdam

van der Staay GW and Staehelin LA (1994). Biochemical characterization of protein composition and protein phosphorylation patterns in stacked and unstacked thylakoid membranes of the prochlorophyte *Prochlorothrix hollandica*. J Biol Chem 269: 24834–24844

van der Staay GW, Yorkova N and Green B (1998) The 38 kDa chlorophyll *a*/*b* protein of the prochlorophyte *Prochlorothrix hollandica* is encoded by a divergent *pcb* gene. Plant Mol Biol 36: 709–716

Walsby AE (1986) Prochlorophytes: origin of chloroplasts. Nature 320: 212

Withers NW, Alberte RS, Lewin RA, Thornber P, Britton G and Goodwin TW (1978) Photosynthetic unit size, carotenoids, and chlorophyll–protein composition of *Prochloron* sp., a prokaryotic green alga. Proc Natl Acad Sci USA 75: 2301–2305

Wolfe GR, Cunningham D, Durnford D, Green B and Gantt E (1994) Evidence for a common origin of chloroplasts with light-harvesting complexes of different pigmentation. Nature 367: 566–568

Yeremenko N, Kouril R, Ihalainen JA, D'Haene S, van Oosterwijk N, Andrizhiyevskaya EG, Keegstra W, Dekker HL, Hagemann M, Boekema EJ, Matthijs HCP and Dekker JP (2004) Supramolecular organization and dual function of the IsiA chlorophyll-binding protein in cyanobacteria. Biochemistry 43: 10308–10313

Zouni A, Witt HT, Kern J, Fromme P, Krauß N, Saenger W and Orth P (2001) Crystal structure of photosystem II from *Synechococcus elongatus* at 3.8 Å resolution. Nature 409: 739–774

Chapter 10

LHCI: The Antenna Complex of Photosystem I in Plants and Green Algae

Roberta Croce
Istituto di Biofisica, Consiglio Nazionale della Ricerche, via Sommarive 18, 38100 Povo, Trento, Italy

Tomas Morosinotto and Roberto Bassi*
Dipartimento Scientifico e Tecnologico, Università di Verona, Strada Le Grazie 15, I-37134 Verona, Italy
CEA/Cadarache, DSV, DEVM, Laboratoire de Génétique et Biophysique des Plantes, UMR, 163 CEA-CNRS-Univ. Méditérranée, 163 avenue de Luminy, 13288 Marseille, France

* Author for correspondence, email: bassi@sci.univr.it

John H. Golbeck (ed): Photosystem I: The Light-Driven Plastocyanin:Ferredoxin Oxidoreductase, 119–137.

Summary

In this chapter we summarize the results of reports published since 1979 on the Chl *a*/*b*-binding light-harvesting complex of PS I. In the first part of this chapter, we review the results that led to our current knowledge of the biochemical properties of the individual gene products constituting LHCI, in particular, the presence and distribution of red-shifted spectral forms and the idea that LHCI, different from LHCII, is organized into heterodimeric complexes. Recent developments based on EM and X-ray crystallography have been reported, which led to the understanding that LHCI is bound to only one side of the PS I–LHCI supramolecular complex rather than surrounding the reaction center as was recently found in bacterial photosystems. The evidence that each Lhca subunit is present in a single copy per reaction center is also reported as compared with the data leading to a previous model with two copies of Lhca polypeptides. In the second part of this chapter, we focus on the origin of the peculiar characteristic of LHCI: the red-shifted Chl spectral forms. First, the evidence for their origin from Chl–Chl interactions is reviewed; second, the different models for the organization of the chromophores involved in these interactions, which have been recently proposed, are discussed. We conclude that present evidence favors the origin of red forms from Chl *a*–Chl *a* excitonic interaction between chromophores localized in binding sites A5 and possibly B5 of the Lhca proteins, while the evidence for involvement of additional chromophores such as Chl *b* are consistent with an indirect structural role of the ligand in site B6.

I. Introduction: LHCI Within the PS I Supercomplex

Photosystem I (PS I) is a multisubunit complex located in the stroma lamellae of thylakoid membranes, which functions as light-dependent plastocyanin/ferredoxin oxidoreductase. In higher plants and green algae this supramolecular complex is composed by two chlorophyll (Chl) binding moieties: (i) the core complex and (ii) the external antenna, encoded by either chloroplast or nuclear genes, respectively. The core is composed by 14 subunits, among which PsaA and PsaB bind the primary donor P700, and cofactors of the electron transport chain up to F_X as well as the greatest portion of the 96–103 Chl *a* and 22 β-carotene molecules. In fact, only a few Chls are bound to the minor subunits of the core complex (Jordan et al., 2001; Scheller et al., 2001; Ben Shem et al., 2003; see also Fromme and Grotjohann, this volume, Chapter 6; Nelson and Ben-Shem, this volume, Chapter 7). In addition to the inner antenna Chls bound to the core moiety, plant PS I is equipped with a peripheral antenna system in which Chl *a*, Chl *b*, and carotenoid molecules are bound to four polypeptides, namely Lhca1–4, with molecular weights between 21 and 24 kDa (Haworth et al., 1983; Bassi and Simpson, 1987; Jansson, 1994). The polypeptide composition of PS I–LHCI, PS I-core, and LHCI is shown in Fig. 1.

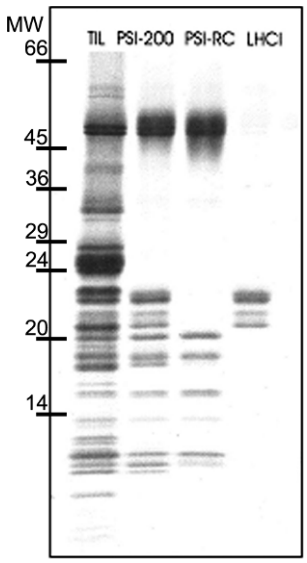

Fig. 1. Polypeptide composition of the PS I–LHCI supercomplex and its two moieties: the PS I-core complex binding Chl *a* and β-carotene and the LHCI moiety binding also Chl *b* and the xanthophylls lutein and violaxanthin. The separation was performed by SDS–urea PAGE. Source: Croce et al. (2002).

The topological organization of the LHCI moiety within the PS I supercomplex remained obscure until recent electron microscope (EM) studies by single particle analysis (Boekema et al., 2001b) showed that the Lhca subunits are located asymmetrically, on one side only, of a monomeric core complex. This organization is in contrast to that of PS II, in which a dimeric core

Abbreviations: α (β)-DM – *n*-dodecyl-α(β)-D-maltoside; β-car – β-carotene; Car – carotenoid; CD – circular dichroism; Chl – chlorophyll; EM – electron microscope; FWHM – full width half maximum; LD – linear dichroism; Lhc – light-harvesting complex; OGP – *n*-octyl-β-D-glucopyranoside; PS I(II) – photosystem I(II); Viola – violaxanthin; WT – wild type.

Fig. 2. Localization of LHCI polypeptides within the PS I–LHCI complex resolved by X-ray diffraction. Top (stromal) view of the PS I–LHCI complex is shown. The four Lhca subunits are aligned into a crescent-like structure on the lower part of the figure. Subunits exclusive of eukaryotic PS I complex are also indicated. Figure was reproduced from Ben Shem et al. (2003) with permission of the authors.

complex is symmetrically surrounded by peripheral antenna proteins that bind at multiple sites (Boekema et al., 1999). Nearest-neighbor analysis was performed both by covalent cross-linking and by observing the loss of Lhca components upon knockout or antisense depletion of individual core complex subunits. On this basis it was proposed that Lhca3 may interact with PsaK, Lhca2 with PsaG, and Lhca1/Lhca4 with PsaF and PsaJ (Jansson et al., 1996; Jensen et al., 2000; Scheller et al., 2001). Moreover, it was also suggested that each Lhca component is in contact with two others (Jansson et al., 1996).

An alternative model has been recently proposed based on the 4.4 Å crystal structure of PS I–LHCI complex from pea (Ben Shem et al., 2003). Lhca complexes were localized asymmetrically on one side of the core complex moiety, aligned in a crescent-like structure (Fig. 2). The only clear interaction could be observed between the helix C of Lhca1 and PsaG, while Lhca2, Lhca3, and Lhca4 subunits are proposed to interact with the core components trough small binding surfaces at their stromal-exposed regions. Both structural and biochemical data support the view of a LHCI antenna moiety arranged on one side only of the PS I-core complex. This arrangement is rather unusual among photosynthetic systems that are generally characterized by a circular or symmetrical arrangement of antenna subunits around the reaction center complex (Bibby et al., 2001; Boekema et al., 2001a; Roszak et al., 2003). The reason for this topological organization appears to be a structural adaptation to allow State I–State II transitions (Allen, 1992). This mechanism provides a balance in energy transfer to PS II versus PS I by transfer of phosphorylated LHCII subunits to stroma lamellae, where they serve to increase the antenna size for PS I. The docking of LHCII to the PS I-core complex has been reported to be mediated by the PsaH subunit (Lunde et al., 2000), which is located on the LHCI-free side of the PS I-core and is thus accessible for binding the phosphorylated LHCII.

From a spectroscopic point of view, the most streaking feature of PS I is the presence of Chls that absorb at

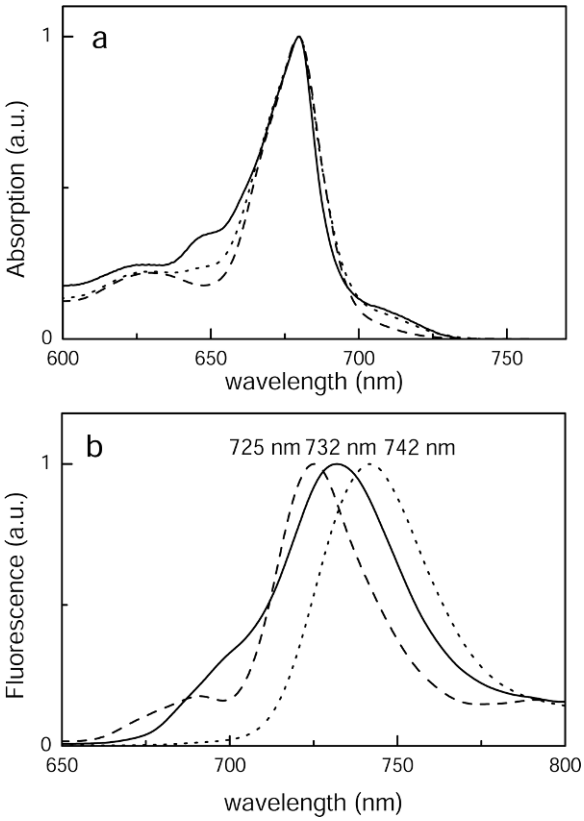

Fig. 3. Spectroscopic properties of LHCI (solid), PS I-core (dashes), PS I–LHCI (dots). (a) Absorption spectra at 77 K (b) Fluorescence spectra at 77 K, emission maxima are also reported.

energy lower than P700, the reaction center trap (Butler and Norris, 1963). This is clearly visible in the fluorescence emission spectra of the PS I–LHCI complex peaking at approximately 740 nm. The absorption and emission spectra of PS I–LHCI, PS I-core, and LHCI are reported in Fig. 3. The absorption spectra show that the Chl *b*, which is responsible for the absorption at 475 and 650 nm, is associated with LHCI proteins, as are the absorption forms at wavelengths >700 nm, which form the red-most tail in the spectra.

The fluorescence emission spectra of the PS I–LHCI supercomplex and of its two moieties reflect the distribution of red-most absorption forms. Thus, PS I–LHCI, PS I-core, and LHCI exhibit their fluorescence emission peaks at 740, 720, and 735 nm, respectively (Mullet et al., 1980b).

It has been demonstrated that at physiological temperatures, 80–90% of the excited states in the system reside in the red-shifted forms (Croce et al., 1996). This implies that to be used for charge separation, most of the excitation energy in PS I has to be transferred uphill from red absorption forms to P700, the reaction center trap.

II. Characterization of LHCI

A. Identification of Lhca Genes with Their Gene Products

Lhca proteins are encoded by the nuclear genome, synthesized by cytoplasmic ribosomes, imported across the two membranes of the chloroplast envelope, and finally inserted into the thylakoid membrane (Lubben et al., 1988). Lhca gene sequences are now available from different organisms, thanks to the work of sequencing projects (e.g., see TIGR web site, http://www.tigr.org/tdb/tgi/plant.shtml).

In vascular plants, six classes of Lhca genes have been identified, namely *Lhca1–6*. Moreover, several copies of the same gene can be found, depending on the species (see, e.g., Jansson, 1994 and references therein). In Fig. 4A, the alignment of protein sequences of Lhca from *Arabidopsis thaliana* is shown (Jansson, 1994). Biochemical studies on Arabidopsis as well as on other plants have shown that only the proteins encoded by genes *Lhca1–4* are expressed under the different experimental conditions investigated (see section II.B and references therein). No information is at present available for the products of the genes *Lhca5* and *Lhca6* except that they are transcribed at a very low level (Jansson, 1999). However, the possibility that Lhca5 and Lhca6 are expressed under special environmental conditions or developmental states cannot be ruled out. Lhca6, which is highly homologous to Lhca2, was proposed to be a pseudogene (Jansson, 1999).

The Lhca genes belong to the Lhc multigenic family, which also includes the genes for the outer antenna of PS II, namely *Lhcb1–6* (Jansson, 1999). In Fig. 4B an unrooted cladogram created by ClustalX of all Lhc deduced protein sequences from Arabidopsis is shown. Antenna proteins of PS I cluster together, being more homologous to each other than to the Lhcb PS II components. Interesting exceptions from this general trend are Lhca1, which is more related to Lhcb4 that to Lhca2–4, and Lhcb6, which is intermediate between the two clusters. Evolutionary studies on the Lhc multigenic family confirmed a separation between Lhca and Lhcb proteins; in fact, Durnford et al. (1999) proposed that Lhca and Lhcb proteins diverged before the separation of different Lhca and Lhcb complexes. Thus, Lhca and Lhcb proteins are separate groups within the Lhc family, suggesting they have specific properties and

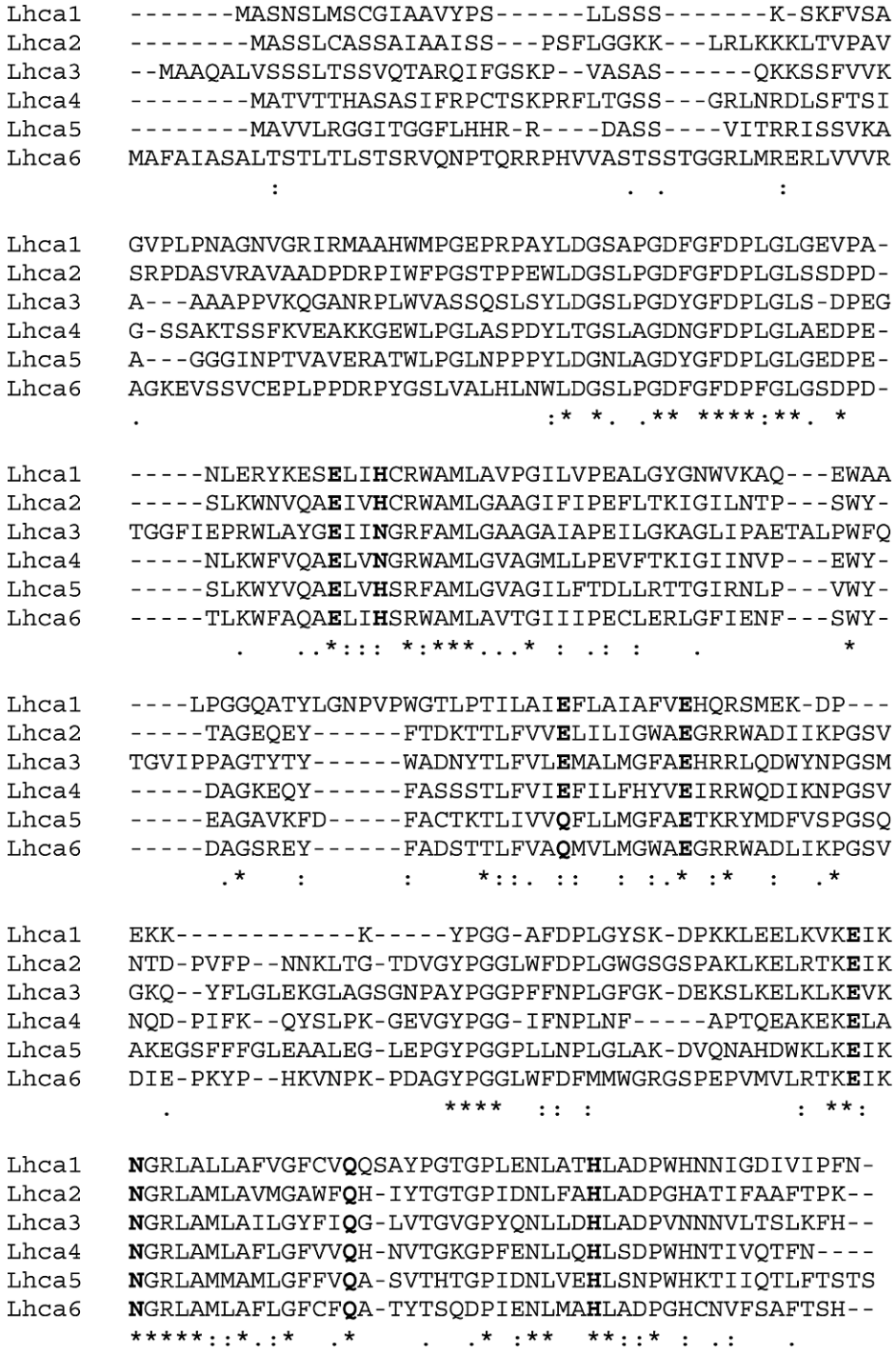

Fig. 4. (A) Alignment of protein sequences of Lhca1–6 from *Arabidopsis thaliana*. Chl binding residues are indicated in bold.

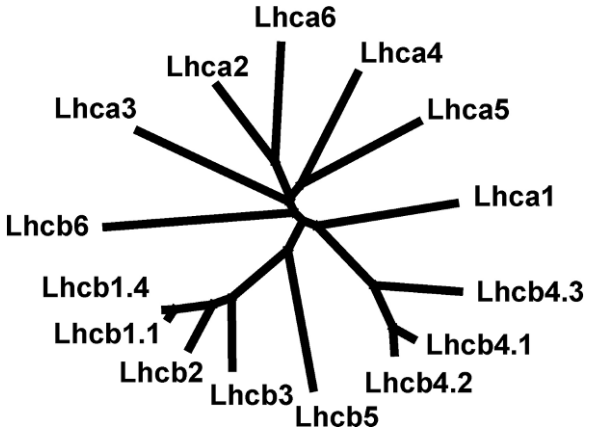

Fig. 4. (B) An unrooted cladogram of deduced protein sequences of Lhc proteins of *A. thaliana*.

functions, probably adapted to the characteristics of the photosystems that they serve.

B. Differential Characterization of Individual Lhca Gene Products

The first evidence for the presence of a Chl *a*/*b* antenna in higher plants PS I came from the work of Mullet et al. (1980b), who purified PS I complexes that differed in antenna size and in the presence of four polypeptides with molecular mass between 20 and 24 kDa, thereafter identified as the outer antenna system of PS I.

To purify the individual Lhca complexes and to determine their biochemical and spectroscopic characteristics, different approaches have been used: purification of LHCI from plants, reverse genetics, and refolding *in vitro*. In the following section, the main steps in the determination of the properties of the individual Lhca complexes are summarized.

1. Fractionation of LHCI – Native LHCI

a. Purification

LHCI complexes were first purified from pea by Haworth et al. (1983) using sucrose gradient ultracentrifugation. The authors isolated a fraction containing four polypeptides with molecular weights between 20 and 24 kDa, and with a Chl *a*/*b* ratio of 3.7. In the following years, several attempts to further purify LHCI complexes were performed using different methods including sucrose gradient ultracentrifugation (Kuang et al., 1984; Lam et al., 1984b; Bassi and Simpson, 1987; Ikeuchi et al., 1991a; Schmid et al., 2002b), nondenaturing electrophoresis (Kuang et al., 1984; Lam et al., 1984a; Bassi et al., 1985; Dunahay and Staeheli, 1985; Vainstein et al., 1989; Knoetzel et al., 1992; Preiss et al., 1993), and perfusion chromatography (Tjus et al., 1995).

In 1984 Lam et al. (1984a) purified two Lhca fractions from spinach by sucrose gradient ultracentrifugation. The upper band contained the 22 and 23 kDa polypeptides (Lhca2 and Lhca3), while the lower was enriched in the 20 kDa polypeptides (Lhca1 and Lhca4). The fractions showed similar Chl *a*/*b* ratio (3.5 ± 0.5), but differed substantially in their spectroscopic properties, with the upper band emitting at 680 nm and the lower and emitting at 730 nm. On the basis of these results, LHCI fractions were named according to their emission peaks at low temperature: LHCI-730 and LHCI-680 (Bassi et al., 1985) and this nomenclature was used in most of the papers that followed this work. From these early experiments it was concluded that the red forms were associated with the 20 and 21 kDa polypeptides (Lhca1 and Lhca4), rather than with the heavier subunits (Lhca2 and Lhca3). The polypeptide composition of LHCI-680 and LHCI-730 varied, however, in the different preparations. LHCI-730 in some preparations contained only Lhca1 and Lhca4 (Knoetzel et al., 1992; Tjus et al., 1995; Schmid et al., 2002b), while in others all four Lhca polypeptides were present (Bassi et al., 1985; Bassi and Simpson, 1987; Ikeuchi et al., 1991b). Typically, the LHCI-730 fraction had an absorption peak in the Q_y region of Chl *a* at 670–676 nm and a 77 K fluorescence emission peak at 730 nm. LHCI-680 was enriched in Lhca2 and Lhca3 polypeptides; it showed a lower sedimentation rate in a sucrose gradient and a higher mobility by nondenaturing electrophoresis (green gels) as compared to LHCI-730, indicating a lower aggregation state. LHCI-680 had an absorption peak in the Q_y region of Chl *a* at 668–670 nm and a 77 K fluorescence emission peak at 678–680 nm (Lam et al., 1984a; Knoetzel et al., 1992; Tjus et al., 1995). Exceptions to this pattern suggested a further grade of heterogeneity among the individual gene products: the "LHCI-680" isolated by Bassi and Simpson (1987) from barley contained a single polypeptide, Lhca2, and had a Chl *a*/*b* ratio of 2.0. Its absorption peak was at 674 nm and its fluorescence emission peaked at 690 nm. The LHCI-680 preparation described by Ikeuchi et al. (1991b), was enriched in Lhca2 and Lhca3. Whereas showing the maximum fluorescence emission occurred at 680 nm, it had a prominent shoulder above 700 nm suggesting the presence of red-shifted spectral forms in either Lhca2 or Lhca3. In other reports, the fractionation of the PS I–LHCI complex did not yield a LHCI-680

Table 1. Pigment composition of LHCI

Plant material	Fraction	Chl *a*/*b*	Chl tot	Viola	Lutein	β-car	References
Pea	LHCI	3.7					Haworth et al. (1983)
	680/730	3.5					Lam et al. (1984a)
Spinach	680	3.1					Palsson et al. (1995)
	730	3.2					Palsson et al. (1995)
Barley	680[a]	2.0					Bassi and Simpson (1987)
	730	2.2					Bassi and Simpson (1987)
Tomato	680	2.5	8.99	0.43	0.92	0.4	Schmid et al. (2002b)
	730	2.57	7.17	0.39	0.84	0.18	Schmid et al. (1997)
		2.48	11.41	0.54	0.99	0.42	Schmid et al. (2002b)
Maize	LHCI	3.8	10	0.55	1.2	0.4	Croce and Bassi (1998)
	680	4–5					Vainstein et al. (1989)
	730	2–2.5					Vainstein et al. (1989)
	Lhca2/Lhca3	3.8	10	0.5–0.6	1.1–1.2	0.5–0.65	Croce (1997)
	Lhca1/Lhca4	3.6–3.8	10	0.6–0.7	1.3–1.4	0.36–0.4	Croce (1997)
Arabidopsis	LHCI	3.3	10	0.6	1.1	0.45	Croce et al. (2002)
Spinach[b]		3.0	92	7	12	8	Damm et al. (1990)

Data shown were obtained with different purification methods and from different plant species (see section II.B).
[a] This preparation contained only Lhca2.
[b] Data were obtained by difference between the pigment composition of PS I-200 and PS I-core.

fraction. Haworth's preparation (1983) showed an emission at 730 nm and contained all four Lhca polypeptides. Also, the LHCI preparation by Croce et al. (1998) did not contain a LHCI-680 fraction but only a LHCI-730 fraction in a dimeric aggregation state. From the latter preparation, two emissions were resolved, peaking at 702 and 730 nm (Ihalainen et al., 2000). It was suggested that the LHCI-680 fraction contains complexes that are not in their fully native state. This is consistent with the blue-shifted absorption peaks (668–670 nm) and the fluorescence emission from partially disconnected Chls (Palsson et al., 1995) that have longer fluorescence lifetimes with respect to LHCI-730. Thus, it appears that Lhca2 and Lhca3 can migrate either as monomers, in the LHCI-680 fraction, or as dimers, in the LHCI-730 fraction, exhibiting spectroscopic differences depending on aggregation state: a longer lifetime emission and a blue-shifted absorption in LHCI-680 with respect to LHCI-730. This might be due to higher sensitivity to detergent treatment of Lhca2 and Lhca3 with respect to Lhca1 and Lhca4, as suggested by Lam et al. (1984a).

An attempt to purify Lhca2 and Lhca3 in the native state was made by Croce et al. (Croce and Bassi, 1998; Croce et al., 2002) using nondenaturing IEF. In this work, fractions containing dimeric complexes were purified either enriched in Lhca2/Lhca3 or in Lhca1/Lhca4. Red emission forms were retained, not only in Lhca4 containing fractions, but also in those in which Lhca2/Lhca3 was predominant, thus suggesting that one or both of these two subunits also accommodate red-shifted Chl forms.

b. Pigment Content

The purification of individual Lhca complexes in their native state by classical biochemical methods has proven very difficult due to the strong association between the external antenna and the core complex. Thus, harsh detergent treatment is required for dissociation. Nevertheless, information about the average biochemical and spectroscopic characteristics of the LHCI complexes was obtained in several plant species.

A summary of LHCI preparations is presented in Table 1. The pigment composition of the complexes is also reported.

The Chl *a*/*b* ratio values obtained from the different preparations vary considerably, with tomato and barley showing the lowest values, 2.5, and maize and pea the highest, 4. Both the methods of preparation and the intrinsic differences in the Chl *b* content of LHCI from different species might be the cause for these differences as judged by the finding that the same procedures applied to maize and Arabidopsis yielded *a*/*b* ratios of 3.8 and 3.3, respectively (Croce et al., 2002). Preparations involving the use of Triton X-100 appear to undergo partial Chl loss. More consistent are the data on the carotenoid composition: Lhca complexes bind violaxanthin and lutein, similar to Lhcb proteins (Bassi et al., 1993). However, they do not bind neoxanthin. β-carotene, which is not bound to Lhcb proteins, instead appears as a minor but genuine chromophore for Lhca proteins.

Thus, biochemical fractionation, although not yielding purified, individual, undenatured, Lhca gene

products, allowed characterization of the overall properties of LHCI. Moreover, evidence was provided for heterogeneity of the four Lhca components with respect to both pigment composition and enrichment in red-shifted absorption forms.

2. Reverse Genetic and Chlorina Mutants

An alternative approach to clarify the properties of Lhca complexes has been the analysis of plants lacking one or more Lhca gene products. The barley *Chlorina* mutant collection (Simpson et al., 1985) has first been used, followed by knockout mutants or antisense plants.

The *Chlorina f2* mutant lacking Chl *b* was analyzed by Mullet et al. (1980a) to support Chl *b* binding to LHCI complexes and their content in red emission forms. The preferential failure of *Clo-f2* to accumulate Lhca4 led to the conclusion that the red forms are associated to this subunit (Bossmann et al., 1997; Knoetzel et al., 1998). This suggestion was supported by Zhang et al. (1997), who produced antisense Arabidopsis plants lacking Lhca4, showing a 6 nm blue shift in the fluorescence emission peak. Antisense plants lacking Lhca2 and Lhca3 (Ganeteg et al., 2001) led the authors conclude that absorption forms at 695 and 715 nm, connected to emissions at 702 and 735 respectively, were associated to Lhca2 and Lhca3. Thus the use of mutant plants lacking one or more Lhca proteins showed to be valuable in establishing the relation between gene products and the associated absorption and fluorescence forms, thereby overcoming the problems due to the partial denaturation of pigment–proteins during purification.

3. Recombinant Proteins

A third approach to the study of PS I antenna system has been the *in vitro* production of Lhca holoproteins by overexpression of the apoproteins in bacteria and reconstitution *in vitro* with purified pigments. This approach, first introduced by Plumley and Schmidt (1987), exploits the ability of Lhc proteins to fold *in vitro* in the presence of Chls and carotenoids. This procedure was first applied to Lhcb proteins, which can be purified more easily than Lhca subunits from thylakoids. Comparison of native and recombinant proteins showed that reconstitution *in vitro* yielded complexes indistinguishable by biochemical and spectroscopic analysis (Giuffra et al., 1996; Pascal et al., 2001; Croce et al., 2003).

In 1997 Schmid et al. (1997) reconstituted Lhca1 and Lhca4 using tomato genes and showed that the two complexes, although homologous, had distinct properties, with Lhca4 emitting at 730 nm and Lhca1 at 686 nm. These experiments provided a direct demonstration that the red-most forms were associated to Lhca4. The same procedure was later applied to Lhca2 and Lhca3 from tomato (Schmid et al., 2002b) and to the four Lhca gene products from Arabidopsis (Croce et al., 2002; Castelletti et al., 2003). It was shown that red-shifted forms are a common characteristic of Lhca proteins, their amplitude and wavelength of emission increasing in the order Lhca1 > 2 > 3 and 4 (Castelletti et al., 2003).

Table 2. Pigment composition of reconstituted Lhca complexes from *Arabidopsis thaliana*

Sample	Chl *a*	Chl *b*	Viola	Lutein	β-car
Lhca1	8 ± 0.04	2 ± 0.04	1.05	1.81	–
Lhca2	6.5 ± 0.2	3.5 ± 0.2	0.47	1.52	–
Lhca3	8.6 ± 0.2	1.4 ± 0.2	0.66	1.62	0.57
Lhca4	7.0 ± 0.2	3 ± 0.2	0.5	1.5	–

Data shown are from Castelletti et al. (2003).

The pigment content of the four Lhca complexes from Arabidopsis is reported in Table 2. All Lhca were estimated to coordinate 10 Chls per polypeptide, while differing sensibly in their Chl *a* to Chl *b* ratio. In particular, a higher Chl *b* content was found in Lhca2 (Chl $a/b = 1.8$), while the lowest was found in Lhca3 (Chl $a/b = 6$). The carotenoid content was found to be either two (in Lhca2 and Lhca4) or three (in Lhca1 and Lhca3). Reconstitution *in vitro* confirmed that neoxanthin is not a component of the antenna system of PS I. In fact, although present in the reconstitution mixture during refolding, it was never bound in the complexes. Lhca3 has the peculiar feature of binding β-carotene in its monomeric state (Croce et al., 2002; Castelletti et al., 2003). While the results on tomato Lhca differ slightly, the trend in both Chl *a*/*b* and carotenoids binding (Schmid et al., 2002b) is consistent with the data found using Arabidopsis genes. Reconstitution in the absence of individual pigment species revealed that Lhca1 and Lhca3 need Chl *a*-only for folding, while Chl *b* is, in addition, essential for the stability of Lhca2 and Lhca4 (Schmid et al., 2002b), consistent with the different affinity of the complexes for the two Chl species.

The possibility to prepare homogeneous preparations of each Lhca complex allowed their spectroscopic properties to be determined. The analysis of the emission spectra at low temperature showed that all Lhca complexes contained emission forms at wavelengths longer than 700 nm. In particular Lhca4 showed an emission maximum at 733 nm, Lhca3 at 725 nm, Lhca2

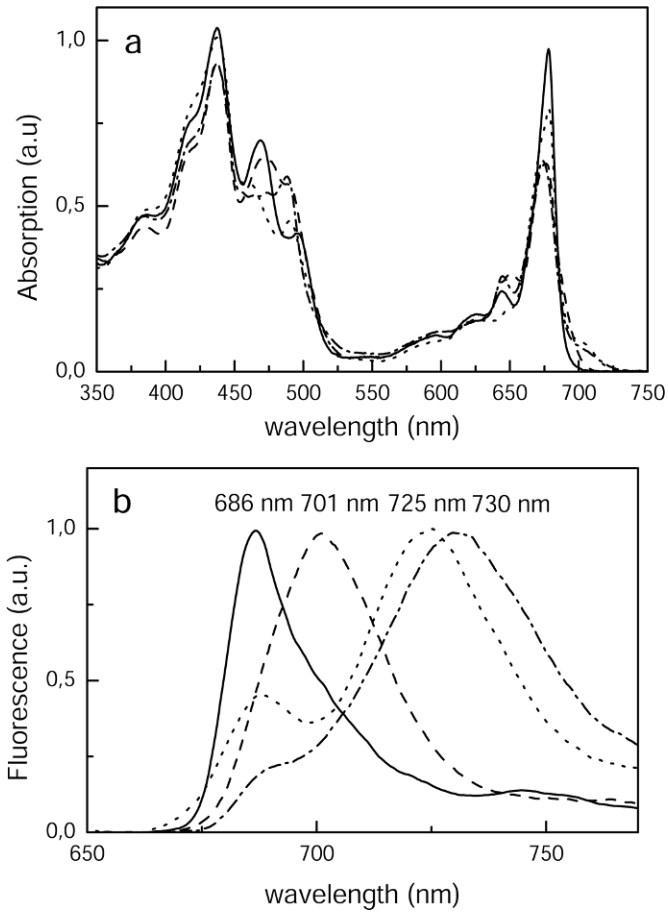

Fig. 5. (a) Absorption and (b) fluorescence emission spectra at 77 K of recombinant Lhca complexes: Lhca1 (solid), Lhca2 (dashes), Lhca3 (dots), Lhca4 (dash-dots). All genes are from *Arabidopsis thaliana*. Emission maxima are also reported.

at 702 nm. The Lhca1 emission peak was at 690 nm but a shoulder was also present at 701 nm (Fig. 5b). The absorption spectra of individual Lhca proteins (Fig. 5a) demonstrated that each of them has peculiar characteristics and a different distribution of the absorption forms. The Q_y absorption peaks of Lhca1, Lhca2, and Lhca3 are found at around 680 nm, strongly red shifted with respect to Lhcb complexes. This is not the case for Lhca4, for which the Q_y absorption peak was found at 676 nm (Fig. 5b).

A comparison between the pigment organization in Lhca and Lhcb complexes can be had by analyzing the CD and LD spectra of the complexes. A red shift in both CD and LD is observed for Lhca complexes as compared to Lhcb, which indicates that the red forms contribute to the dichroic spectra. Interestingly, in the region in which carotenoids absorb, the spectra showed larger differences, thus supporting the hypothesis that the xanthophylls in Lhca complexes are differently organized/oriented than in Lhcb complexes (Croce et al., 2002; Castelletti et al., 2003; Morosinotto et al., 2003).

In vitro reconstitution resulted in a major contribution to the detailed knowledge of the biochemical and spectroscopic characteristics of individual Lhca complexes. It was clear that the four Lhca complexes, despite their high sequence homology, strongly differ in their pigment binding affinity and in the distribution of the absorption forms. Strongly shifted fluorescence emissions were associated with both Lhca4 and Lhca3 monomers, while Lhca1 and Lhca2 had a limited shift of their red-most spectral forms.

III. Models of LHCI Polypeptides

A. Polypeptide Structure

The structure of one member of Lhc family, the main antenna complex of PS II, LHCII, has been solved using

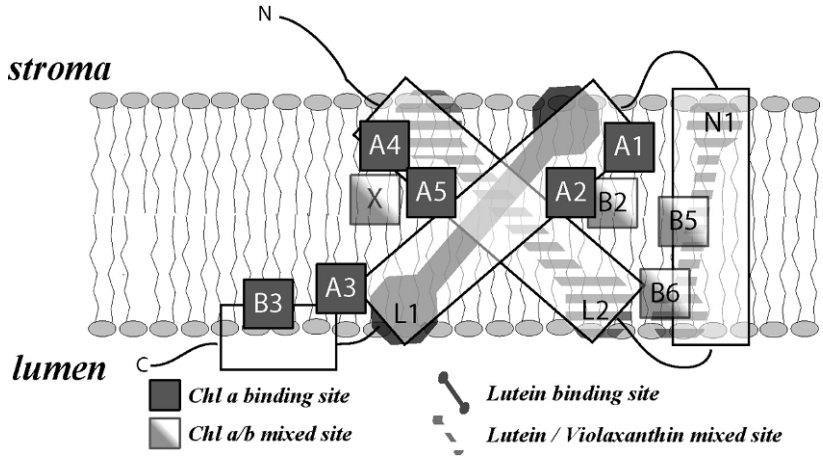

Fig. 6. Schematic 2D representation of Lhca structure, based on reconstitution experiments. Conserved Chl and xanthophyll binding sites are indicated, using the nomenclature proposed by Kühlbrandt et al. (1994). Residues directly coordinating chlorophylls are also indicated.

2D crystals and electron crystallography (Kühlbrandt et al., 1994). The high sequence homology between the members of the Lhc multifamily (Durnford et al., 1999) suggested that they share the same structural organization (Green and Durnford, 1996). This was confirmed by the structure of the PS I–LHCI complex, in which the 3D organization of Lhca polypeptides was solved. Superimposition of the structure of the transmembrane domain of Lhca complexes with LHCII showed an almost perfect match, with three transmembrane helices and one amphipatic helix exposed on the lumenal side of the membrane (Ben Shem et al., 2003). The N-terminus is exposed to the stroma and the C-terminus is exposed to the thylakoid lumen (Fig. 6; Kühlbrandt et al., 1994; Ben Shem et al., 2003).

Less information is at present available about the organization of loops connecting α-helices, which are not resolved in the 2D crystals of LHCII. An analysis of the primary structure reveals differences between the Lhc proteins in the length of the loops connecting the transmembrane helices. In this respect, Lhca1 is similar to Lhcb4, having the stromal and the lumenal loops of the same length (23–25 amino acids). Lhca2, Lhca3, and Lhca4 have longer stromal loops of 41 (Lhca2), 43 (Lhca3), and 36 residues (Lhca4), and shorter lumenal loops of 17 (Lhca2), 26 (Lhca3), and 17 residues (Lhca4), making these complexes more similar to Lhcb6. Structural data suggest that these differences do not influence the packing of the transmembrane domain, but might be involved in interactions with core complex subunits (Ben Shem et al., 2003).

B. Chlorophyll Binding

1. How Many Chls are Bound to Each Lhca Complex?

A pigment determination on a purified LHCI fraction containing all four Lhca complexes showed that there are, on average, 10 Chls per polypeptide (Croce and Bassi, 1998). This value was consistently found in fractions enriched in Lhca2–3 or Lhca1–4. In the PS I–LHCI structure (Ben Shem et al., 2003), the authors observed 56 Chls associated with the external antenna, 14 Chls per each Lhca complex. However, Lhca proteins appear to be embedded in a sort of "pigment bed" composed of Chls either tightly bound to Lhca proteins or bound at the interface between two neighbor Lhca polypeptides or filling the gap between the LHCI crescent-like structure and the PS I-core complex. A portion of the Chls loosely associated with LHCI thus appear to be prone to dissociation during solubilization, thus leaving 10 Chls bound to each Lhca polypeptide as determined from both the Chl-to-polypeptide ratio and the carotenoid to Chl ratio. The latter parameter, in particular, appears to be reliable due to the inner location of three carotenoid binding sites in Lhc proteins (Croce et al., 2002; Castelletti et al., 2003).

2. Chlorophyll Organization

From the structure of LHCII complex, eight amino acid residues were indicated as Chl ligands, while the

Table 3. Biochemical and spectroscopic properties of the Chls in each binding site for Lhcb1 and Lhca1

Site	Lhcb1	Lhca1
A1	Chl *a* (679 nm)	Chl *a* (nd)
A2	Chl *a* (681 nm)	Chl *a* (682 nm)
A3	Chl *a*/Chl *b* (662/650 nm)	Chl *a* (663–681 nm)
A4	Chl *a* (674 nm)	Chl *a* (678–679 nm)
A5	Chl *a* (674 nm)	Chl *a* (675–679 nm)
B3	Chl *a*/Chl *b* (665/650 nm)	Chl *a* (663 nm), traces Chl *b*
B5	Chl *b* (652 nm)	Chl *a*/Chl *b* 644/(668–686/644 nm)
B6	Chl *b* (652 nm)	Chl *a*/Chl *b* 644/(668–686/644 nm)
B1	Chl *a* (679.4 nm)	–
B2	Chl *b* (644 nm)	Chl *a*/Chl *b* (650/682 nm)
A6/A7	0.5 Chl *a*/1.5 Chl *b* (679/652 nm)	–
X[a]	–	Chl *a*/Chl *b* (644/ND)

Data shown are from Remelli et al. (1999) and Morosinotto et al. (2002). The site nomenclature used here is derived from the LHCII nomenclature proposed by Kühlbrandt et al. (1994). It indicates the position of the chlorophyll in the structure. The A and B prefix is not meant here as indication of the Chl *a*/Chl *b* occupancy of the site.

[a] This site seems do not be present in Lhcb1 complex. In Lhca this Chl is lost together with Chl A5.

mode of binding of the remaining four Chl molecules remained unclear. Mutation analysis confirmed that all eight Chl binding residues were indeed able to coordinate the central Mg^{2+} of the Chls in LHCII. It was suggested that the additional four Chls were positioned by interaction with other chromophores, although the involvement of residues in the intra-helices loops could not be excluded (Kühlbrandt et al., 1994; Remelli et al., 1999). Primary structure comparison between LHCII and the Lhca complexes showed that all of the Chl binding residues present in LHCII are conserved in Lhca proteins, with a few substitutions: (i) Chl B6 is coordinated by a Gln in LHCII, while this position is occupied by a Glu in all Lhca proteins; (ii) an Asn residue is present at site A5 in Lhca3 and Lhca4, while in LHCII as well as in all other antenna complexes the ligand for Chl A5 is a His. Mutation analysis confirmed that these residues coordinate Chls as well as all other conserved amino acids (Morosinotto et al., 2002, 2003).

To assign the Chl occupancy to the individual sites and to determine the spectroscopic properties of each Chl, a detailed study of the pigment organization was performed by mutation analysis on Lhca1 (Morosinotto et al., 2002). The results are summarized in Table 3, in which the attribution of chromophores to different sites in Lhca1 is compared to that in Lhcb1.

The results indicate that the occupancy of most of the sites in Lhca1 is similar to Lhcb1, the major differences being due to the increased affinity for Chl *a* vs. Chl *b* of the sites showing mixed Chl *a* and Chl *b* occupancy. Interestingly, in Lhca1 most of the mutations caused the loss of more than one pigment in a manner different from that observed in Lhcb1 and Lhcb4, while several interactions between chromophores were spectroscopically detected in LHCI (Bassi et al., 1999; Remelli et al., 1999). This different pattern of responses suggests that pigment–pigment interactions are stronger in Lhca proteins as compared to Lhcb proteins. The crystal structure shows that the plane of the tetrapyrrole is differently oriented in at least three Chls within Lhca complexes as compared to LHCII, namely Chls in sites B5 (or A5), A7, and A3 (Ben Shem et al., 2003).

C. Carotenoid Binding

The carotenoid organization in Lhca1 was not resolved in the crystal structure, thus information is restricted to data from mutational analysis. Most of the mutations to the Chl binding residues also yielded loss of carotenoid molecules. This was useful for localizing the xanthophyll binding sites within Lhca1 and for determining their affinity for ligands. Three carotenoids are tightly bound to Lhca1 as well as to Lhcb1, and they are likely to be located at the same three binding sites, namely L1 and L2, nearby helices A and B, and N1 near helix C. The affinity of each site for the individual xanthophyll species is not the same: neoxanthin, which is accommodated in the site N1 of Lhcb1 (Croce et al., 1999) is absent in Lhca1 and is substituted by violaxanthin and lutein. Lutein is conserved as a ligand for site L1 in all Lhc complexes analyzed thus far. However, while the occupancy of site L1 is essential for Lhcb protein folding, in Lhca1, lutein is lost on mutating site A3 without destabilizing the complex (Bassi et al., 1999; Remelli

et al., 1999). Site L2 accommodates both lutein and violaxanthin with similar affinities.

On the basis of the results of the mutational analysis, a model for the chromophore organization in Lhca1 can be drawn (Fig. 6).

Preliminary results on the mutational analysis of Lhca2, Lhca3, and Lhca4 suggest that all Lhca proteins share a similar pigment organization with the exception of the number of bound xanthophylls: two in Lhca2 and Lhca4, three in Lhca 1 and 3. Lutein is in site L1, while site L2 is occupied by both lutein and violaxanthin. Lhca3 was shown to coordinate also β-carotene (Schmid et al., 2002b; Castelletti et al., 2003), but its binding site is not yet clear.

The structure of Lhca complexes is similar to LHCII with respect to both apoprotein and chromophores organization. However, differences can be observed in the affinity of the pigment binding sites for the individual chromophores. Small differences in the pigment organization can be detected both by mutational analysis and by X-ray diffraction, suggesting that the peculiar spectroscopic characteristics of Lhca complexes might be due to small changes in inter-chromophore distance and orientation, particularly in the domain including the stromal side of helices A and C.

IV. Dimerization of Lhca Proteins

It is now accepted that all Lhca complexes are present in dimeric form *in vivo* (Croce and Bassi, 1998; Croce et al., 2002). This suggestion was first made by Kuang et al. (1984) and by Bassi (1985) from their apparent mobility as a 40 kDa band in nondenaturing electrophoresis. A similar suggestion was also made based on sucrose gradient ultracentrifugation (Ikeuchi et al., 1991a) and by nearest-neighbor analysis (Jansson et al., 1996) that yielded cross-linking products between 40 and 45 kDa.

The suggestion that Lhca1 and Lhca4 form heterodimers (Knoetzel et al., 1992) was later confirmed by *in vitro* reconstitution (Schmid et al., 1997). In the Lhca1–4 heterodimer there is complete energy transfer between Lhca1 and Lhca4, as demonstrated by the single 733 nm emission peak in the spectrum of the dimer. The CD and the LD spectra of the dimer also showed that the dimerization influenced the pigment organization, especially of Chl *b* (Schmid et al., 1997; Croce et al., 2002). Moreover, the heterodimer was more stable to heat denaturation than the two monomers. Dimerization also involved the binding of β-carotene, probably at the subunit interface (Croce et al., 2002).

Consistent with the *in vitro* data, analysis of *Chlorina* mutants (Knoetzel et al., 1998) and of Lhca4 antisense plants (Zhang et al., 1997) showed that although Lhca1 is maintained in the absence of Lhca4, its stoichiometry with respect to PS I RC is decreased, suggesting that they form dimers *in vivo*.

The results on Lhca2 and Lhca3 are less clear: they do not dimerize *in vitro* (Schmid et al., 2002b) but antisense plants lacking either Lhca2 or Lhca3 showed relevant reduction of Lhca3 and Lhca2, respectively, thus suggesting that the two subunits are connected (Ganeteg et al., 2001). Moreover, partial purification of LHCI by preparative isoelectrofocusing yields both dimers enriched in Lhca1–4 and in Lhca2–3, suggesting their association (Croce et al., 2002). Evidence for Lhca2 homodimers was obtained by analyzing a native LHCI preparation containing all Lhca complexes: two different emissions, at 702 and 733 nm were detected (Ihalainen et al., 2000), which is predicted only if dimers of Lhca2 cannot transfer energy to Lhca3, whose red-most transition is at far lower energy (Castelletti et al., 2003).

The dimerization of Lhca1 and Lhca4 has been studied *in vitro*, producing proteins modified by deletions or point mutagenesis. It has been shown that the Trp residue at position 4 of Lhca1 is involved in dimerization together with an additional Trp residue localized at the C-terminus of the same protein. Lhca4 C- and N-termini are not involved in strong interactions with Lhca1 since Lhca1–4 dimerization was broken only after complete deletion of the N- and C-terminal sequences (Schmid et al., 2002a). This is consistent with the X-ray data showing that Lhca1 binds to the C-helix and to the lumenal loop of Lhca4.

We can conclude that Lhca complexes are present as heterodimers *in vivo* with the Lhca1–4 pair being more stable than the Lhca2–3 dimer. More experiments are needed to elucidate the interaction between Lhca2 and Lhca3 and to determine the spectroscopic characteristics of this heterodimer.

V. PS I–LHCI Stoichiometry

The number of antenna proteins bound to PS I has, for long time, been a matter of debate. It was believed that there were eight Lhca per P700. This figure was derived from EM analysis (Boekema et al., 1990), and it was in good agreement with pigment stoichiometry data that attributed 80 Chls to the LHCI moiety and 10 Chls to each polypeptide (see above). However, a more detailed electron microscopic analysis suggested

that the surface occupied by LHCI in projection with the PS I–LHCI complex could accommodate four to five Lhca per reaction center (Boekema et al., 2001b). The 3D structure of the PS I–LHCI complex supports a stoichiometry of four Lhca per PS I. The structure also allowed the discrepancy between the pigment stoichiometry and the structural data to be explained. In fact, linker Chls are present in between the Lhca complexes and the core and in between the individual Lhca subunits. These Chls could be lost upon separation of LHCI from the core, thus influencing estimations of stoichiometry based on the pigment content of individual polypeptides.

Thus, four Lhca complexes are present in the PS I–LHCI supercomplex, and are connected to the core by linker Chls that are lost upon dissociation of the LHCI fraction from the core moiety.

VI. Energy Transfer

Analysis of the excitation spectra of Lhca complexes reveals that the carotenoid transfers energy to the Chls with 65%, efficiency, a value lower than in Lhcb complexes (70–80%, Croce et al., 2002; Castelletti et al., 2003). The energy transfer pathways in Lhca complexes are reviewed in Karapetyan et al. (this volume, Chapter 13), where the reader is provided more details. Here, we stress that the value obtained from time-resolved data indicate that the energy transfer within LHCI complexes is very similar to that observed within Lhcb complexes. The only difference is represented by the energy transfer component in the red absorbing forms, which takes place in approximately 5 psec. We note that a similar lifetime has been associated with the Chl *a*–Chl *a* equilibration in LHCII and in CP29 (Van Amerongen and van Grondelle, 2001; Croce et al., 2003). The energy transfer between monomers within the dimeric complex is slower than the energy transfer between individual subunits in LHCII trimers (30 psec vs. 12 psec, Kleima et al., 1997). These results suggests that the pigment organization in Lhca complexes is not very different compared to Lhcb with the exception of the presence of the red forms, while the monomers in the dimer seem to be less strongly associated with respect to the trimer of LHCII.

VII. On the Origin of Red Absorption Forms

Following characterization of individual LHCI components, the elucidation of the structural features responsible for the huge shift in the Chl fluorescence emission has been the target of research on LHCI. In higher plant photosynthetic complexes, the Q_y absorption band of Chl is in the 640–660 nm range for Chl *b* and between 660 and 682 nm for Chl *a*. In the case of the red forms, the Chls involved are expected to absorb above 700 nm, and are thus energetically far apart from the bulk Chls. It has been proposed that the red forms represent the low energy band of an excitonic interaction between two or more Chl molecules (Gobets et al., 1994). In the following we will address some detailed questions about red forms:

A. Which complex(es) coordinate the red Chls?
B. Which are the absorption characteristics of the red forms?
C. How many Chls absorb in the red?
D. Which are the Chls involved?
E. Where are the red Chls located within the Lhca complexes?
F. What is the role played by the protein in modulating the absorption of the red Chls in the four Lhca complexes?
G. What mechanism is responsible for the large absorption shift of the red forms as compared to the bulk Chls?

A. Which Complexes Coordinate the Red Chls

The dissociation of PS I-200 into PS I-core and LHCI complexes resulted in the conclusion that the most red forms are associated with the outer antenna system in higher plants. This is in contrast with other organisms, in which the red emission originates from Chls associated with the PS I-core [see Gobets and van Grondelle (2001) for a review].

In vitro reconstitution of individual Lhca complexes yielded the emission spectra of individual Lhca complexes, showing that the emissions at 4 K for Lhca4, Lhca3, Lhca2, and Lhca1 were at 733, 725, 702, and 690 nm, respectively (Castelletti et al., 2003). The Lhca1–4 heterodimer showed the same fluorescence emission as the Lhca4 monomer, indicating complete energy transfer from Lhca1 to the red forms of Lhca4 (Schmid et al., 1997).

B. Which are the Absorption Characteristics of the Red Forms?

While the red forms can be easy detected by fluorescence, especially at low temperature, a determination of

the absorption forms responsible for the red emission is not straightforward since the red pigments represent, at most, the 5% of the total absorption in the Q_y region (Ihalainen et al., 2000). Although these forms are expected to be energetically distant from the bulk Chls, it was not possible to detect a clear band, even at 4 K, due to the lack of structure in the spectra. This suggests that these forms are largely inhomogeneously broadened. From an early analysis of the 735 nm emission of chloroplasts (Butler et al., 1979) it was proposed that the origin of the red emission was an absorption band at 705 nm (Boardman et al., 1978). Site-selected fluorescence measurements on a PS I-200 preparations indicated 716 nm as the upper limit for the maximum of the band responsible for the long wavelength emission (Gobets et al., 1994). Similar work on a purified dimeric LHCI fraction shifted this estimation to 711 nm (Ihalainen et al., 2000). The bandwidth of the 711 nm absorption was suggested to be 356 cm^{-1} by Gaussian deconvolution of the red tail of LHCI absorption spectra, while site-selected fluorescence analysis showed that the contribution of the homogeneous and inhomogeneous broadening to the bandwidth were 210 and 290 cm^{-1}, respectively. Consistently, an electron–phonon coupling value of 2.7 was derived from fluorescence line-narrowing experiments (Ihalainen et al., 2003): the stronger coupling found in photosynthetic antenna complexes. From these values the FWHM of the red band in LHCI of 30 nm and the Stokes shift of 35 nm could be calculated.

Analysis of the reconstituted Lhca complexes at 77 K, by Gaussian deconvolution of difference absorption spectra (see below), suggested that the absorption is located between 700 and 705 nm for both Lhca3 and Lhca4 (Morosinotto et al., 2003). The origin band for the 702 nm emission of Lhca1 and Lhca2 complexes was located at 686–688 nm by comparison of the spectra of WT and point mutant proteins (Morosinotto et al., 2002, unpublished).

C. How Many Chls Absorb in the Red?

In LHCI preparations it was estimated that the red absorption represents 5% of the total absorption in the Q_y band, which translates to 0.5 Chls per complex or 1 Chl molecule per dimer. Analysis of the absorption spectra of reconstituted complexes at low temperature suggested that in both Lhca3 and Lhca4 the red tail represents roughly the absorption of one Chl molecule (Morosinotto et al., 2003), in agreement with the analysis on the native complex. Due to the difficulties associated with the determination of the actual band shape of the low energy absorption forms, this value has to be taken as a rough estimate. However, the value suggests that the Chls involved in the excitonic interaction that yield the red forms are not in the head-to-tail arrangement, but instead their dipole transition vectors are organized almost perpendicular to each other.

D. Which Chl Specie(s) is Involved in Red Forms?

Mukerji and Sauer (1990) observed that excitation of Chl *b* increased the amplitude of red emission as compared to excitation of Chl *a*, and thus concluded that Chl *b* is closely connected to red-shifted chromophores. A suggestion of a direct involvement of Chl *b* in the red forms was also made by Schmid et al. (2001) based on the observation that reconstitution of Lhca4 in the absence of Chl *b* caused a loss of red forms. However, Chl *a*-only Lhca3 (Castelletti et al., 2003) retained the red-shifted emission while Chl *a*-only Lhca4, although reducing the amplitude of red emission, still retained in part this spectral feature. It was shown that by increasing the Chl *b* content in Lhca4 above the control level, a progressive blue shift from 733 to 722 nm resulted in the emission peak. This result was interpreted as evidence that a Chl *a*–Chl *a* interaction was substituted by a Chl *b*–Chl *a* interaction, thus yielding a smaller emission shift due to the larger difference in the transition energy level of interacting monomers (see below). These results show that the interacting Chls responsible for red forms are in fact Chl *a* molecules, while suggesting that Chl *b* is possibly needed to maintain the conformation of chromophores responsible for the red forms.

E. Where are the "Red Chls" Located in the Lhca Architecture?

The mutation of Chl binding residues in Lhca complexes allows determination of the binding sites responsible for the red forms. Mutational analysis of Lhca1 (see section III.B) revealed that the 702 nm fluorescence emission component is lost on mutating sites A5, B5, and B6. On the basis of the occupancy of these sites (Chl *a* for A5, mixed site for B5 and Chl *b* for B6), it was proposed that the red emission originated from a Chl *a*–Chl *a* interaction between Chls located in sites A5 and B5, while the presence of a Chl in site B6 stabilized the conformation leading to the red forms. The mixed occupancy of site B5 explains the presence of the 690 nm fluorescence component: when Chl *b* is accommodated in site B5 the Chl *a*–Chl *a* interaction

that yields the red form is lost, yielding instead, the 690 nm bulk emission (Morosinotto et al., 2002).

The involvement of the A5 B5 domain in the origin of red forms was confirmed in all Lhca complex by constructing mutants at the Chl binding site A5, B5, and B6 (Morosinotto et al., unpublished). In all complexes the absence of Chl A5 and B5 led to the complete disappearance of red emission. B6 mutants, instead, have a slightly different phenotype, especially in Lhca3 and Lhca4: red emission is strongly reduced but not abolished.

From the analysis of the Lhca mutants two conclusions have been drawn: (i) the red forms originate from the same chromophores in all Lhca complexes; (ii) the model proposed for the origin of red forms by excitonic interactions of two Chl *a* molecules in the sites A5 and B5, proposed after the analysis of mutations in Lhca1 is probably maintained in all Lhca proteins.

An alternative hypothesis was recently proposed suggesting that a new Chl binding site, whose ligand residue would be a His belonging to helix C, is responsible for the red forms by establishing excitonic interactions with both Chl A5 and Chl B5 (Melkozernov and Blankenship, 2003). This hypothesis is not consistent with the previous report that Lhca3 has a strong red-shifted emission (Schmid et al., 2002b; Castelletti et al., 2003) and yet lacks the putative Chl binding His residue. Moreover, the recent structure of Lhca4 does not show the presence of an additional Chl coordinated to this particular residue (Ben Shem et al., 2003).

F. What is the Role of the Polypeptide Chain in Modulating the Absorption of the Red Chls in the Four Lhca Complexes?

Primary sequence analysis shows a strong homology between Lhca2 and Lhca4. Lhca1 and Lhca3 are also closely related. This clustering extends to the Chl *a*/*b* ratio and to the number of xanthophylls per polypeptide. However, the distribution of red forms is not consistent with the pattern being associated mainly with Lhca3 and Lhca4. Rather, it correlates with a specific substitution in the ligand of Chl A5: an asparagine in Lhca1 and Lhca3 versus a histidine in Lhca1–2 and in the rest of Lhcb proteins, which are depleted in red forms. A mutation at the A5 ligand (Asn > His) in Lhca3 and Lhca4 led to a loss of the red forms without affecting the pigment composition. The importance of the presence of Asn as a ligand in site A5 for the formation of red forms was confirmed by the reverse mutation on Lhca1: the His > Asn mutant gained red-shifted emission (Morosinotto et al., 2003).

G. What is the Mechanism Responsible for the Large Absorption Shift of the Red Forms Compared to the Bulk Chls?

The type of interaction between the chromophores responsible for the large absorption shift of the red forms has been investigated (Morosinotto et al., 2003) by comparing the absorption spectra of mutants lacking the red forms with the spectra of WT complexes. It was shown that in the His 97 mutant of Lhca4, two absorption forms at 682 and 703 nm were lost, while absorption at 675 nm was gained. This spectrum was interpreted as the loss of an excitonic interaction, having the high-energy term at 682 nm and the low energy contribution at 703 nm, while the 675 nm was representing the absorption of the noninteracting monomers. This was consistent with the analysis of the CD spectra (Morosinotto et al., 2003).

On this basis, it was proposed that part of the large shift of the red absorption band could be associated with the interaction energy (around 200 cm^{-1}). However, the energy associated with this interaction does not fully account for the large red shift of the absorption. Possibly, the presence of the Asn in this position directly influences the properties of the Chl ligand by changing the geometry of the tetrapyrrole or otherwise leading to a different folding of the protein domain that favors the red absorption.

The absence of the red emission in the Asn > His mutants of Lhca4 and Lhca3 was thus interpreted as the loss of the excitonic interaction between Chl A5 and Chl B5. Two parameters influence the interaction, the distance between the chromophores and the orientation of their dipole moments. LD spectra showed no changes in the chromophores orientation, thus suggesting that the substitution of Asn with His increased the distance between the two interacting Chls, thereby lowering the interaction energy (Morosinotto et al., 2003).

VIII. Lhca Proteins in *Chlamydomonas reinhardtii*

The first evidence for the presence of a Chl *b* containing antenna in LHCI was obtained in *Chlamydomonas reinhardtii* (Wollman and Bennoun, 1982). Evolutionary studies on Lhc complexes led to the conclusion that Lhca proteins diverged more than Lhcb during evolution (Durnford et al., 1999). The antenna complex of *C. reinhardtii* has recently been the subject of two electron microscopy studies (Germano et al., 2002;

Table 4. Lhca polypeptides identified in *Chlamydomonas* and their homologous in vascular plants

Chlamydomonas reinhardtii protein	Homologous in vascular plants	Nomenclature from Bassi et al. (1992)
Lhca1	Lhca1	p22.1
Lhca2	Lhca2	p19
Lhca3	Lhca3	p14.1
Lhca4	Lhca2 or Lhca4	p14
Lhca5	Lhca2 or Lhca4	p15.1
Lhca6	Lhca2 or Lhca4	p18.1
Lhca7	Lhca5	p15
Lhca8	Lhca5	p18
Lhca9	Lhca2	p22.2

The correspondence is derived from Stauber et al. (2003). The older nomenclature, used in previous work on *C. reinhardtii* (Bassi et al., 1992) is also reported.

Kargul et al., 2003). In these studies, the authors analyzed the structure of PS I–LHCI by single particle analysis and were led to the conclusion that in PS I between 11 and 14 Lhca subunits are bound to the core complex (Germano et al., 2002; Kargul et al., 2003). These data are consistent with a larger surface occupied by LHCI in *C. reinhardtii* as compared to spinach (Germano et al., 2002). Consequently, *C. reinhardtii* LHCI was shown to contain either seven (Bassi et al., 1992) or nine (Stauber et al., 2003) distinct polypeptides. These values, integrated with sequence data available in databases, allowed the identification of at least nine distinct polypeptides that compose the LHCI complex of PS I in *C. reinhardtii*. These polypeptides have been named Lhca1–9, but these names do not exactly reflect homology to higher plants genes. In particular, five different groups have been identified based on homology with vascular plants Lhca. This is summarized in Table 4 (Stauber et al., 2003).

The biochemical and spectroscopic properties of LHCI are known in less detail in *C. reinhardtii* than in vascular plants. Bassi et al. (1992) identified two LHCI populations, one emitting at 680 nm and the other at 705 nm. Similar purifications of LHCI from higher plants yielded LHCI-680 and LHCI-730 described above (see section II.B). Thus, the red forms of LHCI are not red shifted to the same extent as in vascular plants (Wollman and Bennoun, 1982).

Recently, Kargul et al. (2003) isolated PS I–LHCI complexes from *C. reinhardtii* showing a fluorescence emission maximum at 715 nm. Unfortunately it is not clear if this red emission originated from the antenna or from the core complex.

Pigment binding properties of LHCI of *C. reinhardtii* have not been analyzed in detail. The recent availability of protein sequences, however, shows that all eight Chl binding residues present in higher plant Lhcs are conserved in the *C. reinhardtii* proteins, strongly suggesting that these complexes bind at least eight Chls each. Xanthophyll binding has not been studied. Indirect evidence suggests that the xanthophyll binding properties of LHCI in *C. reinhardtii* are similar to those in vascular plants as deduced from the observation that *C. reinhardtii* mutants depleted in lutein, violaxanthin, and neoxanthin, thus leaving only zeaxanthin and β-carotene as carotenoid species available, were found to retain a stable LHCI. In these conditions Lhcb proteins were severely affected (Polle et al., 2001). The same phenotype was observed the Arabidopsis *npq2-lut2* mutant (Havaux et al., 2004).

From the comparison of Lhca sequences from Arabidopsis and *C. reinhardtii*, some interesting observations can be made. Lhca1 and Lhca3 from Arabidopsis and the corresponding genes from *C. reinhardtii* are highly homologous, while Lhca2 and Lhca4 from higher plants do not have closely related genes in *C. reinhardtii*. Moreover, it is interesting to note that in *C. reinhardtii* there exist two genes homologous to Lhca5 and one of them, Lhca8, is expressed at high levels (Stauber et al., 2003). This suggests that Lhca8 have a physiological function in *C. reinhardtii* that could possibly be maintained by the Lhca5 gene in Arabidopsis.

It has been observed that LHCI from *C. reinhardtii* showed reduced red forms as compared with higher plants. A possible explanation for these characteristics of algal LHCI can be found in the observation that genes highly homologous to higher plant Lhca4 and Lhca3, in fact, have His as the Chl A5 ligand. Asn however, is present at site A5 in three Lhca polypeptides of *C. reinhardtii* (Lhca2, Lhca4, Lhca9). Thus suggesting they may be responsible for the 705–715 nm fluorescence emission.

Acknowledgment

We want to thank Prof. Nelson from the Tel Aviv University for the reproduction of Fig. 2.

References

Allen JF (1992) How does protein phosphorylation regulate photosynthesis? Trends Biochem Sci 17: 12–17

Bassi R (1985) Spectral properties and polypeptide composition of the chlorophyll–proteins from thylakoids of granal and agranal chloroplasts of maize (*zea mays* L.). Carlsberg Res Commun 50: 127–143

Bassi R and Simpson D (1987) Chlorophyll–protein complexes of barley photosystem I. Eur J Biochem 163: 221–230

Bassi R, Machold O and Simpson D (1985) Chlorophyll–proteins of two photosystem I preparations from maize. Carlsberg Res Commun 50: 145–162

Bassi R, Soen SY, Frank G, Zuber H and Rochaix JD (1992) Characterization of chlorophyll-*a*/*b* proteins of photosystem-I from *Chlamydomonas reinhardtii*. J Biol Chem 267: 25714–25721

Bassi R, Pineau B, Dainese P and Marquardt J (1993) Carotenoid-binding proteins of Photosystem-II. Eur J Biochem 212: 297–303

Bassi R, Croce R, Cugini D and Sandona D (1999) Mutational analysis of a higher plant antenna protein provides identification of chromophores bound into multiple sites. Proc Natl Acad Sci USA 96: 10056–10061

Ben Shem A, Frolow F and Nelson N (2003) Crystal structure of plant photosystem I. Nature 426: 630–635

Bibby TS, Nield J and Barber J (2001) Iron deficiency induces the formation of an antenna ring around trimeric photosystem I in cyanobacteria. Nature 412: 743–745

Boardman NK, Anderson JM and Goodchild DJ (1978) Chlorophyll–protein complexes and structure of mature and developing chloroplast. In: Sanadi DR and Vernon LP (eds) Current Topics in Bioenergeties, Vol 8, pp 35–109. Academic Press, New York

Boekema EJ, Wynn RM and Malkin R (1990) The structure of spinach photosystem I studied by electron microscopy. Biochim Biophys Acta 1017: 49–56

Boekema EJ, van Roon H, Calkoen F, Bassi R and Dekker JP (1999) Multiple types of association of photosystem II and its light-harvesting antenna in partially solubilized photosystem II membranes. Biochemistry 38: 2233–2239

Boekema EJ, Hifney A, Yakushevska AE, Piotrowski M, Keegstra W, Berry S, Michel KP, Pistorius EK and Kruip J (2001a) A giant chlorophyll–protein complex induced by iron deficiency in cyanobacteria. Nature 412: 745–748

Boekema EJ, Jensen PE, Schlodder E, van Breemen JF, van Roon H, Scheller HV and Dekker JP (2001b) Green plant photosystem I binds light-harvesting complex I on one side of the complex. Biochemistry 40: 1029–1036

Bossmann B, Knoetzel J and Jansson S (1997) Screening of chlorina mutants of barley (*Hordeum vulgare* L.) with antibodies against light-harvesting proteins of PS I and PS II: absence of specific antenna proteins. Photosynth Res 52: 127–136

Butler WL and Norris KH (1963) Lifetime of the long-wavelength chlorophyll fluorescence. Biochim Biophys Acta 66: 72–77

Butler WL, Tredwell CJ, Malkin R and Barber J (1979) The relationship between the lifetime and yield of the 735 nm fluorescence of chloroplasts at low temperatures. Biochim Biophys Acta 545: 309–315

Castelletti S, Morosinotto T, Robert B, Caffarri S, Bassi R and Croce R (2003) Recombinant Lhca2 and Lhca3 subunits of the photosystem I antenna system. Biochemistry 42: 4226–4234

Croce R (1997) Il fotosistema I delle piante superiori: studi biochimici e spettroscopici. Ph.D. thesis, Universitá di Milano, Milano

Croce R and Bassi R (1998) The light-harvesting complex of photosystem I: pigment composition and stoichiometry. In: Garab G (ed) Photosynthesis: Mechanisms and Effects, Vol 1, pp 421–424. Kluwer Academic Press, Dordrecht

Croce R, Zucchelli G, Garlaschi FM, Bassi R and Jennings RC (1996) Excited state equilibration in the photosystem I light-harvesting I complex: P700 is almost isoenergetic with its antenna. Biochemistry 35: 8572–8579

Croce R, Zucchelli G, Garlaschi FM and Jennings RC (1998) A thermal broadening study of the antenna chlorophylls in PSI-200, LHCI, and PSI core. Biochemistry 37: 17255–17360

Croce R, Remelli R, Varotto C, Breton J and Bassi R (1999) The neoxanthin binding site of the major light harvesting complex (LHC II) from higher plants. FEBS Lett 456: 1–6

Croce R, Morosinotto T, Castelletti S, Breton J and Bassi R (2002) The Lhca antenna complexes of higher plants photosystem I. Biochim Biophys Acta 1556: 29–40

Croce R, Muller MG, Bassi R and Holzwarth AR (2003) Chlorophyll *b* to chlorophyll *a* energy transfer kinetics in the CP29 antenna complex: a comparative femtosecond absorption study between native and reconstituted proteins. Biophys J 84: 2508–2516

Damm I, Steinmetz D and Grimme LH (1990) Multiple functions of β-carotene in Photosystem I. In: Baltscheffsky M (ed) Current Research in Photosynthesis, pp 607–610. Kluwer Academic Press, Dordrecht

Dunahay TG and Staehelin A (1985) Isolation of photosystem I complexes from octyl glucoside/sodium dodecyl sulfate solubilized spinach thylakoids. Characterization and reconstitution into liposomes. Plant Physiol 78: 606–613

Durnford DG, Deane JA, Tan S, McFadden GI, Gantt E and Green BR (1999) A phylogenetic assessment of the eukaryotic light-harvesting antenna proteins, with implications for plastid evolution. J Mol Evol 48: 59–68

Ganeteg U, Strand A, Gustafsson P and Jansson S (2001) The properties of the chlorophyll *a*/*b*-binding proteins Lhca2 and Lhca3 Studied *in vivo* using antisense inhibition. Plant Physiol 127: 150–158

Germano M, Yakushevska AE, Keegstra W, van Gorkom HJ, Dekker JP and Boekema EJ (2002) Supramolecular organization of photosystem I and light-harvesting complex I in *Chlamydomonas reinhardtii*. FEBS Lett 525: 121–125

Giuffra E, Cugini D, Croce R and Bassi R (1996) Reconstitution and pigment-binding properties of recombinant CP29. Eur J Biochem 238: 112–120

Gobets B and van Grondelle R (2001) Energy transfer and trapping in photosystem I. Biochim Biophys Acta 1057: 80–99

Gobets B, Van Amerongen H, Monshouwer R, Kruip J, Rögner M, van Grondelle R and Dekker JP (1994) Polarized site-selected fluorescence spectroscopy of isolated photosystem I particles. Biochim Biophys Acta 1188: 75–85

Green BR and Durnford DG (1996) The chlorophyll–carotenoid proteins of oxygenic photosynthesis. Annu Rev Plant Physiol Plant Mol Biol 47: 685–714

Havaux M, Dall'Osto L, CuinÈ S, Giuliano G and Bassi R (2004) The effect of zeaxanthin as the only xanthophyll on the structure and function of the photosynthetic apparatus in *Arabidopsis thaliana.* J Biol Chem 279: 13878–13888

Haworth P, Watson JL and Arntzen CJ (1983) The detection, isolation and characterisation of a light-harvesting complex which is specifically associated with photosystem I. Biochim Biophys Acta 724: 151–158

Ihalainen JA, Gobets B, Sznee K, Brazzoli M, Croce R, Bassi R, van Grondelle R, Korppi-Tommola JEI and Dekker JP (2000) Evidence for two spectroscopically different dimers of light-harvesting complex I from green plants. Biochemistry 39: 8625–8631

Ihalainen JA, Rätsep M, Jensen PE, Scheller HV, Croce R, Bassi R, Korppi-Tommola JEI and Freiberg A (2003) Red spectral forms of chlorophylls in green plant PSI – a site-selective and high-pressure spectroscopy study. J Phys Chem B 107: 9086–9093

Ikeuchi M, Hirano A and Inoue Y (1991a) Correspondence of apoproteins of light-harvesting chlorophyll-*a*/*b* complexes associated with photosystem-I to cab genes – evidence for a novel type-IV apoprotein. Plant Cell Physiol 32: 103–112

Ikeuchi M, Nyhus KJ, Inoue Y and Pakrasi HB (1991b) Identities of four low-molecular-mass subunits of the photosystem I complex from *Anabaena variabilis* ATCC 29413. Evidence for the presence of the *psaI* gene product in a cyanobacterial complex. FEBS Lett 287: 5–9

Jansson S (1994) The light-harvesting chlorophyll *a*/*b*-binding proteins. Biochim Biophys Acta 1184: 1–19

Jansson S (1999) A guide to the Lhc genes and their relatives in Arabidopsis. Trends Plant Sci 4: 236–240

Jansson S, Andersen B and Scheller HV (1996) Nearest-neighbor analysis of higher-plant photosystem I holocomplex. Plant Physiol 112: 409–420

Jensen PE, Gilpin M, Knoetzel J and Scheller HV (2000) The PSI-K subunit of photosystem I is involved in the interaction between light-harvesting complex I and the photosystem I reaction center core. J Biol Chem 275: 24701–24708

Jordan P, Fromme P, Witt HT, Klukas O, Saenger W and Krauß N (2001) Three-dimensional structure of cyanobacterial photosystem I at 2.5 Å resolution. Nature 411: 909–917

Kargul J, Nield J and Barber J (2003) Three-dimensional reconstruction of a light-harvesting complex I–photosystem I (LHCI–PSI) supercomplex from the green alga *Chlamydomonas reinhardtii* – insights into light harvesting for PSI. J Biol Chem 278: 16135–16141

Kleima FJ, Gradinaru CC, Calkoen F, van Stokkum IHM, van Grondelle R and Van Amerongen H (1997) Energy transfer in LHCII monomers at 77 K studied by sub-picosecond transient absorption spectroscopy. Biochemistry 36: 15262–15268

Knoetzel J, Svendsen I and Simpson DJ (1992) Identification of the photosystem-I antenna polypeptides in barley – isolation of 3 pigment-binding antenna complexes. Eur J Biochem 206: 209–215

Knoetzel J, Bossmann B and Grimme LH (1998) *Chlorina* and *viridis* mutants of barley (*Hordeum vulgare* L.) allow assignment of long-wavelength chlorophyll forms to individual Lhca proteins of photosystem I *in vivo*. FEBS Lett 436: 339–342

Kuang T-Y, Argyroudi-Akoyunoglou JH, Nakatani HY, Watson J and Arntzen CJ (1984) The origin of the long-wavelength fluorescence emission band (77K) from photosystem I. Arch Biochem 235: 618–627

Kühlbrandt W, Wang DN and Fujiyoshi Y (1994) Atomic model of plant light-harvesting complex by electron crystallography. Nature 367: 614–621

Lam E, Ortiz W and Malkin R (1984a) Chlorophyll *a*/*b* proteins of photosystem I. FEBS Lett 168: 10–14

Lam E, Ortiz W, Mayfield S and Malkin R (1984b) Isolation and characterization of a light-harvesting chlorophyll *a*/*b* protein complex associated with photosystem I. Plant Physiol 74: 650–655

Lubben TH, Theg SM and Keegstra K (1988) Transport of proteins into chloroplasts. Photosynth Res 17: 173–194

Lunde C, Jensen PE, Haldrup A, Knoetzel J and Scheller HV (2000) The PSI-H subunit of photosystem I is essential for state transitions in plant photosynthesis. Nature 408: 613–615

Melkozernov AN and Blankenship RE (2003) Structural modeling of the Lhca4 subunit of LHCI-730 peripheral antenna in photosystem I based on similarity with LHCII. J Biol Chem 278: 44542–44551

Morosinotto T, Castelletti S, Breton J, Bassi R and Croce R (2002) Mutation analysis of Lhca1 antenna complex. Low energy absorption forms originate from pigment–pigment interactions. J Biol Chem 277: 36253–36261

Morosinotto T, Breton J, Bassi R and Croce R (2003) The nature of a chlorophyll ligand in Lhca proteins determines the far red fluorescence emission typical of photosystem I. J Biol Chem 278: 49223–49229

Mukerji I and Sauer K (1990) A spectroscopic study of a photosystem I antenna complex. Curr Res Photosynth Vol 2, 321–324

Mullet JE, Burke JJ and Arntzen CJ (1980a) A developmental study of photosystem I peripheral chlorophyll proteins. Plant Physiol 65: 823–827

Mullet JE, Burke JJ and Arntzen CJ (1980b) Chlorophyll proteins of photosystem I. Plant Physiol 65: 814–822

Palsson LO, Tjus SE, Andersson B and Gillbro T (1995) Ultrafast energy-transfer dynamics resolved in isolated spinach light-harvesting complex-I and the Lhc-I-730 subpopulation. Biochim Biophys Acta 1230: 1–9

Pascal A, Gastaldelli M, Ceoldo S, Bassi R and Robert B (2001) Pigment conformation and pigment–protein interactions in the reconstituted Lhcb4 antenna protein. FEBS Lett 492: 54–57

Plumley FG and Schmidt GW (1987) Reconstitution of chlorophyll *a*/*b* light-harvesting complexes: xanthophyll-dependent assembly and energy transfer. Proc Natl Acad Sci USA 84: 146–150

Polle JEW, Niyogi KK and Melis A (2001) Absence of lutein, violaxanthin and neoxanthin affects the functional chlorophyll antenna size of photosystem-II but not that of photosystem-I in the green alga *Chlamydomonas reinhardtii*. Plant Cell Physiol 42: 482–491

Preiss S, Peter GF, Anandan S and Thornber JP (1993) The multiple pigment–proteins of the photosystem-I antenna. Photochem Photobiol 57: 152–157

Remelli R, Varotto C, Sandona D, Croce R and Bassi R (1999) Chlorophyll binding to monomeric light-harvesting complex. A mutation analysis of chromophore-binding residues. J Biol Chem 274: 33510–33521

Roszak AW, Howard TD, Southall J, Gardiner AT, Law CJ, Isaacs NW and Cogdell RJ (2003) Crystal structure of the RC-LH1 core complex from *Rhodopseudomonas palustris*. Science 302: 1969–1972

Scheller HV, Jensen PE, Haldrup A, Lunde C and Knoetzel J (2001) Role of subunits in eukaryotic photosystem I. Biochim Biophys Acta 1507: 41–60

Schmid VHR, Cammarata KV, Bruns BU and Schmidt GW (1997) *In vitro* reconstitution of the photosystem I light-harvesting complex LHCI-730: heterodimerization is required for antenna pigment organization. Proc Natl Acad Sci 94: 7667–7672

Schmid VH, Thome P, Ruhle W, Paulsen H, Kuhlbrandt W and Rogl H (2001) Chlorophyll *b* is involved in long-wavelength

spectral properties of light-harvesting complexes LHC I and LHC II. FEBS Lett 499: 27–31

Schmid VHR, Paulsen H and Rupprecht J (2002a) Identification of N- and C-terminal amino acids of Lhca1 and Lhca4 required for formation of the heterodimeric peripheral photosystem I antenna LHCI-730. Biochemistry 41: 9126–9131

Schmid VHR, Potthast S, Wiener M, Bergauer V, Paulsen H and Storf S (2002b) Pigment binding of photosystem I light-harvesting proteins. J Biol Chem 277: 37307–37314

Simpson DJ, Machold O, Hoyer-hansen G and von Wettstein D (1985) *Chlorina* mutants of barley (*Hordeum vulgare* L.). Carlsberg Res Commun 50: 223–238

Stauber EJ, Fink A, Markert C, Kruse O, Johanningmeier U and Hippler M (2003) Proteomics of *Chlamydomonas reinhardtii* light-harvesting proteins. Eukaryot Cell 2: 978–994

Tjus SE, Roobolboza M, Palsson LO and Andersson B (1995) Rapid isolation of photosystem-I chlorophyll-binding proteins by anion-exchange perfusion chromatography. Photosynth Res 45: 41–49

Vainstein A, Peterson CC and Thornber JP (1989) Light-harvesting pigment–proteins of photosystem I in maize. Subunit composition and biogenesis. J Biol Chem 264: 4058–4063

Van Amerongen H and van Grondelle R (2001) Understanding the energy transfer function of LHCII, the major light-harvesting complex of green plants. J Phys Chem B 105: 604–617

Wollman F-A and Bennoun P (1982) A new chlorophyll-protein complex related to photosystem I in *Chlamydomonas reinhardtii*. Biochim Biophys Acta 680: 352–360

Zhang H, Goodman HM and Jansson S (1997) Antisense inhibition of the photosystem I antenna protein Lhca4 in *Arabidopsis thaliana*. Plant Physiol 115: 1525–1531

Chapter 11

The Low Molecular Mass Subunits in Higher Plant Photosystem I

Anna Haldrup, Poul Erik Jensen and Henrik Vibe Scheller*
Plant Biochemistry Laboratory, Department of Plant Biology, The Royal Veterinary and Agricultural University, 40 Thorvaldsensvej, DK-1871 Frederiksberg C, Denmark

Summary

Photosystem I (PS I) in plants contains 18 different protein subunits. Only three subunits are directly involved in electron transport, while the remaining subunits have a multitude of other functions. Although the PS I complex in plants shows many specific adaptations, it is fascinating that the overall structure and function has been extremely well conserved through the billion years of evolution that separates plants and cyanobacteria. Important roles of the small accessory subunits include efficient docking of the electron donor plastocyanin and the electron acceptor ferredoxin. These functions are conserved between plants and cyanobacteria but plant PS I has a number of specific adaptations, particularly the PS I-N subunit, which is only present in eukaryotes and is involved in the efficient oxidation of plastocyanin. The eukaryote-specific PS I-G subunit is also involved in the binding of

* Author for correspondence, email: hvs@kvl.dk

John H. Golbeck (ed): Photosystem I: The Light-Driven Plastocyanin:Ferredoxin Oxidoreductase, 139–154.

plastocyanin. Another important role of small PS I subunits in plants is the interaction with peripheral antenna proteins. Three conserved subunits PS I-J, -K, and -F together with PS I-G have the role of binding "light-harvesting complex I," which is specific for PS I. Two conserved subunits PS I-I and -L together with the eukaryote-specific PS I-H and -O have the role of binding "light-harvesting complex II" under certain physiological conditions. The plant PS I complex is more stable than the cyanobacterial counterpart, a difference related to structural modifications of the PS I-D and -E subunits, which are located peripherally on the stromal side. The increased stability may be related to a high susceptibility of plants to damage caused by reactive oxygen species generated at the reducing side of PS I.

I. Introduction

Photosystem I (PS I) from higher plants is a supramolecular complex consisting of at least 18 different polypeptides located in the non appressed thylakoid membranes (Scheller et al., 2001; Jensen et al., 2003). The core of PS I consists of at least 14 different subunits named PS I-A to -L, -N, and -O. Two subunits present in cyanobacteria, PS I-M and -X, are absent in plants. The major subunits of PS I, -A, and -B, have a molecular mass of 82–84 kDa and are homologous. They form a heterodimer, which binds components of the electron transfer chain: the primary electron donor P700 and the electron acceptors A_0, A_1, and, F_x (Golbeck, 1992; Jordan et al., 2001; Scheller et al., 2001). The remaining electron acceptors, F_A and F_B (both [4Fe–4S] clusters), are bound to the 9 kDa PS I-C subunit. The remaining 11 subunits of the PS I core have molecular masses ranging between 4 and 18 kDa and do not bind electron acceptors. Figure 1 shows a schematic model of PS I with its subunits and electron acceptors. Table 1 summarizes the subunits and their functions in plant PS I.

The low molecular mass subunits of PS I can be divided into three main groups. The first group consists of the stromal subunits PS I-C, -D, and -E, which are involved in electron transport and docking of ferredoxin. The second group consists of the membrane integral subunits PS I-F, -G, -H, -I, -J, -K, -L, and -O, whose main function is stabilization of the core antenna system and interaction with the peripheral antenna. PS I-F and -G have the additional function of interaction with plastocyanin (Pc). The third group consists of the luminal subunit PS I-N, which is involved in electron transport from Pc. The subunits PS I-G, -H, -N, and -O are unique to higher plants and algae. In the recent 4.4 Å structure of plant PS I the positions of the PS I-G and -H subunits are clearly identified, but PS I-N and -O are not resolved (Ben-Shem et al., 2003; see Nelson and Ben-Shem, this volume, Chapter 7).

PS I of cyanobacteria contains 96 Chl *a* molecules and 22 β-carotene molecules (Jordan et al., 2001; see Fromme and Grotjohann, this volume, Chapter 6). Out of the 96 chlorophylls only three are missing in the plant PS I reaction center: two bound to PS I-M and -X, and one bound to PS I-J (Ben-Shem et al., 2003). From the remaining 93 chlorophylls, 92 are identified at the same position as in the cyanobacterial reaction center. Approximately, 83 of the chlorophyll molecules are bound to the PS I-A/B heterodimer and the remaining are bound to the minor subunits PS I-J (2), -K (4), -L (3), -H (1), and -G (0 or 1).

Light-harvesting complex I (LHCI) is also specific for higher plants and algae. This peripheral antenna is, at least in higher plants, composed of the products of four nuclear genes, *Lhca1–4*, with molecular masses of 20–24 kDa. A fifth protein, Lhca5, has been deduced from EST clones (Jansson, 1999) and recently the protein has been detected in PS I of *Arabidopsis thaliana* in small amounts (Ganeteg et al., 2004; Croce et al., this volume, Chapter 10). In contrast to the trimeric LHCII, the major light-harvesting complex of PS II, Lhca1/Lhca4, and Lhca2/Lhca3 form heterodimers (Ben-Shem et al., 2003). In PS I, two dimers are arranged so that the individual proteins are in series creating a crescent-shaped belt adjacent to the core complex on the PS I-F side (Ben-Shem et al., 2003). This arrangement maximizes the number of LHCI chlorophylls facing the core. Interestingly, the contact site between LHCI and the PS I core resembles the contact site between the IsiA antenna proteins and the PS I core in iron-starved cyanobacteria (Bibby et al., 2001; Boekema et al., 2001b). However, this is an example of convergent evolution since there is no homology between IsiA and Lhca proteins. LHCI binds, according to the structure published by

Abbreviations: Chl – chlorophyll; Cyt – cytochrome; Fd – ferredoxin; FNR – ferredoxin $NADP^+$ oxidoreductase; LHC – light-harvesting complex; NPQ – nonphotochemical quenching; Pc – plastocyanin; PS – photosystem; PS I-A to PS I-O – Alternative higher plant nomenclature for PS I polypeptides.

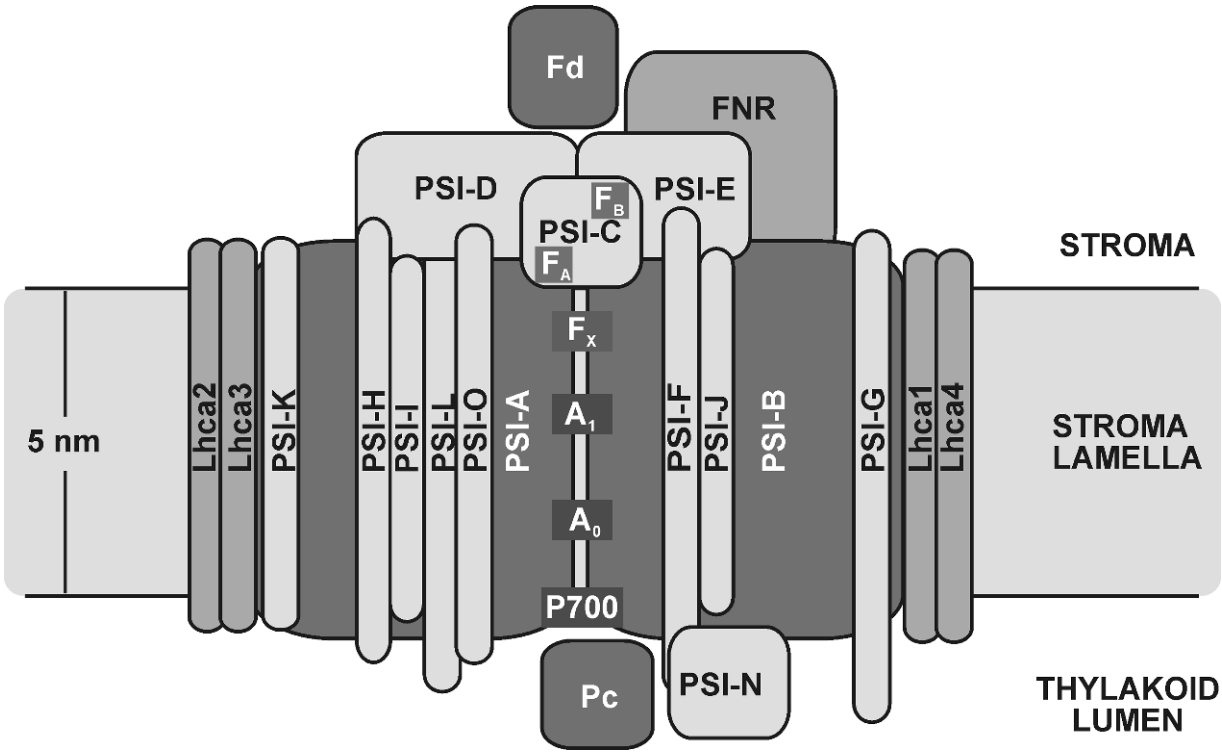

Fig. 1. Schematic model of plant PS I.

Ben-Shem et al. (2003), 56 Chl *a* and Chl *b* molecules per P700 besides lutein, violaxanthin, and small amount of β-carotene (Croce et al., 2002; Schmid et al., 2002). Between the individual Lhca monomers and between the two dimers in LHCI eight linker chlorophylls are found, and between the core and the peripheral antenna are 10 so-called gap chlorophylls, which are not an intrinsic part of LHCI or the reaction center. Thus, plant PS I with its full complement of peripheral antenna binds a total of approximately 167 Chl *a* and *b* molecules (Ben-Shem et al., 2003). Figure 2 shows the arrangement of the core subunits and LHCI in the PS I complex.

The 4.4 Å structure has a geometrical arrangement in excellent agreement with electron microscopy and single particle analysis (Boekema et al., 2001a; Boekema et al., this volume, Chapter 5). These studies indicate a constant size of PS I. However, other studies have shown that the relative content of different Lhca proteins in the thylakoid membrane is variable depending on growth conditions (Bailey et al., 2001). Whether this variability at the thylakoid level reflects variability at the level of PS I complexes has not been determined.

II. The Acceptor Side of PS I: PS I-C, -D, -E, and Electron Donation from PS I to Ferredoxin

A. Topology and Location in PS I

Three small subunits, PS I-C, -D, and -E, are situated at the stromal side of PS I. These three subunits do not contain transmembrane α-helices (Fromme, 2001; Ben-Shem et al., 2003). The three polypeptides form a compact interconnected structure known as the stromal ridge (Kruip et al., 1997; Klukas et al., 1999; Jordan et al., 2001; Antonkine et al., 2003). The subunits are close together and arranged as a crescent (Fig. 2), with PS I-D closest to the PS I-H, -I, -L, -O side, PS I-C in the middle and PS I-E to the PS I-F, -J side (Jordan et al., 2001).

PS I-C is necessary for the stable association of PS I-D, -E, and -L (Mannan et al., 1994; Yu et al., 1995). A knock-out mutant of *psaC* demonstrates a difference between cyanobacteria and green algae. *Anabaena variabilis* ATCC 29413 lacking PS I-C assembled and accumulated a PS I complex with functional P700 (Mannan et al., 1991) and *Synechocystis* sp. PCC

Table 1. Composition of PS I in higher plants. The location of the gene in plants in the chloroplasts (C) or nucleus (N) is indicated together with the number of genes encoding the subunit in *Arabidopsis*. Electron transfer cofactors and pigments attached to the individual subunits and function of the individual subunits in PS I are also indicated (question marks indicate that the assignment of cofactors is not confirmed experimentally)

Gene and subunit	Location of the gene[a]	Molecular mass (kDa)[b]	Cofactors[c]	Function
PsaA, PS I-A	C	83.2	≈79 Chl *a*, ≈22 β-carotene, P700, A_0, A_1, F_X	Light-harvesting, Charge separation
PsaB, PS I-B	C	82.5		Electron transport
PsaC, PS I-C	C	8.9	F_A, F_B	Electron transport
PsaD, PS I-D	N (2)	17.8/17.7		Binding of ferredoxin Binding of PS I-C
PsaE, PS I-E	N (2)	10.4/10.5		Binding of ferredoxin and FNR
PsaF, PS I-F	N	17.3		Binding of plastocyanin Binding of LHCI
PsaG, PS I-G	N	11.0	1–2 β-carotene	Stabilization of LHCI Interaction with plastocyanin
PsaH, PS I-H	N (2)	10.4/10.4	1 Chl *a*	Binding of LHCII Stabilization of PS I-D
PsaI, PS I-I	C	4.1		Stabilization of PS I-L
PsaJ, PS I-J	C	5.0	2–3 Chl *a*	Stabilization of PS I-F
PsaK, PS I-K	N	8.5	2–4 Chl *a*	Binding of LHCI
PsaL, PS I-L	N	18.0	3 Chl *a*	Stabilization of PS I-H and PS I-O
PsaN, PS I-N	N	9.7		Docking of plastocyanin
PsaO, PS I-O	N	10.1	Chl *a* ?	Binding of LHCII (state transitions)
Lhca1, Lhca1	N	21.5	14 Chl, ≈2 carotenoids	Light-harvesting, LHCI-730
Lhca2, Lhca2	N	23.2	14 Chl, ≈2 carotenoids	Light-harvesting, LHCI-680B
Lhca3, Lhca3	N	24.9	14 Chl, ≈2 carotenoids	Light-harvesting, LHCI-680A
Lhca4, Lhca4	N	22.3	14 Chl, ≈2 carotenoids	Light-harvesting, LHCI-730
Lhca5, Lhca5	N	23.2	≈14Chl ?, ≈2 carotenoids ?	Light-harvesting,?

[a]Number in brackets indicate the cases where there is more than one nuclear gene in the *Arabidopsis* genome encoding the subunit.
[b]The predicted molecular mass of the mature *Arabidopsis* protein.
[c]The number of pigment molecules bound to the subunits are from Jordan et al. (2001) and Ben-Shem et al. (2003) except for the plant specific PS I-H and -G where the numbers are from Ihalainen et al. (2002).

6803 lacking PS I-C assembled a PS I subcomplex devoid of PS I-D and -E (Yu et al., 1995). In contrast, a knock-out mutant of *psaC* in *Chlamydomonas reinhardtii* resulted in complete destabilization of the PS I complex, which did not accumulate (Takahashi et al., 1991). No plants lacking PS I-C have been reported.

PS I-D has been shown to interact with PS I-A/B, -C, -E, -L, and -H (Merati and Zanetti, 1987; Zanetti and Merati, 1987; Zilber and Malkin, 1988; Andersen et al., 1992; Armbrust et al., 1996; Jansson et al., 1996). In cyanobacteria, the loop segment in the C-terminus of PS I-D is attached by numerous hydrogen bonds to the stromally exposed sides of PS I-C and -E and seems to help in the positioning of these subunits (Jordan et al., 2001; Antonkine et al., 2003). This is in excellent agreement with the importance of PS I-D for the *in vitro* reconstitution of electron transfer from F_X to F_A/F_B in plants (Naver et al., 1995). An N-terminal extension of PS I-D in plants stabilizes the interaction of PS I-C with the rest of the PS I core and this can explain why the stromal side of PS I in plants is more stable than in cyanobacteria (Naver et al., 1995). Cross-linking experiments carried out with barley PS I have suggested that PS I-D exerts its stabilizing effect via an interaction with PS I-H (Naver et al., 1995). This suggestion is supported by the analysis of transgenic *Arabidopsis* lines cosuppressed for PS I-H, in which PS I-C is not as tightly bound to the PS I core as in the wild-type (Naver et al., 1999).

In *Arabidopsis*, PS I-D is encoded by two homologous genes, *psaD1* and *psaD2* (Haldrup et al., 2003). The two PS I-D proteins are identical in the highly conserved C-terminal region and the differences are only found in the variable N-terminal region. Overexpression analysis has indicated that the products of the two *psaD* genes have redundant functions and can compensate for each other (Ihnatowicz et al., 2004). However, it is possible that the two genes respond to

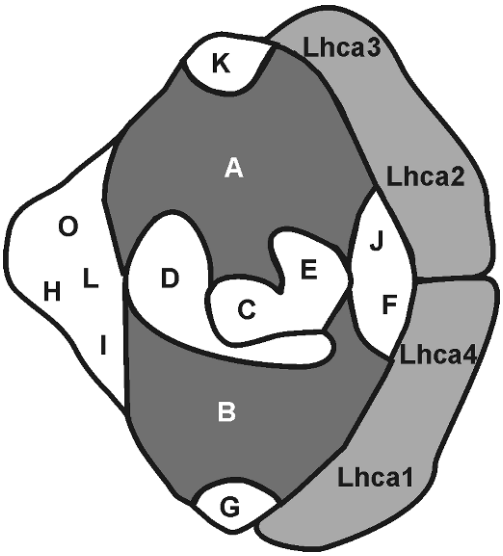

Fig. 2. Schematic view of plant PS I viewed from the stromal side. The outline is modeled on the pea PS I (Ben-Shem et al., 2003) and the plant specific subunits are shown in the deduced positions with approximately the correct size. The position of PS I-O is not resolved in the pea PS I structure and has been inferred from cross-linking data and phenotype of PS I-O mutants. The relative position of the Lhca1/Lhca4 dimer and, Lhca2/Lhca3 dimer has not been experimentally determined but reflects the most likely position based on secondary effects of removing other subunits.

different signal transduction pathways, thus allowing the plant cell to respond more flexibly to environmental stimuli, as found in *Nicotiana sylvestris* (Yamamoto et al., 1993). Recently, PS I-D in *Arabidopsis* was shown to be phosphorylated on a threonine residue close to the N-terminus (Hansson and Vener, 2003). However, this residue is not conserved in PS I-D from many other species and it is an open question if the phosphorylation has an important role in the function of PS I-D.

PS I-E is, like PS I-D, a hydrophilic subunit exposed to the stroma and also encoded by two genes in *Arabidopsis*. However, in barley there appears to be only one *psaE* gene (Okkels et al., 1988). The plant PS I-E subunit has, like PS I-D, an N-terminal extension compared to cyanobacterial proteins and a more conserved C-terminus (Varotto et al., 2000).

B. The Role of PS I-C, -D, and -E in the Docking and Reduction of Ferredoxin

Ferredoxin is reduced at the stromal side of PS I by PS I-C. Cross-linking experiments have shown that PS I-D serves as a docking site for ferredoxin during photoreduction (Zanetti and Merati, 1987; Zilber and Malkin, 1988) and PS I-D is indispensable for the productive interaction of PS I with ferredoxin (Lelong et al., 1994; W Xu et al., 1994; Chitnis et al., 1996). When ferredoxin is chemically cross-linked at the docking site of PS I, electron transport can still take place and the position of ferredoxin in these cross-linked complexes has been identified by electron microscopy (Lelong et al., 1996). The PS I-E subunit interacts with FNR via its N-terminal extension (Andersen et al., 1992) and is important for efficient $NADP^+$ reduction (Naver et al., 1995). In cyanobacteria, photoautotropic growth is barely affected in the absence of PS I-E (Rousseau et al., 1993; W Xu et al., 1994). In contrast, plants lacking PS I-E exhibit severely reduced growth (Varotto et al., 2000; Scheller et al., 2004). Extensive kinetic analysis has so far not been performed with PS I from plants down-regulated in PS I-D or -E.

C. The Role of PS I-D in Assembly of PS I

By the use of antisense technique, *Arabidopsis* plants with only 5–60% of wild-type PS I-D content were generated (Haldrup et al., 2003). Plants with low levels of PS I-D (approximately 5%) were small and struggled to survive and plants totally lacking PS I-D were not found. Also, knock-out mutants of *psaD1-1* with 40% PS I-D remaining and *psaD2-1* mutants with 90% PS I-D remaining have been generated (Ihnatowiez et al., 2003). The growth of the *psaD1-1* mutant was substantially reduced relative to *psaD2-1* and wild-type plants. The *psaD1-1 psaD2-1* double mutants did not survive when grown in soil, but could be propagated in sterile culture supplemented with sucrose, indicating that PS I-D function is essential for photosynthesis (Ihnatowicz et al., 2004). Antisense plants with only about 10% PS I-D present compared to the wild-type were very small, grew very slowly, showed light-green leaf coloration, and set seeds very late (Haldrup et al., 2003). Analysis of other PS I subunits showed a similar decrease in all the subunits including LHCI. Thus, the *Arabidopsis* plants with only 10% PS I-D contained only about 10% of PS I, but all the PS I present had a normal composition including functional LHCs (Haldrup et al., 2003). *In vitro* experiments have confirmed the requirement for PS I-D for stable binding of PS I-C in both cyanobacteria (Li et al., 1991) and plants (Naver et al., 1995, 1996). Considering this knowledge about PS I assembly, the most obvious conclusion is that in the absence of PS I-D in plants, the PS I-C protein cannot be properly assembled with PS I and this results in degradation of the incorrectly assembled complexes.

Degradation products of PS I-E were detected in plants down-regulated in PS I-D (Haldrup et al., 2003). In conclusion, PS I-D plays an essential role for the assembly and stability of PS I in plants. This is different from the situation in *Synechocystis* sp. PCC 6803, where PS I complexes devoid of PS I-D but containing other small subunits are present in *psaD* deletion strains (W Xu et al., 1994).

D. Instability at the Stromal Side Causes Photoinhibition

With low amounts of PS I, the antisense PS I-D plants were able to survive but suffered naturally from low photosynthetic rates and highly unbalanced redox conditions. Plants down-regulated in PS I-D became light-stressed even in low light although they exhibited high non photochemical quenching (NPQ) (Haldrup et al., 2003). The high NPQ was generated by up-regulating the level of violaxanthin de-epoxidase and PsbS, and increasing the level of xanthophyll pigments (Haldrup et al., 2003; Ihnatowicz et al., 2004) that are essential components of NPQ (Niyogi, 1999). The redox state of thioredoxin was also affected. During the normal light cycle thioredoxin becomes increasingly oxidized in plants with low amounts of PS I-D (Haldrup et al., 2003). The change in the thiol disulfide redox state might be fatal for the PS I-D less plants, because reduction of thioredoxin is one of the main switches for the initiation of CO_2 assimilation and photoprotection upon exposure to light.

Recent investigations have shown that PS I-E has a very significant role in plants. *Arabidopsis* plants have been created in which one of the two *psaE* genes was inactivated by transposon tagging (Varotto et al., 2000; Pesaresi et al., 2002). The plants contained about 40% PS I-E compared to the wild-type and an approx 50% decrease in PSI-C, -D, -H, and -L was observed. The plants contained wild-type amounts of most other PS I subunits. The plants with less PS I-E were pale green and exhibited high chlorophyll fluorescence, i.e., lower photochemical quenching, indicating a disturbed redox balance of the intersystem chain. Under greenhouse conditions, the plants showed a 50% decrease in growth rate and susceptibility to photoinhibition. Similar results have been obtained in our laboratory with *Arabidopsis* plants in which PS I-E was down-regulated by antisense suppression (Scheller et al., 2004). These plants were down-regulated to 5–50% of wild-type levels and exhibited severe effects especially in the later stages of development; many plants did not survive to set seeds. Consequently, the plants containing very low amounts of PS I-E were only found in the first generation, whereas the second generation only yielded plants with more than 50% PS I-E. A fraction of LHCII seemed to be stably associated with PS I when plants with low content of PS I-E were exposed to low-light conditions (Pesaresi et al., 2002). The formation of this LHCII-PS I complex was associated with an almost complete suppression of state transitions and a drastic increase in the levels of phosphorylated LHCII. The moderate importance of PS I-E for ferredoxin reduction would not appear to explain the pronounced phenotypic effect of the reduced amount of PS I-E. Plants lacking PS I-H or -N also have a decreased rate of ferredoxin reduction (see below) but they compensate by increasing the PS I/PS II ratio and show virtually no growth phenotype. Such compensation appears to be insufficient in plants lacking PS I-E. Most likely, PS I-E is important for the stability of the reducing side of PS I. Possibly, the lack of PS I-E in plants leads to a high susceptibility to photodamage of the PS I complex. Reduced levels of PS I-E may limit the reduction of ferredoxin and lead to over reduction of the iron–sulfur centers F_A/F_B. This will in turn lead to O_2 reduction by PS I, generating superoxide anion radical and other reactive oxygen species, and causing damage to the photosynthetic apparatus.

III. The Donor Side of PS I: PS I-F, -J, -N, and Electron Donation from Plastocyanin to P700

A. Topology and Location in PS I

Regions of PS I-F are highly conserved between species, but eukaryotic PS I-F has an N-terminal extension (Farah et al., 1995). PS I-F is anchored in the thylakoids with a transmembrane helix and is exposed both to the lumen and to the stroma. The large positively charged N-terminal domain is situated in the lumen and contributes to the structural features of the surface of PS I toward the lumen (Jordan et al., 2001; Ben-Shem et al., 2003). PS I-F and luminal interhelical loops of PS I-A and -B form a docking site for Pc or Cyt c_6 (Farah et al., 1995; Hippler et al., 1997, 1998, 2002; Sommer et al., 2002). The C-terminus forms contacts with PS I-E (Fromme, 2001).

PS I-N is the only subunit located entirely in the thylakoid lumen. It can be dissociated from the PS I complex at high ionic strength and therefore has been

concluded to be located externally in the complex (He and Malkin, 1992). Cross-linking revealed little interaction between PS I-N and other small PS I subunits even though putative cross-linking products with PS I-G and -F were found (Jansson et al., 1996). Unfortunately, the 4.4 Å structure (Ben-Shem et al., 2003) does not reveal the position of PS I-N.

PS I-J is a small hydrophobic subunit with one transmembrane helix that is located close to PS I-F and (Jordan et al., 2001) the N-terminus of PS I-J is located in the stroma, the C-terminus is located in the lumen (Fromme et al., 2001).

B. The Role of PS I-F and -N in the Docking of Plastocyanin

Pc has been regarded the only mobile electron donor to PS I in higher plants. Recently, a Cyt c_6-like protein was identified in higher plants (Gupta et al., 2002; Wastl et al., 2002). Biochemical and genetic analyses suggested that the Cyt c_6-like protein was targeted to the thylakoid lumen where it could replace Pc in reducing PS I (Gupta et al., 2002). However, Weigel et al. (2003) showed that *Arabidopsis* plants deleted in both of the two Pc-encoding genes but with functional Cyt c_6 could not grow photoautotrophically because of a complete block in light-driven electron transport suggesting that only Pc can donate electrons to PS I *in vivo*.

The *psaF* gene was successfully inactivated in *Chlamydomonas* and this confirmed that in eukaryotes PS I-F has a role in docking of Pc (Farah et al., 1995) – a function suggested already 26 years ago by Bengis and Nelson (1977). Introduction of a modified PS I-F containing the N-terminal part of *Chlamydomonas* PS I-F into *Synechococcus elongatus* led to a large increase in the rate of oxidation of Pc and Cyt c_6 (Hippler et al., 1999). Although, the lack of PS I-F had a significant effect on Pc docking in *Chlamydomonas,* the algae devoid of PS I-F were almost unaffected in photoautotrophic growth under normal light conditions. Only in high light did the algae lacking PS I-F become photoinhibited (Hippler et al., 2000). In contrast, *Arabidopsis* plants devoid of PS I-F were barely able to survive even at low-light intensity (Haldrup et al., 2000). In plants lacking PS I-F the electron transfer from Pc to the reaction center of PS I was reduced to the same extent as in *Chlamydomonas*.

PS I-N has been investigated with a cosuppression approach in *Arabidopsis* (Haldrup et al., 1999). The plants lacking any detectable PS I-N were essentially indistinguishable from the wild-type in terms of growth and photosynthesis. Careful analysis revealed a 50% decrease in the rate of Pc oxidation and the steady-state reduction of $NADP^+$. The plants seemed to compensate for the lower activity of PS I by increasing the PS I/PS II ratio. Thus, plants lacking PS I-N had about 20% higher content of PS I on a chlorophyll basis. However, under conditions of sufficient light, this difference did not result in any measurable decrease in photosynthesis. Under light-limited conditions, a 10% decrease in quantum yield of oxygen evolution was observed but this effect was observed with plants acclimatized to a much higher light intensity. When the antisense PS I-N plants were grown under very low light they did not show any growth defect. Apparently, the plants adjust well to any nonfluctuating light condition to which they are exposed. In general, the physiological significance of many of the small subunits may only be apparent under conditions of stress or fluctuating light. The role of PS I-N might be mediated through a direct interaction with Pc or through a modifying effect on PS I-F. In this connection it is interesting to note that transgenic *Arabidopsis* plants lacking PS I-F have a secondary loss of PS I-N (Haldrup et al., 2000).

In cyanobacteria PS I-J interacts with PS I-F (Q Xu et al., 1994). PS I particles isolated from a *Synechocystis* sp. PCC 6803 mutant with deletion of *psaJ* contained only about 20% of the PS I-F subunit compared to the wild-type (W Xu et al., 1994). In contrast, *Chlamydomonas* chloroplast transformants with an inactivated *psaJ* gene contained wild-type levels of PS I-F and were able to grow photosynthetically, while a large fraction of mutant PS I complex displayed slow kinetics of electron donation from Pc or Cyt c_6 to P700 (Fischer et al., 1999). Thus PS I-J does not appear to participate directly in binding of Pc and Cyt $c_6$but plays a role in maintaining a precise recognition site of the N-terminal domain of PS I-F required for fast electron transfer from Pc and Cyt c_6 (Hippler et al., 2002; Hippler and Drepper, this volume, Chapter 29). As PS I-J is chloroplast-encoded and mutants are not readily available, the function of this subunit in higher plants has so far not been analyzed. We are currently investigating the role of PS I-J in transgenic tobacco plants lacking this subunit (P. E. Jensen and J. Meurer, unpublished).

C. Energy Transfer and Photoinhibition

Plants lacking PS I-F were severely affected in energy transfer from LHCI (Haldrup et al., 2000). Thus, although Lhca1 and Lhca4 remain in the PS I complex, they could not efficiently transfer energy to the reaction

center in the absence of PS I-F. This suggests that PS I-F in LHCI-containing plants and perhaps, also green algae should have regions optimized for the interaction with LHCI. This is in agreement with results from electron microscopy and single particle analysis of PS I from spinach, which show that the LHCI complexes only binds to the core complex at the PS I-F side of PS I (Boekema et al., 2001a). A direct contact of PS I-F with plant light-harvesting systems had been suggested earlier by experiments in which plant subunit PS I-F was isolated as a chlorophyll–protein complex with LHCI proteins (Anandan et al., 1989). With the crystal structure of plant PS I, it has now been proven that LHCI is in contact with PS I-F, and it was suggested that Lhca4 is the subunit interacting directly with PS I-F (Ben-Shem et al., 2003).

In cyanobacteria PS I-J binds three chlorophylls (Jordan et al., 2001). In plant PS I-J only two chlorophylls are bound, which are probably important for the energy transfer between LHCI and the PS I core (Ben-Shem et al., 2003).

The inefficiency in the peripheral antenna in plants lacking PS I-F does not explain the severe change in phenotype. Presumably, the lack of PS I-F lead to loss of the stromal subunits PS I-C, -D, and -E, which is accelerated by the generation of active oxygen at the reducing side of PS I. This cascade of events may be similar to the photoinhibitory effects that takes place in plants lacking PS I-D and -E. In all these cases, the phenotypes are much more severe than would be expected from the cyanobacterial counterparts or from the primary decrease in electron transport rates. Apparently, plants are much more sensitive to reactive oxygen formed at the reducing side of PS I than cyanobacteria and even green algae. Perhaps, the difference is related, to the compromise between transpiration and photosynthesis in land plants, which often results in limited availability of electron sinks.

IV. PS I-G and -K and Interaction with LHCI

A. Topology and Location in PS I

PS I-K is a 9 kDa subunit containing two transmembrane α-helices connected by a stromal loop (Jordan et al., 2001; Mant et al., 2001). In the 2.5 Å structure of PS I from *S. elongatus*, PS I-K appears to be the least ordered subunit in the PS I complex (Jordan et al., 2001). The 4.4 Å structure of plant PS I cannot unambiguously assign PS I-K within the PS I complex but PS I-K is proposed to retain its cyanobacterial position in plant PS I. This is also in agreement with cross-linking studies with PS I of higher plants, which showed that PS I-K only cross-links to PS I-A or -B and not to any of the other small intrinsic subunits, suggesting that PS I-K should be located distant from the twofold symmetry axis (Jansson et al., 1996). PS I-G and -K share 30% sequence identity and a similar topology with two transmembrane helices connected by a stromal loop (Mant et al., 2001; Rosgaard et al., 2005). This is in agreement with the topology of PS I-K in the *S. elongatus* structure (Fromme et al., 2001; Jordan et al., 2001) confirming that the higher plant PS I-K is the structural equivalent of the cyanobacterial PS I-K.

B. The Role of PS I-G and -K in Energy Transfer

In cyanobacteria, PS I-K clearly plays a role in proper function of the core antenna system since PS I-K binds two Chl *a* molecules and forms contacts with carotenoids (Jordan et al., 2001). The higher plant PS I-K binds four chlorophylls and was suggested to be involved in binding of Lhca3 (Ben-Shem et al., 2003). Furthermore, PS I-K is part of a contact region between the core and the peripheral antenna. In this region, the interpigment distances are sufficiently short (10–15 Å) to allow efficient energy transfer (Ben-Shem et al., 2003).

The involvement of PS I-K in binding of LHCI in higher plants has been analyzed both by using antisense suppression and disruption of the gene encoding PS I-K (Jensen et al., 2000; Varotto et al., 2002). In both cases it was found that the plants specifically devoid of PS I-K have a secondary loss of ∼20–30% of the Lhca2 protein and ∼30–40% of the Lhca3 protein resulting in a ∼15–20% reduction of the PS I antenna size (Jensen et al., 2002). Thus, PS I-K clearly has a role in the interaction with Lhca2 and/or Lhca3 but PS I-K is not strictly needed for binding of these proteins since they are still present in PS I in the complete absence of PS I-K although in reduced amounts.

The role of PS I-G has also been analyzed in plants in which the *psaG* gene expression has been either suppressed by antisense technology or eliminated by transposon tagging (Jensen et al., 2002; Varotto et al., 2002). The PS I antenna size was determined from flash-induced P700 absorption changes and it was found that the absence of PS I-G does not affect the PS I

antenna size, whereas in the absence of PS I-K there was a 15–20% decrease in size (Jensen et al., 2002). Moreover, PS I-200 particles without PS I-G have a normal content of all LHCI proteins and a Chl *a*/*b* ratio identical to wild-type PS I-200, though under mildly denaturing conditions a more unstable interaction between the PS I core and the LHCI antenna was seen (Jensen et al., 2002). It therefore seems that PS I-G is not needed for binding and function of the peripheral antenna but plays a role in stabilizing the peripheral antenna. According to the plant PS I structure, PS I-G is also part of a contact region between the core and the peripheral antenna located at the opposite end of LHCI compared to PS I-K (Ben-Shem et al., 2003). Most interactions between the core and the LHCI proteins are through small binding surfaces at their stromal-exposed regions but a strong interaction between a transmembrane helix in an LHCI protein (suggested to be Lhca1) and the two transmembrane helices of PS I-G is evident from the 4.4 Å structure. It is therefore surprising that elimination of PS I-G from plant PS I does not lead to a more severe effect on LHCI binding and function. This suggests that binding of the Lhca1/Lhca4 dimer is mainly via direct interactions with the core and that the interaction with PS I-G is less important for binding.

Pigment analysis and 5 K absorption spectra of PS I-200 particles without PS I-G indicate that the PS I-G subunit binds one or two red-shifted β-carotene molecules with a absorption maximum at 5 K of ~506 nm (Ihalainen et al., 2002). There is no evidence for chlorophyll binding to PS I-G, although the binding of a single chlorophyll molecule cannot be excluded. The resolution of the plant PS I structure is unfortunately not detailed enough to give any further insight into the pigment binding properties of PS I-G.

Excitation energy transfer and trapping dynamics were analyzed in PS I-200 particles from wild-type and mutants lacking PS I-G or -K by measuring fluorescence decay kinetics at room temperature (Ihalainen et al., 2002). In both wild-type and the two mutants two fast phases (5 and 15 psec) could, at least in part, be attributed to the excitation equilibration between bulk chlorophyll and red chlorophyll forms, though the 15 psec phase also contains a contribution from trapping by charge separation. Two other phases (50 and 120 psec) predominantly reflect trapping by charge separation in the PS I reaction center. The trapping of excitation energy that takes place within the 15 psec phase probably arises from photons absorbed in the core antenna, whereas trapping of excitation energy within the 50 psec phase is dominated by photons absorbed by Lhca2 and Lhca3 and trapping within the 120 psec phase is dominated by photons absorbed by Lhca1 and Lhca4 (Ihalainen et al., 2002). In agreement with a role of PS I-K and -G in the interaction between core and the peripheral antenna proteins, more excitations are trapped in the 15 psec phase and less in the 50 psec and 120 psec phases in PS I particles without the PS I-K or -G proteins.

The exact location of the two Lhca dimers (one Lhca1/Lhca4 dimer and one Lhca2/Lhca3 dimer) on the PS I core is not known in detail and a resolution of 4.4 Å does not allow unambiguous identification of individual Lhca proteins in the LHCI part of the structure. Suppression of either Lhca2 or Lhca3 by antisense technology clearly indicates that the contents of these proteins are interdependent (Ganeteg et al., 2001). A similar interdependence between Lhca2 and Lhca3 is also indicated from work on plants devoid of PS I-K (Jensen et al., 2000; Varotto et al., 2002). Furthermore, removal of Lhca1 and Lhca4 also affects Lhca2 and Lhca3, suggesting that the two Lhca dimers are adjacent to each other in the PS I holocomplex (Ganeteg et al., 2001). This is in perfect agreement with the structure of plant PS I obtained by electron microscopy, in which protein densities on the PS I-F/J side of PS I were suggested to represent LHCI (Boekema et al., 2001a), an observation recently confirmed by the X-ray crystal structure of plant PS I (Ben-Shem et al., 2003).

C. A Newly Discovered Role for PS I-G in Interaction with Plastocyanin

Plants with no detectable content of PS I-G were indistinguishable from wild-type when grown under growth chamber conditions (Jensen et al., 2002), but showed a decrease in mean size when grown under greenhouse conditions (Varotto et al., 2002). However, in the absence of PS I-G there was a 40% reduction of PS I on a chlorophyll basis (Table 2; Jensen et al., 2002). This reduced PS I content was compensated for by a more effective PS I since the light-dependent reduction of $NADP^+$ *in vitro* was 48% higher (Jensen et al., 2002).

The location of PS I-G in the PS I complex is at the periphery of the complex and therefore it is surprising that PS I-G can affect the electron transport through PS I. Most likely, PS I-G somehow affects the interaction either with ferredoxin on the stromal side or Pc on the luminal side. The kinetics of the Pc–PS I interaction were analyzed by flash-induced P700 absorption transients as a function of varying concentrations of Pc. All

Table 2. Secondary effects of removing a PS I subunit on the other subunits in PS I. Primary removal of a subunit has been accomplished by down-regulation using antisense, co-suppression or RNA interference, or by gene disruption. For references see the text

Plant line	Primary loss	Secondary loss
PsaD	PS I-D1 and -D2	A general reduction of PS I-LHCI corresponding to the residual amount of PS I-D ~20% LCHII
PsaE	PS I-E1 and -E2	40–80% loss of PS I-C, -D, -H, and -L
PsaF	PS I-F	~80% loss of PS I-C, -D, -E, -F, -K, -N, and -O ~50% Lhca1 –3
PsaG	PS I-G	A general 40% reduction in PS I
PsaH	PS I-H1 and -H2	~50% PS I-L, ~80% PS I-O
PsaL	PS I-L	~80 – 90% PS I-H and -O
PsaO	PS I-O	None
PsaN	PS I-N	None
PsaK	PS I-K	~30% Lhca2, ~40% Lhca3

the rate constants of the reaction between Pc and P700 were calculated and the dissociation constant (K_D) was found to be three times higher in wild-type plants (K_D = 30 μM) than in ΔPS I-G plants (K_D = 9.7 μM), indicating that the affinity of P700 for Pc is higher in the absence of PS I-G (Zygadlo et al., 2005). Thus, PS I-G is involved in the interaction between PS I and Pc, but it cannot be concluded whether the interaction is direct or indirect through an effect on the conformation of PS I-F or -N. An interaction between PS I-G and -N is suggested by a putative cross-linking product between the two proteins (Jansson et al., 1996).

V. The PS I-H, -I, -L, -O side of PS I

A. Topology and Location in PS I

Cyanobacterial PS I contains the subunits PS I-L and -I, which are located close to each other near the threefold symmetry axis in PS I trimers (Fromme et al., 2001). The PS I-L subunit is required for the interactions between PS I monomers in the trimers. In plants, the situation is different. First, there is no indication for the presence of PS I trimers, and therefore PS I-L must have a different role. Second, plant PS I contains additional subunits PS I-H and -O, which are located in the same region of PS I. The PS I-H subunit has been known for a long time and topological studies have showed that this subunit is in proximity with PS I-L and -I since these three subunits can all be cross-linked with each other by chemical cross-linkers (Jansson et al., 1996). In agreement with this, a single transmembrane helix adjacent to PS I-L has been assigned to PS I-H in the plant PS I structure (Ben-Shem et al., 2003). The three subunits were also shown by chemical cross-linking to be located close to PS I-D (Andersen et al., 1992; Jansson et al., 1996). More recently, the subunit designated PS I-O was discovered and identified in *Arabidopsis*, barley and spinach (Knoetzel et al., 2002). Open reading frames or mRNAs encoding similar proteins have been reported in many different plant species, in mosses and in green algae. No proteins similar to PS I-O are present in cyanobacteria.

The proximity of the PS I-H, -L, and -O proteins has been supported by the similarity in phenotype of knock-out mutants (see below). In addition, the secondary loss of one subunit as a consequence of a primary deficiency in another subunit confirms the interaction between these proteins (Table 2). Interestingly, the primary deficiency of PS I-L has the strongest secondary effect on the other proteins. Thus, plants down-regulated in the PS I-L protein have only about 10–20% PS I-H (Lunde et al., 2000) and virtually no PS I-O (Jensen et al., 2004). In contrast, primary down-regulation of PS I-H has a much smaller effect on PS I-O and -L (Lunde et al., 2000), and a primary down-regulation of PS I-O has virtually no effect on the content of PS I-H and -L (Jensen et al., 2004). This behavior of the three proteins fits very well with the PS I-L protein being the most ancient and conserved subunit closest to the reaction center and the eukaryotic PS I-H and -O proteins being later additions located more peripherally in the complex. The PS I-I protein is also ancient but its interactions with the other subunits are less well understood for two reasons. First, the quantitative analysis of this small subunit by immunoblotting is technically difficult, and second, no plant knock out of the *psaI* gene has been investigated. The *psaI* gene is located in the chloroplast and knock out of plastid genes does not work well in plants except for tobacco. We are currently investigating the function of PS I-I and its interaction with other proteins in transgenic tobacco.

PS I-H, -I, -L, and -O are all transmembrane proteins. The PS I-L protein in cyanobacteria has three membrane-spanning α-helices and the PS I-I protein has one transmembrane helix. These two proteins are highly conserved between prokaryotes and eukaryotes and we can safely assume that the topology in plants must be the same as in the cyanobacterial PS I, and at

least the three membrane-spanning α-helices of PS I-L are clearly resolved in the plant PS I structure (Ben-Shem et al., 2003). PS I-H is a 10-kDa protein containing one transmembrane α-helix and a 20 Å-long helix lying parallel to the membrane (Ben-Shem et al., 2003). The PS I-O protein has two predicted transmembrane α-helices separated by a luminal loop (Knoetzel et al., 2002). The predicted topology has been confirmed by import experiments (Knoetzel et al., 2002). Because PS I-O was discovered only recently, its interactions with other PS I proteins have not been reported. Recent experiments in our group have shown that PS I-O can be chemically cross-linked with PS I-L in agreement with PS I-O being located near PS I-L (Jensen et al., 2004) but PS I-O is not present or not resolved in the 4.4 Å plant structure (Ben-Shem et al., 2003).

B. Involvement of the PS I-H, -I, -L, and -O Subunits in State Transitions

A "state transition" is a mechanism that allows plants to redistribute some of the light-harvesting antenna proteins between PS II and PS I depending on light conditions and metabolic requirements (Haldrup et al., 2001; Allen, 2003). The major light-harvesting antenna of PS II (LHCII) is composed of trimers of Lhcb1 and Lhcb2 in varying proportions. Some of the trimers appear to be tightly associated with PS II but others are more weakly bound and may dissociate from PS II. Under those conditions, LHCII may then associate with PS I. The condition in which LHCII dissociates from PS II and associates with PS I is known as State 2 and occurs when a reduced plastoquinone pool indicates an imbalance between the two photosystems, with PS I being limiting. The reduced plastoquinone pool leads to activation of a kinase, which phosphorylates LHCII, and this results in transition to State 2. The increase in PS I antenna size and decrease in PS II antenna size will tend to reoxidize the plastoquinone pool. The transition to State 1 takes place when the plastoquinone pool is oxidized and involves dephosphorylation of LHCII by a phosphatase; unlike the kinase the phosphatase activity appears not to be redox regulated. The overall function of state transitions is a negative feedback that tends to keep intersystem electron transport chain in redox homeostasis despite changes in light quality. Most likely, state transitions are most important for the plant at rather low-light intensities when light is limiting. A function of state transitions in photoprotection has also been proposed, but this seems less likely since reversible LHCII phosphorylation does not take place at high-light intensities. State transitions could also play a role in regulating the relative antenna size of PS I and PS II depending on the requirement for cyclic versus linear electron transport.

The dissociation of LHCII from PS II in State 2 has been known for a long time and is easily detected by fluorescence measurements. The association of LHCII with PS I under the same conditions has attracted much less attention. However, there is little doubt that the antenna size of PS I increases in State 2. Until recently, little was known about the point of interaction between LHCII and PS I. Bassi and Simpson (1987) showed that LHCII could not attach to PS I particles from which LHCI had been dissociated with detergents and concluded that LHCII most likely connect to PS I via LHCI. However, the detergent treatment used to remove LHCI is very likely also to have removed PS I core subunits that were not known at the time. More recently, the PS I-H subunit was shown to be directly involved in state transitions (Lunde et al., 2000). *Arabidopsis* plants with co-suppression of the *psaH* genes and containing almost no PS I-H showed almost complete absence of state transitions. LHCII was phosphorylated normally by the kinase under State 2 conditions but LHCII remained bound to PS II and the antenna size of PS I remained the same as in State 1. The wild-type plants in contrast showed an increase in PS I antenna size of about 30% in State 2 compared to State 1.

Plants lacking PS I-L also showed a decrease in state transitions, but this decrease correlated with the secondary loss of PS I-H observed in these plants (Lunde et al., 2000). Therefore, PS I-H was concluded to be the subunit directly responsible for interaction with LHCII. Subsequent studies have shown that also plants lacking PS I-O are highly deficient in state transitions (Jensen et al., 2004). PS I-I could possible be involved in state transitions also, but since no PS I-I knock out has yet been investigated in plants or in green algae, this is not known.

The proposed binding of LHCII to PS I-H was based on studies of mutants and a direct interaction had not been demonstrated. However, recently we have shown that LHCII does in fact interact physically with exactly the part of PS I suggested from the mutant studies (Zhang and Scheller, 2004). In this study, PS I particles were isolated under very mild conditions and it was shown that LHCII could be chemically cross-linked to PS I-H, -L, and -I. No cross-linking of LHCII to PS I-O was found, but this does not necessarily mean that the proteins are not in contact with each other. The studies also showed that PS I particles isolated from mutants

lacking PS I-H, -O, or -L had a much decreased content of LHCII and were similar to PS I particles isolated from the wild-type in State 1.

The emerging picture from studies of the *Arabidopsis* mutants and transformants is that PS I-H, -L, -O, and possibly -I constitute one domain, and are all responsible for state transitions. Some of the proteins interact directly with LHCII and others may just be required for the stability or assembly of the domain. The PS I-L protein originally served the function of interaction between PS I monomers in the trimers, but in eukaryotes that function has changed to interaction with LHCII during state transitions. In the evolution of this changed function, the additional subunits PS I-H and -O were acquired.

C. Pigment Binding of the PS I-H, -L, and -O Subunits

PS I-L in *S. elongatus* binds three Chl *a* molecules (Fromme et al., 2001) and a similar number has been indicated for the plant PS I-L (Ben-Shem et al., 2003). Absorbance spectroscopy of PS I isolated from antisense plants down-regulated in PS I-L showed a decreased content of Chl *a* corresponding to about five molecules per P700 (Ihalainen et al., 2002). Since PS I in the *psaL* antisense plants have lost most of PS I-H, it was suggested that PS I-L binds three chlorophyll molecules as in cyanobacteria while PS I-H would bind the remaining two molecules (Ihalainen et al., 2002). In the recent plant structure, PS I-H binds only one chlorophyll molecule (Ben-Shem et al., 2003). Since we now know that also the content of PS I-O is very low in PS I from antisense *psaL* plants, it is therefore possible that PS I-O also bind one chlorophyll molecule. Because down-regulation of PS I-O does not result in secondary loss of any other subunits, absorption spectroscopy of PS I from PS I-O mutants should resolve this issue. The pigments in the three subunits will of course contribute to the total antenna of PS I. However, we can imagine that these particular pigment molecules are important for the energy transduction from LHCII to P700. A high-resolution structure of eukaryotic PS I and site-directed mutagenesis of the small proteins will be required to determine the significance of these pigment molecules.

D. Other Functions of the PS I-H, -I, -L, and -O Subunits

As stated above, PS I-L is involved in trimer formation in cyanobacteria, but this role has been lost in plants. PS I-I is involved in the stabilization of PS I-L in cyanobacteria and the absence of PS I-I therefore affects trimer formation indirectly (Xu et al., 1995). Given the conservation of the PS I-L and -I proteins it seems likely that PS I-I would have a similar stabilizing role in plants, but whether this is the case is not known. Similarly, the PS I-H protein has a stabilizing role on the other proteins in the domain. However, this mutual stabilization can all be seen as part of the primary function of interaction with LHCII during state transitions. More interesting are the additional functions of PS I-H unrelated to state transitions. In the absence of PS I-H, steady-state electron transport through PS I is decreased (Naver et al., 1999). A thorough kinetic analysis is still lacking but the data suggest that absence of PS I-H affects the binding of ferredoxin. PS I-H has not been shown to interact directly with ferredoxin but it interacts with PS I-D, and this subunit interacts directly with ferredoxin during electron transfer (see section II.B). PS I-H has a relatively large stromal domain and it may be this domain that interacts with PS I-D and stabilizes the binding of ferredoxin. PS I-H also stabilizes the stromal subunits PS I-C, -D, and -E directly (Naver et al., 1999). The three stromal subunits are more strongly bound to eukaryotic PS I than to cyanobacterial PS I, but in the absence of PS I-H they are easily removed. The stabilizing effect of PS I-H on the stromal subunits appear to be of minor importance *in vivo*, since no degraded or inactive PS I was recovered from transformants with a virtual absence of PS I-H (Naver et al., 1999).

E. The Significance of the Subunits In Vivo

As mentioned above, the significance of state transitions for plant growth and development has not been completely clear. While a role in optimizing photosynthesis to changing light composition at low-light intensities seems most likely, a role in photoprotection has also been proposed. It would seem that the mutants lacking some of the PS I subunits responsible for state transitions would be ideal for investigating this idea. However, a clear-cut result has been difficult to obtain. The cosuppression of PS I-H is variable and is absent in very young plants. Hence, the plants must be grown to a certain size and each plant must then be tested individually for the content of PS I-H. Obviously, this limits the scale of growth experiments. Nevertheless, we have grown plants lacking PS I-H or -L under a variety of constant light conditions, both low light and high light with significant photoinhibition. In none of the conditions could we detect any effect on plant growth

(Lunde et al., 2003). One problem with this kind of experiment is that the plants will quickly adjust to any constant growth condition and the significance of an inability to perform dynamic adjustments such as state transitions will not be seen. Therefore, we have also grown plants lacking PS I-H under conditions where the light constantly varied between State 1 and State 2 or between low and high light. With variations between low and high light the plants lacking PS I-H did produce 10% less seeds than the wild-type plants (Lunde et al., 2003). However, it must be emphasized that the lower seed set was not considered statistically significant.

F. The PS I-M Subunit

In cyanobacteria the PS I-M subunit is located in contact with PS I-I. PS I-M is the smallest subunit in PS I consisting of a single transmembrane helix with short domains in the ends. Genes encoding a similar protein have been found in various algae, including green algae, and in *Marchantia polymorpha* but the presence of the PS I-M protein has not been confirmed in any eukaryote. Two *psaM* genes are annotated in the inverted repeat regions of the *Pinus thunbergii* chloroplast genome at a position corresponding to the *psaM* genes in *Marchantia*. However, the putative PS I-M sequences from *Pinus* are virtually impossible to align with PS I-M from other species. Also, no nucleotide sequence from any other plant appears to encode a protein with even remote resemblance to PS I-M. Therefore, in our opinion there is no PS I-M protein in plants and the genes in *Pinus* are most likely not expressed. It may be imagined that the position of PS I-M in cyanobacterial PS I has been taken over by PS I-O in plants. However, green algae appear to contain both PS I-M and -O since the predicted proteins are well conserved.

VI. Concluding Remarks

The subunit composition of plant PS I is essentially known. Since an additional subunit, PS I-O, was discovered relatively recently and 10 years after the discovery of PS I-N, we should be careful in excluding the possibility that there are no additional subunits. However, it is very unlikely that there will be any major additions to the subunit inventory of PS I. An unresolved question is the stoichiometry of the LHCI proteins. The LHCI content and composition in the thylakoid membranes is somewhat variable but it is unclear how that relates to differences in the PS I complexes. The major challenge for the future lies in an understanding of how the subunits interact with each other, especially during assembly and turnover and during dynamic changes in the PS I complex. We know almost nothing about how the PS I complex with all its cofactors is assembled and even less about how the complex is turned over for example after photodamage. Another major challenge is to determine the structure of the plant PS I complex at a higher resolution that presently available.

Acknowledgments

The Danish National Research Foundation, the Nordic Joint Committee for Agricultural Research, and the Danish Veterinary and Agricultural Research Council are thanked for supporting this work.

References

Allen JF (2003) State transitions – a question of balance. Science 299: 1530–1532

Anandan S, Vainstein A and Thornber JP (1989) Correlation of some published amino acid sequences for photosystem I polypeptides to a 17 kDa LHCI pigment–protein and to subunits III and IV of the core complex. FEBS Lett 256: 150–154

Andersen B, Scheller HV and Møller BL (1992) The PSI-E subunit of photosystem I binds ferredoxin:NADP+ oxidoreductase. FEBS Lett 311: 167–173

Antonkine ML, Jordan P, Fromme P, Krauß N, Golbeck JH and Stehlik D (2003) Assembly of protein subunits within the stromal ridge of photosystem I. Structural changes between unbound and sequentially PS I-bound polypeptides and correlated changes of the magnetic properties of the terminal iron sulfur clusters. J Mol Biol 327: 671–697

Armbrust TS, Chitnis PR and Guikema JA (1996) Organization of photosystem I polypeptides examined by chemical cross-linking. Plant Physiol 111: 1307–1312

Bailey S, Walters RG, Jansson S and Horton P (2001) Acclimation of *Arabidopsis thaliana* to the light environment: the existence of separate low light and high light responses. Planta 213: 794–801

Bassi R and Simpson D (1987) Chlorophyll–protein complexes of barley photosystem I. Eur J Biochem 163: 221–230

Bengis C and Nelson N (1977) Subunit structure of chloroplast photosystem I reaction center. J Biol Chem 252: 4564–4569

Ben-Shem A, Frolow F and Nelson N (2003) Crystal structure of plant photosystem I. Nature 426: 630–635

Bibby TS, Nield J and Barber J (2001) Iron deficiency induces the formation of an antenna ring around trimeric photosystem I in cyanobacteria. Nature 412: 743–745

Boekema EJ, Jensen PE, Schlodder E, van Breemen JFL, van Roon H, Scheller HV and Dekker JP (2001a) Green plant photosystem I binds light-harvesting complex I on one side of the complex. Biochemistry 40: 1029–1036

Boekema EJ, Hifney A, Yakushevska AE, Piotrowski M, Keegstra W, Berry S, Michel K-P, Pistorius EK and Kruip J (2001b) A giant chlorophyll–protein complex induced

by iron deficiency in cyanobacteria. Nature 412: 745–748

Chitnis VP, Jung YS, Albee L, Golbeck JH and Chitnis PR (1996) Mutational analysis of photosystem I polypeptides. J Biol Chem 271: 11772–11780

Croce R, Morosinotto T, Castelletti S, Breton J and Bassi R (2002) The Lhca antenna complexes of higher plants photosystem I. Biochim Biophys Acta 1556: 29–40

Farah J, Rappaport F, Choquet Y, Joliot P and Rochaix J-D (1995) Isolation of a *psaF*-deficient mutant of *Chlamydomonas reinhardtii*: efficient interaction of plastocyanin with the photosystem I reaction center is mediated by the PsaF subunit. EMBO J 14: 4976–4984

Fischer N, Boudreau E, Hippler M, Drepper F, Haehnel W and Rochaix J-D (1999) A large fraction of PsaF is nonfunctional in photosystem I complexes lacking the PsaJ subunit. Biochemistry 38: 5546–5552

Fromme P, Jordan P and Krauß N (2001) Structure of photosystem I. Biochim Biophys Acta 1507: 5–31

Ganeteg U, Strand Å, Gustafsson P and Jansson S (2001) The properties of the chlorophyll *a*/*b*-binding proteins Lhca2 and Lhca3 studied *in vivo* using antisense inhibition. Plant Physiol 127: 150–158

Ganeteg U, Klimmek F and Jansson S (2004) Lhca5 – an LHC-type protein associated with Photosystem I. Plant Mol Biol 54: 641–651

Golbeck JH (1992) Structure and function of photosystem I. Annu Rev Plant Physiol Plant Mol Biol 43: 293–324

Gupta R, He Z and Luan S (2002) Functional relationship of cytochrome c_6 and plastocyanin in Arabidopsis. Nature 417: 567–571

Haldrup A, Naver H and Scheller HV (1999) The interaction between plastocyanin and photosystem I is inefficient in transgenic *Arabidopsis* plants lacking the PSI-N subunit of photosystem I. Plant J 17: 689–698

Haldrup A, Simpson JD and Scheller HV (2000) Down-regulation of the PSI-F subunit of Photosystem I in *Arabidopsis thaliana*. The PSI-F subunit is essential for photoautotrophic growth and antenna function. J Biol Chem 275: 31211–31218

Haldrup A, Jensen PE, Lunde C and Scheller HV (2001) Balance of power: a view of the mechanism of photosynthetic state transitions. Trends Plant Sci 6: 301–305

Haldrup A, Lunde C and Scheller HV (2003) *Arabidopsis thaliana* plants lacking the PSI-D subunit of photosystem I suffer severe photoinhibition, have unstable photosystem I complexes and altered redox homeostasis in the chloroplast stroma. J Biol Chem 278: 33276–33283

Hansson M and Vener AV (2003) Identification of three previously unknown *in vivo* protein phosphorylation sites in thylakoid membranes of *Arabidopsis thaliana*. Mol Cell Proteomics 2: 550–559

He WZ and Malkin R (1992) Specific release of a 9-kDa extrinsic polypeptide of photosystem-I from spinach-chloroplasts by salt washing. FEBS Lett 308: 298–300

Hippler M, Drepper F, Farah J and Rochaix J-D (1997) Fast electron transfer from cytochrome c_6 and plastocyanin to photosystem I of *Chlamydomonas reinhardtii* requires PsaF. Biochemistry 36: 6343–6349

Hippler M, Drepper F, Haehnel W and Rochaix J-D (1998) The N-terminal domain of PsaF: precise recognition site for binding and fast electron transfer from cytochrome c(6) and plastocyanin to photosystem I of *Chlamydomonas reinhardtii*. Proc Natl Acad Sci USA 95: 7339–7344

Hippler M, Drepper F, Rochaix JD and Mühlenhoff U (1999) Insertion of the N-terminal part of PsaF from *Chlamydomonas reinhardtii* into photosystem I from *Synechococcus elongatus* enables efficient binding of algal plastocyanin and cytochrome c_6. J Biol Chem 274: 4180–4188

Hippler M, Biehler K, Krieger-Liszkay A, van Dillewjin J and Rochaix J-D (2000) Limitation in electron transfer in photosystem I donor side mutants of *Chlamydomonas reinhardtii* – lethal photo-oxidative damage in high light is overcome in a suppressor strain deficient in the assembly of the light harvesting complex. J Biol Chem 275: 5852–5859

Hippler M, Rimbault B and Takahashi Y (2002) Photosynthetic complex assembly in *Chlamydomonas reinhardtii*. Protist 153: 197–220

Ihalainen JA, Jensen PE, Haldrup A, van Stokkum IHM, van Grondelle R, Scheller HV and Dekker JP (2002) Pigment organization and energy transfer dynamics in isolated photosystem I (PSI) complexes from *Arabidopsis thaliana* depleted of the PSI-G, PSI-K, PSI-L, or PSI-N subunit. Biophys J 83: 2190–2201

Ihnatowicz A, Pesaresi P, Varotto C, Richly E, Schenider A, Jahns P, Salamini F and Leister D (2004) Mutants for photosystem I subunit D of *Arabidopsis thaliana*: effects on photosynthesis, photosystem I stability and expression of nuclear genes for chloroplast functions. Plant J 37: 839–852

Jansson S (1999) A guide to the *Lhc* genes and their relatives in *Arabidopsis*. Trends Plant Sci 4: 236–240

Jansson S, Andersen B and Scheller HV (1996) Nearest neighbor analysis of higher-plant photosystem I holocomplex. Plant Physiol 12: 409–420

Jensen PE, Gilpin M, Knoetzel J and Scheller HV (2000) The PSI-K subunit of photosystem I is involved in the interaction between light-harvesting complex I and the photosystem I reaction core. J Biol Chem 275: 24701–24708

Jensen PE, Rosgaard L, Knoetzel J and Scheller HV (2002) Photosystem I activity is increased in the absence of the PSI-G subunit. J Biol Chem 277: 2798–2803

Jensen PE, Haldrup A, Rosgaard L and Scheller HV (2003) Molecular dissection of photosystem I in higher plants: topology, structure and function. Physiol Plant 119: 313–321

Jensen PE, Haldrup A, Zhang S and Scheller HV (2004) The PSI-O subunit of plant photosystem I is involved in balancing the excitation pressure between the two photosystems. J Biol Chem 279: 24212–24217

Jordan P, Fromme P, Witt HT, Klukas O, Saenger W and Krauß N (2001) Three-dimensional structure of cyanobacterial photosystem I at 2.5 Å resolution. Nature 411: 909–917

Klukas O, Schubert WD, Jordan P, Krauß N, Fromme P, Witt HT and Senger W (1999) Photosystem I, an improved model of the stromal subunits PsaC, PsaD, and PsaE. J Biol Chem 274: 7351–7360

Knoetzel J, Mant A, Haldrup A, Jensen PE and Scheller HV (2002) PSI-O, a new 10-kDa subunit of eukaryotic photosystem I. FEBS Lett 510: 145–148

Kruip J, Chitnis PR, Lagoutte B, Rogner M and Boekema EJ (1997) Structural organization of the major subunits in cyanobacterial photosystem I. Localization of subunits PsaC, -D, -E, -F, and -J. J Biol Chem 272: 17061–17069

Lelong C, Sétif P, Lagoutte B and Bottin H (1994) Identification of the amino acids involved in the functional interaction between photosystem I and ferredoxin from *Synechocystis* sp. PCC 6803 by chemical cross-linking. J Biol Chem 269: 10034–10039

Lelong C, Boekema EJ, Kruip J, Bottin H, Rögner M and Sétif P (1996) Characterization of a redox active cross-linked complex between cyanobacterial photosystem I and soluble ferredoxin. EMBO J 15: 2160–2168

Li N, Zhao J, Warren PV, Warden JT, Bryant DA and Golbeck JH (1991) PsaD is required for the stable binding of PsaC to the photosystem I core protein of *Synechococcus* sp. PCC 6301. Biochemistry 30: 7863–7872

Lunde C, Jensen PE, Haldrup A, Knoetzel J and Scheller HV (2000) The PSI-H subunit of photosystem I is essential for state transition in plants. Nature 408: 613–615

Lunde C, Jensen PE, Rosgaard L, Haldrup A, Gilpin MJ and Scheller HV (2003) Plants impaired in state transitions can to a large degree compensate for their defect. Plant Cell Physiol 44: 44–54

Mannan RM, Whitmarsh J, Nyman P and Pakrasi HB (1991) Directed mutagenesis of an iron–sulfur protein of the Photosystem I complex in the filamentous cyanobacterium *Anabaena variabilis* ATCC 29413. Proc Natl Acad Sci USA 88: 10168–10172

Mannan RM, Pakrasi HB and Sonoike K (1994) The PsaC protein is necessary for the stable association of the PsaD, PsaE, and PsaL proteins in the photosystem I complex: analysis of a cyanobacterial mutant strain. Arch Biochem Biophys 315: 68–73

Mant A, Woolhead CA, Moore M, Henry R and Robinson C (2001) Insertion of PsaK into the thylakoid membrane in a "horseshoe" conformation occurs in the absence of signal recognition particle, nucleoside triphosphates, or functional Albino3. J Biol Chem 276: 36200–36206

Merati G and Zanetti G (1987) Chemical cross-linking of ferredoxin to spinach thylakoids. FEBS Lett 215: 37–40

Naver H, Schott MP, Andersen B, Møller BL and Scheller HV (1995) Reconstitution of barley photosystem I reveals that the N-terminus of the PSI-D subunit is essential for tight binding of PSI-C. Physiol Plant 95: 19–26

Naver H, Scott MP, Golbeck JH, Møller BL and Scheller HV (1996) Reconstitution of barley photosystem I with modified PSI-C allows identification of domains interacting with PSI-D and PSI-A/B. J Biol Chem 271: 8996–9001

Naver H, Haldrup A and Scheller HV (1999) Cosuppression of photosystem I subunit PSI-H in *Arabidopsis thaliana*. Efficient electron transfer and stability of photosystem I is dependent upon the PSI-H subunit. J Biol Chem 274: 10784–10789

Niyogi KK (1999) Photoprotection revisited: genetic and molecular approaches. Ann Rev Plant Physiol Plant Mol Biol 50: 333–359

Okkels JS, Jepsen LB, Hønberg LS, Lehmbeck J, Scheller HV, Brandt P, Høyer-Hansen G, Stummann B, Henningsen KW, von Wettstein D and Møller BL (1988) A cDNA clone encoding a 10.8-kDa photosystem I polypeptide of barley. FEBS Lett 237: 108–112

Pesaresi P, Lunde C, Jahns P, Tarantino D, Meurer J, Varotto C, Hirtz R-D, Soave C, Scheller HV, Salamini F and Leister D (2002) A stable LHCII–PSI aggregate and suppression of photosynthetic state transitions in the *psae1-1* mutant of *Arabidopsis thaliana*. Planta 215: 940–948

Rosgaard L, Zygadlo A, Scheller HV, Mant A and Jensen PE (2005) Insertion of the plant photosystem I subunit G into the thyklakoid membrane: *in vitro* and *in vivo* studies of wild-type and tagged versions of the protein. FEBS J 272: 4002–4010

Rousseau F, Sétif P and Lagoutte B (1993) Evidence for the involvement of PSI-E subunit in the reduction of photosystem I. EMBO J 12: 1755–1765

Scheller HV, Jensen PE, Haldrup A, Lunde C and Knoetzel J (2001) Role of subunits in eukaryotic PSI. Biochim Biophys Acta 1507: 41–60

Scheller HV, Lunde C, Haldrup A and Jensen, PE (2004) Functional characterization of the photosynthetic apparatus in *Arabidopsis thaliana*. In: Leister D (ed) Plant Functional Genomics, pp 393–429. The Haworth's Press, Binghamton, New York

Schmid VHR, Potthast S, Wiener M, Bergauer V, Paulsen H and Storf S (2002) Pigment binding of photosystem I light-harvesting proteins. J Biol Chem 277: 37307–37314

Sommer F, Drepper F and Hippler M (2002) The luminal helix l of PsaB is essential for recognition of plastocyanin or cytochrome c(6) and fast electron transfer to photosystem I in *Chlamydomonas reinhardtii*. J Biol Chem 277: 6573–6581

Takahashi Y, Goldschmidt-Clermont M, Soen SY, Franzen LG and Rochaix J-D (1991) Directed chloroplast transformation in *Chlamydomonas reinhardtii*: insertional inactivation of the *psaC* gene encoding the iron sulfur protein destabilizes photosystem I. EMBO J 10: 2033–2040

Varotto C, Pesaresi P, Meurer J, Oelmuller R, Steiner-Lange S, Salamini F and Leister D (2000) Disruption of the *Arabidopsis* photosystem I gene *psaE1* affects photosynthesis and impairs growth. Plant J 22: 115–124

Varotto C, Pesaresi P, Jahns P, Lessnick A, Tizzano M, Schiavon F, Salamini F and Leister D (2002) Single and double knockouts of the genes for photosystem I subunits G, K, and H of *Arabidopsis*. Effects on photosystem I composition, photosynthetic electron flow, and state transitions. Plant Physiol 129: 616–624

Wastl J, Bendall DS and Howe CJ (2002) Higher plants contain a modified cytochrome c_6. Trends Plant Sci 7: 244–245

Weigel M, Pesaresi P and Leister D (2003) Tracking the function of the cytochrome c_6-like protein in higher plants. Trends Plant Sci 8: 513–517

Xu Q, Yu L, Chitnis VP and Chitnis PR (1994) Function and organization of photosystem I in a cyanobacterial mutant strain that lacks PsaF and PsaJ subunits. J Biol Chem 269: 3205–3211

Xu Q, Hoppe D, Chitnis VP, Odom WR, Guikema JA and Chitnis PR (1995) Mutational analysis of Photosystem I polypeptides in the cyanobacterium *Synechocystis* sp. PCC 6803 – targeted inactivation of *psaI* reveals the function of PsaI in the structural organization of PSI. J Biol Chem 270: 16243–16250

Xu W, Jung YS, Chitnis VP, Guikema JA, Golbeck JH and Chitnis PR (1994) Mutational analysis of photosystem I polypeptides in the cyanobacterium *Synechocystis* sp. PCC 6803. J Biol Chem 269: 21512–21518

Yamamoto Y, Tsuji H and Obokata J (1993) Structure and expression of a nuclear gene for the PSI-D subunit of photosystem I in *Nicotiana sylvestris*. Plant Mol Biol 22: 985–994

Yu J, Smart LB, Jung YS, Golbeck J and McIntosh L (1995) Absence of PsaC subunits allows assembly of Photosystem I core but prevents the binding of PsaD and PsaE in *Synechocystis* sp. PCC 6803. Plant Mol Biol 29: 331–342

Zanetti G and Merati G (1987) Interaction between photosystem I and ferredoxin. Identification by chemical cross-linking of the polypeptide which binds ferredoxin. Eur J Biochem 169: 143–146

Zhang S and Scheller HV (2004) Light harvesting complex II binds to several small subunits of PSI. J Biol Chem 279: 3180–3187

Zilber AL and Malkin R (1988) Ferredoxin cross-links to a 22-kDa subunit of photosystem I. Plant Physiol 88: 810–814

Zygadlo A, Jensen PE, Leister D and Scheller HV (2005) Photosystem I lacking the PSI-G subunit has higher affinity for plastocyanin and is sensitive to photodamage. Biochim Biophys Acta 1708: 154–163

Chapter 12

Ultrafast Optical Spectroscopy of Photosystem I

Sergei Savikhin*
Department of Physics, Purdue University, West Lafayette, IN 47907, USA

Summary

This review discusses energy and electron transfer in Photosystem I (PS I) complexes by means of ultrafast time-resolved optical techniques. In particular, this article addresses directly observable initial (sub)picosecond electronic excitation equilibration among different antenna chlorophyll forms and energy trapping by the charge separation process followed by picosecond electron transfer to the secondary electron acceptor A_1. There is still no general agreement on the energy trapping classification in PS I; the validity of diffusion-limited, trap-limited, and mixed-energy trapping models is tested against the available experimental data. Ultrafast experiments on branch-specific complementary mutants of the reaction center open the unique possibility of differentiating between the two highly symmetrical branches of the reaction center, revealing the directionality of electron transfer in PS I. Finally, the most recent optical data questions the conventional sequence of electron transfer steps, and suggests the intriguing possibility that one additional intermediate radical pair may exist that was not previously observed.

I. Introduction

A. General Remarks

Photosystem I (PS I) is a chlorophyll–protein complex that uses light energy to reduce ferredoxin in cyanobacteria and plants (Brettel, 1997). The primary events triggered by light absorption in the core antenna–reaction center of PS I complexes have been intensively studied by ultrafast spectroscopy since the mid-1980s (van Grondelle et al., 1994). Recent determination and subsequent refinements of the X-ray crystal structure of the PS I core antenna–reaction center (RC) complex from the cyanobacterium *Synechococcus elongatus* (Krauß et al., 1993, 1996; Klukas et al., 1999; Jordan et al., 2001) and from a higher plant

* Author for correspondence, email: sergei@physics.purdue.edu

John H. Golbeck (ed): Photosystem I: The Light-Driven Plastocyanin:Ferredoxin Oxidoreductase, 155–175.

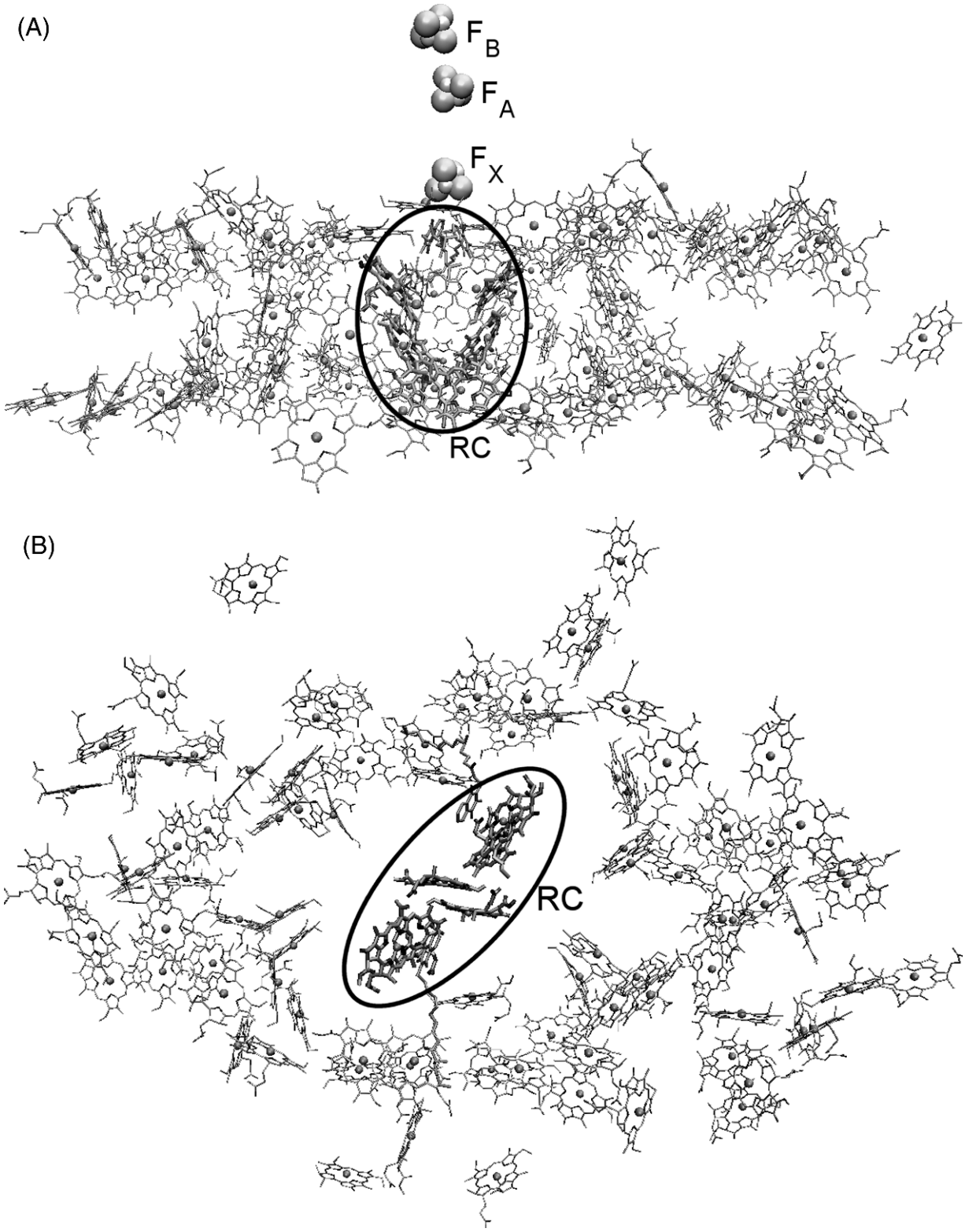

Fig. 1. Arrangement of the pigments and iron–sulfur cofactors within the PS I core complexes from *Synechococcus elongatus*. (A) Side view. (B) Top view (Jordan et al., 2001).

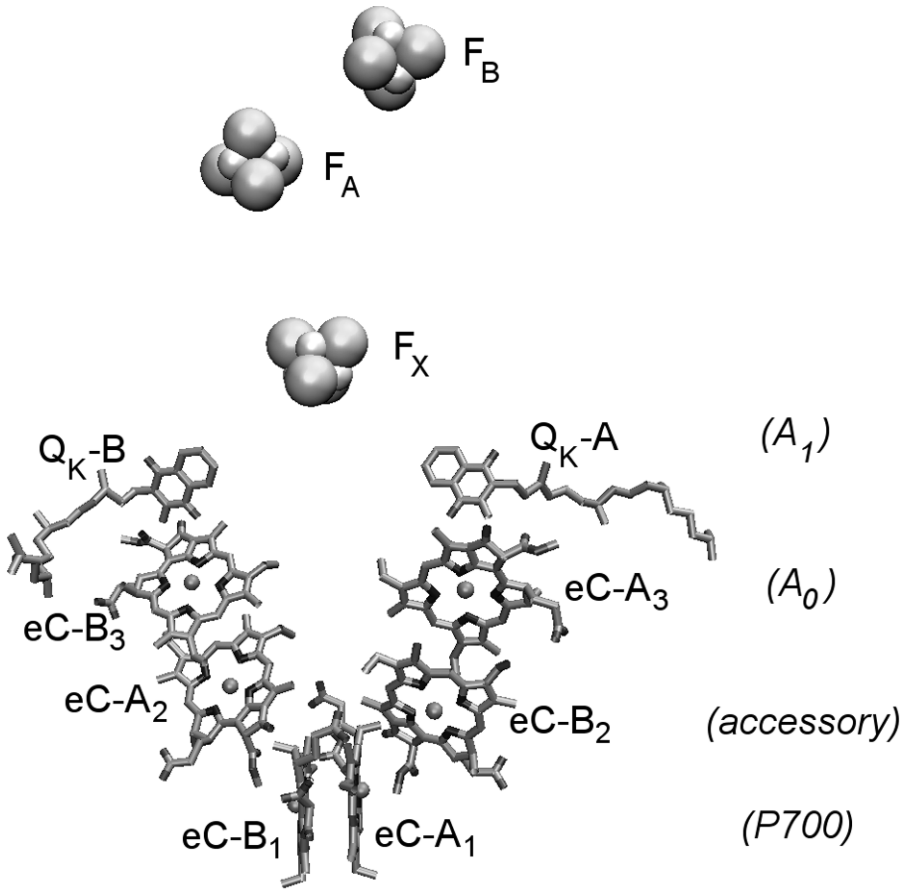

Fig. 2. Arrangement of electron transfer cofactors in PS I (Jordan et al., 2001).

(Ben-Shem et al., 2003) has prompted a resurgence of interest in primary processes in PS I and made structure-based modeling of energy and electron transfers possible in this photosynthetic complex. These simulations, while leading to a deeper molecular understanding of the structure–function relationships in PS I, rely heavily on the available experimental data on the dynamics of the modeled processes. Energy transfer, charge separation, and primary electron transfer (ET) steps in PS I all occur competitively during the first 20–50 psec after absorption of a photon and can be best monitored by means of ultrafast optical spectroscopy.

In this chapter, we summarize investigations of the ultrafast dynamics of electronic energy transfer from the PS I antenna to the PS I RC followed by rapid charge separation and the first electron transfer step.

Abbreviations: Chl – chlorophyll; DAS – decay-associated spectrum; ESA – excited state absorption; ET – electron transfer; PB – photobleaching; PS – photosystem; RC – reaction center; SE – stimulated emission.

B. The Structure of the PS I Complex

According to the latest X-ray data, the cyanobacterial PS I core complex contains one chlorophyll (Chl) *a*′ and 95 Chl *a* pigments, which are coordinated by several protein subunits (Jordan et al., 2001; see Fromme and Grotjohann, this volume, Chapter 6). Most of the pigments function as light-harvesting antenna, capturing light excitation and transferring it to the RC located in the middle of the PS I complex. The antenna pigments are arranged in a quasielliptical manner (Fig. 1A) around the reaction center with the only hint of pseudo-C_2 symmetry. The side view (Fig. 1B) reveals that 79 of all identified Chls form two distinct layers near and parallel to the stromal and lumenal membrane surfaces, respectively. The RC is located in the middle of the complex and is comprised of six Chl cofactors (Fig. 2):

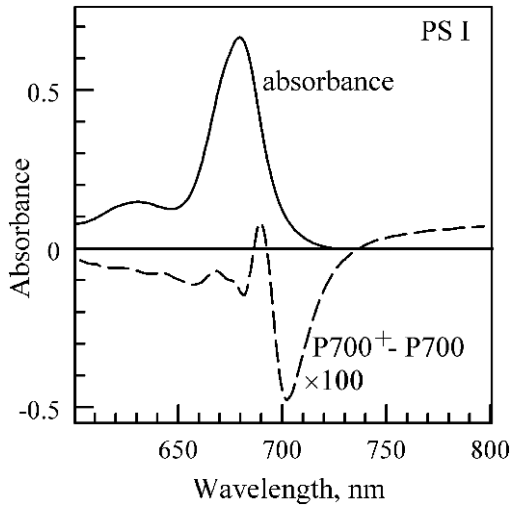

Fig. 3. Steady-state absorption (solid line) and ($P700^+ - P700$) absorption difference spectrum (dashed) of PS I core complexes from *Synechocystis* sp. at room temperature.

the primary electron donor P700 (a heterodimer of Chl a' and a denoted as eC-A_1 and eC-B_1, respectively), two accessory Chls (eC-B_2 and eC-A_2), and two chlorophylls denoted as eC-A_3 and eC-B_3, of which one or both are believed to serve as primary electron acceptor A_0. According to the conventional model, in the PS I RC, primary charge separation leads to the reduction of A_0, creating the radical ion-pair $P700^+A_0^-$. The unpaired electron migrates first to the phylloquinone secondary acceptor A_1 (Q_K-A and/or Q_K-B), then to the [4Fe–4S] center F_X, and finally to the terminal iron–sulfur centers F_A and F_B before being transferred to ferredoxin (Brettel, 1997; Brettel and Leibl, 2001).

The mean distance from any of the antenna pigments to its nearest neighbor in the PS I core complex is 9.9 Å, and the average distance to the second- and third-nearest pigments are 12.2 and 14.3 Å, respectively. Such close proximity of antenna pigments to each other ensures rapid and efficient excitation energy equilibration between antenna pigments and excitation transfer to the RC. A simple estimate based on the Förster energy transfer theory (Struve, 1995) predicts that the single-energy transfer step between the neighboring pigments in PS I occurs in 100–200 fsec. The overall lifetime of electronic excitation in the antenna has been shown to be ~20–60 psec depending on the species (Holzwarth et al., 1998; Karapetyan et al., 1999; Gobets and van Grondelle, 2001; Melkozernov, 2001), which implies that ~100 single-energy transfer steps occur before the electronic excitation reaches the RC and gets trapped, forming the $P700^+A_0^-$ charge separated state. Experimental observation of each individual energy transfer step in such a complex system is impossible; instead, only a small number of average kinetic processes can be distinguished.

Optical transition energies of Chl *a* pigments in PS I strongly overlap—the Q_y absorption band measured for PS I complexes is ~30 nm wide (Fig. 3), while an individual Chl *a* molecule yields an absorption band which is only three times narrower at room temperature. Such spectral congestion, combined with uncertainties in optical transition energies, further complicates detailed analysis of experimental data and modeling of the energy transfer process in PS I. The exact transition energies have only been measured for the special pair P700 and the primary electron acceptor A_0. The former is characterized by a broad (~30 nm fwhm) absorption band centered at ~700 nm, and the latter has been measured to absorb at ~686 nm and has an absorption bandwidth of ~10 nm (Hastings et al., 1994b; Savikhin et al., 2001). Spectral positions of other Chls have recently been derived using structure-based theoretical simulations (Byrdin et al., 2002; Damjanovic et al., 2002), though these predictions could not be experimentally verified. One of the striking features of all PS I complexes is the presence of a relatively small number of Chls that absorb at energies lower than that of the primary electron donor P700 (Shubin et al., 1991; Wittmershaus et al., 1992; van der Lee et al., 1993; Gobets et al., 1994; Pålsson et al., 1996, 1998; Melkozernov et al., 2000; see Karapetyan et al., this volume, Chapter 13). Although the number of these low energy Chls is small, they have a pronounced effect on the overall energy transfer and trapping process since an energy transfer from these "red" pigments to the primary electron donor P700 occurs uphill and is therefore relatively slow.

The primary charge separation in PS I is followed by a rapid electron transfer step from A_0^- to the secondary electron acceptor A_1^-. The intrinsic rate of this electron transfer step (~0.03–0.1 $psec^{-1}$)is comparable to the antenna lifetime and cannot be directly observed in experiments. The formation of $P700^+A_0A_1^-$ concludes the sequence of events, which can be monitored by ultrafast spectroscopy techniques. The subsequent electron transfer steps occur on a time scale of >10 nsec and will be not addressed in this chapter.

II. Ultrafast Optical Spectroscopy Techniques

During past decades, energy and electron transfer in PS I have been studied by several ultrafast

spectroscopy techniques: pump–probe absorption spectroscopy (Holzwarth et al., 1993; Kumazaki et al., 1994a; Hastings et al., 1994b; Hastings et al., 1995b; Melkozernov et al., 2000; Savikhin et al., 2000; Kumazaki et al., 2001; Savikhin et al., 2001; Müller et al., 2003), single-photon counting (Werst et al., 1992; Holzwarth et al., 1993; Turconi et al., 1993; Pålsson et al., 1995), fluorescence upconversion (Du et al., 1993; Kennis et al., 2001), and synchroscan streak camera techniques (Gobets et al., 2001).

In a typical pump–probe absorption experiment, a short laser pulse (pump pulse) is used to excite one of the pigments (typically Chl) within the PS I complex. As the pigment is promoted into an excited state the absorption spectrum of the whole PS I complex changes, reflecting the optical properties of the excited molecule. The resulting difference between the absorption spectrum before excitation and that after excitation (ΔA) is then probed as a function of wavelength and time by a second light pulse (probe pulse). When the excitation energy is transferred between spectrally distinct molecules or is trapped, the dynamics of this process is reflected in the dynamics of the ΔA signal. There are three major contributions to the absorption difference signal when a molecule is excited: photobleaching (PB) of the original absorption spectrum of the excited molecule, excited state absorption (ESA) that arises from the transitions in the excited molecule to higher excited states, and stimulated emission (SE) due to the stimulated transition from the excited state to the ground state of the excited molecule. These three components of the ΔA signal are superimposed on each other and, in general, cannot be measured independently in a pump–probe experiment. The time resolution of a modern ultrafast pump–probe spectrometer is determined only by the duration of the laser pulse and can be better than 100 fsec—a resolution sufficient to resolve a single-energy transfer step in PS I. The sensitivity of the ΔA signal to both the ground and excited state populations allows not only detection of excitation energy transfer dynamics, but also electron transfer kinetics which involve optically visible cofactors such as P700, A_0, and phylloquinone A_1 (the latter has a distinct absorption band at ~380 nm). However, the primary electron transfer steps occur within the same time range as excitation energy transfer processes, and separating the signals due to the different processes is not straightforward.

Single-photon counting, fluorescence upconversion, and synchroscan streak camera techniques all detect transient fluorescence and therefore can monitor only the dynamics of optically active excited states. The main difference between these methods lies in their light sensitivity and time resolution. Single-photon counting and the synchroscan streak camera can both work with very low fluorescence intensities, but their time resolution is limited to ~10 and ~1 psec, respectively. In contrast, fluorescence upconversion techniques can deliver time resolution better than 100 fsec, but have poor light sensitivity due to the non-linear process utilized in the detection scheme.

A single PS I complex contains a coupled network of 96 Chls. Under natural sunlight intensities, a single Chl molecule gets excited less than 10 times per second, and there is never more than one excitation at a time in a single PS I complex. Creating two or more excitations in a PS I complex in experiments utilizing short laser pulses may lead to an effect called singlet–singlet annihilation (van Grondelle, 1985; Valkunas et al., 1995b; Gobets and van Grondelle, 2001), which can seriously distort experimental data. Due to efficient energy transfer, two excitations can collide at a single chlorophyll, promoting it to its second excited state. The following rapid internal conversion to the lowest excited state effectively quenches one of the excitations, adding a nonphysiological component to the measured signal. Alternatively, even if one of the excitations is trapped in a normal way and initiates electron transfer, the oxidation of P700–$P700^+$ effectively closes the normal physiological trapping path for the second excitation, resulting in similar artifacts in the measured transient signal. It was shown, for example, that under intense excitation conditions when 4–8 excitations were created per a single PS I complex, annihilation shortened the natural excitation lifetime in the antenna from 20–30 to 4–5 psec (Hastings et al., 1994b). Due to the probabilistic nature of the excitation process, it is not sufficient to simply match the number of absorbed photons to the number of complexes in the same volume. One can easily show that the ratio of excitations in multiple excited complexes to the total number of excitations is given by $n_{\mathrm{mult}}/n_{\mathrm{tot}} = 1 - (1 - p)^{N-1}$, where $N = 96$ is the number of molecules in a single complex, and p is the absolute fraction of excited Chl molecules. In the case of $p = 1/96$ (i.e., one excitation is created per single complex on average), the fraction of multiple excitations contributing to annihilation artifacts is 63%. To keep this fraction below 10%, each laser shot should excite not more than one out of ~10 PS I complexes. In practice, this implies that excitation pulse energies must be of the order of a *nJ* and the detection system should be capable of detecting absorption changes ΔA smaller than 10^{-3}.

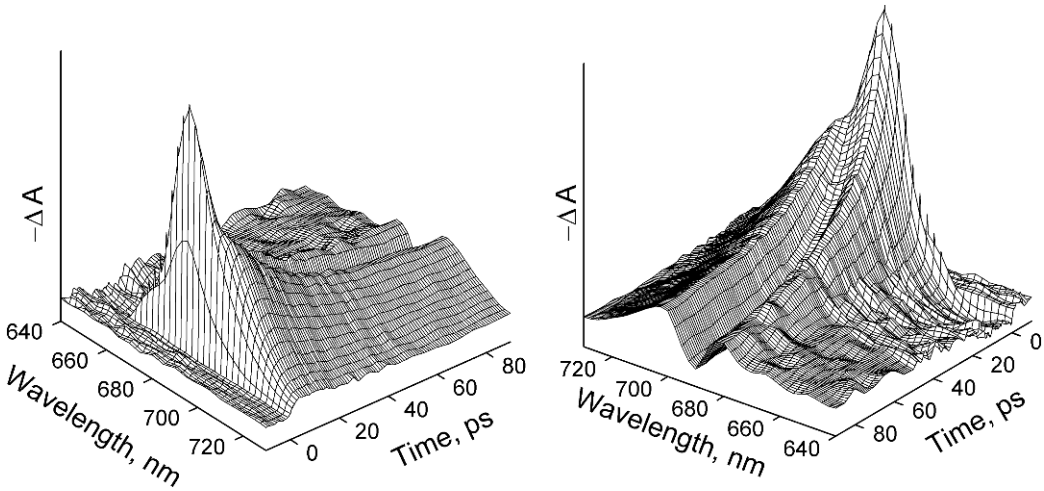

Fig. 4. Two different perspectives of ΔA versus time and wavelength surfaces for PS I core complexes from *Synechocystis* sp. measured at room temperature upon excitation at 660 nm.

Excitation trapping in the PS I complex switches the special pair from the neutral P700 state to the oxidized $P700^+$ state, often referred to as the open and closed states of the RC (or PS I), respectively. When the RC is in a closed state, the normal charge separation function of PS I is disrupted and electronic excitation in the PS I antenna is quenched by a nonphysiological process. To avoid this, sufficient time must be allowed between the consequent excitation pulses to ensure full recovery of the RC to its open state, or, alternatively, a sample should be physically circulated through the laser beam rapidly enough to ensure that every light pulse excites fresh complexes with open RCs. It has been shown that recombination between $P700^+$ and the reduced terminal acceptor $[F_A/F_B]^-$ occurs within 45 msec (Hiyama and Ke, 1971). However, after each excitation, a fraction of electrons on the terminal electron acceptors are scavenged from the PS I complexes (Diaz-Quintana et al., 1998) before recombination can occur, and in the absence of an external reductant, all PS I complexes soon switch to the closed RC state and can remain in that state for hours. Addition of 20 mM of sodium ascorbate provides an alternative channel for $P700^+$ reduction through direct electron donation from ascorbate, which occurs with 120 sec kinetics (Savikhin et al., 2001). Addition of 150 μM phenazine methosulfate along with the ascorbate further shortens this reduction time to ∼2 msec (Byrdin et al., 2000), limiting the excitation pulse repetition rate to <500 Hz for static samples. Higher laser pulse repetition rates require the use of spinning samples (Savikhin et al., 1993) or flow cells and allow pulse repetition rates in the range of 1 – 100 kHz, resulting in higher sensitivity of the experimental setup.

III. Ultrafast Spectroscopy of PS I Core Complexes

Figure 4 shows the three-dimensional plot of ΔA measured by optical pump–probe techniques for PS I core complexes from *Synechocystis* sp. PCC 6803 at room temperature as described in detail in (Savikhin et al., 2000). The ΔA signals were inverted to ease visual perception of the three-dimensional surface. In this experiment, PS I trimeric complexes were excited by ∼100 fsec long pulses into the blue edge of Q_y absorption band at 660 nm (Fig. 3), and the absorption changes were probed by a second ∼100 fsec pulse across the entire PS I Q_y absorption band as a function of the time delay between pump-probe pulses. The initial PB signal created by excitation at 660 nm rapidly (<1 psec) transforms into a strong PB maximum at ∼685 nm, which roughly corresponds to the PS I absorption maximum in the steady-state spectrum (Fig. 3) and is an indication of a rapid subpicosecond excitation energy transfer to the most numerous Chl *a* pigments, which absorb in this spectral region. The time-dependent ΔA signals probed at wavelengths above 700 nm maximize ∼3 psec after initial excitation, reflecting much slower energy transfer to red-most Chl pigments. The slow kinetics of the latter process is a natural consequence of a small number of red-most Chls—many single-transfer steps are required before excitation can “find” those

pigments. Excitation equilibration is essentially complete a few psec after excitation and the subsequent changes in ΔA signal reflect the excitation energy trapping by the special pair and the formation of the $P700^+$ state. At times >50 psec after excitation the energy transfer and charge separation processes are essentially complete with an electron residing on phylloquinone A_1, the ΔA signal at its residual value and its spectral shape mimicking that of the ($P700^+ - P700$) difference spectrum shown in Fig. 3. Since phylloquinone and iron sulfur cluster do not absorb in the Q_y region of Chl, the consequent nanosecond electron transfer from A_1 to F_X is not expected to directly induce any changes in the time-dependent ΔA signals. However, noticeable nanosecond-scale changes in ΔA signals have been recently detected (Savikhin et al., 2001) and attributed to an electrochromic shift of the absorption bands of a few antenna Chls in the changing electric field of the extra electron moving from A_1 to F_X (Dashdorj et al., 2004).

The ΔA dynamics measured in pump-probe experiments is a result of tens or even hundreds of individual energy transfer steps (hops). A detailed model of energy transfer would require consideration of $\sim 10^4$ energy transfer channels between all possible excitation donor-acceptor pairs formed from PS I antenna Chls. It would be impossible to extract reliable information about every single-energy transfer step from the measured ΔA profiles. Instead, the kind of data shown in Fig. 4 is often analyzed in terms of decay-associated spectra (DAS). In this analysis, the experimental time-dependent ΔA slices at all wavelengths are fitted globally with a small number of exponential components. The decay times τ_i (or rates $k_i = 1/\tau_i$) for each component are assumed to be wavelength-independent, while the amplitudes A_i are optimized independently for each individual time-dependent ΔA profile and the data is fitted using the following equation:

$$\Delta A(\lambda, t) = \sum_{i=1}^{N} A_i(\lambda) e^{-\frac{t}{\tau_i}}, \qquad (1)$$

where λ is the probe pulse wavelength, and N is the number of decay components used to fit the data. In this model, each decay component is characterized by a unique wavelength dependent DAS $A_i(\lambda)$.

Figure 5 shows DAS obtained by global analysis of the pump–probe data presented in Fig. 4 (Savikhin et al., 2000). A good fit to the time-dependent profiles at all wavelengths could be obtained with a set of only four exponential components with decay times 530 fsec, 2.3 psec, 23.6 psec and a slow >1 nsec component that could not be resolved in the 200 psec time frame of the experiment.

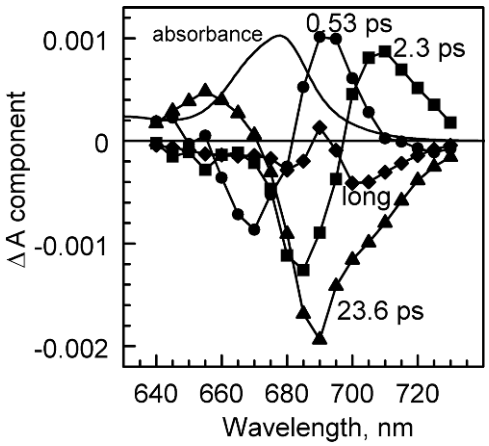

Fig. 5. Decay-associated spectra (DAS) from global analysis of the data shown in Fig. 4: 0.53 psec ( ), 2.3 psec ( ), 23.6 psec ( ), and long component ( ). The solid positive line with no symbols represents scaled down steady-state absorption spectrum of PS I for a reference (Savikhin et al., 2000).

A. Excitation Energy Equilibration in the PS I Antenna

1. Subpicosecond Equilibration Among Bulk Chls

The 530 fsec DAS (Fig. 5) has a negative amplitude at ~670 nm, which represents a PB/SE decay and reflects the decrease of excited Chl *a* molecules absorbing at the blue edge of the PS I absorption band. This decay is mirrored by a PB/SE rise occurring at ~690 nm that has the same absolute amplitude and kinetics and represents a simultaneous increase in the number of excited Chl molecules absorbing at longer wavelengths. Such sigmoidal DAS is a typical signature of a downhill energy transfer. Thus, the 530 fsec component arises from spectral equilibration between bulk Chl forms absorbing at ~670 and those absorbing at ~690 nm. A similar subpicosecond energy equilibration component of 360–500 fsec has been revealed by several groups using pump–probe spectroscopy (Melkozernov et al., 2000; Gibasiewicz et al., 2002), as well as fluorescence upconversion (Kennis et al., 2001) for PS I core complexes from *Synechocystis* sp., *Synechococcus elongatus* and *Chlamydomonas reinhardtii*. Recently, Müller et al. (2003) performed a global analysis of the data similar to the one shown in Fig. 4 for PS I core complexes from *C. reinhardtii* in terms of a lifetime density map with the number $N = 70$–100 in Eq. (1) (Croce et al., 2001), and found that it revealed two subpicosecond

components (300 and 800 fsec) in the initial energy equilibration dynamics.

Since the individual energy transfer hops are predicted to be in the order of 100–200 fsec, the observed 300–800 fsec equilibration requires in average 2–8 elementary energy transfer steps. Inability to distinguish a shorter component in isotropic experiments indicates that the first energy transfer step occurs predominantly between Chl molecules with similar optical properties (i.e., with similar absorption and emission spectra) and therefore does not lead to detectable spectral changes in ΔA or fluorescence signals. However, energy transfer between spectrally equivalent molecules with drastic orientations of optical transition moments could be revealed by studying the time-dependent anisotropy $r(t)$ of ΔA or fluorescence signals after exciting a sample using polarized light pulses:

$$r(t) = \frac{S_{||}(t) - S_{\perp}(t)}{S_{||}(t) + 2S_{\perp}(t)}, \tag{2}$$

where $S_{||}(t)$ and $S_{\perp}(t)$ are ΔA or fluorescence signals detected with light polarization parallel or perpendicular to that of the excitation pulse. Using anisotropic fluorescence upconversion techniques the single step transfer in the PS I core antenna complex was measured to be between 100 and 200 fsec (Du et al., 1993; Kennis et al., 2001). The presence of a similar fast component in pump–probe anisotropies at 680 nm was also indicated in (Savikhin et al., 1999b), but the decay time of that component was not quantified.

2. Picosecond Equilibration with Red Chl Forms

The 2.3 psec DAS (Fig. 5) has a bimodal shape similar to the 530 psec DAS and is attributed to the energy equilibration between the bulk Chls and the "red" Chls absorbing at ~710 nm. It is no surprise that energy transfer to these Chls takes so long as their number is small and 10–20 single-energy transfer hops are required for the excitation to "find" a red Chl.

The number of red Chl forms in PS I complexes and their spectral positions have been found to be species-dependent (Shubin et al., 1991; Wittmershaus et al., 1992; van der Lee et al., 1993; Gobets et al., 1994, 2001; Pålsson et al., 1996). This leads to a wide spread of picosecond energy equilibration times resolved for PS I complexes in different organisms. There is no clear agreement on the number of red Chl forms in PS I complexes from *Synechocystis* sp. Gobets et al. proposed that there is only one red form absorbing at 706 nm (Gobets and van Grondelle, 2001; Gobets et al., 2001). This is consistent with the single red absorption band observed in low-temperature steady-state absorption spectra of PS I complexes (Rätsep et al., 2000; Gobets et al., 2001) as well as with the single 2.3 psec DAS component (Fig. 5) associated with energy equilibration between bulk and red antenna Chls. A similar single-energy equilibration component of 2–5 psec was reported by several groups using various ultrafast optical techniques (Hastings et al., 1995b; Turconi et al., 1996; Melkozernov et al., 2000; Gobets et al., 2001). However, hole burning experiments performed by Hayes et al. (2000) suggested the presence of two distinct red Chl spectral forms absorbing at 706 and 714 nm, respectively. Savikhin et al. (1999b) also reported the presence of two energy equilibration components (2 and 6.5 psec) in DAS of PS I complexes. However, the latter results were obtained on PS I complexes with closed reaction centers, and the presence of the second energy equilibration component was not confirmed in the later experiments on complexes with open RCs (Savikhin et al., 2000).

A single-energy equilibration component of ~2 psec was also recently reported for PS I complexes from *C. reinhardtii* (Gibasiewicz et al., 2002; Müller et al., 2003). The absorption spectrum of PS I complexes from *C. reinhardtii* shows the least content of red Chls as compared to the PS I complexes from other species (Gibasiewicz et al., 2002).

PS I complexes from *Synechococcus elongatus* and *Spirulina platensis* each, exhibit two distinct forms of red Chls (Gobets et al., 2001) and as a result two different equilibration components were observed, with lifetimes ~4 and 10–15 psec (Gobets et al., 2001; Kennis et al., 2001).

The rate of energy equilibration between the bulk antenna Chls and the red Chl forms is clearly dependent on the energy gap between excited states of the antenna and that of the red Chls—larger energy gaps lead to slower equilibration times. The longest equilibration time of 15.1 psec was reported for the *Spirulina platensis* trimeric core complex (Gobets et al., 2001), which contains red Chls absorbing at wavelengths as far as 740 nm. Equilibration with the 708 nm Chl spectral forms in the same complexes occurs within 4.3 psec. This trend is qualitatively consistent with the Förster energy transfer theory, which predicts lower transfer rates as the spectral overlap between donor and acceptor molecules decreases.

B. Excitation Energy Trapping

The shape of the 23.6 psec DAS (Fig. 5) is consistent with the overall decay of a population of excited Chls in PS I antenna caused by excitation trapping at

the reaction center and the formation of $P700^+$ as a result of charge separation. While the 23.6 psec DAS exhibits considerable PB/SE decay amplitude in the red antenna Chl spectral region (>700 nm), it also shows an intense signal at 680–690 nm, overlapping the positive segments of 530 fsec and 2.3 psec DAS. Bulk → red antenna transfers are thus not irreversible; a dynamic equilibrium is reached among the red Chl forms and the bulk antenna. Similar conclusions have been reported by other groups (e.g., Owens et al., 1988; Holzwarth et al., 1990; Werst et al., 1992; Hastings et al., 1995a).

The excitation trapping time was shown to be species-dependent. A trapping time of 20–25 psec was measured for PS I complexes from both *Synechocystis* sp. and *C. reinhardtii* (Hecks et al., 1994; Hastings et al., 1994a; DiMagno et al., 1995; Hastings et al., 1995b; Turconi et al., 1996; Gobets et al., 1998b, Melkozernov et al., 1998a, 2000; Savikhin et al., 2000; Gobets and van Grondelle, 2001; Gobets et al., 2001; Gibasiewicz et al., 2002). A somewhat longer trapping time of 30 psec was reported by Melkozernov et al. (1997) for *C. reinhardtii*. PS I complexes from *Synechococcus elongatus* exhibit trapping times of 30–38 psec (Holzwarth et al., 1993; Byrdin et al., 2000; Gobets et al., 2001; Kennis et al., 2001). The longest energy trapping times of 38–69 psec have been observed in PS I core complexes from *Spirulina platensis* (Karapetyan et al., 1997; Gobets et al., 2001). The increase in energy trapping time in these species correlates with the increased content of red Chl forms combined with the larger spectral shifts of these forms with respect to the energies of the bulk Chls and is consistent with the Förster energy transfer theory.

The validity of the 20–25 psec component assignment to the energy trapping process in *C. reinhardtii* (and perhaps in other species) was recently questioned by Müller et al. (2003). In this work, the authors used a pump–probe technique to obtain data similar to those shown in Fig. 4, but extended the range of probe wavelengths up to 760 nm and analyzed the data in terms of a lifetime density map. The analysis revealed a new component at 6–9 psec which is especially pronounced at wavelengths above 720 nm, and a longer component of ∼20–30 psec similar to the one conventionally assigned to the energy trapping process. The authors proposed that the newly discovered 6–9 psec component is the dominant energy trapping time due to charge separation, and that the longer lifetime represents the consequent electron transfer process, and not trapping as suggested by earlier papers. The new data also suggest that the conventional electron transfer sequence needs to be revised and a new intermediate radical pair state introduced into the kinetic model (see sections "C" and "V" below for further discussion). The new energy/electron transfer kinetic model is intriguing but its validity still needs to be tested by independent experiments.

The DAS of the long >1 nsec component (Fig. 5) represents the $P700^+$ state that is formed as a result of energy trapping and that has a lifetime many orders of magnitude longer than the time window span covered by ultrafast optical experiments. This DAS coincides with a ΔA spectrum measured at a fixed 200 psec delay and is almost superimposable on the steady-state spectrum of the ($P700^+ - P700$) difference spectrum shown in Fig. 3. Slight differences between the steady-state ($P700^+ - P700$) and the ΔA spectrum measured at a fixed 200 psec delay as observed in (Savikhin et al., 2001) were explained by the presence of the electric field of an extra electron, which still resides on the secondary electron acceptor A_1 200 psec after excitation and causes a slight electrochromic shift of the absorption bands of the Chls positioned near A_1 (Dashdorj et al., 2004).

High quantum efficiency of the photosynthetic process implies that the main excitation quenching mechanism in PS I is charge separation initiated when the electronic excitation reaches the special pair. Once charge separation is complete, the special pair switches into its closed (or oxidized) $P700^+$ state and one should expect the excitation lifetime in the antenna to increase substantially (up to the free Chl fluorescence lifetime of ∼4.5 nsec) as the physiological quenching mechanism by charge separation would be blocked. However, extensive evidence suggests that the antenna kinetics are essentially unaffected by the P700 oxidation state (Nuijs et al., 1986; Shuvalov et al., 1986; Owens et al., 1988; Klug et al., 1989; Holzwarth et al., 1993; Turconi et al., 1993; Hastings et al., 1994b; Dorra et al., 1998; Savikhin et al., 2000), and only a slight change in fluorescence quantum yield and fluorescence lifetime for the PS I complex in the closed state was observed (Ikegami, 1976; Telfer et al., 1978; Trissl, 1997; Byrdin et al., 2000). On this basis, the oxidized electron donor $P700^+$ is widely considered to be as good a quencher as the reduced donor P700, although neither the reason nor the physiological significance for this are yet understood. The similarity of antenna kinetics in open and closed PS I complexes opens the unique possibility of comparing the dynamics of excitation in two well-defined redox states of P700, and this strategy has been used by several groups to obtain important information on various aspects of the energy and electron transfer (Shuvalov et al., 1986; Hastings et al., 1994b; White et al., 1996; Byrdin et al., 2000; Savikhin et al., 2001).

Excitation energy trapping by photosynthetic reaction centers is often discussed in terms of "diffusion-limited" or "trap-limited" models (Amesz and Neerken, 2002). In the case of the diffusion-limited model (also called transfer-to-trap-limited model) the rate of trapping is determined only by the rate of diffusion of the excitation energy through antenna pigments to the trap (reaction center), which will only occur if the trap is fully irreversible, i.e., excitation, once transferred to the trap, will not be able to escape back to the antenna. In contrast, the trap-limited model implies that the reaction center is visited by an excitation several times before trapping occurs and the rate of trapping would therefore depend primarily on the trap efficiency.

There is currently no clear agreement on the classification of energy trapping in PS I complexes. On the basis of experimental data and kinetic modeling, several groups argued that the excitation-trapping process in PS I complexes is essentially trap-limited (Holzwarth et al., 1993; Turconi et al., 1993; Hastings et al., 1994a; Kumazaki et al., 1994b; Laible et al., 1994, White et al., 1996; Melkozernov et al., 1997; Beddard, 1998; Dorra et al., 1998). To test the dependence of the energy-trapping rate on the trap efficiency, Melkozernov et al. (1997, 1998b) introduced a site-specific substitution of His-656 residue of PsaB subunit for Asp in the PS I core complexes from *C. reinhardtii*. According to the X-ray structure, the His-656 residue is an immediate ligand to one of the Chls in the special pair and its substitution leads to an increase in redox potential of P700 (Webber et al., 1996) and a change in the P700 photooxidation spectrum. The change in redox potential could cause a decrease in the free energy gap between the primary donor excited state P700* and the primary charge separated state $P700^+A_0^-$, resulting in lower trap efficiency (slower intrinsic charge separation rate). The authors observed the doubling of trapping time in the mutant (~65 psec) as compared to that in wild type PS I, which is consistent with the trap-limited model of energy transfer. However, due to spectral congestion, direct measurement of the intrinsic charge-separation rate in PS I is a challenging task, and one cannot exclude the possibility that the slow excitation trapping rate observed in the mutant may have been caused by the decreased spectral overlap of the primary electron donor P700 with the surrounding antenna.

Back-transfer of excitation from P700* to the antenna is also an indicator of a trap-limited process and has been reported by several groups. White et al. (1996) excited PS I complexes from higher plants at 708 nm in an attempt to create the P700* state directly and observe the consequent formation of $P700^+$, but were forced to conclude that energy transfer from P700* to the antenna is faster than the intrinsic primary charge separation time, which was estimated to be ~1.3 psec. Kumazaki et al. (1998, 2001) studied PS I complexes from higher plants containing only 12–13 Chls per special pair, with the majority of the antenna Chls removed chemically. Both fluorescence upconversion and absorption pump–probe experiments indicated that at least half of the excitations created initially on the special pair escape into the remaining pool of antenna Chls instead of being trapped by the charge separation process. The intrinsic charge-separation time was estimated to be ~1.3–2 psec, while the excitation back-transfer component of ~0.3 psec was observed in fluorescence upconversion experiments (Kumazaki et al., 1998), and an even shorter ~0.1 psec process was detected in the later study using absorption pump–probe techniques (Kumazaki et al., 2001). However, the latter 0.l psec process could be caused by coherent nuclear vibration of P700*, and the presented pump–probe data was in general more consistent with the back-transfer rate being almost equal to the intrinsic charge separation rate. It should be noted here that chemically treated PS I complexes are not equivalent to native complexes, as the removal of a significant number of antenna Chls would necessarily alter the dynamics of the energy equilibration process between antenna Chls and the special pair and may also lead to structural damage of these pigment–protein complexes.

The independence of the effective excitation trapping time on the excitation wavelength (see, e.g., Pålsson et al., 1998; Melkozernov et al., 2000) is also indicative of the trap-limited description of excitation dynamics in PS I.

An alternative transfer-to-trap-limited model of energy trapping in PS I was proposed by several groups (van Grondelle et al., 1994; Valkunas et al., 1995a; Croce et al., 1996; Jennings et al., 1997; Trissl, 1997; Gobets et al., 1998a,b; Pålsson et al., 1998). The transfer-to-trap-limited model implies that while Boltzmann equilibration within the antenna is reached, there is no equilibrium between the antenna and the RC. As a criterion for the Boltzmann equilibrium, the so-called Stepanov–Kennard relation was applied to study the extent of thermal equilibration in PS I-200 particles from higher plants (Croce et al., 1996; Jennings et al., 1997). It was found that the fluorescence yield observed in the experiment was lower than calculated according to the Stepanov–Kennard relation. This was interpreted as an indication that the excitation is trapped by the RC faster than excitation equilibration can be established. However, care should be taken when applying these

results to the core complexes as the PS I-200 particles still contain the outer light-harvesting antenna complex (LHCI), which slows down the overall trapping process. Pålsson et al. (1998) used a similar thermalization approach to study PS I core complexes from *Synechococcus elongatus* and suggested that at low temperatures the rate of primary charge separation is much faster than the back-transfer of the excitation energy from P700* to the neighboring antenna pigments. They also proposed that at room temperature ~50% of photochemical trapping might occur from the red pigments to P700, in which case the latter energy transfer process would represent a bottleneck process. Gobets et al. (1998a,b) modeled time-resolved fluorescence data obtained for PS I core complexes from *Synechococcus elongatus* and *Synechocystis* sp. and suggested that the slow energy transfer from the red pigments located on the periphery of the complex limits the trapping.

Drastically different conclusions reached by various groups on the classification of energy transfer process in PS I complexes are based on essentially similar experimental data. The key factor preventing unanimous agreement in the interpretation of the experimental data is the complexity of the system. Even though the structure of PS I has been determined to high precision, the spectral positions of most of the Chls constituting the PS I antenna are unknown and modeling includes a lot of guessing. Moreover, the measured optical signals are caused by a mixture of many energy (electron) transfer steps, occurring concurrently, and extracting individual (intrinsic) kinetic parameters becomes tricky. It is very possible that energy trapping in PS I is neither of the extreme cases discussed above, but rather an intermediate case where both excitation energy diffusion from the antenna to the special pair and the intrinsic charge separation rate influence the energy trapping in a balanced way (Trinkunas and Holzwarth, 1996; Holzwarth et al., 1998; Karapetyan et al., 1999; Byrdin et al., 2000, 2002).

Trinkunas and Holzwarth (1996) analyzed the available experimental fluorescence data using a genetic algorithm and various kinetic models and reported that the data were inconsistent with both purely transfer-to-trap- and purely trap-limited models. For PS I complexes from *Spirulina platensis*, a new model was suggested with nearly trap-limited excitation transfer from bulk antenna to P700 and a diffusion-limited excitation transfer from the red Chl pools via the bulk antenna (Holzwarth et al., 1998; Karapetyan et al., 1999).

Byrdin et al. (2000) used the latest 2.5 Å structure of PS I (Jordan et al., 2001) to build a detailed model that would reproduce static optical properties of PS I complexes from *Synechococcus elongatus* (steady-state absorption, linear, and circular dichroism) along with excitation transfer and trapping dynamics observed experimentally. The model predicts that electronic light excitation visits P700 an average of six times before being trapped photochemically and creating a charge separated state. Therefore, the overall energy trapping rate must depend on the trap efficiency. Indeed, the two-fold increase or decrease in the intrinsic charge separation rate in respect to its original value of 0.87 psec^{-1} resulted in 23 and 56 psec trapping lifetimes instead of the original 34 psec. On the other hand, similar variations in the Förster parameter R_0, which governs excitation energy transfer rate between Chls, rendered lifetimes of 28 and 45 psec. The authors concluded that the antenna excited state decay lifetime (and trapping) depended on all key parameters of the model—the intrinsic charge separation rate, the transfer-to-the trap rate, and the transfer rate between individual antenna Chls—and that the excited state dynamics is neither pure trap-limited, nor pure transfer-to-trap-limited.

C. Charge Separation and Electron Transfer Kinetics

When discussing the dynamics of charge separation and consequent electron transfer processes in a photosynthetic system, it is important to clearly differentiate between the "effective" transfer rates and the "intrinsic" rate constants. To avoid possible ambiguity, we will adhere to the terminology defined in (Gatzen et al., 1996; Müller et al., 2003). The term "intrinsic rate constant for electron transfer" will be used exclusively to denote the kinetic rate of an individual electron transfer step from a particular electron donor molecule to a particular acceptor molecule in the assumption that all other transfer processes are blocked. The "effective rate constant" (sometimes referred to as "apparent rate constant") is defined as the rate at which a certain redox state is populated (or depopulated). Thus, the energy trapping time of 20–65 psec observed in experiments as the decay of antenna excitation is equivalent to the *effective* charge separation time (time = 1/rate), since excitation trapping leads to the creation of the radical pair(s) and is a consequence of many individual energy transfer steps followed by a single electron transfer step. In contrast, the *intrinsic* charge separation time in PS I represents the kinetics of charge separation in the case when excitation is created directly on P700 and back-transfer from P700 to the antenna, as well as charge recombination are blocked. Since for the PS I complex the described conditions cannot be achieved, the intrinsic

rate constant cannot be directly observed in experiment and is usually obtained via model simulations.

There is unanimous agreement that the intrinsic charge separation rate in PS I RC is much faster than the observed effective excitation trapping rate. Most of the studies put the intrinsic charge separation step in PS I RC in the 0.5–3 psec time range, and the consequent electron transfer from primary electron acceptor A_0 to the secondary electron acceptor A_1 is believed to occur in 10–50 psec (Brettel and Leibl, 2001). However, the precise measurement of these important kinetic parameters presents a challenging problem. Isolation of the RC cofactors from PS I is impossible as the two main protein subunits PsaA and PsaB that coordinate the cofactors also bind most of the antenna Chls. The presence of antenna pigments and spectral congestion among reaction center cofactors precludes selective excitation of P700 and complicates the isolation of the optical signals arising from the electron transfer process from the signals stemming from the excitation energy transfer.

Kumazaki et al. (1994a,b, 2001) tried to minimize the contribution of antenna processes to the measured transient absorption and fluorescence signals by chemical treatment of PS I complexes from spinach that removed most of the antenna Chls from complexes, leaving only 12–14 Chls per P700. Due to the small amount of antenna Chls, preferential excitation of P700 became possible. The authors found that the effective primary charge separation kinetics in these complexes could be described by two components of equal amplitudes with time constants of 0.8 ± 0.1 and 9 ± 1 psec (Kumazaki et al., 2001). The short 0.8 psec component was ascribed to the formation of the charge separated state generated directly from the initially excited P700*, and the relatively slow 9 psec component was assumed to stem from excitations which escaped from P700* to the surrounding pigments and were recaptured at later times. A kinetic model revealed that the observed data could be reproduced with an intrinsic charge separation time of 0.5–0.8 psec.

Several groups (Nuijs et al., 1986; Shuvalov et al., 1986; Wasielewski et al., 1987; Hastings et al., 1994b; Kumazaki et al., 1994b; White et al., 1996; Savikhin et al., 2001) proposed a strategy for isolating the reaction center kinetics by obtaining time-resolved absorption difference profiles for PS I core complexes with open and closed reaction centers. Since extensive experimental evidence suggests that the antenna kinetics are unaffected by the P700 oxidation state, the difference $\Delta\Delta A$ between absorption difference profiles for open and closed RCs ($\Delta\Delta A = \Delta A_{\text{openRC}} - \Delta A_{\text{closedRC}}$) should isolate the electron transfer processes, since they occur only in complexes with open RCs. Hastings et al. (1994b) applied this method to study PS I complexes from *Synechocystis* sp. The experimental $\Delta\Delta A$ profiles probed at 686 nm exhibited an initial PB rise feature of ~4 psec followed by ~21 psec PB decay. This probe wavelength corresponds to the maximum position of the A_0 absorption band, and the observed kinetics were attributed to the formation and decay of the A_0^- state. The authors concluded that the ~4 psec rise represented the effective energy-trapping time, which was significantly shortened as a result of annihilation caused by the use of high-excitation pulse intensities, and that the 21 psec component characterized the intrinsic rate of the $A_0 \rightarrow A_1$ electron transfer step. Savikhin et al. (2001) have further extended this method and studied annihilation-free $\Delta\Delta A$ profiles probed in a wide spectral range with significantly lowered noise levels (Fig. 6). Assuming that all of the antenna kinetics were canceled by the (open-closed) subtraction procedure, the shown $\Delta\Delta A$ profiles should reflect the formation and decay dynamics of only three states:

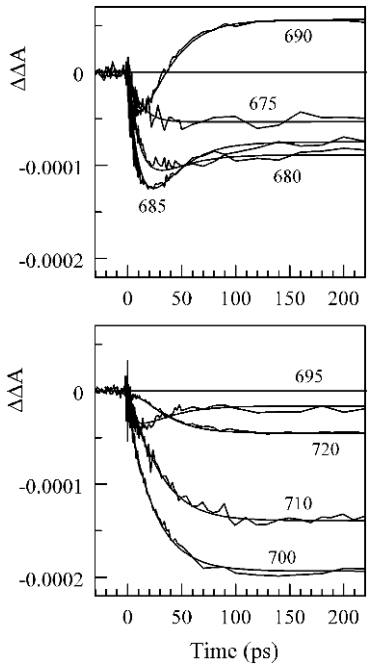

Fig. 6. Time-resolved (open-closed) absorption difference profiles for PS I complexes from *Synechocystis* sp. excited at 660 nm and probed at specified wavelengths. Noisy curves are experimental. Smooth curves are the results of global fit with only two free parameters – intrinsic charge separation and first electron transfer step times; all amplitudes were fixed as described in (Savikhin et al., 2001).

$P700^*A_0A_1$, $P700^+A_0^-A_1$, and $P700^+A_0A_1^-$. Using a simple sequential model of electron transfer, all of the curves shown in Fig. 6 were fitted globally with only two free parameters, resulting in the intrinsic times for charge separation and the following $A_0 \rightarrow A_1$ electron transfer step of 1.3 and 13 psec, respectively. White et al. (1996) applied a similar approach to study dynamics of electron transfer process in PS I complexes from spinach. Using simple models of energy migration, the intrinsic rates of charge separation and primary electron transfer step were estimated to be 1.4 and 20 psec, respectively. It was also found that even when the femtosecond pulses were tuned to preferentially excite P700, only a small fraction of the initially excited P700* led to the charge separated state while the rest of the excitations escaped to the antenna.

The formation and decay kinetics of A_1^- can be monitored directly in its broad near-UV absorption band around 380–390 nm (Brettel et al., 1986; Brettel, 1988; Lüneberg et al., 1994; Brettel and Vos, 1999). At this probe wavelength, Brettel and Vos (1999) observed ΔA transient for *Synechocystis* sp., which could be described by two exponentials with time constants of 7 and 28 psec. The shorter component was attributed to the antenna processes presumably accelerated by an annihilation artifact due to high excitation levels, and the longer component was interpreted as the intrinsic time of $A_0 \rightarrow A_1$ electron transfer step. However, the observed build-up of the A_1^- state was probably delayed by the preceding antenna equilibration and charge separation steps and the reported 28 psec time is likely to be an overestimate. While annihilation phenomenon shortens the antenna excitation lifetime, it also precludes precise measurement of the effective trapping time, since the observed antenna excitation decay is not caused by merely charge separation process anymore. To avoid complications arising from annihilation processes, we performed a similar experiment under low excitation levels. Figure 7A (upper line) shows ΔA kinetics probed at 390 nm after exciting open PS I complexes at 660 nm (N. Dashdorj and S. Savikhin, unpublished). The measured annihilation-free pump–probe profile could be described with a single PB exponent with a time constant of 30 ± 3 psec followed by a non-decaying positive component. In the absence of annihilation, the (effective) trapping that precedes $A_0 \rightarrow A_1$ electron transfer step occurs in 23 psec, which implies that the intrinsic $A_0 \rightarrow A_1$ transfer step is significantly faster than the measured 30 psec time constant. Moreover, the 390 nm signal is initially dominated by the photobleaching of the antenna Chl *a* pigments, and the formation and decay of the reduced A_0^- state may also

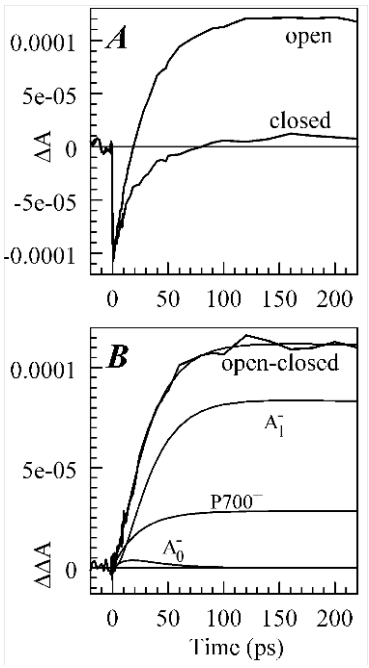

Fig. 7. Time-resolved absorption difference profiles for WT PS I complexes from *Synechocystis* sp. excited at 660 nm and probed at 390 nm. (A) ΔA profiles obtained for PS I complexes with open and closed RCs. (B) Time-resolved (open-closed) absorption difference profile, and the optimized fit to it. Signal contributions due to formation of $P700^+$, A_0^-, and A_1^- are also shown. (Dashdorj et al., 2005)

contribute to the signal. To simplify the analysis, the $\Delta\Delta A$ profile was obtained by subtraction of the ΔA profile for the closed RC from that for the open RC (Fig. 7B). As a result, the early time negative component that stems from excited antenna pigments was canceled (Savikhin et al., 2001), and the resulting profile was fitted using a simple sequential electron transfer model:

$$(\text{Antenna} + P700)^* \xrightarrow{\tau_1} (P700^+A_0^-A_1) \xrightarrow{\tau_2} (P700^+A_0A_1^-)$$

The effective charge separation time τ_1 was fixed at 23 psec (the measured antenna excitation decay time), and a good fit to the data could be obtained with the intrinsic electron transfer time τ_2 varied in the range of 8–15 psec. Similar τ_2 could be obtained by fitting the original unprocessed pump–probe profile for open PS I complexes (Fig. 7A, upper line) and modeling the uncanceled signal contribution due to the antenna excitation decay by a single 23 psec PB component.

The build-up of the positive ΔA signal in the 380–390 nm region upon the formation of $P700^+A_1^-$

observed by Brettel et al. (1999) and our group is, however, not consistent with the picosecond transient absorption measurements by Mi et al. (1999), who reported that the ($P700^+A_1^- - P700A_1$) difference spectrum for *Synechocystis* sp. is negative in this spectral range. The source of this discrepancy is not clear.

A different electron transfer scenario was proposed recently by Müller et al. (2003) on the basis of pump-probe data obtained after exciting PS I complexes from *C. reinhardtii* at 670 and 700 nm. The number of "red" pigments in PS I complexes from these species is small and 700 nm pump pulses excite predominantly P700 dimer directly, while the 670 nm excitation represents the contrasting case when all of the electronic excitations are initially created in the antenna. By comparing pump–probe data measured in these different excitation regimes and analyzing the data in terms of species-associated difference spectra, the authors found that the experimental results could be explained only if one additional radical pair was introduced to the conventional scheme of electron transfer. According to the most probable scenario proposed in the paper, the intrinsic charge separation time is 2.9 psec, which is combined with the backward recombination process with intrinsic time of ~40 psec. Primary charge separation is followed by two fast electron transfer steps with intrinsic times of 13 and 35 psec, respectively, which lead to the formation of $P700^+A_1^-$. The first 13 psec electron transfer step is in good agreement with the result reported by Savikhin et al. (2001), although according to the latter group, the 13 psec transfer step already leads to the formation of $P700^+A_1^-$. Müller et al. (2003) proposed an intriguing possibility that the additional radical pair involves the accessory pigment A_{acc} and that the primary charge separated state may be not $P700^+A_0^-$, but $P700^+A_{acc}^-$ or $A_{acc}^+A_0^-$ (A_{acc} is used to denote one of the accessory Chls, Fig. 2). Formation of the former charge separation state would be reminiscent of the main electron transfer mechanism in the bacterial RC (Woodbury and Allen, 1995).

D. Directionality of Electron Transfer

The presence of two highly symmetrical branches in the RC of PS I raises the question of directionality of the ET in this complex. Evidence for bidirectional ET has mainly been obtained for PS I of eukaryotes such as the alga *Chlorella sorokiniana* (Joliot and Joliot, 1999) and *C. reinhardtii* (Boudreaux et al., 2001; Fairclough et al., 2001; Guergova-Kuras et al., 2001; Muhiuddin et al., 2001), while evidence for more asymmetric electron transfer in PS I has been reported for prokaryotes such as the cyanobacterium *Synechocystis* sp. PCC 6803 (Golbeck et al., 2001; Xu et al., 2003a,b). The conclusions about the electron transfer pathway in PS I are based primarily on studies involving specific mutations around the respective phylloquinone (A_1) binding sites on the PsaA and PsaB polypeptides (Joliot and Joliot, 1999; Boudreaux et al., 2001; Guergova-Kuras et al., 2001; Muhiuddin et al., 2001). The advantage of these mutations is that the spectral and functional changes they induce are so subtle that they do not influence the charge separation. The disadvantage is that the subtle nature of the changes induced by the mutations leaves some ambiguity in the interpretation of the spectral data. Moreover, these experiments have been focusing primarily on the measurements of the changes in the ET kinetics (optical and EPR), which reflect relatively slow nanosecond electron transfer from the A_1 to F_X. In this case, the electron acceptor is common for both branches and the mutational changes around A_1 (which is close to F_X) in one branch can influence the properties of F_X and through that ET kinetics through the other branch.

Recently, Cohen et al. (2004) constructed identical mutations in both the PsaA-side and the PsaB-side at the corresponding A_0 sites modifying the properties of the primary electron acceptor in PS I complexes from *Synechocystis* sp.PCC 6803. In particular, the methionines in $M688_{PsaA}$ or $M668_{PsaB}$ positions were replaced by leucine or asparagine. These methionines are proposed to provide the axial ligands to the respective Mg^{2+} ions of the two A_0 chlorophylls and a change in the ligand would be expected to alter the mid point potential of the A_0^-/A_0 redox pair, causing changes in electron transfer dynamics. Nanosecond optical and EPR experiments revealed significant differences between the PsaA-branch and the PsaB-branch mutants which were more consistent with the assumption that ET occurs primarily along A-branch of the RC (Cohen et al., 2004). These measurements, however, did not have time resolution sufficient to detect changes in the first two electron transfer steps, which directly involve A_0 and would be naturally affected by such point mutations. We have recently performed a series of ultrafast pump–probe experiments on the same samples and supported their findings (Dashdorj et al., 2005). Figures 8A,B show the A_1^- formation dynamics probed at 390 nm for PS I complexes with point mutations in PsaA- and PsaB-branch, respectively, along with the analogous data obtained in native complexes shown previously in Fig. 7. Mutations in PsaB-branch had essentially no effect on electron transfer, while the $A_0 \rightarrow A_1$ electron transfer in PsaA-branch mutants increased

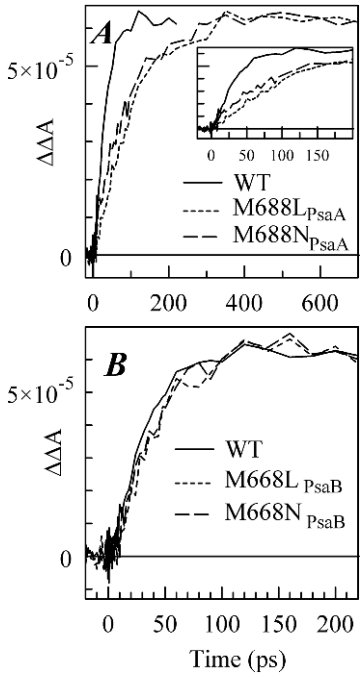

Fig. 8. Time-resolved (open-closed) absorption difference profiles for WT, $M668L_{PsaB}$, and $M668N_{PsaB}$ mutants (A), and for WT, $M688L_{PsaA}$ and $M688N_{PsaA}$ mutants (B). All samples were excited at 660 nm and absorption differences were probed at 390 nm. (Dashdorj et al., 2005)

to ~100 psec. The presented data suggests that in PS I complexes from *Synechocystis* sp., electron transfer preferably occurs along the PsaA-branch of the RC, and that the function of the primary electron acceptor A_0 is served by Chl denoted as eC-A_3 in Fig. 2.

Different results were reported by Ramesh et al. (2004) for PS I complexes from *C. reinhardtii.* These authors introduced branch-specific mutations replacing the methionine residue that provides axial bond to eC-A_3 in the PsaA or eC-B_3 in the PsaB-branch by histidine (see Fig. 2). According to ultrafast pump–probe absorption difference data, the long-lived ($A_0^- - A_0$) difference signal accumulates at ~686 nm in complexes with mutation in either branch, demonstrating that electron transfer between A_0^- and A_1 is blocked or significantly slowed down by this substitution and suggesting that electron transfer occurs along both branches concurrently. These findings support earlier conclusions on bidirectionality of electron transfer in *C. reinhardtii* (Boudreaux et al., 2001; Fairclough et al., 2001; Guergova-Kuras et al., 2001; Muhiuddin et al., 2001).

The contrasting results on directionality of electron transfer may indicate that the electron transfer path in PS I is species-dependent and that relatively small changes in PS I protein structure expected for these organisms may have a significant impact on the details of the electron transfer process.

E. Excitonic Coupling in a PS I Core Complex

The close proximity of pigments to each other in PS I leads to strong excitonic coupling between nearby Chls, altering optical properties of single pigment transitions and further complicating the analysis of transient signals. Excitonic states can be recognized by their distinct signatures in ΔA spectra. Upon excitation into an excitonic band, the early time ΔA spectra typically spread far beyond the excitation pulse bandwidth and exhibit rich spectral structure. Moreover, while the initial anisotropy $r(0)$ of ΔA signals following excitation of an ensemble of single molecules is typically close to 0.4, the $r(0)$ values of excitonic transitions depend strongly on wavelength and may take any value (see the underlying theory in Savikhin et al., 1999a).

It is widely accepted that the close spacing of the two Chls forming P700 leads to excitonic coupling and results in a broad absorption band observed at ~700 nm in ($P700^+ - P700$) spectra (Fig. 3). Gibasiewicz et al. (2002) resolved a highly structured instant ΔA spectrum upon exciting PS I complexes from *C. reinhardtii* at 10 K with 700 nm light pulses that targeted primarily the P700 optical transition. They observed four positive bands accompanied by four negative bands spread over the range of 634–695 nm, far beyond the spectral width of the excitation pulse. The quantity of the observed bands indicated that excitonic coupling spreads over more than just the two pigments forming P700. The observed ΔA spectrum was explained in terms of an excitonic system consisting of all six pigments constituting the RC. For such a system, one should expect six excitonic PB bands combined with 15 excitonic ESA bands and one SE band (Savikhin et al., 1999a). The lower number of the observed features may stem from the low intensity of some of the excitonic transitions and/or overlapping bands.

Savikhin et al. (1999b, 2000) studied PS I complexes from *Synechocystis* sp. by means of the pump–probe technique. Upon exciting complexes at 710 or 720 nm they observed "anomalous" negative initial anisotropies $r(0) \sim -0.5$, which suggest the presence of mutually orthogonally polarized components near ~718 and 680 nm, suggesting that the red-most Chl antenna transition(s) arise from two (or more) strongly coupled Chls. This interpretation is in line with hole-burning experiments (Hayes et al., 2000;

Rätsep et al., 2000; Zazubovich et al., 2002), Stark effect measurements (Frese et al., 2002), and fluorescence line-narrowing studies (Gobets et al., 1994). Several strongly coupled pairs have been proposed to serve as the red-most pigments based on the available X-ray structure (Jordan et al., 2001; Byrdin et al., 2002; Damjanovic et al., 2002; Dashdorj et al., 2004).

IV. Ultrafast Spectroscopy of PS I–LHCI Supercomplexes

In plants and green algae, the PS I core complex is surrounded by the Chl *a*/*b* containing light-harvesting complex (LHC) I that serves as peripheral antenna, increasing the efficiency of the system by capturing additional light and guiding its energy to the PS I core complex antenna (Gobets and van Grondelle, 2001; Melkozernov, 2001; Ben-Shem et al., 2003). The recent 4.4 Å resolution X-ray structure of the PS I–LHCI from pea (Ben-Shem et al., 2003) shows a layer of four evenly spaced monomeric LHCI proteins (Lhca1, 2, 3, and 4) which are in structural contact with PS I and increase the antenna size to 167 Chls per RC (see Nelson and Ben-Shem, this volume, Chapter 7). The structural details of PS I–LHCI supercomplex from green algae are still unknown, but the available low-resolution electron microscopy of *C. reinhardtii* predicts binding of 11–14 Lhca proteins (Germano et al., 2002; Kargul et al., 2003), resulting in an even larger antenna size.

The presence of additional antenna components in PS I–LHCI supercomplexes results in significant heterogeneity of the Chl excitation dynamics and leads to a slower energy trapping process but does not affect the consequent electron-transfer steps (van Grondelle et al., 1994; Pålsson et al., 1995; Croce et al., 2000; Melkozernov, 2001; Melkozernov et al., 2004). Croce et al. (2000) used a single-photon counting technique to resolve the fluorescence dynamics of intact PS I–LHCI supercomplexes from higher plants (PS I-200 particles) and found that excitation trapping could be described by two components of 57 and 130 psec. A single 67 psec excitation trapping component in PS I-200 complexes was measured by Gobets et al. (2001) using a synchroscan streak camera. In comparison, excitation trapping in plant core complexes that miss the peripheral antenna is much faster and occurs in 22 psec (Gobets and van Grondelle, 2001). A similar effect was reported by Melkozernov et al. (2004), who studied excitation transfer and trapping dynamics in PS I–LHCI supercomplexes from a green alga *C. reinhardtii* by means of pump–probe and fluorescence spectroscopy. The excitation trapping was found to be biphasic, with the shorter 25 ± 3 psec component ascribed to photochemical trapping in the PS I core antenna, and the longer 104 ± 20 psec component attributed to excitation trapping occurring from the peripheral LHCI complexes. The slow 104 psec process suggests the presence of a slow energy-transfer pathway from the LHCI to the PS I core and indicates that excitation trapping from the peripheral antenna is diffusion-limited.

The energy equilibration and trapping processes in PS I–LHCI supercomplexes are addressed in more detail by Karapetyan et al., this volume, Chapter 13.

V. Concluding Remarks

The extensive experimental data on the dynamics of energy and electron transfer in PS I core complexes is summarized in the compartment model shown in Fig. 9A. Here, the effective (observable) transfer/equilibration times are labeled in italic, and the intrinsic transfer times are labeled in bold. The antenna is represented as three pools of Chls that are grouped by their Q_y optical transition energies and absorb at ~660, ~680, and >705 nm, respectively. Introduction of three pools is necessary to account for two energy equilibration processes observable in ultrafast optical experiments—or the 300–800 fsec equilibration between Chls absorbing at ~660 and Chls absorbing at ~680 nm, and 2–5 psec equilibration with the small pool of red Chls absorbing at >705 nm. The energy transfer rates from the antenna pigments to the special pair P700 and possible back-transfer rates are model dependent. In the case of a diffusion-limited transfer model, the back-transfer rate from P700 to antenna is negligible and the forward energy transfer rate is essentially equal to the observable effective energy-trapping time. In the case of a trap-limited model, the choice of a unique pair of forward and back-transfer rates is not straightforward since many combinations of forward and backward transfer rates can reproduce the effective excitation trapping rate observed experimentally. The model depicted in Fig. 9A represents a conventional sequence of electron transfer steps, which involves two radical pairs ($P700^+A_0^-\ A_1F_X$) and ($P700^+A_0A_1^-\ F_X$) that precede the relatively slow nanosecond formation of the ($P700^+A_0A_1F_X^-$) state. Figure 9B shows one of the alternative compartment models proposed recently by Müller et al. (2003), which models antenna with only two pools of pigments but adds one more intermediate radical pair to the conventional sequence of electron transfer. The exact nature of the additional radical pair

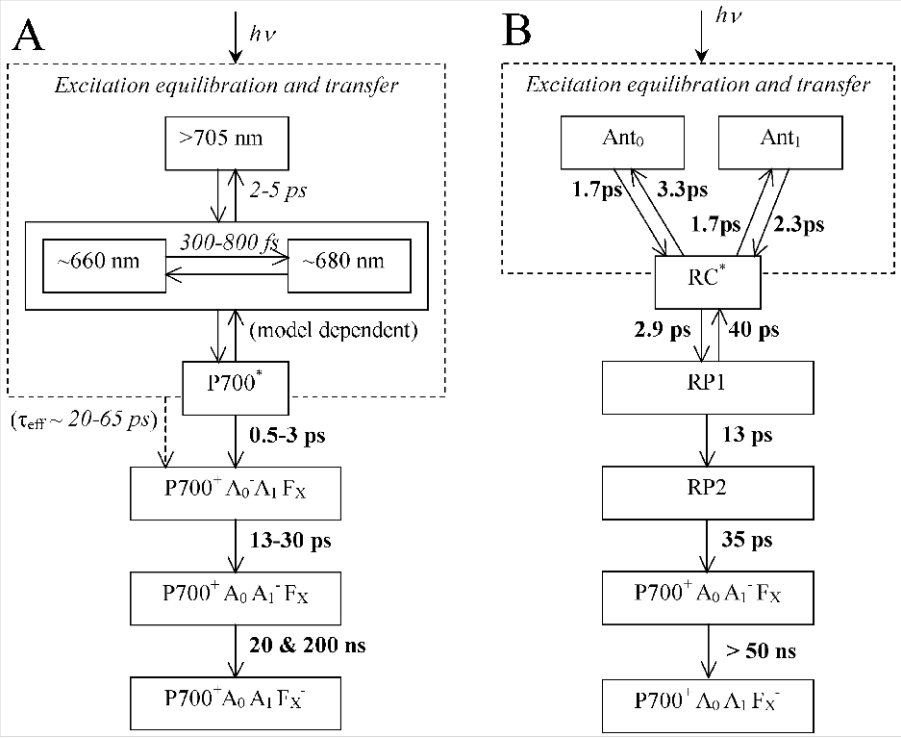

Fig. 9. (A) Compartment model of energy and electron transfer in PS I core complexes consistent with the data presented in Figs. 4 and 6. (B) One of the alternative compartment models with an extra radical pair proposed by Müller et al. (2003). The intrinsic transfer times are printed using bold typeface. In scheme (B) the original transfer rates were converted to lifetimes (time = 1/rate) for easier comparison.

is not known, but it would most probably involve oxidation or reduction of the accessory Chl.

The compartment models shown in Fig. 9 do not exhaust all possible arrangements used to model the results of ultrafast optical experiments (see, e.g., White et al., 1996; Gobets et al., 2001; Kumazaki et al., 2001; Müller et al., 2003). However, while compartment models of excitation transfer and equilibration significantly simplify the analysis of the observable kinetics, they are inherently only approximations of the real processes. Dividing antenna Chls into pools based on their spectroscopic properties ignores the fact that Chls belonging to different spectral pools do not form spatially separated groups but are most probably randomly mixed (interlaced), forming a strongly coupled net of pigments. Availability of high resolution X-ray structure of PS I opens the excellent possibility of building a complete model of energy transfer in this complex that would include excitation transfer between all antenna pigments, or between all excitonic states formed by all strongly coupled antenna pigments (see, e.g., Byrdin et al., 2002). However, for precise simulations, these models require knowledge of Q_y transition energies of each of the pigments in the antenna. Due to spectral congestion, the transition energies of most of the antenna pigments are not accessible in optical experiments—to date, only spectra of P700 and A_0 have been measured reliably. Alternatively, the spectral positions of Chls in antenna could be predicted by performing molecular simulations based on the known local protein structure around each pigment (Damjanovic et al., 2002), though the results of such calculations are difficult to verify.

Acknowledgments

I gratefully thank the following coworkers with whom some of the work discussed in this chapter has been developed: Dr. Walter S. Struve, Dr. Parag R. Chitnis, Dr. Wu Xu, Dr. Peter Martinsson, Dr. John H. Golbeck, and Naranbaatar Dashdorj. I am also indebted to Dr. Stephen M. Durbin for useful comments on the manuscript. Some of the work reported in this chapter was supported by Purdue Research Foundation grant 6903680.

References

Amesz J and Neerken S (2002) Excitation energy trapping in anoxygenic photosynthetic bacteria. Photosynth Res 73: 73–81

Beddard GS (1998) Excitations and excitons in photosystem I. Phil Trans R Soc London 356: 421–448

Ben-Shem A, Frolow F and Nelson N (2003) Crystal structure of plant photosystem I. Nature 426: 630–635

Boudreaux B, MacMillan F, Teutloff C, Agalarov R, Gu F, Grimaldi S, Bittl R, Brettel K and Redding K (2001) Mutations in both sides of the photosystem I reaction center identify the phylloquinone observed by electron paramagnetic resonance spectroscopy. J Biol Chem 276: 37299–37306

Brettel K (1988) Electron transfer from A_1^- to an iron–sulfur center with $t_{1/2}$ = 200 ns at room temperature in photosystem I. Characterization by absorption spectroscopy. FEBS Lett 239: 93–98

Brettel K (1997) Electron transfer and arrangement of the redox cofactors in photosystem I. Biochim Biophys Acta 1318: 322–373

Brettel K and Leibl W (2001) Electron transfer in photosystem I. Biochim Biophys Acta 1507: 100–114

Brettel K and Vos MH (1999) Spectroscopic resolution of the picosecond reduction kinetics of the secondary electron acceptor A_1 in photosystem I. FEBS Lett 447: 315–317

Brettel K, Sétif P and Mathis P (1986) Flash-induced absorption changes in photosystem I at low temperature: evidence that the electron acceptor A_1 is vitamin K_1. FEBS Lett 203: 220–224

Byrdin M, Rimke I, Schlodder E, Stehlik D and Roelofs TA (2000) Decay kinetics and quantum yields of fluorescence in photosystem I from *Synechococcus elongatus* with P700 in the reduced and oxidized state: are the kinetics of excited state decay trap-limited or transfer-limited? Biophys J 79: 992–1007

Byrdin M, Jordan P, Krauß N, Fromme P, Stehlik D and Schlodder E (2002) Light harvesting in photosystem I: modeling based on the 2.5-Å structure of photosystem I from *Synechococcus elongatus*. Biophys J 83: 433–457

Cohen R, Shen G, Golbeck JH, Xu W, Chitnis PR, Valieva A, van der Est A, Pushkar J and Stehlik D (2004) Evidence for asymmetric electron transfer in cyanobacterial photosystem I: analysis of a methionine to leucine mutation of the ligand to the primary electron acceptor A_0. Biophys J 43: 4741–4754

Croce R, Zucchelli G, Garlaschi FM, Bassi R and Jennings RC (1996) Excited state equilibration in the photosystem I light harvesting complex: P700 is almost isoenergetic with its antenna. Biochemistry 35: 8572–8579

Croce R, Dorra D, Holzwarth AR and Jennings RC (2000) Fluorescence decay and spectral evolution in intact photosystem I of higher plants. Biochemistry 39: 6341–6348

Croce R, Müller MG, Bassi R and Holzwarth AR (2001) Carotenoid-to-chlorophyll energy transfer in recombinant major light-harvesting complex (LHC II) of higher plants. I. Femtosecond transient absorption measurements. Biophys J 80: 901–915

Damjanovic A, Vaswani HM, Fromme P and Fleming GR (2002) Chlorophyll excitations in photosystem I of *Synechococcus elongatus*. J Phys Chem B 106: 10251–10262

Dashdorj N, Xu W, Martinsson P, Chitnis PR and Savikhin S (2004) Electrochromic shift of chlorophyll absorption in photosystem I from *Synechocystis* sp. PCC 6803: a probe of optical and dielectric properties around the secondary electron acceptor. Biophys J 86: 3121–3130

Dashdorj N, Wu W, Cohen RO, Golbeck JH and Savikhin S (2005) Asymmetric electron transfer in cyanobacterial Photosytem I: charge separation and secondary electron transfer dynamics in mutations near the primary electron acceptor A_0. Biophys J 88: 1238–1249

Diaz-Quintana A, Leibl W, Bottin W and Sétif P (1998) Electron transfer in photosystem I reaction centers follows a linear pathway in which iron–sulfur cluster F_B is the immediate electron donor to soluble ferredoxin. Biochemistry 37: 3429–3439

DiMagno L, Chan C-K, Jia Y, Lang MJ, Newman JR, Mets L, Fleming GR and Haselkorn R (1995) Energy transfer and trapping in photosystem I reaction centers from cyanobacteria. Proc Natl Acad Sci USA 92: 2715–2719

Dorra D, Fromme P, Karapetyan NV and Holzwarth AR (1998) Fluorescence kinetics of photosystem I: multiple fluorescence components. In: Garab G (ed) Photosynthesis: Mechanisms and Effects, pp 587–590. Kluwer Academic Publishers, Dordrecht, The Netherlands

Du M, Xie X, Jia Y, Mets L and Fleming GR (1993) Direct observation of ultrafast energy transfer in PSI core antenna. Chem Phys Lett 201: 535–542

Fairclough WV, Evans MCW, Purton S, Jones S, Rigby SEJ and Heathcote P (2001) Site-directed mutagenesis of PsaA: M684 in *Chlamydomonas reinhardtii*. In: PS2001 Proceedings: 12th International Congress on Photosynthesis. CSIRO Publishers, Melbourne, Australia

Frese RN, Palacios MA, Azzizi A, van Stokkum IHM, Kruip J, Rögner M, Karapetyan NV, Schlodder E, van Grondelle R and Dekker JP (2002) Electric field effects on red chlorophylls, β-carotenes and P700 in cyanobacterial Photosystem I complexes. Biochim Biophys Acta 1554: 180–191

Gatzen G, Müller MG, Griebenow K and Holzwarth AR (1996) Primary processes and structure of the photosystem II reaction center. 3. Kinetic analysis of picosecond energy transfer and charge separation processes in the D1-D2-cyt-b_{559} complex measured by time resolved fluorescence. J Phys Chem 100: 7269–7278

Germano M, Yakushevska AE, Keegstra W, van Gorkom HJ, Dekker JP and Boekema EJ (2002) Supramolecular organization of photosystem I and light-harvesting complex I in *Chlamydomonas reinhardtii*. FEBS Lett 525: 121–125

Gibasiewicz K, Ramesh VM, Lin S, Woodbury NW and Webber AN (2002) Excitation dynamics in eukaryotic PS I from *Chlamydomonas reinhardtii* CC 2696 at 10 K. Direct detection of the reaction center exciton states. J Phys Chem B 106: 6322–6330

Gobets B and van Grondelle R (2001) Energy transfer and trapping in photosystem I. Biochim Biophys Acta 1507: 80–99

Gobets B, van Amerongen H, Monshouwer R, Kruip J, Rögner M, van Grondelle R and Dekker JP (1994) Polarized site-selected fluorescence spectroscopy of isolated photosystem I particles. Biochim Biophys Acta 1188: 75–85

Gobets B, Dekker JP and van Grondelle R (1998a) Transfer-to-the-trap limited model of energy transfer in photosystem I. In: Garab G (ed) Photosynthesis: Mechanisms and Effects, pp 503–508. Kluwer Academic Publishers, Dordrecht, The Netherlands

Gobets B, van Stokkum IHM, van Mourik F, Rögner M, Kruip J, Dekker JP and van Grondelle R (1998b) Time-resolved fluorescence measurements of photosystem I from *Synechocystis*

PCC 6803. In: Garab G (ed) Photosynthesis: Mechanisms and Effects, pp 571–574. Kluwer Academic Publishers, Dordrecht, The Netherlands

Gobets B, van Stokkum IHM, Rögner M, Kruip J, Schlodder E, Karapetyan NV, Dekker JP and van Grondelle R (2001) Time-resolved fluorescence emission measurements of photosystem I particles of various cyanobacteria: a unified compartmental model. Biophys J 81: 407–424

Golbeck J, Xu W, Zybailov B, van der Est A, Pushkar J, Zech S, Stehlik D and Chitnis PR (2001) Electron transfer through the quinone acceptor in cyanobacterial Photosystem I. In: PS2001 Proceedings: 12th International Congress on Photosynthesis. CSIRO Publishing, Melbourne, Australia

Guergova-Kuras M, Boudreaux B, Joliot A, Joliot P and Redding K (2001) Evidence for two active branches for electron transfer in photosystem I. Proc Natl Acad Sci USA 98: 4437–4442

Hastings G, Kleinherenbrink FAM, Lin S and Blankenship RE (1994a) Time-resolved fluorescence and absorption spectroscopy of photosystem I. Biochemistry 33: 3185–3192

Hastings G, Kleinherenbrink FAM, Lin S, McHugh TJ and Blankenship RE (1994b) Observation of the reduction and reoxidation of the primary electron acceptor in photosystem I. Biochemistry 33: 3193–3200

Hastings G, Hoshina S, Webber AN and Blankenship RE (1995a) Universality of energy and electron transfer processes in photosystem I. Biochemistry 34: 15512–15522

Hastings G, Reed LJ, Lin S and Blankenship RE (1995b) Excited state dynamics in photosystem I: effects of detergent and excitation wavelength. Biophys J 69: 2044–2055

Hayes JM, Matsuzaki S, Rätsep M and Small GJ (2000) Red chlorophyll *a* antenna states of photosystem I of the cyanobacterium *Synechocystis* sp. PCC 6803. J Phys Chem B 104: 5625–5633

Hecks B, Wulf K, Breton J, Leibl W and Trissl H-W (1994) Primary charge separation in photosystem I – a two step electrogenic charge separation connected with $P^{+}_{700}\,A^{-}_{0}$ and $P700^{+}A^{-}_{1}$ formation. Biochemistry 33: 8619–8624

Hiyama T and Ke B (1971) A further study of P430: a possible primary electron acceptor of Photosystem I. Arch Biochem Biophys 147: 99–108

Holzwarth AR, Haehnel W, Ratajczak R, Bittersmann E and Schatz G (1990) Energy transfer kinetics in photosystem I particles isolated from *Synechococcus* sp. and from higher plants. In: Baltscheffsky M (ed) Current Research in Photosynthesis, pp 611–614. Kluwer Academic Publishers, Dordrecht, The Netherlands

Holzwarth AR, Schatz G, Brock H and Bittersmann E (1993) Energy transfer and charge separation kinetics in photosystem I Part I: picosecond transient absorption and fluorescence study of cyanobacterial photosystem I particles. Biophys J 64: 1813–1826

Holzwarth AR, Dorra D, Müller MG and Karapetyan NV (1998) Structure–function relationships and excitation dynamics in photosystem I. In: Garab G (ed) Photosynthesis: Mechanism and Effects, pp 497–502. Kluwer Academic Publishers, Dordrecht, The Netherlands

Ikegami I (1976) Fluorescence changes related to the primary photochemical reaction in the P700 enriched particles isolated from spinach chloroplasts. Biochim Biophys Acta 449: 245–258

Jennings RC, Zucchelli G, Croce R, Valkunas L, Finzi L and Garlaschi FM (1997) Model studies on the excited state equilibrium perturbation due to reaction centre trapping in photosystem I. Photosynth Res 52: 245–253

Joliot P and Joliot A (1999) *In vivo* analysis of the electron transfer within photosystem I: are the two phylloquinones involved? Biochemistry 38: 11130–11136

Jordan P, Fromme P, Witt HT, Klukas O, Saenger W and Krauß N (2001) Three-dimensional structure of cyanobacterial photosystem I at 2.5 Å resolution. Nature 411: 909–917

Karapetyan NV, Dorra D, Schweitzer G, Bezsmertnaya IN and Holzwarth AR (1997) Fluorescence spectroscopy of the long-wave chlorophylls in trimeric and monomeric photosystem I complexes from the cyanobacterium *Spirulina platensis*. Biochemistry 36: 13830–13837

Karapetyan NV, Holzwarth AR and Rögner M (1999) The photosystem I trimer of cyanobacteria: molecular organization, excitation dynamics and physiological significance. FEBS Lett 460: 395–400

Kargul J, Nield J and Barber J (2003) Three-dimensional reconstruction of a light-harvesting complex I- photosystem I (LHCI–PSI) supercomplex from the green alga *Chlamydomonas reinhardtii*. Insights into light harvesting for PSI. J Biol Chem 278: 16135–16141

Kennis JTM, Gobets B, van Stokkum IHM, Dekker JP, van Grondelle R and Fleming GR (2001) Light harvesting by chlorophylls and carotenoids in the photosystem I core complex of *Synechococcus elongatus*: a fluorescence upconversion study. J Phys Chem B 105: 4485–4494

Klug DR, Giorgi LB, Crystal B, Barber J and Porter G (1989) Energy transfer to low energy chlorophyll species prior to trapping by P700 and subsequent electron transfer. Photosynth Res 22: 277–284

Klukas O, Schubert W-D, Jordan P, Krauß N, Fromme P, Witt HT and Saenger W (1999) Photosystem I, an improved model of the stromal subunits PsaC, PsaD, and PsaE. J Biol Chem 274: 7351–7360

Krauß N, Hinrichs W, Witt. I, Fromme P, Pritzkow W, Dauter Z, Betzel C, Wilson KS, Witt HT and Saenger W (1993) Three-dimensional structure of system I of photosynthesis at 6 Å resolution. Nature 361: 326–331

Krauß N, Schubert WD, Klukas O, Fromme P, Witt HT and Saenger W (1996) Photosystem I at 4 Å resolution represents the first structural model of a joint photosynthetic reaction centre and core antenna system. Nat Struct Biol 3: 965–73

Kumazaki S, Iwaki M, Ikegami I, Kandori H, Yoshihara K and Itoh S (1994a) Rates of primary electron transfer reactions in the photosystem I reaction center reconstituted with different quinones as the secondary acceptor. J Phys Chem 98: 11220–11225

Kumazaki S, Kandori H, Petek H, Yoshihara I and Ikegami I (1994b) Primary photochemical processes in P700-enriched photosystem I particles – trap-limited excitation decay and primary charge separation. J Phys Chem 98: 10335–10342

Kumazaki S, Furusawa H, Yoshihara I and Ikegami I (1998) Excitation wavelength dependence of the excitation transfer in photosystem I reaction center with reduced number of antenna chlorophylls. In: Garab G (ed) Photosynthesis: Mechanisms and Effects, pp 575–578. Kluwer Academic Publishers, Dordrecht, The Netherlands

Kumazaki S, Ikegami I, Furusawa H, Yasuda S and Yoshihara K (2001) Observation of the excited state of the primary electron donor chlorophyll (P700) and the ultrafast charge separation

in the spinach photosystem I reaction center. J Phys Chem B 105: 1093–1099

Laible PD, Zipfel W and Owens TG (1994) Excited state dynamics in chlorophyll-based antennae: the role of transfer equilibrium. Biophys J 66: 844–860

Lüneberg J, Fromme P, Jekow P and Schlodder E (1994) Spectroscopic characterization of PS I core complexes from thermophilic *Synechococcus* sp.: identical reoxidation kinetics of A_1^- before and after removal of the iron–sulfur-clusters F_A and F_B. FEBS Lett 338: 197–202

Melkozernov AN (2001) Excitation energy transfer in photosystem I from oxygenic organisms. Photosynth Res 70: 129–153

Melkozernov AN, Su H, Lin S, Bingham S, Webber AN and Blankenship RE (1997) Specific mutations near the primary donor in photosystem I from *Chlamydomonas reinhardtii* alters trapping time and spectroscopic properties of P700. Biochemistry 36: 2898–2907

Melkozernov AN, Lin S and Blankenship RE (1998a) Energy equilibration in the antenna of photosystem I from cyanobacterium *Synechocystis* sp. PCC 6803. In: Garab G (ed) Photosynthesis: Mechanisms and Effects, pp 405–408. Kluwer Publishers, Dordrecht, The Netherlands

Melkozernov AN, Su H, Webber AN and Blankenship RE (1998b) Excitation energy transfer in thylakoid membranes from *Chlamydomonas reinhardtii* lacking chlorophyll *b* and with mutant photosystem I. Photosynth Res 56: 197–207

Melkozernov AN, Lin S and Blankenship RE (2000) Excitation dynamics and heterogeneity of energy equilibration in the core antenna of Photosystem I from the cyanobacterium *Synechocystis* sp. PCC 6803. Biochemistry 39: 1489–1498

Melkozernov AN, Kargul J, Lin S, Barber J and Blankenship RE (2004) Energy coupling in the PSI–LHCI supercomplex from the green alga *Chlamydomonas reinhardtii*. J Phys Chem. 108: 10547–10555

Mi D, Lin S and Blankenship RE (1999) Picosecond transient absorption spectroscopy in the blue spectral region of photosystem I. Biochemistry 38: 15231–15237

Muhiuddin IP, Heathcote P, Carter S, Purton S, Rigby SEJ and Evans MCW (2001) Evidence from time resolved studies of the $P700^+/A_1^-$ radical pair for photosynthetic electron transfer on both the PsaA and PsaB branches of the Photosystem I reaction centre. FEBS Lett 503: 56–60

Müller MG, Niklas J, Lubitz W and Holzwarth AR (2003) Ultrafast transient absorption studies on photosystem I reaction centers from *Chlamydomonas reinhardtii*. 1. A new interpretation of the energy trapping and early electron transfer steps in photosystem I. Biophys J 85: 3899–3922

Nuijs AM, Shuvalov VA, van Gorkom HJ, Plijter JJ and Duysens LNM (1986) Picosecond absorbance difference spectroscopy on the primary reactions and the antenna-excited states in photosystem I particles. Biochim Biophys Acta 850: 310–318

Owens TG, Webb SP, Alberte RS, Mets L and Fleming GR (1988) Antenna structure and excitation dynamics in photosystem I. I. Studies of detergent-isolated photosystem I preparations using time-resolved fluorescence analysis. Biophys J 53: 733–745

Pålsson L-O, Tjus SE, Andersson B and Gillbro T (1995) Energy transfer in photosystem I. Time resolved fluorescence of the native photosystem I complex and its core complex. Chem Phys 194: 291–302

Pålsson L-O, Dekker JP, Schlodder E, Monshouwer R and van Grondelle R (1996) Polarized site-selective fluorescence spectroscopy of long-wavelength emitting chlorophylls in isolated photosystem I particles of *Synechococcus elongatus*. Photosynth Res 48: 239–246

Pålsson L-O, Flemming C, Gobets B, van Grondelle R, Dekker JP and Schlodder E (1998) Energy transfer and charge separation in photosystem I: P700 oxidation upon selective excitation of the long-wavelength antenna chlorophylls of *Synechococcus elongatus*. Biophys J 74: 2611–2622

Ramesh VM, Gibasiewicz K, Lin S, Bingham SE and Webber AN (2004) Bidirectional electron transfer in photosystem I: accumulation of A_0 in A-side and B-side mutants of the axial ligand to chlorophyll A_0. Biochemistry 43: 1369–1375

Rätsep M, Johnson TW, Chitnis PR and Small GJ (2000) The red-absorbing chlorophyll *a* antenna states of photosystem I: a hole-burning study of *Synechocystis* sp. PCC 6803 and its mutants. J Phys Chem B 104: 836–847

Savikhin S, Wells T, Song P-S and Struve WS (1993) Ultrafast pump–probe spectroscopy of native etiolated phytochrome. Biochemistry 32: 7512–7518

Savikhin S, Buck DR and Struve WS (1999a) The Fenna-Matthews-Olson protein: a strongly coupled photosynthetic antenna. In: Andrews DL and Demidov AA (eds) Resonance Energy Transfer, pp 399–434. John Wiley & Sons, New York

Savikhin S, Xu W, Soukoulis V, Chitnis PR and Struve WS (1999b) Ultrafast primary processes in photosystem I of the cyanobacterium *Synechocystis* sp. PCC 6803. Biophys J 76: 3278–3288

Savikhin S, Xu W, Chitnis PR and Struve WS (2000) Ultrafast primary processes in PS I from *Synechocystis* sp. PCC 6803: roles of P700 and A_0. Biophys J 79: 1573–1586.

Savikhin S, Xu W, Martinsson P, Chitnis PR and Struve WS (2001) Kinetics of charge separation and $A_0^- - > A_1$ electron transfer in photosystem I reaction centers. Biochemistry 40: 9282–9290

Shubin VV, Murthy SDS, Karapetyan NV and Mohanty P (1991) Origin of the 77 K variable fluorescence at 758 nm in the cyanobacterium *Spirulina platensis*. Biochim Biophys Acta 1060: 28–36

Shuvalov VA, Nuijs AM, van Gorkom HJ, Smit HWJ and Duysens LNM (1986) Picosecond absorbance changes upon selective excitation of the primary electron donor P700 in photosystem I. Biochim Biophys Acta 850: 319–323

Struve WS (1995) Theory of electronic energy transfer. In: Blankenship RE, Madigan MT and Bauer CE (eds) Anoxygenic Photosynthetic Bacteria, pp 297–313. Kluwer Academic Publishers, Dordrecht, The Netherlands

Telfer A, Barber J, Heathcote P and Evans MCW (1978) Variable chlorophyll *a* fluorescence from P700 enriched photosystem I particles dependent on the redox state of the reaction centre. Biochim Biophys Acta 504: 153–164

Trinkunas G and Holzwarth AR (1996) Kinetic modeling of exciton migration in photosynthetic systems. 3. Application of genetic algorithms to simulations of excitation dynamics in three dimensional photosystem core reaction center complexes. Biophys J 71: 351–364

Trissl H-W (1997) Determination of the quenching efficiency of the oxidized primary donor of photosystem I, $P700^+$: implications for the trapping mechanism. Photosynth Res 54: 237–240

Turconi S, Schweitzer G and Holzwarth AR (1993) Temperature-dependence of picosecond fluorescence kinetics of a cyanobacterial photosystem-I particle. Photochem Photobiol 57: 113–119

Turconi S, Kruip J, Schweitzer G, Rönger M and Holzwarth AR (1996) A comparative fluorescence kinetics study of photosystem I monomers and trimers from *Synechocystis* PCC 6803. Photosynth Res 49: 263–268

Valkunas L, Liuolia V, Dekker JP and van Grondelle R (1995a) Description of energy migration and trapping in photosystem I by a model with 2 distance scaling parameters. Photosynth Res 43: 149–154

Valkunas L, Trinkunas G, Liuolia V and van Grondelle R (1995b) Nonlinear annihilation of excitations in photosynthetic systems. Biophys J 69: 1117–1129

van der Lee J, Bald D, Kwa SLS, van Grondelle R, Rönger M and Dekker JP (1993) Steady-state polarized-light spectroscopy of isolated photosystem-I complexes. Photosynth Res 35: 311–321

van Grondelle R (1985) Excitation energy transfer, trapping and annihilation in photosynthetic systems. Biochim Biophys Acta 811: 147–195

van Grondelle RJ, Dekker JP, Gillbro T and Sundstrom V (1994) Energy trapping and transfer in photosynthesis. Biochim Biophys Acta 1187: 1–65

Wasielewski MR, Fenton JM and Govindjee (1987) The rate of formation of $P700^{+} - A_0^{-}$ in photosystem I particles from spinach as measured by picosecond transient absorption spectroscopy. Photosynth Res 12: 181–190

Webber AN, Su H, Bingham SE, Käss H, Krabben L, Kuhn M, Jordan R, Schlodder E and Lubitz W (1996) Site-directed mutations affecting the spectroscopic characteristics and midpoint potential of the primary donor in photosystem I. Biochemistry 35: 12857–12863

Werst M, Jia Y, Mets L and Fleming GR (1992) Energy transfer and trapping in the photosystem I core antenna. A temperature study. Biophys J 61: 868–878

White NTH, Beddard GS, Thorne JRG, Feehan TM, Keyes TE and Heathcote P (1996) Primary charge separation and energy transfer in the photosystem I reaction center of higher plants. J Phys Chem 100: 12086–12099

Wittmershaus BP, Woolf VM and Vermaas WFJ (1992) Temperature dependence and polarization of fluorescence from photosystem I in the cyanobacterium *Synechocystis* sp PCC 6803. Photosynth Res 31: 75–87

Woodbury NW and Allen JP (1995) The pathway, kinetics and thermodynamics of electron transfer in wild type and mutant reaction centers of purple nonsulfur bacteria. In: Blankenship RE, Madigan MT and Bauer CE (eds) Anoxygenic Photosynthetic Bacteria. Kluwer Academic Publishers, Dordrecht, The Netherlands

Xu W, Chitnis PR, Valieva A, van der Est A, Brettel K, Guergova-Kuras M, Pushkar YN, Zech SG, Stehlik D, Shen G, Zybailov B and Golbeck JH (2003a) Electron transfer in cyanobacterial photosystem I: II. Determination of forward electron transfer rates of site-directed mutants in a putative electron transfer pathway from A_0 through A_1 to F_X. J Biol Chem 278: 27876–27887

Xu W, Chitnis PR, Valieva A, van der Est A, Pushkar YN, Krzystyniak M, Teutloff C, Zech SG, Bittl R, Stehlik D, Zybailov B, Shen G and Golbeck JH (2003b) Electron transfer in cyanobacterial photosystem I: I. Physiological and spectroscopic characterization of site-directed mutants in a putative electron transfer pathway from A_0 through A_1 to F_X. J Biol Chem 278: 27864–27875

Zazubovich V, Matsuzaki S, Johnson TW, Hayes JM, Chitnis PR and Small GJ (2002) Red antenna states of photosystem I from cyanobacterium *Synechococcus elongatus*: a spectral hole burning study. Chem Phys 275: 47–59

Chapter 13

The Long Wavelength Chlorophylls of Photosystem I

Navassard V. Karapetyan*
A.N. Bakh Institute of Biochemistry, Russian Academy of Sciences, 119071 Moscow, Russia

Eberhard Schlodder
Max-Volmer-Laboratory of Biophysical Chemistry, Technical University, 10623 Berlin, Germany

Rienk van Grondelle and Jan P. Dekker
Division of Physics and Astronomy, Free University, 1081 HV Amsterdam, The Netherlands

Summary

In cyanobacteria, long wavelength chlorophylls (LWC) are located in the Photosystem I (PS I) core complex, whereas in plants and algae they are distributed between the PS I core and the light-harvesting complexes (LHC I). LWC are most probably aggregates of (excitonically) coupled chlorophylls, mainly dimers or trimers. The total number of LWC is rather small ($\leq$10% of the total chlorophylls). Depending on their location in the PS I antenna and their distance from P700, they can play a crucial role in the kinetics of energy transfer and in the trapping of the excitation energy by charge separation. Energy absorbed by LWC is transferred uphill to P700 with high efficiency at room temperature, thereby increasing the cross-section for the absorption of red light. LWC are involved also in the dissipation of excess energy, thus protecting the reaction center. Under physiological conditions, the excitations within the PS I antenna are nearly thermally equilibrated over the different spectral forms and the excitation energy is efficiently trapped via charge separation in the reaction center. When the photochemistry in the reaction center is blocked, the excitations migrate to the LWC and are quenched either by $P700^+$ or by the P700 triplet state depending on the state of P700.

* Author for correspondence, email: nkarap@inbi.ras.ru

John H. Golbeck (ed): Photosystem I: The Light-Driven Plastocyanin:Ferredoxin Oxidoreductase, 177–192.

I. Introduction

A unique property of PS I of higher plants, algae, and cyanobacteria is the relatively high content of the so-called long wavelength chlorophylls (LWC), red, or low energy chlorophylls (Chls) that are located on the PS I core complex and/or the peripheral light-harvesting complex (LHC I). We define the LWC on the basis of their spectral properties: LWC are those antenna Chls that absorb wavelengths longer than P700, the primary electron donor of the reaction center, i.e., the lowest excited state energy of the LWC are below that of P700. The presence of LWC in almost all types of PS I complexes indicates their functional importance.

LWC were observed for the first time in green bean leaves as an emission band at 735 nm in the 77 K fluorescence spectra (Litvin and Krasnovsky, 1957) and in the algae *Chlorella* and *Porphyridium cruentum* as an emission band at 720 nm (Brody, 1958). Since a concentrated solution of Chl *a* shows a low temperature fluorescence band at 715 nm, it was suggested that a Chl aggregate (dimer) is responsible for the long wavelength emission (Brody, 1958). Until now, the origin of red-shifted Chls in photosynthetic organisms was not clear. The spectral characteristics of antenna Chls *in vivo* are already red shifted by up to about 15 nm relative to a solution of pure Chl in organic solvents, indicating the involvement of pigment–protein interactions. The optical properties of antenna Chls are highly heterogeneous and, especially at low temperature, spectrally different Chl forms can be distinguished according to the position of the red absorption peak in photosynthetic cells (Krasnovsky, 1960). LWC absorbing at wavelengths longer than 700 nm have also been observed in solutions and films. The Chls in films obtained by evaporation of an alcoholic extract of Chl had spectral characteristics similar to Chls in cells. The fluorescence of these Chl films is effectively quenched as it is *in vivo*. It was shown that exposure of Chl films to water vapor at 50˚C resulted in an additional red shift to 740 nm (for review see Katz et al., 1991), indicating the role of water molecules in that phenomenon. Water-treated films of bacteriochlorophyll *a* (Bchl) and Bchl *c* showed large red shifts relative to their solutions in polar organic solvents. Infra-red spectroscopic investigations of Chl (Bchl) films provided evidence that two types of aggregation can occur in solid pigment films: direct Chl–Chl interactions resulting from keto C=O . . . Mg interactions, and coordination interactions of the keto C=O group that are mediated by water, coordinated to the central Mg atom of another molecule (Krasnovsky and Bystrova, 1986; Katz et al., 1991). These two modes of aggregation generate aggregates with very different optical and magnetic resonance properties. The idea was developed that an aggregation of pigments is involved in both the red shift and the fluorescence quenching of Chls *in vivo*. The fact that water molecules have been found close to antenna Chl dimers or trimers in the X-ray structure of PS I (Jordan et al., 2001) may help to establish the possible role of water molecules in LWC.

The fluorescence yield of LWC strongly increases at low temperatures because excitation energy not utilized by the reaction center (RC) migrates predominantly to LWC. Similar to P700, the LWC serve as terminal energy trap and therefore have a pronounced effect on energy transfer and trapping. It was expected that LWC serve to increase the trapping time and decrease the quantum yield of charge separation. However, the decrease in the quantum yield of primary photochemistry by LWC is compensated by the efficient uphill energy transfer from LWC to bulk Chls at physiological temperatures, and by the increase of the absorption cross-section. Note that the mechanism of efficient uphill energy transfer in the PS I antenna is not yet clear. Probably, even a small overlap between the emission band of the LWC and the absorption band of the primary electron donor is enough for efficient energy transfer.

LWC of PS I may play different roles in photosynthesis depending on their location in antenna, and therefore on the distance between the red Chls and P700 (Karapetyan et al., 1999a). It was suggested that LWC may concentrate energy on P700 by decreasing the amount of energy transfer in bulk Chls (Holzwarth et al., 1993; White et al., 1996); however, recent data have shown that LWC slow down the trapping rate (Gobets et al., 2001b). Red Chls may increase the absorption cross-section under conditions of low-intensity light in the course of cyanobacteria cultivation (Trissl, 1993; Shubin et al., 1995) and plant growth (Rivadossi et al., 1999), or protect RC against excess energy (Mukerji and Sauer, 1989; Karapetyan et al., 1999a,b). LWCs compete with P700 for excitation energy (especially at low temperature), thus affecting the efficiency of charge separation (Palsson et al., 1998). The quantum yield of

Abbreviations: Chl(s) – chlorophyll(s); Bchl – bacteriochlorophyll; C708 (C719, C740, etc.) – Chls with absorption band peak at 708 nm (719, 740, etc.); CD – circular dichroism; DAS – decay associated spectrum; F720 (F735, F760, etc.) – Chls with fluorescence maximum at 720 nm (735, 760, etc.); FWHM – full width at half maximum; LD – linear dichroism; LWC(s) – long wavelength Chl(s); PS I – photosystem I; P700 ($P700^+$) – primary electron donor of PS I in reduced (oxidized) state; ^{3}P700 – P700 in triplet state; RC – reaction center.

P700 oxidation is independent of the wavelength of the excitation, even at wavelengths of up to 760 nm as a result of uphill energy migration to bulk Chl and then to P700 (Shubin et al., 1995; Dorra et al., 1998; Holzwarth et al., 1998; Palsson et al., 1998; Gobets et al., 2003b).

The LWC of PS I have been discussed in several recent reviews (Karapetyan, 1998; Karapetyan et al., 1999a; Gobets and van Grondelle, 2001; Melkozernov, 2001; Fromme et al., 2003). In this chapter, the spectral properties of LWCs, their possible origin, their location in the antenna, and their influence on the energy transfer and trapping kinetics will be discussed.

II. Spectral Characteristics of Long Wavelength Chlorophyll in PS I

Absorbance spectra of PS I exhibit a large spectral heterogeneity in the Q_y region that is probably the result of strong pigment–pigment interactions of tightly coupled Chls and site-energy differences that arise from pigment–protein interactions. At low temperature, absorbance bands are clearly resolved at wavelengths >700 nm. They are attributed to antenna (exciton) states (so-called LWC), which absorb at energies below that of the primary electron donor P700. The number of Chls contributing to the far-red absorption bands can be estimated from the ratio of the integrated intensity of the long wavelength absorption bands in the 5 K spectrum to the total integrated intensity of the Q_y band and the number of Chls per PS I. The number and the spectral characteristics of LWC are species-dependent. Trimeric PS I complexes contain usually more LWC than monomers. Spectral properties of the LWC of cyanobacterial PS I have been described and analyzed in several studies (Shubin et al., 1991, 1993; van der Lee et al., 1993; Gobets et al., 1994, 2001b; Woolf et al., 1994; Palsson et al., 1996, 1998; Turconi et al., 1996; Karapetyan et al., 1997, 1999a; Wittmershaus et al., 1998; Kruip et al., 1999; Cometta et al., 2000; Hayes et al., 2000; Melkozernov et al., 2001; Zazubovich et al., 2002; for more recent reviews see Gobets and van Grondelle, 2001).

Figure 1 shows, as an example, the 5 K absorption spectra of monomeric and trimeric PS I complexes from *Thermosynechoccus elongatus* and *Arthrospira platensis* between 650 nm and 750 nm (see note of Table 1 for changes in names of cyanobacteria). The spectra are dominated by the absorption of the bulk antenna Chls centered at about 678 nm. It should be noted

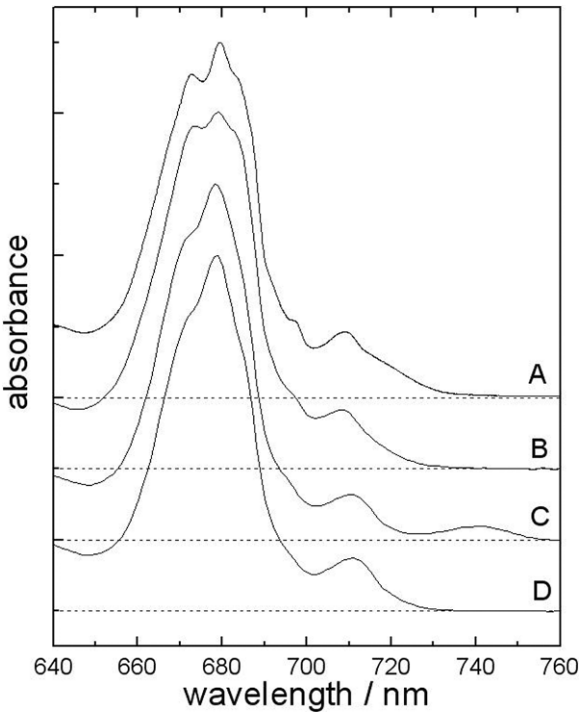

Fig. 1. 5 K absorption spectra of trimeric and monomeric PS I complexes from *T. elongatus* (A and B) and *A. platensis* (C and D). (Gobets et al., 2001b)

that this already corresponds to a red shift of about 15 nm compared to the absorption spectrum of Chl *a* in an organic solvent. Above 700 nm, the spectrum of trimeric PS I complexes from *T. elongatus* (Fig. 1A) shows absorption bands at about 708 and 719 nm with an oscillator strength corresponding to that of ~5 and ~4 Chls, respectively. The monomers contain a lower number (~2) of C719 pigments (Fig. 1B). The notation Cxxx represents LWC with a low temperature Q_y absorption maximum at xxx nm. The maxima of the low temperature emission are 730 nm for monomeric and 732 nm for trimeric PS I complexes from *T. elongatus*. Monomeric PS I complexes from *T. elongatus*, prepared either from a *psaL*$^-$ strain or by dissociation of trimers, lack the PsaL subunit. PsaL forms most of the contact sites within the trimerization domain and coordinates three antenna chlorophylls (Jordan et al., 2001). Therefore, it has been suggested that some of the C719 pigments are located close to the connecting domain of the monomeric PS I complexes within the trimer (Palsson et al., 1998). On the basis of hole-burning experiments, a third spectral form with absorption maximum at 715 nm at low temperature was recently suggested (Zazubovich et al., 2002).

Table 1. Absorption maxima (nm) of LWC in PS I complexes from cyanobacteria at 5 or 77 K; the oscillator strength of the respective absorption bands corresponds to the given number of Chl *a* molecules per P700 (in brackets). The spectral forms of LWC summarized in the table are determined by the deconvolution of low temperature absorption spectra with the minimum number of Gaussian bands

Species	Spectral forms of LWC (nm)		References
Thermosynechococcus elongatus – monomers[a]	708 (5)	719 (2)	Palsson et al. (1998)
Thermosynechococcus elongatus – trimers	708 (5)	719 (4)	Palsson et al. (1998), Byrdin et al. (2000)
Arthrospira platensis – monomers[a]	708 (7)		Gobets et al. (2001b), Schlodder et al. (2005)
Arthrospira platensis – trimers	708 (7)	740 (3)	Gobets et al. (2001b), Schlodder et al. (2005)
Synechocystis sp. – monomers[b]	708 (3)		Melkozernov et al. (2001), Gobets et al. (2001b)
Synechocystis sp. – trimers	708 (5)		Gobets et al. (2001b)
Synechococcus 7942−trimers	703 (2)		Andrizhiyevskaya et al. (2004)

[a]Old name of *Thermosynechococcus elongatus* was *Synechococcus elongatus*, and that of *Arthrospira platensis* was *Spirulina platensis*.
[b]*Synechocystis* sp. is *Synechocystis* sp. PCC 6803.

PS I trimers of *A. platensis* contain the red-most Chl *a* antenna state reported in any PS I complex (Shubin, et al., 1992). The 5 K spectrum exhibits a band at 740 nm (C740, corresponding to about three Chl *a*) (Fig. 1C). In addition, PS I trimers contain a LWC form with an absorption maximum at 708 (corresponding to about seven Chls). PS I monomers show only the LWC form with an absorption maximum at 708 nm (corresponding to about seven Chls) (Fig. 1D). On the basis of a deconvolution with a larger number of Gaussian bands, four to five LWC forms in PS I trimers and three in monomers have been suggested (Karapetyan et al., 1997; Cometta et al., 2000). The maxima of the low-temperature emission are 730 nm for monomeric and 760 nm for trimeric PS I complexes from *A. platensis*. It has been shown that C740 in PS I trimers of *A. platensis* emerges upon trimerization of isolated monomeric PS I complexes (Kruip et al., 1999) indicating that about three Chls of each monomer are red-shifted due to interactions and/or changes in pigment organization induced by the trimerization. Therefore, it has been proposed that C740 originates from pigment–pigment interactions of peripherally located Chls associated with different monomers within the trimeric complex. In the context of the 2.5 Å structure of trimeric PS I complex from *T. elongatus* (Jordan et al., 2001) this is difficult to rationalize because the shortest center-to-center distance between Chls of different monomers is 13.4 Å, which is the distance between aC-M1 and aC-PG1 (nomenclature of Jordan et al., 2001).

The formation of trimers changes not only the spectral characteristics of the Chls, but also those of the carotenoids (Fig. 2): The optical activity of carotenoids in the wavelength region between 480 and 530 nm of the circular dichroism (CD) spectra is higher in PS I trimers than in monomers (Shubin et al., 1993).

PS I trimers and monomers of *Synechocystis* sp. exhibit at 5 K a strongly broadened absorption band at 708 nm (corresponding to about five and three Chls, respectively) (Gobets et al., 2001a,b). Hole-burning experiments (Hayes et al., 2000; Raetsep et al., 2000) indicated that PS I monomers of *Synechocystis* sp. might contain a LWC form with an absorption maximum at 706 nm (three Chls), while PS I trimers contain two forms with an absorption maxima at 708 (two Chls) and 714 nm (two Chls). The maximum of the low-temperature emission is 724 nm for monomeric and trimeric PS I complexes from *Synechocystis* sp. PS I trimers of *Synechococcus* sp. PCC 7942 contain according to our knowledge the lowest number of LWC; the PS I complexes exhibit one red-antenna state with absorption maximum at 703 nm and an oscillator strength corresponding to about two Chls (Andrizhiyevskaya et al., 2002, 2004).

Higher plants and some algae contain the red-most Chls in the light-harvesting complex LHC I associated with Lhca3 and Lhca4), which give rise to the emission at 730–735 nm at low temperature (Croce et al., 2000, 2002; Morosinotto et al., 2002). The LWC in the PS I core absorb around 705 nm and emit at 720 nm.

Upon increasing the temperature, the absorption bands of the LWC, which are resolved well at 5 K, transform into a long, featureless red tail that is observed in the room temperature spectrum. More detailed studies of the temperature dependence of the absorbance spectrum show that a blue shift of the peak position and a

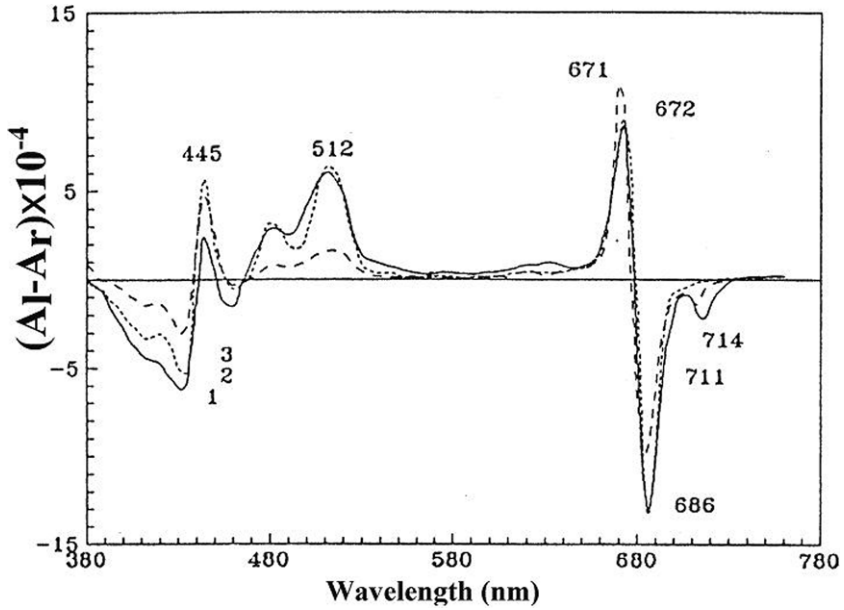

Fig. 2. CD spectra of the *A. platensis* isolated membranes (1) and trimeric (2) and monomeric (3) PS I complexes at 77 K. (Shubin et al., 1993)

broadening of the LWC bands occur when the temperature is raised from 5 K to room temperature (Cometta et al., 2000; Schlodder et al., 2005). The room temperature absorption and emission properties of the LWC have also been estimated from the target analysis of time-resolved fluorescence data (Gobets et al., 2001b). The pronounced peaks of F730 for PS I trimers and F715 for PS I monomers of *A. platensis* at 295 K (Fig. 3) provide evidence that LWC exists under physiological conditions (Karapetyan et al., 1997).

In addition to the strong red shift, other spectroscopic properties of the LWC have been shown to be

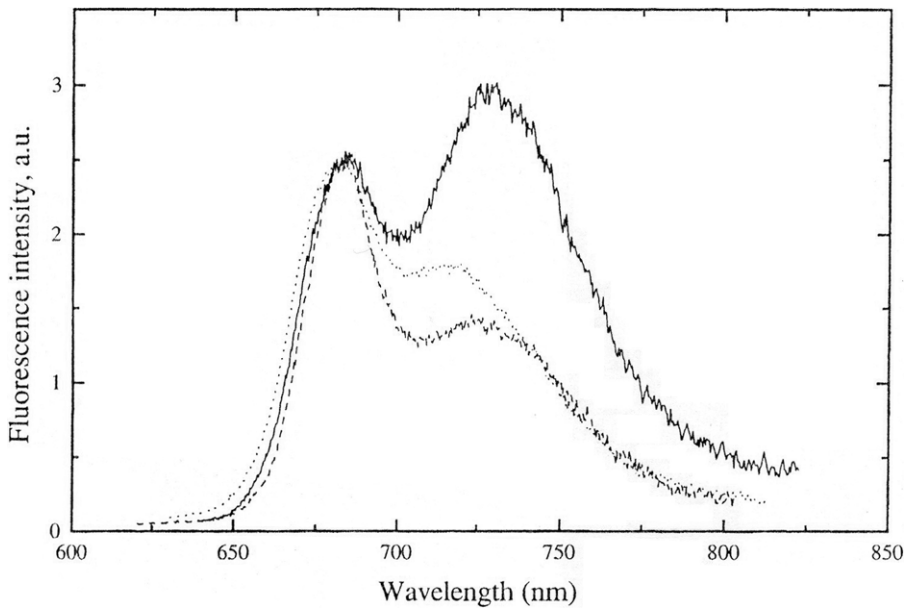

Fig. 3. Fluorescence emission spectra of membranes (dashed) and PS I trimeric (solid) and monomeric (dotted) complexes from *A. platensis* at 295 K. Spectra are normalized at their shortwave band, excitation wavelength 440 nm. (Karapetyan et al., 1997)

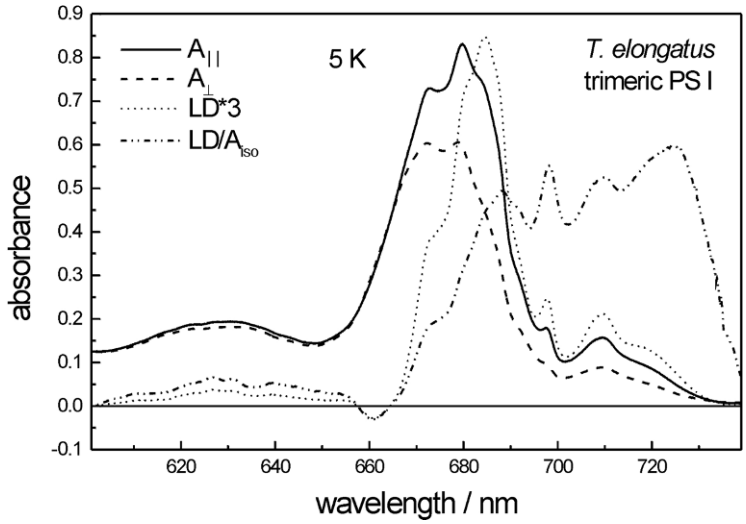

Fig. 4. Linear dichroism of trimeric PS I from *T. elongatus*: Steady-state polarized absorption ($A_{||}$ and $A_{\perp}$), LD = $A_{||} - A_{\perp}$ and reduced LD (=$LD/A_{isotropic}$) spectra of trimeric PS I complexes at 5 K. The LD spectrum is multiplied by a factor of 5.

different from those of the bulk antenna chlorophylls by hole-burning and fluorescence line-narrowing experiments at low temperature. The red-antenna states are characterized by a large Stokes shift of about 200 cm^{-1} due to strong electron–phonon coupling and by a large inhomogeneous broadening of 200–400 cm^{-1} (Gobets et al., 1994; Cometta et al., 2000; Raetsep et al., 2000). The FWHM of absorption and fluorescence bands of the extreme LWC in PS I trimers of *A. platensis* is, for example, about 20 nm as compared to 7–8 nm for bulk Chls. Stark spectroscopy revealed permanent dipole changes between the ground and excited state, which are about a factor of 3–5 larger than that of monomeric chlorophyll (Frese et al., 2002; Zazubovich et al., 2002). The red-most states in *T. elongatus* C719 and in *A. platensis* C740 are furthermore characterized by very large polarizability differences $\Delta\alpha$ between the ground and excited state with values of $f^2 \cdot Tr(\Delta\alpha)$ up to 600 $Å^3$ (f is the local field correction factor). High-pressure hole-burning experiments demonstrated large linear pressure-shift rates of about -0.45 $cm^{-1}MPa^{-1}$ for the red-most states in *T. elongatus* and *Synechocystis* sp. (Zazubovich et al., 2002). These unusual spectroscopic properties provide evidence that strongly excitonically coupled Chls are responsible for the long wavelength absorption and emission, respectively. Indeed, the very large polarizability differences $\Delta\alpha$ of the red-most states C719 of *T. elongatus* and C740 of *A. platensis*, which is similar to those of the special pair of the purple bacterial reaction center, may indicate the mixing of charge transfer states into the excited excitonic state. CD spectroscopy provided evidence that C708 of monomeric and trimeric PS I complexes from *A. platensis* is formed by excitonically coupled Chls (see Fig. 2 and Engelmann et al., 2001). The CD spectrum of the trimeric PS I complex from *T. elongatus* at 77 K also shows a separate band that has been attributed to the low energy exciton band of coupled Chls that give rise to long wavelengths absorption (Byrdin et al., 2002). No CD signal has been resolved thus far for C708 of *Synechocystis* sp. (van der Lee et al., 1993) and C740 of trimeric PS I from *A. platensis* (see Fig. 2) (Shubin et al., 1993; Engelmann et al., 2001). This might be the result of the specific organization of the excitonically coupled Chls. Calculations based on the 2.5 Å structure of trimeric PS I complex from *T. elongatus* (Jordan et al., 2001) show that the lowest exciton bands of the chlorophyll trimers A31A32B7 and B31B32B33 (see below) have small rotational strengths of less than 0.3 $D \cdot \mu_B$.

Information on the orientation of the transition dipole moments of the LWC relative to the membrane plane has been obtained by linear dichroism (LD) spectra. Figure 4 shows, as an example, the polarized absorption ($A_{||}$ and $A_{\perp}$), LD and reduced LD (LD/A_{iso}) spectra of trimeric PS I complexes from *T. elongatus* at 5 K. On the long wavelength side of the main peak in the LD spectrum distinct bands at about 698, 709, and about 720 nm are well resolved. The $LD/A_{isotropic}$ ratio is maximal for the red-most band at 720 nm ($LD/A_{iso} \approx 0.6$). With an orientation factor of about 0.4–0.45, the angle ϑ between the

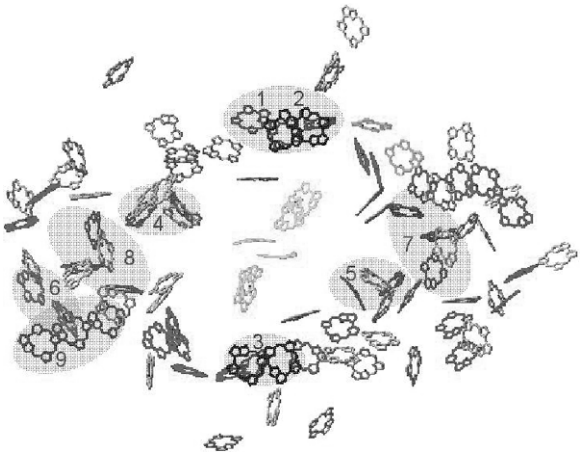

Fig. 5. The arrangement of Chls in one PS I monomer of *T. elongatus*. Only the ring planes of the Chls are shown for clarity. The strongest coupled Chls with an interaction energy $\geq$100 cm^{-1} are depicted in grey. See Color Plate 9, Fig. 1.

transition dipole moment of C719 and the normal to the membrane plane can be calculated using the equation $LD/(3\cdot A_{iso}) = -\langle 0.5\cdot(3\cdot\cos^2\vartheta - 1\rangle \cdot \Phi(n)$ to $80^\circ < \vartheta < 100^\circ$, i.e., the transition moment of the red-most state is oriented virtually parallel to the membrane plane (Schlodder et al., 2005). The reduced LD is only slightly lower for the absorbance band around 708 nm, demonstrating that the transition moments of C708 lie also preferentially parallel to the membrane plane. LD studies of PS I complexes from other species demonstrated also that the transition dipole moments of LWC are almost parallel to the membrane plane (Duval et al., 1986; van der Lee et al., 1993; Schlodder et al., 2005).

III. Localization of Long Wavelength Chlorophyll in Antenna

A. PS I Core Complex

The only PS I complex from cyanobacteria for which a high-resolution X-ray structure is available is the trimeric PS I complex from *T. elongatus* (Jordan et al., 2001) (see Fromme and Grotjohann, this volume, Chapter 6). In the present chapter we will only discuss which of the 96 Chls identified in the structure might be responsible for the long wavelength absorption. On the basis of the spectroscopic properties of LWC described in section II, it has been proposed that red antenna states originate from strongly excitonically coupled Chls. Therefore, we address first the excitonic interactions between the Chls in the trimeric PS I complex from *T. elongatus* (for a more detailed discussion see Byrdin et al., 2002). The mean center-to-center distance between neighboring Chls in the cyanobacterial PS I is 9.9 Å, which is only slightly more than the diameter of the chlorin ring. This dense packing indicates that excitonic interactions play an important role. From the mean nearest neighbor distance an average interaction energy between neighboring Chls of $\sim$70 cm^{-1} is calculated, which corresponds to $\sim$6 nm splitting between the upper and lower excitonic bands.

Figure 5 shows the arrangement of the Chls in one monomer of PS I [pdb file 1JB0]. The strongest coupled Chls with an interaction energy $\geq$100 cm^{-1} are depicted in color. Reddish tones are used if virtually all oscillator strength of the coupled Chls is concentrated in the red-shifted lowest exciton state. If the oscillator strength of the coupled Chls is more equally distributed between upper and lower exciton states, the coupled Chls are represented in green. There are two pairs in blue (A38-A39 and B37-B38 (the nomenclature of Jordan et al., 2001 is used for naming Chls). In these cases, the upper exciton state carries most of the oscillator strength. The ratio between the oscillator strengths of the lower and upper exciton states is about 0.2. In the extended dipole approximation, the strongest couplings ($\sim$250 cm^{-1}) have been calculated for the trimers B7-A32-A31 and B31-B32-B33. It should be noted that upon application of the point dipole approximation, the strongest coupling of 415 cm^{-1} is found between the two pigments that constitute the special pair of P700, corresponding to an excitonic splitting of $\sim$39 nm. It is obvious that excitonic interactions alone cannot explain the strong red shift of LWC. Most probably pigment–protein interactions, which give rise to lower individual site energies of the involved Chls, contribute to the red shift. Furthermore, charge transfer interactions have to be taken into account as well, especially in view of the fact that the edge-to-edge distances between strongly coupled Chls (closest contacts of the π-systems) are close to van der Waals contact.

Although the LWC in PS I from *T. elongatus* (C708 and C719) and the number of Chls contributing to these red-antenna states are known (see Table 1), it is difficult to ascribe the various structurally defined aggregates to specific spectral forms of LWC. Even if we take into consideration that the transition moments of the red-most states are oriented virtually parallel to the membrane plane, any spectral/structural assignment is rather speculative. The coupled Chls circled by elliptical rings in Fig. 5 are possible candidates: (1) A31-A32-B7 with $\vartheta = 95.5^\circ$ (ϑ is the angle between the transition moment of the lower exciton transition and the normal

to the membrane plane) and N = 1.5 (N represents the number of Chls contributing to low energy exciton transition); (2) B18-B19 with $\vartheta = 85^\circ$ and N = 1.9; (3) A26-A27 with $\vartheta = 90.2^\circ$ and N = 0.8; (4) B24-B25 with $\vartheta = 85.5^\circ$ and N = 0.8; (5) B37-B38 with $\vartheta = 91.3^\circ$ and N = 0.4, (6) A38-A39 with $\vartheta = 96.1^\circ$ and N = 0.8; (7) A16-A17-A25 with $\vartheta = 107.6^\circ$ and N = 1.6; (8) B14-B15-B23 with $\vartheta = 107.9^\circ$ and N = 1.6; and (9) B31-B32-B33 with $\vartheta = 111.5^\circ$ and N = 2.9. Interestingly, more than one strongly coupled aggregate is required to match the observation that the oscillator strength of C719 (C708) corresponds to four (five) Chls. The assignment by Zazubovich et al. (2002) that A38-A39 represents C715 and B37-B38 represents C719 would explain only about 15% of the oscillator strength of the red-most transitions. On the basis of modeling of time-resolved fluorescence data at room temperature (Gobets et al., 2003b) it has been proposed that the trimer B31-B32-B33 with $\vartheta = 111.5^\circ$ and N = 2.9 is involved in the C719 spectral form. However, this assignment is not in agreement with the above-described LD experiment at 5 K. The latest data accept that the strongly coupled aggregate (A31-A32-B7) located on the lumenal side close to the trimerization domain of the trimeric complexes and forming hydrophobic contacts with PsaL may represent the C719 (Byrdin et al., 2002; Sener et al., 2002). Obviously, this location is very sensitive both to the lack of the PsaL subunit in a deletion mutant and to the loss of PsaL by detergent treatment, which could explain the lower number of C719 in monomeric PS I (see Table 1). Additionally, B7 is unique for this side of the complex and has no C_2-symmetry analogue on the opposite side.

The dimers A33-A34 and A24-A35 have been suggested to represent C715, while the dimer B22-B34 has been suggested to represent C708 (Sener et al., 2002). The dimer A33-A34 can be excluded because of $\vartheta = 69.7^\circ$. A24-A35 and B22-B34 are not colored in Fig. 5 because these dimers are not strongly coupled.

It is interesting to compare the organization of the Chls in the 2.5 Å structure from *T. elongatus* (Jordan et al., 2001) with those observed in the 4.4 Å structure from pea (Ben-Shem et al., 2003), also because the latter complex does not contain C719, but only C708. Though the latter structure is still at intermediate resolution, it appears that the positions and orientations of most Chls are conserved between cyanobacteria and higher plants. One of the rare differences is Chl B33, which is in significantly different orientations in both organisms. This suggests that the trimer B31/B32/B33 located on the periphery of PS I core antenna could be involved in the C719 spectral form in *T. elongatus*. Note that 92 Chls in the plant PS I core are indicated at the same position as that in the PS I core of cyanobacteria (Jordan et al., 2001; Ben-Shem et al., 2003).

B. LHC I

The PS I complex of higher plants and algae (PS I-200) consists of the PS I core complex and the peripheral LHC I. In higher plants and algae, several Lhca complexes are connected to each PS I monomer (Jansson, 1994; Fromme et al., 2003). Electron microscopic characterization of green plant PS I indicates that LHC I binds to the core complex only on the side of the subunits PsaF/PsaJ and thus does not cause structural hindrances for possible trimerization (Boekema et al., 2001) (see Haldrup et al., this volume, Chapter 11). Recently, a crystal structure at 4.4 Å resolution was published of PS I-200 from pea (Ben-Shem et al., 2003), revealing the binding of four LHC I proteins in a half-moon shape at the PsaF/PsaJ side of the complex (see Nelson and Ben-Shem, this volume, Chapter 7). Green algae such as *Chlamydomonas reinhardtii* bind larger numbers of LHC I proteins (Germano et al., 2002; Kargul et al., 2003). The Lhca1 and Lhca4 proteins of LHC I form a heterodimer in solution (Schmid et al., 1997), which gives rise to a 77 K emission band peaking at about 730 nm and is generally referred to as F730. It was shown that most of the long wavelength emission originates from Lhca4. Lhca2 and Lhca3 were thought to give rise to a 77 K emission peak at 680 nm (the same maximum as observed for all PS II-associated Chl *a*/*b* binding proteins) and could therefore be responsible for LHC I-680, but recent experiments suggested that LHC I-680 could also be a product of the monomerization of the LHC I-730 dimer (Croce et al., 2002). Instead, Lhca2 and/or Lhca3 were shown to give to rise to F702, which originates from an absorption band peaking between 690 and 695 nm (Ihalainen et al., 2000, 2003).

More information on the origin of F730 was recently obtained by Morosinotto et al. (2003). These authors used *in vitro* reconstitution to obtain monomers of Lhca1–4, of which Lhca1 and Lhca2 were shown to give rise to F702, and Lhca3 and Lhca4 to F730 (Morosinotto et al., 2002; Schmid et al., 2002). It appears that Lhca3 and Lhca4 have Asn as the ligand for Chl A5 instead of His, the ligand for Chl A5 in Lhca1, Lhca2, and all Lhcb proteins of PS II, which all show no or a low amounts of LWC. It was shown by site-directed mutagenesis that Asn as ligand for Chl *a* in the A5 binding site is essential for the formation of F730, whereas a substitution of Asn to His ligand in Lhca3 and Lhca4

resulted in a clearly blue-shifted emission (Morosinotto et al., 2003). These results indicate that a pair of Chls bound at the A5 and B5 sites is responsible for F730 in LHC I. The recent finding that the A5 and/or B5 Chls are tilted in LHC I compared to LHC II (Ben-Shem et al., 2003) can be in line with this suggestion.

IV. Dissipation of Excess Energy in PS I via Long Wavelength Chlorophyll

LWC of PS I compete with P700 for excitation energy, and therefore may serve as indicators of energy utilization by the RC. The fluorescence yield of LWC in the PS I antenna is strongly quenched at room temperature and becomes visible in plants and algae only at 77 K as an intense band F735 emanated from LWC of LHC I absorbing at 705–710 nm, or as F720 emitted by LWC of PS I core antenna absorbing around 705 nm (Fromme et al., 2003). Unicellular cyanobacteria such as *Synechocystis* sp. PCC 6803 show the 77 K fluorescence band F720 emitted by PS I core LWC absorbing at 708 nm (van der Lee et al., 1993; Palsson et al., 1996). In addition to F730, the PS I trimers of the cyanobacterium *A. platensis* at 77 K exhibit extremely red-shifted fluorescence F760 emitted by core C740 (Shubin et al., 1992; Karapetyan et al., 1997).

Remarkably, the fluorescence lifetime and yield, respectively, were found to be very similar in PS I with P700 in the reduced ("open RC") and oxidized ("closed RC") states at room temperature. A small amount of light-induced fluorescence enhancement (~5%) of PS I at room temperature for PS I enriched particles isolated from bean chloroplasts was attributed to $P700^+$ accumulation (Karapetyan et al., 1973). A larger (~12%) light-induced increase of long wave fluorescence as a result of $P700^+$ accumulation was observed at room temperature for PS I trimers of the cyanobacterium *T. elongatus* (Byrdin et al., 2000). The invariance of PS I fluorescence was explained as a quenching of the fluorescence of PS I antenna by P700 and $P700^+$ with equal efficiency (Shubin et al., 1995; Karapetyan 1998).

At 77 K, accumulation of $P700^+$ was accompanied by a light-induced decrease of fluorescence in PS I enriched particles (Ikegami, 1976), PS I trimers of the cyanobacterium *A. platensis* (Shubin et al., 1992) and in *T. elongatus* (Byrdin et al., 2000). No fluorescence changes dependent on P700 redox state have been found in PS I trimers of the cyanobacterium *Synechocystis* sp. (van der Lee et al., 1993). The absence of

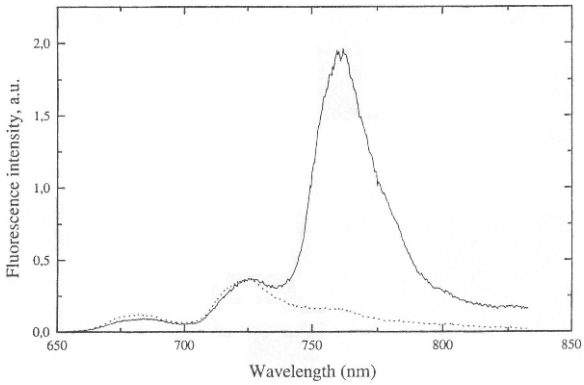

Fig. 6. Fluorescence emission spectra of *A. platensis* PS I trimers for P700 in the reduced (solid) and oxidized (dotted) state (77 K), excitation 440 nm. (Karapetyan et al., 1997)

variable F735 nm in PS I of plants may be due to by the large distance between P700 and the LWC localized on LHC I (about 65 Å, according to Dorra et al., 1998). Note that the intensity of F760 in PS I trimers of *A. platensis* (Fig. 6) as F730 in PS I trimers of *T. elongatus* strongly depends on the P700 redox state at 77 K: it is maximal with P700 is reduced, and minimal with P700 oxidized (Shubin et al., 1993; Karapetyan et al., 1997; Byrdin et al., 2000). $P700^+$ quenches F760 in PS I trimers of *A. platensis* more than one order of magnitude, while F725 of PS I monomers is independent of the P700 redox state (Karapetyan et al., 1997). Quenching of F730 by $P700^+$ in PS I trimers of *T. elongatus* at 5 K was less efficient than that in PS I trimers of *A. platensis* (Byrdin et al., 2000).

The low yield of variable fluorescence of PS I under physiological conditions results from the fact that may different types of energy dissipation in open and closed PS I centers (quenching by charge separation and quenching by chlorophyll cation radicals) are functioning with almost the same quenching efficiency. At low temperature, the strong F760 quenching in PS I trimers of *A. platensis* can be attributed to the direct energy transfer from the LWC absorbing at 740 nm to $P700^+$ (Shubin et al., 1995). The value of the Förster overlap integral between F760 and the absorption band of $P700^+$ in PS I trimers of *A. platensis* is about two orders of magnitude higher than that for P700 (Dorra et al., 1998). This value compensates for the large distance of about 42 Å between P700 and LWC emitting F760 (Dorra et al., 1998; Karapetyan et al., 1999a); a more correct evaluation provides a distance of 32 Å (Schlodder et al., 2005). At the same time, the values of the overlap integral between F730 and $P700/P700^+$ in PS I monomers of cyanobacteria and PS I complexes of

higher plants are equal. Quenching of the long wavelength fluorescence of Bchls by cation radical of the primary electron donor of RC was observed also for the heliobacterium *Heliobacterium chlorum* (Deinum et al., 1991) and the purple bacterium *Rhodopseudomonas viridis* (Kleinherenbrink et al., 1992). The higher values of the overlap integral between the emission band of long wavelength Bchl with the absorption band of cation radicals ($P965^+$ or $P798^+$) as compared with that of reduced primary donors has suggested a similar type of quenching mechanism.

Evidence for an energy exchange between antenna Chls of monomers within a PS I trimer of *A. platensis* has been derived from simultaneously-measured kinetics of P700 oxidation and the light-induced decrease of F760 at 77 K (Karapetyan et al., 1999b). Although the decrease of F760 nm was ascribed to a stronger quenching effect of $P700^+$ on F760 than of reduced P700 (Shubin et al., 1995; Dorra et al., 1998), the light-induced F760 decrease in trimers was faster than P700 oxidation (Karapetyan et al., 1999b). The nonlinear relationship between the variable part of F760 and the fraction of reduced P700 is considered to be the result of an energetic connectivity of the antenna of monomeric complexes within a trimer. When one of the P700 centers in PS I trimers of *A. platensis* is oxidized, the energy from an antenna of monomers with reduced P700 may migrate to a subunit with $P700^+$ and be quenched there. The energy exchange between the antenna of monomers within a PS I trimer stimulates quenching of F760 by $P700^+$ was confirmed by a difference in the midpoint potentials (E_m) between P700 and F760 (Schlodder et al., 2005). The relationship between the values of E_m of F760 and P700 also indicates that about 30% of $P700^+$ (i.e., when one monomer within each trimer on the average has $P700^+$) causes the quenching of about 70% of F760, and 60% of $P700^+$ quenches about 90% of F760 as a result of such energy exchange between monomers within a trimer. A model was presented describing the energetic interaction of antenna of monomeric complexes within the PS I trimer via C740 (Karapetyan et al., 1999b). The intermonomer energy exchange provides no gain in photochemistry, but it stimulates the dissipation of excess energy as heat and therefore protects the RC against photodestruction. PS I trimers are more stable to the light excitation as compared with monomers: According to the X-ray structure of PS I trimers of *T. elongatus*, carotenoids are located close to LWC and in the region of monomer interaction of trimer (Fromme et al., 2001; Jordan et al., 2001).

Under highly reducing conditions, excess energy is also dissipated efficiently. The triplet state of P700 ($^3P700$) is formed when A_1 is prereduced by dithionite. Under these conditions, when electron transport to A_1 is blocked, the primary radical pair $P700^+ A_0^-$ recombines to $^3P700$ which decays with a half-life of $t_{1/2} \sim$ 1.1 msec at 5 K in PS I trimers of *A. platensis* (Witt et al., 2003). The formation and decay of $^3P700$ at 5 K could also be recorded by flash-induced changes of the fluorescence intensity at 760 nm in PS I trimers from *A. platensis*. The flash-induced decrease of F760 attributed to the formation of $^3P700$ decays with virtually the same kinetics as $^3P700$. This provides direct kinetic evidence that $^3P700$ is also an effective quencher of F760 (Schlodder et al., 2005). Thus, dependent on the redox state of P700 and PS I cofactors, fluorescence of the LWC is quenched efficiently under all conditions investigated thus far: either by P700 or by $P700^+$ and $^3P700$, respectively.

V. Energy Transfer and Trapping in PS I

A. Time-Resolved Spectroscopy

The core antenna of PS I is intimately bound to the RC of PS I and consequently time-resolved experiments on native PS I need to be performed on systems with a large number (about 100) of Chls all connected via efficient energy transfer. During the past decade, PS I complexes of a wide variety of species have been studied using (sub-)picosecond time-resolved techniques, including pump-probe, single photon timing, fluorescence upconversion and with the use of a synchroscan streak camera. For most of these PS I cores it was found that the trapping time was in the few 10s of picoseconds range and increasing for systems that contained an increasing complement of red pigments: *Synechococcus* sp. PCC 7942: 19 psec, *Synechocystis* sp. PCC 6803 and plant cores: 22 psec, *T. elongatus*: 36 psec, *A. platensis*: 51 psec. In addition to these "slow" trapping times a number of faster events could be distinguished that all reflected various stages of equilibration (see Savikhin, this volume, Chapter 12).

Figure 7 shows the decay associated spectra (DASes) of PS I core of trimer of *T. elongatus* (Gobets et al., 2001b). Two distinct energy transfer components of 3.8 and 9.6 psec can be distinguished for C708 and C719. The 3.8 psec equilibration component exhibits a DAS, which shows the equilibration between bulk Chls of PS I and C708 (which peaks at 702 nm at room temperature). The spectrum is more or less conservative,

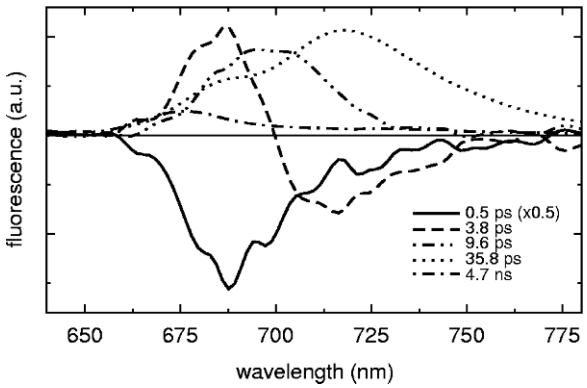

Fig. 7. DAS of fluorescence decay of PS I trimers of *T. elongatus* at 295 K, excitation at 400 nm. (Gobets et al., 2001b)

indicating that in the trimeric core of *T. elongatus* the amount of trapping that occurs with the 3.8 psec time constant is negligible. In contrast, the 9.6 psec DAS is highly nonconservative and basically consists of a broad positive contribution that peaks around 700 nm. This spectrum suggests that during the 9.6 psec component both trapping by charge separation and further equilibration between the bulk/C708 and the C719 pools of Chls is taking place.

B. Modeling Energy Transfer and Trapping in the PS I core

The kinetic model of the fluorescence spectral dynamics of a variety of PS I cores was developed by Gobets and coworkers (2001b). The model discussed here mainly for the PS I core of *T. elongatus* includes ultrafast relaxation from the Soret to the Q_y region, followed by relaxation between the various pools of Chls (bulk, C708, C719) and trapping (Fig. 8). An important result of the kinetic modeling was that a trapping time of 18 psec could be estimated for a hypothetical PS I core without red pigments. Earlier attempts to understand energy transfer and trapping in PS I on the basis for instance of lattice models all suffered from the problem of locating the red pigments. A combination of the charge separation time and (average) single-site lifetime (defined as the time it takes to "hop" away from a certain pigment) result in a 18 psec trapping time of a PS I core "without red pigments." Realistic estimates for the single-site lifetime (τ_{ss}) and the charge separation time (τ_{cs}) are 150 fsec and 1 psec, respectively (note that it is assumed that charge separation may occur from both Chls in P700). The (almost) linear relation between τ_{ss} and τ_{cs} could be explained using a relatively simple perturbed two-level model. This model led to an estimation of the first passage time (fpt) of about 8.5 psec (Gobets et al., 2003a). This implies that on the average an excitation is trapped on the second visit to the RC. The value of the fpt is almost identical to the average time needed for an excitation to reach one of red Chl pools in *T. elongatus*, corroborating experimental evidence that these two processes compete in an approximately 1:1 ratio.

The probability of escaping from the RC after reaching it for the first time is about 50% but most of these excitations are trapped on subsequent revisits. Making the bulk antenna inhomogeneous has some effect on these parameters (for instance the probability of escaping increases), but the general conclusions remain unchanged. To compare the estimated value of τ_{ss} with an experiment, the polarized fluorescence of PS I cores was studied using fluorescence upconversion (Kennis et al., 2001). The anisotropic decay showed a major component of ~150 fsec, most likely reflecting the decay in polarization due to a single energy-transfer step

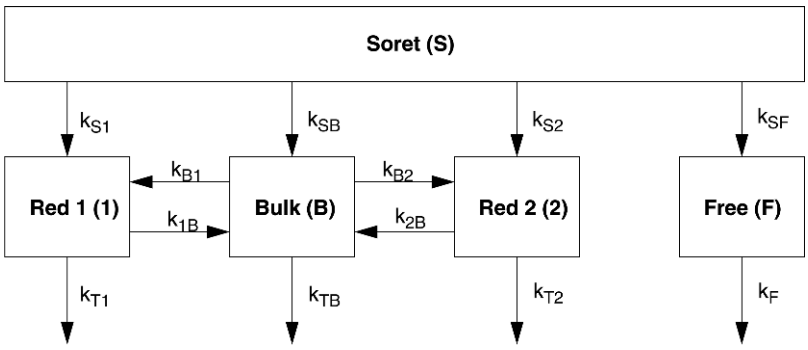

Fig. 8. Compartmental model describing the kinetics of PS I trimeric complex of *T. elongatus* upon excitation at 400 nm. Red 1 represents the pool of C708 and Red 2 represents the pool of the most-red Chls (C719 or C740), Free represents some uncoupled Chls.

in the bulk antenna and consistent with the modeling result. Another important conclusion that follows from the kinetic model (Fig. 8) is that trapping (and thus transfer to the RC) takes place both from the bulk Chls and from the red Chl pools. Comparing the trapping rates relative to the spectral overlap of their emission with the absorption spectrum of P700 indicates that the red Chls in the C708 pool are neither close to the RC nor very distant. For the C719 Chls a more distant location could not be ruled out.

Having accurate estimates for τ_{ss} and the charge separation rate, k_{cs}, the only thing that is required to calculate the dynamics of the PS I core of *T. elongatus* is to assign the C708 and C719 pools in the structure. Since the red pigments are thought to consist of dimers or larger aggregates of Chls, strongly coupled Chl aggregates in the structural model are the prime candidates for these pools. There exist various possible choices for the dimers (Jordan et al., 2001; Sener et al., 2002; Gobets et al., 2003b); assigning any triplet combination these dimers to the C708 species gave good results. In contrast, the C719 species was best represented by the trimer consisting of the Chls designated as aC-B31, aC-B32, and aC-B33. Any other choice could not reproduce the distinct 10 psec equilibration phase.

The amplitudes of the contributions to the DASes of each of the five pools of Chls (bulk, C708, C719, P700, and A_0; A_0 is a Chl *a* monomer, and the primary electron acceptor of PS I) for each of the 96 lifetimes in the system have been studied. Remarkably, only a few (clusters) of the 96 lifetimes correspond to DASes with significant amplitude. Four clusters of lifetimes dominate the dynamics of the system for all excitation conditions: 37.5, 10.9, ~3, and <1.5 psec. First of all we note the excellent correspondence between the lifetimes from the modeling with those from the experiment. Second, the spectrum of the 35–38 psec component is independent of the excitation wavelength, consistent with the experimental trapping spectrum (Gobets et al., 2003b). Note that the amplitude of this spectrum does depend on the excitation wavelength due to the fact that there is significant nonequilibrium trapping upon bulk excitation, but much less when the red pools are excited. Third, the 10.9 psec component clearly reflects energy transfer between the bulk/C708 pools and C719, while the group of ~3 psec components mainly display energy transfer between bulk and C708. Finally, the amplitudes of the <1.5 psec components are small, since they are associated mainly with transfer within the bulk pool, and thus do not lead to spectral changes. The sum of the large number of ultrafast components, however, does show a significant amount of equilibration between the bulk and red pools, especially for selective excitation of the red Chls, consistent with the (sub)-picosecond components that were found for such excitation conditions (Gobets et al., 2003b). Using the emission spectra for the various spectral forms extracted from these data in combination with the kinetic model (Gobets et al., 2003a) one can reconstruct the DASes of each of the four lifetime components. Notably, the very nonconservative character of the 10 psec component is reproduced in the simulation.

The assignment of the Chl trimer to C719 was essential in reproducing the 10 psec equilibration component. The use of any of the dimers (either alone or in combination with another dimer) to represent C719 did not result in a distinct separation of a ~10 psec transfer component from the faster ones. It thus appears that C719 needs to be located in one single cluster on the periphery of the antenna. The assignment of the Chl trimer to the C719 pool is supported by structural and biochemical data for *T. elongatus* and *Synechocystis* sp. PCC 6803, where PS I of the latter organism lacks C719. The lumenal loop in PsaB, which stabilizes the Chl trimer in *T. elongatus*, is shorter in *Synechocystis* sp.; subunit PsaX, which interacts with one of the Chls of the trimer is probably not present in *Synechocystis* sp. PCC 6803; and the axial ligand to aC-B31 (His-B740) is not conserved in *Synechocystis* sp. PCC 6803. Therefore, the presence of a Chl trimer like in PS I of *T. elongatus* is unlikely for PS I of *Synechocystis* sp. PCC 6803 (N. Krauß, P. Jordan, and P. Fromme, personal communication).

It has been speculated that the linker Chls, aC-A40 and aC-B39, play a bridging role in energy transfer from the antenna to the RC (Jordan et al., 2001). However, a simulation of the excitation transfer under conditions in which these linker Chls were removed showed that the dominant lifetimes were only slightly increased. For instance, the trapping time was slowed down by only 2%. Therefore, it is concluded that the linker Chls do not perform a special role in light-harvesting in PS I.

C. Energy Transfer and Trapping in LHC I and PS I-200

The main function of LHC I is to absorb light and transfer the excited state energy to the core of PS I. The excited state decay in a mixture of isolated dimers of LHC I was investigated using fluorescence upconversion and a synchroscan streak camera (Gobets et al., 2001a), while the reconstituted monomeric Lhca4 and

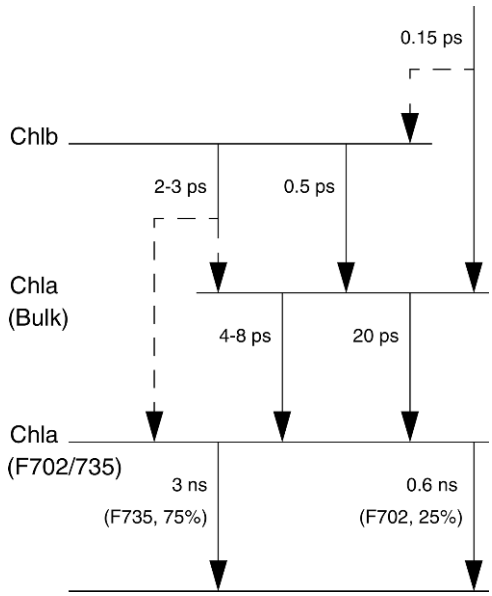

Fig. 9. Scheme of energy-transfer pathways in LHC I. Dashed lines indicate the pathways that presently cannot be decided upon based on our data.

the heterodimer Lhca1/Lhca4 were studied with single photon counting and transient absorption (Melkozernov et al., 1998, 2000c).

In the dimers of LHC I the energy transfer from the carotenoid excited S_2 states to predominantly Chl *a* was found to take place within 150 fsec; whether the S_1 state is involved in slower energy transfer is unknown. Energy transfer from Chl *b* to Chl *a* occurs with two distinct lifetimes, 0.5 and 2–3 psec. The 0.5 psec component mainly reflects energy transfer to the bulk Chl *a*, whereas the 2–3 psec component may also account for direct energy transfer from Chl *b* to the special red-shifted Chl *a* forms. Equilibration between the bulk Chl *a*s and these red-shifted Chl *a* forms displays various lifetimes ranging at 4–8 psec, while a slower phase occurs with about 20 psec. Since the 4–8 psec component was also observed in monomer Lhca4 (Melkozernov et al., 2000c), while the slower phase only appeared in the heterodimer, the 4–8 psec phase probably reflects intramonomer equilibration, while the 20 psec component is energy transfer between the two monomers. Figure 9 summarizes the energy transfer pathways in LHC I.

The fluorescence of these LHC I dimers decays bi-exponentially. The largest fraction of excitations (75–80%), which decays with a 3 nsec time constant, is attributed to the Lhca1/Lhca4 heterodimer and a homodimer of either Lhca2 or Lhca3, whereas the remaining fraction, which decays in 0.6 nsec, is assigned to the remaining homodimer. Large PS I particles show an average fluorescence decay time of about 80 psec (van Grondelle et al., 1994). Faster phases were ascribed to equilibration. A full global analysis of the room temperature fluorescence decay of pea chloroplasts recorded at a variety of wavelengths, led to the assignment of a 10–20 psec phase to equilibration, followed by a 80–120 psec trapping process in PS I. A recent streak-camera study of PS I-200 of *Arabidopsis thaliana* gave lifetimes of 5, 15, 50, and 120 psec (Ihalainen et al., 2002). The 5 and 15 psec phase could at least in part be attributed to the excitation equilibration between bulk and red Chl forms, though the 15 psec phase also contains a contribution from nonequilibrium trapping, similar to the 10 psec phase observed in the PS I cores of *T. elongatus*. The 50 and 120 psec phases have all-positive spectra and correspond to the trapping of the excitations. Very similar kinetics has been reported for PS I-200 from maize (Croce et al., 2000) and spinach (Turconi et al., 1994). A straightforward explanation for the two phases could be that the 50 psec phase, which peaks at 720 nm, reflects the trapping from the PS I core, while the 120 psec phase, which peaks above 725 nm contains a large contribution from the peripheral antenna LHC I, in particular from Lhca1/Lhca4 (Ihalainen et al., 2002).

Acknowledgments

This work was supported by the Russian Academy of Sciences, program Molecular and Cellular Biology (NK), by a grant from the Deutsche Forschungsgemeinschaft, Sfb 498 TP A6 (ES) and by the Netherlands Organization for Scientific Research (NWO) through the Foundation of Life and Earth Sciences (ALW), and by the European Union through the PSICO Research Training Network (RvG and JPD).

References

Andrizhiyevskaya EG, Schwabe TME, Germano M, D'Haene S, Kruip J, van Grondelle R and Dekker JP (2002) Spectroscopic properties of PS I–IsiA supercomplexes of the cyanobacterium *Synechococcus* PCC 7942. Biochim Biophys Acta 1556: 265–272

Andrizhiyevskaya EG, Frolov D, van Grondelle R and Dekker JP (2004) Energy transfer and trapping in the photosystem I complex of *Synechococcus* PCC 7942 and in its supercomplex with IsiA. Biochim Biophys Acta 1656: 104–113

Ben-Shem A, Frolow F and Nelson N (2003) Crystal structure of plant photosystem I. Nature 426: 630–635

Boekema EJ, Jensen PE, Schlodder E, van Breemen JFL, van Roon H, Scheller HV and Dekker JP (2001) Green plant photosystem I binds light-harvesting complex I on one side of the complex. Biochemistry 40: 1029–1036

Brody SS (1958) New excited state of chlorophyll. Science 128: 838–839

Byrdin M, Rimke I, Schlodder E, Stehlik D and Roelofs TA (2000) Decay kinetics and quantum yields of fluorescence in photosystem I from *Synechococcus elongatus* with P700 reduced and oxidized state: are the kinetics of excited state decay trap-limited or transfer-limited? Biophys J 79: 992–1007

Byrdin M, Jordan P, Krauß N, Fromme P, Stehlik D and Schlodder E (2002) Light harvesting in photosystem I: modelling based on 2.5 Å structure of photosystem I from *Synechococcus elongatus*. Biophys J 83: 433–457

Cometta A, Zucchelli G, Karapetyan NV, Engelmann E, Garlashi FM and Jennings RC (2000) Thermal behavior of long wavelength absorption transitions in *Spirulina platensis* photosystem I trimers. Biophys J 79: 3235–3243

Croce R, Dorra D, Holzwarth AR and Jennings RC (2000) Fluorescence decay and spectral evolution in intact photosystem I of higher plants. Biochemistry 39: 6341–6348

Croce R, Morosinotto T, Castelletti S, Breton J and Bassi R (2002) The Lhca antenna complexes of higher plants photosystem I. Biochim Biophys Acta 1556: 29–40

Deinum G, Kramer H, Aartsma TJ, Kleinherenbrink FAM and Amesz J (1991) Fluorescence quenching in *Heliobacterium chlorum* by reaction centers in the charge separated state. Biochim Biophys Acta 1058: 339–44

Dorra D, Fromme P, Karapetyan NV and Holzwarth AR (1998) Fluorescence kinetics of photosystem I: multiple fluorescence components. In: Garab G (ed) Photosynthesis: Mechanisms and Effects, Vol 1, pp 587–590. Kluwer, Dordrecht

Duval J-C, Thomas J-C and Choquet Y (1986) 77 K fluorescence quenching induced by reduction of photosystem I primary electron acceptors in a cyanobacterium. Biochim Biophys Acta 848: 352–358

Engelmann E, Tagliaube T, Karapetyan NV, Garlaschi FM, Zucchelli Z and Jennings RC (2001) CD spectroscopy provides evidence for excitonic interactions involving red-shifted chlorophyll forms in photosystem I. FEBS Lett 499: 112–115

Frese RN, Palacios MA, Azzizi A, van Stokkum IHM, Kruip J, Roegner M, Karapetyan NV, Schlodder E, van Grondelle R and Dekker JP (2002) Electric field effects on red chlorophylls, β-carotenes and P700 in cyanobacterial photosystem I complexes. Biochim Biophys Acta 1554: 180–191

Fromme P, Jordan P and Krauß N (2001) Structure of photosystem I. Biochim Biophys Acta 1507: 5–31

Fromme P, Schlodder E and Jansson S (2003) Structure and function of the antenna system in photosystem I. In: Green BR and Parson WW (eds) Light-Harvesting Antennas in Photosynthesis, pp 253–279. Kluwer, Dordrecht

Germano M, Yakushevska AE, Keegstra W, van Gorkom HJ, Dekker JP and Boekema EJ (2002) Supramolecular organization of photosystem I and light-harvesting complex I in *Chlamydomonas reinhardtii*. FEBS Lett 525: 121–125

Gobets B and van Grondelle R (2001) Energy transfer and trapping in photosystem I. Biochim Biophys Acta 1507: 80–99

Gobets B, van Amerongen H, Monshower R, Kruip J, Rögner M, van Grondelle R and Dekker JP (1994) Polarized site-selected fluorescence spectroscopy of isolated photosystem I particles. Biochim Biophys Acta 1188: 75–85

Gobets B, Kennis JTM, Ihalainen JA, Brazzoli M, Croce R, van Stokkum IHM, Bassi R, Dekker JP, van Amerongen H, Fleming GR and van Grondelle R (2001a) Excitation energy transfer in dimeric light-harvesting complex I: a combined streak-camera/fluorescence upconversion study. J Phys Chem B 105: 10132–10139

Gobets B, van Stokkum IHM, Rögner M, Kruip J, Schlodder E, Karapetyan NV, Dekker JP and van Grondelle R (2001b) Time-resolved fluorescence emission measurements of photosystem I particles of various cyanobacteria: a unified compartmental model. Biophys J 81: 407–424

Gobets B, Valkunas L and van Grondelle R (2003a) Bridging the gap between structural and lattice-models: a parametrization of energy transfer and trapping in photosystem I. Biophys J 85: 3872–3882

Gobets B, van Stokkum IHM, van Mourik F, Dekker JP and van Grondelle R (2003b) Excitation wavelength dependence of the fluorescence kinetics in photosystem I particles from *Synechocystis* PCC 6803 and *Synechococcus elongatus*. Biophys J 85: 3883–3898

Golbeck JH (1994) Photosystem I of cyanobacteria. In: Bryant DA (ed) The Molecular Biology of Cyanobacteria, pp 319–360. Kluwer, Dordrecht

Hayes JM, Matsuzaki S, Raetsep M and Small GJ (2000) Red chlorophyll *a* antenna states of photosystem I of the cyanobacterium *Synechocystis* sp. PCC 6803. J Phys Chem B 104: 5625–5633

Holzwarth AR, Schatz G, Brock H and Bittersmann E (1993) Energy transfer and charge separation kinetics in photosystem I. 1. Picosecond transient absorption and fluorescence study of cyanobacterial photosystem I particles. Biophys J 64: 1813–1826

Holzwarth AR, Dorra D, Mueller MG and Karapetyan NV (1998) Structure–function relationships and excitation dynamics in photosystem I. In: Garab G (ed) Photosynthesis: Mechanisms and Effects, Vol 1, pp 497–502. Kluwer, Dordrecht

Ikegami I (1976) Fluorescence changes related in the primary photochemical reaction in the P700-enriched particles isolated from spinach chloroplasts. Biochim Biophys Acta 449: 245–258

Ihalainen JA, Gobets B, Sznee K, Brazzoli M, Croce R, Bassi R, van Grondelle R, Korppi-Tommola JEI and Dekker JP (2000) Evidence for two spectroscopically different dimers of light-harvesting complex I from green plants. Biochemistry 39: 8625–8631

Ihalainen JA, Jensen PE, Haldrup A, van Stokkum IHM, van Grondelle R, Scheller HV and Dekker JP (2002) Pigment organization and energy transfer dynamics in isolated photosystem I (PS I) complexes from *Arabidopsis thaliana* depleted of the PS I-G, PS I-K, PS I-L, or PS I-N subunit. Biophys J 83: 2190–2201

Ihalainen JA, Raetsep M, Jensen PE, Scheller HV, Croce R, Bassi R, Korppi-Tommola JEI and Freiberg A (2003) Red spectral forms of chlorophylls in green plant PS I – a site-selective and high-pressure spectroscopy study. J Phys Chem B 107: 9086–9093

Jansson S (1994) The light-harvesting chlorophyll *a*/*b*-binding proteins. Biochim Biophys Acta 1184: 1–19

Jordan P, Fromme P, Klukas O, Witt HT, Saenger W and Krauß N (2001) Three-dimensional structure of cyanobacterial photosystem I at 2.5 Å resolution. Nature 411: 909–917

Karapetyan NV (1998) Organization and role of the longwave chlorophylls in the photosystem I of the cyanobacterium *Spirulina*. Membr Cell Biol 12: 571–584

Karapetyan NV, Klimov VV and Krasnovsky AA (1973) Light-induced changes in the fluorescence yield of particles obtained by digitonin fragmentation of chloroplasts. Photosynthetica 7: 330–337

Karapetyan NV, Dorra D, Schweitzer G, Bezsmertnaya IN and Holzwarth AR (1997) Fluorescence spectroscopy of the long-wave chlorophylls in trimeric and monomeric photosystem I core complexes from the cyanobacterium *Spirulina platensis*. Biochemistry 36: 13830–13837

Karapetyan NV, Holzwarth AR and Rögner M (1999a) The photosystem I trimer of cyanobacteria: molecular organization, excitation dynamics and physiological significance. FEBS Lett 460: 395–400

Karapetyan NV, Shubin VV and Strasser RJ (1999b) Energy exchange between the chlorophyll antenna of monomeric subunits within the photosystem I trimeric complex of the cyanobacterium *Spirulina*. Photosynth Res 61: 291–301

Kargul J, Nield J and Barber J (2003) Three-dimensional reconstruction of a light-harvesting complex photosystem I (LHC I-PS I) supercomplex from the green alga *Chlamydomonas reinhardtii*. J Biol Chem 278: 16135–16141

Katz JJ, Bowman MK, Michalski TJ and Worchester DL (1991) Chlorophyll aggregation: chlorophyll/water micelles as models for *in vitro* long-wavelength chlorophyll. In: Scheer H (ed) Chlorophylls, pp 211–235. CRC Press, Boca Raton

Kennis JTM, Gobets B, van Stokkum IHM, Dekker JP, van Grondelle R and Fleming GR (2001) Light harvesting by chlorophylls and carotenoids in the photosystem I core complex of *Synechococcus elongatus*: a fluorescence upconversion study. J Phys Chem B 105: 4485–4494

Kleinherenbrink FAM, Deinum G, Otte CCM, Hoff AJ and Amesz J (1992) Energy transfer from long-wavelength absorbing antenna bacteriochlorophylls to the reaction center. Biochim Biophys Acta 1099: 175–181

Krasnovsky AA (1960) The primary processes of photosynthesis in plants. Annu Rev Plant Physiol 11: 363–410

Krasnovsky AA and Bystrova MI (1986) Self-assembly of chlorophyll aggregated structures. Biosystems 12: 181–194

Kruip J, Karapetyan NV, Terekhova IV and Rögner M (1999) *In vitro* oligomerization of a membrane protein complex. Liposome-based reconstitution of trimeric photosystem I from isolated monomers. J Biol Chem 274: 18181–18188

Litvin FF and Krasnovsky AA (1957) Investigation by fluorescence spectra of intermediate stages of chlorophyll biosynthesis in etiolated leaves. Dokl AN SSSR (Russ) 117: 106–109

Melkozernov AN (2001) Excitation energy transfer in photosystem I from oxygenic organisms. Photosynth Res 70: 129–153

Melkozernov AN, Schmid VHR, Schmidt GW and Blankenship RE (1998) Energy redistribution in heterodimeric light-harvesting complex LHCI-730 of photosystem I. J Phys Chem B 102: 8183–8189

Melkozernov AN, Lin S and Blankenship RE (2000a) Femtosecond transient spectroscopy and excitonic interactions in photosystem I. J Phys Chem B 104: 1651–1656

Melkozernov AN, Lin S and Blankenship RE (2000b) Excitation dynamics and heterogeneity of energy equilibration in the core antenna of photosystem I from the cyanobacterium *Synechocystis* sp. PCC 6803. Biochemistry 39: 1489–1498

Melkozernov AN, Lin S, Schmid VHR, Paulsen H, Schmidt GW and Blankenship RE (2000c) Ultrafast excitation dynamics of low energy pigments in reconstituted peripheral light-harvesting complexes of photosystem I. FEBS Lett 471: 89–92

Melkozernov AN, Lin S, Blankenship RE and Valkunas L (2001) Spectral inhomogeneity of photosystem I and its influence on excitation equilibration and trapping in the cyanobacteriun *Synechocystis* sp. PCC 6803 at 77 K. Biophys J 81: 1144–1154

Morosinotto T, Casteletti S, Breton J, Bassi R and Croce R (2002) Mutation analysis of Lhca1 antenna complex – Low energy absorption forms originate from pigment–pigment interactions. J Biol Chem 277: 36253–36261

Morosinotto T, Breton J, Bassi R and Croce R (2003) The nature of a chlorophyll ligand in Lhca proteins determines the far red fluorescence emission typical of photosystem I. J Biol Chem 278: 49223–49229

Mukerji I and Sauer K (1989) Temperature-dependent steady-state and picosecond kinetic fluorescence measurements of a photosystem I preparation from spinach. In: Briggs WR (ed) Photosynthesis. Plant Biology, Vol 8, pp 105–122. Alan R Liss, New York

Palsson L-O, Dekker JP, Schlodder E, Monshouwer R and van Grondelle R (1996) Polarized site-selective fluorescence spectroscopy of the long-wavelength emitting chlorophylls in isolated photosystem I particles of *Synechococcus elongatus.* Photosynth Res 48: 239–262

Palsson L-O, Flemming C, Gobets B, van Grondelle R, Dekker JP and Schlodder E (1998) Energy transfer and charge separation in photosystem I: P700 oxidation upon selective excitation of the long-wavelength antenna chlorophylls of *Synechococcus elongatus*. Biophys J 74: 2611–2622

Raetsep M, Johnson TW, Chitnis PR and Small GJ (2000) The red-absorbing chlorophyll *a* antenna states of photosystem I: a hole-burning study of *Synechocystis* sp. PCC 6803 and its mutants. J Phys Chem 104B: 836–847

Rivadossi A, Zucchelli G, Garlaschi FM and Jennings RC (1999) The importance of PSI chlorophyll red forms in light-harvesting by leaves. Photosynth Res 60: 209–215

Schlodder E, Cetin M, Byrdin M, Terekhova IN and Karapetyan N. (2005) $P700^+$- and $^3P700$-induced quenching of the fluorescence at 760 nm in trimeric photosystem I complexes from the cyanobacterium*Arthrospira platensis.* Biochim Biophys Acta 1706: 53–67

Schmid VHR, Cammarata KV, Bruns BU and Schmidt GW (1997) *In vitro* reconstitution of the photosystem I light-harvesting complex LHCI-730: heterodimerization is required for antenna pigment organization. Proc Natl Acad Sci USA 94: 7667–7672

Schmid VHR, Potthast S, Wiener M, Bergauer V, Paulsen H and Storf S (2002) Pigment binding of photosystem I light-harvesting proteins. J Biol Chem 277: 36707–36714

Sener MK, Lu DY, Ritz T, Park S, Fromme P and Schulten K (2002) Robustness and optimality of light harvesting in cyanobacterial photosystem I. J Phys Chem B 106: 7948–7960

Shubin VV, Murthy SDS, Karapetyan NV and Mohanty P (1991) Origin of the 77 K variable fluorescence at 758 nm in the cyanobacterium *Spirulina platensis*. Biochim Biophys Acta 1060: 28–36

Shubin VV, Bezsmertnaya IN and Karapetyan NV (1992) Isolation from *Spirulina* membranes of two photosystem I-type complexes, one of which contains chlorophyll responsible for the 77 K fluorescence band at 760 nm. FEBS Lett 309: 340–342

Shubin VV, Tsuprun VL, Bezsmertnaya IN and Karapetyan NV (1993) Trimeric forms of the photosystem I reaction center complex pre-exist in the membranes of the cyanobacteriun *Spirulina platensis.* FEBS Lett 334: 79–82

Shubin VV, Bezsmertnaya IN and Karapetyan NV (1995) Efficient energy transfer from the long-wavelength antenna chlorophylls to P700 in photosystem I complexes from *Spirulina platensis*. J Photochem Photobiol B 30: 153–160

Trissl H-W (1993) Long-wavelength absorbing antenna pigments and heterogeneous absorption bands concentrate excitons and increase absorption cross-section. Photosynth Res 35: 247–263

Turconi S, Weber N, Schweitzer G, Strotmann H and Holzwath A (1994) Energy transfer and charge separation kinetics in photosystem I. 2. Picosecond fluorescence study of various PSI particles and light-harvesting complex isolated from higher plants. Biochim Biophys Acta 1187: 324–334

van der Lee J, Bald D, Kwa SLS, van Grondelle R, Rögner M and Dekker JP (1993) Steady-state polarized-light spectroscopy of isolated photosystem I complex. Photosynth Res 35: 311–321

van Grondelle R, Dekker JP, Gilbro T and Sundstroem V (1994) Energy transfer and trapping in photosynthesis. Biochim Biophys Acta 1187: 1–65

White NTH, Beddard GS, Thorne JR, Feeban TM, Keyes TA, Heathcote P (1996) Primary charge separation and energy transfer in the photosystem I reaction center of higher plants. J Phys Chem B 100: 12086–12099

Witt H, Bordignon E, Carbonera D, Dekker JP, Karapetyan NV, Teutloff C, Webber A, Lubitz W and Schlodder E (2003) Species-specific differences of the spectroscopic properties of P700: analysis of the influence of non-conserved amino acid residues by site-directed mutagenesis of photosystem I from *Chlamydomonas reinhardtii*. J Biol Chem 278: 46760–46771

Wittmershaus BP, Tran TD and Panaia B (1998) Fluorescence from low-energy chlorophylls in photosystem I of *Synechocystis* sp. PCC 6803 at physiological temperatures. Photosynth Res 57: 29–39

Woolf VM, Wittmershaus BP, Vermaas WFJ and Tran TD (1994) Resolution of low-energy chlorophylls in photosystem I of *Synechocystis* sp. PCC 6803 at 77 and 295 K through fluorescence excitation anisotropy. Photosynth Res 40: 21–34

Zazubovich V, Matsuzaki S, Johnson TW, Hayes JM, Chitnis PR and Small GJ (2002) Red antenna states of photosystem I from cyanobacterium *Synechococcus elongatus*: a spectral hole-burning study. Chem. Physics 275: 47–59

Chapter 14

Mutagenesis of Ligands to the Cofactors in Photosystem I

Andrew N. Webber* and Velupillaimani M. Ramesh
School of Life Sciences and Center for Early Events in Photosynthesis, Arizona State University, P.O. Box 874501, Tempe, AZ 85287-4501, USA

Summary

The electron transfer chain of Photosystem I (PS I) is made up of six chlorophylls (P_{700}, A, and A_0), two quinones (A_1), and three iron–sulfur centers (F_X, F_A, and F_B). The chlorophylls and quinones form two potential pathways for electron transfer from P_{700} to F_X. The electron transfer chain chlorophylls are also excitonically coupled as indicated by the spectrally broad transient bleaching observed between 660 and 700 nm upon initial excitation. This article reviews how specific mutagenesis of the ligands of each cofactor is being used to address some of the outstanding questions raised by the structural model of Photosystem I.

I. Introduction

Mutagenesis of ligands to various cofactors has been a useful tool for understanding structure function questions related to Photosystem I (PS I). Prior to a detailed structure of PS I, site-directed mutagenesis was used to address questions related to identifying ligands to specific cofactors, in particular the primary donor and the iron–sulfur centers F_X, F_A, and F_B. As the structure of PS I has gained in resolution, the specific questions that can be addressed using well-designed mutants have increased in sophistication, such that now a combination of mutagenesis and spectroscopic analysis provides a very powerful approach for understanding excitation energy and electron transfer processes. This chapter reviews the major questions that have been or are being addressed by mutagenesis of ligands to the PS I cofactors.

II. Chlorophylls of the Electron Transfer Chain

A. Primary Donor, P_{700}

Some of the earliest work involving specific mutagenesis of PS I *in vivo* was aimed toward identifying the axial ligands to P_{700}. In the absence of any detailed

* Author for correspondence, email: andrew.webber@asu.edu

Abbreviations: ETC – electron transfer chain; EPR – electron paramagnetic resonance; ENDOR – electron-nuclear double resonance; ESEEM – electron spin echo envelope modulation; PSI – Photosystem I.

John H. Golbeck (ed): Photosystem I: The Light-Driven Plastocyanin:Ferredoxin Oxidoreductase, 193–204.

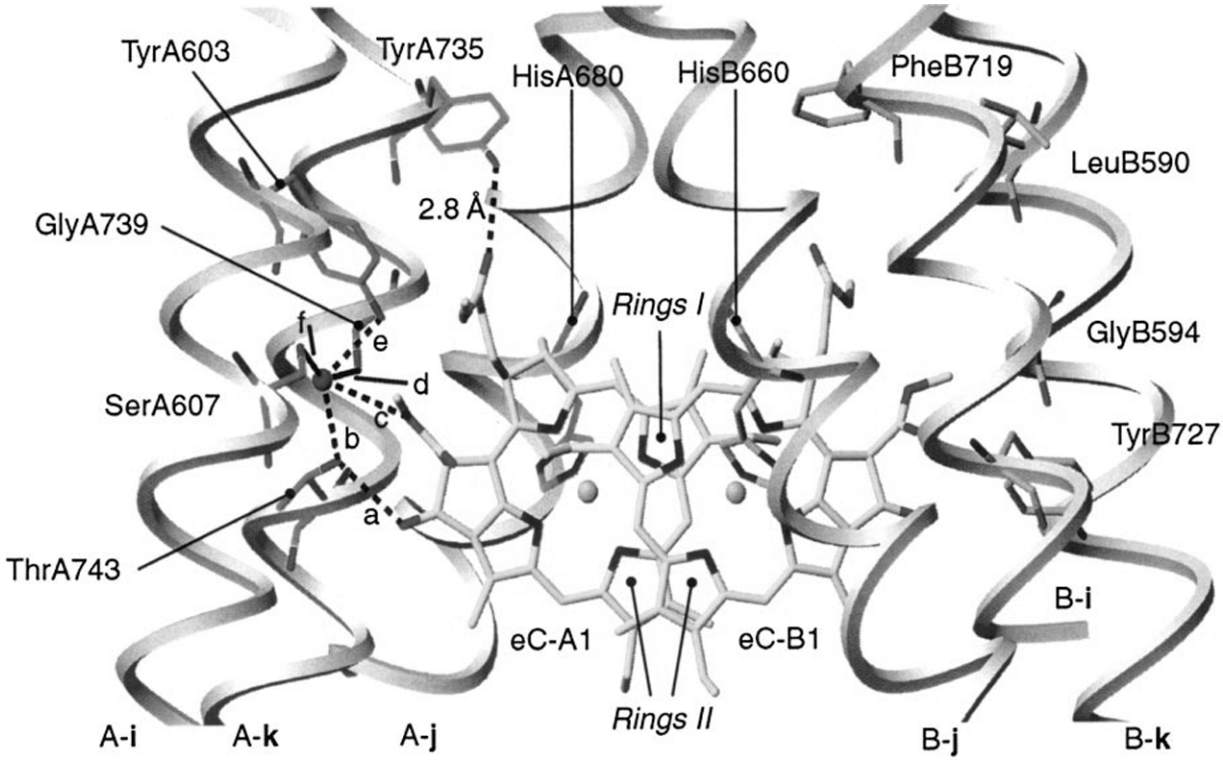

Fig. 1. The primary donor P_{700} and its protein environment. See Color Plate 9, Fig. 2.

structural information, it was assumed that the axial ligand would be a histidine, similar to the case of the purple bacterial reaction center, a hypothesis that was supported by selective isotopic labeling and electron-nuclear double resonance (ENDOR) and electron spin echo envelope modulation (ESEEM) spectroscopy. Changing one particular histidine (His 656 of PsaB) to asparagine or serine was found to result in significant changes in the optical and ENDOR spectra, as well as the redox potential, of P_{700} (Webber et al., 1996), whereas changes in other conserved His residues of PsaB or PsaA had no effect on the spectroscopic properties of P_{700} (Cui et al., 1995; Redding et al., 1998).

The axial ligand mutants have been useful for examining a number of questions related to P_{700}, in particular the issue of whether or not P_{700}^{+} is a monomer or a dimer; which chlorophyll carries the spin density in P_{700}^{+}; and what role the protein environment plays in determining the redox potential of P_{700}. The crystal structure of PS I clearly shows that P_{700} is a chlorophyll *a*′/chlorophyll *a* dimer (Fig. 1). However, a large body of spectroscopic information indicates that P_{700}^{+} is a chlorophyll *a* monomer. In particular, ENDOR spectroscopy of single crystals of PS I from *Thermosynechococcus elongatus* indicates that greater than 80% of the spin distribution in P_{700}^{+} is located on a single chlorophyll. ENDOR studies of the various P_{700} mutants of *Chlamydomonas reinhardtii* have been performed in detail (Webber et al., 1996; Krabben et al., 2000). In all these mutants, only mutations of the PsaB subunit were found to alter the ^{1}H-ENDOR spectra of $P_{700}^{+\cdot}$ and no significant change in the hyperfine couplings were found for the PsaA mutants. The small magnitude of the effect of the mutations was not that surprising given that the spin density at the Mg^{2+} ion coordinated by the axial ligand is probably very small. The surprising observation was that predominantly only one single hfc of the methyl group at position 12 was affected by each of the PsaB mutations (Webber et al., 1996; Krabben et al., 2000). Studies of modified chlorophyll *a in vitro* have shown that the hyperfine coupling of this methyl group is very sensitive to small structural changes and so the increased hyperfine coupling of this methyl group is probably caused by a movement of the chlorophyll *a* or a change in its conformation as a result of substitution of the axial ligand with shorter or nonligating residues (Krabben et al., 2000). These ENDOR results were interpreted to indicate that the PsaB side chlorophyll *a* carries the electron spin density in $P_{700}^{+\cdot}$.

The reason why P_{700} has a highly reducing potential compared to chlorophyll *a* in solution is pretty much unknown. Factors that may contribute to the unusual potential of P_{700} include interaction with the protein environment (Fig. 1). An interesting observation is that decreasing the polarizability of the amino acid ligands to P_{700} results in an increase in the redox potential (Webber et al., 1996; Krabben et al., 2000). This would then suggest that the unpaired electron of the His axial ligand stabilizes the charge on P_{700}^{+} thereby lowering the redox potential. Other factors that will contribute to the redox potential of P_{700}/P_{700}^{+} include the H-bonding the PsaA-side chlorophyll a' at the 13^1-keto carbonyl. Mutation of Thr 739, the H-bond donor to the 13′-keto, in *C. reinhardtii* to Ala was shown to decrease the potential by 32 mV (Witt et al., 2002).

The altered potential of P_{700} in the axial ligand mutants has also been used to examine electron transfer between plastocyanin and P_{700}. Increasing the potential of P_{700} would be expected to increase the driving force for electron transfer between plastocyanin and P_{700}. Indeed, this was found to be the case, and in P_{700} axial ligand mutants that increase the potential of P_{700} there is an also increase the rate of electron transfer from PC to P_{700} (Ramesh et al., 2002). Exploiting "Dutton's ruler" to estimate the distance between two cofactors based upon the rate of electron transfer, it was estimated that the distance between the edge of P_{700} and the Cu of plastocyanin was 15 Å. This estimate fits well with the hypothesis that plastocyanin binds to the lumen side of PS I in a site formed by the *ij* helices of PsaA/B. It has also been suggested that conserved Trp residues on the surface-exposed *ij* loops of PsaA and PsaB may be important for electron transfer from plastocyanin to P_{700}. Mutation of the B-side Trp resulted in PS I complexes that lack the fast phase of electron transfer from P_{700} to PS I supporting the notion that these residues are required for rapid electron transfer within the predocked complex (Sommer et al., 2002, 2004).

B. The Accessory Chlorophylls, A

The two chlorophylls, eC-A2 and eC-B2, are located between P_{700} and eC-A3 and eC-B3 (Jordan et al., 2001). The axial ligand to both of these chlorophylls is a water molecule that is hydrogen bonded to an asparagine. They are located very close to the P_{700} chlorophylls and the eC-A3/B3 chlorophylls. Calculations indicate that eC-A2 and eC-B2 are strongly excitonically coupled to eC-A3 and eC-B3, the chlorophylls expected to represent A_0 (Gibasiewicz et al., 2003). These accessory chlorophylls were first identified from the PS I structure at 6 Å, but have never been detected spectroscopically and so have not been directly implicated in the primary charge separation. However, on the basis of their close proximity and the extent of excitonic coupling it is very unlikely that they are not directly involved. Indeed, based on kinetic modeling of ultrafast absorbance changes thought to represent initial electron transfer events and their insensitivity to redox state of P_{700}, it has been suggested that primary charge separation could initiate at eC-A2 or eC-B2, and that the positive charge subsequently retracts to P_{700} (Gibasiewicz et al., 2003; Muller et al., 2003). At this time this is somewhat speculative, but there is precedent for a similar charge separation mechanism in Photosystem II and purple bacteria.

C. The Primary Acceptor (s), A_0

Spectroscopic analysis has identified the primary electron acceptor, A_0, as a chlorophyll *a* monomer. In the X-ray structure, one or both the chlorophylls eC-A3 and eC-B3 are assumed to be A_0 (Fig. 2). The axial ligands to eC-A3 and eC-B3 are Met688 of PsaA and Met668 of PsaB, respectively (Jordan et al., 2001). Ligation of a hard acid like Mg^{2+} by the soft base sulfur is very surprising and could account for the unusual redox potential of the A_0 chlorophyll. The chlorophyll eC-A3 has two H-bonds, one between the keto oxygen of ring V and Tyr696 of PsaA and a second between the phytyl ester carbonyl and the backbone oxygen of Ser429 of PsaB (Jordan et al., 2001). The chlorophyll eC-B3 has only one H-bond between the keto oxygen of ring V and Tyr676 of PsaB (Jordan et al., 2001).

The very symmetrical nature of the electron transfer chain (ETC) chlorophylls raises the question as to whether both eC-A3 and eC-B3 are involved in electron transfer, or if only a single chlorophyll represents A_0. This question has been addressed in *C. reinhardtii* by site-directed mutagenesis, where the Met ligands have been changed to His, Ser, or Leu (Fairclough et al., 2003; Ramesh et al., 2004). These mutants have been studied by electron paramagnetic resonance (EPR) and ENDOR and by ultrafast optical spectroscopy.

Ultrafast absorption spectroscopy cannot normally resolve bleaching due to reduction of A_0 because of the fast electron transfer to A_1. However, under conditions that doubly reduce the phylloquinones the absorption spectra between 660 and 720 nm measured 200 psec after flash illumination contains contributions from P_{700}^{+} and A_0^{-}. Subtraction of the P_{700}/P_{700}^{+} difference spectra

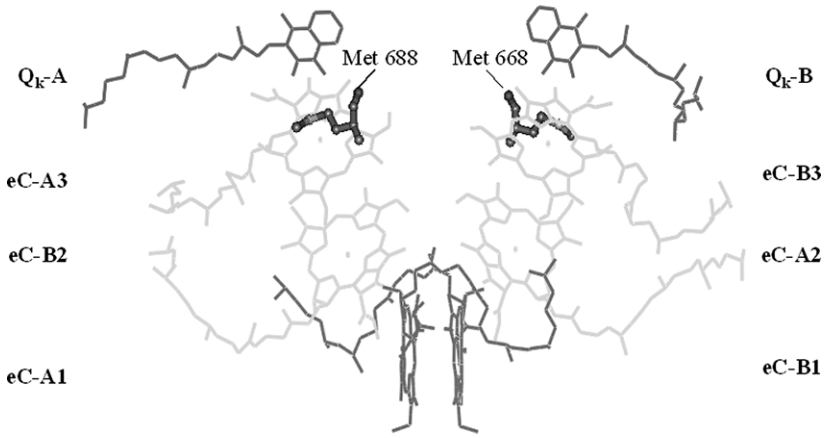

Fig. 2. The chlorophyll cofactors eC-A1, eC-B2, eC-A3, and eC-B1, eC-A2, and eC-B3 of the A- and B-branches of the ETC. The primary electron acceptors eC-A3 and eC-B3 are axially ligated by Met A688 and Met 668, respectively. Source: Ramesh VM, Gibasiewicz G, Lin S, Bingham SE and Webber AN Unpublished.

from the P_{700}^+/A_0^- spectra yields an absorption spectra for A_0^- (Fig. 3) with a maximum bleaching at 682 nm (Hastings et al., 1994, 1995). In the PsaA and PsaB mutants of Met axial ligands, the P_{700}/P_{700}^+ difference spectra is clearly different from the wild-type, indicating a contribution from A_0^- in the spectra (Ramesh et al., 2004). When the P_{700}/P_{700}^+ spectra from wild-type is subtracted from the spectrum from the mutant PS I, a spectrum identical to A_0^- is obtained (Fig. 3) (Ramesh et al., 2004). This data strongly supports the hypothesis that both branches of the electron transfer chain function in forward electron transfer at least to A_0 in *C. reinhardtii*. The amplitude of the bleaching signal attributed to A_0^- is approximately half that from wild-type for both mutants (Ramesh et al., 2004). This indicates that electron transfer occurs along either branch to approximately the same extent. When measured on a longer timescale, it has recently been possible to resolve a component that decays with a lifetime of 1700 psec and which has a shape identical to A_0^- (Ramesh and Webber, unpublished). This indicates that electron transfer from A_0^- to A_1 is slowed from approximately 20 psec in wild-type, to ~1700 psec in the A_0 mutants (Fig. 4).

Time resolved EPR spectroscopy of the decay of the geminate P_{700}^+/A_1^- radical has been used to study forward electron transfer from A_1 to F_X. In wild-type *C. reinhardtii*, the electron spin polarized signal measured at room temperature decays in approximately 350 nsec and has been shown to monitor forward electron transfer from the PsaA-side phylloquinone to F_X (Muhiuddin et al., 2001). This signal was not detected in the PsaA Met mutant indicating that electron transfer from P_{700} to A_1 is blocked (Fairclough et al., 2003). At 100 K in samples reduced with sodium ascorbate and phenazine methosulfate, or sodium dithionite, the rate of decay of the correlation of the $P_{700}^+A_1^-$ radical pair that is thought to reflect the environment of the PsaA is absent in the PsaA Met mutant, with just a fast phase detected (Fairclough et al., 2003). In wild-type cells the fast phase is only detected when F_X is reduced by photoaccumulation (Muhiuddin et al., 2001; Fairclough et al., 2003). Their interpretation is that since the slow phase is missing and since A-side electron transfer is blocked, the fast decay of the correlation of the radical pair must reflect B-side electron transfer. This is apparently supported by the fact that the fast phase of the decay of the spin correlation is absent in the PsaB side Met mutant. However, these interpretations are confused by the fact that the PsaB side mutants also affect the rate of decay of the $P_{700}^+A_1^-$ signal at room temperature, which reflects electron transfer on the A-branch. The difficulty in interpreting these EPR results is that they are not directly monitoring rates of electron transfer but rather the effect of mutations on the decay of radical pair signals decaying by processes other than electron transfer (F_X needs to be prereduced to observe biphasic kinetics in wild-type cells).

Overall the optical and EPR studies lend credence to the hypothesis that both eC-A3 and eC-B3 participate in electron transfer in *C. reinhardtii*. However, the results are still not totally satisfying given the fact that PsaB mutants show an effect on electron transfer events that have been clearly shown to be associated with the A-branch of the ETC. A systematic study of these mutants using optical and EPR techniques is required to understand the impact of mutations on specific electron transfer steps in this organism.

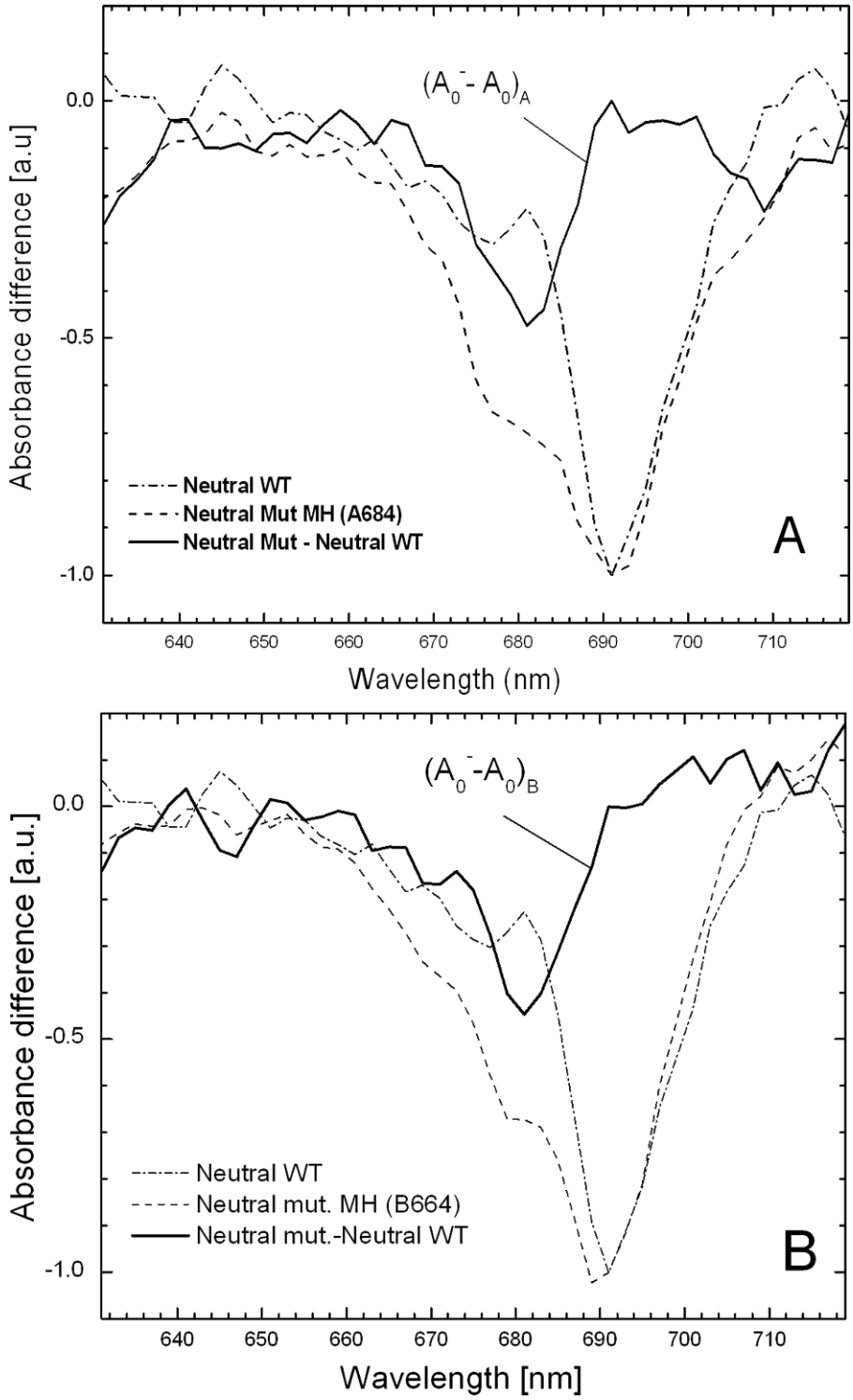

Fig. 3. Accumulation of ($A_0^- - A_0$) absorbance difference spectra in the MH(A684) (A) and MH(B664) (B) mutant PS I from *C. reinhardtii* at room temperature under neutral conditions. The spectra presented were recorded 200–300 psec after ~150 fsec-excitation at 695 nm (Ramesh et al., 2004).

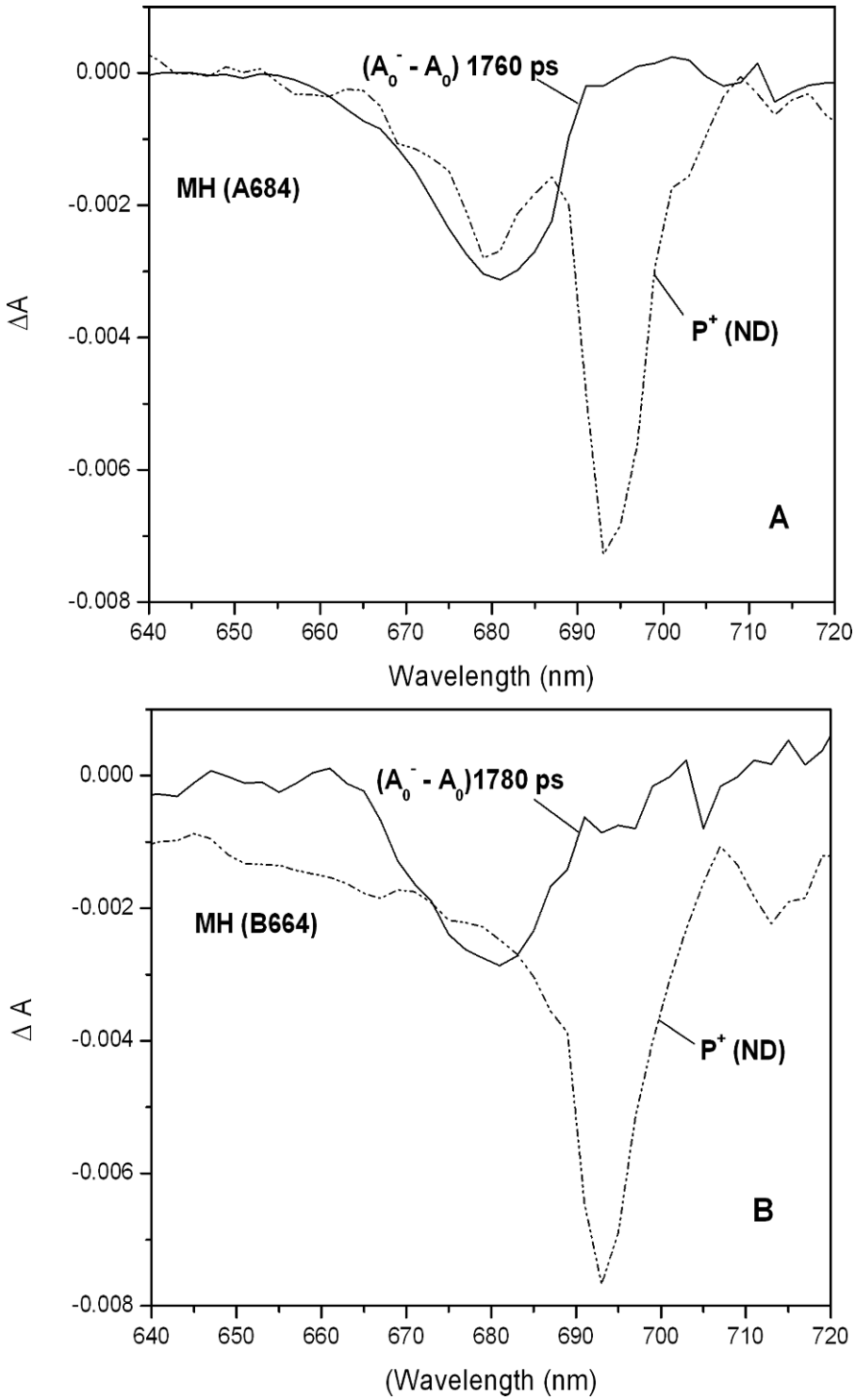

Fig. 4. Decay associated spectra (DAS) of the 1700 psec (solid) and non-decaying (dashed) components obtained from global analysis of data measured under neutral condition in Photosystem I from MH(A684) and MH(B664) mutants of *C. reinhardtii*. Data were collected on a 4 nsec timescale, using high intensity excitation pulses at 695 nm. Source: Ramesh VM, Gibasiewicz G, Lin S, Bingham SE and Webber AN Unpublished.

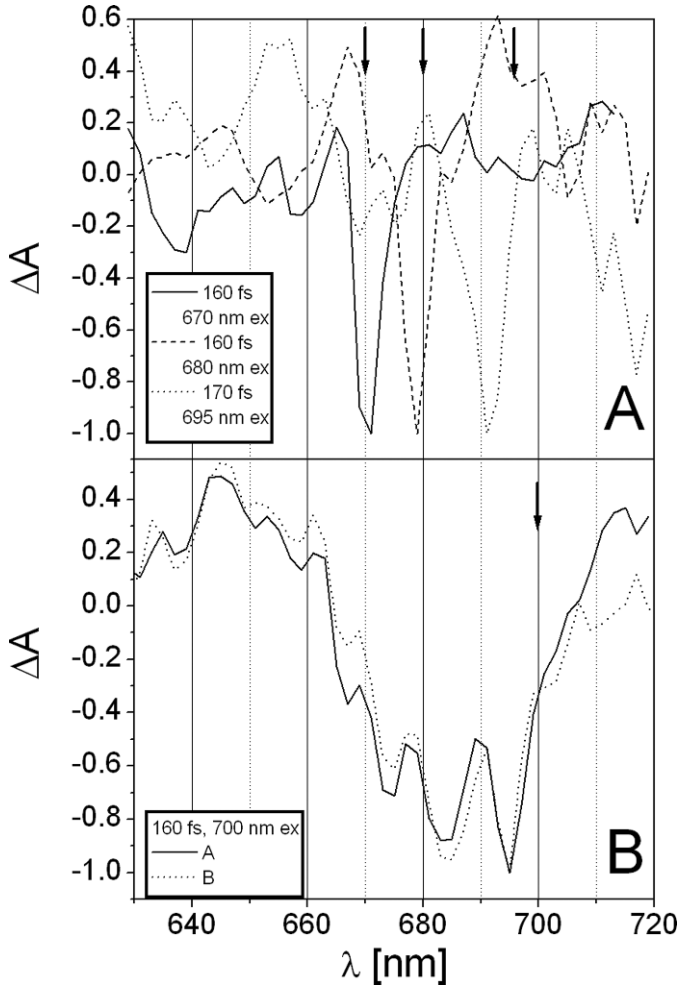

Fig. 5. Comparison of the initial time resolved spectra recorded after a pump-probe delay time of ~160 fsec at excitation wavelengths of 670, 680, and 695 nm (A), and 700 nm (B). Traces A and B in panel B are from two independent experiments. Excitation wavelengths are indicated by arrows. Source: Gibasiewicz K, Ramesh VM, Lin S, Woodbury NW and Webber AN (2002) Excitation dynamics in eukaryotic PS I from *Chlamydomonas reinhardtii* CC 2696 at 10 K. Direct detection of the reaction center exciton states. J Phys Chem B 106: 6322–6330.

D. Excitonic Coupling Between the ETC Chlorophylls

A feature that has emerged from both an analysis of transient (subpicosecond) absorption changes and from modeling chlorophyll interactions based on the 2.5 Å structure is that there is considerable excitonic interaction between the chlorophylls of the ETC (Melkozernov et al., 2000; Byrdin et al., 2002; Gibasiewicz et al., 2002). The extent of the interaction probably needs to result in a reappraisal of our thinking about the nature of the individual chlorophylls of the ETC—they are clearly not isolated molecules but are a connected network that may extend beyond the ETC and include at least the connecting chlorophylls (Gibasiewicz et al., 2003). The nature of the excitonic coupling between chlorophylls of the ETC has been extensively investigated in mutants of *C. reinhardtii* (Gibasiewicz et al., 2003). *C. reinhardtii* has been particularly useful in this regard because the PS I core complexes lack the red-shifted chlorophylls that absorb at 700 nm and longer (Gibasiewicz et al., 2002). This allows for direct excitation of the ETC chlorophylls and therefore a study of the earliest events associated with light absorption. Excitation of the red edge of the Q_y transition band in *C. reinhardtii* PS I using excitation of 700 nm leads to wide transient (subpicosecond) absorption changes with a positive ΔA between 635 and 665 nm and four negative ΔA bands at 667, 675, 685, and 695 nm (Fig. 5). The wide structure of this absorption

band was attributed to excitonic coupling (Gibasiewicz et al., 2002, 2003). The negative bands were ascribed to photobleaching of the transitions to four different one-exciton states, and the positive bands to excited state absorption from the lowest one-exciton state to four different two-exciton states. Calculation of interaction energies between the six ETC chlorophylls based on the 2.5 Å model indicated that the six ETC chlorophylls can be considered as a set of three dimers: eC-A1/A2, eC-A2/eC-A3, and eC-B2/eC-B3 (Gibasiewicz et al., 2003). Because of the symmetry in the structure there is degeneracy in the one-exciton states so that instead of six states there are four. However, the calculated splitting of the lower and upper states was too large to explain the experimental data. Including the connecting chlorophylls in the calculation was shown to predict eight one-exciton levels of which five were well-separated and could be expected to appear in the experimental results (Gibasiewicz et al., 2003). The contribution of each of these chlorophylls to the excitonic coupling was tested by analysis of *C. reinhardtii* mutants that alter the axial ligand to the two connecting chlorophylls (a HL(A730)/HL(B714) double mutant) (Redding et al., 1998; Gibasiewicz et al., 2003) and to the eC-A3 and eC-B3 chlorophylls (Gibasiewicz et al., 2003).

In the HL(A730)/HL(B714) double mutant the band at 683 nm was absent as predicted if the connecting chlorophylls were left out of the calculation (Gibasiewicz et al., 2003). This supported the hypothesis that the connecting chlorophylls significantly contribute to the excitonically coupled network of chlorophylls even though the calculated interaction energy between the connecting chlorophylls and A_0 were small. In the mutants that have changed the axial Met ligand of A_0 to His, the amplitudes of the band attributed to A_0 interacting with A, at 675, and the band attributed to A_0 interacting with the connecting chlorophyll, at 683 nm, were both reduced by half (Gibasiewicz et al., 2003; Ramesh et al., 2004). This was predicted based on calculated interaction energies when either eC-A3 or eC-B3 were removed from the calculations. While the model of interaction between at least eight chlorophylls fits the early absorption spectra discussed here, it remains to be seen if it will also predict other spectroscopic data, such as T-S spectra and P_{700} difference spectra.

The data described in this section supports the hypothesis that the ETC chlorophylls are part of an excitonically coupled system. The resulting wide and structured spectrum of the ETC chlorophylls may be of great significance for the effectiveness of energy transfer from the antenna to the reaction center. It is expected to increase the range of spectral overlap between these two pools of chlorophylls, thus possibly promoting the effective energy transfer between different spectral forms of antenna chlorophylls and ETC chlorophylls (Gibasiewicz et al., 2002, 2003).

III. The Quinone Acceptors, A_1

It is very clear from the current structural model that there are two quinones in symmetrically related positions, completing the bifurcated chain of potential electron carries between $P_{700}$and F_X. Again, as with the A_0 chlorophylls, it is relevant to address whether one or both are active in electron transfer. Optical kinetic measurements of forward electron transfer from A_1^- to F_X show a fast (∼10 nsec**) and a slow phase (∼200 nsec) (Joliot and Joliot, 1999; Guergova-Kuras et al., 2001). Transient EPR measurements, on the other hand, only confirm the presence of the slow phase (Boudreaux et al., 2001; Xu et al., 2003b), reviewed in Golbeck (2003). The two kinetic phases may reflect two separate electron transfer events, one from each quinone bound by PsaA or PsaB, thus inferring bidirectional electron transfer. Alternatively (see Agalarov and Brettel, 2003 for discussion), it has been suggested that the biphasic kinetics arise from unidirectional electron transfer in two distinct PS I populations with different kinetics of forward electron transfer. A third proposal is that there is a quasi-equilibrium between A_1^- and F_X^- that would give rise to a fast A_1^- reoxidation and a slower phase due to depopulation of the quasi-equilibrium state by electron transfer to F_A.

The role of the two quinones has been addressed by a specific mutagenesis of the quinone binding pocket of PsaA and PsaB in attempts to modify electron transfer between one of the quinones and F_X. The first reported mutations were of the π-stacked Trp residues (Fig. 6) that were changed to Phe in *C. reinhardtii* (Boudreaux et al., 2001; Guergova-Kuras et al., 2001). More recently, the analogous π-stacked quinones were also change to Phe in *Synechocystis sp.* PCC 6803, as well as changes to Ser residues that are involved in H-bonding (Golbeck, 2003; Xu et al., 2003a,b). In *C. reinhardtii*, mutation of the PsaB-side Trp slowed the 18 nsec fast phase to 97 nsec while the analogous PsaA-side mutation slowed the 218 nsec slow phase to 609 nsec. Although in *Synechocystis sp.* PCC 6803 the fast phase of A_1 reoxidation only represents a small fraction of the total amplitude of the signal in

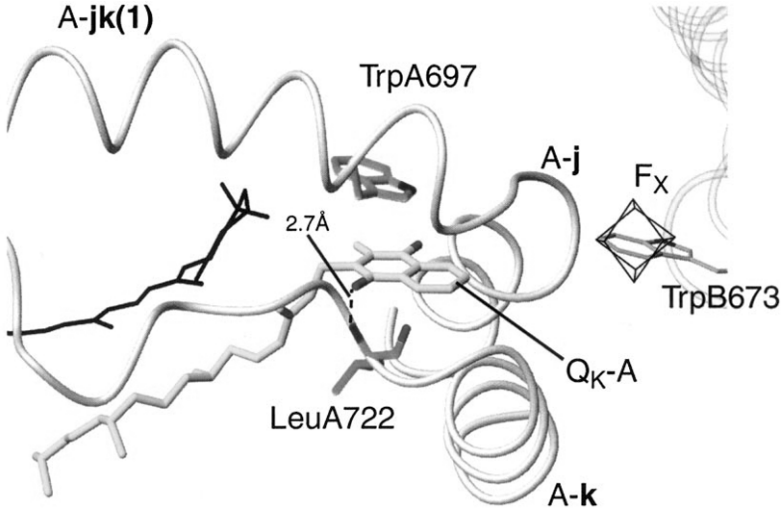

Fig. 6. The environment of the phylloquinone Q_K-A. View direction from the stromal side onto the membrane plane into the phylloquinone binding site at the A-branch of the ETC. The ribbon represents the main chain of PsaA, the residues of which form the binding pocket of Q_K-A. LeuA722 and TrpA697 interact with the quinone. On the left-hand side a carotenoid located near the quinone is drawn in black. On the right-hand side the [4Fe–4S] cluster F_X is shown. TrpB673 is located toward the lumenal side of the F_X cluster. (Modified from Fromme et al., 2001, with permission.)

wild-type, compared to *C. reinhardtii*, the analogous mutations of the Trp residues produced similar results (Xu et al., 2003b). These results are most easily explained by a bidirectional model of electron transfer involving both quinones in forward electron transfer to F_X, although it is not possible to rule out that other factors could be leading to the biphasic kinetics, as mentioned above and discussed in detail in Agalarov and Brettel (2003). Also, the site-directed mutations could have more global effects such that mutation of one specific cofactor could influence other cofactors, as evidenced by the fact that mutation of eC-B3 alters the decay of the spin correlated signal at room temperature, which has been attributed solely to electron transfer along the A-branch (Fairclough et al., 2003).

Characterization of these same mutants by EPR spectroscopy leads to different conclusions compared to those obtained by optical spectroscopy. There is clear agreement that the slow kinetic phase of electron transfer is detected by transient EPR and that this kinetic phase is associated with the same quinone that is detected by EPR photoaccumulation experiments. This is clearly supported by the mutants of the πtstacked tryptophan mutants, WF(A697) in *Synechosystis* sp. PCC 6803 and the WH(A693), WL(A693), and WF(A693) mutants of *C. reinhardtii*. In all cases the mutations effect the photoaccumulation of A_1 and the EPR detected transient $P_{700}^{+}A_1^{-}$ state (Boudreaux et al., 2001; Xu et al., 2003b). Interestingly, none of these parameters are affected by the analogous B-side mutations. The only exception to these observations is that in the WL(B693) mutant of *C. reinhardtii* that has been prereduced by dithionite and subsequently illuminated at 205 K, reducing F_X, the decay of the spin correlated $P_{700}^{+}A_1^{-}$ germinate radical pair is monophasic, rather than the biphasic decay (fast and slow phases) observed in wild-type (Fairclough et al., 2003).

IV. The Iron–sulfur Center, F_X

Most of the mutagenesis work on the ligands to the iron–sulfur center F_X, which were some of the first reported PS I mutants, were performed prior to the availability of a high resolution structure. At that time it was not clear which residues were involved in coordinating the [4Fe–4S] cluster or which residues provided a docking site for PsaC. The presence of two highly conserved sequences containing equally spaced cysteines in PsaA and PsaB (Phe-Pro-Cys-Asp-Gly-Pro-Gly-Arg-Gly-Gly-Thr-Cys), located in loop regions predicted to lie on the stromal side of the membrane, led to the proposal that F_X was an interpolypetide [4Fe–4S] cluster coordinated by two cysteines from PsaA and two cysteines from PsaB. To test this hypothesis the PsaB cysteines were changed to Ser, Asp, and His. The Ser and His mutants of *Synechocystis* sp. PCC 6803 (Smart et al., 1993; Warren et al., 1993), and the His mutant

of *C. reinhardtii* (Webber et al., 1993) resulted in very reduced levels of PS I, suggesting that Asp or His is not able to replace Cys as a ligand to F_X. The Ser mutants of *Synechocystis* sp. PCC 6803 accumulated more substantial PS I and were found to have a reduced the anisotropy of the EPR spectrum of F_X and increased rates in the back reaction from F_X^- and A_1^- (Warren et al., 1993)

Each of the F_X binding regions contain two conserved Pro residues. A Pro adjacent to Cys is found in nearly all [4Fe–4S] proteins involved in electron transfer reactions, suggesting some critical function for this motif. However, when the Pro residues of the PsaB-side loop were changed to Leu there was no effect on PS I accumulation or function (Webber et al., 1993). The stability of the PS I complex from the various proline mutants of PsaB in *C. reinhardtii* was investigated by measuring the extent and rate of dissociation of the PS I reaction center following treatment with urea and subsequent reconstitution of the urea-treated complex with PsaC expressed in *E. coli* (Rodday et al., 1995). The extent of dissociation and reconstitution was followed spectrophotometrically by measuring the recombination kinetics between P_{700}^+ and F_A/F_B^- following a brief activating flash. In wild-type, the half-time for decay of the flash induced absorption change was approximately 30 msec, which is diagnostic for charge recombination between F_A/F_B^- and P_{700}^+. The two PsaB proline mutants, PA(B560) and PL(B560), both displayed a half-time for recombination of 30 msec indicating complete electron transfer to the F_A/F_B acceptors on PsaC (Rodday et al., 1995). The flash transient from PL(B560) showed a minor contribution of a faster msec phase indicating some disruption in electron transfer between F_X and F_A/F_B (Rodday et al., 1995). Following dissociation of the reaction center with urea, the PA(B560) and PL(B560) mutants reconstituted poorly with PsaC indicating that the interaction with PsaC was impaired (Rodday et al., 1995). Similar results were observed following mutagenesis of proline residues in ferredoxin of *Clostridium pasterianium*—the redox properties of the iron–sulfur centers were not affected but the centers were significantly destabilized at increased temperatures (Quinkal et al., 1994). NMR studies of the mutants showed that destabilization was due to changes in hydrogen bonding within the cluster (Quinkal et al., 1994). It was suggested that the proline mutations in PsaB of PS I also led to altered hydrogen bonding in the F_X-domain causing decreased stability (Rodday et al., 1995). A detailed analysis of the 2.5 Å structure of the F_X region (Golbeck, 2003) identifies a complex series of H-bonding and salt bridges in this region, and in particular that the Pro B564 of *T. elongatus* is H-bonded to Arg B712 and thus ties together two transmembrane *a*-helices.

V. The Iron–sulfur Centers, F_A and F_B

The F_A and F_B centers are coordinated by PsaC, a small 9 kDa polypeptide located on the stromal side of PS I. The protein contains two classic [4Fe–4S] binding motifs that bind the F_A and F_B centers. The earlier low-resolution crystal structure of PS I shows a local pseudo-C_2 symmetry around both the iron–sulfur centers, which led to much of the PsaC research focusing on two important questions—which cluster represents F_A and which cluster F_B, and which cluster is proximal to F_X and which cluster is distal to F_X and represents the donor to ferredoxin?

To address the first of these questions site-directed mutagenesis was used to produce mutants of PsaC in which the second Cys ligand in each [4Fe–4S] center was changed to Asp. Following overexpression of the mutant PsaC proteins in *E. coli*, the iron–sulfur clusters were inserted *in vitro*, and the reconstituted proteins were added to $P_{700}^-F_X$ core preparations in the presence of PsaD. EPR spectroscopy revealed that in the C51 mutant there was an intact cluster identified as F_B and a [3Fe–4S] cluster in the other site. In the C14 mutant the intact cluster had an EPR signature identical to that of F_A. On the basis of these results it was predicted that Cys 21, 48, 51, and 54 ligate F_A and that Cys 11, 14, 17, and 58 ligate F_B (Zhao et al., 1992).

The second question, which cluster is proximal to F_X, arose because the orientation of PsaC in the lower resolution structure, which places one of the [4Fe–4S] cluster closer to F_X, could not differentiate F_A and F_B. Chemical inactivation studies supported the hypothesis that F_B was the distal cluster. This was also supported by analysis of site-directed mutants of PsaC in *C. reinhardtii*. Acidic residues located adjacent and upstream of the first cysteine ligand of either F_A or F_B were changed to neutral or basic residues. Only changes of residues near F_B were shown to have an effect on the ferredoxin affinity (Fischer et al., 1999). These results are now all confirmed by the latest PS I structure (Jordan et al., 2001).

References

Agalarov R and Brettel K (2003) Temperature dependence of biphasic forward electron transfer from the phylloquinone(s)

A_1 in photosystem I: only the slower phase is activated. Biochim Biophys Acta 1604: 7–12

Boudreaux B, MacMillan F, Teutloff C, Agalarov R, Gu F, Grimaldi S, Bittl R, Brettel K and Redding K (2001) Mutations in both sides of the photosystem I reaction center identify the phylloquinone observed by electron paramagnetic resonance spectroscopy. J Biol Chem 276: 37299–37306

Byrdin M, Jordan P, Krauß N, Fromme P, Stehlik D and Schlodder E (2002) Light harvesting in photosystem I: modeling based on the 2.5-Å structure of photosystem I from *Synechococcus elongatus*. Biophys J 83: 433–457

Cui L, Bingham SE, Kuhn M, Kass H, Lubitz W and Webber AN (1995) Site-directed mutagenesis of conserved histidines in the helix VIII domain of PsaB impairs assembly of the photosystem I reaction center without altering spectroscopic characteristics of P700. Biochemistry 34: 1549–1558

Fairclough WV, Forsyth A, Evans MC, Rigby SE, Purton S and Heathcote P (2003) Bidirectional electron transfer in photosystem I: electron transfer on the PsaA side is not essential for phototrophic growth in *Chlamydomonas*. Biochim Biophys Acta 1606: 43–55

Fischer N, Sétif P and Rochaix JD (1999) Site-directed mutagenesis of the PsaC subunit of photosystem I. F_B is the cluster interacting with soluble ferredoxin. J Biol Chem 274: 23333–23340

Fromme P, Jordan P and Krauß N (2001) Structure of photosystem I. Biochim Biophys Acta 1507: 5–31

Gibasiewicz K, Ramesh VM, Lin S, Woodbury NW and Webber AN (2002) Excitation dynamics in eukaryotic PS I from *Chlamydomonas reinhardtii* CC 2696 at 10 K. Direct detection of the reaction center exciton states. J Phys Chem B 106: 6322–6330

Gibasiewicz K, Ramesh VM, Lin S, Redding K, Woodbury NW and Webber AN (2003) Excitonic interactions in wild-type and mutant PSI reaction centers. Biophys J 85: 2547–2559

Golbeck JH (2003) The binding of cofactors to photosystem I analyzed by spectroscopic and mutagenic methods. Annu Rev Biophys Biomol Struct 32: 237–256

Guergova-Kuras M, Boudreaux B, Joliot A, Joliot P and Redding K (2001) Evidence for two active branches for electron transfer in photosystem I. Proc Natl Acad Sci USA 98: 4437–4442

Hastings G, Kleinherenbrink FA, Lin S, McHugh TJ and Blankenship RE (1994) Observation of the reduction and reoxidation of the primary electron acceptor in photosystem I. Biochemistry 33: 3193–3200

Hastings G, Hoshina S, Webber AN and Blankenship RE (1995) Universality of energy and electron transfer processes in photosystem I. Biochemistry 34: 15512–15522

Joliot P and Joliot A (1999) *In vivo* analysis of the electron transfer within photosystem I: are the two phylloquinones involved? Biochemistry 38: 11130–11136

Jordan P, Fromme P, Witt HT, Klukas O, Saenger W and Krauß N (2001) Three-dimensional structure of cyanobacterial photosystem I at 2.5 Å resolution. Nature 411: 909–917

Krabben L, Schlodder E, Jordan R, Carbonera D, Giacometti G, Lee H, Webber AN and Lubitz W (2000) Influence of the axial ligands on the spectral properties of P700 of photosystem I: a study of site-directed mutants. Biochemistry 39: 13012–13025

Melkozernov AN, Lin S and Blankenship RE (2000) Femtosecond transient spectroscopy and excitonic interactions in photosystem I. J Phys Chem B 104: 1651–1656

Muhiuddin IP, Heathcote P, Carter S, Purton S, Rigby SE and Evans MC (2001) Evidence from time resolved studies of the $P700^+/A_1^-$ radical pair for photosynthetic electron transfer on both the PsaA and PsaB branches of the photosystem I reaction centre. FEBS Lett 503: 56–60

Muller MG, Niklas J, Lubitz W and Holzwarth AR (2003) Ultrafast transient absorption studies on photosystem I reaction centers from *Chlamydomonas reinhardtii*. 1. A new interpretation of the energy trapping and early electron transfer steps in photosystem I. Biophys J 85: 3899–3922

Quinkal I, Davasse V, Gaillard J and Moulis JM (1994) On the role of conserved proline residues in the structure and function of *Clostridium pasteurianum* 2[4Fe–4S] ferredoxin. Protein Eng 7: 681–687

Ramesh VM, Guergova-Kuras M, Joliot P and Webber AN (2002) Electron transfer from plastocyanin to the photosystem I reaction center in mutants with increased potential of the primary donor in *Chlamydomonas reinhardtii*. Biochemistry 41: 14652–14658

Ramesh VM, Gibasiewicz K, Lin S, Bingham SE and Webber AN (2004) Bidirectional electron transfer in photosystem I: accumulation of A_0^- in A-side or B-side mutants of the axial ligand to chlorophyll A_0. Biochemistry 43: 1369–1375

Redding K, MacMillan F, Leibl W, Brettel K, Hanley J, Rutherford AW, Breton J and Rochaix JD (1998) A systematic survey of conserved histidines in the core subunits of photosystem I by site-directed mutagenesis reveals the likely axial ligands of P700. EMBO J 17: 50–60

Rodday SM, Webber AN, Bingham SE and Biggins J (1995) Evidence that the F_X domain in photosystem I interacts with the subunit PsaC: site-directed changes in PsaB destabilize the subunit interaction in *Chlamydomonas reinhardtii*. Biochemistry 34: 6328–6334

Smart LB, Warren PV, Golbeck JH and McIntosh L (1993) Mutational analysis of the structure and biogenesis of the photosystem I reaction center in the cyanobacterium *Synechocystis* sp. PCC 6803. Proc Natl Acad Sci USA 90: 1132–1136

Sommer F, Drepper F and Hippler M (2002) The luminal helix l of PsaB is essential for recognition of plastocyanin or cytochrome c_6 and fast electron transfer to photosystem I in *Chlamydomonas reinhardtii*. J Biol Chem 277: 6573–6581

Sommer F, Drepper F, Haehnel W and Hippler M (2004) The hydrophobic recognition site formed by residues PsaA-Trp651 and PsaB-Trp627 of photosystem I in *Chlamydomonas reinhardtii* confers distinct selectivity for binding of plastocyanin and cytochrome c_6. J Biol Chem 279: 20009–20017

Warren PV, Smart LB, McIntosh L and Golbeck JH (1993) Site-directed conversion of cysteine-565 to serine in PsaB of photosystem I results in the assembly of [3Fe–4S] and [4Fe–4S] clusters in F_X. A mixed-ligand [4Fe–4S] cluster is capable of electron transfer to F_A and F_B. Biochemistry 32: 4411–4419

Webber AN, Gibbs PB, Ward JB and Bingham SE (1993) Site-directed mutagenesis of the photosystem I reaction center in chloroplasts. The proline-cysteine motif. J Biol Chem 268: 12990–12995

Webber AN, Su H, Bingham SE, Kass H, Krabben L, Kuhn M, Jordan R, Schlodder E and Lubitz W (1996) Site-directed mutations affecting the spectroscopic characteristics and midpoint potential of the primary donor in photosystem I. Biochemistry 35: 12857–12863

Witt H, Schlodder E, Teutloff C, Niklas J, Bordignon E, Carbonera D, Kohler S, Labahn A and Lubitz W (2002) Hydrogen bonding to P700: site-directed mutagenesis of threonine A739 of photosystem I in *Chlamydomonas reinhardtii*. Biochemistry 41: 8557–8569

Xu W, Chitnis P, Valieva A, van der Est A, Pushkar YN, Krzystyniak M, Teutloff C, Zech SG, Bittl R, Stehlik D, Zybailov B, Shen G and Golbeck JH (2003a) Electron transfer in cyanobacterial photosystem I: I. Physiological and spectroscopic characterization of site-directed mutants in a putative electron transfer pathway from A_0 through A_1 to F_X. J Biol Chem 278: 27864–27875

Xu W, Chitnis PR, Valieva A, van der Est A, Brettel K, Guergova-Kuras M, Pushkar YN, Zech SG, Stehlik D, Shen G, Zybailov B and Golbeck JH (2003b) Electron transfer in cyanobacterial photosystem I: II. Determination of forward electron transfer rates of site-directed mutants in a putative electron transfer pathway from A_0 through A_1 to F_X. J Biol Chem 278: 27876–27887

Zhao J, Li N, Warren PV, Golbeck JH and Bryant DA (1992) Site-directed conversion of a cysteine to aspartate leads to the assembly of a [3Fe–4S] cluster in PsaC of photosystem I. The photoreduction of F_A is independent of F_B. Biochemistry 31: 5093–5099

Chapter 15

Genetic Manipulation of Quinone Biosynthesis in Cyanobacteria

Yumiko Sakuragi and Donald A. Bryant*
Department of Biochemistry and Molecular Biology, The Pennsylvania State University, University Park, PA 16801, USA

Summary

Isoprenoid quinones (phylloquinone, plastoquinone) and their derivatives (α-, β-, and γ-tocopherol) play crucial roles in oxygenic photosynthesis. Phylloquinone (vitamin K_1) and plastoquinone-9 are cofactors of Photosystem I (PS I) and Photosystem II (PS II) complexes, respectively, and mediate electron transfer within and between complexes, while the roles of tocopherols are yet to be fully identified. Traditionally, the biosynthetic pathways of these quinones have been studied by direct enzymatic assays or, since the late 1960s, by using isotopic tracer compounds. Recent progress in the genome sequencing of 14 cyanobacteria has provided a new tool for the identification of genes encoding enzymes of the biosynthetic pathways of these quinones; comparative genomics, in combination with reverse genetics, has recently provided a wealth of new information. With the exception of *Gloeobacter violaceus*, phylloquinone biosynthesis in cyanobacteria has been shown to be very similar to menaquinone biosynthesis in *Escherichia coli*. Metabolic engineering of the pathway resulted in the incorporation of a variety of quinone species of either biotic or abiotic origin into the A_1 site of Photosystem I, and the resulting strains are important tools for the investigation of electron transfer around the A_1 quinone. Plastoquinone-9 biosynthesis in cyanobacteria differs from that in higher plants. Comparative genome analysis has revealed the presence of conserved open reading frames, which encode proteins that share sequence similarity with those required for ubiquinone biosynthesis in *E. coli*. Possible applications of metabolic engineering of the plastoquinone-9 and α-tocopherol biosynthetic pathways for studies of oxygenic photosynthesis are also discussed.

* Author for correspondence, email: dab14@psu.edu

John H. Golbeck (ed): Photosystem I: The Light-Driven Plastocyanin:Ferredoxin Oxidoreductase, 205–222.

I. Introduction

Oxygenic photosynthesis transforms CO_2 and water into biomass using light as an energy source and concomitantly releases molecular oxygen as a waste product (Barber and Anderson, 2002). The ability to perform this remarkable process is unique to cyanobacteria and their chloroplast-containing descendants, the algae, and higher plants. Since their first appearance more than 3 billion years ago (Schopf, 1993 and references therein), cyanobacteria have affected, and are continuing to affect, our environment. The production of molecular oxygen has transformed the atmosphere of our planet from an extremely reducing to a rather oxidizing environment, and this change supported the evolution of diverse forms of life on Earth. Since about half of the global CO_2 fixation known to occur on Earth is carried out by cyanobacteria (Falkowski, 2002; Bryant, 2003), these organisms today attract even more attention because of concerns about global warming.

Much has been learned about the molecular mechanisms of oxygenic photosynthesis owing to decades of study by many scientists, who have dissected and solved much of the mystery of water oxidation and the detailed electron-transport functions of the photosynthetic apparatus from the viewpoint of protein function (Deisenhofer and Norris, 1993; Bryant, 1994; Ort and Yocum, 1996; Ke, 2001). Such a perspective, however, has generally overlooked the biological importance of non-proteinous molecules that play roles in these processes. Quinones are cofactor molecules of this type. This class of compounds includes phylloquinone (PhyQ, 2-methyl-3-phytyl-1,4-naphthoquinone, also known as vitamin K_1); menaquinone (MQ, 2-methyl-3-polyprenyl-1,4-naphthoquinone), also known as vitamin K_2; and plastoquinone-9 (PQ-9, 2,3-dimethyl-6-solanyl-1,4-benzoquinone). All of these compounds are composed of a quinonoid nucleus with a polyprenyl substituent (Fig. 1). Two types of quinoid substructures occur naturally: 1,4-naphthoquinone (1,4-NQ), and 1,4-benzoquinone (1,4-BQ). PhyQ is a methyl- and phytyl-substituted 1,4-NQ, while PQ-9 is a methyl- and solanyl-substituted 1,4-BQ. The phytyl substituent is a partially saturated tetra-isoprene unit (equivalent to 20 carbon atoms), while the solanyl substituent is a nona-isoprene unit (equivalent to 45 carbon atoms). MQ has a polyprenyl substituent that can have 4 to ~10 isoprene units (20–50 carbons). α-Tocopherol (2,5,7,8-tetramethyl-6-chromanol, also known as vitamin E) is a highly methylated derivative of a phytyl-substituted 1,4-BQ and contains a tetramethyl-substituted, chromanol quinoid nucleus (Fig. 1). PhyQ, PQ-9, and α-tocopherol are only synthesized in oxygenic phototrophs (Threlfall and Whistance, 1971; Collins and Jones, 1981), and their functions are tightly connected to oxygenic photosynthesis. For example, PhyQ and PQ-9 are bound cofactors of the PS I and PS II reaction center complexes, respectively, and in this context they mediate electron transfer within these complexes as one-electron carriers (see below). In both the photosynthetic electron transport and the respiratory electron transport chains, PQ-9 serves as a membrane-associated carrier of two electrons and two protons. α-Tocopherol, on the other hand, is thought to provide protection against oxidative stress in animals and plants, although its role(s) in cyanobacteria has not yet been demonstrated (see below). In this review, our current understandings of these quinones are summarized. Because PS I structure and function are the principal subjects of this book, this chapter will emphasize the pathway for PhyQ biosynthesis and will only briefly describe the plastoquinone and α-tocopherol pathways. Genetic manipulation of this pathway has been used to create modified PS I complexes that have been used to modify the electron-transfer properties of this reaction center.

It is now accepted that PhyQ serves as the secondary electron acceptor in PS I. Briefly, each PS I monomer of *Synechococcus elongatus* consists of

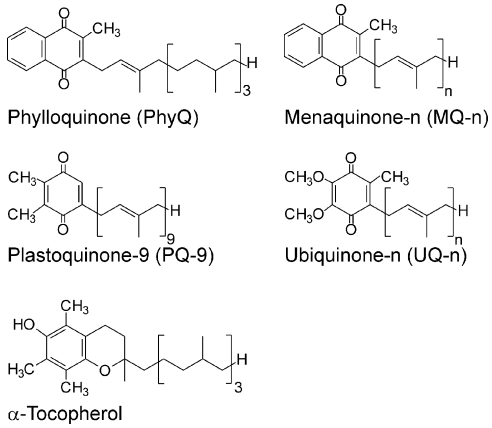

Fig. 1. Structures of isoprenoid quinones.

Abbreviations: AQ – anthraquinone; Chl *a* – chlorophyll *a*; DHNA – 1,4-dihydroxy-2-naphthoate; DMPBQ – 2,3-dimethyl-6-phytyl-1,4-benzoquinone; MPBQ – 2-methyl-6-phytyl-1,4-benzoquinone; MSBQ – 2-methyl-6-solanyl-1,4-benzoquinone; MQ – menaquinone; NQ – naphthoquinone; PhyQ – phylloquinone; PQ – plastoquinone; PS I – Photosystem I; PS II – Photosystem II; UQ – ubiquinone.

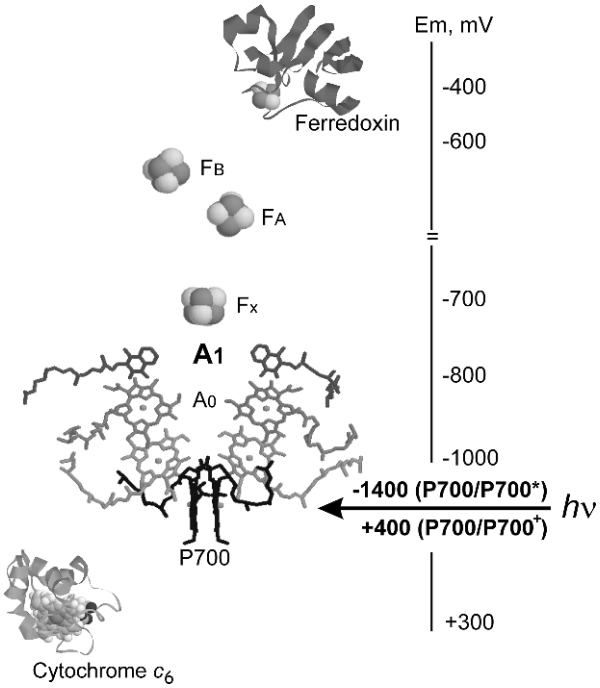

Fig. 2. Electron-transfer cofactors and their redox potentials in PS I, cytochrome c_6 and ferredoxin.

12 protein subunits, 96 chlorophyll *a* (Chl *a*) molecules, 22 β-carotene molecules, 2 PhyQ molecules, 3 [4Fe–4S] clusters, 4 structural lipids, and a large number of water molecules (Jordan et al., 2001; see reviews by Fromme et al., 2001, 2003; see also Fromme and Grotjohann, this volume, Chapter 6). The core structure of the PS I complexes of higher plants appears to be very similar; it lacks two polypeptides (PsaM and PsaX) and lacks only three of the Chl *a* molecules found in the cyanobacterial complex; however, it has four complex-specific subunits (PsaG, PsaH, PsaN, and PsaO) (Ben-Shem et al., 2003, 2004; see also Nelson and Ben-Shem, this volume, Chapter 7). Tightly bound electron-transfer cofactors are associated with the PsaA and PsaB polypeptides that form the cores of both types of PS I complex (Jordan et al., 2001; see reviews by Golbeck, 1994, 2003; Fromme et al., 2001, 2003). These include a Chl *a*–Chl *a′* dimer (P700), two Chl *a* monomers (A_0), two PhyQ molecules (A_1), and three [4Fe–4S] clusters (denoted F_X, F_A, F_B). These cofactors are arranged in two branches related by C_2 symmetry. The spatial arrangement of these cofactors and their estimated *in situ* redox potentials are shown in Fig. 2. Upon photoexcitation, the primary donor P700 reduces the primary acceptor, A_0, resulting in the initial charge-separated state $P700^+A_0^-$. Subsequent electron transfer to the secondary acceptor A_1 stabilizes the charge-separated state $P700^+A_0A_1^-$ and minimizes the rapid charge recombination that occurs between $P700^+$ and A_0^-. The electron is subsequently transferred to F_X producing $P700^+A_0A_1F_X^-$, and finally to the terminal acceptors producing $P700^+A_0A_1F_XF_A^-$ and $P700^+A_0A_1F_XF_AF_B^-$. The F_A and F_B [4Fe–4S] clusters are bound by the peripheral PsaC subunit, which is found on the stromal surface of the PS I complex. The reduction of ferredoxin or flavodoxin takes place upon direct protein–protein interaction between these soluble electron acceptors and the three stromal proteins: PsaC, PsaD, and PsaE (Zhao et al., 1990, 1993; N Li et al., 1991; Golbeck, 1994; Mühlenhoff et al., 1996a,b; Sétif, 2001; Fromme et al., 2003). Photooxidized $P700^+$ accepts an electron from reduced cytochrome c_6 or plastocyanin on the lumenal side of the thylakoid membrane to complete the electron-transfer events and to reset PS I for a new round of photochemistry (Durán et al., 2004).

II. The Phylloquinone Biosynthetic Pathway

A. Historical Perspective

Since the initial discovery of PhyQ in oxygenic phototrophs by Dam in 1941 (cited in Hauska, 1988), the role of PhyQ in PS I was obscure for more than two decades. In the 1970s Thornber et al. (1976) showed that PhyQ copurifies with PS I, and in the 1980s it was established that PhyQ is exclusively associated with PS I (Takahashi et al., 1985; Schoeder and Lockau, 1986). Spin-polarized EPR analyses (Petersen et al., 1987) and kinetic optical spectroscopy (Brettel et al., 1987; see also reviews by Brettel, 1997; Golbeck, 1994, 2003; Brettel and Leibl, 2001) then showed that PhyQ participates in electron transfer in PS I. Further more, supporting evidence for the participation of PhyQ in PS I electron transfer was derived from solvent-extraction studies. Extraction of PhyQ from PS I with hexane or ether resulted in a rapid, nanosecond-scale charge recombination between $P700^+$ and A_0^-. Stable charge separation could be restored by the addition of exogenous PhyQ (Biggins and Mathis, 1988; Itoh and Iwaki, 1989a). It is now accepted that PhyQ is the secondary electron acceptor A_1 and that this quinone plays a crucial role in photosynthesis as a PS I cofactor by mediating electron transfer between the primary acceptor A_0 (Chl *a*) and the tertiary, core-intrinsic acceptor F_X (a [4Fe–4S] cluster) after photoexcitation of the primary

donor P700 (Golbeck, 1994, 2003; Brettel, 1997; Brettel and Leibl, 2001).

The *in vitro* reconstitution method was subsequently used to study the structural and thermodynamic requirements for A_1 by the introduction of diverse quinones, including BQs, NQs, and anthraquinones (AQs) of abiotic origin and with various ring substitutions, into the A_1 site (Itoh and Iwaki, 1989a,b, 1991; Iwaki and Itoh, 1989, 1991; see also review by Itoh et al., 2001). These authors concluded that the successful restoration of stable charge separation occurs only when quinones with redox potentials between those of A_0 and F_X are used. In addition to this, they found that the structure of the head group is not important and that the phytyl tail is not essential, although it contributes to tighter binding to the quinone-binding pocket (Iwaki and Itoh, 1989). This conclusion contradicted earlier studies, in which the presence of the phytyl tail was shown to be essential when hexane/hexane–methanol-extracted PS I complexes were studied (Biggins and Mathis, 1988; Biggins, 1990). These contradictory interpretations imply that different solvent-extraction methods affect the architecture of PS I differently; hence, the inconsistencies in the conclusions might reflect artifacts of the methods employed. Such artifacts can be avoided if "biologically" or "physiologically" modified complexes are used. Complexes that have not gone through harsh extraction processes, which probably result in the extraction of other important PS I constituents such as water, Chl *a*, carotenoid, and lipid molecules (Biggins and Mathis, 1988; Itoh and Iwaki, 1989a,b; Biggins, 1990; Itoh et al., 2001), should produce more consistent and interpretable results. Some of these extractable molecules are located in the vicinity of the quinone-binding site. In particular, as revealed by the 2.5 Å-resolution crystal structure of PS I (Fromme et al., 2001; Jordan et al., 2001), β-carotenes and chlorophylls form hydrophobic contacts with the phytyl side chain of PhyQ and seem to provide structural stability for this important electron carrier.

A genetic method was therefore sought to eliminate PhyQ selectively *in vivo* from the A_1 site of PS I. Since its first introduction by Chitnis and Golbeck, this biological methodology, when employed alone or in combination with reconstitution or exchange procedures, has provided a robust method for the incorporation of a wide range of quinones of biotic or abiotic origin into the A_1 sites of PS I complexes (Johnson et al., 2000). The following sections summarize the identification of the PhyQ biosynthetic pathway in oxygenic phototrophs and progress in using genetic engineering approaches to alter PhyQ biosynthesis and thereby modify PS I.

B. Comparative Genome Analyses and Reverse Genetics

The Gram-negative bacterium *Escherichia coli* synthesizes menaquinone (MQ), whose molecular structure is striking similar to that of PhyQ. The only difference is the length and saturation level of the isoprenoid substituent at the C_3 position (see Fig. 1). MQ biosynthesis in Gram-negative and Gram-positive bacteria is reasonably well understood at both the enzymatic and the genetic levels (see reviews by Meganathan, 1996, 2001). MQ biosynthesis occurs through eight enzymatic steps that are summarized in Fig. 3. The first committed step is the isomerization of chorismate to isochorismate by isochorismate synthase (MenF); the ensuing reaction is the condensation of isochorismate and thiamine-pyrophosphate–succinic semialdehyde, which is catalyzed by 2-succinyl-6-hydroxy-2,4-cyclohexadiene-1-carboxylate synthase (MenD). Dehydration of 2-succinyl-6-hydroxy-2,4-cyclohexadiene-1-carboxylate is catalyzed by *o*-succinylbenzoate synthase (MenC) and the subsequent CoA thioesterification occurs through the activity of *o*-succinylbenzoate-CoA synthetase (MenE). The ring cyclization reaction is catalyzed by 1,4-hydroxynaphthoyl-CoA synthase (MenB), and de-esterification of this product, either by 1,4-hydroxynaphthoyl-CoA thioesterase (MenH) or a spontaneous reaction, results in formation of 1,4-dihydroxy-2-naphthoic acid (DHNA). DHNA polyprenyltransferase (MenA) catalyzes the condensation of DHNA and polyprenyl diphosphate, yielding 2-polyprenyl-1,4-naphthoquinone (demethylmenaquinone). The final methylation reaction is performed by 2-polyprenyl-1,4-naphthoquinone methyltransferase (MenG), with *S*-adenosyl-L-methinone as the methyl donor, and results in the production of MQ. PhyQ and MQ have very similar molecular structures (Fig. 1). However, PhyQ has a partially saturated, C_{20} phytyl substituent while MQ, which is widely distributed among bacteria, has an unsaturated polyprenyl substituent that typically consists of 30–50 carbon units (Collins and Jones, 1981). Interestingly, MenG is a multifunctional methyltransferase and is also responsible for the *C*-methylation reaction that occurs in ubiquinone biosynthesis in *E. coli* (Lee et al., 1997).

PhyQ biosynthesis in higher plants and cyanobacteria is expected to occur by a pathway that is similar to the MQ biosynthetic pathway of bacteria. Indeed, cell extracts from the plants *Morinda lucida* and *Gallium mollugo* have been shown to convert α-[C^{14}] ketoglutarate to 2-succinyl-6-hydroxy-2,4-cyclohexadiene-1-carboxylate and *o*-succinylbenzoate in a thyamine-

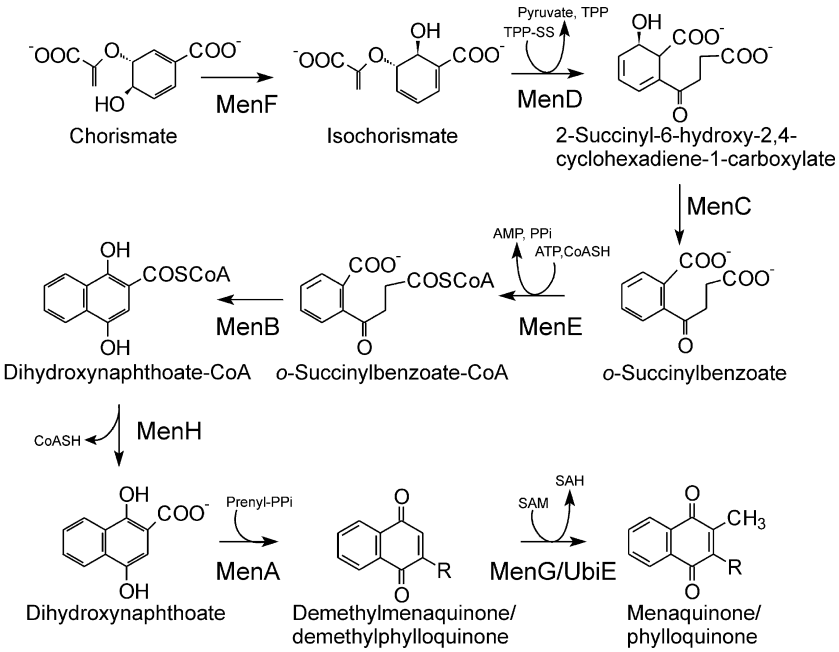

Fig. 3. Menaquinone biosynthesis pathway. SAM – *S*-adenosyl-L-methionine; TPP-SS – thiamine-pyrophosphate–succinic semialdehyde. The MenH-catalyzed reaction can also occur spontaneously (see reviews by Meganathan, 1996, 2001).

pyrophosphate- and isochorismate-dependent manner (see review by Pennock and Threlfall, 1981; Simantiras and Leistner, 1991; Swiezewska, 2004). As of November 17, 2004, complete genomic sequences of six cyanobacteria and one higher plant are available. Complete sequences exist for the cyanobacteria *Synechocystis* sp. PCC 6803 (Kaneko et al., 1996), *Nostoc* sp. PCC 7120 (Kaneko et al., 2001), *Thermosynechococcus elongatus* BP-1 (Nakamura et al., 2002), *Gloeobacter violaceus* (Nakamura et al., 2003), *Prochlorococcus marinus* MED4 and *Prochlorococcus marinus* MIT9313 (Rocap et al., 2003), *Prochlorococcus marinus* SS120 (Dufresne et al., 2003), *Synechococcus* sp. WH8102 (Palenik et al., 2003), and the higher plant *Arabidopsis thaliana*. Incomplete sequences exist for *Synechococcus* sp. PCC 7002 (Marquardt et al., unpublished), *Nostoc punctiforme* (Gene Bank accession number: NZ_AAAY00000000), *Trichodesmium erythraeum* (Gene Bank accession number: NZ_AABK00000000), *Synechococcus elongatus* sp. PCC 7942 (Gene Bank accession number: NZ_AADZ01000001), *Anabaena variabilis* ATCC 29413 (Gene Bank accession number: NZ_AAEA01000001), and *Crocosphaera watsonii* WH8501 (Gene Bank accession number: NZ_AADV01000004). Similarity searches with the MenA through MenH protein sequences of *E. coli* as queries were performed against each genome and the results are summarized in Table 1. Of the organisms examined, 11 cyanobacteria and *A. thaliana* were shown to possess the complete set of eight Men protein homologs. No homologs of MenD (*A. variabilis*) or MenC and MenF (*C. watsonii*) have been identified to date, but these genomes are not yet completely sequenced. Similarities based on amino acid sequences were typically in the range of 30–70%, although MenB sequences were very highly conserved among a wide range of organisms including cyanobacteria, the γ-proteobacterium *E. coli*, the green sulfur bacterium *Chlorobium tepidum*, the Gram-positive bacterium *Bacillus subtilis*, and the archeon *Halobacterium* sp. NRC-1 (similarity >70%).

G. violaceus stands as a notable exception to this highly conserved pattern. In the genome of this organism, only homologs of MenA and MenG were detected while MenB, MenC, MenD, MenE, and MenF are absent. When the *Synechocystis* sp. PCC 6803 MenB sequence was used to search the *G. violaceus* genome database, the best hit was Gll2549 with only 38% similarity. Further database searching has revealed that Gll2549 is highly similar to 6-oxo camphor hydrolase in *Rhodococcus* sp. NCIMB 9784 (69%). When *Synechocystis* sp. PCC 6803 MenC, MenD, MenE, and MenF sequences were used to search the *G. violaceus* database, the best hits were Gll3099 (35%), Gll2804 (44%), Glr1146 (45%), and Gll0757 (43%), respectively. These ORFs also showed significantly higher similarities to other putative proteins: Gll3099 is more

Table 1. Whole genome analyses for the MQ/PhyQ biosynthesis enzymes in 14 cyanobacteria, *E. coli*, *B. subtilis*, *C. tepidum*, and *Halobacterium* sp. NRC-1. Similarity to *Synechocystis* sp. PCC 6803 proteins are shown in parentheses (%). The similarity is based pairwise alignment of the entire sequences constructed by BLOSUM30

	S.6803	*S*.7002	*Nostoc*	*T. ery*	*N. pun*	*A. var*	*C. wat*	*S. elo*	*T. elo*
MenA	Slr1518	(67%)[a]	Alr0033 (70%)	Tery1070 (73%)	Npun0604 (70%)	Avar026348 (68%)	Cwat143901 (34%)[b]	Selo020647 (66%)	Tlr2196 (70%)
MenB	Sll1127	(89%)[a]	All2347 (91%)	Tery1085 (83%)	Npun2498 (91%)	Avar413601 (91%)	Cwat159701 (91%)	Selo187301 (89%)	Tll2458 (88%)
MenC	Sll0409	(52%)[a]	Alr0034 (54%)	Tery1067 (54%)	Npun0605 (52%)	Avar026382 (54%)	–	Selo020304 (50%)	Tlr1174 (55%)
MenD	Sll0603	(62%)[a]	Alr0312 (61%)	Tery1075 (61%)	Npun2496 (59%)	–	Cwat131201 (61%)	Selo02718 (61%)	Tll0130 (56%)
MenE	Slrl0492	(44%)[a]	Alr0035 (56%)	Tery1066 (56%)	Npun0606 (54%)	Avar026381 (52%)	Cwat026026 (52%)	Selo02305 (45%)	Tll1221 (50%)
MenF	Slr0817	(54%)[a]	All0032 (58%)	Teryal71 (57%)	Npun0603 (60%)	Avar026437 (58%)	–	Selo021474 (53%)	Tll1213 (54%)
MenG	Slr1653	(70%)[a]	Alr5252 (72%)	Tery3321 (63%)	Npun3758 (65%)	Avar287101 (48%)[b]	Cwat179201 (68%)	Selo020383 (66%)	Tll2373 (63%)
MenH	Sll1916	(43%)[a]	All0111 (68%)	Tery1986 (46%)	Npun0061 (55%)	Avar513701 (65%)	Cwat024832 (45%)	Selo020062 (52%)	Tlr2066 (43%)
	G. vio	*S*.8102	*P*.MED4	*P*. MIT	*P*.SS120	*Arabidopsis*	*E. coli*	*C. tep*	*B. sub*
MenA	Gll1578 (53%)	Synw2307 (56%)	Pmm0176 (58%)	Pmt2059 (55%)	Pro0201 (55%)	At1g60600 (55%)	B3930 (47%)	CT11511 (44%)	Bsu38490 (41%)
MenB	–	Synw0998 (80%)	Pmm0608 (77%)	Pmt0405 (79%)	Pro1053 (79%)	At1g60550 (78%)	B2262 (78%)	CT1846 (77%)	Bsu3075 (81%)
MenC	–	Synw2306 (39%)	Pmm0175 (41%)	Pmt2058 (43%)	Pro0200 43%)	At1g68900 (46%)	B2261 (38%)	CT1847 (35%)	Bsu30780 (35%)
MenD	–	Synw0997 (46%)	Pmm0607 (46%)	Pmt0406 (47%)	Pro1054 (46%)	At1g68890 (45%)	B2264 (43%)	CT1839 (44%)	Bsu3077 (49%)
MenE	–	Synw2305 (35%)	Pmm0174 (34%)	Pomt2057 (36%)	Pro0199 (35%)	At3g48990 (43%)	B2260 (46%)	CT1848 (39%)	Bsu3074 (39%)
MenF	–	Synw2308 (42%)	Pmm0177 (48%)	Pmt2060 (47%)	Pro0202 (47%)	At1g74710 (51%)	B2265 (44%)	CT1838 (44%)	Bsu3078 (47%)
MenG	Gll0127 (53%)	Synw1674 (56%)	Pmm0431 (51%)	Pmt0276 (37%)	Pro0427 (57%)	At1g23360 (50%)	B3833 (47%)	CT0462 (52%)	Bsu22750 (45%)
MenH	–	Synw0681 (38%)	Pmm1628 (35%)	Pmt0128 (38%)	Pro1790 (40%)	At5g38520 (43%)	B2263 (35%)	CT1845 (31%)	Bsu3076 (34%)

S.6803 –*Synechocystis* sp. PCC 6803; *S*.7002 –*Synechococcus* sp. PCC 7002; *Nostoc* –*Nostoc* sp. PCC 7120; *N. pun* –*Nostoc punctiforme*; *T. elo* –*T. elongatus* BP-1; *T. ery* – *Trichodesmium erythraeum*; *G. vio* – *G. violaceus* PCC 7421; *A. var* – *Anabaena variabilis* ATCC 29413; *S. elo* – *Synechococcus elongatus* sp. 7942; *C. wat* – *Crocosphaera watsonii* WH8501; *S*.8102 – *Synechococcus* sp. WH8102; *P*.MED4 – *Prochlorococcus marinus* MED4; *P*.MIT – *Prochlorococcus marinus* MIT9313; *P*.SS120 –*Prochlorococcus marinus* SS120; *Arabidopsis* –*Arabidopsis thaliana*; *E. coli* –*Escherichia coli*; *C. tep* – *Chlorobium tepidum*; *B. sub* – *Bacillus subtilis*.
[a]No locus tags are available.
[b]N-terminal sequence was truncated.

similar to chloromuconate cycloisomerase in *Clostridium acetobutylicum* (57%); Gll2804 is more similar to acetolactate synthase in *Synechocystis* sp. PCC 6803 (Sll1981, 86%); Glr1146 is more similar to a long-chain fatty-acid CoA ligase in *Bacillus cereus* (54%); and Gll0757 is similar to more anthranilate synthase component I in *Synechocystis* sp. PCC 6803 (Slr1979, 66%). The apparent absence of the MenB, MenC, MenD, MenE, and MenF homologs in *G. violaceus* might suggest that *G. violaceus* does not synthesize PhyQ. Previous studies have shown that PhyQ-less mutants (the *menA* and *menB* mutant of *Synechocystis* sp. PCC 6803; see below) recruit PQ into the A_1 site of PS I, and despite a slightly lower catalytic efficiency for PS I as measured by the flavodoxin reduction rate, the cells are able to grow photoautotrophically (Johnson et al., 2000). One could therefore speculate that PQ-9 functionally replaces PhyQ in PS I in this organism. However, based on the observation that *G. violaceus* synthesizes MQ-4 that most likely functions as the A_1 quinone in PS I (Sakuragi, 2004), this hypothesis has probably been invalidated. Instead, these observations

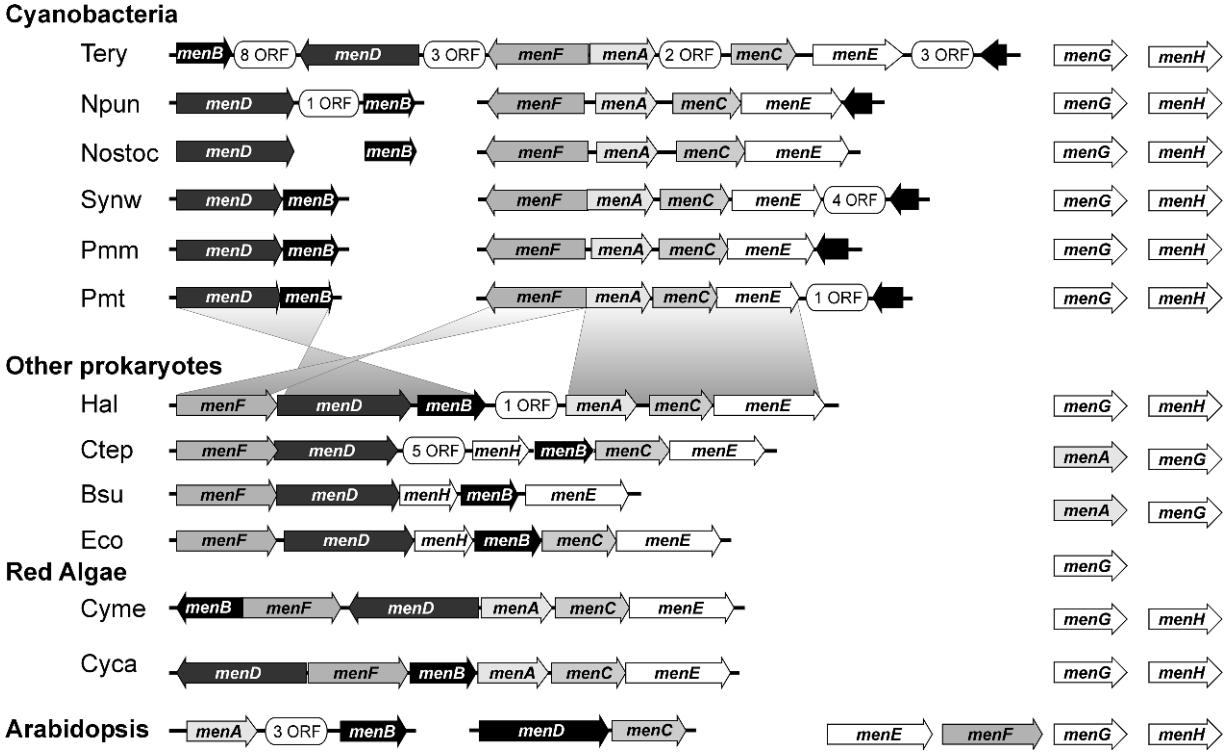

Fig. 4. The *men* gene clusters. Nostoc – *Nostoc* sp. PCC 7120; Bsu – *Bacillus subtilis*; Ctep – *Chlorobium tepidum*; Eco – *Escherichia coli*; Hal – *Halobacterium* sp. NRC-1; Arabidopsis – *A. thaliana*; Cyme – *Cyanidioschyzon merolae*; Cyca – *Cyanidium caldarium*; Npun – *Nostoc punctiforme*; Pmm – *Prochlorococcus marinus* MED4; Pmt – *P. marinus* MIT9313; Synw – *Synechococcus* sp. WH8102; Tery – *Trichodesmium erythraeum*. *P. marinus* SS220 has the same arrangement as Pmm.

strongly suggest that *G. violaceus* has a novel pathway for the synthesis of 1,4-dihydroxy-2-naphthoic acid.

Some of the *men* genes involved in PhyQ biosynthesis are found to form clusters, or possibly operons, in several cyanobacterial genomes. A cluster composed of *menF*, *menA*, *menC*, and *menE* is conserved in *T. erythraeum*, *N. punctiforme*, *Nostoc* sp. PCC 7120, *Synechococcus* sp. WH8102, and all three *Prochlorococcus* species (Fig. 4). In a separate region of the genome, *menD* and *menB* are also found to form a cluster. The observed gene arrangements in these cyanobacteria are similar to parts of the gene clusters found in *E. coli*, *C. tepidum*, *B. subtilis*, and *Halobacterium* sp. NRC-1 (Fig. 4). Combined with the conservation of the amino acid sequences among Men proteins, the conserved arrangements of the *men* genes are strong indications that PhyQ biosynthesis in cyanobacteria evolved from the MQ pathway of other bacteria. The *menF*, *menD*, *menH* and *menB, menC, menE* genes tend to be organized as clusters, while the *menA* and *menG* genes typically are not clustered with other *men* genes. It should be noted that an ORF immediately downstream of *menA* in *E. coli*, which was originally annotated as *menG*, is now characterized as a regulator of RNase E activity A (RraA) and thus is not the authentic *menG* (Monzingo et al., 2003). No *men* gene clusters were found in *Synechocystis* sp. PCC 6803 and *Thermosynechococcus elongatus* BP-1.

In eukaryotic phototrophs, the distribution of the *men* genes is rather incoherent. In the unicellular red algae *Cyanidioschyzon merolae* and *Cyanidium caldarium,* most of the *men* genes (*menA*, *menB*, *menC*, *menD*, *menE*, and *menF*) are found in their chloroplast genomes and form a single cluster (see Fig. 4; Glockner et al., 2000; Ohta et al., 2003). The gene arrangement within these clusters is somewhat similar to those in prokaryotes with characteristic subclusters formed by *menC* and *menE* and by *menB*, *menD*, and *menF*. This may be reflection of the evolution of the PhyQ/MQ-4 biosynthetic pathways, which are probably derived from those in prokaryotes. The *menG* and *menH* genes are expected to be present in the nuclear genomes, and analysis of the *C. merolae* nuclear genome indicates

that is probably the case (Matsuzaki et al., 2004). In more complex red algae, including the multicellular *Porphyra purpurea* and the cryptomonad *Guillardia theta*, the *men* genes are absent from the chloroplast genomes.

In the green lineage of eukaryotic phototrophs, no *men* genes are found in any chloroplast genome. Therefore, one would expect that these genes are encoded by the nuclear genome, and, indeed, in *A. thaliana*, all of the *men* gene homologs are detected in nucleus (Table 1). While most of the *men* genes (*menA*, *menB*, *menC*, *menD*, *menF*, and *menG*) are located in chromosome I, only *menA* and *menB*, and *menC* and *menD* are found to form clusters (Fig. 4). The *menE* gene, which typically is clustered with other *men* genes, occurs alone on chromosome III, and *menH* is encoded on chromosome V. However, it should be noted that the arrangement of the *men* genes appears quite different in *A. thaliana* as compared to those in prokaryotes and in the unicellular red algae. This apparent lack of conservation of the *men* gene arrangement may derive from the possible gene shuffling between the plastid and the nuclear genomes in all green and some red lineages of eukaryotic phototrophs. It is highly likely that, after the unique acquisition of an ancestral chloroplast by the host eukaryotic cell through endosymbiosis (Margulis, 1970), the *men* genes were transferred from the plastid to the nuclear genomes through gene shuffling between the two cellular compartments (Delwiche and Palmer, 1997; Douglas, 1998; Martin et al., 1998).

As noted above, in *E. coli* MenG functions in both the MQ and ubiquinone biosynthesis pathways (Lee et al., 1997). This is not the case in *Synechocystis* sp. PCC 6803 and *Synechococcus* sp. PCC 7002, as no synthesis of ubiquinone occurs in any cyanobacterium known to date and null mutations in the *menG* genes of these two organisms produce no discernible alteration in PQ-9 biosynthesis (Sakuragi, 2004).

Targeted inactivation of the *menA*, *menB*, *menD*, *menE*, and *menG* genes in *Synechocystis* sp. PCC 6803 (Johnson et al., 2000, 2003; Sakuragi et al., 2002) and the *menB*, *menF*, and *menG* genes in *Synechococcus* sp. PCC 7002 (Sakuragi, 2004) has been performed by insertion of antibiotic resistant cartridges into the coding regions of these genes. In all cases, the resulting mutants were unable to synthesize PhyQ. These results provide conclusive evidence that these genes are required for PhyQ or MQ-4 (see below) biosynthesis in cyanobacteria and establish a clear evolutionary relationship between MQ biosynthesis in other prokaryotes and PhyQ biosynthesis in cyanobacteria and higher plants.

C. Distribution of Phylloquinone and Derivatives

Although PhyQ is the major naphthoquinoid species that is synthesized by oxygenic phototrophs and utilized as a cofactor in PS I, there have been sporadic reports of the occurrence of other PhyQ derivatives in this group of organisms. The presence of demethylphylloquinone was reported in spinach chloroplasts 40 years ago (McKenna et al., 1964) but the physiological function of this molecule is still unclear. The synthesis of both PhyQ and 5′-monohydroxyphylloquinone has been reported in the eukaryotic flagellate *Euglena gracilis* Klebs (strain Z) (Ziegler et al., 1989) and the cyanobacterium *Synechococcus* sp. PCC 6301 (Allen et al., 1967; Ziegler et al., 1989). Additionally, a recent study has shown that the red alga *Cyanidium caldarium* synthesizes MQ-4 and utilizes it in its PS I complexes (Yoshida et al., 2003). Two cyanobacteria, *Synechococcus* sp. PCC 7002 and *G. violaceus,* have also been found to synthesize MQ-4 instead of PhyQ (Sakuragi, 2004). Therefore, MQ-4 synthesis and utilization in PS I may occur more widely than is presently realized among oxygenic phototrophs. MQ-4 and 5′-monohydroxyphylloquinone exhibit the same basic molecular structure as PhyQ, with only a modification either in the level of saturation or the presence of a hydroxyl substituent in the alkyl side chain; these molecules have been reported to provide the same functionality as PhyQ in the PS I (Ziegler et al., 1989; Sakuragi, 2004). *G. violaceus*, which lacks thylakoids and exhibits other structural and biochemical differences from most cyanobacteria, is thought to be one of the earliest diverging lineages of the cyanobacteria (Nelissen et al., 1995; Honda et al., 1999). It is therefore highly plausible that ancestral cyanobacteria synthesized MQ-4 and that PhyQ biosynthesis evolved from MQ-4 biosynthesis in cyanobacteria. While this is likely to be the case, the absence of most *men* genes in *G. violaceus* is a finding that certainly warrants additional biochemical studies, since this organism seems to possess a novel pathway for the synthesis of the quinoid head group.

III. Genetic Manipulation of the A_1 Quinone

As the PhyQ/MQ-4 biosynthetic pathway was being nearly completely verified, it was shown that genetic manipulation of the PhyQ pathway in cyanobacteria can also be used to place quinones of biotic or abiotic

origin into the A_1 site of PS I. The type of quinone that can be inserted into the A_1 site depends on the nature of the intermediate that accumulates after the manipulation of the pathway, or it depends upon further chemical treatment and/or reconstitution of the isolated PS I complexes.

A. *The* menA *and* menB *Mutants*

It has been demonstrated that the *menA*, *menB*, *menD*, and *menE* mutants of *Synechocystis* sp. PCC 6803, and *menB* and *menF* mutants of *Synechococcus* sp. PCC 7002 are no longer capable of PhyQ or MQ-4 biosynthesis, respectively, but that they still accumulate a UV-absorbing compound in PS I (Johnson et al., 2000, 2003; Sakuragi et al., 2002; Sakuragi, 2004). This compound has been identified as PQ-9 based on its absorption spectrum, its characteristic retention time in HPLC analysis, and its m/z ratio in mass spectrometric analysis. The orientation of the carbonyl bonds relative to the membrane normal and the distance from $P700^+$ were shown to be the same as those of PhyQ in the wild-type PS I by continuous-wave EPR, electron spin-polarized transient EPR, and electron-spin-echo modulation experiments (Zybailov et al., 2000). In the PS I complexes from such mutants, PQ-9 was shown to participate in electron transfer from A_0 to F_X (Semenov et al., 2000; Zybailov et al., 2000), and this quinone can support nearly 85% of the wild-type, electron-transfer activity of PS I as measured by the rate of cytochrome c_6:flavodoxin oxidoreduction (Johnson et al., 2000). Although they grow at a significantly slower rate than the wild-type strain, the *menA* and *menB* mutants are capable of photoautotrophic growth at low light intensity (20 $\mu E\ m^{-2}\ sec^{-1}$); these results conclusively demonstrate that PQ-9 can functionally replace PhyQ in PS I.

Given the difference in the one-electron reduction potentials between PhyQ (-465 mV vs. NHE, Prince et al., 1983) and PQ-9 (-369 mV vs. NHE, Prince et al., 1986) in dimethylformamide, an alteration of kinetic properties of electron transport for reactions involving A_1 was expected in PS I complexes containing PQ-9. Semenov et al. (2000) demonstrated that charge recombination occurs with a lifetime of 3 msec, which is nearly 25 times faster than the rate for wild-type PS I complexes, between $P700^+$ and the [4Fe–4S] clusters of PS I complexes isolated from the *menA* and *menB* mutants. The forward electron transfer from A_1 to the [4Fe–4S] clusters occurs with lifetimes of $\sim$15 and $\sim$300 μsec, which are 100–1,000 slower than the rates for wild-type PS I complexes. These kinetic data have been used to estimate the *in situ* Gibbs free energy difference between A_1 and F_X, which is ~ -100 mV in wild-type but $\sim +100$ mV in the *menA* and *menB* mutants. Shinkarev et al. (2002) refined their model and calculated that the redox midpoint potential of PQ-9 at the A_1 site is about 135 mV more oxidizing than PhyQ. If this model is correct, the redox potential of PQ-9 at the A_1 site would be more oxidizing than F_X, and the consequence of this would be that thermodynamically unfavorable, up-hill electron transfer from PQ to F_x must occur in the PS I complexes of the *menA* and *menB* mutants. Despite the unfavorable conditions for maintaining stable charge separation, the PQ-9-containing PS I complexes are nearly as active in catalyzing electron transfer as the PhyQ-containing wild-type PS I complexes.

B. *The* menG *Mutant*

Demethylphylloquinone- or demethylmenaquinone-containing PS I complexes have been obtained by construction of the *menG* mutants in *Synechocystis* sp. PCC 6803 and *Synechococcus* sp. PCC 7002, respectively (Sakuragi et al., 2002; Sakuragi, 2004). Unlike the *menA*, *menB*, *menD*, *menE*, and *menF* mutants, PS I complexes isolated from these *menG* mutants contained demethylphylloquinone or demethylmenaquinone-4 in the A_1 site. This clearly indicates that these prenyl naphthoquinones have a higher affinity for the A_1-binding site than PQ-9. Kinetically, the forward electron transfer from A_1 to the [4Fe–4S] clusters is about threefold slower, and correspondingly the rate of charge recombination between FeS^- and $P700^+$ is approximately fourfold faster, in PS I complexes containing demethylphylloquinone than in wild-type PS I complexes containing PhyQ. These results have been interpreted thermodynamically as being due to an alteration of the Gibbs free energy difference between A_1 and F_X (Sakuragi et al., 2002). The kinetic data allow one to estimate that demethylphylloquinone at the A_1 site is about 50 mV more oxidizing than PhyQ. This result is in excellent agreement with the predicted difference based on the redox potentials of the PhyQ analogs 2,3-dimethyl-1,4-naphthoquinone and 2-methyl-1,4-naphthoquinone, in dimethylformamide (Sakuragi et al., 2002). When the PS I activity was measured by the light-dependent rate of flavodoxin reduction using reduced cytochrome c_6 as the electron donor, PS I complexes containing demethylphylloquinone were equally active as the wild-type PS I complexes containing PhyQ. These results indicate that the threefold reduction of the forward electron-transfer rate

is not the rate-limiting step for the reduction of flavodoxin. Because PS I complexes containing demethylphylloquinone function similarly to wild-type PS I complexes, the question then arises as to why the methyl group is present at all. Although no completely satisfying answer to this question is currently available, it is nevertheless possible that the methyl group may play a conditionally important structural role. Indeed, the PS I content of the *menG* mutant cells grown at a moderately high light intensity ($\sim 250\ \mu E\ m^{-2}\ sec^{-1}$) is about 20% lower than that of the wild-type control. The full role(s) of the methyl group is yet to be identified, but it is possible that the absence of this methyl group adversely affects either the stability or the assembly of the PS I complexes.

C. Recruitment of Other Quinones

Attempts have been made to place quinones other than PQ-9 and demethylphylloquinone/demethylmenaquinone into the A_1 site of PS I by supplementing the growth medium for selected cyanobacterial mutants with various quinones of abiotic origin. The first such attempt involved supplementing the medium for a *Synechocystis* sp. PCC 6803 *menB* mutant culture with naphthoquinones (NQ). Of the many quinones tested, 2-carboxyl-1,4-NQ, which is an intermediate of PhyQ biosynthesis, and 2-methyl-1,4-NQ were shown to be phytylated *in vivo* (and methylated in the case of the former) and resulted in the presence of PhyQ in the PS I complexes of the mutant (Johnson et al., 2001). PhyQ was shown to replace PQ-9 at efficiency of ca. 90%, and as a result, the *menB* mutant regained the ability to grow photoautotrophically with a rate nearly equal to that of the wild-type strain (Johnson et al., 2001). When the growth medium of the *menA* mutant was similarly supplemented with intermediates of PhyQ biosynthesis or with other quinones, photoautotrophic growth was not restored. Therefore, it appears that the presence of the phytyl substituent is essential for the displacement of PQ-9 by the exogenously added quinone. Other naphthoquinones tested so far either partially restored the photoautotrophic growth of the *menB* mutant (1,4-NQ, 2-hydroxyl-1,4-NQ, 2-hydroxyl-3-prenyl-1,4-NQ), produced no effect on its growth (2-carboxyl-3,5-NQ, 2-carboxyl-3,7-NQ, 1,2-NQ), or were toxic (5-hydroxy-1,4-NQ, 2-methyl-5-hydroxyl-1,4-NQ, 2,3-dichloro-1,4-NQ).

In light of these findings, medium supplementation of the *menB* mutant with various substituted AQs was also tested (Zybailov, 2003). Of the compounds tested, 9,10-AQ, 2-amino-9,10-AQ, 2,6-diamino-9,10-AQ, 2,3-dimethyl-9,10-AQ, and tertbutyl-9,10-AQ were shown to improve the photoautotrophic growth of the *menB* mutant. Further studies are required to assess the efficiency of the incorporation of these AQs into the A_1 site. In general, the redox potential of AQs are lower than those of NQs in organic solvent (Prince et al., 1982). Therefore, it is reasonably anticipated that the presence of these quinones in the A_1 site would alter thermodynamics of the electron transfer between the cofactors. This would easily be detectable by changes in the rates of the forward and reverse electron-transfer reactions.

Two conclusions can be drawn based on the results obtained from the *in vivo* and *in vitro* quinone replacement studies: (i) a wide variety of quinoid structures can functionally replace PhyQ at the A_1 site, and (ii) a wide range of quinone derivatives can support PS I activity and their effectiveness correlates well with the redox potentials of the molecules examined. As was effectively demonstrated for the studies of the *menA*, *menB*, and *menG* mutants (see above), the obvious advantage of the *in vivo*, genetic manipulation of the PhyQ pathway and growth medium-supplementation method is that it provides a biological and physiological system in which the effect of the quinone alteration can be assessed within the context of the overall photosynthetic activities of the organism. A disadvantage is that apparently only substituted naphthoquinones appear to be able to efficiently displace PQ-9. This limitation has recently been overcome by using PS I complexes isolated from a *rubA menB* double mutant of *Synechococcus* sp. PCC 7002 (Sakuragi et al., 2005). The *rubA* gene encodes a membrane-associated rubredoxin, which is absolutely required for insertion of [4Fe–4S] clusters into PS I (Shen et al., 2002a,b). A *rubA* null mutant, constructed by insertional inactivation of the coding sequence of this gene, produces PS I complexes that are completely devoid of [4Fe–4S] clusters and lacking the PsaC, PsaD, and PsaE stromal surface polypeptides (Shen et al., 2002a,b). The *rubA menB* double mutant therefore produces PS I complexes containing PQ-9 but lacking [4Fe–4S] clusters, including F_X. Intriguingly, when PS I complexes isolated from *rubA menB* double mutant were incubated with AQ and then extensively washed, both PQ-9 and AQ were removed and PS I complexes with apparently empty A_1 sites were produced (Sakuragi et al., 2005). The potential uses and significance of this system are enormous. By using PS I complexes devoid of quinone and iron–sulfur clusters, the inherent rate of charge recombination between A_0 and P700 can be evaluated in complexes that have not been harshly extracted with solvents. Reconstitution of the

A_1 site with a variety of quinones should also be possible without the obstacle of the added molecule having to out-compete PQ-9 for the A_1 sites. It should also now be possible to produce complete PS I complexes with any desired quinone that can be stably bound at the A_1 site by first reconstituting the F_X cluster (Golbeck, 1995; Shen et al., 2002b) and then by adding recombinant PsaC, containing F_A and F_B (Zhao et al., 1992; Mehari et al., 1995; Golbeck, 1998; Vassiliev et al., 2001), and PsaD (Zhao et al., 1990; N Li et al., 1991).

IV. The Plastoquinone Biosynthetic Pathway

The successful delineation of the pathway for PhyQ biosynthesis and genetic manipulation of this pathway as a mechanism for modifying and probing PS I function encourages an extension of this methodology to other quinone biosynthetic pathways. There are at least four reasons to manipulate PQ-9 biosynthesis by a similar strategy. First, the pathway for the synthesis of plastoquinone is presently unknown in cyanobacteria, and it is only known that this pathway differs from that in higher plants (Dähnhardt et al., 2002; Cheng et al., 2003). Second, if a strain mutated in both a *men* gene and a gene encoding an appropriate enzyme in plastoquinone biosynthesis could be constructed, this would allow further manipulation of the quinone species found in the A_1 site of PS I. Third, it would allow manipulation of the quinone species in PS II complexes and would facilitate detailed studies of the kinetics involving Q_A and Q_B *in vivo*. Fourth, it is reasonable to assume that a modified quinone species in the membrane quinone pool would affect the redox state of the electron-transport chain, which would probably alter the redox-dependent expression of some genes that encode components of the photosynthetic apparatus (Escoubas et al., 1995; Alfonso et al., 2000; H Li and Sherman, 2000; see also a review by Allen and Pfannschmidt, 2000 and references therein). Such an experimental system would thus provide a completely novel way to analyze redox effects on photosynthetic gene expression *in vivo*.

Studies of PQ-9 biosynthesis have been carried out in higher plants since the 1960s by using isotopic tracers and direct enzyme activity assays (see a review by Threlfall and Whistance, 1971; Pennock and Threlfall, 1981; Swiezewska, 2004) and only more recently by genetic methods (Collakova and DellaPenna, 2001; Shintani et al., 2002; Cheng et al., 2003). The combined results have shown that in plants PQ is synthesized from homogentisate after two further enzymatic reactions: first, the condensation of solanyl diphosphate and homogentisate by a solanyl transferase resulting in 2-methyl-6-solanyl-1,4-benzoquinone (MSBQ), and second, a methylation reaction at the C_3 position of the benzoquinoid ring system by MSBQ methyltransferase. This MSBQ methyltransferase is also responsible for methylation of 2-methyl-6-phytyl-1,4-benzoquinone (MPBQ) in α-tocopherol biosynthesis, and therefore it is a bifunctional enzyme in higher plant (Shintani et al., 2002; Cheng et al., 2003). Given the frequent similarity of biochemical pathways in plants and cyanobacteria, it would have been logical to assume that the same pathway functions in cyanobacteria. However, recent studies have shown that neither the synthesis of homogentisate nor the presence of MPBQ methyltransferase activity is required for PQ-9 biosynthesis in the cyanobacterium *Synechocystis* sp. PCC 6803 (Dähnhardt et al., 2002; Cheng et al., 2003). These results indicate that PQ-9 biosynthesis in cyanobacteria is distinctly different from that in higher plants and that the PQ-9 biosynthetic pathways may have evolved convergently in cyanobacteria and higher plants (Cheng et al., 2003).

How is PQ synthesized in cyanobacteria? Comparative genome analysis of 14 cyanobacteria revealed the presence of ORFs that show sequence similarity to some of the enzymes responsible for ubiquinone-8 (UQ-8, 2,3-dimethoxy-5-methyl-6-octaprenyl-1,4-benzoquinone) biosynthesis. UQ-8 biosynthesis in *E. coli* occurs as shown in Fig. 5 (see the review by Meganathan, 2001 and references therein). The first committed step of the pathway is the aromatization of chorismate to 4-hydroxybenzoate, which is catalyzed by chorismate-pyruvate lyase (UbiC). Prenylation by 4-hydroxybenzoate octaprenyltransferase (UbiA) and decarboxylation by isofunctional 3-octaprenyl-4-hydroxybenzoate decarboxylases (UbiD and UbiX) results in the synthesis of 2-octaprenyl-phenol, which is converted into UQ after three hydroxylation reactions that alternate with three methylation reactions. A hydroxyl group is first introduced by 2-octaprenyl-phenol monooxygenase (UbiB) (at the position *ortho* to the C_1 OH), which is subsequently methylated by an *O*-methyltransferase (UbiG) resulting in 2-methoxy-6-octaprenyl-phenol. Second, a hydroxyl group is introduced by a monooxygenase (UbiH) at the position *para* to the C_1 hydroxyl group, resulting in the synthesis of 2-methoxy-6-octaprenyl-1,4-benzoquinol. UbiE, a *C*-methyltransferase, delivers a methyl group to a position *ortho* to the C_6 prenyl side chain, resulting

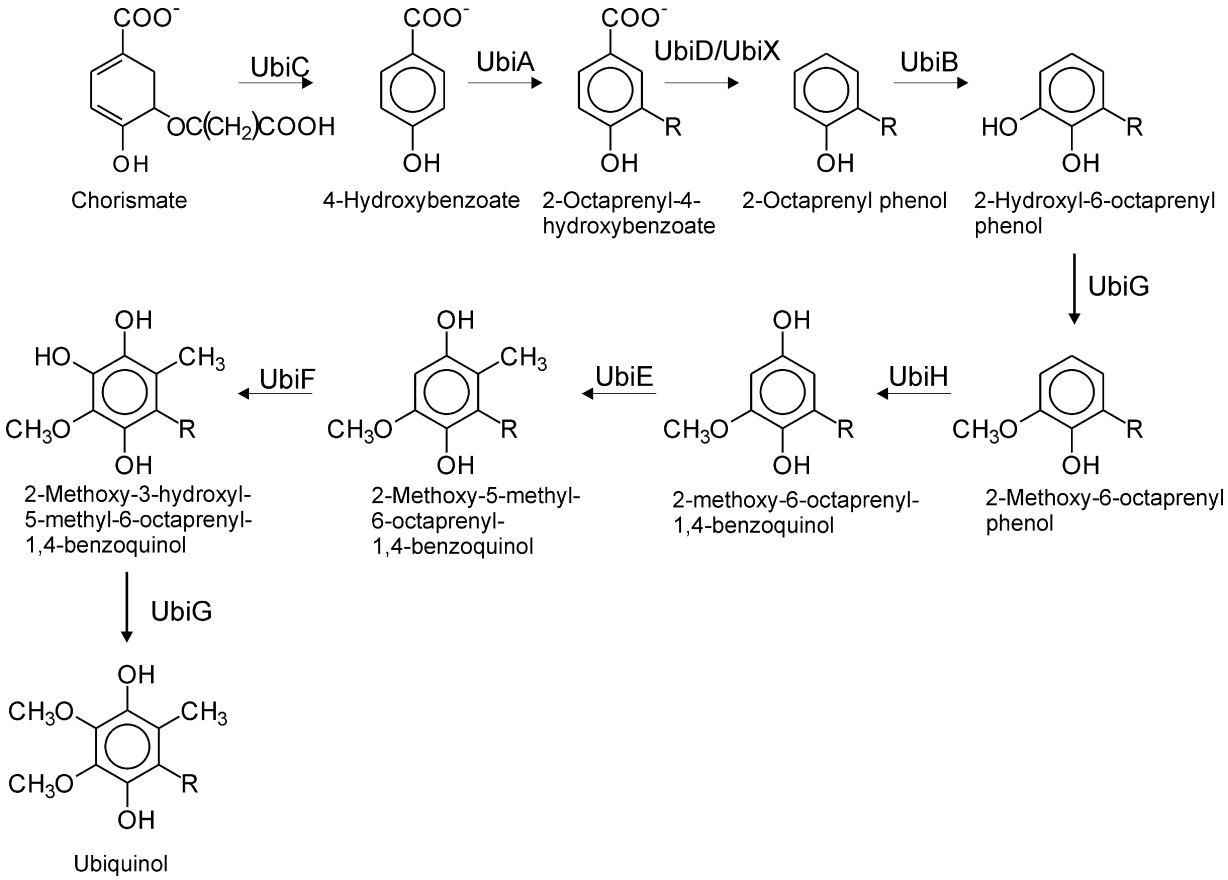

Fig. 5. Ubiquinone biosynthesis pathway in *Escherichia coli*.

in the synthesis of 2-methoxy-5-methyl-6-octaprenyl-1,4-benzoquinol. Further hydroxylation by a monooxygenase (UbiF) and methylation by UbiG at the C_3 position of the ring system results in UQ-8.

UbiA, UbiD, UbiE, UbiH, and UbiX homologs were conserved in 14 cyanobacterial genomes (Sakuragi, 2004). In the structure of PQ-9 the two methoxy groups are replaced by two methyl groups, and no additional methyl group is present at the ring position *ortho* to the prenyl side chain. Therefore, it is possible that PQ-9 biosynthesis occurs by a pathway that is similar to the UQ-8 biosynthesis pathway in proteobacteria, as proposed in Fig. 6. The proposed pathway is most similar to that for UQ-8 in the portion leading to the formation of the prenyl benzoquinone.

Efforts to verify the proposed biosynthetic pathway have been made by attempting to inactivate the *ubiA*, *ubiH*, and *ubiX* genes in *Synechocystis* sp. PC 6803. These attempts, however, resulted in incomplete segregation of the mutant and wild-type alleles, demonstrating that these genes are essential for the survival of this organism (Sakuragi, 2004). Heterologous expression of cyanobacterial homologs in *ubi* mutants of *E. coli* would perhaps resolve the validity of the proposed pathway, and such studies are underway.

As noted above, UbiC, chorismate-pyruvate lyase, is responsible for the first committed step in the UQ biosynthetic pathway in *E. coli* (Fig. 5). In cyanobacteria, however, no obvious *ubiC* homolog was found. This appeared to indicate that a homolog to this gene was absent in cyanobacteria, and that the synthesis of 4-hydroxybenzoate must occur through an alternative pathway. In higher plants, 4-hydroxybenzoate is derived from the amino acids tyrosine and phenylalanine through 4-coumarate and 4-cinnamate intermediates (Threlfall and Whistance, 1971; Pennock and Threlfall, 1981). It is, therefore, possible that the synthesis of PQ-9 in cyanobacteria occurs via one or both of these amino acids. Comparative genome analysis, on the other hand, has recently revealed the presence of an ORF, which shows weak similarity to the UbiC sequences of *E. coli* (<30%) and which is conserved among all

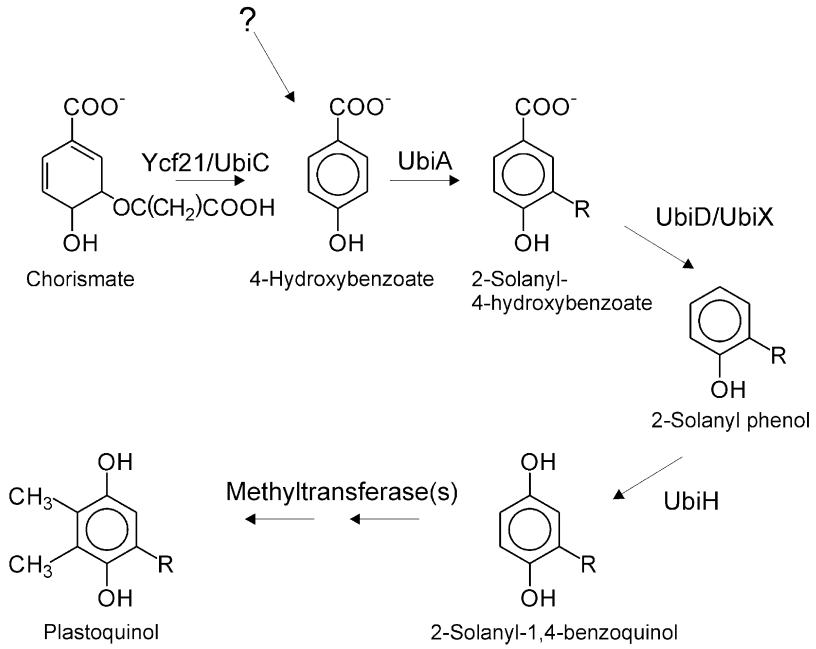

Fig. 6. Proposed plastoquinone biosynthetic pathway in cyanobacteria. The question mark indicates the possibility that an alternative route exists for 4-hydroxybenzoate synthesis.

cyanobacteria (50–80%) (Sakuragi, 2004). This ORF shows a high degree of amino acid sequence similarity to Ycf21 proteins, which are found in the plastid genomes of eukaryotic phototrophs including *Porphyra purpurea* and *Cyanophora paradoxa.* Therefore, it is also possible that these Ycf21 homologs catalyze the conversion of chorismate to 4-hydroxybenzoate in cyanobacteria. This possibility could be tested by complementation of an *ubiC* mutant of *E. coli* with a cyanobacterial *ycf21* gene.

In the genome of *Synechocystis* sp. PCC 6803, there are several homologs of *menG*/*ubiE*, the gene encoding the enzyme responsible for the methylation reactions in both ubiquinone and menaquinone biosynthesis in *E. coli*. These are *sll1653*/*menG* (Sakuragi et al., 2002), *sll0418* [encoding 2-methyl-6-phytyl-1,4-benzoquinone methyltransferase (Shintani et al., 2002; Cheng et al., 2003)], *slr0089* [encoding γ-tocopherol methyltransferase (Shintani and DellaPenna, 1998)], *slr1618*, *slr0407*, *slr1039*, *sll0487*, and *sll0829*. Of all of these putative methyltransferase genes, only *menG* and *sll0418* are highly conserved throughout the sequenced cyanobacterial genomes, suggesting they could be the responsible methyltransferases in PhyQ and PQ-9 biosynthesis, respectively. However, null mutations of these genes, either individually or in combination with mutations in these other methyltransferase genes (up to triple mutations), did not affect the synthesis of PQ-9, indicating that functional redundancy for this reaction may occur in this cyanobacterium (Sakuragi, 2004). Thus, it is possible that *ubiE* homologs are not required for the methylation reactions in PQ-9 biosynthesis, and the identity of the responsible methyltransferase(s), or the appropriate biosynthetic intermediate, is currently unknown.

V. The α-Tocopherol Biosynthetic Pathway

The biosynthetic pathway for α-tocopherol is largely identical in cyanobacteria and higher plants (Fig. 7; Threlfall and Whistance, 1971; d'Harlingue and Camara, 1985; Norris et al., 1998; Shintani and DellaPenna, 1998; Collakova and DellaPenna, 2001, 2003; Schledz et al., 2001; Dähnhardt et al., 2002; Porfirova et al., 2002; Savidge et al., 2002; Shintani et al., 2002; Cheng et al., 2003; Koch et al., 2003; Sattler et al., 2003). Briefly, the precursor homogentisate is converted by homogentisate phytyltransferase to 2-methyl-6-phytyl-1,4-benzoquinone (MPBQ) (Collakova and DellaPenna, 2001, 2003; Schledz et al., 2001; Savidge et al., 2002), which is methylated by MPBQ methyltransferase resulting in 2,3-dimethyl-6-phytyl-1,4-benzoquinone (DMPBQ) (Soll et al., 1985; Shintani et al., 2002; Cheng et al. 2003). DMPBQ

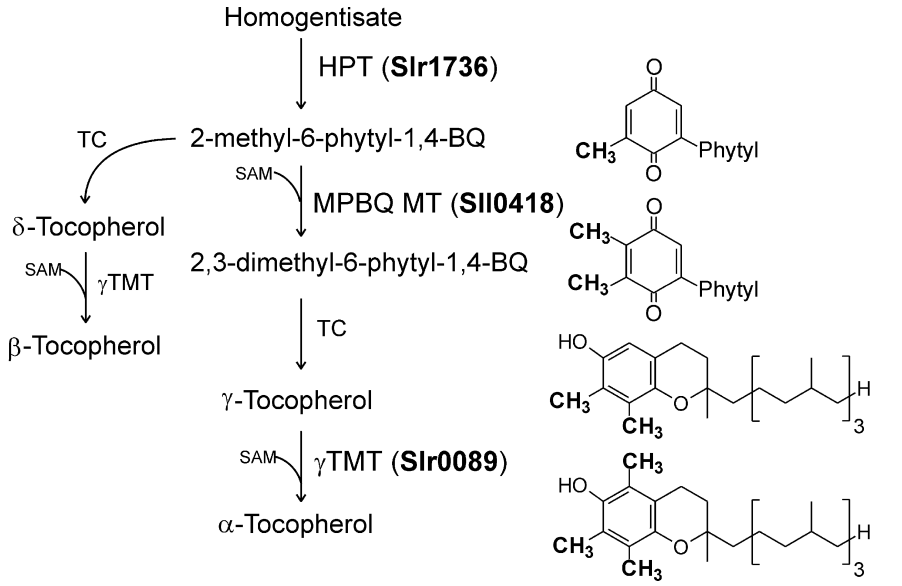

Fig. 7. α-Tocopherol biosynthetic pathway in cyanobacteria. HTP – homogentisate phytyltransferase; MPBQ – 2-methyl-6-phytyl-1,4-benzoquinone; SAM – *S*-adenosyl-L-methionine; TC – tocopherol cyclase; γ TMT – γ-tocopherol methyltransferase.

undergoes cyclization by tocopherol cyclase resulting in γ-tocopherol (Soll et al., 1985; Porfirova et al., 2002; Sattler et al., 2003), which is further methylated by γ-tocopherol methyltransferase to produce α-tocopherol (Soll et al., 1980; d'Harlingue and Camara, 1985; Shintani and DellaPenna, 1998; Koch et al., 2003). Homogentisate is derived from 4-hydroxyphenylpyruvate by 4-hydroxyphenylpyruvate dioxygenase (Norris et al., 1998; Dähnhardt et al., 2002).

DMPBQ is a subject of interest for studies of PS I. This molecule possesses a dimethyl-1,4-benzoquinoid head group and is structurally identical to PQ-9 except that it carries a C-20 phytyl side chain rather than a C-45 solanesyl side chain. It has been demonstrated that a null mutation of *slr1737*, encoding tocopherol cyclase, results in the accumulation of DMBQ in the cells of *Synechocystis* sp. PCC 6803 (Sattler et al., 2003). Therefore, it is reasonable to expect that this molecule could compete effectively with PQ-9 for binding to the A_1 site and occupy this site in PS I in strains carrying mutations in *menB* or other *men* genes. A detailed analysis of such a mutant, in comparison to the wild-type and other *men* mutants, should allow one to assess the structural requirement(s) of the alkyl substituent for proper association of the quinone with PS I.

The role(s) of α-tocopherol in oxygenic phototrophs has been a mystery for more than 80 years since the first discovery of this compound as an essential factor for pregnancy in rats (Evans and Bishop, 1992). Based on results gathered in animals, animal cell cultures, and artificial membranes, it has been shown that tocopherols function as antioxidants and scavenge or quench various reactive oxygen species and lipid oxidation byproducts that would otherwise propagate lipid peroxidation chain reactions in membranes (Kamal-Eldin and Appelqvist, 1996). This antioxidant role of α-tocopherol has now been demonstrated in eukaryotic phototrophs owing to studies in the past several years. The herbicide-mediated interruption of the α-tocopherol biosynthetic pathway has been shown to render PS II more susceptible to oxidative stress at extremely high light intensities in the green alga *Chlamydomonas reinhardtii* (Trebst et al., 2002). Moreover, the presence of α-tocopherol has been shown to suppress the propagation of lipid peroxidation during seed germination in *A. thaliana* (Sattler et al., 2004). Thus, there is little doubt that α-tocopherol can function as a bulk antioxidant in eukaryotic phototrophs as well as in animals. The antioxidant role of α-tocopherol is also being investigated in the cyanobacterium *Synechocystis* sp. PCC 6803, and the results obtained so far also support a role for α-tocopherol as an antioxidant in this organism (Maeda et al., unpublished results). In addition to its role as an antioxidant, however, recent studies have demonstrated a second role, which apparently does not involve its antioxidant properties, for α-tocopherol in *Synechocystis* sp. PCC 6803. The tocopherol-less mutant strain was unable to grow in the presence of glucose at pH 7.4 or below, although the wild-type grows

normally under these conditions (Sakuragi, 2004). Under these conditions, cells became chlorotic and PS II activity was completely lost within 24 h. The transcription of some important metabolic and regulatory genes was altered upon loss of α-tocopherol. The expression of some genes was constitutively altered (e.g., *slr2031*, *ndhF3*, *ndhR*, and *sbtA*), and the expression of other genes was conditionally altered (e.g., *sigA*, *sigG*, *rbcL*, *ccmK*, *ndhF4*). These results suggest that α-tocopherol functions as a signaling molecule and regulator of transcription in cyanobacteria. A similar transcriptional regulatory role of α-tocopherol has been reported in animal systems (see reviews by Azzi et al., 2002; Ricciarelli et al., 2002 and references therein). Whether there is a common underlying mechanism between these two evolutionarily distinct systems is an intriguing subject for future study.

Acknowledgments

We thank Prof. Dean DellaPenna of Michigan State University for sharing his ideas and for helpful discussions concerning the functional roles of α-tocopherol and metabolic engineering of its biosynthetic pathway.

References

Alfonso M, Perewoska I and Kirilovsky D (2000) Redox control of *psbA* gene expression in the cyanobacterium *Synechocystis* PCC 6803. Involvement of the cytochrome b_6/f complex. Plant Physiol 122: 505–516

Allen JF and Pfannschmidt T (2000) Balancing the two photosystems: photosynthetic electron transfer governs transcription of reaction centre genes in chloroplasts. Phil Trans R Soc Lond B Biol Sci 355: 1351–1359

Allen CF, Franke H and Hirayama O (1967) Identification of plastoquinone and two naphthoquinones in *Anacystis nidulans* by NMR and mass spectroscopy. Biochem Biophys Res Commun 26: 562–568

Azzi A, Ricciarelli R and Zingg JM (2002) Non-antioxidant molecular functions of α-tocopherol (vitamin E). FEBS Lett 519: 8–10

Barber J and Anderson JM (2002) Introduction. Phil Trans R Soc Lond B 357: 1325–1328

Ben-Shem A, Frolow F and Nelson N (2003) Crystal structure of plant photosystem I. Nature 426: 630–635

Ben-Shem A, Frolow F and Nelson N (2004) Evolution of photosystem I – from symmetry through pseudosymmetry to asymmetry. FEBS Lett 564: 274–280

Biggins J (1990) Evaluation of selected benzoquinones, naphthoquinones, and anthraquinones as replacements for phylloquinone in the A_1 acceptor site of the Photosystem I reaction center. Biochemistry 29: 7259–7264

Biggins J and Mathis P (1988) Functional role of vitamin K_1 in Photosystem I of the cyanobacterium *Synechocystis* 6803. Biochemistry 27: 1494–1500

Brettel K (1997) Electron transfer and arrangement of the redox cofactors in photosystem I. Biochim Biophys Acta 1318: 322–373

Brettel K and Leibl W (2001) Electron transfer in Photosystem I. Biochim Biophys Acta 1507: 100–114

Brettel K, Sétif P and Mathis P (1987) Flash-induced absorption changes in Photosystem I at low temperature: evidence that the electron acceptor A_1 is vitamin K_1. FEBS Lett 203: 220–224

Bryant DA (1994) The Molecular Biology of Cyanobacteria. Kluwer Academic Publisher, Dordrecht

Bryant DA (2003) The beauty in small things revealed. Proc Natl Acad Sci USA 17: 9647–9649

Cheng Z, Sattler S, Maeda H, Sakuragi Y, Bryant DA and DellaPenna D (2003) Highly divergent methyltransferase catalyzes a conserved reaction in tocopherol and plastoquinone synthesis in cyanobacteria and photosynthetic prokaryotes. Plant Cell 15: 2343–2356

Collakova E and DellaPenna D (2001) Isolation and functional analysis of homogentisate phytyltransferase from *Synechocystis* sp. PCC 6803 and Arabidopsis. Plant Physiol 127: 1–12

Collakova E and DellaPenna D (2003) Homogentisate phytyltransferase activity is limiting for tocopherol biosynthesis in Arabidopsis. Plant Physiol 131: 632–642

Collins MD and Jones D (1981) Distribution of isoprenoid quinone structural types in bacteria and their taxonomic implications. Microbiol Rev 45: 316–354

Dähnhardt D, Falk J, Appel J, van der Kooij TAW, Schulz-Friedrich R and Krupinska K (2002) The hydroxyphenylpyruvate dioxygenase from *Synechocystis* sp. PCC 6803 is not required for plastoquinone biosynthesis. FEBS Lett 523: 177–181

Deisenhofer J and Norris JR (1993) The Photosynthetic Reaction Center, Vol 1. Academic Press, San Diego

Delwiche FC and Palmer JD (1997) The origin of plastids and their spread via secondary endosymbiosis. In: Bhattacharya D (ed) Origins of Algae and Their Plastids, pp 53–86. Springer-Verlag, New York

d'Harlingue A and Camara B (1985) Plastid enzymes of terpenoid biosynthesis. J Biol Chem 260: 15200–15203

Douglas SD (1998) Plastid evolution: origins, diversity, trends. Curr Opin Genet Dev 8: 655–661

Dufresne A, Salanoubat M, Partensky F, Artiguenave F, Axmann IM, Barbe V, Duprat S, Galperin MY, Koonin EV, Le Gall F, Makarova KS, Ostrowski M, Oztas S, Robert C, Rogozin IB, Scanlan DJ, Tandeau de Marsac N, Weissenbach J, Wincker P, Wolf YI and Hess WR (2003) Genome sequence of the cyanobacterium *Prochlorococcus marinus* SS120, a nearly minimal oxyphototrophic genome. Proc Natl Acad Sci USA 100: 9647–9649

Durán RV, Hervás M, de la Rosa MA and Navarro JA (2004) The efficient functioning of photosynthesis and respiration in *Synechocystis* sp. PCC 6803 strictly requires the presence of either cytochrome c_6 or plastocyanin. J Biol Chem 279: 7229–7233

Escoubas JM, Lomas M, LaRoche J and Falkowski PG (1995) Light intensity regulation of *cab* gene transcription is signaled by the redox state of the plastoquinone pool. Proc Natl Acad Sci USA 92: 10237–10241

Evans HM and Bishop BKS (1922) Fetal resorption. Science 55: 650

Falkowski PG (2002) The ocean's invisible forest. Sci Am 287: 54–61

Fromme P, Jordan P and Krauß N (2001) Structure of photosystem I. Biochim Biophys Acta 1507: 5–31

Fromme P, Melkozernov A, Jordan P and Krauß N (2003) Structure and function of photosystem I: interactions with its soluble electron carriers and external antenna systems. FEBS Lett 555: 40–44

Glockner G, Rosenthal A and Valentin K (2000) The structure and gene repertoire of an ancient red algal plastid genome. J Mol Evol 51: 382–390

Golbeck JH (1994) Photosystem I in cyanobacteria. In: Bryant DA (ed) The Molecular Biology of Cyanobacteria, pp 319–360. Kluwer Academic Publishers, Dordrecht

Golbeck JH (1995) Photosystem I and its bacterial counterparts. In: Song PS and Horspool W (eds) CRC Handbook of Organic Photochemistry and Photobiology, pp 1407–1419. CRC Press, Boca Raton, FL

Golbeck JH (1998) Comparison of *in vitro* and *in vivo* mutants of PsaC in photosystem I: protocols for mutagenesis and techniques for analysis. Methods Enzymol 297: 95–123

Golbeck JH (2003) The binding of cofactors to Photosystem I analyzed by spectroscopic and mutagenic methods. Annu Rev Biophys Biomol Struct 32: 237–256

Hauska G (1988) Phylloquinone in Photosystem I. Are quinones the secondary-electron acceptors in all types of photosynthetic reaction centers. Trends Biochem Sci 13: 415–416

Honda D, Yokota A and Sugiyama J (1999) Detection of seven major evolutionary lineages in cyanobacteria based on the 16S rRNA gene sequence analysis with new sequences of five marine *Synechococcus* strains. J Mol Evol 48: 723–739

Itoh S and Iwaki M (1989a) Vitamin K_1 (phylloquinone) restores the turnover of FeS centers in the ether-extracted spinach PS I particles. FEBS Lett 243: 47–52

Itoh S and Iwaki M (1989b) New herbicide-binding site in the photosynthetic electron-transport chain. Competitive herbicide binding at the photosystem I phylloquinone-(vitamin K_1)-binding site. FEBS Lett 250: 441–447

Itoh S and Iwaki M (1991) Full replacement of the function of the secondary electron acceptor phylloquinone (=vitamin K_1) by non-quinone carbonyl compounds in green plant Photosystem I photosynthetic reaction center. Biochemistry 30: 5340–5346

Itoh S, Iwaki M and Ikegami I (2001) Modification of Photosystem I reaction center by the extraction and exchange of chlorophylls and quinones. Biochim Biophys Acta 1507: 115–138

Iwaki M and Itoh S (1989) Electron transfer in spinach Photosystem I reaction center containing benzo-, naphtho- and anthraquinones in place of phylloquinone. FEBS Lett 256: 11–16

Iwaki M and Itoh S (1991) Structure of the phylloquinone-binding (Qϕ) site in green plant Photosystem I reaction centers: the affinity of quinones and quinoid compounds for Qϕ site. Biochemistry 30: 5347–5352

Johnson TW, Shen G, Zybailov B, Folling D, Reategui R, Beauparlant S, Vassiliev IR, Bryant DA, Jones AD, Golbeck JH and Chitnis PR (2000) Recruitment of a foreign quinone into the A_1 site of Photosystem I: I. Genetic and physiological characterization of phylloquinone biosynthetic pathway mutants in *Synechocystis* sp. PCC 6803. J Biol Chem 275: 8523–8530

Johnson TW, Zybailov B, Jones AD, Bittl R, Zech S, Stehlik D, Golbeck JH and Chitnis PR (2001) Recruitment of a foreign quinone into the A_1 site of Photosystem I: *in vivo* replacement of plastoquinone-9 by media-supplemented naphthoquinones in phylloquinone biosynthetic pathway mutants of *Synechocystis* sp. PCC 6803. J Biol Chem 276: 39512–39521

Johnson TW, Naithani S, Stewart C Jr, Zybailov B, Jones AD, Golbeck JH and Chitnis PR (2003) The *menD* and *menE* homologs code for 2-succinyl-6-hydroxyl-2,4-cyclohexadiene-1-carboxylate synthase and O-succinylbenzoic acid-CoA synthase in the phylloquinone biosynthetic pathway of *Synechocystis* sp. PCC 6803. Biochim Biophys Acta 1557: 67–76

Jordan P, Fromme P, Witt HT, Klukas O, Saenger W and Krauß N (2001) Three-dimensional structure of cyanobacterial Photosystem I at 2.5 Å resolution. Nature 411: 896–899

Kamal-Eldin A and Appelqvist L-A (1996) The chemistry and antioxidant properties of tocopherols and tocotrienols. Lipids 31: 671–701

Kaneko T, Sato S, Kotani H, Tanaka A, Asamizu E, Nakamura Y, Miyajima N, Hirosawa M, Sugiura M, Sasamoto S, Kimura T, Hosouchi T, Matsuno A, Muraki A, Nakazaki N, Naruo K, Okumura S, Shimpo S, Takeuchi C, Wada T, Watanabe A, Yamada M, Yasuda M and Tabata S (1996) Sequence analysis of the genome of the unicellular cyanobacterium *Synechocystis* sp. strain PCC6803. II. Sequence determination of the entire genome and assignment of potential protein-coding regions. DNA Res 3: 109–136

Kaneko T, Nakamura Y, Wolk CP, Kuritz T, Sasamoto T, Watanabe A, Iriguchi M, Ishikawa M, Kawashima M, Kimura T, Kishida Y, Kohara M, Matsumoto M, Matsuno A, Muraki A, Nakazaki N, Shimpo S, Sugimoto M, Takazawa M, Yamada M, Yasuda M and Tabata S (2001) Complete genomic sequence of the filamentous nitrogen-fixing cyanobacterium *Anabaena* sp. strain PCC 7120. DNA Res 8: 205–213

Ke B (2001) Photosynthesis: Photobiochemistry and Photobiophysics. Kluwer Academic Publishers, Dordrecht

Koch M, Lemke R, Heise K and Mock H (2003) Characterization of γ-tocopherol methyltransferase from *Capsicum annuum* L. and *Arabidopsis thaliana*. Eur J Biochem 270: 84–92

Lee PT, Hsu AY, Ha HT and Clarke CF (1997) A *C*-methyltransferase involved in both ubiquinone and menaquinone biosynthesis: isolation and identification of *Escherichia coli ubiE* gene. J Bacteriol 179: 1748–1754

Li H and Sherman LA (2000) A redox-responsive regulator of photosynthesis gene expression in the cyanobacterium *Synechocystis* sp. Strain PCC 6803. J Bacteriol 182: 4268–4277

Li N, Zhao JD, Warren PV, Warden JT, Bryant DA and Golbeck JH (1991) PsaD is required for the stable binding of PsaC to the Photosystem I core protein of *Synechococcus* sp. PCC 6301. Biochemistry 30: 7863–7872

Margulis L (1970) Origin of Eukaryotic Cells. Yale University Press, New Haven

Martin W, Stoebe B, Gremykin V, Hapsmann S, Hasegawa M and Kowallik KV (1998) Gene transfer to the nucleus and the evolution of chloroplast. Nature 393: 162–165

Matsuzaki M, Misumi O, Shin-IT, Maruyama S, Takahara M, Miyagishima SY, Mori T, Nishida K, Yagisawa F, Nishida K, Yoshida Y, Nishimura Y, Nakao S, Kobayashi T, Momoyama Y, Higashiyama T, Minoda A, Sano M, Nomoto H, Oishi K, Hayashi H, Ohta F, Nishizaka S, Haga S, Miura S, Morishita T, Kabeya Y, Terasawa K, Suzuki Y, Ishii Y, Asakawa S, Takano H, Ohta N, Kuroiwa H, Tanaka K, Shimizu N, Sugano S, Sato N, Nozaki H, Ogasawara N, Kohara Y and Kuroiwa T (2004)

Genome sequence of the ultrasmall unicellular red alga *Cyanidioschyzon merolae* 10D. Nature 428: 653–657

McKenna M, Henninger MD and Crane FL (1964) A second naphthoquinone in spinach chloroplasts. Nature 203: 524–525

Meganathan R (1996) Biosynthesis of the isoprenoid quinones-menaquinone (vitamin K_2) and ubiquinone (coenzyme Q). In: Neidhardt FC (ed) *Escherichia coli* and *Salmonella* – Cellular and Molecular Biology, Vol 2, pp 642–656. ASM press, Washington, DC

Meganathan R (2001) Biosynthesis of menaquinone (vitamin K_2) and ubiquinone (coenzyme Q): a perspective on enzymatic mechanisms. Vitam Horm 61: 173–218

Mehari T, Qiao F, Scott MP, Nellis DF, Zhao J, Bryant DA and Golbeck JH (1995) Modified ligands to F_A and F_B in Photosystem I. I. Structural constraints for the formation of iron–sulfur clusters in free and rebound PsaC. J Biol Chem 270: 28108–29117

Monzingo AF, Gao J, Qiu J, Georgiou G and Robertus JD (2003) The X-ray structure of *Escherichia coli* RraA (MenG), a protein inhibitor of RNA processing. J Mol Biol 332: 1015–1024

Mühlenhoff U, Kruip J, Nitschke W, Bryant DA, Rögner M, Sétif P and Boekema E (1996a) Characterization of a redox active cross-linking complex between cyanobacterial photosystem I and its physiological acceptor flavodoxin. EMBO J 15: 488–497

Mühlenhoff U, Zhao J and Bryant DA (1996b) Interaction of Photosystem I and flavodoxin from the cyanobacterium *Synechococcus* sp. PCC 7002 as revealed by chemical cross-linking. Eur J Biochem 325: 324–331

Nakamura Y, Kaneko T, Sato S, Ikeuchi M, Katoh H, Sasamoto S, Watanabe A, Iriguchi M, Kawashima K, Kimura T, Kishida Y, Kiyokawa C, Kohara M, Matsumoto M, Matsuno A, Nakazaki N, Shinpo S, Sugimoto M, Takeuchi C, Yamada M and Tabata S (2002) Complete genome structure of the thermophilic cyanobacterium *Thermosynechococcus elongatus* BP-1. DNA Res 9: 123–130

Nakamura Y, Kaneko T, Sato S, Mimuro M, Miyashita H, Tsuchiya T, Sasamoto S, Watanabe A, Kawashima K, Kishida Y, Kiyokawa C, Kohara M, Matsumoto M, Matsuno A, Nakazaki N, Shimpo S, Takeuchi C, Yamada M and Tabata S (2003) Complete genome structure of *Gloeobacter violaceus* PCC 7421, a cyanobacterium that lacks thylakoids. DNA Res 10: 137–145

Nelissen B, Van de Peer Y, Wilmotte A and De Wachter R (1995) An early origin of plastids within the cyanobacterial divergence is suggested by evolutionary trees based on complete 16S rRNA sequences. Mol Biol Evol 12: 1166–1173

Norris SR, Shen X and DellaPenna D (1998) Complementation of the Arabidopsis *pds1* mutation with the gene encoding *p*-hydroxyphenylpyruvate dioxygenase. Plant Physiol 117: 1317–1323

Ohta N, Matsuzaki M, Misumi O, Miyagishima SY, Nozaki H, Tanaka K, Shin-IT, Kohara Y and Kuroiwa T (2003) Complete sequence and analysis of the plastid genome of the unicellular red alga *Cyanidioschyzon merolae*. DNA Res 10: 67–77

Ort DR and Yocum CF (1996) Oxygenic Photosynthesis: The Light Reactions. Kluwer Academic Publishers, Dordrecht

Palenik B, Brahamsha B, Larimer FW, Land M, Hauser L, Chain P, Lamerdin J, Regala W, Allen EE, McCarren J, Paulsen I, Dufresne A, Partensky F, Webb EA and Waterbury J (2003) The genome of a motile marine *Synechococcus*. Nature 424: 1037–1042

Pennock JF and Threlfall DR (1981) Biosynthesis of ubiquinone and related compounds. In: Porter JW and Spurgeon SL (eds) Biosynthesis of Isoprenoid Compounds, Vol 2, pp 191–303. John Wiley & Sons, New York

Petersen J, Stehlik D, Gast P and Thurnauer M (1987) Comparison of the electron spin polarized spectrum found in plant Photosystem I and in iron-depleted bacterial reaction centers with time-resolved K-band EPR; evidence that the Photosystem I acceptor A_1 is a quinone. Photosynth Res 14: 15–29

Porfirova S, Bergmuller E, Tropf S, Lemke R and Dormann P (2002) Isolation of an *Arabidopsis* mutant lacking vitamin E and identification of a cyclase essential for all tocopherol biosynthesis. Proc Natl Acad Sci USA 99: 12495–12500

Prince RC, Gunner MR and Dutton PL (1982) Quinones of value to electron-transfer studies: oxidation–reduction potentials of the first reduction step in an aprotic solvent. In: Trumpower BL (ed) Function of Quinones in Energy Conserving Systems, pp 29–33. Academic Press, New York

Prince RC, Dutton PL and Bruce JM (1983) Electrochemistry of ubiquinones: menaquinones and plastoquinones in aprotic solvents. FEBS Lett 160: 273–276

Prince RC, Lloyd-Williams P, Bruce JM and Dutton PL (1986) Voltammetric measurements of quinones. Methods Enzymol 125: 109–119

Ricciarelli R, Zingg J-M and Azzi A (2002) The 80th anniversary of vitamin E: beyond its antioxidant properties. Biol Chem 383: 457–465

Rocap G, Larimer FW, Lamerdin J, Malfatti S, Chain P, Ahlgren NA, Arellano A, Coleman M, Hauser L, Hess WR, Johnson ZI, Land M, Lindell D, Post AF, Regala W, Shah M, Shaw SL, Steglich C, Sullivan MB, Ting CS, Tolonen A, Webb EA, Zinser ER and Chisholm SW (2003) Genome divergence in two *Prochlorococcus* ecotypes reflects oceanic niche differentiation. Nature 424: 1042–1047

Sakuragi Y (2004) Cyanobacterial quinomics – studies of quinones in cyanobacteria. PhD Thesis. The Pennsylvania State University

Sakuragi Y, Zybailov B, Shen G, Jones AD, Chitnis PR, van der Est A, Bittl R, Zech S, Stehlik D, Golbeck JH and Bryant DA (2002) Insertional inactivation of the *men*G gene, encoding 2-phytyl-1,4-naphthoquinone methyltransferase of *Synechocystis* sp. PCC 6803, results in the incorporation of 2-phytyl-1,4-naphthoquinone into the A_1 site and alteration of the equilibrium constant between A_1 and F_X in Photosystem I. Biochemistry 41: 394–405

Sakuragi Y, Zybailov B, Shen G, Bryant DA, Golbeck, JH, Diner BA, Karygina I, Pushkar Y and Stehlik D (2005) Recruitment of a foreign quinone into the A_1 site of photosystem I. Characterization of a *menB rubA* double deletion mutant in *Synechococcus* sp. PCC 7002 devoid of F_X, F_A, and F_B and containing plastoquinone or exchanged 9,10-anthraquinone. J Biol Chem 280: 12371–12381

Sattler S, Cahoon EB, Coughlan SJ and DellaPenna D (2003) Characterization of tocopherol cyclases from higher plants and cyanobacteria. Evolutionary implications for tocopherol synthesis and function. Plant Phys 132: 2184–2195

Sattler S, Gillilanda LU, Magallanes-Lundback M, Pollard M and DellaPenna D (2004) Vitamin E is essential for seed longevity and preventing lipid peroxidation during germination. Plant Cell 16: 1419–1432

Savidge B, Weiss JD, Wong YH, Lassner NW, Mitsky TA, Shewmaker CK, Post-Beittenmiller D and Valentin HE (2002)

Isolation and characterization of homogentisate phytyltransferase genes from *Synechocystis* sp. PCC 6803 and Arabidopsis. Plant Physiol 129: 321–332

Schledz M, Seidler A, Beyer P and Neuhaus G (2001) A novel phytyltransferase from *Synechocystis* sp. PCC 6803 involved in tocopherol biosynthesis. FEBS Lett 499: 15–3589

Schoeder H-U and Lockau W (1986) Phylloquinone copurified with the large subunits of Photosystem I. FEBS Lett 199: 23–27

Schopf JW (1993) Microfossils of the early archean apex chert: new evidence of the antiquity of life. Science 260: 640–646

Semenov AY, Vassiliev IR, van der Est A, Mamedov MD, Zybailov B, Shen G, Stehlik D, Diner BA, Chitnis PR and Golbeck JH (2000) Recruitment of a foreign quinone into the A_1 site of Photosystem I: altered kinetics of electron transfer in phylloquinone biosynthetic pathway mutants studied by time-resolved optical, EPR, and electromagnetic techniques. J Biol Chem 275: 23429–23438

Sétif P (2001) Ferredoxin and flavodoxin reduction by photosystem I. Biochim Biophys Acta 1507: 161–179

Shen G, Zhao J, Reimer SK, Antonkine ML, Cai Q, Weiland SM, Golbeck JH and Bryant DA (2002a) Assembly of Photosystem I: I. Inactivation of the *rubA* gene encoding a membrane-associated rubredoxin in the cyanobacterium *Synechococcus* sp. PCC 7002 causes a loss of Photosystem I activity. J Biol Chem 277: 20343–20354

Shen G, Antonkine ML, van der Est A, Vassiliev IR, Brettel K, Bittl R, Zech SG, Zhao J, Stehlik D, Bryant DA and Golbeck JH (2002b) Assembly of Photosystem I. II. Rubredoxin is required for the *in vivo* assembly of F_X in *Synechococcus* sp. PCC 7002 as shown by optical and EPR spectroscopy. J Biol Chem 277: 20355–20366

Shinkarev VP, Zybailov B, Vassiliev IR and Golbeck JH (2002) Modeling of the $P700^+$ charge recombination kinetics with phylloquinone and plastoquinone in the A_1 site of Photosystem I. Biophys J 83: 2885–2897

Shintani D and DellaPenna D (1998) Elevating the vitamin E content of plants through metabolic engineering. Science 282: 2098–2100

Shintani D, Cheng Z and DellaPenna D (2002) The role of 2-methyl-6-phytyl-benzoquinone methyltransferase in determining tocopherol composition in *Synechocystis* sp. PCC 6803. FEBS Lett 511: 1–5

Simantiras M and Leistner E (1991) Cell free synthesis of ortho-succinylbenzoic acid in protein extracts from anthraquinone and phylloquinone (vitamin K_1) producing plant-cell suspensions cultures – occurrence of intermediates between isochorismic and ortho-succinylbenzoic acid. Z Naturforsch C 46: 364–370

Soll J, Kemmerling M and Schultz G (1980) Tocopherol and plastoquinone synthesis in spinach chloroplasts subfractions. Arch Biochem Biophys 204: 544–550

Soll J, Schultz G, Joyard J, Douce R and Block MA (1985) Localization and synthesis of prenylquinones in isolated outer and inner envelope membranes from spinach chloroplast. Arch Biochem Biophys 238: 290–299

Swiezewska E (2004) Ubiquinone and plastoquinone metabolism in plants. Methods Enzymol 378: 124–131

Takahashi Y, Hirota K and Katoh S (1985) Multiple forms of P700-chlorophyll *a*–protein complex from *Synechococcus* sp.: the iron, quinone and carotenoid contents. Photosynth Res 6: 183–192

Thornber JP, Alberte RS, Hunter FA, Shiozawa JA and Kan K-S (1976) The organization of chlorophyll in the plant photosynthetic unit. Brookhaven Symp Biol 28: 132–148

Threlfall DR and Whistance GR (1971) Biosynthesis of isoprenoid quinones and chromanols. In: Goodwin TW (ed) Aspects of Terpenoid Chemistry and Biochemistry, Vol 12, pp 357–404. Academic Press, New York

Trebst A, Depka BM and Hollander-Czytko H (2002) A specific role for tocopherol and of chemical singlet oxygen quenchers in the maintenance of Photosystem II structure and function in *Chlamydomonas reinhardtii*. FEBS Lett 516: 156–160

Vassiliev IR, Antonkine ML and Golbeck JH (2001) Iron–sulfur clusters in type I reaction centers. Biochim Biophys Acta 1507: 139–160

Yoshida E, Nakamura A and Watanabe A (2003) Reversed-phase HPLC determination of chlorophyll a′ and naphthoquinones in Photosystem I of red algae: existence of two menaquinone-4 molecules in Photosystem I of *Cyanidium caldarium*. Anal Sci 19: 1001–1005

Zhao JD, Warren PV, Li N, Bryant DA and Golbeck JH (1990) Reconstitution of electron transport in Photosystem I with PsaC and PsaD proteins expressed in *Escherichia coli*. FEBS Lett 276: 175–180

Zhao J, Li N, Warren PV, Golbeck JH and Bryant DA (1992) Site-directed conversion of a cysteine to aspartate leads to the assembly of a [3Fe–4S] cluster in PsaC of Photosystem I. The photoreduction of F_A is independent of F_B at low temperature. Biochemistry 31: 5093–5099

Zhao J, Snyder WB, Mühlenhoff U, Rhiel E, Warren PV, Golbeck JH and Bryant DA (1993) Cloning and characterization of the *psaE* gene of the cyanobacterium *Synechococcus* sp. PCC 7002: characterization of a *psaE* mutant and overproduction of the protein in *Escherichia coli*. Mol Microbiol 9: 183–194

Ziegler K, Maldener I and Lockau W (1989) 5′-Monohydroxyphylloquinone as a component of Photosystem I. Z Natuforsch C 44: 468–472

Zybailov B (2003) Modified quinone acceptor in photosystem I. PhD Thesis. The Pennsylvania State University

Zybailov B, van der Est A, Zech SG, Teutloff C, Johnson TW, Shen G, Bittle R, Stehlik D, Chitnis PR and Golbeck JH (2000) Recruitment of a foreign quinone into the A_1 site of Photosystem I: II. Structural and functional characterization of phylloquinone biosynthetic pathway mutants by electron paramagnetic resonance and electron-nuclear double resonance spectroscopy. J Biol Chem 275: 8531–8539

Chapter 16

Optical Measurements of Secondary Electron Transfer in Photosystem I

Fabrice Rappaport*
Laboratoire de Physiologie membranaire et moléculaire du Chloroplaste, UMR 7141 CNRS-Univ. Paris 6, Institut de Biologie Physico-Chimique, 13 rue Pierre et Marie Curie, 75005 Paris, France

Bruce A. Diner
Central Research and Development, Experimental Station, E. I. du Pont de Nemours & Co., Wilmington, DE 19880-017, USA

Kevin Redding
Department of Chemistry, University of Alabama, Tuscaloosa, AL 35487-0336, USA

*Author for correspondence, email: rappaport@ibpc.fr

John H. Golbeck (ed): Photosystem I: The Light-Driven Plastocyanin:Ferredoxin Oxidoreductase, 223–244.

Summary

All known photosynthetic reaction centers have symmetric structures, using two similar or identical integral membrane subunits to form a dimeric core, which binds the cofactors through which electrons are shuttled across the membrane. This symmetric arrangement gives rise to two similar branches of cofactors, down which light-driven electron transfer could proceed. The first three members of each branch are chlorins, while the third is a quinone. It is known that the initial electron transfer occurs almost exclusively along one of the two branches in the well-characterized Type 2 reaction centers, although the origins of this strong asymmetry are still debated. Photosystem I is the best characterized representative of the Type 1 reaction centers, but many aspects of electron transfer directionality remain unresolved. Recent time-resolved absorption studies suggest that electron transfer can make use of both cofactor branches of Photosystem I at room temperature. Here, we will present the results that led to this proposal and discuss this model in the light of the recent studies aimed at testing its validity.

I. Introduction

In the past few years a considerable number of new results have improved and challenged our understanding of structure/function relationships in Photosystem I (PS I). The determination at atomic resolution of its three-dimensional structure is certainly not the least (see Fromme and Grotjohann, this volume, Chapter 6; Nelson and Ben-Shem, this volume, Chapter 7; Antonkine and Golbeck, this volume, Chapter 8). It set the basis for detailed calculations as well as experimental assessment of the excitonic coupling of the hundreds of chlorophylls that act as light-harvesting pigments (see Savikhin, this volume, Chapter 12; Karapetyan et al., this volume, Chapter 13; Schlodder and Renger, this volume, Chapter 35) and significantly boosted the site-directed mutagenesis strategy aimed at elucidating the physico-chemical properties, as well as the eventual participation, of the different redox cofactors involved in the various electron transfer (ET) reactions (see Webber and Ramesh, this volume, Chapter 14; van der Est, this volume, Chapter 25). In this article we will focus on the ET reaction between the quinones, which serve as secondary electron acceptors, and the iron–sulfur clusters, which serve as terminal electron acceptors. These reactions have been mostly studied by time-resolved absorption spectroscopy and transient EPR spectroscopy. We will focus on the results obtained with the former approach. As will be argued, we feel that this approach yields a fairly consistent picture but we refer the reader to Stehlik (this volume, Chapter 23) and Redding and van der Est (this volume, Chapter 24) for a comprehensive review of the results obtained by transient EPR spectroscopy, from which significantly different conclusions are drawn. Please note that unless stated otherwise, the numbering of the amino acids in the PsaA and PsaB subunits refers to that of *Thermosynechococcus elongatus*.

Abbreviations: A_0 – primary electron acceptor composed of chlorophyll monomer; A_{0A} – primary electron acceptor bound to PsaA; A_{0B} – primary electron acceptor bound to PsaB; A_1 – secondary electron acceptor composed of phylloquinone(s); PhQ_A – phylloquinone bound to PsaA; PhQ_B – phylloquinone bound to PsaB; Chl – chlorophyll; ENDOR – electron-nuclear double resonance; EPR – electron paramagnetic resonance; ET – electron transfer; PS I – Photosystem I; PS II – Photosystem II; PsaA and PsaB – heterodimeric core subunits of Photosystem I.

II. Secondary Electron Transfer: Are the Two Phylloquinones Involved?

The reoxidation kinetics of the quinone A_1^- have been studied essentially by two techniques: optical spectroscopy, the time resolution of which is presently unequaled, and time-resolved EPR spectroscopy. Both techniques have been extensively used since 1988 and have provided an increasingly refined characterization of the kinetics of forward ET between the reduced phylloquinone and the Fe_4S_4 clusters.

A. Monophasic Versus Biphasic Kinetics

The first evidence for biphasic kinetics with half times of 20 and 150 nsec came from a study of the flash-induced absorption changes in the near UV in PS I complexes from spinach (*Spinacia oleracea*) (Sétif and Brettel, 1993). The relative amplitudes of these two phases were found, however, to vary between 2:1 and 1:2 for different preparations. Since the relative amplitude of the fast phase rose with increasingly harsh solubilization treatment, it was proposed that the reoxidation of A_1^- was intrinsically monophasic and slow, and that the fast phase was a consequence of the purification procedure. This hypothesis was consistent with

the earlier finding of essentially monophasic A_1^- reoxidation kinetics in PS I from cyanobacteria ($t_{1/2} \sim 200$ nsec) (Brettel, 1988). The reoxidation of the reduced quinones may also be studied by transient EPR spectroscopy. Indeed, the relatively long lifetime of electron spin correlation in the light-induced charge separated state allows one to detect the spin polarization changes associated with ET reactions. It is noteworthy, however, that the time resolution of this latter approach is not sufficient to allow one to observe directly changes in the light-induced spin polarization signals in the tens of nanosecond time range. Yet, as discussed in van der Est (2001), the fast phase has a clear signature, since it significantly affects the transients. Indeed, an increase in the relative amplitude of the fast phase results in a significant decrease of the relative amplitude of the absorptive part of the transient spectrum ascribed to the $P_{700}^+A_1^-$ state, due to overlap with the emissive spectrum ascribed to the $P_{700}^+FeS^-$ state (see van der Est, this volume, Chapter 24). Despite the inferiority of the time resolution of transient EPR spectroscopy with respect to optical spectroscopy, the former technique has the great advantage in allowing study of the spin polarization changes in PS I with no interference from PS II, even in samples that have not been subjected to any biochemical treatment, such as whole cells or chloroplasts (see van der Est, 2001). This differs from the earlier studies using optical spectroscopy, which were restricted, for technical reasons, to detergent-solubilized PS I particles. A thorough analysis of the ET reaction from A_1^- to the iron–sulfur centers has been made by transient EPR in a series of PS I preparations from cyanobacteria ranging from whole cells to core particles. The decay of the signal ascribed to the $P_{700}^+A_1^-$ state was found to be monophasic in intact samples; the biphasicity became manifest in PS I particles (van der Est et al., 1994), supporting the idea that the fast phase was an artifact and that forward ET from A_1^- to the iron–sulfur cluster was monophasic with a half time of ~200 nsec as observed in PS I from cyanobacteria. This view was challenged by studies using refined optical spectroscopy. Using an instrument with an improved time resolution of 2 nsec, Brettel could resolve a fast phase ($t_{1/2} \sim 7$ nsec, relative amplitude 30%) in PS I from the cyanobacterium *Synechocystis* sp. PCC 6803 (Brettel, 1998). However, this finding did not settle the controversy, since these results were obtained with PS I particles. A significant breakthrough came with the development of a new spectrophotometer with a time resolution of 5 nsec and a signal-to-noise ratio high enough to allow one to study A_1^- reoxidation kinetics in whole cells (Béal et al., 1999). Using this technique, Joliot and Joliot confirmed the existence of two phases with half times of 15 and 150 nsec, respectively (relative amplitude 45%, 55%), in whole cells of a PS II-depleted mutant from *Chlorella sorokiniana* (Joliot and Joliot, 1999). Thus, despite the effect of biochemical purification, the fast phase can be considered as an inherent kinetic feature of intact PS I. Interestingly, no fast phase was detected by time-resolved photovoltage measurements, although this technique is ideally suited for monitoring charge transfer with a significant component perpendicular to the membrane plane. A fast instrument-limited phase ascribed to the formation of $P_{700}^+A_1^-$, followed by a monophasic rise (ascribed to ET from A_1^- via F_x to F_A and possibly F_B) with $t_{1/2}$ ~150 nsec accounting for 35–40% of the total amplitude was found in membranes from *Synechocystis* sp. PCC 6803 (Hecks et al., 1994; Leibl et al., 1995). The biphasic nature of A_1^- reoxidation is, however, now well established from optical measurements as an intrinsic feature of forward ET to the iron–sulfur clusters. Yet, it is widely recognized, as well, that the overall kinetics of quinone reoxidation may be artificially accelerated by biochemical treatments such as detergent solubilization using Triton X-100 (Sétif and Brettel, 1993). Moreover, the relative amplitude of the fast and slow phases are species dependent. Indeed, the relative amplitude of the fast phase was found to be consistently smaller in cyanobacteria (amplitude ratio 1:3–4) than in eukaryotic organisms (amplitude ratio about 1:1–2) (see Xu et al., 2003b for a discussion and references therein).

B. The Origin of the Biphasic Kinetics

Multiphasic or dispersed kinetics is a commonly observed feature in condensed phase systems in general and in biological systems in particular. When discussing such features, it should be kept in mind that distinguishing more than two exponentials with half times differing by less than a factor of 5 is a difficult task. In the present case of the two phases of A_1^- reoxidation, the half times differ by about one order of magnitude. They can thus be distinguished with confidence. Yet, although fitting with three exponentials rather than two does not significantly improve the quality of the fit, the occurrence of other phases may not be excluded. We will assume the presence of only two exponential decay components for the present discussion, and take up the case of additional component(s) later (see below). Several models have been proposed to account for the biphasicity. As one possible explanation, Sétif and Brettel proposed that the difference in free energy

between the $P_{700}^{+}A_1^{-}$ and the $P_{700}^{+}F_X^{-}$ states is small enough that a quasi-equilibrium is reached between these two states before ET proceeds further to F_A/F_B (Sétif and Brettel, 1993). The fast phase would correspond to the establishment of this equilibrium, the slow one to the oxidation of F_X^{-}. Since ET from A_1^{-} to F_X is electrogenic (Leibl et al., 1995), the equilibrium constant of this ET reaction, and hence the relative amplitude of the fast phase, would be expected to be modulated by a transmembrane electric field. Joliot and Joliot tested the above model by measuring the kinetics of A_1^{-} reoxidation under varying transmembrane electric fields, and concluded that the relative amplitudes of the two phases were not sensitive to the transmembrane electric field (Joliot and Joliot, 1999). On these grounds, they proposed two alternative models to account for the biphasicity of the A_1^{-} reoxidation kinetics: (i) two different conformational states of the same reduced phylloquinone differing in their A_1^{-} reoxidation rates, (ii) two different reduced quinones with different reoxidation rates. The essential difference between these two models is that the former assumes that only one of the two ET branches is active whereas the latter is based on a bi-directional ET model. Indeed, to reduce the two quinones with similar yields, both branches would have to be similarly efficient. This proposal has significantly revised the way one envisions the function of PS I in particular and photosynthetic electron transport in general.

III. Uni-Directional or Bi-Directional Electron Transfer in Reaction Centers

All known photosynthetic reaction centers share the common structural feature of a pseudo-C_2 symmetry. Yet, the two types of reaction centers are distinguished on the basis of their terminal electron acceptors. In Type 2 reaction centers, these terminal electron acceptors are quinones and the last one in the chain may be doubly reduced and doubly protonated to a quinol, which can exchange with an oxidized quinone from the membrane. In Type 1 reaction centers, the terminal electron acceptors are iron–sulfur clusters and the quinones are "merely" electron carriers in the chain leading to these iron–sulfur clusters. Type 2 reaction centers have been examined using highly sophisticated biophysical methods. These have allowed one to identify, long before the three-dimensional structure was solved, the different redox cofactors involved in photosynthetic charge separation, and moreover, to show that they were present in duplicate. In Type 2 reaction centers it is well known, however, that functional symmetry does not follow from the structural symmetry. Direct measurement of absorption changes reflecting the state of the primary acceptor, which is a pheophytin (Pheo), have shown that the primary charge separation involves ET almost exclusively down one of the two branches (forming the $P^{+}Pheo_A^{-}$ state). Photopumping measurements have demonstrated, however, that it is possible to form the spectrally distinguishable $P^{+}Pheo_B^{-}$ state (Kellogg et al., 1989), indicating that it does not lie very far above P* in energy. Numerous unsuccessful attempts have been made to reverse the functional asymmetry (i.e., to force the ET to proceed down the "nonfunctional" branch with a similar yield as that observed for the "functional one") by mutagenesis of the protein environment of the primary donor or acceptor. The paucity of success, even when P was converted to a Chl:Pheo heterodimer (Kirmaier et al., 1988) or $Pheo_A$ to a Chl (Kirmaier et al., 1991), indicates that other factors must be important in determining the functional asymmetry. Stark effect spectroscopy (Steffen et al., 1994) and global energy profile calculations (Gunner et al., 1996) have suggested that the origin of this effect may be ascribed to differences in electrostatic properties between the two branches. Interestingly, a recent study of a *Rhodobacter sphaeroides* reaction center mutant shows that a stable radical pair state may be formed even in the absence of the primary quinone, Q_A (Laible et al., 2003; Wakeham et al., 2003). The mere formation of this radical pair state identified as $P^{+}Q_B^{-}$ (Laible et al., 2003) shows that ET may occur down the "inactive branch." A similar observation was made in Q_A-lacking mutants even in the absence of any mutation or pigment modification at the level of the primary charge separation (Wakeham et al., 2003). This points to bi-directionality of the ET as being, on kinetic grounds, an inherent feature of photosynthetic reaction centers. The functional asymmetry observed in Type 2 reaction centers would then essentially reflect the strong difference in the yield of the ET sequence down either one of the two branches. As alluded to above, the study of the ET yield down either of the two symmetrically arranged cofactor branches in Type 2 bacterial reaction centers has taken advantage of the different spectroscopic signatures of the different cofactors. Such differences allow one to confidently map the level of participation in ET of these various redox cofactors. Until the recent characterization of different site-directed mutants of PS I, no such information was available for Type 1 reaction centers.

IV. A Mutagenesis Survey of the Two Phases Ascribed to A_1^- Reoxidation

A. Mutations Affecting the Quinone Binding Pocket

Here, again, EPR and ENDOR spectroscopy have set the foundation of most of our knowledge on the local environment of the reduced quinone (see Rigby et al., 2001; van der Est, 2001 for reviews). The recent determination of the three-dimensional structure of the PS I reaction center from the cyanobacterium *Thermosynechococcus elongatus* has provided further details on the dark-adapted state of the reaction center (Jordan et al., 2001).

1. The PsaA-W697 and PsaB-W677 Mutants

A coplanar arrangement of the quinone headgroup with the aromatic ring of a Trp was found in both the dark-adapted state (Jordan et al., 2001) and the reduced state (Hanley et al., 1997; van der Est et al., 1997). Moreover, the crystal structure has shown that both PhQ_A and PhQ_B are involved in π–π stacking with a nearby Trp (PsaA-W697 and PsaB-W677, respectively). These residues were targeted by site-directed mutagenesis and substituted for Phe in PS I from the green alga *Chlamydomonas reinhardtii*. These mutations significantly altered the kinetics of quinone reoxidation, as observed by time-resolved UV–visible absorption spectroscopy. In the PsaA-W697F mutant only the half time of the slow phase was decreased, whereas in the symmetric PsaB-W677F mutant only the half time of the fast phase was decreased. Moreover, the relative amplitudes of the two phases were unchanged. Furthermore, the effect of the mutations proved additive, since in the double mutant PsaA-W697F/PsaB-W677F the half time of both phases was decreased (Guergova-Kuras et al., 2001). Last but not least, the spectra of the absorption changes associated with the two phases had a similar overall shape to those observed in the WT strain, indicating that the local environment of the two quinones was not greatly perturbed by the mutation. These results clearly showed that the two phases do not reflect two sequential events, since it proved possible to slow down the fast phase to a rate close to that of the slow phase without affecting the latter. Furthermore, they made possible the identification of the first spectroscopic signatures of the two quinones since they allowed one to ascribe the fast and slow phases to the reoxidation of PhQ_B and PhQ_A, respectively. This latter assignment has been supported by the study of the forward ET from A_1 to F_X in the PsaA W697H or PsaA W697L mutants by transient EPR spectroscopy (Purton et al., 2001). As alluded to above, only the slow phase may be directly detected by this technique. Here again, the decrease of the rate of decay of the spin polarized signal suggested that the slow phase is specifically associated with the quinone bound to PsaA. Similar findings were recently reported from *Synechocystis* sp. PCC 6803 mutants in which the homologous tryptophans of both the PsaA and PsaB subunits were changed to Phe. Here again, time-resolved spectroscopy showed that the PsaA-W697F mutations specifically affected the slow phase, whereas in the symmetric mutant, PsaB-W677F, only the fast phase was slowed (Xu et al., 2003b). Despite the overall consistency between the UV–visible absorption spectroscopy results obtained with PS I from *Synechocystis* sp. PCC 6803 or *C. reinhardtii* PS I, it has been argued that only the slow phase could be ascribed with confidence to the reoxidation of the quinone bound to PsaA, since transient EPR spectroscopy failed to confirm the kinetic effect of the PsaB-W677F mutation but supported that of PsaA-W697F (Xu et al., 2003b). On these grounds, it seems fair to say that the assignment of the fast phase to the reoxidation of the quinone bound to PsaB, initially proposed by Joliot, Redding and colleagues, is still controversial, but that agreement has been reached on the assignment of the slow phase to the reoxidation of the quinone bound to PsaA. As will be discussed below, several other studies have provided further support of the latter assignment.

In addition to providing an unambiguous assignment of at least one of the two phases, these data provided new insights into the unusually negative midpoint potential of the quinone in PS I. Since the finding that phylloquinone acts as secondary electron acceptor in PS I, it has been largely recognized that its midpoint potential should be about −700 mV (see Brettel, 1997 for a review and references therein). Among the different factors that control the midpoint potential of redox cofactors in proteins, interaction with side chain residues may play crucial roles. Iwaki and Itoh (1991) pointed out that π–π stacking between the indole ring of a tryptophan and the aromatic ring of a quinone should destabilize the reduced form (i.e., lower its reduction potential). It is noteworthy that the kinetic consequences of the disruption of this stacking, the strength of which is peculiar to PS I, agree nicely with this hypothesis. Indeed, the replacement of the indole ring with an aliphatic chain (PsaA-W697L), an imidazole ring

(PsaA-W697H) or even a phenyl ring (PsaA-W697F) are expected, according to this hypothesis, to make the reduction potential of the quinone more positive (i.e., decrease the driving force of ET between the quinone and the F_X iron–sulfur cluster). Thus, in the framework of Marcus theory, the rate of this reaction is expected to decrease, as observed, provided $-\Delta G < \lambda$ (where ΔG and λ are the driving force and reorganization energy of the reaction, respectively) (Marcus and Sutin, 1985). Interestingly, Boudreaux et al. (Boudreaux et al., 2001) observed that the conversion of the indole ring to a phenyl group speeds up the $P_{700}^{+}F_{AB}^{-}$ charge recombination. This is also consistent with a decreased free energy gap between $P_{700}^{+}A_1^{-}$ and $P_{700}^{+}F_X^{-}$, since charge recombination is thought to involve the thermally activated repopulation of these two states (the increase in rate of charge recombination was proposed to reflect a decrease by 60–80 meV of this free energy difference). In this framework, the fact that both the PsaA-W697F and PsaB-W677F single mutations resulted in an increased rate of charge recombination of the $P_{700}^{+}F_{AB}^{-}$ state and that the double mutant showed an even faster rate, is consistent with the model according to which PS I may make use of both ET branches for charge recombination (Boudreaux et al., 2001).

2. More Mutants in the Quinone Binding Pocket

As shown by the three-dimensional crystal structure, the PsaA-W697F and PsaB-W677F side chains are by far the most obvious residues to target so as to attempt to modify specifically the quinone binding sites. H-bonds are also known to play an important role in determining the physico-chemical properties of redox cofactors. Unfortunately, the N–H group involved in a H-bond with the C=O group of either quinone is not provided by a side chain residue but by the backbone amide of either the PsaA-L722 or PsaB-L706, preventing facile modulation of the strength of this H-bond by site-directed mutagenesis (Jordan et al., 2001). According to Heathcote and colleagues, the ENDOR spectrum of the semiquinone suggests that the singly reduced quinones are involved in a second H-bond (Rigby et al., 2001). Yet, the assignment of the hyperfine coupling constants is still controversial and in any case the eventual H-bond donor has not been identified. Several other mutants have been constructed recently, however, to modify the local environment of both quinones either in *Synechocystis* sp. PCC 6803 or in *C. reinhardtii*. Both the PsaA and PsaB subunits bear a serine (PsaA-S692, PsaB-S672) whose hydroxyl side chain accepts a H-bond from the indole nitrogen of the nearby Trp (PsaA-W697 and PsaB-W677, respectively). Site-directed replacement of these residues may alter the π–π stacking between the quinone and the Trp and hence have similar effects as replacing the Trp itself. Similarly, the backbone carbonyl group of the leucine (PsaA-L722 and PsaB-L706), whose backbone amide group is involved in a H-bond with the quinone, forms a H-bond with the side chain of an Arg residue (PsaA-R694 and PsaB-R674, respectively). Here, again, mutating these Arg residues may alter the H-bond network in which the quinone is involved and hence its redox properties. Furthermore, these Arg residues tie together the two binding sites of the quinones and the Fe/S cluster F_X by providing a H-bond network that acts as a bridge between the loop containing PsaA-L722 (PsaB-L706) and the F_X binding loop. Finally, a Gly residue is found at position 693 in the PsaA subunit, whereas a Trp is found at the symmetric PsaB position. In an attempt to investigate the origin of the different rates of reoxidation of the two quinones, this Gly was changed to a Trp (PsaA-G693W).

The results from time-resolved absorption spectroscopy (at 380 nm) are presented in Table 1, in terms of half times and relative amplitude of the two phases. Except for the PsaA-R694A and PsaB-R674A mutants, which will be discussed below, all of these various mutants yielded results fully consistent with those obtained using the Trp mutations. Briefly, the mutations affecting the environment of the quinone bound to PsaA subunit resulted in a decreased rate of the slow phase with no effect on the fast phase, whereas mutations affecting the immediate environment of the quinone bound to the PsaB subunit provoked the converse effect. Remarkably, the relative amplitudes of the two phases were hardly changed. The rate of the slow ET phase in the cyanobacterial mutants measured by transient EPR spectroscopy were in good agreement with absorption spectroscopy (Xu et al., 2003b). It is noteworthy, however, that the PsaB-S672C (in *Synechocystis* sp. PCC 6803) or PsaB-S672A (in *C. reinhardtii*) mutations had a much smaller effect than the symmetric mutations (PsaA-S692C or PsaA-S692A), whereas the kinetic effects were of similar magnitude for PsaA-W697F and PsaB-W677F. In fact, these latter mutations are much less conservative than those targeting the Ser. Indeed the Ser mutations may be expected to modify indirectly the stacking between the tryptophans and the quinone rings by altering the H-bond network of the sites, whereas in the case of the tryptophan mutations the π–π stacking is directly perturbed.

Table 1. Half times in nsec and relative amplitude of the two phases ascribed to the reoxidation of A_1^- measured at 380 nm. In bold are indicated the major mutation induced changes with respect to the control strain. The numbering of the amino acid residues corresponds to that of *Thermosynechococcus elongatus*

	Synechocystis sp. PCC 6803		*Chlamydomonas reinhardtii*	
Mutated residue	$t_{1/2}$ (rel. amp.)	$t_{1/2}$ (rel. amp.)	$t_{1/2}$ (rel. amp.)	$t_{1/2}$ (rel. amp.)
Control	8 (0.25)	166 (0.75)	13.5 (0.31)	140 (0.69)
Psa**A**-W697F	6.3 (0.26)[a]	**500** (0.74)[a]	15 (0.34)[b]	**490** (0.66)[b]
Psa**B**-W677F	**23** (0.24)[a]	180 (0.76)[a]	**73** (0.33)[b]	140 (0.67)[b]
Psa**A**-W697F/Psa**B**-W677F	–	–	**73 (0.49)**[b]	**485 (0.51)**[b]
Psa**A**-S692A	–	–	9 (0.33)[c]	**673** (0.67)[c]
Psa**B**-S672A			**18** (0.34)[c]	140 (0.64)[c]
Psa**A**-S692A/Psa**B**-S672A	–	–	**17** (0.28)[c]	**714** (0.72)[c]
Psa**A**-S692C	8.3 (0.29)[a]	**720** (0.71)[a]	–	–
Psa**B**-S672C	**17.3** (0.26)[a]	194 (0.74)[a]	–	–
Psa**B**-R674A	8 (0.30)[a]	**901** (0.7)[a]	–	–
Psa**A**-G693W	–	–	12 (0.33)[c]	**690** (0.67)[c]

[a] Xu et al. (2003b).
[b] Guergova-Kuras et al. (2001).
[c] Rappaport et al. (unpublished).

In this context, it should be pointed out that the kinetic consequences of a change in the driving force of the ET reaction between the quinone and the F_X iron–sulfur cluster may be expected to be significantly different depending on which quinone is involved. Indeed, as will be discussed below, Agalarov and Brettel recently reported that whereas the rate of the slow phase decreases with temperature, that of the fast phase is relatively temperature independent (Agalarov and Brettel, 2003). Incorporating this finding into the model according to which the fast and slow phases reflects ET from PhQ_B to F_X and from PhQ_A to F_X respectively, they proposed that the former is exergonic and the latter endergonic. In this framework, making the reduction potential of PhQ_A or PhQ_B more positive is expected to result in significantly different kinetic changes. Indeed, making the reduction potential of PhQ_B more positive by 60 mV is expected to decrease by the same value the exergonicity of the ET from PhQ_B to F_X. According to Marcus ET theory, such a change yields a threefold decreased rate in the range where $-\Delta G$ is small with respect to the reorganization energy λ (and where $\Delta G \approx 0$) and an even smaller change in rate if $-\Delta G$ is close to λ. Conversely, in the model proposed by Agalarov and Brettel, a similar change of the reduction potential of PhQ_A would increase the endergonicity of the ET between PhQ_A^- and F_X. A 60-mV upshift in the reduction potential of PhQ_A may yield up to a 10-fold decrease of the apparent rate of ET to F_X. In a sense, the ET rate from PhQ_B to F_X would be expected, in this model, to be less sensitive to relatively small changes of the PhQ_B reduction potential than its counterpart involving reduction of F_X at the expense of PhQ_A. The similar effect of the PsaA-W697 and PsaB-W677 mutations on the rates of both the fast and slow phases would then be coincidental and/or reflect subtle structural changes beyond mere shifts in redox potentials. As a hint in favor of different structural effects of the PsaA-S692 and PsaA-W697 mutations, EPR and ENDOR spectra from these mutants reveal significantly different features. Indeed, despite a similar effect on the rate of the slow phase, the spectra of these mutants displayed significant but opposite changes with respect to the WT. The PsaA-W697F mutant displayed a marked shoulder in the low field region of the absorptive part of the X-band spin polarized transient EPR spectra (Boudreaux et al., 2001; Xu et al., 2003a), whereas in the PsaA-S692C/A mutants this shoulder was less pronounced (Xu et al., 2003a; Gu et al., unpublished). The hyperfine coupling pattern of PhQ_A^- was also studied by ENDOR. Here again, the edges of the methyl hyperfine powder pattern were shifted in both mutants, but the shifts were in the opposite direction (Xu et al., 2003a; MacMillan et al., unpublished).

The results obtained with time-resolved absorption spectroscopy are, with the exception of those observed with the PsaB-R674A mutant, easily accounted for in the bi-directional model according to which both quinones are reduced and transfer their electron to F_X with a specific rate. The PsaB-R674A mutation, however, resulted in a slowing down of the slow phase (Xu et al., 2003b) rather than that of the fast one, as would be expected if the quinone bound to PsaB were characterized by a fast reoxidation rate. This result was supported by transient EPR measurements, although the half time of the slow phase was found to be smaller than that

measured by time-resolved absorption spectroscopy [680 and 900 nsec respectively (Xu et al., 2003b)]. Strikingly, the symmetric mutation in PsaA also resulted in slowing down of the slow phase as seen by EPR spectroscopy (Xu et al., 2003b). Taken together, these results seem to challenge the assignment of the fast phase to the reoxidation of the PhQ_B^-. It is noteworthy, however, that neither the PsaA-R694 nor the PsaB-R674 mutation are very much likely to affect significantly the local environment of either of the two quinones and hence their physico-chemical properties. The arginine side chain is involved in a H-bond with the carbonyl backbone group of the Leu, the backbone amide group of which is involved in a H-bond with the C=O group of the quinone. The interaction between the Arg side chain and the quinone is thus most indirect. Much more direct is the involvement of these Arg residues in the scaffold that bears the F_X iron–sulfur cluster. It could thus be argued that the cofactor which is most affected by these mutation is the F_X iron–sulfur, rather than the quinones, as discussed by (Xu et al., 2003b). Interestingly enough, the three-dimensional structure suggests a similar effect upon F_X expected for the PsaA-R694 and PsaB-R674 mutations. To account for the slowing of the slow phase, one would have to assume, in the framework of the bi-directional model, that either of the two mutations induces a more negative reduction potential of the F_X cluster. This would increase the endergonicity of the ET reaction between PhQ_A and F_X and hence slow its rate. Conversely, the free energy change associated with the reduction of F_X by PhQ_B^- would be become less negative, but, as discussed above, the consecutive change in ET rate might be small enough to escape detection. According to this hypothesis, one would expect the $P_{700}^+F_X^-$ charge recombination rate to be affected by both of these mutations, a point that still awaits experimental confirmation. Despite the large amount of recent data that supports the bi-directional hypothesis, a single set of data may be enough to challenge the whole model. However, we feel that more work is required on the PsaA-R694 and PsaA-R674 mutants before a definitive conclusion may be drawn.

Until now we have mostly focused on the site-directed mutagenesis strategy that targeted the quinone binding sites. An alternative strategy for testing the validity of the bi-directional model involves the construction of site-directed mutations that target the redox cofactors upstream of the quinones in the two proposed ET chains. The rationale behind this strategy is that such mutations could affect the relative yield of the two branches and hence the probability to reduce either of the two quinones. The experimental signature of such effects would be a modification of the relative amplitude of one of the two phases ascribed to the reoxidation of PhQ_A^- and PhQ_B^-. It is noteworthy, that, in contrast to the mutations affecting the quinone binding sites, the relative amplitudes are expected to be modified whereas the rates of the two phases should remain unchanged.

B. Mutations Along the Electron Transfer Branches Upstream of the Quinones

In this extensive survey, numerous mutants have been constructed to be able to modify the physico-chemical properties of the different chlorophylls along both chains. In each of these mutants the kinetics of ET between the quinones and the iron–sulfur clusters have been studied by time-resolved absorption spectroscopy at 380 nm. The results are presented in Table 2.

1. Mutations Affecting A_{0A} or A_{0B}

Until now, two residues have been targeted in order to alter the physico-chemical properties of the two A_0 chlorophylls: the two Met residues that provide the axial ligands of the A_{0A} and A_{0B} chlorophylls, and the two symmetric Tyr residues, the phenol ring of which forms an H-bond with the 13^1-keto oxygen of ring V of the chlorophylls (Jordan et al., 2001).

Since H-bonds are known to play a crucial role in determining the redox potential of electron carriers, substitution of one of these two Tyr residues with Phe was expected to alter the redox properties of its associated chlorophyll, which would act as primary electron acceptor of that specific branch in the bi-directional model. As shown in Fig. 1, these different mutations resulted in marked changes in the kinetics of absorption changes as measured at 380 nm, in whole cells of *C. reinhardtii*. In the PsaA-Y696F, PsaA-M688L, or PsaA-M688H mutants, which affect the A_{0A} binding pocket, the overall kinetics were significantly faster than in WT, whereas it was slower in the symmetric A_{0B} mutants. The fit of the data with two exponentials yielded similar half times as the wild type but the amplitude of the fast phase was increased in the PsaA mutants, whereas it was decreased in the PsaB mutants (see Table 2). These results provide further evidence in favor of the bi-directional model, since they show that modifying the physico-chemical properties of electron carriers located upstream of the quinones makes it possible to change the relative amplitude of both phases without affecting their rates. In the case of

Table 2. Half times in nsec and relative amplitudes of the two phases ascribed to the reoxidation of A_1^- measured at 380 nm. In bold are indicated the major mutation induced changes with respect to the control strain. The numbering of the amino acid residues corresponds to that of *Thermosynechococcus elongatus*

	Synechocystis sp. PCC 6803		*Chlamydomonas* reinhardtii	
Mutated residue	$t_{1/2}$ (rel. amp.)	$t_{1/2}$ (rel. amp.)	$t_{1/2}$ (rel. amp.)	$t_{1/2}$(rel. amp.)
Control	8 (0.25)	166 (0.75)	13.5 (0.31)	140 (0.69)
Psa**A**-Y696F	–	–	15 **(0.55)**[a]	150**(0.45)**[a]
Psa**B**-Y676F	–	–	14**(0.17)**[a]	140 **(0.83)**[a]
Psa**A**-M688L	15**(0.58)**[b]	200 **(0.42)**[b]	15**(0.69)**[b]	150**(0.31)**[b]
Psa**A**-M688H	–	–	15 **(0.76)**[b]	180**(0.24)**[b]
Psa**B**-M668H	–	–	15 (0.13)[b]	**220 (0.87)**[b]
Psa**B**-M668L	15**(0.13)**[b]	200 **(0.87)**[b]	–	–
Psa**B**-N591D	–	–	12 (0.37)[b]	150 (0.63)[b]
Psa**A**-T743A	–	–	14 (0.31)[c]	140 (0.69)[c]

[a]Li et al., 2006.
[b]Rappaport et al. (unpublished data).
[c]Li et al., 2006.

the PsaA-Y696F and PsaB-Y676F mutations we have checked that the spectra of the absorption changes associated with either of the two phases were similar to those found with the WT (Li et al., 2006), despite a significant change in their amplitudes. It is noteworthy that both types of mutations resulted in an increase of the relative amplitude of the component ascribed to the reoxidation of the quinone bound to the subunit that does not bear the mutation. In the bi-directional framework this suggests that the mutations affecting A_{0A} decrease the yield of the ET down the A branch and that, conversely, the mutations affecting A_{0B} decrease the yield of the ET down the B branch. Based on these simple results, however, it is impossible to discriminate between two fundamentally different models. In the first one, two different subpopulations of PS I reaction centers can be considered. Due to structural heterogeneity, in each subpopulation ET would be

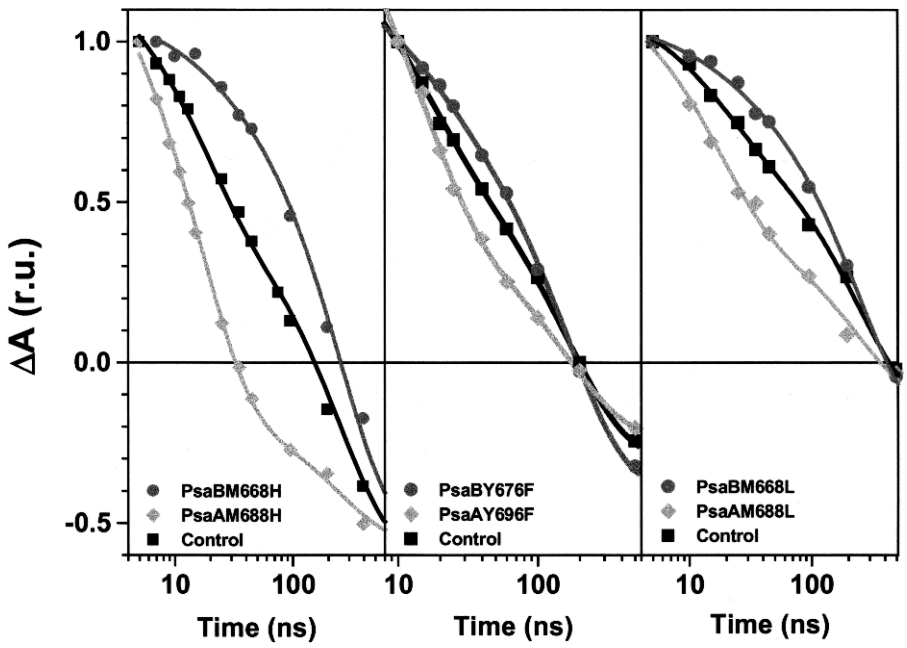

Fig. 1. Kinetics of absorption changes at 380 nm in various PS I mutants. Left and middle panel: *Chlamydomonas reinhardtii* PS I mutants. Right panel: *Synechocystis* sp. PCC 6803 PS I mutants. The data were normalized to the absorption changes measured 7 nsec after the actinic flash. (F. Rappaport, P. Heathcote, J. Golbeck, and K. Redding, unpublished)

intrinsically uni-directional and the relative amplitude of the two phases of reoxidation of the quinones would reflect the relative size of each subpopulation before charge separation occurs. While the effect of the mutations would thus be to shift the equilibrium constant between the two subpopulations, the direction of the shift is difficult to predict in the absence of precise knowledge about the nature of this heterogeneity. As will be discussed below, low-temperature experiments suggest that this model applies, at least at temperatures below 150 K (Schlodder et al., 1998). The main constraint of this model is that the thermodynamic equilibrium between these two subpopulations must be slow with respect to charge separation to be able to account for the observed biphasicity in the reoxidation of the quinones. The least one can say is that this is obviously not a very severe constraint, considering the ultra-fast time range of charge separation compared to protein dynamics.

In the second model, ET in PS I is inherently bi-directional. In other words, in each PS I reaction center, the reduction of A_{0A} or A_{0B} occurs with a certain probability. In this model, a mutation of the A_{0A} binding pocket would modify specifically the probability of reducing A_{0A}. As an indirect consequence, the probability of reducing A_{0B} would change in a compensatory manner. Decreasing the probability of reducing A_{0A} would effectively redirect electrons down the B branch and *vice versa*. The results obtained with the Tyr mutants may be readily, although not exclusively, accounted for by this model. Indeed, as mentioned above, disrupting an H-bond usually results in a more reducing redox potential. For example, such an increase in the reduction potential of A_{0A} would be expected to decrease the free energy difference between P^*_{700} and $P^+_{700}A^-_{0A}$, leaving unchanged the free energy difference between P^*_{700} and $P^+_{700}A^-_{0B}$. This should increase the probability for charge separation to occur down the B branch at the expense of its occurrence down the A branch.

It is more difficult to predict reliably the expected effects of the Met mutations. Indeed, one does not know the ligation state of the A_{0A} or A_{0B} Chls in the mutants. It seems reasonable to assume that, in the Met → Leu mutants a water molecule provides a ligand, or that in the Met → His mutants a nitrogen atom of the imidazole ring provides the fifth ligand. In both cases the strength of the ligation (i.e., the strength of the interaction with the Mg^{2+}, a hard Lewis acid) might be stronger, as oxygen and nitrogen are harder Lewis bases than sulfur. Yet, since the strength of the ligation is also dependent on the distance between the coordinating atom and the Mg^{2+}, the question of whether the ligand is effectively stronger or weaker is difficult to address in the absence of a detailed structure of the mutants PS I. As discussed in Fromme et al. (2001), the lack of a strong fifth ligand might be responsible for the remarkably low redox potential reported for the A_0/A_0^- redox couple (Kleinherenbrink et al., 1994; Brettel, 1997 for a review. Hence, although the mutations are likely to induce a shift in the reduction potential of either of the two A_0 Chls, the direction of the shift is hard to predict. A stronger ligand would make the reduction potential more positive, whereas a weaker ligand would have the opposite effect. If the latter case applied, the situation would be similar to the Tyr mutants in which an H-bond is broken and the interpretation discussed above of the observed changes in relative amplitude of the two phases would also apply. If the ligand were stronger, the free energy change associated with the reduction of the Chl with a mutated ligand would increase. Such an increase would be expected to favor reduction of this Chl at the expense of the other one, assuming that the reduction of A_0 lies in the normal region of the Marcus curve (i.e., $-\Delta G < \lambda$, where ΔG and λ are the free energy change and the reorganization energy of this reaction). If it lies in the inverted region (i.e., $-\Delta G > \lambda$ the reduction yield of the Chl with a mutated ligand would be, as in the previous case, decreased. If the reduction yield of the Chl with a mutated ligand were increased, then one would expect, in the bi-directional mode, that the relative reduction yield of the quinone downstream of this Chl to increase, which is at variance with the results presented in Table 2.

However, it is possible that the shift in redox potential resulting from the Met → Leu or Met → His mutations is such that the free energy level of the $P^+_{700}A^-_0$ lies below that of the $P^+_{700}PhQ^-$ state. In this case, the formation of the latter state at the expense of the former would be significantly slowed down with respect to WT or even blocked. This model is supported by the recent findings by Heathcote and coworkers that the PsaA-M688H mutations blocks ET to PhQ_A at 265 K as well as photoaccumulation of PhQ_A^-, and that the symmetric PsaB-M668H mutations blocks ET to PhQ_B at 100 K but not its photoaccumulation (Fairclough et al., 2003). In line with these results, Ramesh et al. (2003) reported that, indeed, a $P^+_{700}A^-_0$ state may be observed in the PsaA-M688H or PsaB-M668H mutants with a lifetime longer than 300 psec [as compared to the time constant of ~30 psec reported for the reduction of the quinones (Hastings et al., 1994; Hecks et al., 1994)]. The study of similar mutants from *Synechocystis* sp. PCC 6803 showed that the

PsaA-M688L or PsaA-M688N mutations also results in a ten-fold slowing down of A_1 reduction, yet the symmetric PsaB-M688L or PsaB-M688N mutations induced no significant kinetic changes (Dashdorj et al., 2005). In any case, if ET down either of the two branches were blocked, then the overall quinone reduction yield should be decreased. Furthermore, one would expect to observe absorption changes associated with charge recombination of the long-lived $P_{700}^{+}A_0^{-}$ state. In this case, the changes in the relative amplitude of the two phases reported in Table 2 would reflect this specific block, rather than a redirection of electrons to either of the two branches at the expense of the other. Our preliminary results suggest that, in the PsaA-M688L or PsaA-M688H mutants from *C. reinhardtii*, 20–25% of the PS I reaction centers were unable to form P_{700}^{+} with a lifetime longer than 2 μsec. A larger value (45%) was found in *Synechocystis* sp. PCC 6803 by Cohen et al. (2004). In this fraction of centers it seems likely that charge recombination between P_{700}^{+} and A_{0A}^{-} occurs, thereby decreasing the relative amplitude of the phase ascribed to PhQ_A^{-} reoxidation. Consistent with this, Cohen et al. observed a significant increase in the P_{700}^{T} triplet formation yield in the PsaA-M688L mutants from *Synechocystis* sp. PCC 6803 (Cohen et al., 2004). In this case, the observation reported by Fairclough et al. (2003) of a blockage of the ET down the branch containing the Chl with a mutated ligand to the downstream quinone would suggest that the ET reaction may not only be severely slowed down by the mutation at room temperature but may become thermally activated, rendering the reduction of the downstream quinone barely possible at the temperature of the transient EPR measurement (265 K). In any case, whether ET down the mutated branch is blocked or whether it is redirected down the other branch, the results reported in Table 2 are consistent with the assignment of the fast and slow phases to the reoxidation of PhQ_B^{-} and PhQ_A^{-}, respectively. Yet the question as to whether the relative reduction yield of the two quinones is effectively changed by the PsaA-M688L and PsaB-M668L mutations remains open.

2. Mutations Upstream of A_0

To date, several mutants have been constructed to change the relative yield of the two ET branches by altering the physico-chemical properties of either P_{700} or the "accessory Chls." The crystal structure has revealed that P_{700} is a heterodimer comprised of a Chl *a* and a Chl *a′*, the former bound to PsaB and the latter to PsaA (Fromme et al., 2001; Jordan et al., 2001). The charge or spin distribution between these two Chls in the P_{700}^{+} state has been studied by various spectroscopic techniques. Magnetic resonance (ENDOR and high field EPR) studies have led to the conclusion that the spin distribution is strongly asymmetric in P_{700}^{+} and that the Chl *a* bound to PsaB bears most of the spin (Webber et al., 1996; Krabben et al., 2000; Petrenko et al., 2004; see Webber and Lubitz, 2001 for a review). Breton and coworkers, however, concluded, on the basis of the FTIR difference spectra that the hole resulting from P_{700} oxidation is almost equally shared by the two Chls (Breton et al., 1999, 2002). To date this controversy is still unsettled and we refer the reader to Lubitz (this volume, Chapter 17) and Breton (this volume, Chapter 18) for further discussion. In addition to the different chemical nature of the two Chls that form P_{700}, another potential cause of asymmetry lies in the existence of an H-bond between the 13^1-keto of the Chl *a′* and the side chain of a threonine (Jordan et al., 2001). Interestingly the Chl *a* is not H-bonded. Recent studies suggest that disrupting this H-bond by replacing this threonine (PsaA-T743) with various apolar residues induced a small redistribution of the spin density (Witt et al., 2002; Li et al., 2004). Furthermore, the redox potential of the P_{700}^{+}/P_{700} couple was shifted downward by up to ∼30 mV as expected from the removal of a single H-bond (Witt et al., 2002). To investigate whether these changes might affect the relative yield of ET down the two branches, we measured the kinetics of reoxidation of the quinones at 380 nm in the PsaA-T743A mutant. The results were identical to those obtained with the WT suggesting that the directionality of ET is unchanged by the mutation (Table 2). It is crucial to mention that the state involved in the early charge separation process, at which level the directionality is likely to be determined, is P_{700}^{*} rather than P_{700}^{+}. How much the energetics and charge/spin distribution of P_{700}^{+} measured in a relaxed state reflects the early charge separation events is an open question. The dramatic changes induced by the mutation in the (P_{700}^{+}/P_{700}) absorption spectra, together with the down-shift of the redox potential of the P_{700}^{+}/P_{700} couple (Witt et al., 2002; Li et al., 2004) make likely, however, a change in the redox potential of the P_{700}^{+}/P_{700}^{*} couple and hence in the free energy change associated with charge separation. Such a change should similarly affect the free energy change associated with the reduction of A_{0A} or A_{0B}. As an alternative hypothesis, P_{700}^{*} might not in fact be the primary donor, as has been recently proposed for bacterial reaction centers and PS II (Van Brederode et al., 1997; Diner et al., 2001; Diner and Rappaport, 2002). In such a model, charge separation would

effectively occur between an "accessory Chl" and A_0, and P_{700} would act as a secondary electron donor to the oxidized Chl. Obviously, the charge or spin distribution within the oxidized state of P_{700} would then give an extremely distant picture of charge separation. There is no doubt whatsoever that the "accessory Chls" are involved in the charge separation process either as the primary electron acceptor or primary electron donor (or even in a superexchange mechanism which would facilitate ET from P^*_{700} to A_0, (see Parson, 1996 for a discussion of this mechanism in bacterial reaction centers). Thus, as for A_0, modification of their local environment might be expected to modify the relative yield of ET down the two branches. The "accessory Chl" in the A branch is coordinated by the side chain of Asn 591 (*C. reinhardtii* numbering) of the PsaB subunit *via* a water molecule. This Asn has been converted to an Asp residue. As presented in Table 2, the kinetics of reoxidation of the quinones in this mutant were indistinguishable from those in WT. This negative result should obviously not be taken as an indication that these cofactors are not involved in the initial events that determine the directionality. Indeed, since this cofactor is deeply buried in the protein, it is likely that the carboxylic side chain introduced at this position is protonated. The P^+_{700}/P_{700} FTIR difference spectra of this mutant are consistent with this hypothesis (Hastings et al., unpublished). Since it is the oxygen of the Asn amide to which the water is H-bonded, rather than the nitrogen, its replacement with a carboxylic acid (not a carboxylate) would have little effect. The H-bond network to which the water molecule that serves as ligand to the Chl participates would be conserved and no significant effect on directionality would be expected.

To summarize the results from this mutagenesis survey up to this point, single point mutations in the A_0 binding pockets have proved very effective in changing the relative amplitude of the two components ascribed to ET down the two branches. The physico-chemical parameters that control the relative yields remain to be identified. In light of the results obtained with the A_0 mutants, a choice between the different mechanisms proposed awaits further characterization.

V. Spectroscopic Features Specific to the Spectra of the Fast and Slow Phase in the 320–540 nm Region

After having discussed the kinetics of reoxidation of the quinones, we would like to focus on the spectroscopic characteristics of the absorption changes associated with the fast and slow phases, as they set the groundwork for their assignment to quinone reoxidation. As first shown by Brettel et al., the flash-induced absorption changes associated with the reduction of A_1 at 10 K display features in the 240–430 nm region, which resemble the *in vitro* difference spectrum of a phyllosemiquinone (Brettel et al., 1986). This qualitative agreement has been taken as evidence that A_1 is a phylloquinone. A transient spectrum formed in less than 5 nsec and decaying in the hundreds of nsec time range was later reported at room temperature with similar features (Brettel, 1988; Mathis and Sétif, 1988). Here again the spectrum of these transient absorption changes showed convincing similarities in the 330–410 nm region with the *in vitro* spectrum of a phyllosemiquinone (Brettel, 1988). These spectroscopic features, combined with the detection of vitamin K_1 at stoichiometric amounts in PS I (Takahashi et al., 1985), led to the identification of A_1 as a phylloquinone, consistent with transient EPR studies (Thurnauer and Gast, 1985). In the 420–500 nm region, where the semiquinone difference absorption spectrum is featureless, features that cannot attributed to the semiquinone are consistently observed (see Brettel, 1997 for a review). In this region a bleaching at 450 nm, together with an overall absorption increase around 480 nm, has been observed and ascribed to an electrochromic bandshift undergone by a nearby carotenoid (Brettel, 1988; Sétif and Brettel, 1993). Interestingly, very similar spectra were found in PS I from spinach (Sétif and Brettel, 1993) and from cyanobacteria (Brettel, 1988) although the fast and slow phases were predominant in the former and the latter, respectively. The similarity between these spectra suggests that they reflect the same reaction. With improved time resolution, however, Brettel observed subtle differences in the 450–500 nm region between the spectra of the fast and slow phases from *Synechocystis* sp. PCC 6803 PS I (Brettel, 1998). Joliot and Joliot observed a similar trend with PS I in whole cells of *Chlorella sorokiniana* (Joliot and Joliot, 1999).

In Fig. 2 (left panel) are shown the spectra of the fast and slow phases assigned to quinone reoxidation in the 300–540 nm region of *Synechocystis* sp. PCC 6803 (Bautista et al., 2005). These results are in good agreement with the spectra found in the literature, but the wider spectral range allows one to identify significant differences, despite the overall similarity. These differences are most obvious in the 430–540 nm region. The bleaching observed around 450 nm is redshifted in the spectrum of the slow phase with respect to that of the fast phase. Furthermore, new peaks are

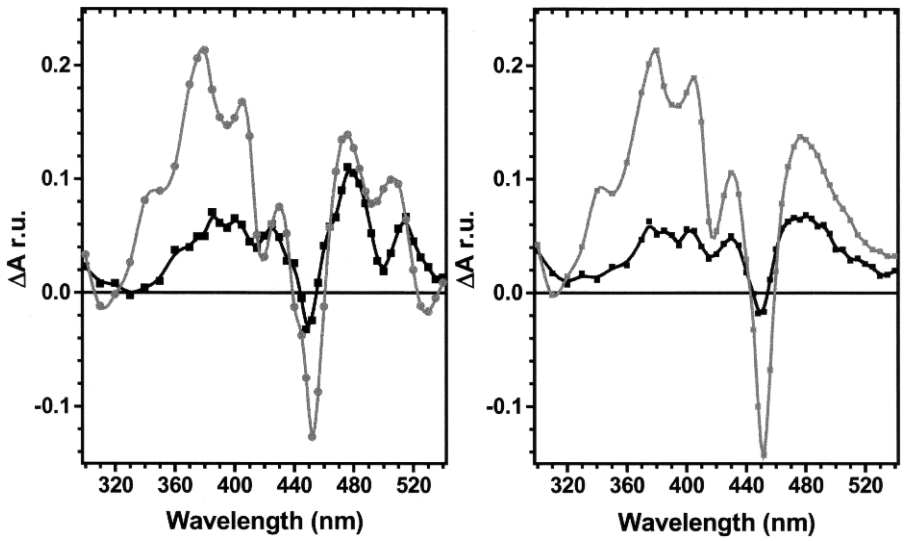

Fig. 2. Decay-associated spectra of the fast (black) and slow (gray) phases ascribed to A_1^- reoxidation. Left panel: PS I particles from the WT strain of *Synechocystis* sp. PCC 6803. Right panel: PS I particles from a mutant strain of *Synechocystis* sp. PCC 6803 in which the zeta-carotene desaturase gene was deleted (Bautista et al., 2005).

resolved at 505 and 515 nm in the spectrum of the slow and fast phases, respectively. As shown in Figs. 2 and 3, the UV regions of the two spectra also display significant differences. As previously observed by Brettel (1998) and later by Joliot and coworkers (Joliot and Joliot, 1999; Guergova-Kuras et al., 2001), the slow-phase spectrum displays a clear peak around 380 nm and a marked shoulder at 405 nm, whereas these

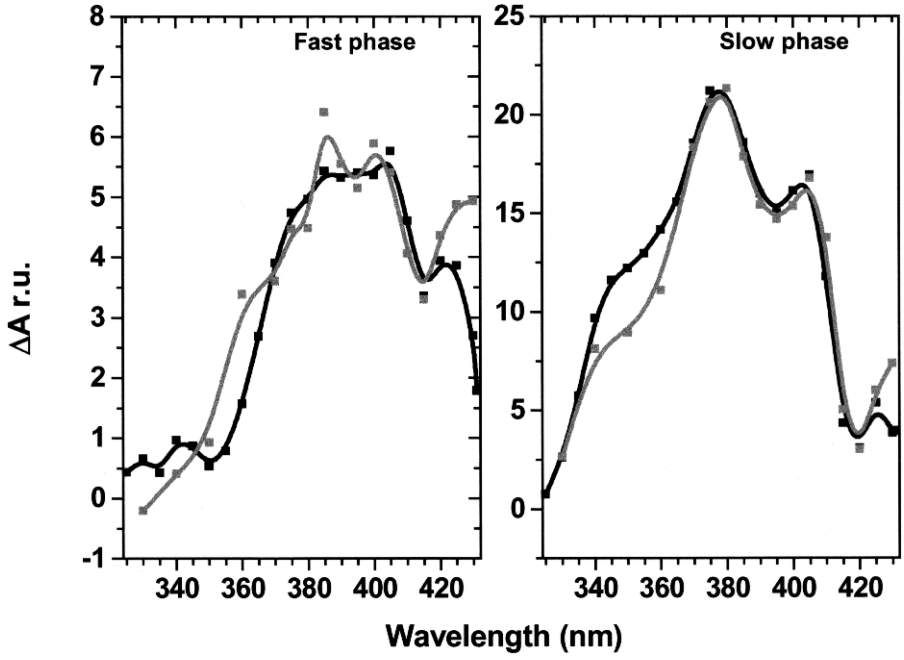

Fig. 3. Decay-associated spectra of the fast and slow phases ascribed to A_1^- reoxidation. In black are decay-associated spectra observed in whole cells of *C. reinhardtii*; in gray are decay-associated spectra observed in PS I particles from WT *Synechocystis* sp. PCC 6803. The spectra were normalized to the amplitude at 380 nm. (F. Rappaport, B. A. Diner, and K. Redding, unpublished)

features are much less distinct, if even present, in the fast-phase spectrum. This latter spectrum peaks around 400 nm, in good agreement with *in vitro* spectrum of the phylloquinone radical. Furthermore, the fast-phase spectrum shows only little absorption in the 350–380 nm region, whereas an absorption increase is still observed in this region of the slow-phase spectrum. As shown in Fig. 3, the specific features of the spectra of the two phases that have just been described seem remarkably well conserved between *Synechocystis* sp. PCC 6803 and *C. reinhardtii*. Two different and nonexclusive hypotheses may be proposed to interpret these specific features, both in the visible and near UV range: (i) As discussed above, the two phases reflect the reoxidation of the two different quinones. Thus, although their chemical nature is identical, the absorption changes associated with their reduction and reoxidation may somehow differ owing to differences in their respective binding pockets. (ii) Since these spectra reflect the absorption changes occurring during a certain kinetic phase one cannot exclude the possibility that, other processes occur in a similar temporal regime and also contribute, at least in some wavelength region(s), to the overall absorption changes. In this case, the spectra of the fast and slow phases would be a combination of the absorption changes associated with these different reactions. We will now discuss both hypotheses in the light of recent observations.

A. Spectroscopic Features Specific to the Spectra of the Fast and Slow Phase in the 420–540 nm Region

The *in vitro* difference spectrum of the phyllosemiquinone does not display any absorption changes above 450 nm (Romijn and Amesz, 1977). Consequently, the bands and trough observed in the spectra of the fast and slow phases in the 420–500 nm region were ascribed to local electrochromic shifts of nearby pigments, proposed to be carotenoids (Brettel, 1988; Sétif and Brettel, 1993; Joliot and Joliot, 1999). PS I reaction centers from *T. elongatus* bear, beside the 6 Chls involved in ET, 90 Chl *a* and 22 carotenoids that participate in the light-harvesting process (Fromme et al., 2001). Diner and coworkers have recently succeeded in disrupting, in *Synechocystis sp* PCC 6803, the biosynthetic pathway leading to the synthesis of β-carotene, known to be the dominant carotenoid in PS I (Fromme et al., 2001) and references therein). The light-induced absorption changes in PS I reaction centers purified from these cells have been analyzed to be able to investigate further the assignment of the spectroscopic features in the visible region. Similar to the WT, two exponentials were required to fit the data in the whole 320–540 nm region. The spectra of these two phases are shown in Fig. 2 (right panel). In the near-UV range (320–420 nm) region they are nearly identical to those from WT, indicating that they may safely be ascribed to the same ET reaction. Surprisingly, the trough observed in both spectra at about 450 nm was conserved in the mutant, indicating that it does not result from an electrochromic shift of a carotenoid. Thus, it seems most likely to be due to an electrochromic shift of nearby Chl *a* molecule(s). The features observed above 470 nm in both the fast and slow-phase spectra from WT were totally absent in the mutant spectra, however, allowing one to ascribe them to electrochromic bandshifts. The fact that the wavelength maxima and minima of these shifts differ between the fast and slow phases suggest that (at least) two different carotenoids contribute to this feature in the 2 nsec decay components. This may be taken as an indication that the two phases result from redox changes of two different species in the vicinity of spectroscopically distinct set of pigments further supporting the assignment of the fast and slow phase to the reoxidation of the two quinones (Bautista et al., 2005).

B. Spectroscopic Features Specific to the Spectra of the Fast and Slow Phase in the 320–420 nm Region

On the basis of the *in vitro* semiquinone spectrum (Romijn and Amesz, 1977), the absorption increase in the 320–420 nm region of the fast and slow phases spectra may be thought to directly reflect the redox state of the quinones. Yet we recently observed significant differences with the *in vitro* spectrum (see Fig. 3), in good agreement with previous findings (Brettel, 1998). The slow-phase spectrum displays two peaks, a major one at 380 nm and another at 405 nm; whereas the fast-phase spectrum has a broader major peak at 400 nm and a second one at 425 nm. In addition, the slow-phase spectrum shows absorption changes in the 320–360 nm region, whereas the fast-phase spectrum does not. Could this be taken as an indication that that the fast-phase spectrum is red-shifted by about 20 nm with respect to the slow phase one? The structure of the quinone binding pockets provides no obvious rationale to support such a shift. The possibility remains, however, that the two semiquinones interact differently with the protein matrix as suggested by recent theoretical calculations (Ishikita and Knapp, 2003).

Various spectroscopic results also support this hypothesis. From the crystal structure the distance

between F_X and PhQ_A or F_X and PhQ_B are identical. Thus, despite the extreme sensitivity of electron transfer rates to donor–acceptor distances (Moser et al., 1992), this factor does not account for the 10-fold difference between the reoxidation rates of the two quinones. In the bi-directional model, either the free energy associated with each reaction or the reorganization energy of the two reactions must differ. Consistent with this view is the finding that each reaction has a significantly different activation energy (Agalarov and Brettel, 2003). One must also account for the number of bands found in the FTIR difference spectra of $(A_1^- - A_1)$, which seems too large to result from a single species (Hastings and Sivakumar, 2001). In the bi-directional model, the differences in the FTIR difference spectra of each of the two quinones are a consequence of their residence in different binding pockets. In the case of bacterial reaction centers, the FTIR spectra associated with the reduction of Q_A or Q_B was also found to be significantly different (Breton et al., 1994, 1995; Brudler et al., 1994, 1995) despite a similar structure of the binding pockets, as seen by X-ray crystallography (Allen et al., 1987). Finally, ENDOR spectroscopy of biosynthetically deuterated PS I allowed the identification of ENDOR features arising from the hyperfine coupling of the proton involved in a hydrogen bond (Rigby et al., 1996). The ENDOR spectrum of the semiquinone was interpreted as showing two hydrogen bonded protons (see Rigby et al., 2001), in contrast with the X-ray crystal structure of the dark-adapted state, which shows a single H-bond between a backbone amide group and one carbonyl group of each quinone. More recently, Heathcote and coworkers managed to resolve the ENDOR spectra resulting from the reduction of either PhQ_A or PhQ_B (Rigby et al., 2002; Fairclough et al., 2003). The ENDOR spectra were interpreted in terms of both semiquinones being H-bonded, despite the fact that there were differences in the magnitude of the hfcs assigned to them. To reconcile these data with the X-ray data, one would have to resort either to a structural rearrangement upon reduction or to the presence of a water molecule not visible in the current structure but acting as a H-bond donor (Rigby et al., 2002). Based on these different studies, it thus seems conceivable that the interaction between each semiquinone and its respective binding pocket is different. Whether these differences are sufficient to account for the different absorption difference spectra assigned to the two phases remains to be addressed.

As discussed previously, one should keep in mind that the absorption spectra of the two phases reflect nothing more than the absorption changes associated with a given kinetic component. The assignment of these two phases was based on the differential effects of the PsaA-W697 and PsaB-W677 mutations on the rates of the slow and the fast phases, respectively (Guergova-Kuras et al., 2001; Muhiuddin et al., 2001). It is noteworthy that, despite the significant effects on rate, the difference spectra in both mutants were very similar to those of WT, suggesting that these phases could be confidently ascribed solely to ET between either of the two quinones and F_X (Guergova-Kuras et al., 2001). Owing to technical limitations, however, the reported spectra did not extend below 375 nm, a region where the differences in the two spectra are most marked. The question that we want to address now is whether other ET reactions may proceed concomitantly to one (or both) of the phases and give rise to absorption changes that would then contribute to the spectrum of this phase. If this were indeed the case, it is of note that this reaction would have to be an ET reaction occurring within the PS I reaction center, since similar spectra were found in whole cells of *C. reinhardtii* and PS I complexes from *Synechocystis* sp. PCC 6803. A second requirement is that this hypothetical ET reaction would have to occur downstream of the F_X cluster to proceed concomitantly with one of the two quinone oxidation steps. Altogether, these two requirements make ET between the iron-sulfur clusters the best possible candidates for this reaction. Unfortunately, the available data on the rate of ET between the three different iron-sulfur clusters are scarce. The three reduced iron–sulfur clusters are not readily distinguishable on the basis of their time-resolved X-band EPR spectra (Kandrashkin et al., 1998), precluding the characterization of the ET rate between them. Yet, there is indirect evidence suggesting that the terminal iron-sulfur cluster, identified as F_B (Diaz-Quintana et al., 1998; Vassiliev et al., 1998; Fischer et al., 1999; Lakshmi et al., 1999), is reduced in the hundreds of nsec time range. Photovoltage measurements indicated a phase with a half time of 150 nsec, which was ascribed to the ET between A_1^- and F_A/F_B, as its amplitude (40% of the total flash-induced electrogenicity) was much larger than that expected for the reduction of F_X at the expense of A_1^-. Furthermore, removal of F_A and F_B resulted in a two-fold decrease of its amplitude but left its time constant unchanged (Leibl et al., 1995; Diaz-Quintana et al., 1998). Because the half time found for this overall reaction matches that observed by optical spectroscopy for the reoxidation of PhQ_A^-, it was proposed that the ET between F_X and the terminal iron-sulfur clusters occurred with a rate equal or faster than $(50\ \text{nsec})^{-1}$ (Leibl et al., 1995;

Diaz-Quintana et al., 1998). Consistent with this hypothesis, the fastest first-order rate constant found for ferredoxin reduction is about $(400\ \text{nsec})^{-1}$ (Sétif and Bottin, 1995; Sétif, 2001). Since F_B must be reduced before ET to ferredoxin occurs, this finding allows one to put a lower limit of about $(400\ \text{nsec})^{-1}$ for the rate of F_B reduction. Thus, it seems highly likely that the absorption changes associated with ET between F_X and $F_{A/B}$ contribute to the spectrum of the slow phase of A_1^- oxidation. Does such a contribution account for the differences between the spectra of the two phases? Lüneberg et al. characterized the absorption changes associated with the formation of the $P_{700}^+F_{A/B}^-$ and $P_{700}^+F_x^-$ states in the 350–460 nm range using particles that either contained or lacked the PsaC subunit, respectively (Lüneberg et al., 1994). These two spectra are very similar, except for a larger absorption increase between 350 and 390 nm and a smaller absorption increase between 445–470 nm in the $P_{700}^+F_X^-$ spectrum. This observation suggests that ET from F_X to the terminal iron–sulfur cluster(s) should induce a slight absorption decrease in the 350–390 nm region and a slight increase in the 445–470 nm region. Such absorption changes are, however, rather featureless (see Fig. 4) in Lüneberg et al., 1994) and are thus unlikely to account for all of the pronounced differences between the fast and slow components described previously (Fig. 3). Interestingly, these authors also compared the flash-induced absorption decays at 384 nm in the absence and presence of the terminal iron–sulfur cluster (F_A/F_B). Although the half time of the decay was found to be identical (180 nsec), its overall amplitude was slightly diminished after removal of F_A/F_B, further supporting the idea that small but observable absorption changes in this wavelength region are expected to result from ET between the iron–sulfur clusters.

This hypothesis may also reconcile the finding of Fairclough et al. of a blockage in ET down the A branch in the PsaA-M684H mutant (Fairclough et al., 2003) with the observation reported here that the absorption changes are still biphasic in this mutant, with the slow phase having a half time similar to that generally ascribed to the reoxidation of PhQ_A (see Table 2). Indeed, one may propose that, in this mutant, this phase does not reflect the reoxidation of PhQ_A, whose reduction is mostly blocked according to (Fairclough et al., 2003), but rather is due to ET from F_X^- (which is reduced by PhQ_B in tens of nsec) to the terminal iron–sulfur clusters. Obviously, this point deserves a careful spectroscopic analysis. Interestingly, this hypothesis has at least one corollary that, if demonstrated, could provide further support for the bi-directional model discussed above. In the mutants where the slow phase ascribed to the reoxidation of PhQ_A is either retarded, because of alteration of the PhQ_A site, or does not occur, because ET has been redirected toward the B branch, one would expect the ET reaction between the Fe/S clusters to become directly observable with less complication of the reaction between PhQ_A and F_X. Indeed, such mutations would open the 100–200 nsec time window and allow one to resolve sequential ET from $PhyQ_B$ to F_X, which is thought to proceed with a half time of 10–15 nsec, and the subsequent ET to the terminal Fe/S clusters, which should occur in the hundreds of nsec time range. Hopefully, a combination of time-resolved EPR and optical spectroscopy will allow one to address this issue.

VI. Energetic Picture of Quinone Reoxidation via Forward or Backward Electron Transfer

We now turn to a discussion of factors that determine the rates of the reaction occurring on the acceptor side of PS I. An important question that remains to be addressed is the 10-fold difference in rate of ET between PhQ_A and F_X or PhQ_B and F_X. The structure of PS I does not provide any obvious clue that could rationalize this 10-fold difference: the edge to edge distances between F_X and either of the two quinones are very similar and the binding pockets do not display any major structural differences (Fromme et al., 2001). A recent study points to the energetic parameters of these reactions as being the main factors that accounts for the difference. Agalarov and Brettel measured the temperature dependence of the slow and fast phases of quinone reoxidation. They observed that the slow phase is thermally activated, in agreement with the previous finding of Schlodder et al. (1998) [although the activation energy of 110 meV reported in (Agalarov and Brettel, 2003) is smaller than the 220 meV found in (Schlodder et al., 1998)]. In contrast, the rate of the fast phase is almost temperature-independent (Agalarov and Brettel, 2003). According to ET theory, ET rates are expected to be essentially temperature-independent when the characteristic energy $h\omega$ of the nuclear vibrational mode coupled to ET is larger than the thermal energy k_BT (Hopfield, 1974; Jortner, 1976 and see Moser and Dutton, 1996 for a discussion). This has been shown to apply for ET between quinones in *Rhodobacter sphaeroides* reaction centers (Gunner and Dutton, 1988), in which the temperature and free energy dependence of the ET rate could be described with a single characteristic energy of 70 meV (i.e., three times the thermal

energy at room temperature). If such is also the case for ET between the quinones and F_X, then the temperature dependence of the slow phase suggests that this reaction is uphill ($\Delta G > 0$), whereas the temperature independence of the fast phase suggests it is downhill. On the basis of these results Agalarov and Brettel proposed two alternative models: in line with the bi-directional hypothesis, ET from PhQ_B would be downhill and temperature independent, whereas ET from PhQ_A to F_X would be uphill and thermally activated (note that in the latter case, overall ET from PhQ_A to F_A/F_B would be favorable). This model is supported by recent calculation of the redox potentials of the two quinones. According to these estimates the redox potential of PhQ_B would be more negative than that of PhQ_A by about 150 mV (Ishikita and Knapp, 2003).

In an alternative model, ET from P_{700} would be unidirectional down the B-branch and only PhQ_B would be initially reduced. ET to F_X would proceed in the 10-nsec time range. At this stage, two downhill reactions would compete: ET to F_A on the one hand, and ET to PhQ_A on the other hand. PhQ_A^- would ultimately be reoxidized by thermally activated ET via F_X to F_A (Agalarov and Brettel, 2003). This latter model seems unlikely since recent findings discussed above support the involvement of both A_0 Chls in charge separation. In addition, it is clear that the PhQ of the $P_{700}^+PhQ^-$ radical pair observed by transient EPR is PhQ_A (Boudreaux et al., 2001; Purton et al., 2001; Xu et al., 2003b); transfer through two more intermediates would most likely cause loss of spin correlation, which is not observed. In either of the two models, the observed rate constant of the slow phase would be strongly dependent upon the ΔG of the ET reaction between PhQ_A and F_X (see discussion above). Because this reaction is electrogenic, this observed rate should still be significantly decreased in the presence of external transmembrane electrical potential, which is at variance with the results of Joliot and Joliot (Joliot and Joliot, 1999). Furthermore, this lack of a kinetic effect of the external transmembrane electric field suggests that both the fast and slow phases of A_1^- reoxidation reflect exergonic ET reactions. To reconcile the finding of a significant activation energy with a decrease in free energy, one may propose that a significant increase in entropy occurs upon the $P_{700}^+PhQ_A^- \rightarrow P_{700}^+F_X^-$ ET reaction, so that $\Delta G = \Delta H - T\Delta S < 0$ even though $\Delta H > 0$. Recent photoacoustic experiments might support this hypothesis; approximately half of the free energy change associated with $P_{700}^* \rightarrow P_{700}^+(F_A/F_B)^-$ at room temperature is from the entropic term ($-T\Delta S$) (Hou et al., 2001).

The evidence in support of the bi-directional model is steadily increasing. As described above, this evidence now includes the specific kinetic effect on the fast and slow phases of A_1^- reoxidation by mutations altering the binding sites of either quinone, the likely involvement of both A_{0A} and A_{0B} in charge separation, the difference in the absorption changes associated with each phase and reports of different energetic parameters for the two phases. However, charge recombination of the $P_{700}^+A_1^-$ state provides a significant challenge to this model: In the simple bi-directional model, charge separation occurs with a certain probability down each of the ET branches. Consequently, each quinone is reduced with this same probability. In the absence of forward ET from A_1^-, the $P_{700}^+A_1^-$ state decays through charge recombination to the ground state. This process has been shown to proceed, after removal of all three iron–sulfur clusters, *via* a pathway involving direct electron tunneling between the electron donor A_1^- and P_{700}^+ (Warren et al., 1993; Brettel and Golbeck, 1995). As the two quinones have different reduction potentials, the free energy change associated with charge recombination should be different if the electron donor is PhQ_A^- or PhQ_B^-. Thus, assuming that $-\Delta G \neq \lambda$, the observed charge recombination should be biphasic.

The bi-directional model further predicts that the amplitude of each of the two phases of charge recombination should match the amplitude of each of the two phases observed during the forward ET from A_1^-, since these are determined by the initial charge separation event in each case (assuming that the conditions used to block forward ET from A_1 do not affect the branching ratio). Lastly, as the spectra of the two phases observed during forward ET are different, the spectra of the two phases observed during charge recombination should also display similar distinct features. Among these various expectations, a biphasicity is in fact observed for $P_{700}^+A_1^-$ charge recombination. A refined study of PS I particles from *Synechococcus* sp. PCC 6301 showed clearly that, after removal of the three iron–sulfur clusters, at least two exponentials are required to fit satisfyingly the decay of $P_{700}^+A_1^-$ (Brettel and Golbeck, 1995). The faster phase ($t_{1/2} \approx 10$ μsec) accounted for ~70% of the total amplitude (at 380 nm) and the slower one ($t_{1/2} \approx 10$ μsec) accounted for ~25% of the total amplitude. In PS I reaction centers purified from a *Synechococcus* sp. PCC 7002 mutant in which the F_X, F_B, and F_B clusters were genetically prevented from assembling, Shen et al. also observed a biphasic charge recombination with similar half times, but the relative amplitude of the two phases were significantly

different: 45% and 55% for the fast and slow phase, respectively (Shen et al., 2002).

The question then arises as to whether it is possible in the framework of the bi-directional model to ascribe these two phases to the charge recombination from the $P_{700}^{+}PhQ_{A}^{-}$ and $P_{700}^{+}PhQ_{B}^{-}$ states. As discussed above, two different approaches led to the conclusion that the free energy level of these two states are different: Thus, the free energy difference between either of these states and the ground state is expected to be different (that associated with the decay of $P_{700}^{+}PhQ_{B}^{-}$ to the ground state by direct electron tunneling being larger than that associated with $P_{700}^{+}PhQ_{A}^{-}$ to the ground state) (Agalarov and Brettel, 2003; Ishikita and Knapp, 2003). To infer from these conclusions which of these two states would be expected to decay faster, one must know in which region of the Marcus curve these reactions occur. On the basis of the estimated ΔG of the charge recombination process, Brettel (1997) argued that direct ET between the semiquinones and P_{700}^{+} is likely to lie in the inverted region of the Marcus curve. The calculated reduction potential of the two quinones (-531 mV for PhQ_A and -686 mV for PhQ_B) are significantly less negative than the values used by Brettel to draw this conclusion (-850 mV, taken from Vos and van Gorkom, 1988) but Brettel argued that this value was not fully reliable (Brettel, 1997). Taking the recently calculated values of the phylloquinone reduction potentials (Ishikita and Knapp, 2003) (which have the merit of being consistent with the estimated activation energy of the ET from the quinones to the F_X iron-sulfur cluster, as discussed above) and the reduction potential of the P_{700}^{+}/P_{700} couple (450 mV), we can estimate a free energy change of about -1000 meV associated with charge recombination. In *Rhodobacter sphaeroides* reaction centers, the reorganization energy of the $P^{+}Q_{A}^{-}$ charge recombination was found to be about 900 meV (Lin et al., 1994). If such a value also applies to the PS I reaction center, then this would put the $P_{700}^{+}A_{1}^{-}$ charge recombination in the inverted region of the Marcus curve, but close to its maximum. In this case, a 150-meV difference between the ΔG of the two reactions would not be sufficient to account for the ratio of about 10 between the two rates. It is conceivable that the reorganization energy of charge recombination between the quinones and P^{+} is smaller in PS I than in the Type 2 bacterial reaction centers. Indeed, the acceptor side of the Type 2 reaction centers is likely to be more polar than in Type 1 reaction centers, since proton transfer involving H-bond networks is associated with the reduction of the quinones, whereas in Type 1 reaction centers the quinone binding sites lie deeply buried within the protein protected from water and protons. In this case, the $P_{700}^{+}A_{1}^{-}$ charge recombination would lie further in the inverted region of the Marcus curve, where increases in ΔG of the reaction would slow the rate more acutely. By this argument the fast and slow phases of charge recombination would be attributed to the decay of $P_{700}^{+}PhyQ_{A}^{-}$ and $P_{700}^{+}PhyQ_{B}^{-}$, respectively. According to this assignment, the bi-directional model predicts, in the absence of F_X, F_A, and F_B, that the fast recombination phase should have the same relative amplitude as that of the slow phase observed in the forward ET reaction from A_{1}^{-} to F_X. The previous finding by Brettel and Golbeck that the fast recombination phase accounts for about 70% of the total decay (Brettel and Golbeck, 1995) would be more or less consistent with the relative amplitude of the slow phase in cyanobacteria (about 75%, see Table 1). However, in PS I from a mutant altered in the biosynthetic pathway for iron–sulfur cluster, the relative amplitude of the fast recombination phase was found to be somewhat smaller (55% at 380 nm) (Shen et al., 2002). The reasons for this discrepancy remains unclear, although these measurement were made in different species. The above assignment might be supported by the spectra of the two recombination phases. Whereas, Brettel and Golbeck found no significant differences between the spectra of the two recombination phases at room temperature (Brettel and Golbeck, 1995), the spectra found by Shen et al. in the rubredoxin mutant display different features (Shen et al., 2002), which are more or less consistent with those observed in the spectra of the forward ET reactions: in the 350–405 nm region the spectrum of the fast component has two peaks (although of similar amplitude) whereas that of the slow component is more flat, in the 450–490 nm region the trough around 460 nm and peak around 480 nm are slightly redshifted with respect to that observed in the slow component spectrum. Furthermore, it is of note that, from a kinetic standpoint, both the PsaA-W697F and PsaB-W677F mutations induced an increase in the rate of charge recombination between $F_A F_B^{-}$ and P_{700}^{+}, consistent with the hypothesis that both quinones may be involved in this recombination process (Boudreaux et al., 2001).

The last point that we want to discuss is the strong heterogeneity between PS I reaction centers that is observed at low temperature. Since the early studies by Sétif et al., it has been known that forward electron transfer is blocked in a fraction of centers at temperature below 150 K (Sétif et al., 1984). At 77 K, ET downstream of A_{1}^{-} is blocked in 65% of the centers. In this fraction of centers, charge recombination

between P_{700}^{+} and A_1^{-} occurs with a half time of 170 μsec (similar to that of the slow phase of recombination at room temperature) (Schlodder et al., 1998). Obviously, the recent finding that the slow phase of forward ET is thermally activated provides a rationale for this observation, yet we note that this observation implies that, in a given fraction of centers, charge separation must occur only down one branch (at temperatures below 150 K), otherwise the totality of the centers would eventually be trapped in the same state. This would be one of the predictions of the hypothesis whereby both quinones may be reduced from a statistical standpoint, but that in a given reaction centers charge separation is inherently unidirectional (discussed in greater detail in Redding and van der Est, this volume, Chapter 25).

VII. Conclusions

Based on a review of the kinetic, energetic, and spectroscopic features of the two phases ascribed to A_1^{-} reoxidation, we have argued that they most probably reflect ET between either PhQ_B and F_X or PhQ_A and F_X. The assignment of the fast and slow phase to the former and latter reactions respectively, which originated from the specific effects of site-directed mutations in the binding pocket of PhQ_A or PhQ_B, is further supported by the recent results obtained in site-directed mutants targeting residues interacting with redox cofactors located upstream of the quinones. Although these results strengthen the hypothesis that both quinones may indeed be reduced in PS I, the precise mechanism by which they are reduced still need to be unraveled. We are confident that the constantly renewed dynamism of the various players in the field will lead to new experimental approaches designed to address these issues.

Acknowledgments

B.A.D. gratefully acknowledges the support of the NRICGP/USDA (2001-35318-11270). K.R. acknowledges support from the U.S. Dept. of Energy (DE-FG02-00ER15097) and the National Science Foundation (MCB-0347935). F.R. is grateful to the C.N.R.S and the French Ministry of Research for financial support. F.R. wishes to thank Klaus Brettel, Pierre Sétif, P. Joliot, and M. Byrdin for fruitful and stimulating discussions.

References

Agalarov R and Brettel K (2003) Temperature dependence of biphasic forward electron transfer from the phylloquinone(s) A1 in photosystem I: only the slower phase is activated. Biochim Biophys Acta 1604: 7–12

Allen JP, Feher G, Yeates TO, Komiya H and Rees DC (1987) Structure of the reaction center from *Rhodobacter sphaeroides* R–26: the cofactors. Proc Natl Acad Sci USA 84: 5730–5734

Bautista JA, Rappaport F, Guergova-Kuras M, Cohen RO, Golbeck JH, Wang JY, Beal D and Diner BA (2005) Biochemical and biophysical characterization of photosystem I from phytoene desaturase and zeta-carotene desaturase deletion mutants of *Synechocystis* sp. PCC 6803: Evidence for PsaA- and PsaB-side electron transport in cyanobacteria. J Biol Chem 280: 20030–20041

Béal D, Rappaport F and Joliot P (1999) A new high-sensitivity 10-ns time-resolution spectrophotometric technique adapted to *in vivo* analysis of the photosynthetic apparatus. Rev Sci Instrum 70: 202–207

Boudreaux B, MacMillan F, Teutloff C, Agalarov R, Gu F, Grimaldi S, Bittl R, Brettel K and Redding K (2001) Mutations in both sides of the photosystem I reaction center identify the phylloquinone observed by electron paramagnetic resonance spectroscopy. J Biol Chem 276: 37299–37306

Breton J, Burie JR, Berthomieu C, Berger G and Nabedryk E (1994) The binding sites of quinones in photosynthetic bacterial reaction centers investigated by light-induced FTIR difference spectroscopy: assignment of the Q(A) vibrations in *Rhodobacter sphaeroides* using O-18 or C-13 labeled ubiquinone and vitamin K. Biochemistry 33: 4953–4965

Breton J, Boullais C, Berger G, Mioskowski C and Nabedryk E (1995) Binding sites of quinones in photosynthetic bacterial reaction centers investigated by light-induced FTIR difference spectroscopy: symmetry of the carbonyl interactions and close equivalence of the Q_B vibrations in *Rhodobacter sphaeroides* and *Rhodopseudomonas viridis* probed by isotope labeling. Biochemistry 34: 11606–11616

Breton J, Nabedryk E and Leibl W (1999) FTIR study of the primary electron donor of photosystem I (P700) revealing delocalization of the charge in $P700^{+}$ and localization of the triplet character in $^{3}P700$. Biochemistry 38: 11585–11592

Breton J, Xu W, Diner BA and Chitnis PR (2002) The two histidine axial ligands of the primary electron donor chlorophylls (P700) in photosystem I are similarly perturbed upon $P700^{+}$ formation. Biochemistry 41: 11200–11210

Brettel K (1988) Electron transfer from A-1 to an iron—sulfur center with $t_{1/2} = 200$ nsec at room temperature in photosystem I. FEBS Lett 239: 93–98

Brettel K (1997) Electron transfer and arrangement of the redox cofactors in photosystem I. Biochim Biophys Acta 1318: 322–373

Brettel K (1998) Electron transfer from acceptors A_1 to the iron–sulfur clusters in Photosystem I measured with a time resolution of 2 ns. In: Garab G (ed) Photosynthesis: Mechanism and Effects, Vol I, pp 611–614. Kluwer Academic Publishers Dordrecht, The Netherlands

Brettel K and Golbeck JH (1995) Spectral and kinetic characterization of electron acceptor A_1 in a Photosystem 1 core devoid of iron–sulfur centers F_X, F_A, F_B. Photosynth Res 45: 183–193

Brettel K, Sétif P and Mathis P (1986) Flash-induced absorption changes in photosystem I at low temperature: evidence that the electron acceptor A_1 is a vitamin K_1. FEBS Lett 203: 220–224

Brudler R, de Groot HJM, Vanliemt WBS, Steggerda WF, Esmeijer R, Gast P, Hoff AJ, Lugtenburg J and Gerwert K (1994) Asymmetric binding of the 1- and 4-C=0 groups of Q_A in *Rhodobacter sphaeroides* R26 reaction centres monitored by Fourier transform infra-red spectroscopy using site-specific isotopically labelled ubiquinone-10. EMBO J 13: 5523–5530

Brudler R, de Groot HJ, van Liemt WB, Gast P, Hoff AJ, Lugtenburg J and Gerwert K (1995) FTIR spectroscopy shows weak symmetric hydrogen bonding of the Q_B carbonyl groups in *Rhodobacter sphaeroides* R26 reaction centres. FEBS Lett 370: 88–92

Cohen RO, Shen G, Golbeck JH, Xu W, Chitnis PR, Valieva AI, van der Est A, Pushkar Y and Stehlik D. (2004) Evidence for asymmetric electron transfer in cyanobacterial photosystem I: analysis of a methionine-to-leucine mutation of the ligand to the primary electron acceptor A_0. Biochemistry 43: 4741–4754

Dashdorj N, Xu W, Cohen RO, Golbeck JH and Savikhin S (2005) Asymmetric electron transfer in cyanobacterial Photosystem I: charge separation and secondary electron transfer dynamics of mutations near the primary electron acceptor A_0. Biophys J 88: 1238–1249

Diaz-Quintana A, Leibl W, Bottin H and Sétif P (1998) Electron transfer in photosystem I reaction centers follows a linear pathway in which iron–sulfur cluster F_B is the immediate electron donor to soluble ferredoxin. Biochemistry 37: 3429–3439

Diner BA and Rappaport F (2002) Structure, dynamics, and energetics of the primary photochemistry of photosystem II of oxygenic photosynthesis. Annu Rev Plant Biol 53: 551–580

Diner BA, Schlodder E, Nixon PJ, Coleman WJ, Rappaport F, Lavergne J, Vermaas WF and Chisholm DA (2001) Site-directed mutations at D1-His198 and D2-His197 of photosystem II in *Synechocystis* sp. PCC 6803: sites of primary charge separation and cation and triplet stabilization. Biochemistry 40: 9265–9281

Fairclough WV, Forsyth A, Evans MC, Rigby SE, Purton S and Heathcote P (2003) Bidirectional electron transfer in photosystem I: electron transfer on the PsaA side is not essential for phototrophic growth in *Chlamydomonas*. Biochim Biophys Acta 1606: 43–55

Fischer N, Sétif P and Rochaix JD (1999) Site-directed mutagenesis of the PsaC subunit of photosystem I F(b) is the cluster interacting with soluble ferredoxin. J Biol Chem 274: 23333–23340

Fromme P, Jordan P and Krauß N (2001) Structure of photosystem I. Biochim Biophys Acta 1507: 5–31

Guergova-Kuras M, Boudreaux B, Joliot A, Joliot P and Redding K (2001) Evidence for two active branches for electron transfer in photosystem I. Proc Natl Acad Sci USA 98: 4437–4442

Gunner MR and Dutton PL (1988) Temperature and $-\Delta G^{\circ}$ dependence of the electron transfer to and from QA in reaction center protein from *Rhodobacter sphaeroides*. In: Breton J and Verméglio A (eds) The Photosynthetic Bacterial Reaction Center, pp 259–269. Plenum Press, New York, London

Gunner MR, Nicholls A and Honig B (1996) Electrostatic potentials in *Rhodopseudomonas viridis* reaction centers: implications for the driving force and directionality of electron transfer. J Phys Chem 100: 4277–4291

Hanley J, Deligiannakis Y, MacMillan F, Bottin H and Rutherford AW (1997) ESEEM study of the phyllosemiquinone radical A_1^- in ^{14}N- and ^{15}N-labeled photosystem I. Biochemistry 36: 11543–11549

Hastings G and Sivakumar V (2001) A Fourier transform infrared absorption difference spectrum associated with the reduction of A_1 in photosystem I: are both phylloquinones involved in electron transfer? Biochemistry 40: 3681–3689

Hastings G, Kleinherenbrink FAM, Lin S, McHugh TJ and Blankenship RE (1994) Observation of the reduction and re-oxidation of the primary electron acceptor in photosystem I. Biochemistry 33: 3193–3200

Hecks B, Breton J, Leibl W, Wulf K and Trissl H-W (1994) Primary charge separation in photosystem I: a picosecond two-step electrogenic charge separation connected with $P700^+A_0^-$- and $P700^+A_1^-$ formation. Biochemistry 33: 8619–8624

Hopfield JJ (1974) Electron transfer between biological molecules by thermally activated tunneling. Proc Natl Acad Sci USA 71: 3640–3644

Hou JM, Boichenko VA, Wang YC, Chitnis PR and Mauzerall D (2001) Thermodynamics of electron transfer in oxygenic photosynthetic reaction centers: a pulsed photoacoustic study of electron transfer in photosystem I reveals a similarity to bacterial reaction centers in both volume change and entropy. Biochemistry 40: 7109–7116

Ishikita H and Knapp EW (2003) Redox potential of quinones in both electron transfer branches of photosystem I. J Biol Chem 278: 52002–52011

Iwaki M and Itoh S (1991) Structure of the phylloquinone-binding (Q phi) site in green plant photosystem-I reaction centers: the affinity of quinones and quinonoid compounds for the Q phi site. Biochemistry 30: 5347–5352

Joliot P and Joliot A (1999) *In vivo* analysis of the electron transfer within photosystem I: are the two phylloquinones involved? Biochemistry 38: 11130–11136

Jordan P, Fromme P, Witt HT, Klukas O, Saenger W and Krauß N (2001) Three-dimensional structure of cyanobacterial photosystem I at 2.5 Å resolution. Nature 411: 909–917

Jortner J (1976) Temperature dependent activation energy for electron transfer between biological molecules. J Chem Phys 64: 4860–4867

Kandrashkin YE, Salikhov KM, van der Est A and Stehlik D (1998) Electron Spin Polarization in consecutive spin-correlated radical pairs: application to short-lived and long-lived precursors in type 1 photosynthetic reaction centres. Appl Magn Res 15: 417–444

Kellogg EC, Kolaczkowski S, Wasielewski MR and Tiede DM (1989) Measurement of the extent of electron-transfer to the bacteriopheophytin in the M-subunit in reaction centers of *Rhodopseudomonas viridis*. Photosynth Res 22: 47–59

Kirmaier C, Holten D, Bylina EJ and Youvan DC (1988) Electron transfer in a genetically modified bacterial reaction center containing a heterodimer. Proc Natl Acad Sci USA 85: 7562–7566

Kirmaier C, Gaul D, Debey R, Holten D and Schenck CC (1991) Charge separation in a reaction center incorporating bacteriochlorophyll for photoactive bacteriopheophytin. Science 251: 922–927

Kleinherenbrink FAM, Hastings G, Wittmershaus BP and Blankenship RE (1994) Delayed fluorescence from Fe–S type photosynthetic reaction centers at low redox potential. Biochemistry 33: 3096–3105

Krabben L, Schloddr E, Jordan R, Carbonera D, Giacometti G, Lee H, Webber AN and Lubitz W (2000) Influence of the axial ligands on the spectral properties of P_{700} of photosystem I: a study of site-directed mutants. Biochemistry 39: 13012–13025

Laible PD, Kirmaier C, Udawatte CS, Hofman SJ, Holten D and Hanson DK (2003) Quinone reduction via secondary B-branch electron transfer in mutant bacterial reaction centers. Biochemistry 42: 1718–1730

Lakshmi KV, Jung YS, Golbeck JH and Brudvig GW (1999) Location of the iron–sulfur clusters F_A and F_B in photosystem I: an electron paramagnetic resonance study of spin relaxation enhancement of P700+. Biochemistry 38: 13210–13215

Leibl W, Toupance B and Breton J (1995) Photoelectric characterization of forward electron transfer to iron–sulfur centers in photosystem I. Biochemistry 34: 10237–10244

Li Y, Lucas MG, Konovalova T, Abbott B, MacMillan F, Petrenko A, Sivakumar V, Wang R, Hastings G, Gu F, van Tol J, Brunel LC, Timkovich R, Rappaport F and Redding K. (2004) Mutation of the putative hydrogen-bond donor to P700 of photosystem I. Biochemistry 43: 12634–12647

Li Y, van der Est A, Lucas MG, Ramesh VM, Gu F, Petrenko A, Lin S, Webber AN, Rappaport F and Redding K (2006) Directing electron transfer within Photosystem I by breaking H-bonds in the cofactor branches. Proc Natl Acad Sci USA 103: 2144–2149

Lin X, Murchison HA, Nagarajan V, Parson WW, Allen JP and Williams JC (1994) Specific alteration of the oxidation potential of the electron donor in reaction centers from *Rhodobacter sphaeroides*. Proc Natl Acad Sci USA 91: 10265–10269

Lüneberg J, Fromme P, Jekow P and Schlodder E (1994) Spectroscopic characterization of PS I core complexes from thermophilic *Synechococcus* sp. Identical reoxidation kinetics of A_1^- before and after removal of the iron–sulfur-clusters F_A and F_B. FEBS Lett 338: 197–202

Marcus RA and Sutin N (1985) Electron transfers in chemistry and biology. Biochim Biophys Acta 811: 265–322

Mathis P and Sétif P (1988) Kinetic studies on the function of A_1 in the photosystem I reaction center. FEBS Lett 237: 65–68

Moser CC and Dutton PL (1996) Outline of theory of protein electron transfer. In: Bendall DS (ed) Protein Electron Transfer, pp 1–21. BIOS Scientific Publishers, Oxford

Moser CC, Keske JM, Warncke K, Farid RS and Dutton PL (1992) Nature of biological electron transfer. Nature 355: 796–802

Muhiuddin IP, Heathcote P, Carter S, Purton S, Rigby SE and Evans MC (2001) Evidence from time resolved studies of the $P700^+/A_1^-$ radical pair for photosynthetic electron transfer on both the PsaA and PsaB branches of the photosystem I reaction centre. FEBS Lett 503: 56–60

Parson WW (1996) Photosynthetic bacterial reaction centers. In: Bendall DS (ed) Protein Electron Transfer, pp 125–160. BIOS Scientific Publishers Ltd, Oxford

Petrenko A, Maniero AL, van Tol J, MacMillan F, Li Y, Brunel L-C and Redding K (2004) A high-field EPR study of $P_{700}^{+\cdot}$ in wild-type and mutant Photosystem I from *Chlamydomonas reinhardtii*. Biochemistry 43: 1781–1786

Purton S, Stevens DR, Muhiuddin IP, Evans MC, Carter S, Rigby SE and Heathcote P (2001) Site-directed mutagenesis of PsaA residue W693 affects phylloquinone binding and function in the photosystem I reaction center of *Chlamydomonas reinhardtii*. Biochemistry 40: 2167–2175

Ramesh VM, Gibasiewicz K, Lin S, Bingham SE and Webber AN (2003) Bi-directional electron transfer in Photosystem I: accumulation of A_0^- in A-side or B-side mutants of the axial ligand to chlorophyll A_0. Biochemistry 43: 1369–1375

Rigby SE, Evans MC and Heathcote P (1996) ENDOR and special triple resonance spectroscopy of A_1^- of photosystem 1. Biochemistry 35: 6651–6656

Rigby SE, Evans MC and Heathcote P (2001) Electron nuclear double resonance (ENDOR) spectroscopy of radicals in photosystem I and related Type 1 photosynthetic reaction centres. Biochim Biophys Acta 1507: 247–259

Rigby SE, Muhiuddin IP, Evans MC, Purton S and Heathcote P (2002) Photoaccumulation of the PsaB phyllosemiquinone in photosystem I of *Chlamydomonas reinhardtii*. Biochim Biophys Acta 1556: 13–20

Romijn JC and Amesz J (1977) Purification and photochemical properties of reaction centers of *Chromatium vinosum*. Evidence for the photoreduction of a naphthoquinone. Biochim Biophys Acta 461: 327–338

Schlodder E, Falkenberg K, Gergeleit M and Brettel K (1998) Temperature dependence of forward and reverse electron transfer from A_1^-, the reduced secondary electron acceptor in photosystem I. Biochemistry 37: 9466–9476

Sétif P (2001) Ferredoxin and flavodoxin reduction by photosystem I. Biochim Biophys Acta 1507: 161–179

Sétif P and Bottin H (1995) Laser flash absorption spectroscopy study of ferredoxin reduction by photosystem I: spectral and kinetic evidence for the existence of several photosystem I–ferredoxin complexes. Biochemistry 34: 9059–9070

Sétif P and Brettel K (1993) Forward electron transfer from phylloquinone A_1 to iron sulfur centers in spinach photosystem I. Biochemistry 32: 7846–7854

Sétif P, Mathis P and Vanngard T (1984) Photosystem I photochemistry at low temperature. Heterogeneity in pathways for electron transfer to the secondary acceptors and for recombination processes. Biochim Biophys Acta 767: 404–414

Shen G, Antonkine ML, van der Est A, Vassiliev IR, Brettel K, Bittl R, Zech SG, Zhao J, Stehlik D, Bryant DA and Golbeck JH (2002) Assembly of photosystem I. II. Rubredoxin is required for the in vivo assembly of F_X in *Synechococcus* sp. PCC 7002 as shown by optical and EPR spectroscopy. J Biol Chem 277: 20355–20366

Steffen MA, Lao KQ and Boxer SG (1994) Dielectric asymmetry in the photosynthetic reaction center. Science 264: 810–816

Takahashi Y, Hirota K and Katoh S (1985) Multiple forms of P700-chlorophyll a–protein complexes from *Synechococcus* sp.: the iron, quinone and carotenoid contents. Photosynth Res 6: 183–192

Thurnauer MC and Gast P (1985) Q-band (35 GHz) EPR results on the nature of A_1 and the electron spin polarization in photosystem I particles. Photobiochem Photobiophys 9: 29–38

Van Brederode ME, Jones MR, Van Mourik F, Van Stokkum IH and Van Grondelle R (1997) A new pathway for transmembrane electron transfer in photosynthetic reaction centers of *Rhodobacter sphaeroides* not involving the excited special pair. Biochemistry 36: 6855–6861

van der Est A (2001) Light-induced spin polarization in type I photosynthetic reaction centres. Biochim Biophys Acta 1507: 212–225

van der Est A, Bock C, Golbeck J, Brettel K, Sétif P and Stehlik D (1994) Electron transfer from the acceptor A_1 to the

iron–sulfur centers in photosystem I as studied by transient EPR spectroscopy. Biochemistry 33: 11789–11797

van der Est A, Prisner T, Bittl R, Fromme P, Lubitz W, Mobius K and Stehlik D (1997) Time-resolved X-, K-, and W-Band EPR of the radical pair state $P_{700}^{+}A_1^{-}$ of Photosystem I in comparison with $P_{865}^{+}Q_A^{-}$ in bacterial reaction centers. J Phys Chem B 101: 1437–1443

Vassiliev IR, Jung YS, Yang F and Golbeck JH (1998) PsaC subunit of photosystem I is oriented with iron–sulfur cluster F_B as the immediate electron donor to ferredoxin and flavodoxin. Biophys J 74: 2029–2035

Vos MH and van Gorkom HJ (1988) Thermodynamics of electron transport in photosystem I by electric field-stimulated charge recombination. Biochim Biophys Acta 934: 293–302

Wakeham MC, Goodwin MG, McKibbin C and Jones MR (2003) Photo-accumulation of the $P+Q_B^{-}$ radical pair state in purple bacterial reaction centres that lack the Q_A ubiquinone. FEBS Lett 540: 234–240

Warren PV, Golbeck JH and Warden JT (1993) Charge recombination between $P700^{+}$ and A_1^{-} occurs directly to the ground state of P700 in a photosystem I core devoid of F_X, F_B, and F_A. Biochemistry 32: 849–857

Webber AN and Lubitz W (2001) P700: the primary electron donor of photosystem I. Biochim Biophys Acta 1507: 61–79

Webber AN, Su H, Bingham SE, Kass H, Krabben L, Kuhn M, Jordan R, Schlodder E and Lubitz W (1996) Site-directed mutations affecting the spectroscopic characteristics and midpoint potential of the primary donor in photosystem I. Biochemistry 35: 12857–12863

Witt H, Schlodder E, Teutloff C, Niklas J, Bordignon E, Carbonera D, Kohler S, Labahn A and Lubitz W (2002) Hydrogen bonding to P700: site-directed mutagenesis of threonine A739 of photosystem I in *Chlamydomonas reinhardtii*. Biochemistry 41: 8557–8569

Xu W, Chitnis P, Valieva A, van der Est A, Pushkar YN, Krzystyniak M, Teutloff C, Zech SG, Bittl R, Stehlik D, Zybailov B, Shen G and Golbeck JH (2003a) Electron transfer in cyanobacterial photosystem I: I. Physiological and spectroscopic characterization of site-directed mutants in a putative electron transfer pathway from A_0 through A_1 to F_X. J Biol Chem 278: 27864–27875

Xu W, Chitnis PR, Valieva A, van der Est A, Brettel K, Guergova-Kuras M, Pushkar YN, Zech SG, Stehlik D, Shen G, Zybailov B and Golbeck JH (2003b) Electron transfer in cyanobacterial photosystem I: II. Determination of forward electron transfer rates of site-directed mutants in a putative electron transfer pathway from A_0 through A_1 to F_X. J Biol Chem 278: 27876–27887

Chapter 17

EPR Studies of the Primary Electron Donor P700 in Photosystem I

Wolfgang Lubitz*
Max-Planck-Institut für Bioanorganische Chemie, Stiftstraße 34-36, D-45470, Mülheim an der Ruhr, Germany

Summary

The primary donor P700 in Photosystem I (PS I) is a heterodimer comprised of a chlorophyll *a* and a chlorophyll *a*′. The electronic structure of this species, which is related to its function *in vivo*, can be studied by EPR techniques applied to the paramagnetic states $P700^{\cdot+}$ (cation radical) and $^3P700$ (triplet state) of the primary donor. In the case of $P700^{\cdot+}$ observables are the electronic *g* tensor and the electron-nuclear hyperfine and nuclear quadrupole coupling tensors; in the case of $^3P700$ the electron–electron dipolar coupling tensor serves as an additional probe. In this contribution, the determination of the magnetic resonance parameters by EPR techniques are described. Conclusions about the electronic structure, in particular about the spin and charge density distribution in this species, are drawn. The results are corroborated by studies of model systems and of the primary donor in genetically modified photosystem I preparations, which gives information on the effect of the protein surroundings. Emphasis is placed on a theoretical description of P700 in its various states, which is based on a comparison with molecular orbital calculations. Implications of the experimental findings for the functional properties of the primary donor in photosystem I are discussed.

*Author for correspondence, email: lubitz@mpi-muelheim.mpg.de

John H. Golbeck (ed): Photosystem I: The Light-Driven Plastocyanin:Ferredoxin Oxidoreductase, 245–269.

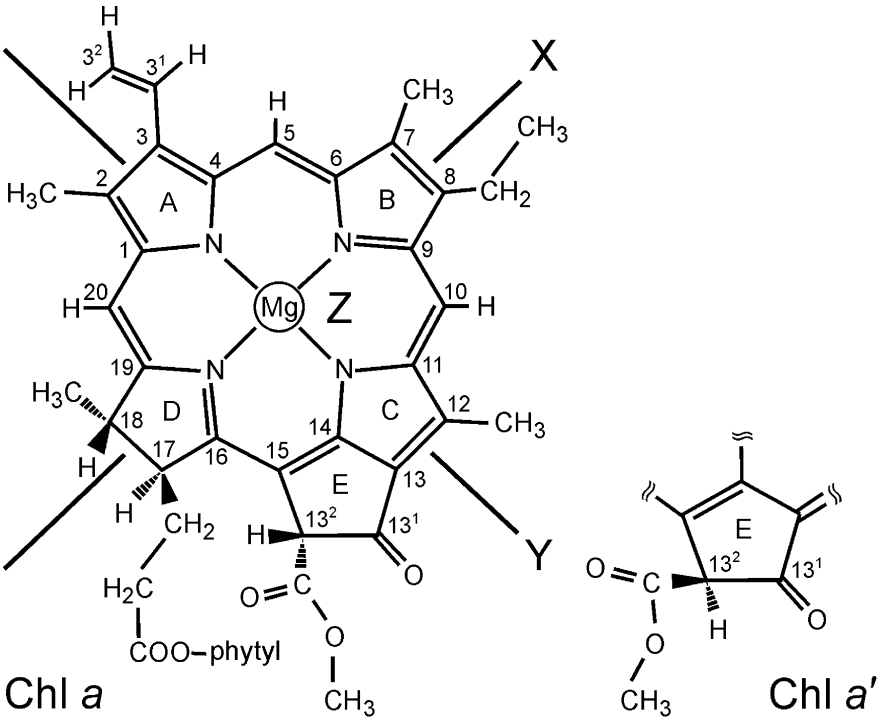

Fig. 1. Molecular structure of Chl *a* with numbering scheme (IUPAC). The molecular axes (X, Y, Z) are indicated. Chl *a′* (right) is the 13^2 epimer of Chl *a*.

I. Introduction

The primary electron donor in photosynthetic reaction centers is of great importance since this species is located at the interface of exciton transfer in the antenna system and electron transfer in the reaction center. In photosystem PS I of oxygenic photosynthesis the primary donor was identified as a pigment absorbing near 700 nm (Kok, 1956, 1957) and was therefore called P700. The light reaction generates the singlet excited state, ^{1}P700*, probably the most powerful reductant in natural systems ($E_m \approx -1.2$ V), which is crucial for the function of the electron transport in photosynthesis, for reviews see Brettel (1997) and Brettel and Leibl (2001). ^{1}P700* loses an electron to an electron transport chain, thereby creating cation and anion radicals, i.e., radical pair states. EPR spectroscopy has been instrumental in studying these paramagnetic species in PS I. It played an important role in the early detection and identification of the "light products," among these the primary electron donor radical cation $P700^{\cdot+}$ (Commoner et al., 1956).

P700 has long been known to be a chlorophyll (Chl) species (Fig. 1) (Kok, 1961; Witt et al., 1961) and based on optical data it was suggested already in 1968 that P700 may be an excitonically coupled Chl dimer (Döring et al., 1968). The exact composition of P700 remained a matter of considerable debate for several decades (Deligiannakis and Rutherford, 2001; Webber and Lubitz, 2001). In addition to Chl dimers (Norris et al., 1971) and monomers (O'Malley and Babcock, 1984), a Chl enol (Wasielewski et al., 1981b), a Chl epimer (Kobayashi et al., 1988), and even a chlorinated Chl *a* (Dörnemann and Senger, 1986) have been proposed to function as primary donor.

The X-ray crystallographic analysis of single crystals of PS I from the cyanobacterium *Thermosynechococcus elongatus* (Fromme et al., 2001; Jordan et al., 2001) revealed that P700 is indeed a Chl dimer. Surprisingly, it was shown to be comprised of one Chl *a* and one Chl *a′*, the 13^2 epimer of Chl *a*, in which the two substituents at position $C13^2$ are interchanged, causing the carbomethoxy group to be positioned on the same side of the chlorine macrocycle as the phytyl

Abbreviations: EPR – electron paramagnetic resonance; PS I – photosystem I.

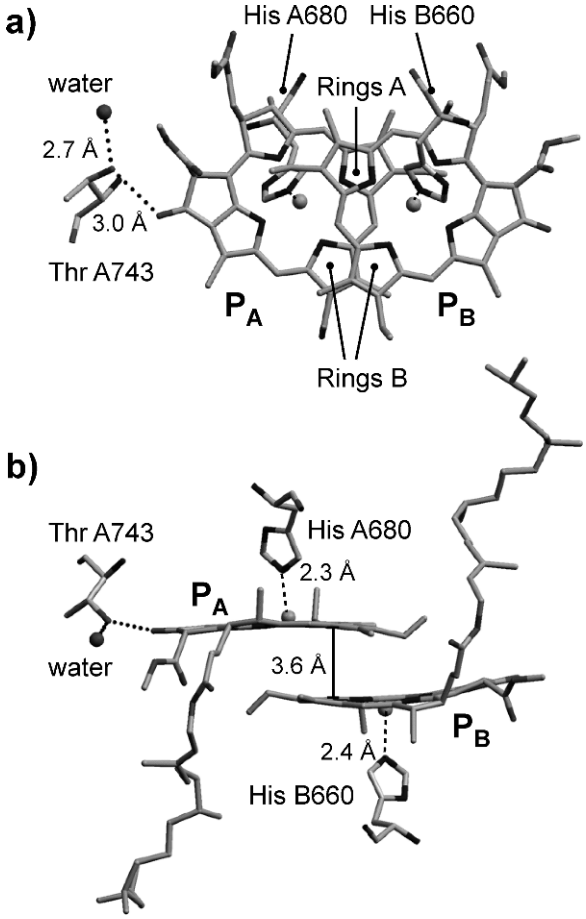

Fig. 2. Geometrical structure of P700 according to the X-ray crystallographic structure of *T. elongatus* (Jordan et al., 2001) with local environment including only the directly interacting amino acids Thr A743 (H-bond to Chl *a*′, dotted line), a nearby water molecule, and His A680 and His B660, (ligands of the Mg atoms, dashed lines). P_A = Chl *a*′ and P_B = Chl *a*. Further hydrogen bonds (not shown) are formed between amino acid residues and oxygen atoms of Chl *a*′ which are not conjugated to the π-system (see Fig. 3 in Jordan et al., 2001). (A) View perpendicular to the chlorin planes. (B) View along the pseudo-C_2-axis. (Adapted from Plato et al., 2003.) Note that in *C. reinhardtii* the two histidine ligands are H(A676) and H(B656) and the threonine is T(A739).

chain (Fig. 1). The existence of Chl *a*′ in PS I had already been proposed earlier (Kobayashi et al., 1988; Nakamura and Watanabe, 1998). As shown in Fig. 2 the two chlorin rings are approximately parallel to each other and overlap at the pyrrole rings A and B. They are separated by an average interplanar distance of 3.6 ± 0.1 Å. Both Chls show a dome-like deviation from planarity. There are no other significant structural differences from the X-ray structure, excluding the protein surroundings. In the PS I protein (Jordan et al., 2001) each chlorophyll is positioned on either side of an approximate C_2 symmetry axis that runs through P700 and the first [4Fe–4S] cluster F_X of the ET chain (see Fromme and Grotjohann, this volume, Chapter 6). This arrangement is highly conserved also in higher plants as recently shown by the X-ray crystallographic structure of plant PS I (Ben-Shem et al., 2003; see Nelson and Ben-Shem, this volume, Chapter 7). In *T. elongatus* PS I the central magnesium atoms of both Chls of P700, P_A and P_B, have an axial ligand provided by a histidine residue from the PsaA and PsaB subunits, respectively (Jordan et al., 2001). The axial ligand to Chl *a*′ (P_A) is provided by His(A680) and that to Chl *a* (P_B) by His(B660). This mode of ligation has been postulated earlier on the basis of spectroscopic studies of PS I mutants from *Chlamydomonas reinhardtii* (Webber et al., 1996; Redding et al., 1998; Krabben et al., 2000; see Webber and Ramesh, this volume, Chapter 14). Whereas there are no hydrogen bonds to the Chl *a*, the Chl *a*′ participates in H-bonding from amino acid side chains and water (Jordan et al., 2001). The 13^1-keto group carbonyl oxygen at ring E is an acceptor of a H-bond from threonine, Thr(A743), see Fig. 2. The phytyl ester carbonyl oxygen is a H-bond partner of Tyr(A735). In addition, the carboxy ester oxygen of the 13^2-carbomethoxy group is H-bonded by water, probably stabilizing incorporation of Chl *a*′ into the PsaA site (Jordan et al., 2001; Webber and Lubitz, 2001). Three other amino acids, Tyr(A603), Ser(A607), Thr(A743) are putative hydrogen bond partners of this water molecule. The amino acid residues involved in this pattern are found in many diverse species suggesting that the structure and structural interaction of P700 with its surrounding is evolutionary highly conserved.

The physicochemical properties of the Chls are determined by the electronic structure of their macrocycles and their substituents. However, evidence that the properties of the cofactors are also affected by pigment–pigment and pigment–protein interactions has accumulated. Striking examples are the primary donors of PS I (P700) and PS II (P680). Although both are constituted of Chl *a* molecules, the midpoint potentials differ by ∼0.7 V [E_m(P700) ≤ +0.5 V, E_m (P680) ≥ +1.1 V] (Watanabe and Kobayashi, 1991). Specific interactions with the protein take place via the coordinating ligands and hydrogen bonding with the peripheral substituents of the Chls. Studies with genetically modified bacterial reaction centers (RCs) have shown that hydrogen bonding of the protein to the carbonyl group of the 3-acetyl and the 13^1-keto group, which are both part of the conjugated π-system, has a

significant influence on the electronic structure and redox potential (Allen and Williams, 1995; Mattioli et al., 1995; Rautter et al., 1995).

Clearly, knowledge of the electronic structure of the primary donor is of importance for an understanding of the functional properties of PS I. In particular, it is important to know whether P700 is also electronically a dimer, which must be described by a wave function extending over both dimer halves as found for the bacteriochlorophyll dimers in bacterial RCs. For the paramagnetic oxidized state $P700^{\cdot+}$ created in the electron transfer (ET) process, such information can be deduced from electron paramagnetic resonance (EPR), electron-nuclear-double resonance (ENDOR), and electron-spin-echo-envelope-modulation (ESEEM) experiments (for details of techniques see Kurreck et al., 1988; Dikanov and Tsvetkov, 1992; Atherton, 1993; Amesz and Hoff 1995; Schweiger and Jeschke, 2001). However, the spectroscopic data obtained in the past have been interpreted quite differently and various models have been proposed for the primary donor $P700^{\cdot+}$ in PS I ranging from a symmetric dimer (Norris et al., 1971, 1975), via asymmetric dimer models (Davis et al., 1993; Rigby et al., 1994; Käss et al., 1995, 1996; Krabben et al., 2000) to Chl monomers (Wasielewski et al., 1981a,b; O'Malley and Babcock, 1984; Mac et al., 1998). On the basis of more recent experimental studies on PS I single crystals and PS I mutants (Krabben et al., 2000; Käss et al., 2001; Webber and Lubitz, 2001; Witt et al., 2002) and independent data from FTIR spectroscopy (Breton, 2001; Hastings et al., 2001; Wang et al., 2003) it can be concluded that $P700^{\cdot+}$ is also electronically a dimeric species with the spin density predominantly located on the Chl *a* half of the dimer.

For the second paramagnetic state, the primary donor triplet $^3P700$, less information is available from EPR spectroscopy. The existing EPR data indicate a localization of the triplet exciton on one chlorophyll at cryogenic temperatures and an evolving delocalization over both halves of the dimer at higher temperatures (Sieckmann et al., 1993; J. Niklas and W. Lubitz, 2004, unpublished data).

In this chapter data obtained from EPR techniques applied to $P700^{\cdot+}$ and $^3P700$ in PS I of various species are reviewed and compared to monomeric models of Chl $a^{\cdot+}$ and ^{3}Chl *a* in organic solvents. On the basis of these results and concomitant molecular orbital calculations a consistent picture of the electronic structure of the primary donor in PS I is now emerging.

II. The Primary Donor Radical Cation $P700^{\cdot+}$

A. Generation of $P700^{\cdot+}$

Illumination of PS I preparations leads to charge separation

$$PA_0A_1F \xrightarrow{h\nu} {}^1P^*A_0A_1F \rightarrow P^{\cdot+}A_0^{\cdot-}A_1F \rightarrow P^{\cdot+}A_0A_1^{\cdot-}F \rightarrow P^{\cdot+}A_0A_1F^{red}$$

in which P is the primary donor, A_0 the first chlorophyll acceptor, A_1 is phylloquinone, and F stands for the iron–sulfur centers F_x, F_A, and F_B (Brettel, 1997; Brettel and Leibl, 2001). In this process a quite stable radical cation $P700^{\cdot+}$ is formed due to the slow charge recombination with the terminal electron acceptors. $P700^{\cdot+}$ can be obtained by illumination of various PS I preparations including single crystals, chloroplasts, or even whole leaves with (white) light during freezing or by illumination of dark-adapted samples at low temperatures. *In situ* illumination in the EPR cavity is also possible and allows the observation of the radical at ambient temperatures. Since $P700^{\cdot+}$ is rather stable, it can be studied by conventional cw EPR and ENDOR techniques. Chemical oxidation of PS I preparations, using $K_3[Fe(CN)_6]$, is also possible and leads to high yields of $P700^{\cdot+}$ with spectroscopic properties identical to those of the light-induced state (Käss, 1995).

As a model system the Chl *a* radical cation is studied in organic solvents, which are selected to prevent aggregation in solution (e.g., CH_2Cl_2/THF or CH_2Cl_2/CH_3OH). The radical is usually generated by iodine oxidation (Scheer et al., 1977; Lubitz, 1991; Käss et al., 1998).

B. The Electronic g Tensor

At standard X-band frequencies ($\nu_{mw} \approx 9$ GHz) $P700^{\cdot+}$ shows a single EPR line, from which only an effective electronic *g*-factor of $g = 2.0025(1)$ and a Gaussian linewidth (0.70–0.71 mT) are available. Experiments performed on $P700^{\cdot+}$ in PS I from different organisms show very little variation of this signal, indicating a stable well-defined species embedded in a highly conserved protein environment. For monomeric Chl $a^{\cdot+}$ the same *g*-factor as for $P700^{\cdot+}$ was reported (Lubitz, 1991).

The electronic *g*-factor is an easily accessible integral property of a radical. Its magnitude depends on spin–orbit coupling of the distributed unpaired electron

in the molecule. According to simple g-factor theory (Stone, 1963a,b) large values are obtained when the spin density is high at atoms with large spin–orbit coupling like oxygen or heavier atoms and small if only carbon atoms are involved. Furthermore, the g value is an anisotropic quantity. In planar organic π radicals one finds g_x, $g_y > g_z = g_e$, where g_e is the free electron values (2.00232), and g_x and g_y show only a small deviation from g_e ($<10^{-2}$). The tensor axis of g_z is oriented parallel to the normal of the π-system, whereas g_x and g_y lie in the molecular plane.

The g anisotropy of $P700^{\cdot+}$ is very small and typical for a planar delocalized carbon π-radical. It cannot be resolved at the low microwave frequencies used in standard EPR instruments (X and Q band). With the advent of high-field/high-frequency EPR techniques this situation changed. Prisner et al. (1993) were the first to completely resolve the g tensor of $P700^{\cdot+}$ using deuterated PS I from *T. elongatus* at a frequency of 140 GHz. The use of even higher microwave frequencies allows the resolution of the g values without resorting to an elaborate deuteration of the sample (Bratt et al., 1997).

A typical EPR spectrum of $P700^{\cdot+}$, obtained at a microwave frequency of ~330 GHz, in wild type and mutants of PS I of the green algae *Chlamydomonas reinhardtii* (Petrenko et al., 2004), is shown in Fig. 3. The g tensor is fully resolved in all cases and shifts of g tensor components are observed. Figure 3 also shows a spectrum of a Chl $a_z^{\cdot+}$ species in PS II, which is known to result from a monomeric protein-bound chlorophyll. Differences between g components of $P700^{\cdot+}$ and this preparation were clearly observed (Table 1), and tentatively explained by effects resulting from dimerization of the chlorophylls in $P700^{\cdot+}$. However, for Chl $a^{\cdot+}$ in organic solvents somewhat larger g value components were observed than for Chl $a_z^{\cdot+}$ (Bratt et al., 2000; Poluektov et al., 2002). In the work of Bratt et al. (1997) it was found that the largest g value (g_x) of $P700^{\cdot+}$ is temperature dependent (Table 1). This was interpreted as resulting from a structural change or a redistribution of spin density, which could easily occur in a dimeric species. At present, these differences make it difficult to draw conclusions from a comparison between the g tensors of $P700^{\cdot+}$ and the Chl $a^{\cdot+}$ model systems.

Table 1 also contains g tensor data from some mutants in which the surroundings of P700 have been altered (Petrenko et al., 2004). In these mutants the histidines (H) ligating the two Mg atoms of the chlorophylls forming the primary donor are exchanged against glutamines (Q) [mutants HQ(A676) and HQ(B656)]. A pronounced effect on the g tensor could only be observed when the ligand on the P_B-side was replaced. The authors (Petrenko et al., 2004) concluded that their results agree with a model for $P700^{\cdot+}$ with an asymmetric spin density distribution, in which the spin is mainly localized on P_B. Furthermore, a deviation of the P_B chlorophyll structure from planarity due to the axial ligation or vinyl group rotation was postulated. Replacement of the threonine residue hydrogen bonded to the 13^1-keto group of P_A also changed one g

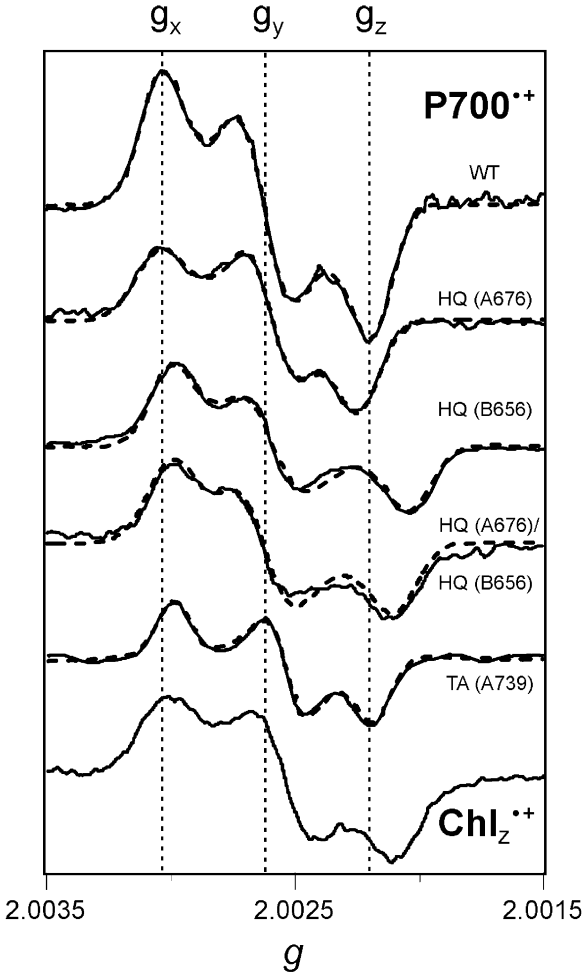

Fig. 3. High-field EPR spectra of $P700^{\cdot+}$ in wild type and several mutants of PS I from *C. reinhardtii* at T = 10 K and a field strength of 11.6–11.7 T (324–327 GHz). The experimental spectra (solid line) were scaled for better comparison, the dashed lines show simulations. The vertical dotted lines indicate the principal g tensor values of $P700^{\cdot+}$ in wild type, for data see Table 1. (Adapted from Petrenko et al., 2004, with permission from the American Chemical Society. © 2002.)

Table 1. Experimental *g* tensor principal values of the primary donor cation radical $P700^{\cdot+}$ from different species (wild type and mutants)

			T/K	ν_{mw}/GHz	g_x	g_y	g_z	References
$P700^{\cdot+}$	*T. elongatus*[a]		290	140	2.00304	2.00262	2.00232	Prisner et al. (1993)
	T. elongatus[a]		80	94	2.00308	2.00264	2.00226	Zech et al. (2000)
	T. elongatus[b]		80	94	2.00309	2.00260	2.00223	Zech et al. (2000)
	pea		200	325	2.00307	2.00260	2.00226	Bratt et al. (1997)
	pea		40	325	2.00317	2.00264	2.00226	Bratt et al. (1997)
	s. lividus[a]		70	130	2.00329	2.00282	2.00246	Poluektov et al. (2002)
	C. reinhardtii	WT	10	330	2.00304	2.00262	2.00220	Petrenko et al. (2004)
	C. reinhardtii	HQ(A676)	10	330	2.00305	2.00260	2.00224	Petrenko et al. (2004)
	C. reinhardtii	HQ(B656)	10	330	2.00301	2.00260	2.00205	Petrenko et al. (2004)
	C. reinhardtii	HQ(B656) HQ(A676)	10	330	2.00300	2.00261	2.00210	Petrenko et al. (2004)
	C. reinhardtii	TA(A739)	10	330	2.00301	2.00255	2.00220	Petrenko et al. (2004)
Chl $a^{\cdot+}$[c]			10	330	2.00329	2.00275	2.00220	Bratt et al. (2000)
$Chl_Z^{\cdot+}$	Spinach	Photosystem II	10	330	2.00304	2.00252	2.00213	Petrenko et al. (2004)

[a] Obtained from fully deuterated PS I.
[b] Obtained from the analysis of PS I single crystal spectra.
[c] Obtained from deuterated Chl *a*.

component. This indicates that some spin density must also reside on the P_A half of the $P700^{\cdot+}$ dimer. All these findings agree with earlier interpretations based on hyperfine data (Krabben et al., 2000; Käss et al., 2001; Witt et al., 2002).

An important additional piece of information is the orientation of the *g* tensor axes in the molecule that also depends on the details of the electron spin density distribution in $P700^{\cdot+}$. The first EPR experiments on $P700^{\cdot+}$ in PS I single crystals from *T. elongatus* performed at 94 GHz (W band) were reported by Zech et al. (2000). Typical spectra obtained by rotation in one of the crystallographic planes are depicted in Fig. 4. The analysis, together with additional orientation information from spin-polarized high frequency spectra of the secondary radical pair, $P700^{\cdot+}A_1^{\cdot-}$, yielded *g* tensor values identical within error to those reported by most other groups (Table 1) and an orientation of the *g* tensor that is shown in Fig. 4. It is evident that the *g* tensor axes are not related to any of the molecular axes (Fig. 1) known from the X-ray crystallographic structure (Jordan et al., 2001). This has also been observed for the *g* tensor of the primary donor $P865^{\cdot+}$ in RCs of the bacterium *Rhodobacter sphaeroides*, which was studied earlier in RC single crystals using W-band EPR (Klette et al., 1993). In the latter system this has been explained by a different rotation of the acetyl groups of the two BChl *a* moieties forming $P865^{\cdot+}$ (Plato and Möbius, 1995). However, such acetyl groups are not present in Chl *a*, which has instead a vinyl group (Fig. 1). The 13^1-keto group of Chl *a* does not show rotational freedom. A reason could lie in the different interaction with the environment of the two moieties forming P700, Chl *a*, and Chl *a*′ (Fig. 2).

At present the variations of the *g* tensor principal values and axes of $P700^{\cdot+}$ are not well understood due to the lack of reliable *g* tensor calculations. The future interpretation of the *g* tensor magnitudes and orientations based on advanced theoretical models would certainly contribute to a basic understanding of the electronic structure of $P700^{\cdot+}$ and its changes in different environments. However, knowledge of the *g* tensor alone will never be sufficient to predict electronic structure, additional information about the electron-nuclear hyperfine interactions of the individual magnetic nuclei is required. This is described in the following section.

C. Electron Spin Density Distribution: The Hyperfine Coupling Constants

At X-band frequencies the inhomogeneously broadened linewidth of $P700^{\cdot+}$ is 0.70 to 0.71 mT; the broadening is mainly caused by unresolved electron-nuclear hyperfine coupling constants (hfcs). For Chl $a^{\cdot+}$ larger values were reported, ranging from 0.78 mT to 0.92 mT depending on the solvent (Davis et al., 1979; Lubitz, 1991). The smaller linewidth of $P700^{\cdot+}$ was attributed to a change of the magnitude of the hfcs and the number of contributing nuclei to each hfc due to formation of a dimer. The original "special pair" model of Norris et al. (1971) for the primary donor in PS I was based on this EPR line-narrowing effect. For a fully symmetric dimer a line narrowing, as compared with the monomer, by a factor $1/\sqrt{2} \cong 0.71$ is theoretically expected. For asymmetric dimer models the line narrowing is less pronounced (Lendzian et al., 1993).

From the crystal structure alone, no information on the electronic structure, i.e., the distribution of the

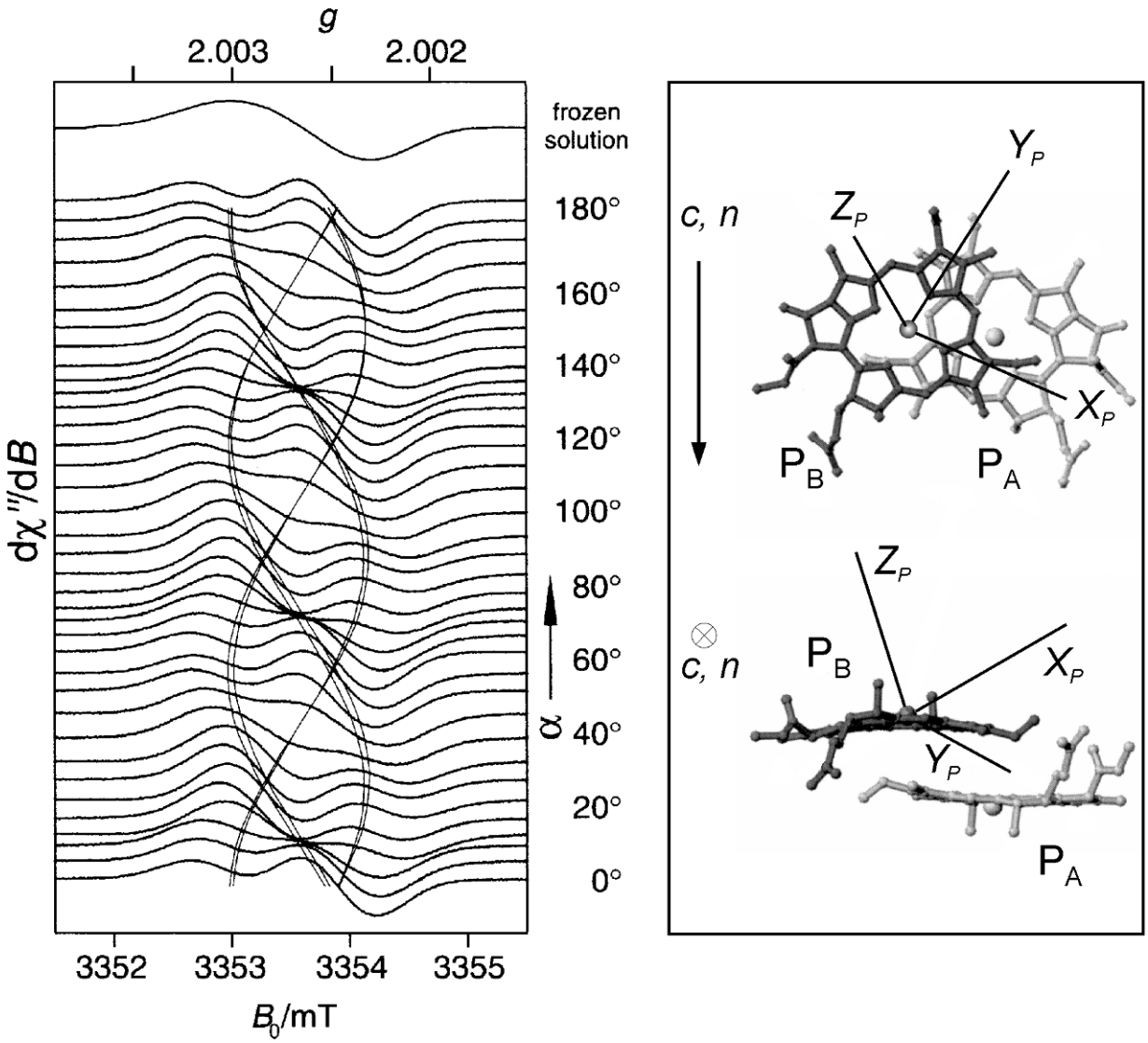

Fig. 4. Left: Angular dependence of the EPR spectra of $P700^{\cdot+}$ photochemically generated in a PS I single crystal ($P6_3$ space group) at 94 GHz; rotation axis approximately parallel to the crystallographic c-axis, leading to a pairwise degeneracy of the six expected lines and resulting effectively in a 2:2:2 line structure with 60° periodicity. All spectra are normalized. For other orientations see Zech et al. (2000). Right: Orientation of principal axes of the g tensor of $P700^{\cdot+}$ with respect to the molecular frame of the Chl *a* molecule (P_B) carrying most of the spin. Top: View direction perpendicular to the crystallographic c-axis, which is parallel to the thylakoid membrane normal n (parallel to the average plane normal of the chlorophyll); Bottom: view parallel to the c-axis (along the membrane normal). Note that for example the angle between the g_z and the molecular Z-axis of the spin-carrying chlorophyll P_B is 30°. For further details see Zech et al. (2000).

valence electrons, is available. This can be obtained from the measured and assigned electron-nuclear hyperfine coupling constants (hfcs) of $P700^{\cdot+}$. In such a radical the unpaired electron is delocalized in the π-system of the chlorophyll(s) and interacts with the various magnetic nuclei (mainly ^1H and ^{14}N). This hyperfine interaction usually splits the EPR line (Atherton, 1993). In the case of many interacting nuclei, the hfcs cannot be resolved and lead to inhomogeneous line broadening in the EPR spectrum. This is demonstrated for the chlorophyll *a* radical cation, Chl $a^{\cdot+}$, in Fig. 5A. To retrieve the hfcs from the EPR line, more advanced methods with higher spectral resolution must be applied, such as ENDOR or ESEEM. In an ENDOR experiment the NMR transitions of individual nuclei in a radical are observed via intensity

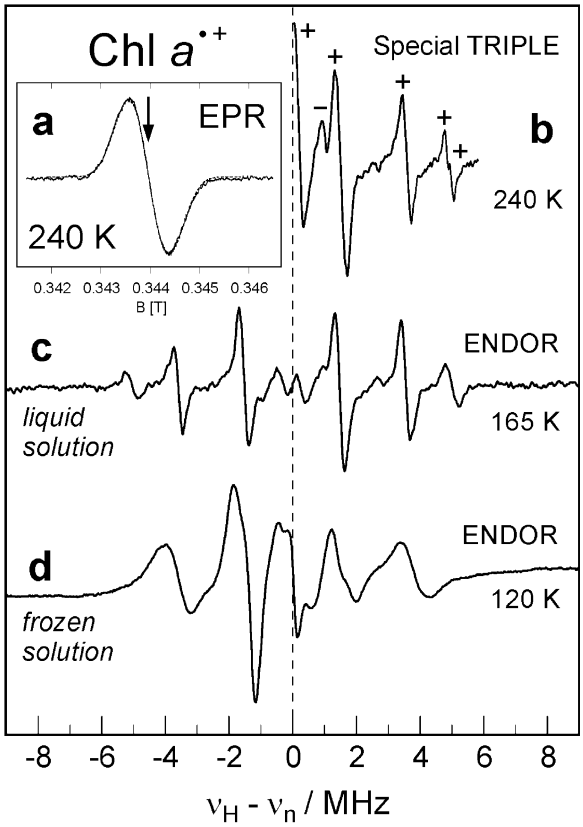

Fig. 5. EPR, ENDOR, and Special TRIPLE resonance spectra of Chl $a^{\cdot+}$ in CH_2Cl_2/THF (10:1) solution. (a) Gaussian EPR line exhibiting a width of 0.79 mT (liquid solution, 240 K) (0.98 mT in frozen solution, 10 K) showing no resolved hyperfine structure. (b) Special TRIPLE resonance of Chl $a^{\cdot+}$ showing six resolved line (isotropic hfcs see Table 2), the signs of the hfcs are indicated on the respective lines (from General TRIPLE resonance). (c) ENDOR in liquid solution (165 K). (d) ENDOR in frozen solution (glass state, 120 K); for details see text. (Spectra adapted from Huber et al., 1986; Möbius and Lubitz, 1987; Käss, 1995; Käss et al., 1998.)

changes of the monitored EPR transition. This experiment can be performed both in cw (continuous wave) (Kurreck et al., 1988) and pulsed mode (Schweiger and Jeschke, 2001). The first order resonance condition $\nu^{\pm}_{\mathrm{ENDOR}} = |\nu_{\mathrm{n}} \pm A/2|$ shows that line pairs are expected to be symmetrically spaced around the nuclear Larmor frequency ν_{n} and split by the respective hfc A. By application of electron-nuclear-nuclear TRIPLE resonance a significant increase in signal amplitude can be obtained (Special TRIPLE) and the relative signs of the hfcs become accessible (General TRIPLE) (Kurreck et al., 1988).

In Fig. 5 an example of cw EPR/ENDOR/TRIPLE is shown for the Chl *a* radical cation, Chl $a^{\cdot+}$, in solution. In liquid solution, the molecules tumble fast enough to average out all anisotropic hfcs, and the isotropic (Fermi contact) hfcs (A_{iso}) are directly obtained. A_{iso} is proportional to the spin density at the nucleus and can be related to the π-spin density. Thus, a map of the distribution of the unpaired electron in the molecule can be constructed from the measured and assigned isotropic hfcs, which can also be obtained theoretically, see e.g., Sinnecker et al., 2002. In the EPR spectrum (Fig. 5a) no hfcs are resolved. ENDOR in liquid solution (Fig. 5c) yields four pronounced line pairs symmetrically spaced around the proton Larmor frequency $\nu_{\mathrm{H}} \approx 14.5$ MHz at X band; their distance directly yields the isotropic hfcs in frequency units. In the Special TRIPLE resonance experiment (Fig. 5b) low- and high-frequency ENDOR transitions are simultaneously irradiated, yielding an increase in sensitivity and resolution, showing six resolved lines for Chl $a^{\cdot+}$ under optimized experimental conditions. The data are collected in Table 2. Special TRIPLE is often used to detect spectra of weak paramagnetic centers in complex proteins in solution. It even works at elevated temperatures where the ENDOR enhancement is usually very small (Lendzian et al., 1993).

Freezing of the liquid solution leads to immobilization of the radicals and typical powder EPR and ENDOR spectra are observed. In the ENDOR trace of Chl $a^{\cdot+}$ at T = 120 K (Fig. 5d) only line pairs belonging to proton hfcs of the freely rotating methyl groups are observed that have a small anisotropy. Such protons can thus be easily identified (Hyde and Rist, 1968) and are often used as probes for the electronic structure (Rautter et al., 1995; Rigby et al., 2001; Müh et al., 2002). Other protons with larger anisotropy are smeared out over a larger spectral range and become quite weak.

The small g anisotropy of Chl radicals prevents the detection of orientation-selected and single crystal type ENDOR spectra that can be obtained by selecting specific field positions in the EPR spectrum (Schweiger and Jeschke, 2001). A way out of this dilemma is either the application of high-field EPR/ENDOR techniques, which leads to an increased Zeeman interaction, or the use of single crystals. In this way the full anisotropic hfc tensors with principal components $A_{\mathrm{i}}(i = x, y, z)$ are detected (Lubitz and Lendzian, 1996). The purely dipolar part of the hf interaction, $A'_{\mathrm{i}} = A_{\mathrm{i}} - A_{\mathrm{iso}}$, with $A_{\mathrm{iso}} = {}^1/_3 \,\mathrm{Tr}\,\mathbf{A}$, reflects spin density in non-spherically symmetric orbitals near the nucleus and contains geometric information about the radical. Thus, the hfcs are ideal probes for studying the intimate details of the electronic and geometric structure of a radical, and they react in a very sensitive way to structural changes of the molecule and its surrounding.

Table 2. ^{1}H Hyperfine couplings (MHz) of Chl $a^{\cdot+}$ and of P700$^{\cdot+}$ in PS I of different organisms determined by ENDOR spectroscopy in frozen solutions. A comparison of data from the literature

Chl $a^{\cdot+}$	P700$^{\cdot+}$						Assignment position[a] (group)
CH_2Cl_2/THF[b] $T = 200$ K	*T. elongatus*[c] $T = 100$ K	*Chlorella vulgaris*[d] $T = 100$ K	Spinach[e] $T = 77$ K	Spinach[f] $T = 123$ K	*Scenedesmus obliquus*[g] $T = 210$ K	Spinach[h] $T = 10$ K	
3.0[i]	2.9 (2.80)	–	2.7	2.6	2.8	2.6	2^1 (CH_3)
3.0[i]	3.5 (3.40)	3.6	3.4	3.3	3.3	3.4	7^1 (CH_3)
7.1	5.3 (5.15)	5.3	5.2	5.3[j]	5.0	5.6	12^1 (CH_3)
10.1	7.7	–	7.5	7.5	7.5	7.2	17, 18 (βH)
10.3	9.6	–	–	–	–	–	17, 18 (βH)
2.2[k]	1.8	1.7	–	1.9	1.4	1.8	
0.6	0.8	–	–	0.8	0.7	0.9	

[a] For numbering of positions see Fig. 1. The assignment is based on the single crystal ENDOR spectra (Käss et al., 2001). For possible assignments of the two small hfcs see text and Table 8.
[b] Huber et al. (1986).
[c] Käss et al. (2001). Note that for the CH_3 protons the isotropic hfcs are given and not the individual tensor components for better comparison with the average powder ENDOR data found in the literature. The values in bracket are derived from experiments on PS I single crystal (Käss et al., 2001). The complete A(CH_3) tensors are 2^1: 2.55, 2.35, 3.55; 7^1: 3.15, 2.80, 4.20; 12^1: 4.70, 4.65, 6.10 (all values in MHz).
[d] Norris et al. (1975).
[e] Hoff (1979).
[f] O'Malley and Babcock (1984).
[g] Lendzian (1982).
[h] Rigby et al. (1994). Note that these data were obtained at very low temperature at which some of the hfcs might be influenced by dynamic effects (see text), this is particularly important for the hfc at position 12^1.
[i] These hfcs are split in 3-acetyl Chl $a^{\cdot+}$ (Käss et al., 1998) showing that they are degenerate in Chl $a^{\cdot+}$, see also Scheer et al. (1977). The use of CH_2Cl_2/CH_3OH as solvent mixture did not significantly change the hfcs (Käss, 1995).
[j] The authors gave two hfcs (5.0 and 5.9 MHz). Here these were assigned to the tensor components $A_\perp$ and $A_{||}$ of the 12^1 CH_3 protons. The value of 5.3 is the respective isotropic hfc.
[k] This hfc has a negative sign, it is hard to detect in frozen solutions (Käss et al., 1998) and is probably not detected in P700$^{\cdot+}$. Note that the data given in this column were obtained in liquid (isotropic) solution (Huber et al., 1986).

The ESEEM technique (Dikanov and Tsvetkov, 1992; Schweiger and Jeschke, 2001) can only be used in the solid state (powders, frozen solutions, single crystals). In principle, ESEEM allows the determination of dipolar and quadrupolar hyperfine interactions from a careful simulation of the modulation of the electron spin echo. This pulse EPR technique is complementary to ENDOR and is used mainly for the detection of insensitive magnetic nuclei with small Larmor frequencies and small hfcs that are otherwise difficult to detect (here ^{2}H, ^{14}N, ^{15}N). A recent review on technique, methodology, and applications of ESEEM to radicals in PS I has been published by Deligiannakis and Rutherford (2001).

For P700$^{\cdot+}$ in PS I complexes it has been shown that even at room temperature in liquid aqueous solution isotropic EPR and ENDOR spectra cannot be obtained. This is due to the large particle size of the trimeric PS I complexes of ∼1000 kDa, which prevents tumbling of the protein in solution that is fast enough to average out the anisotropic *g* and hyperfine contributions (Käss et al., 2001). Thus, powder-type ENDOR spectra are measured that are quite similar in liquid and frozen solutions. Such spectra of P700$^{\cdot+}$ have been obtained by many authors (Norris et al., 1975; Hoff, 1979; Lendzian, 1982; O'Malley and Babcock, 1984; Möbius and Lubitz, 1987; Rigby et al., 1994; Käss et al., 2001), see Table 2. All research groups basically measured the same hf splittings, but often a different number of hfcs was detected, and the assignment of the hfcs to molecular positions varied. This led to quite different views of the spin density distribution in P700$^{\cdot+}$ ranging from symmetric (Norris et al., 1971, 1975) to very asymmetric dimers, (Rigby et al., 1994; Käss et al., 2001) to a Chl monomer (O'Malley and Babcock, 1984).

In principle, a decision about the monomeric or dimeric nature of P700$^{\cdot+}$ is possible on the basis of the measured and assigned hyperfine coupling constants of P700$^{\cdot+}$. The firm assignment of a dimeric species requires, however, the detection of hfcs from *both* dimer halves as has been shown for the primary donor in bacterial reaction centers (Lendzian et al.,

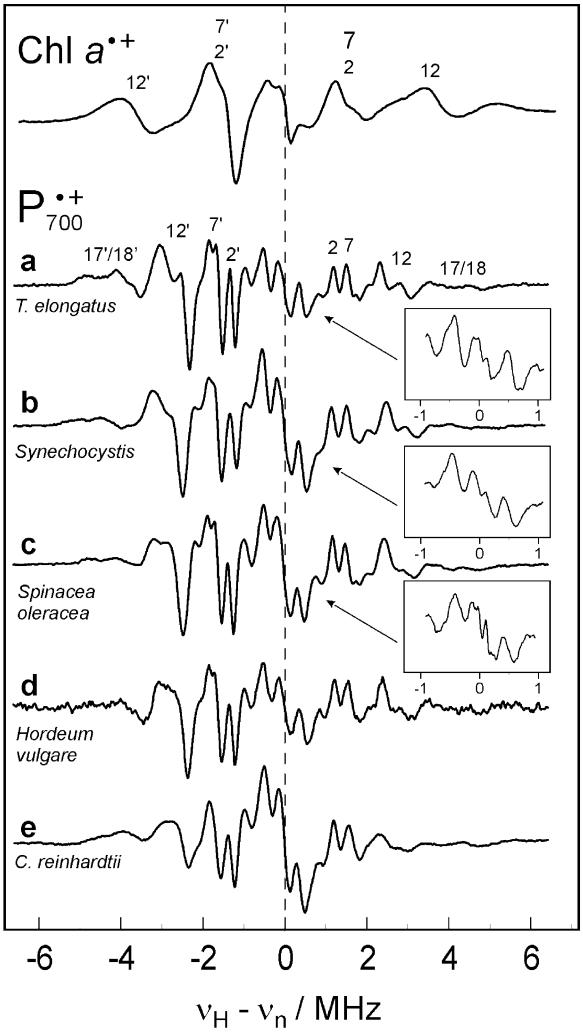

Fig. 6. Comparison of frozen solution ^{1}H ENDOR spectra of Chl $a^{\cdot+}$ (120 K, cf. Fig. 5) and of P700$^{\cdot+}$ in different species (a, b: cyanobacteria; c, d: higher plants; e: green algae) at T = 120 K (a–d) and 160 K (e). For Chl $a^{\cdot+}$ and P700$^{\cdot+}$ (top trace) the assignment of ENDOR line pairs to specific molecular positions of the Chl *a* macrocycle (Fig. 1) is given. The insert shows the region of small hf splittings for (a) to (c) under high resolution conditions. Note that the P700$^{\cdot+}$ spectra are all very similar. (Adapted from Käss, 1995; see also Witt et al., 2003.)

1993). Unfortunately, an unequivocal assignment of experimental ^{1}H hfcs to a second dimer half has not been achieved thus far for P700$^{\cdot+}$, making a final decision difficult.

An alternative approach to decide on the nature of the spin density distribution in P700$^{\cdot+}$ is to compare the hfc data with those of monomeric Chl $a^{\cdot+}$ in organic solvents. A comparison of the ENDOR spectra of Chl $a^{\cdot+}$ and of P700$^{\cdot+}$ in PS I from various species (cyanobacteria, higher plants, and green algae) is shown in Fig. 6. In earlier work performed on the radical cations of Chl *a* and various differently substituted and labeled chlorophyll species (Scheer et al., 1977; Huber et al., 1986; Käss et al., 1998), the three methyl groups at positions 12, 7, and 2 (Figs. 1 and 6) could be safely assigned; one data set is shown in Table 2. The powder-type cw ENDOR spectra of P700$^{\cdot+}$ (Fig. 6) show only very small variations among the different species (Käss, 1995; Witt et al., 2003) and the hfcs are nicely resolved for the protons of the three methyl groups (positions 2, 7, 12) and the β-protons (positions 17, 18). It could also be shown that the hfcs exhibit no large-temperature dependence, apart from a freezing of the methyl group rotation at very low temperatures (Käss et al., 2001). This result shows that structural changes of this radical species upon freezing do not occur. For P700$^{\cdot+}$ effects from the detergent used for PS I isolation on the ENDOR spectra have not been observed (Käss, 1995). Such effects were detected for P865$^{\cdot+}$ in the bacterial reaction center (bRC) where they lead to drastical changes of the EPR/ENDOR and the optical spectra (Müh et al., 1998).

In Table 2 a representative data set obtained for P700$^{\cdot+}$ of *T. elongatus* is given and compared to data collected in various other laboratories. Considering the error margins and the different species used this comparison shows a good agreement of the data. In P700$^{\cdot+}$ the respective values for $A_{CH_3}(12^1)$ and $A_{CH_3}(2^1)$ are reduced as compared with Chl $a^{\cdot+}$, whereas that for $A_{CH_3}(7^1)$ is increased. The two β-proton hfcs assigned to ring D (17, 18) are also clearly reduced in P700$^{\cdot+}$, but these proton hfcs are very sensitive to geometrical changes of the hydrogenated ring D. On the basis of a comparison of the three large methyl hfcs in P700$^{\cdot+}$ and Chl $a^{\cdot+}$ (Table 2), it has been argued (Käss, 1995) that at least 85% of the spin is located on one dimer half, i.e., on the "spin-carrying" Chl molecule. However, this estimate is not very reliable since the electronic structure of Chl $a^{\cdot+}$ is influenced by solvent, counterion, and temperature leading to a variation of the hfcs and of the EPR linewidth (Davis et al., 1979); for a compilation of hfc data see Table 3 in Lubitz (1991).

Additional information has been obtained from ENDOR studies of P700$^{\cdot+}$ in single crystals of PS I from *T. elongatus* (Käss et al., 2001). Some spectra obtained by rotation of the crystals (hexagonal space group $P6_3$) in one crystallographic plane are shown in Fig. 7, together with the powder spectrum. In these spectra, three hf tensors could be clearly resolved and safely assigned to the protons of the three methyl groups at positions 12, 7, and 2 belonging to one Chl *a*

Table 3. ^{14}N-Hyperfine coupling (A) and quadrupole coupling parameters (K, η) of Chl $a^{\cdot+}$ determined by ESEEM[a]

	A			B			C			D			
	A	K	η	A	K	η	A	K	η	A	K	η	References
Exp.	2.10[b]			2.86[b]			2.30[b]			2.86[b]			Astashkin et al. (1987)
				3.18	0.67	0.60				2.95	0.80	0.50	Dikanov et al. (1983)
					0.66	0.60					0.81	0.49	Käss et al. (1996)
Calc. DFT	−2.16	0.67	0.52	−3.25	0.65	0.70	−2.35	0.66	0.70	−2.77	0.71	0.57	Sinnecker et al. (2002)
													Sinnecker et al. (unpubl. data)

[a] A and K are given in MHz. An assignment is made to the four nitrogens in the pyrrole rings A to D, based on the DFT calculations.
[b] Values converted from ^{15}N hfcs by $\gamma(^{15}N)/\gamma(^{14}N) = 1.4$.

molecule (Table 2). The observed larger hfcs belong to the β-protons (positions 17, 18) of the same Chl. In the range of the smaller hfcs strong resonances were observed and were tentatively assigned by Käss (1995) to methyl protons of the second Chl half of the P700$^{\cdot+}$ dimer. If this assignment is correct, a spin-density distribution between the two halves of the dimer would range from 75:25 to 70:30. However, an assignment of the small hfcs to protons from the surrounding amino acids or to smaller hfcs of the spin-carrying *Chl a* itself cannot be completely excluded.

An alternative interpretation of the experimental data has been given by O'Malley and Babcock (1984), see also Mac et al. (1998) and O'Malley and Collins (2001). They explained the observed changes of the hfcs in P700$^{\cdot+}$ as compared with Chl $a^{\cdot+}$ as arising from a redistribution of spin density in a monomeric chlorophyll using a hybrid orbital model. This approach is based on an admixture of the first excited doublet state into the doublet ground state of the radical, which is brought about by interaction of the molecule with the protein surrounding (see below). The number of different ^{1}H nuclei coupled to a Chl $a^{\cdot+}$ monomer or even to a dimer is very large and leads to complex ^{1}H ENDOR spectra. Consequently, attempts have been undertaken to measure the hyperfine tensors of nitrogen nuclei in Chl $a^{\cdot+}$ and P700$^{\cdot+}$. Here the number of hfcs (4 versus 8) should allow a clear decision upon the monomeric or dimeric character of P700$^{\cdot+}$. Both hfcs from ^{14}N and ^{15}N nuclei in respectively labeled materials were measured, using ENDOR and ESEEM techniques (Astashkin et al., 1987; Davis et al., 1993; Käss et al., 1995; Käss and Lubitz, 1996; Käss et al., 1996; Mac et al., 1998).

Nitrogen hfc data obtained by various groups are collected in Table 3 for Chl $a^{\cdot+}$ and in Table 4 for P700$^{\cdot+}$. The comparison of the measured ^{14}N hfcs of monomeric Chl $a^{\cdot+}$ and P700$^{\cdot+}$ shows that, in general, the values for the latter are smaller. This decrease of the spin density, which was also observed for the proton hfcs, has let several groups to postulate that P700$^{\cdot+}$ is indeed a dimeric species, albeit with a significant asymmetry (Davis et al., 1993; Käss et al., 1995; Käss and Lubitz, 1996; Käss et al., 1996). As pointed out above the comparison with Chl $a^{\cdot+}$ is, however, problematic since it might not be a good model system for the chlorophyll dimer in PS I. Furthermore, the fraction of the total spin density present at the nitrogens is very small (<1%) (Deligiannakis and Rutherford, 2001). It is only created via spin polarization from the large spin density present at the neighboring carbon atoms (cf. Fig. 1) and will therefore be very sensitive even to small local structural changes. A much stronger argument for spin delocalization over more than one chlorophyll would be the detection of more than four nitrogen hfcs. Käss et al. provided three lines of evidence for a weak fifth nitrogen coupling based on ^{15}N ENDOR studies on ^{15}N-P700$^{\cdot+}$ and ^{15}N-Chl $a^{\cdot+}$ (Käss et al., 1995), concomitant HYSCORE spectroscopy of the ^{15}N-labeled species (Käss and Lubitz, 1996) and ESEEM studies of PS I single crystals (Käss et al., 1996). The authors assigned the fifth nitrogen hfc to the second half of the putative P700$^{\cdot+}$ dimer and considered this as strong evidence for the spin delocalization model. The data (see Table 4) have been critically reviewed (Deligiannakis and Rutherford, 2001).

This view has been challenged by Mac et al. who detected only four sets of nitrogen couplings and assigned them to one monomeric Chl $a^{\cdot+}$ forming the primary donor (Table 4) (Mac et al., 1998). In their model the observed changes of spin densities are interpreted within the hybrid orbital model, (O'Malley and Babcock, 1984), which predicts an admixture of the first excited state (by e.g., 25%) to the ground state in monomeric Chl $a^{\cdot+}$. A specific feature of this model is the decrease of spin density at several carbon (proton) positions and the significant increase at the central Mg and at two of the nitrogens. For the latter this causes a change of the sign of the respective hfcs. However, such a sign change could not be detected for the

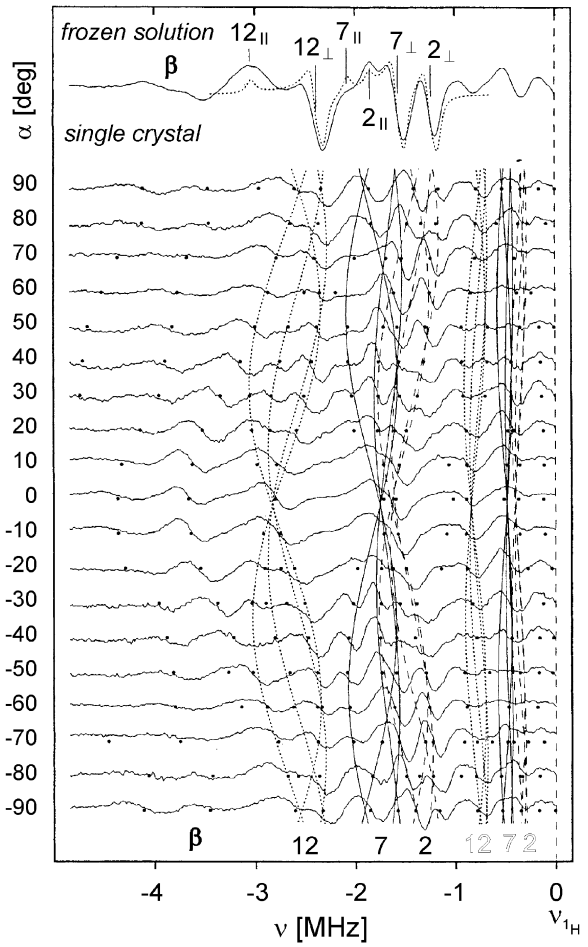

Fig. 7. Set of ^{1}H ENDOR spectra of $P700^{\cdot+}$ (low frequency part below ν_{1_H}) for rotation of a PS I single crystal ($P6_3$ space group) perpendicular to its crystallographic c-axis. The line positions obtained from spectral deconvolution are marked by black dots (•). The individual rotation patterns shown are assigned to the methyl group protons at positions 12, 7, 2 (P_B-side). Together with the experimental spectrum of $P700^{\cdot+}$ in frozen solution (top) a simulation is shown using the methyl proton hfc tensors taken from the single crystal spectra (see Table 2). The position of the respective hfc tensor components, assuming axial symmetry, is also indicated. Furthermore, the position of the β-proton hfcs (positions 17, 18) are marked. Rotation patterns for the small hfcs in the spectra are also indicated (open symbols) that were tentatively assigned to the methyl groups (12, 7, 2) of the other dimer half (P_A), see Käss (1995). (Adapted from Käss et al., 2001; Webber and Lubitz, 2001).

nitrogen (^{15}N) couplings in the ENDOR/TRIPLE resonance experiments performed by Käss et al. (1995) on ^{15}N-$P700^{\cdot+}$, i.e., the spin density at the nitrogens is negative. It has also been argued (Käss, 1995) that other properties of this radical would be expected to change if the hybrid orbital model would hold, such as the *g* tensor and the relaxation behavior, which was not observed in any of the experiments. It is therefore unlikely that the hybrid orbital model plays a role for $P700^{\cdot+}$, see also Sun et al. (2004).

Furthermore, ESEEM and ENDOR work by Babcock and coworkers (Mac et al., 1996, 1998) identified one additional nitrogen coupling and assigned it by use of ^{15}N-labeled histidine (and with ^{14}N-labeled His in an ^{15}N-labeled background) to interaction of the spin-carrying monomeric Chl $a^{\cdot+}$ with a histidine residue axially bound to the Mg atom. Histidine binding to the chlorophylls of P700 has also been concluded from mutagenesis studies (Cui et al., 1995; Webber et al., 1996; Redding et al., 1998; Krabben et al., 2000) as discussed below, and was also found in the recent X-ray crystallographic structure (Fromme et al., 2001; Jordan et al., 2001).

D. Electric Field Gradients: Nuclear Quadrupole Coupling Constants

The nuclear quadrupole couplings (nqc) of nuclei with $I \geq 1$ close to a spin center are, in principle, accessible by ENDOR spectroscopy in addition to the electron-nuclear hfcs. Advantageously 3- or 4-pulse ESEEM techniques have been used for small hyperfine couplings provided that the cancellation condition is fulfilled $|\nu_n \pm |A|/2| < K$ (Käss et al., 1996). This implies that the nuclear Zeeman and electron–nuclear hf interactions approximately cancel each other in one m_s manifold, so that the level splittings are primarily determined by the nqc. This results in three sharp lines at $\nu_0 = 2K\eta$, $\nu_- = K(3 - \eta)$, $\nu_+ = K(3 + \eta)$, where $4K = e^2qQ/h$ is the nqc and η is the asymmetry parameter of the traceless quadrupole tensor. The hfc can be estimated from the much broader double quantum transition observed from the other m_s manifold in the ESEEM spectrum $\nu_{dq} \approx 2\,[(\nu_n + |A|/2)^2 + K^2(3 + \eta^2)]^{1/2}$, where A represents an effective component of the hfc tensor, which is mainly determined by A_{iso}.

The nqc is related to the electric field gradient and is therefore probing the distribution of electrical charges around the nucleus. Its value is sensitive to the specific bonding situation. For ^{14}N nuclei, the nqc and η values attain characteristic values for a quadrupole nucleus in a specific molecule and allow an assignment of the observed nucleus (Lucken, 1969).

For Chl $a^{\cdot+}$ the observed values for two of the pyrrole rings (Table 3) are in good agreement with recent density functional theory calculations. On the basis of calculations, the nqcs for the other two rings are not expected to significantly deviate from these values.

Table 4. ^{14}N-Hyperfine coupling (A) and quadrupole coupling parameters (K, η) of $P700^{\cdot+}$ determined by ESEEM[a]

I			II			III			IV			V			
A	K	η	A	K	η	A	K	η	A	K	η	A	K	η	References
2.19	0.70	0.70	2.13	0.67	0.87	2.06	0.78	0.20	1.95	0.67	0.87	–			Mac et al. (1998)
2.51[b]			2.07[b]			1.20[b]			0.71[b]			0.26[b]			Käss and Lubitz (1996)
–	0.75	0.73	–	0.70	0.81	–	0.67	0.83		0.66	0.77	–	0.63	0.77	Käss et al. (1996)
2.38	0.68	0.73	2.23	0.74	0.78	–			–			–			Davis et al. (1993)

[a] A and K in MHz. No assignment to nitrogen positions in $P700^{\cdot+}$ has been made here, the ^{14}N couplings are given in order of decreasing magnitude (columns I to V); for a possible assignment of hfcs see Table 8. Note that Mac et al. (1998) proposed some assignments of their values to rings A to D in a chlorophyll monomer.
[b] Values converted from ^{15}N data by $\gamma(^{15}N)/\gamma(^{14}N) = 1.4$.

For $P700^{\cdot+}$ Mac et al. (1998) determined four sets of nqc values and assigned them to the four nitrogen in a monomeric Chl $a^{\cdot+}$. The data lie in the expected range, except for one very small η value (Table 4). Käss et al. (1996) obtained five sets of nqc values from an analysis of three-pulse ESEEM and HYSCORE experiments performed on PS I single crystals (Table 4). All K values lie in the range 0.65–0.78 MHz and the asymmetry parameters between 0.73 and 0.83. Good agreement is obtained with an earlier analysis of PS I in frozen solution by Davis et al. (1993), who measured the nqc of two nitrogens. All K values actually agree quite well with those found for Chl $a^{\cdot+}$ (Table 3). However, the asymmetry parameters are somewhat larger in $P700^{\cdot+}$ indicating some local differences of the charge-density distribution around the nitrogens, which may be caused by the protein surrounding. On the basis of these results the fifth nitrogen coupling measured by Käss et al. (1996) should belong to the Chl macrocycle and not to an imidazole nitrogen (i.e., ligating histidine). This assignment is, however, still controversial and is discussed in the literature (Mac et al., 1998; Deligiannakis and Rutherford, 2001).

E. Orientation of the Primary Donor

The ^{1}H ENDOR experiments on $P700^{\cdot+}$ in single crystals (Käss et al., 2001) also yielded the tensor axes of the three methyl groups of the spin-carrying Chl *a*. The axis of the major tensor component is related to the C–CH_3 bond direction (Atherton, 1993). This information allowed the determination of the angle between the C–CH_3 bonds and the crystallographic axes. For example, the main principal axis of the methyl groups tensor at position 12 makes an angle of $33 \pm 5^\circ$ with the crystallographic c-axis. The other angles are 54° (position 7) and 30° (position 2), which allowed an unequivocal assignment of these couplings (Käss et al., 2001). The molecular plane of the Chl *a* molecule in $P700^{\cdot+}$ could also be determined and proved to be parallel to the crystallographic c-axis. The orientation of this Chl *a* carrying most of the unpaired spin density could thus be fully determined (Käss, 1995; Käss et al., 2001). It was later found to be in excellent agreement with the crystallographic structure of P700 (P_B half) (Jordan et al., 2001). The crystallographic c-axis is parallel to the pseudo-C_2-axis of the PS I protein that relates the two cofactor branches of PS I to each other and the second Chl half is expected to be also approximately parallel to this axis. Due to the lack of assigned hfcs from the second half of $P700^{\cdot+}$, the orientation of the Chl *a′* (P_A) could not be determined by ENDOR spectroscopy.

The geometrical results obtained from ENDOR on $P700^{\cdot+}$ are consistent with EPR results on the triplet state ^{3}P700 (Rutherford and Sétif, 1990; Sieckmann et al., 1993) and with the structure obtained for P700 from X-ray crystallography (Jordan et al., 2001). Furthermore, results derived from quantum beat oscillations of the radical pair $P700^{\cdot+}$ $A_1^{\cdot-}$ are discussed in Thurnauer et al. (this volume, Chapter 22).

F. Interaction of $P700^{\cdot+}$ with the Protein Surroundings

Another chance to decide on the dimeric or monomeric nature of $P700^{\cdot+}$ lies in the exchange of specific amino acids in the surroundings of the donor, i.e., near P_A or P_B, by site-directed mutagenesis. These residues are expected to interact with P700 and should thus lead to shifts of the spin- and charge-density distribution and to changes of the hfcs, nqcs, and other physical properties of the donor. Such effects have been detected earlier, e.g., for $P865^{\cdot+}$ in bacterial RCs, see e.g., Rautter et al. (1995), Johnson et al. (2002), and Müh et al. (2002).

Several groups have used site-directed mutagenesis of the PsaA and PsaB subunits in *C. reinhardtii* to identify histidines that might function as ligands to P700

Table 5. Comparison of selected isotropic hyperfine couplings constants (MHz) of $P700^{\cdot+}$ from wild type and mutants of *C. reinhardtii*

	Hfc[a]			
Species	$12^1(CH_3)$	$7^1(CH_3)$	$2^1(CH_3)$	17,18 (β)[b]
$P700^{\cdot+}$				
Wild type	5.32	3.65	2.93	8.7/7.2
TV(A739)	4.85	3.55	2.83	8.2/6.8
TH(A739)	5.04	3.7	2.9	8.4/7.0
TY(A739)	5.04	3.65	2.89	8.4/6.9
HQ(A676)	5.30	3.43	2.95	–
HS(A676)	5.37	3.63	2.97	–
HQ(B656)	5.63	3.70	3.02	–
HC(B656)	5.98	3.57	2.97	–
HG(B656)	6.00	3.61	3.07	–
HS(B656)	6.08	3.61	2.97	–
HN(B656)	6.32	3.78	3.10	–

[a] Threonine mutants from Witt et al. (2002), Histidine mutants from Krabben et al. (2000); for details see text. The error in hfcs in ±0.1 MHz (CH_3) and ±0.2 MHz (β-protons). The A_{iso} values of the methyl hfcs were calculated from the $A_{||}$ and $A_{\perp}$ features in the powder ENDOR spectra using $A_{iso} = 1/3\ (A_{||} + 2A_{\perp})$.

[b] For the histidine mutants the β-proton hfcs could not be determined with confidence.

and to determine the influence of axial ligands on the specific properties of P700 (Cui et al., 1995; Webber et al., 1996; Redding et al., 1998; Krabben et al., 2000). Of all histidines conserved in both PsaA and PsaB, only specific mutation of residues in the membrane spanning helices j or j′ altered the spectroscopic properties of P700. This led to the conclusion that the axial ligands to P700 are His(A676) and His(B656) in *C. reinhardtii* (Cui et al., 1995; Webber et al., 1996; Redding et al., 1998; Krabben et al., 2000).

ENDOR studies of these histidine mutants have been performed on $P700^{\cdot+}$ (Krabben et al., 2000). Mutations of the PsaB subunit were observed to alter the ENDOR spectra of $P700^{\cdot+}$ with no significant change in hfcs being found in the PsaA mutants. The observed small magnitude of the effect of the PsaB mutations is probably due to the fact that other residues or water molecules are ligating the Mg atoms in these mutants, as observed for the donor in bacterial RCs (Goldsmith et al., 1996). Furthermore, the spin density at the Mg ions is expected to be very low. The surprising observation was that predominantly only one hfc, that of the methyl group (position 12) was affected by the PsaB mutations (see Table 5). Studies of modified Chl *a in vitro* have, however, shown that the hfc of this methyl group is especially sensitive even to small structural changes (Käss, 1995; Käss et al., 1998). Furthermore, the resonances from the other methyl groups are expected to strongly overlap with other lines, in particular from a putative second dimer half. Shifts of hfcs are therefore more difficult to detect. The ENDOR results were interpreted to indicate that P_B carries the majority of the electron spin density in $P700^{\cdot+}$. Krabben et al. (2000) have also carried out redox titration, optical, and functional studies on the histidine mutants. For all mutants an increase of the oxidation potential $E_m^{ox}(P)$ has been observed that was most pronounced for the B-side mutations. As in the case of the bacterial RC (Plato et al., 1988a) it is expected that in PS I the axial histidine lowers the energy level of $P700^{\cdot+}$ due to interaction with the positive charge on the chlorin dimer. The extent of interaction between $P700^{\cdot+}$ and any substituted amino acid will therefore depend on the distance and polarizability of the side chain. This reasoning was used to explain the effect of different amino acids on the $E_m^{ox}(P)$. From the observed effects it was concluded that spin and positive charge mainly resides on P_B, and P_A has only a minor effect. The results demonstrate a role of the axial ligands in fine-tuning of the potential of P700.

A sensitive probe for the electrostatic interactions with the surrounding of a radical ion is also the *g* tensor. In Fig. 3 the effects of the His mutations on the *g* anisotropy of $P700^{\cdot+}$ are shown. The strongest effect was observed for the B-side mutant HQ(B656), whereas the respective A-side mutant HQ(676) showed only a minor, and opposite, effect. The respective double mutant is dominated by the B-side (see also Table 1). This again shows that most of the spin/charge density must be on P_B.

Interesting observations have been made by Witt et al. (2002) upon replacement of Thr(A739). This amino acid is hydrogen bonded to the 13^1-keto group of P_A and is H-bonded to a structural water molecule (Fig. 2). Exchange of this threonine to other amino acids is expected to change the H-bond situation and thereby alter the electronic structure and the physical properties. This assumption is based on the extensive work on hydrogen bond mutants of the bacterial RC (Rautter et al., 1995; Müh et al., 2002; Reimers and Hush, 2004). However, effects would only be expected when P_A participates electronically in the dimer formation.

Witt et al. (2002) have studied P700 wild type and three mutants of *C. reinhardtii*, in which Thr(A739) was exchanged with valine (V), histidine (H), and tyrosine (T). The ENDOR spectra showed clear changes of the major hfcs; in contrast to the histidine mutants, the hfcs are decreased. The values measured from the powder ENDOR spectra are collected in Table 5. The hfcs assigned to the β-protons (position 17, 18) and to the

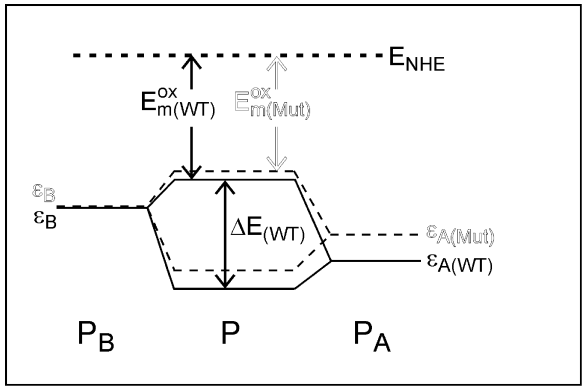

Fig. 8. Molecular orbital (MO) model for the primary donor P in PS I. P_A and P_B stand for the two dimer halves, E_m^{ox} denotes the oxidation potential of the dimer, and ε_A and ε_B are the energies of P_A and P_B, respectively. ΔE is the energetic difference between the MOs of the dimer P and is calculated according to $\Delta E = [(\Delta\alpha)^2 + (2\beta)^2)]^{1/2}$ where $\Delta\alpha = \varepsilon_A - \varepsilon_B$ signifies the difference between the HOMO energies of P_A and P_B, and β (resonance integral) describes the strength of the electronic coupling between the two dimer halves. Removal of the hydrogen bond to the 13^1-keto group of P_A in the respective mutants leads to an increase in the HOMO energy of P_A which results in a decrease of the oxidation potential of the dimer P, and in a more equal spin density distribution in the dimer.

12-CH_3 group are significantly smaller, the observed decrease of the other two methyl hfcs (7-CH_3 and 2-CH_3) is small and close to the error limit. Changes of the remaining smaller hfcs, which might belong to a second Chl half, could not be detected with confidence. Effects of the exchange of Thr(A739) have also been studied by many other techniques, for details see Witt et al. (2002). For example, the oxidation potential of all mutants was found to be lower than that of WT, for TV(A739) by −32 mV. A similar mutant, TA(A739), has also been shown to have different *g*-tensor components than WT in *C. reinhardtii* (Petrenko et al., 2004), indicating an impact of this mutation on the all-over electronic structure of $P700^{\cdot+}$.

In summary, there is now good evidence that P_A is electronically coupled to P_B and is thus involved in P700. The decrease in spin density on P_B (Table 5) in all mutants can be interpreted as a spin density shift from P_B towards P_A. This view has been fully supported by recent FTIR results (Wang et al., 2003). The effect of H-bonding to P700 shows entirely the same characteristics as for P865 in the bacterial RC of *R. sphaeroides* [replacement of Leu(M160) with His] (Rautter et al., 1995). This shows that $P700^{\cdot+}$ is indeed a dimer with a spin density distribution over the two halves.

The impact on the electronic structure affecting the oxidation potential and the electron spin distribution can be explained within a simple molecular orbital (MO) model introduced by Plato et al. (1992) and Parson et al. (1992) for the bacterial RC (Müh et al., 2002), which is shown in Fig. 8. In this MO scheme ε_A and ε_B are the site energies of the isolated monomeric chlorophylls P_A and P_B, respectively, which are assumed to be different ($\varepsilon_A - \varepsilon_B = \Delta\alpha$). The electronic coupling β between the two chlorophylls constituting P700 yields two molecular orbitals of the dimer. Their energetic difference is given by $\Delta E = [(\Delta\alpha)^2 + (2\beta)^2]^{1/2}$. The oxidation potential of P700, E_m^{ox}, is related to the HOMO energy level of the dimer as indicated.

From the scheme it is clear that the E_m^{ox} of P700 is lower than that of the monomeric chlorophylls and depends on the magnitude of $\Delta\alpha$ and on the coupling β. In the figure $\varepsilon_B > \varepsilon_A$, i.e., the spin density distribution will be asymmetric with more spin on P_B [ε_B and ε_{HOMO}(P) are closer in energy]. Note that P_A is stabilized by H-bonding to the Chl *a*′. Removal of this H-bond results in a destabilization and increase of ε_A, leading to an increase of ε_{HOMO} (P) and to a less positive oxidation potential of P700 ($E_{m\,(Mut)}^{ox} < E_{m\,(WT)}^{ox}$). Another consequence of the increase in the energy of the highest occupied π-orbital (HOMO) of P_A would be a decrease in the site energy difference ($\Delta\alpha$) between P_A and P_B. This leads to a more symmetric charge distribution and a shift of the spin density from P_B to P_A, as observed experimentally.

III. The Primary Donor Triplet State ^{3}P700

A. Generation of ^{3}P700

If in the charge separation process electron transfer in PS I beyond the first acceptor A_0 is blocked by treatment with sodium dithionite at high pH and illumination, which reduces the iron–sulfur centers F and the quinone A_1, the triplet state of the donor, ^{3}P700, is obtained via radical pair recombination from the triplet RP according to:

$$PA_0A_1^{red} \xrightarrow{h\nu} {}^1P^*A_0A_1^{red} \rightarrow {}^1(P^{\cdot+}A_0^{\cdot-})\,A_1^{red} \overset{\omega}{\rightleftharpoons} {}^3(P^{\cdot+}A_0^{\cdot-})A_1^{red} \rightarrow {}^3PA_0A_1^{red}.$$

Other pathways of ^{3}P700 formation have also been discussed (Brettel, 1997). The RP mechanism initially only populates the T_0 triplet sublevel in the external strong magnetic field, and therefore, leads to a characteristic EPR spin polarization AEE AAE (A = enhanced absorption, E = stimulated emission) (Angerhofer, 1991). ^{3}P700 was first observed by Frank et al.

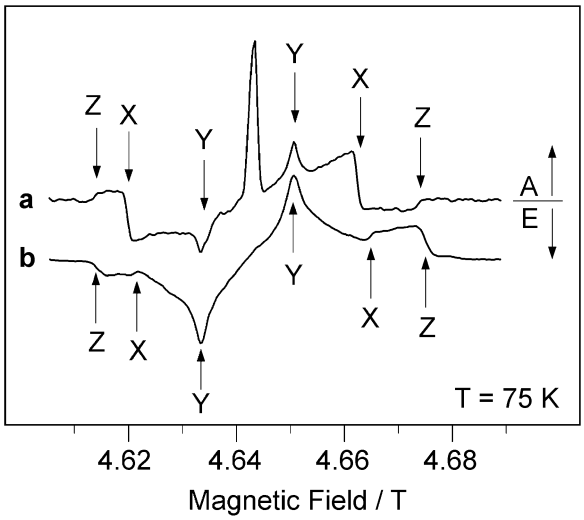

Fig. 9. Spin-polarized pulse EPR spectra of the light-induced triplet state ^{3}P700 in deuterated PS I from *Synechococcus lividus* (a) and of ^{3}Chl *a* in illuminated toluene/pyridine (9:1) solution (b). Arrows indicate the turning points in the spectra, which correspond to the principal orientations of the zero-field tensor. A and E indicate absorptive and emissive lines in the spectra. The strong absorption in the center of trace (a) is due to the cation radical $P700^{\cdot+}$. (Adapted from Poluektov et al., 2002, with permission from the American Chemical Society. © 2002.)

(1979). ^{3}P700 is short-lived ($\leq$1 ms) and is thus studied by time-domain techniques like transient and pulse EPR (Stehlik and Möbius, 1997). If only the iron–sulfur centers are prereduced, the radical pair $P700^{\cdot+}A_1^{\cdot-}$ is formed. It can be studied by EPR and ENDOR techniques.

As a model system the triplet state of monomeric chlorophylls is studied. ^{3}Chl *a* can be generated by illumination of Chl *a* dissolved in an organic glass, where it is populated *via* intersystem crossing (ISC) from the singlet excited state (Budil and Thurnauer, 1991; Angerhofer, 1991). This species also shows a spin polarization of the EPR spectrum. Since the mechanism of triplet formation is different, the polarization pattern is different from that of ^{3}P700 (Thurnauer et al., 1975).

B. Information from the g Tensor

The g-tensor components are usually not resolved for a triplet state of a porphyrin or chlorin molecule at X- and Q-band frequencies and only the zero field splitting (ZFS) parameters are obtained. This situation changed with the advent of high-field/high-frequency EPR techniques. The first data of ^{3}P700 and ^{3}Chl *a* were published by Poluektov et al. (2002), the respective spectra are shown in Fig. 9. The obtained data (Table 6) clearly show that the g anisotropy of the triplet states is larger than that of the respective cation radicals (Table 1). A similar effect has been observed for the triplet states of the primary donors in PS II (Pashenko et al., 2003) and in the bacterial RC (Labahn and Huber, 2001; Pashenko et al., 2001; Zeng et al., 2003). This can be explained by the fact that the triplet electrons probe the spin distribution in two different orbitals (HOMO and LUMO), and the latter has a rather large spin density at the nitrogens and the central magnesium, cf. O'Malley (2000) and Sinnecker et al. (2002), by which the spin–orbit coupling and the g-anisotropy is increased.

Comparison of the g-tensors of ^{3}P700 and ^{3}Chl *a* shows interesting differences with respect not only to magnitude but also to axes orientation. The analysis yielded a switching between the g_x and g_y axes with respect to the orientation of the ZFS tensor (Poluektov et al., 2002). For ^{3}P700 a rotation of the ZFS axes with respect to the singlet and triplet–triplet optical transition moments has also been reported (Vrieze et al., 1996). The observed effect indicates a significant change of the electronic structure, which needs to be corroborated by additional data obtained in single crystals before a final interpretation can be attempted.

C. Zero Field Splitting

The triplet state EPR spectrum of ^{3}P700 in Fig. 9 shows the characteristic spin polarization (AEEAAE), which is different from that of ^{3}Chl *a* (EAEAEA) (Poluektov et al., 2002). The spectrum is dominated by the dipolar interaction of the two unpaired electrons leading to zero field splitting (ZFS) or fine structure, described by the parameters $|D|$ and $|E|$, that reflect the energy differences between the triplet sublevels in zero-magnetic field (Atherton, 1993). Whereas $|D|$ is proportional to the third power of the reciprocal distance of the two unpaired electrons in the extended π-orbitals of a Chl, $|E|$ characterizes the deviation from axial symmetry of the electronic system. Here, the respective magnetic axes are chosen such that z is perpendicular to the π-plane of the Chl ($D > 0$) and x, y lie in this plane (sign of E depends on choice of axes).

The $|D|$ and $|E|$ values for ^{3}P700 in PS I and ^{3}Chl *a* have been measured at low temperatures by optical detection of magnetic resonance (ODMR) (Angerhofer, 1991; Hoff, 1996; Carbonera et al., 1997) and EPR techniques (Angerhofer, 1991; Budil and Thurnauer, 1991) for a variety of species. A comparison of the $|D|$ and $|E|$ values of monomeric ^{3}Chl *a* and ^{3}P700 at low

Table 6. Experimental g tensor and ZFS tensor principal values of the primary donor triplet state ^{3}P700 and ^{3}Chl a at T = 75 K and $\nu_{mw} = 130$ GHz, from Poluektov et al. (2002)

	g_x	g_y	g_z	$\lvert D\rvert \times 10^{-4}$ cm^{-1}	$\lvert E\rvert \times 10^{-4}$ cm^{-1}
^{3}Chl a[a]	2.00344	2.00383	2.00265	284 ± 1[d]	41.3 ± 0.2[d]
^{3}P700[b]	2.00369	2.00323	2.00252	280 ± 1[e]	39.0 ± 0.2[e]
Chl $a_z^{\cdot+}$[c]	2.00332	2.00280	2.00225	–	–

[a] From deuterated Chl a.
[b] From PS I of fully deuterated *S. lividus.*
[c] In PS II (*S. lividus*), note differences to values in Table 1 (Petrenko et al., 2004).
[d] Values reported for ^{3}Chl a (in different solvents) range from 275 × 10^{-4}cm^{-1} to 299 × 10^{-4} cm^{-1} for |D| and from 35 × 10^{-4} cm^{-1} to 44 × 10^{-4} cm^{-1} for |E| (Angerhofer, 1991).
[e] Values reported for ^{3}P700 range from 278× 10^{-4} cm^{-1} to 287 × 10^{-4} cm^{-1} for |D| and from 38× 10^{-4} cm^{-1} to 44 × 10^{-4} cm^{-1} for |E| (Angerhofer, 1991).

temperatures shows no significant difference (Table 6), indicating to first order a localization of the triplet exciton on a monomeric Chl a – or on *one* half of a dimeric ^{3}P700. Assuming that P700 is a dimer, the triplet state, ^{3}P700, can be described by a linear combination of two local excitations, $^3P_AP_B$ and $P_A{}^3P_B$, and two charge transfer (CT) states, $^3(P_A^+P_B^-)$ and $^3(P_A^-P_B^+)$. Considering only local excitations, the $|D|$ value will not be changed significantly in a coplanar Chl a dimer with respect to monomeric Chl a, but a reduction of $|E|$ is generally expected. Inclusion of CT states will reduce $|D|$ (Angerhofer, 1991). At room temperature, Stehlik and coworkers (Sieckmann et al., 1993) reported a reduction of $|E|$ for ^{3}P700, whereas $|D|$ remained the same as found at low temperatures. These experiments were recently repeated, yielding basically the same results (Niklas et al., unpublished). The authors interpreted their findings as resulting from triplet delocalization over two coplanar Chl a molecules at elevated temperatures. The magnetic z-axes of the two chlorophylls are parallel and their magnetic x (and y) axes form an angle of approximately 55°. In addition, the orientation dependence of the triplet state showed that the plane of the Chl, which carries the triplet at low temperature, is oriented perpendicular to the membrane (Rutherford and Sétif, 1990), i.e., the triplet state must be located on P_A or P_B.

The $|D|$ and $|E|$ values for ^{3}P700 in PS I mutants of *C. reinhardtii*, in which the histidines ligating the Mg atoms of P_A and P_B and the hydrogen bond to P_A were altered, indicate that the triplet state remains trapped on a single Chl (Krabben et al., 2000; Witt et al., 2002). In this context it should be noted that $|D|$ and $|E|$ values of ^{3}Chl are solvent dependent *in vitro* and the variations of up to 10% have been related to changes of the Chl ligation (Angerhofer, 1991). Analysis of triplet-minus-singlet absorbance difference spectra indicated that the triplet state at low temperature is localized on P_B as found for the cationic state in P700$^{\cdot+}$ (Krabben et al., 2000; Witt et al., 2002). This result is still controversial and is discussed in the literature (Breton et al., 2002; see also Breton, this volume, Chapter 18).

Further information on ^{3}P700 is at present sparse since no single crystal studies have been performed and hyperfine data from ENDOR are not available. Thus, our understanding of the P700 triplet state is far from being complete. However, the available data indicate that the triplet exciton in ^{3}P700 is probably delocalized in the P_AP_B heterodimer at ambient temperature but is trapped on one half of the dimer at cryogenic temperature. This important result is in support of a dimeric electronic structure of P700.

IV. MO Calculations of the Electronic Structure of P700$^{\cdot+}$

A. Calculation of the g Tensor

The first successful calculation of g tensors of Chl pigments has been reported by Plato and Möbius (1995), who used a semiempirical MO method (RHF-INDO) based on Stone's g-factor theory (Stone, 1963a,b). Recently, a similar semiempirical approach (ZINDO) was applied by Bratt et al. (2000) to geometry optimized Chl $a^{\cdot+}$ in an effective solvent field, and magnitude and orientation of the g tensor was obtained. The agreement between the experimental (2.00329, 2.00275, 2.00220) and calculated g tensor magnitude for the geometry optimized Chl $a^{\cdot+}$ in a dielectric environment representative of CH_2Cl_2 (2.00301, 2.00287, 2.00223) is quite satisfying, the largest deviation occurs for Δg_x with 28 × 10^{-5}. The prediction of the isotropic g-value g_{iso} = 1/3 Tr **g** is also very good (2.00270 versus 2.00275 in the experiment) (Bratt et al., 2000).

Additional information is obtained for the g-tensor orientation, which is largely determined by the shape of the frontier orbitals that enter with the largest weight

into the estimation of g. As expected the g_z value is approximately parallel to the normal (Z) of the chlorophyll plane (4° deviation); g_x and g_y are rotated with respect to the molecular axes X, Y (Fig. 1) by approximately 17° (Bratt et al., 2000). However, this value is strongly dependent on the orientation of the various substituents on the chlorine macrocycle. The approximate orientation of the largest g value (g_x) along the molecular Y-axis (along the N_A–N_C direction, see Fig. 1) is in agreement with earlier estimates on the bacterial system (Möbius and Plato, 1996).

To the best of our knowledge a calculation of the g tensor of $P700^{\cdot+}$ has not been successfully performed so far. The measured g tensor of $P700^{\cdot+}$ in single crystals (Zech et al., 2000) showed that g_z is not perpendicular to the average plane of the two macrocycles indicating deviations from planarity, or specific rotations of substituents caused by interactions with the environment. Furthermore, the g_x, g_y values are rotated away from the molecular axes (Fig. 4). At present, these effects cannot be interpreted. The results of an improved g tensor calculation should shed light on the unusual g tensor orientation and help to relate the g tensor magnitude to the electronic and spatial structure of this species *in vivo*.

B. Spin Density Distribution

Truncated models of the chlorophyll *a* radical cation have been calculated by O'Malley and coworkers using density functional theory (DFT) (O'Malley, 2000; O'Malley and Collins, 2001) yielding information on the spin distribution in the chlorin macrocycle and on the effect of axial Mg ligation. The first DFT calculation on a complete, structurally optimized monomeric Chl $a^{\cdot+}$ (only phytyl chain truncated) was reported by Sinnecker et al. (2002). The hyperfine coupling constants of all magnetic nuclei and the spin density distribution were obtained and compared with earlier semiempirical approaches using the RHF-INDO/SP method (Käss et al., 1998). The agreement with the experimental data (Table 2) is very satisfying. It was also found that the coupling constants of a completely geometry optimized radical cation of the epimer (Chl a') are barely distinguishable from those of Chl $a^{\cdot+}$ (Sinnecker et al., 2002). Noticeable differences were calculated only for the large coupling constants of the β-hydrogens. This is mainly caused by a somewhat different geometry of the hydrogenated rings. Hence, a distinction between Chl $a^{\cdot+}$ and the corresponding epimer radical cation based on EPR/ENDOR data will be rather difficult. This is particularly true when these species are embedded in a protein environment, where pigment–protein interaction can easily change the geometry and electronic structure of the cofactor in question.

It has been proposed by Wasielewski et al. (1981b) that enolic forms of Chl *a* could occur in the primary donor P700 of PS I of plants. In particular, the low-oxidation potential of $P700/P700^{\cdot+}$ as compared to that of monomeric Chl *a* in solution (Watanabe and Kobayashi, 1991) could arise from such an enolization process. DFT calculations were performed on various geometry optimized enols of monomeric Chl $a^{\cdot+}$.They are characterized by strongly altered hfcs in comparison with Chl $a^{\cdot+}$. This is due to the different π electron delocalization in the enols for which the electronic and geometrical structure of ring E is significantly changed. The calculations show that the SOMO for all enol forms is quite different from that of the keto form and the spin-density distributions of the enolic forms are very different from those observed in ENDOR experiments performed on $P700^{\cdot+}$ (Sinnecker et al., 2002). It was concluded that an enolic form of Chl *a* is unlikely to significantly contribute to P700. Recently, Sun et al. (2004) reported DFT calculations on Chl $a^{\cdot+}$, where they probed axial ligation of the Mg and hydrogen bonding to the 13^1 carbonyl oxygen. This work shows that H-bonding can significantly affect the spin density distribution, which will play a role for $P700^{\cdot+}$.

Calculations on Chl dimers, in particular with partial inclusion of the amino acid surroundings, still present a challenge for DFT and *ab initio* methods. In the past semiempirical methods have, however, been used quite successfully, e.g., the RHF-INDO/SP method introduced by Plato et al. (1991). On the basis of geometry provided by the X-ray structure analysis of PS I single crystals of *T. elongatus* (see Fig. 2) (Jordan et al., 2001) a series of RHF-INDO/SP calculations was performed on the bare dimer (including some geometry optimization) and also on dimers including several of the surrounding amino acids that interact with P700 (Plato et al., 2003). The aim of this work was to show the validity of the dimer model for the primary donor in PS I and to analyze theoretically in more detail the effects of the various structural features of P700 and its surrounding on the spin- and charge-density distribution, the possible occurrence of enols or related forms, and the energetic properties of the system. The latter is important for understanding the quite low oxidation potential of $P700/P700^{\cdot+}$. The following observations were made.

Table 7. Spin density ratios of $P700^{\cdot+}$ for different geometrical cases based on RHF-INDO/SP calculations[a]

	Case[b]	$R_{B/A}$[c]	$R^0_{B/A}$[d]
I	Bare dimer P	2.83	1.72
II	I + H-bond (Thr A743)	4.46	2.22
III	II + Mg-ligands (His A680, His B660)	4.62	2.25
IV	III + 43 AARs (426 point charges)	3.33	1.87
V	III + geometry optimization (vinyl groups)	7.70	3.10
VI	Bare dimer P with P_B as enol	0.27	0.53

[a] Data from Plato et al. (2003).
[b] The numbering of amino acids refers to PS I of *T. elongatus*, AAR = amino acid residue.
[c] $R_{B/A}$ = ratio of spin densities on P_B and P_A with spin polarization.
[d] $R^0_{B/A}$ = ratio of spin densities on P_B and P_A without spin polarization (identical to charge density distribution, $Q_{B/A}$).

- The calculation shows a delocalization of the spin/charge density over both halves of the dimer P_A and P_B.
- Theory predicts an intrinsic electronic asymmetry of the spin density distribution of P_B over P_A, yielding a ratio $R_{B/A} \cong 2.8$ for the "bare" dimer (case I). This asymmetry cannot be traced to a specific structural feature of either half P_A (Chl *a*′) or P_B (Chl *a*).
- The stepwise inclusion of various interactions of the dimer with its nearest surrounding (cases II, III in Table 7) leads to a systematic enhancement of the electronic asymmetry in favor of P_B. The hydrogen bond between P_A and ThrA743 has a significant effect, whereas the two histidine ligands (His A680, His B660) of the Mg atoms exhibit only a small effect due to their highly symmetric arrangement.
- The inclusion of interactions with more remote amino acid residues (case IV) and with the two accessory chlorophylls (charge distributions) have only small effects on the asymmetry if dielectric shielding effects are taken into account.
- Among several geometry optimizations the largest contribution to the electronic asymmetry was found by a rotation of the conjugated vinyl groups of P_A and P_B (case V).
- The possible occurrence of enol forms of P_B (case VI) could be fully ruled out for $P700^{\cdot+}$ by energetic considerations and by a detailed comparison of experimental and calculated hfcs. This conclusion fully agrees with earlier DFT results on the monomeric Chl$a^{\cdot+}$ (Sinnecker et al., 2002).
- In Table 7, for the different cases I to VI, the ratio of spin density on P_B and P_A is given with and without spin polarization by $R_{B/A}$ and $R^0_{B/A}$, respectively; $R^0_{B/A}$ is identical to the charge density distribution $Q_{B/A}$ in the dimer. The calculations show that due to spin polarization the spin asymmetry is significantly larger than any charge asymmetry in the $P700^{\cdot+}$ dimer (see Table 3). EPR and ENDOR is probing the spin-density distribution ($R_{B/A}$), whereas vibrational frequencies (FTIR, Raman) are affected by changes of the charge distribution ($Q_{B/A}$). This finding sheds light on the different interpretations of the electronic structure asymmetry of $P700^{\cdot+}$ based on EPR and FTIR data (Breton et al., 1999; Breton, 2001; Hastings et al., 2001; Breton et al., 2002; Wang et al., 2003; see also Breton, this volume, Chapter 18).

The calculated isotropic ^{1}H and ^{14}N hfcs of the final partially dressed dimer (case III) and locally geometry optimized dimer (case V) are compared to experimental values (Käss et al., 2001) in Table 8. The agreement is remarkably good not only for the proton but also for the nitrogen hfcs. However, a few discrepancies remain, particularly with regard to the small ^{1}H hfcs of P_A (Chl *a*′). Up to now, the assignment of these small hfcs in the experiment is only tentative. According to the calculations the smallest ^{14}N hfc must be reassigned to P_B, whereas the fourth largest belongs to P_A. These assignments are partially contrasted by the proposal that the smallest ^{14}N hfc belongs to a nitrogen from a histidine ligand (Mac et al., 1996). The RHF-INDO/SP calculations show that the spin density at the two histidine ligands of P700 are vanishingly small. The p_z (π) spin density distributions for these two cases (III and V) are shown in graphical form in Fig. 10A,B.

The presented theoretical results clearly show that P700 is also electronically a "supermolecule" consisting of two Chl *a*-type molecules. This is similar to the case of the BChl dimers found in reaction centers of all nonsulfur and sulfur purple bacteria (Müh et al., 2001). The detailed geometry of the dimer and its interactions with the surrounding in PS I is, however, different from those found in the BChl dimers.

Table 8. Comparison of theoretical and experimental isotropic proton hyperfine couplings of the dimer $P700^{\cdot+}$ in MHz. RHF-INDO/SP calculations based on X-ray structural data

		III[a]		V[a]			
		Dressed dimer: H-bond + Mg-ligands		Dressed dimer + vinyl group rotation		Exp[b]	
Nucleus	Position	P_A	P_B	P_A	P_B	P_A	P_B
^1H	2[c]	+0.53	+2.07	+0.74	+2.61	0.8[d]	+2.9
	7[c]	+1.57	+3.80	+1.35	+4.71	1.8[d]	+3.5
	12[c]	+1.88	+4.92	+1.70	+7.12	1.8[d]	+5.3
	5	+0.57	+1.05	+0.50	+1.17	0.8[d]	1.8[d]
	10	+1.64	+3.76	+1.28	+3.94	1.8[d]	3.5[d]
	15	−1.16	−4.25	−1.08	−4.00		
	17	+4.28	+14.3	+3.04	+14.3		9.6
	18	+1.94	+7.55	+1.80	+10.3		7.7
^{14}N	A	−0.20	−0.26	−0.23	−0.34		0.27
	B	−0.68	−1.75	−0.54	−1.91		−2.07
	C	−0.75	−1.96	−0.64	−2.12	0.71	−2.51
	D	−0.40	−1.27	−0.35	−1.41		1.20

[a] Theoretical isotropic proton hyperfine couplings of the dimer $P700^{\cdot+}$ in MHz for two selected cases, see Plato et al. (2003). The two dimer halves are denoted P_A and P_B (Fig. 2), for numbering of positions see Fig. 1.
[b] ^1H: From Käss et al. (2001); ^{14}N: from Käss and Lubitz (1996); signs of hfcs were only determined for the methyl hfcs and the two large nitrogen hfcs via General TRIPLE as given in Käss et al. (1995).
[c] Methyl proton hfcs were averaged for fast rotation.
[d] Tentative assignment of experimental hfcs, see Käss et al. (2001), Webber and Lubitz (2001).

C. Estimation of the Oxidation Potential

Experimental values of the midpoint potential E_m^{ox} for monomeric Chl *a* in different solvents range between +0.74 and +0.93 V vs. NHE (Watanabe and Kobayashi, 1991). For P700 in the PS I protein this value is significantly lower, e.g., +0.45 to +0.47 V have been reported for *C. reinhardtii* (Krabben et al., 2000; Witt et al., 2002).

It is known from extensive work on the BChl-dimer in bacterial-reaction centers (Müh et al., 2002) that formation of a dimer leads to a reduction of the donor potential E_m^{ox} by

$$E_m^{ox}(P) = E_m^{ox}(P_A) - |\beta|\sqrt{Q_{B/A}}$$

where $E_m^{ox}(P)$ and $E_m^{ox}(P_A)$ are the oxidation potentials of the dimer P700 and the monomeric half P_A (Chl *a*′), β is the resonance integral and $Q_{B/A}$ the charge density distribution of the dimer. Using $|\beta| = 0.12$ eV and $Q_{B/A} = 2.25$ and assuming the lower monomeric value (+0.74 V) one obtains E_m^{ox} (P) = +0.56 V. Thus, the dimerization causes a decrease of the oxidation potential by ∼25%. Additional effects from the surrounding dielectric medium not accounted for in this simple model could lead to a further decrease of E_m^{ox} (P) in PS I (Datta et al., 2001).

V. Conclusion: Electronic Structure of the Primary Donor and Implications for its Function

EPR and related techniques have led to the following conclusions about the primary donor.

(i) According to the EPR spectroscopic results on $P700^{\cdot+}$ in different species (plants, green algae, cyanobacteria), the structure of P700 and its interaction with the protein surrounding is highly conserved.
(ii) $P700^{\cdot+}$ is a noncovalently bound dimeric supermolecule with a wave function extending over both halves of a heterodimer comprising one Chl *a* and one Chl *a*′ molecule. On the basis of accumulated knowledge, the earlier discussed monomeric models for $P700^{\cdot+}$ with an altered electronic (hybrid orbital model) or geometrical structure (e.g., enol forms) do not provide a correct description of the experimental data.
(iii) The spin-density distribution of the radical cation $P700^{\cdot+}$ is asymmetric with more spin density on P_B (Chl *a*). Temperature changes have only a minor effect on the spin delocalization. The asymmetry is probably not determined by the heterodimeric character of P700

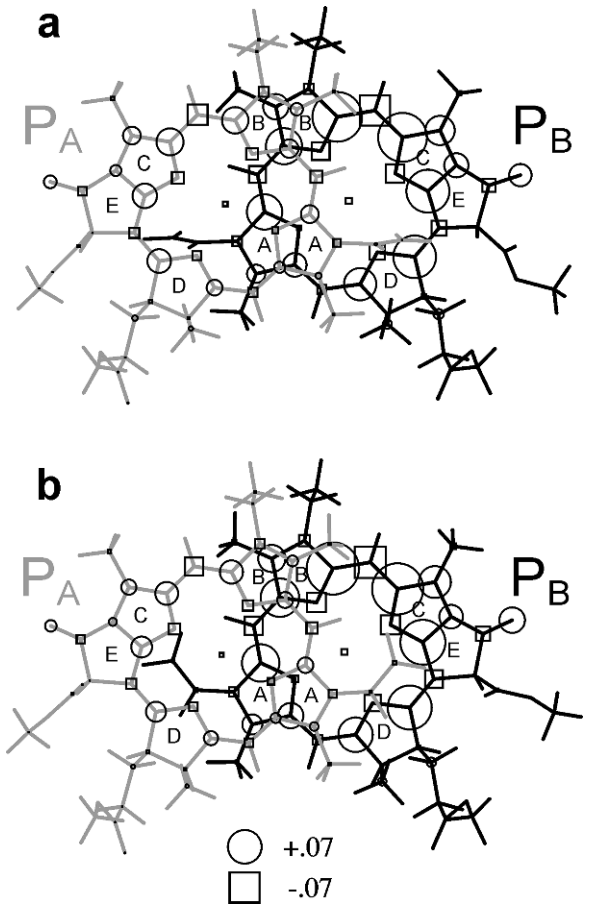

Fig. 10. Plot of calculated $p_z(\pi)$ spin densities of $P700^{\cdot+}$ for two geometries (see text): (a) case III ($R_{B/A} = 4.62$) and (b) case V ($R_{B/A} = 7.70$), see text and Table 4. Areas of the circles and squares represent positive and negative spin density values, respectively. The dimer half P_A ($\equiv$ Chl a') is given in gray, P_B ($\equiv$ Chl a) in black.

but is rather caused by inherent structural features and interactions with the surroundings (asymmetric hydrogen bonding). The fairly large asymmetry is due to spin polarization effects in $P700^{\cdot+}$. This determines the magnitude of the hyperfine couplings and the appearance of the EPR, ENDOR, and ESEEM spectra.

(iv) The charge-density distribution of $P700^{\cdot+}$ is, according to calculations, much less asymmetric. This effect is less pronounced for $P865^{\cdot+}$ in bacterial reaction centers. The charge-density distribution determines the effects observed in vibrational spectra and the electron transfer rates (electronic matrix elements) (Plato et al., 1988b).

(v) The triplet state of the primary donor $^3P700$ is localized on a single chlorophyll at cryogenic temperatures. Studies on PS I mutants indicate that it is also trapped on P_B. However, this is still a controversial point. At higher temperatures the triplet state becomes more delocalized. According to current models this delocalization involves two chlorophylls with approximately parallel planes of the macrocycle, i.e., P_A and P_B of P700.

The determination of details of the spatial and electronic structure of the primary donor in PS I has clearly made great progress, in particular with respect to the radical cation and the triplet state. Much less information is available on the electronic and spatial structure of the first singlet excited state $^1P700^*$. According to the recent X-ray crystallographic structure the Chl pigments in the PS I core (the reaction center) are strongly excitonically coupled, so that excitation transfer from the antenna system will certainly lead to an excited singlet state delocalized over all six chlorophylls. This explains the large susceptibility of the optical properties to slight structural differences between various species (Witt et al., 2003), which was not observed for the cation radical, where the charge/spin is more localized on one species. Charge separation from the excited delocalized singlet state could, in principle, occur from any of the Chls. In the past it was always assumed that a Chl dimer, i.e., "P700," is the primary donor but other Chls (e.g., the "accessory" Chl) have recently also been considered to initiate the charge separation (Müller et al., 2003). Apart from these very early events, there is no doubt from various studies that after a very short time the radical cation is formed on the two plane parallel Chls denoted P_A (Chl a') and P_B (Chl a). Here the positive charge is stabilized by delocalization in the (hetero)dimer which leads to a less positive oxidation potential of this species as compared to monomeric Chl. This adjustment of the potential is obviously required for optimizing the electron transfer from a docked plastocyanin (in plants) or cytochrome c_6 (in cyanobacteria) to reduce $P700^{\cdot+}$ to P700 and prepare the RC for the next turnover.

An important point is also the very strong reducing power of the excited state $^1P700^*$. A full molecular description of this state has also not been given to date, it might involve more than just two chlorophylls due to excitonic coupling in the PS I reaction center. The specific arrangement of the pigments and the resulting electronic structure of the excited state will determine

the redox potential of ^{1}P700*. By EPR only the excited triplet state ^{3}P700 is accessible. Interestingly this state is localized on one chlorophyll at low temperatures and shows delocalization probably involving the two dimer halves P_A and P_B at ambient temperature. More information on this important state is expected from ENDOR and related spectroscopies, which is at present not available. A more profound understanding of the triplet state ^{3}P700 is necessary to better understand subsequent reactions that lead to damage of the photosystems, in particular in the presence of oxygen.

Acknowledgments

All collaborators are gratefully acknowledged who contributed to the author's work and who are cited in the references. Mikhail Antonkine, Jens Niklas, and Sebastian Sinnecker are thanked for critically reading the manuscript. Special thanks go to Birgit Deckers and Bärbel Plaschkies for their great help in preparing the figures and typing the manuscript. This work was supported by Deutsche Forschungsgemeinschaft and Max Planck Society.

References

Allen JP and Williams JC (1995) Relationship between the oxidation potential of the bacteriochlorophyll dimer and electron transfer in photosynthetic reaction centers. J Bioenerg Biomembr 27: 275–283

Amesz J and Hoff AJ (eds) 1995. Biophysical Techniques in Photosynthesis. Kluwer Academic Publishers, Dordrecht

Angerhofer A (1991) Chlorophyll triplets and radical pairs. In: Scheer H (ed) Chlorophylls, pp 945–991. CRC Press, Boca Raton, FL

Astashkin AV, Dikanov SA, Tsvetkov YD and Goldfeld MG (1987) Comparative analysis of ESE modulation from oxidized chlorophyll *a* and P700 centers in chloroplasts containing N-15 nuclei. Chem Phys Lett 134: 438–443

Atherton NM (1993) Principles of Electron Spin Resonance. Ellis Horwood PTR, Prentice Hall, New York

Ben-Shem A, Frolow F and Nelson N (2003) Crystal structure of plant photosystem I. Nature 426: 630–635

Bratt PJ, Rohrer M, Krzystek J, Evans MCW, Brunel L-C and Angerhofer A (1997) Submillimeter high-field EPR studies of the primary donor in plant photosystem I $P700^+$. J Phys Chem 101: 9686–9689

Bratt PJ, Poluektov OG, Thurnauer MC, Krzystek J, Brunel L-C, Schrier J, Hsiao Y-W, Zerner M and Angerhofer A (2000) The g-factor anisotropy of plant chlorophyll $a^{\cdot+}$. J Phys Chem B 104: 6973–6977

Breton J (2001) Fourier transform infrared spectroscopy of primary electron donors in type I photosynthetic reaction centers. Biochim Biophys Acta 1507: 180–193

Breton J, Nabedryk E and Leibl W (1999) FTIR Study of the primary electron donor of photosystem I (P700) revealing delocalization of the charge in $P700^+$ and localization of the triplet character in ^{3}P700. Biochemistry 38: 11585–11592

Breton J, Xu W, Diner BA and Chitnis P (2002) The two histidine axial ligands of the primary electron donor chlorophylls (P700) in photosystem I are similarly perturbed upon $P700^+$ formation. Biochemistry 41: 11200–11210

Brettel K (1997) Electron transfer and arrangement of the redox cofactors in photosystem I. Biochim Biophys Acta 1318: 322–373

Brettel K and Leibl W (2001) Electron transfer in photosystem I. Biochim Biophys Acta 1507: 100–114

Budil DE and Thurnauer MC (1991) The chlorophyll triplet state as a probe of structure and function in photosynthesis. Biochim Biophys Acta 1057: 1–41

Carbonera D, Collareta P and Giacometti G (1997) The P700 triplet state in an intact environment detected by ODMR. A well resolved triplet minus singlet spectrum. Biochim Biophys Acta 1322: 115–128

Commoner B, Heise JJ and Townsend J (1956) Light-induced paramagnetism in chloroplasts. Proc Natl Acad Sci USA 42: 710–718

Cui LY, Bingham SE, Kuhn M, Käss H, Lubitz W and Webber AN (1995) Site-directed mutagenesis of conserved histidines in the helix-VIII domain of PsaB impairs assembly of the photosystem-I reaction-center without altering spectroscopic characteristics of P-700. Biochemistry 34: 1549–1558

Datta SN, Parandekar PV and Lochan RC (2001) Identity of green plant reaction centers from quantum chemical determination of redox potentials of special pairs. J Phys Chem B 105: 1442–1451

Davis MS, Forman A and Fajer J (1979) Ligated chlorophyll cation radicals: their function in photosystem II of plant photosynthesis. Proc Natl Acad Sci USA 76: 4170–4174

Davis IH, Heathcote P, MacLachlan DJ and Evans MCW (1993) Modulation analysis of the electron-spin echo signals of *in vivo* oxidized primary donor N-14 chlorophyll centers in bacterial, P870 and P960, and plant photosystem-I, P700, reaction centers. Biochim Biophys Acta 1143: 183–189

Deligiannakis Y and Rutherford AW (2001) Electron spin echo envelope modulation spectroscopy in photosystem I. Biochim Biophys Acta 1507: 226–246

Dikanov SA and Tsvetkov YD (1992) Electron Spin Echo Envelope Modulation (ESEEM) Spectroscopy. CRC Press, Boca Raton, FL, USA

Dikanov SA, Astashkin AV, Tsvetkov YD and Goldfeld MG (1983) Comparative modulation analysis of electron spin echo signals from oxidized chlorophyll *a in vitro* and P700 centres in chloroplasts. Chem Phys Lett 101: 206–210

Döring G, Bailey JL, Kreutz W, Weikard J and Witt HT (1968) The action of two chlorophyll-$a_{|}$ molecules in light reaction I of photosynthesis. Naturwissenschaften 55: 219–220

Dörnemann D and Senger H (1986) The structure of chlorophyll-RC-I – a chromophore of the reaction center of photosystem-I. Photochem Photobiol 43: 573–581

Frank HA, McLean MB and Sauer K (1979) Triplet states in photosystem I of spinach chloroplasts and subchloroplast particles. Proc Natl Acad Sci USA 76:5124–5128

Fromme P, Jordan P and Krauß N (2001) Structure of photosystem I. Biochim Biophys Acta 1507: 5–31

Goldsmith JO, King B and Boxer SG (1996) Mg coordination by amino acid side chains is not required for assembly and function of the special pair in bacterial photosynthetic reaction centers. Biochemistry 35: 2421–2428

Hastings G, Ramesh VM, Wang R, Sivakumar V and Webber A (2001) Primary donor photo-oxidation in photosystem I: a re-evaluation of (P700(+) − P700) Fourier transform infrared difference spectra. Biochemistry 40: 12943–12949

Hoff AJ (1979) Applications of ESR in photosynthesis. Phys Rep 54: 75–200

Hoff AJ (1996) Optically detected magnetic resonance (ODMR) of triplet states in Photosynthesis. In: Amesz J and Hoff AJ (eds) Biophysical Techniques in Photosynthesis, Advances in Photosynthesis, Vol 3, pp 277–295. Kluwer, Dordrecht

Huber M, Lendzian F, Lubitz W, Tränkle E, Möbius K and Wasielewski MR (1986) ENDOR and triple resonance in solutions of the chlorophyll-*a* and bis(chlorophyll)cyclophane radical cations. Chem Phys Lett 132: 467–473

Hyde JS and Rist GH (1968) Endor of methyl, matrix, and α protons in amorphous and polycrystalline matrices. J Phys Chem B 72: 4269–4276

Johnson ET, Müh F, Nabedryk E, Williams JC, Allen JP, Lubitz W, Breton J and Parson WW (2002) Electronic and vibronic coupling of the special pair of bacteriochlorophylls in photosynthetic reaction centers from wild-type and mutant strains of *Rhodobacter sphaeroides*. J Phys Chem B 106: 11859–11869

Jordan R, Fromme P, Witt HT, Klukas O, Saenger W and Krauß N (2001) Three-dimensional structure of cyanobacterial photosystem I at 2.5 Å resolution. Nature 411: 909–917

Käss H (1995) Die Struktur des primären Donators P700 in photosystem I: Untersuchungen mit Methoden der stationären und gepulsten Elektronspinresonanz. Dissertation. Technische Universität Berlin

Käss H and Lubitz W (1996) Evaluation of 2D-ESEEM data of N-15-labeled radical cations of the primary donor P-700 in photosystem I and chlorophyll *a*. Chem Phys Lett 251: 193–203

Käss H, Bittersmann-Weidlich E, Andréasson L-E, Bönigk B and Lubitz W (1995) ENDOR and ESEEM of the N-15 labelled radical cations of chlorophyll-*a* and the primary donor P-700 in photosystem-I. Chem Phys Lett 194: 419–432

Käss H, Fromme P and Lubitz W (1996) Quadrupole parameters of nitrogen nuclei in the cation radical $P700^{\cdot+}$ determined by ESEEM of single crystals of photosystem I. Chem Phys Lett 257: 197–206

Käss H, Lubitz W, Hartwig G, Scheer H, Noy D and Scherz A (1998) ENDOR studies of substituted chlorophyll cation radicals. Spectrochim Acta 54A: 1141–1156

Käss H, Fromme P, Witt HT and Lubitz W (2001) Orientation and electronic structure of the primary donor radical cation $P\text{-}700^{\cdot+}$ in photosystem I: a single crystals EPR and ENDOR study. J Phys Chem B 105: 1225–1239

Klette R, Törring JT, Plato M, Möbius K, Bönigk B and Lubitz W (1993) Determination of the g tensor of the primary donor cation radical in single-crystals of *Rhodobacter-sphaeroides* R-26 reaction centers by 3-mm high-field EPR. J Phys Chem 97: 2015–2020

Kobayashi M, Watanabe T, Nakazato M, Ikegami I, Hiyama T, Matsunaga T and Murata N (1988) Chlorophyll *a* /P-700 and pheophytin a/P-680 stoichiometries in higher plants and cyanobacteria determined by HPLC analysis. Biochim Biophys Acta 936: 81–89

Kok B (1956) On the reversible absorption change at 705 mμ in photosynthetic organisms. Biochim Biophys Acta 22: 399–401

Kok B (1957) Absorption changes induced by the photochemical reaction of photosynthesis. Nature 179: 583–584

Kok B (1961) Partial purification and determination of oxidation reduction potential of photosynthetic chlorophyll complex absorbing at 700 mμ. Biochim Biophys Acta 48: 527–533

Krabben L, Schlodder E, Jordan R, Carbonera D, Giacometti G, Lee H, Webber AN and Lubitz W (2000) Influence of the axial ligands on the spectral properties of P700 of photosystem I: a study of site-directed mutants. Biochemistry 39: 13012–13025

Kurreck H, Kirste B and Lubitz W (1988) Electron Nuclear Double Resonance Spectroscopy of Radicals in Solution – Applications to Organic and Biological Chemistry. VCH Publishers, Inc., Deerfield Beach, Florida

Labahn A and Huber C (2001) The *g*-tensor anisotropy of the triplet state of the primary electron donor in the photosynthetic bacterium *Rhodobacter sphaeroides* by high-field (95 GHz) EPR. Appl Magn Reson 21: 381–387

Lendzian F (1982) Elektron-Kern-Mehrfachresonanz an Primärprodukten der Photosynthese. Dissertation. Technische Universität Berlin

Lendzian F, Huber M, Isaacson RA, Endeward B, Plato M, Bönigk B, Möbius K, Lubitz W and Feher G (1993) The electronic-structure of the primary donor cation-radical in *Rhodobacter-sphaeroides* R-26 – ENDOR and triple-resonance studies in single-crystals of reaction centers. Biochim Biophys Acta 1183: 139–160

Lubitz W (1991) EPR and ENDOR studies of chlorophyll cation and anion radicals. In: Scheer H (ed) Chlorophylls, pp 903–944. CRC Press, Inc., Boca Raton, FL

Lubitz W and Lendzian F (1996) ENDOR spectroscopy. In: Amesz J and Hoff AJ (eds) Biophysical Techniques in Photosynthesis, Advances in Photosynthesis, Vol 3, pp 255–275. Kluwer, Dordrecht

Lucken EAC (1969) Nuclear Quadrupole Couplings Constants. Academic Press, London

Mac M, Tang X-S, Diner BA, McCracken J and Babcock GT (1996) Identification of histidine as an axial ligand to $P700^{\cdot+}$. Biochemistry 35: 13288–13293

Mac M, Bowlby NR, Babcock GT and McCracken J (1998) Monomeric spin density distribution in the primary donor of photosystem I as determined by electron magnetic resonance: functional and thermodynamic implications. J Am Chem Soc 120: 13215–13223

Mattioli TA, Lin X, Allen JP and Williams JC (1995) Correlation between multiple hydrogen-bonding and alteration of the oxidation potential of the bacteriochlorophyll dimer of reaction centers from *Rhodobacter sphaeroides*. Biochemistry 34: 6142–6152

Möbius K and Lubitz W (1987) ENDOR Spectroscopy in Photobiology and Biochemistry. In: Berliner LJ and Reuben J (eds) Biological Magnetic Resonance, Vol 7, pp 129–247. Plenum Press, New York

Möbius K and Plato M (1996) Structure information on the bacterial primary donor $P^{\cdot+}$, acceptor $Q_A^{\cdot-}$, and radical Pair $P^{\cdot+}Q_A^{\cdot-}$ as obtained from high-field EPR/ENDOR and MO studies. In: Michel-Beyerle MB (ed) The Reaction Center of Photosynthetic Bacteria, pp 63–80. Springer-Verlag, Berlin, Heidelberg, New York

Müh F, Schulz C, Schlodder E, Jones MR, Rautter J, Kuhn M and Lubitz W (1998) Effects of zwitterionic detergents on the electronic structure of the primary donor and the charge recombination kinetics of $P^+Q_A^-$ in native and mutant reaction centers from *Rhodobacter sphaeroides*. Photosynth Res 55: 199–205

Müh F, Gardiner AT, Witt H, Schulz C, Imhoff JF, Cogdell RJ and Lubitz W (2001) Conserved electronic structure of the primary donor in reaction centers of sulfur and non-sulfur purple bacteria. Proceedings of the 12th International Congress on Photosynthesis, Brisbane, Australia. CSIRO Publishing (S7-005)

Müh F, Lendzian F, Roy M, Williams JC, Allen JP and Lubitz W (2002) Pigment–protein interactions in bacterial reaction centers and their influence on oxidation potential and spin density distribution of the primary donor. J Phys Chem B 106: 3226–3236

Müller M, Niklas J, Lubitz W and Holzwarth AR (2003) Ultrafast transient absorption studies on photosystem I reaction centers from *Chlamydomonas reinhardtii*. 1. A new interpretation of the energy trapping and early electron transfer steps in photosystem I. Biophys J 85: 3899–3822

Nakamura A and Watanabe T (1998) HPLC determination of photosynthetic pigments during greening of etiolated barley leaves. FEBS Lett 426: 201–204

Norris JR, Uphaus RA, Crespi HL and Katz JJ (1971) Electron spin resonance of chlorophyll and origin of signal-I in photosynthesis. Proc Natl Acad Sci USA 68: 625–628

Norris JR, Scheer H and Katz JJ (1975) Models for antenna and reaction center chlorophylls. Ann NY Acad Sci 244: 260–280

O'Malley PJ (2000) The effect of oxidation and reduction of chlorophyll *a* on its geometry, vibrational and spin density properties as revealed by hybrid density functional methods. J Am Chem Soc 122: 7798–7801

O'Malley PJ and Babcock GT (1984) Electron nuclear double resonance evidence supporting a monomeric nature for $P700^{\cdot+}$ in spinach chloroplasts. Proc Natl Acad Sci USA 81: 1098–1101

O'Malley PJ and Collins SJ (2001) The effect of axial Mg ligation on the geometry and spin density distribution of chlorophyll cation free radical models: a density functional study. J Am Chem Soc 123: 11042–11046

Parson WW, Nabedryk E, and Breton J (1992) Mid- and near-IR electronic transitions of $P^{\cdot+}$: new probes of resonance interactions and structural asymmetry in reaction centers. In: Breton J and Verméglio A (eds) The Photosynthetic Bacterial Reaction Center II, pp 79–88. Plenum Press, New York

Pashenko SV, Gast P and Hoff AJ (2001) A D-band (130 GHz) EPR study of the primary electron donor triplet state in photosynthetic reaction centers of *Rhodobacter sphaeroides* R26. Appl Magn Reson 21: 325–334

Pashenko SV, Proskuryakov II, Germano M, van Gorkom HJ and Gast P (2003) Triplet state in photosystem II reaction centers as studied by 130 GHz EPR. Chem Phys 294: 439–449

Petrenko A, Maniero AL, van Tol J, MacMillan F, Li Y, Brunel L-C and Redding K (2004) A high-field EPR study of $P700^{\cdot+}$ in wild-type and mutant photosystem I from *Chlamydomonas reinhardtii*. Biochemistry 43: 1781–1786

Plato M and Möbius K (1995) Structural characterization of the primary donor in photosynthetic bacteria by its electronic g-tensor. Chem Phys 197: 289–295

Plato M, Lubitz W, Lendzian F and Möbius K (1988a) Magnetic resonance and molecular orbital studies of the primary donor cation radical $P960^{\cdot+}$ in the photosynthetic bacterium *Rhodopseudomonas viridis*. Isr J Chem 28: 109–119

Plato M, Möbius K, Michel-Beyerle MB, Bixon M and Jortner J (1988b) Intermolecular electronic interactions in the primary charge separation in bacterial photosynthesis. J Am Chem Soc 110: 7279–7285

Plato M, Möbius K, and Lubitz W (1991) Molecular orbital calculations on chlorophyll radical ions. In: Scheer H (ed) Chlorophylls, pp 1015–1046. CRC Press Inc., Boca Raton, FL

Plato M, Lendzian F, Lubitz W, and Möbius K (1992) Molecular orbital study of electronic asymmetry in primary donors of bacterial reaction centers. In: Breton J and Verméglio A (eds) The Photosynthetic Bacterial Reaction Center II, pp 109–118. Plenum Press, New York

Plato M, Krauß N, Fromme P and Lubitz W (2003) Molecular orbital study of the primary electron donor P700 of photosystem I based on a recent X-ray single crystal structure analysis. Chem Phys 294: 483–499

Poluektov OG, Utschig LM, Schlesselman SL, Lakshmi KV, Brudvig GW, Kothe G and Thurnauer MC (2002) Electronic structure of the P700 special pair from high-frequency electron paramagnetic resonance spectroscopy. J Phys Chem B 106: 8911–8916

Prisner T, McDermott AE, Un S, Norris JR, Thurnauer MC and Griffin RG (1993) Measurement of the g-tensor of the $P700^{\cdot+}$ signal from deuterated cyanobacterial photosystem-I particles. Proc Natl Acad Sci USA 90: 9485–9788

Rautter J, Lendzian F, Schulz C, Fetsch A, Kuhn M, Lin X, Williams JC, Allen JP and Lubitz W (1995) ENDOR studies of the primary donor cation-radical in mutant reaction centers of *Rhodobacter sphaeroides* with altered hydrogen-bond interactions. Biochemistry 34: 8130–8143

Redding K, MacMillan F, Leibl W, Brettel K, Hanley J, Rutherford AW, Breton J and Rochaix J-D (1998) A systematic survey of conserved histidines in the core subunits of photosystem I by site-directed mutagenesis reveals the likely axial ligands of P_{700}. EMBO J. 17: 50–60

Reimers JR and Hush NS (2004) A unified description of the electrochemical, charge distribution, and spectroscopic properties of the special-pair radical cation in bacterial photosynthesis. J Am Chem Soc 126: 4132–4144

Rigby SEJ, Nugent JHA and O'Malley PJ (1994) ENDOR and special triple resonance studies of chlorophyll cation radicals in photosystem 2. Biochemistry 33: 10043–10050

Rigby SEJ, Evans MCW and Heathcote P (2001) Electron nuclear double resonance (ENDOR) spectroscopy of radicals in photosystem I and related type I photosynthetic reaction centres. Biochim Biophys Acta 1507: 247–259

Rutherford AW and Sétif P (1990) Orientation of P700, the primary electron-donor of photosystem I. Biochim Biophys Acta 1019: 128–132

Scheer H, Katz JJ and Norris JR (1977) Proton–electron hyperfine coupling constants of the chlorophyll *a* cation radical by ENDOR spectroscopy. J Am Chem Soc 99: 1372–1381

Schweiger A and Jeschke G (2001) Principles of Pulse Electron Paramagnetic Resonance. Oxford University Press, Oxford

Sieckmann I, Brettel K, Bock H, van der Est A and Stehlik D (1993) Transient electron paramagnetic resonance of the triplet state of P700 in photosystem I. Evidence for triplet

delocalization at room temperature. Biochemistry 32: 4842–4847

Sinnecker S, Koch W and Lubitz W (2002) Chlorophyll a radical ions: a density functional study. J Phys Chem B 106: 5281–5288

Stehlik D and Möbius K (1997) New EPR methods for investigating photoprocesses with paramagnetic intermediates. Annu Rev Phys Chem 48: 745–784

Stone AJ (1963a) g-Factors of aromatic free radicals. Mol Phys 6: 509–515

Stone AJ (1963b) Gauge invariance of g-tensor. Proc R Soc Lond A 271: 424–424

Sun Y, Wang H, Zhao F and Sun J (2004) The effect of axial Mg^{2+} ligation and peripheral hydrogen bonding on chlorophyll *a*. Chem Phys Lett 387: 12–16

Thurnauer MC, Katz JJ and Norris JR (1975) The triplet state in bacterial photosynthesis: possible mechanisms of the primary photo-act. Proc Natl Acad Sci USA 72:3270–3274

Vrieze J, Gast P and Hoff AJ (1996) Structure of the reaction center of photosystem I of plants. An investigation with linear-dichroic absorbance-detected magnetic resonance. J Phys Chem 100: 9960–9967

Wang R, Sivakumar V, Li Y, Redding K and Hastings G (2003) Mutation induced modulation of hydrogen bonding to P700 studied using FTIR difference spectroscopy. Biochemistry 42: 9889–9897

Wasielewski MR, Norris JR, Crespi HL and Harper J (1981a) Photoinduced ESR signals from the primary electron donors in deuterated highly ^{13}C enriched photosynthetic bacteria and algae. J Am Chem Soc 103: 7664–7665

Wasielewski MR, Norris JR, Shipman LL, Lin C-P and Svec WA (1981b) Monomeric chlorophyll a *enol*: evidence for its possible role as the primary electron donor in photosystem I of plant photosynthesis. Proc Natl Acad Sci USA 78: 2957–2961

Watanabe T and Kobayashi M (1991) Electrochemistry of chlorophylls. In: Scheer H (ed) Chlorophylls, pp 287–315. CRC Press Inc., Boca Raton, FL

Webber AN and Lubitz W (2001) P700: the primary electron donor of photosystem I. Biochim Biophys Acta 1507: 61–79

Webber AN, Su H, Bingham SE, Käss H, Krabben L, Kuhn M, Jordan R, Schlodder E and Lubitz W (1996) Site-directed mutations affecting the spectroscopic characteristics and midpoint potential of the primary donor in photosystem I. Biochemistry 35: 12857–12863

Witt H, Müller A and Rumberg B (1961) Oxidized cytochrome and chlorophyll in photosynthesis. Nature 192: 967–969

Witt H, Schlodder E, Teutloff C, Niklas J, Bordignon E, Carbonera D, Kohler S, Labahn A and Lubitz W (2002) Hydrogen bonding to P700: site-directed mutagenesis of threonine A739 of photosystem I in *Chlamydomonas reinhardtii*. Biochemistry 41: 8557–8569

Witt H, Bordignon E, Carbonera D, Dekker JP, Karapetyan N, Teutloff C, Webber A, Lubitz W and Schlodder E (2003) Species specific differences of the spectroscopic properties of P700 – analysis of the influence of non-conserved amino acid residues investigated by site-directed mutagenesis of photosystem I from *Chlamydomonas reinhardtii*. J Biol Chem 278: 46760-46771

Zech S, Hofbauer W, Kamlowski A, Fromme P, Stehlik D, Lubitz W and Bittl R (2000) A structural model for the charge separated state $P700^{\cdot+}A_1^{\cdot-}$ in photosystem I from the orientation of the magnetic interaction tensors. J Phys Chem B 104: 9728–9739

Zeng RH, van Tol J, Deal A, Frank HA and Budil DE (2003) Temperature dependence of the primary donor triplet state g-tensor in photosynthetic reaction centers of *Rhodobacter sphaeroides* R-26 observed by transient 240 GHz electron paramagnetic resonance. J Phys Chem B 107: 4624–4631

Chapter 18

FTIR Studies of the Primary Electron Donor, P700

Jacques Breton*
Service de Bioénergétique, Bât. 532, CEA-Saclay, 91191 Gif-sur-Yvette, France

Summary

Over the last two decades FTIR difference spectroscopy has emerged as a prominent technique to investigate the electronic structure and the bonding interactions of P700, the primary electron donor of photosystem I. In this chapter, the advances in the field during this period are reviewed and discussed in the light of the structural model of P700 derived from X-ray crystallography. The effect on the FTIR difference spectra of mutations of the axial ligands of the chlorophyll molecules in P700 as well as of amino acid residues in hydrogen bonding interaction with the carbonyl groups of P700 is analyzed. The results of both global and selective isotope labeling studies are

*Author for correspondence, email: cadara3@dsvidf.cea.fr

John H. Golbeck (ed): Photosystem I: The Light-Driven Plastocyanin:Ferredoxin Oxidoreductase, 271–289.

presented. Special emphasis is given at analyzing the agreements and the discrepancies between the assignments of the various vibrational bands in the FTIR difference spectra recorded upon P700 photooxidation that are available in literature. The reasons behind the strong disagreement between the results of FTIR spectroscopy and of magnetic resonance techniques such as ADMR and ENDOR with regard to the localization of the triplet character in ^{3}P700 and the extent of charge versus spin distribution in P700$^+$ are critically discussed.

I. Introduction

The key steps of photosynthesis occur in specific membrane proteins called reaction centers (RCs), where the initial separation of electric charges and their subsequent stabilization across the membrane take place. This process starts from the excited state of a special dimer of chlorophyll (Chl) or bacteriochlorophyll (BChl) molecules called primary electron donor (P). Owing to this important role, the structure of the primary donors in their neutral, triplet, and cationic states has been investigated in great detail using optical, vibrational, and magnetic resonance spectroscopic techniques. These studies have led to models for the organization of the pigments within the dimer and the distribution of charge and spin in the oxidized and triplet states of the primary donors.

In the last two decades, X-ray crystallographic models of RC proteins have provided an invaluable source of information to complement the data obtained by spectroscopy alone, notably, when the resolution of the structures becomes sufficient to identify the amino acid side chains interacting with the pigments through hydrogen bonds to the carbonyl groups or axial ligation to the central Mg atoms of the (B)Chl molecules. In this case, site-directed mutagenesis becomes the method of choice to perturb selectively the pigment–protein interactions, therefore providing RCs with modified primary donors, the structure and function of which can be probed by spectroscopy. While X-ray crystallography provides key information on the identity of the H-bond partners and some details on the structure of these H-bonds in the ground state of the primary donors, it remains silent on several important aspects of the electronic structure of the special pair after charge separation occurs, such as the localization of the triplet state in ^{3}P or the hydrogen bonding status of the Chls and the charge distribution in P$^+$.

Abbreviations: PS – photosystem; P – primary electron donor; P700 – primary electron donor of PS I; (B)Chl – (bacterio)chlorophyll; RC – reaction center; FTIR – Fourier transform infrared; ADMR – absorption detected magnetic resonance; ENDOR – electron nuclear double resonance; Hfcs – hyperfine coupling constants.

Among the spectroscopic tools that can bring specific information on structure–function relationships in both native and genetically modified RCs, light-induced FTIR difference spectroscopy has emerged as a prominent technique (Mäntele, 1993; Breton and Nabedryk, 1996; Nabedryk, 1996; Breton, 2001). The complementarity of this spectroscopic approach and of X-ray crystallography has been initially encountered in the field of purple photosynthetic bacteria, where the first X-ray structural model of RC has appeared in 1984. It is now advancing at great strides for photosystem I (PS I) and is also developing in the case of photosystem II (PS II). The present chapter will review the structural and functional information that has been obtained on P700 by FTIR difference spectroscopy over the last two decades.

II. FTIR Studies of P700 Prior to the High-Resolution X-Ray Structure of PS I

A. Early Studies

The first light-induced FTIR difference spectrum of P700 photooxidation was obtained at room temperature on PS I particles isolated from pea (Tavitian et al., 1986). A control of the reaction was performed in parallel on the same sample by measuring the kinetics at 706 and 820 nm. In the absence of IR spectra of isolated Chl a^+, the interpretation of the P700$^+$/P700 FTIR difference spectra was limited to that of the negative bands, i.e., the bands that pertain to the Chl(s) in P700. A large negative band at ~1,700 cm^{-1} was proposed to correspond to the 9-keto C=O group of the Chl *a* molecule(s) of P700 having no bonding interactions with the protein (see Fig. 1 for the structural formula and labeling of Chl *a*), while the two negative bands at 1,749 and 1,735 cm^{-1} were tentatively assigned to ester C=O groups (Tavitian et al., 1986).

To assist the assignment of the bands in the P700$^+$/P700 FTIR difference spectra (Fig. 2a), cation-minus-neutral FTIR difference spectra of Chl *a* and pyroChl *a* (Chl *a* lacking the 10a-ester carbonyl) in organic solvents were generated electrochemically in

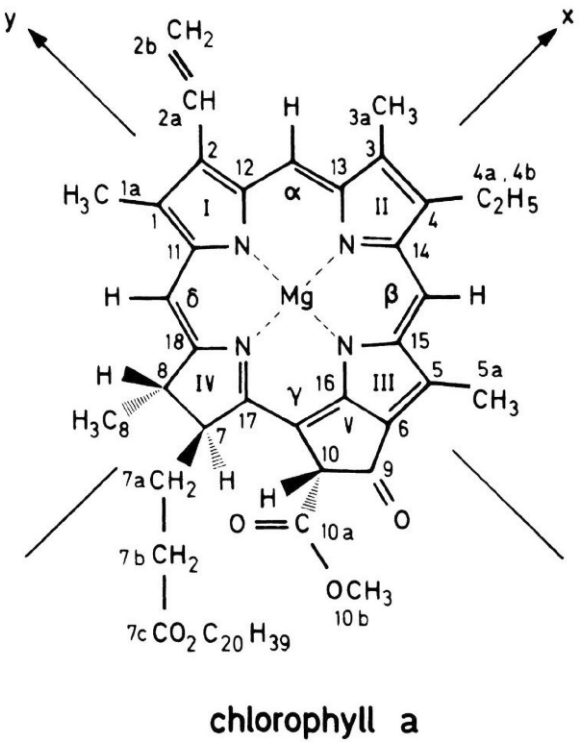

Fig. 1. Structural formula of chlorophyll *a*.

a thin IR cell (Mäntele et al., 1988). For both Chl *a* and pyroChl *a* in tetrahydrofuran, the 9-keto C=O was observed to upshift by 25–26 cm^{-1} upon cation formation. This upshift has been rationalized on the basis of density functional calculations (O'Malley, 2000). Furthermore, the lack of an IR signal in the C=O ester region of the cation-minus-neutral difference spectrum for pyroChl *a* demonstrated that the differential feature at 1,751(+)/1,738(−) cm^{-1} in the cation-minus-neutral difference spectrum of Chl *a* was due solely to the 10a-ester C=O with no significant contribution from the 7c-ester C=O (Nabedryk et al., 1990). The striking similarity between the large differential signals at 1,718/1,698 and 1,718/1,693 cm^{-1} in the $P700^+$/P700 and Chl a^+/Chl *a* difference spectra (Fig. 2), respectively, led to the assignment of the former to the frequency upshift upon photooxidation of the 9-keto group of the Chl *a* molecule(s) in P700 (Nabedryk et al., 1990). As already mentioned, the high frequency of the 9-keto vibration in P700 indicates an absence of bonding interaction with the PS I protein. The two differential signals observed at 1,754/1,749 and 1,742/1,735 cm^{-1} in the $P700^+$/P700 FTIR difference spectrum were tentatively assigned to 10a-ester C=O groups in inequivalent environments.

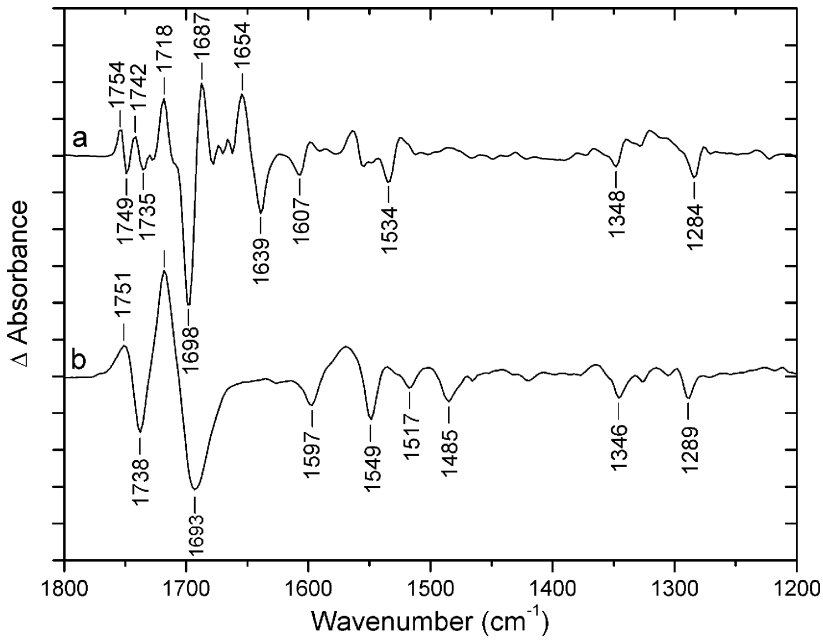

Fig. 2. (a) Light-induced $P700^+$/P700 FTIR difference spectrum of the photooxidation of a dry film of PS I particles from *Synechocystis* sp. PCC 6803 at 5°C. (b) Redox-induced Chl a^+/Chl *a* FTIR difference spectrum of chlorophyll *a* cation formation at U = +0.8 V in deuterated tetrahydrofuran at 20°C. Peak-to-peak amplitudes are 2×10^{-3} and 6×10^{-2} absorbance units in (a) and (b), respectively. (From Breton, J (2001))

B. Search for the Axial Ligands to the P700 Chls

In the RC of purple photosynthetic bacteria, the central Mg atom of the two BChl molecules constituting the primary electron donor are liganded to homologous His residues. This observation led to the search of the potential axial ligands of the P700 Chls by identifying the conserved His residues at homologous positions in the transmembrane helices of the PsaA and PsaB polypeptides that constitute the core of PS I.

Six pairs of His were targeted by site-directed mutagenesis and changed to pairs of Gln side chains in the green alga *Chlamydomonas reinhardtii* (Redding et al, 1998). The mutation of the His pair in helix 10 (HisA676 and HisB656) was the only one to result in a perturbed $P700^+$/P700 light-induced FTIR difference spectrum. Notably, a 4–5 cm^{-1} upshift of the main negative band at 1,700 cm^{-1} was observed upon the double mutation. All of the other double substitution mutants showed FTIR difference spectra very similar to that of wild type. Single His to Gln mutations were introduced at each one of these two sites and the change at HisA676 was found to be responsible for most of the effect on the FTIR difference spectrum of the HisA676/HisB656 double Gln mutant (Redding et al., 1998). The conclusion that HisA676 and HisB656 are the axial ligands to the Chl of P700 was further supported by the strong perturbation of the $P700^+$/P700 FTIR difference spectrum of a mutant in which HisB656 is changed for a Leu residue (Leibl et al., 1998).

C. Identification of Carbonyl Modes of P700 by Isotope Labeling

In principle, the carbonyl groups of Chl can be distinguished from those of the protein by using global isotope labeling. The rationale is that the small coupling of the C=O and N–H vibrations within the amide bond leads to a 1–3 cm^{-1} downshift of the amide I band around 1,650 cm^{-1} upon global ^{15}N-labeling while the Chl C=O vibrations are essentially unaffected by this label. On the other hand, global ^2H-labeling leads to a small downshift of the C=O vibrations of both the protein and the Chl. Upon ^2H-labeling, the 10a-ester C=O group of isolated Chl downshifts by $\sim$5 cm^{-1}, whereas the 9-keto C=O carbonyl downshifts by only $\sim$3 cm^{-1}. Applying this approach to $P700^+$/P700 FTIR difference spectra of *Synechocystis* sp. PCC 6803 at 90 K, it was concluded that the two negative bands at 1,697 and 1,637 cm^{-1} were likely to correspond to Chl 9-keto groups (Breton et al., 1999). Furthermore, the two negative bands at 1,749 and 1,733 cm^{-1} could be assigned to 10a-ester C=O vibrations from the P700 Chls on the basis of their $\sim$5 cm^{-1} isotopic shift upon ^2H-labeling, equivalent to that observed for the same group in isolated Chl *a*. Similarly, the isotope effects observed on the positive bands at 1,754, 1,740, 1,717, and 1,656 cm^{-1} favored their assignment to the upshifted vibrations in $P700^+$ associated with the four negative Chl C=O bands of P700 at 1,749, 1,733, 1,697, and 1,637 cm^{-1}, respectively.

A comparable approach using selective labeling of the 10a-ester C=O group of the Chls of P700 has been exploited by feeding *Synechocystis* sp. PCC 6803 with ^2H-labeled methionine (Kim and Barry, 2000). Although intrinsically more specific than the global ^2H-labeling (Breton et al., 1999), this selective approach leads to a ^1H-minus-^2H double-difference spectrum that is very close to ours in the range 1,760–1,710 cm^{-1}. Notably, positive bands at 1,754, 1,745, 1,730, and 1,720 cm^{-1} and negative bands at 1,750, 1,737, 1,726, and 1,714 cm^{-1} in Kim and Barry (2000) are located within less than 2–3 cm^{-1} of analogous peaks in Breton et al. (1999). This similarity is to be expected as in both experiments the methyl of the 10a-carbomethoxy group is labeled with ^2H. The two main differential features at 1,754/1,749 and 1,740/1,733 cm^{-1} in the $P700^+$/P700 difference spectrum of the unlabeled sample were therefore also interpreted as originating from the 10a-ester C=O vibrations from the two Chls in P700 (Kim and Barry, 2000).

It was further proposed that additional derivative signals at 1,730/1,726 and 1,720/1,714 cm^{-1} in their ^1H-minus-^2H double-difference spectrum should also be assigned to 10a-ester C=O groups (Kim and Barry, 2000). This interpretation of the 1,730/1,726 cm^{-1} signal is supported by recent experiments on *Synechocystis* sp. PCC 6803 bearing mutations on the PsaA residues involved in hydrogen bonding to the 10a-ester C=O group of the PsaA Chl of P700 (Pantelidou et al., 2004). On the other hand, we have suggested that the small 1,720/1,714 cm^{-1} differential signal that they observe under the 1,717 cm^{-1} positive peak of the $P700^+$/P700 difference spectrum of the unlabeled sample is rather to be assigned to the 9-keto C=O of one of the Chl in $P700^+$ that is affected by the ^2H-labeling of the 10a-carbomethoxy group through vibrational coupling (Breton, 2001). This proposal relies on the observation that global ^2H-labeling induces a $\sim$3 cm^{-1} downshift of the 9-keto frequency in isolated Chl *a* (Breton et al., 1999). The latter phenomenon could also help rationalize the unexplained weak isotope effects

on bands underlying the main 1,697 cm^{-1} band reported in Kim and Barry (2000). However, to firm up these interpretations, it would be necessary to measure the frequency of the 9-keto C=O band in the IR absorption spectrum of the isolated Chl with the 10a-carbomethoxy group selectively labeled with ^2H and to compare it with that of the globally ^2H-labeled Chl where not only the 10a-carbomethoxy group but also the hydrogen atom at C_{10} is labeled.

D. Mid-IR Electronic Transition of $P700^+$

The presence of an electronic transition absorbing in the mid-IR and characteristic of delocalization of the hole over the two BChl molecules in P^+ has been initially predicted on theoretical grounds (Parson et al., 1990) and was first observed in the P^+/P FTIR difference spectra of purple bacteria as a broad band peaking at 2,650 cm^{-1} (Breton et al., 1992). Electronic transitions of the same nature (hole-transfer bands) and with absorption maxima in the 2,800–1,900 cm^{-1} range have been observed as broad bands in the P^+/P FTIR difference spectra of the photooxidation of P in green bacteria, heliobacteria, and PS II (Nabedryk et al., 1996; Breton, 2001 and references therein).

In the early studies of P700 photooxidation, a significant amplitude of the $P700^+$ electronic transition could not be detected in the 2,800–1,900 cm^{-1} frequency range in the $P700^+/P700$ FTIR difference spectra (Hamacher et al., 1996; Nabedryk et al., 1996). However, several technical improvements allowed a search over a broader spectral range and led to the discovery of such a broad electronic transition in the $P700^+/P700$ FTIR difference spectrum (Breton et al., 1999). In PS I preparations from *Synechocystis* sp. PCC 6803 and spinach, this band peaks around 3,300–3,100 cm^{-1} and, as expected for an electronic transition, it is not shifted by global labeling with ^{15}N nor with ^2H (Breton et al., 1999). Such an electronic transition would not be expected if $P700^+$ were monomeric. This band exhibits a different shape and its maximum is downshifted to ~2,700 cm^{-1} in the case of PS I from *C. reinhardtii* (Leibl et al., 1998; Hastings et al., 2001), a surprising observation when considering that the $P700^+/P700$ FTIR difference spectra in the usual 1,800–1,000 cm^{-1} range are highly comparable among various species including *C. reinhardtii* (Breton, 2001). Nevertheless, the presence of an electronic transition in the $P700^+/P700$ FTIR difference spectra of all the investigated species shows that the unpaired electron is distributed amongst at least two Chl molecules in $P700^+$.

E. Comparison of $P700^+/P700$ and $^3P700/P700$ FTIR Spectra. Assignment Scheme of Breton et al. (1999)

One major difficulty in the identification of the 9-keto C=O vibrations of the (B)Chl pigments of primary electron donors (P) in FTIR difference spectra of the photooxidation of P is the likely possibility that the positive charge on P^+ could perturb the vibrations of the nearby protein amide I modes that absorb in the same frequency range. Such a difficulty is absent when analyzing the triplet state of P (^3P) because this species is electroneutral and therefore should leave the protein vibrations unperturbed. In addition, the direct comparison of P^+/P and $^3P/P$ FTIR difference spectra measured under comparable conditions provides a means to identify the C=O vibrations of the neutral (B)Chl(s) of P as the common negative bands in the carbonyl frequency range of the two spectra. This approach was first applied to P870, the primary electron donor in *Rhodobacter (Rb.) sphaeroides*, where negative bands at 1,692 and ~1,682 cm^{-1} that are common to both the $P870^+/P870$ and $^3P870/P870$ FTIR difference spectra could be identified as the 9-keto C=O vibrations of the two BChls in P870 (Breton and Nabedryk, 1993). More recently, the same approach has been applied to the primary electron donor P840 of the green bacterium *Chlorobium tepidum* (Mezzetti et al., 2003).

The $^3P700/P700$ difference spectrum generated at 90 K on PS I particles from *Synechocystis* sp. PCC 6803 (Fig. 3a) exhibits a main negative band at 1,637 cm^{-1} associated to a positive band at 1,594 cm^{-1} (Breton et al., 1999). These two bands can be assigned to the 9-keto C=O of a Chl *a in vivo* on the basis of the comparable frequency downshift observed for the 9-keto C=O upon triplet formation of Chl *a* in tetrahydrofuran (Breton et al., 1999). The frequency of the negative band at 1,637 cm^{-1} in the $^3P700/P700$ spectrum (Fig. 3a) closely matched that of a negative band in the $P700^+/P700$ difference spectrum (Fig. 3b), this band was attributed to the 9-keto C=O mode of one of the Chl *a* that constitutes P700 (Breton et al., 1999) and that was denoted P_1 [at that time only a structural model of PS I at 4 Å resolution had been reported (Krauß et al., 1996), preventing a nomenclature of the two Chls of P700 with reference to the PsaA and PsaB polypeptides]. The $^3P700/P700$ FTIR difference spectrum also shows a small negative band at 1,733 cm^{-1} matching a negative band at the same frequency in the $P700^+/P700$

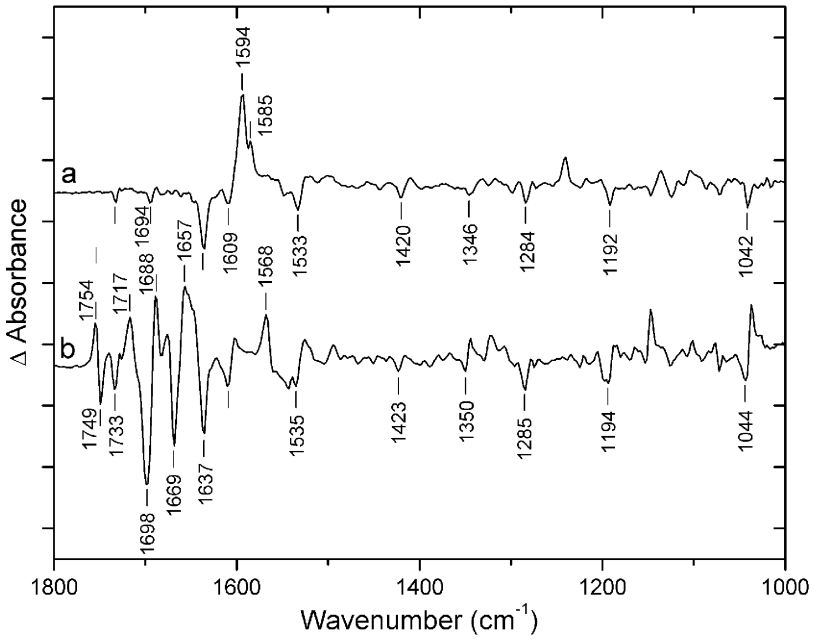

Fig. 3. Light-induced FTIR difference spectra of PS I particles from *Synechocystis* sp. PCC 6803 at 90 K. (a) ^{3}P700/P700 triplet-minus-singlet spectrum on FeS-depleted PS I. (b) P700$^+$/P700 spectrum on native PS I. Peak-to-peak amplitudes are 4×10^{-4} and 6×10^{-4} absorbance units in (a) and (b), respectively. (From Breton, J (2001))

spectrum (Fig. 3), which was assigned to the 10a-ester C=O of P_1. For this Chl molecule of P700, the down-shifted IR frequencies compared to isolated Chl *a* in tetrahydrofuran show that both the 9-keto and the 10a-ester C=O groups are hydrogen bonded. The second Chl *a* molecule of P700, denoted P_2, with its 9-keto and 10a-ester C=O vibrations at 1,697 and 1,749 cm^{-1}, respectively, is free from interactions with the protein. Although P_2 is practically unaffected by the formation of ^{3}P700, it makes a large contribution to the P700$^+$/P700 difference spectrum (Breton et al., 1999). When the high-resolution X-ray structure appeared (Jordan et al., 2001), it became clear that the description of the interactions of the 9-keto and 10a-ester C=O of P_1 and P_2 derived from our FTIR experiments was in excellent agreement with the structural data provided P_1 and P_2 were identified with the PsaA and PsaB Chls of P700, respectively (Table 1; Breton, 2001). In the following, these two Chls will be identified as P_A and P_B, respectively.

In both the ^{3}P700/P700 and the P700$^+$/P700 difference spectra, marker bands at ~1,610 and 1,535 cm^{-1} are typical for five-coordination of the central Mg atom (Fujiwara and Tasumi, 1986). The absence of six-coordinated Mg marker bands at around 1,600 and 1,515 cm^{-1} in the P700$^+$/P700 spectrum indicates that each of the Chl *a* molecules in P700 has only one axial ligand (Breton et al., 1999). These ligands have been previously identified as HisA676 and HisB656 in *C. reinhardtii* (Redding et al., 1998).

Table 1. Assignments of carbonyl stretching frequencies (cm^{-1}) of the two chlorophylls of P700 in *Synechocystis* sp. PCC 6803 at 90 K (Breton et al., 1999; Breton, 2001)

	Carbonyl	P700	P700$^+$	^{3}P700
P_A	10a-ester	1733	~1740	~1728
	9-keto	1637	1656	1594
P_B	10a-ester	1749	1754	
	9-keto	1697	1717	

F. Localization of ^{3}P700 and Charge Distribution in P700$^+$

While ^{3}P700 at low temperature is found to reside exclusively on the P_A Chl, the positive charge in P700$^+$ is shared amongst P_A and P_B (Breton et al., 1999; Breton, 2001). In an attempt to estimate the distribution of the charge between P_A^+ and P_B^+, it was noticed that upon photooxidation of P700 at 90 K the 9-keto C=O of P_A at 1,637 cm^{-1} and P_B at 1,697 cm^{-1} both upshifted by the same amount (19–20 cm^{-1}), which allowed the peak-to-peak amplitude of the 1,717/1,697 and 1,656/1,637 cm^{-1} differential signals to be used

Table 2. Sequence numbering of some PsaA and PsaB amino acids in close proximity of P700 in *Synechococcus elongatus*, *Synechocystis* sp. PCC 6803, and *Chlamydomonas reinhardtii*

	S. elongatus	*Synechocystis*	*C. reinhardtii*
Axial ligands to P700	HisA680	HisA676	HisA676
	HisB660	HisB651	HisB656
Vicinity of 9-keto C=O of P700	ThrA743	ThrA739	ThrA739
	TyrB727	TyrB718	TyrB723
Vicinity of 10a-ester C=O of P700	SerA607, TyrA603	SerA603, TyrA599	
	GlyB594, LeuB590	GlyB585, LeuB581	
Vicinity of 7c-ester C=O of P700	TyrA735	TyrA731	
	PheB719	PheB710	

as a crude estimate of the charge distribution on the 9-keto group of the two molecules. This amplitude is generally somewhat smaller for P_A than for P_B although this effect is less pronounced at ambient temperature. Upon assuming the same extinction coefficient for the two 9-keto carbonyl groups, a global analysis of all our $P700^+$/P700 FTIR difference spectra obtained at both room temperature and low temperature on various PS I preparations from cyanobacteria, unicellular algae, and higher plants (Breton, 2001) leads to an amplitude ratio varying from 1:1 to 2:1 in favor of P_B. Comparable amplitude ratios are estimated when analyzing the relative contributions of the 10a-ester C=O groups of P_A and P_B (Breton et al., 1999; Breton, 2001). Therefore, the extent of charge distribution in $P700^+$ is probed equally well by the IR absorbance changes experienced by each of the two carbonyl groups attached to ring V of the two Chls. Because ring V is fully conjugated to the Chl macrocycle, it was concluded from the FTIR data to a strong delocalization of the positive charge over the two halves of the $P700^+$ dimer with a charge distribution ranging from 1:1 to 2:1 in favor of P_B (Breton et al., 1999; Breton, 2001). This conclusion was at variance from that derived from advanced magnetic resonance techniques from which a strong localization of the positive charge, with at least 85% of the spin residing on one Chl in $P700^+$, was determined (Weber and Lubitz, 2001 and references therein; see also Lubitz, this volume, Chapter 17).

G. Comparison with the High-Resolution Structure of PS I

When the crystallographic structure of PS I at 2.5 Å resolution appeared (Jordan et al., 2001), it became immediately clear that it was directly relevant to several issues of the organization of the two Chl molecules in P700 as deduced from FTIR difference spectroscopy. Notably, the conclusion that the histidine side chains of HisA676 and HisB656 in *C. reinhardtii* are the axial ligands to the Chl of P700 (Redding et al., 1998) has been confirmed (for the various amino acid residues that are discussed in this chapter, see Table 2 for the correspondence of their numbering in the sequences of *C. reinhardtii*, *Synechococcus elongatus*, and *Synechocystis* sp. PCC 6803). Furthermore, the strong inequivalence of the hydrogen bonding pattern of the carbonyl groups of the two Chl molecules in P700, that had been initially inferred from FTIR spectroscopy (Breton et al., 1999), is also apparent in the new crystallographic structure (Jordan et al., 2001). The structure shows one Chl molecule having no hydrogen bond, while the other has three hydrogen bonds that include those at the 9-keto and 10a-carbomethoxy positions previously determined in the FTIR study (Breton et al., 1999). Additional important information that is provided by the new crystallographic study includes the determination that P_A, the strongly hydrogen bonded Chl half of P700, is actually a Chl *a′* molecule (epimer of Chl *a* at C_{10}; the stereochemistry of Chl *a* at C_{10} is shown in Fig. 1).

In the structural model (Jordan et al., 2001), the 9-keto of P_A is hydrogen bonded to the ThrA743 side chain and the 10a-carbomethoxy group is hydrogen bonded to a water molecule (H_2O-19) interacting with the same Thr side chain as well as with several other residues. It should be noted that the present description of this water donating a hydrogen bond to the methoxy oxygen atom of the 10a-carbomethoxy group (Jordan et al., 2001) differs slightly from that deduced from the FTIR study that shows a perturbation of the IR frequency of the C=O double bond of the 10a-carbomethoxy ester group (Breton et al., 1999). The third hydrogen bond, located between the 7c-ester C=O and a Tyr residue, was not detected by FTIR, an observation essentially consistent with the lack of conjugation with the Chl macrocycle of this ester group (Nabedryk et al., 1990). P_B, on the other hand, is free from hydrogen bond interaction. Therefore, the new data on the axial Mg ligands and on the bonding pattern of the carbonyls of P700 obtained from X-ray

crystallography are in excellent agreement with the conclusions previously derived from FTIR difference spectroscopy (Breton et al., 1999; Breton, 2001).

III. FTIR Studies of P700 Following the High-Resolution X-Ray Structure of PS I

A. Effects of Mutations of the Axial Ligands to P700 in C. reinhardtii

Our conclusion from FTIR spectroscopy that the ^{3}P700 triplet is fully localized on P_A while the charge in P700$^+$ is shared between P_A and P_B (Breton et al., 1999) was at odds with the interpretations proposed for the effect of substitution of the histidine axial ligands of P700 on the redox potential of P^+/P, the P700$^+$/P700 optical spectra at ambient temperature, the ENDOR spectra of P700$^+$ measured at 150 K, and the triplet-minus-singlet electronic absorption measured by ADMR at 1.8 K (Krabben et al., 2000; Weber and Lubitz, 2001). From these studies, it was concluded that the triplet character in ^{3}P700 is mainly localized on P_B, i.e., the same Chl molecule that, according to ENDOR measurements, also carries all or most of the spin in P700$^+$. This strong discrepancy was not likely to be due to a difference in the temperature at which the two experiments are conducted as the P700$^+$/P700 spectra are very comparable at 280 and 90 K (Figs. 2A and 3B) and the P700$^+$/P700 and ^{3}P700/P700 FTIR difference spectra are almost unchanged when the temperature is lowered from 100 to 10 K (J. Breton and W. Leibl, unpublished results). As previously discussed (Breton, 2001), such a large disagreement cannot be blamed on some unusual vibrational property of porphyrin as changes of bond order occurring upon triplet or cation formation for (B)Chl *a* in solution have been extensively documented using both FTIR and Raman spectroscopies. In addition, the suggestion was put forward in (Krabben et al., 2000) that the FTIR data on P700$^+$/P700 in (Breton et al., 1999) could be explained by considering that the unpaired electron localized on one of the Chl in P700$^+$ electrostatically influences the frequency of the carbonyl of the neighboring neutral Chl. This interpretation appears unlikely as the frequency upshift observed upon P700$^+$ formation is the same for the 9-keto vibration of P_A (19 cm^{-1}) and P_B (20 cm^{-1}) and is close to that (25 cm^{-1}) observed for isolated Chl *a* in tetrahydrofuran (Breton et al., 1999). A more detailed discussion of this point has been reported (Pantelidou et al., 2004).

B. Assignment Scheme of Hastings et al. (2001)

The large discrepancy between the interpretation of the results of magnetic resonance and FTIR experiments led Hastings et al. (2001) to analyze the P700$^+$/P700 FTIR difference spectra of *C. reinhardtii* and to propose an assignment of bands for the 9-keto C=O group of P_A that differs considerably from the previous interpretation of the FTIR data (Breton et al., 1999) but that is more in line with the conclusions derived from magnetic resonance spectroscopy (Weber and Lubitz, 2001). However, the FTIR assignments in Hastings et al. (2001) are based on the perturbation of the 9-keto carbonyl frequency in a single mutant modified at the His axial ligand of P_A by replacement with a Ser side chain, and they do not take into account the comparison of the P700$^+$/P700 and ^{3}P700/P700 FTIR difference spectra that was at the root of the previous assignments (Breton et al., 1999). On the other hand, the P700$^+$/P700 FTIR difference spectra of *C. reinhardtii* and of *Synechocystis* sp. PCC 6803 are close enough in the frequency range of absorption of the 10a-ester and 9-keto C=O vibrations of Chl (Breton, 2001; Hastings et al., 2001) that any interpretation of the P700$^+$/P700 FTIR differential signals in terms of detailed bonding interactions should be valid for both species.

In the scheme of Hastings et al. (2001), the 10a-ester C=O groups of P_A and P_B as well as the 9-keto C=O of P_B all upshift in frequency upon P700$^+$ formation and receive the same assignment as in Breton et al. (1999). On the other hand, the 9-keto C=O of P_A is proposed to contribute to the large negative band at 1,700 cm^{-1} and to downshift to 1,686 cm^{-1} in P_A^+. No explanation was provided for the physical process underlying this downshift of a Chl 9-keto C=O vibration upon P700$^+$ formation, a behavior that has never been reported when cations of Chl or BChl are generated either *in vivo* or *in vitro*. At this stage it can be conjectured that such a downshift could be caused by an electrochromic effect of the positive charge on P_B affecting the IR mode of P_A. This model does not require P_A to bear a positive charge in P700$^+$ to contribute to the P700$^+$/P700 FTIR difference spectrum and therefore would be consistent with the conclusions from ENDOR experiments (Krabben et al., 2000; Weber and Lubitz, 2001). One difficulty with this model is that the 10-ester C=O group of P_A upshifts upon P700$^+$ formation and therefore experiences a very different electric field compared to that felt by the nearby 9-keto C=O group on the same Chl.

An alternative interpretation would be to consider that a very strong hydrogen bond is established between the 9-keto carbonyl of P_A and the nearby PsaA Thr upon $P700^+$ formation. This strong hydrogen bond would be needed to be able to offset and even overcompensate the normal frequency upshift of the 9-keto carbonyl of Chl occurring upon cation formation. Although this seems to be the explanation preferred in Hastings et al. (2001), there are two main difficulties with this model. First, the frequency of 1,697 cm^{-1} proposed for the 9-keto C=O group of P_A in wild type is characteristic of a carbonyl in an apolar environment and free from hydrogen bonding interactions with the protein, which contradicts the model derived from X-ray crystallography (Jordan et al., 2001). Second, in the curve fitting analysis of the $P700^+$/P700 FTIR difference spectra in the 1,720–1,680 cm^{-1} spectral range to estimate the contributions of P_A, P_A^+, P_B, and P_B^+ (Hastings et al., 2001), the bands of P_A and P_A^+ have an amplitude approximately half or equal to that of the bands of P_B and P_B^+. Taken together with the very comparable amplitudes of the differential signals assigned to the contribution of the 10a-ester C=O group of the two Chls of P700, this observation would be consistent with the conclusions from the ENDOR studies (Krabben et al., 2000; Weber and Lubitz, 2001) only under the assumption of a much larger extinction coefficient for the two carbonyls of P_A than for those of P_B, an issue which is not addressed in Hastings et al. (2001).

On the basis of the effect of the mutation H(A676)S in *C. reinhardtii*, the large 1,652(+)/1,636(−) cm^{-1} differential signal in the $P700^+$/P700 FTIR spectrum of wild type was assigned to the imidazole C_4=C_5 mode from the two His axial ligands (Hastings et al., 2001). Such a frequency for an imidazole C_4=C_5 mode for His protonated at the Nπ site and with a metal bound at the Nτ site would be strongly outside the usual frequency range of 1,606–1,593 cm^{-1} observed for this mode (Hasegawa et al., 2002). In addition, the amplitude of the differential signals centered around 1,645 cm^{-1} in the $P700^+$/P700 FTIR difference spectra is extremely large compared to the usual small magnitude of the FTIR contributions from His modes in biological reactions (Hasegawa et al., 2002 and references therein). As will be shown below, the $P700^+$/P700 FTIR difference spectrum of *Synechocystis* sp. PCC 6803 PS I in which all the His have been uniformly labeled with ^{13}C is strictly incompatible with the assignment of the 1,652(+)/1,636(−) cm^{-1} differential signal to imidazole C_4=C_5 modes as proposed in Hastings et al. (2001).

C. Mutations of the His Axial Ligands of P700 in Synechocystis *sp. PCC 6803*

1. Effect of the Mutations on the Chl Vibrations

The $P700^+$/P700 FTIR difference spectra of three mutants of *Synechocystis* sp. PCC 6803 in which HisB651, the axial ligand of P_B, is replaced by Cys, Gln, or Leu have been reported (Breton et al., 2002). They show only very small shifts (at most 2 cm^{-1}) of the frequency of Chl carbonyl vibrations compared to wild type. Therefore, the hydrogen bonding status of these C=O groups in both the neutral and oxidized states of P700 appear robust to changes of the axial ligand. However, the relative amplitude of the differential signals assigned to frequency upshifts of the 9-keto and 10a-ester C=O groups of the P700 Chls upon photooxidation varies within a factor of ∼2 as a function of the mutation. The conclusion that the charge of $P700^+$ is delocalized is supported by the presence of a broad positive band around 3,000 cm^{-1} in the $P700^+$/P700 FTIR difference spectra of the mutants. A similar observation has also been reported for the H(A676)S mutant of *C. reinhardtii* (Hastings et al., 2001). Finally, the Chl C=C modes at 1,608 and 1,533 cm^{-1}, which are characteristic of penta-coordination of the central Mg atom (Fujiwara and Tasumi, 1986), are left unperturbed by the mutations, indicating that in each mutant a fifth axial ligand must replace the mutated His residue. At least for the Leu mutant, a water molecule probably takes the place of the His side chain, as originally proposed for *Rb. sphaeroides* RC mutants in which the His axial ligands of the BChl molecules of P were replaced by Gly (Goldsmith et al., 1996).

By analogy with the results of a comparable FTIR study on the photooxidation of P in a series of mutants at HisM202, which is the axial ligand of the BChl interacting with the M-polypeptide in *Rb. sphaeroides* (Nabedryk et al., 2000), it has been proposed that the variations in the frequency and intensity of the 9-keto and 10a-ester C=O bands of Chl observed in the $P700^+$/P700 FTIR difference spectra of all the His axial ligand mutants in *Synechocystis* sp. PCC 6803 are due primarily to repositioning of the P700 dimer in the protein cavity generated by the mutation (Breton et al., 2002). This proposal, which applies as well to *C. reinhardtii* (Leibl et al., 1998; Redding et al., 1998; Hastings et al., 2001) can also explain how two equivalent mutations at homologous sites, such as H(B656)Q in *C. reinhardtii* and H(B651)Q in

Synechocystis sp. PCC 6803, have somewhat different effects on the $P700^+$/P700 FTIR difference spectra in different species (Redding et al., 1998; Breton et al., 2002). Minute differences in the shape of the protein cavity for P700 in the two species can become important factors for the conformation and/or environment of the Chl carbonyl groups.

2. Effect of the Mutations on the His Vibrations

FTIR spectroscopy is well suited to investigate the protonation and ligation states of the two nitrogen atoms of the imidazole group of His side chains in proteins. The relatively intense C_5–Nτ stretching mode around 1,100 cm^{-1} was found to be a good marker of the protonation and coordination state of the histidine side chain. When a metal is coordinated at Nτ, the C_5–Nτ stretching mode depends whether the Nπ site is protonated or not and occurs in the characteristic ranges of ∼1,115–1,100 cm^{-1} and ∼1,100–1,090 cm^{-1}, respectively (Hasegawa et al., 2002).

The first indication that a His C_5–Nτ stretching mode could be identified in the $P700^+$/P700 FTIR difference spectra of *Synechocystis* sp. PCC 6803 came from global ^{15}N-labeling experiments where a small differential signal negative at 1,108 cm^{-1} and positive at 1,102 cm^{-1} downshifted by 8–9 cm^{-1} upon labeling (Breton et al., 2002). The frequency position at 1,108 cm^{-1} and the magnitude of the shift were consistent with such an assignment. Confirmation of this assignment was obtained by comparing the $P700^+$/P700 FTIR difference spectra of PS I core complexes isolated from a culture of *Synechocystis* sp. PCC 6803 having incorporated histidine either unlabeled (Fig. 4a) or uniformly labeled with ^{13}C (Fig. 4b). In this case the 1,102/1,108 cm^{-1} differential signal is downshifted by 15–16 cm^{-1} for the ^{13}C-histidine and the double-difference spectrum (Fig. 4c) shows that this is the most affected mode in the 1,200–1,000 cm^{-1} spectral range.

In the spectral range 1,200–1,000 cm^{-1}, the 1,102/1,108 cm^{-1} differential signal was still present in the spectra of the *Synechocystis* sp. PCC 6803 mutants at HisB651, albeit with a reduced amplitude and a frequency downshift of ∼1 cm^{-1}. A closer analysis of the double-difference spectra, in which the spectrum of the ^{13}C-labeled His sample from wild type was subtracted from each of the individual spectra of the mutant, indicated that the 1,102/1,108 cm^{-1} signal of wild type is, in fact, the resultant of two differential signals of roughly equal amplitudes at ∼1,101/1,107 and

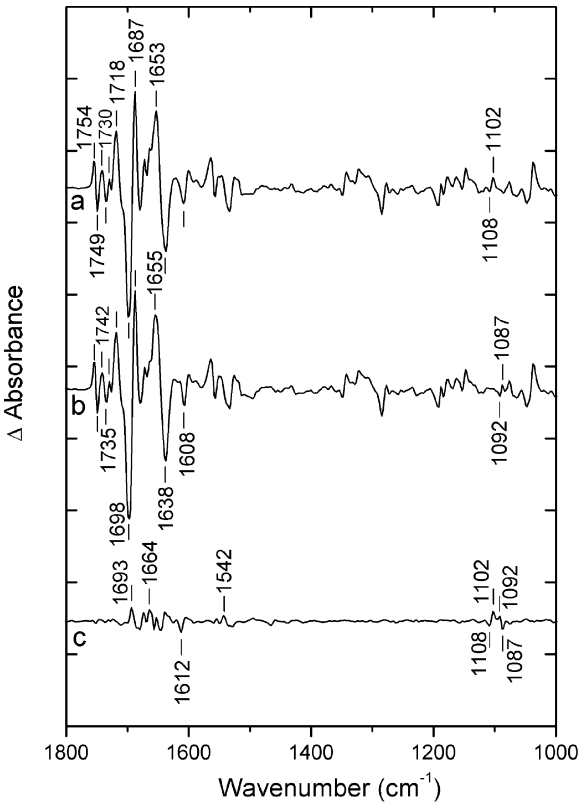

Fig. 4. Light-induced $P700^+$/P700 FTIR difference spectra of the photooxidation of PS I particles from *Synechocystis* sp. PCC 6803 at 5°C containing (a) unlabeled His and (b) uniformly ^{13}C-labeled His. (c) Double-difference spectrum unlabeled-minus-uniformly ^{13}C-labeled His. (Breton, J. unpublished)

at ∼1,103/1,109 cm^{-1}. These features were therefore assigned to the C_5–Nτ mode of HisA676 and HisB651, respectively (Breton et al., 2002).

In the assignment scheme of Breton et al. (1999), the interpretation of the FTIR data as showing a rather symmetrical distribution of the positive charge on the two Chl molecules in $P700^+$ (Breton et al., 1999; Breton, 2001) rests on the reasonable assumption that the extinction coefficients for the 9-keto and 10a-ester C=O groups of the two Chl molecules of P700 are not vastly different due to differences in their hydrogen bonding state, environment, or chemical nature (Jordan et al., 2001). The observation that the C_5–Nτ modes of each of the His axial ligands of the two Chl molecules in P700 are also perturbed to a similar extent upon $P700^+$ formation, although the histidines are not conjugated to the Chl macrocycles circumvents this concern and provides independent and compelling evidence to reinforce our conclusion that the charge in $P700^+$ is distributed approximately equally over the two Chl

molecules of the PS I primary electron donor (Breton et al., 1999; Breton, 2001).

Finally, the $P700^+/P700$ FTIR difference spectra of *Synechocystis* sp. PCC 6803 containing the uniformly ^{13}C-labeled His has been used to search for the imidazole $C_4{=}C_5$ stretching mode which is also a good marker for the state of protonation and coordination of His (Hasegawa et al., 2002). This mode is observed at ~1,612 cm^{-1} with an amplitude about 1.5–2 times that of the 1,108 cm^{-1} C_5–Nτ mode (Fig. 4). This frequency is slightly above but close to the upper limit of the 1,606–1,593 cm^{-1} frequency range characteristic of 4-methyl imidazole protonated at the Nπ site and coordinated to a metal atom at Nτ (Hasegawa et al., 2002). As can be seen in Fig. 4, the imidazole $C_4{=}C_5$ stretching mode does not contribute appreciably to the large differential signal 1,653(+)/1,638(−) cm^{-1}. This observation rules out the proposed assignment of Hastings et al. (2001) that HisA676 and HisB656 are responsible for the differential signal at 1,652(+)/1,636(−) cm^{-1} in *C. reinhardtii*. This differential signal has been assigned to the 9-keto C=O group of P_A^+/P_A (Breton et al., 1999; Breton, 2001). The set of bands observed within the envelope of the amide I band in the unlabeled minus ^{13}C-labeled double-difference spectrum (Fig. 4c) are assigned for the most part to vibrations of the PsaA and PsaB polypeptide backbone involving the amide bond sustaining the His residues.

D. Effect of Mutations Affecting the Carbonyls of Ring V of the PsaA Chl of P700

1. Study by Witt et al. (2002)

In the first investigation by FTIR difference spectroscopy of mutations affecting the hydrogen bonds to the carbonyls of P_A, the residue ThrA739 in *C. reinhardtii* was replaced by Tyr, His, or Val (Witt et al., 2002). All three mutations induce large perturbations of the wild type spectrum in the 1,720–1,600 cm^{-1} frequency range. Smaller effects are observed in the region 1,730–1,760 cm^{-1}, probably at least in part as a consequence of the normalization procedure that was constrained to this small frequency window. While the positive band at ~1,688 cm^{-1} in wild type increases its amplitude by more than a factor of two in the three mutants, even larger perturbations are found between 1,680 and 1,620 cm^{-1} with the spectrum of each mutant differing from that of wild type (Witt et al., 2002). These spectral alterations upon mutation occur within the main range of the amide I C=O vibrations and should be related, at least in part, to protein conformational changes. For $P700^+/P700$ FTIR difference spectra, contributions from amide I and II vibrations have been detected by global isotopic labeling experiments (Breton et al., 1999, 2002). Hastings et al. (2001) have attributed the whole 1,652/1,636 cm^{-1} differential signal in their $P700^+/P700$ spectrum of wild type *C. reinhardtii* to protein contributions from the two His axial ligands. Surprisingly, the possibility that the protein contributes to the IR absorption changes observed by Witt et al. (2002) in the 1,620–1,680 cm^{-1} frequency range was not considered and the authors made the statement that their observations provide the first direct evidence that the 1,634 cm^{-1} band can be ascribed to the 9-keto group of P_A. It has been stressed that in the absence of isotope labeling experiments or of an analysis of $^3P700/P700$ FTIR difference spectra, it is not possible to discriminate between Chl 9-keto C=O and protein C=O groups in the whole range of the amide I absorption (Breton et al., 2002). Therefore, the data presented in Witt et al. (2002) provide no direct clues to support their assignment of the 1,634 cm^{-1} band to a Chl 9-keto C=O vibration.

Although the $P700^+/P700$ FTIR difference spectra of the Thr A739 mutants reported by Witt et al. (2002) do not provide an unambiguous assignment of the 9-keto C=O vibration of P_A, they certainly bring supporting evidence in favor of the existence of a hydrogen bond to the 9-keto C=O group of this Chl in *C. reinhardtii*. Notably, the strong perturbation of the 1,656(+)/1,634(−) cm^{-1} differential in the spectra of all the Thr A739 mutants firms up the assignment previously made to the 9-keto C=O vibrational mode of P_A^+/P_A in wild type (Breton et al., 1999; Breton, 2001) and provides the first evidence that the hydrogen bond to this residue has been affected by the mutations.

2. Study by Wang et al. (2003)

In another investigation, the residue ThrA739 was replaced by Ala in *C. reinhardtii* (Wang et al., 2003). The $P700^+/P700$ FTIR difference spectrum closely resembles that of the T(A739)V mutant of Witt et al. (2002). Furthermore, the mutant spectra are analyzed by calculating double-difference spectra with wild type. Large changes are observed, notably for the 1,654(+)/1,637(−) cm^{-1} differential signal of wild type, which is replaced by a mostly positive band of reduced amplitude at 1,652 cm^{-1} in the spectrum of the mutant. As already noticed in the T(A739)V mutant (Witt et al., 2002) negative and positive bands appears at 1,672 and 1,688 cm^{-1}, respectively. These spectral changes give rise to two differential signals of equal

Table 3. Frequencies (cm^{-1}) of the $P700^+/P700$ bands assigned to the 9-keto and 10a-ester C=O carbonyls of P_A and P_B in WT and Thr A739 mutants in *Chlamydomonas reinhardtii* (Wang et al., 2003) and in *Synechocystis* sp. PCC 6803 (Pantelidou et al., 2004)

		Chlamydomonas reinhardtii		*Synechocystis* sp. PCC 6803	
		WT	T(A739)A	WT	T(A739)F
P_A^+/P_A	10a-ester C=O	1741/1734	1743/1734	1742/1735	1742/1736
	9-keto C=O	1686/1695	1688/1699	1660/1637	1689/1676
P_B^+/P_B	10a-ester C=O	1753/1748	1752/1748	1754/1749	1754/1749
	9-keto C=O	1716/1704	1713/1704	1718/1698	1717/1698

amplitude but of opposite signs at 1,690(−)/1,672(+) and 1,660(+)/1,636(−) cm^{-1}, which are the most prominent features in the double-difference spectrum.

These spectral changes could be readily explained in the assignment scheme of Breton et al. (Breton et al., 1999; Breton, 2001; Witt et al., 2002) by assuming that the 1,660(+)/1,636(−) cm^{-1} differential signal due to the 9-keto C=O vibrational mode of P_A^+/P_A in wild type upshifts by 30–36 cm^{-1} when the hydrogen bond to the Thr A739 in *C. reinhardtii* is perturbed by the mutation. However, Wang et al. (2003) rather assign the changes upon the T(A739)A mutation observed in the 1,665–1,620 cm^{-1} frequency range to the imidazole C_4=C_5 stretching mode of the two His axial ligands of P700. They rationalize the differences between the contributions of the two His residues in the $P700^+/P700$ FTIR spectra of the wild type and the mutant in this region by invoking some redistribution of the positive charge from P_B^+ to P_A^+ upon mutation, which would change the relative weight of the two His residues. As discussed above, these assignments are compatible neither with the current literature on IR vibrations of His side chains (Hasegawa et al., 2002 and references therein) nor with the $P700^+/P700$ FTIR difference spectra on *Synechocystis* sp. PCC 6803 PS I core complexes containing uniformly ^{13}C-labeled His (Fig. 4; Breton et al., 2002).

In the assignment scheme of Hastings et al. (2001), the impact of the T(A739)A mutation on the 9-keto C=O vibration of P_A and P_A^+ is actually very modest. This vibrational mode upshifts upon mutation by only 4 cm^{-1} from 1,695 to 1,699 cm^{-1} in P_A and by 2 cm^{-1} from 1,686 to 1,688 cm^{-1} in P_A^+ (Table 3; Wang et al., 2003). Taking these assignments at face value, the straightforward interpretation of the 9-keto C=O frequencies proposed for P_A and P_A^+ would be to consider that P_A is free from bonding interactions in both wild type and mutant and that a very strong hydrogen bond to P_A^+ is essentially unchanged upon mutation. The effect of the mutation on the 9-keto C=O vibration of P_B and P_B^+ and on the 10a-ester C=O modes are either absent or very minor and the corresponding bands keep the same assignments as proposed previously (Breton et al., 1999; Breton, 2001; Hastings et al., 2001). On the other hand, the small band observed around 1,730 cm^{-1} in the region of absorption of the C=O esters of Chl (Kim and Barry, 2000), which is affected by the T(A739)A mutation, is tentatively assigned to the 7c-ester C=O of P_A (Wang et al., 2003). Note that the latter assignment is not consistent with the effect of selective labeling of the 10a-ester C=O group (Kim and Barry, 2000).

In their analysis of the effect of the T(A739)A mutation on the $P700^+/P700$ FTIR difference spectrum, Wang et al. (2003) discuss three distinct reasons why the 1,654(+)/1,637(−) cm^{-1} differential signal of wild type *C. reinhardtii* should not be assigned to the 9-keto C=O group of P_A^+/P_A, as proposed in Breton et al. (1999) and Breton (2001). First, they state that the strong hydrogen bond needed to explain the observed low frequency of the 1,637 cm^{-1} vibration should lead to a considerable downshift of this mode upon uniform ^2H-labeling. As such sensitivity was not observed (Breton et al., 1999), they reject the interpretation. This is a surprising statement because it is established that C=O groups in strong bonding interactions with H-bond donors show only minor shifts upon ^2H-labeling. A well-known case is the amide I vibration in α-helices, which exhibits small downshifts by only a few wave numbers upon $^1H/^2H$ exchange. Other examples in the bacterial RCs are for example the 9-keto C=O group of the active bacteriopheophytin interacting with the side chain of GluL104 or the C=O group of the quinone Q_A in very strong bonding interaction with the imidazole NH of HisM219, which are both almost insensitive to $^1H/^2H$ exchange (Breton et al., 1997) although ENDOR experiments have shown the exchange to take place at these sites. Second, Wang et al. (2003) reject an interpretation within our assignment scheme (Breton et al., 1999; Breton, 2001) of the effect of the T(A739)A mutation on the $P700^+/P700$ FTIR difference spectrum of *C. reinhardtii* on the basis of the

magnitude of the frequency upshift of the 9-keto and 10a-ester C=O vibrations upon $P700^+$ in wild type and mutant. They propose that minute frequency shifts (by about 1 cm^{-1}) of the 10a-ester C=O vibrations of P_A^+ and P_B^+ upon mutation correspond to a redistribution of the charge from P_B^+ to P_A^+ and they argue that the 9-keto vibrations do not follow the same quantitative pattern because the cation-induced upshift is smaller in the mutant than in wild type.

However, they do not take into account the effect of the environment, and notably of mutation-induced variations in the strength of the hydrogen bonds, on the frequency of those vibrations. This is surprising when considering that their whole model relies on the presence of a very strong hydrogen bond responsible for a downshift by ~10 cm^{-1} upon P_A^+ formation of the 9-keto C=O vibration of a Chl, while this vibration has been shown to upshift by ~15–30 cm^{-1} in all of the other reported cases of (B)Chl cation formation both *in vivo* and *in vitro*. Finally, they argue that a frequency of 1,672 cm^{-1} for the 9-keto C=O vibration of P_A in the mutant is too low for a free group without considering that a water molecule or a suitable hydrogen bond donor could take the place of the OH group of the Thr side chain in the mutant. Therefore, none of the three points listed above appear to bring significant weight to their assignment scheme where the 9-keto C=O vibration of P_A is proposed to absorb at 1,695 cm^{-1} when in hydrogen bonding interaction with ThrA739, and at 1699 cm^{-1} when free from this interaction (Wang et al., 2003).

3. Study by Pantelidou et al. (2004)

In the structural model of P700 (Jordan et al., 2001), the 9-keto of P_A is hydrogen bonded to the ThrA743, side chain and the 10a-carbomethoxy group is hydrogen bonded to a water molecule (H_2O-19) interacting with ThrA743, as well as with TyrA603 and SerA607 (*S. elongatus* numbering, see Table 2 for the homologous residues in PsaB and for the correspondence with *Synechocystis* sp. PCC 6803). Recently, a single T(A739)F mutation as well as a set of three mutations aimed at altering the hydrogen bonding pattern of the 9-keto and 10a-ester C=O groups of P_A by making it similar to the environment of the symmetry-related P_B that exhibits no hydrogen bonding interaction with the protein were devised in *Synechocystis* sp. PCC 6803. The triple mutant containing the changes T(A739)Y, S(A603)G, and Y(A599)L was analyzed by FTIR difference spectroscopy and was compared to the T(A739)F single mutant (Pantelidou et al., 2004).

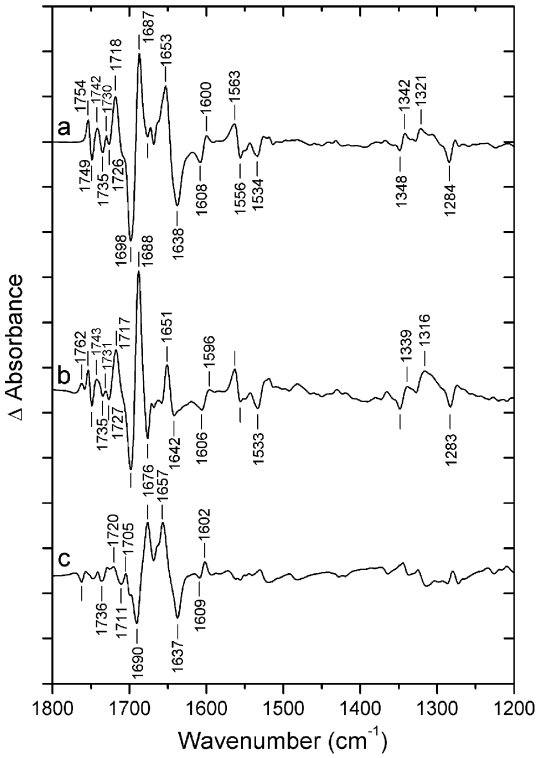

Fig. 5. Light-induced $P700^+$/P700 FTIR difference spectra of the photooxidation of PS I particles from *Synechocystis* sp. PCC 6803 at 5°C for (a) WT and (b) a triple mutant containing the changes T(A739)Y, S(A603)G, and Y(A599)L. (c) Double-difference spectrum WT-minus-mutant. (From Pantelidou M, et al. (2004))

The largest impact of the mutations at ThrA739 on the $P700^+$/P700 FTIR spectrum occurs in the spectral range characteristic of the 9-keto C=O of the Chls of P700 and $P700^+$ between 1,720 and 1,635 cm^{-1}. The 1,653(+)/1,638(−) cm^{-1} differential signal in the spectrum of wild type (Fig. 5a) is replaced by another one of much reduced amplitude and mostly positive at 1,651(+)/1,642(−) cm^{-1} in the spectrum of T(A739)F and of the triple mutant (Fig. 5b). This is accompanied by the development of a negative band at 1,676 cm^{-1} in the mutants and of a positive one at 1,688 cm^{-1} that overlaps with a preexisting positive band at 1,687 cm^{-1} in wild type. Together these changes contribute two large differential signals of comparable amplitudes but of opposite signs at 1,690(−)/1,676(+) and 1660–1657(+)/1,637(−) cm^{-1}, which constitute the major features of the double-difference spectra (Fig. 5c). These features that are closely comparable to those observed at 1,690(−)/1,672(+) and 1,660(+)/1,636(−) cm^{-1} for the T(A739)A mutant in *C. reinhardtii* (Wang et al., 2003), are readily

explained in the assignment scheme of Breton et al. (Breton et al., 1999; Breton, 2001; Witt et al., 2002) by assuming that the 1660–1657(+)/1,637(−) cm^{-1} differential signal due to the 9-keto C=O vibrational mode of P_A^+/P_A in wild type upshifts by ∼30–40 cm^{-1} when the hydrogen bond to ThrA739 is perturbed by the mutations. The amplitude of the 1,718/1,698 cm^{-1} signal in the spectrum of the control is somewhat reduced in the mutants, which would be consistent with a slight redistribution of the positive charge from P_B^+ to P_A^+ upon mutation.

It is worth noting that only about 50–60% of the 1,653(+)/1,638(−) cm^{-1} differential signal in the $P700^+$/P700 FTIR difference spectrum of wild type upshifts upon mutation (Fig. 5). The remaining 1,651(+)/1,642(−) cm^{-1} signal could have at least two main origins. It could represent the amide I signature of a protein conformational and/or electrostatic change or it could correspond to the upshift upon P700 photooxidation of the 9-keto C=O carbonyl group of P_A in hydrogen bonding interaction with the OH group of a water molecule (or of the Tyr side chain introduced at the PsaA739 site). To test between these two possibilities, global ^{15}N-labeling of the triple mutant was performed. A ∼1–2 cm^{-1} downshift upon global ^{15}N-labeling was observed for the 1,651(+)/1,642(−) cm^{-1} signal in the $P700^+$/P700 FTIR spectrum of the triple mutant which is therefore preferentially assigned to a protein conformational change rather than to the 9-keto C=O of P_A (Pantelidou et al., 2004). This conclusion reinforces our earlier observation (Breton et al., 2002) that it was somewhat hazardous to assign the differential signal centered around 1,645 cm^{-1} in the $P700^+$/P700 FTIR spectrum of wild type solely on the effect of mutations (Witt et al., 2002). It is interesting to note that global ^{15}N-labeling has also a small effect on the large $P700^+$/P700 bands located around 1,680–1,690 cm^{-1}. Comparable effects have been detected previously for wild type (Breton et al., 1999). It is therefore likely that the positive band at 1,688 cm^{-1} in $P700^+$/P700 FTIR spectra of both the mutants and wild type contains some contributions from protein amide I modes.

In the frequency range typical of the 10a-ester C=O above 1,720 cm^{-1}, very little difference is observed between the spectrum of wild type and that of the T(A739)F single mutant except for a ∼1 cm^{-1} upshift upon mutation of the small differential signal at 1,735(−)/1,730(+) cm^{-1} (Pantelidou et al., 2004). This is taken to indicate that the water molecule H_2O-19, which is held by several residues, including ThrA739, and is proposed to be the hydrogen bond donor to the bridging oxygen of the 10a-carbomethoxy group of P_A (Jordan et al., 2001), is probably still present and is almost unperturbed by the T(A739)F mutation. Furthermore, the differential signal at 1,754(+)/1,749(−) cm^{-1} is not affected by the mutation, consistent with its assignment to the free 10a-ester C=O of P_B^+/P_B (Breton et al., 1999; Breton, 2001). In contrast, a significant alteration of the $P700^+$/P700 FTIR spectrum is detected upon the triple mutation (Fig. 5). Notably, a complex set of two negative bands at 1,735 and 1,726 cm^{-1} with a positive band located in between at 1,730 cm^{-1} in the wild type spectrum is strongly affected, while a new positive band appears at 1,762 cm^{-1} in the triple mutant. These observations clearly show that a perturbed 10a-ester C=O group of P_A absorbing at a lower frequency than unbound Chl 10a-ester carbonyls becomes free of interaction when TyrA599, SerA603, and ThrA739 in *Synechocystis* sp. PCC 6803 are simultaneously replaced by their PsaB homologs Leu, Gly, and Tyr, respectively. This suggests that in the triple mutant, the H_2O-19 water is either no longer present in the site or, at least, is interacting much less with the 10a-carbomethoxy group of P_A. Previously, a 1,740(+)/1,733(−) cm^{-1} differential signal in the $P700^+$/P700 FTIR difference spectrum of *Synechocystis* sp. PCC 6,803 at 90 K was assigned to the upshift upon photooxidation of the 10a-ester C=O group of P_A (Breton et al., 1999; Breton, 2001). Thus, the frequency upshift of a bound 10a-ester C=O group upon removal of the hydrogen bonds to water H_2O-19 observed in the present study also supports our previous assignment (Breton et al., 1999; Breton, 2001).

One interesting observation for both the single T(A739)F and the triple mutants is a 2–3 cm^{-1} downshift of the macrocycle C=C marker mode of five-coordinated Chl at 1,608 cm^{-1} compared to wild type. A comparable perturbation of this mode was previously noticed in the T(A739) A mutant in *C. reinhardtii* (Wang et al., 2003). Such a perturbation could indicate a constrained conformation of the P_A macrocycle in wild type which would be released when the strong hydrogen bond to the 9-keto carbonyl group is modified by the T(A739)Y mutation.

IV. Other FTIR Studies of P700

A. Redox-Induced and Perfusion-Induced FTIR Spectra of P700 Oxidation

Electrochemically induced $P700^+$/P700 FTIR difference spectra have been generated in *Synechocystis* sp.

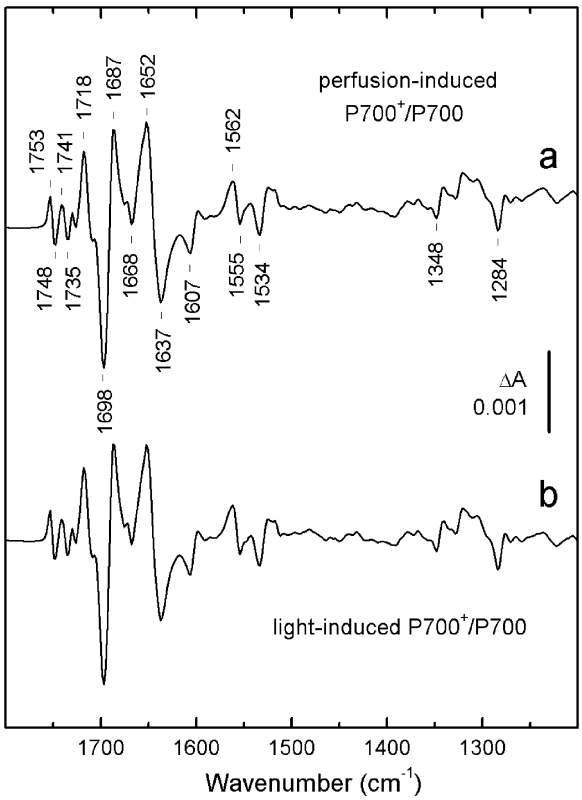

Fig. 6. Perfusion-induced (a) and light-induced (b) ATR–FTIR difference spectra of $P700^+/P700$ of PSI particles from *Synechocystis*. The perfusion-induced difference spectrum was obtained by switching solutions of buffers containing 3 mM ferricyanide for oxidation and 3 mM ferrocyanide for the reduction. The light-induced difference spectrum was obtained in a buffer containing 2.5 mM ferrocyanide and 0.5 mM ferricyanide. (From Iwaki M, et al. (2002))

PCC 6803 and the effect of $^1H/^2H$ exchange has been investigated (Hamacher et al., 1996). The probable presence of small contributions from oxidized antenna Chls has been discussed previously (Breton, 2001).

Recently, the approach of perfusion-induced FTIR difference spectroscopy on the oxidation of P700 using ferricyanide- or ferrocyanide-containing buffers has demonstrated that the quality of the perfusion-induced spectra was equivalent to that of the light-induced spectra (Fig. 6; Iwaki et al., 2002).

B. Effect of $^1H/^2$ H Exchange on the $P700^+/P700$ FTIR Difference Spectra

Several studies have demonstrated that $^1H/^2H$ exchange has only limited effects in the 1760–1600 cm^{-1} frequency range of the $P700^+/P700$ FTIR difference spectra from various organisms (Tavitian et al., 1986; Hamacher et al., 1996; Breton et al., 1999; Kim et al., 2002; Sivakumar et al., 2003) but, in our opinion, few useful interpretations have been obtained from these observations.

In a related study, Kim et al. (2002) have reported the perturbation of a nonexchangeable S–H vibration from a cysteine residue upon P700 photooxidation. Surprisingly, the 2,551(+)/2,560(−) cm^{-1} differential signal assigned to this mode decreases in amplitude by ∼50% upon $^1H/^2H$ exchange but does not show the downshift by ∼900 cm^{-1} expected for the S–D vibration.

C. FTIR of P740 Photooxidation in Acaryochloris marina

PS I from this organism contains Chl *d* in which a formyl replaces the vinyl group at position 2 of Chl *a*. The $P740^+/P740$ FTIR difference spectrum bear many similarities with the $P700^+/P700$ FTIR difference spectrum of *Synechocystis* sp. PCC 6803 including a mid-IR electronic transition (Hastings, 2001; Sivakumar et al., 2003). The $P740^+/P740$ spectrum is more sensitive to $^1H/^2H$ exchange than the $P700^+/P700$ spectrum and bands at 2,727 and 2,715 cm^{-1} were tentatively assigned to the formyl group of the two Chl *d* molecules in P740.

V. Comparison of the Results of FTIR and of Magnetic Resonance Spectroscopy

A. The Localization of $^3P700$

From FTIR spectroscopy of $^3P700$ (Breton et al., 1999) and comparison with the PS I structural model (Jordan et al., 2001), it has been concluded that $^3P700$ is fully localized on P_A (Breton, 2001). The opposite conclusion that $^3P700$ is mainly localized on P_B has been reached from magnetic resonance experiments investigating the effect of mutants on the axial ligands of P700 (Krabben et al., 2000; Weber and Lubitz, 2001). Recently, the later conclusion has been called into question on the basis of the observation that the degree of coupling of the pigments in the PS I RC is larger than previously assumed in the analysis of the ADMR data and it was stated that straightforward conclusions cannot be drawn from this technique concerning the localization of the triplet (Witt et al., 2002). It was also suggested that the observation that the $P700^+/P700$ and the $^3P700/P700$ ΔA spectra are affected in a similar way by each of the various mutations (Krabben et al., 2000; Witt et al., 2002) indicates that the triplet state and the

positive charge are located on the same Chl. As discussed previously (Breton et al., 2002), it therefore follows from the statements in Witt et al. (2002) that the results of ADMR and ΔA spectroscopy of P700 no longer contradict the finding from FTIR spectroscopy that ^{3}P700 is fully localized on P_A (Breton et al., 1999; Breton, 2001).

B. The Issue of Charge/Spin Distribution in P700$^+$

Knowledge of the electronic structure of P700 and $P700^+$ is important to better understand the functional properties of PS I. For example it is of interest to determine where in the $P700^+$ dimer is localized the excess positive charge as this is an important parameter related to the mid-point redox potential, the charge transfer properties of P700 and also, possibly, to the mechanism of initial charge separation and the issue of unidirectionality versus bidirectionality of electron transfer in PS I. For these reasons, the structure of $P700^+$ has received considerable attention over the last 30 years. Notably, a large number of investigations have been performed with a variety of magnetic resonance techniques. However, the conclusions have evolved over a wide range of structures from symmetrical dimers to fully localized monomers (see, e.g., Weber and Lubitz, 2001). Up to now ENDOR has emerged as one of the most prominent technique to address this issue with the most detailed experimental work, performed on oriented single crystals of PS I, leading to the conclusion that P_B carries all or most (more than 85%) of the spin density in $P700^+$ while P_A carries no or little (up to 15%) spin density (Käss et al., 2001; Weber and Lubitz, 2001). Clearly, this conclusion is difficult to reconcile with our interpretation of the FTIR data that concludes to a charge distribution between P_A^+ and P_B^+ ranging from 1:1 to 2:1 in favor of P_B (Breton et al., 1999, 2002; Breton, 2001; Pantelidou et al., 2004).

In the FTIR experiments, the charge density distribution between P_A^+ and P_B^+ has been assessed by the relative magnitudes of signals assigned to the change of bond order of the 9-keto and 10a-ester C=O groups of the two Chls of P700 upon photooxidation (Breton et al., 1999; Breton, 2001). This conclusion of a rather symmetrical charge distribution in $P700^+$ has been further supported by an independent FTIR measurement of the relative perturbation of the imidazole C_5–Nτ stretching mode of the His axial ligand of P_A and P_B (Breton et al., 2002). Moreover, the assignment scheme used to interpret the FTIR spectra (Table 1; Breton et al., 1999; Breton, 2001) has been supported by the results of studies of mutants at the ThrA739 site (Witt et al., 2002; Pantelidou et al., 2004). On the other hand, the conclusion that P_B carries most of the spin density in $P700^+$ while P_A carries no or little (up to 15%) spin density derived from ENDOR is based essentially on the comparison of the sum of the assigned proton hfcs of three methyl groups in $P700^+$ with those in isolated Chl a^+ (Käss et al., 2001).

While seeking an explanation for such a stringent discrepancy between the results of FTIR and of ENDOR, it was realized that several difficulties preventing an unambiguous analysis of the ENDOR data on $P700^+$ had been discussed by the authors of the magnetic resonance studies (Breton et al., 2002). These difficulties were related, notably, to the lack of an assignment for the hfcs corresponding to the methyl groups of P_A^+ and to the unreliable comparison with Chl a^+ in solution (Käss et al., 2001; Weber and Lubitz, 2001). Additional complexity in the analysis of the ENDOR data on the P700 axial mutants in *C. reinhardtii* was the unexpected observation that only the hfcs assigned to the methyl group attached to ring III of the Chl are affected in the His PsaB axial ligand mutants while the hfcs assigned to the methyl groups on rings I and II are not affected (Krabben et al., 2000). This was taken to indicate a modification in the local environment of the ring III methyl group caused by a movement of P_B or a change in its conformation. Further complications were noticed with the ThrA739 mutants where significant changes of the hfcs of the ring III methyl group were observed (Witt et al., 2002). For the first time a mutation affecting P_A led to changes of the hfcs of P_B, which, according to (Witt et al., 2002), may be interpreted as a spin density shift from P_B^+ to P_A^+ and indicates electronic coupling between the two halves of the $P700^+$ dimer in wild type.

Our initial estimate of the charge distribution in $P700^+$ from FTIR measurements (Breton et al., 1999) was based on the perturbation upon P700 photooxidation of the 10a-ester and 9-keto C=O groups, which are partially and fully conjugated to the P700 Chl macrocycles, respectively. As previously discussed (Breton et al., 2002), the hfcs of the methyl group on ring III being very sensitive to modifications of the neighboring exocyclic ring V (Krabben et al., 2000), it is therefore conceivable that a small change of the geometry or of the local electrostatic interactions in this region of $P700^+$ upon various mutations may affect the minute amount of spin localized on this specific methyl group. Similarly, the unusually strong downshift of the frequency of the 9-keto C=O group of P_A indicates a

drastic perturbation of ring V of this Chl. Such perturbation may be responsible for the difficulties in assigning the methyl group on ring III of P_A.

Finally, the possibility that the spin distribution derived from the proton ENDOR hfcs of three of the methyl groups of P_B^+ diverges strongly from the actual charge distribution on the two Chls of $P700^+$ is a question that seems to have been raised only very recently (Plato et al., 2003). This is an important issue to assess the extent to which the present ENDOR data can be used to derive information on the overall electronic structure of $P700^+$ and, notably, on the average distribution of the unpaired electron between P_A^+ and P_B^+. This essential question also bears directly on the pertinence of comparing the results of FTIR and ENDOR spectroscopy of $P700^+$. Using semiempirical quantum chemical calculations and the available coordinates (Jordan et al., 2001), it has been recently concluded that, due to spin polarization effects, the spin asymmetry could be significantly larger than the charge asymmetry in $P700^+$ (Plato et al., 2003). It should be noticed, however, that such calculations on proton hfcs in $P700^+$ were performed using a structure of the neutral state of P700 and not of $P700^+$. In the structure at 2.5 Å resolution, the positions of the hydrogen atoms are not available and the geometry of the 10a-carbomethoxy group of P_A, as defined by the X-ray coordinates (Jordan et al., 2001), is somewhat uncertain (N. Krauß, personal communication). Therefore, these calculations required some adjustment of input parameters (e.g., orientation of the vinyl groups, length of C–CH_3 bonds). Finally, it should also be noted that there seem to be controversial aspects in such calculations, at least for the case of Chl a^+ (O'Malley and Collins, 2001). In conclusion, we are confident that FTIR difference spectroscopy, which provides direct experimental information on the charge distribution between P_A^+ and P_B^+, will prove a useful approach to further elucidate the electronic structure of $P700^+$ in PS I of both native and mutant organisms.

VI. Addendum

After submission of this Chapter two new publications from the group of Hastings on the $P700^+$/P700 FTIR difference spectra of PS I have appeared (Li et al., 2004; Wang et al., 2004). Several points or issues raised in these publications have not been dealt with in the present chapter and are worth a brief discussion. In Wang et al. (2004) the $P700^+$/P700 FTIR difference spectra of PS I from *Synechocystis* sp. PCC 6803 globally labeled with either ^2H or ^{15}N was investigated. These global labels are the same as those used by us previously for the purpose of tentative identification of carbonyl modes from protein and Chl (Breton et al., 1999).

Wang et al. (2004) state that in the $^3P700$/P700 difference spectrum generated at 90 K on PS I particles from *Synechocystis* sp. PCC 6803 (Breton et al., 1999) it has never been shown that the triplet state was associated with one of the Chl of P700. However, the use of standard procedures and the control kinetics measured in the visible (Breton et al., 1999) have shown that the species investigated has the same properties as those of the $^3P700$ species previously characterized by EPR and ADMR. The authors also stress that the conclusions from the FTIR studies of Breton et al. (1999) that $^3P700$ is localized on P_A and that the charge in $P700^+$ is distributed between P_A and P_B are inconsistent with the previous conclusions from magnetic resonance (Weber and Lubitz, 2001). However, the validity of the latter conclusions has been recently challenged by the authors of the relevant studies themselves (Witt et al., 2002; Plato et al., 2003).

Wang et al. (2004) interpret all the features in the ^2H-minus-^1H double-difference spectra between 1,720 and 1,670 cm^{-1} as originating exclusively from contributions from 9-keto C=O groups of the P700 Chl. They do not take into account the likely possibility that some of these features are due to protein C=O bands shifting upon $^1H/^2H$ exchange of the NH group. Upon making the hypothesis that the 1,639 cm^{-1} band is due to the 9-keto group of P_A, they calculate that $^1H/^2H$ exchange of the OH group of Thr A739 should lead to a 2–3 cm^{-1} downshift of the 9-keto mode of P_A and they indeed observe a downshift by 3 cm^{-1} of the 1,639 cm^{-1} band. It is therefore difficult to understand why they reject the assignment of the 1,639 cm^{-1} band to the 9-keto group of P_A. We also note that the result of this calculation contrasts their previous assertion that the latter mode "should downshift considerably upon uniform ^2H-labeling of PS I" (Wang et al., 2003).

The results of the global labeling study led Wang et al. (2004) to reject their previous assignment of the 1,655/1,639 cm^{-1} differential signal to the C_4=C_5 imidazole mode of the two His side chains acting as axial ligands to the P700 Chls. However, no alternative assignment for this large signal is provided. Furthermore, it is surprising that this signal is still considered as originating from a perturbation of the C_4=C_5 imidazole mode in the most recent publication from the same group (Li et al., 2004).

A FTIR study of the effect of mutations targeting the side chains of PsaB amino acids close to P700 has been recently reported (Breton et al., 2005). In this work, the residue Tyr B718 of *Synechocystis* sp. PCC 6803, homologous to the Thr A739 residue donating a strong hydrogen bond to the 9-keto carbonyl of P_A, was changed for a Thr side chain. The $P700^+$/P700 FTIR difference spectrum of this mutant provides evidence that the 9-keto carbonyl of P_B and P_B^+ engages a relatively strong hydrogen bond in a significant fraction (40 ± 10%) of the reaction centers. Additional mutations on the two PsaB residues homologous to those involved in the main interactions between the PsaA polypeptide and the 10a-carbomethoxy groups of P_A affect only marginally the vibrational frequency of the 10a-ester C=O group of P_B. The FTIR data on single, double, and triple mutants at these PsaB sites indicate a plasticity of the interactions of the carbonyl groups of P_B with the surrounding protein. However, these mutations do not perturb the hydrogen bonding interactions assumed by the 9-keto and 10a-ester C=O groups of P_A and P_A^+ with the protein and have only a limited effect on the relative charge distribution between P_A^+ and P_B^+.

References

Breton J (2001) Fourier transform infrared spectroscopy of primary electron donors in type I photosynthetic reaction centers. Biochim Biophys Acta 1507: 180–193

Breton J and Nabedryk E (1993) $S_0 \rightarrow T_1$ infrared difference spectrum of the triplet state of the primary electron donor in *Rb. sphaeroides* photosynthetic reaction centers. Chem Phys Lett 213: 571–575

Breton J and Nabedryk E (1996) Protein-quinone interactions in the bacterial photosynthetic reaction center: light-induced FTIR difference spectroscopy of the quinone vibrations. Biochim Biophys Acta 1275: 84–90

Breton J, Nabedryk E and Parson WW (1992) A new electronic transition of the oxidized primary electron donor in bacterial reaction centers: a way to assess resonance interactions between the bacteriochlorophylls. Biochemistry 31: 7503–7510

Breton J, Nabedryk E, Allen JP and Williams JC (1997) Electrostatic influence of Q_A reduction on the IR vibrational mode of the 10-a ester C=O of H_A demonstrated by mutations at residues Glu L104 and Trp L100 in reaction centers from *Rhodobacter sphaeroides*. Biochemistry 36: 4515–4525

Breton J, Nabedryk E and Leibl W (1999) FTIR study of the primary electron donor of photosystem I (P700) revealing delocalization of the charge in $P700^+$ and localization of the triplet character in ^{3}P700. Biochemistry 38: 11585–11592

Breton J, Xu W, Diner BA and Chitnis P (2002) The two histidine axial ligands of the primary electron donor chlorophylls (P700) in photosystem I are similarly perturbed upon $P700^+$ formation. Biochemistry 41: 11200–11210

Breton J, Chitnis P and Pantelidou M (2005) Evidence for hydrogen bond formation to the PsaB chlorophyll of P700 in photosystem I mutants of *Synechocystis* sp. PCC 6803. Biochemistry 44: 5402–5408

Fujiwara M and Tasumi M (1986) Metal-sensitive bands in the Raman and infrared spectra of intact and metal-substituted chlorophyll *a*. J Phys Chem 90: 5646–5650

Goldsmith JO, King B and Boxer SG (1996) Mg coordination by amino acid side chains is not required for assembly and function of the special pair in the photosynthetic reaction center. Biochemistry 35: 2421–2428

Hamacher E, Kruip J, Rögner M and Mäntele W (1996) Characterization of the primary electron donor of photosystem I, P700, by electrochemistry and Fourier transform infrared (FTIR) difference spectroscopy. Spectrochim Acta A 52: 107–121

Hasegawa K, Ono T and Noguchi T (2002) *Ab initio* density functional theory calculations and vibrational analysis of zinc-bound 4-methylimidazole as a model of a histidine ligand in metalloenzymes. J Phys Chem A 106: 3377–3390

Hastings G (2001) Time-resolved step-scan Fourier transform infrared and visible absorption difference spectroscopy for the study of photosystem I. Appl Spectrosc 55: 894–900

Hastings G, Ramesh VM, Wang R, Sivakumar V and Weber A (2001) Primary donor photo-oxidation in photosystem I: a re-evaluation of ($P700^+ -$ P700) Fourier transform infrared difference spectra. Biochemistry 40: 12943–12949

Iwaki M, Andrianambinintsoa S, Rich P and Breton J (2002) Attenuated total reflection Fourier transform infrared spectroscopy of redox transitions in photosynthetic reaction centers: comparison of perfusion- and light-induced difference spectra. Spectrochim Acta A 58: 1523–1533

Jordan P, Fromme P, Witt HT, Klukas O, Saenger W and Krauß N (2001) Three-dimensional structure of cyanobacterial photosystem I at 2.5 Å resolution. Nature 411: 909–917

Käss H, Fromme P, Witt HT and Lubitz W (2001) Orientation and electronic structure of the primary donor radical cation $P_{700}^{+\cdot}$ in photosystem I: a single crystal EPR and ENDOR study. J Phys Chem B 105: 1225–1239

Kim S and Barry BA (2000) Identification of carbonyl modes of P700 by *in situ* chlorophyll labeling in photosystem I. J Am Chem Soc 122: 4980–4981

Kim S, Sacksteder CA, Bixby KA and Barry BA (2002) A reaction-induced FT-IR study of cyanobacterial photosystem I. Biochemistry 40: 15384–15395

Krabben L, Schlodder E, Jordan R, Carbonera D, Giacometti G, Lee H, Weber AN and Lubitz W (2000) Influence of the axial ligands on the spectral properties of P700 of photosystem I: a study of site-directed mutants. Biochemistry 39: 13012–13025

Krauß N, Schubert W-D, Klukas OP, Fromme P, Witt HT and Saenger W (1996) Photosystem I at 4 Å resolution represents the first structural model of a joint photosynthetic reaction centre and core antenna system. Nature Struct Biol 3: 965–973

Leibl W, Brettel K, Nabedryk E, Breton J, Rochaix J-D and Redding K (1998) Effect of PsaB-His656→Leu mutation on optical and infrared difference spectra of P700 photooxidation. In: Garab G (ed) Photosynthesis: Mechanisms and Effects, Vol I, pp 595–598. Kluwer Academic Publishers, Dordrecht, The Netherlands

Li Y, Lucas M-G, Konovalova, T, Abbott B, MacMillan F, Petrenko A, Sivakumar V, Wang R, Hastings G, Gu F, van Tol J, Brunel L-C, Timkovich R, Rappaport F and Redding K (2004)

Mutations of the putative hydrogen-bond donor to P700 of photosystem I. Biochemistry 43: 12634–12647

Mäntele W (1993) Infrared vibrational spectroscopy of the photosynthetic reaction center. In: Deisenhofer H and Norris JR (eds) The Photosynthetic Reaction Center, Vol II, pp 239–283. Academic Press, San Diego

Mäntele W, Wollenweber A, Rashwan F, Heinze J, Nabedryk E, Berger G and Breton J (1988) Fourier transform infrared spectroelectrochemistry of the bacteriochlorophyll *a* anion radical. Photochem Photobiol 47: 451–455

Mezzetti A, Seo D, Leibl W, Sakurai H and Breton J (2003) Time-resolved step-scan FTIR investigation of the reaction center from the green sulfur bacterium *Chlorobium tepidum*. Photosynth Res 75: 161–169

Nabedryk E (1996) Light-induced Fourier transform infrared difference spectroscopy of the primary electron donor in photosynthetic reaction centers. In: Mantsch HH and Chapman D (eds) Infrared Spectroscopy of Biomolecules, pp 39–81. Willey-Liss, New York

Nabedryk E, Leonhard M, Mäntele W and Breton J (1990) Fourier transform infrared difference spectroscopy shows no evidence for an enolization of chlorophyll *a* upon cation formation either in vitro or during P700 photooxidation. Biochemistry 29: 3242–3247

Nabedryk E, Leibl W and Breton J (1996) FTIR spectroscopy of primary donor photooxidation in photosystem I, *Heliobacillus mobilis*, and *Chlorobium limicola*. Comparison with purple bacteria. Photosynth Res 48: 301–308

Nabedryk E, Schulz C, Müh F, Lubitz W and Breton J (2000) Heterodimeric versus homodimeric structure of the primary electron donor in *Rhodobacter sphaeroides* reaction centers genetically modified at position M202. Photochem Photobiol 71: 582–588

O'Malley PJ (2000) The effect of oxidation and reduction of chlorophyll *a* on its geometry, vibrational and spin density properties as revealed by hybrid density functional methods. J Am Chem Soc 122: 7798–7801

O'Malley PJ and Collins SJ (2001) The effect of axial Mg ligation on the geometry and spin density distribution of chlorophyll and bacteriochlorophyll cation free radical models: a density functional study. J Am Chem Soc 123: 11042–11046

Pantelidou M, Chitnis P and Breton J (2004) FTIR spectroscopy of *Synechocystis* 6803 mutants affected on the hydrogen bonds to the carbonyl groups of the PsaA chlorophyll of P700 supports a model of extensive delocalization of the charge in $P700^+$. Biochemistry 43: 8380–8390

Parson WW, Chu Z-T and Warshel A (1990) Electrostatic control of charge separation in bacterial photosynthesis. Biochim Biophys Acta 1017: 251–272

Plato M, Krauß N, Fromme P and Lubitz W (2003) Molecular orbital studies of the primary electron donor P700 of photosystem I based on a recent X-ray single crystal analysis. Chem Phys 294: 483–499

Redding K, MacMillan F, Leibl W, Brettel K, Hanley J, Rutherford AW, Breton J and Rochaix J-D (1998) A systematic survey of conserved histidines in the core subunits of photosystem I by site-directed mutagenesis reveals the likely axial ligands of P_{700}. EMBO J 17: 50–60

Sivakumar V, Wang R and Hastings G (2003) Photooxidation of P740, the primary electron donor in photosystem I from *Acaryochloris marina*. Biophys J 85: 3162–3172

Tavitian B, Nabedryk E, Mäntele W and Breton J (1986) Light-induced Fourier transform infrared (FTIR) spectroscopic investigations of primary reactions in photosystem I and photosystem II. FEBS Lett 201: 151–157

Wang R, Sivakumar V, Li Y, Redding K and Hastings G (2003) Mutation induced modulation of hydrogen bonding to P700 studied using FTIR difference spectroscopy. Biochemistry 42: 988–9897

Wang R, Sivakumar V, Li Y, Johnson TW and Hastings G (2004) FTIR difference spectroscopy in combination with isotope labeling for identification of the carbonyl modes of P700 and $P700^+$ in photosystem I. Biophys J 86: 1061–1073

Weber AN and Lubitz W (2001) P700: the primary electron donor of photosystem I. Biochim Biophys Acta 1507: 61–79

Witt H, Schlodder E, Teutloff C, Niklas J, Bordignon E, Carbonera D, Kohler S, Labahn A and Lubitz W (2002) Hydrogen bonding to P700: site-directed mutagenesis of threonine A739 of photosystem I in *Chlamydomonas reinhardtii*. Biochemistry 41: 8557–8569

Chapter 19

Primary Charge Separation Between P700* and the Primary Electron Acceptor Complex A-A_0: A Comparison with Bacterial Reaction Centers

Vladimir A. Shuvalov*, Andrei G. Yakovlev
Laboratory of Photobiophysics, Belozersky Institute of Chemical and Physical Biology of Moscow State University, Moscow 119899, Russia

L. G. Vasilieva, Anatoly Ya. Shkuropatov
Institute of Basic Biological Problems, Russian Academy of Sciences, Pushchino, Moscow Region 142290, Russia

Summary

The mechanism of charge separation and the stabilization of separated charges in photosystem I (PS I) is considered in comparison with reaction centers (RCs) in bacteria. The analysis of the X-ray crystal structures of the RCs together with psec and fsec studies of charge separation coupled to nuclear motion in the system provides new insight into the problem. A psec study of PS I RCs has shown that the primary charge separation takes place between P700* and the A-A_0 complex. The three-dimensional structure of both the primary electron donor and acceptor shows a possible pathway for electron transfer between P700 and the A-A_0 complex that is governed by nuclear motions. A fsec study of a coherent formation of the nuclear wavepacket on the potential energy surface of the excited state of the primary electron donor P* and of the charge separated state P^+A^- (where A is the primary electron acceptor) in native, pheophytin-modified and mutant reaction centers of *Rhodobacter spaeroides* was compared with X-ray and psec data for PS I RCs. A mechanism of the charge separation and stabilization of separated charges in PS I RCs is proposed.

I. Introduction

The primary charge separation in reaction centers (RCs) of oxygenic organisms and photosynthetic bacteria occurs between the excited state of the primary

*Author for correspondence, email: shuvalov@issp.serpukhov.su

John H. Golbeck (ed): Photosystem I: The Light-Driven Plastocyanin:Ferredoxin Oxidoreductase, 291–300.

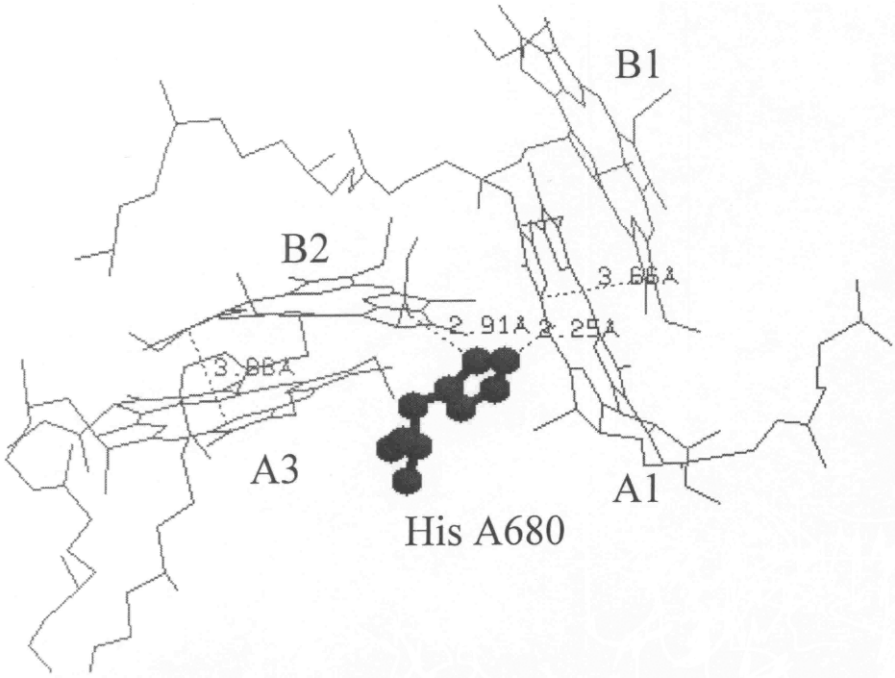

Fig. 1. The mutual arrangement of the Chl molecules of the primary electron donor P700 (A1 and B1) and the primary electron acceptor complex A − A_0 (B2 and A3) according to X-ray structure (Jordan et al., 2001). Central Mg ions of A1 and B1 are ligated to histidines A680 and B660, respectively. The Mg ion of B2 is coordinated to the water molecule hydrogen-bonded to side chains of Asn B591 (not shown). The central Mg ion of A3 is coordinated to the sulfur atom of Met B668 (not shown). Numbers show the distances in Å.

electron donor [the chlorophyll (Chl) dimer P700 in photosystem I (PS I), P680 in photosystem II (PS II), and the bacteriochlorophyll (BChl) dimer P870 in bacteria] and the primary chlorophyll electron acceptor [A_0(Chl-690) in PS I (Shuvalov et al., 1986), Chl–pheophytin in PS II (Klimov et al., 1977; Shuvalov and Heber, 2003) and BChl-800 in bacteria (Shuvalov et al., 1978), respectively]. These electronic interactions are consistent with the X-ray structure analysis of PS I (Jordan et al., 2001), PS II (Kamiya and Shen, 2003), and purple bacterial RCs (Michel et al., 1986; Komiya et al., 1988), showing a close proximity between the primary electron donor and the monomeric Chl in PS I and PS II, and the monomeric BChl in bacterial RCs. In contrast to PS II and bacterial RCs, in which (bacterio)pheophytin ((B)Pheo) functions as the electron acceptor, in PS I the primary electron transfer cofactors are entirely Chls.

II. Mutual Arrangement and Spectral Properties of the Primary Electron Donor and Acceptors

The P700 Chl molecules (B1 is a Chl *a* and A1 is a C-13^2 Chl *a* epimer designated *a*′) are located in close proximity to the C_2 axis near the lumenal side of PS I (Fig. 1). The perpendicular plane-to-plane distance between two Chls in P700 is 3.6 Å (Jordan et al., 2001). Rings I and II of these molecules overlap partially with the Mg^{2+} ions, which are separated by 6.3 Å. The perfect overlap of rings I of the two Chls is a characteristic feature of P700. The central Mg^{2+} atoms of the Chls constituting P700 as well as of other PS I Chls are coordinated by axial ligands provided by two protein subunits PsaA and PsaB (Jordan et al., 2001). For P700, these ligands are HisA680 and HisB660. This type of coordination is similar to that found for P870 BChls in bacterial RCs. Interestingly, the transmembrane α-helices A-i and A-k and the water molecule in

Abbreviations: A1 and B1 – chlorophyll molecules of the primary electron donor P700 in photosystem I; B2 and A3 – chlorophyll molecules of A-A_0 electron acceptor complex in photosystem I, respectively; B_A and H_A – bacteriochlorophyll and bacteriopheophytin molecules, respectively, of primary and secondary electron acceptors in bacterial reaction centers; PA and PB – bacteriochlorophylls of the primary electron donor P870.

PS I can donate hydrogen bonds to PA1, whereas no hydrogen bonding to PB1 is found. The latter molecule is populated by ~80% of the spin density localized on $P700^+$ (Kass et al., 2001). In contrast, PA1 should have maximal electron spin density in the excited state $P700^*$ according to calculations by Plato et al. (1988). All these features are similar to those observed for bacterial P870.

A second pair of Chls (nearest to P700), called the accessory Chls, or A2 and B2, are located about 7 Å toward the central part of the membrane (Jordan et al., 2001). They are ~10 Å distant from the C_2 axis, and their porphyrin planes show similar angles of 27° and 31° relative to the membrane normal, respectively. The center-to-center distances between the P700 Chls and the accessory Chls are 11–12 Å. The mutual orientation of accessory Chls with respect to P700 is very similar to that of the accessory BChls-800 (B_A and B_B) in bacterial RCs (Michel et al., 1986; Komiya et al., 1988). The A2 and B2 chlorophylls are not involved in any hydrogen bonds. Their Mg^{2+} ions are unusually coordinated by water molecules hydrogen-bonded to side chains of AsnA640 and AsnB591, respectively (Jordan et al., 2001).

Recent measurements of the formation of the 1,020-nm absorption band characteristic of the radical anion band of BChl (B_A) have provided clear evidence that Ba is the primary electron acceptor in purple bacterial RCs (Arlt et al., 1993; Schmidt et al., 1995; Kennis et al., 1997; Yakovlev et al., 2002, 2003; Shuvalov and Yakovlev, 2003). The spectroscopic data obtained on PS I have indicated that the $(A_0^- - A_0)$ absorption difference spectrum had some contribution from A2 and B2 (Hastings et al., 1995). This observation is consistent with the 3.9 Å distance between rings I of B2 and A3 (of the third pair of Chl molecules called the electron acceptor A_0) both representing an acceptor complex A-A_0 (Fig. 1; Jordan et al., 2001).

The third pair of Chls A3 and B3 has the closest edge-to-edge distance of 13 Å with respect to Chls of P700 and are located close to the central part of the thylakoid membrane (Jordan et al., 2001). These positions are similar to those occupied by BPheo molecules in bacterial RCs, one of which, BPheo H_A, serves as the secondary electron acceptor (Shuvalov and Klimov, 1976). A_0 is thought to be a first spectroscopically-resolved electron acceptor in PS I (Shuvalov et al., 1986). Notably, the A_0 Chl molecules of both pigment branches are unusually coordinated by the sulfur atoms of MetA688 and MetB668 (distance Mg–S is about 2.6 Å), respectively (Jordan et al., 2001). This type of coordination together with hydrogen bonding between the hydroxyl groups of tyrosine YA696 and YB676 and the keto-oxygens of rings V of A3 and B3 (Jordan et al., 2001) may determine the unusual low-redox potential of A_0 of about −1.02 V (Brettel, 1997). The specific spectroscopic properties of A_0 (the position of the central absorption band around 685–695 nm (Shuvalov et al., 1986; Fig. 2) suggests that it is not a monomeric pigment but most likely a product of a resonance interaction between B2 and A3 and between A2 and B3 (Fig. 1). The findings that the components of these pigment pairs are in close contact with each other (ring I-to-ring I distance of 3.9 Å) and that their chlorin planes are roughly parallel (Fig. 1) would be consistent with such a suggestion.

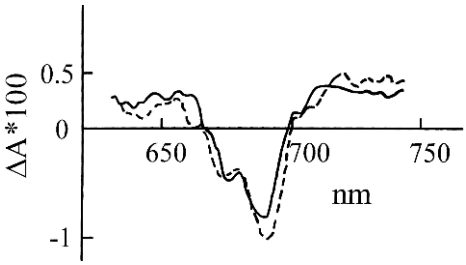

Fig. 2. Difference absorption spectra of $(A_0^- - A_0)$ obtained by subtraction of the spectrum of $(P700^+ - P700)$ from the psec difference spectra measured at 21 psec in the presence of neutral electron acceptors (dashed) and at 370 psec in the presence of reduced electron acceptors (A_1 and Fe–S centers) (solid) in photosystem I complexes excited at 710 nm and at 293 K. (From Shuvalov et al. (1986))

III. Kinetics of Primary Charge Separation and Secondary Electron Transfer

The kinetics of formation and decay of $P700^+A_0^-$ have been measured using different approaches. The papers in the field reveal common features in spite of differences in the preparations (PS I samples from cyanobacteria, green algae, and higher plants were employed). From optical measurements, it has been concluded that in spinach PS I particles, the formation and decay of $P700^+A_0^-$ occurs in less than 10 psec and within 32 psec, respectively (Shuvalov et al., 1986). The decay of $P700^+A_0^-$ in a PS II deletion mutant from the cyanobacteria *Synechocystis* sp. occurred within 21 psec under high excitation-intensity conditions (Hastings et al., 1994). For three species of PS I, the equilibration process between energy transfer and charge separation was

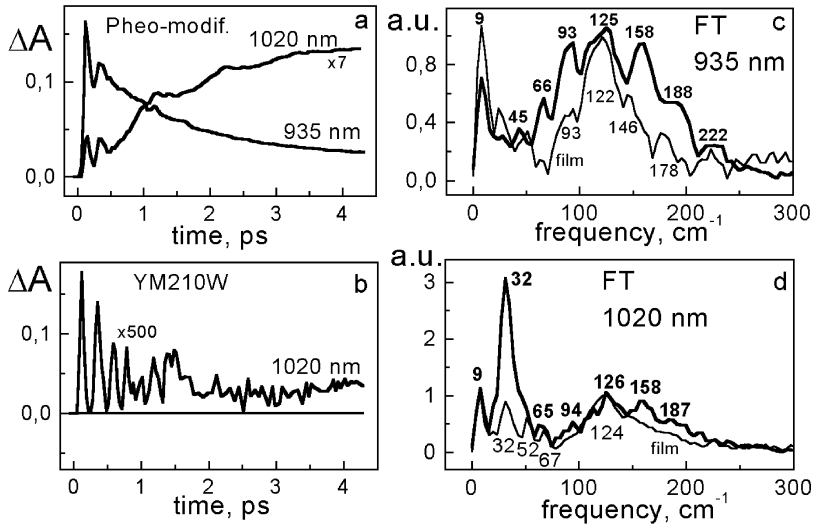

Fig. 3. (a) Kinetics of the 935-nm band of the P* stimulated emission and of the 1,020-nm absorption band of the state $P^+B_A^-$ in Pheo-modified *Rb. sphaeroides* R-26 RCs. (b) Kinetics of the 1,020-nm band of the $P^+B_A^-$ state in the YM210W mutant RCs of *Rb. sphaeroides* and in their dry film (close to zero line). (c) Spectra of Fourier transform of the oscillatory part of the 935-nm kinetics for Pheo-modified RCs of *Rb. sphaeroides* R-26 (thick curve) and for their dry film (thin curve). (d) Spectra of Fourier transform of the oscillatory part of the 1,020-nm kinetics for Pheo-modified R-26 RCs (thick) and for their dry film (thin). Measurements were performed at 90 K using 20-fsec excitation at 870 nm. (From Yakovlev et al. (2002b))

found to be within 3.7–7.5 psec, and reoxidation of A_0^- within 20 psec (Hastings et al., 1995). The charge separation time was estimated to be 1–4 psec in a *Synechocystis* sp. PCC 6803 mutant, in which PS I was the sole chromophore in the photosynthetic membrane (DiMango et al., 1995). The primary charge separation rate in PS I of maize was estimated to be 1–2 $psec^{-1}$ (Croce et al., 1996). The radical pair $P700^+A_0^-$ formed with the 1.3 psec rise kinetics after creation of P700* and decayed within ~13 psec in *Synechocystis* sp. PCC 6803 (Savikhin et al., 2001) (see Savikhin, this volume, Chapter 12). This decay kinetics is faster than that found by other groups. In spinach PS I particles containing only 12–13 Chls per P700 the rise time of $P700^+$ was biphasic: 0.8 psec (50%) and 9 psec (50%) (Kumazaki et al., 2001). In PS I of *Acaryochloris marina* that contains Chl *d* instead of Chl *a*, the rise and decay of the primary charge separation proceed with time constants of 7.2 and 50 psec, respectively (Kumazaki et al., 2002). The study of the primary charge separation by ps photovoltage measurements revealed the rise and decay time of $P700^+A_0^-$ within 22 and 50 psec, respectively (Hecks et al., 1994). The longer rise time for $P700^+A_0^-$ formation could be due to a limited time resolution of the photovoltage experiments. The average values for the rise and decay time of $P700^+A_0^-$, calculated from all above-mentioned data, are about 3.7 and 33 psec, respectively. The charge separation time in PS I is consistent with that observed for bacterial RCs between P870* and B_A [about 3.5 psec at room temperature (Yakovlev et al., 2002a)].

IV. The Comparison of Mechanisms of the Primary Charge Separation in Photosystem I and Bacterial Reaction Centers

A. A Possible Electron Transfer Pathway

The close similarity of the mutual arrangements of the pigments in PS I and in bacterial RCs suggests a common mechanism of charge separation and stabilization of separated charges. Therefore, it is reasonable to consider these mechanisms for PS I in comparison with those studied intensively in purple bacteria, for which the positions of all atoms in the RC are known (Michel et al., 1986; Komiya et al., 1988).

Vos and coauthors (1993, 1994, 2000) have suggested to use laser pulses with duration of less than 30 fsec to produce nuclear wavepackets on the potential energy surface of the excited state P*, thereby providing a powerful tool to study electron transfer (ET) reactions between pigments. Coherent fsec spectroscopy offers also the possibility to register vibrational and rotational modes of some molecular groups involved in charge separation. Thus low frequency modes in the

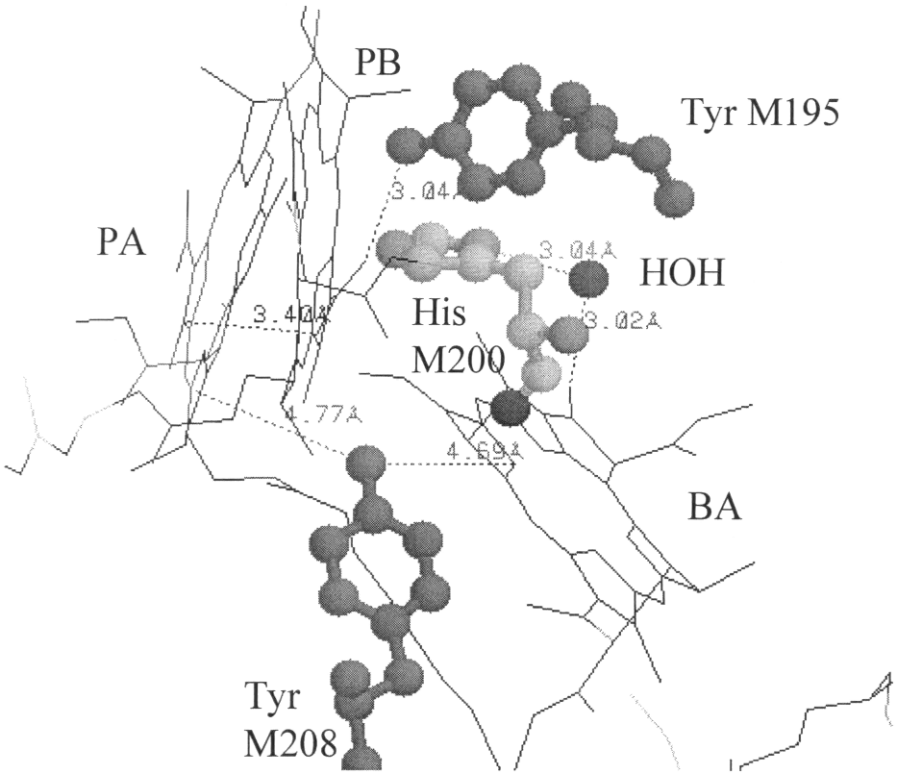

Fig. 4. View (Brookhaven Protein Data Bank, number 1PRC) of special pair of bacteriochlorophylls PA and PB, monomeric bacteriochlorophyll B_A of *Rps. viridis* RCs. His M200, liganding the Mg ion of PB, is connected by hydrogen bond via H_2O to oxygen of the keto carbonyl group of ring V of B_A. Thus PB is connected to B_A via a sequence of the following polar groups: $Mg(P_B)$–N–C–N(His M200)–H–O–H(water)–O=B_A which could represent a pathway for the electron transfer from P* to B_A. The rotation of the water molecule in such a system with 32 cm^{-1} frequency and its overtones is induced by the electron flow from P* to B_A. Oxygen of acetyl group of ring I of PB is hydrogen-bonded to oxygen of Tyr M195 (analogous to M197 in *Rb. sphaeroides* RCs). The distance between oxygen of Tyr M208 (analogous to M210 in *Rb. sphaeroides* RCs) is about 4.7 Å from PA and B_A atoms having maximal electron spin density for P^+ and B_A^- (see text for details). Numbers show the distances in Å.

range of 10–500 cm^{-1} were found in the oscillatory part of the kinetics of the decay of the stimulated emission from P870*. Further developments of these studies are provided by the measurements of fsec oscillations in the product kinetics at 1,020 nm, representing the formation of the radical anion of the primary electron acceptor Ba [BChl monomer in the photoactive A-branch absorbing at 800 nm in *Rhodobacter* (*Rb*) *sphaeroides* RCs] (Yakovlev et al., 2002a,b, 2003; Shuvalov and Yakovlev, 2003). It has been found that fsec oscillations in the product kinetics are in phase with fsec oscillations in the decay kinetics of the P* stimulated emission in the long-wavelength band at 940 nm and out-of-phase with those of the short-wavelength emission of P* at 900 nm. The Fourier transform of the oscillatory part of the kinetics at 940 and 1,020 nm includes two main bands, one of which belongs to the vibrational mode at ∼130 cm^{-1} and another associated with the water HOH55 rotational mode at 32 cm^{-1} with its overtones (Fig. 3).

The activation of the 32 cm^{-1} rotation mode with its overtones has been suggested to be due to the electron transfer from P* to Ba via a set of polar groups N–Mg(PB)–N–C–N(HisM202)–HOH55–O=(Ba), containing water molecule at the position 55 (see Brookhaven Protein Data Bank, 1AIJ; Fig. 4). This chain seems *not* to be conserved in PS I RCs (Jordan et al., 2001).

The vibrational mode at ∼130 cm^{-1} represents some nuclear motions that are of particular interest. Water evaporation from *Rb. sphaeroides* RCs is accompanied by a considerable decrease of the 32 cm^{-1} mode and its higher overtones both in the decay kinetics of stimulated emission from P* and in the product kinetics at 1,020 nm (Fig. 3). Remarkably, the mode at 130 cm^{-1} was not influenced by water removal. A similar mode at 150 cm^{-1} has also been observed in the YM210L mutant of *Rb. sphaeroides* in which the rate of primary charge separation was strongly slowed down by replacement of tyrosine M210 for leucine. The mutation

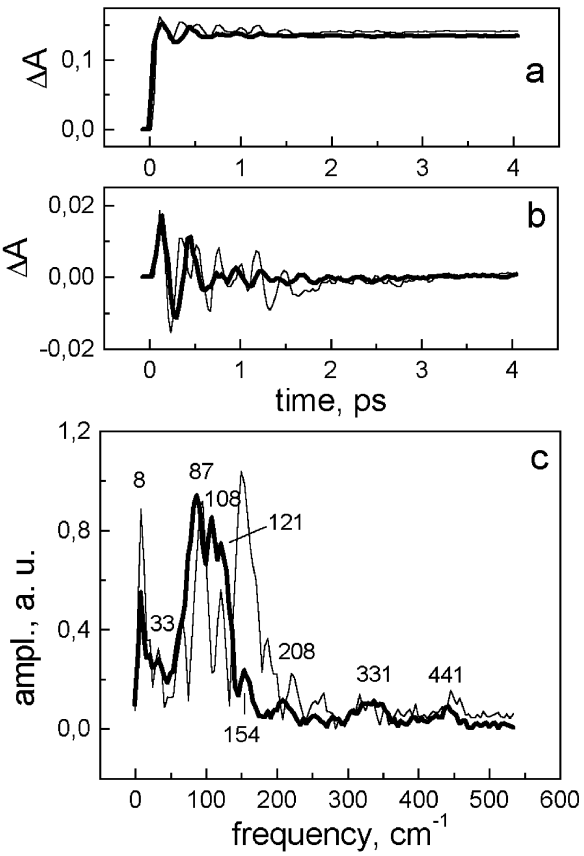

Fig. 5. Femtosecond kinetics of ΔA (a), its oscillatory part (b), and the spectrum of Fourier transform of the oscillatory part (c) for the 935-nm band in RCs of mutant YM210L (thin) and double mutant YM210L/FM197Y (thick) of *Rb. sphaeroides* in glycerol-TT buffer at 90 K. RCs were excited by 20-fsec pulses at 870 nm. Figure for YM210L mutant is from Yakovlev et al. (2003).

YM210L leads to the simplest pattern of the oscillations in the kinetics at 940 and at 1,020 nm, showing a reversible electron transfer between P* and B_A in the absence of the stabilization of separated charges in the state $P^+B_A^-$ (Yakovlev et al., 2003; see Fig. 5). These facts suggest that the 130–150 cm^{-1} mode is not related to ET reactions but reflects properties of the primary electron donor P870.

To obtain more information on the origin of the 130–150 cm^{-1} mode, we studied fsec oscillations in RCs of the double mutant YM210L/FM197Y of *Rb. sphaeroides.* In addition to the simplification of the kinetics caused by the YM210L mutation, the second mutation introduced a new tyrosine residue at the position M197 that was found to donate a hydrogen bond to the acetyl carbonyl group of ring I of PB (Kuglstatter et al., 1999). Note that a similar bond is naturally observed in RCs from *Rps. viridis* (Fig. 4; Michel et al., 1986), in which primary ET rates are even higher than in *Rb. sphaeroides* RCs. One could suggest that the new hydrogen bonding to PB provided by the FM197Y mutation might affect the vibrational modes activated by light excitation of P (Fig. 4).

Figures 5 and 6 show that in the YM210L/FM197Y double mutant RCs, the frequency of the initial oscillations in the kinetics of P* stimulated emission at 940 nm and in the product kinetics at 1,020 nm are shifted from 150⁻ to ∼100 cm^{-1}. This frequency shift to a lower value seems to result from an increase of the effective mass of some part of the oscillating molecular group (retarding its motion) and can be tentatively rationalized in terms of hydrogen bond formation. An increase of the effective mass of the acetyl group of the pyrrol ring I of PB is because of its involvement in the hydrogen bond with OH-TyrM197 would mean that the pyrrol ring I of PB is involved in the nuclear motion induced by fsec excitation of P. A similar low-frequency shift has been observed for the P* stimulated emission in RCs of the FM197H mutant of *Rb. sphaeroides* (Vos et al., 1993, 1994, 2000) due possibly to formation of a new hydrogen bond between the acetyl carbonyl of ring I of PB and HisM197 (Michel et al., 1986). In the symmetrical HL168F mutant, in which the natural hydrogen bond between the acetyl carbonyl group of ring I of PA and HL168 was removed, the frequency changes were not so evident (Rischel et al., 1998).

In the light of this assumption, the fsec oscillations with the frequencies in the range of 130–150 cm^{-1} found in the kinetics of both stimulated emission from P* and the product $P^+B_A^-$ reflect the motion of PB with respect to PA in the space of overlapping of rings I of PA and PB. One of the consequences of this motion might be the formation of an excited molecular complex by a charge transfer interaction similar to the well-known appearance of excimer and exciplex complexes between aromatic cycles of excited dyes in a solution (Beens and Weller, 1975). These molecular dimers formed in the excited state of dyes are characterized by a parallel orientation of conjugated electron systems of two molecules with a partial charge transfer from one molecule to another. Eximer and exciplex formation is accompanied by a long-wavelength shift of the fluorescence with respect to the monomeric dyes. It is reasonable to expect the formation of such excited dimers between two (B)Chls in P870 and P700 when ring I of PB is in a position closest to ring I of PA. The appearance of the long-wavelength stimulated emission from P* at 940 nm could be interpreted as a result

of a "dynamic" formation of the exciplex between PA and PB.

Using theoretical calculations, it has been found (Plato et al., 1988) that in the excited state P* the charge between PA and PB is not equally distributed, but is shifted from PA to PB in the proportion of 0.74–0.24 (see Lubitz, this volume, Chapter 17). This would mean that when wavepacket is created on the P* potential energy surface the nuclear motion of PB with respect to PA is accompanied by a long-wavelength shift of stimulated emission and by charge transfer from PA to PB. When the distance between the pyrrol rings I of PA and PB is the closest, the maximal electron spin density displacement from PA to PB occurs, and the maximal long-wavelength shift of the stimulated emission from P* takes place.

The measurements of the product kinetics at 1,020 nm provide new insight to this problem. The similarity of the FT spectra for the 935 and 1,020 nm kinetics in the YM210L mutant and their similar changes in the double mutant YM210L/FM197Y show that the low frequency modes seen in the P* stimulated emission are active in the ET process between P* and B_A. The appearance of the stimulated emission at 940 nm is accompanied by the appearance of an electron on the B_A molecule (Figs. 5 and 6). This can be taken as an additional indication of the charge redistribution between PA and PB ($PA^{\delta+}PB^{\delta-}$) in P*. In other words, it is reasonable to suggest that the formation of a component with the $PA^{\delta+}PB^{\delta-}$ character in the P* state leads to ET from $PB^{\delta-}$ to B_A via a polar bridge N–Mg(PB)–N–C–N(HisM202)–HOH55–O=(B_A) connecting PB and B_A (see Fig. 4).

A detailed inspection of the mutual arrangement of the Chls of P700, including the B1 and A1 molecules, and of the electron acceptor complex $A-A_0$ including B2 and A3 demonstrates that both the donor and acceptor are constituted by a Chl dimer with perfect overlap of rings I in each case (Fig. 1). This is a striking, new feature of the arrangement of the primary electron donor and acceptor systems in PS I RCs that is not realized in bacterial (Michel et al., 1986) and PS II (Kamiya and Shen, 2003) RCs. In bacterial RCs the overlap of any of the rings of B_A and H_A is not observed (Michel et al., 1986; Komiya et al., 1988). The mutual arrangement of donor and acceptor Chl dimers in PS I (Jordan et al., 2001) can suggest a possible mechanism of charge separation between P700* and the $A-A_0$ complex.

The question about the pathway of the electron transfer from P700 to $A-A_0$ is of interest for further discussion. The closest distance of 3.7 Å between the two dimers is represented by the distance between the two methyl groups of ring I of A1 and ring III of B2 (Fig. 1). However, both groups are hydrophobic and not involved in the conjugated systems of macrocycles of A1 and B2. According to calculations of Plato et al. (1988), the maximal electron spin density in the excited state of dimer P* is located on the nitrogen atoms of rings II and III of PB in bacterial RCs or correspondingly of A1 in PS I RCs (Kass et al., 2001). Then, the most effective pathway for ET from P700* to A_0 would be as follows: N(II, IV)–Mg(A1)–NCH(His A680)–O(B2). From Fig. 1, one can find that His A680 closest to nitrogen atoms coordinating Mg^{2+} of A1 (N atoms of rings II and IV are mostly populated by electron spin density in P* according to Plato et al., 1988) is surrounded by three oxygen atoms of ring

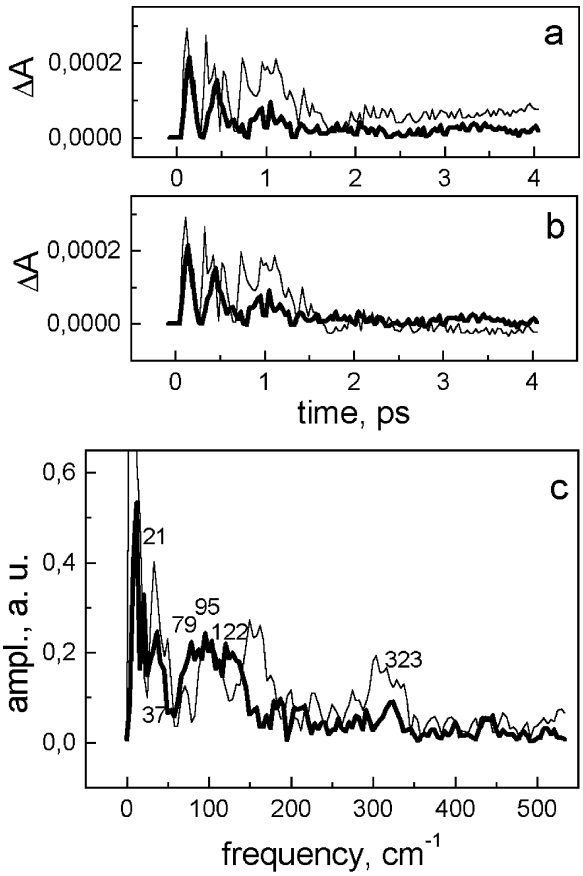

Fig. 6. Femtosecond kinetics of ΔA (a), its oscillatory part (b), and the spectrum of Fourier transform of the oscillatory part (c) for the 1,020-nm band in RCs of mutant YM210L (thin) and double mutant YM210L/FM197Y (thick) of *Rb. sphaeroides* in glycerol-TT buffer at 90 K. RCs were excited by 20-fsec pulses at 870 nm. Figure for YM210L mutant is from Yakovlev et al. (2003).

V of B2 with minimal distance of 2.9 Å between His A680 and B2. If H atom of the CH group of His is taken into consideration, then this distance can be decreased by 1 Å. Thus, the ET from P700* to A_0 might be carried out via His A680 collecting an electron density of A1 in P700* and transmitting it to the oxygen atoms of ring V of B2.

B. Stabilization of Separated Charges in Photosystem I and Bacterial Reaction Centers

In bacterial RCs, the stabilization of separated charges on $P870^+$ and B_A^- was considered in terms of the participation of the OH group of TyrM210 (Shuvalov and Yakovlev, 2003; Yakovlev et al., 2003). In fact, TyrM210 (M208 in *Rps. viridis*) is separated by 4.8 Å from the closest C atom of ring IV of PA, having maximal electron spin density on $P870^+$ and by 4.7 Å from the N atom of ring II of B_A, having maximal spin density on the radical anion B_A^-, according to (Plato et al., 1988).

As mentioned above, fsec oscillations in the kinetics at 935 and 1,020 nm are observed in the mutant YM210W at 90 K; these oscillations demonstrate the simplest pattern observed until now (Fig. 3). The decay of the stimulated emission at 935 nm and the accumulation of the state $P^+B_A^-$ are considerably delayed, especially at low temperature (up to ~300 psec at 90 K) in agreement with earlier observations (see Vos et al., 1996 for refs.). Even in this case, seven peaks of fsec oscillations with a low amplitude are observed in both kinetics with a period of ~215 fsec and a frequency of ~145 cm^{-1} (Figs. 5 and 6).

For a dynamic stabilization of $P^+B_A^-$ two possibilities can be considered. (i) An electron from P* is transferred to the higher vibrational level on the $P^+B_A^-$ potential energy surface followed by vibrational relaxation to the lowest level according to well-known models (see Bixon et al., 1988 for refs.). (ii) Stabilization takes place due to a reorientation of surrounding groups when $P^+B_A^-$ is reversibly formed. In the latter case, the symmetrical arrangement of the potential surfaces of P* and $P^+B_A^-$ can be realized with the maximal possible rate of ET from P* to B_A. When the nuclear wavepacket motion on the P* surface approaches the intercrossing point between two surfaces, both states, P* and $P^+B_A^-$, are registered. The wavepacket goes back to the P* surface if there are no additional changes in the nuclear position. However, these changes can be induced by reorientation of the surrounding polar group such as $O^{\delta-}H^{\delta+}$ of TyrM210 (TyrM208 in *Rhodopseudomonas viridis*; Fig. 4). In the absence of YM210, the oscillations with period of 215 fsec at 1,020 nm are not perturbed within ~1.5 psec (Fig. 3b). It would mean that the motion of $H^{\delta+}$of OH-TyrM210 toward B_A^- could lower the energy of $P^+B_A^-$ with respect to that of P*, thus stopping coherent oscillations in the system (the oscillations are suppressed within 0.5 psec, not shown).

The estimations of the energy difference in the system were performed (Yakovlev et al., 2003) for two positions of $H^{\delta+}$ of OH-TyrM210 with respect to P_A and B_A having mostly positive and negative charges, respectively, in $P^+B_A^-$ (Plato et al., 1988). In the first position, a dipole $O^{\delta-}H^{\delta+}$ of TyrM210 is perpendicular to a line running between C–N(IV) of P_A and N(II) of B_A, which are the closest neighbors to TyrM210 and mostly populated by positive and negative charges, respectively, in the state $P^+B_A^-$ (Plato et al., 1988). This position was suggested to correspond to the neutral states PB_A or P^*B_A. In the second position, $H^{\delta+}$ of OH-TyrM210 is on a line connecting $O^{\delta-}$ of OH-TyrM210 and N(II) of B_A. This position is assumed to be realized when $H^{\delta+}$ is attracted and repulsed by B_A^- and P_A^+, respectively, in the stabilized state $P^+B_A^-$. The energy difference between two positions was estimated to be ~890 cm^{-1}. The experimental energy difference between P* and $P^+B_A^-$ in the stabilized state $P^+B_A^-$ in Pheo-modified RCs was found to be 350–550 cm^{-1} (Shuvalov and Yakovlev, 1998). Thus, the energy of 890 cm^{-1} is enough to stabilize an electron on B_A^- if $H^{\delta+}$ of OH-TyrM210 is shifted to B_A direction during charge separation.

The presence of a similar tyrosine in the structure of PS I RC is not evident. Indeed, TyrA735 and TyrA603 (and ThrA743) (Jordan et al., 2001) are too far from B2 and A3 to influence considerably the free energy of $P700^+A_0^-$. Other candidates for a stabilizing function might be water molecules coordinating Mg^{2+} in B2 and A2 (Jordan et al., 2001). The most interesting process that could participate in the charge stabilization between $P700^+$ and $A–A_0^-$ might be related to the change in the distance between overlapping rings I of B2 and A3 when an electron is transferred to $A-A_0$ complex. However, the mechanism of the stabilization of the separated charges in PS I needs to be clarified.

Acknowledgments

We thank V. A. Shkuropatova and T. I. Bolgarina for help in RCs preparation. Support by Russian Basic

Research Foundation, INTAS, NWO (The Netherlands), ISTS (N2296) and PCB RAS grants are gratefully acknowledged.

References

Arlt T, Schmidt S, Kaiser W, Lauterwasser C, Meyer M, Scheer H and Zinth W (1993) The accessory bacteriochlorophyll: a real electron carrier in primary photosynthesis. Proc Natl Acad Sci USA 90: 11757–11761

Beens H and Weller A (1975) Excited molecular π-complexes in solution. In: Birks JB (ed) Organic Molecular Photophysics, Vol 11, pp 159–215. John Willey & Sons, London

Bixon M, Jortner J, Plato M, and Michel-Beyerle ME (1988) Mechanism of the primary charge separation in bacterial photosynthetic reaction centers. In: Breton J and Vermeglio A (eds) The Photosynthetic Bacterial Reaction Center: Structure and Dynamics, pp 379–388. Plenum Press, New York

Brettel K (1997) Electron transfer and arrangement of the redox cofactors in photosystem I. Biochim Biophys Acta 1318: 322–373

Croce R, Zucchelli G, Garlaschi FM, Bassi R and Jennings RC (1996) Excited state equilibration in the photosystem I-light-harvesting I complex: P700 is almost isoenergetic with its antenna. Biochemistry 35: 8572–8579

DiMagno L, Chan CK, Jia Y, Lang MJ, Newman JR, Mets L, Fleming GR and Haselkorn R (1995) Energy transfer and trapping in photosystem I reaction centers from cyanobacteria. Proc Natl Acad Sci USA 92: 2715–2719

Hastings G, Kleinherenbrink FAM, Lin S, McHugh TJ and Blankenship RE (1994) Observation of the reduction and re-oxidation of the primary electron acceptor in photosystem I. Biochemistry 33: 3193–3200

Hastings G, Hoshina S, Webber AN and Blankenship RE (1995) Universality of energy and electron transfer processes in photosystem I. Biochemistry 34: 15512–15522

Hecks B, Wulf K, Breton J, Leibl W and Trissl H-W (1994) Primary charge separation in photosystem I: a two step electrogenic charge separation connected with $P700^+A_0^-$ and $P700^+A_1^-$ formation. Biochemistry 33: 8619–8624

Jordan P, Fromme P, Witt HT, Klukas O, Saenger W and Krauß N (2001) Three-dimensional structure of cyanobacterial photosystem I at 2.5 Å resolution. Nature 411: 909–917

Kamiya N and Shen J-R (2003) Crystal structure of oxygen-evolving photosystem II from *Thermosynechococcus vulcanus* at 3.7-Å resolution. Proc Natl Acad Sci USA 100: 98–103

Kass H, Fromme P, Witt HT and Lubitz W (2001) Orientation and electronic structure of the primary donor radical cation $P700^+$ in photosystem I: a single crystal EPR and ENDOR study. J Phys Chem B 105: 1225–1239

Kennis JTM, Shkuropatov AY, Stokkum IHM, Gast P, Hoff AJ, Shuvalov VA and Aartsma TJ (1997) Formation of a long-lived $P^+B_A^-$ state in plant pheophytin-exchanged reaction centers of *Rhodobacter sphaeroides* R26 at low temperature. Biochemistry 36: 16231–16238

Klimov VV, Klevanik AV, Shuvalov VA and Krasnovsky AA (1977) Reduction of pheophytin in the primary light reaction of photosystem II. FEBS Lett 82: 183–186

Komiya H, Yeates TO, Rees DC, Allen JP and Feher G (1988) Structure of the reaction center from *Rhodobacter sphaeroides* R-26 and 2.4.1: symmetry relations and sequence comparisons between different species. Proc Natl Acad Sci USA 85: 9012–9016

Kuglstatter A, Hellwig P, Fritzsch G, Wachtveitl J, Oesterhelt D, Mantele W and Michel H (1999) Identification of a hydrogen bond in the Phe M197→Tyr mutant reaction center of the photosynthetic purple bacterium *Rhodobacter sphaeroides* by X-ray crystallography and FTIR spectroscopy. FEBS Lett 463: 169–174

Kumazaki S, Ikegami I, Furusava H, Yasuda S and Yoshikhara K (2001) Observation of the excited state of the primary electron donor chlorophyll (P700) and the ultrafast charge separation in the spinach photosystem I reaction center. J Phys Chem B 105: 1093–1099

Kumazaki S, Abiko K, Ikegami I, Iwaki M and Itoh S (2002) Energy equilibration and primary charge separation in chlorophyll *d*-based photosystem I reaction center isolated from *Acaryochloris marina*. FEBS Lett 530: 153–157

Michel H, Epp O and Deisenhofer J (1986) Pigment–protein interactions in the photosynthetic reaction centre from *Rhodopseuudomonas viridis*. EMBO J 5: 2445–2451

Plato M, Lendzian F, Lubitz W, Trankle E and Mobius K (1988) Molecular orbital studies on the primary donor P960 in bacterial centers of *Rps. viridis.* In: Breton J and Vermeglio A (eds) The Photosynthetic Bacterial Reaction Center: Structure and Dynamics, pp 379–388. Plenum Press, New York

Rischel C, Spiedel D, Ridge JP, Jones MR, Breton J, Lambry J-L, Martin J-L and Vos MH (1998) Low frequency vibrational modes in protein: charges induced by point-mutations in the protein–cofactor matrix of bacterial reaction centers. Proc Natl Acad Sci USA 95: 12306–12311

Savikhin S, Xu W, Martinsson P, Chitnis PR and Struve WS (2001) Kinetics of charge separation and $A_0^- \rightarrow A_1$ electron transfer in photosystem I reaction centers. Biochemistry 40: 9282–9290

Schmidt S, Arlt T, Hamm P, Huber H, Nagele T, Wachtveitl J, Zinth W, Meyer M and Scheer H (1995) Primary electron-transfer dynamics in modified bacterial reaction centers containing pheophytin-a instead of bacteriopheophytin-a. Spectrochimica Acta part A 51: 1565–1578

Shuvalov VA and Heber U (2003) Photochemical reactions in dehydrated photosynthetic organisms, leaves, chloroplasts and photosystem II particles: reversible reduction of pheophytin and chlorophyll and oxidation of β-carotene. Chem Phys 294: 227–237

Shuvalov VA and Klimov VV (1976) The primary photoreactions in the complex cytochrome-P890 P760 (bacteriopheophytin-760) of *Chromatium minutissimum* at low redox potentials. Biochim Biophys Acta 440: 587–599

Shuvalov VA and Yakovlev AG (1998) Energy level of P^+B^- with respect to P^* found from recombination fluorescence measurements in pheophytin-modified reaction centers. Membr Cell Biol (Moscow) 12: 563–569

Shuvalov VA and Yakovlev AG (2003) Coupling of nuclear wavepacket motion and charge separation in bacterial reaction centers. FEBS Lett 540: 26–34

Shuvalov VA, Klevanik AV, Sharkov AJ, Matveetz A and Krukov PG (1978) Picosecond detection of BChl-800 as an intermediate electron carrier between selectively-excited P870

and bacteriopheophytin in *Rhodospirillum rubrum* relaction centers. FEBS Lett 91: 135–139

Shuvalov VA, Nuijs AM, van Gorkom HJ, Smit HW and Duysens LNM (1986) Picosecond absorbance changes upon selective excitation of the primary electron donor P700 in photosystem I. Biochim Biophys Acta 850: 319–323

Vos MH, Rappoport F, Lambry J-C, Breton J and Martin J-L (1993) Visualization of coherent nuclear motion in a membrane protein by femtosecond spectroscopy. Nature 363: 320–325

Vos MH, Jones MR, Hunter CN, Breton J, Lambry J-C and Martin J-L (1994) Coherent dynamics during the primary electron-transfer reaction in membrane-bound reaction centers of *Rhodobacter sphaeroides*. Biochemistry 33: 6750–6757

Vos MH, Jones MR, Breton J, Breton J, Lambry J-C and Martin J-L (1996) Vibrational dephasing of long- and short-lived primary donor excited states in mutant reaction centers of *Rhodobacter sphaeroides*. Biochemistry 35: 2687–2692

Vos MH, Rischel C, Jones MR and Martin J-L (2000) Electrochromic detection of a coherent component in the formation of the charge pair $P^+H_L^-$ in bacterial reaction centers. Biochemistry 39: 8353–8361

Yakovlev AG, Shkuropatov AY and Shuvalov VA (2002a) Nuclear motion between P^* and $P^+B_A^-$ potential surface with a subsequent electron transfer to H_A in bacterial reaction centers. 1. Room temperature. Biochemistry 41: 2667–2674

Yakovlev AG, Shkuropatov AY and Shuvalov VA (2002b) Nuclear motion between P^* and $P^+B_A^-$ potential surface with a subsequent electron transfer to H_A in bacterial reaction centers at 90 K; possible electron transfer pathway. Biochemistry 41: 14019–14027

Yakovlev AG, Vasilieva LG, Shkuropatov AY, Bolgarina TI, Shkuropatova VA and Shuvalov VA (2003) Mechanism of charge separation and stabilization of separated charges in reaction centers of *Chloroflexus aurantiacus* and of YM210W(L) mutants of *Rhodobacter sphaeroides* excited by 20 fs pulses at 90 K. J Phys Chem A 107: 8330–8338

Chapter 20

Fourier Transform Infrared Studies of the Secondary Electron Acceptor, A_1

Gary Hastings*
Department of Physics and Astronomy, Georgia State University, Atlanta, GA 30303, USA

Summary

Fourier transform infrared (FTIR) difference spectroscopy is a useful tool for the study of the structural details of electron transfer cofactors (and their binding sites) in photosynthetic complexes. To date, most FTIR difference spectroscopic studies of photosynthetic complexes have been static experiments in the sense that a steady-state population of an excited state species is photo-accumulated. In intact Photosystem I (PS I) particles the $P700^+A_1^-$ state is short-lived, and not easily studied using static FTIR difference techniques. Time-resolved techniques are required. In this article the use of time-resolved step-scan FTIR difference spectroscopy for the study of the $P700^+A_1^-$ state in intact PS I particles from cyanobacteria is described. With reliable $P700^+A_1^-$ FTIR difference spectra it is possible to construct A_1^-/A_1 FTIR difference spectra. The main obstacle to obtaining reliable A_1^-/A_1 FTIR difference spectra is the sensitivity of the time-resolved step-scan FTIR approach. Until now, no A_1^-/A_1 FTIR difference spectra have been obtained using intact PS I particles. In this article, recent work in our lab is described where we have used low-temperature (77 K), time-resolved step-scan FTIR difference spectroscopy to generate A_1^-/A_1 FTIR difference spectra for intact cyanobacterial PS I particles that are unlabeled, deuterated,

*Author for correspondence, email: ghastings@gsu.edu

John H. Golbeck (ed): Photosystem I: The Light-Driven Plastocyanin:Ferredoxin Oxidoreductase, 301–318.

^{15}N, and ^{13}C labeled. From a consideration of the isotope-induced band-shifts, assignments for specific bands in the difference spectra are proposed.

I. Electron Transfer Processes in PS I

Knowledge of the timescales of the various electron transfer (ET) processes in Photosystem I (PS I) under various sets of conditions is essential for deciding which approach to take in time-resolved step-scan FTIR difference spectroscopic (TRSS FTIR DS) measurements (see section IV). Therefore, a very brief summary of the time constants governing relevant ET processes in PS I will be presented.

Upon photo-excitation of P700 an electron is transferred to a nearby Chl-*a* acceptor called A_0 (Brettel, 1997). The photo-generated radical pair is stabilized by further ETs. From A_0 an electron is transferred to A_1 [a phylloquinone (PhQ) molecule, also called vitamin K_1], then to F_x (an iron sulfur cluster) and then to a terminal set of iron-sulfur clusters designated $F_{A/B}$ (Brettel, 1997).

In PS I two symmetrical sets of ET cofactors are bound to the two membrane-spanning protein subunits called PsaA and PsaB. In this article the cofactors that are bound to PsaA and PsaB will be distinguished. The PhQs bound to PsaA and PsaB will be called A_{1-A} and A_{1-B}, respectively. Similarly, the primary electron accepting chlorophyll cofactors will be called A_{0-A} and A_{0-B}. Finally, the pigments of P700 bound to PsaA and PsaB will be called P_A and P_B, respectively.

In cyanobacterial PS I particles from *Synechocystis* sp. PCC 6803 at room temperature (RT) forward ET from A_1^- to F_X is characterized by time constants of ~10 and ~280 ns (Xu et al., 2003b). Both the fast and slow phases are observable at low temperature. The fast phase is temperature independent (Agalarov and Brettel, 2003). Since the fast phase has a lifetime of ~10 ns, it is impossible to study this transient species at any temperature using TRSS FTIR DS (see below). The slow phase shows a pronounced slowing as the temperature is decreased, with an activation energy of 110–220 meV (Schlodder et al., 1998). As the temperature is lowered, forward ET from A_1^- to F_X slows and is eventually replaced by $P700^+A_1^-$ recombination. At 77 K the slower phase has a lifetime of ~245 μs, and can be studied using TRSS FTIR instrumentation with 5 μs time resolution (see below).

In cyanobacterial PS I at RT $P700^+F_{A/B}^-$ recombines in tens to hundreds of milliseconds. At 77 K the $P700^+F_{A/B}^-$ state is formed irreversibly in ~35% of PS I particles (Schlodder et al., 1998). In ~20% of the PS I particles the radical pair states $P700^+F_X^-$ recombines in ~5–100 ms, while in ~35% of the particles $P700^+A_1^-$ recombines in ~245 μs (Schlodder et al., 1998). In static photo-accumulation experiments at 77 K, it is mainly the $P700^+F_X^-$ and $P700^+F_{A/B}^-$ states that are accumulated. The iron sulfur clusters do not contribute to FTIR DS in the 2,000–1,000 cm^{-1} region (Hastings et al., 2001). Therefore, the FTIR DS photo-accumulated at 77 K is purely due to P700 and $P700^+$, and will be simply referred to as the $P700^+$/P700 FTIR DS.

Up until recently it had been assumed that ET in PS I was unidirectional, as is the case in PS II and purple bacteria. Recently, however, it has been suggested that ET is bidirectional in PS I from *Chlamydomonas reinhardtii* (Guergova-Kuras et al., 2001). In PS I from *C. reinhardtii* forward ET from A_1^- to F_X is biexponential, and characterized by time constants of 13 and 143 ns that represent ET down both branches (Guergova-Kuras et al., 2001). From the amplitudes of the two kinetic phases it was suggested that there is approximately an equal amount of ET down each branch (Guergova-Kuras et al., 2001). In contrast, in cyanobacterial PS I particles from *Synechocystis* sp. PCC 6803, ET proceeds with lifetimes of 10 and 280 ns. However, ET is dominated by the slow phase, which represents ET down PsaA (Xu et al., 2003a,b). This fact, along with the results of Schlodder et al. (1998), indicate that the recombination reaction observed at 77 K is between $P700^+$ and A_{1-A}^-. So, TRSS FTIR DS measurements with 5 μs time resolution can be used to directly study A_{1-A} in cyanobacterial PS I at 77 K. This is in fact a useful and quite fortuitous result. The A_1^-/A FTIR DS will contain contributions from only one, rather than

Abbreviations: ADC – analog to digital converter; AU – absorbance units; A_{0-A} – primary electron acceptor in photosystem I bound to PsaA; A_{1-A} – secondary electron acceptor in photosystem I bound to PsaA; Chl-*a* – chlorophyll-*a*; C=O – carbonyl; C–O – semiquinone carbonyl; DS – difference spectra, spectrum, spectroscopic, or spectroscopy; ET – electron transfer; FTIR – Fourier transform infrared; μs – microsecond; ns – nanosecond; H-bond – hydrogen bond; P_A – chlorophyll of P700 bound to PsaA; PS I – photosystem I; PBRCs – purple bacterial reaction centers; PhQ – phylloquinone (2-methyl-3-phytyl-1,4-naphthoquinone); *Rb. – Rhodobacter; Rps. – Rhodopseudomonas* (now known as *Blastochloris*); RT – room temperature; TR – time-resolved; TRSS – time-resolved step-scan.

two, quinones. Therefore, analysis of the spectra will be considerably simplified.

II. Instrumentation for TRSS FTIR DS

FTIR DS has been applied to a number of large protein complexes (>100 kDa) (Braiman and Rothschild, 1988), including photosynthetic complexes (Mäntele, 1993, 1995; Nabedryk, 1996; Breton, 2001). Modern FTIR difference techniques routinely have sufficient sensitivities to detect single bonds in large proteins (Mäntele, 1993, 1995; Nabedryk, 1996; Breton, 2001). Most of the FTIR studies performed to date on pigment–protein complexes are static experiments in the sense that a steady-state population of an excited state species is accumulated. For example, at 77 K, $P700^+F_X^-$ recombines in 5–100 ms, and a static population can be easily photo-accumulated. For studies of transient intermediates with lifetimes in the nano-microsecond regime, static photo-accumulation experiments are difficult, if not impossible, and several new time-resolved approaches to FTIR DS have appeared (Gerwert, 2001). One of the most useful approaches is time-resolved step-scan FTIR difference spectroscopy (TRSS FTIR DS) (Uhmann et al., 1991). In this type of experiment, the interferometer mirror moves in discrete jumps, instead of moving smoothly and continuously as in normal FTIR experiments. At each discrete mirror position, samples are excited by a pulsed laser, for example, and a temporally digitized transient is obtained. Usually, the results of several laser flashes are averaged at each mirror step, to improve the signal-to-noise ratio. For studies of PS I in our lab, we typically average only 10–20 laser flashes at each step. The laser flash repetition rate is usually 10 Hz. Therefore, any single TRSS FTIR DS experiment requires accumulating results from typically thousands of laser flashes. TRSS FTIR DS requires that the systems studied must fully recover prior to each laser flash. A method for using TRSS FTIR DS to study irreversible systems has been outlined (Rammelsberg et al., 1999). However, this approach is difficult to implement and, so far, no other TRSS FTIR DS studies of irreversible systems have been reported.

A. Data Acquisition Times, Spectral Coverage, and Spectral Filtering

In TRSS FTIR DS the number of mirror steps depends on: (1) The spectral resolution required. (2) Whether single or double-sided interferograms are collected. (3) The spectral region one wishes to cover. For studies of PS I at 77 K (see below), we typically collect double-sided interferograms, with spectral resolution set at 4 cm^{-1}, covering the 2,105–1,060 cm^{-1} spectral region. This requires sampling the interferogram 946 times (946 mirror steps). If the laser is fired at 10 Hz, and the results of 20 laser flashes are coadded, then a single TRSS FTIR experiment requires 18,920 laser flashes, which requires at least 31.5 min to collect. For PS I we also typically average the results of 30–60 TRSS FTIR experiments. Thus the spectra from TRSS FTIR DS shown below have taken 15.75–31.5 h to collect. We have also undertaken TRSS FTIR DS experiments over the whole of the 5,000–1,000 cm^{-1} region (Anderson et al., 2001, 2002). In these experiments data was collected at a spectral resolution of 32 cm^{-1} or 64 cm^{-1}, to reduce the number of mirror steps (and hence the acquisition time) required to complete a step-scan run.

A crucial point for FTIR DS in general is that no probing light at frequencies outside the spectral region covered should reach the detector. Light with frequencies outside the spectral region covered are sampled (by the interferometer) and appear to have a frequency that is within the spectral region covered. This process is known as "folding" (Griffiths and de Haseth, 1986) and it leads to artifacts in the resulting spectra. To overcome this folding problem, optical filters are used to totally block light outside the spectral region of interest. If this light cannot be blocked, then the spectral region covered should be increased accordingly. For studies of PS I at 77 K, we typically filter the IR beam using two 2,000–1,000 cm^{-1} band-pass filters (Fig. 1). One is placed before the sample while the other is mounted directly onto the detector. The later filter prevents actinic laser light from reaching the detector. We also incorporate six CaF_2 windows into the system (two 4 mm thick windows to seal the interferometer sample compartment, two 4 mm thick windows for the cryostat shroud, and two 2 mm thick windows for the sample). These CaF_2 windows totally block all light below $\sim$1,200 cm^{-1}.

B. Factors Limiting Time Resolution in TRSS FTIR DS

The different setups for μs and ns TRSS FTIR DS are shown in Figs. 1A,B, respectively. The time resolution is determined by: (1) The laser pulse-width. (2) The detector response time. (3) The bandwidth of the analog to digital converter (ADC). Aspects of these three devices are discussed below.

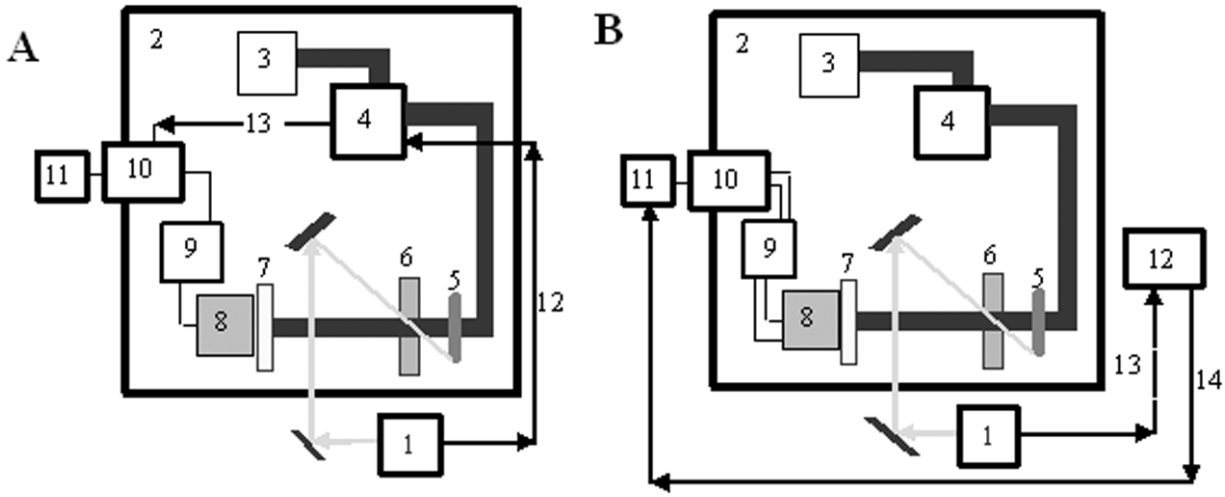

Fig. 1. Experimental Layout For (A) 5 μs and (B) 10 ns TRSS FTIR Measurements.
(A) 1. Q-Switched Nd:YAG laser. 8 ns pulses at 355, 532 and 1,064 nm. A 532 nm pumped. OPO is mounted inside the laser, and pulses from 680 to 2,200 nm can be produced; 2. FTIR spectrometer. Chamber is continuously purged with nitrogen gas; 3. Infrared output beam from a globar; 4. Interferometer equipped with KBr beamsplitter; 5. 1,000–2,000 cm^{-1} band-pass filter; 6. Sample; 7. 1,000–2,000 cm^{-1} band-pass filter; 8. MCT detector; 9. Fast preamplifier which can be AC or DC coupled. The DC coupled preamplifier has a variable offset; 10. 16-bit, 200 kHz ADC; 11. Computer; 12. Laser lamp firing triggers interferometer mirror to step; 13. Interferometer settles and triggers acquisition electronics. There is a 135 or 180 μs delay between the lamp firing and the laser pulse reaching the sample. (B) Components 1–7 are the same as A; 8. 200 MHz MCT detector with dual AC and DC coupled preamplifier outputs. The DC preamplifier also has variable offset; 9. AC and DC coupled amplifiers; 10. 100 or 40 MHz ADC boards; 11. Computer; 12. Stanford Research Systems Digital Delay generator; 13. Laser lamp firing sends a TTL signal to digital delay generator (12); 14 .Delay generator sends a trigger pulse to the acquisition electronics after a variable time delay, for example ∼179 μs. The interferometer mirror is also signaled to step. If the laser pulse is delayed 180 μs after the laser lamp fire, the laser pulse reaches the sample ∼1 μs after the acquisition has started.

1. Typically, Q-switched YAG lasers (coupled to a dye laser or optical parametric oscillators to generate excitation pulses with variable wavelength) are used in TRSS FTIR DS experiments. These lasers generally have pulse-widths of 5–10 ns and are not a major factor limiting time resolution.

2. The detector response is an important factor in TRSS FTIR DS experiments, with different detectors generally being used for μs and ns TRSS FTIR experiments. For μs TRSS FTIR experiments typically a mercury cadmium telluride (MCT) detector, with 0.2–1 MHz bandwidth, is used. In our lab we use a photoconductive MCT detector (Graseby D313). The detector surface area is 1 mm^2, and coupling the IR light into the detector is straightforward. The detector is connected to a 200 kHz preamplifier with both AC and DC coupled outputs. The DC offset can also be manually adjusted.

   For nanosecond time resolution higher bandwidth detectors are required. The bandwidth is limited by the detector RC time constant, so the detector element is smaller to overcome limitations imposed by the capacitance of the detector. In our laboratory and others, a 50 MHz photovoltaic MCT detector (Kolmar Technologies Model KMPV50-0.5-J2) is used. The detector element has a surface area of 0.5 mm^2, imposing slightly more restrictive specifications on the optical geometry. With the use of high-power parabolic or elliptical-turning mirrors this limitation is easily overcome, however. The detector is supplied with both AC and DC coupled outputs and the DC output can be manually offset. In our lab the DC signals are amplified using a fast preamplifier (Stanford Research Systems Model SR445) with $\times 125$ amplification possible. The preamplifier output is limited to ± 1 V, however. The AC signals can also be amplified. In our laboratory we use two 100 MHz $\times 10$ amplifiers (Kolmar Technologies mode KA100-2). In this case the amplified output can be up to ± 10 V.

3. In TRSS FTIR DS, time resolution is limited primarily by the analog to digital converter (ADC).

For 5 μs or 10 ns TRSS FTIR DS experiments typically 200 kHz, 16-bit or 100 MHz, 8-bit transient digitizers are used, respectively. These digitizers limit the time resolution to 5 μs or 10 ns, respectively. Transient digitizers can only offer 10 ns time resolution by sacrificing dynamic range or bit resolution (only 8-bit digitizers exist for 10 ns sampling intervals). This fact considerably complicates 10 ns TRSS FTIR DS (see section III.C).

C. Nanosecond TRSS FTIR DS

Interferometry requires very high dynamic range (Uhmann et al., 1991; Johnson and Zachmann, 2000), and any type of FTIR experiment is simplified considerably if a 16-bit digitizer can be used. Since only 8/12-bit digitizers are available for 10/40 ns TRSS FTIR DS, this represents a serious problem. A second problem is that 8/12-bit digitizers can only accept signals in the $\pm 1/\pm 4$ V range, whereas 16-bit digitizers can accept signals in the ± 10 V range. The effects on spectra resulting from data collected with ADCs with different dynamic ranges has been discussed (Griffiths and de Haseth, 1986). In addition, Johnson and Zachmann (2000), discuss the use of ADCs in TRSS FTIR spectroscopy. Finally, the noise level in an experiment also increases as the square root of the electronic bandwidth. The noise level is therefore higher for shorter timescale measurements. In summary, TRSS FTIR DS experiments with 10–40 ns time resolution are considerably more difficult than 5 μs time-resolved experiments: The dynamic range is reduced, the increased bandwidth increases the intrinsic noise level and the intensity of signals that can be accommodated by the ADC is reduced.

In TRSS FTIR experiments it is necessary to collect data with the detector output DC coupled (Johnson and Zachmann, 2000). Therefore, the smallest change in the interferogram measurable using an 8-bit or 12-bit digitizer (without considering noise) is ~0.39% or 0.025%, respectively. For PS I, many of the light-induced signals are likely to result in changes in the interferogram that are considerably less than 0.025% (see below). It is therefore obvious that TRSS FTIR DS experiments on PS I cannot easily be undertaken using a DC coupled detector with an 8- or 12-bit digitizer. In an attempt to overcome the limitations imposed in ns TRSS FTIR experiments a new electronic coupling scheme has been developed (Fig. 1B) (Uhmann et al., 1991; Hu et al., 1996). The basic idea is to AC couple the detector and measure only the flash-induced change in the intensity of the interferogram at each mirror step. The AC coupled signals can then be amplified to utilize the full dynamic range of the digitizer. However, the DC coupled signals are also required for Fourier transformation (Uhmann et al., 1991), so the step-scan measurement has to be repeated and data obtained with the detector DC coupled. In Uhmann et al. (1991), the DC and AC signals are monitored simultaneously using a novel, home-built, switching amplifier. However, for standard Bruker software and instrumentation, the AC and DC coupled TRSS FTIR measurements need to be performed separately. In addition, the precise amplification of the DC and AC signals needs to be known, and then used to correct the resultant single beam spectra. The change in absorption as a function of time can then be calculated using the equation; $\Delta A(\nu, t) = -\ln(1 + c\Delta I(\nu, t)/dI(\nu))$. Where c and d are the amplification factors applied to the AC and DC coupled signals. $I(\nu)$ is the static single beam spectrum, collected with the detector DC coupled. If the amplification factors c and d are not known precisely a baseline shift in the spectra will result. The fact that there is a significant delay between the collection of the DC and AC coupled signals is also disadvantageous, as baseline drift in the spectrometer will lead to noise in the resulting spectra.

For ns TRSS FTIR experiments in our laboratory, synchronization of the laser lamp firing to laser pulse emission and spectrometer data acquisition are controlled using a Stanford Research Systems digital delay generator (DCR35) (Fig. 1B).

Given the difficulties of ns TRSS FTIR DS, only a few reports have appeared describing its use for the study of large pigment–protein complexes (Hage et al., 1996; Hu et al., 1996; Rammelsberg et al., 1997, 1998). Previously, we have also described the use of ns TRSS FTIR DS (10 ns time resolution) for the study of intact PS I particles from *Synechocystis* sp. PCC 6803 at RT (Hastings, 2001). Using an 8-bit digitizer within the experimental scheme shown in Fig. 1B, over the first 500 ns we could only achieve a noise level of $\sim \pm 3.5 \times 10^{-4}$ [in absorbance units (AU)] with ~5 h of signal averaging at 10 Hz. This is inadequate for studies of A_1 reduction in PS I (see section IV.F).

D. Microsecond TRSS FTIR DS

Figure 1A shows an outline of instrumentation for 5 μs TRSS FTIR DS. Generally, a 16-bit, 200 kHz ADC is used, which limits the time resolution to 5 μs. No 16-bit ADCs with higher bandwidth are available. For 5 μs TRSS FTIR DS the DC coupled detector is connected

to an amplifier with variable offset. In our laboratory, for measurements over ~1 ms, we use the lamp firing of a Q-switched laser to synchronize the detection electronics to the laser pulse (the time between laser lamp firing and Q-switch triggering is variable, and can also be used to control the output pulse energy). Data acquisition is triggered by the laser lamp firing. After 135–180 μs the Q-switch is triggered and the laser pulse impinges on the sample. Therefore, at 5 μs time resolution, ~27–36 spectra are collected prior to sample excitation. This is ideal for measurements over 1–2 ms. For measurements over longer timescales (say 100 ms) the synchronization of the laser pulse and detector electronics will need to be controlled using a digital delay generator (Fig. 1B). For studies of PS I at 77 K we typically collect data over 1 ms. That is, 200 single-beam spectra are collected, 27–36 of which are prior to the laser flash. The single-beam spectra collected prior to the laser flash are averaged. This averaged spectrum is then ratioed directly against all single-beam spectra collected before and after the laser flash. In this way transmission difference spectra are obtained, which are then converted to absorption difference spectra. All spectral manipulations are undertaken using OPUS 4.0 software from Bruker Optics.

In our laboratory we have found that the procedure described above for 5 μs TRSS FTIR DS is the simplest approach. This approach has also been used for the study of other biological systems (Contzen and Jung, 1998; Koutsoupakis et al., 2002, 2003). Other authors have used the AC/DC coupling scheme, in combination with a 16-bit ADC (Mezzetti et al., 2003). In theory, this is a valid approach. However, we have found that, given similar data acquisition times, this approach always produces spectra of lower sensitivity when compared to spectra obtained using the simpler approach described above.

E. Instrumental Testing

Carbonmonoxy-myoglobin is a useful system for testing ns and μs TRSS FTIR DS instrumentation (Plunkett et al., 1995). Upon laser excitation of CO-myoglobin the CO dissociates from the heme and then recombines on the ms timescale (Plunkett et al., 1995). Heme bound CO absorbs at 1,944 cm^{-1} while free CO absorbs above 2,100 cm^{-1}. Thus laser excitation of CO-myoglobin results in sub-nsec bleaching at 1,944 cm^{-1} followed by a recovery on the ms timescale. Figure 2A shows the laser induced spectral changes in the 1,980–1,910 cm^{-1} region for CO-myoglobin. Figure 2B,C compares the μs and ns kinetics at 1,944 cm^{-1}. The noise level in the kinetics are described in the legend. Clearly TRSS FTIR DS with 10 ns resolution, in the 1,980–1,910 cm^{-1} region, is easily implemented if signals greater than $\sim 10^{-3}$ are to be detected. For 5 μs TRSS FTIR DS in the 1,980–1,910 cm^{-1} region, if signals are greater than $\sim 10^{-3}$ then very highly resolved kinetic information can be obtained. In the amide I region, where both protein and water absorb significantly, experiments are more difficult but still straightforward (Plunkett et al., 1995; Hu et al., 1996). In Fig. 2C it appears that the noise level is considerably increased during the first 500 ns. This is precisely the time region that high sensitivity is required for studies of intact PS I particles at RT, since forward ET from $P700^+A_1^-$ occurs in ~280 ns (Xu et al., 2003b).

F. Considerations Regarding the Production of $P700^+A_1^-/P700A_1$ TRSS FTIR DS

In static $P700^+$/P700 FTIR DS obtained using cyanobacterial PS I particles at RT, the most intense difference band is observed at 1,698(−)/1,718(+) cm^{-1}, with a peak to peak intensity of $\sim 2.5 \times 10^{-3}$ (in AU) (Hastings et al., 2001) at 80–90 K this band decreases in intensity to $\sim 0.5 \times 10^{-3}$ (Breton et al., 1999b; Kim et al., 2001). For PS I from *C. reinhardtii* at RT a maximal difference band is observed at 1,700(−)/1,716(+) cm^{-1}, with a peak to peak intensity of $\sim 0.6 \times 10^{-3}$ (Hastings et al., 2001). At 77 K this band decreases in intensity to $\sim 0.2 \times 10^{-3}$ (data not shown). Taking into account that; (1) the decay of a band needs to be measured in TRSS FTIR DS experiments, (2) the kinetics of lower amplitude difference bands also need to be measured, and (3) at 77 K, with a laser repetition rate of 10 Hz, there may be increased contributions from irreversibly oxidized P700, a useful TRSS FTIR DS for PS I at 77 K would require a sensitivity of ~20–40 times higher than the largest signal in the $P700^+$/P700 FTIR DS. That is, a noise level of ~3–1.5 $\times 10^{-5}$ or 10–5 $\times 10^{-6}$ is required for TRSS FTIR DS studies of PS I from *Synechocystis* sp. PCC 6803 or *C. reinhardtii*, respectively. These numbers can be approximately doubled for measurements at RT. However, in this case $P700^+A_1^-$ decays in less than 300 ns. From previous 10 ns TRSS FTIR DS measurements on PS I particles from *Synechocystis* sp. PCC 6803 at RT, we have shown that it is practically impossible to reach a noise level of 6×10^{-5} using an 8-bit ADC (Hastings, 2001). Previous ns TRSS FTIR DS studies on other biological systems also indicate that this is the case (Hu et al., 1996). However, it is feasible to

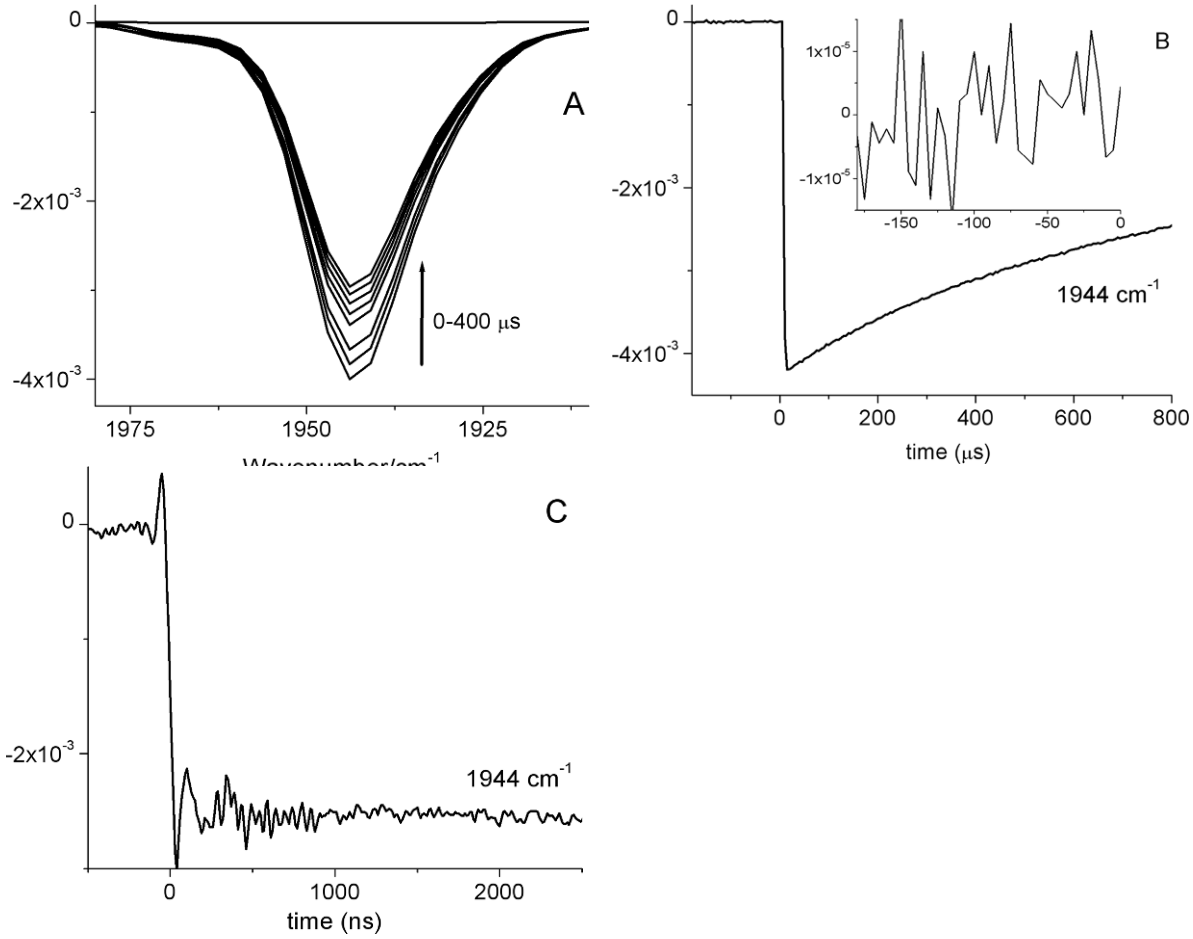

Fig. 2. (A) TRSS FTIR DS obtained following a 532 nm laser flash of carbonmonoxy-myoglobin in the 1,980–1,910 cm^{-1} region. At each mirror step the results of 40 laser flashes were averaged. Data collected using a 16-bit digitizer with time resolution set at 5 μs. A spectrum is shown every 50 μs. Data was collected in ∼1 h. (B) Time course of absorption changes at 1,944 cm^{-1}. The inset shows an expanded view of the portion of the kinetic prior to the laser flash, and indicates that the noise level is $\pm 1.5 \times 10^{-5}$ AU. (C) Time course of absorption changes at 1,944 cm^{-1} in carbonmonoxy-myoglobin, obtained using an 8-bit digitizer. Data was collected in 10 ns increments using the scheme outlined in Fig. 1B. The trace is the average of 14 measurements, each of which took 1 h. The noise level is ± 3–4×10^{-4} AU in the first 500 ns and less than $\pm 1 \times 10^{-4}$ beyond ∼1 μs. (G. Hastings, unpublished)

reach a noise level of 1.5×10^{-5} in 5 μs TRSS FTIR DS measurements using a 16-bit ADC (Fig. 2B). So, if the $P700^+A_1^-$ state can be made to decay with a lifetime greater than 5 μs, highly resolved TRSS FTIR DS can be produced. Although the $P700^+A_1^-$ radical pair state decays in ∼245 μs in cyanobacterial PS I at 77 K (Schlodder et al., 1998), this allows the possibility of recording highly sensitive TRSS $P700^+A_1^-/P700A_1$ FTIR DS. So A_1 reduction in PS I is most easily studied using TRSS FTIR DS at or near 77 K. In PS I from *C. reinhardtii* the FTIR difference signals are about a factor of three smaller than the corresponding signals obtained using PS I from *Synechocystis* sp. PCC 6803. To achieve similar signal to noise ratios in *C. reinhardtii* and *Synechocystis* sp. PCC 6803 FTIR DS the signal averaging would need to be increased by a factor of nine for experiments on *C. reinhardtii*. For 5 μs TRSS FTIR DS measurements of PS I from *Synechocystis* sp. PCC 6803 we typically signal average for 15–30 h. So for studies of PS I from *C. reinhardtii* we would need to signal average 135–270 h (5.6–11.2 days). So TRSS FTIR DS studies of A_1 reduction in PS I from *C. reinhardtii* are quite impractical, although not impossible.

For the reasons outlined above we have concentrated our TRSS FTIR DS studies of A_1 reduction using cyanobacterial PS I from *Synechocystis* sp. PCC 6803 and *Synechococcus* sp. PCC 7002. Since charge separation is mainly unidirectional down the A-branch in

cyanobacterial PS I, TRSS FTIR DS studies at 77 K will probe A_{1-A}.

III. Previous TRSS FTIR DS Studies of Photosynthetic Systems

TRSS FTIR DS has not been widely used to study the reaction dynamics in photosynthetic systems. TRSS FTIR DS at a temporal resolution of 10 μs was used to study the $P^+Q_A^-$ and ^3P states in PBRCs from *Rhodobacter (Rb) sphaeroides* at 90 K (Burie et al., 1993). Since these spectra can be obtained using static FTIR DS (Breton and Nabedryk, 1993), this report merely demonstrates that TRSS FTIR DS might be a useful tool. Brudler and Gerwert (1998) have also used TRSS FTIR DS to study $P^+Q_A^-$ and $P^+Q_B^-$ in PBRCs from *Rb. sphaeroides.* Again, these spectra are of limited value, since they are easily obtained using static, or rapid-scan FTIR DS (Mezzetti et al., 2002). Recently, we reported on the use of ns and μs TRSS FTIR DS for the study of PS I (Hastings, 2001). In this report it was shown that it is doubtful that ns TRSS FTIR DS will be useful for studies of PS I. The reported experiments on PS I were conducted at RT, so the only state being studied in the 5 μs TRSS FTIR DS experiments is P700. These TRSS FTIR DS are also of limited value since $P700^+$/P700 FTIR DS can be obtained using static FTIR DS. However, these RT studies allowed stringent instrumental testing as the signals are considerably weaker than those obtained using PBRCs. More recently, a preliminary report on the use of 5 μs TRSS FTIR DS for the study of A_1 in intact PS I from *Synechocystis* sp. PCC 6803 at 77 K was reported (Hastings and Sivakumar, 2001). In these experiments some baseline drift of the TRSS FTIR DS was observed that was related, at least in part, to the laser pulse heating the sample. However, we also showed that precise kinetic information could still be derived from the data. Since then these difficulties have been overcome by using very low laser excitation intensities (<1 mJ per pulse, spread out over a spot diameter of 1 cm) and/or by changing the excitation wavelength to 700 nm.

TRSS FTIR DS at a temporal resolution of 5 μs has also been used to study the $P^+_{840}FeS^-$ and $^3P_{840}$ states in the green sulfur bacterium *Chlorobium tepidum* (Mezzetti et al., 2003). The $^3P_{840}$ state was generated using particles stripped of their terminal iron sulfur clusters. The iron sulfur clusters were removed by incubating the intact particles in high concentrations of urea. The AC/DC coupling scheme described in section III.C below was used with a 16-bit ADC. As described above, it is doubtful if this is a wise approach. These authors do not mention if or how the different amplifications of the AC and DC signals are corrected to produce absorbance difference spectra. Possibly not surprisingly, kinetic data at various IR wavelengths were not presented in this study.

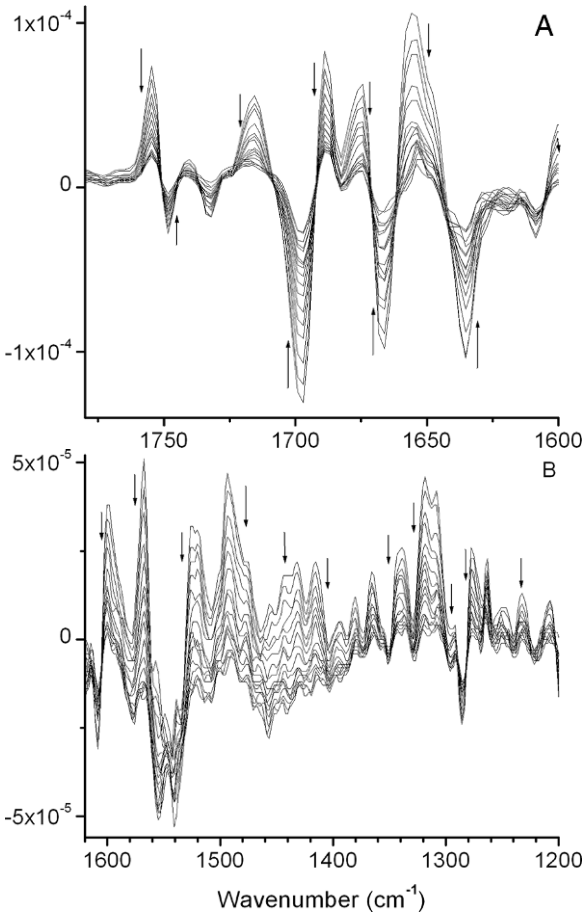

Fig. 3. TRSS $P700^+A_1^-$/$P700A_1$ FTIR DS obtained in the 1,780–1,600 (*top*) and 1,620–1,200 (*bottom*) cm^{-1} regions following 532 nm laser excitation of trimeric PS I particles from *Synechococcus* sp. PCC 7002 at 77 K. Each spectrum is the average of nine spectra collected in 5 μs increments. Thus each spectrum in the figure is separated by 45 μs. The arrows show the direction in which the difference bands are decaying. The spectra are the average of 36 TRSS FTIR experiments on three different samples. Adapted from Sivakumar et al., 2005.

IV. TRSS A_1^-/A_1 FTIR DS Obtained Using Intact Cyanobacterial PS I Particles

Figure 3A,B shows TRSS $P700^+A_1^-$/$P700A_1$ FTIR DS in the 1,770–1,250 cm^{-1} region obtained using PS I

particles from *Synechococcus* sp. PCC 7002 at 77 K. Clearly, even the decay of the weaker bands are easily discernible in the spectra. Each spectrum is the average of nine spectra collected in 5 μs increments. Figure 4 shows the time course of the absorption changes at 1,754, 1,748, and 1,495 cm^{-1}. The kinetics shown are for specific wavelengths that are limited only by the instrumental resolution. Only three frequencies are shown in Fig. 4. However, kinetics have been obtained every 2.06 cm^{-1}, at over 500 frequencies. The kinetic data show the absorption change in each 5 μs interval, and have not been averaged over longer temporal intervals, unlike the spectra in Fig. 3. In addition, the data in Fig. 4 have not been averaged over larger spectral intervals, as we have done previously (Hastings and Sivakumar, 2001). Finally, no baseline correction has been applied to any of the data in Figs. 3 or 4.

Figure 5 demonstrates one method for construction of pure A_1^-/A_1 FTIR DS from static and TRSS FTIR DS obtained using intact PS I particles from *Synechococcus* sp. PCC 7002 at 77 K. The $P700^+A_1^-/P700A_1$ FTIR DS shown in Fig. 5 is the first spectrum after the laser flash in Fig. 3. The $P700^+/P700$ FTIR DS was obtained separately in a static photo-accumulation experiment. The two spectra were normalized so that the 1,716(+)/1,698(−) cm^{-1} difference bands were similar in amplitude. The spectrum that results from direct subtraction of the $P700^+/P700$ FTIR DS from the $P700^+A_1^-/P700A_1$ FTIR DS is also shown in Fig. 5, and is labeled as the A_1^-/A_1 FTIR DS.

Figure 6, spectra b and a, shows ^1H and ^2H *Synechococcus* sp. PCC 7002 A_1^-/A_1 FTIR DS, respectively. The A_1^-/A_1 FTIR DS were normalized so that the 1,677(+)/1,666(−) and 1,669(+)/1,652(−) cm^{-1} difference bands were similar in intensity. Figure 6, spectra c, d, and e show trimeric ^1H, ^{15}N, and ^{13}C *Synechocystis* sp. PCC 6803 A_1^-/A_1 FTIR DS, respectively.

The ^1H A_1^-/A_1 FTIR DS for PS I from *Synechococcus* sp. PCC 7002 and *Synechocystis* sp. PCC 6803 (Fig. 6, spectra b and c) share many similar features. First, in both spectra a difference band is observed at ∼1,754(+)/1,748(−) cm^{-1}. The kinetic data in Fig. 4A indicates that this difference band is very well resolved. Second, a lower intensity difference band is observed at ∼1,733(−)/1,726(+) cm^{-1} in both spectra. The 1,754(+)/1,748(−) and 1,733(−)/1,726(+) cm^{-1} difference bands are also observed at in the ^{15}N *Synechocystis* sp. PCC 6803A_1^-/A_1 FTIR DS. Third, a broad, structured negative absorption band is observed near 1,550 cm^{-1}. For *Synechococcus* sp. PCC 7002 a peak is observed at 1,549(−) cm^{-1}, with a shoulder at 1,559(−) cm^{-1}. For *Synechocystis* sp. PCC 6803, two

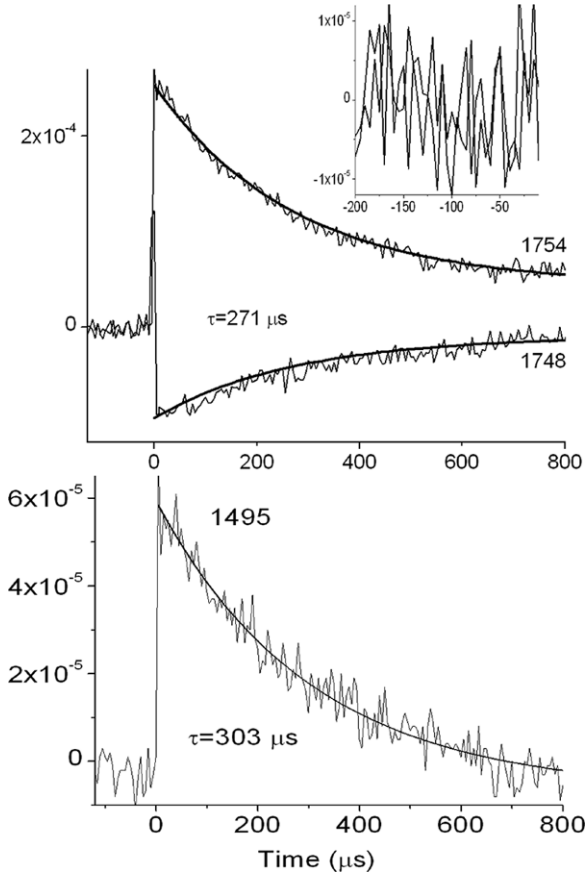

Fig. 4. Absorption changes observed at 1,754, 1,748, and 1,495 cm^{-1} following laser flash excitation of PS I particles from *Synechococcus* sp. PCC 7002 at 77 K. The inset shows the data before the laser flash. This data indicates that the noise level is below $\pm 1 \times 10^{-5}$ in arbitrary units. The kinetics were fitted to a single exponential component plus a constant. In (top) the two curves were fitted simultaneously and an exponential time constant of 271 μs is found. In (bottom) the time constant is found to be 303 μs. Within error, this is the same as in (top). Adapted from Sivakumar et al., 2005.

distinct peaks are observed at 1,546(−) and 1,559(−) cm^{-1}. Fourth, both spectra show positive absorption bands at ∼1,495(+) and 1,414(+) cm^{-1}. The kinetic in Fig. 4B indicates that these positive difference bands are well resolved.

Spectra b and c in Fig. 6 also show some differences in the amide I region. For *Synechococcus* sp. PCC 7002, an intense derivative feature is observed at 1,676(+)/1,666(−) cm^{-1}. For *Synechocystis* sp. PCC 6803, a similar shaped feature is observed at 1,674(+)/1,656(−) cm^{-1}. At first sight it appears somewhat surprising that such differences exist in the A_1^-/A_1 FTIR DS for PS I from *Synechocystis* sp. PCC 6803 and *Synechococcus* sp. PCC 7002. However, PS

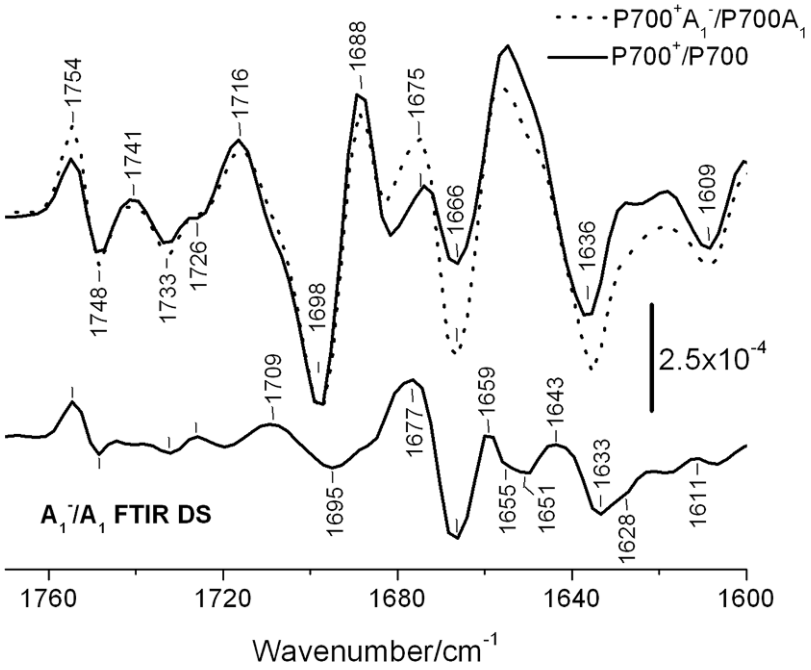

Fig. 5. Dotted line: Average of nine time-resolved FTIR DS, collected in 5 μs increments between 5 and 50 μs, for trimeric PS I particles from *Synechococcus* sp. PCC 7002 incubated in H_2O at 77 K (the first spectrum after the laser flash in Fig. 3). *Solid line:* Static $P700^+/P700$ FTIR DS at 77 K. The difference between the two spectra is also shown and labeled the A_1^-/A_1 FTIR DS. Adapted from Sivakumar et al., 2005.

I from *Synechocystis* sp. PCC 6803 contains PhQ in the A_1 site, while PS I from *Synechococcus* sp. PCC 7002 contains menaquinone-4 (MQ-4) (Sakuragi et al., 2005). MQ-4 and PhQ have the same napthoquinone head group, and differ only in the degree of saturation of the chain attached at position 3. It is not clear if this could explain the differences in the *Synechocystis* sp. PCC 6803 and *Synechococcus* sp. PCC 7002 A_1^-/A_1 FTIR DS.

V. Discussion of Features in A_1^-/A_1 FTIR DS

In FTIR DS negative bands are due to ground state modes while positive bands are due to the same modes in the excited state. $P700^+/P700$ FTIR DS contain contributions from molecular groups of P700, nearby amino acids and the protein backbone. Difference bands will result from cation-induced changes as well as electrochromic shifts that arise because of the positive charge on P700. In the $P700^+A_1^-/P700A_1$ FTIR DS bands associated with both P700 and A_1 contribute to the spectrum. In addition, molecular modes impacted electrochromically by the charge-separated state will also contribute. It is assumed that by subtracting the static $P700^+/P700$ FTIR DS from the $P700^+A_1^-/P700A_1$ FTIR DS that all contributions to the DS from P700 (and F_X) will cancel out. If the charge distribution over the pigments in the $P700^+$ and $P700^+A_1^-$ states is different then these differences will also manifest themselves in the A_1^-/A_1 FTIR DS.

A. The 13^3 ester C=O Mode of A_{0-A} Contributes to A_1^-/A_1 FTIR DS

In the $P700^+A_1^-/P700A_1$ FTIR DS in Fig. 5 the difference band at 1,754(+)/1,748(−) cm^{-1} is considerably more intense than the band at the same frequency in the $P700^+/P700$ FTIR DS. This leads to a difference band at 1,754(+)/1,748(−) cm^{-1} in the A_1^-/A_1 FTIR DS in Fig. 5. A similar derivative feature is observed at the same frequency in ^1H and ^{15}N *Synechocystis* sp. PCC 6803 A_1^-/A_1 FTIR DS (Fig. 6A, spectra c and d). In ^2H *Synechococcus* sp. PCC 7002 A_1^-/A_1 FTIR DS this difference band down-shift ~5 cm^{-1} [at least the 1,754(+) cm^{-1} band does, Fig. 6A, spectrum a], while upon ^{13}C labeling it down-shifts 43–44 cm^{-1} (Fig. 6A, spectrum e). A frequency of 1,754(+)/1,748(−) cm^{-1}, as well as all of the labeling induced band-shifts are most

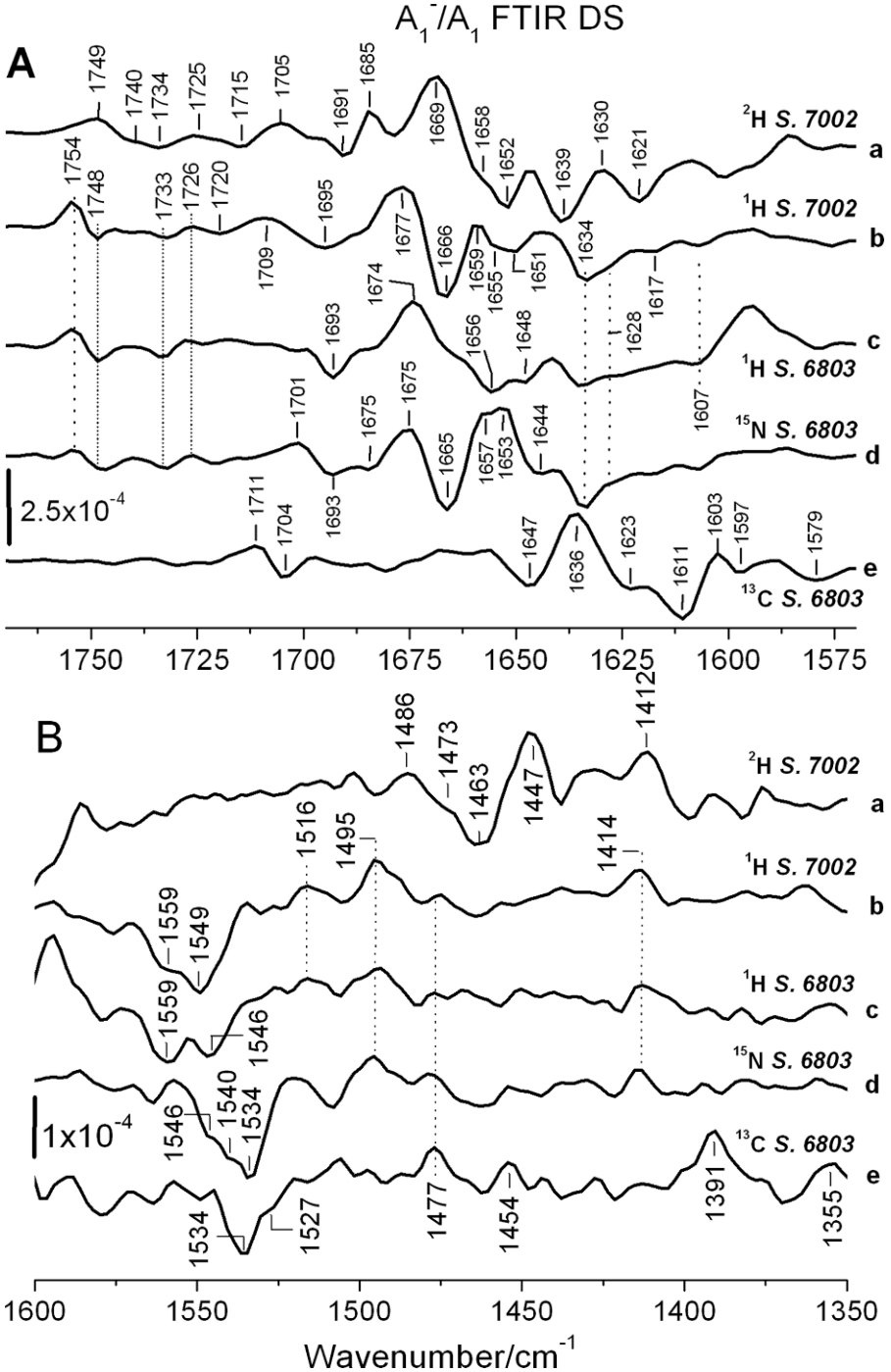

Fig. 6. A_1^-/A_1 FTIR DS in the (A) 1,770–1,570 and (B) 1,600–1,250 cm^{-1} spectral regions obtained using trimeric PS I particles from *Synechococcus* sp. PCC 7002 and monomeric PS I particles from *Synechocystis* sp. PCC 6803. Spectra c and b are for unlabeled PS I particles from *Synechocystis* sp. PCC 6803 and *Synechococcus* sp. PCC 7002, respectively. Spectrum a is for fully deuterated PS I particles from *Synechococcus* sp. PCC 7002. Spectra d and e are for ^{15}N and ^{13}C labeled PS I particles from *Synechocystis* sp. PCC 6803, respectively. *Synechococcus* sp. PCC 7002 and *Synechocystis* sp. PCC 6803 are abbreviated as *S*. 7002 and *S*. 6803. Adapted from Sivakumar et al., 2005.

consistent with the 1,754(+)/1,748(−) cm^{-1} band in the ^1H A_1^-/A_1 FTIR DS being due to a 13^3 ester C=O mode of a chlorophyll *a* molecule.

In ^1H $P700^+/P700$ FTIR DS (Fig. 5) the difference band at 1,754(+)/1,748(−) cm^{-1} is due to the 13^3 ester C=O mode of P_B. The only way this mode could give rise to the 1,754(+)/1,748(−) cm^{-1} band in the A_1^-/A_1 FTIR DS is if there was an increase in intensity of the whole difference band in the $P700^+A_1^-$ state, compared to the $P700^+$ state. This is not possible since the ground state is the same in both the static and time-resolved experiments.

The 1,754(+)/1,748(−) cm^{-1} band could be due to a carboxylic acid C=O mode, since such modes are generally found in the 1,770–1,720 cm^{-1} region (Hastings and Sivakumar, 2001; Smith, 1999). GluA702 and GluA699 are near A_{1-A} (see Fromme and Grotjohann, this volume, Chapter 6) and could be impacted by the electrostatic field generated upon A_1 reduction. One argument against this proposal is that carboxylic acid C=O modes are known to down-shift >10 cm^{-1} upon deuteration (Siebert et al., 1982; Nabedryk et al., 1995), which is not observed here.

It is very unlikely that the 1,754(+)/1,748(−) cm^{-1} band in the A_1^-/A_1 FTIR DS is due to an amide I mode, as these modes generally absorb well below ∼1,700 cm^{-1}. In addition, from the infrared absorption spectra of PS I we have found that the amide I and II absorption bands down-shift 38 and 13 cm^{-1} respectively, upon ^{13}C labeling (data not shown). Here we observe that the 1,754(+)/1,748(−) cm^{-1} band in the A_1^-/A_1 FTIR DS down-shifts 43–44 cm^{-1} upon ^{13}C labeling, this also supports the notion that the 1,754(+)/1,748(−) cm^{-1} difference band is not due to an amide I mode.

The most likely conclusion is that 1,754(+)/1,748(−) cm^{-1} difference band in the A_1^-/A_1 FTIR DS is due to a 13^3 ester C=O mode of A_{0-A}, that is impacted by the presence of a negative charge on A_{1-A} [this hypothesis takes into account the fact that ET occurs predominantly down the A-branch in cyanobacterial PS I (Xu et al., 2003a,b)]. All of the isotope induced band-shifts support this hypothesis. Several further observations also suggest that this is an appropriate hypothesis. (1) A_{1-A} is coupled to A_{0-A} through the protein. The 13^3 ester C=O of A_{0-A} is 8.28 Å from the closest carbonyl oxygen of A_{0-A} and 3.47 Å from TrpA697, which is π-stacked upon A_{1-A} (Fromme et al., 2001; Jordan et al., 2001). (2) In FTIR DS studies of PBRCs from *Rps. viridis* (Breton and Nabedryk, 1995, 1998; Breton et al., 1999a) and *Rb. sphaeroides* (Breton and Nabedryk, 1995; Breton et al., 1997) it is well established that the 13^3 ester C=O of H_A (the electron accepting bacteriopheophytin) is impacted by the electrostatic field generated upon Q_A^- formation, as bands associated with the H_A 13^3 ester C=O are clearly present in Q_A^-/Q_A FTIR DS [the 13^3 ester C=O of H_A in *Rp. viridis* is also impacted by the electrostatic field generated upon Q_B^- formation (Breton and Nabedryk, 1998)]. In PBRCs, Q_A is >10 Å from H_A. This distance is considerably larger than the distance between the 13^3 ester carbonyl oxygen of A_{0-A} and the closest carbonyl oxygen of A_{1-A}. The data from Q_A^-/Q_A FTIR DS obtained using PBRCs then suggest that it is very likely that there will be a long-range electrostatic interaction between A_0 and A_1^- in PS I. (3) Long range electrostatic effects in PS I are also well known. For instance, a carotenoid absorption band is shifted upon A_1 reduction (Brettel, 1988). This electrochromic band-shift is most clearly observed at ∼480 nm in time-resolved pump–probe measurements (Agalarov and Brettel, 2003). The PhQ carbonyl oxygens are between 7–9 Å from the ring atoms of the closest β-carotene (labeled BCR4014 in 1JB0).

Finally, the 13^3 ester C=O mode of H_A, observed at 1,736(−) cm^{-1} in Q_A^-/Q_A FTIR DS from *Rps. viridis, down-shifts* ∼6 cm^{-1} upon Q_A reduction (Breton et al., 1999a). In contrast, the 1,754(+)/1,748(−) cm^{-1} band observed in A_1^-/A_1 FTIR DS indicates a 6 cm^{-1} *up-shift*. It is not clear if the electrochromic response of the 13^3 ester C=O mode of A_{0-A} to A_{1-A} reduction should lead to a down-shift or up-shift. The direction of the shift will depend on the geometry of the C=O mode relative to the geometry of the negative charge on the PhQ. This idea is exemplified by the observation that the 13^1 keto C=O mode of H_A, observed at 1,676(−) cm^{-1} in Q_A^-/Q_A FTIR DS from *Rps. viridis*, *up-shifts* ∼9 cm^{-1} upon Q_A reduction (Breton et al., 1999a).

B. Does the 13^1 keto C=O Mode of A_{0-A} Contribute To A_1^-/A_1 FTIR DS

If a 13^3 ester C=O mode of A_{0-A} contributes to the ^1H A_1^-/A_1 FTIR DS in Fig. 6, it is reasonable to suggest that 13^1 keto C=O mode of A_{0-A} should also contribute to the DS. The 13^1 keto carbonyl oxygen of A_{0-A} is H-bonded to TyrA696, and is 8.97 Å from the closest carbonyl oxygen of A_{1-A} (Fromme et al., 2001; Jordan et al., 2001).

In the ^1H and ^2H *Synechococcus* sp. PCC 7002 A_1^-/A_1 FTIR DS, bands are observed at

1,709(+)/1,695(−) and 1,705(+)/1,691(+) cm^{-1}, respectively. The 1,691(−) cm^{-1} band in the ^2H A_1^-/A_1 FTIR DS is obscured by a positive feature at 1,685 cm^{-1} that is absent in the ^1H spectrum. However, the suggestion is that the 1,709(+)/1,695(−) cm^{-1} difference band down-shifts 4 cm^{-1} upon deuteration. In ^1H and ^{15}N *Synechocystis* sp. PCC 6803 A_1^-/A_1 FTIR DS, a negative band is observed at 1,693 cm^{-1}, but no clear positive band is observed near 1,709 cm^{-1}. Notwithstanding this complication, we associate the 1,693(−) cm^{-1} bands in ^1H and ^{15}N *Synechocystis* sp. PCC 6803 A_1^-/A_1 FTIR DS with the 1,695(−) and 1,691(−) cm^{-1} bands in ^1H and ^2H *Synechococcus* sp. PCC 7002 A_1^-/A_1 FTIR DS. Upon ^{13}C labeling, one possibility is that the 1,693(−) cm^{-1} band in ^1H *Synechocystis* sp. PCC 6803 A_1^-/A_1 FTIR DS down-shifts 46–1,647 cm^{-1}.

Down-shifts of the negative band at 1,693–1,695 cm^{-1} by 4/0/47 cm^{-1} upon $^2H/^{15}N/^{13}C$ labeling is consistent with this band being due to a 13^1 keto C=O mode (Breton, 2001; Kimura et al., 2003; Wang et al., 2003). However, the 13^1 keto C=O group of A_{0-A} is H-bonded to TyrA696, whose hydroxyl side-chain is also impacted upon deuteration. So, it is not entirely clear what should happen to the 13^1 keto C=O mode of A_{0-A} upon deuteration or ^{13}C labeling. Because of these difficulties it is only very tentatively suggested that the 1,693–1,695(−) cm^{-1} band in A_1^-/A_1 FTIR DS is due to the 13^1 keto C=O mode of A_{0-A}. Another observation that may appear to be incompatible with this assignment is that a frequency of 1,695(−) cm^{-1} for a 13^1 keto C=O mode suggests that it is free or only very weakly H-bonded. Our tentative interpretation would then suggests that TyrA696 may be only weakly H-bonded (if at all) to the 13^1 keto C=O of A_{0-A}.

In FTIR studies of PBRCs from *Rps. viridis* (Breton and Nabedryk, 1995, 1998; Breton et al., 1999a) and *Rb. sphaeroides* (Breton and Nabedryk, 1995; Breton et al., 1997) it has also been established that the 13^1 keto C=O of H_A is impacted upon Q_A^- formation. In *Rps. viridis* the keto C=O of H_A is H-bonded to GluL104 and absorbs at 1,676 cm^{-1}. Upon Q_A^- formation this band up-shifts 9–1,685 cm^{-1}. In the A_1^-/A_1 FTIR DS in the 1,680–1,650 cm^{-1} region many difference bands appear to contribute (see section VII.D), thus definitive assignment of bands to 13^1 keto C=O modes is difficult based upon the data presented here. Ambiguity in assigning bands to the 13^1 keto C=O mode of A_{0-A} could possibly be removed by producing A_1^-/A_1 FTIR DS using PS I particles in which TyrA696 has been mutated to a non-H-bonding residue.

C. Amide II Modes in A_1^-/A_1 FTIR DS

In the ^1H *Synechococcus* sp. PCC 7002 A_1^-/A_1 FTIR DS a negative band is observed at 1,549(−) cm^{-1}, with a shoulder at 1,558 cm^{-1} (Fig. 6B, spectrum b). These negative bands are completely absent in the ^2H *Synechococcus* sp. PCC 7002 A_1^-/A_1 FTIR DS (Fig. 6B, spectrum a). In the ^2H A_1^-/A_1 FTIR DS, an intense negative band is observed at 1,463 cm^{-1}, with a shoulder at 1,473 cm^{-1}. These bands are absent in the ^1H *Synechococcus* sp. PCC 7002 A_1^-/A_1 FTIR DS. These ^2H induced changes are typical of the behavior of amide II modes, which generally occur near 1,550 cm^{-1} and down-shift up to 100 cm^{-1} upon deuteration (Sivakumar et al., 2003).

In Q_B^-/Q_B FTIR DS obtained using PBRCs incubated in H_2O and D_2O (with ∼70% exchange), a difference band at 1,537(−) cm^{-1} was found to down-shift ∼68–1,469 cm^{-1} upon deuteration (Nabedryk et al., 1995). In the case presented here, absorption bands at 1,549/1,558 cm^{-1} down-shift 85/86 cm^{-1}, to 1,463/1,473 cm^{-1}, upon deuteration. This is strong evidence supporting the idea that the band at 1,549 cm^{-1} and the shoulder at 1,558 cm^{-1} in the ^1H *Synechococcus* sp. PCC 7002 A_1^-/A_1 FTIR DS are due to amide II modes.

In the ^1H *Synechocystis* sp. PCC 6803 A_1^-/A_1 FTIR DS two negative bands are observed at 1,559 and 1,546 cm^{-1}. These bands likely correspond to the 1,549(−) cm^{-1} band, and the shoulder at 1,558(−) cm^{-1}, in the ^1H *Synechococcus* sp. PCC 7002 A_1^-/A_1 FTIR DS. Upon ^{15}N labeling of PS I from *Synechocystis* sp. PCC 6803 a broad negative band with a peak at 1,534 cm^{-1} and shoulders at 1,540 and 1,546 cm^{-1} are observed. From this data the suggestion is that the 1,558(−) and 1,546(−) cm^{-1} bands in the unlabeled spectrum down-shift 12 cm^{-1} to ∼1,546(−) and 1,534(−) cm^{-1} upon ^{15}N labeling. Amide II absorption bands down-shifts ∼14 cm^{-1} upon ^{15}N labeling (Wang et al., 2003), so it would be appropriate to assign the 1,558(−) and 1,546(−) cm^{-1} bands in the ^1H *Synechocystis* sp. PCC 6803 A_1^-/A_1 FTIR DS to amide II modes. However, upon ^{13}C labeling, a negative band is observed at 1,536 cm^{-1}, with a shoulder at 1,528 cm^{-1}. Since amide II modes down-shift ∼13 cm^{-1} upon ^{13}C labeling (Kimura et al., 2003) it would appear that the 1,558(−) cm^{-1} band in the ^1H *Synechocystis* sp. PCC 6803 A_1^-/A_1 FTIR DS cannot be due to an amide II

mode, as it would have to down-shift ~23 cm^{-1} upon ^{13}C labeling. However, the 1,546(−) cm^{-1} band could be due to an amide II mode as it down-shifts ~10 cm^{-1} upon ^{13}C labeling.

D. Amide I Modes in A_1^-/A_1 FTIR DS

Since amide II difference bands clearly contribute to A_1^-/A_1 FTIR DS, amide I difference bands should also contribute. The most obvious candidates for amide I difference bands in the ^1H *Synechococcus* sp. PCC 7002 and *Synechocystis* sp. PCC 6803 A_1^-/A_1 FTIR DS are the bands at 1,677(+)/1,666(−) and 1,674(+)/1,656(−) cm^{-1}, respectively. Upon ^2H labeling the 1,677(+)/1,666(−) cm^{-1} difference band is considerably impacted, and an intense difference feature is observed at 1,669(+)/1,652(−) cm^{-1}, with a shoulder at 1,658(−) cm^{-1}. If the 1,677(+)/1,666(−) cm^{-1} feature in the ^1H *Synechococcus* sp. PCC 7002 A_1^-/A_1 FTIR DS corresponds to the 1,669(+)/1,652(−) cm^{-1} feature in the ^2H A_1^-/A_1 FTIR DS then the ^2H induced down-shift is 8/14 cm^{-1}. A 14 cm^{-1} ^2H induced down-shift is very large, probably too large, for an amide I absorption band [in RT infrared absorption spectra of the *Synechococcus* sp. PCC 7002 PS I particles it is found that the amide I absorption band down-shifts 9 cm^{-1} upon ^2H labeling (data not shown)]. However, the 1,658(−) cm^{-1} shoulder in the ^2H A_1^-/A_1 FTIR DS could be the feature that is due to amide I. In this case the 1,677(+)/1,666(−) cm^{-1} band in the ^1H A_1^-/A_1 FTIR DS down-shifts 8/8 cm^{-1} upon deuteration, which is then consistent with the 1,677(+)/1,666(−) cm^{-1} difference band being due to amide I modes.

In Q_B^-/Q_B FTIR DS obtained using PBRCs incubated in H_2O and D_2O unambiguous identification of amide I absorption bands in WT spectra was not possible. However, bands at 1,667(+) and 1,657(−) cm^{-1} in mutant Q_B^-/Q_B FTIR DS were assigned to amide I modes as they down-shifted ~3 cm^{-1} upon deuteration (Nabedryk et al., 1995).

The 1,674(+) cm^{-1} band in ^1H *Synechocystis* sp. PCC 6803 A_1^-/A_1 FTIR DS down-shifts 38–1,636 cm^{-1} upon ^{13}C labeling, and is probably only slightly affected by ^{15}N labeling. A 38 cm^{-1} ^{13}C induced shift is expected for an amide I mode, but it is 6–8 cm^{-1} lower than would be expected for a C=O mode. Therefore, we assign the 1,674(+) cm^{-1} band in unlabeled *Synechocystis* sp. PCC 6803 A_1^-/A_1 FTIR DS to an amide I mode.

The negative band at 1,656(−) cm^{-1} in the ^1H *Synechocystis* sp. PCC 6803 A_1^-/A_1 FTIR DS down-shifts 33 or 45 cm^{-1} to 1,623 or 1,611 cm^{-1} upon ^{13}C labeling. Thus it is difficult to distinguish if the 1,656 cm^{-1} band is associated with a C=O mode or amide I mode. This difficulty in assigning the 1,656(−) cm^{-1} band arises in part because the changes in the A_1^-/A_1 FTIR DS, in the 1,670–1,640 cm^{-1} region, upon ^{15}N labeling are complex. Since we assign the 1,666(−) cm^{-1} band in *Synechococcus* sp. PCC 7002 A_1^-/A_1 FTIR DS to an amide I mode, and if we can associate the 1,666(−) cm^{-1} band in the ^1H *Synechococcus* sp. PCC 7002 A_1^-/A_1 FTIR DS with the 1,656(−) cm^{-1} band in the ^1H *Synechocystis* sp. PCC 6803 A_1^-/A_1 FTIR DS, we can then, albeit very tentatively, assign the 1,656(−) cm^{-1} band in the *Synechocystis* sp. PCC 6803 A_1^-/A_1 FTIR DS to an amide I mode also.

The 1,674(+)/1,656(−) cm^{-1} band in the ^1H *Synechocystis* sp. PCC 6803 A_1^-/A_1 FTIR DS is considerably modified upon ^{15}N labeling. The 1,674(+) cm^{-1} band appears unaltered upon ^{15}N labeling. However, the 1,656(−) cm^{-1} band is considerably altered, with a complicated set of features appearing at 1,657(+)/1,653(+)/1,644(−)/1,634(−) cm^{-1}. These features could suggest the appearance of a new band at ~1,654(−)/1,667(+) cm^{-1} upon ^{15}N labeling. The changes appear to be too complex to be due solely to a few amide I modes. So the ^{15}N induced changes are probably related to other modes, in addition to amide I modes. Side-chain modes of tryptophan (Trp) residues will be impacted upon ^{15}N labeling. Since Trp residues are very close to the PhQs in PS I, it could be possible that changes in Trp residues also contribute to the complicated ^{15}N induced changes. However, Trp CN or NH modes are not expected in the 1,660–1,630 cm^{-1} region (Barth, 2000). Complicating issues further are: (1) The possibility that a serine residue could be (partially) H-bonded to the tryptophan indole nitrogen. (2) C=O modes of PhQ may also give rise to absorption bands in the 1,660–1,640 cm^{-1} region. This later point suggests that if the ^{15}N label impacts the nearby indole nitrogen of TrpA697, then it is likely that the C=O modes of PhQ will be modified. The above described factors indicate that complex ^{15}N induced changes are in fact likely in A_1^-/A_1 FTIR DS in the 1,665–1,650 cm^{-1} region.

E. PhQ Ground State Absorption Difference Bands

PhQ C=O and C=C modes are expected to give rise to negative difference bands in the A_1^-/A_1 FTIR DS, in the ~1,680–1,580 cm^{-1} region. In both Q_A^-/Q_A and

Q_B^-/Q_B FTIR DS from PBRCs, bands due to protein modes dominate the difference spectra in the 1,750–1,610 cm^{-1} region. These observations indicate that it may be difficult to observe modes of PhQ in the 1,680–1,590 cm^{-1} region in A_1^-/A_1 FTIR DS.

For PhQ *in vitro* an absorption band is observed at 1,662 cm^{-1}, and is due to both C=O modes. Bands due to C=C modes are found at 1,618 and 1,597 cm^{-1} (Breton et al., 1994). From Q_A^-/Q_A FTIR DS obtained using PBRCs from *Rb. sphaeroides* reconstituted with PhQ, it was suggested that bands associated with the C=O modes are found at 1,651 and 1,640 cm^{-1}, while bands associated with the C=C modes are found at 1,608 and 1,588 cm^{-1} (Breton et al., 1994). So, the bands associated with the C=O modes of PhQ reconstituted into the Q_A site are asymmetrically bonded, compared to PhQ *in vitro*. This is expected since the quinone carbonyls are differently H-bonded in the Q_A site in PBRCs. For PhQ in PS I, the C=O modes are also differentially H-bonded (Fromme et al., 2001; Jordan et al., 2001), so one might expect to observe two negative bands associated with C=O modes, and two to four negative bands associated with C=C modes of PhQ in A_1^-/A_1 FTIR DS. Therefore, one possible set of band assignments in the ^1H, *Synechococcus* sp. PCC 7002, A_1^-/A_1 FTIR DS is: (1) The bands at 1,655(−) and 1,651(−) cm^{-1} are due to a PhQ C=O modes. (2) The band at 1,633(−) and the shoulder at 1,628 cm^{-1} are due to PhQ C=C modes. (3) The 1,617(−) and 1,607(−) cm^{-1} bands are also due to PhQ C=C modes. However, it is also possible that one or both of the bands at 1,655(−) and 1,651(−) cm^{-1} are due to C=C modes, while one or more of the bands at 1,633(−), 1,628(−), 1,617(−), and 1,607(−) cm^{-1} are due to C=O modes. Similar interpretations may hold for the negative bands at 1,656(−), 1,648(−), 1,633(−), and 1,628 cm^{-1} in the ^1H, *Synechocystis* sp. PCC 6803, A_1^-/A_1 FTIR DS. However, it was suggested above that the 1,656(−) cm^{-1} band is due to an amide mode.

Deuterium exchange leads to considerable modification of the *Synechococcus* sp. PCC 7002, A_1^-/A_1 FTIR DS in the 1,660–1,610 cm^{-1}, region and so the above interpretations are still ambiguous upon comparison of the ^1H and ^2H *Synechococcus* sp. PCC 7002, A_1^-/A_1 FTIR DS.

The bands at 1,633(−) and 1,628 cm^{-1} in the ^1H, *Synechocystis* sp. PCC 6803, A_1^-/A_1 FTIR DS appear to be little affected by ^{15}N labeling. However, the 1,633–1,628 cm^{-1} bands may down-shift ∼31–36 or ∼49–55 cm^{-1} to 1,597 or 1,579 cm^{-1} upon ^{13}C labeling. The former suggests that the 1,635–1,628 cm^{-1} bands are due to amide modes while the later suggests that the 1,635–1,628 cm^{-1} bands are associated with C=C modes, and probably not C=O modes.

Unambiguous identification of PhQ C=O and C=C modes will most likely require the incorporation of specifically labeled quinones into PS I. Such work is beginning in our laboratory.

F. Phyllosemiquinone Difference Bands

Semiquinone C···O and C···C modes are expected to show up as positive difference bands in the ∼1,520–1,380 cm^{-1} region. In Q_A^-/Q_A FTIR DS obtained using *Rps. viridis* RCs (Q_A is menaquinone-9 in *Rps. viridis*) and *Rb. sphaeroides* RCs reconstituted with PhQ into the Q_A site, three well-separated bands are observed at 1,478(+), 1,444–1,438(+), and 1,394–1,392(+) cm^{-1} (Breton et al., 1994). These bands are nearly as intense as the bands that are observed in the 1,600–1,700 cm^{-1} region. The 1,478(+) and 1,394–1,392(+) cm^{-1} bands were assigned to C···C modes while the 1,444–1,448(+) cm^{-1} band is assigned to a C···O mode coupled to a C···C vibration (Breton et al., 1994). This is somewhat different from conclusions drawn from spectro-electrochemical FTIR studies of 2-methyl-1,4-naphthoquinone in acetonitrile (Breton et al., 1991b), in which anion bands at 1,502, 1,444, and ∼1,380 cm^{-1} were assigned to C···O, C···C, and C···O modes, respectively. Q_A^-/Q_A FTIR DS have been obtained using *Rps. viridis* and *Rb. sphaeroides* (either reconstituted with vitamin K_1 or with ubiquinone in the Q_A site) RCs that have been ^1H and ^2H labeled (Breton and Nabedryk, 1995). The 1,444–1,438(+) cm^{-1} band is the one predominantly affected by ^2H exchange. This supports the idea that this band is due to a, possibly H-bonded C···O mode.

In ^1H, *Synechococcus* sp. PCC 7002 A_1^-/A_1 FTIR DS prominent positive bands are observed at 1,516(+), 1,493(+), and 1,414(+) cm^{-1}. Three bands are also observed with similar frequency in the ^1H *Synechocystis* sp. PCC 6803 A_1^-/A_1 FTIR DS. In *Synechococcus* sp. PCC 7002 A_1^-/A_1 FTIR DS the 1,494(+) cm^{-1} band is considerably impacted by deuteration, while the 1,414(+) cm^{-1} band-shifts less than 2 cm^{-1}. These observations suggests that the 1,495(+) and 1,414(+) cm^{-1} bands are due to C···O and C···C modes of A_1^-, respectively. Upon ^{13}C labeling, it could be possible that part of the 1,495(+) cm^{-1} band down-shifts ∼38–1,454(+) cm^{-1}. Such a shift could be consistent with the idea that the 1,494(+) cm^{-1} band is due to a semiquinone C···O mode. Upon ^{13}C labeling, it could

also be possible that part of the 1,414(+) cm^{-1} band down-shifts ~58–1,355(+) cm^{-1}. Such a shift is consistent with the idea that the 1,414(+) cm^{-1} band is due to a semiquinone C···C mode. In Q_A^-/Q_A FTIR DS obtained using *Rb. sphaeroides* RCs reconstituted with Q_8, a band at 1,466(+) cm^{-1} in unlabeled Q_A^-/Q_A FTIR DS was found to down-shift 59 cm^{-1}, to 1,407 cm^{-1} upon uniform ^{13}C labeling of Q_8. This again is consistent with the assignment of the 1,466(+) cm^{-1} band (in unlabeled Q_A^-/Q_A FTIR DS of RCs reconstituted with Q_8) to a C···C mode.

The unlabeled and labeled spectra are extremely complex in the 1,500–1,300 cm^{-1} region, and we have outlined only a few possible band assignments. For unambiguous assignment, specific types of labeling strategies will be required to deconvolute the complex spectra. Such work is just beginning in our laboratory.

VI. Conclusions

It has been shown that TRSS FTIR instrumentation can reach a very high level of sensitivity. This sensitivity allows the collection of reliable A_1^-/A_1 FTIR DS in intact cyanobacterial PS I particles. However, the level of sensitivity obtainable is still inadequate to obtain reliable A_1^-/A_1 FTIR DS for intact PS I particles from *C. reinhardtii*. The collection of A_1^-/A_1 FTIR DS for unlabeled and uniformly isotope-labeled PS I particles has allowed some solid and unambiguous band assignments to be made. Many other tentative band assignments were suggested, that remain to be tested using specific labeling strategies, site-directed mutagenesis, and foreign quinone incorporation studies. Such studies have already been undertaken in the quest to understand both the Q_A and Q_B binding sites in PBRCs.

VII. Addendum

1. After submission of this work it was found that A_1^-/A_1 FTIR DS obtained using trimeric PS I particles from *Synechocystis* sp. PCC 6803 and *Synechococcus* sp. PCC 7002 are very similar. The spectra in Fig. 6, b/c were obtained using trimeric/monomeric PS I particles from *Synechococcus* sp. PCC 7002/*Synechocystis* sp. PCC 6803, respectively. The differences in Fig. 6, spectra b and c are therefore likely due to the use of monomeric or trimeric PS I particles. The above observation also led us to suspect that the 1,656(−) cm^{-1} band in the *Synechocystis* sp. PCC 6803, ^1H A_1^-/A_1 FTIR DS (Fig. 6, spectrum c) is not due to an amide I mode.

2. Recently, we have obtained A_1^-/A_1 FTIR DS using trimeric PS I particles from *Synechocystis* sp. PCC 6803 in which the methionine axial ligands to A_{0-A} and A_{0-B} have been changed to leucine. Upon changing the A_{0-A} methionine ligand the 1,754(−)/1,748(−) cm^{-1} band disappears. Changing the A_{0-B} methionine ligand, however, has little impact on the spectra. These observations are in keeping with the band assignments proposed above.

Acknowledgments

This work was supported by the United State Department of Agriculture, Grant #35318-10894. Other support for this work came from start-up funds, a quality improvement grant and a research initiation grant from Georgia State University. Velautham Sivakumar undertook most of the TRSS FTIR experiments described in this article.

References

Agalarov R and Brettel K (2003) Temperature dependence of biphasic forward electron transfer from the phylloquinone(s) A_1 in photosystem I: only the slower phase is activated. Biochim Biophys Acta 1604: 7–12

Anderson NA, Hao EC, Ai X, Hastings G and Lian TQ (2001) Ultrafast and long-lived photoinduced charge separation in MEH-PPV/nanoporous semiconductor thin film composites. Chem Phys Lett 347: 304–310

Anderson NA, Hao EC, Ai X, Hastings G and Lian TQ (2002) Sub-picosecond photoinduced electron transfer from a conjugated polymer to SnO_2 semiconductor nanocrystals. Physica E 14: 215–218

Barth A (2000) The infrared absorption of amino acid side chains. Prog Biophys Mol Biol 74: 141–173

Braiman MS and Rothschild KJ (1988) Fourier transform infrared techniques for probing membrane protein structure. Annu Rev Biophys Biophys Chem 17: 541–570

Breton J (2001) Fourier transform infrared spectroscopy of primary electron donors in type I photosynthetic reaction centers. Biochim Biophys Acta 1507: 180–193

Breton J and Nabedryk E (1993) S_0–T_1 infrared difference spectrum of the triplet-state of the primary electron-donor in *Rhodobacter-sphaeroides* photosynthetic bacterial reaction centers. Chem Phys Lett 213: 571–575

Breton J and Nabedryk E (1995) Protein and bacteriopheophytin response to Q_A reduction in photosynthetic bacterial reaction centers from *Rb. sphaeroides* and *Rp. viridis* investigated

by $^1H/^2H$ Exchange and light-induced FTIR difference spectroscopy. In: Mathis P (ed) Photosynthesis: From Light to the Biosphere, pp 395–400. Kluwer Academic Publishers, Dordrecht, Boston

Breton J and Nabedryk E (1998) Electrostatic influence Of Q_A and Q_B reduction on the 10a-ester C=O vibration In *Rp. viridis*. In: Garab G (ed) Photosynthesis: Mechanisms and Effects, pp 687–692. Kluwer Academic Publishers, Dordrecht, Boston

Breton J, Bauscher M, Berthomieu C, Thibodeau DL, Andrianambinintsoa S, Dejonghe D, Mantele, W and Nabedryk E (1991) FTIR difference spectroscopy of menaquionone photoreduction in bacterial reaction centers. In: Spectroscopy of Biological Molecules. Hester RE and Girling RB, Eds. Royal Society of Chemistry: Cambridge, England, p 43–46

Breton J, Burie JR, Berthomieu C, Berger G and Nabedryk E (1994) The binding sites of quinones in photosynthetic bacterial reaction centers investigated by light-induced FTIR difference spectroscopy: assignment of the Q_A vibrations in *Rhodobacter sphaeroides* using ^{18}O- or ^{13}C-labeled ubiquinone and vitamin K_1. Biochemistry 33: 4953–4965

Breton J, Nabedryk E, Allen JP and Williams JC (1997) Electrostatic influence of Q_A reduction on the IR vibrational mode of the 10a-ester C=O of H_A demonstrated by mutations at residues Glu L104 and Trp L100 in reaction centers from *Rhodobacter sphaeroides*. Biochemistry 36: 4515–4525

Breton J, Bibikova M, Oesterhelt D and Nabedryk E (1999a) Conformational heterogeneity of the bacteriopheophytin electron acceptor H_A in reaction centers from *Rhodopseudomonas viridis* revealed by Fourier transform infrared spectroscopy and site-directed mutagenesis. Biochemistry 38: 11541–11552

Breton J, Nabedryk E and Leibl W (1999b) FTIR study of the primary electron donor of photosystem I (P700) revealing delocalization of the charge in P700(+) and localization of the triplet character in (3)P700. Biochemistry 38: 11585–11592

Brettel K (1988) Electron transfer room A_1 to an iron–sulfur center with $t_{1/2}$ = 200 ns at room temperature in Photosystem I. Characterization by flash absorption spectroscopy. FEBS Lett 239: 93–98

Brettel K (1997) Electron transfer and arrangement of the redox cofactors in photosystem I. Biochim. Biophys. Acta 1318: 322–373

Brudler R and Gerwert K (1998) Step-scan FTIR spectroscopy resolves the $Q_A^-Q_B^- > Q_AQ_B^-$ transition in *Rb-sphaeroides* R26 reaction centres. Photosynth Res 55: 261–266

Burie JR, Leibl W, Nabedryk E and Breton J (1993) Step-scan FT-IR spectroscopy of electron-transfer in the photosynthetic bacterial reaction-center. Appl Spectrosc 47: 1401–1404

Contzen J and Jung C (1998) Step-scan time-resolved FTIR spectroscopy of cytochrome P-450cam carbon monoxide complex: a salt link involved in the ligand-rebinding process. Biochemistry 37: 4317–4324

Fromme P, Jordan P and Krauß N (2001) Structure of photosystem I. Biochim Biophys Acta 1507: 5–31

Gerwert K (2001) Time-resolved FT-IR difference spectroscopy: a tool to monitor molecular reaction mechanisms of proteins. In: Gremlich H and Yan B (eds) Infrared and Raman Spectroscopy of Biological Materials, pp 193–230. Marcel Dekker, New York

Griffiths P and de Haseth J (1986) Fourier Transform Infrared Spectroscopy, pp 58–80. John Wiley and Sons, New York

Guergova-Kuras M, Boudreaux B, Joliot A, Joliot P and Redding K (2001) Evidence for two active branches for electron transfer in photosystem I. Proc Natl Acad Sci USA 98: 4437–4442

Hage W, Kim M, Frei H and Mathies RA (1996) Protein dynamics in the bacteriorhodopsin photocycle: a nanosecond step-scan FTIR investigation of the KL to L transition. J Phys Chem 100: 16026–16033

Hastings G (2001) Time-resolved step-scan Fourier transform infrared and visible absorption difference spectroscopy for the study of photosystem I. Appl Spectrosc 55: 894–900

Hastings G and Sivakumar V (2001) Time-resolved Fourier transform infrared difference spectroscopy for the study of A_1 reduction in intact Photosystem I. In: Critchley C (ed) PS2001: 12th International Conference in Photosynthesis, Abstract S6-017. CSIRO Publishing, Melbourne, Australia

Hastings G, Ramesh VM, Wang R, Sivakumar V and Webber A (2001) Primary donor photo-oxidation in photosystem I: a re-evaluation of ($P700^+ - P700$) Fourier transform infrared difference spectra. Biochemistry 40: 12943–12949

Hu X, Frei H and Spiro TG (1996) Nanosecond step-scan FTIR spectroscopy of hemoglobin: ligand recombination and protein conformational changes. Biochemistry 35: 13001–13005

Johnson T and Zachmann G (2000) Introduction to Step-Scan FTIR, pp 1–94. Bruker Optics

Jordan P, Fromme P, Witt HT, Klukas O, Saenger W and Krauß N (2001) Three-dimensional structure of cyanobacterial photosystem I at 2.5 Ångstrom resolution. Nature 411: 909–917

Kim S, Sacksteder CA, Bixby KA and Barry BA (2001) A reaction-induced FT-IR study of cyanobacterial photosystem I. Biochemistry 40: 15384–15395

Kimura Y, Mizusawa N, Ishii A, Yamanari T and Ono TA (2003) Changes of low-frequency vibrational modes induced by universal (15)N- and (13)C-isotope labeling in S(2)/S(1) FTIR difference spectrum of oxygen-evolving complex. Biochemistry 42: 13170–13177

Koutsoupakis K, Stavrakis S, Pinakoulaki E, Soulimane T and Varotsis C (2002) Observation of the equilibrium CuB-CO complex and functional implications of the transient heme a_3 propionates in cytochrome ba_3-CO from *Thermus thermophilus*. Fourier transform infrared (FTIR) and time-resolved step-scan FTIR studies. J Biol Chem 277: 32860–32866

Koutsoupakis C, Soulimane T and Varotsis C (2003) Docking site dynamics of ba_3-cytochrome c oxidase from *Thermus thermophilus*. J Biol Chem 278: 36806–36809

Mäntele W (1993) Infrared vibrational spectroscopy of photosynthetic reaction centers. In: Deisenhofer J and Norris J (ed) The Photosynthetic Reaction Center, pp 239–283. Academic Press, San Diego

Mäntele W (1995) Infrared vibrational spectroscopy of reaction centers. In: Blankenship RE, Madigan MT and Bauer CE (eds) Anoxygenic Photosynthetic Bacteria, pp 627–647. Kluwer Academic Publishers, Dordrecht, Boston

Mezzetti A, Nabedryk E, Breton J, Okamura MY, Paddock ML, Giacometti G and Leibl W (2002) Rapid-scan Fourier transform infrared spectroscopy shows coupling of GLu-L212 protonation and electron transfer to Q_B in *Rhodobacter sphaeroides* reaction centers. Biochim Biophys Acta 1553: 320–330

Mezzetti A, Seo D, Leibl W, Sakurai H and Breton J (2003) Time-resolved step-scan FTIR investigation on the primary

donor of the reaction center from the green sulfur bacterium *Chlorobium tepidum*. Photosynth Res 75: 161–169

Nabedryk E (1996) Light-induced Fourier transform infrared difference spectroscopy of the primary electron donor in photosynthetic reaction centers. In: Mantsch HH and Chapman D (eds) Infrared Spectroscopy of Biomolecules, pp 39–81. Wiley-Liss, New York

Nabedryk E, Breton J, Hienerwadel R, Fogel C, Mantele W, Paddock ML and Okamura MY (1995) Fourier transforms infrared difference spectroscopy of secondary quinone acceptor photoreduction in proton transfer mutants of *Rhodobacter sphaeroides*. Biochemistry 34: 14722–14732

Plunkett SE, Chao JL, Tague TJ and Palmer RA (1995) Time-resolved step-scan RT-IR spectroscopy of the photodynamics of carbonmonoxymyoglobin. Appl Spectrosc 49: 702–708

Rammelsberg R, Hessling B, Chorongiewski H and Gerwert K (1997) Molecular reaction mechanisms of proteins monitored by nanosecond step-scan FT-IR difference spectroscopy. Appl Spectrosc 51: 558–562

Rammelsberg R, Huhn G, Lubben M and Gerwert K (1998) Bacteriorhodopsin's intramolecular proton-release pathway consists of a hydrogen-bonded network. Biochemistry 37: 5001–5009

Rammelsberg R, Boulas S, Chorongiewski H and Gerwert K (1999) Set-up for time-resolved step-scan FTIR spectroscopy of noncyclic reactions. Vib Spectrosc 19: 143–149

Sakuragi Y, Zybailov B, Shen G, Bryant DA, Golbeck JH, Diner BA, Karygina I, Pushkar Y and Stehlik D (2005) Recruitment of a foreign quinone into the A_1 site of Photosystem I. Characterization of a *menB rubA* double deletion mutant in *Synechococcus* sp. PCC 7002 devoid of F_X, F_A, and F_B and containing plastoquinone or exchanged 9,10-anthraquinone. J Biol Chem 280: 12371–12381

Schlodder E, Falkenberg K, Gergeleit M and Brettel K (1998) Temperature dependence of forward and reverse electron transfer from A_1^-, the reduced secondary electron acceptor in photosystem I. Biochemistry 37: 9466–9476

Siebert F, Mantele W and Kreutz W (1982) Evidence for the protonation of two internal carboxylic groups during the photocycle of bacteriorhodopsin. FEBS Lett 141: 82–87

Sivakumar V, Wang R and Hastings G (2003) Photo-oxidation of P740, the primary electron donor in Photosystem I from *Acaryochloris marina.* Biophys J 85: 3162–3172

Sivakumar V, Wang R and Hastings G (2005) A_1 reduction in intact cyanobacterial Photosystem I particles studies using time-resolved step-scan Fourier transform infra-red difference spectroscopy and isotope labeling. Biochem 44: 1880–1893

Smith BC (1999) Infrared Spectral Interpretation: A Systematic Approach. CRC Press, Boca Raton

Uhmann W, Becker A, Taran C and Siebert F (1991) Time-resolved FT-IR absorption spectroscopy using a step-scan interferometer. Appl Spectrosc 45: 390–397

Wang R, Sivakumar V, Johnson T and Hastings G (2003) FTIR difference spectroscopy in combination with isotope labeling for identification of the carbonyl modes of P700 and $P700^+$ in Photosystem I. Biophys J 86: 1061–1073

Xu W, Chitnis P, Valieva A, van der Est A, Pushkar YN, Krzystyniak M, Teutloff C, Zech SG, Bittl R, Stehlik D, Shen, G, Zybailov B and Golbeck JH (2003a) Electron transfer in cyanobacterial photosystem I: I. Physiological and spectroscopic characterization of site-directed mutants in a putative electron transfer pathway from A_0 through A_1 to F_X. J Biol Chem 278: 27864–27875

Xu W, Chitnis PR, Valieva A, van der Est A, Brettel K, Guergova-Kuras M, Pushkar YN, Zech SG, Stehlik D, Shen G and Golbeck JH (2003b) Electron transfer in cyanobacterial photosystem I: II. Determination of forward electron transfer rates of site-directed mutants in a putative electron transfer pathway from A_0 through A_1 to F_X. J Biol Chem 278: 27876–27887

Chapter 21

Electrogenic Reactions Associated with Electron Transfer in Photosystem I

Alexey Yu. Semenov*, Mahir D. Mamedov
A.N. Belozersky Institute of Physico-Chemical Biology, Moscow State University, Moscow, Russia

Sergey K. Chamorovsky
Department of Biophysics, Faculty of Biology, Moscow State University, Moscow, Russia

Summary

Photoelectric methods to study charge transfer processes in photosynthetic organisms are reviewed along with comparative analyses of photoelectric reactions in Photosystem I, Photosystem II, and the reaction center of purple bacteria. Particular emphasis is placed on a comparison of dielectrically weighted photoelectric signal amplitudes with local structural parameters obtained from the X-ray diffraction data. This analysis demonstrates that the

*Author for correspondence, email: semenov@genebee.msu.su

John H. Golbeck (ed): Photosystem I: The Light-Driven Plastocyanin:Ferredoxin Oxidoreductase, 319–338.

effective dielectric constant (ε) is distributed heterogeneously over the pigment–protein complexes of Photosystem I, Photosystem II, and the bacterial reaction center. The electrogenicity in the Photosystem I complex and its interaction with natural donors (plastocyanin, cytochrome c_6), natural acceptors (ferredoxin, flavodoxin), and artificial acceptors and donors (methyl viologen and other redox dyes) were studied. The profile of distribution of the dielectric constant along the stretch of the complexes was calculated. It was found that the ε value is minimal at the core of the complexes and gradually increases toward the periphery. To a first approximation, the hierarchy of the dielectric constant values derived from photoelectric experiments qualitatively correlates with the hierarchy of the rate constants of charge transfer reactions along the photosynthetic electron transport chain. The fastest primary reactions of charge separation and stabilization of separated charges occur in the core of the complexes in the picosecond time range, whereas slower secondary reactions take place on the periphery of the complexes in the microsecond to millisecond time range. The correlation between the local dielectric constant and the electron transfer rate constant at a corresponding chain segment is discussed in terms of mechanism. It is suggested that these mechanisms are specified by the dielectric reorganization and relaxation of the medium.

I. Structure and Function of PS I

The primary processes of light energy conversion in photosynthetic organisms take place in special pigment–protein complexes that mediate transmembrane charge separation with high quantum and energy efficiencies. The transmembrane charge separation itself initiates further biochemical reactions in the cell. The chlorophyll (Chl)–protein complexes of Photosystem I (PS I) from cyanobacteria, algae, and higher plants, in which low-potential iron–sulfur clusters (F_A/F_B) are the terminal electron acceptors, belong to the Type I class of photosynthetic reaction centers (RC). In terms of evolution, PS I complexes are close to the RC of green sulfur bacteria and heliobacteria. These Type I complexes share many structural and functional similarities (Golbeck and Bryant, 1991).

PS I mediates photoinduced transfer of an electron from plastocyanin (Pc) to ferredoxin (Fd). Cytochrome (cyt) c_6 and flavodoxin (Fld), serve as an alternative electron donor and acceptor, respectively, in cyanobacteria. The three-dimensional structure of PS from the thermophilic cyanobacterium *Synechococcus elongatus* has been solved by X-ray diffraction at a resolution of 2.5 Å (Jordan et al., 2001). PS I complexes in higher plants are monomers, whereas they are trimers in many species of cyanobacteria (Karapetyan et al., 1999; see Karapetyan et al., this volume, Chapter 13). Each monomer (∼300 kD) contains a copy of 12 different protein subunits. The core of the PS I complex consists of two large subunits (products of the expression of the *psaA*, *psaB*, and *psaC* genes), which bind 96 molecules of Chl *a*, 22 molecules of β-carotene, two molecules of phylloquinone, and an interpolypeptide iron–sulfur center F_X. The majority of Chl *a* molecules serve as antenna pigments. The terminal iron–sulfur clusters F_A/F_B ([4Fe–4S] clusters) are bound to the peripheral stromal subunit PsaC, which has a molecular weight of ∼9 kD.

A scheme showing the mutual arrangement of electron transport cofactors and subunits PsaA, PsaB, and PsaC, which constitute the PS I core complex, is shown in Fig. 1. The stromal subunits PsaD and PsaE do not contain redox cofactors, yet they are required to provide binding and effective interaction of PS I with Fd and Fld. The primary electron donor P700 comprises two Chl molecules (eC-A1/eC-B1), the porphyrin planes of the molecules being parallel to one another (distance, 3.6 Å) and perpendicular to the membrane plane. The X-ray diffraction analysis of crystals of the PS I complex also revealed two domains of high electron density that were attributed to Chl *a* molecules in positions corresponding to accessory bacteriochlorophyll molecules in the RC of purple bacteria (eC-A2/eC-B2), two Chl *a* molecules in positions corresponding to bacteriopheophytin molecules in the RC of purple bacteria (Deisenhofer et al., 1985; Allen et al., 1987) (eC-A3

Abbreviations: Δψ – transmembrane electric potential difference; ε – effective dielectric constant; A_0 – monomer chlorophyll acceptor; A_1 – phylloquinone; ALM – artificial lipid membrane; bRC – bacterial photosynthetic reaction centers; Chl – chlorophyll; cyt – cytochrome; DCMU – 3-(3,4-dichlorophenyl)-1,1-dimethylurea; DCPIP – 2,6-dichlorophenol–indophenol; Fd – ferredoxin; Fld – flavodoxin; F_X, F_A, and F_B – 4Fe–4S clusters; MV – methyl viologen; P680 – primary donor of photosystem II; P700 – primary donor of photosystem I; P960 (P870) – primary donor of bacterial reaction center; Pc – plastocyanin; Pheo – pheophytin; PMS – phenazine methosulfate; PS I – Photosystem I; PS II – Photosystem II; Q_A – primary quinone acceptor; Q_B – secondary quinone acceptor; RC – reaction center; TMPD – *N*,*N*,*N*′,*N*′-tetramethyl-*p*-phenylendiamine; Y_Z – redox-active Tyr 161 of photosystem II D1 protein.

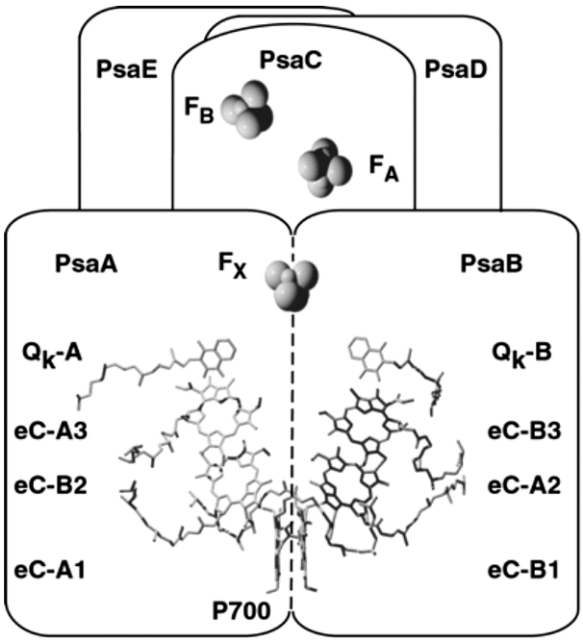

Fig. 1. Arrangement of electron transfer cofactors based on the X-ray diffraction analysis of PS I crystals (Jordan et al., 2001).

and eC-B3), and two phylloquinone molecules (Qk-A and Qk-B).

Pairs of Chl and phylloquinone molecules are located in nearly symmetric electron transport branches A and B, which are bound to subunits PsaA and PsaB, respectively. Branch A incorporates Chl molecules eC-A1, eC-B2, eC-A3, and phylloquinone Qk-A, whereas branch B incorporates Chl molecules eC-B1, eC-A2, eC-B3, and phylloquinone Qk-B. The cofactors forming each branch are crossed rather than exclusively bound to one PS I subunit (eC-B2 belongs to branch A, whereas eC-A2 belongs to branch B). The PS I electron transport chain includes P700, A_0 (one or the two Chl monomer molecules denoted as eC-A3/eC-B3), A_1 (one or the two molecules of phylloquinone Qk-A/Qk-B), and iron–sulfur clusters F_X, F_A, and F_B. Whether one or both of the two symmetric branches of cofactors are involved in electron transfer from P700 to F_X is not completely solved (Guergova-Kuras et al., 2001; Xu et al., 2003).

The spatial arrangement of electron transfer cofactors and antenna Chl molecules in the photosynthetic membrane is shown in Fig. 2. The majority of antenna Chl molecules are arranged in two parallel layers. The boundary of the lower layer is slightly below the level of P700, whereas the boundary of the upper layer is near the level of iron–sulfur cluster F_X. This arrangement of the antenna Chl molecules delineates an arbitrary borderline of the lipid bilayer, thereby inferring the topography of the PS I electron carriers in the membrane.

A diagram of the electron transport reactions in PS I, along with lifetimes of the direct and back reactions as well as midpoint potentials (E_m) of the redox cofactors, is shown in Fig. 3. Upon absorbing a light quantum, the primary electron donor becomes an excited state P700*, which is followed by the act of charge separation between P700* and the primary acceptor A_0 and the subsequent formation of the intermediate state $P^+A_0^-$ within <20 psec. After 50 psec, the electron is transferred to the phylloquinone A_1 and within $\leq$200 nsec to the iron–sulfur clusters F_X and F_A/F_B. Furthermore, electron transfer to the natural acceptor Fd (Fld) occurs within 0.5–100 μsec. In the absence of an electron acceptor, the kinetics of the back reactions of the electron from F_X^- and $(F_A/F_B)^-$ to $P700^+$ are characterized by lifetimes of 0.5–5 and 30–100 msec, respectively. In the presence of the native secondary donor Pc (cyt c_6), the fast reduction of photooxidized P700 prevents charge recombination between F_X^- or $(F_A/F_B)^-$ and $P700^+$ (see Brettel and Leibl, 2001, for review).

II. Methods of Measurement of Membrane Potentials

According to the widely accepted chemiosmotic principle of energy coupling through a proton-motive force as suggested by P. Mitchell, membrane proteins and vectorial metabolic reactions play a key role in the primary processes of energy accumulation in biological membranes (see Mitchell and Pasternak, 1992, for review). Redox components comprising electron transport chains in coupled membranes are located asymmetrically in membrane proteins, thereby providing a basis for transmembrane vectorial charge transfer. Light-dependent charge transfer in RCs of photosynthetic organisms is accompanied by the generation of a transmembrane electric potential difference ($\Delta\psi$). The relative contribution of individual reactions to the total amplitude of ψ is dielectrically weighted, i.e., it is determined not only by the projection of the cofactor-to-cofactor distance onto the perpendicular to the membrane plane but also by the dielectric properties of the environment at the protein site between the redox centers. In addition, conformational changes of charged amino acid residues and redox centers that accompany transmembrane charge transfer may also contribute to generation of $\Delta\psi$. Both the slowest kinetic stages of

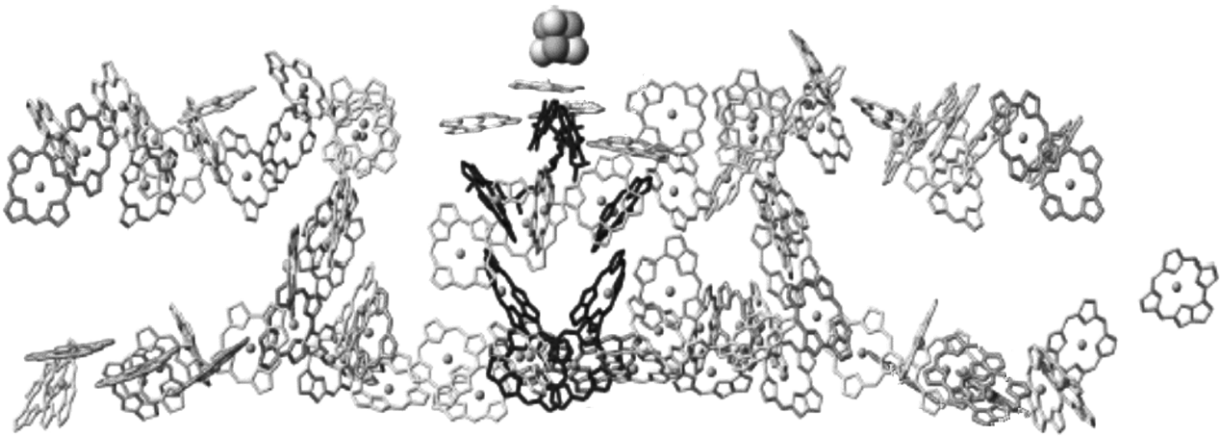

Fig. 2. Topography of redox carriers and PS I Chl antenna molecules in the membrane. The electron transfer cofactors and Chl molecules are highlighted in black and gray, respectively. The iron–sulfur cluster F_X is shown as a group of spheres (adapted from Jordan, 2001).

the generation of $\Delta\psi$ and the steady-state level of $\Delta\psi$ depend on the ion permeability of the membrane, the membrane integrity, and the electric resistance.

A method based on the detection of the absorption changes of carotenoids is commonly used for measuring $\Delta\psi$ in membranes of photosynthetic organisms. Absorption changes of carotenoids in photosynthetic membranes are due to an electrochromic shift of maximums of their absorption spectra (Junge and Witt, 1968). It was shown that the amplitude of the absorption change induced by an electric field is a linear function of the transmembrane potential (Junge and Witt, 1968; Jackson and Crofts, 1969). This method has been widely used in studies of electrogenic reactions in chromatophores of purple bacteria and thylakoids of chloroplasts. However, this method proved to be ineffective in studies of cyanobacteria and isolated pigment–protein complexes in model systems. In addition, the carotenoid method is characterized by a relatively low signal-to-noise ratio, which requires signal averaging of the kinetic records. It should be noted, however, that Joliot and Joliot (1984) have developed a kinetic spectrophotometer that achieves a high signal-to-noise ratio by utilizing differential optics and a series of relatively intense light pulses from a flashlamp instead of a continuous beam to probe the sample.

A microelectrode method permits the direct measurement of $\Delta\psi$. A capillary microelectrode was

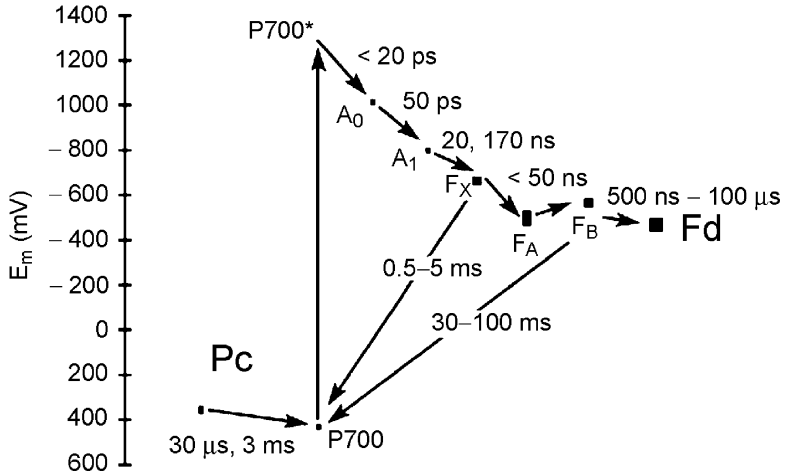

Fig. 3. Diagram of the forward and back reactions of electron transfer in PS I with lifetimes and midpoint redox potential (E_m) values of the cofactors.

inserted into the giant chloroplast in a eukaryotic alga (Bulychev et al., 1972), and it was thereby shown that the electrogenic activity (i.e., activity accompanied by the generation of an electric potential difference) of PS I was higher than the electrogenic activity of PS II. However, it should be noted that the microelectrode technique could be used to measure the membrane potential in only a few naturally occurring organisms. In addition, the high ohmic resistance of microelectrodes reduces the time resolution of the method to ~1 msec.

The generation of $\Delta\psi$ in PS I complexes under conditions of pulse laser excitation is due to the transfer of an electron through the dielectric layer of the membrane protein from the natural donors (Pc or cyt c_6) through P700, A_0, A_1, F_X, F_A, and F_B to the exogenous acceptors Fd or Fld. Because this review is focused on fast electrogenic reactions in isolated PS I complexes, we will describe in detail the photoelectric methods designed to measure $\Delta\psi$ with a high time resolution.

A. Measurement of the Generation of the Electric Potential Difference at the Heptane/Water Interface

When chloroplasts are positioned at a heptane/water interface, the thylakoid membranes are ruptured and the components of the membrane are oriented at the interface according to their hydrophobic/hydrophilic properties. If the chloroplasts, which are spread over the heptane/water interface, are illuminated with a flash of light, a photovoltage of about 2 mV can be measured using a high-resolution capacitive electrode (Trissl and Gräber, 1980). It was shown that the amplitude of the photoelectric signal was decreased by about one-half in the presence of 3-(3,4-dichlorophenyl)-1,1-dimethylurea (DCMU), an inhibitor of electron transport through PS II. From these data, it was concluded that the amplitude of the photoelectric signal generated by PS I contributed about one-half of the total photoelectric signal of the thylakoid membrane. The rise-time of the photoelectric signal was measured in these experiments to be less than 1 nsec. It should be noted, however, that charge transfer to F_A/F_B in PS I occurs within the time interval of about 200 nsec, whereas electron stabilization in the subnanosecond time range occurs only in the phylloquinone A_1 molecule (see Brettel and Leibl, 2001, for review).

Double-flash experiments with PS I vesicles exposed to the heptane/water interface revealed that the lifetime (τ) of the back reaction was ~65 msec, which corresponds to the kinetics of charge recombination between $P700^+$ and terminal iron–sulfur acceptors $(F_A/F_B)^-$. It should be noted that exposure of chloroplasts or PS I vesicles to the heptane/water interface is accompanied by partial extraction and denaturation of pigment–protein complexes. Perhaps this disadvantage does not permit the method of measurement of $\Delta\psi$ generation at a heptane/water interface to be used more widely.

B. Measurement of Electric Potential Generated by a Light Gradient in Chloroplast Suspensions

When a suspension of chloroplasts is exposed to a nonsaturating flash, a transient electric potential difference can be measured between two electrodes immersed in the suspension, provided that the electrodes are separated along the direction of the light beam propagation (Witt and Zickler, 1973; Fowler and Kok, 1974). This effect represents the transient processes of the generation of the transvesicular $\Delta\psi$. Because of the lack of light saturation, a larger number of charge separations occur at the light entry side of the vesicle as compared to the light exit side (see scheme in Fig. 4).

Because charge transfer is directed from the inside to the outside of the vesicle, an array of oriented dipoles is generated with the negative sign at the light entrance side of the vesicle. Therefore, the additive effect of all thylakoids located along the light path allows the $\Delta\psi$ to be measured with two macroscopic electrodes inserted at different depths into the apparatus containing the suspension of thylakoids. The direction of the primary photosynthetic electron transport can be determined from the polarity of the photovoltage. This method has been given the name "the light gradient method." With this method it was shown that the polarity of the potential generated by inside-out thylakoids was opposite to the polarity of intact chloroplasts (Gräber, 1987). Double-flash experiments with the light gradient method in chloroplasts also demonstrated the possibility of detecting $P700^+$ reduction kinetics.

C. Measurement of the Electric Potential Difference in Oriented Multilayers

A further upgrade to the light gradient method was made in the laboratory of H. -W. Trissl on the basis of the formation of a multilayer of PS I-containing membrane fragments electrically oriented in a low-impedance capacitive microcoaxial cell (Deprez et al., 1986; Hecks et al., 1994). This allowed the rise-time of the electrogenic phase to be resolved with picosecond time resolution. These measurements revealed the photovoltage generation steps accompanying electron

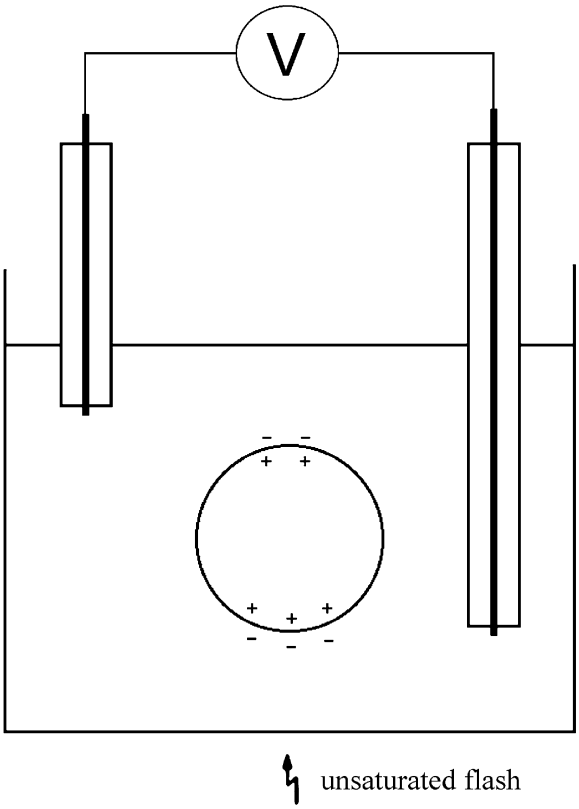

Fig. 4. Schematic diagram of the light gradient method for detection of electric signals in chloroplasts (adapted from Gräber, 1987).

transfer between P700 and A_0 ($\tau < 22$ psec) and between A_0 and A_1($\tau \sim 50$ psec). However, the time window of the low-impedance measurements did not extend longer than 1–2 nsec and was limited by the parameters of the input *RC*-circuit. A variant of this method using a high-input impedance amplifier allowed the time window of detection to be extended up to 50 nsec (Trissl et al., 1987).

A further extension of the time window was achieved by calculating the ideal photovoltage $\Delta\psi$ rise-time as the integral of the displacement current and the removal of the decay due to ionic relaxation by a numerical deconvolution procedure. This procedure allowed an electrogenic phase with $\tau \sim 220$ nsec to be resolved. This phase was ascribed to electron transfer from A_1 to F_X and further to F_A/F_B (Leibl et al., 1995). However, this method is not applicable to the measurement of the amplitude and kinetics of slower electrogenic phases because the kinetic phase with $\tau \sim 220$ nsec was obtained as a decay-cleared trace rather than actually measured kinetic transient. Therefore, it is appropriate to develop another method of detection of $\Delta\psi$ generation within the time range from 200 nsec to ~100 msec. The system based on phospholipid-impregnated collodion film developed in our laboratory seems to be well-suited for the measurement of photovoltage kinetics on the microsecond to millisecond time scale. This system was used earlier in our laboratory to study bacteriorhodopsin and bacterial photosynthetic reaction centers. It was later used to study electrogenic reactions in PS I complexes.

D. The Direct Electrometrical Method

The method of direct measurement of the electrical activity of membrane enzymes was first used in studies of electrogenesis in membranes of proteoliposomes containing bacteriorhodopsin and a number of mitochondrial energy–transformation complexes (Drachev et al., 1974). The principles of this method are based on the association of closed lipid–protein membrane vesicles (proteoliposomes) with an artificial lipid membrane (ALM) and measurement of $\Delta\psi$ in the system using macroelectrodes immersed in a buffer electrolyte solution at the two sides of the ALM. The macroelectrodes are connected to an electrometric voltmeter (or to a broad-band operating amplifier when detecting fast kinetics). The incubation of proteoliposomes for ~1 h at room temperature in the presence of the cations Ca^{2+}or Mg^{2+} (incubation is required to neutralize negative charges at the surfaces of the contacting membranes) gives rise to the association of proteoliposomes with the ALM. The ALM-bound proteoliposomes are retained the inner aqueous phase, which was confirmed by electron microscopy and by experiments with gramicidin (Drachev et al., 1976).

Thick membranes formed from an asolectin (phosphatidylcholine type II-S) solution in *n*-decane in a 1-mm hole in a Teflon film that separates two compartments of the measuring system were used in early experiments as the ALM. A further methodological upgrade of the measuring system included the use of porous filters as an ALM frame (Drachev et al., 1979). However, the low electric capacitance of a thick ALM is a disadvantage because it results in distortion of the $\Delta\psi$ kinetics.

Let us consider a simplified equivalent electrical circuit of the proteoliposome–ALM measuring system put forward by L. A. Drachev (Fig. 5; Drachev et al., 1981a). According to the equivalent electric circuit,

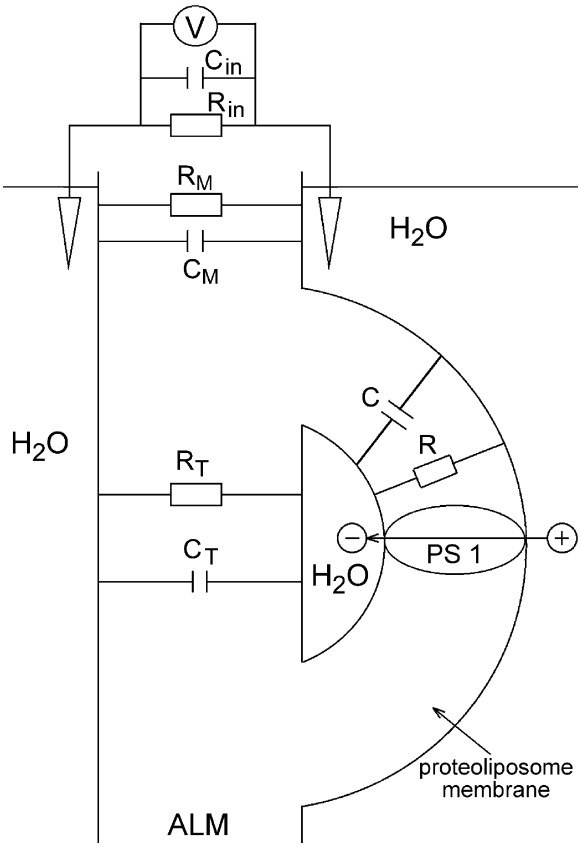

Fig. 5. Schematic diagram of the direct electrometrical method of measurement of the electric potential difference in the proteoliposome–ALM system. Explanations are given in the text (adapted from Drachev et al., 1981).

the electrical voltage measured with the voltmeter V is less than the voltage generated across the proteoliposome membrane associated with ALM because the voltmeter V is connected to the generator (e.g., PS I) through a voltage divider formed by resistances R_T and R_m and capacitances C_T and C_m. This voltage divider is compensated (its coefficient of attenuation does not depend on the signal frequency) because the time-constants C_pR_p and C_mR_m are equal to one another (the two regions are parts of the same ALM). Therefore, the photoelectric signal generated in a proteoliposome membrane should be transmitted to the electrodes with a lower amplitude but without a distortion of the signal shape. This is indeed observed provided the input resistance of the voltmeter (or operational amplifier) R_{in} is larger and the input capacitance C_{in} is significantly lower than the resistance and capacitance of the proteoliposome-ALM system, respectively.

The actual equivalent circuit of this system is more complicated than the circuit considered above. The resistances and capacitances of the ALM/H_2O interface were found to be significantly larger than the resistance and capacitance of phospholipid solution because ordered lipid layers are formed at the border zones, whereas disordered phospholipid molecules dissolved in *n*-decane are located in the bulk ALM. Therefore, the boundary ALM layers are simulated by *RC*-chains with larger capacitances and resistances than in *RC*-chain that simulate the inner ALM layers. As a result, the capacitance of the system measured within the low-frequency range corresponds to the bilayer lipid membrane capacitance, whereas the capacitance of the system measured at higher frequencies is comparable to the amplifier C_{in}. This causes a distortion of the photoelectric kinetics from the true value. To increase the capacitance of the inner ALM layer, the thickness of the artificial membrane should be decreased and its area increased as much as possible.

A thin but sufficiently strong collodion (nitrocellulose) film impregnated with phospholipid solution was used in our experiments for detecting fast stages of $\Delta\psi$ generation (Drachev et al., 1981a). The resistance of the collodion film was significantly lower than the amplifier R_{in}, whereas its capacitance (5000 pF) was three orders of magnitude larger than the operating amplifier C_{in}. The use of the phospholipid-impregnated collodion film as ALM provided an opportunity to detect undistorted electric signals with a time resolution ~200 nsec. The time resolution of measurement was limited by parameters of the signal recording hardware. After completion of the process of ALM association with proteoliposomes, the incubation medium in the two compartments of the Teflon measuring cell was replaced with fresh buffer medium containing neither proteoliposomes nor divalent metal cations. Light-dependent reactions in this system were induced by laser flashes (wavelength, 532 nm; pulse halfwidth, 15 nsec), which provided synchronous single-turnover photoexcitation of PS I complexes. Photoelectric signals were detected using an operational amplifier with a frequency bandwidth of 8 MHz and an amplification coefficient 100. The electric signals from the operational amplifier output were applied to a transient recorder and stored in computer memory. To analyze the kinetics of the $\Delta\psi$ signal rise and decay in the same record, the photoelectric signal was recorded using two different time sweeps in one kinetic curve. The resulting curve was expanded into exponential components using computer programs GIM (developed by A. L. Drachev) and DISCRETE.

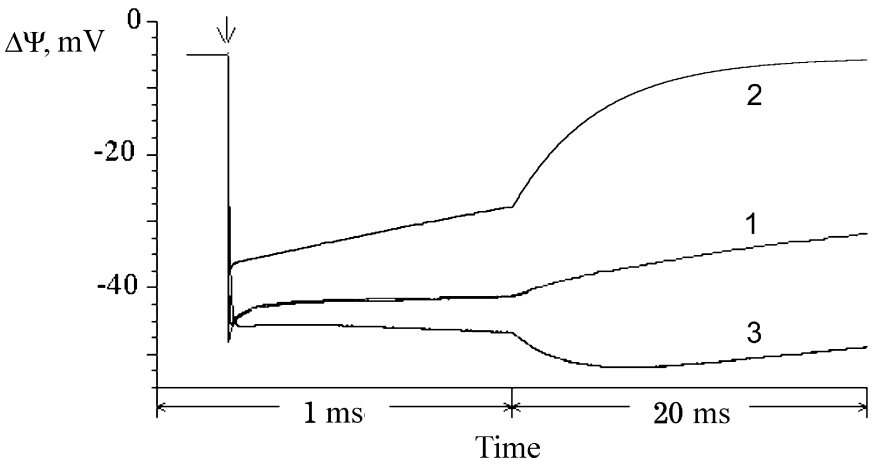

Fig. 6. Photoelectric responses of proteoliposomes containing PS I. Photoelectric responses were recorded using the direct electrometrical method: (1) in the absence of additions; (2) in the presence of 100 mM sodium dithionite; (3) in the presence of 10 mM sodium ascorbate and 0.4 mM Pc (adapted from Mamedov et al., 1998, 2001).

III. Electrogenic Reactions in PS I

A. Electrogenic Reactions on the Acceptor Side of PS I

1. Electrogenicity Accompanies Photoreduction of Iron–Sulfur Clusters F_A and F_B in PS I

In the absence of soluble electron donors and acceptors, the kinetics of the dark reduction of $P700^+$ are characterized by back reactions from one of the bound electron acceptors (Vassiliev et al., 1997). The direct electrometrical method developed in our laboratory (Drachev et al., 1974, 1979, 1981b; Dracheva et al., 1988) was used to monitor the flash-induced photoelectric responses of the proteoliposomes containing PS I complexes from the cyanobacterium *Synechocystis* sp. PCC 6803 adsorbed on the surface of a phospholipid-impregnated collodion film. The formation of the transmembrane electric potential difference corresponded to the negative charging of the interior of the proteoliposomes (Mamedov et al., 1996). According to the negative sign of the photoelectric response and the effect of the nonpenetrating oxidizing agent potassium ferricyanide on the amplitude of the flash-induced $\Delta\psi$, the orientation of P700 in the proteoliposome membrane was estimated to be >95% facing the external aqueous phase (Mamedov et al., 1996). The main component of the $\Delta\psi$ decay kinetics with a lifetime of ~100 msec corresponded to the charge recombination between $P700^+$ and $(F_A/F_B)^-$, whereas the minor faster components were attributed to back reactions from F_X^- and A_1^- in a fraction of the PS I complexes with impaired forward electron transfer to F_A/F_B (Vassiliev et al., 1997).

The kinetics of forward electron transfer from A_1^- to the Fe/S clusters in PS I is approximated by two components with τ ~20 and τ ~200 nsec (see Joliot and Joliot, 1999; Brettel and Leibl, 2001 and references therein). On the basis of photoelectric measurements on electrically oriented PS I-containing membrane fragments, it was concluded that the overall electron transfer from A_1^- to F_B was limited by the step from A_1^- to F_X (Diaz-Quintana et al., 1998). Because the lifetime of the $\Delta\psi$ generation measured by Joliot and Joliot (1999) fell within a time interval shorter than the instrument-limited response time of our instrumentation (200 nsec), neither the 20 nor 200 nsec kinetic phases of forward electron transfer between A_1 and F_A/F_B were resolved (Fig. 6, trace 1). Therefore, to estimate the relative contribution of electron transfer reactions between iron–sulfur clusters to the overall electrogenesis, we used an indirect approach. Our strategy was based on the following assumptions: (i) sodium dithionite is able to reduce F_A and F_B and (ii) treatment with $HgCl_2$ causes selective extraction of the F_B cluster (Kojima et al., 1987). A comparison of the dithionite-induced decrease in the magnitude of the total photoelectric responses obtained with control and F_B-less ($HgCl_2$-treated) PS I complexes provides an independent approach to the elucidation of the relative contribution of $F_X \rightarrow F_B$ and $F_X \rightarrow F_A$ electron transfer reactions to the overall electrogenesis within the PS I complex.

The initial amplitude of $\Delta\psi$ can be determined by extrapolating the $\Delta\psi$ decay kinetics. The main decay pathway of the flash-induced $\Delta\psi$ that is built-up across the membrane is the charge recombination between $P700^+$ and the photoreduced terminal acceptors F_A^- and F_B^- (whose lifetime ranges between 30 and 100 msec (Vassiliev et al., 1997; see also Brettel and Leibl, 2001, for review). To determine the initial amplitude of $\Delta\psi$ we took into account only the charge separation between components with lifetimes longer than 400 μsec, i.e., the components related to electron transfer steps at distances larger than between P700 and A_1. This excluded contributions from centers with impaired electron transfer between A_1 and F_X. On the basis of room-temperature kinetics of P700 absorption changes in isolated PS I complexes, the amount of dithionite used (100 μM) was found to be sufficient to chemically reduce F_A and F_B without any noticeable reduction of F_X. As expected, the addition of dithionite led to an acceleration of the $\Delta\psi$ decay kinetics (Fig. 6, trace 2), which was mainly due to the back-reaction from F_X^- (lifetime ranging between 0.5 and 5 msec). The deconvolution of the kinetic curves shows a ~30% decrease in the amplitude of the photoelectric response in the presence of dithionite, which occurs due to the blockage of the electron transfer between F_X and F_A/F_B.

Treatment of cyanobacterial PS I complexes with $HgCl_2$ results in >95% destruction of the F_B cluster and retention of >90% of the F_A cluster (Jung et al., 1995). For the $HgCl_2$-treated (F_B-free) samples, we performed similar multiexponential analysis of the decay kinetics in the absence and in the presence of dithionite, and determined the initial amplitudes of $\Delta\psi$ after subtracting the fast phases with lifetimes shorter than 400 μsec. The addition of dithionite to both the control and $HgCl_2$-treated samples resulted in similar acceleration of the $\Delta\psi$ kinetics, but the decrease of the initial $\Delta\psi$ amplitude associated with the blockage of electron transfer from F_X to F_A was less significant in $HgCl_2$-treated samples (15–17%). It should be noted that Diaz-Quintana et al. (1998) observed a decrease in the amplitude of the electrogenic phase corresponding to the $A_1 \rightarrow F_A/F_B$ electron transfer in $HgCl_2$-treated sample compared to the control. However, this decrease was attributed in (Diaz-Quintana et al., 1998) to the treatment-induced destruction of ~30% of F_A. Note that no such $HgCl_2$-induced degradation of the F_A iron–sulfur clusters was observed in our experiments (Mamedov et al., 1998). The discrepancy could be due to the differences in PS I preparations, in the $HgCl_2$-treatment procedure, and in the techniques used to measure the electrogenic changes (PS I-containing proteoliposomes adsorbed onto the phospholipid collodion membrane (Mamedov et al., 1998) versus electrically oriented multilayer membrane fragments adsorbed onto a platinum electrode (Diaz-Quintana et al., 1998).

The data obtained unambiguously indicate that the voltage changes on the reducing side of PS I are related to the electron transfer between F_X and F_A as well as between F_A and F_B. On the basis of the electrogenic nature of the latter reaction, we concluded that F_B rather than F_A was the electron acceptor distal to F_X (Mamedov et al., 1998).

2. Electron Transfer from the Terminal Cluster F_B to External Acceptors is Electrically Silent

The electrometrical technique was also used to investigate electron transfer between the terminal iron–sulfur centers F_A/F_B and external electron acceptors in PS I complexes isolated from the cyanobacterium *Synechococcus* sp. PCC 6301 and from spinach (Mamedova et al., 1999). The photoelectric responses were monitored in PS I-containing proteoliposomes either in the absence or the presence of Fd, Fld, and methyl viologen (MV) entrapped in phospholipid vesicles. The increase in the relative contribution of the slow components of the $\Delta\psi$ decay kinetics in the presence of both native (Fd, Fld) and artificial (MV) electron acceptors indicates that the interaction between the terminal Fe/S cluster and acceptors is effective. The lack of additional electrogenicity under conditions of effective electron transfer from the F_B redox center to soluble acceptors implies that this reaction is electrically silent. Similar data were obtained using proteoliposomes containing spinach PS I complexes, where the orientation of the complexes was opposite. The finding that F_A fails to donate electrons to Fld in the F_B-deficient ($HgCl_2$-treated) PS I complexes suggests that F_B is the direct electron donor to Fld (Mamedova et al., 1999). This conclusion is in line with the data obtained by monitoring the kinetics of re-reduction of the photooxidized P700 in the presence of Fd and Fld (Vassiliev et al., 1998) and the kinetics of Fd reduction (Diaz-Quintana et al., 1998) by control and F_B-deficient PS I complexes. Although the F_B-free PS I complexes, which almost completely lost the ability to donate electron to Fld, were still capable of reducing MV, the effective concentration in this case was much higher than the concentration required to provide interaction with intact PS I complexes. The fact that the concentration of MV required to accept an

electron from F_A is higher than that for F_B implies that the $F_A$cluster is sterically hindered relative to the F_B site (Vassiliev et al., 1998).

The finding that F_B is the distal cluster to F_X and that it serves as the immediate electron donor to Fd/Fld unequivocally indicates that the electron transfer on the acceptor side of PS I is arranged as in the following series: $F_X \rightarrow F_A \rightarrow F_B \rightarrow$ Fd/Fld (see Golbeck, 1999, for review).

B. Electrogenicity Accompanying Reduction of Photooxidized P700 by Electron Donors

1. Electrogenic Reduction of P700 by Plastocyanin and Cytochrome c_6

The accessibility of $P700^+$ to the external aqueous phase makes PS I-containing proteoliposomes a convenient system for studying electron donation from nonpenetrating hydrophilic donors. As mentioned above, cyt c_6 and Pc are alternative native secondary electron donors to photooxidized P700 in cyanobacteria. The addition of a donor capable of donating an electron to $P700^+$ more rapidly than the photoreduced acceptor gives rise to competitive substitution of recombination by direct electron transfer.

The addition of reduced Pc in a gradually increasing concentration experiment resulted in slowing down of the $\Delta\psi$ decay due to competition with $(F_A/F_B)^-$ for reduction of $P700^+$. At a Pc concentration above 50 μM, an additional $\Delta\psi$ rise phase is observed in the kinetics of the photoelectric response. The maximal amplitude makes up ~20% of the amplitude of the fast phase attributed to $P700^+(F_A/F_B)^-$ charge separation (Fig. 6, trace 3), whereas the apparent pseudo-first-order rate constant exhibits a saturation profile at increasing Pc concentrations, thereby suggesting the formation of a transient complex with PS I. Additionally, a small but detectable fast electrogenic phase was observed at high Pc concentrations. The rate constant of this phase was independent of Pc concentration, indicating that it is related to a first-order process. The $\Delta\psi$ rise kinetics at a Pc concentration of 400 μM is clearly biphasic: the small fast component is characterized by $\tau \sim 30$ μs and the large slow one, by $\tau \sim 3$ msec (Mamedov et al., 2001).

A comparative kinetic analysis of electron transfer between Pc and photooxidized P700 in a variety of evolutionary-differentiated organisms led to the proposal of different reaction mechanisms for PS I reduction (Hervas et al., 1995). In most primitive cyanobacteria, such as *Synechocystis* sp. PCC 6803 and *Synechococcus elongatus*, a linear Pc-concentration dependence of the rate constant of $P700^+$ reduction was observed (Hervas et al., 1994). This type of behavior corresponds to a simple bimolecular collisional mechanism (type I). In the other cyanobacteria, such as *Anabaena* sp. PCC 7119 and *Pseudanabaena* sp. PCC 6903 and in hybrid systems composed of eucaryotic PS I and cyanobacterial Pc, a saturation profile in the Pc-concentration dependence uncovered a pseudo-first-order rate constant of $P700^+$ reduction. This profile was attributed to a two-step mechanism (type II), which involved complex formation prior to the electron transfer. The kinetic profiles of the type I and type II mechanisms were monophasic, with no detectable fast phases. The electron transfer kinetics between Pc and PS I in higher plants and eucaryotic algae was shown to be bi-exponential with a fast first-order rate constant ($t_{1/2}$ = 10–20 μsec) and a slower second-order rate constant. A three-step kinetic mechanism (type III), involving a rate-limiting conformational change within the Pc–PS I complex prior to intracomplex electron transfer was suggested to explain the experimental data at saturating Pc concentrations.

The data presented in our experiments seem to be consistent with a type III mechanism. Indeed, in the presence of Pc, the kinetics of $\Delta\psi$ generation contained two exponential phases: (i) a small component with a fast first-order rate constant and (ii) a large component with a slow second-order rate constant that exhibited a saturation profile.

The addition of cyt c_6 also caused a decrease in the $\Delta\psi$ decay rate and changed the kinetics of the $\Delta\psi$ generation. In addition to the kinetically unresolvable fast phase of the photoelectric response, slower phases in the submillisecond time scale appeared. These phases can be assigned to electron transfer from cyt c_6 to $P700^+$. The amplitudes of these phases accounted for 20% of the fast phase amplitude, and the kinetics were approximated by two exponents with lifetimes of 25 and 200 μsec in an amplitude ratio of 2:3. The kinetics of the former rather than the latter phase did not depend on cyt c_6 concentration, indicating the formation of a specific complex between cyt c_6 and P700 (Mamedov et al., 1996).

2. Electrogenic Reduction of P700 by Redox Dyes

Reduced forms of redox-mediators such as N,N, N', N'-tetramethyl-*p*-phenylendiamine (TMPD), 2,6-dichlorophenol–indophenol (DCPIP), and phenazine

methosulfate (PMS) have been widely used as artificial secondary electron donors, in particular for the photooxidized bacteriochlorophyll dimer in bacterial photosynthetic reaction centers (bRC) and for the Chl dimer (P700) in PS I complexes (Drachev et al., 1985; Gourovskaya et al., 1997). The decay kinetics slowed down upon increasing the concentration of the redox dye. At a certain concentration, the fast component of the membrane potential related to electron transfer between P700 and the terminal iron–sulfur acceptor F_B was followed by a new electrogenic phase in the millisecond time domain, which contributed approximately 20% to the overall photoelectric response. The reduced form of PMS was a more effective electron donor to $P700^+$ than TMPD or DCPIP. This new kinetic phase was attributed to the vectorial transfer of an electron from the reduced form of the redox dye to the protein-embedded Mg-porphyrin ring of $P700^+$ (Gourovskaya et al., 1997).

These results suggest that the electrogenic nature of the electron donation to $P700^+$ is not specific for cyt c_6 and Pc, the native electron donors. Moreover, the electrogenic response observed in the presence of artificial donors was approximately equal to the contribution of the phase observed in the presence of Pc or cyt c_6, (~20% to the overall photoelectric response). Therefore, it is safe to conclude that the electrogenic reduction of $P700^+$ *in vivo* occurs as a result of vectorial electron transfer within the PsaA/PsaB heterodimer rather than within the cyt c_6-P700 or Pc–P700 complexes.

IV. Profile of Changes of the Effective Dielectric Constant along the Photosynthetic Electron Transfer Complex

A. Photosystem I

Because the photoelectric signal amplitude is proportional to the dielectrically weighted distances, a comparison of the projections of the distance vectors between redox cofactors onto the membrane normal with the relative photovoltage amplitudes provides a unique opportunity to estimate the profile of distribution of the dielectric constant (ε) values along the whole stretch of the PS I protein complex. The dielectric constants estimated from photoelectric experiments are effective values determined with respect to the time scale of the corresponding reaction. In terms of dielectric environment, the ε values related to membrane-embedded protein-bound cofactors are presumably determined by local structural properties of the protein matrix, whereas in case of electron carriers exposed to polar aqueous medium, the aqueous phase surrounding the membrane may also contribute to the ε value. Strictly speaking, the dielectric constant is a macroscopic characteristic determined by the atomic state of the surrounding medium. However, it has been demonstrated in various model systems (including genetically modified proteins) that the macroscopic estimates of dielectric parameters did not change drastically on the Ångstrom scale (Fersht, 1999).

The prerequisite for the estimation of ε is the knowledge of the three-dimensional structure of the protein. Although this information was not available at the time of the first photoelectric measurements on PS I (Trissl et al., 1987; Hecks et al., 1994), these experiments provided valuable structural information about the relative transmembrane positions of the cofactors. To interpret the results of the fast photoelectric measurements on oriented multilayer membrane fragments, it was originally assumed that the dielectric environment was homogeneous, at least for the part of the PS I complex inside the protein/lipid layer (Trissl et al., 1987; Leibl et al., 1995). However, it was found later that this assumption needed to be revised at least in the case of the bRC (Dracheva et al., 1988). It is not also supported by the general three-phase model of membrane proteins, which assumes the increase of effective ε value in the direction from the central hydrophobic part of the protein toward the periphery of the protein/lipid layer (Cherepanov and Krishtalik, 1990).

Let the electron transfer reactions in the complex be denoted as A→B→C. Given the fact that the electron transfer reactions in the complex are essentially irreversible, the relationship of the ratio between the mean ε values corresponding to B→C and A→B electron transfer stages ($\varepsilon_{BC}/\varepsilon_{AB}$) with the photovoltage drop between B and C (ψ_{BC}) and between A and B (ψ_{AB}) can be described by the following approximate equation:

$$(\varepsilon_{BC}/\varepsilon_{AB}) = (D_{BC}/D_{AB})/(\psi_{BC})/(\psi_{AB})$$

where D_{BC} and D_{AB} are the projections for the B→C and A→B distance vectors to the membrane normal, respectively. Taking into account the distances between the PS I cofactors (Jordan et al., 2001) and the structural model of the Fd (Fromme, 1994) and Pc (Fromme, 1994; Myshkin et al., 2002) docking sites, as well as relative contributions of the electron transfer reactions P700 → A_0 and A_0 → A_1 (Hecks et al., 1994), A_1 → F_X (Leibl et al., 1995; Diaz-Quintana, 1998), F_X →

Table 1. Calculation of the effective dielectric constant values in the protein domains between redox cofactors of PS I

PS I protein domains between redox cofactors	Projections of the distance vectors (D) Å	Relative photovoltages, (ψ)	Effective dielectric constant values (ε)
Pc–P700	~ 20	0.155[a]	9.7
P700–A_0	15.5	0.38	3
A_0–A_1	7.2	0.095	5.4
A_1–F_X	8.5	0.12	5.4
F_X–F_A	14.1	0.125	8.7
F_A–F_B	7.4	0.125	4.6
F_B–Fld	11	<0.02[b]	>42

[a] Experimental error in determination of value of ψ in different experiments did not exceed $\pm$10%. Because geometrical parameters were estimated from the X-ray diffraction (Jordan et al., 2001) with sufficiently high accuracy, the sum error of the calculation of ε was $\pm$10%.
[b] This value was taken from the previously estimated lower limit for a detectable relative photovoltage measured by the direct electrometrical technique (see Semenov, 1991, for review).

F_A and $F_A \rightarrow F_B$ (Mamedov et al., 1998), Pc $\rightarrow$ P700 (Mamedov et al., 2001) and $F_B \rightarrow$Fld (Mamedova et al., 1999) to the overall electrogenesis provided by the PS I complex, the following suggestions can be made:

1. Let the minimal value of the dielectric constant for the P700$\rightarrow A_0$ protein region be $\varepsilon \sim 3$. Then, the ε value for the $A_0 \rightarrow A_1$ and $A_1 \rightarrow F_X$ domains can be estimated to be ~5.4;

2. On the acceptor side, the ε value further increases along the PsaC subunit to ~8.7 at the $F_X \rightarrow F_A$ site and then decreases to ~4.6 at the $F_A \rightarrow F_B$ site;

3. On the donor side between the Pc binding site and P700 Mg-porphyrin rings embedded into PsaA/PsaB heterodimer (Pc$\rightarrow$P700), the mean ε value is equal to 9.7.

The results of calculation of the effective ε values in the protein domains between redox cofactors are presented in Table 1, whereas the profile of variation of ε along the PS I complex is shown in Fig. 7. The large value of ε on the donor side between the Pc binding site and the P700 Mg-porphyrin rings is not very surprising because in contrast to the PS I complex, the plastocyanin/cytochrome subunit is exposed to the polar aqueous medium. A gradual increase in the value of ε from ~3 at the center of the protein globule to ~10 at its periphery has also been observed in globular proteins (see Mertz and Krishtalik, 2000, for review).

The relative contributions of electrogenic reactions associated with the $F_X \rightarrow F_A$ and $F_A \rightarrow F_B$ electron transfer reactions to the overall electrogenesis are virtually equal to one another (Mamedov et al., 1998), whereas the projections of the center-to-center vectors from F_X to F_A and from F_A to F_B to the membrane normal differ almost twofold (14.1 and 7.4 Å, respectively). This finding assumes that the average effective dielectric constant value in the $F_A \rightarrow F_B$ domain is about 1.9 times lower relative to the $F_X \rightarrow F_A$ domain. This result seems to be fairly surprising in terms of the three-phase model, according to which the redox centers more remote from the hydrophobic inner part of the membrane protein should be located in the protein domains with ε values similar to or higher than that of the inner part of the membrane. However, there are at least two noticeable exceptions to this general rule:

(i) The primary (Q_A) and secondary (Q_B) quinone acceptors in the photosynthetic bRC are located at the same distance from the border of the protein dielectric (Allen et al., 1988; Okamura et al., 1992). However, Q_B is surrounded by a larger number of charged amino acid residues and water molecules than Q_A, which leads to a higher dielectric constant in the vicinity of Q_B as compared to Q_A (Ermler et al., 1994; Stowell et al., 1997).

(ii) Substantially higher effective dielectric constants were suggested in the vicinity of the redox cofactors of the functional branch than that for the nonfunctional branch of *Rhodobacter sphaeroides* RCs (Steffen et al., 1994).

Taking into account these considerations, it is safe to speculate that the observed decrease of the effective dielectric constant in the $F_A \rightarrow F_B$ domain compared to

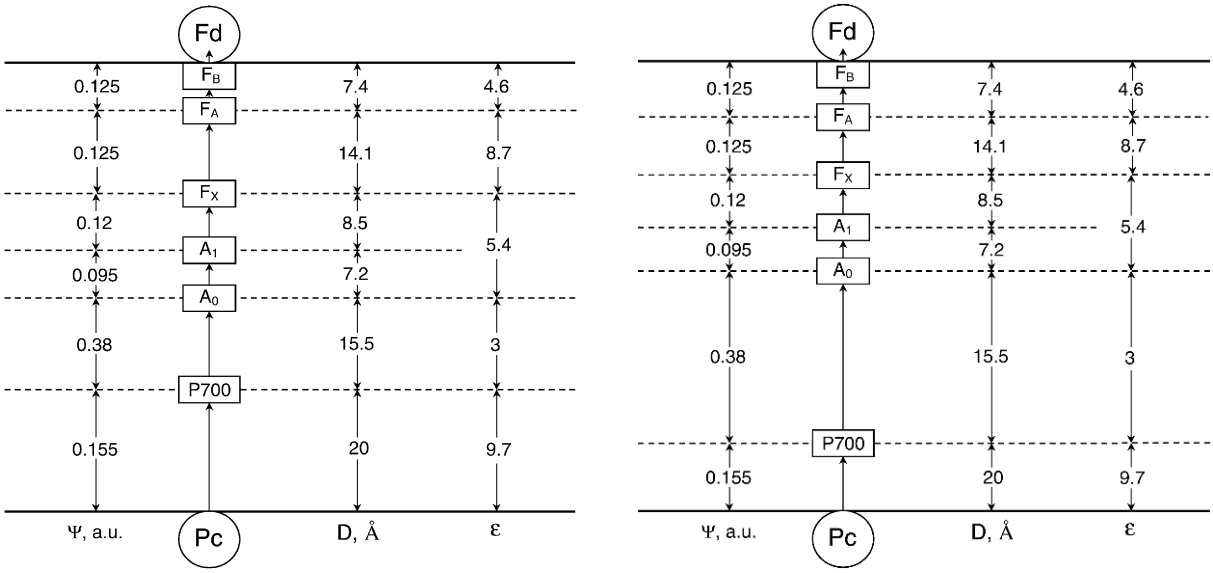

Fig. 7. Dielectric properties of PS I complex. Relative contribution of individual reactions of electron transfer to net electrogenesis (ψ, arb. units); projections of distance vectors between redox cofactors in PS I onto the normal to the membrane plane (D, Å); and mean values of effective dielectric constant (ε) at the protein sites between redox cofactors: (A) cofactors spaced in proportion with the distances projected onto the normal to the membrane plane; (B) cofactors spaced at their dielectrically weighted distances. Horizontal solid lines show arbitrary interfaces between hydrophobic and hydrophilic phases of pigment–protein complex. The other symbols are denoted in text.

$F_X \rightarrow F_A$ domain can be due to a more polar surrounding of the F_X-proximal F_A compared to the F_X-distal F_B cluster. This explanation is confirmed by the comparison of the relative hydrophobicity of the F_X, F_A, and F_B protein environment. Indeed, according to the X-ray structure of PS I (Jordan et al., 2001), the number of hydrophilic charged amino acid residues (Asp, Glu, Lys, Arg, and His) counted with regard to the effect of compensation of closely located opposite charges (distance <3.5 Å) (Antonkine et al., 2003) in the vicinity of F_A is about three times larger than that in the vicinity of F_B (see Table 2 for more detail). Moreover, the number of tightly-bound water molecules in the vicinity of F_X and F_A is also larger than that around F_B. Thus, both amino acid and water surrounding F_X, F_A, and F_B indicate that the environment of the former two clusters is more polar as compared to the latter. This estimate is in line with the assumption made above that the average effective dielectric constant value in the $F_X \rightarrow F_A$ domain is about twice larger than in the $F_A \rightarrow F_B$ protein domain.

It should be noted that there is a hierarchy of the rate constants of the reactions of charge transfer along the photosynthetic electron transport chain. The fastest picosecond primary reactions of charge separation and stabilization of separated charges occur in the photosynthetic reaction center core, whereas slower (within microsecond to millisecond time range) secondary reactions occur on the periphery of the complex. To a first approximation, this hierarchy qualitatively correlates with the hierarchy of the dielectric constant values calculated from our experiments (Fig. 7). Indeed, the fastest and slower processes were found to be related to regions with low and high values of ε, respectively (see Semenov et al., 2003, for minireview of results obtained in PS I).

B. The Bacterial Reaction Center

Although the PS I complex differs significantly from the RC of purple photosynthetic bacteria, there are remarkable similarities between PS I and the bRC, especially in the RC core and donor sites. Estimates of the value of the effective dielectric constant for the bRC of *Blastochloris* (formerly *Rhodopseudomonas*) *viridis* are given in Table 3. It was shown in our earlier studies that electrogenic reduction of the photooxidized bacteriochlorophyll dimer, P960, by the immediate electron donor, a high-potential cyt c_{559}, and further electron transfer from the second high-potential cyt c_{556} to oxidized cyt c_{559} account for 15 and 5% of the overall photoresponse amplitude, respectively (Dracheva et al.,

Table 2. Distances D from iron–sulfur centers to closest ($D < 10$ Å) polar amino acid residues and water molecules in PS I complexes

Iron-sulfur centers	Amino acid residues												Water		
	ASP (–)		GLU (–)		LYS (+)		ARG (+)		HIS (+ at pH = 6.0)		Total $D < 11$ Å	Total $D < 11$ Å with regard to compensation			
	No.	D, Å	No.	D, Å	No.	D, Å	No.	D, Å	No.	D, Å			No.	D, Å	Total
Fx	575	6.6	54[a]	10.8	51[a]	9.0	728[b]	5.1			13	5	162	4.2	20
	579[c]	8.3	62[c]	14.2			712[d]	5.6					43	5.3	
	566[a]	8.6					694	9.4					12	5.3	
	593[b]	8.6					674	9.6					190	6.0	
	580[d]	9.2					583[c]	9.7					73	6.3	
	568[c]	14.2					570[a]	10.5					37	6.4	
							65[a]	11.2					67	6.4	
							52[c]	12.0					6	6.6	
													26	6.9	
													145	7.0	
													36	7.0	
F_A	579[c]	7.3	54[a]	7.3	51[a]	8.4	583[c]	6.9	2	7.0	15	9	167	6.5	11
	23	8.3	62[c]	8.1	5	8.9	52[c]	7.7					25	6.6	
	46[e]	9.6	45	10.7			60	9.6					6.6	6.8	
	568[c]	11.3	71	10.7			43	9.9					145	6.8	
	566[a]	11.4					65[a]	10.2					76	8.0	
							570[a]	12.0					89	8.4	
							74[e]	12.6					165	8.4	
													166	8.6	
													34	8.8	
													119	9.4	
													120	10.4	
F_B	8	10.4	54[a]	10.1	51[a]	13.2	18	9.4			3	3	182	6.9	8
	566[a]	13.4					65[a]	11.4					126	7.1	
							570[a]	11.7					82	7.8	
													184	9.0	

The structure file was taken from RCSB Protein Data Bank, PDB ID: 1JB0 (Jordan et al., 2001). Distance measurements were performed using VMD 1.7.1 software (Theoretical Biophysics Group, Beckman Institute for Advanced Science and Technology, University of Illinois).

Distance D from amino acid residue to iron–sulfur center was measured as the shortest distance between the charged residue and the closest iron atom of the center. Groups of residues compensating each other are denoted as:

[a]ASP 566, GLU 54, LYS 51, ARG 570, ARG 65; net charge +1.

[b]ASP 593, ARG 728; net charge 0.

[c]ASP 579, ASP 568, GLU 62, ARG 583, ARG 52; net charge –1.

[d]ASP 580, ARG 712; net charge 0.

[e]ASP 46, ARG 74; net charge 0.

Table 3. Calculation of effective dielectric constant values in the protein domains between redox cofactors of bacterial photosynthetic reaction centers from *Blastochloris viridis*

bRC protein domains between redox cofactors	Projections of distance vectors (D) Å[a]	Relative photovoltages, (ψ)[b]	Effective dielectric constant values (ε)
Cyt c_{556}–cyt c_{559}	24	0.05	34
Cyt c_{559}–P960	21	0.15	9.8
P960–BPheo	15	0.35	3
Pheo–Q_A	15	0.35	3
Q_B-protein–water boundary	39	0.1	23

[a] The distances along the axis normal to the membrane plane are given according to the X-ray data of Deisenhofer et al. (1984).

[b] Relative contributions of partial reactions to the overall electrogenesis were revealed in Dracheva et al. (1988) and Deprez et al. (1986).

1988). The same relative photovoltages and effective dielectric constant values were obtained for the donor sites of the *Rhodospirillum rubrum* and *R. sphaeroides* bRC (see Semenov, 1991, for review). A comparison of the distance vector projections onto the membrane normal with the relative photovoltage amplitudes in PS I and the bRC demonstrated that the ε values corresponding to electron transfer from the native donor proteins to P700 and P960 (or P870 in case of the other bRC species) were close to one another. Note that the electron transport reactions at the donor side of PS I and bRC share the following similarities: (i) the Gibbs energy difference (ΔG) between Pc/cyt c_6 and P700 is close to the value of ΔG between cyt c_2 and P870; (ii) the electron transfer kinetics and the proposed reaction mechanisms are very similar.

The main electrogenic step on the acceptor side of the bRC is due to protonation of the doubly reduced secondary quinone Q_B (Kaminskaya et al., 1986). The ε value in this region is ∼20 (Shinkarev et al., 1993), which is about three times larger than that in the acceptor region of PS I. Note also that the thermodynamic and kinetic properties of the terminal acceptors in the two complexes essentially differ. The redox midpoint potential (E_m) values of the Q_A/Q_A^- and Q_B/Q_B^- redox couples in the bRC are in the range of −50 to +100 mV, whereas the E_m values of F_X, F_A, and F_B in PS I are much more negative (in the range of −500 mV to −700 mV). The lifetimes of the electron-and-proton transfer reactions on the acceptor side of the bRC (in the submillisecond time range) are at least three orders of magnitude lower than those values in the domain of the iron–sulfur clusters in PS I (in the range of tens to hundreds nanoseconds). Perhaps the three-order-of-magnitude difference between the rate constants of charge transfer on the acceptor side of the bRC and PS I, and the threefold increase in the estimated value of ε reflects a correlation between the reaction rates and the dielectric properties of the corresponding protein domains between redox cofactors.

C. Photosystem II

Recently determined X-ray crystal structures of the PS II core complex from the cyanobacteria *Synechococcus elongatus* and *Thermosynechoccus vulcanus* (Zouni et al., 2001; Kamiya and Shen, 2003) were resolved at 3.8 and 3.7 Å resolution, respectively. It follows from these data that the arrangement of the electron transfer cofactors in PS II is rather similar to that in RCs of purple nonsulfur bacteria. The cofactors form two branches organized symmetrically along the pseudo-C_2 axis. This symmetry is broken at the lumenal side of the D1 protein by the redox-active Tyr 161 (Y_Z) and the manganese cluster $[Mn]_4$, which is located ∼15 Å off the pseudo-C2 axis.

The kinetics and the yield of primary charge separation in pea chloroplasts has been studied using the light-gradient technique (Trissl and Leibl, 1989). Charge separation occurs with two electrogenic phases: the faster phase with a rise-time <50 psec was ascribed to electron transfer from the primary donor Chl dimer P680 to the intermediary acceptor pheophytin (Pheo), while the slower phase (∼500 psec) was attributed to electron transfer from Pheo to the primary quinone acceptor Q_A. The relative photovoltage contributions of the faster and slower phases were approximately equal to one another.

Fast photovoltage measurements using PS II membranes electrically oriented in a microcoaxial cell (Pokorny et al., 1994) and using PS II-containing proteoliposomes attached to a planar phospholipid membrane (Mamedov et al., 1995; Haumann et al., 1997) showed that electron transfer from Y_Z to $P680^+$ spanned a dielectrically weighted distance of 13–18% of the distance between P680 and Q_A. The dielectrically weighted distance of the electron transfer from $[Mn]_4$ to Y_Z^{ox} ($S_1 \rightarrow S_2$ transition of the oxygen-evolving complex) was estimated to be less than 3.5% (Haumann et al., 1997; Mamedov et al., 1999). Larger electrogenic components (about 7%) were attributed to proton transfer from the oxidized cofactor "X" to the lumen phase during the transition $S_2 \rightarrow S_3$ (Haumann et al., 1997).

The charge transfer reaction associated with protonation of double-reduced secondary plastoquinone Q_B^{2-} at the acceptor side contributes about 5% to the overall electrogenesis in PS II (Hook and Brzezinski, 1994; Mamedov et al., 1994). However, it should be noted that this estimate most probably represents the lower limit of the relative contribution of this reaction, because: (i) there were some indications that the reconstruction of the Q_B function in the PS II particles used in these experiments was incomplete (Mamedov et al., 1994) and (ii) slow component (lifetime ∼1 sec) of $\Delta\psi$ decay contributed only ∼50% to the overall laser flash-induced $\Delta\psi$ decay. These findings indicate that about one-half of the oxygen-evolving complexes are inactive (Hillmann et al., 1995). Therefore, it is safe to suggest that the dielectric properties in the Q_B-protein boundary domain of PS II are similar to that of the bRC. It was shown recently in our laboratory using PS II preparations in which the contribution of the slow component of the $\Delta\psi$ decay reached ∼90% that the amplitude of the electrogenic phase attributed to Q_B^{2-} protonation

Table 4. Calculation of effective dielectric constant values in the protein domains between redox cofactors of PS II

PS II protein domains between redox cofactors	Projections of distance vectors (D) Å[a]	Relative photovoltages, (ψ)[b]	Effective dielectric constant values (ε)
$[Mn]_4$–Y_Z	9.4	0.03	7.4
Y_Z–P680	5.5	0.12	4.7
P680–Pheo	12.3	0.43	3
Pheo–Q_A	10	0.36	3
Q_B-protein/water boundary	12	0.06	23

[a] The projection values were calculated from the atomic coordinates deposited in the Protein Data Bank [accession numbers 1FE1 (Zouni et al., 2001) and 1IZL (Kamiya and Shen, 2003)].
[b] The average relative photovoltage values were calculated on the basis of data taken from (Trissl and Leibl, 1989; Pokorny et al., 1994; Mamedov et al., 1995; Haumann et al., 1997; Mamedov et al., 1999; Mamedov et al., 2005).

was ~11% of total amplitude of $\Delta\psi$ (Mamedov et al., 2005).

The data shown in Table 4 provide a comparison of the distance vectors between the redox cofactors in PS II and relative photovoltages that accompany corresponding charge transfer reactions. As in the case of the bRC (see Table 3), the ε value in the protein domain between the Chl (bacteriochlorophyll) dimer and Q_A is the lowest, whereas it gradually increases both at the donor and the acceptor sides. The dielectric properties in the Q_B-protein boundary domain of PS II are similar to that of BRC (Tables 3 and 4). A similar increase in the effective dielectric constant is observed on the donor side of PS I (Table 1). Note that the ε value in the domain between Y_Z and P680 is only ~1.5 times higher than that in the P680-Q_A region, while the ε values in the Pc-P700 and cyt c_{559}-P960 protein regions of PS I and the bRC increase about threefold relative to the hydrophobic core domains (Tables 1, 3, and 4), which is seemingly consistent with a higher electron transfer rate (30 nsec, according to Pokorny et al., 1994) as compared to that at the donor sides of PS I and bRC (microsecond-to-millisecond lifetime range). On the other hand, the values of ε calculated for the $[Mn]_4$-Y_Z, Pc-P700, and cyt c_{559}-P960 protein regions were larger than that for Y_Z-P680, and comparable with each other, which seems to be consistent with similar rate constants of corresponding electron transfer reactions.

D. Possible Mechanisms Underlying the Correlation Between the Dielectric Constant and the Rate of Charge Transfer

The process of charge transfer proceeds in several stages including medium reorganization and electron tunneling. The efficiency of the process crucially depends on the dielectric reorganization of the medium. Effective relaxation processes (e.g., polarization) of the milieu of the reacting groups are required to provide charge stabilization. Perhaps, the correlation between the dielectric constant values and the rate constants of electron transfer reactions in photosynthetic complexes is conditioned by the processes of relaxation.

According to the Marcus theory (Marcus, 1996), the activation energy of the elementary act of charge transfer is determined by two parameters, the reorganization energy and the free energy difference of the elementary act. The two parameters can be represented as the sum of the structure-dependent and the polarization-dependent components. In the simplest case of charge transfer in a homogeneous medium, the polarization-dependent component of the reorganization energy is proportional to the so-called coupling constant $C = 1/\varepsilon_0 - 1/\varepsilon_S$, where ε_0 and ε_S are the optical and low-frequency dielectric constants, respectively (Parson et al., 1998; Krishtalik and Topolev, 2000). The value of ε_0 for proteins was shown to be constant (about 2.5) (Krishtalik and Topolev, 2000). If the value of the effective dielectric constant deduced from our experiments were proportional to the polarization-dependent component, the variability of the ε value at different sites of the electron transport chain would correspond to a considerable (threefold to fourfold) variability of the coupling constant value.

It should be noted that fast charge separation reactions are activationless (at least in case of the bRC). The primary photoproducts are created very close to the free energy level of the excited bacteriochlorophyll dimer and relax to the final state on the picosecond and nanosecond time scales (Woodbury and Parson, 1984; Peloquin et al., 1994; Holzwarth and Muller, 1996). These properties require that the reorganization energy

should be comparable in magnitude to the free energy change.

A dynamic solvation model of relaxation processes was suggested in (Peloquin et al., 1994) to explain the temperature dependence of the complex exponential kinetics of the bRC fluorescence decay on the picosecond to nanosecond time scale. This model was later refined on the basis of fast nanosecond photoelectric measurements performed in chromatophores of purple bacteria (Trissl et al., 2001). These experiments revealed that under reducing conditions, the photovoltage signal decayed significantly faster than the spectroscopically detected recombination of separated charges. This implies the occurrence of considerable dielectric relaxation at the primary radical pair site. It was suggested that these relaxations could be ascribed to protein solvation processes that decrease the Gibbs free energy. Possible molecular candidates that might contribute to the primary radical pair relaxation in the bRC were suggested to be two water molecules near the intermediate bacteriochlorophyll acceptor, amino acid residues hydrogen-bonded to the acceptor, and a collectively acting ensemble of amino acids. Medium relaxation associated with electron transfer to the primary quinone Q_A in bRC was suggested to be relevant to water molecules and certain molecular groups exposed to the membrane/water interface (Trissl et al., 2001).

On the other hand, it was shown in (Krishtalik, 1996) that the exact compensation of the ε_S-dependent components of reorganization and reaction energies was inherent in the charge separation process alone and that it did not take part in other charge transfer processes. The problem of a correlation between the relaxation processes and the kinetics of charge stabilization requires further theoretical and experimental elucidation.

V. Concluding Remarks

A comparison of the dielectrically weighted photoelectric signal amplitude with local structural parameters obtained from the X-ray diffraction data demonstrates that the effective dielectric constant ε is distributed heterogeneously over the pigment–protein complexes involved in photosynthetic charge transfer (PS I, PS II, bRC) and provides the opportunity to estimate the profile of distribution of the dielectric constant value in the complexes. It was found that the ε value is minimal at the core of the complexes and gradually increases toward their periphery. To a first approximation, the hierarchy of the dielectric constant values derived from photoelectric experiments qualitatively correlates with the hierarchy of rate constants of the reactions involving charge transfer along the photosynthetic electron transport chain. Indeed, the fastest primary reactions of charge separation and stabilization of separated charges occur in the core of the complexes within a picosecond time scale, whereas slower secondary reactions take place at the periphery of the complexes within the microsecond to millisecond time scale. It was suggested that mechanisms underlying the correlation between the dielectric constant and the rate constant of charge transfer are determined by the processes of dielectric reorganization and relaxation of the medium. However, further experimental and theoretical research is required to provide a deeper insight into these mechanisms.

Acknowledgments

The authors are grateful to Prof. J. H. Golbeck and Prof. L. I. Krishtalik for valuable discussions and to Mr. C. S. Chamorovsky for help in preparation of the manuscript. This study was supported by a Grant from the International Science and Technology Center (ISTC) 2296 (to A.Y.S.), Grant 01-483 from the INTAS (to A.Y.S.), Grants from the Russian Foundation for Basic Research 03-04-49219 (to S.K.C.), 03-04-48983 (to A.Y.S.), and 04-04-49441 (to M.D.M.), and Grant RC1-2400-MO-02 (to A.Y.S.) from the Civilian Research and Development Foundation (CRDF).

References

Allen JP, Feher G, Yeates TO, Komiya H and Rees DC (1987) Structure of the reaction center from *Rhodobacter sphaeroides* R-26: the cofactors. Proc Natl Acad Sci USA 84:5730–5734

Allen JP, Feher G, Yeates TO, Komiya H and Rees DC (1988) Structure of the reaction center from *Rhodobacter sphaeroides* R-26: protein – cofactor (quinones and Fe^{2+}) interactions. Proc Natl Acad Sci USA 85: 8487–8491

Antonkine ML, Jordan P, Fromme P, Krauß N, Golbeck JH and Stehlik D (2003) Assembly of protein subunits within the stromal ridge of photosystem I. Structural changes between unbound and sequentially PS I-bound polypeptides and correlated changes of the magnetic properties of the terminal iron–sulfur clusters. J Mol Biol 327: 671–697

Brettel K and Leibl W (2001) Electron transfer in photosystem I. Biochim Biophys Acta 1507: 100–114

Bulychev AA, Andrianov VK, Kurella GA and Litvin FF (1972) Micro-electrode measurements of the transmembrane potential of chloroplasts and its photoinduced changes. Nature 236: 175–177

Cherepanov DA and Krishtalik LI (1990) Intramembrane electric fields: a single charge, protein α-helix, photosynthetic reaction center. Bioelectrochem Bioenerg 24: 113–127

Deisenhofer J, Epp O, Miki K, Huber R and Michel H (1985) Structure of the protein subunits in the photosynthetic reaction center of *Rhodopseudomonas viridis* at 3 Å resolution. Nature 318: 618–624

Deprez J, Trissl HW and Breton J (1986) Excitation trapping and primary charge stabilization in *Rhodopseudomonas viridis* cells, measured electrically with picosecond resolution. Proc Natl Acad Sci USA 83: 1699–1703

Diaz-Quintana A, Leibl W, Bottin H and Sétif P (1998) Electron transfer in photosystem I reaction centers follows a linear pathway in which iron-sulfur cluster F_B is the immediate electron donor to soluble ferredoxin. Biochemistry 37: 3429–3439

Drachev LA, Jasaitis AA, Kaulen AD, Kondrashin AA, Liberman EA, Nemecek IB, Ostroumov SA, Semenov AY and Skulachev VP (1974) Direct measurement of electric current generation by cytochrome oxidase, H^+-ATPase and bacteriorhodopsin. Nature 249: 321–324

Drachev LA, Frolov VN, Kaulen AD, Kondrashin AA, Samuilov VD, Semenov AY and Skulachev VP (1976) Generation of electric current by chromatophores of *Rhodospirillum rubrum* and reconstitution of electrogenic function in subchromatophore pigment–protein complexes. Biochim Biophys Acta 440: 637–660

Drachev LA, Kaulen AD, Semenov AY, Severina II and Skulachev VP (1979) Lipid-impregnated filters as a tool for studying the electric current-generating proteins. Analyt Biochem 96: 250–262

Drachev LA, Kaulen AD, Khitrina LV and Skulachev VP (1981a) Fast stages of photoelectric processes in biological membranes. I. Bacteriorhodopsin. Eur J Biochem 117: 461–470

Drachev LA, Semenov AY, Skulachev VP, Smirnova IA, Chamorovsky SK, Kononenko AA, Rubin AB and Uspenskaya NYa (1981b) Fast stages of photoelectric processes in biological membranes. III. Bacterial photosynthetic redox system. Eur J Biochem 117: 483–489

Drachev LA, Kaminskaya OP, Konstantinov AA, Semenov AY, Skulachev VP (1985) Electrogenic reduction of *Rhodospirillum rubrum* reaction centre bacteriochlorophyll $P870^+$ by redox dyes. Indication of intraprotein electron transfer. FEBS Lett 189: 45–49

Dracheva SM, Drachev LA, Konstantinov AA, Semenov AY, Skulachev VP, Arutyunian AM, Shuvalov VA and Zaberezhnaya SM (1988) Electrogenic steps in the redox reactions catalyzed by photosynthetic reaction-centre complex from *Rhodopseudomonas viridis.* Eur J Biochem 171: 253–264

Ermler U, Fritzsch G, Buchanan SK and Michel H (1994) Structure of the photosynthetic reaction center from *Rhodobacter sphaeroides* at 2.65 Å resolution: cofactors and protein-cofactor interactions. Structure 2: 925–936

Fersht A (1999) Structure and Mechanism in Protein Science: A Guide to Enzyme Catalysis and Protein Folding. WH Freeman, New York

Fowler CF and Kok B (1974) Direct observation of a light-induced electric field in chloroplasts. Biochim Biophys Acta 357: 308–318

Fromme P, Schubert WD and Krauß N (1994) Structure of photosystem I: suggestions on the docking sites for plastocyanin, ferredoxin and the coordination of P700. Biochim Biophys Acta 1187: 99–105

Golbeck JH (1999) A comparative analysis of the spin state distributions of *in vitro* and *in vivo* mutants of PsaC. A biochemical argument for the sequence of electron transfer as $F_X \rightarrow F_A \rightarrow F_B \rightarrow$ ferredoxin. Photosynth Res 61: 107–144

Golbeck JH and Bryant DA (1991) Photosystem I. In: Lee CP (ed) Light-Driven Reactions in Bioenergetics. Current Topics in Bioenergetics, Vol 16, pp 83–177. Academic Press, New York

Gourovskaya KN, Mamedov MD, Vassiliev IR, Golbeck JH and Semenov AY (1997) Electrogenic reduction of the primary electron donor $P700^+$ in photosystem I by redox dyes. FEBS Lett 414: 193–196

Gräber P (1987) Primary charge separation and energy transduction in photosynthesis. In: Milazzo G and Blanks M (eds) Bioelectrochemistry II, pp 381–429. Plenum Publishing Corporation, New York

Guergova-Kuras M, Boudreaux B, Joliot A, Joliot P and Redding K (2001) Evidence for two active branches for electron transfer in photosystem I. Proc Natl Acad Sci USA 98: 4437–4442

Haumann M, Mulkidjanian A and Junge W (1997) Electrogenicity of electron and proton transfer at the oxidizing side of photosystem II. Biochemistry 36: 9304–9315

Hecks B, Wulf K, Breton J, Leibl W and Trissl HW (1994) Primary charge separation in photosystem I: a two-step electrogenic charge separation connected with $P700^+A_0^-$ and $P700^+A_1^-$ formation. Biochemistry 33: 8619–8624

Hervas M, Ortega JM, Navarro JA, De la Rosa MA and Bottin H (1994) Laser flash kinetic analysis of *Synechocystis* PCC 6803 cytochrome c_6 and plastocyanin oxidation by photosystem I. Biochim Biophys Acta 1184: 235–241

Hervas M, Navarro JA, Diaz A, Bottin H and De la Rosa MA (1995) Laser-flash kinetic analysis of the fast electron transfer from plastocyanin and cytochrome c_6 to photosystem I. Experimental evidence on the evolution of the reaction mechanism. Biochemistry 34: 11321–11326

Hillmann B, Brettel K, van Mieghem F, Kamlowski A, Rutherford AW and Schlodder E (1995) Charge recombination reactions in photosystem II. 2. Transient absorbance difference spectra and their temperature dependence. Biochemistry 34: 4814–4827

Holzwarth AR and Muller MG (1996) Energetics and kinetics of radical pairs in reaction centers from *Rhodobacter sphaeroides*. A femtosecond transient absorption study. Biochemistry 35: 11820–11831

Hook F and Brzezinski P (1994) Light-induced voltage changes associated with electron and proton transfer in photosystem II core complexes reconstituted in phospholipid monolayers. Biophys J 66: 2066–2072

Jackson JB and Crofts AR (1969) The high energy state in chromatophores from *Rhodopseudomonas sphaeroides*. FEBS Lett 4: 185–189

Joliot P and Joliot A (1984) Electron transfer between the two photosystems. I. Flash excitation under oxidizing conditions. Biochim Biophys Acta 765: 210–218

Joliot P and Joliot A (1999) *In vivo* analysis of the electron transfer within photosystem I: are the two phylloquinones involved? Biochemistry 38: 11130–11136

Jordan P (2001) Rontgenstrukturanalyse des Trimeren Photosystems I aus dem Cyanobakterium *Synechococcus elongatus* bei 2.5 A Auflosung. PhD Thesis. Free University, Berlin

Jordan P, Fromme P, Witt HT, Klukas O, Saenger W and Krauß N (2001) Three-dimensional structure of cyanobacterial photosystem I at 2.5 Å resolution. Nature 411: 909–917

Jung Y-S, Yu L and Golbeck JH (1995) Reconstitution of iron–sulfur center F_B results in complete restoration of $NADP^+$ photoreduction in Hg-treated Photosystem I complexes from *Synechococcus* sp. PCC 6301. Photosynth Res 46: 249–255

Junge W and Witt HT (1968) On the ion transport system of photosynthesis. Investigations on a molecular level. Z Naturforsch 23b: 244–246

Kaminskaya OP, Drachev LA, Konstantinov AA, Semenov AY and Skulachev VP (1986) Electrogenic reduction of the secondary quinone acceptor in chromatophores of *Rhodospirillum rubrum.* Rapid kinetic measurements. FEBS Lett 2: 224–228

Kamiya N and Shen JR (2003) Crystal structure of oxygen-evolving photosystem II from *Thermosynecoccus vulcanus* at 3.7 Å resolution. Proc Natl Acad Sci USA 100: 98–103

Karapetyan NV, Holzwarth AR and Rögner M (1999) The photosystem I trimer of cyanobacteria: molecular organization, excitation dynamics and physiological significance. FEBS Lett 460: 395–400

Kojima Y, Niinomi Y, Tsuboi S, Hiyama T and Sakurai H (1987) Destruction of photosystem I iron-sulfur centers of spinach and *Anacystis nidulans* by mercurials. Bot Mag 100: 243–253

Krishtalik LI (1996) Intramembrane electron transfer: processes in the photosynthetic reaction center. Biochim Biophys Acta 1273: 139–149

Krishtalik LI and Topolev VV (2000) Effects of medium polarization and pre-existing field on activation energy of enzymatic charge-transfer reactions. Biochim Biophys Acta 1459: 88–105

Leibl W, Toupance B and Breton J (1995) Photoelectric characterization of forward electron transfer to iron-sulfur centers in photosystem I. Biochemistry 34: 10237–10244

Mamedov MD, Beshta OE, Samuilov VD and Semenov AY (1994) Electrogenicity at the secondary quinone acceptor site of cyanobacterial photosystem II. FEBS Lett 350: 96–98

Mamedov MD, Lovyagina EP, Verkhovsky MI, Semenov AY, Cherepanov DA and Shinkarev VP (1995) Generation of the electrical potential difference by photosystem II from thermophilic cyanobacteria. Biochemistry (Moscow) 59: 327–341

Mamedov MD, Gadjieva RM, Gourovskaya KN, Drachev LA and Semenov AY (1996) Electrogenicity at the donor/acceptor sides of cyanobacterial photosystem I. J Bioenerg Biomembr 28: 517–522

Mamedov MD, Gourovskaya KN, Vassiliev IR, Golbeck JH and Semenov AY (1998) Electrogenicity accompanies photoreduction of the iron-sulfur clusters F_A and F_B in photosystem I. FEBS Lett 431: 219–223

Mamedov MD, Beshta OE, Gourovskaya KN, Mamedova AA, Neverov KD, Samuilov VD and Semenov AY (1999) Photoelectric responses of oxygen-evolving complexes of photosystem II. Biochemistry (Moscow) 64: 606–611

Mamedov MD, Mamedova AA, Chamorovsky SK, Semenov AY (2001) Electrogenic reduction of the primary electron donor $P700^+$ by plastocyanin in photosystem I complexes. FEBS Lett 500: 172–176

Mamedov MD, Tyunyatkina AA and Semenov AY (2005) Electrogenic protonation of the secondary quinone acceptor Q_B in spinach photosystem II complexes incorporated into lipid vesicles. Biochemistry (Moscow) 70: 1639–1645

Mamedova AA, Mamedov MD, Gourovskaya KN, Vassiliev IR, Golbeck JH and Semenov AY (1999) Electrometrical study of electron transfer from the terminal F_A/F_B iron-sulfur clusters to external acceptors in photosystem I. FEBS Lett 462: 421–424

Marcus R (1996) Electron transfer reactions in chemistry. Theory and experiment. In: Bendall DS (ed) Protein Electron Transfer, pp 249–272. Bios Scientific Publishers, Oxford

Mertz EL and Krishtalik LI (2000) Low dielectric response in enzyme active site. Proc Natl Acad Sci USA 97: 2081–2086

Mitchell P and Pasternak CA (eds) (1992) Perspectives in Vectorial Metabolism and Osmochemistry. Glynn Research Foundation, Glynn, U.K.

Myshkin E, Leontis NB and Bullerjahn S (2002) Computational simulation of the docking of *Prochlorothrix hollandica* plastocyanin to photosystem I: modeling the electron transfer complex. Biophys J 82: 3305–3313

Okamura MY and Feher G (1992) Proton transfer in reaction centers from photosynthetic bacteria. Annu Rev Biochem 61: 861–896

Parson WW, Chu ZT and Warshel A (1998) Reorganization energy of the initial electron-transfer step in photosynthetic bacterial reaction centers. Biophys J 74: 182–191

Peloquin JM, Williams JC, Lin XM, Alden RG, Taguchi AKW, Allen JP and Woodbury NW (1994) Time-dependent thermodynamics during early electron transfer in reaction centers from *Rhodobacter sphaeroides*. Biochemistry 33: 8089–8100

Pokorny A, Wulf K and Trissl H-W (1994) An electrogenic reaction associated with the re-reduction of P680 by Tyr Z in photosystem II. Biochim Biophys Acta 1184: 65–70

Semenov AY (1991) Electrogenic reactions in photosynthetic reaction centres of purple bacteria. In: Skulachev VP (ed) Soviet Scientific Reviews/Section D, Vol 10, pp 45–75. Harwood Academic Publishers, U.K.

Semenov AY, Mamedov MD and Chamorovsky SK (2003) Photoelectric studies of the transmembrane charge transfer reactions in photosystem I pigment-protein complexes. FEBS Lett 553: 223–228

Shinkarev VP, Drachev LA, Mamedov MD, Mulkidjanian AYa, Semenov AY and Verkhovsky MI (1993) Effect of pH and surface potential on the rate of electric potential generation due to proton uptake by secondary quinone acceptor of reaction centers in *Rhodobacter sphaeroides* chromatophores. Biochim Biophys Acta 1144: 285–294

Steffen MA, Lao K and Boxer SG (1994) Dielectric asymmetry in the photosynthetic reaction center. Science 264: 810–815

Stowell MHB, McPhillips TM, Rees DC, Soltis SM, Abresch E and Feher G (1997) Light-induced structural changes in photosynthetic reaction center: implications for mechanism of electron-proton transfer. Science 276: 812–816

Trissl HW and Gräber P (1980) II. Electrical measurements in the nanosecond range of the charge separation from chloroplasts spread at a heptane-water interface. Application of a novel capacitive electrode. Biochim Biophys Acta 595: 96–108

Trissl HW and Leibl W (1989) Primary charge separation in photosystem II involves two electrogenic steps. FEBS Lett 244: 85–88

Trissl HW, Leibl W, Deprez J, Dobek A and Breton J (1987) Trapping and annihilation in the antenna system of photosystem I. Biochim Biophys Acta 893: 320–332

Trissl HW, Bernhardt K and Lapin M (2001) Evidence for protein dielectric relaxations in reaction centers associated with the primary charge separation detected from *Rhodospirillum rubrum* chromatophores by combined photovoltage and absorption measurements in the 1–15 ns time range. Biochemistry 40: 5290–5298

Vassiliev IR, Jung Y-S, Mamedov MD, Semenov AY and Golbeck JH (1997) Near-IR absorbance changes and electrogenic reactions in the microsecond-to-second time domain in photosystem I. Biophys J 72: 301–315

Vassiliev IR, Jung Y-S, Yang F and Golbeck JH (1998) PsaC subunit of photosystem I is oriented with iron-sulfur cluster F_B as the immediate electron donor to ferredoxin and flavodoxin. Biophys J 74: 2029–2035

Witt HT and Zickler A (1973) Vectorial electron flow across the thylakoid membrane. Further evidence by kinetic measurements with an electrochromic and electrical method. FEBS Lett 37: 307–310

Woodbury NW and Parson WW (1984) Nanosecond fluorescence from isolated photosynthetic reaction centers of *Rhodopseudomonas sphaeroides*. Biochim Biophys Acta 767: 345–361

Xu W, Chitnis P, Valieva A, van der Est A, Brettel K, Guergova-Kuras M, Pushkar J, Zech SG, Stehlik D, Shen G, Zybailov B and Golbeck JH (2003) Electron transfer in cyanobacterial photosystem I: II. Determination of forward electron transfer rates of site-directed mutants in a putative electron transfer pathway from A_0 through A_1 to F_X. J Biol Chem 278: 27876–27887

Zouni A, Witt H-T, Kern J, Fromme P, Krauß N, Saenger W and Orth P (2001) Crystal structure of photosystem II from *Synechococcus elongatus* at 3.8 Å resolution. Nature 409: 739–743

Chapter 22

High-Field EPR Studies of Electron Transfer Intermediates in Photosystem I

Marion C. Thurnauer*, Oleg G. Poluektov
Chemistry Division, Argonne National Laboratory, 9700 S. Cass Ave., Argonne, IL 60439, USA

Gerd Kothe
Department of Physical Chemistry, University of Freiburg, Albertstrasse 21, D-79104 Freiburg, Germany

Summary

High-field frequency EPR and multifrequency quantum beat studies of the electron transfer intermediates in Photosystem I reveal new details of structure and function that could not be obtained without the enhanced resolution, both spectral and temporal, and sensitivity of these advanced spectroscopic techniques. The results of careful measurements and analyses of the resolved *g*-tensors of the primary donor cation radical and excited triplet state show that their electronic structures differ from those of monomeric chlorophyll *a*. Multifrequency time-resolved EPR, which includes high-field EPR, has made it possible to determine the structure of the transient charge-separated state $P_{700}^{+}A_{1}^{-}$ and its orientation in the thylakoid membrane. High-field EPR studies are just beginning to have an impact on photosynthesis research, as the technique has only been widely accessible for the last few years. There are several important advantages of high-field EPR spectroscopy. First is the high *g*-tensor resolution. This makes it possible to resolve lines from different radicals with close *g*-factors. It also allows complete resolution of the weak anisotropy of the g-tensors and a recording of a single-crystal-like spectrum. Second is a high nuclear *g*-value resolution in the high frequency ENDOR spectrum. Third is the possibility to observe and analyze paramagnetic

*Author for correspondence, email: mariont@anl.gov

John H. Golbeck (ed): Photosystem I: The Light-Driven Plastocyanin:Ferredoxin Oxidoreductase, 339–360.

centers with large zero-field splittings. Fourth is a high absolute sensitivity, which is of a special significance for biochemical and biophysical studies, in which often only small amounts of material are available. We expect that high-field EPR techniques will continue to advance our understanding of the particular interactions in photosynthetic proteins that result in control and optimization of electron transfer leading to efficient charge separation.

I. Introduction

Since the first observations of light-induced paramagnetism in chloroplasts (Commoner et al., 1954, 1956; Sogo et al., 1959) electron paramagnetic resonance (EPR) and associated spectroscopies have been among the most important tools for unraveling structure–function relationships in photosynthetic proteins. Besides the obvious inherent property of this spectroscopy as a tool to study paramagnetic species, EPR has a number of advantages for monitoring the intermediates that are formed during the initial electron transfer reactions leading to photochemical energy conversion, i.e., the separation of a positively charged electron donor and negatively charged electron acceptor across a biological membrane. (See Fig. 1 for a reaction scheme of Photosystem I primary photochemistry.) Samples can range from the intact cells of, for example, cyanobacteria, to isolated reaction center (RC) proteins, the units of which contain the cofactors that participate in the initial photochemistry. Additionally, the EPR properties of the paramagnetic intermediates formed in RCs can be compared to those of the oxidized or reduced states of isolated cofactors in varied environments. The impact on our understanding of the initial photosynthetic energy conversion steps from developments and improvements in magnetic-resonance methods during the last fifty years have been significant (Warden, 1978; Hoff and Deisenhofer, 1997). This continues with the current developments in high-field EPR (HFEPR) spectroscopy and its applications to study photosynthetic systems (Stehlik and Möbius, 1997; Möbius, 2000).

EPR studies of photosynthesis have revealed striking similarities between the initial photochemistries of purple photosynthetic bacteria (PBa) and Photosystems I (PS I) and II (PS II) of cyanobacteria, algae, and green plants. For example, comparisons of the EPR linewidths of the oxidized primary electron donors in PS I and PBa to those of the cation radicals of chlorophyll *a* (Chl *a*) and bacteriochlorophyll *a* (Bchl *a*), respectively, led to the suggestion that the primary donors are molecular dimers of Chl *a* and Bchl *a*, respectively (Norris et al., 1971; Feher et al., 1975). Further EPR studies combined with careful biochemistry showed that the "primary acceptor" in PBa is a reduced quinone (Q_a) interacting magnetically with a non-heme iron; (Clayton and Straley, 1972; Feher et al., 1972; Loach and Hall, 1972; Okamura et al., 1975) while in PS I three iron–sulfur centers were observed as "primary and secondary acceptors" (Bearden and Malkin, 1972a,b; Evans et al., 1972, 1974, 1975; Ke et al., 1973; Evans and Cammack, 1975; McIntosh et al., 1975).

Applications of magnetic-resonance techniques were instrumental in revealing that there are necessarily intermediate acceptor(s) between the primary electron donors and the "primary acceptors." When RCs of PBa, in which Q_a was reduced, were irradiated at low temperature in an EPR cavity, an EPR signal, characteristic of a triplet state was observed (Dutton et al., 1972, 1973; Leigh and Dutton, 1974). This signal exhibited so-called "T_0" electron spin-polarization (ESP), i.e., a characteristic non-Boltzmann spin population distribution. From analysis of this signal, particularly by comparison with that of the photoexcited triplet state EPR signal from isolated Bchl *a*, it was suggested that the triplet state resides on the primary donor, P_{865}, and the ESP in RCs was the result of radical pair intersystem crossing, requiring an intermediate electron acceptor (bacteriopheophytin) (Thurnauer et al., 1975; Thurnauer, 1979; Budil and Thurnauer, 1991). Subsequently "T_0" ESP triplet state signals were observed in reduced RCs of PS I and PS II (Frank et al., 1979; Rutherford and Mullet, 1981; Rutherford et al., 1981). These results, together with photoaccumulation experiments, verified the existence of intermediate electron acceptors (identified as A_0 and A_1) between the primary electron donor, P_{700}, and iron–sulfur centers in PS I (Bonnerjea and Evans, 1982; Gast et al., 1983).

Continuous wave and pulsed time-resolved (TR) EPR techniques were initially developed in the mid-1970s (Trifunac and Norris, 1978; Trifunac et al., 1978; Kim and Weissman, 1979; Trifunac and

Abbreviations: A_1 – PS I quinone secondary electron acceptor; Bchl – bacteriochlorophyll; Chl – chlorophyll; ENDOR – electron nuclear double resonance; EPR – electron paramagnetic resonance; ESP – electron spin-polarization; HFEPR – high-field/frequency EPR; P – general primary electron donor; P_{700} – PS I primary electron donor; P_{865} – primary electron donor in *Rhodobacter sphaeroides*; PBa – purple photosynthetic bacteria; PS I – Photosystem I; PS II – Photosystem II; Q_a – primary quinone electron acceptor in PBa; RCs – reaction centers; SCRP – spin-correlated radical pair; *S. lividus* – *Synechococcus lividus.*

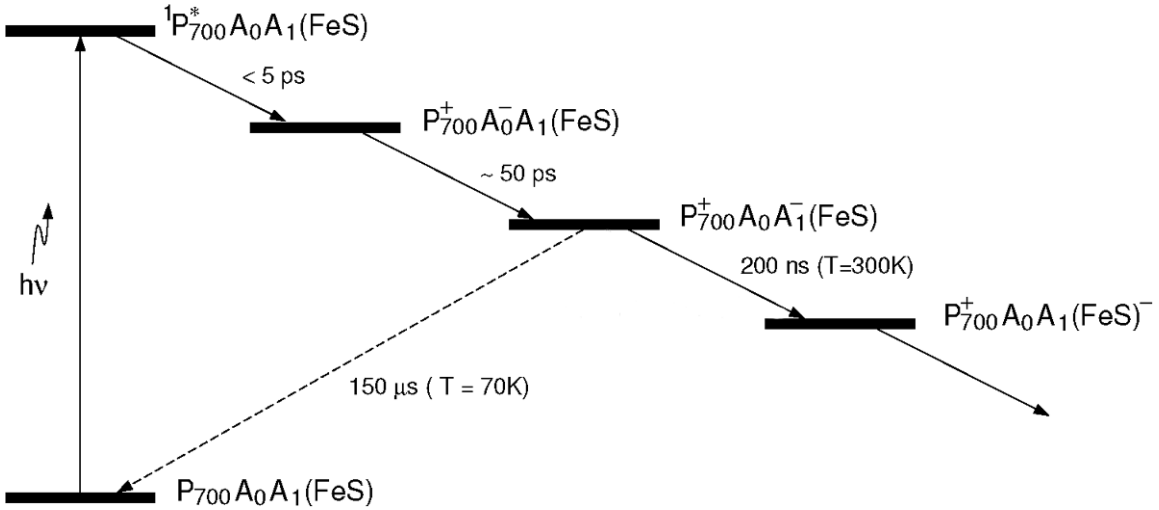

Fig. 1. Charge separation in PS I is initiated by photoexcitation of the primary chlorophyll donor, P_{700} (Golbeck and Bryant, 1991; Jordan et al., 2001). An electron is transferred from the excited singlet state of P_{700} to a phylloquinone acceptor (Rustandi et al., 1990; Snyder et al., 1991), A_1, through an intervening chlorophyll acceptor, A_0. The radical pair $P^+_{700}A^-_1$ is the first intermediate detectable by time-resolved EPR. At room temperature, $P^+_{700}A^-_1$ decays in about 200 nsec by forward electron transfer to the next acceptor (Thurnauer et al., 1982; Brettel, 1988) an iron–sulfur (FeS) center (Golbeck and Bryant, 1991; Jordan et al., 2001). At low temperature, the lifetime of $P^+_{700}A^-_1$ is about 150 μsec, and it decays primarily by charge recombination (Sétif et al., 1984).

Thurnauer, 1979). Not surprisingly, these methods have been extensively used to monitor the primary photochemistry in RCs of PBa, PS I, and PS II (McIntosh and Bolton, 1979; Blankenship, 1981; Snyder and Thurnauer, 1993; Stehlik and Möbius, 1997). In these experiments EPR signals of the transient charge-separated states between the oxidized chlorophyll electron donors P^+ and the reduced quinone electron acceptor, Q^-_a in PBa and PS II, and A^-_1 in PS I are observed. In fact, TR EPR experiments on PS I were employed to assign phylloquinone as the electron acceptor A_1 (Rustandi et al., 1990, 1992; Snyder et al., 1991).

The charge-separated state monitored with TR EPR exhibits ESP which can be explained by the so-called spin-correlated radical pair polarization (SCRP) (Thurnauer and Norris, 1980; Buckley et al., 1987; Closs et al., 1987; Stehlik et al., 1989). Based on the SCRP model several interesting spin-phenomena have been explained and/or predicted, i.e., quantum beats, observed at short delay times after optical excitation (Salikhov et al., 1990; Bittl and Kothe, 1991; Kothe et al., 1991); out of phase modulation of the electron spin echo signal, which is due to dipole–dipole and exchange interactions in the SCRP and allows for distance measurements (Salikhov et al., 1992; Tang et al., 1994; Dzuba et al., 1995); multiple quantum coherence in photo-induced radical pairs, which allows for direct measurements of coherence decays (Tang and Norris, 1995; Borovykh et al., 2001); sequential electron transfer polarization mechanism, which allows for study of the electron transfer dynamics (Norris et al., 1990; Morris et al., 1995).

In the forgoing, the shared characteristics of photosynthetic RCs revealed through magnetic resonance indicate underlying *fundamental structural and energetic requirements for efficient charge separation*. Indeed, duplication of either the triplet "T_0" ESP or SCRP ESP via control of the photophysics and photochemistry of model systems remains a rigorous criterion for designing and synthesizing a "working" electron transfer system (Wasielewski et al., 1990; Wasielewski, 1995; Hasharoni et al., 1995; Carbonera et al., 1998; Steinberg-Yfrach et al., 1998; Wiederrecht et al., 1999).

Although the photosynthetic RCs of oxygenic photosynthesis and purple bacteria have similar organizations, the mechanisms involved in excitation energy and electron transfer are necessarily optimized differently in the respective systems, to accommodate their varied "functional" roles (Krauß, 2003). For example, whereas PS II is optimized for its role in facilitating water oxidation, PS I provides the free energy to reduce $NADP^+$. Thus, even though the primary donors of PS I and PS II are both chlorophyll molecule(s), their redox properties differ considerably.

The differences in the interactions in the photosynthetic proteins that result in this optimization are apparent in a number of observations from magnetic-resonance studies. Yet, they are still not well

understood. For example, the crystal structures of the RC proteins confirmed the conclusion, originally proposed from EPR results, that the primary chlorophyll electron donors of PBa, PS I, and PS II RCs are structural dimers (Diesenhofer et al., 1984; Ermler et al., 1994; Jordan et al., 2001; Zouni et al., 2001). However, to what degree the cations or triplet states of the primary donors are electronic dimers is still not well defined, particularly in the cases of PS I and PS II (Krauß, 2003; Plato et al., 2003). This information is relevant to determining what factors affect the redox properties of the cofactors in the RC proteins.

Much information about the subtleties of the interactions in the photosynthetic proteins can be extracted from TR EPR experiments. In principle, detailed structures of RC photoexcited states (as opposed to the equilibrium structures) can be derived from the TR EPR experiments, allowing for comparisons between the RC proteins. In addition, the array of spin-phenomena (mentioned above) exhibited by the SCRP monitored in these experiments contain detailed information on dynamics, and energetics. For example, the sequential electron transfer polarization analysis of the SCRP in PBa observed at high field/frequency EPR demonstrated the importance of protein reorganization energy in controlling electron transfer (Tang et al., 1999).

However, revealing the information from TR EPR is not a trivial task as (i) donor and acceptor signals strongly overlap, particularly when recorded at conventional X-band EPR (Furrer and Thurnauer, 1983; Thurnauer and Gast, 1985), and (ii) a large number of parameters are required to model experimental data (Hore, 1989; Morris et al., 1995; Tang et al., 1999), so that solutions are not unique. Thus new approaches, based on modern EPR techniques with enhanced spectral and temporal resolution are absolutely necessary to advance our understanding of photosynthetic electron transfer.

In this chapter we describe how the high spectral resolution of high-field/frequency EPR (HFEPR) spectroscopy in combination with time-resolved multifrequency EPR spectroscopy can provide unique information on the geometries and electronic structures of the cofactors involved in the photosynthetic electron-transfer reactions in PS I. The development of HFEPR spectroscopy in the late 1970s (Grinberg et al., 1976; Lebedev, 1990) has had important impacts on photosynthetic research owing to the following advantages. First, it can provide a complete resolution of the *g*-tensor components of the radical species involved in the electron transfer pathways and thus identification of these species. Second, small changes in the magnetic-resonance parameters, which can be detected only by HFEPR, reveal information on the weak interactions between active radicals and the protein environment, i.e., hydrogen bonding, or effects of protein mutations as well as dynamics of the paramagnetic species. Third, high spectral resolution allows for recording single-crystal-like spectra and for performing orientation selection experiments, which otherwise is possible only from single-crystal samples. A fourth advantage is a high absolute sensitivity, which is of special significance for biochemical research where often only small amounts of material are available.

The enhanced spectral resolution of HFEPR allows detailed *g*-tensor analysis of the paramagnetic states in PS I. This analysis has been made for the cation radical and triplet state of the primary donor in PS I (P_{700}) compared to the same species from Chl *a in vitro*. The data prove that the electronic structures of the primary donor cation radical and triplet state are different from those of monomeric Chl *a*. A comprehensive model for the ESP EPR spectra observed in PS I has been developed by using a multifrequency approach, which includes HFEPR. As for HFEPR spectroscopy, two microwave frequencies were used in this study: D-band EPR, operating at 130 GHz and 4.6 T, and W-band EPR, operating at 95 GHz and 3.3 T. Two conventional EPR bands referred to in this chapter are Q-band EPR (35 GHz/1.2 T) and X-band, EPR (9.5 GHz/0.35 T). The cells of the photosynthetic cyanobacteria align in the magnetic field of the HFEPR spectrometer, and this alignment allows us to determine the orientation of the primary donor cation radical, P_{700}^{+}, and reduced electron acceptor, A_1^{-}, with respect to the membrane in which the RC resides. We describe how HFEPR of a magnetically aligned sample in combination with the study of quantum beat oscillations represents a powerful tool for obtaining structure of the short-lived radical pair intermediates of photosynthesis.

II. Electronic Structure of the PS I Primary Donor

A. Background

Recently, 2.5 Å resolution X-ray diffraction analysis (Jordan et al., 2001) confirmed the presence of the structural Chl *a* dimer in PS I photosynthetic RC proteins. The crystal structure revealed that P_{700} is a Chl *a*/Chl *a*′ "heterodimer," where Chl *a*′ is the $C13^2$ epimer of Chl *a* (Jordan et al., 2001). X-ray analysis, however, cannot provide information on the electronic coupling or electronic structure of the chlorophyll dimers.

Importantly, the electronic structure of the primary donors determines their redox properties. The oxidation potential of the primary donors in photosynthetic RCs is considerably higher than those of the respective monomeric chlorophyll molecules, Bchl *a* and Chl *a* *in vitro*. This is believed to be due to the pairing of the chlorophyll molecules which, in turn, facilitates an efficient charge separation in the RC proteins. Thus, the electronic structures of the primary donors, particularly in their active states (excited singlet and triplet, and oxidized – P^*, P^T, P^+, respectively), have been the focus of much research. In particular, the excited triplet and oxidized states have been studied extensively with EPR spectroscopy.

In the case of the bacterial RCs from *Rhodobacter sphaeroides*, it has been established that the primary donors are "real" dimers, i.e., excitation in P^* and densities of unpaired electrons in P^+ and P^T states are delocalized over both chlorophyll molecules, with an asymmetry 2:1 (Norris et al., 1971; Feher et al., 1975; Lubitz, 1991; Artz et al., 1997). As for the primary donor in PS I, data confirming either monomeric or dimeric electronic structures are very controversial. The initial interpretation of EPR data on P_{700}^+ suggested that this species is an electronically coupled dimer (Norris et al., 1971). However, later results and interpretations claimed both monomeric or dimeric electronic structures (Wasielewski et al., 1981b; Käss and Lubitz, 1996; Mac et al., 1998; Breton et al., 1999; Krabben et al., 2000). Thus, the question is still not resolved. A detailed chronological review of this controversy concerning the electronic structure of P_{700} is presented in a recent article devoted to this problem (Käss et al., 2001) (for additional details, see Lubitz, this volume, Chapter 17). The main contradiction is that from the magnetic-resonance studies [EPR, electron nuclear double resonance (ENDOR), electron spin echo envelope modulation (ESEEM)] a pure monomeric (Wasielewski et al., 1981a) or very asymmetric (>6:1) (Käss and Lubitz, 1996; Mac et al., 1998; Krabben et al., 2000; Käss et al., 2001) spin density distribution in P_{700}^+ is found, while optical data reveal a dimer structure with a symmetric distribution of the spin density (Breton et al., 1999) (for further details, see Breton, this volume, Chapter 18). For the triplet state P_{700}^T (Frank et al., 1979), there is evidence from EPR experiments that at room temperature triplet excitation is delocalized over the two halves of a chlorophyll dimer (Sieckmann et al., 1993) but localized on one of the chlorophyll molecules at low temperature (Rutherford and Sétif, 1990; Budil and Thurnauer, 1991). This conclusion is based on the experimental findings that the zero-field splitting parameters of P_{700}^T compared to those of Chl a^T are the same at low temperatures and slightly smaller at room temperature.

HFEPR spectroscopy, providing high spectral resolution, can offer an independent view on this controversial problem since the *g*-tensor is a fingerprint of the electronic structure of a paramagnetic center. The *g*-tensors of P_{700}^+ and Chl a^+ were measured at HFEPR by a number of groups (Prisner et al., 1993; Bratt et al., 1997, 2000; MacMillan et al., 1998; Lakshmi et al., 2000). These data were collected under different experimental conditions (temperatures, magnetic fields, microwave cavities, microwave powers, modulation amplitudes) and with different *g*-value calibration procedures. The latter, in combination with lineshape distortions owing to fast-passage effects (Bratt et al., 2000; Lakshmi et al., 2000), is the main source of errors in the *g*-value measurements. This leads to the large scatter of the experimental *g*-values that are found in the literature. While the reported anisotropy of the *g*-tensors, or relative measurements of the *g*-values within one spectrum, are very similar, the absolute *g*-values are often outside the claimed experimental errors, making comparison difficult. To minimize the error and make the absolute g-values comparable, we measured the magnetic-resonance parameters of P_{700}^+, Chl a^+, P_{700}^T, and Chl a^T under the same experimental conditions, using the same calibration procedure and g-value reference marker.

To improve spectral resolution, deuterated samples with their consequent EPR linewidth narrowing were used. Deuterated Chl *a* was extracted from 99% deuterated cells of *Scenedesmus obliquus* (Svec, 1978). Deuterated PS I and PS II complexes were isolated from deuterated cells of *Synechococcus lividus* using the procedure described in Lakshmi et al. (2000).

B. P_{700} and Chlorophyll a Cation Radicals

We were unable to record a well-resolved EPR spectrum of deuterated Chl *a* cation radical in methylene chloride or toluene/pyridine solutions as the linewidths of the canonical components of Chl a^+ are always broader *in vitro* than those observed in the protein environment. This was previously reported for protonated Chl a^+ (Bratt et al., 2000) and explained by the *g*-strain effect. The strain is caused by heterogeneity in either chlorophyll–solvent interactions or conformational structures of chlorophyll molecules. These observations demonstrate that the protein environment has a high homogeneity, and the spread in the conformational structures is very small compared to the glassy state of the isotropic solvents. The same conclusion on

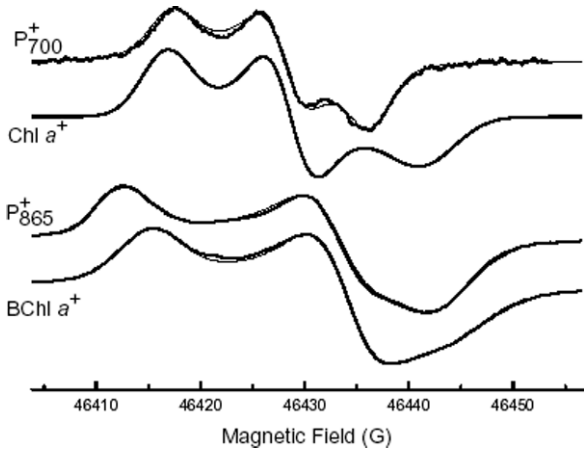

Fig. 2. D-band EPR spectra recorded at 70 K: (P^+_{700}) – cation radical of primary donor P_{700} in deuterated Photosystem I; (Chl a^+) – simulated spectrum of the deuterated Chl *a* cation radical obtained from the deconvolution of overlapping chlorophyll/carotenoid signals in photosystem II (for details see Stewart et al., 1998); (P^+_{865}) – cation radical of primary donor P_{865} in deuterated bacterial reaction center protein from *Rhodobacter sphaeroides*; (BChl a^+) – cation radical of the deuterated BChl *a* in toluene solution (0.5 mM). Dashed lines are theoretical fits. Source: Poluetkov et al., 2002.

the homogeneity of the bacterial RC proteins has been made from the analysis of the linewidth of the primary donor and chlorophyll triplet states (Budil and Thurnauer, 1991).

Therefore we used a different strategy to record the spectrum of monomeric Chl a^+. In PS II, when the electron transfer from the water-oxidizing center to the oxidized primary electron donor (P^+_{680}) is blocked, an alternate secondary electron pathway that quenches P^+_{680} becomes active. Under these conditions, a monomeric chlorophyll *a* cation radical [Chl(z)$^+$] and a carotenoid cation radical are trapped at low temperature. Although the EPR signals of these species overlap, the enhanced resolution achieved by deuteration and HFEPR allows for detailed g-tensor analysis (Lakshmi et al., 2000). Thus, as discussed below, the Chl(z) cation radical is used to obtain the g-tensor of monomeric Chl a^+.

D-band EPR spectra of the cation radicals P^+_{700} and Chl(z)$^+$ are shown in Fig. 2 (Poluektov et al., 2002). The spectrum of Chl(z)$^+$ is a simulated spectrum, which was obtained from the deconvolution of the Chl(z)/carotenoid (Car) cation radical signal recorded in PS II as described in Lakshmi et al. (2000). Note that the chemical structure of Chl(z) is identical to the structure of Chl *a* (Stewart et al., 1998). The relative *g*-values or *g*-value anisotropy (i.e., the $g_{xx} - g_{zz}$ and $g_{yy} - g_{zz}$ values) are in agreement with the data obtained for deuterated Chl a^+ in methylene chloride at 327 GHz EPR frequency (Bratt et al., 2000). Relative *g*-value measurements are more accurate than absolute measurements, as the accuracy of the absolute *g*-value measurements is usually restricted by the linewidth ΔH, whereas relative measurements depend upon the simulation of the spectral lineshape and thus are more precise. The similar anisotropy of the *g*-tensors obtained for Chl(z)$^+$ and Chl a^+ (see Table 1) proves the identity of the Chl(z)$^+$ and Chl a^+ electronic structures. This also indicates that the protein environment is very similar to the low molecular weight glassy environment.

Recording the EPR spectra of P^+_{700} and Chl a^+ under similar experimental conditions and with the same *g*-marker signal allows us to make a comparative analysis of their *g*-values. The results presented in the Table 1 and Fig. 2 show that the anisotropy of the P^+_{700} signal is considerably smaller than that of Chl a^+. The most important observation is that the g-tensor components of P^+_{700} are shifted from those of Chl a^+, with the g_{zz} component having the largest shift. This shift of 21×10^{-5} is considerably greater than the accuracy of the absolute g-tensor measurements, which we estimate to be 5×10^{-5}. The value of the g_{zz}-shift and the fact that the g_{zz} component has the largest perturbation for P^+_{700} cannot be explained assuming that the cation radical is localized on one of the Chl *a* molecules and that the electronic structure of Chl *a* is not disturbed. Indeed, Stone's classical theory of *g*-values (Stone, 1963) predicts shifts of the radical *g*-values due to interactions with the surrounding environment. Interaction with the environment leads to the unpaired electron spin density redistribution and changes in the energy of the occupied and unoccupied orbitals. According to Stone's theory, the shift in the g_{zz} component, the component whose value is closest to the free electron value of 2.0023, is a second-order effect (order of magnitude smaller) compared to the shifts of the g_{xx} and g_{yy} components. On the contrary, the experimentally observed shifts of the g_{xx} and g_{yy} peaks of P^+_{700} compared to Chl a^+ are smaller than the shift of g_{zz}. The main conclusion from these observations is that the electronic structure of the primary donor cation P^+_{700} differs from the electronic structure of monomeric Chl a^+ and environmental effects, even specific interactions, such as hydrogen bonding, cannot explain this difference.

A possible explanation of the deviation of the P^+_{700} electronic structure from its monomeric analog could be a delocalization of the spin density of the unpaired electron between the two chlorophyll molecules of P_{700}. This can account for the observed shift of g_{zz} and decrease in the anisotropy of the *g*-tensor in P^+_{700} compared to Chl a^+. In this case, the *g*-values are effectively

Table 1. Magnetic-resonance parameters of P_{700}^{+}, Chl a^{+}, P_{700}^{T}, and Chl a^{T} obtained by simulation of the experimental D-band EPR spectra presented in Figs. 2 and 3

Sample	g_{xx}	g_{yy}	g_{zz}	$g_{xx} - g_{zz}$ [10^{-5}]	$g_{xx} - g_{yy}$ [10^{-5}]	$g_{yy} - g_{zz}$ [10^{-5}]	D [10^{-4} cm^{-1}]	E [10^{-4} cm^{-1}]
P_{700}^{+a}	2.00329	2.00282	2.00246	83	47	36		
Chl $a^{+a,b}$	2.00332	2.00280	2.00225	107	52	55		
P_{700}^{Tc}	2.00369	2.00323	2.00252	117	46	71	280 ± 1	39.0 ± 0.2
Chl a^{T}	2.00344	2.00382	2.00265	79	−38	117	284 ± 1	41.3 ± 0.2

[a] The notation of the g-tensor axes *X*, *Y*, and *Z* is a standard one and counts from the smaller to higher magnetic field, respectively. The error in the absolute measurements of the g-values is $\pm 5 \times 10^{-5}$. The relative measurements of Δg within one radical is more accurate, $\pm 2 \times 10^{-5}$, as it is based on the simulation of the lineshape of the spectrum.

[b] The data were collected for the Chl(z) cation radical which has a chemical structure identical to Chl *a* (see explanation in the text) (Stewart et al., 1998).

[c] The notation of *X*, *Y*, and *Z* axes is standard for triplet sublevels with positive D: the sublevel energy in the zero-field approximation is increasing from *Z* to *X*. The g-tensor is measured as a middle point between respective zero-field components. The error in the absolute and relative g-values is $\pm 9 \times 10^{-5}$. It is larger than for the cation radicals due to the broad linewidth and wide spread of the spectra.

averaged between the two molecules, leading to a decrease of the total *g*-value anisotropy. The shift of the g_{zz} component may be the same order of magnitude or even higher than for the g_{xx} and g_{yy} components.

According to the X-ray diffraction crystal data (Deisenhofer et al., 1984; Ermler et al., 1994; Jordan et al., 2001; Zouni et al., 2001), from the series of photosynthetic RC proteins of PS I, PBa, and PS II, the separation between the central Mg^{2+} ions increases from 6.3 to 7.6 Å and 10 Å, respectively. As the separation between the chlorophylls decreases, the overlap increases (Jordan et al., 2001) and, as a consequence, π–π interactions are assumed to be stronger. Note that in PBa the unpaired electron spin density of P_{865}^{+} is believed to be delocalized, whereas in PS II it is believed to be localized. Thus, it is logical that in PS I, with the smallest separation between chlorophyll molecules, the spin density in P_{700}^{+} is delocalized.

Another indication of the delocalization of the spin density in P_{700}^{+} comes from analysis of the spectral linewidth. The g_{zz} component of P_{700}^{+} has a surprisingly small linewidth. From the simulation of the P_{700}^{+} spectrum, the Gaussian linewidth of the g_{zz} component is $\Delta H_Z = 3.8$ G, the same as for g_{yy}: $\Delta H_Y = 3.8$ G, and smaller than for g_{xx}: $\Delta H_X = 4.2$ G. On the other hand one would expect for chlorophyll cation radicals that the linewidth, ΔH_Z, being determined by the unresolved ^{14}N hyperfine couplings, should be the largest. These hyperfine couplings are anisotropic and have the largest value along the *z*-axis, which is perpendicular to the chlorin plane (Vrieze et al., 1996; Zech et al., 2000; Link et al., 2001). This is indeed the case for Bchl a^{+}, as well as for the primary donor in *Rb. sphaeroides* PBa, P_{865}^{+}, and Chl a^{+} (Bratt et al., 2000) (see Fig. 2). In these cases ΔH_Z is 1.5–2 times greater than ΔH_X and ΔH_Y. The simulated Chl a^{+} spectrum presented in Fig. 2 displays the same trend: $\Delta H_Z = 6.4$ G, $\Delta H_Y = 4.0$ G, and $\Delta H_X = 4.7$ G. An averaging of the magnetic-resonance parameters between the two halves of a P_{700} dimer could be responsible for the relatively small linewidth of the g_{zz} component in P_{700}^{+}.

On the other hand, the observed difference in the electronic structures of P_{700}^{+} and Chl a^{+} could be explained by trapping of the cation state on a molecule whose structure is different from Chl *a* or is a highly distorted Chl *a*. Evidence that a reversible rearrangement of the geometric and electronic structure of Chl *a* can account for the observed differences in the magnetic resonance and redox properties between P_{700}^{+} and Chl a^{+} *in vitro* has been previously reported (Wasielewski et al., 1981b). The authors proposed that an enolization of the ring V β-keto ester of Chl *a* is responsible for the change of the electronic properties of P_{700}^{+}. Support for this hypothesis came recently from the X-ray crystal structure of PS I (Jordan et al., 2001). In this publication, a strong hydrogen bond with a keto group of ring V was reported for only one of the chlorophylls – Chl *a*′. The possibility of hydrogen bonding was excluded for Chl *a*. This latter conclusion is based on the fact that no H atoms are observed in the vicinity close to the oxygen of the keto group of ring V for Chl *a*. One plausible explanation for this could be that hydrogen is already covalently bound to the oxygen of Chl *a*, thus forming an enol. If this is the case then a number of controversial data including magnetic-resonance parameters of P_{700}^{+} and, optical and redox properties of P_{700} could be explained assuming localization of the active species on Chl *a*-enol. It should be noted, however, that recent molecular orbital calculations of P_{700}^{+} do not bear out this Chl *a*-enol model (Plato et al., 2003).

As an alternative explanation we have to keep in mind that chlorophyll molecules, as was mentioned above, demonstrate broad heterogeneity due to

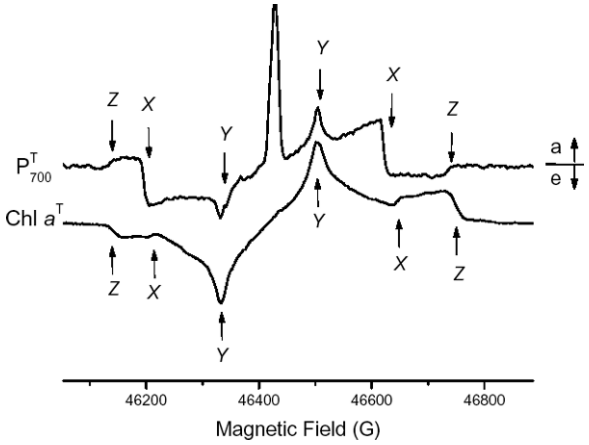

Fig. 3. Time-resolved D-band polarized EPR spectra of the triplet states of primary donor P_{700} in deuterated Photosystem I and of deuterated Chl *a* in toluene/pyridine (90:10) solvent, recorded by pulsed EPR technique. The microwave pulse sequence used in the experiment was $t_{p1} - \tau - t_{p2} = 40\text{-}300\text{-}60$ns, DAF (delay after flash) time equals 3 μsec, optical excitation wavelength $\lambda = 550$ nm, temperature = 75 K. *X*, *Y*, and *Z* in combination with arrows indicate positions of the turning points in the spectra, which correspond to the main components of the zero-field tensor. **a** and **e** indicate absorption and emission parts of the spectra, respectively. Source: Poluektov et al., 2002.

chlorophyll–solvent interactions. In addition such interactions could lead to formation of a set of conformation substates of chlorophyll molecules (Budil and Thurnauer, 1991; Bratt et al., 2000). The protein environment might fix the structure of P_{700} in unusual conformational substates and thus considerably change the electronic properties of one or both chlorophyll molecules in P_{700}.

C. P_{700} and Chlorophyll a Triplet States

The observed difference of the electronic properties of the primary donor P_{700} from Chl *a* molecules should be revealed in the triplet state of P_{700} as well. However, the reported magnetic-resonance parameters of P^T_{700} are the same as those of Chl a^T at low temperatures. To examine this conclusion we recorded the HFEPR spectra of the P^T_{700} and Chl a^T triplet states (see Fig. 3).

For the preparation of the triplet state P^T_{700}, the PS I complex was treated with dithionite (pH 10) and preilluminated at 75 K which leads to the reduction of iron–sulfur centers and A_1 (phylloquinone). To detect the triplet states of Chl *a* and P_{700}, samples were illuminated in the cavity of the EPR spectrometer and EPR spectra were recorded using the TR pulsed HFEPR by monitoring the electron spin echo (ESE) intensity as a function of the scanned magnetic field (Fig. 3; Poluektov et al., 2002).

The positions of the canonical components corresponding to the main orientations of the zero-field tensor are marked by arrows in Fig. 3. The splitting between these arrows is defined by the zero-field splitting parameters D and E: 2D for the *Z*-axis, D – 3E for the *Y*-axis and D + 3E for the *X*-axis in the standard notation of the triplet sublevels in the low-field approximation (Budil and Thurnauer, 1991). These parameters are summarized in Table 1 and are in agreement with previously reported data (Frank et al., 1979; Rutherford and Sétif, 1990; Budil and Thurnauer, 1991; Krabben et al., 2000). The spectra of P^T_{700} and Chl a^T triplet states exhibit electron spin-polarization (ESP). The so-called "T_0" ESP of the P^T_{700} has been explained by the radical pair mechanism of the triplet formation and the ESP pattern of the Chl a^T by spin–orbit induced intersystem crossing (Budil and Thurnauer, 1991).

Recording the triplet state EPR spectra at high magnetic field allows direct measurement of the projection of the *g*-tensor component on the direction of the zero-field axes. Analysis of the data, presented in the Table 1, demonstrates a striking effect. The ordering of the g_{xx} and g_{yy} components is switched between P^T_{700} and Chl a^T (Poluektov et al., 2002). This effect is clearly seen in spite of the fact that, due to the large spread of the triplet spectrum and relatively broad linewidth of the canonical components, the absolute error in the g-value measurement is $\sim 9 \times 10^{-5}$, which is higher than for the cation radicals.

The effect can only be explained by having a different orientation of the zero-field axes with respect to the *g*-tensor main axes in P^T_{700} compared to Chl a^T. This means that, while the values of the zero-field parameters of these two triplet states are very close, the distributions of the spin densities are very different. The conclusion that the spin density is localized on one of the two chlorophylls in the triplet state of the P_{700} primary donor was based on the similarities of the magnetic parameters (Rutherford and Sétif, 1990; Budil and Thurnauer, 1991). Thus, in contrast to this previous analysis, HFEPR spectra indicate that the triplet state of P^T_{700} deviates considerably from Chl a^T.

Again, a reasonable explanation for the switching between the *X*- and *Y*-axes may be either the delocalization of the electron spin density over the two chlorophyll species assigned to the primary donor or a deviation of the structure of the molecule, with a trapped triplet state, from Chl *a*. To answer these questions, an extended theoretical study of these systems is needed.

Thus, the HFEPR data on the P_{700}^{+} and P_{700}^{T} states in PS I in comparison with that of the Chl a^{+} and Chl a^{T} states present unambiguous proof that the electronic structures of the primary donor cation radical and triplet state are different from those of monomeric Chl *a*. However, on the basis of present data we cannot distinguish between two possible explanations, i.e., delocalization of the spin density in P_{700}^{+} and P_{700}^{T} over two chlorophyll molecules or reversible rearrangement of the geometric and electronic structure of Chl *a* molecules, i.e., enolization, freezing of a conformational substate.

III. Structure of the $P_{700}^{+}A_{1}^{-}$ Radical Pair Intermediate from Magnetically Aligned Samples and Multifrequency Quantum Beat Oscillations

A. Background

The three-dimensional structure of the radical pair $P_{700}^{+}A_{1}^{-}$ with respect to the membrane in which the RC resides can be derived with transient EPR data. This is possible because during the course of HFEPR experiments on whole cells of the cyanobacterium *Synechococcus lividus*, we discovered (Berthold et al., 1999) that the ESP pattern of the EPR spectra is sensitive to the alignment of the cells in the magnetic field of the spectrometer. Our strategy for obtaining structure of the short-lived radical pair intermediates involves a multifrequency EPR approach with data collection at three microwave frequencies as follows. The orientation of the magnetic tensors of $P_{700}^{+}A_{1}^{-}$ is obtained from analysis of the pronounced anisotropy of the zero quantum electron coherences in a transient Q-band EPR experiment. The orientation of the cofactors of the primary donor is then determined by analyzing transient X-band EPR spectra, extracted from a two-dimensional data set. Finally, transient W-band spectra of a magnetically aligned sample provide detailed information on the cofactor arrangement of $P_{700}^{+}A_{1}^{-}$ in the photosynthetic membrane. These experiments were performed using *deuterated* and ^{15}*N-substituted* cyanobacteria *Synechococcus lividus*. Deuteration provides enhanced spectral resolution, particularly in the case of SCRP ESP, and ^{15}N substitution facilitates analysis of the nuclear quantum beats at X-band frequency. In section III.B we describe the analysis and explanation of the magnetic field alignment of whole cells of cyanobacteria, in section III.C we briefly discuss the method of analysis of quantum beat oscillations and in section III.D we present the multifrequency approach for obtaining detailed structural information.

B. High-Field EPR of Magnetically Oriented Cyanobacteria

HFEPR spectra from samples frozen in the presence of the magnetic field indicate an anisotropic distribution of the radical pair with respect to the laboratory frame (Berthold et al., 1999; Heinen et al., 2003a,b). In a typical experiment, the sample is aligned in the static magnetic field (3.3 T) of a W-band EPR spectrometer at room temperature and then cooled to low temperatures. Representative results are shown in Fig. 4 (solid lines). To establish the field-induced alignment of the reaction centers, the EPR spectra were recorded at two different orientations of the frozen sample. The EPR spectrum in Fig. 4a reflects the original sample orientation immediately after cooling ($\rho = 0^{\circ}$). The spectrum in Fig. 4b, was taken after the frozen sample was rotated by 90° about an axis perpendicular to the magnetic field ($\rho = 90^{\circ}$) (Berthold et al., 1999). Pronounced spectral differences are observed particularly in the high-field region. If, however, the sample was cooled in the absence of the magnetic field, two identical lineshapes were detected (results not shown).

Previously this type of alignment was demonstrated for whole cells of green algae and photosynthetic bacteria, using fluorescence polarization and linear dichroism measurements (Geacintov et al., 1972; Breton, 1974). The physical origin of this magneto-orientation is an anisotropy in the diamagnetic susceptibility of the photosynthetic system. Assuming that the susceptibility tensor is axially symmetric in its principal axis system, $\mathbf{X}'$,$\mathbf{Y}'$,$\mathbf{Z}'$ (see Fig. 5), the orientational distribution function of the symmetry axis $\mathbf{Z}'$ can be written as (Geacintov, 1972)

$$f(\beta) = N \exp(A \cos^2 \beta), \tag{1}$$

$$A = \frac{1}{2}\Delta\chi V B_0^2/(\mu_0 kT). \tag{2}$$

Here, N is a normalization constant, $\Delta\chi$ is the anisotropy in the volume diamagnetic susceptibility, V is the effective volume, μ_0 is the vacuum permeability, k is the Boltzmann constant, and T is the absolute temperature of the Boltzmann distribution. The angle β denotes the angle between the principal axis of the susceptibility tensor and the sample axis, $\mathbf{z}''$, determined by the magnetic field direction during sample orientation (see Fig. 5). Thus, $\mathbf{z}''$ specifies the macroscopic axis of symmetry of the angular distribution. The coefficient

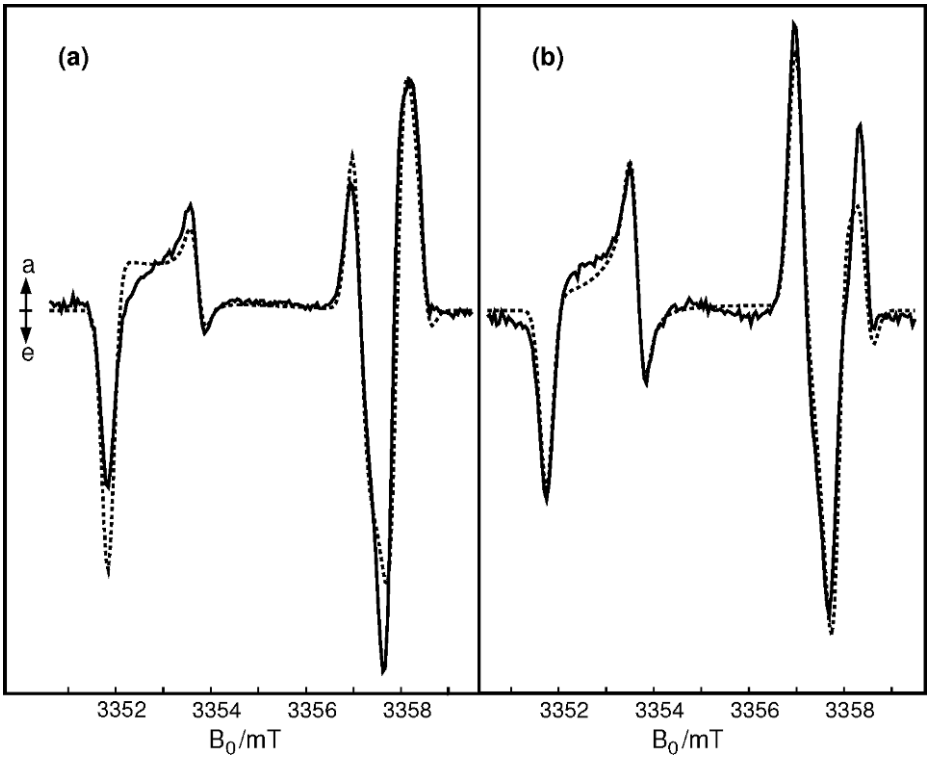

Fig. 4. Transient W-band EPR spectra of the light-induced radical pair $P_{700}^{+}A_1^{-}$ in Photosystem I at two different orientational distributions with respect to the laboratory frame. Positive, **a**, and negative, **e**, signals indicate absorptive and emissive polarizations, respectively. (a) Sample axis parallel to the magnetic field, $\rho = 0^{\circ}$. (b) Sample axis perpendicular to the magnetic field, $\rho = 90^{\circ}$. Full lines: Experimental spectra from deuterated and ^{15}N-substituted cyanobacteria *Synechococcus lividus* measured at temperature = 90 K. Magneto-orientation of the sample is achieved with an alignment field of $B_0 = 3.35$ T. The signal intensity is averaged in the time window 0.4–2.4 μs. Microwave field: $B_1 = 0.01$ mT. Microwave frequency: $\omega/2\pi = 94.1163$ GHz. Dashed lines: Best-fit simulations. Source: Heinen et al., 2004a, 2004b.

A in Eq. (1) characterizes the magnetic field-induced alignment of the susceptibility tensor axes relative to the sample axis, $\mathbf{z}''$, while the angle ρ specifies the orientation of $\mathbf{z}''$ in the laboratory frame (see Fig. 5). The orientational order parameter, $S_{Z'Z'}$, is related to the coefficient A by a mean value integral,

$$S_{Z'Z'} = \frac{1}{2}\int_0^{\pi} (3\cos^2\beta - 1) f(\beta) \sin\beta d\beta \qquad (3)$$

Since the susceptibility tensor has a fixed orientation, ϑ,ψ, with respect to the molecular reference system, **X, Y**,**Z**, it is possible to express $\cos\beta$ as a function of the Euler angles Φ, Θ, Ψ and (see Fig. 5; Berthold et al., 1999; Heinen et al., 2004a):

$$\begin{aligned}\cos\beta = &-\sin\rho\sin\vartheta\cos\Theta\cos\Psi\cos(\psi+\Phi)\\ &+\sin\rho\sin\vartheta\sin\Psi\sin(\psi+\Phi)\\ &-\sin\rho\cos\vartheta\sin\Theta\cos\Psi - \cos\rho\sin\vartheta\sin\Theta\\ &\cos(\psi+\Phi) + \cos\rho\cos\vartheta\cos\Theta.\end{aligned} \qquad (4)$$

Equations (4) and (1) can be used to evaluate the statistical weight for the EPR spectrum of a given molecular orientation specified by the Euler angles $\Omega = (\Phi, \Theta, \Psi)$. Integration over all possible orientations, Ω, then yields the anisotropic "powder" lineshape. The free adjustable parameters are $S_{Z'Z'}$, ϑ and ψ.

Values for these parameters were determined by a simultaneous fit of two experimental high-field EPR spectra of $P_{700}^{+}A_1^{-}$ measured with the sample axis either parallel ($\rho = 0^{\circ}$) or perpendicular ($\rho = 90^{\circ}$) to the magnetic field (Berthold et al., 1999; Heinen et al., 2004a). The results of these fits, performed at W-band (95 GHz) and D-band (130 GHz) frequencies, were verified by repeating the fit procedure for a large number of different starting values covering the whole parameter space. In the majority of all test runs, the same global minimum values were obtained, including a small *positive* value for the order parameter $S_{Z'Z'}$ (Berthold et al., 1999; Heinen et al., 2004a). The *positive* sign of $S_{Z'Z'}$ implies that the susceptibility tensor axes $\mathbf{Z}'$ orient preferentially parallel to the magnetic field. This is clear evidence for membrane proteins being the major source of the anisotropy in the diamagnetic

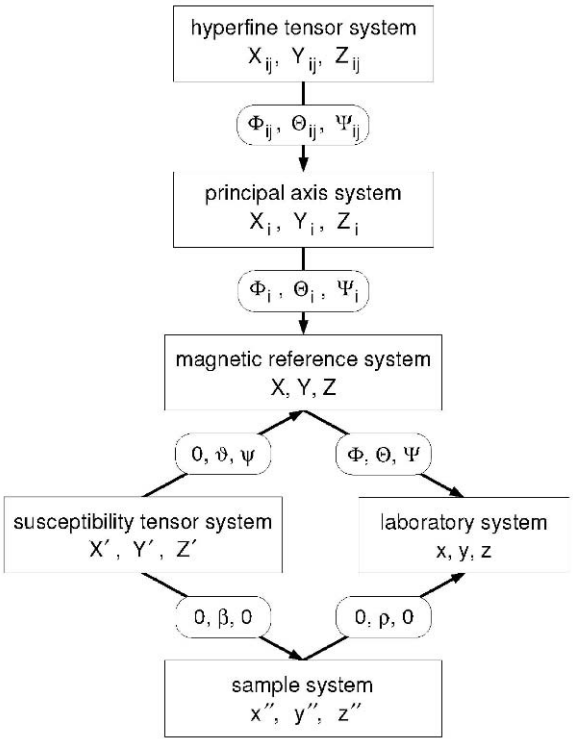

Fig. 5. Notation for coordinate systems and Euler transformations used in the EPR model. $\mathbf{X}_{ij}$, $\mathbf{Y}_{ij}$, $\mathbf{Z}_{ij}$ = principal axis system of the hyperfine tensor of nucleus j coupled to radical i. $\mathbf{X}_i$, $\mathbf{Y}_i$, $\mathbf{Z}_i$ = principal axis system of the g-tensor of the primary donor ($i = 1$) and of the g-tensor of the quinone acceptor ($i = 2$). $\mathbf{X}$, $\mathbf{Y}$, $\mathbf{Z}$ = magnetic reference system (g-tensor of the reduced quinone acceptor). $\mathbf{z}$ = magnetic field direction, $\mathbf{Z}'$ = symmetry axis of the susceptibility tensor (membrane normal), $\mathbf{z}''$ = sample axis (magnetic field direction during sample orientation).

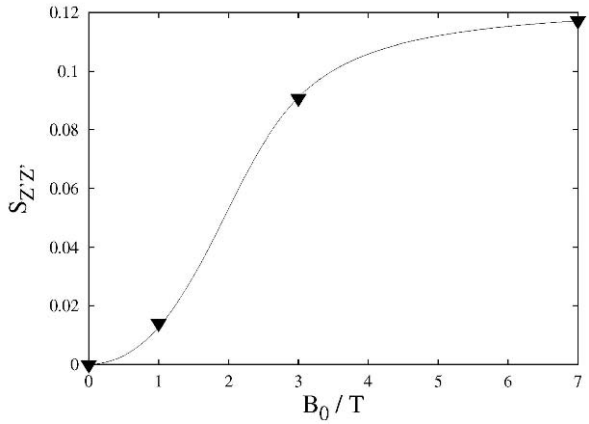

Fig. 6. Magnetic field dependence of the order parameter, $S_{Z'Z'}$, characterizing the alignment of the symmetry axis of the susceptibility tensor relative to the magnetic field. The experimental values (solid triangles) are extracted from spin polarized D-band EPR spectra of the light-induced radical pair, $P_{700}^{+}A_1^{-}$ in Photosystem I. The solid line represents a best-fit simulation using a simple model for magneto-orientation. The extracted value for the anisotropy of the diamagnetic susceptibility is $\Delta\chi V = 5.7 \times 10^{-27}\mathrm{m}^3$. Source: Heinen et al., 2004a.

susceptibility (Worcester, 1978; Pauling, 1979). If lipid membranes were the dominant source for the susceptibility anisotropy, one would expect that the susceptibility tensor axes $\mathbf{Z}'$ orient mainly perpendicular to the magnetic field, i.e., the order parameter $S_{Z'Z'}$ is negative (Scholz et al., 1984).

In cyanobacteria, the photosynthetic proteins are embedded within the thylakoid membranes, which consist of mostly parallel glycolipid bilayers. Theoretical studies indicate that peptide bonds are a source of anisotropic diamagnetic susceptibility responsible for the alignment of the helix axis parallel to the magnetic field (Worcester, 1978; Pauling, 1979). In cyanobacterial PS I as well as in many other membrane proteins, a total of about 30 transmembrane α-helices are aligned to within a small angle of the membrane normal (Jordan et al., 2001), which thus represents a natural choice for the principal axis of the susceptibility tensor, $\mathbf{Z}'$. Furthermore, any anisotropy in the plane of the membrane will be averaged out for such an arrangement. It is therefore reasonable to identify the symmetry axis of the susceptibility tensor with the membrane normal.

To obtain further information on the mechanism of the magneto-orientation process, the order parameter $S_{Z'Z'}$ was evaluated as a function of the applied magnetic field (Heinen et al., 2004a). For this purpose, spin polarized D-band EPR spectra of the radical pair $P_{700}^{+}A_1^{-}$ were measured for four different alignment fields varying between 0 and 7 T. A computer analysis of the observed angular-dependent lineshapes then provided values for the order parameter $S_{Z'Z'}$. In Fig. 6 this order parameter is plotted as a function of the alignment field. The experimental values (solid triangles) refer to the cyanobacterium *S. lividus*. One sees that $S_{Z'Z'}$ first increases gradually, then rises steeply and finally levels off to a constant limiting value. Thus, the magnetic field dependence of $S_{Z'Z'}$ can be described by a saturation curve, as defined in the Eqs. (1–3). The free adjustable parameters of this curve, $\Delta\chi V$ and $(S_{Z'Z'})_{limit}$ were determined by fitting calculated order parameters $S_{Z'Z'}$, to the experimental ones. The solid line in Fig. 6 represents the best-fit simulation based on the parameter values (Heinen et al., 2004a) $\Delta\chi V = 5.7 \times 10^{-27}\,\mathrm{m}^3$; $(S_{Z'Z'})_{\mathrm{limit}} = 0.12 \pm 0.02$.

The large value for the anisotropy of the diamagnetic susceptibility of $\Delta\chi V = 5.7 \times 10^{-27}\,\mathrm{m}^3$, extracted from the saturation curve, suggests that whole cells might be oriented by the magnetic field. To check

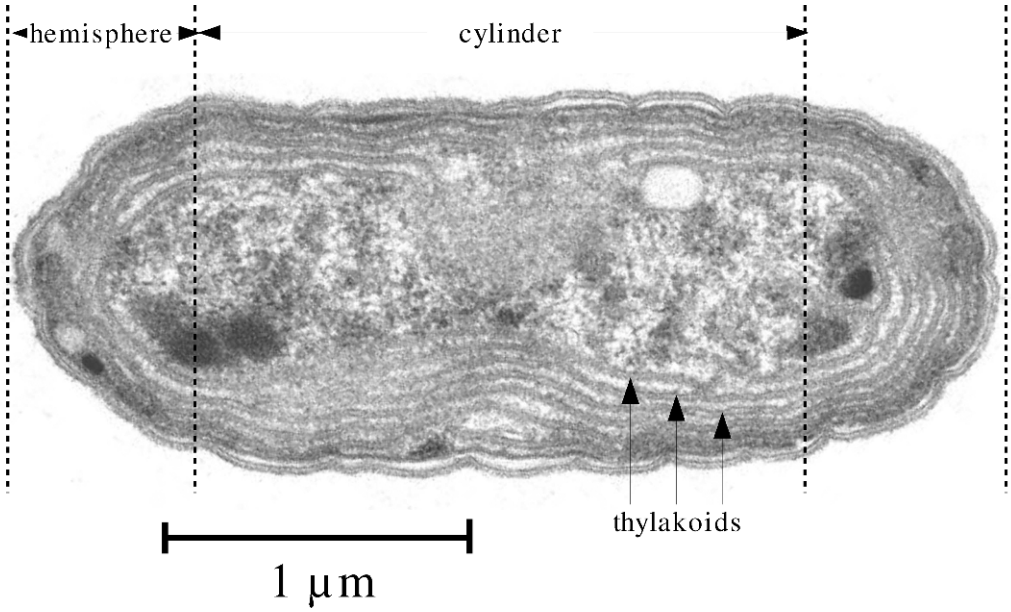

Fig. 7. Electron micrograph of an ultrathin section of a *S. lividus* cell at high magnification. Note that the thylakoid membranes are arranged in several layers running parallel to the cell envelope which has a regular cylindrical shape. By courtesy of J. R. Golecki.

this possibility, model calculations were performed for $\Delta\chi V$ using structural information from a recent electron microscopy study (Heinen et al., 2004b). Figure 7 depicts an electron micrograph of a *S. lividus* cell at high magnification. One sees that the thylakoid membranes are arranged in several layers running parallel to the cell envelope. According to morphometric measurements, an average cell contains thylakoids with a total membrane area of $\sim 9.8 \times 10^{-11} m^2$. Of this, about 50% are covered by membrane proteins, i.e., 4.9×10^{-11} m^2 (Heinen et al., 2004b). Taking PS I as a representative example, we estimate that a typical membrane protein covers an area of 1.0×10^{-16} m^2 (Jordan et al., 2001). Thus, on the average, a cyanobacterial cell contains about 4.9×10^5 membrane proteins within its thylakoid system.

Let us now estimate the susceptibility anisotropy of a single membrane protein such as PS I. In cyanobacterial PS I, there are 30 parallel transmembrane α-helices (Jordan et al., 2001), which define the symmetry axis of the susceptibility tensor. Assuming alignment parallel to the magnetic field, we estimate a susceptibility anisotropy of 5.0×10^{-32} m^3. The value is based on quantum chemical calculations of the susceptibility anisotropy of peptide bonds (Pauling, 1979) arranged in α-helices (Worcester, 1978). To calculate the susceptibility anisotropy of a whole cyanobacterial cell, we have to consider that the membrane proteins are not all aligned parallel to the magnetic field but are distributed according to an order parameter of $S_{Z'Z'} = 0.12$. This leads to an estimated total susceptibility anisotropy of $(\Delta\chi V)_{calc} = (4.9 \times 10^5) \times (5 \times 10^{-32}\ m^3) \times 0.12 = 2.9 \times 10^{-27}\ m^3$. In view of the approximations used in the derivation, the estimated value is in surprisingly good agreement with the observed value of $\Delta\chi V = 5.7 \times 10^{-27} m^3$. Evidently, whole cells are aligned in the magneto-orientation process.

A prerequisite for the alignment is an anisotropic shape of the bacterial cell and the thylakoid system. Inspection of Fig. 7 reveals that the thylakoid membranes in *S. lividus* cyanobacteria form regular cylinders with hemispherical caps on both ends. If the long axes of the cells were oriented parallel to the magnetic field, all bilayer normals in the cylinder part would be orthogonal to the field implying a negative order parameter $S_{Z'Z'}$. This is not observed in the HFEPR experiments of $P_{700}^+A_1^-$. We, therefore, conclude that the cyanobacterial cells align perpendicular to the magnetic field.

Figure 8 depicts a schematic of the magneto-orientation process, as revealed by time-resolved D-band EPR of the radical pair $P_{700}^+A_1^-$ (Heinen et al., 2004a). Spectral analysis indicates that membrane proteins are mainly responsible for the anisotropy of the diamagnetic susceptibility. In cyanobacterial PS I, as well as in many other membrane proteins, a large

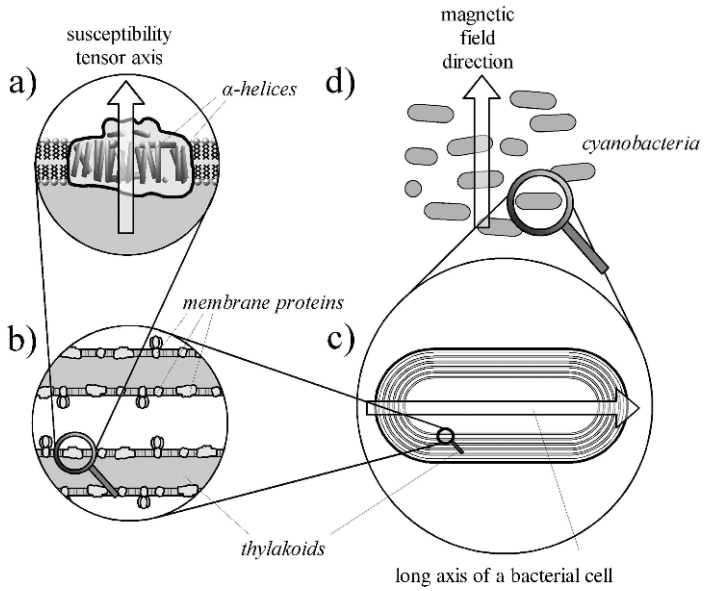

Fig. 8. Schematic of the magneto-orientation process proposed for the photosynthetic reaction centers in cyanobacteria. (a) Arrangement of the reaction center protein in the photosynthetic membrane. (b) Structure of the thylakoid membranes. (c) Structure of a cyanobacterial cell. (d) Alignment of the cyanobacterial cells in a strong magnetic field.

number of transmembrane α-helices are aligned to within a small angle of the membrane normal, which thus defines the symmetry axis of the susceptibility tensor (see Fig. 8a). The membrane proteins are embedded within the thylakoid membranes consisting of mostly parallel glycolipid bilayers (see Fig. 8b). The whole thylakoid system has a regular three-dimensional structure that closely follows the shape of the cyanobacterial cell (see Fig. 8c). If a magnetic field of sufficient strength is applied, the cyanobacterial cells align with their long axes perpendicular to the field (see Fig. 8d).

On the basis of this model, we now rationalize the extracted value for the order parameter $S_{Z'Z'}$. Let us assume that the distribution of the bilayer normals in the laboratory frame can be described by a convolution of two axially symmetric distribution functions f_1 and f_2 as given in Eq. (1) (Heinen et al., 2004b). Specifically, we assume that the function f_1 characterizes the distribution of the bilayer normals with respect to the symmetry axis of the cyanobacterial cell and the function f_2 describes the distribution of these axes relative to the magnetic field. Under these conditions, the order parameter S of the bilayer normals relative to the magnetic field can be written as a product of the two order parameters S_1 and S_2, each defined according to Eq. (3).

Inspection of Fig. 8 reveals that the order parameter S_1 is completely determined by the shape of the cyanobacterial cell. Using morphometric data from the electron microscopy study of the *S. lividus* cells, we estimate a value of $S_1 \approx -0.34$ (Heinen et al., 2004b). For the order parameter S_2 a strong dependence on the alignment field is expected. Assuming complete alignment for $B_0 = 7$ T, the order parameter S_2 can be assessed to $S_2 \approx -0.5$. This gives a total order parameter of $S = S_1 S_2 \approx 0.17$, which compares favorably with the limiting order parameter of $S_{Z'Z'} = 0.12$ observed by D-band EPR (Fig. 6). We, therefore, conclude that the evaluated mechanism for magneto-orientation of photosynthetic RCs is correct.

Thus, HFEPR of a magnetically aligned sample can provide the orientation of the membrane normal, ϑ and ψ, in a magnetic reference system. This structural information is unique as it is not easily available by other EPR techniques. Knowledge of this orientation makes it possible to determine the three-dimensional structure of the $P_{700}^{+}A_1^{-}$ radical pair intermediate in its native membrane. The structural analysis requires analysis of the quantum beat oscillations observed for a SCRP. Therefore, we first briefly describe this analysis in section III.C, and in section III.D we present the multifrequency approach for determining the structure of the SCRP. Thus, one also obtains the cofactor arrangement of the radical pair with respect to the membrane.

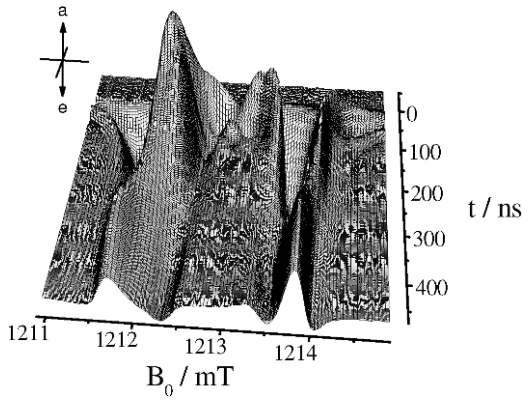

Fig. 9. Transient Q-band EPR data set of the light-induced radical pair $P_{700}^{+}A_1^{-}$ in Photosystem I of deuterated and ^{15}N-substituted cyanobacterium *Synechococcus lividus*. Positive, **a**, and negative, **b**, signals indicate absorptive and emissive polarizations, respectively. Microwave frequency: $\omega/2\pi$ = 33.9893 GHz. Microwave field: B_1 = 0.029 mT. Temperature = 70 K. Source: Link et al., 2001.

C. Analysis of Quantum Beat Oscillations from Spin-Correlated Radical Pairs

In transient EPR experiments, the sample is irradiated with a short laser pulse and the time evolution of the magnetization is detected in the presence of a weak microwave magnetic field. Generally, a complete data set consists of transient signals taken at equidistant field points covering the total spectral width. This yields a two-dimensional variation of the signal intensity with respect to both the magnetic field and the time axis (see van der Est, this volume, Chapter 24). Such a complete data set for $P_{700}^{+}A_1^{-}$ measured at Q-band microwave frequency (35 GHz) is shown in Fig. 9. Transient spectra can be extracted from this plot at any fixed time after the laser pulse as slices parallel to the magnetic field axis. Likewise, the time evolution of the transverse magnetization may be obtained for any given field as a slice along the time axis.

Note the pronounced modulations in the transverse magnetization. These consist of fast initial oscillations which disappear 100 nsec after the laser flash, and slow persisting oscillations with frequencies of a few MHz. The formation of these coherences can be rationalized in terms of an analytical EPR model developed for the light-induced radical pairs of photosynthesis (Kothe et al., 1998). The model is based on the density matrix approach,

$$\rho(\Omega, t) = \exp[-(i/\hbar)H(\Omega)t].\rho(\Omega, 0).\exp[(i/\hbar)H(\Omega)t], \quad (5)$$

where $\rho(\Omega, 0)$ specifies the initial configuration of the radical pair immediately after the laser pulse. The spin Hamiltonian employed,

$$H(\Omega) = H_Z(\Omega) + H_{EX} + H_D(\Omega) + H_{HF}(\Omega) + H_{NZ}, \quad (6)$$

considers Zeeman, exchange, dipolar, hyperfine, and nuclear Zeeman interactions of the radical pair. For computational simplicity, hyperfine interactions are restricted to one $I = 1/2$ nucleus in the donor (Kothe et al., 1998). In the presence of a microwave field, a microwave term, H_{MW}, must be added to the static Hamiltonian.

The crucial point is the specification of the initial condition of the radical pair at the instant of the laser pulse. In native photosynthetic reaction centers, the lifetime of the primary radical pair ($P_{700}^{+}A_0^{-}$) is short (see Fig. 1). Thus, even the secondary radical pair ($P_{700}^{+}A_1^{-}$) is generated in a virtually pure singlet state,

$$\rho(\Omega, 0) = \frac{1}{2}\left\{\left|S+\frac{1}{2}\right\rangle\left\langle S+\frac{1}{2}\right| + \left|S-\frac{1}{2}\right\rangle\left\langle S-\frac{1}{2}\right|\right\} n(\Omega), \quad (7)$$

determined by the spin multiplicity of the excited primary donor (see Fig. 1). The analysis shows that such a singlet radical pair is created with spin-correlated population of only four of the eight eigenstates. This gives rise to high optical spin-polarization (Thurnauer and Norris, 1980; Closs et al., 1987; Buckley et al., 1987), which has been exploited in structural studies of $P_{700}^{+}A_1^{-}$ using time-resolved EPR at different microwave frequencies (Stehlik et al., 1989; Fuechsle et al., 1993; van der Est et al., 1997; Kamlowski et al., 1998; Zech et al., 2000). In addition, there are coherences between the eigenstates of the radical pair. Analysis reveals that zero quantum electron (Salikhov et al., 1990; Bittl and Kothe, 1991; Kothe et al., 1991, 1994a,b, 1998; Zwanenburg and Hore, 1993; Bittl et al., 1994; Kiefer et al., 1999; Link et al., 2001; Heinen et al., 2002) and single quantum nuclear coherences (Weber et al., 1995; 1997; Jeschke, 1997; Kothe et al., 1998) are involved.

Light generation of these coherences can be rationalized in terms of the nonadiabatic change of the spin Hamiltonian at the instant of the laser pulse. At time zero, the radical pair is created in a singlet state as a consequence of spin conservation in an ultrafast photochemical reaction (see Fig. 1). Since the singlet is not an eigenstate of the corresponding spin

Hamiltonian,

$$[\rho(\Omega, 0), H(\Omega)] \neq 0, \tag{8}$$

the radical pair starts out in a coherent superposition of eigenstates, which can manifest itself as quantum beats in an EPR experiment with adequate time resolution (Kothe et al., 1991, 1994a,b, 1998; Bittl et al., 1994; Weber et al., 1995; Kiefer et al., 1999; Link et al., 2001; Heinen et al., 2002).

The continuous microwave field, applied in transient EPR, has two effects. First, it converts the longitudinal magnetization associated with the population differences between neighboring eigenstates into transverse magnetization (Zwanenburg and Hore, 1993). This gives the Torrey oscillations (Torrey, 1949). Secondly, it converts the zero quantum electron and nuclear coherences into observable single quantum precessions or quantum beats. Under slow-motional conditions, the frequency ω_{ZQ} of the zero quantum electron precessions critically depends on the orientation, $\Omega = (\Phi, \Theta, \Psi)$, of the radical pair in the laboratory frame, **x**, **y**, **z** (see Fig. 5). As shown previously (Kothe et al., 1994a,b; Kiefer et al., 1999; Link et al., 2001; Heinen et al., 2002), ω_{ZQ} is given by

$$\begin{aligned}\omega_{ZQ} = (1/\hbar)\{&[2/3D^{zz}(\Omega) - 2J_{ex}]^2 \\ &+ [(g_1^{zz}(\Omega) - g_2^{zz}(\Omega))\mu_B B_0 \\ &+ \sum\nolimits_k A_{1k}^{zz}(\Omega)M_{1k}^i - \sum\nolimits_l A_{2l}^{zz}(\Omega)M_{2l}^j]^2\}^{1/2},\end{aligned} \tag{9}$$

where $D^{zz}(\Omega)$, J_{ex}, $g_i^{zz}(\Omega)$, μ_B, B_0, and are the zz component of the dipolar coupling tensor, the strength of the isotropic exchange interaction, the zz component of the g-tensor of radical i, the Bohr magneton, the static magnetic field and the secular part of the hyperfine interaction between nucleus j and radical i, respectively. The weak B_1 field, commonly employed in transient EPR, allows for only a small range of orientations to meet the resonance condition. Consequently, the phase and frequency of the quantum beats vary significantly with B_0 across the powder spectrum. This pronounced variation can be used to extract the geometry of the radical pair intermediates in photosynthetic reaction centers (Kothe et al., 1991, 1994a,b; Kiefer et al., 1999; Link et al., 2001; Heinen et al., 2002).

D. Cofactor Arrangement of the $P_{700}^+ A_1^-$ Radical Pair

Figure 10 depicts the short-time behavior of the transverse magnetization of $P_{700}^+A_1^-$ measured at Q-band frequency (35 GHz) and four selected field positions along the powder spectrum [(a)–(d)] (Link et al., 2001). As noted above (section III.C) the transient signals contain fast oscillations, associated with the spin-correlated generation of the radical pair, which disappear 100 nsec after the laser pulse. Basically, these oscillations represent Q-band quantum beats [Eq. (9)], and their frequency varies significantly across the powder spectrum. Generally, oscillation frequencies from 10 to 50 MHz can be extracted from the corresponding power spectra.

The pronounced variation of the Q-band quantum beats can be employed to evaluate the orientation of the magnetic tensors in $P_{700}^+A_1^-$ (Link et al., 2001). Calculated time profiles covering the total spectral width that are simulated by varying the parameters of the tensor orientations provide five Euler angles, characterizing the orientation of the magnetic tensors of $P_{700}^+A_1^-$ (g-tensor of P_{700}^+, dipolar tensor) with respect to a magnetic reference frame (g-tensor of A_1^-). Dashed lines in Fig. 10 represent best-fit simulations.

The cofactor orientation of the primary donor in the g-tensor system of P_{700}^+ can be determined by analyzing transient X-band (9.5 GHz) EPR spectra. At this frequency anisotropic ^{15}N hyperfine interactions give rise to nuclear modulations in the transverse magnetization (Weber et al., 1995; 1997; Jeschke, 1997; Kothe et al., 1998). In the analysis presented here only four ^{15}N hyperfine tensors, whose symmetry axes are collinear, were considered. The orientation of this axis in the g-tensor system of P_{700}^+ is characterized by the Euler angles, Θ_{1j} and ψ_{1j} (Fig. 5).

Typical X-band lineshapes of $P_{700}^+A_1^-$, observed 50, 70, and 200 nsec after the laser pulse, are shown in Fig. 11 (solid lines) (Link et al., 2001). The variation was used to extract values for Θ_{1j} and ψ_{1j} Typically, a set of 27 calculated spectra, selected at various times after the laser pulse, was simultaneously fitted to the experimental spectra by varying Θ_{1j} and Ψ_{1j}. Dashed lines in Fig. 11 represent best-fit simulations. Note that the evaluated Euler angles, Θ_{1j} and ψ_{1j}, characterize the orientation of the symmetry axis of the ^{15}N hyperfine tensors in the g-tensor system of P_{700}^+. Because of the local character of the hyperfine interactions, it is reasonable to identify this symmetry axis with the chlorophyll normal. The two-dimensional Q- and X-band experiments provide seven Euler angles, characterizing the mutual orientation of P_{700}^+ and A_1^-.

Analysis of the transient W-band lineshapes of $P_{700}^+A_1^-$ was performed using the model outlined in the section III.B. The parameters of the orientational distribution function, ϑ, ψ, $S_{Z'Z'}$, were determined by simultaneously fitting the two angular-dependent spectra, measured with the sample axis either parallel

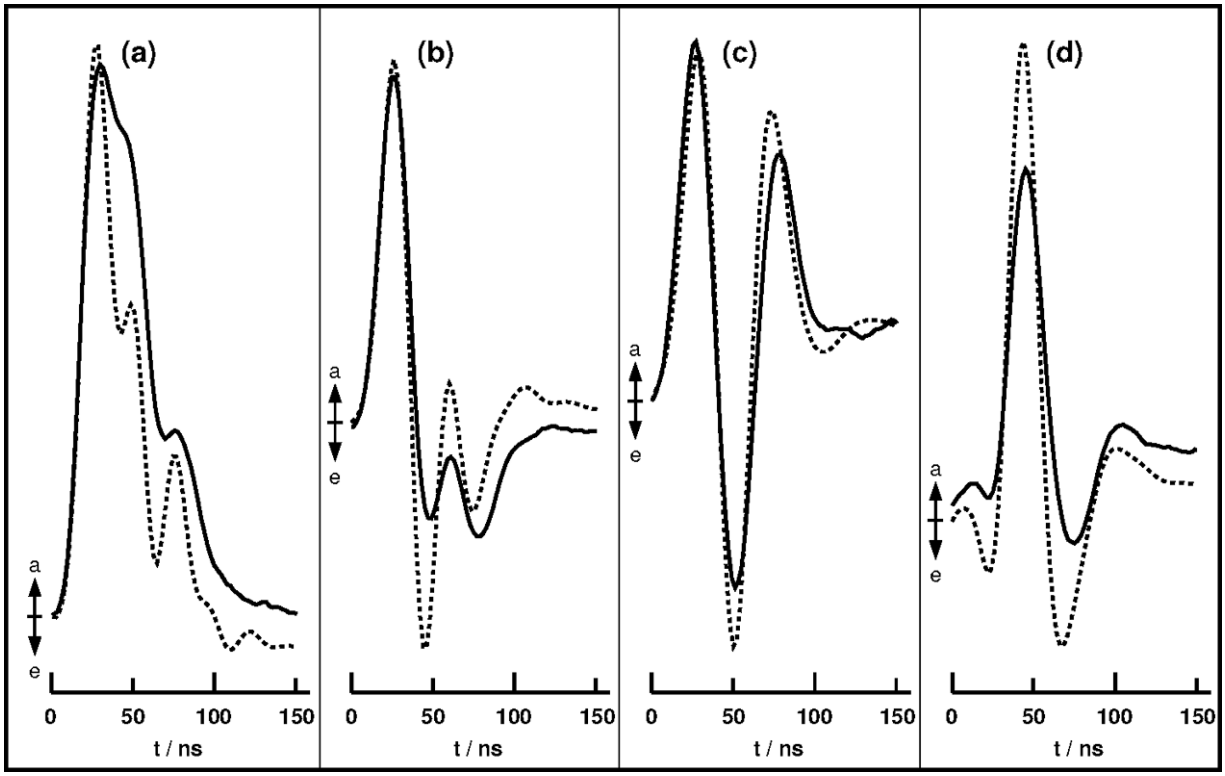

Fig. 10. Time evolution of the transverse magnetization of the light-induced radical pair $P_{700}^{+}A_1^{-}$ in Photosystem I measured at Q-band. The time profiles refer to four selected field positions (a), (b), (c), and (d), along the powder spectrum. Positive and negative signals indicate absorptive and emissive polarizations, respectively. Microwave frequency: $\omega/2\pi = 33.9893$ GHz. Microwave field: B_1 = 0.029 mT. Full lines: Experimental time profiles from the deuterated and ^{15}N-substituted cyanobacterium *Synechococcus lividus* measured at temperature = 70 K. Dashed lines: Best-fit simulations. Source: Link et al., 2001.

($\rho = 0^\circ$) or perpendicular ($\rho = 90^\circ$) to the magnetic field (Berthold et al., 1999). The dashed lines in Fig. 4 represent best-fit simulations. Generally, the agreement achieved is good. The obtained Euler angles, ϑ and ψ, characterize the orientation of the membrane normal in the g-tensor system of the primary donor. Knowledge of this orientation makes it possible to depict the three-dimensional structure of the radical pair intermediate $P_{700}^{+}A_1^{-}$ in its native membrane, as shown in Fig. 12. The structural model, describing the orientation of the *g*-tensor of P_{700}^{+} as well as the position and orientation of A_1^{-}, is in substantial agreement with recent EPR (Zech et al., 2000) and crystallographic results (Jordan et al., 2001), based on PS I single crystals. Note that values for all nine Euler angles, characterizing the geometry of the charge-separated state, have been obtained. The geometry is based on the analysis of quantum beat oscillations in combination with high-field EPR and a magnetically aligned sample.

Let us first discuss the *g*-tensor orientation of P_{700}^{+}. To describe this orientation, we define the chlorophyll-based reference system, $\mathbf{X}_{chl}$, $\mathbf{Y}_{chl}$, $\mathbf{Z}_{chl}$. The Z_{chl}-axis is the chlorophyll normal; the Y_{chl} -axis is the projection of the membrane normal onto the chlorophyll plane. The X_{chl} -axis then lies in the chlorophyll plane perpendicular to $\mathbf{Y}_{chl}$. Figure 13 depicts a three-dimensional representation of the *g*-tensor orientation of P_{700}^{+}. For simplicity, we show only one of the two chlorophyll molecules of the primary donor, which is the chlorophyll *a* species coordinated by the PsaB protein subunit (Krabben et al., 2000; Link et al., 2001).

In simple π radicals, the principal direction corresponding to the smallest g-tensor component, g^Z, is expected to lie near the normal of the molecular plane (Stone, 1963). Inspection of Fig. 13 reveals a significant deviation of $\Theta_{1j} = 29^\circ$ between $\mathbf{Z}$ and $\mathbf{Z}_{chl}$ (Link et al., 2001), in reasonable agreement with recent EPR results based on PS I single crystals (Zech et al., 2000). This deviation is difficult to explain if we assume that the spin density of the unpaired electron is completely localized on one of the chlorophyll molecules of the P_{700}^{+} dimer. On the other hand, this observation is in agreement with the asymmetric delocalization of the

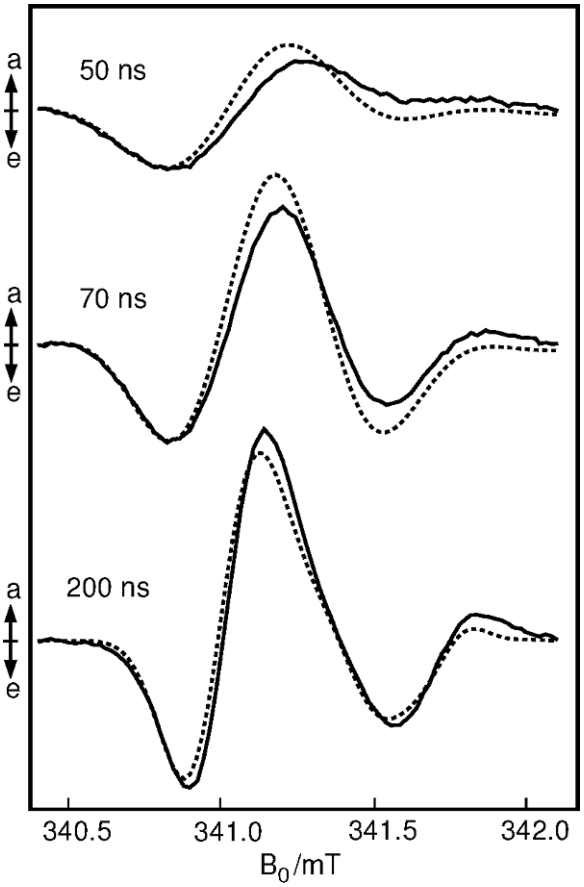

Fig. 11. Transient X-band EPR spectra of the light-induced radical pair $P_{700}^{+}A_1^{-}$ in Photosystem I at various times after the laser pulse. Positive and negative signals indicate absorptive and emissive polarizations, respectively. Microwave frequency: $\omega/2\pi = 9.57375$ GHz. Microwave field: $B_1 = 0.020$ mT. Full lines: Experimental spectra from deuterated and ^{15}N-substituted cyanobacterium *Synechococcus lividus* measured at temperature = 70 K. Dashed lines: Best-fit simulations. Source: Link et al., 2001.

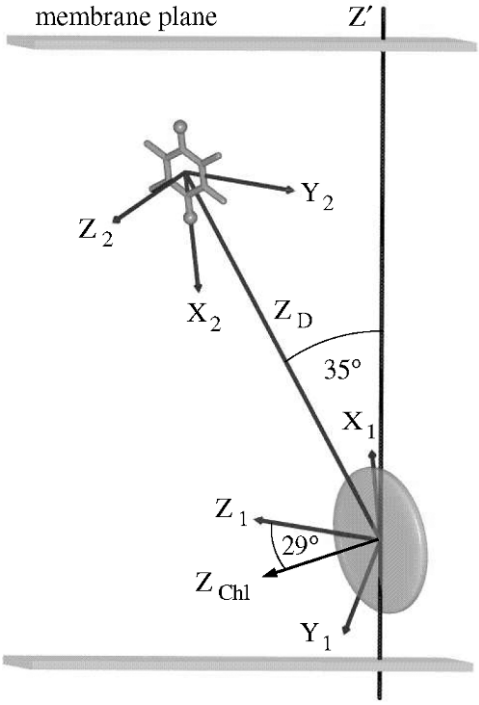

Fig. 12. Structure of the secondary pair $P_{700}^{+}A_1^{-}$ in Photosystem I as determined by high time resolution multifrequency EPR, employing quantum beat oscillations and a magnetically aligned sample. The view direction is parallel to the membrane plane. The shaded disk represents one of two chlorophyll molecules of the primary donor, which carries the major part of the unpaired spin. $\mathbf{X}_1, \mathbf{Y}_1, \mathbf{Z}_1$ = principal axis system of the g-tensor of P_{700}^{+}. $\mathbf{X}_2, \mathbf{Y}_2, \mathbf{Z}_2$ = principal axis system of the g-tensor of A_1^{-}. $\mathbf{Z}_D$ = symmetry axis of the dipolar tensor. $\mathbf{Z}'$ = membrane normal.

spin density between two halves of the P_{700}^{+} dimer or strong distortion of the electronic structure of the Chl *a*, which was discussed in section II.

Figure 14 shows a structural model for the reduced quinone acceptor, A_1^{-}, based on the nine Euler angles discussed above (Link et al., 2001). In this model, the quinone plane of A_1^{-} is found to be inclined by 68° relative to the membrane plane, while the O–O axis makes an angle of 23° with the membrane normal. These values are in substantial agreement with those reported in the high-resolution X-ray structure (Jordan et al., 2001). Nevertheless, some characteristic deviations exist. They might reflect a reorientation of the reduced quinone in its binding pocket. It should be noted that the depicted geometry refers to the charge-separated state, $P_{700}^{+}A_1^{-}$, observed at low temperature, where forward electron transfer is partially blocked (Sétif et al., 1984; Schlodder et al., 1998).

IV. Conclusion

We have presented examples of recent HFEPR and multifrequency quantum beat studies of the electron transfer intermediates in PS I. These studies reveal new details of structure and function that could not be obtained without the enhanced spectral and temporal resolution, and sensitivity of these advanced spectroscopic techniques.

The results of careful measurements and analyses of the resolved *g*-tensors of the primary donor cation radical and excited triplet state show that their electronic structures differ from those of monomeric chlorophyll *a*. The observed differences cannot be explained by environmental effects. These observations can be interpreted either as (i) delocalization of the spin density of the unpaired electron between the two chlorophyll molecules of P_{700}^{+} or by (ii) trapping of the cation radical

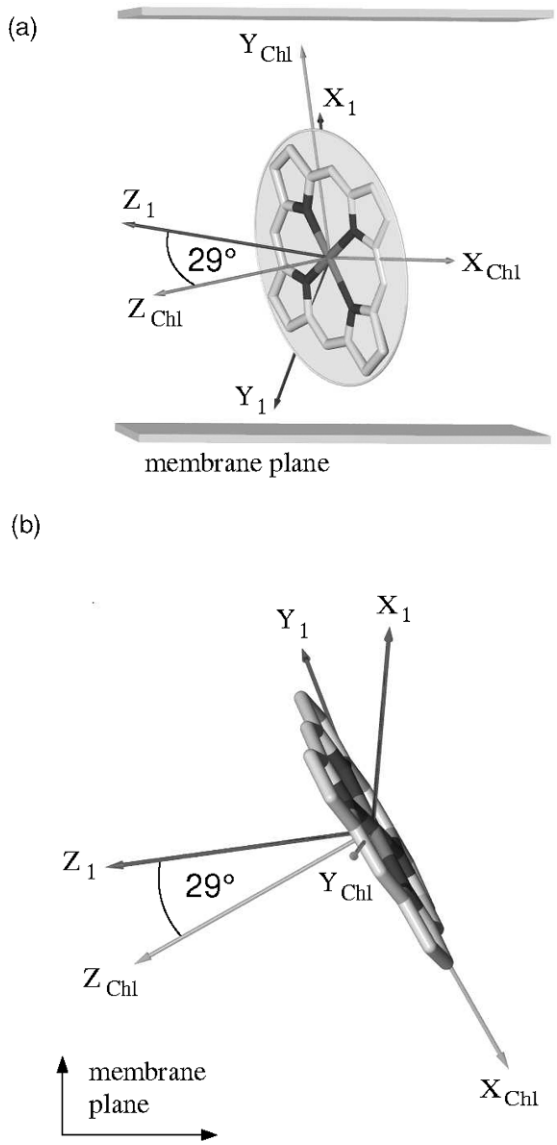

Fig. 13. Orientation of the g-tensor of the primary donor P_{700}^{+} in Photosystem I as determined by high time resolution multifrequency EPR, employing quantum beat oscillations and a magnetically aligned sample. For simplicity, we show only one of the two chlorophyll molecules, which carries the major part of the unpaired spin. (a) View direction parallel to the membrane plane. (b) View direction onto the membrane plane. $\mathbf{X}_1$, $\mathbf{Y}_1$, $\mathbf{Z}_1$ = principal axis system of the g-tensor of P_{700}^{+}. $\mathbf{X}_{chl}$, $\mathbf{Y}_{chl}$, $\mathbf{Z}_{chl}$ = chlorophyll-based reference system. The orientation of the chlorophyll molecule in the ($\mathbf{X}_{chl}$, $\mathbf{Y}_{chl}$) plane has been chosen according to a recent X-ray structure of Photosystem I at 2.5 Å resolution (Jordan et al., 2001).

state on a molecule different from nondistorted chlorophyll *a*. Multifrequency time-resolved EPR which includes HFEPR has made it possible to determine the structure of the transient charge-separated state $P_{700}^{+}A_1^{-}$ and its orientation in the thylakoid membrane.

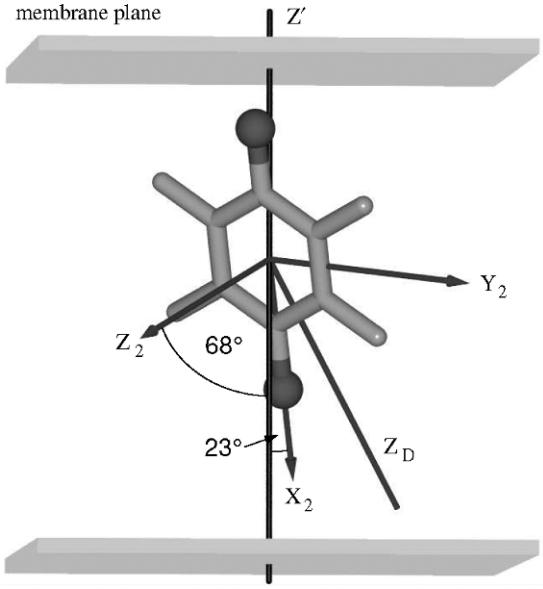

Fig. 14. Structural model for the reduced quinone acceptor A_1^{-} in Photosystem I as determined from low temperature transient EPR experiments, employing quantum beat oscillations and a magnetically aligned sample. The view direction is parallel to the membrane plane. $\mathbf{X}_2$ = quinone O–O axis. $\mathbf{Y}_2$ = phylloquinone long axis. $\mathbf{Z}_2$ = quinone plane normal. $\mathbf{Z}_D$ = symmetry axis of the dipolar tensor. $\mathbf{Z}'$ = membrane normal.

HFEPR studies are just beginning to have an impact on photosynthesis research, as the technique has only been widely accessible for the last few years. These new capabilities will continue to provide information that cannot otherwise be obtained. We have recently demonstrated in studies of purple photosynthetic bacteria that time-resolved high-field ENDOR on SCRPs has the potential to provide details of the electron transfer pathways in photosynthetic proteins (Poluektov et al., 2004). Application of this method to PS I may contribute to our understanding of the possible bidirectional electron transfer pathways in PS I (Brettel and Leibl, 2001 Shen et al., 2002; Cohen et al., 2004; Poluektov et al., 2005; Santabarbara et al., 2005). Thus, we expect that HFEPR techniques will significantly advance our understanding of the particular interactions in photosynthetic proteins that result in control and optimization of electron transfer leading to efficient charge separation.

Acknowledgments

We would like to acknowledge our coworkers whose contributions are essential for our HFEPR research of the photosynthetic systems: L. Utschig, J. Tang, S. Schlesselman, A. M. Wagner, G. Link, U. Heinen,

T. Berthold. Work at Argonne was supported by the U.S. Department of Energy, Office of Basic Energy Sciences, Division of Chemical Sciences, Geosciences, and Biosciences, under contract W-31-109-Eng-38 (ANL). GK acknowledges support by the DFG Priority Program "High-Field EPR in Biology, Chemistry and Physics" (SPP 1051).

References

Artz K, Williams JC, Allen JP, Lendzian F, Rautter J and Lubitz W (1997) Relationship between the oxidation potential and electron spin density of the primary electron donor in reaction centers from *Rhodobacter sphaeroides*. Proc Natl Acad Sci USA 94: 13582–13587

Bearden AJ and Malkin R (1972a) The bound ferredoxin of chloroplasts: a role as the primary electron acceptor of photosystem I. Biochim Biophys Res Comm 46: 1299–1305

Bearden AJ and Malkin R (1972b) Quantitative EPR studies of the primary reaction of photosystem I in chloroplasts. Biochim Biophys Acta 283: 456–468

Berthold T, Bechtold M, Heinen U, Link G, Poluektov O, Utschig L, Tang J, Thurnauer MC and Kothe G (1999) Magnetic field induced orientation of photosynthetic reaction centers as revealed by time-resolved W-band EPR of spin-correlated radical pairs. J Phys Chem B 103: 10733–10736

Bittl R and Kothe G (1991) Transient EPR of radical pairs in photosynthetic reaction centers: prediction of quantum beats. Chem Phys Lett 177: 547–553

Bittl R, van der Est A, Kamlowski A, Lubitz W and Stehlik D (1994) Time-resolved EPR of the radical pair $P_{865}^{+\cdot}Q_A^-$ in bacterial reaction centers. Observation of transient nutations, quantum beats and envelope modulation effects. Chem Phys Lett 226: 349–358

Blankenship RE (1981) Chemically induced magnetic polarization in photosynthetic systems. Acc Chem Res 14: 163–170

Bonnerjea J and Evans MCW (1982) Identification of multiple components in the intermediary electron carrier complex of photosystem I. FEBS Lett 148: 313–316

Borovykh IV, Kulik LV, Dzuba SA and Hoff AJ (2001) Selective excitation in pulsed EPR of spin-correlated radical pairs: electron–electron interactions, zero-, single-, and double-quantum relaxation and spectral diffusion. Chem Phys Lett 338: 173–179

Bratt PJ, Rohrer JK, Evans MCW, Brunel L-C and Angerhofer A (1997) Submillimeter high-field EPR studies of the primary donor in plant photosystem I P_{700}^+. J Phys Chem B 101: 9686–9689

Bratt PJ, Poluektov OG, Thurnauer MC, Krzystek J, Brunel L-C, Schrier J, Hsiao Y-W, Zerner M and Angerhofer A (2000) The *g*-factor anisotropy of plant chlorophyll $a^{\cdot+}$. J Phys Chem B 104: 6973–6977

Breton J (1974) The state of chlorophyll and carotenoid *in vivo*. II – a linear dichroism study of pigment orientation in photosynthetic bacteria. Biochim Biophys Res Comm 59: 1011–1017

Breton J, Nabedryk E and Leibl W (1999) FTIR study of the primary electron donor of photosystem I (P700) revealing delocalization of the charge in $P700^+$ and localization of the triplet character in ^{3}P700. Biochemistry 38: 11585–11592

Brettel K (1988) Electron transfer from A_1^- to an iron-sulfur center with $t_{1/2} = 200$ ns at room temperature in photosystem I. Characterization by flash absorption spectroscopy. FEBS Lett 239: 93–98

Brettel K and Leibl W (2001) Electron transfer in photosystem I. Biochim Biophys Acta 1507: 100–114

Buckley CD, Hunter DA, Hore PJ and McLauchlan KA (1987) ESR of spin-correlated radical pairs. Chem Phys Lett 135: 307–312

Budil DE and Thurnauer MC (1991) The chlorophyll triplet state as a probe of structure and function in photosynthesis. Biochim Biophys Acta 1057: 1–41

Carbonera D, DiValentin M, Corvaja C, Agostini G, Giacometti G, Liddell PA, Kuciauskas D, Moore AL, Moore TA and Gust D (1998) EPR investigation of photoinduced radical pair formation and decay to a triplet state in a carotene-porphyrin-fullerene triad. J Am Chem Soc 120: 4398–4405

Clayton RK and Straley SC (1972) Photochemical electron transport in photosynthetic reaction centers. IV. Observations related to the reduced photoproducts. Biophys J 12: 1221–1234

Closs GL, Forbes MDE and Norris JR (1987) Spin-polarized electron paramagnetic resonance spectra of radical pairs in micelles. Observation of electron spin–spin interactions. J Phys Chem 91: 3592–3599

Cohen RO, Shen G, Golbeck JH, Xu W, Chitnis PR, Valieva AI, van der Est A, Pushkar Y, and Stehlik D (2004) Evidence for asymmetric electron transfer in cyanobacterial photosystem I: Analysis of a methionine-to-leucine mutation of the ligand to the primary electron acceptor A_0. Biochemistry 43: 4741–4754

Commoner B, Townsend J and Pake GE (1954) Free radicals in biological materials. Nature (London) 174: 689–691

Commoner B, Heise JJ and Townsend J (1956) Light-induced paramagnetism in chloroplasts. Proc Natl Acad Sci USA 42: 710–718

Deisenhofer J, Epp O, Miki K, Huber R and Michel H (1984) X ray structure analysis of a membrane protein complex. Electron density map at 3 Å resolution and a model of the chromophores of the photosynthetic reaction center of *Rhodopseudomonas viridis*. J Mol Biol 180: 385–398

Dutton PL, Leigh JS and Seibert M (1972) Primary processes in photosynthesis: in situ ESR studies on the light induced oxidized and triplet state of reaction center bacteriochlorophyll. Biochim Biophys Res Comm 46: 406–413

Dutton PL, Leigh JS and Reed DW (1973) Primary events in the photosynthetic reaction centre from *Rhodopseudomonas sphaeroides* Strain R26: triplet and oxidized states of bacteriochlorophyll and the identification of the primary electron acceptor. Biochim Biophys Acta 292: 654–664

Dzuba SA, Gast P and Hoff AJ (1995) ESEEM study of spin–spin interactions in spin-polarised $P^+Q_A^-$ pairs in the photosynthetic purple bacterium *Rhodobacter sphaeroides* R26. Chem Phys Lett 236: 595–602

Ermler U, Fritzsch G, Buchanan SK and Michel H (1994) Structure of the photosynthetic reaction centre from *Rhodobacter sphaeroides* at 2.65 Å resolution: cofactors and protein-cofactor interactions. Structure 2: 925–936

Evans MCW and Cammack R (1975) The effect of the redox state of the bound iron-sulfur centers in spinach chloroplasts on the reversibility of P700 photooxidation at low temperatures. Biochim Biophys Res Comm 63: 187–193

Evans MCW, Telfer A and Lord AV (1972) Evidence for the role of a bound ferredoxin as a primary electron acceptor of

photosystem I in spinach chloroplasts. Biochim Biophys Acta 267: 530–537

Evans MCW, Reeves SG and Cammack R (1974) Determination of the oxidation-reduction potential of the bound iron-sulfur proteins of the primary electron acceptor complex of photosystem I in spinach chloroplasts. FEBS Lett 49: 111–114

Evans MCW, Sihra CK, Bolton J and Cammack R (1975) Primary electron acceptor complex of photosystem I in spinach chloroplasts. Nature (London) 256: 668–670

Feher G, Okamura MY and McElroy JD (1972) Identification of an electron acceptor in reaction centers of *Rhodopseudomonas sphaeroides* by EPR spectroscopy. Biochim Biophys Acta 267: 222–226

Feher G, Hoff AJ, Isaacson RA and Ackerson LC (1975) ENDOR experiments on chlorophyll and bacteriochlorophyll in vitro and in the photosynthetic unit. Ann NY Acad Sci USA 244: 239–259

Frank HA, McLean MB and Sauer K (1979) Triplet states in photosystem I of spinach chloroplasts and subchloroplast particles. Proc Natl Acad Sci USA 76: 5124–5128

Fuechsle G, Bittl R, van der Est A, Lubitz W and Stehlik D (1993) Transient EPR spectroscopy of the charge separated state P^+Q^- in photosynthetic reaction centers. Comparison of Zn-substituted *Rhodobacter sphaeroides* R-26 and photosystem I. Biochim Biophys Acta 1142: 23–25

Furrer R and Thurnauer MC (1983) Resolution of signals attributed to photosystem I primary reactants by time-resolved EPR at K band. FEBS Lett 153: 399–403

Gast P, Swarthoff T, Ebskamp FCR and Hoff AJ (1983) Evidence for a new early acceptor in photosystem I of plants; an ESR investigation of reaction center triplet yield and of the reduced intermediary acceptors. Biochim Biophys Acta 722: 163–175

Geacintov NE, van Nostrand F, Becker JF and Tinkel JB (1972) Magnetic field induced orientation of photosynthetic systems. Biochim Biophys Acta 267: 65–79

Golbeck JH and Bryant DA (1991) Photosystem I. Curr Top Bioenerg 16: 83–177

Grinberg OY, Dubinski AA, Shuvalov VF, Oranskii LG, Kurochkin VI and Lebedev YS (1976) Submillimeter ESR spectroscopy of free-radicals. Dokl Phys Chem (Engl Transl) 230: 923–928

Hasharoni K, Levanon H, Greenfield SR, Gosztola DJ, Svec WA and Wasielewski MR (1995) Mimicry of the radical pair and triplet states in photosynthetic reaction centers with a synthetic model. J Am Chem Soc 30: 8055–8056

Heinen U, Berthold T, Kothe G, Stavitski E, Galili T, Levanon H, Wiederrecht G and Wasielewski MR (2002) High time resolution Q-band EPR study of sequential electron transfer in a triad oriented in a liquid crystal. J Phys Chem A 106: 1933–1937

Heinen U, Poluektov O, Stavitski E, Berthold T, Ohmes E, Schlesselman SL, Golecki JR, Moro GJ, Levanon H, Thurnauer MC and Kothe G (2004a) Magnetic field induced orientation of photosynthetic reaction centers as revealed by time-resolved D-band EPR of spin-correlated radical pairs. II. Field dependence of the alignment. J Phys Chem B 108: 9498–9504

Heinen U, Golecki JR, Poluektov O, Berthold T, Schlesselman SL, Frezzato D, Ohmes E, Moro GJ, Thurnauer MC and Kothe G (2004b) Magnetic field induced orientation of photosynthetic reaction centers as revealed by time-resolved W-band EPR of spin-correlated radical pairs. Development of a molecular model. Appl Magn Reson 26: 99–115

Hoff AJ and Deisenhofer J (1997) Photophysics of photosynthesis. Structure and spectroscopy of reaction centers of purple bacteria. Phys Rep 287: 1–248

Hore PJ (1989) Analysis of polarized EPR spectra. In: Hoff AJ (ed) Advanced EPR, Application in Biology and Biochemistry, pp 405–440. Elsevier, Amsterdam

Jeschke G (1997) Electron-electron-nuclear three-spin mixing in spin-correlated radical pairs. J Chem Phys 106: 10072–10086

Jordan P, Fromme P, Witt HT, Klukas O, Saenger W and Krauß N (2001) Three-dimensional structure of cyanobacterial photosystem I at 2.5 Å resolution. Nature 411: 909–917

Kamlowski A, Zech SG, Fromme P, Bittl R, Lubitz W, Witt H-T and Stehlik D (1998) The radical pair state $P_{700}^+ A_1^-$ in photosystem I single crystals: orientation dependence of the transient spin-polarized EPR spectra. J Phys Chem B 102: 8266–8277

Käss H and Lubitz W (1996) Evaluation of 2D-ESEEM of the ^{15}N-labeled radical cations of the primary donor P700 in photosystem I and chlorophyll *a*. Chem Phys Lett 251: 193–203

Käss H, Fromme P, Witt HT and Lubitz W (2001) Orientation and electronic structure of the primary donor radical cation P_{700}^+ in photosystem I: a single crystals EPR and ENDOR study. J Phys Chem B 105: 1225–1239

Ke B, Hansen RE and Beinert H (1973) Oxidation-reduction potentials of bound iron-sulfur proteins of photosystem I. Proc Acad Sci USA 70: 2941–2945

Kiefer AM, Kast SM, Wasielewski MR, Laukenmann K and Kothe G (1999) Exploring the structure of a photosynthetic model by quantum-chemical calculations and time-resolved Q-band electron paramagnetic resonance. J Am Chem Soc 121: 188–198

Kim SS and Weissman SI (1979) Transient magnetization following photoexcitation, Rev Chem Intermed 3: 10–120

Kothe G, Weber S, Bittl R, Ohmes E, Thurnauer MC and Norris JR (1991) Transient EPR of light-induced radical pairs in plant photosystem I: observation of quantum beats. Chem Phys Lett 186: 474–480

Kothe G, Weber S, Ohmes E, Thurnauer MC and Norris JR (1994a) Transient EPR of light-induced spin-correlated radical pairs: manifestation of zero quantum coherence. J Phys Chem 98: 2706–2712

Kothe G, Weber S, Ohmes E, Thurnauer MC and Norris JR (1994b) High time resolution electron paramagnetic resonance of light-induced radical pairs in photosynthetic bacterial reaction centers: observation of quantum beats. J Am Chem Soc 116: 7729–7734

Kothe G, Bechtold M, Link G, Ohmes E and Weidner J-U (1998) Pulsed EPR detection of light-induced nuclear coherences in photosynthetic reaction centers. Chem Phys Lett 283: 51–60

Krabben L, Schlodder E, Jordan R, Carbonera D, Giacometti G, Lee H, Webber AN and Lubitz W (2000) Influence of the axial ligands on the spectral properties of P700 of photosystem I: a study of site-directed mutants. Biochemistry 39: 13012–13025

Krauß N (2003) Mechanisms for photosytems I and II. Curr Opin Chem Biol 7: 540–550

Lakshmi KV, Reifler MJ, Brudvig GW, Poluektov OG, Wagner AM and Thurnauer MC (2000) High-field EPR study of carotenoid and chlorophyll cation radicals in photosystem II. J Phys Chem B 104: 10445–10448

Lebedev YaS (1990) High-frequency continuous-wave electron spin resonance. In: Kevan L and Bowman MK (eds) Modern

Pulsed and Continuous-Wave Electron Spin Resonance, pp 365–404. Wiley, New York

Leigh JS and Dutton PL (1974) Reaction center bacteriochlorophyll triplet states: redox potential dependence and kinetics. Biochim Biophys Acta 357: 67–77

Link G, Berthold T, Bechtold M, Weidner J-U, Ohmes E, Tang J, Poluektov O, Utschig L, Schlesselman SL, Thurnauer MC and Kothe G (2001) Structure of the $P_{700}^{+}A_{1}^{-}$ radical pair intermediate in photosystem I by high time resolution multifrequency electron paramagnetic resonance: analysis of quantum beat oscillations. J Am Chem Soc 123: 4211–4222

Loach PA and Hall RL (1972) The question of the primary electron acceptor in bacterial photosynthesis. Proc Natl Acad Sci USA 69: 786–790

Lubitz W (1991) EPR and ENDOR studies of chlorophyll cation and anion radicals. In: Scheer H (ed) Chlorophylls, pp 903–944. CRC Press, Boca Raton, Florida

Mac M, Bowlby NR, Babcock GT and McCracken J (1998) Monomeric spin density distribution in the primary donor of photosystem I as determined by electron magnetic resonance: functional and thermodynamic implications. J Am Chem Soc 120: 13215–13223

MacMillan F, Rohrer M, Krzystek J and Brunel L-C (1998) A high-field/high-frequency EPR characterisation of the primary donor ($P^{+\cdot}$) in bacterial and plant photosynthetic reaction centres. In: Garab G (ed) Photosynthesis: Mechanisms and Effects, Vol II, pp 715. Kluwer Academic Publishers, Dordrecht

McIntosh AR and Bolton JR (1979) CIDEP in the photosystems of green plant photosynthesis. Rev Chem Intermed 3: 121–129

McIntosh AR, Chu M and Bolton JR (1975) Flash photolysis electron spin resonance studies of the electron acceptor species at low temperatures in photosystem I of spinach subchloroplast particles. Biochim Biophys Acta 376: 308–314

Möbius K (2000) Primary processes in photosynthesis: what do we learn from high-field EPR spectroscopy? Chem Soc Rev 29: 129–139

Morris AL, Snyder SW, Zhang Y, Tang J, Thurnauer MC, Dutton PL, Robertson DE and Gunner MR (1995) An electron spin polarization model applied to sequential electron transfer in iron-containing photosynthetic bacterial reaction centers with different quinones as Q_A. J Phys Chem 99: 3854–3866

Norris JR, Uphaus RA, Crespi HL and Katz JJ (1971) Electron spin resonance of chlorophyll and the origin of signal I in photosynthesis. Proc Natl Acad Sci USA 68: 625–628

Norris JR, Uphaus RA and Katz JJ (1975) ESR of triplet states of chlorophylls a, b, c_1, c_2 and bacteriochlorophyll a. Applications of ZFS and electron spin polarization in photosynthesis. Chem Phys Lett 31: 157–161

Norris JR, Morris AL, Thurnauer MC and Tang J (1990) A general model of electron spin polarization arising from the interactions within radical pairs. J Chem Phys 92: 4239–4249

Okamura MY, Isaacson RA and Feher G (1975) Primary acceptor in bacterial photosynthesis: obligatory role of ubiquinone in photoactive reaction centers of *Rhodopseudomonas sphaeroides*. Proc Natl Acad Sci USA 72: 3491–3495

Pauling L (1979) Diamagnetic anisotropy of the peptide group. Proc Natl Acad Sci USA 76: 2293–2294

Plato M, Krauß N, Fromme P and Lubitz W (2003) Molecular orbital study of the primary electron donor P_{700} of photosystem I based on a recent x-ray single crystal structure analysis. Chem Phys 294: 483–499

Poluektov OG, Utschig LM, Schlesselman SL, Lakshmi KV, Brudvig GW, Kothe G and Thurnauer MC (2002) Electronic structure of the P_{700} special pair from electron paramagnetic resonance spectroscopy. J Phys Chem B 106: 8911–8916

Poluektov OG, Utschig LM, Dubinskij AA and Thurnauer MC (2004) ENDOR of spin-correlated radical pairs in photosynthesis at high magnetic field: a tool for mapping electron transfer pathways. J Am Chem Soc 126: 1644–1645

Poluektov OG, Paschenko SV, Utschig LM, Lakshmi KV and Thurnauer MC (2005) Bidirectional electron transfer in photosystem I: direct evidence from high-frequency time-resolved EPR spectroscopy. J Am Chem Soc 127: 11910–11911

Prisner TF, McDermott AE, Un S, Norris JR, Thurnauer MC and Griffin RG (1993) Measurement of the *g*-tensor of the P_{700}^{+} signal from deuterated cyanobacterial photosystem I particles. Proc Natl Acad Sci USA 90: 9485–9488

Rustandi RR, Snyder SW, Feezel LL, Michalski TJ, Norris JR, Thurnauer MC and Biggins J (1990) Contribution of vitamin K_1 to the electron spin polarized signal in photosystem I. Biochemistry 29: 8030–8032

Rustandi RR, Snyder SW, Biggins J, Norris JR and Thurnauer MC (1992) Reconstitution and exchange of quinones at the A_1 site in photosystem I. An electron spin polarization electron paramagnetic resonance study. Biochim Biophys Acta 1101: 311–320

Rutherford AW and Mullet JE (1981) Reaction center triplet states in photosystem I and photosystem II. Biochim Biophys Acta 635: 225–235

Rutherford AW and Sétif P (1990) Orientation of P_{700}, the primary electron donor of photosystem I. Biochim Biophys Acta 1019: 128–132

Rutherford AW, Paterson DR and Mullet JE (1981) A light induced spin-polarized triplet detected by EPR in photosystem II reaction centers. Biochim Biophys Acta 635: 205–214

Salikhov KM, Bock CH and Stehlik D (1990) Time development of electron spin polarization in magnetically coupled, spin correlated radical pairs. Appl Magn Reson 1: 195–211

Salikhov KM, Kandrashkin Yu E and Salikhov AK (1992) Peculiarities of free induction and primary spin echo signals for spin-correlated radical pairs. Appl Magn Reson 3: 199–216

Santabarbara S, Kuprov I, Fairclough WV, Purton S, Hore PJ, Heathcote P and Evans MC (2005) Bidirectional electron transfer in photosystem I: Determination of two distances between P_{700}^{+} and A_{1}^{-} in spin-correlated radical pairs. Biochemistry 44: 2119–2128

Schlodder E, Falkenberg K, Gergeleit M and Brettel K (1998) Temperature dependence of forward and reverse electron transfer from A_{1}^{-}, the reduced secondary electron acceptor in photosystem I. Biochemistry 37: 9466–9476

Scholz F, Boroske E and Helfrich W (1984) Magnetic anisotropy of lecithin membranes. A new anisotropy susceptometer. Biophys J 45: 589–592

Sétif P, Mathis P and Vänngard T (1984) Photosystem I photochemistry at low temperature. Heterogeneity in pathways for electron transfer to the secondary acceptors and for recombination processes. Biochim Biophys Acta 767: 404–414

Shen G, Antonkine ML, van der Est A, Vassiliev IR, Brettel K, Bittl R, Zech SG, Zhao J, Stehlik D, Bryant DA, and Golbeck JH (2002) Assembly of photosystem I. II. Rubredoxin is required for the *in vivo* assembly of F_X in *Synechococcus* sp. PCC 7002 as shown by optical and EPR spectroscopy. J Biol Chem 277: 20355–20366

Sieckmann I, Brettel K, Bock C, van der Est A and Stehlik D (1993) Transient electron paramagnetic resonance of the triplet state of P_{700} in photosystem I: evidence for triplet delocalization at room temperature. Biochemistry 32: 4842–4847

Snyder SW and Thurnauer MC (1993) Electron spin polarization in photosynthetic reaction centers. In: Deisenhofer H and Norris JR (eds) The Photosynthetic Reaction Center, Vol 2, pp 285–329. Academic Press, New York

Snyder SW, Rustandi RR, Biggins J, Norris JR and Thurnauer MC (1991) Direct assignment of vitamin K_1 as the secondary acceptor A_1 in photosystem I. Proc Natl Acad Sci USA 88: 9895–9896

Sogo P, Jost M and Calvin M (1959) Free radical production in photosynthesizing systems. Radiat Res (Suppl I): 511–518

Stehlik D and Möbius K (1997) New EPR methods for investigating photoprocesses with paramagnetic intermediates. Ann Rev Phys Chem 48: 745–784

Stehlik D, Bock CH and Petersen J (1989) Anisotropic electron spin polarization in photosynthetic reaction centers. J Phys Chem 93: 1612–1619

Steinberg-Yfrach G, Rigaud J-L, Durantini EN, Moore AL, Gust D and Moore TA (1998) Light-driven production of ATP catalysed by F_0F_1-ATP synthase in an artificial photosynthetic membrane. Nature 392: 479–482

Stewart DH, Cua A, Chisholm DA, Diner BA, Bocian DF and Brudvig GW (1998) Identification of histidine 118 in the D1 polypeptide of photosystem II as the axial ligand to chlorophyll z. Biochemistry 37: 10040–10046

Stone AJ (1963) G-tensors of aromatic hydrocarbons. Mol Phys 7: 311–316

Svec WA (1978) The isolation, preparation, characterization, and estimation of the chlorophylls and the bacteriochlorophylls. In: Dolphin D (ed) The Porphyrins, Vol V, pp 341–399. Academic Press, New York

Tang J and Norris JR (1995) Multiple-quantum EPR coherence in a spin-correlated radical pair system. Chem Phys Lett 233: 192–200

Tang J, Thurnauer MC and Norris JR (1994) Electron spin echo modulation due to exchange and dipolar interactions in a spin-correlated radical pair. Chem Phys Lett 219: 283–290

Tang J, Utschig LM, Poluektov O and Thurnauer MC (1999) Transient W-band EPR study of sequential electron transfer in photosynthetic bacterial reaction centers. J Phys Chem B 103: 5145–5150

Thurnauer MC (1979) ESR study of the photoexcited triplet state in photosynthetic bacteria. Rev Chem Intermed 3: 197–230

Thurnauer MC and Gast P (1985) Q-band (35 GHz) EPR results on the nature of A_1 and the electron spin polarization in photosystem I particles. Photobiochem Photobiophys 9: 29–38

Thurnauer MC and Norris JR (1980) An electron spin echo phase shift observed in photosynthetic algae. Possible evidence for dynamic radical pair interactions. Chem Phys Lett 76: 557–561

Thurnauer MC, Katz JJ and Norris JR (1975) The triplet state in bacterial photosynthesis: possible mechanisms of the primary photo-act. Proc Natl Acad Sci USA 72: 3270–3274

Thurnauer MC, Rutherford AW and Norris JR (1982) The effect of ambient redox potential on the transient ESE signals observed in chloroplasts and photosynthetic algae. Biochim Biophys Acta 682: 332–338

Torrey HC (1949) Transient nutations in nuclear magnetic resonance. Phys Rev 76: 1059–1072

Trifunac AD and Norris JR (1978) Nanosecond time resolved EPR spectroscopy. EPR time profile via electron spin echo. CIDEP. Chem Phys Lett 59: 140–142

Trifunac AD and Thurnauer MC (1979) Time-resolved electron spin resonance of transient radicals. In: Kevan L and Schwartz RN (eds) Time Domain Electron Spin Resonance, Chapter 4, pp 107–152. John Wiley & Sons, New York

Trifunac AD, Thurnauer MC and Norris JR (1978) Submicrosecond time-resolved EPR in laser photolysis. Chem Phys Lett 57: 471–473

van der Est A, Prisner T, Bittl R, Fromme P, Lubitz W, Möbius K and Stehlik D (1997) Time-resolved X-, K-, and W-band EPR of the radical pair state P_{700}^{+} A_1^{-} of photosystem I in comparison with P_{865}^{+} Q_A^{-} in bacterial reaction centers. J Phys Chem B 101: 1437–1443

Vrieze J, Gast P and Hoff AJ (1996) Structure of the reaction center of photosystem I of plants. An investigation with linear-dichroic absorbance-detected magnetic resonance. J Phys Chem 100: 9960–9967

Warden JT (1978) Paramagnetic intermediates in photosynthetic systems. In: Berliner LJ and Reuben J (eds) Biological Magnetic Resonance, Vol 1, pp 239–275. Plenum, New York

Wasielewski MR (1995) Photogenerated spin-correlated radical ion pair in photosynthetic model systems. Spectrum 8: 8–12

Wasielewski MR, Norris JR, Crespi HL and Harper J (1981a) Photoinduced ESR signals from the primary electron donors in deuterated highly ^{13}C enriched photosynthetic bacteria and algae. J Am Chem Soc 103: 7664–7665

Wasielewski MR, Norris JR, Shipman LL, Lin C-P and Svec WA (1981b) Monomeric chlorophyll *a enol*: evidence for its possible role as the primary electron donor in photosystem I of plant photosynthesis. Proc Natl Acad Sci USA 78: 2957–2961

Wasielewski MR, Gaines III GL, O'Neil MP, Svec WA and Niemczyk MP (1990) Photoinduced spin-polarized radical ion pair formation in a fixed-distance photosynthetic model system at 5K. J Am Chem Soc 112: 4559–4560

Weber S, Ohmes E, Thurnauer MC, Norris JR and Kothe G (1995) Light-generated nuclear quantum beats: a signature of photosynthesis. Proc Natl Acad Sci USA 92: 7789–7793

Weber S, Kothe G and Norris JR (1997) Transient nutation electron spin resonance spectroscopy on spin-correlated racial pairs: a theoretical analysis of hyperfine-induced nuclear modulations. J Chem Phys 106: 6248–6261

Wiederrecht GP, Svec WA, Wasielewski MR, Galili T and Levanon H (1999) Triplet states with unusual spin polarization resulting from radical ion pair recombination at short distances. J Am Chem Soc 121: 7726–7727

Worcester DL (1978) Structural origins of diamagnetic anisotropy in proteins. Proc Natl Acad Sci USA 75: 5475–5477

Zech SG, Hofbauer W, Kamlowski A, Fromme P, Stehlik D, Lubitz W and Bittl R (2000) A structural model for the charge separated state $P_{700}^{+\cdot}$ $A_1^{-\cdot}$ in photosystem I from the orientation of the magnetic interaction tensors. J Phys Chem B 104: 9728–9739

Zouni A, Witt H-T, Kern J, Fromme P, Krauß N, Saenger W, and Orth P (2001) Crystal structure of photosystem II from Synechococcus elongatus at 3.8 Å resolution. Nature 409: 739–743

Zwanenburg G and Hore PJ (1993) EPR of spin-correlated radical pairs. Analytical treatment of selective excitation including zero quantum coherence. Chem Phys Lett 203: 65–74

Chapter 23

Transient EPR Spectroscopy as Applied to Light-Induced Functional Intermediates Along the Electron Transfer Pathway in Photosystem I

Dietmar Stehlik*
Fachbereich Physik, Freie Universität Berlin, Arnimallee 14, D-14195 Berlin, Germany

Summary

In the pursuit to understand biological function in fundamental processes such as photo-induced charge separation along a chain of electron carriers as in Photosystem I (PS I), detailed knowledge of protein-cofactor interactions is desired in real time. Today, every promising time resolved molecular spectroscopic method is scrutinized, adapted, and exploited to provide that knowledge. The primary processes in photosynthetic charge separation involve the sequential generation of paramagnetic intermediates in the form of radical ion pairs. Hence, magnetic resonance techniques are a specific method of choice and promise the most detailed insight into protein-induced molecular interactions. This chapter reviews the potential of transient EPR spectroscopy and its specific application to PS I. It

*Author for correspondence, email: stehlik@physik.fu-berlin.de

John H. Golbeck (ed): Photosystem I: The Light-Driven Plastocyanin:Ferredoxin Oxidoreductase, 361–386.

attempts to span the full range of processes from the initial generation of a correlated radical ion pair as a fundamental quantum physics phenomenon to the evaluation of essential magnetic interaction tensor parameters and their correlation to structural and dynamic properties of the specific protein-cofactor interactions in control of function. In particular, the detailed molecular information available on key interactions such as protein-induced hydrogen-bonding, π-stacking, and electrostatic interactions are collected for the quinone electron acceptor in PS I. Initial answers are at hand to essential functional questions, for example: how can similar and even identical quinone acceptors operate at vastly different redox levels in type I (PS I) and type II (pbRC and PS II) reaction centers? The interactive concerted use of the impressive toolbox of modern molecular biology, biochemistry, and spectroscopy provides the possibility of detailed tests at atomic detail in experiment and in theoretical analysis.

I. Introduction

Light-induced biological processes are of particular interest to spectroscopists because the kinetics as well as the structure, dynamics, and molecular characteristics can be accessed following pulsed laser excitation. Ideally, all transient intermediates in a sequence of reaction steps can be followed in real time. While optical spectroscopy is able to explore ultrashort kinetics down to the femtosecond range, other techniques, in particular magnetic resonance spectroscopy, yield significantly more information on the molecular and electronic structure of the intermediate states but with the drawback of a slower rising instrumental response function, typically suited for the 10 nsec kinetic range and longer. In addition, magnetic resonance spectroscopy requires paramagnetic intermediates for detection. However, they are native to many elementary biological processes. In particular, light-induced charge separation by electron transfer (ET) during the primary processes of photosynthesis is associated with a sequence of paramagnetic intermediates. The most commonly applied methods to follow the time course of these paramagnetic transient states are optical spectroscopy (mainly absorption difference and luminescence) and magnetic resonance spectroscopy. The disadvantage of a slower time resolution for the latter is compensated by the advantage that the spectra, as governed by the various magnetic interactions, contain in principle complete information on the molecular and electronic structure of the intermediates. In addition, multifrequency and multiple resonance techniques are available to increase the spectral resolution to determine the full set of parameters required to characterize the relevant magnetic interactions (Zeeman or ***g***-tensors, fine and hyperfine and quadrupole coupling tensors, dipolar and other intra- and intermolecular magnetic interactions, etc.).

The purpose of this chapter is to give an account of the main knowledge gathered thus far from the application of time resolved (transient as well as pulsed) TR EPR (electron paramagnetic or spin resonance) spectroscopy to Photosystem I (PS I) and how it has contributed (often in combination with a variety of advanced EPR and other spectroscopic techniques) to a better understanding of the cofactor-protein interactions that control function in PS I. The latter is the best characterized type I photosynthetic reaction center (RC), the only one for which an X-ray crystal structure at atomic detail is available. A comparison with the more extensively studied type II reaction center of purple bacteria (pbRC) and recently that of Photosystem II (PS II) is particularly attractive because in spite of similar cofactors in similar structural environments substantially different functional properties are realized. This includes very different redox potentials, even for identical cofactors, in the two types of reaction centers (RCs). With the advent of the first X-ray crystal structure at atomic detail for a type I RC [(Jordan et al., 2001), PDB code: 1JB0, and subsequent structure- and mutant-based studies)] these comparisons are now possible at a more advanced interpretive level. Many details of the differences in specific protein-cofactor interactions have emerged and can be correlated to differences in functional properties. In the case of the first quinone acceptor site, PS I appears to be the simpler RC to analyze for specific protein-cofactor interactions (a single dominant H-bond to the protein backbone, a strong π-stacking interaction, specific electrostatic interactions, etc.). It could well

Abbreviations: Chl – chlorophyll; CRP – correlated radical ion pair; CW – continuous wave; DD – direct detection (no magnetic field modulation); ESR/EPR – electron spin resonance/electron paramagnetic resonance; ESP – electron spin polarization; ENDOR – electron-nuclear double resonance; ESEEM – electron spin echo envelope modulation; ET – electron transfer; Hfc – hyperfine coupling; NQ – naphthoquinone; PS – photosystem; PhQ – phylloquinone or 2-methyl-3-phytyl-1,4-naphthoquinone or 2-methyl-3-(3,7,11,15-tetramethyl-2-hexadecenyl)-1,4-naphthalenedione; RC(s) – reaction center(s); RP – radical ion pair; pbRC – purple bacterial RC.

develop as the preferred system for tests of advanced theoretical models and as a guideline for the interpretation of the structurally better-resolved pbRC, which is a more complicated case due to the partly competing and compensating multiple protein-cofactor interactions present in type II RCs. These recently emerging aspects give added value to studies of PS I. Moreover, it is important to note that the X-ray structures generally concern structural details available for the ground state but that transient spectroscopies extend this knowledge to the functionally relevant transient states as they are occupied sequentially during the series of charge separation processes following initial pulsed light excitation. This chapter intends to highlight these recent developments.

The TR EPR techniques employed have not experienced fundamentally new developments since their introduction to the study of photochemical reactions. Therefore, reference to earlier reviews is quite appropriate, e.g., Stehlik et al. (1989). However, multifrequency capabilities have been expanded considerably, in particular, toward the high-frequency range up to several hundred GHz, and special pulsed EPR and multiple resonance techniques (see Jeschke et al., 1998; Prisner et al., 2001) have advanced at a rapid pace. Applications to PS I have been reviewed mostly up to the advent of the X-ray structural model at 2.5 Å resolution (e.g., Hoff and Deisenhofer, 1997; Stehlik and Möbius, 1997). More recent reviews include among others (van der Est, 2001; Möbius, 2003; Bittl and Weber, 2005). Plenty of new data have become available, in particular from TR EPR spectroscopy. With this new information, a consistent picture begins to emerge concerning key protein-cofactor interactions in control of function. At the same time, a number of instances of conflicting data exist from various experimental groups and these need to be sorted out. Concerning both aspects, a critical summary is intended in this chapter.

As a time resolved technique TR EPR spectroscopy inherently delivers kinetic information concerning the transient states under study. Kinetic data certainly provide an essential identifying property of the transient state to be characterized. Otherwise, however, kinetics will not be dealt with here, but separately in the following chapters of this book (see van der Est, this volume, Chapter 24). A controversially debated issue concerns the directionality of electron transfer (ET) in PS I (see Redding and van der Est, this volume, Chapter 25). The arrangement of two quasi C_2 symmetric branches, with three acceptors each (A_{-1}, A_0, and A_1)$_{A/B}$ connecting the common excited primary donor $^*P_{700}$ near the lumen with the centrally located terminal Fe/S cluster F_X, followed by F_A and F_B on the stromal side of the membrane, neither offers a structural nor functional hint for uni-directional ET as encountered in type II RCs. For the latter, the functional requirement of double reduction (and protonation) of the terminal acceptor, the secondary quinone, Q_B, and thus the need of two successive electron transfer processes from the donor P via the one-electron gate, the primary quinone, Q_A, to the Q_B site can only be fulfilled with uni-directional electron flow along the A-branch. As a consequence, the directionality of ET is an issue of functional significance in type II RCs but not in PS I. Hence, in this chapter, the directionality issue plays only an indirect role in branch-identification. Otherwise, this chapter focuses on protein-cofactor interactions in active intermediates and their functional significance in sequential ET processes.

II. Materials and Methods

A. Material Aspects

Transient or time resolved (TR) EPR spectroscopic results presented in this chapter concern PS I preparations from cyanobacterial systems. For protocols and sample characterization specific reference will be given to the relevant literature. Note that the best available type I X-ray crystal structure at atomic detail (1JB0) concerns PS I from *Thermosynechococcus elongatus*, while the best developed mutagenesis systems concern different species, but with high sequence similarity: *Synechocystis* sp. PCC 6803 and *Synechococcus* sp. PCC 7002. Another well-developed mutagenesis system derives from the eukaryotic algae *Chlamydomonas reinhardtii*. Transient spectroscopy data for the latter system will be compared in the concluding paragraph.

Detailed molecular structures of the relevant cofactors are found in the PS I review literature. The bulk of the TR EPR results presented in this chapter concerns the first quinone acceptor site in PS I. For convenience, Fig. 1 collects the molecular structures and axes of the native quinones found in the three best characterized RCs. Note that in addition to the native PhQ, the other two quinones have been shown to function when reconstituted into the A_1 site of PS I.

B. TR EPR Techniques

Standard steady state continuous wave (cw) EPR techniques have been used early on to follow (slow) concentration changes of paramagnetic intermediates during

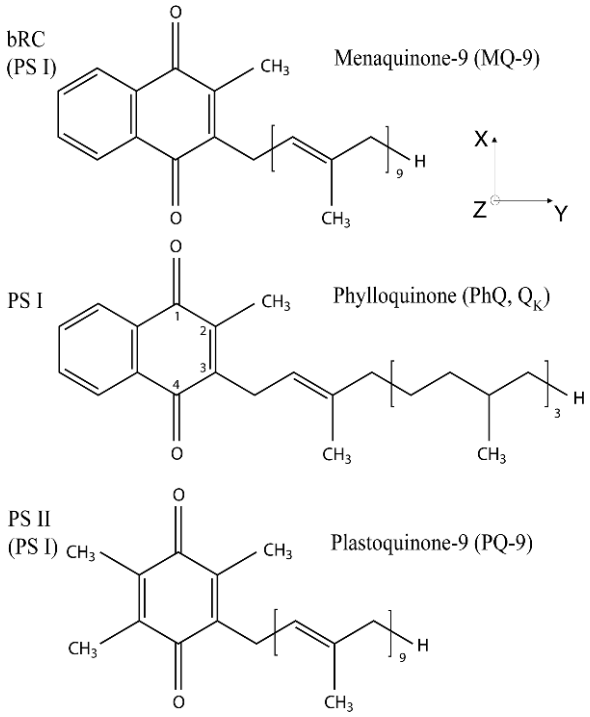

Fig. 1. Molecular structure and molecular axes of native quinones used as first electron acceptors in the three most thoroughly studied photosynthetic reaction centers. The *middle* one (PhQ) is the native quinone in the $A_1(Q_K)$ site of Photosystem I (PS I). The *top* one (MQ-9) and *bottom* one (PlQ-9) are the native quinones in the Q_A site of type II RCs of purple bacteria (*Rhodopseudomonas viridis*, top) and of Photosystem II (bottom). The C–O bond direction, i.e., the short in-plane axis of naphthoquinone (NQ) is defined as $\mathbf{x}_Q$, the other (long) in-plane as $\mathbf{y}_Q$ and the out-of-plane axis as $\mathbf{z}_Q$. The numbering in the quinone ring has the methyl group in the ring position 2 while the tail is in position 3.

the course of photochemical processes. The usual magnetic field modulation, applied together with phase sensitive narrow band detection for increased sensitivity, has an inherent time resolution corresponding to roughly the inverse of the modulation frequency (commonly 100 kHz in commercial instruments). Increased modulation frequency (up to several MHz), with its unavoidable trade-off in sensitivity, has also been used to push the time resolution into the μsec range. In the case of photoprocesses, additional modulation of the exciting light intensity was recognized to provide the decisive advantage of discriminating against all light-independent paramagnetic impurities. To go the next step in time resolution, field modulation and the sensitivity advantage that accompanies it, had to be abandoned. Direct detection (DD) of the transient (TR) EPR signal at a fixed magnetic field in response to a sufficiently "sudden" exposure of spin magnetization to a resonant microwave (mw) field in combination with a fast data acquisition system is the simplest extension of standard cw EPR instrumentation. In fact, the method was introduced, fully analyzed as well as experimentally demonstrated, in the very first years of nuclear magnetic resonance (NMR) by Torrey, in 1949. With the advent of Fourier-transform spectroscopy, the method lost practical importance in NMR. In comparison, it is still of interest in EPR as reviewed previously (Stehlik et al., 1989). The main reasons for this assessment are restated here:

(i) In the case of photoreactions, the requirement of a fast turn-on of the microwave (mw) field (usually associated with unavoidable problems of electronic ringing and instability) is by-passed elegantly because the paramagnetic intermediates of interest can be generated suddenly by a short laser pulse. Therefore, the light-induced paramagnetic species, and only those, experience suddenly the mw field, which can be operated continuously, and this is obviously equivalent to the sudden turning on of a mw field in the normal Torrey experiment.

(ii) Photoreactions and light-induced charge separation in photosynthetic RCs in particular are associated with characteristic electron spin polarization (ESP) (for further details see below and van der Est, this volume, Chapter 24). The accompanying signal-enhancement factor largely compensates for the loss of sensitivity by broadband detection required for fast time resolution.

(iii) As a key advantage in the EPR regime, the signal rise time turns out to be independent of the mw field strength if it is determined by the inverse linewidth. Because broad lines are rather the rule than the exception in EPR, which is particularly true in frozen solution or large protein complexes, time resolution is mainly limited by the instrumental rise time (on the order of 10 nsec).

The basics of the transient EPR technique have not changed a lot since the previous review (Stehlik et al., 1989). The application to light-induced processes has the important advantage that cw microwave irradiation of standard EPR instrumentation can be used. The "sudden" turn-on of the microwave field is replaced by the equivalent "sudden" generation of spin magnetism by a light pulse. The time dependence of the

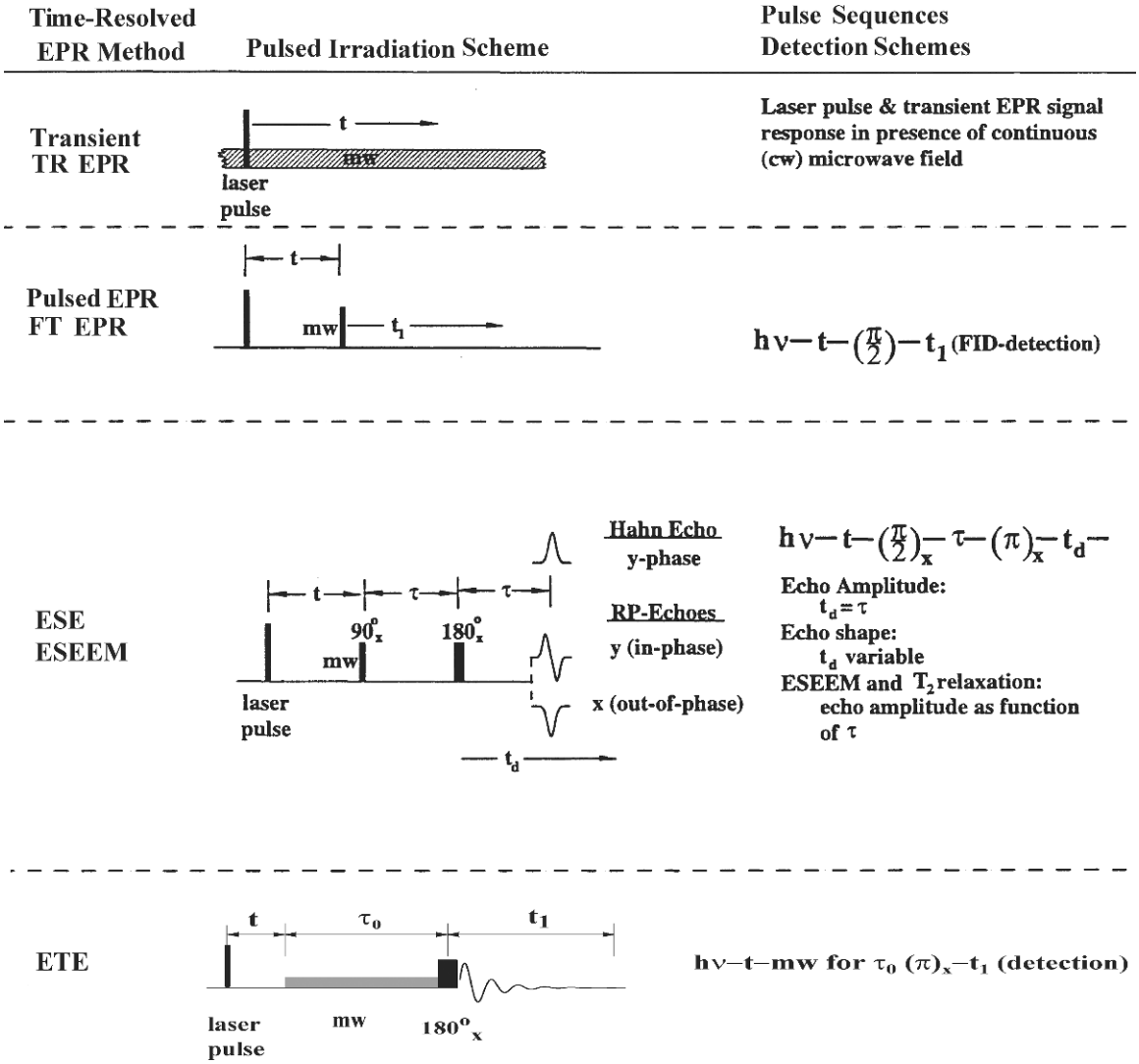

Fig. 2. Microwave (mw)-irradiation schemes of commonly used time resolved EPR (TR EPR) techniques as applied to the study of photoactive proteins. The initial laser excitation pulse sets the common time zero reference. See text for description and references of the various selected mw-irradiation schemes.

transient EPR signal is followed as a function of time *t* after the laser pulse, see Fig. 2, first line, and stored in, for instance, a transient recorder. In addition to improvements in the resonator design and detection electronics, progress has been achieved in the recent years in the extension of the TR EPR technique to high field/high frequency, see contributions in Grinberg and Berliner (2004). As experienced in the development of NMR decades ago, the pulse methods begin to dominate the EPR field as well. Figure 2 includes a couple of pulsed irradiation schemes: the Fourier-transform (FT) EPR and the electron spin echo (ESE) technique. A decisive advantage of such pulse EPR techniques is their ability to extent readily to multiple resonance techniques. The radiation field-free intervals between the pulses or between pulse and echo offer the possibility to introduce an irradiation interval for an additional microwave (mw) or radio frequency (rf) field and thus exploit the increased spectral resolution of electron-electron (ELDOR) or electron-nuclear double resonance (ENDOR) methods. The expanding range of these advanced pulse schemes is presented elegantly in Schweiger and Jeschke (2001). It includes the hybrid extended time excitation (ETE) scheme depicted in the bottom line of Fig. 2. The time incremental data collection of an ESE envelope modulation (ESEEM) is

replaced for ETE by a continuous refocusing scheme. This selection of time resolving EPR techniques in Fig. 2 includes essentially all methods applied to study the primary processes in photosynthetic reaction centers.

C. Concept of the Correlated Radical Ion Spin Pair (CRP) Mechanism

The primary process of charge separation starts with light excitation of the primary donor P from its diamagnetic ground state to an excited singlet state *P. The most efficient decay process is electron transfer (ET) to a series of acceptors (A_n), i.e., generation of a series of radical ion spin pair $P^{\cdot+}A_n^{\cdot-}$ states. The transferred electron adds an electron to the acceptor A (reduces it) and leaves a hole at the donor P (oxidizes it). This hole state is associated with a now unpaired partner electron at P. According to the Pauli principle, this electron spin of $P^{\cdot+}$ and the one transferred to $A_n^{\cdot-}$ are strictly anticorrelated. The first RP state is typically generated on a psec time scale and will remain correlated until individual spin relaxation (μsec time scale) sets in as a result of interaction of each electron spin with its respective surrounding. Depending on the time scale after a fast (sub-psec) laser pulse initiation of the CRP a series of spin dynamics phenomena can evolve. They are briefly mentioned here to the extent they may be useful for a better insight into the functional details of the photosynthetic primary processes.

1. Relation to Basic Quantum Physics Experiments

At first sight it appears to be of purely academic interest, but at its origin CRP generation includes all aspects of the famous Einstein-Podolsky-Rosen–Gedanken experiment of 1935 based on a correlated two-particle concept. Indeed, if charge separation occurs on a time scale fast compared to that associated with the inter RP spin interaction, it is a straightforward example of Bohm's spin version (Bohm, 1951), also cited with brilliant analysis in Bell (1993). For actual experiments with correlated photon systems see reviews such as Zeilinger (1999). As a key feature correlated particles in an entangled quantum state may be separated over large distances and thus open intriguing experimental test cases for the foundations of quantum physics. Indeed, photosynthetic charge separation separates correlated electron spins over some distance, albeit only the thickness of a bilayer membrane (order of 3 nm). In spite of several speculations, there is no experimental indication that entangled states are used for functional purposes in photosynthesis neither in excitation energy transfer nor in charge separation. However, the potential of quantum teleportation of arbitrary quantum state information across a bilayer membrane with the help of the CRP generated efficiently by the primary process of charge separation in a natural membrane spanning photosynthetic RC complex (such as PS I) is an intriguing idea. Arbitrary input quantum state information could be encoded via an auxiliary spin center placed near the primary donor. If this auxiliary spin is designed to recombine with the $P^{\cdot+}$ radical ion of the CRP (which includes the selection rule of just singlet state recombination), the initially encoded quantum information on the auxiliary spin is instantly encoded also on the correlated $A_n^{\cdot-}$ radical ion state. Thus it can be decoded at the other side of the membrane by a refocusing pulse at the $A_n^{\cdot-}$-specific resonance frequency. Quantum information would be teleported across a membrane.

2. Observed Phenomena: Electron Spin Polarization (ESE) and Quantum Beats

The CRP state discussed thus far is that of a pair of strictly correlated, spatially separated, and noninteracting spins. With the onset of the weak magnetic interactions between the separated CRP spins and with the respective protein environment, these characteristic initial CRP features are lost. The time scale is given by the inverse of such interactions in frequency units, typically of the order of nsec or faster, too fast for direct TR EPR detection. However, now the weakly interacting RP, still populated only in the initial noneigenstate (singlet state) has to evolve into the eigenstates of the acting spin Hamiltonian. The corresponding spin dynamics has been worked out at various levels of sophistication. An early review (Hore, 1989) focuses on the explanation of the experimentally observable spin polarized transient EPR spectra in real photosynthetic RCs. In addition, electron and nuclear coherences have been analyzed and observed as a result of the spin dynamics due to the time evolution of singlet-triplet spin state mixing (Salikhov et al., 1990; Bittl and Kothe, 1991; Kothe et al., 1991; Bittl et al., 1994; Kothe et al., 1994). At this stage the understanding of the various spin dynamics phenomena was a prime research issue. Additional motivation came from their potential for more and independent experimental details on structure-function relations to advance the understanding of the mechanisms at work during photosynthetic charge separation.

Useful algorithms have been developed for the simulation of both the quantum beat as well as the spin polarization phenomena. Convenient summary descriptions and in particular sets of the relevant interaction parameters for PS I are found for instance in Zech et al. (2000), Link et al. (2001), and Salikhov et al. (2002a,b). The latter reference includes transient effects due to a third observer spin present during the time evolution of the CRP. Another important extension concerns the treatment of consecutive CRPs as they may occur in sequential ET steps in RCs (Tang et al., 1999; Kandrashkin et al., 2002; Salikhov et al., 2003).

Following this survey of the more advanced efforts to simulate observable spin polarized CRP spectra, for the benefit of the less spectroscopy-oriented reader Fig. 3 collects a few plausible arguments and facts to introduce the origin of the electron spin polarization (ESP) pattern in TR EPR spectra as they are actually observed for the $P^{\cdot+}A_1^{\cdot-}$ state of PS I (see results). The four energy levels scheme shown in Fig. 3 (top) represents a two spin 1/2 system with a spin Hamiltonian reduced to just the two Zeeman energies of the two spins with different Larmor frequencies $g_i\beta B_0$ and the inter spin coupling composed of exchange (main parameter J) and dipolar coupling (D). The four (partially allowed) EPR transitions are indicated as arrows connecting the energy levels in Fig. 3 (top). The four transition frequencies are given in the middle part of Fig. 3 and are arranged as a stick spectrum (left) showing the resonance positions (ω_{ij}) on a magnetic field or g-factor scale. For weak (fixed) inter spin coupling, $2(J - d) \ll \Delta g$, the transitions group in pairs around the resonance Zeeman positions $g_i\beta B_0$. Because only the two middle levels in Fig. 3 (top) have singlet character and therefore can be populated during CRP generation, the pair of lines around $g_i\beta B_0$ must be oppositely polarized as indicated by negative (E for emissive) and positive (A for absorptive) line intensity. Finally, each of the resonance positions $g_i\beta B_0$ has to be spread out on the spectral scale according to the **g**-tensor anisotropy assuming a statistical distribution of orientations of the **g**-tensor axes with respect to the external magnetic field B_0. This corresponds to the typical sample case of a liquid (or frozen) solution of photosynthetic RCs. Some inhomogeneous broadening is added using a Gaussian line shape with orientation independent linewidth. With the appropriate choice of the relevant interaction parameters the four pairwise oppositely polarized contributions (Fig. 3, bottom A) add up to the observable TR EPR pattern B. This calculated spectral pattern simulates well the actually observed ESP pattern of the $P^{\cdot+}A_1^{\cdot-}$ state of fully deuterated PS I at high field/high frequency (95 GHz) (Zech et al., 2000). Successful simulation of the measured TR EPR spectral patterns and their time development is the basis for the subsequent interpretation in terms of structural and functional conclusions as described in the next section for selected experimental results.

III. Experimental Results in Photosystem I

A. The Earliest TR EPR Studies of Paramagnetic Intermediates in PS I

The very first light-induced EPR signal observed in photosynthetic material (chloroplasts) was reported in the early seventies (Dutton et al., 1972) and turned out to be due to PS I. Standard cw EPR was used, but with the significant modification of adding modulation of the exciting light intensity. Phase-sensitive detection with respect to the light-modulation frequency assured selective observation of only the light-induced paramagnetic states that contribute to the signal intensity and varied in population together with the modulated light intensity. Steady state (light-independent) paramagnetic species (also those with lifetimes long compared to the inverse light-modulation frequency) will not contribute to the signal intensity. In this manner, these early results qualify as the first (slow time resolution) TR EPR observation of PS I.

The observed signal could be identified as the triplet state $^3P_{700}$ of the primary donor in PS I. The zero-field splitting parameters correspond to those of a chlorophyll (Chl) species. The signal-to-noise for ^3P detection was significantly increased by the occurrence of light-induced spin polarization. The relevant spin polarization mechanism provided a unique signature to identify the observed ^3P state as a recombination product of the primary charge separated radical ion pair state, provided further electron transfer is inhibited or blocked. With this original discovery, ^3P EPR spectroscopy was introduced as a versatile tool to probe the electronic structure and molecular environment of the primary donor Chl in photosynthetic RCs (reviewed in Budil and Thurnauer, 1991; Angerhofer and Bittl, 1996). With the help of highly oriented thylakoid membranes, it was possible to locate the low temperature recombinant $^3P_{700}$ state on one Chl half of the P_{700} Chl dimer (Rutherford and Sétif, 1990). Thermal

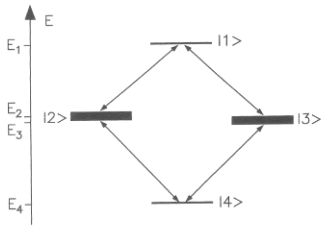

energies (in freq. units)

$E_1 = \omega_0 - (J - d)/2$

$E_2 = \Omega + (J - d)/2$

$E_3 = -\Omega + (J - d)/2$

$E_4 = -\omega_0 - (J - d)/2$

parameters

$\omega_0 = 1/2\,(g_1 + g_2)\beta B_0$

$\Delta\omega = 1/2\,(g_1 - g_2)\beta B_0$

$d = 1/3\,D\,(3\cos^2\vartheta - 1)$

$\Omega^2 = \Delta\omega^2 + (J + d/2)^2$

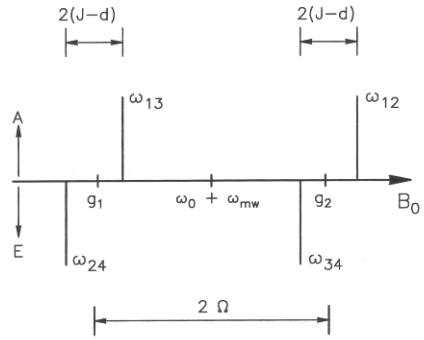

transition frequencies

$\omega_{12} = E_1 - E_2 = \omega_0 - (J - d) - \Omega$

$\omega_{34} = E_3 - E_4 = \omega_0 + (J - d) - \Omega$

$\omega_{13} = E_1 - E_3 = \omega_0 - (J - d) + \Omega$

$\omega_{24} = E_2 - E_4 = \omega_0 + (J - d) + \Omega$

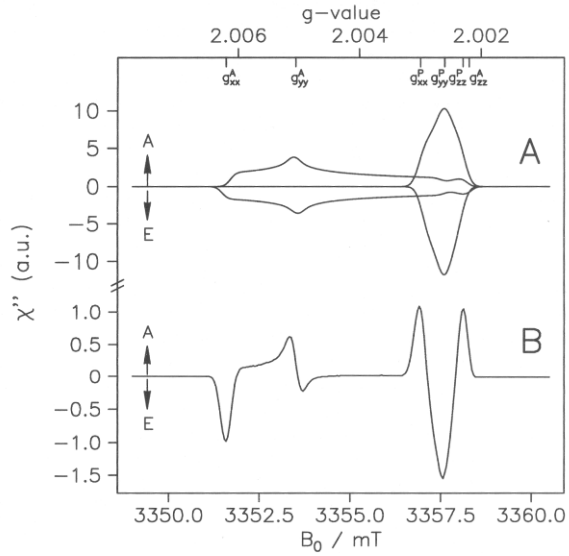

Fig. 3. Essential elements of the correlated radical pair (CRP) electron spin polarization (ESP) mechanism. *Top*: energy level scheme of a weakly coupled two spin 1/2 system. The double arrows indicate the possible single quantum transitions. The CRP is generated as pure singlet state; hence initial population is only in the middle levels (heavy energy level bars). The key parameters determining the energies are the average Zeeman frequency ω_0 and the difference $\Delta\omega$ between the two radical Zeeman frequencies. The interaction between the radical spins is exchange (J) and dipolar coupling (d). With $\Delta\omega$ they determine the singlet–triplet mixing frequency Ω. *Middle*: transition intensities and resonance positions as a "stick spectrum" on a magnetic field (B_0) or *g*-parameter or frequency (ω) scale at the four possible transition frequencies given at the right side. A fixed set of interaction parameters g_1, g_2, J, and d is assumed with weak coupling $2(J - d) \ll \Delta g$; a pair of oppositely polarized transition groups around each of the resonance positions g_1 and g_2. *Bottom*: statistical distribution of all orientations with respect to the fixed magnetic field B_0 is assumed for powder spectra (top) of each of the four transitions (middle spectrum) according to the g-tensor anisotropies indicated by the g-tensor principal *g*-values for acceptor (A) and donor (P) at the top, magnetic field scale at the bottom. The sum of the four contributions (bottom) corresponds to a simulation of the actually observed TP EPR spectrum of the $P_{700}^{+\cdot}\,A_1^{-\cdot}$ state of deuterated PS I.

delocalization over the two dimer halves was observed at ambient temperatures (Sieckmann et al., 1993).

Improved time resolution with directly detected (DD) EPR or pulsed EPR led to the observation of additional light-induced transient EPR spectra with their own characteristic spin polarization patterns (for an early review see Hoff, 1984). In clear contrast to the wide triplet spectra mentioned previously, these spectra are confined to a narrower magnetic field range around g = 2, which is typical for organic radical ions. Comparison of EPR data at different field/frequencies (Furrer and Thurnauer, 1983) provided clear evidence for characteristic g-anisotropy in these spectra and thus for a contribution of a reduced quinone acceptor in the electron transfer chain of PS I. Given the fact that even the existence of quinone as an electron acceptor in PS I was questioned in the early 1980s from biochemical data, see, e.g., Evans and Nugent (1993) such TR EPR results for functional charge-separated states were significant and, together with optical and cw EPR studies, provided ample evidence for the identification of a quinone as the A_1 acceptor in PS I (reviewed in Golbeck 1987; Stehlik et al., 1989).

At the time of the earliest TR EPR results with either direct detected EPR (Blankenship et al., 1975) or pulsed EPR (Thurnauer and Norris, 1980), possible mechanisms for the origin of the observed spin polarization pattern were suggested but not yet fully quantified. The quantitative correlated radical ion pair (CRP) concept (briefly outlined in II. C) was first used to explain the spin polarized EPR spectra associated with light-induced radical pair generation in micelles (Buckley et al., 1987; Closs et al., 1987). On the basis of the CRP concept, the TR EPR spectra observed in PS I up to this point could be simulated and interpreted satisfactorily by the end of the 1980s (for reviews see Stehlik et al., 1989; Hore, 1989). The next stage of TR EPR studies pursued mainly two aims: first, to confirm the CRP concept in more detail and in all its aspects; second, to achieve reliable simulations of the observed spectral patterns with the aim of obtaining relevant structural and dynamic information on the RC under investigation. Independent information on as many relevant magnetic interaction tensor parameters as possible was needed. Only this way, critical PS I-specific structural (dipolar coupling and relative tensor orientations) and kinetic information could be extracted from the simulated spectra. This program focused mainly on the functional charge separated $P_{700}^{+}A_1^{-}$ state because it is directly accessible by TR EPR studies in native PS I under physiological conditions. In particular, the next section emphasizes what independent structural information could be obtained from TR EPR results prior (BC) to the first X-ray crystal structure at atomic detail (Jordan et al., 2001). As in other cases of membrane proteins, the latter event represented a turning point in PS I research as well.

B. Experimental Confirmation of the CRP Concept and EPR Structure Model for $P_{700}^{+}A_1^{-}$

The time range for the appearance and decay of the $P_{700}^{+}A_1^{-}$ charge-separated radical ion pair state following light-pulse excitation was reported in the late 1980s to have the following limits: less than 100 psec for the rise time, and a few 100 nsec for the lifetime at ambient temperature [for a review concerning the results of sub-nsec and nsec resolution optical absorption difference spectroscopy in the blue (380 nm), considered to be most sensitive to A_1^{-} reduction and reoxidation, see Brettel, 1997]. This putative time range combines decisive advantages for TR EPR detection in real time. (1) The sub-100 psec rise time is clearly much faster than the inverse of the relevant magnetic interaction terms (order of 1 GHz or 1 $nsec^{-1}$) and assures that no spin dynamics (singlet-triplet mixing) occur prior to $P_{700}^{+}A_1^{-}$ formation. As a consequence, the $P_{700}^{+}A_1^{-}$ state is born as a pure singlet radical ion pair state. A well-defined initial condition exists. However, it should be mentioned that the time range in which spin dynamics mixes singlet and triplet to various degrees, between the two extremes of <0.5 nsec (pure singlet state) and >5 nsec (complete singlet-triplet mixing), offers another kinetic window for (indirect) TR EPR detection because the ESP pattern of the $P_{700}^{+}A_1^{-}$ state varies with the lifetime of the precursor RP state (see section II and experimental example in section III.3). (2) A lifetime of the $P_{700}^{+}A_1^{-}$ state of several hundred nsec is conveniently long compared to the instrumental rise time (typically 10-50 nsec) and falls in the middle of the direct TR EPR observation time window, which is limited at long times by the spin relaxation time (a few μsec to several hundred μsec depending on temperature and other sample conditions). An observation time of about 100 nsec or longer simplifies the analysis. Not only has singlet-triplet mixing been completed, also spin coherence effects have died out and phase relaxation has taken place. Therefore, reaction kinetics and/or spin relaxation determine the time course of the TR EPR signal intensity of the $P_{700}^{+}A_1^{-}$ state.

Compared to other RCs these favorable conditions for TR EPR detection are unique to PS I. The presence of a non-heme iron (Fe^{2+}) near the quinone acceptors in

type II RCs, and with it the presence of an efficient spin polarization relaxer, suppresses TR EPR detectability of the corresponding $P^+Q_A^-$ state in native type II RCs. Conversely, the absence of such a relaxer in PS I does not only allow full access to the $P_{700}^{\cdot+}A_1^{\cdot-}$ state kinetics within the TR EPR observation time window, but the suppression of any competing signals from type II RCs permits TR EPR studies of PS I in whole cells, algae, or thylakoid membrane fragments without the need of isolation and purification of PS I.

Comparable TR EPR studies for type II RCs require the replacement of the non-heme iron by a diamagnetic ion such as Zn^{2+} (or others). This is the reason why detailed TR EPR characterization of charge separated P^+Q^- states started out with application to PS I. The requirement of a substantial biochemical modification caused a delay of TR EPR studies in the pbRC. On the other hand, spectroscopic results for pbRC (and comparable type II RCs) could be interpreted at a much more advanced level because an X-ray crystal structure at atomic detail existed for the pbRC since 1985 (for a review see Hoff and Deisenhofer, 1997).

With the CRP concept, the first satisfactory simulations of the spin polarization patterns of the $P_{700}^{\cdot+}A_1^{\cdot-}$ state were achieved (Bock et al., 1989; reviewed in Chapters 12 and 11 in Hore, 1989; Stehlik et al., 1989). Some key structural properties could be determined for the A_1 site. Note that this concerns the functional charge separated $P_{700}^{\cdot+}A_1^{\cdot-}$ state. The most detailed structural information comes from the relative orientations of the **g**-tensors $\mathbf{g}(P_{700}^{\cdot+})$, $\mathbf{g}(A_1^{\cdot-})$, and the dipolar coupling tensor between the two radical pair (RP) spins, mainly its principal axis $\mathbf{z}_D$ connecting the donor and acceptor spin density centers. Initially, appropriate accuracy was obtained for one specific structural piece of information: the g_{xx} (A_1^-) axis (essentially the quinone molecular axis along the C–O bonds) and the dipolar axis z_D are nearly parallel. Note that this early structural assessment has not required any further refinement. On the other hand, this particular property could not be revealed in the earlier X-ray structure studies; only the latest structural model (1JBO) at 2.5 Å resolution (Jordan et al., 2001) was able to confirm it.

Another early result is worth noting. Recall that TR EPR records both spectral and time resolved information within the same data set. Thus, the kinetics of the ET step from A_1^- to the first Fe/S cluster and the structural properties inherent in the spectral patterns of the $P_{700}^{\cdot+}A_1^{\cdot-}$ state are directly correlated. This applies in particular to native PS I in normal aqueous medium and under physiological conditions at ambient temperature during which TR EPR can be applied (Bock et al., 1989). Within experimental accuracy the ET kinetics do not deviate from a single exponential, in agreement with parallel kinetic studies with nsec optical difference spectroscopy in the UV on the same samples (Brettel, 1988). From these early results until the present, structural details as well as magnetic interaction parameters were obtained as a unique set of values. In combination with single exponential ET kinetics, this is a strong indication that only a single $P_{700}^{\cdot+}A_1^{\cdot-}$ state was observed, in contrast to a superposition of two states as expected from inequivalent A_1 sites for each of the C_2 symmetric branches of cofactors.

While it is satisfying that basic initial structural and kinetic PS I properties from TR EPR turned out to be correct, the emphasis of further spectroscopic studies was equally on confirming the CRP concept including additional dynamic aspects and the extraction of complete sets of principal values and orientational parameters of additional magnetic interaction tensors. These data were substantially refined in the 1990s. Advances in TR EPR techniques, complementary information from independent spectroscopic and structural techniques, and last but not least improvement in sample preparation and in particular site-directed mutation and modification protocols all contributed. The state of knowledge to the mid-1990s has been reviewed, see for example Angerhofer and Bittl (1996), Hoff and Deisenhofer (1997), and Stehlik and Möbius (1997). Here the intent is to focus on what structural and functional model could be evaluated from TR EPR data for the A_1 site in PS I by 2000, i.e., prior to the first X-ray structure at atomic detail (Jordan et al., 2001). Some selected experimental data are presented to illustrate how primary spectroscopic information translates into structural and mechanistic information for the quinone site in PS I. In addition it will be pointed out how specific advanced TR EPR methods helped to fill in essential independent information.

One of the important experimental extensions in the 1990s was expanded multifrequency TR EPR capacity toward high field/frequency with typical sets of Zeeman resonance frequencies covering 9 (X-), 24 (K-), 35 (Q-), and 94 GHz (W-band), with higher frequencies available at the present time up to several hundred GHz. Optimal conditions can be chosen for the determination of magnetic interaction tensor parameters. Magnetic field dependent interactions (Zeeman, **g**-tensors) are best resolved with sufficiently high field/frequency EPR. For that the anisotropic Zeeman interaction ($\Delta g \cdot B_0$) has to exceed the usually inhomogeneous line broadening ($g_{iso} \cdot \Delta B_{1/2}$). On the other hand, field-independent interactions such as hyperfine and inter spin exchange

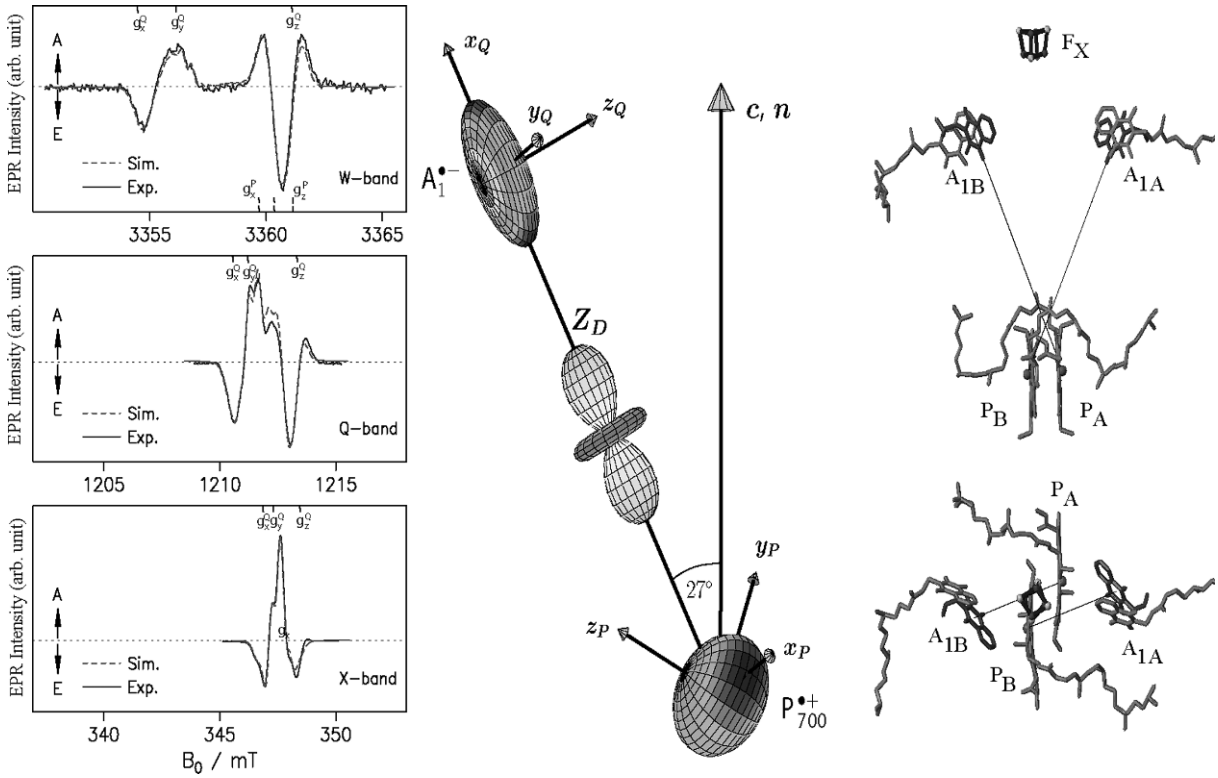

Fig. 4. From the TR EPR spin polarization patterns (left) via the relevant magnetic interaction tensors (middle) to an EPR-based structural model of the A_1-binding site in PS I (right). *Left:* Spin polarization pattern of the transient $P_{700}^{+}A_1^{-}$ radical ion pair state of PS I at three mw-frequencies (94, 35, 9 GHz, top to bottom). The arrows at the left of each spectrum indicate absorptive (A) and emissive (E) signal amplitude. The **g**-tensor principal values used for the simulated spectra (dotted line) are marked at the top and/or bottom of the spectra. *Middle:* EPR-based structural information resides mostly in the relative orientation of the depicted respective **g**-tensor ellipsoids and axes (P_{700}^{+} and A_1^{-}) and the dipolar magnetic interaction tensor with the principal axis $\mathbf{z}_D$, connecting the spin density centers of donor P_{700}^{+} and acceptor A_1^{-} radical ion. With oriented PS I samples (the membrane normal **n** or crystal axis **c** can be oriented with respect to the magnet field $\mathbf{B}_0$), the angle ($\mathbf{z}_D$, **c**) has been determined to $27 \pm 3°$. *Right*: The position and orientation of the quinone molecule in the A_1 site as derived from EPR data (darker gray) is compared with the X-ray structure model (PDP code: 1JB0) (light gray); from the cofactors only the C_2-symmetric electron donor P_{700} (P_A and P_B) and the electron acceptors A_1 (A_{1A} and A_{1B}) and F_X are shown. The view is along the membrane plane (top) and perpendicular to it (bottom). The thin lines represent the possible dipolar axis $\mathbf{z}_D$ vector connecting the spin density centers of P_{700}^{+} and A_1^{-}. *Note:* Independent information from mutants in the P_{700} environment locates the spin density of P_{700}^{+} mainly in the center of P_B. As a consequence, it is the A_{1A}^{-} site which is detected by TR EPR. Note: The protein-derived quasi C_2-symmetry axis passes through the center of F_x (not P_{700}). Source: Salikhov et al., 1999.

(scalar) and dipolar interactions parameters are more readily extracted from lower field EPR spectra for which the **g**-tensor anisotropy can be ignored. Further separation of multiple hyperfine and inter spin interactions has been greatly advanced with improved multiple resonance (ENDOR, ELDOR, etc.) methods which are now also available for orientation dependent studies even in isotropic (frozen) solutions by taking advantage of orientation selection due to the **g**-tensor resolution at sufficiently high field/frequency. The rapid development of pulsed EPR techniques includes these multiple resonance methods and is of particular interest here because transient states can be studied also. In addition, specific pulsed EPR techniques such as ESEEM (electron spin echo envelope modulation) can be adapted to improve separation of specific magnetic interactions, ESEEM for small hyperfine couplings and out-of-phase ESEEM for accurate determination of inter spin couplings in correlated radical pairs (Bittl and Zech, 2001). The advanced EPR techniques just mentioned are reviewed in monographs such as Schweiger and Jeschke (2001). Most are also described separately in other chapters of this book, including more detailed technical references and with the decisive advantage of their focus on application to PS I.

The development from the TR EPR spectra of the $P_{700}^{+}A_1^{-}$ state to a structural model for the A_1 site from these data is illustrated in Fig. 4. In the left panel,

multi-frequency TR EPR spectra of the functional $P_{700}^{\cdot+}A_1^{\cdot-}$ state of (protonated) PS I are displayed together with simulations based on the CRP concept and the same parameter set for all field/frequencies. Satisfactory simulations are achieved for both protonated (Kamlowski et al., 1998) and deuterated PS I samples (Zech et al., 2000). They demonstrate the validity of the underlying CRP concept as well as the reliability of the parameter set used, in particular the relevant structural parameters. The principal values of the $\mathbf{g}_Q$-tensor are clearly resolved at W-band (95 GHz), see Fig. 4 (top left). For deuterated PS I, comparable resolution can already be achieved at Q-band, see Fig. 1 of Zech et al. (2000), because the inhomogeneous linewidth due to unresolved proton hyperfine coupling is significantly reduced by deuteration. For deuterated PS I, even the $\mathbf{g}_P$-tensor is sufficiently resolved at W-band to measure the $\mathbf{g}_P$-tensor orientation in PS I single crystals (Zech et al., 2000).

Structural information can be extracted from the relative orientations of the magnetic interaction tensors. The middle panel of Fig. 4 illustrates the relative orientations of the tensors $\mathbf{g}(P_{700}^{+})$, $\mathbf{g}(A_1^{-})$, represented as ellipsoids, and the dipolar interaction tensor (with principal axis $\mathbf{z}_D$) as coupling between them. The dipolar coupling strength and with it the distance between the spin density centers of $P_{700}^{\cdot+}$ and $A_1^{\cdot-}$ is determined independently from a purpose-designed pulse EPR experiment, out-of-phase ESEEM (Bittl and Zech, 1997). The orientation of the dipolar axis $\mathbf{z}_D$ to the crystal axis **c** (also membrane normal **n**) comes from single crystal data. It is important to note that the relative orientations of these tensors will be the same for all the sites per unit cell. This fact provides a convenient way to assign the observed inequivalent **g**-tensors to the respective independent sites per unit cell. Orientation of **g**-tensors to the membrane plane has also be obtained independently from measurements on PS I-containing membrane fragments oriented either by attachment to mylar sheets (MacMillan et al., 1997) or by high magnetic fields (Heinen et al., 2004a,b), but requires additional simulation parameters to account for any degree of incomplete ordering.

In addition, strong hyperfine coupling (hfc) may be resolved directly in the EPR spectra. An example is the hfc due to the methyl substituent of the quinone acceptor (see the X-band spectrum in Fig. 4). The orientation of the methyl hfc tensor determines the position of the respective quinone substituent in the A_1 site. Finally, a key problem for the structural model is the question whether the observed single A_1 site is located on the A- or B-branch of cofactors. Obviously, this cannot be answered from EPR data alone because the C_2 symmetry renders the two sites magnetically equivalent; note the equivalent possibilities of dipolar connecting lines in the right panel of Fig. 4. However, selective mutation of the histidine ligand to the central Mg ion of either of the two Chl constituents of P_{700} (P_A or P_B) provided independent evidence that the spin density center is located on P_B (Krabben et al., 2000). With this additional information, the TR EPR observed functional $P_{700}^{\cdot+}A_1^{\cdot-}$ state can be assigned in the structural model as the A_{1A} site (Zech et al., 2000).

In Fig. 4 (right panel) the EPR-based structural model of the functional $P_{700}^{\cdot+}A_1^{\cdot-}$ state is also compared with the first X-ray ground state structure at 2.5 Å resolution (Jordan et al., 2001), PDB code 1JB0. The two structures are aligned for the same orientation of the *c*-axis (or the parallel membrane normal **n**) and the same positions of the central Mg atoms of P_A and P_B. The agreement concerning the quinone ring orientation and individual ring substituent positions is excellent. The distances between the molecular centers of P_{700} and A_1 also agree very well. The apparent differences in the quinone ring positions are well within the experimental error for mainly the angle between $\mathbf{z}_D$ and $\mathbf{c}||\mathbf{n}$. The otherwise close (and independently confirmed) agreement between the structural properties of the A_1 site for ground state (X-ray) and functional charge separated $P_{700}^{\cdot+}A_1^{\cdot-}$state (TR EPR) is not at all trivial. The strong electric field associated with the generation of the charge-separated state provides a potent force for possible structural rearrangements. For example, the kinetic "Kleinfeld-effect," observed in the pbRC (Kleinfeld et al., 1984), was interpreted initially as evidence for structural rearrangement due to the light-induced electric field, although alternative interpretations are possible. In any case for PS I, the structural properties available from EPR for the A_1 site do not provide any indication for conformational changes due to charge separation (see also independent distance measurement Bittl and Zech, 1997).

Another important possibility after the achievement of a structural model for PS I is the comparison of the TR EPR results for the $P_{700}^{\cdot+}A_1^{\cdot-}$ state in PS I with those for the $P_{700}^{\cdot+}Q_A^{\cdot-}$ state of pbRC of purple bacteria, i.e., type II RCs with detailed X-ray structures available (for an earlier review see Hoff and Deisenhofer, 1997). As mentioned previously, TR EPR application to pbRC requires the replacement of the non-heme iron by a diamagnetic ion such as Zn^{2+}; it could be verified that this has no significant influence on the X-ray structure. A direct comparison of multiple frequency TR EPR data, reviewed for example with Fig. 3 in

Stehlik and Möbius (1997), permits some significant conclusions:

(i) Similar orientation of the $\mathbf{g}(P^+)$ tensors, but different orientation of $\mathbf{g}(Q^-)$ tensors in the respective binding site with respect to a RC fixed axis such as the P^+Q^- interconnecting distance vector $\mathbf{z}_D$ or the membrane normal. The quinone g_{xx} principal axis, which is nearly identical with the C–O bond direction (short in-plane axis of the NQ ring plane), is oriented close to parallel to the membrane plane for pbRC while it is oriented parallel to $\mathbf{z}_D$ or within 30° perpendicular to the membrane plane for PS I.

(ii) Compared to the $\mathbf{g}(Q^-)$ tensor parameters in frozen solution, the $\mathbf{g}(A_1^-)$ tensor in PS I displayed a larger g-anisotropy while it remained nearly the same for $\mathbf{g}(Q_A^-)$ in pbRC, a first indication of different protein-cofactor interactions in the respective quinone binding sites.

In addition a useful concept for the assignment of magnetic interaction tensors to the inequivalent centers per unit cell of single crystals could be exemplified.

The fixed orientation between the tensors $\mathbf{g}(P^+)$, $\mathbf{g}(Q^-)$, and $\mathbf{H}_{DD}$ (or $\mathbf{z}_D$) in every RC can be used as decisive information to determine which of the $\mathbf{g}(P^+)$ tensors determined in any single crystal orientation patterns, e.g., in the case of pbRC (Klette et al., 1993; Prisner et al., 1995), belongs to which of the inequivalent RCs per unit cell. This is a generally applicable concept. It has been utilized for instance to distinguish the six inequivalent RCs per unit cell in PS I single crystals via the fixed tensor relation between the two [4Fe–4S] centers per PsaC subunit in the stromal ridge complex (Kamlowski et al., 1997a,b). The procedure can be of help in present day studies on PS II single crystals when $\mathbf{g}$ and hfi tensors associated with the Mn_4 cluster need to be assigned to the different PS II RCs per unit cell and additional rotation patterns associated with other magnetic interaction tensors such as $\mathbf{g}(Y_D^+)$ can be measured for the same crystals.

C. Selected Recent Structure- and Mutant-Based TR EPR Studies in PS I

1. Remarks Concerning Structural and Functional Issues Relevant to the TR EPR Studies

The advent of the first X-ray structural model at atomic detail marks always a key point in the understanding of structure-function relations of complex protein systems, and of membrane-bound systems in particular. For PS I this mark was set in 2001 (Jordan et al., 2001); the structure coordinates are available as PDB entry 1JB0. As usual, the emphasis of spectroscopic studies shifts to a large extent from structural to functional and dynamic issues; the latter may involve related structural changes. As was demonstrated in Fig. 4 the pre X-ray structure model derived from TR EPR data for the A_1 site of PS I (concerning the functional charge-separated state as pointed out previously) turned out to be in good agreement with the ground state X-ray structure model (1JB0). Hence, this finding provides the following favorable conditions for further analysis: the EPR data can be interpreted in the first approximation on the basis of the far more detailed X-ray structure model for the ground state; in addition, TR EPR is able to observe certain essential structural features together with correlated kinetic and dynamical properties even under physiological conditions. Therefore, the results can be interpreted directly in terms of structure-function relations but also to a good approximation in the broader context of the full X-ray structure model. These introductory remarks are further intended to highlight essential structural features in the context of key functional issues pursued in today's PS I research with the intention of specifying the context and relevance of the selected TR EPR data that contribute to these issues.

a. Quasi C_2 symmetry of the PS I reaction center and the directionality of ET

An obvious feature of the PS I structure is the quasi C_2 symmetry of the RC core. It concerns primarily the PsaA/PsaB heterodimer protein framework and as a consequence also the arrangement of the two branches of electron acceptors $(A_{-1}, A_0, A_1)_{A/B}$ as an integral structural part of the core structure. The two acceptor branches originate at the common primary donor P_{700}, a Chl *a*/Chl *a*′ pair, located close to the lumen membrane surface. The arrangement is quite similar in type II RCs, both in the well-resolved structure of RCs of purple bacteria (pbRC, we will refer to the most detailed pbRC structure of *Rhodobacter sphaeroides*, PDB code: 1PCR) and to the recent medium-resolution structures of PS II (Zouni et al., 2001; Kamiya and Shen, 2003; Ferreira et al., 2004) (1S5L), (Zouni et al., 2004). Common in both types of RCs is a first quinone acceptor, A_1 (PhQ in PS I) and Q_A (UQ-10 or MQ-9 in pbRC, PQ-9 in PS II, see Fig. 1 for the molecular structure and axes of these native quinones). In both types of RCs the first quinone acceptor functions as one electron

gate. However, the two types of RCs differ significantly with respect to the ET steps past the first quinone acceptor. In type II RCs, the final ET step proceeds from Q_A to Q_B parallel to the membrane plane from one acceptor branch to the other. In the end, Q_B accepts sequentially two electrons and two protons to be released from its binding site into the membrane as protonated Q_BH_2. Deprotonation in the bulk phase (quinone pool) and rebinding to the Q_B binding site complete the Q_B cycle. This well-established cycle is mentioned here only because it constitutes a clear functional requirement for unidirectional electron flow along the branch binding Q_A (L-branch). Indeed, ET unidirectionality is experimentally well-verified and theoretically understood for type II RCs.

In contrast, in PS I the terminal electron acceptors are arranged in a perpendicular direction to the membrane plane as a triangle of three consecutive [4Fe–4S] clusters (F_X, F_A, and F_B), starting with F_X and its center of mass located directly on the quasi C_2 symmetry axis; the two cofactor branches converge at this central F_X acceptor. Therefore, a specific functional requirement for uni-directional ET as in type II RCs cannot be identified for PS I. Nevertheless, it is conceivable that the same quasi C_2 symmetric heterodimer arrangement has been retained in PS I as well as in PS II simply because evolution-wise they both originate from a common ancestor (similar to purple bacteria), in which unidirectionality was already established as a functional requirement. In any case, for PS I, uni- and bi-directionality appear both to be functionally equivalent. Even without a functional requirement, it is certainly worth asking whether unidirectionality of ET has been maintained in PS I during evolution. A preference for one branch would be quite consistent with the multiple deviations from C_2 symmetry retained in the PS I protein core heterodimer. On the other hand it is equally conceivable that bi-directionality has reevolved without the evolutionary pressure of a functional requirement. Obviously, the same aspects become even more relevant in the case of homodimeric type I RCs as identified in *Chlorobium* and *Heliobacteria* (for a review see Nitschke and Rutherford, 1991; Amesz, 1995). Recently, the stability and the handling of RC complexes from *Heliobacterium modesticaldum* (HbRC) have advanced significantly (Heinnickel et al., 2005). A thorough study of the directionality issue can be foreseen to be carried out soon for homodimeric type I RCs.

In conclusion, the question of uni- or bi-directionality is not a functional issue in PS I research. Instead, the relevant question in the further investigation of homo- as well as heterodimeric type I RCs and their comparison with type II RC is likely to be: what specific properties of protein-cofactor interactions determine ET directionality and how can directionality be controlled?

b. What is the significance of the directionality issue for this chapter?

In spite of the fact that the directionality issue is not associated with a functional requirement for PS I, in contrast to type II RCs, a considerable amount of experimental effort has been devoted to verify bi-directionality in PS I and to determine the degree of branching of ET along the A- and B-branches. In the 1980s it was shown that an additional (fast) optical phase in the A_1^- reoxidation kinetics of spinach PS I can be induced by detergent treatment of PS I preparations (Brettel, 1988). However, with sufficient time resolution it is now well-established that the nsec A_1^- reoxidation kinetics includes a fast minority contribution in the 10 nsec range, also in intact PS I preparations from cyanobacteria and eukaryotes such as *C. reinhardtii* (for review see Brettel and Leibl, 2001 and other chapters in this book). The most appealing interpretation for this multiexponential kinetics is bi-directional electron flow along the two acceptor branches. This assessment has been backed up by branch-specific A_1 mutant studies (Xu et al., 2003b). In addition, confirmation in intact cells exclude any preparation-induced origin of the bi-exponential A_1^- reoxidation kinetics (Joliot and Joliot, 1999; Guergova-Kuras et al., 2001). For a further development of the bi-directional ET model in the light of recent experimental evidence see Santabarbara et al. (2005) and Chapter 25, this volume.

A final decisive step would be to demonstrate the feasibility of redirection or control of directionality of ET along either of the two branches in PS I. This has failed so far in PS I but was demonstrated for type II pbRC. However, it required a combination of at least four mutations in the primary donor and acceptor environments (see Kirmaier et al., 2003; Haffa et al., 2004; Paddock et al., 2005). In that respect, it is not surprising that the single (and double) mutants, tested so far in the P_{700} environment of PS I, have failed to produce significant changes in the observable believed to indicate bi-directionality.

The status of the directionality studies was reviewed briefly here to establish that the TR EPR results presented in this chapter for type I RCs are not able to contribute much to a solution to this problem. It turns out that the conditions of the TR EPR experiment favor the detection of the intermediate $P_{700}^{+\cdot}A_1^{-\cdot}$ state in

the A-branch. B-branch ET cannot be detected directly. However, even if the time resolution for direct real-time TR EPR detection is insufficient, indirect contributions to the spin polarization pattern of the common $P_{700}^{+}F_{X}^{-}$ state should be able to detect a B-branch ET contribution of more than 20% (see van der Est, this volume, Chapter 24). It will become clear that the TR EPR data presented in this chapter concern ET intermediates along the A-branch only. Note that kinetic data concerning these A-branch ET intermediates agree well with those from other methods, in particular optical studies. A-branch ET represents the dominant ET pathway in all data, in particular under physiological conditions at ambient temperatures. The possible inability of TR EPR to detect a faster minor ET phase due to time resolution constraints can also be seen as an advantage: it discriminates against faster kinetic contributions and thus assures "clean" spectra of the majority A-branch transient intermediates.

c. TR EPR data for cyanobacterial PS I concern PsaA branch and A_{1A} site only

For cyanobacterial PS I, it was shown that the TR EPR structural model in Fig. 4, combined with independent information from selective mutations of either of the P_{700} histidine ligands, permits the assignment of the TR EPR observable state to the A_{1A} site within the PsaA branch (Zech et al., 2000). Since then, an ever-increasing number of branch-specific site-directed mutants concerning all cofactor sites in each of the branches from P_{700} via A_{-1}, A_0, A_1 to F_X have been constructed and studied. They confirm the above assignment and correlate the A_{1A} site with the slow A_1 reoxidation rate, with respect to which the TR EPR and optical kinetics show satisfactory agreement (see Xu et al., 2003a,b and references therein). Independent of the ongoing disputes concerning directionality and branch-specific photoaccumulation of reduced cofactors, all published mutant-based studies agree with respect to specific statements and these are of particular relevance for this chapter:

(i) All directly observed TR EPR spectral and kinetic data concern the A_{1A} site only; and
(ii) ET along the A-branch is the dominant pathway under physiological conditions.

(Concerning the nomenclature of A- and B-branches a reminder may be appropriate: of course, the definition of A- and B-branches has been done independently in PS I and previously in type II pbRCs. It is just by accident that the TR EPR active A_{1A} site in PS I corresponds in its function as one electron gate to the primary quinone Q_A site in pbRC.)

The two statements (i) and (ii) apply to both temperature ranges typically used in experiments: *High T*: in fact the ambient temperature range (in aqueous solution above 240 K including room temperature). As key functional criterion, the A_1 to F_X ET is fully operational and observed for all photoexcited PS I RCs. *Low T* (<200 K): in frozen aqueous medium two fractions of PS I particles are found (Schlodder et al., 1998). One involves cyclic ET from P_{700} to A_1 and back, because forward-ET past A_1 to the Fe/S centers is blocked for these PS I complexes. The other involves stable charge separation to F_A/F_B, i.e., the charges will be trapped as P_{700}^{+} and F_A/F_B^{-}, at least on the time scale of typical repetition rates used in TR EPR experiments. Again, within experimental accuracy, the directly observable TR EPR radical ion pair state concerns the A-branch quinone only.

In addition, for cyanobacterial PS I, conditions can be established that only the A-branch quinone site is photoaccumulated to a stable A_1^{-}. In this case of a stable radical ion state, the full range of advanced EPR techniques including pulsed EPR and multiple resonance techniques can be applied for further spectroscopic characterization of the photoaccumulated steady state.

d. Protein-cofactor interactions in the A_1 binding site from X-ray structure model

Since 2001, spectroscopic studies of PS I can be based on an X-ray structure model at atomic detail. The essential structural details for just the A_{1A} binding site are presented in Fig. 5. Side chains are shown for those residues that are involved in protein-quinone interactions. All of the specified amino acids have been subjected to branch-specific mutations to investigate their influence on A_{1A} site properties. Obvious protein-quinone interactions include: (i) Highly *asymmetric H-bonding* to one quinone C–O group only; the H-bond is provided by the backbone N–H group of the LeuA722 residue, which is close by as part of the return loop from the stromal surface helix A-**jk**(1) before it enters the transmembrane k-helix. The second quinone C–O group is believed to lack an H-bond; instead an H-bond network connects the potential donor candidate in the SerA692 side chain with the backbone of MetA688 (which ligates the cofactor) and the N–H group of the TrpA697 residue. (ii) The latter Trp aromatic side chain is positioned in favorable π-*stacking* configuration,

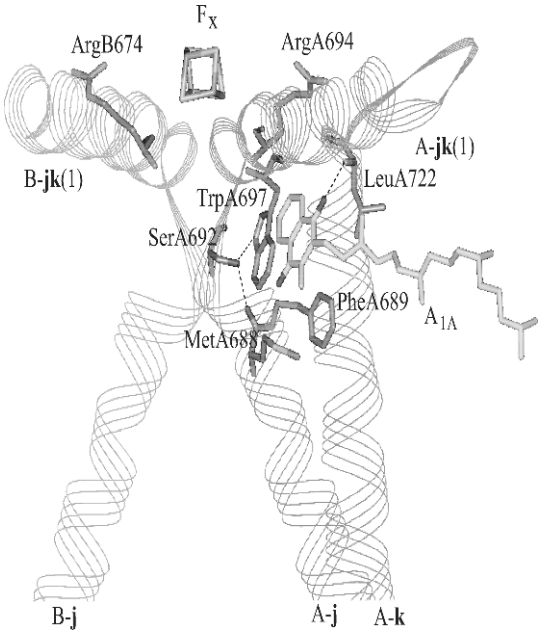

Fig. 5. The A_{1A} binding site is shown with relevant elements of the protein environment as extracted from the X-ray structure model (1JB0). Identified protein-quinone interactions are π-stacking with the TrpA697 residue and H-bonding (dotted line) to the top- or stroma-facing quinone C–O group from the backbone amid (NH) group of the LeuA722 residue. The second C–O group is not H-bonded according to the X-ray structure model, instead the close by amino acids residues establish an H-bond network with the SerA692 C–O group in the middle connecting to the MetA688 backbone C–O group on the one side and the N–H group of the TrpA697 five ring on the other side. The latter establishes a π-stacking configuration to the quinone ring system.

possibly stabilized by the above H-bond network. (iii) Partial charges of cofactors (F_X) and side chains and/or protonable groups introduce *electrostatic interactions*. The symmetric residues ArgA694 and ArgB674 are depicted as examples. However, their proximity to F_X and their involvement in inter protein subunit contacts hint at a predominant influence on the properties of F_X, as was shown by experiments. Many other candidates potentially contribute to electrostatic interactions and will be mentioned later.

Within this structure- and function-based framework, the rest of this section summarizes results achieved up to the present and concerned with the characterization of protein-cofactor interactions for the quinone acceptor in the A_{1A} site of PS I. Although modifications of the quinone cofactor turn out to have minor consequences on the structural and functional properties of the A_{1A} site, the major influence comes from the protein environment. These results will be further discussed in the context of other literature results and in particular with respect to a comparison with different types of RCs (section IV).

2. Detailed TR EPR Spectroscopic Properties of the A_{1A} Site in Cyanobacterial PS I

All significant A_{1A} site properties will be summarized as obtained from structure- and mutant-based investigations in recent years. Even for the native PS I some new information on the A_{1A} site properties has been added since 2001, partially due to more refined pulsed EPR techniques, partially also due to more elaborate interpretation of existing data. Here, the focus is on information obtained from systematic modification of the quinone acceptor and in particular of the relevant protein environment. Modification of the quinone acceptor requires first extraction of the native PhQ from the A_{1A} site and subsequent replacement with a target quinone. In this case, it is mandatory to test whether the integrity of the A_{1A} site has been maintained during the extraction/replacement procedure. It is further necessary to ask which elements of the molecular structure of the replacement quinone acceptor are necessary such that it enters the native PhQ site with identical structural properties as native PhQ. Subsequently, the modification of the A_{1A} site environment aims to identify features of the protein environment (i.e., the PsaA and PsaB subunits of the PS I core), which determine and control the structural and functional properties of the A_1 site via specific protein-cofactor interactions.

a. The A_{1A} site properties are retained when the substitute quinone has specific molecular features

Two methods have been tested thoroughly that allow replacement of the quinone in the A_1 site: (i) The native quinone is extracted from the A_1 site by organic solvents. (Biggins and Mathis, 1988). This harsh procedure is known to affect other cofactor sites and is likely to modify further structural and functional properties as well. (ii) The most bio-compatible method available uses biosynthetic phylloquinone pathway mutations that block production of the native PhQ during cell growth (Zybailov et al., 2000). The A_1 site is found to be filled with a more weakly bound quinone, identified as PQ-9, the native quinone in the $Q_{A/B}$ site of PS II, which has been recruited into the A_1 site. For both kinds of PhQ-less PS I preparations (i) and (ii), selected target quinones can be either reconstituted or

biochemically exchanged into the A_1 site occupied by the PQ-9 instead of the more tightly bound native PhQ.

In spite of the fundamental differences of the two quinone displacement methods it comes as a pleasant surprise that in both cases equivalent TR EPR features are recorded concerning the structural and functional integrity of the A_1 site. Therefore, the following results for a series of specific replacement quinones should be considered to apply to both methods of PS I preparation (i) and (ii).

- Identical TR EPR derived structural properties of the transient A_{1A} site were observed when the native PhQ is replaced either by dephytylated 2-methyl 1,4-NQ (VK_3), i.e., PhQ without phytyl tail (Johnson et al., 2001; Pushkar et al., 2002) or by demethylated PhQ (*men*G mutant) (Sakuragi et al., 2002). Hence, the common notion of the phytyl tail as an "anchor" in the protein matrix is not based on experimental evidence. On the other hand, at least one asymmetric substituent to the NQ head group appears to be required for full structural A_{1A} site integrity, as can be concluded from uncertain A_{1A} site properties observed when symmetrically substituted or plain 1,4-NQ is used for the replacement. The suitability of the singly substituted 2-methyl 1,4-NQ as a PhQ replacement offers a convenient method to introduce isotopically labeled quinones into the A_{1A} site. Specific spin markers in critical quinone ring positions have been introduced to map out the spin density distribution of the radical ion in the A_{1A} site, which in turn yields valuable information on the quinone-protein interactions that control biological function.
- Quinone replacement has been extended to a large variety of quinones (Iwaki and Itoh, 1991) as reviewed in Itoh et al. (2001). This method will be discussed later as a way of introducing small specific changes of the quinone redox potential in the A_{1A} site. The major contributions to the quinone redox potential come from the specific protein environment.

b. Protein-quinone interaction in the A_{1A} site: H-bonding

The X-ray structure model suggests a single H-bond from the backbone NH group of the LeuA722 residue to the PhQ carbonyl group that is in meta-position to the phytyl tail (see Fig. 5). Before the functional significance of this H-bonding asymmetry (concerning the C_2 symmetry around the long NQ in-plane axis) can be assessed it is important to clarify whether it applies only to the ground state or also to the functional charge separated $P_{700}^{+}A_1^{-}$ state (as well as the photoaccumulated A_1^{-} state). The short answer is yes. However, contradictory literature data (for details see below) require first a consistent account of recent data that assure the correctness of the short answer, at least for the case of cyanobacterial PS I. Even before the X-ray structure in 2001, evidence for a highly asymmetric H-bond pattern was concluded from the **g**-tensor data, and in particular from the large proton hyperfine coupling, measured for the single methyl group attached to position 2 of the NQ core of PhQ (for molecular structure see Fig. 1). The EPR-based structural model summarized in section III.B and in Fig. 4 was largely based on these results. The large methyl hfc position of the NQ core radical cation due to asymmetric H-bonding, and with it a highly asymmetric spin density distribution over the ring, can be rationalized on the basis of a valence bond model (for a summary see Fig. 14 in Lubitz and Feher, 1999). In Fig. 6 it is adapted to PS I as reproduced from Pushkar et al. (2004b). Compared to the symmetric H-bonding situation for the NQ core radical cation in isotropic solution, this model predicts an alternating, highly asymmetric spin density distribution. Specifically, the spin density is increased for the NQ ring position of the methyl group in meta-position to the C–O group with the dominant H-bond as well as for the carbon of the H-bonded C–O and the oxygen of the C–O group with no or very weak H-bond. The increase of the hyperfine splitting due to the three equivalent methyl protons is large enough that it is directly observable as (partially resolved) hfc in the TR EPR spectral pattern of the $P_{700}^{+}A_{1A}^{-}$ state of PS I. The same applies for the above-mentioned carbon and oxygen positions if isotopic labeling with spin carrying nuclei (^{13}C, ^{17}O) introduces an additional large hyperfine interaction. The advantage of direct hfc observation in the TR EPR spectrum and hence direct spectra interpretation permits the rare chance of direct documentation of the essential results as shown in Fig. 7.

The top spectrum shows a clearly resolved quartet of lines (1:3:3:1) as it is characteristic for three equivalent protons of a methyl group. Note that the resolution is slightly better for VK_3 than for PhQ in the A_1 site of PS I (see Fig. 4, left) because the extra line broadening due to unresolved hfc of the protons of the phytyl tail is removed with VK_3. Direct observation of such selectively increased hfc values can be exploited further. As demonstrated with the middle spectrum of Fig. 7,

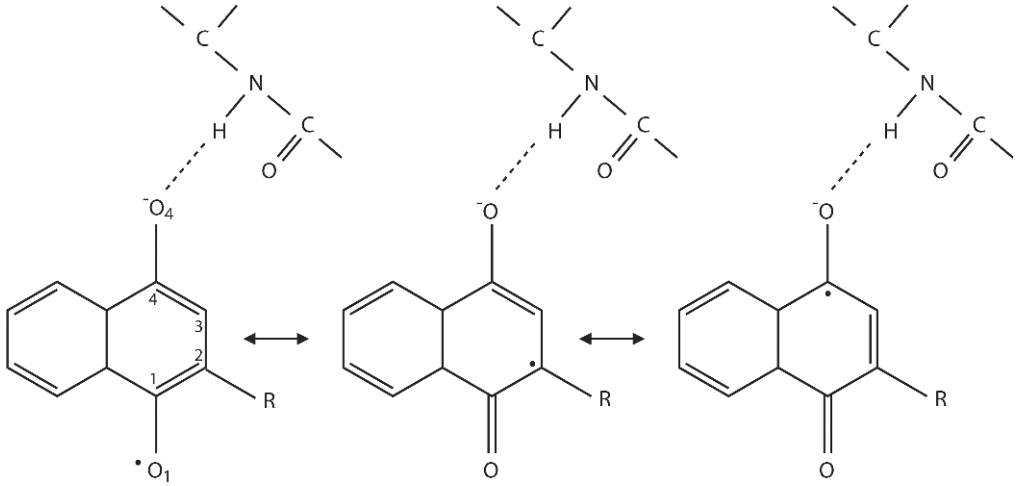

Fig. 6. Basic valence bond model: the single H-bond from the backbone NH group redistributes the unpaired π-electron spin density of the $NQ^{\bullet -}$ radical ion across the quinone ring according to the three resonance structures shown. Alternating spin density changes are predicted with increased spin density at the ring carbon positions 2 and 4 as well as at the O_1 oxygen (without H-bond), and decreased density in between.

a well-resolved (1:2:1) hfc multiplet due to two equivalent protons is observed when the single substituent of 1,4-NQ is a $–(CH_2)_{(n-1)}CH_3$ *n*-alkyl chain of variable length. The shortest chain (ethyl, $n = 2$) contains a single CH_2 group the two protons of which are responsible for the observed (1:2:1) hfc pattern. Nearly identical spectra have been obtained for alkyl chains up to $n = 7$ (Pushkar et al., 2002). While the hfc pattern is readily interpreted, the consequence is surprising: in the A_1 site of PS I an alkyl tail is found in the position of the CH_3 group and not in that of the phytyl tail for wild type PS I. The details of the protein-chain interactions responsible for this observation are not yet fully understood. The early part of the more flexible *n*-alkyl tail appears to fit better into the phytyl binding channel when the A_{1A} site configuration is altered compared to the wild type. The single double bond (third bond) along the phytyl tail may play a relevant role. When selected 1,4-NQs with a tail substituent with a double bond in this place (e.g., lapacol) are placed into the A_{1A} site, the tail indeed takes up the position characteristic for the native phytyl tail. The bottom spectrum of Fig. 7 demonstrates a substantially altered hfc pattern when a single ^{13}C spin is introduced into the H-bonded C_4–O group. The spectra contain all information about the full ^{13}C hfc tensor as evaluated in Pushkar et al. (2004a). The results are in good agreement with the predictions of the valence bond model of Fig. 6 with the assumption of a highly asymmetric H-bonding to one quinone C–O group only. To test the third position with increased spin density, ^{17}O labeling has been carried out (Pushkar et al., 2005). Surprisingly, the inequivalence of the hfc values observed for the two ^{17}O positions associated with the two quinone C–O groups was found to be quite small, even smaller than for the two sided H-bond scheme established for the Q_A site of pbRC (Lubitz and Feher, 1999). However, this is not in contradiction with the conclusion of a highly asymmetric H-bonding in the A_1 site because the ^{17}O hfc tensor is known to be largely insensitive to the strength of the H-bond to the C–O group under investigation (Reiter et al., 1990). Note that so far only the high spin density positions have been studied. Certainly, the low spin density positions should be investigated as well. However, apart for the required isotopic labeling effort, the analysis of the hfc tensors can be expected to be more complicated, in particular for the highly asymmetric H-bond situation encountered for the A_1 site. Contributions from the neighboring high spin density ring positions to the measured hfcs will play a significant role. In summary, the hfc tensors have been determined for all significant (high spin density) positions of the quinone ring in the A_1 site. The relevant tensor parameters and the interrelation with the spin density distribution have been collected in the tables presented in Pushkar et al. (2004a, 2005) and references therein. They are in good agreement with the single sided H-bond pattern shown in the scheme of Fig. 6.

A further essential experiment is the determination of the proton hfc tensor associated with the single dominant H-bond to the quinone in the A_1 site. Different and even contradictory assignments of the H-bond

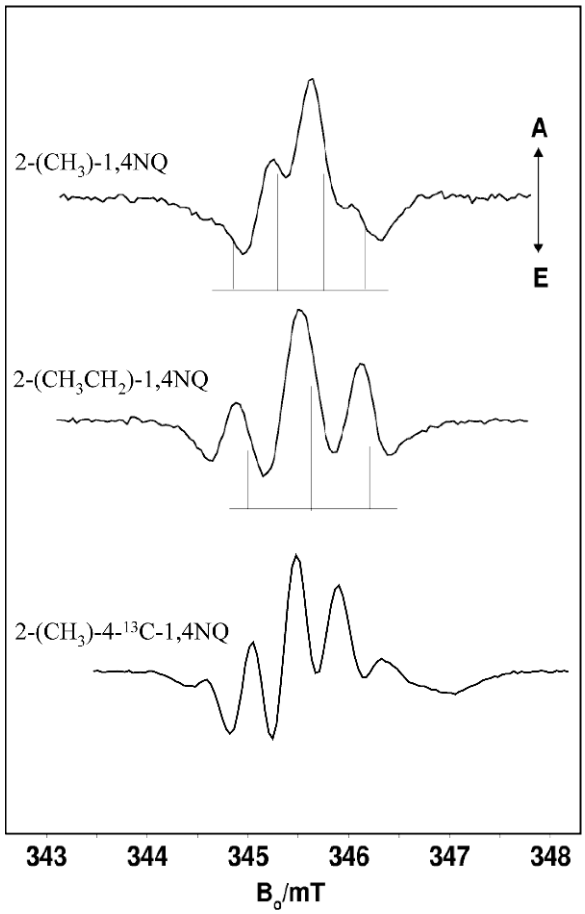

Fig. 7. TR EPR spectra at X-band for three PS I samples with two artificial quinones, 2-(methyl)-1,4 NQ (top and bottom) and 2-(ethyl)-1,4 NQ (middle) in the A_1site. For the bottom spectrum a ^{13}C isotopic nuclear spin marker is placed in the C_4 ring position. The increased spin density in the respective ring positions due to asymmetric H-bonding to O_4 is directly recognized in the partially resolved characteristic hyperfine patterns of the 1:3:3:1 multiplet associated with a methyl group (top), a 1:2:1 triplet due to the CH_2 group attached in ring position C_2 and the additional splitting due to the strong hfc of the ^{13}C spin $^1/_2$ in position C_4 (bottom). Source: Pushkar et al., 2002; Pushkar et al., 2004a.

tensor(s) are offered in the literature, including a double H-bond pattern with one H-bond hfc tensor to each of the C–O groups, even for both possible photoaccumulated A_1^-states, one located on the PsaA- the other on the PsaB-branch (Rigby et al., 2002). Such an H-bond scheme would contradict the H-bond asymmetry indicated by the X-ray structure model for the ground state (see Fig. 5) and the TR EPR data summarized above for the charge separated state. This confusing situation can be clarified, at least for cyanobacterial PS I, by simplifying the interpretation with the use of deuterated quinone, i.e., proton spins attached to NQ in the A_1 site will exist only in exchangeable H-positions such as H-bonds. Exactly one H-bond hfc tensor has been observed for the photoaccumulated A_{1A}^-state (Pushkar et al., 2004b). The observed hfc tensor has the typical dipolar characteristics expected for an H-bond and qualifies as a strong H-bond, fully consistent with the asymmetric H-bonding situation according to the X-ray structure prediction for the A_1 site in Fig. 5.

The assignment of a single strong H-bond hfc tensor stimulates a revisit of prior ENDOR results obtained for point mutants directed toward the A_1 binding site, see Fig. 5. In Fig. 8, TR ENDOR spectra of Xu et al. (2003a) are reproduced for the $P_{700}^+A_{1A}^-$ state of point mutants concerning the π-stacking Trp (A-W697F), the H-bond network constituent Ser (A-S692C), and the equivalent Arg residues (A-R694A; B-R674A); the latter connect to the F_X binding loop provided from the partner PsaA/PsaB subunit and are expected to affect the F_X properties equally. In Fig. 8, the B-side *Trp* and *Ser* mutants show identical spectra, which also represent the wild type spectrum. In contrast, the A-side mutants show characteristic changes in the hfc tensor values. The spectral contributions of the nearly axially symmetric hfc tensor of the methyl group in ring position 2 are clearly identified and marked as spectral edge features in Fig. 8. Both characteristic hfc values are seen to increase for the A-W697F mutant but decrease for A-S692C. In addition, only for the latter mutant, a further change is noticed in the ENDOR spectrum and is marked by symmetric arrows below the spectra. With the H-bond hfc tensor now assigned (Pushkar et al., 2004b) the observed changes concern the $A_{perpendicular}$ component of the H-bond hfc tensor. Interestingly, a change of the π-stacking for the *Trp* mutant does not change the H-bond properties. In contrast both the methyl and H-bond hfc values decrease for the *Ser* mutant. This is consistent with a weaker H-bond asymmetry induced by the alteration of the Ser-based H-bond network (see Fig. 5). In case of the kinetically equivalent F_X mutants A-R694A/B-R674A (Xu et al., 2003a), only the A-side mutant A-R694A shows an analogous decrease of the quinone associated proton hfc values. A molecular mechanistic basis may be suggested to explain this result. SerA692 and ArgA694 are next nearest neighbors in the A-**j** helix (Fig. 5) and are members of a connecting bond chain extending from A_0 to F_X part of which is shown with the H-bonds indicated as dotted lines in Fig. 5. If a connection is broken as for the A-R694A mutant, this may affect the H-bond network around SerA692 as well.

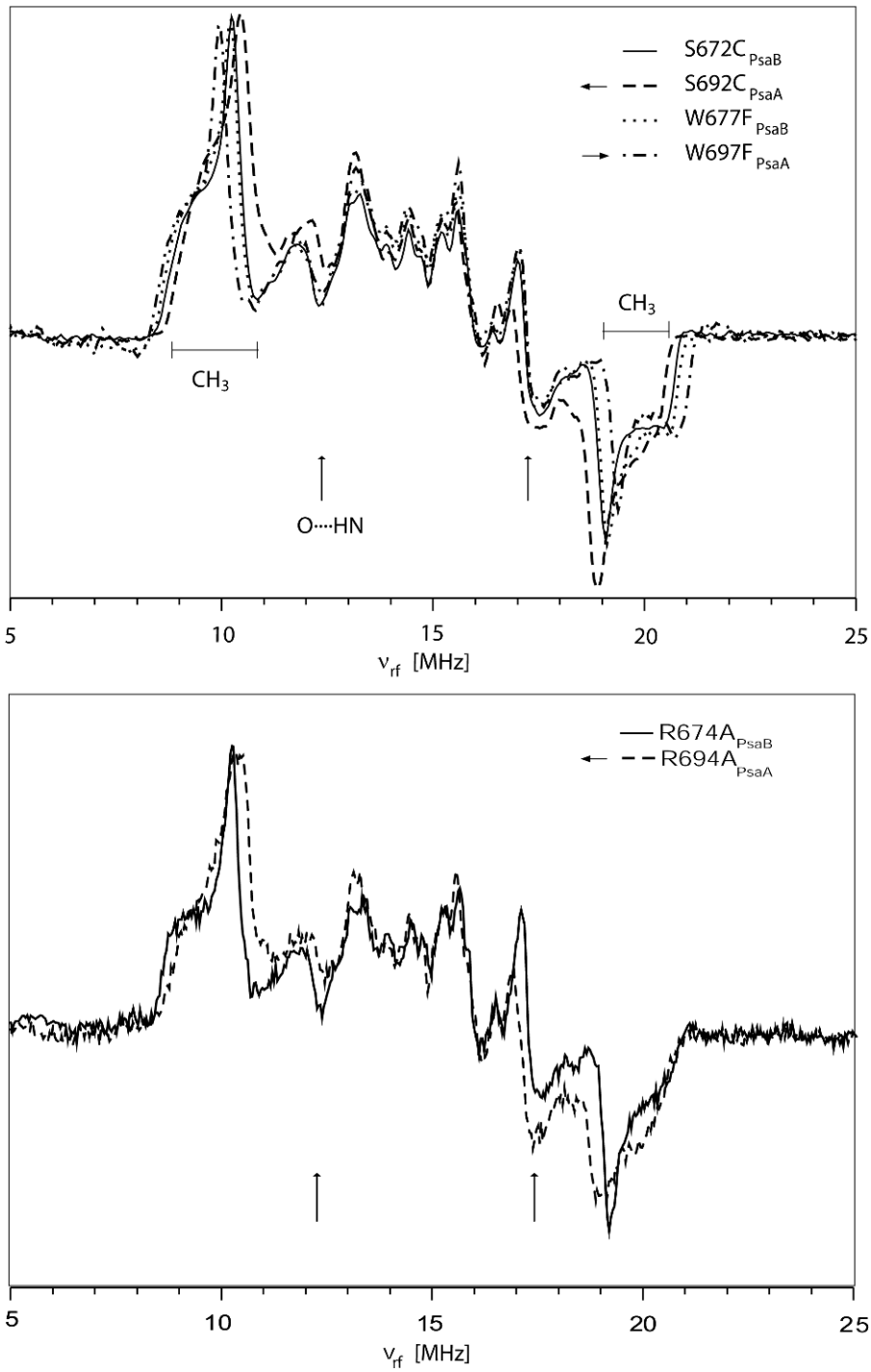

Fig. 8. Pulsed ENDOR spectra of the transient $P_{700}^{+}A_1^{-}$ state of selected PS I point mutants; for experimental and interpretational details see Xu et al. (2003a). The outside features (low- and up-frequency end of the spectrum) are readily assigned to the axially symmetric hfc tensor of the CH_3 group in ring position 2. In addition to the readily interpretable hfc tensor of the CH_3 group, the resonance positions marked by arrows below the spectra can now be associated with the hfc of the proton in the H-bond (O···HN) to the C–O group in ring position 4 (Pushkar et al., 2004b). See text for further interpretational details. Source: Xu et al., 2003a.

In summary, the highly asymmetric H-bond pattern is not only consistent with the X-ray structural model for the ground state, it is also shown to apply for the functional charge separated state as concluded from the TR EPR/ENDOR work just summarized. Furthermore, the clear confirmation of a one-side H-bonded quinone binding site for PS I provides the best test case for advanced theoretical calculations in comparison with the more elaborate double but still asymmetric H-bond network for pbRC (Lubitz and Feher, 1999) and the perhaps even more H-bonded Q_H binding site of quinole oxidase (Grimaldi et al., 2003).

c. Protein-quinone interaction in the A_{1A} site: ππ-stacking

π-Stacking is known to influence the observable **g**-tensor anisotropy of the quinone radical ion. It is convenient to express it as the deviation Δg from the free electron g_e-value (2.00232). The perturbation approach of Stone (1963), Angstl (1990), Huber et al. (1995), and subsequent refinements provide a convenient base for qualitative interpretation of the **g**-tensor data collected for the $P_{700}^{+}A_{1A}^{-}$ state of PS I, see Fig. 4 (middle) for a pictorial representation of the **g**-tensor data (as ellipsoids including their determined relative orientations). An example for a qualitative interpretation is found for instance in van der Est et al. (1995). At that time, only the structure of the quinone binding site in the pbRC was known. In comparison, the **g**-tensor data for PS I indicated a stronger π-stacking for the quinone, as confirmed later by the X-ray structure. In fact, the EPR results stimulated a search for a suitable candidate in the A_1 environment. The Trp residue (TrpA697 for the PsaA side) could be suggested by structural model building under the constraints of the EPR data (Kamlowski et al., 1998; Zech et al., 2000). Independent evidence was provided from ESEEM data. Hyperfine coupling to a near ^{14}N spin and its quadrupole coupling yield a fingerprint for an interacting Trp residue (Hanley et al., 1997), as reviewed in Deligiannakis and Rutherford (2001).

However, for conclusions from just **g**-tensor data a word of caution is appropriate. Generally, π-stacking and H-bonding will both influence the **g**-tensor anisotropy, e.g., increased π-stacking as well as weaker H-bonding tend to increase the **g**-anisotropy. Even with the advanced calculation approaches available now, the weak and partly compensating effects make it difficult to disentangle the contributions due to different protein-cofactor interactions. However, in combination with a sufficiently large data set from independent EPR methods, the **g**-tensor data constitute a major contributor.

The measurement and evaluation of the considerably smaller **g**-tensor anisotropy of P_{700}^{+} and other naturally occurring Chl-type radical ions and neutral radicals have become an important domain of high field/frequency EPR (see, e.g., Bratt et al., 1997, for review Möbius et al., 2004).

Now, as X-ray structures at (nearly) atomic detail become available for the three main photosynthetic reaction centers: pbRC, PS I, and PS II, it is indeed clear that the strongest π-stacking is realized for the A_1 site in PS I. Another special feature is the strongest asymmetry in H-bonding: only one strong H-bond to just one quinone C–O group is observed (see section III.C.2.b). Moreover, the A_1 site in PS I has the most negative midpoint potential among all other well-characterized quinone binding sites. The identification of possible contributors from the A_1 environment as well as their control will be addressed next.

d. Protein-quinone interaction in the A_{1A} site: electrostatic interactions

Little experimental information is available concerning the number and significance of factors that contribute to the redox potential of protein-bound ET cofactors. These factors are difficult to separate and experimental access to them is limited. The PS I and PS II RCs of oxygenic photosynthesis (as well as other type I and type II RCs) represent an outstanding case, allowing one to probe the influence of the protein environment on cofactors within structurally partly homologous yet functionally very different membrane-bound complexes. The influence of the molecular identity of the quinone cofactor is minor and can be determined separately. For example, the same plastoquinone (PQ-9) acceptor, which is native to the Q_A site of PS II, has been shown to function also in the A_1 site of PS I (*menB* mutant) (Semenov et al., 2000). The key question is: how does the protein control the remaining large potential difference of ∼600 mV for PQ-9 in the A_1 site of PS I versus Q_A site of PS II? Some steps have been taken toward an answer. In general, the large potential difference appears to be composed of many small factors that add up. This makes the identification of individual contributions more difficult, but explains readily the general robustness of PS I against changes.

The first test is to introduce a small but systematic change in the redox potential for the quinone in the A_1 site. Anthraquinone (AQ) inserted into PS I is expected

to introduce a more negative redox potential in the A_1 site (see Iwaki and Itoh, 1991; Itoh et al. 2001). The energy difference between A_1 and F_X will increase, and ET between them speeds up. Correspondingly, the energy difference between A_0 and A_1 decreases and ET between them slows down. Indeed, for the first time consecutive forward-ET steps from A_0 to A_1 to F_X become observable by TR EPR spectroscopy (Sakuragi et al., 2005). Some key results are: (i) within experimental accuracy, AQ does not alter the structural integrity of the A_1 site. The relevant structural properties and protein–cofactor interactions parameters remain the same as observed for native PhQ. (ii) The slow down of the A_0 to A_1 kinetics is sufficient to be determined by the altered spin polarization pattern of the directly observed $P_{700}^{+}A_{1A}^{-}$ state. Forward-ET from A_1 to F_X is faster by an order of magnitude. The temperature dependence can be measured in a wider range. Reliable activation energies can be determined. (iii) Most important, access to the A_0 to A_1 kinetics opens a way to measure the influence of the presence or absence of the nominal negative charge $[Fe_4S_4(SCH_3)_4]^{2-}$ associated with F_X. Indeed, the largely compensated negative charge yields a more negative redox potential of AQ in the A_1 site. However the electrostatic calculations (Ishikita and Knapp, 2003) appear to overestimate the influence.

The essential contributions to the specific redox potential of the A_1 site come from the protein environment. The various site-directed mutants (tryptophan, serine, arginine) near the A_{1A} site produced only small changes in the midpoint potential (Xu et al., 2003a,b). All of them slow down the A_1-F_X ET kinetics, therefore they decrease the energy difference between the consecutive charge separated states, but only slightly. With increasing number of H-bonds to the Q acceptor (one in PS I *versus* two in type II RCs), the mid-point potential is predicted to be less reducing. The data indicate a much smaller effect (Pushkar et al., 2004b) as compared to the 100 up to 250 mV per H-bond noted at times in the general literature. Most attention focuses on differences in the wider electrostatic environment, for instance uncompensated charges, protonable groups, etc. Structure-based electrostatic calculations have advanced significantly. A key advantage is that individual mutational changes can be incorporated one by one; each respective contribution to the redox potential can be calculated separately. Predictions are available from a first set of electrostatic calculations (Ishikita and Knapp, 2003). Some of them have already been subjected to experimental test; others yield a guideline for further experimental tests.

So far, the mutant and cofactor changes studied up to now have resulted mostly in smaller changes of redox potential in experiment than predicted by the calculations.

IV. Concluding Remarks

This chapter has focused on how TR EPR spectroscopy is able to determine detailed properties of protein–cofactor interactions. An extensive database has been obtained for the quinone acceptor in the A_{1A} site of PS I. Note that mutually consistent data are available for the transient active $P_{700}^{\cdot+}A_{1A}^{\cdot-}$ as well as for the trapped photoaccumulated individual radical ion $A_{1A}^{\cdot-}$ state. Moreover, consequences concerning structural properties of the A_{1A} binding site as well as specific protein-quinone interactions (like H-bonding and π-stacking) agree well with the X-ray structure model (1JB0) for the ground state, see also Fig. 5. Certainly, models (like the valence bond model in Fig. 6) for the correlation between measured hyperfine tensor parameters and details of the H-bonding pattern to the protein environment still need refinement but essential conclusions such as highly asymmetric H-bonding, its geometry, and the differences to the A_{1A} site in pbRC are well confirmed.

The prime significance of such spectroscopic information is whether it can advance a better understanding of ET function in the photosynthetic RC. First, it needs to be assured that the PsaA branch is involved in ET function. Indeed, all spectroscopy- and mutant-based studies, including Guergova-Kuras et al. (2001) and Xu et al. (2003a,b), agree that under physiological conditions the PsaA branch dominates ET activity in PS I. Hence, the observed A_{1A} site properties are relevant to the question how ET function is affected by them. Of particular interest is a comparison to the Q_A site in pbRC. Both quinone sites function as one-electron gate in the primary charge separation event. As example one question may be specified to which TR EPR results can contribute significantly: Can the specific protein-cofactor interactions be identified, characterized, and possibly modified that control the mid-point (redox) potential of the first quinone acceptor? The significance of the question is most obvious when the (identical) quinone acceptor is observed to operate at a much more reducing (more negative) midpoint potential E_m when placed into the specific protein environment of the A_{1A} site of PS I in comparison to the Q_A site of type II RCs (pbRC or PS II) with a mid-point potential at least 0.5V more positive (see, e.g., Blankenship, 1992). Details

of protein-quinone interactions as collected in this chapter for the A_{1A} site in PS I can be compared with those available for the Q_A site of pbRC as reviewed in Lubitz and Feher (1999). Emerging structure-based electrostatic calculations (Ishikita and Knapp, 2003) can serve as a guideline to check for specific contributors to the very negative redox potential in the A_{1A} site of PS I. With the TR EPR data collected in this chapter some specific contributors can be already identified:

- One versus two H-bonds from the protein to the quinone in the A_{1A} versus Q_A site, but the difference in redox potential contribution is quite small.
- The nominal charges associated with the $[Fe_4S_4(SCH_3)_4]^{2-}$ clusters in PS I and the non-heme Fe^{2+} in pbRC do contribute, but less (Sakuragi et al., 2005) than expected from the electrostatic calculation (Ishikita and Knapp, 2003).
- The degree of protonation of specific residues is predicted to depend critically on the specific protein environment. With site-directed mutants the individual redox potential contributions can be measured individually.

All results available so far have in common that each of the specified contributions is significantly smaller than predicted by the cited calculations. Therefore, the large difference in redox potential between A_{1A} versus Q_A site is likely to be the sum of even more small contributions. Such a strategy is well in line with the general quality of robustness of PS I against changes.

The demonstrated ability to exchange the quinone in the A_1 site gently and with full site integrity concerning structural properties opens fine possibilities for further studies. With a systematic shift of the A_1 redox potential, the kinetics of the A_0 to A_1 to F_X electron transfer steps can be adjusted to the limited time window of the TR EPR spectroscopy. This will be needed to get access to these kinetic processes in the important class of homodimeric type I reaction centers or in direct detection of ET along the PsaB branch if control of the ET branching at the primary donor P_{700} will be possible as so far realized only for pbRC so far.

Acknowledgments

Sincere thanks go to the present and past members of my research group at the Free University Berlin for their dedicated research work and a highly motivating yet relaxed group atmosphere. Equally thankful we all are for the long standing invaluable cooperation with the members of our interdisciplinary partner labs of John Golbeck (PennState Univ.), Kev Salikhov (Russian Acad. of Sciences in Kazan), Art van der Est (Brock Univ. Canada), and many other international friends. The essential contributions of all the unnamed collaborators become apparent with the cited publications. Special thanks to Sabine Simon for her patient help with the many technical aspects of this manuscript. Generous DFG funding is acknowledged in recent years through Sfb 498 (project A3).

References

Amesz J (1995) The heliobacteria, a new group of photosynthetic bacteria. J Photochem Photobiol B 30: 89–96

Angerhofer A and Bittl R (1996) Radicals and radical pairs in photosynthesis. Photochem Photobiol 63: 11–38

Angstl R (1990) Calculation of molecular g tensors. Comparison of Rayleigh–Schroedinger and Hartree–Fock perturbation theory. Chem Phys 145: 413–426

Bell J (1993) Bertlmann‘s socks and the nature of reality. In: Bell J (ed) Speakable and Unspeakable in Quantum Mechanics, pp 139–158. Cambridge University Press, Cambridge

Biggins J and Mathis P (1988) Functional role of vitamin K_1 in photosystem I of the cyanobacterium *Synechocystis* 6803. Biochemistry 27: 1494–1500

Bittl R and Kothe G (1991) Transient EPR of radical pairs in photosynthetic reaction centers – prediction of quantum beats. Chem Phys Lett 177: 547–553

Bittl R and Weber S (2005) Transient radical pairs studied by time-resolved EPR. Biochim Biophys Acta 1707: 117– 126

Bittl R and Zech SG (1997) Pulsed EPR study of spin-coupled radical pairs in photosynthetic reaction centers: measurement of the distance between P_{700}^+ and A_1^- in photosystem I and between P_{865}^+ and Q_A^- in bacterial reaction centers. J Phys Chem B 101: 1429–1436

Bittl R and Zech SG (2001) Pulsed EPR spectroscopy on short-lived intermediates in Photosystem I. Biochim Biophys Acta 1507: 194–211

Bittl R, van der Est A, Kamlowski A, Lubitz W and Stehlik D (1994) Time-resolved EPR of the radical pair $P_{865}^+Q_A^-$ in bacterial reaction centers. Observation of transient mutations, quantum beats and envelope modulation effects. Chem Phys Lett 226: 349–358

Blankenship R (1992) Origin and early evolution of photosynthesis. Photosynth Res 33: 91–111

Blankenship R, McGuire A and Sauer K (1975) Chemically induced dynamic electron polarization in chloroplasts at room temperature: evidence for triplet state participation in photosynthesis. Proc Natl Acad Sci USA 72: 4943–4947

Bock CH, van der Est AJ, Brettel K and Stehlik D (1989) Nanosecond electron transfer kinetics in photosystem I as obtained from transient EPR at room temperature. FEBS Lett 247: 91–96

Bohm D (1951) Quantum Theory, pp. 611–623. Englewood-Cliff, New York

Bratt PJ, Rohrer M, Krzystek J, Evans MCW, Brunel LC and Angerhofer A (1997) Submillimeter high-field EPR studies of the primary donor in plant photosystem I P700. J Phys Chem B 101: 9686–9689

Brettel K (1988) Electron transfer from A_1^- to an iron–sulfur center with $t_{1/2} = 200$ ns at room temperature in Photosystem I. FEBS Lett 239: 93–98

Brettel K (1997) Electron transfer and arrangement of the redox cofactors in photosystem I. Biochim Biophys Acta 1318: 322–373

Brettel K and Leibl W (2001) Electron transfer in Photosystem I. Biochim Biophys Acta 1507: 100–114

Buckley CD, Hunter DA, Hore PJ and McLauchlan KA (1987) Electron spin resonance of spin-correlated radical pairs. Chem Phys Lett 135: 307–312

Budil DE and Thurnauer MC (1991) The chlorophyll triplet state as a probe of structure and function in photosynthesis. Biochim Biophys Acta 1057: 1–41

Closs GL, Forbes MDE and Norris JR (1987) Spin-polarized electron paramagnetic resonance spectra of radical pairs in micelles. Observation of electron spin–spin interactions. J Phys Chem 91: 3592–3599

Deligiannakis Y and Rutherford AW (2001) Electron spin echo envelope modulation spectroscopy in photosystem I. Biochim Biophys Acta 1507: 226–246

Dutton P, Leigh JS and Seibert M (1972) Primary processes in photosynthesis. In situ ESR studies on the light-induced oxidized and triplet state of reaction center bacteriochlorophyll. Biochem Biophys Res Commun 46: 406–413

Evans MCW and Nugent JHA (1993) Structure and function of the reaction center cofactors in oxygenic organisms. In: Deisenhofer J and Norris J (eds) The Photosynthetic Reaction Center. Academic Press, San Diego

Ferreira KN, Iverson TM, Maghlaoui K, Barber J and Iwata S (2004) Architecture of the photosynthetic oxygen-evolving center. Science 303: 1831–1838

Furrer R and Thurnauer MC (1983) Resolution of signals attributed to Photosystem-I primary reactants by time-resolved electron-paramagnetic-resonance at K-band. FEBS Lett 153: 399–403

Golbeck JH (1987) Structure, function and organization of the Photosystem I reaction center complex. Biochim Biophys Acta 895: 167–204

Grimaldi S, Ostermann T, Weiden N, Mogi T, Miyoshi H, Ludwig B, Michel H, Prisner T and MacMillan F (2003) Asymmetric binding of the high-affinity $QH^{\cdot -}$ ubisemiquinone in quinol oxidase (b_{o3}) from *Escherichia coli* studied by multifrequency electron paramagnetic resonance spectroscopy. Biochemistry 42: 5632–5639

Grinberg O and Berliner L (2004) Very High Frequency (VHF) ESR/EPR. Kluwer/Plenum Publishers, New York

Guergova-Kuras M, Boudreaux B, Joliot A, Joliot P and Redding K (2001) Evidence for two active branches for electron transfer in Photosystem I. Proc Natl Acad Sci USA 98: 4437–4442

Haffa ALM, Lin S, Williams JC, Bowen BP, Taguchi AKW, Allen JP and Woodbury NW (2004) Controlling the pathway of photosynthetic charge separation in bacterial reaction centers. J Phys Chem 108: 4–7

Hanley J, Deligiannakis Y, MacMillan F, Bottin H and Rutherford AW (1997) ESEEM study of the phyllosemiquinone radical $A_1^{\cdot -}$ in ^{14}N- and ^{15}N-labeled Photosystem I. Biochemistry 36: 11543–11549

Heinen U, Golecki JR, Poluektov OG, Berthold T, Schlesselman SL, Frezzato D, Ohmes E, Moro GJ, Thurnauer M and Kothe G (2004a) Magnetic field induced orientation of photosynthetic reaction centers as revealed by time-resolved W-band EPR of spin-correlated radical pairs. III. Development of a molecular model. Appl Magn Reson 26: 99–115

Heinen U, Poluektov OG, Stavitski E, Berthold T, Ohmes E, Schlesselman SL, Golecki JR, Moro GJ, Levanon H, Thurnauer M and Kothe G (2004b) Magnetic field induced orientation of photosynthetic reaction centers as revealed by time-resolved D-band EPR of spin-correlated radical pairs. II. Field dependence of the alignment. J Phys Chem B 108: 9498–9504

Heinnickel M, Shen G, Agalarov R and Golbeck JH (2005) Resolution and reconstitution of a bound Fe–S protein from the photosynthetic reaction center of *Heliobacterium modesticaldum*. Biochemistry 44: 9950–9960

Hoff A (1984) Electron spin polarization of photosynthetic reactants. Q Rev Biophys 17: 153–282

Hoff A and Deisenhofer J (1997) Photophysics of photosynthesis. Structure and spectroscopy of reaction centers of purple bacteria. Phys Rep 287: 1–247

Hore PJ (1989) Analysis of polarized EPR spectra. In: Hoff AJ (ed) Advanced EPR in Biology and Biochemistry, Chapter 12, pp 405–440. Elsevier, Amsterdam

Huber M, Törring J, Plato M, Fink U, Lubitz W, Feick R, Schenck C and Möbius K (1995) Investigation of the electronic structure of the primary electron donor in bacterial photosynthesis – measurements of the anisotropy of the electronic g-tensor using high-field/high-frequency EPR. Sol Energy Mater Sol Cells 38: 119–126

Ishikita H and Knapp EW (2003) Redox potential of quinones in both electron transfer branches of photosystem I. J Biol Chem 278: 52002–52011

Itoh S, Iwaki M and Ikegami I (2001) Modification of Photosystem I reaction center by the extraction and exchange of chlorophylls and quinones. Biochim Biophys Acta 1507: 115–138

Iwaki M and Itoh S (1991) Structure of the phylloquinone-binding Q_{Ph} site in green plant photosystem I reaction centers: the affinity of quinones and quinoid compounds for the Q_{Ph} site. Biochemistry 30: 5347–5352

Jeschke G, Rakhmatullin R and Schweiger A (1998) Sensitivity enhancement by matched microwave pulses in one- and two-dimensional electron spin echo envelope modulation spectroscopy. J Magn Reson 131: 261–271

Johnson TW, Zybailov B, Jones AD, Bittl R, Zech S, Stehlik D, Golbeck JH and Chitnis PR (2001) Recruitment of a foreign quinone into the A_1 site of Photosystem I – *in vivo* replacement of plastoquinone-9 by media-supplemented naphthoquinones in phylloquinone biosynthetic pathway mutants of *Synechocystis* sp PCC 6803. J Biol Chem 276: 39512–39521

Joliot P and Joliot A (1999) In vivo analysis of the electron transfer within Photosystem I: are the two phylloquinones involved? Biochemistry 38: 11130–11136

Jordan P, Fromme P, Witt HT, Klukas O, Saenger W and Krauß N (2001) Three dimensional structure of Photosystem I at 2.5 Å resolution. Nature 411: 909–917

Kamiya N and Shen JR (2003) Crystal structure of oxygen-evolving photosystem II from *Thermosynechococcus vulcanus* at 3.7 Å resolution. Proc Natl Acad Sci USA 100: 98–103

Kamlowski A, van der Est A, Fromme P, Krauß N, Schubert WD, Klukas O and Stehlik D (1997a) The structural organization of the PsaC protein in Photosystem I from single crystal EPR and x-ray crystallographic studies. Biochim Biophys Acta 1319: 199–213

Kamlowski A, van der Est A, Fromme P and Stehlik D (1997b) Low temperature EPR on Photosystem I single crystals: orientation of the iron–sulfur centers F_A and F_B. Biochim Biophys Acta 1319: 185–198

Kamlowski A, Altenberg-Greulich B, van der Est A, Zech SG, Bittl R, Fromme P, Lubitz W and Stehlik D (1998) The quinone acceptor A_1 in photosystem I: binding site, and comparison to Q_A in purple bacteria reaction centers. J Phys Chem B 102: 8278–8287

Kandrashkin YE, Vollmann W, Stehlik D, Salikhov K and van der Est A (2002) The magnetic field dependence of the electron spin polarization in consecutive spin correlated radical pairs in type I photosynthetic reaction centres. Mol Phys 100: 1431–1443

Kirmaier C, Laible PD, Hanson DK and Holten D (2003) B-side charge separation in bacterial photosynthetic reaction centers: nanosecond time scale electron transfer from H_B^- to Q_B. Biochemistry 42: 2016–2024

Kleinfeld D, Okamura MY and Feher G (1984) Electron-transfer kinetics in photosynthetic reaction centers cooled to cryogenic temperatures in the charge-separated state: evidence for light-induced structural changes. Biochemistry 23: 5780–5786

Klette R, Törring J, Plato M, Möbius K, Boenigk B and Lubitz W (1993) Determination of the g tensor of the primary donor cation radical in single crystals of *Rhodobacter sphaeroides* R-26 reaction centers by 3-mm high-field EPR. J Phys Chem 97: 2015–2020

Kothe G, Weber S, Bittl R, Ohmes E, Thurnauer M and Norris J (1991) Transient EPR of light-induced radical pairs in plant photosystem: I. Observation of quantum beats. Chem Phys Lett 186: 474–480

Kothe G, Weber S, Ohmes E, Thurnauer MC and Norris JR (1994) High time resolution electron paramagnetic resonance of light-induced radical pairs in photosynthetic bacterial reaction centers: observation of quantum beats. J Am Chem Soc 116: 7729–7734

Krabben L, Schlodder E, Jordan R, Carbonera D, Giacometti G, Lee H, Webber AN and Lubitz W (2000) Influence of the axial ligands on the spectral properties of P700 of Photosystem I: a study of site-directed mutants. Biochemistry 39: 13012–13025

Link G, Berthold T, Bechtold M, Weidner JU, Ohmes E, Tang J, Poluektov O, Utschig L, Schlesselman SL, Thurnauer MC and Kothe G (2001) Structure of the $P_{700}^+A_1^-$ radical pair intermediate in photosystem I by high time resolution multifrequency electron paramagnetic resonance: analysis of quantum beat oscillations. J Am Chem Soc 123: 4211–4222

Lubitz W and Feher G (1999) The primary and secondary acceptors in bacterial photosynthesis III. Characterization of the quinone radicals Q_A^- and Q_B^- by EPR and ENDOR. Appl Magn Reson 17: 1–48

MacMillan F, Hanley J, vanderWeerd L, Knupling M, Un S and Rutherford AW (1997) Orientation of the phylloquinone electron acceptor anion radical in photosystem I. Biochemistry 36: 9297–9303

Möbius K (2003) Multifrequency EPR and ENDOR on transient radicals and radical pairs in liquid crystals and proteins: structure and dynamics of cofactors in natural and artificial photosynthesis. Mol Cryst Liq Cryst 394: 1–17

Möbius K, Savitsky A and Fuchs M (2004) Primary processes in photosynthesis: what do we learn from high-field EPR spectroscopy? In: Grinberg O and Berliner L (eds) Very High Frequency (VHF) ESR/EPRL, pp 45–93. Kluwer/Plenum Publisher, New York

Nitschke W and Rutherford AW (1991) Photosynthetic reaction centres: variations on a common structural theme? Trends Biochem Sci 16: 241–245

Paddock ML, Chang C, Xu Q, Abresch EC, Axelrod HL, Feher G and Okamura MY (2005) Quinone (Q_B) reduction by B-branch electron transfer in mutant bacterial reaction centers from *Rhodobacter sphaeroides*: quantum efficiency and X-ray structure. Biochemistry 44: 6920–6928

Prisner TF, van der Est A, Bittl R, Lubitz W, Stehlik D and Möbius K (1995) Time-resolved W-band (95 GHz) EPR spectroscopy of Zn-substituted reaction centers of *Rhodobacter sphaeroides* R-26. Chem Phys 194: 361–370

Prisner T, Rohrer M and MacMillan F (2001) Pulsed EPR spectroscopy: biological applications. Annu Rev Phys Chem 52: 279–313

Pushkar YN, Zech SG, Stehlik D, Brown S, van der Est A, and Zimmermann H (2002) Orientation and protein–cofactor interactions of monosubstituted *n*-alkyl naphthoquinones in the A_1 binding site of photosystem I. J Phys Chem B 106: 12052-12058.

Pushkar YN, Golbeck JH, Stehlik D and Zimmermann H (2004a) Asymmetric hydrogen-bonding of the quinone cofactor in Photosystem I probed by ^{13}C labeled naphthoquinones. J Phys Chem B 108: 9439–9450

Pushkar YN, Stehlik D, van Gastel M and Lubitz W (2004b) An EPR/ENDOR study of the asymmetric hydrogen bond between the quinone electron acceptor and the protein backbone in Photosystem I. J Mol Struct 700: 233–241

Pushkar YN, Karyagina I, Stehlik D, Brown S and van der Est A (2005) Recruitment of a foreign quinone into the A_1 site of photosystem I. Consecutive forward electron transfer from A_0 to A_1 to F_X with anthraquinone in the A_1 site as studied by transient EPR. J Biol Chem 280: 12382–12390

Reiter RC, Stevenson GR and Wang ZY (1990) Total π spin density mapping as a function of hydrogen bonding involving an anion radical. J Phys Chem 94: 5717–5720

Rigby SEJ, Muhiuddin IP, Evans MCW, Purton S and Heathcote P (2002) Photoaccumulation of the PsaB phyllosemiquinone in Photosystem I of *Chlamydomonas reinhardtii*. Biochim Biophys Acta 1556: 13–20

Rutherford AW and Sétif P (1990) Orientation of P_{700}, the primary electron donor of photosystem I. Biochim Biophys Acta 1019: 128–132

Sakuragi Y, Zybailov B, Shen GZ, Jones AD, Chitnis PR, van der Est A, Bittl R, Zech S, Stehlik D, Golbeck JH and Bryant DA (2002) Insertional inactivation of the *menG* gene, encoding 2-phytyl-1,4-naphthoquinone methyltransferase of *Synechocystis* sp PCC 6803, results in the incorporation of 2-phytyl-1,4-naphthoquinone into the A_1 site and alteration of the equilibrium constant between A_1 and F_X in Photosystem I. Biochemistry 41: 394–405

Sakuragi Y, Zybailov B, Shen G, Bryant DA, Golbeck JH, Diner BA, Karyagina I, Pushkar Y and Stehlik D (2005) Characterization of a foreign quinone into the A_1 site of photosystem I. Characterization of a *menB rubA* double deletion mutant in

Synechococcus sp. PCC 7002 devoid of F_X, F_A and F_B and containing plastoquinone or exchanged 9,10-anthraquinone. J Biol Chem 280: 12371–12381

Salikhov KM, Bock CH and Stehlik D (1990) Time development of electron spin polarization in magnetically coupled, spin correlated radical pairs. Appl Magn Reson 1: 195–211

Salikhov KM, van der Est AJ and Stehlik D (1999) The transient EPR spectra and spin dynamics of coupled three-spin systems in photosynthetic reaction centres. Appl Mag Res 16: 101–134

Salikhov KM, Zech SG and Stehlik D (2002a) Light induced radical pair intermediates in photosynthetic reaction centres in contact with an observer spin label: spin dynamics and effects on transient EPR spectra. Mol Phys 100: 1311–1321

Salikhov KM, Zech SG and Stehlik D (2002b) Light induced radical pair intermediates in photosynthetic reaction centres in contact with an observer spin label: spin dynamics and effects on transient EPR spectra. Mol Phys 100: 3331–3331

Salikhov KM, Pushkar YN, Golbeck JH and Stehlik D (2003) Interpretation of multifrequency transient EPR spectra of the $P^+_{700}A_0Q^-_K$ state in Photosystem I complex with a sequential correlated radical pair model: wild type versus A_0 mutants. Appl Magn Reson 24: 467–482

Santabarbara S, Kuprov I, Fairclough WV, Purton S, Hore P, Heathcote P and Evans MC (2005) Bidirectional electron transfer in Photosystem I: determination of two distances between P^+_{700} and A^-_1 in spin-correlated radical pairs. Biochemistry 44: 2119–2128

Schlodder E, Falkenberg K, Gergeleit M and Brettel K (1998) Temperature dependence of forward and reverse electron transfer from A^-_1, the reduced secondary electron acceptor in photosystem I. Biochemistry 37: 9466–9476

Schweiger A and Jeschke G (2001) Principles of Pulse Electron Paramagnetic Resonance Spectroscopy. Oxford University Press, Oxford

Semenov AY, Vassiliev IR, van der Est A, Mamedov MD, Zybailov B, Shen GZ, Stehlik D, Diner BA, Chitnis PR and Golbeck JH (2000) Recruitment of a foreign quinone into the A_1 site of Photosystem I – altered kinetics of electron transfer in phylloquinone biosynthetic pathway mutants studied by time-resolved optical, EPR, and electrometric techniques. J Biol Chem 275: 23429–23438

Sieckmann I, Brettel K, Bock C, van der Est A and Stehlik D (1993) Transient electron-paramagnetic-resonance of the triplet-state of P_{700} in Photosystem I. Evidence for triplet delocalization at room-temperature. Biochemistry 32: 4842–4847

Stehlik D and Möbius K (1997) New EPR methods for investigating photoprocesses with paramagnetic intermediates. Annu Rev Phys Chem 48: 745–784

Stehlik D, Bock CH and Thurnauer MC (1989) Transient EPR-spectroscopy of photoinduced electronic spin states in rigid matrices. In: Hoff AJ (ed) Advanced EPR in Biology and Biochemistry, pp 371–403. Elsevier, Amsterdam

Stone A (1963) Gauge invariance of the g tensor. Proc R Soc Lond Ser A 271: 424

Tang J, Utschig LM, Poluektov O and Thurnauer MC (1999) Transient W-band EPR study of sequential electron transfer in photosynthetic bacterial reaction centers. J Phys Chem B 103: 5145–5150

Thurnauer MC and Norris JR (1980) An electron-spin echo phase-shift observed in photosynthetic algae – possible evidence for dynamic radical pair interactions. Chem Phys Lett 76: 557–561

van der Est A (2001) Light-induced spin polarization in type I photosynthetic reaction centres. Biochim Biophys Acta 1507: 212–225

van der Est A, Sieckmann I, Lubitz W and Stehlik D (1995) Differences in the binding of the primary quinone acceptor in Photosystem-I and reaction centers of *Rhodobacter sphaeroides*- R26 studied with transient EPR spectroscopy. Chem Phys 194: 349–359

Xu W, Chitnis P, Valieva A, van der Est A, Pushkar YN, Krzystyniak M, Teutloff C, Zech SG, Bittl R, Stehlik D, Zybailov B, Shen GZ and Golbeck JH (2003a) Electron transfer in cyanobacterial Photosystem I – I. Physiological and spectroscopic characterization of site-directed mutants in a putative electron transfer pathway from A_0 through A_1 to F_X. J Biol Chem 278: 27864–27875

Xu W, Chitnis PR, Valieva A, van der Est A, Brettel K, Guergova-Kuras M, Pushkar YN, Zech SG, Stehlik D, Shen GZ, Zybailov B and Golbeck JH (2003b) Electron transfer in cyanobacterial photosystem I – II. Determination of forward electron transfer rates of site-directed mutants in a putative electron transfer pathway from A_0 through A_1 to F_X. J Biol Chem 278: 27876–27887

Zech SG, Hofbauer W, Kamlowski A, Fromme P, Stehlik D, Lubitz W and Bittl R (2000) A structural model for the charge separated state $P^+_{700}A^-_1$ in photosystem I from the orientation of the magnetic interaction tensors. J Phys Chem B 104: 9728–9739

Zeilinger A (1999) Experiment and the foundations of quantum physics. Rev Modern Phys 71: 288–297

Zouni A, Witt HT, Kern J, Fromme P, Krauß N, Saenger W and Orth P (2001) Crystal structure of photosystem II from *Synechococcus elongatus* at 3.8 Ångstrom resolution. Nature 409: 739–743

Zouni A, Biesiadka J, Loll B, Kern J and Irrgang K (2004) Crystal structure of cyanobacterial photosystem II at 3.2 Å resolution: a closer look at the Mn cluster. Phys Chem Chem Phys 6: 4733–4736

Zybailov B, van der Est A, Zech SG, Teutloff C, Johnson TW, Shen GZ, Bittl R, Stehlik D, Chitnis PR and Golbeck JH (2000) Recruitment of a foreign quinone into the A_1 site of photosystem I – II. Structural and functional characterization of phylloquinone biosynthetic pathway mutants by electron paramagnetic resonance and electron-nuclear double resonance spectroscopy. J Biol Chem 275: 8531–8539

Chapter 24

Electron Transfer Involving Phylloquinone in Photosystem I

Art van der Est*
Department of Chemistry, Brock University, 500 Glenridge Avenue, St. Catharines, Ontario, Canada L2S 3A1

Summary

This chapter focuses on the kinetics of electron transfer through A_1 in Photosystem I. The techniques used to study this step are described and their relative advantages and disadvantages are discussed. This is followed by a review of recent results that have been obtained since the publication of the 2.5 Å resolution X-ray structure. Older results are also presented where they are relevant to the new data. However, this chapter is not meant as an exhaustive review of the literature, and interested readers are directed to earlier reviews and other chapters in this volume where appropriate. The main focus of the chapter is the factors such as the energetics and structural arrangement of the cofactors that determine the kinetics of the electron transfer through phylloquinone. These topics are discussed

* Author for correspondence, email: avde@brocku.ca

John H. Golbeck (ed): Photosystem I: The Light-Driven Plastocyanin:Ferredoxin Oxidoreductase, 387–411.

primarily in terms of recent results, which have lead to advances in our understanding of how electron transfer is governed. A large portion of the chapter necessarily deals with the question of the activity of the two phylloquinones in Photosystem I, and the data supporting the unidirectional and bi-directional models are compared and contrasted.

I. Introduction

The Photosystem I (PS I) enzyme functions as an oxidoreductase, oxidizing plastocyanin, or cytochrome c_6 on the lumenal side of the thylakoid membrane and reducing soluble ferrodoxin or flavodoxin on the stromal side. This is achieved via a light-induced electron transfer reaction, which produces the oxidant P_{700}^{+} (a chlorophyll cation radical) and the strong reductant F_B^{-} (a reduced iron–sulfur cluster). Phylloquinone acts as a protein-bound intermediate known as A_1 in this electron transfer reaction, re-oxidizing the primary electron acceptor A_0^{-} and reducing the first iron–sulfur cluster F_X. This is a somewhat unusual function for a quinone, since their primary roles in energy transducing membranes are as mobile lipophilic proton and electron carriers (Cramer and Knaff, 1990). In the thylakoid membrane, for example, the most prevalent quinone, plastoquinone, transports electrons from Photosystem II (PS II) to the cytochrome b_6/f complex and carries protons from the stroma to the lumen. Plastoquinone also acts as the bound electron acceptor Q_A in PS II but its reduction midpoint potential (Rappaport et al., 2002) is 600–800 mV more positive than that of phylloquinone in PS I (see Brettel, 1997 for a discussion of the midpoint potential of A_1). The unusually negative reduction midpoint potential of phylloquinone in PS I is due largely to the influence of the protein environment. This is illustrated by the difference in midpoint potential observed for quinones in the A_1 binding site of PS I and the Q_A binding site in PS II. This comparison shows that when plastoquinone is introduced into the A_1 binding site in PS I its midpoint potential is estimated to be 550–600 mV more negative than in the Q_A site in PS II (Johnson et al., 2000; Semenov et al., 2000; Zybailov et al., 2000). Much of the research on electron transfer in PS I has been fueled by a desire to understand such effects and their role in determining the function of the enzyme. Because of the large influence of the protein on the properties of phylloquinone in PS I and because it can be observed spectroscopically with relative ease, it is among the most widely studied components of PS I.

Despite the large body of research on the electron transfer kinetics involving phylloquinone, there are still a number of unresolved issues. One of the most interesting of these has arisen from the fact that the X-ray structure (Klukas et al., 1999; Fromme et al., 2001; Jordan et al., 2001) reveals two symmetry-related phylloquinone molecules (see Fig. 1). There are no obvious features in the structure to suggest whether only one or both of the quinones is active and whether their electron transfer kinetics are distinguishable. Moreover, the presence of two branches of cofactors is intriguing since there is no apparent advantage or disadvantage to such an arrangement in PS I. With the resolution of the amino acid side groups in the X-ray structure (Klukas et al., 1999; Fromme et al., 2001; Jordan et al., 2001), it has become possible to interpret the results of point mutation studies on the basis of specific expected structural changes. This has allowed the electron transfer pathway to be studied at a level of detail that was previously not possible. Moreover, it has allowed the role of the protein environment in determining the function to be investigated both experimentally and theoretically.

In this chapter, recent developments in our understanding of the electron transfer through the phylloquinone in PS I will be summarized and discussed. The discovery of the electron transfer intermediate A_1 and its identification as phylloquinone are reviewed by Mathis and Sauer (this volume, Chapter 4) and elsewhere (Golbeck, 1989; Golbeck and Bryant, 1991). Hence, they will not be presented in detail here. This chapter is intended to complement previous review articles on the function of PS I (Golbeck, 1989; 1992; Brettel, 1997; Brettel and Leibl, 2001), in which mutagenesis and structure based studies are either not discussed or are only mentioned briefly as an emerging area of interest. Because many of these studies address the issue of directionality, it is a central theme of the chapter. However, the main focus is on electron transfer through phylloquinone; the review by Redding and van der Est (this volume, Chapter 25) will address question of directionality in general.

A. Types of Photosynthetic Reaction Centers

Photosynthetic reaction centers are generally divided up into two types on the basis of the nature of terminal acceptors (Blankenship, 2002). One class has iron–sulfur clusters as terminal acceptors, which reduce water-soluble acceptors such as ferredoxin. The

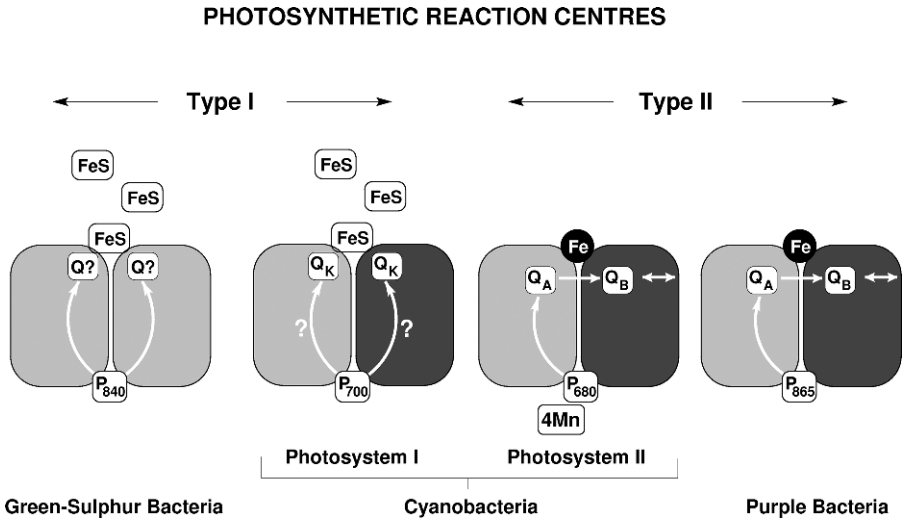

Fig. 1. Schematic representation of the reaction centers of different classes of photosynthetic bacteria. The shaded ovals represent the protein dimer of the reaction center core. In the reaction centers of green sulfur bacteria, the two subunits are identical and hence the same shading is used for both. In the other reaction centers, the two proteins are different and thus they are shaded differently. The arrows represent the known or postulated pathway of electron transfer from the primary donor P to the quinones Q. FeS = iron–sulfur clusters, Fe = non-heme iron, 4Mn = Manganese containing water-splitting-complex of PS II.

other class has a lipophylic quinone as the terminal acceptor, which diffuses out of the reaction centers upon double reduction and protonation. In the first case, the reaction centers are referred to as iron–sulfur type or Type I because PS I belongs to this class. In the second case they are called iron–quinone or Type II because of the presence of a non-heme iron atom in the reaction center and the fact that PS II belongs to this class. Despite these differences, the general features and overall structure of the reaction centers of various organisms are quite similar (Schubert et al., 1998). In all cases, the reaction center core consists of a protein dimer and the primary electron donor is a (bacterio)chlorophyll dimer. The two proteins forming the dimer bind two branches of cofactors, which extend across the membrane from the donor. Figure 1 shows a schematic diagram of this arrangement in the reaction centers of several species of photosynthetic bacteria. The proteins are depicted as shaded ovals and the thick arrows indicate the pathway (as far as it is known) of electron transfer from the donor P, to the quinone acceptors, Q. In Type II reaction centers, shown on the right of Fig. 1, the dimer is made up of two different protein subunits as indicated by the different shading. In these types of reaction centers, electron transfer is biased very strongly toward the branch containing the nonmobile quinone Q_A, which (upon accepting an electron) then reduces the mobile quinone Q_B in the other branch. In Type I reaction centers, the situation is less clear with the two branches of cofactors converging at the iron–sulfur cluster (FeS) bound by both subunits. In green sulfur bacteria and heliobacteria (Fig. 1 left), the two protein subunits of the dimer are identical and the two branches of cofactors are indistinguishable to the best of our knowledge. Conflicting evidence for the participation of a quinone in electron transfer has been reported for these reaction centers, with kinetic measurements pointing toward no involvement (Brettel et al., 1998; van der Est et al., 1998), while photoaccumulation studies show that semiquinone radicals can be trapped (Kjaer et al., 1998; Muhiuddin et al., 1999). PS I is an interesting intermediate case with two distinguishable electron transfer pathways, both of which contain a quinone acceptor. However, unlike the Type II reaction centers, in which two electrons must be accumulated on Q_B, there is no obvious need to bias the electron transfer towards one branch or the other.

The electron transfer through the quinones in PS I, presents an intriguing problem. This is not only a question of whether they are both active or not but also how the relatively subtle differences in the structure of the two protein subunits influences the properties of the two quinones.

B. Overview of Electron Transfer Kinetics in Photosystem I

Figure 2 shows an approximate energy and kinetic scheme for electron transfer in PS I based on literature values of the midpoint potentials of the cofactors

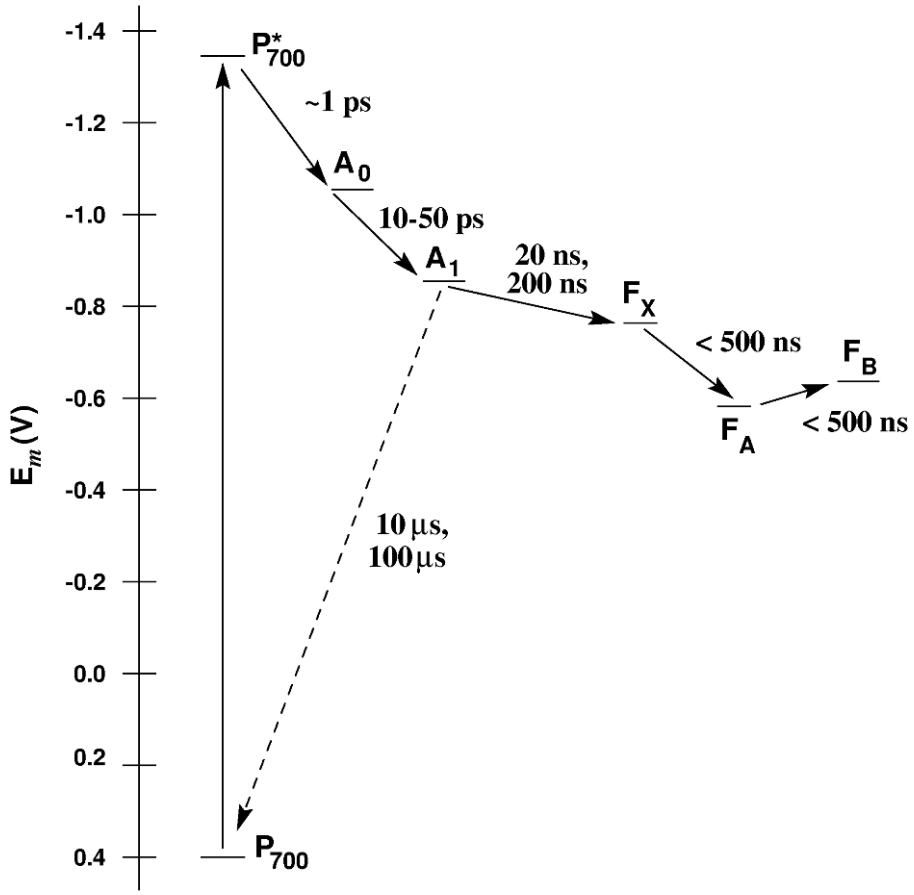

Fig. 2. Approximate electron transfer lifetimes and mid-point potentials of cofactors in PS I. The figure has been adapted from similar schemes given in Semenov et al. (2000) and Brettel and Leibl (2001). The lifetimes and potentials are average values from the literature.

and lifetimes of the intermediates. Here, only a brief overview is presented and the interested reader is referred to previous reviews (Brettel, 1997; Brettel and Leibl, 2001) for a more detailed discussion of the redox potentials and kinetics (see Shinkarev, this volume, Chapter 36). However, particular steps in the kinetic scheme shown in Fig. 2 will be discussed at length later in the chapter. Following excitation of P_{700}, either directly or by energy transfer from the antenna, an electron is transferred from P^*_{700} to A_0. All spectroscopic and structural data point to A_0^- being a chlorophyll *a* radical anion (Brettel and Leibl, 2001; Fromme et al., 2001) while P^+_{700} is the cation radical of a chlorophyll dimer (Fromme et al., 2001; Webber and Lubitz, 2001). At present it is unclear whether P^*_{700} is localized on the same chlorophylls as P^+_{700} and whether the charge separation occurs directly between P^*_{700} and A_0 or via an intermediate chlorophyll acceptor. The lifetime of the initial charge separation is difficult to determine because the overall trapping time of the excitation is considerably longer. Thus, it is necessary to either subtract the antenna excited state dynamics in the spectral data or to model the energy transfer and include the charge separation lifetime as a parameter. Several recent studies place the lifetime of the initial charge separation at roughly 1 ps (Savikhin et al., 2001; Byrdin et al., 2002; Yang et al., 2003) in general agreement with earlier work (see Gobets and van Grondelle, 2001 and Brettel and Leibl, 2001 for reviews of the literature up to 2001; see Savikhin, this volume, Chapter 12).

Electron transfer from A_0^- to the phylloquinone acceptor A_1 stabilizes the charge separation. The lifetime of this step has been determined to be ~30 ps by a number of authors (Hastings et al., 1994; Hecks et al., 1994; Brettel and Vos, 1999; Mi et al., 1999; Savikhin et al., 2001), although there is some variation in values obtained as a result of differences in the details of data analysis and techniques used. The subsequent

reoxidation of A_1^- has been measured by a number of different techniques and two lifetimes of approximately 20 and 200 ns (Brettel, 1988; Bock et al., 1989; Sétif and Brettel, 1993; Leibl et al., 1995; Schlodder et al., 1998; Joliot and Joliot, 1999) have been found. Although the spectroscopic data suggest electron transfer to an iron–sulfur cluster, none of these experiments clearly identifies the acceptor following A_1. This question has been answered by experiments in which the three iron–sulfur clusters were selectively removed. Three independent studies showed that the rate of forward electron transfer past A_1 was unaffected by removal of F_A and F_B but that it was blocked by the removal of F_X indicating that it is the subsequent acceptor (Luneberg et al., 1994; Moenne-Loccoz et al., 1994; van der Est et al., 1994). Below the glass transition temperature of the protein, forward transfer past A_1 is blocked in approximately one half of the reaction centers and stable formation of $P_{700}^+F_A^-$ occurs in the other half (Brettel, 1997). When the iron–sulfur clusters are absent, charge recombination from A_1 takes place with lifetimes of ~10 and 100 μs (Brettel and Golbeck, 1995; Shen et al., 2002a). At present it is unknown whether a correlation exists between the two fractions observed at low temperature, the two kinetic phases of forward electron transfer and the two back reaction rates.

Electron transfer through the iron–sulfur clusters is not well characterized. The order of F_A and F_B was a controversial topic for many years. However, there is now consensus that F_B is the terminal acceptor and that the electron transfer proceeds from F_X to F_A to F_B (see Vassiliev et al., 2001 for a review). Although, the order of the clusters in the electron transfer chain has now been established, the kinetics of the electron transfer is not certain. Photovoltage measurements and studies of the reduction of ferredoxin suggest an overall lifetime for electron transfer to F_B of less than 500 ns (Brettel and Leibl, 2001). However, at present accurate values of the lifetimes of the individual steps are not available (see Semenov et al., this volume, Chapter 21).

C. Location and Structure of the Phylloquinone Binding Site

Figure 3 shows the overall arrangement of the electron transfer cofactors in the 2.5 Å resolution X-ray structure of PS I (Jordan et al., 2001) viewed along the plane of the thylakoid membrane. Light excitation of the complex leads to electron transfer along one or

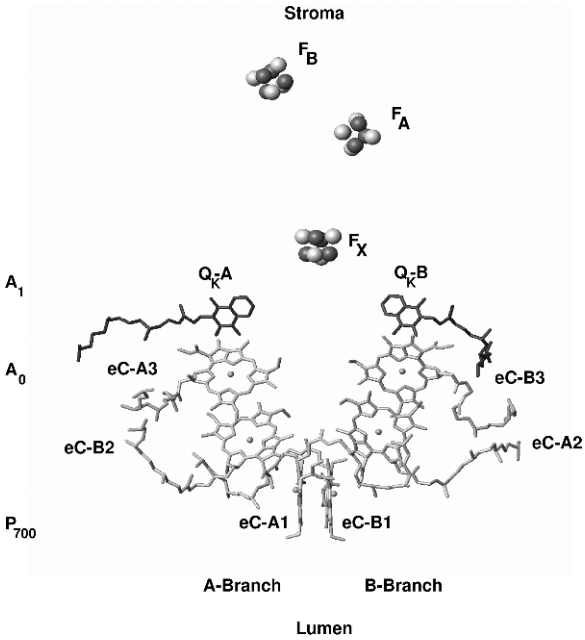

Fig. 3. Arrangement of the electron transfer cofactors of PS I. from the 2.5 Å resolution X-ray structure (Jordan et al., 2001) (pdb entry **1JB0**). The complex is shown from a direction roughly parallel to the membrane plane and the cofactors are labeled using the naming scheme given in Jordan et al. (2001). The two branches of cofactors are referred to as the A-branch and B-branch as indicated. On the left of the figure the spectroscopic names of the electron transfer components are given. Because the assignment of the spectroscopic species is still under debate the labels have been place adjacent to the A- and B-branch cofactors thought to be associated with them. The figure was constructed using the program MOLMOL (Koradi et al., 1996).

both of the branches of cofactors extending from the chlorophyll dimer (eC-A1, eC-B1) on the lumenal side of the membrane to the iron–sulfur clusters on the stromal side. The presence of two branches creates a problem in devising a consistent naming scheme because of the ambiguity in assigning the spectroscopic species to the structure. Hence, in the literature, the term A_1 is generally used to refer to one or both of the phylloquinones in connection with spectroscopic data, while Q_K-A and Q_K-B refer to the two phylloquinones bound to the PsaA and PsaB protein subunits, respectively. In Fig. 3 the structure is viewed such that the A- and B-branches of cofactors are on the left and right, respectively, as indicated by the label under each branch. The individual cofactors are labeled with their structural names, while the spectroscopic terms are given on the left and are not associated with either branch. The structural labels, eC-A1, eC-B1, etc., for the chlorophyll molecules indicate that they belong to the electron

transfer chain and gives the subunit to which they are bound, e.g., eC-A1 is bound to PsaA and eC-B1 is bound to PsaB. Note, however, that the protein subunit does not always correspond to the branch. For example, chlorophyll eC-B2 is bound to PsaB but is in the A-branch and chlorophyll eC-A2 is bound to PsaA but is in the B-branch. Despite the apparent C_2 rotational symmetry of the complex there are some notable differences between the two branches. The most striking of these is that eC-A1 and eC-B1 are different stereoisomers of chlorophyll *a* with significantly different binding pockets (Fromme et al., 2001; Jordan et al., 2001).

Figure 4 shows a closer view of the quinone binding region in the two branches. In the upper part of the figure, which shows the A-branch binding site, the structure is viewed from approximately the same perspective as in Fig. 3. In the bottom part of Fig. 4, the direction along which the structure is viewed is rotated by 180° about the normal to the membrane (crystallographic *c*-axis). If the structure had perfect C_2 symmetry, the two views would be identical. As is evident from Fig. 4 this is nearly the case. However, careful inspection reveals some small differences, for example, the conformation of the phytyl tails of Q_K-A and Q_K-B is different. Because of their proximity to the respective phylloquinones and in analogy to the pheophytin in Type II reaction centers, one or both of chlorophylls eC-A3 and eC-B3 is assumed to be the acceptor A_0. However, this assignment has not yet been demonstrated conclusively. The three cofactors A_0, A_1, and F_X are linked by a network of contacts and hydrogen bonds, which bind them to the protein and may promote electron transfer between them. Methionine $M688_{PsaA}$ ($M668_{PsaB}$) is the axial ligand to chlorophyll eC-A3 (eC-B3) and is also H-bonded via its backbone oxygen to $S692_{PsaA}$ ($S672_{PsaB}$). The side chain oxygen of $S692_{PsaA}$ ($S672_{PsaB}$) is also H-bonded to the ring nitrogen of $W697_{PsaA}$ ($W677_{PsaB}$). This tryptophan is π-stacked with the phylloquinone Q_K-A (Q_K-B), which is H-bonded to $L722_{PsaA}$ ($L706_{PsaB}$). In turn, the backbone oxygen of $L722_{PsaA}$ ($L706_{PsaB}$) is H-bonded to the F_X binding loop through $R694_{PsaA}$ ($R674_{PsaB}$).

The two most striking features of the quinone binding pocket are the close π-stacked arrangement with $W697_{PsaA}$ ($W677_{PsaB}$) and the lack of a hydrogen bond to an amino acid side chain. Both of these features would be expected to destabilize a negative charge on the quinone and undoubtedly contribute to its very negative redox potential. Because of their, apparent involvement in quinone binding and possible significance for electron transfer these residues have been targeted for site-directed mutagenesis studies (Evans et al., 1999; Boudreaux et al., 2001; Guergova-Kuras et al., 2001; Cohen et al., 2003; Fairclough et al., 2003; Gong et al., 2003; Xu et al., 2003a,b).

II. Techniques for Studying Electron Transfer Through Phylloquinone

A. Direct Methods

1. Flash Absorption Spectroscopy

Flash absorbance spectroscopy has provided much of the kinetic data regarding electron transfer through the quinone(s) in PS I. In most set-ups (see, e.g., Brettel et al., 1998), the absorbance of the sample is monitored using a single, weak measuring beam, which is of low intensity and is usually pulsed to minimize actinic effects. A short, relatively intense laser pulse is then applied and the resulting absorbance change is followed as a function of time. Time traces of the absorbance changes can be analyzed to determine the lifetimes associated with the electron transfer and absorbance difference spectra can be constructed by varying the wavelength of the measuring beam. Electron transfer to phylloquinone leads to an increase in absorbance in the near UV. The spectrum of the absorbance change in this region is broad and relatively featureless with a maximum at ∼380 nm. This band is assigned to changes in the phylloquinone absorbance because it resembles the phyllo-semiquinone-minus-phylloquinone difference spectrum in solution (Brettel et al., 1986). In the visible region there is also an absorbance decrease at ∼450 nm and an absorbance increase at ∼480 nm. The origin of these features is not known with certainty but the position and shape of the band suggests that they may be due to a carotenoid electrochromic bandshift (Brettel, 1988). This suggestion is consistent with the presence of carotenoids close to Q_K-A and Q_K-B revealed in the 2.5 Å resolution X-ray structure (Jordan et al., 2001). See Brettel (1988) for a more detailed discussion of the spectral shape. The kinetics of these changes can be followed on timescales as short as a few nanoseconds, depending on the width of the actinic pulse and the detection system.

One of the most important limitations of flash absorbance spectroscopy as described above is the time resolution, which is limited by the detection system to times on the order of ∼1 ns. A further restriction is the requirement of samples with relatively low optical density because of the necessity of working with a weak measuring beam. These two limitations preclude

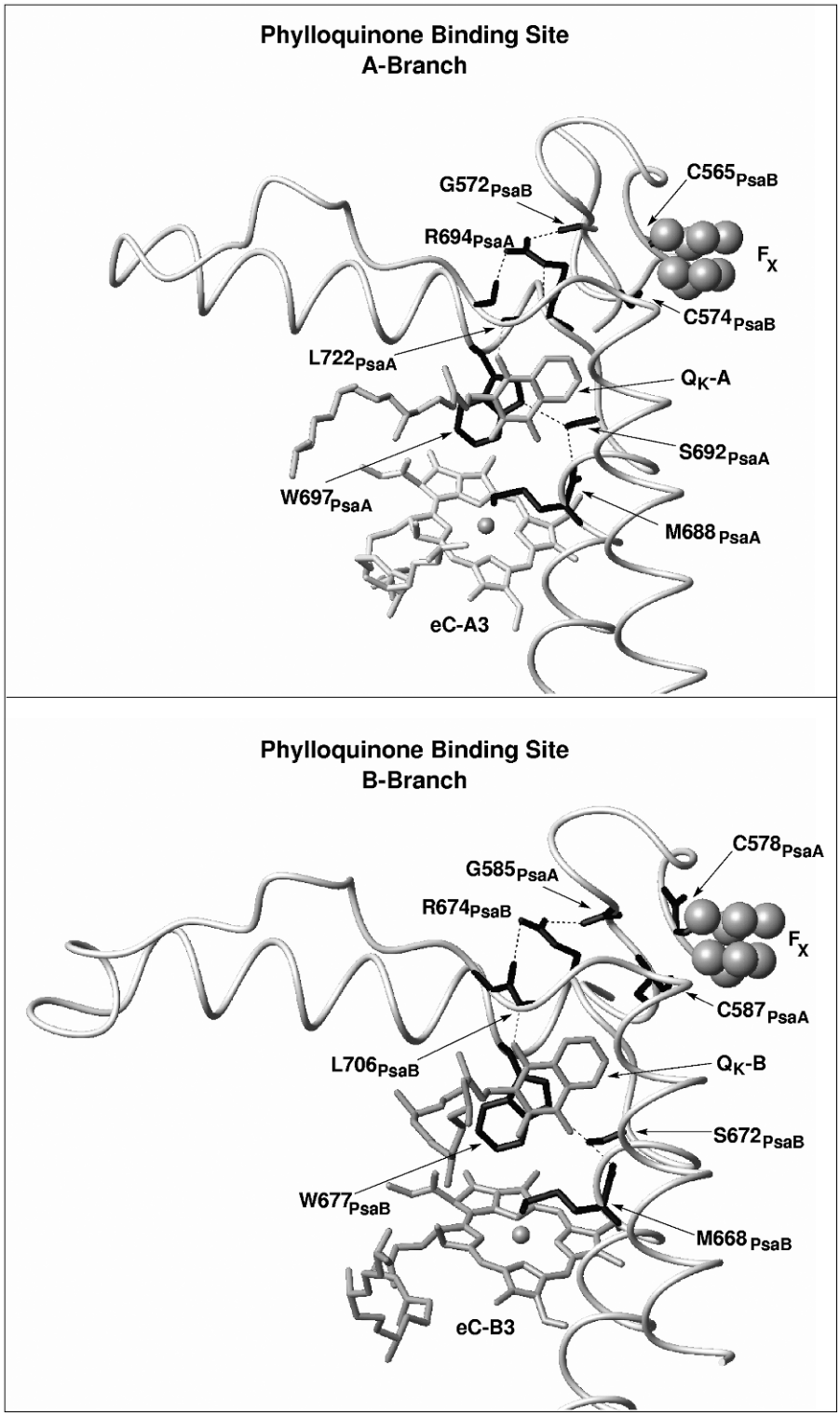

Fig. 4. The PsaA and PsaB branch phylloquinone binding sites in PS I from the 2.5 Å X-ray structure (Jordan et al., 2001) (pdb entry **1JB0**). The two binding sites are viewed from two different perspectives both approximately in the membrane plane and related by a rotation of ∼180˚ about the membrane normal. The amino acids chosen for mutation studies because of their apparent interactions with the cofactors are shown in black. The figure was constructed using the program MOLMOL (Koradi et al., 1996).

measurement of the electron transfer kinetics from A_0 to A_1 and experiments on fully intact samples; the former because the kinetics are too fast, the latter because the optically density is too high. Both of these problems can be overcome using pump–probe techniques, in which two laser pulses with a variable delay between them are applied to the sample. The intensity of the probe pulse is then measured as a function of the delay between pump and probe. Thus, the pulse width and the accuracy of the delay, and not the detector, limit the time resolution. The narrow width of the detection pulse also allows higher intensities to be used (Béal et al., 1999). Spectrometers of this type with subpicosecond time resolution have been used to measure the electron transfer from A_0^- to A_1 (Hastings et al., 1994; Brettel and Vos, 1999; Savikhin et al., 2001). In these experiments the repetition rate of the laser flashes is usually much faster than the turnover rate of PS I. Thus, to ensure that every flash is effective in generating electron transfer the sample is either spun or pumped through the cuvette.

The problem of working with optically dense samples has recently been solved by Joliot and coworkers (Béal et al., 1999) who have designed a spectrometer, which uses the pump–probe technique and short relatively intense probe pulses. Samples with an optical density as high as three can be studied with this set-up, which has made it possible to measure the kinetics of A_1 to F_X electron transfer in whole cells of green algae (Joliot and Joliot, 1999; Guergova-Kuras et al., 2001) and cyanobacteria (Xu et al., 2003b) (see Rappaport et al., this volume, Chapter 16). This is a very important advancement since previous studies had shown a strong dependence of the electron transfer kinetics on the isolation procedures used (Sétif and Brettel, 1993). The time resolution of the set-up used in Joliot and Joliot (1999) and Guergova-Kuras et al. (2001) is limited by the width of the detection pulse, ~6 ns, and is slightly lower than that of the 2 ns resolution of the flash absorption set-up described in Brettel (1998). Moreover, whole cells are expected to be inherently inhomogeneous due to the presence of partially assembled and damaged complexes. Hence, a combination of both pump–probe measurements of whole cells and continuous detection on particles such as used in Xu et al. (2003b) provides a more complete picture of the absorbance changes associated with the electron transfer kinetics.

In PS I, it is difficult to relate spectral changes to specific properties of the cofactors or their surroundings and the severe spectral overlap of the chlorophylls presents a problem when energy transfer or other relaxation processes occur at the same time electron transfer. Hence, it is important to complement the optical methods with other techniques that reflect different properties of the system.

2. Photoelectric Techniques

Photovoltage measurements provide one such alternative. The technique measures the photoelectric response of oriented membranes and both the kinetics of the electron transfer as well as the dielectrically weighted transmembrane distance of the charge separation can be obtained from such measurements (see Semenov et al., this volume, Chapter 21). The membranes are oriented between two capacitive electrodes either using an applied voltage (Trissl and Wulf, 1995) or by adsorbing them onto a film (Mamedov et al., 1996). The voltage between the electrodes in then measured as a function of time following flash illumination of the cell. A full description of the experimental details of one such set-up can be found in Trissl and Wulf (1995). A weakness of the method is that the species involved can only be inferred from the signal amplitude and kinetics and by comparison to spectroscopic data. The technique is particularly well suited for measuring the kinetics of the electron transfer through A_1 (Hecks et al., 1994; Leibl et al., 1995; Semenov et al., 2000) because PS I containing membrane fragments are easily oriented and the position of the cofactors are known. Hence, a strong photoelectric response can be measured and the observed kinetic phases can be assigned with a reasonable degree of confidence to particular electron transfer steps. In PS I, the kinetics of both the electron transfer from A_0 to A_1 (Hecks et al., 1994) as well as from A_1 to the iron–sulfur clusters (Leibl et al., 1995; Semenov et al., 2000) have been determined from such measurements. On a slower timescale, the back reaction through A_1 (Vassiliev et al., 1997) has also been studied. The lifetimes determined by these photovoltage measurements are in reasonable agreement with those obtained by other methods; however, there are some differences.

3. Time Resolved Electron Paramagnetic Resonance

Electron paramagnetic resonance (EPR) spectroscopy is one of the most widely used techniques for studying phylloquinone in PS I (see Hoff, 1993; Snyder and Thurnauer, 1993; Angerhofer and Bittl, 1996; Stehlik and Möbius, 1997; Möbius, 2000; Bittl and Zech, 2001; van der Est, 2001 for a series of reviews). The strength

of EPR is that it detects the magnetic moments of the unpaired electrons generated by light-induced electron transfer. Hence, only the species directly involved in the electron transfer are observed. Moreover, the magnetic moments are very sensitive to the local environment and the interactions are tensorial so that the radicals can be identified unambiguously and geometric and kinetic information is obtained simultaneously. Two significant limitations of the method, however, are its poor sensitivity and comparatively low time resolution (on the order of tens of nanoseconds). These limitations are compensated for to some extent by the spin polarization associated with light-induced radical pairs. This increases the signal strength by several orders of magnitude and makes the spectra sensitive to short-lived precursors that cannot be detected directly. The vast majority of EPR studies of phylloquinone in PS I involve the radical pair $P_{700}^{+}A_1^{-}$ at low temperature or photoaccumulated A_1^{-}. These types of studies have provided an enormous amount of detailed information about the geometry and environment of A_1^{-}. However, they do not depend directly on the electron transfer kinetics.

Two main EPR techniques exist for measuring the electron transfer through A_1, both of which take advantage of the light-induced spin polarization of the states $P_{700}^{+}A_1^{-}$ and $P_{700}^{+}F_X^{-}$. Transient EPR is the simplest of these (see Stehlik and Möbius, 1997 for a review of EPR methods for investigating photoprocesses with paramagnetic intermediates; see Stehlik, this volume, Chapter 23). The sample is irradiated continuously with low power microwaves and the transient EPR response is measured as a function time following a laser flash. The transients are then collected over a range of magnetic field positions generating a time/field data set from which the EPR spectra at a given time can be extracted. At physiological temperatures, PS I samples give two sequential spectra corresponding to the states $P_{700}^{+}A_1^{-}$ and $P_{700}^{+}(Fe/S)^{-}$. Although it is known that electron transfer from A_1 proceeds via F_X (Luneberg et al., 1994; Moenne-Loccoz et al., 1994; van der Est et al., 1994), the term Fe/S is used to represent one of the three iron–sulfur clusters and to allow for the possibility that electron transfer from F_X to F_A/F_B is faster than from A_1 to F_X. The spin polarization patterns of these states and their dependence on the lifetimes and magnetic properties of the radical pairs are well understood (see van der Est, 2001 for a recent review). Hence, they can be used to study both the electron transfer kinetics and the interactions of the cofactors with their surroundings.

The second technique uses high power pulsed microwave irradiation to detect the radical pair states (Bittl and Zech, 2001; see Thurnauer et al., this volume, Chapter 22). The microwave pulses are given at a variable delay time relative to the laser flash and generate a spin echo. The amplitude of the echo is then monitored as a function of the delay time between the laser flash, the separation between the microwave pulses and/or the magnetic field. In a spin correlated radical pair generated from a singlet state precursor, the spin echo is phase shifted by 90° compared to that of a stable radical. Indeed in PS I, the observation of this phase shift by Thurnauer and Norris (1980) was an important step in identifying the spin polarized EPR signals as arising from radical pairs. This technique has been applied primarily at low temperature using conditions under which the decay of the signals due to $P_{700}^{+}A_1^{-}$ is determined by spin relaxation and using pulse sequences, which produce a modulation of the echo amplitude. The modulation arises from the spin–spin coupling between the radicals and can be analyzed to give very accurate values of the distance between them (see Bittl and Zech, 2001 for a review). However, the out-of-phase echo can also be used to measure the electron transfer kinetics (Thurnauer and Norris, 1980; Thurnauer et al., 1982; Moenne-Loccoz et al., 1994; Muhiuddin et al., 2001; Fairclough et al., 2003). The phase shift in the echo is due to the fact that the coupled electron spins of the radical pair have purely dipolar order. Since this order is lost during the electron transfer from A_1^{-} to F_X, the echo decay reflects the electron transfer kinetics if it faster than the loss of the correlation between the spin due to relaxation effects. Compared to transient EPR, this approach has the advantage that only the first radical pair is detected and hence contributions from $P_{700}^{+}A_1^{-}$ and $P_{700}^{+}(Fe/S)^{-}$ do not need to be separated from one another. However, this also has the drawback that contributions from the fast phase of electron transfer to the iron–sulfur clusters are not observed. Another important consideration for modified PS I preparations is that the amplitude of the out-of-phase echo is sensitive to the extent of singlet–triplet mixing during the lifetime of $P_{700}^{+}A_0^{-}$. Hence, the echo amplitude is not a good quantity for monitoring the extent of forward electron transfer in samples in which the lifetime of $P_{700}^{+}A_0^{-}$ is altered.

B. Indirect Methods

In addition to the direct methods, discussed above a range of techniques exist in which the electron transfer involving A_1 can be inferred from signals which arise either from other species or which do not directly reflect the kinetics.

1. Spin Dynamics

The transient EPR techniques discussed above are only able to resolve kinetics on the timescale of tens of nanoseconds. Hence, the ∼10 ns component of electron transfer from A_1 to F_X^- is not resolved. Similarly, the electron transfer from A_0^- to A_1 is also too fast to be observed. This limitation can be partially overcome using the memory effect in the coherent motion of the spins, which is arguably the most important aspect of any magnetic resonance method. This is the basis, for example, of the vast array of NMR methods in which pulses are used to first generate coherent oscillations of the spin system and then transfer them to the observable component of the magnetization. In many respects the electron transfer steps in a series of sequential radical pairs influence the spin system like a series of pulses causing sudden changes in the magnetic interactions. The overall result is that the spin polarization pattern at a given time reflects the history of the spin system (Pedersen, 1979; Norris et al., 1990; Morris et al., 1995; Hore, 1996; Kandrashkin et al., 1997). In PS I, the series of sequential radical pairs is initially in a pure singlet state because the electron transfer is generated from the excited singlet state of P_{700}. During the lifetime of each radical pair, singlet–triplet mixing takes place, which is reflected in the spin polarization patterns of all subsequent radical pairs. This is demonstrated in Fig. 5. In the upper and lower parts of the figure the net polarization of P_{700}^+, which develops as a result of singlet–triplet mixing in $P_{700}^+A_1^-$ (upper curve) and $P_{700}^+A_0^-$ (lower curve), is shown as a function of the lifetime of the respective radical pairs. The filled circles show their lifetimes in wild type PS I. The two insets show the shape of the polarization pattern of P_{700}^+ that would be caused by mixing in the respective radical pairs for arbitrarily assumed lifetimes (see figure caption). The spectra are plotted such that negative features represent emission and positive features represent absorption. In both cases, a pattern of emission/absorption is generated by the singlet–triplet mixing. However, the polarization arising from mixing in $P_{700}^+A_0^-$ upper spectrum has stronger absorption on the upfield (right hand) side, while the pattern arising from $P_{700}^+A_1^-$ has a stronger emission on the downfield side. This difference arises because of the opposite signs of the spin–spin coupling in the two radical pairs. In native PS I, no polarization is generated due to mixing in $P_{700}^+A_0^-$ because its lifetime is too short as can be seen from the position of the filled circle in the left of the figure. For $P_{700}^+A_1^-$ the lifetime is sufficiently long that it generates a polarization pattern similar to that on the right of Fig. 5 when the electron is transferred to F_X.

From knowledge of the polarization generated by this effect the patterns can be used to deduce properties of the precursors. In principle, this could be used to determine the lifetimes of precursor radical pairs with only the precession of the spins as a limiting factor for the time resolution. For the primary radical pair in reaction centers, this places a lower limit on the measurable lifetime of ∼500 ps for experiments at X-band as can be seen on the left of Fig. 5. However, in practice the uncertainty in the properties of the radical pairs hampers accurate determination of the lifetimes. This technique has been used extensively to study slowing of the electron transfer rate from pheophytin to Q_A in modified reaction centers of purple bacteria (Norris et al., 1990; Snyder et al., 1993; Morris et al., 1995; Tang et al., 1996; Utschig et al., 1997; Hulsebosch et al., 1999; Tang et al., 1999) and these studies have firmly established the relationship between the polarization patterns and the precursor lifetime. Despite these advances and the availability of experimental data on sequential radical pairs in PS I (Blankenship et al., 1975; McIntosh et al., 1979a,b; Thurnauer, 1980; Manikowski et al., 1984; Bock et al., 1989), detailed calculations of their spin polarization patterns were not carried out until the late 1990s because reliable values for the magnetic interaction parameters, distances, and geometries for the cofactors were lacking. With the availability of high field EPR, PS I single crystals, pulsed ENDOR, and other advanced techniques, these parameters are now available. The large body of EPR work on which they are based is covered by Lubitz (this volume, Chapter 17) Thurnauer et al. (this volume, Chapter 22), and Stehlik (this volume, Chapter 23). Using these data to fix the parameters and assuming at most a small contribution from the fast phase of electron transfer, the room temperature polarization patterns from cyanobacteria are reproduced very well (Kandrashkin et al., 2002). In contrast, the spin polarization patterns from eukaryotic PS I show a significant influence of the fast phase (Kandrashkin and van der Est, 2002). This difference is shown in Fig. 6. Thus, although the fast component cannot be resolved kinetically, transient EPR can reveal its presence. In native PS I, the influence of singlet–triplet mixing in the primary radical pair is minimal because of its short lifetime. However, in other Type I reaction centers, i.e., from green sulfur bacteria and heliobacteria, it has a significant effect on the polarization patterns (van der Est et al., 1998; Kandrashkin et al., 2002), which can be explained.

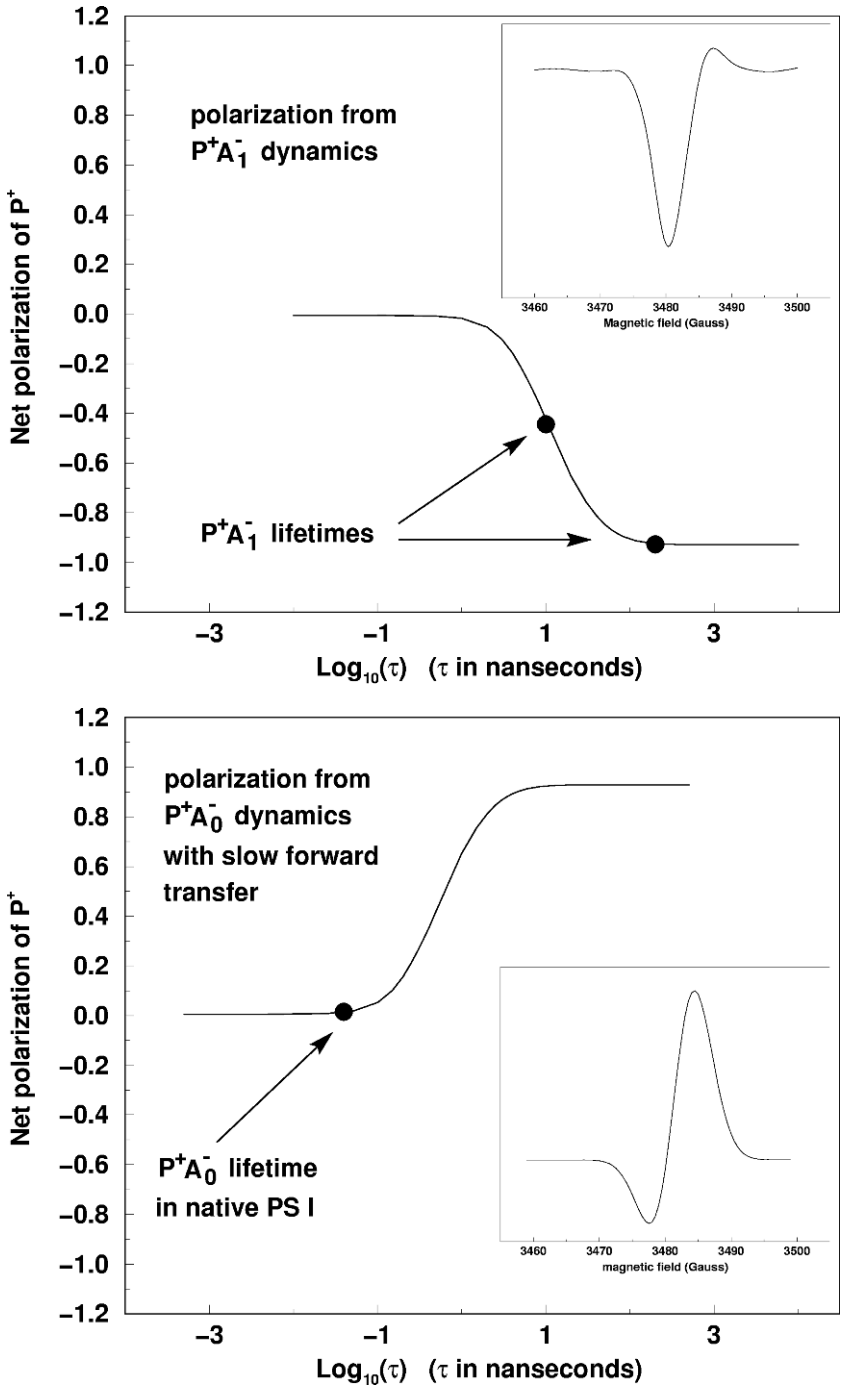

Fig. 5. The effect of singlet–triplet mixing on the spin polarization of P_{700}^{+} in PS I. Top: The expected polarization of P_{700}^{+} in subsequent radical pairs as a result of singlet–triplet mixing in $P_{700}^{+}A_{1}^{-}$. The curve is the net polarization of P_{700}^{+} plotted as a function of the lifetime of $P_{700}^{+}A_{1}^{-}$ and the solid circles show the points on the curve corresponding to the lifetimes of the two kinetic phases of A_{1}^{-} to F_X electron transfer. The inset is the contribution from P_{700}^{+} to the EPR spectrum of $P_{700}^{+}(Fe/S)^{-}$ for a lifetime of 200 ns for A_1. Bottom: The corresponding polarization generated due spin dynamics in $P_{700}^{+}A_{0}^{-}$. The solid circle shows the point on the curve for the lifetimes of $P_{700}^{+}A_{0}^{-}$ in native PS I. The inset shows the contribution of P_{700}^{+} to the spectrum of $P_{700}^{+}A_{1}^{-}$ which would be generated by spin dynamics in $P_{700}^{+}A_{0}^{-}$ if it had a lifetime of $\sim$1 ns.

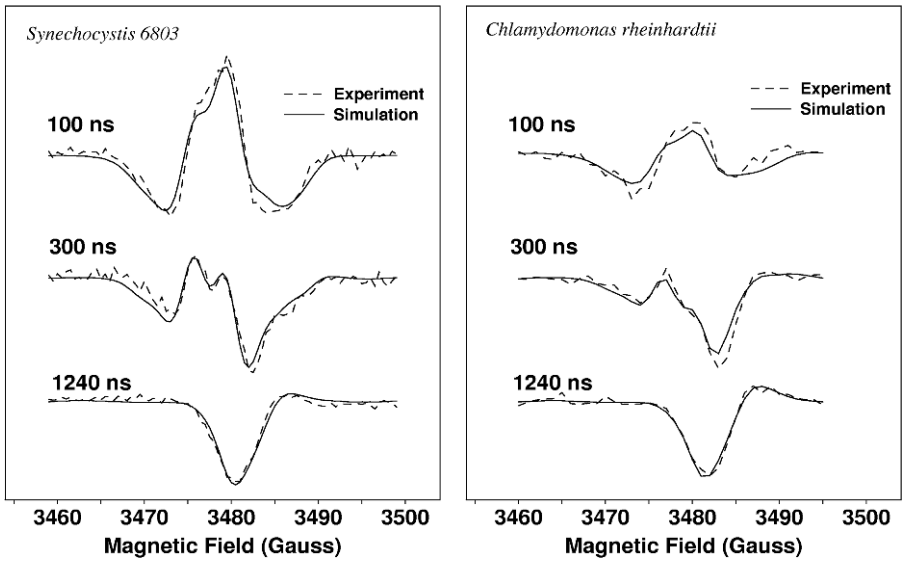

Fig. 6. Comparison of the room temperature spin polarization patterns of PS I from the cyanobacterium *Synechocystis* sp. PCC 6803 (left) and from the green algae *C. reinhardtii* (right). The spectra from top to bottom show the development of the spin polarization as the electron is transferred from A_1 to F_X. The three spectra correspond to a time window centered at the delay times after the laser indicated in the figure. The dashed curves are simulations based on parameters from the literature given in Kandrashkin et al. (2002) and van der Est et al. (2003). In the simulation of the sample from *Synechocystis* sp. PCC 6803 (left) the fast component accounts for 15% of the electron transfer while in the simulation of the sample from *C. reinhardtii,* it accounts for 45% of the electron transfer.

2. Photoaccumulation

Another well-established method for determining the activity of a particular species or pathway in photosynthetic reaction centers is to trap electrons on the acceptors. This can be accomplished by chemically reducing the terminal acceptors and then using continuous illumination in the presence of an electron donor to back-up the electron transfer chain. By freezing the sample during this process the reduced acceptors are trapped and can be studied using standard EPR and ENDOR techniques. In PS I this techniques provided some of the first evidence for the acceptor A_1^- (Bonnerjea and Evans, 1982; Gast et al., 1983) and is now routinely used to study the properties of phylloquinone. The advantage and at the same time disadvantage of this method is that it relies on multiple turnovers of the reaction center. On the one hand this ensures that trapped radicals can be produced even if the single flash quantum yield is low. However, this very fact means that it is possible in principle, to accumulate radicals via functionally irrelevant pathways. Moreover, the conditions required to trap electrons on phylloquinone in PS I (Heathcote et al., 1996) are very far from physiological.

III. Recent Structure Based Results

Since the publication of the 2.5 Å resolution X-ray structure (Jordan et al., 2001), there have been a considerable number of spectroscopic and theoretical studies that have addressed aspects of the electron transfer through phylloquinone. In the following sections the results of these studies will be discussed. Although much of this work gives a clear, consistent picture of the electron transfer, there are a number of aspects, such as the origin of the biphasic kinetics, which are not yet well understood. An effort will be made to point out these aspects and indicate the differences in the various methods and possible models.

A. Forward Electron Transfer Pathway

1. Deletion Mutants

Many of the recent structure-based studies have attempted to assign the various spectroscopic signatures of A_1 to one or both of the phylloquinones. The first study of this type pre-dates the 2.5 Å resolution X-ray structure and involved peripheral subunit deletion

mutants (Yang et al., 1999). With the determination of the X-ray structure at 4 Å resolution (Krauß et al., 1996; Schubert et al., 1997), the location of the peripheral subunits within the PS I complex became known. It became apparent that they are arranged asymmetrically with respect to the electron transfer chain and that this provided a possibility for selectively influencing the two sides of the reaction center. The approach taken by Yang et al. (1999) was to selectively delete various combinations of the genes for encoding the polypeptides PsaE, PsaF, and PsaI through PsaM. The premise of the experiments was that if removing one or a combination of polypeptides influenced the properties of A_1 the location of the corresponding phylloquinone in the A-branch or B-branch could be deduced from the location of the polypeptides. Photoaccumulation of A_1^- and the back reaction were used to monitor the properties of A_1. It was found that PsaE and PsaF were the only subunits that had an influence on these properties and that when they were absent, A_0^- was accumulated bythe protocol that trapped A_1^- in all of the other samples. This effect was observed only when Triton X-100 was used to isolate the PS I particles. This is consistent with earlier observations that Triton X-100 can be used to extract PsaF (Bengis and Nelson, 1977) in higher plants. It also known to lead to changes in the ratio of the kinetic phases of forward electron transfer kinetics through A_1 (Sétif and Brettel, 1993) and to differences in the appearance of the photoaccumulated spectrum of A_1^- (Heathcote et al., 1993; Heathcote et al., 1996) in eukaryotic PS I. In other respects, the PS I particles from the PsaE, PsaF deletion mutants were similar to those of wild type. In particular, it was shown that there was no loss of phylloquinone and no change in the recombination kinetics. Some change in the ability of the particles to reduce flavodoxin was observed but there was no correlation with the photoaccumulation behavior. From simulations of the Q-band EPR spectra, it was concluded that at most *one* phylloquinone radical could be photoaccumulated per reaction center and that any additional spins were derived from A_0^-. These results were interpreted as indicating that electron transfer occurs predominantly in the branch of cofactors closest to PsaE and PsaF. It was postulated that in the absence of these two polypeptides, the detergent altered the environment of the quinone in this branch allowing it to be more easily doubly reduced. At the time, it was not known which of the two branches, A or B, was closest to PsaE and PsaF. In the meantime it has been identified as the A-branch.

2. Quinone Binding Site Point Mutants

The obvious drawback to the deletion mutant studies is that the removal of an entire protein subunit represents a major perturbation of the system and the possible effects may not be restricted to a small area of the complex. However, with the elucidation of the 2.5 Å resolution X-ray structure, amino acids in the phylloquinone binding site could be identified and targeted for site-directed mutagenesis studies. An important aspect of these studies is that they have been carried out on both the eukaryotic organism, *Chlamydomonas reinhardtii* (Boudreaux et al., 2001; Fairclough et al., 2001; Guergova-Kuras et al., 2001; Purton et al., 2001; Redding et al., 2001; Fairclough et al., 2003) and the prokaryote *Synechocystis* sp. PCC 6803 (Golbeck et al., 2001; Xu et al., 2003a,b). The first of these studies (Purton et al., 2001) showed that when tryptophan[1] $W693_{PsaA}$ was changed to a histidine or a leucine, the lifetime of the out-of-phase echo signal due to $P_{700}^+A_1^-$ at 260 K was increased by approximately a factor of three. The ENDOR spectra of photoaccumulated A_1^- in these samples were also interpreted as indicating a change in the electronic structure of the phylloquinone radical. In contrast, little or no change was observed when the same mutations were made to tryptophan $W702_{PsaA}$. Although mutations were only made in one of the two branches, the change in the forward electron transfer kinetics suggested that electron transfer occurred in the A-branch, in agreement with the deletion mutant studies.

A more complete study of mutations in both phylloquinone binding sites in *C. reinhardtii* (Guergova-Kuras et al., 2001) showed a similar decrease in the electron transfer rate when $W693_{PsaA}$ was altered but also provided evidence for electron transfer in both branches. The forward electron transfer was monitored in whole cells using the pump–probe technique (Béal et al., 1999) described above. Phenylalanine mutations of $W693_{PsaA}$ and $W673_{PsaB}$ led to complementary changes in the two kinetic phases of electron transfer such that the slow phase was slowed in the $W693F_{PsaA}$ mutant, the fast phase became slower in the $W673F_{PsaB}$ mutant, and both phases were slowed in a double mutant. The relative amplitudes of the two phases did not change in any of the mutants. The straightforward

[1] Note that the numbering of the amino acids is species-dependent and $W693_{PsaA}$ in *C. reinhardtii* corresponds to $W697_{PsaA}$ shown in Fig. 4 for *S. elongatus*

explanation for this result is that the two kinetic phases represent electron transfer in the two branches and that mutations in a given branch alter the rate of electron transfer in that branch.

A further set of experiments on the same mutants (Boudreaux et al., 2001) revealed a more complicated picture of the electron transfer. The A-branch mutant, $W693F_{PsaA}$ and double mutant $W693F_{PsaA}/W673F_{PsaB}$ both had clearly altered spin polarized EPR spectra of $P_{700}^{+}A_1^{-}$ recorded at 80 K, while the spectrum of the corresponding B-branch mutant $W673F_{PsaB}$ was indistinguishable from that of the wild type. Photoaccumulation studies were also carried out on these samples and, similar to the deletion mutants described above, varying amounts of A_0^{-} and A_1^{-} were observed. In the A-branch mutant only A_0^{-} was accumulated while the B-branch mutant showed less A_0^{-} than in the wild type. The double mutant, on the other hand, had no effect. On the basis of the observed changes in the spin polarization patterns and photoacumulated A_1^{-} spectra, it was concluded in Boudreaux et al. (2001) that both EPR signals arise from the phylloquinone in the PsaA branch.

A more extensive investigation of this type has been carried on the cyanobacterium *Synechocystis* sp. PCC 6803 (Xu et al., 2003a,b). In many respects, the results mirror those found for *C. reinhardtii*, however some significant differences are also observed. The residues involved in the H-bond network shown in Fig. 4 were altered to investigate the pathway of electron transfer from A_0 through A_1 to F_X and the possible role of hydrogen bonding in this process. Mutations were made to $W697_{PsaA}$, $W677_{PsaB}$, $S692_{PsaA}$, $S672_{PsaB}$ and $R694_{PsaA}$, $R674_{PsaB}$ in the two branches. The electron transfer was characterized using Q-band EPR to measure photoaccumulated A_1^{-}; X-band transient EPR at room temperature to measure the sequential radical pairs $P_{700}^{+}A_1^{-}$ and $P_{700}^{+}(Fe/S)^{-}$; X-, Q-, and W-band EPR at 80 K to measure $P_{700}^{+}A_1^{-}$, pulsed ENDOR at 80 K to measure hyperfine couplings in $P_{700}^{+}A_1^{-}$ and flash-induced absorbance changes in both the visible and UV on both whole cells and isolated PS I complexes. All of the EPR and ENDOR data consistently showed changes as a result of mutations in the A-branch, while they were unaffected by mutations in the immediate vicinity of the B-branch quinone. An important aspect of the results is that the spectral changes observed in both the photoaccumulation experiments and transient EPR measurements are consistent with changes in the hyperfine coupling seen very clearly in the pulsed ENDOR measurements. From this result it was concluded that at low temperature, the cyclic electron between P_{700} and A_1 occurs along the A-branch of cofactors and that the mutations altered the spin density distribution on the A-branch phyllo-semiquinone. The changes in the hyperfine splittings were also apparent in the room temperature spin polarization patterns of $P_{700}^{+}A_1^{-}$. Moreover, the flash-induced absorbance change measurements and EPR kinetic traces at room temperature both showed that the 200 ns phase of electron transfer from A_1^{-} to F_X was consistently slowed by mutations near either the A-branch quinone or F_X. In all of the data, this fraction represented the majority of the electron transfer. Hence, it was concluded that the slow phase represents electron transfer along the A-branch and that the electron transfer in cyanobacterial PS I is biased toward this branch.

An unresolved issue from this study, was the fate of the remaining fraction. Similar to the findings for *C. reinhardtii*, the fast phase of electron transfer measured in flash-induced absorbance experiments was slowed by some of the mutations in the B-branch and was unaffected by mutations in the A-branch. This correlation suggests that a minor fraction of electrons is transferred along the B-branch. However, the correlation is ambiguous in some of the data reported in Xu et al. (2003b). No change in the fast phase was observed for mutation of $R674_{PsaB}$, which is located directly between Q_K-B and F_X (see Fig. 3) and mutation of $S672_{PsaB}$ caused no change in the fast phase in whole cells, although it was slowed in isolated particles. Independent evidence for the assignment of the fast phase to the B-branch could not be found in any of the other spectroscopic data. In particular, a contribution to the spin polarized EPR spectra is expected from this fraction. Although, the spin polarization patterns reported in Xu et al. (2003a,b) do not completely rule out a small fraction of fast electron transfer to F_X, its influence is not apparent in the data from cyanobacteria. This can be seen in Fig. 6, left. The spectrum in a time window $\sim$100 ns after the laser flash is dominated by $P_{700}^{+}A_1^{-}$ and has roughly equal amounts of emission and absorption. This is in contrast to samples from *C. reinhardtii*, shown on the right of Fig. 6, in which the influence of the fast phase is clearly evident in the early spectrum. The simulations in Fig. 6 predict that if the fast component accounts for 45% of the electron transfer, the early spectrum should be purely emissive due to the overlap of contributions from $P_{700}^{+}A_1^{-}$ and $P_{700}^{+}(Fe/S)^{-}$. At present, the origin of the differences in the polarization patterns in the two species shown in Fig. 6 is not clear. Because of the ambiguities in the correlation between the fast phase and mutations in the B-branch and the lack of a clear contribution to the spin polarization

from this phase, its assignment was left as an open question in Xu et al. (2003a,b).

3. The Search for EPR Signatures of Electron Transfer Through Q_K-B

The observation that B-branch mutations affect the fast phase while they have no influence on the 80 K transient EPR spectra suggests that at low temperature, the B-branch is either inactive or leads to irreversible charge separation. In the latter scenario, only the fraction undergoing cyclic electron transfer to A_1 in the A-branch would contribute to the low temperature EPR spectrum. This possibility has led to investigations of samples in which electron transfer past A_1 is blocked. The premise of the experiment is that if electron transfer past A_1 cannot occur, electrons being transferred along the B-branch possible should also contribute to the EPR signals. In Muhiuddin et al. (2001) electron transfer past A_1 was blocked by reduction of the iron–sulfur clusters. Samples containing dithionite at high pH were illuminated at 200 K for various periods of time, cooled to 100 K and measured using pulsed EPR. It was found that the decay of the out-of-phase echo was biexponential with lifetimes of ~25 and ~2.5 μs and that the relative amplitudes of the two components depended on the illumination time at 200 K. In the absence of dithionite and without illumination, only the slower of the two phases was observed, while in the presence of dithionite at pH 8 the relative amount of the fast component increased with increasing illumination times at 200 K. In the $W693H_{PsaA}$ mutant, freezing in the dark in the presence of dithionite abolished the out-of-phase signal but when the sample was illuminated at 200 K, the echo reappeared and only the shorter of the two lifetimes was found. These results were interpreted in terms of a bi-directional model and the fast decaying component of the echo was assigned to electron transfer in the B-branch. However, no explanation of why the echo decay should differ in the two branches was given.

In Shen et al. (2002a,b) it was shown that PS I complexes isolated from *rubA* deletion mutants of *Synechococcus* sp. PCC 7002 completely lacked the stromal subunits PsaC, PsaD, and PsaE and the iron–sulfur clusters F_X, F_B, and F_A Thus, this mutant provides a very elegant way of producing PS I core complexes lacking all three iron–sulfur clusters. The low temperature spin polarized EPR spectra at X-, Q-, and W-band and the out-of-phase echo signals from such particles (Shen et al., 2002a) were approximately three times more intense but were otherwise indistinguishable from those of PS I from the wild type. The increase in signal strength in the *rubA* mutant is due to the fact that none of the reaction centers are trapped in the state $P_{700}^+(F_A/F_B)^-$ and only reversible electron transfer to A_1 takes places. Thus, if electron transfer along the B-branch were taking place, Q_K-B would be expected to contribute the EPR signals of $P_{700}^+A_1^-$. The fact that the spin polarized EPR spectra and echo modulation curves are identical to the wild type, clearly show that any contribution from B-branch electron transfer is either extremely small or produces identical signals to those of the A-branch. Since the spin density on P_{700}^+ is very asymmetrically distributed over the two chlorophylls (Käss et al., 2001; Webber and Lubitz, 2001) the two radical pairs $P_{700}^+Q_K$-A^- and $P_{700}^+Q_K$-B^- would be expected to give significantly different spin polarized transient EPR spectra. This is demonstrated in Fig. 7, which shows calculated and experimental W-band spectra of $P_{700}^+A_1^-$. The top part of Fig. 7 shows that the shape of the experimental spectra from the *rubA* mutant and wild type PS I are virtually identical as reported in Shen et al. (2002a). Note that the two spectra have been normalized to the same amplitude in Fig. 7. As discussed in Shen et al. (2002a) the intensity of the *rubA* spectrum before normalization is much larger than that of the wild type. The middle trace in Fig. 7 shows a comparison of the experimental spectrum from the *rubA* mutant and the calculated spectrum of $P_{700}^+Q_K$-A^-, i.e., assuming uni-directional electron transfer in the A-branch. In the bottom trace, the spectrum from the *rubA* mutant is compared to a calculated spectrum comprised of 60% $P_{700}^+Q_K$-A^- and 40% $P_{700}^+Q_K$-B^-, i.e., assuming bi-directional electron transfer. Clearly, the agreement is better when uni-directional electron transfer is assumed. More importantly, the simulations show that the W-band $P_{700}^+A_1^-$ spectrum is sensitive to changes in the relative amounts of $P_{700}^+Q_K$-A^- and $P_{700}^+Q_K$-B^-. Hence, the fact that the spectra of the *rubA* mutant and the wild type are identical indicates that the relative amounts of the two radical pairs is unaffected by the removal of the iron–sulfur clusters. Combined with the point mutation results in Xu et al. (2003a) the data from the *rubA* mutant therefore suggest that the electron transfer in cyanobacterial PS I is very strongly biased toward the A-branch at low temperature.

The marked difference between the observations with prereduced samples versus those lacking F_X suggests an alternative interpretation of the data from the prereduced samples. It is important to note that the fast decay component of the out-of-phase echo has only been reported in samples in which F_X is reduced (Muhiuddin et al., 2001). It is not found in the *rubA*

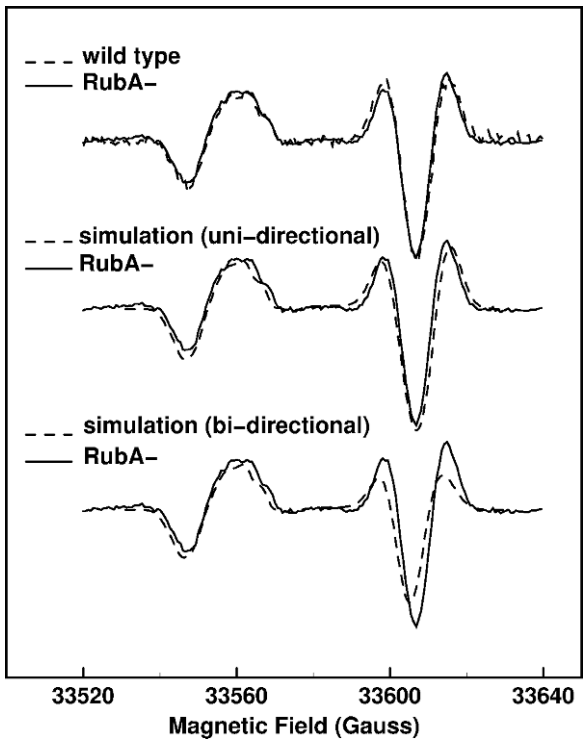

Fig. 7. Low temperature W-band spin polarization pattern of PS I from the *rubA*$^-$ mutant of the cyanobacterium *Synechococcus* sp. PCC 7002. Top: Comparison of the *rubA*$^-$ mutant (solid curve) with the corresponding spectrum of the wild type (dashed curve). Middle: Comparison of the *rubA*$^-$ mutant (solid curve) with a simulation (dashed curve) assuming unidirectional electron transfer in the A-branch. Bottom: Comparison of the *rubA*$^-$ mutant (solid curve) with a simulation (dashed curve) assuming 60% electron transfer in the A-branch and 40% in the B-branch. The experimental spectra are taken from Shen et al. (2002a) and the simulations are based on parameters from the literature given in Kandrashkin et al. (2002) and van der Est et al. (2003). The Euler angles between gP and the dipolar coupling vector to Q_K-B were calculated as: $\alpha, \beta, \gamma = 101^\circ, 80^\circ, -220^\circ$ from the X-ray structure.

mutant (Shen et al., 2002a) nor in PS I containing foreign quinones, some of which are incapable of transferring electrons to F_X (Dzuba et al., 1997; Zech et al., 1997; Zybailov et al., 2000; Johnson et al., 2001). Thus, it is much more likely that the changes in the echo decay observed after illumination in the presence of dithionite at high pH are due to the influence of a spin on F_X^-. Recently, the properties of three-spin systems like $P_{700}^+ A_1^- F_X^-$ consisting of a radical pair in the presence of an observer spin have been investigated theoretically (Salikhov et al., 2002). This study shows that the observer spin has a significant influence on the spin polarized EPR spectrum and the spin dynamics. This, combined with the fact that the relaxation of F_X^- is known to be fast clearly suggests that F_X^- induces the fast decay of the out-of-phase echo.

In contrast to the low temperature behavior, the room temperature transient EPR spectra of $P_{700}^+ A_1^-$ are affected by removal of F_X either chemically (van der Est et al., 1994) or by deleting the *rubA* gene (Shen et al., 2002a), but the interpretation of this result remains unclear. Two obvious possible explanations for the changes are that either (i) removal of F_X might lead to structural changes of the A_1 site at room temperature as suggested in van der Est et al. (1994a) or (ii) the spectra might contain a contribution from $P_{700}^+ Q_K B^-$. However, both of these explanations have somewhat unlikely consequences. If the differences were the result of structural changes in the quinone binding site, the altered structure would only be present at room temperature. On the other hand, if the changes were due electron transfer in the B-branch its activity would have to be strongly temperature dependent. This is difficult to reconcile with the fast rate associated with the initial charge separation.

Another approach to the search for EPR signatures of electron transfer through Q_K-B has been photoaccumulation experiments. The premise of these experiments is that if the B-branch is active in electron transfer then it should be possible to photoaccumulate the semiquinone in this branch. In principle, several pieces of evidence for such a scenario are possible in the spectra of the photoaccumulated radicals. First, if more than one semiquinone radical is accumulated per P_{700}, one could conclude that both quinones are reduced, at least in a fraction of the reaction centers. Second, if the properties of the two quinones differ then changes in the semiquinone spectrum might be observed if different protocols are used to accumulate the radicals. Finally, if it is possible to reduce both quinones in the same reaction center, then the spin–spin coupling between the two radicals should be observable. This has been demonstrated recently in purple bacterial reaction centers in which both Q_A and Q_B are reduced (Calvo et al., 1999, 2000). In eukaryotic PS I, accumulation of up to four spins per P_{700} has been reported (Heathcote et al., 1993; Rigby et al., 2002) following illumination at pH 10 and 220–230 K. However, in cyanobacterial PS I, various accumulation protocols produced no more than one semiquinone spin per P_{700}^+ (MacMillan et al., 1997; Teutloff et al., 1998; Yang et al., 1998). The origin of this difference is not clear. Nonetheless, the results in eukaryotic PS I suggests that it might be possible to accumulate electrons on both quinones in these species. A fundamental difficulty with determining the

number of photo-accumulated electrons is the coupling between the spins. If the reported maximum of four spins (Heathcote et al., 1993; Rigby et al., 2002) are accumulated on the acceptors it creates a spin system with $S = 2$. Based on the distances between the acceptors, the zero-field splitting of the spectrum should be on the order of a few tens of Gauss and the exchange interactions are of the similar magnitude or larger. The spin system should therefore have several paramagnetic multiplet states, which could potentially contribute to the spectrum. The intensity of such a spectrum is not related in a simple way to the number of spins involved, hence the reported value of four spins/reaction center should be treated with caution.

In Rigby et al. (2002) it was shown that both the EPR and ENDOR spectra obtained from PS I from *C. reinhardtii* after photo-accumulation at pH 10 and 220 K differed from those taken after illumination at pH 8 and 220 K or at pH 10 and 205 K. The difference was attributed to a contribution from the B-side semiquinone when the photoaccumulation was performed at pH 10 and 220 K. However, this assignment is far from certain because there are 15 possible ways to place between one and four electrons on the four acceptors Q_K-A, Q_K-B, eC-A3, and eC-B3 and all of these states could potentially contribute to the spectrum. Many of them are extremely unlikely, but even if only the most probably states are considered there are still a fairly large number possibilities. The EPR and ENDOR spectra obtained by illumination at pH 8 and 220 K were subtracted from those accumulated at pH 10 and 220 K and the resulting difference spectra were assigned to Q_K-B^- (Rigby et al., 2002). For this assignment to be correct, a number of conditions must be met: (i) the amount of Q_K-A^- must be the same for both illumination protocols, (ii) there must no contribution from reaction centers with both quinones reduced because the coupling between the radicals would change the Q_K-A^- contribution, and (iii) any contamination of the signals from other radicals such as A_0^- (Rigby et al., 2003) must not change and must not alter the Q_K-A^- spectrum. It is very unlikely that these conditions are fulfilled in Rigby et al. (2002) and thus it is not clear whether Q_K-B^- contributes to the spectra or not.

Recently, the hyperfine couplings associated with photoaccumulated A_1^- have been separated from other contributions to the spectra using a combination of selective deuteration and Q-band pulsed ENDOR (Pushkar et al., 2004). In these experiments a fully deuterated quinone was introduced into the A_1 binding site and proton Q-band ENDOR was carried out on the photo-accumulated spectrum. The goal of these experiments was to measure the strength of the hyperfine coupling to the proton involved in the hydrogen bond to the backbone nitrogen of leucine $L722_{PsaA}$ ($L706_{PsaB}$). The higher spectral resolution possible at Q-band allows the observed hyperfine couplings to be correlated with regions of the EPR spectrum associated with either A_1^- or A_0^-. The results show that some of the couplings previously assigned to the A_1^- hydrogen bonded proton only appear in regions of the spectrum associated with A_0^-. Hence, it would appear that contamination of the A_1^- spectrum by contributions from A_0^- may be a problem in many earlier studies.

B. Factors Controlling Electron Transfer from A_1 to F_X

1. Energetics

An adequate description of the energetics of the electron transfer from A_1^- to F_X in PS I has proven to be a surprisingly elusive goal. For other electron transfer steps in photosynthetic reaction centers, the energetics are often treated using the semiclassical Marcus equation (Marcus and Sutin, 1985), which predicts a temperature-dependent rate given by:

$$k_{et} = \frac{2\pi |V|^2}{\hbar\sqrt{4\pi k_B T}} \exp\left\{-(\Delta G + \lambda)^2/4\lambda k_B T\right\} \quad (1)$$

where ΔG is the free energy difference and λ is the reorganization energy, V is the electronic tunneling matrix element between the donor and acceptor. The rate has its maximum value and is nearly independent of temperature when $\Delta G = -\lambda$, while it is less than the maximum and strongly temperature-dependent when ΔG is much larger or much smaller than $-\lambda$. A crucial element of Eq. (1) is that it assumes a single, classical Hooke's Law potential for the mode of motion, which is coupled to the electron transfer. This is clearly an oversimplification and there is a large body of literature devoted to the development of more sophisticated models (see Jortner and Bixon, 1999a,b for an exhaustive review). The earliest of these introduced a quantum mechanical treatment and the possibility of coupling to modes of different frequency (Jortner, 1976; Devault, 1980). For coupling to a single mode, the quantum mechanical treatment converged to the classical expression at high temperature but became temperature-independent when the energy of the mode was much smaller than kT. Hence, the temperature dependence of the rate depends not only on the relative magnitudes of ΔG and λ but also on the coupling of the electron transfer to the vibrational modes. Another

important feature of Eq. (1) is the electronic coupling, V, which is expected to fall off exponentially with the distance between the donor and acceptor. Based on this idea, Moser and Dutton have proposed a semiempirical form of Eq. (1) that has been shown to reproduce the measured rates for a wide range of electron transfer reaction in oxidoreductases (Moser and Dutton, 1992; Page et al., 1999):

$$\log_{10} k_{et} = 15 - 0.6R - 3.1(\Delta G + \lambda)^2/\lambda \qquad (2)$$

where R is the edge-to-edge distance between the donor and acceptor in Å. The temperature dependence is incorporated into the numerical constants in Eq. (2), which have been calculated for 300 K. For A_1 and F_X a value of R= 6.8 Å was determined for both Q_K-A and Q_K-B from the 2.5 Å resolution X-ray structure (Jordan et al., 2001). In Eq. (2) this gives a rate of $k_{et} = (12\ \text{ps})^{-1}$ which is 3–4 orders of magnitude faster than the measured rates. From this, it is clear that ΔG must be very different from -λ and therefore in a regime in which the predicted rate depends strongly on the values of ΔG and λ. In principle ΔG can be estimated from the reduction midpoint potentials of A_1 and F_x, however, both of these potentials are very negative making them difficult to determine accurately (see Brettel, 1997; Brettel and Leibl, 2001 for a detailed discussion). The existing estimates in the literature point to a value for ΔG on the order of ±0.1 eV (see Brettel, 1997; Semenov et al., 2000 for a discussion). This is considerably smaller than λ, which is usually taken to be in the range of 0.7–1.0 eV, and suggests that the electron transfer from A_1 to F_x is not at the maximum of the Marcus curve (1). Hence, according to the classical Marcus Eq. (1), it is predicted to have a significant activation energy and an Arrhenius type temperature dependence. Consistent with this, the slow kinetic component is known to be strongly temperature dependent (Schlodder et al., 1998; Agalarov and Brettel, 2003). A number of recent studies have addressed the problem of the energetics in connection with the analysis of new kinetic data. In Semenov et al. (2000), Shinkarev et al. (2000), Zybailov et al. (2000), Sakuragi et al. (2002), Shinkarev et al. (2002), and Agalarov and Brettel (2003) the effect of replacing phylloquinone with nonnative quinones was investigated. Interruption of the biosynthetic pathway to phylloquinone results in mutants with either plastoquinone (Johnson et al., 2000) or 2-phytyl-1,4-naphthoquinone (Sakuragi et al., 2002) in the A_1 site. In both cases, the midpoint potential of the nonnative quinone was estimated to be more positive than that of phylloquinone. The analysis of the observed forward and back reaction rates suggested that this leads to an energetically uphill step from the nonnative quinones to F_X. The energetics of the A_1 to F_X electron transfer in native PS I are less clear. Studies on PS I complexes devoid of PsaC (Luneberg et al., 1994; Moenne-Loccoz et al., 1994; van der Est et al., 1994; Brettel and Golbeck, 1995; Yu et al., 1995; Shinkarev et al., 2002) show that the rate of forward electron transfer to F_X is the same as in the wild type and that the back reaction occurs primarily from F_X. These two observations suggest that removal of PsaC does not affect the redox potential of F_X and that the equilibrium $P_{700}^+ A_1^- F_X \leftrightarrow P_{700}^+ A_1 F_X^-$ lies well to the right. This, in turn, implies that the electron transfer from A_1 to F_X in native PS I is energetically downhill (Shinkarev et al., 2002). However, two recent studies (Agalarov and Brettel, 2003; Gong et al., 2003) show that the situation is more complex than this and illustrate the difficulties in determining the relative energies of A_1 and F_X. In the first study (Gong et al., 2003), it was found that a significant fraction (∼80%) of the complexes from a PsaC deletion mutant were unable to transfer electrons to F_X. In contrast, earlier work (Yu et al., 1995) on a similar PsaC deletion mutant showed no evidence for significant loss of F_X reduction in thylakoid membranes. The difference in the results of these two studies is most likely due to differences in sample preparation which suggests that in the absence of PsaC, the stromal side of the PS I complex is susceptible to preparation dependent heterogeneity. Hence, it is difficult to interpret the loss of electron transfer to F_X in samples devoid of PsaC in terms of the relative energies of A_1 and F_X in native PS I. In the second study (Agalarov and Brettel, 2003), the temperature dependence of the two kinetic phases of A_1^- to F_X electron transfer was studied. The fast phase was found to be essentially independent of temperature while the slow phase showed Arrhenius type behavior as had been demonstrated earlier by Schlodder et al. (1998). The temperature-independence of the fast component cannot be explained using a classical treatment of the vibrational modes since it requires that $\Delta G = -\lambda$. If this were true, then the rate should be governed by the matrix element V and based on the distance between A_1 and F_X would be many orders of magnitude faster than observed. In a quantum mechanical treatment of the vibrations, temperature-independent electron transfer can occur for $\Delta G \neq \lambda$ if the energy of the mode(s) coupled to electron transfer is (are) much smaller than kT. This suggests that, at least for the fast component, the electron transfer is coupled to one or more high frequency mode(s). In Agalarov and Brettel (2003) two alternative models were proposed to reconcile the

different electron transfer rates and their temperature dependencies. The main feature of both models was that the two rates of electron transfer were accounted for by proposing two different relative energies for A_1 and F_X. For the fast component, A_1 was suggested to lie energetically higher than F_X, while for the slow component, the electron transfer was proposed to be uphill to account for its temperature dependence. Furthermore, the two components were assigned to electron transfer in the two branches with the fast component being associated with the PsaB branch and the slow component being associated with the PsaA branch. The two models proposed that either (i) the electron transfer occurs with 70% probability in the A-branch and 30% probability in the B-branch or (ii) electron transfer occurs only in the B-branch but Q_K-A is reduced by F_X in a fraction of the reaction centers during this process. Although both models are consistent with the observed kinetics, they are difficult to reconcile with a number of other experimental findings. First, two recent studies of A_0 point mutants (Cohen et al., 2003; Fairclough et al., 2003) suggest that the slow phase of electron transfer is unaffected by mutations in the PsaB branch, while significant effects are seen for mutations in the PsaA-branch. Moreover, removal of F_X does not have any influence on the shape of the observed spin polarization pattern of $P_{700}^{+}A_1^{-}$ (Shen et al., 2002a). These two findings essentially rule out model (ii). Model (i) is more compatible with the spin polarization patterns, provided that the spin polarization is associated with the 30% of electrons proceeding along the B-branch is negligible. Although it is possible that this is the case in cyanobacteria, it is rather unlikely given the fact that a significant contribution from the fast phase is observed in preparations from *C. reinhardtii* (Fig. 6).

2. The Role of the Stromal Subunits and Detergent Effects

The proposal that the two kinetic phases of forward electron transfer from A_1 to F_X correspond to the two branches raises a number of interesting questions. If this assignment is correct, a change in the relative amplitudes of the two phases implies a change in the fraction of electrons that are transferred along the two branches. It has been known for many years that this ratio is quite sensitive to the method used to isolate PS I from spinach and that harsher treatments produce larger amounts of fast electron transfer (Sétif and Brettel, 1993). Because of this, it was generally thought that the fast phase was probably a preparation artifact until Joliot and Joliot showed that it is present in whole cells (Joliot and Joliot, 1999). In spinach PS I preparations, strong detergent treatments lead to reduced amounts proteins of mass of 8, 16.5, and 20–22 kDa (Lagoutte et al., 1984), which suggests that some of the peripheral subunits are being lost. The fact that these types of preparations typically show larger amounts of fast electron transfer to F_X, suggests that the change in kinetics might be related to the loss of the peripheral subunits. Based on this observation, a study of the effect on the A_1 to F_X electron transfer of removing some of the stromal subunits was investigated in van der Est et al. (2003). It was shown that removal of PsaF in particular makes PS I particles from cyanobacteria susceptible to a detergent-induced contribution to the fast phase. Although the origin of this contribution could not be determined unambiguously, the fact that PsaF has a large number of contacts with PsaA near the Q_K-A binding site and none near P_{700} nor Q_K-B suggests that the detergent can induce fast electron transfer in the A-branch when PsaF is absent.

3. The Role of F_X

In another recent study of electron transfer through phylloquinone the effect of alterations in the environment of F_X were investigated (Gong et al., 2003). The double mutation $C565S_{PsaB}/D566E_{PsaB}$ in the F_X binding pocket caused 10-fold decrease in the rate of electron transfer from A_1 to F_X but caused little or no blockage of electron transfer. The result was rationalized in terms of postulated changes in the redox potential of F_X in response to changes in the environment and it was suggested that F_X plays a major role in controlling the electron transfer. An intriguing feature of the absorbance change curves from the double mutant is that electron transfer between A_1 and F_X becomes essentially monophasic. Thus, the mutation either slows both phases found in the wild type such that their rates become equal in the mutant or it abolishes one of the two phases and slows the other. These two possibilities cannot be distinguished on the basis of the data but it is important to note that changes on the stromal side of the complex again lead to a change in the relative amplitudes of the two kinetic phases.

4. The Influence of Specific Amino Acids

As discussed above, excitation of PS I generates a strong reducing potential and it is therefore perhaps somewhat surprising that it contains a quinone acceptor. The protein environment of A_1 clearly imparts

an unusually negative redox potential to the quinone. However, how this occurs is not yet well understood. With the availability of the 2.5 Å X-ray structure it has become possible to investigate this question theoretically using models of the electrostatic environment. In one of the first of these studies, the influence of the π-stacked tryptophan was investigated (Kaupp, 2002). The phylloquinone and its binding site were modeled by various indole–quinone and indole–semiquinone complexes to investigate the differences in energy and optimal geometry for the reduced and oxidized forms. It was found that geometry optimization of the indole–quinone complexes lead to the expected π-stacked arrangement. In contrast, semiquinone radical anions were found to adopt a T-stacked conformation with significant N–H–π hydrogen bonding interactions. It was proposed that in PS I, the interaction of the quinone side chain with the protein prevents such an arrangement which corresponds to a lowering of the midpoint potential of A_1. An implied consequence of this finding is that a weakening of the π–π interaction would be expected to push the midpoint potential of the quinone more positive. Consistent with this, mutations in the A_1 binding site such as $W693F_{PsaA}$ and $S692_{PsaA}$, which are expected to disturb the π-stacked arrangement also slow the forward electron transfer. Two other studies (Ishikita and Knapp, 2003; Ivashin and Larsson, 2003) investigated possible sources for the bi-exponential electron transfer. In Ivashin and Larsson (2003) it was proposed that the two electron transfer rates might be due to different electronic coupling between Q_K and F_X and in the two branches. This presupposes a bi-directional model. The only significant asymmetry found in the calculated electronic couplings was between $W673_{PsaB}$ and the two quinones. This is because this residue is not conserved in PsaA and PsaB. The calculation suggests that suggest that $W673_{PsaB}$ may act as a bridge between Q_K-B and F_X. Because the corresponding residue in PsaA is a glycine, the overall coupling between Q_K-A and F_X is predicted to be smaller. However, to date there is no experimental confirmation of such an effect, for example through mutation of these residues.

In the other study of this type (Ishikita and Knapp, 2003), it was proposed that the differences in rates is perhaps due to difference in the redox potentials of the two quinones as suggested in Agalarov and Brettel (2003). Again, presupposing a bi-directional model, the authors suggest that the negative midpoint potential of A_1 in PS I is primarily because of the influence of F_X rather than the π-stacked tryptophan as suggested by Kaupp (2002). The reduction potentials of the two quinones were found to differ in the calculation as a result of structural differences in the conformation of the protein backbone and it was suggested that Asp-B575 changes its protonation state upon reduction of either quinone. However, preliminary studies of point mutants of Asp-B575 show no correlation between the pKa of the residue at this position and the rate of forward electron transfer (van der Est et al., unpublished results).

C. Back Reaction Kinetics

Although charge recombination is not directly involved in the function of PS I, the back reaction kinetics nonetheless play an important role. In terms of the function of the reaction center unproductive charge recombination must be avoided. In terms of characterization of PS I, the back reaction kinetics provide additional data from which properties of the cofactors can be deduced. Formation of P_{700}^+ leads to an absorbance increase at ∼820 nm in the near IR, which can be used to conveniently measure the charge recombination. Alternatively, the EPR signal from P_{700}^+ can be followed as a function of time. In isolated PS I particles at ambient temperature, the main decay component has a lifetime on the order of ∼100 ms. Studies of modified PS I in which some or all of the iron–sulfur clusters are removed have shown that this component is due to back reaction from F_A/F_B (Brettel and Golbeck, 1995; Yu et al., 1995). Backreaction from F_X is found to occur with lifetimes of ∼0.2 and ∼2 ms (Vassiliev et al., 1997), whereas in samples devoid of all three iron–sulfur clusters two back reaction lifetimes of ∼10 and ∼100 μs are found (Brettel and Golbeck, 1995). However, samples containing nonnative quinones also show altered back reaction rates, demonstrating that the back reaction pathway involves the quinone (Semenov et al., 2000; Sakuragi et al., 2002). Kinetic modeling of these data can then be used to estimate electron transfer rates, equilibrium constants, and redox potentials, associated with the electron transfer steps through the quinone (Shinkarev et al., 2002; see Shinkarev, this volume, Chapter 36). Thus the question of directionality is also an issue for the backreaction. It is important to note however, that the two possible paths diverge at F_X for the back reaction, while the partitioning occurs at P_{700} for the forward reaction. Thus, the activity of the two branches in the forward and back reaction are likely to be different. However, this aspect of the electron transfer has not yet been investigated in detail. The assignment of specific kinetic phases of the back reaction to a specific quinone would provide an addition

piece of information to fit into the overall picture of their function.

IV. Concluding Remarks

Despite the enormous progress which has been made in since the elucidation of the X-ray structure of PS I, understanding the details of the electron transfer through phylloquinone remains ones of the most challenging aspects of research on PS I. The two main issues are the energetics of the quinones and their involvement in forward electron transfer. There is general agreement that the slow phase of forward electron transfer is associated with the PsaA branch and it is also clear that cyclic electron transfer at low temperature also occurs in the PsaA branch. However, there are still a considerable number of unresolved or uncertain issues. There is a significant body of evidence pointing toward participation of Q_K-B in forward electron transfer but this is difficult to reconcile with the presence of two fractions of reaction centers at low temperature. In one fraction, illumination at low temperature leads to stable reduction of F_A/F_B. In the other it leads to cyclic electron transfer in the PsaA branch. Superficially, the presence of these two fractions would appear to be consistent with two possible electron transfer pathways. However, the fact that PS I samples can be illuminated for days at 50 K without a significant change in the amplitude of the cyclic fraction presents a problem. There are two possible interpretations or this result: (i) the two fractions are not related to the two possible pathways but rather are the result of a distribution of activation energies for electron transfer past A_1 (ii) the two fractions correspond to electron transfer in the two branches and occur because of the different temperature dependencies of the two phases of A_1 to F_X electron transfer. To be consistent with EPR data from point mutants, the first explanation requires that electron transfer must be very strongly biased toward the A-branch at low temperature but does not rule out a small fraction of electron transfer in the B-branch provided it does not lead to stable charge separation. The second explanation requires that for the fraction undergoing cyclic electron transfer, the probability of electron transfer occurring in the B-branch is effectively zero, otherwise prolonged illumination would lead to disappearance of the cyclic fraction.

The key to this issue is most likely associated with F_X. In most discussions of the electron transfer, it is implicitly assumed that F_X behaves in much the same way as any other cofactor. However, the electronic structure of the iron–sulfur clusters is very different from that of an organic compound and it is well-known that their redox potentials are extremely sensitive to changes in the protein structure in the immediate vicinity. Moreover, F_X is located at the interface between three protein subunits PsaA, PsaB, and PsaC. Thus, it is likely that this region of the protein is structurally unstable with the probable consequence of a distribution of redox potentials for F_X. To date there have been few studies directed toward understanding the role of F_X in determining the rates of electron transfer and the relative amounts of trapped and cyclic electron transfer at low temperature. The few data, which do exist (see, e.g., Zeng et al., 2002; Gong et al., 2003) clearly point to an important but complex role for F_X.

References

Agalarov R and Brettel K (2003) Temperature dependence of biphasic forward electron transfer from the phylloquinone(s) A_1 in photosystem I: only the slower phase is activated. Biochim Biophys Acta 1604: 7–12

Angerhofer A and Bittl R (1996) Radicals and radical pairs in photosynthesis. Photochem Photobiol 63: 11–38

Béal D, Rappaport F and Joliot P (1999) A new high-sensitivity 10-ns time-resolution spectrophotometric technique adapted to *in vivo* analysis of the photosynthetic apparatus. Rev Sci Instrum 70: 202–207

Bengis C and Nelson N (1977) Subunit structure of chloroplast Photosystem-I reaction center. J Biol Chem 252: 4564–4569

Bittl R and Zech SG (2001) Pulsed EPR spectroscopy on short-lived intermediates in photosystem I. Biochim Biophys Acta 1507: 194–211

Blankenship RE (2002) Molecular Mechanisms of Photosynthesis. Blackwell Science Inc, Oxford

Blankenship R, McGuire A and Sauer K (1975) Chemically-induced dynamic electron polarization in chloroplasts at room-temperature – evidence for triplet-state participation in photosynthesis. Proc Natl Acad Sci USA 72: 4943–4947

Bock CH, van der Est AJ, Brettel K and Stehlik D (1989) Nanosecond electron transfer kinetics in Photosystem I as obtained from transient EPR at room temperature. FEBS Lett 247: 91–96

Bonnerjea J and Evans MCW (1982) Identification of multiple components in the intermediary electron carrier complex of Photosystem-I. FEBS Lett 148: 313–316

Boudreaux B, MacMillan F, Teutloff C, Agalarov R, Gu FF, Grimaldi S, Bittl R, Brettel K and Redding K (2001) Mutations in both sides of the Photosystem I reaction center identify the phylloquinone observed by electron paramagnetic resonance spectroscopy. J Biol Chem 276: 37299–37306

Brettel K (1988) Electron transfer from A_1^- to an iron–sulfur center with $t_{1/2} = 200$ ns at room temperature in Photosystem I characterization by flash absorption spectroscopy. FEBS Lett 239: 93–98

Brettel K (1997) Electron transfer and arrangement of the redox cofactors in Photosystem I. Biochim Biophys Acta 1318: 322–373

Brettel K (1998) Electron transfer from acceptor A_1 to the iron–sulfur clusters in Photosystem I measured with a time resolution of 2 ns. In: Garab G (ed) Photosynthesis Mechanisms and Effects, Vol I, pp 611–614. Kluwer Academic Publishers, Dordrecht/Boston/London

Brettel K and Golbeck JH (1995) Spectral and kinetic characterization of electron acceptor A_1 in a Photosystem I core devoid of iron–sulfur centers F_X, F_B and F_A. Photosynth Res 45: 183–193

Brettel K and Leibl W (2001) Electron transfer in Photosystem I. Biochim Biophys Acta 1507: 100–114

Brettel K and Vos MH (1999) Spectroscopic resolution of the picosecond reduction kinetics of the secondary electron acceptor A_1 in Photosystem I. FEBS Lett 447: 315–317

Brettel K, Sétif P and Mathis P (1986) Flash-induced absorption changes in Photosystem-I at low-temperature – evidence that the electron acceptor-A_1 is vitamin-K_1. FEBS Lett 203: 220–224

Brettel K, Leibl W and Liebl U (1998) Electron transfer in the heliobacterial reaction center: evidence against a quinone-type electron acceptor functioning analogous to A_1 in photosystem I. Biochim Biophys Acta 1363: 175–181

Byrdin M, Jordan P, Krauß N, Fromme P, Stehlik D and Schlodder E (2002) Light harvesting in Photosystem I: modeling based on the 2.5-Ångstrom structure of Photosystem I from *Synechococcus elongatus*. Biophys J 83: 433–457

Calvo R, Hofbauer W, Lendzian F, Lubitz W, Paddock ML, Abresch EC, Isaacson RA, Okamura MY and Feher G (1999) Magnetic coupling between Q_A^- and Q_B^- in RCs of *Rb. Sphaeroides* determined by EPR spectroscopy at 95 GHz. Biophys J 76: A392–A392

Calvo R, Abresch EC, Bittl R, Feher G, Hofbauer W, Isaacson RA, Lubitz W, Okamura MY and Paddock ML (2000) EPR study of the molecular and electronic structure of the semiquinone biradical $Q_A^{-\cdot}Q_B^{-\cdot}$ in photosynthetic reaction centers from *Rhodobacter sphaeroides*. J Am Chem Soc 122: 7327–7341

Cohen R, Shen G, Golbeck J, Xu W, Chitnis P, Valieva A, van der Est A, Pushkar YN and Stehlik D (2003) Evidence for asymmetric electron transfer in cyanobacterial Photosystem I: analysis of a methionine to leucine mutation of the ligand to the primary electron acceptor A_0. Biochemistry 43,4741–4754

Cramer WA and Knaff DB (1990) Energy Transduction in Biological Membranes. Springer, New York

Devault D (1980) Quantum-mechanical tunnelling in biological-systems. Q Rev Biophys 13: 387–564

Dzuba SA, Hara H, Kawamori A, Iwaki M, Itoh S and Tsvetkov YD (1997) Electron spin echo of spin-polarised radical pairs in intact and quinone-reconstituted plant Photosystem I reaction centers. Chem Phys Lett 264: 238–244

Evans MCW, Purton S, Patel V, Wright D, Heathcote P and Rigby SEJ (1999) Modification of electron transfer from the quinone electron carrier, A_1, of Photosystem 1 in a site directed mutant D576L within the Fe-S_x binding site of PsaA and in second site suppressors of the mutation in *Chlamydomonas reinhardtii*. Photosynth Res 61: 33–42

Fairclough WV, Evans MCW, Purton S, Jones S, Rigby SEJ and Heathcote P (2001) Site-directed mutagenesis of PsaA:M684 in *Chlamydomonas reinhardtii*. In: Critchley C (ed) PS2001: 12th International Congress on Photosynthesis, pp S6–022. CSIRO Publishers, Melbourne Australia.

Fairclough WV, Forsyth A, Evans MCW, Rigby SEJ, Purton S and Heathcote P (2003) Bidirectional electron transfer in Photosystem I: electron transfer on the PsaA side is not essential for phototrophic growth in *Chlamydomonas*. Biochim Biophys Acta 1606: 43–55

Fromme P, Jordan P and Krauß N (2001) Structure of Photosystem I. Biochim Biophys Acta 1507: 5–31

Gast P, Swarthoff T, Ebskamp FCR and Hoff AJ (1983) Evidence for a new early acceptor in Photosystem-I of plants – an electron-spin-resonance investigation of reaction center triplet yield and of the reduced intermediary acceptors. Biochim Biophys Acta 722: 163–175

Gobets B and van Grondelle R (2001) Energy transfer and trapping in Photosystem I. Biochim Biophys Acta 1507: 80–99

Golbeck JH (1989) Structure, function and organization of the Photosystem I reaction center complex. Biochim Biophys Acta 895: 167–204

Golbeck JH (1992) Structure and function of Photosystem I. Annu Rev Plant Physiol Plant Mol Biol 43: 293–324

Golbeck JH and Bryant DA (1991) Photosystem I. Curr Top Bioenerg 16: 83–177

Golbeck J, Xu W, Zybailov B, van der Est A, Pushkar J, Zech S, Stehlik D and Chitnis P (2001) Electron transfer through the quinone electron acceptor in Photosystem I. In: Critchley C (ed) PS2001: 12th International Congress on Photosynthesis, pp S6–006. CSIRO Publishing, Melbourne, Australia

Gong XM, Agalarov R, Brettel K and Carmeli C (2003) Control of electron transport in Photosystem I by the iron–sulfur cluster F_X in response to intra- and intersubunit interactions. J Biol Chem 278: 19141–19150

Guergova-Kuras M, Boudreaux B, Joliot A, Joliot P and Redding K (2001) Evidence for two active branches for electron transfer in Photosystem I. Proc Natl Acad Sci USA 98: 4437–4442

Hastings G, Kleinherenbrink FAM, Lin S, McHugh TJ and Blankenship RE (1994) Observation of the reduction and reoxidation of the primary electron acceptor in Photosystem I. Biochemistry 33: 3193–3200

Heathcote P, Hanley JA and Evans MCW (1993) Double-reduction of A_1 abolishes the EPR signal attributed to A_1^-: evidence for C_2 symmetry in the Photosystem I reaction center. Biochim Biophys Acta 1144: 54–61

Heathcote P, MoenneLoccoz P, Rigby SEJ and Evans MCW (1996) Photoaccumulation in photosystem I does produce a phylloquinone (A_1^-) radical. Biochemistry 35: 6644–6650

Hecks B, Wulf K, Breton J, Leibl W and Trissl HW (1994) Primary charge separation in Photosystem I – a 2-step electrogenic charge separation connected with $P_{700}^+A_0^-$ and $P_{700}^+A_1^-$ formation. Biochemistry 33: 8619–8624

Hoff A (1993) Time resolved EPR methods. In: Deisenhofer J and Norris JR (eds) The Photosynthetic Reaction Center, Vol II, pp 331–386. Academic Press, San Diego/London

Hore PJ (1996) Transfer of spin correlation between radical pairs in the initial steps of photosynthetic energy conversion. Mol Phys 89: 1195–1202

Hulsebosch RJ, Borovykh IV, Paschenko SV, Gast P and Hoff AJ (1999) Radical pair dynamics and interactions in quinone-reconstituted photosynthetic reaction centers of *Rb. sphaeroides* R26: a multifrequency magnetic resonance study. J Phys Chem B 103: 6815–6823

Ishikita H and Knapp EW (2003) Redox potential of quinones in both electron transfer branches of photosystem I. J Biol Chem 278: 52002–52011

Ivashin N and Larsson S (2003) Electron transfer pathways in photosystem I reaction centers. Chem Phys Lett 375: 383–387

Johnson TW, Shen GZ, Zybailov B, Kolling D, Reategui R, Beauparlant S, Vassiliev IR, Bryant DA, Jones AD, Golbeck JH and Chitnis PR (2000) Recruitment of a foreign quinone into the A_1 site of Photosystem I – I. Genetic and physiological characterization of phylloquinone biosynthetic pathway mutants in *Synechocystis* sp PCC 6803. J Biol Chem 275: 8523–8530

Johnson TW, Zybailov B, Jones AD, Bittl R, Zech S, Stehlik D, Golbeck JH and Chitnis PR (2001) Recruitment of a foreign quinone into the A_1 site of Photosystem I – in vivo replacement of plastoquinone-9 by media-supplemented naphthoquinones in phylloquinone biosynthetic pathway mutants of *Synechocystis* sp. PCC 6803. J Biol Chem 276: 39512–39521

Joliot P and Joliot A (1999) In vivo analysis of the electron transfer within Photosystem I: are the two phylloquinones involved? Biochemistry 38: 11130–11136

Jordan P, Fromme P, Witt HT, Klukas O, Saenger W and Krauß N (2001) Three-dimensional structure of cyanobacterial Photosystem I at 2.5 Ångstrom resolution. Nature 411: 909–917

Jortner J (1976) Temperature dependent activation energy for electron transfer between biological molecules. J Chem Phys 64: 4860–4867

Jortner J and Bixon M (eds) (1999a) Electron transfer – from isolated molecules to biomolecules, Part One. Advances in Chemical Physics, Vol 106. John Wiley & Sons, Inc, New York

Jortner J and Bixon M (eds) (1999b) Electron transfer – from isolated molecules to biomolecules, Part Two. Advances in Chemical Physics, Vol 107. John Wiley & Sons, Inc., New York

Kandrashkin Y and van der Est A (2002) Electron spin polarization in photosynthetic reaction centers: strategies for extracting structural and functional information. RIKEN Rev 44: 124–127

Kandrashkin YE, Salikhov KM and Stehlik D (1997) Spin dynamics and EPR spectra of consecutive spin-correlated radical pairs. Model calculations. Appl Magn Reson 12: 141–166

Kandrashkin YE, Vollmann W, Stehlik D, Salikhov K and Van der Est A (2002) The magnetic field dependence of the electron spin polarization in consecutive spin correlated radical pairs in type I photosynthetic reaction centers. Mol Phys 100: 1431–1443

Käss H, Fromme P, Witt HT and Lubitz W (2001) Orientation and electronic structure of the primary donor radical cation P_{700}^{+} in Photosystem I: a single crystals EPR and ENDOR study. J Phys Chem B 105: 1225–1239

Kaupp M (2002) The function of photosystem I. Quantum chemical insight into the role of tryptophan–quinone interactions. Biochemistry 41: 2895–2900

Kjaer B, Frigaard NU, Yang F, Zybailov B, Miller M, Golbeck JH and Scheller HV (1998) Menaquinone-7 in the reaction center complex of the green sulfur bacterium *Chlorobium vibrioforme* functions as the electron acceptor A_1. Biochemistry 37: 3237–3242

Klukas O, Schubert WD, Jordan P, Krauß N, Fromme P, Witt HT and Saenger W (1999) Localization of two phylloquinones, Q_K and Q_K', in an improved electron density map of Photosystem I at 4 Ångstrom resolution. J Biol Chem 274: 7361–7367

Koradi R, Billeter M and Wuthrich K (1996) MOLMOL: a program for display and analysis of macromolecular structures. J Mol Graphics 14: 51–55, 29–32

Krauß N, Schubert WD, Klukas O, Fromme P, Witt HT and Saenger W (1996) Photosystem I at 4 Å resolution represents the first structural model of a joint photosynthetic reaction center and core antenna system. Nat Struct Biol 3: 965–973

Lagoutte B, Sétif P and Duranton J (1984) Tentative identification of the apoproteins of iron–sulfur centers of Photosystem I. FEBS Lett 174: 24–29

Leibl W, Toupance B and Breton J (1995) Photoelectric characterization of forward electron transfer to iron–sulfur centers in Photosystem I. Biochemistry 34: 10237–10235

Luneberg J, Fromme P, Jekow P and Schlodder E (1994) Spectroscopic characterization of PS I core complexes from thermophilic *Synechococcus* sp.: identical reoxidation kinetics of A_1^- before and after removal of the iron–sulfur clusters F_A and F_B. FEBS Lett 338: 197

MacMillan F, Hanley J, vanderWeerd L, Knupling M, Un S and Rutherford AW (1997) Orientation of the phylloquinone electron acceptor anion radical in photosystem I. Biochemistry 36: 9297–9303

Mamedov MD, Gadzhieva RM, Gourovskaya KN, Drachev LA and Semenov AY (1996) Electrogenicity at the donor acceptor sides of cyanobacterial photosystem I. J Bioenerg Biomembr 28: 517–522

Manikowski H, McIntosh AR and Bolton JR (1984) A study of chemically-induced dynamic electron polarization (CIDEP) in Photosystem-I of whole algal cells at ambient-temperatures. Biochim Biophys Acta 765: 68–73

Marcus RA and Sutin N (1985) Electron transfers in chemistry and biology. Biochim Biophys Acta 811: 265–322

McIntosh AR, Manikowski H and Bolton JR (1979a) Observations of chemically-induced dynamic electron polarization in Photosystem-I of green plants and algae. J Phys Chem 83: 3309–3313

McIntosh AR, Manikowski H, Wong SK, Taylor CPS and Bolton JR (1979b) CIDEP observations in Photosystem-I of green plant and algal photosynthesis. Biochem Biophys Res Commun 87: 605–612

Mi DH, Lin S and Blankenship RE (1999) Picosecond transient absorption spectroscopy in the blue spectral region of Photosystem I. Biochemistry 38: 15231–15237

Möbius K (2000) Primary processes in photosynthesis: what do we learn from high-field EPR spectroscopy? Chem Soc Rev 29: 129–139

Moenne-Loccoz P, Heathcote P, Maclachlan DJ, Berry MC, Davis IH and Evans MCW (1994) Path of electron transfer in Photosystem 1 – direct evidence of forward electron transfer from A_1 to Fe-S_x. Biochemistry 33: 10037–10042

Morris AL, Snyder SW, Zhang YN, Tang J, Thurnauer MC, Dutton PL, Robertson DE and Gunner MR (1995) Electron-spin polarization model applied to sequential electron-transfer in iron-containing photosynthetic bacterial reaction centers with different quinones as Q(a). J Phys Chem 99: 3854–3866

Moser CC and Dutton PL (1992) Engineering protein-structure for electron-transfer function in photosynthetic reaction centers. Biochim Biophys Acta 1101: 171–176

Muhiuddin IP, Rigby SEJ, Evans MCW, Amesz J and Heathcote P (1999) ENDOR and special TRIPLE resonance spectroscopy

of photoaccumulated semiquinone electron acceptors in the reaction centers of green sulfur bacteria and heliobacteria. Biochemistry 38: 7159–7167

Muhiuddin IP, Heathcote P, Carter S, Purton S, Rigby SEJ and Evans MCW (2001) Evidence from time resolved studies of the $P_{700}^{+}A_1^{-}$ radical pair for photosynthetic electron transfer on both the PsaA and PsaB branches of the Photosystem I reaction center. FEBS Lett 503: 56–60

Norris JR, Morris AL, Thurnauer MC and Tang J (1990) A general-model of electron-spin polarization arising from the interactions within radical pairs. J Chem Phys 92: 4239–4249

Page CC, Moser CC, Chen XX and Dutton PL (1999) Natural engineering principles of electron tunnelling in biological oxidation–reduction. Nature 402: 47–52

Pedersen JB (1979) Determination of the primary reactions of photosynthesis from transient ESR signals. FEBS Lett 97: 305–310

Purton S, Stevens DR, Muhiuddin IP, Evans MCW, Carter S, Rigby SEJ and Heathcote P (2001) Site-directed mutagenesis of PsaA residue W693 affects phylloquinone binding and function in the photosystem I reaction center of C*hlamydomonas reinhardtii*. Biochemistry 40: 2167–2175

Pushkar YN, Stehlik D, Lubitz W and van Gastel M (2004) An EPR/ENDOR study of the asymmetric hydrogen bond between the quinone electron acceptor and the protein backbone in Photosystem I. J Mol Struct 700: 233–241

Rappaport F, Guergova-Kuras M, Nixon PJ, Diner BA and Lavergne J (2002) Kinetics and pathways of charge recombination in Photosystem II. Biochemistry 41: 8518–8527

Redding K, Guergova-Kuras M, MacMillan F, Bittl R, Brettel K, Boudreaux B, Gu FF, Joliot A, Joliot P, Grimaldi S, Teutloff C and Agalarov R (2001) Mutational analysis of the binding sites of the active phylloquinones in PS I. In: Critchley C (ed) PS2001: 12th International Congress on Photosynthesis, pp S6–029. CSIRO Publishers, Melbourne, Australia

Rigby SEJ, Muhiuddin IP, Evans MCW, Purton S and Heathcote P (2002) Photoaccumulation of the PsaB phyllosemiquinone in Photosystem I of *Chlamydomonas reinhardtii*. Biochim Biophys Acta 1556: 13–20

Rigby SEJ, Muhiuddin IP, Santabarbara S, Evans MCW and Heathcote P (2003) Proton ENDOR spectroscopy of the anion radicals of the chlorophyll primary electron acceptors in type I photosynthetic reaction centers. Chem Phys 294: 319–328

Sakuragi Y, Zybailov B, Shen GZ, Jones AD, Chitnis PR, van der Est A, Bittl R, Zech S, Stehlik D, Golbeck JH and Bryant DA (2002) Insertional inactivation of the *menG* gene, encoding 2-phytyl-1,4-naphthoquinone methyltransferase of *Synechocystis* sp. PCC 6803, results in the incorporation of 2-phytyl-1,4-naphthoquinone into the A_1 site and alteration of the equilibrium constant between A_1 and F_x in Photosystem I. Biochemistry 41: 394–405

Salikhov KM, Zech SG and Stehlik D (2002) Light induced radical pair intermediates in photosynthetic reaction centers in contact with an observer spin label: spin dynamics and effects on transient EPR spectra. Mol Phys 100: 1311–1321

Savikhin S, Xu W, Martinsson P, Chitnis PR and Struve WS (2001) Kinetics of charge separation and $A_0^{-} \rightarrow > A_1$ electron transfer in photosystem reaction centers. Biochemistry 40: 9282–9290

Schlodder E, Falkenberg K, Gergeleit M and Brettel K (1998) Temperature dependence of forward and reverse electron transfer from A_1^{-}, the reduced secondary electron acceptor in Photosystem I. Biochemistry 37: 9466–9476

Schubert WD, Klukas O, Krauß N, Saenger W, Fromme P and Witt HT (1997) Photosystem I of *Synechococcus elongatu*s at 4 Ångstrom resolution: comprehensive structure analysis. J Mol Biol 272: 741–769

Schubert WD, Klukas O, Saenger W, Witt HT, Fromme P and Krauß N (1998) A common ancestor for oxygenic and anoxygenic photosynthetic systems: a comparison based on the structural model of photosystem I. J Mol Biol 280: 297–314

Semenov AY, Vassiliev IR, van der Est A, Mamedov MD, Zybailov B, Shen GZ, Stehlik D, Diner BA, Chitnis PR and Golbeck JH (2000) Recruitment of a foreign quinone into the A_1 site of Photosystem I – altered kinetics of electron transfer in phylloquinone biosynthetic pathway mutants studied by time-resolved optical, EPR, and electrometric techniques. J Biol Chem 275: 23429–23438

Sétif P and Brettel K (1993) Forward electron transfer from phylloquinone A_1 to iron–sulfur centers in spinach Photosystem I. Biochemistry 32: 7846–7854

Shen GZ, Antonkine ML, van der Est A, Vassiliev IR, Brettel K, Bittl R, Zech SG, Zhao JD, Stehlik D, Bryant DA and Golbeck JH (2002a) Assembly of photosystem I. II. Rubredoxin is required for the *in vivo* assembly of F_x in *Synechococcus* sp. PCC 7002 as shown by optical and EPR spectroscopy. J Biol Chem 277: 20355–20366

Shen GZ, Zhao JD, Reimer SK, Antonkine ML, Cai Q, Weiland SM, Golbeck JH and Bryant DA (2002b) Assembly of photosystem I. I. Inactivation of the *rubA* gene encoding a membrane-associated rubredoxin in the cyanobacterium *Synechococcus* sp. PCC 7002 causes a loss of Photosystem I activity. J Biol Chem 277: 20343–20354

Shinkarev VP, Vassiliev IR and Golbeck JH (2000) A kinetic assessment of the sequence of electron transfer from F_X to F_A and further to F_B in photosystem I: the value of the equilibrium constant between F_X and F_A. Biophys J 78: 363–372

Shinkarev VP, Zybailov B, Vassiliev IR and Golbeck JH (2002) Modeling of the $P700^{+}$ charge recombination kinetics with phylloquinone and plastoquinone-9 in the A_1 site of photosystem I. Biophys J 83: 2885–2897

Snyder SW and Thurnauer M (1993) Electron spin polarization in photosynthetic reaction centers. In: Deisenhofer J and Norris JR (eds) The Photosynthetic Reaction Center, Vol II, pp 285–330. Academic Press, San Diego/London

Snyder SW, Morris AL, Bondeson SR, Norris JR and Thurnauer MC (1993) Electron-spin polarization in sequential electron transfer – an example from iron-containing photosynthetic bacterial reaction center proteins. J Am Chem Soc 115: 3774–3775

Stehlik D and Möbius K (1997) New EPR methods for investigating photoprocesses with paramagnetic intermediates. Annu Rev Phys Chem 48: 745–784

Tang J, Bondeson S and Thurnauer MC (1996) Effects of sequential electron transfer on electron spin polarized transient EPR spectra at high fields. Chem Phys Lett 253: 293–298

Tang J, Utschig LM, Poluektov O and Thurnauer MC (1999) Transient W-band EPR study of sequential electron transfer in photosynthetic bacterial reaction centers. J Phys Chem B 103: 5145–5150

Teutloff C, MacMillan F, Bittl R, Lendzian F and Lubitz W (1998) A comparative study of A_1^{-} in PS I from cyanobacteria, green

plants and algae using EPR and ENDOR spectroscopy. In: Garab G (ed) Photosynthesis: Mechanisms and Effects, Vol I, pp 607–610. Kluwer Academic Publishers, Dordrecht, The Netherlands

Thurnauer MC and Norris JR (1980) An electron-spin echo phase-shift observed in photosynthetic algae – possible evidence for dynamic radical pair interactions. Chem Phys Lett 76: 557–561

Thurnauer MC, Rutherford AW and Norris JR (1982) The effect of ambient redox potential on the transient electron-spin echo signals observed in chloroplasts and photosynthetic algae. Biochim Biophys Acta 682: 332–338

Trissl HW and Wulf K (1995) Fast photovoltage measurements in photosynthesis. II. Experimental methods. Biospectroscopy 1: 71–82

Utschig LM, Greenfield SR, Tang J, Laible PD and Thurnauer MC (1997) Influence of iron-removal procedures on sequential electron transfer in photosynthetic bacterial reaction centers studied by transient EPR spectroscopy. Biochemistry 36: 8548–8558

van der Est A (2001) Light-induced spin polarization in type I photosynthetic reaction centers. Biochim Biophys Acta 1507: 212–225

van der Est A, Bock C, Golbeck J, Brettel K, Sétif P and Stehlik D (1994) Electron transfer from acceptor A_1 to the iron–sulfur centers in Photosystem I as studied by transient EPR spectroscopy. Biochemistry 33: 11789–11797

van der Est A, Hager-Braun C, Leibl W, Hauska G and Stehlik D (1998) Transient electron paramagnetic resonance spectroscopy on green-sulfur bacteria and heliobacteria at two microwave frequencies. Biochim Biophys Acta 1409: 87–98

van der Est A, Valieva A, Kandrashkin Y, Shen G, Bryant D and Golbeck J (2003) Removal of PsaF alters forward electron transfer in Photosystem I: evidence for fast reoxidation of Q_K-A in subunit deletion mutants of *Synechococcus* sp. PCC 7002. Biochemistry 43: 1264–1275

Vassiliev IR, Jung YS, Mamedov MD, Semenov AY and Golbeck JH (1997) Near-IR absorbance changes and electrogenic reactions in the microsecond-to-second time domain in photosystem I. Biophys J 72: 301–315

Vassiliev IR, Antonkine ML and Golbeck JH (2001) Iron–sulfur clusters in type I reaction centers. Biochim Biophys Acta 1507: 139–160

Webber AN and Lubitz W (2001) P700: the primary electron donor of Photosystem I. Biochim Biophys Acta 1507: 61–79

Xu W, Chitnis P, Valieva A, van der Est A, Pushkar YN, Krzystyniak M, Teutloff C, Zech SG, Bittl R, Stehlik D, Zybailov B, Shen GZ and Golbeck JH (2003a) Electron transfer in cyanobacterial Photosystem I – I. Physiological and spectroscopic characterization of site-directed mutants in a putative electron transfer pathway from A_0 through A_1 to F_x. J Biol Chem 278: 27864–27875

Xu W, Chitnis PR, Valieva A, van der Est A, Brettel K, Guergova-Kuras M, Pushkar YN, Zech SG, Stehlik D, Shen GZ, Zybailov B and Golbeck JH (2003b) Electron transfer in cyanobacterial photosystem I – II. Determination of forward electron transfer rates of site-directed mutants in a putative electron transfer pathway from A_0 through A_1 to F_X. J Biol Chem 278: 27876–27887

Yang F, Shen GZ, Schluchter WM, Zybailov BL, Ganago AO, Vassiliev IR, Bryant DA and Golbeck JH (1998) Deletion of the PsaF polypeptide modifies the environment of the redox-active phylloquinone (A_1). Evidence for unidirectionality of electron transfer in photosystem I. J Phys Chem B 102: 8288–8299

Yang F, Shen GZ, Schluchter WM, Zybailov BL, Ganago AO, Vassiliev IR, Bryant DA and Golbeck JH (1999) Structural and functional analyses of cyanobacterial Photosystem I: the directionality of electron transfer. In: Peschek GA, Loeffelhardt W and Schmetterer G (eds) The Phototrophic Prokaryotes. Plenum Press, New York

Yang M, Damjanovic A, Vaswani HM and Fleming GR (2003) Energy transfer in photosystem I of cyanobacteria *Synechococcus elongatus*: model study with structure-based semi-empirical Hamiltonian and experimental spectral density. Biophys J 85: 140–158

Yu JP, Smart LB, Jung YS, Golbeck J and McIntosh L (1995) Absence of PsaC subunit allows assembly of the Photosystem-I core but prevents the binding of PsaD and PsaE in *Synechocystis* sp. PCC 6803. Plant Mol Biol 29: 331–342

Zech SG, van der Est AJ and Bittl R (1997) Measurement of cofactor distances between P_{700}^+ and A_1^- in native and quinone-substituted Photosystem I using pulsed electron paramagnetic resonance spectroscopy. Biochemistry 36: 9774–9779

Zeng MT, Gong XM, Evans MCW, Nelson N and Carmeli C (2002) Stabilization of iron–sulfur cluster F_X by intra-subunit interactions unraveled by suppressor and second site-directed mutations in PsaB of Photosystem I. Biochim Biophys Acta 1556: 254–264

Zybailov B, van der Est A, Zech SG, Teutloff C, Johnson TW, Shen GZ, Bittl R, Stehlik D, Chitnis PR and Golbeck JH (2000) Recruitment of a foreign quinone into the A_1 site of photosystem I – II. Structural and functional characterization of phylloquinone biosynthetic pathway mutants by electron paramagnetic resonance and electron-nuclear double resonance spectroscopy. J Biol Chem 275: 8531–8539

Chapter 25

The Directionality of Electron Transport in Photosystem I

Kevin Redding*
Departments of Chemistry and Biological Sciences, The University of Alabama, 206 Shelby Hall, 500 Campus Drive, Tuscaloosa, AL 35487-0336, USA

Art van der Est
Department of Chemistry, Brock University, 500 Glenridge Avenue, St. Catharines, Ontario, Canada L2S 3A1

* Author for correspondence, email: kredding@bama.ua.edu

John H. Golbeck (ed): Photosystem I: The Light-Driven Plastocyanin:Ferredoxin Oxidoreductase, 413–437.

Summary

Photosynthetic reaction centers are the membrane–protein complexes responsible for the capture and storage of light energy in photosynthetic organisms. These proteins contain a large number of cofactors, mostly chlorophylls, which absorb light and transfer the energy to the core of the complex, where it is used to drive a transmembrane electron transfer reaction. Since the discovery that these complexes are dimeric structures with two virtually identical branches of cofactors extending across the membrane from the primary donor, the focus of a large body of research has been directed toward understanding to what extent electron transfer occurs in the two branches. The ultimate goal of this work is to understand the factors that govern the directionality and to learn how it can be influenced. This problem has been studied for many years in the reaction centers of purple bacteria (pbRC). However, because electron transfer is very strongly biased toward one of the two branches in these systems, it is relatively difficult to perturb the system to change its directionality, making it hard to draw conclusions about the importance of various factors. Recently, these types of studies have become possible in Photosystem I (PS I), because the X-ray crystal structure has been solved to 2.5-Å resolution. The structure reveals which amino acid residues interact with the electron transfer cofactors so that site-directed mutagenesis can be used to selectively influence the two branches of cofactors. Although many open questions remain, it has become clear that the behavior of PS I and pbRCs are remarkably different. There is a growing body of evidence to suggest that both branches may be active in PS I and that it may be possible to redirect the electron transfer by altering the protein environment. However, at present many aspects of the electron transfer in PS I are still unclear and there is no model that is consistent with all of the experimental data. The goal of this review is to summarize both older and more recent experimental data on the directionality issue and to show where there is general agreement and where open questions still remain.

I. Introduction

A. The Concept of Directionality

The reaction centers of all known photosynthetic organisms share a common structural theme, with two branches of electron acceptors extending across the photosynthetic membrane from a chlorophyll (or bacteriochlorophyll) dimer that acts as the electron donor. This arrangement can be seen in Fig. 1, which shows the crystal structures of the electron transfer (ET) cofactors of PS I from the cyanobacterium

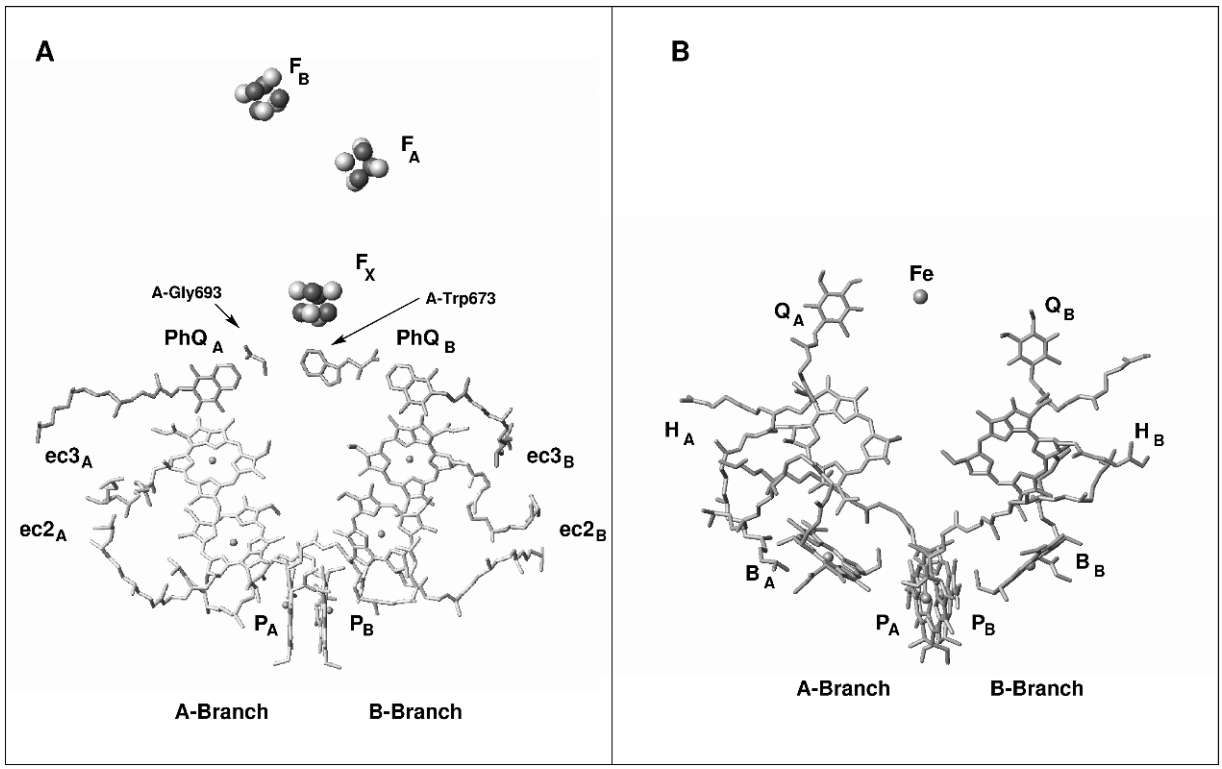

Fig. 1. The arrangement of cofactors in PS I with suggested nomenclature (A) and the pbRC (B). The asymmetric residues PsaA-Gly693 and PsaB-Trp673 are indicated in panel A.

Thermosynechococcus elongatus and of the reaction center of the purple bacterium *Rhodobacter sphaeroides*. The structure is presented with the respective primary donors at the bottom with the two branches extending upward. The electron transfer is deemed unidirectional if it occurs in only one of the two branches, and bidirectional if both pathways are used. However, this simple definition becomes somewhat less clear in practice, because absolute unidirectionality and bidirectionality are two endpoints of a continuum. Generally, the terms "unidirectional" and "bidirectional" are used to mean near-exclusive use of one pathway or near-equal use of both, respectively. The dividing line between the two is usually determined by the experimental error of the techniques used to determine the activity of the two pathways. Typically this lies in the range of 1–10%. This definition implies that the two pathways must be distinguishable in much the same way that asymmetric synthesis is only meaningful for reactions that can produce two stereoisomers. Hence the concept of directionality breaks down for totally symmetric reaction centers, such as those of heliobacteria and green sulfur bacteria, in which the two branches are bound to identical polypeptides (Büttner et al., 1992; Liebl et al., 1993) and are thus indistinguishable. Such RCs likely have two active branches, but they would be operationally unidirectional. However, this issue does not arise for PS I and pbRCs, because the two protein subunits are distinct and the interaction of the cofactors with their surroundings creates local differences between the two branches, despite the high overall symmetry.

Abbreviations: B – monomeric bacteriochlorophyll in the pbRC; BChl – bacteriochlorophyll; Bpheo – bacteriopheophytin; Chl – chlorophyll; DAS – decay-associated spectrum/spectra; DS – difference spectroscopy/spectrum/spectra; ec1 – chlorophyll of P_{700}; ec2 – second chlorophyll of electron transfer branch; ec3 – third chlorophyll of electron transfer branch; ENDOR – electron-nuclear double resonance; EPR – electron paramagnetic resonance; ET – electron transfer; F_A – terminal Fe_4S_4 cluster (in PsaC); F_B – terminal Fe_4S_4 cluster (in PsaC); F_X – intermediate Fe_4S_4 cluster (between quinone and F_A); FTIR – Fourier transform infra-red; H – bacteriopheophytin in the pbRC; Pheo – pheophytin; pbRC – purple bacterial (proteobacterial) RC; PELDOR – pulsed electron double resonance; PhQ – phylloquinone; $PhQH_2$ – phylloquinol; PQ – plastoquinone; PS I – Photosystem I; PS II – Photosystem II; Q – generic quinone (or for Type II RCs); RC – reaction center; TR – time-resolved or transient; WT – wild type.

B. Directionality in the Two Types of RCs

Photosynthetic RCs can be grouped into two general classes according to the nature of their terminal acceptors. The Type I RCs have iron–sulfur clusters and are sometimes referred to as "Fe/S-type" RCs. The Type II RCs, on the other hand, use a mobile quinone as the terminal acceptor and have (bacterio)pheophytin as an intermediate acceptor. Hence, they are also called "Pheo-Q type" RCs. The two reaction centers in Fig. 1 (PS I and pbRCs) are the best-characterized representatives of the two general classes and they have been most widely used to address the issue of directionality. Most of this review will focus on PS I. However, we will begin by summarizing the basic properties of the two types of RCs, partly for historical reasons, but also to illustrate the differences between the classes.

1. Type II RCs (pbRC)

In Type II RCs, the quinone Q_B serves as the terminal acceptor of the RC and as a mobile electron and proton carrier between the RC and a cyt *bc* complex. Two turnovers of the reaction center lead to double reduction of Q_B and, after taking up two protons, it diffuses out of the binding site into the lipid bilayer and a new quinone takes its place. The symmetry-related quinone, Q_A, is tightly bound. The issue of directionality is therefore to what extent reduction of Q_B occurs via Q_A or via H_B, the bacteriopheophytin (BPheo) in the B-branch. This question has been answered primarily using pump–probe spectroscopy, taking advantage of the different absorption properties of bacteriochlorophyll (BChl) and BPheo in the Q_X region of the optical spectrum. This difference makes it possible to observe the reduction of H_A and H_B without interference from BChl absorbance changes. Moreover, due to slight differences in their environments, H_A and H_B have different absorption maxima: 545 nm for H_A and 530 nm for H_B (Lin et al., 2001). Thus, it is possible to distinguish electron transfer to H_A and H_B. Q_A and Q_B are also spectroscopically distinct (Woodbury and Allen, 1995), but not as convenient for determining the ET pathway because the absorbance changes associated with $P^+Q_B^-$ formation do not reveal the pathway taken. Therefore, ultrafast pump–probe measurements of H_A and H_B have been most widely used to assess the directionality. In native pbRCs very little reduction of H_B is observed, with estimates of the ratio of A-side/B-side ET ranging from ~4:1 to ~200:1 (reviewed by Woodbury and Allen, 1995). Thus, there is general consensus that ET in Type II RCs is unidirectional along the A-branch of cofactors. This reason for the unidirectionality appears to be the fact that it minimizes the potential for damage when the Q_B site is unoccupied.

2. Type I RCs (PS I)

The most striking difference between PS 1 and pbRCs (Fig. 1) is the presence of the iron–sulfur clusters (F_X, F_A, and F_B)on the stromal side of the complex. F_A and F_B are bound by the extrinsic subunit, PsaC, while F_X is located on the symmetry axis of the complex at the interface of the two related subunits PsaA and PsaB. One immediate consequence of this is that there is no apparent reason *a priori* why electron transfer should be directed along one branch or the other. Unlike the situation in the pbRC, in which the two possible pathways to Q_B involve a different sequence of acceptors, the two pathways to F_X in PS I involve the same series of chemically equivalent acceptors. Hence, any asymmetry must be due to differences between PsaA and PsaB. Although PS I is a heterodimeric system, the PsaA and PsaB polypeptides that comprise the core have a higher degree of similarity (45–50%) than the L and M polypeptides of the pbRC or D1 and D2 polypeptides of PS II (~30–35%). Thus they might be regarded as an intermediate between the homodimeric Type I RCs and the Type II RCs. Much of this review is devoted to the central question: are these differences great enough to make ET within PS I unidirectional or are they only sufficient to make the two branches distinct?

In addressing this issue it is important to have a clear and consistent naming scheme for the cofactors. A number of such schemes have been developed for PS I, however all of them present some difficulties when discussing directionality. The most commonly used names (P_{700}, A_0, A_1, F_X, F_A, and F_B) refer to the spectroscopic signatures of the cofactors. However, in the cases of A_0 and A_1, the assignment of the spectroscopic properties to specific cofactors in the structure is still ambiguous. With the determination of the 2.5-Å resolution X-ray structure an alternative naming scheme was suggested and each cofactor was given a unique label (Fromme et al., 2001). Although this scheme removes the ambiguities associated with the spectroscopic names, the membership of some of the cofactors in a specific branch and their chemical identity is not reflected transparently in their given names. Therefore we will modify this nomenclature here to bring it more into line with that used for the pbRC. The Chls of each branch will be referred to as ec1, ec2, and ec3 (for electron transfer chain chlorophyll)

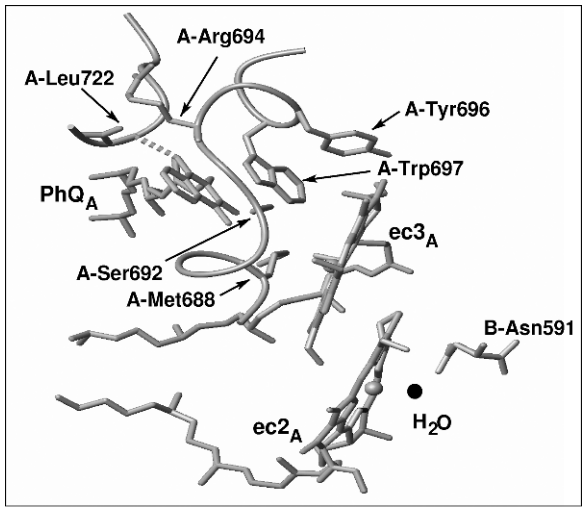

Fig. 2. The environments of the ec2, ec3, and PhQ cofactors (A-side). This view is from behind the PhQ_A headgroup in order to see its interactions with Trp697 (π-stack), Ser692 (H-bond to Trp697), and Leu722 (H-bond). Also shown are the axial ligand (Met688) and H-bond donor (Tyr696) to $ec3_A$, as well as the water molecule that serves as axial ligand to $ec2_A$ and the residue (PsaB-Asn591) coordinating it.

with a subscript to denote their branch. For example, $ec3_A$ is the third chlorophyll in the A-branch. This is essentially the same scheme used in Jordan et al. (2001) except that we assign each chlorophyll to branch A or B, based upon the polypeptide that contributes the *majority* of the interactions, rather than the axial ligand. Thus, we assign chlorophyll $ec2_A$ to the A-branch, even though a water molecule bound to PsaB provides the axial ligand (see Fig. 2). The $ec1_A$ and $ec1_B$ Chls, which compose P_{700}, will also be referred to as P_A and P_B in analogy to the naming scheme for pbRC. The two phylloquinones will be referred to as PhQ_A and PhQ_B. We will continue to use the spectroscopic names when the assignment to a particular cofactor is ambiguous or to distinguish between *in vitro* and *in vivo* properties.

II. Models for the Use of the Two Branches in PS I

Most of the spectroscopic and kinetic data for PS I is analogous to that from Type II RCs and can be adequately explained without invoking anything beyond a simple unidirectional model. Hence, in much of the literature it is implicitly assumed that the electron transfer is either unidirectional or the two paths are indistinguishable. More recently however, several studies, particularly dealing with PhQ reoxidation, suggest that the situation is more complex. It has been known for many years that electron transfer from PhQ to F_X is biphasic (Sétif and Brettel, 1993; Brettel, 1998; Joliot and Joliot, 1999; Agalarov and Brettel, 2003). Comparison of the kinetics in a wide range of PS I preparations pointed toward the fast component being a preparation artifact that was introduced when PS I particles were isolated from spinach using harsher procedures (Sétif and Brettel, 1993). However, the recent observation of biphasic electron transfer in whole cells (Joliot and Joliot, 1999) demonstrates convincingly that it is an intrinsic feature of PS I. Moreover, point mutation studies (Guergova-Kuras et al., 2001; Xu et al., 2003b) have shown that the two kinetic phases can be influenced selectively by mutations in the vicinity of PhQ_A and PhQ_B. This has sparked a debate about the directionality of electron transfer through PhQ and several models have been suggested.

A. Unidirectional Models

In the unidirectional models, the biphasic kinetics of PhQ^- reoxidation can be explained in two main ways. The simplest is that it reflects structural heterogeneity, as has been observed in pbRC (Woodbury and Allen, 1995). Thus, electrons are assumed to take the single active branch to a unique quinone. However, variations in conformation, solvation, or other environmental factors in the PhQ/F_X vicinity are proposed to result in a distribution of $PhQ \rightarrow F_X$ ET rates with two dominant components. The other possibility, suggested by Brettel (1997), is that the forward and back ET rates between PhQ and F_X might be similar given the small free energy difference between $P_{700}^+PhQ^-$ and $P_{700}^+F_X^-$. If the back-reaction rate is of similar magnitude to the rate of forward ET past F_X, the overall reoxidation of PhQ^- is predicted to be bi-exponential. In both cases, detergent-induced alteration of the stromal side of the PS I complex could explain the preparation-dependent variation in the ratio of the two kinetic components.

B. Bidirectional Models

The bidirectional models envision ET within both branches of PS I. The asymmetry of the protein environment and the cofactors is assumed to be too small to bias the charge separation strongly toward either branch, and therefore ET would occur with similar probability in the two branches. In these models, the two PhQ^- reoxidation rates are assigned to the two quinones, implying that the protein imparts different redox

potentials to PhQ_A and PhQ_B (see also Moser and Dutton, this volume, Chapter 34). Usually such models also assume that P^*_{700} serves as an electron donor to $ec3_A$ or $ec3_B$, and that the divergence between the two branches takes place at the level of initial charge separation. As has been discussed elsewhere (Klukas et al., 1999), the long distance (~20 Å) between P_{700} and the ec3 Chl suggests that the ec2 Chl should be involved, either as a real or virtual intermediate. Hence, the relative use of the two branches would be determined by: (i) the electronic asymmetry within P^*_{700}; (ii) differences in energy between $P^+_{700}ec2^-_A$ and $P^+_{700}ec2^-_B$ or between $P^+_{700}ec3^-_A$ and $P^+_{700}ec3^-_B$; (iii) differences in electronic coupling between P_{700} and the ec2 Chls or between the ec2–ec3 pairs; (iv) differences in charge distribution and or dielectric strength within the two pathways; (v) differences in distances between cofactors. In the pbRC, the corresponding differences are all relatively small, yet ET is strongly biased to the A-branch. Therefore, small alterations of any of these factors could lead to significant changes in the use of the two branches.

C. Alternate Charge Separation Model

The nature of the initial charge separation in PS I has not yet been firmly established and recently it was proposed (Müller et al., 2003) that it might occur between the ec2 and ec3 Chls to generate an $ec2^+ec3^-$ state, followed rapidly by ET from P_{700} to give rise to $P^+_{700}ec3^-$(see Savikhin, this volume, Chapter 12). A similar notion has also been advanced for the Type II RCs (cf. Prokhorenko and Holzwarth, 2000; Diner and Rappaport, 2002). The model is supported by the fact that the ec2–ec3 pairs interact much more intimately than the corresponding B–H pairs in pbRCs, as borne out by the X-ray structure (Jordan et al., 2001) and recent calculations of electron transfer integrals (Petrenko and Redding, 2004). In this model, the role of P_{700} would be as secondary electron donor, and it would play little role in directing charge separation to one branch or the other. Instead the relative use of each branch would be a reflection of the ability of each ec2–ec3 pair to function as a photochemical trap. Hence, this model is compatible with either unidirectional or bidirectional ET, with many of the same factors mentioned above (e.g., differences in energy of $ec2^+_Aec3^-_A$ *vs.* $ec2^+_Bec3^-_B$, etc.) playing a role in determining the relative activity of the branches. An interesting feature of this model is that it introduces the possibility that the RC could trap two photons leading to double oxidation of the lumenal side of the complex. However, there is no experimental evidence showing that this occurs with anything but a very low probability.

D. Hybrid Model

Finally, we come to a model that incorporates elements of both the unidirectional and bidirectional models. In this hybrid model, two populations of PS I RCs are postulated with structural heterogeneity at the level of the early cofactors. Differences between the two conformations bias ET strongly toward the A-branch in one population and toward the B-branch in the other. As in the bidirectional model, differences between the two PhQ sites would result in two distinct rates of PhQ reoxidation. Although both branches of PS I are used in this model, the charge separation is unidirectional *within each population*. The relative populations of the two structural conformations would determine the relative use of each branch. These would likely be in equilibrium, although the rate of interconversion, like typical protein conformational changes, would likely be slower than the rate of charge separation. This model will become important later when discussing results from experiments conducted at low temperature, where the rate of interconversion would become very slow. The nature of conformation differences is left unspecified, but they could include the distribution of conformers of P_{700} or the ec2–ec3 Chl pairs. The distribution of charges (e.g., produced by chains of H-bonded ionized residues) could also give rise to concerted changes in the overall electric field experienced by the early cofactors.

III. Strategies for Studying Directionality

The goal of studies of the directionality in PS I has been to distinguish between the various models presented above. A wide range of techniques has been used to study ET in PS I and most of them can be used to address this issue of directionality. However, this presents a significant challenge because, unlike the situation in pbRCs, none of the spectroscopic signatures of PS I can be unambiguously assigned to one branch or the other, although in some instances it is at least possible in principle. The various techniques are described in detail in other chapters in this volume and we will not review them here. Rather we will discuss the different strategies that have been adopted to garner information about the directionality and will refer to the appropriate chapters for more details on the spectroscopic techniques involved.

A. Selective Alteration of the Two Branches

1. Point Mutagenesis

Site-specific mutagenesis of individual amino acids offers an attractive way to overcome the lack of reliable spectroscopic markers in the individual branches. The premise of such experiments is that by changing amino acids close to the ET cofactors, their properties can be selectively altered. However, a number of conditions must be met if this premise is to be valid. First, the location of the individual amino acids relative to the cofactors must be known. This problem has been largely solved with the advent of the 2.5-Å resolution crystal structure (Jordan et al., 2001). Rigorously speaking, information about the relative positions of the cofactors and amino acids is only available for the species for which X-ray structural data exist. However, the high level of conservation of RC core polypeptides across wide phylogenetic distances suggests that one can safely assume that the known structure is an adequate model for all species. The recent 4.4-Å structure of pea PS I (Ben-Shem et al., 2003) confirms that this is almost certainly true for the core cofactors, although minor differences cannot be ruled out. Second, the mutations must produce an observable effect, yet not perturb the system too strongly. For example, it is difficult to infer the behavior of the native system based on the effect of a mutation that completely alters the yield and directionality of the electron transfer. In general, conservative mutations can be expected to cause relatively minor effects and by basing conclusions on several mutations of several neighboring residues, these problems can be minimized. A more serious issue is the possibility of remote effects. If ET were unidirectional, but mutations in one branch could cause changes in the other branch, one might wrongly conclude that both branches were active. Use of a series of conservative mutations should minimize the likelihood of such remote effects distorting the conclusions. In addition, one needs to carefully analyze the consequences of similar mutations in both branches: the "direct effect" of a mutation in the active branch should not necessarily resemble the "remote effect" of a mutation in the inactive branch.

2. Subunit Deletion

Subunit deletion mutants can provide an important complement to point mutations. One advantage is that detailed knowledge of the structure is not required and hence they were used before the 2.5-Å resolution structure was determined. Although deletion of one or more entire subunits is a fairly drastic change to the reaction center, these changes can be made relatively far from the electron transfer chain, so that the overall effect on ET might be fairly subtle. The tendency of cells to degrade the partially assembled photosystem also presents a problem in isolating PS I from such mutants, particularly in eukaryotic systems (Takahashi et al., 1991; Redding et al., 1998). Despite these challenges, analyses of a series of a series of deletion mutants in cyanobacteria has proved very informative (c.f. Yang et al., 1998).

B. Slowing or Blockage of Electron Transfer Past PhQ

An alternative to changing the protein to selectively alter electron transfer in each branch is simply to slow forward ET past PhQ. The idea behind such an approach is to increase the lifetime of the radical pair in the part of the RC with two branches. This then allows application of techniques, such as pulsed EPR, ENDOR, and FTIR, which can provide very detailed information about the cofactors. Such studies are also important for testing kinetic models of ET.

1. Quinone Replacement

One of the first such manipulations was to use solvent extraction to remove the PhQs and then to incorporate foreign quinones by incubating them with the extracted PS I (Itoh et al., 1987; Biggins and Mathis, 1988). A more subtle way of accomplishing the same end is to use mutants in the phylloquinone biosynthetic pathway (see Sakuragi and Bryant, this volume, Chapter 15). Deletion of the genes encoding the phytyl transferase (*menA*) or 1,4-dihydroxy-2-naphthoate synthase (*menB*) in *Synechocystis* sp. PCC 6803 resulted in abrogation of phylloquinone synthesis and replacement of PhQ in PS I with plastoquinone (PQ) (Johnson et al., 2000). A number of quinones were found to displace PQ when PS I from *menA* or *menB* was incubated with an excess of the quinone (Pushkar et al., 2002). A mutant in the 2-phytyl-1,4-naphthoquinone methyl transferase (*menG*) produced PS I containing 2-phytyl-1,4-naphthoquinone (i.e., demethylPhQ) in place of PhQ (Sakuragi et al., 2002). In almost all cases, incorporation of a foreign quinone slowed forward ET.

2. Removal of the Iron–Sulfur Clusters

The goal of slowing or blocking electron transfer past PhQ can be achieved by removing or altering the iron-sulfur clusters. The PsaC subunit containing the F_A and F_B clusters can be removed from the PS I core by washing particles or membranes with ~7 M urea (Parrett et al., 1989). The F_X cluster can also be destroyed by subsequent treatment with ferricyanide in the presence of urea (Warren et al., 1990). The *rubA* mutant of *Synechococcus* sp. PCC 7002 blocks assembly of all three Fe/S clusters of PS I (Shen et al., 2002a,b), and allows creation of PS I particles containing no Fe/S clusters without resorting to such harsh treatments. One can also pre-reduce the terminal Fe/S clusters by treatment with dithionite at elevated pH (Hanley et al., 1992).

3. Temperature Dependence

One of the easiest ways to block electron transfer past PhQ is simply to lower the temperature, and a great deal of information has been gained in this way. However, electron transfer is blocked in only a fraction of PS I RCs. This so-called "cycling fraction" can be studied by repetitive laser-flash measurements at low temperature. In the other fraction, electron transfer proceeds irreversibly to the terminal Fe/S clusters after the first charge separation. The origin of the two fractions is not well understood, but it is an important part of the behavior of PS I and must be included in the various directionality models.

4. Photoaccumulation

A well-established technique for determining the number and identity of the electron acceptors is to back the electron transport chain up and trap the accumulated radicals by freezing in the presence of a strong reductant. The trapped radicals can then be measured using EPR and ENDOR. In PS I, a variety of photoaccumulation protocols have been established to selectively trap electrons on each of the acceptors from A_0 to F_B. This technique can be useful for measuring the throughput of electrons to F_A and F_B and studying the effects of mutations on the spectroscopic properties of the accumulated species. The fact that it relies on multiple turnovers of the RC can be seen as both an advantage and disadvantage for studying directionality. In contrast to single-turnover flash experiments, it does not depend on the lifetime of a particular species; thus, the existence of short-lived intermediates that may be hard to detect kinetically can be demonstrated. Conversely, the multiple turnovers mean that the accumulation of an intermediate does not depend strongly on the quantum yield of the reaction producing it. Hence, even if ET in a particular branch has a very low quantum yield, it might be possible to trap electrons on its cofactors. Thus, lack of accumulation in a particular branch might provide good evidence for a very low quantum yield.

IV. Summary of Recent Spectroscopic Data Under Different Conditions

We now turn to a consideration of the experimental evidence supporting the various models. This section will be divided into separate discussion of different types of preparations, starting with trapped radicals, moving through cyclic fractions at low temperature, and ending with PS I RCs performing forward ET at ambient temperatures.

A. Steady-State Experiments

1. Character of P_{700}^+

Directionality of ET cannot be deduced directly from measurements on P_{700}^+, since it is the point at which the two branches diverge. However, the properties of the primary electron donor are expected to play a decisive role in determining the directionality. The X-ray structure (Jordan et al., 2001) reveals considerable asymmetry in P_{700} and its environment. Firstly, it is a heterodimer composed of Chl *a* (P_B) and Chl *a*′ (P_A), the 13^2-epimer of Chl *a*. Secondly, P_A appears to be involved in a H-bonding network, while P_B is not. Strong localization of spin density to one Chl of the P_{700}^+ cation radical has been revealed by ENDOR spectroscopy (reviewed by Webber and Lubitz, 2001). By EPR and ENDOR analysis of mutants in the axial ligands to P_A and P_B, this Chl was assigned to P_B (Webber et al., 1996; Redding et al., 1998; Krabben et al., 2000). A recent analysis of axial ligand mutants by high-field EPR (Petrenko et al., 2004) gave the same conclusion. In contrast, from interpretation of the $P_{700}^+ - P_{700}$ FTIR difference spectrum, Breton and colleagues concluded that charge is shared almost equally between the two Chls of P_{700}^+ (reviewed by Breton, 2001, however see Hastings et al., 2001 for an alternate view). Both interpretations agree that the triplet is strongly localized in $^3P_{700}$, but they disagree on the placement. On the basis of the effect of the P_B axial ligand mutants upon the $^3P_{700} - P_{700}$ absorption-detected magnetic

resonance spectrum, Krabben et al. (2000) assigned it to P_B. Breton et al. (1999), however, assigned it to P_A, based upon the fact that one of the major bleaching bands, assumed to be from the 13^1-keto group, was downshifted from a free ketone and therefore H-bonded. Interestingly, mutation of the H-bond donor to P_A, while lowering the reduction potential of P_{700}^+/P_{700}, does not much alter the spin density distribution in P_{700}^+ as seen by ENDOR spectroscopy (Witt et al., 2002; Li et al., 2004). Together these results point to strong asymmetry in P_{700}, but it is not clear whether a similarly strong asymmetry exists within P_{700}^* nor what effect, if any, this has on the directionality. The reader is referred to Lubitz (this volume, Chapter 17) and Breton (this volume, Chapter 18), respectively, for more detailed information on P_{700}.

2. Photoaccumulation of PhQ^- and Chl^- Radicals

Photo-accumulation of PhQ^- is discussed in detail elsewhere (Rigby et al., 2001; see also van der Est, this volume, Chapter 24). Hence we will touch only briefly on this subject here and summarize the main conclusions from recent results. In cyanobacteria, there is general consensus that the photoaccumulated phyllosemiquinone is exclusively PhQ_A^-. This is based on the fact that at most one PhQ^- radical can be accumulated per reaction center (MacMillan et al., 1997) and the intensity and shape of its EPR spectrum are affected only by alteration of the PsaA side of the complex (Yang et al., 1998; Xu et al., 2003a). For eukaryotic PS I the situation is less clear. The results of a point mutant study of *C. reinhardtii* (Boudreaux et al., 2001) parallel those in cyanobacteria quite closely. However, there have also been reports that up to four spins/P_{700} can be trapped in spinach PS I (Heathcote et al., 1993) and signal contributions assigned to PhQ_A^- (Rigby et al., 2002) and PhQ_B^- (Fairclough et al., 2003) have been reported for *C. reinhardtii*. The latter result is controversial and attempts to reproduce the finding that four spins can be trapped in PS I have been unsuccessful (Redding and MacMillan, unpublished results). Moreover, recent Q-band ENDOR data (Pushkar et al., 2004) suggests that some of the signals assigned to PhQ^- in Rigby et al. (2002) are due to Chl^- (see Stehlik, this volume, Chapter 23).

The chlorophyll radical anion that arises during photoaccumulation experiments has not been as well characterized. It is assumed that this species corresponds to A_0^- but it is not known which of the ec2 or ec3 Chls it represents. This question was recently addressed using pulsed electron double resonance (PELDOR), which allows the distances between radicals to be estimated from the spin–spin coupling (see Jeschke et al., 2000 for an overview). PELDOR data from PS I particles from *Synechocystis* sp. PCC 6803 with spins photo-accumulated on PhQ^- and Chl^- gave an estimate of 22–23 Å between the PhQ^- and Chl^- radicals (MacMillan and Redding, manuscript in preparation). Since the phylloquinone radical is known to be PhQ_A^-, the PELDOR distance can be compared to the distance between PhQ_A and the possible locations of the Chl^- radical in the X-ray structure. This comparison suggests that the Chl^- radical is $ec3_B^-$ and that the two trapped radicals therefore reside in different branches. In contrast, recent high-field EPR measurements of the Chl^- radical photo-accumulated in PS I after intentional double reduction of PhQ are consistent with its assignment as $ec3_A^-$, since this spectrum was altered by mutation of the Tyr donating a H-bond to $ec3_A$ (Luthra et al., manuscript in preparation). In both experiments, it is difficult to interpret the results in terms of directionality, because the pathway to trapping of the Chl radical is not known.

3. Steady-State FTIR Results

New results from FTIR of PS I are also relevant to this discussion. Hastings and Sivakumar (2001) collected light - dark FTIR difference spectra (FTIR DS) of three types of PS I preparations: intact ($P_{700}-F_{AB}$), after removal of PsaC ($P_{700}-F_X$), and after removal of PsaC and destruction of F_X (P_{700}-PhQ). The FTIR DS attributed to $P_{700}^+ - P_{700}$ and P_{700}^+ $PhQ^- - P_{700}$ PhQ were subtracted to obtain a $PhQ^- -$ PhQ FTIR DS. The authors interpreted the data as arising from two quinones in different environments, each giving rise to a distinct set of bands. This result is consistent with the idea that the biphasic PhQ^- reoxidation kinetics is related to two different quinone environments. However, it is also known that the extensive manipulation of the RCs required to generate these samples induces changes in the PhQ region of the transient EPR spectra (van der Est et al., 1994). Hence the authors warn that the two sets of bands could due to preparation-induced structural heterogeneity (Hastings and Sivakumar, 2001; see Hastings, this volume, Chapter 20).

B. Time-Resolved Experiments at Low Temperature

At low temperature, optical and EPR data show that in PS I samples at least two fractions exist; one in which

stable charge separation to F_A/F_B occurs and one in which electron transfer past PhQ is blocked (see Brettel, 1997 for an extensive review). The origin of these two fractions is not known. However, the energy barrier for ET past PhQ obviously plays a role.

1. Optical Measurements

Schlodder et al. (1998) found that the slow phase of forward ET from PhQ to F_X slows with decreasing temperature, while Agalarov and Brettel found that the fast phase is practically temperature-independent (Agalarov and Brettel, 2003). This suggests that the fraction manifesting fast ET from PhQ might correlate with stable charge separation, while the fraction showing slow ET would perform back-reaction from PhQ at low temperature. If this is correct, the behavior of the two fractions has important consequences for the directionality models. The fact that both fractions are stable for extended periods shows that there is no interconversion between them at low temperature, otherwise every PS I RC would eventually be trapped as $P_{700}^+F_{A/B}^-$. The temperature range in which bifurcation into two fractions occurs correlates strongly with the amount of glycerol and therefore the glass transition temperature of the buffer (Schlodder et al., 1998). Hence, it is likely that reorganization of the protein plays a role in determining whether forward ET to $F_{A/B}$ can occur. The reversible fraction can be further subdivided into two populations: a major one (~45% of total) giving rise to a faster backreaction (~170 μs) attributed to $P_{700}^+PhQ^-$ and a minor one (~20% of total) giving rise to a slower backreaction (~5–100 ms) attributed to $P_{700}^+F_X^-$.

2. Time-Resolved EPR and ENDOR Measurements

Much of the transient or time-resolved EPR and ENDOR work on PS I has been performed at low temperature. This is primarily because the dielectric losses due to microwave absorption by water are greatly reduced and the rapid backreaction from the quinone allows a high flash repetition rate with accompanying rapid data acquisition. The stability of the frozen samples also improves reproducibility during experiments requiring long accumulations. However, since such experiments are only sensitive to those RCs undergoing reversible charge separation, it is very important to distinguish between studies carried at low temperature, in which this occurs in only a fraction of the PS I complexes, and those carried out at higher temperatures, in which the entire PS I population can be observed.

In the majority of time-resolved EPR and ENDOR studies of PS I at low temperature, the goal has been to determine the geometry and magnetic parameters of the charge-separated state $P_{700}^+PhQ^-$. A review of all of these is beyond the scope of this chapter and we refer interested readers to (van der Est, 2001) for an overview of transient EPR on PS I and (Bittl and Zech, 2001) for a similar review of pulsed EPR experiments (see also Stehlik, this volume, Chapter 23; van der Est, this volume, Chapter 24). For the discussion of directionality, the crucial result of this large body of work is that all of the data for $P_{700}^+PhQ^-$ in native PS I can be interpreted as arising from a single radical pair. Point mutation studies of *C. reinhardtii* (Boudreaux et al., 2001) and *Synechocystis* sp. PCC 6803 (Xu et al., 2003a) both demonstrated that PhQ_A is the acceptor at low temperature. In addition, the finding that the spin density in P_{700}^+ is localized mainly on P_B (Webber et al., 1996; Redding et al., 1998; Krabben et al., 2000; Webber and Lubitz, 2001) leads to the conclusion that the radical pair observed by time-resolved EPR at low temperature should be assigned to $P_B^+PhQ_A^-$. Thus, there is consensus that reversible electron transfer to PhQ occurs exclusively in the A-branch at low temperature. However, this result does not resolve the question of the directionality, because the pathway leading to stable charge separation is still unknown.

This pathway can be investigated by time-resolved EPR if electron transfer past PhQ is blocked by removing F_X or by changing the quinone in the PhQ site. As discussed extensively in van der Est (this volume, Chapter 24) the results of all such studies are also consistent with a single radical pair species, just as in native PS I. In particular, the data from the *rubA* mutant, which lacks the iron–sulfur clusters F_A, F_B, and F_X are identical to those of wild type PS I, apart from an increase in signal intensity (Shen et al., 2002a). Hence, there is no evidence for any contribution from ET in the B-branch at low temperature in this mutant. Likewise, the distance between P_{700}^+ and Q^- estimated from out-of-phase echo-modulation experiments does not depend on the presence or absence of F_X nor on which quinone occupies the PhQ binding site, irrespective of the method by which it has been introduced. Based on the positions of the two quinones relative to P_B in the X-ray structure the two radical pairs are predicted to have clearly distinguishable spin-polarization patterns and echo-modulation curves. Hence, these data all suggest

that ET in PS I is unidirectional in the A-branch at low temperature.

An alternative to removal of F_X or replacement of PhQ is prereduction of the iron–sulfur clusters. Normally the spin-polarized EPR signal (presumably due to $P_{700}^+PhQ^-$) decays with a time constant of ~20 μs in *C. reinhardtii* PS I, but illumination in the presence of dithionite induced the appearance of a faster decay component (~2.5 μs; Muhiuddin et al., 2001; Fairclough et al., 2003). This was attributed to decay of the $P_{700}^+PhQ_B^-$ radical pair signal, and this assignment was supported by studies with mutants near the ec3 Chls and PhQs (Muhiuddin et al., 2001; Fairclough et al., 2003). However, this work leaves many unanswered questions, such as whether the spectra associated with the signal decay are also consistent with the assignment to $P_{700}^+PhQ_B^-$ and why its rate of spin-polarization decay should be so much faster. Moreover, the fact that such behavior is not observed in any of the other samples in which electron transfer past PhQ is blocked suggests that the observed effects may be induced by the reduction of F_X.

3. Time-Resolved FTIR

The first time-resolved FTIR study of PS I has been carried out recently by Hastings and co-workers (see Sivakumar et al., 2005; see Hastings, this volume, Chapter 20). This was performed at 77 K on cyanobacterial PS I particles using a μs-resolution step-scan apparatus with laser flashes to initiate charge separation. To facilitate assignment of the bands, they used cyanobacterial PS I particles that were labeled with ^2H, ^{15}N, or ^{13}C (Wang et al., 2004). The time constant for decay of the laser-generated FTIR DS was ~300 μs, consistent with back-reaction of $P_{700}^+PhQ^-$ at cryogenic temperature. The decay-associated FTIR DS could be extracted from the kinetic data and assigned to $(P_{700}^+PhQ^-) - (P_{700}PhQ)$. Using standard photoaccumulation techniques, they were also able to produce $P_{700}^+ - P_{700}$ FTIR DS, and thus by subtraction they could generate the $PhQ^- - PhQ$ difference spectrum. One interesting hypothesis resulting from this work is that the $PhQ^- - PhQ$ FTIR DS contains significant contributions from the nearby $ec3_A$ Chl. In addition, modes consistent with the H-bonded and non-H-bonded quinone carbonyls were identified. Further work, including specific isotopic substitutions of the PhQ and site-directed mutations in the vicinity of $ec3_A$ and PhQ_A will be required to test the hypotheses generated by this first effort.

4. Summary of Low-Temperature Time-Resolved Data

In none of the cases mentioned above was it necessary to include ET to a second quinone in order to explain the data. In fact, the site-directed mutagenesis data seem to say very clearly that the radical pair seen at low temperature is $P_{700}^+PhQ_A^-$. Thus, ET to PhQ_B does not appear to occur in the fraction observed by time-resolved methods at low temperature. Moreover, most of the data from altered samples in which this is the only fraction do not show evidence for involvement of the B-branch quinone.

C. Time-Resolved Experiments at Ambient Temperature

We now turn to experiments in which forward ET past PhQ occurs in all fractions of the sample and does not lead to trapping of $P_{700}^+(F_A/F_B)^-$. We will refer to this temperature regime as ambient temperature, although it includes data taken down to ~240 K.

1. Forward Electron Transfer from PhQ to Fe/S Clusters

At these temperatures, ET from the PhQ(s) to and through the Fe/S clusters occurs in the ns to μs time region. Optical and EPR studies in this region have provided the bulk of the evidence for and against the various models of the directionality. However, there are apparent contradictions in some of the data and open questions of interpretation, so that no unique picture of ET in PS I has emerged yet.

a. Laser-flash optical studies

The literature on optical changes attributed to reduction and reoxidation of PhQ in PS I RCs has been well reviewed (Brettel, 1997; Brettel and Leibl, 2001). However, we will summarize some aspects that are important for the discussion of the directionality models. One of the principle observations supporting the bidirectional model is the two kinetic components with decay times of ~15–25 and ~150–250 ns. Both components have positive amplitude in the 350–400 nm region (see Fig. 3), corresponding to reoxidation of PhQ^-. In addition, both components have a bleaching around 450 nm and an absorption increase around 480 nm, which were attributed to electrochromic bandshifts of nearby pigments. As discussed above, it was thought for many

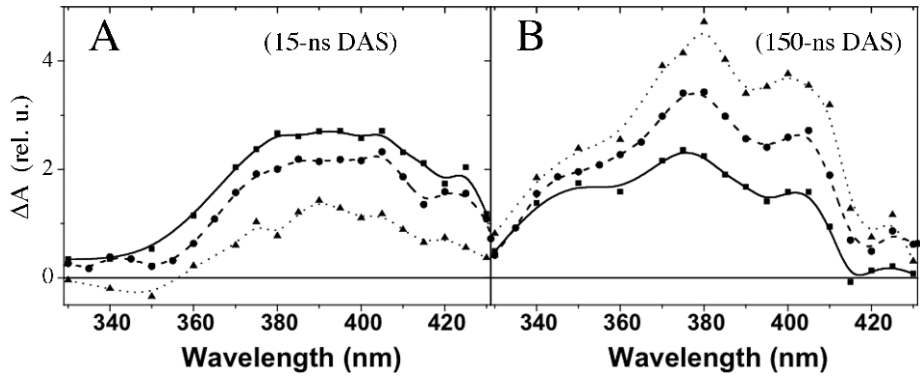

Fig. 3. The *in vivo* DAS of the fast (A) and slow (B) components in WT (circles, dashed line), PsaA-Y696F (squares, solid line), and PsaB-Y676F (triangles, dotted line). The strains used here contained no PS II and low amounts of antenna complexes in order to simplify analysis, but it was performed essentially as previously described (Guergova-Kuras et al., 2001). Spectra of the various components were obtained by the global fit analysis with three exponentials and were normalized to the amplitude of the 4-μs component at 430 nm (not shown).

years that the fast component was probably a detergent-induced artifact, because it is largest when harsher detergents are used to isolate PS I (Sétif and Brettel, 1993) and/or stromal subunits are lost (van der Est et al., 2004). However, it is now known to occur *in vivo* in whole cells (Joliot and Joliot, 1999; Guergova-Kuras et al., 2001; Xu et al., 2003b) and is therefore an inherent property of PS I. Brettel and Sétif (Brettel, 1988) showed that biphasic kinetics would be a natural consequence of a small energy difference between $P_{700}^{+}PhQ^{-}$ and $P_{700}^{+}F_{X}^{-}$. This would allow a pseudo-equilibrium to be formed (the fast component), which would be drained by forward and irreversible ET from F_X to F_A/F_B (the slow component). Under such a scheme the detergent effects can be easily rationalized, since a shift in the equilibrium would lead to a change in the relative amplitudes of the two phases. Joliot and Joliot (1999) reasoned that such a shift would also be expected *in vivo* under conditions that abolished the transmembrane electric field. They tested this idea by examining the kinetics of PhQ^{-} reoxidation under such conditions and found that the amplitudes and rates of the two decay components were insensitive to the field strength. Hence, they suggested that the biphasic kinetics were instead due to ET involving PhQ in two different environments. They favored a model in which the two rates correspond to the two quinones (bidirectional model). However, the two environments could also have corresponded to two different populations of the same quinone.

The shapes of the decay-associated spectra (DAS) also provide some clues about the origin of the two kinetic phases. In *Chlorella sorokiniana*, *C. reinhardtii*, and *Synechocystis* sp. PCC 6803, the shape of the DAS are all very similar (Joliot and Joliot, 1999; Guergova-Kuras et al., 2001; Agalarov and Brettel, 2003; see Rappaport et al., this volume, Chapter 16). In all cases, there are clear differences in the amplitude and shape of the spectra of the two kinetic components, particularly in the "electrochromic bandshift region" (~450–500 nm). This suggested that the two phases might correspond to quinones in which the optical properties of the surrounding pigments differ. The bandshift was generally assumed to be due to carotenoids, in which case the differences in the bandshift region might be due to differences in the conformation of the carotenoids near the two quinones. Recent work on *Synechocystis* sp. PCC 6803 mutants lacking β-carotene has shown that at least some of this feature is also due to Chls (Bautista et al., 2005; see Rappaport et al., this volume, Chapter 16). Interestingly, the remaining electrochromic bandshift in the two DAS become very similar in these mutants, indicating that differences between them are primarily due to carotenoids. This observation is most easily explained by the bidirectional model, since the arrangement and number of carotenes close to PhQ_A or PhQ_B are quite different, while the nearby Chls are more highly conserved (Jordan et al., 2001). To explain the distinct DAS of the two components by a unidirectional model requires postulating that the structural inhomogeneity near PhQ_A/F_X affecting the rate of ET also extends to encompass the neighboring pigments and that its effect on the spectral properties of the carotenes is larger than on the Chls.

Agalarov and Brettel (2003) assessed the temperature dependence of the two phases in *Synechocystis* sp. PCC 6803. In agreement with previous studies (Schlodder et al., 1998) they found that the slow component

is strongly temperature dependent, with an estimated activation energy in the range of 100–200 meV. In contrast, the fast component was almost temperature-independent, with an estimated activation energy of ∼15 meV (Agalarov and Brettel, 2003). These authors explained these results in terms of a model where the fast component corresponds to a downhill ET event, while the slow component represents an uphill ET. However, they also presented an interesting alternative model, in which ET was unidirectional *along the B-branch*, leading to reduction of PhQ_B, and thence to F_X, after which a bifurcation was possible with downhill ET either to F_A or PhQ_A. Electrons taking the latter path would proceed to F_X and then to F_A, via a thermally activated ET corresponding to the slow component. However, this model is difficult to reconcile with the observed electron spin polarization and the low-temperature data discussed above.

b. Time-resolved EPR studies

The use of transient EPR to study forward ET from PhQ has been reviewed recently (van der Est, 2001; see also van der Est, this volume, Chapter 24). Above ∼240 K two sequential spin-polarized spectra attributed to $P^+_{700}PhQ^-$ and $P^+_{700}Fe/S^-$ are seen. [The notation Fe/S^- is used to allow for the possibility that ET from F_X to F_A/F_B may be faster than from PhQ to F_X (van der Est, 2001).] The lifetime of $P^+_{700}PhQ^-$ obtained from such data is consistent with that of the slow phase obtained from transient optical absorption experiments. The subsequent decay of the late spectrum in the microsecond timescale is primarily due to loss of spin polarization by spin–lattice relaxation. An important issue for transient EPR studies of directionality in PS I is whether the fast component seen optically can be detected. As discussed in van der Est (this volume, Chapter 24) the temporal resolution of ∼50 ns precludes direct observation of the fast component. However, it has a clear and well-understood influence on the spin-polarization patterns. Kandrashkin et al. (2002) have recently published a thorough theoretical analysis of the early and late spectra and their magnetic-field dependence, including simulations with the inclusion of a fast component of forward ET. Based upon this, they estimated that no more than 20% of the *Synechocystis* sp. PCC 6803 PS I RCs could be exhibiting such a fast phase. In contrast, similar simulations of room-temperature data from PS I particles of *C. reinhardtii* (Kandrashkin and van der Est, 2002) and subunit deletion mutants of *Synechococcus* sp. PCC 7002 (van der Est et al., 2004) show much larger fractions of fast component.

c. Site-directed mutations near PhQ_A and PhQ_B

Although the data from native PS I provide some clues about the possible involvement of the two quinones in forward ET, point mutation studies give much more direct evidence both for and against such a scheme. Guergova-Kuras et al. (2001) analyzed forward ET in whole cells of *C. reinhardtii* in which the π-stacking tryptophans near PhQ_A and PhQ_B had been converted to phenylalanine. They found that the decay rate of the slower component (∼200-ns) was decreased in the PsaA-W697F mutant (to ∼700 ns) without effect upon the faster component (∼19-ns). In the PsaB-W677F mutant, however, the decay of the absorption in both the PhQ^- and electrochromic bandshift regions could be fit, albeit poorly by a single exponential decay with $\tau \approx \sim 160$ ns. The situation was clarified by examination of the double mutant (PsaA-W697F/PsaB-W677F). In this mutant, there were clearly two decay components with time constants of ∼100 and ∼700 ns. If the A-side mutation was assumed to specifically slow the slow component ∼3.5-fold and the B-side mutation had a similar effect (approximately five-fold slowing) upon the fast component, decay components of ∼100 and ∼200 ns are expected for the PsaB-W677F mutant. These lifetimes are not sufficiently different to be distinguished reliably, but they gave better agreement than the best fit to a single component.

An important issue for such studies is what fraction of RCs is associated with each phase and whether the mutations alter this ratio. Because the DAS of the two phases differ and the changes in rates are also accompanied by changes in the DAS, it is difficult to answer this question quantitatively. However, the fast component accounts for about 1/3 of the total amplitude between 475 and 415 nm in all three spectra reported in Guergova-Kuras et al. (2001), hence the mutations did not induce any drastic change in the ratio of the kinetic components. At the same time, the DAS of the slow component in the PsaA-W697F mutant appeared to be altered such that the absorbance increase at 400 nm was larger relative to that at 390 nm while the spectrum of the fast component was unchanged. In the double mutant, the DAS of both phases were altered such that the absorbance change at 400 nm was increased relative to that at 390 nm. These results are most easily explained with a bidirectional model in which the two mutations have specific and similar effects on the respective quinones. Although the results can be rationalized with a unidirectional ET model that explains

biphasic kinetics by structural heterogeneity in the PhQ_A/F_X region, a number of unlikely coincidences must be assumed to explain the specific and similar effects caused by each mutation.

Similar results were obtained for a larger set of mutants in *Synechocystis* sp. PCC 6803 (Xu et al., 2003a) using data from several spectroscopic techniques. Absorbance difference spectroscopy *in vivo* on whole cells and *in vitro* on isolated PS I particles both showed that the PsaA-W697F mutation causes a three- to four-fold increase in the lifetime of the slow component with no discernible effect upon the lifetime of the fast component. In the PsaB-W677F mutant, the converse was observed: the fast component was slowed approximately threefold, while the slow component was unaffected. In all cases, the amplitude ratio was not changed by either mutation. The transient EPR data for the PsaA-W697F mutant was consistent with the optical data showing a slowing of forward ET by about a factor of 3. The corresponding mutation near PhQ_B, however, had no discernible effect by this technique.

Purton et al. (2001) also measured the kinetics of forward ET in several mutants of PsaA-Trp697 and PsaB-Trp677 using pulsed EPR at 260 K. At this temperature, they found a time constant of ~450 ns in WT, which is shorter than the value of ~1 μs (Schlodder et al., 1998) obtained from optical absorbance changes and ~800 ns (Xu et al., 2003b) from transient EPR. In the PsaA-W697L and PsaA-W697H mutants, the rate was slowed significantly (τ = ~1,200 and ~1,500 ns, respectively), consistent with the observations for the PsaA-W697F mutant (Guergova-Kuras et al., 2001; Xu et al., 2003b). The pulsed EPR measurements did not detect a faster component, despite the lowered temperature, consistent with the weak temperature dependence seen in optical measurements (Agalarov and Brettel, 2003). However, in contrast to the transient EPR data for PsaB-W677F, which were indistinguishable from the wild type, Fairclough et al. (2003) reported a single ~800-ns component for PsaB-W677L. The authors explained this either as an indirect effect upon ET in the A-branch or by a slowing of ET from PhQ_B to a τ > 500 ns that could not be resolved from the 450-ns component. Both of these explanations would require a dramatic difference in the behavior of the PsaB-W677L mutant compared to PsaB-W677F, despite the fact that the behavior of the corresponding A-branch mutations are essentially identical.

Serines PsaA-Ser692 and PsaB-Ser672, which are near the PhQs and appear to H-bond with the Trp (Jordan et al., 2001), have also been altered by mutagenesis. Xu et al. (2003b) analyzed Cys mutants of these resides and observed a dramatic slowing of the slow component in the PsaA-S692C mutant, both *in vivo* (τ = ~1,300 ns) and *in vitro* (τ = ~1,000 ns), with no effect upon the faster component. However, for the B-branch mutant (PsaB-S672C), the decays *in vivo* were not significantly different from WT (~13 and ~210 ns). Again, the transient EPR data showed a slowing of electron transfer to F_X for the PsaA mutant, while the PsaB mutant showed no effect. Alanine mutations of the corresponding residues in *C. reinhardtii* were not very different (Gu et al., 2005). The PsaA-S692A mutation had a bigger effect upon the slow component than the PsaA-W697F mutation and little effect upon the fast component (~970 and ~13 ns). In this case, the PsaB-S672A mutant did give a detectable slowing of the fast component *in vivo* (~26 ns), but the effect was very modest. Moreover, the shapes of the DAS and the amplitudes of the components were much the same as in WT (see Rappaport et al., this volume, Chapter 16).

Xu et al. (2003b) also investigated mutants of PsaA-Arg694 and PsaB-Arg674, which are located in the region between F_X and PhQ_A or PhQ_B, respectively. The transient EPR data showed that both mutants lead to a slowing of forward ET, as might be expected for mutants in the vicinity of F_X. However, analysis of the 380-nm decay of the PsaB-R674A mutant *in vivo* demonstrated the slowing of the slow phase seen by transient EPR was not accompanied by a change in the fast phase.

The residues PsaA-Gly693 and PsaB-Trp673 point toward each other in the region between the two PhQs and are directly above F_X (Fig. 1). This structural arrangement explains why they are so well conserved between species, despite the fact that they represent the same position when PsaA and PsaB are aligned, as it would seem unlikely that two Trps could be accommodated in the space. However, contrary to expectations, mutation of PsaA-Gly693 to Trp allows PS I to accumulate. *In vivo* analysis of PhQ^- reoxidation in this mutant revealed a specific and large effect upon the slow component but none upon the fast one (17 and 1,000 ns; Gu et al., 2005). Unfortunately, the converse mutation (PsaB-W673G) did not allow PS I to accumulate.

d. Loss of peripheral subunits

Much of the data presented above provides evidence that the two phases of PhQ reoxidation might be associated with electron transfer in the two branches. One consequence of invoking such an assignment of the two

kinetic phases is that it implies that the extent of ET in the two branches is somehow preparation-dependent, since it is well known that using harsh detergents to isolate PS I can increase the fraction of the fast phase (Sétif and Brettel, 1993). However, it is difficult to understand how such treatment could alter the initial charge separation and increase the fraction of ET in the B-branch. The observation that PsaF appears to be missing in many of the preparations exhibiting a large fraction of fast phase led to an investigation of the ratio of the two phases in mutants of *Synechococcus* sp. PCC 7002 mutants lacking PsaF (and/or PsaE) (van der Est et al., 2004). It was found that the fraction of fast component was indeed larger in the mutants and the effect was much stronger in particles that had been isolated with Triton X-100. The fact that the vast majority of contacts between the PsaF subunit and PsaA and PsaB are very close to the PhQ_A binding site led the authors to postulate that the detergent effect is probably due to alteration of ET in A-branch rather than redirection toward the B-branch. If this interpretation is correct, care must be taken in interpreting the effect of mutations on the ratio of the fast and slow components. It is also possible that, to explain both the subunit deletion results and *in vivo* optical data on mutants near PhQ and ec3 cofactors, structural heterogeneity in the PhQ/F_X region may have to be included in every model considered.

e. A possible phase for F_X to F_A/F_B

In *C. reinhardtii* PhQ_A-site mutants in which the ~200-ns component is slowed greater than threefold, it is possible to resolve a new component with $\tau \approx 100$ ns (Byrdin et al., 2005). The shape of the DAS is rather featureless, with broad positive amplitude at ~330–400 nm and broad negative amplitude at ~430–470 nm. After the results of Lüneberg et al. (1994), this is rather what one would expect for an ET from F_X to F_A/F_B. Furthermore, it is in the time range expected for this ET event. Under normal conditions, therefore, the ~200-ns component would actually represent two different components that overlap temporally. However, if one can observe an $F_X \rightarrow F_{A/B}$ ET event with $\tau \approx 120$ ns under conditions in which ET from PhQ_A to F_X has been slowed to $\tau > 600$ ns, then the electrons must have been delivered to F_X earlier than 100 ns, implicating the faster component. More work needs to be done here, but confirmation of this hypothesis would provide conclusive evidence that the fast component does indeed represent ET from a PhQ to F_X.

f. Summary of data on ET from PhQ to Fe/S clusters

All of the above studies of the ET kinetics at ambient temperature consistently show that mutations expected to affect PhQ_A influence the slow kinetic phase. Thus the assignment of the slow phase to the A-branch seems well founded. The correlation between mutations in the B-branch and changes in the kinetics is less clear. Some of the data favors an assignment of the fast phase to the B-branch, but some of the mutations that would be expected to influence electron transfer in the B-branch showed no effect or altered the slow phase. These results are puzzling when they are rationalized in terms of any of the models. In the bidirectional model they imply that equivalent mutations in the two branches have different effects upon the respective PhQ sites, while in the unidirectional model they would have different effects upon F_X in the two conformations. This clearly illustrates the limitation of using point mutants to deduce the electron transfer pathway. For example, based on the X-ray structure, mutation of PsaA-Ser692 might be expected to have a similar but smaller effect upon reoxidation of PhQ_A compared to mutation of the PsaA-Trp697. On the other hand, mutation of PsaB-Arg674 would be expected to either affect both phases in a similar manner or only affect ET in the B-branch. The fact that the results do not correspond to these expectations shows that simple predictions of the effect of a given mutation based on the structure and basic chemical principles are not always adequate.

However, given the fact that some of the mutants do not affect the fast component, it is worth considering the possibility that it might not correspond to electron transfer. While optical studies consistently show this phase to be present, the photoelectric and TR-EPR work on native PS I from cyanobacteria have found no evidence of such a component. The lack of evidence for a fast component in cyanobacteria from EPR and photoelectric measurements is probably due to the shorter lifetime and smaller amplitude in these organisms. Moreover, the presence of the fast component is clearly evident in the TR-EPR data from eukaryotic PS I (see van der Est, this volume, Chapter 25). It is nonetheless surprising that none of the mutations that affect the lifetime of the fast component have yet shown any effect in the transient EPR at room temperature. Moreover, it is clear that a fast component can be induced by harsh treatment of PS I particles, and it would seem that eukaryotic PS I is more susceptible to this phenomenon. Thus, one must interpret with caution the results on fast components, especially *in vitro*.

For this reason, the *in vivo* optical data has great potential value. The optical results with the Trp mutants seem to say quite clearly that the two PhQs are reduced and then reoxidized by F_X, but it is true that of all the mutations made near PhQ_B, the PsaB-W697F mutation has the greatest effect so far. Had the Ser mutants been measured first, in which the PsaA-S692C/A mutant(s) had a large effect upon the slow component and the PsaB-S672C/A mutant(s) had a much smaller effect upon the fast component, the initial conclusion might well have been the opposite. However, if one assumes that ET from PhQ_B is downhill and ET from PhQ_A is uphill, as has been proposed (Agalarov and Brettel, 2003), then PhQ_A might be more sensitive to changes in redox potential than PhQ_B. Thus, even if symmetric mutations had the same effect upon each PhQ, one might expect a greater change in the rate of ET from PhQ_A. In this case, the important question would not be why the PsaB-S672C/A mutations had such a small effect, but why the PsaB-W697F mutation had such a large effect upon the fast phase.

2. Forward Electron Transfer from P_{700} to PhQ

There is an extensive literature on energy transfer and the charge separation from P_{700} via A_0 to PhQ. The majority of this work involves ultrafast optical pump–probe spectroscopy in the fs–ps timescale (Gulotty et al., 1985; Hastings et al., 1994, 1995; Pälsson et al., 1995; White et al., 1996; Melkozernov et al., 1997; Mi et al., 1999; see also Savikhin, this volume, Chapter 11; Shuvalov et al., this volume, Chapter 18). Photoelectric techniques have also been used to follow the reduction of PhQ on the ps timescale (Hecks et al., 1994; see also Semenov et al., this volume, Chapter 21). In quinone-exchanged PS I, forward ET is slowed and transient absorption techniques in the ns regime can be used (see Itoh et al., 2001 for a review). None of these data on native or quinone-exchanged PS I gives any clear indication, such as biphasic kinetics or two distinct A_0 or PhQ spectra, to suggest bidirectional ET. However, the inherent differences between the two branches might be too small to detect easily, and therefore site-directed mutagenesis has again been used to selectively alter the individual branches.

a. Site-directed mutations near $ec3_A$ and $ec3_B$

The methionines PsaA-Met688 and PsaB-Met668, which act as axial ligands to the ec3 Chls, are the most obvious targets for mutation. Other candidates are tyrosines PsaA-Tyr696 and PsaB-Tyr676, which are H-bonded to the ec3 Chls, and asparagines PsaA-Asn611 and PsaB-Asn591, which coordinate the water molecules that act as axial ligand to the ec2 Chls (see Fig. 2). Alteration of any of these residues is expected to change the rate of electron transfer through A_0 and/or the yield of ET in the branch carrying the mutation. Changes in the reduction and reoxidation kinetics of A_0 require ultra-fast techniques or indirect detection (e.g., in the spin polarization of subsequent radical pairs). The yield of ET in the two branches can be monitored using the spectroscopic signatures of either A_0 or PhQ.

(i) Studies in the nanosecond to microsecond range

The results obtained from mutants of PsaA-Met688 and PsaB-Met668 reported to date do not give a consistent picture of the activity of the two branches. In *C. reinhardtii*, the PsaA-M688H mutant gave no out-of-phase spin echo decay at 265 K (Fairclough et al., 2003), while the PsaB-M668H mutation was reported to slow the echo decay approximately twofold. The first observation was explained as a result of blockage of forward ET from $ec3_A$ to PhQ_A. However, a recent attempt to confirm this (McConnell et al., 2005) showed the presence of a spin-polarized EPR spectrum from the PsaA-M668H mutant at 150 K and no evidence for slowing of the forward ET from PhQ to F_X at room temperature in the PsaB-M668H mutant. The latter data are more in line with the results of a study of the PsaA-M688L and PsaB-M668L mutants in *Synechocystis* sp. PCC 6803 (Cohen et al., 2004). The early and late spectra observed in the PsaB-M668L mutant, as well as the kinetics of their production and decay, were virtually indistinguishable from the WT. In contrast, the PsaA-M688L mutation had several obvious effects. Its early spectrum (60–160 ns) was drastically altered, with no midfield absorptive peak and an absorptive rather than emissive feature in the high-field region, while its late spectrum had a prominent high-field absorptive peak. These aspects were explained in terms of a longer lifetime of the $P_{700}^+ec3_A^-$ state, leading to greater singlet–triplet mixing before forward ET from this state to produce $P_{700}^+PhQ_A^-$. However, both qualitative examination of the transients and a quantitative analysis of the kinetics showed that the rate of forward ET in PsaA-M688L was the same as in WT, indicating no effect upon PhQ_A or F_X. Consistent with the observed slowing of forward ET to PhQ, the spectrum of $^3P_{700}$ formed by radical pair recombination was clearly produced by a laser flash in the PsaA-M688L mutant, while it was not seen in WT

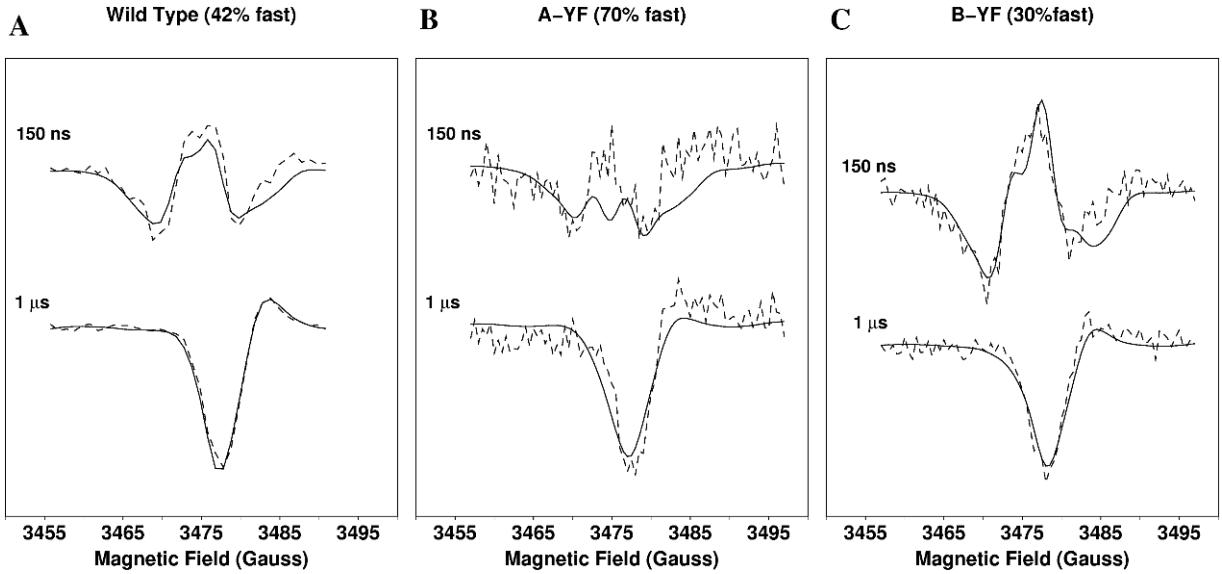

Fig. 4. TR-EPR data on the WT (A), PsaA-Y696F (B), and PsaB-Y676F (C) mutants. Experimental and calculated spectra (dashed and solid curves, respectively) are shown at early (150 ns) and late (1 μs) times. The experimental data are boxcar spectra extracted from the full time/field datasets of thylakoid membranes of *C. reinhardtii* devoid of PS II (as in Fig. 3). The calculated spectra are fits to the complete datasets in which only the relative amounts of the fast and slow components of ET from PhQ to Fe/S clusters were varied. The lifetimes of the two phases were fixed at 20 and 250 ns, the remaining parameters were held fixed at the values given in van der Est et al. (2004) and it was assumed that no significant singlet–triplet mixing occurred during the lifetime of $P^+A_0^-$.

or the PsaB-M668L mutant. The possibility that this occurred due to partial loss of PhQ_A was ruled out by checking the quinone content of the samples. Interestingly, the effect on the spin-polarization patterns ascribed to singlet–triplet mixing in the $P^+_{700}ec3^-_A$ state became weaker upon lowering the temperature from 295 to 240 K. This effect was rationalized as resulting from heterogeneity in ET rate from $ec3_A$ to PhQ_A, which was exacerbated by the introduction of the Leu side chain near $ec3_A$.

At the time of writing, optical studies of the electron transfer from PhQ to F_X for mutants of residues near $ec3_A$ and $ec3_B$ are in progress but have not yet been published (see Rappaport et al., this volume, Chapter 16). In *C. reinhardtii*, these data show that such mutations cause little or no change in the rates of both the fast and slow components but significant changes in their relative amplitudes. All mutations of residue PsaA-Met688 resulted in a large increase in the fast component and a decrease in the slow one, to the point where the fast component was the major one (accounting for ∼60–75% of the 380-nm decay). In contrast, the PsaB-M668H mutation resulted in the opposite effect, with the amplitude of the fast component dropping approximately twofold. Mutation of the tyrosines that donate an H-bond to the ec3 Chls in *C. reinhardtii* produced a similar effect, although not as drastic. Both transient absorption data (Fig. 3) and transient EPR data (Fig. 4) show that the PsaA-Y696F mutation resulted in a greater proportion of fast decay, while the PsaB-Y676F mutation resulted in a smaller proportion of fast decay, compared to WT. Although the relative amplitudes of the two fractions predicted from EPR differ somewhat from those obtained from the optical data, the same trend is observed in both experiments.

As with the PhQ-site mutants, it is difficult to explain all of these results by any of the simple directionality models. The facts that the mutations are located in the middle of the respective branches and that they have complementary effects in some of the experiments suggest a bidirectional model. On the other hand, the data reported in (Cohen et al., 2004) suggest a strong asymmetry in electron transfer. In the bidirectional model, the changes in the amplitudes of the two phases of PhQ^- reoxidation observed optically are explained as resulting from changes in the yield of ET in the two branches. This implies that the mutations affect the initial charge separation and therefore that ec3 is involved. Thus, the initial charge separation would have to follow either the dual-trap model, in which the first charge-separated state is $ec2^+ec3^-$, or a model in which the ec2 and ec3 chlorophylls are strongly coupled and act together as the primary

acceptor. No matter which model of initial charge separation is correct, the ec2 Chl(s) should play some role. Therefore, one would expect that mutations of PsaA-Asn611 and PsaB-Asn591, which coordinate the water molecules ligated to the ec2 Chls, to influence the quantum yield of the initial charge separation in the two branches. However, conversion of either of these residues to an Asp had no effect upon the relative amplitudes of the two components of PhQ^- reoxidation (see Rappaport et al., this volume, Chapter 16). The structure suggests that the carbonyl oxygen of the Asn side chain interacts with the water molecule. Since Asp side chain has an analogous carbonyl group, the main effect of the mutation was expected to arise from the difference in charge between neutral Asn and negatively charged Asp. FTIR analysis of P_{700}^+/P_{700} in the PsaB-N591D mutant showed shifts consistent with replacement of an amide by a carboxylic acid as expected for replacement of Asn by Asp, but no changes indicative of introduction of a negative charge were found (Hastings and Redding, unpublished data). This suggests that the Asp might be protonated and would therefore not induce any significant effect. Clearly, a better understanding of the nature of the initial charge separation and a more complete series of mutations is needed to interpret the changes in the relative amplitudes of the two kinetic phases.

(ii) Studies in the femtosecond to picosecond range

Recently, two ultrafast pump–probe studies of mutants in which the ec3 axial ligands have been converted from Met to His in *C. reinhardtii* (Ramesh et al., 2004) or to Leu and Asn in *Synechocystis* sp. PCC 6803 (Dashdorj et al., 2005) have been published. Again, the results give very different pictures of the directionality.

The absorbance difference spectra of the *C. reinhardtii* mutants were taken 200–300 ps after a femtosecond laser flash (Ramesh et al., 2004). Only a strong bleaching due to P_{700}^+ is observed in this time window in WT PS I, but both mutants showed an additional bleaching with a maximum at ∼681 nm. The kinetic behavior of the absorbance changes was not reported in this study. Because bleaching in the region around ∼685 nm has been observed when electron transfer past A_0 is blocked (Melkozernov et al., 1997), the additional bleaching in the mutants suggests the presence of a long-lived (several hundred ps) contribution from A_0^-. Under the assumption that the $P_{700}^+ - P_{700}$ spectrum was unaltered in the mutants, given that the mutations were relatively far from P_{700}, the spectrum of the additional species was obtained by subtracting the WT spectrum. The resulting DS was very similar to that expected for $A_0^- - A_0$ and by comparing the spectra obtained under neutral and reducing conditions, it was estimated that roughly one half of the A_0^- was long-lived in each of the mutants. These results were interpreted to mean that charge separation in PS I is inherently bidirectional and that mutation of the axial ligand to one of the ec3 Chls did not alter the quantum yield of ET to that Chl, but impaired forward ET from it to the neighboring PhQ.

A very different picture emerged from the analogous study of Met to Asn or Leu mutants in *Synechocystis* sp. PCC 6803 (Dashdorj et al., 2005; see Savikhin, this volume, Chapter 12). Pump–probe absorbance measurements in the picosecond range were made at 390 nm and from 640 to 720 nm. The reduction of PhQ contributes strongly to the absorbance changes at 390 nm, while A_0^- formation is observed most clearly in the red region, which is dominated by the Chls. Qualitatively, the PsaB mutants were almost indistinguishable from the wild type, while the kinetics were clearly altered in the PsaA mutants. A global analysis of the time traces in which antenna processes were subtracted, yielded an A_0^- lifetime of 12.5 ± 2.5 ps in the WT and both PsaB mutants, while values of 112 ± 10 and 100 ± 10 ps were obtained in the PsaA-M688N and PsaA-M688L mutants, respectively. The data clearly suggest that electron transfer is strongly asymmetric and biased toward the A-branch. After fitting the data with a bidirectional model, the authors concluded that no more than ∼20% of the electrons could proceed along the B-branch.

Thus, the two studies come to very different conclusions about the directionality. It is possible that this is due to species-specific differences, but further work is needed to rule out other explanations. An important observation in Dashdorj et al. (2005) is that the steady-state light-minus-dark spectrum usually attributed to $P_{700}^+ - P_{700}$ is altered by the mutations. The differences are larger for the PsaA mutant and occur exclusively below 690 nm. Several possible explanations were offered for this behavior, including a more symmetric distribution of the charge over the two chlorophylls in P_{700}^+, a change in an electrochromic bandshift of chlorophylls near P_{700}, or a change in the excitonic coupling between P_{700} and neighboring chlorophylls. In Ramesh et al. (2004) it was assumed that such changes were negligible and did not contribute to the absorbance differences attributed to long-lived A_0^-. More extensive studies of the *C. reinhardtii*

mutants are in progress to clarify whether this assumption is valid (Ramesh et al., 2005).

b. Mutations in the vicinity of the P_{700} Chls

In the case of bidirectional ET, mutations near the primary donor might be expected to affect the extent of electron transfer to the two possible acceptors. Very little work has been done to investigate this. However, one study mutation of the H-bond donor to P_A in *C. reinhardtii* (PsaA-T743A) was found to produce no changes in the relative amplitudes of the two components of PhQ^- reoxidation (Li et al., 2004). This suggests that the mutation does not affect the directionality, but the reason for this is not clear. One possibility is that ET is unidirectional as in the pbRC and the changes induced by the mutation are not sufficient to force ET down the inactive branch. Alternatively, the electron transfer might be bidirectional, but the influence of the mutation on P^*_{700} might be too small to cause a significant change in the ratio of electron transfer in the two branches. Both of these possibilities would be consistent with the fact that the mutation does not greatly change the asymmetric character of P^+_{700} (Li et al., 2004). Another alternative is the dual-trap model in which P_{700} is not involved in the initial charge separation. In this case, mutations near P_{700} would not be expected to have a large effect upon directionality.

3. Back-Reactions at Ambient Temperature

The backreaction kinetics and their associated spectra also provide an avenue through which the directionality may be studied. However, if the backreaction occurs from the iron–sulfur clusters, the activity of the two branches may be different from that in forward transfer, because the bifurcation points for the forward and backward reactions are different. Hence, to obtain information about the directionality of forward ET from the backreactions, the iron–sulfur clusters must first be removed or inactivated.

In the *rubA* mutant, which lacks all three Fe/S clusters, the near-IR absorbance change due to P^+_{700} formation was found to decay with two major components of similar amplitude and time constants of 13 and 86 μs (Shen et al., 2002a). Analogous behavior was observed in both PS I particles and membranes, indicating that the two lifetimes were not induced by detergent treatment. When transient optical changes were measured in the near-UV region, a similar picture emerged: two major kinetic components of similar amplitude and spectral shape with time constants of 15 and 95 μs. The decay-associated spectra (DAS) and decay times were similar to those observed previously in PS I RCs that had been stripped of Fe/S clusters by chemical treatments (Brettel and Golbeck, 1995). The spectral features attributed to P^+_{700} (large central trough centered at 430 nm) were identical in the two DAS. However, those assigned to PhQ^- (absorbance increase at 360–400 nm) and electrochromic bandshift(s) of nearby pigments (absorbance increase at 460–500 nm) were subtly different for the two kinetic phases. The difference in decay rate and spectral shape suggests that backreaction is occurring from PhQ(s) in different environments. This is also supported by the fact that the transient EPR spectrum at ambient temperature shows some evidence for heterogeneity. However, the origin of this heterogeneity is unclear. It could represent backreaction from a single species (PhQ_A) in two different environments or from the two PhQs (PhQ_A and PhQ_B).

Under strongly reducing conditions, ET past PhQ is also prevented, but the back-reaction produces the excited triplet-state of P_{700} (Mathis and Sétif, 1988; Sétif and Brettel, 1990) rather than the ground state. A detailed investigation of the temperature dependence of the recombination kinetics under such conditions revealed several kinetic phases (Polm and Brettel, 1998). The main phase, attributed to P^+PhQ^- recombination, had a half-life of ∼200 ns at room temperature and was found to be an activated process. The authors explained this behavior with a model in which recombination was proposed to occur via thermal repopulation of $P^+_{700}A^-_0$. The model assumed recombination from a single P^+PhQ^- species. However, the possibility that both quinones might be active is difficult to assess in such experiments, because the pre-reduction protocol inevitably leads to incomplete reduction of F_X and partial reduction of PhQ. Hence, it is not clear whether the observed multiphasic kinetics arise because both PhQs are active or because of heterogeneity introduced by the reduction protocol.

V. Theoretical Work

With the publication of the 2.5-Å structural model of PS I, the range of feasible theoretical calculations related to ET in PS I has expanded greatly. A thorough review of this work and related issues is presented by Moser and Dutton (this volume, Chapter 34). Here we will review only cursorily some aspects, which are relevant to the issue of directionality. Central to all of the models concerning directionality is a rationalization

of the biphasic electron transfer kinetics from PhQ to F_X. In the bidirectional model, the two phases are assigned to electron transfer in the two branches, while the unidirectional model invokes structural heterogeneity. However, it is necessary to explain why the rates should differ in the two branches or two conformations. This question has been addressed in two recent publications (Ishikita and Knapp, 2003; Ivashin and Larsson, 2003) both of which assume a bidirectional model and attempt to explain why the rates of forward ET from the two PhQs would be so different. Ivashin and Larsson (2003), calculated electronic couplings between cofactors using mainly semiempirical methods. They calculated similar couplings ($\sim$0.3 cm^{-1}) for ET from either PhQ to F_X. They suggested, however, that the Trp unique to the B-side (PsaB-Trp673) mediates the ET reaction from PhQ_B to F_X but not from PhQ_A. The fact that conversion of the corresponding residue (PsaA-Gly693) to Trp did not accelerate ET from PhQ_A, but rather slowed it considerably, does not seem to support this hypothesis (Gu et al., 2005). However, it is unclear whether the position and orientation of the introduced Trp are analogous to those of PsaB-Trp673.

A crucial feature of such calculations is the values of the redox potentials of the cofactors involved. Because the measured or estimated redox potentials are not known accurately, Ishikita and Knapp (2003) calculated them on purely electrostatic grounds using the X-ray crystal structure coordinates (Jordan et al., 2001). They arrived at semiquinone/quinone midpoint potentials of -531 mV for PhQ_A and -686 mV for PhQ_B. The large difference was attributed to two main factors: (i) the protonation state of PsaB-Asp575 was proposed to change upon reduction of either quinone but to be more strongly coupled to PhQ_A than PhQ_B, (ii) the backbone conformation of the protein was proposed to stabilize PhQ_A^- and PhQ_B^- by different amounts. Recently, the first proposal, which was suggested to be the larger effect, has been tested by re-examining mutants in which PsaB-Asp575 was converted to Lys or Ala (Vassiliev et al., 1999). The side chains in this series (Asp, Ala, Lys) cover a pK_a range of $\sim$4–10 and should provide a good test of the role of this residue's protonation state on the rate of ET. Both mutations lead to a slight slowing of ET similar to the effects observed for PhQ-site mutations (van der Est et al., unpublished results), suggesting that the side chain pKa of residue PsaB-575 does not play a significant role in determining this rate. Based on the calculated redox potentials for the quinones and experimental estimates of the redox potential of F_X^-/F_X around -650 to -705 mV, Ishikita and Knapp (2003) concluded that ET from PhQ_A is endothermic, as suggested previously by Brettel (1997). ET from PhQ_B, on the other hand, was predicted to be exothermic or very slightly endothermic. While such an arrangement is consistent with the difference in rates and the temperature dependencies of the two kinetic components in a bidirectional model (Agalarov and Brettel, 2003), it is difficult to reconcile with the transient EPR data. This is because electron transfer in the B-branch could lead to reduction of PhQ_A via PhQ_B and F_X. However, there is no evidence for a contribution to the spin polarization of the radical pair from such a pathway.

Finally, we note that the ec2–ec3 Chls are much more intimately paired than are the corresponding B–H pair in the pbRC (Fig. 1). The macrocyclic rings are practically parallel, and there is substantial overlap between them, which may be important for determining how initial charge separation occurs. The semiempirical calculations of Ivashin and Larsson (2003) found a large coupling between these Chls, and recent *ab initio* calculations have come to similar conclusions (Petrenko and Redding, 2004). In the latter calculation, a fourfold larger coupling was found for $ec2_A$–$ec3_A$ than for $ec2_B$–$ec3_B$, because of minor differences in how these pairs are arranged in *T. elongatus*. It is not immediately clear what influence this would have on the yield of electron transfer in the two branches, but it suggests that A-branch ET would probably be more efficient in this organism. It also suggests that the relative efficiency of ET in the two branches might be strongly species dependent, because the coupling between the ec2 and ec3 Chls is very sensitive to their structural arrangement.

VI. Main Unresolved Issues, Final Thoughts, and Speculations

From the preceding overview of recent results it is apparent that no completely consistent picture of directionality in PS I has emerged from the data. However, it is encouraging that some important aspects of ET in PS I have been established. For example, all of the data consistently show that the slow kinetic phase of PhQ to F_X electron transfer and cyclic electron transfer at low temperature are associated with the A-branch. Moreover, all of the data show that this is the dominant ET pathway. Thus, ET is clearly biased to some extent toward the A-branch. However, there is still a great deal of uncertainty and conflicting data regarding the activity of the B-branch. Some of the data, particularly from point mutations in the PhQ sites, argue strongly for the involvement of the B-branch, while other data, primarily from cyanobacterial mutants in the ec3 sites,

argue against such a scheme. To arrive at a final answer to this question, there are a number of important issues regarding ET in PS I that must be resolved.

A. Nature of the Initial Charge Separation

We do not yet know which cofactors compose the primary radical pair after charge separation. Although it has widely been assumed to be $P_{700}^{+}ec2^{-}$, other scenarios such as the dual-trap model are also consistent with the data. Answering this question is crucial to understanding why ET would be unidirectional or bidirectional and which factors would be likely to control it.

It is also important to note that there are discrepancies within various proposals that invoke bidirectional ET to explain different experimental data. For example, the ultra-fast results of Ramesh et al. (2004) seem to indicate that the amount of charge separation making use of the A-branch or B-branch is not affected by the mutations to the ec3 axial ligands. However, results with the mutations to the H-bond donor to the ec3 Chls appear to argue that one can modulate the use of one branch or another (Figs. 3 and 4; Li et al., 2006). Furthermore, the low-temperature results from the Heathcote group on PS I with pre-reduced Fe/S clusters (Muhiuddin et al., 2001; Fairclough et al., 2003) was interpreted in terms of the hybrid model (see section II.D), in which different conformational states are frozen in by low temperature and ET is unidirectional within each population, but in opposite branches. This model predicts that the relative use of each pathway would be determined by the equilibrium between these conformational states. However, this model provides no apparent reason why or how any mutation should influence this equilibrium and therefore change the relative amplitudes of the two kinetic phases of ET from PhQ to F_X.

B. Low-Temperature Effects

An adequate description of the temperature dependence of ET in PS I is also an important missing piece of the puzzle. At present it is not known what factors determine the two low-temperature fractions ("cycling" and "irreversible") and how they relate, if at all, with the activity of the two branches. The evidence that the two kinetic phases of ET from PhQ to F_X correspond to the two branches, and the fact that they have different activation energies, suggests that the two low-temperature fractions may be a result of bidirectional ET. On the other hand, there is some evidence that only the A-branch is active at low temperature. The observation that the amplitude of the fast component decreases as the temperature is lowered (Agalarov and Brettel, 2003) suggests that ET to PhQ_B might be temperature dependent, if this component is assigned to ET *from* PhQ_B. In this case, the two fractions would both arise from ET in the A-branch and would be caused by heterogeneity on the stromal side of the complex, one conformation blocking ET from PhQ_A and the other allowing irreversible ET to F_A/F_B.

C. Species Dependence

Another open question is whether there is any significant difference in the directionality between prokaryotic and eukaryotic PS I. On the basis of the high degree of sequence homology between various species, such an effect would be unexpected. However, it is well-known that the fraction of fast ET from PhQ is generally larger and has a longer lifetime in eukaryotic PS I compared to prokaryotic PS I. Moreover, there is a marked difference in the sensitivity of the ratio of the two components to preparation conditions, with harsher treatments required to induce a significant fast component in prokaryotic PS I (e.g., removal of PsaF and treatment with Triton X-100; van der Est et al., 2004).

D. Possible Advantages of Bidirectional Electron Transfer for the Organism

Because the properties of the PS I reaction center have evolved by natural selection, it is reasonable to assume that the directionality of the ET is determined by selective advantage to the organism. Although the evolutionary trajectory of PS I is still unknown, it seems likely that it evolved from a homodimeric ancestor, with the *psaA* and *psaB* genes diverging after a gene duplication event occurring >1 billion years ago. In a homodimeric RC, the ET can only be biased toward one branch by some asymmetry in the tertiary structure. Hence, it seems highly likely that both branches would be used in such a system. Thus, the proposal that PS I evolved from a homodimeric RC raises two intriguing questions: (i) Which factors led to the evolution of a heterodimeric Type I RC? (ii) Is the asymmetry of the heterodimeric PS I RC sufficient to bias electron transfer to one branch? It is only possible to speculate about the first question. However, it seems likely that it is related to factors other than ET, such as binding the electron donor and acceptors or antenna proteins, since there is no obvious advantage or need for two

distinct pathways in Type I RCs. Despite this lack of an apparent functional advantage to a heterodimeric RC, the high degree of sequence conservation between PsaA (and PsaB) polypeptides of cyanobacteria, algae, and plants suggests that the core of PS I has been highly optimized. The second question is partially answered by the data reviewed in this chapter, showing that the ET is biased toward the A-branch, although the extent of this bias and its functional significance have not been established. Hence, we can only speculate about possible advantages of maintaining a significant level of activity in the B-branch. If the changes in the amplitudes of the two kinetic phases are interpreted as changes in the efficiency in the two pathways, it implies that the relative use of the two branches can be altered by relatively minor perturbations of the RC. This in turn implies that there was indeed some selective value in retaining both pathways. One possible reason is that having two pathways allows the RC to function even if one pathway is damaged. Although this is thought to be a relatively rare event, and there is no direct experimental evidence showing that having two branches compensates for damage to one of them, there are some observations that suggest that it might play a role. For example, it is known that exogenous PhQ can exchange with bound PhQ *in vitro* (Ostafin and Weber, 1997), and it is likely that this occurs *in vivo* as well. During the exchange process, which might be used to get rid of rarely produced $PhQH_2$, the PhQ site would be unoccupied for some period of time, rendering its branch inactive. In a unidirectional model, this would lead to complete loss of activity during exchange of the active quinone, while in a bidirectional model ET in the other branch would still be possible.

Acknowledgments

This work was supported by grants from the U.S. Department of Energy (DE-FG02-00ER15097) and U.S. National Science Foundation (MCB-0347935) to KR and by a grant from the Canadian Natural Sciences and Engineering Research Council (NSERC) and a Chancellor's Chair Research Excellence Award to AvdE.

References

Agalarov R and Brettel K (2003) Temperature dependence of biphasic forward electron transfer from the phylloquinone(s) A_1 in photosystem I: only the slower phase is activated. Biochim Biophys Acta 1604: 7–12

Bautista JA, Rappaport F, Guergova-Kuras M, Cohen RO, Golbeck JH, Wang JY, Beal D and Diner BA (2005) Biochemical and biophysical characterization of photosystem I from phytoene desaturase and zeta-carotene desaturase deletion mutants of *Synechocystis* sp. PCC 6803: evidence for PsaA- and PsaB-side electron transport in cyanobacteria. J Biol Chem 280: 20030–20041

Ben-Shem A, Frolow F and Nelson N (2003) Crystal structure of plant photosystem I. Nature 426: 630–635

Biggins J and Mathis P (1988) Functional role of vitamin K in photosystem I of the cyanobacterium *Synechocystis* 6803. Biochemistry 27: 1494–1500

Bittl R and Zech SG (2001) Pulsed EPR spectroscopy on short-lived intermediates in photosystem I. Biochim Biophys Act 1507: 194–211

Boudreaux B, MacMillan F, Teutloff C, Agalarov R, Gu F, Grimaldi S, Bittl R, Brettel K and Redding K (2001) Mutations in both sides of the photosystem I reaction center identify the phylloquinone observed by electron paramagnetic resonance spectroscopy. J Biol Chem 276: 37299–37306

Breton J (2001) Fourier transform infra-red spectroscopy of primary electron donors in type I photosynthetic reaction centers. Biochim Biophys Acta 1507: 180–193

Breton J, Nabedryk E and Leibl W (1999) FTIR study of the primary electron donor of photosystem I (P700) revealing delocalization of the charge in $P700^+$ and localization of the triplet character in $^3P700$. Biochemistry 38: 11585–11592

Brettel K (1988) Electron transfer from A_1^- to an iron–sulfur center with $t_{1/2} = 200$ ns at room temperature in photosystem I. Characterization by flash absorption spectroscopy. FEBS Lett 239: 93–98

Brettel K (1997) Electron transfer and arrangement of the redox cofactors in photosystem I. Biochim Biophys Acta 1318: 322–373

Brettel K (1998) Electron transfer from acceptor A_1 to the iron–sulfur clusters in photosystem I measured with a time resolution of 2 ns. In: Garab G (ed) Photosynthesis: Mechanisms and Effects, Proceedings of 11th International Congress on Photosynthesis, Vol 1, pp 611–614. Kluwer Academic Publishers, Dordrecht

Brettel K and Golbeck JH (1995) Spectral and kinetic characterization of electron acceptor A_1 in a Photosystem I core devoid of iron–sulfur centers F_X, F_B and F_A. Photosynth Res 45: 183–193

Brettel K and Leibl W (2001) Electron transfer in Photosystem I. Biochim Biophys Acta 1507: 100–114

Büttner M, Xie DL, Nelson H, Pinther W, Hauska G and Nelson N (1992) The photosystem I-like P840-reaction center of green S-bacteria is a homodimer. Biochim Biophys Acta 1101: 154–156

Byrdin M, Cohen R, Fairclough W, Gu F, Golbeck J, Heathcote P, Redding K and Rappaport F (2005) Secondary electron transfer in photosystem I: what transient absorption can tell. In: van der Est A and Bruce D (eds) Photosynthesis: Fundamental Aspects to Global Perspectives, pp 36–38. Allen Press, Lawrence, Kansas

Cohen RO, Shen G, Golbeck JH, Xu W, Chitnis PR, Valieva AI, van der Est A, Pushkar YN and Stehlik D (2004) Evidence for asymmetric electron transfer in cyanobacterial Photosystem I: analysis of a methionine to leucine mutation of the ligand to the primary electron acceptor A_0. Biochemistry 43: 4741–4754

Dashdorj N, Xu W, Cohen R, Golbeck J and Savikhin S (2005) Asymmetric electron transfer in cyanobacterial Photosystem I: charge separation and secondary electron transfer dynamics of mutations near the primary electron acceptor A_0. Biophys J 88: 1238–1249

Diner BA and Rappaport F (2002) Structure, dynamics, and energetics of the primary photochemistry of photosystem II of oxygenic photosynthesis. Annu Rev Plant Biol 53: 551–580

Fairclough WV, Forsyth A, Evans MCW, Rigby SEJ, Purton S and Heathcote P (2003) Bidirectional electron transfer in Photosystem I: electron transfer on the PsaA side is not essential for phototrophic growth in *Chlamydomonas*. Biochim Biophys Acta 1606: 43–55

Fromme P, Jordan P and Krauß N (2001) Structure of Photosystem I. Biochim Biophys Acta 1507: 5–31

Gibasiewicz K, Ramesh VM, Lin S, Redding K, Woodbury NW and Webber AN (2003) Excitonic interactions in wild-type and mutant PSI reaction centers. Biophys J 85: 2547–2559

Gu F, Byrdin M, Rappaport F, van der Est A, MacMillan F and Redding K (2005) Mutational analysis of the two phylloquinones in Photosystem I. In: van der Est A and Bruce D (eds) Photosynthesis: Fundamental Aspects to Global Perspectives, pp 101–103. Allen Press, Lawrence, Kansas

Guergova-Kuras M, Boudreaux B, Joliot A, Joliot P and Redding K (2001) Evidence for two active branches for electron transfer in photosystem I. Proc Natl Acad Sci USA 98: 4437–4442

Gulotty RJ, Mets L, Alberte RS and Fleming GR (1985) Picosecond fluorescence study of photosynthetic mutants of *Chlamydomonas-reinhardtii* – origin of the fluorescence decay kinetics of chloroplasts. Photochem Photobiol 41: 487–496

Hanley JA, Kear J, Bredenkamp G, Li G, Heathcote P and Evans MCW (1992) Biochemical evidence for the role of bound iron–sulfur Center A and Center B in $NADP^+$ reduction by Photosystem I. Biochim Biophys Acta 10899: 152–156

Hastings G and Sivakumar V (2001) A Fourier transform infrared absorption difference spectrum associated with the reduction of A_1 in photosystem I: are both phylloquinones involved in electron transfer? Biochemistry 40: 3681–3689

Hastings G, Kleinherenbrink FA, Lin S, McHugh TJ and Blankenship RE (1994) Observation of the reduction and reoxidation of the primary electron acceptor in photosystem I. Biochemistry 33: 3193–3200

Hastings G, Hoshina S, Webber AN and Blankenship RE (1995) Universality of energy and electron transfer processes in photosystem I. Biochemistry 34: 15512–15522

Hastings G, Ramesh V, Wang R, Sivakumar V and Webber A (2001) Primary donor photo-oxidation in Photosystem I: a reevaluation of (P^+_{700}-P_{700}) Fourier transform infrared difference spectra. Biochemistry 40: 12943–12949

Heathcote P, Hanley JA and Evans MCW (1993) Double-reduction of A_1 abolishes the EPR signal attributed to A_1^-: evidence for C_2 symmetry in the Photosystem I reaction center. Biochim Biophys Acta 1144: 54–61

Hecks B, Wulf K, Breton J, Leibl W and Trissl H-W (1994) Primary charge separation in Photosystem I: a two-step electrogenic charge separation connected with $P^+_{700}A^-_0$ and $P^+_{700}A^-_0$ formation. Biochemistry 33: 8619–8624

Ishikita H and Knapp EW (2003) Redox potential of quinones in both electron transfer branches of photosystem I. J Biol Chem 278: 52002–52011

Itoh S, Iwaki M and Ikegami I (1987) Extraction of vitamin K_1 from photosystem I particles by treatment with diethyl ether and its effects on the A_1^--EPR signal and system I photochemistry. Biochim Biophys Acta 893: 508–516

Itoh S, Iwaki M and Ikegami I (2001) Modification of photosystem I reaction center by the extraction and exchange of chlorophylls and quinones. Biochim Biophys Acta 1507: 115–138

Ivashin N and Larsson S (2003) Electron transfer pathways in photosystem I reaction centers. Chem Phys Lett 375: 383–387

Jeschke G, Pannier M and Spiess H (2000) Double electron–electron resonance. In: Berliner L, Eaton S and Eaton G (eds) Biological Magnetic Resonance, Vol 19, pp 493–512. Kluwer Academic/Plenum Publishers, New York

Johnson TW, Shen GZ, Zybailov B, Kolling D, Reategui R, Beauparlant S, Vassiliev IR, Bryant DA, Jones AD, Golbeck JH and Chitnis PR (2000) Recruitment of a foreign quinone into the A_1 site of photosystem I – I. Genetic and physiological characterization of phylloquinone biosynthetic pathway mutants in *Synechocystis* sp PCC 6803. J Biol Chem 275: 8523–8530

Joliot P and Joliot A (1999) In vivo analysis of the electron transfer within photosystem I: are the two phylloquinones involved? Biochemistry 38: 11130–11136

Jordan P, Fromme P, Witt HT, Klukas O, Saenger W and Krauß N (2001) Three-dimensional structure of cyanobacterial photosystem I at 2.5 Å resolution. Nature 411: 909–917

Kandrashkin Y and van der Est A (2002) Electron spin polarization in photosynthetic reaction centres: strategies for extracting structural and functional information. RIKEN Rev. 44: 124–127

Kandrashkin YE, Vollmann W, Stehlik D, Salikhov K and Van der Est A (2002) The magnetic field dependence of the electron spin polarization in consecutive spin correlated radical pairs in type I photosynthetic reaction centres. Mol Phys 100: 1431–1443

Klukas O, Schubert WD, Jordan P, Krauß N, Fromme P, Witt HT and Saenger W (1999) Localization of two phylloquinones, Q_K and Q'_K, in an improved electron density map of photosystem I at 4-Å resolution. J Biol Chem 274: 7361–7367

Krabben L, Schlodder E, Jordan R, Carbonera D, Giacometti G, Lee H, Webber AN and Lubitz W (2000) Influence of the axial ligands on the spectral properties of P700 of photosystem I: a study of site-directed mutants. Biochemistry 39: 13012–13025

Kumazaki S, Ikegami I, Furusawa H, Yasuda S and Yoshihara K (2001) Observation of the excited state of the primary electron donor chlorophyll (P700) and the ultrafast charge separation in the spinach photosystem I reaction center. J Phys Chem B 105: 1093–1099

Li Y, Lucas MG, Konovalova T, Abbott B, MacMillan F, Petrenko A, Sivakumar V, Wang RL, Hastings G, Gu F, van Tol J, Brunel LC, Timkovich R, Rappaport F and Redding K (2004) Mutation of the putative hydrogen-bond donor to P-700 of photosystem I. Biochemistry 43: 12634–12647

Li Y, van der Est A, Lucas MG, Ramesh VM, Gu F, Petrenko A, Lin S, Webber AN, Rappaport F and Redding K (2006) Directing electron transfer within Photosystem I by breaking H-bonds in the cofactor branches. Proc Natl Acad Sci USA 103: 2144–2149

Liebl U, Mockensturm-Wilson M, Trost J, Brune D, Blankenship R and Vermaas W (1993) Single core polypeptide in the reaction center of the photosynthetic bacterium *Heliobacillus mobilis*: structural implications and relations to other photosystems. Proc Natl Acad Sci USA 90: 7124–7128

Lin S, Katilius E, Haffa ALM, Taguchi AKW and Woodbury NW (2001) Blue light drives B-side electron transfer in

bacterial photosynthetic reaction centers. Biochemistry 40: 13767–13773

Lüneberg J, Fromme P, Jekow P and Schlodder E (1994) Spectroscopic characterization of PS I core complexes from thermophilic *Synechococcus* sp.: identical reoxidation kinetics of A_1^- before and after removal of the iron sulfur clusters F_A and F_B. FEBS Lett 338: 197–202

MacMillan F, Hanley J, van der Weerd L, Knüpling M, Un S and Rutherford AW (1997) Orientation of the phylloquinone electron acceptor anion radical in Photosystem I. Biochemistry 36: 9297–9303

Mathis P and Sétif P (1988) Kinetic studies on the function of A_1 in the photosystem I reaction center. FEBS Lett 237: 65–68

McConnell MD, Wyndhamn I, Brown SAE, Ramesh VM, van der Est A and Webber AN (2005) Directionality of electron transfer in Photosystem I of *Chlamydomonas reinhardtii* probed by electron paramagnetic resonance. In: van der Est A and Bruce D (eds) Photosynthesis: Fundamental Aspects to Global Perspectives, pp 68–70. Allen Press, Lawrence, Kansas

Melkozernov AN, Su H, Lin S, Bingham S, Webber AN and Blankenship RE (1997) Specific mutation near the primary donor in photosystem I from *Chlamydomonas reinhardtii* alters the trapping time and spectroscopic properties of P-700. Biochemistry 36: 2898–2907

Mi DH, Lin S and Blankenship RE (1999) Picosecond transient absorption spectroscopy in the blue spectral region of Photosystem I. Biochemistry 38: 15231–15237

Muhiuddin IP, Heathcote P, Carter S, Purton S, Rigby SEJ and Evans MCW (2001) Evidence from time resolved studies of the $P_{700}^+A_1^-$ radical pair for photosynthetic electron transfer on both the PsaA and PsaB branches of the Photosystem I reaction centre. FEBS Lett 503: 56–60

Müller MG, Niklas J, Lubitz W and Holzwarth AR (2003) Ultrafast transient absorption studies on Photosystem I reaction centers from *Chlamydomonas reinhardtii*. 1. A new interpretation of the energy trapping and early electron transfer steps in Photosystem I. Biophys J 85: 3899–3922

Ostafin AE and Weber S (1997) Quinone exchange at the A_1 site in Photosystem I in spinach and cyanobacteria. Biochim Biophys Acta 1320: 195–207

Pälsson LO, Tjus SE, Andersson B and Gillbro T (1995) Ultrafast energy-transfer dynamics resolved in isolated spinach light-harvesting complex-I and the LHC-I-730 subpopulation. Biochim Biophys Acta 1230: 1–9

Parrett KG, Mehari T, Warren PG and Golbeck JH (1989) Purification and properties of the intact P-700 and F_X-containing Photosystem-I core protein. Biochim Biophys Acta 973: 324–332

Petrenko A and Redding K (2004) Intermolecular electron transfer and exchange integrals in photosystem I. Chem Phys Lett 400: 98–103

Petrenko A, Maniero AL, van Tol J, MacMillan F, Li YJ, Brunel LC and Redding K (2004) A high-field EPR study of P-700$^+$ in wild-type and mutant photosystem I from *Chlamydomonas reinhardtii*. Biochemistry 43: 1781–1786

Polm M and Brettel K (1998) Secondary pair charge recombination in photosystem I under strongly reducing conditions: temperature dependence and suggested mechanism. Biophys J 74: 3173–3181

Prokhorenko VI and Holzwarth AR (2000) Primary processes and structure of the photosystem II reaction center: a photon echo study. J Phys Chem B 104: 11563–11578

Purton S, Stevens DR, Muhiuddin IP, Evans MC, Carter S, Rigby SE and Heathcote P (2001) Site-directed mutagenesis of *psaA* residue W693 affects phylloquinone binding and function in the photosystem I reaction center of *Chlamydomonas reinhardtii*. Biochemistry 40: 2167–2175

Pushkar YN, Zech SG, Stehlik D, Brown S, van der Est A and Zimmermann H (2002) Orientation and protein–cofactor interactions of monosubstituted *n*-alkyl naphthoquinones in the A_1 binding site of photosystem I. J Phys Chem B 106: 12052–12058

Pushkar YN, Golbeck JH, Stehlik D and Zimmermann H (2004) Asymmetric hydrogen-bonding of the quinone cofactor in photosystem I probed by C^{13}-labeled naphthoquinones. J Phys Chem B 108: 9439–9448

Ramesh VM, Gibasiewicz K, Lin S, Bingham SE and Webber AN (2004) Bidirectional electron transfer in photosystem I: accumulation of A_0^- in A-side or B-side mutants of the axial ligand to chlorophyll A_0. Biochemistry 43: 1369–1375

Ramesh V, Gibasiewicz K, Lin S, Bingham SE and Webber AN (2005) Evidence for bi-directional electron transfer in *Chlamydomonas* PS I: analysis of mutants of the axial ligands to Chl A_0. In: van der Est A and Bruce D (eds) Photosynthesis: Fundamental Aspects to Global Perspectives, pp 79–83. Allen Press, Lawrence, Kansas

Redding K, MacMillan F, Leibl W, Brettel K, Hanley J, Rutherford AW, Breton J and Rochaix JD (1998) A systematic survey of conserved histidines in the core subunits of Photosystem I by site-directed mutagenesis reveals the likely axial ligands of P700. EMBO J 17: 50–60

Rigby SEJ, Evans MCW and Heathcote P (2001) Electron nuclear double resonance (ENDOR) spectroscopy of radicals in photosystem I and related Type 1 photosynthetic reaction centres. Biochim Biophys Acta 1507: 247–259

Rigby SEJ, Muhiuddin IP, Evans MCW, Purton S and Heathcote P (2002) Photoaccumulation of the PsaB phyllosemiquinone in Photosystem I of *Chlamydomonas reinhardtii*. Biochim Biophys Acta 1556: 13–20

Sakuragi Y, Zybailov B, Shen GZ, Jones AD, Chitnis PR, van der Est A, Bittl R, Zech S, Stehlik D, Golbeck JH and Bryant DA (2002) Insertional inactivation of the *menG* gene, encoding 2-phytyl-1,4-naphthoquinone methyltransferase of *Synechocystis* sp PCC 6803, results in the incorporation of 2-phytyl-1,4-naphthoquinone into the A_1 site and alteration of the equilibrium constant between A_1 and F_x in Photosystem I. Biochemistry 41: 394–405

Savikhin S, Xu W, Soukoulis V, Chitnis PR and Struve WS (1999) Ultrafast primary processes in photosystem I of the cyanobacterium *Synechocystis* sp. PCC 6803. Biophys J 76: 3278–3288

Savikhin S, Xu W, Martinsson P, Chitnis PR and Struve WS (2001) Kinetics of charge separation and $A_0^- \rightarrow A_1$ electron transfer in photosystem reaction centers. Biochemistry 40: 9282–9290

Schlodder E, Falkenberg K, Gergeleit M and Brettel K (1998) Temperature dependence of forward and reverse electron transfer from A_1^-, the reduced secondary electron acceptor in photosystem I. Biochemistry 37: 9466–9476

Sétif P and Brettel K (1990) Photosystem-I photochemistry under highly reducing conditions – study of the P700 triplet-state formation from the secondary radical pair ($P700^+ - A_1^-$). Biochim Biophys Acta 1020: 232–238

Sétif P and Brettel K (1993) Forward electron transfer from phylloquinone A_1 to iron–sulfur centers in spinach Photosystem I. Biochemistry 32: 7846–7854

Shen GZ, Antonkine ML, van der Est A, Vassiliev IR, Brettel K, Bittl R, Zech SG, Zhao JD, Stehlik D, Bryant DA and Golbeck JH (2002a) Assembly of photosystem I. II. Rubredoxin is required for the *in vivo* assembly of F_x in *Synechococcus* sp. PCC 7002 as shown by optical and EPR spectroscopy. J Biol Chem 277: 20355–20366

Shen GZ, Zhao JD, Reimer SK, Antonkine ML, Cai Q, Weiland SM, Golbeck JH and Bryant DA (2002b) Assembly of photosystem I. I. Inactivation of the *rubA* gene encoding a membrane-associated rubredoxin in the cyanobacterium *Synechococcus* sp. PCC 7002 causes a loss of Photosystem I activity. J Biol Chem 277: 20343–20354

Sivakumar V, Wang R and Hastings G (2005) A_1 reduction in intact cyanobacterial photosystem I particles studied by time-resolved step-scan Fourier transform infrared difference spectroscopy and isotope labeling. Biochemistry 44: 1880–1893

Takahashi Y, Goldschmidt-Clermont M, Soen SY, Franzen LG and Rochaix JD (1991) Directed chloroplast transformation in *Chlamydomonas reinhardtii*: insertional inactivation of the *psaC* gene encoding the iron sulfur protein destabilizes photosystem I. EMBO J 10: 2033–2040

van der Est A (2001) Light-induced spin polarization in type I photosynthetic reaction centres. Biochim Biophys Acta 1507: 212–225

van der Est A, Bock C, Golbeck J, Brettel K, Sétif P and Stehlik D (1994) Electron transfer from the acceptor A_1 to the iron–sulfur centers in Photosystem I as studied by transient EPR spectroscopy. Biochemistry 33: 11789–11797

van der Est A, Valieva AI, Kandrashkin YE, Shen GZ, Bryant DA and Golbeck JH (2004) Removal of PsaF alters forward electron transfer in photosystem I: evidence for fast reoxidation of Q_K-A in subunit deletion mutants of *Synechococcus* sp. PCC 7002. Biochemistry 43: 1264–1275

Vassiliev IR, Yu JP, Jung YS, Schulz R, Ganago AO, McIntosh L and Golbeck JH (1999) The cysteine-proximal aspartates in the F_X-binding niche of photosystem I – effect of alanine and lysine replacements on photoautotrophic growth, electron transfer rates, single-turnover flash efficiency, and EPR spectral properties. J Biol Chem 274: 9993–10001

Wang R, Sivakumar V, Johnson TW and Hastings G (2004) FTIR difference spectroscopy in combination with isotope labeling for identification of the carbonyl modes of P700 and P700+ in photosystem I. Biophys J 86: 1061–1073

Warren PV, Parrett KG, Warden JT and Golbeck JH (1990) Characterization of a Photosystem-I core containing P700 and intermediate electron acceptor-A_1. Biochemistry 29: 6545–6550

Webber A and Lubitz W (2001) P700: the primary electron donor of Photosystem I. Biochim Biophys Acta 1507: 61–79

Webber AN, Su H, Bingham SE, Käss H, Krabben L, Kuhn M, Jordan R, Schlodder E and Lubitz W (1996) Site-directed mutations affecting the spectroscopic characteristics and midpoint potential of the primary donor in photosystem I. Biochemistry 35: 12857–12863

White NTH, Beddard GS, Thorne JRG, Feehan TM, Keyes TE and Heathcote P (1996) Primary charge separation and energy transfer in the photosystem I reaction center of higher plants. J Phys Chem 100: 12086–12099

Witt H, Schlodder E, Teutloff C, Niklas J, Bordignon E, Carbonera D, Kohler S, Labahn A and Lubitz W (2002) Hydrogen bonding to P700: site-directed mutagenesis of threonine A739 of photosystem I in *Chlamydomonas reinhardtii*. Biochemistry 41: 8557–8569

Woodbury NW and Allen JP (1995) The pathway, kinetics and thermodynamics of electron transfer in wild type and mutant reaction centers of purple non-sulfur bacteria. In: Blankenship RE, Madigan MT and Bauer CE (eds) Anoxygenic Photosynthetic Bacteria, pp 527–557. Kluwer Academic Press, Dordrecht, the Netherlands

Xu W, Chitnis P, Valieva A, van der Est A, Pushkar YN, Krzystyniak M, Teutloff C, Zech SG, Bittl R, Stehlik D, Zybailov B, Shen G and Golbeck JH (2003a) Electron transfer in cyanobacterial photosystem I: I. Physiological and spectroscopic characterization of site-directed mutants in a putative electron transfer pathway from A_0 through A_1 to F_X. J Biol Chem 278: 27864–27875

Xu W, Chitnis PR, Valieva A, van der Est A, Brettel K, Guergova-Kuras M, Pushkar YN, Zech SG, Stehlik D, Shen G, Zybailov B and Golbeck JH (2003b) Electron transfer in cyanobacterial photosystem I: II. Determination of forward electron transfer rates of site-directed mutants in a putative electron transfer pathway from A_0 through A_1 to F_X. J Biol Chem 278: 27876–27887

Yang F, Shen GZ, Schluchter WM, Zybailov BL, Ganago AO, Vassiliev IR, Bryant DA and Golbeck JH (1998) Deletion of the PsaF polypeptide modifies the environment of the redox-active phylloquinone (A_1) evidence for unidirectionality of electron transfer in photosystem I. J Phys Chem B 102: 8288–8299

Chapter 26

Electron Transfer from the Bound Iron–Sulfur Clusters to Ferredoxin/Flavodoxin: Kinetic and Structural Properties of Ferredoxin/Flavodoxin Reduction by Photosystem I

Pierre Sétif*
Commissariat à l'Energie Atomique, Département de Biologie Joliot Curie, Service de Bioénergétique and URA CNRS 2096, 91191 Gif sur Yvette, France

Summary

In oxygen-evolving organisms, Photosystem I (PS I) catalyzes the light-driven reduction of ferredoxin, a small acidic soluble protein containing a low-potential [2Fe–2S] cluster. Under conditions of iron deprivation, flavodoxin, which contains a FMN cofactor, can replace ferredoxin in some algae and cyanobacteria. The reduction kinetics of ferredoxin and flavodoxin by (PS I) have been studied over the last 10 years with the unique technique of flash-absorption spectroscopy. This chapter describes and discusses the kinetic aspects of these processes, using data obtained *in vitro* with wild type systems as well as with mutants. A detailed summary of all the available kinetic data concerning the effects of the mutations is provided. In the case of the three stromal subunits PsaC, PsaD, and PsaE, this allows one to define structurally the region of the reaction center that is involved in ferredoxin docking, using the 2.5 Å structure of PS I from the cyanobacterium *Thermosynechococcus elongatus*.

I. Introduction

Photosystem I (PS I) operates as a light-driven oxidoreductase in the photosynthetic membrane of oxygen-evolving organisms, i.e., cyanobacteria, algae, and plants. After charge separation and stabilization, it oxidizes plastocyanin (or cytochrome c_6) on the lumenal side of the membrane and reduces ferredoxin (Fd) on the stromal (cytoplasmic) side of the membrane. Flavodoxin (Fld) can substitute Fd under conditions of

*Author for correspondence, email: pierre.setif@cea.fr
Abbreviations: Chlamydomonas reinhardtii – C. reinhardtii; ET – electron transfer; Fd – ferredoxin; Fld – flavodoxin; FMN – flavin mononucleotide; FNR – ferredoxin-$NADP^+$-oxidoreductase; K_d – dissociation constant; k_{ET} – electron transfer rate; k_{on} – second-order rate constant; PsaC, PsaD, and PsaE: – the three extrinsic subunits of photosystem I; PS I – photosystem I; *Thermosynechococcus elongatus – T. elongatus*; WT – wild type.

John H. Golbeck (ed): Photosystem I: The Light-Driven Plastocyanin:Ferredoxin Oxidoreductase, 439–454.

iron deprivation in most cyanobacteria and some algae (Rogers, 1987; Straus, 1994). The crystallographic structure of PS I from the thermophilic cyanobacterium *Thermosynechococcus elongatus* is known at present at a resolution of 2.5 Å (Jordan et al., 2001; see Fromme and Grotjohann, this volume, Chapter 6). More recently, the structure of a higher plant PS I has been obtained with a resolution of 4.4 Å (Ben Shem et al., 2003; see Nelson and Ben-Shem, this volume, Chapter 7). Three-dimensional structures of several plant-type Fds and Flds are known (Drennan et al., 1999; Morales et al., 1999 and references therein).

The initial photoinduced charge separation in PS I is stabilized by several steps of secondary electron transfer (ET) processes involving different electron acceptors such as chlorophyll(s), quinone(s), and three different [4Fe–4S] clusters, named F_X, F_A, and F_B. Cluster F_X makes a bridge between the two large membrane subunits PsaA and PsaB, with each of these two polypeptides providing two cysteine ligands to the cluster. The center of F_X is located on the C_2 pseudo-symmetry axis of the core of PS I, which is perpendicular to the membrane and passes as well between the two chlorophylls *a* that make up the primary electron donor P700. The terminal electron acceptors F_A or F_B are bound to the extrinsic subunit PsaC, the fold of which is similar to that of bacterial ferredoxins containing 2[4Fe–4S] clusters. Subunit PsaC has local C_2 pseudo-symmetry and this C_2-axis makes an angle of 62° with the membrane normal, which makes cluster F_A closer to F_X and cluster F_B closer to the surface of the PS I complex, in line with F_B being the partner of the [2Fe–2S] cluster of soluble ferredoxin during ET (Sétif, 2001). Therefore, ET involving iron–sulfur clusters occurs most probably according to the successive steps: $F_X \rightarrow F_A \rightarrow F_B \rightarrow$ [2Fe–2S] of Fd. In addition to PsaC, PS I contains two other stromal subunits named PsaD and PsaE, which do not contain any cofactors. The PsaC, PsaD, and PsaE subunits, which are the only purely extrinsic subunits found in cyanobacterial and chloroplastic PS I structures (Jordan et al., 2001; Ben Shem et al., 2003), form a ridge at the stromal surface of PS I and are potentially involved in the interaction of PS I with Fd and Fld (see Antonkine and Golbeck, this volume, Chapter 8).

Fd and Fld can both sustain cyclic (see Joliot et al., this volume, Chapter 37) as well as linear electron flow. During linear electron flow, reduced Fd (Fld) provides the electrons necessary for $NADP^+$ reduction in a reaction catalyzed by ferredoxin-$NADP^+$-oxidoreductase (FNR) (see Hurley et al., this volume, Chapter 27). Fd serves also as an electron donor to a number of soluble enzymes involved in nitrogen metabolism, sulfur metabolism, and the regulation of carbon metabolism (Knaff, 1996; see Hase et al., this volume, Chapter 28). Fld may be efficient in reducing most or all of these soluble enzymes.

ET from PS I to Fd/Fld has been observed directly for the last 10 years. The only technique used for characterizing the kinetics of this process has been flash-absorption spectroscopy. One difficulty in using this technique is that the three different iron–sulfur clusters of PS I have similar absorption properties, so that the kinetic steps preceding immediately Fd/Fld reduction cannot be spectrally distinguished. Photoelectric measurements, i.e., the measurement of electric fields created by ET in membrane fragments or vesicles containing PS I, does not suffer from the same limitation and was extremely useful in the study of ET steps within PS I (Brettel and Leibl, 2001). However, Fd (Fld) reduction from F_B^- appears to be electrically silent (Semenov et al., 2003; see Semenov et al., this volume, Chapter 21).

Ferredoxin and flavodoxin reduction by PS I (Sétif, 2001) as well as the Fd docking site of PS I (Sétif et al., 2002) have been reviewed recently. In the present chapter, I will focus on the kinetic and structural aspects of these processes, summarizing the available data that have been discussed in these recent reviews while incorporating the scarce new data that appeared more recently.

II. Electron Transfer from PS I to Ferredoxin in Wild Type Systems

As mentioned above, flash-absorption spectroscopy seems, up to now, the only available method for monitoring directly the kinetics of Fd reduction by PS I. Experiments were performed in the 460–600 nm region, taking advantage of the fact that reduction of the [2Fe–2S] cluster of Fd leads to a larger bleaching than single reduction of the terminal [4Fe–4S] clusters F_A and F_B of PS I (Sétif and Bottin, 1995). A relatively slow process of Fd reduction ($k < 280\ sec^{-1}$ i.e., $t_{1/2} > 2.5$ msec) has been observed for Fd reduction using spinach PS I and Fd from either the green alga *Monoraphidium braunii* (Hervas et al., 1992) or the cyanobacterium *Anabaena* sp. PCC 7120 (Navarro et al., 1995). In these reports, a single phase was observed with a rate increasing nonlinearly with the Fd concentration. Parameters k_{ET} (electron transfer rate; half-time $t_{1/2}$), k_{on} (second-order rate constant), and K_d (dissociation constant) were estimated assuming a two-step mechanism

(formation of a PS I/Fd complex followed by ET within the complex) and following a numerical analysis, which is valid under the steady-state approximation (Tollin et al., 1986) (Table 1). Note, however, that this last approximation is disputable, as previously noted (Hope, 2000), in the case of flash-induced measurements which inherently lead to an out-of-equilibrium initial state and with rates of association, dissociation, and ET in the same time range.

These observations of only relatively slow processes constitute a complete discrepancy with the fast Fd reduction that has been measured in kinetic studies made by myself and colleagues, with first-order half-times in the submicrosecond and microsecond ranges and half-times corresponding to second-order processes that can be observed below a few hundreds of microseconds (Table 1; see e.g., Sétif and Bottin, 1995; Fischer et al., 1997). This discrepancy seems difficult to ascribe to the use of biological materials from different organisms as fast kinetics could be observed in any type of PS I/Fd system yet studied. Our measurements of ET between isolated PS I and Fd have been studied with proteins purified from cyanobacteria, mostly *Synechocystis* sp. PCC 6803 (Sétif and Bottin, 1994, 1995) but also *T. elongatus* (Sétif and Bottin, 1994), from spinach (Sétif and Bottin, 1995), and from the green alga *Chlamydomonas reinhardtii* (Fischer et al., 1998). Cyanobacterial systems were studied in the 460–600 nm region but kinetics were reported only at 580 nm for chloroplastic PS I due to the larger absorption of the antenna system, which makes studies at shorter wavelengths more difficult. A detailed summary of the properties of these systems (either homologous or heterologous) can be found in (Sétif, 2001). The main conclusions that can be drawn from these kinetic studies are the following:

1) Several kinetic components are present in the submicrosecond and microsecond time ranges. The rates of the fastest components do not depend upon the concentrations of the reaction partners and these components are therefore first-order ($t_{1/2}$ in Table 1). Their amplitude increases with the ferredoxin concentration and saturates at high ferredoxin concentrations. The slowest component is second-order. Its rate depends linearly on Fd concentration when Fd is in large excess compared to PS I, which allows a second-order rate constant k_{on} to be derived.
2) The first-order phases are thought to correspond to ET occurring within PS I/Fd complexes, which are preformed before flash excitation, assuming that the association/dissociation processes are much slower than the first-order reduction of Fd.
   a) A dissociation constant K_d (Table 1) for the PS I/Fd complex, which deals with the oxidized partners, can be calculated from the dependence of the first-order phase amplitudes upon the Fd concentration, assuming a simple binding equilibrium.
   b) The fastest of the first-order phases is submicrosecond ($t_{1/2} \approx 0.5$ μsec when measured, i.e., in the case of *Synechocystis* sp. PCC 6803). It is present in all systems studied thus far and contributes to about 30% of the absorption changes ascribed to Fd reduction. This component is preceded with a lag phase following flash excitation lasting for about 200 nsec (Sétif and Bottin, 1994). The existence of a lag is expected as ET along the chain of acceptors must occur before Fd is reduced by F_B^-. Such a lag is consistent with the known kinetics within the PS I acceptors, with the rate-limiting step being presumably ET from the phylloquinone in the A-branch to cluster F_X ($t_{1/2} \approx 200$ nsec) (Brettel and Leibl, 2001; see Rappaport et al., this volume, Chapter 16; Stehlik, this volume, Chapter 23). In accordance with photoelectric measurements, the available kinetic data of Fd reduction obtained with WT and some PS I mutants support submicrosecond ($F_X \rightarrow F_A$) and ($F_A \rightarrow F_B$) ET (Sétif, 2001; Semenov et al., 2003).
   c) A microsecond phase (with $t_{1/2}$ from 4 to 20 μsec) is always present. A third phase ($t_{1/2} \approx 100$ μsec) has been found up to now only with PS I from cyanobacteria (Sétif and Bottin, 1994). The heterogeneity of first-order ET kinetics was ascribed to different conformations of the PS I/Fd complex. (Sétif and Bottin, 1995; Sétif, 2001). It cannot be excluded from the available data that Fd binding in some conformation(s) slows down ET between F_A and F_B, which could then occur in the microsecond time range and be rate-limiting (discussed in Sétif, 2001). Alternatively, ET from F_B^- to Fd itself may occur in the microsecond time range in some conformation(s), due, e.g., to larger distances between F_B and Fd. Another explanation might be proposed from recent observations by X-ray diffraction, which shows

Table 1. Kinetic parameters of ferredoxin reduction in wild type systems

PS I organism	Ferredoxin organism	First-order phases			Second-order phase, k_{on} ($M^{-1} sec^{-1}$)	References
		K_d (μM)	Number of phases	$t_{1/2}$ of phases		
Synechocystis sp. PCC 6803	*Synechocystis* sp. PCC 6803	0.2–0.4	3	0.5 μsec/13–20 μsec/85–120 μsec	$3.5 \pm 1.5 \times 10^8$	Sétif and Bottin (1994, 1995)
Synechocystis sp. PCC 6803	*C. reinhardtii*	1.8	3	<1 μsec/20 μsec/100 μsec	nd[a]	Sétif and Bottin (1994)
Synechocystis sp. PCC 6803	Spinach	4–6	2	<1 μsec/4–6 μsec	5.6×10^8	Sétif and Bottin (1995)
C. reinhardtii	*C. reinhardtii*	6–9	2	<1 μsec/3–6 μsec	$2.3 \pm 0.5 \times 10^8$	Fischer et al. (1998)
C. reinhardtii	*Synechocystis* sp. PCC 6803	6	2	<1 μsec/9–13 μsec	3.5×10^8	Fischer et al. (1997)
Spinach	Spinach	<3	2	<1 μsec/4–6 μsec	nd	Sétif and Bottin (1995)
Spinach	Spinach	nd	1	5 msec	0.3×10^8	Hervas et al (1992)[b]
Spinach	*Monoraphidium braunii*	nd	1	3.9 msec	0.33×10^8	Hervas et al (1992)[b]
Spinach	*Anabaena* sp. PCC 7120 (vegetative form)	1.1	1	4 msec	0.7×10^8	Navarro et al. (1995)[b]

[a] nd: not determined.

[b] A single phase was observed. The data were analyzed assuming a two-step mechanism (formation of a PS I/Fd complex followed by ET within the complex).

evidence for a redox-linked conformational change in a cyanobacterial ferredoxin from *Anabaena* sp. PCC 7120 (Morales et al., 1999). This change concerns mainly the orientation of the peptide bond linking two residues (Cys46 and Ser47) which are located close to the reducible iron at the Fd surface, and involves at least two other essential residues, Phe65 and Glu94 (using the numbering of *Anabaena* sp. PCC 7120 Fd; Morales et al., 2002; Pizzitutti et al., 2003). The relative stability of the two conformations and the activation barrier between them appear to be modulated by the distance between Ser47 and Glu94 (Pizzitutti et al., 2003). Heterogeneity of binding leading to various distances and/or relaxation between such conformations are other possible interpretations for the existence of the complex kinetics of Fd reduction. Further work is needed to support or eliminate these possibilities.

3) The second-order phase (k_{on} in Table 1) corresponds to a diffusion-limited ET process between PS I and Fd. The PS I reaction centers involved in this reaction do not bind Fd at the time of flash excitation. After charge separation, they bear $(F_A,F_B)^-$ and the partners in this reaction are therefore PS I with reduced terminal acceptors and oxidized Fd.

The change in Gibbs energy associated with Fd reduction can be estimated from the midpoint potentials of the ET partners. Several genes and isoforms of plant-like Fds are present in oxygen-evolving organisms, the midpoint potentials of which span a large midpoint potential region, in the range of −300 to −450 mV. Among these, the major isoforms of ferredoxins present in leaves of higher plants, in algae, and cyanobacteria, are partners of PS I and exhibit redox potentials around −420 mV. For the two organisms, which have been studied kinetically for Fd reduction (*Synechocystis* sp. PCC 6803 and *C. reinhardtii*), the redox potentials of free Fd are −412 and −445 mV, respectively (Bottin and Lagoutte, 1992; Garcia-Sanchez et al., 2000). The midpoint potentials of the terminal acceptors of PS I have been measured by titrating the EPR signals of F_A^- and F_B^- at low temperature, giving values of −590 to −540 mV (Brettel, 1997). From these values, one may conclude that Fd reduction by $(F_A,F_B)^-$ is almost complete within a complex. However, caution must be taken with this assessment: (1) Higher values in the range of −480 to −440 mV have been measured at room temperature for the redox potential of the highest potential PS I acceptor (either F_A or F_B; Jordan et al., 1998; see Brettel, 1997 for discussion). (2) The redox potentials of (F_A, F_B) and Fd within the complex may be different from their values in the free forms, as was found, e.g., for the cofactors in the Fd/FNR complex (Pueyo et al., 1992).

Despite the above uncertainties, two conclusions were previously drawn from a careful examination of the available experimental data (Sétif, 2001):

- though F_B reduction probably occurs in the submicrosecond time range in free PS I, this may not hold in 100% of the PS I/Fd complexes, where, in a fraction of these, it may occur in the microsecond time range and could be a limiting step for Fd reduction. Whether the microsecond first-order kinetics of Fd reduction can be ascribed to ($F_A \rightarrow F_B$) or to ($F_B \rightarrow$ Fd) ET is therefore still an unresolved issue.
- from the available kinetic data in the 460–600 nm region, it was assumed that at least 80% of Fd is reduced within the *Synechocystis* sp. PCC 6803 PS I/Fd complex (with submicrosecond and microsecond kinetics). A similar conclusion could not be drawn in the case of *C. reinhardtii* due to insufficient data (Sétif, 2001).

III. Electron Transfer from PS I to Flavodoxin in Wild Type Systems

The FMN cofactor of flavodoxins can undergo two successive single electron reductions. Oxidized Fld is first reduced to a protonated semiquinone form ($FMNH^{\cdot}$) and then reduced to a hydroquinone form ($FMNH^-$). For flavodoxins found in photoautotrophic organisms, the corresponding midpoint potentials are in the −180/−240 mV region for the FMN/$FMNH^{\cdot}$ couple (at pH 7) and in the −370/−470 mV region for the $FMNH^{\cdot}$/$FMNH^-$ couple (Sykes and Rogers, 1984). Reduction of the Fld semiquinone occurs therefore at about the same redox potential as reduction of Fd. This might imply that only the second wave of Fld reduction is involved in shuttling electrons between PS I and soluble acceptors, in line with the EPR detection of the Fld semiquinone in cyanobacterial cells in darkness (Norris et al., 1972) and with the relatively high stability of the semiquinone (Mühlenhoff and Sétif, 1996). However, in some species, the midpoint potentials of the two waves might be rather close at pH 8 or above, values

that can occur *in vivo* in the light, so that a physiological role for the oxidized-semiquinone couple cannot be excluded (Rogers, 1987).

A. Reduction of Oxidized Flavodoxin

In vitro measurements of the kinetics of oxidized Fld photoreduction were measured with different cyanobacterial Flds and PS I from either cyanobacteria or chloroplasts (spinach and *C. reinhardtii*) (see parameters k_{ET}, K_d, and k_{on} in Table 2). In all cases, formation of semireduced Fld occurs in the millisecond time range with a single exponential component. The rate of this component increases nonlinearly with the Fld concentration and levels off at high Fld concentrations to an asymptotic value which is taken as the ET rate k_{ET}. The absence of a domain of linear dependence at low Fld concentrations impedes a direct estimation of a second-order rate constant corresponding to complex formation. However, this second-order rate constant was estimated in some publications (Medina et al., 1992; Navarro et al., 1995) assuming a two-step mechanism (formation of a PS I/Fld complex followed by ET within the complex; see paragraph above). It was proposed in Mühlenhoff and Sétif (1996) that reduction of oxidized Fld, which is relatively slow compared to reduction of semireduced Fld (see below and Table 2), might be rate-limited by protonation of FMN. Evidence against this proposal has been provided recently, as the rate of Fld semiquinone protonation following its reduction by the 5-deazariboflavin radical is about the same in several mutants of Fld (410–730 sec^{-1}), whereas large differences were found in k_{ET} rates for reduction by PS I (Casaus et al., 2002; see below and Table 5). An alternative explanation could be that the PS I/Fld complexes have different conformations when Fld is oxidized or semireduced (see below), with a larger edge-to-edge distance between F_B and FMN when Fld is oxidized (Page et al., 1999). To my knowledge, the only available evidence, which could support this hypothesis is the small structural difference observed between Fld structures (of the non-photosynthetic type) in the oxidized and semireduced states (flipping of a peptide bond in the vicinity of FMN; Smith et al., 1977; Watt et al., 1991; Romero et al., 1996).

B. Reduction of Semireduced Flavodoxin

The kinetics of the second wave of Fld reduction by PS I ($FMNH^{\cdot}$ to $FMNH^{-}$) were observed in two homologous cyanobacterial systems as well as with PS I from *C. reinhardtii* and a cyanobacterial Fld (see parameters K_d, $t_{1/2}$, and k_{on} in Table 2) under conditions where most of Fld was reduced to the semiquinone form before flash excitation. In the two homologous systems (Mühlenhoff and Sétif, 1996; Meimberg et al., 1998), a fast phase is present with $t_{1/2} = 10$–13 μsec. Its kinetics are independent on the Fld concentration and its size increases with concentration. These characteristics are consistent with a first-order process of ET within a preformed PS I/(semireduced Fld) complex. The fast phase is followed by a slower phase with a rate depending linearly on the Fld concentration, thus allowing a second-order rate constant k_{on} to be derived. This rate reflects presumably the association (rate-limiting for ET) between PS I and semireduced Fld. With PS I from *C. reinhardtii*, only the slowest second-order phase was detected with no observable microsecond ET (Meimberg et al., 1999). This can be ascribed to a relatively low affinity of semireduced Fld for the algal PS I, in line with the probable absence of Fld in *C. reinhardtii* (Meimberg et al., 1999). The absence of a functional complex was also observed when PS I and semireduced Fld originate from two different cyanobacterial strains (*T. elongatus* and *Synechocystis* sp. PCC 7002, respectively), which suggests that the recognition process depends strongly either on details of the PS I structure or on a precise and organism-dependent complementarity between the two partners (Meimberg et al., 1998). This is opposite to Fd binding, which was not found to be much dependent on homologous systems (Table 1; Sétif and Bottin, 1994). In the two homologous cyanobacterial systems, it has been found that the amplitude of the first-order fast phase represents, at saturating concentrations of semireduced Fld, only about 65% of the total amplitude of $FMNH\cdot$ reduction. Two possible explanations were proposed for this effect, either an incomplete reduction due to redox equilibrium within the complex, or the presence of a fraction of PS I/(semireduced Fld) not competent for fast ET (Mühlenhoff and Sétif, 1996).

IV. Ionic Strength Dependence of Ferredoxin/Flavodoxin Reduction

The ionic strength dependence of Fd and Fld reduction by PS I has been studied with several systems (Hervas et al., 1992; Medina et al., 1992; Sétif and Bottin, 1994; Navarro et al., 1995; Mühlenhoff and Sétif, 1996). In all cases, a bell-shaped dependence was observed with a rate increase at low ionic strength and a rate decrease at high ionic strength. The rate decrease at high ionic strength is consistent with opposite charges borne by

Table 2. Kinetic parameters of flavodoxin reduction in wild type systems

		Reduction of oxidized flavodoxin			Reduction of semireduced flavodoxin			
					First-order component		Second-order component	
PS I organism	Flavodoxin organism	k_{ET} (sec^{-1})	K_d (μM)	k_{on} ($M^{-1}sec^{-1}$)	K_d (μM)	$t_{1/2}$ (μsec)	k_{on}(M^{-1} sec^{-1})	References
Synechococcus sp. PCC 7002	*Synechococcus* sp. PCC 7002	600	nd[a]	nd	2.6	10	1.7×10^8	Mühlenhoff et al. (1996)
Synechocystis sp. PCC 6803	*Synechocystis* sp. PCC 6803	500	nd	nd	2.0	13	2.2×10^8	Meimberg et al. (1998)
Chlam. reinhardtii	*Synechocystis* sp. PCC 6803	670	nd	nd	>>60	nd	1.0×10^8	Meimberg et al. (1999)
Spinach	*Anabaena* sp. PCC 7119	270	nd	3.6×10^7	nd	nd	nd	Medina et al. (1992)[b]
Spinach	*Anabaena* sp. PCC 7120	310	4.3	4.9×10^7	nd	nd	nd	Navarro et al. (1995)[b]
Anabaena sp. PCC 7119	*Anabaena* sp. PCC 7119	500	1.7	nd	nd	nd	nd	Casaus et al. (2002)[b]

[a] nd: not determined.

[b] Only reduction of oxidized flavodoxin was observed. The data were analyzed assuming a two-step mechanism (formation of a PS I/Fld complex followed by ET within the complex).

Fd/Fld and the stromal ridge of PS I, with rate enhancement due to electrostatic attraction between the two partners and steering of the soluble partner in the electrostatic field of PS I. The rate increase at low ionic strength has been explained by a rearrangement process (Meyer et al., 1993): at low salt concentration, the partners are locked, due to large electrostatic interactions, in a relative position that is not optimal or is even unfavorable for electron transfer. Rearrangement to a more favorable conformation is enhanced at higher salt concentration, which then allows faster ET. The two regimes of salt dependence thus define a salt concentration optimal for fast ET.

V. The Ferredoxin Docking Site

The approximate docking sites of Fd and Fld onto PS I were first deduced from electron microscopy measurements of PS I/Fd and PS I/Fld functional covalent complexes (Mühlenhoff et al., 1996; Lelong et al., 1996) and from modeling (Fromme et al., 1994), both methods being applied with cyanobacterial PS I. These first data supported the view that the docking site is very similar for Fd and Fld, both partners binding to the side of the ridge formed by the three extrinsic stromal subunits PsaC, PsaD, and PsaE of PS I. In a more recent electron microscopy study of a covalent PS I/Fd complex with spinach PS I, Fd was found to bind to the top of the stromal ridge (Ruffle et al., 2000). The kinetics of Fd reduction were also studied by flash-absorption spectroscopy in many mutants of the three PS I extrinsic subunits. The results of these studies will be summarized below using the available PS I structure at 2.5 Å resolution (Jordan et al., 2001). It may be useful to recall here that the K_d determinations correspond to functional PS I/Fd complexes which undergo fast (submicrosecond and microsecond) Fd reduction.

PsaC mutants were obtained from the green alga *C. reinhardtii* whereas PsaD and PsaE mutants were obtained from the cyanobacterium *Synechocystis* sp. PCC 6803. Modified kinetics and affinities were found with mutants from the three subunits and allowed the identification of residues important for Fd reduction. These results are summarized in Table 3 and Fig. 1. Table 3 recapitulates all the available data (parameters K_d and k_{on}) concerning PS I mutations that lead to change of at least a factor of 2 in the dissociation constant K_d of the PS I/Fd complex. A detailed discussion of some of the mutations together with a list of PS I mutations with little change in K_d can be found elsewhere (Sétif et al., 2002). The deletion of either PsaD or PsaE was found to decrease considerably the affinity of Fd for PS I, though a complex was still observable in both cases, as found from the presence of fast Fd reduction at large ferredoxin concentrations. A comparison of the two types of deleted mutants led to the suggestion that PsaD might be more involved in guiding Fd to its binding site whereas PsaE might be more involved in controlling the lifetime of the PS I/Fd complex (Barth et al., 1998). The other mutations are dealing with substitutions of residues leading to a change in the charge or the charge distribution in PS I. Their effects on K_d are plotted in Fig. 1, in which it was assumed that the acidic or basic residues are in their charged state at pH 8.0, where all measurements were performed. This choice of mutations was made on the basis of the assumption that electrostatic interactions are essential for Fd/Fld binding, as indicated by the effects of salts (see section IV) and as suggested by the acidic nature of Fd and Fld. It was also later recognized from the PS I structure that the solvent-accessible surface of the three PS I stromal subunits is positively charged (Jordan et al., 2001), in accordance with a charge complementarity between PS I and Fd. Electrostatic attraction between PS I and Fd is clearly confirmed from Fig. 1, where only two quadrants are filled with experimental points. The upper left quadrant corresponds to PS I being less positive and Fd affinity being smaller than in the wild type, whereas the lower right quadrant corresponds to PS I being more positive and Fd affinity being larger. The existence of PsaC and PsaD mutants with a much larger affinity for Fd than the wild type suggests that this affinity is tuned to an optimal value (in the micromolar range), allowing an efficient turnover of Fd reduction.

Figure 2 exhibits a stereo side view (parallel to the membrane) of the stromal part of PS I from *T. elongatus*. The mutations giving rise to the largest changes in K_d are circled in Fig. 1 and the side chains of the corresponding residues are arrowed in Fig. 2. In addition to these residues, residue K104 is also shown in Fig. 2 as it has been shown to be covalently bound to an acidic residue of Fd in the functional covalent PS I/Fd complex from *Synechocystis* sp. PCC 6803 (Lelong et al., 1994) (K106 in the numbering of *Synechocystis* sp. PCC 6803). The PS I residues shown in Fig. 2 belong to the three stromal subunits of PS I and allow to define the approximate docking site for Fd at the PS I surface. This region fits nicely with previous data from electron microscopy data of a covalent complex (Lelong et al., 1996) as well from a study modeling the Fd docking site from the PS I structure at 6 Å resolution (Fromme et al., 1994). It corresponds to the region where the outermost cluster F_B lies closer to the PS I surface,

Table 3. Kinetic parameters of ferredoxin reduction for strongly affected photosystem I mutants ($K_{d(mutant)}/K_{d(WT)}$ <0.5 or > 2)[a]

Subunit	Mutation	Organism	Corresponding residue in PS I of *T. elongatus*	$K_{d(mutant)}/K_{d(WT)}$	$k_{on(mutant)}/k_{on(WT)}$	References
PsaC	K35E	*Chlamydomonas reinhardtii*	K34	>35	0.012	Fischer et al. (1998)
PsaC	K35D	*Chlamydomonas reinhardtii*	K34	>35	0.027	Fischer et al. (1998)
PsaC	K35T	*Chlamydomonas reinhardtii*	K34	>35	0.20	Fischer et al. (1998)
PsaC	K35T/S37K[b]	*Chlamydomonas reinhardtii*	K34/G36	21	0.35[c]	Sétif et al. (2002)
PsaC	V49I/K52T/R53Q	*Chlamydomonas reinhardtii*	V48/K51/R52	2.8	0.9	Fischer et al. (1999)
PsaC	S37K[b]	*Chlamydomonas reinhardtii*	G36	0.35	1.5[c]	Sétif et al. (2002)
PsaC	I12V/T15K/Q16R	*Chlamydomonas reinhardtii*	I11/T14/Q15	0.017	nd[f]	Fischer et al. (1999)
PsaD	Deletion	*Synechocystis* sp. PCC 6803	–	26	0.08	Barth et al. (1998)
PsaD	H97E	*Synechocystis* sp. PCC 6803	H95	8	nd	Hanley et al. (1996)
PsaD	K106C	*Synechocystis* sp. PCC 6803	K104	5.5	nd	Hanley et al. (1996)
PsaD	K106A	*Synechocystis* sp. PCC 6803	K104	2	nd	Hanley et al. (1996)
PsaD	R111C	*Synechocystis* sp. PCC 6803	R109[d]	4.5	nd	Hanley et al. (1996)
PsaD	E109K[e]	*Synechocystis* sp. PCC 6803	K107	0.3	nd	Bottin et al. (2001)
PsaD	D100S	*Synechocystis* sp. PCC 6803	D98	0.3	nd	Bottin et al. (2001)
PsaD	D100K	*Synechocystis* sp. PCC 6803	D98	0.12	nd	Bottin et al. (2001)
PsaD	E105Q	*Synechocystis* sp. PCC 6803	E103	0.04	nd	Bottin et al. (2001)
PsaE	Deletion	*Synechocystis* sp. PCC 6803	–	100	0.43	Barth et al. (1998)
PsaE	R39E	*Synechocystis* sp. PCC 6803	R39	>450	0.07	Barth et al. (2000)
PsaE	R39D	*Synechocystis* sp. PCC 6803	R39	>450	0.10	Barth et al. (2000)
PsaE	R39Q	*Synechocystis* sp. PCC 6803	R39	250	0.31	Barth et al. (2000)
PsaE	R39H	*Synechocystis* sp. PCC 6803	R39	140	0.32	Barth et al. (2000)
PsaE	R39K	*Synechocystis* sp. PCC 6803	R39	7	1.1	Barth et al. (2000)

[a] For each of the three subunits PsaC, PsaD, and PsaE, the mutants are generally ordered by increasing Fd affinity (when compared to the respective WT).
[b] The corresponding residue is a lysine residue in most plants and in some red algae. In other species, it is replaced by alanine, asparagine, glycine, glutamine, or serine.
[c] Fischer et al. (unpublished data).
[d] The side chain of R109 is only partially exposed to the solvent in the *T. elongatus* structure. It is located beneath D98 in the top view of PS I (see Fig. 3).
[e] This residue is not conserved. It is glutamate in several cyanobacterial species, but alanine and proline are also found, these two substitutions being found in most eukaryotic species. The presence of a lysine in *T. elongatus* represents an exception.
[f] nd: not determined.

which is favorable for fast ET. This can be seen in Fig. 2 where two inorganic sulfur atoms (colored in yellow) belonging to F_B can be seen between the side chains of residues I11 and Q15 of PsaC whereas the β carbon of a cysteine residue liganding F_B (C13 in the *T. elongatus* numbering) lies between these two side chains (shown by an asterisk). The approximate contours of the PsaA, PsaF, and PsaJ subunits are also shown in Fig. 2. Although the possible participation of PsaA in Fd binding still awaits experimental support, mutants of *C. reinhardtii* deleted in either PsaF or PsaJ exhibit no significant modification in Fd binding (Sétif et al., 2002).

Figure 3 exhibits a stereo top view (perpendicular to the membrane) of the stromal part of PS I from *T. elongatus*. The same side chains as those shown in Fig. 2 are also shown, when visible. Some additional side chains are designated as well: The colored ones correspond to positions for which functionally significant mutations have been studied (see Table 3), whereas the black ones correspond to positions where mutations do not give rise to any significant effect on K_d, in line with their location on the side of the stromal ridge opposite to the proposed Fd docking site. The residues $G36_C$, $D98_D$, and $K107_D$ (numbering of *T. elongatus*), which correspond to positions with significant effects of mutations (see Table 1), are located on the top of the stromal ridge and therefore outside the docking site as defined above. It has been recently hypothesized that the effects of these mutations are related to a role of the upper side of the stromal ridge in steering electrostatically Fd toward its final binding site (Sétif et al., 2002), which would be consistent with the location of Fd in a covalent complex from spinach (Ruffle et al., 2000). Cyanobacterial PS I/Fd cocrystals have been obtained recently with a 7–8 Å resolution (Fromme et al., 2002). A deeper knowledge of the PS I/Fd structure is expected from the determination of the structure of

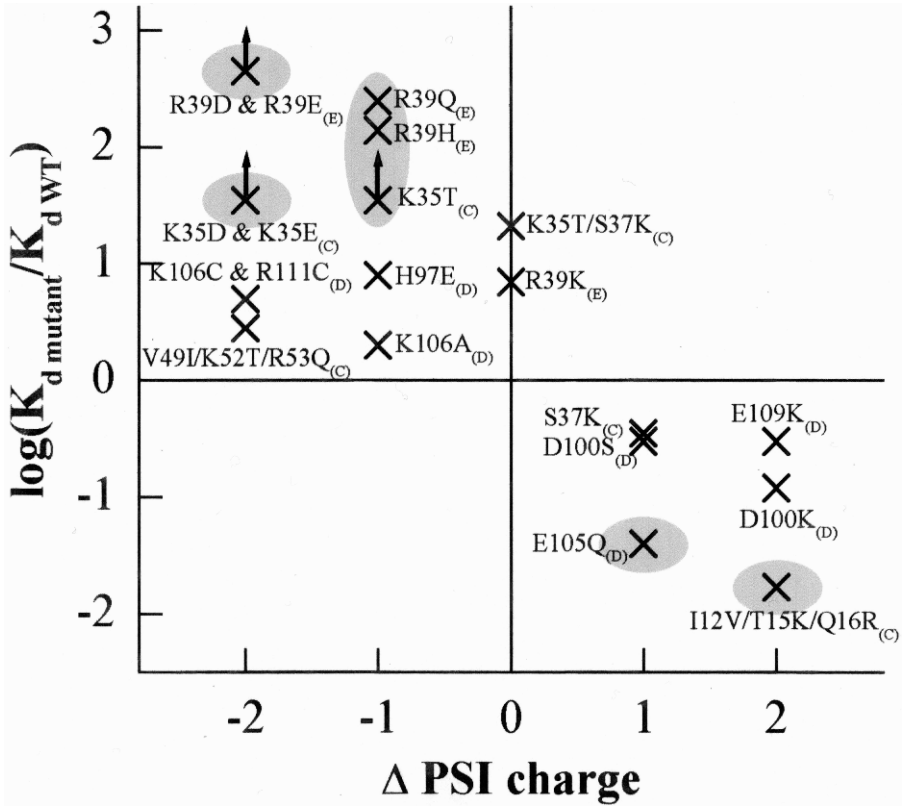

Fig. 1. Changes in the dissociation constant K_d of the photosystem I/ferredoxin complex in mutants of the PsaC, PsaD, and PsaE subunits of photosystem I. The ratio of K_ds between the mutated and the WT PS Is is plotted on a logarithmic vertical scale. Numbering of the residues is made according to the PsaC sequence of *C. reinhardtii* and of the PsaD and PsaE sequences of *Synechocystis* sp. PCC 6803. Numbering of the corresponding mutated residues of *T. elongatus* can be found from Table 1. Subscript characters refer to the PS I subunit (PsaC, PsaD, or PsaE). The vertical arrows indicate that only a lower limit of the ratio $K_{d(mutant)}/K_{d(WT)}$ was measured. The mutations giving rise to the largest effects are surrounded by shaded ellipses and the corresponding residues are arrowed in Fig. 2.

PS I/Fd cocrystals when better resolution will become available.

Since the publication of the structure of pea PS I at a 4.4 Å resolution (Ben-Shem et al., 2003; see also Nelson and Ben-Shem, this volume, Chapter 7), comparison between cyanobacterial and higher plant PS I can now be performed on a structural basis. With regard to Fd/Fld reduction, one relevant issue is whether the N-terminal extensions found in the PsaD and PsaE subunits of higher plant PS I may be involved in binding the soluble partners. It appears that the N-terminal extension of PsaD extends outside the proposed Fd binding site (Ben Shem et al., 2003) whereas the PsaE extension is not reported in the pea structure, though it has been identified in isolated pea PS I (Dunn et al., 1988).

Significant effects of PS I mutations on Fld reduction have been reported only in two cases, both with Fld from *Synechocystis* sp. PCC 6803 (Table 5). The first mutation was deletion of the PsaE subunit in PS I from *Synechocystis* sp. PCC 6803. The behavior of this mutant almost parallels that of Fd reduction (Meimberg et al., 1998; see section V and Table 3). The second mutation was K35E of the PsaC subunit in *C. reinhardtii*. The mutant exhibited a large decrease in the second-order rate constant of the reduction of the semireduced Fld (Meimberg et al., 1999), as was also the case for Fd reduction. No docking site for Fld can be proposed from these scarce data and a similarity in the docking sites for Fd and Fld can be inferred only from studies of covalent complexes by electron microscopy (Lelong et al., 1996; Mühlenhoff et al., 1996). In this context, it can be noted that the presence of all three extrinsic subunits PsaC, PsaD, and PsaE has been confirmed in PS I cyanobacterial trimers surrounded by a ring of light-harvesting subunits, a supercomplex

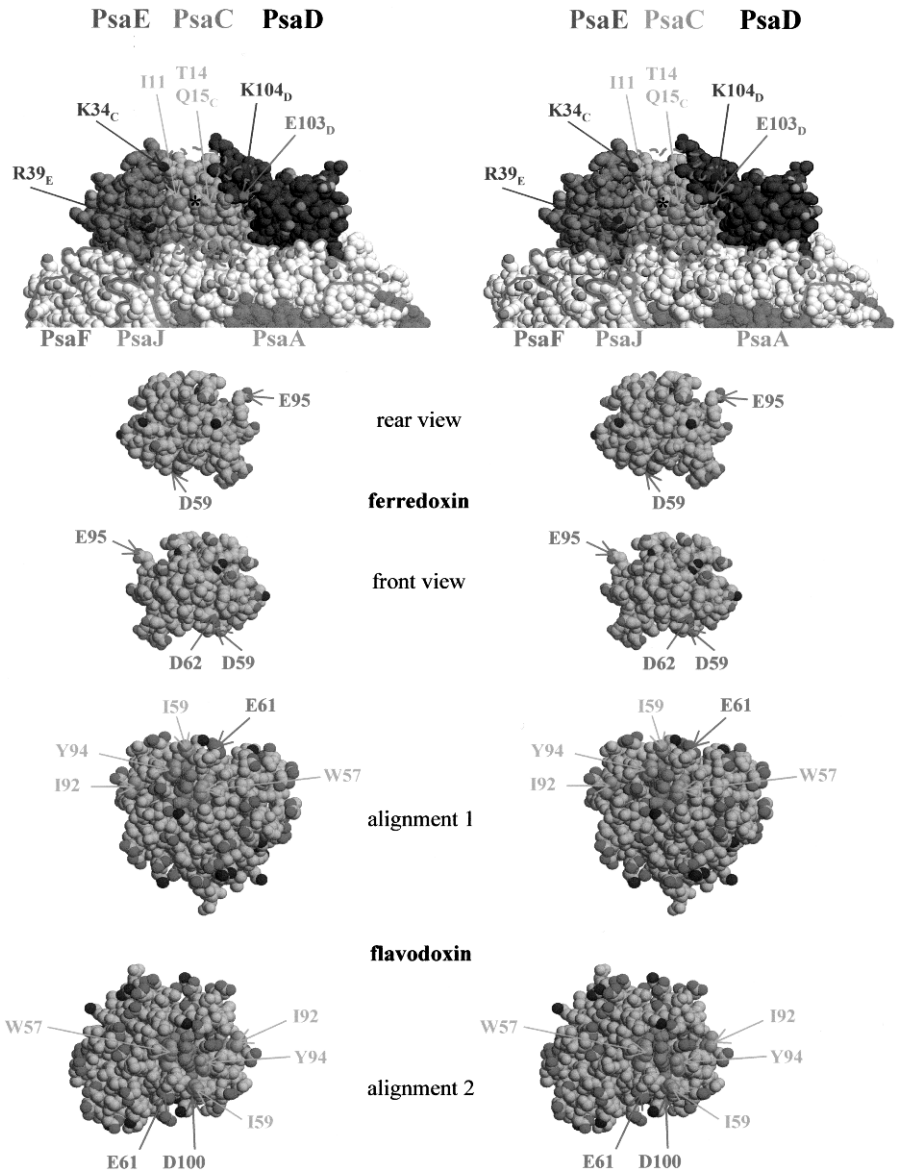

Fig. 2. Stereo views of photosystem I, ferredoxin and flavodoxin (crossed eyes). See Color Plate 10, Fig. 1.

structure which is present under conditions of iron deficiency (Nield et al., 2003; see Barber et al., this volume, Chapter 9).

VI. Ferredoxin and Flavodoxin Mutants

A. Ferredoxin Mutants

The Fd mutations giving the most significant effects on the affinity for PS I are summarized in Table 4 ($K_{d(mutant)}/K_{d(WT)} > 2$). With one exception (Navarro et al., 1995), they were all obtained with Fd from *Synechocystis* sp. PCC 6803 (Poncelet et al., 1998; Guillouard et al., 2000). As mentioned above, K_d was measured from the amount of functional complex taken from the size of the first-order ET components corresponding to intracomplex ET. In the single case of the mutation E95K of *Anabaena* sp. PCC 7120 Fd, fast first-order ET was not observed and the K_d was obtained from an analysis of the dependence of Fd reduction upon Fd concentration (Navarro et al., 1995). The side chains of the residues mentioned in Table 4 are indicated in Fig. 2 showing the X-ray Fd structure

Table 4. Kinetic parameters of Fd reduction for strongly affected ferredoxin mutants ($K_{d(mutant)}/K_{d(WT)} > 2$)

Mutation	Organism	Corresponding residue in Fd of *Spirulina platensis*	$K_{d(mutant)}/K_{d(WT)}$	References
D57K/D60K	*Synechocystis* sp. PCC6803	D59/D62	18	Guillouard et al. (2000)
D57R/D60R	*Synechocystis* sp. PCC6803	D59/D62	15	Guillouard et al. (2000)
D60K	*Synechocystis* sp. PCC6803	D62	6	Guillouard et al. (2000)
D60R	*Synechocystis* sp. PCC6803	D62	3.5	Guillouard et al. (2000)
D57K	*Synechocystis* sp. PCC6803	D59	4.5	Guillouard et al. (2000)
D57R	*Synechocystis* sp. PCC6803	D59	4.2	Guillouard et al. (2000)
D57A	*Synechocystis* sp. PCC6803	D59	2.5	Guillouard et al. (2000)
D57A	*Synechocystis* sp. PCC6803	D59	2.5	Guillouard et al. (2000)
E93A	*Synechocystis* sp. PCC6803	E95	2.0	Poncelet et al. (1998)
E95K	*Anabaena* sp. PCC 7120	E95	2.5	Navarro et al. (1995)[a]

[a] No fast first-order component of ferredoxin reduction was observed. The K_d was deduced from the dependence of the observed rate on the ferredoxin concentration.

from *Spirulina platensis* (Fukuyama et al., 1995), the sequence of which is very similar to that of *Synechocystis* sp. PCC 6803. Residue E95 (numbering of *S. platensis*) was found to be covalently bound to K104 of PsaD (numbering of *T. elongatus*) in a covalent functional PS I/Fd complex (Lelong et al., 1994). Some other Fd mutants have been studied with no significant change in the affinity (Navarro et al., 1995; Poncelet et al., 1998; Guillouard et al., 2000).

The Fd structure shown in Fig. 2 was rotated in such a way that, in the rear view, the side chain of E95 lies close to the side chain of K104 of PsaD with the reducible iron of Fd located approximately above the F_B cluster. The contour of Fd in this position is shown superimposed on the PS I structure. The front view of Fd is also shown after a rotation of 180° around the vertical axis. The ferredoxin position shown here is only illustrative and should be taken with much caution: First, much work is further needed to identify more precisely the docking site(s); second there may be a multitude of PS I/Fd complexes allowing efficient ET so that a static picture may be misleading.

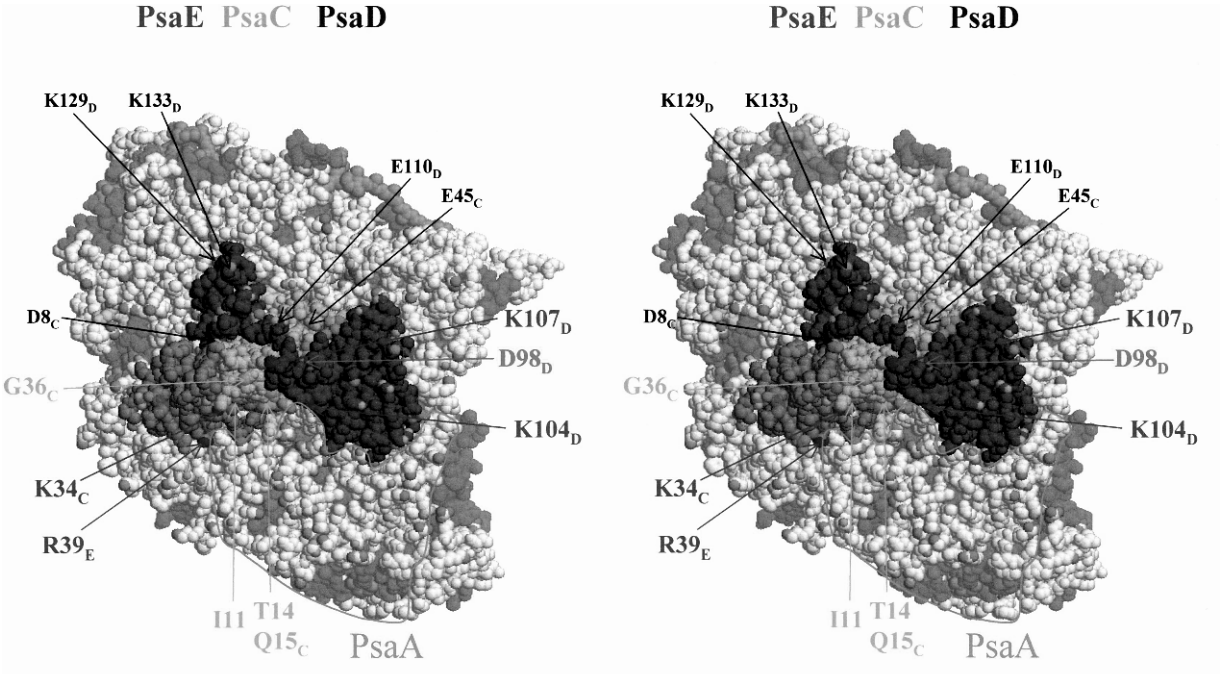

Fig. 3. Stereo top view of photosystem I. This stereo view (crossed eyes) shows PS I from the stromal side perpendicularly to the membrane plane. See Color Plate 11, Fig. 1.

Table 5. Kinetic parameters of flavodoxin reduction for strongly affected photosystem I and flavodoxin mutants (any parameter, K_d, k_{ET}, or k_2 with $value_{(mutant)}/value_{(WT)} < 0.5$ or >2)

		Reduction of oxidized flavodoxin				Reduction of semireduced flavodoxin		
PS I: organism/ mutation	Flavodoxin: organism/mutation	$k_{ET(mutant)}/k_{ET(WT)}$	$K_{d(mutant)}/K_{d(WT)}$	$k_{on(mutant)}/k_{on(WT)}$	E_m (pH 7.0) mV	First-order component: $K_{d(mutant)}/K_{d(WT)}$	Second-order component: $k_{on(mutant)}/k_{on(WT)}$	References
Synechocystis 6803/PsaE minus	*Synechocystis* sp. PCC 6803/WT	1.8	nd[a]	nd	−238	>25	0.68	Meimberg et al. (1998)
Chlam. reinh. PsaC: K35E	*Synechocystis* sp. PCC 6803/WT	0.40	nd	nd	−238	nd	0.05	Meimberg et al. (1999)
Spinach/WT	*Anabaena* sp. PCC 7120/D100N	0.86	2.9	1.9	nd	nd	nd	Navarro et al. (1995)
Spinach/WT	7120/W57L	0.62	2.3	1.3	−212[b] (-212 for WT)	nd	nd	Navarro et al. (1995)
Spinach/WT	7120/E61Q	0.89	0.45	0.37	nd	nd	nd	Navarro et al. (1995)
Anabaena sp. PCC 7119/WT	*Anabaena* sp. PCC 7119/Y94A	11	0.86	nd	−203(−212 for WT)	nd	nd	Casaus et al. (2002)
7119/WT	7119/Y94F	0.27	0.75	nd	−186	nd	nd	Casaus et al. (2002)
7119/WT	7119/Y94W	<0.2	nd	nd	−182	nd	nd	Casaus et al. (2002)
7119/WT	7119/W57F	6	2.0	nd	−152	nd	nd	Casaus et al. (2002)
7119/WT	7119/W57L	1.9	6	nd	−212	nd	nd	Casaus et al. (2002)
7119/WT	7119/W57A	3.0	1.0	nd	−173	nd	nd	Casaus et al. (2002)
7119/WT	7119/W57Y	0.2	1.5	nd	−139	nd	nd	Casaus et al. (2002)
7119/WT	7119/I59K	3.8	2.2	nd	−223	nd	nd	Nogues et al. (2003)
7119/WT	7119/I92K	nd	nd	nd[c]	−190	nd	nd	Nogues et al. (2003)

[a] nd: not determined.

[b] Identical to the E_m values determined for *Anabaena* sp. PCC 7119 Fld (Casaus et al., 2002) as the amino acid sequence is identical.

[c] The k_{on} parameter was not determined in the case of the wild type. A value of 1.6×10^7 $M^{-1}sec^{-1}$ was measured for the I92K mutant from a linear dependence of k_{on} versus [Fld]. This linear dependence impeded the determination of k_{ET} and K_d (no saturation pattern). One can note that this linear dependence was not observed in any other case of reduction of oxidized flavodoxin (see text for discussion).

B. Flavodoxin Mutants

Table 5 summarizes the kinetic parameters obtained for reduction of mutated Flds, when significant modifications were observed. Flds were from *Anabaena* sp. PCC 7119 or 7120 (identical sequences) and only reduction of oxidized Fld was reported in all cases (Navarro et al., 1995; Casaus et al., 2002; Nogues et al., 2003). These studies allowed to emphasize the importance of two aromatic residues, W57 and Y94, which sandwich the flavin ring (Casaus et al., 2002), and of two acidic residues, E61 and D100, located near the solvent-exposed edge of the flavin (Navarro et al., 1995). Replacement of leucines by lysines at positions 59 and 92 also leads to modification in reduction of oxidized Fld (Nogues et al., 2003). In the latter study, the most striking modification was obtained with mutant I92K, which exhibited a linear dependence of the observed rate with the Fld concentration. This behavior is unique as it has never been observed in any other study of reduction of oxidized Fld. This was interpreted as due to a modification of the reduction mechanism with no formation of a stable transient complex. It is also interesting to note that the observed rates, and therefore the k_{ET} rates (corresponding to the asymptotic value of the rates at saturating Fld concentration) observed in several mutants, are larger than in the wild type. This effect seems not related to a change in the Fld redox potentials which are not considerably modified by the mutations (Table 5). In the case of the aromatic residues W57 and Y94, it was interpreted as due to a modification in the accessibility of the flavin ring. More generally, a conformational change in the PS I/Fld complex leading to a smaller edge-to-edge distance between F_B and oxidized FMN could explain these effects. A structural alignment of Fd and Fld was performed on the basis of the electrostatic potentials, from which two different alignments were proposed (Ullmann et al., 2000). Taking Fd orientation as given in Fig. 2 as a reference (front view), and the structure of Fld from *Anabaena* sp. PCC 7120 (Burkhart et al., 1995), these two alignments were used to display in the bottom part of Fig. 2 the approximate positions of Fld while showing the side chains of the substituted residues mentioned in Table 5.

References

Barth P, Lagoutte B and Sétif P (1998) Ferredoxin reduction by photosystem I from *Synechocystis* sp. PCC 6803: toward an understanding of the respective roles of subunits PsaD and PsaE in ferredoxin binding. Biochemistry 37: 16233–16241.

Barth P, Guillouard I, Sétif P and Lagoutte B (2000) Essential role of a single arginine of photosystem I in stabilizing the electron transfer complex with ferredoxin. J Biol Chem 275: 7030–7036.

Ben Shem A, Frolow F and Nelson N (2003) Crystal structure of plant photosystem I. Nature 426: 630–635.

Bottin H and Lagoutte B (1992) Ferredoxin and flavodoxin from the cyanobacterium *Synechocystis* sp. PCC 6803. Biochim Biophys Acta 1101: 48–56.

Bottin H, Hanley J and Lagoutte B (2001) Role of acidic amino acid residues of PsaD subunit on limiting the affinity of photosystem I for ferredoxin. Biochem Biophys Res Commun 287: 833–836.

Brettel K (1997) Electron transfer and arrangement of the redox cofactors in photosystem I. Biochim Biophys Acta 1318: 322–373.

Brettel K and Leibl W (2001) Electron transfer in photosystem I. Biochim Biophys Acta 1507: 100–114.

Burkhart BM, Ramakrishnan B, Yan H, Reedstrom RJ, Markley JL, Straus NA and Sundaralingam M (1995) Structure of the trigonal form of recombinant oxidized flavodoxin from *Anabaena* 7120 at 1.40 Å resolution. Acta Crystallogr D 51: 318–330.

Casaus JL, Navarro JA, Hervas M, Lostao A, De la Rosa MA, Gomez-Moreno C, Sancho J and Medina A (2002) *Anabaena* sp PCC 7119 flavodoxin as electron carrier from photosystem I to Ferredoxin-$NADP^+$ reductase – role of TRP^{57} and TYR^{94}. J Biol Chem 277: 22338–22344.

Drennan CL, Pattridge KA, Weber CH, Metzger AL, Hoover DM and Ludwig ML (1999) Refined structures of oxidized flavodoxin from *Anacystis nidulans*. J Mol Biol 294: 711–724.

Dunn PPJ, Packman LC, Pappin D and Gray JC (1988) N-terminal amino acid sequence analysis of the subunits of pea photosystem I. FEBS Lett 228: 157–161.

Fischer N, Sétif P and Rochaix J-D (1997) Targeted mutations in the *psaC* gene of *Chlamydomonas reinhardtii*: preferential reduction of F_B at low temperature is not accompanied by altered electron flow from photosystem I to ferredoxin. Biochemistry 36: 93–102.

Fischer N, Hippler M, Sétif P, Jacquot J-P and Rochaix J-D (1998) The PsaC subunit of photosystem I provides an essential lysine residue for fast electron transfer to ferredoxin. EMBO J 17: 849–858.

Fischer N, Sétif P and Rochaix J-D (1999) Site-directed mutagenesis of the PsaC subunit of photosystem I – F_B is the cluster interacting with soluble ferredoxin. J Biol Chem 274: 23333–23340.

Fromme P, Schubert WD and Krauß N (1994) Structure of photosystem I: suggestions on the docking sites for plastocyanin and ferredoxin, and the coordination of P700. Biochim Biophys Acta 1187: 99–105.

Fromme P, Bottin H, Krauss N and Sétif P (2002) Crystallization and electron paramagnetic resonance characterization of the complex of photosystem I with its natural electron acceptor ferredoxin. Biophys J 83: 1760–1773.

Fukuyama K, Ueki N, Nakamura H, Tsukihara T and Matsubara H (1995) Tertiary structure of [2Fe–2S] ferredoxin from *Spirulina platensis* refined at 2.5 Å resolution: structural comparisons of plant-type ferredoxins and an electrostatic potential analysis. J Biochem (Tokyo) 117: 1017–1023.

Garcia-Sanchez MI, Diaz-Quintana A, Gotor C, Jacquot JP, De la Rosa MA and Vega JM (2000) Homology predicted structure

and functional interaction of ferredoxin from the eukaryotic alga *Chlamydomonas reinhardtii* with nitrite reductase and glutamate synthase. J Biol Inorg Chem 5: 713–719.

Guillouard I, Lagoutte B, Moal G and Bottin H (2000) Importance of the region including aspartates 57 and 60 of ferredoxin on the electron transfer complex with photosystem I in the cyanobacterium *Synechocystis* sp. PCC 6803. Biochem Biophys Res Commun 271: 647–653.

Hanley J, Sétif P, Bottin H and Lagoutte B (1996) Mutagenesis of photosystem I in the region of the ferredoxin crosslinking site: modifications of positively charged amino acids. Biochemistry 35: 8563–8571.

Hervas M, Navarro JA and Tollin G (1992) A laser flash spectroscopy study of the kinetics of electron transfer from spinach photosystem I to spinach and algal ferredoxins. Photochem Photobiol 56: 319–324.

Hope AB (2000) Electron transfers amongst cytochrome f, plastocyanin and photosystem I: kinetics and mechanisms. Biochim Biophys Acta 1456: 5–26.

Jordan R, Nessau U and Schlodder E (1998) Charge recombination between the reduced iron–sulphur clusters and $P700^+$. In: Garab G (ed) Photosynthesis: Mechanisms and Effects, pp 663–666. Kluwer Academic Publishers, Dordrecht.

Jordan P, Fromme P, Witt HT, Klukas O, Saenger W and Krauß N (2001) Three-dimensional structure of cyanobacterial photosystem I at 2.5 Å resolution. Nature 411: 909–917.

Knaff DB (1996) Ferredoxin and ferredoxin-dependent enzymes. In: Ort DR and Yocum C (eds) Oxygenic Photosynthesis: The Light Reactions, pp 333–361. Kluwer Academic Publishers, The Netherlands.

Lagoutte B, Hanley J and Bottin H (2001) Multiple functions for the C terminus of the PsaD subunit in the cyanobacterial photosystem I complex. Plant Physiol 126: 307–316.

Lelong C, Sétif P, Lagoutte B and Bottin H (1994) Identification of the amino acids involved in the functional interaction between photosystem I and ferredoxin from *Synechocystis* sp. PCC 6803 by chemical crosslinking. J Biol Chem 269: 10034–10039.

Lelong C, Boekema EJ, Kruip J, Bottin H, Rögner M and Sétif P (1996) Characterization of a redox active crosslinked complex between cyanobacterial photosystem I and soluble ferredoxin. EMBO J 15: 2160–2168.

Medina M, Hervas M, Navarro JA, De la Rosa MA, Gomez-Moreno C and Tollin G (1992) A laser flash absorption spectroscopy study of *Anabaena* sp. PCC 7119 flavodoxin photoreduction by photosystem I particles from spinach. FEBS Lett 313: 239–242.

Meimberg K, Lagoutte B, Bottin H and Mühlenhoff U (1998) The PsaE subunit is required for complex formation between photosystem I and flavodoxin from the cyanobacterium *Synechocystis* sp. PCC 6803. Biochemistry 37: 9759–9767.

Meimberg K, Fischer N, Rochaix JD and Mühlenhoff U (1999) Lys35 of PsaC is required for the efficient photoreduction of flavodoxin by photosystem I from *Chlamydomonas reinhardtii*. Eur J Biochem 263: 137–144.

Meyer TE, Zhao ZG, Cusanovich MA and Tollin G (1993) Transient kinetics of electron transfer from a variety of *c*-type cytochromes to plastocyanin. Biochemistry 32: 4552–4559.

Morales R, Charon MH, Hudry-Clergeon G, Pétillot Y, Norager S, Medina M and Frey M (1999) Refined X-ray structures of the oxidized, at 1.3 Å, and reduced, at 1.17 Å, [2Fe–2S] ferredoxin from the cyanobacterium *Anabaena* PCC7119 show redox-linked conformational changes. Biochemistry 38: 15764–15773.

Morales R, Frey M and Mouesca JM (2002) An approach based on quantum chemistry calculations and structural analysis of a [2Fe–2S] ferredoxin that reveal a redox-linked switch in the electron-transfer process to the Fd-$NADP^+$ reductase. J Am Chem Soc 124: 6714–6722.

Mühlenhoff U and Sétif P (1996) Laser flash absorption spectroscopy study of flavodoxin reduction by photosystem I in *Synechococcus* sp. PCC 7002. Biochemistry 35: 1367–1374.

Mühlenhoff U, Kruip J, Bryant DA, Rögner M, Sétif P and Boekema E (1996) Characterization of a redox-active crosslinked complex between cyanobacterial photosystem I and its physiological acceptor flavodoxin. EMBO J 15: 488–497.

Navarro JA, Hervas M, Genzor CG, Cheddar G, Fillat MF, De la Rosa MA, Gomez-Moreno C, Cheng H and Xia B (1995) Site-specific mutagenesis demonstrates that the structural requirements for efficient electron transfer in *Anabaena* ferredoxin and flavodoxin are highly dependent on the reaction partner: kinetic studies with photosystem I, ferredoxin:$NADP^+$ reductase, and cytochrome *c*. Arch Biochem Biophys 321: 229–238.

Nield J, Morris EP, Bibby TS and Barber J (2003) Structural analysis of the photosystem I supercomplex of cyanobacteria induced by iron deficiency. Biochemistry 42: 3180–3188.

Nogues I, Martinez-Julvez M, Navarro JA, Hervas M, Armenteros L, De la Rosa MA, Brodie TB, Hurley JK, Tollin G, Gomez-Moreno C and Medina M (2003) Role of hydrophobic interactions in the flavodoxin mediated electron transfer from photosystem I to ferredoxin-$NADP^+$ reductase in *Anabaena* PCC 7119. Biochemistry 42: 2036–2045.

Norris JR, Crespi HL and Katz JJ (1972) Characterization of a new photo-ESR signal associated with photosynthesis. Biochem Biophys Res Commun 49: 139–146.

Page CC, Moser CC, Chen XX and Dutton PL (1999) Natural engineering principles of electron tunnelling in biological oxidation-reduction. Nature 402: 47–52.

Pizzitutti F, Sétif P and Marchi M (2003) Theoretical Investigation of the "CO in"–"CO out" isomerization in a [2Fe–2S] ferredoxin: free energy profiles and redox states. J Am Chem Soc 125: 15224–15232.

Poncelet M, Cassier-Chauvat C, Leschelle X, Bottin H and Chauvat F (1998) Targeted deletion and mutational analysis of the essential (2Fe–2S) plant-like ferredoxin in *Synechocystis* PCC 6803 by plasmid shuffling. Mol Microbiol 28: 813–821.

Pueyo JJ, Revilla C, Mayhew SG and Gomez-Moreno C (1992) Complex formation between ferredoxin and ferredoxin-$NADP^+$ reductase from *Anabaena* PCC 7119: cross-linking studies. Arch Biochem Biophys 294: 367–372.

Rogers LJ (1987) Ferredoxins, flavodoxins and related proteins: structure, function and evolution. In: Fay P and Van Baalen C (eds) The Cyanobacteria, pp 35–67. Elsevier, Amsterdam.

Romero A, Caldeira J, LeGall J, Moura I, Moura JJ and Romao MJ (1996) Crystal structure of flavodoxin from *Desulfovibrio desulfuricans* ATCC 27774 in two oxidation states. Eur J Biochem 239: 190–196.

Ruffle SV, Mustafa AO, Kitmitto A, Holzenburg A and Ford RC (2000) The location of the mobile electron carrier ferredoxin in vascular plant photosystem I. J Biol Chem 275: 36250–36255.

Semenov AY, Mamedov MD and Chamorovsky SK (2003) Photoelectric studies of the transmembrane charge transfer reactions in photosystem I pigment-protein complexes. FEBS Lett 553: 223–228.

Sétif P (2001) Ferredoxin and flavodoxin reduction by photosystem I. Biochim Biophys Acta 1507: 161–179.

Sétif P and Bottin H (1994) Laser flash absorption spectroscopy study of ferredoxin reduction by photosystem I in *Synechocystis* sp. PCC 6803: evidence for submicrosecond and microsecond kinetics. Biochemistry 33: 8495–8504.

Sétif P and Bottin H (1995) Laser flash absorption spectroscopy study of ferredoxin reduction by photosystem I: spectral and kinetic evidence for the existence of several photosystem I-ferredoxin complexes. Biochemistry 34: 9059–9070.

Sétif P, Fischer N, Lagoutte B, Bottin H and Rochaix JD (2002) The ferredoxin docking site of photosystem I. Biochim Biophys Acta 1555: 204–209.

Smith WW, Burnett RM, Darling GD and Ludwig ML (1977) Structure of the semiquinone form of flavodoxin from *Clostridium* MP. Extension of 1.8 Å resolution and some comparisons with the oxidized state. J Mol Biol 117: 195–225.

Straus NA (1994) Iron deprivation: physiology and gene regulation. In: Bryant DA (ed) The Molecular Biology of Cyanobacteria, pp 731–750. Kluwer Academic Publishers, Dordrecht.

Sykes GA and Rogers LJ (1984) Redox potentials of algal and cyanobacterial flavodoxins. Biochem J 217: 845–850.

Tollin G, Meyer TE and Cusanovich MA (1986) Elucidation of the factors which determine reaction-rate constants and biological specificity for electron-transfer proteins. Biochim Biophys Acta 853: 29–41.

Ullmann GM, Hauswald M, Jensen A and Knapp EW (2000) Structural alignment of ferredoxin and flavodoxin based on electrostatic potentials: implications for their interactions with photosystem I and ferredoxin-NADP reductase. Proteins: Struct, Funct, Genet 38: 301–309.

Watt W, Tulinsky A, Swenson RP and Watenpaugh KD (1991) Comparison of the crystal structures of a flavodoxin in its three oxidation states at cryogenic temperatures. J Mol Biol 218: 195–208.

Chapter 27

Electron Transfer From Ferredoxin and Flavodoxin to Ferredoxin:NADP$^+$ Reductase

John K. Hurley and Gordon Tollin*
Department of Biochemistry and Molecular Biophysics, University of Arizona, Tucson, AZ 85721, USA

Milagros Medina and Carlos Gómez-Moreno
Departmento de Bioquímica y Biología Molecular y Celular, Universidad de Zaragoza, 50009 Zaragoza, Spain

*Author for correspondence, email: gtollin@u.arizona.edu

John H. Golbeck (ed): Photosystem I: The Light-Driven Plastocyanin:Ferredoxin Oxidoreductase, 455–476.

Summary

An overview is presented of structure/function relationships in the interactions between the small electron transfer proteins ferredoxin (Fd) and flavodoxin (Fld) and the flavoprotein enzyme ferredoxin:$NADP^+$ reductase (FNR), primarily emphasizing the proteins from the cyanobacterium, *Anabaena*, and the higher plant, spinach. Results are summarized from experiments utilizing rapid-reaction kinetic methods (stopped-flow spectrophotometry and laser flash photolysis) involving wild-type and site-specific mutants of these proteins, redox potential determinations, and X-ray crystallography, including the crystal structure of a Fd/FNR complex. These have provided detailed insights into the protein–protein recognition and electron transfer mechanisms utilized by these systems. Fd and Fld bind to FNR within a concave region of the FNR surface that contains the exposed dimethylbenzene ring of the FAD cofactor. In the Fd case, electron transfer between the iron–sulfur and flavin centers proceeds with a maximum rate constant of 5,500 sec^{-1} via a direct outer-sphere mechanism. Both electrostatic and hydrophobic interactions occur between the proteins, resulting in a precise surface complementarity.

I. Introduction

The primary function of Photosystem I (PSI) in oxygenic photosynthetic organisms (plants, algae, and cyanobacteria) is to reduce $NADP^+$ to NADPH for use in the reductive pentose phosphate cycle (Calvin cycle). This occurs via reduction of the soluble [2Fe–2S] protein Fd (Shin et al., 1963). Fd_{red} interacts (in two one-electron steps) with FNR, an FAD-containing flavoprotein, which reduces $NADP^+$ to NADPH according to Eq. (1):

$$2Fd_{red} + NADP^+ + H^+ \rightarrow 2Fd_{ox} + NADPH \quad (1)$$

It is the interaction between FNR_{ox} and Fd_{red} (Eq. 2) that is the primary subject of this chapter.

$$Fd_{red} + FNR_{ox} \overset{K_d}{\leftrightarrow} [Fd_{red} \text{---} FNR_{ox}] \overset{k_{et}}{\rightarrow} Fd_{ox} + FNR_{red} \quad (2)$$

We will mainly consider structure–function studies of the proteins from the cyanobacterium *Anabaena variabilis* and from spinach, as these are the most thoroughly investigated systems. In Eq. (2), K_d corresponds to the dissociation constant of the intermediate ET complex and k_{et} is the ET rate constant. Note that k_{et} can include protein structural rearrangements and changes in hydration of the proteins occurring upon redox state changes and complex formation, as well as the actual ET step. In most cyanobacteria and some algae Fld (an FMN flavoprotein) can substitute for Fd under low iron conditions (Smillie, 1965; Rogers, 1987). We will also review the interaction of *Anabaena* Fld with *Anabaena* FNR.

The X-ray crystal structure of a complex between Fd_{ox}:FNR_{ox} from *Anabaena* PCC 7119 has been solved at 2.4 Å resolution (Fig. 1; the interfacial region of this complex is shown in Fig. 2; Morales et al., 2000) and will be discussed. The structure of a complex of the proteins from maize leaf has also been reported (Kurisu et al., 2001) and will be compared with the structure of the *Anabaena* complex. Some of this material has been presented in previous reviews (Holden et al., 1994; Knaff, 1996; Hurley et al., 2002; Carrillo and Ceccarelli, 2003).

II. Ferredoxin Structure and Properties

Fds comprise a class of low molecular weight (6–14 kDa) highly acidic ET proteins found ubiquitously in nature (Johnson, 1994; Knaff, 1996; Beinert et al., 1997; Sticht and Rösch, 1998; Beinert and Kiley, 1999). Aside from photosynthetic ET, they also participate in nitrate reduction and in carbon and sulfur metabolism (Lovenberg, 1973, 1974, 1977; Knaff, 1996). In heterocyst cells of N_2-fixing cyanobacteria, an isoform of veg Fd, known as het Fd, donates electrons to nitrogenase (Böhme and Schrautemeier, 1987; Böhme and Haselkorn, 1988). Het AnFd has 51% sequence identity to the vegetative form and its three-dimensional structure has also been determined (Jacobson et al., 1993). The α-carbon backbone of the

Abbreviations: AnFd – *Anabaena* 7120 ferredoxin; AnFld – *Anabaena* 7119 flavodoxin; AnFNR – *Anabaena* 7119 ferredoxin: $NADP^+$ reductase; ET – electron transfer; Fd – ferredoxin; Fd_{ox} – oxidized Fd; Fd_{red} – reduced Fd; FNR – ferredoxin: $NADP^+$ reductase; FNR_{ox} – oxidized FNR; FNR_{red}, FNR_{hq} – fully reduced, hydroquinone FNR; FNR_{sq} – semiquinone FNR; het – heterocyst; LFP/TRA – laser flash photolysis/time resolved absorbance; μ – ionic strength; PSI – Photosystem I; RMSD – root-mean-square deviation; spFd – spinach ferredoxin; spFNR – spinach FNR; veg – vegetative; wt – wild-type.

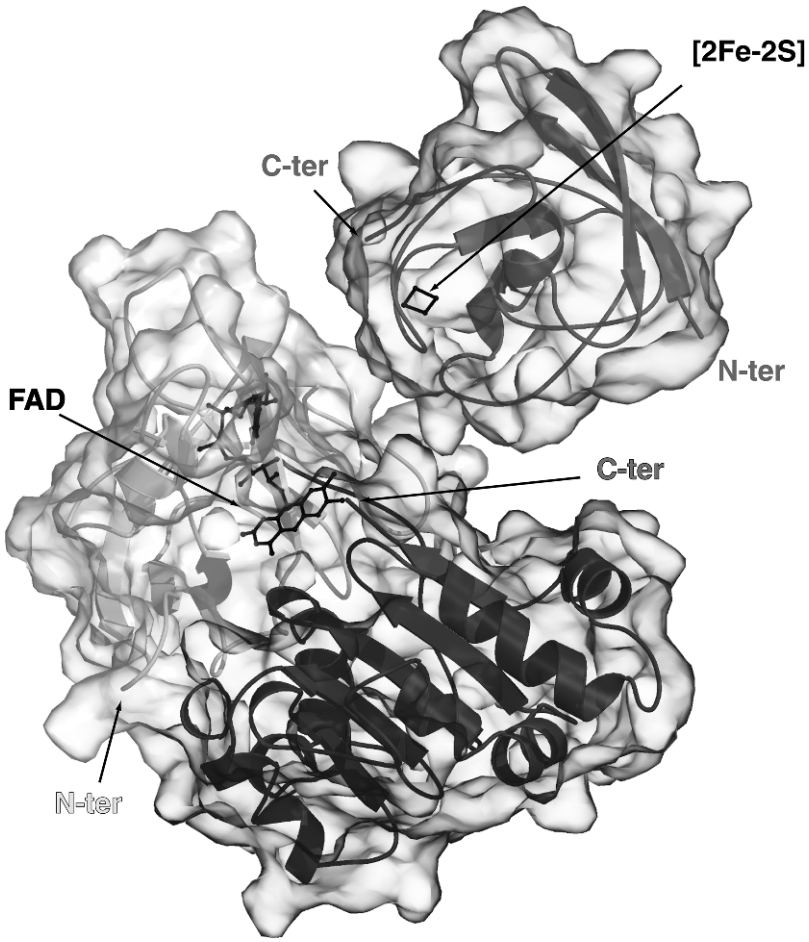

Fig. 1. Structure of the *Anabaena* Fd/FNR complex with the Fd molecule (uppermost protein) moved away from the FNR molecule to which it binds. This figure was kindly provided by Dr. Renaud Morales.

het AnFd superimposes with that of the veg AnFd with a root-mean-square deviation (RMSD) of 1.0 Å, although there are some interesting substitutions of otherwise highly conserved residues at positions Arg42 (His42), Glu95 (Pro95), and Tyr98 (Ala98). The only significant differences in the polypeptide backbone are in the loop delineated by Ile9 and Thr24 and the three C-terminal amino acids. Excluding these regions the backbones superimpose with a RMSD of 0.45 Å. Also, three other residues (Ser43, Leu76, and Leu78) that are conserved in nonhalophilic Fds (Matsubara and Hase, 1983) are not retained in het AnFd. Despite these differences, het AnFd can transfer electrons to AnFNR with essentially the same efficiency as wt veg AnFd (Hurley et al., 1993a). Fd also functions in cyclic photophosphorylation, transferring electrons from PSI to cytochrome b_6f (and not to FNR), either directly or indirectly, yielding ATP as the only product (Malkin, 1996).

The so-called "plant-type" Fds contain a single [2Fe–2S] cluster (the redox site) in an 11 kDa peptide chain having 93–99 amino acids and they are all homologous, particularly around the [2Fe–2S] cluster, indicating that they have been highly conserved over 1.5 billion years (Matsubara and Saeki, 1992). The reduction potentials of these Fds range from −305 to −455 mV (Cammack et al., 1977). The value for spinach Fd (spFd) was reported to be −420 mV (Tagawa and Arnon, 1962, 1968), placing this protein amongst the most highly reducing in nature. The reduction potential of the veg AnFd has been determined to be −384 mV (Hurley et al., 1997a). Each iron atom in the cluster is approximately tetrahedrally coordinated by four sulfur atoms, by two inorganic sulfides bridging the two irons, and by two cysteinyl sulfurs contributed by the protein. It has been shown by NMR that the backbone amide of Arg42 hydrogen bonds to one of the sulfides in both the oxidized and reduced forms of

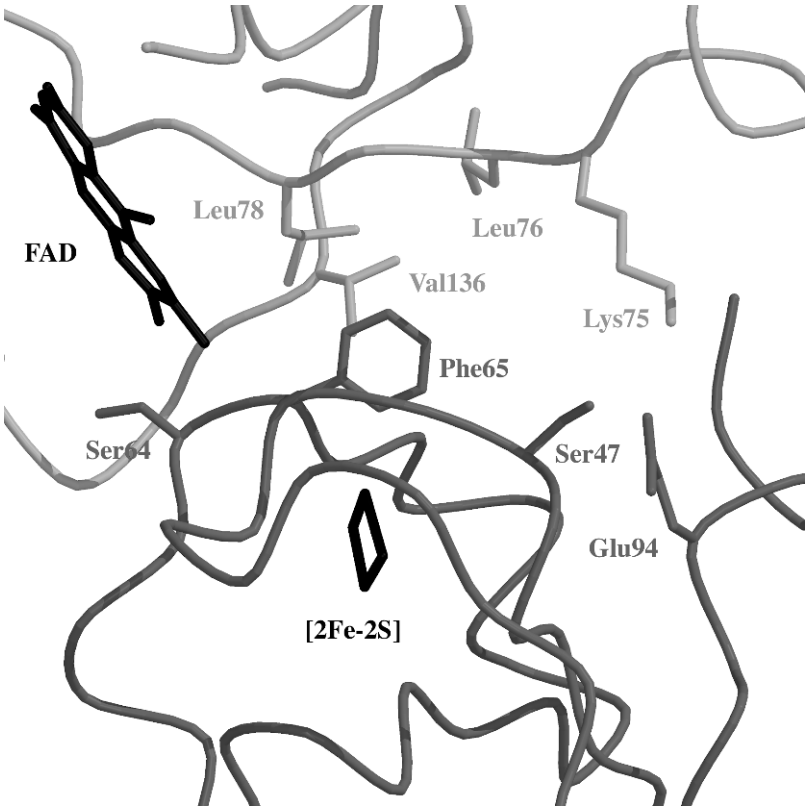

Fig. 2. Close-up view of the protein–protein interface of the *Anabaena* Fd/FNR complex in the region of the redox cofactors. Several of the residues important for ET between the two proteins are labeled. Fd is depicted in the darker shade of gray and FNR in the lighter shade. This figure was kindly provided by Dr. Renaud Morales.

veg AnFd (Cheng et al., 1995). The [2Fe–2S] cluster in all known structures of plant-type Fds lies quite close to the surface of the protein. In veg AnFd, the cluster is bound in a structurally conserved loop that extends as much as 9 Å from the main body of the protein (Holden et al., 1994). This cluster-binding loop, which also contains an evolutionarily conserved hydrogen-bonding pattern, undoubtedly helps to maintain the overall three-dimensional integrity of the protein by tethering to the short C-terminal α-helix (Holden et al., 1994).

In Fd_{ox}, the [2Fe–2S] cluster consists of two nonequivalent antiferromagnetically coupled, high-spin (S = 5/2) ferric ions, producing a diamagnetic spin state (S = 0). Upon one-electron reduction, the cluster contains one high-spin ferrous ion (S = 2) antiferromagnetically coupled to a high-spin ferric (S = 5/2) ion, giving the cluster a paramagnetic spin state of S = 1/2 (Palmer, 1973; Sands and Dunham, 1975; Fu et al., 1992; Johnson, 1994). In $spFd_{red}$ (Tsukihara et al., 1990) and veg $AnFd_{red}$ (Rypniewski et al., 1991; Skjeldal et al., 1991) it has been shown that it is the Fe atom closer to the molecular surface that is reduced (Dugard et al., 1990). The UV-vis spectrum of veg AnFd has peaks at 276, 330, 422, and 463 nm and the 422 nm extinction coefficient is 9.7 $mM^{-1}cm^{-1}$ (Böhme and Haselkorn, 1989).

Structures of a number of plant-type Fds have been solved by X-ray crystallography or NMR. The main chain foldings of all these ferredoxins are essentially the same (Fukuyama et al., 1995). A ribbon diagram of the veg An 7120 Fd (Rypniewski et al., 1991) is shown in Fig. 3A. The major secondary structural elements are three α-helices comprising residues 26–32, 68–73, and 94–98, and five β-strands comprising residues 1–9, 14–20, 50–55, 75–78, and 87–91. The structure of $AnFd_{red}$ (Morales et al., 1999) showed that the peptide bond linking C46 and S47 points its carbonyl oxygen away from the nearby cluster S2 atom in the reduced Fd and toward it in the oxidized protein. It was suggested that such a peptide "flip" occurring upon reduction could trigger the dissociation of the Fd_{ox}–FNR_{sq} complex.

Although the three-dimensional structure of wt spFd has yet to be determined, its E92K mutant has a

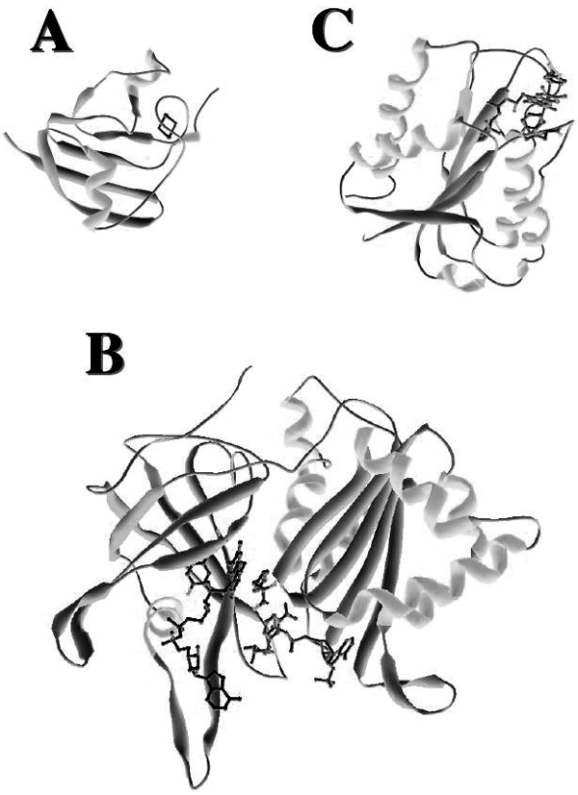

Fig. 3. Ribbon diagrams of (A) *Anabaena* 7120 vegetative Fd, (B) *Anabaena* 7119 vegetative FNR in a cocrystallized complex with NADP$^+$, and (C) *Anabaena* 7119 Fld. α-Helices are represented as coils and β-sheets as arrows. The [2Fe–2S] center in Fd, the FAD, and FMN groups in FNR and Fld, respectively, and the residues sandwiching the flavin rings in FNR and Fld, and the NADP$^+$ coenzyme of FNR are in ball and stick representation.

structure similar to the plant-type Fds (Binda et al., 1998). This mutation most likely has negligible effects on the main chain fold, inasmuch as the C^α backbone of the corresponding mutant in veg AnFd (E94K) superimposes with that of the wt veg AnFd with an RMSD of 0.40 Å (Hurley et al., 1997a). The E92K mutant in spFd does, however, show a slight change in the geometry of the [2Fe–2S] cluster as determined by EPR spectrometry (Aliverti et al., 1995a). This change also affects the redox potential of the mutant.

III. Ferredoxin:NADP$^+$ Reductase Structure and Properties

FNR has noncovalently bound FAD as a redox cofactor. Flavin cofactors commonly participate in ET reactions mainly because they have a very low redox potential (comparable to that of Fd) and also because they can transfer either one or two electrons. The transfer of one electron to the oxidized flavin group generates the semiquinone species, a form that is not stable when the cofactor is free in solution. However, it can be observed in the protein-bound cofactor, which demonstrates the influence of the polypeptide chain on the redox properties of the cofactor. The semiquinone can either be anionic or neutral, depending upon whether or not a proton transfer accompanies the ET. The addition of a second electron (usually coupled with a proton transfer) generates the fully reduced flavin. The versatility of the flavin cofactor provides flavoproteins with the ability to participate in many biological ET processes, such as those in which electrons have to be transferred between NADPH or NADH and iron–sulfur or heme metalloproteins. Protein/flavin interactions have also been shown to influence the redox potential of flavoproteins and to determine their reactivity. For example, flavoproteins have potentials ranging from below −400 mV, as in Flds (Pueyo et al., 1991), to positive values as for thiamine oxidase (Gómez-Moreno et al., 1979). For AnFNR, the two one-electron potentials are close to one another (approximately −300 mV; see below). The UV-visible spectrum of veg AnFNR has peaks at 274, 390, and 458 nm and the extinction coefficient at 458 nm is 9.4 $mM^{-1}cm^{-1}$ (Pueyo and Gómez-Moreno, 1991).

The first three-dimensional structure obtained for an FNR was for the protein from spinach. This showed two different domains, one of which binds FAD and the other NADP$^+$, each corresponding to approximately half of the polypeptide chain in the protein (Fig. 3; Karplus et al., 1991). The structure of AnFNR resembles that of spFNR, the main differences being an additional short α-helix that is present in AnFNR and also some residues involved in the interaction with NADP$^+$ that are different in both enzymes (Serre et al., 1996). The general fold found in FNR is also present in other sequence-related enzymes and has led to the proposal that this protein is the structural prototype of a family of enzymes, including cytochrome P450 reductases, cytochrome b_5 reductase, nitrate reductase, and sulfite reductase. However, other NAD(P)H-dependent enzymes very closely related functionally, such as adrenodoxin and putidaredoxin reductases, do not belong to this family.

The FAD-binding domain in AnFNR includes residues 1–138 and is made up of a scaffold of six antiparallel β-strands arranged in two perpendicular β-sheets having a short α-helix at the bottom and another helix and a long loop that is maintained by

a small two-stranded antiparallel β-sheet at the top. The $NADP^+$-binding domain includes residues 139–303 and consists of a core of five parallel β-strands surrounded by seven α-helices that is a variant of the Rossmann fold characteristic of dinucleotide-binding enzymes (Serre et al., 1996). The interaction of the AnFNR with its ET protein substrates takes place in the area where the FAD is located as well as in a large surface that belongs to the two domains of the protein (Martínez-Júlvez et al., 1999).

IV. Flavodoxin Structure and Properties

Flds are small flavoproteins that contain a noncovalently bound FMN cofactor as the redox center. They are mainly prokaryotic proteins with only a few exceptions, e.g., the green alga *Chlorella fusca* (Peleato et al., 1994) and two red algae, *Chondrus crispus* (Rogers, 1987), and *Porphyra umbilicalis* (Price et al., 1992). As in other flavoproteins, the FMN in AnFld can exist in three different oxidation states: oxidized, neutral semiquinone, and hydroquinone; the semiquinone form in Flds is exceptionally stable even in the presence of oxygen. The midpoint redox potentials of Fld are quite negative, as expected for proteins that can replace Fd. In the case of AnFld, the values are −212 mV for the oxidized/semiquinone reaction and −436 mV for the semiquinone/hydroquinone reaction (Pueyo et al., 1991). Fld replaces Fd in most of the reactions in which this protein participates by exchanging electrons between the semiquinone and the hydroquinone forms. It is now well established, and assumed to be true in other flavoproteins, that the redox potential of the different forms of Fld is a direct consequence of the different stability of the oxidized, semiquinone, and reduced apoflavodoxin–FMN complexes, i.e., the apoprotein binds the redox forms of FMN with different affinities and this modifies the redox potentials of the bound FMN (Swenson and Krey, 1994; Lostao et al., 1997). In most Flds the isoalloxazine ring of FMN is sandwiched between two aromatic residues located in loops at the C-terminus of the β-sheet (Fig. 3). In AnFld one of the residues is Tyr94 that makes extensive contacts with the isoalloxazine ring, while the other is Trp57 that interacts less tightly. It has been established that the interaction of those residues with the redox center of Fld determines the redox potential of FMN (Swenson and Krey, 1994; Lostao et al., 1997). The UV-visible spectrum of veg AnFld has peaks at 274, 390, and 464 nm and the extinction coefficient at 458 nm is 9.4 $mM^{-1}cm^{-1}$ (Pueyo and Gómez-Moreno, 1991).

The structures of several Flds in their oxidized states have been obtained by X-ray crystallography (Fukuyama et al., 1992; Rao et al., 1992; Ludwig et al., 1997; Walsh et al., 1998; Drennan et al., 1999; Freigang et al., 2002), while several others have been solved by NMR (van Mierlo et al., 1990; Knauf et al., 1993). They all show the same general folding pattern consisting of a five-stranded parallel β-sheet sandwiched by five α-helices. The FMN group is located at the edge of the globular protein exposing its two isoalloxazine methyl groups to the solvent (Fig. 3). Fld has a large excess of acidic residues (20 Asp, 11 Glu, 4 Arg, and 10 Lys in AnFld) distributed asymmetrically on the surface of the protein. This produces a dipole that influences the interaction with its protein partners. There are some areas on the surface of AnFld where there is a concentration of negative charges, e.g., amino acids 72–77, where 1 Glu and 3 Asp are present, and 144–146 where there are 2 Asp and 1 Glu.

V. The Catalytic Cycle

Using difference spectroscopy it was shown (Foust and Massey, 1967; Shin and San Pietro, 1968; Nelson and Neuman, 1968; Foust et al., 1969) that $spFNR_{ox}$ forms a 1:1 complex with $spFd_{ox}$ (see San Pietro, this volume, Chapter 1). Complex formation was influenced by ionic strength (μ) (Foust et al., 1969), consistent with electrostatic interactions. Complex formation has also been observed between FNR and $NADP^+$ (Shin and San Pietro, 1968). In addition, a ternary Fd-FNR-$NADP^+$ complex was reported (Batie and Kamin, 1984a). Thus, $NADP^+$ is able to occupy a site on FNR without displacing Fd, as was also suggested by cross-linking studies of the spinach proteins (Zanetti et al., 1984). During catalysis the order of addition of substrate is not important (Batie and Kamin, 1984a), although Fd lowers the affinity for $NADP^+$ and occupation of the $NADP^+$-binding site weakens the Fd:FNR complex. Thus, the two binding sites are not completely independent. Furthermore, spectral changes associated with the 1:1 Fd:FNR complex were the same whether or not $NADP^+$ was present, indicating that the Fd occupied the same site in the binary and ternary complexes, although interactions were weaker in the ternary complexes. Similar arguments made it unlikely that $NADP^+$ has more than one binding site.

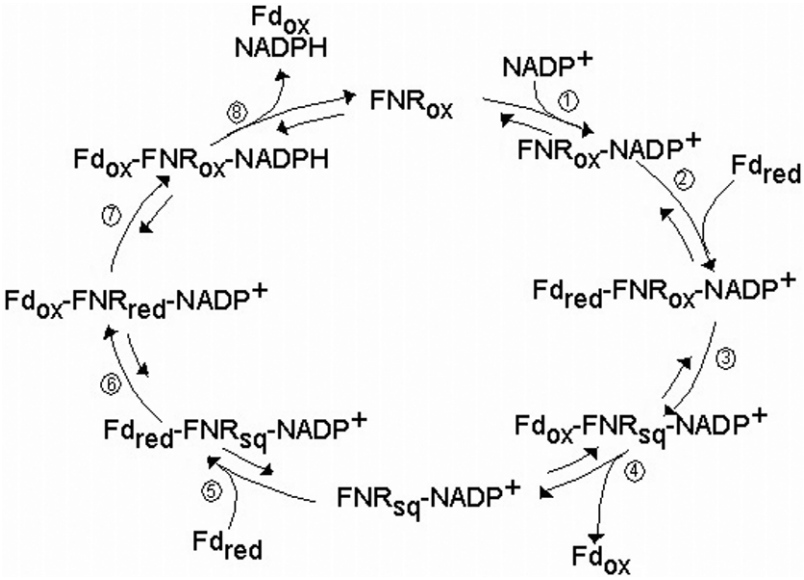

Fig. 4. The catalytic cycle for the two-electron reduction of spFNR by spFd. (Adapted from Batie and Kamin, 1984.)

Extensive rapid-reaction studies aimed at determining the catalytic mechanism have been carried out (Batie and Kamin, 1984b), and combined with the steady-state work of Masaki et al. (1982a,b) on the *Spirulina platensis* proteins, the mechanism shown in Fig. 4 was proposed. Ternary complex formation with NADP$^+$ was found to increase the rate of ET by facilitating dissociation of the product (Fd$_{ox}$). The rate-limiting step in the mechanism was not determined. Recent structural studies also confirm the existence of the ternary complex (Hermoso et al., 2002; Carrillo and Ceccarelli, 2003).

VI. Structure–Function Studies of Ferredoxin and Ferredoxin:NADP$^+$ Reductase

These studies have mainly utilized site-specific mutagenesis in order to elucidate the roles of specific amino acid side chains in the ET process. As will be shown in sections B and C below, redox potential shifts or large structural perturbations have been ruled out as the cause of impaired reactivity of Fd and FNR mutants. UV-vis and CD spectroscopy indicated no large structural changes for all mutants, which was confirmed in all those mutants whose X-ray structure has been determined (Hurley et al., 1997a,b; Mayoral et al., 2000; Martínez-Júlvez et al., 2001; Faro et al., 2002b).

A. The Effect of Mutations and Complexation on Redox Potentials

1. Reduction Potentials of WT Spinach Fd

The reduction potential for spFd was reported to be −432 mV (Tagawa and Arnon, 1962) and later −420 mV (Tagawa and Arnon, 1968). In the latter study, the redox potential of spFd was shown to be invariant over the pH range studied (pH 6.67–7.41). In later work, potential values −428 mV at pH 7.0 (Stombaugh et al., 1976), −415 mV at pH 8.0 (Cammack et al., 1977), −420 mV at pH 8.4 (Batie and Kamin, 1981), −401 mV (Aliverti et al., 1995a), and −405 mV over the pH range 6.0–10.5 (Verhagen et al., 1995) were reported. Differences in the above values can be mostly attributed to methodology differences and point to the difficulty of measuring such low potentials. Batie and Kamin (1981) showed that the reduction potential of Fd decreased by 90 mV upon complexation with FNR, while that of FNR increased by 20 mV, whereas Smith et al. (1981) reported that upon complex formation the potential of Fd decreased by 22 mV while that of FNR increased by 23 mV.

For spFNR the reduction potentials for the two individual one-electron steps ($E_{ox/sq}$ and $E_{sq/hq}$) were found to be −320 and −400 mV ($E_m = -360$ mV), respectively, at pH 7 (Keirns and Wang, 1972). Smith et al. (1981) reported an E_m value of −372 mV at pH 7.3 and Corrado et al. (1996) obtained an E_m value of −342

Table 1. Influence of complex formation on the reduction potentials of wt AnFNR and AnFd mutants[a]

	[2Fe–2S] of Fd (mV)	FAD of FNR (mV)		
Ferredoxin	$E_m^{\circ\prime}$	$E_1^{\circ\prime}$	$E_2^{\circ\prime}$	$E_m^{\circ\prime}$
None	–	−331	−314	−323
Fd alone	−384	–	–	–
Complexed	−372	−291	−300	−298
ΔE	+12	+40	+14	+25
F65I alone	−328	–	–	–
Complexed	−338	−277	−273	−274
ΔE	−10	+54	+41	+49
E94K alone	−304	–	–	–
Complexed	−298	−291	−286	−282
ΔE	+15	+40	+28	+41
S47A alone	−337	–	–	–
Complexed	−336	−269	−282	−273
ΔE	+1	+62	+32	+50

[a] Adapted from Hurley et al. (1997a); pH = 7.5, T = 4°C. For the complexed proteins, μ = 12 mM; for the uncomplexed proteins, μ= 100 mM. Uncertainty in the measurements is ±1–3 mV; values relative to the standard hydrogen electrode.

mV at pH 7. The latter workers calculated the two one-electron steps to have potentials of −350 and −335 mV, respectively. An E_m value of −442 mV at pH 8.4 was measured by Batie and Kamin (1981). The latter value seems to be inconsistent with the first three values listed above; the reason for this is unclear. However, it is clear that the two one-electron potentials are close together and that complexation makes ET thermodynamically more favorable.

2. Reduction Potentials of Mutant Spinach Fds

The reduction potentials (Piubelli et al., 1996) of the E92K, E92Q, and E92A (equivalent to E94 in AnFd) mutants of spFd at pH 7.4 were 93, 73, and 78 mV more positive than the wt spFd ($E_m = -401$ mV). These values are comparable in magnitude to the changes seen for the E94K and E94Q AnFd mutants (Table 1). They were not, however, measured in the Fd:FNR complex. These altered potentials were used to explain the reduced activity of these mutants (Piubelli et al., 1996).

3. Reduction Potentials of WT Anabaena Fd and FNR

The reduction potential for the wt veg AnFd was reported to be −440 mV (Hurley et al., 1993a) and −408mV (Pueyo et al., 1992). Two values, −406 and −439 mV, were also reported by Vidakovic et al. (1995), depending on the method used. For the *Anabaena variabilis* vegFd, which differs from the *Anabaena* 7120 protein by only one residue, a value of −433 mV was measured (Böhme and Schrautemeier, 1987). The *variabilis* Fd potential was also measured to be −355 mV by Cammack et al. (1977). The reason for the discrepancy is not known at present. The veg AnFd was again measured by Stankovich and coworkers (Hurley et al., 1997a) and determined to be −384 mV at pH 7.5 (Table 1). It was further shown that the potential of veg AnFd increased by 12 mV upon complexation with wt AnFNR.

The E_m value for *A. variabilis* FNR was −344 mV at pH 7 (Sancho et al., 1988) and that for AnFNR was −320 mV at pH 7 (Pueyo et al., 1991). From this value and using the estimated semiquinone formation constant, AnFNR $E_{ox/sq}$ and $E_{sq/hq}$ were calculated to be −370 and −270 mV, respectively. Recently, $E_{ox/rd} = -325$ mV has been reported for recombinant AnFNR, with the calculated redox potentials for the two individual ET processes $E_{ox/sq} = -338$ mV and $E_{sq/rd} = -312$ mV at pH 8.0 and 10°C (Martínez-Júlvez et al., 2001; Faro et al., 2002a). Despite the differences in buffer composition, temperature, or pH, the values are in good agreement with each other and also with those for enzymes from other species. Upon complexation, the AnFd potential became 15 mV more negative and that of AnFNR became 27–40 mV more positive (Hurley et al., 1997a). Thus, as was seen with the spinach protein, complexation makes ET between the wt *Anabaena* proteins thermodynamically more favorable. For all the structure–function studies discussed here, it is the $E_1^{\circ\prime}$ value that is of interest since in almost every case, the FNR cycled between the oxidized and semiquinone states.

4. Reduction Potentials of Mutant Anabaena Fds and FNRs

The $E^{\circ\prime}$ values for wt and AnFd mutants and $E_m^{\circ\prime}$ values for wt and AnFNR mutants from the studies of Hurley et al. (1997a), Martínez-Júlvez et al. (2001), and Faro et al. (2002a) are presented in Table 2 and the results for those proteins that were measured in the complex are given in Table 1. Comparing the $E_1^{\circ\prime}$ values for wt and mutant AnFNRs to the $E^{\circ\prime}$ value of wt AnFd shows that there are no thermodynamic barriers for ET from Fd to FNR for any of the AnFNR mutants (Table 1). Thus, K75E, L76E, L78D, L78F, and V136S had $E_{ox/rd}$ midpoint redox potentials about 20 mV more positive than that of the wt protein (Martínez-Júlvez et al., 2001; Faro et al., 2002a). Major changes were observed in the case of the E301A and L76S mutants,

Table 2. One-electron reduction potentials of wt and mutant AnFd and midpoint two-electron reduction potentials of wt and mutant AnFNR[a]

Ferredoxin	$E^{\circ\prime}$ (mv)	Ferredoxin	$E^{\circ\prime}$ (mv)	FNR	$E_m^{\circ\prime}$ (mv)
wtFd[b]	−384	F65I[b]	−328	wtFNR[c]	−323
R42H[d]	−382	F65Y[b]	−390	K75E[e]	−305
A43S[d]	−381	D68K[b]	−380	L76D[c]	−330
A45S[d,f]	−375	Q70K[b]	−382	L76F[c]	−333
C46S[g]	−381	T78A[d]	−345	L76S[c]	−305
S47A[b]	−337	T78I[d]	−337	L76D/L78D[c]	−317
S47T[b]	−438	T78S[d]	−378	L78D[c]	−302
T48A[d]	−382	E94D[b]	−367	L78F[c]	−307
T48S[d]	−401	E94K[b]	−304	L78S[c]	−286
C49S[g]	−329	E94Q[b]	−319	V136S[c]	−305
D62K[b]	−373	E95K[b]	−372	E139K[e]	−326
F65A[b]	−291			E301A[e]	−284

[a] Uncertainty in the measurements is ±1–3 mV; values relative to the standard hydrogen electrode.
[b] Hurley et al. (1997a); pH = 7.5, T = 4°C, μ = 100 mM.
[c] Martínez-Júlvez et al. (2001); 50 mM Tris/HCl buffer, pH = 8, T = 10°C.
[d] Weber-Main et al. (1998); 50 mM potassium phosphate buffer, pH = 7.5, T = 4°C.
[e] Faro et al. (2002a); 50 mM Tris/HCl buffer, pH = 8, T = 10°C.
[f] In agreement with Vidakovic et al. (1995).
[g] Hurley et al. (1997b). Conditions as in footnote b.

since their $E_{ox/rd}$ midpoint potential were 40 mV more positive than those of the WT. Moreover, in the case of the E301A a complete lack of stabilization of the semiquinone state was observed, apparently produced by a shift in the redox potential value of the sq/rd couple, estimated as $E_{sq/rd} = -210$ mV (Faro et al., 2002a). Comparing the $E_1^{\circ\prime}$ values of wt AnFNR to the $E^{\circ\prime}$ value of mutant AnFds (Table 1) reveals that small thermodynamic barriers exist for ET from E94K and F65A AnFd mutants to wt AnFNR. However, upon complex formation, the ET reaction of E94K to wt AnFNR becomes thermodynamically favored by 67 mV. The reaction of F65I is approximately isopotential with wt AnFNR in the isolated proteins, but the driving force for ET for this highly impaired AnFd mutant becomes thermodynamically favored by 61 mV in the complex. A similar effect is found for the AnFd mutant. Thus, unfavorable redox potential changes are not the reason for the extremely low ET reactivity of these mutants. The reduction potentials of two other highly impaired AnFd mutants, F65A, and E94Q, were not measured in their complexes, nor was that of the moderately impaired C49S mutant. However, inspection of Table 1 shows that the potential of the Fd shifts to a relatively small degree in either direction, whereas the $E_1^{\circ\prime}$ values of the AnFNRs shift to much larger extents and always in the thermodynamically favorable direction for ET. As noted below, it thus appears that disruption of the precise surface complementarity at the protein–protein interface in the impaired mutants is the primary cause of decreased reactivity.

B. Interaction of WT Fd with WT FNR

Batie and Kamin (1984a) postulated the existence of a cluster of positive charge on FNR at the Fd-binding site. Later chemical modification studies identified an Arg residue (Sancho et al., 1990; Medina et al., 1992a) and two Lys residues (Medina et al., 1992b) in AnFNR that were involved in binding veg AnFd. In addition, from the surface charge distribution of Fd from different species, a molecular dipole moment can be calculated (De Pascalis et al., 1993). This allowed calculation of the orientation of that dipole moment for spFNR (Jelesarov et al., 1993), which was shown to cross the FNR surface near Val151 (equivalent to Val136 in AnFNR), with the negative end close to the [2Fe–2S] cluster. Electrostatic surface potentials for *A. variabilis* and *Spirulina platensis* Fds indicated that a similar dipole vector would be expected. The positive end of the dipole moment calculated for spFNR (Jelesarov et al., 1993) was shown to cross the FNR surface near Val151 (equivalent to Val136 in AnFNR) and the negative end near Phe231 (equivalent to Tyr220 in AnFNR). It was proposed that the "large dipole moment of 58 Debye will provide electrostatic guidance and facilitate orientation of Fd."

In agreement with the aforementioned studies, the effects of ionic strength on the kinetics of ET from spFd to spFNR using LFP/TRA measurements (Bhattacharyya et al., 1986; Walker et al., 1991) indicated a strong influence of complementary electrostatic charges on complex formation and stabilization and on

ET rate constants. Many subsequent results from the laboratories of Tollin and Medina and Gómez-Moreno (see below) are also consistent with a plus–minus electrostatic interaction between the proteins from *Anabaena*.

In LFP/TRA studies (Hurley et al., 1996a), the ionic strength dependence of k_{obs} for the ET interaction between native veg AnFd or its recombinant counterpart and AnFNR was shown to be biphasic. The values increased with increasing μ, with maximum k_{obs} values of similar magnitude obtained at $\mu = 40$ and 110 mM for the native and recombinant Fd, respectively, and then decreased as expected for the interaction of oppositely-charged proteins. It was suggested that the drop-off in k_{obs} at low values of μ was due to the formation of a tight complex having a nonoptimal mutual orientation. As the salt concentration was increased, electrostatic interactions were weakened, which allowed the proteins to attain a more effective orientation. It was also suggested that the more pronounced effect at low μ for recombinant Fd was due to the presence of six extra amino acids (TQAKAK) at the N-terminus, two of which are positively charged, that were proteolytically cleaved during isolation of the native Fd. The crystal structure of the Fd/FNR complex (Morales et al., 2000) shows that although the N-terminal region of FNR is positioned outside of the protein–protein interface, it is close enough to interact electrostatically with a negatively charged region of Fd (D67, D68, D69). Biphasic ionic-strength dependencies had also been observed previously (Nakamura and Kimura, 1971a,b; Masaki et al., 1982a) for the diaphorase and cytochrome *c* reductase activities. The NADPH-cytochrome *c* reductase activity of a chimeric protein containing spFd and spFNR in one polypeptide chain, as well as that of the dissociable complex of the spinach proteins, also showed a biphasic dependence on ionic strength (Aliverti and Zanetti, 1997). The LFR/TRA studies described below were performed at the optimal μ values in experiments with native and recombinant FNR, respectively. Transient kinetic experiments on the ET reaction from Fd to *Anabaena* FNR (Walker et al., 1991; Hurley et al., 1993a) were consistent with the (minimal) two-step mechanism shown in Eq. (2) above.

Thermodynamic studies have shown that hydrophobic effects, suggested to originate from dehydration of the protein–protein interface, also make a large contribution to complex stability in the spinach proteins (Jelesarov and Bosshard, 1994). Differences between experimental and theoretical complex stability constants as a function of μ also have been attributed to hydrophobic interactions in the *Anabaena* proteins (Hurley et al., 1996a). Consistent with this, in the crystal structure of the *Anabaena* Fd/FNR complex the molecular interface includes a hydrophobic core involving F65 from Fd and L76, L78, and V136 from FNR (Morales et al., 2000).

C. Interaction of Mutant Fds with WT FNR

Both AnFd 7120 (Alam et al., 1986; Böhme and Haselkorn, 1989) and AnFNR 7119 (Fillat et al., 1991, 1994; Gómez-Moreno et al., 1995) have been cloned and overexpressed in *Escherichia coli* and the X-ray crystal structures have been solved to high resolution (Rypniewski et al., 1991; Serre et al., 1996). This has allowed the use of site-directed mutagenesis to investigate the roles of specific amino acid residues in ET. In addition, two covalent cross-linking studies have implicated several acidic spFd residues within the regions 20–30, 65–70, and 92–94 (corresponding to regions 22–32, 67–72, and 94–96 in veg AnFd) in binding to spFNR (Vieira et al., 1986; Zanetti et al., 1988). Computer modeling also pointed to acidic residues in these segments of the Fd molecule (Karplus, 1991). Differential chemical modification of spFd implicated acidic residues D28, E31, E32, D36, and D67 (AnFd numbering) in complex formation with spFNR (De Pascalis et al., 1993).

1. Critical Fd Residues

LFP/TRA studies showed that residues E94, F65, and S47 in AnFd (Hurley et al., 1993a, 1997a) were critical to the Fd/FNR ET interaction. Thus, the mutants E94K, E94Q, F65A, F65I, and S47A had k_{obs} values that were approximately four orders of magnitude smaller than wt AnFd in their ET reactions with wt AnFNR. Steady-state kinetic measurements of AnFNR reduction by these mutants also showed them to be highly impaired (Schmitz et al., 1998), although to a lesser degree. In contrast, the mutants F65W and F65Y (Hurley et al., 1993b), E94D (Hurley et al., 1994), and S47T (Hurley et al., 1997a) reacted very much like wt AnFd. This suggested that an aromatic amino acid is required at position 65, a negative charge is required at position 94 and a hydroxyl-bearing amino acid is required at position 47 for rapid ET to AnFd. The S47T result also pointed to the importance of the hydrogen bond between S47 and E94, that is part of a larger hydrogen-bonding network that tethers the [2Fe–2S] cluster to the C-terminal α-helix, helping to stabilize an otherwise highly flexible region of the protein (Holden et al., 1994). Disruption of this could block the ET pathway out of Fd, as well as

perturb the normal binding modes between the proteins that allow formation of a productive ET complex.

E94 has been shown to hydrogen bond with K75 of AnFNR in the crystalline complex of the *Anabaena* proteins (Morales et al., 2000) and this hydrogen bond is apparently crucial to ET-competent complex formation. Interestingly, the adjacent E95K mutant was shown to react like wt AnFd. Such a dramatic difference between mutations at adjacent sites suggests that a very precise surface complementarity must be maintained for efficient ET.

The equivalent residue to E94 in spFd is E92. EPR spectroscopy, electrochemistry, and steady-state kinetic studies have been carried out on the E92K, E92Q, and E92A mutants (Aliverti et al., 1995a, 1997; Piubelli et al., 1996). The E92K mutation did not impair ET in a nonphysiological assay in which ET occurs in the opposite direction. In contrast, in photoreduction of FNR by thylakoid membranes (Piubelli et al., 1996), E92Q, and E92A were approximately 50% as effective as wt spFd, whereas E92K was only 30% as effective. This was attributed to a less negative reduction potential for these spFd mutants. However, in such steady-state experiments, it is not known what the rate-determining step is, and thus it is possible that the observed rates do not reflect the Fd_{red} to FNR ET step. Furthermore, it is not known to what extent redox potential shifts occur upon complex formation in these proteins (see section A above). Based on the X-ray structure of the E92K mutant (Binda et al., 1998), modeling a Glu residue at position 92 showed that the acidic side chain could hydrogen bond with S45 (equivalent to S47 in *Anabaena*). Loss of this hydrogen bond in the mutant protein may have a deleterious effect on the functionality of the spinach protein, similar to that observed for *Anabaena* Fd. EPR experiments on the E92 mutants of spFd revealed small changes in the [2Fe–2S] geometry (Aliverti et al., 1995a). E92 in spFd may be one of the residues modified in the aforementioned studies of Vieira et al. (1986) and Zanetti et al. (1988).

In the maize protein complex, in contrast to *Anabaena*, the side chain of Y63 in Fd, which is the equivalent of F65 in AnFd, is neither in close contact with the [2Fe–2S] cluster, nor does it lie between the two prosthetic groups. Also, E92 (the equivalent of AnFd E94) does not interact with FNR (Kurisu et al., 2001).

2. Moderately Important Fd Residues

AnFd residues whose mutation resulted in proteins that were 20–67% as effective in ET with AnFNR were considered moderately important (Hurley et al., 2002). Among these were C41, C46, and C49 (each mutated to Ser), three of the four cysteine residues that ligate the [2Fe–2S] cluster, and E32, F39, S40, R42, T48, D62, D67, D69, and Q70. Instability of the C79S mutant precluded studies of its ET reactivity, and instability of C41S prevented measurement of its reduction potential. The ET reactivity of the three Cys mutants (Hurley et al., 1997a) did not correlate with the K_d value determined for the transient ET complex (Fd_{red}:FNR_{ox}). ^{1}H NMR spectroscopy has also been carried out on these mutants (including C79S; Cheng et al., 1994), demonstrating that *in vitro* selfassembly of the iron-sulfur cluster occurs upon addition of iron- and inorganic sulfur to the apoprotein. Thus, Ser can substitute for Cys as one of the ligands to the iron-sulfur cluster. However, the stability of the cluster as well as the ET reactivity is clearly diminished by such substitution.

The UV-vis (Cheng et al., 1994) and CD spectra (Hurley et al., 1997b) of the Cys mutants are different from each other and from wt AnFd. This is a consequence of perturbations of the electronic character of the [2Fe–2S] cluster, due to altered symmetry and to different energies of the ligand → Fe charge-transfer transitions, caused by substitution of oxygen for sulfur as one of the ligands to the cluster. Such electronic alterations may also play a part in the moderately reduced ET reactivity of these mutants with FNR, as well as in the altered reduction potential measured for the C49S mutant.

E32 was judged to be moderately important since the E31K/E32K double mutant was only 54% as reactive in ET as wt Fd, whereas E31K was unaltered in its reactivity (Hurley et al., 2002). Similarly, in a steady-state cytochrome *c* reductase assay, the double mutant E31Q/E32Q was only 69% as active as wt AnFd (Schmitz and Böhme, 1995). Altered redox potential or binding properties may be a factor, inasmuch as E32 is not at the complex interface in the crystal structure (Morales et al., 2000). Thus, it is possible that the double charge-reversal mutation alters the molecular dipole of the Fd such that the mutual orientation of the two proteins is adversely affected.

F39A was observed to have an ET reactivity that was 65% of wt AnFd (Hurley et al., 2002). Consistent with this, the crystal structure shows that the local secondary structure of the [2Fe–2S] cluster-binding loop forces F39 of AnFd into a solvent-exposed position, and it was suggested that "one potential role of such a conserved, solvent-exposed aromatic amino acid may be in redox partner recognition" (Holden et al., 1994).

R42 hydrogen bonds through its amide nitrogen with one of the inorganic sulfurs of the [2Fe–2S] cluster

(Skjeldal et al., 1991), and is also involved in a salt bridge with E31 as part of the [2Fe–2S] cluster-binding loop (Holden et al., 1994). It has been suggested that R42 might play an important role in physiological functioning and in the proper folding of the Fd molecule (Tsukihara et al., 1982). The R42A, R42H, and R42E mutants were, respectively 154%, 54%, and 117% as effective as wt AnFd in ET with AnFNR (Hurley et al., 2002), implying that neither the presence of a positive charge at this position nor the R42–E31 salt linkage is required for rapid ET with FNR. This is in agreement with the *Anabaena* Fd/FNR complex structure (Morales et al., 2000) which shows that the R42 side chain is not involved in the interaction. The lowered reactivity observed for the R42E mutant may be due to a long-range repulsive electrostatic interaction that alters the mutual orientation between the proteins in the intermediate complex. The crystallographic structure of the FNR/Fd complex from maize (Kurisu et al., 2001) shows that Arg40 (equivalent to Arg42 in AnFd) and Glu 29 (equivalent to Glu31 in AnFd) of the Fd molecule form an intermolecular salt bridge with Lys304 of FNR (Lys293 in *Anabaena*). It was proposed that this structural feature may be related to the redox potential shift observed in the free spFd relative to that found in the FNR-bound state. An earlier chemical modification study of Arg40 in spFd showed that the modified Arg did not impair ET to spFNR (Vieira and Davis, 1986). The reason for the decrease in reactivity of the R42H mutant is not clear.

The T48A mutant was only 58% as effective as wt AnFd in its ET reactivity with AnFNR (Weber-Main et al., 1998). T48 is part of the cluster-binding loop of Fd and this may be the cause of its lowered reactivity. Altered complex stability or protein–protein orientation in the transient ET complex could also be responsible.

D62K was only 35% as effective as wt AnFd in ET to AnFNR (Hurley et al., 1997a). The K_d value determined for the intermediate ET complex was somewhat smaller than that for wt AnFd, showing that decreased binding affinity is not the cause of the reduced reactivity. D62 is part of the complex interface (Morales et al., 2000) and the reduced ET reactivity can be attributed to the charge reversal at this position causing alterations in protein–protein orientation. Stereochemical factors may also play a role.

The D67K and D69K mutants were respectively 43% and 57% as effective as wt AnFd in their ET interactions with AnFNR (Hurley et al., 2002). This is in contrast to D68K, which was 20% more reactive than wt AnFd. Again, such distinctly opposite effects for the same mutation at contiguous sites along the peptide chain suggests that a very precise surface complementarity at the interprotein interface must be maintained for efficient ET interaction. Interestingly, at low μ values, the impairment due to the D69K mutation was partially overcome by the D68K substitution in the D68K/D69K double mutant (Hurley et al., 1996b). However, including the D68K mutation in a triple mutant, D67K/D68K/D69K, did not overcome the impairment caused by the D67K and D69K mutations. The K_d values for complexes with $AnFNR_{ox}$ measured for each of these oxidized mutant proteins (except D67K/D68K/D69K, for which no binding was observed) showed that binding was at least as tight as it was for wt AnFd (Hurley et al., 1996b). Schmitz and Böhme (1995) found D67N/D68N and D67N to be 62% and 66%, respectively, as active as wt AnFd in a Fd-dependent steady-state assay. D67 and D69 are at the edge of the interface in the crystalline complex (Morales et al., 2000; Hurley et al., 2002), and it had been observed earlier by chemical modification and cross-linking (Vieira et al., 1986) that acidic residues in the region 63–68 (AnFd numbering) were involved in the Fd:FNR interaction. Thus, it is not surprising that D67K and D69K have an effect on ET reactivity. It is likely that electrostatic effects are operative, although again stereochemical factors may be involved. The increase observed with D68K is most likely due to electrostatic effects that lead to a more efficient interprotein orientation.

The S40A mutant reacted about 60% as well as wt AnFd (Hurley et al., 2002). The reason for this is not clear, although this residue is part of the [2Fe–2S] binding loop. The reactivity of Q70K was reduced to 59% that of wt AnFd and the K_d value for the intermediate complex was approximately 50% smaller than the value for wt AnFd (Hurley et al., 1997a). Thus, Q70 moderately influences the Fd/FNR interaction, although again the reason for its effect is not known. Mutations at a number of other residues of AnFd (D28, E31, D36, A43, A45, D68, T78, H92, E95, and Y98) showed these not to be important in the ET interaction (Hurley et al., 2002).

D. Interaction of Mutant FNRs with WT Fd

1. Critical FNR Residues

Hurley et al. (2002; see also Medina and Gómez-Moreno, 2004) have also studied AnFNR mutants in their ET interactions with wt AnFd using LFP/TRA. Thus, the reactivity toward wt $AnFd_{red}$ of mutants

having nonconservative mutations at R16, K72, K75, L76, L78, and E301 was only 10%, 13%, 0.7%, 4%, 13%, and 1%, respectively, that of wt AnFNR. The ET reactivity of the R16 and K75 mutants correlated well with K_d values measured for complex formation between the oxidized proteins at $\mu = 12$ mM, suggesting that impaired binding was involved (Martínez-Júlvez et al., 1998a, 1999; Hurley et al., 1999). Steady-state NADP$^+$ photoreduction assays also showed the reactivities of R16E, K72E, and K75E to be significantly lowered (Gómez-Moreno et al., 1995; Schmitz et al., 1998). The equivalent of K72 in spFNR (K88) was mutated to a Gln and was 60% as active as wt spFNR in a steady-state cytochrome *c* reductase assay (Aliverti et al., 1994).

The electrostatic interactions beween the R16E, K72E, and K75E mutants and AnFd were altered such that the biphasic μ dependencies were eliminated. Thus, R16E and K75E were more reactive at $\mu = 12$ mM than wt AnFNR, although again reactivity dropped-off rapidly at increasing μ values. Electrostatic surface potential calculations (Hurley et al., 1999) showed that R16, K72, and K75 lie in a region of the protein surface where positive charge predominates, and charge reversal would therefore have a large effect on the local surface electrostatic potential. The large effects on ET reactivity of mutations in these residues are consistent with the major role of the N-terminal domain (residues 1–138) of FNR in the interaction with Fd within the crystalline complex (Morales et al., 2000). The conservative mutant K75R reacted much like wt AnFNR, whereas K75Q and K75S were only moderately hindered. Steady-state kinetic studies, utilizing the diaphorase activity with DCPIP, also showed the requirement of a positive charge at position 75, i.e., the reaction was not measurable for the K75E mutant (Martínez-Júlvez et al., 1998a). K75 forms a salt bridge with Fd E94 at the periphery of the interface in the crystalline complex (Morales et al., 2000), and this charge-pair plays a structural role in the association. Thus, these results, along with the greatly diminished ET reactivity of the E94K mutant, clearly indicate that the charge complementarity of FNR K75 and Fd E94 is critical for binding Fd and FNR during ET. It is noteworthy, however, that ET reactivity was not restored when E94K Fd was reacted with K75E FNR (Hurley et al., unpublished observations). This may be because charges surrounding the mutation sites in the two proteins disrupted the attractive electrostatic interaction between the mutated residues.

Among a large series of mutations made at L76, the strongly diminished reactivity of L76D in ET measured by LFP/TRA is most striking (Martínez-Júlvez et al., 2001). Stopped-flow kinetic experiments, as well as the diaphorase and NADPH-dependent cytochrome *c* reductase steady-state assays also showed a high degree of impairment of the reactions between L76D and Fd. The K_d values measured for complexation of the oxidized Ser, Ala, Val, and Phe mutants at position 76 with $AnFd_{ox}$ varied by less than a factor of three from the value obtained for wt AnFNR. In contrast, the binding of L76D to Fd could not be detected. Similarly, an Asp substitution at position L78 was shown by LFP/TRA to cause a high degree of impairment in the ET interaction with AnFd. Other more conservative mutations at this position caused only small to moderate reductions in ET reactivity. L78D was also shown to be highly impaired by stopped-flow kinetic experiments as well as by steady-state diaphorase and NADPH-dependent cytochrome *c* reductase activities. As for L76D, no binding to Fd could be detected by difference spectroscopy for L78D. These mutations introduce a negatively charged side chain in an area near the FAD cofactor that is involved in hydrophobic contacts at the Fd/FNR interface in the crystalline complex (Morales et al., 2000). This would be expected to be disruptive, consistent with the importance of hydrophobic forces in the protein–protein interaction.

Double mutations at positions L76 and L78 were produced by the simultaneous introduction of two Asp or two Phe residues. The introduction of two negatively charged residues at these positions inhibited complex formation and ET with AnFd completely. This is consistent with a major alteration in the electrostatic surface potential calculated for the enzyme near the flavin ring using the three-dimensional structure of the mutant (Martínez-Júlvez et al., 2001). The L76F/L78F mutant was, however, still able to interact with AnFd, although its complex with AnFd is less effective for ET, presumably due to an altered mutual orientation of the cofactors caused by steric interferences (Martínez-Júlvez et al., 2001).

The E301A mutant was only 1% as active as wt AnFNR in its ET interaction with AnFd (Medina et al., 1998). However, the steady-state photoreduction of NADP$^+$ was not impaired to this same extent, presumably because the rate-limiting step in the more complex steady-state system is something other than ET. Complex formation with AnFd was diminished by a factor of two, but this is too small to account for the decrease in ET reactivity measured by LFP/TRA. Steady-state experiments demonstrated that the semiquinone state of the FAD was significantly destabilized in the E301A mutant relative to wt AnFNR (Medina et al., 1998).

This had also been observed in three of the four mutants made at E312 in spFNR (Aliverti et al., 1998) but not to the same extent as determined for the *Anabaena* protein. Thus, lack of stabilization of the semiquinone state of the E301A mutant of AnFNR is probably the principal reason for the highly decreased ET reactivity.

It was suggested by the X-ray crystal structure of spFNR (Bruns and Karplus, 1995) that E312 might be involved in proton transfer via S96 to the N-5 position of the isoalloxazine ring of FAD during semiquinone formation. In AnFNR, E301 appeared to be a good candidate to transfer protons to FAD via S80 (Serre et al., 1996). However, subsequent kinetic characterization and X-ray crystal structure determinations of E312 mutant proteins (Zanetti et al., 1997; Aliverti et al., 1998) led to the conclusion that this residue does not act as a proton donor during catalysis in spFNR, but is involved in binding NADP(H). It was further determined that the charge of E312 contributes to establishing the redox potential of the FAD semiquinone, and that the side chain of E312 has little effect on the affinity of spFNR for spFd, but does influence ET between the two proteins. In AnFNR, although it is clear that E301 is a critical residue in the AnFd/AnFNR interaction (Medina et al., 1998), whether or not it is involved in transferring protons to the FAD could not be determined. In the AnFd/AnFNR crystalline complex (Morales et al., 2000), although the carboxylic group of Glu301 is no longer exposed to solvent, it is hydrogen bonded to the hydroxyl oxygen of Ser64 of Fd, which is exposed to solvent. This suggests a possible pathway for proton transfer between the external medium and the AnFNR isoalloxazine N5 via Ser64 of AnFd and the Glu301 and Ser80 side chains of AnFNR. Further work is needed to test this possibility.

In the crystal structure of the AnFNR E301A mutant, although no significant folding differences were observed relative to wt FNR (Mayoral et al., 2000), conformational differences were observed for the side chain of a nearby residue, E139. In the mutant, this side chain points toward the FAD, is stabilized by a network of five hydrogen bonds to several H_2O molecules, and is connected to the S80 side chain through a series of three H_2O molecules. It was suggested that in the mutant the E139 side chain may perform some of the functions of the E301 side chain in wt AnFNR. As described below, mutation of E139 has unusual effects on ET kinetics.

2. Moderately Important FNR Residues

Nonconservative mutations of K138, E139, R264, K290, and K294 in AnFNR caused the ET reactivity with $AnFd_{red}$ to be reduced to 18–40% of that observed with wt protein (Hurley et al., 2002). K138E was also shown to have diminished reactivity by steady-state and stopped-flow methods (Schmitz et al., 1998; Martínez-Júlvez et al., 1999). The decreased ET reactivity of K138E correlated with increased K_d values for AnFd complex formation with the oxidized protein at μ = 12 mM. LFP/TRA showed E139K to be significantly impaired in its ET interaction with $AnFd_{red}$ (Hurley et al., 2002). This residue is located at the periphery of the interaction site in the crystalline complex (Morales et al., 2000). Although no direct contact occurs with Fd, the distance from FNR E139 Oε to the Fd S61 main chain carbonyl oxygen is 4.6 Å. This allows it to be mutated to a Lys or a Gln without sterically impairing the AnFd/AnFNR association. However, the change in charge in the E139K and E139Q mutations would adversely affect the electrostatic interactions of the proteins. At μ = 12 mM, the ET interaction with Fd was highly impaired, and the k_{obs} vs. FNR concentration dependence showed strong upward curvature at FNR concentrations >10 μM (Hurley et al., 2000). At values of μ > 200 mM, the ET reaction rates approached those observed with wt AnFNR and the expected saturation kinetics were obtained. The E139Q mutant was also less reactive at low values of μ and low protein concentrations but showed a smaller degree of upward curvature in its k_{obs} dependency on FNR concentration. Like E139K, this mutant showed the expected saturation kinetics at higher values of μ. The E139D mutant, as well as the wt AnFNR (which was reevaluated after the E139K results were obtained), also showed a small extent of upward curvature at AnFNR concentrations > 30 μM at μ = 12 mM, and showed saturation at higher values of μ.

The explanation given for the unusual kinetic behavior of the E139K mutant was as follows (Hurley et al., 2000). At low μ values, the proteins form a complex in which the mutual orientation of the redox cofactors is so far from optimal that they are almost ET unreactive. As the E139K concentration was increased, the added FNR was able to oxidize the bound $AnFd_{red}$ in the slowly reacting complex because the iron–sulfur center was oriented away from the FNR surface. This ternary reaction was the source of the upward curvature in the FNR concentration dependence. The degree of diminished reactivity observed at low values of μ depended on the particular amino acid substitution, with E139K being by far the most unreactive. Only a small amount of non-linearity was observed at the highest FNR concentrations for wt AnFNR. As the value of μ was increased, electrostatic forces involved in stabilizing the complex were weakened, allowing the proteins to rearrange to a more reactive ET complex in which

the iron–sulfur center was pointed toward the FNR surface. Thus,electrostatic interactions were responsible for controlling the specific geometry at the interface between the proteins, which in turn determined the rates of ET occurring within the complex. Ternary reactions involving ET proteins are not unique to this protein pair and have been previously described for the cytochrome *c*: cytochrome *c* peroxidase system (Kang et al., 1977; Nuevo et al., 1993; Mauk et al., 1994; Zhou et al., 1995). There was no evidence for a stable ternary complex formed between AnFd and two molecules of E139K and the reaction was assumed, therefore, to proceed via a collisional interaction. These results demonstrate the importance of E139 for competent complex formation between AnFd and AnFNR, as well as the strong influence of electrostatic interactions on the ET behavior of this protein pair.

It was previously suggested that R264 played a role in AnFd recognition (Serre et al., 1996). In support of this, LFP/TRA, stopped-flow, and steady-state kinetic measurements (Martínez-Júlvez et al., 1998b) showed R264E to have appreciably diminished ET reactivity. The K_d values for complex formation to $AnFd_{ox}$ between both the oxidized and reduced forms of R264E were similar to those for wt FNR. The dependence of k_{obs} on μ, however, indicated that electrostatic interactions were weakened in the complex leading to more productive ET complexes at lower salt concentrations compared to wt AnFNR. Electrostatic surface potential calculations revealed a significant change in the FAD environment, which was proposed to have a destabilizing effect on the complex (Martínez-Júlvez et al., 1998b). R264 is one of the most important interface residues in the Fd/FNR crystalline complex (Morales et al., 2000), having 12 van der Waals contacts and two direct H-bonds. However, since this residue is located at the periphery of the interaction site, mutation to Glu would not sterically impair the formation of the complex, although it would greatly decrease the number of van der Waals contacts and eliminate the hydrogen bonds. These factors apparently result in a nonoptimal interprotein orientation in the complex.

The ET interactions of K290E and K294E with $AnFd_{ox}$ were evaluated by LFP/TRA, stopped-flow and steady-state techniques (Schmitz et al., 1998; Hurley et al., 1999; Martínez-Júlvez et al., 1999), demonstrating that these mutants were moderately impaired. The K_d values for the oxidized proteins at $\mu = 12$ mM correlated well with the ET reactivity.

Charge-reversal mutations at K138, R264, K290, and K294 altered the electrostatic forces stabilizing the ET complexes such that the biphasic μ dependency observed for wt AnFNR was eliminated or minimized (Hurley et al., 1999). As a result, the ET complexes that were formed at low values of μ were more reactive. Electrostatic calculations revealed these four residues to lie in regions of the protein that have a large negative surface potential (Hurley et al., 1999). Thus, introduction of additional negative charge in these areas would be expected to have relatively small effects, as observed.

There are five cysteine residues in spFNR (C42, C114, C132, C127, and C272, corresponding to V25, C98, C117, T22, and C261 in AnFNR) and each of these have been individually mutated to Ser (Aliverti et al., 1993). Of these, C42S could not be expressed in *E. coli*, and C132S and C272S were moderately impaired in the Fd-dependent cytochrome *c* reductase activity. C272 is part of the NADP(H)-binding site while the other cysteine residues in spFNR are part of the FAD-binding domain. The K_d values for the oxidized forms of these two mutants with wt $spFd_{ox}$ were identical to that of wt FNR. AnFNR contains only three Cys residues and none of these have been mutated. R100 and V136 in AnFNR (Hurley et al., 2002) and S96 (equivalent to S80 in AnFNR) in spFNR (Aliverti et al., 1995b) were shown to be unimportant in the Fd:FNR interaction.

E. Insights from Fd: FNR Crystalline Complexes

In the crystal structure of the AnFd/AnFNR complex (Fig. 1) Fd is seen to bind to the concave surface of the FNR molecule from which the exposed dimethylbenzene portion of the isoalloxazine ring projects. The closest distance from the [2Fe–2S] cluster to the flavin is 7.4 Å (from the S2 atom of the cluster to the C8-methyl of the FAD), consistent with evidence indicating that the C8-methyl group of the isoalloxazine ring is involved in flavoprotein ET (Fritz et al., 1973). There is little steric hindrance to electron flow between the cofactors, suggesting a relatively rapid direct outer-sphere electron transfer between them, which is consistent with the observed maximal k_{et} of 5,500 $sec^{-}1$ (Hurley et al., 1996a). The redox-linked conformational change that occurs in AnFd upon ET (Morales et al., 1999, 2000) is centered at the core of the Fd/FNR interfacial region in the *Anabaena* complex and thus may be involved in the separation of the two proteins subsequent to ET. Similarly, in the maize complex, the C8-methyl group of the FAD is 6.0 Å from the Fe1 atom of the [2Fe–2S] cluster, sufficiently close for direct and rapid ET between the cofactors.

Only a relatively small number of mutations resulted in large kinetic effects on the ET reaction between the

Anabaena proteins. In AnFd (see Fig. 1A in Hurley et al., 2002), several of the critical residues lie close to the partially exposed [2Fe–2S] cluster, with the region immediately below the cluster being the most important (S47, F65, E94). In AnFNR (see Fig. 1C in Hurley et al., 2002), the most important residues lie within and at the right-hand periphery of the concave cavity of the AnFNR surface that contains the exposed edge of the flavin isoalloxazine ring (R16, K72, K75, L76, L78, E301). It is important to note that all of these residues are found at the FNR-Fd interface in the crystalline complex (Morales et al., 2000; see Fig. 1 in Hurley et al., 2002).

The interprotein interface in the crystalline *Anabaena* complex contains a core of hydrophobic side chains (including F65 of Fd and L76, L78, and V136 of FNR), as well as acidic residues of Fd (D62, D67, E94) and acidic (E267, E301) and basic (R16, K75, R264, K294) residues of FNR. These groups interact with each other either directly or through bridging water molecules. Thus, D67 interacts with R16; D62 hydrogen bonds with R264; E94 of AnFd forms a salt linkage with K75. The interface between the *Anabaena* proteins is also stabilized by hydrophobic interactions involving long side chains such as R264 of FNR (which makes 11 van der Waals contacts with Fd), and the loss of about 10 water molecules upon complex formation (Morales et al., 2000). This latter point is in agreement with calorimetric experiments on the spinach protein complex (Jelesarov et al., 1993).

Of the 11 van der Waals contacts with AnFNR made by F65 of Fd, seven are with L78 and two are with V136. The decreases observed for ET reactivity for mutants in which an Asp substitution at L78 and a Ser substitution at V136 are made are consistent with a disruption of these hydrophobic interactions, as are the Ala and Ile substitutions of F65. An Asp substitution at L76 also severely impairs ET to Fd; although L76 does not directly contact F65, it does lie within the complex interface. In addition, the critical S47 residue of Fd, as well as the moderately important C46, is positioned in front of AnFNR in the complex, although there is a "cavity" separating these residues from direct contact with the FNR surface. The K72 residue in FNR, which was shown to be crucial for ET, is not located at the complex interface and the impaired reactivity of the K72E mutant can be attributed to a disruptive long-range electrostatic interaction with the negatively charged Fd surface (Hurley et al., 2002). Similar long-range electrostatic effects may explain why some additional residues located close to but not within the complex interface in AnFNR (K290 and K294) and in AnFd (Q70) showed moderate impairment in ET reactivity upon nonconservative mutation. Other amino acids in this category are F39, S40, and T48 of AnFd, all of which show moderate impairment in ET upon nonconservative mutation, but are not directly located at the complex interface. These latter three residues, however, are part of the [2Fe–2S] cluster-binding loop, and are located 4.5–5.0 Å from the cluster. A direct effect on the properties of the cluster may thus be involved in their influence on reactivity. Based on these correlations, Hurley et al. (2002) concluded that the crystalline *Anabaena* Fd/FNR complex is a viable model for a productive intermediate formed during ET.

The X-ray crystal structure of the maize Fd/FNR complex (Kurisu et al., 2001) also shows an interface consisting of both electrostatic and hydrophobic interactions near the prosthetic groups, the latter involving mainly V92, L94, and V151. However, superposition of the FNR molecules of each of the two complexes reveals that the Fd molecules are rotated by an angle of 96°, indicating that many of the specific interactions within the complexes are not the same. In particular, Y63, which corresponds to the critical F65 residue of AnFd, is no longer located between the prosthetic groups of the two proteins and is involved to a lesser extent in hydrophobic interactions with FNR. Also, E92, the maize equivalent of the critical E94 residue of AnFd, is not involved at all in the FNR interaction. We point out that kinetic studies have shown significant differences between the *Anabaena* and spinach protein systems in the relative contributions of electrostatic and hydrophobic interactions during ET (Walker et al., 1991), indicating that species-specific differences in the protein–protein interactions do occur. However, the comparison demonstrates that the major features shared by the *Anabaena* and maize Fd/FNR crystalline complexes are several complementary electrostatic interactions, a hydrophobic patch centered on FNR that provides a non-polar environment during ET, and close proximity of the two redox centers, which allows fast ET. Thus, despite their structural differences, both complexes may represent functional ET intermediates.

VII. Structure–Function Studies of Flavodoxin and Ferredoxin:NADP$^+$ Reductase

A. Interaction of Mutant Flds with WT FNR

Since in some photosynthetic systems (e.g., various algae and cyanobacteria) Fld can efficiently replace Fd

in the ET process, a careful analysis of the FNR:Fld interaction has been carried out (Martínez-Júlvez et al., 1998a, 1999; Nogués et al., 2003). However, no critical residue on AnFld has thus far been identified. Chemical modification studies suggested the involvement of some negatively charged regions on the AnFld surface (D123, D126, D129, D144, E145, and D146) in the interaction with AnFNR (Medina et al., 1992c). Although Fd and Fld are of different size and structure and have a different redox cofactor, they still are expected to interact at the same site on the reductase, suggesting that comparison of the interface area in both proteins could provide important information about the determinants for molecular recognition. Analysis of site-directed mutants at positions (E61, E67, D100, D126, D144, and E145) suggested by such chemical modification studies, and by analysis of the three-dimensional AnFld structure, indicated that none of these appear to be critical for the complex formation and ET processes between Fld and its substrates (Navarro et al., 1995; Jenkins et al., 1997). In an attempt to look for the AnFNR hydrophobic counterpart region on the AnFld surface, replacement of the only two non-polar residues on the AnFld surface near the FMN (I59 and I92) by a Lys suggests that these two hydrophobic residues are also not critical in the interaction and ET processes (Nogués et al., 2003).

The influence of the amino acid residues sandwiching the FMN ring in AnFld (W57 and Y94) in complex formation and ET with FNR has also been examined in several mutants (Casaus et al., 2002). The ability to form complexes with FNR is similar to that of wt Fld and the slightly altered ET kinetics can be explained in terms of altered flavin accessibility and/or thermodynamic parameters (Casaus et al., 2002). Thus, W57 and Y94 do not play an active role in Fld interaction and ET with FNR.

B. Interaction of Mutant FNRs with WT Fld

1. Critical FNR Residues

Analysis of several charge-reversal mutants on the AnFNR surface indicated that the positively charged residues that have been shown to be critical for achieving maximal ET rates with AnFd (R16, K72, and particularly K75) are also determinants for an efficient interaction with AnFld (Martínez-Júlvez et al., 1999; 1998a). In addition, E139 in AnFNR has been shown to play an active role in the AnFld interaction (Faro et al., 2002b), although this residue behaves differently with the two ET proteins. Thus, although removal of the negative charge produces a deleterious effect on ET reactions with AnFd, it appears to enhance the ET process with AnFld. With regard to the hydrophobic interactions, ET with Fld is almost completely lost upon introduction of negatively charged side chains at the hydrophobic patch formed by L76, L78, and V136 in AnFNR, whereas, as in the reaction with Fd, more conservative changes modulate the ET rates by altering the binding constants and the midpoint redox potentials of the flavin group (Nogués et al., 2003). Therefore, it is concluded that these non-polar residues participate in the establishment of interactions with both AnFld and AnFd.

2. Moderately Important FNR Residues

Mutations of the positively charged AnFNR residues in the NADP$^+$-binding domain have shown that the K138 and R264 side chains are more important in establishing interactions with AnFld than with AnFd (Martínez-Júlvez et al., 1999; 1998b). As was the case with Fd, E301 in AnFNR is not involved in complex formation with Fld, but rather plays a role in the catalytic process via semiquinone stabilization (Medina et al., 1998; Mayoral et al., 2000; Faro et al., 2002a).

In summary, since most of the mutations in AnFNR produced somewhat different behaviors with both ET proteins, it can be concluded that although AnFld occupies the same region as AnFd during its interaction with the reductase, individual residues on the AnFNR surface do not participate to the same extent in the processes with the two proteins (Martínez-Júlvez et al., 1999, 2001; Nogués et al., 2003). Moreover, analysis of Fd and Fld surface electrostatic potentials also shows overlap, suggesting a similar mechanism of interaction (Ullmann et al., 2000).

C. Insights from Fld:FNR Crystallographic Complexes

Despite much effort, the three-dimensional structure of the AnFNR:AnFld complex remains unsolved, suggesting that the interactions formed between FNR and Fld are short-lived and of low stability, perhaps to favor a fast ET process. However, the three-dimensional structure reported for microsomal NADPH-cytochrome P450 reductase (CPR) can be used as a model for the FNR:Fld interaction (Wang et al., 1997). This enzyme contains both FAD and FMN and is composed of four structural domains, in which the FMN-binding domain is similar to Fld, and the FAD- and NADPH-binding domains are similar to

FNR. The connecting domain is responsible for ensuring the proper orientation of the two flavins for efficient ET. In this structure the two flavin isoalloxazine rings are juxtaposed, with the closest distance between them being 4 Å. Therefore, simple superposition of FNR and Fld onto the CPR structure would place the flavin redox centers much closer than observed in the FNR:Fd structures (about 7.6 Å) (Morales et al., 2000; Kurisu et al., 2001). Such a putative closer proximity of the flavin rings in the FNR:Fld interaction might favor ET over the FNR:Fd interaction. Additionally, the partial exposure of the flavin rings in FNR and Fld would allow multiple orientations of the Fld to occur on the same FNR surface without affecting the relative distance between the cofactors. Such observations are in agreement with the fact that whereas multiple chemical modifications produced Fld forms less suitable for ET than the unmodified protein (Medina et al., 1992c), site-directed mutagenesis has not revealed any critical residue on the Fld surface for the interaction with FNR. Therefore, a less specific interaction between FNR and Fld relative to the FNR/Fd interaction might be expected. However, further work must be done in order to clarify this point.

Acknowledgments

This research was supported by grants from the National Institutes of Health (DK15057 to GT), Comisión Interministerial de Ciencia y Tecnología (CICYT, Grant BIO2000-1259 to C. G.-M. and Grant BQU2001-2520 to M.M.) and by CONSI+D (DGA, Grant P006/2000 to M.M.).

References

Alam J, Whitaker RA, Krogman DW and Curtis SE (1986) Isolation and sequence of the gene for ferredoxin I from the cyanobacterium *Anabaena* sp. strain PCC 7120. J Bact 168: 1265–1271

Aliverti A and Zanetti G (1997) A three-domain iron-sulfur flavoprotein obtained through gene fusion of ferredoxin and ferredoxin $NADP^+$ reductase from spinach leaves. Biochemistry 36: 14771–14777

Aliverti A, Piubelli L, Zanetti G, Lübberstedt T, Herrmann RG and Curti B (1993) The role of cysteine residues of spinach ferredoxin reductase as assessed by site-directed mutagenesis. Biochemistry 32: 6374–6380

Aliverti A, Corrado ME and Zanetti G (1994) Involvement of lysine-88 of spinach ferredoxin:$NADP^+$ reductase in the interaction with ferredoxin. FEBS Lett 343: 247–250

Aliverti A, Hagen WR and Zanetti G (1995a) Direct electrochemistry and EPR spectroscopy of spinach ferredoxin mutants with modified electron transfer proteins. FEBS Lett 368: 220–224

Aliverti A, Bruns CM, Pandini VE, Karplus PA, Vanoni MA, Curti B and Zanetti G (1995b) Involvement of serine 96 in the catalytic mechanism of ferredoxin:$NADP^+$ reductase: structure-function relationship as studied by site-directed mutagenesis and x-ray crystallography. Biochemistry 34: 8371–8379

Aliverti A, Livraghi A, Piubelli L and Zanetti G (1997) On the role of the acidic cluster Glu 92-94 of spinach ferredoxin I. Biochim Biophys Acta 1342: 45–50

Aliverti A, Deng Z, Ravasi D, Piubelli L, Karplus PA and Zanetti G (1998) Probing the function of the invariant glutamyl residue 312 in spinach ferredoxin:$NADP^+$ reductase. J Biol Chem 273: 34008–34015

Batie CJ and Kamin H (1981) The relation of pH and oxidation-reduction potential to the association state of the ferredoxin:ferredoxin:$NADP^+$ reductase complex. J Biol Chem 256: 7756–7763

Batie CJ and Kamin H (1984a) Ferredoxin:$NADP^+$ oxidoreductase. Equilibria in binary and ternary complexes with $NADP^+$ and ferredoxin. J Biol Chem 259: 8832–8839

Batie CJ and Kamin H (1984b) Electron transfer by ferredoxin:$NADP^+$ reductase. Rapid-reaction evidence for participation of a ternary complex. J Biol Chem 259: 11976–11985

Beinert H and Kiley PJ (1999) Fe-S proteins in sensing and regulatory functions. Curr Opin Chem Biol 3: 152–157

Beinert H, Holm RH and Münck E (1997) Iron-sulfur clusters: nature's modular, multipurpose structures. Science 277: 653–659

Bhattacharyya AK, Meyer TE and Tollin G (1986) Reduction kinetics of the ferredoxin-ferredoxin-$NADP^+$ reductase complex. Biochemistry 25: 4655–4661

Binda C, Coda A, Aliverti A, Zanetti G and Mattevi A (1998) Structure of the mutant E92K of [2Fe-2S] ferredoxin I from *Spinacia oleracea* at 1.7 Å resolution. Acta Cryst D54: 1353–1358

Böhme H and Haselkorn R (1988) Molecular cloning and nucleotide sequence analysis of the gene coding for the heterocyst ferredoxin from the cyanobacterium *Anabaena* sp. strain PCC 7120. Mol Gen Genet 214: 278–285

Böhme H and Haselkorn R (1989) Expression of *Anabaena* ferredoxin genes in *Escherichia coli*. Plant Mol Biol 12: 667–672

Böhme H and Schrautemeier B (1987) Comparative characterization of ferredoxin from heterocysts and vegetative cells of *Anabaena variabilis*. Biochim Biophys Acta 891: 1–7

Bruns CM and Karplus PA (1995) Refined crystal structure of spinach ferredoxin reductase at 1.7 Å resolution: oxidized, reduced and 2′-phospho-5′-AMP bound states. J Mol Biol 247: 125–145

Cammack R, Rao KK, Bargeron CP, Hutson KG, Andrew PW and Rogers LJ (1977) Midpoint redox potentials of plant and algal ferredoxins. Biochem J 168: 205–209

Carrillo N and Ceccarelli EA (2003) Open questions in ferredoxin-$NADP^+$ reductase catalytic mechanism. Eur J Biochem 270: 1900–1915

Casaus JL, Navarro JA, Hervas M, Lostao A, De la Rosa MA, Gomez-Moreno C, Sancho J and Medina M (2002) *Anabaena* sp. PCC 7119 flavodoxin as electron carrier from

photosystem I to ferredoxin-NADP$^+$ reductase. Role of Trp(57) and Tyr(94). J Biol Chem 277: 22338–22344

Cheng H, Xia B, Reed GH and Markley JL (1994) Optical, EPR, and ^{1}H NMR spectroscopy of serine-ligated [2Fe-2S] ferredoxins produced by site-directed mutagenesis of cysteine residues in recombinant *Anabaena* 7120 vegetative ferredoxin. Biochemistry 33: 3155–3164

Cheng H, Westler WM, Oh B-H and Markley JL (1995) Protein expression, selective isotopic labeling, and analysis of hyperfine-shifted NMR signals of *Anabaena* 7120 vegetative [2Fe-2S] ferredoxin. Arch Biochem Biophys 316: 619–634

Corrado ME, Aliverti A, Zanetti G and Mayhew SG (1996) Analysis of the oxidation-reduction potentials of recombinant ferredoxin-NADP$^+$ reductase from spinach chloroplasts. Eur J Biochem 239: 662–667

De Pascalis AR, Jelesarov I, Ackermann F, Koppenol WH, Hirasawa M, Knaff DB and Bosshard HR (1993) Binding of ferredoxin to ferredoxin:NADP$^+$ reductase: the role of carboxyl groups, electrostatic surface potential, and molecular dipole moment. Protein Sci 2: 1126–1135

Drennan CL, Pattridge KA, Weber CH, Metzger AL, Hoover DM and Ludwig ML (1999) Refined structures of oxidized flavodoxin from *Anacystis nidulans*. J Mol Biol 294: 711–724

Dugard LB, La Mar GN, Banci L and Bertine L (1990) Identification of localized redox states in plant-type two-iron ferredoxins using the nuclear overhauser effect. Biochemistry 29: 2263–2271

Faro M, Gómez-Moreno C, Stankovich M and Medina M (2002a) Role of critical charged residues in reduction potential modulation of ferredoxin-NADP$^+$ reductase. Differential stabilization of FAD redox forms. Eur J Biochem 269: 2656–2661

Faro M, Frago S, Mayoral T, Hermoso JA, Sanz-Aparicio J, Gómez-Moreno C and Medina M (2002b) Probing the role of the glutamic 139 residue in *Anabaena* ferredoxin-NADP$^+$ reductase in its interaction with substrates. Eur J Biochem 269: 4938–4947

Fillat MF, Borrias WE and Weisbeek PJ (1991) Cloning of the ferredoxin-NADP$^+$-oxidoreductase gene and overexpression of a synthetic flavodoxin gene from the cyanobacteria *Anabaena* PCC 7119. In: Curti B, Ronchi S and Zanetti G (eds) Flavins and Flavoproteins 1990, pp 445–448. Walter de Gruyter & Co., Berlin

Fillat MF, Pacheco MC, Peleato ML and Gómez-Moreno C (1994) Overexpression of ferredoxin-NADP$^+$ reductase from *Anabaena* sp. PCC 7119 in *E. coli.* In: Yagi K (ed) Flavins and Flavoproteins 1993, pp 447–450. Walter de Gruyter & Co., Berlin

Foust GP and Massey V (1967) Studies of ferredoxin-TPN reductase and ferredoxin from spinach. Fed Proc 26: 732

Foust GP, Mayhew SG and Massey V (1969) Complex formation between ferredoxin triphosphopyridine nucleotide reductase and electron transfer proteins. J Biol Chem 244: 964–970

Freigang J, Diederichs K, Schaefer KP, Welte W and Paul R (2002) Crystal structure of oxidized flavodoxin, an essential protein in *Helicobacter pylori*. Protein Sci 11: 253–261

Fritz J, Müller F and Mayhew SG (1973) Electron-nuclear double resonance study of flavodoxin from *Peptostreptococcus elsdenii*. Helv Chim Acta 56: 2250–2254

Fu W, Drozdzewski PM, Davies MD, Sligar SG and Johnson MK (1992) Resonance Raman and magnetic circular dichroism studies of reduced [2Fe-2S] proteins. J Biol Chem 267: 15502–15510

Fukuyama K, Matsubara H and Rogers LJ (1992) Crystal structure of oxidized flavodoxin from a red alga *Chondrus crispus* refined at 1.8 A resolution. Description of the flavin mononucleotide binding site. J Mol Biol 225: 775–789

Fukuyama K, Ueki N, Nakamura H, Tsukihara T and Matsubara H (1995) Tertiary structure of [2Fe-2S] ferredoxin from *Spirulina platensis* refined at 2.5 Å resolution: structural comparisons of plant-type ferredoxins and electrostatic potential analysis. J Biochem 117: 1017–1023

Gómez-Moreno C, Choy M and Edmondson DE (1979) Purification and properties of the bacterial flavoenzyme thiamine dehydrogenase. J Biol Chem 254: 7630–7635

Gómez-Moreno C, Martínez-Júlvez M, Fillat MF, Hurley JK and Tollin G (1995) Molecular recognition in electron transfer proteins. In: Mathis P (ed) Photosynthesis: From Light to Biosphere, Vol II, pp 627–632. Kluwer Academic Publishers, The Netherlands

Hermoso JA, Mayoral T, Faro M, Gómez-Moreno C, Sanz-Aparicio J and Medina M (2002) Mechanism of coenzyme recognition and binding revealed by crystal structure analysis of ferredoxin-NADP$^+$ reductase complexed with NADP$^+$. J Mol Biol 319: 1133–1142

Holden HM, Jacobson BL, Hurley JK, Tollin G, Oh B-H, Skjeldal L, Chae YK, Cheng H, Xia B and Markley JL (1994) Structure-function studies of [2Fe-2S] ferredoxins. J Bioenerg Biomembr 26:67–88

Hurley JK, Salamon Z, Meyer TE, Fitch JC, Cusanovich MA, Markley JL, Cheng H, Xia B, Chae YK, Medina M, Gómez-Moreno C and Tollin G (1993a) Amino acid residues in *Anabaena* ferredoxin crucial to interaction with ferredoxin-NADP$^+$ reductase: site-directed mutagenesis and laser flash photolysis. Biochemistry 32: 9346–9354

Hurley JK, Cheng H, Xia B, Markley JL, Medina M, Gómez-Moreno C and Tollin G (1993b) An aromatic amino acid is required at position 65 in *Anabaena* ferredoxin for rapid electron transfer to ferredoxin:NADP$^+$ reductase. J Am Chem Soc 115: 11698–11701

Hurley JK, Medina M, Gómez-Moreno C and Tollin G (1994) Further characterization by site-directed mutagenesis of the protein–protein interface in the ferredoxin/ferredoxin:NADP$^+$ system from *Anabaena*: requirement for a negative charge at position 94 in ferredoxin for rapid electron transfer. Arch Biochem Biophys 312: 480–486

Hurley JK, Fillat MF, Gómez-Moreno C and Tollin G (1996a) Electrostatic and hydrophobic interactions during complex formation and electron transfer in the ferredoxin/ferredoxin:NADP$^+$ reductase system from *Anabaena.* J Am Chem Soc 118: 5526–5531

Hurley JK, Schmeits JL, Genzor C, Gómez-Moreno C and Tollin G (1996b) Charge reversal mutations in a conserved acidic patch in *Anabaena* ferredoxin can attenuate or enhance electron transfer to ferredoxin:NADP$^+$ reductase by altering protein/protein orientation within the intermediate complex. Arch Biochem Biophys 333: 243–250

Hurley JK, Weber-Main AM, Stankovich MT, Benning MM, Thoden JB, Vanhooke JL, Holden HM, Chae YK, Xia B, Cheng H, Markley JL, Martínez-Júlvez M, Gómez-Moreno C, Schmeits JL and Tollin G (1997a) Structure-function relationships in *Anabaena* ferredoxin: correlations between x-ray crystal structures, reduction potentials, and rate

constants for electron transfer to ferredoxin:NADP$^+$ reductase for site-specific ferredoxin mutants. Biochemistry 36: 11100–11117

Hurley JK, Weber-Main AM, Hodges AE, Stankovich MT, Benning MM, Holden HM, Cheng H, Xia B, Markley JL, Genzor C, Gómez-Moreno C, Hafezi R and Tollin G (1997b) Iron-sulfur cluster cysteine-to-serine mutants of *Anabaena* [2Fe-2S] ferredoxin exhibit unexpected redox properties and are competent in electron transfer to ferredoxin:NADP$^+$ reductase. Biochemistry 36: 15109–15117

Hurley JK, Hazzard JT, Martínez-Júlvez M, Medina M, Gómez-Moreno C and Tollin G (1999) Electrostatic forces involved in orienting *Anabaena* ferredoxin during binding to *Anabaena* ferredoxin:NADP$^+$ reductase: site-specific mutagenesis, transient kinetic measurements, and electrostatic surface potentials. Protein Sci 8: 1614–1622

Hurley JK, Faro M, Brodie TB, Hazzard JT, Medina M, Gómez-Moreno C and Tollin G (2000) Highly nonproductive complexes with *Anabaena* ferredoxin at low ionic strength are induced by nonconservative amino acid substitutions at Glu 139 in *Anabaena* ferredoxin:NADP+ reductase. Biochemistry 39: 13695–13702

Hurley JK, Morales R, Martínez-Júlvez M, Brody TB, Medina M, Gómez-Moreno C and Tollin G (2002) Structure-function relationships in *Anabaena* ferredoxin/ferredoxin:NADP$^+$ electron transfer: insights from site-directed mutagenesis, transient absorption measurements and X-ray crystallography. Biochim Biophys Acta 1554: 5–21

Jacobson BL, Chae YK, Markley JL, Rayment I and Holden HM (1993) Molecular structure of the oxidized, recombinant, heterocyst [2Fe-2S] ferredoxin from *Anabaena* 7120 determined to 1.7-Å resolution. Biochemistry 32: 6788–6793

Jelesarov I and Bosshard HR (1994) Thermodynamics of ferredoxin binding to ferredoxin:NADP$^+$ reductase and the role of water at the complex interface. Biochemistry 33: 13321–13328

Jelesarov I, De Pascalis AR, Koppenol WH, Hirasawa M, Knaff DB and Bosshard HR (1993) Ferredoxin binding site on ferredoxin:NADP$^+$ reductase. Differential chemical modification of free and ferredoxin-bound enzyme. Eur J Biochem 216: 57–66

Jenkins CM, Genzor, CG, Fillat MF, Waterman MR and Gómez-Moreno M (1997) Negatively charged *Anabaena* flavodoxin residues (Asp144 and Glu145) are important for reconstitution of cytochrome P450 17 alpha-hydroxylase activity. J Biol Chem 36: 22509–22513

Johnson MK (1994) Iron-sulfur proteins. In: King RB (ed) Encyclopedia of inorganic chemistry, pp 1896–1915. John Wiley and Sons, New York

Kang CH, Ferguson-Miller S and Margoliash E (1977) Steady state kinetics and binding of eukaryotic cytochromes *c* with yeast cytochrome *c* peroxidase. Biochemistry 252: 919–926

Karplus PA (1991) Structure/function of spinach ferredoxin:NADP$^+$ oxidoreductase. In: Curti B, Ronchi S and Zanetti G (eds) Flavins and Flavoproteins 1990, pp 449–455. Walter de Gruyter & Co., Berlin

Karplus PA, Daniels MJ and Herriot JR (1991) Atomic structure of ferredoxin-NADP$^+$ reductase: prototype for a structurally novel flavoenzyme family. Science 251: 60–66

Keirns JJ and Wang JH (1972) Studies on nicotinamide adenine dinucleotide phosphate reductase from spinach chloroplasts. J Biol Chem 22: 7374–7382

Knaff DB (1996) Ferredoxin and ferredoxin-dependent enzymes. In: Ort DR and Yocum CF (eds) Oxygenic Photosynthesis: The Light Reactions, pp 333–361. Kluwer Academic Publishers, Dordrecht

Knauf MA, Lohr F, Curley GP, O'Farrell P, Mayhew SG, Muller F and Ruterjans H (1993) Homonuclear and heteronuclear NMR studies of oxidized *Desulfovibrio vulgaris* flavodoxin. Sequential assignments and identification of secondary structure elements. Eur J Biochem 213: 167–184

Kurisu G, Kusunoki M, Katoh E, Yamazaki T, Teshima K, Onda Y, Kimata-Ariga Y and Hase T (2001) Structure of the electron transfer complex between ferredoxin and ferredoxin-NADP$^+$ reductase. Nat Struct Biol 8: 117–121

Lostao A, Gómez-Moreno C, Mayhew SG and Sancho J (1997) Differential stabilization of the three FMN redox forms by tyrosine 94 and tryptophan 57 in flavodoxin from *Anabaena* and its influence on the redox potentials. Biochemistry 36: 14334–14344

Lovenberg W (ed) (1973) (1974) (1977) Iron-Sulfur Proteins, Vol. I, II, III. Academic Press, New York

Ludwig ML, Pattridge KA, Metzger AL, Dixon MM, Eren M, Feng Y and Swenson RP (1997) Control of oxidation-reduction potentials in flavodoxin from *Clostridium beijerinckii*: the role of conformation changes. Biochemistry 36: 1259–1280

Malkin R (1996) Photosystem I electron transfer reactions – components and kinetics. In: Ort DR and Yocum CF (eds) Oxygenic Photosynthesis: The Light Reactions, pp 333–361. Kluwer Academic Publishers, Dordrecht

Martínez-Júlvez M, Medina M, Hurley JK, Hafezi R, Brodie TB, Tollin G and Gómez-Moreno C (1998a) Lys 75 of *Anabaena* ferredoxin-NADP$^+$ reductase is a critical residue for binding ferredoxin and flavodoxin during electron transfer. Biochemistry 37: 13604–13613

Martínez-Júlvez M, Hermoso J, Hurley JK, Mayoral T, Sanz-Aparicio J, Tollin G, Gómez-Moreno C and Medina M (1998b) Role of Arg100 and Arg264 from *Anabaena* PCC 7119 ferredoxin-NADP$^+$ reductase: binding and electron transfer. Biochemistry 37: 17680–17691

Martínez-Júlvez M, Medina M and Gómez-Moreno C (1999) Ferredoxin-NADP$^+$ reductase uses the same site for the interaction with ferredoxin and flavodoxin. J Biol Inorg Chem 4: 568–578

Martínez-Júlvez M, Nogués I, Faro M, Hurley JK, Brodie TB, Mayoral T, Sanz-Aparicio J, Hermoso JA, Stankovich MT, Medina M, Tollin G and Gómez-Moreno C (2001) Role of a cluster of hydrophobic residues near the FAD cofactor in *Anabaena* PCC 7119 ferrredoxin-NADP$^+$ reductase for optimal complex formation and electron transfer to ferredoxin. J Biol Chem 276: 27498–27510

Masaki R, Yoshikawa S and Matsubara H (1982a) Steady-state kinetics of oxidation of reduced ferredoxin with ferredoxin-NADP$^+$ reductase. Biochim Biophys Acta 700: 101–109

Masaki R, Matsumoto M, Yoshikawa S and Matsubara H (1982b) Steady state and transient kinetics of reduced ferredoxin with ferredoxin-NADP$^+$ reductase. In: Massey V and Williams CH (eds) Flavins and Flavoproteins, pp 675–678. Elsevier, North Holland

Matsubara H and Hase T (1983) Phylogenetic consideration of ferredoxins sequences in plants, particularly algae. In: Jensen U and Fairbrothers DE (eds) Proteins and Nucleic Acids in Plant Systematics, pp 168–181. Springer-Verlag, Berlin

Matsubara H and Saeki K (1992) Structural and functional diversity of ferredoxins and related proteins. In: Cammack R and Sykes AG (eds) Advances in Inorganic Chemistry, Iron-Sulfur Proteins, Vol 38, pp 223–280. Academic Press, Inc., San Diego, CA

Mauk MR, Ferrer JC and Mauk AG (1994) Proton linkage in formation of the cytochrome *c*-cytochrome *c* peroxidase complex: electrostatic properties of the high- and low-affinity cytochrome binding sites on the peroxidase. Biochemistry 33: 12609–12614

Mayoral T, Medina M, Sanz-Aparicio J, Gómez-Moreno C and Hermoso JA (2000) Structural basis of the catalytic role of Glu301 in *Anabaena* PCC 7119 ferredoxin-NADP$^+$ reductase revealed by X-ray crystallography. Proteins: Struct Funct Gen 38: 60–69

Medina M and Gómez-Moreno C (2004) Interaction of ferredoxin-NADP+ reductase with its substrates: optimal interaction for efficient electron transfer. Photosynth Res 79: 113–131.

Medina M, Méndez E and Gómez-Moreno C (1992a) Identification of arginyl residues involved in the binding of ferredoxin-NADP$^+$ reductase from *Anabaena* sp. 7119 to its substrates. Arch Biochem Biophys 299: 281–286

Medina M, Méndez E and Gómez-Moreno C (1992b) Lysine residues on ferredoxin-NADP$^+$ reductase from *Anabaena* sp. 7119 involved in substrate binding. FEBS Lett 298: 25–28

Medina M, Peleato ML, Mendez E and Gómez-Moreno C (1992c) Identification of specific carboxyl groups on *Anabaena* PCC 7119 flavodoxin which are involved in the interaction with ferredoxin-NADP$^+$ reductase. Eur J Biochem 203: 373–379

Medina M, Martínez-Júlvez M, Hurley JK, Tollin G and Gómez-Moreno C (1998) Involvement of glutamic acid 301 in the catalytic mechanism of ferredoxin-NADP$^+$ reductase from *Anabaena* PCC 7119. Biochemistry 37: 2715–2728

Morales R, Charon M-H, Hudry-Clergeon G, Pétillot Y, Norager S, Medina M and Frey M (1999) Refined X-ray structures of the oxidized, at 1.3 Å, and reduced, at 1.17 Å, [2Fe-2S] ferredoxin from the cyanobacterium *Anabaena* PCC7119 show redox-linked conformational changes. Biochemistry 38: 15764–15773

Morales R, Charon M-H, Kacholova G, Serre L, Medina M, Gómez-Moreno C and Frey M (2000) A redox-dependent interaction between two electron-transfer partners involved in photosynthesis. EMBO Rep 1: 271–276

Nakamura S and Kimura T (1971a) A possible regulation of activity of ferredoxin-NADP$^+$ reductase and ferredoxin system by ionic strength: catalytic significance of the one to one complex. FEBS Lett 15: 352–354

Nakamura S and Kimura T (1971b) Studies on spinach ferredoxin-nicotinomide adenine dinucleotide phosphate reductase. FEBS Lett 15: 352–354

Navarro JA, Hervas M, Genzor CG, Cheddar G, Fillat MF, de la Rosa MA, Gómez-Moreno C, Cheng H, Xia B, Chae YK, Yan H, Wong B, Straus A, Markley JL, Hurley JK and Tollin G (1995) Site-specific mutagenesis demonstrates that the structural requirements for efficient electron transfer in *Anabaena* ferredoxin and flavodoxin are highly dependent on the reaction partner: kinetic studies with photosystem I, ferredoxin:NADP$^+$ reductase, and cytochrome *c*. Arch Biochem Biophys 321: 229–238

Nelson N and Neumann J (1968) Interaction between ferredoxin and ferredoxin-NADP$^+$ reductase from chloroplasts. Biochem Biophys Res Comm 30: 142–147

Nogués I, Martínez-Júlvez M, Navarro JA, Hervás M, Armenteros L, de la Rosa MA, Brodie TB, Hurley JK, Tollin G, Gómez-Moreno C and Medina M (2003) Role of hydrophobic interactions in the flavodoxin mediated electron transfer from Photosystem I to ferredoxin-NADP$^+$ reductase in *Anabaena* PCC 7119. Biochemistry 42: 2036–2045

Nuevo MR, Chu H-H, Vitello LB and Erman JE (1993) Salt-dependent switch in the pathway of electron transfer from cytochrome *c* to cytochrome *c* reductase compound I. J Am Chem Soc 115: 5873–5874

Palmer G (1973) Current insights into the active center of spinach ferredoxin and other iron-sulfur proteins. In: Lovenberg W (ed) Iron-Sulfur Proteins, Vol 2, pp 285–325. Academic Press, New York

Peleato ML, Ayora S, Inda LA and Gómez-Moreno C (1994) Isolation and characterization of two different flavodoxins from the eukaryotic alga *Chlorella fusca*. Biochem J 302: 807–811

Piubelli L, Aliverti A, Bellintani F and Zanetti G (1996) Mutations of Glu92 in ferredoxin I from spinach leaves produces proteins fully functional in electron transfer but less efficient in supporting NADP$^+$ photoreduction. Eur J Biochem 236: 465–469

Price NT, Smith AJ and Rogers LJ (1992) Relationship of the flavodoxin isoforms from *Porphyra umbilicalis*. Phytochemistry 30: 2835–2839

Pueyo JJ and Gómez-Moreno C (1991) Purification of ferredoxin-NADP$^+$ reductase, flavodoxin and ferredoxin from a single batch of the cyanobacterium *Anabaena* PCC7119. Prep Biochem 21: 191–204

Pueyo JJ, Gómez-Moreno C and Mayhew SG (1991) Oxidation-reduction potentials of ferredoxin-NADP$^+$ reductase and flavodoxin from *Anabaena* PCC 7119 and their electrostatic and covalent complexes. Eur J Biochem 202: 1065–1071

Pueyo JJ, Revilla C, Mayhew SG and Gómez-Moreno C (1992) Complex formation between ferredoxin and ferredoxin-NADP$^+$ reductase from *Anabaena* PCC 7119: cross-linking studies. Arch Biochem Biophys 294: 367–372

Rao ST, Shaffie F, Yu C, Satyshur KA, Stockman BJ, Markley JL and Sundarlingam M (1992) Structure of the oxidized long-chain flavodoxin from *Anabaena* 7120 at 2 Å resolution. Protein Sci 1: 1413–1427

Rogers LJ (1987) Ferredoxins, flavodoxins and related proteins: structure, function and evolution. In: Fay P and Van Baalen C (eds) The Cyanobacteria, pp 35–67. Elsevier, Amsterdam

Rypniewski WR, Breiter DR, Benning MM, Wesenberg G, Oh B-H, Markley JL, Rayment I and Holden HM (1991) Crystallization and structure determination to 2.5-Å resolution of the oxidized [2Fe-2S] ferredoxin from *Anabaena* 7120. Biochemistry 30: 4126–4131

Sancho J, Peleato ML, Gómez-Moreno C and Edmondson DE (1988) Purification and properties of ferredoxin-NADP$^+$ oxidoreductase from the nitrogen-fixing cyanobacteria *Anabaena variabilis*. Arch Biochem Biophys 260: 200–207

Sancho J, Medina M and Gómez-Moreno C (1990) Arginyl groups involved in the binding of *Anabaena* ferredoxin-NADP$^+$ reductase to NADP$^+$ and to ferredoxin. Eur J Biochem 187: 39–48

Sands RH and Dunham WR (1975) Spectroscopic studies on two-iron ferredoxins. In: Engström A, Ehrenberg A, Keynes

RD and Felsenfeld G (eds) Quarterly Reviews of Biophysics, Vol 7, pp 443–504. Cambridge University Press, Cambridge

Schmitz S and Böhme H (1995) Amino acid residues involved in functional interaction of vegetative cell ferredoxin from the cyanobacterium *Anabaena* sp. PCC 7120 with ferredoxin:$NADP^+$ reductase, nitrite reductase and nitrate reductase. Biochim Biophys Acta 1231: 335–341

Schmitz S, Martínez-Júlvez M, Gómez-Moreno C and Böhme H (1998) Interaction of positively charged amino acid residues of recombinant, cyanobacterial ferredoxin:$NADP^+$ reductase with ferredoxin probed by site-directed mutagenesis. Biochim Biophys Acta 1363: 85–93

Serre L, Vellieux FMD, Medina M, Gómez-Moreno C, Fontecilla-Camps JC and Frey M (1996) X-ray structure of the ferredoxin:$NADP^+$ reductase from the cyanobacterium *Anabaena* PCC 7119 at 1.8 Å resolution, and the crystallographic studies of $NADP^+$ binding at 2.25 Å resolution. J Mol Biol 263: 20–39

Shin M and San Pietro A (1968) Complex formation of ferredoxin-NADP reductase with ferredoxin and with NADP. Biochem Biophys Res Comm 33: 38–42

Shin M, Tagawa K and Arnon DI (1963) Crystallization of ferredoxin-TPN reductase and its role in the photosynthetic apparatus of chloroplasts. Biochem Zeitsch 338: 84–96

Skjeldal L, Westler WM, Oh B-H, Krezel AM, Holden HM, Jacobson BL, Rayment I and Markley JL (1991) Two-dimensional magnetization exchange spectroscopy of *Anabaena* 7120 ferredoxin. Nuclear overhauser effect and electron self-exchange cross peaks from amino acid residues surrounding the 2Fe-2S cluster. Biochemistry 30: 7363–7368

Smillie RM (1965) Isolation of phytoflavin, a flavoprotein with chloroplast ferredoxin activity. Plant Physiol 40: 1124–1165

Smith JM, Smith WH and Knaff DB (1981) Electrochemical titrations of ferredoxin-ferredoxin:$NADP^+$ oxidoreductase complex. Biochim Biophys Acta 635: 405–411

Sticht H and Rösch P (1998) The structure of iron-sulfur proteins. Progr Biophys Mol Biol 70, 95–136

Stombaugh NA, Sundquist JE, Burris RH and Orme-Johnson WH (1976) Oxidation-reduction properties of several low potential iron-sulfur proteins and of methylviologen. Biochemistry 15: 2633–2641

Swenson RP and Krey GD (1994) Site-directed mutagenesis of tyrosine-98 in the flavodoxin from *Desulfovibrio vulgaris* (Hildenborough): regulation of oxidation-reduction properties of the bound FMN cofactor by aromatic, solvent, and electrostatic interactions. Biochemistry 33: 15298–15308

Tagawa K and Arnon DI (1962) Ferredoxins as electron carriers in photosynthesis and the biological production and consumption of hydrogen gas. Nature 195: 537–543

Tagawa K and Arnon DI (1968) Oxidation reduction potentials and stoichiometry of electron transfer in ferredoxins. Biochim Biophys Acta 153: 602–613

Tsukihara T, Kobayashi M, Nakamura M, Katsube Y, Fukuyama K, Hase T and Matsubara H (1982) Structure-function relationship of [2Fe-2S] ferredoxins and design of a model molecule. Biosystems 15: 243–257

Tsukihara T, Fukuyama K, Mizushima M, Harioka T, Kusunoki M, Katsube Y, Hase T and Matsubara H (1990) Structure of the [2Fe-2S] ferredoxin I from blue-green alga *Aphanothece sacrum.* J Mol Biol 216: 399–410

Ullmann GM, Hauswald M, Jensen A and Knapp EW (2000) Structural alignment of ferredoxin and flavodoxin based on electrostatic potentials: implications for their interactions with photosystem I and ferredoxin-$NADP^+$ reductase. Proteins 38: 301–309

van Mierlo CP, Muller F and Vervoort J (1990) Secondary and tertiary structure characteristics of *Megasphaera elsdenii* flavodoxin in the reduced state as determined by two-dimensional 1H NMR. Eur J Biochem 189: 589–600

Verhagen MFJM, Link TA and Hagen WR (1995) Electrochemical study of the redox properties of [2Fe-2S] ferredoxins. Evidence of superreduction of the rieske [2Fe-2S] cluster. FEBS Lett 361: 75–78

Vidakovic M, Fraczkiewicz G, Dave BC, Czernuszewicz RS and Germanas J (1995) The environment of [2Fe-2S] clusters in ferredoxins: the role of residue 45 probed by site-directed mutagenesis. Biochemistry 34: 13906–13913

Vieira BJ and Davis DJ (1986) Interaction of ferredoxin with ferredoxin:NADP reductase: effects of chemical modification of ferredoxin. Arch Biochem Biophys 247: 140–146

Vieira BJ, Colvert KK and Davis DJ (1986) Chemical modification and cross-linking as probes of regions on ferredoxin involved in interaction with ferredoxin:NADP reductase. Biochim Biophys Acta 851: 109–122

Walker MC, Pueyo JJ, Navarro JA, Gómez-Moreno C and Tollin G (1991) Laser flash photolysis studies of reduction of ferredoxins and ferredoxin-$NADP^+$ reductases from *Anabaena* PCC 7119 and spinach: electrostatic effects on intracomplex electron transfer. Arch Biochem Biophys 287: 351–358

Walsh MA, McCarthy A, O'Farrell PA, McArdle P, Cunningham PD, Mayhew SG and Higgins TM (1998) X-ray crystal structure of the *Desulfovibrio vulgaris* (Hildenborough) apoflavodoxin-riboflavin complex. Eur J Biochem 258: 362–371

Wang M, Roberts DL, Paschke R, Shea TM, Masters BS and Kim JJ (1997) Three-dimensional structure of NADPH-cytochrome P450 reductase: prototype for FMN- and FAD-containing enzymes. Proc Natl Acad Sci USA 94: 8411–8416

Weber-Main AM, Hurley JK, Cheng H, Xia B, Chae YK, Markley JL, Martínez-Júlvez M, Gómez-Moreno C, Stankovich MT and Tollin G (1998) An electrostatic, kinetic and spectroscopic characterization of [2Fe-2S] vegetative and heterocyst ferredoxins from *Anabaena* 7120 with mutations in the cluster binding loop. Arch Biochem Biophys 355: 181–188

Zanetti G, Aliverti A and Curti B (1984) A cross-linked complex between ferredoxin and ferredoxin-$NADP^+$ reductase. J Biol Chem 259: 6153–6157

Zanetti G, Morelli D, Ronchi S, Negri A, Aliverti A and Curti B (1988) Structural studies on the interaction between ferredoxin and ferredoxin:$NADP^+$ reductase. Biochemistry 27: 3753–3759

Zanetti G, Aliverti A, Ravasi D, Curti B, Deng Z and Karplus PA (1997) On the role of glutamate 312 of spinach ferredoxin:$NADP^+$ reductase. In: Stevenson KJ, Massey V and Williams CH Jr (eds) Flavins and Flavoproteins 1996, pp 509–512. University of Calgary Press, Calgary, Alberta

Zhou J, Nocek JM, DeVan ML and Hoffman BM (1995) Inhibitor-enhanced electron transfer: copper cytochrome c as a redox-inert probe of ternary complexes. Science 269: 204–207

Chapter 28

The Interaction of Ferredoxin with Ferredoxin-Dependent Enzymes

Toshiharu Hase
Institute for Protein Research, Osaka University, 3-2 Yamadaoka, Suita, Osaka 565-0871

Peter Schürmann
Laboratoire de Biochimie Végétale, Université de Neuchâtel, CH-2007 Neuchâtel, Switzerland

David B. Knaff*
Department of Chemistry and Biochemistry, Texas Tech University, Lubbock, TX 79409-1061, USA

Summary

Ferredoxin, reduced by Photosystem I (PS I) in the light, serves as the electron donor for the reduction of NADP$^+$ to NADPH, of sulfite to sulfide, of nitrite to ammonia and for the reductant-requiring of glutamate and 2-oxoglutarate to glutamate in all oxygenic photosynthetic organisms. Reduced ferredoxin also serves as the electron donor for the reduction of nitrate to nitrite in cyanobacteria. In addition to its role in supplying a source of electrons for the net reduction of oxidized species in reductant-requiring assimilatory pathways, reduced ferredoxin plays an important role, via the ferredoxin/thioredoxin system, in the regulation of carbon assimilation and other pathways. This chapter focuses on the interactions between ferredoxin and six enzymes that utilize reduced ferredoxin as an electron donor (NADP$^+$ reductase, nitrate reductase, nitrite reductase, glutamate synthase, sulfite reductase, and thioredoxin reductase). The mechanisms of several of these enzymes will also be discussed.

*Author for correspondence, email:david.knaff@ttu.edu

John H. Golbeck (ed): Photosystem I: The Light-Driven Plastocyanin:Ferredoxin Oxidoreductase, 477–498.

I. Introduction

Ferredoxin serves as the ultimate electron acceptor for all of the electrons that enter the photosynthetic electron transfer chain, as a result of the oxidation of water to oxygen, in oxygenic photosynthetic organisms (for the sake of simplicity, this chapter will not treat situations in which flavodoxin replaces ferredoxin in some organisms under iron-limiting conditions). Most of the reduced ferredoxin generated by the light-reaction of Photosystem I is used to reduce $NADP^+$, in a reaction catalyzed by ferredoxin:$NADP^+$ oxidoreductase, hereafter abbreviated FNR. The NADPH produced by this FNR-catalyzed reaction serves as the electron donor for the single reductant-requiring step in the pathway of CO_2 assimilation in C3 plants, the reduction of 1,3-bisphosphoglyceric acid to glyceraldehyde-3-phosphate (Hoober, 1984). Reduced ferredoxin also serves as the electron donor for the reduction of nitrite to ammonia, the reductive conversion of 2-oxoglutarate plus glutamine to glutamate, the reduction of sulfite to sulfide, and the reduction of two proteins that regulate carbon assimilation, thioredoxins *m* and *f* (Knaff, 1996; Jacquot et al., 1997a). In oxygenic photosynthetic eukaryotes, all of these reactions are catalyzed by enzymes located in the chloroplast stromal space. Although the first step in nitrate assimilation in photosynthetic eukaryotes, the two-electron reduction of nitrate to nitrite, utilizes reduced pyridine nucleotide as the electron donor, in cyanobacteria the reduction of nitrate to nitrite is also ferredoxin-dependent (Flores and Herrero, 1994; Knaff, 1996). In addition to serving as the electron donor for the noncyclic electron acceptors listed above, reduced ferredoxin serves as an electron carrier for cyclic electron flow, which provides a portion of the ATP utilized for CO_2 assimilation.

Ferredoxins found in cyanobacteria and in the chloroplasts of algae and higher plants are acidic, monomeric proteins with molecular masses of ~11 kDa (Holden et al., 1994; Knaff, 1996). All ferredoxins contain a single $[2Fe–2S]^{+1,+2}$ cluster that serves as a one-electron carrier, operating at low redox potentials (E_m values range from −300 to −460 mV, Holden et al., 1994; Knaff, 1996). Amino acid sequences are known for a large number of these "plant-type" ferredoxins and several regions of the protein are highly conserved (Matsubara and Hase, 1983; Holden et al., 1994). Three-dimensional structures are available for at least ten of these ferredoxins (including proteins from cyanobacteria, algae, and higher plants). Most of these structures, all of which are quite similar, were obtained by X-ray crystallography but solution structures obtained by NMR spectroscopy are also available (Holden et al., 1994; Fukuyama, 2004). The major secondary structural features of ferredoxins have been presented by Sétif (this volume, Chapter 26), and so they will not be discussed again in detail in this chapter. Readers are referred also to the recent review by Fukuyama (2004) for more information about these structures.

A large body of data, obtained from chemical modification studies, cross-linking experiments, site-directed mutagenesis, and computer modeling, supported the hypothesis that electrostatically stabilized complexes between ferredoxin (hereafter abbreviated as Fd) and Fd-dependent enzymes play an important role in the electron transfer from reduced Fd to these enzymes (Knaff, 1996). As might be expected from the fact that ferredoxins are highly acidic proteins, these data suggest that, for the most part, Fd supplies the negatively charged groups and the enzymes supply the positively charged groups involved in complex formation (Knaff, 1996). This chapter will focus on the details of the interactions between Fd and six enzymes that use reduced Fd as an electron donor. In the case of one of these enzymes, ferredoxin:$NADP^+$ oxidoreductase, the prosthetic group content, redox properties, and reaction mechanism are extensively discussed by Hurley et al. (this volume, Chapter 27). In the cases of the other five enzymes to be discussed in this chapter (i.e., nitrate reductase, nitrite reductase, glutamate synthase, sulfite reductase, and thioredoxin reductase), brief descriptions of the prosthetic group contents and mechanisms will be presented in addition to descriptions of what is known about the protein–protein interactions that occur in the complexes of these enzymes with Fd. As the kinetics of Fd reduction by the PS I reaction center have been presented in extensive detail by Sétif (this volume, Chapter 26), the discussions of enzymes that use reduced Fd as an electron donor presented below will start from the point where reduced Fd is already available.

II. Ferredoxin:$NADP^+$ Oxidoreductase

The kinetics of FNR reduction by reduced Fd and the identity of several amino acids that appear to play important roles in optimizing the interactions between the

Abbreviations: 2-IG – 2-iminoglutarate; 2-OG – 2-oxoglutarate; DON – 6-diazo-5-oxo-L-norleucine; E_m – midpoint oxidation–reduction potential; Fd – ferredoxin; FNR – ferredoxin:$NADP^+$; FTR – ferredoxin:thioredoxin reductase; L-Gln – L-glutamine; L-Glu – L-glutamate; ONL – 5-oxo-L-norleucine; Trx – thioredoxin.

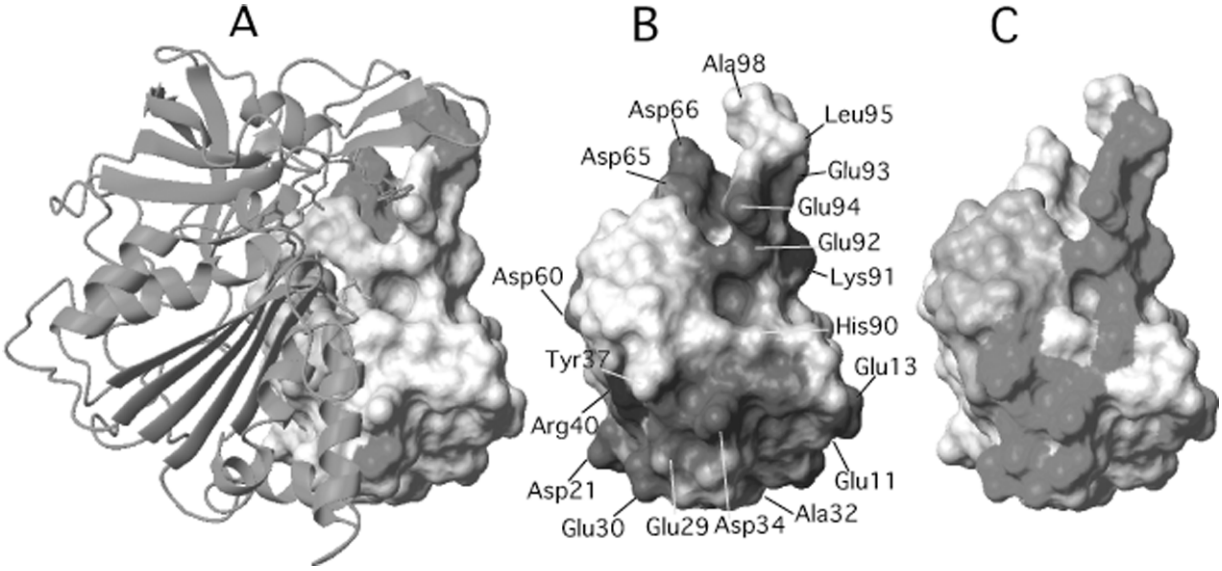

Fig. 1. NMR chemical shift perturbation of Fd upon complex formation with FNR or SiR were determined by measuring 2D ^{1}H–^{15}N HSQC spectra of ^{15}N labeled Fd. See Color Plate 11, Fig. 2.

two proteins for productive electron transfer have been discussed by Sétif (this volume, Chapter 26) and by Hurley et al. (this volume, Chapter 27). Thus, the discussion of the interactions between Fd and FNR in this chapter will focus on structural aspects of the complex between the proteins. Recently, the three-dimensional structure of maize leaf Fd-FNR complex at 2.59 Å resolution was determined (Kurisu et al., 2001) and the detailed geometry of the complex is now available (Fig. 1A). The surface electrostatic potential distribution of Fd is shown in Fig. 1B. As ferredoxins typically have isoelectric points of 3.5 or less, Fd has a substantial net negative charge at pH values near neutrality and regions of negative potential dominate most of its surface. Thus, as might be expected, the intermolecular electrostatic interactions between Fd and FNR involve mainly negative charges on Fd and positive charges on FNR, i.e., salt bridge pairs between Glu29-Lys304, Asp60-Lys33, Asp65-Lys91, and Asp66-Lys88 (the Fd amino acid is listed first in each case). There is one exception, i.e., a salt bridge between the positively charged side chain of Arg40 on Fd and the negatively charged side chain of Glu154 on FNR. The crystal structure of the Fd/FNR complex formed by the proteins from the cyanobacterium *Anabaena* sp. PCC 7119 also reveals the presence of a number of electrostatic interactions between the two proteins. However, there are some significant differences between the structures of the two complexes (see Hurley et al., this volume, Chapter 27 for a detailed discussion). One significant difference between the complexes is that a highly conserved glutamate residue near the C-terminus of Fd (it is Glu94 in the *Anabaena* protein) that had been implicated by site-directed mutagenesis studies as playing an important role in forming a Fd/FNR complex that is productive for electron transfer, does indeed interact with FNR in the complex between the *Anabaena* proteins (Morales et al., 2000) but the equivalent residue in maize leaf Fd (Glu92) is not at the protein–protein interface in the complex with maize leaf FNR (Kurisu et al., 2001).

The [2Fe–2S] cluster of Fd and the FAD of FNR are in close proximity in the complex of the maize proteins, with the C8 methyl group of FAD separated by 6.0 Å from the Fe1 of the [2Fe–2S] cluster. The two prosthetic groups are almost as close in the complex between *Anabaena* FNR and Fd, with 7.4 Å separating the C8 methyl group of FNR from the S2 sulfur of the [2Fe–2S] cluster (Morales et al., 2000). These distances are consistent with direct, rapid outersphere electron transfer between the two prosthetic groups. The fact that it is the C8 methyl group of FNRs FAD group that is closest to the [2Fe–2S] cluster of Fd in both complexes is consistent with the suggestion that it is this portion of the FAD isoalloxazine ring that is involved in the electron transfer reaction. It should be pointed out that in the complex of the *Anabaena* proteins, Phe65 of Fd (a residue that mutagenic studies have implicated as playing an important role in electron transfer from Fd to FNR) is close to the [2Fe–2S]

cluster of Fd and is involved in the hydrophobic interactions with FNR at the protein/protein interface. In contrast, the corresponding aromatic residue in maize leaf Fd, Tyr63, is neither in close contact with the [2Fe–2S] cluster of Fd nor is it located between the two prosthetic groups at the protein/protein interface (see Morales et al., 2000; Kurisu et al., 2001; Hurley et al., this volume, Chapter 27).

The protein–protein interface near the prosthetic groups is rather hydrophobic and is occupied largely by uncharged amino acid residues in both the complex between the maize leaf proteins (Kurisu et al., 2001) and the *Anabaena* proteins (Morales et al., 2000). In fact, earlier studies of the effects of ionic strength on the kinetics of electron transfer from *Anabaena* sp. PCC 7120 ferredoxin to *Anabaena* sp. PCC 7119 FNR had indicated that hydrophobic, as well as electrostatic, effects were likely to play an important role in this system (Hurley et al., 1996). In this context, it should be mentioned that a microcalorimetry study of the complex formed between spinach Fd and spinach FNR indicated that ΔH, the change in enthalpy associated with complex formation, is essentially zero. The large, favorable negative ΔG (the free energy change) for complex formation results entirely from the favorable positive ΔS (the entropy change) associated with complex formation (Jelesarov and Bosshard, 1994). These results suggest that the salt bridges present in the complex do not make significant net energetic contributions to stabilizing the Fd/FNR complex. Experiments carried out in mixed solvent systems suggest that the favorable positive ΔS appears to arise instead from the transfer of oriented water molecules, bound to the surfaces of the individual protein, from the protein–protein interface region into the bulk solvent during complex formation (Jelesarov and Bosshard, 1994). In fact, structural studies on the *Anabaena* proteins indicate that approximately 10 ordered water molecules are lost as a result of complex formation.

The maize leaf Fd domains that interact with maize leaf FNR were also analyzed in solution using an NMR chemical perturbation technique in which specific features of the NMR spectrum of [^{15}N] Fd that are altered as a result of complex formation with FNR were assigned to regions on Fd that are involved in interactions with FNR (Kurisu et al., 2001). The areas on Fd that interact with FNR that are detected in the NMR experiment are very similar to those Fd regions implicated in interacting with FNR by the crystallographic data (see Fig. 1A).

Several structural changes occur in both Fd and FNR as a result of complex formation between the leaf proteins. It has also been shown that binding of Fd to FNR results in a negative shift in the E_m value of the [2Fe–2S] cluster of Fd (Smith et al., 1981; Batie and Kamin, 1984). It has been shown that spinach Fd1 (the dominant Fd isoform present in mature leaves) contains an internal salt bridge between the side chains of Glu29 and Arg40 (Binda et al., 1998). Although the structure of uncomplexed maize leaf Fd is not yet available, it is highly likely that this internal salt bridge exists in the highly homologous maize protein. Formation of the complex with FNR breaks this bond and, as described above, two new intermolecular salt bridges are formed, one between Glu29 of Fd and Lys394 of FNR and one between Arg40 of Fd and Glu154 of FNR. This internal salt bridge between Glu29 and Arg40 probably stabilizes the [2Fe–2S] cluster (Teshima et al., 2003), and it therefore is likely that this salt bridge exchange causes the shift in E_m. Such a negative shift in redox potential would make electron transfer from Fd to FNR a thermodynamically more favorable step during the FNR-catalyzed reduction of $NADP^+$. A positive change in the E_m value of the FAD group of FNR has been reported to accompany complex formation between spinach Fd and FNR (Smith et al., 1981), a change that would also make electron transfer from Fd to FNR thermodynamically more favorable. Binding of Fd induces slight movements of both the NADPH-binding and FAD-binding domains of FNR. The most significant movement is that of FNR Glu312. On formation of the complex, the carboxyl group of FNR Glu312 moves 2 Å toward the hydroxyl group of FNR Ser96 (to within hydrogen-bonding distance). Site-directed mutagenesis studies of Glu312 in spinach leaf FNR (Aliverti et al., 1998) documented an important role for this residue in binding of the nicotinamide ring of $NADP^+$ to the enzyme. As this residue is highly conserved, it seems likely that Glu312 plays a similar role in the maize leaf enzyme. Such changes in molecular interactions could alter the microenvironment at the binding site to optimize orientation of $NADP^+$ for productive interaction with the FAD (Deng et al., 1999; Kurisu et al., 2001; Carrillo and Ceccarelli, 2003). Replacement of Glu301 (the corresponding residue in *Anabaena* sp. PC 7119 FNR) by alanine effects electron transfer between this cyanobacterial FNR and *Anabaena* Fd, but the precise role of this glutamate residue in the cyanobacterial system remains to be elucidated (see Medina et al., 1998; Mayoral et al., 2000; see also Hurley et al., this volume, Chapter 27).

In several higher plants, distinct isoforms of Fd (Hase et al., 1991) and FNR (Morigasaki et al., 1990; Ritchie et al., 1994) are present in leaf and root, most

probably playing their unique roles in photosynthetic and nonphotosynthetic metabolism respectively (Green et al., 1991; Neuhaus and Emes, 2000; Yonekura-Sakakibara et al., 2000). Among different combinations of these FNR and Fd isoforms the highest activity occurs with the combination of leaf FNR and leaf Fd when electron transfer is in the photosynthetic direction, i.e., with reduced Fd donating electrons to $NADP^+$, and with the combination of root FNR and root Fd when electron transfer is from NADPH to Fd (Onda et al., 2000; Hanke et al., 2004a). Differences in activity may be explained in part by differences between the E_m values of the different isoforms of Fd, with the root-type Fd having a much more positive value (around −340 mV) than the leaf-type Fd (around -420 mV). This difference makes electron flow from root FNR to root Fd considerably more favorable than is the case for the leaf proteins (Akashi et al., 1999; Aliverti et al., 2001; Hanke et al., 2004a). Protein–protein interaction is another important determinant of electron transfer between Fd and FNR, and dissociation constants measured for different combinations of Fd and FNR point to a high level of isoform-specific recognition (Onda et al., 2000; Aliverti et al., 2001, 2004). Very recently, an X-ray crystal structure of the complex formed between maize root Fd and maize root FNR has been solved (Kurisu et al., submitted). This structure, together with that of the leaf counterpart, will provide us with a valuable opportunity to consider molecular arrangements selected for their efficiency in either photosynthetic or heterotrophic electron cascades [see the recent review by Hanke et al. (2004b) for a discussion of some aspects of this topic].

III. Nitrogen Assimilation

The pathway for nitrogen assimilation in oxygenic photosynthetic organisms (excluding the case of nitrogen-fixing cyanobacteria and plants that have established symbiotic relationships with nitrogen-fixing bacteria) begins with the uptake of nitrate and its two-electron reduction to nitrite, catalyzed by nitrate reductase (see Foyer et al., 2001, for a description of the nitrogen assimilation pathway). This is followed by the six-electron reduction of nitrate to ammonia, catalyzed by nitrite reductase, and the subsequent ATP-dependent incorporation of ammonia into glutamate to form glutamine (a reaction, catalyzed by glutamine synthetase, that does not involve any redox chemistry). The last step in this first stage of nitrogen assimilation involves the conversion of glutamine plus 2-oxoglutarate to two molecules of glutamate, a two-electron reductive reaction catalyzed by glutamate synthase (Suzuki and Knaff, 2005). In oxygenic photosynthetic eukaryotes, two of these redox reactions (those catalyzed by nitrite reductase and glutamate synthase) utilize reduced Fd as the electron donor, while in cyanobacteria all three reactions are ferredoxin-dependent.

A. Ferredoxin-Dependent Nitrite and Nitrate Reductases

1. Nitrate Reductase

The Fd-dependent nitrate reductases of cyanobacteria catalyze the two-electron reduction of nitrate to nitrite. Cyanobacteria are unique among oxygenic photosynthetic organisms in using reduced ferredoxin as the electron donor for the two-electron reduction of nitrate to nitrite (all other oxygenic photosynthetic organisms use NAD(P)H as the electron donor). The soluble Fd-dependent nitrate reductase of the cyanobacterium *Synechococcus* sp. PCC 7942, the product of the *narB* gene, is among the best characterized of the Fd-dependent nitrate reductases (Rubio et al., 1996, 2002). The complete amino acid sequence, deduced from the nucleotide sequence of the *narB* gene, is known for the 76 kDa protein, which has been shown to contain one molybdopterin cofactor (likely to be a *bis*-molybdopterin guanine dinucleotide) and one $[4Fe–4S]^{2+,1+}$ cluster as prosthetic groups (Rubio et al., 2002; Jepson et al., 2004). The native protein and a His-tagged variant, both of which are fully active, can be expressed in *Escherichia coli* and site-directed mutagenesis experiments have identified the four cysteines that are the likely ligands to the iron–sulfur cluster (Rubio et al., 2002). The E_m value of the iron–sulfur cluster is −190 mV and the E_m value of $Mo^{6+/5+}$ couple of the molybdopterin cofactor is −150 mV (Jepson et al., 2004). Although details of the mechanism of the *Synechococcus* sp. PCC 7942 enzyme have not yet been fully elucidated, protein film voltammetry experiments suggest that the catalytic cycle involves nitrate binding to the molybdopterin cofactor of enzyme that has been reduced by two electrons (compared to the air-oxidized, as-isolated enzyme), i.e., in which the enzyme cofactors are in the Mo^{5+} and $[4Fe–4S]^{1+}$ states. As the enzyme appears to contain only a single Fd-binding site (see below), two-electron reduction of the enzyme must involve two sequential and separate electron transfers from reduced Fd, given the fact that reduced Fd is a one-electron donor.

Titrations of nitrate reductase with Fd, using perturbations of both visible-region and CD spectra to monitor interaction between the proteins, are consistent with the formation of a 1:1 complex of very high affinity between the two proteins (Hirasawa et al., 2004a). The observation that these spectral perturbations are observed at low ionic strength, but not at high ionic strength, suggests that electrostatic forces play an important role in the formation of this protein–protein complex. Enzyme activity with Fd as the electron donor (but not with the nonphysiological electron donor, reduced methyl viologen) decreased greatly with increasing ionic strength, suggesting that electrostatic protein–protein interactions are important in catalysis (Schmitz and Böhme, 1995; Hirasawa et al., 2004a). Treatment of nitrate reductase with either the lysine-modifying reagent *N*-acetylsuccinimide or with the arginine-modifying reagent phenylglyoxal produced substantial inhibition of the Fd-dependent activity of the enzyme but had little effect on the reduction of nitrate catalyzed by the enzyme if reduced methyl viologen replaced reduced Fd as the electron donor. Chemical modification also significantly decreased the affinity of Fd binding by the enzyme. These observations, and the fact that formation of a complex between Fd and nitrate reductase completely protected the enzyme against inhibition by *N*-acetylsuccinimide and phenylglyoxal, suggest that one or more lysine and arginine residues are present at the Fd-binding site of this cyanobacterial nitrate reductase. Site-directed mutational replacement of either of two highly conserved glutamate residues near the C-terminus of Fd from the cyanobacterium *Anabaena* sp. PCC 7119, Glu94 or Glu95, by lysine residues dramatically decreased the rate of nitrate reduction catalyzed by the *Synechococcus* sp. PCC 7942 nitrate reductase, implicating the negative charges on these two residues in the interaction between Fd and the enzyme (Hirasawa et al., 2004a). Earlier mutational studies had implicated Glu94 in the interaction of Fd with the nitrate reductase isolated from *Anabaena* sp. PCC 7120 (Schmitz and Böhme, 1995). Mutagenesis experiments also suggest that a conserved aromatic amino acid residue on Fd (it is Phe65 in *Anabaena* sp. PCC 7120 Fd) may play some role in electron transfer from Fd to nitrate reductase (Schmitz and Böhme, 1995). Despite the availability of these important data, it is clear that a great deal of additional work remains to be done, particularly in terms of obtaining structural information, before a detailed picture of the protein/protein interaction domains involved in complex formation between Fd and cyanobacterial nitrate reductases will be available.

2. Nitrite Reductase

Plant, algal, and cyanobacterial nitrite reductases catalyze the six-electron reduction of nitrite to ammonia using reduced ferredoxin as the electron donor. Fd-dependent nitrite reductases have been isolated from several higher plants, algae, and cyanobacteria and characterized. Spinach leaf nitrite reductase is the best characterized of these enzymes, but all of the Fd-dependent nitrite reductases characterized to date are quite similar in molecular mass and catalytic properties. Although it is beyond the scope of this chapter, it should be pointed out that Fd-dependent nitrite reductases, along with other ferredoxin-dependent enzymes like FNR (see above), glutamate synthase, and sulfite reductase (see below), are found in nonphotosynthetic tissues in higher plants. In nonphotosynthetic tissues, such as roots, these enzymes use Fd reduced by NADPH (in a FNR-catalyzed reaction) as a source of reducing power for assimilatory reactions (Morigasaki et al., 1990; Green et al., 1991; Hase et al., 1991; Ritchie et al., 1994; Aoki et al., 1995; Neuhaus and Emes, 2000; Yonekura-Sakakibara et al., 2000).

Fd-dependent nitrite reductases are soluble enzymes that are located in the chloroplast stroma in photosynthetic eukaryotes. They are monomeric proteins with molecular masses ranging from 60 to 63 kDa. In photosynthetic eukaryotes, the genes encoding the enzymes are located in the nucleus and the proteins are synthesized in the cytoplasm as precursor proteins, with an N-terminal signal sequence that targets them for delivery to the chloroplast stroma, which is subsequently cleaved to form the mature-length protein (Back et al., 1988). Amino acid sequences, usually deduced from the corresponding cDNA sequences (including one for the 62,883 Da spinach enzyme), are available and the proteins, regardless of whether they are from cyanobacteria, algae, or higher plants, show significant regions of homology (Back et al., 1988; Luque et al., 1993; Bellissimo and Privalle, 1995; Knaff, 1996; Dose et al., 1997; Hirasawa et al., 1998). The enzymes contain one noncovalently bound siroheme and one low-potential $[4Fe–4S]^{+1,+2}$ cluster as the only prosthetic groups, with nitrite binding occurring at the siroheme iron through the N atom of the substrate (Knaff, 1996; Kuznetsova et al., 2004a,b). The four cysteine residues that bind the four iron atoms of the [4Fe–4S] cluster have been identified by sequence homology arguments (they are Cys473, Cys 479, Cys514, and Cys518 in the spinach enzyme) and the importance of Cys514 and Cys518 has been confirmed by site-directed mutagenesis analysis of the spinach enzyme (Bellissimo and

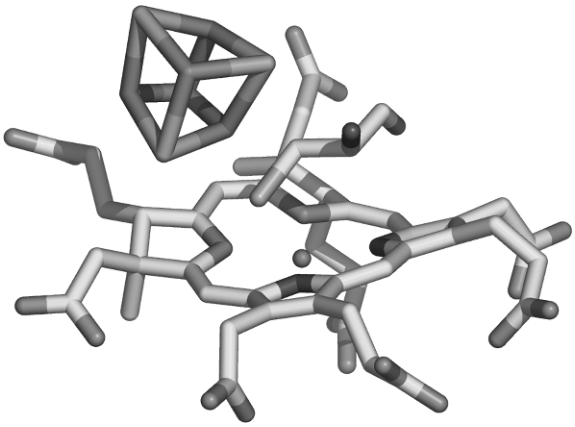

Fig. 2. The active site of spinach nitrite reductase. Shown is part of the current model of the three-dimensional structure of NiR, namely the iron–sulfur cluster, siroheme, and the cysteine, Cys518, that coordinates both cofactors through the iron atoms of each cofactor.

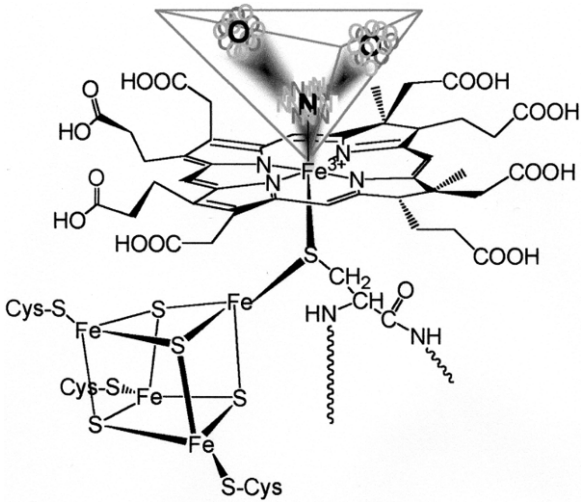

Fig. 3. Nitrite binding at the active site of oxidized spinach nitrite reductase.

Privalle, 1995). Spectroscopic evidence had suggested that the enzyme's two prosthetic groups are electronically coupled, probably through the sharing of a sulfur ligand between the heme iron and the [4Fe–4S] cluster (Wilkerson et al., 1983), an arrangement known to be present in the spectroscopically similar, [4Fe–4S] and siroheme-containing subunit of *E. coli* sulfite reductase (Crane et al., 1995, 1997). Very recently, the three-dimensional structure of spinach Fd-dependent NiR has been solved by X-ray crystallography (Swamy et al., 2005), confirming the prediction that the two prosthetic groups of Fd-dependent nitrite reductase are indeed arranged in a linked fashion (Fig. 2). Despite the fact that the sulfur from a cysteine residue (it is Cys518 in the spinach enzyme) serves as a bridging ligand to both the siroheme iron and one of the iron atoms of the [4Fe–4S] cluster (Fig. 2), the two prosthetic groups titrate as independent one-electron components in equilibrium oxidation–reduction measurements with $E_m$values of −365 and −290 mV for the [4Fe–4S] cluster and siroheme, respectively (Hirasawa et al., 1994a). As might be expected from these $E_m$values, flash photolysis experiments have demonstrated an initial reduction of the [4Fe–4S] cluster, followed by electron transfer from the [4Fe–4S] cluster to the siroheme (Hirasawa et al., 1994a).

As ferredoxin, the physiological electron donor to nitrite reductase, is a one-electron donor and the spinach chloroplast enzyme has only a single binding site for ferredoxin (Mikami and Ida, 1989), the enzyme can accept electrons only one at a time during the six-electron reduction the reduction of nitrite to ammonia catalyzed by the enzyme. A major unsolved aspect of the mechanism of this key enzyme in plant nitrogen assimilation has been the identification of all the partially reduced, enzyme-bound intermediates that are formed during the reduction of nitrite. The as-isolated, resting enzyme contains both prosthetic groups in the oxidized form, with the ferric siroheme in a high-spin hexacoordinate state that contains one weak axial ligand (Kuznetsova et al., 2004a,b). This oxidized form of the enzyme can bind nitrite, to form a six-coordinate low-spin ferric siroheme complex that does not display an EPR signal (Kuznetsova et al., 2004a,b). Figure 3 shows a model for nitrite binding to the oxidized enzyme, based on the resonance Raman spectra of the complex (Kuznetsova et al., 2004b), which indicates that nitrite binding to the siroheme iron is very heterogeneous, i.e., that nitrite does not occupy a single fixed position at the binding site when the enzyme is fully oxidized. This heterogeneity of binding provides an explanation for the fact that no EPR signal is observed for the nitrite complex of the oxidized enzyme (Kuznetsova et al., 2004a,b).

Recent kinetic measurements indicate that nitrite binding by the fully oxidized enzyme is very slow compared to the turnover rate of the enzyme and it is thus likely that nitrite binding follows reduction of the enzyme by ferredoxin during the catalytic cycle (Kuznetsova et al., 2004a,b). Nitrite binding by the oxidized enzyme is also slow compared to the oxidation of photoreduced Fd by oxidized nitrite reductase (Kuznetsova et al., 2004b), an observation that is also consistent with the hypothesis that rapid nitrite binding requires prior reduction of the enzyme as was first suggested by Cammack et al. (1978). A species that has been proposed as an early, reduced intermediate

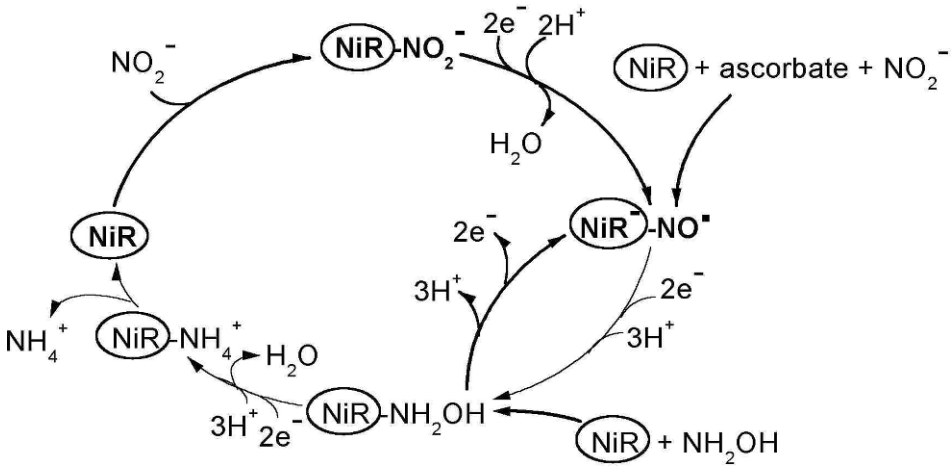

Fig. 4. The catalytic cycle of ferredoxin-dependent nitrite reductase. (This figure is adapted from Kuznetsova et al., 2004a.)

that is a ferrous siroheme/NO complex of the enzyme. This species, in which the [4Fe–4S] cluster is in the oxidized state, was first detected almost 30 years ago (Aparico et al., 1976; Cammack et al., 1978; Lancaster et al., 1979) and evidence has recently been obtained (Kuznetsova et al., 2004a) supporting the earlier proposal (Fry et al., 1980) that the NO complex is a true intermediate. Consistent with the fact that a ferrous siroheme/NO complex is two electrons more reduced than the oxidized enzyme plus nitrite, formation of this species has been shown to require electron donation by two reduced ferredoxins (Kuznetsova et al., 2004a).

Another possible species that has been proposed to play a role as an intermediate in the nitrite reductase-catalyzed conversion of nitrite to ammonia is hydroxylamine, a species that is only two electrons more oxidized than ammonia. The earliest proposal that enzyme-bound hydroxylamine might be a reaction intermediate was based on absorbance difference spectra that were interpreted in terms of the ability of hydroxylamine to form a complex with the siroheme group of the enzyme (Vega and Kmain, 1977). However, recent EPR and resonance Raman studies of the enzyme indicate that incubation of the enzyme with hydroxylamine results in quantitative formation of the ferrous siroheme/NO form of the enzyme (see Fig. 4), in an apparent reversal of a possible step in the forward reaction pathway (Kuznetsova et al., 2004a,b). Thus, the earlier difference spectra that were attributed to the presence of an enzyme complex with hydroxylamine no doubt arose from the ferrous siroheme/NO complex. Nevertheless, the observation that, in a coupled assay system, spinach nitrite reductase can catalyze the Fd-dependent reduction of hydroxylamine (M. Hirasawa and T. Hase, unpublished observations) is consistent with the proposal that hydroxylamine is in fact a reaction intermediate. Figure 4 shows a possible scheme for the catalytic cycle carried out by spinach nitrite reductase and includes the recent observation (Kuznetsova et al., 2004a) that the ferrous siroheme/NO form of the enzyme can be produced by a nonphysiological reduction of nitrite at the active site of the enzyme with ascorbate serving as the reductant.

The 1:1 complex formed between Fd-dependent nitrite reductase and Fd can only be detected at low ionic strengths, consistent with a significant contribution from electrostatic forces in stabilizing the complex (Privalle et al., 1985; Hirasawa et al., 1986; Mikami and Ida, 1989). The observation that the Fd-dependent activity of the enzyme also decreases markedly as the ionic strength of the medium used in steady-state assays is increased (Schmitz and Böhme, 1995; M. Hirasawa, unpublished observations) suggests that electrostatic effects are important in at least one step of the catalytic mechanism. Compared to the detailed picture available about the protein/protein interaction domains involved in the Fd/FNR complex (see above), relatively little is known about the identity of specific amino acids involved in the interaction between Fd and nitrite reductase. However, some information about the groups that may be located at or near the protein/protein interaction domain is available. Chemical modification experiments suggested the possibility that a conserved tryptophan residue, Trp92, is located at or near the Fd-binding site of spinach nitrite reductase and plays a role in at least one-electron transfer step during the reduction of nitrite (Hirasawa et al., 1994b, 1998). Site-specific mutagenesis of the ferredoxin-dependent nitrite reductase from the cyanobacterium *Anabaena* sp. PCC 7120 also points to a role for a tryptophan residue (Trp53, which is the residue in the

cyanobacterial enzyme that corresponds to Trp92 in the spinach enzyme) in catalysis by the enzyme (Curdt et al., 2000). The possibility that aromatic amino acid residues play an important role in electron transfer in the Fd/nitrate reductase reaction is supported by the observations that replacement of a conserved aromatic residue in cyanobacterial Fd (Phe65 in *Anabaena* Fd) by a non-aromatic amino acid dramatically decreases the steady-state rate of the Fd-dependent reactions catalyzed by nitrite reductases from both *Anabaena* (Schmitz and Böhme, 1995) and spinach (M. Hirasawa and J. Tripathy, unpublished observations).

Chemical modification (Hirasawa et al., 1986) and site-directed mutagenesis studies (Schmitz and Böhme, 1995; García-Sánchez et al., 1997, 2000; Kim et al., unpublished observations) have implicated negatively charged residues on Fd as participants in complex formation with nitrite reductase. In all cases tested, site-directed replacement of a conserved glutamate residue near the C-terminus of Fd by an uncharged or positively charged amino acid produces a significant decrease in the steady-state rate of the Fd-dependent reactions catalyzed by nitrite reductases isolated from either a cyanobacteria, a green alga, or a higher plant. Mutagenesis studies have also implicated a second acidic region on Fd (consisting of Asp25, Glu28, and Glu29 in *Chlamydomonas reinhardtii* Fd) in binding to nitrite reductase. Chemical modification (Hirasawa et al., 1993) and site-directed mutagenesis (Curdt et al., 2000) studies have also implicated positively charged residues on the enzyme in Fd binding. Peptide mapping experiments had identified two specific arginine residues (Arg357 and Arg556) and one lysine residue (Lys436) that are likely to be involved in supplying positive charges on spinach nitrite reductase that participate in Fd binding (Dose et al., 1997) and site-directed mutagenesis experiments suggest that the corresponding residues in *Anabaena* nitrate reductase, along with other basic residues, are also likely to play a role in binding Fd (Curdt et al., 2000). However, the recently published structure of spinach nitrite reductase (Swamy et al., 2005) suggests that Trp92, Lys436, Arg357, and Arg556 are not likely to be part of the Fd-binding domain and that the chemical modifications of these residues mentioned above arise from secondary effects. Progress in solving the complete three-dimensional structure of spinach nitrite reductase (J. P. Allen, personal communication) and the possibility of using the NMR interaction technique described above in the section on Fd-FNR interaction, to examine the binding domain on Fd for nitrite reductase will hopefully lead to a more exact mapping of the protein–protein interaction domains involved in complex formation between Fd and nitrite reductase in the near future. In fact, a computer docking model of the 1:1 complex between spinach nitrite reductase and spinach Fd1 suggests that Fd fits into a pocket in nitrite reductase that brings the electron-donating [2Fe–2S] cluster of Fd to within 11 Å of the electron-accepting [4Fe–4S] cluster of nitrite reductase. The putative complex is stabilized by interactions between Lys80, Lys83, and Lys100 of nitrite reductase with Glu93 and Ser43 of Fd, a salt bridge between Arg504 of nitrite reductase and Asp60 of Fd and a H-bond from Lys100 of nitrite reductase to Ser43 of Fd (Swamy et al., 2005).

B. Ferredoxin-Dependent Glutamate Synthase

Fd-dependent glutamate synthases catalyze the two-electron reductive conversion of glutamine plus 2-oxoglutarate to two molecules of glutamate. The key role of this enzyme in nitrogen assimilation by oxygenic higher plants has been extensively documented (Suzuki and Knaff, 2005) and so will not be reviewed here, but it is worth mentioning that the enzyme also plays a major role in nitrogen assimilation in cyanobacteria (Okuhara et al., 1999). Glutamate synthases in bacteria most commonly use NADPH as the electron donor and contain two types of subunits, one of which displays significant similarities to the single type of peptide found in Fd-dependent enzymes in terms of prosthetic group content and catalytic mechanism. A comparison of the NADPH-dependent and Fd-dependent glutamate synthases is beyond the scope of this article but excellent recent reviews on the bacterial enzymes are available (Vanoni and Curti, 1999; van den Heuvel et al., 2004; Vanoni et al., 2005). The Fd-dependent glutamate synthases are soluble, monomeric proteins with molecular masses near 170 kDa and are found in the chloroplast stromal space in photosynthetic eukaryotes. In most oxygenic photosynthetic eukaryotes the enzymes are encoded by nuclear genes and synthesized as preproteins with N-terminal signal sequences that targets them for delivery to the chloroplast stroma (Suzuki and Knaff, 2005). However, in at least one red alga the enzyme is plastid encoded (Valentin et al., 1993).

The enzymes all contain only two prosthetic groups, a [3Fe–4S] cluster (which is coordinated by three conserved cysteine residues) and a noncovalently bound FMN (Knaff, 1996). Oxidation–reduction titrations of the $[3Fe–4S]^{0,+1}$ cluster in the spinach enzyme gave an excellent fit to the Nernst equation for a one-electron redox couple with an E_m value of -170 ± 10 mV and titrations of the FMN gave an excellent fit to the Nernst equation for a two-electron redox couple with an E_m

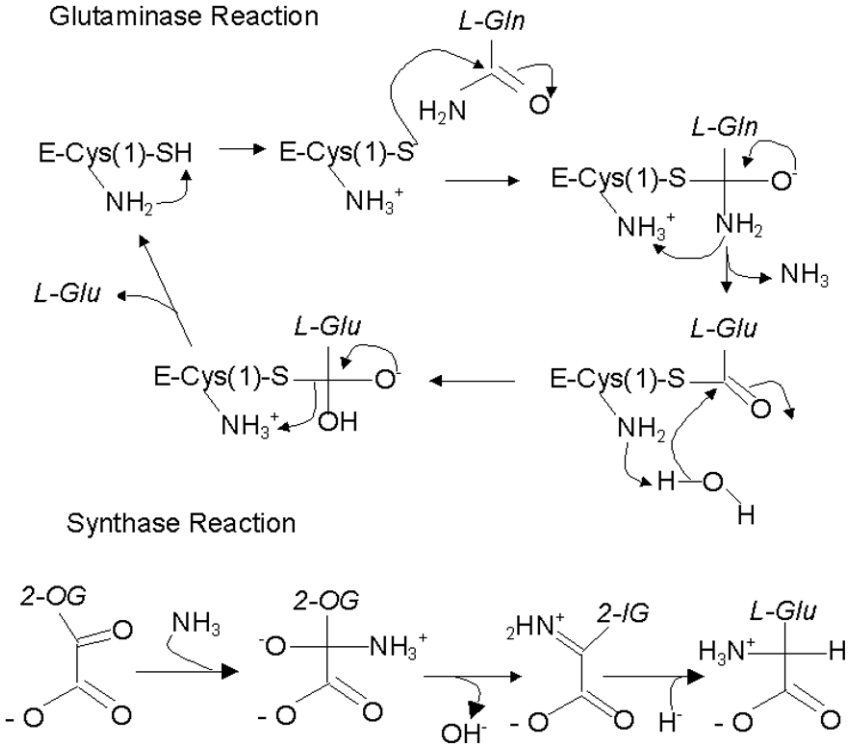

Fig. 5. The steps of the glutamate synthase-catalyzed reaction. Only the parts of L-glutamine (L-Gln), 2-oxoglutarate (2-OG), 2-iminoglutarate (2-IG), and L-glutamate (L-Glu) that participate in the reaction are shown. (This figure is reproduced, with permission, from Vanoni et al., 2005. © Springer.)

value of -180 ± 10 mV (Hirasawa et al., 1992). Thus, within the experimental uncertainties of the measurements, the two prosthetic groups of the enzyme are isopotential. Neither visible-region absorbance spectra nor EPR spectra, measured during the titrations, showed any evidence for detectable amounts of the one-electron reduced FMN semiquinone (Hirasawa et al., 1992). A cyclic voltammetry investigation of the redox properties of spinach glutamate synthase also demonstrated that the two prosthetic groups of the enzyme are isopotential, although this technique gave a somewhat more negative E_m value of -225 mV for both groups (Hirasawa et al., 1996). Thus, unlike the case for nitrite reductase where the E_m values of the two prosthetic groups differ by 75 mV, it is not possible to predict the likely sequence of electron transfer events between the two prosthetic groups of glutamate synthase on thermodynamic grounds alone. Titrations of the FMN in the Fd-dependent glutamate synthase from *Synechocystis* sp. PCC 6803 gave a good fit to the two-electron Nernst equation with $E_m = -200 \pm 25$ mV at pH 7.5 (Navarro et al., 2000). As was the case for the spinach Fd-dependent glutamate synthase, no evidence for the presence of a flavin semiquinone was observed in the course of titrations of the FMN group of the *Synechocystis* sp. PCC 6803 enzyme, suggesting that the two one-electron E_m values for the oxidized semiquinone and semiquinone fully reduced FMN couples differ by at least 100 mV (Ravasio et al., 2002). An estimation of the E_m value of the $[3Fe–4S]^{0,+1}$ cluster in the *Synechocystis* sp. PCC 6803 enzyme from absorbance changes observed during an anaerobic titration of the enzyme with sodium dithionite suggested that the E_m value of the cluster was 40–50 mV more positive than that of the enzyme's FMN group, putting the E_m of the $[3Fe–4S]^{0,+1}$ cluster at the rather positive value of -150 to -160 mV (Ravasio et al., 2002). Given the experimental uncertainties in these measurements and the fact that E_m values are quite sensitive to experimental conditions (such as pH, temperature, and ionic strength), it is perhaps more important to stress on the similarities in these E_m values, rather than the relatively small differences. It also should be pointed out that E_m values may be affected by complex formation (Knaff, 1996) and thus the thermodynamics of electron transfer between the two prosthetic groups may be different within a glutamate synthase/Fd complex than is the case for the isolated enzyme.

The reaction catalyzed by glutamate synthases consists of two separate partial reactions, as shown in Fig. 5.

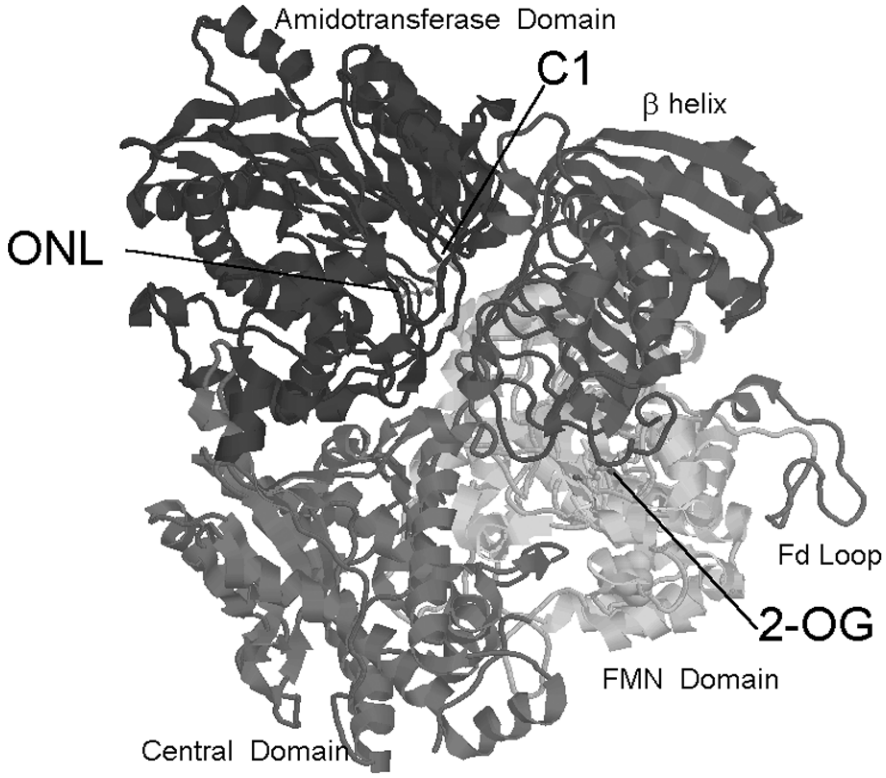

Fig. 6. The structure of the Fd-dependent glutamate synthase from the cyanobacterium *Synechocystis* sp. PCC 6820. See Color Plate 12, Fig. 1.

In the first partial reaction (often referred to as the glutaminase reaction), which occurs at the amidotransferase domain, the active-site Cys1 makes a nucleophilic attack on L-glutamine, releasing ammonia and forming a thioester intermediate which, after reaction with water, produces the first L-glutamate molecule and returns the thiol group of Cys1 to its original state. In the second partial reaction (often referred to as the synthase reaction), which takes place at the FMN-binding domain, the ammonia molecule released in the first step attacks the second substrate, 2-oxoglutarate, with 2-iminoglutarate most likely being formed as an intermediate. The 2-iminoglutarate is then reduced, in a two-electron reaction, by the hydroquinone form cofactor of the enzyme.

Recently, the first three-dimensional structure for a Fd-dependent glutamate synthase has become available (van den Heuvel et al., 2002, 2003). Figure 6 shows the structure of the Fd-dependent glutamate synthase from the cyanobacterium *Synechocystis* sp. PCC 6803, a structure that shows some important similarities to the α subunit of the NADPH-dependent glutamate synthase isolated from *Azospirillum brasilense* (Binda et al., 2000). The structure shown in Fig. 6 indicates the binding site for one of the substrates, 2-oxoglutarate (2-OG), based on the structure of the enzyme/substrate complex (structures of the unliganded enzyme and of a covalently modified form have also been solved and the resolutions of the structures range from 2.0 to 2.7 Å). Figure 6 also shows the structure of the covalent oxonorleucine (ONL) adduct formed when the complex of the enzyme with its substrate 2-oxoglutarate is treated with the covalent inhibitor 5-diazo-5-oxo-L-norleucine (DON) to specifically modify the active-site Cys1. The FMN and [3Fe–4S] clusters are well-defined in the structure and are separated by a distance of 8 Å, in an orientation that is essentially identical to that found in the α subunit of the *A. brasilense* enzyme (van den Heuvel et al., 2002). As is the case in the α subunit of the *A. brasilense* enzyme, a methionine residue (which is strictly conserved in all glutamate synthases) bridges the two prosthetic groups and is likely to be involved in electron transfer between them.

One particularly striking feature of the structure of the S*ynechocystis* sp. PCC 6803 Fd-dependent glutamate synthase, a feature also found in the structure of the α subunit of the NADPH-dependent glutamate synthase from *A. brasilense* is the large distance (ca. 33 Å in the cyanobacterial Fd-dependent enzyme) between the site at which ammonia is released as a result

of the glutaminase reaction and the site where it must react with 2-oxoglutarate, in the synthase reaction, in the FMN domain. In fact, both structures are characterized by the presence of an "ammonia tunnel," formed as a consequence of the arrangement of the four major domains of the enzyme (the N-terminal amidotransferase domain, the FMN-binding domain, a central domain, and a C-terminal domain), that allows the released ammonia to be transferred to the site where it serves as a reactant without being lost to the solvent. The ammonia tunnel in the *Synechocystis* sp. PCC 6803 enzyme contains 10 ordered water molecules, which form an extensive hydrogen-bonded network with amino acids in the tunnel (van den Heuvel et al., 2003, 2004). The amino acid groups that line the tunnel also may function to prevent protonation of ammonia, which is much more reactive in the second partial reaction than is the NH_4^+ ion.

Quite a bit is known about the details of the mechanism of the reaction catalyzed by Fd-dependent glutamate synthase, but as this material has been exhaustively covered in the review articles cited above, it will not be presented here and emphasis will instead be placed on the interaction of the enzyme with Fd. Complex formation between Fd and Fd-dependent glutamate synthase has been shown to occur at low, but not a high, ionic strength, pointing to a contribution from electrostatic forces in Fd binding to the enzyme (Knaff, 1996). It has also been shown, as is the case for the reactions catalyzed by the Fd-dependent nitrate and nitrite reductases, that steady-state activity decreases as the ionic strength of the reaction medium is increased, consistent with the participation of electrostatic forces at some stage in the reaction pathway. As was described above for spinach nitrite reductase, chemical modification studies suggested that negatively charged groups on ferredoxin (Hirasawa et al., 1986) and positively charged groups on spinach glutamate synthase (Hirasawa and Knaff, 1993) are involved in complex formation. Site-directed mutagenesis studies support the hypothesis that conserved acidic residues near the C-terminus of Fd are involved in complex formation with Fd-dependent glutamate synthase (García-Sánchez et al., 1997; Hirasawa et al., 1998; García-Sánchez et al., 2000). The mutational studies involving *C. reinhardtii* Fd have provided evidence that a second acidic region on Fd, containing Asp25, Glu28, and Glu29, also plays a role in binding glutamate synthase (García-Sánchez et al., 2000).

All of the other Fd-enzyme complexes involving proteins from oxygenic photosynthetic organisms that have been characterized to date (i.e., the complexes with FNR, FTR, nitrate reductase, nitrite reductase, and sulfite reductase) exhibit a 1:1 Fd/enzyme stoichiometry. Convincing evidence, obtained by a variety of techniques including X-ray small angle scattering (van den Heuvel et al., 2003) and nanoflow electron spray ionization mass spectrometry (van den Heuvel et al., 2004) has been presented to support a 1:1 Fd/enzyme stoichiometry in the case of the *Synechocystis* sp. PCC 6803 glutamate synthase. However, in the case of the spinach enzyme (Hirasawa et al., 1989, 1991) and Fd-dependent glutamate synthases isolated from the green algae *C. reinhardtii* (63) and *Monoraphidium braunii* (62) cross-linking, spectral perturbation, and membrane ultrafiltration experiments support the presence of two Fd-binding sites on the enzyme. An examination of the structure of the *Synechocystis* sp. PCC 6803 Fd-dependent glutamate synthase (Fig. 6) reveals the presence of a rather long insert (compared to the α subunit of the *A. brasilense* enzyme), running from amino acid 907 to 933 which forms a loop that is not present in the structure of the α subunit of the *A. brasilense* enzyme (van den Heuvel et al., 2004). The fact that this loop is located near the [3Fe–4S] cluster (the distance is ca. 14 Å) and the fact that this insert is conserved in Fd-dependent glutamate synthases suggests that this loop is likely to be involved in binding Fd and thus the feature is labeled the Fd Loop in Fig. 6. Fd binding at this position would imply that reduction of glutamate synthase by reduced Fd would involve an initial reduction of the [3Fe–4S] cluster of the enzyme, followed by electron transfer from the reduced cluster to the enzyme's FMN. It also should be pointed out that there is only one putative Fd-binding loop seen in the structure of the *Synechocystis* sp. PCC 6803 enzyme, an observation that supports the existence of only a single physiologically important binding site for the enzyme's electron donor. It will be of great interest to see if the Fd Loop is also present in spinach glutamate synthase, as would be expected from the similarities of amino acid sequences of the two enzymes in this region, if current attempts to crystallize the spinach enzyme prove successful.

Early circular dichroism studies on the formation of the complex between oxidized spinach Fd and the oxidized spinach Fd-dependent glutamate synthase indicated that complex formation resulted in significant conformational changes in one or both of the proteins (Hirasawa et al., 1989). Recently it has been demonstrated that binding of reduced Fd to the Fd-dependent glutamate synthase from *Synechocystis* sp. PCC 6803 plays an important role in activating the enzyme, presumably as a consequence of

conformational changes in the enzyme that are triggered by Fd binding (Ravasio et al., 2002; van den Heuvel et al., 2002, 2003, 2004). The conformation assumed by the enzyme in the absence of Fd and 2-oxoglutarate is apparently not appropriate for efficient catalysis of the glutaminase reaction, thus preventing any wasteful consumption of L-glutamine when Fd and/or 2-oxoglutarate are not available at the synthase site for productive utilization of ammonia released by the glutaminase reaction. A detailed scheme outlining how the conformational changes, induced by substrate binding, that are involved in synchronizing the activities of the two sites of the Fd-dependent *Synechocystis* sp. PCC 6803 glutamate synthase has been proposed (Ravasio et al., 2002; van den Heuvel et al., 2002, 2003, 2004).

IV. Sulfite Reductase

The assimilatory pathway for sulfur in photosynthetic organisms starts with the ATP-dependent conversion of sulfate to 5′-adenylylsulfate (APS), followed by the two-electron reduction of APS to sulfite plus AMP (Setya et al., 1996). Sulfite is then subsequently reduced to sulfide in a six-electron reaction catalyzed by sulfite reductase (hereafter abbreviated as SiR), and sulfide is subsequently incorporated into a variety of organo-sulfur compounds. The reductant for the APS reductase-catalyzed formation of sulfite is probably reduced glutathione (Setya et al., 1996), while reduced Fd serves as the physiological electron donor for plant and cyanobacterial SiR's. Fd-dependent SiR's are soluble, monomeric enzymes with molecular masses near 65 kDa, that contain one $[4Fe–4S]^{2+,1+}$ cluster and one non-covalently bound siroheme as the only prosthetic groups (Krueger and Siegel, 1982a). The E_m values for the $[4Fe–4S]^{2+,1+}$ cluster and siroheme in maize SiR have been determined to be −400 and −285 mV, respectively (Hirasawa et al., 2004b), in the range where electron flow to the enzyme from reduced Fd's, which have E_m values ranging from −420 to −340 mV (Nakayama et al., 2000; Yonekura-Sakakibara et al., 2000), is thermodynamically favorable. It has also been shown (Hirasawa et al., 2004b) that either replacement of a conserved arginine at the substrate-binding site of maize Fd-SiR or the binding of different ligands to the enzyme's siroheme affect the E_m values of the prosthetic groups.

In contrast to the Fd-dependent SiR's from oxygenic photosynthetic organisms, SiR's found in *E. coli* and other bacteria utilize NADPH as the electron donor for the reduction of sulfite. Bacterial SiR's are heterooctameric enzymes, with a $\alpha_4\beta_4$ composition. The α_4 subunit is a flavoprotein that functions to accept electrons from NADPH and transfer them to the β subunit. The β subunit is the "catalytic subunit" that contains the active site for sulfite reduction to sulfide (Siegel et al., 1982). The catalytic subunit of NADPH-SiR (usually referred to as the hemoprotein subunit) is approximately 30% homologous to Fd-SiR at the amino acid level and contains the same two prosthetic groups as plant SiR (Siegel et al., 1982). X-ray crystallography studies of the hemoprotein subunit have revealed that four cysteines function as ligands to the [4Fe–4S] cluster and that one of the cysteines also serves as an axial ligand to the siroheme (Crane et al., 1995, 1997). This unique structure (see Fig. 2, which shows the very similar structure of the prosthetic groups at the active site of spinach nitrite reductase) provides an explanation for the results of spectroscopic studies that had indicated that the two prosthetic groups of the hemoprotein subunit are magnetically coupled (Christner et al., 1981; Janick and Siegel, 1982). Another notable feature of the structure is the presence, on the distal side of siroheme, of an extensive hydrogen-bonding network among positively charged amino acid side chains, ordered water molecules, siroheme carboxylates, and the substrate sulfite. This structure is considered to be crucial for facilitating the six-electron reduction of sulfite without releasing intermediates during the catalytic reaction (Crane et al., 1995). A proposed mechanism for the reduction of the sulfite anion involves transfer of two electrons from the coupled prosthetic groups to the siroheme-bound anions and the concomitant cleavage of the S–O bonds, leaving the oxygen atom as a water molecule (Crane et al., 1997). Although no three-dimensional structure is currently available for any Fd-SiR, spectroscopic data indicates that the arrangement of the siroheme and [4Fe–4S] cluster prosthetic groups in Fd-SiR is likely to be very similar to that found in the hemoprotein subunit of *E. coli* SiR (Krueger and Siegel, 1982b).

It should be reemphasized that Fd-dependent nitrite reductases have essentially the same prosthetic group arrangement found in Fd-dependent SiR and the hemoprotein subunit of NADPH-dependent SiR (see above). The facts that both Fd-dependent and NADPH-dependent SiR's can catalyze the reduction of nitrite to ammonia and that NiR can catalyze the reduction of sulfite to sulfide (Krueger and Siegel, 1982a), suggests that there are also similarities in the catalytic mechanisms of the two enzymes. Despite these likely

mechanistic similarities, the fact that each enzyme has a K_m for its preferred substrate approximately two orders of magnitude less than the K_m for the alternate substrate indicates the presence of high specificity in substrate recognition. NiR and SiR bind their favored substrates to the siroheme iron through their nitrogen and sulfur atoms, respectively (see the discussion of Fd-NiR above and also Crane et al., 1997). One important consequence of this mode of binding is that the oxygen atoms of the two anionic substrates protrude into the substrate-binding cavities of the enzymes. It might thus be expected that the substrate-binding sites contain positively charged groups that are involved in binding the anionic substrate oxygens in the proper orientation for reduction and, in fact, the crystal structures of the sulfite and nitrite complexes of the hemoprotein subunit of *E. coli* SiR reveals just these sorts of interactions. The fact that the nitrite anion has only two oxygen atoms, while the sulfite anion has three, has important consequences for binding of the two anionic substrates. In fact, the crystal structure of the nitrite complex of the hemoprotein subunit of *E. coli* SiR shows that, while the two oxygens of nitrite occupy positions similar to those occupied by two of the three oxygens in sulfite, an interaction between Arg153 and the third oxygen of sulfite is absent in the nitrite complex. Sequence homology arguments suggest that an equivalent arginine residue is likely be present at the substrate-binding site of Fd-SiR but absent from the substrate-binding site of Fd-NiR (Nakayama et al., 2000). Support for this hypothesis comes from the observation that replacement of a conserved arginine residue at the putative substrate-binding site of maize Fd-SiR (Arg193) with either a neutral or a negatively charged amino acid resulted in almost complete loss of the enzyme's ability to reduce sulfite but produced a large decrease in the K_m for nitrite [the R193A variant of maize Fd-SiR has a K_m value ca. 3.3-fold lower than the K_m value of the wild-type enzyme and the R193E variant has a K_m value ca. 33 time lower than that of the wild-type enzyme (Nakayama et al., 2000)].

In comparison with the detailed knowledge of protein/protein interactions in the Fd/FNR complex (see above and Hurley et al., this volume, Chapter 27), relatively little is known about complex between SiR and Fd. However, it is known that SiR forms an electrostatically stabilized, 1:1 complex with Fd, and that complex formation is likely to be crucial for efficient electron transfer between the two proteins (Hirasawa et al., 1987; Akashi et al., 1999; Nakayama et al., 2000). Crystallographic structures for a Fd-dependent SiR or for a complex between Fd and SiR are not yet available. However, NMR spectroscopy, which is a particularly useful technique for topological analyses of transient protein/protein complexes, has been successfully applied to study the interaction of Fd and SiR at the atomic level (Saito et al., 2005). As shown in Panel C of Fig. 1, chemical shift mapping of Fd in its complex with SiR gives a clear picture of molecular recognition domain on Fd for SiR. Alterations in the NMR spectrum of [^{15}N] Fd that result from complex formation with SiR can be assigned to two regions of Fd, one including Glu29, Glu30, and Asp34, and the other including Glu92, Glu93, and Glu94. The changes in the NMR features can be interpreted as arising either from direct protein–protein interactions or from an alteration in electronic shielding upon complex formation. It is important to note that the mapping patterns of Fd regions affected by complex formation with a Fd-dependent enzyme are significantly different when SiR is the interaction partner than is the case when FNR is the interaction partner (compare Panels A and C of Fig. 1).

V. Ferredoxin:Thioredoxin Reductase

In oxygenic photosynthetic organisms assimilatory photosynthetic pathways coexist with dissimilatory pathways in the same cell compartment, using some of the same enzymes. For an efficient use of photosynthetic energy the simultaneous functioning of these opposing pathways has to be avoided. Therefore, these organisms have developed light-dependent control mechanisms, which allow switching between light and dark metabolism. Light actually activates a number of biosynthetic enzymes and inhibits a key enzyme of carbohydrate degradation, the glucose 6-phosphate dehydrogenase. The regulatory system, which transmits the light signal to specific target enzymes is the Fd/thioredoxin system, composed of the proteins Fd, ferredoxin:thioredoxin reductase (FTR), and thioredoxins (trx). The light signal, in the form of electrons originating in PS I, is transferred by Fd to FTR, which transforms it into a sulfhydryl signal. The thiol signal is then transmitted, through disulfide–dithiol interchange reactions involving thioredoxins, to target proteins, which have one or more regulatory disulfide reduced through the Fd/FTR/thioredoxin system. The catalytic properties of the target enzymes are modified in a manner that depends on their function in the organism's metabolism. Different aspects of this regulatory system have been treated in a number of recent reviews (Jacquot et al., 1997a; Meyer et al., 1999; Ruelland and

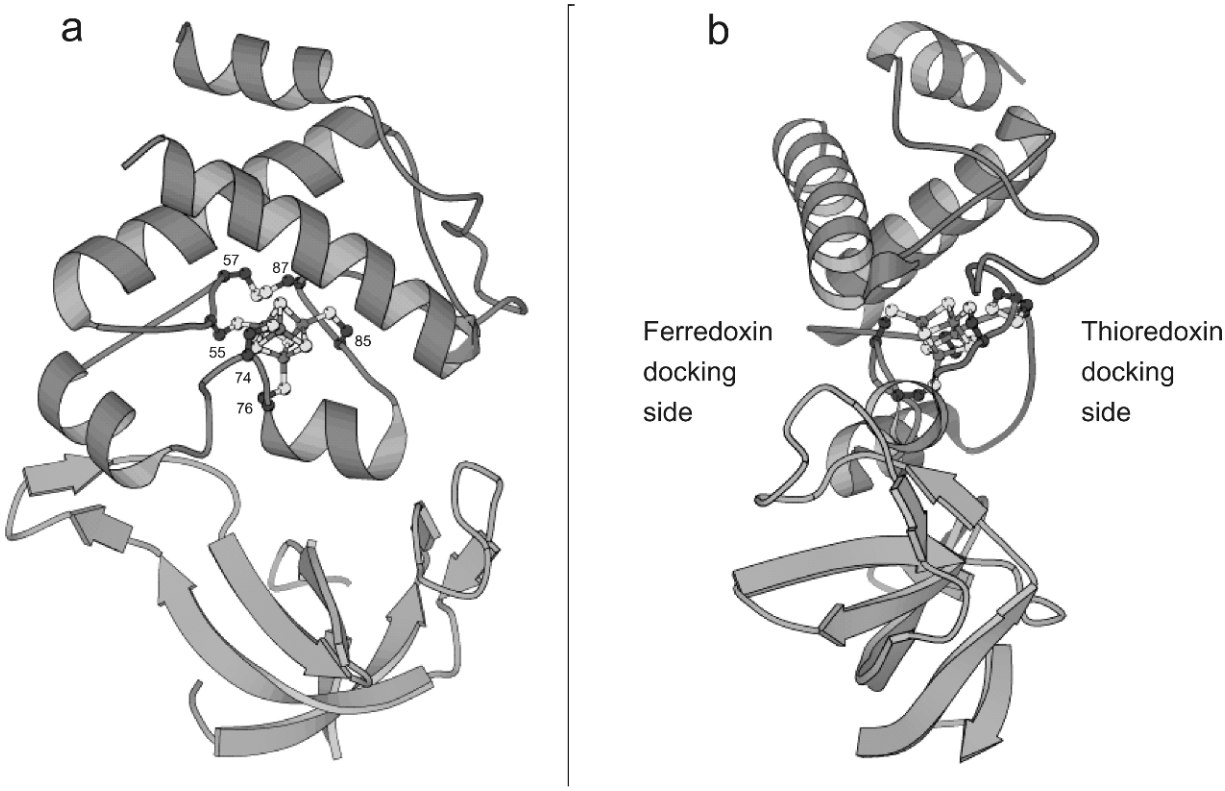

Fig. 7. The structure of the FTR heterodimer. (A) Face view of the molecule with the α-helical catalytic subunit on the top and the β-sheet structure of the variable subunit on the bottom. The [4Fe–4S] cluster and the active-site disulfide are modeled in ball and stick. (B) Side view showing that the FTR is a very thin, concave disk-like molecule with only 10 Å across the center where the iron–sulfur cluster and the disulfide are located. (Adapted from Dai et al., 2000a. © Cambridge University Press.)

Miginiac-Maslow, 1999; Dai et al., 2000a; Follmann, 2000; Schürmann and Jacquot, 2000; Meyer et al., 2001; Schürmann and Buchanan, 2001; Schürmann, 2003a,b; Dai et al., 2004, 2005; Walters and Johnson, 2004). Here we will concentrate on FTR and its interactions with Fd and thioredoxin.

FTR is a unique enzyme, present only in oxygenic photosynthetic cells, that catalyzes the reduction of the disulfide bridge of thioredoxins using electrons donated by reduced Fd. FTR is a relatively small, colored, heterodimeric protein composed of a variable subunit, with only a structural role, and of a catalytic subunit. The primary sequence and the size of variable subunits from different organisms vary considerably (8–13 kDa), whereas the catalytic subunits, which contain a [4Fe–4S] cluster and a redox-active disulfide bridge, are highly conserved and of constant size (∼13 kDa, Schürmann and Buchanan, 2001). The disulfide in FTR has an $E_m$value of −320 mV at pH 7. This is a more negative value than the midpoint potentials of the two thioredoxins that are known to be reduced by FTR, i.e., thioredoxins *f* and *m*, which have $E_m$values (at pH 7.0) of −290 and −300 mV, respectively (Hirasawa et al., 1999; Knaff, 2000). This potential difference makes the reduction of both thioredoxins thermodynamically favorable. The E_m values of the mixed disulfide bonds between FTR and the two thioredoxins in the FTR-thioredoxin covalent complexes are 40–50 mV more positive than the potential of the active-site disulfide of FTR. These significantly more positive E_m values for the one-electron reduced intermediate favor the liberation of reduced thioredoxin, the second step of thioredoxin reduction (Glauser et al., 2004).

The enzymes from spinach and from the cyanobacterium *Synechocystis* sp. PCC 6803 have been cloned and overexpressed (Schwendtmayer et al., 1998; Gaymard et al., 2000). The two enzymes show no functional differences but the *Synechocystis* sp. PCC 6803 FTR is significantly more stable (Manieri et al., 2003) and this enabled its structural analysis by X-ray crystallography (Dai et al., 2000b). The FTR heterodimer is an unusually thin molecule. It is shaped like a concave disk and is only 10 Å across the center of the molecule, where the iron–sulfur center and the disulfide are located (Fig. 7).

The variable subunit, at the bottom of the molecule, is a heart-shaped, open β-barrel structure containing five antiparallel strands (Dai et al., 2000a). On top of it sits the catalytic subunit, which has an α-helical structure containing five helices. The N-terminal half of the subunit, together with the C-terminal helix, forms an α-helical structure covering the iron–sulfur center, while the intervening 40 residues contain all the iron ligands and redox-active cysteines. The four cysteine residues that serve as ligands to the [4Fe–4S] cluster do not follow a typical consensus motif, but show an entirely new arrangement (Chow et al., 1995) with the following fingerprint: **C**PCX$_{16}$**C**P**C**X$_8$**C**HC (cluster ligands are in bold). Two iron atoms are ligated by the cysteines in the central Cys74ProCys76 motif (*Synechocystis* sp. PCC 6803 FTR numbering) and the other two iron atoms are coordinated by Cys55 in the Cys55ProCys57 motif and by Cys85 of the Cys85HisCys87 motif. The remaining two cysteines, Cys57 and Cys87, form the active-site disulfide bridge positioning it right next to the [4Fe–4S] center. The sulfur atom of Cys87 of the disulfide bridge is in van der Waals contact with the iron atom bound by Cys55, with the sulfur atom of Cys55, and with a sulfide ion of the cluster (Dai et al., 2000a). These contacts appear to be very important for the stability of the iron–sulfur cluster. Mutational studies, in which Cys87 was replaced by another amino acid, yielded a significantly less stable cluster in the Cys87Ala variant and a totally unstable protein in the Cys87Ser variant (Manieri et al., 2003; Glauser et al., 2004).

The iron–sulfur cluster is located on one side of the flat molecule, close to the surface of the Fd docking site. The disulfide bridge is accessible from the opposite side, the thioredoxin docking site. This arrangement allows simultaneous docking of Fd, the electron donor, and thioredoxin, the electron acceptor protein, on opposite sides of the FTR and the transfer of an electron across the center of the molecule. This is a prerequisite for the proposed reaction mechanism, which includes the formation of a transient, mixed disulfide between FTR and thioredoxin (Holmgren, 1995; Staples et al., 1998; Dai et al., 2000a; Walters and Johnson, 2004). The docking sites on both sides of the FTR molecule are well adapted for their function and their surface residues are highly conserved. Using monocysteic mutants of thioredoxins it has been possible to stabilize the proposed transient mixed disulfide between FTR and thioredoxin. The fact that this stable disulfide-linked adduct formed a high-affinity complex with Fd (Glauser et al., 2004) presents compelling evidence for the idea that FTR can form a ternary complex with Fd and thioredoxin and that FTR must contain separate binding sites for its two protein substrates.

FTR forms a high-affinity, 1:1 complex with Fd that is stabilized by electrostatic forces (Hirasawa et al., 1988; Glauser et al., 2004). The structural analysis of FTR showed that the Fd interaction area contains three positively charged residues. Together with hydrophobic residues around the iron–sulfur cluster they form a docking area for negatively charged ferredoxins. Furthermore, this Fd docking site has shape that is complementary to the Fd molecule (Dai et al., 2000a). It had been demonstrated earlier that there are two clusters of negative charges, located respectively in helix 1 and the C-terminal helix 3 of Fd, that are essential for the FTR-Fd recognition in spinach (De Pascalis et al., 1994). The essential role of one of the C-terminal glutamate residues (Glu 92 in spinach or the corresponding glutamate residue in *C. reinhardtii* Fd) has been confirmed by chemical derivatization (De Pascalis et al., 1994) or site-directed mutagenesis (Jacquot et al., 1997b) and more recently by structure determination of the *Synechocystis* sp. PCC 6803 Fd-FTR complex (S. Dai, personal communication). The structural studies also revealed that only the catalytic subunit of FTR is involved in the interaction with Fd, which is stabilized by a number of hydrogen bonds and salt bridges between the two proteins as well as by hydrophobic interactions. These various intermolecular contacts and the structural fit combine to contribute the high affinity of the complex between FTR and Fd. These factors are probably also the basis for a certain level of specificity in this interaction as can be seen in the significantly lower affinity in the interaction between spinach Fd and *Synechocystis* sp. PCC 6803 FTR than between the homologous spinach proteins (Schwendtmayer et al., 1998). In contrast *Synechocystis* sp. PCC 6803 Fd displays a high affinity for both spinach and *Synechocystis* sp. PCC 6803 FTR (unpublished observation).

Studies with FTR in which the Fd interaction site has been mutated have not yet been undertaken. However, when the interaction between Fd and the FTR C87A active-site mutant was studied, a degradation of FTR was observed when Fd above an equimolar ratio was added to the FTR. This was interpreted as being the consequence of the rather strong interaction forces between the two proteins. As the contacts between a cluster iron and the sulfur of Cys87 are missing in this FTR variant, the cluster is probably more labile and not able to withstand the slight deformation caused by the electrostatic forces stabilizing the complex (Glauser et al., 2004).

The thioredoxin interaction area on FTR is less charged than the Fd-binding domain and contains mainly hydrophobic residues, which makes the area less selective. This seems to be important *in vivo*,

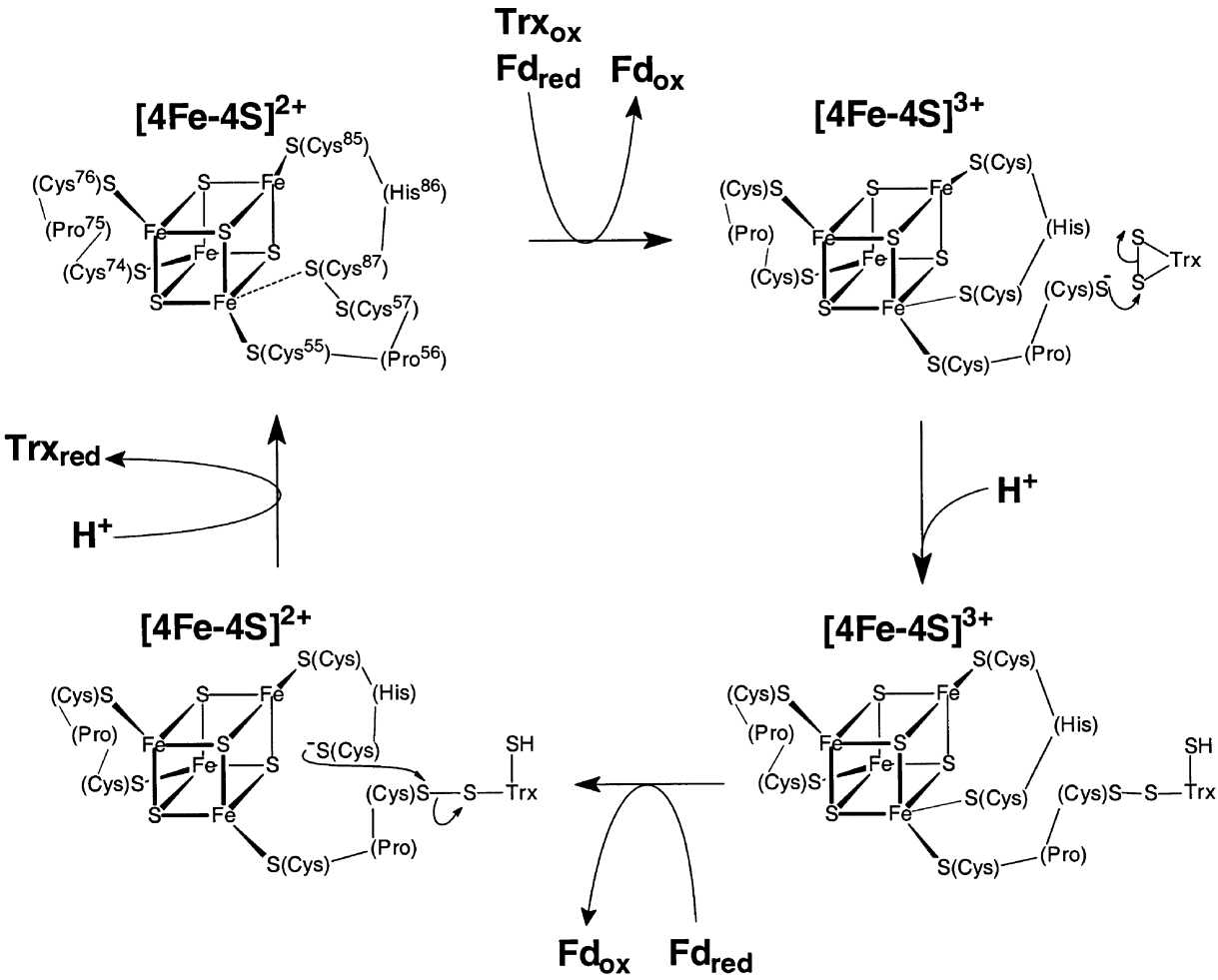

Fig. 8. Proposed catalytic cycle for thioredoxin reduction by FTR. Residues are numbered according to *Synechocystis* sp. PCC 6820 FTR. Fd – ferredoxin; Trx – thioredoxin. (Reproduced with permission from Walters and Johnson, 2004. © Kluwer Academic Publishers.)

where FTR might function in the reduction of several different thioredoxins. This is the case in spinach chloroplasts, where two types of thioredoxins, *m* and *f* are both reduced in FTR-catalyzed reactions. The three-dimensional structures of the FTR-Trx *f* and FTR-Trx *m* complexes demonstrate that there are very few interactions between FTR and either thioredoxin and that the interactions involve only the catalytic subunit of the FTR (Dai et al., 2006). These properties make the FTR a versatile thioredoxin reductase, capable of accepting electrons from diverse ferredoxins, although with different efficiencies, and reducing the disulfides of various thioredoxins.

Full reduction of the disulfide bridge of thioredoxin requires two electrons. However, Fd can provide only one electron at a time. As there is only a single binding site for Fd on FTR, FTR must catalyze the disulfide reduction in two consecutive steps and must stabilize a transiently formed one-electron reduced intermediate. FTR uses its iron–sulfur cluster to cleave and reduce the active-site disulfide, which is possible because of their close proximity. Cys87, the solvent-protected Cys of the active site, already interacts with the closest Fe of the cluster in the resting state of the enzyme, an interaction that plays a crucial role in stabilizing the one-electron reduced intermediate (Jameson et al., 2003).

In the first reduction step (Fig. 8), initiated by an electron delivered by Fd, the active-site disulfide is cleaved forming a thiol, located on the surface exposed Cys57, and a thiyl radical (Cys87). The latter is stabilized by ligation to the cluster, oxidizing it from the $[4Fe–4S]^{2+}$ to the $[4Fe–4S]^{3+}$ state and forming a unique iron–sulfur cluster with five cysteine ligands (Jameson et al., 2003). The exposed Cys57 can now act as an attacking nucleophile and cleave the disulfide of

thioredoxin. This nucleophilic attack results in the formation of a mixed disulfide between FTR and thioredoxin, linked through an intermolecular disulfide bond. Recently, the structure of the FTR-thioredoxin *f* complex has been solved by X-ray crystallography, providing structural evidence for this mixed disulfide intermediate, and clearly showing the presence of a disulfide bond between Cys57 of FTR and Cys46 of thioredoxin *f*. This structure also documents that an iron–sulfur cluster with five cysteine ligands can be formed by FTR as an intermediate during the catalytic cycle (Dai et al., 2006). In a second reduction step, driven by an electron delivered by a second Fd molecule, the bond between a cluster Fe and Cys87 is cleaved and the cluster reduced to its original 2^+ oxidation state. Cys87, which has been converted to the thiol state (or perhaps the thiolate anion state – the protonation state of the sulfur is not known), serves as a nucleophile and attacks the intermolecular disulfide releasing the fully reduced thioredoxin and returning the FTR active site to its disulfide state. This proposed reaction scheme is based on spectroscopic analyses of native and active-site modified FTR (Staples et al., 1996, 1998; Walters and Johnson, 2004) and is entirely compatible with structural models derived from crystallographic data (Dai et al., 2006; Dai, personal communication). The particular, disk-like structure of FTR enables simultaneous docking of Fd and thioredoxin on opposite sides of the molecule, as described in the sequence of interactions, and a rapid transfer of electrons across the center of the FTR.

VI. Conclusion

It has now been close to 40 years since the first demonstration of complex formation between Fd and a Fd-dependent enzyme. The independent discovery, in three separate laboratories, that Fd and FNR formed an electrostatically stabilized complex marked the opening of an important area of investigation in photosynthesis research (Shin and San Pietro, 1968; Foust et al., 1969; Nelson and Neumann, 1969). It soon became clear that FNR was not the only Fd-dependent enzyme to form such complexes and, as can be seen from the description provided above, that formation of such complexes is the rule rather than the exception. Early investigations into the interactions between Fd and its target enzymes, undertaken at a time when little structural or mechanistic information was available, focused on the roles of negatively charged Fd residues and positively charged residues on the enzymes and emphasized the likelihood that the binding site on Fd would not vary appreciably from one Fd-dependent enzyme to another. As can be seen from the material presented in this chapter (and in other chapters as well), a rich vein of mechanistic and structural information about these enzymes is now available, thanks to the successful application of modern structural, kinetic, and spectroscopic approaches (it is also likely that additional structures for Fd-dependent enzymes and for their complexes with Fd will be available soon). It has also become clear that hydrophobic effects and entropy considerations play important roles in the interactions between Fd and these enzymes and that the binding domains on Fd for different Fd-dependent enzymes are in fact not exactly the same for all of these enzymes. Finally, it should be mentioned that the study of Fd-dependent enzymes has provided considerable new insight into the mechanisms by which enzymes that catalyze multi-electron transfer reactions process and store electrons that arrive one at a time. Much remains to be done in this field, not only in understanding the detailed mechanisms by which these Fd-dependent enzymes catalyze these key steps in biosynthetic pathways, but also in trying to elucidate the *in vivo* control mechanisms involved in distributing electrons from reduced Fd between these many different target enzymes. However, considering how much progress has been made in studying these fascinating enzymes in recent years, we can predict with some confidence that the prospects for a continued deepening of our understanding of these key biosynthetic enzymes is excellent indeed.

Acknowledgments

The authors would like to thank James Allen, Guy Hanke, Masakazu Hirasawa, Michael K. Johnson, Masato Nakayama, Tony Mattioli, Pierre Sétif, Akira Suzuki, Saito Takashi, Gordon Tollin, and Maria Vanoni for helpful discussions. Work in the authors' laboratories was supported by grants from the U.S. Department of Energy (DE-FG03-99ER20346 to D.B.K.), the Schweizerischer Nationalfonds (to P.S.), and a Grant-in-Aid for Creative Scientific Research (No. 15GS0320 to T.H.) from the Ministry of Education, Culture, Sports, Science, and Technology of Japan.

References

Akashi T, Matsumura T, Ideguchi T, Iwakiri K, Kawakatsu T, Taniguchi I and Hase T (1999) Comparison of the electrostatic

binding sites on the surface of ferredoxin for two ferredoxin-dependent enzymes, ferredoxin-NADP$^+$ reductase and sulfite reductase. J Biol Chem 274: 29399–29405

Aliverti A, Deng Z, Ravasi D, Piubelli L, Karplus PA and Zanetti (1998) Probing the function of the invariant glutamyl residue 312 in spinach ferredoxin-NADP$^+$ reductase. J Biol Chem 273: 34008–34015

Aliverti A, Faber R, Finnerty CM, Ferioli C, Pandini V, Negri A, Karplus PA and Zanettti G (2001) Biochemical and crystallographic characterization of ferredoxin-NADP$^+$ reductase from nonphotosynthetic tissues. Biochemistry 40: 14501–14508

Aliverti A, Pandini V and Zanetti G (2004) Domain exchange between isoforms of ferredoxin-NADP$^+$ reductase produces a functional enzyme. Biochim Biophys Acta 1696: 93–101

Aoki H, Tanaka K and Ida S (1995) The genomic organization of the gene encoding a nitrate-inducible ferredoxin-NADP$^+$ oxidoreductase from rice roots. Biochim Biophys Acta 1229: 389–392

Aparico PJ, Knaff DB and Malkin R (1975) The role of an iron–sulfur center and siroheme in spinach nitrite reductase. Arch Biochem Biophys 169: 102–107

Back E, Burkhart W, Moyer M, Privalle L and Rothstein S (1988) Isolation of cDNA clones coding for spinach nitrite reductase: complete sequence and nitrate induction. Mol Gen Genet 212: 20–26

Batie CJ and Kamin H (1984) Ferredoxin-NADP$^+$ oxidoreductase. Equilibria in binary and ternary complexes with NADP$^+$ and ferredoxin. J Biol Chem 259: 8832–8839

Bellissimo DB and Privalle LS (1995) Expression of spinach nitrite reductase in *Escherichia coli*: site-directed mutagenesis of predicted active site amino acids. Arch Biochem Biophys 323: 155–163

Binda C, Coda A, Aliverti A, Zanetti G and Mattevi A (1998) Structure of the mutant E92K of [2Fe–2S] ferredoxin from *Spinacia oleracea* at 1.7 Å resolution. Acta Crystallogr D 54: 1353–1358

Binda C, Bossi RT, Wakatsuki S, Artz S, Coda A, Curti B, Vanoni MA and Mattevi A (2000) Cross-talk and ammonia channeling between active centers in the unexpected domain arrangement of glutamate synthase. Structure 6: 1299–1308

Cammack R, Hucklesby DP and Hewitt EJ (1978) Electron-paramagnetic-resonance studies of the mechanism of leaf nitrite reductase. Biochem J 171: 519–526

Carrillo N and Ceccarelli EA (2003) Open questions in ferredoxin-NADP$^+$ reductase catalytic mechanism. Eur J Biochem 270: 1900–1915

Chow L-P, Iwadate H, Yano K, Kamo M, Tsugita A, Gardet-Salvi L, Stritt-Etter A-L and Schürmann P (1995) Amino acid sequence of spinach ferredoxin:thioredoxin reductase catalytic subunit and identification of thiol groups constituting a redox active disulfide and a [4Fe–4S] cluster. Eur J Biochem 231: 149–156

Christner JA, Münck E, Janick PA and Siegel LM (1981) Mössbauer spectroscopic studies of *Escherichia coli* sulfite reductase. J Biol Chem 256: 2089–2101

Crane BR, Siegel LM and Getzoff ED (1995) Sulfite reductase structure at 1.6 Å: evolution and catalysis for reduction of inorganic anions. Science 270: 59–67

Crane BR, Siegel LM and Getzoff ED (1997) Probing the catalytic mechanism of sulfite reductase by X-ray crystallography: structures of the *Escherichia coli* hemoprotein in complex with substrates, inhibitors, intermediates, and products. Biochemistry 36: 12120–12137

Curdt I, Singh BB, Jakoby M, Hachtel W and Böhme H (2000) Identification of amino acid residues of nitrite reductase from *Anabaena* sp. PCC 7120 involved in ferredoxin binding. Biochim Biophys Acta 1543: 60–68

Dai S, Schwendtmayer C, Johansson K, Ramaswamy S, Schürmann P and Eklund H (2000a) How does light regulate chloroplast enzymes? Structure–function studies of the ferredoxin/thioredoxin system. Q Rev Biophys 33: 67–108

Dai S, Schwendtmayer C, Schürmann P, Ramaswamy S and Eklund H (2000b) Redox signaling in chloroplasts: cleavage of disulfides by an iron–sulfur cluster. Science 287: 655–658

Dai S, Johansson K, Miginiac-Maslow M, Schürmann P and Eklund H (2004) Structural basis of redox signaling in photosynthesis: structure and function of ferredoxin:thioredoxin reductase and target enzymes. Photosynth Res 79: 233–248

Dai S, Halberg K, Schürmann P and Eklund H (2006) Light/dark regulation of chloroplast metabolism. In: Wise RR and Hoober JK (eds) Structure and Function of Plastids, pp 221–236. Springer, Dordrecht, The Netherlands

Deng Z, Aliverti A, Zanetti G, Arakaki AK, Ottado J, Orellano EG, Calcaterra NB, Ceccarelli EA, Carrillo N and Karplus PA (1999) A productive NADP$^+$ binding mode of ferredoxin-NADP$^+$ reductase revealed by protein engineering and crystallographic studies. Nat Struct Biol 6: 847–853

De Pascalis AR, Schürmann P and Bosshard HR (1994) Comparison of the binding sites of plant ferredoxin for two ferredoxin-dependent enzymes. FEBS Lett 337: 217–220

Dose MM, Hirasawa M, Kleis-SanFrancisco S, Lew EL and Knaff DB (1997) The ferredoxin-binding site of ferredoxin:nitrite oxidoreductase. Plant Physiol 114: 1047–1053

Flores E and Herrero A (1994) Assimilatory nitrogen metabolism and its regulation. In: Bryant DA (ed) The Molecular Biology of Cyanobacteria, pp 487–517. Kluwer Academic Publishers, Dordrecht, The Netherlands

Follmann H (2000) Light-dark and thioredoxin-mediated metabolic redox control in plant cells. In: Vanden Driessche T, Guisset J-L and Petiau-de Vries GM (eds) The Redox State and Circadian Rhythms, pp 59–83. Kluwer Academic Publishers, The Netherlands

Foust GP, Mayhew SG and Massey V (1969) Complex formation between ferredoxin triphosphopyridine nucleotide reductase and electron transfer proteins. J Biol Chem 244: 964–970

Foyer CH, Ferrario-Méry S and Noctor G (2001) Interactions between carbon and nitrogen assimilation. In Lea PJ and Morot-Gaudry JF (eds) Plant Nitrogen, pp 237–254. Springer, Berlin

Fry IV, Cammack, R, Hucklesby DP and Hewitt EJ (1980) Stability of the nitrosyl-heme complex of plant nitrite reductase, investigated by EPR spectroscopy. FEBS Lett 111: 377–380

Fukuyama K (2004) Structure and function of plant type ferredoxins. Photosynth Res 81: 289–301

Fukuyama K, Hase T, Matsumoto S, Tsukihara T, Katsube Y, Tanaka N, Kakudo M, Wada K and Matsubara H (1980) Structure of *S. platensis* (2Fe–2S) ferredoxin and evolution of chloroplast-type ferredoxin. Nature 286: 522–523

García-Sánchez MI, Gotor C, Jacquot J-P, Stein M, Suzuki A and Vega JM (1997) Critical residues of *Chlamydomonas reinhardtii* ferredoxin for interaction with nitrite reductase and glutamate synthase revealed by site-directed mutagenesis. Eur J Biochem 250: 364–368

García-Sánchez MI, Díaz-Quintana A, Gotor C, Jacquot J-P, De la Rosa MA and Vega JM (2000) Homology predicted structure and functional interaction of ferreodxin from the eukaryotic alga *Chlamydomonas reinhardtii* with nitrite reductase and glutamate synthase. J Biol Inorg Chem 5: 713–719

Gaymard E, Franchini L, Manieri W, Stutz E and Schürmann P (2000) A dicistronic construct for the expression of functional spinach chloroplast ferredoxin:thioredoxin reductase in *E. coli*. Plant Sci 158: 107–113

Glauser DA, Bourquin F, Manieri W and Schürmann P (2004) Characterization of ferredoxin:thioredoxin reductase (FTR) modified by site-directed mutagenesis. J Biol Chem 279: 16662–16669

Green LS, Yee BC, Buchanan BB, Kamide K, Sanada Y and Wada K (1991) Ferredoxin and ferredoxin-$NADP^+$ reductase from photosynthetic and non-photosynthetic tissues of tomato. Plant Physiol 96: 1207–1213

Hanke G, Kimata-Ariga Y, Taniguchi I and Hase T (2004a) A post genomic characterization of *Arabidopsis* ferredoxins. Plant Physiol 134: 255–264

Hanke G, Kurisu G, Kusunoki M and Hase T (2004b) Fd:FNR electron transfer complexes: evolutionary refinement of structural interactions. Photosynth Res 81: 317–327

Hase T, Kimata Y, Matsumura T and Sakakibara H (1991) Molecular cloning and differential expression of the maize ferredoxin family. Plant Physiol 96: 77–83

Hirasawa M and Knaff DB (1993) The role of lysine and arginine residues at the ferredoxin-binding site of spinach glutamate synthase. Biochim Biophys Acta 1144: 85–91

Hirasawa M, Boyer JM, Gray KA, Davis DJ and Knaff DB (1986) The interaction of ferredoxin with chloroplast ferredoxin-linked enzymes. Biochim Biophys Acta 851: 23–28

Hirasawa M, Boyer JM, Gray KA, Davis DJ and Knaff DB (1987) The interaction of ferredoxin-linked sulfite reductase with ferredoxin. FEBS Lett 221: 343–348

Hirasawa M, Droux M, Gray KA, Boyer JM, Davis DJ, Buchanan BB and Knaff DB (1988) Ferredoxin-thioredoxin reductase: properties of its complex with ferredoxin. Biochim Biophys Acta 935: 1–8

Hirasawa M, Chang K-T, Morrow KJ and Knaff DB (1989) Circular dichroism, binding and immunological studies on the interaction between spinach ferredoxin and glutamate synthase. Arch Biochem Biophys 977: 150–156

Hirasawa M, Chang K-T and Knaff DB (1991) The interaction of ferredoxin and glutamate synthase: cross-linking and immunological studies. Arch Biochem Biophys 286: 171–177

Hirasawa M, Robertson DE, Ameyibor E, Johnson MK and Knaff DB (1992) Oxidation–reduction properties of the ferredoxin-linked glutamate synthase from spinach leaf. Biochim Biophys Acta 1100: 105–108

Hirasawa M, de Best JH and Knaff DB (1993) The effect of lysine- and arginine-modifying reagents on spinach ferredoxin:nitrite oxidoreductase. Biochim Biophys Acta 1140: 304–312

Hirasawa M, Tollin G, Salamon Z and Knaff DB (1994a) Transient kinetic and oxidation–reduction studies of spinach ferredoxin:nitrite oxidoreductase. Biochim Biophys Acta 1185: 80–85

Hirasawa M, Proske PA and Knaff DB (1994b) The role of tryptophan in the reaction catalyzed by spinach ferredoxin-dependent nitrite reductase. Biochim Biophys Acta 1187: 80–88

Hirasawa M, Hurley JK, Salamon Z, Tollin G, and Knaff DB (1996) Oxidation-reduction and transient kinetic studies of spinach ferredoxin-dependent glutamate synthase. Arch Biochem Biophys 330: 209–215

Hirasawa M, Dose MM, Kleis-SanFrancisco S, Hurley JK, Tollin G and Knaff DB (1998) A conserved tryptophan at the ferredoxin-binding site of ferredoxin:nitrite oxidoreductase. Biochim Biophys Acta 354: 95–101

Hirasawa M, Schürmann P, Jacquot J-P, Manieri W, Jacquot P, Keryer E, Hartman FC and Knaff DB (1999) Oxidation–reduction properties of chloroplast thioredoxins, ferredoxin:thioredoxin reductase and thioredoxin *f*-regulated enzymes. Biochemistry 38: 5200–5205

Hirasawa M, Rubio LM, Griffin JL, Flores E, Herrero A, Li J, Kim H-K, Hurley JK, Tollin G and Knaff DB (2004a) Complex formation between ferredoxin and *Synechococcus* ferredoxin:nitrate oxidoreductase. Biochim Biophys Acta 1608: 155–162

Hirasawa M, Nakayama M, Hase T and Knaff D (2004b) Oxidation–reduction properties of maize chloroplast ferredoxin sulfite oxidoreductase. Biochim Biophys Acta 1608: 140–148

Holden HM, Jacobsen BL, Hurley JK, Tollin G, Oh B-H, Skeldal L, Chao YK, Xia B and Markley JL (1994) Structure–function studies of [2Fe–2S] ferredoxins. J Bioenerg 26: 67–87

Holmgren A (1995) Thioredoxin structure and mechanism: conformational changes on oxidation of the active-site sulfhydryls to a disulfide. Structure 3: 239–243

Hoober JK (1984) Chloroplasts. Plenum Press, New York

Hurley JK, Fillat MF, Gómez-Moreno C and Tollin G (1966) Electrostatic and hydrophobic interactions during complex formation and electron transfer in ferredoxin/ferredoxin:$NADP^+$ reductase system from *Anabaena*. J Am Chem Soc 118: 5526–5531

Jacquot J-P, Lancelin J-M and Meyer Y (1997a) Thioredoxins: structure and function in plant cells. New Phytol 136: 543–570

Jacquot J-P, Stein M, Suzuki K, Liottet S, Sandoz G and Miginiac-Maslow M (1997b) Residue Glu-91 of *Chlamydomonas reinhardtii* ferredoxin is essential for electron transfer to ferredoxin-thioredoxin reductase. FEBS Lett 400: 293–296

Jameson GNL, Walters EM, Manieri W, Schürmann P, Johnson MK and Huynh BH (2003) Spectroscopic evidence for site specific chemistry at a unique iron site of the [4Fe–4S] cluster in ferredoxin:thioredoxin reductase. J Am Chem Soc 125: 1146–1147

Janick PA and Siegel LM (1982) Electron paramagnetic resonance and optical spectroscopic evidence for interaction between siroheme and Fe_4S_4 prosthetic groups in *Escherichia coli* sulfite reductase hemoprotein subunit. Biochemistry 21: 3538–3547

Jelesarov I and Bosshard HR (1994) Thermodynamics of ferredoxin binding to ferredoxin:$NADP^+$ reductase and the role of water at the complex interface. Biochemistry 33: 13321–133328

Jepson BJN, Anderson LJ, Rubio LM, Taylor CJ, Butler CS, Flores E, Herrero A, Butt JN and Richardon DJ (2004) Tuning a nitrate reductase for function: the first spectro-potentiometric characterization of a bacterial assimilatory nitrate reductase reveals novel redox properties. J Biol Chem 279: 32212–32218

Knaff DB (1996) Ferredoxin and ferredoxin-dependent enzymes. In: Ort DR and Yocum CF (eds) Oxygenic Photosynthesis: The Light Reactions, pp 333–361. Kluwer Academic Publishers, Dordrecht, The Netherlands

Knaff DB (2000) Oxidation–reduction properties of thioredoxins and thioredoxin-regulated enzymes. Physiol Plant 110: 309–313

Krueger RJ and Siegel LM (1982a) Spinach siroheme enzymes: isolation and characterization of ferredoxin-sulfite reductase and comparison with properties with ferredoxin-nitrite reductase. Biochemistry 21: 2892–2904.

Krueger RJ and Siegel LM (1982b) Evidence for siroheme–Fe_4S_4 interaction in spinach ferredoxin-sulfite reductase. Biochemistry 21: 2905–2909

Kurisu G, Kusunoki M, Katoh E, Yamazaki T, Teshima K, Onda Y, Kimata-Ariga Y and Hase T (2001) Structure of the electron transfer complex between ferredoxin and ferredoxin-$NADP^+$ reductase. Nat Struct Biol 8: 117–121

Kuznetsova S, Knaff DB, Hirasawa M, Lagoutte B and Sétif P (2004a) Mechanism of spinach chloroplast ferredoxin-dependent nitrite reductase: spectroscopic evidence for intermediate states. Biochemistry 43: 510–517

Kuznetsova S, Knaff DB, Hirasawa M, Sétif P and Mattioli TA (2004b) Reactions of spinach nitrite reductase with its substrate, nitrite, and a putative intermediate, hydroxylamine. Biochemistry 43: 10765–10774

Lancaster JR, Vega JM, Kamin H, Orme-Johnson NR, Orme-Johnson WH, Krueger RJ and Siegel LM (1979) Identification of the iron–sulfur center of spinach ferredoxin-nitrite reductase as a tetranuclear center, and preliminary EPR studies of mechanism. J Biol Chem 254: 1268–1272

Luque I, Flores E and Herrero A (1993) Nitrite reductase gene from *Synechococcus* sp. PCC 7942: homolgy between cyanobacterial and higher-plant nitrite reductase. Plant Mol Biol 21: 1201–1205

Manieri W, Franchini L, Raeber L, Dai S, Stritt-Etter A-L and Schürmann P (2003) N-terminal truncation of the variable subunit stabilizes spinach ferredoxin:thioredoxin reductase. FEBS Lett 549: 167–170

Matsubara H and Hase T (1983) Phylogenetic consideration of ferredoxin sequences in plants, particularly algae. In: Jensen U and Fairbrother DE (eds) Proteins and Nucleic Acids in Plant Systematics, pp 168–181. Springer-Verlag, Berlin, Germany

Mayoral T, Medina M, Sanz-Aparicio J, Gomez-Moreno C and Hermoso J (2000) Structure basis of the catalytic role of Glu301 in *Anabaena* PCC 7119 ferredoxin-$NADP^+$ reductase revealed by X-ray crystallography. Proteins 38: 60–69

Medina M, Martinez-Julvez M, Hurley JK, Tollin G and Gomez-Moreno (1998) Involvement of glutamic acid 301 in the catalytic mechanism of ferredoxin-$NADP^+$ reductase from *Anabaena* PCC 7119. Biochemistry 37: 2715–2728

Meyer Y, Verdoucq L and Vignols F (1999) Plant thioredoxins and glutaredoxins: identity and putative roles. Trends Plant Sci 4: 388–394

Meyer Y, Miginiac-Maslow M, Schürmann P and Jacquot J-P (2001) Protein–protein interactions in the plant thioredoxin dependent systems. In: McManus MT, Laing W and Allan A (eds) The Annual Plant Reviews, pp 1–29. Sheffield Academic Press, Sheffield, England

Mikami B and Ida S (1989) Spinach ferredoxin-nitrite reductase: characterization of catalytic activity and interaction of the enzyme with substrates. J Biochem 105: 47–50

Morales R, Charon M-H, Kachaova G, Serre L, Medina M, Gómez-Moreno C and Frey M (2000) A redox-dependent interaction between two electron-transfer partners involved in photosynthesis. EMBO Rep 1: 271–276

Morigasaki S, Takata K, Suzuki T and Wada K (1990) Purification and characterization of a ferredoxin-$NADP^+$ oxidoreductase-like enzyme from radish root tissues. Plant Physiol 93: 896–901

Nakayama M, Akashi T and Hase T (2000) Plant sulfite reductase molecular structure, catalytic function and interaction with ferredoxin. J Inorg Biochem 82: 27–32

Navarro F, Martín-Figueroa E, Candau P and Florencio FJ (2000) Ferredoxin-dependent iron–sulfur flavoprotein glutamate synthase (GlsF) from the cyanobacterium *Synechocystis* sp. PCC 6803: expression and assembly in *Escherichia coli*. Arch Biochem Biophys 379: 267–276

Nelson N and Neumann J (1969) Interaction between ferredoxin and ferredoxin nicotinamide dinucleotide phosphate reductase in pyridine nucleotide photoreduction and some partial reactions. J Biol Chem 244: 1932–1936

Neuhaus HE and Emes MJ (2000) Nonphotosynthetic metabolism in plastids. Annu Rev Plant Physiol Plant Mol Biol 51: 111–140

Okuhara H, Matsumura T, Fujita Y and Hase T (1999) Cloning and inactivation of genes encoding ferredoxin- and NADH-dependent glutamate synthases in the cyanobacterium *Plectonema boryanum*. Imbalances in nitrogen and carbon assimilations caused by deficiency of the ferredoxin-dependent enzyme. Plant Physiol 120: 33–41

Onda Y, Matsumura T, Kimata-Ariga Y, Sakakibara H, Sugiyama T and Hase T (2000) Differential interaction of maize root ferredoxin:$NADP^+$ oxidoreductase with photosynthetic and non-photosynthetic ferredoxin isoproteins. Plant Physiol 123: 1037–1045

Privalle LS, Privalle CT, Leonardy NJ, and Kamin H (1985) Interactions between spinach ferredoxin-nitrite reductase and its substrates. Evidence for the specificity of ferredoxin. J Biol Chem 260: 14344–14350

Ravasio S, Dossena l, Martin-Figueroa E, Florencio FJ, Mattevi A, Morandi P, Curti B and Vanoni MA (2002) Properties of recombinant ferredoxin-dependent glutamate synthase of *Synechocystis* PCC 6803. Comparison with the *Azospirillum brasilense* NADPH-dependent enzyme and its isolated α subunit. Biochemistry 41: 8120–8133

Ritchie SW, Redinbaugh MG, Shiraishi N, Vrba JM and Campbell WH (1994) Identification of a maize root transcript expressed in the primary response to nitrate: characterization of a cDNA with homology to ferredoxin-$NADP^+$ oxidoreductase. Plant Mol Biol 26: 678–690

Rubio LM, Herrero A and Flores E (1996) A cyanobacterial *narB* gene encodes a ferredoxin-dependent nitrate reductase. Plant Mol Biol 30: 845–850

Rubio LM, Flores E and Herrero A (2002) Purification, cofactor analysis, and site-directed mutagenesis of *Synechococcus* ferredoxin-nitrate reductase. Photosynth Res 72: 13–26

Ruelland E and Miginiac-Maslow M (1999) Regulation of chloroplast enzyme activities by thioredoxins: activation or relief from inhibition? Trends Plant Sci 4: 136–141

Saito T, Toyota H, Nakayama M, Ilegami T, Kurisu G and Hase T (2005) NMR study of the interaction between plant sulfite reductase and ferredoxin. In: Saito K, de Kok LJ, Stulen I,

Hawkesford MJ, Schnug E, Sirko A and Rennenberg H (eds) Sulfur Transport and Assimilation in the Post-Genomic Era, pp 87–89. Proceedings of 6th International Workshop on Plant Sulfur Metabolism. Backhuys Pub., Leiden

Schmitz S and Böhme H (1995) Amino acid residues involved in functional interaction of vegetative cell ferredoxin from the cyanobacterium *Anabaena* sp. PCC 7120 with ferredoxin:NADP reductase, nitrite reductase and nitrate reductase. Biochim Biophys Acta 1231: 335–341

Schürmann P (2003a) Redox signaling in the chloroplast – the ferredoxin/thioredoxin system. Antioxid Redox Signal 5: 69–78

Schürmann P (2003b) The ferredoxin/thioredoxin system. A light-dependent redox regulatory system in oxygenic photosynthetic cells. In: Gitler C and Danon A (eds) Cellular Implications of Redox Signaling, pp 73–98. World Scientific Publishing Co Pte Ltd, Singapore

Schürmann P and Buchanan BB (2001) The structure and function of the ferredoxin/thioredoxin system in photosynthesis. In: Aro E-M and Andersson B (eds) Advances in Photosynthesis and Respiration, pp 331–361. Kluwer Academic Publishers, Dordrecht, The Netherlands

Schürmann P and Jacquot J-P (2000) Plant thioredoxin systems revisited. In: Jones RL, Bohnert HJ and Delmer DP (eds) Annual Review of Plant Physiology and Plant Molecular Biology, pp 371–400. Annual Reviews, Inc., Palo Alto, USA

Schwendtmayer C, Manieri W, Hirasawa M, Knaff DB and Schürmann P (1998) Cloning, expression and characterization of ferredoxin:thioredoxin reductase from *Synechocystis* sp. PCC 6803. In: Garab G (ed) Photosynthesis: Mechanisms and Effects, Vol 3, pp 1927–1930. Kluwer Academic Publishers, Dordrecht

Setya A, Murillo M and Leustek T (1996) Sulfate reduction in higher plants: molecular evidence for a novel 5′-adenylylsulfate reductase. Proc Natl Acad Sci USA 93: 13383–13388

Shin M and San Pietro A (1968) Complex formation between ferredoxin-NADP reductase with ferredoxin and with NADP. Biochem Biophys Res Comm 33: 38–42

Siegel LM, Rueger DC, Barber MJ, Krueger RJ, Orme-Johnson NR and Orme-Johnson WH (1982) *Escherichia coli* sulfite reductase hemoprotein subunit. Prosthetic groups, catalytic parameters and ligand complexes. J Biol Chem 257: 6343–6350

Smith JM, Smith WH and Knaff DB (1981) Electrochemical titrations of a ferredoxin-ferredoxin-NADP$^+$ reductase complex. Biochim Biophys Acta 635: 405–411

Staples CR, Ameyibor E, Fu W, Gardet-Salvi L, Stritt-Etter A-L, Schürmann P, Knaff DB and Johnson MK (1996) The nature and properties of the iron–sulfur center in spinach ferredoxin:thioredoxin reductase: a new biological role for iron–sulfur clusters. Biochemistry 35: 11425–11434

Staples CR, Gaymard E, Stritt-Etter AL, Telser J, Hoffman BM, Schürmann P, Knaff DB and Johnson MK (1998) Role of the [Fe_4S_4] cluster in mediating disulfide reduction in spinach ferredoxin:thioredoxin reductase. Biochemistry 37: 4612–4620

Suzuki A and Knaff DB (2005) Nitrogen metabolism and roles of glutamate synthase in higher plants. Photosyn Res 83: 191–217

Swamy U, Wang M, Tripathy JN, Kim SK, Hirasawa M, Knaff DB, and Allen JP (2005) Structure of spinach nitrite reductase: implications for multi-electron reactions by the iron–sulfur:siroheme cofactor. Biochemistry 44: 16054–16063

Teshima K, Fujita S, Hirose S, Nishiyama S, Kurisu G, Kusunoki M, Kimata-Ariga Y and Hase T (2003) A ferredoxin Arg–Glu pair important for efficient electron transfer between ferredoxin and ferredoxin-NADP$^+$ reductase. FEBS Lett 546: 189–194

Valentin K, Kostrzewa M and Zetsche K (1993) Glutamate synthase is plastid-encoded in a red alga: implications for the evolution of glutamate synthases. Plant Mol Biol 23: 77–85

van den Heuvel RHH, Ferrari D, Bossi RT, Ravasio S, Curti B, Vanoni MA, Florencio FJ and Mattevi A (2002) Structural studies on the synchronization of catalytic centers in glutamate synthase. J Biol Chem 277: 24579–24583

van den Heuvel RHH, Svergun DI, Petoukhov MV, Coda A, Curti B, Ravasio S, Vanoni MA and Mattevi A (2003) The active conformation of glutamate synthase and its binding to ferredoxin. J Mol Biol 330: 113–128

van den Heuvel RHH, Curti B, Vanoni MA and Mattevi A (2004) Glutamate synthase: a fascinating pathway from L-glutamine to L-glutamate. Cell Mol Life Sci 61: 669–681

Vanoni MA and Curti B (1999) Glutamate synthase: a complex iron–sulfur flavoprotein. Cell Mol Life Sci 55: 617–638

Vanoni MA, Dossena L, van den Heuvel R and Curti B (2005) Structure–function studies on the complex iron–sulfur flavoprotein glutamate synthase: the key enzyme of ammonia assimilation. Photosynth Res 83: 219–238

Vega JM and Kamin H (1977) Spinach nitrite reductase. Purification and properties of a siroheme-containing iron–sulfur enzyme. J Biol Chem 252: 896–909

Vigara AJ, García-Sánchez MI, Gotor C and Vega JM (1996) Interaction between glutamate synthase and ferredoxin from *Monoraphidium braunii*. Chemical modification and cross-linking studies. Plant Physiol Biochem 34: 707–711

Walters EM and Johnson MK (2004) Ferredoxin:thioredoxin reductase: disulfide reduction catalyzed via novel site-specific [4Fe–4S] cluster chemistry. Photosynth Res 79: 249–264

Wilkerson JO, Janick PA and Siegel LM (1983) Electron paramagnetic resonance and optical spectroscopic evidence for interaction between siroheme and tetranuclear iron–sulfur center prosthetic groups in spinach ferredoxin-nitrite reductase. Biochemistry 22: 5048–5054

Yonekura-Sakakibara K, Onda Y, Ashikari T, Tanaka Y, Kusumi T and Hase T (2000) Analysis of reductant supply systems for ferredoxin-dependent sulfite reductase in photosynthetic and nonphotosynthetic organs in maize. Plant Physiol 122: 887–894

Chapter 29

Electron Transfer Between Photosystem I and Plastocyanin or Cytochrome c_6

Michael Hippler*
Department of Biology, University of Pennsylvania, Philadelphia, PA 19104, USA

Friedel Drepper
Biochemie der Pflanzen, Universität Freiburg, Schänzlestr, 179104 Freiburg, Germany

Summary

Electron transfer between photosystem I (PS I) and its soluble lumenal electron donors plastocyanin (pc) or cytochrome c_6 (cyt c_6) is an essential reaction in photosynthetic electron transport that is required to reduce the photooxidized primary donor $P700^+$. PS I is an integral light driven plastocyanin (cytochrome c_6):ferredoxin oxidoreductase that is embedded in the thylakoid membrane, which uses light energy to transport electrons from a lumenal, soluble electron carrier across the membrane to the stromal, soluble electron acceptor ferredoxin. Two types of interactions between PS I and soluble electron transfer donors can be distinguished, namely interactions that are based on electrostatic attraction and hydrophobic contact. Although the hydrophobic binding site within PS I, formed by the lumenal loops i/j of PsaA and PsaB, appears to be similar in prokaryotic and eukaryotic organisms, the structural elements required for the electrostatic interactions were forced to incur either large changes or were

*Author for correspondence, email: mhippler@sas.upenn.edu

John H. Golbeck (ed): Photosystem I: The Light-Driven Plastocyanin:Ferredoxin Oxidoreductase, 499–513.

even invented during evolution. An insertion of a positively charged domain in eukaryotic PsaF, which is absent in cyanobacterial PsaF, led to an efficient electrostatic interaction between the oxidizing side of PS I and the negatively charged donor molecules. The resulting differences in binding between the donor side of PS I and the electron transfer donors are reflected in differences in the dissociation constants found for the electron transfer reaction between pc or cyt c_6 and PS I in prokaryotic and eukaryotic organisms. In several prokaryotic organisms the binding constant is rather high and is found in the mM range whereas in eukaryotic organisms this value can be lower than 10 μM, demonstrating that the affinity between the donors and the oxidizing site of PS I is much larger in chloroplast-based than in most prokaryotic oxygenic photosynthetic organisms. Other kinetic parameters defined for the electron transfer reaction between the soluble donors and PS I and differences in kinetic behavior between cyanobacteria and green plants are also discussed.

I. Donor Side of PS I

From the crystal structures of the cyanobacterial and plant PS I it appears that the flat lumenal surface of the donor side of PS I is mainly formed by the loop regions that connect the transmembrane domains of subunits PsaA and PsaB (Jordan et al., 2001; Ben-Shem et al., 2003; see Fromme and Grotjohann, this volume, Chapter 6; Nelson and Ben-Shem, this volume, Chapter 7). The lumenal loops of PsaA/B as well as the subunit PsaF contribute significant structural elements to this side. Light-induced charge separation in PS I leads to the formation of $P700^+$. The oxidized primary donor is then reduced by electron transfer from the lumenal electron donors pc or cyt c_6. Pc can be replaced by cyt c_6 in some cyanobacteria and green algae when the availability of copper is limiting (Wood, 1978; Ho and Krogmann, 1984; Merchant and Bogorad, 1986). The lumenal loops i/j of PsaA and PsaB play an important role in binding and electron transfer between PS I and the lumenal electron donors pc or cyt c_6 in both prokaryotic and eukaryotic organisms. In contrast, a structural element formed by the PsaF subunit provides an essential recognition site for efficient binding and electron transfer between PS I and the electron donors in eukaryotic organisms (see below).

Recently a modified cyt c_6 was discovered in several vascular plants that possesses an extra loop of 12 residues that is a unique feature of the plant heme protein. However, physicochemical, structural, and functional analysis of the vascular plant cyt c_6 revealed that it cannot replace pc in electron transport to PS I (Gupta et al., 2002; Molina-Heredia et al., 2003; Weigel et al., 2003). Therefore, the function of this cytochrome is not discussed further in this review.

Abbreviations: WT – wild-type; K_D – dissociation constant; pc – plastocyanin; cyt c_6 – cytochrome c_6; E – Einstein; PS – photosystem.

A. Electrostatic Interactions Guiding the Formation of Productive Electron Transfer Complexes

1. Electrostatic Interaction Between the Soluble Donors and the Core of PS I

In cyanobacteria electrostatic interactions between the electron donors and the oxidizing side of PS I appear to be independent of PsaF (see below) or any other peripheral PS I subunit. However, site-directed mutagenesis of pc or cyt c_6 from *Synechocystis* sp. PCC 6803 and *Anabaena* sp. PCC 7119 and analysis of binding and electron transfer between the altered donors and cyanobacterial PS I revealed that a positively charged amino acid located at the "northern face" of either pc or cyt c_6 is crucial for the interaction with the reaction center (De la Cerda et al., 1999; Molina-Heredia et al., 1999, 2001; see also below). Interestingly, an equivalent positively charged exposed amino acid is present in cyt c_6 from *Chlamydomonas reinhardtii* (Kerfeld et al., 1995) but absent from pc of *C. reinhardtii* and other eukaryotic pc structures (see Fig. 1). It is tempting to speculate that this positively charged amino acid that is expressed by pc or cyt c_6 in cyanobacteria is important for an electrostatic recognition of a negatively charged amino acid present in the core subunits PsaA or PsaB and thereby helps the formation of an electron transfer complex. From an evolutionary point of view it is remarkable that eukaryotic pc structures are lacking this positively charged residue. However, as discussed below, in eukaryotic organisms a positively charged domain within the PsaF subunit is crucial for the electrostatic interaction between the negatively charged donors and PS I, which indicates that this interaction has overcome the prokaryotic binding mechanism. The recent crystal structure of plant PS I (Ben-Shem et al., 2003) conforms this view and shows that the N-terminal extension of PsaF exceeds into the lumenal space to allow binding and guidance of pc and

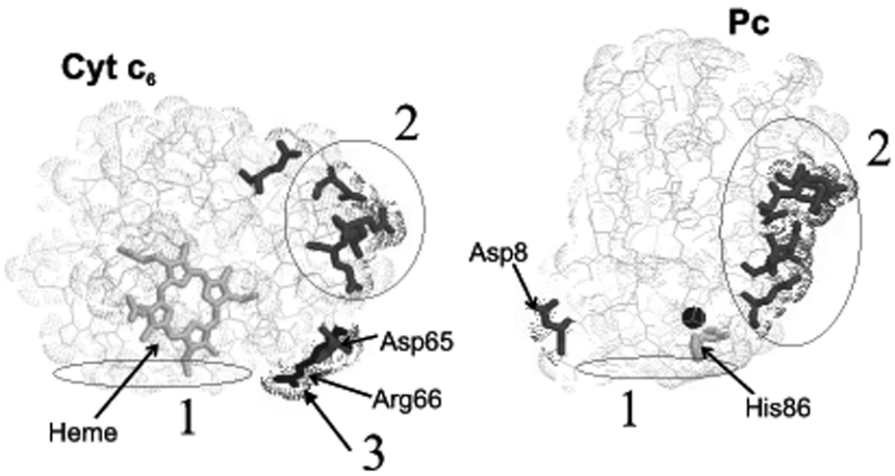

Fig. 1. Crystal structures of *Chlamydomonas reinhardtii* cyt c_6 at a resolution of 1.6 Å (Kerfeld et al., 1995) and pc at 1.5 Å (Redinbo et al., 1994). See Color Plate 12, Fig. 2.

cyt c_6 into the final electron transfer position, enabling fast and efficient electron transfer to $P700^+$.

2. The Positively Charged N-Terminal Domain of PsaF that is Present in Eukaryotic but Absent in Prokaryotic Organisms Forms a Specific Recognition Site for Binding of pc and cyt c_6 to PS I

More than 25 years ago, the pioneering work of Bengis and Nelson (1977) provided evidence that a peripheral subunit of PS I, namely subunit III, is required for binding and efficient electron transfer between pc and PS I. Later it was shown that subunit III can be cross-linked to pc (Wynn and Malkin, 1988; Hippler et al., 1989) in a manner that μsec electron transfer from pc to the photooxidized $P700^+$ is preserved within the cross-linked complex (Hippler et al., 1989). It was further shown that subunit III is identical to the *psaF* gene product (Hippler et al., 1989), indicating that PsaF is the pc binding subunit of green plants. Another major step in understanding of the function of PsaF was through the deletion of the *psaF* gene in *C. reinhardtii*. The analysis of the resulting PsaF-deficient strains helped to define the role of the PsaF subunit in electron transfer to PS I in eukaryotic organisms (Farah et al., 1995). The mutant still assembles a functional PS I complex and grows photoautotrophically, although it is sensitive to high light [>400 $\mu E/m^2/sec$; (Hippler et al., 2000)]. However the rate of electron transfer from pc to PS I as revealed by *in vivo* flash-induced spectrometric measurements is reduced 20-fold as compared to wild-type, indicating that the PsaF subunit is important for docking pc to the PS I complex. *In vitro* studies have supported these results and have shown that PsaF is, in addition, important for binding and electron transfer between cyt c_6 and PS I, since electron transfer rates for pc and cyt c_6 were 80 and 40 times slower, respectively, as compared to the wild-type (Hippler et al., 1997). Its function in vascular plants was also analyzed in a reverse genetic experiment that used an antisense strategy to lower the levels of PsaF in Arabidopsis (Haldrup et al., 2000).This approach resulted in PS I complexes that were largely depleted in PsaF (Haldrup et al., 2000). Functional analysis of these plants showed that the depletion of PsaF strongly impairs the binding and electron transfer between PS I and pc. In contrast to eukaryotic organisms, efficient binding and electron transfer between PS I and pc or cyt c_6 does not depend on the PsaF subunit in cyanobacteria, since the specific deletion of the *psaF* gene in *Synechocystis* sp. PCC 6803 did not affect photoautotrophic growth (Chitnis et al., 1991) and the *in vivo* measured electron transfer rate between cyt c_{553} and PS I was the same as in the wild-type (Xu et al., 1994). *In vitro* measurements revealed that even at high concentrations of pc or cyt c_6, no difference in electron transfer rates could be measured between the donor proteins and PS I isolated from wild-type or the PsaF-deficient *Synechocystis* sp. PCC 6803 mutant (Hippler et al., 1998).

The PsaF subunit of eukaryotic photosynthetic organisms contains a positively charged N-terminal domain with a putative amphipathic α-helical structure which is missing in cyanobacteria (Hippler et al., 1996). Experiments using the reagents EDC and NHS showed that for the formation of a cross-linked product,

negatively charged amino acids residues provided by pc and positively charged amino acid residues of PsaF were required (Hippler et al., 1996). To determine the amino acid residues that were cross-linked between pc and PsaF, the cross-linked PsaF–pc product was excised after SDS–PAGE fractionation, digested with trypsin and the resulting peptides were separated and analyzed by liquid chromatography coupled to mass spectrometry. As a result, cross-linked peptides were identified with a covalent link between the positively charged N-terminal domain of PsaF and conserved acidic amino acids of pc (Hippler et al., 1996), implicating that the evolution of this N-terminal charged domain allowed a stable complex formation between pc and PS I, thereby enabling fast inter-molecular electron transfer. In a reverse genetic experiment the role of the Lys residues within the N-terminal domain of PsaF was further analyzed by taking advantage of the PsaF-deficient mutant 3bF of *C. reinhardtii*. Evaluation of possible secondary structures of the N-terminal domain of PsaF indicated that it may form a amphipathic α-helical structure with five lysine residues that point in one direction. All five lysine residues were altered by site-directed mutagenesis of the *psaF* gene. To obtain nuclear transformants, the PsaF-deficient strain 3bF was cotransformed with the respective *psaF* genes carrying a specific point mutation together with a plasmid containing the *CRY1* [which confers resistance to cryptopleurine and emetine (Nelson et al., 1994)] or the *ble* gene [which confers resistance to phleomycin and zeomycin (Stevens et al., 1996; Hippler et al., 1998)]. The subsequent screening of the transformants resulted in four strains that stably expressed the altered PsaF. These strains had the following changes in the N-terminal domain of PsaF Lys12Pro, Lys16Gln, Lys23Gln, and Lys30Gln, respectively. The Lys23Gln change drastically affected binding of pc and cyt c_6 to PS I and the cross-linking of pc to PS I. Smaller effects were found for the mutations Lys16Gln and Lys30Gln, whereas in Lys12Pro no difference in the rate of electron transfer was detected relative to wild-type PS I. Interestingly, the fast 3 μsec electron transfer phase was not changed in these mutants, indicating that the overall conformation of PsaF is not altered [the rate of electron transfer is very sensitive to changes in distance between electron transfer partners (Marcus and Suttin, 1985)]. Because these single amino acid changes within the N-terminal domain of PsaF did show differential effects on binding of both electron donors, this strongly points to the existence of a rather precise recognition site for pc and cyt c_6 formed by the N-terminal domain of PsaF. We can conclude that this binding motif leads to the stabilization of the final electron transfer complex through electrostatic interactions. It is of note that although pc and cyt c_6 have different primary structures and carry distinct redox cofactors, both donors bind to a similar recognition site within the N-terminal part of PsaF. Concerning the binding and electron transfer, the effect of the mutations always impaired the interaction between pc and PS I more strongly than the interaction between cyt c_6 and PS I, which indicates that the electrostatic guidance provided by the N-terminal domain of PsaF is more important for pc than for cyt c_6. How can this discrepancy in binding of pc and cyt c_6 to PS I been explained? As pointed out above, *C. reinhardtii* cyt c_6 still possesses the positively charged residue in the northern face of the molecule that facilitates binding of the cyanobacterial donor to PS I and it is tempting to speculate that this motif helps cyt c_6 to bind to the core of PS I to form a productive electron transfer complex. On the contrary, *C. reinhardtii* pc more strongly depends on the recognition by the positively charged domain of PsaF. Nevertheless, we can conclude from the site-directed mutagenesis and cotransformation experiments that Lys23 and Lys16 of the N-terminal domain of PsaF are the most important determinants of this recognition site and are likely to stabilize the electron transfer complex through electrostatic interactions. Importantly the α-helical structure of the N-terminal domain of PsaF is supported by the first plant PS I crystal structure and appears to be oriented in a way that Lys23 and Lys16 can interact with the conserved negatively charged residues present in pc or cyt c_6 (Ben-Shem et al., 2003).

To test the impact of the eukaryotic basic N-terminal domain of PsaF from *C. reinhardtii* for efficient electron transfer between pc or cyt c_6 and PS I in cyanobacteria a chimeric protein consisting of the first 83 amino acids of PsaF of *C. reinhardtii* fused to the C-terminal part of PsaF from the cyanobacterium *Synechococcus elongatus* (since renamed *Thermosynechococcus elongatus*) was constructed (Hippler et al., 1999). The chimeric construct was transformed into a PsaF-deficient strain of *S. elongatus*. Analysis of transformants that expressed this chimeric protein showed that it was inserted into the PS I complex of the PsaF-deficient mutant, thus allowing functional analysis. *In vitro* flash-induced absorbance measurements showed that the rate of electron transfer between the chimeric PS I complex and pc or cyt c_6 from *C. reinhardtii* increased by two or three orders of magnitude in 30% of the complexes. These results clearly demonstrate that the insertion of the positively charged N-terminal domain of PsaF from *C. reinhardtii* into cyanobacterial PS I changes the prokaryotic binding mechanism to an eukaryotic type of binding, leading to an

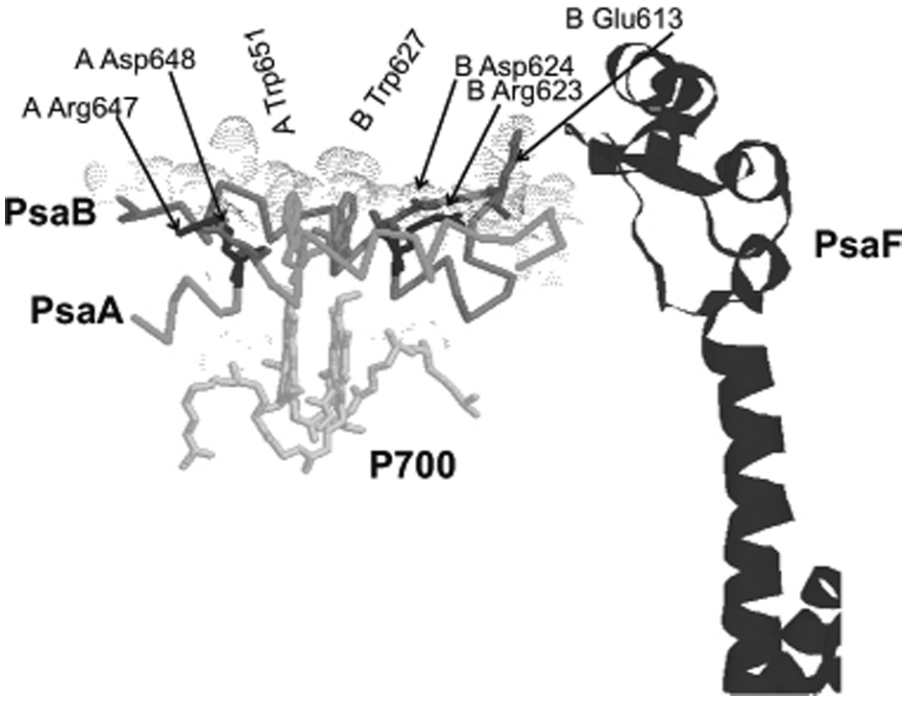

Fig. 2. Part of the crystal structure of *Synechococcus elongatus* PS I at 2.5 Å (Jordan et al., 2001) in a view along the membrane plane. The numbering for all residues corresponds to the positions in *Chlamydomonas reinhardtii*. The PsaF subunit in eukaryotic PS I contains an N-terminal extension on the lumenal side of PS I presenting patches of positively charged residues which have been shown to interact with the negatively charged patches on the both donors and is orientated through close electrostatic interactions with PsaB-Glu613 (Sommer et al., 2002).

enhanced interaction between the algal donors and this chimeric PS I complex (Hippler et al., 1999). Interestingly, binding of both algal donors to the chimeric PS I is greatly enhanced, but only cyt c_6 is capable of forming an inter-molecular electron transfer complex with the chimeric PS I (Hippler et al., 1999) that leads to μsec electron transfer kinetics within the complex. This demonstrates that cyt c_6 from *C. reinhardtii* recognizes chimeric cyanobacterial PS I as well as *C. reinhardtii* PS I, whereas pc does not, which implies that (i) along with the evolution of PS I, structural elements of pc changed to improve binding to the positively charged element within PsaF present in eukaryotic organisms and (ii) that cyt c_6 is regarding its binding mechanism to PS I an evolutionary intermediate between cyt c_6 from *S. elongatus* and pc from *C. reinhardtii* (Hippler et al., 1999) as discussed above.

B. Binding of the Soluble Donors to the Core of PS I

From site-directed mutagenesis of pc and analysis of the binding and electron transfer between the altered pc and PS I (Haehnel, 1984; Nordling et al., 1991; Lee et al., 1995; Hippler et al., 1996) it has been suggested for eukaryotic organisms that in addition to the long-range electrostatic interaction between the positively charged PsaF and the negative patches of pc, a second recognition site is required, which brings the flat hydrophobic surface of pc in close contact with the core of PS I to allow efficient electron transfer from copper *via* the "northern face" of the molecule to $P700^+$ (see Fig. 2). According to the three-dimensional structure of PS I, the primary photosynthetic electron donor P700 is localized near the lumenal surface. The lumenal surface of PS I is mainly build up by loop regions that connect transmembrane α-helices of subunits PsaA and PsaB. Part of the loops i/j of PsaA/B form two α-helices that are parallel to the membrane and in which two conserved Trp residues PsaA655 and PsaB631 are located (Fig. 2). It is assumed that these loops are involved in docking of the soluble donors pc and cyt c_6 (Schubert et al., 1997; Sun et al., 1999; Jordan et al., 2001; Sommer et al., 2002, 2004). Sun et al. (1999) generated site-directed mutants in the lumenal loop j of the PsaB protein in *Synechocystis sp.* PCC 6803 and, consistent with the previous hypothesis, the double mutant Trp622Cys/Ala632Arg

strongly affected the interaction between the altered PS I and the electron donors. The high resolution structural data on PS I (Jordan et al., 2001) show that Trp631 (corresponding to Trp627 in *C. reinhardtii*) from helix l of PsaB together with Trp655 (corresponding to Trp651 in *C. reinhardtii*) from PsaA, form a sandwich, with their indole groups stacked at van der Waals distance (Jordan et al., 2001), and directly situated above P700. This view is confirmed by the structural data on PS I from pea (Ben-Shem et al., 2003). The function of these two Trp residues in electron transfer between the two donors and PS I was questioned in a reverse genetic experiment in *C. reinhardtii*. The Trp residues were altered by site-directed mutagenesis and, by transformation of PsaA- and PsaB-deficient strains, the mutant strains PsaATrp651Phe, PsaATrp651Ser, and PsaBTrp627Phe (corresponding to PsaATrp655 PsaBTrp631 in *Synechococcus elongatus*) were generated (Sommer et al., 2002, 2004). The change of either of the two PsaA or PsaB Trp residues to Phe abolished the formation of an inter-molecular electron transfer complex between PS I and pc, indicating that PsaATrp651, as well as PsaBTrp627 of loops i/j are part of the suggested hydrophobic recognition site required for binding of pc to the core of PS I. Thus, binding of pc to this structural element possibly allows electron transfer from His87 of pc via the π-electron of the aromatic Trp residues directly to $P700^+$. The mutation of Trp to Phe decreases the hydrophobic surface that is exposed into the putative binding site from a value of about 255–210 $Å^2$ (Chothia, 1975). This change is apparently too large to allow a hydrophobic contact sufficient for the stable formation of an electron transfer complex between the northern face of pc and the altered PS I.

Interestingly, for cyt c_6, mutations at PsaATrp651 had a much larger impact on binding and electron transfer with PS I than did the mutation of PsaBTrp627, whereas for pc it was contrariwise (Sommer et al., 2002, 2004). The binding constant for the electron transfer between cyt c_6 and the altered PsaATrp651Ser is greater than 2 mM compared to less than 200 μM for PsaB-Trp627Phe and to about 80 μM found for wild-type PS I. In contrast the binding constant for the electron transfer between pc and the altered PsaBTrp627Phe appears to be in the mM range compared to about 500 μM for PsaATrp651Ser and to 83 μM for wild-type PS I. The same tendency is seen for the second-order electron transfer constants as measured for the electron transfer between the two donors and the altered PS I (Sommer et al., 2004). It is of note that the rate of electron transfer within the inter-molecular complex between cyt c_6 or pc and the mutated PsaATrp651Ser or PsaBTrp627Phe PS I is about 10 times slower as compared to the wild-type. Given that the rate of electron transfer is very sensitive to changes in distance between electron transfer partners (Marcus and Suttin, 1985), this implies that the orientation and/or conformation of the pc- or cyt c_6–PS I complex is altered in comparison to the wild-type, Thus Trp residues PsaA651 and PsaB627 are required for the formation of the inter-molecular electron transfer complex competent in the 3 μsec kinetic component of the electron transfer.

In summary, we propose that Trp651 from PsaA and Trp627 from PsaB form the specific hydrophobic recognition site of the core of PS I. This site is required for effective binding and electron transfer, as well as stable complex formation, between pc or cyt c_6 and PS I, and is important for proper electron transfer within the inter-molecular complex of donor molecules and PS I (see Fig. 2). In addition, we suggest that the PsaA-Trp651 side is more important for the binding of cyt c_6, whereas the PsaBTrp627 side is more crucial for the binding of pc to PS I, indicating that the binding of pc or cyt c_6 to the core of PS I is slightly different. This suggests that the hydrophobic recognition site formed by residues PsaA-W651 and PsaB-W627 confers a distinct selectivity for the binding of pc and cyt c_6.

How can this be rationalized? From a structural point of view (Fig. 2), other highly conserved residues on PsaA and PsaB, namely PsaA-D648 and PsaA-R647 as well as PsaB-D624 and PsaB-R623 are exposed into the lumenal space. These charge-compensated pairs are close to PsaA-W651 and PsaB-W627 and enframe the Trp dimer. An equivalent charge-compensated pair is located at the northern face of cyt c_6 in *C. reinhardtii* [Asp65 and Arg66 (Kerfeld et al., 1995), see above] and of pc and cyt c_6 in cyanobacteria. As already mentioned above, the positively charged residue on the northern face of the cyanobacterial donor molecule in either pc or cyt c_6 is crucial for the interaction with the PS I complex (De la Cerda et al., 1999; Molina-Heredia et al., 1999, 2001). An equivalent positively charged, exposed amino acid is absent in pc of *C. reinhardtii* (Fig. 1) and in other pc structures from eukaryotes. By comparing the geometry and the distances obtained from the structural data, electrostatic interaction between Arg66/Asp65 of cyt c_6 and Asp624/Arg623 on PsaB appears to be feasible. On the other hand, an interaction of Asp8 on pc and Arg647 on PsaA might be possible. Interestingly, the geometry and distances are very similar for the conserved triplets PsaA-Trp651/B-Asp624/PsaB-Arg623 or PsaB-Trp627/PsaA-Asp648/A-Arg647. In the case

of prokaryotic PS I and prokaryotic donors, where the orientation for binding of the donors to the PS I is not restricted by correct interaction with the PsaF subunit, two symmetric orientations for the donor binding would be possible, favoring either of the two triplets. In such a way, the shape of the binding pocket would have changed from a symmetric to an asymmetric interface. The loss of the positively charged residue at the "northern face" of eukaryotic pc is in line with this assessment. Cyt c_6 from *C. reinhardtii* would therefore represent the ancient donor, whereas pc from *C. reinhardtii* would represent the donor that is optimized to interact with the eukaryotic oxidizing side of PS I, which is characterized by the presence of the positively charged N-terminal domain of PsaF.

C. Stabilization and Orientation the N-Terminal Domain of PsaF in Eukaryotic Organisms

PsaF can be cross-linked to PsaJ, a small hydrophobic subunit with a single transmembrane domain, suggesting an interaction between these two PS I subunits (Jansson et al., 1996). To analyze the function of PsaJ, the chloroplast encoded *psaJ* gene of *C. reinhardtii* was inactivated (Fischer et al., 1999). PsaJ-deficient cells grow photoautotrophically and accumulate normal levels of PS I. Electron transfer measurements by flash absorption spectroscopy were performed to determine whether PsaJ has an impact on electron transfer between pc or cyt c_6 and PS I. These measurements revealed that only 30% of the PsaJ-deficient PS I complexes oxidize pc or cyt c_6 with kinetics identical to the wild-type. The remaining 70% displayed only a slow kinetic phase similar to that observed with PsaF-deficient PS I complexes, even though PsaF accumulates in normal amounts in the mutant PS I. Cross-linking between PsaF and pc or cyt c_6 occurred to the same extent as with wild-type PS I, indicating that the binding of the two donors to PsaF is not disturbed. It was therefore suggested that PsaJ may help to maintain PsaF in an orientation that its N-terminal domain can serve as a docking site for the soluble donor proteins, thus mediating fast electron transfer to $P700^+$.

Site-directed mutagenesis of residues within the inter-helical-region of the lumenal loop j, that connects transmembrane helices k and m of the PsaB protein in *C. reinhardtii* resulted in the mutant strain PsaBGlu613Lys. This strain is strongly impaired in electron transfer between PS I and the two donor proteins as investigated by *in vitro* flash-induced absorption spectroscopy (Sommer et al., 2002). The electron transfer rates for the mutant Glu613Lys PS I and the donors pc or cyt c_6 were about two orders of magnitude lower as compared to wild-type. These values are comparable to values obtained for electron transfer between PS I from the PsaF-deficient mutant and the two donors. Another mutation of PsaBGlu613 to Asn had an opposite effect. It resulted in a clear acceleration of electron transfer rates, as well as improved binding of both donors to the altered PS I as compared to wild-type. From the structural data it seems to be clear that the negative charge provided by residue PsaBGlu613 is exposed on the surface of PS I (see Fig. 2). Thus, a change of Glu to Asn could lead to a tighter binding of the donors to PS I in mutant PsaBGlu613Asn because this mutation decreases the electrostatic repulsion between the negatively charged donors and PS I. On the other hand PsaBGlu613 of *C. reinhardtii* is in close proximity to the N-terminus of the PsaF subunit of cyanobacterial PS I. The N-terminal domain of PsaF in *C. reinhardtii* is largely positively charged so that that mutation PsaBGlu613Lys may cause a distortion of that domain by charge repulsion. This in turn would lead to a disorientation of the N-terminal domain of PsaF and thereby to a loss of affinity for binding of the two donors to PS I. The salt dependence of electron transfer between the donors and the PsaBGlu613Lys PS I was comparable to that measured for the PsaF-deficient mutant, which indicates that although PsaF was present, the electrostatic attraction for binding the donors was lost, suggesting that the N-terminal domain of PsaF is indeed disoriented in that mutant. We propose that residue PsaBGlu613 supports unbinding of the two donors from PS I by electrostatic repulsion and orientates the positively charged N-terminal domain of PsaF in a way that it allows efficient binding of the donors to PS I.

D. Does PsaN Contribute to the Binding of pc?

The PsaN subunit of PS I is localized on the lumenal side of the thylakoids and is only present in eukaryotic organisms. To analyze the function of PsaN, an antisense strategy was pursued in Arabidopsis (Haldrup et al., 1999). Antisense plants without detectable amounts of PsaN assemble functional PS I complexes and grow photoautotrophically. The rate of electron transfer between the PsaN-deficient PS I and pc as well as the steady-state $NADP^+$ reduction rate are twofold lower as compared to the wild-type. These data indicate that PsaN may contribute to the binding of pc to the donor side of PS I. However, these data do not

allow one to distinguish whether PsaN is directly involved in the binding of pc or whether the lack of PsaN causes a conformational change of PsaF, which in turn would have an impact on the binding of pc to PS I.

E. The Oxidizing Side of PS I Modulates the Electron Transfer Within the Inter-Molecular Complex of pc and PS I

The reaction between soluble pc and the PS I complex can be stabilized in a functional conformational state by chemical cross-linking (Hippler et al., 1989, 1997; Drepper et al., 1996). The cross-linked complex is therefore an attractive system for studying the mechanism of electron transfer within interprotein complexes. The cross-linked complex can be isolated and separated from free non-cross-linked pc so that electron transfer between the bound pc and PS I can be analyzed in detail. The amplitude of the μsec electron transfer kinetic phase within the cross-linked complex was measured as a function of the ambient redox potential. Interestingly it was found that the redox midpoint potential of bound pc is about 50–60 mV higher as compared to free pc (Drepper et al., 1996; see also below). The shift in the midpoint potential of pc upon binding to PS I is confirmed in the better binding of soluble, reduced pc to PS I as compared to oxidized pc, indicating that the oxidizing side of PS I stabilizes and promotes the binding of the reduced over oxidized donor (see also below). To further evaluate the question of how the donor side of PS I modulates the redox properties of bound pc, the cross-linked complex between pc and PS I was used to investigate the effect of pH and temperature on electron transfer of bound and unbound pc.

1. pH-Dependence of Electron Transfer

The three-dimensional structures of reduced pc by X-ray crystallography at several pH values (Guss et al., 1986) reveals that there are two distinct pH-dependent conformations of the copper center. The pH 7.0 form is similar to that of oxidized pc (Guss and Freeman, 1983), whereas in the pH 3.8 form His87 is protonated, which results in the break of the Cu-His87 bond. The liganding geometry of the copper ion at low pH is trigonal-planar, which stabilizes the reduced copper form (Guss et al., 1986), resulting in a pH-dependent redox midpoint potential. Guss et al. (1986) suggested that the protonation of pc results in a redox-inactive form of pc. Measurements of free pc at various pH values showed that the midpoint potential increases with lower pH values, with a slope of about 55 mV/pH unit and a pK value of about 5.6 (Katoh et al., 1962; Armstrong et al., 1985). According to NMR studies, the pK value of His87 appears to be 4.9 in spinach (Markley et al., 1975; Sinclair-Day et al., 1985).

It is of physiological interest whether pc is redox-inactive at low pH values. The pH of the lumenal space of the thylakoid membrane in which pc is located may drop to a value of about pH 6 and may even decrease further to values around pH 5 (Juensch and Gräber, 1987; Renganathan et al., 1993). The electron transfer rate of $P700^+$ reduction by pc shows a clear pH dependence, having a maximal rate constant at about pH 5.0 (Hope, 2000), thus indicating that pc is redox-active at these pH values. According to the structural data (Guss et al., 1986), a shift of the pK value of His87 to a lower value upon binding of pc to PS I may explain the fact that pc is still redox-active at pH 5.0. Indeed, redox titrations of the amplitude of the μsec kinetic phase of electron transfer within the cross-linked complex between pc and PS I as a function of pH show (see Fig. 3A) that the E_m value of bound pc remains constant to a pH value as low as pH 4.75 and only slightly increases to 438 mV at pH 4.5 (Hippler et al., 1995). The redox midpoint potential of PS I is not affected by the change in pH. The pK value of reduced pc bound to PS I can be calculated (Dutton and Wilson, 1974). This equation predicts that at a pH equal to that of the pK value of the redox-active group, the redox midpoint potential of the electron transfer component will increase by about 17 mV. Thus, from the pH dependence of the E_m values of pc bound to PS I, a pK value as low as 4.5 can be estimated. For comparison, the redox midpoint potential of free pc increases from 360 mV at pH 7 to 430 mV at pH 4.5 (see Fig. 3A), consistent with previous data (see above), indicating a pK value of soluble pc of about 5.5 with a rising midpoint potential of about 58 mV/pH. It is obvious that the pK values of bound and free pc vary at least by one pH unit. From the structural data as well as from the data obtained by analysis of site-directed mutants it appears that the hydrophobic northern face involving His87 of pc binds to the hydrophobic Trp dimer that is formed by the lumenal loops i/j of subunits PsaA/B. It is tempting to speculate that such a hydrophobic protein–protein interaction excludes solvent molecules, which in turn would lower the pK value of His87 when reduced pc binds to PS I. This would lead to a deprotonation that thereby shifts the geometry of the copper ligands from a trigonal-planar conformation to a tetragonal one, which in turn allows oxidation of the reduced pc and electron transfer to $P700^+$.

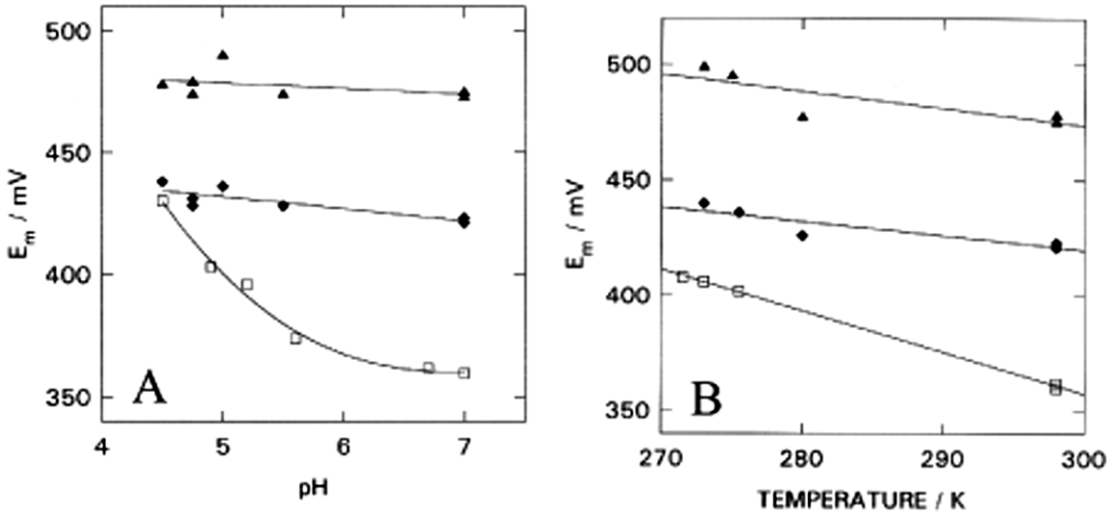

Fig. 3. The dependence of the redox midpoint potentials of P700 (triangles, up), pc cross-linked to PS I (diamonds), and pc (open squares) on the pH (A) and temperature (B). (Reproduced from Hippler et al., 1995.)

2. Temperature Dependence of Electron Transfer

The effect of temperature on the electron transfer kinetics within the inter-molecular complex of pc and PS I was studied to determine the thermodynamic parameters for this reaction. The kinetics of $P700^+$ reduction was measured within the range 300–200 K (Hippler et al., 1995). Pc cross-linked to PS I donates electrons to $P700^+$ with a halftime of 14 μsec at 304 K and 92 μsec at 202 K. The resulting slope of an Arrhenius plot of the $P700^+$ reduction rate yields an activation energy of about 9.0 kJ/mol (see Fig. 3B), which is similar to the activation energy of about 10 kJ/mol which is similar to the activation energy of about 10 kJ/mol that can be calculated from the data for the temperature dependence of the reaction rate between soluble pc and PS I.

The properties of bound and soluble pc were further investigated by measuring the effect of temperature on midpoint potential (Hippler et al., 1995). Over the temperature range investigated, the change in the midpoint potential of pc bound to PS I was very small (see Fig. 3C). In contrast, the slope for soluble pc is about two times higher. From the temperature dependence of the midpoint potentials, the standard entropy of reduction ΔS° and the standard enthalpy ΔH° can be evaluated, which resulted in values for ΔS° and ΔH° of 0.64 and -612 meV for bound pc and values of 1.81 and -900 meV for soluble pc, respectively (Hippler et al., 1995). A possible explanation for the differences observed between bound and soluble pc could be the protection of bound pc from solvent molecules in the binding pocket of PS I. Such an exclusion of solvent molecules would result in a decrease in standard entropy of reduction ΔS° of bound compared to soluble pc mainly from changes in freedom of the rotation and liberation of the solvent molecules which surround the reaction partners (Marcus and Sutin, 1985).

The thermodynamic parameters obtained for the electron transfer between bound pc and PS I with $\Delta G = -55$ meV, $\Delta H^\circ = -86$ meV, and $\Delta H^* = 69$ meV were used to calculate a reorganization energy λ of about 418 meV for the intermolecular electron transfer between pc and PS I (Hippler et al., 1995). The rather small value for the reorganization energy is consistent with a rather hydrophobic environment at the contact side of both proteins. This indicates that electron transfer between pc and PS I is coupled to a small reorganization of solvent molecules that thereby supports fast interprotein electron transfer in spite of the relatively low driving force.

These thermodynamic parameters can be used to estimate the edge-to-edge distance of the redox centers of pc and PS I. Using an empirical approximation for intra-protein electron transfer that was developed by Moser and Dutton (1992), an edge-to-edge distance of 14.5 Å can be calculated.

A similar estimate for this distance has been made in an independent study using a reverse genetic approach (Ramesh et al., 2002). In a series of site-directed mutants of *C. reinhardtii* in which the histidyl axial ligand to the Mg^{2+} of the P700 chlorophyll *a* has been altered to different amino acids, the dependence of the

$P700^+$/P700 midpoint potential on kinetics of $P700^+$ reduction has been examined *in vivo*. The rate of reduction of $P700^+$ by pc changed in response to changes in the $P700^+$/P700 midpoint potential in the various mutant strains. Using approximations of Marcus electron transfer theory, it was possible to calculate a reorganization energy, λ, of about 545 mV, which results in a distance between the copper of pc and P700 of about 15 Å.

Does this distance fit with the distance between the redox centers of PS I and pc deduced from the structural data? The structures of the redox centers of pc and PS I must first be considered. The Cu liganding $N\delta_1$ of His87, which is suggested to be involved in the electron transfer route from the copper to P700 (Nordling et al., 1991; Haehnel et al., 1994), is the atom of the π-system that is expected to be nearest to P700 in the inter-molecular electron transfer complex. The distance of $N\delta_1$ of His87 to the copper center derived from the X-ray structure of pc (Guss and Freemann, 1983) is measured to be about 4.4 Å. Based on the structure of PS I (Jordan et al., 2001; Ben-Shem et al., 2003) and on site-directed mutagenesis data, which show that PsaATrp651 and PsaBTrp627 in PS I from *C. reinhardtii* are essential for efficient electron transfer and probably directly engaged in binding of both electron donors (Sommer et al., 2002, 2004), the edge-to-edge distance between the chlorophyll-dimer of P700 and the copper center of pc should be a distance of about 14.1 Å. This estimate fits well to the distance calculated from the empirical approximation for inter-molecular protein electron transfer. This strongly supports our view that electron transfer from the copper center of pc to $P700^+$ occurs in a rather hydrophobic environment, most likely through binding of the northern face of the pc molecule to the Trp dimer formed by the PsaA/PsaB loops i/j. This leads to an exclusion of solvent molecules to support fast and efficient electron transfer.

II. Kinetic Analysis of Electron Transfer Between Soluble Donors and PS I

A. Electron Transfer Needs a Transient Complex Between the Donor and PS I

In plants and green algae, electron donation from pc or cyt c_6 to P700 after its photooxidation by a short flash of light generally displays two distinct kinetic phases (Haehnel et al., 1980; Bottin and Mathis, 1985, 1987; Haehnel et al., 1989; Nordling et al., 1991; Drepper et al., 1996). A simple explanation for this biphasic kinetic scheme was that those PS I complexes that had already formed a stable complex with the donor give rise to the fast, microsecond kinetic phase of intra-complex electron transfer. The remaining PS I complexes are rereduced by the soluble donor in a bimolecular reaction with second-order kinetics. Evidence for such a stable pre-formed complex was only found in the presence of the eukaryotic positively charged domain of subunit PsaF (see above).

In early studies on cyanobacteria with acidic donors to PS I, monophasic kinetics were reported with a rate ~2 orders of magnitude slower than in green algae and higher plants. Moreover, the rate was independent of the presence of the PsaF subunit (Hatanaka et al., 1993; Xu et al., 1994; Hippler et al., 1996). The absence of a first-order electron transfer was interpreted in terms of a collisional mechanism for the bimolecular reaction (Hervas et al., 1995, 1996; Navarro et al., 1997). However, a microsecond first-order electron transfer can be observed at higher (millimolar) concentrations of the donor from *S. elongatus* with PS I *in vitro* (F. Drepper and W. Haehnel, unpublished) and has been observed *in vivo* (Baymann et al., 2001). This suggests that although the on-rate is slower in these cyanobacteria, they have already evolved the formation of a transient complex that has a lifetime being about 10- to 20-fold longer than the half-life of intra-complex electron transfer (F. Drepper and W. Haehnel, unpublished).

In Anabaena species, both cyt c_6 and pc carry a net positive charge. Early studies on *Anabaena* sp. PCC 7119 (Hervas et al., 1995) showed biphasic kinetics *in vitro,* indicating complex formation between cyt c_6 and PS I. By analogy to the binding mechanism for eukaryotic PS I, it was tempting to propose that the negatively charged PsaF subunit of *Anabaena* sp. PCC 7119 PS I (Nyhus et al., 1992; Ziegler et al., 1995; see also Golbeck, 1994) may help to attract the positively charged donor (Navarro et al., 1997). However, studies on *Anabaena variabilis* mutants that lack subunits PsaF and PsaJ have shown that both cyt c_6 and pc donate electrons with microsecond first-order kinetics to PS I in a manner similar to wild-type PS I (Drepper et al., manuscript in preparation). Thus, these net positively charged donors are attracted most probably by the negatively charged surface of the PS I core and not by subunit PsaF.

B. Evidence for the Formation of One Specific Electron Transfer Complex

For eukaryotic donors, the binding to PS I has been shown to involve a precise recognition site: electrostatic interaction with subunit PsaF and a hydrophobic

surface patch around the exposed part of the redox center of the donors (see above). Hydrophobic surface patches are a common motif in many soluble electron carriers. For pseudoazurin and cytochrome c_{550}, complementary hydrophobic surface regions have been proposed to provide a "pseudo specific" docking to a wide range of structurally different donors and acceptors in the bacterial periplasm (Williams et al., 1995). The role of PsaF in the kinetics of binding of electron donors to PS I suggests that algae and higher plants have adapted the motif of a hydrophobic surface patch to guide the donor into *one specific* docking position optimized for fast electron transfer to $P700^+$.

Several observations suggest that cyanobacteria may have evolved a binding motif that leads to a preferential docking of the donor into one position at PS I that is optimal for fast electron transfer. First, for both acidic and basic cyanobacterial donors a similar first-order phase of microsecond electron transfer kinetics to $P700^+$ is discernible. Second, the structures of cyanobacterial pc [e.g., from *Synechococcus* sp. PCC 7942, Inoue et al. (1999)] and cyt c_6 [e.g., from *S. elongatus*, Beissinger et al. (1998)] are similar to their eukaryotic homologs and exhibit a hydrophobic surface region (that is oriented toward the bottom in Fig. 1). One important difference is the presence of one basic residue, an arginine, at position 87 of Pc and 66 of cyt c_6 (numbering for equivalent residues from *C. reinhardtii*). These residues protrude at the edge of this surface. In both proteins, the respective position of these residues relative to the proposed electron transfer site via the copper liganding histidine of Pc and the exposed heme edge of cyt c_6 is very similar. A structural alignment of the two analogous donors that superimpose the hydrophobic surfaces as well as the position of the positive arginine residue supports their functional equivalence. A short-range interaction of these positive residues with a hydrophilic group at the binding site of PS I can be expected to cause a specific molecular recognition (see also above). Third, it is of note that an alignment proposed previously for pc and cyt c_6 from *C. reinhardtii* (Frazao et al., 1995) that was based on the location of the acidic patches and the resulting dipole moment yielded similar relative orientations between the two eukaryotic donors as that mentioned above for the cyanobacterial donors. This suggests that although the main electrostatic features that are involved in the recognition at PS I have been changed from the prokaryotic to the eukaryotic donors, the relative orientation of pc and cyt c_6 in specific complexes with their reaction partners has been conserved. This may suggest that the specificity of the complex formation was already achieved by cyanobacteria before endosymbiosis occurred and the subsequent introduction of a new binding domain in eukaryotic PsaF.

C. Does the Docking Need a Rearrangement of an Initial Encounter Complex?

The effect of donor concentration has been extensively studied *in vitro* to elucidate the mechanisms of binding and electron donation under various conditions with proteins from various organisms. For the analysis of flash-induced optical absorbance changes, a kinetic model must be applied that best describes the data and additionally allows the rate constants for individual kinetic steps to be deduced. To decide which kinetic model best describes the data, many investigators have used the limiting half-life of the slower kinetic component as well as the saturation behavior of the amplitude of the fast kinetic component at high donor concentrations. The latter approaches a limit, the value of which depends in many cases on the methods used for the isolation of PS I. For spinach PS I particles and pc, values were in the range from 60–70% (Bottin and Mathis, 1987; Nordling et al., 1991; Sigfridsson et al., 1995, 1996) to 80–90% (Drepper et al., 1996). It has been found that PS I particles with a Chl *a*/*b* ratio of ~10 generally exhibited slightly higher saturation values than PS I with lower Chl *a*/*b* ratios (Drepper et al., 1996). In intact spinach chloroplasts, 90–95% of P700 becomes reduced with first-order microsecond kinetics (Haehnel et al., 1989). For binding of pc or cyt c_6 to wild-type PS I from *C. reinhardtii,* values of 60–70% have been observed (Hippler et al., 1998). Similar values were found in recent studies of the binding of acidic and basic donors from cyanobacteria, ~70% *in vivo* in the cyanobacterium *Synechococcus* sp. PCC 7002 (Baymann et al., 2001) and ~85% for cyt c_6 from *A. variabilis* (Drepper et al., manuscript in preparation). In many cases, a decrease in the maximum fraction of the functional complex was found after mutations (Sigfridsson et al., 1995, 1996) or for heterologous reaction partners (Hervas et al., 1995).

A simple two-step kinetic model as suggested by Nordling et al. (1991) is depicted in the left part of scheme (1a). It consists of an equilibrium complex formation (rate constants k_{on} and k_{off}) between the reduced donor (D^{red}) and PS I (P, or P^+ when P700 is photooxidized) and subsequent intra-complex electron transfer from the donor to P700 (rate constant k_{et}). However, this simple model is not sufficient to describe biphasic kinetics at high concentrations of the donor. Therefore, alternative models have been applied. An additional rate-limiting step has been introduced by Bottin

and Mathis (1985, 1987, see scheme 1b) which may reflect a necessary structural rearrangement after formation of the initial encounter complex ($D^{red}\ldots P^{+}$) in order to form the productive electron transfer complex ($D^{red}.P^{+}$). The equilibrium of the rearrangement is given by two additional rate constants k_d and k_c. A detailed description for the determination of rate constants from kinetic data has been given by Sigfridsson et al. (1995, 1996). It has been argued that the appearance of such a conformational change may be related to an evolution from a simple (collision) reaction mechanism as proposed for some cyanobacteria to a more elaborate process in plants involving PsaF as a donor-binding subunit (Hervas et al., 1995, 2003; Navarro et al., 1997). At variance with this view, there are no clear differences in the limiting amplitude of the first-order component between many cyanobacterial systems and the behavior in higher plants and green algae.

$$D^{red} + P^{+} \left[\begin{array}{c} \xrightarrow{k_{on}} \\ \xleftarrow{k_{off}} \end{array}\right] D^{red}.P^{+} \begin{array}{c} \xrightarrow{k_{et}} \\ \xleftarrow{k_{bet}} \end{array} D^{ox}.P \begin{array}{c} \xrightarrow{k_{off}^{ox}} \\ \xleftarrow{k_{on}^{ox}} \end{array} D^{ox} + P \quad \text{(1a)}$$

$$\left[\begin{array}{c} \xrightarrow{k'_{on}} \\ \xleftarrow{k'_{off}} \end{array} D^{red}\ldots P^{+} \begin{array}{c} \xrightarrow{k_d} \\ \xleftarrow{k_c} \end{array}\right] \quad \text{(1b)}$$

$$\left[\begin{array}{c} \xrightarrow{k_{on}} \\ \uparrow\downarrow \xleftarrow{k_{off}} \\ D^{red}\vdots P^{+} \end{array}\right] \quad \text{(1c)}$$

So far, in the two-step model (left part of 1a) and the three-step model (1b), the equilibrium of electron transfer between P700 and its donor and the release of the oxidized donor (see right part of 1a) have been neglected in the kinetic analysis. Using flash-induced absorption measurements in the presence of both reduced and oxidized pc, it has been shown (Drepper et al., 1996) that the electron transfer equilibrium can be expected to contribute to the kinetics and can be measured in independent experiments, e.g., in redox titrations. The equilibrium constant for electron transfer within the complex of spinach pc and PS I was found to be only ~10, i.e., the rate of backward electron transfer (k_{bet}) is not negligible. The equilibrium constant is lower than expected from redox midpoint potentials of the isolated reaction partners due to a positive shift of the midpoint potential of pc Cu^{II}/Cu^{I} upon binding to PS I. As a consequence, oxidized pc is less tightly bound to PS I than reduced pc. This shift decreases the driving force of the electron transfer but was shown to lead to a rapid dissociation of the oxidized product and therefore may optimize the turnover of PS I. Evidence for such a stabilization of the Cu^{I} form of Pc upon binding to PS I came from independent measurements (Danielsen et al., 1999). These authors used Ag- and Cd-substituted Pc to model the Cu^{I} and Cu^{II} form of Pc and the technique of perturbed angular correlation spectroscopy to probe the binding to PS I.

The hypothesis that unbinding of oxidized pc from PS I is important to optimize turnover of PS I was challenged *in vivo* (Finazzi et al., 2005). Hereby different Chlamydomonas strains with a modified oxidizing side of PS I were analyzed by fast absorbance spectroscopy. By comparing the kinetic properties of mutants in which either the k_{on} or the k_{off} for pc binding to PS I was affected, it was concluded that unbinding of oxidized pc from PS I represents the limiting step of electron transfer between cyt b_6/f complex and PS I *in vivo* and is therefore crucial for efficient electron transfer between both complexes.

Which model best describes the kinetics of the binding of donors to PS I may depend on the details of the system under investigation. The closer the experimental conditions are chosen to native conditions, the less appears the electron donation to be governed by a rate-limiting step during binding. This suggests that most physiological systems are rather optimized to ensure that the donor gets correctly oriented by electrostatic forces during its approach to the binding site, and to prevent it from binding in less productive or even inhibitory conformations (for a discussion, compare, e.g., Northrup et al., 1987). Obviously, with mutated or heterologous reaction partners, and possibly in some native situations, electron donation becomes limited by the binding process at high donor concentrations. However, the proposed three-step model, which includes a rate-limiting step that reflects a rearrangement during the binding (scheme 1b), is not the only, and certainly not the simplest, extension to the minimal two-step model. Alternatives, such as a mutual hindrance of donors or formation of substrate inhibition complexes at the binding site at high donor concentrations have not been tested thoroughly. The formation of inhibitory complexes by binding of the donor in a non-productive complex ($D^{red}|P^{+}$) is depicted in scheme (1c). A careful comparison of different models and a model selection based on their ability to explain experimental data, especially with mutated or heterologous reaction partners, is still missing.

References

Armstrong FA, Hill HAO, Oliver N and Whitford D (1985) Direct electrochemistry of the photosynthetic blue copper protein plastocyanin. Electrostatic promotion of rapid charge transfer at an edge-oriented pyrolytic graphite electrode. J Am Chem Soc 107: 1473–1477

Baymann F, Rappaport F, Joliot P and Kallas T (2001) Rapid electron transfer to photosystem I and unusual spectral features of cytochrome c_6 in *Synechococcus* sp. PCC 7002 *in vivo*. Biochemistry 40: 10570–15077

Beissinger M, Sticht H, Sutter M, Ejchart A, Haehnel W and Rosch P (1998) Solution structure of cytochrome c_6 from the thermophilic cyanobacterium *Synechococcus elongatus.* EMBO J 17: 27–36

Bengis C and Nelson N (1977) Subunit structure of chloroplast photosystem I reaction center. J Biol Chem 252: 4564–4569

Ben-Shem A, Frolow F and Nelson N (2003) Crystal structure of plant photosystem I. Nature 426: 630–635

Bottin H and Mathis P (1985) Interaction of plastocyanin with photosystem I reaction center: a kinetic study by flash absorption spectroscopy. Biochemistry 24: 6453–6460

Bottin H and Mathis P (1987) Turn-over of electron-donors in Photosystem-I – double-flash experiments with pea-chloroplasts and Photosystem-I particles. Biochim Biophys Acta 892: 91–98

Chitnis PR, Purvis D and Nelson N (1991) Molecular cloning and targeted mutagenesis of the gene psaF encoding subunit III of photosystem I from the cyanobacterium *Synechocystis* sp. PCC 6803. J Biol Chem 266: 20146–20151

Chothia C (1975) The nature of the accessible and buried surfaces in proteins. J Mol Biol 105: 1–14

Danielsen E, Scheller HV, Bauer R, Hemmingsen L, Bjerrum MJ and Hansson O (1999) Plastocyanin binding to photosystem I as a function of the charge state of the metal ion: effect of metal site conformation. Biochemistry 38: 11531–11540

De la Cerda B, Diaz-Quintana A, Navarro JA, Hervas M and De la Rosa MA (1999) Site-directed mutagenesis of cytochrome c_6 from *Synechocystis* sp. PCC 6803. The heme protein possesses a negatively charged area that may be isofunctional with the acidic patch of plastocyanin. J Biol Chem 274: 13292–13297

Drepper F, Hippler M, Nitschke W, and Haehnel W (1996) Binding dynamics and electron transfer between plastocyanin and photosystem I. Biochemistry 35: 1282–1295

Dutton PL and Wilson DF (1974) Redox potentiometry in mitochondrial and photosynthetic bioenergetics. Biochim Biophys Acta 346: 165–212

Farah J, Rappaport F, Choquet Y, Joliot P and Rochaix JD (1995) Isolation of a *psaF*-deficient mutant of *Chlamydomonas reinhardtii*: efficient interaction of plastocyanin with the photosystem I reaction center is mediated by the PsaF subunit. EMBO J 14: 4976–4984

Finazzi G, Sommer F and Hippler M (2005) Release of oxidized plastocyanin from photosystem I limits electron transfer between photosystem I and cytochrome b_6f complex *in vivo*. Proc Natl Acad Sci USA 102: 7031–7036

Fischer N, Boudreau E, Hippler M, Drepper F, Haehnel W and Rochaix JD (1999) A large fraction of PsaF is nonfunctional in photosystem I complexes lacking the PsaJ subunit. Biochemistry 38: 5546–5552

Frazao C, Soares CM, Carrondo MA, Pohl E, Dauter Z, Wilson KS, Hervas M, Navarro JA, De la Rosa MA and Sheldrick GM (1995) *Ab initio* determination of the crystal structure of cytochrome c_6 and comparison with plastocyanin. Structure 3: 1159–1169

Golbeck JH (1994) Photosystem I in cyanobacteria. In: Bryant DA (ed) The Molecular Biology of Cyanobacteria, pp 319–360. Kluwer Academic Publishers, Dordrecht, The Netherlands

Gupta R, He Z and Luan S (2002) Functional relationship of cytochrome c_6 and plastocyanin in Arabidopsis. Nature 417: 567–571

Guss JM and Freeman HC (1983) Structure of oxidized poplar plastocyanin at 1.6 Å resolution. J Mol Biol 169: 521–563

Guss JM, Harrowell PR, Murata M, Norris VA and Freeman HC (1986) Crystal structure analyses of reduced (CuI) poplar plastocyanin at six pH values. J Mol Biol 192: 361–387

Haehnel W (1984) Photosynthetic electron transport in higher plants. Ann Rev Plant Physiol 35: 659–693

Haehnel W, Propper A and Krause H (1980) Evidence for complexed plastocyanin as the immediate electron donor of P-700. Biochim Biophys Acta 593: 384–399

Haehnel W, Ratajczak R and Robenek H (1989) Lateral distribution and diffusion of plastocyanin in chloroplast thylakoids. J Cell Biol 108: 1397–1405

Haehnel W, Jansen T, Gause K, Klosgen RB, Stahl B, Michl D, Huvermann B, Karas M, and Herrmann RG (1994) Electron transfer from plastocyanin to Photosystem I. EMBO J 13: 1028–1038

Haldrup A, Naver H and Scheller HV (1999) The interaction between plastocyanin and photosystem I is inefficient in transgenic Arabidopsis plants lacking the PSI-N subunit of photosystem I. Plant J 17: 689–698

Haldrup A, Simpson DJ and Scheller HV (2000) Down-regulation of the PSI-F subunit of photosystem I (PSI) in *Arabidopsis thaliana*. The PSI-F subunit is essential for photoautotrophic growth and contributes to antenna function. J Biol Chem 275: 31211–31218

Hatanaka H, Sonoike K, Hirano M and Katoh S (1993) Small subunits of Photosystem I reaction center complexes from *Synechococcus elongatus*. I. Is the *psaF* gene product required for oxidation of cytochrome c-553? Biochim Biophys Acta 1141: 45–51

Hervas M, Navarro JA, Diaz A, Bottin H and De la Rosa MA (1995) Laser-flash kinetic analysis of the fast electron transfer from plastocyanin and cytochrome c_6 to photosystem I. Experimental evidence on the evolution of the reaction mechanism. Biochemistry 34: 11321–11326

Hervas M, Navarro JA, Diaz A and De la Rosa MA (1996) A comparative thermodynamic analysis by laser-flash absorption spectroscopy of photosystem I reduction by plastocyanin and cytochrome c_6 in *Anabaena* PCC 7119, *Synechocystis* PCC 6803 and spinach. Biochemistry 35: 2693–2698

Hervas M, Navarro JA and De La Rosa MA (2003) Electron transfer between membrane complexes and soluble proteins in photosynthesis. Acc Chem Res 36: 798–805

Hippler M, Ratajczak R and Haehnel W (1989) Identification of the plastocyanin binding subunit of photosystem I. FEBS Lett 250: 280–284

Hippler M, Drepper F and Haehnel W (1995) The oxidizing site of Photosystem I modulates the electron transfer from plastocyanin to P700+. In: Mathis P (ed) From Light to Biosphere, pp 99–102. Kluwer Academic Publishers, Amsterdam, NL

Hippler M, Reichert J, Sutter M, Zak E, Altschmied L, Schröer U, Herrmann RG and Haehnel W (1996) The plastocyanin binding domain of photosystem I. EMBO J 15: 6374–6384

Hippler M, Drepper F, Farah J and Rochaix JD (1997) Fast electron transfer from cytochrome c_6 and plastocyanin to photosystem I of *Chlamydomonas reinhardtii* requires PsaF. Biochemistry 36: 6343–6349

Hippler M, Drepper F, Haehnel W and Rochaix JD (1998) The N-terminal domain of PsaF: precise recognition site for binding and fast electron transfer from cytochrome c_6 and plastocyanin to photosystem I of *Chlamydomonas reinhardtii*. Proc Natl Acad Sci USA 95: 7339–7344

Hippler M, Drepper F, Rochaix JD and Mühlenhoff U (1999) Insertion of the N-terminal part of PsaF from *Chlamydomonas reinhardtii* into photosystem I from *Synechococcus elongatus* enables efficient binding of algal plastocyanin and cytochrome c_6. J Biol Chem 274: 4180–4188

Hippler M, Biehler K, Krieger-Liszkay A, van Dillewjin J and Rochaix JD (2000) Limitation in electron transfer in photosystem I donor side mutants of *Chlamydomonas reinhardtii*. Lethal photo-oxidative damage in high light is overcome in a suppressor strain deficient in the assembly of the light harvesting complex. J Biol Chem 275: 5852–5829

Ho KK and Krogmann DW (1984) Electron donors to P700 in cyanobacteria and algae: an instance of unusual genetic variability. Biochim Biophys Acta 766: 310–316

Hope AB (2000) Electron transfers amongst cytochrome f, plastocyanin and photosystem I: kinetics and mechanisms. Biochim Biophys Acta 1456: 5–26

Inoue T, Sugawara H, Hamanaka S, Tsukui H, Suzuki E, Kohzuma T and Kai Y (1999) Crystal structure determinations of oxidized and reduced plastocyanin from the cyanobacterium *Synechococcus* sp. PCC 7942. Biochemistry 38: 6063–6069

Jansson S, Andersen B and Scheller HV (1996) Nearest-neighbor analysis of higher-plant photosystem I holocomplex. Plant Physiol 112: 409–420

Jordan P, Fromme P, Witt HT, Klukas O, Saenger W and Krauß N (2001) Three-dimensional structure of cyanobacterial photosystem I at 2.5 Å resolution. Nature 411: 909–917

Juensch U and Gräber P (1987) Influence of the redox state and the activation of the chloroplast ATP synthase on proton-transport-coupled ATP synthesis/hydrolysis. Biochim Biophys Acta 893: 275–288

Katoh S, Shiratori I and Takamiya A (1962) Purification and some properties of spinach plastocyanin. J Biochem 51: 32–40

Kerfeld CA, Anwar HP, Interrante R, Merchant S and Yeates TO (1995) The structure of chloroplast cytochrome c_6 at 1.9 Å resolution: evidence for functional oligomerization. J Mol Biol 250: 627–647

Lee BH, Hibino T, Takabe T, Weisbeek PJ and Takabe T (1995) Site-directed mutagenetic study on the role of negative patches on silene plastocyanin in the interactions with cytochrome f and photosystem I. J Biochem (Tokyo) 117: 1209–1217

Marcus RA and Suttin N (1985) Electron transfer in chemistry and biology. Biochim Biophys Acta 811: 265–322

Markley JL, Ulrich EL, Berg SP and Krogmann DW (1975) Nuclear magnetic resonance studies of the copper binding sites of blue copper proteins: oxidized, reduced, and apoplastocyanin. Biochemistry 14: 4428–4433

Merchant S and Bogorad L (1986) Regulation by copper of expression of plastocyanin and cytochrome c_{552} in *Chlamydomonas reinhardtii*. Mol Cell Biol 6: 462–469

Molina-Heredia FP, Diaz-Quintana A, Hervas M, Navarro JA and De La Rosa MA (1999) Site-directed mutagenesis of cytochrome c_6 from *Anabaena* sp. PCC 7119. Identification of surface residues of the hemeprotein involved in photosystem I reduction. J Biol Chem 274: 33565–33570

Molina-Heredia FP, Hervas M, Navarro JA and De la Rosa MA (2001) A single arginyl residue in plastocyanin and in cytochrome c_6 from the cyanobacterium *Anabaena* sp. PCC 7119 is required for efficient reduction of photosystem I. J Biol Chem 276: 601–605

Molina-Heredia FP, Wastl J, Navarro JA, Bendall DS, Hervas M, Howe CJ and De La Rosa MA (2003) Photosynthesis: a new function for an old cytochrome? Nature 424: 33–34

Moser CC and Dutton PL (1992) Engineering protein structure for electron transfer function in photosynthetic reaction centers. Biochim Biophys Acta 1101: 171–176

Navarro JA, Hervas M and DelaRosa MA (1997) Co-evolution of cytochrome c_6 and plastocyanin, mobile proteins transferring electrons from cytochrome b_6f to photosystem I. J Biol Inorg Chem 2: 11–22

Nelson JAE, Savereide PB and Lefebvre PA (1994) The CRY1 gene in *Chlamydomonas reinhardtii*: structure and use as a dominant selectable marker for nuclear transformation. Mol Cell Biol 14: 4011–4019

Nordling M, Sigfridsson K, Young S, Lundberg LG and Hansson O (1991) Flash-photolysis studies of the electron transfer form genetically modified spinach plastocyanin to photosystem I. FEBS Lett 291: 327–330

Northrup SH, Boles JO and Reynolds JCL (1987) Electrostatic effects in the Brownian dynamics of association and orientation of heme-proteins. J Phys Chem 91: 5991–5998

Nyhus KJ, Ikeuchi M, Inoue Y, Whitmarsh J and Pakrasi HB (1992) Purification and characterization of the photosystem I complex from the filamentous cyanobacterium *Anabaena variabilis* ATCC 29413. J Biol Chem 267: 12489–12495

Ramesh VM, Guergova-Kuras M, Joliot P and Webber AN (2002) Electron transfer from plastocyanin to the photosystem I reaction center in mutants with increased potential of the primary donor in *Chlamydomonas reinhardtii*. Biochemistry 41: 14652–14658

Redinbo MR, Yeates TO and Merchant S (1994) Plastocyanin: structural and functional analysis. J Bioenerg Biomembr 26: 49–66

Renganathan M, Pfündel E and Dilly A (1993) Thylakoid lumenal pH determination using a fluorescent dye: correlation of lumen pH and gating between localized and delocalized energy coupling. Biochim Biophys Acta 1142: 277–292

Schubert W, Klukas O, Krauß N, Saenger W, Fromme P and Witt H (1997) Photosystem I of *Synechococcus elongatus* at 4 Å resolution: comprehensive structure analysis. J Mol Biol 272: 741–769

Sigfridsson K, Hansson O and Brzezinski P (1995) Electrogenic light reactions in photosystem I: resolution of electron-transfer rates between the iron–sulfur centers. Proc Natl Acad Sci USA 92: 3458–3462

Sigfridsson K, Young S and Hansson O (1996) Structural dynamics in the plastocyanin–photosystem 1 electron-transfer complex as revealed by mutant studies. Biochemistry 35: 1249–1257

Sinclair-Day JD, Sisley MJ, Sykes AG, King GC and Wright PE (1985) Acid dissociation constants for plastocyanin in the Cu I state. J Chem Soc Chem Commun 1985: 505–507

Sommer F, Drepper F and Hippler M (2002) The luminal helix l of PsaB is essential for recognition of plastocyanin or cytochrome c_6 and fast electron transfer to photosystem I in *Chlamydomonas reinhardtii*. J Biol Chem 277: 6573–6581

Sommer F, Drepper F, Haehnel W and Hippler M (2004) The hydrophobic recognition site formed by residues PsaA-Trp651 and PsaB-Trp627 of photosystem I in *Chlamydomonas reinhardtii* confers distinct selectivity for binding of plastocyanin and cytochrome c_6. J Biol Chem 279: 20009–20017

Stevens D, Rochaix JD and Purton S (1996) The bacterial phleomycin resistance gene *ble* as a dominant selectable marker in Chlamydomonas. Mol Gen Genet 251: 23–30

Sun J, Xu W, Hervas M, Navarro JA, Rosa MA and Chitnis PR (1999) Oxidizing side of the cyanobacterial photosystem I. Evidence for interaction between the electron donor proteins and a luminal surface helix of the PsaB subunit. J Biol Chem 274: 19048–19054

Weigel M, Pesaresi P and Leister D (2003) Tracking the function of the cytochrome c_6-like protein in higher plants. Trends Plant Sci 8: 513–517

Williams PA, Fulop V, Leung YC, Chan C, Moir JW, Howlett G, Ferguson SJ, Radford SE and Hajdu J (1995) Pseudospecific docking surfaces on electron transfer proteins as illustrated by pseudoazurin, cytochrome c_{550} and cytochrome cd_1 nitrite reductase. Nat Struct Biol 2: 975–982

Wood PM (1978) Interchangeable copper and iron proteins in algal photosynthesis. Studies on plastocyanin and cytochrome c_{552} in *Chlamydomonas*. Eur J Biochem 87: 9–19

Wynn RM and Malkin R (1988) Interaction of plastocyanin with photosystem I: a chemical cross-linking study of the polypeptide that binds plastocyanin. Biochemistry 27: 5863–5869

Xu Q, Odom WR, Guikema JA, Chitnis VP and Chitnis PR (1994) Targeted deletion of *psaJ* from the cyanobacterium *Synechocystis* sp. PCC 6803 indicates structural interactions between the PsaJ and PsaF subunits of photosystem I. Plant Mol Biol 26: 291–302

Ziegler K, Schuetz M, Zimmermann R and Lockau W (1995) EMBL GenBank database Entry Id AVPSAFJ

Chapter 30

Genetic Dissection of Photosystem I Assembly and Turnover in Eukaryotes

Jean-David Rochaix*
Departments of Molecular Biology and Plant Biology, University of Geneva, 30 Quai Ernest Ansermet, 1211 Geneva 4, Switzerland

Summary

The photosystem I (PS I) complex of plants and algae is a large multisubunit protein complex consisting of nucleus- and chloroplast-encoded subunits. Besides its redox cofactors P700, A_0, A_1, F_X, F_A, and F_B, the PS I complex also contains a core antenna consisting of 90 chlorophyll and 22 carotenoid molecules. An extensive forward and reverse genetics approach in *Chlamydomonas* and *Arabidopsis* has provided important insights into the mechanisms of synthesis of the subunits and their assembly into a functional complex. The picture which emerges from these studies is that a surprisingly large number of nucleus-encoded factors are involved in several post-transcriptional steps of expression of the two large chloroplast-encoded reaction center subunits PsaA and PsaB. Thus 14 factors are required for the maturation of the *psaA* mRNA through two *trans*-splicing reactions, two factors are required for the translation of the *psaB* mRNA, and one is required for *psaB* mRNA stability in *Chlamydomonas*. Several additional factors, including Ycf3 and Ycf4, are specifically required for the assembly of the PS I complex. With its three [4Fe–4S] clusters, PS I constitutes an important sink for iron. Its specific and early loss following iron deprivation is a phylogenetically conserved process and is preceded by a remodeling of the PS I antenna. Coupled genetic and biochemical approaches have revealed a new link between PS I assembly and the chlorophyll biosynthetic pathway through the identification of Crd1, a di-iron enzyme possibly involved in the aerobic oxidative cyclase reaction of chlorophyll synthesis that is essential for PS I and LHCI accumulation under copper deprivation.

*Author for correspondence, email: jean-david.rochaix@molbio.unige.ch

John H. Golbeck (ed): Photosystem I: The Light-Driven Plastocyanin:Ferredoxin Oxidoreductase, 515–527.

I. Introduction

The determination of the atomic structure of the cyanobacterial Photosystem I (PS I) core complex at a resolution of 2.5 Å (Jordan et al., 2001; see Fromme, this volume, Chapter 6) and the recent crystal structure of plant PS I with its four light-harvesting proteins at 4.4 Å resolution (Ben-Shem et al., 2003; see Nelson and Ben-Shem, this volume, Chapter 7) have provided important new insights into the organization of the multiple subunits, cofactors, and pigments of this large membrane complex. The core complex is similar between cyanobacteria, plants, and algae. The reaction center consists of the two large PsaA and PsaB subunits which contain eleven transmembrane domains each and which provide the ligands of the chlorophyll dimer P700, of the primary acceptor chlorophyll A_0, the secondary acceptor phylloquinone A_1, the [4Fe–4S] center F_X, and of the numerous chlorophylls of the core antenna. The other two [4Fe–4S] centers F_A and F_B are bound to the smaller peripheral PsaC subunit (see Antonkine and Golbeck, this volume, Chapter 8). These three subunits together with the smaller PsaI and PsaJ subunits are encoded by the chloroplast genome of plants and green algae (for review see Scheller et al., 2001; see Haldrup et al., this volume, Chapter 11). Moreover the PsaM subunit first identified in cyanobacteria is also chloroplast-encoded in several algae and gymnosperms, but absent in angiosperms. In eukaryotic photosynthetic organisms the remaining nine subunits PsaD, PsaE, PsaF, PsaG, PsaH, PsaK, PsaL, PsaN, and PsaO are nucleus-encoded, translated in the cytosol and imported into the chloroplast and targeted to the thylakoid membrane. PS I of land plants is connected to the LHCI antenna consisting of the four chlorophyll binding proteins Lhca1-4 (Scheller et al., 2001). In *C. reinhardtii* at least seven distinct LHCI polypeptides have been identified (Bassi et al., 1992). Although a great deal is known about the organization of these polypeptides within the PS I complex and on their respective functions, the molecular mechanisms underlying PS I synthesis and assembly within the thylakoid membrane of photosynthetic eukaryotic organisms are still largely unknown.

This chapter presents an overview of the assembly process of PS I from the level of gene expression to the integration and assembly of the PS I subunits into the thylakoid membrane in green algae and land plants. Biosynthesis of the PS I complex depends on the coordinated expression of nuclear and chloroplast genes, the targeting of subunits to their proper location within the chloroplast, the association of the different redox cofactors and the assembly of the subunits into a functional complex (Fig. 1; Table 1). Moreover the light-harvesting complex I (LHCI) has to be properly connected to PS I to allow for efficient transfer of light excitation energy to the PS I reaction center. The unicellular alga *Chlamydomonas reinhardtii* has proven to be a powerful model system for studying the assembly and function of the photosystem I (PS I) complex. An important feature of this alga is that its photosynthetic function is dispensable when the cells are grown in the presence of acetate. It is thus relatively easy to isolate and to maintain mutants deficient in photosynthetic activity and to analyze them by genetic means (see Harris, 1989). Moreover, efficient transformation methods are available for both the nuclear and chloroplast genome. In particular, mutants can be complemented by transformation with ordered cosmid libraries. Finally, the sequences of the chloroplast and most of the nuclear genome have been determined recently and a large EST collection is available (http://www.biology.duke.edu/chlamy_genome/est.html). Besides *C. reinhardtii*, *Arabidopsis thaliana* has emerged as another powerful model organism for studying PS I function and assembly through reverse genetics with the availability of a large collection of T-DNA insertion lines and antisense and RNA interference technology (Scheller et al., 2001).

Mutants of *C. reinhardtii* deficient in PS I accumulation have been invaluable for understanding the biosynthesis of PS I. A remarkable feature of this alga is its ability to synthesize chlorophyll in a light-independent manner. This property is particularly important for the functional study of PS I because PS I mutants are usually highly sensitive to light and are able to grow only under dim light or in the dark. The ability of synthesizing chlorophyll in the dark is therefore crucial for assembly of the PS I complex in these mutants.

II. Synthesis and Assembly of PS I

A. Expression of the psaA *and* psaB *Genes*

Control of chloroplast gene expression occurs mainly at the posttranscriptional level. However transcriptional control has also been documented for *psaA* and *psaB* especially during acclimation to changes in light

Abbreviations: DCMU – 3-(3,4-dichlorophenyl)-1,1-dimethylurea; LHCI – light-harvesting system of photosystem I; PS I – photosystem I; TPR – tetratricopeptide repeat.

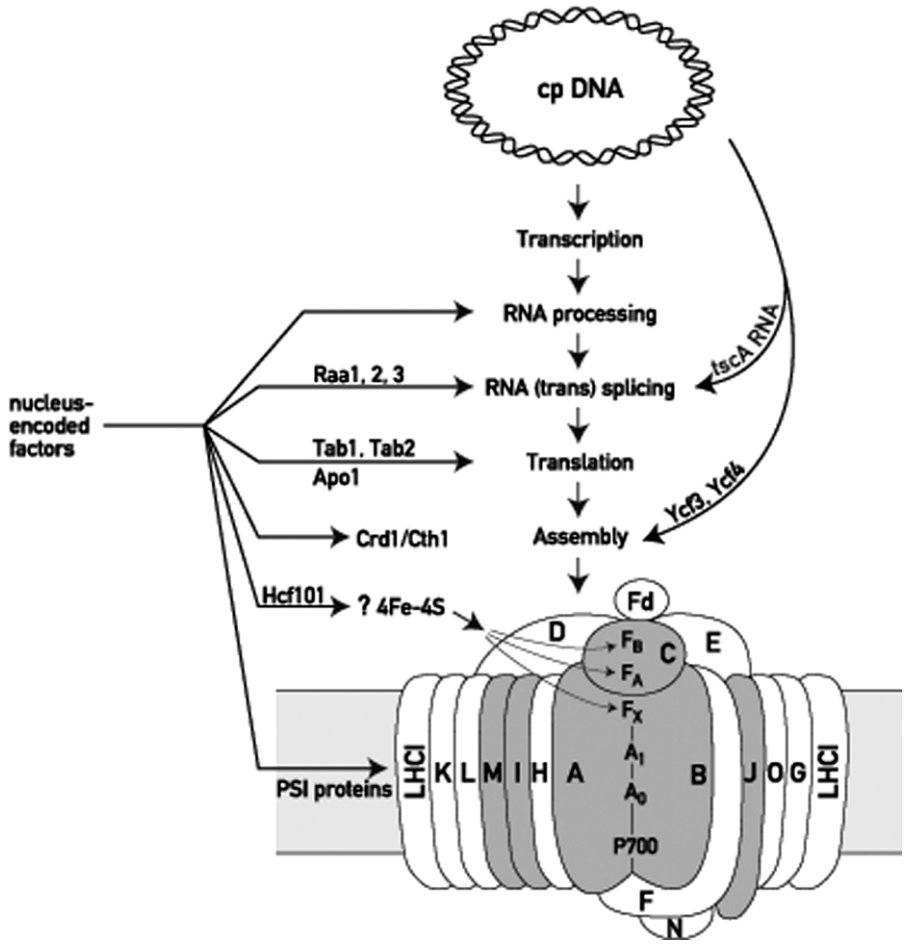

Fig. 1. Scheme of biosynthesis of PS I. The PS I complex is shown schematically at the bottom with the chloroplast-encoded subunits PsaA, PsaB, PsaC, PsaI, PsaJ, and PsaM shaded and the nucleus-encoded subunits PsaD, PsaE, PsaF, PsaG, PsaH, PsaK, PsaL, PsaN, and PsaO unshaded. The light-harvesting system of PS I (LHCI) is also shown. The redox cofactors of PS I are indicated: P700, a chlorophyll dimer that acts as primary electron donor of PS I; the primary acceptor A_0 (chlorophyll), the secondary acceptor A_1 (phylloquinone); the three [4Fe–4S] centers F_X, liganded by PsaA and PsaB and F_A, F_B liganded by PsaC. Fd indicates ferredoxin. Both chloroplast-encoded factors (tscA RNA, assembly factors Ycf3, Ycf4) and nucleus-encoded factors are involved in the different chloroplast post-transcriptional steps that include RNA processing, *trans*-splicing, translation, and assembly as indicated: Raa1, Raa2, and Raa3 are factors required for *psaA* RNA *trans*-splicing, Tab1 and Tab2 are involved in *psaB* mRNA translation. Hcf101 is likely to play a role in [4Fe–4S] assembly; Crd1/Cth1 are di-iron enzymes required for the accumulation of both PS I and LHCI in the absence and presence of copper, respectively.

conditions. In mustard seedlings the levels of PS II and PS I respond in a complementary way to light preferentially absorbed by each of the two photosystems (Pfannschmidt and Allen, 1999). The initial response to this altered excitation energy distribution between the photosystems involves changes in the transcription rates of the genes encoding the reaction center subunits of PS II and PS I. These changes appear to be governed by the redox state of the plastoquinone pool such that reduced plastoquinone resulting from the preferential light-stimulation of PS II induces PS I and represses PS II (Pfannschmidt and Allen, 1999). Oxidized plastoquinone resulting from preferential light-stimulation of PS I induces the reverse response. Thus reduced activity of PS I relative to that of PS II leads to an increase in transcription of the *psaA* and *psaB* genes. However, a similar transcriptional response of the *psaA* and *psaB* genes to changes in the redox state of the plastoquinone pool resulting from mutations affecting PS I could not be detected in *Chlamydomonas* cells (Stampacchia et al., 1997).

A large number of mutants deficient in PS I have been identified in *Chlamydomonas*. These mutants are easy to recognize because of their high chlorophyll

Table 1. Role of the PS I subunits in PS I assembly and function

Subunit	Gene location	Cyanobacteria	State transition	Function	Assembly of PS I		Photoautotrophic growth	
					Cr	At	Cr	At
PsaA	C	+	−	Reaction center	−	−	−	−
PsaB	C	+	−	Reaction center	−	−	−	−
PsaC	C	+	−	Reaction center	−	+	−	−
PsaD	N	+	(+)	Docking of Fd		−		−
PsaE	N	+				+[a]		+
PsaF	N	+			+	−[b]	+	+
PsaG	N	−	(+)	LHCI binding		+	+	+
PsaH	N	−	−					
PsaI	C	+						
PsaJ	C	+						
PsaK	N	−	(+)	LHCI binding				
PsaL	N	+						
PsaM[c]	C	+						
PsaN	N	+	+	Lumenal extrinsic				
PsaO	N	+						
PsaX[d]	–	+						

Cr, *C. reinhardtii*; At, *A. thaliana*.
[a] *A. thaliana* contains two *PsaE* genes. Only one copy, *PsaE1* was inactivated.
[b] The inactivation of *PsaF* in *C. reinhardtii* leads to a weaker phenotype than in *A. thaliana*.
[c] Present in gymnosperms and in several algae taxa, but not in angiosperms.
[d] Not present in eukaryotes.

fluorescence. Because the subunits of the photosynthetic complexes are amongst the most abundant thylakoid polypeptides, their rate of synthesis can be readily determined by protein pulse-labeling in the presence of cycloheximide to block cytosolic protein synthesis (Girard-Bascou et al., 1987; Girard-Bascou et al., 1992). In this way many mutants unable to synthesize PsaA or PsaB have been identified (Table 2). They constitute the majority of the PS I mutants of *C. reinhardtii*. In the absence of either of these proteins, the other subunits are rapidly degraded and they do not accumulate. Mutants deficient in *psaA* expression appear at a particularly high frequency in *C. reinhardtii*. This is due to the unusual structure of *psaA* on the chloroplast genome of this alga. The gene consists of three exons that are widely separated on the chloroplast genome and that are transcribed independently giving rise to three *psaA* precursor transcripts (Fig. 2) (Kück et al., 1987; Choquet et al., 1988). Each exon is flanked by group II intron sequences. Thus production of the mature *psaA* mRNA requires two *trans*-splicing reactions. Many mutants deficient in *psaA* *trans*-splicing have been characterized (Goldschmidt-Clermont et al., 1990). They fall into three phenotypic classes: Class A mutants are specifically deficient in *trans*-splicing of exons 2 and 3 whereas class C mutants are deficient in the *trans*-splicing of exons 1 and 2. Class B mutants are deficient in both *trans*-splicing reactions. An extensive genetic analysis of mutants deficient in *psaA trans*-splicing has revealed that the mutations fall into at least 14 nuclear complementation groups (Goldschmidt-Clermont et al., 1990). Moreover a chloroplast locus, *tscA*, is also involved in the first *trans*-splicing reaction. It encodes a small RNA that represents the middle part of intron 1 (Goldschmidt-Clermont et al., 1991). This intron is therefore at least tri-partite. At this time three nuclear genes involved in *trans*-splicing have been isolated through either genomic complementation of the mutants with a genomic cosmid library or through gene tagging by transformation. Raa1 and Raa2 are *trans*-acting factors that are involved in the second *psaA trans*-splicing reaction (Perron et al., 1999; M. Goldschmidt-Clermont, unpublished). Raa2 is related to pseudouridine synthase, an enzyme that is usually involved in tRNA base modification. Mutations of residues known to be critical for pseudouridylation do not interfere with *trans*-splicing indicating that the former process is not required for the latter (Perron et al., 1999). Raa1 is a 205 kDa protein that is unrelated to any known protein in the database (M. Goldschmidt-Clermont, unpublished). However, it contains five short repeats that are related to repeats previously found in some chloroplast translation factors. Raa1 and Raa2 form a high molecular weight 400–500 kDa complex that is absent or altered in some of the other *trans*-splicing

Table 2. *Trans*-acting factors involved in post-transcriptional steps of PS I synthesis

Mutant	Org	Protein	Pt step	Specific target	Features	References
314B	Cr	Raa1	*Trans*-splicing	Pre-*psaA* RNA		M. Goldschmidt-Clermont (unpublished)
A18	Cr	Raa2	*Trans*-splicing	Pre-*psaA* RNA	ψ -uridine synthase	Perron et al. (1999)
M18	Cr	Raa3	*Trans*-splicing	Pre-*psaA* RNA	Pyridoxamine 5′P oxidase	Rivier et al. (2001)
F15-tab1	Cr	Tab1	Translation	*psaB* mRNA	Lipase domain	Stampacchia et al. (1997), F. Laroche and J. D. Rochaix (unpublished)
F14-tab2	Cr	Tab2	Translation	*psaB* mRNA	RNA binding	Dauvillee et al. (2003)
Apo1	At	Apo1	Translation	*psaA-psaB-rps14* RNA		J. Meurer (unpublished)
Hcf101	At	Hcf101	Assembly	[4Fe–4S] center?	P-loop ATPase	Lezhneva et al. (2003)
Crd1	Cr	Crd1	Assembly		Di-iron binding motif	Moseley et al. (2000), Tottey et al. (2003)
ΔYcf3	Cr, Nt	Ycf3	Assembly		TPR domains	Boudreau et al. (1997), Ruf et al. (1997)
ΔYcf4	Cr, Sy	Ycf4	Assembly			Wilde et al. (1995), Boudreau et al. (1997)
ΔBtpa	Sy	BtpA	Accumulation			Bartsevich and Pakrasi (1997)

CR, *C. reinhardtii*; At, *A. thaliana*; Nt, *Nicotiana tabacum*; Sy, *Synechocystis* sp. PCC 6803; org, organism; pt, post-transcriptional.

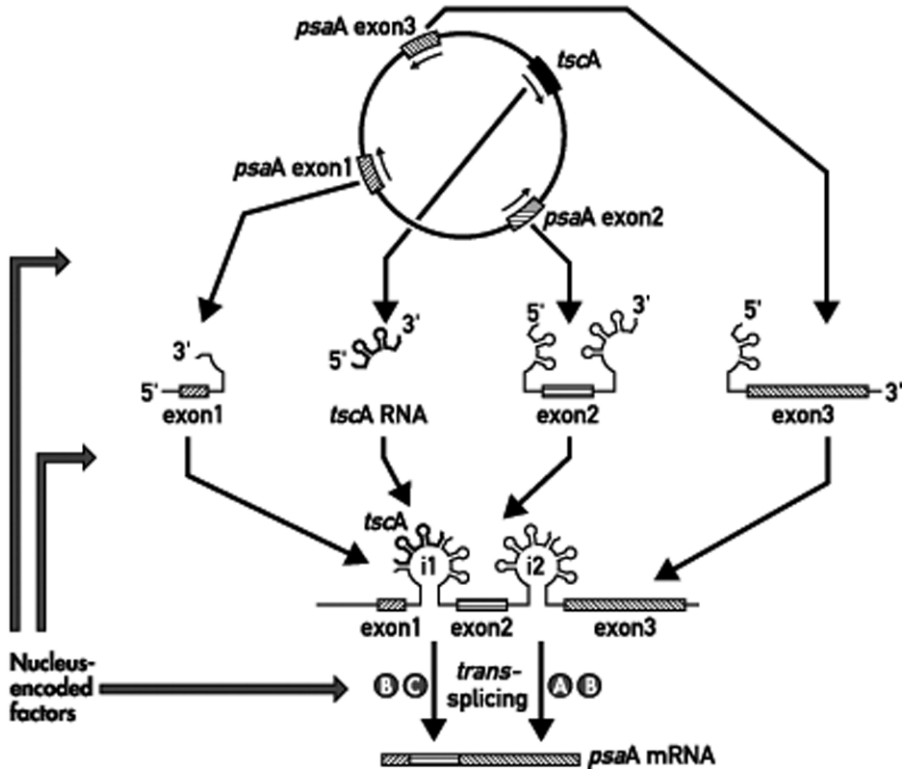

Fig. 2. Maturation of the *psaA* mRNA of *C. reinhardtii*. The three exons of *psaA* with their flanking group II intron sequences are transcribed independently on the chloroplast genome and the three resulting transcripts are spliced in *trans* in two independent reactions. A fourth locus on the chloroplast genome, *tscA*, encodes a RNA that completes the structure of intron 1. Mutants deficient in *psaA trans*-splicing fall into three phenotypic classes: class A mutants are deficient in exon 2–exon 3 splicing, class C mutants are deficient in exon 1–exon 2 splicing and class B mutants are deficient in both *trans*-splicing reactions. These mutations fall into 14 nuclear complementation groups (from Goldschmidt-Clermont, 1998, with permission).

mutants (K. Perron, M. Goldschmidt-Clermont, and J. D. Rochaix, unpublished). These mutations affect genes that could encode factors that are either part of the same complex or that are required for its synthesis. Moreover, Raa1 is also part of a larger complex that contains RNA.

Raa3 is required for the first *trans*-splicing reaction. Together with *tscA* RNA and the *psaA* exon 1 transcript, it forms a large protein–RNA complex of 1,700 kDa (Rivier et al., 2001). Thus at least three distinct high molecular weight complexes involved in *psaA trans*-splicing have been identified. They could represent spliceosomal subparticles in the chloroplast. It is interesting that insertion of a continuous *psaA* gene into the chloroplast of *C. reinhardtii* abrogates the dependence of photoautotrophic growth on the nucleus-encoded factors involved in *trans*-splicing indicating that they do not have any essential role besides *trans*-splicing (C. Rivier, M. Goldschmidt-Clermont, and J. D. Rochaix, unpublished).

In contrast to *psaA*, the *psaB* gene of *C. reinhardtii* is continuous. One mutant, *F*24, is specifically deficient in *psaB* mRNA accumulation (Girard et al., 1980). Several mutants deficient in translation of the *psaB* mRNA have been identified. The *F15-tab1* and *F14-tab2* PS I-deficient mutants have been characterized in some detail. In both mutants, protein pulse-labeling reveals that PsaA and PsaB are no longer detectable while the *psaB* mRNA accumulates at close to wild-type levels suggesting a translational defect. This was further confirmed by inserting a chimeric gene consisting of the *psaB* 5′ UTR fused to the *aadA* coding sequence. This chimeric gene is expressed and confers spectinomycin resistance in a wild-type background. However, it is no longer expressed in the presence of the mutant *tab1-F15* or *tab2-F14* alleles indicating that at least one target site of the factors affected by the mutations is within the *psaB* 5′UTR and that these factors act at the level of initiation of translation (Stampacchia et al., 1997; Dauvillée et al., 2003). The *tab1-F15* mutation can be suppressed by a chloroplast mutation within the *psaB* 5′UTR further confirming that translation initiation is affected in the mutant. Comparison of mutants deficient in *psaA* and *psaB* expression shows that there is a one-sided dependence on their expression. Mutants unable to produce PsaB are also deficient in PsaA synthesis based on pulse-labeling experiments. In contrast mutants deficient in PsaA expression are still able to synthesize PsaB although the protein is rather unstable and does not accumulate to detectable levels (Girard-Bascou et al., 1987; Stampacchia et al., 1997). The dependence of PsaA expression on that of PsaB has been explained within the frame of the CES model (control by epistasy of synthesis) based on studies of the biosynthesis of the cytochrome b_6f complex (Choquet et al., 1998). It was shown that in this case translation but not stability of cytochrome *f* depends on the assembly state of the complex. In the absence of either cytochrome b_6 or subunit IV (PetD), synthesis of cytochrome *f* is markedly reduced. It was furthermore shown that the unassembled C-terminal end of free cytochrome *f* acts negatively on the *petA* 5′UTR most likely through a *trans*-acting factor. Recent experiments based on the use of chimeric genes containing the *psaA* 5′UTR fused to a reporter gene indicate that expression of the chimeric gene is reduced in mutants deficient in PsaB synthesis (Choquet et al., 2001). However, other explanations are possible. PsaB could be the anchor protein that needs to be inserted first into the thylakoid membrane before PsaA can be properly integrated and stably assembled. In the absence of PsaB, PsaA would be rapidly degraded and undetectable by pulse-labeling.

The *tab1* gene has been cloned and shown to encode a large polypeptide with five putative transmembrane domains in the N-terminal half and a lipase domain in its C-terminal part (F. Laroche and J. D. Rochaix, unpublished). Analysis of truncated versions of this protein indicate that the transmembrane domains are not essential for *psaB* mRNA translation. However, the C-terminal part including the lipase domain is essential. The lipase activity is not essential for *psaB* mRNA translation because mutations known to block lipase activity do not inhibit translation. It is noteworthy that amongst the translation factors identified so far in *Chlamydomonas* and land plants, Tab1 is the first integral membrane protein.

The *tab2* gene encodes a chloroplast soluble protein that interacts directly and specifically with the *psaB* 5′UTR. The protein is associated with a high molecular mass protein complex containing the *psaB* mRNA (Dauvillée et al., 2003). It represents a new type of RNA binding protein that is conserved in all oxygenic photosynthetic organisms, in particular land plants and cyanobacteria. It is clearly involved in the translation of *psaB* mRNA, but it could also be required for the first assembly steps of PS I. Interestingly, mutants of *Arabidopsis* deficient in the orthologous gene have a strong albino phenotype suggesting that this factor may have other roles besides its requirement for PS I assembly (F. Barnèche and J. D. Rochaix, unpublished results). Tab2 could act early in the PS I assembly pathway by binding to *psaB* mRNA. It could then target this RNA to the thylakoid membrane perhaps in close cooperation

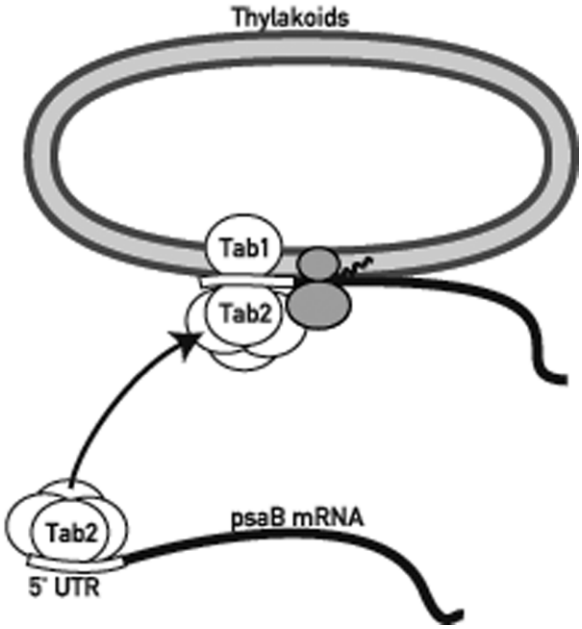

Fig. 3. Model for the role of Tab1 and Tab2 in the initiation of translation of *psaB* mRNA. Tab2 is part of a large complex and binds specifically to the *psaB* 5′ UTR (indicated by an open box). It may bind to the nascent *psaB* RNA chain and guide the RNA to the thylakoid membrane perhaps by interacting with Tab1 which acts as a translational activator.

with Tab1 and promote initiation of translation (Fig. 3). Tab2 must be released from the *psaB* mRNA shortly after initiation of translation because it is not associated with polysomes.

Nuclear mutants deficient in PS I accumulation have also been characterized in *Arabidopsis*. It is interesting that some of the mutations act specifically on single plastid transcripts as observed in *Chlamydomonas*. Thus, the *hcf145* mutant is specifically deficient in the stability of the tricistronic *psaA-psaB-rps14* transcript that encodes the two PS I reaction center subunits and the S14 peptide of the small ribosomal subunit (Lezhneva and Meurer, 2004). All of the PS I subunits are drastically reduced whereas the composition and activity of the other photosynthetic complexes are not affected in this mutant. The LHCI levels are only mildly reduced indicating that the PS I core complex is not required for stabilizing the antenna complex as also observed in the barley mutant *viridis-zb*^{63} (Nielsen et al., 1996) and in the *Chlamydomonas* mutants deficient in PS I (Girard-Bascou et al., 1987). It cannot be excluded that Hcf145 has additional roles in translation of the *psaA-psaB-rps14* transcripts and in the assembly of its products. Another PS I-deficient mutant of *A. thaliana*, *apoI*, is specifically deficient in the translational elongation of the *psaA-psaB-rps14* transcript (Amann et al., 2004). Moreover, this mutant fails to accumulate LHCI and to form grana stacks suggesting additional roles of Apo1 in thylakoid biogenesis. The Apo1 gene belongs to a new gene family present exclusively in vascular plants.

Light regulation of PS I gene expression at the level of translation occurs in spinach seedlings. The mRNAs of the PS I subunits PsaD, PsaF, and PsaL are associated with polyribosomes in the light, but not in the dark (Sherameti et al., 2002). This association is blocked by inhibitors of photosynthetic electron flow such as DCMU. Moreover, in the case of the *PsaD* mRNA, this response is mediated through its 5′ UTR as shown by the similar response in the expression of a reporter fused to this sequence, thus strongly suggesting that the control occurs at the level of translation initiation.

Chloroplast reverse genetics has been used extensively in *Chlamydomonas* and to some extent in tobacco to assess the roles of the chloroplast-encoded PS I subunits in assembly and stability of the complex. Mutants lacking either PsaA or PsaB do not accumulate the other subunits of PS I presumably because unassembled subunits are rapidly degraded (Redding et al., 1998). Inactivation of *psaC* in *C. reinhardtii* leads to destabilization of the PS I complex; in particular the levels of PsaA and PsaB are strongly reduced (Takahashi et al., 1991a). In contrast, in cyanobacteria *psaC* inactivation is less severe and both PsaA and PsaB accumulate to detectable levels although PS I is inactive (Yu et al., 1995). Inactivation of *psaI* in *C. reinhardtii* does not affect PS I accumulation and has only a mild effect on the electron transfer from the soluble donor proteins plastocyanin and cytochrome c_6 to $P700^+$ (Fischer et al., 1999).

B. Reverse Genetics of PS I in Arabidopsis

Reverse nuclear genetics of PS I has been rather successfully used in *Arabidopsis* using either antisense, cosuppression, RNA interference or gene disruption (Scheller et al., 2001). *Arabidopsis* plants lacking the peripheral PsaD subunit involved in the docking of ferredoxin to PS I are considerably affected in the accumulation of PS I and the light-harvesting system. They suffer severe photoinhibition and undergo a change in the thiol redox state which greatly affects the light-dependent modulation of several key enzymes of the Calvin cycle (Haldrup et al., 2003). The antisense plants examined accumulate 5–60% of PS I with a corresponding reduction of all PS I subunits including the light-harvesting complex. No plant was recovered

lacking PsaD entirely suggesting that this subunit is essential for PS I assembly and/or stability. In striking contrast, inactivation of PsaD in cyanobacteria does not prevent the accumulation of PsaA and PsaB (Chitnis et al., 1989). However, the minor PS I subunits are undetectable. Interestingly, cyanobacterial PS I lacking PsaD is unable to transfer electrons to ferredoxin, but can reduce flavodoxin with a low efficiency.

Arabidopsis plants contain two copies of the *psaE* gene. Disruption of the *psaE1* gene leads to a significant reduction of PsaE as well as PsaC and PsaD which together form the stromal ridge substructure of PS I (Varotto et al., 2000). The mutant plants display increased sensitivity to light and photoinhibition and a decrease in growth rate. Moreover, the formation of an abnormal stable LHCII–PS I in the mutant correlates with its inability to perform state transition, with an increase in the level of phosphorylated LHCII and with a permanent reduction in PS II antenna size (Pesaresi et al., 2002). State transition involves a redistribution of light excitation energy between the two photosystems in response to changes in the spectral composition of light which leads to an optimal quantum yield. This process is governed by the redox state of the plastoquinone pool and the occupancy of the Q_0 site of the cytochrome b_6f complex by plastoquinol. As a result of these interactions a kinase is activated that phosphorylates LHCII. The latter process is correlated with a displacement of the LHCII antenna to PS I and corresponds to a transition from state I to state II.

The PsaH subunit forms a subdomain of PS I together with PsaI, PsaL, and PsaD. Mutants lacking PsaH are blocked in state I although they are still able to phosphorylate LHCII (Lunde et al., 2000). Thus the cross-section of the PS I antenna size remains constant irrespective of the light conditions suggesting that PsaH could play a role in the binding of the mobile part of LHCII to PS I. Interestingly, the crystal structure of PS I reveals that LHCI is located on the opposite side of PS I (Ben-Shem et al., 2003; see also Nelson and Ben-Shen, this volume, Chapter 7).

The sequences of PsaG and PsaK are similar and the two subunits are localized on opposite sides of PS I. In contrast cyanobacterial PS I contains a single subunit that is related to PsaG and PsaK. Loss of either PsaG or PsaK leads to an impairment in state transition in plants. These two subunits have distinct roles as shown by the fact that reduction of PsaK leads to a decrease of Lhca2 and Lhca3, but Lhca1 and Lhca4 are not reduced (Jensen et al., 2000). A similar decrease of LHCI is not observed in the absence of PsaG (Jensen et al., 2002). However the crystal structure of plant PS I shows that the binding of LHCI to the reaction center is asymmetric and that it is much stronger on the side of PsaG (Ben-Shem et al., 2003). Plants lacking PsaK compensate by producing 20% more PS I (Jensen et al., 2000). An interesting feature is that the 40% decrease of PS I in the PsaG-deficient strain is compensated by a higher *in vitro* PS I activity suggesting that PsaG may regulate electron transport. Although PsaK and PsaG are equally similar to the cyanobacterial PsaK subunit and have evolved from the same ancestral protein, they have different functions.

In the case of loss of PsaN, PsaH, or PsaL, PS I activity is diminished and a compensation occurs through an increase in PS I levels. It thus appears that sensing mechanisms occur to fine-tune PS I activity either by changing the levels or the activity of PS I with the end result that a normal phenotype is preserved under optimal growth conditions (Lunde et al., 2000; Jensen et al., 2002).

Inactivation of specific PS I subunits can have rather different effects on the accumulation and function of PS I in cyanobacteria, green algae, and land plants as shown for mutants deficient in PsaF. In cyanobacteria, loss of PsaF still allows for photoautotrophic growth with no apparent deficiency in photosynthetic activity (Chitnis et al., 1991). *C. reinhardtii* cells lacking PsaF accumulate PS I to the same level as in the wild type and grow photoautotrophically. However, loss of PsaF leads to a drastic reduction in the rate of electron transfer from plastocyanin to $P700^+$ (Farah et al., 1995). Moreover, the PsaF-deficient *C. reinhardtii* mutant is sensitive to high light (>400 $\mu Em^{-2}sec^{-1}$) under aerobic conditions (Hippler et al., 2000; see also Hippler and Drepper, this volume, Chapter 29).

In contrast to algae and cyanobacteria, the down-regulation of PsaF in land plants has a considerably stronger phenotype. *Arabidopsis* antisense lines with reduced amounts of PsaF grow much more slowly than the wild type and are severely dwarfed (Haldrup et al., 2000). The strongly reduced levels of the stromal subunits PsaD, PsaC, and PsaD in the PsaF-deficient plants may explain why they have a severe phenotype. Also, energy transfer from LHCI is considerably reduced.

III. PS I Assembly Factors

A. The Ycf3 and Ycf4 Factors

Considering the complexity of PS I it is not surprising that its assembly requires specific factors. Three thylakoid proteins, BtpA (Bartsevich and Pakrasi, 1997), Ycf3 (Boudreau et al., 1997; Ruf et al., 1997), and Ycf4 (Wilde et al., 1995; Boudreau et al., 1997) required for

the accumulation of PS I in cyanobacteria, algae, and land plants have been identified. The BtpA factor is an extrinsic membrane protein located on the cytoplasmic side of the cyanobacterial thylakoid membrane, and it appears to act at the level of PS I stabilization (Zak et al., 1999; Zak and Pakrasi, 2000). Inactivation of the *ycf3* or *ycf4* gene leads to the loss of PS I (Boudreau et al., 1997; Ruf et al., 1997). Both factors act at a posttranslational level based on the fact that translation of the two PS I reaction center polypeptides PsaA and PsaB is not affected in mutant strains lacking *ycf3* or *ycf4* (Boudreau et al., 1997; Ruf et al., 1997). However Ycf3 and Ycf4 do not cofractionate with PS I upon solubilization of the thylakoid membrane. Ycf3 is loosely associated with the thylakoid membrane and can be released from the membrane by carbonate treatment. This protein consists of three tetratricopeptide repeat (TPR) domains. Several mutations were produced in the first and second TPR domains (Naver et al., 2001). They lead to a small decrease in PS I, but they prevent photoautotrophic growth and cause enhanced light sensitivity although the accumulated PS I complex appears to be fully functional. The phenotype appears to be due to photooxidative damage because it can be reversed under anaerobic conditions. Temperature-sensitive *ycf3* mutants have been used to show that the mutant PS I assembled under permissive conditions is as stable as the wild-type complex upon transfer to restrictive temperature conditions. In contrast, accumulation of newly synthesized PS I is decreased significantly in the mutant after the shift to the restrictive temperature indicating that Ycf3 is required for the assembly of PS I rather than for its stability. Moreover Ycf3 interacts specifically with the PsaA and PsaD subunits, but not with subunits of other complexes. It may act as a PS I-specific chaperone and assist the assembly of PsaA and PsaB that carry most of the PS I redox cofactors. Its TPR domains could be the site of interaction between Ycf3 and additional assembly factors, perhaps those involved in the assembly of the redox cofactors. In contrast to Ycf3, Ycf4, which contains one transmembrane domain, is firmly bound to the thylakoid membrane. It is associated with a large molecular weight complex upon solubilization of the thylakoid membrane (Boudreau et al., 1997). Pulse chase experiments indicate that newly synthesized PS I subunits are associated transiently with the Ycf4 complex before they are incorporated into PS I (Y. Takahashi and J. D. Rochaix, unpublished). This suggests that Ycf4 may be involved in the early steps of PS I assembly.

Careful membrane fractionations in cyanobacteria have revealed that the initial steps of PS I biogenesis occur on the plasma membrane rather than on the thylakoid membrane (Zak et al., 2001). In particular the PS I assembly factors Ycf3 and Ycf4 are associated with the plasma membrane. Moreover PS I components are assembled into protein–pigment complexes on the plasma membrane. Partially assembled PS I core complex undergoes light-induced charge separation in the plasma membrane (Zak et al., 2001). These data suggest that in cyanobacteria, the plasma membrane is the site for several of the early steps of assembly of the PS I reaction center complex. In contrast in algae, Ycf3 and Ycf4 are associated exclusively with the thylakoid membrane (Boudreau et al., 1997). However, some of the *trans*-acting factors required for chloroplast post-transcriptional steps required for PS I biogenesis have been localized on a low density membrane system in *C. reinhardtii* (Zerges and Rochaix, 1998; Perron et al., 1999). It is not yet clear whether this membrane system represents a subfraction of the inner envelope membrane, a pre-compartment of the thylakoids or a vesicle system (Westphal et al., 2001).

B. Genetic Analysis of LHCI Assembly

The high light sensitivity of the *C. reinhardtii* PsaF-deficient mutant strain has been used for isolating high light-resistant suppressor strains which have a high chlorophyll *a*/*b* ratio and which are deficient in the assembly of LHC (Hippler et al., 2000). Although the light-harvesting capacity of photosynthetic cells can be adapted to avoid overexcitation of the antennae, in the case of the PsaF-deficient strain such an adaptation mechanism is not sufficient to protect the strain from photo-oxidative damage under high light. In one of the suppressor strains, the light-harvesting polypeptides are not correctly integrated within the thylakoid membrane: LHCP trimers are absent from thylakoids, the LHC polypeptides are highly sensitive to mild protease digestion, and the PS I reaction center is not stably associated with LHCI. This suggests that the nuclear mutation that suppresses the phenotype of the PsaF deletion very probably affects a factor that is important for the integration of the LHCI and LHCII polypeptides into the thylakoid membrane (Hippler et al., 2000).

C. Assembly of [4Fe–4S] Centers of PS I

With its three [4Fe–4S] centers PS I constitutes an important iron sink in the chloroplast. How iron is recruited and assembled into [4Fe–4S] clusters is still largely unknown. It has been possible to reconstitute the F_A and F_B [4Fe–4S] centers in the cyanobacterial PsaC protein *in vitro* using $FeCl_3$, Na_2S, and β-mercaptoethanol (Mehari et al., 1991). In the presence

of the reconstituted PsaC holoprotein, the PsaD and PsaE protein rebind to the PS I core. However, the assembly of these [4Fe–4S] clusters is likely to require several factors *in vivo*. Two of these factors have been identified in nitrogen-fixing bacteria, NifS, a cysteine desulfurase and NifU that binds to nascent Fe/S clusters before they are transferred to the nitrogenase. In yeast mitochondria the NfuI protein shares significant sequence identity with the C-terminal domain of NifU. NfuI is also related to the cyanobacterial *nifU* product which contains the same conserved 50 amino acid NFU domain (see also Shen and Golbeck, this volume, Chapter 31).

Takahashi et al. (1991b) first showed that chloroplast extracts are capable to convert apo- into holoferredoxin using cysteine as sulfur donor. In *Arabidopsis*, five NFU-like genes have been identified, three of which are localized in the chloroplast and two in the mitochondria (Leon et al., 2003). Moreover, NifS and IscA-like proteins have been identified chloroplasts (Leon et al., 2002). IscA has been proposed to act as an alternative scaffold protein to IscU in *E. coli*. Taken together these data suggest that mitochondria and chloroplasts each contain their own Fe/S assembly system. It remains to be explored how iron is partitioned between the different chloroplast Fe/S complexes and whether specific factors exist that are required for the assembly and integration of F_X, F_A, and F_B into PS I. In this respect a highly interesting *Arabidopsis* mutant, *hcf101*, was recently characterized (Lezhneva et al., 2004). This seedling lethal nuclear mutant is specifically deficient in PS I activity. The other photosynthetic complexes are unaffected. The *psaA* and *psaB* mRNAs accumulate normally and they are translated at wild-type rates, but are unstable. Besides their inability to accumulate PS I, mutant plants also fail to accumulate ferredoxin–thioredoxin reductase, a stromal protein with [4Fe–4S] clusters, to normal levels. The mutation affects specifically assembly of [4Fe–4S] clusters because proteins with [2Fe-2S] clusters accumulate normally. The Hcf101 protein is localized in the chloroplast and is part of an ancient and widespread family of P-loop ATPases.

IV. Adaptation of the PS I–LHCI Complex to Fe-Deficiency

Copper is known to be essential for the stable accumulation and function of plastocyanin, the electron carrier between the cytochrome b_6f complex and PS I. In green algae and cyanobacteria, copper deprivation leads to the degradation of plastocyanin and to the synthesis of cytochrome c_6, the alternate electron carrier (Merchant and Bogorad, 1986). Although copper is not a cofactor of PS I, mutant strains of *C. reinhardtii* have been isolated that fail to accumulate PS I and LHCI under copper deprivation, but that are able to form these complexes in the presence of copper (Moseley et al., 2000). All of the 12 independently isolated *crd* (copper response defect) mutations fall into the same complementation group defining the Crd1 locus. This locus encodes a hydrophilic protein with a consensus carboxylate-bridged di-iron binding site. Recently it was shown that Chl27, the *Arabidopsis* homologue to *Chlamydomonas* Crd1, is a candidate subunit of the aerobic oxidative cyclase involved in the cyclization of the propionate side chain for formation of the fifth ring typical of all chlorophyll molecules. Chl27 has been localized both in the envelope and thylakoid fractions (Tottey et al., 2003). In *C. reinhardtii* Cth1 is an isoform of Crd1 and is only expressed under copper replete conditions. The two forms have overlapping, but not identical functions because of the inability of Cth1 to completely compensate for the loss of Crd1 in copper-replete Crd1 cells (Moseley et al., 2002a,b).

Fe-deficiency in algae and vascular plants induces a stress response, which leads to the proteolytic degradation of components of the photosynthetic apparatus and finally to chlorosis. Changes in the association of the LHCI antenna to PS I are apparent before the chlorosis becomes detectable in *Chlamydomonas* cells (Moseley et al., 2002a,b). The level of the peripheral chlorophyll binding subunit PsaK is reduced under these conditions. Because this subunit is involved in the binding of Lhca3 homodimer to PS I, the association of Lhca3 to PS I is diminished resulting in an uncoupling of LHCI from PS I. In addition new LHCI proteins are induced by the Fe-deficiency indicating that the adaptation to Fe-deficiency involves a remodeling of the PS I–LHCI complex (Moseley et al., 2002a,b). Interestingly, the accumulation of PsaK is modulated post-transcriptionally by the activity of Crd1 that has been proposed to be a key target of Fe-deficiency (Moseley et al., 2002a,b). One possibility is that the chlorophyll binding sites of PsaK are sensitive to flux through the chlorophyll biosynthetic pathway which depends on the activity of the Fe-requiring aerobic oxidative cyclase, one of the subunits of which has been proposed to be Crd1 (Moseley et al., 2002a,b). Thus, this model proposes that the adaptation to Fe-deficiency of the photosynthetic apparatus is determined by the activity of the aerobic oxidation cyclase in chlorophyll synthesis and thereby explains the connection between the loss of

photosynthetic function induced by Fe-deficiency and the loss of chlorophyll biosynthetic activity which has been known for a long time.

V. Degradation of PS I

Regulated protein degradation appears to be involved in the adaptation to Fe-deficiency. Degradation of Lhca3 from thylakoid membranes isolated from Fe-replete cells occurs upon addition of thylakoids from Fe-deficient cells (Moseley et al., 2002a,b). It will be interesting to identify the protease which is either activated or newly expressed during Fe-deficiency.

PS I disassembly and degradation has also been examined *in vitro* with purified thylakoid membranes of *C. reinhardtii* (Henderson et al., 2003). First a rapid decrease in PS I photochemical activity occurs followed by a slower disassembly of the PS I chlorophyll–protein complex and by proteolysis of the reaction center subunits. Degradation does not require soluble proteins, ATP or GTP. Proteolysis is inhibited by chelation with divalent cations and can be partially restored by addition of metal ions implicating a membrane-bound metallo-protease in this process.

VI. Conclusions

The synthesis and assembly of the PS I complex in the thylakoid membrane involves a large number of steps. In eukaryotic photosynthetic organisms the process starts with the transcription of the nuclear and chloroplast genes of the PS I subunits. Some of these early steps in the chloroplast appear to be modulated by the redox state of the plastoquinone pool and are followed by complex RNA maturation processes involving specific endo- and exo-nucleolytic RNA processing and, in *C. reinhardtii*, *trans*-splicing events. A striking example is provided by the maturation of the *psaA* mRNA in *C. reinhardtii* which depends on two plastid *trans*-splicing reactions with the participation of a least 14 nucleus-encoded factors. Amongst the post-transcriptional steps, translation appears to be an important control site as shown for the light regulation of the cytoplasmic *psbD* mRNA and of the plastid *psaA* and *psaB* mRNAs. Moreover, additional control steps appear to exist in which translation of *psaA* mRNA depends on the assembly stage of PS I and which ensures a coordinate expression of the principal PS I reaction center subunits. Finally, the stoichiometric accumulation of the PS I subunits depends on post-translational proteolytic steps which are still poorly understood.

While the molecular mechanisms underlying the synthesis of the PS I subunits are at least partially understood, we know very little on how these subunits are assembled into a functional complex. Although several specific PS I assembly factors such as BtpA, Ycf3, and Ycf4 have been identified and characterized to some extent, their precise mode of action is still unknown. It is also not clear how the three [4Fe–4S] clusters of PS I are assembled although some potential factors involved in this process have been recently identified.

Reverse genetics approaches have provided important new insights not only into the functional role of the various PS I subunits, but also on their importance for maintaining PS I stability. While either of the two reaction center subunits are essential for stable accumulation of the other subunits in both prokaryotic and eukaryotic organisms capable of photosynthesis, the loss of some of the other subunits can have very different effects as shown for PsaF whose absence has only mild effects in cyanobacteria and green algae, but severe effects in land plants. The reason for these different phenotypes are not clear. It could be that loss of PsaF in land plants alters the conformation of the other subunits in such a way that they are prone to a proteolytic clearing system which is unique to land plants.

A particularly fascinating area of research is to understand how the PS I–LHCI complex adapts to changes in light and nutrient conditions. Genetic analysis of the response to copper deprivation in *Chlamydomonas* has provided new important insights into the role of copper in the assembly of PS I and LHCI and its link to the chlorophyll biosynthetic pathway through Crd1, a strong candidate for the Fe-dependent aerobic cyclase. Although the study of PS I acclimation to changing environmental conditions is still at an early stage, it has already led to unexpected findings and it is likely that more surprises lie ahead.

Acknowledgments

I thank M. Goldschmidt-Clermont for helpful comments, J. Meurer for communicating unpublished results, and N. Roggli for the drawings. The work in the author's laboratory was supported by grant 3100-067763.02 from the Swiss National Science Foundation.

References

Amann K, Lezhneva L, Wanner G, Herrmann RG and Meurer J (2004) ACCUMULATION OF PHOTOSYSTEM ONE1, a

member of a novel gene family, is required for accumulation of [4Fe–4S] cluster-containing chloroplast complexes and antenna proteins. Plant Cell 16: 3084–3097

Bartsevich VV and Pakrasi HB (1997) Molecular identification of a novel protein that regulates biogenesis of photosystem I, a membrane protein complex. J Biol Chem 272: 6382–6387

Bassi R, Soen SY, Frank G, Zuber H and Rochaix JD (1992) Characterization of chlorophyll a/b proteins of photosystem I from *Chlamydomonas reinhardtii*. J Biol Chem 267: 25714–25721

Ben-Shem A, Frolow F and Nelson N (2003) Crystal structure of plant photosystem I. Nature 426: 630–635

Boudreau E, Takahashi Y, Lemieux C, Turmel M and Rochaix JD (1997) The chloroplast *ycf3* and *ycf4* open reading frames of *Chlamydomonas reinhardtii* are required for the accumulation of the photosystem I complex. EMBO J 16: 6095–6104

Chitnis PR, Reilly PA and Nelson N (1989) Insertional inactivation of the gene encoding subunit II of photosystem I from the cyanobacterium *Synechocystis* sp. PCC 6803. J Biol Chem 264: 18381–18385

Chitnis PR, Purvis D and Nelson N (1991) Molecular cloning and targeted mutagenesis of the gene *psaF* encoding subunit III of photosystem I from the cyanobacterium *Synechocystis* sp. PCC 6803. J Biol Chem 266: 20146–20151

Choquet Y, Goldschmidt-Clermont M, Girard-Bascou J, Kück U, Bennoun P and Rochaix JD (1988) Mutant phenotypes support a *trans*-splicing mechanism for expression of the tripartite *psaA* gene in the *C. reinhardtii* chloroplast. Cell 52: 903–913

Choquet Y, Stern DB, Wostrikoff K, Girard-Bascou J and Wollman FA (1998) Translation of cytochrome *f* is autoregulated through the 5' untranslated region of *petA* mRNA in *Chlamydomonas* chloroplasts. Proc Natl Acad Sci USA 95: 4380–4385

Choquet Y, Wostrikoff K, Rimbault B, Zito F, Girard-Bascou J, Drapier D and Wollman FA (2001) Assembly-controlled regulation of chloroplast gene translation. Biochem Soc Trans 29: 421–426

Dauvillée D, Stampacchia O, Girard-Bascou J and Rochaix JD (2003) Tab2 is a novel conserved RNA binding protein required for translation of the chloroplast *psaB* mRNA. EMBO J 22: 6378–6388

Farah J, Rappaport F, Choquet Y, Joliot P and Rochaix JD (1995) Isolation of a *psaF*-deficient mutant of *Chlamydomonas reinhardtii*: efficient interaction of plastocyanin with the photosystem I reaction center is mediated by the PsaF subunit. EMBO J 14: 4976–4984

Fischer N, Boudreau E, Hippler M, Drepper F, Haehnel W and Rochaix JD (1999) A large fraction of PsaF is nonfunctional in photosystem I complexes lacking the PsaJ subunit. Biochemistry 38: 5546–5552

Girard J, Chua NH, Bennoun P, Schmidt G and Delosme M (1980) Studies on mutants deficient in photosystem I reaction centers in *Chlamydomonas reinhardtii*. Curr Genet 2: 489–495

Girard-Bascou J, Choquet Y, Schneider M, Delosme M and Dron M (1987) Characterization of a chloroplast mutation in the *psaA2* gene of *Chlamydomonas reinhardtii*. Curr Genet 12: 489–495

Girard-Bascou J, Pierre Y and Drapier D (1992) A nuclear mutation affects the synthesis of the chloroplast *psbA* gene production in *Chlamydomonas reinhardtii*. Curr Genet 22: 47–52

Goldschmidt-Clermont M (1998) Coordination of nuclear and chloroplast gene expression in plant cells. Int Rev Cytol 177: 115–180

Goldschmidt-Clermont M, Girard-Bascou J, Choquet Y and Rochaix JD (1990) *Trans*-splicing mutants of *Chlamydomonas reinhardtii*. Mol Gen Genet 223: 417–425

Goldschmidt-Clermont M, Choquet Y, Girard-Bascou J, Michel F, Schirmer-Rahire M and Rochaix JD (1991) A small chloroplast RNA may be required for *trans*-splicing in *Chlamydomonas reinhardtii*. Cell 65: 135–143

Haldrup A, Simpson DJ and Scheller HV (2000) Down-regulation of the PSI-F subunit of photosystem I (PSI) in *Arabidopsis thaliana*. The PSI-F subunit is essential for photoautotrophic growth and contributes to antenna function. J Biol Chem 275: 31211–31218

Haldrup A, Lunde C and Scheller HV (2003) *Arabidopsis thaliana* plants lacking the PSI-D subunit of photosystem I suffer severe photoinhibition, have unstable photosystem I complexes, and altered redox homeostasis in the chloroplast stroma. J Biol Chem 278: 33276–33283

Harris EH (1989) The *Chlamydomonas* Source Book: A Comprehensive Guide to Biology and Laboratory Use. Academic Press, Inc., San Diego, CA

Henderson JN, Zhang J, Evans BW and Redding K (2003) Disassembly and degradation of photosystem I in an *in vitro* system are multievent, metal-dependent processes. J Biol Chem 278: 39978–39986

Hippler M, Biehler K, Krieger-Liszkay A, van Dillewjin J and Rochaix JD (2000) Limitation in electron transfer in photosystem I donor side mutants of *Chlamydomonas reinhardtii*. Lethal photo-oxidative damage in high light is overcome in a suppressor strain deficient in the assembly of the light harvesting complex. J Biol Chem 275: 5852–5859

Jensen PE, Gilpin M, Knoetzel J and Scheller HV (2000) The PSI-K subunit of photosystem I is involved in the interaction between light-harvesting complex I and the photosystem I reaction center core. J Biol Chem 275: 24701–24708

Jensen PE, Rosgaard L, Knoetzel J and Scheller HV (2002) Photosystem I activity is increased in the absence of the PSI-G subunit. J Biol Chem 277: 2798–2803

Jordan P, Fromme P, Witt HT, Klukas O, Saenger W and Krauß N (2001) Three-dimensional structure of cyanobacterial photosystem I at 2.5 Å resolution. Nature 411: 909–917

Kück U, Choquet Y, Schneider M, Dron M and Bennoun P (1987) Structural and transcriptional analysis of two homologous genes for the P700 chlorophyll *a*-apoproteins in *Chlamydomonas reinhardtii*: evidence for *in vivo trans* splicing. EMBO J 6: 2185–2195

Leon S, Touraine B, Briat JF and Lobreaux S (2002) The AtNFS2 gene from *Arabidopsis thaliana* encodes a NifS-like plastidial cysteine desulphurase. Biochem J 366: 557–564

Leon S, Touraine B, Ribot C, Briat JF and Lobreaux S (2003) Iron–sulphur cluster assembly in plants: distinct NFU proteins in mitochondria and plastids from *Arabidopsis thaliana*. Biochem J 371: 823–830

Lezhneva L and Meurer J (2004) The nuclear factor HCF145 affects chloroplast *psaA-psaB-rps14* transcript abundance in *Arabidopsis thaliana*. Plant J 38: 740–753

Lezhneva L, Amann K, Martin W and Meurer J (2004) The universally conserved HCF101 protein is involved in assembly of 4Fe–4S-cluster containing complexes in *Arabidopsis* chloroplasts. Plant J 37: 174–185

Lunde C, Jensen PE, Haldrup A, Knoetzel J and Scheller HV (2000) The PSI-H subunit of photosystem I is essential for state transitions in plant photosynthesis. Nature 408: 613–615

Mehari T, Parrett KG, Warren PV and Golbeck JH (1991) Reconstitution of the iron–sulfur clusters in the isolated F_A/F_B protein: ESR characterization of same-species and cross-species photosystem I complexes. Biochim Biophys Acta 1056: 139–148

Merchant S and Bogorad L (1986) Regulation by copper of the expression of plastocyanin and cytochrome c_{552} in *Chlamydomonas reinhardi*. Mol Cell Biol 6: 462–469

Moseley J, Quinn J, Eriksson M and Merchant S (2000) The *crd1* gene encodes a putative di-iron enzyme required for photosystem I accumulation in copper deficiency and hypoxia in *Chlamydomonas reinhardtii*. EMBO J 19: 2139–2151

Moseley JL, Allinger T, Herzog S, Hoerth P, Wehinger E, Merchant S and Hippler M (2002a) Adaptation to Fe-deficiency requires remodeling of the photosynthetic apparatus. EMBO J 21: 6709–6720

Moseley JL, Page MD, Alder NP, Eriksson M, Quinn J, Soto F, Theg SM, Hippler M and Merchant S (2002b) Reciprocal expression of two candidate di-iron enzymes affecting photosystem I and light-harvesting complex accumulation. Plant Cell 14: 673–688

Naver H, Boudreau E and Rochaix JD (2001) Functional studies of Ycf3: its role in assembly of photosystem I and interactions with some of its subunits. Plant Cell 13: 2731–2745

Nielsen VS, Scheller HV and Moller BL (1996) The photosystem I mutant *viridis-zb*^{63} of barley (*Hordeum vulgare*) contains low amounts of active but unstable photosystem I. Physiol Plant 98: 637–644

Perron K, Goldschmidt-Clermont M and Rochaix JD (1999) A factor related to pseudouridine synthases is required for chloroplast group II intron trans-splicing in *Chlamydomonas reinhardtii*. EMBO J 18: 6481–6490

Pesaresi P, Lunde C, Jahns P, Tarantino D, Meurer J, Varotto C, Hirtz RD, Soave C, Scheller HV, Salamini F and Leister D (2002) A stable LHCII–PSI aggregate and suppression of photosynthetic state transitions in the *psae1-1* mutant of *Arabidopsis thaliana*. Planta 215: 940–948

Pfannschmidt T and Allen JF (1999) Photosynthetic control of chloroplast gene expression. Nature 397: 625–628

Redding K, MacMillan F, Leibl W, Brettel K, Hanley J, Rutherford AW, Breton J and Rochaix JD (1998) A systematic survey of conserved histidines in the core subunits of photosystem I by site-directed mutagenesis reveals the likely axial ligands of P700. EMBO J 17: 50–60

Rivier C, Goldschmidt-Clermont M and Rochaix JD (2001) Identification of an RNA–protein complex involved in chloroplast group II intron trans-splicing in *Chlamydomonas reinhardtii*. EMBO J 20: 1765–1773

Ruf S, Kossel H and Bock R (1997) Targeted inactivation of a tobacco intron-containing open reading frame reveals a novel chloroplast-encoded photosystem I-related gene. J Cell Biol 139: 95–102

Scheller HV, Jensen PE, Haldrup A, Lunde C and Knoetzel J (2001) Role of subunits in eukaryotic Photosystem I. Biochim Biophys Acta 1507: 41–60

Sherameti I, Nakamura M, Yamamoto YY, Pfannschmidt T, Obokata J and Oelmuller R (2002) Polyribosome loading of spinach mRNAs for photosystem I subunits is controlled by photosynthetic electron transport. Plant J 32: 631–639

Stampacchia O, Girard-Bascou J, Zanasco JL, Zerges W, Bennoun P and Rochaix JD (1997) A nuclear-encoded function essential for translation of the chloroplast *psaB* mRNA in *Chlamydomonas*. Plant Cell 9: 773–782

Takahashi Y, Goldschmidt-Clermont M, Soen SY, Franzen LG and Rochaix JD (1991a) Directed chloroplast transformation in *Chlamydomonas reinhardtii*: insertional inactivation of the *psaC* gene encoding the iron sulfur protein destabilizes photosystem I. EMBO J 10: 2033–2040

Takahashi Y, Mitsui A and Matsubara H (1991b) Formation of Fe–S cluster of ferredoxin in lysed spinach chloroplasts. Plant Physiol 95: 97–103

Tottey S, Block M, Allen M, Westergren T, Albrieux C, Scheller HV, Merchant S and Jensen PE (2003) *Arabidopsis* CHL27, located in both envelope and thylakoid membranes, is required for the synthesis of protochlorophyllide. Proc Nat Acad Sci USA 100: 16119–16124

Varotto C, Pesaresi P, Meurer J, Oelmuller R, Steiner-Lange S, Salamini F and Leister D (2000) Disruption of the *Arabidopsis* photosystem I gene *psaE1* affects photosynthesis and impairs growth. Plant J 22: 115–124

Westphal S, Soll J and Vothknecht UC (2001) A vesicle transport system inside chloroplasts. FEBS Lett 506: 257–261

Wilde A, Hartel H, Hubschmann T, Hoffmann P, Shestakov SV and Borner T (1995) Inactivation of a *Synechocystis* sp. strain PCC 6803 gene with homology to conserved chloroplast open reading frame 184 increases the photosystem II-to-photosystem I ratio. Plant Cell 7: 649–658

Yu J, Smart LB, Jung YS, Golbeck J and McIntosh L (1995) Absence of PsaC subunit allows assembly of photosystem I core but prevents the binding of PsaD and PsaE in *Synechocystis* sp. PCC 6803. Plant Mol Biol 29: 331–342

Zak E and Pakrasi HB (2000) The BtpA protein stabilizes the reaction center proteins of photosystem I in the cyanobacterium *Synechocystis* sp. PCC 6803 at low temperature. Plant Physiol 123: 215–222

Zak E, Norling B, Andersson B and Pakrasi HB (1999) Subcellular localization of the BtpA protein in the cyanobacterium *Synechocystis* sp. PCC 6803. Eur J Biochem 261: 311–316

Zak E, Norling B, Maitra R, Huang F, Andersson B and Pakrasi HB (2001) The initial steps of biogenesis of cyanobacterial photosystems occur in plasma membranes. Proc Natl Acad Sci USA 98: 13443–13448

Zerges W and Rochaix J-D (1998) Low density membranes are associated with RNA-binding proteins and thylakoids in the chloroplast of *Chlamydomonas reinhardtii*. J Cell Biol 140: 101–110

Chapter 31

Assembly of the Bound Iron–Sulfur Clusters in Photosystem I

Gaozhong Shen*
Department of Biochemistry and Molecular Biology, The Pennsylvania State University, University Park, PA 16802, USA

John H. Golbeck
Department of Biochemistry and Molecular Biology, Department of Chemistry, The Pennsylvania State University, University Park, PA 16802, USA

*Author for correspondence, email: gxs22@psu.edu

John H. Golbeck (ed): Photosystem I: The Light-Driven Plastocyanin:Ferredoxin Oxidoreductase, 529–547.

Summary

The first attempts to elucidate the molecular mechanisms that function in the bioassembly of the bound Fe/S clusters in Photosystem I (PS I) are discussed. Fe/S proteins participate in a wide variety of processes, the most important of which in photosynthetic organisms are light-mediated electron transport and stress-induced regulation of genes. One of the last steps in the biogenesis of PS I involves the assembly of the three bound [4Fe–4S] clusters F_X, F_A, and F_B. It has been shown that the proteins encoded by the *suf* regulon are involved in the assembly and repair of the bound Fe/S clusters in cyanobacteria. The SUF system of Fe/S cluster assembly is localized in the chloroplasts of plants; however, no homologs of the *suf* genes have been identified in nonphotosynthetic eukaryotes. The expression of the *suf* genes in cyanobacteria is subject to control by the transcription factor SufR, which is regulated, in turn, by oxidative stress and iron stress. On the basis of the commonality of the major components, the SUF system in cyanobacteria and chloroplasts may employ a mechanism similar to that described in nonphotosynthetic bacteria to assemble Fe/S clusters. SufS, a cysteine desulfurase, functions in close cooperation with SufE to mobilize sulfur. SufC functions as a versatile orphan ATPase, and may work together with SufB and SufD in iron assimilation. Although SufA has been proposed to function as a scaffold protein for Fe/S cluster assembly in nonphotosynthetic bacteria, it is not essential in cyanobacteria. The scaffold function may, instead, be carried out by NFU. Oxygenic photosynthetic organisms may require additional factors for the insertion and maturation of the Fe/S clusters into photosynthetic complexes. One example is RubA, a membrane-associated rubredoxin, which plays a role in the assembly of F_X in PS I.

I. Introduction

Proteins that contain iron–sulfur (Fe/S) clusters are ubiquitous in living organisms. A major role of Fe/S clusters is in mediating one-electron transfers such as those carried out in the respiratory and photosynthetic electron transport chains. The chemical versatility of iron and sulfur allows for the biosynthesis of a variety of Fe/S cluster types that span a wide range of oxidation–reduction potentials. Fe/S clusters also function in binding and activation of substrates at the unique iron site in certain catalytic reactions such as in aconitase (Beinert et al., 1996) and in coupling electron transfer to proton transport (Duff et al., 1996). Fe/S clusters have structural roles within proteins, such as in endonuclease III, as well as serving as a bridge between two proteins, such as in the Fe-protein of nitrogenase and F_X of Photosystem I (PS I). Fe/S clusters are involved in gene regulation and serve as sensors of oxidative stress and iron deficiency (for recent reviews, see Johnson, 1998; Beinert and Kiley, 1999). Examples include the regulatory proteins SoxR (Gaudu and Weiss, 1996; Pomposiello and Demple, 2001), IscR (Schwartz et al., 2001), and SufR (Wang et al., 2004). The oxidative state of Fe/S clusters can also serve as a switch in response to the changes of the levels of iron, O_2, CO_2, and NO (Drapier, 1997; Khoroshilova et al., 1997; Beinert and Kiley, 1999).

In cyanobacteria and higher plants, Fe/S clusters serve as electron transfer cofactors in photosynthesis,

Abbreviations: ATP – adenosine triphosphate; EPR – electron paramagnetic resonance; Fe/S – iron–sulfur; FTR – ferredoxin–thioredoxin reductase; HCF – high chlorophyll fluorescence; PLP – pyridoxal 5′-phosphate; PS I – photosystem I.

not only in soluble ferredoxin, but also in the cytochrome b_6f-Rieske complex and in PS I as the terminal acceptors F_X, F_B, and F_A. PS I in cyanobacteria and higher plants catalyze the light-induced transfer of an electron from plastocyanin or cytochrome c_6 to ferredoxin or flavodoxin. The kinetics and energetics of electron transfer in PS I have been investigated by a wide variety of spectroscopic techniques over the last several decades (see Golbeck, 1999; Brettel and Leibl, 2001 for reviews). The recent high-resolution structure of PS I has further improved our understanding of the ligands that bind the cofactors in PS I (Schubert et al., 1997; Jordan et al., 2001; see Grotjohann and Fromme, this volume, Chapter 6). PS I is multisubunit protein–pigment complex that consists of 12 subunits in cyanobacteria and 13 subunits in higher plants, however only the PsaA, PsaB, and PsaC subunits harbor the electron transfer cofactors that are involved in light-induced charge separation and charge stabilization (Golbeck, 1994). The central core of PS I is formed by six chlorophylls and two phylloquinones arranged as two nearly symmetrical branches of cofactors. These branches join at F_X, which is a [4Fe–4S] cluster coordinated by four cysteines, two of which are contributed by PsaA and two of which are contributed by PsaB. Therefore, in addition to its role in electron transfer, F_X may also play a structural role in the PsaA and PsaB heterodimer.

The membrane-associated PsaC subunit harbors the two terminal [4Fe–4S] clusters F_A and F_B. PsaC displays structural similarities to soluble bacterial dicluster ferredoxins, including a similar molecular mass, a common Fe/S cluster-binding motif (CxxCxxCxxxCP), and a pseudo-twofold symmetry axis (see Antonkine and Golbeck, this volume, Chapter 8). The identity of the cysteine ligands to F_A and F_B were first identified by site-directed mutagenesis (summarized in Golbeck, 1999), and later confirmed by NMR solution studies of unbound PsaC (Antonkine et al., 2000, 2002). In this review, we describe the mechanism of assembly of the Fe/S clusters in biological organisms, focusing especially on the F_X, F_A, and F_B clusters in PS I of cyanobacteria and higher plants.

II. PS I Biogenesis and the Bound Fe/S Clusters

A. Biogenesis of the PS I Reaction Center

The biogenesis of fully functional PS I requires the assembly of F_X, F_A, and F_B, which are [4Fe–4S] clusters, and the [2Fe–2S] cluster in soluble ferredoxin. The insertion of the metal or metal cluster is usually the key step in the posttranslational maturation of metalloproteins. As found in a study of the *rubA* null mutant, trimeric PS I can be assembled in thylakoid membranes even in the absence of F_X (Shen et al., 2002a,b). However, the PsaA/PsaB heterodimer cannot bind PsaC (and two other stromal subunits, PsaD and PsaE) unless F_X is present. Similarly, the PsaC cannot bind to the PsaA/PsaB heterodimer unless F_A and F_B are present. Indeed, when the second Cys in the CxxCxxCxxxCP motif of PsaC is altered to alanine, an amino acid without a suitable ligand for iron, the mutant PsaC lacks the [4Fe–4S] cluster(s) and is unable to bind to the PsaA/PsaB heterodimer (reviewed by Golbeck, 1999). These results show that in the biogenesis of the PS I core, the process of protein translation and protein folding are independent of the final maturation step, which involves the insertion of the F_X cluster and the attachment of the PsaC, PsaD, and PsaE subunits (see also Fish et al., this volume, Chapter 32). The bound Fe/S clusters are therefore the key to the final steps in the biogenesis of PS I.

B. Fe/S Clusters in Biological Systems

Although cysteine is one of the least abundant amino acids, it plays an important role in proteins because of its unique metal binding properties. In proteins that contain [2Fe–2S] and [4Fe–4S] clusters, the iron atoms are bridged by inorganic sulfur atoms (via μ-sulfido bridges) and are ligated to the protein by the thiolate side chains of cysteine residues. Each cysteine sulfur is attached to one atom of Fe, with the four iron atoms forming an irregular tetrahedron at an Fe–Fe distance of 2.67–2.81 Å. The four inorganic sulfur atoms (S^{2-}) form an interpenetrating tetrahedron 3.49–3.61 Å on a side with each of sulfur atoms bonded to three iron atoms (see Vassiliev et al., 2001). The identity of the amino acids in the surrounding environment and the spacing of cysteine residues in the binding pocket are among the factors that define the wide range of electronic and chemical properties available to Fe/S clusters in proteins.

It has been shown that [2Fe–2S] and [4Fe–4S] clusters can be reconstituted chemically into Fe-free apoferredoxins by the addition of inorganic sulfide and ferric ion in the presence of an organic thiolate such as 2-mercaptoethanol (Malkin and Rabinowitz, 1966). This procedure also reconstitutes the [4Fe–4S] clusters into the empty F_X, F_B, and F_A sites of PS I (reviewed by Golbeck, 1995, 1999). It is thought that

water-soluble [2Fe–2S] and [4Fe–4S] clusters are formed with 2-mercaptoethanol as ligands, and that a facile 2-mercaptoethanol–cysteine exchange mechanism allows insertion of the Fe/S core into the target apoprotein. The insertion process can be quantitative in the presence of excess reagent and is most likely entropically driven by the substitution of four independent 2-mercaptoethanol ligands for the four cysteine ligands on a single apoprotein (Mehari et al., 1991). However, biological Fe/S clusters are not formed spontaneously nor in this manner. Free iron is damaging to cells due to its ability to create hydoxy radicals from H_2O_2 via the Fenton reaction, and free sulfide is highly toxic. As a result, the assembly, insertion, and maturation of Fe/S clusters occur within the highly protected environment of proteins. Indeed, Fe/S cluster assembly has been found to be a complex process that involves several distinct systems and many highly conserved proteins.

The first biological system found to carry out Fe/S cluster assembly was described in the biogenesis of nitrogenase in *Azotobacter vinelandii*. The NItrogen Fixation (NIF) system plays a specific role in the assembly of Fe/S clusters destined for the nitrogenase enzyme. A series of elegant genetic and biochemical studies showed that NifS and NifU are essential factors in the assembly of the Fe/S clusters (Jacobson et al., 1989; Dean et al., 1993; Zheng et al., 1993). Considering the diversity in the structure and function of Fe/S proteins in the three major life processes of photosynthesis, respiration, and nitrogen fixation, it might be predicted that different factors would be required for the biogenesis of different Fe/S proteins. Indeed, recent progress in genomic sequencing and genetic studies have provided detailed information on the fundamental mechanisms of metalloprotein assembly in all living cells, and shows that there exist two independent systems for assembling Fe/S clusters.

III. Two Fe/S Biogenesis Systems in Oxygenic Photosynthetic Organisms

A. Aerobic and Anaerobic Environments for Photosynthesis and Respiration

In oxygenic photosynthetic organisms, Fe/S proteins are involved in two of the most important energy-generating processes in the cell: photosynthesis and respiration. In higher plants, these processes take place in different organelles, the plastid and the mitochondrion, which are highly divergent with respect to oxygen metabolism. In cyanobacteria (which is considered the ancestor of the plastid) and in plastids of higher plants, oxygen evolution is the consequence of the H_2O-splitting activity of Photosystem II. In the mitochondria of higher plants, oxygen consumption is the consequence of respiration. Accordingly, plastids and mitochondria operate near the extremes of two unlike environments: aerobic and anaerobic. Among other proteins, Fe/S clusters are present in ferredoxin and PS I in chloroplasts, and in NADH dehydrogenase and fumarase in mitochondria. The Fe/S proteins that function in photosynthesis and respiration appear to utilize different bioassembly systems for Fe/S cluster assembly, insertion, and maturation. These two genetic systems have been identified in Fe/S cluster assembly and repair in bacteria: the Isc proteins encoded by the *isc* gene cluster and the Suf proteins encoded *suf* gene cluster. Apparently, because of their specificity in functioning in anaerobic and aerobic environments, the ISC and SUF systems were adopted for Fe/S cluster assembly in mitochondria and chloroplasts of higher plants, respectively.

B. The ISC System: Mitochondrial-Type Machinery

1. Composition and Mechanism in Prokaryotes

A gene cluster composed of *iscR–iscS–iscU–iscA–hscB–hscA–fdx–ORF3* was shown to function in generalized Iron–Sulfur Cluster assembly (ISC) in *Azotobacter vinelandii* (Zheng et al., 1998). A similar *isc* operon has since been identified in *Escherichia coli* (Nakamura et al., 1991; Takahashi and Nakamura, 1999; Tokumoto et al., 2002) and other bacteria. The ISC system has been widely studied using genetic, biochemical, and biophysical approaches (reviewed by Frazzon et al., 2002; Mihara and Esaki, 2002; Frazzon and Dean, 2002, 2003; Lill and Mühlenhoff, 2005; Johnson et al., 2005). The ISC system shares a high degree of similarity with the NIF system in terms of genes and proteins. The best-studied component, IscS, is a NifS homolog, which functions as cysteine desulfurase (Flint, 1996; Zheng et al., 1998). IscU corresponds to the N-terminal domain of NifU (Fig. 1). Three conserved Cys residues in IscU have been suggested to serve as ligands for a proposed scaffold in the assembly of nascent Fe/S clusters (Agar et al., 2000) and for mediated delivery to the target apoprotein as first proposed for NifU (Smith et al., 2000; Yuvaniyama et al., 2000). In *E. coli*, IscU and IscS interact and form a complex (Kato et al., 2002). On the basis of both its ability to bind

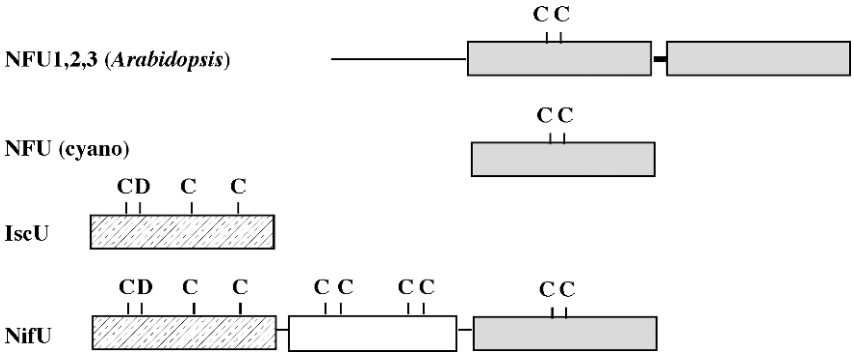

Fig. 1. Structural comparison of the NFU, IscU, and NifU proteins. The NSU proteins from cynaobacteria and higher plants are related to the C-terminal domain of NifU (*from A. vinelandii* and other nitrogen-fixation organisms). The *Arabidopsis* AtNFU1,2,3 proteins contain a plastid-targeting transit sequence and an extra C-terminal extension that exhibit high sequence similarity to NFU, but without presence of the CXXC motif. IscU is homologous to the N-terminal domain of NifU, which has three conserved Cys residues and binds a labile [2Fe–2S] cluster. The central domain of NifU binds a permanent [2Fe–2S] cluster that is essential for its function.

a [2Fe–2S] cluster, and on its homology to ^{Nif}IscA in the *nif* operon, IscA was proposed to function as a alternative Fe/S cluster scaffold protein (Krebs et al., 2001). However, IscA may also be involved in a regulatory process as suggested from studies on a *Xenorhabdus nematophila* mutant with a colonization defect caused by a Tn10 insertion in the *iscA–hscBA–fdx* locus (Martens et al., 2003). Its insertion between the *iscA* and *hscBA–fdx* loci did not attenuate the expression of the *hscBA* genes, rather it disrupted the coordination of expression of the *iscA* gene and the *hscBA* genes. Using biochemical copurification methods and a genetic approach with the yeast two-hybrid system, it was reported that IscA interacts with HscA. Also, interactions were observed for the combinations of IscS–IscU, HscA–HscB, and IscU–HscB (Tokumoto et al., 2002). However, there is also evidence of a specific relationship of IscA with ferredoxin (Fdx) and a possible role for IscA in transferring iron and sulfur to Fdx (Ollagnier-de-Choudens et al., 2001). The Fdx encoded by the *fdx* gene in the *isc* operon binds a [2Fe–2S] cluster. By examining the co-expression of the *fdx* gene using the *isc* gene cluster as a reporter, it was shown that *iscS*, *hscA*, *hscB*, and *ORF3* were required for the assembly of the [2Fe–2S] cluster in Fdx. Fdx was therefore proposed to be an intermediate site for Fe/S cluster assembly (Takahashi and Nakamura, 1999). However, this conclusion may be premature given that a tightly bound [2Fe–2S] cluster is unlikely to be a good candidate for an Fe/S cluster intermediate. HscA and HscB are homologs of the bacterial DnaK and DnaJ molecular chaperones (Vickery et al., 1997). HscB functions as a specific cochaperone that regulates the ATP-dependent activity of HscA (Takahashi and Nakamura, 1999; Tokumoto and Takahashi, 2001). HscAB may serve as molecular chaperone by assisting the folding Fe/S protein or the transfer of [2Fe–2S] clusters. Indeed, IscU was found to interact with HscA and HscB (Hoff et al., 2000; Silberg et al., 2001).The *iscR* gene (which has no counterpart in the *nif* operon) was found to be a negative regulator of the *isc* operon in *E. coli* (Schwartz et al., 2000). When *iscR* repression is relieved by exposure to H_2O_2, the *iscSU* genes are induced, while the *hscBA–fdx* genes are not (Zheng et al., 2001). Thus, IscR does not appear to coregulate the *hscBA–fdx* genes with the upstream *isc* genes. X-ray crystal structures are available for IscS (Cupp-Vickery et al., 2003), HscA with the IscU recognition peptide ELPPVKIHL (Cupp-Vickery et al., 2004a,b), and IscA (Bilder et al., 2004; Cupp-Vickery et al., 2004a,b), and an NMR solution structure is available for IscU (Ramelot et al., 2004).

2. Localization and Activity in Mitochondria of Eukaryotes

The genes that comprise the ISC machinery are conserved from bacteria through eukaryotes (Schilke et al., 1999; Lill and Mühlenhoff, 2005). In eukaryotes, yeast mitochondria have been shown to host the ISC machinery for Fe/S cluster assembly (reviewed by Lill and Kispal, 2000; Mühlenhoff and Lill, 2000; Lill and Mühlenhoff, 2005). The mitochondrion contains all of the major components of the ISC system, including IscS-like Nfs1p, IscU-like IscU1p and IscU2p, IscA-like Isa1p and Isa2p, Fdx-like Yah1p, HscA-like Ssq1, and HscB-like Jac1 in the matrix. In addition, several new proteins have been identified in the Fe/S cluster assembly and export machineries and found to be

Table 1. Assignment of Fe/S cluster biogenesis genes in *Synechocystis* sp. PCC 6803 and homologs in *Synechococcus* sp. PCC 7002

Name	ORF[a]	Proposed function	Mutant
Isc system			
IscR	*slr0846*	Regulatory repressor	Not essential
IscS1	*slr0387*	Cysteine desulfurase	Not essential[b]
IscS2	*sll0704*	Cysteine desulfurase	Not essential[b]
IscA	*slr1565*	Iron or Fe/S scaffold	Not essential[c]
HscA	*sll0170*	Molecular chaperone	(Not studied)
HscB	*sll0169?*	Molecular chaperone	(Not studied)
Fdx	*slr0148*	Electron transfer	Not essential
Suf system			
SufR	*sll0088*	Regulatory repressor	Not essential
SufA	*slr1417*	Assembly scaffold	Not essential[c]
SufB	*slr0074*	ABC transporter?	Essential
SufC	*slr0075*	ATPase?	Essential
SufD	*slr0076*	Iron mobilization?	Essential
SufS	*slr0077*	Cysteine desulfurase	Essential
SufE	*slr1419*	Enhances SufS activity	Essential
Unclassified			
NFU	*ssl2667*	Assembly scaffold	Essential
C-DES	*slr2143*	Cyst(e)ine desulfurase	(Not studied)
RubA	*slr2033*	Electron transfer	Essential for F_X

[a] *In Synechocystis sp. PCC 6803.*
[b] *iscS1/iscS2* double mutant also not essential.
[c] *sufA/iscA* double mutant is also not essential.

mitochondrial-specific, including Arh1, Atm1, Erv1p, Yfh1/frataxin, Grx5, and Mge1 (Lill and Kispal, 2000; Gerber and Lill, 2002; Lill and Mühlenhoff, 2005). Yeast mitochondria use the ISC machinery to synthesize their own Fe/S proteins, and quite likely, to export Fe/S clusters for cytosolic proteins.

3. The ISC System in Cyanobacteria and Higher Plants

A database search shows that homologs of *iscR*, *iscA*, *iscU*, *iscS*, *hscB*, *hscA*, and *fdx* can are present in the genome of the higher plant *Arabidopsis thaliana*. IscS (the product of *slr0387* in *Synechocystis* sp. PCC 6803) is annotated as AtNFS1 and has been located in the mitochondrion of *A. thaliana* (Kushnir et al., 2001). Two *iscU* homologs identified in the genome of *A. thaliana* (NFU4 and NFU5) have been located in the mitochondrial matrix (Léon et al., 2003). Plant mitochondria also possess an Atm1p-like ABC transporter system similar to that found in yeast mitochondria (Kushnir et al., 2001). It is therefore likely that higher plants utilize the ISC machinery for Fe/S cluster assembly in their mitochondria as do other eukaryotes. All components of the ISC system except for IscU can be identified in the sequenced genomes of cyanobacteria (Table 1). However, in cyanobacteria, the *isc* genes are dispensable. For example, no phenotype can be observed in fully segregated mutants of *slr0387* (*iscS*) or *sll0704* (an *iscS* homolog) in *Synechocystis* sp. PCC 6803 or in a fully segregated mutant of *iscS* in *Synechococcus* sp. PCC 7002 (Shen et al., 2004). A *slr0387/sll0704* double mutant in *Synechocystis* sp. PCC 6803 also grows photoautotrophically under normal growth conditions. These results show that the ISC machinery cannot be the major Fe/S cluster biogenesis system in cyanobacteria.

C. The SUF System: Chloroplast-Type Machinery

The presence of Fe/S cluster assembly machinery in chloroplasts has been verified in a series of studies on the [2Fe–2S] cluster plant ferredoxin (Takahashi et al., 1986, 1991a,b; Li et al., 1990). Cysteine was found to be the source of sulfur for Fe/S cluster assembly and for the Fe/S cluster insertion into ferredoxin in lysed chloroplasts (Takahashi et al., 1991a) and isolated intact chloroplasts (Takahashi et al., 1991b). It was shown that this process requires the presence of light or adenosine triphosphate (ATP) and reduced nicotanamide adenine dinucleotide phosphate (NADPH). Although no candidate enzymes were identified, the unique substrate requirements were the first indication that the machinery of Fe/S cluster assembly in plastids may be different from that in mitochondria.

1. Assembly and Stabilization of Fe/S Clusters in PS I and the suf Operon

A gene cluster composed of *sufA–sufB–sufC–sufD–sufS–sufE* that had been previously identified as the Sulfur Utilization Factor (SUF) was found to code for proteins involved in a second Fe/S cluster assembly system in *E. coli* (Takahashi and Tokumoto, 2002). Evidence for a connection between the SUF system and the biogenesis of PS I came about from the identification of the *sll0088* gene in *Synechocystis* sp. PCC 6803, which was discovered by screening pseudorevertants of *psaC* site-directed mutants (Yu et al., 2003). The PsaC mutants C51D (an altered ligand to F_A) and C14S (an altered ligand to F_B) failed to grow photoautotrophically and were sensitive to higher light intensities, even though electron transfer in isolated PS I complexes occurred at near wild-type rates (Yu et al., 1997). Screening of PsaC mutants under increased light intensities resulted in the appearance of pseudorevertant colonies that were able to grow photoautotrophically. Two intragenic suppressor strains, C14S-R62 and C14S-R18, were

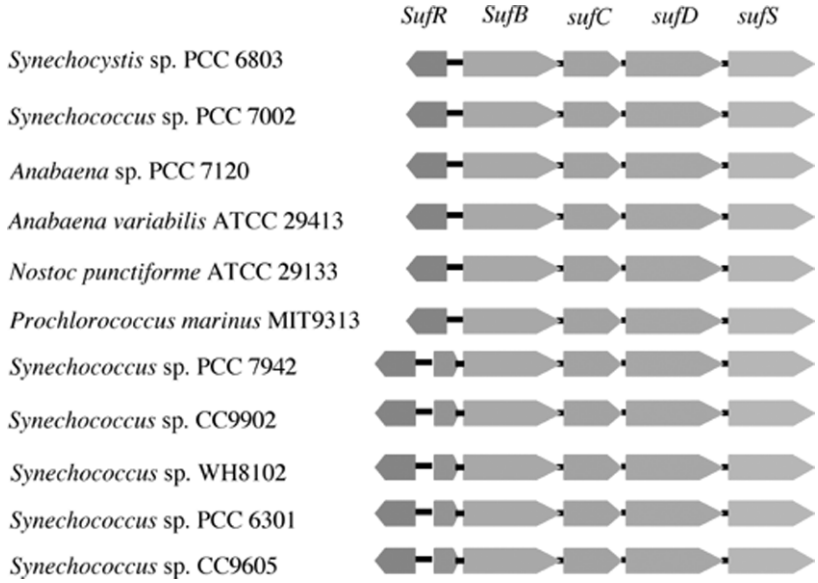

Fig. 2. Comparison of the gene organization of *sufR* and the *sufBCDS* operon in the genomes of sequenced cyanobacteria. The direction of the block arrow indicates the transcription orientation.

isolated that retained the primary mutation, which was verified through amplification of the *psaC* gene fragment by PCR and sequencing. Suppressor mutations were located to a specific ORF, *sll0088*, by phenotypic complementation and identified by DNA sequencing (Yu et al., 2003). The mutations involved the substitution of a Pro for Arg161 due to a G482C mutation and the insertion of a GlyTyrPhe following Cys321 due to a TGGTTAATTT duplication at T698, both of which are likely to break the function of the Sll0088 protein. The involvement of Sll0088 in repair and stabilization of the Fe/S clusters in PsaC was verified through characterization of an *sll0088* null mutant in *Synechococcus* sp. PCC 7002 (Wang et al., 2004). As discussed later in greater detail, a gene expression assay has shown that the *sll0088* gene serves as a negative transcriptional regulator in the *suf* regulon. The gene has therefore been labeled "*sufR*," for "repressor" of the *suf* regulon. Identical to a *sufR* null mutant, the expression of the nonfunctional SufR mutant proteins in the PsaC pseudorevertants resulted in the overexpression of the *suf* genes, which function in the assembly and transfer of Fe/S clusters to PsaC. As shown in Fig. 2, comparative genomics analysis shows that a *sufR*-like gene can be identified directly upstream of the conserved *sufBCDS* operon in several sequenced cyanobacterial genomes. Interestingly, the *ftrC* gene, encoding the beta chain of the ferredoxin-thioreductase, is sometimes inserted between the *sufR* gene and the *sufBCDS* operon. In all cases, the *sufR* gene is transcribed in the direction opposite to the *suf* genes.

2. Suf Proteins: Location in the Plastids of Higher Plants

a. Gene localization and plastids

In the genomes of cyanobacteria, the arrangement of the *sufB*, *sufC*, *sufD*, and *sufS* genes suggest that they comprise an operon. Indeed, the cotranscription of the *sufB*/*sufC*/*sufD*/*sufS* genes has been verified in *Synechococcus* sp. PCC 7002 (Wang et al., 2004). Cyanobacteria are considered the evolutionary ancestors of plastids. Therefore, the occurrence of *suf* genes in cyanobacteria implies that they should be located in the plastids of higher plants. A search of the database shows that homologs of *sufB* and *sufC*, named *ycf24* and *ycf16*, have been located in the plastidic chromosome of the red alga *Porphyra purpurea* (Reith and Munholland, 1995), *Cyanidium caldarium* (Glockner et al., 2003), and *Cyanidioschyzon merolae* (Ohta et al., 2003), the Chl $a + c$-containing centric diatom *Odontella sinensis* (Kowallik et al., 1995), the cyanelle of *Cyanophora paradoxa* (Stirewalt et al., 1995), and the cryptomonad *Guillardia theta* (Douglas and Penny, 1999). Also, the *sufA* gene has been identified as the *ycf83* gene in *Porphyra purpurea* (Reith and Munholland, 1995), *Cyanidioschyzon merolae* (Ohta et al., 2003), and *Galdieria sulphuraria* (Whitney and Andrews, 2001). In *A. thaliana*, the *sufB*, *sufC*, *sufD*, and *sufS* genes are nuclear-encoded. However, the existence of a transit peptide in the predicted sequences of SufC, SufD, and SufS of *A. thaliana* indicate that

they are plastid-targeted (Emanuelsson and von Heijine, 2001) Our attempts to inactivate the *sufD* and *sufS* genes in *Synechococcus* sp. PCC 7002 have been unsuccessful; hence, the *suf* genes appear to be essential in cyanobacteria (Shen et al., 2004). This result hints suggest the *suf* genes should be essential in the plastids of higher plants, but this has yet to be established experimentally.

b. Protein localization and activity in plastids

Studies on SufS provided the first biochemical evidence for the presence of the SUF system in plastids. Cysteine was identified as the sulfur source for Fe/S cluster formation in the plastid (Takahashi, 1986, 1991a,b). Seleno-cysteine desulfurase activity was later detected in plastids of *Arabidopsis* (Pilon-Smits et al., 2002). From the sequenced genome of *Arabidopsis*, the At1g08490 gene (accession number AAF22900) can be identified as the *sufS* gene. It has been shown that the SufS protein (also named AtNFS2) can be addressed to chloroplasts as an AtNFS2-GFP chimeric fusion protein (Léon et al., 2002a). Targeting of *Arabidopsis* SufS into chloroplasts has also been studied using *in vitro* plastid uptake experiments. A radiolabeled 47 kD SufS precursor was incubated with purified intact chloroplasts in the light and in the presence of ATP. Import and intraorganellar routing was monitored by reisolation of the plastids, protease treatment, and fractionation into a soluble-stroma fraction and membranes. SufS accumulated in chloroplasts, specifically in the chloroplast stroma, with a mature size of 43 kDa (Pilon-Smits et al., 2002). Characterization of the *Arabidopsis* mutant *laf6* led to the identification a plastidic ABC protein (AtABC1), which was later shown to be a homolog of SufB (Møller et al., 2001). The plastidic localization of the *Arabidopsis* AtNAP7 (SufC) protein was suggested by its N-terminal extension. Using a construct of AtNAP7 cDNA fused to YFP to transiently express the protein in tobacco leaves, it has also been shown that AtNAP7 (SufC) is localized to the chloroplast (Xu and Møller, 2004). The plastidic localization of SufD has been verified by transient expression of the *Arabidopsis* AtNAP6(SufD)/GFP fusion protein in leaf cell protoplasts from *A. thaliana* (Hjorth et al., 2005). In immunogold-labeling experiments, binding of the SufD antibody was found preferentially in the tips of plastids of cryptophyte *Guillardia theta*. By fusing the predicted chloroplast transit sequence of SufA homolog CpIscA to GFP (green fluorescence protein), green fluorescence from the SufA transit peptide and GFP could be localized to the chloroplast stroma (Abdel-Ghany et al., 2005). These results firmly establish that the SUF system has an important role in Fe/S cluster assembly in plastids.

3. Why Does the SUF System Exist in Non-Photosynthetic Organisms?

As discussed above, the ISC system is responsible for the biogenesis of Fe/S proteins necessary for respiratory and other metabolism processes in the mitochondria. The ISC system has also proven to be the major housekeeping system for Fe/S cluster assembly in non-photosynthetic bacteria. In *E. coli*, genetic studies indicate that the genes in the *isc* operon play a central role in Fe/S cluster formation (Schwart et al., 2000; Tokumoto and Takahashi, 2001; Mihara et al., 2002). Nevertheless, a modest amount of Fe/S cluster assembly persists in an *iscS* null mutant, which suggests that SufS or perhaps other proteins with desulfurase activity may account for residual Fe/S cluster assembly (Schwart et al., 2000). It was not possible to delete the *iscS* gene in *A. vinelandii*, indicating that it plays an essential role (Zheng et al., 1998). However, it should be noted that this organism does not contain the SUF system. In contrast, the *suf* genes are dispensable in *E. coli* (Patzer and Hantke, 1999; Takahashi and Tokumoto, 2002) and the plant pathogen *Erwinia chrysanthemi* (Nachin et al., 2001, 2003). It has been reported that expression of the *suf* genes is under control by oxidative stress and iron limitation in *E. coli*. It has also been reported that overexpression of the *suf* operon can restore the activity of Fe/S proteins in an *iscSUA* mutant (Takahashi and Tokumoto, 2002). Therefore, in non-photosynthetic organisms, the SUF system may be invoked under conditions such as oxidative stress and iron stress, which would involve biogenesis of Fe/S proteins and repair of oxidatively damaged Fe/S clusters. We should mention that no homologs of SufB and SufC could be identified in non-photosynthetic eukaryotes; thus only the ISC system appears to assemble Fe/S clusters in these organisms.

IV. Function of Suf proteins and Assembly of Fe/S Clusters

A. Function of SufS and SufE in Mobilizing Sulfur

1. SufS: Structure and Mechanism

The X-ray crystal structure of SufS from *E. coli* (Fujii et al., 2000; Lima, 2002) and *Synechocystis* sp. PCC

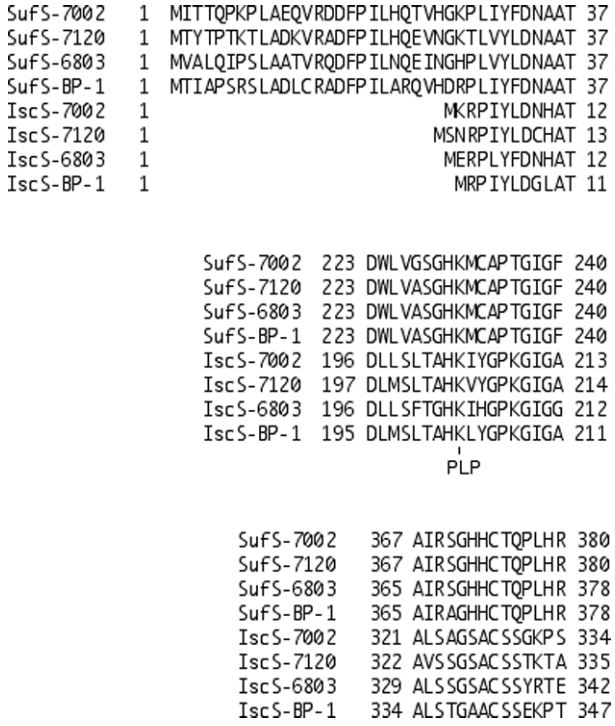

Fig. 3. Difference between SufS and IscS proteins from cyanobacteria in their N-terminal region, pyridoxal phosphate binding region, and the active site.

6803 (Tirupati et al., 2004) has been solved to atomic resolution. SufS is structurally similar to IscS (Cupp-Vickery et al., 2003) and NifS (Kaiser et al., 2000); it is a homodimeric, pyridoxal 5′-phosphate (PLP)-dependent cysteine desulfurase that catalyzes the conversion of cysteine to alanine and sulfane sulfur, as illustrated first in studies of NifS (Zheng et al., 1993) and IscS (Flint, 1996). The desulfuration of cysteine is initiated by the formation of a Schiff base with PLP. The specific cysteine residue is highly conserved in all cysteine desulfurase homologs (SufS, IscS, and NifS), acting as nucleophile to attack the sulfhydryl group of substrate cysteine persulfide intermediate.

In spite of their structural and functional similarities, significant differences exist between SufS and IscS. As indicated in Fig. 3, one difference concerns the region around the active cysteine: in SufS, a different amino acid sequence exists in the pocket and a much shorter extended lobe harbors the catalytic cysteine. This difference may account for the different catalytic efficiencies in the desulfuration of cysteine and seleno-cysteine (Mihara et al., 1999; Tachezy et al., 1999; Behshad et al., 2004). In addition, SufS has an extended N-terminus, which may assume a specific function in protein–protein interactions.

Unlike SufS and IscS, C-DES (a cystine desulfurase) is missing the largely conserved active-site cysteine (Clausen et al., 2000). C-DES produces ammonium pyruvate and sulfide from cysteine, and has a strong substrate preference for cystine over cysteine. This distinct L-cysteine/L-cystine C-S lyase has been shown to participate in Fe/S cluster assembly in cyanobacterial apoferredoxin (Lang and Kesseler, 1999). Sequence analysis suggests that C-DES proteins are more closely related to SufS proteins than to IscS proteins.

2. SufE and its Cooperation with SufS

SufE is a cytosolic protein with a highly conserved Cys residue (Outten et al., 2003). A homolog of *sufE* can be identified in the genome of the higher plant *Arabidopsis* where the predicted SufE protein possesses a typical N-terminal extension for plastid-targeting. The recent determined X-ray crystal structure of SufE from *E. coli* (Goldsmith-Fischman et al., 2004) shows that the protein is a homodimer containing a novel fold consisting of both α-helices and β-sheets. Two distinct Cys51 active sites are positioned on opposing sides of the SufE dimer, but packed inward into the hydrophobic core. This might indicate that SufE is in an inactive conformation as a homodimer. SufS and SufE interact each other to form a complex (Loiseau et al., 2003; Outten et al., 2003). SufE stimulates the cysteine desulfurase

activity of SufS and accepts the sulfane sulfur from SufS (Loiseau et al., 2003; Outten et al., 2003). The highly conserved Cys residue in SufE was shown to be essential for sulfur transfer (Outten et al., 2003). Cyanobacterial SufE can also interact with SufS to facilitate transfer of sulfide (Tirupati et al., unpublished results). Therefore, SufE functions as a universal sulfur acceptor protein. However, SufE is selective in mobilizing sulfur from SufS; it was shown that SufE cannot accept mobilized sulfur from IscS or NifS (Outten et al., 2003).

B. SufBCD: A Function in Mobilizing Iron?

1. SufB and SufD

SufB is annotated as the membrane component of an ABC-type transporter. Although the primary amino acid sequence shows no indication that it is an intrinsic membrane protein, SufB was found to be associated with the chloroplast membranes of *Arabidopsis* (Møller et al., 2001). Thus, the opportunity exists to interact with the membrane-bound PS I complex during Fe/S cluster assembly. It appears that SufB is comprised of several domains; in particular, the highly conserved UPF0051 domain in the C-terminus shares homology with that of SufD. This may account for known interaction of SufB and SufD (Loiseau et al., 2003). The C-terminal domain of SufB is predicted to form an extensive set of short β-strands followed by three small terminal α-helices, which may provide transporter-like properties.

2. SufC

SufC contains a conserved ABC motif for ATP-binding that is readily folded *in silico* to the archetypal structure of the membrane-associated, ATP-binding subunit of the ABC transporter as HisP (Watanabe et al., 2005). The three motifs typical of the ATP-hydrolyzing domains of ABC ATPases can be identified in SufC: Walker sites A and B as well as motif C. The hydrolytic activity of SufC as an ATPase has been established using expressed recombinant SufC from *Thermotoga maritima* (Rangachari et al., 2002) and *E. chrysanthemi* (Nachin et al., 2003). Therefore, SufC functions as a versatile orphan ATPase in the Fe/S cluster assembly machinery. As shown in isolated intact chloroplasts and lysed chloroplasts, ATP is required for the insertion of the Fe/S cluster into ferredoxin (Takahashi et al., 1991b). The ATP hydrolysis activity of SufC appears to be central to iron mobilization and formation of the Fe/S cluster.

3. The Interaction of SufC with SufB and/or SufD

The *sufB* and *sufC* genes are the best conserved *suf* genes in cyanobacteria and plants. In fact, *sufB* and *sufC* invariably occur together in cyanobacteria, and are also found in the chloroplast DNA of *Porphyra purpurea* and *Guillardia theta* as *ycf24-ycf16* or in the nucleus, the products being directed to the organelle in the later case. SufB and SufC were shown to interact with each other in immunolocalization assays (Rangachari et al., 2002) as well as in a yeast two-hybrid assay (Nachin et al., 2003; Xu et al., 2005). SufB and SufC can be expressed and isolated as a complex (Wilson et al., 2002; Loiseau et al., 2003). The ability of ATP to bind to SufC was enhanced in a SufB/SufC complex, as shown using stopped-flow fluorescence anisotropy experiments (Wilson et al., 2002). SufC has also been shown to interact with SufB and SufD by affinity chromatography (Nachin et al., 2003). SufB/SufC/SufD can be copurified as a complex when expressed together using a s*ufABCDSE* construct (Outten et al., 2003). These results indicate that SufB, SufC, and SufD work closely together in Fe/S cluster assembly. The SufB/SufC/SufD complex enhances the activity of SufS/SufE in sulfur mobilization, most likely due to their coordinated activity in Fe/S cluster assembly. The enhancement of SufS activity by the SufB/SufC/SufD complex does not require ATP hydrolysis (Outten et al., 2003). In contrast, the release of strongly bound Fe^{3+} from storage proteins and their subsequent transport requires energy. The hydrolysis of ATP may therefore be required for iron acquisition rather than Fe/S cluster assembly. Reverse genetics has shown that the *sufB* and *sufC* genes are important in iron metabolism and oxidative stress in *E. chrysanthemi* (Nachin et al., 2001). Therefore, the SufBCD complex plays an important role as an ATP-dependent energizer in iron metabolism and Fe/S cluster formation. A mutation in *sufD* resulted in an increased sensitivity to oxidative stress and a mutation in *sufC* resulted in increased intra-cellular accumulation of free iron. It has been reported that *Arabidopsis* plants deficient in the SufC homolog AtNAP7 exhibit lethality in embryogenesis (Xu and Møller, 2004), suggesting an essential role for SufC in plastidic Fe/S cluster assembly and repair during *Arabidopsis* seed viability and normal embryo development. SufB, SufC, and SufD were found to be essential in the utilization of ferric chrysobactin in *E. chrysanthemi* (Masclaux and Expert, 1995). The role of SufB and SufC in the maintenance of iron homeostasis was also inferred from a *sufB* homolog mutant of *Arabidopsis* (named as atABC1), which

accumulated the heme/chlorophyll precursor PPIX. This can be explained as a result of a deficiency in Fe-assimilation.

C. SufA May Assume a Regulatory Function

1. Is SufA a Scaffold Protein for Fe/S Cluster Assembly?

Following a similar proposal for IscA, SufA in *E. chrysanthemi* (Choudens et al., 2003) and cyanobacteria (Wollenberrg et al., 2003) has been proposed to function as a scaffold protein similar to that of NifU or IscU in the assembly of a transient [2Fe–2S] cluster. If SufA is indeed a scaffold protein, it should also play this role in the chloroplast-type SUF system. To probe the function of SufA in *Synechococcus* sp. PCC 7002, we constructed interruption mutants of *sufA* using a variety of antibiotic resistance cartridge genes (Balasubramanian et al., 2006). Compared to the wild-type strain, the *sufA* mutant showed no phenotype under photoautotrophic growth conditions, which suggests that the *sufA* gene is not essential. Nevertheless, it is possible that IscA might complement the role of the missing SufA. To test this possibility, double mutants were generated in *Synechococcus* sp. PCC 7002 in which both the *sufA* and *iscA* genes were inactivated. In the absence of SufA and IscA, the double mutant strains still showed no phenotype under normal photoauototrophic growth conditions. Thus, we question whether SufA functions as a scaffold protein for generalized Fe/S cluster assembly in cyanobacteria.

2. Specificity of the SufA Protein

SufA shares a high degree of homology with IscA, a component of the mitochondrial ISC system (Kaut et al., 2000), indicating that the two proteins may be similar in structure and function. SufA, which is encoded by the *slr1417* gene in *Synechocystis* sp. PCC 6803, harbors an unstable [2Fe–2S] cluster (Morimoto et al., 2002; Wollengerg et al., 2003). An unstable [2Fe–2S] cluster has also been identified in IscA of *Synechocystis* sp. PCC 6803 (Morimoto et al., 2002) as well as in ^{Nif}IscA of *Azotobacter vinelandii* (Krebs et al., 2001) and IscA of *E. coli* (Ollagnierde-Chaudens et al., 2001). Cyanobacterial SufA (*slr1417* in *Synechocystis* sp. PCC 6803) was found to bind iron ions as well as an unstable [2Fe–2S] cluster (Morimoto et al., 2002).

SufA in cyanobacteria and higher plants shows two significant differences compared to IscA: the presence of two additional conserved cysteine residues in the N-terminal domain as well as an N-terminal extension (Balasubramanian et al., 2006). It is reported that only two cysteine residues in the C-terminal domain are involved in binding the [2Fe–2S] cluster between the two protomers of SufA (Wollengerg et al., 2003). It is possible that the two extra cysteine residues are involved either in the coordination of iron or that they function as redox sensors through disulfide bond formation (as in the regulator OxyR). In the *suf* operon of bacteria, the *sufA* gene is organized together with *sufBC*, a possible ABC transporter system in iron mobilization for Fe/S cluster assembly. Likewise, in the *isc* operon of bacteria, *iscA* is conservatively organized with *hscBA* genes as a *iscA–hscBA–fdx* gene cluster. The *hscBA* genes encode Hsc66 and Hsc20, respectively, which are typical chaperonine proteins. The expression of the *sufA* gene is under the control of Fe stress in cyanobacteria (Balasubramanian et al., 2006), similar to other bacteria (Zheng et al., 2001). Although much remains to be done in elucidating its function, we are exploring the possibility that SufA serves a role in regulating Fe metabolism in cyanobacteria.

D. RubA and the Assembly of the F_X Cluster in PS I

1. RubA: A Chloroplast-Specific Factor

Based on the conservation of the major components, the SUF system may adapt a similar molecular mechanism to assemble Fe/S clusters in photosynthetic and non-photosynthetic organisms. However, oxygenic photosynthetic organisms require additional factors that may work together with the SUF system in the maturation of particular Fe/S proteins. One such additional factor is the membrane-associated rubredoxin (RubA) found in cyanobacteria (Shen et al., 2002a). This protein is found in oxygen-evolving photosynthetic organisms, such as in the nucleomorph of the cryptomonad *G. theta* (Wastl et al., 2000) and in *Arabidopsis* (At1g54500). RubA is a small non-heme iron protein (Fig. 3) that contains a domain of about 50 amino acids with a very high similarity to the rubredoxins of anaerobic bacteria and archaea. RubA also contains a region of about 50 amino acids that is predicted to form a flexible hinge and a transmembrane α-helix at the C-terminus as a thylakoid membrane anchor. The localization of RubA in chloroplasts can be predicted by its presence of plastid-targeting leader sequence, and has been confirmed by immunoelectron microscopy (Wastl et al., 2000). Our studies demonstrate that RubA is

associated with thylakoid membranes and is transiently associated with monomeric PS I complexes (Shen et al., 2002a).

2. RubA and the Assembly of the [4Fe–4S] Cluster in F_X

At least one function of the *rubA* gene, the biogenesis of the F_X cluster in PS I, has been elucidated through reverse genetics (Shen et al., 2002a). Inactivation of the *rubA* gene of *Synechococcus* sp. PCC 7002 produced a mutant unable to grow photoautotrophically and led to a complete loss of PS I electron transport activity. Although trimeric PS I could be assembled at reduced levels, PS I complexes of the *rubA* mutant were lacking the stromal subunits PsaC, PsaD, and PsaE. Low temperature electron paramagnetic resonance (EPR) spectroscopy shows that not only are F_A and F_B missing, as would be expected from the loss of PsaC, but F_X is also missing (Shen et al., 2002b). This was true in whole cells, thylakoids, and PS I complexes of the *rubA* mutant, indicating that the loss of F_X was not the result of damage incurred during isolation. The absence of F_X was confirmed in PS I complexes by time-resolved optical spectroscopy and spin-polarized EPR measurements. Consequently, flash-induced charge separation and recombination occurs between P700 and A_1. Because F_X is required for PsaC to bind, it is uncertain whether the lack of F_A and F_B is a direct consequence of the lack of RubA or whether it is indirect result of the absence of F_X. Nevertheless, RubA appears to be specifically required for the assembly of F_X.

It is interesting that we found no other growth phenotype in the RubA null mutant. Hence, the Fe/S proteins involved in sulfur and nitrogen metabolism, in respiration, and other vital functions of the cell appear to be unaffected. The question, then, becomes one of asking what is unique about F_X that requires the participation of a protein whose only known function is in electron transfer? The answer may lie in the knowledge that F_X, F_B, and F_A are the last components to be assembled during the biogenesis of PS I. We can safely assume that the bioassembly of PS I occurs in the light during all stages in the growth and reproductive stages of the cell. Hence, in this nascent PS I complex, all of the chlorophylls, carotenoids, and quinones are present prior to the insertion of the Fe/S clusters. Charge separation would therefore take place between P700 and A_1 during the time that the Fe/S cluster is assembled and inserted into the F_X site. The assembly process is likely to require delicate biochemistry, requiring the proper redox states of the iron atoms, i.e., fully assembled F_X has two ferrous and two ferric ions in the oxidized state. The redox potential of A_1^-/A_1 is -710 to -730 mV vs the normal hydrogen electrode, making it one of the most reducing potentials in all of biology. Our hypothesis is that the membrane-bound rubredoxin functions as an electron shunt during the process of F_X assembly, vectoring electrons out of A_1^- to a harmless oxidant so that the correct redox environment exists for the assembly and insertion of the $[4Fe–4S]^{2+}$ cluster into the F_X site (Fig. 4). Once F_X is present, PsaC, PsaD, and PsaE can bind, and PS I can be considered fully assembled. According to this scenario, if rubredoxin is not present, the F_X cluster will not assemble, and the development of PS I will be arrested. Because ferredoxin and flavodoxin cannot be reduced by A_1^-, the organism cannot grow photoautotrophically. It is significant that at this stage, i.e., with A_1 as the terminal electron acceptor, the attenuated PS I core is not recognized as damaged, and it accumulates in the cell. Indeed, the availability of a biologically prepared P700-A_1 core has been used to great advantage in the study of the primary and secondary electron acceptors in PS I (Sakuragi et al., 2005).

E. HCF101: A New Factor Involved in Fe/S Cluster Assembly in PS I?

HCF101 was initially identified through characterization of an *Arabidopsis* high-chlorophyll-fluorescence (HCF) mutant (Lezhneva et al., 2004; Stöckel and Oelmüller, 2004). High chlorophyll fluorescence originates from an inefficiency in excitation energy transfer from light-harvesting chlorophylls, which may be due to impairment of electron transport from PS II to PS I as occurs, for instance, in mutants deficient in PS I (Shen et al., 1993; Shen and Bryant, 1995). Therefore, high chlorophyll fluorescence can serve as a useful phenotypic marker for screening mutant strains. Indeed, an impairment in PS I assembly and function was found in the *Arabidopsis* HCF101 mutant (Stöckel and Oelmüller, 2004). The HCF101 protein belongs to the family of P-loop ATPases, which is ubiquitous distributed in all organisms, both photosynthetic and non-photosynthetic. However, the HCF101 proteins from cyanobacteria and higher plants can be classified into a subgroup based on an characteristic N-terminal feature (Lezhneva et al., 2004). The predicted transit peptide of HCF101 suggests a localization in the chloroplast, which has been verified by cell fractionation and immunodetection (Lezhneva et al., 2004; Stöckel and Oelmüller, 2004). On the basis of involvement of HCF101 in PS I biogenesis or stabilization, the HCF101 protein is proposed to assist either

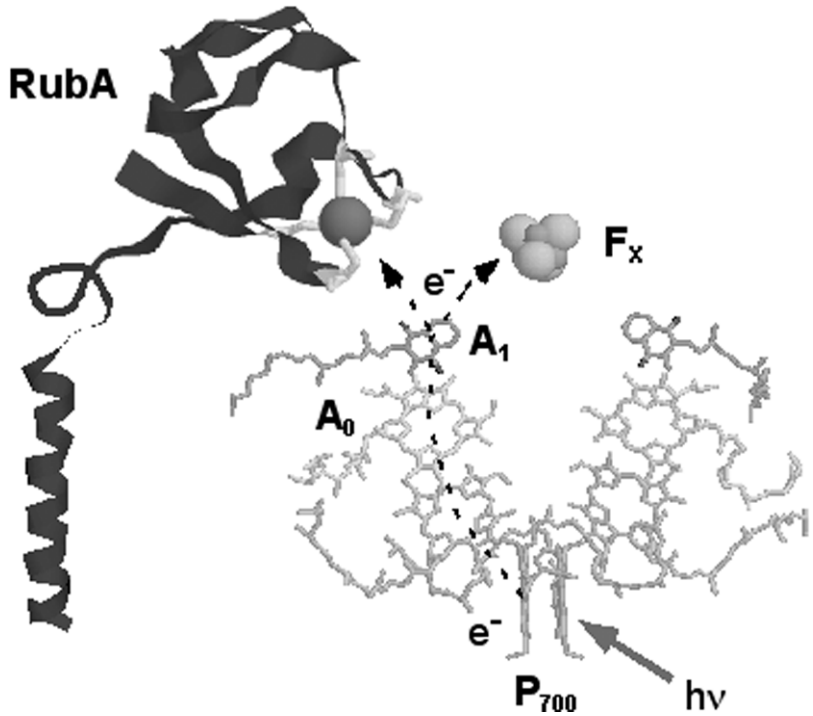

Fig. 4. Hypothetical model for the function of the RubA protein in insertion of the F_X cluster during PS I biogenesis. The membrane-localized RubA is postulated to intercept electrons from reduced phylloquinone A_1 and thus prevent reduction of intermediates during the assembly of the intersubunit [4Fe–4S] cluster (Shen et al., 2002a,b).

in PsaA/PsaB folding or in cofactor delivery (Stöckel and Oelmüller, 2004), and quite possibly Fe/S cluster assembly (Lezhneva et al., 2004).

V. Mechanism of the SUF System in Oxygenic Photosynthetic Organisms

A. The Conversion of 2[2Fe–2S]$^{1+}$ Clusters into [4Fe–4S] $^{2+}$ Clusters

The modular structures of Fe/S clusters are supported by their remarkable facility for conversion and interconversion in both the free and protein-bound forms. Ligand exchange reactions and oxidative denaturation of Fe/S clusters play an important role in their regulatory functions. A facile $[4Fe–4S]^{2+}$ and $2[2Fe–2S]^{1+}$ + $2e^-$ cluster conversion was reported in *E. coli* FNR (fumarate nitrate reduction protein) with the oxidative process mediated by O_2 (Khoroshilova et al., 1997), resulting in the conversion of the transcriptionally active $[4Fe–4S]^{2+}$ form to the transcriptionally inactive $[2Fe–2S]^{2+}$ form. The oxygen-labile [4Fe–4S] cluster in FNR therefore functions as a transcriptional regulator that controls the switch from aerobic to anaerobic metabolism. This mechanism is further supported by observation of a $2[2Fe–2S]^{1+}$ to $[4Fe–4S]^{2+}$ conversion in synthetic complexes (Beinert et al., 1997). The near-stoichiometric conversion of two $[2Fe–2S]^{2+}$ clusters to form one S = 0 $[4Fe–4S]^{2+}$ cluster with complete cysteinyl-S coordination under reducing conditions was observed using optical absorbance and resonance Raman studies in *E. coli* biotin synthase (Duin et al., 1997). Despite the diversity of Fe/S cluster proteins, especially in structure and electronic properties, it is possible that most, if not all, polynuclear [Fe/S] clusters are assembled from [2Fe–2S] precursors. In this conversion model, Fe_2S_2 rhombs provide the basic building block of all mature Fe/S clusters. As proposed for the NifU protein, the scaffold protein serves as a platform for harboring a transient [2Fe–2S] cluster and then transferring it into the target Fe/S apoprotein.

B. NFU Genes in Cyanobacteria and Higher Plants

1. Specificity of the NFU Protein

In cyanobacteria and higher plants, NFU shares sequence similarity with the C-terminal domain of NifU

from *A. vinelandii*. As shown in Fig. 1, this domain is about 50 amino acids in length and contains a conserved CXXC motif. Analysis of the genome of *Arabidopsis* reveals the existence of five genes encoding NFU-like proteins; they are named AtNFU1-5 and can be divided into two distinct classes. AtNFU4 and AtNFU5 share sequence similarity with the yeast mitochondrial protein ScNFU1, and contain mitochondria-targeting sequences in their N-terminal regions (Schilke et al., 1999). AtNFU1-3, in contrast, share sequence similarity with the NFU-like protein of cyanobacteria, which contain an additional sequence located downstream of the NFU domain but without the CXXC motif. A plastid-targeting sequence is located for the sequence located upstream of the NFU domain of the AtNFU1-3 proteins. Therefore, AtNFU1-3 are predicted to be localized in plastids with typical plastid-specific features. It will be important to explore the function and specificity of each of three AtNFU proteins. At this time, only AtNFU2 and AtNFU3 can be found in the plastid by immunodetection (Leon et al., 2003). Searches in the database reveal that NFU is present in other higher plants such as rice (Accession Number AB096013). Thus, two different Fe/S cluster assembly systems exist in two distinct compartments in higher plant cells.

2. Can NFU Assume the Role of NifU?

The NFU protein of *Synechocystis* sp. PCC 6803 and the AtNFU2 protein of *Arabidopsis* (Leon et al., 2003) harbor a labile [2Fe–2S] cluster (Nishio and Nakai, 2000). Based on its ability to transfer a [2Fe–2S] cluster to apoferredoxin (Nishio and Nakai, 2000), cyanobacterial NFU has been suggested to function as a scaffold for Fe/S cluster assembly, similar to the roles proposed for NifU and IscU in *E. coli* and yeast, It is not possible to inactivate the *nfu* gene in *Synechococcus* sp. PCC 7002 in either the wild-type strain or in a PS I-less strain (Balasubramanian et al., 2006), suggesting that NFU has an essential function in cyanobacteria. That it is required even in the PS I-less background indicates that NFU is involved in non-photosynthetic functions. It is perhaps significant that a homolog of the IscU-like domain of NifU, which is the platform that harbors the labile [2Fe–2S] cluster for transfer, cannot be identified in cyanobacteria or in the chloroplasts of higher plants. Based its localization in the *Arabidopsis* plastid, it is likely that NFU may functions alongside the SUF system in Fe/S cluster biogenesis in cyanobacteria and plastids of higher plant. Although it is unknown how the three AtNfu proteins coordinate their roles in plastidic Fe/S cluster assembly, it has been reported that the inactivation of the *AtNfu2* gene leads to a reduction in PS I activity along with a decrease in the activity of sulfite reductase, which is involved in the sulfur assimilation pathway (Touraine at al., 2004).

3. Is a Scaffold Protein Necessary for Fe/S Cluster Assembly in the SUF System?

The central tenent in the field of Fe/S cluster assembly is the presence of external scaffold protein on which a labile [2Fe–2S] or [4Fe–4S] cluster is built prior to transfer to the target apoprotein. An interesting case involves the study of the bioassembly of HiPIP in *Chromatium vinosum* using NMR spectroscopy (Natarajan and Cowan, 1997). Incubation of the apoprotein with Fe^{2+} and dithiothreitol led to the appearance of assignable crosspeaks in the ^{1}H–^{15}N HSQC spectrum, indicating the presence of a 4Fe-containing center as a relatively stable intermediate. The NMR study shows that the protein is largely correctly folded. It is suggested that the 4Fe-containing intermediate contains an Fe-cluster that lacks sulfide bridges but is stabilized by ligation to Cys thiolates from the protein and from DTT. The native Fe/S clusters form upon addition of sulfide. Even in bacterial systems, it has been proposed that the SUF system may assemble Fe/S clusters within the apoprotein itself without an external scaffold (Outten et al., 2003).

Considering the [2Fe–2S] to [4Fe–4S] conversion model for ISC system, there could be two possible routines in the final step of cluster maturation: either direct transfer or degradation and reassembly of the binuclear entity into the apoprotein target. Even for direct transfer, additional factors might be required to unload the preassembled [2Fe–2S] clusters from the scaffold protein and reinstall them into the target apoprotein. Therefore, one scenario is that the SUF system follows a two-step procedure: apoprotein → [4Fe] → [4Fe–4S]. A similar protocol might occur in the assembly of PS I-bound [4Fe–4S] clusters. Certainly, chloroplast-specific factors, such as RubA, are already known to play additional roles in insertion, and maturation of the F_X cluster in PS I.

VI. Regulation of the SUF System

A. SufR: Regulation of Fe/S Cluster Assembly in PS I

A variety of physiological and environmental input signals regulate the genes involved in the biogenesis

and/or repair of Fe/S proteins. In cyanobacteria, the expression of the *suf* genes is subject to the regulation of *sufR* (Wang et al., 2004). The SufR protein contains a DNA-binding domain that is composed of a basic region and a putative helix–loop–helix motif, a typical feature of negative transcriptional regulators. The regulatory role of *sufR* on the expression of the *sufBCDS* genes has been studied in a *sufR* null mutant in *Synechococcus* sp. PCC 7002. The transcript levels of the *suf* genes are consistently higher in the mutant, which indicates that the *suf* operon is negatively regulated by SufR (Wang et al., 2004). Our working model is that SufR functions as a repressor when the Fe/S cluster is present. The Fe/S cluster, which is coordinated by the conserved cysteine motif near the C-terminus, may sense oxidative stress and decompose, thereby controlling the expression of the *suf* regulon.

There exist similarities between the SUF and ISC systems in terms of gene regulation. The IscR protein of *E. coli* functions as a transcriptional repressor of the *iscRSUA* operon in *E. coli* (Schwartz et al., 2001). The presence of a [2Fe–2S] cluster on the IscR protein may serve as the sensor in an autoregulatory mechanism, and thereby assume a function similar to the SoxR transcriptional regulator (Pomposiello and Demple, 2001). At the first level of approximation, if the [2Fe–2S] cluster is present, then transcription is attenuated, and when the [2Fe–2S] cluster is absent, then transcription is permitted.

B. Stress and the Regulation of the suf *Genes*

The s*uf* genes are up-regulated in cyanobacterial cells under conditions of oxidative stress and Fe starvation. When cells are grown in normal media and treated with 3-(3′,4′-dichlorphenyl)-1,1-dimethylurea (DCMU, an inhibitor of Photosystem II), 2,5-dibromo-3-methyl-6-isopropylbenzoquinone (DBMIB, an inhibitor of cytochrome b_6/f), H_2O_2, or subject to iron deprivation, transcript levels of *sufB* and *sufS* are increased more than 3–4 times (Wang et al., 2004). The expression levels of the *suf* genes are also reported to be upregulated under conditions of oxidative stress in nonphotosynthetic organisms, such as in the plant pathogen *E. chrysanthemi* (Nachin et al., 2001) and in *E. coli* (Zheng et al., 2001). However, in non-photosynthetic bacteria, the *suf* operon is regulated by factors such as SoxR (Hidalgo et al., 1997) and OxyR, probably in response to their different physiological niches. Transcription factors OxyR (in *E. coli*, Zheng et al., 2001) and SoxR (in *E. chrysanthemi*, Nachin et al., 2001) have been found to function as redox-responding regulators in controlling expression of the *suf* genes. SoxR and OxyR are two well-defined redox-responsive transcriptional activators in *E. coli* (see review by Pomposiello and Demple, 2001). However, no homologs of SoxR and OxyR can be identified in the sequenced genomes of cyanobacteria and the higher plant *Arabidopsis*. Conversely, *sufR* is not present in organisms other than cyanobacteria and a certain class of microbial pathogens. Thus, different factors are involved in gene regulation in response to oxidative stress in oxygenic photosynthetic vs. nonphotosynthetic organisms.

C. Light and Fe/S Cluster Biogenesis

It is well known that the biogenesis of plastids is regulated by light, mostly through regulation of the expression of photosynthetic genes. The formation of Fe/S clusters in lysed chloroplasts is dependent on both ATP and illumination; the reaction does not occur in the dark even in the presence of added ATP (Takahashi et al., 1991a). In higher plants, transport of the nuclear-encoded SufS into the chloroplast stroma is a light-stimulated process (Pilon-Smits et al., 2002). Light stimulation of Fe/S cluster formation is likely to be related to the biogenesis of the photosynthetic complexes, especially PS I. As shown in Fig. 2, the *ftrC* gene is located between *sufR* and the *sufBCDS* operon in several genomes of *Synechococcus* strains, and is most likely co-transcribed with the *sufBCDS* genes. The *ftrC* gene encodes the catalytic chain of heterodimeric ferredoxin–thioredoxin reductase (FTR) (see Hase et al., this volume, Chapter 28). FTR is unique to oxygenic photosynthetic cells. It converts an electron signal (photoreduced ferredoxin) to a chemical signal (reduced thioredoxin), thereby regulating enzymes by the reduction of specific disulfide groups. The light-dependent FTR system is involved in regulating the activity of many key photosynthetic regulatory enzymes by a light-driven reduction of disulfide bonds (reviewed by Schürmann and Buchanan, 2001). Therefore, a connection of the *ftrC* gene with the *sufR* and *suf* operon suggests that the expression of the *suf* genes might be subject to the FTR system involved light regulation.

VII. Concluding Remarks

Two major systems are responsible for the biogenesis and repair of Fe/S clusters in oxygenic photosynthetic organisms. In higher plants, the ISC system functions to assemble Fe/S clusters destined for Fe/S proteins

present in mitochondria, and by analogy with yeast, for Fe/S proteins that are present in the cytoplasm. The SUF system functions to assemble Fe/S clusters destined for Fe/S proteins present in the plastid, including the assembly and repair of PS I-bound Fe/S clusters. In cyanobacteria, the ISC system is present, but all of the genes can be deleted without loss of viability. The SUF system, however, is linked closely to the assembly of Fe/S clusters destined for the photosynthetic apparatus, particularly the bound Fe/S clusters in PS I, and is indispensable. Several reports support the [2Fe–2S] to [4Fe–4S] conversion model in the biosynthesis of Fe/S clusters. Nevertheless, with the exception of the similar cysteine desulfurases IscS and SufS, in the ISC and SUF systems, respectively, there are strong indications that the process of Fe/S cluster assembly occurs by fundamentally different mechanisms in these two systems. Indeed, the near-anaerobic environment of the mitochondria and the oxygen-saturated environment of the chloroplast may require fundamentally different mechanisms for Fe/S cluster assembly. The expression of the *suf* genes in cyanobacteria is subject to the regulation by the transcription factor SufR, and to regulation by oxidative stress and iron stress. On the basis of the conservation of the major components, the SUF system may adopt a similar fundamental molecular mechanism in the formation of Fe/S cluster in photosynthetic and non-photosynthetic organisms. However, additional chloroplast-specific factors are known to be involved in Fe/S clusters destined for PS I. One these factors is the membrane-associated RubA protein, which has been found to be essential for the assembly of the F_X cluster in PS I. Additional research is needed to identify any chloroplast-specific regulators that might mediate Fe/S protein biogenesis in higher-plant chloroplasts.

Acknowledgments

The preparation of this review was supported by grants from NSF (MCB-0117079) and USDA (2005-35318-15284) to JHG.

References

Abdel-Ghany SE, Ye H, Garifullina GF, Zhang L, Pilon-Smits EAH and Pilon M (2005) Iron–sulfur cluster biogenesis in chloroplasts. Involvement of the scaffold protein CpIscA. Plant Physiol 138: 161–172

Agar JN, Zheng L, Cash VL and Dean DR (2000) Role of the IscU protein in iron–sulfur cluster biosynthesis: IscS-mediated assembly of a [Fe2–S2] cluster in IscU. J Am Chem Soc 122: 2136–2137

Antonkine ML, Bentrop D, Bertini I, Luchinat C, Shen G, Bryant DA, Stehlik D and Golbeck JH (2000) Paramagnetic H^1 NMR spectroscopy of the reduced, unbound Photosystem I subunit PsaC: sequence specific assignment of contact-shifted resonances and identification of mixed- and equal-valence Fe–Fe pairs in [4Fe–4S] centers F_A^- and F_B^-. J Biol Inorg Chem 5: 381–392

Antonkine ML, Liu G, Bentrop D, Bryant DA, Bertini I, Luchinat C, Golbeck JH and Stehlik D (2002) Solution structure of the bound, oxidized photosystem I subunit PsaC, containing [4Fe–4S] clusters F_A and F_B: a conformational change occurs upon binding to Photosystem I. J Biol Inorg Chem 7: 461–472

Balasubramanian R, Shen G, Bryant DA and Golbeck, JH (2006) Regulatory roles for IscA and SufA in iron homeostasis and redox stress responses in the cyanobacterium *Synechococcus* sp. strain PCC 7002. J Bacteriol 188: 3182–3191

Behshad E, Parkin SE and Bollinger JM (2004) Mechanism of cysteine desulfurase Slr0387 from *Synechocystis* sp. PCC 6803: kinetic analysis of cleavage of the persulfide intermediate by chemical reductants. Biochemistry 43: 12220–12226

Beinert H and Kiley PJ (1999) Fe/S proteins in sensing and regulatory functions. Curr Opin Chem Biol 3: 152–157

Beinert H, Kennedy CD and Stout CD (1996) Aconitase as iron–sulfur protein, enzyme and iron-regulatory protein. Chem Rev 96: 2335–2373

Beinert H, Holm RH and Münck E (1997) Iron–sulfur clusters: nature's modular, multipurpose structures. Science 277: 653–659

Bilder PW, Ding H and Newcomer ME (2004) Crystal structure of the ancient, Fe-S scaffold IscA reveals a novel protein fold. Biochemistry 43: 133–139

Brettel K and Leibl W (2001) Electron transfer in photosystem I. Biochim Biophys Acta 1507: 100–114

Choudens SO, Nachin L, Sanakis Y, Loiseau L, Barras F and Fontecave M (2003) SufA from *Erwinia chrysanthemi*. Characterization of a scaffold protein required for iron–sulfur cluster assembly. J Biol Chem 278: 17993–18001

Clausen T, Kaiser JT, Steegborn C, Huber R and Kessier D (2000) Crystal structure of the cystine C-S lyase from *Synechocystis*: stabilization of cysteine persulfide for FeS cluster biosynthesis. Proc Natl Acad Sci USA 97: 3856–3861

Cupp-Vickery JR, Urbina H and Vickery LE (2003) Crystal structure of IscS, a cysteine desulfurase from *Escherichia coli*. J Mol Biol 330: 1049–1059

Cupp-Vickery JR, Silberg J, Ta DT and Vickery LE (2004a) Crystal structure of IscA, an iron–sulfur cluster assembly protein from *Escherichia coli*. J Mol Biol 338: 127–137

Cupp-Vickery JR, Peterson JC, Ta DT and Vickery LE (2004b) Crystal structure of the molecular chaperone HscA substrate binding domain complexed with the IscU recognition peptide ELPPVKIHC. J Mol Biol 342: 1265–1278

Dean DR, Bolin JT and Zheng L (1993) Nitrogenase metalloclusters: structures, organization, and synthesis. J Bacteriol 175: 6737–6744

Douglas SE and Penny SL (1999) The plastid genome of the cryptophyte alga, *Guillardia theta*: complete sequence and conserved synteny groups confirm its common ancestry with red algae. J Mol Evol 48: 236–244

Drapier JC (1997) Interplay between NO and [Fe–S] clusters: relevance to biological systems. Methods 11: 319–329

Duff JLC, Breton JLJ, Butt JN, Armstrong FA and Thomson AJ (1996) Novel redox chemistry of the [3Fe–4S] clusters: electrochemical characterization of all-Fe(II) form of the [3Fe–4S] cluster generated reversibly in various proteins and its spectroscopic investigation in *Sulfolobus acidocaldarius* ferredoxin. J Am Chem Soc 118: 8593–8603

Duin EC, Lafferty ME, Crouse BR, Allen RM, Sanyal I, Flint DH and Johnson MK (1997) [2Fe–2S] to [4Fe–4S] cluster conversion in *Escherichia coli* biotin synthase. Biochemistry 36: 11811–11820

Emanuelsson O and von Heijne G (2001) Prediction of organellar targeting signals. Biochim Biophys Acta 1541: 114–119

Flint DH (1996) *Escherichia coli* contains a protein that is homologous in function and N-terminal sequence to the protein encoded by the *nifS* gene of *Azotobacter vinelandii* and that can participate in the synthesis of the Fe/S cluster of dihydroxy-acid dehydratase. J Biol Chem 271: 16068–16074

Frazzon J and Dean DR (2002) Biosynthesis of the nitrogenase iron-molybdenum-cofactor from *Azotobacter vinelandii*. Met Ions Biol Syst 39: 163–186

Frazzon J and Dean DR (2003) Formation of iron–sulfur clusters in bacteria: an emerging field in biological chemistry. Curr Opin Chem Biol 7: 166–173

Frazzon J, Fick JR and Dean DR (2002) Biosynthesis of iron–sulphur clusters is a complex and highly conserved process. Biochem Soc Trans 30: 680–685

Fujii T, Maeda M, Mihara H, Kurihara T, Esaki N and Hata Y (2000) Structure of a NifS homologue: X-ray structure analysis of CsdB, an *Escherichia coli* counterpart of mammalian selenocysteine lyase. Biochemistry 39: 1263–1273

Gaudu P and Weiss B (1996) SoxR, a [2Fe–2S] transcription factor, is active only in its oxidized form. Proc Natl Acad Sci USA 93: 10094–10098

Gerber J and Lill R (2002) Biogenesis of iron–sulfur proteins in eukaryotes: components, mechanism and pathology. Mitochondria 2: 71–86

Glockner G, Rosenthal A and Valentin K (2003) The structure and gene repertoire of an ancient red algal plastid genome. J Mol Evol 51: 382–390

Golbeck JH (1994) Photosystem I in cyanobacteria. In: Bryant DA (ed) The Molecular Biology of Cyanobacteria, pp 319–360. Kluwer Academic Publishers, Dordrecht

Golbeck JH (1995) Resolution and reconstitution of Photosystem I. In: Song PS and Horspools WM (eds) CRC Handbook of Organic Photochemistry and Photobiology, pp. 1407–1419. CRC Press, Boca Raton

Golbeck JH (1999) A comparative analysis of the spin state distribution of *in vivo* and *in vitro* mutants of PsaC. A biochemical argument for the sequence of electron transfer in Photosystem I as $F_X \rightarrow F_A \rightarrow F_B \rightarrow$ ferredoxin/flavodoxin. Photosynth Res 61: 107–149

Goldsmith-Fischman S, Kuzin A, Edstrom WC, Benach J, Shastry R, Xiao R, Acton TB, Honig B, Montelione GT and Hunt JF (2004) The SufE sulfur-acceptor protein contains a conserved core structure that mediates interdomain interactions in a variety of redox protein complexes. J Mol Biol 344: 549–565

Hidalgo EH, Ding G and Demple B (1997) Redox signal transduction via iron–sulfur clusters in the SoxR transcription activator. Trends Biochem Sci 22: 207–210

Hjorth E, Hadfi K, Zauner S and Maier UG (2005) Unique genetic compartmentalization of the SUF system in cryptophytes and characterization of a SufD mutant in *Arabidopsis thaliana*. FEBS Lett 579: 1129–1135

Hoff KG, Silberg JJ and Vickery LE (2000) Interaction of the iron–sulfur cluster assembly protein IscU with the Hsc66/Hsc20 molecular chaperone system of *Escherichia coli*. Proc Natl Acad Sci USA 97: 7790–7795

Jacobson MR, Cash VL, Weiss MC, Laird NF, Newton WE and Dean DR (1989) Biochemical and genetic analysis of the NifUSVWZM cluster from *Azotobacter vinelandii*. Mol Gen Genet 219: 49–57

Johnson MK (1998) Iron–sulfur proteins: new roles for old clusters. Curr Opin Chem Biol 2: 173–181

Johnson D, Dean DR, Smith AD and Johnson MK (2005) Structure, function and formation of biological iron–sulfur clusters. Annu Rev Biochem 74: 247–281

Jordan P, Fromme P, Witt HT, Klukas O, Saenger W and Krauβ N (2001) Three-dimensional structure of cyanobacterial photosystem I at 2.5 Å resolution. Nature 411: 909–917

Kaiser JT, Clausen T, Bourenkow GP, Bartunik HD, Steinbacher S and Huber R (2000) Crystal structure of a NifS-like protein from *Thermotoga maritime*: implications for iron sulfur cluster assembly. J Mol Biol 297: 451–464

Kato S, Mihara H, Kurihara T, Takahashi Y, Tokumoto U, Yoshimura T and Esaki N (2002) Cys-328 of IscS and Cys-63 of IscU are the sites of disulfite bridge formation in a covalently bound IscS/IscU complex: implications for the mechanism of iron–sulfur cluster assembly. Proc Natl Acad Sci USA 99: 5948–5952

Kaut A, Lange H, Diekert K, Kispal G and Lill R (2000) Isa1p is a component of the mitochondrial machinery for maturation of cellular iron–sulfur proteins and requires conserved cysteine residues for function. J Biol Chem 275: 15955–15961

Khoroshilova N, Popescu C, Munck E, Beinert H, Kiley PJ (1997) Iron–sulfur cluster disassembly in the FNR protein of *Escherichia coli* by O_2: [4Fe–4S] to [2Fe–2S] conversion with loss of biological activity. Proc Natl Acad Sci USA 94: 6087–6092

Kowallik KV, Stobe B, Schaffran I, Kroth-Pancic P and Freier U (1995) The chloroplast genome of a chlorophyll $a + c$-containing alga, *Odontella sinensis*. Plant Mol Biol Rep 13: 336–342

Krebs C, Agar JN, Smith AD, Frazzon J, Dean DR, Huynh BH and Johnson MK (2001) IscA, an alternate scaffold for Fe/S cluster biosynthesis. Biochemistry 40: 14069–14080

Kushnir S, Babiyachuk E, Storozhenko S, Davey M, Papenbrock J, De Rycke RR, Engler G, Stephan U, Lange H, Kispal G, Lill R and Montagu MV (2001) A mutation of the mitochondrial ABC transporter Sta1 leads to dwarfism and chlorosis in the *Arabidopsis* mutant *Starik*. Plant Cell 13: 89–100

Lang T and Kesseler D (1999) Evidence for cystine persulfide as reaction product of L-cyst(e)ine C-S-lyase (C-DES) from *Synechocystis*. Analysis using cystine analogues and recombinant C-DES. J Biol Chem 274: 189–195

Léon S, Touraine B, Briat JF and Lobreaux. S (2002) The AtNFS2 gene from *Arabidopsis thaliana* encodes a NifS-like plastidial cysteine desulphurase. Biochem J 366: 557–564

Léon S, Touraine B, Ribot C, Briat JF and Lobreaux S (2003) Iron–sulfur cluster assembly in plants: distinct NFU proteins in mitochondria and plastids from *Arabidopsis thaliana*. Biochem J 371: 823–830

Lezhneva L, Amann K and Meurer J (2004) The universally conserved HCF101 protein is involved in assembly of [4Fe–4S]-cluster-containing complexes in *Arabidopsis thaliana* chloroplasts. Plant J 37: 174–185

Li H, Theg SM, Bauerle CM and Keegstra K (1990) Metal-ion-center assembly of ferredoxin and plastocyanin in isolated chloroplasts. Pro Natl Acad Sci USA 87: 6748–6752

Lill R and Kispal G (2000) Maturation of cellular Fe/S proteins: the essential function of mitochondria. Trends Biochem Sci 25: 352–356

Lill R and Mühlenhoff U (2005) Iron–sulfur-protein biogenesis in eukaryotes. Trends Biochem Sci 30: 133–141

Lima CD (2002) Analysis of the *E. coli* NifS CsdB protein at 2.0 Å reveals the structure basis for perselenide and persulfide intermediate formation. J Mol Biol 315: 1199–1208

Loiseau L, Ollagnier-De-Choudens S, Nachin L, Fonteave M and Barras F (2003) Biogenesis of Fe/S cluster by the bacterial Suf system. SufS and SufE form a new type of cysteine desulfurase. J Biol Chem 278: 38352–38359

Malkin R and Rabinowitz J (1966) The reconstitution of Clostridial ferredoxin. Biochem Biophys Res Commun 23: 822–827

Martens EC, Gawronski-salerno J, Vokal DL, Pellitteri MC, Menard ML and Goodrich-Blair H (2003) *Xenorhabdus nematophila* required an intact *iscRSUA-hscBA-fdx* operon to colonize *Steinernema carpocapsae* Nematodes. J Bacteriol 185: 3678–3682

Masclaux C and Experts D (1995) Signalling potential of iron in plant microbe interactions: the pathogenic switch of iron transport in *Erwinia chrysanthemi*. Plant J 7: 121–128

Mehari TK, Parrett G, Warren PV and Golbeck JH (1991) Reconstitution of the iron–sulfur clusters in the isolated F_A/F_B protein: EPR spectral characterization of same-species and cross-species Photosystem I complexes. Biochim Biophys Acta 1056: 139–148

Mihara H and Esaki N (2002) Bacterial cysteine desulfurase: their function and mechanisms. Appl Microbiol Biotechnol 60: 12–23

Mihara K, Maeda M, Fujii T, Kurihara T, Hata Y and Esaki N (1999) A *nifS*-like gene, *csdB*, encodes an *Escherichia coli* counterpart of mammalian slenocysteine lyase. Gene cloning, purification, characterization and preliminary X-ray crystallographic studies. J Biol Chem 274: 14768–14772

Mihara H, Kato S-I, Lacouriere GM, Stadtman TC, Kennedy RA, Kurihara T, Tokumoto U, Takahashi Y and Esaki N (2002) The *iscS* gene is essential for the biosynthesis of 2-selenouridine in tRNA and selenocysteine-containing formate dehydrogenase H. Proc Natl Acad Sci USA 99: 6679–6683

Møller SG, Kunkel T and Chau NH (2001) A plastidic ABC protein involved in intercompartmental communication of light signaling. Genes Dev 15: 90–103

Morimoto K, Nishio K and Nakai M (2002) Identification of a novel prokaryotic HEAT-repeats-containing protein which interacts with a cyanobacterial IscA homolog. FEBS Lett 519: 123–127

Mühlenhoff U and Lill R (2000) Biogenesis of iron–sulfur proteins in eukaryotes: a novel task of mitochondria that is inherited from bacteria. Biochim Biophys Acta 1459: 370–382

Nachin L, Hassouni M, Loiseau L, Expert LD and Barras F (2001) SoxR-dependent response to oxidative stress and virulence of *Erwinia chrysanthemi*: the key role of SufC, an orphan ABC ATPase. Mol Microbiol 39: 960–972

Nachin L, Loiseau L, Expert LD and Barras F (2003) SufC: an unorthodox cytoplasmic ABC/ATPase required for [Fe/S] biogenesis under oxidative stress. EMBO J 22: 427–437

Nakamura M, Saeki K and Takahashi Y (1999) Hyperproduction of recombinant ferredoxins in *Escherichia coli* by co-expression of the ORF1–ORF2–*iscS–iscU–iscA–hscB–hscA–fdx*--ORF3 gene cluster. J Biochem 126: 10–18

Natarajan K and Cowan JA (1997) Identification of a key intermediate of relevance to iron–sulfur cluster biosynthesis. Mechanism of cluster assembly and implication for protein folding. J Am Chem Soc 119: 4082–4083

Nishio K and Nakai M (2000) Transfer of iron–sulfur cluster from NifU to apoprotein. J Biol Chem 275: 22615–22618

Ohta N, Matsuzaki M, Misumi O, Miyagishima SY, Nozaki H, Tanaka K, Shin-I T, Kohara Y and Kuroiwa T (2003) Complete sequence and analysis of the plastid genome of the unicellular red alga *Cyanidioschyzon merolae*. DNA Res 10: 67–77

Ollagnier-de-Choudens S, Mattioli T, Takahashi Y and Fontecave M (2001) Iron–sulfur cluster assembly. Characterization of IscA and evidence for a specific and functional complex with ferredoxin. J Biol Chem 276: 22604–22607

Outten FW, Wood MJ, Munoz FM and Storz G (2003) The SufE protein and the SufBCD complex enhance SufS cysteine desulfurase activity as part of a sulfur transfer pathway for Fe/S cluster assembly in *E. coli.* J Biol Chem 278: 45713–45719

Patzer SI and Hantke K (1999) SufS is a NifS-like protein, and SufD is necessary for stability of the [2Fe–2S] FhuF protein in *Escherichia coli*. J Bacteriol 181: 3307–3309

Pilon-Smits EA, Garifullina GF, Abdel-Ghany S, Kato S, Mihara H, Hale KL, Burkhead J, Esaki N, Kurihara T and Pilon M (2002) Characterization of a NifS-like chloroplast protein from *Arabidopsis*. Implications for its role in sulfur and selenium metabolism. Plant Physiol 130: 1309–1318

Pomposiello PJ and Demple B (2001) Redox-operated genetic switches: the SoxR and OxyR transcription factors. Trends Biotechnol 19: 109–114

Ramelot TA, Cort JR, Goldsmith-Fischman S, Kornhaber GJ, Xiao R, Shastry R, Acton TB, Honig B, Montelione GT and Kennedy MA (2004) Solution NMR structure of the iron–sulfur cluster assembly protein U (IscU) with zinc bound at the active site. J Mol Biol 344: 567–583

Rangachari K, Davis CT, Eccleston JF, Hirst EMA, Saldanha JW, Strath M and Wilson RJM (2002) SufC hydrolyzes ATP and interacts with SufB from *Thermotoga maritime*. FEBS Lett 514: 225–228

Reith ME and Munholland J (1995) Complete nucleotide sequence of the *Porphyra purpurea* chloroplast genome. Plant Mol Biol Rep 13: 333–335

Sakuragi Y, Zybailov B, Shen G, Bryant DA, Golbeck JH, Diner BA, Karygina I, Pushkar Y and Stehlik D. (2005) Recruitment of a foreign quinone into the A_1 site of Photosystem I. Characterization of a *menB rubA* double deletion mutant in *Synechococcus* sp. PCC 7002 devoid of F_X, F_A, and F_B and containing plastoquinone or exchanged 9,10-anthraquinone. J. Biol Chem 280: 12371–12381

Schilke B, Voisine H and Craig E (1999) Evidence for a conserved system for iron metabolism in the mitochondria of *Saccharomyces cerevisiae*. Proc Natl Acad Sci USA 96: 10206–10211

Schubert WD, Klukas O, Krauß N and Saenger W (1997) Photosystem I of *Synechococcus elongatus* at 4 Å resolution: comprehensive structure analysis. J Mol Biol 272: 741–769

Schürmann P and Buchanan BB (2001) The structure and function of the ferredoxin/thioredoxin system in photosynthesis. In: Aro EM and Andersson B (eds) Regulation of Photosynthesis, pp 331–361. Kluwer Academic Publishers, The Netherlands

Schwartz CJ, Djaman O, Imlay JA and Kiley PJ (2000) The cysteine desulfurase, IscS, has a major role in *in vivo* Fe/S cluster formation in *Escherichia coli*. Proc Natl Acad Sci USA 97: 9009–9014

Schwartz CJ, Giel JL, Patschkowski T, Luther TC, Ruzicka FJ, Beinert H and Kiley PJ (2001) IscR, an Fe/S cluster-containing transcription factor, represses expression of *Escherichia coli* genes encoding Fe/S cluster assembly proteins. Proc Natl Acad Sci USA 98: 14895–14900

Shen G and Bryant DA (1995) Characterization of a *Synechococcus* sp. strain PCC 7002 mutant lacking Photosystem I. Protein assembly and energy distribution in the absence of the Photosystem I reaction center core complex. Photosynth Res 44: 41–53

Shen G, Boussiba S and Vermaas WFJ (1993) *Synechocystis* sp. PCC 6803 strains lacking Photosystem I and phycobilisome function. Plant Cell 5: 1853–1863

Shen G, Zhao J, Reimer SK, Antonkine ML, Cai Q, Weiland SM, Golbeck JH and Bryant DA (2002a) Assembly of Photosystem I. I. Inactivation of the *rubA* gene encoding a membrane-associated rubredoxin in the cyanobacterium S*ynechococcus* sp. PCC 7002 causes a loss of photosystem I activity. J Biol Chem 277: 20343–20354

Shen G, Antonkine ML, van der Est A, Vassiliev IR, Brettel K, Bittl R, Zech SG, Zhao J, Stehlik D, Bryant DA and Golbeck JH (2002b) Assembly of Photosystem I. II. Rubredoxin is required for the *in vivo* assembly of F_X in *Synechococcus* sp. PCC 7002 as shown by optical and EPR spectroscopy. J Biol Chem 277: 20355–20366

Shen G, Balasubramanian R, Wang T, Tirupati B, Bollinger JM, Golbeck JH and Bryant DA (2004) Functional genomics of genes for the biogenesis of Fe/S proteins in cyanobacteria. In: van der Est R and Bruce D (eds) Photosynthesis: Fundamental Aspects to Global Perspectives, Vol II, pp 882–884. Alliance Communication Group Publisher

Silberg JJ, Hoff KG, Tapley TL and Vickery LE (2001) The Fe/S assembly protein IscU behaves as a substrate for the molecular chaperone Hsc66 from *Escherichia coli*. J Biol Chem 276: 1696–1700

Smith AD, Agar JN, Johnson KA, Frazzon J, Amster IJ, Dean DR, and Johnson MK (2001) Sulfur transfer from IscS to IscU: the first step in iron–sulfur cluster biosynthesis. J Am Chem Soc 123: 11103–11104

Stirewalt VL, Michalowski CB, Löffelhardt W, Bohnert HJ and Bryant DA (1995) Nucleotide sequence of the cyanelle genome from *Cyanophora paradoxa*. Plant Mol Biol Rep 13: 327–332

Stöckel J and Oelmüller R (2004) A novel protein for photosystem I biogenesis. J Biol Chem 279: 10243–10251

Tachezy J, Sanchez LB and Muller M (2001) Mitochondrial type iron–sulfur cluster assembly in the amitochondriate eukaryotes *Trichomonas vaginalis* and *Giardia intestinalis*, as indicated by the phylogeny of IscS. Mol Biol Evol 18: 1919–1928

Takahashi Y and Nakamura M (1999) Functional assignment of the ORF2–*iscR–iscS–iscU–iscA–hscBhscA–fdx*–ORF3 gene cluster involved in the assembly of Fe/S clusters in *Escherichia coli*. J Biochem 126: 917–926

Takahashi Y and Tokumoto U (2002) A third bacterial system for the assembly of iron–sulfur clusters with homologs in archaea and plastids. J Biol Chem 277: 28380–38383

Takahashi Y, Mitsui A and Matsubara H (1986) Formation of the iron–sulfur cluster of ferredoxin in isolated chloroplasts. Proc Natl Acad Sci USA 83: 2434–2437

Takahashi Y, Mitsui A and Matsubara H (1991a) Formation of the iron–sulfur cluster of ferredoxin in lysed spinach chloroplasts. Plant Physiol 95: 97–103

Takahashi Y, Mitsui A, Fujita Y and Matsubara H (1991b) Roles of ATP and NADPH in formation of the Fe/S cluster of spinach ferredoxin. Plant Physiol 95: 104–110

Tirupati B, Vey JL, Drennan CL and Bollinger JM (2004) Kinetics and structural characterization of Slr0077/SufS, the essential cysteine desulfurase from *Synechocystis* sp. PCC 6803. Biochemistry 43: 12210–12219

Tokumoto U and Takahashi Y (2001) Genetic analysis of the *isc* operon in *Escherichia coli* involved in the biogenesis of cellular iron–sulfur proteins. J Biochem 130: 63–71

Tokumoto U, Nomura S, Minami Y, Mihara H, Kato S, Kurihara T, Esaki N, Kanazawa H, Matsubara H and Takahashi Y (2002) Network of protein–protein interactions among iron–sulfur cluster assembly proteins in *Escherichia coli*. J Biochem 131: 713–719

Touraine B, Boutin JP, Marion-Poll A, Briat JF, Peltier G and Lobreaux S (2004) Nfu2: a scaffold protein required for [4Fe–4S] and ferredoxin iron–sulfur cluster assembly in *Arabidopsis* chloroplasts. Plant J 40: 101–111

Vassiliev IR, Antonkine ML and Golbeck JH (2001) Iron–sulfur clusters in type I reaction centers. Biochim Biophys Acta 1507: 139–160

Vickery IE, Silberg JJ and Ta DT (1997) Hsc66 and Hsc20, a new heat shock cognate molecular chaperone system from *Escherichia coli*. Protein Sci 6: 1047–1056

Wang T, Shen G, Balasubramanian R, McIntosh L, Bryant DA and Golbeck JH (2004) The *sufR* gene (*sll0088* in *Synechocystis* sp. PCC 6803) functions as a repressor of the *sufBCDS* operon in iron–sulfur cluster biogenesis in cyanobacteria. J Bacteriol 186: 956–967

Wastl J, Duin EC, Iuzzolino L, Dörner W, Link T, Hoffmann S, Sticht H, Dau H, Lingelbach K and Maier UG (2000) Eukaryotically encoded and chloroplast-located rubredoxin is associated with photosystem II. J Biol Chem 275: 30058–30063

Watanabe S, Kita A and Miki K (2005) Crystal structure of atypical cytoplasmic ABC-ATPase SufC from *Thermus thermophilius* HB8. J Mol Biol 353: 1043–1054

Whitney SM and Andrews J (2001) Gene Bank Accession #AAF81679

Wilson RJM, Rangachari K, Saldanha JW, Rickman L, Buxton RS and Eccleston JF (2002) Parasite plastids: maintenance and functions. Phil Trans Res Soc Lond B 358: 155–164

Wollenberg M, Berndt C, Bill E, Schwenn JD and Seidler A (2003) A dimer of the FeS cluster biosynthesis protein IscA from cyanobacterial binds a [2Fe2S] cluster between two protomers and transfer it to [2Fe–2S] and [4Fe–4S] apo proteins. Eur J Biochem 270: 1662–1671

Xu X and Møller SG (2004) AtNAP7 is a plastidic SufC-like ATP-binding cassette/ATPase essential for Arabidopsis embryogenesis. Proc Natl Acad Sci USA 101: 9143–9148

Xu XM, Adams S, Chau NH and Møller SG (2005) AtNAP1 represents an atypical SufB protein in *Arabidopsis* plastids. J Biol Chem 280: 6648–6654

Yu J, Shen G, Wang T, Bryant DA, Golbeck JH and McIntosh L (2003) Suppressor mutations in the study of Photosystem I biogenesis: *sll0088* is a previously unidentified gene involved in reaction center accumulation in *Synechocystis* sp. strain PCC 6803. J Bacteriol 185: 3878–3887

Yu J, Vassiliev IR, Jung YS, Golbeck JH and McIntosh L (1997) Strains of *Synechocystis* sp. PCC 6803 with altered PsaC. J Biol Chem 272: 8032–8039

Yuvaniyama P, Agar JN, Cash VL, Johnson MK and Dean DR (2000) NifS-directed assembly of a transient [2Fe–2S] cluster within the NifU protein. Proc Natl Acad Sci USA 97: 599–604

Zheng L, White RH, Cash VL, Jack RF and Dean DR (1993) Cysteine desulfurase activity indicates a role for NIFS in metallocluster biosynthesis. Proc Natl Acad Sci USA 90: 2754–2758

Zheng L, Cash, VL, Flint DH and Dean DR (1998) Assembly of iron–sulfur clusters. Identification of an *iscSUA-hscBA-fdx* gene cluster from *Azotobacter vinelandii*. J Biol Chem 273: 13264–13272

Zheng M, Wang X, Temleton LJ, Smulski DR, LaRossa RA and Storz G (2001) DNA microarray-mediated transcriptional profiling of the *Escherichia coli* response to hydrogen peroxide. J Bacteriol 183: 4562–4570

Chapter 32

The Assembly of Photosystem I Reducing Site

Alexander Fish, Konstantin Kogan and Rachel Nechushtai*
Department of Plant Sciences and The Wolfson Centre for Applied Structural Biology, The Hebrew University of Jerusalem, The Edmond J. Safra Campus, Givat Ram, Jerusalem 91904, Israel

Summary

This chapter underlines the knowledge accumulated on the assembly of the reducing site of Photosystem I (PS I). A brief description of the biochemical and molecular characteristics of the reducing-site members, the peripheral, cytosol/stromal facing, PsaC, PsaD, and PsaE subunits is followed by their functional characterizations as individual subunits and as members of a cooperative entity. The main focus of the chapter is the current knowledge on the PsaC, PsaD, and PsaE assembly processes to form the fully functional "stromal ridge." The accepted scenario, in which a sequential assembly of the three subunits occurs, is described in detail. Accordingly, the formation of the "stromal ridge" initiates when the PsaC subunit associates with the PsaA–PsaB heterodimer that has already assembled in the thylakoids with its pigments and electron acceptors, including F_X. Concomitantly with, or right after the PsaC association, a set of interactions with the PsaA/PsaB heterodimer, is formed. The latter, and the subsequent binding of PsaD, impose conformation changes on the F_A and F_B iron–sulfur clusters of PsaC. The PsaD association with PS I is stabilized by its interactions with PsaC and with the PsaA/PsaB. The last subunit of the "stromal ridge" to assemble is PsaE which in the assembled-PS I complex maintains a structure that is very similar to the free/soluble PsaE. This currently accepted scenario describes the formation/development of the reducing site and not its steady-state maintenance. It relies on structural information of the free/soluble proteins before their assembly and their structures in the fully assembled-PS I, i.e., after the processes involved in their assembly has been accomplished. That means that we understand the beginning and end states. Information and knowledge on the dynamics of the assembly process, especially during steady-state turnover conditions, are still missing. This chapter highlights the known and accepted data as well as the issues and unanswered questions that still comprise the missing parts of the puzzle.

*Author for correspondence, email: rachel@vms.huji.ac.il

John H. Golbeck (ed): Photosystem I: The Light-Driven Plastocyanin:Ferredoxin Oxidoreductase, 549–569.

I. Introduction

The high resolution three-dimensional structure of Photosystem I (PS I) from a cyanobacterium (Jordan et al., 2001) and the recently reported structure of the holo-PS I from a higher plant (Ben-Shem et al., 2003), have proved that the core PS I complex subunits are organized into the following three subcompartments:

- Membranal core formed by PsaA/PsaB, each having 11 membrane-spanning helices, and the small subunits PsaI–PsaM each with at least one membrane transverse helix. This hydrophobic core, mainly PsaA/PsaB, binds all the photosynthetic pigments and most of the electron carriers (Vallon and Bogorad, 1993; Chitnis, 2001; Jordan et al., 2001).
- Luminal-oxidative site includes PsaF and PsaN. In plants and algae, PsaF has been shown to be involved in plastocyanin (PC) docking to PS I (Farah et al., 1995; Hibino et al., 1996; Hippler et al., 1996, 1997, 1998; see Hippler and Drepper, this volume, Chapter 29). In cyanobacteria, PsaF has been shown to contain a transmembranal helix and not to be involved in docking cytochrome c_6 to PS I (Chitnis et al., 1991; Fromme et al., 2001; Jordan et al., 2001).
- Reducing site includes the cytosol/stromal facing subunits PsaC, PsaD, and PsaE (Xu et al., 1994a,b) that are involved in the electron transfer (ET) from PS I to its electron acceptor ferredoxin (Fd) (Knaff and Hirasawa, 1991; Fromme et al., 2001) and/or flavodoxin (Fld) in cyanobacteria under specific conditions. These subunits, PsaC, PsaD, and PsaE, are homologous in all oxygenic PS I photosynthetic complexes. The three proteins have been shown to have a synergetic operation in carrying out the reducing-site function, i.e., ET to Fd and/or Fld. The two final electron carriers of PS I, namely the iron–sulfur (Fe/S) clusters – F_A and F_B, located in PsaC (Jordan et al., 2001), transfer the electrons to the water soluble Fd/Fld. The reducing-site subunits PsaD and PsaE have been shown to be involved in the docking of Fd (Zanetti and Merati, 1987; Cohen et al., 1993; Lelong et al., 1994; Xu et al., 1994a,b; Hanley et al., 1996; Barth et al., 1998) and that of Fld (Xu et al., 1994a,b; Mühlenhoff et al., 1996a,b; Nield et al., 2003), and in strengthening the binding of PsaC to PS I (Hanley et al., 1996). The detailed interaction of Fd with the reducing site of PS I has been studied in detail in recent years. We refer the readers to Sétif (2001) and Sétif et al. (2002).

The aim of the present article is to present events and steps involved in the assembly of the reducing-site subunits PsaC, PsaD, and PsaE, as individuals and as components that have to be bound together to jointly form the assembled site. The latter involves the formation of numerous contacts between the PsaC, PsaD, and PsaE subunits themselves and between these and other subunits of PS I, mainly the PsaA and PsaB heterodimer. These are extremely important to allow the formation of the reducing site in a way that secures the function of ET in the most efficient manner. In the last years the study of the assembly of the reducing-site subunits has entered into a new phase for two major reasons: First, the remarkable development of the structural biology knowledge of both the assembled-PS I and of different subunits of the reducing site in their free/soluble form before their integration into the thylakoids. Second, the assembly of the reducing-site proteins has greatly benefited from the implementation of genome sequencing and different genetic approaches. In recent years, the most significant insights into the reducing-site assembly have come from comparing the phenotype of mutants resulting from gene disruptions or site-directed mutagenesis in the reducing-site subunits of prokaryotes and eukaryotes. These approaches, together with the availability of *in vitro* expression and assembly assays, have paved the way for the refined studies of the assembly pathways and steps. In this chapter we will cover these recent developments and highlight the questions that are still open. The different issues of the reducing-site assembly as a whole and of its individual subunits, and their organization to a fully functional entity will be analyzed under what may be regarded as *formation/developmental* conditions. The questions yet to be answered lie in the different steps concerning the *steady-state* maintenance of the fully functional site; i.e., how does the maintenance of the site take place? How are the different subunits replaced when the PS I undergoes turnover? Is their assembly sequential or they assemble all together when the site is under its continuous maintenance (turnover)? i.e., is the assembly of each of the subunits an

Abbreviations: CCM – CO_2-concentrating mechanism; CD – circular dichroism; DCMU – 3-(3′,4′-dichlorophenyl)-1,1′-dimethyl urea; EPR – electron paramagnetic resonance; ET – electron transfer; Fe/S – iron–sulfur; Fd – ferredoxin; Fld – flavodoxin; FMN – flavin mononucleotide; FNR – Fd-NADP reductase; PC – plastocyanin; PS I – photosystem I; TPR – tetratrico peptide repeats.

```
M. laminosus          SHTVKIYDTCIGCTQCVRACPTDVLEMVPWDGCKAQQIASSPRTEDCVGCKRCETACPTD 60
S. elongatus          AHTVKIYDTCIGCTQCVRACPTDVLEMVPWDGCKAGQIASSPRTEDCVGCKRCETACPTD 60
Anabaena sp.          SHTVKIYDTCIGCTQCVRACPTDVLEMVPWDGCKAAQVASSPRTEDCVGCKRCETACPTD 60
Synechocystis sp.     SHSVKIYDTCIGCTQCVRACPLDVLEMVPWDGCKAAQIASSPRTEDCVGCKRCETACPTD 60
C. reinhardtii        AHIVKIYDTCIGCTQCVRACPLDVLEMVPWDGCKASQMASAPRTEDCVGCKRCETACPTD 60
S. oleracea           SHSVKIYDTCIGCTQCVRACPTDVLEMIPWDGCKAKQIASAPRTEDCVGCKRCESACPTD 60
                      :* ***************** *****:******* *:**:*************:*****

M. laminosus          FLSIRVYLGAETTRSMGLAY 80
S. elongatus          FLSIRVYLGAETTRSMGLAY 80
Anabaena sp.          FLSIRVYLGAETTRSMGLAY 80
Synechocystis sp.     FLSIRVYLGAETTRSMGLAY 80
C. reinhardtii        FLSVRVYLGSESTRSMGLSY 80
S. oleracea           FLSVRVYLWHETTRSMGLGY 80
                      ***:****  *:******.*
```

Fig. 1. Sequence alignment of the PsaC subunit from different photosynthetic organisms. PsaC from two thermophilic cyanobacteria: *Mastigocladus laminosus* and *Synechococcus elongatus*; two mesophilic cyanobacteria: *Anabaena* sp. PCC 7120 and *Synechocystis* sp. PCC 6803; the green alga *Chlamydomonas reinhardtii*; and the higher plant *Spinacia oleracea*, were aligned. Identical residues in the six PsaC proteins are indicated by an asterisk (*), highly similar residues are indicated by two dots (:), and similar by one point (.). Sequence alignment was made using ClustalW (Thompson et al., 1994).

independent process or is there a cooperative concert process?

These different topics will be discussed further after the description of the current knowledge on the reducing-site proteins and their function as individuals and as a part of a cooperative site.

II. The Composition of the Reducing Site: Protein Subunits and Co-Factors

As stated above, the three subunits that comprise the reducing site, PsaC, PsaD, and PsaE are highly homologous in all oxygenic photosynthetic organisms. The following information underlines the current knowledge on the important characteristics of each of these proteins.

A. The PsaC Subunit

Among the three reducing-site proteins, PsaC has the lowest molecular weight of about 9 kDa. PsaC is an extremely conservative protein; More than 84% identity and 92% homology exists between PsaC of different photosynthetic oxygenic organisms from cyanobacteria to higher plants (Fig. 1). In eukaryotic organisms, the *psaC* gene encoding the PsaC protein is chloroplast encoded. The localization of the *psaC* gene differs in the case of the chloroplast of vascular plants and that of cyanobacteria. In the former, it is cotranscribed with two adjacent *ndh* genes (Hayashida et al., 1987), whereas in the latter it is transcribed as a monocistronic mRNA in *Synechococcus* sp. PCC 7002 (Rhiel et al., 1992) and *Synechocystis* sp. PCC 6803 (Steinmuller, 1992).

The PsaC protein contains the two terminal electron carriers of PS I, namely the Fe/S clusters – F_A and F_B (Oh-oka et al., 1987, 1988; Wynn and Malkin, 1988), from which the electrons are transferred to the Fd and/or Fld. F_A has been identified as the cluster proximal to F_X of PsaA and PsaB (Vassiliev et al., 1998; Golbeck, 1999; Klukas et al., 1999a,b) and the ET sequence has been concluded to be $F_X \rightarrow F_A \rightarrow F_B \rightarrow$ Fd/Fld (Diaz-Quintana et al., 1998; Vassiliev et al., 1998, 2001; Fischer et al., 1999). The important function of PsaC in hosting the two final electron acceptors of PS I, and the relatively low molecular weight of the protein, may explain the high degree of conservation in its primary, secondary, and tertiary structures in all species.

B. The PsaD Subunit

PsaD is a ~16–18 kDa subunit that is involved in the docking of Fd to the "stromal ridge" formed by the reducing-site subunits. In eukaryotes, the PsaD encoding gene *psaD*, has been transferred to the nucleus and a transit/leader peptide of ~2–5 KDa has been added to its N-terminus. Hence, PsaD of eukaryotes is synthesized in the cytoplasm as a precursor that is targeted to the chloroplast by its leader/transit peptide. There, the leader peptide is cleaved by a stromal processing

```
M. laminosus          ------------------------------------------------------------
S. elongatus          ------------------------------------------------------------
Anabaena sp.          ------------------------------------------------------------
Synechocystis sp.     ------------------------------------------------------------
C. reinhardtii        ----------------MAVMMRTQAPAATRASSRVAVAARPAARRAVVVRAEAEAAPAAA 44
S. oleracea           MAMATQATLFSPSSLSSAKPIDTRLTTSFKQPSAVTFASKPASRHHSIRAAAAAEGKAAA 60

M. laminosus          -----------MAETLSGQT--PIFGGSTGGLLKKAEVEEKYAITWTSPKEQVFEMPTGG 47
S. elongatus          ------------TTLTGQP--PLYGGSTGGLLSAADTEEKYAITWTSPKEQVFEMPTAG 45
Anabaena sp.          -----------MAETLSGKT--PLFAGSTGGLLTKAVEEEKYAITWTSPKAQVFELPTGG 47
Synechocystis sp.     ------------TELSGQP--PKFGGSTGGLLSKANREEKYAITWTSASEQVFEMPTGG 45
C. reinhardtii        KKAAEKP--AWTVPTLNPDTPSPIFGGSTGGLLRKAQTEEFYVITWEAKKEQIFEMPTGG 102
S. oleracea           ATETKEAPKGFTPPELDPNTPSPIFAGSTGGLLRKAQVEEFYVITWESPKEQIFEMPTGG 120
                                    *  ..  * :.*******  *  ** *.*** : . *:**:**.*

M. laminosus          AAKMRQGQNLLYLARKEQCIALGS-QLRRL---KITDYKIYRIYPNGETAYIHPADGVFP 103
S. elongatus          AAVMREGENLVYFARKEQCLALAAQQLRPR---KINDYKIYRIFPDGETVLIHPKDGVFP 102
Anabaena sp.          AATMHEGENLLYIARKEYGIALGG-QLRKF---KITNYKIYRILPSGETTFIHPADGVFP 103
Synechocystis sp.     AAIMNEGENLLYLARKEQCLALGT-QLRTKFKPKIQDYKIYRVYPSGEVQYLHPADGVFP 104
C. reinhardtii        AAIMRQGPNLLKFGKKEQCLALTT-QLRNK---FKLTPCFYRVFPDGKVQYLHPADGVYP 158
S. oleracea           AAIMREGPNLLKLARKEQCLALGT-RLRSK---YKIKYQFYRVFPSGEVQYLHPKDGVYP 176
                      ** *.:* **: :.:**  :**   :**           :**: *.*:.  :** ***:*

M. laminosus          EKVNPGRQKVRYNDRRIGQNPDPAKLKFSGVATYDAPNP 142
S. elongatus          EKVNKGREAVNSVPRSIGQNPNPSQLKFTGKKPYDP--- 138
Anabaena sp.          EKVNAGREKVRFNARSIGENPNPSQVKFSGKATYDA--- 139
Synechocystis sp.     EKVNEGREAQGTKTRRIGQNPEPVTIKFSGKAPYEV--- 140
C. reinhardtii        EKVNAGRVGANQNMRRIGQNVNPIKVKFSGRMMSPAEI- 196
S. oleracea           EKVNPGRQGVGLNMRSIGKNVSPIEVKFTGKQPYDL--- 212
                      **** **       * **:* .*  :**:*
```

Fig. 2. Sequence alignment of the PsaD subunit from different photosynthetic organisms. PsaD from four cyanobacteria: *Mastigocladus laminosus*, *Synechococcus elongatus*, *Anabaena* sp. PCC 7120, and *Synechocystis* sp. PCC 6803; and the precursor of PsaD (pre-PsaD) from the green alga *Chlamydomonas reinhardtii* and the higher plant *Spinacia oleracea*, were aligned. Identical residues of the six proteins are indicated by an asterisk (*), highly similar residues are indicated by two dots (:), and similar residues by one point (.). Sequence alignment was made using ClustalW (Thompson et al., 1994).

peptidase (Cohen and Nechushtai, 1992), thus allowing to obtain the mature-PsaD which is the form found in the assembled-PS I complex within the thylakoid membranes (Minai et al., 1996). The mature part of PsaD shows a 49% identity and a 70% similarity between different organisms (Fig. 2). PsaD does not contain any electron acceptor, i.e., it does not participate in the ET process, nevertheless; chemical cross-linking experiments have revealed a direct interaction between PsaD and Fd (Zanetti and Merati, 1987; Hirasawa et al., 1988; Lelong et al., 1994), thereby PsaD is considered as the docking site for Fd in the reducing site. In addition, PsaD has been proven to be a key subunit in the assembly, stability, and functionality of PS I. It is the first nuclear-encoded subunit to accumulate in the thylakoid membranes during the greening of etiolated seedlings (Nechushtai and Nelson, 1985; Lotan et al., 1993). The other nuclear-encoded PS I subunits accumulated in the thylakoids in a sequential manner with PsaD being the first nuclear-encoded subunit to be detected. At the level of mRNA accumulation, it was reported that the expression of the *psaD* gene shows minor circadian rhythm and that red light as well as blue light mediate *psaD* gene expression (Giuliano et al., 1988; Oelmuller et al., 1989). On the basis of experiments in transgenic tobacco it was concluded that an intron sequence contributes to the light-dependent expression of the *psaD* gene (Flieger et al., 1994; Bolle et al., 1996). Moreover, only in the light, the PsaD mRNA was found associated with the polysomal fraction and the PsaD polypeptide is accumulated (Lotan et al., 1993). Additional experiments with photosynthetic electron transport inhibitor 3-(3′,4′-dichlorophenyl)-1,1′-dimethyl urea (DCMU) demonstrated that both levels of regulation are controlled by diverse light quality-dependent redox signals from the plastids during photosystem stoichiometry adjustment (Pfannschmidt et al., 2001; Sherameti et al., 2002).

```
M. laminosus          ------------------------------------------------------------
S. elongatus          ------------------------------------------------------------
Anabaena sp.          ------------------------------------------------------------
Synechocystis sp.     ------------------------------------------------------------
C. reinhardtii        MQALSSRVNIAA----------KPQRAQRLVVR-AEEVKAAPKKE-------------- 34
S. oleracea           MASIASSVAVRLGLTQVLPNKNFSSPRSTRLVVRAAEEAAAAPAAASPEGEAPKAAAKPP 60

M. laminosus          --MVQRGSKVRILRPESYWFQDIGTVASIEQGGTIRYPVIVRFDKVNY-------AGVNT 51
S. elongatus          ---VQRGSKVKILRPESYWYNEVGTVASVDQTPGVKYPVIVRFDKVNYTGYSGSASGVNT 57
Anabaena sp.          --MVQRGSKVRILRPESYWFQDVGTVASVDQSG-IKYPVIVRFDKVNY-------AGINT 50
Synechocystis sp.     --ALNRGDKVRIKRTESYWYGDVGTVASVEKS-GILYPVIVRFDRVNYNGFSGSASGVNT 57
C. reinhardtii        -VGPKRGSLVKILRPESYWFNQVGKVVSVDQS-GVRYPVVVRFENQNY-------AGVTT 85
S. oleracea           PIGPKRGSKVRIMRKESYWYKGVGSVVAVDQDPKTRYPVVVRFNKVNY-------ANVST 113
                         :**. *:* * ****:  :*.*.::::     ***:***:. **       :.:.*

M. laminosus          NNFAEYELVEVEAPKAKPKK 71
S. elongatus          NNFALHEVQEVAPP-KKGK- 75
Anabaena sp.          NNFAVDELIEVEAPKAKAKK 70
Synechocystis sp.     NNFAENELELVQAA-AK--- 73
C. reinhardtii        NNYALDEVVAAK-------- 97
S. oleracea           NNYALDEIQEVA-------- 125
                      **:*  *:  . ... . ..
```

Fig. 3. Sequence alignment of the PsaE subunit from different photosynthetic organisms. PsaE from four cyanobacteria: *Mastigocladus laminosus*, *Synechococcus elongatus*, *Anabaena* sp. PCC 7120, and *Synechocystis* sp. PCC 6803; and the precursor PsaE (pre-PsaE) from the green alga *Chlamydomonas reinhardtii* and the higher plant *Spinacia oleracea*, were aligned. Identical residues of the six proteins are indicated by an asterisk (*), highly similar residues are indicated by two dots (:), and similar residues by one point (.). Sequence alignment was made using ClustalW (Thompson et al., 1994).

PsaD has also been shown to be essential for the stable assembly of PsaC and PsaE into the PS I complex (Zhao et al., 1990; Li et al., 1991; Chitnis et al., 1996; Naver et al., 1996). In the cyanobacteria *Synechocystis* sp. PCC 6803, the photoautotrophic growth of a mutant strain lacking PsaD has been found to be much slower than that of wild-type cells (Chitnis et al., 1989).

C. The PsaE Subunit

PsaE is a ~8–10 KDa subunit that together with PsaD has been shown to shield the PsaC subunit (Jordan et al., 2001). PsaE has been shown to be involved in the docking of Fd (Kruip et al., 1997) and Fld (Mühlenhoff et al., 1996a,b) and in strengthening the binding of PsaC to PS I (Weber and Strotmann, 1993; Hanley et al., 1996; Klukas et al., 1999a,b). In eukaryotes, as for PsaD, the PsaE encoding gene, *psaE*, has been transferred to the nucleus and a transit/leader peptide of ~5 kDa has been added to its N-terminus. PsaE of eukaryotes is synthesized in the cytoplasm as a precursor that undergoes import to the chloroplast and processing by a stromal processing peptidase (Chitnis et al., 1995) to obtain the mature form detected in the assembled-PS I. The mature part of PsaE shows a 49% identity and 85% similarity between different organisms, thus making this protein, like PsaD, a much less conservative one than PsaC (Fig. 3).

PsaE has been shown to have specific interactions with Fd only in barley (Rousseau et al., 1993). In cyanobacteria, PsaE is postulated to be involved in the docking and binding of both Fd and Fld to PS I (Mühlenhoff et al., 1996a,b; Meimberg et al., 1998). PsaE has also been shown to be involved in the cyclic electron flow occurring around the PS I complex both *in vivo* (L. Yu et al., 1993) and *in vitro* (Barth et al., 1998). This function is directly related to the process known in cyanobacteria as CO_2—concentrating mechanism (CCM), thus the energy required for HCO_3^- uptake is supplied by the PsaE — mediated cyclic electron pathway (Xu et al., 1994a,b).

III. The Function of the Reducing Site: ET from PS I to Fd/Fld

In the PS I reducing site the ET to Fd/Fld occurs. Both these electron acceptors, Fd and Fld, can sustain cyclic as well as linear electron flow (Sétif, 2001; Sétif et al., 2002). From them, the electrons are transferred to a number of soluble enzymes involved in different metabolic reactions. Due to their reduction properties,

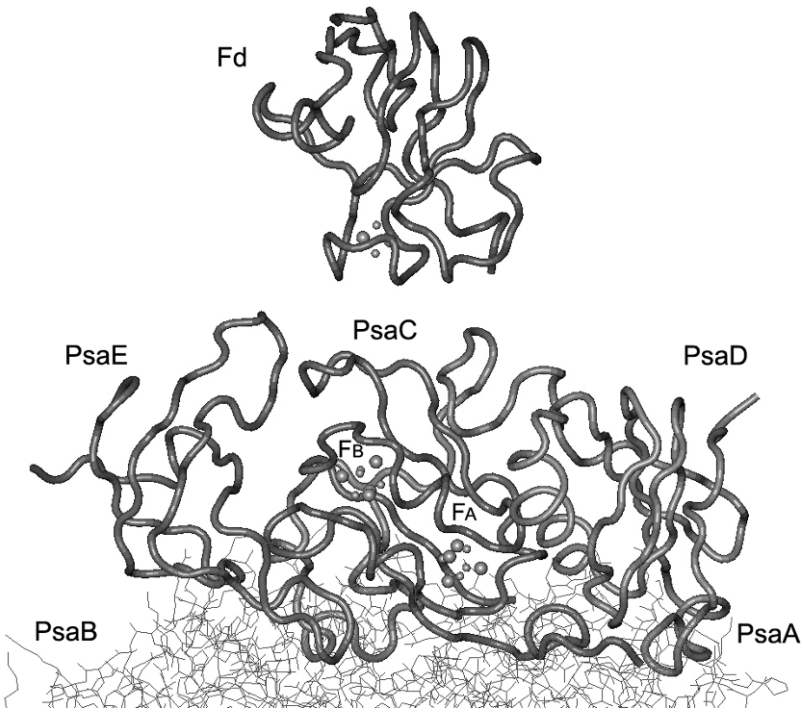

Fig. 4. Structural representation of the subunits of PS I reducing site and their electron acceptor, Fd. See Color Plate 13, Fig. 1.

Fd/Fld serve as the electron donor in various important reactions such as $NADP^+$ reduction, where Fd-NADP reductase (FNR) is the active enzyme, carbon assimilation, nitrite reduction for nitrogen assimilation, sulfite reduction, glutamate synthesis, and thioredoxin reduction for metabolic regulation (Knaff and Hirasawa, 1991; Knaff, 1996; see Hase et al., this volume, Chapter 28).

The PS I reducing site is composed of PsaC, PsaD, and PsaE that together form a ridge on the stromal site of PS I, where the PsaC is located between the PsaD and PsaE subunits (Kruip et al., 1997). The three proteins function together to execute the ET from PS I to its acceptor(s). Interactions of the reducing-site subunits with Fd/Fld have been studied for the past two decades (for review see Sétif et al., 2002). These interactions are basically between four proteins, two of which, PsaD and PsaE are very positively charged, i.e., electrostatic interactions probably enable the docking and association of the negatively overall charged Fd/Fld to the reducing-site subunit PsaC from where it has to receive the electrons. Figure 4 indicates the four players in these interactions – PsaC, PsaD, PsaE, and Fd.

To allow the function of the reducing site to be accomplished, ET from PS I to Fd/Fld, three different steps need to take place:

1. Association/docking/binding of Fd/Fld to the reducing site.

2. ET from the PsaC [4Fe–4S] clusters to the [2Fe–2S]/flavin mononucleotide (FMN) cluster of the soluble Fd/Fld respectively.

3. Dissociation of the reduced Fd/Fld from the PS I reducing site to enable its function as electron donor in numerous metabolic reactions.

Several experimental techniques have been used to elucidate how the above-described steps take place. One should note, though, that none of the methods could address all the three steps in one experimental system. To detect docking/binding/association of Fd/Fld, mainly cross-linking has been used (Zanetti and Merati, 1987; Andersen et al., 1992; Fischer et al., 1998). To characterize the ET itself, the kinetics of Fd/Fld photoreduction has been studied in native and mutants of the reducing-site subunits PsaC, PsaD, and PsaE by flash absorption and electron paramagnetic resonance (EPR) spectroscopy (Sétif and Bottin, 1994, 1995; Fischer et al., 1997; Sétif et al., 2002; see Sétif, this volume, Chapter 26). The direct evidence for dissociation of Fd from the PS I reducing-site subunits has

been detected with BIACOR where K_{on} and K_{off} has been obtainable (Lushy et al., 2000).

Attempts to pinpoint the residues involved in the association/dissociation of – and ET to – Fd/Fld, in each of the reducing-site proteins relied mainly on site-directed mutagenesis studies. Such mutagenesis studies on PsaC have shown that only K35 of PsaC is essential for cross-linking with Fd, hence; K35 has been concluded to be an interaction site between PsaC and its redox partner Fd (Fischer et al., 1998). A successive study indicated that the same residue, K35, plays a strikingly similar role in ET from PS I to Fld (Meimberg et al., 1999). To prove which of the Fe/S clusters (F_A or F_B) of PsaC is involved in the ET to Fd/Fld, positively charged residues have been introduced close to the F_B cluster. In the cyanobacterium *Synechococcus* sp. PCC 6301 flash absorption spectroscopy has been used to determine that the PsaC is being oriented with F_A as the cluster proximal to F_X and F_B as the distal cluster that donates electrons to ferredoxin (Vassiliev et al., 1998). In the green alga, *Chlamydomonas reinhardtii* the triple mutant (I12V/T15K/Q16R) has resulted in a 60-fold increase of Fd affinity to PS I as measured by flash absorption spectroscopy and a larger amount of PsaC-Fd cross-linking product. These data indicate that F_B is the cluster interacting with Fd and, therefore, the outermost iron–sulfur cluster of PS I (Vassiliev et al., 1998; Fischer et al., 1999; Golbeck, 1999).

Although PsaC is the only protein involved in the ET per-se, an important role has also been assigned for PsaD and PsaE. Whenever Fd photo-reduction was followed by PS I of *psaD* and *psaE* less mutants from *Synechocystis* sp. PCC 6803, significant changes in the association and dissociation of Fd from their PS I complex have been reported. Based on such studies, the researchers have concluded that PsaD is important for the guiding of Fd to its binding site, i.e., it mainly affects the association rate, whereas PsaE seems to control the PS I/Fd complex lifetime, i.e., it mainly affects the dissociation rate. The effect of different pH on the ET from PS I to Fd has also been studied. In the PsaE deleted mutant as in the wild-type, the change of pH from 8.0 to 5.8 induces a 10-fold increase in affinity of Fd for PS I. In the absence of PsaD, this pH effect is not observed, this indicating that the PsaE subunit is the one mostly responsible for the increase in affinity at low pH (Barth et al., 1998).

Direct association of Fd with PsaD has been shown in cross-linking experiments for native PsaD (Mühlenhoff et al., 1996a,b; Ruffle et al., 2000) and recombinant PsaD (Pandini et al., 1999). Recombinant PsaD of spinach has been produced in *Escherichia coli* as a soluble protein that has been purified to homogeneity. The interaction of the PsaD subunit with Fd has been investigated by three different approaches: chemical cross-linking between the two purified proteins in solution, affinity chromatography of the PsaD subunit on a Fd-coupled resin, and titration with Fd of the protein fluorescence of the PsaD subunit. All these studies have indicated that the isolated PsaD in solution has a definite conformation and it maintains the ability to bind Fd with high affinity and specificity. The K_D value of the complex of PsaD and Fd has been reported to be in the nanomolar range. The ionic strength dependence of the K_D suggests that the protein–protein interaction is at least partially electrostatic in nature. Nevertheless, none of the glutamate residues of the acidic cluster of residues 92–94 of Fd have proven to be essential for PsaD binding. This conclusion is in agreement with the one obtained with the E93-95 mutant of *Synechococcus elongatus* which has shown that cross-linking to PsaD is possible (Floss et al., 1997).

These results contradict those obtained on PS I/Fd covalent complex prepared from *Synechocystis* sp. PCC 6803, where K106 from PsaD has been found to be cross-linked to E93 of Fd (Lelong et al., 1994). Mutagenesis studies in which K106 has been substituted have indicated a significant, though not essential, role of K106 (Sykes and Rogers, 1984; Chitnis et al., 1996; Mühlenhoff and Sétif, 1996a,b). Other mutagenesis studies in *S. elongatus* have indicated that another electrostatic contact, away from K106, is responsible for the interactions that exist between Fd and PsaD (Floss et al., 1997). Mutagenesis studies in the same organism in the sequence extending from His97 to Arg119, have predicted that the residues responsible for the protein–protein interactions of PsaD-Fd, are specifically His97 and R111 and the acidic amino acids D100, E105, and E109 (Hanley et al., 1996; Bottin et al., 2001; Lagoutte et al., 2001). Most single replacements of the acidic residues by neutral amino acids have increased the affinity for Fd, indicating the existence of a negative control for Fd binding (Bottin et al., 2001; Lagoutte et al., 2001).

Site-directed mutants of the PsaE subunit have been obtained only in *Synechocystis* sp. (Rousseau et al., 1993; Barth et al., 2000). Only in mutants of R39 (Barth et al., 2000) have the kinetics of Fd photoreduction been strongly affected. These researchers have proposed that the role of the positive charge at position 39 is to control the lifetime of the complex (rate K_{off}) with Fd. A model suggested by the authors has shown that the side chain of the R39 is exposed

to the stroma and is in a favorable position to interact with Fd and perform the suggested role of facilitation of the Fd dissociation (Sétif, 2001; Sétif et al., 2002). In the cyanobacterial system it has been shown that *psaE* deleted mutants are also affected during the dissociation of ferredoxin/FNR complex. This transient complex of PS I/ferredoxin/FNR formed during linear electron transport which is PsaE-dependent, is affected during its dissociation (van Thor et al., 1999).

In experiments using the BIACORE® technique, the role suggested for PsaE by these researchers has been confirmed. This technique enables the determination of real-time biomolecular interaction analysis (BIA) by surface plasmon resonance (SPR) technology (Jonsson et al., 1991). Real-time BIA monitors the formation and dissociation of biomolecular complexes on a sensor surface as the interaction occurs. By attaching one molecule (the ligand) to the surface, the binding of another molecule in solution (the analyte) with the ligand is followed. The preliminary data obtained (Lushy et al., 2000), has shown similar K_D values for PsaD-Fd; PsaE-Fd and the entire PS I-Fd associations as measured by the other techniques described above (Barth et al., 1998, 2000; Pandini et al., 1999).

Several mutants have also been generated in Fd/Fld to analyze the amino acids important in the acceptors for the interactions with PS I. Out of several mutants generated in *Synechocystis* sp. PCC 6803 (Poncelet et al., 1998; Guillouard et al., 2000), the ones having the larger decrease in the affinity of Fd to PS I have been found in the double mutant D57R/D60R and D57K/D60K(Guillouard et al., 2000).

Taken together, the vast information in recent years on the involvement of specific residues in the reducing-site-Fd/Fld ET, have indicated the central role of K35 of PsaC, R39 of PsaE, and E105 of PsaD in the PS I reducing site, and D57/D60 in Fd. These mutations and the PS I structure (Jordan et al., 2001) have allowed the definition of the docking site for the acceptors, with Fd binding at the edge of the "stromal ridge" formed by its three peripheral membrane PsaC, PsaD, and PsaE subunits (Sétif et al., 2002). Nevertheless, all the mutagenesis studies have been mapped onto the PS I structure solved with the native proteins (Jordan et al., 2001). More direct structural information is required that will enlighten us with more exact interactions and geometry. Currently, the only structural information known comes from electron microscopy and modeling studies. The former study characterized cross-linked complexes of PS I with either Fd (Lelong et al., 1996; Ruffle et al., 2000) or Fld (Mühlenhoff et al., 1996a,b) and the latter study modeled the interactions of Fd from *Spirulina platensis* to the 4 Å electron density map of PS I from *S. elongatus* (Fromme, 1996). Both studies have suggested that the binding site of Fd is located close to the terminal [4Fe–4S] cluster of PS I. Nevertheless, the low resolution nature of these studies has not permitted detailed information on the complex geometry. There is no doubt that a structure of a cocrystal that contains Fd with the reducing-site subunits and/or PS I is essential in order to understand the precise interactions and geometry. Such a crystal has been studied recently for its EPR characteristics (Fromme et al., 2002). Unfortunately, these crystals diffracted X-rays to a resolution of only 7 Å, which has not permitted the determination of their atomic structure.

IV. The Organization of the Reducing-Site Subunits

To be able to carry out the function of ET to Fd/Fld; i.e., the association/binding of Fd/Fld to the reducing-site ridge, the ET to Fd/Fld, and the dissociation of the reduced Fd/Fld; the different members of the reducing site have to integrate into the thylakoids, specifically into PS I, and to retain the proper conformation in the "stromal ridge" that secures their proper functionality. Several experimental systems have been developed to follow the steps involved in this assembly/organizational process. These include *in vitro* assembly assays in which native and mutated PsaD and/or PsaE have been expressed and/or over-expressed and introduced into isolated thylakoids and/or purified PS I complexes. *In vivo* systems, like those of cyanobacteria or green algae (Chitnis et al., 1996; Fischer et al., 1997, 1999; Meimberg et al., 1999) have enabled one to follow the effects of different mutations on the stable assembly of the PsaC/D/E proteins by detecting their presence and functionality in thylakoids isolated from intact cells (J. Yu et al., 1995; Gong et al., 2003). In recent years, the availability of structural information on the structure of the different subunits in their soluble form, i.e., before their integration into the PS I on the one hand, and their available structures in the assembled-PS I structure on the other hand, has provided a new insight that has permitted a better understanding of the conformational changes and protein–protein interactions occurring during the assembly processes. To simplify the issues relating to the integration and the folding to retain the proper conformation, we will first describe the current available information on the assembly of each of the reducing-site subunits. In these individual sections the questions still opened

regarding each of the subunits will be discussed. After the detailed information on each of the proteins, we will address the issues that are still needed to be resolved to enable a more global understanding of the assembly of the entire site.

A. Assembly of the PsaC Subunit

The central role of PsaC in the assembly of the PS I reducing site was first reported in cyanobacteria. A strain of *Anabaena variabilis T398* was generated in which the *psaC* gene encoding the PsaC protein was insertionally inactivated. The PS I complex isolated from the generated *T398* strain has retained a functionally active P_{700}. However, this purified PS I complex lacked the PsaD, PsaE, and PsaL polypeptides. Western analysis with polyclonal antibodies raised against these proteins has indicated that the two reducing-site polypeptides, PsaD and PsaE, are absent in isolated thylakoid membranes from *T398* cells. The PsaL polypeptide was detected at a level comparable to that in wild-type thylakoid membranes, but it is absent in the PS I preparation from the mutant strain (Mannan et al., 1994).

In another cyanobacterium, *Synechocystis* sp. PCC 6803, insertion of a gene encoding kanamycin resistance into the *psaC* gene resulted in a photosynthesis-deficient strain, *CDK25*, lacking the PsaC, PsaD, and PsaE polypeptides in isolated thylakoid membranes, while the PsaA/PsaB and PsaF subunits were found to be present. Growth of the mutant cells under light-activated heterotrophic growth was undistinguished from that of the wild-type. A reversible P_{700}^{+} signal was detected but the EPR signals attributed to F_A and F_B are absent in the mutant strain. The addition of PsaC and PsaD proteins to the thylakoids restored the EPR resonance characteristic of an interaction-type spectrum of F_A^- and F_B^-. This study has demonstrated that in PS I of *Synechocystis* sp. PCC 6803 the PsaC polypeptide is necessary for stable assembly of PsaD and PsaE into PS I complex *in vivo*. Moreover, it has indicated that PsaC, PsaD, and PsaE are not needed for the assembly of PsaA–PsaB dimer and electron transport from P_{700} to F_X (L. Yu et al., 1995). A recent study of the same cyanobacterium *Synechocystis* sp. PCC 6803 has further strengthened these findings. In the latter, the *psaC* gene has been interrupted and a similar phenotype has been obtained, i.e., cells cannot grow under photosynthetic conditions when subunit PsaC has been deleted, yet the PsaC-deficient mutant cells grow under heterotrophic conditions and assemble the core subunits of PS I in which light-induced electron transfer from P_{700} to A_1 are detected. Yet in this mutant, the photo-reduction of F_X has been largely inhibited, as seen from direct measurement of the extent of electron transfer from A_1 to F_X. The availability of the atomic structure of PS I (Jordan et al., 2001), has allowed these researchers to propose that the removal of subunits PsaC, PsaD, and PsaE in the PsaC-deficient mutant causes the breaking of bridges between these subunits and PsaA and PsaB, which causes the formation of a net of negative surface charges on PsaA/PsaB. They have suggested that these surface charges induce a potential on F_X that inhibits the electron transport to it from the quinone (A_1) (Gong et al., 2003). Although the two groups report a similar phenotype, L. Yu et al. (1995) found that the absence of PsaC (and PsaD/PsaE) did not prevent the reversible reduction of F_x. From these studies it is clear that the absence of PsaC subunit allows assembly of photosystem I core but prevents the binding of PsaD and PsaE in *Synechocystis* sp. PCC 6803.

The effects of the salt bridges and other protein–protein interactions on the stable assembly of PsaC, the proper integration of its iron–sulfur clusters F_A and F_B and the ET to them and from them to the soluble Fd, have been the focus of several studies in the recent few years. From the X-ray structure of *S. elongatus* (Jordan et al., 2001) it is evident that PsaC is located at the center of the stromal ridge and is surrounded by PsaD and PsaE. PsaC seems to be the situated at the top of the core of the pseudo-C_2 symmetric reaction center heterodimer of PS I formed by the main membrane-spanning PsaA and PsaB subunits. Indeed, the recent very extensive study (Antonkine et al., 2003) has indicated that PsaC is the reducing-site subunit that forms the most extensive network of protein–protein interactions with the surface of PsaA and PsaB. The latter, and the inner location of PsaC within the "stromal ridge," are no doubt key factors that affect the proper assembly of PsaC in the reducing-site complex. There is the question of PsaC integration into its inner position. Under steady-state conditions, when PsaC needs to undergo a turnover, the formation of the network of numerous interactions to obtain the optimized conformation for its function is an issue to be addressed, as is the question of the release of PsaC from its inner location. Another question is the need for the achievement of the proper assembly of the PsaC iron–sulfur clusters F_A and F_B, that must gain a proper conformation to allow their optimal function in ET to Fd/Fld. Because of their central functional role in the electron transfer process, the assembly of these [4Fe–4S] clusters of PsaC has been studied by biochemical and spectroscopic methods that followed their magnetic resonance properties

(Golbeck, 1999; Vassiliev et al., 2001). These studies have indicated that PsaC can be overexpressed as a free/soluble protein; to this free apo-protein the Fe/S clusters F_A and F_B are integrated. As a result, the protein backbone in the core of PsaC, i.e., the region that surrounds the clusters, is folded into a defined three-dimensional conformation (Golbeck, 1999; Vassiliev et al., 2001; Antonkine et al., 2002). This proper integration and assembly of the Fe/S clusters and the folding of the PsaC core occurs before the integration of PsaC into the thylakoids/PS I. The question of whether the proper integration of the clusters into PsaC is a prerequisite to enable the protein to assemble into the PS I heterodimer has been addressed in a successive study. The researchers have used the strain of the *psaC* deletion mutant of *Synechocystis* sp. PCC 6803, into which they have incorporated site-specific amino acid substitutions in the cysteine residues that ligate the F_A and F_B iron–sulfur clusters. The results have shown that only those PsaC proteins that contain the two [4Fe–4S] clusters properly integrated, can assemble properly into the PS I (Jung et al., 1997).

Nevertheless, in this free/soluble PsaC, that contains the F_A and F_B and is capable of assembly into PS I, the magnetic resonance properties of the clusters differ from their properties in the PS I-assembled PsaC. In the free/soluble PsaC, the magnetic characteristics of the F_A cluster have been found to be basically equivalent to those of F_B (Golbeck, 1999). Taken together, these results led to the view that before the integration of PsaC into PS I, the F_A, and F_B have to be integrated into the protein. The effect of the integration of F_A and F_B on the structure of PsaC was addressed in a recent report on three-dimensional NMR solution structure of recombinant, oxidized, unbound PsaC from *Synechococcus* sp. PCC 7002. The latter has indeed indicated significant differences between the unbound PsaC structure and the available X-ray structure of PS I-assembled PsaC (Antonkine et al., 2002). These differences mainly concern the arrangement of the N- and C-termini with respect to the [4Fe–4S] core domain. In the NMR solution structure of PsaC, the C-terminal region assumes a disordered helical conformation that is clearly different from the extended coil conformation, which is one of the structural elements required to anchor PsaC to the PS I core heterodimer. In solution, the N-terminus of PsaC is in contact with the pre-C-terminal region; it slides in between the latter and the iron–sulfur core region of the protein. Together, these features result in a concerted movement of the N-terminus and pre-C-terminal region away from the F_A binding site, accompanied by a bending of the N-terminus. In the PS I-assembled PsaC, the same terminal regions are positioned much closer to F_A and have an antiparallel β-sheet conformation. These reported conformational changes between bound and unbound PsaC correlate with the differences reported earlier for the EPR spectra of reduced F_A and F_B in assembled versus free/soluble PsaC (Li et al., 1991). The researchers have shown that the structural changes of free PsaC *vs.* PS I-assembled PsaC, and the differences in the magnetic properties of F_A and F_B are affected by, or related to, the assembly of PsaC to PS I. Upon the binding of the free/soluble PsaC to the PS I heterodimer, PsaA, and PsaB subunits, a change of the magnetic properties of F_A and F_B occurs. The amino acid motif surrounding the F_A creates the F_A binding site of PsaC with the P700-F_X core. It has been suggested that these charged amino acid residues of the PsaC F_A binding motif play a crucial role in the intersubunit binding network of PsaC to PS I. The K51 and R52 residues of PsaC have been suggested as being the most important ones in this binding (Antonkine et al., 2003). The association of PsaC with the PsaA and PsaB heterodimer is the first assembly step that affects the magnetic characteristics of the clusters. Further changes occur following the binding of PsaD to the assembled PsaC–PS I-core (Li et al., 1991; Chitnis et al., 1996). The PsaC D46 residue in front of the F_A binding motif has been pointed out as being involved in the contact formed by PsaC with PsaD (Antonkine et al., 2003). The different findings indicate that both the PsaC conformation and the magnetic properties of its iron–sulfur clusters are reaching similar characteristics as reported for the PS I-assembled PsaC only after PsaD gets assembled to the PsaC–PS I-heterodimer complex (Li et al., 1991). The recent study described in Antonkine et al. (2003) has provided a solid explanation to these previous observations. In this study the X-ray structural information on the PS I-assembled "stromal ridge" subunits has been compared to the soluble structures of free/soluble PsaC, PsaD, and PsaE. Moreover, in this recent report the biochemical and spectroscopic studies have been analyzed in light of the structural contact analysis. The researchers related the contact information based on the assembled-PS I structure to conformational changes in the proteins occurring concomitantly with their assembly. Their analysis accepted the suggested sequential assembly of the subunits of the "stromal ridge" of PS I suggested by Golbeck and coworkers (Golbeck, 1999). As for PsaC, three assembly stages were suggested to take place: firstly, PsaC is in solution as a free protein into which the iron cluster are integrated; secondly PsaC binds to the PsaA–PsaB heterodimer ("PsaC-only") and

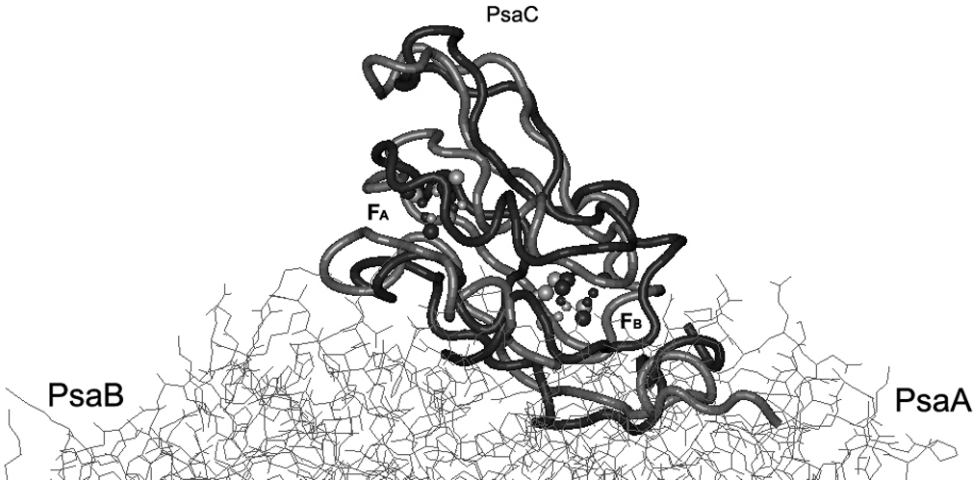

Fig. 5. Association of PsaC with the PS I complex. See Color Plate 13, Fig. 2.

following the binding of PsaD, the PsaC reaches its final PS I-assembled conformation termed by them: "PsaC (PS I)" (Antonkine et al., 2003).

Figure 5 shows the changes in PsaC structures upon assembly based on currently available structural information (step 1 and step 3 mentioned above). The structure of PsaC (free) — in blue, taken from (PDB entry 1K0T) and described in details in Antonkine et al. (2002), is superimposed on the structure of PsaC (PS I) — cyan, taken from (PDB entry 1JB0) and described in details in Jordan et al. (2001). The stromal exposed area of the PsaA and PsaB structures is presented in the background. The view presented is parallel to the thylakoids. Figure 5 clearly demonstrates the conformational changes detected for PsaC.

A recent study has indicated an assembly governed regulation of the synthesis of the chloroplast-encoded PS I subunits. It shows that the presence of PsaB is required for significant rate of synthesis of PsaA which is required for synthesis of PsaC (Wostrikoff et al., 2004). This study suggests that the regulation of assembly of PsaC may occur as early as its translation step.

B. Assembly of the PsaD Subunit

The assembly of PsaD was initially studied in eukaryotic systems where it was shown to play a key role in the assembly of the entire PS I (Nechushtai and Nelson, 1981, 1985). As shown in Fig. 2, PsaD of eukaryotes is longer than PsaD of cyanobacteria. The eukaryotic PsaD is synthesized in the cytoplasm as a precursor with a leader peptide at its N-terminus, pre-PsaD, which targets it to the chloroplast. There, the leader peptide is cleaved by a stromal processing peptidase (Cohen et al., 1992), thus allowing PsaD to assemble properly into the PS I complex within the thylakoid membranes (Minai et al., 1996). The assembly of PsaD into the thylakoid membrane requires neither the presence of ATP nor the presence of a stromal component (Chitnis and Nelson, 1992; Cohen et al., 1992). PsaD assembles specifically into the PS I complex. No association of the newly integrated protein subunit with any other membrane complex has been observed (Chitnis and Nelson, 1992; Cohen et al., 1992). Moreover, pre-PsaD can also assemble into isolated PS I complexes. Upon addition of the stromal fraction, the pre-PsaD, bound to the isolated PS I can be correctly processed by the stromal processing peptidase (Cohen and Nechushtai, 1992). Although the assembly of the pre-PsaD into the thylakoids is not affected by the presence of salts, the mature form that resembles the cyanobacterial PsaD cannot assemble into the membrane at high salt concentrations (Minai and Nechushtai, 1995). This form of mature-PsaD becomes resistant to proteolysis only when properly assembled into the thylakoids in low ionic strength (Minai et al., 1996). The assembly of pre-PsaD/PsaD into the PS I complex is led by the C-terminus of the protein, which is phyla specific (Cohen et al., 1995; Minai and Nechushtai, 2001).

Taken together, the observations on the assembly of eukaryotic PS I argue for the involvement of at least two steps in the assembly process of pre-PsaD. As a first step, pre-PsaD binds to PS I probably in an extended conformation that is responsible for its proteolytic susceptibility. The extended conformation, which maybe similar to that of pre-PsaD in a soluble environment, is probably caused by the presence of the leader peptide. Then, in a second step of the assembly process,

the pre-PsaD is processed to its mature form. The latter step is most likely accompanied by a conformational change, thus allowing the formation of associations/contacts/bindings between PsaD and other PS I subunits. This intracomplex association secures the assembly of PsaD in PS I at the stromal surface of the thylakoid membranes and provides the PsaD protection against proteolytic digestion (Minai et al., 1996; Wollman et al., 1999).

An *in vitro* comprehensive study has involved the characterization of the assembly of plants (spinach), green algae (*C. reinhardtii*), and cyanobacterial (*Mastigocladus laminosus*) PsaD. The study has aimed at unraveling the mechanism by which the PsaD assembly takes place. Mature-PsaD of spinach and PsaD of the cyanobacterium *M. laminosus*, have been over-expressed, purified to homogeneity and introduced to isolated PS I complexes. The findings have indicated that an exchange mechanism enables the assembly of a newly introduced PsaD into PS I. The latter replaces the PsaD subunit that is present *in situ* within the complex.

In vivo studies that have followed the assembly of PsaD in *C. reinhardtii* cells have supported this *in vitro* characterized exchange mechanism. In *C. reinhardtii* in the absence of synthesis and assembly of new PS I complexes, newly synthesized PsaD assembled into pre-existing PS I complexes (Minai et al., 2001). Cyanobacterial experimental systems have enabled to characterize the assembly of wild-type and mutants of PsaD *in vivo*. To determine the function of the basic region in PsaD, site-directed mutagenesis studies of the cyanobacterium *Synechocystis* sp. PCC 6803 have taken place. Five mutant strains have been generated in which one or more charged residues have been altered. The results have indicated that the basic residues in the central region of PsaD, especially K74, are crucial in the assembly of PsaD into the PS I complex (Chitnis et al., 1997).

Several methods have been used to analyze the structural elements in free/soluble PsaD that play a role in its assembly into the PS I complex. The over-expressed soluble PsaD of *M. laminosus* can assemble into the PsaD-less PS I. While some of the residues C66, K21, R118, and R119 have been identified as being exposed on the surface of soluble PsaD, others like K129 and K131 residues have not been exposed on the surface, indicating a distinct conformation that "buries" them inside the protein. Circular dichroism (CD) spectroscopy has revealed that the free/soluble PsaD contains a small proportion of α-helical conformation (Jin et al., 1999). Another study on the free/soluble PsaD of *Synechocystis* sp. PCC 6803 has indicated that only 11% of the protein is in a defined conformation (β-sheet), and PsaD exists in two or more conformations whose distribution is affected by pH (Xia et al., 1998). These researchers have also found that in solution, as free protein, PsaD is a stable dimer, and they assume that the core of PS I might induce dimer/monomer transition. The dimeric form of PsaD has also been reported for *M. laminosus* PsaD (Minai et al., 2001). In the recent study of Antonkine et al. (2003), the researchers took the available limited structural information from the NMR study of free/soluble PsaD (Xia et al., 1998) as evidence of a nonstructured PsaD in the free/soluble state. This assumption contradicts the conclusions from assembly assays. In the section described above, it has been shown that in extended conformation, PsaD is susceptible to proteolysis. So without a defined conformation, it is difficult to envision how PsaD reaches the PS I complex in the thylakoids after being soluble, non-structured protein in mediums (cytoplasm and/or stroma) enriched with proteolytic enzymes. Further contradicting evidence comes from the study done by Chitnis and Nelson (1992) who studied the assembly of different deletion mutants of PsaD. They showed that the deletions prevented the incorporation of the deleted-PsaD into the thylakoids and its proper assembly into PS I. They suggested that probably the overall conformation of PsaD, rather than a specific targeting sequence, is required for PsaD assembly into PS I. It may very well be that to-date a defined three-dimensional structure for the free/soluble PsaD has not been reported, rather, the results are from experimental conditions rather than from a truly non-structured free/soluble PsaD.

The recent detailed analysis (Antonkine et al., 2003) of all the contacts formed by PsaD in the PS I-assembled complex aimed at understanding the assembly process of PsaD with respect to its conformation. These researchers suggested that the contacts formed by PsaD and the P_{700}-F_x/PsaC core containing the PsaA and PsaB subunits, are responsible for the formation of the tertiary structures of PsaD. Initially they suggest the formation of contacts of the N-terminal residues of PsaD (residues 12, 14, and 16 that bind to PsaA and 17 and 19 to PsaB) as well as the other set of contacts binding to PsaA (residues 40, 46, 60, and 62 of PsaD) are suggested to be responsible for positioning different elements of the secondary structure of the N-terminus of PsaD with respect to one another and with respect to the stromal exposed PsaA surface. These contacts, on the other hand, involve tertiary structural features of other PS I subunits, like PsaC. The extended conformation of the PsaC C-terminus and its interactions with PsaB are

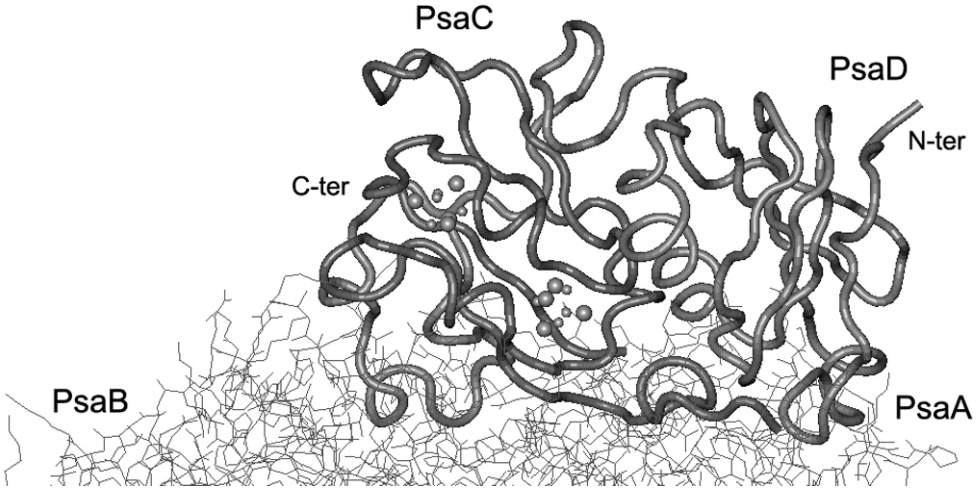

Fig. 6. Assembly of PsaD in the PS I complex. See Color Plate 14, Fig. 1.

stabilized by PsaD binding. These researchers suggest that the binding of PsaD even induces the formation of some intra-PsaC contacts, which have been revealed in the X-ray structure of assembled-PS I (Jordan et al., 2001), but have not been observed in free PsaC (Antonkine et al., 2002). Another important interaction of PsaD with PsaC occurs in the region of the C-clamp of PsaD. The C-clamp contacts with PsaC not only determine the position of the C-clamp, but also initialize the formation and stabilization of the anti-parallel β-sheet arrangement of the N- and C-terminal regions of PsaC. After all the sets of contacts of the C-clamp around PsaC are present, the proper position of the C-terminus of PsaD forms its specific contact network to the PsaB subunit. Finally, these researchers have concluded that the contacts formed by PsaD with PsaA, PsaB, and with PsaC are the ones that dictate the final conformation of the PsaD within the assembled-PS I complex (Jordan et al., 2001), an antiparallel four-stranded β-sheet followed by a second two-stranded β-sheet. A short loop connects the fourth β-strand to the only α-helix in PsaD. Figure 6 indicates the addition of the PsaD in its final conformation that also locks the PsaC in its final conformation taken from (PDB entry 1JB0) and described in details in Jordan et al. (2001).

C. Assembly of the PsaE Subunit

In cyanobacteria, *in vivo* experimental systems have been used to follow the assembly of PsaE into thylakoids isolated from mutant strains that lack specific PS I subunits. It has been found that the PsaE incorporated into membranes isolated from the wild-type cells, is resistant to chaotropic agents and proteolytic digestion. Susceptibility to proteolysis and/or removal by chaotropic agents has been detected while the newly assembled PsaE integrated into the thylakoids of different mutants. The results have suggested that PsaD and PsaF/PsaJ interact with PsaE to stabilize its assembly into the assembled-photosystem I complex (Cohen et al., 1993).

In a recent study the introduction of purified PsaE protein to thylakoids isolated from *M. laminosus* was conducted by following the assembly of overexpressed and purified PsaE from this cyanobacterium. The purification of the different thylakoid protein complexes has indicated that PsaE accumulates specifically in its functional location, the PS I complex. A similar stable assembly has been detected when PsaE is introduced into purified PS I complexes, i.e., in the absence of other thylakoid components. The latter strongly indicates that the information for the stable assembly of PsaE into PS I lies within the polypeptide itself and within other subunits of the PS I complex that interact with it. To determine the nature of these interactions, the assembly reaction has been performed in conditions affecting the ionic and/or osmotic strength. It has been found that altering the ionic strength significantly affects the capability of PsaE to assemble into isolated thylakoids or PS I complexes, strongly supporting the notion that electrostatic interactions are formed between PsaE and other PS I subunits. Moreover, the data suggest that the formation of electrostatic interactions occurs concomitantly with an exchange step in which newly introduced PsaE replaces the subunit present *in situ* (Lushy

et al., 2002). These results imply that the PsaE assembly mechanism is by an exchange mechanism resembling those described above for PsaD (Minai et al., 2001), which would make the exchange mechanism, under steady-state conditions, a general one for the assembly of the reducing-site subunits.

Site-directed mutagenesis study of basic residues of the PsaE in *Synechocystis* sp. PCC 6803, have shown that some of the mutants were impaired for PsaE integration into PS I, with phenotypes identical to the *psaE*-deleted mutant (Rousseau et al., 1993). These observations have confirmed that important changes in either of the two terminal sequences of the PsaE impair its correct integration into PS I.

In vivo studies in which the genes encoding PsaE have been disrupted in plants have been performed in *Arabidopsis*. The *psae1-1* mutant, in one of two *Arabidopsis* genes that encode PsaE, has been identified. In this mutant, a significantly altered steady-state redox level and the rate of reoxidation of P_{700} have been found. An additional mutant allele, *psae1-2*, has been identified by reverse genetics. In wild-type plants, the *psaE1* transcript is expressed at a higher level than *psaE2* mRNA. In the mutants, however, the *psaE1* transcript has barely been detectable, and has been expressed only in small groups of wild-type cells resulting from somatic reversions. As a consequence, the amount of PsaE protein present in the mutant is significantly reduced. Concomitantly, the levels of other stromal photosystem I subunits (PsaC and PsaD) are also affected. Mutant plants have shown a marked increase in light sensitivity and photoinhibition. Additional effects of the *psae1* mutation include light green pigmentation, an increase in chlorophyll fluorescence and a decrease of ~50% in growth rate under greenhouse conditions (Varotto et al., 2000). These observations clearly indicate that in plants the assembly of all subunits of the reducing site PsaC, PsaD, and PsaE is well co-ordinated and that disruption of one of them affects the others as well.

In recent years, several reports on the three-dimensional structure of over-expressed purified PsaE as a soluble/free protein have been reported. The researchers all used solution NMR as the methodology to determine the structure. The initial report of (Falzone et al., 1994) has indicated that the PsaE protein isolated from the cyanobacterium *Synechococcus* sp. PCC 7002 adopts the β topology of an SH3 domain, with five β-strands (βA through βE) and a turn of 3(10) helix between strands βD and βE.

A few years later, the same group reported on the NMR structure of PsaE from the cyanobacterium *Nostoc* sp. PCC 8009 (Mayer et al., 1999). These researchers claimed that although the primary structure of the PsaE protein is strongly conserved across all oxygen-evolving photosynthetic organisms, variability in loop lengths, as well as N- or C-terminal extensions exist. The latter may affect the structure of the protein; therefore, they decided to determine the solution structure of PsaE from *Nostoc* sp. PCC 8009. The obtained family of 20 NMR structures of *Nostoc sp.* PCC 8009 have been compared to the structure of PsaE from *Synechococcus* sp. PCC 7002. The comparison has indicated that *Nostoc* sp. PCC 8009 PsaE has a seven-residue deletion in the loop connecting strands βC and βD, and an eight-residue C-terminal extension. Differences between the two cyanobacterial proteins are mostly confined to the CD loop region and the C-terminal disordered extension (Mayer et al., 1999).

Recently, a third NMR solution structure of PsaE from the cyanobacterium *Synechocystis* sp. PCC 6803 has been reported (Barth et al., 2002). The overall fold of this structure is highly similar to previous structures of PsaE (Falzone et al., 1994; Mayer et al., 1999). These results have also indicated that a well-defined central core consists of a five-stranded β-sheet (+1, +1, +1, −4x), characteristic of PsaE structure. Four loops (designated as AB, BC, CD, and DE loops) connect these β-strands, and the overall resulting structure being that of an SH3-like domain. As compared to previously determined PsaE structures, conformational differences are observed in the first three loops. The flexibility of the loops has been shown to be small in amplitude for the AB and BC loops, but large for the CD loop (Barth et al., 2002).

The availability of three-dimensional structures of PsaE as a free/soluble protein, have enabled the comparison of the nonbound, free PsaE before its integration to PS I, to that of the assembled PsaE structure as reported in the high resolution X-ray structure of PS I (Jordan et al., 2001). Figure 7 indicates the changes of the two PsaE structures; the free/soluble PsaE structure from *Synechococcus* sp. PCC 7002 (PDB code 1PSF), colored purple, compared with the structure of PsaE in the assembled-PS I (PDB code 1JB0), colored pink. This comparison indicates the differences between free/soluble PsaE and the protein bound to the PS I. Analysis of the latter with regards to the insertion process and the function(s) of PsaE in the assembled-PS I can be performed. Such analysis was presented in the recent study of Antonkine et al. (2003) that indicated that for PsaE, the three-dimensional structure is very similar in solution and in the PS I-bound form, with the exception of two loop regions BC and CD. They

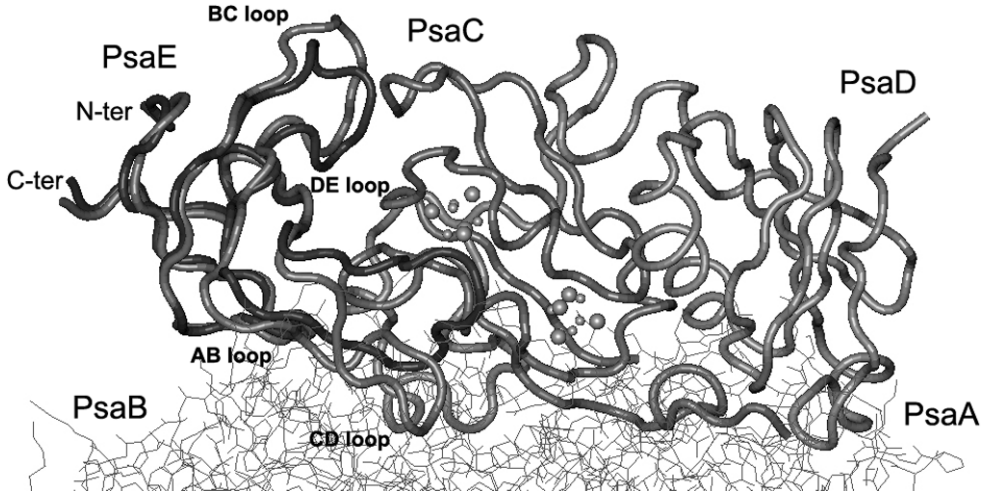

Fig. 7. Association of PsaE with the PS I complex. See Color Plate 14, Fig. 2.

have suggested that these changes in the structures of PsaE are caused by the sequential formation of multiple networks of contacts between the polypeptides of the stromal ridge and between those polypeptides and the PsaA/PsaB core polypeptides, where the BC- and CD-loop region play a important structural role. CD-loop, together with AB-loop, form contacts with the PsaA/PsaB core and stromal interface. The location of PsaE covers the stromal surface immediately above the Q_K-A binding site. The removal of PsaE together with PsaF influences the photoaccumulation of reduced A_1^- radical by facilitation solvent access to Q_K-A (Yang et al., 1998). The researchers (Antonkine et al., 2003) have also proposed that Y45 (CD-loop) and Y15 (AB-loop) of PsaD, which are, located close to the Q_K-A binding site, function as H-bond donor and H-bond acceptor, respectively. They suggested that the later may influence the unusually low reducing potential of the phylloquinone in PS I. The BC-loop is involved in the PsaE interaction to PsaC and these contacts help to stabilize this part of PsaE structure (Antonkine et al., 2003).

V. Other Proteins Involved in the Assembly of the PS I Reducing Site

We have described the assembly of the PsaC, PsaD, and PsaE subunits of the PS I reducing site as it depends only on the conformation of these proteins and the formation of contacts between them and other PS I proteins. However, we would like to draw the readers' attention to the accumulating evidence in recent years, which indicates that proteins that do not belong to PS I affect the assembly of the reducing site as well.

By reverse genetics, the function of Ycf3 and Ycf4 has been established (see Rochaix, this volume, Chapter 30). The genes encoding these proteins have been found to be present in cyanobacteria, green algae, and plants (Wilde et al., 1995). Disruption of the *ycf3* gene in tobacco (Ruf et al., 1997) and in *C. reinhardtii* (Boudreau et al., 1997) has led to complete loss in the assembled-PS I core complex. Disruption of the *ycf4* gene had a similar effect in *C. reinhardtii* and in *Synechocystis* sp. PCC 6803; it caused a 50% loss in assembled-PS I (Wilde et al., 1995). The Ycf3 and Ycf4 have been found in thylakoids of *C. reinhardtii* with Ycf3 predicted to be present in the stromal side of the membranes (Boudreau et al., 1997). A recent study has indicated that the Ycf3 protein is essential for the accumulation of the PS I complex and that it acts at a post-translational level. The sequence of Ycf3 has been conserved in cyanobacteria, algae, and plants and contains three tetratrico peptide repeats (TPR). TPRs have been shown to function as sites for protein–protein interactions. A temperature-sensitive *ycf3* mutant, generated by random mutagenesis of a conserved region near the N-terminal end of Ycf3, has been used in temperature-shift experiments to show that Ycf3 is required for PS I assembly (Rochaix et al., 2004) but not for its stability. Immunoblot analysis of thylakoid membranes separated by two-dimensional gel electrophoresis and immunoprecipitations shows that Ycf3 interacts directly with the PS I subunits PsaA and PsaD, but not with subunits from other photosynthetic complexes. Thus, Ycf3 appears to act as a chaperone that interacts directly and specifically with at least two of the PS I

subunits during assembly of the PS I complex (Naver et al., 2001).

Another protein that influences the PS I assembly is RubA that contains a domain of ~50 amino acids with very high similarity to the rubredoxins of anaerobic bacteria and archaea (see Shen and Golbeck, this volume, Chapter 31). It also contains a region of about 50 amino acids that is predicted to form a flexible hinge and a transmembrane α-helix at its C-terminus. Inactivation of the *rubA* gene of *Synechococcus* sp. PCC 7002 has produced a mutant that is unable to grow photoautotrophically. PS I complexes can be isolated from the *rubA* mutant. These PS I complexes completely lack the stromal subunits PsaC, PsaD, and PsaE but contain all membrane-intrinsic subunits. Loss of the RubA causes the complete loss of PS I activity as well as the destabilization of the three peripheral polypeptides, PsaC, PsaD, and PsaE (Shen et al., 2002a,b). EPR spectroscopy at low temperature shows that the three terminal Fe/S clusters, F_X, F_A, and F_B, are missing in whole cells, thylakoids, and PS I complexes of the *rubA* mutant (Shen et al., 2002a,b). It is proposed that RubA is specifically required for the assembly of the F_X iron–sulfur cluster but that F_X is not required for the biosynthesis of P700-A_1 cores. Since the PsaC protein requires the presence of F_X for binding to the PsaA–PsaB heterodimer, the absence of F_A and F_B may be an indirect result of the absence of F_X (Shen et al., 2002a,b).

Of additional importance is the stabilization of the assembled proteins and their turnover. A random screen for photosynthesis-deficient mutants from *Synechocystis* sp. PCC 6803 has identified the *btpA* gene that encodes a 30-kDa polypeptide. Mutations in this gene significantly affect accumulation of the reaction center proteins of PS I in *Synechocystis* sp. PCC 6803 (Bartsevich and Pakrasi, 1997). Immunolocalization in *Synechocystis* sp. PCC 6803 cells has demonstrated that the BtpA protein is tightly associated with the thylakoid membranes. Treatments of inside-out and right-side-out thylakoid vesicles from *Synechocystis* sp. PCC 6803 with different salts and proteases have shown that the BtpA protein is an extrinsic membrane protein which is exposed to the cytoplasmic face of the thylakoid membrane (Zak et al., 1999). The BtpA protein has been found to be a necessary regulatory factor for stabilization of the PsaA and PsaB proteins by lowering the rates of degradation of the PsaA and PsaB proteins, under low-temperature conditions. A *btpA* deletion mutant strain of *Synechocystis* sp. PCC 6803 cannot grow photoautotrophically at low temperature, and has exhibited rapid degradation of the PS I complex after transfer of the cells from normal to low temperature (Zak and Pakrasi, 2000). The molecular mechanism of action of the BtpA protein is unknown, however, (Zak and Pakrasi, 2000) hypothesize that the BtpA protein may function as a chaperone, directly interacting with the PsaA and/or PsaB proteins. In particular, BtpA may be involved in the insertion/assembly of co-factors in PS I, such as iron–sulfur centers or phylloquinones.

Recently in the *pgsA* mutant of *Synechocystis* sp. PCC 6803, it was shown that long term depletion of phosphatidylglycerol (PG) resulted in a dramatic decrease of assembly and major structural changes of PS I (Domonkos et al., 2004). Another group of proteins, recently shown to affect the assembly of PS I, are proteins involved in Fe/S cluster biogenesis. The *Arabidopsis* NifU like protein, AtCnfU-V, has been shown to drastically impair PS I accumulation, as well as Fd (Yabe et al., 2004).

VI. Concluding Remarks

This chapter outlines the current knowledge on the assembly of the reducing site of PS I as studied in the past decade. It describes the accepted scenario in which a sequential assembly of PsaC that is followed by PsaD is followed by PsaE.

This scenario, in principle, addresses the process of the formation of PS I and not the steady-state maintenance of the complex.

Accordingly, the formation of the "stromal ridge" initiates when the PsaC subunit, the first of the three subunits, associates with the PsaA/PsaB heterodimer which has already been assembled in the thylakoids with its chlorophylls and electron acceptors, including F_X, which has also already been assembled (Antonkine et al., 2003). PsaC that associates with the PsaA and PsaB contains the F_A and F_B clusters with the inner structure of the protein fixed by these two Fe/S clusters. The C-terminus of the free/soluble PsaC has a disordered helical conformation, while the N-terminal end bends and slides between the pre-C-terminus and the iron–sulfur core. Concomitantly with, or right after the PsaC associates with the PsaA/PsaB heterodimer, a set of ionic interactions is formed. The latter, and the subsequent binding of PsaD, impose conformation changes on the F_A and F_B iron–sulfur clusters as indicated by the alteration of their magnetic resonance characteristics. The N- and C-termini of PsaC also undergo a conformational change. The association of PsaD with PS I is stabilized by interactions with PsaC and with the PsaA/PsaB as well as with PsaL, another membrane-spanning subunit of PS I. The last subunit of the "stromal ridge" to associate with PS I is PsaE, which in the

assembled-PS I complex maintains a structure that is very similar to the free/soluble PsaE.

This sequential formation of the "stromal ridge" where PsaC is followed by PsaD, which is followed by PsaE, as described in details in Antonkine et al. (2003), is challenged by the results of two different experimental systems: the disassembly studies of PS I and the *in vitro* assembly assays in which purified PsaD/PsaE were introduced to fully assembled, preexisting PS I complexes. The results of the former system indicate that in the case of the disassembly of the "stromal ridge," PsaE is the first to leave the reducing site, followed by PsaC and the last to leave is PsaD. If the disassembly is a mirror image of the assembly process, how can the most buried and the first to assemble PsaC subunit leave before PsaD, which according to the sequential scenario is the second one to assemble?

Moreover, the *in vitro* assembly assays have shown that both PsaD and PsaE assemble into PS I in an exchange mechanism where the newly introduced protein replaces the same subunit present *in situ* in the assembled-PS I complex. How can PsaD assemble with PsaE being present?

In summary, we strongly believe that the currently available information describes the states of the "stromal ridge" subunits before and after their assembly. The structural information of the free/soluble PsaC and PsaE and the structures of PsaC, PsaD, and PsaE after assembly in the fully assembled-PS I, shed light on the beginning and end states. Moreover, the structure in the assembled-PS I, enables the characterization of the contacts formed in the final step; after the assembly process is completed.

Experimental data on the dynamics of the assembly process, especially during steady-state conditions, are still lacking; i.e., how the subunits of fully assembled-PS I "stromal ridge" undergo turnover and what happens during their assembly, as opposed to before and after. We strongly believe that the next decade will be devoted to the developing of the experimental tools and methodologies that will enable the understanding of the assembly dynamics. The encouraging progress made with the PS I – "stromal ridge" subunits in the past few years, provides a strong basis for the belief that the dynamics of the assembly enigma will be unraveled.

Acknowledgments

We wish to acknowledge. Dorit Michaeli and Lilya Vorchovsky for their assistance in experimental work mentioned in this chapter. Mezi Berman is acknowledged for her constructive remarks on the writing of the chapter.

References

Andersen B, Scheller HV and Møller BL (1992) The PSI-E subunit of photosystem I binds ferredoxin:NADP+ oxidoreductase. FEBS Lett 311: 169–173

Antonkine ML, Liu G, Bentrop D, Bryant DA, Bertini I, Luchinat C, Golbeck JH and Stehlik D (2002) Solution structure of the unbound, oxidized Photosystem I subunit PsaC, containing [4Fe–4S] clusters F_A and F_B: a conformational change occurs upon binding to photosystem I. J Biol Inorg Chem 7: 461–472

Antonkine ML, Jordan P, Fromme P, Krauß N, Golbeck JH and Stehlik D (2003) Assembly of protein subunits within the stromal ridge of photosystem I. Structural changes between unbound and sequentially PS I-bound polypeptides and correlated changes of the magnetic properties of the terminal iron sulfur clusters. J Mol Biol 327: 671–697

Barth P, Lagoutte B and Sétif P (1998) Ferredoxin reduction by photosystem I from *Synechocystis* sp. PCC 6803: toward an understanding of the respective roles of subunits PsaD and PsaE in ferredoxin binding. Biochemistry 37: 16233–16241

Barth P, Guillouard I, Sétif P and Lagoutte B (2000) Essential role of a single arginine of photosystem I in stabilizing the electron transfer complex with ferredoxin. J Biol Chem 275: 7030–7036

Barth P, Savarin P, Gilquin B, Lagoutte B and Ochsenbein F (2002) Solution NMR structure and backbone dynamics of the PsaE subunit of photosystem I from *Synechocystis* sp. PCC 6803. Biochemistry 41: 13902–13914

Bartsevich VV and Pakrasi HB (1997) Molecular identification of a novel protein that regulates biogenesis of photosystem I, a membrane protein complex. J Biol Chem 272: 6382–6387

Ben-Shem A, Frolow F and Nelson N (2003) Crystal structure of plant photosystem I. Nature 426: 630–635

Bolle C, Herrmann RG and Oelmuller R (1996) Intron sequences are involved in the plastid- and light-dependent expression of the spinach *psaD* gene. Plant J 10: 919–924

Bottin H, Hanley J and Lagoutte B (2001) Role of acidic amino acid residues of PsaD subunit on limiting the affinity of photosystem I for ferredoxin. Biochem Biophys Res Commun 287: 833–836

Boudreau E, Takahashi Y, Lemieux C, Turmel M and Rochaix J-D (1997) The chloroplast *ycf3* and *ycf4* open reading frames of *Chlamydomonas reinhardtii* are required for the accumulation of the photosystem I complex. EMBO J 16: 6095–6104

Chitnis PR (2001) Photosystem I: function and physiology. Annu Rev Plant Physiol Plant Mol Biol 52: 593–626

Chitnis PR and Nelson N (1992) Assembly of two subunits of the cyanobacterial photosystem I on the N-side of thylakoid membranes. Plant Physiol 99: 239–246

Chitnis PR, Reilly PA and Nelson N (1989) Insertional inactivation of the gene encoding subunit II of photosystem I from the cyanobacterium *Synechocystis* sp. PCC 6803. J Biol Chem 264: 18381–18385

Chitnis PR, Purvis D and Nelson N (1991) Molecular cloning and targeted mutagenesis of the gene *psaF* encoding subunit III of photosystem I from the cyanobacterium *Synechocystis* sp. PCC 6803. J Biol Chem 266: 20146–20151

Chitnis PR, Xu Q, Chitnis VP and Nechushtai R (1995) Function and organization of photosystem I polypeptides. Photosynth Res 44: 23–40

Chitnis VP, Jungs YS, Albee L, Golbeck JH and Chitnis PR (1996) Mutational analysis of photosystem I polypeptides. Role of PsaD and the lysyl 106 residue in the reductase activity of the photosystem I. J Biol Chem 271: 11772–11780

Chitnis VP, Ke A and Chitnis PR (1997) The PsaD subunit of photosystem I. Mutations in the basic domain reduce the level of PsaD in the membranes. Plant Physiol 115: 1699–1705

Cohen Y and Nechushtai R (1992) Assembly and processing of subunit II (PsaD) precursor in the isolated photosystem-I complex. FEBS Lett 302: 15–17

Cohen Y, Steppuhn J, Herrmann RG, Yalovsky S and Nechushtai R (1992) Insertion and assembly of the precursor of subunit II into the photosystem I complex may precede its processing. EMBO J 11: 79–85

Cohen Y, Chitnis VP, Nechushtai R and Chitnis PR (1993) Stable assembly of PsaE into cyanobacterial photosynthetic membranes is dependent on the presence of other accessory subunits of photosystem I. Plant Mol Biol 23: 895–900

Cohen Y, Nelson N, Chitnis PR and Nechushtai R (1995) The carboxyl-terminal region of the spinach PsaD subunit contains information for its specific assembly into plant thylakoids. Photosynth Res 44: 157–164

Diaz-Quintana A, Leibl W, Bottin H and Sétif P (1998) Electron transfer in photosystem I reaction centers follows a linear pathway in which iron–sulfur cluster F_B is the immediate electron donor to soluble ferredoxin. Biochemistry 37: 3429–3439

Domonkos I, Malec P, Sallai A, Kovacs L, Itoh K, Shen G, Ughy B, Bogos B, Sakurai I, Kis M, Strzalka K, Wada H, Itoh S, Farkas T and Gombos Z (2004) Phosphatidylglycerol is essential for oligomerization of photosystem I reaction center. Plant Physiol 134: 1471–1478

Falzone CJ, Kao YH, Zhao J, Bryant DA and Lecomte JT (1994) Three-dimensional solution structure of PsaE from the cyanobacterium *Synechococcus* sp. strain PCC 7002, a photosystem I protein that shows structural homology with SH3 domains. Biochemistry 33(20): 6052–6062

Farah J, Rappaport F, Choquet Y, Joliot P and Rochaix JD (1995) Isolation of a *psaF*-deficient mutant of *Chlamydomonas reinhardtii*: efficient interaction of plastocyanin with the photosystem I reaction center is mediated by the PsaF subunit. EMBO J 14 (20): 4976–4984

Fischer N, Sétif P and Rochaix JD (1997) Targeted mutations in the *psaC* gene of *Chlamydomonas reinhardtii*: preferential reduction of F_B at low temperature is not accompanied by altered electron flow from photosystem I to ferredoxin. Biochemistry 36: 93–102

Fischer N, Hippler M, Sétif P, Jacquot JP and Rochaix JD (1998) The PsaC subunit of photosystem I provides an essential lysine residue for fast electron transfer to ferredoxin. EMBO J 17: 849–858

Fischer N, Sétif P and Rochaix JD (1999) Site-directed mutagenesis of the PsaC subunit of photosystem I. F_B is the cluster interacting with soluble ferredoxin. J Biol Chem 274: 23333–23340

Flieger K, Wicke A, Herrmann RG and Oelmuller R (1994) Promoter and leader sequences of the spinach PsaD and PsaF genes direct an opposite light response in tobacco cotyledons: PsaD sequences downstream of the ATG codon are required for a positive light response. Plant J 6: 359–368

Floss B, Igloi GL, Cassier-Chauvat C and Muhlenhoff U (1997) Molecular characterization and overexpression of the *petF* gene from *Synechococcus elongatus*: evidence for a second site of electrostatic interaction between ferredoxin and the PS I-D subunit. Photosynth Res 54: 63–71

Fromme P (1996) Structure and function of photosystem I. Curr Opin Struct Biol 6: 473–484

Fromme P, Jordan P and Krauß N (2001) Structure of photosystem I. Biochim Biophys Acta 1507: 5–31

Fromme P, Bottin H, Krauß N and Sétif P (2002) Crystallization and electron paramagnetic resonance characterization of the complex of photosystem I with its natural electron acceptor ferredoxin. Biophys J 83: 1760–1773

Giuliano G, Hoffman NE, Ko K, Scolnik PA and Cashmore AR (1988) A light-entrained circadian clock controls transcription of several plant genes. EMBO J 7: 3635–3642

Golbeck JH (1999) A comparative analysis of the spin state distribution of *in vitro* and *in vivo* mutants of PsaC. A biochemical argument for the sequence of electron transfer in Photosystem I as $F_X \rightarrow F_A \rightarrow F_B \rightarrow$ ferredoxin/flavodoxin. Photosynth Res 61: 107–144

Gong XM, Agalarov R, Brettel K and Carmeli C (2003) Control of electron transport in photosystem I by the iron–sulfur cluster F_X in response to intra- and intersubunit interactions. J Biol Chem 278: 19141–19150

Guillouard I, Lagoutte B, Moal G and Bottin H (2000) Importance of the region including aspartates 57 and 60 of ferredoxin on the electron transfer complex with photosystem I in the cyanobacterium *Synechocystis* sp. PCC 6803. Biochem Biophys Res Commun 271: 647–653

Hanley J, Sétif P, Bottin H and Lagoutte B (1996) Mutagenesis of photosystem I in the region of the ferredoxin cross-linking site: modifications of positively charged amino acids. Biochemistry 35: 8563–8571

Hayashida N, Matsubayashi T, Shinozaki K, Sugiura M, Inoue K and Hiyama T (1987) The gene for the 9 kd polypeptide, a possible apoprotein for the iron–sulfur centers A and B of the photosystem I complex, in tobacco chloroplast DNA. Curr Genet 12: 247–250

Hibino T, Lee BH, Yajima T, Odani A, Yamauchi O and Takabe T (1996) Kinetic and cross-linking studies on the interactions of negative patch mutant plastocyanin from *Silene pratensis* with photosystem I complexes from cyanobacteria, green algae, and plants. J Biochem (Tokyo) 120: 556–563

Hippler M, Reichert J, Sutter M, Zak E, Altschmied L, Schroer U, Herrmann RG and Haehnel W (1996) The plastocyanin binding domain of photosystem I. EMBO J 15: 6374–6384

Hippler M, Drepper F, Farah J and Rochaix JD (1997) Fast electron transfer from cytochrome c_6 and plastocyanin to photosystem I of *Chlamydomonas reinhardtii* requires PsaF. Biochemistry 36: 6343–6349

Hippler M, Drepper F, Haehnel W and Rochaix JD (1998) The N-terminal domain of PsaF: precise recognition site for binding and fast electron transfer from cytochrome c_6 and plastocyanin to photosystem I of *Chlamydomonas reinhardtii*. Proc Natl Acad Sci USA 95: 7339–7344

Hirasawa M, Sung JD, Malkin R, Zilber A, Droux M and Knaff DB (1988) Evidence for the presence of a [2Fe–2S] ferredoxin in bean sprouts. Biochim Biophys Acta 934: 169–176

Jin P, Sun J and Chitnis PR (1999) Structural features and assembly of the soluble overexpressed PsaD subunit of photosystem I. Biochim Biophys Acta 1410: 7–18

Jonsson U, Fagerstam L, Ivarsson B, Johnsson B, Karlsson R, Lundh K, Lofas S, Persson B, Roos H, Ronnberg I, Sjolander S, Stenberg E, Stahlberg R, Urbaniczky C, Ostlin H and Malmqvist M (1991) Real-time biospecific interaction analysis using surface plasmon resonance and a sensor chip technology. Biotechniques 11: 620–627

Jordan P, Fromme P, Witt HT, Klukas O, Saenger W and Krauß N (2001) Three-dimensional structure of cyanobacterial photosystem I at 2.5 Å resolution. Nature 411: 909–917

Jung YS, Vassiliev IR, Yu J, McIntosh L and Golbeck JH (1997) Strains of *Synechocystis* sp. PCC 6803 with altered PsaC. II. EPR and optical spectroscopic properties of F_A and F_B in aspartate, serine, and alanine replacements of cysteines 14 and 51. J Biol Chem 272: 8040–8049

Klukas O, Schubert WD, Jordan P, Krauß N, Fromme P, Witt HT and Saenger W (1999a) Photosystem I, an improved model of the stromal subunits PsaC, PsaD, and PsaE. J Biol Chem 274: 7351–7360

Klukas O, Schubert W-D, Jordan P, Krauß N, Fromme P, Witt HT and Saenger W (1999b) Localization of two phylloquinones, Q_K and $Q_{K'}$, in an improved electron density map of photosystem I at 4-Å resolution. J Biol Chem 274: 7361–7367

Knaff DB (1996) Ferredoxin and ferredoxin-dependent enzymes. In: Ort DR and Yocum C (eds) Oxygenic Photosynthesis: The Light Reactions, pp. 333–361. Kluwer Academic Publishers, Dordrecht

Knaff DB and Hirasawa M (1991) Ferredoxin-dependent chloroplast enzymes. Biochim Biophys Acta 1056: 93–125

Kruip J, Chitnis PR, Lagoutte B, Rögner M and Boekema EJ (1997) Structural organization of the major subunits in cyanobacterial photosystem 1. Localization of subunits PsaC, -D, -E, -F, and -J. J Biol Chem 272: 17061–17069

Lagoutte B, Hanley J and Bottin H (2001) Multiple functions for the C terminus of the PsaD subunit in the cyanobacterial photosystem I complex. Plant Physiol 126: 307–316

Lelong C, Sétif P, Lagoutte B and Bottin H (1994) Identification of the amino acids involved in the functional interaction between photosystem I and ferredoxin from *Synechocystis* sp. PCC 6803 by chemical cross-linking. J Biol Chem 269: 10034–10039

Lelong C, Boekema EJ, Kruip J, Bottin H, Rogner M and Sétif P (1996) Characterization of a redox active cross-linked complex between cyanobacterial photosystem I and soluble ferredoxin. EMBO J 15: 2160–2168

Li N, Zhao JD, Warren PV, Warden JT, Bryant DA and Golbeck JH (1991) PsaD is required for the stable binding of PsaC to the photosystem I core protein of *Synechococcus* sp. PCC 6301. Biochemistry 30: 7863–7872

Lotan O, Cohen Y, Michaeli D and Nechushtai R (1993) High levels of photosystem I subunit II (PsaD) mRNA result in the accumulation of the PsaD polypeptide only in the presence of light. J Biol Chem 268: 16185–16189

Lushy A, He Z, Fish A, Darash-Yahana M, Minai L, Verchovsky L, Michaeli D and Nechushtai R (2000) An insight into the assembly and organization of photosystem I complex in the thylakoid membranes of the thermophilic cyanobacterium, *Mastigocladus laminosus*. Indian J Biochem Biophys 37: 405–417

Lushy A, Verchovsky L and Nechushtai R (2002) The stable assembly of newly synthesized PsaE into the photosystem I complex occurring via the exchange mechanism is facilitated by electrostatic interactions. Biochemistry 41: 11192–11199

Mannan RM, Pakrasi HB and Sonoike K (1994) The PsaC protein is necessary for the stable association of the PsaD, PsaE, and PsaL proteins in the photosystem I complex: analysis of a cyanobacterial mutant strain. Arch Biochem Biophys 315: 68–73

Mayer KL, Shen G, Bryant DA, Lecomte JT and Falzone CJ (1999) The solution structure of photosystem I accessory protein E from the cyanobacterium *Nostoc* sp. strain PCC 8009. Biochemistry 38: 13736–13746

Meimberg K, Lagoutte B, Bottin H and Mühlenhoff U (1998) The PsaE subunit is required for complex formation between photosystem I and flavodoxin from the cyanobacterium *Synechocystis* sp. PCC 6803. Biochemistry 37: 9759–9767

Meimberg K, Fischer N, Rochaix JD and Mühlenhoff U (1999) Lys35 of PsaC is required for the efficient photoreduction of flavodoxin by photosystem I from *Chlamydomonas reinhardtii*. Eur J Biochem 263: 137–144

Minai L and Nechushtai R (1995) Electrostatic interactions are involved in the assembly of PsaD into Photosystem I. The Xth International Photosynthesis Congress. Kluwer Academic Publishers, Montpellier, France

Minai L and Nechushtai R (2001) The specific assembly of the peripheral PsaD subunit into the photosystem I complex of different organisms. PS2001 Proceedings: 12th International Congress on Photosynthesis. CSIRO Publishing, Melbourne, Australia

Minai L, Cohen Y, Chitnis PR and Nechushtai R (1996) The precursor of PsaD assembles into the photosystem I complex in two steps. Proc Natl Acad Sci USA 93: 6338–6342

Minai L, Fish A, Darash-Yahana M, Verchovsky L and Nechushtai R (2001) The assembly of the PsaD subunit into the membranal photosystem I complex occurs via an exchange mechanism. Biochemistry 40: 12754–12760

Mühlenhoff U and Sétif P (1996) Laser flash absorption spectroscopy study of flavodoxin reduction by photosystem I in *Synechococcus* sp. PCC 7002. Biochemistry 35: 1367–1374

Mühlenhoff U, Kruip J, Bryant DA, Rogner M, Sétif P and Boekema E (1996a) Characterization of a redox-active cross-linked complex between cyanobacterial photosystem I and its physiological acceptor flavodoxin. EMBO J 15: 488–497

Mühlenhoff U, Zhao J and Bryant DA (1996b) Interaction between photosystem I and flavodoxin from the cyanobacterium *Synechococcus* sp. PCC 7002 as revealed by chemical cross-linking. Eur J Biochem 235: 324–331

Naver H, Scott MP, Golbeck JH, Møller BL and Scheller HV (1996) Reconstitution of barley photosystem I with modified PSI-C allows identification of domains interacting with PSI-D and PSI-A/B. J Biol Chem 271: 8996–9001

Naver H, Boudreau E and Rochaix JD (2001) Functional studies of Ycf3: its role in assembly of photosystem I and interactions with some of its subunits. Plant Cell 13: 2731–2745

Nechushtai R and Nelson N (1981) Purification properties and biogenesis of *Chlamydomonas reinhardtii* photosystem I reaction center. J Biol Chem 256: 11624–11628

Nechushtai R and Nelson N (1985) Biogenesis of photosystem I reaction center during greening of oat, bean and spinach leaves. Plant Mol Biol 4: 377–384

Nield J, Morris EP, Bibby TS and Barber J (2003) Structural analysis of the photosystem I supercomplex of cyanobacteria induced by iron deficiency. Biochemistry 42: 3180–3188

Oelmuller R, Kendrick RE and Briggs WR (1989) Blue-light mediated accumulation of nuclear-encoded transcripts coding for proteins of the thylakoid membrane is absent in the phytochrome-deficient aurea mutant of tomato. Plant Mol Biol 13: 223–232

Oh-oka H, Takahashi Y, Wada K, Matsubara H, Ohyama K and Ozeki H (1987) The 8 kDa polypeptide in photosystem I is a probable candidate of an iron–sulfur center protein coded by the chloroplast gene *frxA*. FEBS Lett 218: 52–54

Oh-oka H, Takahashi Y, Kuriyama K, Saeki K and Matsubara H (1988) The protein responsible for center A/B in spinach photosystem I: isolation with iron–sulfur cluster(s) and complete sequence analysis. J Biochem 103: 962–968

Pandini V, Aliverti A and Zanetti G (1999) Interaction of the soluble recombinant PsaD subunit of spinach photosystem I with ferredoxin I. Biochemistry 38: 10707–10713

Pfannschmidt T, Schutze K, Brost M and Oelmuller R (2001) A novel mechanism of nuclear photosynthesis gene regulation by redox signals from the chloroplast during photosystem stoichiometry adjustment. J Biol Chem 276: 36125–36130

Poncelet M, Cassier-Chauvat C, Leschelle X, Bottin H and Chauvat F (1998) Targeted deletion and mutational analysis of the essential (2Fe–2S) plant-like ferredoxin in *Synechocystis* PCC 6803 by plasmid shuffling. Mol Microbiol 28: 813–821

Rhiel E, Stirewalt VL, Gasparich GE and Bryant DA (1992) The *psaC* genes of *Synechococcus* sp. PCC 7002 and *Cyanophora paradoxa:* cloning and sequence analysis. Gene 112: 123–128

Rochaix JD, Perron K, Dauvillee D, Laroche F, Takahashi Y and Goldschmidt-Clermont M (2004) Post-transcriptional steps involved in the assembly of photosystem I in *Chlamydomonas*. Biochem Soc Trans 32: 567–570

Rousseau F, Setif P and Lagoutte B (1993) Evidence for the involvement of PSI-E subunit in the reduction of ferredoxin by photosystem I. EMBO J 12: 1755–1765

Ruf S, Kossel H and Bock R (1997) Targeted inactivation of a tobacco intron-containing open reading frame reveals a novel chloroplast-encoded photosystem I-related gene. J Cell Biol 139: 95–102

Ruffle SV, Mustafa AO, Kitmitto A, Holzenburg A and Ford RC (2000) The location of the mobile electron carrier ferredoxin in vascular plant photosystem I. J Biol Chem 275: 36250–36255

Sétif P (2001) Ferredoxin and flavodoxin reduction by photosystem I. Biochim Biophys Acta 1507: 161–179

Sétif PQ and Bottin H (1994) Laser flash absorption spectroscopy study of ferredoxin reduction by photosystem I in *Synechocystis* sp. PCC 6803: evidence for submicrosecond and microsecond kinetics. Biochemistry 33: 8495–8504

Sétif PQ and Bottin H (1995) Laser flash absorption spectroscopy study of ferredoxin reduction by photosystem I: spectral and kinetic evidence for the existence of several photosystem I–ferredoxin complexes. Biochemistry 34: 9059–9070

Sétif P, Fischer N, Lagoutte B, Bottin H and Rochaix JD (2002) The ferredoxin docking site of photosystem I. Biochim Biophys Acta 1555: 204–209

Shen G, Antonkine ML, van der Est A, Vassiliev IR, Brettel K, Bittl R, Zech SG, Zhao J, Stehlik D, Bryant DA and Golbeck JH (2002a) Assembly of photosystem I. II. Rubredoxin is required for the *in vivo* assembly of F_X in *Synechococcus* sp. PCC 7002 as shown by optical and EPR spectroscopy. J Biol Chem 277: 20355–20366

Shen G, Zhao J, Reimer SK, Antonkine ML, Cai Q, Weiland SM, Golbeck JH and Bryant DA (2002b) Assembly of photosystem I. I. Inactivation of the *rubA* gene encoding a membrane-associated rubredoxin in the cyanobacterium *Synechococcus* sp. PCC 7002 causes a loss of photosystem I activity. J Biol Chem 277: 20343–20354

Sherameti I, Nakamura M, Yamamoto YY, Pfannschmidt T, Obokata J and Oelmuller R (2002) Polyribosome loading of spinach mRNAs for photosystem I subunits is controlled by photosynthetic electron transport. Plant J 32: 631–639

Steinmuller K (1992) Identification of a second *psaC* gene in the cyanobacterium *Synechocystis* sp. PCC 6803. Plant Mol Biol 20: 997–1001

Sykes GA and Rogers LJ (1984) Redox potentials of algal and cyanobacterial flavodoxins. Biochem J 217: 845–850

Thompson JD, Higgins DG and Gibson TJ (1994) CLUSTAL W: improving the sensitivity of progressive multiple sequence alignment through sequence weighting, position-specific gap penalties and weight matrix choice. Nucleic Acids Res 22: 4673–4680

Tsukihara T, Fukuyama K, Mizushima M, Harioka T, Kusunoki M, Katsube Y, Hase T and Matsubara H (1990) Structure of the [2Fe–2S] ferredoxin I from the blue-green alga *Aphanothece sacrum* at 2.2 Å resolution. J Mol Biol 216: 399–410

Vallon O and Bogorad L (1993) Topological study of PSI-A and PSI-B, the large subunits of the photosystem-I reaction center. Eur J Biochem 214: 907–915

van Thor JJ, Geerlings TH, Matthijs HC and Hellingwerf KJ (1999) Kinetic evidence for the PsaE-dependent transient ternary complex photosystem I/ferredoxin/ferredoxin: NADP(+) reductase in a cyanobacterium. Biochemistry 38: 12735–12746

Varotto C, Pesaresi P, Meurer J, Oelmuller R, Steiner-Lange S, Salamini F and Leister D (2000) Disruption of the Arabidopsis photosystem I gene *psaE1* affects photosynthesis and impairs growth. Plant J 22: 115–124

Vassiliev IR, Jung Y-S, Yang F and Golbeck JH (1998) PsaC subunit of photosystem I is oriented with iron–sulfur cluster F_B as the immediate electron donor to ferredoxin and flavodoxin. Biophys J 74: 2029–2035

Vassiliev IR, Antonkine ML and Golbeck JH (2001) Iron–sulfur clusters in type I reaction centers. Biochim Biophys Acta 1507: 139–160

Weber N and Strotmann H (1993) On the function of subunit PsaE in chloroplast Photosystem I. Biochim Biophys Acta 1143: 204–210

Wilde A, Hartel H, Hubschmann T, Hoffmann P, Shestakov SV and Borner T (1995) Inactivation of a *Synechocystis* sp. strain PCC 6803 gene with homology to conserved chloroplast open reading frame 184 increases the Photosystem II-to-Photosystem I ratio. Plant Cell 7: 649–658

Wollman FA, Minai L and Nechushtai R (1999) The biogenesis and assembly of photosynthetic proteins in thylakoid membranes. Biochim Biophys Acta 1411: 21–85

Wostrikoff K, Girard-Bascou J, Wollman FA and Choquet Y (2004) Biogenesis of PSI involves a cascade of translational autoregulation in the chloroplast of Chlamydomonas. EMBO J 23: 2696–2705

Wynn RM and Malkin R (1988) Characterization of an isolated chloroplast membrane FeS protein and its identification as the photosystem I FeS_A/FeS_B binding protein. FEBS Lett 229: 293–297

Xia Z, Broadhurst RW, Laue ED, Bryant DA, Golbeck JH and Bendall DS (1998) Structure and properties in solution of PsaD, an extrinsic polypeptide of photosystem I. Eur J Biochem 255: 309–316

Xu Q, Guikema JA and Chitnis PR (1994a) Identification of surface-exposed domains on the reducing side of photosystem I. Plant Physiol 106: 617–624

Xu Q, Jung YS, Chitnis VP, Guikema JA, Golbeck JH and Chitnis PR (1994b) Mutational analysis of photosystem I polypeptides in *Synechocystis* sp. PCC 6803. Subunit requirements for reduction of NADP+ mediated by ferredoxin and flavodoxin. J Biol Chem 269: 21512–21518

Yabe T, Morimoto K, Kikuchi S, Nishio K, Terashima I and Nakai M (2004) The Arabidopsis chloroplastic NifU-like protein CnfU, which can act as an iron–sulfur cluster scaffold protein, is required for biogenesis of ferredoxin and photosystem I. Plant Cell 16: 993–1007

Yang F, Shen G, Schluchter WM, Zybailov BL, Ganago AO, Vassiliev IR, Bryant DA and Golbeck JH (1998) Deletion of the PsaF polypeptide modifies the environment of the redox-active phylloquinone (A_1) Evidence for unidirectionality of electron transfer in Photosystem I. J Phys Chem B 102: 8288–8299

Yu L, Zhao J, Mühlenhoff U, Bryant DA and Golbeck JH (1993) PsaE Is required for *in vivo* cyclic electron flow around Photosystem I in the cyanobacterium *Synechococcus* sp. PCC 7002. Plant Physiol 103: 171–180

Yu J, Smart LB, Jung YS, Golbeck J and McIntosh L (1995) Absence of PsaC subunit allows assembly of photosystem I core but prevents the binding of PsaD and PsaE in *Synechocystis* sp. PCC 6803. Plant Mol Biol 29: 331–342

Zak E and Pakrasi HB (2000) The BtpA protein stabilizes the reaction center proteins of photosystem I in the cyanobacterium *Synechocystis* sp. PCC 6803 at low temperature. Plant Physiol 123: 215–222

Zak E, Norling B, Andersson B and Pakrasi HB (1999) Subcellular localization of the BtpA protein in the cyanobacterium *Synechocystis* sp. PCC 6803. Eur J Biochem 261: 311–316

Zanetti G and Merati G (1987) Interaction between photosystem I and ferredoxin. Identification by chemical cross-linking of the polypeptide which binds ferredoxin. Eur J Biochem 169: 143–146

Zhao JD, Warren PV, Li N, Bryant DA and Golbeck JH (1990) Reconstitution of electron transport in photosystem I with PsaC and PsaD proteins expressed in *Escherichia coli*. FEBS Lett 276: 175–180

Chapter 33

Thermodynamics of Photosystem I

David Mauzerall*
Rockefeller University, 1230 York Avenue, New York, NY 10021-6399, USA

Summary

Methods of obtaining the free energy and enthalpy of the steps of electron transfer through the Photosystem I reaction center are presented. The values are tabulated and discussed from the viewpoint of efficiency of the process. The bacterial system resembles Photosystem I but Photosystem II is quite different. It appears that more energy is lost

*Author for correspondence, email: mauzera@mail.rockefeller.edu

John H. Golbeck (ed): Photosystem I: The Light-Driven Plastocyanin:Ferredoxin Oxidoreductase, 571–581.

than strictly required by thermodynamics. A greater understanding is obtained by decomposing the free energy into its components of enthalpy and entropy. These identify changes in bonding energy in contrast to changes in structure/ordering of the system. It is found that the contribution of entropy to these processes is substantial. In fact, the A_1 to $F_{A/B}$ step is entropy driven. The volume changes associated with these electron transfer steps give information on the effective dielectric coefficient of the reaction center protein and show fairly large effects of substituting plastoquinone for phylloquinone at the A_1 site. They provide confirmation that the electron is delocalized over the complete $Fe_4S_4(Cys)_4$ complex. Thus, these thermodynamic measurements can contribute significantly to our understanding of the remarkable process of photosynthesis.

I. Introduction

Knowledge of both the thermodynamics and the kinetics of a process are required for its full understanding. Extensive spectroscopic investigations have led to good knowledge of the intermediates in the process of Photosystem I (PS I) and the kinetics of the intermediate steps (see Chapters 16–29 of this volume). The successful determination of the structure of reaction centers and antenna proteins (see Chapters 6–8 of this volume) has added much to our understanding of the process. However, knowledge of the thermodynamics of the process is far less well advanced. Since the early photosynthetic reactions are electron transfer processes, the focus has been on the redox potentials of the intermediates. As discussed below, these values are not known at all well. There are two reasons to wish to know these values more accurately. One is the question of efficiency of the process. This word is used in different contexts with quite different meanings. It often refers to the efficiency of utilization of solar energy. This is a small and variable number. It is small because about half the solar energy is in the near and far infra-red regions which are not used in photosynthesis and because all the photon energy greater than the trap energy is rapidly degraded to heat. The trap energy is the energy of the excited state of the pigment(s) in the reaction center that do the first charge separation step. The theoretical efficiency is that fraction of the trap energy that is stored in the particular intermediates under consideration. It is thus a function of time, reaching a minimum when the final products of photosynthesis are reached. It is the prime subject of this chapter. The second reason to know the thermodynamics of a process is the far greater understanding obtained by breaking up the free energy into its components: enthalpy and entropy. From the viewpoint of statistical mechanics, a further breakdown into the change in heat capacity at each step is the most useful. Unfortunately, we are still quite a ways from the precise measurements required for this much knowledge of the intermediates. Knowledge of the components of the free energy allows us to separate this energy into its bonding or enthalpy and structural or entropy components. The latter is often a small component in many chemical reactions at normal temperature, ~300 K. However, in structured environments such as proteins and the particular solvent, water, the contribution of entropy can be the determining factor. This is exemplified in the denaturation of proteins where the massive configuration entropy determines the thermal reaction.

Abbreviations: A_0 – primary acceptor of PS I, chlorophyll; A_1 – secondary acceptor in PS I, phylloquinone; A_P – secondary acceptor in PS I, *menA,B* mutants, plastoquinone; B_{860} – trap of bacterial photosystem; DMF – dimethylformamide; EPR – electron paramagnetic resonance; $F_{A/B}$ – second and third Fe/S cluster acceptors in PS I; Fd – ferredoxin; FNR-Fd – ferredoxin nucleotide reductase—ferredoxin complex; F_X – first Fe/S cluster acceptor in PS I; P_{700} – trap of PS I; PS I – photosystem I; PS II – photosystem II; Q_A – primary quinone acceptor in bacterial photosystem; RC – reaction center.

II. Components of Photosystem I

It was not long after the discovery of P_{700}, the primary photoreactant of Photosystem I (PS I) by absorption spectroscopy (Kok, 1957; Ke, this volume, Chapter 3) that its redox potential was determined (Kok, 1961). The redox potential with a change of units is the free energy of the reaction: $\Delta G^\circ = -nFE^\circ$, where n is the number of electrons exchanged and F is the Faraday constant. Since it is the Gibbs free energy that determines the equilibrium of a reaction, interest in thermodynamics of electron transfer reactions has often stopped there and the focus has been on the kinetics of the processes. This attitude has been reinforced by the success of the Marcus theory (Marcus and Sutin, 1985; Moser and Dutton, this volume, Chapter 34) in correlating the kinetics of electron transfer with the free energy of the reaction. However, a much greater understanding of the process can be obtained by decomposing the free energy into its components of enthalpy and entropy. The former is a measure of the change in bonding

interactions, while the latter is a measure of the probability of the state. For simple chemical reactions the entropy contribution is small, but for structured material such as liquid water and proteins the entropy can determine the change in free energy. I will outline what is known of the thermodynamics of PS I and discuss our measurements of the enthalpy and volume changes of these reactions using photoacoustics. By combining knowledge of changes in free energy and enthalpy, one can obtain the change in entropy via the Gibbs relation: $\Delta G = \Delta H - T\Delta S$.

There are many excellent reviews of the structure and function of PS I (Fromme et al., 2000; Chitnis, 2001; Heathcote et al., 2003) including this very book. Spectroscopic methods have established the kinetics over the entire time range and the crystal structure determinations have fixed the location and orientation of molecules previously inferred from complex spectroscopic measurements. I will only outline the known steps of the electron transfer chain and discuss the energetics of these steps.

2 psec 30 psec 10 nsec to 100 nsec 1 μsec

$P^*_{700} \rightarrow A_0 \rightarrow A_1 \rightarrow F_X \rightarrow F_A/F_B \rightarrow F_d$

-1.25 -1.05 -0.85 -0.7 -0.5 -0.4 V

P^*_{700} is the excited state of the photoreactive or trap chlorophyll in the reaction center; A_0 is the primary chlorophyll acceptor; A_1 is the secondary acceptor, a phylloquinone; F_X is the first iron–sulfur complex; F_A/F_B is the pair of iron–sulfur complexes thought to be in equilibrium; and F_d is ferredoxin. The times shown are rough approximations. The detailed kinetics are described in Chapters 24–29 of this volume. The numbers below the components are their approximate potentials. Since these are the crux of the matter, I will discuss the methods of obtaining their values. The potentials are relative to the standard hydrogen electrode and the free energies are relative to the reduced P_{700}, oxidized acceptors state. I will use eV (understood/molecule) as the unit of energy (1 eV = 23 kcal/mol or 99.6 kJ/mol) as the unit of energy since it is so directly related to the potentials, V, involved.

III. Methods of Determining Redox Potentials

A. Direct Method

One establishes a fixed redox potential with mediators (small redox molecules of suitable potential that react with the preparation) or directly with electrodes in the case of bacterial reaction centers. The ratio of reduced to oxidized species is determined, usually by absorption or EPR spectroscopy. The fixed potential is varied and the midpoint potential, E_m, is determined. This very general method has been used for most intermediates in the photosynthetic electron transfer pathways. As pointed out by Brettel (1997), this method measures a single potential of the pair formed photochemically. Electrostatic interaction between the donor and acceptor can shift the ΔG by 0.1–0.2 V, depending on their separation and the effective dielectric coefficient. Our estimate of the effective dielectric coefficient in the bacterial reaction center, 4 ± 1 with separation of 28 Å (Mauzerall et al., 2002), leads to a correction of 0.1 V. In addition there may be changes in the protein, and the reduced and oxidized species are necessarily measured under different conditions. The method is inherently slow and so the totally relaxed state is measured. Thus reactions occurring on the psec–nsec time scales may not be fully relaxed and so may have a higher potential than that measured at equilibrium. For these reasons, the quoted values of the potentials may have larger error than the simple measurement error.

B. Indirect Methods

1. Rates

An empirical relation between rates and free energies of reaction can be used to estimate ΔG. The Moser–Dutton relation between distance and rates based on the Marcus equation relating rates with ΔG and a reorganization energy is often used (see Moser and Dutton, this volume, Chapter 34). This method involves several ad hoc assumptions and results in uncertainties larger than the above method. The results should be taken as rough estimates. A better method is to assume equilibrium among the components of the chain and to use the observed forward rate constants together with estimates of the reverse rate constants obtained from the lifetime of the state under consideration, when further electron transfer is prohibited, to estimate the equilibrium constant and thus the ΔG of the step under consideration. Since the distances are large, direct electron tunneling in the reverse step is likely slower than the thermal climb through the intermediates at 300 K. The total free energy gap from the measured species to P^+_{700} is obtained and can be decomposed into other steps by further measurements. A detailed example is given by Shinkarev et al. (2002); see Shinkarev (this volume, Chapter 36).

2. Fluorescence

The ratio of delayed to prompt fluorescence in reaction centers of *Rhodobacter sphaeroides* was used by Arata and Parson (1981a) to estimate the free energy of the B^*_{860} to Q_A electron transfer. The weak fluorescence of PS I seems to have hindered the use of this method.

C. Experimental Free Energies

The data in this section are largely taken from the reviews by Brettel (1997), Brettel and Leibl (2001), and Fromme et al. (2000).

1. $P^*_{700} \rightarrow A_0$

Kleinherenbrink et al. (1994) estimated a ΔG of -0.25 eV for this reaction from the ratio of prompt fluorescence to that at 35 nsec, the lifetime of A_0. The measurement required double reduction of A_1, which may well lessen the gap. Assuming the (free) energy of P^*_{700} is 1.77 eV ($E_{h\nu}$ of 700 nm) the ΔG of $P^+_{700}A^-_0$ is 1.52 eV above the ground state.

2. $A_0 \rightarrow A_1$

The A_1/A_1^- potential was indirectly estimated at -0.81 V by the effect of an electric field on the kinetics of luminescence (Vos and Van Gorkum, 1990) and is quoted as -0.76 V by Shinkarev et al. (2002). This is 0.3 V more negative than in DMF and reflects the large influence of the protein by lowering the effective dielectric coefficient and minimizing hydrogen bonding (Chitnis, 2001). The redox potentials of quinones are known to be sensitive to their environment (Prince et al., 1981). Taking the potential of P^+_{700} as +0.5 V, the ΔG of $P^+_{700}A^-_1$ is -1.3 eV. Analysis of the temperature dependence of the slow recovery kinetics of A_1^- (Sétif and Brettel, 1993) also gave a ΔG for $A_0 \rightarrow A_1$ of -0.2 eV. However, more recent analysis (Agalarov and Brettel, 2003) gave -0.1 eV for this value. They suggested that the two relaxation times and redox potentials refer to the A and B chains of the cofactors in the PS I RC but this is still uncertain (see Van der Est, this volume, Chapter 24).

3. $P^*_{700} \rightarrow A_P$

The *menA* and *menB* mutants of *Synechocystis* sp. PCC 6803 (Semenov et al., 2000) insert plastoquinone into the A_1 pocket when the synthesis of phylloquinone is inhibited. The mutant can grow photosynthetically in dim light but the electron transfer to the F_X acceptor is slowed 1,000-fold. The ΔG of A_0^- to A_P has been estimated by the rate method (Shinkarev et al., 2002) to be -0.4 eV, i.e., to be 0.2 eV below that of the phylloquinone, i.e., to have a potential of ~ -0.6 V. If the 1,000-fold slowing of electron transfer to F_X is simply interpreted as an increased activation energy, one estimates an energy difference of 0.18 eV. The redox potential of plastoquinone in the A_1 site of PS I is another example of the strong influence of the protein: it is -0.13 V in the Q_A site of PS II and -0.04 V in the Q_B site. The availability of hydrogen bonds is a critical component of this influence.

4. $A_1 \rightarrow F_X$

Various redox titrations of F_X lead to a potential of -0.73 V (Sétif and Brettel, 1993; reviewed by Brettel, 1997). Again, the succeeding components, $F_{A/B}$ are in the reduced state, which may affect the potential. Indeed the redox potential of F_X in the absence of PsaC (hence, in the absence of F_A and F_B) was measured to be 0.06 V more positive than in the control (Parrett et al., 1989). The ΔG of $P^+_{700}F^-_X$ is -1.2 eV and that of $A_1 \rightarrow F_X$ is -0.1 eV. Shinkarev et al. (2002) obtained the same value by analysis of rates of re-oxidation of F_X^-.

5. $A_P \rightarrow F_X$

Given the estimated potential of A_P as -0.67 V, the ΔG for this step is $\sim +0.1$ eV and partly accounts for the 1,000-fold slowing of this step relative to the wild type.

6. $F_X \rightarrow F_A/F_B$

Redox titrations of F_A and F_B lead to potentials of -0.54 and -0.59 V (reviewed by Brettel, 1997). The ΔG of $P^+_{700}F^-_{A/B}$ is -1.0 eV and that of $F_X \rightarrow F_A/F_B$ is -0.2 eV. Shinkarev et al. (2000) obtained a value of -0.1 eV for this step using the rate of re-oxidation of F_A/F_B. This may be an example of the difference between estimates of ΔG from redox measurements of single components and from rate measurements.

7. $F_A/F_B \rightarrow F_d$

The potential of F_d is -0.42 V, so ΔG of $P^+_{700}F^-_d$ is -0.9 eV and that of $F_A/F_B \rightarrow F_d$ is -0.1 to -0.2 eV.

I conclude that the redox potentials (free energies) of the steps in the PS I electron transfer pathway are only known to within ± 0.05 V (eV) because of the

limitations of methodology and variability of the preparations. The ΔG of some individual steps may be more accurately known and these seem to be in the 0.1–0.2 eV range. They are a compromise between retaining energy efficiency and the flow to products (see below). A recent review by Santabarbara et al. (2005) indicates possible complex equilibria between A_1 and $F_{A/B}$ intermediates.

IV. Decomposition of ΔG into ΔH and ΔS

Since entropy meters are hard to come by, a simple method is to measure ΔH and calculate ΔS by difference with ΔG. Before discussing the actual methods, I make a few comments.

1. The photosynthetic system is obviously "open," i.e., energy flows through the sequence of steps, yet we are treating it as a closed system at equilibrium. This is a good approximation for light intensities below saturation or for single turnover flashes where only one electron per unit is being transferred. The electron flow will lead to a potential drop across the organized system. The components span a biological membrane in their *in vivo* state. For liposomal or *in vivo* systems, the resulting transmembrane potential must be included in the estimated potential. There is also the question of the "relaxed" or complete equilibrium state of the system between each electron transfer step mentioned above. If this equilibrium state is reached, then all is well. If not, then a new state must be defined. Since the thermalization time in condensed phases is very fast, any step beyond a few psec can be defined as an "equilibrium" state. For faster times, the problem becomes one of kinetics and their best representation.

2. Since it is the changes of the thermodynamic parameters that occupy our attention, it is only the scale of the parameters and not their absolute values that are relevant. It is important to remember that these potentials are a function of temperature, pH, ionic strengths and, unfortunately, the particular preparation. For this reason *in vivo* measurements are very useful.

3. All of these thermodynamic parameters can be related to the changes in heat capacity, ΔCp. Unfortunately the time resolution of present, sensitive heat capacity measurements is insufficient for the transient intermediates under discussion.

A. Methods of Measuring Enthalpy

1. Indirect Method

The dependence on temperature of the yield of delayed light from previously excited reaction centers of *R. sphaeroides* has been used by Arata and Parson (1981b) to estimate the enthalpy of the charge separation reaction. The basic assumption is that the ion pair is in equilibrium with the singlet excited state. However, there are many other states, such as triplets involved and the detailed kinetics are always observed to be rather complex. This method has been criticized by Brettel (1997) and by McMahon et al. (1998). In any case the low fluorescence yield of PS I seems to have discouraged its use.

2. Direct Method

One directly measures the heat evolved in the reaction with pulsed photoacoustics. The method is well described in the literature (Braslavsky and Heibel, 1992; Feitelson and Mauzerall, 1996; Gensch and Viappiani, 2003) and I will only give an outline. A short pulse of light shaped as a sheet into a simple cell (Mauzerall et al., 1995) or onto a front face (Arnaut et al., 1992) cell generates a plane sound wave that is detected by a piezoelectric element. The volume change, which generates the pressure wave, has two sources. One is the thermal expansion (or contraction for water below its temperature of maximum density) caused by the desired heat flux. The second is any inherent volume change of the reaction itself. Prominent among the latter in photosynthetic primary reactions is a shrinkage caused by electrostriction on charge separation. Using the magic property of water referred to above, at the temperature of maximum density the thermal expansivity, α, is zero and so only inherent volume changes are observed. Assuming that ΔH and ΔV do not change over the small ($\sim$20°C) range of temperature, they are readily separated. To optimize signal-to-noise, one averages many weak flashes of light and plots the data, corrected for any changes in compressibility, versus the thermal expansivity of the particular medium used. By normalizing to the reference (see below) the slope of this line is $\Delta H/E_{h\nu}$ and the intercept is $\Delta V/\alpha\ E_{h\nu}$. Details are given in our papers (Edens et al., 2000; Hou et al., 2001a) and possible errors are discussed in Edens et al. (2000). The use of whole cells requires a

correction for their internal medium (see Boichenko et al., 2001). The time resolution depends on the thickness of the wave-forming volume. It is about 1 μsec for a 1 mm thickness. Deconvolution procedures allow measurement of 10% of this resolution (Feitelson and Mauzerall, 1996). We have resolved the 10 nsec lifetime of the B_{860} cation–bacteriopheophytin anion in quinone-less bacterial reaction centers in a 0.1 mm cell (Edens and Mauzerall, in preparation). All measurements are normalized to a reference, which absorbs the same as the sample at the working wavelength and degrades the absorbed photon to heat in less than the resolving time of the apparatus. Photosynthetic systems have an internal normalization when they are light-saturated. The absorption remains the same because of the large excess of antennae pigments over the reaction center pigments and the weak PA pulse is now the reference. This internal reference is very useful as it allows a calibration without changing the sample.

The long time range is limited to about 10 μsec because the pressure wave is proportional to the rate of volume change and thus decreases with this rate. For a given ΔV, a microvolt signal in 1 μsec becomes a nanovolt signal in 1 msec. In addition, reflections from any air boundaries in a reasonably sized apparatus lead to a confused signal within a few tens of μsec. An air microphone can be used to measure in the 10 msec time range and it determines heat only. However, it is principally sensitive to surface effects and thus is ideal for leaves. A synthetic leaf of algae on a Millipore filter has been used and given results in agreement with solution measurements for *Chlorella vulgaris* (Cha and Mauzerall, 1992) and for *Synechococcus* sp. PCC 7002 (Charlebois and Mauzerall, 1999).

We have now developed a cell which measures the pressure change directly and is useful in the 50 μsec to 1 sec time range (Edens et al., 2003; Mauzerall et al., 2003). Arata and Parson (1981b) used a capacitor cell to make similar measurements but their results could not be repeated. Their cell was far too sensitive to vibration and electrical interference. Our cell is more robust and the enthalpy and volume changes of intermediates in the photocycle of bacteriorhodopsin have been obtained (Liu et al., in preparation).

Given these difficulties, why measure enthalpy?

a. Separation of ΔG into ΔH and $T\Delta S$ defines the basic driving force of the reaction. If ΔH is the larger, the driving force is bonding, if $T\Delta S$ is the larger, it is the number of states or the occupation of low frequency modes, i.e., weak intermolecular interactions. For simple chemical reactions, ΔH usually predominates, but for reactions in the complex solvent water or with proteins, $T\Delta S$ can be very large because of structural changes and ensuing changes in the number of occupied states.
b. Comparison of ΔG and ΔH immediately distinguishes simple and complex reactions. If $\Delta G \sim \Delta H$ then $T\Delta S \sim 0$ and there are little structural changes or relaxations. But if not, then the reaction may be complex.
c. Reactions with small ΔG are often considered to be trivial: nothing much happens, one is near equilibrium. However, if one finds a large ΔH (of either sign) then there must be a corresponding large $T\Delta S$ of the same sign. Thus the small ΔG may hide large bonding and structural changes which would be missed without this added information. I give an example of this in the A_1^- to $F_{A/B}$ reaction below.

B. Measured Enthalpy and Volume, General Results

The results of our measurements on PS I are given in Table 1 along with data from bacterial reaction centers and PS II for comparison. The large volume decreases can be assigned to electrostriction and their analysis leads to a value of 4 ± 1 for the *effective* dielectric coefficient in the bacterial centers (Mauzerall et al., 2002). Here I will focus on the enthalpy data.

The volume and enthalpy changes of bacterial and PS I RC's are remarkably similar even though the bacterial RC is usually associated with PS II because of the quinone intermediate acceptor rather than the PS I Fe/S acceptors. In fact, the structures of all the RC's are very similar and the PS I centers have a phylloquinone secondary acceptor. The small volume change in PS II is caused either by the tyrosine donor, Y_Z, being already anionic and thus no charge is separated, or by a rapid proton transfer to the polar region where the electrostriction is much less (Hou et al., 2001b). The enthalpy of the PS I RC reaction, -0.4 eV, is much smaller than that previously estimated by the change of delayed light with temperature, -0.7 eV (Arata and Parson, 1981a). Brettel (1997) and McMahon et al. (1998) have given a critical discussion of the difficulties in using this method. It is possible that the free energy change could be smaller on the nsec–μsec time scale of the PA experiment and relax to a larger value at the ~100 msec time scale of the delayed light measurement. While relaxations on the psec–nsec time scale and the Q_B structural change (~100 μsec) in bacterial RC are well documented, changes on the time scale of

Table 1. Thermodynamic parameters of photosynthesis, 25°C

Reaction	Preparation	pH	ΔV (Å^3)	ΔH (eV)	ΔG (eV)	TΔS (eV)
$B^*_{860} \rightarrow Q_A$	RC[a]	8	−28	−0.44	−0.86	+0.42
$P^*_{700} \rightarrow F_{A/B}$	RC, PS I[b]	7	−26	−0.40	−0.74	+0.35
$P^*_{700} \rightarrow F_{A/B}$	WC, PS I[c]	7	−27	−0.32	−0.74	+0.4
$P^*_{700} \rightarrow A_1$	RC, PS I[d]	7	−23	−0.8	−0.6	−0.2
$A_1^- \rightarrow F_{AB}$	RC, PS I[d]	7	−3	+0.4	−0.2	+0.6
$P^*_{700} \rightarrow A_P$	RC, *menA*[e]	7	−17	−0.7	−0.67	−0.05
$A_P^- \rightarrow F_{AB}$	RC, *menA*[e]	7	−9	+0.3	−0.07	+0.4
Cyt $b_6/f \rightarrow$ Fd	WC, PS I[f]	8	–	−1.1	∼ −0.8	+0.3
$P^*_{680} \rightarrow Y_Z$	RC, PS II[g]	6	−9	−0.9	−0.77	−0.1
$P^*_{680} \rightarrow Y_Z$	RC, PS II[g]	9	−3	−1.15	−0.92	−0.2
$P^*_{680} \rightarrow Y_Z$	WC, PS II[c]	7	−1	−1	−0.77	−0.2
S state $\rightarrow Q_B$	WC, PS II[f]	8	–	−0.8	∼ −1.0	+0.2

Error: ΔV, ±1 Å^3, ΔH, ±0.1 eV except Boichenko et al. (2001) and Cha and Mauzerall (1992), ±0.2 eV. Time scale 1 μsec, all except Cha and Mauzerall (1992).
[a] *Rb. sphaeroides*, Edens et al. (2000).
[b] *Synechocystis sp*. PCC 6803, Hou et al. (2001a).
[c] *Synechocystis sp*. PCC 6803, whole cells, Boichenko et al. (2001).
[d] *Synechocystis sp*. PCC 6803, Hou et al. (in preparation).
[e] *Synechocystis sp*. PCC 6803, *menA*/*B* mutants, Hou et al. (in preparation).
[f] *C. vulgaris*, whole cells, air microphone, time scale 10 msec, Cha and Mauzerall (1992).
[g] *Synechocystis* sp. PCC 6803, Hou et al. (2001b).

interest in PS I are not known. Note that if the free energy is mistaken, then the myriad fits of electron transfer rates to the Marcus theory using these values are in error.

We have chosen to interpret the difference between the observed values of ΔG and ΔH as TΔS in energy units. This is the simplest interpretation and serves to focus attention on entropy, a rather neglected aspect of bio-thermodynamics. It is a good way to encapsulate the problem and suggests definite experimental checks. The difference in both bacterial RC and PS I is about 0.4 eV of positive entropy. A tentative explanation is the liberation of bound counter ions when the charge separation approximately cancels charges in the proteins near to the surface (Edens et al., 2000; Hou et al., 2001a). This hypothesis could be verified by an increase in ionic conductivity following charge separation. An alternative, and not exclusive possibility, is the loosening of the structure with the formation of a dozen low, from high, frequency vibrations in binding sites. The different occupation of the vibrational levels changes the heat capacity and thus the entropy.

The smaller ΔH for the primary stabilized reaction in PS I (−0.4 eV) than in PS II (−1 eV) means that more energy of the photon is stored in PS I than in PS II. This is the opposite of previous interpretations, since it was believed that more energy was needed to oxidize water to oxygen than to reduce carbon dioxide. However, ATP is also required for this reaction and it is formed via proton gradients. The extra energy in PS I is easily sufficient to generate a gradient of two to three protons per electron as required by the cyt *b*/*c*-Q cycle. Our measurements of the energy stored in PS I in *C. vulgaris* on the 8 msec time scale using the air microphone was 0.7 eV, corresponding to an enthalpy change of −1.1 eV (Cha and Mauzerall, 1992). This stored energy roughly agrees with the difference of redox potentials of cyt b_6/f and the FNR-Fd complex. The values do indicate that large changes in enthalpy occur on the time scale of 10 μsec to 10 msec.

The enthalpy change inferred for PS II on this long time scale was −0.8 eV, within the error of that observed on the 1 μsec time scale, Table 1. This indicates that little change in enthalpy occurs between these time scales, supporting the hypothesis that the oxygen formation cycle works on the minimal energy path, i.e., each step requires only the average free energy of the process. The difference from the estimated free energy, TΔS, is −0.2 eV, but again the error is large.

C. Measured Enthalpy and Volume Changes in Steps of PS I Electron Transfer

1. $P^*_{700} \rightarrow F_{A/B}$

The volume change for the A_1 reaction is the same as that in the bacterial RC, −26 Å^3. We estimate a value of −28 Å^3 using the Drude–Nernst equation

and the same parameters as the bacterial system (Hou et al., 2001a). This close result is only obtained if one uses the radius of the large $Fe_4S_4(Cys)_4$ complex (8 Å) with its charge change of -1 to -2. Use of the smaller Fe_4S_4 complex (5 Å) with charge change of +3 to +2 would predict an increase of volume, the opposite of that observed. The charge must be distributed over all of the sulfur atoms of the complex as anticipated. Thus even molecular details can be obtained from these thermodynamic measurements.

The measured ΔH, -0.4 eV, is only about half of the estimated ΔG, so there is +0.4 eV of $T\Delta S$, again similar to the bacterial system. The explanation we offer is the same (see above). The ΔH of $P^+_{700}F^-_{A/B}$ was estimated to be -1.1 eV from the temperature dependence of the luminescence of this state (Shuvalov et al., 1976) but the objections to this kind of measurement were given in Brettel (1997) and in McMahon et al. (1998).

2. $P^*_{700} \rightarrow A_1$

On increasing the time resolution of the PA apparatus we obtained evidence of the ~100 nsec step in the pathway (Hou and Mauzerall, 2006; 13th International Congress of Photosynthesis, Montreal, 2004, abstract no. 25). The volume change to the phylloquinone is -21 Å^3, as expected (calculated ΔV, -21 Å^3). However, the measured ΔH is a surprising -0.8 eV. Together with the estimated ΔG of -0.6 eV (see above), a $T\Delta S$ of -0.2 eV is estimated. These large values may be characteristic of reduction of quinones (Feitelson and Mauzerall, 2002). The ultimate cause may be the concentration of charge on the oxygen atoms of the quinone. This leads to increased hydrogen bonding or even protonation with large negative ΔH and increased orientation of polar residues with negative ΔS. The ΔG is a balance between large and opposing ΔH and $-T\Delta S$. Note that this may be a case where energy is stored as negative entropy.

3. $P^*_{700} \rightarrow A_P$

The *menA* and *menB* mutants were found to have the same values of ΔV, -17 Å^3, and ΔH, -0.7 eV (Table 1). Since the quinone nucleus of plastoquinone is smaller than that of phylloquinone, we might expect a larger negative ΔV in the mutant. The contrary probably reflects the concentration of charge on the oxygen atoms versus the carbon rings. The smaller volume decrease may be caused by a decreased compressibility (κ) or an increased effective dielectric coefficient (ε) since these enter the Drude–Nernst equation as κ/ε. The larger tail of the plastoquinone may not fit well in the A_1 pocket and thus decrease κ. More likely, the A_P site may be more polar than the A_1 site. In fact the plastoquinone is easily exchanged and replaced by other quinones (Johnson et al., 2001).

The measured ΔH, -0.7 eV, is 0.4 eV below that of the wild type. Together with the estimated ΔG, the estimated $T\Delta S$ is only -0.05 eV. The enthalpy is large as expected for a quinone reduction but the poorer fit of the phylloquinone may reduce the interaction energy. Similarly this poorer fit may not allow much of the increased orientation and higher vibrational frequencies responsible for the large negative entropy in the case of the plastoquinone.

4. $A^-_1 \rightarrow F_{A/B}$

The volume change for the ~100 nsec reaction measured in the fast PA cell is only -3 Å^3 and the calculated value is -2 Å^3. This agreement again only occurs if the large $Fe_4S_4(Cys)_4$ complex is used as the acceptor. The measured enthalpy, however is positive, $+0.4\pm$ 0.3 eV, i.e., the reaction absorbs heat from the bath. Together with the estimated ΔG of -0.14 eV leads to a $T\Delta S$ of $+0.5\pm$ 0.3 eV. This is a clear example of an entropy-driven reaction. In such a reaction the increase in the degrees of freedom outweighs the decrease in bonding or other interaction energies. These new degrees of freedom must center on the loss of the increased orientation and increased frequency of vibrational coupling of the quinone anion with its environment. We estimate that the loss of a dozen of these modes would account for these observations. The enthalpy of reduction of low potential FeS_4Cys_4 ferredoxins are positive (Battistuzi et al., 2000). If these proteins are similar to PS I, the Fe/S centers may contribute to the positive enthalpy.

5. $A^-_P \rightarrow F_{A/B}$

A larger volume decrease for this reaction, -9 Å^3 is inferred for both the *menA* and *menB* mutants. The larger value follows from the more positive volume change of formation of the plastoquinone anion compared to that of the phylloquinone and assuming that of $F_{A/B}$ does not change.

The inferred enthalpy change is a more modest, but still positive, +0.3 eV. With the estimated ΔG of -0.1 eV, one obtains a $T\Delta S$ of +0.4 eV, again an

entropy-driven reaction. The more limited coupling of the phylloquinone with its environment leads to these smaller but still impressive thermodynamic values.

V. Efficiency

The quantum and reaction yields in the PS I RC are close to unity (Hou et al., 2001a). The efficiency of storage of free energy from the trap state P^*_{700} to P^+_{700} $F^-_{A/B}$ is 58%, 1.03 eV out of 1.77 eV for an energy loss of 0.74 eV assuming no entropy in the excited state. That of the enthalpy is 77%, 1.37 eV out of 1.77 eV. The bacterial system stores only 0.45 eV out of 1.3 eV, or 35%, for an energy loss of 0.86 eV. There is no thermodynamic reason that the efficiency could not be 100% if no flow of energy was required and the lifetime of the excited state were infinite. For a lifetime of excited singlet states of 1 nsec, a primary reaction time of ∼10 psec is required for a reaction yield of 99%. This is in fact close to the observed ∼3 psec for the primary electron transfer. Since these one-electron transfers are inherently reversible, the reverse reaction can be slowed by a loss of free energy. Thermal excitation would then be required for reversal. A general discussion of deterring reverse electron transfer has been presented (Mauzerall, 1988). Assuming the Boltzmann distribution, a gap, or energy loss, of 0.2 eV is required to keep the lifetime of the charge-separated state at ∼1 nsec and its yield at 99%. A longer life of the charge-separated state requires a larger energy loss. If we take the lifetime of 1 μsec for the P^+_{700} $F^-_{A/B}$ state and a lifetime of the excited state energy as 1 nsec, then a factor of 10^5 is required for a yield of 99%. This translates to an energy gap of ∼0.3 V at 300 K. It seems that the observed gap of 0.75 V is a bit wasteful. However, the complete separation of charge across the membrane in vivo creates a transmembrane potential that adds to the energy storage. This can amount to ∼0.2 eV and so decreases the observed difference to 0.25 eV. Since photosynthetic systems are only rarely photon limited, the balance between rates and energy storage achieved in the evolution of RC's may not only be determined by efficiency but by molecular availability and thus by historical accidents.

The crucial step in photosynthesis is in arranging to separate the charges through the RC, i.e., across the lipid bilayer (∼25 A), before appreciable charge recombination takes place. The long distance cannot be accomplished in one tunneling act in the required time and is achieved by dividing it into several segments. Each segment can be fast because of the exponential dependence of rate of transfer on distance. The bacterial system accomplishes this in two steps but PS I takes four to five steps, but through twice the distance, ∼55 Å.

It is interesting to compare the effects of the product of oxygenic photosynthesis on the system itself. Quantum mechanics highly favors single electron transfer reactions and reactions from short lived excited states that are almost exclusively of this kind. Before oxygen accumulated on earth, the reactive one-electron intermediates in photochemical reactions could react at their leisure. However, with the present atmospheric pressure of oxygen, the reduced species can live only ∼1 μsec before being oxidized. Note that the oxidized porphyrin radicals are stable to oxygen, a reason for their choice by evolution (Fuhrhop and Mauzerall, 1969). Thus the anaerobic bacterial RC can afford a lifetime of >0.1 msec for a semiquinone intermediate before conversion to a stable protonated hydroquinone. In attempting to reach a more negative operating potential, PS I used the more negative potential of the Fe/S clusters to overlap with ferredoxin:$NADP^+$ reductase. Note that once the two-electron plus proton stage of NADPH or hydroquinone is reached, both the thermal back reaction and the reaction with oxygen become negligible. However, this choice for PS I required a shortening of distance of electron transfer (12–15 Å from 25 Å, via chlorophylls) since the overlaps of the π orbitals of a quinone and the d-π orbitals of the Fe/S complex are limited. Together with the longer total distance to accommodate the FNR complex, more steps were required to retain energy utilization. The requirement of two electrons to stabilize the product, NADPH, may be a reason for the presence of trimers in PS I. This would triple the probability of supplying two electrons to the local ferredoxin in a given time period and would be particularly useful at low-light intensities.

VI. Conclusions

Far too little is reliably known of the thermodynamics of this photosynthetic system notwithstanding the enormous amount of research effort in this field. This is because most of the effort has concentrated on kinetics and on structure. But some solid thermodynamic underpinnings are required for an understanding of the complete process. The crucial free energies of the reaction steps or potentials of the reacting pairs must be better defined. The photoacoustic and similar methodologies

are excellent ways to learn of the enthalpy and volume changes over extended time scales. The following results have already been established:

1. The enthalpy of the photosynthetic reaction steps can differ considerably from earlier indirect estimates. In particular PS I and PS II differ by 0.6 eV on the 1 μsec time scale with PS II being more negative. On the msec time scale they differ by about 0.3 eV, with PS I being more negative.

2. The contribution of entropy to the free energy of these reactions is often large and can be determining. The $A_1^- \rightarrow F_{A/B}$ reaction is entropy driven.

3. The volume changes give information on the compressibility and dielectric coefficient of the RC proteins. The changes for the Fe/S clusters require charge delocalization over the large $Fe_4S_4(Cys)_4$ cluster. They also show appreciable effects of substituting plastoquinone for phylloquinone at the A_1 site.

Acknowledgment

I thank Dr. J. Golbeck for many useful comments.

References

Agalarov R and Brettel W (2003) Temperature dependence of biphasic forward electron transfer from the phylloquinone(s) A_1 in photosystem I: only the slower phase is activated. Biochim Biophys Acta 1604: 7–12

Arata H and Parson W (1981a) Delayed fluorescence from *Rhodopseudomonas sphaeroides* reaction centers: enthalpy and free energy changes accompanying electron transfer from P-870 to quinones. Biochim Biophys Acta 638: 201–209

Arata H and Parson W (1981b) Enthalpy and volume changes accompanying electron transfer from P-870 to quinones in *Rhodopseudomonas sphaeroides* reaction centers. Biochim Biophys Acta 636: 70–81

Arnaut LG, Caldwell RA, Elbert JE and Melton LS (1992) Recent advances in photoacoustic calorimetry: theoretical basis and improvements in experimental design. Rev Sci Instrum 63: 5381–5389

Battistuzzi G, D'Onofrio M, Borsari M, Sola M, Macedo AL, Moura JJG, Rodriges P (2000) Redox thermodynamics of low-potential iron–sulfur proteins. J Biol Inorg Chem 5: 748–760

Boichenko V, Hou J and Mauzerall D (2001) Thermodynamics of electron transfer in oxygenic photosynthetic reaction centers: volume change, enthalpy, and entropy of electron-transfer reactions in the intact cells of the cyanobacterium *Synechocystis* PCC 6803. Biochemistry 40: 7126–7132

Braslavsky SE and Heibel GE (1992) Time-resolved photothermal and photoacoustic methods applied to photoinduced processes in solution. Chem Rev 92: 1381–1410

Brettel K (1997) Electron transfer and arrangement of the redox cofactors in photosystem I. Biochim Biophys Acta 1318: 1869–1877

Brettel K and Leibl W (2001) Electron transfer in photosystem I. Biochim Biophys Acta 1507: 100–114

Cha Y and Mauzerall DC (1992) Energy storage of linear and cyclic electron flows in photosynthesis. Plant Physiol 100: 1869–1877

Charlebois D and Mauzerall D (1999) Energy storage and optical cross-section of PS I in the cyanobacterium *Synechococcus* PCC 7002 and a *psaE*$^-$ mutant. Photosynth Res 59: 27–38

Chitnis PR (2001) Photosystem I: function and physiology. Annu Rev Plant Physiol Plant Mol Biol 52: 593–626

Edens GJ, Gunner MR, Xu Q and Mauzerall D (2000) The enthalpy and entropy of reaction for formation of P^+Q_A- from excited reaction centers of *Rhodobacter sphaeroides*. J Am Chem Soc 122: 1479–1485

Edens GJ, Liu Y, Grzymski J and Mauzerall D (2003) Pressure cell for time-resolved calorimetric measurements of photoinitiated reactions on the fractional millisecond and longer time scale. Rev Sci Instrum 74: 2523–2529

Feitelson J and Mauzerall D (1996) Photoacoustic evaluation of volume and entropy changes in energy and electron transfer. Triplet state porphyrin with oxygen and naphthoquinone-2-sulfonate. J Phys Chem 100: 7698–7703

Feitelson J and Mauzerall D (2002) Enthalpy and electrostriction in the electron-transfer reaction between triplet zinc uroporphyrin and ferricyanide. J Phys Chem B 106: 9674–9678

Fromme P, Jordan P and Krauß N (2000) Structure of photosystem I. Biochim Biophys Acta 1507: 5–31

Fuhrhop J-H and Mauzerall D (1969) The one-electron oxidation of metalloporphyrins. J Am Chem Soc 91: 4174–4181

Gensch T and Viappiani C (2003) Time-resolved photothermal methods: accessing time-resolved thermodynamics of photoinduced processes in chemistry and biology. Photochem Photobiol Sci 2: 699–721

Heathcote P, Jones MR and Fyfe PK (2003) Type I photosynthetic reaction centers: structure and function. Philos Trans R Soc Lond B Biol Sci 358 (1429): 231–243

Hou H J and Mauzerall D (2006) The A-F_x to $F_{A/B}$ step in *Synechocystis* 6803 Photosystem I is entropy driven. J Am Chem Soc 128, 1580–1586

Hou J, Boichenko VA, Wang Y-C, Chitnis PR and Mauzerall D (2001a) Thermodynamics of electron transfer in oxygenic photosynthetic reaction center: a pulsed photoacoustic study of electron transfer in photosystem I reveals a similarity to bacterial reaction centers in both volume change and entropy. Biochemistry 40: 7109–7116

Hou J-M, Boichenko VA, Diner, BA and Mauzerall D (2001b) Thermodynamics of electron transfer in oxygenic photosynthetic reaction center: volume change, enthalpy and entropy of electron-transfer reactions in manganese-depleted photosystem II core complexes. Biochemistry 40: 7117–7125

Johnson TW, Zybailov B, Jones AD, Bittl R, Zech S, Stehlik D, Golbeck JH and Chitnis PR (2001) Recruitment of a foreign quinone into the A_1 site of photosystem I. *In vivo* replacement of plastoquinone-9 by media-supplemented

naphthoquinones in phylloquinone biosynthetic pathway mutants of *Synechocystis* sp. PCC 6803. J Biol Chem 276: 39512–39521

Kleinherenbrink FAM, Hastings G, Wittmershaus BP and Blankenship RE (1994) Delayed fluorescence from Fe–S type photosynthetic reaction centers at low redox potential. Biochemistry 33: 3096–3105

Kok B (1957) Absorption changes induced by the photochemical reaction of photosynthesis. Nature 179: 583–584

Kok B (1961) Partial purification and determination of oxidation–reduction potential of the photosynthetic chlorophyll complex absorbing at 700 nm. Biochim Biophys Acta 48: 527–533

Marcus RA and Sutin N (1985) Electron transfers in chemistry and biology. Biochim Biophys Acta 811: 265–322

Mauzerall D (1988) Circumventing reverse electron transfer. In: Chanon M and Fox MA (eds) Photoinduced Electron Transfer, Part A, pp 228A–244A. Elsevier Science, Amsterdam

Mauzerall D, Gunner MR and Zhang JW (1995) Volume contraction on photoexcitation of the reaction center from *Rhodobacter sphaeroides* R-26: internal probe of dielectrics. Biophys J 68: 275–280

Mauzerall D, Hou J-M and Boichenko VA (2002) Volume changes and electrostriction in the primary photoreactions of various photosynthetic systems: estimation of dielectric coefficient in bacterial reaction centers and of the observed volume changes with the Drude–Nernst equation. Photosynth Res 74: 173–180

Mauzerall D, Liu Y, Edens GJ and Grzymski J (2003) Measurement of enthalpy and volume changes in photoinitiated reactions on the ms timescale with a novel pressure cell. Photobiol Sci 2: 788–790

McMahon BH, Müller JD, Wraight CA and Nienhaus GU (1998) Electron transfer and protein dynamics in the photosynthetic reaction center. Biophys J 74: 2567–2587

Parrett, KG, Mehari T, Warren PG and Golbeck JH (1989) Purification and properties of the intact P-700 and Fx-containing photosystem I core protein. Biochim Biophys Acta 973: 324–332

Prince RC, Gunner MR, Dutton PL (1981) Quinones of value to electron transfer studies: oxidation–reduction potentials of the first reduction steps in an aprotic solvent. In: Trumpower BL (ed) Function of Quinines in Energy Conserving Systems, pp 29–34. Academic Press, New York

Santabarbara S, Heathcote P and Evans M C (2005) Modelling of the electron transfer reactions in Photosystem I by electron tunnelling theory: the phylloquinones bound to the PsaA and the PsaB reaction centre subunits of PS I are almost isoenergetic to the iron–sulfur cluster F_x. Biochim Biophys Acta 1708: 283–310

Semenov AY, Vassiliev IR, van der Est A, Mamedov MD, Zybailov B, Shen G, Stehlik D, Diner BA, Chitnis PR and Golbeck JH (2000) Recruitment of a foreign quinone into the A_1 site of photosystem I. Altered kinetics of electron transfer in phylloquinone biosynthetic pathway mutants studied by time-resolved optical, EPR, and electrometric techniques. J Biol Chem 275: 23429–23438

Sétif P and Brettel K (1993) Forward electron transfer from phylloquinone A_1 to iron–sulfur centers in spinach photosystem I. Biochemistry 32: 7846–7854

Shinkarev VP, Vassiliev IR and Golbeck JH (2000) A kinetic assessment of the sequence of electron transfer from F_X to F_A and further to F_B in photosystem I: the value of the equilibrium constant between F_X and F_A. Biophys J 78: 363–372

Shinkarev VP, Zybailov B, Vassiliev IR and Golbeck JH (2002) Modeling of the $P700^+$ charge recombination kinetics with phylloquinone and plastoquinone-9 in the A_1 site of photosystem I. Biophys J 83: 2885–2897

Shuvalov V A, Klimov V V and Krasnovskii A A (1976) Study of primary photoprocesses in the light fragments of chloroplasts. Molek Biol 10: 326–339

Vos MH and van Gorkom HJ (1990) Thermodynamical and structural information on photosynthetic systems obtained from electroluminescence kinetics. Biophys J 58: 1547–1555

Chapter 34

Application of Marcus Theory to Photosystem I Electron Transfer

Christopher C. Moser* and P. Leslie Dutton
Department of Biochemistry and Biophysics, 1005 Stellar-Chance Labs, University of Pennsylvania, Philadelphia, PA 19104-6059, USA

Summary

To understand the engineering of light induced electron transfer and energy conversion, photosystem I (PS I) has been extensively reshaped by isolation, removal of protein subunits, and redox cofactors and in some cases reconstitution of exotic redox centers. Such manipulations together with Marcus theory and its biologically focused empirical derivations show that electron tunneling dominated electron transfer kinetics are established principally by the natural selection of distance between redox centers; the driving force and reorganization energy of each electron transfer step falls within a range that assures robust function, despite the repeated impact of mutation and change during evolution. Relatively simple empirical expressions for determining electron tunneling rates are more than adequate to understand the operation of PS I, especially since kinetic and preparative heterogeneity is common. Unlike other photosystems, the typical twofold symmetry of redox centers translates into a functionally relevant, near-symmetric two-branch pattern of electron transfer that culminates in the ability of the quinone on either branch to reduce the first redox center in the terminal iron–sulfur chain. Relatively small differences apparent in the kinetics of the two branches may reflect the tolerance of evolutionary drift in the thermodynamic properties of individual redox centers. Calculation suggests that productive charge separation, while slightly favoring the B chain chlorins, initially reduces both quinones roughly equally; long-term redox equilibration and short-circuiting charge recombination, however, tend to favor electron return through the A-branch.

I. Electron Tunneling Parameters

Before crystal structures of PS I were well resolved, a number of laboratories used their measurements of electron transfer rates between the various redox centers in this photosynthetic electron transfer chain to provide some structural estimates of the distances between cofactors (Golbeck, 1993; Séitif and Brettel, 1993; Kumazaki et al., 1994). Such estimates presumed, as is often the case, that intraprotein electron transfers were limited by electron tunneling. Since this tunneling is reasonably well described by a simple exponential

*Author for correspondence, email: moserc@mail.med.upenn.edu

John H. Golbeck (ed): Photosystem I: The Light-Driven Plastocyanin:Ferredoxin Oxidoreductase, 583–594.

decay with distance, with a typical exponential decay coefficient (β) of 1.4 $Å^{-1}$ (Moser et al., 1992; Page et al., 1999), then the minimum tunneling distance separating redox centers are easily calculated according to the expression

$$\log_{10} k_{et}^{exer} = 13 - 0.6\,(R - 3.6) \quad (1)$$

where k_{et} is in units of per second, R is the edge-to-edge distance between redox cofactors in Ångstoms, and 3.6 represents van der Waals contact. The electron tunneling rate will dependent on driving force (ΔG°) as well, and this can be estimated from the difference in redox midpoint potential values (E_m) between donor and acceptor, assuming that redox centers are not so close to one another that there is a lot of electrostatic charge–charge interaction between them. The natural design of PS I includes a number of redox centers with redox midpoint potentials so negative that they are, unfortunately, very difficult to measure in straightforward redox titrations. Even with those centers where it seems possible to do redox titrations, there is often a range of midpoint values reported in the literature (see Table 1). On the right are E_m values that we have used in this chapter to evaluate the application of Marcus theory to PS I.

There is another energetic term that affects tunneling rates and hence distance estimates, the reorganization energy (λ), which reflects the amount of energy required to distort the nuclear geometry of the reactants before electron transfer so that they resemble the equilibrium nuclear geometry of the products after electron transfer. This takes the form of small changes in bond lengths and reorientation of dipoles around the redox centers to reflect the new pattern of electric fields before and after electron transfer. It can be viewed as an indirect measure of the activation energy of the electron transfer reaction. If the exergonic driving force of the reaction matches the reorganization energy for the reactions ($\Delta G = -\lambda$), then the tunneling rate will be activationless and as fast as possible and described by Eq. (1). If the driving force is different from this optimal value, either less exergonic (Marcus normal region) or more exergonic (Marcus inverted region) (Marcus, 1956; Marcus and Sutin, 1985), the electron tunneling rate will decrease in an approximately Gaussian dependence of rate on driving force. An empirical estimate of this rate at room temperature is given by

$$\log_{10} k_{et}^{exer} = 13 - 0.6\,(R - 3.6) - 3.1\,(\Delta G + \lambda)^2/\lambda \quad (2)$$

where R is in Å, and ΔG and λ are in eV (Moser and Dutton, 1992; Moser et al., 1992).

Reorganization energies are even more difficult to measure experimentally than E_m values. One common method measures the temperature dependence of the electron transfer reaction and extracts a reorganization energy consistent with this activation energy. This method tends to be fraught with difficulties, because for a biological electron transfer the temperature dependence may not reflect the activation energy for a tunneling event. For example, changing the temperature can change a rate limited by electron tunneling to a rate limited by a gating event, such as a conformational change that modulates the energetics of the electron transfer, and lead to an overestimate of the reorganization energy. On the other hand, if electron tunneling is coupled to large quantized nuclear vibrations, then the temperature sensitivity will tend to underestimate the reorganization energy. One sure way of measuring the reorganization energy associated with tunneling is to manipulate the driving force of the electron transfer, and to examine the effect at different temperatures (Gunner and Dutton, 1989). This will reveal whether the rate approximates the classical Gaussian dependence on driving force described by Marcus (1956), or the somewhat broader rate dependence on driving force described by quantum modifications of the Marcus model (Levich and Dogonadze, 1959; Hopfield, 1974; Moser et al., 1992). Systematic changes in driving force can be accomplished by mutational changes in amino acid residues that surround redox cofactors and change the E_m, for example by changing hydrogen bond patterns, or by changing the redox centers themselves, for example by genetic manipulation to truncate the synthetic pathways leading to the native redox center, and so forcing a non-native redox center to take its place, or by extracting the native redox center and

Abbreviations: A – auxiliary chlorophyll electron acceptor/donor; A_0 – primary chlorophyll electron acceptor; A_1 – quinone redox center; $BChl_2$ – bacteriochlorophyll dimer in purple bacterial reaction centers; BPh – bacteriopheophytin; Chl – chlorophyll; E_m – oxidation reduction midpoint potential; eV – electron volts; F_X, F_A, F_B – terminal iron–sulfur centers; P700 – central pair of chlorophylls forming light excited electron donor; PS I – photosystem I; Q_A, Q_B – primary and secondary quinone acceptor in purple bacterial reactioncenters; R – edge-to-edge distance between redox centers; RC – reaction center; T – temperature; ΔG – driving force for electron transfer; $\hbar\omega$ – characteristic frequency of vibration coupled to electron transfer; λ – reorganization energy; ρ – densities of the protein medium between redox centers.

Table 1. A sampling of reported redox midpoint values for redox cofactors of PS I

Redox center	E_m (V SHE)	Method	E_m simulation
P700	0.447	Visible redox titration	0.447
$P700^{1*}$	−1.32	Subtract 700 nm photon from P700 (Krabben et al., 2000)	−1.32
$P700^{3*}$	−0.82	Subtract 1.27 eV from P700	−0.82
A_a and A_b	−1.29	Small energy drop from P700* (Shuvalov, 1976)	−1.29
A_{0a} and A_{0b}	−1.05	0.25 eV less than P700* by delayed fluorescence (Kleinherenbrink et al., 1994)	−1.05
A_{0a} and A_{0b}	−1.01	Electroluminescence (Vos and van Gorkom, 1988)	
A_{1a} and A_{1b}	−0.74 or −0.75	Recombination from F_A, F_B, assuming 150 μsec direct A_1 recombination (Brettel, 1997)	$-0.74\,A_{1b}$, $-0.70\,A_{1a}$
A_{1a} and A_{1b}	<−0.79	Recombination when F_X pre-reduced places A_1 more negative than triplet (Sétif and Bottin, 1989)	
A_{1a} and A_{1b}	<−0.80	Electroluminescence kinetics (Vos and Van Gorkom, 1990)	
F_X	−0.705	Gold electrode, low temperature EPR (Chamorovsky and Cammack, 1982)	−0.70
F_X	−0.67	Room temperature optical redox titration P700-F_X cores (Parrett et al., 1989)	
F_A	−0.54	Low temperature EPR (Evans and Heathcote, 1980)	−0.49
F_A	−0.44	Room temperature optical charge recombination $P700^+$ (Jordan et al., 1998)	
F_B	−0.56	Low temperature EPR (Evans and Heathcote, 1980)	−0.51
F_B	−0.465	Room temperature charge recombination $P700^+$ (Jordan et al., 1998)	

replacing it with exotic chemically synthesized analogues. All of these have been done in PS I. The driving force of the electron transfer from plastocyanin to PS I in *Chlamydomonas reinhardtii* was systematically made more exothermic, from a ΔG of −77 to −213 mV, in a series of mutants that raised the E_m of P700 (Ramesh et al., 2002), increasing the rate of electron transfer by a factor of 5. While this free energy range was not a large enough to identify the leveling off of rate with driving force that is characteristic of reaching the reorganization energy rate optimum in a Marcus description, it did allow the authors to estimate a reorganization energy of about 545 meV, similar to the value estimated for the corresponding electron transfer from cytochrome c_2 to P+ in purple bacterial reaction centers (Lin et al., 1994). The native phylloquinone of center A_1 has been subjected to biosynthetic changes (Zybailov et al., 2000; Sakuragi et al., 2002) or to extraction and reconstitution (Iwaki and Itoh, 1989; Itoh et al., 2001). The latter both increased and decreased the driving force of the native A_0–A_1 electron transfer and covered an impressive 1,200 meV range, clearly revealing a free energy optimum near the 300 meV natural driving force with phylloquinone (Itoh et al., 2001). This range is much larger than that explored with the corresponding BPh to Q_A electron transfer in the purple bacterial reaction center (Fig. 1; Gunner and Dutton, 1989).

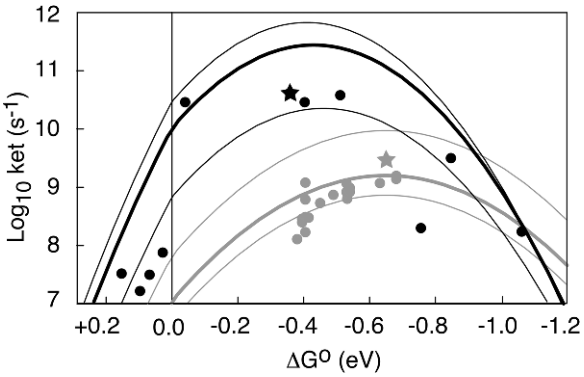

Fig. 1. Effect of quinone substitution modulated driving force on electron transfer rate from A_0 to A_1 in PS I (black) and from BPh to Q_A in purple bacterial RC (gray). Native quinones shown starred. Thick lines represent theoretical curves using Eq. (2) and distances in structures 1JB0 and 1PCR. Thin lines represent Eq. (3) with packing densities estimated from these pdb files (upper) or best fit (lower).

II. Symmetric PS I Redox Cofactor Geometry

When the structure of PS I was resolved fine enough to identify all the redox centers (Klukas et al., 1999) it turned out that many of these rate-based structural estimates were quite good (see Fig. 2). Like the purple sulfur bacterial reaction centers, there was a central pair

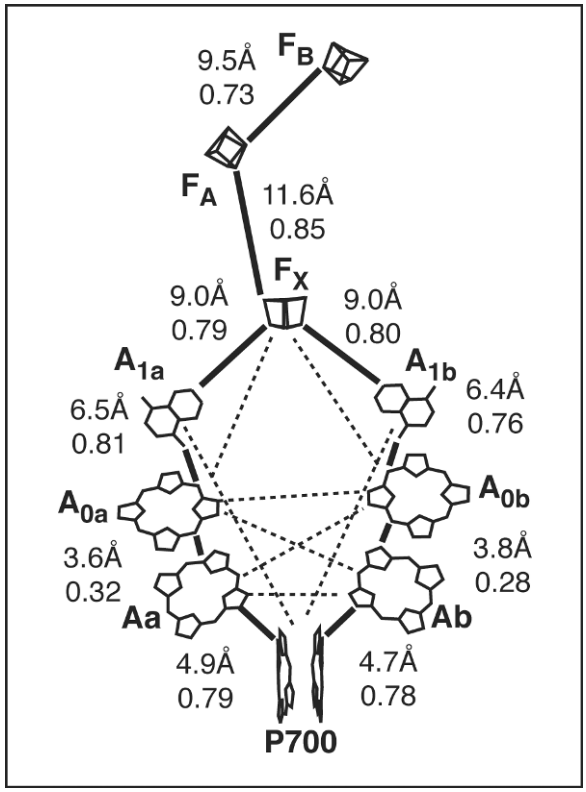

Fig. 2. PS I cofactor structure (1JB0) with edge-to-edge distances (in Å) and packing densities for the productive electron transfer reactions. Simulations of tunneling kinetics of the PS I system also include the unproductive electron transfers (dashed lines).

of chlorophylls (P700), in this case made of Chl and Chl a′, four other chlorophylls (A and A_0) symmetrically placed in A- and B-branches on either side leading to quinone acceptors (A_1). However, unlike the purple bacterial reaction centers, both quinone redox centers were the same distance from the subsequent acceptor, iron–sulfur center F_X placed right on the symmetry axis of PS I and ligated equally by amino acids from the two symmetric protein subunits. Thus, unlike the purple bacterial reaction center, where charge separation occurs essentially exclusively down the A-branch cofactor chain, it seemed from a structural point of view that both sides of PS I could reasonably participate in productive photosynthetic electron transfer. Indeed, simulation of electron tunneling from center to center using the nearly completely symmetric A- and B-branch distances of the high resolution structure 1JB0 and a symmetric set of redox properties based on estimates of Table 1 and the tunneling relationship of Eq. (2), shows that a symmetric PS I reaction center will separate charge quite efficiently and robustly (see Fig. 3).

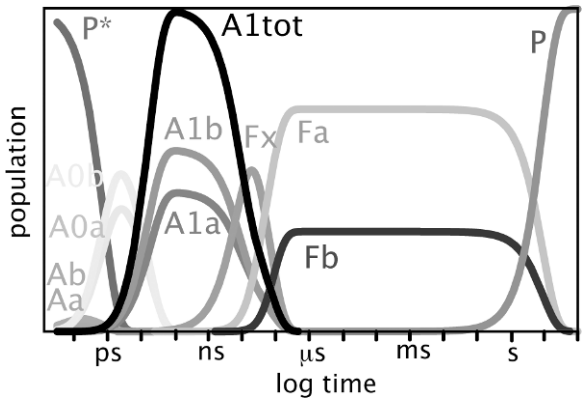

Fig. 3. PS I electron tunneling kinetics with symmetric energetics (but structure-based distances and packing). In this simulation, the midpoint potentials of A_{1a} and A_{1b} are set equal at −0.74 V. Electron transfers occur at rates at roughly comparable with experimental values, and energy wasting short-circuits are not a problem.

Figure 3 simulates the approximately picosecond decay of the excited state of the central Chl pair (P* red) to transiently form a small population of reduced Chl A, which goes on to reduce A_0 Chl on both branches. Within 10 psec this begins to decay and populate reduced phylloquinone A_1 on both branches, with minor deviations from a 50:50 mix due to small distance asymmetries between the branches. Both branches contribute to partial F_X reduction on a 10 nsec timescale. Reduced F_X in turn reduces F_A and F_B on the 10–100 nsec timescale. The unequal sharing of the electron between the two Fe/S centers is a simple reflection of the small E_m difference between the centers. In the natural system, $P700^+$ would be rereduced by plastocyanin, but in this simulation of isolated PS I, short-circuit of the electron from F_A and F_B via thermal repopulation of A_1 to $P700^+$ would take place on a 1–10 sec timescale. Quantum yield is near 100% in this simulation. We note that Savikhin et al., using a distance of 4.5–5 Å, found that these tunneling equations overestimated the electron rate between A_0 and A_1 at 0.8 psec and concluded that the equations were inappropriate (Savikhin et al., 2001). However, by using the 6.4 and 6.5 Å edge-to-edge distances derived from the 1JB0 crystal structures, we find that the tunneling calculations estimate a remarkably good rate around 10 psec.

III. Asymmetric PS I Electron Transfer Kinetics

Although energy transduction by a symmetric PS I would function perfectly well, there is good

experimental evidence in the natural PS I for significant energetic asymmetry between the A- and B-branches, at least at the level of the quinones A_1. This asymmetry was suggested by a conspicuous fast (~20 nsec) and slow (~200 nsec) biphasic quality of A_1 reoxidation, as monitored in the visible spectrum (Sétif and Brettel, 1993; Joliot and Joliot, 1999). Further support was provided by mutation of the individual tyrosines near either A_{1a} or A_{1b} that selectively slowed either the slow or fast phase, respectively (Guergova-Kuras et al., 2001). It is also clear that separate mutations in the amino acids ligating the primary acceptor chlorophylls A_0 in either the A- or B-branch, that are presumably part of the redox chain that would lead to either A_{1a} or A_{1b}, are both capable of transferring electrons as far as the Fe/S centers, although with altered kinetics of intermediate A_1 reduction (Fairclough et al., 2003). On the basis of these mutational experiments, it seems unlikely that the quinone on only one branch is active, and that at least part of the explanation of the kinetic heterogeneity can be ascribed to differences in the two quinones.

With virtually identical edge-to-edge distances between the quinone and the F_X, it is conceivable that a difference in electron transfer rate could reflect differences in the effective tunneling barrier of the intervening medium. A volume with a greater density of atoms and bonds will tend to present a lower barrier to a tunneling electron than a region with a low density of atoms and bonds. One measure of this is provided by packing density (ρ). Adding the effect of variations in packing density to Eq. (2) gives

$$\log_{10} k_{et}^{exer} = 13 - (1.2 - 0.8\rho)(R - 3.6) - 3.1\,(\Delta G + \lambda)^2/\lambda \qquad (3)$$

Edge-to-edge distances are well defined for all cofactors with the possible exception of the native phylloquinone, which has an aromatic ring extending toward the F_X center. Since substitutions of the aromatic ring of naphthoquinones clearly have dramatic effect on the redox properties of the quinones (Ashnagar et al., 1984; Braun et al., 1986; Warncke and Dutton, 1993), it seems reasonable that a significant amount of the wavefunction of the quinone electrons is delocalized over the carbons atoms in this ring. Thus we include these atoms when defining the quinone edge.

A packing density analysis between the quinones and F_X (Fig. 2) shows unremarkable and virtually identical packing; this strongly suggests that tunneling barrier differences are not the source of any rate heterogeneity. A similar conclusion was reached in a pathway analysis to examine the effect of the intervening protein medium on the electronic wavefunction coupling between A_{1a} or A_{1b} with F_X (Ivashin and Larsson, 2003). Surprisingly, this group indicates that the only factor of Eq. (2) of any importance in determining the rate of electron transfer between π-systems is the edge-to-edge distance, apparently not considering the ΔG and λ terms. To find an explanation for the heterogeneous kinetics, this group proposes that a Trp residue that was closer to A_{1b} (5.3 Å) than A_{1a} (6.6 Å) might act as a redox intermediate in electron transfer at about the same redox potential as A_1 and thus speed B-branch electron transfer. Introducing another redox center shortens the electron transfer distance dramatically, making the electron transfer between A_{1b} and Trp even shorter than electron transfer from A_0 to A_1. In our view, moving the oxidant of A_{1b} 3.7 Å closer and leaving a short 4.1 Å hop from Trp to F_X, should raise the rate of A_{1b} reoxidation by a conspicuous two orders of magnitude into the subnanosecond time domain, inconsistent with observed rates of A_1 reoxidation, unless the electron transfer from A_{1b} to Trp had a substantially uphill energetic penalty. However, a substantially uphill step would make the fast phase of A_1 reoxidation dramatically more temperature sensitive than the slow phase, contrary to observation (see below) (Agalarov and Brettel, 2003).

It seems more likely that the PS I has evolved an A-branch versus B-branch energetic asymmetry, either in E_m or λ. Considering first the reorganization energy, the last term in Eqs. (2) or (3) suggests that when $-\Delta G << \lambda$, the electron tunneling rate will fall by an order of magnitude if the λ rises by about 0.3 eV. This would be comparable to purple bacterial reaction centers, which display such a difference in reorganization energy between Q_A and Q_B charge recombination to ground state $BChl_2$ (Moser et al.). If in PS I the redox midpoints of both A_{1a} and A_{1b} are assumed to be the same as the reported -0.74 V (Brettel, 1997) and F_X has the reported midpoint of -0.70 V (Chamorovsky and Cammack, 1982), then reorganization energies of A_{1a} and A_{1b} to F_X electron transfer can be adjusted to 1.1 and 0.8 eV to model the reported biphasic rates of electron transfer (see Table 2; Agalarov and Brettel, 2003). The eventual approximately 100 msec charge recombination from F_A and F_B through F_X and A_1 will also be modeled if the redox midpoints of F_A and F_B are -0.54 and -0.56 V, at the negative end of the reported range (Evans et al., 1974).

Although reorganization energy differences between quinones is observed in the purple bacterial reaction center and can be understood by their quite different environments, there is no obvious difference in the

Table 2. A_1 reoxidation temperature dependence. Electron tunneling expected from Eq. (4) and fit to two exponential decays (rates k_1 and k_2 in natural log units and relative extents in parentheses), compared with experiment (Agalarov and Brettel, 2003). In these experiments all Fe/S centers are oxidized and electron transfer competent. Simulations of electron transfer kinetics show that A-branch versus B-branch asymmetry in either the reorganization energy or the driving force (derived from redox midpoint values) will give similar, appropriate biphasic kinetics. With the redox midpoints of A_{1a} and A_{1b} the same at −0.74 V (Brettel, 1997), and the redox midpoint of F_X at −0.70 V (Chamorovsky and Cammack, 1982), the appropriate reorganization energies are 1.1 and 0.8 eV. With the reorganization energies the same at 0.85 eV, the appropriate redox midpoints are about −0.70 and −0.74 V respectively

Temperature (K)	Meas/calc	Fast phase ln k_1	Slow phase ln k_2
295	Meas	18.3 (0.4)	14.9 (0.6)
295	Calc	18.3 (0.42)	14.8 (0.58)
223	Meas	17.9 (0.3)	13.5 (0.7)
223	Calc	17.6 (0.45)	14.1 (0.55)

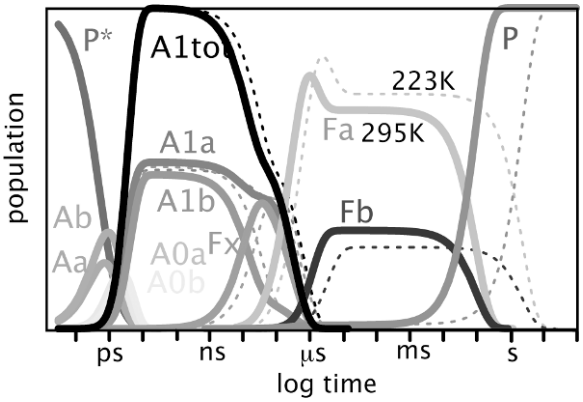

Fig. 4. Simulation of temperature dependent PS I electron tunneling kinetics with asymmetric energetics described in Table 1, distances and packing described in Fig. 2, using Eq. (4) with a characteristic frequency of 50 meV and reorganization energies described in the text.

polarity of the amino acid environment around the two quinones which might lead to a similar reorganization energy difference in PS I. In PS I, the source of the biphasic A_{1a} kinetics could just as easily come from differences in redox midpoint values rather than reorganization energy. Indeed, an E_m difference between the quinones has the great advantage that it explains the old observation that A_{1a} can be photo-accumulated much easier than A_{1b} (Heathcote et al., 1993; Fairclough et al., 2003). Photoaccumulation suggests that A_{1a} reduction is favored by at least a 40 mV more positive E_m. On the other hand, the E_m of A_{1a} can not be too much more positive than the E_m of F_X, or the electron transfer from A_{1a} to F_X will be slowed too much by the uphill electron transfer from A_{1a} to F_X. The rate of an uphill electron tunneling reaction (Page et al., 1999) can be estimated by calculating the downhill electron tunneling rate of the reverse reaction, and then applying a Boltzmann penalty, which is an order of magnitude slowing for every 60 mV uphill at room temperature. If there is a connection between the thermodynamic asymmetry between A_{1a} and A_{1b} and the observation that total A_{1a} oxidation is biphasic, with a slow phase that is about an order or magnitude slower than the fast phase, then we expect the E_m of A_{1a} to be no more than 60 mV positive of the E_m of F_X.

A better appreciation of the practical limits on the E_m values of A_{1a} and A_{1b} can be seen by simulation using the tunneling expression of Eq. (3). Beginning with reported midpoint values of −0.74 V (Brettel, 1997) for A_1 in a thermodynamically symmetric PS I (Fig. 3), which is only 40–80 mV more negative than the reported E_m of F_X (Chamorovsky and Cammack, 1982; Parrett et al., 1989), we can observed the appearance of a second slower phase as we raise the E_m for A_{1a} toward the E_m of F_X. As A_{1a} approaches within about 30 mV of F_X, the Nernst relation indicates that A_{1a} and F_X tend to share the electron between them and the slow phase begins to reflect the inherent rate of electron transfer from F_X to the next acceptor F_A (see Fig. 4 for the simple case in which the E_m of A_{1a} and F_X are the same). Equation (3) yields a tunneling rate between F_X and F_A surprisingly similar to the reported slow phase of A_1 oxidation, when the distances and packing density of the crystal structure (Fig. 2), the reported E_m differences between F_X and F_A (Evans and Heathcote, 1980; Jordan et al., 1998), and typical reorganization energies (Moser et al., 1992) are used. Thus it seems quite likely that the biphasic A_1 oxidation reflects an asymmetry in the A_{1a} and A_{1b} energetics that slightly raises the E_m of A_{1a} and brings it close enough to the E_m of F_X to allow significant sharing of the electron between F_X and A_{1a} before electron transfer to F_A completes the oxidation of both. Using the reported E_m of F_X of -0.70 V, a similar E_m for A_{1a}, E_m values of F_A and F_B in the middle of their reported range together with reorganization energies of 0.85 eV for A_1 to F_X electron transfer and 1.1 eV for electron transfer between the various Fe/S centers, gives fast and slow phases for A_1 oxidation that match reported analysis (Table 2; Agalarov and Brettel, 2003).

Electron transfer kinetics measured in PS I are often significantly nonexponential, and experimental rates often include multiple phases, sometimes described as

Table 3. Charge recombination to $P700^+$ in PS I with various complements of Fe/S centers active and native phylloquinone at A_1. Measured rates are the mean of the stretched exponentials (Shinkarev et al., 2002). Calculations use Eq. (4) and fit to two exponentials. Redox midpoint values as in Table 1, and reorganization energies as described in the text

Quinone	Fe/S present	Meas/calc	First phase rate (extent)	Second phase rate (extent)	Third phase rate (extent)
PhylloQ	F_X F_A F_B	Meas	2.2 msec (5)	107 msec (64)	2.0 sec (25)
PhylloQ	F_X F_A F_B	Calc		102 msec	
PlastoQ	F_X F_A F_B	Meas	4.1 μsec (13)	2.9 msec (87)	
PlastoQ	F_X F_A F_B	Calc	7.7 μsec (13)	8.3 msec (87)	
PhylloQ	F_X	Meas	11.6 μsec (24)	192 μsec (24)	971 μsec (52)
PhylloQ	F_X	Calc	22 μsec (9)	37 μsec (91)	
PlastoQ	F_X	Meas	3.0 μsec (4)	26 μsec (25)	584 μsec (55)
PlastoQ	F_X	Calc		11 μsec	
PhylloQ	None	Meas	12.6 μsec (50)	80.7 μsec (50)	
PhylloQ	None	Calc	15 μsec (40)	76 μsec (59)	
PlastoQ	None	Meas	2.5 μsec (18)	26 μsec (18)	362 μsec (63)
PlastoQ	None	Calc	8 μsec (49) λ 0.6 eV, 70 μsec (26) λ 0.5 eV	51 μsec (51) λ 0.6 eV, 200 μsec (74) λ 0.5 eV	

stretched exponentials (Shinkarev et al., 2002). Putting aside the problem of synchronously activating subpicosecond charge separation when energy transfer from the antennae itself stretches over tens of picoseconds, it seems that the size and complexity of the PS I complex and a potential sensitivity to change during isolation and study, conspire to make electron transfer kinetics in an ensemble of PS I particles inherently heterogeneous. Without more control over the experimental system and good measures of the driving forces of the electron transfer reactions, there seems little point to the use of tunneling treatments more sophisticated than those described here. Yet even if each PS I were chemically and physically homogeneous, simulation of the electron transfer kinetics using these tunneling expressions (as in Figs. 3 and 4) demonstrate that PS I kinetics should be conspicuously nonexponential-certain redox centers are transiently reduced and reoxidized at nearly the same rate, while redox centers on different branches with different kinetics sometimes blend together in a single experimental spectral change. To make comparison with experiment, the nonexponential kinetics of the simulations have been fit in Tables 2 and 3 to two single exponentials. Over any time range, a biphasic fit may appear quite good, but it is important to understand that the fit parameters will dependent more or less on the range of time selected for the fit, and that exponential rate values assigned to a nonexponential process are inherently uncertain.

One of the peculiarities of having different redox midpoint potentials for the quinones A_{1a} and A_{1b} that emerges from our modeling, is that charge separation is likely to take a different branch than charge recombination. Because of small asymmetries in the edge-to-edge distances between redox centers, the B-branch chlorins and quinone are very slightly favored for charge separation. However, given the proximity and roughly similar redox potentials of the chlorins and the tendency of the electron to be partly shared by all the chlorins, the A-side quinone could be favored if it is sufficiently more positive than the B-side quinone. The potentials chosen to fit the temperature dependent kinetics suggest a roughly similar initial reduction of both quinones. The more positive redox potential means the A-side quinone will be favored at long redox equilibration times, and charge recombination, which includes uphill steps that are quite sensitive to differences in driving force, will be strongly dominated by A_{1a}.

IV. Temperature Dependence of Electron Tunneling

One test of the validity of the choice of E_m values and reorganization energies in the simulations is the temperature dependence of the reactions. Uphill electron transfer reactions in particular should show extra sensitivity because of the Boltzmann term. In addition the downhill electron tunneling terms will have some temperature sensitivity due to their coupling to vibrational modes. These can be described by Eq. (4) (Moser et al., 1992, 2001) which is an adaptation of the room temperature Eq. (3) that includes an explicit reference to the temperature T, and the characteristic frequency of the vibrations coupled to the electron transfer ($\hbar\omega$) in a

semiclassical form (Hopfield, 1974):

$$\log_{10} k_{et}^{exer} \cong 13 - (1.2 - 0.8\rho)(R - 3.6) - 0.22(\Delta G + \lambda)^2/\lambda\hbar\omega Coth[\hbar\omega/2k_B T] \quad (4)$$

Previous analysis of the simultaneous free energy dependence and temperature dependence of electron tunneling in biological systems suggests that the characteristic frequency coupled to electron tunneling may be around 50–70 meV (Moser et al., 1992, 2001), although because of the challenge of designing these experiments the natural range of this characteristic frequency is uncertain. Although it has been suggested that a characteristic frequency above the Boltzmann thermal energy at room temperature $k_B T$ of about 25 meV should not be temperature dependent (Agalarov and Brettel, 2003), the use of the semiclassical expression of Eq. (4) can retain noticeable temperature dependence, albeit considerably less than the fully classical original Marcus expression (Marcus, 1956). Other quantized versions of the Marcus expression have been used to model kinetics in PS I, including an exact expression assuming a single quantum harmonic oscillator coupled to electron transfer (Schlodder et al., 1998). Such an analysis leads to a different, smaller frequency coupled to electron transfer (about 25 meV) than the Hopfield expression which, as an approximation for a complex biological system, has many vibrations integral to the reorganization coupled to electron transfer with the reorganization weighted average around 50 meV.

The dashed lines in Fig. 4 show the expected change in electron transfer that accompanies a drop from room temperature (295 K) to a low temperature that is still above the glass phase transition (223 K). All rates after initial quinone reduction are noticeably slowed, including the fast phase of A_1 reoxidation, even when A_{1a} and F_X have the same E_m and no net driving force for electron transfer. The rates that show the greatest change are those that involve substantial uphill electron transfer steps, which include in this simulation the uphill electron transfer from F_A and F_B to F_X and A_{1a} leading to downhill short-circuiting electron transfer to the ground-state oxidized P700. Recovery of ground state should occur nearly two orders of magnitude more slowly at 223 K compared to room temperature.

A comparison of the rates and extents of a fit of the simulation to biphasic decays with experiment (Table 2) shows that the extents and rates correlate well at both room temperature and 223 K, especially considering the uncertainties involved in a biphasic fit to nonexponential kinetics. Experiment does show a slightly greater slowing of the slow phase, suggesting that the electron transfer from A_{1a} to F_X may be slightly uphill and thus slightly more temperature dependent than assumed in this simple, equal E_m simulation.

Simulation of kinetics at temperature lower than 223 K is problematic because functional heterogeneity in PS I seems enhanced by passing below the glass phase transition temperature (Schlodder et al., 1998). For example, upon repeated illumination, about a third of the PS I particles at 77 K form reduced F_A and F_B and get trapped there as reverse uphill electron transfer is extremely slow, while the rest seem capable of charge recombination through A_1 (Schlodder et al., 1998). It would appear that the redox centers in PS I are naturally in a dynamic fluctuation that rapidly modulates the redox properties of the centers about some average E_m at room temperature, but that as the temperature falls, especially below the glass transition, these fluctuations slow and heterogeneity becomes more conspicuous. Modeling this cryogenic change in heterogeneity is not attempted here.

V. Plastoquinone/Phylloquinone Substitution and Fe/S Removal

The near matching E_m values of native A_1 and F_X suggested by the simulations has also been indicated by experiments that alter the redox properties of the quinone at A_1, either through genetic manipulation of the quinone biosynthetic sequence (Zybailov et al., 2000; Sakuragi et al., 2002) or by extraction and replacement of the quinone itself (Iwaki and Itoh, 1989; Itoh et al., 2001). Figure 5 compares the effects of substituting plastoquinone for the native phylloquinone under a series of experimentally relevant conditions in which the Fe/S chain is fully oxidized, partly reduced or fully reduced before flash activation. The structural and energetic parameters are the same as Fig. 4, but with the E_m of the quinones raised by 50 mV to reflect the new redox properties of plastoquinone. Table 3 shows a comparison of the multiphasic fits to the rereduction of the $P700^+$ ground state under these various Fe/S redox state conditions for both experiment and tunneling simulation.

Aside from the somewhat larger kinetic heterogeneity observed in natural PS I preparations, the basic tunneling simulation does a reasonably good job at matching the kinetics and extents under this wide range of conditions, suggesting that we have a good functional picture of the parameters that determine quinone

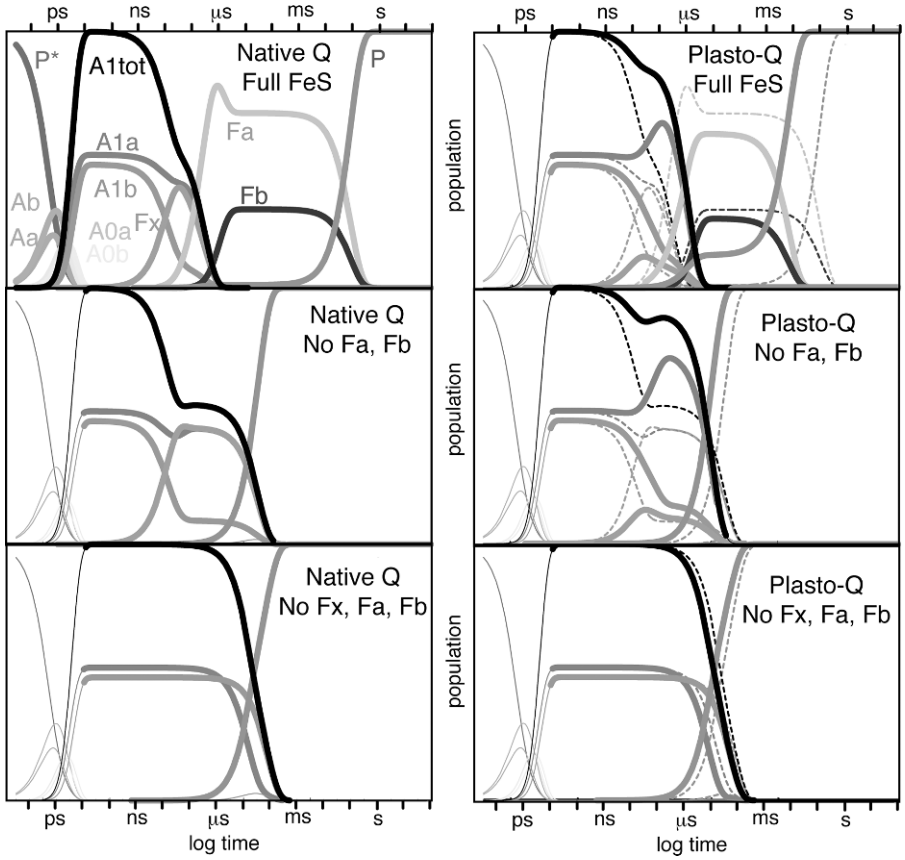

Fig. 5. Electron tunneling kinetics with different complements of Fe/S and different quinones using electron tunneling parameters described in the text. One the right, a comparison of native phylloquinone (dashed) with plastoquinone (solid). See Color Plate 15, Fig. 1.

related electron tunneling in PS I. Figure 5 shows that with the plastoquinone substitution, the electron tends to accumulate and linger on the A_{1a} whenever F_X is present. The population of F_X reduced at any time, already less than 50% in wild type PS I is smaller still in the plastoquinone PS I. Short-circuit charge recombination reactions are generally accelerated, by almost two orders of magnitude in the case of PS I with the full complement of Fe/S centers.

The increase in short-circuit rate is least affected in PS I core particles in which all the Fe/S centers have been removed and the direct short-circuit is maximal. The more positive E_m of plastoquinone relative to the native phylloquinone will decrease the driving force for this direct long-distance charge recombination between A_{1a} and $P700^+$ from about 1.15 eV to about 1.10 eV. Given the distance of 18.1 Å and the unusually high packing density of 0.88 in this region of the protein, in order to have the recombination rate slow enough to be consistent with experiment, the reorganization energy must be about 0.6 eV, thereby placing the recombination well into the inverted region and somewhat counter-intuitively, slowing the short-circuit reaction. As has been pointed out (Shinkarev et al., 2002), the smaller driving force of the plastoquinone charge recombination will slightly increase the electron transfer reaction rate of an inverted region electron transfer, as indeed our simulations show. However, experiment shows that with inactivated Fe/S centers much of the recombination with plastoquinone is *slower* than with phylloquinone.

In order to realize a slowing after quinone substitution in PS I core particles without Fe/S centers, some change in the parameters of electron tunneling besides a small rise in midpoint potential of the quinone must take place. Given the chemical similarity of the phylloquinone and plastoquinone, it seems unlikely that the recombination observed with plastoquinone is slowed by assuming a structural position some 1.4 Å further from P700. A number of different quinone substitutions

have shown no change in the EPR determined distance between reduced A_1^- and oxidized $P700^+$, while others have shown that the orientation of plastoquinone-9 radical is the same as the native phylloquinone (Zybailov et al., 2000). At best there is likely to be on minor distance changes, as pulsed EPR indicates that the benzoquinone duroquinone is 0.3 Å further way from P700 than the native phylloquinone (Zech et al., 1997), potentially slowing charge recombination by only twofold, not the fivefold change observed experimentally (Shinkarev et al., 2002). On the other hand, if plastoquinone were for some reason to have a lower reorganization energy for charge recombination, this would slow the rate, as shown in Table 3. Such a reorganization energy drop runs counter to intuition, however, since plastoquinone is smaller than phylloquinone, and substitution in the A_1 sites would be normally be expected to make the site more mobile and likely to increase the reorganization energy.

Aside from the unexpected slowing of charge recombination in plastoquinone substituted PS I with inactive F_X, the most noticeable deviation of simulated versus experimental kinetics appears when the centers F_A and F_B have been stripped by removal of PsaC using urea. The calculations match the fast phase, and show the appropriate acceleration when plastoquinone replaces the native phylloquinone, but the calculations do not reveal the approximately 10 times slower slow phase. Once again, it seems unlikely that distances between redox centers have changed significantly. Possibly some of the slow phase is a remnant of incomplete removal of F_A and F_B or a change in reorganization energy for at least some of the F_X on removal of the PsaC protein subunit. On the other hand, it has been reported that removal of the stromal extrinsic subunits depleting F_A and F_B may increase the redox potential of F_X (Brettel, 1997). This will tend to slow the recombination rates if F_X to A_1 electron transfer is now more uphill.

VI. PS I Robustness

In spite of descriptions of PS I as "highly optimized" (Itoh et al., 2001), we find that simple distance between the various cofactors contributes to a collective robustness of PS I function that does not require a great deal of fine tuning of the energetic and packing parameters that influence electron tunneling rates. Even without including the stabilizing effect of plastocyanin electron transfer to $P700^+$, the architecture of PS I favors a high yield of light induced charge separation over wasteful charge recombination. Itoh and Iwaki's very extensive range of quinone substitutions for A_1 indicates that the driving force for the native A_0–A_1 electron transfer rather closely matches the unusually small reorganization energy for this reaction, and that this may represent an element of evolutionary design to optimize this reaction. However, simulations show that the system can tolerate rather large changes in this reorganization energy, which can rise from optimal values near 0.3 eV to a value as large as 1.2 eV before charge recombination through the formation of triplet state P700 begins to be a problem. Similarly, quinone substitutions for A_1 that drop the redox midpoint as low as -1 V (much lower than the -0.74 to -0.70 V that seems to be displayed by the native system), can be tolerated by PS I, before the electron begins to be shared significantly between the quinones and the chlorophylls. On the other hand, the redox potential of A_1 cannot rise to a value much beyond the E_m of F_X, or the electron will tend to remain on A_1 long enough for direct charge recombination to the ground state to become a problem. Thus there seems to be a broad tolerance of E_m ranges of the quinones A_{1a} and A_{1b}, and it may be fair to say that the observed asymmetry in the electron transfer kinetics of the two branches does not reflect an advantageous design feature of PS I, but merely a tolerable evolutionary drift that has little effect on performance. Perhaps more surprising is why the natural redox midpoint of F_X should be as negative as it is, which forces the design of a quinone binding site to keep the midpoint potential of the quinone at an unusually low value below about -0.70 V. Certainly, the system could tolerate a rise of 0.1 V in the F_X midpoint potential and still keep the electrons on F_A and F_B, ready for subsequent reduction of ferredoxin. The present redox properties of F_X may represent the adoption of a "good enough" electron transfer system, in which the position of the F_X on the symmetry axis of PS I with good proximity to A_{1a}, A_{1b}, and F_A secures the single most important parameter in determining the electron tunneling rates.

It appears that PS I, perhaps even in the native membrane, may be prone to an inherent heterogeneity in redox potentials and perhaps reorganization energies that leads to non-ideal multiphasic electron transfer behavior. Indeed, it may be the very robustness of the PS I design that allows kinetic hetereogeniety to be functionally well tolerated. It makes little sense to apply more sophisticated quantum analysis to this electron tunneling problem when basic issues such as heterogeneity of driving force are so poorly defined. In the

end, Marcus theory and tunneling analysis may provide the best measure of the thermodynamic heterogeneity present in this photosynthetic system.

Acknowledgments

The authors gratefully acknowledge the support of the National Institute of Health GM41048.

References

Agalarov R and Brettel K (2003) Temperature dependence of biphasic forward electron transfer from the phylloquinone(s) A_1 in photosystem I: only the slower phase is activated. Biochim Biophys Acta 1604: 7–12

Ashnagar A, Bruce JM, Dutton PL and Prince RC (1984) One- and two-electron reduction of hydroxy-1,4-naphthoquinones and hydroxy-9,10-anthraquinones. The role of internal hydrogen bonding and its bearing on the redox chemistry of the anthracycline antitumour quinones. Biochim Biophys Acta 801: 351–359

Braun BS, Benbow U, Lloyd-Williams P, Bruce JM and Dutton PL (1986) Determination of partition coefficients of quinones by high-performance liquid chromatography. Methods Enzymol 125: 119–129

Brettel K (1997) Electron transfer and arrangement of the redox cofactors in photosystem I. Biochim Biophys Acta 1318: 322–373

Chamorovsky SK and Cammack R (1982) Direct determination of the midpoint potential of the acceptor-X in chloroplast photosystem-I by electrochemical reduction and electron-spin-resonance spectroscopy. Photobiochem Photobiophys 4: 195–200

Evans MCW and Heathcote P (1980) Effects of glycerol on the redox properties of the electron-acceptor complex in spinach photosystem-I particles. Biochim Biophys Acta 590: 89–96

Evans MCW, Reeves SG and Cammack R (1974) Determination of oxidation-reduction potential of bound iron-sulfur proteins of primary electron-acceptor complex of photosystem-I in spinach-chloroplasts. FEBS Lett 49: 111–114

Fairclough WV, Forsyth A, Evans MCW, Rigby SEJ, Purton S and Heathcote P (2003) Bidirectional electron transfer in photosystem I: electron transfer on the *psaA* side is not essential for phototrophic growth in *Chlamydomonas*. Biochim Biophys Acta 1606: 43–55

Golbeck JH (1993) The structure of photosystem-I. Curr Opin Struct Biol 3: 508–514

Guergova-Kuras M, Boudreaux B, Joliot A, Joliot P and Redding K (2001) Evidence for two active branches for electron transfer in photosystem I. Proc Natl Acad Sci USA 98: 4437–4442

Gunner MR and Dutton PL (1989) Temperature and -delta-g-degrees dependence of the electron-transfer from BPh^- to Qa in reaction center protein from *Rhodobacter-sphaeroides* with different quinones as Qa. JACS 111: 3400–3412

Heathcote P, Hanley JA and Evans MCW (1993) Double-reduction of A_1abolishes the EPR signal attributed to A_1: evidence for C_2 symmetry in the photosystem I reaction centre. Biochim Biophys Acta 1144: 54–61

Hopfield JJ (1974) Electron transfer between biological molecules by thermally activated tunneling. Proc Natl Acad Sci USA 71: 3640–3664

Itoh S, Iwaki M and Ikegami I (2001) Modification of photosystem I reaction center by the extraction and exchange of chlorophylls and quinones. Biochim Biophys Acta 1507: 115–138

Ivashin N and Larsson S (2003) Electron transfer pathways in photosystem I reaction centers. Chem Phys Lett 375: 383–387

Iwaki M and Itoh S (1989) Electron transfer in spinach photosystem I reaction center containing benzo-, naphtho- and anthraquinones in place of phylloquinone. FEBS Lett 256: 11–16

Joliot P and Joliot A (1999) In vivo analysis of the electron transfer within photosystem I: are the two phylloquinones involved? Biochemistry 38: 11130–11136

Jordan R, Nessau U and Schlodder E (1998) Charge recombination between reduced iron–sulfur clusters and $P700^+$. In: Garab G (ed) Photosynthesis: Mechanisms and Effects. Pp 663–666 Kluwer Academic Publishers, Dordrecht

Kleinherenbrink FAM, Hastings G, Wittmershaus BP and Blankenship RE (1994) Delayed fluorescence from Fe-S type photosynthetic reaction centers at low redox potential. Biochemistry 33: 3096–3105

Klukas O, Schubert WD, Jordan P, Krauß N, Fromme P, Witt HT and Saenger W (1999) Localization of two phylloquinones, Q_K and Q_K', in an improved electron density map of photosystem I at 4-Ångstrom resolution. J Biol Chem 274: 7361–7367

Krabben L, Schlodder E, Jordan R, Carbonera D, Giacometti G, Lee H, Webber AN and Lubitz W (2000) Influence of the axial ligands on the spectral properties of P700 of photosystem I: a study of site-directed mutants. Biochemistry 39: 13012–13025

Kumazaki S, Iwaki M, Ikegami I, Kandori H, Yoshihara K and Itoh S (1994) Rates of primary electron-transfer reactions in the photosystem-I reaction-center reconstituted with different quinones as the secondary acceptor. J Phys Chem 98: 11220–11225

Levich VG and Dogonadze RR (1959) Teiriya bezizluchatelnikh electronnikh perekhodov mezhdu ionami v rastvorakh. Dokl Akad Nauk SSSR 124: 123–126

Lin X, Williams JC, Allen JP and Mathis P (1994) Relationship between rate and free-energy difference for electron-transfer from cytochrome c (2) to the reaction-center in *Rhodobacter sphaeroides*. Biochemistry 33: 13517–13523

Marcus RA (1956) On the theory of oxidation-reduction reactions involving electron transfer: I. J Chem Phys 24: 966–978

Marcus RA and Sutin N (1985) Electron transfers in chemistry and biology. Biochim Biophys Acta 811: 265–322

Moser CC and Dutton PL (1992) Engineering protein structure for electron transfer function in photosynthetic reaction centers. Biochim Biophys Acta 1101: 171–176

Moser CC, Keske JM, Warncke K, Farid RS and Dutton PL (1992) Nature of biological electron transfer. Nature 355: 796–802

Moser CC, Page CC and Dutton PL (2001). Photosynthesis: bacterial reaction center. In: Balzani V (ed) Electron Transfer in Chemistry, pp 24–38. Wiley-VCH, New York

Page CC, Moser CC, Chen X and Dutton PL (1999) Natural engineering principles of electron tunneling in biological oxidation-reduction. Nature 402: 47–52

Parrett KG, Mehari T, Warren PG and Golbeck JH (1989) Purification and properties of the intact P-700 and F_X-containing

photosystem-I core protein. Biochim Biophys Acta 973: 324–332

Ramesh VM, Guergova-Kuras M, Joliot P and Webber AN (2002) Electron transfer from plastocyanin to the photosystem I reaction center in mutants with increased potential of the primary donor in *Chlamydomonas reinhardtii*. Biochemistry 41: 14652–14658

Sakuragi Y, Zybailov B, Shen GZ, Jones AD, Chitnis PR, van der Est A, Bittl R, Zech S, Stehlik D, Golbeck JH and Bryant DA (2002) Insertional inactivation of the *menG* gene, encoding 2-phytyl-1,4-naphthoquinone methyltransferase of *Synechocystis* sp. PCC 6803, results in the incorporation of 2-phytyl-1,4-naphthoquinone into the A_1 site and alteration of the equilibrium constant between A_1 and F_X in photosystem I. Biochemistry 41: 394–405.

Savikhin S, Xu W, Martinsson P, Chitnis PR and Struve WS (2001) Kinetics of charge separation and $A_0 \rightarrow A_1$ electron transfer in photosystem reaction centers. Biochemistry 40: 9282–9290

Schlodder E, Falkenberg K, Gergeleit M and Brettel K (1998) Temperature dependence of forward and reverse electron tranfer from A_1^-, the reduced secondary electron acceptor in photosystem I. Biochemistry 37: 9466–9476

Sétif P and Bottin H (1989) Identification of electron-transfer reactions involving the acceptor-A_1 of photosystem-I at room-temperature. Biochemistry 28: 2689–2697

Sétif P and Brettel K (1993) Forward electron transfer from phylloquinone A_1 to iron-sulfur centers in spinach photosystem I. Biochemistry 32: 7846–7854

Shinkarev VP, Zybailov B, Vassiliev IR and Golbeck JH (2002) Modeling of the $P700^+$ charge recombination kinetics with phylloquinone and plastoquinone-9 in the A_1 site of photosystem I. Biophys J 83: 2885–2897

Shuvalov VA (1976) The study of the primary photoprocesses in photosystem I of chloroplasts recombination luminescence, chlorophyll triplet state and triplet-triplet annihilation. Biochim Biophys Acta 430: 113–121

Vos MH and van Gorkom HJ (1988) Thermodynamics of electron transport in photosystem I studied by electric field-stimulated charge recombination. Biochim Biophys Acta 934: 293–302

Vos MH and Van Gorkom HJ (1990) Thermodynamical and structural information on photosynthetic systems obtained from electroluminescence kinetics. Biophys J 58: 1547–1555

Warncke K and Dutton PL (1993) Influence of Qa site redox cofactor structure on equilibrium binding, in situ electrochemistry, and electron-transfer performance in the photosynthetic reaction center protein. Biochemistry 32: 4769–4779

Zech SG, van der Est AJ and Bittll R (1997) Measurement of cofactor distances between $P700^+$ and A_1^- in native and quinone-substituted photosystem I using pulsed electron paramagnetic resonance spectroscopy. Biochemistry 36: 9774–9779

Zybailov B, van der Est A, Zech SG, Teutloff C, Johnson TW, Shen G, Bittl R, Stehlik D, Chitnis PR and Golbeck JH (2000) Recruitment of a foreign quinone into the A_1 site of photosystem I-II. Structural and functional characterization of phylloquinone biosynthesis pathway mutants by electron paramagnetic resonance and electron-nuclear double resonance spectroscopy. J Biol Chem 275: 8531–8539

Chapter 35

Modeling of Optical Spectra and Light Harvesting in Photosystem I

Thomas Renger
Institut für Chemie (Kristallographie), Freie Universität Berlin, Takustr. 6, D-14195 Berlin, Germany

Eberhard Schlodder*
Max-Volmer-Laboratorium für Biophysikalische Chemie, Fakultät II, Technische Universität Berlin, Straße des 17 Juni 135, D-10623 Berlin, Germany

Summary

In this chapter, structure-based modeling of excitation energy transfer and trapping in Photosystem I (PS I) core complexes will be addressed. The prerequisite for modeling is the knowledge of the spatial arrangement of the pigments (distances between pigments, orientation of their transition dipole moments) and the understanding of the spectral properties of the core antenna and the reaction center. The former is provided by the X-ray structure of trimeric photosystem I core complexes from *Thermosynechococcus elongatus* (formerly *Synechococcus elongatus*)

* Author for correspondence, email: eberhard.schlodder@tu-berlin.de

John H. Golbeck (ed): Photosystem I: The Light-Driven Plastocyanin:Ferredoxin Oxidoreductase, 595–610.

at 2.5 Å resolution (Jordan et al., 2001). The spectral properties are determined by the local transition energies of the pigments, the pigment–pigment interactions and the coupling of the electronic pigment transitions with pigment and protein vibrations. The simultaneous description of the dynamics of excitation energy transfer and of the spectral properties of PS I is a major challenge for the theory. In this chapter, recent theoretical attempts in the literature and our own work are described. The focus is put on the question of how the different approaches relate to experimental data.

I. Introduction

Photosystem I (PS I) captures solar energy by a large antenna system consisting of chlorophylls (Chls) and carotenoids and transfers the energy to the reaction center of the complex where the excitation energy is used to create a charge separated state. PS I is characterized by a high stability against photodestruction and a high efficiency of energy conversion. The quantum yield for the formation of the charge separated state is about 98%.

The 2.5 Å X-ray structure of trimeric PS I core complexes from the thermophilic cyanobacterium *Thermosynechococcus elongatus* (formerly *Synechococcus elongatus*) identifies 12 protein subunits, 96 chlorophyll molecules (Chls), 22 carotenoids (Car), 2 phylloquinones, and 3 iron–sulfur clusters (Jordan et al., 2001; see Fromme and Grotjohann, this volume, Chapter 6). The two largest subunits (PsaA and PsaB) bind most of the antenna and all of the reaction center pigments. The following cofactors constitute the reaction center: The primary electron donor P700 is a heterodimer of chlorophyll *a* (eC-B1), P_B and *a′* (eC-A1), P_A. Two branches of cofactors related by pseudo-C_2 symmetry connect P700 and the first [4Fe–4S] cluster F_X. Each branch is composed of two chlorophylls [Acc-A (eC-B2) and A_0-A (eC-A3) in the A-branch and Acc-B (eC-A2) and A_0-B (eC-B3) in the B-branch] and one phylloquinone (Q_K-A and Q_K-B, respectively) (see Fig. 1).

The core antenna of PS I consisting of the remaining 90 Chl *a* and 22 carotenoid molecules surrounds the reaction center. Most of the chlorophylls are located near the stromal and lumenal membrane surface. Within these two layers a ring-shaped arrangement of antenna chlorophylls is visible (Byrdin et al., 2002). The Chls of these two rings are well connected among each other via Chls located in the membrane-integral part of the protein and with chlorophylls located peripherally on the stromal and lumenal side, respectively. The center-to-center distance between any core antenna Chl and the reaction center Chls is greater than 18 Å except for the two so-called connecting Chls (Jordan et al., 2001) that seem to provide a link between the antenna system and the reaction center. The mean center-to-center distance between neighboring Chls is 9.9 Å, which is only about 30% larger than the diameter of the chlorin ring. This dense packing indicates that excitonic interactions have to be taken into account for a description of the spectral and functional properties of PS I. The arrangement of the Chls indicates clusters consisting of 2–12 moderately or strongly interacting pigments (Byrdin et al., 2002). The interaction between Chls belonging to different clusters is weak. In addition, there are Chls that are rather isolated at the periphery of the PS I complex.

Strong pigment–pigment interactions are most probably also the reason for so-called red antenna states or long-wavelength chlorophylls (see Karapetyan et al., this volume, Chapter 13), which absorb at energies below that of the primary electron donor P700. PS I of *T. elongatus* contains about 10 red Chls per PS I monomer as shown by spectroscopic investigations (Pålsson et al., 1998). The low temperature absorption spectrum exhibits bands at about 708 nm (C708) and 719 nm (C719) with oscillator strengths corresponding to approximately six and four Chls, respectively.

The recent 4.4 Å X-ray structure of PS I from pea reveals that 92 Chls in the core of PS I from plants are at the same position as the Chls in PS I from *T. elongatus*. Three Chls are missing (M1, X1, and J3) and there is only one other Chl (B33) of which the position and orientation is significantly modified (Ben-Shem et al., 2003; see Nelson and Ben-Shem, this volume, Chapter 7). Taking into consideration the conservation

Abbreviations: Chl(s) – chlorophyll(s); C708 (C719 etc) – Chls with low temperature absorption maximum at the respective wavelength; CD – circular dichroism; DAS – decay-associated spectrum; LD – linear dichroism; P700 – chlorophyll heterodimer comprised of Chl *a* (eC-A1), P_A and Chl *a′* (eC-B1), P_B; PS I – Photosystem I; RC – reaction center; Acc-A, Acc-B – accessory Chl of the A-branch and B-branch; A_0-A, A_0-B – Chl *a* monomer of the A-branch and B-branch, intermediate electron acceptor; Q_K-A, Q_K-B – phylloquinone of the A-branch and B-branch; A_1 – spectroscopically identified secondary electron acceptor in PS I which is assigned to one or both of the phylloquinones.

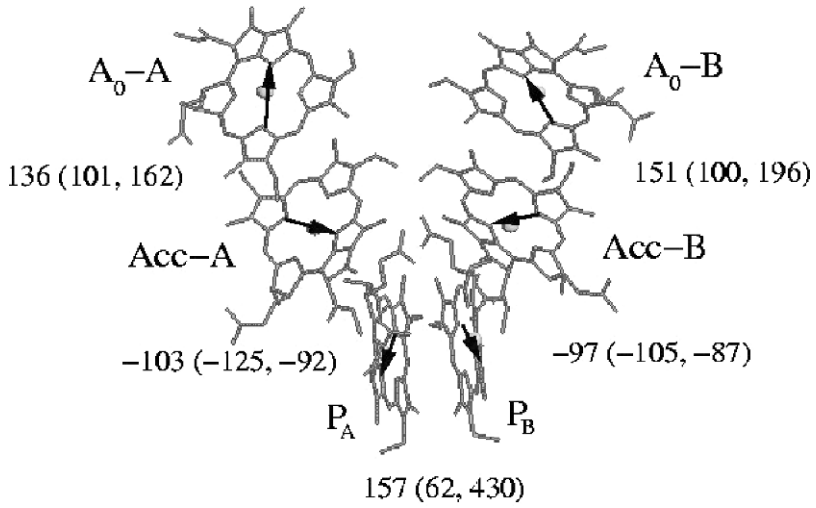

Fig. 1. Structural arrangement of reaction center pigments. Arrows indicate the geometry of optical transition dipole moments. The nearest neighbor couplings are indicated, values obtained within extended dipole approximation are compared to those obtained using transition monopole method (first number in bracket) and point-dipole approximation (second number in bracket). The amount of the partial charges, used in the extended dipole approximation is 0.16 e, and the length of the dipole was 5.7 Å, resulting in an effective transition dipole strength of 19 D^2 [We used $\varepsilon_r = 1$ in Eq. (3)].

of the pigment organization in the PS I core it is interesting to note that the number and spectral characteristics of red antenna states are highly species dependent.

The excited-state dynamics of PS I complexes have been studied intensively by time-resolved absorption and fluorescence spectroscopy. The average rate constant for energy transfer (hopping) between two Chls has been estimated to be about $(100\ \text{fsec})^{-1}$ (Du et al., 1993; Kennis et al., 2001). Energy equilibration between bulk antenna Chls occurs probably in less than 1 psec. In PS I from *T. elongatus*, a ca. 4 psec component has been attributed to energy transfer from bulk antenna Chls to red Chls giving rise to a decay-associated spectrum with positive amplitudes below 700 nm and negative amplitudes at wavelengths longer than 700 nm. In addition, a 9.6 psec component peaks around 700 nm and barely drops below zero. This component has been assigned to a slower energy-transfer process, during which trapping occurs to a great extent (Gobets et al., 2001). The decay of the excitation energy due to trapping by charge separation occurs in about 35 psec, determined in good agreement by various groups (Holzwarth et al., 1993; Dorra et al., 1998; Byrdin et al., 2000; Gobets et al., 2001; Kennis et al., 2001). The spectrum associated with the trapping was reported to be virtually independent of the excitation wavelength (Hastings et al., 1995; Gobets et al., 2003). It resembles closely the steady-state emission spectrum, which exhibits a maximum at 721 nm and a shoulder at 685 nm at room temperature in PS I from *T. elongatus*. This result indicates that the largest part of the fluorescence is emitted from the long-wavelength Chls. Time-resolved fluorescence measurements in species that have different contents of "red" Chls show clearly that these Chls slow down the trapping (Gobets et al., 2001). The increase of the trapping lifetime from 23 to 50 psec is correlated with the amount and the transition energies of the long-wavelength Chls in the different species.

The theory of optical spectra and excitation energy transfer of photosynthetic pigment–protein complexes must describe the couplings between pigments and between pigments and protein. If the pigment–pigment interaction dominates, the absorption of light leads to a delocalized excited state in the complex and the pigment–protein coupling causes relaxation between such delocalized states. If, on the other hand, the pigment–protein coupling dominates, localized excitations are formed in the complex and those local excitations move incoherently between the pigments due to the interpigment Coulomb coupling. A challenging theoretical problem is the intermediate regime, where both types of couplings are of similar magnitude. In this case the excited states are partially delocalized and thus show features of localized states as vibrational sidebands in optical spectra and features of delocalized states as global changes of the absorption spectrum upon changing the absorption of a single pigment as seen, for example, in hole-burning spectroscopy and triplet-minus-singlet spectroscopy.

The pigment–protein coupling causes a modulation of optical transition energies of the pigments. Owing to a different protein environment, pigments in different binding sites have different transition energies. Even site energies of pigments in the same binding sites (but in different complexes in the sample) may differ because of conformational motion of the protein. The fast protein motion leads to a dynamic modulation of pigment transition energies and is included explicitly in the dynamic theory, whereas the slow motion can be treated as static disorder. The timescales of slow and fast motion are defined with respect to the lifetime of the exciton (fsec up to nsec). The dynamic modulation of pigment energies allows the protein to form a heat bath that exchanges energy with excitons on their way from the antenna to the reaction center.

When modeling optical spectra and light harvesting in PS I, one is faced with the following difficulties:

(i) The number of pigments is much larger than in other antenna or reaction center complexes. This large number makes it very difficult, if not impossible, to extract optical transition energies of pigments in their local protein environments from independent experiments. An alternative way chosen by the Fleming group is a quantum chemical calculation of those transition energies (Damjanovic et al., 2002). Nevertheless, it is difficult to judge the outcome of those calculations for a complex as large as PS I.
(ii) PS I contains a number of so-called red chlorophylls that absorb at lower energies than the reaction center. It is very likely that the red shift occurs because of a mixing of optical transitions with intermolecular charge transfer states. There is no standard theory of optical spectra that considers such a mixing.
(iii) There are weakly as well as strongly coupled pigments in PS I and there is no standard theory that is valid for the whole range of couplings.

The remaining of this chapter is organized in the following manner. First, the different types of interactions present in photosynthetic pigment–protein complexes are described in detail and are related to theories of optical spectra and excitation energy transfer. Recent applications of those theories to describe optical spectra (absorption, linear dichroism, circular dichroism, steady-state, and time-resolved fluorescence) and excitation energy transfer and trapping in PS I are discussed. Next, recent extensions of the standard theories, the Modified Redfield theory and a non-Markovian density matrix theory, are described, that allow one to treat exciton relaxation and optical spectra of aggregates with strongly coupled pigments and strong couplings to vibrations. Finally, an application of the theory is given to extract optical transition energies of the pigments in the PS I reaction center from optical difference spectra.

II. Interactions in Pigment–Protein Complexes

A. Site Energies, Static, and Dynamic Disorder

Due to different protein environments, pigments in different binding sites have different optical transition energies. The latter are called site energies. The following protein–cofactor interactions influence the energetic and spectroscopic properties of the Chls: (a) differences in the dielectric constant of the local environment, (b) electrostatic interactions with charged amino acid side chains (Eccles and Honig, 1983), and (c) differences in Mg^{2+}-ligation, H-bonding, and deviations from planarity of the chlorine ring induced by the protein binding site (Gudowska-Nowak et al., 1990). Because of the complexity of these interactions, the transition energies cannot be derived directly from the structure. A microscopic calculation of site energies is difficult (Damjanovic et al., 2002) since both the conformation of the pigment and the electrostatic coupling of the pigment with its protein environment have to be taken into account. In addition, some of the protein residues, the titratable groups, might occur in a protonated or unprotonated form and thus an average over the possible titration states of the titratable groups is necessary. Often, therefore, the site energies are used as parameters that are determined from the calculation of optical spectra (e.g., Byrdin et al., 2002).

Usually experiments are done on ensembles of pigment–protein complexes. Due to different conformational substates of the protein, pigments bound at the same site in different complexes in the sample will absorb at different energies. This effect is termed diagonal disorder. For the calculation of experimental signals, therefore, an average over the conformational substates of the protein is necessary. If the diagonal disorder is weak compared to the excitonic coupling the disorder can be described by a perturbation theory (e.g., Dempster et al., 2001). In many pigment–protein complexes the diagonal disorder is comparable in magnitude or even of larger magnitude than the excitonic couplings. In this case a numerical Monte Carlo method

can be used to treat the disorder non-perturbatively (e.g., Renger et al., 2001).

In addition to static disorder in site energies there is also a dynamic modulation caused by the vibrational motion of the protein environment. The latter leads to dissipation of electronic excess energy and determines the overlap integrals appearing in standard transfer theories and the homogeneous broadening of optical spectra, as will be discussed in detail later.

B. Pigment–Pigment Coupling/ Excitons/Gaussian Dressed Exciton Stick Spectra

The pigment–pigment coupling mainly involves the Coulomb coupling between a pigment in an excited electronic state and another pigment in the ground state. This so-called excitonic coupling between the pigments leads to a nonradiative transition of excitation energy between the pigments (Förster, 1948), in photosynthetic antennae and reaction center complexes. The matrix element V_{mn} represents the interaction energy between an excited pigment m and a pigment n in the ground state

$$V_{mn} = \left\langle \phi_m^{(e)} \phi_n^{(g)} | \, V_{Coulomb} | \phi_m^{(g)} \phi_n^{(e)} \right\rangle \tag{1}$$

where $\phi_m^{(e)}$ and $\phi_n^{(e)}$ denote the excited-state wave functions of pigments m and n, $\phi_m^{(g)}$ and $\phi_n^{(g)}$ are the ground-state wave functions of pigments m and n, and $V_{Coulomb}$ is the Coulomb coupling between the electrons and nuclei of the two pigments.

1. Point-Dipole Approximation

If the extension of the electronic wave functions of the pigments is small when compared to the center-to-center distance between the pigments, $V_{Coulomb}$ can be expanded in a Taylor series and the first nonvanishing element of that series is the well-known point-dipole approximation (e.g., van Amerongen et al., 2000)

$$V_{mn} = \frac{1}{4\pi\varepsilon_0\varepsilon_r} \left(\frac{\vec{\mu}_m \vec{\mu}_n}{R_{mn}^3} - 3\frac{(\vec{\mu}_m \vec{R}_{mn})(\vec{\mu}_n \vec{R}_{mn})}{R_{mn}^5} \right) \tag{2}$$

where $\vec{\mu}_m$ and $\vec{\mu}_n$ are the optical transition dipoles of the two pigments and $\vec{R}_{mn}$ is the center-to-center spatial vector between the two pigments. The above formula expresses the excitonic coupling as the dipole–dipole coupling between optical transition dipoles.

The orientations of transition dipoles $\vec{\mu}_m$ of photosynthetic pigments and distance vectors $\vec{R}_{mn}$ can be obtained from structural data and the dipole strengths $|\mu_m|^2$ can be determined from optical spectra of chlorophylls in solution. Therefore, Eq. (2) provides a very practical tool to estimate excitonic couplings. The screening effects of the Coulomb coupling are included by the dielectric constant ε_r, the precise value of which is not clear in proteins. In addition to screening effects there are also local field corrections (for a discussion of the latter see, e.g., van Amerongen et al., 2000) that were neglected in the above equation. In applications, the dipole strengths are often treated as effective dipole strengths that include screening and local field corrections in an effective way and in this case one would set $\varepsilon_r = 1$ in the above equation.

2. Extended–Dipole Approximation

Within the above point-dipole approximation the optical transition dipoles of the pigments are treated as ideal point-dipoles. A first correction of this approximation, that can take into account a certain extension of the electronic wave functions of the pigments, is the extended dipole approximation where the optical transition dipoles of the pigments are described by two charges of opposite sign $\delta q_m^{(+)} = \delta q$ and $\delta q_m^{(-)} = -\delta q$ that are placed along the direction of the optical transition dipoles of the pigments. The distance l between the two charges effectively describes the extension of the electronic wave functions. The charges δq are chosen such as to result in a dipole strength $|\mu_m|^2 = (\delta q)^2 l^2$ estimated from measurements in solution. The dipole strength is assumed to be the same for all pigments, i.e., independent on index m'. The excitonic coupling is then obtained from the Coulomb interaction between the point charges of the two pigments

$$V_{mn} = \frac{1}{4\pi\varepsilon_0\varepsilon_r} \sum_{i,j=+,-} \frac{\delta q_m^{(i)} \delta q_n^{(j)}}{r_{mn}^{(ij)}} \tag{3}$$

where $r_{mn}^{(ij)}$ is the distance between $\delta q_m^{(i)}$ and $\delta q_n^{(j)}$.

3. Transition Density Quantum Chemical Methods

If the closest distance between pigments becomes comparable or smaller than the extension of their electronic wave functions the above approximations become invalid and the excitonic coupling has to be calculated by a quantum chemical method. For this purpose the coupling V_{mn} is written in terms of a Coulomb coupling between transition densities

$$V_{mn} = \langle \rho_m | \, V_{Coulomb} \, | \rho_n \rangle \tag{4}$$

where the transition density ρ_m of pigment m is defined as the product of the ground- and excited-state wave functions

$$\rho_m = \left(\phi_m^{(e)}\right)^* \phi_m^{(g)} \tag{5}$$

Once those transition densities were calculated by a quantum chemical method, different ways exist to evaluate the excitonic coupling V_{mn}. One way is to approximate this coupling by the Coulomb interaction between transition charges of the two pigments that are obtained from the transition densities by integration over certain volume elements.

In the transition monopole method (Chang, 1977) the transition charges are obtained for every atom of a pigment by integration over the transition density of that particular atom. In the transition density cube method (Krueger et al., 1998) the space around each pigment is divided into cubes by a three-dimensional grid. The transition charge in a cube is then obtained by integration of the transition density within this cube and this charge is put in the center of the respective cube.

We note that for small interpigment distances, besides the excitonic coupling, additional interactions between pigments occur. Intermolecular charge transfer states can be formed and have an influence on position and widths of optical lines. Although this topic is of some relevance for the unusual behavior of the red chlorophylls in PS I, we do not go into more details here.

4. Delocalized Excited States

If the excitonic couplings V_{mn} are large compared to the static and dynamic disorder, the excited states $|M\rangle = \sum_m c_m^{(M)} |m\rangle$ are delocalized and are given in terms of a linear combination of localized excited states $|m\rangle$, where the eigencoefficients $c_m^{(M)}$ and exciton-(eigen)-energies ε_M are obtained by solving $H_{ex} |M\rangle = \varepsilon_M |M\rangle$ with the excitonic Hamiltonian

$$H_{ex} = \sum_m E_m |m\rangle \langle m| + \sum_{m \neq n} V_{mn} |m\rangle \langle n|. \tag{6}$$

Here, E_m is the site energy of pigment m (strictly defined as the vertical transition energy of the pigment at the equilibrium position of nuclei in the electronic ground state of the aggregate) and V_{mn} is the excitonic coupling between pigments m and n, introduced above. If the dynamic pigment–protein coupling is neglected, the absorption spectrum is obtained as

$$\alpha(\omega) \propto \omega \sum_M |\mu_M|^2 \delta(\omega - \omega_M), \tag{7}$$

where the transition dipole of exciton state M,

$$\vec{\mu}_M = \sum_m c_m^{(M)} \vec{\mu}_m, \tag{8}$$

is given in terms of the exciton coefficients $c_m^{(M)}$ and local transition dipoles $\vec{\mu}_m$ and $\omega_M = \varepsilon_M/\hbar$, the eigenfrequency of exciton state M. The spectrum is sometimes called stick spectrum, because it can be visualized by vertical lines of height $|\mu_M|^2$ at position $\omega = \omega_M$. No homogeneous broadening is included so far (but will be discussed later).

We note that in analogy to the above equation for absorption the linear dichroism spectrum $LD(\omega) = \alpha_{||}(\omega) - \alpha_\perp(\omega)$, as the difference in absorption measured parallel ($\alpha_{||}$) and perpendicular ($\alpha_\perp$) to the membrane is obtained as

$$LD(\omega) \propto \frac{3}{2}\omega \sum_M |\mu_M|^2 \times (1 - 3\cos^2(\theta_M))\delta(\omega - \omega_M), \tag{9}$$

where θ_M is the angle between $\vec{\mu}_M$ and the normal of the membrane. The circular dichroism spectrum

$$CD(\omega) \propto \omega \sum_M r_M \delta(\omega - \omega_M), \tag{10}$$

contains the rotational strength

$$r_M = \sum_{m>n} c_m^{(M)} c_n^{(M)} \vec{R}_{mn} (\vec{\mu}_m \otimes \vec{\mu}_n), \tag{11}$$

where $\otimes$ denotes a cross product. The fluorescence spectrum $I(\omega)$ is obtained as

$$I(\omega) \propto \omega^3 \sum_M f(M) |\mu_M|^2 \delta(\omega - \omega_M), \tag{12}$$

where $f(M) = \exp(-\varepsilon_M/kT)/\sum_N \exp(-\varepsilon_N/kT)$ is a Boltzmann factor that takes into account that fluorescence starts from an electronically relaxed excited state. We note that no Stokes shift is included, since the vibrations are neglected. However, in some approaches the Stoke shift is included in an effective way by including a shift Δ in the transition energies, i.e., replacing $\delta(\omega - \omega_M)$ in Eq. 12 by $\delta(\omega + \Delta - \omega_M)$.

In simple models of static disorder a Gaussian distribution function $P_{inh}(\omega_M - \bar{\omega}_M)$ of exciton transition frequencies, centered around a mean transition frequency $\hbar\bar{\omega}_M$ is assumed and the absorption $\alpha(\omega)$ in this case is obtained from an average of the homogeneous absorption spectrum given above with respect to this distribution function.

$$\alpha(\omega) \propto \omega \sum_M |\mu_M|^2 \int d\omega_M P_{inh}(\omega_M - \bar{\omega}_M)\delta(\omega - \omega_M) \propto \omega \sum_M |\mu_M|^2 P_{inh}(\omega - \bar{\omega}_M) \tag{13}$$

Here, the same distribution function was assumed for all exciton states, for simplicity.

In more realistic, although numerically more involved, approaches a distribution of local site energies is assumed and a Monte Carlo scheme is used to calculate the spectra. Within this method different configurations of site energies of the pigments are generated randomly from a given distribution function. The experimental signal then is calculated for every configuration of site energies and an average is performed. Usually, a Gaussian distribution function is used for every site and the fluctuations at different sites are assumed to be uncorrelated. In such calculations the mean site energies and the width of the distribution function for the site energies are fit parameters. The Monte Carlo approach includes the so-called resonance energy-transfer narrowing, i.e., a narrowing of the distribution of exciton energies with respect to the distribution of pigment energies that is due to the excitonic couplings (e.g., Knapp, 1984).

III. Theory of Excitation Energy Transfer

A. Transfer Between Weakly Coupled Pigments – Förster Theory

If the disorder is much stronger than the excitonic coupling the excited states are localized on single pigments and the transfer starts from a vibrationally relaxed excited state of a pigment. In this case, a second-order perturbation theory in the excitonic coupling is used to obtain a Förster type rate constant $k_{m\to n}$ for excitation energy transfer between pigments m and n. The rate constant

$$k_{m\to n} = 2\pi \frac{|V_{mn}|^2}{\hbar^2} \int_{-\infty}^{\infty} d\omega D_I^{(m)}(\omega) D_\alpha^{(n)}(\omega) \qquad (14)$$

is given as the product of the square of the point-dipole excitonic coupling and an overlap integral of the fluorescence lineshape function $D_I^{(m)}(\omega)$ of the donor and the absorption lineshape function $D_\alpha^{(n)}(\omega)$ of the acceptor. Within a linear model for the coupling between vibrational coordinates and pigment transition energies the lineshape functions are related to a spectral density $J(\omega)$ by (Lax, 1952; May and Kühn, 2000)

$$D_I^{(m)}(\omega) = \frac{1}{2\pi} \int_{-\infty}^{\infty} dt e^{-i(\omega-\tilde{\omega}_m)t} e^{G(t)-G(0)} \qquad (15)$$

$$D_\alpha^{(n)}(\omega) = \frac{1}{2\pi} \int_{-\infty}^{\infty} dt e^{i(\omega-\tilde{\omega}_n)t} e^{G(t)-G(0)} \qquad (16)$$

where the function $G(t)$

$$G(t) = \int_0^{\infty} d\omega J(\omega) \times \left\{(1+n(\omega))e^{-i\omega t} + n(\omega)e^{i\omega t}\right\}, \qquad (17)$$

contains the spectral density $J(\omega)$ and the mean number $n(\omega)$ of vibrational quanta that are excited in a vibrational mode of frequency ω at a given temperature T,

$$n(\omega) = \frac{1}{e^{\hbar\omega/kT} - 1}. \qquad (18)$$

The spectral density

$$J(\omega) = \sum_\xi g_\xi^2 \delta(\omega - \omega_\xi) \qquad (19)$$

contains the density of vibrational modes weighted by the constants g_ξ^2 that describe the coupling strength between the vibrational mode $\xi$and the optical transition of the pigment. The $J(\omega)$ can be extracted from optical spectra as will be discussed below. The frequencies $\tilde{\omega}_m = (E_m - E_\lambda)/\hbar$ and $\tilde{\omega}_n = (E_n - E_\lambda)/\hbar$ that enter the lineshape functions in Eqs. (15) and (16) are transition frequencies between the minima of the ground- and excited-state potential energy surfaces, they are obtained from the site energies E_m and E_n and the reorganization energy

$$E_\lambda = \hbar \int_0^{\infty} d\omega J(\omega)\omega. \qquad (20)$$

Noting, that the experimental fluorescence signal of the donor $I_m(\omega)$ is proportional to $\omega^3 D_I^{(m)}(\omega)$ and the absorption signal of the acceptor $\alpha_n(\omega)$ is proportional to $\omega D_\alpha^{(n)}(\omega)$ (Lax, 1952), the rate constant $k_{m\to n}$ can be expressed in terms of those experimental quantities as

$$k_{m\to n} = 2\pi \frac{|V_{mn}|^2}{\hbar^2} \frac{\int_0^{\infty} d\omega I_m(\omega)\alpha_n(\omega)\omega^{-4}}{\int_0^{\infty} d\omega I_m(\omega)\omega^{-3} \int_0^{\infty} d\omega \alpha_n(\omega)\omega^{-1}}. \qquad (21)$$

In the original expression for the rate constant (Förster, 1965) the explicit calculation of the excitonic coupling V_{mn} was avoided by expressing its square as $|V_{mn}|^2 = \frac{1}{4\pi\varepsilon_0\varepsilon_r} |\mu_m|^2 |\mu_n|^2 \kappa_{mn}^2 / R_{mn}^6$ and including the dipole strengths $|\mu_m|^2$of the donor and $|\mu_n|^2$of the acceptor in the radiative lifetime τ_m of the donor and in the molar extinction coefficient $\varepsilon_n(\upsilon)$ of the acceptor, respectively. The orientational factor $\kappa_{mn} = \vec{e}_m\vec{e}_n - 3(\vec{e}_m\vec{e}_{mn})(\vec{e}_n\vec{e}_{mn})$ contains the unit vectors $\vec{e}_m$ along the transition dipole $\vec{\mu}_m$, $\vec{e}_n$ along $\vec{\mu}_n$, and $\vec{e}_{mn}$ along $\vec{R}_{mn}$. The rate constant is then obtained in dependence on the overlap between $\varepsilon_n(\upsilon)$ and the normalized

fluorescence spectrum $I_m(\upsilon)$ as (Förster, 1965)

$$k_{m\to n} = \frac{\kappa_{mn}^2}{R_{mn}^6} \frac{9c^4 \ln(10)}{128\pi^5 n^4 N_L \tau_m} \times \int_0^\infty d\upsilon\, I_m(\upsilon)\varepsilon_n(\upsilon)\upsilon^{-4}, \quad (22)$$

where the experimental spectra are given as a function of frequency $\upsilon = \omega/2\pi$, c, n, and N_L being the velocity of light, index of refraction, and Loschmidt's number, respectively.

B. Transfer Between Aggregates of Strongly Coupled Pigments

If the transfer occurs between aggregates with strong excitonic couplings between pigments in the same aggregate and weak couplings between pigments in different aggregates, Förster theory can be generalized to describe this situation (Fetisova et al., 1996; Mukai et al., 1999; Sumi, 1999). In this case the transfer starts from an electronically and vibrationally relaxed aggregate state and the rate constant contains a thermal distribution of exciton states of the donor aggregate, a generalized matrix element of the dipole–dipole interaction and a generalized overlap integral of fluorescence and absorption. Those quantities are generalized in the sense that they depend not only on local pigment properties but also on the coefficients of excitonic wave functions of the aggregates. In particular excitation energy transfer can involve optically dark states. We discuss here for simplicity the case where the transfer occurs between a localized donor state m and a delocalized aggregate state N. The rate constant $k_{m\to N}$ then is obtained as (Fetisova et al., 1996; Mukai et al., 1999)

$$k_{m\to N} = 2\pi \frac{|V_{mN}|^2}{\hbar^2} \int_{-\infty}^{\infty} d\omega D_I^{(m)}(\omega) D_\alpha^{(N)}(\omega), \quad (23)$$

where the excitonic coupling V_{mN} between the monomer state m and the aggregate state N is given as a sum of the point-dipole couplings V_{mN} (Eq. 12) between the individual pigments (counted by index n) of the aggregate and the monomer m, weighted by the exciton coefficient $c_n^{(N)}$ of pigment n, i.e.,

$$V_{mN} = \sum_n c_n^{(N)} V_{mn}. \quad (24)$$

The lineshape functions $D_\alpha^{(N)}(\omega)$of the aggregate in general contains vibrational sidebands of exciton transitions and a lifetime broadening that is due to exciton relaxation. A theory for the excitonic lineshape function $D_\alpha^{(N)}(\omega)$ will be given below. Here, we note that in the simplest approach those lineshape functions are approximated by local lineshape functions of the pigments. The extension to the case of transfer between two delocalized states in different aggregates with strong intra-aggregate couplings and weak inter-aggregate coupling is straightforward (Fetisova et al., 1996).

IV. Application to Photosystem I

Using the theory described above several attempts have been performed to model energy transfer and trapping in PS I core complexes. The first structure-based model calculations of excitation energy transfer of PS I (White et al., 1996; Beddard, 1998; Gobets et al., 1998; Byrdin et al., 2000) were performed on the basis of the crystal structure at 6 Å resolution (Krauß et al., 1993) and 4 Å resolution (Schubert et al., 1997), respectively. The 2.5 Å X-ray structure (Jordan et al., 2001) opened up the possibility to calculate the excitonic interactions in a more realistic way by taking into account the center-to-center distance R_{mn} and the orientational factor κ_{mn}. Other important parameters are not precisely known including the Förster overlap integrals due to lack of knowledge of the site-specific spectral properties of the 96 Chls and the local dielectric constant of the protein environment.

Model calculations on the basis of the 2.5 Å crystal structure have been reported first by Byrdin et al. (2002). In their work, optical spectra of the PS I complex from *T. elongatus* (absorption, linear and circular dichroism, and emission) and the energy-transfer kinetics were simultaneously simulated with a common set of parameters. The excitonic interactions in the PS I complex were analyzed using the point-dipole and the extended dipole approximation. It turned out that several aggregates of moderately or strongly interacting pigments (e.g., the tetramer A31-A32-B7-B6, the trimer B31-B32-B33 and several dimers including P700) are present in the PS I core, along with Chls that are rather isolated at the periphery of the PS I complex (Byrdin et al., 2002). Figure 1 shows the arrangement of the six chlorophylls within the reaction center. The Q_y transition dipole moments are represented by arrows lying on the axis connecting N atoms of ring I and III ($N_B - N_D$ in the nomenclature of the Brookhaven protein data bank). The excitonic couplings between neighboring pigments are also indicated. They were calculated using the extended dipole approximation. The numbers in brackets give the results obtained by the transition monopole (Chang, 1977) and the

point-dipole approximations. The extended dipole approximation gives couplings that are between those obtained in the transition monopole approach and the simple point-dipole approximation. Interestingly, by far the largest deviations (a factor of 7) result for the coupling of P_A and P_B, whereas all other coupling strengths differ by less than a factor of 2 in the three approximations. Within extended dipole approximation, the coupling energies between all neighboring Chls in the reaction center become comparable. More sophisticated quantum chemical methods for the calculation of the coupling strengths have been applied by Damjanovic et al. (2002) and Sener et al. (2002). The results are somewhat disappointing so far because the couplings calculated by the various methods differ considerably.

Excitonic coupling contributes considerably to both the broadening and red shift of the Q_Y absorption band of PS I as compared to that of Chl *a* in organic solvents. In addition, a distribution of site energies with a width of about 300 cm^{-1} (FWHM) around 675 nm is required for the simulation of the inhomogeneously broadened Q_Y absorption band of PS I (Byrdin et al., 2002). To simulate the long, featureless red tail of the room temperature absorption spectrum, for six Chls, the wavelength of the Q_y transition had to be chosen larger than 700 nm.

The assignment of transition energies to all the structurally defined Chls was obtained by simultaneous fitting of available optical spectra and of the excitation transfer dynamics. The long-wavelength absorption was assigned to the tightly coupled cluster of four Chls near the trimerization domain (A31-A32-B7-B6) and the A38/39 and B37/38 dimers, which also are strongly coupled and are close to the linker Chls A40 and B39 (Byrdin et al., 2002). It should be noted that the contribution of the dimers A38/39 and B37/38 to the long-wavelength absorption is small because they have most of their dipole strength (80% and 85%, respectively) in the high-energy exciton transition. Figure 2 compares the experimental steady-state spectra [absorption, linear dichroism (LD), circular dichroism (CD), and fluorescence spectra] (dotted lines) with the simulated spectra. Excellent agreement between simulation and experiment was obtained for the absorption and the LD spectrum. For the CD spectrum, which displays the difference in the absorption of left and right circularly polarized light, the agreement between simulation and experiment is less satisfying. The deviations may have several causes. It is a specific property of excitonically coupled transitions, that they show *conservative* CD spectra, i.e., $\int d\omega CD(\omega) = 0$. The measured CD signal is clearly nonconservative, which

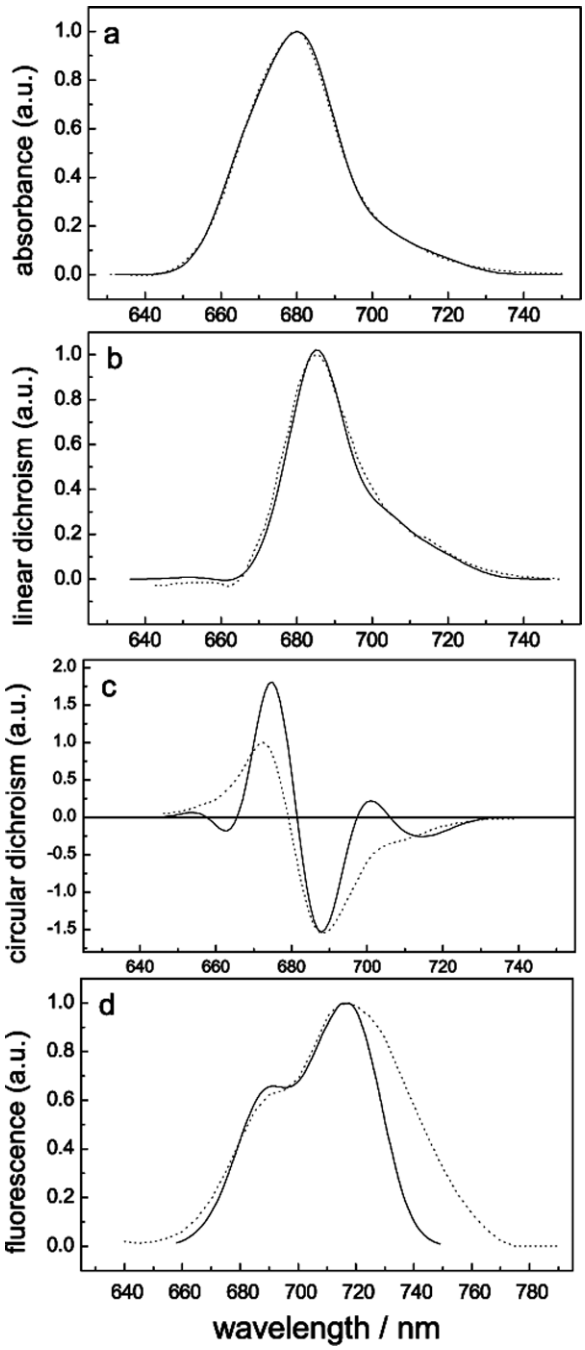

Fig. 2. Comparison of simulated (solid lines) and measured (dotted lines) steady-state spectra of trimeric PS I core complexes from *T. elongatus* (A) absorption, (B) linear dichroism, (C) circular dichroism, and (D) fluorescence. Whereas (A) and (B) show rather good agreement, (C) and (D) cannot reproduce the width of the experimental spectra, possibly due to the simple Gaussian dressing method used. The simulations take into account the site energies of the Chls given in Byrdin et al. (2002) and all excitonic interactions as calculated from the 2.5 Å structure.

might be due to mixing with higher excited states, the so-called "hyperchromism" (Scherz and Parson, 1984). As the simulation was limited to pure Q_Y states, this effect was not taken into account. The simple Gaussian dressing of the stick spectra is probably the reason that the widths of the bands in the CD and fluorescence spectra are not correctly reproduced.

Assuming the same site energy for all pigments, the walk of excitations through the antenna will be random. The time constant for trapping in such a system was calculated to be about 60 psec, which is longer than the time observed experimentally (∼35 psec). Excitonic coupling between neighboring Chls introduces spectral heterogeneity by energy splitting and gives rise to the reorientation of transition dipoles and to the redistribution of dipole strength. By all three effects transfer rates are modified. The detailed analysis shows that the reorientation of transition dipoles due to excitonic coupling leads to an enhancement of transfer rates (Byrdin et al., 2002). Using the spectral/spatial assignments derived from the simulation of the optical spectra the low-energy exciton band of P700 in *T. elongatus* is located at 703 nm. Hence, the absorption of P700 occurs at longer wavelengths than the absorption of all the other Chls except the red Chls. The resulting energy gradient toward the photochemical trap imposes a directionality and is calculated to speed up trapping to about 20 psec if the wavelengths of the red Chls are set to 680 nm. A trapping time of 20 psec is similar to that observed in PS I complexes with the fewest red Chls. If the long-wavelength absorption of PS I from *T. elongatus* attributed to the tetramer (A31-A32-B7-B6) and to the two linker dimers (A38/39 and B37/38) is also taken into account, the calculated trapping time increases and agrees well with the experimental value of 35 psec (Byrdin et al., 2002). Excitation energy redistribution between bulk and red chlorophylls toward a thermally equilibrated state was calculated to occur within about 4 psec as experimentally observed in recent studies with high time resolution (Gobets et al., 2001; Kennis et al., 2001). The parameters used in this modeling assume both fast transfer between Chls (Förster radius = 78 Å), and fast trapping (intrinsic rate constant for primary charge separation = 0.87 psec^{-1}). The effects of varying these parameters indicate that the excited-state dynamics is not limited exclusively by either the rate constant for electron transfer ("trap-limited") or the rate of energy transfer to the trap ("transfer-limited").

Gobets et al. (2003) used Förster theory to calculate excitation energy-transfer rates. Spectral heterogeneity induced by the excitonic coupling are included in an effective way be assigning low site energies to strongly coupled pigments. Individual site energies were assigned to the P700 (698 nm) and the A_0 (686 nm) chlorophylls. On the basis of their spectral characteristics the red chlorophylls are assigned to strongly coupled dimers or larger aggregates. The remaining Chls are assumed to absorb at 680 nm. The delocalized nature of the excited states of aggregates with strong pigment interactions were not taken into account. In this simple approach Gobets et al. successfully modeled the kinetics of the excited-state dynamics and the decay-associated spectra of the 3, 11, and 37 psec components. They concluded that the red most absorption has to be assigned to the trimer of chlorophylls B31-B32-B33 (for a more detailed discussion see Karapetyan et al., this volume, Chapter 13).

An interesting aspect of these structure-based modeling studies is the possibility to analyze situations in which the arrangement of the Chls is modified within the calculation, for example by removal of the linker and/or the linker dimer Chls, removal of outlying Chls in the small subunits to simulate deletion mutants, or removal of antenna Chls located in middle of the membrane (Byrdin et al., 2002; Sener et al., 2002). Interestingly, removing the linker Chls has almost no effect on the calculated trapping time, indicating that these Chls are not required for an efficient trapping (Byrdin et al., 2002; Sener et al., 2002; Gobets et al., 2003). Of course, one can also study the influence of various spectral/spatial assignments. The variation of the trapping time found in these calculations is rather small. The values differ only by about a factor of 3, corresponding to a difference in quantum efficiency of only 3% between ∼98% and ∼95%. This result indicates that the system is optimized for robustness (Byrdin et al., 2002; Sener et al., 2002).

V. Exciton Relaxation Within Aggregates of Strongly Coupled Pigments

A. Redfield Theory and Limitations

If the excitonic coupling is stronger than the modulation of site energies by vibrations and the static disorder, exciton relaxation between partially delocalized exciton states occurs. A second order perturbation theory in the exciton-vibrational coupling, within Markov approximation, yields the rate constant for exciton relaxation between states M and N(see e.g., Renger et al., 2001)

$$k_{M\to N} = 2\pi\gamma_{MN}\omega_{MN}^2 \times \{J(\omega_{MN})(1+n(\omega_{MN})) + J(\omega_{NM})n(\omega_{NM})\} \quad (25)$$

We note that $J(\omega)$ for negative ω is zero and

$$\omega_{MN} = (\varepsilon_M - \varepsilon_N)/\hbar \quad (26)$$

is the transition frequency between the two states. The function

$$\gamma_{MN} = \sum_{m,n} e^{-R_{mn}/R_c} |c_m^{(M)}|^2 |c_n^{(N)}|^2 \tag{27}$$

contains the overlap of electronic wave function of the two exciton states and a correlation radius of protein vibrations that describes in an effective way how the fluctuations of site energies at different sites are correlated (Renger et al., 2001). Redfield theory was used by Brüggemann et al. (2004) to study linear optical spectra and excitation relaxation in Photosystem I. The approximations of the Redfield theory are (i) a perturbative treatment of the exciton-vibrational coupling and (ii) a Markov approximation. The latter assumes that vibrational relaxation in the states M and N is fast compared to the transfer. The first approximation neglects reorganization effects of the vibrations during the transfer, i.e., the potential energy surfaces of states M and N are treated as unshifted along the vibrational coordinates. This approximation can be tested by using a theory that describes the diagonal part of the exciton-vibrational coupling in a nonperturbative manner. Such a theory is described next.

B. Modified Redfield Theory – Application to PS I

In the presence of static disorder it can be assumed that the diagonal part of the exciton-vibrational coupling (diagonal in the representation of delocalized exciton states) is larger than the off-diagonal part and the former can be used to construct excitonic potential energy surfaces (PES). Taking into account the diagonal part nonperturbatively the following rate constant is obtained when an harmonic oscillator description is used for the vibrations (Renger and Marcus, 2003)

$$k_{M\to N} = \int_{-\infty}^{\infty} dt e^{i\tilde{\omega}_{MN}t} e^{\phi_{MN}(t)-\phi_{MN}(0)} \times \left([\lambda_{MN}/\hbar + G_{MN}(t)]^2 + F_{MN}(t) \right) \tag{28}$$

with the time-dependent functions

$$\phi_{MN}(t) = \sum_m \left[\left(c_m^{(M)}\right)^2 - \left(c_m^{(N)}\right)^2 \right]^2 \phi_0(t) \tag{29}$$

$$G_{MN}(t) = \sum_m \left[\left(c_m^{(M)}\right)^3 c_m^{(N)} - \left(c_m^{(N)}\right)^3 c_m^{(M)} \right] \phi_1(t) \tag{30}$$

$$F_{MN}(t) = \sum_m \left(c_m^{(M)}\right)^2 \left(c_m^{(N)}\right)^2 \phi_2(t) \tag{31}$$

where the function $\phi_n(t)(n = 0, 1, 2)$ in Eqs 29–31 is given by

$$\phi_n(t) = \int_{-\infty}^{\infty} d\omega \omega^n e^{-i\omega t}(1 + n(\omega)) \times [J(\omega) - J(-\omega)]. \tag{32}$$

The $\tilde{\omega}_{MN}$ in Eq. (28) is the transition frequency between the minima of the two excitonic potential energy surfaces, $\tilde{\omega}_{MN} = \omega_{MN} - (\gamma_{MM} - \gamma_{NN})E_\lambda$, with the γ_{MN} and the E_λ in Eqs. (27) and (20), respectively.

A similar, but somewhat more complicated expression was derived earlier by Mukamel and coworkers (Zhang et al., 1998), using a Brownian oscillator description. This theory, that was termed Modified Redfield Theory (Yang and Fleming, 2002), was applied recently to study exciton relaxation within strongly coupled pigments in PS I (Yang et al., 2003). Besides the use of the Modified Redfield theory for exciton relaxation between strongly coupled pigments, another new aspect in this application was the use of different lineshape functions for the red chlorophylls, taking into account a stronger exciton-vibrational coupling of those states in an effective way. Experimental evidence for a stronger exciton-vibrational coupling of the red chlorophylls and the primary donor P700 in the PS I reaction center was reported in hole-burning studies (Gillie et al., 1989; Zazubovich et al., 2002).

In the calculations of the trapping time it was found that the energies of the reaction center pigments have a large influence and that the energies of the antenna pigments are less important for the calculated trapping time (Yang et al., 2003). It was suggested that the transition energies of reaction center pigments calculated earlier (Damjanovic et al., 2002) are optimized for efficient trapping of excitation energy. We have some doubts concerning this suggestion because there is no experimental evidence for the site energy of P_A calculated to be the red-most chlorophyll in PS I. This problem was already discussed by Damjanovic et al. (2002). The site energy might indeed have been calculated incorrectly because of a mistake in the coordinates of the 1JB0.pdb file (Norbert Krauß, personal communication). In addition, we were not able to find agreement between calculated and experimental difference spectra of PS I reaction centers using those transition energies (even if we correct the site energy of the Chl *a* epimer, that was calculated incorrectly because of wrong structural data).

We have chosen an alternative strategy to obtain the optical transition energies of PS I reaction centers. They are used as fit parameters in the calculation of difference spectra as discussed in detail below.

VI. Outlook

A. Theory of Optical Lineshapes of Aggregates with Strongly Coupled Pigments

In the case of strongly coupled pigments delocalized exciton states are excited in the aggregate and the homogeneous absorption spectrum, within secular approximation, is given in terms of excitonic lineshape functions $D_M(\omega)$ as

$$\alpha(\omega) \propto \omega \sum_M |\mu_M|^2 \, D_M(\omega). \tag{33}$$

In the simplest case, neglecting any exciton-vibrational coupling, there is no homogeneous broadening and so the lineshape function is a delta-function $D_M(\omega) = \delta(\omega - \omega_M)$, as discussed before in Eq. (7).

In the following, more realistic lineshape functions are given that include homogeneous broadening and are based on a linear model for the local coupling of optical transitions to vibrational coordinates.

1. Redfield Theory – Markovian Lineshapes

Using standard Redfield theory a Lorentzian lineshape function $D_M(\omega)$ is obtained for the optical transitions between the ground- and exciton-state M (e.g., Renger et al., 2001)

$$D_M(\omega) = \frac{\tau_M^{-1}}{(\omega - \tilde{\omega}_M)^2 + \tau_M^{-2}}. \tag{34}$$

The homogeneous broadening is determined by the lifetime of exciton state M that follows from the rate constants of exciton relaxation between this state and all other states

$$\tau_M^{-1} = \frac{1}{2} \sum_N k_{M \to N}, \tag{35}$$

with the $k_{M \to N}$ in Eq. (25).

The peak position of $D_M(\omega)$ occurs at $\omega = \tilde{\omega}_{M0}$ where a renormalization of the exciton energy ω_{M0} by the diagonal (the γ_{MM} term) and the off-diagonal part (the γ_{MK} term) of the exciton-vibrational coupling is taken into account (Renger and Marcus, 2002):

$$\tilde{\omega}_M = \omega_M - E_\lambda \gamma_{MM} - \sum_{K \neq M} \gamma_{MK} \wp \times \wp \int_{-\infty}^{\infty} d\omega \frac{\omega^2 \{(1 + n(\omega))J(\omega) + n(-\omega)J(-\omega)\}}{\omega_{MK} - \omega} \tag{36}$$

In the above equation $\wp$ denotes the principal part of the integral and γ_{MK} and E_λ are given in Eqs. (27) and (20).

2. Non-Markovian Lineshapes – Inclusion of Vibrational Sidebands

For the inclusion of vibrational sidebands a non–Markovian density matrix theory (Renger and Marcus, 2002) is used for the diagonal parts of the exciton-vibrational coupling and the off-diagonal parts are described within Markov approximation as before. In this case the lineshape function is obtained as (Renger and Marcus, 2002)

$$D_M(\omega) = \Re \int_0^\infty dt e^{i(\omega - \tilde{\omega}_M)t} e^{G_M(t) - G_M(0)} e^{-t/\tau_M}, \tag{37}$$

where $\Re$ denotes the real part, the time dependent function $G_M(t)$ is

$$G_M(t) = \gamma_{MM} G(t), \tag{38}$$

and the τ_M^{-1} is given in Eq. (35).

The function $G(t)$ determines the local lineshape function of the pigments as was shown before in Eqs. (15) and (16). The difference in displacements of potential energy surfaces of local excited states and delocalized excited states is treated by the γ_{MM} factor in Eq. (20). For localized states γ_{MM} becomes one as expected, for delocalized states it is smaller than one indicating that a delocalized electronic state couples weaker to vibrations than a localized state.

The present lineshape function contains both, vibrational sidebands that occur because of the displacement of the excitonic with respect to the ground-state potential energy surface [described by $G_M(t)$] and lifetime broadening due to exciton relaxation (described by τ_M).

B. Description of Optical Properties of the Reaction Center

For the trapping of excitation energy by the reaction center in PS I the site energies of the reaction center pigments are of particular importance (Yang et al., 2003).

In the spectra discussed below, the difference in absorption of a PS I complex in the ground state and a PS I complex with oxidized primary donor or with a reaction center pigment converted into the triplet state, is studied. Because of the difference, only those pigments contribute to the spectra that are coupled strongly, either directly or via other pigments, to the pigment that changed its electronic state. In the calculations we use

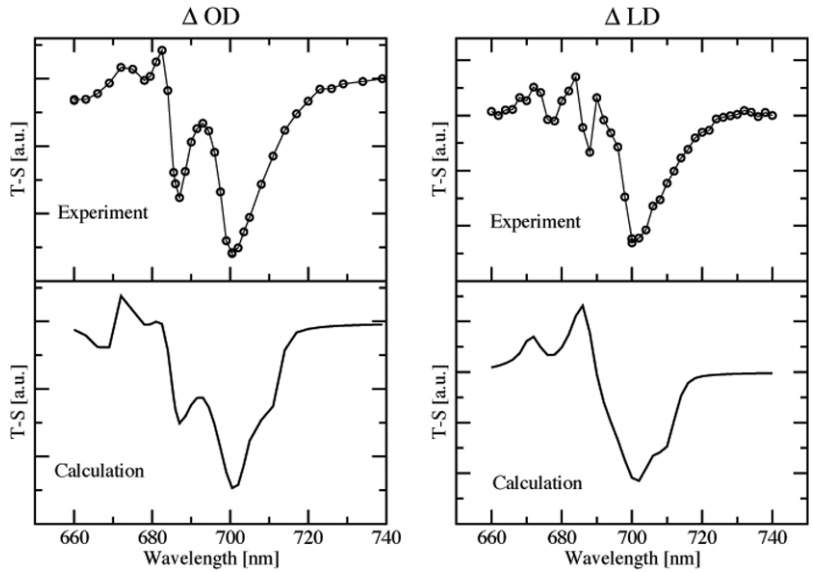

Fig. 3. Comparison of experimental (upper part) and calculated (lower part) triplet-minus-singlet spectra of trimeric PS I core complexes from *T. elongatus* at 5 K. Left part contains the difference in absorption and right part the difference in linear dichroism of the complex with P700 in the triplet and in the singlet state. In the calculations the following site energies were used: P_A – 1.810 eV (685 nm), P_B – 1.802 eV (688 nm), Acc-A – 1.834 eV (676 nm), Acc-B – 1.794 eV (691 nm), A_0-A – 1.831 eV (677 nm), A_0-B – 1.784 eV (695 nm). The Huang–Rhys factors of P_B and A_0-B were increased by a factor of four with respect to those of the other pigments.

the fact that the pigment–pigment couplings inside the reaction center are larger than between the reaction center and the antenna. Therefore, in good approximation the difference spectra can be calculated by taking into account only the six reaction center pigments, instead of the 96 chlorophylls of the PS I core complex.

From the complex shape of the experimental triplet-minus-singlet spectrum (upper parts of Fig. 3) direct evidence for the strong coupling between the reaction center pigments and hence delocalization of excited states is obtained. If there were only weak coupling there would appear just a simple negative band at the position of the site energy of the pigment that changed its electronic state. Because of the strong coupling, the excitonic structure of the whole spectrum is changed upon converting one pigment into a different state.

Käß et al. (2001) concluded from EPR/ENDOR experiments that the cation is mainly localized on one of the Chls constituting P700. Virtually identical zero-field-splitting (ZFS) parameters of ^{3}P700 and of monomeric ^{3}Chl *a* or ^{3}Chl *a*′ in organic solvents at low temperature (Witt et al., 2002) were taken as evidence that the triplet state of P700 is mainly localized on one chlorophyll. In addition, the orientation dependence of the triplet state showed that the plane of the Chl which carries the triplet state is oriented perpendicular to the membrane (Rutherford and Sétif, 1981), i.e., the triplet state should be localized on P_A or P_B.

Whether the triplet state and the cation are located on the same or on different pigments is an open question. Hole-burning studies show that the lowest state of the reaction center is homogeneously broadened (Gillie et al., 1989).

In short, the following scheme was used for the calculation of the spectra: The theory that includes vibrational sidebands, described above, was used and the Huang–Rhys factor of two low energy pigments were increased with respect to the Huang–Rhys factors of the other pigments in order to describe the homogeneous broadening of the lowest exciton state. The Huang–Rhys factor of the remaining pigments was set to 1.3, as obtained from $\int_0^\infty d\omega J(\omega)$ using the spectral density

$$J(\omega) = \sum_{i=1,2} \frac{s_i}{7!2\omega_i^4} \omega^3 e^{-(\omega/\omega_i)^{1/2}} \tag{39}$$

that was extracted (Renger and Marcus, 2002) from fluorescence line narrowing spectra of B777-complexes. The parameters in Eq. (39) are $s_1 = 0.8, s_2 = 0.5$, $\hbar\omega_1 = 0.069\,\text{meV}$, $\hbar\omega_2 = 0.24\,\text{meV}$. The maxima of the two contributions in Eq. (39) occur at frequencies $36 \cdot \omega_i$, i.e., at 20 and 70 cm^{-1}.

To obtain the spectrum after formation of the triplet state, the pigment, that was assumed to carry the triplet

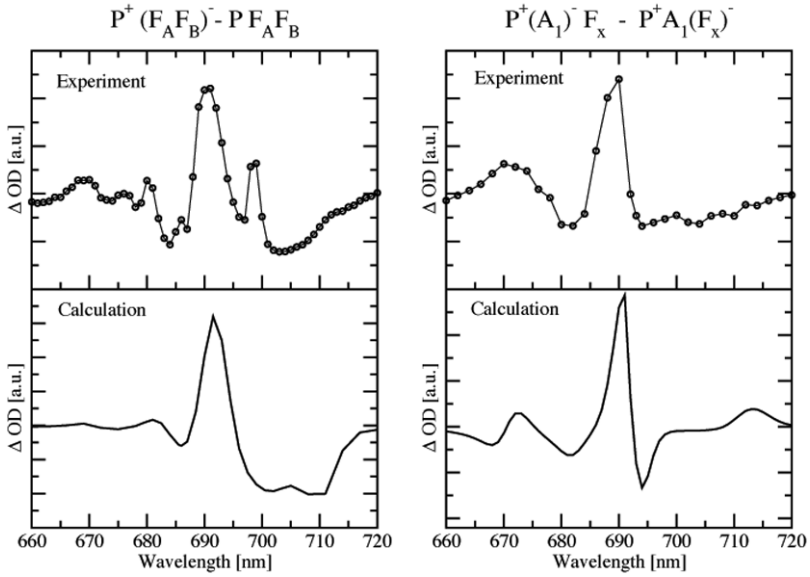

Fig. 4. Comparison of experimental (upper part) and calculated (lower part) absorption difference spectra of trimeric PS I core complexes from *T. elongatus* at 5 K. Left part contains the difference in absorption of the complex in the charge separated state $P700^+$ $(F_AF_B)^-$ and in the ground state and right part the difference in absorption for oxidized state P700 and different locations of the anion $[(A_1)^-$ and $(F_x)^-]$. In the calculations the same parameters as in Fig. 3 were used.

state was simply removed from the calculation of exciton states and optical spectra. In the same way, the spectrum of the PS I reaction center with oxidized primary donor ($P700^+$) was calculated. In addition, the electrochromic shifts of the site energies of the remaining pigments were taken into account in the following way. The positive charge was evenly distributed over the atoms of the π-system of the cation pigment and the electrochromic shifts were obtained from the Coulomb interaction between the partial charges δq_i of the cation with the difference permanent dipole moment $\Delta\vec{\mu} = \vec{\mu}_e - \vec{\mu}_g$ of the excited and ground state of the remaining pigments. The latter is known to be oriented approximately along the N_D–N_B axis of the chlorophylls and its magnitude is about 1 Debey (Krawczyk, 1991). A genetic algorithm was used to optimize the six site energies from a simultaneous fit of the T-S absorption and linear dichroism spectrum at 6 K. It was assumed that the triplet is localized on one of the two special pair pigments P_A or P_B. The spectra obtained for the optimized site energies are shown in the lower part of Fig. 3. The optimal site energies of the pigments of one branch are found to be red shifted with respect to the site energies of the pigments in the other branch (see caption of Fig. 3) and the triplet is located on the special pair pigment of the branch with larger site energies. Because of the symmetric structure of the reaction center it is not possible to identify the high- and low-energy branches from the present calculations. However, from the calculation of triplet-minus-singlet spectra of PS I mutants where the H-bond donor Thr(A739) to P_A was replaced by valine, there is some evidence that the B-branch is the low energy branch and that the triplet state therefore is located at the special pair pigment P_A of the A branch (data not shown).

In the calculations of the $P^+ - P$ spectrum, the site energies determined from the T-S spectra were used and again two situations were investigated: cation localized on P_A or P_B. The calculated $P^+ - P$ spectrum is shown in the lower left part of Fig. 4. The experimental spectra can only be described if the cation is assumed to be located on the special pair pigment that does not carry the triplet state, i.e., the one of the low-energy branch, most likely P_B. This result is a consequence of the strong excitonic coupling, electrochromic effects are found of minor importance for the qualitative shape of the spectra. The very different shapes of the experimental T-S spectra in Fig. 3 and the $P700^+ - P700$ spectrum in Fig. 4 can only be described by assuming that the triplet and the cation are localized on different pigments. The calculated spectra are in qualitative agreement with the experimental data. Further more, support for the extracted site energies is obtained from calculations of difference spectra that involve a reduction of the iron–sulfur cluster and the phylloquinone. The calculated spectra are compared in the right part

of Fig. 4 with experimental data. The maximum absorbance difference measured in this spectrum is about a factor of 5 smaller than the difference detected in the $P^+ - P$ spectrum (left part of Fig. 4), since in the latter the bleaching of a pigment and change in excitonic couplings contribute whereas the former is determined solely by electrochromic effects.

We believe that the present site energies, which are different from any values used in the literature so far, provide a basis for more realistic calculations of excitation energy trapping by the PS I reaction center. For a better quantitative agreement of the calculated and measured spectra, we think, an explicit inclusion of charge transfer states in the theory of optical spectra will be helpful.

Acknowledgments

This work was supported by the Deutsche Forschungsgemeinschaft through an Emmy Noether grant RE 1610 and through the Sonderforschungsbereich 498, TP A6 and A7. We thank Enrica Bordignon for a collaboration on the calculation of optical spectra and for stimulating discussions.

References

Beddard GS (1998) Excitations and excitons in photosystem I. Phil Trans R Soc Lond A 356: 421–448

Ben-Shem A, Frolow F and Nelson N (2003) Crystal structure of plant photosystem I. Nature 426: 630–635

Brüggemann B, Sznee K, Novoderezhkin V, van Grondelle R and May V (2004) From structure to dynamics: Modeling excition dynamics in the photosynthetic antenna PS I. J Phys Chem B 108: 13536–13546

Byrdin M, Rimke I, Schlodder E, Stehlik D and Roelofs TA (2000) Decay kinetics and quantum yields of fluorescence in photosystem I from *Synechococcus elongatus* with P700 in the reduced and oxidized state: are the kinetics of excited state decay trap-limited or transfer-limited? Biophys J 79: 992–1007

Byrdin M, Jordan P, Krauß N, Fromme P, Stehlik D and Schlodder E (2002) Light harvesting in photosystem I – modeling based on the 2.5 Å structure of photosystem I from *Synechococcus elongatus*. Biophys J 83: 433–457

Chang JC (1977) Monopole effects on electronic excitation interactions between large molecules. I. Application to energy transfer in chlorophylls. J Chem Phys 67: 3901–3909

Damjanovic A, Vaswani HM, Fromme P and Flemming GR (2002) Chlorophyll excitations in Photosystem I of *Synechococcus elongatus*. J Phys Chem B 106: 10251–10262

Dempster S, Jang S and Silbey R (2001) Single molecule spectroscopy of disordered circular aggregates: A perturbation analysis. J Chem Phys 114: 10015–10023

Dorra D, Fromme P, Karapetyan NV and Holzwarth AR (1998) Fluorescence kinetics of photosystem I: multiple fluorescence components. In: Garab G (ed) Proceedings of the XIth International Photosynthesis Congress, pp 587–590. Kluwer Academic Publishers, Dordrecht

Du M, Xie X, Jia Y, Mets L and Fleming GR (1993) Direct observation of ultrafast energy transfer in PS I core antenna. Chem Phys Lett 201: 535–542

Eccles J and Honig B (1983) Charges amino acids as spectroscopic determinants for chlorophyll *in vivo*. Proc Natl Acad Sci USA 80: 4959–4962

Fetisova Z, Freiberg A, Mauring K, Novoderezhkin V, Taisova A and Timpmann K (1996) Excitation energy transfer in chlorosomes of green bacteria: theoretical and experimental studies. Biophys J 71: 995–1010

Förster T (1948) Zwischenmolekulare Energiewanderung und Fluoreszenz. Ann Phys (Leipzig) 2: 47–54

Förster T (1965) Delocalized excitation and excitation transfer. In: Sinnanoğlu O (ed) Modern Quantum Chemistry, Vol IIIB, pp 93–137. Academic Press, New York

Gillie JK, Lyle PA, Small GJ and Golbeck JH (1989) Spectral holeburning of the primary electron donor state of Photosystem I. Photosynth Res 22: 233–246

Gobets B, Dekker JP and van Grondelle R (1998) Transfer-to-the-trap limited model of energy transfer in photosystem I. In: Garab G (ed) Proceedings of the XIth International Photosynthesis Congress, pp 503–508. Kluwer Academic Publishers, Dordrecht

Gobets B, van Stokkum IHM, Rögner M, Kruip J, Schlodder E, Karapetyan NV, Dekker JP and van Grondelle R (2001) Time resolved fluorescence emission measurements of photosystem I particles of various cyanobacteria: a unified compartmental model. Biophys J 81: 407–424

Gobets B, van Stokkum IHM, van Mourik F, Rögner M, Kruip J, Dekker JP and van Grondelle R (2003) Excitation wavelength dependence of the fluorescence kinetics in photosystem I particles from *Synechocystis* sp. PCC 6803 and *Synechococcus elongatus*. Biophys J 85: 3883–3898

Gudowska-Nowak E, Newton MD and Fajer J (1990) Conformational and environmental effects on bacteriochlorophyll optical spectra: correlations of calculated spectra with structural results. J Phys Chem 94: 5795–5801

Hastings G, Reed LJ, Lin S and Blankenship B (1995) Excited state dynamics in photosystem I: effects of detergent and excitation wavelength. Biophys J 69: 2044–2055

Holzwarth AR, Schatz G, Brock H and Bittersmann E (1993) Energy transfer and charge separation kinetics in photosystem I. Part I: picosecond transient absorption and fluorescence study of cyanobacterial photosystem I particles. Biophys J 64: 1813–1826

Jordan P, Fromme P, Klukas O, Witt HT, Saenger W and Krauß N (2001) Three-dimensional structure of cyanobacterial photosystem I at 2.5 Å resolution. Nature 411: 909–917

Käß H, Fromme P, Witt HT and Lubitz W (2001) Orientation and electronic structure of the primary electron donor radical cation in photosystem I: a single crystal EPR and ENDOR Study. J Phys Chem B 105: 1225–1239

Kennis JTM, Gobets B, van Stokkum IHM, Dekker JP, van Grondelle R and Flemming GR (2001) Light harvesting by chlorophylls and carotenoids in the photosystem I core complex of *Synechococcus elongatus*: a fluorescence upconversion study. J Phys Chem 105: 4485–4494

Knapp EW (1984) Lineshape of molecular aggregates. Exchange narrowing and intersite correlation. Chem Phys 85: 73–82

Krauß N, Hinrichs W, Witt I, Fromme P, Pritzkow W, Dauter Z, Betzel C, Wilson KS, Witt HT and Saenger W (1993) 3-Dimensional structure of system-I of photosynthesis at 6 Å resolution. Nature 361: 326–331

Krawczyk S (1991) Electrochromism of chlorophyll *a* monomer and special pair dimer. Biochim Biophys Acta 1056: 64–70

Krueger BP, Scholes GD and Fleming GR (1998) Calculation of couplings and energy-transfer pathways between the pigments of LH2 by the ab initio transition density cube method. J Phys Chem 102: 5378–5386

Lax E (1952) The Franck–Condon principle and its application to crystals. J Chem Phys 20: 1752–1760

May V and Kühn O (2000) Charge and Energy Transfer Dynamics in Molecular Systems. Wiley-VCH, Berlin, Germany

Mukai K, Abe S and Sumi H (1999) Theory of rapid excitation-energy transfer from B800 to optically forbidden exciton states of B850 in the antenna system LH2 of photosynthetic purple bacteria. J Phys Chem B 103: 6096–6102

Pålsson LO, Flemming C, Gobets B, van Grondelle R, Dekker JP and Schlodder E (1998) Energy transfer and charge separation in photosystem I: P700 oxidation upon selective excitation of the long-wavelength antenna chlorophylls of *Synechococcus elongatus*. Biophys J 74: 2611–2622

Renger T and Marcus RA (2002) On the relation of protein dynamics and exciton relaxation in pigment–protein complexes: an estimation of the spectral density and a theory for the calculation of optical spectra. J Chem Phys 116: 9997–10019

Renger T and Marcus RA (2003) Variable range hopping electron transfer through disordered bridge states: application to DNA. J Phys Chem A 107: 8404–8419

Renger T, May V and Kühn O (2001) Ultrafast excitation energy transfer dynamics in photosynthetic pigment–protein complexes. Phys Rep 343: 138–254

Rutherford AW and Sétif P (1990) Orientation of P700, the primary electron donor of photosystem I. Biochim Biophys Acta 1019: 128–132

Scherz A and Parson WW (1984) Exciton interactions in dimers of bacteriochlorophyll and related molecules. Biochim Biophys Acta 766: 666–678

Schubert WD, Klukas O, Krauß N, Saenger W, Witt HT, Fromme P and Witt HT (1997) Photosystem I of *Synechococcus elongatus* at 4 Å resolution: comprehensive structure analysis. J Mol Biol 272: 741–769

Sener MK, Lu DY, Ritz T, Park S, Fromme P and Schulten K (2002) Robustness and optimality of light harvesting in cyanobacterial Photosystem I. J Phys Chem B 106: 7948–7960

Sumi H (1999) Theory on rates of excitation-energy transfer between molecular aggregates through distributed dipoles with application to the antenna system in bacterial photosynthesis. J Phys Chem B 103: 252–260

van Amerongen H, Valkunal L and van Grondelle R (2000) Photosynthetic Excitons. World Scientific, London, U.K.

White NTH, Beddard GS, Thorne JRG, Feehan TM, Keyes TE and Heathcote P (1996) Primary charge separation and energy transfer in the photosystem I reaction center of higher plants. J Phys Chem 100: 12086–12099

Witt H, Schlodder E, Teutloff C, Niklas J, Bordignon E, Carbonera D, Kohler S, Labahn A and Lubitz W (2002) Hydrogen bonding to P700 – site-directed mutagenesis of threonine A739 of photosystem I in *Chlamydomonas reinhardtii.* Biochemistry 41: 8557–8569

Yang M and Fleming GR (2002) Influence of phonons on exciton transfer dynamics: comparison of the Redfield, Förster, and modified Redfield equations. Chem Phys 282: 163–180

Yang M, Damjanovic A, Vaswani HM and Fleming GR (2003) Energy transfer in Photosystem I of cyanobacteria *Synechococcus elongatus*: model study with structure-based semi-empirical Hamiltonian and experimental spectral density. Biophys J 85: 140–158

Zazubovich V, Matsuzaki S, Johnson TW, Hayes JM, Chitnis PR and Small GJ (2002) Red antenna states of Photosystem I from cyanobacterium *Synechococcus elongatus*: a spectral hole burning study. Chem Phys 275: 47–59

Zhang WM, Meier T, Chernyak V and Mukamel S (1998) Exciton migration and three pulse femtosecond optical spectroscopies of photosynthetic antenna complexes. J Chem Phys 108: 7763–7774

Chapter 36

Functional Modeling of Electron Transfer in Photosynthetic Reaction Centers

Vladimir Shinkarev*
Department of Biochemistry; University of Illinois at Urbana-Champaign; Urbana, IL 61801, USA

*Author for correspondence, email: vshinkar@uiuc.edu

John H. Golbeck (ed): Photosystem I: The Light-Driven Plastocyanin:Ferredoxin Oxidoreductase, 611–637.

Summary

In recent years significant progress has been made in gaining insight into the structure and function of the reaction centers (RCs) of plants, algae, and photosynthetic bacteria. All RCs with known structures have a porphyrin–quinone core. This core is coupled with specific donors, acceptors, and light-harvesting antenna. RCs can use both water-soluble and lipid-soluble donors and acceptors. The electron exchange of RCs with these donors and acceptors occurs via specialized processing sites, which are responsible for recognition of respective donor-acceptor, and for channeling the electrons and protons in and out of the complex. The purpose of this chapter is to describe some simple kinetic models of flash-induced electron transfer in these RCs. In our consideration we try to find the balance between *analytical* solutions for the simplest models and *numerical* calculations for a detailed quantitative description of electron transfer in RCs. The quantitative description of flash-induced relaxation of RCs begins with a simple two-state model. Then we introduce the *spreading of equilibrium* model. According to this model, the time evolution of RCs after primary charge separation occurs via waves of quasi-equilibrium. By choosing the certain time scale of consideration one can describe the electron transport using simple two-state approximation. Analysis of the relaxation of charge-separated states in RCs explicitly includes all parallel pathways of electron transfer from reduced acceptor species to the oxidized primary donor. This model applied for the quantitative description of the flash-induced kinetics of Photosystem (PS) I that contains either an intact set or a subset of iron–sulfur clusters F_X, F_A, and F_B. RCs of PS II and purple bacteria include multielectron carriers at the donor and acceptor sides. As a result, activation of such RCs with multiple flashes initiates periodic oscillations of the state of these carriers. Here we consider the quantitative description of flash-induced binary oscillations of the state of secondary quinone acceptor and quaternary oscillations of oxygen-evolving complex in PS II. The quantitative models considered here constitute a basis for the analytical description of flash-induced kinetics of electron transfer in native and mutant RCs. However, when more precise analysis is needed one should use specific numerical approaches for solving differential equations needed to describe the time evolution of RCs. Such approach is illustrated here for the analysis of the flash-induced electron transfer in PS I.

I. Introduction

A. Reaction Centers of Known Structure

The initial events of photosynthesis occur in membrane-bound pigment–protein complexes called reaction centers (RCs). RCs of photosynthesis in plants, algae, and a variety of bacterial species are integral membrane proteins that are responsible for the conversion of light energy into chemical-free energy. Significant progress has been made in recent years in the biochemical and biophysical characterization of RCs. Several RCs from different sources, including Photosystem II (PS II) and Photosystem I (PS I), have been crystallized and their structures have been determined at atomic resolution. As a result, cofactors of the RC proteins were localized and the role of the individual amino acid residues in cofactor binding has been made certain.

Abbreviations: BChl – bacteriochlorophyll; Chl – chlorophyll; D1 and D2 – polypeptides of the Photosystem II (PS II) reaction center; DCPIP – 2,6-dichlorophenol-indophenol; DM – *n*-dodecyl-β-D-maltoside; F_A, F_B – [4Fe–4S] iron–sulfur centers associated with PsaC subunit of PS I; Fd – ferredoxin; F_X – [4Fe–4S] iron–sulfur center bound to PsaA and to PsaB subunits of PS I; L, M – polypeptides of the reaction center from purple bacteria; L_{XA} – the equilibrium constant of electron transfer between F_X and F_A; OEC – oxygen-evolving complex; P680 – primary electron donor in Photosystem II; P700 – primary donor of electrons in Photosystem I; P870 – primary electron donor of *Rhodobacter sphaeroides* reaction center; PC – plastocyanin; Pheo – pheophytin; PQ – plastoquinone; PS I – Photosystem I; PS II – Photosystem II; PsaA, PsaB, PsaC – main subunits of PS I which bind all cofactors active in electron transfer; Q_A – primary acceptor quinone; Q_B – secondary acceptor quinone; QH_2 – quinol; $r \equiv [(\alpha-\beta)^2+\gamma^2]^{1/2}$; RC – photosynthetic reaction center; *rubA* – mutant with interrupted *rubA* gene in *Synechococcus* sp PCC 7002; s_i – initial conditions for i-th S-state, $s_0 = s_0(0)$, $s_1 = s_1(0)$, $s_2 = s_2(0)$, $s_3 = s_3(0)$; $s_i(n)$ – the probability (fraction) of the S_i state after the flash n; S_n – redox states of the OEC, where $n = 0, 1, 2, 3, 4$ represents the number of oxidizing equivalents; TX – Triton X100; wild-type PS I – PS I complex, containing phylloquinone, F_X, F_A, and F_B clusters, isolated using DM; $x \equiv s_0 - s_2$ (Eq. 30); $y \equiv s_3 - s_1$ (Eq. 30); Y(n) – oxygen yield after n-th flash; Y_D – redox-active tyrosine slowly interacting with S-states; Y_Z – redox-active tyrosine, fast electron donor to P680; $z \equiv s_0 - s_1 + s_2 - s_3$ (Eq. 30); α – traditionally used notation for the miss (zero-step advancement) in the Kok model; β – traditionally used notation for the double hit (two-step advancement) in the Kok model; γ – traditionally used notation for the hit (one-step advancement) in the Kok model; $\mu \equiv \alpha - \gamma + \beta$; σ – stretch factor providing a measure of the heterogeneity of kinetics; φ – angle in Eq. (30), $\varphi \equiv \arcsin(\gamma/r)$.

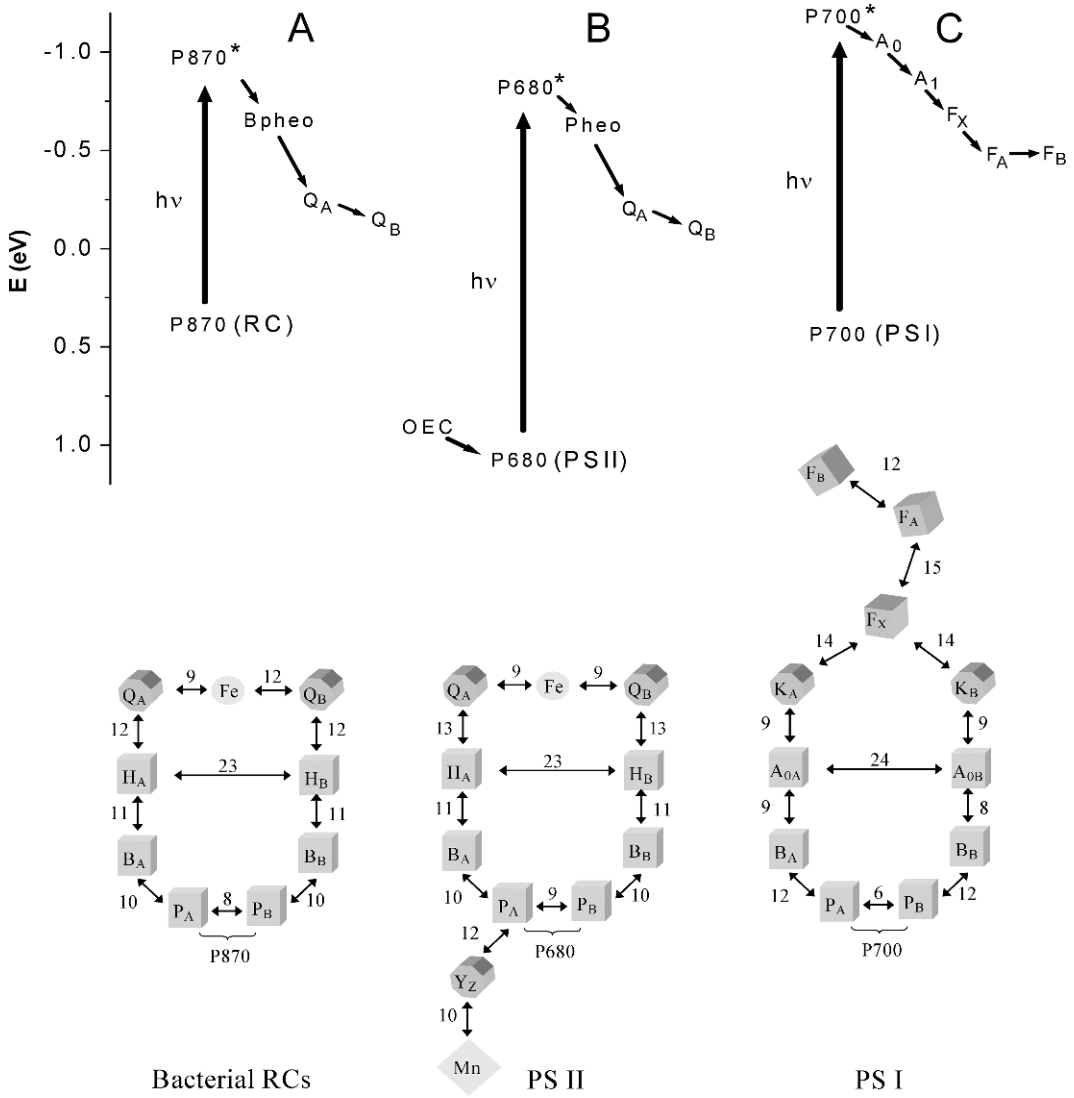

Fig. 1. Primary reactions (top) and approximate center-to-center distances (in Å) between cofactors (bottom) in the RCs from purple bacteria (A), PS II (B), and PS I (C). The figure is based on the coordinates of Jordan et al. (2001) for PS I, of Zouni et al. (2001) and Ferreira et al. (2004) for PS II and of Ermler et al. (1994) for the bacterial RC. BChl – bacteriochlorophyll; Bpheo – bacteriopheophytin; Chl – chlorophyll; F_A, F_B – iron–sulfur centers associated with PsaC subunit; F_X – iron–sulfur center bound to PsaA and to PsaB subunits; OEC – oxygen-evolving complex; P680 – primary electron donor in PS II; P700 – primary electron donor in PS I; P870 – primary electron donor of reaction center in purple bacteria; Pheo – pheophytin; PS I – Photosystem I; PS II – Photosystem II; Q_A – primary acceptor quinone; Q_B – secondary acceptor quinone; RC – photosynthetic reaction center; Y_Z – redox-active tyrosine of the D1 polypeptide. B_A, B_B – (bacterio)chlorophyll molecules in the branches A and B, respectively; H_A, H_B – (bacterio)pheophytin molecules in the branches A and B, respectively; P_A, P_B – (bacterio)chlorophyll molecules, components of primary electron donor; K_A, K_B – phylloquinone (vitamin K_1) molecules in the branches A and B of PS I. A_{0A}, A_{0B} – chlorophyll molecules in the branches A and B of PS I functioning as A_0 acceptor.

It was found that photosynthetic RCs differ significantly in their composition and in the nature of the terminal donors and acceptors. In spite of these differences, all known types of photosynthetic RCs show significant similarity in the arrangement of their cofactors involved in the light-induced transmembrane charge separation (Fig. 1, bottom). In all studied cases, the general outline of RCs includes two symmetrically arranged branches of six porphyrin derivatives and two quinones. With this general outline, RCs in different organisms were able to accommodate (by changing the type of quinone and porphyrin cofactors, or by

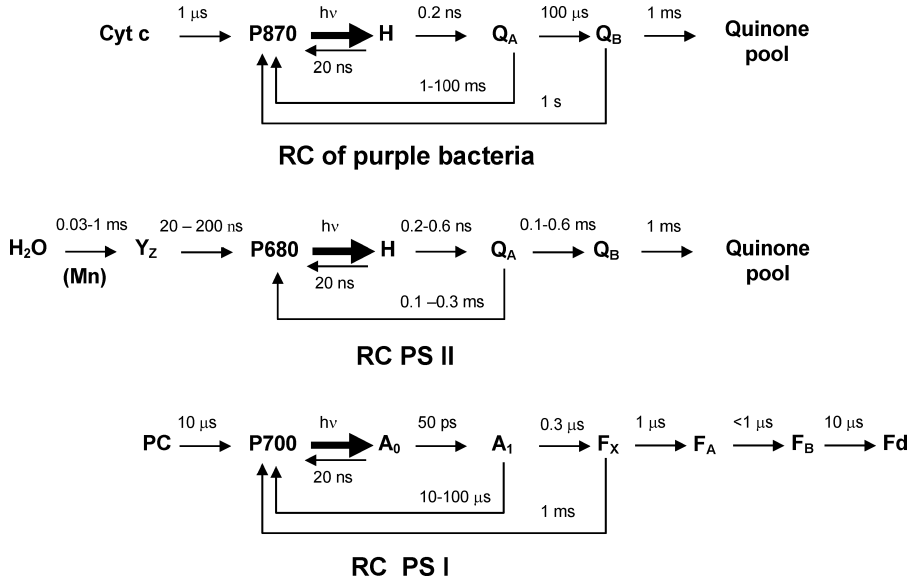

Fig. 2. Simplified schemes of electron transfer in different photosynthetic RCs. The lifetimes are taken from the current literature and provide general guidance rather than exact values. A_0 – chlorophyll molecule in PS I functioning as electron acceptor; F_A, F_B – iron–sulfur centers associated with PsaC subunit; Fd – ferredoxin; F_X – iron–sulfur center bound to PsaA and to PsaB subunits; H – (bacterio)pheophytin molecule; P680 – primary electron donor of PS II; P700 – primary electron donor in PS I; P870 – primary electron donor of reaction center of purple bacteria; PC – plastocyanin; PS I – Photosystem I; PS II – Photosystem II; Q_A – primary acceptor quinone; Q_B – secondary acceptor quinone; RC – photosynthetic reaction center; Y_Z – redox-active tyrosine of the D1 polypeptide.

modifying specific protein–cofactor interactions) different donors and acceptors.

1. Reaction Centers from Purple Bacteria

RCs from purple bacteria use the energy of light to transfer electrons from water-soluble cytochrome to quinone (reviewed in Shinkarev and Wraight, 1993a; Woodbury and Allen, 1995; Okamura et al., 2000; Ke, 2001; Lancaster and Michel, 2001; Blankenship, 2002).

Detailed atomic structures of many RCs have been determined in recent years (reviewed in Lancaster and Michel, 2001). Cofactors in the RC are arranged in two symmetrical branches. In spite of the symmetry of this arrangement, electron transfer occurs predominantly through only one branch, first to Q_A and then to Q_B (Fig. 2).

The RC complex of purple photosynthetic bacteria consists of three subunits (usually referred to as L, M, and H). The functional core of the RC is formed by the L and M subunits which bind all of the cofactors active in electron transfer, namely four bacteriochlorophylls (Bchl), two bacteriopheophytins (Bpheo), two quinones (Q), and one non-heme iron atom (Fe). In addition to these three subunits, some species also have a tightly bound multiheme cytochrome (reviewed in Lancaster and Michel, 2001).

After light activation of the RC, an electron is transferred from the excited state of dimer of bacteriochlorophylls to bacteriopheophytin ($Bpheo_A$) in ~3 psec. The electron is then transferred to Q_A in ~0.2 nsec. From Q_A, the electron can be transferred to Q_B in 10–400 μsec (reviewed in Ke, 2001). Electron transfer to Q_A leads to the stabilization of the separated charges in a millisecond time domain. Transfer of the electron to Q_B leads to further charge stabilization.

The primary acceptor quinone, Q_A, functions under physiological conditions as one-electron carrier. The secondary acceptor quinone, Q_B, functions as a two-electron carrier. The coupling of the two-electron Q_B with the one-electron Q_A occurs via step-by-step flash-induced reduction Q_B by Q_A^-. The first flash leads to the formation of Q_B semiquinone, while the second flash leads to the formation of quinol, Q_BH_2. The semiquinone Q_B^- is sufficiently stable to wait until the arrival of the second-light activation of the RC, which enables transfer of the second electron to Q_B^-. In contrast to the semiquinone form, the neutral forms of quinone (Q, QH_2) are loosely bound to the Q_B binding site (reviewed in Shinkarev and Wraight, 1993a). They can exchange rapidly ($\leq$1 msec) with quinones from

the membrane pool. The semiquinone stabilization and the exchange of the neutral forms of quinone with the membrane pool are the most significant aspects of the two-electron gate at the acceptor side of the RC.

2. Photosystem II

PS II is a light-driven water:plastoquinone oxidoreductase, an enzyme that uses light energy to oxidize water and to reduce plastoquinone (reviewed in Ke, 2001; Blankenship, 2002). PS II is the main source of atmospheric oxygen. A complex multisubunit structure is needed to couple together the capture of light energy, oxidation of water, reduction of plastoquinone, formation of a transmembrane proton gradient, and to regulate photon, electron, and proton fluxes.

A detailed molecular structure of PS II from *Synechococcus elongatus*, active in water oxidation, has now been determined (Zouni et al., 2001; Kamiya and Shen, 2003; Ferreira et al., 2004). All of the cofactors involved in the primary charge separation in PS II are bound within the D1 and D2 subunits. The general architecture of the RC of PS II is similar to that for purple bacteria, but there are some significant differences (Zouni et al., 2001; Kamiya and Shen, 2003; Ferreira et al., 2004). In particular, two Chl molecules forming P680 have a Mg–Mg distance of 8–10 Å (Zouni et al., 2001; Ferreira et al., 2004) which is larger than the respective Mg–Mg distance in RCs of purple bacteria.

Light activation of PS II induces the electron transfer from the primary donor (P680) to the pheophytin (Pheo). This is followed by electron transfer to the primary quinone acceptor (Q_A) and then to the secondary quinone acceptor (Q_B). In PS II, the one-electron photochemistry is coupled with multielectron charge accumulation at the donor and acceptor sides. The acceptor quinone complex of PS II functions similarly to that of purple bacteria and releases electrons from the RC only after each second flash (Bouges-Bocquet, 1973; Hangulov et al., 1974; Velthuys and Amesz, 1974).

The catalytic site of the oxygen-evolving (and water oxidizing) complex (OEC) contains cluster of four Mn that interacts with a redox-active tyrosine Y_Z, which, in turn, can be oxidized by $P680^+$. The light activation of the core of PS II leads to the accumulation of oxidizing equivalents by the OEC that is needed for water oxidation. Recently, Ferreira et al. (2004) suggested that OEC is, in fact, Mn_3CaO_4 cluster linked to a fourth Mn by a mono-μ-oxo bridge.

3. Photosystem I

PS I of oxygenic photosynthesis uses the energy of light to transfer electrons from plastocyanin (or cytochrome c_6) to ferredoxin (or flavodoxin). Reduced ferredoxin is a low-potential water-soluble electron carrier that can either reduce $NADP^+$ or components of the cytochrome b_6f complex (reviewed in Ke, 2001, Blankenship, 2002; Golbeck, 2003).

The recent 2.5 Å crystal structure of PS I from the thermophilic cyanobacterium *Synechococcus elongatus* showed an extremely complex enzyme. PS I forms a trimer, where each unit includes 12 protein subunits carrying 96 chlorophylls, 2 phylloquinones (vitamin K_1), 3 [4Fe–4S] clusters, 22 carotenoids, and at least 4 specific lipids (Fromme et al., 2001; Jordan et al., 2001; Krauß, 2003).

Each unit of the PS I includes: (i) two main subunits PsaA and PsaB, which carry P700, A_0, A_1, and F_X, (ii) subunit PsaC carrying the two [4Fe–4S] centers (F_A and F_B), and (iii) nine smaller subunits (Fromme et al., 2001; Jordan et al., 2001). The primary electron carriers are arranged in two branches, to have a set of six chlorophyll molecules, two phylloquinones, and three iron–sulfur clusters (Fig. 1C). In the absence of ferredoxin (flavodoxin), [4Fe–4S] clusters F_A and F_B operate as the terminal electron acceptors.

B. Generalized Functional View of a Reaction Center

The examples considered above indicate that all RCs with known structure have a porphyrin–quinone core. This core is coupled with specific donors, acceptors, and light-harvesting antenna. RCs can use both water-soluble and lipid-soluble donors and acceptors. The electron exchange of RCs with these donors and acceptors occurs via specialized processing sites (sometimes called binding or docking sites), which are responsible for recognition of respective donor-acceptor, and for channeling the electrons and protons in and out of the complex. For example, a PS I monomer has one ferredoxin processing site and one plastocyanin (cytochrome *c*) processing site. To quantitatively characterize electron transport in RCs it is necessary to provide kinetic descriptions of electron transfer in the RC core complemented by quantitative description of such specialized binding sites. Similarly, RCs have very specific light-processing sites, which are commonly referred to as light-harvesting antenna. Figure 3 shows

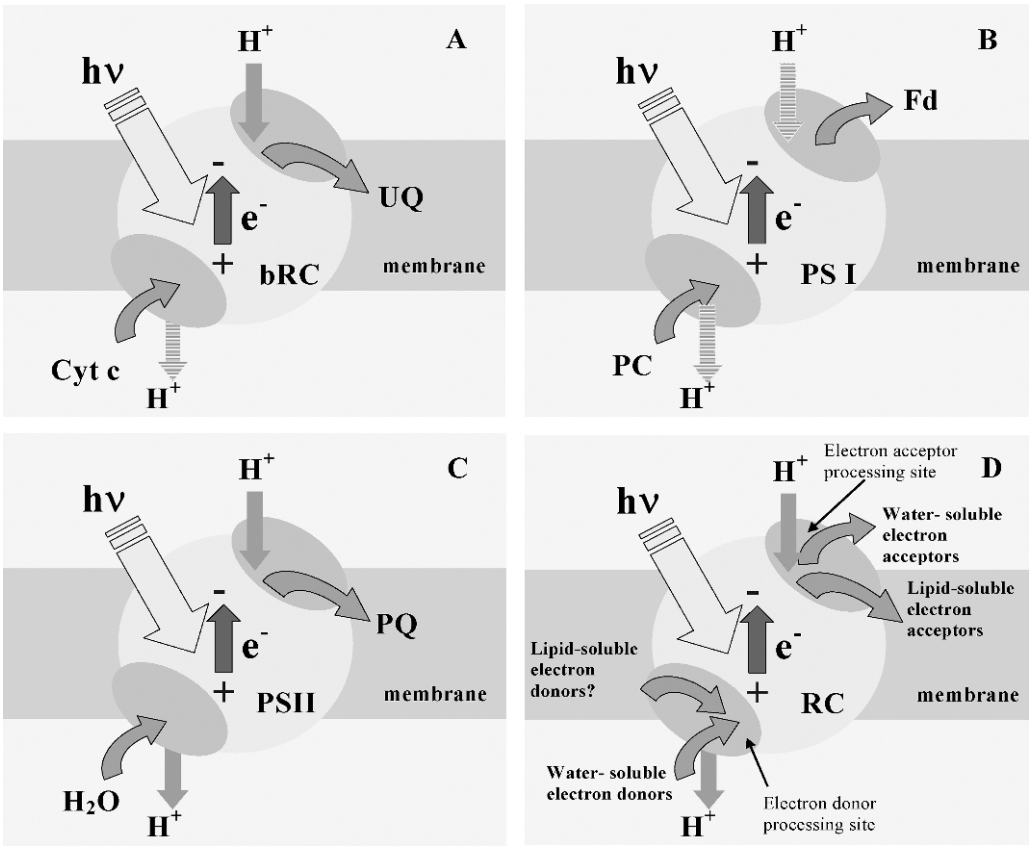

Fig. 3. Light-induced electron transfer in the bacterial RC (A), PS I (B), PS II (C), and in "generalized" RC (D), presented as transmembrane nanodevice designed for coupling together photon, electron and proton fluxes. The exchange of RCs with respective donors and acceptors occurs via specialized binding sites (shown by dark gray ovals), which are responsible for recognition of respective donor/acceptor, and for channeling the electrons and protons in and out of the complex. These processing sites are the targets for specific inhibitors. The light activation of the RCs occurs via light-processing site (light-harvesting antenna). Thus, generalized reaction center has porphyrin–quinone core, coupled with specific donors, acceptors, and light-harvesting antenna (not shown).

simplified view of different RCs that can be used for their functional modeling.

C. Approaches Used for Quantitative Analysis of Electron Transfer in Reaction Centers

1. Electron Transfer in Complexes

Construction of the appropriate quantitative model must recognize two main approaches to the description of electron transport in energy transducing membranes. One is based on the assumption that carriers are mobile and their interactions occur according to the mass action law. The other is based on the assumption that carriers are arranged into multienzyme complexes. These approaches are not necessarily exclusive, and it is often appropriate to use them in parallel, depending on the application. Here we consider briefly the specifics of electron transfer in complexes (reviewed in Rubin and Shinkarev, 1984; Joliot et al., 1993).

In the case where electron carriers are organized into molecular complexes, the kinetic equations describing the electron transfer are significantly different from those used to describe the mobile carriers (see, e.g., Hill, 1977; Shinkarev and Venediktov, 1977; Rubin and Shinkarev, 1984; Joliot et al., 1993; Shinkarev, 1998).

Let $S_1, S_2, \ldots, S_n$ (1, 2, 3, . . . , n) be the states of the complex, and let $P(S_i,t) = p_i(t)$ be the probability of being in the state S_i at time t. In many cases it is useful to consider the transitions between states of the complex as a Markov's process (Shinkarev and Venediktov, 1977). In this case the dynamics of electron transport in complexes can be described by a set of ordinary

differential equations:

$$\frac{dp_i}{dt} = \sum_{j=1}^{n} (p_j k_{ji} - p_i k_{ij})$$
$$p_i(0) = b_i \qquad \left(b_i \geq 0, \sum_{i=1}^{n} b_i = 1 \right) \tag{1}$$

or in a vector form

$$\frac{dp}{dt} = K^T \mathbf{p}, \mathbf{p}(0) = \mathbf{b} \tag{2}$$

Here $\mathbf{p} = (p_1, p_2, \ldots, p_n)$ is a column-vector; K^T is a matrix transposed to matrix $K = \{k_{ij}\}$ each element of which, k_{ij} $(i \neq j)$, represents the rate constant for the complex transition from the i-th to j-th state; $k_{ii} = -\sum_j k_{ij}$; $\mathbf{b} = (b_1, b_2, \ldots, b_n)$ is the vector of initial probabilities for the complex, $\sum_j b_j = 1$, $b_j \geq 0$.

As example, let consider molecular complex of two carriers C_1 and C_2 interacting according to scheme below

$$\xrightarrow{k_1} \boxed{C_1 \underset{k_{-2}}{\overset{k_2}{\rightleftharpoons}} C_2} \xrightarrow{k_3} \tag{3}$$

The transitions of a complex of these two carriers can be presented as follows:

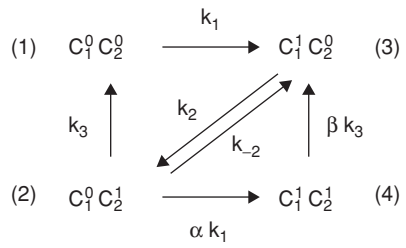

(4)

Here the superscripts "0" and "1" denote the oxidized and reduced state of a carrier, respectively. $C_1^1 C_2^0$ is the state of the complex where C_1 is in the reduced and C_2 is in the oxidized form. Numbers in brackets enumerate the states of the complex. k_1 and k_3 are pseudomonomolecular rate constants for electron exchange interactions with the environment. In the simplest case, k_1 is proportional to the concentration of the donor D in the reduced form and k_3 to that of the acceptor A in the oxidized form. k_2 is the monomolecular rate constant for intraprotein electron transfer. In general, rate constants may depend on states of the carriers of the complex (cooperative effect). Cooperative effects in the system are reflected by the coefficients α and β.

A set of differential equations describing the time dependence of the probabilities of states of the complex, p_i, within the framework of scheme (4), can be written (in the absence of cooperative effects, i.e., $\alpha = \beta = 1$) in the form:

$$\begin{aligned} dp_1/dt &= k_3 p_2 - k_1 p_1 \\ dp_2/dt &= k_2 p_3 - (k_1 + k_{-2} + k_3) p_2 \\ dp_3/dt &= k_1 p_1 + k_{-2} p_2 + k_3 p_4 - k_2 p_3 \\ dp_4/dt &= k_1 p_2 - k_3 p_4 \\ p_1 + p_2 + p_3 + p_4 &= 1, p_i(0) = b_i \end{aligned} \tag{5}$$

Having obtained p_i from Eq. (5), probabilities of states for individual carriers can be found by summing up the probabilities of complex states for which the carrier of interest is in the respective state, for example, $P(C_1^1) = p_3 + p_4$.

2. Kinetic Description of Processing Sites

The exchange of RCs with respective donors and acceptors occurs via specialized processing (binding) sites, which are responsible not only for recognition of respective donor-acceptor, but also for channeling the electrons and protons in and out of the complex. As a rule, RCs have two different processing sites. One of them is located on the donor side or RC and another on the acceptor side. In case of the RC from purple bacteria there is one quinone-processing site (Q_B) and one cytochrome *c* processing site. To characterize electron transport in RCs it is necessary to incorporate kinetic descriptions of such specialized binding sites. For quantitative description of such binding sites, one should consider the different states of occupancy of the binding site by different intermediates, as well as concentrations of free donor and acceptor molecules (in solution or in the membrane). For example, quantitative analysis of the quinone-processing sites in PS II should incorporate at least four different states of the binding site (vacant, occupied by quinone, semiquinone, or quinol). An example of such an analysis of a quinone-processing site can be found in Shinkarev (1998).

D. General Problems of Kinetic Description of Reaction Centers

Until recently, significant uncertainty existed concerning the nature of cofactors involved in the electron transport in different types of RCs. As a result, the functional modeling of electron transfer in RCs was significantly limited. The availability of structural information for different types of RCs created a solid background for the functional modeling of electron transport and coupled processes.

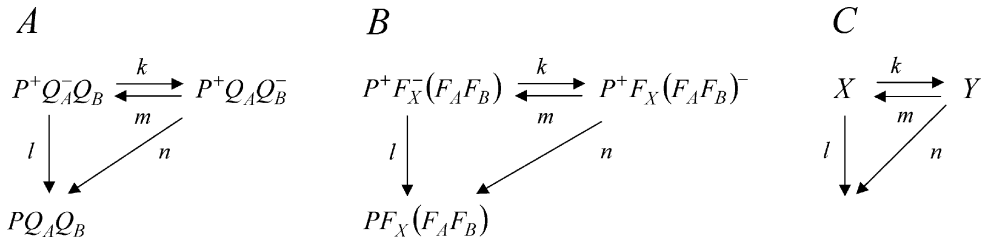

Fig. 4. Schemes of dark relaxation of RC of purple bacteria (A) and PS I (B), and the two-state model of the RC (C). Here X and Y are states of RC, and k, m, l, and n are respective rate constants. Notations as in Fig. 1.

The emerging quantitative description of RCs should overcome principal difficulties in the functional modeling of electron transport that arise from the large number of interacting cofactors, nonlinear interactions between some electron carriers, coupling of electron transport with generation of a proton gradient, and necessity of parallel consideration of different interacting processes at molecular, intermolecular, and membrane levels.

General problems of functional modeling of electron transfer in wild-type and mutant photosynthetic RCs include:

(i) building a realistic mathematical model of RCs that takes into account current knowledge of their structure and function;
(ii) predicting the time dependence of all cofactors in RC induced by different types of light activation (single and multiple flashes, steady state, periodic light activation, etc.);
(iii) quantitative kinetics description of different processing sites of RCs;
(iv) analysis of consistency of different sets of rate and equilibrium constants in a RC;
(v) quantitative description of effect of different factors governing the kinetics of electron transfer in RCs, such as temperature, pH, ionic strength, state of aggregation, etc.;
(vi) increasing our understanding of how all the parts of photosynthesis work together.

II. Simple Analytical Models for Single-Turnover Reaction Center Transitions

A. Two-State Model

The model considered in this paragraph is frequently used to describe the kinetics of electron transfer in different RCs. Figure 4 shows examples of the schemes of the dark relaxation of RC from purple bacteria (A) and PS I (B), which can be described by the two-state model. The system of differential equations describing transitions in the two-state systems shown in Fig. 4 can be solved analytically. We will use this analytical solution later to describe the kinetics of $P700^+$ dark relaxation.

The system of linear differential equations describing transitions in Fig. 4C can be written as follows:

$$\begin{aligned} \dot{x} &= -(k+l)x + my \\ \dot{y} &= kx - (m+n)y \end{aligned} \tag{6}$$

We will assume arbitrary initial conditions for X and Y: $x(0) = x_0 \geq 0$, $y(0) = y_0 \geq 0$, $x_0 + y_0 = 1$.

The general solution of this system of differential equations with constant coefficients can be written in following simple form (assuming that $\lambda \neq \mu$)

$$\begin{aligned} x &= Ae^{\lambda t} + Be^{\mu t} \\ y &= Ce^{\lambda t} + De^{\mu t} \end{aligned} \tag{7}$$

where
$\lambda = -p - \sqrt{p^2 - q}$, $\mu = -p + \sqrt{p^2 - q}$, $p = (k + l + m + n)/2$, $q = kn + lm + ln$, $A = m[x_0 b(\mu) - y_0]/(\mu - \lambda)$, $B = m[y_0 - x_0 b(\lambda)]/(\mu - \lambda)$, $C = b(\lambda)A$, $D = b(\mu)B$, $b(u) \equiv (u + k + l)/m$.

We consider here only the approximation $p^2 \gg q$ of this general solution. In this case both characteristic values λ and μ are real and can be approximated as follows:

$$-\lambda = p + \sqrt{p^2 - q} \approx k + l + m + n \quad \text{(fast component)} \tag{8}$$

$$-\mu \approx q/2p = (kn + lm + ln)/(k + l + m + n) \quad \text{(slow component)} \tag{9}$$

When $l = 0$, $n = 0$ (equilibrium between X and Y), the solution (7) for x and y can be written in the form:

$$\begin{aligned} x &= \bar{x} + (x_0 - \bar{x})e^{-(k+m)t}, \\ y &= \bar{y} + (y_0 - \bar{y})\, e^{-(k+m)t} \end{aligned} \tag{10}$$

where $\bar{x}, \bar{y}$ are equilibrium values of x and y: $\bar{x} = 1/(K+1)$, $\bar{y} = K/(K+1), K = k/m$. When initially system is not in equilibrium, it exponentially approaches equilibrium state with lifetime $\sim 1/(k+m)$.

When $k, m \gg l$, $n > 0$ ("leaking" rate constants l and n are significantly less than the rate constants of electron transfer between X and Y), one can write the following approximation for the characteristic values:

$$-\lambda \approx k + m \tag{11}$$

$$-\mu \approx (kn + lm)/(k+m) \approx n\frac{k}{k+m} + l\frac{m}{k+m} \equiv n\tilde{y} + l\tilde{x}, \tag{12}$$

where $\tilde{x}, \tilde{y}$ are the values of steady-state solution in scheme assuming the equilibrium between X and Y (calculated with zero rate constants l and n). One can interpret fast characteristic value (here $-\lambda$) as rate of establishing the equilibrium between X and Y. The slow characteristic value (here $-\mu$) characterizes "leaking" of electrons from acceptors X and Y and is calculated as mean value of the rate constants n and l. Equation (12) indicates that the value of μ can be calculated by assuming that X and Y are at equilibrium during this slow "leaking" process.

B. The Model of Spreading Equilibrium

1. Introduction to the Model

The model of spreading equilibrium considered below can frequently describe the flash-induced kinetics in RCs. The model takes into account the observation that, as a rule, the closer the reaction to the primary charge separation step, the larger is its rate constant. This is illustrated in Fig. 5, which shows profiles of rate constants at the acceptor side of different types of RCs. Such organization of the RC allows it to effectively couple fast processes of light-induced charge separation that occur on the time scale of picoseconds with slower processes of substrate transformation and exchange that occur on the time scale of milliseconds or seconds. Additionally, the model takes into account that at each stage the forward rate constant of electron transfer, as a rule, is larger than rate constants of backreactions, both direct (via tunneling), and indirect (via reversion of the reaction involving earlier intermediates). Such hierarchy provides a quantum yield of charge separation close to 1.

Consequently, electron transfer in an RC after primary charge separation can be considered as occurring via well-defined steps in each of which all previous

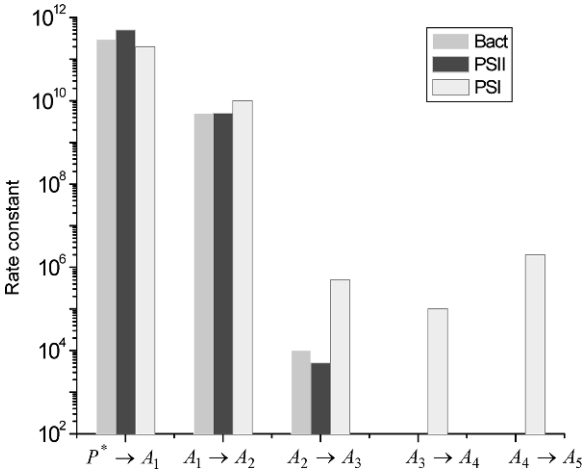

Fig. 5. Profile of rate constants at the acceptor side of different types of RCs, purple bacteria (Bact), PS II, and PS I. Note that A_1 here is the stable acceptor like bacteriopheophytin in bacterial RCs, pheophytin in PS II, or A_0 in PS I.

steps are at (quasi)equilibrium. Such equilibriums are spreading sequentially from processes that occur in the picosecond time domain to those in the microsecond–millisecond time domain. The equilibrium of all earlier processes allows their effective replacement by a single (quasi)state. Thus, by changing the scale of consideration one can describe such electron transfer as occurring only between two (quasi)states. This simple model allows the introduction of certain time domains for each of which the kinetics of electron transfer in RCs can be described with reasonable accuracy.

The hierarchy of the values of rate constants determines the effectiveness of the procedure of the isolation of quasi-states. The larger is the difference in the rate constants, the better the functioning of the complex could be described by means of the quasi-states.

It is obvious that the less is the time interval in question, the less is the number of RC states that can be achieved from some initial state. After estimating the time of output from a quasi-equilibrium state, it is possible to indicate quasi-states, which are accessible to the complex during the time of consideration. Consequently, the set of states that need to be taken into account to describe the functioning of the RC complex after the flash depends both on the initial conditions and on the time of observation of the RC (Fig. 6).

Thus, for the short time intervals it is sufficient to consider only small number of states, which can be reached for this time. In case of the large time intervals, the number of states that can be reached by the RC increases; however, the introduction of quasi-states

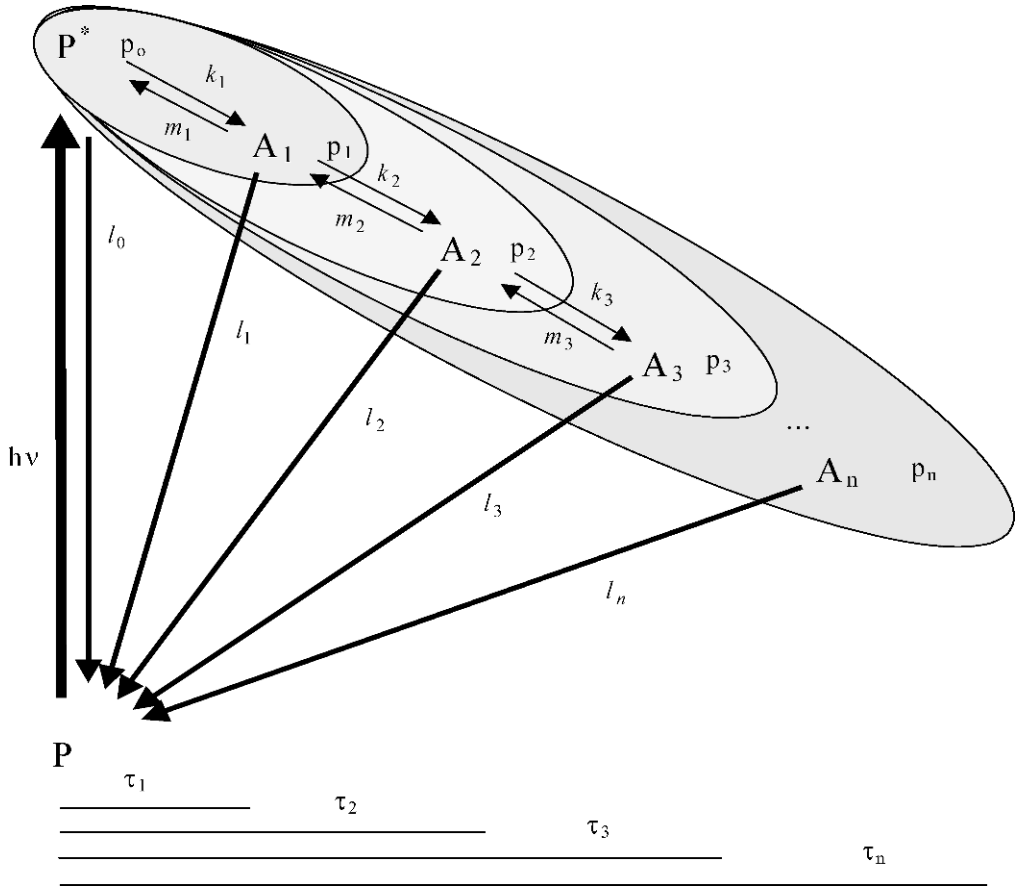

Fig. 6. Schematic presentations of waves of equilibrium in RC after the flash. Due to the hierarchy of rate constants, the process of electron transfer at the acceptor side can be presented as occurring on well-separated time scales (here $\tau_1, \tau_2, \ldots$).

(group of fast-equilibrating states) significantly simplifies the analysis. Therefore, in spite of an increase in the number of states accessible to the RC with time, it is possible to effectively decrease the number of independent variables by introducing quasi-states.

2. Time Dependent Two-State Approximation

Let us consider the scheme shown in Fig. 6. For the time scale ($0 \le \tau < 1/(m_1 + k_1 + l_0) \sim 1/k_1$) only P^* and A_1 are changing with time. All other states are not yet accessible. Thus, here we can consider only the transition between these two states quantitatively characterized above. From this point on, we use the notation according to which $p_0(t)$ is the probability of the excited state of the primary electron donor, and $p_i(t)$ is the probability (fraction) of finding electron on A_i (i.e., $P^+A_i^-$) at time t after the flash. We can write solution for the fractions of first two states in the form (assuming that $p_0(0) = 1$, $p_1(0) = 0$):

$$p_0(t) \approx \frac{1}{1+K_1} + \frac{K_1}{1+K_1} e^{-(k_1+m_1)t}, \tag{13}$$

$$p_1(t) \approx \frac{K_1}{1+K_1}(1 - e^{-(k_1+m_1)t}), \tag{14}$$

where $K_1 = k_1/m_1$. Note that here we ignored the transition via l_0 to ensure that quantum yield is close to 1 for this time scale. Yet, the transitions with this rate constant can be significant at a longer time scale. These expressions indicate that both p_0 and p_1 exponentially approach their (quasi)steady states that are determined by the value of equilibrium constant only.

We can see that for the time $\sim 1/k_1$, electron is partitioned between first two states according to the equilibrium constant K_1. This equilibrium partitioning between P^* and A_1 continue to be valid during further RC relaxation.

The existence of equilibrium between first two states does not mean that there are not any further processes

of relaxation in the RC. Indeed, we know that later the electron will move to the next electron acceptor. However, this transition will occur with both first states being in (quasi)equilibrium. As a result, the kinetics of electron transfer between A_1 and A_2 on the time scale $1/k_1 \le \tau < 1/k_2$ can be described by the following scheme:

$$\underbrace{\left(P^* \underset{}{\overset{K_1}{\rightleftarrows}} A_1\right)}_{\text{(Quasi) equilibrium}} \underset{m_2}{\overset{k_2}{\rightleftarrows}} A_2 \tag{15}$$

which can be presented as a two-state transition:

$$B_1 \underset{m_2}{\overset{\bar{k}_2}{\rightleftarrows}} A_2 \tag{16}$$

where $B_1 = P^* + A_1$. We can write down the equations for the transition of B_1 and A_2 (we use symbol q_1 for B_1, symbol $\bar{k}_2$ for new rate constant for $B_1 \to A_2$ transition, and $\bar{K}_2 \equiv \bar{k}_2/m_2$ for new equilibrium constant)

$$q_1(t) \approx \frac{1}{1+\bar{K}_2} + \frac{\bar{K}_2}{1+\bar{K}_2} e^{-\bar{k}_2 t} \qquad \text{(for } B_1\text{)} \tag{17}$$

$$p_2(t) \approx \frac{\bar{K}_2}{1+\bar{K}_2}(1 - e^{-\bar{k}_2 t}) \qquad \text{(for } A_2\text{)} \tag{18}$$

The apparent rate constant $\bar{k}_2$ for $B_1 \to A_2$ transition is determined by electron partitioning between P^* and A_1 according to the equilibrium constant K_1. It can be presented [see Eq. (12)] as product of equilibrium fraction A_1 and rate constant k_2:

$$\bar{k}_2 = k_2 \cdot \bar{p}_1 = k_2[K_1/(K_1+1)] \overset{K_1 \gg 1}{\approx} k_2 \tag{19}$$

In case when $K_1 \gg 1$, we can ignore the difference between k_2 and $\bar{k}_2$.

In the general case, each transition effectively can be considered on the time scale of transition from the group of states, which are at equilibrium to another state, i.e., effectively we have transition between two (quasi)states:

$$\underbrace{\left(P^* \underset{m_0}{\overset{k_0}{\rightleftarrows}} A_1 \underset{m_1}{\overset{k_1}{\rightleftarrows}} \cdots \underset{m_{l-1}}{\overset{k_{l-1}}{\rightleftarrows}} A_l\right)}_{\text{(Quasi) equilibrium for time} > 1/k_l} \underset{m_l}{\overset{k_l}{\rightleftarrows}} A_{l+1} \tag{20}$$

This can be iterated further to take into account more electron acceptors, until final quasi-equilibrium is established between all states of acceptor side of the RC.

This simple model of electron transfer in RC allows one to characterize the main steps of electron transfer in the RC before all states reach (quasi)equilibrium. After that the time dependence of acceptors will be determined by the "leaking" of the electron from acceptor side to the donor side of the RC, or by donation of electrons to the exogenous electron acceptor.

Similar considerations could be used for the processes occurring at the donor side of RC (see, e.g., Rubin and Shinkarev, 1984; Shinkarev and Wraight, 1993b).

3. General Expression for the Rate Constant of the Flash-Induced Dark Reduction of P^+

In previous paragraph we described the kinetics of electron transfer to the terminal acceptors. Here we consider slower process of dark reduction of P^+ after electron has reached terminal acceptor of the RC.

We will assume that during dark reduction different states of RC are in (quasi)equilibrium. The assumption of the (quasi)equilibrium between different states of the RC is frequently used for the analysis of the electron transfer in different RCs (see, e.g., Rubin and Shinkarev, 1984; Iwaki and Itoh, 1994; Brettel, 1997; Shinkarev and Wraight, 1993a,b). Using such assumption, the observed rate constant of P^+ dark reduction can be described by the following general expression (Shinkarev and Wraight, 1993a):

$$k_P \approx k_{PP}[P^*] + k_{A_1P}[A_1^-] + k_{A_2P}[A_2^-] + \cdots + k_{A_nP}[A_n^-] \tag{21}$$

Here k_{PP} is the rate constant for P^*deexcitation; k_{A_1P} is the rate constant of *direct* electron transfer from A_1^- to P^+; k_{A_2P} is the rate constant of *direct* electron transfer from A_2^- to P^+; etc.

Square brackets in Eq. (21) indicate the *relative* (per RC) concentrations of the different states of RC. Assuming quasi-equilibrium between different states during dark reduction, the relative concentrations of the components can be found as function of an equilibrium constant of electron transfer between the components:

$$[P^*] \approx 1/Z, [A_1^-] \approx K_{PA_1}/Z, \ldots, [A_n^-] \approx K_{PA_n}/Z, Z \approx 1 + K_{PA_1} + K_{PA_2} + \cdots + K_{PA_n} \tag{22}$$

Here K_{PA_1} is the equilibrium constant for electron transfer from P^* to A_1, $K_{A_1A_2}$ is the equilibrium

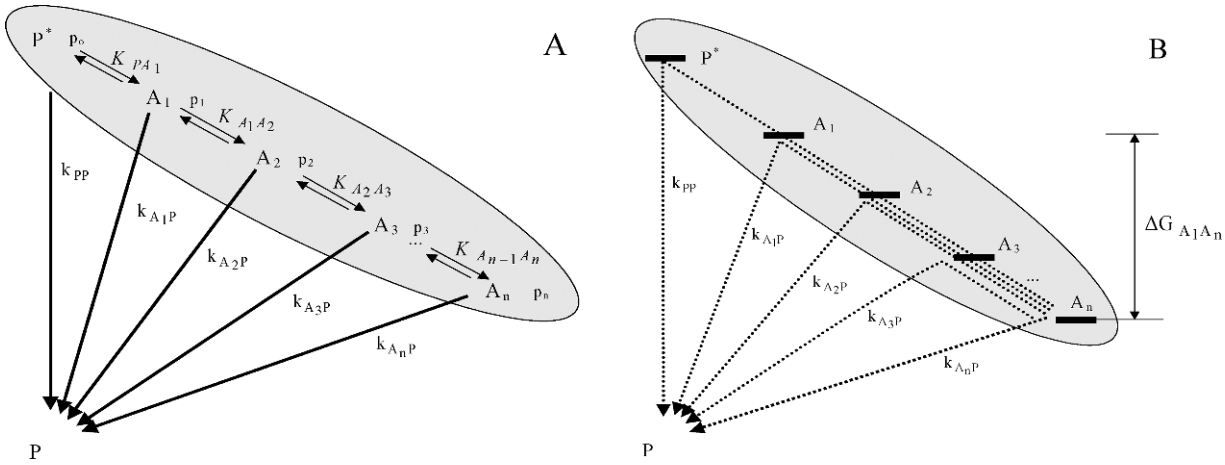

Fig. 7. Schemes of dark relaxation of the RC after establishing (quasi)steady state. (A) General case; (B) Scheme illustrating different pathways of electron return from A_n to P^+ that contribute to the effective rate constant of P^+ decay given by Eq. (27).

constant for electron transfer from A_1 to A_2, etc.

$$K_{PA_2} \approx K_{PA_1} K_{A_1A_2},$$
$$K_{PA_3} \approx K_{PA_1} K_{A_1A_2} K_{A_2A_3}, \ldots,$$
$$K_{PA_n} \approx K_{PA_1} K_{A_1A_2} K_{A_2A_3} \ldots K_{A_{n-1}A_n} \quad (23)$$

(see Fig. 7 for a notation of the equilibrium constants between electron carriers).

Inserting the solution (22) into Eq. (21) gives:

$$k_P \approx \frac{k_{PP} + k_{A_1P}K_{PA_1} + k_{A_2P}K_{PA_2} + \cdots + k_{A_nP}K_{PA_n}}{1 + K_{PA_1} + K_{PA_2} + \cdots + K_{PA_n}} \quad (24)$$

This equation can be rewritten via the relevant free-energy differences, $\Delta G_{XY} = -RT\ln(L_{XY})$:

$$k_P \approx (k_{pp} + k_{A_1P}e^{-\Delta G_{PA_1}/RT} + k_{A_2P}e^{-\Delta G_{PA_2}/RT} + \cdots + k_{A_nP}e^{-\Delta G_{PA_n}/RT}/Z \quad (25)$$

In case when concentration of terminal acceptor A_n is significantly higher than concentrations of all other acceptors, the Eq. (24) allows simple interpretation. Indeed, in this case we can assume that all relaxation of RC occurs from the terminal acceptor A_n and terms in Eq. (24) correspond to different pathways of electron return from A_n to P^+ that contribute to the effective rate constant of P^+ decay. Let assume that $K_{PA_n} \gg K_{PA_k}$ ($1 \le k < n$). In this case Eq. (24) can be simplified as follows:

$$k_P \approx k_{PP}/K_{PA_n} + k_{A_1P}/K_{A_1A_n} + k_{A_2P}/K_{A_2A_n} + \cdots + k_{A_nP} \quad (26)$$

where we used Eq. (23) to replace K_{PA_k}/K_{PA_n} by $1/K_{A_kA_{k+1}} \cdot \cdots \cdot K_{A_{n-1}A_n} \equiv 1/K_{A_kA_n}$. The Eq. (26) written via free energies takes the form:

$$k_p \approx \underbrace{k_{PP}e^{\Delta G_{PA_n}/RT}}_{A_n \to A_{n-1} \to \cdots A_1 \to P^* \to P} + \underbrace{k_{A_1P}e^{\Delta G_{A_1A_n}/RT}}_{A_n \to A_{n-1} \to \cdots A_1 \to P} + \cdots + \underbrace{k_{A_{n-1}P}e^{\Delta G_{A_{n-1}A_n}/RT}}_{A_n \to A_{n-1} \to P} + \underbrace{k_{A_nP}}_{A_n \to P} + \quad (27)$$

These routes include the thermal repopulation of P^* from A_n, followed by transition from P^* to P (the term $k_{PP}e^{\Delta G_{PA_n}/RT}$), thermal repopulation of A_1 from A_n, followed by direct electron transfer from A_1 to P^+ (the term $k_{A_1P}e^{\Delta G_{A_1A_n}/RT}$), etc (see Fig. 7).

This formalism, especially in its simplest form, has wide application for analysis of electron transfer in different types of RCs (see, e.g., Shinkarev and Wraight, 1993a; Shinkarev et al., 2002). It is also complimentary to the method of Parson and coworkers, who have used delayed fluorescence emission to monitor the P^* population in equilibrium with lower lying charge separated states (see, e.g., Arata and Parson, 1981; Woodbury and Parson, 1984). Below we will use this formalism for the analysis of kinetics of electron transfer in PS I.

4. Expression for the Ratio of Two Different Pathways of P^+ Dark Reduction

The relative contribution of each route is quite sensitive to the values of energy differences between different states. Indeed, from Eq. (27) we can write the ratio of two different pathways of the P^+ dark reduction as

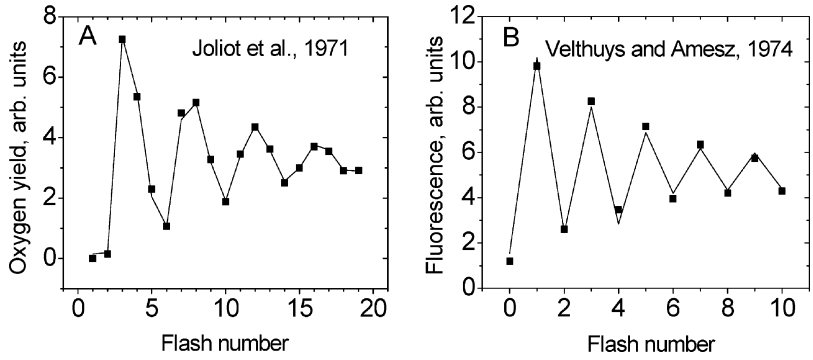

Fig. 8. Classical experiments describing flash-induced charge accumulation at the donor (A) and acceptor (B) sides of PS II. (A) Flash-induced O_2 evolution in spinach chloroplasts measured by Joliot et al. (1971). (B) Flash-induced binary oscillations of fluorescence measured by Velthuys and Amesz (1974).

follows (we assume that $j \geq k$ here):

$$\frac{\text{Pathway via } A_j}{\text{Pathway via } A_k} = \frac{k_{A_jP} \cdot e^{\Delta G_{A_jA_n}/RT}}{k_{A_kP} \cdot e^{\Delta G_{A_kA_n}/RT}} \equiv \left(\frac{k_{A_jP}}{k_{A_kP}}\right) e^{\Delta G_{A_jA_k}/RT} \quad (28)$$

Thus, the ratio of two different pathways of P^+ dark reduction depends on the free energy difference between these two acceptors and ratio of the rate constants of direct electron transfer from these acceptors to P^+. Changes in the free energy gaps between different states can cause noticeable differences in the observed time of the P^+decay and change the contribution of different routes. These two pathways are equal when $(k_{A_jP}/k_{A_kP}) \cdot e^{\Delta G_{A_jA_k}/RT} = 1$. One should expect that the changing the midpoint potential of the acceptor can lead to significant redistribution of different pathways.

III. Simple Analytical Models for Multiple-Turnover RC Transitions

A. Charge Accumulation at the Processing Sites of Reaction Centers

Light-activated primary charge separation in RCs is one-electron process. Therefore, in case when RC has multielectron donors and acceptors, one can assume some kind of charge accumulation. One significant difference with PS I is that RCs of PS II use charge accumulation both at the donor and acceptor sides. Multiple flash activation of such RCs initiates periodic oscillations of the state of their processing sites (Fig. 8). To quantitatively describe such oscillations one should consider different states of the processing site. In case of the Q_B processing site they include a vacant processing site and a site occupied by quinone, semiquinone, or quinol. Similarly, to describe the water oxidizing processing site (water-oxidized complex), one needs to take into account its different states.

A mathematical model of binary oscillations that describe the two-electron gate on the acceptor side of purple bacteria and PS II has been known for over 20 years (Shinkarev et al., 1981). At the same time the analytical solution for the period four oscillations at the donor side of PS II was obtained only recently (Shinkarev, 2003, 2005). Here we shortly consider the quantitative description of flash-induced charge accumulation at the donor and acceptor sides of PS II.

B. Binary Oscillations of the Q_B Semiquinone

In the simplest case, when there is no dark oxidation of semiquinone between two consecutive flashes, and only two states of the Q_B site are considered, the fraction of the Q_B semiquinone after the n-th flash, $q_B^-(n)$, is given by (Shinkarev et al., 1981; Verkhovsky et al., 1981):

$$q_B^-(n) = \frac{\rho}{\rho + \sigma}[1 - (1 - \rho - \sigma)^n] \quad (29)$$

where ρ and σ are "hit" probabilities for different states of Q_B. If Q_B is oxidized before the flash, the Q_B semiquinone will be formed with probability ρ. Similarly, if Q_B is in the semiquinone state before the flash, it will be converted to the oxidized form with probability σ.

Figure 8B shows theoretical curve (solid lines) described by Eq. (29). One can see that Eq. (29) reproduces main features of experimentally observed binary oscillations (squares). Other examples of binary

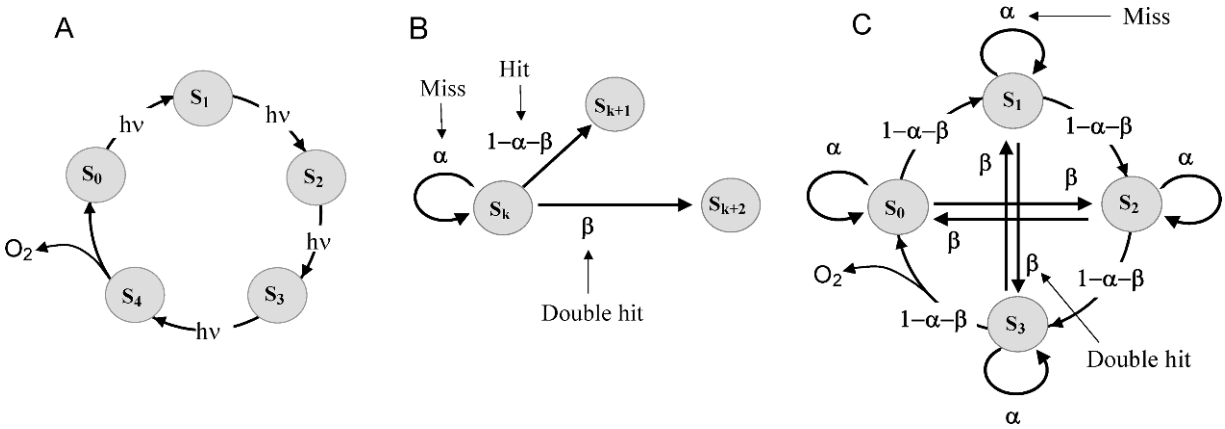

Fig. 9. Kok model of oxygen evolution in PS II. (A) Light-induced transitions between different S-states. (B) Transition probabilities for each S_k-th state. (C) Mathematical representation of the Kok model via transition probabilities.

oscillation patterns (arising from the Kok model of oxygen evolution) are shown in Figs. 12 and 13 below.

More advanced kinetic models have been developed to take into account different factors that govern flash-induced binary oscillations in PS II and bacterial RCs (see, e.g., Shinkarev et al., 1981; Shinkarev and Wraight, 1993a; Shinkarev, 1998).

C. The Kok Model of the Flash-Induced Oxygen Evolution

1. The Formulation of the Model

The activation of dark-adapted PS II by a series of single-turnover actinic flashes leads to oxygen evolution with a periodicity of four (Joliot et al., 1969; Kok et al., 1970; Joliot et al., 1971). Figure 8A shows such flash-induced oscillations of oxygen evolution. Almost no oxygen evolution is observed after first and second flashes. The largest oxygen evolution is observed after the third flash. Kok et al. (1970) explained this periodicity by introducing the concept of the S-states (S_n, where n = 0, 1, 2, 3, 4) of the oxygen-evolving complex, where each S-state has a different number (n) of stored oxidizing equivalents. During $S_4 \rightarrow S_0$ transition oxygen is released and S_0 is regenerated. The kinetic model of oxygen evolution and its mathematical representation are shown in Fig. 9.

To quantitatively describe the damping of the period four oscillations of oxygen evolution, the Kok model includes so called misses, which describe failure to advance the S-states after the flash, and the so called double hits, which describe double advances of S-states (Fig. 9B). Double hits are mainly due to actual double turnovers during a long flash and can be minimized by using laser activation (see, e.g., Weiss and Sauer, 1970; Joliot et al., 1971; Joliot and Kok, 1975).

The period four oscillations are purely kinetic phenomena arising from synchronous light activation of different RCs. Kok et al. (1970) used such oscillations in the oxygen yields for finding the information about oxygen evolution in term of misses, double hits, and initial conditions. In an alternative approach, Shinkarev and Wraight (1993b,c) used known PS II kinetic and thermodynamic data to reconstruct the period four oscillations in oxygen evolution. This approach allowed mechanistic interpretation of misses. It also allowed one to estimate conditions under which the Kok model of oxygen evolution is valid.

2. Analytical Solution for the S-states

The Kok model (Fig. 9), with equal misses for each transition, has been successfully used over 30 years for interpretation of experimental data in photosynthesis. However, there has been no simple analytical solution for it. Recently such solution was found for any initial conditions. The probabilities of individual S-states after n-th flash, $s_i(n)$, are described by the following surprisingly simple equations (Shinkarev, 2003, 2005):

$$\begin{aligned}
4s_0(n) &= 1 + \mu^n z + 2r^n(x\cos(n\varphi) + y\sin(n\varphi)) \\
4s_1(n) &= 1 - \mu^n z + 2r^n(-y\cos(n\varphi) + x\sin(n\varphi)) \\
4s_2(n) &= 1 + \mu^n z + 2r^n(-x\cos(n\varphi) - y\sin(n\varphi)) \\
4s_3(n) &= \underbrace{1 - \mu^n z}_{\text{Binary term}} + \underbrace{2r^n(y\cos(n\varphi) - x\sin(n\varphi))}_{\text{Quaternary term (damped sine)}},
\end{aligned} \tag{30}$$

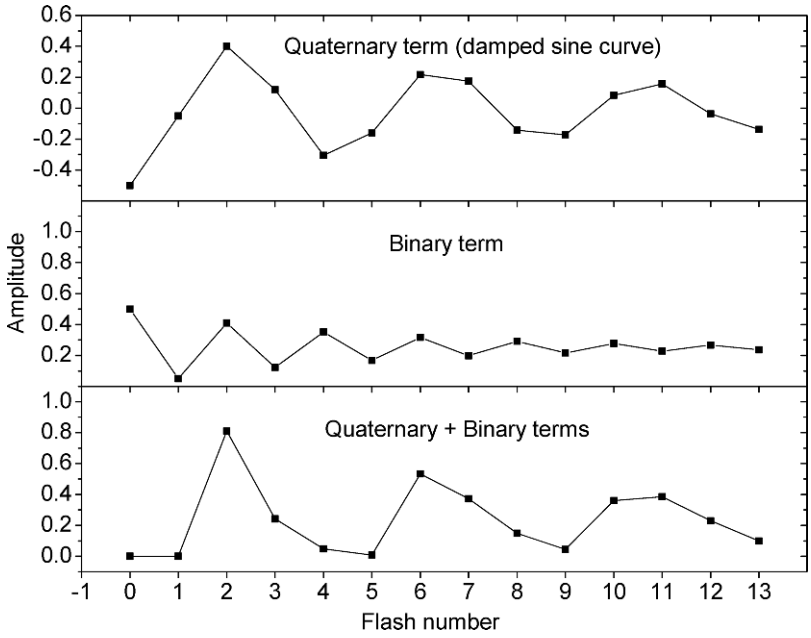

Fig. 10. Different components of general solution given by Eq. (30).

where α, γ, and β, are miss, hit, and double hit, respectively, $\mu \equiv \alpha - \gamma + \beta$, $r \equiv [(\alpha - \beta)^2 + \gamma^2]^{1/2}$, $\varphi \equiv \arcsin(\gamma/r)$, n – number of the flashes, $s_i = s_i(0)$ are initial conditions for S_i, $x \equiv s_0 - s_2$, $y \equiv s_3 - s_1$, $z \equiv s_0 - s_1 + s_2 - s_3$.

A similar analytical solution can be obtained for the extended Kok model that includes misses, double hits, inactivation, and backward transitions (Shinkarev, 2005).

Equation (30) describes the flash number dependence of individual S-states as function of miss, double hit, and initial conditions for the S-states. The general structure of the solution is illustrated in Fig. 10.

According to the Kok model oxygen evolution after n-th flash can be determined by the fraction of PS II in S_3 and S_2 states before the $(n-1)$-th flash:

$$\begin{aligned} Y(n) &= s_3(n-1)\cdot(\text{hit} + \text{double hit}) \\ &\quad + s_2(n-1)\cdot \text{double hit} \\ &= (\gamma+\beta)s_3(n-1) + \beta s_2(n-1) \end{aligned} \tag{31}$$

where $s_2(n-1)$, $s_3(n-1)$ are given by Eq. (30).

Figure 11 shows flash-induced oxygen evolution calculated from Eq. (31) for different values of miss (A) and double hit (B). Increase of miss (at zero double hit) leads to damping of oscillations. The increase of double hit (at zero miss) leads to disappearance of oscillations and to increase of the amplitude of oxygen yield after the second flash. Other than that, the effects of miss and double hit on pattern of oscillations are similar.

3. Binary Oscillations in the Kok Model

The same light activates the donor and acceptor sides of PS II. Therefore, there should be significant correlation in accumulation charges at the donor and acceptor sides of PS II. In the case when slowly rereduced components of PS II can be excluded from consideration, this correlation leads to the existence of two parallel cycles of O_2 evolution (Shinkarev and Wraight 1993b). In each cycle, a single turnover of the oxygen-evolving complex is accompanied by two turnovers of the acceptor quinone complex. As a result, the kinetic behavior of the acceptor side of PS II can be obtained by summing the solutions for respective S-states. For example, by adding s_0 and s_2 from Eq. (30) one can obtain the equation for the fraction of the Q_B semiquinone after the n-th flash, (Shinkarev, 1996, 2003):

$$q_B^-(n) = s_0(n) + s_2(n) = 0.5\cdot[1 + \mu^n z] \tag{32}$$

where, as before, α, γ, and β, are miss, hit, and double hit, respectively, $\mu \equiv \alpha - \gamma + \beta$, $s_i = s_i(0)$, $z \equiv s_0 - s_1 + s_2 - s_3$.

Figure 12 shows the binary oscillations of Q_B^- described by Eq. (32) as well as probabilities for S_0 and

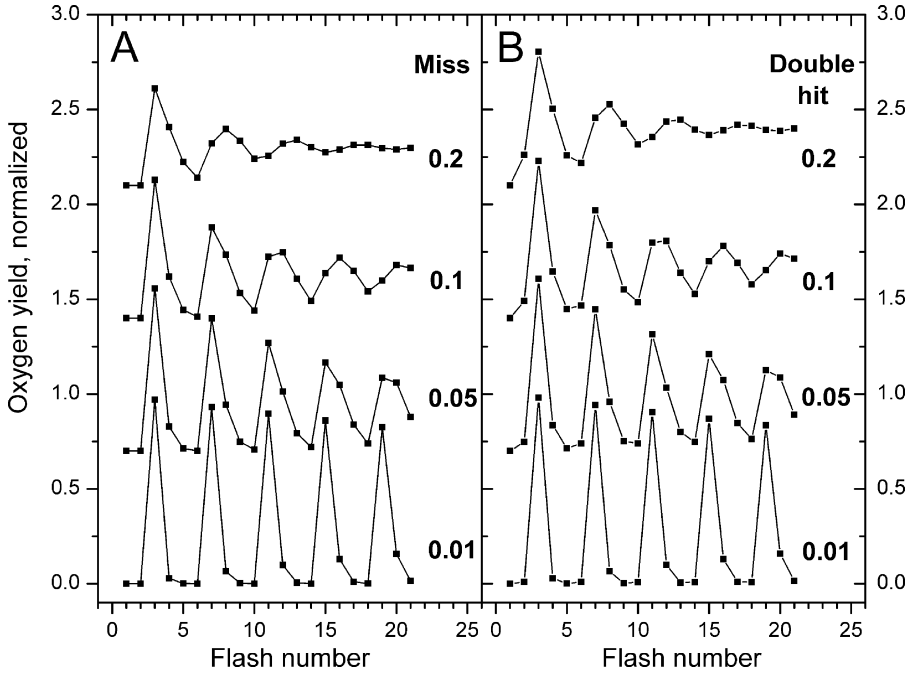

Fig. 11. Oxygen evolution calculated from Eq. (31) for different miss (panel A) and double hit (panel B) parameters. In panel A, the value of double hit (β) is 0. In the panel B the value of miss (α) is 0. During calculations it was assumed that $s_1 = 1$ for both panels. Traces are shifted vertically to improve their visibility.

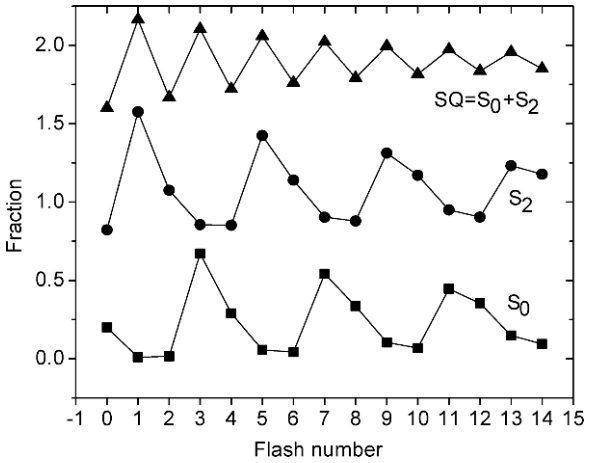

Fig. 12. Flash number dependence of the semiquinone Q_B^-, calculated using Eq. (32). Fractions of S_0 and S_2 states were calculated using Eq. (30) for $\alpha = 0.05$, $\beta = 0.01$. It is assumed that at the beginning of the flash series, 80% of PS II are in the S_1 state and 20% are in the S_0 state. Traces are shifted up to improve their visibility.

S_2. This figure illustrates how adding two quaternary oscillations leads to the period two oscillations.

Figure 13 shows Q_B^- binary oscillations for different initial conditions (panel B) and for different values of misses (panel A). Depending on initial conditions, oscillations can change their direction, or even disappear.

4. Finding Parameters Governing Oxygen Evolution and Semiquinone Oscillations

The developed equations significantly simplify the fitting of experimental data via standard non-linear regression analysis and make unnecessary the use of many previously developed methods for finding parameters of the Kok model. Fitting the experimental points of Fig. 8A with Eqs. (30) and (31) gave the following parameters: $\alpha = 0.12$, $\beta = 0.02$, $s_0 = 0.32$, $s_1 = 0.68$, $s_2 = 0$. Fitting the experimental points for flash-induced binary oscillations in Fig. 8B (shown by solid lines) with Eq. (32) (plus trend) gave $\alpha + \beta = 0.09$.

IV. Dark Relaxation in PS I After Flash Activation

Here we analyze the kinetics of $P700^+$ dark reduction observed after single-turnover flash activation of PS I. This analysis closely follows the paper by Shinkarev et al. (2002). Figure 14 shows the generally accepted scheme of flash-induced electron transfer in PS I. The

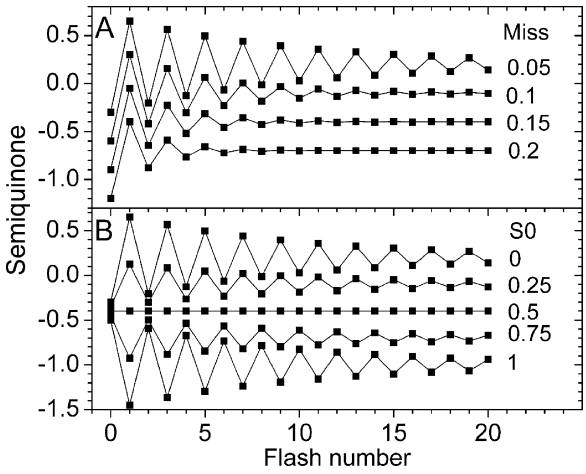

Fig. 13. Dependence of binary oscillations of semiquinone on the miss factor and initial conditions. (A) Effect of miss on the flash number dependence of Q_B^-, calculated using Eq. (32). Initial conditions $s_0 = 0$, $s_1 = 1$. Double hit is zero. (B) Effect of initial conditions on the flash number dependence of the relative concentrations Q_B^-. Traces are calculated from Eq. (32). Right hand numbers indicate initial conditions for S_0. It is assumed that $s_1 = 1 - s_0$, $\alpha = 0.05$, $\beta = 0$. Traces are shifted vertically to improve their visibility.

rate constants and respective midpoint potentials are taken from the current literature and provide general guidance rather than exact values. They can be adjusted to fit the kinetics in a particular sample, if needed.

As in the general case considered in section II above, we can assume the (quasi)equilibrium between different states of the PS I complex during dark reduction. Such assumption is frequently used previously for the analysis of the electron transfer in PS I (see, e.g., Iwaki and Itoh, 1994; Brettel, 1997). Using such assumption, the observed rate constant of P^+ dark reduction can be described by the following expression (Shinkarev et al., 2002):

$$k_P \approx k_{PP}[P^*] + k_{A_0P}[A_0^-] + k_{A_1P}[A_1^-] + k_{F_XP}[F_X^-] + k_{F_AP}[F_A^-] + k_{F_BP}[F_B^-] \quad (33)$$

Here k_{PP} is the rate constant for P^* deexcitation; k_{A_0P} is the rate constant of *direct* electron transfer from A_0^- to $P700^+$; k_{A_1P} is the rate constant of *direct* electron transfer from A_1^- to $P700^+$; k_{F_XP} is the rate constant of *direct* electron transfer from F_X^- to $P700^+$; k_{F_AP} is the rate constant of *direct* electron transfer from F_A^- to $P700^+$; and k_{F_BP} is the rate constant of *direct* electron transfer from F_B^- to $P700^+$.

A. The Relationship Between Electron Transfer Rate and Distance Between Electron Carriers

The rate of electron transfer between electron carriers decreases exponentially with distance and this dependence has been tabulated for different reactions in proteins (see, for example, Likhtenshtein, 1988; Moser et al., 1995; Gray and Winkler, 1996; see also Moser and Dutton, this volume, Chapter 34). According to Moser et al. (1995), the logarithm of the rate constant of *intraprotein* electron transfer between two electron carriers with edge to edge distance R can be described

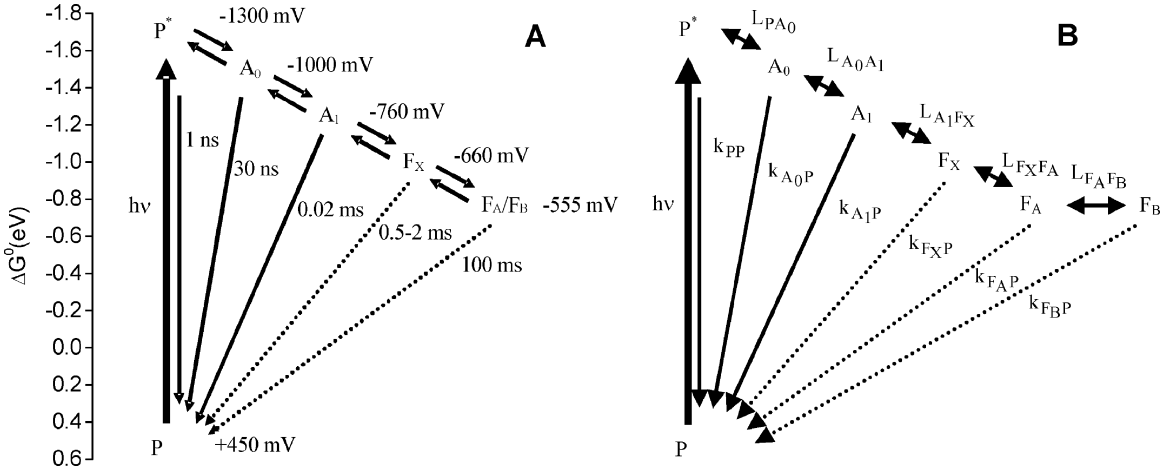

Fig. 14. (A) Scheme of electron transport in PS I (reviewed in Brettel, 1997, Ke, 2001, Brettel and Leibl, 2001). Note that in panel A we show lifetimes of *direct* electron transfer for reactions $A_0 \rightarrow P$, $A_1 \rightarrow P$. The indicated time for the reaction $F_A/F_B \rightarrow P$ corresponds to the *indirect* electron transfer via F_X, A_1, etc. (B) Notations used for the rate and equilibrium constants in PS I. Adapted from Shinkarev et al. (2002).

by the following equation:

$$\log k = 15 - 0.6 \times R - 3.1(\Delta G^{\circ} + \lambda)^2/\lambda \qquad (34)$$

where R is in Å, ΔG° is the standard reaction free energy in eV and λ is the reorganization energy in eV.

Schlodder et al. (1998) estimated from temperature dependence of electron transport that reorganization energy for the reaction between A_1 and F_X has value of ca. 1 eV. In further considerations we assume $\lambda = 1$ eV for reactions between all iron–sulfur clusters in PS I.

The distance between $F_A(F_B)$ and P700 provided by the X-ray crystal structure is so large (>30 Å, Jordan et al., 2001) that based on Eq. (34), we can ignore direct electron transfer between them and $P700^+$ on a millisecond time scale. Thus, electron transfer from F_A^- and F_B^- to $P700^+$ occurs indirectly via thermal repopulation of F_X, F_A, etc. Similarly, the edge-to-edge distance of 26–27 Å between F_X and P700 also indicate that the time of electron transfer from F_X^- to $P700^+$ should be seconds. Therefore, we should ignore direct electron transfer from F_X, F_A, and F_B to $P700^+$, i.e., $k_{FAP} \sim 0$, $k_{FBP} \sim 0$, and $k_{FXP} \sim 0$.

Assuming $k_{FAP} = 0$, $k_{FBP} = 0$, and $k_{FXP} = 0$, Eq. (33) for the observed rate constant of $P700^+$ dark decay can be rewritten in the following simple form:

$$k_P \approx k_{PP}[P^*] + k_{A_0P}[A_0^-] + k_{A_1P}[A_1^-] \qquad (35)$$

B. Heterogeneity in the Kinetics of $P700^+$ Dark Reduction

1. Two Different Explanations of Heterogeneity

One would expect that in a simplest case the monomolecular backreaction between a particular acceptor and $P700^+$ should follow monoexponential kinetics. However, in most cases the experimental data clearly show the presence of two or more kinetic components (see, e.g., Vassiliev et al., 1997), indicating some kind of heterogeneity. The nature of this heterogeneity in the dark relaxation of $P700^+$ is not fully understood, but it may have two fundamentally different sources. (i) it could be due to the presence of a mixture (discrete or continuous) of different populations of PS I complexes, or (ii) it could be due to internal heterogeneity of each RC.

Heterogeneity in purified PS I complexes can originate from differences in protein composition, bound cofactors, lipid, and detergent. The proposed participation of two different branches of cofactors in electron transport in PS I can also lead to heterogeneity of the measured kinetics (Guergova-Kuras et al., 2001; Agalarov and Brettel, 2003).

The existence of different conformational (sub)states in the PS I complex can also be the source of heterogeneity (Vassiliev et al., 1997). Such heterogeneity has been reported in PS I (Schlodder et al., 1998) and RCs from purple bacteria (Kleinfeld et al., 1984; McMahon et al., 1998).

One can also expect the presence of continuous distribution of rate constants due to a distribution of energy gaps, distances, or reorganization energies. Such distributions of rate constants have been considered for PS I (Ke et al., 1979; Zamaraev et al., 1985) and purple bacteria (Kleinfeld et al., 1984; McMahon et al., 1998; Kriegl et al., 2003).

2. Stretched Exponentials

Many different approaches have been developed to decrease the influence of heterogeneity in the case of closely spaced kinetic components. In some cases such kinetics components can be approximated with single exponential (Shinkarev et al., 2000), with a rate constant (lifetime) equal to the weighted average of the two or more rate constants (lifetimes). For example, in case of three components, the average time is determined as $(\tau_1 A_1 + \tau_2 A_2 + \tau_3 A_3)/(A_1 + A_2 + A_3)$, where τ_i are the lifetimes and A_i are the amplitudes of the single exponentials, corresponding to the *same* reaction of P^+ dark reduction. The disadvantage of such approach is uncertainty in choosing the components needed to be aggregated.

Wong and Angell (1976) indicated that sum of exponentials $\sum_k a_k e^{-\lambda_k t}$ can be approximated by the stretched exponential function, $e^{-(kt)^{\sigma}}$, which sometimes called Kohlrausch function, or Kohlrausch–Williams–Watts function (see, e.g., Williams and Watts, 1970; Alvarez et al., 1991; Phillips, 1996; Sturman et al., 2003). The stretch factor, σ ($0 < \sigma \leq 1$) provides a measure of the heterogeneity of the kinetics. Vassiliev et al. (2001a,b) used stretched exponentials to reduce number of closely spaced kinetic components, without losing the quality of the fit (see also Fig. 15 below).

The stretched exponential function is a Weibull distribution that has multiple applications in the reliability theory and statistics (see, e.g., Gnedenko et al., 1969; Murthy et al., 2003).

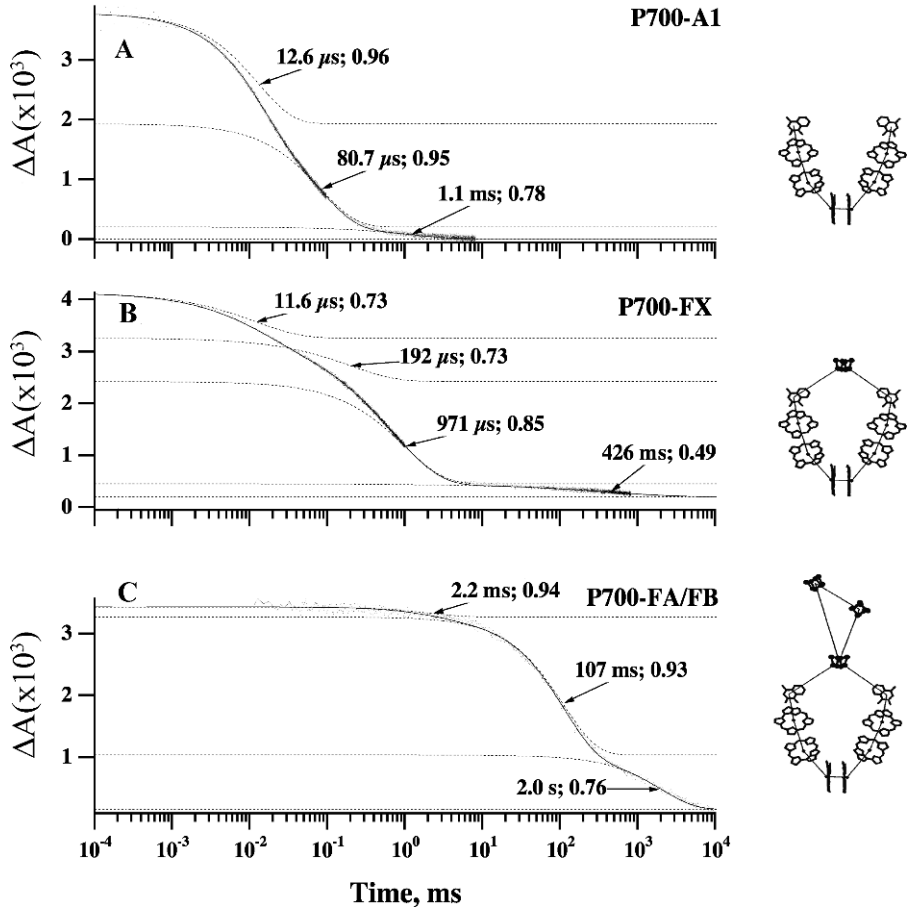

Fig. 15. Kinetics of flash-induced P700 changes in PS I complexes with different subsets of iron–sulfur clusters [none – (panel A), F_X only (panel B), and intact set (panel C)] (adapted from Shinkarev et al., 2002). Schemes indicate active iron–sulfur clusters. (A) PS I core lacking F_X, F_A, and F_B (prepared from the *rubA* mutant of *Synechococcus* sp.PCC 7002). (B) Wild-type PS I core lacking F_A and F_B (prepared by chemically removing PsaC from *Synechococcus* sp. PCC 6301 PS I complexes with urea). (C) Wild-type PS I complex from *Synechocystis* sp. PCC 6803 with F_X, F_B, and F_A present. Reaction medium: 25 mM Tris buffer (pH 8.3), 0.04% *n*-dodecyl-β-D-maltoside, 4 μM DCPIP, and 10 mM sodium ascorbate. Each individual component of the stretched multiexponential fit is plotted with a vertical offset relative to the next component (with a longer lifetime) or the baseline, the offset being equal to the amplitude of the latter component. The values indicate the (1/e) lifetime and the stretch parameter (separated by semicolon from lifetime). Adapted from Shinkarev et al. (2002).

C. Kinetics of $P700^+$ in PS I Complexes with Different Subsets of Iron–Sulfur Clusters

Figure 15A shows the kinetics of flash-induced absorbance changes in a PS I core isolated from the *rubA* mutant that is devoid of the F_X, F_A, or F_B iron–sulfur clusters, but contains phylloquinone in the A_1 site. Using optical and EPR spectroscopy Shen et al. (2002a) showed that rubredoxin is required for assembly of the iron–sulfur clusters in PS I. The stretched multiexponential fit of the kinetics shows three different components with lifetimes of 12.6 μsec (0.96), 80.7 μsec (0.95), and 1.1 msec (0.78) with relative amplitudes of 49.7%, 43.1%, and 4.1%, respectively. Stretch factors are shown in parentheses. As have been shown by optical and EPR spectroscopy, the two main μsec components represent the backreaction of $P700^+$ with A_1^- (Shen et al., 2002b). These lifetimes are similar to the ca. 10 and 110 μsec lifetimes measured in a chemically prepared P700-A_1 core that also lacks F_X, F_A, and F_B. Both kinetic phases show spectral signatures in the near-UV characteristic of the semiquinone anion radical (Brettel and Golbeck, 1995). Thus, in both the chemically prepared P700-A_1 core, and the *rubA* mutant devoid of the F_X, F_A, or F_B iron–sulfur clusters the backreaction of $P700^+$ with A_1^- shows lifetimes of

ca. 10 and 100 μsec with approximately equal amplitude and stretch factors close to 1. The nature of the observed heterogeneity is not clear. One can speculate that these components could originate from independent backreaction in the A and B branches.

Figure 15B shows the flash-induced kinetics of $P700^+$ in a wild-type PS I core devoid of the F_A and F_B iron–sulfur clusters (prepared by chemically removing PsaC from the wild-type with urea). The stretched multiexponential fit of the kinetics shows 4 different components with lifetimes of 11.6 μsec (0.73), 192 μsec (0.73), 971 μsec (0.85), and 426 msec (0.49), and amplitudes ca. 20%, 20%, 48%, and 5%, respectively.

The main kinetic phase with ~1.0 msec lifetime has been shown by optical and EPR spectroscopy to represent the backreaction of $P700^+$ with F_X^- (Golbeck, 1995), and agrees with the lifetime of $P700^+$ measured in a *psaC* interruption mutant in *Synechocystis* sp. PCC 6803 (Yu et al., 1995). The kinetic phases of 12 and ca. 200 μsec in a 1:1 ratio represents the backreaction of $P700^+$ with A_1^- (Vassiliev et al., 1997) in PS I complexes in which F_X has inadvertently been destroyed. The small kinetic phase with lifetime of 426 msec probably represents a population of PS I complexes in which PsaC has not been removed.

Figure 15C shows the kinetics of flash-induced changes of P700 in wild-type (phylloquinone-containing) PS I complexes from *Synechocystis* sp. PCC 6803. When fitted with the stretched exponentials, the kinetics show three components with lifetimes of 2.2 msec (0.94), 107 msec (0.93) and 2.0 sec (0.76) with relative amplitudes of ca. 5%, 68%, and 28%, respectively. The main 107 msec component is due to the backreaction of $P700^+$ with $[F_A/F_B.]^-$. The minor, 2.2 msec kinetic phase may be due to PS I complexes in which PsaC has been lost during isolation (compare with panel B). The 2.0 s kinetic phase is due to forward electron donation by DCPIP in PS I complexes in which the electron has been lost from the iron–sulfur clusters (Vassiliev et al., 1997).

By comparing the results of three data sets shown in Fig. 15, one can see a progressive acceleration of the $P700^+$ dark relaxation with increasing the number of iron–sulfur clusters inactivated. The lifetime of $P700^+$ dark relaxation is changing from ~0.1 sec in the integral complex with all iron–sulfur clusters present to ~ 0.3 msec in PS I complexes without F_A and F_B and to ~20 μsec in PS I complexes without any of the iron–sulfur clusters. The significant difference between these lifetimes allows the identification of similar components in mutant PS I complexes.

1. Flash-Induced Reactions of PS I in the Absence of All of the Iron–Sulfur Clusters

In the case where all iron–sulfur clusters including F_X are removed, A_1 serves as the terminal electron acceptor. In this case Eq. (27) can be written as follows:

$$(k_P)_{noF_X} \approx \underbrace{k_{PP} e^{\Delta G_{PA_1}/RT}}_{A_1 \to A_0 \to P^* \to P} + \underbrace{k_{A_0P} e^{\Delta G_{A_0A_1}/RT}}_{A_1 \to A_0 \to P} + \underbrace{k_{A_1P}}_{A_1 \to P} \quad (36)$$

Setting here the rate constants and free energy gaps shown in Fig. 14 ($1/k_{PP} = 1$ nsec; $1/k_{A_0P} = 30$ nsec; $1/k_{A_1P} = 21$ μsec; $\Delta G_{PA_1} = -550$ mV; $\Delta G_{A_0A_1} \approx -250$ mV), gives the following estimate for the rate constant of $P700^+$ dark reduction in the absence of F_X:

$$(k_P)_{noF_X} \approx \underbrace{0.68}_{A_1 \to A_0 \to P^* \to P} + \underbrace{2271}_{A_1 \to A_0 \to P} + \underbrace{47619}_{A_1 \to P} \approx 5 \cdot 10^4\ \mathrm{sec}^{-1} \quad (37)$$

Thus, for this set of values, the main route of backreaction is the direct electron transfer from A_1 to $P700^+$ with lifetime of ~20 μsec.

The presence of two components of backreaction in $P700^+$ dark relaxation with lifetimes of ca. 10 and 100 μsec with approximately equal amplitude (Fig. 15A) could indicate that both branches are active in the backward electron transfer. The closeness of the stretch factors for each of these to 1 also indicate that observed kinetics could originate from mixture of two independent populations. Figure 16 shows possible origin of the two components of $P700^+$ dark relaxation in the absence of all iron–sulfur clusters.

2. Kinetics of $P700^+$ in the Presence of F_X Only

In the absence of PsaC, F_X serves as the terminal electron acceptor. In our kinetic analysis of the reactions in PS I we assume, for simplicity, that the absence of PsaC does not influence the thermodynamic or kinetic properties of F_X, and that the absence of F_X does not influence the thermodynamic and kinetic properties of A_1. Figure 17 shows the scheme of respective flash-induced transitions.

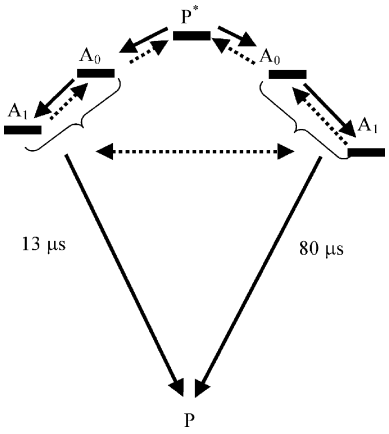

Fig. 16. Scheme indicating the possible origin of the two components of $P700^+$ reduction in wild-type PS I in the absence of the iron–sulfur clusters.

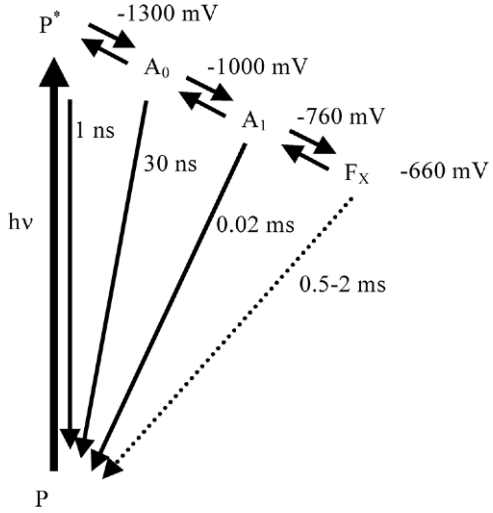

Fig. 17. Scheme of $P700^+$ dark reduction in wild-type PS I in the absence of PsaC.

In the case when F_X serves as the terminal electron acceptor, the Eq. (27) transforms as follows:

$$(k_P)_{noF_AF_B} \approx \underbrace{k_{PP}e^{\Delta G_{PF_X}/RT}}_{F_X\to A_1\to A_0\to P^*\to P} + \underbrace{k_{A_0P}e^{\Delta G_{A_0F_X}/RT}}_{F_X\to A_1\to A_0\to P} + \underbrace{k_{A_1P}e^{\Delta G_{A_1F_X}/RT}}_{F_X\to A_1\to P} \quad (38)$$

As before, this equation indicates the various routes of electron transfer that contribute to the $P700^+$ decay. In further calculations, following values for the rate constants and free energy gaps shown in Fig. 14 were used: $1/k_{PP} = 1$ nsec; $1/k_{A_0P} = 30$ nsec; $1/k_{A_1P} = 21$ μsec; $\Delta G_{PF_X} = -650$ mV; $\Delta G_{A_0F_X} = -350$ mV; $\Delta G_{A_1F_X} = -100$ mV.

The kinetics of the $A_1^- \to P^+$ transition are described by two components with ca. 10 and 100 μsec lifetimes (see Fig. 15, panel A). The nature of these components is not clear. As an initial approximation, we can use the average time for the $A_1^- \to P^+$ transition, obtained according to equation $1/\tau^{av}_{A_1P} = k^{av}_{A_1P} = (k^1_{A_1P}\cdot p_1 + k^2_{A_1P}\cdot p_2)/(p_1+p_2)$, where $\tau^1_{A_1P} = 1/k^1_{A_1P}$, $\tau^2_{A_1P} = 1/k^2_{A_1P}$ are time constants of the stretched multiexponential fit of the kinetics of $P700^+$ reduction by A_1^-, and p_1, p_2 are their amplitudes. The $\tau^{av}_{A_1P}$ is 20.7 μsec for a PS I core from the *rubA* mutant lacking F_X, F_A, and F_B (Fig. 15A). Thus, we employ 21 μsec for the $A_1^- \to P^+$ transition.

Setting these parameters in Eq. (38), gives the following estimate for the rate constant of $P700^+$ dark reduction in the absence of F_A and F_B:

$$(k_P)_{noF_AF_B} \approx \underbrace{0.01}_{F_X\to A_1\to A_0\to P^*\to P} + \underbrace{49}_{F_X\to A_1\to A_0\to P} + \underbrace{1026}_{F_X\to A_1\to P} \approx 1075 \quad (39)$$

Equation (39) shows that the main route of the P^+ dark reduction ($\geq$90%) is due to electron transfer from A_1^- to $P700^+$. The estimated rate constant $(k_P)_{noF_AF_B}$ corresponds to a lifetime of ca. 1 msec, which is identical to the measured value in a PsaC-deficient PS I core (Fig. 15B). Thus, in the PS I complexes in the absence of F_A and F_B, Eq. (38) is simplified significantly:

$$(k_P)_{noF_A/F_B} \approx k_{A_1P}e^{\Delta G_{A_1F_X}/RT} \quad (40)$$

3. Kinetics in the Presence of All of the Iron–Sulfur Clusters

Assuming for simplicity that $\Delta G_{PF_A} \approx \Delta G_{PF_B}$, we can write Eq. (27) in the form (Shinkarev et al., 2002):

$$2(k_P)_{F_AF_B} \approx \underbrace{k_{pp}e^{\Delta G_{PF_A}/RT}}_{F_A\to F_X\to A_1\to A_0\to P^*\to P} + \underbrace{k_{A_0P}e^{\Delta G_{A_0F_A}/RT}}_{F_A\to F_X\to A_1\to A_0\to P} + \underbrace{k_{A_1P}e^{\Delta G_{A_1F_A}/RT}}_{F_A\to F_X\to A_1\to P} \quad (41)$$

Setting rate constants and free energy gaps shown in Fig. 14A ($1/k_{PP} = 1$ nsec; $1/k_{A_0P} = 30$ nsec; $1/k_{A_1P} = 21$ μsec; $\Delta G_{PF_A} = -755$ mV; $\Delta G_{A_0F_A} = -455$ mV; $\Delta G_{A_1F_A} = -205$ mV) in Eq. (41), gives the following

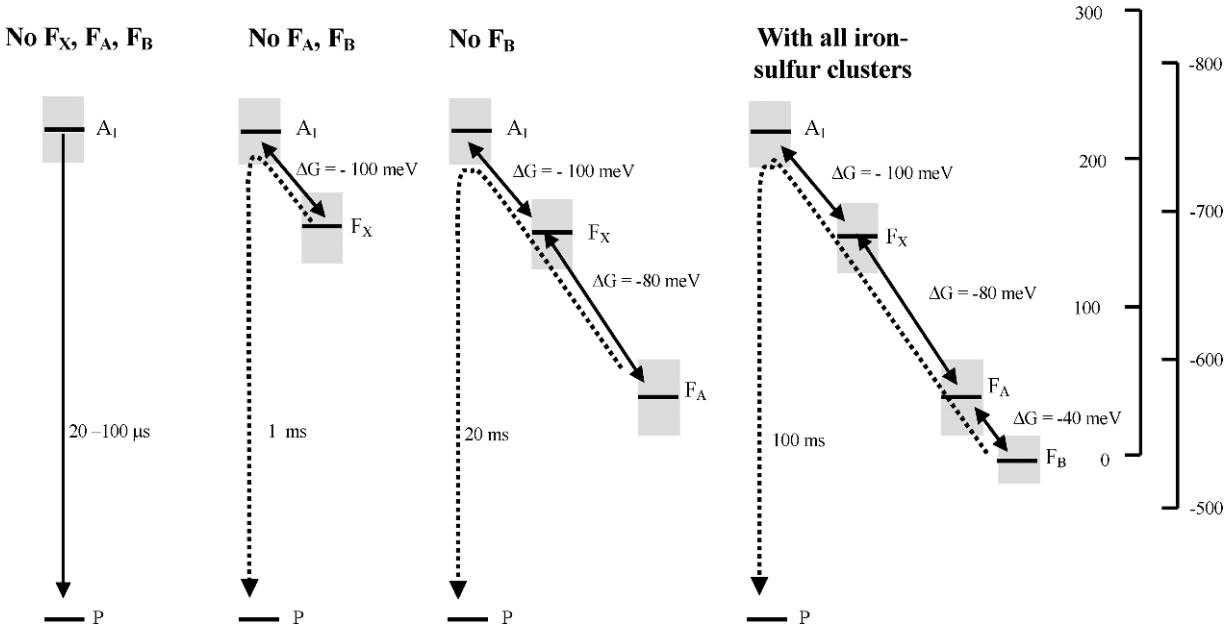

Fig. 18. Schemes of electron transport in wild-type PS I complexes with different subsets of iron–sulfur clusters at room temperature based on the analysis of the $P700^+$ dark relaxation. Two different energetic scales are shown. One is the relative scale with zero at the level of F_B. Only this scale is determined from the kinetics of $P700^+$ dark reduction considered here. The other is an absolute (but less certain) scale. This scale takes into account the known midpoint potential of F_B independently determined by redox titration. The subdivision of the free energy difference of ca. −200 meV between A_1 and F_A/F_B into smaller free energy differences is based on the effect of mercury chloride on the kinetics $P700^+$ (see, e.g., Shinkarev et al., 2000). Shaded boxes indicate the uncertainty in the values of the estimated midpoint redox potentials due to the heterogeneity of the observed kinetics.

estimate for the rate:

$$(k_P)_{F_AF_B} \approx (0 + \underbrace{0.9}_{F_A/F_B\to F_X\to A_1\to A_0\to P} + \underbrace{18.2}_{F_A/F_B\to F_X\to A_1\to P})/2 \approx 9.6\,\mathrm{sec}^{-1} \quad (42)$$

Equation (42) shows that the main route of the P^+ dark reduction is due to electron transfer from F_A/F_B to A_1 and then to P700, whereas the routes involving A_0 and P^* constitute less than 10%. The lifetime given by Eq. (42) is ca. 105 msec, which is close to the 107 msec value shown experimentally (Fig. 15C).

Thus, in case of wild-type PS I in the presence of DCPIP and ascorbate, Eq. (41) is simplified to the following approximate expression for the rate constant of $P700^+$ dark reduction:

$$(k_P)_{F_AF_B} \approx \frac{k_{A_1P}e^{\Delta G_{A_1F_A}/RT}}{2} \quad (43)$$

Using this equation we can estimate free energy gap between A_1 and F_A/F_B for $1/(k_P)_{F_AF_B} = 108$ msec and $1/k_{A_1P} = 0.021$ msec:

$$\Delta G_{A_1F_A} \approx 60 \cdot \log\left(\frac{2(k_P)_{F_AF_B}}{k_{A_1P}}\right) \approx -205\,\mathrm{mV} \quad (44)$$

Figure 18 shows estimated free energy differences in wild-type PS I complexes with different subsets of iron–sulfur clusters at room temperature based on the analysis of the $P700^+$ dark relaxation.

D. Numerical Modeling of Electron Transfer in PS I

While an analytical solution of respective differential equations can give significant insight into the general principles of RC operation, it frequently cannot be used for detailed description of electron transport in RCs, because the used approximations do not work, or too detailed information is needed. In this case, an analytical analysis should be complemented with a numerical analysis of the respective differential equations. We used such an approach to describe electron transport in wild-type PS I complexes with an intact set or a subset of iron–sulfur clusters F_X, F_B, and F_A^*.

*Figure 18 reflects the observation that $HgCl_2$ accelerates the kinetics of dark relaxation of $P700^+$. In a control sample, the lifetime of the main component is ∼107 msec, while in the $HgCl_2$ treated sample the lifetime is shortened to ∼20 msec. If we

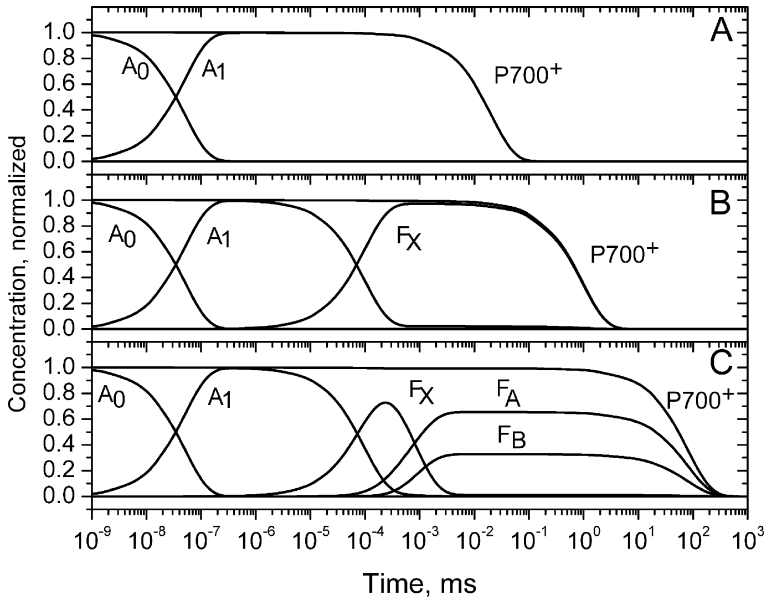

Fig. 19. The theoretical time dependence of the relative concentrations of different electron carriers of the PS I complexes with different subsets of iron–sulfur clusters [none – (panel A), F_X only – (panel B), and intact set – (panel C)]. Rate and equilibrium constants used in calculation are shown in Table 1. The rate constant for the backward transition between two states was calculated from the forward rate constant and the respective equilibrium constant, which was estimated from the free energy difference for these two states. In simulating the effect of the removal of PsaC, we assume $k_{F_XF_A} = 0$ to reflect that both F_A and F_B are absent. Similarly, we assume $k_{A_1F_X} = 0$ in the case when all iron–sulfur clusters are absent. Adapted from Shinkarev et al. (2002).

Figure 19 shows a series of theoretical curves calculated by solving a respective system of linear differential equations that describe the flash-induced transitions between different states in PS I depicted in Fig. 14:

$$d[A_1^-]/dt = -(k_{A_1P} + k_{A_1A_0} + k_{A_1F_X})[A_1^-] + k_{A_0A_1}[A_0^-] + k_{F_XA_1}[F_X^-], \text{ etc.}, \quad (45)$$

where $[A_0^-]$, $[A_1^-]$, $[F_X^-]$ are the relative (per PS I complex) concentrations of the PS I states with reduced A_0, A_1, and F_X, respectively. This system of stiff differential equations was solved using Matlab software. As initial conditions for this system, we assumed that A_0 is completely reduced after the short flash of light, i.e., $[A_0^-(0)] = 1$. The values of rate constants and free energy differences used for calculations are summarized in Table 1.

Table 1. Values of the time constants and free energy differences for PS I, used in the calculations of Fig. 19

	WT with F_X, F_B, F_A	WT with F_X only	RubA (no F_X, F_B, F_A)
$1/k_{PP}$	1 nsec	1 nsec	1 nsec
$1/k_{A_0A_1}$	50 psec	50 psec	50 psec
$1/k_{A_1F_X}$	100 nsec	100 nsec	0
$1/k_{F_XF_A}$	800 nsec	0	–
$1/k_{F_AF_B}$	500 nsec	500 nsec	500 nsec
$1/k_{F_BF_A}$	250 nsec	–	–
$1/k_{A_0P}$	30 nsec	30 nsec	30 nsec
$1/k_{A_1P}$	21 μsec	21 μsec	21 μsec
$1/k_{F_XP}$	500 msec	500 msec	–
$\Delta G_{A_0A_1}$	−250 mV	−250 mV	−250 mV
$\Delta G_{A_1F_X}$	−100 mV	−100 mV	–
$\Delta G_{F_XF_A}$	−105 mV	–	–

The numerical solution of the respective system of differential equations for particular set of rate and equilibrium constants for PS I with different sets of iron–sulfur clusters allows visualization of general behavior of acceptor side of PS I and is in semiquantitative agreement with experimental results depicted in Fig. 15.

interpret the acceleration of P700 dark relaxation in the $HgCl_2$ treated sample as indication of the difference in the midpoint potentials of F_A and F_B, we can estimate that equilibrium constant between F_A and F_B is approximately 105/20∼5. This corresponds to the energy difference of ∼40 mV at room temperature, as shown in the figure. This value evidently contradicts to the low-temperature measurements where the potential for F_B is lower than that for F_A.

V. Conclusions

The initial events of photosynthesis occur in specialized membrane-bound pigment–protein complexes called RCs. The structures of RCs, including PS II and PS I, have been determined at atomic resolution. All RCs with known structure have a porphyrin–quinone core. The general outline of photosynthetic RCs includes two symmetrically arranged branches of six porphyrin derivatives and two quinones. The porphyrin–quinone core in different RCs is coupled with specific donors, acceptors, and light-harvesting antenna. RCs can use both water-soluble and lipid-soluble donors and acceptors. The electron exchange of RCs with these donors and acceptors occurs via specialized processing sites responsible for recognition of respective donor-acceptor, and for channeling the electrons and protons in and out of the complex.

A construction of the appropriate quantitative model should recognize two different approaches to the description of electron transport. One is based on the assumption that carriers are mobile and their interactions occur according to the mass action law. The other, predominantly used for analysis of RCs, is based on the assumption that carriers are arranged in complexes. These approaches are not necessarily exclusive, and it is often appropriate to use them in parallel, depending on the application, especially for quantitative description of electron exchange with an RC.

The quantitative models considered here constitute a basis for the analytical and numerical description of flash-induced kinetics of electron transfer in native and mutant RCs.

In many cases the two-state model provides quite accurate insight into the flash-induced relaxation of RCs. The two main advantages of the two-state model are its simplicity and the availability of an exact analytical solution.

We considered here the *spreading of equilibrium* model, according to which the time evolution of RCs after primary charge separation occurs via waves of quasi-equilibrium. By choosing the certain time scale of consideration one can effectively describe the kinetics of flash-induced electron transport in RCs.

In our analysis of the relaxation of charge-separated states in RCs we included all parallel pathways of electron transfer from reduced acceptor species to the oxidized primary donor. This approach has wide applications for the description of the flash-induced kinetics of primary donor in RCs of purple bacteria and PS I. Here we used this approach to describe the kinetics of $P700^+$ in different PS I preparations that contains either an intact set, or a subset, of iron–sulfur clusters.

Among all RCs the only PS II can use light energy to oxidize water (with the release of oxygen and protons) and to reduce plastoquinone (with the uptake of protons). The Kok model, which describes the period four oscillations in oxygen evolution, has been successfully used for over 30 years for the interpretation of experimental data. Because a simple analytical solution for the Kok model was unknown, many indirect quantitative methods were developed to estimate the values of the parameters of the Kok model. Here we described a recently found simple analytical solution for the Kok model. The solution significantly simplifies the fitting of the experimental data via non-linear regression analysis. Using the Kok model we were able to quantitatively describe binary oscillations of the secondary acceptor semiquinone at the acceptor side of the RC of PS II and the release of reducing equivalents to the b_6f complex. The developed models for the simultaneous description of the individual S-states, oxygen evolution and states of acceptor quinones constitute a basis for quantitative analysis of the charge accumulation processes at the donor and acceptor sides of PS II.

The analytical description of the kinetics in RCs can be complemented by a numerical analysis of the respective differential equations. Here we used such an approach to describe electron transport in PS I complexes with an intact set or a subset of iron–sulfur clusters F_X, F_B, and F_A.

Acknowledgments

I am grateful to John Golbeck and Ilya Vassiliev for many stimulating discussions. This work was partially supported by NIH grant GM 53508.

References

Agalarov R and Brettel K (2003) Temperature dependence of biphasic forward electron transfer from the phylloquinone(s) A_1 in Photosystem I: only the slower phase is activated. Biochim Biophys Acta 1604: 7–12

Alvarez F, Alegría A and Colmenero J (1991) Relationship between the time-domain Kohlrausch–Williams–Watts and frequency-domain Havriliak–Negami relaxation functions. Phys Rev B 44: 7306–7312

Arata H and Parson WW (1981) Delayed fluorescence from *Rhodopseudomonas sphaeroides* reaction centers: enthalpy and free energy changes accompanying electron transfer from P870 to quinone. Biochim Biophys Acta 638: 201–209

Blankenship RE (1992) Origin and early evolution of photosynthesis. Photosynth Res 33: 91–111

Blankenship RE (2002) Molecular Mechanisms of Photosynthesis. Blackwell Science, Oxford

Bouges-Bocquet B (1973) Electron transfer between the two photosystems in spinach chloroplasts. Biochim Biophys Acta 314: 250–256

Brettel K (1997) Electron transfer and arrangement of the redox cofactors in Photosystem I. Biochim Biophys Acta 1318: 322–373

Brettel K and Golbeck JH (1995) Spectral and kinetic characterization of electron acceptor A_1 in a Photosystem I core devoid of iron–sulfur clusters F_X, F_B and F_A. Photosynth Res 45: 183–193

Brettel K and Leibl W (2001) Electron transfer in Photosystem I. Biochim Biophys Acta 1507: 100–114

Ermler U, Fritzsch G, Buchanan SK and Michel H (1994) Structure of the photosynthetic reaction centre from *Rhodobacter sphaeroides* at 2.65 Å resolution: cofactors and protein–cofactor interactions. Structure 2: 925–936

Ferreira KN, Iverson TM, Maghlaoui K, Barber J and Iwata S (2004) Architecture of the photosynthetic oxygen-evolving center. Science 303: 1831–1838

Fromme P, Jordan P and Krauß N (2001) Structure of Photosystem I. Biochim Biophys Acta 1507: 5–31

Gnedenko B, Belyayev Y and Solovyev AD (1969) *Mathematical Methods of Reliability Theory*. Academic Press, New York

Golbeck JH (1995) Resolution and reconstitution of Photosystem I. In: Song PS and Horspeels W (eds) CRC Handbook of Organic Photochemistry and Photobiology, pp 1423–1433. CRC Press Boca Raton, FL

Golbeck JH (1999) A comparative analysis of the spin state distribution of *in vivo* and *in vitro* mutants of PsaC. A biochemical argument for the sequence of electron transfer in Photosystem I as $F_X \rightarrow F_A \rightarrow F_B \rightarrow$ ferredoxin/flavodoxin. Photosynth Res 61: 107–149

Golbeck JH (2003) The binding of cofactors to Photosystem I analyzed by spectroscopic and mutagenic methods. Annu Rev Biophys Biomol Struct 32: 237–256

Gray HB and Winkler JR (1996) Electron transfer in proteins. Annu Rev Biochem 65: 537–561

Guergova-Kuras M, Boudreaux B, Joliot A, Joliot P and Redding K (2001) Evidence for two active branches for electron transfer in photosystem I. Proc Natl Acad Sci USA 98: 4437–4442

Hangulov SV, Golfield MG and Blumenfeld LA (1974) To mechanism of phototransfer of electron in plant chloroplasts. Proc Natl Acad Sci USSR 218: 726–730

Hill TL (1977) Free Energy Transduction in Biology. Academic Press, New York

Itoh S, Iwaki M and Ikegami I (1987) Extraction of vitamin K_1 from Photosystem I particles by treatment with diethyl ether and its effects on the A_1^- EPR signal and system I photochemistry. Biochim Biophys Acta 893: 508–516

Iwaki M and Itoh S (1991a) Function of quinones and quinonoids in green-plant Photosystem I reaction center. Adv Chem Ser 228: 163–178

Iwaki M and Itoh S (1991b) Structure of the phylloquinone-binding (Q_ϕ) site in green plant photosystem I reaction centers: the affinity of quinones and quinonoid compounds for the Q_ϕ site. Biochemistry 30: 5347–5352

Iwaki M and Itoh S (1994) Reaction of reconstituted acceptor quinone and dynamic equilibration of electron transfer in the photosystem I reaction center. Plant and Cell Physiol 35: 983–993

Iwaki M, Kumazaki S, Yoshihara S, Erabi T and Itoh S (1996) ΔG° dependence of the electron transfer rate in the photosynthetic reaction center of plant Photosystem I: natural optimization of reaction between chlorophyll a (A_0) and quinone. J Phys Chem B 100: 10802–10809

Johnson TW, Shen G, Zybailov B, Kolling D, Reategui R, Beauparlant S, Vassiliev IR, Bryant DA, Jones AD, Golbeck JH and Chitnis PR (2000) Recruitment of a foreign quinone into the A1 site of photosystem I. I. Genetic and physiological characterization of phylloquinone biosynthetic pathway mutants in *Synechocystis* sp. PCC 6803. J Biol Chem 275: 8523–8530

Johnson TW, Zybailov B, Jones AD, Bittl R, Zech S, Stehlik D, Golbeck JH and Chitnis P (2001) Recruitment of a foreign quinone into the A_1 site of Photosystem I. *In vivo* replacement of plastoquinone-9 by media-supplemented naphthoquinones in phylloquinone biosynthetic pathway mutants of *Synechocystis* sp. PCC 6803. J Biol Chem 24: 39512–39521

Joliot P and Kok B (1975) Oxygen evolution in photosynthesis. In: Govindjee (ed) Bioenergetics of Photosynthesis, pp 388–413. Academic Press, New York

Joliot P, Barbieri G and Chabaud R (1969) Un nouveau modèle des centers photochimiques du système II. Photochem Photobiol 10: 309–329

Joliot P, Joliot A, Bouges B and Barbieri G (1971) Studies of system II photocenters by comparative measurements of luminescence, fluorescence and oxygen emission. Photochem Photobiol 14: 287–305

Joliot P, Vermeglio A and Joliot A (1993) Supramolecular membrane protein assemblies in photosynthesis and respiration. Biochim Biophys Acta 1141: 151–174

Jordan P, Fromme P, Witt HT, Klukas O, Saenger W and Krauß N (2001) Three dimensional structure of Photosystem I at 2.5 Å resolution. Nature 411: 909–917

Kamiya N and Shen JR (2003) Crystal structure of oxygen-evolving Photosystem II from *Thermosynechococcus vulcanus* at 3.7 Å resolution. Proc Natl Acad Sci USA 100: 98–103

Ke B (2001) Photosynthesis: Photobiochemistry and Photobiophysics. Advances in Photosynthesis and Respiration. Kluwer Academic Publishers, Dordrecht, The Netherlands

Ke B, Demeter S, Zamaraev KI and Khairutdinov RF (1979) Charge recombination in Photosystem I at low temperatures. Kinetics of electron tunneling. Biochim Biophys Acta 545: 265–284

Kleinfeld D, Okamura MY and Feher G (1984) Electron-transfer kinetics in photosynthetic reaction centers cooled to cryogenic temperatures in the charge-separated state: Evidence for light-induced structural changes? Biochemistry 23: 5780–5786

Klukas O, Schubert WD, Jordan P, Krauß N, Fromme P, Witt HT and Saenger W (1999a) Localization of two phylloquinones, Q_K and Q'_K, in an improved electron density map of photosystem I at 4-Å resolution. J Biol Chem 274: 7361–7367

Klukas O, Schubert WD, Jordan P, Krauß N, Fromme P, Witt HT and Saenger W (1999b) Photosystem I, an improved model of the stromal subunits PsaC, PsaD, and PsaE. J Biol Chem 274: 7351–7360

Kohlrausch R (1854) Theorie des elektrischen Rückstandes der Leidner Flasche. Poggendorf Ann Phys Chem 91: 56–82

Kohlrausch R (1863) Über die elastiche Nachwirkung bei der Torsion. Poggendorf Ann Phys Chem 119: 337–368

Kok B, Forbush B and McGloin M (1970) Cooperation of charges in photosynthetic O_2 evolution – I. A linear four step mechanism. Photochem Photobiol 11: 467–475

Krauß N (2003) Mechanisms for Photosystems I and II. Curr Opin Chem Biol 7: 540–550

Kriegl JM, Forster FK and Nienhaus GU (2003) Charge recombination and protein dynamics in bacterial photosynthetic reaction centers entrapped in a sol–gel matrix. Biophys J 85: 1851–1870

Lancaster CRD and Michel H (2001) Photosynthetic reaction centers of purple bacteria. In: Messerschmidt A, Huber R, Poulos T and Wieghardt K (eds) Handbook of Metalloproteins, pp 119–135. John Wiley & Sons, Ltd, Chichester

Likhtenshtein GI (1988) Chemical Physics of Redox Metalloenzyme Catalysis. Springer-Verlag, Berlin

Marcus RA and Sutin N (1985) Electron transfer in chemistry and biology. Biochim Biophys Acta 811: 265–322

McMahon BH, Muller JD, Wraight CA and Nienhaus GU (1998) Electron transfer and protein dynamics in the photosynthetic reaction center. Biophys J 74: 2567–2587

Moser CC, Page CC, Farid R and Dutton PL (1995) Biological electron transfer. J Bioenerg Biomembr 27: 263–274

Murthy DNP, Xie M and Jiang R (2004) Weibull Models. John Wiley & Sons, Inc, Hoboken, New Jersey

Okamura MY, Paddock ML, Graige MS and Feher G (2000) Proton and electron transfer in bacterial reaction centers. Biochim Biophys Acta 1458: 148–163

Phillips JC (1996) Stretched exponential relaxation in molecular and electronic glasses. Rep Prog Phys 59: 1133–1207

Rubin AB and Shinkarev VP (1984) Electron Transfer in Biological Systems. Nauka, Moscow (in Russian)

Schlodder E, Falkenberg K, Gergeleit M and Brettel K (1998) Temperature dependence of forward and reverse electron transfer from A_1^-, the reduced secondary electron acceptor in photosystem I. Biochemistry 37: 9466–9476

Semenov AY, Vassiliev IR, van der Est A, Mamedov MD, Zybailov B, Shen G, Stehlik D, Diner BA, Chitnis PR and Golbeck JH (2000) Recruitment of a foreign quinone into the A_1 site of photosystem I. Altered kinetics of electron transfer in phylloquinone biosynthetic pathway mutants studied by time-resolved optical, EPR, and electrometric techniques. J Biol Chem 275: 23429–23438

Shen G, Zhao J, Reimer S, Cai Q, Golbeck JH and Bryant DA (2002a) Assembly of [4Fe–4S] clusters in Photosystem I. I. Inactivation of the gene encoding a membrane-associated rubredoxin in the cyanobacterium *Synechococcus* sp. PCC 7002. J Biol Chem 277: 20343–20354

Shen G, Antonkine ML, van der Est AJ, Vassiliev IR, Brettel K, Zhao J, Stehlik D, Bryant D and Golbeck JH (2002b) Assembly of [4Fe–4S] clusters in Photosystem I. II. Rubredoxin is required for assembly of F_X as shown by optical and EPR spectroscopy. J Biol Chem 277: 20355–20366

Shinkarev VP (1990) Function of quinones in bacterial photosynthesis. In: Advances in Science and Technology, Biophysics Series, Chamorovsky, SK (ed) Vol 35, pp 1–205. VINITI, Moscow (in Russian)

Shinkarev VP (1996) Binary oscillations in the Kok model of oxygen evolution in oxygenic photosynthesis. Photosynth Res 48: 411–417

Shinkarev VP (1998) The general kinetic model of electron transfer in photosynthetic reaction centers activated by multiple flashes. Photochem Photobiol 67: 683–699

Shinkarev VP (2003) Oxygen evolution in photosynthesis: simple analytical solution for the Kok model. Biophys J 85: 435–441

Shinkarev VP (2005) Flash-induced oxygen evolution in photosynthesis. Simple solution for the extended S-state model that includes misses, double hits, inactivation and backward transitions. Biophys J 88: 412–421

Shinkarev VP and Venediktov PS (1977) Stochastic description of the processes of electron transfer in molecular complexes. Biophysics (USSR) 22: 413–417

Shinkarev VP and Wraight CA (1993a) Electron and proton transfer in the acceptor quinone complex of reaction centers of phototrophic bacteria. In: Deisenhofer J and Norris J (eds) The Photosynthetic Reaction Center, Vol 1, pp 193–255. Academic Press, New York

Shinkarev VP and Wraight CA (1993b) Oxygen evolution in photosynthesis: from unicycle to bicycle. Proc Natl Acad Sci USA 90: 1834–1838

Shinkarev VP and Wraight CA (1993c) Kinetic factors in the bicycle model of oxygen evolution by Photosystem II. Photosynth Res 38: 315–321

Shinkarev VP, Verkhovsky MI, Kaurov BS and Rubin AB (1981) The kinetic model of two-electron gate in photosynthetic RCs of purple bacteria. Mol Biol (USSR) 15: 1069–1082

Shinkarev VP, Vassiliev IR and Golbeck JH (2000) A kinetic assessment of the sequence of electron transfer from F_X to F_A and further to F_B in Photosystem I. The value of the equilibrium constant between F_X and F_A. Biophys J 78: 363–372

Shinkarev VP, Zybailov B, Vassiliev IR and Golbeck JH (2002) Modeling of the $P700^+$ charge recombination kinetics with phylloquinone and plastoquinone-9 in the A_1 site of Photosystem I. Biophys J 83: 2885–2897

Sturman B, Podivilov E and Gorkunov M (2003) Origin of stretched exponential relaxation for hopping-transport models. Phys Rev Lett 19 (17): 176602

Vassiliev IR, Jung YS, Mamedov MD, Semenov AY and Golbeck JH (1997) Near-IR absorbance changes and electrogenic reactions in the microsecond-to-second time domain in photosystem I. Biophys J 72: 301–315

Vassiliev IR, Antonkine M and Golbeck JH (2001a) Iron–sulfur clusters in type I reaction centers. Biochim Biophys Acta 1507: 139–160

Vassiliev IR, Kjær B, Schorner G, Scheller HV and Golbeck JH (2001b) Photoinduced transient absorbance spectra of P840/$P840^+$ and the FMO protein in reaction centers of *Chlorobium vibrioforme*. Biophys J 81: 382–393

Velthuys BR and Amesz J (1974) Charge accumulation at the reducing side of Photosystem 2 of photosynthesis. Biochim Biophys Acta 333: 85–94

Verkhovskii MI, Kaurov BS, Rubin AB and Shinkarev VP (1981) Kinetics of ubisemiquinone redox changes in primary reactions of bacterial photosynthesis. Mol Biol (USSR) 15: 589–600

Weiss C and Sauer K (1970) Activation kinetics of photosynthetic oxygen evolution under 20–40 nanosecond laser flashes. Photochem Photobiol 11: 495–501

Williams G and Watts DC (1970) Non-symmetrical dielectric relaxation behavior arising from a simple empirical decay function. Trans Faraday Soc 66: 80–83

Wong J and Angell CA (1976) Glass Structure by Spectroscopy. Dekker, New York

Woodbury NW and Allen JP (1995) The pathway, kinetics and thermodynamics of electron transfer in wild type and mutant bacterial reaction centers of purple nonsulfur bacteria. In: Blankenship RE, Madigan MT and Bauer CE (eds) Anoxygenic Photosynthetic Bacteria, pp 527–557. Kluwer Academic Publishers, Dordrecht

Woodbury NW and Parson WW (1984) Nanosecond fluorescence from isolated photosynthetic reaction centers of *Rhodopseudomonas sphaeroides*. Biochim Biophys Acta 769: 345–361

Yu J, Smart LB, Jung YS, Golbeck JH and McIntosh L (1995) Absence of PsaC subunit allows assembly of photosystem I core but prevents binding of PsaD and PsaE in *Synechocystis* sp. PCC 6803. Plant Mol Biol 29: 311–342

Zamaraev KI, Khairutdinov RF and Zhadanov VP (1985) Electron Tunneling in Chemistry. Nauka, Novosibirsk (in Russian)

Zouni A, Witt HT, Kern J, Fromme P, Krauß N, Saenger W and Orth P (2001) Crystal structure of Photosystem II from *Synechococcus elongatus* at 3.8 Ångstrom resolution. Nature 409: 739–743

Zybailov B, van der Est A, Zech SG, Teutloff C, Johnson TW, Shen G, Bittl R, Stehlik D, Chitnis PR and Golbeck JH (2000) Recruitment of a foreign quinone into the A_1 site of Photosystem I. II. Structural and functional characterization of phylloquinone biosynthetic pathway mutants by electron paramagnetic resonance and electron-nuclear double resonance spectroscopy. J Biol Chem 275: 8531–8539

Chapter 37

Cyclic Electron Transfer Around Photosystem I

Pierre Joliot* and Anne Joliot
CNRS UMR 7141, Institut de Biologie Physico-Chimique, 13, rue Pierre et Marie Curie, 75005 Paris, France

Giles Johnson
University of Manchester, School of Biological Sciences, 3.614 Stopford Building, Oxford Road, Manchester, M13 9PT, UK

Summary

Cyclic electron transport around Photosystem I remains one of the last great enigmas in photosynthesis research. Although first described in 1955 by Arnon and coworkers, the molecular details of the pathway, its physiological role and even its very occurrence remain in question. Nevertheless, significant progress is starting to be made in our understanding of this process. At least two pathways of cyclic electron transport appear to operate, one involving the transfer of electrons from NADPH to plastoquinone and the other operating via the donation of electrons from ferredoxin to plastoquinone. The relative importance of these two pathways seems to vary between cyanobacteria, unicellular green algae and higher plants as do many details concerning the regulation of the pathway and its functional organization in the thylakoid membrane. Two distinct functions for cyclic electron transport can be defined — the generation of ATP and, in higher plants, the generation of ΔpH to regulate light harvesting. These two functions give rise to the need for different regulatory processes to control the ratio of cyclic and linear electron flow. We discuss recent findings that cast new light on how cyclic electron transport is regulated under a range of physiological conditions.

*Author for correspondence, email: pjoliot@ibpc.fr

John H. Golbeck (ed): Photosystem I: The Light-Driven Plastocyanin:Ferredoxin Oxidoreductase, 639–656.

I. Introduction

The concept of cyclic electron transport (ET) around Photosystem (PS) I is sufficiently established that it features in the diagrams of photosynthetic electron transport found in every undergraduate biochemistry textbook. In spite of this celebrity, the redox components involved, the functional importance, the regulation and, indeed, even the very occurrence of this pathway all remain unclear. Part of the problem in studying cyclic ET has been, that, by its very nature, it is difficult to quantify — as a cycle it involves no net flux and so we are forced to resort to use indirect means to deduce its existence. There is now growing evidence, however, that cyclic ET does indeed occur in a variety of organisms under a wide range of conditions, fulfilling at least two distinct functions. Here, we present a review of this evidence, focusing in particular on advances over the last decade and identifying the challenges that remain. For more detailed coverage of earlier work and alternative views on the subject, a number of good reviews are available (Heber and Walker, 1992; Fork and Herbert, 1993; Bendall and Manasse, 1995; Heber, 2002; Allen, 2003).

II. Early Observations of Cyclic Electron Transfer

Photosynthetic phosphorylation (photophosphorylation) was discovered in 1954 by Arnon et al. (1954) who established that illumination of isolated chloroplasts in the presence of oxygen-induced ATP synthesis. As this process was not associated with oxygen formation or consumption, the contribution of a respiratory chain could be excluded. Later, it was established that the dependence of photophosphorylation on oxygen can be abolished by the addition of vitamin K or other naphthoquinones (Arnon, 1955). This experiment marks the discovery of the cyclic phosphorylation process, (reviewed in Arnon et al., 1961). The reaction previously characterized in 1954 by Arnon and coworkers appears now to be a pseudocyclic process in which electrons are transferred from water to O_2 (Mehler, 1951) via the linear electron transfer chain. Subsequently, nonphysiological compounds, such as phenazine methosulfate (PMS), were shown to catalyze cyclic photophosphorylation more efficiently than vitamin K (Jagendorf and Avron, 1958).

The anaerobic cyclic phosphorylation identified in chloroplasts appeared analogous to a cyclic phosphorylation process previously identified in chromatophores from photosynthetic bacteria (Frenkel, 1954). In *Rhodospirillum rubrum*, this cyclic process was observed to involve cytochrome (cyt) *c* (Smith and Baltscheffsky, 1959); in chloroplasts cyt *f* is involved (Arnon, 1959). In 1960, Hill and Bendall put forward a model describing the linear electron transfer chain involving both the photoreactions PS II and PS I working in series (Hill and Bendall, 1960). It became clear, however, that cyclic photophosphorylation involves only PS I, as it operates in the presence of specific inhibitors of oxygen evolution, such as 3-(3,4-dichloro-phenyl)-1,1-dimethylurea (DCMU). Tagawa et al. (1963b) established that ferredoxin (Fd) was able to catalyze cyclic phosphorylation. This provided evidence for a physiological catalyst of cyclic ET, making it seems likely that this process was more than an artifact of *in vitro* conditions.

III. Possible Pathways of Electron Flow in Cyclic Electron Transfer

There is a general agreement that both PS I and the cyt b/f complex are obligatory involved in cyclic electron flow — cyclic ET is efficiently driven by far-red light and is sensitive to inhibitors of the cyt b/f complex, such as 2,5-dibromo-3-methyl-6-isopropyl-*p*-benzoquinone (DBMIB) and stigmatellin — however, the electron pathway from the acceptor side of PS I back to the cyt b/f complex has not yet been clearly elucidated. Cyclic ET, as conventionally measured, leads to the generation of a trans-thylakoid pH gradient. Thus, whatever the pathway involved a proton-pumping step involving the cyt b/f complex must be postulated.

Based mainly on studies of the effects of the inhibitor antimycin A, it has been postulated that at least two pathways exist. Experiments performed on isolated chloroplasts showed that antimycin inhibits cyclic flow in the presence of Fd (Tagawa et al., 1963b) but not in the presence of vitamin K or PMS (Whatley et al., 1959). Hosler and Yocum (1985) measured the ratio of P/O in the presence of Fd, using oxygen as a terminal electron acceptor and found this to be sensitive to antimycin. They explained this effect as being due to the

Abbreviations: cyt – cytochrome; DBMIB – 2,5-dibromo-3-methyl-6-isopropyl-*p*-benzoquinone; DCMU – 3-(3,4-dichloro-phenyl)-1,1-dimethylurea; ET – electron transport; ETC – electron transfer chain; Fd – ferredoxin; FNR – ferredoxin: NADP oxidoreductase; FQR – ferredoxin: plastoquinone reductase; HQNO – 2-heptyl-4-hydroxy-quinoline N-oxide; NDH – NADH dehydrogenase; PC – plastocyanin; PMS – N-methylphenazonium-3-sulfonate; PQ – plastoquinone; PQH_2 – plastoquinol; PS – Photosystem; RC – reaction center.

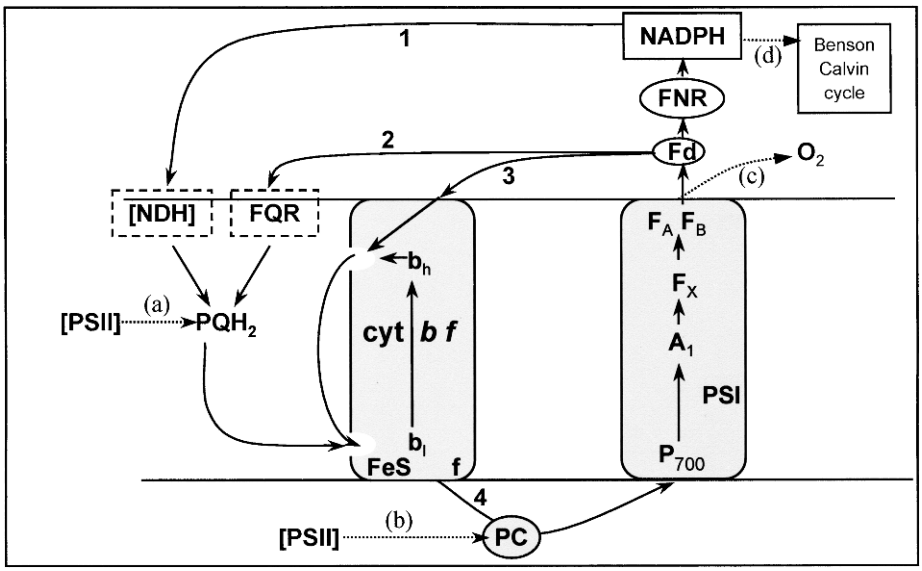

Fig. 1. Possible pathways for cyclic electron flow.

inhibition of cyclic ET. By contrast, when the same experiment was performed using NADP as an electron acceptor, the P/O ratio was high and antimycin-insensitive (Hosler and Yocum, 1985). Scheller (1996) measured the rereduction of P700 following light flashes in the presence of DCMU and noted an antimycin-insensitive portion in Fd-mediated cyclic ET, possibly suggesting a third pathway (Scheller, 1996). However, the very slow rate of this, barely distinguishable from the DBMIB-inhibited rate, makes it hard to separate this from background redox equilibration of the sample. Cleland and Bendall (1992) measured the oxidation of reduced Fd following illumination of DCMU-poisoned thylakoids and found this rate to be inhibited by antimycin A as completely as by stigmatellin (Cleland and Bendall, 1992). One can thus conclude that several mechanisms could be involved in a cyclic ET.

In a conventional Q-cycle process (Mitchell, 1975; Crofts et al., 1983), electrons are transferred to the cyt b/f complex via a reduced quinone that binds site Q_o, on the lumenal side of this complex. Assuming this is the step generating ΔpH in the cyclic process, we need to invoke an enzyme that is able to transfer electrons from NADP or Fd to plastoquinone (PQ), with the resultant plastoquinol (PQH_2) being protonated on the stromal side of the membrane. In cyanobacteria, the presence of respiratory and photosynthetic electron transport chains in the same membrane means that this function could be fulfilled by a respiratory NADH dehydrogenase (NDH; complex I). Genes coding for such an enzyme have also been identified in the chloroplast genome of higher plants (Shinokazi et al., 1986), which is a likely candidate to be involved in the cyclic electron transfer chain (ETC) (Fig. 1, pathway 1).

Moss and Bendall (1984) noted that, whilst both Fd-mediated and artificially mediated cyclic ET are sensitive to the cyt *b* inhibitor 2-heptyl-4-hydroxy-quinoline N-oxide (HQNO), only Fd-mediated cyclic ET was sensitive to antimycin (Moss and Bendall, 1984). This led them to suggest an alternative site for antimycin inhibition on an enzyme distinct from the b/f complex, termed ferredoxin:plastoquinone oxidoreductase (FQR) (Fig. 1, pathway 2).

The involvement of ferredoxin:NADP oxidoreductase (FNR) in cyclic ET has been much discussed. Its involvement in the NADP-dependent pathway is presumed; however, a role in the Fd-dependent pathway has also been postulated. The observation that this enzyme is stoichiometrically bound to the cyt b/f complex in spinach provides an intriguing indication of an additional role, other than that of linear electron transport (Zhang et al., 2001). It is suggested that FNR mediates the transfer of electrons from ferredoxin to site Q_i (Fig. 1, pathway 3).

The mechanisms involved in these different pathways will be discussed in more detail below.

IV. Redox Poising of the Cyclic Electron Transfer Chain

Photochemical charge separation at the level of a reaction center (RC) requires the presence of a reduced primary donor and an oxidized electron acceptor.

Over-reduction or overoxidation of the cyclic chain will thus inhibit this process. The concept of redox poising of the cyclic ETC was introduced to explain the oxygen requirement of cyclic phosphorylation (Tagawa et al., 1963a; Whatley, 1963; reviewed in Allen, 1983). Later, Arnon and Chain (1977) established that a maximum efficiency of the cyclic ET in the presence of oxygen is observed in the presence of NADPH and subsaturating concentrations of DCMU that impose an optimal redox poise of the carriers involved in the cyclic chain (Arnon and Chain, 1977).

Redox poising is determined by the relative rate of electron efflux or influx from or toward the carriers belonging to the cyclic electron transfer chain. Both efflux and influx will occur preferentially at the level of mobile carriers that are common to linear and cyclic chains. PS II will be the main source of reductive power (Fig. 1, pathways a and b) while electron efflux will occur at the level of PS I acceptors toward O_2 and the Benson–Calvin cycle (Fig. 1, pathways c and d, respectively). If we assume that cyclic and linear pathways are connected, i.e., share the same mobile carriers, the redox poise of the cyclic chain will be controlled by the electron flow through the linear chain. Under strong illumination, given under condition where the Benson–Calvin cycle is inhibited (e.g., in isolated thylakoids or dark-adapted leaves), PS II will induce an overreduction of the cyclic chain, via pathway a or b (Fig. 1). Conversely, under conditions where PS II is inhibited or under far-red light, the electron efflux via pathway c or d will induce an overoxidation of the cyclic chain. On the other hand, if the cyclic and linear chains are structurally separated, the redox poise of the cyclic chain will be controlled by the rate of slow electron leaks that occur between carriers involved in both processes. We thus conclude that the structural organization of membrane proteins that controls the localization of the cyclic and linear chains within the membrane may play an essential role in the control of the efficiency of the cyclic process.

V. Structural Organization of Thylakoid Membranes – Consequences for Cyclic Electron Transfer

Oxygenic photosynthetic organisms — higher plants, unicellular algae, and cyanobacteria — differ substantially in the supramolecular organization of their photosynthetic membranes and these differences may have important consequences for the pathway and regulation of cyclic ET.

In higher plants, PS II and PS I are localized in different membrane regions (Andersson and Anderson, 1980). Most of PS II is localized in the appressed regions of the grana stacks while PS I is localized in the stroma lamellae and in the granal end membranes. Unlike PS II and PS I, cyt b/f complex is distributed across all membrane regions (Cox and Andersson, 1981). An open question concerns a possible localization of PS I centers in the margin of the grana stacks (Webber et al., 1988; Anderson, 1989; Albertsson, 1995). Albertsson (2001) put forward the hypothesis that PS I localized in the margin and ends of the grana stacks contributes to the linear pathway while PS I localized in the stroma lamellae contributes to the cyclic pathway (Albertsson, 2001). The localization of PS I and PS II in different membrane regions requires long-range diffusion of the mobile carriers PQ or plastocyanin (PC). A detailed analysis of the kinetics of electron transfer reaction between PS II and the PQ pool has shown that diffusion of PQ is restricted to small heterogeneous domains including an average of three to four RC, a membrane surface much smaller than the size of a grana disk (Joliot et al., 1992; Lavergne et al., 1992; Kirchhoff et al., 2000). It is assumed that the membrane proteins, which occupy more than half of the membrane surface, limit the diffusion of PQ. This implies that PQ is not involved in long distance transfer and that the linear process exclusively involves cyt b/f complexes localized close to PS II, i.e., in the appressed regions. Conversely, the sole role of the cyt b/f complexes localized in the stroma region might be to participate in the cyclic process ("cyclic cyt b/f").

It worth pointing out that, if the photosynthetic apparatus were exclusively devoted to a linear process, one would expect that its optimization during evolution would have led to a random distribution of RCs within the membrane. Such a distribution would minimize the distance between membrane proteins, leading to faster electron exchanges mediated by PQ or PC. Thus, the segregation of PS I and PS II centers in different membrane regions can be taken as a way to separate the carriers involved in the cyclic and the linear flows, which limits redox cross-talk between the cyclic and linear chains. Structural separation between the linear and cyclic processes is pushed to an extreme in the case of C4 plants, in which only a cyclic process operates in bundle sheath cells that mainly include PS I centers (Bassi et al., 1985).

In green unicellular algae, the supramolecular organization of thylakoid membranes significantly differs from that in higher plants. Thylakoid membranes

consist of long flat vesicles (disks) that are generally stacked in groups of 2–4, a much smaller number than that seen in higher plants. Freeze-fracture images suggest that appressed and nonappressed regions are more widely connected than is the case in chloroplasts of higher plants, which are connected by narrow fret junctions. This membrane organization suggests that cyclic and linear pathways could interact more in green algae than in higher plants.

In cyanobacteria, thylakoids membranes are unstacked and appear as isolated flat vesicles. The organization of these membranes differs between species but concentric arrangements of thylakoids are often seen in rod-shaped cells as *Synechococcus* sp. PCC 6803 or filamentous species such as *Phormidium laminosum*. There is evidence from freeze-fracture images of cyanobacterial thylakoid membranes that PS I and PS II are typically found in the same membrane regions — see Mullineaux (1999), although Sherman et al. (1994) noted a slight asymmetry in the distribution of complexes in *Synechococcus* sp. PCC 6803, suggesting a concentration of PS I near to the plasma membranes. Spatial segregation of linear and cyclic chains is thus very unlikely and one expects these pathways to share the same electron carriers. In contrast to photosynthetic eukaryotes, thylakoids in cyanobacteria include a respiratory chain that shares the PQ pool and the cyt b/f complex with the photosynthetic chain (for a review see Schmetteter, 1994). Thus, redox poising of a putative cyclic chain could be controlled by interaction with the linear photosynthetic chain as well as with the respiratory chain. An open question is the nature of the substrate of the NDH enzymes of the respiratory chain—NADH or NADPH—localized in the thylakoids. NADPH-PQ reductase, present at high concentration in the chloroplasts, could itself contribute efficiently to a cyclic process (Fig. 1, pathway 1).

VI. Occurrence of Cyclic Flow in Higher Plants

Work establishing the existence of pathways for cyclic ET has largely been performed in isolated systems, usually thylakoid membranes (broken chloroplasts), with addition of natural or artificial mediators. While such studies are essential in characterizing the pathway of cyclic ET, they leave open the question; does this pathway actually operate under *in vivo* conditions? More specifically, if we are to understand the function of cyclic ET it must be established whether it occurs under normal physiological conditions, where linear ET is also possible.

Many of the studies that have indicated the presence of cyclic ET in intact leaves have used rather indirect means, typically involving conditions that largely or totally suppress PS II turnover. While such studies are valuable, especially in trying to understand the regulation of the cyclic pathway, they do not, in themselves, show that this pathway is able to compete with linear ET.

One commonly used assay taken as evidence for cyclic flux is the measurement of the relaxation of $P700^+$ following illumination of a leaf with a period of far-red light ($\lambda > 695$ nm) or in the presence of a PS II inhibitor, such as DCMU (Maxwell and Biggins, 1976). When a leaf is exposed to far-red light to oxidize P700 and then that light is abruptly cut, typically at least two phases of $P700^+$ reduction can be detected. The half time for the *fast* phase is typically of the order of 200–1,000 msec (Joët et al., 2002). By comparison, in white light, under conditions where PS II is turning over normally, the half time for $P700^+$ reduction is of the order of 10–20 msec. Thus, it seems immediately unlikely that cyclic ET could ever compete effectively with a linear flow that is 10–50 times faster. However, measurements made in the absence of PS II turnover will tend to result the accumulation of electron transfer components (including Fd and NADP) in the oxidized state and so, the half times measured probably represent a gross underestimate of the maximum rate of electron flow from the stroma to $P700^+$. The rate of $P700^+$ reduction varies between different groups of organisms, being slow in plants and especially slow in C3 plants (Herbert et al., 1990; Joët et al., 2002). The rate can, however, be accelerated under certain conditions, for example under anaerobiosis (Joët et al., 2002) or following heat stress (Maxwell and Biggins, 1976; Burrows et al., 1998; Bukhov et al., 1999). The former probably reflects an increase in the reduction state of the chloroplast in the dark, increasing the supply of reductant to re-reduce $P700^+$. In the latter case, it is less clear what gives rise to the effect, it may relate to a temperature induced shift in redox poise or to an "opening up" of redox components to the surrounding medium accelerating their reduction. Recently, Golding et al. (2004), examining the relaxation of $P700^+$ in the presence of the PS II inhibitor DCMU, observed that preillumination of leaves eliminates the fast component of $P700^+$ reduction but that this effect is removed if the leaves are experiencing drought stress. It is suggested that a transient "cyclic-enabled" state existing in the dark is stabilized under drought conditions (Johnson, 2005).

Another parameter that has been taken to indicate cyclic ET is the presence of a transient rise in fluorescence following illumination (Asada et al., 1993; Burrows et al., 1998). When actinic light is removed, the fluorescence yield falls, due to the oxidation of Q_A^-. In some conditions, the yield of fluorescence is seen to rise transiently and then fall again. This effect is attributed to the reduction of the PQ pool by electrons originating from the stroma, indicating that a pathway exists between the stroma and the electron transport chain that could participate in cyclic ET. Such measurements can be made following conditions of steady-state white light, so may reflect better the normal physiological state of the leaf but, as with the decay of $P700^+$, involve processes that are far too slow (several tens of seconds) for them to be supposed to be involved in efficient cyclic ET in competition with linear ET. As with the decay of $P700^+$ following far-red light, this effect is enhanced by exposing plants to heat stress (Sazanov et al., 1998).

Although cyclic ET involves no net flux that can be measured, it does nonetheless have "products" that are measurable, notably the formation of a pH gradient across the thylakoid membrane, which can be evidenced using optical spectroscopy and the storage of light energy, which is measured using the technique of photoacoustics.

Two absorbance signals have been used as indicators of the pumping of protons across the thylakoid membrane during cyclic ET: Proton translocation results in the formation of a transmembrane electrical potential, which can be measured as an apparent absorbance change around 515 nm; and the swelling of the thylakoid membrane that occurs when a ΔpH is generated induces a change in its light scattering properties, giving an apparent absorbance change in the region of 535 nm. Both of these absorbance changes can be observed when leaves are illuminated with far-red light, indicating that cyclic ET is occurring and is generating ΔpH. However, the conditions needed to observe such changes are often quite specific, so again it is difficult to be certain whether the cycling observed is relevant to conditions of steady-state photosynthesis.

Photoacoustics measures pressure waves produced in samples in response to light, which can be interpreted to provide information on energy storage and gas exchange. Photoacoustic signals are complex, with a number of different processes contributing, so it is necessary to design experiments carefully to give any information on cyclic ET. As with most other methods, this often means using far-red light to avoid any contribution from PS II photochemistry. A large number of studies have been published using this approach, often in combination with other approaches. For example (Joët et al., 2002), recently combined measurements of photoacoustics with relaxation of $P700^+$ to investigate the functioning of cyclic ET in tobacco.

In spite of the array of different methods that have been applied in an attempt to determine whether cyclic ET occurs in higher plants, the question still remains controversial. A clear case where cyclic ET is thought to be the norm is in the bundle sheath cells of certain C4 plants, including maize (Herbert et al., 1990; Asada et al., 1993; Joët et al., 2002). In such cells, PS II is largely absent, yet these cells are responsible for the fixation of CO_2 through normal Benson–Calvin cycle activity. By contrast, photosynthesis (and specifically PS II) is not responsible for generating the reducing potential required to drive CO_2 fixation, since this is generated through the oxidation and decarboxylation of malate imported from the mesophyll. Cyclic ET is thought to provide the ATP. Studies using photoacoustics and $P700^+$ reduction kinetics have both provided support for the occurrence of cyclic ET in maize bundle sheath chloroplasts (Herbert et al., 1990; Joët et al., 2002) as have combined measurements of P700 and chlorophyll fluorescence under combinations of far-red and red light (Asada et al., 1993).

In C3 plants, the situation is less clear. As early as 1978, Heber et al. (1978) observed the presence of far red-induced light scattering changes in spinach leaves. This scattering was slow to form however and was inhibited by oxygen. The latter observation can easily be explained in terms of the ability of oxygen to oxidize the acceptor side of PS I. If PS II activity is suppressed, then electrons taking part in the cyclic pathway that are leaked to oxygen cannot be replaced. The cyclic ETC will rapidly become completely oxidized and cyclic ET will stop. This contrasts with the situation in C4 bundle sheath cells, where reductant is available from the decarboxylation of malate, such that, even in the absence of PS II activity, electrons can be reinjected in to the cyclic pathway.

A number of studies have, however, indicated that efficient far red-induced cyclic ET can occur in C3 leaves, however, this requires careful selection of conditions. For example, Katona et al. (1992) observed that, under conditions of CO_2 free air, far-red light was able to efficiently energize chloroplasts in cabbage leaves, as indicated by light scattering changes. This effect was however suppressed by O_2 or CO_2. Heber et al. (1992) performed similar experiments on ivy leaves and reached similar conclusions, with the CO_2 concentration again being crucial. By contrast, the combination of *red* light

(rather than far-red) and low CO_2 and O_2 did not result in chloroplast energization. In other words, conditions giving rise to PS II turnover in the absence of any terminal electron acceptor result in the rapid total reduction of the ETC. Under such conditions, no further electron transport, linear or cyclic, is possible (see section on redox poising above). Taking an alternative approach, Cornic and colleagues observed the effects of periods of actinic illumination on the ability of limiting levels of far-red light to oxidize P700. Even short periods of high light were found to be sufficient to reduce the effectiveness of far-red light in oxidizing P700. This was interpreted as being due to an activation of cyclic ET during high light, feeding electrons back into the ETC via an efficient cyclic pathway (Cornic et al., 2000).

While the above discussion leads to the conclusion that cyclic ET *can* be induced in the leaves of higher plants, it does not tell us whether it *does* occur under conditions of steady-state photosynthesis. Given the low rates of ET that have been measured and the careful poising that is often needed to observe cyclic ET, it is not at all clear that this pathway can compete under conditions where linear ET is feeding electrons into the ETC. To determine whether or not cyclic is a real physiological phenomenon, we need to be able to measure it under conditions of normal photosynthesis.

The most common approach evidencing cyclic ET under conditions of steady-state photosynthesis is to examine the relationship between PS I and PS II electron transport. Given that cyclic ET involves only PS I and linear both PS I and PS II, any change in cyclic ET, *relative to* linear ET will give a change in the ratio of the flux of the two photosystems. Measurements of PS II flux are usually made using analysis of chlorophyll fluorescence. The quantum efficiency of PS II is measured as the parameter ΦPS II (Genty et al., 1989). Multiplying this parameter by the light intensity gives a measure of relative flux. Provided light interception by the PS II antenna remains constant (which might not be the case, e.g., due to state transitions) this parameter is thought to give a robust relative measure of the PS II electron transport rate.

In vivo measurements of PS I electron transport under conditions of steady-state photosynthesis have proved more controversial. A commonly used approach has been to measure the redox state of the P700 pool and to take the extent of reduction of this pool as a measure of the quantum efficiency of PS I. Comparisons of PS I turnover measured in this way with PS II turnover measured by fluorescence have been made at a variety of irradiances and CO_2 concentrations (Harbinson and Foyer, 1991; Harbinson, 1994). These studies have found the relationship between these two parameters to be linear. Thus, it has been concluded that, under most physiological conditions, cyclic ET is either absent in the presence of light or forms a constant proportion of the linear flux. More recent data have however found clear evidence for cyclic electron transport using this approach (Clark and Johnson, 2001; Miyake et al., 2004; Miyake et al., 2005a,b).

The contradictions between the above studies have not yet been fully explained however probably relate to the measuring conditions or the physiological status of the plants concerned. Observations of cyclic ET have been made under conditions where the supply of CO_2 to the leaf is restricted. For example, Harbinson and Foyer (1991) observed that the relationship between PS I and PS II quantum efficiency (using light as a variable) was different in CO_2 free air to that seen in the presence of CO_2. Gerst et al. (1995) observed that, upon imposing drought stress upon a leaf in the light, PS II was more sensitive to inhibition than PS I. By contrast, however, in experiments where a leaf was exposed to varying CO_2, the relationship between PS I and PS II efficiency was found to be linear, extrapolating to the origin (Harbinson, 1994). Thus any cyclic flow that occurs must be in proportion to linear flow. In a similar experiment, Golding and Johnson (2003) noted that, although the total amount of reduced P700 was proportional to PS II efficiency, this relationship did not extrapolate to the origin, giving space for a constant rate of cyclic ET (Golding and Johnson, 2003). In addition, however, these authors applied the method of Klughammer and Schreiber (1994), to estimate the proportion of PS I in an "active" state. This measurement is performed by superimposing a saturating flash of white light on top of background actinic illumination and then transferring the sample directly to darkness, taking the total signal following the flash-to-dark transition as a measure of active centers. In the study of Klughammer and Schreiber (1994), the loss of active centers was supposed to be related to a limitation on the acceptor side of PS I, preventing centers from turning over. Surprisingly, Golding and Johnson (2003) noted that active PS I *rose* at low CO_2 (i.e., under conditions where PS I is most likely to be acceptor-side limited). They suggested that a distinct population of PS I centers exists that is largely or wholly involved in cyclic ET. This "cyclic-only" pool is activated at low concentrations of CO_2 and under high light. Thus, the contradictions in earlier measurements might be related to the way in which CO_2 limitation was applied and whether these "cyclic" centers were already activated or not.

In measurements of cyclic ET in far-red light it has been common to take the rate of $P700^+$ reduction as an indicator of PS I turnover (Maxwell and Biggins, 1976). Essentially, the same approach can be applied in white light conditions. This relies on the limiting step in electron transport lying prior to PS I, which is usually the case under physiological conditions, such that the flow of electrons to P700 can be measured and reflects the overall flux through PS I. A potential problem with this method was noted by Sacksteder and Kramer (2000), who noted that a net reduction of cyt *f*, measured at the time the light is switched off, might have to be taken into account to determine the electron flux toward P700 (Sacksteder and Kramer, 2000). Strictly, there should be no net reduction of cyt *f* at the moment when the light is switched off, as at steady-state the rate of oxidation and reduction are identical and neither of these are instantly affected by cutting the light. Practically, given the time resolution and sensitivity of most instruments, this may be a problem but only under low light conditions where P700 is largely reduced but cyt *f* oxidized, giving rise to a short time lag in the reduction of cyt *f*. Sacksteder and Kramer (2000) have compared the turnover of PS I and PS II in greenhouse grown sunflowers. They observed a linear relationship between PS I and PS II ET, implying no (or a constant proportion of) cyclic ET, the same conclusion as reached by Harbinson and colleagues using P700 redox state to measure PS I turnover (Harbinson et al., 1990; Harbinson, 1994). In contrast, Clarke and Johnson compared the rates of PS I and PS II turnover across a range of temperatures and light intensities in barley grown in a growth cabinet. They observed that PS II photochemistry saturated at lower irradiances and was more sensitive to low temperature than PS I. Thus, they concluded that high light and low temperatures lead to enhancement of cyclic ET (Clarke and Johnson, 2001). The contradiction between these two studies may reflect a species difference, but is more likely explained by the range of light intensities used in each case. In the experiments of Sacksteder and Kramer, the highest light intensities used were just saturating, whereas for Clarke and Johnson light intensities were used that went well above saturating for PS II electron transport (though not necessarily for PS I). Thus it appears that cyclic ET is a characteristic of saturating light, although a low rate at subsaturating light cannot be excluded, if this forms a constant proportion of the linear flux. A similar approach by Golding and Johnson (2003) drew the same conclusion concerning responses to low CO_2 and drought.

A new technical approach, based on membrane potential measurements (Joliot and Joliot, 2002, 2004) has been developed to determine the absolute rate of the cyclic and linear pathways whatever the intensity of illumination. In this method, the sum of the rates of photochemical reactions I and II is measured by the difference in the rate of membrane potential changes determined immediately before or after switching off the light. Experiments were performed under strong light excitation in the presence of air, with dark-adapted spinach (Joliot and Joliot, 2002) or *Arabidopsis thaliana* leaves (Joliot and Joliot, 2004), i.e., in conditions where the Benson–Calvin cycle and thus, the linear ET, is mainly inactive. Under saturating illumination, rate of the cyclic flow is estimated to $\sim$130 sec^{-1} and remains roughly constant during the first 10 sec of illumination. Unexpectedly, this cyclic process is not inhibited by antimycin (Joliot and Joliot, 2002). Under the same conditions, fluorescence induction kinetics shows that a pool of soluble PS I acceptors (Fd, FNR and NADP) of approximately nine electron equivalents is reduced in less than 100 msec via the linear pathway. This implies that, even in dark-adapted leaves, PS I remains able to transfer electrons to a pool of oxidized PS I acceptors. In the presence of DCMU, where the linear flow is fully inhibited, a similar rate of the cyclic flow is measured during the first seconds of illumination. This rate progressively drops to zero in $\sim$7 sec, due to slow electron leaks that lead to the oxidation of the carriers involved in the cyclic chain.

After 100 msec of illumination at an intensity that is saturating for the cyclic process, most of P700 is reduced (Harbinson and Hedley, 1993; Strasser et al., 2001; Joliot and Joliot, 2002; Schankser et al., 2003) implying that a fast charge recombination between $P700^+$ and reduced acceptors will occur. In agreement with this assumption, it is observed that the kinetics of the membrane potential displays a fast decaying phase of small amplitude, which is completed in $\sim$500 μsec. The amplitude of this phase is roughly proportional to the light intensity. This phase correlates with a reduction phase of $P700^+$ (measured by the absorption changes at 810 nm) and has been ascribed to a charge recombination between $P700^+$ and most probably the iron-sulfur carrier F_X (Joliot and Joliot, 2002). It can be thus concluded that most of the carriers of the linear and cyclic chains are poised in their reduced state. A small fraction of "cyclic PS I" centers includes $P700^+$ and a single negative charge on the F_A/F_B cluster. For these RCs, the rate of $P700^+$ reduction via the cyclic pathway is faster than the rate of charge recombination between $P700^+$ and $(F_A/F_B)^-$ ($t_{1/2} \sim 45$ msec; Hiyama and Ke, 1971).

A charge recombination process is also observed in the presence of DCMU, the amplitude of which is half

that measured in its absence. This is explained by the fact that illumination induces the oxidation of all the carriers of the linear chain, while the carriers involved in the cyclic pathway are transitorily poised at a potential able to induce the reduction of most of the F_A/F_B acceptors (<-600 mV). In the 1–7 sec time range, the decrease in the rate of the cyclic flow is associated with a corresponding decrease in the amplitude of the charge recombination phase. This parallel decrease reveals a progressive oxidation of all the carriers involved in the cyclic process, associated with a slow electron leak toward O_2 or the Benson–Calvin cycle.

VII. Pathway of Cyclic Flow in Higher Plants

Work described above leads us to conclude that cyclic ET is a real physiological phenomenon, though perhaps only occurring under a limited range of conditions. The question then arises, what is (are) the physiological pathway(s) for this electron flow. Early work indicating two pathways of cyclic ET in isolated systems were mainly based on measurements of chloroplasts isolated from C3 plants. We would therefore expect to see evidence for both the ferredoxin-linked antimycin-sensitive and the NADPH-linked antimycin-insensitive pathways in whole leaves. The *in vivo* data on the effect of antimycin A are however, ambiguous. Joët et al. (2002) reported a slow cyclic ET measured under far-red excitation is stimulated in anaerobiosis but also in the presence of inhibitors of the respiratory chain, including antimycin. In the same way, antimycin does not inhibit the fast cyclic flow measured under strong illumination of dark-adapted leaves (Joliot and Joliot, 2002). In both cases, it was proposed that the effect of antimycin is related to the inhibition of the respiratory chain, which increases the reducing power in chloroplasts via mitochondria–chloroplast interactions. Further confusion might arise in *in vivo* measurements because of other functions of antimycin, notably its ability to inhibit nonphotochemical quenching (Oxborough and Horton, 1987). We thus conclude that effect of antimycin is not a decisive test in proposing or excluding the occurrence of cyclic electron flow.

A. NADPH-Dependent Cyclic Electron Transfer

The more convincing arguments that favor the involvement of NADPH:PQ reductase (NDH) in the cyclic pathway come from the analysis of mutants lacking this enzyme. NDH-dependent cyclic ET reported in the literature appears as a slow process that is very likely related to the low concentration of NDH [$\sim$1% of that of the photosynthetic chain (Sazanov et al., 1995)]. Levels of this complex are seen to increase under conditions of stress, suggesting a role in survival under conditions of oxidative stress (Casano et al., 2000; Teicher et al., 2000; Lascano et al., 2003), however, to what extent this increases the flux through the NDH complex remains unclear. Burrows et al. (1998) observed that plants lacking the NDH complex lacked the transient fluorescence rise seen following illumination. Hashimoto et al. (2003) were recently able to use this characteristic to identify a new mutant of *A. thaliana*, CRR2, which lacks a nuclear encoded factor that seems to be essential for NDH expression. However, the absence of a fluorescence rise in NDH-less mutants seems to be highly sensitive to the developmental and metabolic status of the leaf (A. Krieger-Liszkay, personal communication.), supporting the idea that this is not the only route for reduction of the PQ pool by stromal factors. Evidence has also been published that the reduction of $P700^+$ following far-red light is affected in plants lacking the NDH complex (Joët et al., 2002). Involvement of NDH in the fast cyclic ET measured in dark-adapted leaves submitted to strong illumination (Joliot and Joliot, 2002, 2004) appears unlikely as this enzyme, which is present at low concentration, would have to operate at rate as high as $\sim 10^4$ sec^{-1} to sustain a rate of electron flow of 130 sec^{-1}.

B. Ferredoxin-Dependent Cyclic Electron Transfer

If rapid rates of cyclic ET cannot be sustained by the NDH complex, then we must consider the likely involvement of a ferredoxin pathway. Electrons maybe directly transferred from Fd either directly to cyt b/f (Fig. 1, pathway 3) or via a FQR (Fig. 1, pathway 2; Bendall and Manasse, 1995). In Fig. 2, a mechanism is proposed that results in the pumping of one proton per electron transferred, but differs from conventional Q-cycle process (Joliot and Joliot, 2004). FNR is known to copurify with the cyt b/f complex (Clark et al., 1984) and provides a binding site for Fd (Zhang et al., 2001). It seems likely that the electron pathway between Fd and site Q_i involves the covalently bound cyt c' (cyt c_i) recently characterized in the structure of cyt b/f complex in *Chlamydomonas reinhardtii* (Stroebel et al., 2003) and in cyanobacteria (Kurisu et al., 2003). On the other hand, it has been proposed that an electron carrier G (Lavergne, 1983; Joliot and Joliot, 1988), is localized on the stromal side of the cyt b/f complex and able to exchange electrons with cyt

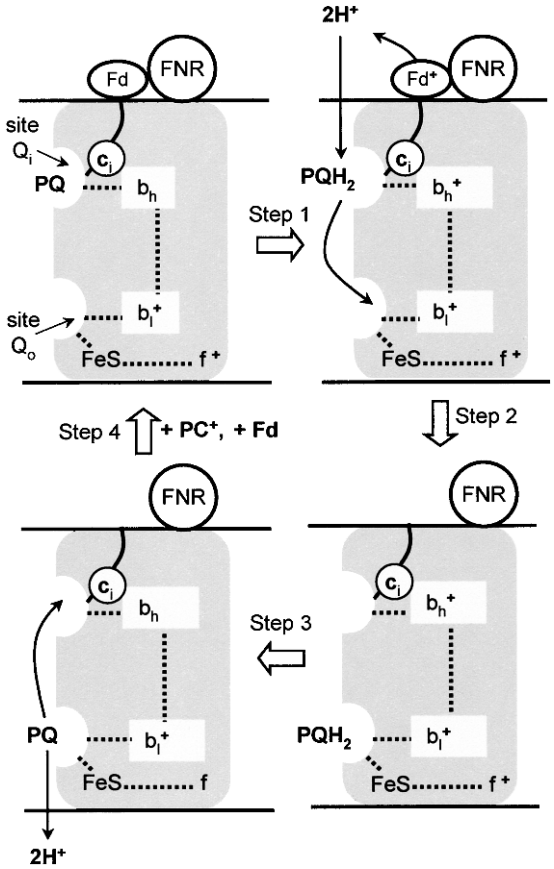

Fig. 2. A mechanism for the ferredoxin-dependent electron transfer.

b_h. This carrier G has been now identified as cyt c_i (Alric et al., 2005). According to Fig. 2, sites Q_i and Q_o behave quite symmetrically. At site Q_i, reduction of PQ involves the transfer of one electron from Fd and one electron from cyt b_h; at site Q_o, oxidation of PQH_2 involves the transfer of one electron to cyt f via the Rieske Fe/S protein and one electron to cyt b_l. It worth noting that, in the dark, reduction of the PQ pool could be induced by the sequential transfer of electrons from Fd to site Q_i and the cyt b/f complex would then behave as a FQR. Evidence for a distinct FQR, independent of the Q_i site, is related to the effect of antimycin compared to HQNO (Moss and Bendall, 1984). This evidence only rules out a role for antimycin in blocking the Q_i site and does not rule out the involvement of that site, if it does not bind antimycin.

It has been proposed that the small hydrophilic polypeptide PGR5 is required in a process of proton gradient generation and could be involved in FQR activity (Munekage et al., 2002). At present, very little information on this mutant is available and a better characterization of its function is required. PGR5 lacks a metal binding motif that might implicate it in a direct role in electron transfer, however it might play a secondary role, e.g., in being involved in the binding of FNR to the cyt b/f complex. The published evidence that PGR5 is involved in cyclic ET is based on the observation that NADPH and Fd-dependent reduction of PQ pool, measured by chlorophyll fluorescence is impaired in PGR5 mutant. This observation needs to be considered with care, however, since the effect on the kinetics of PQ reduction and the sensitivity to antimycin appear to be qualitatively the same, with only the amplitude of the fluorescence rise being changed (Munekage et al., 2002). Since the latter might be sensitive to other factors, for example the presence of photoinhibited PS II centers in the thylakoid membrane, this result is not conclusive.

The fraction of PS I centers that operate according to the cyclic or linear mode has been determined by measuring P700 and PC oxidation under weak far-red excitation (8 photons / PSI / s), a photochemical rate constant well below the rate constant of the limiting steps of cyclic or linear flow (Joliot and Joliot, 2005). Far-red illumination of a dark-adapted leaf induces a slow oxidation of P700 and PC that is completed in 10–20 sec. During this oxidation phase, the number of PS I turnovers is much larger than the number of electrons stored in the primary and secondary PS I donors. It implies that most of the electrons formed on the stromal side of PS I are transferred back to PS I via the cyt b/f complex (cyclic electron flow). Slow electron leaks, probably toward the Benson-Calvin cycle, result in a progressive oxidation of most of the carriers involved in the cyclic pathway, including P700. When the same leaf is first preilluminated for several minutes under green light that excites both photosystems and activates the Benson-Calvin cycle, P700 oxidation induced by far-red excitation is a much faster process completed in less than 3 sec. The kinetics of P700 oxidation measured with a preilluminated leaf is close to that measured in the presence of methyl viologen, an efficient PS I electron acceptor. It implies that, in preilluminated leaves, most of the electrons reaching the stromal size of PS I are transferred to the Benson-Calvin cycle via FNR and NADP (linear electron flow). Using the same approach, the transition from a cyclic (dark-adapted leaf) to a linear mode (preilluminated leaf) has been recently analyzed during the course of the green preillumination (P. Joliot, unpublished data). For the first minute of illumination, most of PS I centers contribute to cyclic electron flow. During the subsequent period of illumination (1–10 min), activation of the

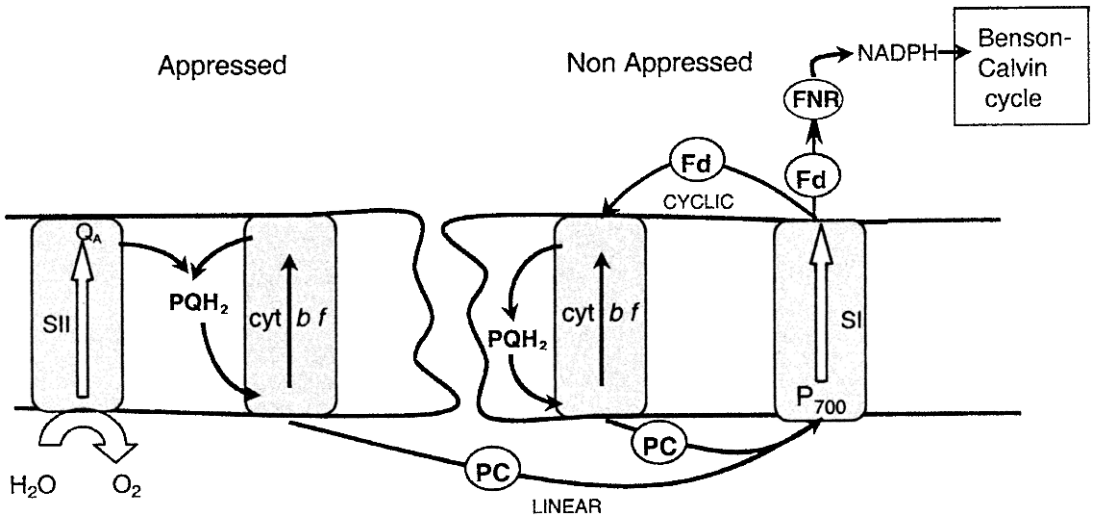

Fig. 3. A model for the structural organization of linear and cyclic ways within the photosynthetic membrane.

Benson-Calvin cycle, as shown by the increase in the rate of linear flow, correlates with a decrease in the rate of the cyclic flow. In the same way, the slowdown of the linear flow induced by a lack of CO_2 is associated with an increase of the rate of the cyclic flow, as previously proposed by Heber and co-workers (Hauser et al., 1995). These results suggest that linear and cyclic pathways be in permanent competition for the reoxidation of Fd. The relative efficiency of cyclic and linear pathways is suggested to be determined by the probability of Fd binding either to a site localized on the stromal site of the cyt b/f complex or to an 'active' FNR. This we define as an FNR molecule to which $NADP^+$ is bound. Activation of cyclic flow is thus associated with the reduction of $NADP^+$ and the competition between cyclic and linear mode will be controlled by the redox state of NADP which depends upon the degree of activation of the Benson-Calvin cycle. In dark-adapted leaves, illumination first induces the reduction of the small pool of acceptors present in their oxidized state (FNR and $NADP^+$). When this pool is fully reduced, Fd in excess is available to bind the stromal site of cyt b/f, which initiates cyclic electron flow.

In the model depicted in Fig. 3, Fd is presumed to freely diffuse in the stromal compartment. This contrasts with models in which the cyclic chain is organized in supercomplexes that associate 1 PS I center / a cyt b/f 1 PC / 1 Fd (Carillo and Vallejos, 1983; Laisk et al., 1992; Laisk, 1993; Joliot and Joliot, 2002). In this hypothesis, the concentration of PS I included in the supercomplex cannot be larger than that of cyt b/f complex localized in the non-appressed region of the membrane. As most of PS I can be involved in cyclic electron flow (Joliot and Joliot, 2005) and only ~50% of cyt b/f complex is localized in the non-appressed region Albertsson, 2001), the obligatory formation of supercomplexes for cyclic electron flow can be excluded.

VIII. Cyclic Flow in Green Unicellular Algae

There is a general consensus that a cyclic electron flow operates in algae, at least under anaerobic conditions, when PS II activity is mainly inhibited due to the reduction of Q_A. It worth pointing out that, in contrast to higher plants, anaerobiosis is a common occurrence for many algae in their natural environment. Anaerobiosis is known to induce state 1 to state 2 transition associated with changes in the distribution of the membrane complexes (Bulté et al., 1990) to a much larger extent than those induced by chromatic adaptation (Bonaventura and Myers, 1969). Anaerobiosis, like all treatments that decrease the ATP content of the cell (mitochondrial inhibitors, uncouplers, ATP-synthase inhibitors), induces the transfer of most of the light harvesting complex LHC II (Bulté et al., 1990) and of a fraction of cyt b/f complexes (Vallon et al., 1991) from the appressed to the nonappressed region of the thylakoids. On the basis of measurements of the turnover rate of cyt f, Finazzi et al. (1999) concluded that only linear ET is active in the presence of O_2 (state 1 conditions), while cyclic electron flow operates in state 2 conditions (anaerobiosis or presence of uncouplers), where the linear process is fully inhibited. The rate of cyclic flow measured in state 2 conditions is similar to that

measured for the linear flow at the same light intensity in state 1 conditions. One can thus conclude that in anaerobic conditions, most of the antennae is involved in the cyclic process with ~80% of the light collected by the "cyclic PS I." In these conditions, unicellular algae may behave in a similar way to the green bacteria with type I photosystems, with a photosynthetic process entirely devoted to ATP synthesis. The cyclic process in algae thus appears fundamentally different from that in higher plants, which occurs in the presence of O_2 and state 1 conditions.

A. Mechanisms of Cyclic Flow in Algae

Complexes containing PS I and cyt b/f complexes have been observed in solubilized membranes of *C. reinhardtii* (Wollman and Bulté, 1989) possibly pointing to the presence of supercomplexes in this organism. On the other hand, the analysis of ET kinetics in state 2 conditions in a mutant with a low cyt b/f content has shown that PC is able to freely diffuse from any PS I center to cyt f (Finazzi et al., 2002). This excludes the presence of functional supercomplexes, including a trapped PC. In state 2 conditions, a spatial separation between the linear and cyclic chains results from the transfer of a large fraction of the stromal cyt b/f complexes from the appressed to the nonappressed region. Thus, one expects that, even in the absence of supercomplexes, an efficient cyclic ET will occur in the nonappressed region that includes the PS I centers and most of the cyt b/f complexes.

The electron pathway from PS I to the cyt b/f complex has not been identified. While no gene encoding for an enzyme similar to NDH has been identified in the chloroplast of algae, the presence of a PQ reductase is suggested by the slow reduction of PQ pool in the appressed region, which has been observed in the presence of O_2 (Diner and Mauzerall, 1973). One expects that such an enzyme would operate at a much higher rate in anaerobic conditions. This enzyme could be involved in a cyclic process if it were present in the nonappressed region. Another possible pathway is a direct ET from PS I to cyt b/f complex, as depicted in Fig. 1 (pathway 3). It worth pointing out that, to our knowledge, complexes that associate FNR and the cyt b/f complex have not been identified in *C. reinhardtii*.

IX. Cyclic Flow in Cyanobacteria

In cyanobacteria, the presence of respiratory and photosynthetic electron transport chains in the same membrane system, to the point where the two share redox components (Scherer, 1990), means that the cyclic ET occurs in an environment very different to that in plants and algae. A common feature to most of cyanobacteriae is the large excess of PS I as compared to PS II centers (Fujita et al., 1994). This suggests that even under steady-state condition of illumination, a fraction of PS I centers could be involved in cyclic ET. On the other hand, in cyanobacteria, PS I centers are organized in trimers, which exclude the formation of supercomplexes that associate PS I centers with the cyt b/f complex.

After illumination in the presence of DCMU or after far-red excitation, reduction of $P700^+$ occurs with $t_{1/2} \sim 500$ msec, taken to be indicative of cyclic ET (Maxwell and Biggins, 1976; Mi et al., 1992a,b; Yu et al., 1993). At the same time, measurements of energy storage via photoacoustics point to the occurrence of cyclic ET under such conditions. However, it can be assumed that, in dark-adapted samples, the PQ pool will be maintained in a relatively reduced state due to respiratory electron flow. It needs to be shown, therefore, that electron transport from the acceptor side of PS I back into the PQ pool occurs and is maintained under conditions where PS II is active. (Sandmann and Malkin, 1983, 1984) were able to observe that, while respiration was inhibited in the light, due to competition with photosynthesis, NAD(P)H oxidation by spheroplasts from *Aphanocapsa* was less affected. The addition of DCMU did not enhance NAD(P)H oxidation, suggesting no competition between NDH and PS II for PQ reduction. However, as pointed out by Mi et al. (2000), the organization of the membrane systems in cyanobacteria may be substantially disturbed in isolated systems. As far as we are aware, these results have not yet been confirmed in intact cells.

Measurements on mutants lacking the NDH complex suggest this is generally the primary route for cyclic ET (Yu et al., 1993; Mi et al., 2000). Mutants lacking *ndhF* of the NDH complex and *psaE* in PS I, show inhibited growth at low-light intensities, but are unaffected at high light. Cyclic ET in cyanobacteria has been implicated in providing energy for CO_2 concentrating mechanisms. Growth of *Synechocystis* at low CO_2 results in upregulation of NDH subunits (Deng et al., 2003). Mutants lacking the NDH complex have a reduced ability to tolerate growth under limiting CO_2 conditions (Ogawa, 1991). On the other hand, it has been reported that *Synechocystis* sp. PCC 6803 contains a succinate quinol oxidoreductase that is suggested to contribute to cyclic electron flow (Cooley et al., 2000). This enzymatic activity would, however,

involve a more complex cyclic pathway than so far considered and it is questionable whether it can still be regarded as cyclic electron flow.

Exposure to high salt concentrations leads to an activation of a cyclic ET pathway that does not require NDH (Jeanjean et al., 1998). The details of this pathway remain unclear but probably involve FNR (van Thor et al., 2000; Matthijs et al., 2002). Binding of the FNR to the membrane is facilitated by an N-terminal domain which is absent in the higher plant enzyme (van Thor et al., 2000). Low concentrations of sodium bisulfite have also recently been suggested to stimulate cyclic ET (Wang et al., 2003).

X. Functions and Regulation of Cyclic Electron Transfer

The primary role of cyclic ET has always been supposed to be the generation of ATP, either to support CO_2 fixation or for other metabolic processes. The requirement for cyclic ET to balance the production of reductant and ATP in normal CO_2 fixation conditions has been widely debated. Structural analysis of the electrical rotor of the chloroplast ATP-synthase has shown that it is made up of 14 polypeptides (Seelert et al., 2000). One thus expects that a complete rotation of the rotor, which induces the synthesis of 3 ATP, is associated with the transfer of 14 protons across the membrane that leads to H^+/ATP ratio of $14/3 = 4.7$. Assuming that 3 protons are pumped per electron transferred via the linear chain, the number of ATP synthesized per electron is $3/4.7 = 0.64$ or $\sim$2.55 ATP per CO_2, a value over-estimated as ion leaks through the membrane are not taken into account. This amount of ATP is definitely lower than that required by the Benson–Calvin cycle (3 ATP/CO_2). It is thus likely that, even in light-adapted conditions, a small fraction of PS I contributes to a cyclic flow to satisfy the ATP requirement of the Benson–Calvin cycle. This could explain why the minimum quantum requirement of the photosynthetic process measured under weak excitation (10–12 quanta/O_2) is significantly larger than the theoretical value of eight quanta/O_2.

If cyclic ET is contributing ATP to drive CO_2 fixation and assuming that this is regulated in a way that ensures that the ATP supply is maintained at a constant level, then we would expect that under steady-state condition of illumination, the rate of cyclic ET would parallel the rate of linear ET. Thus, it is perhaps unsurprising that light-limited steady-state measurements, which rely on comparing PS I and PS II ET, have typically found no evidence for this cyclic flow (Harbinson et al., 1990; Sacksteder and Kramer, 2000). By contrast, when the ATP consumption is not directly coupled to CO_2 fixation, we would expect to find discrepancies between PS I and PS II turnover. This would certainly be the case in C4 bundle sheath cells, where the reductant required for CO_2 fixation is not provided by linear ET. It would also be the case during the first few seconds of illumination, during which time a trans-thylakoid pH gradient must be established before ATP synthesis can begin (Joliot and Joliot, 2002).

In green algae, reducing conditions (anaerobiosis) result in a large state transition, with phosphorylation of LHC II resulting in its migration to PS I, pushing the chloroplast into a "cyclic-only" state. Under anaerobiosis, mitochondrial respiration will be inhibited, leading to a deficit of ATP and possibly also to a rise in the concentration of NADH. A shift from linear to cyclic photosynthetic ET would counteract this effect, lowering the production of reducing potential in favor of ATP synthesis. Thus the redox regulation of state transitions in algae and the resultant regulation of cyclic ET is a mechanism for balancing the overall cellular ATP/NAD(P)H ratio.

In higher plants, state transitions are less prominent and their regulation in response to redox potential very different. Reducing conditions induced by anaerobiosis do not give rise to state 1 to state 2 transitions but they are inhibited under conditions, where the Benson–Calvin cycle is active, though the action of thioredoxin (Aro and Ohad, 2003). On the other hand, and in contrast to algae, efficient cyclic ET operates during the first seconds of illumination of dark-adapted leaves (Joliot and Joliot, 2002), i.e., in pure state 1 conditions, and there is no evidence that state transitions lead to an increase in cyclic ET, rather they are thought to balance excitation of PS I and PS II for optimal linear ET. The small state transitions that do occur are seen at very low light and depend on the redox state of the PQ pool. On the other hand, the observation that *A. thaliana* grown under very low-light increase PS I relative to PS II might suggest a role for cyclic ET under such conditions, implying a switch from CO_2 fixation to ATP synthesis (Bailey et al., 2001).

A notable difference between higher plants, some algae and cyanobacteria is in their ability to protect themselves from high light through the process of high energy state quenching (qE). This process, which is linked to the presence of the carotenoid zeaxanthin, is driven by ΔpH. It was first suggested some years ago that the ΔpH required to generate this quenching was generated by cyclic ET (Heber and Walker, 1992); however, it is only recently that direct evidence for its

requirement has been obtained. The PGR5 mutant of *A. thaliana* that is thought to be deficient in cyclic ET, was isolated using a screen that selected for a deficiency in quenching (Munekage et al., 2002). Golding and Johnson observed a quantitative link between the extent of non-photochemical quenching (NPQ) and the extent of cyclic ET under conditions of low CO_2 and drought (Golding and Johnson, 2003).

Given the dual function of cyclic ET in higher plants, it is tempting to suggest that the different pathways of cyclic ET may be fulfilling different functions and therefore be differentially regulated. Upregulation of cyclic at low CO_2 correlates with a downregulation of the cyt b/f complex, inhibiting linear ET (Golding and Johnson, 2003). This downregulation of linear ET has been suggested to be regulated via thioredoxin (Johnson, 2003). Thus, upregulation of cyclic ET in response to reducing conditions seems likely, although the mechanism involved is different to that seen in green algae.

Joliot and Joliot (2002) suggested that the cyclic ET seen following a dark to light transition in dark-adapted leaves maybe regulated by the ATP/ADP ratio in the chloroplast. This is a reasonable suggestion, if we accept that this cyclic is required to kick-start ATP synthesis. On the other hand, the cyclic ET seen under such conditions has a short lag period, during which time the Fd and NADPH pools are likely to become reduced, in agreement with a redox regulation process. After a preillumination, the transition from the linear to the cyclic mode requires more than 1 hour of dark adaptation (Golding et al., 2004; Joliot and Joliot, 2005). Deactivation of the Benson-Calvin cyclic following illumination is slow, taking up to 3 hours or more in some species. Thus the long period of time required for the induction of a cyclic activated state might be explained simply by this deactivation, though changes in the energy status of the cell, related to the consumption of carbohydrate reserves might also play a role.

Given the low requirement for additional ΔpH arising from CO_2 fixation, it might be speculated that the capacity of NDH pathway is sufficient to support this. However, mutants lacking NDH are clearly not deficient in CO_2 fixation. It may be however that a normally stress (redox) activated cyclic pathway becomes partially activated under conditions where NDH is lacking, compensating for the lack of this pathway. There is little evidence that the NDH pathway contributes to photoprotection. Ndh-less mutants have normal levels of NPQ and are not more susceptible to photoinhibition either of PS I or PS II at ambient or low temperature (Barth and Krause, 2002). On the other hand, there are some indications that plants lacking NDH are more sensitive to water stress (Horvath et al., 2000).

In cyanobacteria, there is a large amount of data that link the NDH complex to CO_2 concentrating mechanisms. It seems that there are distinct forms of the complex that are involved in this process, with there possibly being a direct role of NDH in the formation of HCO_3^- from CO_2. It is not clear how this relates cyclic ET however, i.e., whether this reaction depends on electron transport occurring through PS I (see discussion in Badger and Price, 2003).

XI. Conclusion

The pathway of linear electron transport has been clearly established for many years. Cyclic ET on the other hand remains enigmatic. Nevertheless, this is an area in which significant progress is beginning to be made. The establishment of new methods for the quantitation of cyclic flow, such as those outlined here, will help in this progress. Clearer ideas on the function of cyclic ET will also help in the identification of the proteins involved in this pathway, either through conventional screening approaches or through reverse genetics, examining the effects of knockout mutations on cyclic electron transport.

Acknowledgments

We would like to thank Dr. Giovanni Finazzi (IBPC, Paris, France) and Dr. Conrad Mullineaux (University College, London, UK) for useful discussions and Prof. Toshiharu Shikanai (Nara Institute of Science and Technology, Japan) for providing a reprint of his work.

References

Albertsson PA (1995) The structure and function of the chloroplast photosynthetic membrane – a model for the domain organization. Photosynth Res 46: 141–149

Albertsson PA (2001) A quantitative model of the domain structure of the photosynthetic membrane. Trends Plant Sci 6: 349–354

Alric J, Pierre Y, Picot D, Lavergne J and Rappaport F (2005) Spectral and redox characterization of the heme c_i of the cytochrome b_6f complex. Proc Natl Acad Sci USA 102: 15860–15865

Allen JF (1983) Regulation of photosynthetic phosphorylation. CRC Crit Rev Plant Sci 1: 1–22

Allen JF (2003) Cyclic, pseudocyclic and noncyclic photophosphorylation: new links in the chain. Trends Plant Sci 8: 15–19

Anderson JM (1989) The grana margins of plant thylakoid membranes. Physiol Plant 76: 243–248

Andersson B and Anderson JM (1980) Lateral heterogeneity in the distribution of chlorophyll–protein complexes of the thylakoid membranes of spinach chloroplasts. Biochim Biophys Acta 593: 427–440

Arnon DI (1955) The chloroplast as a complete photosynthetic unit. Science 122: 9–16

Arnon DI (1959) Conversion of light into chemical energy in photosynthesis. Nature 184: 10–21

Arnon DI and Chain RK (1977) Role of oxygen in ferredoxin-catalyzed cyclic photophosphorylation. FEBS Lett 82: 297–302

Arnon DI, Allen MB and Whatley FR (1954) Photosynthesis by isolated chloroplasts. Nature 174: 394–396

Arnon DI, Losada M, Nozaki M and Tagawa K (1961) Photoproduction of hydrogen, photofixation of nitrogen and a unified concept of photosynthesis. Nature 190: 601–606

Aro EM and Ohad I (2003) Redox regulation of thylakoid protein phosphorylation. Antioxid Redox Signal 5: 55–67

Asada K, Heber U and Schreiber U (1993) Electron flow to the intersystem chain from stromal components and cyclic electron flow in maize chloroplasts, as detected in intact leaves by monitoring redox change of P700 and chlorophyll fluorescence. Plant Cell Physiol 34: 39–50

Badger M and Price GD (2003) CO_2 concentrating mechanisms in cyanobacteria: molecular components, their diversity and evolution. J Exp Botany 54: 609–622

Bailey S, Walters RG, Jansson S and Horton P (2001) Acclimation of *Arabidopsis thaliana* to the light environment: the existence of separate low light and high light responses. Planta 213: 794–801

Barth C and Krause GH (2002) Study of tobacco transformants to assess the role of chloroplastic NAD(P)H dehydrogenase in photoprotection of photosystems I and II. Planta 216: 273–279

Bassi R, dal Belin Peruffo A, Barbato R and Ghisi R (1985) Differences in chlorophyll–protein complexes and composition of polypeptides between thylakoids from bundle sheaths and mesophyll cells in maize. Eur J Biochem 146: 589–595

Bendall DS and Manasse RS (1995) Cyclic photophosphorylation and electron transport. Biochim Biophys Acta 1229: 23–38

Bonaventura C and Myers J (1969) Fluorescence and oxygen evolution from *Chlorella pyrenoidosa*. Biochim Biophys Acta 189: 366–383

Bukhov NG, Wiese C, Neimanis S and Heber U (1999) Heat sensitivity of chloroplasts and leaves: leakage of protons from thylakoids and reversible activation of cyclic electron transport. Photosynth Res 59: 81–93

Bulté L, Gans P, Rebéillé F and Wollman F-A (1990) ATP control on state transitions in vivo in *Chlamydomonas reinhardtii.* Biochim Biophys Acta 1020: 72–80

Burrows PA, Sazanov LA, Svab Z, Maliga P and Nixon PJ (1998) Identification of a functional respiratory complex in chloroplasts through analysis of tobacco mutants containing disrupted plastid *ndh* genes. EMBO J 17: 868–876

Carillo N and Vallejos RH (1983) The light-dependent modulation of photosynthetic electron transport. TIBS February 1983: 52–56

Casano LM, Zapata JM, Martin M and Sabater B (2000) Chlororespiration and poising of cyclic electron transport – plastoquinone as electron transporter between thylakoid NADH dehydrogenase and peroxidase. J Biol Chem 275: 942–948

Clark RD, Hawkesford MJ, Coughlan SJ, Bennett J and Hind G (1984) Association of ferredoxin $NADP^+$ oxidoreductase with the chloroplast cytochrome b–f complex. FEBS Lett 174: 137–142

Clarke JE and Johnson GN (2001) *In vivo* temperature dependence of cyclic and pseudocyclic electron transport in barley. Planta 212: 808–816

Cleland RE and Bendall DS (1992) Photosystem-I cyclic electron transport – measurement of ferredoxin-plastoquinone reductase activity. Photosynth Res 34: 409–418

Cooley JW, Howitt CA and Vermaas WFJ (2000) Succinate:quinol oxidoreductase in the cyanobacterium *Synechocystis* sp. Strain PCC 6803: presence and function in metabolism and electron transport. J Bacteriol 182: 714–722

Cornic G, Bukhov NG, Wiese C, Bligny R and Heber U (2000) Flexible coupling between light-dependent electron and vectorial proton transport in illuminated leaves of C-3 plants. Role of photosystem I-dependent proton pumping. Planta 210: 468–477

Cox RP and Andersson B (1981) Lateral and transverse organisation of cytochromes in the chloroplast thylakoid membrane. Biochem Biophys Res Commun 103: 1336–1342

Crofts AR, Meinahrdt SW, Jones KR and Snozzi M (1983) The role of the quinone pool in the cyclic electron-transfer chain of *Rhodopseudomonas sphaeroides*. A modified Q-cycle mechanism. Biochim Biophys Acta 723: 202–218

Deng Y, Ye JY and Mi H (2003) Effects of low CO_2 on NAD(P)H dehydrogenase, a mediator of cyclic electron transport around Photosystem I in the cyanobacterium *Synechocystis* PCC 6803. Plant Cell Physiol 44: 534–540

Diner B and Mauzerall D (1973) Feedback controlling oxygen production in a cross-reaction between two photosystems in photosynthesis. Biochim Biophys Acta 305: 329–352

Finazzi G, Furia A, Barbagallo RP and Forti G (1999) State transitions, cyclic and linear electron transport and photophosphorylation in *Chlamydomonas reinhardtii*. Biochim Biophys Acta 1413: 117–129

Finazzi G, Rappaport F, Furia A, Fleischmann M, Rochaix JD, Zito F and Forti G (2002) Involvement of state transitions in the switch between linear and cyclic electron flow in *Chlamydomonas reinhardtii*. EMBO Rep 3: 280–285

Fork DC and Herbert SK (1993) Electron transport and photophosphorylation by Photosystem I in vivo in plants and cyanobacteria. Photosynth Res 36: 149–168

Frenkel AW (1954) Light induced phosphorylation by cell-free preparations of photosynthetic bacteria. J Am Chem Soc 76: 5568–5569

Fujita Y, Murakami A, Aizawa K and Ohki K (1994) Short-term and long-term adaptation of the photosynthetic apparatus: homeostatic properties of thylakoids. In: Bryant DA (ed) The Molecular Biology of Cyanobacteriae, Vol 1, pp 677–692. Kluwer Academic Publishers, Dordrecht

Genty B, Briantais J-M and Baker NR (1989) The relationship between the quantum yield of photosynthetic electron transport and quenching of chlorophyll fluorescence. Biochim Biophys Acta 990: 87–92

Gerst U, Schreiber U, Neimanis S and Heber U (1995) Photosystem I dependent cyclic electron flow contributes to control of Photosystem II in leaves when stomata close under water stress. In: Mathis P (ed) Photosynthesis: From Light to

Biosphere, Proceedings of the Xth International Photosynthesis Congress, Vol II, pp 835–838. Kluwer Academic Publishers, Montpellier

Golding AJ and Johnson GN (2003) Down-regulation of linear and activation of cyclic electron transport during drought. Planta 218: 107–114

Golding AJ, Finazzi G and Johnson GN (2004) Reduction of the thylakoid electron transport chain by stromal reductants–evidence for activation of cyclic electron transport upon dark adaptation or under drought. Planta 220: 356–363

Harbinson J (1994) The responses of thylakoid electron transport and light utilization efficiency to sink limitation of photosynthesis. In: Baker NR and Bowyer JR (eds) Photoinhibition of Photosynthesis, from Molecular Mechanisms to the Field, pp 273–295. BIOS scientific publishers Springer, The Netherlands

Harbinson J and Foyer CH (1991) Relationships between the efficiencies of Photosystem-I and Photosystem-II and stromal redox state in CO_2-free air – evidence for cyclic electron flow *in vivo*. Plant Physiol 97: 41–49

Harbinson J and Hedley CL (1993) Changes in P-700 oxidation during the early stages of the induction of photosynthesis. Plant Physiol 103: 649–660

Harbinson J, Genty B and Baker NR (1990) The relationship between CO_2 assimilation and electron transport in leaves. Photosynth Res 25: 213–224

Hashimoto M, Endo T, Peltier G, Tasaka M and Shikanai T (2003) A nucleus-encoded factor, CRR2, is essential for the expression of chloroplast *ndhB* in *Arabidopsis*. Plant J 36: 541–549

Hauser M, Eichelmann H, Oja V, Heber U and Laisk A (1995) Stimulation by light of repid pH regulation in the chloroplast stroma *in vivo* as indicated by CO_2 solubilization in leaves. Plant Physiol 108: 1059–1066

Heber U (2002) Irrungen, Wirrungen? The Mehler reaction in relation to cyclic electron transport in C3 plants. Photosynth Res 73: 223–231

Heber U and Walker D (1992) Concerning a dual function of coupled cyclic electron-transport in leaves. Plant Physiol 100: 1621–1626

Heber U, Egneus H, Hanck U, Jensen M and Koster S (1978) Regulation of photosynthetic electron transport and phosphorylation in intact chloroplasts and leaves of *Spinacia oleracea L*. Planta 143: 41–49

Heber U, Neimanis S, Siebke K, Schonknecht G and Katona E (1992) Chloroplast energization and oxidation of P700 and plastocyanin in illuminated leaves at reduced levels of CO_2 or oxygen. Photosynth Res 34: 433–447

Herbert SK, Fork DC and Malkin R (1990) Photoacoustic measurements *in vivo* of energy storage by cyclic electron transport in algae and higher plants. Plant Physiol 94: 926–934

Hill R and Bendall F (1960) Function of the two cytochrome components in chloroplasts: a working hypothesis. Nature 186: 136–137

Hiyama T and Ke B (1971) A further study of P430. A possible primary acceptor of photosystem I. Arch Biochem Biophys 147: 99–180

Horvath EM, Peter SO, Joet T, Rumeau D, Cournac L, Horvath GV, Kavanagh TA, Schafer C, Peltier G and Medgyesy P (2000) Targeted inactivation of the plastid *ndhB* gene in tobacco results in an enhanced sensitivity of photosynthesis to moderate stomatal closure. Plant Physiol 123: 1337–1349

Hosler JP and Yocum CF (1985) Evidence for 2 cyclic photophosphorylation reactions concurrent with ferredoxin-catalyzed non-cyclic electron-transport. Biochim Biophys Acta 808: 21–31

Jagendorf AT and Avron M (1958) Cofactors and rates of photosynthetic phosphorylation by spinach chloroplasts. J Biol Chem 231: 277–290

Jeanjean R, Bedu S, Havaux M, Matthijs HCP and Joset F (1998) Salt-induced photosystem I cyclic electron transfer restores growth on low inorganic carbon in a type 1 NAD(P)H dehydrogenase deficient mutant of *Synechocystis* PCC 6803. FEMS Microbiol Lett 167: 131–137

Joët T, Cournac L, Peltier G and Havaux M (2002) Cyclic electron flow around photosystem I in C-3 plants. *In vivo* control by the redox state of chloroplasts and involvement of the NADH-dehydrogenase complex. Plant Physiol 128: 760–769

Johnson GN (2003) Thiol regulation of the thylakoid electron transport chains: a missing link in the regulation of photosynthesis? Biochemistry 42: 3040–3044

Johnson GN (2005) Cyclic electron transport in C_3 plants: fact or artefact? J Exp Bot 56: 407–416

Joliot P and Joliot A (1988) The low-potential electron-transfer chain in the cytochrome b/f complex. Biochim Biophys Acta 933: 319–333

Joliot P and Joliot A (2002) Cyclic electron transfer in plant leaf. Proc Natl Acad Sci USA 99: 10209–10214

Joliot P and Joliot A (2004) Cyclic electron flow under saturating excitation of dark-adapted Arabidopsis leaves. Biochim Biophys Acta 1656: 166–176

Joliot, P and Joliot A (2005) Quantification of cyclic and linear flows in plants. Proc Natl Acad Sci USA 102: 4913–4918

Joliot P, Lavergne J and Béal D (1992) Plastoquinone compartmentation in chloroplasts. 1. Evidence for domains with different rates of photo-reduction. Biochim Biophys Acta 1101: 1–12

Joliot P, Beal D and Joliot A (2004) Cyclic electron flow under saturating excitation of dark-adapted Arabidopsis leaves. Biochim Biophys Acta 1656: 166–176

Katona E, Neimanis S, Schonknecht G and Heber U (1992) Photosystem I-dependent cyclic electron-transport is important in controlling Photosystem-II activity in leaves under conditions of water-stress. Photosynth Res 34: 449–464

Kirchhoff H, Horstmann S and Weis E (2000) Control of the photosynthetic electron transport by PQ diffusion microdomaines in thylakoids of higher plants. Biochim Biophys Acta 1459: 148–168

Klughammer C and Schreiber U (1994) An improved method, using saturating light-pulses, for the determination of Photosystem-I quantum yield via P^{+}_{700}- absorbency changes at 830 nm. Planta 192: 261–268

Kurisu G, Zhang HM, Smith JL and Cramer WA (2003) Structure of the cytochrome $b_6 f$ complex of oxygenic photosynthesis: tuning the cavity. Science 302: 1009–1014

Laisk A (1993) Mathematical modelling of free-pool and channelled electron transport in photosynthesis: evidence for a functional supercomplex around photosystem 1. Proc R Soc Lond B 251: 243–251

Laisk A, Oja V and Heber U (1992) Steady-state and induction kinetics of the photosynthetic electron transport related to donor side oxidation and acceptor side reduction of photosystem 1 in sunflower leaves. Photosynthetica 27: 449–463

Lascano HR, Casano LM, Martin M and Sabater B (2003) The activity of the chloroplastic Ndh complex is regulated by phosphorylation of the NDH-F subunit. Plant Physiol 132: 256–262

Lavergne J (1983) Membrane potential-dependent reduction of cyt $b_6$in algal mutant lacking Photosystem I centers. Biochim Biophys Acta 725: 25–33

Lavergne J, Bouchaud JP and Joliot P (1992) Plastoquinone compartmentation in chloroplasts. 2. Theoretical aspects. Biochim Biophys Acta 1101: 13–22

Matthijs HCP, Jeanjean R, Yeremenko N, Huisman J, Joset F and Hellingwerf KJ (2002) Hypothesis: versatile function of ferredoxin-NADP(+) reductase in cyanobacteria provides regulation for transient photosystem I-driven cyclic electron flow. Funct. Plant Biol. 29: 201–210

Maxwell PC and Biggins J (1976) Role of cyclic electron transport in photosynthesis as measured by photoinduced turnover of P700 *in vivo*. Biochemistry 15: 3975–3981

Mehler AT (1951) Studies on reactions of illuminated chloroplasts. I. Mechanism of the reduction of oxygen and other Hill reagents. Arch Biochem Biophys 33: 65–77

Mi HL, Endo T, Schreiber U and Asada K (1992a) Donation of electrons from cytosolic components to the intersystem chain in the cyanobacterium *Synechococcus* sp PCC 7002 as determined by the reduction of $P700^+$. Plant Cell Physiol 33: 1099–1105

Mi HL, Endo T, Schreiber U, Ogawa T and Asada K (1992b) Electron donation from cyclic and respiratory flows to the photosynthetic intersystem chain is mediated by pyridine-nucleotide dehydrogenase in the cyanobacterium *Synechocystis* PCC 6803. Plant Cell Physiol 33: 1233–1237

Mi HL, Klughammer C and Schreiber U (2000) Light-induced dynamic changes of NADPH fluorescence in *Synechocystis* PCC 6803 and its *ndhB*-defective mutant M55. Plant Cell Physiol 41: 1129–1135

Miyake C, Shinzaki Y, Miyata M and Tomizawa K (2004) Enhancement of cyclic electron flow around PSI at high light and its contribution to the induction of non-photochemical quenching of chl fluorescence in intact leaves of tobacco plants. Plant Cell Physiol 45: 1426–1433

Miyake C, Horiguchi S, Makino A, Shinzaki Y, Yamamoto H and Tomizawa K (2005a) Effects of light intensity on cyclic electron flow around PS I and its relationship to non-photochemical quenching of Chl fluorescence in tobacco leaves. Plant Cell Physiol 46: 1819–1830

Miyake C, Miyata M, Shinzaki Y and Tomizawa K (2005b) CO_2 response of cyclic electron flow around PS I (CEF-PS I) in tobacco leaves–relative electron fluxes through PS I and PS II determine the magnitude of non-photochemical quenching (NPQ) of Chl fluorescence. Plant Cell Physiol 46: 629–637

Mitchell P (1975) The protonmotive Q cycle: a general formulation. FEBS Lett 59: 137–199

Moss DA and Bendall DS (1984) Cyclic electron transport in chloroplasts. The Q-cycle and the site of action of antimycin. Biochim Biophys Acta 767: 389–395

Mullineaux CW (1999) The thyalkoid membranes of cyanobacteria: structure dynamics and function. Aust J Plant Physiol 26: 671–677

Munekage Y, Hojo M, Meurer J, Endo T, Tasaka M and Shikanai T (2002) PGR5 is involved in cyclic electron flow around photosystem I and is essential for photoprotection in *Arabidopsis*. Cell 110: 361–371

Ogawa T (1991) Cloning and inactivation of a gene essential to inorganic carbon transport of *Synechocystis* PCC 6803. Plant Physiol 96: 280–284

Oxborough K and Horton P (1987) Characterisation of the effects of antimycin A upon high-energy-state quenching of chlorophyll fluorescence (qE) in spinach and pea chloroplasts. Photosynth Res 12: 119–128

Sacksteder A and Kramer DM (2000) Dark-interval relaxation kinetics (DIRK) of absorbance changes as a quantitative probe of steady-state electron transfer. Photosynth Res 66: 145–158

Sandmann G and Malkin R (1983) NADH and NADPH as electron donors to respiratory and photosynthetic electron transport in the blue-green alga *Aphanocapsa*. Biochim Biophys Acta 725: 21–224

Sandmann G and Malkin R (1984) Light inhibition of respiration is due to a dual function of the cytochrome $b_6 f$ complex and the plastocyanin/cytochrome c-533 pool in *Aphanocapsa*. Arch Biochem Biophys 234: 105–111

Sazanov LA, Burrows P and Nixon PJ (1995) Presence of a large protein complex containing the *ndhK* gene product and possessing NADH-specific dehydrogenase activity in thylakoid membranes of higher plant chloroplasts. In: Mathis P (ed) Photosynthesis: From Light to Biosphere Xth International Congress on Photosynthesis, Vol 2, pp 705–708. Kluwer Academic Publishers, Montpellier, France

Sazanov LA, Burrows PA and Nixon PJ (1998) The chloroplast Ndh complex mediates the dark reduction of the plastoquinone pool in response to heat stress in tobacco leaves. FEBS Lett 429: 115–118

Schankser G, Srivastava A, Govindjee and Strasser RJ (2003) Characterisation of the 820-nm transmission signal paralleling the chlorophyll *a* fluorescence rise (OIJP) in pea leaves. Funct Plant Biol 30: 785–796

Scheller H (1996) *In vitro* cyclic electron transport in barley thylakoids follows two independent pathways. Plant Physiol 110: 187–194

Scherer S (1990) Do photosynthetic and respiratory electron transport chains share redox proteins? TIBS 15: 458–462

Schmetteter G (1994) Cyanobacterial respiration. In: Bryant DA (ed) The Molecular Biology of Cyanobacteria, Vol 1, pp 409–435. Kluwer Academic Publishers, Dordrecht

Seelert H, Poetsch A, Dencher NA, Engel A, Stahlberg H and Muller DJ (2000) Structural biology. Proton-powered turbine of a plant motor. Nature 405: 418–419

Sherman DM, Troyan TA and Sherman LA (1994) Localization of membrane proteins in the cyanobacterium *Synechococcus sp*. PCC 7942. Plant Physiol 106: 251–262

Shinokazi K, Ohme M, Tanaka M, Wakasuki T, Hayashida N, Matsubayashi T, Zaita N, Chunwongse J, Obokata J, Yamaguchi-Shinokazi K, Ohto C, Torazawa K, Meng BY, Sugita M, Deno H, Kamogashira T, Yamada K, Kusuda J, Takaiwa F, Kato A, Tohdoh N, Shimada H and Sugiura M (1986) The complete nucleotide sequence of the tobacco chloroplast genome: its gene organization and expression. EMBO J 5: 2043–2049

Smith L and Baltscheffsky M (1959) Respiration and light-induced phosphorylation in extracts of *Rhodospirillum rubrum*. J Biol Chem 234: 1575–1579

Strasser RJ, Schansker G, Srivastava A and Govindjee (2001) Simultaneous measurement of Photosystem I and Photosystem

II probed by modulated transmission at 820 nm and by chlorophyll a fluorescence in the sub ms to second time range. In: Critchley C (ed) PS2001 12th International Congress on Photosynthesis, pp S14–003. CSIRO Publishers, Brisbane, Australia

Stroebel D, Choquet Y, Popot J-L and Picot D (2003) An atypical haem in the cytochrome b_6f complex. Nature 426: 413–418

Tagawa K, Tsujimoto HY and Arnon DI (1963a) Analysis of photosynthetic reactions by the use of monochromatic light. Nature 199: 1247–1252

Tagawa K, Tsujimoto HY and Arnon DI (1963b) Role of chloroplast ferredoxin in the energy conversion process of photosynthesis. Proc Natl Acad Sci USA 49: 567–572

Teicher BH, Moller BL and Scheller HV (2000) Photoinhibition of Photosystem I in field-grown barley (*Hordeum vulgare* L.): induction, recovery and acclimation. Photosynth Res 64: 53–61

Vallon O, Bulte L, Dainese P, Olive J, Bassi R and Wollman FA (1991) Lateral redistribution of cytochrome b_6/f complexes along thylakoid membranes upon state transitions. Proc Natl Acad Sci USA 88: 8262–8266

van Thor JJ, Jeanjean R, Havaux M, Sjollema KA, Joset F, Hellingwerf KJ and Matthijs HCP (2000) Salt shock-inducible Photosystem I cyclic electron transfer in *Synechocystis* PCC 6803 relies on binding of ferredoxin:NADP(+) reductase to the thylakoid membranes via its CpcD phycobilisome-linker homologous N-terminal domain. Biochim Biophys Acta 1457: 129–144

Wang HW, Mi HL, Ye JY, Deng Y and Shen YK (2003) Low concentrations of $NaHSO_3$ increase cyclic photophosphorylation and photosynthesis in cyanobacterium*Synechocystis* PCC 6803. Photosynth Res 75: 151–159

Webber AN, Platt-Aloia KA, Heath RL and Thomson WW (1988) The marginal regions of thylakoid membranes: a partial characterization by polyoxyethylene sorbitane monolaurate (Tween 20) solubilization of spinach thylakoids. Physiol Plant 72: 288–297

Whatley FR (1963) Some effects of oxygen in photosynthesis by chloroplast preparations. In: Kok B and Jagendorf A (eds) Photosynthetic Mechanisms of Green Plants, pp 243–250. National Academy of Sciences – National Research Council, Washington, DC

Whatley FR, Allen MB and Arnon DI (1959) Photosynthesis by isolated chloroplasts. VII. Vitamin K and Riboflavin Phosphate as cofactors of cyclic photophosphorylation. Biochim Biophys Acta 32: 32–46

Wollman F-A and Bulté L (1989) Toward an understanding of the physiological role of state transitions. In: Hall DO and Grassi G (eds) Photoconversion Processes for Energy and Chemicals, pp 198–207. Elsevier, Amsterdam

Yu L, Zhao JD, Muhlenhoff U, Bryant DA and Golbeck JH (1993) PsaE is required for *in vivo* cyclic electron flow around Photosystem-I in the cyanobacterium *Synechococcus* sp. PCC-7002. Plant Physiol 103: 171–180

Zhang HM, Whitelegge JP and Cramer WA (2001) Ferredoxin:NADP(+) oxidoreductase is a subunit of the chloroplast cytochrome b(6)f complex. J Biol Chem 276: 38159–38165

Chapter 38

Photoinhibition and Protection of Photosystem I

Kintake Sonoike*
Department of Integrated Biosciences, Graduate School of Frontier Sciences, University of Tokyo, Kashiwanoha 5-1-5, Kashiwa-shi, Chiba 277-8562, Japan

Summary

Photosystem I (PS I) had been believed to be stable under almost all kinds of environmental stresses, but research in the last 10 years has revealed that PS I is sensitive to photooxidative stress. When combined with low temperature stress, PS I is the main target of photoinhibition, which limits not only overall photosynthesis but also subsequent growth following the application of stress. The molecular mechanism of inhibition is being clarified, and the elucidation of the mechanism of protection from photoinhibition is in progress. Recent advances in the understanding of the photoinhibition of PS I will be discussed in connection with the protection mechanism from inhibition.

*Author for correspondence, email: sonoike@k.u-tokyo.ac.jp

John H. Golbeck (ed): Photosystem I: The Light-Driven Plastocyanin:Ferredoxin Oxidoreductase, 657–668.

I. Introduction

Light is essential for plants as the driving force of photosynthesis. However, everything has two sides, and light is no exception. Too much light causes a decrease in photosynthetic activity, the phenomenon of so-called photoinhibition. The term photoinhibition was originally defined by Kok (1956), who is also a discoverer of the absorption change due to P700, the reaction center chlorophyll of photosystem I (PS I) (Kok, 1957). His group determined the site of photoinhibition using spinach thylakoid membranes and found that, apparently, both PS I and photosystem II (PS II) were inactivated by the photoinhibitory treatment (Jones and Kok, 1966). Since light of very high intensity (more than 15 times of direct sun light) was used for the inactivation of photosynthesis in their experiments, we cannot say whether or not this first observation of photoinhibition of PS I had physiological relevance. Subsequent analysis by Satoh (1970a,b,c) using spinach thylakoid membranes revealed that both PS I and PS II were photoinhibited by a more or less physiological intensity of light. Although there appeared several more reports on the photoinhibition of PS I *in vitro* (e.g., Inoue et al., 1986, 1989), there was substantially no report on the photoinhibition of PS I in intact leaves of higher plant species before 1994. Powles stated in his review (Powles, 1984) that the site of photoinhibition is PS II, and this statement was widely accepted by researchers in photosynthesis.

A turning point came in 1994 when reports on the *in vivo* photoinhibition of PS I appeared (Havaux and Davaud, 1994; Sonoike and Terashima, 1994; Terashima et al., 1994). After 1994, a number of papers appeared on PS I photoinhibition both *in vivo* and *in vitro* (for reviews, see Sonoike, 1996a, 1998a; Hihara and Sonoike, 2001). It is now established that PS I can be a site of photoinhibition. The phenomenon seems to be associated with environmental stress such as low temperature, and the involvement of reactive oxygen species was suggested. Although the precise relationship between inhibition, temperature stress, or reactive oxygen species is not yet fully elucidated, substantial information has been accumulated in these 10 years. In this article, the recent progress in the study of the photoinhibition of PS I will be reviewed in connection with the mechanism of protection from the inhibition.

Abbreviations: PS I – photosystem I; PS II – photosystem II; DCMU – 3-(3,4-dichlorophenyl)-1,1-dimethylurea; DBMIB – 2,5-dibromo-3-methyl-6-isopropyl-*p*-benzoquinone; EPR – electron paramagnetic resonance; P700 – primary electron donor; F_X, F_A, and F_B – terminal electron acceptor iron–sulfur centers.

II. Requirements for the Photoinhibition of PS I

A. Plant Species

Selective photoinhibition of PS I *in vivo* was first reported in cucumber (Sonoike and Terashima, 1994; Terashima et al., 1994) and potato (Havaux and Davaud, 1994) by the moderate light treatment of intact leaves at chilling temperatures. Although there is no further report on the inhibition in potato, many other groups confirmed that PS I is more sensitive to light/chilling stress than PS II in cucumber (e.g., Barth and Krause, 1999; Kim et al., 2001; Jun et al., 2001; Choi et al., 2002). The photoinhibition of PS I itself was also reported for many other plant species: common bean (Sonoike et al., 1995a), spinach, pumpkin, and tobacco (Barth and Krause, 1999), winter rye (Ivanov et al., 1998), barley (Tjus et al., 1998, 1999), maize (Kingston-Smith et al., 1999), coffee (Ramalho et al., 1999), sweet pepper (Li et al., 2003), and cotton (Kornyeyev et al., 2003a,b). In these cases, the extent of the inhibition is not always greater in PS I than in PS II. Moderate light irradiance of cotton at chilling temperatures (Kornyeyev et al., 2003a,b) or high light irradiance of coffee with a low nitrogen supply (Ramalho et al., 1999) preferentially inactivated PS I just as in the case of cucumber, while PS I and PS II are similarly inhibited in spinach, pumpkin, or tobacco (Barth and Krause, 1999). Apparently, the sensitivity of PS I to light stress varies depending on the plant species used or on the experimental conditions employed. Moreover, the mechanism of the inhibition itself may be different depending on the plant species. As described in the next section, there exists evidence that electron flow from PS II is necessary for the inhibition of PS I (Havaux and Davaud, 1994; Sonoike, 1995). On the other hand, it was reported that PS I was degraded in bundle sheath cells of maize (Kingston-Smith et al., 1999) even though PS II is absent in bundle sheath cells of NADP-ME type C4 plants (Ku et al., 1974; Hatch and Osmond, 1976). Apparently, the reducing pressure on the oxidizing side of PS I, not the presence of PS II itself, is important for the inhibition of PS I. The reducing power in bundle sheath cells may be supplied from NADPH imported from mesophyll cells in the form of malate.

The photoinhibition of PS I is induced in chilling-tolerant plants as well as in chilling-sensitive plants. In the case of cucumber, the inhibition of growth and the inhibition of photosynthesis were reported to show a significant correlation (Aoki et al., 1989). Furthermore, genotypic variation of the chilling sensitivity within cucumber could be explained by the variation of the sensitivity of PS I to photoinhibition (Yu et al., 2002). At least in cucumber, photoinhibition of PS I limits photosynthesis, and thereby limits growth.

There are also a few reports of PS I photoinhibition in several algae (Harvey and Bishop, 1978; Gerber and Burris, 1981; Martin et al., 1997). However, there is no report of PS I photoinhibition in cyanobacteria. In cyanobacteria, the photosynthetic electron transport chain shares the plastoquinone pool and the cytochrome b/f complex with the respiratory electron transport chain (Aoki and Katoh, 1982). The presence of an alternative electron sink may function as a protective mechanism against the photoinhibition of PS I in cyanobacteria.

B. Light and Temperature

The photoinhibition of PS I was first reported in the chilling treatment of cucumber, a chilling-sensitive plant, under moderate light (Terashima et al., 1994). Although the plant species that showed the inhibition of PS I was not restricted to chilling-sensitive plants as described above, the inhibition was observed most often when leaves were illuminated at chilling temperatures. Chilling alone does not cause any inhibition in PS I. Dark-chilling treatment of chilling-sensitive plants causes the overreduction and subsequent release of Mn atoms in PS II oxygen-evolving complexes (Kaniuga et al., 1978; Shen et al., 1990; Higuchi et al., 2003). On the other hand, PS I was not inhibited in the dark and inhibition was only observed under illumination (Sonoike and Terashima, 1994; Terashima et al., 1994; Sonoike et al., 1995b; Jun et al., 2001). Therefore, light is an essential factor in the inhibition of PS I. Chilling stress, however, does not seem to be essential for the inhibition. Nitrogen-deficient conditions under high light were reported to cause selective inhibition of PS I at normal temperatures in coffee (Ramalho et al., 1999). When isolated thylakoid membranes were illuminated by moderate light, the photoinhibition of PS I occurred both in chilling-sensitive plants and in chilling-tolerant plants irrespective of the temperature during the treatment (Sonoike, 1995). PS I itself seems to be sensitive to light, and the stability of PS I in intact leaves must be due to some protective mechanisms *in vivo*. The difference in the chilling sensitivity is attributed to a difference in the protective mechanism such as a scavenging system of reactive oxygen species, but not to PS I itself. The role of temperature in the photoinhibition of PS I seems to be related to the readiness of the generation and/or scavenging of reactive oxygen species.

C. Oxygen

Another essential factor for PS I photoinhibition is the presence of oxygen. A decrease in the quantum yield of PS I could not be induced under a nitrogen atmosphere in cucumber (Terashima et al., 1994). Similarly, the fragmentation of the reaction center subunits of PS I was not observed under a nitrogen atmosphere in cucumber (Sonoike and Terashima, 1994), and the decrease of the photooxidation of P700 was suppressed in 2% oxygen (Havaux and Davaud, 1994). A requirement of oxygen for inhibition was also observed in the photoinhibition of PS I in isolated spinach thylakoid membranes (Sonoike, 1995), making the presence of oxygen a fundamental factor in the photoinhibition of PS I. This also suggests the involvement of reactive oxygen species in the process of PS I photoinhibition.

D. Active Electron Transport from PS II

Another factor reported to be necessary for PS I photoinhibition is the presence of active PS II. When PS II was inactivated by the addition of DCMU, photoinhibition of PS I was not observed in chilled potato leaves (Havaux and Davaud, 1994). The protective effect of DCMU was also observed in the photoinhibitory treatment of isolated thylakoid membranes *in vitro* (Sonoike, 1995). DBMIB, which is an inhibitor of cytochrome b/f complex, is also effective in protecting thylakoid membranes (Sonoike, 1995) meaning that electron transfer from PS II (i.e., excitation pressure to PS I) must be necessary for the inhibition of PS I. In addition, chilling pre-treatment of cucumber leaves in the dark, which inhibits PS II (Higuchi et al., 2003) protects PS I from photoinhibition by subsequent chilling treatment in the light (Kudoh and Sonoike, 2002b). However, the correlation between excitation pressure at the plastoquinone pool and the extent of PS I photoinhibition is low, while excitation pressure well explains the extent of PS II photoinhibition (Sonoike, 1999). The extent of the inhibition in PS I seems to be dependent on other factor(s) than excitation pressure at the plastoquinone pool. If PS II is necessary for the inhibition

of PS I, the inhibition should not be observed in isolated PS I complexes. In fact, the photon flux density necessary for the inhibition of isolated PS I complexes is much higher than is necessary for the inhibition of intact leaves or thylakoid membranes (e.g., Yu et al., 2000; Rajagopal et al., 2002). Low photon flux density is enough to inactivate PS I in the presence of PS II, whereas high photon flux density is necessary to inactivate PS I in the absence of PS II. The mechanism of inhibition seems to be different in these two cases. As mentioned in section II.A, the mechanism of inhibition is also different for photoinhibition in bundle sheath cells of maize, where the content of PS II is negligible.

E. Other Environmental Factors

There are a few reports on the inhibition of PS I by other stresses. Ozone fumigation was reported to induce inhibition of both PS I and PS II (Ranieri et al., 2000, 2001). It was also reported that incubation of cyanobacterial cells in 0.5 M NaCl inactivated PS I (Allakhverdiev et al., 2000). Dark-induced senescence of attached wheat leaves also induced inhibition of PS I activity (Misra and Biswal, 1982). At present, it is difficult to understand the relationship between these results and other reports on the photoinhibition of PS I.

F. Mutation in PS I

There are several reports showing the degradation of PS I in mutants of PS I. The degradation of the PsaB subunit was observed under normal growth conditions in a mutant of *Arabidopsis thaliana* with 5% PsaF, the plastocyanin docking subunit (Haldrup et al., 2000). The degradation of the PsaA and PsaD subunits was also observed under high light in mutants of *Chlamydomonas reinhardtii*, which had defects in either on the donor side (PsaF or lumenal loop of PsaB) or on the acceptor side (PsaC) of PS I (Sommer et al., 2003). The acceptor side mutants are apparently light sensitive due to the increased production of reactive oxygen species. The donor side mutants also showed light sensitivity, although to a lesser extent than the acceptor side mutants. The mechanism of photosensitivity may be different between donor side mutants and acceptor side mutants. The *in vitro* stability of the PS I complex itself was not affected by the lack of PsaF in *C. reinhardtii* (Hippler et al., 2000).

III. Mechanism of the Photoinhibition of PS I

A. Direct Cause of Inhibition

Considering the factors to induce the inhibition of PS I, i.e., light, oxygen, and the input of electrons from PS II, it is natural to assume that reactive oxygen species brought about by the reduction of oxygen is the direct cause of inhibition. One-electron reduction of oxygen produces the superoxide anion radical, which could dismutate and be converted into hydrogen peroxide. In the presence of reduced metal ions, hydrogen peroxide is converted to hydroxyl radical, which is highly reactive and destroys biological components within the diffusion limit (Asada, 1999). Interestingly, *in vitro* experiments with isolated thylakoid membranes revealed that the addition of methyl viologen, which accepts electrons from PS I and reduces oxygen to the superoxide anion radical, protects PS I from photoinhibition rather than enhances it (Sonoike, 1996b). It was also found that addition of hydrogen peroxide in the dark did not cause any inhibition of PS I (Sonoike et al., 1997). Thus, superoxide or hydrogen peroxide could not be the reactive oxygen species that are directly responsible for the inhibition of PS I. The addition of hydrogen peroxide during illumination of thylakoid membranes, however, caused the complete loss of the photooxidation of P700 (Sonoike et al., 1997). These results suggest that the photoreduction of the iron–sulfur centers on acceptor side of PS I by light illumination is the key to the problem. Hydroxyl radical, a most reactive species of active oxygen, is usually generated by a reaction between hydrogen peroxide and a reduced metal ion in a process called the Fenton reaction. It is plausible to assume that the hydroxyl radical, which is generated by the reaction between hydrogen peroxide and photoreduced iron–sulfur centers, destroys PS I at the site of production of hydroxyl radicals. This scheme was supported by the fact that *n*-propyl gallate, a scavenger of hydroxyl radical, partially protect PS I from photoinhibition (Sonoike, 1996b).

B. Cause of the Increase in Reactive Oxygen Species

A direct determination of the concentration of hydrogen peroxide supported the mechanism of PS I photoinhibition described above. Light/chilling treatment of cucumber leaves resulted in a temporal increase of hydrogen peroxide and in a decrease of ascorbate (Terashima et al., 1998). This temporal increase of

hydrogen peroxide could be explained by an initial increase of the production rate of hydrogen peroxide due the lowered activity of ascorbate peroxidase at chilling temperatures and a subsequent decrease due to the lower rate of electron transfer through photoinhibited PS I (Terashima et al., 1998). In another report, a decrease of the activity of chloroplastic ascorbate peroxidase was observed in cucumber but not in sweet pepper, which is less sensitive to photoinhibition than cucumber (Li et al., 2003). Inactivation of ascorbate peroxidase could be also induced during photooxidative stress by methyl viologen and light (Mano et al., 2001). Chilling of maize caused the accumulation of hydrogen peroxide in leaves (Kingston-Smith and Foyer, 2000). Since the decrease in the activity of ascorbate peroxidase was observed in coffee upon high light irradiance with low nitrogen (Ramalho et al., 1998), the change in ascorbate peroxidase is induced not only by chilling but also by high light. There is a report that the activity of Cu/Zn-superoxide dismutase, not of ascorbate peroxidase, decreased by light/chilling stress in cucumber leaves, concomitant with the increase in the leaf concentration of hydrogen peroxide (Choi et al., 2002). In some cases, however, an increase, not a decrease, in the activity of Cu/Zn-superoxide dismutase by photoinhibitory condition was reported (Ramalho et al., 1998; Li et al., 2003). Since superoxide dismutase produces hydrogen peroxide rather than scavenges it, the inactivation of superoxide dismutase would be the result of an increase in hydrogen peroxide concentration rather than the cause of it. The resulting inactivation of Cu/Zn-superoxide dismutase should further enhance the inhibition of PS I through the suppression of the water–water cycle. In fact, it was reported that the inactivation of Cu/Zn-superoxide dismutase by the copper chelator dimethyldithiocarbamate in spinach leaf discs inhibited PS I activity (Hwang et al., 2004). If we assume that the decrease in the activity of ascorbate peroxidase at chilling temperatures, or the inhibition of the enzyme due to oxidative stress, is the initial step of the photoinhibition, the inhibition of other components such as PS I and Cu/Zn-superoxide dismutase could be explained as follows. The increase of hydrogen peroxide resulting from the inhibition of ascorbate peroxidase at chilling temperature would lead to the production of hydroxyl radicals that inactivate PS I or to the inactivation of Cu/Zn-superoxide dismutase and other enzymes that are sensitive to hydrogen peroxide.

Interestingly, selective excitation of PS I is damaging not only to PS I but also to PS II (Tjus et al., 2001). Concomitant with the decrease of the PS II activity, some conformational change of D1 protein seemed to be induced, judging from the shift of mobility in electrophoresis. Apparently, localized production of superoxide on PS I could be also damaging to PS II as well as the production of singlet oxygen within PS II complexes.

C. Site of Inhibition and Degradation

The initial site of PS I photoinhibition was found to be the iron–sulfur centers on the acceptor side. This was first suggested by the discrepancy in the amount of P700 determined chemically and photochemically (Sonoike and Terashima, 1994). The destruction of iron–sulfurs, F_A, F_B, and F_X is directly shown by EPR measurements and determination of charge recombination kinetics (Sonoike et al., 1995b; Tjus et al., 1999; Teicher et al., 2000). P700, the reaction center chlorophyll of PS I, could be destroyed under higher photon flux densities (Terashima et al., 1994).

Concomitant with the inhibition, the degradation of PS I subunits was also reported. The reaction center subunits of PS I were degraded upon photoinhibition in cucumber leaves (Sonoike and Terashima, 1994) and in spinach thylakoid membranes (Sonoike, 1996b). One of the sites of cleavage was determined as between Ala^{500} and Val^{501} of the PsaB protein, and another as on the stromal loop between helices 8 and 9, which contains the ligands for iron–sulfur center F_X (Sonoike et al., 1997). The PsaA protein and some other small subunits, as well as PsaB protein, can be also degraded in barley (Tjus et al., 1999; Teicher et al., 2000). In the case of maize, the PsaB protein was degraded upon chilling, while the PsaA protein was degraded upon methyl viologen treatment (Kingston-Smith et al., 1999; Kingston-Smith and Foyer, 2000). The fragmentation of PsaA/B was also observed in the green algae, *Dunaliella salina*, grown under high light conditions (Polle and Melis, 1999).

Light-dependent fragmentation was also reported in wheat chloroplasts for the large subunit of Rubisco (Ishida et al., 1997, 1998). This degradation was completely suppressed by the addition of DCMU or methyl viologen (Ishida et al., 1998), just as in the case of the PsaB protein of PS I (Sonoike, 1996b). The degradation of Rubisco is also observed in the exposure of the protein to a hydroxyl radical generating system (Ishida et al., 1999), and the site of cleavage was around the active site of the enzyme (Luo et al., 2002). These results indicate that Rubisco is inactivated by hydroxyl radical produced by the Fenton reaction between hydrogen peroxide and a reduced metal ion, both produced by photosynthetic electron transfer through PS I. It was also

reported that illumination of the chloroplast lysate caused the degradation of glutamine synthetase (Thoenen and Feller, 1998; Palatnik et al., 1999). This degradation is suppressed by the addition of *n*-propyl gallate, and is enhanced by the generating system of hydroxyl radical (Ishida et al., 2002). Furthermore, fragmentation of Rubisco was also reported upon the light/chilling treatment of cucumber leaves *in vivo*, a condition in which PS I is photoinhibited (Nakano et al., 2006). The fragmentation occurred several hours after the photoinhibition of PS I, and the fragmentation was suppressed by the addition of deferoxamine, a specific chelator of iron, or of *n*-propyl gallate (Nakano et al., 2006). Rubisco itself does not contain iron, but several divalent cations including iron could bind to the enzyme to activate it in place of magnesium (Christeller, 1981) forming a metal-substrate complex at the active site of the enzyme (Brändén et al., 1984). Since the site of cleavage of Rubisco *in vivo* was also very specific and might be near the active site of the enzyme (Nakano et al., 2006), it is tempting to assume that the iron, which is released from iron–sulfur centers of PS I to stroma upon photoinhibition of PS I, binds to Rubisco in the place of magnesium and triggers the degradation of the enzyme.

IV. Protection of PS I from Photoinhibition

A. Scavenging Enzymes for Reactive Oxygen Species

As discussed in sections III.A and III.B, reactive oxygen species are responsible for the inhibition of PS I. If this is true, it is expected that the inactivation of the genes encoding the scavenging enzymes for reactive oxygen species would enhance the inhibition, while the overproduction of those genes would suppress the inhibition. In fact, cotton plants that overexpressed genes encoding chloroplast-targeted antioxidant enzymes (superoxide dismutase, ascorbate peroxidase, and glutathione reductase) showed suppression of the decrease of oxygen evolution upon photoinhibitory treatment at chilling temperatures but not of F_v/F_m (Kornyeyev et al., 2001; Payton et al., 2001). Since photochemical quenching was decreased (i.e., the plastoquinone pool became more reduced) in the transformants after the photoinhibitory treatment, downstream of PS II should be inhibited by the light/chilling treatment. Cotton leaves with overproduced ascorbate peroxidase showed less H_2O_2 content and less photoinhibition of PS I and PS II compared with the parent strain upon photoinhibitory treatment at a chilling temperature. However, the correlation between H_2O_2 content and the extent of the inactivation of PS I was not observed (Kornyeyev et al., 2003a). Overproduction of glutathione reductase in cotton partially protects PS I and PS II from photoinhibition (Kornyeyev et al., 2003b).

B. Cyclic Electron Transport and Charge Recombination

As protective mechanisms in PS I, cyclic electron transport around PS I and charge recombination within PS I were proposed. Both processes would lead to a decreased rate of oxidation of P700 upon excitation and an increased rate of rereduction of P700 in the dark. Such kinetics of P700 have been commonly observed under photoinhibitory conditions in chilled potato leaves (Havaux and Davaud, 1994), chilled cucumber leaves (Sonoike, 1998b; Kim et al., 2001), chilled tobacco leaves (Barth and Krause, 2002), overwintering Scots pine (Ivanov et al., 2001), and even in a cyanobacterium grown at 17˚C (Thomas et al., 1999). Cold stress enhanced cyclic electron transfer around PS I leads to a 3.7-fold higher intersystem electron pool size and a fivefold increase in the stromal electron pool available for $P700^+$ reduction in Scots pine (Ivanov et al., 2001). A lowered efficiency of P700 oxidation led to the necessity of a higher intensity of far-red light for the oxidation of P700 (Sonoike, 1998b; Barth et al., 2001; Krause et al., 2003). All of the observed phenomena appear similar, but the explanation for the underlining mechanism is somewhat controversial.

In the case of cucumber leaves chilled for 5 h, the light saturation curve for P700 oxidation determined *in vivo* was almost linear in far-red light up to 15 W/m^2, which is opposite in the case of untreated leaves, which shows saturation by the same far-red light. The difference in the light saturation curves between control and chilling conditions vanished when it was determined *in vitro* with isolated thylakoid membranes (Sonoike, 1998b). Thus, the difference could not be ascribed to an alteration in antenna size or in the rate of charge recombination within the PS I complex. This result suggests that enhanced cyclic electron transfer may be the cause of the faster reduction of P700 in the dark. On the other hand, Kim et al. (2001) proposed that the charge recombination within PS I complexes, not cyclic electron transfer, was the predominant factor for the accelerated rereduction of P700 in chilled cucumber leaves. This proposal is based on the fact that the effect of methyl viologen, which would diminish both cyclic electron

transfer and charge recombination, was observed in the presence of DCMU, which may disturb the proper redox poising of the interphotosystem electron carriers in favor of cyclic electron transport. More direct evidence for the involvement of other factors than cyclic electron transfer in the increased rate of P700 ressreduction came from an NDH deficient mutant. NDH was proposed as a component of cyclic electron transport (Mi et al., 1995; Burrows et al., 1998; Shikanai et al., 1998; Teicher and Scheller, 1998), and the *ndhCKJ*$^{-}$ mutant should have decreased activity of NDH and cyclic electron transfer. However, the light saturation curve for P700 oxidation was similar between the mutant and wild type plants (Barth and Krause, 2002). Thus, cyclic electron transfer could not be a sole factor for the increased rate of P700 re-reduction. A decrease of the efficiency of P700 oxidation upon photoinhibition may be based on an accelerated charge recombination in PS I, and could facilitate thermal dissipation of excessive light energy in these cases. It was also proposed that $P700^{+}$ accumulated under high light stress, which may contribute to photoprotection (Barth et al., 2001).

Cyclic electron transfer, however, seems to play an important role at least in the long-term acclimation of barley leaves. It was found that high light and cold acclimated barley plants showed an increase in the amount of NDH complex and corresponding NADPH dehydrogenase activity (Teicher et al., 2000). If the enhancement of cyclic electron transfer has a protective role from high light or low temperature, the mutants defective in cyclic electron transfer would be expected to show an increased sensitivity to stress. It was reported that F_v/F_m, a measure of PS II quantum yield, decreased more in the tobacco *ndhB*$^{-}$ mutant than in the WT when illuminated at 3,000 μmol/m^{2}sec for 20 min (Endo et al., 1999). The absorption change due to P700 after the treatment is smaller in the *ndhB*$^{-}$ mutant, but this could be explained by charge recombination due to overreduction (Endo et al., 1999; Li et al., 2004). An *ndhCKJ*$^{-}$ mutant was also characterized, but the extent of inhibition of PS I or PS II under photoinhibitory conditions at 20˚C or 4˚C was not affected by the mutation (Barth and Krause, 2002). Similarly, the deletion mutants of *ndhB* and *psaE* and the WT strain of *Synechocystis* sp. PCC 6803 did not show any difference in the extent of photoinhibition of PS I (Thomas et al., 2001), although these genes were reported to play an important role in cyclic electron transfer around PS I in cyanobacteria.

In contrast to these reports, a very clear phenotype was reported for the *Arabidopsis* mutant of *PGR5*, which is a newly identified component of the cyclic electron transfer pathway, which may be redundant with the NDH-mediated pathway (Munekage et al., 2002). The mutant showed the reduction of P700 under high light, which resulted from charge recombination due to an overreduction of the acceptor side of PS I. Exposure of the mutant to high light (1,500 μmol/m^{2}sec) for 15 min resulted in a 70% decrease in the P700 content, while a decrease of less than 30% was observed in PS II quantum yield (Munekage et al., 2002). The results clearly demonstrate that cyclic electron transport is essential for the protection of PS I from photoinhibition, and that the *PGR5* pathway, not the NDH pathway, is the main route for cyclic electron flow around PS I (see also Joliot et al., this volume, Chapter 37).

C. Other Factors

Xanthophyll cycle pigments are known to play important role in energy dissipation and to protect PS II from photooxidative stress. It was also reported that some osmoprotectants are effective in stabilizing conformation and activity of PS II. In the case of PS I, the protective role of these components have not been proven *in vivo*, but an *in vitro* study revealed that PS I could be protected from stress by osmoprotectants. Glycinebetaine was shown to stabilize PS I electron transport against heat inactivation of thylakoid membranes or PS I-enriched membranes (Allakhverdieva et al., 1999). Sucrose, as well as glycinebetaine, was also reported to protect PS I submembrane particles from photoinhibition (Rajagopal and Carpentier, 2003). The activity of *S*-adenosylmethionine decarboxylase, which functions in the synthesis of polyamines, increased at chilling temperatures, and the inhibition of the enzyme resulted in an enhanced inhibition of PS I and PS II at chilling temperatures (He et al., 2002). As reported for other proteins, these osmoprotectants may protect PS I through the stabilization of the quaternary structure of proteins. As for the xanthophyll cycle pigments, there is no report that clarifies the function in PS I. Xanthophyll cycle pigments are present in LHC I (Thayer and Björkman, 1992; Lee and Thornber, 1995; Färber et al., 1997), although their conversion rate is slower than those present in LHC II (Verhoeven et al., 1999). The role of xanthophyll cycle pigments in PS I should be examined in the future.

V. Recovery from Photoinhibition

More than 30 years ago, it was pointed out that photoinhibition at chilling temperatures is irreversible even

after returning the plants to normal growth temperatures (Lyons, 1973). For example, the damage to the photosynthetic activity of tomato at chilling temperatures was reported to be irreversible (Yakir et al., 1986; Brüggemann et al., 1992). Similarly, expansion of the leaf area after chilling treatment of cucumber was inhibited even after three days (Aoki et al., 1989). The rate of turnover of PS II, especially of the D1 protein of PS II, is very high (Sundby et al., 1993; Neidhardt et al., 1998). The recovery of PS II from photoinhibition became slower after chilling stress, but the quantum yield of PS II still recovered three days after light/chilling treatment (Kudoh and Sonoike, 2002a). This is in contrast to the case of PS I, which showed substantial inhibition even after seven days following the light/chilling treatment (Kudoh and Sonoike, 2002a). The reaction center subunits of PS I, which are not a rapid turnover protein like the D1 protein, were shown to be degraded upon the photoinhibition of PS I as discussed in section III.C. It is reasonable to assume that the inhibition of PS I is irreversible, or at least very slow to recover, due to the slow turnover rate of the PS I reaction center subunits.

In addition to the degradation of the reaction center proteins, the degradation of chlorophyll was observed upon photoinhibition of PS I in attached cucumber leaves. Interestingly, degradation of chlorophyll was observed only after returning to normal growth temperatures (Kudoh and Sonoike, 2002a). The residual amount of chlorophyll on the third day after the treatment closely correlated with the amount of functional PS I. This result indicates that the decrease in chlorophyll content is a consequence of the degradation of irreversibly damaged PS I complexes. The damaged PS I, which is able to harvest light energy but unable to utilize it, is a potential source of the reactive oxygen species. Thus, the prompt degradation of damaged PS I after light/chilling stress should have a protective role in avoiding secondary damage from such reactive oxygen species. The bleaching of chlorophyll after chilling stress has been considered to be a symptom of the damage (Lyons, 1973). Considering the results above, however, the bleaching may not be "damage" but should instead be regarded as one of "emergency measures" upon photoinhibition of PS I to avoid secondary damage to the photosynthetic machinery.

It must be noted that the decrease of the PS I content itself would not be hazardous to photosynthesis. The relative decrease of PS I to PS II may result in an enhanced downregulation of PS II through the reduction of the intersystem electron pool, but such regulation would be advantageous rather than harmful under stress conditions. Upon high light illumination, the PS I content decreased, resulting in the reduction of the plastoquinone pool and the down regulation of electron transport in the cyanobacterium, *Synechocystis* sp. PCC 6803 (Hihara et al., 1998). This down regulation is unfavorable for growth after short-term exposure to high light, but it is important for survival under prolonged high light conditions (Sonoike et al., 2001). A preferential decrease of PS I content was also reported during the forced decrease of chlorophyll content in another cyanobacterium *Plectonema boryanum* (Kada et al., 2003). The relative decrease of PS I to PS II content seems to be based on the principle of "safety first," where the production of active oxygen species is avoided at the cost of decreased activity of electron transport.

VI. Physiological Importance

In the case of cucumber, a chilling-sensitive plant, the first target of photoinhibition at chilling temperatures is PS I (Terashima et al., 1994; Barth and Krause, 1999), and the sensitivity of PS I to light/chilling stress must determine the lower limit of the growth temperature. The photoinhibition of PS I is also induced in field grown barley, which is a chilling-tolerant plant (Teicher et al., 2000). In this case, the inhibition was not selective, and both PS I and PS II were similarly inhibited. When the extent of the damage is similar between PS I and PS II, the effect of the inhibition on the growth of plants depends on the rate of recovery from inhibition. Since the recovery rate of PS I from photoinhibition is very low, as discussed in the previous section, in the final analysis photoinhibition of PS I is more harmful for plants than photoinhibition of PS II. It seems that the photoinhibition of PS II is more of regulation, which is necessary for the normal growth, while that of PS I is more of damage, which should be avoided.

Very recently, the regulation of the dissipation of light energy was also reported at the PS I level. Addition of $NADP^+$ to isolated PS I submembrane fractions induced conformational changes in PS I complexes, resulting in the quenching of the chlorophyll fluorescence of PS I. Under these conditions, 25% of P700 could not be oxidized (Rajagopal et al., 2003). Apparently, some kind of "nonphotochemical quenching" was induced and the quantum yield of P700 photooxidation was decreased by the addition of $NADP^+$. The precise mechanism or the physiological role of this phenomenon is not yet clear. It was speculated that the down regulation of PS I under high $NADP^+$/NADPH conditions *in vivo*

would lead to the proper poising (i.e., partial reduction) of plastoquinone pool, which is reported to be necessary for the operation of cyclic electron transfer (e.g., Arnon and Chain, 1975). The physiological meaning of regulation at the PS I level, including cyclic electron transfer, should be examined in future research.

VII. Concluding Remarks

It is now established that PS I is the site of photoinhibition in many plant species under many different conditions. The mechanism of the inhibition of PS I has been clarified. The inhibition seems to be the consequence of the intrinsic nature of PS I: the low redox potential of the electron acceptors sufficient for the reduction of oxygen, and the presence of a metal in the iron–sulfur centers. Although PS I is readily photoinhibited in isolated thylakoid membranes, PS I is more-or-less protected in intact leaves, suggesting the presence of efficient protective mechanisms *in vivo*. Information on these protective mechanisms is very limited at present, and the next issue in the research of PS I photoinhibition should focus on these protective mechanisms *in vivo*.

Acknowledgments

The author thanks Prof. Terashima and Dr. Hihara for a critical reading of the manuscript and for helpful discussions.

References

Allakhverdieva YM, Mamedov MD, Ferimazova N, Papageorgiou GC and Gasanov RA (1999) Glycinebetaine stabilizes photosystem 1 and photosystem 2 electron transport in spinach thylakoid membranes against heat inactivation. Photosynthetica 37: 423–432

Allakhverdiev SI, Sakamoto A, Nishiyama Y, Inaba M and Murata N (2000) Ionic and osmotic effects of NaCl-induced inactivation of photosystem I and II in *Synechococcus* sp. Plant Physiol 123: 1047–1056

Aoki M and Katoh S (1982) Oxidation and reduction of plastoquinone by photosynthetic and respiratory electron transport in a cyanobacterium *Synechococcus* sp. Biochim Biophys Acta 1141: 307–314

Aoki S, Oda M and Hosino K (1989) Varietal differences in chilling-induced depression of photosynthesis and leaf growth in cucumber seedlings. J Jpn Soc Hort Sci 58: 173–179

Arnon DI and Chain PK (1975) Regulation of ferredoxin-catalyzed photosynthetic phosphorylations. Proc Natl Acad Sci USA 72: 4961–4965

Asada K (1999) The water–water cycle in chloroplasts: scavenging of active oxygens and dissipation of excess photons. Annu Rev Plant Physiol Mol Biol 50: 601–639

Barth C and Krause GH (1999) Inhibition of photosystem I and II in chilling-sensitive and chilling-tolerant plants under light and low-temperature stress. Z Naturforsch 54c: 645–657

Barth C and Krause GH (2002) Study of tobacco transformants to assess the role of chloroplastic NAD(P)H dehydrogenase in photoprotection of photosystem I and II. Planta 216: 273–279

Barth C, Krause GH and Winter K (2001) Responses of photosystem I compared with photosystem II to high-light stress in tropical shade and sun leaves. Plant Cell Environ 24: 163–176

Brändén R, Nilsson T and Styring S (1984) Ribulose-1,5-bisphosphate carboxylase/oxygenase incubated with Cu^{2+} and studied by electron paramagnetic resonance spectroscopy. Biochemistry 23: 4374–4378

Brüggemann W, van der Kooju TAW and van Hasselt PR (1992) Long-term chilling of young plants under low light and subsequent recovery. Planta 186: 172–178

Burrows PA, Sazanov LA, Svab Z, Maliga P and Nixon PJ (1998) Identification of a functional respiratory complex in chloroplasts through analysis of tobacco mutants containing disrupted plastid *ndh* genes. EMBO J 17: 868–876

Choi SM, Jeong SW, Jeong WJ, Kwon SY, Chow WS and Park Y-I (2002) Chloroplast Cu/Zn-superoxide dismutase is a highly sensitive site in cucumber leaves chilled in the light. Planta 216: 315–324

Christeller JT (1981) The effects of bivalent cations on ribulose bisphosphate carboxylase/oxygenase. Biochem J 193: 839–844

Endo T, Shikanai T, Takabayashi A, Asada K and Sato F (1999) The role of chloroplastic NAD(P)H dehydrogenase in photoprotection. FEBS Lett 457: 5–8

Färber A, Young AJ, Ruban AV, Horton P and Jahns P (1997) Dynamics of xanthophyll-cycle activity in different antenna subcomplexes in the photosynthetic membranes of higher plants. Plant Physiol 115: 1609–1618

Gerber DW and Burris JE (1981) Photoinhibition and P-700 in the marine diatom *Amphora* sp. Plant Physiol 68: 699–702

Haldrup A, Simpson DJ and Scheller HV (2000) Down-regulation of the PSI-F subunit of photosystem I (PSI) in *Arabidopsis thaliana*. J Biol Chem 275: 31211–31218

Harvey GW and Bishop NI (1978) Photolability of photosynthesis in two separate mutants of *Scenedesmus obliquus*. Plant Physiol 62: 330–336

Hatch MD and Osmond CB (1976) Compartmentation and transport in C_4 photosynthesis. In: Stocking CR and Hever U (eds) Transport in Plants III: Intracellular Interactions and Transport Processes. Encyclopedia of Plant Physiology, New Series, Vol 3, pp 144–184. Springer-Verlag, Berlin

Havaux M and Davaud A (1994) Photoinhibition of photosynthesis in chilled potato leaves is not correlated with a loss of photosystem-II activity – preferential inactivation of photosystem I. Photosynth Res 40: 75–92

He L, Nada K, Kasukabe Y and Tachibana S (2002) Enhanced susceptibility of photosynthesis to low-temperature photoinhibition due to interruption of chill-induced increase of *S*-adenosylmethionine decarboxylase activity in leaves of spinach (*Spinacia oleracea* L.). Plant Cell Physiol 43: 196–206

Higuchi M, Noguchi T and Sonoike K (2003) Over-reduced state of the Mn-cluster in cucumber leaves induced by dark-chilling treatment. Biochim Biophys Acta 1604: 151–158

Hihara Y and Sonoike K (2001) Regulation, inhibition and protection of photosystem I. In: Aro E-M and Andersson B (eds)

Regulation of Photosynthesis, pp 507–531. Kluwer Academic Publishers, Dordrecht

Hihara Y, Sonoike K and Ikeuchi M (1998) A novel gene, *pmgA*, specifically regulates photosystem stoichiometry in the cyanobacterium *Synechocystis* species PCC 6803 in response to high light. Plant Physiol 117: 1205–1216

Hippler M, Biehler K, Krieger-Liszkay A, van Dillewjin J and Rochaix J-D (2000) Limitation in electron transfer in photosystem I donor side mutants of *Chlamydomonas reinhardtii*. J Biol Chem 275: 5852–5859

Hwang HJ, Kim J-H, Eu Y-J, Moon BY, Cho SH and Lee C-H (2004) Photoinhibition of photosystem I is accelerated by dimethyldithiocarbamate, an inhibitor of superoxide dismutase, during light-chilling of spinach leaves. J Photochem Photobiol B: Biol 73: 79–85

Inoue K, Sakurai H and Hiyama T (1986) Photoinactivation sites of photosystem I in isolated chloroplasts. Plant Cell Physiol 27: 961–968

Inoue K, Fujii T, Yokoyama E, Matsuura K, Hiyama T and Sakurai H (1989) The photoinhibition site of photosystem I in isolated chloroplasts under extremely reducing conditions. Plant Cell Physiol 30: 65–71

Ishida H, Nishimori Y, Sugisawa M, Makino A and Mae T (1997) The large subunit of ribulose-1, 5-bisphosphate carboxylase/oxygenase in fragmented into 37-kDa and 16-kDa polypeptides by active oxygen in the lysates of chloroplasts from primary leaves of wheat. Plant Cell Physiol 38: 471–479

Ishida H, Shimizu S, Makino A and Mae T (1998) Light-dependent fragmentation of the large subunit of ribulose-1,5-bisphosphate carboxylase/oxygenase in chloroplasts isolated from wheat leaves. Planta 204: 305–309

Ishida H, Makino A and Mae T (1999) Fragmentation of the large subunit of ribulose-1,5-bisphosphate carboxylase by reactive oxygen species occurs near Gly-329. J Biol Chem 274: 5222–5226

Ishida H, Anzawa D, Kokubun N, Makino A and Mae T (2002) Direct evidence for non-enzymatic fragmentation of chloroplastic glutamine synthase by a reactive oxygen species. Plant Cell Environ 25: 625–631

Ivanov AG, Morgan RM, Gray GR, Velitchkova MY and Huner NPA (1998) Temperature/light dependent development of selective resistance to photoinhibition of photosystem I. FEBS Lett 430: 288–292

Ivanov AG, Sane PV, Zeinalov Y, Malmberg G, Gardeström P, Huner NPA and Öquist G (2001) Photosynthetic electron transport adjustments in overwintering Scots pine (*Pinus sylvestris* L.). Planta 213: 575–585

Jones LW and Kok B (1966) Photoinhibition of chloroplast reactions. I. Kinetics and action spectra. Plant Physiol 41: 1037–0143

Jun S-S, Kim JM and Lee CB (2001) A comparative study on the effect of chilling treatment in the light and in the dark on subsequent photosynthesis in cucumber. Aust J Plant Physiol 28: 489–496

Kada K, Koike H, Satoh K, Hase T and Fujita Y (2003) Arrest of chlorophyll synthesis and differential decrease of Photosystem I and II in a cyanobacterial mutant lacking light-independent protochlorophyllide reductase. Plant Mol Biol 51: 225–235

Kaniuga Z, Zabek J and Sochanowicz B (1978) Photosynthetic apparatus in chilling-sensitive plants. III. Contribution of loosely bound manganese to the mechanism of reversible inactivation of Hill reaction activity following cold and dark storage and illumination of leaves. Planta 144: 49–56

Kim S-J, Lee C-H, Hope AB and Chow WS (2001) Inhibition of photosystem I and II and enhanced back flow of photosystem I electrons in cucumber leaf discs chilled in the light. Plant Cell Physiol 42: 842–848

Kingston-Smith AH and Foyer CH (2000) Bundle sheath proteins are more sensitive to oxidative damage than those of mesophyll in maize leaves exposed to paraquat or low temperatures. J Exp Bot 51: 123–130

Kingston-Smith AH, Harbinson J and Foyer CH (1999) Acclimation of photosynthesis, H_2O_2 content and antioxidants in maize (*Zea mays*) grown at sub-optimal temperatures. Plant Cell Environ 22: 1071–1083

Kok B (1956) On the inhibition of photosynthesis by intense light. Biochim Biophys Acta 21: 234–244

Kok B (1957) Absorption changes induced by the photochemical reaction of photosynthesis. Nature 179: 583–584

Kornyeyev D, Logan BA, Payton P, Allen RD and Holaday AS (2001) Enhanced photochemical light utilization and decreased chilling-induced photoinhibition of photosystem II in cotton overexpressing genes encoding chloroplast-targeted antioxidant enzymes. Physiol Plant 113: 323–331

Kornyeyev D, Logan BA, Allen RD and Holaday AS (2003a) Effect of chloroplastic overproduction of ascorbate peroxidase on photosynthesis and photoprotection in cotton leaves subjected to low temperature photoinhibition. Plant Sci 165: 1033–1041

Kornyeyev D, Logan BA, Payton PR, Allen RD and Holaday AS (2003b) Elevated chloroplastic glutathione reductase activities decrease chilling-induced photoinhibition by increasing rates of photochemistry, but not thermal energy dissipation, in transgenic cotton. Funct Plant Biol 30: 101–110

Krause GH, Grube E, Virgo A and Winter K (2003) Sudden exposure to solar UV-B radiation reduces net CO_2 uptake and photosystem I efficiency in shade-acclimated tropical tree seedlings. Plant Physiol 131: 745–752

Ku SB, Guttierez M, Kanai R and Edwards GE (1974) Photosynthesis in mesophyll and bundle sheath cells of various type of C_4 plants. II. Chlorophyll and Hill reaction studies. Z Pflanzenphysiol 72: 320–337

Kudoh H and Sonoike K (2002a) Irreversible damage to photosystem I by chilling in the light: cause of the degradation of chlorophyll after returning to normal growth temperature. Planta 215: 541–548

Kudoh H and Sonoike K (2002b) Dark-chilling pretreatment protects PSI from light-chilling damage. J Photosci 9: 59–62

Lee AI-C and Thornber JP (1995) Analysis of the pigment stoichiometry of pigment–protein complexes from barley (*Hordeum vulgare*). The xanthophyll cycle intermediates occur mainly in the light-harvesting complexes of photosystem I and photosystem II. Plant Physiol 107: 565–574

Li X-G, Meng Q-W, Jiang G-Q and Zou Q (2003) The susceptibility of cucumber and sweet pepper to chilling under low irradiance is related to energy dissipation and water–water cycle. Photosynthetica 41: 259–265

Li X-G, Duan W, Meng Q-W, Zou Q and Zhao S-J (2004) The function of chloroplastic NAD(P)H dehydrogenase in tobacco during chilling stress under low irradiance. Plant Cell Physiol 45: 103–108

Luo S, Ishida H, Makino A and Mae T (2002) Fe^{2+}-catalyzed site-specific cleavage of the large subunit of ribulose

1,5-bisphosphate carboxylase close to the active site. J Biol Chem 277: 12382–12387

Lyons JM (1973) Chilling injury in plants. Ann Rev Plant Physiol 24: 443–466

Mano J, Ohno C, Domae Y and Asada K (2001) Chloroplastic ascorbate peroxidase is the primary target of methyl viologen-induced photooxidative stress in spinach leaves: its relevance to monodehydroascorbate radical detected with *in vivo* ESR. Biochim Biophys Acta 1504: 275–287

Martin RE, Thomas DJ, Tucker DE and Herbert SK (1997) The effects of photooxidative stress on photosystem I measured *in vivo* in *Chlamydomonas*. Plant Cell Environ 20: 1451–1461

Mi H, Endo T, Ogawa T and Asada K (1995) Thylakoid membrane-bound, NADPH-specific pyridine nucleotide dehydrogenase complex mediates cyclic electron transport in the cyanobacterium *Synechocystis* sp. PCC 6803. Plant Cell Physiol 36: 661–668

Misra AN and Biswal UC (1982) Differential changes in the electron transport properties of thylakoid membranes during aging of attached and detached leaves, and of isolated chloroplasts. Plant Cell Environ 5: 27–30

Munekage Y, Hojo M, Meurer J, Endo T, Tasaka M and Shikanai T (2002) *PGR5* is involved in cyclic electron flow around photosystem I and is essential for photoprotection in *Arabidopsis*. Cell 110: 361–371

Nakano R, Ishida H, Makino A and Mae T (2006) *In vivo* fragmentation of the large subunit of ribulose-1, 5-bisphosphate carboxylase by reactive oxygen species in an intact leaf of cucumber under chilling-light conditions. Plant Cell Physiol 4: 270–276

Neidhardt J, Benemann JR, Zhang LP and Melis A (1998) Photosystem II repair and chloroplast recovery from irradiance stress: relationship between chronic photoinhibition, light-harvesting chlorophyll antenna size and photosynthetic productivity in *Dunaliella salina* (green algae). Photosynth Res 56: 175–184

Palatnik JF, Carrillo N and Valle EM (1999) The role of photosynthetic electron transport in the oxidative degradation of chloroplastic glutamine synthetase. Plant Physiol 121: 471–478

Payton P, Webb R, Kornyeyev D, Allen R and Holaday AS (2001) Protecting cotton photosynthesis during moderate chilling at high light intensity by increasing chloroplastic antioxidant enzyme activity. J Exp Bot 52: 2345–2354

Polle JEW and Melis A (1999) Recovery of the photosynthetic apparatus from photoinhibition during dark incubation of the green alga *Dunaliella salina*. Aust J Plant Physiol 26: 679–686

Powles SB (1984) Photoinhibition of photosynthesis induced by visible light. Annu Rev Plant Physiol 35: 15–44

Rajagopal S and Carpentier R (2003) Retardation of photo-induced changes in photosystem I submembrane particles by glycinebetaine and sucrose. Photosynth Res 78: 77–85

Rajagopal S, Bukhov NG and Carpentier R (2002) Changes in the structure of chlorophyll–protein complexes and excitation energy transfer during photoinhibitory treatment of isolated photosystem I submembrane particles. J Photochem Photobiol B: Biol 62: 194–200

Rajagopal S, Bukhov NG, Tajmir-Riahi H-A and Carpentier R (2003) Control of energy dissipation and photochemical activity in photosystem I by NADP-dependent reversible conformational changes. Biochemistry 42: 11839–11845

Ramalho JC, Campos PS, Teixeira M and Nunes MA (1998) Nitrogen dependent changes in antioxidant system and in fatty acid composition of chloroplast membranes from *Coffea arabica* L. plants submitted to high irradiance. Plant Sci 135: 115–124

Ramalho JC, Campos PS, Quartin VL, Silva MJ and Nunes MA (1999) High irradiance impairments on photosynthetic electron transport, ribulose-1,5-bisphosphate carboxylase/oxygenase and N assimilation as a function of N availability in *Coffea arabica* L. plants. J Plant Physiol 154: 319–326

Ranieri A, Serini R, Castagna A, Nali C, Baldan B, Lorenzini G and Soldatini GF (2000) Differential sensitivity to ozone in two poplar clones. Analysis of thylakoid pigment–protein complexes. Physiol Plant 110: 181–188

Ranieri A, Giuntini D, Ferraro F, Nali C, Baldan B, Lorenzini G and Soldatini GF (2001) Chronic ozone fumigation induces alterations in thylakoid functionality and composition in two poplar clones. Plant Physiol Biochem 39: 999–1008

Satoh K (1970a) Mechanism of photoinactivation in photosynthetic systems. I. The dark reaction in photoinactivation. Plant Cell Physiol 11: 15–27

Satoh K (1970b) Mechanism of photoinactivation in photosynthetic systems. II. The occurrence and properties of two different types of photoinactivation. Plant Cell Physiol 11: 29–38

Satoh K (1970c) Mechanism of photoinactivation in photosynthetic systems. III. Site and mode of photoinactivation in photosystem I. Plant Cell Physiol 11: 187–197

Shen J-R, Terashima I and Katoh S (1990) Cause for dark, chilling-induced inactivation of photosynthetic oxygen-evolving system in cucumber leaves. Plant Physiol 93: 1354–1357

Shikanai T, Endo T, Hashimoto T, Yamada Y, Asada K and Yokota A (1998) Directed disruption of the tobacco *ndhB* gene impairs cyclic electron flow around photosystem I. Proc Natl Acad Sci USA 95: 9705–9709

Sommer F, Hippler M, Biehler K, Fischer N and Rochaix J-D (2003) Comparative analysis of photosensitivity in photosystem I donor and acceptor side mutants of *Chlamydomonas reinhardtii*. Plant Cell Environ 26: 1881–1892

Sonoike K (1995) Selective photoinhibition of photosystem I in isolated thylakoid membranes from cucumber and spinach. Plant Cell Physiol 36: 825–830

Sonoike K (1996a) Photoinhibition of photosystem I: its physiological significance in the chilling sensitivity of plants. Plant Cell Physiol 37: 239–247

Sonoike K (1996b) Degradation of *psaB* gene product, the reaction center subunit of photosystem I, is caused during photoinhibition of photosystem I: possible involvement of active oxygen species. Plant Sci 115: 157–164

Sonoike K (1998a) Various aspects of inhibition of photosynthesis under light/chilling stress: 'Photoinhibition at chilling temperatures' versus 'Chilling damage in the light'. J Plant Res 111: 121–129

Sonoike K (1998b) Photoinhibition of photosystem I in chilling sensitive plants determined in vivo and in vitro. In: Garab G (ed) Photosynthesis: Mechanisms and Effects, Vol III, pp 2217–2220. Kluwer Academic Publishers, Dordrecht

Sonoike K (1999) The different roles of chilling temperatures in the photoinhibition of photosystem I and photosystem II. J Photochem Photobiol 48: 136–141

Sonoike K and Terashima I (1994) Mechanism of the photosystem I photoinhibition in leaves of *Cucumis sativus* L. Planta 194: 287–293

Sonoike K, Ishibashi M, Watanabe A (1995a) Chilling sensitive steps in leaves of *Phaseolus vulgaris* L. Examination of the effects of growth irradiances on PS I photoinhibition. In: Mathis P (ed) Photosynthesis: From Light to Biosphere, Vol IV, pp 853–856. Kluwer Academic Publishers, Dordrecht

Sonoike K, Terashima I, Iwaki M and Itoh S (1995b) Destruction of photosystem I iron–sulfur centers in leaves of *Cucumis sativus* L. by weak illumination at chilling temperatures. FEBS Lett 362: 235–238

Sonoike K, Kamo M, Hihara Y, Hiyama T and Enami I (1997) The mechanism of the degradation of *psaB* gene product, one of the photosynthetic reaction center subunits of photosystem I, upon photoinhibition. Photosynth Res 53: 55–63

Sonoike K, Hihara Y and Ikeuchi M (2001) Physiological significance of the regulation of photosystem stoichiometry upon high light acclimation of *Synechocystis* sp. PCC 6803. Plant Cell Physiol 42: 379–384

Sundby C, McCaffery S and Anderson JM (1993) Turnover of the photosystem II D1 protein in higher plants under photoinhibitory and nonphotoinhibitory irradiance. J Biol Chem 268: 25476–25482

Teicher HB and Scheller HV (1998) The NAD(P)H dehydrogenase in barley thylakoids is photoactivatable and uses NADPH as well as NADH. Plant Physiol 117: 525–532

Teicher HB, Møller BL and Scheller HV (2000) Photoinhibition of photosystem I in field-grown barley (*Hordeum vulgare* L.): induction, recovery and acclimation. Photosynth Res 64: 53–61

Terashima I, Funayama S and Sonoike K (1994) The site of photoinhibition in leaves of *Cucumis sativus* L. at low temperatures is photosystem I, not photosystem II. Planta 193: 300–306

Terashima I, Noguchi K, Itoh-Nemoto T, Park Y-M, Kubo A and Tanaka K (1998) The cause of PSI photoinhibition at low temperatures in leaves of *Cucumis sativus*, a chilling-sensitive plant. Physiol Plant 103: 295–303

Thayer SS and Björkman O (1992) Carotenoid distribution and deepoxidation in thylakoid pigment–protein complexes from cotton leaves and bundle-sheath cells of maize. Photosynth Res 33: 213–225

Thoenen M and Feller U (1998) Degradation of glutamine synthetase in intact chloroplasts isolated from pea (*Pisum sativum*) leaves. Aust J Plant Physiol 25: 279–286

Thomas DJ, Thomas JB, Pier SD, Nasso NE and Herbert SK (1999) Iron superoxide dismutase protects against chilling damage in the cyanobacterium *Synechococcus* species PCC7942. Plant Physiol 120: 275–282

Thomas DJ, Thomas J, Youderian PA and Herbert SK (2001) Photoinhibition and light-induced cyclic electron transport in *ndhB*$^-$ and *psaE*$^-$ mutants of *Synechocystis* sp. PCC 6803. Plant Cell Physiol 42: 803–812

Tjus SE, Møller BL and Scheller HV (1998) Photosystem I is an early target of photoinhibition in barley illuminated at chilling temperatures. Plant Physiol 116: 755–764

Tjus SE, Møller BL and Scheller HV (1999) Photoinhibition of photosystem I damages both reaction center proteins PS I-A and PS I-B and acceptor-side located small photosystem I polypeptide. Photosynth Res 60: 75–86

Tjus SE, Scheller HV, Andersson B and Møller BL (2001) Active oxygen produced during selective excitation of photosystem I is damaging not only to photosystem I, but also to photosystem II. Plant Physiol 125: 2007–2015

Verhoeven AS, Adams WW III, Demmig-Adams B, Croce R and Bassi R (1999) Xanthophyll cycle pigment localization and dynamics during exposure to low temperatures and light stress in *Vinca major*. Plant Physiol 120: 727–737

Yakir D, Rudich J and Bravdo BA (1986) Adaptation to chilling: photosynthetic characteristics of the cultivated tomato and a high altitude wild species. Plant Cell Environ 9: 477–484

Yu H, Wei J and Carpentier R (2000) Degradation of the photosystem I complex during photoinhibition. Photochem Photobiol 72: 508–512

Yu J-Q, Zhou Y-H, Huang L-F and Allen DJ (2002) Chill-induced inhibition of photosynthesis: genotypic variation within *Cucumis sativus*. Plant Cell Physiol 43: 1182–1188

Chapter 39

Evolutionary Relationships Among Type I Photosynthetic Reaction Centers

Jason Raymond
Microbial Systems Division, Biosciences Directorate, Lawrence Livermore National Laboratory, Livermore, CA 94551, USA

Robert E. Blankenship*
Department of Chemistry and Biochemistry, Arizona State University, Tempe, AZ 85287-1604, USA

Summary

The evolutionary history of photosynthetic reaction centers has been marked by a dramatic increase in subunit and cofactor complexity among the photosystems of oxygenic photosynthetic organisms, including plants, algae, and cyanobacteria. Comparative structural and sequence analysis has made a convincing case for the common ancestry of all tetrapyrrole-based reaction centers, and the combined reaction center family is noteworthy in that multiple evolutionary developmental stages can still be found and studied in extant phototrophs. Photosystem I in particular has expanded from a two-domain homodimeric reaction center with integrated antenna and core electron transfer cofactors, to a multisubunit complex with nearly 130 total cofactors and up to 15 closely interacting subunits in some organisms. Here we discuss some of the notable events in the evolution of Photosystem I that have occurred during this dramatic increase in structural complexity, some of which are lineage-specific while others must have happened before the divergence of plastids and cyanobacteria, possibly with direct relevance to the development of oxygenic photosynthesis.

I. Introduction

The Type I reaction center complexes are found in three distantly separated groups of photosynthetic organisms. The cyanobacteria and related chloroplasts of eukaryotic oxygenic organisms contain Photosystem I (PS I), consisting of a heterodimeric protein core and up to 13 additional protein subunits, not including peripheral antenna complexes. The anoxygenic green sulfur bacteria and heliobacteria are much simpler in structure, both because they contain a homodimeric protein

*Author for Correspondence, email: rblankenship@asu.edu

John H. Golbeck (ed): Photosystem I: The Light-Driven Plastocyanin:Ferredoxin Oxidoreductase, 669–681.

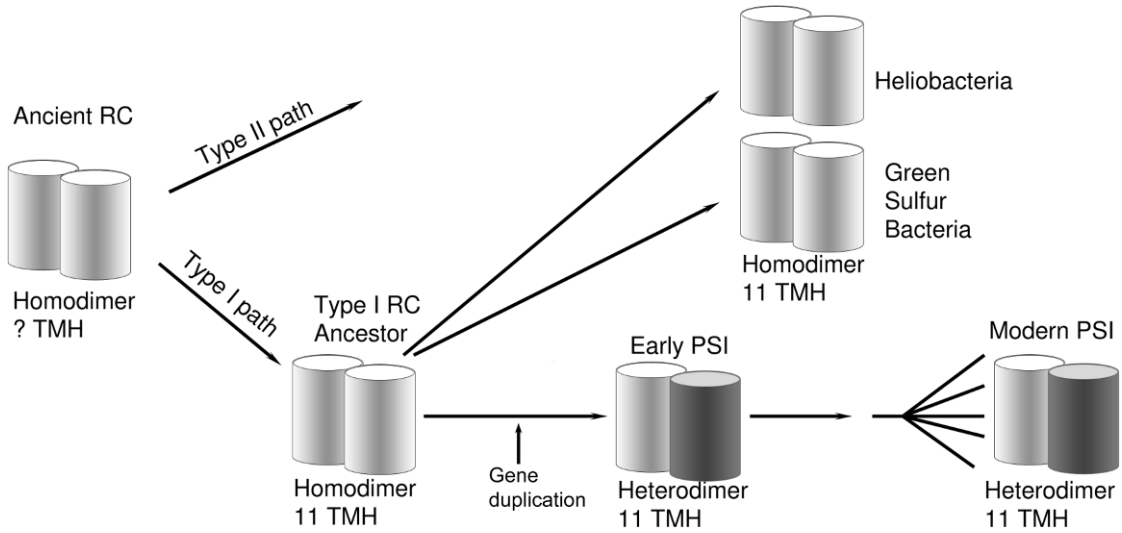

Fig. 1. Schematic of known events in the development of PS I discussed in the text. Proceeding from left to right: an ancient homodimeric reaction center that may have been either five or eleven transmembrane helix; duplication and/or divergence giving rise to two distinct reaction center lineages; divergence of type I RCs through speciation; heterodimerization of the type I reaction center followed by a dramatic increase in subunit complexity specific to modern oxygenic photosynthetic organisms.

core of two identical copies of a single gene product and also because they contain many fewer protein subunits.

This chapter considers some of the evolutionary relationships among the various protein subunits of the Type I reaction center complexes. The overall picture that emerges from this analysis is that the Type I reaction centers have arisen via evolution from an ancient homodimeric complex, that in turn is derived from an even older homodimeric complex that is the ancestor of both the Type I and Type II reaction center complexes. As discussed below, the heterodimeric complex found in oxygenic organisms has undergone a long period of evolution since the gene duplication that gave rise to the heterodimeric structural motif. Figure 1 represents a schematic representation of the overall evolutionary development of the core proteins of the type I reaction centers. There is no indication that any of the other protein subunits have specifically coevolved along with the core from either the ancient ancestor of all reaction centers or from the still ancient, but intermediate ancestor of type I RCs. Instead, it appears that the additional subunits have been acquired over time by gene recruitment from other sources.

The nature of the ancient reaction center that is the ancestor to both type I and II reaction centers has been the subject of considerable discussion, in particular whether it contained five or eleven transmembrane helices. We consider this issue at the end of this chapter, but the available data are not sufficient to come to a reliable conclusion on this point.

II. Evolution of the PS I Core

The overall structure of the PS I reaction center is of a multisubunit integral membrane protein complex (Jordan et al., 2001; see also Fromme and Grotjohann, this volume, Chapter 6). The core of the complex is a heterodimer of two intrinsic subunits, each of which has eleven transmembrane helices. The first six helices form an antenna domain, while the last five helices form the core electron transfer domain.

The core of PS I is comprised of two paralogous subunits, PsaA and PsaB, that comprise the scaffold for electron transfer chain cofactors. The two proteins are clearly related to one another by a gene duplication event that preceded the divergence of known cyanobacterial or plastid lineages, as supported by the presence of homologous homodimeric type I reaction centers in the relatively more primitive photosynthetic apparati of green sulfur bacteria and heliobacteria. In addition to being about 10 amino acids shorter (average 735 residues, though *Gloeobacter violaceus* has an ~140 amino acid C-terminal extension), PsaB also shows slightly better conservation than PsaA, both between plants, algae, and cyanobacteria on the whole or when comparing PsaA and PsaB sequences between the groups individually. Importantly, however, the majority of sequence variability between PsaA and PsaB, as evident in alignments and inferred phylogenies, occurred prior to the divergence of known species of oxyphotobacteria (Fig. 2). This is most explicit in the

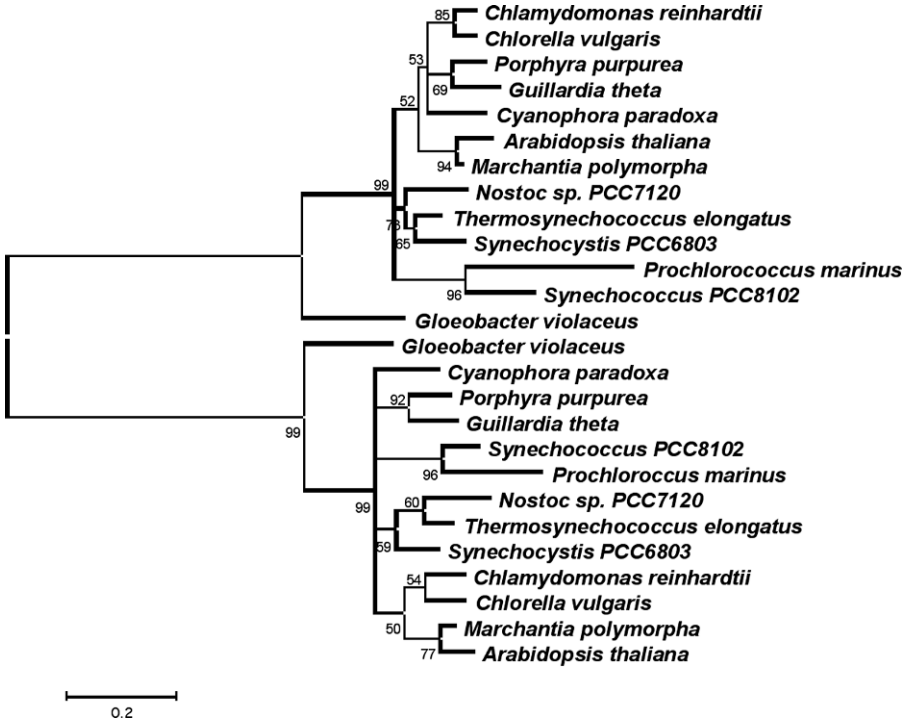

Fig. 2. Rooted maximum likelihood phylogeny of PsaA and PsaB protein sequences from various plants, algae, and cyanobacteria. Scale bar shows number of substitutions per site, numbers at nodes indicate bootstrap support (100 replicates), with nodes having <50% bootstrap support collapsed to denote poor resolution.

shallow branching of PsaA/PsaB clades, which indicates that the two proteins diverged substantially from their common homodimeric ancestor before the earliest true speciation events, subsequent to which the proteins have remained highly conserved. This timing is consistent with that of major events in the development of the Photosystem II (PS II) complex, and both photosystems appear to have developed under strong selective pressure — arguably driven during the transition from anoxygenic to oxygenic photosynthesis — between the emergence of the first primitive, dual-photosystem cyanobacterium, and the plastid endosymbiotic event (Raymond and Blankenship, 2004). While this is typically supported in oxyphototroph phylogenies by the deepest event being the divergence of plastids and cyanobacteria, some trees show conflicting results. Interestingly, the combined PsaA/PsaB phylogeny is one such case, where *Gloeobacter violaceus* consistently and robustly branches prior to the plastid/cyanobacteria split (Fig. 2). However, the primary sequences of PsaA and PsaB from *Gloeobacter* exhibit both unique and chimeric features that could potentially be confounding the observed maximum likelihood topology.

The heterodimeric core of PS I comprises two of the most highly conserved of all photosystem proteins, averaging 59% overall amino acid identity between PsaA and PsaB proteins from a diverse set of sequences spanning cyanobacteria, algae, and plants. Within the respective PsaA and PsaB clades, it is apparent that PsaB proteins are slightly better conserved than PsaA proteins, having an average of 79.4% identity versus 76.3% identity in the latter. In most organisms the *psaA* and *psaB* genes are organized in tandem as a single-copy, cotranscribed bicistron. However, the *psaB* gene (though not *psaA*, barring gene loss) underwent an apparent gene duplication in the common ancestor of order Nostocales (Figs. 2 and 4). It is not clear whether or when this second copy is functional, for example, in differentiated heterocyst cells, or why *psaA* is not maintained in two copies, though overall *psaB2* is more highly conserved among the genomes of *Nostoc punctiforme*, *Nostoc PCC7120*, and *Anabaena variabilis* than the bicistronic *psaB1*.

About 45% of the amino acids in the PsaA and PsaB proteins have not changed since their evolution from a common homodimeric ancestor. The degree of conservation increases moving from the peripheral antenna

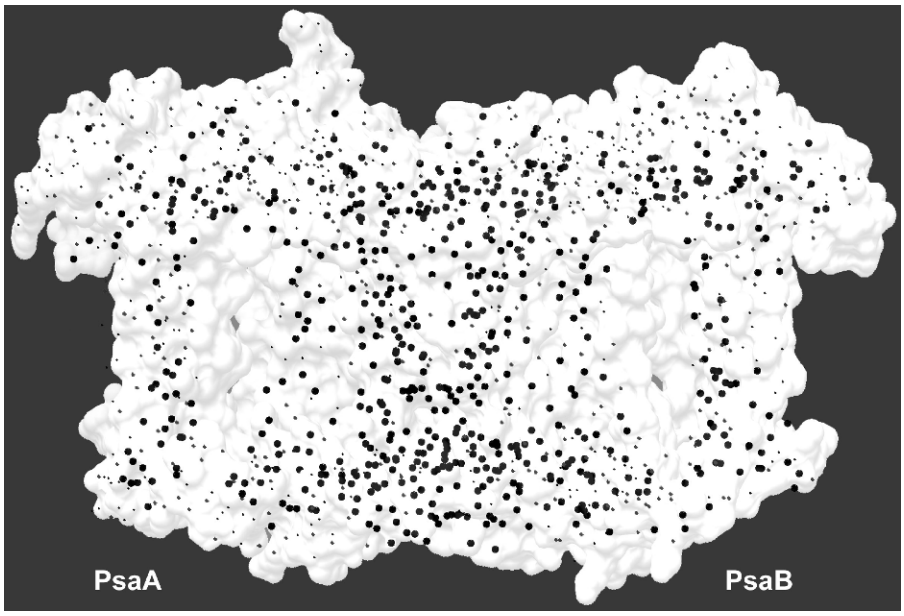

Fig. 3. Conservation of amino acids residues in PsaA and PsaB across cyanobacteria, plants, and algae. Large versus small circles correspond to the position of the C_α carbon of identical and similar residues, respectively, in the *T. elongatus* PS I. Conservation in the heterodimer is highest in and around cofactor binding sites, including the central electron transfer chain and antenna chlorophylls.

domains of the heterodimer toward the core electron transfer chain (ETC) components. For example, superposing the similar and identical residues of photosystem proteins of plants and cyanobacteria back onto the crystal structure of Jordan et al. indicates that residues within a sphere of radius 10 Å of the ETC show 90% or more amino acid similarity (invariant or conservatively substituted) across plants, cyanobacteria, and algae, with 80% of all amino acid residues invariant. Extending outward in 10 Å-incrementing shells, there is 85% overall similarity with 60% of residues invariant between 10 and 20 Å from the ETC, analogous numbers between 30 and 40 Å, 82% similarity but only 45% invariant residues between 40 and 50 Å, and roughly 75% similarity with only 27% of sites invariant around the extended periphery of the heteridimeric core (see Fig. 3). A cursory inspection reveals that the arrangement of invariant and highly conserved residues seems to parallel that of the roughly 90 antenna chlorophyll pigments arranged around the protein scaffold, suggesting that the architecture of antenna pigments presents a strong functional constraint on the evolutionary plasticity of the protein periphery. This notion of an evolutionary history first driven then constrained by cofactor architecture is consistent with ideas advanced in recent structural data indicating almost all of the antenna chlorophylls in PS I have not only been retained but are spatially conserved across cyanobacterial and plastid photosystems (Ben-Shem et al., 2003; see Nelson and Ben-Shem, this volume, Chapter 7). Further support is obtained in looking at the average distance between core chlorophylls and conserved or invariant residues, which shows that the C_α carbon of invariant residues are on average around 15% closer to the nearest chlorophyll Mg atom than variable residues (conserved in less than half of PsaA and PsaB sequences) (data not shown). Furthermore, the number and proportion of invariant residues decreases along outer transmembrane domains of the heterodimer when comparing PsaA and PsaB to one another, though the peripheral residues are indeed strongly conserved *within* the PsaA and PsaB clades. This may reflect the postduplication developmental sequence of the core photosystem, suggesting that while the periphery of the heterodimer has evolved considerably since duplication, the core has changed relatively little at the primary sequence level. This peripheral tuning of the antenna domains around a conserved core may have occurred in tandem with the asymmetric evolution of adjacent photosystem and light harvesting proteins, with some such adaptations being specific to recent emerging lineages and likely coupled to adaptive radiation and colonization of new niches. [See (Ben-Shem et al., 2004) for a well-presented discussion of this so-called "symmetry breaking" in photosystem evolution].

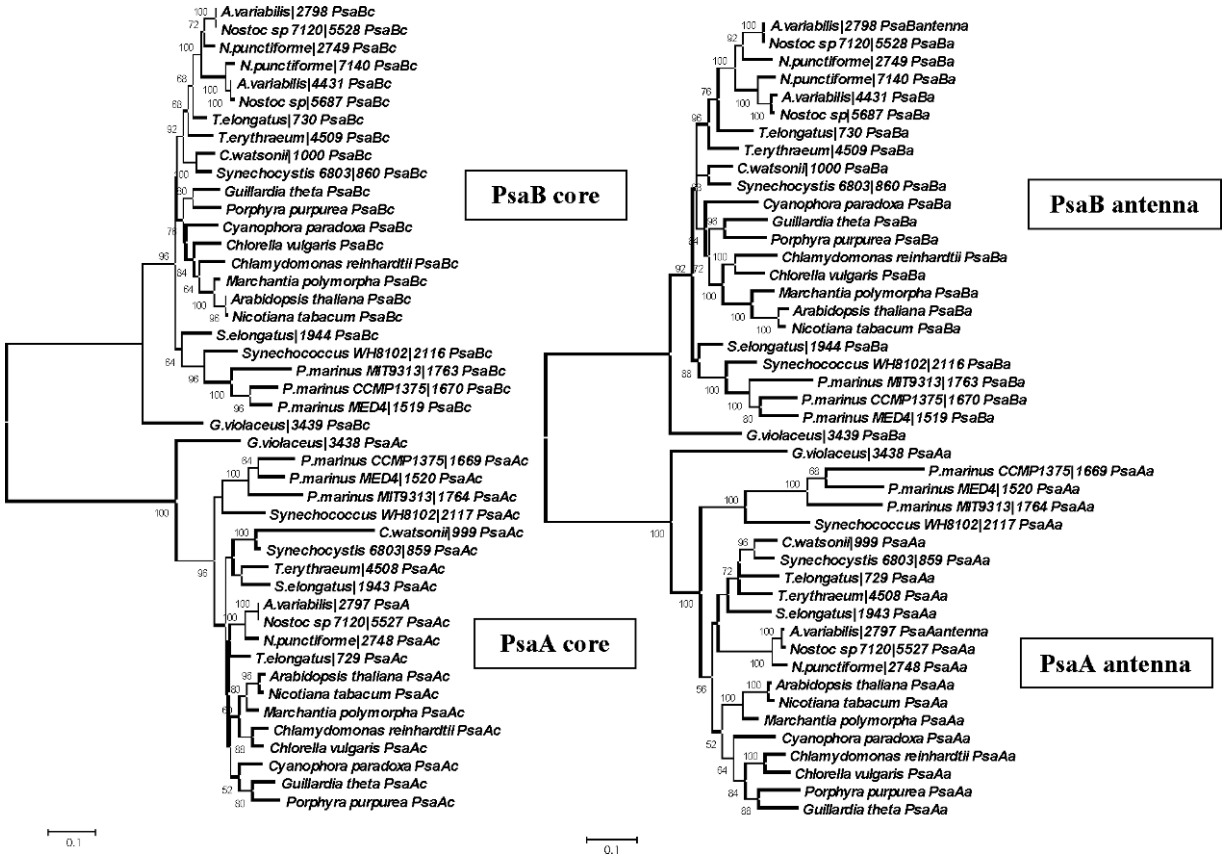

Fig. 4. Individual trees for the core (left) versus antenna (right) domains of PsaB (top clades) and PsaA (bottom clades). Though the two trees are loosely consistent with one another, some differences are clear in the details. Between the PsaA core and antenna domains, the topology differs within both the algae/plant and cyanobacteria clade. The branch lengths of the PsaA antenna domain from prochlorophytes, as well as the PsaA core domain from *C. watsonii*, are uncharacteristically long likely an artifact of the variability in evolutionary rate as discussed in the text and illustrated in Fig. 5. The PsaB core and antenna domains show largely isomorphic topologies, with the exception of the glaucophyte *Cyanophora paradoxa* and the second copy of PsaB in the Nostocales. Both trees are constructed using a neighbor joining algorithm, employing the JTT model of amino acid substitution, percentages of 50 bootstrap replicates are shown at nodes; bootstrap values <50% are not shown, indicating poorly resolved nodes. Numbers following cyanobacterial binomen indicate the approximate position (open reading frame number) within each individual genome.

Further insight into the subtleties of heterodimer divergence is gained in comparing the inferred rate of evolution between the core and antenna domains of PsaA and PsaB, both between and within the two proteins. Figure 4 shows "split" evolutionary tree and Fig. 5 shows a plot of the evolutionary rate in the core versus the antenna domains of PsaA and PsaB from pairwise comparisons of 21 different genomes comprising cyanobacteria, algae, and plants. Each point is taken from corresponding entries in the evolutionary rate matrices for PsaA and PsaB core and antenna proteins. One point, for example, indicates how many amino acid substitutions have occurred between the core domains of PsaA from *Synechocystis* sp. PCC 6803 and *Arabidopsis thaliana*, plotted versus the number of substitutions that have occurred in the PsaB antenna domains from these same two organisms (corrected for length differences). Two proteins or domains that are evolving at identical rates will, for any pair of organisms, show the same number of amino acid substitutions per amino acid site and so would fall along a 45˚ slope. Deviations in evolutionary rate, whether overall between the two proteins or else within specific clades, will manifest as deviations from this ideal slope. Figures 4 and 5 also corroborate the evidence presented above that the antenna domains of PsaA and PsaB are in fact more divergent than their core domains, quantitatively indicating that the antenna domain has undergone roughly 10–20% more substitutions per site than the core domain. Interestingly, the core and

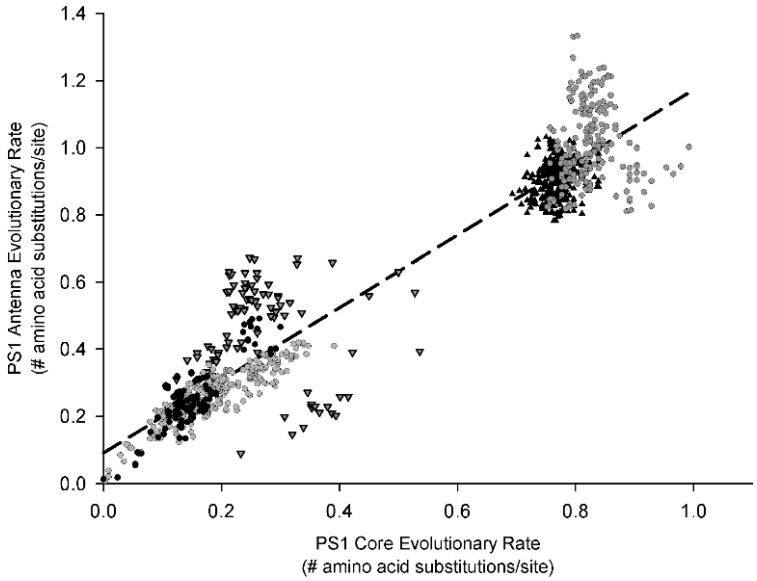

Fig. 5. Strong covariation in the evolutionary rate of the PsaA and PsaB core and antenna domains. Each point plots the evolutionary rate, in number of amino acid substitutions per site, found in the core versus the antenna of PS I between two different oxyphototrophs. The lower left cluster represents ortholog comparisons (PsaA core versus PsaA antenna, PsaB core versus PsaB antenna), while the upper right cluster represents paralog comparisons (PsaA core versus PsaB antenna, and vice versa). PsaB core versus antenna comparisons are gray circles at the lower left, and correlate very strongly. PsaA core versus antenna comparisons correlate most strongly in oxyphototrophs (black circles) after prochlorophyte and *C. watsonii* data are considered separately (inverted triangles). A similar trend is noted in PsaA versus PsaB comparisons comprising the cluster at the upper right; prochlorophyte plus *C. watsonii* data (gray circles) is much more scattered than the same comparisons from other oxyphototrophs (black triangles). The linear regression (dashed line) equation is $y = 1.08x + 0.09 (R^2 = 0.92)$ for all data, though the correlation coefficient improves to 0.96 when prochlorophyte and *C. watsonii* data are omitted. See text for full discussion.

antenna domains of PsaB—as distinct from PsaA—show marked collinearity in their evolutionary rates across all known oxyphototrophs (gray circles, lower left cluster). Conversely, while still positively correlated, there has been some degree of differentiation in the evolution of the antenna versus the core of PsaA, though it is important to note that the phylogeny of the two domains are (topologically) indistinguishable. Principle components analysis indicates that much of the variance observed in PsaA core versus antenna evolutionary rates stems from inclusion of four prochlorophytes and *Crocosphaera watsonii* in the dataset. These five organisms are plotted as inverted triangles in Fig. 5 so as to distinguish them from PsaA core versus antenna plots from other oxyphototrophs (black circles, lower left cluster). Similarly and predictably, these same organisms account for much of the variance when comparing core and antenna domains between PsaA and PsaB (cluster at the upper right of the graph), with the prochlorophyte/*C. watsonii* datasets indicated with black circles as opposed to gray upright triangles for the other oxyphototrophs. This atypical divergence between prochlorophyte PsaA and PsaB proteins has also been noted and detailed in van der Staay et al. (2000).

Given the evidence presented above—that the concerted evolution of PsaB has been less dramatic than that of PsaA—the above data can be summarized as follows. First, as is supported by the structural superposition and also captured in comparison of domain evolutionary rates, the antenna domains of PsaA and PsaB have diverged more than the core domains, due to differences in selective constraints between the two domains. Despite the difference in evolutionary rate, this divergence has been largely collinear since heterodimerization across most phyla of oxyphototrophs, with the noted exception of the prochlorophytes and of *C. watsonii*. The lack of correlation in the core versus antenna domains of these organisms may point to novel functional adaptations or an underlying mode of nonvertical evolution, such as intragenic recombination. Coupling this information to structural data, and comparing it also to PS II antenna and core protein evolution, should be able to provide insight into the nature and timing of photosystem compartmentalization.

Second, the evolution of the core and antenna domains of PsaB has been more tightly coupled than that of the corresponding domains in PsaA. PsaB has been more conserved not only between domains but across known photosynthetic taxa, raising the logical argument that, because PsaB has undergone less overall and change since duplication and heterodimerization, it represents a closer analog to the ancestral homodimer. This difference in the inferred rate of amino acid substitution could result from relatively slow evolution of PsaB, most likely to purifying selection, or from accelerated evolution of PsaA, as would be caused by positive selection. Deciphering where and when these disparities arose within the two halves of the heterodimer, and whether they were coupled to functional development of the photosynthetic apparatus, remains an undertaking of considerable interest.

III. The Soluble Electron Carriers Ferredoxin and Flavodoxin

Following charge separation within the PS I core complex, an electron is transferred to the [4Fe–4S] acceptor contained within the PsaC subunit on the stromal side of the membrane and, ultimately, to ferredoxin or flavodoxin as soluble electron carriers. Extensive deletion, cross-linking, and mutagenesis studies have elucidated PsaC, along with PsaD and PsaE, as primary constituents of the so-called ferredoxin docking site, which guides and stabilizes the interaction of the soluble carrier with the stromal (cytoplasmic) side of the PS I complex (Rousseau et al., 1993; Hanley et al., 1996; Barth et al., 1998). This extrinsic complex has been extensively studied in a number of organisms and appears to be highly conserved evolutionarily. Flavodoxin and ferredoxin appear to be interchangeable as soluble electron carriers in a number of different roles across the tree of life, including that of primary electron acceptor from PS I of cyanobacteria, plants, and algae. In cyanobacteria ferredoxin is found under conditions of iron sufficiency whereas flavodoxin (IsiB) is induced as part of the response to iron deficiency, along with an antenna complex (IsiA) that forms a ring around PS I and increases the overall photon capture cross section by approximately 40% (Leonhardt and Straus, 1992; Bibby et al., 2001; see Barber, this volume, Chapter 9). This permits cells to make fewer PS I complexes, each of which contains 12 Fe atoms, under conditions of iron deficiency.

Ferredoxin and flavodoxin show no clear homology to each other in either sequence or domain structure—ferredoxins are typically small iron–sulfur cluster-containing proteins, whereas flavodoxins are flavoproteins of nearly twice the mass of the [4Fe–4S] ferredoxins they interchange with in oxyphototrophs. Intriguingly, structural alignments of the two proteins on the basis of surface electrostatic potential indicate that the two proteins have significant overlap in critical charged residues and in their active sites. This helps to explain how ferredoxin and flavodoxin are able to substitute for one another effectively in some interactions while still requiring explicit partners in others (Ullmann et al., 2000). The history of these two electron transfer proteins appears to be a remarkable example of evolutionary convergence.

IV. Ferredoxin Docking Site (PsaC, PsaD, PsaE Subunits)

PsaC acts as the central conduit for transferring electrons between F_X of the PS I core to one of the soluble electron carriers ferredoxin or flavodoxin. In association with PsaD and PsaE, PsaC is part of the binding pocket for ferredoxin or flavodoxin and is required for sequential transfer of photoexcited electrons from the PS I core (Fig. 6). PsaC binds two [4Fe–4S] clusters, with the first (F_A) being proximal to F_X within the PS I core and the second (F_B) located closer to the ferredoxin/flavodoxin binding site (Golbeck, 1999). Though PsaC is the link through which electrons flow from PS I, the process of interaction with and charge transfer to the soluble electron carrier is a concerted one, and recent advances in mutagenesis have begun to elucidate residues crucial for correct assembly of the binding pocket, interaction with the soluble carrier, and facilitation of charge transfer (Sétif et al., 2002; see Sétif, this volume, Chapter 26). While *Synechocystis* sp. PCC 6803 PsaD and PsaE knockout mutants are still able to reduce ferredoxin or flavodoxin at a much impaired rate, electron transfer to these proteins is completely obliterated in the absence of PsaC (Sétif, 2001).

On the basis of sequence and structural similarities, PsaC is a member of the ferredoxin superfamily, which includes a remarkably diverse group of electron transfer proteins (see Antonkine and Golbeck, this volume, Chapter 8). As is observed in PsaC, many members of this ferredoxin superfamily contain dicluster binding motifs (CxxCxxCxxxCP, in PsaC and its closest homologs) localized to two tandem stretches of residues separated by a solvent-exposed loop. Note that the first three Cys residues in one motif along with one

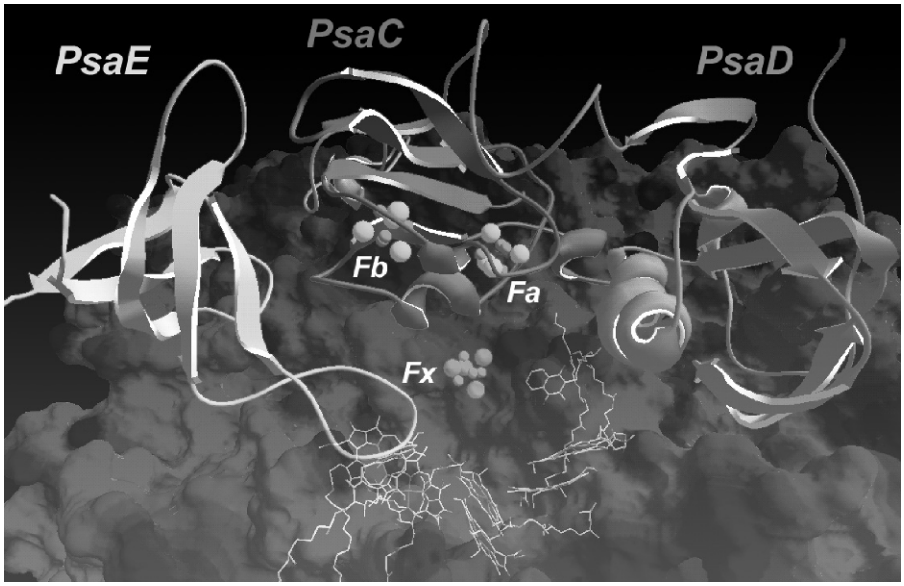

Fig. 6. Looking down at the ferredoxin/flavodoxin binding site, in a cleft bordered by a ~30 Å cytoplasmic extension comprised of PsaC, PsaD, and PsaE. Electron transfer proceeds from the special pair up a chain of secondary acceptors (bottom/distal), to [4Fe–4S] clusters F_X, F_A, and F_B, en route to the soluble electron carrier.

residue from the other motif coordinate one [4Fe–4S] center, while the other motif has the reverse pattern. Several residues within this loop are important in ferredoxin/flavodoxin interaction, as demonstrated by mutagenesis experiments (Fischer et al., 1998). Homologous proteins to PsaC are found throughout the three kingdoms, encompassing a wide swath of known and putative functional roles ranging from ferredoxins to heterodisulfide reductases. Importantly though, the PsaC clade from cyanobacteria and photosynthetic eukaryotes is absolutely distinct in sequence when compared to all other known [4Fe–4S] motif-containing proteins. Known PsaC proteins are very highly conserved in all oxyphototrophs, not just in primary sequence but also in total length – roughly 90% identity (79–100% range) over exactly 81 amino acid residues in all but a single case from SwissProt (PsaC from the marine diatom *Odontella sinensis* has 82 amino acids by way of a single insertion in the C-terminal region). This extreme uniformity is uncharacteristic of photosystem proteins and may reflect a relatively confined geometry within which PsaC functions. The high identity observed in PsaC proteins has the result that phylogenies are confounded by a lack of phylogenetically informative positions. While some taxonomically consistent groups can be discerned on the basis of sequence synapomorphies—for example, the marine prochlorophyte/*Synechococcus* clade is unique at two positions (A4 and D70)—overall the protein is too short and too highly conserved to be robust for resolving phylogenies.

In a mechanism highly analogous to that observed in oxygenic phototrophs, green sulfur bacteria such as *Chlorobium tepidum* transfer electrons via F_X in their homodimeric reaction center to F_A and F_B sites on the so-called PscB protein. However, despite this common electron transfer pathway, the PsaC and PscB proteins are only similar to one another at the C-terminal domain. Beyond the shared, tandem [4Fe–4S] cluster binding motifs, the overall similarity between PscB and PsaC is unremarkable, and both proteins have more closely related ferredoxin-type counterparts in non-photosynthetic organisms. Even among known PscB proteins from green sulfur bacteria, the C-terminal F_A/F_B binding domain is highly conserved whereas the N-terminal domain comprises a highly variable and somewhat unusual looking (with respect to primary sequence) proline- and alanine-rich region with a number of sporadic insertions and deletions. Though the function of this N-terminal extension found in PscB sequences is unclear, pro/ala-rich motifs are thought to be important, for example, as flexible links to membrane anchors, as observed in auracyanin and azurin-like H8 antigen (Bond et al., 2001), and proline-rich domains have been widely implicated as structural motifs coordinating protein–protein interaction and cell membrane localization or translocation of enzymes. The search for the F_A/F_B protein in the other group of type I

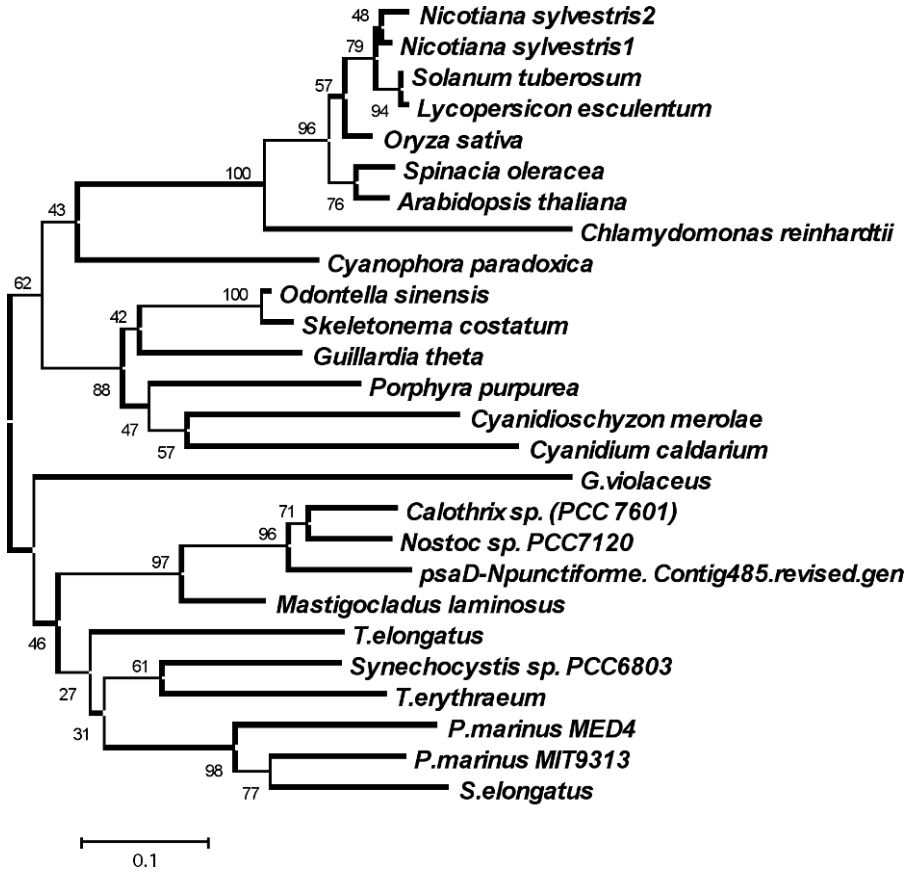

Fig. 7. Neighbor joining phylogeny (JTT matrix, 100 bootstrap replicates) of PsaD proteins presently available in GenBank. Scale bar indicates amino acid substitutions per site.

RC-containing organisms, the heliobacteria, is still ongoing but has yet to produce any primary sequence information for comparison, and whether an analogous or homologous protein to PsaC exists in heliobacteria is still unresolved (Neerken and Amesz, 2001; Heathcote et al., 2003).

PsaD is the largest of the three stromal subunits comprising the ferredoxin/flavodoxin binding site of PS I, though its encoded (preprocessed) size various from around 15 kDa in cyanobacteria to 23 kDa in most eukaryotes, the difference due largely to the plastid-targeting N-terminal extension present in eukaryotic transcripts. The sequence has a number of residues required for proper docking of flavodoxin or ferredoxin at multiple spatially segregated contact points (Sétif, 2001), though PsaD-less mutants are able to reduce ferredoxin with a roughly 100-fold increase in the dissociation constant, supporting the idea of a binding pocket comprised of and extending across multiple proteins (Barth et al., 1998). Furthermore, PsaD appears to impart structural stability not only during assembly of the ferredoxin/flavodoxin docking site (Li et al., 1991; Hanley et al., 1996), but also in the interaction of several peripheral PS-I subunits and in formation of PS-I trimers (Chitnis and Chitnis, 1993; Xu et al., 1994).

Whereas the short overall length and relatively high degree of conservation of PsaC limits its phylogenetic usefulness, the sequence of PsaD carries several distinct markers that allow for a strong reconstruction of known oxyphototroph clades (Fig. 7). This contrasts with the otherwise ambiguous signal in PsaC and PsaE phylogenies (data not shown). For example, as mentioned above, the sequence from plants and *Chlamydomonas reinhardtii* possesses a 50–70 residue N-terminal extension, that clearly demarcates this clade. This extension contains a discernable plastid-targeting motif consistent with a nuclear-encoded, chloroplast-directed eukaryotic gene (also observed for PsaE, though PsaC is plastid-encoded). Roughly 25 amino acids extending beyond the plastid-targeting sequence have been proposed to possibly direct proper cleavage of the transit peptide (Lagoutte et al., 2001).

Table 1. PS I subunits, known or probable function, and distribution in oxyphototrophs

Subunit	Function	Distribution
PsaA	Electron transfer cofactors, core antenna	All oxyphototrophs
PsaB	Electron transfer cofactors, core antenna	All oxyphototrophs
PsaC	Ferredoxin docking, F_A and F_B	All oxyphototrophs
PsaD	Ferredoxin docking	All oxyphototrophs
PsaE	Ferredoxin docking	All oxyphototrophs
PsaF	Plastocyanin docking (algae/plants)	All oxyphototrophs
PsaG	LHC binding	Plastid only
PsaH	LHC binding	Plastid only
PsaI	PsaL interaction, trimerization (cyanobacteria)	Absent in *Gloeobacter violaceus*
PsaJ	Unknown	Absent in *G. violaceus*
PsaK	LHC binding	Absent in *G. violaceus*
PsaL	Trimerization (cyanobacteria), PS I assembly	All oxyphototrophs
PsaM	Unknown	Absent in some prochlorophytes
PsaN	PS I assembly, plastocyanin interaction	Plastid only
PsaO	PS I assembly and function	Plastid only
PsaX	Unknown	Absent in plants and several cyanos

Structural data suggest that this N-terminal extension is distal to, and probably too far removed from the ferredoxin/flavodoxin docking site to play a role in recognition or binding (Fromme et al., 2003). Highly similar duplicate copies of PsaD, indicating a relatively recent gene duplication, have been found in some genomes (e.g., Arabidopsis, spinach), and knockout/complementation studies in spinach have begun to elucidate the important and putatively overlapping function of these PsaD paralogs (Ihnatowicz et al., 2004).

PsaE is approximately 70 residues in cyanobacteria and about 50% larger in plants and algae, again largely accounted for by a plastid-targeting N-terminal extension. Known PsaE proteins are highly conserved across their shared residues though their short overall lengths and lack of informative sites confound phylogenies. Of note is a seven residue insertion largely specific to marine cyanobacteria (*Prochlorococcus* and *Synechococcus* strains) but also found in *Synechocystis* sp. PCC 6803. The solution structure of PsaE determined that the protein shows structural similarity with known SH3 domains (Falzone et al., 1994), found in a diverse set of examples such as the recently determined structure of ferredoxin:thioredoxin oxidoreductase (FTR) (Dai et al., 2000); though the possible functional or evolutionary significance of this similarity has not been further investigated.

V. Peripheral Proteins

The peripheral subunits of PS I are a group of relatively small transmembrane proteins that have differentiated considerably since the divergence of plastids and cyanobacteria, collectively exhibiting considerable plasticity as compared to the highly conserved photosystem core. Several peripheral proteins are exclusive to specific clades of oxyphototrophs, making it likely that they evolved after the cyanobacteria/plastid divergence. PsaG, PsaH, PsaN, and PsaO are found only in algal and plant lineages and at least two of these (PsaG and PsaH) are argued to facilitate binding between the photosystem complex and the chlorophyll *a*/*b* binding light harvesting complexes (LHCs) also specific to these lineages (Ben-Shem et al., 2004; see Nelson and Ben-Shem, this volume, Chapter 7). PsaX, on the other hand, is a 4.8 kDa subunit that appears to be specific to cyanobacteria, though not at all ubiquitous within the clade. At least six other intrinsic subunits, however, are found relatively widely across oxyphototrophs, with a few arguably lineage-specific cases of gene loss as in *Gloeobacter violaceus* or within the reduced genomes of several *prochlorophytes* (Table 1). Detection and analysis of these proteins, both experimentally and computationally, is hindered by their small size, functional variability, and limited distribution among oxyphototrophs and will not be considered at great length here, with the exception of PsaF. While PsaF is in fact present in all oxyphototrophs examined to date, it has nonetheless diverged considerably in function (see Hippler and Drepper, this volume, Chapter 29). In plants, the two-domain protein has an integral transmembrane helix and an extrinsic helix that runs approximately parallel to the membrane plane, with several cis-helical, positively charged lysine residues in that interact with a negative patch on the surface of plastocyanin (Hippler et al., 1998; Fromme

et al., 2001). Along with interactions that may span several other photosystem subunits including PsaB, this domain of PsaF comprises a plastocyanin-recognition site in plants and algae that facilitates electron transfer from plastocyanin to P700 following photooxidation. In cyanobacteria, and in particular in cytochrome c_6 binding in lieu of plastocyanin, the role of PsaF is not analogous to that in plants, as has been demonstrated in $PsaF^-$ mutants and mutagenesis studies. Furthermore, kinetic and structural studies support diffusion-limited hydrophobic interaction (rather than electrostatic interaction) between cytochrome c_6 and PS I (De la Rosa et al., 2002; Fromme et al., 2003). De la rosa et al. (2002) point out the remarkable feature that in numerous organisms with both cytochrome c_6 and plastocyanin, presumed to be expressed in response to changing metal availability, the two proteins appear to have co-evolved to retain very similar characteristics—such as redox potential, mass, and pI—so as to remain indistinguishable to the photosystem complex (see de la Rosa et al., this volume, Chapter 40).

VI. A Brief Discourse on the Nature of Earliest Reaction Center Complex

While the availability of high-resolution structures for photosystem and reaction center proteins has argued resolutely for their common ancestry, unraveling the architecture of the ancestral reaction center has remained elusive. Extensive debate has centered on so-called fusion versus fission hypotheses, which respectively propose that the ancestral RC contained five as opposed to eleven transmembrane helices that were subsequently either joined or split to give rise to the other RC family, and multiple scenarios have been proposed for the origin and subsequent distribution of photosynthetic reaction centers (Olson and Pierson, 1987; Nitschke and Rutherford, 1991; Blankenship, 1992; Baymann et al., 2001; Fyfe et al., 2002; Heathcote et al., 2002; Xiong and Bauer, 2002; Heathcote et al., 2003). Distinguishing between these two hypotheses should provide clues to the function of the earliest RC, for example, whether quinones versus iron–sulfur clusters were used as terminal electron acceptors, and also may have some bearing on whether any modern phototrophs represent relict analogs of the earliest photosynthetic organism.

Following the sweeping impact of rRNA-based molecular taxonomy, there was some notion that insight into the earliest photosystem could be addressed by identifying the earliest emerging family of phototrophs, which, based on the rRNA tree of life, has consistently been phylum Chloroflexi (Oyaizu et al., 1987). However, the remarkable chimeric nature of *Chloroflexus aurantiacus* was noted early on as potentially confounding the phylogenetic picture (Blankenship, 1992), and recent studies have further substantiated that the evolution of photosynthesis has been markedly more complex than the evolution of phototrophs, particularly in light of notable examples of horizontal gene transfer (Xiong et al., 2000; Raymond et al., 2002; Xiong and Bauer, 2002; Boucher et al., 2003). Importantly, this failure of organismal phylogeny in revealing the history of photosynthesis is not characteristic of reaction center phylogenies. Conversely, the evolution of the two RC families has followed a fundamentally linear trajectory (Fig. 1), with representatives from several of the intermediate developmental stages found in different groups of modern phototrophs. The stumbling block in understanding the nature of the ancestral reaction center arises in inferring characteristics at the root of the RC phylogenetic tree, and is an inherent obstacle in most trees comprised of only two paralogous families where parsimony has (by default) the same resolving power as a coin toss.

Many thoughtful schema have arisen nonetheless [recently reviewed in (Olson and Blankenship, 2004)], invoking insights based on, for example, the argued antiquity of iron–sulfur proteins and the apparent primitiveness of homodimeric type I reaction centers (both levied in favor of a type I-early scenario). However, these points each elicit valid counterpoints; as counterexamples to the above points, one can argue that quinone analogs are a common currency in respiratory electron transfer change across all three domains of life and were likely utilized in the prephotosynthesis progenitor of modern organisms (Castresana and Moreira, 1999). Furthermore, while type I reaction centers may appear relatively primitive, they are in fact remarkably complex structures that almost certainly evolved from simpler photosynthetic machinery, quite plausibly proceeding through an earlier developmental stage with discrete core and antenna domains akin to type II reaction centers. The cohesion of type I RC organisms (cyanobacteria, heliobacteria, and green sulfur bacteria), apparent in several different photorespiratory complexes (Schutz et al., 2000), has also been argued to be consistent with RCI as predecessor to RCII, the latter which evolved via gene duplication and fission in an early cyanobacterium before horizontal transfer to proteobacteria and filamentous anoxygenic phototrophs such as *Chloroflexus*. This scenario predicts that in comparing extant type I to type II reaction centers, PS I and PS II from cyanobacteria should be

most similar as being temporally closest to the point of RC duplication. However, quite possibly because of the extensive divergence between the two types of RC's (and minding the old "absence of evidence. . . " adage), there is no such pattern apparent either in sequence or structural data to corroborate this prediction. Another counterexample exists as well, in that this RCI-early scheme can be inverted by the simple assumption RCII had evolved earlier in a photosynthetic proteobacterium, subsequently giving rise to RCI via duplication and divergence in the three type I clades, followed by loss of RCII in heliobacteria and green sulfur bacteria. Because RCII loss is required in green sulfur and heliobacteria in the latter scenario, it is in fact less parsimonious, but garners the benefit of fitting phylogenetic data both from analysis of pigment biosynthesis genes as well as what can be inferred from RC evolutionary trees. Methods based on primary sequence analysis for tackling this issue of the earliest reaction center are still operating under limited data; there simply is not enough signal left at the primary sequence level to infer a robust evolutionary trajectory that connects the two types of RC's. Simply put, the alignments and trees we can build today are no better than they were 15 years ago, even using the most penetrating models that molecular evolutionists can come up with. Importantly, this shroud of data limitation shows some signs of lifting in light of an essential and expanding database of relevant structural data, especially in some clever recent analyses that purport to couple structural evolution with functional divergence in reaction center proteins. Though the two conflicting predominant hypotheses on early RC evolution have remained trenchantly embedded in the status quo for nearly two decades, new investigations are making what were previously untenable forays attempting to integrate information from structural and functional studies of photosynthetic reaction centers within a molecular evolutionary context.

Acknowledgments

The NASA Exobiology Program is gratefully acknowledged for support. JR acknowledges funding through an E.O. Lawrence Fellowship at Lawrence Livermore National Laboratory.

References

Barth P, Lagoutte B and Sétif P (1998) Ferredoxin reduction by Photosystem I from *Synechocystis* sp. PCC 6803: toward an understanding of the respective roles of subunits PsaD and PsaE in ferredoxin binding. Biochemistry 37: 16233–16241

Baymann F, Brugna M, Muhlenhoff U and Nitschke W (2001) Daddy, where did PS-1 come from? Biochim Biophys Acta 1507: 291–310

Ben-Shem A, Frolow F and Nelson N (2003) Crystal structure of plant Photosystem I. Nature 426: 630–635

Ben-Shem A, Frolow F and Nelson N (2004) Evolution of Photosystem I – from symmetry through pseudo-symmetry to asymmetry. FEBS Lett 564: 274–280

Bibby TS, Nield J and Barber J (2001) Iron deficiency induces the formation of an antenna ring around trimeric Photosystem I in cyanobacteria. Nature 412: 743–745

Blankenship RE (1992) Origin and early evolution of photosynthesis. Photosynth Res 33: 91–111

Bond CS, Blankenship RE, Freeman HC, Guss JM, Maher MJ, Selvaraj FM, Wilce MC and Willingham KM (2001) Crystal structure of auracyanin, a "blue" copper protein from the green thermophilic photosynthetic bacterium *Chloroflexus aurantiacus*. J. Mol Biol 306: 47–67

Boucher Y, Douady CJ, Papke RT, Walsh DA, Boudreau ME, Nesbo CL, Case RJ and Doolittle WF (2003) Lateral gene transfer and the origins of prokaryotic groups. Annu Rev Genet 37: 283–328

Castresana J and Moreira D (1999) Respiratory chains in the last common ancestor of living organisms. J Mol Evol 49: 453–460

Chitnis VP and Chitnis PR (1993) PsaL subunit is required for the formation of Photosystem I trimers in the cyanobacterium *Synechocystis* sp. PCC 6803. FEBS Lett 336: 330–334

Dai S, Schwendtmayer C, Schurmann P, Ramaswamy S and Eklund H (2000) Redox signaling in chloroplasts: cleavage of disulfides by an iron–sulfur cluster. Science 287: 655–658

De la Rosa MA, Navarro JA, Díaz-Quintana A, De la Cerda B, Molina-Heredia FP, Balme A, Murdoch PS, Díaz-Moreno I, Durán RV and Hervás M (2002) An evolutionary analysis of the reaction mechanisms of Photosystem I reduction by cytochrome c_6 and plastocyanin. Bioelectrochem 55: 41–45

Falzone CJ, Kao YH, Zhao JD, Bryant DA, and Lecomte J (1994) Three-dimensional solution structure of PsaE from the cyanobacterium *Synechococcus* sp. strain PCC 7002, a photosystem I protein that shows structural homology with SH3 domains, Biochemistry 33: 6052–6062

Fischer N, Hippler M, Sétif P, Jacquot JP and Rochaix JD (1998) The PsaC subunit of Photosystem I provides an essential lysine residue for fast electron transfer to ferredoxin. EMBO J 17: 849–858

Fromme P, Jordan P and Krauß N (2001) Structure of Photosystem I. Biochim Biophys Acta 1507: 5–31

Fromme P, Melkozernov A, Jordan P and Krauß N (2003) Structure and function of Photosystem I: interaction with its soluble electron carriers and external antenna systems. FEBS Lett 555: 40–44

Fyfe PK, Jones MR and Heathcote P (2002) Insights into the evolution of the antenna domains of Type-I and Type-II photosynthetic reaction centres through homology modelling. FEBS Lett 530: 117–123

Golbeck JH (1999) A comparative analysis of the spin state distribution of *in vitro* and *in vivo* mutants of PsaC – a biochemical argument for the sequence of electron transfer in Photosystem I as $F_X \rightarrow F_A \rightarrow F_B \rightarrow$ ferredoxin/flavodoxin. Photosynth Res 61: 107–144

Hanley J, Sétif P, Bottin H and Lagoutte B (1996) Mutagenesis of Photosystem I in the region of the ferredoxin cross-linking site: modifications of positively charged amino acids. Biochemistry 35: 8563–8571

Heathcote P, Fyfe PK and Jones MR (2002) Reaction centres: the structure and evolution of biological solar power. Trends Biochem Sci 27: 79–87

Heathcote P, Jones MR and Fyfe PK (2003) Type I photosynthetic reaction centres: structure and function. Philos Trans R Soc Lond B Biol Sci 358: 231–243

Hippler M, Drepper F, Haehnel W and Rochaix JD (1998) The N-terminal domain of PsaF: precise recognition site for binding and fast electron transfer from cytochrome c_6 and plastocyanin to Photosystem I of *Chlamydomonas reinhardtii*. Proc Natl Acad Sci USA 95: 7339–7344

Ihnatowicz A, Pesaresi P, Varotto C, Richly E, Schneider A, Jans P, Salamini F and Leister D (2004) Mutants for Photosystem I subunit D of *Arabidopsis thaliana*: effects on photosynthesis, Photosystem I stability and expression of nuclear genes for chloroplast functions. Plant J 37: 839–852

Jordan P, Fromme P, Witt HT, Klukas O, Saenger W and Krauß N (2001) Three-dimensional structure of cyanobacterial Photosystem I at 2.5 Å resolution. Nature 411: 909–917

Lagoutte B, Hanley J and Bottin H (2001) Multiple functions for the C terminus of the PsaD subunit in the cyanobacterial Photosystem I complex. Plant Physiol 126: 307–316

Leonhardt K and Straus NA (1992) An iron stress operon involved in photosynthetic electron transport in the marine cyanobacterium *Synechococcus* sp. PCC 7002. J Gen Microbiol 138: 1613–1621

Li N, Zhao JD, Warren PV, Warden JT, Bryant DA and Golbeck JH (1991) PsaD is required for the stable binding of PsaC to the Photosystem I core protein of *Synechococcus* sp. PCC 6301. Biochemistry 30: 7863–7872

Neerken S and Amesz J (2001) The antenna reaction center complex of heliobacteria: composition, energy conversion and electron transfer. Biochim Biophys Acta 1507: 278–290

Nitschke W and Rutherford SW (1991) Photosynthetic reaction centres: variations on a common structural theme? Trends Biochem Sci 16: 241–245

Olson JM and Blankenship RE (2004) Thinking about the evolution of photosynthesis. Photosynth Res 80: 373–386

Olson JM and Pierson BK (1987) Evolution of reaction centers in photosynthetic prokaryotes. Int Rev Cytol 108: 209–248

Oyaizu H, Debrunner-Vossbrinck B, Mandelco L, Studier JA and Woese CR (1987) The green non-sulfur bacteria: a deep branching in the eubacterial line of descent. Syst Appl Microbiol 9: 47–53

Raymond J and Blankenship RE (2004) The evolutionary development of the protein complement of photosystem 2. Biochim Biophys Acta 1655: 133–139

Raymond J, Zhaxybayeva O, Gogarten JP, Gerdes SY and Blankenship RE (2002) Whole-genome analysis of photosynthetic prokaryotes. Science 298: 1616–1620

Rousseau F, Setif P and Lagoutte B (1993) Evidence for the involvement of PSI-E subunit in the reduction of ferredoxin by Photosystem I. EMBO J 12: 1755–1765

Schutz M, Brugna M, Lebrun E, Baymann F, Huber R, Stetter KO, Hauska G, Toci R, Lemesle-Meunier D, Tron P, Schmidt C and Nitschke W (2000) Early evolution of cytochrome *bc* complexes. J Mol Biol 300: 663–675

Sétif P (2001) Ferredoxin and flavodoxin reduction by Photosystem I. Biochim Biophys Acta 1507: 161–179

Sétif P, Fischer N, Lagoutte B, Bottin H and Rochaix JD (2002) The ferredoxin docking site of Photosystem I. Biochim Biophys Acta 1555: 204–209

Ullmann GM, Hauswald M, Jensen A and Knapp EW (2000) Structural alignment of ferredoxin and flavodoxin based on electrostatic potentials: implications for their interactions with Photosystem I and ferredoxin-NADP reductase. Proteins 38: 301–309

van der Staay GWM, Moon-van der Staay SY, Garczarek L and Partensky F (2000) Rapid evolutionary divergence of Photosystem I core subunits PsaA and PsaB in the marine prokaryote Prochlorococcus. Photosynth Res 65: 131–139

Xiong J and Bauer CE (2002) Complex evolution of photosynthesis. Annu Rev Plant Physiol Plant Mol Biol 53: 503–521

Xiong J, Fischer WM, Inoue K, Nakahara M and Bauer CE (2000) Molecular evidence for the early evolution of photosynthesis. Science 289: 1724–1730

Xu Q, Armbrust TS, Guikema JA and Chitnis PR (1994) Organization of Photosystem I polypeptides (a structural interaction between the PsaD and PsaL subunits). Plant Physiol 106: 1057–1063

Chapter 40

Convergent Evolution of Cytochrome c_6 and Plastocyanin

The Evolutionary Pathways of the Two Proteins are Connected to the Geochemical Changes in Iron and Copper Availabilities

Miguel A. De la Rosa*, Fernando P. Molina-Heredia, Manuel Hervás and José A. Navarro
Instituto de Bioquímica Vegetal y Fotosíntesis, Universidad de Sevilla y CSIC, Américo Vespucio 49, 41092 Sevilla, Spain

Summary

Cytochrome c_6 and plastocyanin are an excellent case study of the convergent evolution of proteins. The two molecules differ in their primary sequence and 3D structure but function in a similar way to transfer electrons from cytochrome b_6f to Photosystem I. It seems that cytochrome c_6 was first "discovered" by Nature when iron was much more available than copper because of the reducing character of the Earth's atmosphere. As the atmospheric molecular oxygen concentration began to rise because of photosynthetic activity, the relative bioavailabilities of iron and copper declined and rose, respectively, and cytochrome c_6 was replaced with plastocyanin. Such a transition from the heme protein to the copper protein would have indeed involved an evolution of the reaction mechanism, as inferred

*Address for correspondence, email: marosa@us.es

John H. Golbeck (ed): Photosystem I: The Light-Driven Plastocyanin:Ferredoxin Oxidoreductase, 683–696.

from the comparative analysis of the structure–function relationships of plastocyanin and cytochrome c_6 isolated from a number of differently evolved organisms. Three different kinetic models for the reaction mechanism have been proposed: type I (an oriented collisional model), type II (a minimal two-step mechanism involving formation of a transient complex), and type III (a mechanism requiring an additional rearrangement step to make the redox centers orientate properly within the complex). The mechanism of heuristic searching in molecular recognition is thus a product of evolution rather than an inherent feature of molecular interactions. In plants, cytochrome c_6 is not produced as such but there exists a cytochrome c_6-like protein (herein called cytochrome c_P) that could be phyllogenetically related to cyanobacterial cytochrome c_M.

I. Introduction

The membrane complexes cytochrome b_6f and Photosystem I (PS I) are spatially separated, thereby requiring a diffusible carrier that shuttles electrons between them. The carrier must be suitably small to freely diffuse within the thylakoid compartment, acquiring or donating electrons as it transiently comes into contact with the luminal faces of the two membrane complexes. In plant chloroplasts, the carrier is the copper protein plastocyanin. In eukaryotic algae and many, but not all, cyanobacteria, the carrier is also plastocyanin, but their metabolism is so versatile as to allow them to adapt to changing environments: in copper-sufficient cells, plastocyanin is used, but under copper deficiency it is replaced by another metal-containing protein, cytochrome c_6, as an alternative redox carrier (Wood, 1978; Ho and Krogmann, 1984). In each organism, the synthesis of either cytochrome c_6 or plastocyanin is controlled by copper availability, and so electrons can flow through the heme protein rather than the copper protein when the latter metal is in short supply. Finally, there are some cyanobacteria that can only synthesize cytochrome c_6. For example, the absence of plastocyanin has been reported for a strain of *Arthrospira maxima* from Lake Texcoco (in the broad Valley of Mexico), with a pH greater than 10 — at which copper is insoluble (Cavet et al., 2003). From these findings, a plausible hypothesis is that there has been a gradual transition from cytochrome c_6 to plastocyanin, with the first being replaced by the latter at the end of the evolutionary pathway.

Cytochrome c_6 and plastocyanin are thus two different soluble proteins that can play the same physiological role: the transfer of electrons between the membrane complexes cytochrome b_6f and PS I (see Hervás et al., 2003 and Hippler and Drepper, this volume, Chapter 29, for recent reviews). However, a series of questions arise. Why did photosynthetic organisms "invent" two different proteins for the same function? What was the driving-force? What is the structural basis of such a functional interchangeability? Is cytochrome c_6 still present in plants? (Wastl et al., 2002; Molina-Heredia et al., 2003).

Abbreviations: BYA –billion years ago; K_A – equilibrium constant for complex association; k_{et} – rate constant for electron transfer; k_{obs} – observed pseudo first-order rate constant; K_R – equilibrium constant for complex rearrangement; k_2 – bimolecular rate constant; PS I – photosystem I.

II. Molecular Evolution and Geochemical Environment

Since the origin of life on the planet, microbial life has been able to colonize every habitat where biochemical molecules can function and to generate energy using virtually every thermodynamically favorable energy couple. For most of life's history only prokaryotes have existed, and so microorganisms have probably determined the basic composition of Earth's atmosphere during the first half of Earth's history (Kasting and Seifert, 2003). During the latter half of Earth's history, microorganisms created the breathable, O_2-rich air that we enjoy today.

This accomplishment has been attributed to fundamental connections between the evolution of molecules (mainly, nucleic acids and proteins) and the geochemical environment. However, such a strong interplay of geochemical change and biological evolution raises questions about how new biochemical capabilities arise and spread in response to environmental changes in biogeochemical cycling (Macalady and Banfield, 2003).

A. Changes in Oxygen Content of Earth's Atmosphere

The evolution of Earth's atmosphere is linked tightly to the evolution of its biota. The planet is about 4.6 billion years old, and life (biosphere) appeared about 3.8 billion years ago (3.8 BYA). The biosphere was exclusively unicellular and was dominated by

hyperthermophiles that utilized chemical sources of energy and employed a range of metabolic pathways for CO_2 assimilation (Des Marais, 1998). When the first living organism, unicellular bacteria, appeared on the primitive Earth, molecular oxygen did not exist in the atmosphere. Nonoxygenic photosynthesis arose very early, and the oxygen-evolving process arose later but still prior to 2.7 BYA. It appears that oxygenic photosynthesis, an extremely complex biochemical process, was "invented" only once, and a primitive cyanobacterium was the organism responsible. Cyanobacteria elaborated an efficient light-driven machinery and gradually developed into unicellular and multicellular photosynthetic organisms, which produced more and more molecular oxygen. The transition toward the modern global environment was paced by a decline in volcanic and hydrothermal activity (Des Marais, 1998).

Figure 1 shows the increase in the oxygen content of the atmosphere throughout the Earth's life. During at least 2 billion years of photosynthetic activity, molecular oxygen did not enter the atmosphere and dioxygen concentration remained stable at a low level because it was being used for chemical oxidation of huge amounts of reduced compounds (namely sulfide and ferrous iron) as long as cyanobacteria were producing it. The oxygen concentration began to increase rapidly and the limit marked by the Pasteur point (1% of present level) was reached 0.6 BYA, thus allowing the appearance of eukaryotic organisms. The Pasteur point, which means that respiration consuming molecular oxygen can produce energy much more efficiently than anaerobic fermentation, does represent the minimum to sustain the aerobic life. Thereafter, photosynthetic oxygen concentration increased exponentially to reach the Berkner–Marshall point (10% of present level), which marks the formation of a substantial ozone layer in the upper atmosphere along with the land colonization by plants and animals (Peschek, 1999). Berkner and Marshall (1965) proposed that the invasion of land 0.42 BYA was dependent upon the build-up of atmospheric oxygen and the formation of the ozone shield that would have reduced the ultraviolet flux.

Atmospheric evolution is determined largely by its microbial populations, but also is intimately linked with the evolution of new microbial traits and capabilities. Although multicellular organisms such as fungi, algae, plants, and humans have made a significant mark on Earth's geochemistry, averaged over geologic time, it is clear that the most important agents by far have been unicellular organisms. Microbes affect the chemistry and distribution of nearly all elements in the Periodic Table and, thus, directly influence their bioavailability (Newman and Banfield, 2002).

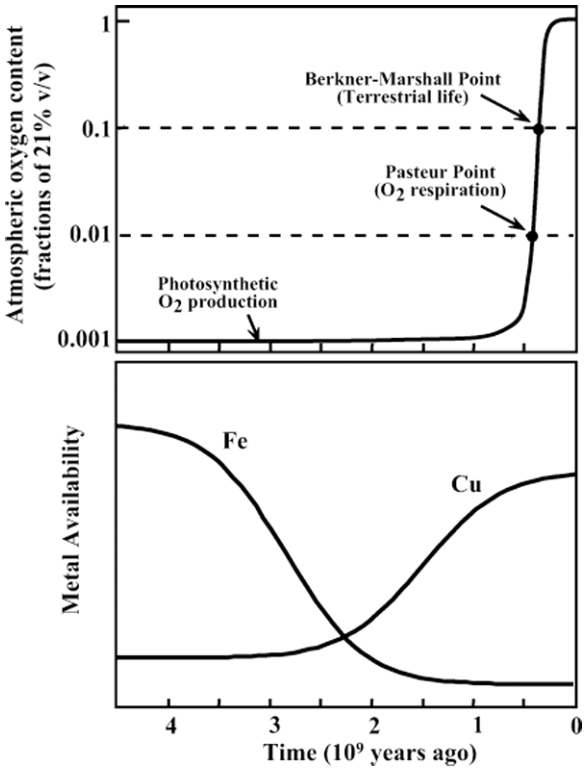

Fig. 1. Time course of changes in atmospheric oxygen content (*upper*) and bioavailability of the chemical elements iron and copper (*lower*) along the Earth's life.

B. Changes in Iron and Copper Bioavailabilities

With the appearance of cyanobacteria and hence dioxygen-generating photosynthesis, the solubility of metals was altered on a global scale as a by-product. The oxygen released changed the world from anaerobic to aerobic and made possible the last great advance in energy-yielding metabolism, aerobic respiration. It should thus be emphasized the role of the environment as the driving force behind the evolution of internal cellular mechanisms (Williams and Fraústo da Silva, 1997).

The advent of oxygen was a catastrophic event for most living organisms, which can be considered to be the first general irreversible pollution of the Earth. On one hand, oxygen acted as a poison for organisms suited to an anaerobic environment, thus being discarded by living cells as a toxic by-product. On the other hand, the slow development of a dioxygen atmosphere had a

gradual effect on many elements of the surface of the Earth and in the sea. In fact, there was a gradual rise in redox potential of the surface of the sea as the partial pressure of O_2 rose. The change was slow and remains far from complete since the reducing components of the early surface and sea formed a large redox buffer, especially through iron sulfides. The elements had to change to higher redox states and some elements, like copper, became more available and some others, like iron, became of greatly reduced availability (Fig. 1) (Williams and Fraústo da Silva, 1997).

Bioavailability of the elements does depend on such variables as their individual solubilities and how in turn these depend on their chemical properties as well as on environmental variables such as temperature. The more soluble a metal complex, the more available it is to life. Sodium, magnesium, calcium, and potassium were very common in the sea and these were used by early life forms. However, copper was relatively unavailable as it had a very low solubility in a reducing environment. Thus early life forms did not use copper in their metabolic processes. As oxygen levels increased, copper became more and more available (Williams and Fraústo da Silva, 1997).

Iron and copper are indeed metals that play an important role in the living world. From a brief consideration of their chemistry and biochemistry it can be concluded that the early chemistry of life used water-soluble ferrous iron while copper was in the water-insoluble Cu(I) state as highly insoluble sulfides. In contrast to the oxidation of iron and its loss of bioavailability as insoluble Fe(III), the oxidation of insoluble Cu(I) led to soluble Cu(II) (Crichton and Pierre, 2001). In summary, life's "addiction" to iron is thought to reflect this early evolution in an iron-rich reducing environment. Large-scale seeding experiments confirm that today iron availability limits growth of oceanic cyanobacteria possibly due to its requirement in photosynthesis and nitrogen fixation (Cavet et al., 2003). On the other hand, copper is contained in a number of enzymes and proteins, but most of them are found only in eukaryotes (Ochiai, 1983).

On the basis of the changing bioavailabilities of iron and copper throughout the Earth's life, the transition form cytochrome c_6 to plastocyanin can be interpreted as a consequence of microbial adaptation to environmental conditions. This means that the first O_2-generating photosynthetic organisms produced the heme protein, as iron was much more abundant than copper, to transfer electrons from cytochrome b_6f to PS I. When copper became available as the atmosphere turn from reducing to oxidizing, the photosynthetic organisms learnt to use such a "novel" metal and incorporated it into proteins to play the same role as some of the "old" iron proteins.

III. Plastocyanin and Cytochrome c_6: Two Structurally Unrelated Proteins

Plastocyanin and cytochrome c_6 are by now well-characterized proteins. A great number of crystal and solution structures are already available for the two molecules from both prokaryotes and eukaryotes. On the basis of such a structural background, a comparative analysis is here performed not only to emphasize the main general features but also to highlight the particular characteristics of each protein depending on the organism from which it is isolated.

A. Description of the Structures

1. Plastocyanin

Plastocyanin, a classical member of the family of type I blue copper proteins, contains a single metal atom bound to a relatively small polypeptide chain (molecular mass, ca. 10.5 kDa) (Sigfridsson, 1998). All plastocyanins from plants, green algae and cyanobacteria possess a similar folding pattern: a β-barrel formed by eight β strands with an additional loop forming in most cases a short α-helix (Guss and Freeman, 1983; Guss et al., 1986; Romero et al., 1998; Kohzuma et al., 1999). According to the typical orientation of the molecule, the copper atom is located at the top of the barrel, thus defining the "northern end" of the molecule (see below), close to the protein surface but not solvent-exposed (Fig. 2). The coordination sphere of the copper atom consists of two histidines, one cysteine, and one methionine in a distorted tetrahedral geometry (Guss and Freeman, 1983; Sigfridsson, 1998). His87 (according to plant residue numbering) is the only ligand exposed to the solvent, thus establishing the electron transfer pathway to and from the metal atom (see below).

The amino acid sequence of plastocyanin is highly conserved in plants and green algae, but shows larger variations in cyanobacteria (Ullmann et al., 1997; Díaz-Quintana et al., 2003). Conserved residues in all plastocyanins include the four copper ligands, whereas the number of acidic and basic residues on the protein surface varies drastically from one organism to another. Actually, the isoelectric point is ca. 4 in eukaryotes (green algae and plants), but in cyanobacteria can vary

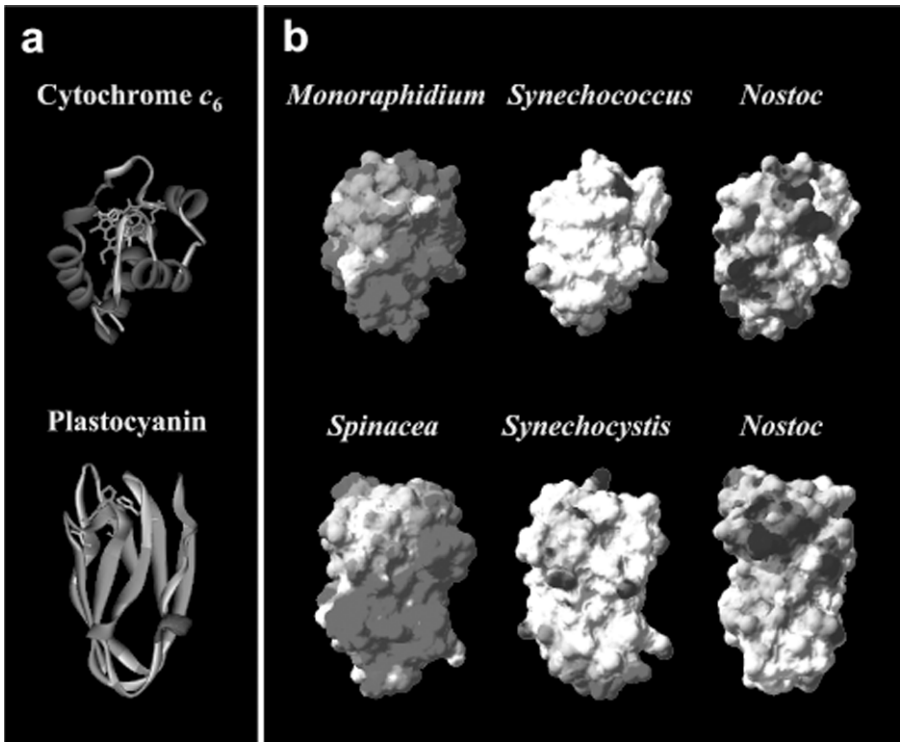

Fig. 2. Overall folding (a) and surface electrostatic potential distribution (b) of cytochrome c_6 (*upper*) and plastocyanin (*lower*) from different organisms. See Color Plate 16, Fig. 1.

from 6 (*Synechocystis* sp. PCC 6803) to 9 (*Nostoc*, formerly *Anabaena* sp. PCC 7119) (De la Rosa et al., 2002).

The first 3D structure of plastocyanin was solved by X-ray crystallography for the protein from poplar (Guss and Freeman, 1983; Guss et al., 1986). Two well-defined areas were identified at the surface level: a flat hydrophobic patch around His87 (the so-called north pole, or site 1), and a negatively charged region around Tyr83 that includes several aspartates and glutamates at positions 42–45 and 59–61 (the so-called east face, or site 2) (Guss et al., 1986; Sigfridsson, 1998). The hydrophobic patch is highly conserved in all plastocyanins, either from eukaryotes or prokaryotes, but the acidic residues of the negative patch are replaced by neutral or positively charged groups in cyanobacteria (Navarro et al., 1997; De la Rosa et al., 2002). Two striking exceptions to this general pattern have been recently reported. The first is plastocyanin from the cyanobacterium *Prochlorothrix hollandica*, whose hydrophobic patch is drastically modified by the presence of proline and tyrosine residues (Babu et al., 1999). The second is fern plastocyanin, which exhibits very distinct electrostatic properties as the acidic region is shifted from the east to the north and surrounds the hydrophobic patch (Kohzuma et al., 1999).

2. Cytochrome c_6

Cytochrome c_6 is a typical class I *c*-type cytochrome, in which the heme group is covalently attached to a single polypeptide chain (molecular mass, ca. 9.5 kDa) with an α-helix folding pattern (Frazão et al., 1995; Kerfeld et al., 1995; Beißinger et al., 1998; Sawaya et al., 2001). According to the residue numbering for the protein from the green alga *Monoraphidium braunii*, the heme iron is axially coordinated by His19 and Met61. The surface exposure of the heme group is ca. 6%, with the edge of pyrrole ring C and the ring D propionic group being solvent accessible and making this area the most probable electron transfer port of the protein (Fig. 2). The heme-binding Cys-Ala-X-Cys-His motif, some of the residues that form the hydrophobic pocket surrounding the heme group and the loop containing the axial ligand Met61 are highly conserved (Kerfeld et al., 1995; Ullmann et al., 1997). Like plastocyanin, cytochrome c_6 from eukaryotes is mostly acidic, whereas the prokaryotic protein can be either neutral or basic. In

fact, a negatively charged area formed by aspartate and glutamate residues at positions 69–72 is well conserved in eukaryotic but not in cyanobacterial cytochrome c_6 (Ullmann et al., 1997; Díaz-Quintana et al., 2003). The relevance of such a parallel diversity in charged groups of plastocyanin and cytochrome c_6 on their physiological function is discussed below.

B. Structural Similarities Between the Two Proteins

Although cytochrome c_6 and plastocyanin are two structurally unrelated proteins, there exist a number of common structural features that explain their functional equivalence, so making the two proteins replace each other inside the cells. First, cytochrome c_6 and plastocyanin exhibit similar values for some physicochemical parameters, namely molecular mass (see above) and midpoint redox potential (ca. 350 mV at pH 7). The isoelectric point is also similar when the two proteins are isolated from the same source, but it can vary accordingly from one organism to another (De la Rosa et al., 2002). Such a difference, which reveals the parallel variation of charged residues at the respective protein surfaces, is one of the most striking aspects of the evolutionary analysis of these two proteins (Fig. 2).

In eukaryotes, the negatively charged area formed by residues 69–72 of cytochrome c_6 (see above) is similar to that at the "east site" of plastocyanin (Frazão et al., 1995; Ullmann et al., 1997; Dikiy et al., 2002). In cyanobacteria, such an equivalent electrostatic area varies in the two proteins in parallel according to their respective isoelectric points. In fact, the electrostatic patch is positively charged in *Nostoc* sp. PCC 7119 and almost neutral in *Synechocystis* sp. PCC 6803 (De la Rosa et al., 2002). The concomitant changes of cytochrome c_6 and plastocyanin at one of their critical functional sites (see below) thus represent an interesting case study of biological evolution at the molecular level that is not only convergent but also parallel: two different proteins that have evolved to play the same physiological role, and so exhibit a number of identical physicochemical properties but show some others that are similar within the same organism and different from one organism to another.

The homology between plastocyanin and cytochrome c_6 does not only relate to the charged groups but can also be extended to the hydrophobic residues. In fact, the hydrophobic patch of plastocyanin around His87 (site 1) is equivalent to that in cytochrome c_6 formed by the hydrophobic residues that surround the heme accessible part, including a hydrophobic residue in position 25 and the conserved Pro59 (Frazão et al., 1995; Ullmann et al., 1997; Dikiy et al., 2002).

The structural comparison between plastocyanin and cytochrome c_6 allowed us to propose that their respective hydrophobic and electrostatic areas, namely sites 1 and 2, are functionally equivalent when these two proteins interact with their two physiological membrane-embedded partners, PS I and cytochrome b_6f (Frazão et al., 1995; Ubbink et al., 1998; Crowley et al., 2002; Díaz-Quintana et al., 2003; Díaz-Moreno et al., 2005). The structural data of the transient complexes formed by cytochrome c_6 and plastocyanin with cytochrome f obtained by NMR spectroscopy (Ubbink et al., 1998; Crowley et al., 2002; Díaz-Moreno et al., 2005), along with the comparative kinetic analysis of the electron transfer from wild-type and mutant species of plastocyanin and cytochrome c_6 to PS I and from cytochrome f to wild-type and mutant plastocyanin (Lee et al., 1995; De la Cerda et al., 1999; Molina-Heredia et al., 1999, 2001; Hart et al., 2003; Albarrán et al., 2005), have unequivocally shown that these two soluble redox carriers use the same areas for interacting with their two physiological counterparts. On the basis of these findings, it has been proposed that the electrostatic patch is responsible for the formation of the transient complex between the membrane system and soluble proteins, whereas the hydrophobic area is used to establish the pathway for electron transfer both to PS I and from cytochrome f. The electrons go into and out the proteins *via* His87 in plastocyanin and the heme accessible ring C in cytochrome c_6 (Frazão et al., 1995; Ubbink et al., 1998; Crowley et al., 2002; Díaz-Moreno et al., 2005).

It is also noteworthy that cyanobacterial plastocyanin and cytochrome c_6 possess just one arginine each that is similarly located between the hydrophobic and electrostatic patches. In plastocyanin, such residue (Arg88) is required for the efficient transfer of electrons from cytochrome f to the copper protein and from it to PS I (Molina-Heredia et al., 2001; Albarrán et al., 2005). The equivalent residue in cytochrome c_6 (Arg67) is also required for the reduction of PS I (see below and Hippler and Drepper, this volume, Chapter 29).

Thus the fine details of the evolutionary trajectories of plastocyanin and cytochrome c_6 at the protein surface level can be quite similar even within a single organism. In fact, the comparison makes evident that these two proteins possess similar interaction areas, thereby explaining their functional equivalence and physiological interchangeability.

IV. Evolution of the Reaction Mechanism of PS I Reduction

The electron transfer from soluble metalloproteins to PS I can be easily observed by following the specific absorbance changes of the special chlorophyll pair P700 in the near infra-red at 820 nm, where it presents an extinction coefficient of 6.5 $mM^{-1}cm^{-1}$ (Mathis and Sétif, 1981). The reaction can be triggered by a short (within the range of nanoseconds), high-energy laser flash at any actinic wavelength. A detailed kinetic study of the interaction between the alternative electron donor proteins (plastocyanin and cytochrome c_6) and PS I has been carried out in an ample variety of differently evolved photosynthetic organisms, ranging from cyanobacteria to plants (see Hope, 2000; Díaz-Quintana et al., 2003; Hervás et al., 2003, for reviews). This comparative evolutionary analysis of PS I reduction by its two donor proteins has provided relevant information on the reaction mechanism and its evolution to improve the kinetic efficiency of the redox reaction.

A. Kinetic Models for the Reaction Mechanism

The reaction course of PS I reduction by plastocyanin and cytochrome c_6 varies drastically among organisms. To simplify the analysis of experimental data, we have proposed (Hervás et al., 1995; De la Rosa et al., 2002) three different kinetic models: type I, when PS I interacts with plastocyanin or cytochrome c_6 by following a collisional reaction mechanism, with no formation of any kinetically detectable transient complex; type II, when an intermediate complex between PS I and its donor protein is detected; and type III, when it is also possible to observe an additional step resulting from the rearrangement of the two redox partners within the complex prior to electron transfer. The three kinetic models are represented in the following scheme:

$$\text{I)}\ \text{PS I}_{ox} + \text{D}_{red} \xrightarrow{k_2} \text{PS I}_{red} + \text{D}_{ox}$$

$$\text{II)}\ \text{PS I}_{ox} + \text{D}_{red} \overset{K_A}{\leftrightarrow} [\text{PS I}_{ox} + \text{D}_{red}] \xrightarrow{k_{et}} \text{PS I}_{red} + \text{D}_{ox}$$

$$\text{III)}\ \text{PS I}_{ox} + \text{D}_{red} \overset{K_A}{\leftrightarrow} [\text{PS I}_{ox} + \text{D}_{red}] \overset{K_R}{\leftrightarrow} [\text{PS I}_{ox} + \text{D}_{red}]^* \xrightarrow{k_{et}} \text{PS I}_{red} + \text{D}_{ox}$$

where PS I and D stand respectively for PS I and donor protein (cytochrome c_6 or plastocyanin), the brackets indicate formation of the transient complex, and the asterisk denotes partners rearrangement within the transient complex. Whichever the kinetic model is applied in every case will depend on the relative values of the equilibrium constants for complex association (K_A) and rearrangement (K_R), as well as of the rate constant for electron transfer itself (k_{et}). As noted by Hope (2000), the Type III model does correspond to the full description of the whole reaction in all systems. The differences among the three kinetic models rather lie on their relative rate-limiting steps, with the kinetics being describable by different equations mainly because of the relative speeds of the electron transfer and rearrangement steps.

The kinetics of PS I reduction are typically monophasic for Type I, either monophasic or biphasic for Type II, and biphasic for Type III. In the two-phase profiles, the lifetime of the first, fast phase is within the range of several microseconds and that of the second, slower phase is usually one or two orders of magnitude higher. For the Type I model, the observed rate constant (k_{obs}) of the monoexponential kinetics increases linearly with increasing protein concentration. For Types II and III models, however, the values for k_{obs} of the slow phase in biphasic kinetics and that for the only phase in monophasic curves show a hyperbolic dependence on the donor protein concentration up to reach a saturating plateau. The value for k_{obs} at such saturating donor protein concentration is assumed to be the rate constant for electron transfer (k_{et}) in Type II but that for donor/PS I complex rearrangement in Type III. In fact, the latter rate constant would be the rate-limiting step for Type III at high donor concentration, with the observed rate constant of the fast phase corresponding to k_{et}. In most donor protein/PS I systems so far analyzed from different organisms, the kinetics of PS I reduction can be well fitted to one of such kinetic models (Hervás et al., 1995; Sigfridsson et al., 1995; Hippler et al., 1997).

B. Evolutionary Optimization of the Reaction Mechanism

On the basis of the above kinetic models for the reaction mechanism of PS I reduction by cytochrome c_6 and plastocyanin, the comparative analysis of the redox reaction in a great number of different organisms — namely, cyanobacteria, green algae, ferns, and plants — shows that the whole process has linearly evolved from Type I to Types II and III up to reach the maximum efficiency (Fig. 3) (Hervás et al., 2003). Thus the type I (or collisional) model is found in some primitive cyanobacteria (*Synechocystis* sp. PCC 6803, *Phormidium laminosum*) with slightly acidic donor proteins, which are unable to form a kinetically detectable transient complex with PS I because of electrostatic

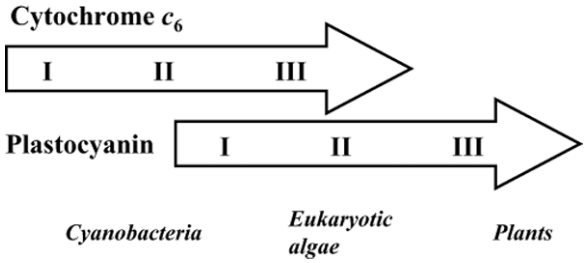

Fig. 3. Scheme showing the evolutionary transition from cytochrome c_6 to plastocyanin in different photosynthetic organisms. The kinetic mechanism of PS I reduction by either cytochrome c_6 or plastocyanin would have evolved from type I to type II and III.

repulsion (Hervás et al., 1994). The Type II model is exhibited by some other cyanobacteria, in which the observed transient complex can be either electrostatic (most cases) or hydrophobic (*Prochlorothrix hollandica* plastocyanin) (Navarro et al., 2001b). Finally, the Type III model is mostly shown by eukaryotic organisms — and some cyanobacteria with positively charged donor proteins (see below) — in which the intermediate complex is first formed by electrostatic attractive forces and further rearranged to establish a hydrophobic interface and accommodate the two redox centers in the right way as to allow a fast electron transfer (Hervás et al., 1995).

The evolutionary story would start with the ancient donor, the heme protein. So the interaction with PS I was first optimized with cyanobacterial cytochrome c_6, which follows a reaction mechanism ranging from Types I to III, whereas cyanobacterial plastocyanins follow a Type I model with no kinetically detectable complex formation (Díaz-Quintana et al., 2003; Durán et al., 2004). In most primitive eukaryotes, namely green algae, plastocyanin started to "learn" to play according to the rules of the Type III model up to be even more efficient than cytochrome c_6, which continued on its own way. Finally, in plants cytochrome c_6 lost its original function and plastocyanin definitely replaced the heme protein as the electron donor for PS I (Fig. 3).

The extensive analyses of the effect of ionic strength on the interactions of cytochrome c_6 and plastocyanin with PS I have yielded relevant information on the nature of the forces involved in the different steps of the whole process. In agreement with the changes in electrostatic properties and isoelectric points of the two metalloproteins (see above), the profiles for the ionic strength dependence of the PS I reduction rate constant are practically identical for the two proteins isolated from the same source, but vary drastically

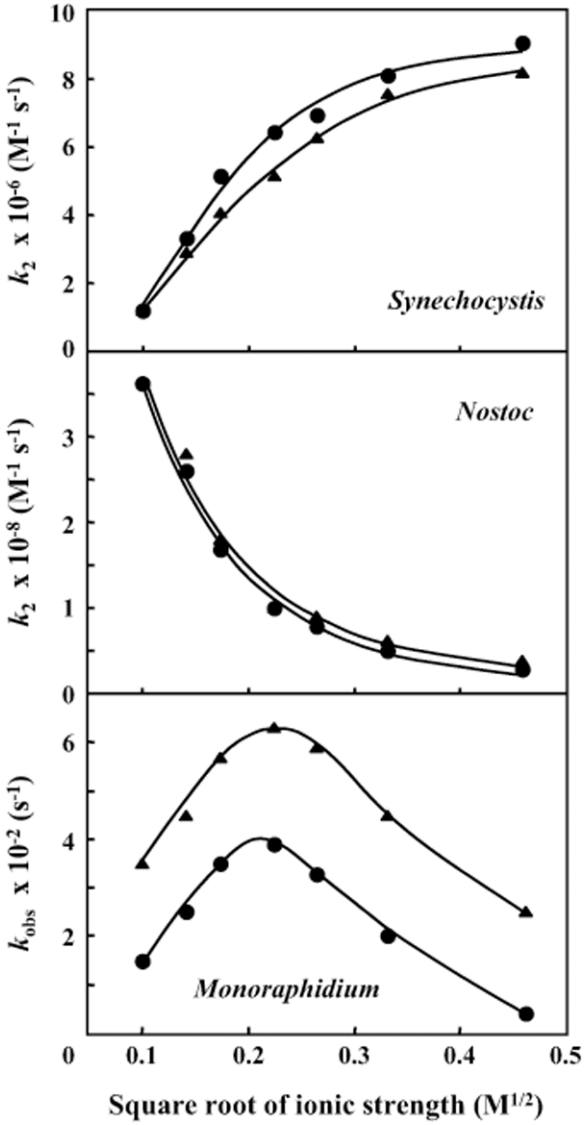

Fig. 4. Dependence on ionic strength of the second-order rate constant (k_2) and the observed rate constant (k_{obs}) for the reduction of PS I by cytochrome c_6 (circles) and plastocyanin (triangles) in *Synechocystis*, *Nostoc* and *Monoraphidium*. In all cases, the ionic strength was adjusted by adding small amounts of a concentrated NaCl solution. The continuous lines correspond to the theoretical fits of experimental data according to the formalism developed by Watkins et al. (1994).

from one organism to another (Fig. 4). In prokaryotes, the ionic strength curves usually vary monotonically although the rate constant can either increase, as is the case with the slightly acidic proteins from *Synechocystis* sp. PCC 6803 and *Phormidium laminosum* (Hervás et al., 1994), or decrease, as is the case with the positively charged donors from *Nostoc* sp. PCC 7119

(Molina-Heredia et al., 1999), with increasing ionic strength. In other cyanobacteria with neutral donor proteins, like *Arthrospira maxima*, the reaction is wholly independent of ionic strength (Hervás et al., 2005). Eukaryotic organisms, by contrast, exhibit a biphasic dependence of the rate constant on ionic strength, with a typical bell-shaped profile (Fig. 4) (Hervás et al., 1995). According to the formalism by Watkins et al. (1994), such a biphasic dependence of eukaryotes could be explained by assuming that the monopolar and dipolar energy terms are of opposite sign but thus is physically unlikely. An alternative explanation is that the electrostatic complex may not be optimized for electron transfer and thus requires certain rearrangement (Type III model) involving hydrophobic interactions.

Hydrophobic forces are non-specific, but ionic bonds exhibit directionality and require matching parts with opposite polarities, just like Velcro fasteners's loops and hooks (Hong, 2004). It is thus the pairing of complementary charges that defines the specificity for molecular recognition. It should also be noted that the asymmetric charge distribution at the protein surface forms an electric dipole (Frazão et al., 1995), with the interaction of two encountering electric dipoles helping the approaching proteins align prior to collision. Thus electrostatic interactions would have a double effect: homing (oriented collision) and defining the specificity of transient complex formation (docking) (Hong, 2004). From an evolutionary point of view, it seems that molecular recognition starts as exploration by means of random diffusion and collisions but further switches to a more deterministic search (see below).

When investigating the cross-reactions between cytochrome c_6 and PS I from different cyanobacteria whose donor proteins are either acidic, neutral, or basic, interesting findings on the evolution of the reaction mechanism can be obtained. In fact, the ionic strength dependence profile of the rate constant for PS I reduction is not determined by PS I but cytochrome c_6 (Hervás et al., 2005). In other words, the specific structural features of each cytochrome c_6 molecule are responsible for the differences in reactivity toward PS I, whereas the cyanobacterial photosystems are structurally quite similar to each other and have no significant effect on the kinetic differences. From an evolutionary point of view, this finding speaks in favor of the hypothesis that PS I is less specific in cyanobacteria — in which the interaction area and binding site are still poorly defined — than in eukaryotes (see below).

With regards to the relative involvement of hydrophobic and/or electrostatic forces in driving the interaction between the donor proteins and PS I throughout evolution, it seems to be clear that the electrostatic attractive movement has gradually gained more relevance in determining complex formation from prokaryotes to eukaryotes, but not within the cyanobacterial group. It is noteworthy that such an evolutionary tendency is not related with the global electrostatic charge of the donor proteins: Both *Arthrospira maxima* cytochrome c_6, which is neutral, and *Prochlorothrix hollandica* plastocyanin, which is a basic protein, interact with PS I by means of hydrophobic forces (Navarro et al., 2001b). We can thus conclude that the predominant use of electrostatic or hydrophobic interactions by the cyanobacterial heme and copper proteins has been evolutionarily driven by environmental factors like temperature, ionic strength, pH, and others.

C. Improvement in Specificity and Efficiency

A number of relevant questions can be addressed when comparing the kinetics of PS I reduction in eukaryotic and prokaryotic organisms: Is the reaction mechanism really different? If the answer is yes, is it due to structural differences? If also yes, could they have any evolutionary implications?

A plausible proposal is that cytochrome c_6 was first "discovered" by Nature, when cyanobacteria started to perform oxygenic-photosynthesis, and its redox interactions with PS I were gradually optimized with time. In seeking for the highest efficiency, the structural core of the heme protein was well preserved along evolution but its surface properties were modified to better recognize and react with the chlorophyll-containing photosystem. The large number of differently evolved cyanobacterial organisms is today reflected by the ample variety we observe in the surface properties of cytochromes c_6 (and plastocyanins). In fact, the interaction area of cyanobacterial PS I is poorly defined, thus consisting of a lumenal region formed by the H loop of the PsaB subunit with some negative residues (Sun et al., 1999; Fromme et al., 2001; Navarro et al., 2001a), whereas the PsaF subunit — which is required for the efficient binding of plastocyanin in plants — does not play any functional role (Chitnis et al., 1991; Xu et al., 1994).

As the primitive cyanobacterial PS I is able to work at a reasonable efficiency, by means of repulsive or attractive interactions with acidic, basic, or even neutral donor proteins, it can be inferred that the hydrophobic patch was developed in cytochrome c_6 and plastocyanin from the very beginning, whereas the electrostatic patch was elaborated later on. The further

evolutionary steps to improve the whole process in eukaryotic organisms would have involved a series of concerted modifications not only in PS I but also in the two donor proteins. On one hand, cytochrome c_6 and plastocyanin would acquire a well-defined negatively charged patch for the electrostatic interaction with PS I. The relevance of such area becomes evident when comparing the kinetics of PS I reduction by plastocyanin from ferns, in which the acidic residues are shifted toward the north site – and plants: the fern system lacks the fast phase of electron transfer and follows a type II kinetic model (Navarro et al., 2004). On the other hand, the PsaF subunit of PS I would develop a lysine-rich (positively charged) patch that could serve as an electrostatically complementary site for binding of the donor protein (Haehnel et al., 1980; Hippler et al., 1997; Sommer et al., 2002), thereby increasing the specificity and efficiency of the eukaryotic systems. Hippler et al. (1999) have modified the PsaF subunit of cyanobacterial PS I by inserting the typical eukaryotic lysine-rich patch, so making the membrane complex recognize and interact efficiently with the eukaryotic donor proteins.

V. Evolution of the Donor Proteins in Plants

It seems that it is the whole process of PS I reduction by either plastocyanin or cytochrome c_6 that has experienced a long evolutionary development involving many structure-based functional changes. In short, the most interesting evolutionary aspects concern the molecular progression which has been mainly convergent (two different proteins adapting to each other to play the same role), but also divergent (the two donor proteins have independently evolved from one organism to another) and parallel (cytochrome c_6 and plastocyanin have accordingly progressed within each organism). The evolutionary development would be linearly aimed at optimizing the electron transfer efficiency, but it should simultaneously have to overcome a series of drawbacks coming from environmental changes. The process has thus leaded to the enhancement of the kinetic behavior, as well as to the definite substitution of cytochrome c_6 by plastocyanin in plants.

For many years, it was widely accepted that plants had lost cytochrome c_6 after living in an environment where copper never is a limiting nutrient, whereas cyanobacteria and green algae would have preserved the capacity to synthesize the heme and copper proteins to tune their metabolism to changing metal bioavailabilities in lakes, rivers, and seas. In 2002, however, two independent groups detected the presence of a cytochrome c_6-like protein in plants (Gupta et al., 2002; Wastl et al., 2002), and a lively debate was launched (Molina-Heredia et al., 2003; Weigel et al., 2003a,b; Wastl et al., 2004a).

A. Cytochrome c_6-like Protein in Plants

In the light of the analysis of cDNA libraries from nonphotosynthetic tissues, the ETS sequences of a cytochrome c_6-like protein in several plants were reported (Wastl et al., 2002). The sequence comparison revealed an additional stretch of 12 amino acids that is highly conserved in the plant protein but absent in all known sequences of cyanobacterial and algal cytochrome c_6, thereby suggesting that such a modified plant heme protein would have lost its original function as electron donor to PS I. On the other hand, Gupta et al. (2002) found a cytochrome c_6-like protein in *Arabidopsis thaliana* when screening for proteins interacting with inmunophilins, and performed a series of genetic and biochemical analyses to demonstrate its capacity to shuttle electrons between cytochrome b_6f and PS I.

The structural and functional comparison of *Arabidopsis* cytochrome c_6-like protein with *Arabidopsis* plastocyanin, and also with *Monoraphidium braunii* cytochrome c_6 allowed us to conclude unequivocally that the heme-protein cannot play in plants the same physiological role as plastocyanin (Molina-Heredia et al., 2003). This assessment was in part attained from the physicochemical features of *Arabidopsis* cytochrome c_6-like protein, but also from its lack of reactivity toward PS I. With a value of 140 mV at pH 7, the midpoint redox potential of *Arabidopsis* cytochrome c_6-like protein is ca. 200 mV lower than that of algal cytochrome c_6 (ca. 350 mV), and so it is thermodynamically incompetent to be efficiently reduced by cytochrome f, with a redox potential of 320 mV (Metzger et al., 1995). Even though *Arabidopsis* cytochrome c_6-like protein could still donate electrons to PS I, the laser flash-induced kinetic analysis demonstrated its lack of reactivity toward the photosystem (Molina-Heredia et al., 2003).

The same conclusion was further inferred from genetic analyses by Weigel et al. (2003b), who reported that the simultaneous mutation of the two plastocyanin-coding genes in *Arabidopsis* promotes a complete blockage of light-driven electron transport in spite of the presence of a functional cytochrome c_6-like protein. Because the function of this cytochrome c_6-like protein of *Arabidopsis* obviously differs from that of cytochrome c_6 from cyanobacteria and algae, its

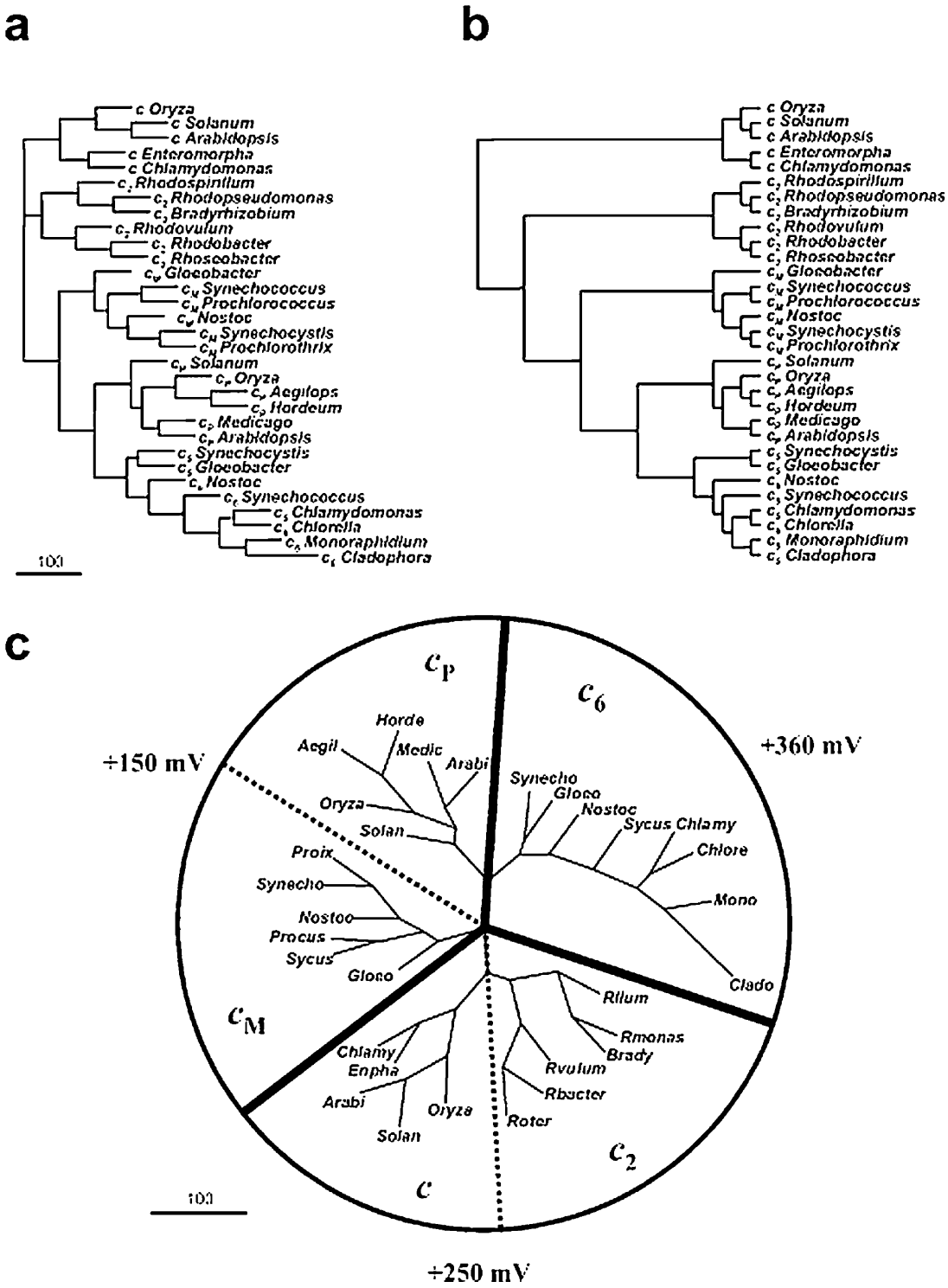

Fig. 5. Phylogenetic trees of soluble monoheme cytochromes with His-Met iron axial coordination in photosynthetic organisms. (A) Rooted tree using respiratory cytochrome *c* as outgroup. (B) Tree drawn as a rectangular cladogram. (C) Radial unrooted tree, in which the bold lines divide the proteins in three major groups according to its redox potential value at pH 7, as indicated, and the dashed lines separate subgroups of proteins inside the same major group according to their typical classification. The trees were constructed by protein maximum likelihood with PROTML (MOLPHY). Branch lengths reflect the estimated number of substitutions/100 sites. Aegil (*Aegilops*), Arabi (*Arabidopsis*), Brady (*Bradyrhizobium*), Chlamy (*Chlamydomonas*), Chlore (*Chlorella*), Clado (*Cladophora*), Enpha (*Enteromorpha*), Gloeo (*Gloeobacter*), Horde (*Hordeum*), Medic (*Medicago*), Mono (*Monoraphidium*), Nostoc (*Nostoc*), Oryza (*Oryza*), Procus (*Prochlorococcus*), Proix (*Prochlorothrix*), Rbacter (*Rhodobacter*), Rllum (*Rhodospirillum*), Rmonas (*Rhodopseudomonas*), Roter (*Rhoseobacter*), Rvulum (*Rhodovulum*), Solan (*Solanum*), Sycus (*Synechococcus*), Synecho (*Synechocystis*).

designation as cytochrome c_6 could be misleading and so the protein will be hereinafter called "cytochrome c_P" (the subscript "P" refer to plants) until its biochemical function is clarified.

The differences between cytochrome c_P and cyanobacterial and algal cytochrome c_6 were first ascribed to the 12 amino acid extra loop of the plant protein (see above). Notwithstanding, we have recently reported that a mutant form of *Arabidopsis* cytochrome c_P in which the entire extension was deleted is still incompetent to transfer electrons to PS I, concluding that the sequence extension in the plant protein has a function that is not yet identified (Wastl et al., 2004a).

As plant cytochrome c_P can interact with chloroplast immunophilin and its extra loop contains two cysteine residues, some authors have proposed that it could serve a regulatory function (Wastl et al., 2002; Weigel et al., 2003a). Whatever the physiological role of plant cytochrome c_P is, the question on its structural and evolutionary relations to algal and cyanobacterial cytochrome c_6 remains unanswered: Is plant cytochrome c_P another member of the cytochrome c_6 family or does it belong to a new group of heme proteins?

B. Where Does Plant Cytochrome c_P Come From?

Preliminary phylogenetic analyses performed by Weigel et al. (2003b) suggested that plant cytochrome c_P is distantly related to cytochrome c_6 from cyanobacteria and green algae, but has diversified in sequence and acquired a new function, other than transferring electrons to PS I.

In order to elucidate its evolutionary origin, we have compared the amino acid sequences of plant cytochrome c_P with those of the four other soluble monoheme cytochromes with His-Met axial metal coordination of photosynthetic organisms: cytochrome c_2 (nonoxygenic bacteria), cytochrome c_M (cyanobacteria), cytochrome c_6 (cyanobacteria and green algae), and respiratory cytochrome c (algal and plant mitochondria). As can be seen in Fig. 5A and B, all plant cytochrome c_P proteins constitute by themselves a new clade as they are all in a single branch that is independent not only of algal and cyanobacterial cytochrome c_6, but also of the other heme proteins. Cytochrome c_6 seems indeed to sequentially evolve in a linear branch from prokaryotes to eukaryotic algae, whereas plant cytochrome c_P would follow another pathway that had previously diverged from cytochrome c_6. This is also in agreement with the different physicochemical properties of cytochromes c_6 and c_P (Molina-Heredia et al., 2003; Wastl et al., 2004a), and so we can conclude that cytochrome c_P is a "novel" heme protein of plants.

When the five c-type cytochromes from photosynthetic organisms are classified according to their respective redox potential values (Fig. 5C), plant cytochrome c_P is surprisingly placed in the same group as cytochrome c_M (E_m, pH 7, ca. 150 mV) (Molina-Heredia et al., 2002), but cytochrome c_6 constitutes an independent group (E_m, pH 7, ca. 350 mV). Along with the phylogenetic data, this finding suggests that plant cytochrome c_P could be evolutionarily closer to cyanobacterial cytochrome c_M and that they could both be functionally related as well.

VI. Addendum

After submission of this manuscript, Wastl et al. (2004b) reported the presence of two different genes in the eukaryotic green alga *Chlamydomonas reinhardtii*, one coding for cytochrome c_6 and the other coding for a heme protein which corresponds to the herein called cytochrome c_P.

Acknowledgments

The authors thank their co-workers and collaborators, listed in the references, for their contributions to this research. Thanks are also due to the Spanish Ministry of Education and Science, Andalusian Government and European Commission for providing financial support.

References

Albarrán C, Navarro JA, Molina-Heredia FP, Murdoch PS, De la Rosa MA and Hervás M (2005) Laser flash-induced kinetic analysis of cytochrome *f* oxidation by wild-type and mutant plastocyanin from the cyanobacterium *Nostoc* sp. PCC 7119. Biochemistry 44: 11601–11607

Babu CR, Volkman BF and Bullerjahn GS (1999) NMR solution structure of plastocyanin from the photosynthetic prokaryote *Prochlorothrix hollandica*. Biochemistry 38: 4988–4995

Beißinger M, Sticht H, Sutter M, Ejchart A, Haehnel W and Rosch P (1998) Solution structure of cytochrome c_6 from the thermophilic cyanobacterium *Synechococcus elongatus*. EMBO J 17: 27–36

Berkner LV and Marshall LC (1965) History of major atmospheric components. Proc Natl Acad Sci USA 53: 1215–1225

Cavet JS, Borrelly GPM and Robinson NJ (2003) Zn, Cu and Co in cyanobacteria: selective control of metal availability. FEMS Microbiol Rev 27: 165–181

Chitnis PR, Purvis D and Nelson N (1991) Molecular cloning and targeted mutagenesis of the gene *psa*F encoding subunit

III of photosystem I from the cyanobacterium *Synechocystis* sp. PCC 6803. J Biol Chem 266: 20146–20151

Crichton RR and Pierre JL (2001) Old iron, young copper: from Mars to Venus. Biometals 14: 99–112

Crowley B, Díaz-Quintana A, Molina-Heredia FP, Nieto P, Sutter M, Haehnel W, De la Rosa MA and Ubbink M (2002) The interactions of cyanobacterial cytochrome c_6 and cytochrome f characterized by NMR. J Biol Chem 277: 48685–48689

De la Cerda B, Díaz-Quintana A, Navarro JA, Hervás M and De la Rosa MA (1999) Site-directed mutagenesis of cytochrome c_6 from *Synechocystis* sp. PCC 6803. The heme-protein possesses a negatively charged area that may be isofunctional with the acidic patch of plastocyanin. J Biol Chem 274: 13292–13297

De la Rosa MA, Navarro JA, Díaz-Quintana A, De la Cerda B, Molina-Heredia FP, Balme A, Murdoch PS, Díaz-Moreno I, Durán RV and Hervás M (2002) An evolutionary analysis of the reaction mechanisms of photosystem I reduction by cytochrome c_6 and plastocyanin. Bioelectrochemistry 55: 41–45

Des Marais DJ (1998) Earth's early biosphere. Gravit Space Biol Bull 11: 23–30

Díaz-Moreno I, Díaz-Quintana A, De la Rosa MA and Ubbink M (2005) Structure of the complex between plastocyanin and cytochrome f from the cyanobacterium *Nostoc* sp. PCC 7119 as determined by paramagnetic NMR. J Biol Chem 280: 18908–18915

Díaz-Quintana A, Navarro JA, Hervás M, Molina-Heredia FP, De la Cerda B and De la Rosa MA (2003) A comparative structural and functional analysis of cyanobacterial plastocyanin and cytochrome c_6 as alternative donors to photosystem I. Photosynth Res 75: 97–110

Dikiy A, Carpentier W, Vandenberghe I, Borsari M, Safarov N, Dikaya A, Beeumen JV and Ciurli S (2002) Structural basis for the molecular properties of cytochrome c_6. Biochemistry 41: 14689–14699

Durán RV, Hervás M, De la Rosa MA and Navarro JA (2004) The efficient functioning of photosynthesis and respiration in *Synechocystis* sp. PCC 6803 strictly requires the presence of either cytochrome c_6 or plastocyanin. J Biol Chem 279: 7229–7233

Frazão C, Soares CM, Carrondo MA, Pohl E, Dauter Z, Wilson KS, Hervás M, Navarro JA, De la Rosa MA and Sheldrick GM (1995) *Ab initio* determination of the crystal structure of cytochrome c_6 and comparison with plastocyanin. Structure 3: 1159–1169

Fromme P, Jordan P and Krauß N (2001) Structure of photosystem I. Biochim Biophys Acta 1507: 5–31

Gupta R, He Z and Luan S (2002) Functional relationship of cytochrome c_6 and plastocyanin in *Arabidopsis*. Nature 30: 567–571

Guss JM and Freeman HC (1983) Structure of oxidized poplar plastocyanin at 1.6 Å resolution. J Mol Biol 169: 521–563

Guss JM, Harrowell PR, Murata M, Norris VA and Freeman HC (1986) Crystal structure analyses of reduced (CuI) poplar plastocyanin at six pH values. J Mol Biol 192: 361–387

Haehnel W, Hesse V and Pröpper A (1980) Electron transfer from plastocyanin to P700. Function of a subunit of photosystem I reaction center. FEBS Lett 111: 79–82

Hart SE, Schlarb-Ridley B, Delon C, Bendall DS and Howe CJ (2003) Role of charges of cytochrome f from the cyanobacterium *Phormidium laminosum* in its interaction with plastocyanin. Biochemistry 42: 4829–4836

Hervás M, Ortega JM, Navarro JA, De la Rosa MA and Bottin H (1994) Laser flash kinetic analysis of *Synechocystis* PCC 6803 cytochrome $c_6$and plastocyanin oxidation by photosystem I. Biochim Biophys Acta 1184: 235–241

Hervás M, Navarro JA, Díaz A, Bottin H and De la Rosa MA (1995) Laser-flash kinetic analysis of the fast electron transfer from plastocyanin and cytochrome c_6 to photosystem I. Experimental evidence on the evolution of the reaction mechanism. Biochemistry 34: 11321–11326

Hervás M, Navarro JA and De la Rosa MA (2003) Electron transfer between soluble proteins and membrane complexes in photosynthesis. Accounts Chem Res 36: 798–805

Hervás M, Díaz-Quintana A, Kerfeld CA, Krogmann DW, De la Rosa MA and Navarro JA (2005) Cyanobacterial photosystem I lacks specificity in its interaction with cytochrome c_6 electron donors. Photosynth Res 83: 329–333

Hippler M, Drepper F, Farah J and Rochaix JD (1997) Fast electron transfer from cytochrome c_6 and plastocyanin to photosystem I of *Chlamydomonas reinhardtii* requires PsaF. Biochemistry 36: 6343–6349

Hippler M, Drepper F, Rochaix JD and Mühlenhoff U (1999) Insertion of the N-terminal part of PsaF from *Chlamydomonas reinhardtii* into photosystem I from *Synechococcus elongatus* enables efficient binding of algal plastocyanin and cytochrome c_6. J Biol Chem 274: 4180–4188

Ho KK and Krogmann DW (1984) Electron donors to P700 in cyanobacteria and algae. An instance of unusual genetic variability. Biochim Biophys Acta 766: 310–316

Hong FT (2004) Molecular electronic switches in photobiology. In: Horspool W and Lenci F (eds) Handbook of Organic Photochemistry and Photobiology, 2nd Edition, Chapter 134. CRC Press, Boca Raton

Hope AB (2000) Electron transfer amongst cytochrome f, plastocyanin and photosystem I: kinetics and mechanisms. Biochim Biophys Acta 1456: 5–26

Kasting JF and Siefert JL (2003) Life and the evolution of Earth's atmosphere. Science 296: 1066–1068

Kerfeld CA, Anwar HP, Interrante R, Merchant S and Yeates TO (1995) The structure of chloroplast cytochrome c_6 at 1.9 Å resolution: evidence for functional oligomerization. J Mol Biol 250: 627–647

Kohzuma T, Inoue T, Yoshizaki F, Sasakawa Y, Onodera K, Nagatomo S, Kitagawa T, Uzawa S, Isobe Y, Sugimura Y, Gotowda M and Kai Y (1999) The structure and unusual pH dependence of plastocyanin from the fern *Dryopteris crassirhizoma*. The protonation of an active site histidine is hindered by π–π interactions. J Biol Chem 274: 11817–11823

Lee BH, Hibino T, Takabe T, Weisbeek PJ and Takabe T (1995) Site-directed mutagenetic study on the role of negative patches on silene plastocyanin in the interactions with cytochrome f and photosystem I. J Biochem Tokyo 117: 1209–1217

Macalady J and Banfield JF (2003) Molecular geomicrobiology: genes and geochemical cycling. Earth Planet Sci Lett 209: 1–17

Mathis P and Sétif P (1981) Near infra-red absorption spectra of the chlorophyll *a* cations and triplet state *in vitro* and *in vivo*. Isr J Chem 21: 316–320

Metzger SU, Pakrasi HB and Whitmarsh J (1995) Characterization of a double deletion mutant that lacks cytochrome c_6 and

cytochrome c_M in *Synechocystis* 6803. In: Mathis P (ed) Photosynthesis: From Light to Biosphere, pp 823–826. Kluwer Academic Publishers, Dordrecht

Molina-Heredia FP, Díaz-Quintana A, Hervás M, Navarro JA and De la Rosa MA (1999) Site-directed mutagenesis of cytochrome c_6 from *Nostoc* species PCC 7119. Identification of surface residues of the hemeprotein involved in photosystem I reduction. J Biol Chem 274: 33565–33570

Molina-Heredia FP, Hervás M, Navarro JA and De la Rosa MA (2001) A single arginyl residue in plastocyanin and cytochrome c_6 from the cyanobacterium *Anabaena* sp. PCC 7119 is required for efficient reduction of photosystem I. J Biol Chem 276: 601–605

Molina-Heredia FP, Balme A, Hervás M, Navarro JA and De la Rosa MA (2002) A comparative structural and functional analysis of cytochrome c_M cytochrome c_6 and plastocyanin from the cyanobacterium *Synechocystis* sp. PCC 6803. FEBS Lett 517: 50–54

Molina-Heredia FP, Wastl J, Navarro JA, Bendall DS, Hervás M, Howe CJ and De la Rosa MA (2003) Photosynthesis: a new function for an old cytochrome? Nature 424: 33–34

Navarro JA, Hervás M and De la Rosa MA (1997) Co-evolution of cytochrome c_6 and plastocyanin, mobile proteins transferring electrons from cytochrome $b_6 - f$ to photosystem I. J Biol Inorg Chem 2: 11–22

Navarro JA, Hervás M, Sun J, De la Cerda B, Chitnis PR and De la Rosa MA (2001a) Negatively charged residues in the H loop of PsaB subunit in photosystem I from *Synechocystis* sp. PCC 6803 appear to be responsible for electrostatic repulsions with plastocyanin. Photosynth Res 65: 63–68

Navarro JA, Myshkin E, De la Rosa MA, Bullerjahn GS and Hervás M (2001b) The unique proline of the *Prochlorothrix hollandica* plastocyanin hydrophobic patch impairs electron transfer to photosystem I. J Biol Chem 276: 37501–37505

Navarro JA, Lowe C, Amons R, Kohzuma T, Canters G, De la Rosa MA, Ubbink M and Hervás M (2004) Functional characterization of the evolutionarily divergent fern plastocyanin. Eur J Biochem 271: 3449–3456

Newman DK and Banfield JF (2002) Geomicrobiology: how molecular-scale interactions underpin biogeochemical systems. Science 296: 1071–1077

Ochiai EI (1983) Copper and the biological evolution. Biosystems 16: 81–86

Peschek G (1999) Photosynthesis and respiration of cyanobacteria. In: Peschek GA, Loeffelhord W and Schmetterer G (eds) The Phototrophic Prokaryotes, pp 201–209. Kluwer Academic/Plenum Publishers, New York

Romero A, De la Cerda B, Varela PF, Navarro, JA, Hervás M and De la Rosa MA (1998) The 2.15 Å crystal structure of a triple mutant plastocyanin from the cyanobacterium *Synechocystis* sp. PCC 6803. J Mol Biol 275: 327–336

Sawaya MR, Krogmann DW, Serag A, Ho KK, Yeates TO and Kerfeld CA (2001) Structures of cytochrome *c*-549 and cytochrome c_6 from the cyanobacterium *Arthrospira maxima*. Biochemistry 40: 9215–9225

Sigfridsson K (1998) Plastocyanin, an electron-transfer protein. Photosynth Res 57: 1–28

Sigfridsson K, Hansson Ö, Karlsson BG, Baltzer L, Nordling M and Lundberg LG (1995) Spectroscopic and kinetic characterization of the spinach plastocyanin mutant Tyr83-His: a histidine residue with a high pK_a value. Biochim Biophys Acta 1228: 28–36

Sommer F, Drepper F and Hippler M (2002) The luminal helix l of PsaB is essential for recognition of plastocyanin or cytochrome c_6 and fast electron transfer to photosystem I in *Chlamydomonas reinhardtii*. J Biol Chem 277: 6573–6581

Sun J, Xu W, Hervás M, Navarro JA, De la Rosa MA and Chitnis PR (1999) Oxidising side of the cyanobacterial photosystem I. Evidence for interaction between the electron donor proteins and a luminal surface helix of the PsaB subunit. J Biol Chem 274: 19048–19054

Ubbink M, Ejdebäck M, Karlsson BG and Bendall DS (1998) The structure of the complex of plastocyanin and cytochrome *f* determined by paramagnetic NMR and restrained rigid-body molecular dynamics. Structure 6: 323–335

Ullmann GM, Hauswald M, Jensen A, Kostic NM and Knapp E-W (1997) Comparison of the physiologically equivalent proteins cytochrome c_6 and plastocyanin on the basis of their electrostatic potentials. Tryptophan 63 in cytochrome $c_6$may be isofunctional with tyrosine 83 in plastocyanin. Biochemistry 36: 16187–16196

Wastl J, Bendall DS and Howe CJ (2002) Higher plants contain a modified cytochrome c_6. Trends Plant Sci 7: 244–245

Wastl J, Molina-Heredia FP, Hervás M, Navarro JA, De la Rosa MA, Bendall DS and Howe CJ (2004a) Redox properties of *Arabidopsis* cytochrome c_6 are independent of the loop extension specific to higher plants. BBA-Bioenergetics 1657: 115–120

Wastl J, Purton S, Bendall DS and Howe CJ (2004b) Two forms of cytochrome c_6 in a single eukaryote. Trends Plant Sci 9: 474–476

Watkins JA, Cusanovich MA, Meyer TE and Tollin G (1994) A "parallel plate" electrostatic model of bimolecular rate constants applied to electron transfer proteins. Protein Sci 3: 2104–2114

Weigel M, Pesaresi P and Leister D (2003a) Tracking the function of the cytochrome c_6-like protein in higher plants. Trends Plant Sci 8: 513–517

Weigel M, Varotto C, Pesaresi P, Finazzi G, Rappaport F, Salamini F and Leister D (2003b) Plastocyanin is indispensable for photosynthetic electron flow in *Arabidopsis* thaliana. J Biol Chem 15: 31286–31289

Williams RJP and Fraústo da Silva JJR (1997) The Natural Selection of the Chemical Elements. Oxford University Press, Oxford

Wood PM (1978) Interchangeable copper and iron proteins in algal photosynthesis. Studies on plastocyanin and cytochrome *c*-552 in *Chlamydomonas*. Eur J Biochem 87: 9–19

Xu Q, Chitnis VP, Yu L and Chitnis PR (1994) Function and organization of photosystem I in a cyanobacterial mutant strain that lacks PsaF and PsaJ subunits. J Biol Chem 269: 3205–3211

Subject Index

Organism Index

Mutant Index

Gene and Gene Product Index

Series editor: Govindjee, University of Illinois, Urbana, Illinois, U.S.A.

1. D.A. Bryant (ed.): *The Molecular Biology of Cyanobacteria*. 1994 ISBN Hb: 0-7923-3222-9; Pb: 0-7923-3273-3
2. R.E. Blankenship, M.T. Madigan and C.E. Bauer (eds.): *Anoxygenic Photosynthetic Bacteria.* 1995 ISBN Hb: 0-7923-3681-X; Pb: 0-7923-3682-8
3. J. Amesz and A.J. Hoff (eds.): *Biophysical Techniques in Photosynthesis.* 1996 ISBN 0-7923-3642-9
4. D.R. Ort and C.F. Yocum (eds.): *Oxygenic Photosynthesis: The Light Reactions.* 1996 ISBN Hb: 0-7923-3683-6; Pb: 0-7923-3684-4
5. N.R. Baker (ed.): *Photosynthesis and the Environment.* 1996 ISBN 0-7923-4316-6
6. P.-A. Siegenthaler and N. Murata (eds.): *Lipids in Photosynthesis: Structure, Function and Genetics.* 1998 ISBN 0-7923-5173-8
7. J.-D. Rochaix, M. Goldschmidt-Clermont and S. Merchant (eds.): *The Molecular Biology of Chloroplasts and Mitochondria in Chlamydomonas.* 1998 ISBN 0-7923-5174-6
8. H.A. Frank, A.J. Young, G. Britton and R.J. Cogdell (eds.): *The Photochemistry of Carotenoids.* 1999 ISBN 0-7923-5942-9
9. R.C. Leegood, T.D. Sharkey and S. von Caemmerer (eds.): *Photosynthesis: Physiology and Metabolism.* 2000 ISBN 0-7923-6143-1
10. B. Ke: *Photosynthesis: Photobiochemistry and Photobiophysics.* 2001 ISBN 0-7923-6334-5
11. E.-M. Aro and B. Andersson (eds.): *Regulation of Photosynthesis.* 2001 ISBN 0-7923-6332-9
12. C.H. Foyer and G. Noctor (eds.): *Photosynthetic Nitrogen Assimilation and Associated Carbon and Respiratory Metabolism.* 2002 ISBN 0-7923-6336-1
13. B.R. Green and W.W. Parson (eds.): *Light-Harvesting Antennas in Photosynthesis.* 2003 ISBN 0-7923-6335-3
14. A.W.D. Larkum, S.E. Douglas and J.A. Raven (eds.): *Photosynthesis in Algae.* 2003 ISBN 0-7923-6333-7
15. D. Zannoni (ed.): *Respiration in Archaea and Bacteria*. Diversity of Prokaryotic Electron Transport Carriers. 2004 ISBN 1-4020-2001-5
16. D. Zannoni (ed.): *Respiration in Archaea and Bacteria*. Diversity of Prokaryotic Respiratory Systems. 2004 ISBN 1-4020-2002-3
17. D. Day, A.H. Millar and J. Whelan (eds.): *Plant Mitochondria*. From Genome to Function. 2004 ISBN 1-4020-2399-5
18. H. Lambers and M. Ribas-Carbo (eds.): *Plant Respiration*. From Cell to Ecosystem. 2005 ISBN 1-4020-3588-8
19. G. Papageorgiou and Govindjee (eds.): *Chlorophyll a Fluorescence*. A Signature of Photosynthesis. 2004 ISBN 1-4020-3217-X
20. Govindjee, J.T. Beatty, H. Gest and J.F. Allen (eds.): *Discoveries in Photosynthesis*. 2005 ISBN 1-4020-3323-0
21. B. Demmig-Adams, W.W. Adams III and A. Mattoo (eds.): *Photoprotection, Photoinhibition, Gene Regulation, and Environment*. 2005 ISBN 1-4020-3564-0

22. T.J. Wydrzynski and K. Satoh (eds.): *Photosystem II*. The Light-Driven Water:Plastoquinone Oxidoreductase. 2005 ISBN 1-4020-4249-3
23. R.R. Wise and J.K. Hoober (eds.): *The Structure and Function of Plastids*. 2006 ISBN 1-4020-4060-1
24. J.H. Golbeck (ed.): *Photosystem I*. The Light-Driven Plastocyanin:Ferrodoxin Oxidoreductase. 2006 ISBN 1-4020-4255-8
25. B. Grimm, R.J. Porra, W. Rüdiger and H. Scheer (eds.): *Chlorophylls and Bacteriochlorophylls*. Biochemistry, Biophysics, Functions and Applications. 2006 ISBN 1-4020-4515-8

For further information about the series and how to order please visit our Website
http://www.springer.com